NAS 1.9/4:33/10
RED SEAL

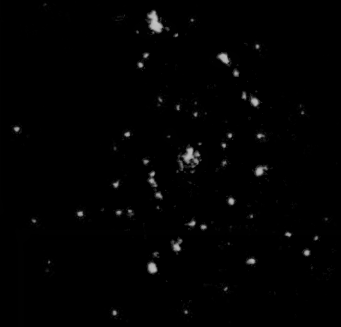

An Abstract Journal

NASA

Volume 33, Number 10
October 1995
N95-28678 to N95-30357

The NASA STI Office ... in Profile

Since its founding, NASA has been dedicated to the advancement of aeronautics and space science. The NASA Scientific and Technical Information (STI) Office plays a key part in helping NASA maintain this important role.

The NASA STI Office provides access to the NASA STI Database, the largest collection of aeronautical and space science STI in the world. The Office is also NASA's institutional mechanism for disseminating the results of its research and development activities.

Specialized services that help round out the Office's diverse offerings include creating custom thesauri, translating material to or from 34 foreign languages, building customized databases, organizing and publishing research results ... even providing videos.

For more information about the NASA STI Office, you can:

- **Phone** the NASA Access Help Desk at (301) 621-0390
- **Fax** your question to the NASA Access Help Desk at (301) 621-0134
- **E-mail** your question via the **Internet** to help@sti.nasa.gov
- **Write** to:

NASA Access Help Desk
NASA Center for AeroSpace Information
800 Elkridge Landing Road
Linthicum Heights, MD 21090-2934

DETROIT PUBLIC LIBRARY
3 5674 02477634 7

Scientific and Technical Aerospace Reports

STAR

Scientific a... ***(STAR)***, is published each month as a major product of the NASA Scientific and Technical Information (STI) Office.

Inside this issue you will find:

- **Front Matter** containing a typical citation and abstract sample explaining the standard format, including codes for ordering reports
- **An Abstract Section** containing citations and abstracts of reports and publications that provide comprehensive coverage of worldwide aerospace-related topics including aeronautics and space science technology. *STAR* lists published and publicly available reports entered into the NASA STI Database during the four weeks preceding publication of this issue. These citations and abstracts are listed by subject categories.
- **An Index Section**
  - Subject
  - Personal author
  - Corporate source
  - Contract number
  - Report number
- **An Appendix** containing a guide for ordering cited reports, registering with the NASA STI Office, and using the available products and services. Additionally, price schedules, phone numbers, and addresses are included in this information packed section.

NASA also sponsors the companion journal, *NASA Open Volumes on Aerospace (NOVA)*, which lists abstracts of the open literature on aerospace subjects available worldwide. *NOVA* is for internal NASA use only, available from the NASA Center for AeroSpace Information (CASI).

Entries found in *STAR* are available through the NASA online retrieval service, RECON.

The NASA STI Office gathers information through national and international agreements and exchanges and makes this information available to the NASA community and to the public in many forms through various outlets.

For additional information on the NASA STI Office, call the NASA Access Help Desk at (301) 621-0390, or write to:

NASA Center for AeroSpace Information
800 Elkridge Landing Road
Linthicum Heights, Maryland 21090-2934

US ISSN 0036-8741

The New NASA Video Catalog is Here

Free!

To order your free copy call
the NASA Access Help Desk at
(301) 621-0390 or
fax to (301) 621-0134 or
e-mail to helpdesk@sti.nasa.gov

EXPLORE THE UNIVERSE

This publication was prepared by the NASA Center for AeroSpace Information,
800 Elkridge Landing Road, Linthicum Heights, MD 21090-2934, (301) 621-0390.

Volume 33 Number 10 / October 1995

TABLE OF CONTENTS

AERONAUTICS For related information see also *Astronautics.*

01 AERONAUTICS (GENERAL) **2477**

02 AERODYNAMICS **2477**
Includes aerodynamics of bodies, combinations, wings, rotors, and control surfaces; and internal flow in ducts and turbomachinery. For related information see also *34 Fluid Mechanics and Heat Transfer.*

03 AIR TRANSPORTATION AND SAFETY **2492**
Includes passenger and cargo air transport operations; and aircraft accidents. For related information see also *16 Space Transportation* and *85 Urban Technology and Transportation.*

04 AIRCRAFT COMMUNICATIONS AND NAVIGATION **2493**
Includes digital and voice communication with aircraft; air navigation systems (satellite and ground based); and air traffic control. For related information see also *17 Space Communications, Spacecraft Communications, Command and Tracking* and *32 Communications and Radar.*

05 AIRCRAFT DESIGN, TESTING AND PERFORMANCE **2495**
Includes aircraft simulation technology. For related information see also *18 Spacecraft Design, Testing and Performance* and *39 Structural Mechanics.* For land transportation vehicles see *85 Urban Technology and Transportation.*

06 AIRCRAFT INSTRUMENTATION **2499**
Includes cockpit and cabin display devices; and flight instruments. For related information see also *19 Spacecraft Instrumentation* and *35 Instrumentation and Photography.*

07 AIRCRAFT PROPULSION AND POWER **2500**
Includes prime propulsion systems and systems components, e.g., gas turbine engines and compressors; and onboard auxiliary power plants for aircraft. For related information see also *20 Spacecraft Propulsion and Power, 28 Propellants and Fuels,* and *44 Energy Production and Conversion.*

08 AIRCRAFT STABILITY AND CONTROL **2501**
Includes aircraft handling qualities; piloting; flight controls; and autopilots. For related information see also *05 Aircraft Design, Testing and Performance.*

09 RESEARCH AND SUPPORT FACILITIES (AIR) **2502**
Includes airports, hangars and runways; aircraft repair and overhaul facilities; wind tunnels; shock tubes; and aircraft engine test stands. For related information see also *14 Ground Support Systems and Facilities (Space).*

ASTRONAUTICS For related information see also *Aeronautics.*

12 ASTRONAUTICS (GENERAL) **2503**
For extraterrestrial exploration see *91 Lunar and Planetary Exploration.*

13 ASTRODYNAMICS **2503**
Includes powered and free-flight trajectories; and orbital and launching dynamics.

14 GROUND SUPPORT SYSTEMS AND FACILITIES (SPACE) ..... **N.A.**
Includes launch complexes, research and production facilities; ground support equipment, e.g., mobile transporters; and simulators. For related information see also *09 Research and Support Facilities (Air).*

15 LAUNCH VEHICLES AND SPACE VEHICLES **2504**
Includes boosters; operating problems of launch/space vehicle systems; and reusable vehicles. For related information see also *20 Spacecraft Propulsion and Power.*

16 SPACE TRANSPORTATION **2504**
Includes passenger and cargo space transportation, e.g., shuttle operations; and space rescue techniques. For related information see also *03 Air Transportation and Safety* and *18 Spacecraft Design, Testing and Performance.* For space suits see *54 Man/System Technology and Life Support.*

17 SPACE COMMUNICATIONS, SPACECRAFT COMMUNICATIONS, COMMAND AND TRACKING **2506**
Includes telemetry; space communications networks; astronavigation and guidance; and radio blackout. For related information see also *04 Aircraft Communications and Navigation* and *32 Communications and Radar.*

N.A.—No abstracts were assigned to this category for this issue.

18 SPACECRAFT DESIGN, TESTING AND PERFORMANCE **2506**
Includes satellites; space platforms; space stations; spacecraft systems and components such as thermal and environmental controls; and attitude controls. For life support systems see *54 Man/System Technology and Life Support.* For related information see also *05 Aircraft Design, Testing and Performance, 39 Structural Mechanics,* and *16 Space Transportation.*

19 SPACECRAFT INSTRUMENTATION **2509**
For related information see also *06 Aircraft Instrumentation* and *35 Instrumentation and Photography.*

20 SPACECRAFT PROPULSION AND POWER **2510**
Includes main propulsion systems and components, e.g., rocket engines; and spacecraft auxiliary power sources. For related information see also *07 Aircraft Propulsion and Power, 28 Propellants and Fuels, 44 Energy Production and Conversion,* and *15 Launch Vehicles and Space Vehicles.*

CHEMISTRY AND MATERIALS

23 CHEMISTRY AND MATERIALS (GENERAL) **2511**

24 COMPOSITE MATERIALS **2513**
Includes physical, chemical, and mechanical properties of laminates and other composite materials. For ceramic materials see *27 Nonmetallic Materials.*

25 INORGANIC AND PHYSICAL CHEMISTRY **2530**
Includes chemical analysis, e.g., chromatography; combustion theory; electrochemistry; and photochemistry. For related information see also *77 Thermodynamics and Statistical Physics.*

26 METALLIC MATERIALS **2535**
Includes physical, chemical, and mechanical properties of metals, e.g., corrosion; and metallurgy.

27 NONMETALLIC MATERIALS **2539**
Includes physical, chemical, and mechanical properties of plastics, elastomers, lubricants, polymers, textiles, adhesives, and ceramic materials. For composite materials see *24 Composite Materials.*

28 PROPELLANTS AND FUELS **2548**
Includes rocket propellants, igniters and oxidizers; their storage and handling procedures; and aircraft fuels. For related information see also *07 Aircraft Propulsion and Power, 20 Spacecraft Propulsion and Power,* and *44 Energy Production and Conversion.*

29 MATERIALS PROCESSING **2549**
Includes space-based development of products and processes for commercial application. For biological materials see *55 Space Biology:*

ENGINEERING For related information see also *Physics.*

31 ENGINEERING (GENERAL) **2549**
Includes vacuum technology; control engineering; display engineering; cryogenics; and fire prevention.

32 COMMUNICATIONS AND RADAR **2551**
Includes radar; land and global communications; communications theory; and optical communications. For related information see also *04 Aircraft Communications and Navigation* and *17 Space Communications, Spacecraft Communications, Command and Tracking.* For search and rescue see *03 Air Transportation and Safety,* and *16 Space Transportation.*

33 ELECTRONICS AND ELECTRICAL ENGINEERING **2560**
Includes test equipment and maintainability; components, e.g., tunnel diodes and transistors; microminiaturization; and integrated circuitry. For related information see also *60 Computer Operations and Hardware* and *76 Solid-State Physics.*

34 FLUID MECHANICS AND HEAT TRANSFER **2568**
Includes boundary layers; hydrodynamics; fluidics; mass transfer and ablation cooling. For related information see also *02 Aerodynamics* and *77 Thermodynamics and Statistical Physics.*

35 INSTRUMENTATION AND PHOTOGRAPHY **2582**
Includes remote sensors; measuring instruments and gauges; detectors; cameras and photographic supplies; and holography. For aerial photography see *43 Earth Resources and Remote Sensing.* For related information see also *06 Aircraft Instrumentation* and *19 Spacecraft Instrumentation.*

36 LASERS AND MASERS **2584**
Includes parametric amplifiers. For related information see also *76 Solid-State Physics.*

37 MECHANICAL ENGINEERING **2588**
Includes auxiliary systems (nonpower); machine elements and processes; and mechanical equipment.

38 QUALITY ASSURANCE AND RELIABILITY **2592**
Includes product sampling procedures and techniques; and quality control.

39 STRUCTURAL MECHANICS **2593**
Includes structural element design and weight analysis; fatigue; and thermal stress. For applications see *05 Aircraft Design, Testing and Performance* and *18 Spacecraft Design, Testing and Performance.*

GEOSCIENCES For related information see also *Space Sciences.*

42 GEOSCIENCES (GENERAL) ..... **N.A.**

43 EARTH RESOURCES AND REMOTE SENSING **2598**
Includes remote sensing of earth resources by aircraft and spacecraft; photogrammetry; and aerial photography. For instrumentation see *35 Instrumentation and Photography.*

44 ENERGY PRODUCTION AND CONVERSION **2602**
Includes specific energy conversion systems, e.g., fuel cells; global sources of energy; geophysical conversion; and windpower. For related information see also *07 Aircraft Propulsion and Power, 20 Spacecraft Propulsion and Power,* and *28 Propellants and Fuels.*

45 ENVIRONMENT POLLUTION **2608**
Includes atmospheric, noise, thermal, and water pollution.

46 GEOPHYSICS **2611**
Includes aeronomy; upper and lower atmosphere studies; ionospheric and magnetospheric physics; and geomagnetism. For space radiation see *93 Space Radiation.*

47 METEOROLOGY AND CLIMATOLOGY **2619**
Includes weather forecasting and modification.

48 OCEANOGRAPHY **2628**
Includes biological, dynamic, and physical oceanography; and marine resources. For related information see also *43 Earth Resources and Remote Sensing.*

LIFE SCIENCES

51 LIFE SCIENCES (GENERAL) **2631**

52 AEROSPACE MEDICINE **2633**
Includes physiological factors; biological effects of radiation; and effects of weightlessness on man and animals.

53 BEHAVIORAL SCIENCES **2638**
Includes psychological factors; individual and group behavior; crew training and evaluation; and psychiatric research.

54 MAN/SYSTEM TECHNOLOGY AND LIFE SUPPORT **2640**
Includes human engineering; biotechnology; and space suits and protective clothing. For related information see also *16 Space Transportation.*

55 SPACE BIOLOGY **2642**
Includes exobiology; planetary biology; and extraterrestrial life.

MATHEMATICAL AND COMPUTER SCIENCES

59 MATHEMATICAL AND COMPUTER SCIENCES (GENERAL) ..... **N.A.**

60 COMPUTER OPERATIONS AND HARDWARE **2642**
Includes hardware for computer graphics, firmware, and data processing. For components see *33 Electronics and Electrical Engineering.*

61 COMPUTER PROGRAMMING AND SOFTWARE **2643**
Includes computer programs, routines, algorithms, and specific applications, e.g., CAD/CAM.

62 COMPUTER SYSTEMS **2657**
Includes computer networks and special application computer systems.

63 CYBERNETICS **2661**
Includes feedback and control theory, artificial intelligence, robotics and expert systems. For related information see also *54 Man/System Technology and Life Support.*

64 NUMERICAL ANALYSIS **2668**
Includes iteration, difference equations, and numerical approximation.

65 STATISTICS AND PROBABILITY **2674**
Includes data sampling and smoothing; Monte Carlo method; and stochastic processes.

66 SYSTEMS ANALYSIS **2676**
Includes mathematical modeling; network analysis; and operations research.

67 THEORETICAL MATHEMATICS **2680**
Includes topology and number theory.

PHYSICS For related information see also *Engineering.*

70 PHYSICS (GENERAL) **2680**
For precision time and time interval (PTTI) see *35 Instrumentation and Photography*; for geophysics, astrophysics or solar physics see *46 Geophysics, 90 Astrophysics*, or *92 Solar Physics.*

71 ACOUSTICS **2682**
Includes sound generation, transmission, and attenuation. For noise pollution see *45 Environment Pollution.*

72 ATOMIC AND MOLECULAR PHYSICS **2690**
Includes atomic structure, electron properties, and molecular spectra.

73 NUCLEAR AND HIGH-ENERGY PHYSICS **2695**
Includes elementary and nuclear particles; and reactor theory. For space radiation see *93 Space Radiation.*

74 OPTICS **2696**
Includes light phenomena and optical devices. For lasers see *36 Lasers and Masers.*

75 PLASMA PHYSICS **2703**
Includes magnetohydrodynamics and plasma fusion. For ionospheric plasmas see *46 Geophysics.* For space plasmas see *90 Astrophysics.*

76 SOLID-STATE PHYSICS **2712**
Includes superconductivity. For related information see also *33 Electronics and Electrical Engineering* and *36 Lasers and Masers.*

77 THERMODYNAMICS AND STATISTICAL PHYSICS **2718**
Includes quantum mechanics; theoretical physics; and Bose and Fermi statistics. For related information see also *25 Inorganic and Physical Chemistry* and *34 Fluid Mechanics and Heat Transfer.*

SOCIAL SCIENCES

80 SOCIAL SCIENCES (GENERAL) **2720**
Includes educational matters.

81 ADMINISTRATION AND MANAGEMENT **2720**
Includes management planning and research.

82 DOCUMENTATION AND INFORMATION SCIENCE **2720**
Includes information management; information storage and retrieval technology; technical writing; graphic arts; and micrography. For computer documentation see *61 Computer Programming and Software.*

83 ECONOMICS AND COST ANALYSIS ..... **N.A.**
Includes cost effectiveness studies.

84 LAW, POLITICAL SCIENCE AND SPACE POLICY ..... **N.A.**
Includes NASA appropriation hearings; aviation law; space law and policy; international law; international cooperation; and patent policy.

85 URBAN TECHNOLOGY AND TRANSPORTATION ..... **N.A.**
Includes applications of space technology to urban problems; technology transfer; technology assessment; and surface and mass transportation. For related information see *03 Air Transportation and Safety, 16 Space Transportation,* and *44 Energy Production and Conversion.*

SPACE SCIENCES For related information see also *Geosciences.*

88 SPACE SCIENCES (GENERAL) ..... **N.A.**

89 ASTRONOMY **2726**
Includes radio, gamma-ray, and infrared astronomy; and astrometry.

90 ASTROPHYSICS **2731**
Includes cosmology; celestial mechanics; space plasmas; and interstellar and interplanetary gases and dust. For related information see also *75 Plasma Physics.*

91 LUNAR AND PLANETARY EXPLORATION **2736**
Includes planetology; and manned and unmanned flights. For spacecraft design or space stations see *18 Spacecraft Design, Testing and Performance.*

92 SOLAR PHYSICS **2737**
Includes solar activity, solar flares, solar radiation and sunspots. For related information see also *93 Space Radiation.*

93 SPACE RADIATION **2739**
Includes cosmic radiation; and inner and outer earth's radiation belts. For biological effects of radiation see *52 Aerospace Medicine.* For theory see *73 Nuclear and High-Energy Physics.*

GENERAL

Includes aeronautical, astronautical, and space science related histories, biographies, and pertinent reports too broad for categorization; histories or broad overviews of NASA programs.

99 GENERAL **2740**

SUBJECT INDEX **I-1**

PERSONAL AUTHOR INDEX **I-127**

CORPORATE SOURCE INDEX **I-139**

CONTRACT NUMBER INDEX **I-157**

REPORT NUMBER INDEX **I-161**

APPENDIX **A-1**

TYPICAL CITATION AND ABSTRACT

NASA SPONSORED — ON MICROFICHE

ACCESSION NUMBER → N95-10148*# National Aeronautics and Space Administration. Lewis Research Center, Cleveland, OH. ← CORPORATE SOURCE

TITLE → **EFFECTS OF A FORWARD-SWEPT FRONT ROTOR ON THE FLOWFIELD OF A COUNTERROTATION PROPELLER**

AUTHORS → M. Nallasamy (NYMA, Inc., Brook Park, OH.) and Gary G. Podboy Aug. 1994 19 p Presented at the 30th Joint Propulsion Conference, Indianapolis, IN, 27-29 Jun. 1994; sponsored by AIAA, ASME, SAE, and ASEE ← PUBLICATION DATE

CONTRACT OR GRANT → (Contract NAS3-27186; RTOP 538-03-11)

REPORT NUMBERS → (NASA-TM-106671; E-8994; NAS 1.15:106671; AIAA Paper 94-2694) Avail: CASI HC A03/MF A01; 6 functional color pages ← AVAILABILITY SOURCE AND PRICE CODE

The effects of a forward-swept front rotor on the flowfield of a counterrotation model propeller at takeoff conditions at zero degree angle of attack are studied by solving the unsteady three-dimensional Euler equations. The configuration considered is an uneven blade count counterrotation model with twelve forward-swept blades on the fore rotor and ten aft-swept blades on the aft rotor. The flowfield is compared with that of a reference aft-swept counterrotation geometry and Laser Doppler Velocimeter (LDV) measurements. At the operating conditions considered, the forward-swept blade experiences a higher tip loading and produces a stronger tip vortex compared to the aft-swept blade, consistent with the LDV and acoustic measurements. Neither the solution nor the LDV data indicated the formation of a leading edge vortex. The predicted radial distribution of the circumferentially averaged axial velocity at the measurement station agreed very closely with LDV data, while crossflow velocities showed poor agreement. The discrepancy between prediction and LDV data of tangential and radial velocities is due in part to the insufficient mesh resolution in the region between the rotors and in the tip region to track the tip vortex. The vortex is diffused by the time it arrives at the measurement station. The uneven blade count configuration requires the solution to be carried out for six blade passages of the fore rotor and five passages of the aft rotor, thus making grid refinement prohibitive.

Author

VOLUME 33 NUMBER 10 / October 1995

Scientific and Technical Aerospace Reports

A Monthly Publication of the National Aeronautics and Space Administration

01 AERONAUTICS (GENERAL)

N95-28816*# National Aeronautics and Space Administration. Ames Research Center, Moffett Field, CA.
INVESTIGATION OF WING UPPER SURFACE FLOW-FIELD DISTURBANCE DUE TO NASA DC-8-72 IN-FLIGHT INBOARD THRUST-REVERSER DEPLOYMENT
Hedayat U. Hamid, Richard J. Margason, and Gordon Hardy Jun. 1995 63 p
(RTOP 505-59-53)
(NASA-TM-110351; A-950060; NAS 1.15:110351) Avail: CASI HC A04/MF A01

An investigation of the wing upper surface flow-field disturbance due to in-flight inboard thrust reverser deployment on the NASA DC-8-72, which was conducted cooperatively by NASA Ames, the Federal Aviation Administration (FAA), McDonnell Douglas, and the Aerospace Industry Association (AIA), is outlined and discussed in detail. The purpose of this flight test was to obtain tufted flow visualization data which demonstrates the effect of thrust reverser deployment on the wing upper surface flow field to determine if the disturbed flow regions could be modeled by computational methods. A total of six symmetric thrust reversals of the two inboard engines were performed to monitor tuft and flow cone patterns as well as the character of their movement at the nominal Mach numbers of 0.55, 0.70, and 0.85. The tufts and flow cones were photographed and video-taped to determine the type of flow field that occurs with and without the thrust reversers deployed. In addition, the normal NASA DC-8 onboard Data Acquisition Distribution System (DADS) was used to synchronize the cameras. Results of this flight test will be presented in two parts. First, three distinct flow patterns associated with the above Mach numbers were sketched from the motion videos and discussed in detail. Second, other relevant aircraft parameters, such as aircraft's angular orientation, altitude, Mach number, and vertical descent, are discussed. The flight test participants' comments were recorded on the videos and the interested reader is referred to the video supplement section of this report for that information. Author

N95-29414# Naval Postgraduate School, Monterey, CA.
AN ANALYSIS OF THE IMPACT OF ASPA ON ORGANIZATIONAL AND DEPOT LEVEL MAINTENANCE M.S. Thesis
Robert G. Ramsey and Leo J. Legidakes Dec. 1994 79 p
(AD-A292670) Avail: CASI HC A05/MF A01

The Aircraft Service Period Adjustment (ASPA) Program was designed to determine the need to induct an aircraft into Standard Depot Level Maintenance (SDLM) based on Period End Date (PED), material condition, flight time and other factors in order to determine if the SDLM could be deferred for one year before reinspection and/or induction. If the SDLM is deferred, the expenditure of depot funds for an aircraft is deferred in the current year. Initially, the program allowed for the extension and deferral of numerous aircraft and did produce a one time saving. However, it has been observed that deferring SDLM, results in the deterioration in aircraft material condition. More over, ASPA brings significant uncertainty in depot parts support and SDLM planning and scheduling. ASPA causes a redundancy of effort in duplicating the aircraft inspections for ASPA and for induction into SDLM. In this research we show that the termination of the ASPA Program will significantly reduce the uncertainty and variability inherent in the Navy depot induction process. With the variability reduced turnaround time, organizational and depot workload, man hours expended and total costs will be improved. DTIC

N95-30229*# National Aeronautics and Space Administration. Lewis Research Center, Cleveland, OH.
LASER DOPPLER VELOCIMETER SYSTEM FOR SUBSONIC JET MIXER NOZZLE TESTING AT THE NASA LEWIS AEROACOUSTIC PROPULSION LAB
Gary G. Podboy, James E. Bridges (NYMA, Inc., Brook Park, OH.), Naseem H. Saiyed, and Martin J. Krupar Jun. 1995 30 p Presented at the 31st Joint Propulsion Conference and Exhibit, San Diego, CA, 10-12 Jul. 1995; sponsored by AIAA, ASME, SAE, and ASEE
(RTOP 538-03-11)
(NASA-TM-106984; E-9753; NAS 1.15:106984; AIAA Paper 95-2787)
Avail: CASI HC A03/MF A01; 4 functional color pages

A laser Doppler velocimeter (LDV) system developed for the Aeroacoustic Propulsion Laboratory (APL) at the NASA Lewis Research Center is described. This system was developed to acquire detailed flow field data which could be used to quantify the effectiveness of internal exhaust gas mixers (IEGM's) and to verify and calibrate computational codes. The LDV was used as an orthogonal, three component system to measure the flow field downstream of the exit of a series of IEGM's and a reference axisymmetric splitter configuration. The LDV system was also used as a one component system to measure the internal axial flow within the nozzle tailpipe downstream of the mixers. These IEGM's were designed for low-bypass ratio turbofan engines. The data were obtained at a simulated low flight speed, high-power operating condition. The optical, seeding, and data acquisition systems of the LDV are described in detail. Sample flow field measurements are provided to illustrate the capabilities of the system at the time of this test, which represented the first use of LDV at the APL. A discussion of planned improvements to the LDV is also included. Author

02 AERODYNAMICS

Includes aerodynamics of bodies, combinations, wings, rotors, and control surfaces; and internal flow in ducts and turbomachinery.

For related information see also *34 Fluid Mechanics and Heat Transfer.*

N95-28708 ESDU International Ltd., London (England).
COMPUTER PROGRAM FOR ESTIMATION OF LEADING-EDGE SUCTION DISTRIBUTION FOR PLANE THIN WINGS AT SUBSONIC SPEEDS
Dec. 1994 5 p
(ISSN 0141-397X)
(ESDU-94038; ISBN-0-856-79925-4) Avail: ESDU

ESDU 94038 introduces a Fortran program, ESDUpac A9438, that calculates the total theoretical leading-edge suction and its normalized spanwise distribution for wings from the tabulated values for the distribution given in ESDU 94037, making any necessary interpolations. It applies to wings with unswept or swept back leading-edges. The input to and output from the program are explained and illustrated by a worked example and the program is provided on disc (uncompiled) in the software volume. ESDU

N95-28720*# Wyle Labs., Inc., Arlington, VA.
THE ACOUSTIC CHARACTERISTICS OF TURBOMACHINERY CAVITIES
Final Contractor Report
M. J. Lucas, R. Noreen, L. D. Southerland, J. Cole, III (Cambridge Acoustical Associates, Inc., Cambridge, MA.), and M. Junger (Cambridge Acoustical Associates, Inc., Cambridge, MA.) Washington NASA May 1995 308 p
(Contract NAS8-37360)
(NASA-CR-4671; M-778; NAS 1.26:4671) Avail: CASI HC A14/MF A03

Internal fluid flows are subject not only to self-sustained oscillations of the purely hydrodynamic type but also to the coupling of the instability with the acoustic mode of the surrounding cavity. This situation is common to turbomachinery, since flow instabilities are confined within a flow path where the acoustic wavelength is typically smaller than the dimensions of the cavity and flow speeds are low enough to allow resonances. When acoustic coupling occurs, the fluctuations can become so severe in amplitude that it may induce structural failure of engine components. The potential for catastrophic failure makes identifying flow-induced noise and vibration sources a priority. In view of the complexity of these types of flows, this report was written with the purpose of presenting many of the methods used to compute frequencies for self-sustained oscillations. The report also presents the engineering formulae needed to calculate the acoustic resonant modes for ducts and cavities. Although the report is not a replacement for more complex numerical or experimental modeling techniques, it is intended to be used on general types of flow configurations that are known to produce self-sustained oscillations. This report provides a complete collection of these models under one cover. Author

N95-28723*# National Aeronautics and Space Administration. Lewis Research Center, Cleveland, OH.
SURFACE MODELING, GRID GENERATION, AND RELATED ISSUES IN COMPUTATIONAL FLUID DYNAMIC (CFD) SOLUTIONS
Yung K. Choo, comp. Mar. 1995 832 p Workshop held in Cleveland, OH, 9-11 May 1995
(RTOP 505-62-52)
(NASA-CP-3291; E-9458; NAS 1.55:3291) Copyright Avail: CASI HC A99/MF A10

The NASA Steering Committee for Surface Modeling and Grid Generation (SMAGG) sponsored a workshop on surface modeling, grid generation, and related issues in Computational Fluid Dynamics (CFD) solutions at Lewis Research Center, Cleveland, Ohio, May 9-11, 1995. The workshop provided a forum to identify industry needs, strengths, and weaknesses of the five grid technologies (patched structured, overset structured, Cartesian, unstructured, and hybrid), and to exchange thoughts about where each technology will be in 2 to 5 years. The workshop also provided opportunities for engineers and scientists to present new methods, approaches, and applications in SMAGG for CFD. This Conference Publication (CP) consists of papers on industry overview, NASA overview, five grid technologies, new methods/ approaches/applications, and software systems. For individual titles, see N95-28724 through N95-28775.

N95-28724*# McDonnell-Douglas Aerospace, Saint Louis, MO.
FUTURE REQUIREMENTS IN SURFACE MODELING AND GRID GENERATION **c34**
Raymond R. Cosner *In* NASA. Lewis Research Center, Surface Modeling, Grid Generation, and Related Issues in Computational Fluid Dynamic (CFD) Solutions Mar. 1995 p 3-13 (For primary document see N95-28723 10-02)
Avail: CASI HC A03/MF A10

The past ten years have seen steady progress in surface modeling procedures, and wholesale changes in grid generation technology. Today, it seems fair to state that a satisfactory grid can be developed to model nearly any configuration of interest. The issues at present focus on operational concerns such as cost and quality. Continuing evolution of the engineering process is placing new demands on the technologies of surface modeling and grid generation. In the evolution toward a multidisciplinary analysis-bascd design environment, methods developed for Computational Fluid Dynamics are finding acceptance in many additional applications. These two trends, the normal evolution of the process and a watershed shift toward concurrent and multidisciplinary analysis, will be considered in assessing current capabilities and needed technological improvements. Derived from text

N95-28725*# Lockheed Aeronautical Systems Co., Marietta, GA.
REQUIREMENTS FOR EFFECTIVE USE OF CFD IN AEROSPACE DESIGN **c34**
Pradeep Raj *In* NASA. Lewis Research Center, Surface Modeling, Grid Generation, and Related Issues in Computational Fluid Dynamic (CFD) Solutions Mar. 1995 p 15-28 (For primary document see N95-28723 10-02)
Avail: CASI HC A03/MF A10

This paper presents a perspective on the requirements that Computational Fluid Dynamics (CFD) technology must meet for its effective use in aerospace design. General observations are made on current aerospace design practices and deficiencies are noted that must be rectified for the U.S. aerospace industry to maintain its leadership position in the global marketplace. In order to rectify deficiencies, industry is transitioning to an integrated product and process development (IPPD) environment and design processes are undergoing radical changes. The role of CFD in producing data that design teams need to support flight vehicle development is briefly discussed. An overview of the current state of the art in CFD is given to provide an assessment of strengths and weaknesses of the variety of methods currently available, or under development, to produce aerodynamic data. Effectiveness requirements are examined from a customer/supplier view point with design team as customer and CFD practitioner as supplier. Partnership between the design team and CFD team is identified as an essential requirement for effective use of CFD. Rapid turnaround, reliable accuracy, and affordability are offered as three key requirements that CFD community must address if CFD is to play its rightful role in supporting the IPPD design environment needed to produce high quality yet affordable designs. Derived from text

N95-28726*# General Electric Co., Schenectady, NY. Research and Development Center.
GRID GENERATION AND SURFACE MODELING FOR CFD **c34**
Stuart D. Connell, Janet S. Sober, and Scott H. Lamson *In* NASA. Lewis Research Center, Surface Modeling, Grid Generation, and Related Issues in Computational Fluid Dynamic (CFD) Solutions Mar. 1995 p 29-43 (For primary document see N95-28723 10-02)
Avail: CASI HC A03/MF A10

When computing the flow around complex three dimensional configurations, the generation of the mesh is the most time consuming part of any calculation. With some meshing technologies this can take of the order of a man month or more. The requirement for a number of design iterations coupled with ever decreasing time allocated for design leads to the need for a significant acceleration of this process. Of the two competing approaches, block-structured and unstructured, only the unstructured approach will allow fully automatic mesh generation directly from a CAD model. Using this approach coupled with the techniques described in this paper, it is possible to reduce the mesh generation time from man months to a few hours on a workstation. The desire to closely couple a CFD code with a design or optimization algorithm requires that the changes to the geometry be performed quickly and in a smooth manner. This need for smoothness necessitates the use of Bezier polynomials in place of the more usual NURBS or cubic splines. A two dimensional Bezier polynomial based design system is described. Author

N95-28727*# Pratt and Whitney Aircraft, East Hartford, CT.
GRID GENERATION: A VIEW FROM THE TRENCHES **c34**
David Ives, Robert Miller, William Siddons, and Kevin VanDyke (Pratt and Whitney Aircraft, West Palm Beach, FL.) *In* NASA. Lewis Research Center, Surface Modeling, Grid Generation, and Related Issues in Computational Fluid Dynamic (CFD) Solutions Mar. 1995 p 45-54 (For primary document see N95-28723 10-02)
Avail: CASI HC A02/MF A10

This paper presents 'A view from the trenches' on CFD grid generation from a Pratt & Whitney perspective. We anticipate that other organizations have similar views. We focus on customer expectations and the consequent requirements. We enunciate a vision for grid generation, discuss issues that developers must recognize. Author

N95-28728*# National Aeronautics and Space Administration. Ames Research Center, Moffett Field, CA.
APPLICATION OF CFD IN AERONAUTICS AT NASA AMES RESEARCH CENTER **c34**

Catherine M. Maksymiuk, Francis Y. Enomoto, and William R. VanDalsem *In* NASA. Lewis Research Center, Surface Modeling, Grid Generation, and Related Issues in Computational Fluid Dynamic (CFD) Solutions Mar. 1995 p 57-67 (For primary document see N95-28723 10-02)
Avail: CASI HC A03/MF A10

The role of Computational Fluid Dynamics (CFD) at Ames Research Center has expanded to address a broad range of aeronautical problems, including wind tunnel support, flight test support, design, and analysis. Balancing the requirements of each new problem against the available resources - software, hardware, time, and expertise - is critical to the effective use of CFD. Several case studies of recent applications highlight the depth of CFD capability at Ames, the tradeoffs involved in various approaches, and lessons learned in the use of CFD as an engineering tool. Derived from text

N95-28729*# National Aeronautics and Space Administration. Langley Research Center, Hampton, VA.
GEOMETRY LABORATORY (GEOLAB) SURFACE MODELING AND GRID GENERATION TECHNOLOGY AND SERVICES c61
Patricia A. Kerr, Robert E. Smith, and Mary-Anne K. Posenau *In* NASA. Lewis Research Center, Surface Modeling, Grid Generation, and Related Issues in Computational Fluid Dynamic (CFD) Solutions Mar. 1995 p 69-86 (For primary document see N95-28723 10-02)
Avail: CASI HC A03/MF A10

The facilities and services of the GEOmetry LABoratory (GEOLAB) at the NASA Langley Research Center are described. Included in this description are the laboratory functions, the surface modeling and grid generation technologies used in the laboratory, and examples of the tasks performed in the laboratory. Author

N95-28730*# National Aeronautics and Space Administration. Langley Research Center, Hampton, VA.
RAPID AIRPLANE PARAMETRIC INPUT DESIGN (RAPID) Abstract Only c05
Robert E. Smith *In* NASA. Lewis Research Center, Surface Modeling, Grid Generation, and Related Issues in Computational Fluid Dynamic (CFD) Solutions Mar. 1995 p 87 (For primary document see N95-28723 10-02)
Avail: CASI HC A01/MF A10

RAPID is a methodology and software system to define a class of airplane configurations and directly evaluate surface grids, volume grids, and grid sensitivity on and about the configurations. A distinguishing characteristic which separates RAPID from other airplane surface modellers is that the output grids and grid sensitivity are directly applicable in CFD analysis. A small set of design parameters and grid control parameters govern the process which is incorporated into interactive software for 'real time' visual analysis and into batch software for the application of optimization technology. The computed surface grids and volume grids are suitable for a wide range of Computational Fluid Dynamics (CFD) simulation. The general airplane configuration has wing, fuselage, horizontal tail, and vertical tail components. The double-delta wing and tail components are manifested by solving a fourth order partial differential equation (PDE) subject to Dirichlet and Neumann boundary conditions. The design parameters are incorporated into the boundary conditions and therefore govern the shapes of the surfaces. The PDE solution yields a smooth transition between boundaries. Surface grids suitable for CFD calculation are created by establishing an H-type topology about the configuration and incorporating grid spacing functions in the PDE equation for the lifting components and the fuselage definition equations. User specified grid parameters govern the location and degree of grid concentration. A two-block volume grid about a configuration is calculated using the Control Point Form (CPF) technique. The interactive software, which runs on Silicon Graphics IRIS workstations, allows design parameters to be continuously varied and the resulting surface grid to be observed in real time. The batch software computes both the surface and volume grids and also computes the sensitivity of the output grid with respect to the input design parameters by applying the precompiler tool ADIFOR to the grid generation program. The output of ADIFOR is a new source code containing the old code plus expressions for derivatives of specified dependent variables (grid coordinates) with respect to specified independent variables (design parameters). The RAPID methodology and software provide a means of rapidly defining numerical prototypes, grids, and grid sensitivity of a class of airplane configurations. This technology and software is highly useful for CFD research for preliminary design and optimization processes. Author

N95-28731*# National Aeronautics and Space Administration. Langley Research Center, Hampton, VA.
ALGORITHMS FOR HIGH ASPECT RATIO ORIENTED TRIANGULATIONS Abstract Only
Mary-Anne K. Posenau *In* NASA. Lewis Research Center, Surface Modeling, Grid Generation, and Related Issues in Computational Fluid Dynamic (CFD) Solutions Mar. 1995 p 88 (For primary document see N95-28723 10-02)
Avail: CASI HC A01/MF A10

Grid generation plays an integral part in the solution of computational fluid dynamics problems for aerodynamics applications. A major difficulty with standard structured grid generation, which produces quadrilateral (or hexahedral) elements with implicit connectivity, has been the requirement for a great deal of human intervention in developing grids around complex configurations. This has led to investigations into unstructured grids with explicit connectivities, which are primarily composed of triangular (or tetrahedral) elements, although other subdivisions of convex cells may be used. The existence of large gradients in the solution of aerodynamic problems may be exploited to reduce the computational effort by using high aspect ratio elements in high gradient regions. However, the heuristic approaches currently in use do not adequately address this need for high aspect ratio unstructured grids. High aspect ratio triangulations very often produce the large angles that are to be avoided. Point generation techniques based on contour or front generation are judged to be the most promising in terms of being able to handle complicated multiple body objects, with this technique lending itself well to adaptivity. The eventual goal encompasses several phases: first, a partitioning phase, in which the Voronoi diagram of a set of points and line segments (the input set) will be generated to partition the input domain; second, a contour generation phase in which body-conforming contours are used to subdivide the partition further as well as introduce the foundation for aspect ratio control, and; third, a Steiner triangulation phase in which points are added to the partition to enable triangulation while controlling angle bounds and aspect ratio. This provides a combination of the advancing front/contour techniques and refinement. By using a front, aspect ratio can be better controlled. By using refinement, bounds on angles can be maintained, while attempting to minimize the number of Steiner points. Derived from text

N95-28732*# National Aeronautics and Space Administration. Lewis Research Center, Cleveland, OH.
SURFACE MODELING AND GRID GENERATION FOR AEROPROPULSION CFD c34
Yung K. Choo, John W. Slater, James Loellbach, and Jinho Lee (NYMA, Inc., Cleveland, OH.) *In its* Surface Modeling, Grid Generation, and Related Issues in Computational Fluid Dynamic (CFD) Solutions Mar. 1995 p 89-103 (For primary document see N95-28723 10-02)
Avail: CASI HC A03/MF A10

The efforts in geometry modeling and grid generation at the NASA Lewis Research Center, as applied to the computational fluid dynamic (CFD) analysis of aeropropulsion systems, are presented. The efforts are mainly characterized by a focus on the analysis of components of an aeropropulsion system, which involve turbulent viscous flow with heat transfer and chemistry. Thus, this discussion will follow that characterization and will sequence through the components of typical propulsion systems consisting of inlets, compressors, combustors, turbines, and nozzles. For each component, some applications of CFD analysis will be presented to show how CFD is used to compute the desired performance information, how geometry modeling and grid generation are performed, and what issues have developed related to geometry modeling and grid generation. The discussion will illustrate the following needs related to geometry modeling and grid generation as observed in aeropropulsion analysis: (1) accurate and efficient resolution of turbulent viscous and chemically-reacting flowfields; (2) easy-to-use interfaces with CAD data for automated grid generation about complex geometries; and (3) automated batch grid generation software for use with design and optimization software. Derived from text

N95-28733*# National Aeronautics and Space Administration. Marshall Space Flight Center, Huntsville, AL.

MARSHALL SPACE FLIGHT CENTER SURFACE MODELING AND GRID GENERATION APPLICATIONS **c20**

Robert W. Williams, Theodore G. Benjamin, and Joni W. Cornelison *In* NASA. Lewis Research Center, Surface Modeling, Grid Generation, and Related Issues in Computational Fluid Dynamic (CFD) Solutions Mar. 1995 p 105-120 (For primary document see N95-28723 10-02)

Avail: CASI HC A03/MF A10

The Solid Rocket Motors (SRM) used by NASA to propel the Space Shuttle employ gimballing nozzles as a means for vehicular guidance during launch and ascent. Gimballing a nozzle renders the pressure field of the exhaust gases nonaxisymmetric. This has two effects: (1) it exerts a torque and side load on the nozzle; and (2) the exhaust gases flow circumferentially in the aft-dome region, thermally loading the flexible boot, case-to-nozzle joint, and casing insulation. The use of CFD models to simulate such flows is imperative in order to assess SRM design. The grids for these problems were constructed by obtaining information from drawings and tabulated coordinates. The 2D axisymmetric grids were designed and generated using the EZ-Surf and GEN2D surface and grid generation codes. These 2D grids were solved using codes such as FDNS, GASP, and MINT. These axisymmetric grids were rotated around the center-line to form 3D nongimballed grids. These were then gimballed around the pivot point and the gaps or overlaps resurfaced to obtain the final domains, which contained approximately 366,000 grid points. The 2D solutions were then rotated and manipulated as appropriate for geometry and used as initial guesses in the final solution. The analyses were used in answering questions about flight criteria. Derived from text

N95-28734*# United Technologies Research Center, East Hartford, CT.

AUTOMATIC BLOCKING FOR COMPLEX THREE-DIMENSIONAL CONFIGURATIONS **c61**

John F. Dannenhoffer, III *In* NASA. Lewis Research Center, Surface Modeling, Grid Generation, and Related Issues in Computational Fluid Dynamic (CFD) Solutions Mar. 1995 p 123-142 (For primary document see N95-28723 10-02)

Avail: CASI HC A03/MF A10

A new blocking technique for complex three-dimensional configurations is described. This new technique is based upon the concept of an abstraction, or squared-up representation, of the configuration and the associated grid. By allowing the user to describe blocking requirements in natural terms (such as 'wrap a grid around this leading edge' or 'make all grid lines emanating from this wall orthogonal to it'), users can quickly generate complex grids around complex configurations, while still maintaining a high level of control where desired. An added advantage of the abstraction concept is that once a blocking is defined for a class of configurations, it can be automatically applied to other configurations of the same class, making the new technique particularly well suited for the parametric variations which typically occur during design processes. Grids have been generated for a variety of real-world, two- and three-dimensional configurations. In all cases, the time required to generate the grid, given just an electronic form of the configuration, was at most a few days. Hence with this new technique, the generation of a block-structured grid is only slightly more expensive than the generation of an unstructured grid for the same configuration. Author

N95-28735*# Program Development Corp., White Plains, NY.

MULTIBLOCK GRID GENERATION WITH AUTOMATIC ZONING **c61**

Peter R. Eiseman *In* NASA. Lewis Research Center, Surface Modeling, Grid Generation, and Related Issues in Computational Fluid Dynamic (CFD) Solutions Mar. 1995 p 143-162 (For primary document see N95-28723 10-02)

Avail: CASI HC A03/MF A10

An overview will be given for multiblock grid generation with automatic zoning. We shall explore the many advantages and benefits of this exciting technology and will also see how to apply it to a number of interesting cases. The technology is available in the form of a commercial code, GridPro(registered trademark)/az3000. This code takes surface geometry definitions and patterns of points as its primary input and produces high quality grids as its output. Before we embark upon our exploration, we shall first give a brief background of the environment in which this technology fits. Derived from text

N95-28736*# National Aeronautics and Space Administration. Langley Research Center, Hampton, VA.

BLOCK-STRUCTURED GRIDS FOR COMPLEX AERODYNAMIC CONFIGURATIONS: CURRENT STATUS **c34**

Veer N. Vatsa, Mark D. Sanetrik (AS&M, Inc., Hampton, VA.), and Edward B. Parlette (Vigyan Research Associates, Inc., Hampton, VA.) *In* NASA. Lewis Research Center, Surface Modeling, Grid Generation, and Related Issues in Computational Fluid Dynamic (CFD) Solutions Mar. 1995 p 163-177 (For primary document see N95-28723 10-02)

Avail: CASI HC A03/MF A10

The status of CFD methods based on the use of block-structured grids for analyzing viscous flows over complex configurations is examined. The objective of the present study is to make a realistic assessment of the usability of such grids for routine computations typically encountered in the aerospace industry. It is recognized at the very outset that the total turnaround time, from the moment the configuration is identified until the computational results have been obtained and postprocessed, is more important than just the computational time. Pertinent examples will be cited to demonstrate the feasibility of solving flow over practical configurations of current interest on block-structured grids. Derived from text

N95-28737*# National Aeronautics and Space Administration. Ames Research Center, Moffett Field, CA.

GRID RELATED ISSUES FOR STATIC AND DYNAMIC GEOMETRY PROBLEMS USING SYSTEMS OF OVERSET STRUCTURED GRIDS **c34**

Robert L. Meakin *In* NASA. Lewis Research Center, Surface Modeling, Grid Generation, and Related Issues in Computational Fluid Dynamic (CFD) Solutions Mar. 1995 p 181-192 (For primary document see N95-28723 10-02)

Avail: CASI HC A03/MF A10

Grid related issues of the Chimera overset grid method are discussed in the context of a method of solution and analysis of unsteady three-dimensional viscous flows. The state of maturity of the various pieces of support software required to use the approach is considered. Current limitations of the approach are identified. Derived from text

N95-28738*# Wright Lab., Eglin AFB, FL.

THE ROLE OF OVERSET GRIDS IN THE DEVELOPMENT OF THE GENERAL PURPOSE CFD CODE **c34**

Davy M. Belk *In* NASA. Lewis Research Center, Surface Modeling, Grid Generation, and Related Issues in Computational Fluid Dynamic (CFD) Solutions Mar. 1995 p 193-204 (For primary document see N95-28723 10-02)

Avail: CASI HC A03/MF A10

A discussion of the strengths and weaknesses of overset composite grid and solution technology is given, along with a sampling of current work in the area. Major trends are identified, and the observation is made that generalized and hybridized overset methods provide a natural framework for combining disparate mesh types and physics models. Because of this, the author concludes that overset methods will be the foundation for the general purpose computational fluid dynamics programs of the future. Derived from text

N95-28739*# National Aeronautics and Space Administration. Lewis Research Center, Cleveland, OH.

A CARTESIAN, CELL-BASED APPROACH FOR ADAPTIVELY-REFINED SOLUTIONS OF THE EULER AND NAVIER-STOKES EQUATIONS **c34**

William J. Coirier and Kenneth G. Powell (Michigan Univ., Ann Arbor, MI.) *In its* Surface Modeling, Grid Generation, and Related Issues in Computational Fluid Dynamic (CFD) Solutions Mar. 1995 p 207-224 (For primary document see N95-28723 10-02)

Avail: CASI HC A03/MF A10

A Cartesian, cell-based approach for adaptively-refined solutions of the Euler and Navier-Stokes equations in two dimensions is developed and tested. Grids about geometrically complicated bodies are generated automatically, by recursive subdivision of a single Cartesian cell encompassing the entire flow domain. Where the resulting cells intersect bodies, N-sided 'cut' cells are created using polygon-clipping algorithms. The grid is stored in a binary-tree data structure which provides a natural means of obtaining cell-to-cell connectivity and of carrying out

solution-adaptive mesh refinement. The Euler and Navier-Stokes equations are solved on the resulting grids using a finite-volume formulation. The convective terms are upwinded: A gradient-limited, linear reconstruction of the primitive variables is performed, providing input states to an approximate Riemann solver for computing the fluxes between neighboring cells. The more robust of a series of viscous flux functions is used to provide the viscous fluxes at the cell interfaces. Adaptively-refined solutions of the Navier-Stokes equations using the Cartesian, cell-based approach are obtained and compared to theory, experiment and other accepted computational results for a series of low and moderate Reynolds number flows. Author

N95-28740*# National Aeronautics and Space Administration. Ames Research Center, Moffett Field, CA.

DEVELOPMENT AND APPLICATION OF A 3D CARTESIAN GRID EULER METHOD **c34**

John E. Melton, Michael J. Aftosmis (Wright Lab., Wright-Patterson AFB, OH.), Marsha J. Berger (New York Univ., New York, NY.), and Michael D. Wong (Sterling Software, Inc., Palo Alto, CA.) *In* NASA. Lewis Research Center, Surface Modeling, Grid Generation, and Related Issues in Computational Fluid Dynamic (CFD) Solutions Mar. 1995 p 225-249 (For primary document see N95-28723 10-02)

(Contracts DE-FG02-88ER-25053; F49620-94-1-0132)

Avail: CASI HC A03/MF A10

This report describes recent progress in the development and application of 3D Cartesian grid generation and Euler flow solution techniques. Improvements to flow field grid generation algorithms, geometry representations, and geometry refinement criteria are presented, including details of a procedure for correctly identifying and resolving extremely thin surface features. An initial implementation of automatic flow field refinement is also presented. Results for several 3D multi-component configurations are provided and discussed. Author

N95-28741*# Lockheed-Fort Worth Co., Fort Worth, TX. Engineering Group.

UNSTRUCTURED CARTESIAN/PRISMATIC GRID GENERATION FOR COMPLEX GEOMETRIES **c61**

Steve L. Karman, Jr. *In* NASA. Lewis Research Center, Surface Modeling, Grid Generation, and Related Issues in Computational Fluid Dynamic (CFD) Solutions Mar. 1995 p 251-270 (For primary document see N95-28723 10-02)

Avail: CASI HC A03/MF A10

The generation of a hybrid grid system for discretizing complex three dimensional (3D) geometries is described. The primary grid system is an unstructured Cartesian grid automatically generated using recursive cell subdivision. This grid system is sufficient for computing Euler solutions about extremely complex 3D geometries. A secondary grid system, using triangular-prismatic elements, may be added for resolving the boundary layer region of viscous flows near surfaces of solid bodies. This paper describes the grid generation processes used to generate each grid type. Several example grids are shown, demonstrating the ability of the method to discretize complex geometries, with very little pre-processing required by the user. Derived from text

N95-28742*# Princeton Univ., NJ. Dept. of Mechanical and Aerospace Engineering.

PROSPECTS AND EXPECTATIONS FOR UNSTRUCTURED METHODS **c34**

Timothy J. Baker *In* NASA. Lewis Research Center, Surface Modeling, Grid Generation, and Related Issues in Computational Fluid Dynamic (CFD) Solutions Mar. 1995 p 273-287 (For primary document see N95-28723 10-02)

Avail: CASI HC A03/MF A10

The last decade has witnessed a vigorous and sustained research effort on unstructured methods for computational fluid dynamics. Unstructured mesh generators and flow solvers have evolved to the point where they are now in use for design purposes throughout the aerospace industry. In this paper we survey the various mesh types, structured as well as unstructured, and examine their relative strengths and weaknesses. We argue that unstructured methodology does offer the best prospect for the next generation of computational fluid dynamics algorithms. Derived from text

N95-28743*# National Aeronautics and Space Administration. Langley Research Center, Hampton, VA.

AN UNSTRUCTURED-GRID SOFTWARE SYSTEM FOR SOLVING COMPLEX AERODYNAMIC PROBLEMS

Neal T. Frink, Shahyar Pirzadeh (Vigyan Research Associates, Inc., Hampton, VA.), and Paresh Parikh (Vigyan Research Associates, Inc., Hampton, VA.) *In* NASA. Lewis Research Center, Surface Modeling, Grid Generation, and Related Issues in Computational Fluid Dynamic (CFD) Solutions Mar. 1995 p 289-308 (For primary document see N95-28723 10-02)

Avail: CASI HC A03/MF A10

A coordinated effort has been underway over the past four years to elevate unstructured-grid methodology to a mature level. The goal of this endeavor is to provide a validated capability to non-expert users for performing rapid aerodynamic analysis and design of complex configurations. The Euler component of the system is well developed, and is impacting a broad spectrum of engineering needs with capabilities such as rapid grid generation and inviscid flow analysis, inverse design, interactive boundary layers, and propulsion effects. Progress is also being made in the more tenuous Navier-Stokes component of the system. A robust grid generator is under development for constructing quality thin-layer tetrahedral grids, along with a companion Navier-Stokes flow solver. This paper presents an overview of this effort, along with a perspective on the present and future status of the methodology. Derived from text

N95-28744*# Texas Univ., Austin, TX. Dept. of Aerospace Engineering and Engineering Mechanics

ADAPTIVE HYBRID PRISMATIC-TETRAHEDRAL GRIDS FOR VISCOUS FLOWS **c34**

Yannis Kallinderis, Aly Khawaja, and Harlan McMorris *In* NASA. Lewis Research Center, Surface Modeling, Grid Generation, and Related Issues in Computational Fluid Dynamic (CFD) Solutions Mar. 1995 p 311-332 (For primary document see N95-28723 10-02)

(Grants NAG1-1459; NSF ASC-93-57677)

Avail: CASI HC A03/MF A10

The paper presents generation of adaptive hybrid prismatic/tetrahedral grids for complex 3-D geometries including multi-body domains. The prisms cover the region close to each body's surface, while tetrahedra are created elsewhere. Two developments are presented for hybrid grid generation around complex 3-D geometries. The first is a new octree/advancing front type of method for generation of the tetrahedra of the hybrid mesh. The main feature of the present advancing front tetrahedra generator that is different from previous such methods is that it does not require the creation of a background mesh by the user for the determination of the grid-spacing and stretching parameters. These are determined via an automatically generated octree. The second development is an Automatic Receding Method (ARM) for treating the narrow gaps in between different bodies in a multiply-connected domain. This method is applied to a two-element wing case. A hybrid grid adaptation scheme that employs both h-refinement and redistribution strategies is developed to provide optimum meshes for viscous flow computations. Grid refinement is a dual adaptation scheme that couples division of tetrahedra, as well as 2-D directional division of prisms. Author

N95-28745*# MDA Engineering, Inc., Arlington, TX.

THREE-DIMENSIONAL HYBRID GRID GENERATION USING ADVANCING FRONT TECHNIQUES **c61**

John P. Steinbrenner and Ralph W. Noack *In* NASA. Lewis Research Center, Surface Modeling, Grid Generation, and Related Issues in Computational Fluid Dynamic (CFD) Solutions Mar. 1995 p 333-356 (For primary document see N95-28723 10-02)

(Contract F08630-93-C-0074)

Avail: CASI HC A03/MF A10

A new 3-dimensional hybrid grid generation technique has been developed, based on ideas of advancing fronts for both structured and unstructured grids. In this approach, structured grids are first generate independently around individual components of the geometry. Fronts are initialized on these structure grids, and advanced outward so that new cells are extracted directly from the structured grids. Employing typical advancing front techniques, cells are rejected if they intersect the existing front or fail other criteria When no more viable structured cells exist further cells are advanced in an unstructured manner to close off the overall domain, resulting in a grid of 'hybrid' form. There are two primary advantages

to the hybrid formulation. First, generating blocks with limited regard to topology eliminates the bottleneck encountered when a multiple block system is used to fully encapsulate a domain. Individual blocks may be generated free of external constraints, which will significantly reduce the generation time. Secondly, grid points near the body (presumably with high aspect ratio) will still maintain a structured (non-triangular or tetrahedral) character, thereby maximizing grid quality and solution accuracy near the surface.

Author

N95-28746*# National Aeronautics and Space Administration. Ames Research Center, Moffett Field, CA.

EMERGING CFD TECHNOLOGIES AND AEROSPACE VEHICLE DESIGN **c34**

Michael J. Aftosmis *In* NASA. Lewis Research Center, Surface Modeling, Grid Generation, and Related Issues in Computational Fluid Dynamic (CFD) Solutions Mar. 1995 p 359-384 Prepared in cooperation with Wright Lab., Wright-Patterson AFB, OH (For primary document see N95-28723 10-02)

Avail: CASI HC A03/MF A10

With the recent focus on the needs of design and applications CFD, research groups have begun to address the traditional bottlenecks of grid generation and surface modeling. Now, a host of emerging technologies promise to shortcut or dramatically simplify the simulation process. This paper discusses the current status of these emerging technologies. It will argue that some tools are already available which can have positive impact on portions of the design cycle. However, in most cases, these tools need to be integrated into specific engineering systems and process cycles to be used effectively. The rapidly maturing status of unstructured and Cartesian approaches for inviscid simulations makes suggests the possibility of highly automated Euler-boundary layer simulations with application to loads estimation and even preliminary design. Similarly, technology is available to link block structured mesh generation algorithms with topology libraries to avoid tedious re-meshing of topologically similar configurations. Work in algorithmic based auto-blocking suggests that domain decomposition and point placement operations in multi-block mesh generation may be properly posed as problems in Computational Geometry, and following this approach may lead to robust algorithmic processes for automatic mesh generation.

Derived from text

N95-28747*# Lockheed Aeronautical Systems Co., Marietta, GA.

AN ASSESSMENT OF UNSTRUCTURED GRID TECHNOLOGY FOR TIMELY CFD ANALYSIS **c34**

Tom A. Kinard and Deanne M. Schabowski (Lockheed-Fort Worth Co., Fort Worth, TX.) *In* NASA. Lewis Research Center, Surface Modeling, Grid Generation, and Related Issues in Computational Fluid Dynamic (CFD) Solutions Mar. 1995 p 385-400 (For primary document see N95-28723 10-02)

Avail: CASI HC A03/MF A10

An assessment of two unstructured methods is presented in this paper. A tetrahedral unstructured method USM3D, developed at NASA Langley Research Center is compared to a Cartesian unstructured method, SPLITFLOW, developed at Lockheed Fort Worth Company. USM3D is an upwind finite volume solver that accepts grids generated primarily from the Vgrid grid generator. SPLITFLOW combines an unstructured grid generator with an implicit flow solver in one package. Both methods are exercised on three test cases, a wing, and a wing body, and a fully expanded nozzle. The results for the first two runs are included here and compared to the structured grid method TEAM and to available test data. On each test case, the set up procedure are described, including any difficulties that were encountered. Detailed descriptions of the solvers are not included in this paper.

Derived from text

N95-28748*# CFD Research Corp., Huntsville, AL.

EVALUATION OF GRID GENERATION TECHNOLOGIES FROM AN APPLIED PERSPECTIVE **c61**

Gary S. Hufford, Vincent J. Harrand, Bhavin C. Patel, and Curtis R. Mitchell *In* NASA. Lewis Research Center, Surface Modeling, Grid Generation, and Related Issues in Computational Fluid Dynamic (CFD) Solutions Mar. 1995 p 401-420 (For primary document see N95-28723 10-02)

Avail: CASI HC A03/MF A10

An analysis of the grid generation process from the point of view of an applied CFD engineer is given. Issues addressed include geometric modeling, structured grid generation, unstructured grid generation, hybrid grid generation and use of virtual parts libraries in large parametric analysis projects. The analysis is geared towards comparing the effective turn around time for specific grid generation and CFD projects. The conclusion was made that a single grid generation methodology is not universally suited for all CFD applications due to both limitations in grid generation and flow solver technology. A new geometric modeling and grid generation tool, CFD-GEOM, is introduced to effectively integrate the geometric modeling process to the various grid generation methodologies including structured, unstructured, and hybrid procedures. The full integration of the geometric modeling and grid generation allows implementation of extremely efficient updating procedures, a necessary requirement for large parametric analysis projects. The concept of using virtual parts libraries in conjunction with hybrid grids for large parametric analysis projects is also introduced to improve the efficiency of the applied CFD engineer.

Author

N95-28749*# Mississippi State Univ., Mississippi State, MS.

THE NATIONAL GRID PROJECT: A SYSTEM OVERVIEW **c61**

Adam Gaither, Kelly Gaither, Brian Jean, Michael Remotigue, John Whitmire, Bharat Soni, Joe Thompson, Dannenhoffer, John (United Technologies Research Center, East Hartford, CT.), and Nigel Weatherill (Wales Univ., Swansea, United Kingdom.) *In* NASA. Lewis Research Center, Surface Modeling, Grid Generation, and Related Issues in Computational Fluid Dynamic (CFD) Solutions Mar. 1995 p 423-446 (For primary document see N95-28723 10-02)

Avail: CASI HC A03/MF A10

The National Grid Project (NGP) is a comprehensive numerical grid generation software system that is being developed at the National Science Foundation (NSF) Engineering Research Center (ERC) for Computational Field Simulation (CFS) at Mississippi State University (MSU). NGP is supported by a coalition of U.S. industries and federal laboratories. The objective of the NGP is to significantly decrease the amount of time it takes to generate a numerical grid for complex geometries and to increase the quality of these grids to enable computational field simulations for applications in industry. A geometric configuration can be discretized into grids (or meshes) that have two fundamental forms: structured and unstructured. Structured grids are formed by intersecting curvilinear coordinate lines and are composed of quadrilateral (2D) and hexahedral (3D) logically rectangular cells. The connectivity of a structured grid provides for trivial identification of neighboring points by incrementing coordinate indices. Unstructured grids are composed of cells of any shape (commonly triangles, quadrilaterals, tetrahedra and hexahedra), but do not have trivial identification of neighbors by incrementing an index. For unstructured grids, a set of points and an associated connectivity table is generated to define unstructured cell shapes and neighboring points. Hybrid grids are a combination of structured grids and unstructured grids. Chimera (overset) grids are intersecting or overlapping structured grids. The NGP system currently provides a user interface that integrates both 2D and 3D structured and unstructured grid generation, a solid modeling topology data management system, an internal Computer Aided Design (CAD) system based on Non-Uniform Rational B-Splines (NURBS), a journaling language, and a grid/solution visualization system.

Derived from text

N95-28750*# National Aeronautics and Space Administration. Ames Research Center, Moffett Field, CA.

A 3DGRAPE/AL: THE AMES/LANGLEY TECHNOLOGY UPGRADE **c61**

Reese L. Sorenson and Stephen J. Alter (Lockheed Engineering and Sciences Co., Hampton, VA.) *In* NASA. Lewis Research Center, Surface Modeling, Grid Generation, and Related Issues in Computational Fluid Dynamic (CFD) Solutions Mar. 1995 p 447-462 (For primary document see N95-28723 10-02)

(Contract NAS1-19000)

Avail: CASI HC A03/MF A10

This paper describes a new three-dimensional structured multiple-block volume grid generator called 3DGRAPE/AL. It is a significantly improved version of the previously-released and widely-distributed program 3DGRAPE, with many of the improvements taken from the grid-generator program 3DMAGGS. It generates volume grids by iteratively solving the Poisson Equations in three-dimensions. The right-hand-side terms are designed so that user-specified grid cell heights and user-specified grid cell skewness near boundary surfaces result automatically, with little user intervention.

Versatility was a high priority in this code's development, and as a result it can generate grids in almost any three-dimensional physical domain. Improvements include added kinds of forcing functions, improved control of cell skewness, improved initial conditions, convergence acceleration, the ability to take as input the output from GRIDGEN, and a simple but powerful graphical user interface (GUI). Derived from text

N95-28751*# Pointwise, Inc., Bedford, TX.
AUTOMATIC STRUCTURED GRID GENERATION USING GRIDGEN (SOME RESTRICTIONS APPLY) **c61**
John R. Chawner and John P. Steinbrenner *In* NASA. Lewis Research Center, Surface Modeling, Grid Generation, and Related Issues in Computational Fluid Dynamic (CFD) Solutions Mar. 1995 p 463-476 (For primary document see N95-28723 10-02)
Avail: CASI HC A03/MF A10

The authors have noticed in the recent grid generation literature an emphasis on the automation of structured grid generation. The motivation behind such work is clear; grid generation is easily the most despised task in the grid-analyze-visualize triad of computational analysis (CA). However, because grid generation is closely coupled to both the design and analysis software and because quantitative measures of grid quality are lacking, 'push button' grid generation usually results in a compromise between speed, control, and quality. Overt emphasis on automation obscures the substantive issues of providing users with flexible tools for generating and modifying high quality grids in a design environment. In support of this paper's tongue-in-cheek title, many features of the Gridgen software are described. Gridgen is by no stretch of the imagination an automatic grid generator. Despite this fact, the code does utilize many automation techniques that permit interesting regenerative features. Derived from text

N95-28752*# ICEM CFD Engineering, Berkeley, CA.
TUNED GRID GENERATION WITH ICEM CFD **c61**
Armin Wulf and Vedat Akdag *In* NASA. Lewis Research Center, Surface Modeling, Grid Generation, and Related Issues in Computational Fluid Dynamic (CFD) Solutions Mar. 1995 p 477-488 (For primary document see N95-28723 10-02)
Avail: CASI HC A03/MF A10

ICEM CFD is a CAD based grid generation package that supports multiblock structured, unstructured tetrahedral and unstructured hexahedral grids. Major development efforts have been spent to extend ICEM CFD's multiblock structured and hexahedral unstructured grid generation capabilities. The modules added are: a parametric grid generation module and a semi-automatic hexahedral grid generation module. A fully automatic version of the hexahedral grid generation module for around a set of predefined objects in rectilinear enclosures has been developed. These modules will be presented and the procedures used will be described, and examples will be discussed. Author

N95-28753*# Mississippi State Univ., Mississippi State, MS. Engineering Research Center for Computational Field Simulation.
GEOMETRY MODELING AND GRID GENERATION USING 3D NURBS CONTROL VOLUME - **c61**
Tzu-Yi Yu, Bharat K. Soni, and Ming-Hsin Shih *In* NASA. Lewis Research Center, Surface Modeling, Grid Generation, and Related Issues in Computational Fluid Dynamic (CFD) Solutions Mar. 1995 p 491-503 Sponsored by NASA. Marshall Space Flight Center (For primary document see N95-28723 10-02)
Avail: CASI HC A03/MF A10

The algorithms for volume grid generation using NURBS -geometric representation are presented. The parameterization algorithm is enhanced to yield a desired physical distribution on the curve, surface and volume. This approach bridges the gap between CAD surface/volume definition and surface/volume grid generation. Computational examples associated with practical configurations have shown the utilization of these algorithms. Author

N95-28754*# McDonnell-Douglas Corp., Saint Louis, MO. Computational Fluid Dynamics Project.
GENERATING GRIDS DIRECTLY ON CAD DATABASE SURFACES USING A PARAMETRIC EVALUATOR APPROACH **c61**
Timothy D. Gatzhe and Thomas G. Melson *In* NASA. Lewis Research Center, Surface Modeling, Grid Generation, and Related Issues in Computational Fluid Dynamic (CFD) Solutions Mar. 1995 p 505-515 (For primary document see N95-28723 10-02)
Avail: CASI HC A03/MF A10

A very important, but often overlooked step in grid generation is acquiring a suitable geometry definition of the vehicle to be analyzed. In the past, geometry was usually obtained by generating a number of cross-sections of each component. A number of recent efforts have focussed on non-uniform rational B-spline surfaces (NURBS) to provide as single type of analytic surface to deal with inside the grid generator. This approach has required the development of tools to read other types of surfaces and convert them, either exactly or by approximation, into a NURBS surface. This paper describes a more generic parametric evaluator approach, which does not rely on a particular surface type internal to the grid generation system and is less restrictive in the number of surface types that can be represented exactly. This approach has been implemented in the McDonnell Douglas grid generation system, MACGS, and offers direct access to all types of surfaces from a Unigraphics part file. Author

N95-28755*# Rockwell International Corp., Seal Beach, CA. North American Aircraft Div.
GRID GENERATION ON TRIMMED BEZIER AND NURBS QUILTED SURFACES **c61**
Chung-Jin Woan, Willard C. Clever, and Clement K. Tam *In* NASA. Lewis Research Center, Surface Modeling, Grid Generation, and Related Issues in Computational Fluid Dynamic (CFD) Solutions Mar. 1995 p 517-534 (For primary document see N95-28723 10-02)
Avail: CASI HC A03/MF A10

This paper presents some recently added capabilities to RAGGS, Rockwell Automated Grid Generation System. Included are the trimmed surface handling and display capability and structures and unstructured grid generation on trimmed Bezier and NURBS (non-uniform rational B-spline surfaces) quilted surfaces. Samples are given to demonstrate the new capabilities. Author

N95-28756*# Pratt and Whitney Aircraft, East Hartford, CT.
GEOMETRIC GRID GENERATION **c61**
David Ives *In* NASA. Lewis Research Center, Surface Modeling, Grid Generation, and Related Issues in Computational Fluid Dynamic (CFD) Solutions Mar. 1995 p 535-557 (For primary document see N95-28723 10-02)
Avail: CASI HC A03/MF A10

This paper presents a highly automated hexahedral grid generator based on extensive geometrical and solid modeling operations developed in response to a vision of a designer-driven one day turnaround CFD process which implies a designer-driven one hour grid generation process. Author

N95-28757*# Centre Europeen Recherche et de Formation Advance en Calcul Scientific, Toulouse (France).
ALGORITHMS FOR THE AUTOMATIC GENERATION OF 2-D STRUCTURED MULTI-BLOCK GRIDS **c61**
Thilo Schoenfeld, Per Weinerfelt (Linkoeping Univ., Sweden.), and Carl B. Jenssen (Selskapet for Industriell og Teknisk Forskning, Trondheim, Norway.) *In* NASA. Lewis Research Center, Surface Modeling, Grid Generation, and Related Issues in Computational Fluid Dynamic (CFD) Solutions Mar. 1995 p 561-580 (For primary document see N95-28723 10-02)
Avail: CASI HC A03/MF A10

Two different approaches to the fully automatic generation of structured multi-block grids in two dimensions are presented. The work aims to simplify the user interactivity necessary for the definition of a multiple block grid topology. The first approach is based on an advancing front method commonly used for the generation of unstructured grids. The original algorithm has been modified toward the generation of large quadrilateral elements. The second method is based on the divide-and-conquer paradigm with the global domain recursively partitioned into sub-domains. For either method each of the resulting blocks is then meshed using transfinite interpolation and elliptic smoothing. The applicability of these methods to practical problems is demonstrated for typical geometries of fluid dynamics. Author

N95-28758*# Rutgers - The State Univ., New Brunswick, NJ. Dept. of Computer Science.

INTELLIGENT AUTOMATED SURFACE GRID GENERATION **c61**

Ke-Thia Yao and Andrew Gelsey *In* NASA. Lewis Research Center, Surface Modeling, Grid Generation, and Related Issues in Computational Fluid Dynamic (CFD) Solutions Mar. 1995 p 581-595 (For primary document see N95-28723 10-02)

(Contract NAG2-645; ARPA-63-93-C-0064; NSF CCR-92-09793)

Avail: CASI HC A03/MF A10

The goal of our research is to produce a flexible, general grid generator for automated use by other programs, such as numerical optimizers. The current trend in the gridding field is toward interactive gridding. Interactive gridding more readily taps into the spatial reasoning abilities of the human user through the use of a graphical interface with a mouse. However, a sometimes fruitful approach to generating new designs is to apply an optimizer with shape modification operators to improve an initial design. In order for this approach to be useful, the optimizer must be able to automatically grid and evaluate the candidate designs. This paper describes and intelligent gridder that is capable of analyzing the topology of the spatial domain and predicting approximate physical behaviors based on the geometry of the spatial domain to automatically generate grids for computational fluid dynamics simulators. Typically gridding programs are given a partitioning of the spatial domain to assist the gridder. Our gridder is capable of performing this partitioning. This enables the gridder to automatically grid spatial domains of wide range of configurations. Author

N95-28759*# Korea Air Force Academy, Cheong-Ju (Korea). Dept. of Aerospace Engineering.

OPTIMAL DOMAIN DECOMPOSITION STRATEGIES **c61**

Yonghyun Yoon and Bharat K. Soni (Mississippi State Univ., Mississippi State, MS.) *In* NASA. Lewis Research Center, Surface Modeling, Grid Generation, and Related Issues in Computational Fluid Dynamic (CFD) Solutions Mar. 1995 p 597-613 (For primary document see N95-28723 10-02)

Avail: CASI HC A03/MF A10

The primary interest of the authors is in the area of grid generation, in particular, optimal domain decomposition about realistic configurations. A grid generation procedure with optimal blocking strategies has been developed to generate multi-block grids for a circular-to-rectangular transition duct. The focus of this study is the domain decomposition which optimizes solution algorithm/block compatibility based on geometrical complexities as well as the physical characteristics of flow field. The progress realized in this study is summarized in this paper. Author

N95-28760*# National Aerospace Lab., Amsterdam (Netherlands).

ELLIPTIC SURFACE GRID GENERATION ON MINIMAL AND PARMETRIZED SURFACES **c61**

S. P. Spekreijse, G. H. Nijhuis, and J. W. Boerstoel *In* NASA. Lewis Research Center, Surface Modeling, Grid Generation, and Related Issues in Computational Fluid Dynamic (CFD) Solutions Mar. 1995 p 617-636 (For primary document see N95-28723 10-02)

Avail: CASI HC A03/MF A10

An elliptic grid generation method is presented which generates excellent boundary conforming grids in domains in 2D physical space. The method is based on the composition of an algebraic and elliptic transformation. The composite mapping obeys the familiar Poisson grid generation system with control functions specified by the algebraic transformation. New expressions are given for the control functions. Grid orthogonality at the boundary is achieved by modification of the algebraic transformation. It is shown that grid generation on a minimal surface in 3D physical space is in fact equivalent to grid generation in a domain in 2D physical space. A second elliptic grid generation method is presented which generates excellent boundary conforming grids on smooth surfaces. It is assumed that the surfaces are parametrized and that the grid only depends on the shape of the surface and is independent of the parametrization. Concerning surface modeling, it is shown that bicubic Hermite interpolation is an excellent method to generate a smooth surface which is passing through a given discrete set of control points. In contrast to bicubic spline interpolation, there is extra freedom to model the tangent and twist vectors such that spurious oscillations are prevented. Author

N95-28761*# Boeing Co., Seattle, WA. Aerodynamics Configuration Computing.

COOPERATIVE SOLUTIONS COUPLING A GEOMETRY ENGINE AND ADAPTIVE SOLVER CODES **c61**

Thomas P. Dickens *In* NASA. Lewis Research Center, Surface Modeling, Grid Generation, and Related Issues in Computational Fluid Dynamic (CFD) Solutions Mar. 1995 p 637-646 (For primary document see N95-28723 10-02)

Avail: CASI HC A02/MF A10

Follow-on work has progressed in using Aero Grid and Paneling System (AGPS), a geometry and visualization system, as a dynamic real time geometry monitor, manipulator, and interrogator for other codes. In particular, AGPS has been successfully coupled with adaptive flow solvers which iterate, refining the grid in areas of interest, and continuing on to a solution. With the coupling to the geometry engine, the new grids represent the actual geometry much more accurately since they are derived directly from the geometry and do not use refits to the first-cut grids. Additional work has been done with design runs where the geometric shape is modified to achieve a desired result. Various constraints are used to point the solution in a reasonable direction which also more closely satisfies the desired results. Concepts and techniques are presented, as well as examples of sample case studies. Issues such as distributed operation of the cooperative codes versus running all codes locally and pre-calculation for performance are discussed. Future directions are considered which will build on these techniques in light of changing computer environments. Author

N95-28762*# Rockwell International Corp., Canoga Park, CA. Rocketdyne Div.

AUTOMATION OF THREE-DIMENSIONAL STRUCTURED MESH GENERATION FOR TURBOMACHINERY BLADE PASSAGES **c61**

Edward P. Ascoli and George H. Prueger *In* NASA. Lewis Research Center, Surface Modeling, Grid Generation, and Related Issues in Computational Fluid Dynamic (CFD) Solutions Mar. 1995 p 647-655 (For primary document see N95-28723 10-02)

Avail: CASI HC A02/MF A10

Hybrid tools have been developed which greatly reduce the time required to generate three-dimensional structured CFD meshes for turbomachinery blade passages. RAGGS, an existing Rockwell proprietary, general purpose mesh generation and visualization system, provides the starting point and framework for tool development. Utilities which manipulate and interface with RAGGS tools have been developed to (1) facilitate blade geometry inputs from point or CAD representations, (2) automate auxiliary surface creation, and (3) streamline and automate edge, surface, and subsequent volume mesh generation from minimal inputs. The emphasis of this approach has been to maintain all the functionality of the general purpose mesh generator while simultaneously eliminating the bulk of the repetitive and tediuos manual steps in the mesh generation process. Using this approach, mesh generation cycle times have been reduced from the order of days down to the order of hours. Author

N95-28763*# Computer Sciences Corp., Hampton, VA.

A GRID GENERATION SYSTEM FOR MULTI-DISCIPLINARY DESIGN OPTIMIZATION **c61**

William T. Jones and Jamshid Samareh-Abolhassani *In* NASA. Lewis Research Center, Surface Modeling, Grid Generation, and Related Issues in Computational Fluid Dynamic (CFD) Solutions Mar. 1995 p 657-667 (For primary document see N95-28723 10-02)

Avail: CASI HC A03/MF A10

A general multi-block three-dimensional volume grid generator is presented which is suitable for Multi-Disciplinary Design Optimization. The code is timely, robust, highly automated, and written in ANSI 'C' for platform independence. Algebraic techniques are used to generate and/or modify block face and volume grids to reflect geometric changes resulting from design optimization. Volume grids are generated/modified in a batch environment and controlled via an ASCII user input deck. This allows the code to be incorporated directly into the design loop. Generated volume grids are presented for a High Speed Civil Transport (HSCT) Wing/Body geometry as well a complex HSCT configuration including horizontal and vertical tails, engine nacelles and pylons, and canard surfaces. Author

N95-28764*# Washington Univ., Seattle, WA. Dept. of Aeronautics and Astronautics.

AUTOMATIC MULTI-BLOCK GRID GENERATION FOR HIGH-LIFT CONFIGURATION WINGS **c61**

Byoungsoo Kim and Scott Eberhardt *In* NASA. Lewis Research Center, Surface Modeling, Grid Generation, and Related Issues in Computational Fluid Dynamic (CFD) Solutions Mar. 1995 p 671-688 Sponsored by NASA. Ames Research Center (For primary document see N95-28723 10-02)

Avail: CASI HC A03/MF A10

A new method for automatic multi-block grid generation is described. The method combines the Modified Advancing Front Method as a Predictor with an elliptic scheme as a corrector. It advances a collection of cells by one cell height in the outward direction using Modified Advancing Front Method, and then corrects newly-obtained cell positions by solving elliptic equations. This predictor-corrector type scheme is repeatedly applied until the field of interest is filled with hexahedral grid cells. Given the configuration surface grid, the scheme produces block layouts as well as grid cells with overall smoothness as its output. The present method saves human-time and reduces the burden on the user in generating grids for general 3-D configurations. It was used to generate multi-block grids for wings in their high-lift configuration. Author

N95-28765*# National Aeronautics and Space Administration. Langley Research Center, Hampton, VA.

MULTILEVEL ELLIPTIC SMOOTHING OF LARGE THREE-DIMENSIONAL GRIDS **c61**

C. Wayne Mastin *In* NASA. Lewis Research Center, Surface Modeling, Grid Generation, and Related Issues in Computational Fluid Dynamic (CFD) Solutions Mar. 1995 p 689-696 (For primary document see N95-28723 10-02)

Avail: CASI HC A02/MF A10

Elliptic grid generation methods have been used for many years to smooth and improve grids generated by algebraic interpolation schemes. However, the elliptic system that must be solved is nonlinear and convergence is generally very slow for large grids. In an attempt to make elliptic methods practical for large three-dimensional grids, a two-stage implementation is developed where the overall grid point locations are set using a coarse grid generated by the elliptic system. The coarse grid is then interpolated to generate a finer grid which is smoothed using only a few iterations of the elliptic system. Author

N95-28766*# National Aeronautics and Space Administration. Lewis Research Center, Cleveland, OH.

ADVANCED METHODOLOGY FOR SIMULATION OF COMPLEX FLOWS USING STRUCTURED GRID SYSTEMS **c34**

Erlendur Steinthorsson and David Modiano *In its* Surface Modeling, Grid Generation, and Related Issues in Computational Fluid Dynamic (CFD) Solutions Mar. 1995 p 697-710 (For primary document see N95-28723 10-02)

Avail: CASI HC A03/MF A10

Detailed simulations of viscous flows in complicated geometries pose a significant challenge to current capabilities of Computational Fluid Dynamics (CFD). To enable routine application of CFD to this class of problems, advanced methodologies are required that employ (a) automated grid generation, (b) adaptivity, (c) accurate discretizations and efficient solvers, and (d) advanced software techniques. Each of these ingredients contributes to increased accuracy, efficiency (in terms of human effort and computer time), and/or reliability of CFD software. In the long run, methodologies employing structured grid systems will remain a viable choice for routine simulation of flows in complex geometries only if genuinely automatic grid generation techniques for structured grids can be developed and if adaptivity is employed more routinely. More research in both these areas is urgently needed. Author

N95-28767*# National Aerospace Lab., Amsterdam (Netherlands).

DEMONSTRATION OF AN AUTOMATED CFD SYSTEM FOR THREE-DIMENSIONAL FLOW SIMULATIONS **c34**

J. W. vanderBurg, J. E. J. Maseland, R. Hagmeijer, and K. M. J. deCock *In* NASA. Lewis Research Center, Surface Modeling, Grid Generation, and Related Issues in Computational Fluid Dynamic (CFD) Solutions Mar. 1995 p 713-730 Sponsored by Netherlands Agency for Aerospace Programs (For primary document see N95-28723 10-02)

Avail: CASI HC A03/MF A10

In this paper the capabilities of an automated CFD system which is currently available at NLR are demonstrated. Transonic flow around the AS28G wing/body configuration and hypersonic flow through a generic three-dimensional mixed-compression airbreathing inlet are simulated. An assessment of the level of automation of the current CFD-system is made. The problem-turnaround time lies within the order of a week for both applications. Author

N95-28768*# National Aeronautics and Space Administration. Ames Research Center, Moffett Field, CA.

A PROCEDURE FOR AUTOMATING CFD SIMULATIONS OF AN INLET-BLEED PROBLEM **c34**

Wei J. Chyu, Mark J. Rimlinger (Carnegie-Mellon Univ., Pittsburgh, PA.), and Tom I.-P. Shih (Carnegie-Mellon Univ., Pittsburgh, PA.) *In* NASA. Lewis Research Center, Surface Modeling, Grid Generation, and Related Issues in Computational Fluid Dynamic (CFD) Solutions Mar. 1995 p 731-749 (For primary document see N95-28723 10-02)

Avail: CASI HC A03/MF A10

A procedure was developed to improve the turn-around time for computational fluid dynamics (CFD) simulations of an inlet-bleed problem involving oblique shock-wave/boundary-layer interactions on a flat plate with bleed into a plenum through one or more circular holes. This procedure is embodied in a preprocessor called AUTOMAT. With AUTOMAT, once data for the geometry and flow conditions have been specified (either interactively or via a namelist), it will automatically generate all input files needed to perform a three-dimensional Navier-Stokes simulation of the prescribed inlet-bleed problem by using the PEGASUS and OVERFLOW codes. The input files automatically generated by AUTOMAT include those for the grid system and those for the initial and boundary conditions. The grid systems automatically generated by AUTOMAT are multi-block structured grids of the overlapping type. Results obtained by using AUTOMAT are presented to illustrate its capability. Author

N95-28769*# United Technologies Research Center, East Hartford, CT.

A TECHNIQUE FOR OPTIMIZING GRID BLOCKS **c61**

John F. Dannenhoffer, III *In* NASA. Lewis Research Center, Surface Modeling, Grid Generation, and Related Issues in Computational Fluid Dynamic (CFD) Solutions Mar. 1995 p 751-762 (For primary document see N95-28723 10-02)

Avail: CASI HC A03/MF A10

A new technique for automatically combining grid blocks of a given block-structured grid into logically-rectangular clusters which are 'optimal' is presented. This technique uses the simulated annealing optimization method to reorganize the blocks into an optimum configuration, that is, one which minimizes a user-defined objective function such as the number of clusters or the differential in the sizes of all the clusters. The clusters which result from applying the technique to two different two-dimensional configurations are presented for a variety of objective function definitions. In all cases, the automatically-generated clusters are significantly better than the original clusters. While this new technique can be applied to block-structured grids generated from any source, it is particularly useful for operating on block-structured grids containing many blocks, such as those produced by the emerging automatic block-structured grid generators. Author

N95-28770*# National Aeronautics and Space Administration. Lewis Research Center, Cleveland, OH.

A COMBINED GEOMETRIC APPROACH FOR COMPUTATIONAL FLUID DYNAMICS ON DYNAMIC GRIDS **c34**

John W. Slater *In its* Surface Modeling, Grid Generation, and Related Issues in Computational Fluid Dynamic (CFD) Solutions Mar. 1995 p 763-780 (For primary document see N95-28723 10-02)

Avail: CASI HC A03/MF A10

A combined geometric approach for computational fluid dynamics is presented for the analysis of unsteady flow about mechanisms in which its components are in moderate relative motion. For a CFD analysis, the total dynamics problem involves the dynamics of the aspects of geometry modeling, grid generation, and flow modeling. The interrelationships between these three aspects allow for a more natural formulation of the problem

and the sharing of information which can be advantageous to the computation of the dynamics. The approach is applied to planar geometries with the use of an efficient multi-block, structured grid generation method to compute unsteady, two-dimensional and axisymmetric flow. The applications presented include the computation of the unsteady, inviscid flow about a hinged-flap with flap deflections and a high-speed inlet with centerbody motion as part of the unstart / restart operation. Author

N95-28771*# AeroHydro, Inc., Southwest Harbor, ME.
PARAMETRIC DESIGN AND GRIDDING THROUGH RELATIONAL GEOMETRY **c61**
John S. Letcher, Jr. and D. Michael Shook *In* NASA. Lewis Research Center, Surface Modeling, Grid Generation, and Related Issues in Computational Fluid Dynamic (CFD) Solutions Mar. 1995 p 783-800 (For primary document see N95-28723 10-02)
(Contract N00167-95-C-0003)
Avail: CASI HC A03/MF A10

Relational Geometric Synthesis (RGS) is a new logical framework for building up precise definitions of complex geometric models from points, curves, surfaces and solids. RGS achieves unprecedented design flexibility by supporting a rich variety of useful curve and surface entities. During the design process, many qualitative and quantitative relationships between elementary objects may be captured and retained in a data structure equivalent to a directed graph, such that they can be utilized for automatically updating the complete model geometry following changes in the shape or location of an underlying object. Capture of relationships enables many new possibilities for parametric variations and optimization. Examples are given of panelization applications for submarines, sailing yachts, offshore structures, and propellers. Author

N95-28772*# Program Development Corp., White Plains, NY.
EXAMPLES OF GRID GENERATION WITH IMPLICITLY SPECIFIED SURFACES USING GridPro (TM)/az3000. 1: FILLETED MULTI-TUBE CONFIGURATIONS **c61**
Zheming Cheng and Peter R. Eiseman *In* NASA. Lewis Research Center, Surface Modeling, Grid Generation, and Related Issues in Computational Fluid Dynamic (CFD) Solutions Mar. 1995 p 801-819 (For primary document see N95-28723 10-02)
Avail: CASI HC A03/MF A10

With examples, we illustrate how implicitly specified surfaces can be used for grid generation with GridPro/az3000. The particular examples address two questions: (1) How do you model intersecting tubes with fillets? and (2) How do you generate grids inside the intersected tubes? The implication is much more general. With the results in a forthcoming paper which develops an easy-to-follow procedure for implicit surface modeling, we provide a powerful means for rapid prototyping in grid generation. Author

N95-28773*# Computer Sciences Corp., Hampton, VA.
GridTool: A SURFACE MODELING AND GRID GENERATION TOOL **c61**
Jamshid Samareh-Abolhassani *In* NASA. Lewis Research Center, Surface Modeling, Grid Generation, and Related Issues in Computational Fluid Dynamic (CFD) Solutions Mar. 1995 p 821-831 (For primary document see N95-28723 10-02)
Avail: CASI HC A03/MF A10

GridTool is designed around the concept that the surface grids are generated on a set of bi-linear patches. This type of grid generation is quite easy to implement, and it avoids the problems associated with complex CAD surface representations and associated surface parameterizations. However, the resulting surface grids are close to but not on the original CAD surfaces. This problem can be alleviated by projecting the resulting surface grids onto the original CAD surfaces. GridTool is designed primary for unstructured grid generation systems. Currently, GridTool supports VGRID and FELISA systems, and it can be easily extended to support other unstructured grid generation systems. The data in GridTool is stored parametrically so that once the problem is set up, one can modify the surfaces and the entire set of points, curves and patches will be updated automatically. This is very useful in a multidisciplinary design and optimization process. GridTool is written entirely in ANSI 'C', the interface is based on the FORMS library, and the graphics is based on the GL library. The code has been tested successfully on IRIS workstations running IRIX4.0 and above. The memory is allocated dynamically, therefore, memory size will depend on the complexity of geometry/grid. GridTool data structure is based on a link-list structure which allows the required memory to expand and contract dynamically according to the user's data size and action. Data structure contains several types of objects such as points, curves, patches, sources and surfaces. At any given time, there is always an active object which is drawn in magenta, or in their highlighted colors as defined by the resource file which will be discussed later. Author

N95-28774*# Program Development Corp., White Plains, NY.
INTERACTIVE HIGH QUALITY GRID GENERATION **c61**
Ning Lu and Peter R. Eiseman *In* NASA. Lewis Research Center, Surface Modeling, Grid Generation, and Related Issues in Computational Fluid Dynamic (CFD) Solutions Mar. 1995 p 833-843 (For primary document see N95-28723 10-02)
Avail: CASI HC A03/MF A10

We generate high quality grids interactively on a computer workstation through optimization for some simple yet commonly encountered geometric shapes. Author

N95-28775*# Computer Sciences Corp., Moffett Field, CA.
NASA-IGES TRANSLATOR AND VIEWER **c61**
Jin J. Chou and Michael A. Logan *In* NASA. Lewis Research Center, Surface Modeling, Grid Generation, and Related Issues in Computational Fluid Dynamic (CFD) Solutions Mar. 1995 p 845-855 (For primary document see N95-28723 10-02)
Avail: CASI HC A03/MF A10

NASA-IGES Translator (NIGEStranslator) is a batch program that translates a general IGES (Initial Graphics Exchange Specification) file to a NASA-IGES-Nurbs-Only (NINO) file. IGES is the most popular geometry exchange standard among Computer Aided Geometric Design (CAD) systems. NINO format is a subset of IGES, implementing the simple and yet the most popular NURBS (Non-Uniform Rational B-Splines) representation. NIGEStranslator converts a complex IGES file to the simpler NINO file to simplify the tasks of CFD grid generation for models in CAD format. The NASA-IGES Viewer (NIGESview) is an Open-Inventor-based, highly interactive viewer/ editor for NINO files. Geometry in the IGES files can be viewed, copied, transformed, deleted, and inquired. Users can use NIGEStranslator to translate IGES files from CAD systems to NINO files. The geometry then can be examined with NIGESview. Extraneous geometries can be interactively removed, and the cleaned model can be written to an IGES file, ready to be used in grid generation. Author

N95-28800 ESDU International Ltd., London (England).
LEADING-EDGE SUCTION DISTRIBUTION FOR PLANE THIN WINGS AT SUBSONIC SPEEDS
Nov. 1994 58 p
(ISSN 0141-397X)
(ESDU-94037; ISBN-0-85679-924-6) Avail: ESDU

ESDU 94037 gives an expression for calculating the total theoretical leading-edge suction force using the lift-curve slope and the lift-dependent drag factor which can be obtained respectively from ESDU 70011 and 74035. The normalized spanwise distribution of suction for plane straight-tapered wings is tabulated, and illustrated in graphs, for a systematic set of planforms that allows the distribution to be obtained for any wing by cross plotting the tabulated results. The results were obtained from runs of a vortex-lattice program but special modelling was necessary for certain difficult planforms such as those of low taper ratio and low aspect ratio, and also in the vicinity of the centre-line chord, to ensure a coherent set of normalized distributions. Details of the corrections are included. A computer program, ESDUpac A9438, is introduced in ESDU 94038, which incorporates all the corrected tabulated data, carries out any interpolation required to obtain the distribution for the chosen planform and calculates the total suction force. The expected accuracy of the results is discussed. Author

N95-28885 ESDU International Ltd., London (England).
INCREMENTS IN AEROFOIL LIFT COEFFICIENT AT ZERO ANGLE OF ATTACK AND IN MAXIMUM LIFT COEFFICIENT DUE TO DEPLOYMENT OF A PLAIN TRAILING-EDGE FLAP, WITH OR WITHOUT A LEADING-EDGE HIGH-LIFT DEVICE, AT LOW SPEEDS

Dec. 1994 15 p
(ISSN 0141-397X)
(ESDU-94028; ISBN-0-85679-915-7) Avail: ESDU

ESDU 94028 presents an estimation method based on first approximations from the theory for a thin hinged plate modified using empirical correlation factors to account for the geometry of practical aerofoils and high-lift devices. To allow for the effects of chord extension, the flap chord ratio and lift coefficients are based on an aerofoil extended chord. The data for aerofoils with trailing-edge flaps deployed from which the methods were developed were extracted from wind-tunnel tests reported in the literature covering a wide range of practical geometries. Fewer data were available for aerofoils with both leading- and trailing-edge devices deployed. The methods apply to Reynolds numbers greater than a million and freestream Mach numbers less than 0.2. The predicted and test data for the lift coefficient increments at zero angle of attack and at maximum lift are correlated to within 20 percent. The use of the methods is illustrated by worked examples. To obtain results for an aerofoil with both leading-edge devices and plain flaps deployed, ESDU 84026 is used in conjunction with this document and ESDU 94027. ESDU

N95-28897 ESDU International Ltd., London (England).
EXCRESCENCE DRAG LEVELS ON AIRCRAFT
Nov. 1994 34 p
(ISSN 0141-4054)
(ESDU-94044; ISBN-0-856-79931-9) Avail: ESDU

ESDU 94044 is based on manufacturer's estimated values for a large number of aircraft as manufactured and provides a guide to standards that have been achieved and a method to obtain a first approximate estimate. In most cases a datum drag parameter is presented at the troposphere and a Mach number of 0.8; a correction factor to other altitudes and speeds whose derivation is included is based on a detailed study of the variation of excrescence drag with Reynolds and Mach numbers. The drag parameter is plotted against wetted area for complete airframes but, for a more detailed estimate, values for some categories of excrescence are also given graphically. They are: surface and control imperfections, air-data systems, lights and beacons, antennas, static discharge wicks, auxiliary power unit, and features required for rain dispersal, for ventilation/cooling, for air-conditioning and for fuel systems. Some information is included on the extent that 'clean-up' has proved possible on several aircraft. Author

N95-28904 ESDU International Ltd., London (England).
SURFACE PRESSURE COEFFICIENT DISTRIBUTIONS FOR AXISYMMETRIC FORECOWLS AT ZERO INCIDENCE (M SUB INFINITY LESS THAN OR EQUAL TO 1.5)
Jun. 1994 78 p
(ISSN 0141-4356)
(ESDU-94015; ISBN-0-85679-902-5) Avail: ESDU

ESDU 94015 presents charts for 20 cowls of the distributions computed from finite difference solutions to the Euler equations for inviscid compressible flow. Computed shock waves are smeared over a few mesh cells which should give correct shock pressure jumps. The results are shown as functions of freestream Mach number and mass flow ratio. Data are presented for the same cowls and flow conditions as in ESDU 94014 which gives corresponding values of coefficients of wave drag, pre-entry force and forecowl pressure force. Sixteen cowls have NACA 1-series external profile, with differing combinations of diameter ratio and fineness ratio. The remaining four have fixed diameter ratio and fineness ratio but external profiles that differ systematically from the NACA I-series profile. Author

N95-28921# Notre Dame Univ., IN. Dept. of Aerospace and Mechanical Engineering.
THE EFFECTS OF THREE-DIMENSIONAL IMPOSED DISTURBANCES ON BLUFF BODY NEAR WAKE FLOWS: EFFECTS OF TAPER AND SPLITTER PLATES ON THE NEAR WAKE CHARACTERISTICS OF A CIRCULAR CYLINDER IN UNIFORM AND SHEAR FLOW Final Report
Elgin A. Anderson and Albin A. Szewczyk Apr. 1994 320 p
(Contract N00014-90-J-4083)
(AD-A292113) Avail: CASI HC A14/MF A03

The near wake characteristics of a circular cylinder were modified by use of splitter plates, cylinder taper, and shear flow to investigate the relationship between the various near wake parameters. The results are based on hot wire and mean pressure measurements, flow visualization of the near wake, and linear stability analysis of the shear layer. The straight cylinder variation in Strouhal number with respect to splitter plate length was divided into four regions identified by the flow phenomenon that dominates the shedding frequency selection namely, stabilizing, shear layer elongation, reduced entrainment, and splitter plate-vortex interaction. A sinuous plate increased the 2-dimensionality of the shear layer compared to the straight plate and affected the spanwise coherence of the Karman vortices. However, within the formation region the sinuous splitter plate produced results similar to those produced by a straight plate of equal average length. DTIC

N95-29091# Washington State Univ., Pullman, WA. Dept. of Mechanical and Materials Engineering.
INTERACTIONS OF SPANWISE AND CHORDWISE VORTICITY ASSOCIATED WITH THREE-DIMENSIONAL DYNAMIC STALL OVER AN OSCILLATING WING Final Report, 15 Feb. 1991 - 15 Aug. 1994
B. R. Ramaprian 15 Oct. 1994 19 p
(Contract DAAL03-91-G-0026)
(AD-A290546; ARO-28159.9-EG) Avail: CASI HC A03/MF A01

This is the final report on the experimental research performed under U.S. Army Research Office Grant No. DAAL 03-91-0026, with Dr. Thomas Doligaiski as the Technical Program Manager. The Principal Investigator was B.R. Ramaprian. The research work involved the measurement of the pressure and velocity fields in the three-dimensional flow field surrounding and in the wake of the tip region of a rectangular wing of NACA 0015 profile. Measurements were made both with the wing stationary and with the wing oscillating sinusoidally in pitch about its quarter-chord axis. Pressure transducers and three-component laser Doppler velocimetry were used in these measurements. The results have been used to understand the vorticity dynamics in three-dimensional steady and unsteady flows. The study is relevant to helicopter rotor aerodynamics. All the data have been archived and are available for use by any interested reader. DTIC

N95-29094 Minnesota Univ., Minneapolis, MN.
STUDIES IN DRAG REDUCTION Ph.D. Thesis
Christodoulos Christodoulou 1994 165 p
Avail: Univ. Microfilms Order No. DA9415476

Drag reduction due to riblets (streamwise longitudinal grooves) in fully developed turbulent flows in pipes and cylindrical Couette flows is established and shown to have similar characteristics. The maximum drag reduction is about eight percent and occurs when the riblet spacing (which in this case is equal to the riblet height) when expressed in wall units is about 11 to 16. This correlates well with the Taylor microscale of the fluctuating velocity gradient in the spanwise direction. The Taylor microscale was shown by Kailasnath and Sreenivasan to be approximately equal to the mean value of the zero-crossing scale of a random signal and our result was interpreted as a signal being influenced most through its zero-crossing scale. The combined effects of riblets and dilute polymer solutions in drag reduction in pipes is examined and the results show a superposition of drag reduction (but not additive) that depends on the kind of polymer used and its concentration. Some additions to the wave speed meter are reported as well as new wave speed data. A possibility of drag reduction in dilute polymer solutions being a change of type phenomenon is stated. Finally friction factors versus Reynolds number curves are computed using the k-e model for perfect core annular flow of water and crude oil in pipes. Dissert. Abstr.

N95-29102 Florida State Univ., Gainesville, FL.
PIV INVESTIGATION OF COMPRESSIBILITY EFFECTS ON DYNAMIC STALL Ph.D. Thesis
William Paul Crisler 1993 164 p
Avail: Univ. Microfilms Order No. DA9413277

An experimental investigation was conducted to study compressibility effects on dynamic stall for an airfoil pitching at a constant rate. Instantaneous, whole field velocity data was acquired using an on-line, video-based particle image velocimetry (PIV) system, which incorporated a passive, optical, displacement bias technique to eliminate the sign ambiguity inherent in PIV measurements of reversed flows. Vorticity data was subsequently computed from the corresponding velocity field. Free stream Mach numbers were 0.23 and 0.45, and corresponding Reynolds numbers were 280,000 and 620,000, respectively. Nondimensional pitch rates were

0.010, 0.030, and 0.060. Although the flow was near sonic in the high speed case, no shocks were observed. The sequence of events at high speed was remarkably similar to that at both low speed and to that observed in water tank experiments. The dynamic stall process is initiated with formation and convection aft of a single, discrete, vortex. Formation and initial release of the structure is probably initiated by a van Dommelen-Shen unsteady separation. A region of closed vorticity forms over the forward portion of the airfoil, caused by periodic reattachment and shedding of discrete vortical structures of positive sign from the leading edge. These structures and the adverse pressure gradient then induce production of negative vorticity near the airfoil surface, which is convected forward and accumulates near the quarter chord. Subsequently, coherent negative vorticity is ejected into the outer flow, isolating the initial structures from the leading edge. Subsequent interaction induces separation from the surface of the dynamic stall vortex, which is composed of several small, interacting structures rather than a single, large structure. The data complement Schlieren and surface pressure investigations, which are useful but provide no information about local flow direction. The data also demonstrate the utility of PIV for investigating highly unsteady, reversed flows with dynamic boundary conditions at compressible or transonic speeds. Dissert. Abstr.

N95-29108 Georgia Inst. of Tech., Atlanta, GA.
A VORTICITY-VELOCITY APPROACH FOR THREE-DIMENSIONAL UNSTEADY VISCOUS FLOW OVER WINGS Ph.D. Thesis
Goo Kim 1993 271 p
Avail: Univ. Microfilms Order No. DA9415648

A computational method for the simulation of three-dimensional unsteady viscous flows is presented in this thesis. Particular attention is given to the three-dimensional application of the integro-differential formulation for the Navier-Stokes flows. This formulation has some salient features, including the capability of the 'zonal solution,' which are believed to be still useful for efficient and accurate computation of three-dimensional flow. Satisfaction of the constraint of no vorticity divergence in computation is emphasized for the stable convergence of a steady flow solution as well as for the physical validity of the solution. It is shown that the constraint can be automatically satisfied if the curl form of the vorticity transport equations are discretized through the use of an appropriate staggered arrangement of the variables. Second-order accurate centered-space differences are used in the discretization, and suitable artificial dissipation terms are added to the difference equations in the manner of not destroying the basic divergence-free property of the resulting numerical scheme. The boundary vorticity is determined by the kinematic integral relationship between the vorticity and velocity distributions, with the vorticity constraint. Based on this method of determination, numerical techniques for efficient and accurate estimation of the boundary vorticity are presented. The surface pressure is also computed accurately using an integral representation for the pressure Poisson's equation. It appears that a solution of the Poisson's equation using the finite difference approximation could suffer from large discretization errors for flows over rapidly moving bodies. The validity of the present method is demonstrated by the application of the method to the problem of external flow past an impulsively starting NACA 0012 wing. Computational results are limited to low Reynolds-number flows in this study. They are investigated in various ways, compared with other numerical and experimental results available. Various important three-dimensional flow features are shown to be well simulated. By virtue of vorticity formulation, computation of dynamic flow about a maneuvering body is already in the scope of applicability of the present method. Also, computation of high Reynolds-number flows can be immediately carried out when an appropriate turbulence model is incorporated in the present solution scheme.
Dissert. Abstr.

N95-29118# University of Southern California, Los Angeles, CA.
AN EXTENSION OF THE CONTINUUM MODEL BY GRAD'S THIRTEEN MOMENT EQUATIONS FOR HYPERSONIC RAREFIED FLOWS Ph.D. Thesis
Eric Y. Wong 1993
Avail: Issuing Activity (Univ. of Southern California, Doheny Library, Micrographics Dept., Los Angeles, CA 90089-0182)

Whereas it is well known that Grad's thirteen moment equations fail to yield solutions for normal shock structures at freestream Mach number larger than 1.65, it is recognized, however, that these equations may be used as an extension of the continuum model behind the shock. In this study, the 13-moment equations are applied to the flow between a strong bow shock and a solid surface under the thin shock layer formalism resulting in greatly simplified constitutive relations. Two dimensional hypersonic flows on the windward side of unaligned flat plates are studied to assess the accuracy of this 13-moment based shock-layer theory. In flows of large translational nonequilibrium, the 13-moment based predictions in heat transfer and skin friction are found to be in agreement with Direct Simulation Monte Carlo results. Comparisons of the parallel and perpendicular distribution functions also show reasonable agreements. Of interest is a correlation principle revealed by this study, which relates gas kinetic based results to corresponding Navier Stokes based solutions. A key to the derivation of the principle is the use of the Von Mises or Dorodnitsyn variables, which enable the reduction of the 13-moment based shock-layer equations to those of the Navier-Stokes based system. A critical test of the principle is conducted by examining the degree of successful correlations for the velocity and enthalpy profiles of a monatomic gas about the unaligned flat plates. Detailed comparisons with DSMC calculations support the viability of the principle. Dissert. Abstr.

N95-29121 Kansas Univ., Lawrence, KS.
NAVIER-STOKES SOLUTION OF WING WAKE STRUCTURE AND ITS PERTURBATION Ph.D. Thesis
Ta-Cheng Lee 1993 134 p
Avail: Univ. Microfilms Order No. DA9425933

A 'flow embedding' method based on Navier-Stokes solutions is developed to calculate detailed wing wake structures. The method allows the calculation to be completed in two stages, first a global solution with a coarse grid and then the embedded solution in a small region with a dense grid. The boundary condition for the latter is obtained from the former. The main advantages of this two-staged scheme are: (1) it provides a very fine grid resolution in the region of interest to capture flow details; and (2) it calculates efficiently without demanding huge computer memory space. This embedded flow method, when comparing the numerical results with available experimental data in the near wake, is shown to produce a detailed and accurate wake structure for a delta wing. The computed results further downstream indicate that there are two concentrated vortices, one being the leading edge vortex, and the other being the trailing vortex, rotating opposite to each other. These two vortices stay strong and well organized from feeding of wake shear layers. Due to this effect, the total pressure and axial velocity of both vortices are increasing in the downstream direction. For the rectangular wing of aspect ratio 6, the calculated results are also compared with near-wake experimental data. Again, two vortices are identified, one being the conventional tip vortex and the other being the trailing vortex. The tip vortex is formed at the wing tip and moves outboard and upward; while the trailing vortex is formed downstream from the roll-up of shear layer and tends to move inboard and downward. The calculated total velocity in the core and the maximum tangential velocity around the trailing vortex core are shown to agree reasonably well with experimental data. The steady-state Navier-Stokes solution of the local wake flow region further serves as a base flow for wake attenuation investigations. An oscillatory disturbance is imposed at the trailing edge of the wing in an attempt to excite the instabilities of the wake flow. Results from the unsteady computations indicate that the current scheme can excite the wake flow with limited success. Dissert. Abstr.

N95-29129 ESDU International Ltd., London (England).
INCREMENTS IN AEROFOIL LIFT COEFFICIENT AT ZERO ANGLE OF ATTACK AND IN MAXIMUM LIFT COEFFICIENT DUE TO DEPLOYMENT OF A TRAILING-EDGE SPLIT FLAP, WITH OR WITHOUT A LEADING-EDGE HIGH-LIFT DEVICE, AT LOW SPEEDS
Dec. 1994 17 p
(ISSN 0141-397X)
(ESDU-94029; ISBN-0-85679-916-5) Avail: ESDU

ESDU 94029 presents an estimation method based on first approximations from the theory for a thin hinged plate modified using empirical correlation factors to account for the geometry of practical aerofoils and high-lift devices. To allow for the effects of chord extension, the flap chord ratio and lift coefficients are based on an aerofoil extended chord. The data for aerofoils with trailing-edge flaps deployed from which the methods were developed were extracted from wind-tunnel tests reported in the literature covering a wide range of practical geometries. Fewer data

were available for aerofoils with both leading- and trailing-edge devices deployed. The methods apply to Reynolds numbers greater than a million and freestream Mach numbers less than 0.2. The predicted and test data for the lift coefficient increment at zero angle of attack correlated to within 10 per cent and for the increment in maximum lift coefficient to within 15 per cent. The use of the methods is illustrated by worked examples. To obtain results for an aerofoil with both leading-edge devices and split flaps deployed, ESDU 84026 is used in conjunction with this document and ESDU 94027. ESDU

N95-29243 Massachusetts Inst. of Tech., Cambridge, MA.
DYNAMIC STALL OF A NACA 0012 AIRFOIL IN LAMINAR FLOW Ph.D. Thesis
Sasi K. Digavalli 1994
Avail: Issuing Activity (MIT Libraries, Rm. 14-0551, Cambridge, MA 02139-4307)

The dynamic stall processes of a NACA 0012 airfoil oscillating sinusoidally in pitch and heave in laminar incompressible flow were investigated. The effects of changing the reduced frequency k from 0.6 to 1.2 and the pivot location x(0)/c from 1/4 to 3/4 were calculated. The nominal angle of incidence on the airfoil oscillated between 6 deg and 18 deg about a mean of 12 deg. The incompressible and inviscid external flow around the body was calculated using unsteady Bernoulli and a conformal transformation. The unsteady boundary layers were analyzed by C.C. Lin's asymptotic method applicable when the reduced frequency is 'large' . An unsteady separation condition, consistent with the Moore-Rott-Sears separation criterion, developed by A. Gioulekas as an extension of Stratford's separation condition for steady flows, was used to calculate the separation points of the boundary layers. The separated free shear layers were represented by discrete vortices. Each vortex was convected force-free (in the inertial frame) throughout the calculation by using the Biot-Savart law. The primary effect of moving the pivot towards the trailing edge is a delay in the onset of dynamic stall. The upstream movement of the separation point and the time of inception of the primary vortex are delayed. The slope of C(L)-alpha curve, the maximum velocity attained near the leading edge and the C(L(max)) decreased. The maximum penetration of the separation point towards the leading edge also decreased. The dwell time of the primary vortex near the leading edge is not altered significantly. Its maximum strength decreased while its average speed increased. Some of these effects of moving the pivot point and increasing k can qualitatively be forecast by analyzing the results from linear potential theory. Such an analysis leads to the definition of 'effective angle of incidence'. Dynamic stall characteristics of a heaving airfoil emulated some of the features of dynamic stall of a pitching airfoil with a rearward-pivot. Namely, upstream movement of the separation point and the inception of the primary vortex are delayed. The process of stall is less abrupt on a heaving airfoil than on a pitching airfoil with a forward pivot. The C(L(max)) and the strength of the primary vortex are both smaller. Some of these effects can also be deduced from an analysis of the simple linear potential theory. The effects of increasing the reduced frequency on the dynamic stalling of a heaving airfoil are similar to those on pitching airfoils.
Dissert. Abstr.

N95-29316# CFD Research Corp., Huntsville, AL.
PRESSURE BASED HIGH ORDER TVD METHODOLOGY FOR DYNAMIC STALL CONTROL Final Report, 30 Sep. 1992 - 30 Sep. 1994
H. Q. Yang, Z. J. Wang, V. J. Harrand, and A. J. Przekwas Nov. 1994 96 p
(Contract F49620-92-C-0070)
(AD-A290149; AFOSR-0020TR) Avail: CASI HC A05/MF A01

The objective was to study various dynamic stall control concepts using a code developed under Phase 1. The concepts studied were: vortex flaps, apex fence flaps, forebody strakes, spanwise blowing, leading edge blowing and suction, and forebody blowing and suction. DTIC

N95-29338*# Texas A&M Univ., College Station, TX.
A TWO ELEMENT LAMINAR FLOW AIRFOIL OPTIMIZED FOR CRUISE M.S. Thesis
Gregory Glen Steen Aug. 1994 175 p
(Grant NAG1-1522)
(NASA-CR-198580; NAS 1.26:198580) Avail: CASI HC A08/MF A02

Numerical and experimental results are presented for a new two-element, fixed-geometry natural laminar flow airfoil optimized for cruise Reynolds numbers on the order of three million. The airfoil design consists of a primary element and an independent secondary element with a primary to secondary chord ratio of three to one. The airfoil was designed to improve the cruise lift-to-drag ratio while maintaining an appropriate landing capability when compared to conventional airfoils. The airfoil was numerically developed utilizing the NASA Langley Multi-Component Airfoil Analysis computer code running on a personal computer. Numerical results show a nearly 11.75 percent decrease in overall wing drag with no increase in stall speed at sailplane cruise conditions when compared to a wing based on an efficient single element airfoil. Section surface pressure, wake survey, transition location, and flow visualization results were obtained in the Texas A&M University Low Speed Wind Tunnel. Comparisons between the numerical and experimental data, the effects of the relative position and angle of the two elements, and Reynolds number variations from 8 x 10(exp 5) to 3 x 10(exp 6) for the optimum geometry case are presented.
Author

N95-29402*# Modern Technologies Corp., Middleburg Heights, OH. Cleveland Office.
THE DECAY OF LONGITUDINAL VORTICES SHED FROM AIRFOIL VORTEX GENERATORS Final Contractor Report
Bruce J. Wendt, Bruce A. Reichert (Kansas State Univ., Manhattan, KS.), and Jeffry D. Foster (Iowa State Univ. of Science and Technology, Ames, IA.) Jun. 1995 13 p Presented at the 13th Applied Aerodynamics Conference, San Diego, CA, 19-22 Jun. 1995; sponsored by AIAA
(Contract NAS3-27377; RTOP 505-62-52)
(NASA-CR-198356; E-9730; NAS 1.26:198356; AIAA Paper 95-1797)
Avail: CASI HC A03/MF A01

An experimental study is conducted to examine the crossplane structure and streamwise decay of vortices shed from airfoil-type vortex generators. The vortex generators are set in a counter-rotating array spanning the full circumference of a straight pipe. The span of the vortex generators above the duct surface, h, is approximately equal to the local turbulent boundary layer thickness, delta. Measurement of three-component mean flow velocity in downstream crossplanes are used to characterize the structure of the shed vortices. Measurements in adjacent crossplanes (closely spaced along the streamwise coordinate) characterize the interaction and decay of the embedded vortices. A model constructed by the superposition of Oseen vortices is compared to the data for one test case. Author

N95-29428# Naval Postgraduate School, Monterey, CA. Dept. of Aeronautics and Astronautics.
COMPRESSIBILITY EFFECTS ON AND CONTROL OF DYNAMIC STALL OF OSCILLATING AIRFOIL Final Report, 14 Mar. 1990 - 30 Jun. 1994
M. S. Chandrasekhara 23 Dec. 1994 52 p
(Contract ARO-MIPR-103-94)
(AD-A291804; ARO-27894.27-EG) Avail: CASI HC A04/MF A01

A three year effort to study the 'Compressibility Effects on the Control of Dynamic Stall of Oscillating Airfoils' was funded by ARO in 1990. A fourth year extension was granted for the project. As part of this research, a new real-time interferometry system known as Point Diffraction Interferometry (PDI) was developed. Several new and exciting details of the dynamic stall flow over an oscillating airfoil such as formation of multiple shocks were captured. The study also addressed the role of transition in influencing the dynamic stall process. A concurrent computational study was carried out to investigate the role of transition. Additionally, LDV measurements of the dynamic stall flow were obtained which support the PDI observations. A high speed PDI 'movie' imaging system was designed to capture events of dynamic stall during a single pitch-up motion of the airfoil. This report describes the significant results obtained from the four year study of dynamic stall over an oscillating airfoil. DTIC

N95-29500# Air Force Inst. of Tech., Wright-Patterson AFB, OH. School of Engineering.
AN EXPERIMENTAL INVESTIGATION OF THE TIME-DEPENDENT SEPARATION OF TANGENT BODIES IN SUPERSONIC FLOW Final Report Ph.D. Thesis
Neal Anthony Mosbarger 1 Dec. 1994 318 p
(AD-A290720; AFIT/DS/AA/94-7) Avail: CASI HC A14/MF A03

An experimental, time-dependent separation of tangent bodies was performed in a supersonic wind tunnel (Mach 1.5 and 1.9) to investigate

the significance of transient effects and the suitability of using steady-state assumptions to predict a dynamic separation event. The model configurations consisted of two bodies placed in a near tangent position. A stationary body, plate or ogive, was instrumented to obtain dynamic surface pressures, while a second body, a wedge attached to an air cylinder, was plunged in a constrained motion away from and towards the stationary model. Three-dimensional flow expansion around the edge of the wedge reduced the strength of the shock waves and created a region of low pressure, near freestream static, on body surfaces between the incident and reflection shock waves. The dynamic motion of the wedge did not significantly affect the shock wave development between the bodies, and steady-state corrections that accounted for the motion-induced wedge angle were appropriate for predicting the time-dependent surface pressures induced by the incident shock wave. DTIC

N95-29640# Tokyo Univ. (Japan). Inst. of Space and Astronautical Science.

TRANSONIC, SUPERSONIC AND HYPERSONIC WIND-TUNNEL TESTS ON AERODYNAMIC CHARACTERISTICS OF REENTRY BODY WITH BLUNTED CONE CONFIGURATION

Kojiro Suzuki and Takashi Abe Mar. 1995 28 p
(ISAS-658) Avail: CASI HC A03/MF A01

The aerodynamic characteristics of the early version of the 'EXPRESS' reentry capsule, having a blunted cone configuration with flat bottom, are investigated experimentally over a wide range of the Mach number from 0.6 to 7.1 by using the transonic, supersonic and hypersonic wind tunnels. The continuity of the experimental data with respect to the Mach number is examined especially at the Mach numbers where the experimental facility is changed from the transonic wind tunnel to the supersonic wind tunnel and from the supersonic wind tunnel to the hypersonic wind tunnel. The experimental data in the supersonic and hypersonic regime show the tendency that when the Mach number becomes large, the aerodynamic characteristics become independent of the Mach number. It is clarified that in the transonic regime the aerodynamic center of the capsule moves forward and the static stability of the vehicle on the pitch plane is significantly reduced. In order to overcome such reduction in the static stability of the vehicle, it is necessary to deploy the parachute behind the capsule by the time when the flight Mach number decreases to the transonic regime and the static stability around the center-of-gravity vanishes. The critical Mach number for the parachute deployment is determined for various center-of-gravity locations. When the center-of-gravity of the capsule is located around the center of the body, the parachute must be deployed at supersonic speed. The effects of the nose shape and the bottom configuration on the aerodynamic characteristics of the capsule are experimentally investigated The validity of the Newtonian flow analysis in prediction of the aerodynamic characteristics of the capsule is assessed by comparisons with the experimental data. Author

N95-29771 Georgia Inst. of Tech., Atlanta, GA.

UNSTEADY PRESSURE AND INFLOW VELOCITY ON A PITCHING ROTOR BLADE IN HOVER Ph.D. Thesis

Mihir Kumar Lal 1993 221 p
Avail: Univ. Microfilms Order No. DA9415649

This dissertation seeks to describe and analyze the measurements of inflow velocity and chordwise distributions of unsteady pressure at three radial locations on a stiff two-bladed teetering helicopter rotor in hover, with the blades executing simple harmonic pitch oscillations about the quarter-chord pitch axis. The objective was to develop viable measurement techniques for determination of unsteady pressure and inflow velocity in the near field of a rotor blade for axial flow, with simple harmonic oscillation in pitch about finite mean values. These techniques enabled measurement of unsteady pressure and inflow velocity for a range of inflow conditions encompassed by the investigation. Two means of changing the mean inflow independent of reduced frequency have been employed, first by an appropriate combination of rotor speed and forcing frequency, and second by changing the mean pitch angle. The phase effects, reduced frequency effects, and the 3-dimensional tip effects on the lifting perturbation pressure have also been demonstrated. The unsteady pressures are correlated with Theodorsen's and Loewy's 2-dimensional incompressible unsteady aerodynamic theories and with Kaladi's pulsating doublet distribution method. The level of agreement between these analytical methods and the experiment has been assessed and guidelines have been provided for their use in order to obtain best possible results under given operating conditions and radial locations. Inflow velocity measured using a Laser Doppler Velocimeter is correlated with Peters' theory. The inflow velocity agrees very well with Peters' theory under steady as well as dynamic pitch. The inflow velocity under dynamic pitch shows velocity perturbation and dependence on the phase of excitation. Spectral analysis shows multiple harmonics of forcing frequency. Hysteresis is observed in inflow velocity which decays towards the tip. Dissert. Abstr.

N95-29788 Iowa State Univ. of Science and Technology, Ames, IA.

COMPUTATION OF THE INTEGRATED AERODYNAMIC AND PROPULSIVE FLOWFIELDS OF A GENERIC HYPERSONIC SPACE PLANE Ph.D. Thesis

Ganesh Wadawadigi 1993 85 p
Avail: Univ. Microfilms Order No. DA9414032

A new upwind, parabolized Navier-Stokes (PNS) code has been developed to compute two- and three-dimensional (3D) chemically reacting, turbulent flows with hydrogen-air chemistry. The code is a modification of the 3D upwind PNS (UPS) airflow code. The code solves the PNS equations using a finite-volume upwind, TVD (Total Variation Diminishing) method based on Roe's approximate Riemann solver that has been modified to account for non equilibrium effects. The fluid medium is assumed to be a chemically reacting mixture of thermally perfect (but calorically imperfect) gases in thermal equilibrium. Two turbulence models have been incorporated into the code including an algebraic model, that has the ability to account for internal flows with multiple walls, and a two-equation kappa-epsilon turbulence model. For the two-equation turbulence model option, the code solves the turbulence transport equations in an uncoupled manner from the fluids equations. With these enhancements, the UPS code is now capable of computing the chemically reacting flow in scramjet (supersonic combustion ramjet) engines. Various component test cases have been used to validate the code. The computed results are in good agreement with the available numerical and analytical solutions and experimental data. Finally, the full capabilities of the new code have been demonstrated with a 3D tip-to-tail numerical calculation of the integrated aerodynamic and propulsive flowfields of a generic hypersonic space plane. Two test cases, one with power-off and one with power-on, were considered to study the flow structure around such a configuration. Both tip-to-tail cases were successfully computed in this study. Dissert. Abstr.

N95-29853# Naval Surface Warfare Center, Dahlgren, VA.

THE 1995 VERSION OF THE NSWC AEROPREDICTION CODE. PART 1: SUMMARY OF NEW THEORETICAL METHODOLOGY Final Report

Frank G. Morre, Roy M. McInville, and Tom Hymer Feb. 1995 111 p
(AD-A291518; NSWCDD/TR-94/379) Avail: CASI HC A06/MF A02

The NSWC Aeroprediction Code has been extended to angles of attack (AOA) greater than 30 deg. To accomplish this, several data bases were used to approximate the nonlinearities in individual missile component aerodynamics. Theoretical aerodynamic methods are used at small AOA. The new semiempirical model was applied to several configurations and the empirical constants adjusted to eliminate some of the errors associated with wind tunnel measurements of individual missile component loads. The new version of the code (AP95) was then applied to several other missile configurations and estimates compared to data and other aerodynamic code calculations. Comparisons were made for Mach numbers 0.1 to 10.0 and AOA of 0 to 90 deg (not all data were available on any single configuration). In general, average accuracy levels of + or - 10 percent could be obtained for axial and normal force coefficient and + or - 4 percent of body length for center of pressure, using the AP95. An exception to this was at AOA above 30 deg and at high supersonic Mach numbers, where nonlinearities caused by internal shock interactions were not accounted for. While these accuracy levels are very encouraging for a semiempirical code, improvements on the AP95 methodology could be made by additional missile-component wind-tunnel data at high AOA. DTIC

N95-29898 ESDU International Ltd., London (England).

INCREMENTS IN AEROFOIL LIFT COEFFICIENT AT ZERO ANGLE OF ATTACK AND IN MAXIMUM LIFT COEFFICIENT DUE TO DEPLOYMENT OF VARIOUS LEADING-EDGE HIGH-LIFT DEVICES AT LOW SPEEDS

Dec. 1994 27 p
(ISSN 0141-397X)
(ESDU-94027; ISBN-0-85678-914-9) Avail: ESDU

ESDU 94027 presents an estimation method based on first approximations from the theory for a thin hinged plate modified using empirical correlation factors to account for the geometry of practical aerofoils and high-lift devices. It applies to plain flaps, drooped leading edges, slats (including sealed slats) and Kruger flaps (including vented Krugers). To allow for the effects of chord extension, the flap chord ratio and lift coefficients are based on an aerofoil extended chord. The data from which the methods were developed were extracted from wind-tunnel tests reported in the literature covering a wide range of practical geometries. However, the methods for Kruger flaps apply only to those cases in which the flap leading-edge radius is the same as that of the basic aerofoil. The methods apply to Reynolds numbers greater than a million and freestream Mach numbers less than 0.2. The predicted and test data for the lift coefficient decrement at zero angle of attack are correlated to within 0.07 and the increment in maximum lift coefficient to within 0.1. The use of the methods is illustrated by worked examples. To obtain results for an aerofoil with both leading- and trailing-edge devices deployed, ESDU 84026 is used in conjunction with results from this document and the appropriate document of ESDU 94027 to 94031 for the contribution of trailing-edge devices.

ESDU

N95-29899 ESDU International Ltd., London (England).
INTRODUCTION TO THE ESTIMATION OF THE LIFT COEFFICIENTS AT ZERO ANGLE OF ATTACK AND AT MAXIMUM LIFT FOR AEROFOILS WITH HIGH-LIFT DEVICES AT LOW SPEEDS
Dec. 1994 12 p
(ISSN 0141-397X)
(ESDU-94026; ISBN-0-85679-913-0) Avail: ESDU

ESDU 94026 discusses the behavior of the lift-curve of an aerofoil depending on its thickness/chord ratio, and the effects on that behavior of the deployment of high-lift devices. It provides an introduction to and a link between ESDU 84026 which predicts lift at zero incidence and maximum lift for the basic aerofoil with high-lift devices undeployed and the series, ESDU 94026 to 94031, which deals with the incremental effects of deployment of the various types of leading-edge and trailing-edge devices. The method of incorporating the incremental effects is explained and illustrated with a worked example, and the applicability and accuracy of the method is discussed.

ESDU

N95-29965 Air Force Inst. of Tech., Wright-Patterson AFB, OH.
AN AERODYNAMIC AND STATIC-STABILITY ANALYSIS OF THE HYPERSONIC APPLIED RESEARCH TECHNOLOGY (HART) MISSILE Ph.D. Thesis
Kenneth John Moran 1994 227 p
(DA9426923) Avail: Issuing Activity (WL/MTPN, Wright-Patterson AFB, OH 45433-6533)

The flow about the complete Hypersonic Applied Research Technology (HART) missile is simulated for inviscid, laminar, and turbulent conditions and Mach numbers from 2 to 6. An explicit, second-order-accurate, flux-difference-splitting, algorithm is implemented and employed to solve the Navier-Stokes equations. The formulation models turbulence with the zero-equation, Baldwin-Lomax turbulence model, accounting for pressure-gradient and compressibility effects. The equations are solved using a finite-volume methodology. In the first part of the study, numerical experiments are performed using an infinitely thin-fin approximation. The aerodynamic and static stability characteristics are investigated to determine if conventional supersonic missile configurations can be flown at Mach numbers higher than 5. The effects of nosetip blunting and boundary-layer condition are demonstrated. In addition, many unresolved issues from experimental testing of the HART missile are addressed. In the second part of the study, the effects of fin thickness and cross section are explored. A comparison is made between thin-fin results and thick-fin results to assess the impact on missile stability. The structure of the flow near the fins is significantly affected by the turbulent transport of momentum in regions of blocked cross flow. Turbulence and the blockage phenomenon cause bleeding around the fin leading edges. Ultimately, this results in lower fin effectiveness and reduced static stability. In addition, the strength and extent of the flow structures that develop in the blocked regions appear to be enhanced by fin thickness. The aerodynamic characteristics of the HART missile are predicted at Mach numbers beyond the experimental free-flight testing capabilities. The current predictions indicate that the pitching-moment coefficient decreases with increasing Mach number much less than previous numerical computations. The present results also suggest that the clipped-delta-fin configuration is stable beyond Mach 7.

Dissert. Abstr.

N95-29972# Princeton Univ., NJ. Dept. of Mechanical and Aerospace Engineering.
COMPUTATIONAL ALGORITHMS FOR AERODYNAMIC ANALYSIS AND DESIGN Annual Report, 1 Oct. 1993 - 30 Sep. 1994
Antony Jameson, James Reuther, and Luigi Martinelli Sep. 1994 13 p
(Grant AF-AFOSR-0391-91)
(AD-A291084; AFOSR-95-0082TR) Avail: CASI HC A03/MF A01

The goal of our research under AFOSR sponsorship is to develop mathematical procedures which can be used to arrive at optimum, or near optimum, aerodynamic shapes by merging techniques from computational fluid dynamics and control theory. With this in mind we have continued to work in two main topics: Development of high resolution shock capturing schemes with low numerical diffusion. Since last year the symmetric limited positive (SLIP) and upstream limited positive (USLIP) schemes have been improved by the introduction of a new flux limiter which guarantees positivity while maintaining good accuracy in smooth flow regions. A comprehensive theory has also been developed for design of numerical fluxes which guarantee stationary discrete shocks with a single interior point. Aerodynamic shape optimization by boundary control progress in aerodynamic shape optimization has been realized on two fronts. First the method has been successfully implemented for two-dimensional lifting potential flows using a general finite volume scheme with numerically generated grids. Secondly, the method has been successfully implemented for three-dimensional wing design using the Euler equations.

DTIC

N95-30091*# National Aeronautics and Space Administration. Lewis Research Center, Cleveland, OH.
USE OF THE PARC CODE TO ESTIMATE THE OFF-DESIGN TRANSONIC PERFORMANCE OF AN OVER/UNDER TURBORAMJET NOZZLE
David W. Lam Jul. 1995 18 p Presented at the 31st Joint Propulsion Conference and Exhibit, San Diego, CA, 10-12 Jul 1995; sponsored by AIAA, ASME, SAE, and ASEE
(RTOP 505-70-62)
(NASA-TM-106924; E-9638; NAS 1.15:106924; AIAA Paper 95-2616)
Avail: CASI HC A03/MF A01

The transonic performance of a dual-throat, single-expansion-ramp nozzle (SERN) was investigated with a PARC computational fluid dynamics (CFD) code, an external flow Navier-Stokes solver. The nozzle configuration was from a conceptual Mach 5 cruise aircraft powered by four air-breathing turboramjets. Initial test cases used the two-dimensional version of PARC in Euler mode to investigate the effect of geometric variation on transonic performance. Additional cases used the two-dimensional version in viscous mode and the three-dimensional version in both Euler and viscous modes. Results of the analysis indicate low nozzle performance and a highly three-dimensional nozzle flow at transonic conditions. In another comparative study using the PARC code, a single-throat SERN configuration for which experimental data were available at transonic conditions was used to validate the results of the over/under turboramjet nozzle.

Author

N95-30235 Ohio State Univ., Columbus, OH.
A NUMERICAL STUDY OF THE SMALL SCALE WING-BODY JUNCTION PROBLEM Ph.D. Thesis
Eun Young Lee 1994 152 p
Avail: Univ. Microfilms Order No. DA9420980

Inspired by asymptotic theory, a solution method has been developed for the calculation of the wing-body junction problem. Some flaws in Smith and Gajjar's theory have been corrected for the linearized solutions. As a part of solution procedure, effective hump shapes are generated using a transformation technique applied to the pressure-displacement relationship. Numerical solutions of the nonlinear triple-deck equations of boundary-layer flow past a smooth, three-dimensional, surface-mounted wing are presented. The results obtained from finite-difference nonlinear solutions are confirmed by linearized fast Fourier transform solutions.

Dissert. Abstr.

N95-30253*# National Aeronautics and Space Administration. Lewis Research Center, Cleveland, OH.
GRID RESOLUTION AND TURBULENT INFLOW BOUNDARY CONDITION RECOMMENDATIONS FOR NPARC CALCULATIONS
Nicholas J. Georgiadis, Julianne C. Dudek, and Thomas P. Tierney (Massachusetts Inst. of Tech., Cambridge, MA.) Jul. 1995 18 p Presented at the 31st Joint Propulsion Conference and Exhibit, San Diego, CA, 10-12 Jul. 1995; sponsored by AIAA; ASME; SAE; and ASEE
(RTOP 537-02-23)
(NASA-TM-106959; E-9711; NAS 1.15:106959; AIAA Paper 95-2613)
Avail: CASI HC A03/MF A01

The effects of grid resolution and specification of turbulent inflow boundary conditions were examined using the NPARC code with the Baldwin-Lomax and Chien k-e turbulence models. Three benchmark turbulent test cases were calculated: two were wall bounded flows and the third was a compressible mixing layer. The wall bounded flows were essentially insensitive to axial grid density; however, the location of the first point off the wall had a substantial effect on flow solutions. It was determined that the first point off the wall must be in the laminar sublayer (y+ less than or equal to 5) for the entire boundary layer. For the compressible mixing layer cases, the axial grid density affected the capturing of oblique shock waves in the mixing region, but the overall mixing rate was not strongly dependent on grid resolution. In specifying the inflow turbulent boundary conditions, it was very important to match the boundary layer and momentum thicknesses of the two flows entering the mixing region; calculations obtained with smaller or no boundary layers resulted in substantially reduced mixing. The solutions were relatively insensitive to freestream turbulence level. Author

N95-30294 Arizona State Univ., Tempe, AZ.
GROWTH AND DEVELOPMENT OF ROUGHNESS-INDUCED STATIONARY CROSSFLOW VORTICES Ph.D. Thesis
Ronald Henry Radeztsky, Jr. 1994 480 p
Avail: Univ. Microfilms Order No. DA9422060

Stability experiments are conducted in the Arizona State University Unsteady Wind Tunnel with a 45 deg swept airfoil model. The pressure field is designed so that crossflow and Tollmien-Schlichting instabilities are weakly amplified. The surface of the airfoil is hand polished to a 0.25 micron finish. Under these conditions, natural stationary crossflow amplitudes are not measurable. This provides an ideal environment for measuring roughness-induced stationary crossflow. Spanwise arrays of 70-150 micron roughness elements are introduced near the attachment line. These elements induce clearly defined stationary crossflow vortices downstream. Detailed hot-wire measurements are taken to document the growth and development of these vortices. Roughness spacing and Reynolds number are varied in order to examine the behavior of all amplified wavelengths. The measurements clearly show that traditional linear stability theory does not accurately predict the growth rates of stationary crossflow under these conditions. Dissert. Abstr.

N95-30349# Deutsche Forschungs- und Versuchsanstalt fuer Luft- und Raumfahrt, Goettingen (Germany). Inst. of Fluid Mechanics.
NUMERICAL SIMULATION AND ANALYSIS OF THE HYPERSONIC TURBULENT FLOW PAST A BLUNT-FIN/RAMP CONFIGURATION Ph.D. Thesis - Rheinisch-Westfaelische Technische Hochschule Aachen [NUMERISCHE SIMULATION UND ANALYSE DER TURBULENTEN HYPERSCHALLSTROEMUNG UM EINEN STUMPFEN FIN MIT RAMPE]
Thomas Gerhold Cologne 1994 159 p In GERMAN
(ISSN 0939-2963)
(DLR-FB-94-19) Avail: CASI HC A08/MF A02

The turbulent hypersonic flow past a blunt-tin/ramp configuration is investigated numerically. The compressible mass-weighted Reynolds-averaged Navier-Stokes equations are solved by an implicit finite-difference algorithm with upwind-discretization and TVD property. Perfect gas is assumed. For the closure of the equations the algebraic turbulence model according to Baldwin & Lomax, as well as different versions of a two-equation kappa-epsilon-model according to Jones & Launder are used. One version of this model accounts for compressibility effects on the turbulence. The influence of the turbulence models on the flow-field simulation is investigated, the grid influence is discussed and the topology of the flow field is depicted by using the results obtained. For validation purposes the results are compared with new experimental data. Finally, the extrapolation to flight of the results is discussed. Author

03 AIR TRANSPORTATION AND SAFETY

Includes passenger and cargo air transport operations; and aircraft accidents.

For related information see also *16 Space Transportation* and *85 Urban Technology and Transportation.*

N95-28811# Dayton Univ., OH. Research Inst.
AN ANALYSIS OF B-1B EXTERIOR JET BLAST WINDSHIELD ANTI-ICING PERFORMANCE USING PRE-COOLED COMPRESSOR BLEED AIR Interim Report, for 1 Mar. - 1 May 1994
D. S. Emmer and M. P. Bouchard Jul. 1994 30 p
(Contract F33615-92-C-3400)
(AD-A292522; UDR-TR-94-94; WL-TR-94-3129) Avail: CASI HC A03/MF A01

This work presents the results of an analytical study designed to evaluate whether the B-1B hot-air windshield deicing/anti-icing system, operating independently from the embedded electrical resistance system, was capable of adequately meeting deicing and anti-icing requirements. Two icing scenarios were considered in loiter, landing, and ground/taxi modes of operation. The results indicate that in a loiter and landing mode, the system capability ranges from marginal to adequate. Additional work is needed to expand the applicability of the analysis mode to ground/taxi conditions. DTIC

N95-29057# Army Aeromedical Research Lab., Fort Rucker, AL.
BIODYNAMIC SIMULATION OF PILOT INTERACTION WITH A HELICOPTER MULTIAIRBAG RESTRAINT SYSTEM
Gregory Strawn and Nabih M. Alem Oct. 1994 37 p
(AD-A290196; USAARL-95-3) Avail: CASI HC A03/MF A01

The introduction of airbags into the helicopter cockpit has raised the issue of acceptable limits on the weights of helmet-supported devices which can be tolerated safely by the aviator. It is hypothesized that, if the acceptable injury risk associated with current helmet-supported weights were reduced with the use of airbags, then an increase in the helmet weight would not necessarily increase the injury risk above what is acceptable without an airbag. To test this hypothesis, a biodynamic simulation software, Dynaman, is used. But first, the data set which describes the crash scenario must be developed. The results of the simulations are described in a separate report. This report describes the input data set required by Dynaman to simulate the interaction of a helicopter pilot with a multiairbag system during a simulated crash. DTIC

N95-29132*# NYMA, Inc., Brook Park, OH.
USERS MANUAL FOR THE IMPROVED NASA LEWIS ICE ACCRETION CODE LEWICE 1.6 Final Report
William B. Wright Jun. 1995 97 p Supersedes N95-14295 and N90-20943
(Contract NAS3-27186; RTOP 505-68-10)
(NASA-CR-198355; E-9729; NAS 1.26:198355) Avail: CASI HC A05/MF A02

This report is intended as an update/replacement to NASA CR 185129 'User's Manual for the NASALewis Ice Accretion Prediction Code (LEWICE)' and as an update to NASA CR 195387 'Update to the NASA Lewis Ice Accretion Code LEWICE'. In addition to describing the changes specifically made for this version, information from previous manuals will be duplicated so that the user will not need three manuals to use this code. Author

N95-29210# Delaware State Coll., Dover, DE.
MODE OF HUMAN IMAGE REPRESENTATION AND ERROR CHECKING STRATEGIES IN COMPLEX VISUAL DISPLAYS Final Technical Report, 30 Sep. 1993 - 29 Sep. 1994
Albert B. Miller 9 Dec. 1994 17 p
(Contract F49620-93-1-0608)
(AD-A290107; AFOSR-95-0005TR) Avail: CASI HC A03/MF A01

Experimental designs are currently being developed which will utilize the laboratory resources obtained under this grant for the purpose of examining error-checking strategies of human observers when monitoring

complex visual displays. Some preliminary software has been developed and it is hoped that this development will be able to continue with the acquisition of research support. During the period of this grant, discussions were held with staff at the National Transportation Safety Board and with staff at the Aviation Safety Reporting System Office at Battelle which provided us with data base searches of human error incidents involved in aircraft accidents. This data has been extremely useful in our preliminary development of experimental protocols which will allow us to develop Department of Defense relevant research studies. DTIC

N95-29448# Federal Aviation Administration, Oklahoma City, OK. Office of Aviation Medicine.

ALTERNATIVE METHODS FOR FLOTATION SEAT CUSHION USE Final Report

Gordon E. Funkhouser and Mark H. George May 1995 9 p
(DOT/FAA/AM-95/20) Avail: CASI HC A02/MF A01

Alternative methods of using flotation seat cushions for water crash survivors were identified at the Civil Aeromedical Institute (CAMI). These methods, tested in the CAMI survival tank and a theme park wave pool, were: (1) two people facing each other, holding two cushions between them; (2) two people facing each other, holding two cushions between them, with a third person held between the two cushions; (3) two people facing each other, holding their cushions on the other person's back; (4) two people facing each other, holding their cushions on the other person's back, with a third person held between the two people; and (5) each person holding a cushion while interlocking arms with adjacent survivors to form a large cluster. The first two methods, using cushions held between two people, are beneficial when linking-up is difficult because of rough seas and when heat loss is not a problem. When seas are calm and the water is cold, the third and fourth methods should retard loss of body heat. The fifth method, where the survivors are clustered together, brings together and connects the survivors who are using the other methods. The cluster allows for more support and help for injured and unconscious survivors. Because individuals tend to separate in the water, the cluster also presents a large visual target for rescuers. Preliminary testing, using a small flotation dummy, suggests that the second method could be used to rescue children by placing them between the cushions held by adults.
Author

N95-29855# Federal Aviation Administration, Atlantic City, NJ.

THE EFFECT OF WEAR ON FIRE-BLOCKING LAYER MATERIAL EFFECTIVENESS

J. M. Barrientos Jan. 1995 19 p
(AD-A291520; DOT/FAA/CT-TN94/16) Avail: CASI HC A03/MF A01

On Apr. 6, 1993, China Airline's MD-11 Flight 583 underwent severe turbulence caused by the inadvertent deployment of the wing leading edge slats. The aircraft experienced three violent pitch oscillations and a loss of altitude of about 5,000 feet which significantly damaged the interior of the cabin. Upon examination of the passenger seats in the cabin interior, excessive wear was noticed with the fire-blocking layer (FBL) material which encapsulates the foam cushions that protect them in the event of a fire. Concerns arose with this FBL material manufactured by Testori of Italy, as well as other FBL material in service, with regard to their effectiveness in protecting the foam cushions from fire. Samples of this type of material underwent several flammability tests at the FAA Technical Center International Airport, NJ, and chemical analysis and microscopic examination at Du Pont Fibers Laboratory in Wilmington, Delaware. DTIC

N95-29873# BioTechnology, Inc., Falls Church, VA.

DEVELOPMENT OF AN INTERVENTION PROGRAM TO ENCOURAGE SHOULDER HARNESS USE AND AIRCRAFT RETROFIT IN GENERAL AVIATION AIRCRAFT: PHASES 1 AND 2 Final Report

James F. Parker, Jr., William T. Shepherd (Federal Aviation Administration, Washington, DC.), Walter J. Gunn (Arlington Associates, Daytona Beach, FL.), and Diane G. Christensen Jan. 1995 64 p
(AD-A290966; DOT/FAA/AM-95/2) Avail: CASI HC A04/MF A01

This report describes a study of shoulder harness installation and use rates in general aviation aircraft. Observations were made at six geographically separate areas to determine estimates of current installation and use rates. An expert panel was employed to identify important factors that affect installation and use of shoulder harnesses in general aviation aircraft. Analyses are presented to explain reasons for shoulder harness installation and use rates. An educational program is proposed to influence pilots to install and/or use shoulder harnesses in their general aviation aircraft.
DTIC

04 AIRCRAFT COMMUNICATIONS AND NAVIGATION

Includes digital and voice communication with aircraft; air navigation systems (satellite and ground based); and air traffic control.

For related information see also *17 Space Communications, Spacecraft Communications, Command and Tracking* and *Communications and Radar.*

N95-28716*# Draper (Charles Stark) Lab., Inc., Cambridge, MA.

ERROR MODELING FOR DIFFERENTIAL GPS M.S. Thesis - MIT, 12 May 1995

Gregory S. Blerman 12 May 1995 93 p
(Contract NAS9-18426)
(NASA-CR-188367; NAS 1.26:288367; CSDL-T-1241) Avail: CASI HC A05/MF A01

Differential Global Positioning System (DGPS) positioning is used to accurately locate a GPS receiver based upon the well-known position of a reference site. In utilizing this technique, several error sources contribute to position inaccuracy. This thesis investigates the error in DGPS operation and attempts to develop a statistical model for the behavior of this error. The model for DGPS error is developed using GPS data collected by Draper Laboratory. The Marquardt method for nonlinear curve-fitting is used to find the parameters of a first order Markov process that models the average errors from the collected data. The results show that a first order Markov process can be used to model the DGPS error as a function of baseline distance and time delay. The model's time correlation constant is 3847.1 seconds (1.07 hours) for the mean square error. The distance correlation constant is 122.8 kilometers. The total process variance for the DGPS model is 3.73 sq meters.
Author

N95-28790# Federal Aviation Administration, Oklahoma City, OK. Civil Aeromedical Inst.

AUTOMATION AND COGNITION IN AIR TRAFFIC CONTROL: AN EMPIRICAL INVESTIGATION Final Report

O. U. Vortac, Mark B. Edwards, Dana K. Fuller, and Carol A. Manning Feb. 1995 17 p Prepared in cooperation with Oklahoma Univ., Norman, Dept. of Psychology
(Contract DTFA02-91-C-91089)
(AD-A291932; DOT/FAA/AM-95/9) Avail: CASI HC A02/MF A01

A simulation of an air traffic control task was the setting for an investigation of the functions of external cues in prospective memory. External cues can support the triggering of an action or memory for the content of the action. We focused on memory for the content and manipulated the temporal characteristics of the external cue to disentangle two possible functions the cue can support: (1) An external cue visible during a retention interval could support rehearsal of the to-be-performed action; and (2) An external cue visible at the end of a retention interval could support retrieval of the to-be-performed action. Two experiments were conducted that converge on the same conclusion: the primary function of an external cue was to support retrieval. implications for the design of a computer interface to present prospective cues are discussed. DTIC

N95-28819# Civil Aeromedical Inst., Oklahoma City, OK.

CONVERSION OF THE TRACON OPERATIONS CONCEPTS DATABASE INTO A FORMAL SENTENCE OUTLINE JOB TASK TAXONOMY Final Report

Mark D. Rodgers and Gena K. Drechsler May 1995 68 p
(DOT/FAA/AM-95/16) Avail: CASI HC A04/MF A01

FAA Air Traffic Control Operations Concepts Volume 8: TRACON Controllers (1989) developed by CTA, Inc., a technical description of the duties of a TRACON air traffic control specialist (ATCS), formatted in User Interface Language, was restructured into a hierarchical formal sentence outline. To ensure that none of the meaning associated with a task or task element was lost during the conversion, the revised document was reviewed by subject matter experts (SMEs) consisting of four groups of six

TRACON controllers and four quality assurance managers. SMEs looked for words, phrases, or acronyms not commonly used by TRACON controllers, and illogical sequencing of duties described in the document. Appropriate suggestions for change were implemented into the document before the next review. Six-hundred seventy-one changes were made to the document, with only seven of these changes made during the final review, confirming that an improved document resulted from the research. The restructured document is intended to assist in the identification of situation awareness information requirements. However, an easily understood, detailed description of duties performed by a TRACON ATCS has potential for use not only by researchers interested in TRACON ATCS tasks, but also by quality assurance investigation teams and training personnel. Author

N95-28887# Connecticut Univ., Storrs, CT.
MATSURV MULTISENSOR AIR TRAFFIC SURVEILLANCE Final Report, May 1993 - Aug. 1994
Murali Yeddanapudi, Yaakov Bar-Shalom, Krishna R. Pattipati, T. Kirubarajan, and Somnath Deb Jan. 1995 40 p
(Contract F30602-93-C-0090)
(AD-A292253; RL-TR-95-4) Avail: CASI HC A03/MF A01

In this report, the results of the work on multisensor air traffic surveillance and a description of MATSurv, a software tool for tracking multiple targets using measurements from asynchronous sensors, are presented. The work addresses the issues of modeling the target motion, estimating target states, and determining a consistent set of measurement-target associations. The specific objectives of this work are to formulate and solve the data association problem for actual tracking scenarios with multiple, multimodality sensor subsystems. Two phases of the work are described, namely, the tuning phase whereby the measurements are associated with the appropriate targets using the known target IDs to tune and validate the tracking filter, and the assignment phase whereby the association is carried out using a two-dimensional assignment algorithm developed at UConn. Also, the performance of the tracking and assignment algorithms using three representative sets of measurements is illustrated. DTIC

N95-29107 Stanford Univ., CA.
WIDE AREA DIFFERENTIAL GPS (WADGPS) Ph.D. Thesis
Changdon Kee 1994 147 p
Avail: Univ. Microfilms Order No. DA9414592

The Global Positioning System (GPS) has proven to be an extremely accurate positioning sensor, with an accuracy of 100 meters, for a wide variety of applications. However in some situations, such as aircraft precision approaches, higher accuracy is required. Conventional Differential GPS (DGPS) usually has an accuracy of 2 to 5 meters within 100 kilometers of the stationary calibration receiver, even with the expected levels of induced Selective Availability (SA) errors. To implement DGPS on a large scale, the total number of monitor stations needed to cover the continental United States to this accuracy would exceed 500. Wide Area Differential GPS (WADGPS) is a system that can limit the number of necessary monitor stations to 15 while achieving the same accuracy. WADGPS can reduce the overall cost and the operation cost of the system dramatically and can also increase the system's reliability and integrity. The WADGPS system comprises a master station and monitor stations distributed across the United States. It calculates and transmits a vector of error corrections to the users preferably via satellite. This correction vector consists of parameters describing the three-dimensional ephemeris errors, the satellite clock offsets including SA, and optionally the ionospheric time delay. The performance of a 15-station WADGPS network was investigated by simulation for users at sites across the United States, and the results indicated that normal GPS positioning errors can potentially be reduced by more than 95 percent using WADGPS. Experimental results from field tests using six monitor stations with a 1632-km minimum baseline from a dual frequency user showed a submeter positioning accuracy with no latency. These results strongly support the potential of WADGPS to give high positioning accuracy at a cost substantially lower than that of conventional DGPS.
Dissert. Abstr.

N95-29542 Ohio Univ., Athens, OH.
AN INVESTIGATION INTO THE USE OF SATELLITE-BASED POSITIONING SYSTEMS FOR FLIGHT REFERENCE/AUTOLAND OPERATIONS Ph.D. Thesis
David William Diggle 1994 146 p
Avail: Univ. Microfilms Order No. DA9424040

An Interferometric Global Positioning System Flight Reference System (IGPS FRS) is implemented and flight tested on a transport category aircraft. This dissertation discusses the IGPS FRS theory and principles of operation, its architecture and integration with the aircraft, and the initial static calibration and flight-test performance results. The validity of the results is established by referencing them to a known ground test point and/or a laser tracking system. The principles underlying the operation of the IGPS FRS are similar to those used for kinematic surveying, and are also referred to as differential carrier-phase tracking with integer ambiguities resolved. Flight Reference System objectives include: 0.1 m accuracy rms (each axis); one or more updates per second; UTC (Universal Time, Coordinated) synchronization better than 0.1 ms; real-time, all-weather operation; and, repeatable flight paths. The latter requirement calls for full integration with the aircraft flight control system and coupled flight. Dissert. Abstr.

N95-29596 Wisconsin Univ., Madison, WI.
MODELING SPATIO-TEMPORAL DATABASES TO MEASURE THE PERFORMANCE OF THE GPS SATELLITE CONSTELLATION Ph.D. Thesis
Wael Mohamed Zakout 1994 226 p
Avail: Univ. Microfilms Order No. DA9417227

The NAVSTAR (NAVigation Satellite Time And Ranging) Global Positioning System (GPS) is a satellite-based positioning system currently under development by the United States Department of Defense. The primary goal of the system is to support the U.S. military and its allies with real-time, all weather global navigational capabilities. For this reason, the system was designed so that at least four satellites are simultaneously in view from every point on the earth's surface. However, since the launch of the first GPS satellites in the late 1970's, numerous new techniques and methods have been developed to utilize the system, and hundreds of civilian applications have been added to those originally considered. GPS user requirements for applications such as navigation, geodetic surveying, time transfer, and photogrammetry vary in both accuracy and reliability. These requirements are a function of location and conditions, e.g., the use of GPS for land navigation in a large city requires more visible satellites than does ocean navigation. In this research investigation, a new technique was developed to incorporate user requirements as a performance measure of the GPS satellite constellation. To do so, a new approach was followed for modeling spatio-temporal databases using existing geo-relational Geographic Information Systems (GIS's). GPS users were sampled and their positional and navigational requirements reviewed. Then, the power of GIS technology was used to map these requirements into spatial data layers. Satellite coverage parameters were mapped into slices of spatial data, each slice representing the number of visible satellites and the corresponding dilution of precision (DOP) factors at a specific instant of time. The feasibility of interpolation between time slices was evaluated. Finally, the spatio-temporal model was tested on several available platforms to measure response times of existing hardware and software configurations. The system developed to measure GPS satellite constellation performance is flexible enough to incorporate additional measurement criteria.
Dissert. Abstr.

N95-29733# Federal Aviation Administration, Washington, DC.
FEDERAL AVIATION ADMINISTRATION PLAN FOR RESEARCH, ENGINEERING AND DEVELOPMENT
Dec. 1994 203 p
(AD-A290952) Avail: CASI HC A10/MF A03

The Federal Aviation Administration (FAA) manages and operates the National Airspace System (NAS), a significant national resource. However, the demands on this system are continuously growing, and changing technologies provide the opportunity to improve system effectiveness and efficiency. Today, 23 of the country's largest airports are plagued by more than 20,000 hours of delay per year, which is projected to grow to 40 major airports by 2000. Nationally, air traffic delays cost the economy an estimated $6 billion in passenger delays and $3 billion in airline operating costs in 1990. At current trends, these costs will increase 50 percent within 10 years. Aviation and related industries are also challenged by energy and environmental factors, Currently, 45 percent of air carrier aircraft operating costs are for fuel, a large portion of which is from imported oil. While reducing fuel usage is a priority in terms of energy conservation, it

is also an increasingly critical environmental issue, based on recent findings relating to nitrogen oxide emissions at high altitudes. Given the projected increases in aviation activity and stringent environmental standards being proposed in Europe and elsewhere, noise and engine emissions reductions are essential to the national aviation industry's viability. DTIC

N95-29880# Federal Aviation Administration, Washington, DC. Office of Aviation Policy and Plans.
TERMINAL AREA FORECASTS-FISCAL YEARS 1993-2010
1 Sep. 1994 557 p
(AD-A290835; FAA-APO-94-11) Avail: CASI HC A24/MF A04

This report contains forecasts of aviation activity of 875 airports in the United States for fiscal years 1993-2010. These include 401 airports with FAA air traffic control towers and radar approach control services and 29 FAA contract towers. For each airport, detailed forecasts are made for the four major users of the air traffic system: air carriers, air taxi/commuters, general aviation, and military. Summary table contain national, FAA regional, and State aviation data and other airport specific highlights. The forecasts have been prepared to meet the budget and planning needs of the FAA and to provide airport specific information that can be used by State and local aviation authorities, the aviation industry, and the general public. DTIC

N95-30031# Federal Aviation Administration, Atlantic City, NJ.
PROTOTYPE STOP BAR SYSTEM EVALUATION AT SEATTLE-TACOMA INTERNATIONAL AIRPORT Final Report
Eric Katz Nov. 1994 81 p
(AD-A290136; DOT/FAA/CT-94/62) Avail: CASI HC A05/MF A01

An interim United States stop bar specification was developed by the Federal Aviation Administration Technical Center. Using the guidance material contained in the interim specification, a full-scale prototype stop bar system was installed to protect runway 16R/34L at the Seattle-Tacoma International Airport (SEA). The system consists of two stop bars which incorporate both inset and elevated red light fixtures. Associated with each stop bar are green inset lead-on lights and microwave detectors that provide for automatic switching of the stop bar/lead-on light segments. Once installed, the SEA stop bar system was operated during air traffic controller training sessions and under actual low-visibility weather conditions for evaluation and user organization familiarization. Air traffic controller and air-carrier pilot questionnaires were distributed and returned to the FAA Technical Center for analysis after completion. The questionnaires were designed to solicit information regarding the effectiveness and reliability of the stop bar system. As a result of the evaluation, the U.S. stop bar lighting configuration, as developed and described in the interim specification, was found to be satisfactory and acceptable to user pilots. DTIC

05 AIRCRAFT DESIGN, TESTING AND PERFORMANCE

Includes aircraft simulation technology.

For related information see also *18 Spacecraft Design, Testing and Performance* and *39 Structural Mechanics*.For land transportation vehicles see *85 Urban Technology and Transportation.*

N95-28704 ESDU International Ltd., London (England).
EJECTORS AND JET PUMPS: COMPUTER PROGRAM FOR DESIGN AND PERFORMANCE FOR STEAM/GAS FLOW
Dec. 1994 61 p
(ISSN 0141-4011)
(ESDU-94046; ISBN-0-85679-933-5) Avail: ESDU

ESDU 94046 introduces a Fortran program (ESDUpac A9446) for ejectors in which the primary and secondary flows are non-reacting gases that can be modelled as real. Three procedures are provided: a Quick Design Procedure, a Detailed Design Procedure and Performance Prediction. The first is based on experimental data obtained for steam ejectors pumping air at 20 degrees C. If other gases are handled the secondary mass flow rate is converted by the program to an equivalent rate based on the molar mass of the secondary gas. For the second the input is a selection of entry and required exit pressures and flow rates, together with estimates of loss coefficients in the primary and secondary nozzles, mixing duct and diffuser. The program will optimize the ejector, calculating the primary nozzle and exit dimensions, and flow conditions throughout. For the third case, the ejector dimensions are input together with the loss factors again and a range of entry flow conditions and the program will calculate flow conditions throughout the ejector and at exit. The equations on which the program is based are fully specified, the input format required is set out in clear tables, and three worked examples illustrate the use of the procedures. Notes are provided on the mechanical design of steam/gas ejectors including the use of multi-stage units and annular- or multi-nozzles. Possible operating problems are discussed. The program is provided on disc (uncompiled) in the software volume, and compiled within ESDUview, a user-friendly shell running under MS-DOS that prompts on screen for input data. ESDU

N95-28707 ESDU International Ltd., London (England).
EFFECTS OF SMALL CHANGES ON RATE OF CLIMB
Oct. 1994 6 p
(ISSN 0141-4054)
(ESDU-94039; ISBN-0-856-79926-2) Avail: ESDU

ESDU 94039 gives simple formulae for the effect of small changes in thrust, power (for propeller-driven aircraft), weight and drag (assuming a parabolic drag law) at constant airspeed and, when divided by the acceleration factor, when airspeed is changing. Rather more complex formulae are also given for the effect of changes in airspeed and relative density. All the equations assume that there are no consequential changes in the other independent variables. Such formulae are useful in the adjustment of measured results to other conditions and in assessing changes required to achieve a specific performance level. ESDU

N95-28820*# National Aeronautics and Space Administration. Langley Research Center, Hampton, VA.
AN EFFICIENCY STUDY OF THE SIMULTANEOUS ANALYSIS AND DESIGN OF STRUCTURES
Alfred G. Striz (Oklahoma Univ., Norman, OK.), Zhiqi Wu (Oklahoma Univ., Norman, OK.), and Jaroslaw Sobieski Apr. 1995 11 p Presented at the 1st World Congress of Structural and Multidisciplinary Optimization, ISSMO, Goslar, Germany, 28 May - 2 Jun. 1995
(RTOP 505-63-50-06)
(NASA-TM-110168; NAS 1.15:110168) Avail: CASI HC A03/MF A01

The efficiency of the Simultaneous Analysis and Design (SAND) approach in the minimum weight optimization of structural systems subject to strength and displacement constraints as well as size side constraints is investigated. SAND allows for an optimization to take place in one single operation as opposed to the more traditional and sequential Nested Analysis and Design (NAND) method, where analyses and optimizations alternate. Thus, SAND has the advantage that the stiffness matrix is never factored during the optimization retaining its original sparsity. One of SAND's disadvantages is the increase in the number of design variables and in the associated number of constraint gradient evaluations. If SAND is to be an acceptable player in the optimization field, it is essential to investigate the efficiency of the method and to present a possible cure for any inherent deficiencies. Author

N95-28851 Defence Science and Technology Organisation, Canberra (Australia). Aeronautical and Maritime Research Lab.
HELICOPTER LIFE SUBSTANTIATION: REVIEW OF SOME USA AND UK INITIATIVES Technical Report
Ken F. Fraser Sep. 1994 27 p Limited Reproducibility: More than 20% of this document may be affected by microfiche quality
(AD-A290045; DSTO-TR-0062; DODA-AR-008-924) Avail: Issuing Activity (Defense Technical Information Center (DTIC))

Military operators normally undertake programs to substantiate the fatigue lives of life-limited components in their major helicopter fleets. During recent visits to military helicopter representatives in the USA and the UK, the author discussed the motivation and the technical approach adopted by these operators for helicopter component life substantiation. Issues and programs of particular relevance to the Australian Defence Force are examined in this document. DTIC

N95-28896 ESDU International Ltd., London (England).
SHEAR FORCE, BENDING MOMENT AND TORQUE OF RIGID AIRCRAFT IN SYMMETRIC STEADY MANEUVERING FLIGHT

Dec. 1994 17 p
(ISSN 0141-3988)
(ESDU-94045; ISBN-0-85679-932-7) Avail: ESDU

ESDU 94045 uses for an aircraft of classical configuration at constant incidence the data identified in ESDU 94009 for aerodynamic load and mass of the components of a wing-filselage-nacelle combination. The wing shear force, bending moment and torque variations along the span are determined relative to a flexural axis for both an unswept high aspect ratio wing and for a swept, medium to high aspect ratio wing. In the former case a straight flexural axis is defined perpendicular to the aircraft plane of symmetry; a load applied to that axis will cause bending only, while a torque applied about it (in a plane normal to it) will cause only twist about it. In the latter case two types of flexural axis are considered: a straight axis parallel to the sweep line of the wing (an effective root chord is thereby defined that is not parallel to the aircraft plane of symmetry) about which the wing is assumed to bend and a curved axis along the span when the wing is assumed to bend and twist in a plane parallel to the aircraft plane of symmetry. For the fuselage the forces and moments are taken along the aircraft centre line in the plane of symmetry and only shear forces and bending moments are determined. Author

N95-28928* Advanced Rotorcraft Technology, Inc., Mountain View, CA.
APPLICATION OF PARALLEL PROCESSING TECHNOLOGY IN COMPLEX HELICOPTER ANALYSIS. PHASE 1 Final Report, 14 Jul. - 9 Dec. 1994
Dharmendra Kumar and Hossein Saberi 9 Dec. 1994 47 p Limited Reproducibility: More than 20% of this document may be affected by microfiche quality
(Contract NAS2-14084)
(NASA-CR-197850; NAS 1.26:197850; AD-A288899; FR7060-001) Avail: Issuing Activity (Defense Technical Information Center (DTIC))

Complex Helicopter Analysis codes, such as the Second Generation Comprehensive Helicopter Analysis System (2GCHAS), have been developed to provide a common framework for interdisciplinary design and analysis of rotorcraft systems. A major limitation on the effectiveness of the second generation comprehensive analysis codes is the slow processing speed that results from the computational intensity of the analysis software. The goal of phase I effort is to carefully define the specification for the parallelization opportunities in 2GCHAS, and apply the parallel processing techniques on a sample analysis to demonstrate a proof of concept. The Onyx Computer System from Silicon Graphics Inc. was chosen as the target machine for this effort as it has 4 processors and was available to ART. The tasks performed during the Phase 1 Base effort went beyond meeting the Phase 1 objectives and included the following: (1) Port of the most recent version of 2GCHAS Analysis to the Silicon Graphics Computer System; (2) Parallelize multicase analysis in 2GCHAS; (3) Choose an appropriate analysis component for parallelization in a single case analysis; (4) Parallelize Linearization Analysis and thereby reduce the overall runtime of a single case Linear System analysis; and (5) Identify candidates for future parallelization in 2GCHAS. In addition, efforts had been made to improve the eigenanalysis solution method. The result obtained from the Phase 1 effort showed over an order of magnitude reduction in the overall runtime for the sample problems due to parallelization, better RDB implementation, less overhead in a process invocation, improved analysis algorithm and faster machine speed. DTIC

N95-28977# Naval Air Warfare Center, Warminster, PA. Air Vehicle and Crew Systems Technology Dept.
EVALUATION OF PROPOSED AGILITY METRICS USING X-31 VS. F/A-18 FLIGHT DATA Final Report, Oct. 1993 - Sep. 1994
Julieta E. Booz 30 Nov. 1994 38 p
(AD-A292573; NAWCADWAR-95012-4.3) Avail: CASI HC A03/MF A01

This report is an evaluation of the specific agility metrics and tactical agility metrics as described in Veda Technical Report 33158-94U/P3553-003, Aircraft Fighter Agility: Theory, Advanced Metrics, and Simulation. The agility metrics were applied to six engagements flown between the X-31 and the F/A-18. A comparison was done to determine if the agility metrics correlated with the results from the engagements flown (e.g. did the more agile aircraft get the win). The results indicate that applying these agility metrics to correlate with the win or loss of an engagement did not provide consistent predictions as to which aircraft would score a win. Evaluation of the data from the engagements indicate that what determined which aircraft achieved the win (by obtaining a missile kill) was that aircraft which was the first to maneuver into an offensive position within the weapons firing solution. This was primarily done by generating the higher acceleration rate or by obtaining a higher initial acceleration value. DTIC

N95-29016 ESDU International Ltd., London (England).
EFFECTS OF CABIN PRESSURE ON CLIMB AND DESCENT RATES
Nov. 1994 6 p
(ISSN 0141-4054)
(ESDU-94040; ISBN-0-856-79927-0) Avail: ESDU

ESDU 94040 discusses how the maximum cabin pressure differential and the rate of change of cabin pressure affect rates of climb and descent, particularly of civil aircraft. The cabin pressure differential is governed by the capability of the air-conditioning system, the strength of the fuselage and the maximum operating altitude of the aircraft. A sketch illustrates how cabin pressure and pressure differential affect operating altitude and indicates where aircraft of various classes operate. Excessive rate of change of pressure can build up a differential pressure across the eardrums and at 0.5 lbf/sq in (3.45 kN/sq m) would cause pain. For civil aircraft restricting the rate of change of cabin pressure is a major factor in determining descent profile and has also to be considered in climb although to a lesser extent. A further sketch illustrates possible climb and descent profiles chosen to maintain cabin pressure and its rate of change within the necessary restrictions while not exceeding cabin differential pressure limits. ESDU

N95-29027*# Lockheed Aeronautical Systems Co., Marietta, GA.
ADVANCED COMPOSITE STRUCTURAL CONCEPTS AND MATERIALS TECHNOLOGIES FOR PRIMARY AIRCRAFT STRUCTURES: ADVANCED MATERIAL CONCEPTS Final Technical Report, Jun. 1989 - Jun. 1992
Kreisler S. Y. Lau (Lockheed Missiles and Space Co., Palo Alto, CA.), Abraham L. Landis (Lockheed Missiles and Space Co., Palo Alto, CA.), Andrea W. Chow (Lockheed Missiles and Space Co., Palo Alto, CA.), and Richard D. Hamlin (Lockheed Missiles and Space Co., Palo Alto, CA.) Feb. 1993 106 p
(Contract NAS1-18888; RTOP 510-02-13-01)
(NASA-CR-4485; NAS 1.26:4485) Avail: CASI HC A06/MF A02

To achieve acceptable performance and long-term durability at elevated temperatures (350 to 600 F) for high-speed transport systems, further improvements of the high-performance matrix materials will be necessary to achieve very long-term (60,000-120,000 service hours) retention of mechanical properties and damage tolerance. This report emphasizes isoimide modification as a complementary technique to semi-interpenetrating polymer networks (SIPN's) to achieve greater processibility, better curing dynamics, and possibly enhanced thermo-mechanical properties in composites. A key result is the demonstration of enhanced processibility of isoimide-modified linear and thermo-setting polyimide systems. Author

N95-29122 Massachusetts Inst. of Tech., Cambridge, MA.
A NUMERICAL METHOD FOR MODELLING WINGS WITH SHARP EDGES MANEUVERING AT HIGH ANGLES OF ATTACK Ph.D. Thesis
Stephane Lucien Mondoloni 1994
Avail: Issuing Activity (MIT Libraries, Rm. 14-0551, Cambridge, MA 02139-4307)

An unsteady, high-order panel method is presented for computing the loading on wings maneuvering at high angles of attack. The method is also applicable to wing-tail combinations. Wakes are allowed to shed from sharp user-prescribed edges. These wakes are model led using desingularized vortex filaments. Global wake properties such as the motion of the centroid and overall extent of the tip vortices agree with experiments, yet predicting the local spiral structure requires more resolution. The effect of the wake desingularization and time stepping scheme on the stability of the discrete vortex sheet is investigated. This yields important information for understanding the behavior of the discretized vortex sheet. Higher core sizes decrease the instabilities, with greatest effect on the smallest wavelength. Unseparated, steady and unsteady calculations of wings with different planforms, and a wing-tail case are compared to experiment, theory and other panel methods with excellent agreement. The initial normal force on impulsively plunged two-dimensional plates and delta wings with separation is shown to be sensitive to the positioning of the shedding vortex. This sensitivity is removed by positioning the shedding vortex along the streakline emanating from the edge, which should prove useful to

users of vortex-filaments trying to capture unsteady loading. An aspect ratio one wing is impulsively plunged with leading-edge separation. The rollup and unsteady loading is sensitive to numerical core size. This sensitivity diminishes as the overall resolution is increased. Steady-state comparisons to theory, experiments and code show good agreement except near the apex region. Dissert. Abstr.

N95-29126# General Accounting Office, Washington, DC. National Security and International Affairs Div.

UNMANNED AERIAL VEHICLES: NO MORE HUNTER SYSTEMS SHOULD BE BOUGHT UNTIL PROBLEMS ARE FIXED

Mar. 1995 19 p

(AD-A292172; GAO-NSIAD-95-52) Avail: CASI HC A03/MF A01

The Hunter is a pilotless aircraft resembling a small airplane that is controlled from a ground station. It is intended to perform reconnaissance, target acquisition, and other military missions by flying over enemy territory and transmitting video imagery back to ground stations for use by military commanders. The Hunter program (formerly called the Short-Range UAV program) began in 1989 as a joint-service effort in response to congressional concern over the proliferation of UAV5 by the different services and the need to acquire UAV5 that could meet the requirements of more than one service. DOD started the program by procuring two candidate systems for competitive testing. In early 1993, after the Hunter was selected as the winning system, DOD approved its low-rate initial production of seven systems and awarded a $171-million contract. DTIC

N95-29282 Air Univ., Maxwell AFB, AL. Airpower Research Inst.

ROLE OF UNMANNED AERIAL VEHICLES IN FUTURE ARMED CONFLICT SCENARIOS

Dana A. Longino Dec. 1994 43 p Limited Reproducibility: More than 20% of this document may be affected by microfiche quality

(AD-A289777; AU-ARI-92-12) Avail: Issuing Activity (Defense Technical Information Center (DTIC))

Unmanned aerial vehicles (UAV) are not something new to write about. Especially since the Gulf War numerous articles on the subject have been published in military and aviation periodicals. The war added significantly to the information available on the capabilities of UAV's and provided increased support for an expanded role for UAV's on the modern battlefield. In a 20 March 1991 interview with Defense News, US Adm David E. Jeremiah, vice chairman of the joint chiefs of staff (JCS), stated, The outcome of Operation Desert Storm might not have been as swift or decisive if U.S. and allied forces had not made use of intelligence-gathering and tactical reconnaissance platforms such as the Israeli-designed Pioneer. We witnessed a high payoff to the commander who's been able to field UAV's. DTIC

N95-29322# Florida Atlantic Univ., Boca Raton, FL.

HIGH-AND LOW-FREQUENCY DYNAMICS OF ISOLATED BLADES AND ROTORS WITH DYNAMIC STALL AND WAKE Final Report, 1 Jan. 1991 - 30 Sep. 1994

Gopal H. Gaonkar 23 Nov. 1994 50 p

(Contract DAAL03-91-G-0007)

(AD-A290358; ARO-28123.10-EG) Avail: CASI HC A03/MF A01

This report investigates the effects of dynamic stall and three-dimensional wake on the trim results of control inputs and periodic responses and on the damping levels of isolated hingeless rotors. The investigation covers three items: (1) the convergence characteristics of trim and damping with respect to the number of harmonics of the wake model in the presence of dynamic stall; (2) a parametric study of trim and damping over a broad range of system parameters such as thrust level and advance ratio; and (3) a comprehensive correlation with the measured lag-regressive-mode damping. The correlation includes near-zero thrust conditions in hover and forward flight to high-thrust and highly stalled conditions in forward flight with advance ratio as high as 0.55 and shaft angle as high as 200. The convergence characteristics and the parametric study are based on a three-bladed isolated rotor in propulsive trim: the cantilever blades have flap bending, lag bending and torsion degrees of freedom. In the correlation study, the root-flexure-blade assembly of the experimental rotor is modeled by an offset-hinged, rigid flap-lag model and by three elastic blade models, which differ in modeling the root flexure The experimental rotor is soft inplane and operated untrimmed. The ONERA dynamic stall models of lift drag and pitching moment and a finite-state three-dimensional wake model are used. The control inputs and periodic responses as well as the Floquet transition matrix about that response are obtained by periodic shooting with damped Newton iteration. The damping levels are generated from a full Floquet analysis that includes all the structural and aerodynamic states in trim analysis and eigenanalysis. For lag damping predictions in the presence of dynamic stall, at least nine wake harmonics are required even for the low frequency lag-regressive mode. DTIC

N95-29362 Defence Science and Technology Organisation, Melbourne (Australia). Aeronautical and Maritime Research Lab.

UNMANNED AERIAL VEHICLE TECHNOLOGY

Keith Cameron Feb. 1995 46 p

(DSTO-GD-0044; AR-008-372) Copyright Avail: Issuing Activity

This document reviews the individual technologies that may be applicable to Unmanned Aerial Vehicles (UAVs). In addition, an overview of UAV systems as a new technology and their integration into the existing ADF (Australian Defence Force) structure is considered. Despite there having been considerable interest in UAVs for at least twenty years they have not as yet become a significant factor in operations outside Israel and possibly the Gulf war. The number of operational systems is limited as is the specific technology base of UAVs. This may be due to the need for a significant market before industry will make the investment needed and to the users not being able to acquire suitable systems. Therefore, it is likely that slow progress will be made until a 'critical mass' is achieved when industry will make the needed investment to produce the range of UAVs required by the users. Author

N95-29426# DACCO SCI, Inc., Columbia, MD.

THE USE OF ELECTROCHEMISTRY AND ELLIPSOMETRY FOR IDENTIFYING AND EVALUATING CORROSION ON AIRCRAFT Final Report, 15 Jun. - 15 Dec. 1994

Chester M. Dacres, Brian C. Taggart, Charles R. Anderson, and Pam Whisnant 15 Dec. 1994 84 p Prepared in cooperation with Marietta Lab.

(Contract F49620-94-C-0042)

(AD-A290249) Avail: CASI HC A05/MF A01

Electrochemical corrosion testing using AC impedance measurement and ellipsometry has been performed on aircraft aluminum 2024-T3 samples. The AC Impedance technique was used to acquire a precise low-frequency impedance signature of corroding painted aircraft aluminum which will be used to develop a simple, yet powerful, sensor for the early detection and measurement of corrosion processes on aircraft. The use of ellipsometry and DC electrochemical techniques, have verified that the low-frequency impedance spectrum obtained from the AC Impedance technique is representative of the corrosion process for painted aircraft aluminum 2024-T3. Based on these findings, several versions of prototype electrode sensors were developed capable of obtaining this signature utilizing a two-electrode approach. These in-situ electrode sensors were extensively tested using AC Impedance, electrochemistry, ellipsometry, and X-ray Photoelectron Spectroscopy. Results indicate the ability of the electrode sensors to non-destructively monitor the corrosion process on aircraft aluminum 2024-T3 and to withstand harsh operating environments. DTIC

N95-29437# Naval Postgraduate School, Monterey, CA.

APPLICATIONS OF DIGITAL VIDEO AND SYNTHETIC ENVIRONMENTS TO UNMANNED AERIAL VEHICLES M.S. Thesis

Franklin J. Tipton Sep. 1994 91 p

(AD-A291875) Avail: CASI HC A05/MF A01

The current Army Unmanned Aerial Vehicle (UAV) system has two problems: (1) it does not provide for the direct distribution of live UAV video throughout command posts across their local area networks; and (2) it lacks an automated trainer. To solve the video distribution problem, I studied the UAV system, video compression techniques, and local area network protocols to develop the video distribution model. The approach taken for developing the simulator included researching the operational characteristics of the UAV system and studying the creation of synthetic environments. This thesis develops an architecture for extending the distribution of live UAV video inside the command post using a local area network. It recommends distributing full-motion UAV video over an Asynchronous Transfer Mode (ATM) local area network using the motion Joint Photographic Expert Group (JPEG) compression technique. Additionally, I created an interactive, UAV Simulator using the IRIS Performer applications

program interface and C++. The simulator is implemented using two networked workstations which replicate the functions of the air vehicle and mission payload operators. The workstations communicate across a local area network using the Distributed Interactive Simulation (DIS) protocol.
DTIC

N95-29445 Defence Science and Technology Organisation, Melbourne (Australia). Aeronautical and Maritime Research Lab.
ESTIMATION OF AERODYNAMIC LOAD DISTRIBUTIONS ON THE F/A-18 AIRCRAFT USING A CFD PANEL CODE
Howard A. Quick Mar. 1995 44 p
(DSTO-TR-0147; AR-008-420) Copyright Avail: Issuing Activity

The computational fluid dynamics panel method code VSAERO has been used to estimate the aerodynamic load distributions on the stabilators, fins and aft fuselage of the F/A-18 aircraft for steady sideslip and steady roll conditions. Three separate VSAERO models have been developed to obtain results for these conditions. These are a symmetric F/A-18 model, a starboard fin model and a starboard stabilator and fin model. Difficulties in modelling the vortices separating from the leading edges of the stabilators and fins at moderate angles of attack have restricted the range of conditions for which the method has been used.
Author

N95-29457 Naval Postgraduate School, Monterey, CA.
DESIGN AND EVALUATION OF A LQR CONTROLLER FOR THE BLUEBIRD UNMANNED AIR VEHICLE M.S. Thesis
Brian T. Foley Sep. 1994 86 p Limited Reproducibility: More than 20% of this document may be affected by microfiche quality
(AD-A289769) Avail: Issuing Activity (Defense Technical Information Center (DTIC))

The modern aerospace controls engineer is provided with a variety of powerful tools to aid in the design and testing of digital flight control systems. The current fiscal environment requires extensive validation of all aerospace based systems through simulation and hardware-in-the-loop testing prior to implementation. This work explores the design and evaluation of an Automatic Flight Control System (AFCS) for the Bluebird Unmanned Aerial Vehicle (UAV). Software tools such as MATLAB and MATRIXx are used to evaluate the dynamic stability of the aircraft model and Linear Quadratic Gaussian algorithms are used to obtain the appropriate controller. Graphical design applications such as SIMULINK and SystemBuild are then used to build a visual block diagram model of the aircraft dynamics and link it with the designed controller. Using this model, the control system response to commanded inputs and external disturbances was evaluated.
DTIC

N95-29503# Advisory Group for Aerospace Research and Development, Neuilly-Sur-Seine (France). Flight Mechanics Panel.
AGARD FLIGHT TEST TECHNIQUES SERIES. VOLUME 13: RELIABILITY AND MAINTAINABILITY [FIABILITE ET MAINTENABILITE]
Jan M. Howell (Test Wing, 0412th, Edwards AFB, CA.) Feb. 1995 63 p
(AGARD-AG-300-Vol-13; ISBN-92-836-1014-8) Copyright Avail: CASI HC A04/MF A01

This AGARDograph outlines the rudiments of reliability and maintainability (R&M) evaluations conducted during initial flight test programs. Many organizations, both military and civilian, prefer to defer R&M evaluations until the new equipment has been delivered to the eventual user. The U.S. Air Force Flight Test Center has long conducted R&M evaluations during initial flight test and has found value in that process. This document discusses, first, the objectives of the early evaluations. Then, the acquisition process and the test planning process, as they relate to R&M evaluations, are presented. The test planning section discusses the data needed for a successful R&M evaluation and the sources of such data. The conduct of the test, analysis of results, and subsequent reporting methods are delineated. Follow-up actions that are needed after the test are considered. In conclusion, the document lists some R&M considerations for the future.
Author

N95-29565# Federal Aviation Administration, Atlantic City, NJ.
AIRCRAFT ADVANCED MATERIALS RESEARCH AND DEVELOPMENT PROGRAM PLAN Final Report
Peter Shyprykevich and Joe Soderquist Nov. 1994 56 p
(AD-A290542; DOT/FAA/CT-94/106) Avail: CASI HC A04/MF A01

This report describes the FAA research and development plan in Aircraft Advanced Materials and Structures. The Aircraft Advanced Materials Research and Development Plan identifies technology issues that must be addressed to accomplish the FAA mission.
DTIC

N95-29787 Yale Univ., New Haven, CT.
AN ANALYTIC MODELING AND SYSTEM IDENTIFICATION STUDY OF HELICOPTER DYNAMICS Ph.D. Thesis
Steven W. Hong 1993 254 p
Avail: Univ. Microfilms Order No. DA9415860

This thesis applies well-known concepts in maximum likelihood estimation theory to the parametric system identification of a high-order state-space model of rotor craft hover dynamics, and describes an analytic modeling investigation which achieves a partial resolution of differences between the identified and theoretical models. A mathematically derived dynamic model was used to generate the time-domain likelihood function. A model parametrization scheme employing equivalent physical coefficients was used in order to avoid the overparametrization of high order state-space models, to permit an examination of analytic modeling assumptions, and to gain physical insight into system dynamics. The likelihood function was optimized by first using the genetic algorithm approach to locate the neighborhood of the global maximum. This method proved highly effective in locating the near-optimum of a highly multimodal parameter space contour, and when used in conjunction with a gradient-based optimization method, has led to an identified state-space model from flight test data which includes coupled fuselage/rotor dynamics, including main rotor inflow. An examination of the estimated equivalent physical coefficients revealed differences between nominal and estimated parameter values, indicating the need for model improvement in several areas. This study provides a rigorous analytic explanation for the estimated parameters in one important case involving main rotor blade structural flexibility. The investigation has shown that including blade flexibility is important in correctly predicting coupled fuselage/rotor dynamics. Blade structural dynamics were modeled using a Lagrangian formulation of the normal modes approach and has resulted in excellent agreement between flight test and theory, especially in the high frequency range.
Dissert. Abstr.

N95-29911# Naval Postgraduate School, Monterey, CA.
AN OPERATIONAL COMPARISON OF THE CH-46E AND HH-60H AS NAVY COMBAT SUPPORT HELICOPTER REPLACEMENT OPTIONS USING THE SIMULATED MOBILITY MODELING AND ANALYSIS TOOLBOX (SMMAT) M.S. Thesis
Timothy M. Wilson Sep. 1994 65 p
(AD-A288494) Avail: CASI HC A04/MF A01

This study is an operational Comparison of the CH-46E and HH-6OH as potential replacements for the CH-46D combat support helicopter. The Comparison is performed as a simulation using the Simulated Mobility Modeling and Analysis Toolbox (SMMAT). The model places each aircraft in a hypothetical CVBG consisting of eight ships, and has it perform a set of logistics missions. The missions are based on an analysis of seven HC detachments in support of Operation Desert Storm, and consist of internal and external cargo delivery, and passenger transport. The study concludes that for the scenario modeled, the CH-46E is a more capable combat support platform, due in large part to its larger internal cargo capacity. Further study is recommended.
DTIC

N95-30226*# National Aeronautics and Space Administration. Langley Research Center, Hampton, VA.
LOW-SPEED WIND-TUNNEL INVESTIGATION OF THE STABILITY AND CONTROL CHARACTERISTICS OF A SERIES OF FLYING WINGS WITH SWEEP ANGLES OF 50 DEG
Scott P. Fears (Lockheed Engineering and Sciences Co., Hampton, VA.), Holly M. Ross, and Thomas M. Moul Jun. 1995 148 p
(RTOP 505-68-30-01)
(NASA-TM-4640; L-17427; NAS 1.15:4640) Avail: CASI HC A07/MF A02

A wind-tunnel investigation was conducted in the Langley 12-Foot Low-Speed Tunnel to study the low-speed stability and control characteristics of a series of four flying wings over an extended range of angle of attack (-8 deg to 48 deg). Because of the current emphasis on reducing the

radar cross section (RCS) of new military aircraft, the planform of each wing was composed of lines swept at a relatively high angle of 50 deg, and all the trailing-edge lines were aligned with one of the two leading edges. Three arrow planforms with different aspect ratios and one diamond planform were tested. The models incorporated leading-edge flaps for improved longitudinal characteristics and lateral stability and had trailing-edge flaps in three segments that were deflected differentially for roll control, symmetrically for pitch control, and in a split fashion for yaw control. Three top body widths and two sizes of twin vertical tails were also tested on each model. A large aerodynamic database was compiled that could be used to evaluate some of the trade-offs involved in the design of a configuration with a reduced RCS and good flight dynamic characteristics. Author

N95-30335*# California Polytechnic State Univ., San Luis Obispo, CA. Dept. of Aeronautical Engineering.
DEVELOPING A WORKSTATION-BASED, REAL-TIME SIMULATION FOR RAPID HANDLING QUALITIES EVALUATIONS DURING DESIGN Final Report
Frederick Anderson and Daniel J. Biezad 1994 10 p
(Contract NCC2-800)
(NASA-CR-198831; NAS 1.26:198831) Avail: CASI HC A02/MF A01

This paper describes the Rapid Aircraft Dynamics AssessmeNt (RADIAN) project - an integration of the Aircraft SYNThesis (ACSTNT) design code with the USAD DATCOM code that estimates stability derivatives. Both of these codes are available to universities. These programs are then linked to flight simulation and flight controller synthesis tools and resulting design is evaluated on a graphics workstation. The entire process reduces the preliminary design time by an order of magnitude and provides an initial handling qualities evaluation of the design coupled to a control law. The integrated design process is applicable to both conventional aircraft taken from current textbooks and to unconventional designs emphasizing agility and propulsive control of attitude. The interactive and concurrent nature of the design process has been well received by industry and by design engineers at NASA. The process is being implemented into the design curriculum and is being used by students who view it as a significant advance over prior methods. Author

N95-28730*# National Aeronautics and Space Administration. Langley Research Center, Hampton, VA.
RAPID AIRPLANE PARAMETRIC INPUT DESIGN (RAPID) Abstract Only
Robert E. Smith *In* NASA. Lewis Research Center, Surface Modeling, Grid Generation, and Related Issues in Computational Fluid Dynamic (CFD) Solutions Mar. 1995 p 87 (For primary document see N95-28723 10-02)
Avail: CASI HC A01/MF A10

N95-28831*# Boeing Commercial Airplane Co., Seattle, WA.
THE EFFECTS OF DESIGN DETAILS ON COST AND WEIGHT OF FUSELAGE STRUCTURES
G. D. Swanson, S. L. Metschan, M. R. Morris, and C. Kassapoglou (Sikorsky Aircraft, Stratford, CT.) *In* NASA. Langley Research Center, Third NASA Advanced Composites Technology Conference, Volume 1, Part 2 Jan. 1993 p 601-622 (For primary document see N95-28823 10-24)
(Contract NAS1-18889)
Avail: CASI HC A03/MF A04

N95-28840*# Boeing Commercial Airplane Co., Seattle, WA.
GLOBAL COST AND WEIGHT EVALUATION OF FUSELAGE KEEL DESIGN CONCEPTS
B. W. Flynn, M. R. Morris, S. L. Metschan, G. D. Swanson, P. J. Smith, K. H. Griess, M. R. Schramm, and R. J. Humphrey *In* NASA. Langley Research Center, Third NASA Advanced Composites Technology Conference, Volume 1, Part 2 Jan. 1993 p 807-836 (For primary document see N95-28823 10-24)
(Contract NAS1-18889)
Avail: CASI HC A03/MF A04

N95-28841*# National Aeronautics and Space Administration. Langley Research Center, Hampton, VA.
DESIGN AND EVALUATION OF A FOAM-FILLED HAT-STIFFENED PANEL CONCEPT FOR AIRCRAFT PRIMARY STRUCTURAL APPLICATIONS
Damodar R. Ambur *In its* Third NASA Advanced Composites Technology Conference, Volume 1, Part 2 Jan. 1993 p 839-857 (For primary document see N95-28823 10-24)
Avail: CASI HC A03/MF A04

N95-29623# Princess Alexandra Hospital, Swindon (England).
A GENERIC SPECIFICATION FOR SPECIAL PURPOSE AEROMEDICAL EQUIPMENT
I. Spencer *In* AGARD, Recent Issues and Advances in Aeromedical Evacuation (MEDEVAC) Feb. 1995 5 p (For primary document see N95-29604 10-66)
Copyright Avail: CASI HC A01/MF A02

06 AIRCRAFT INSTRUMENTATION

Includes cockpit and cabin display devices; and flight instruments.

For related information see also *19 Spacecraft Instrumentation* and *35 Instrumentation and Photography.*

N95-28691 Air Force Inst. of Tech., Wright-Patterson AFB, OH.
THREE-D WEATHER DISPLAYS FOR AIRCRAFT COCKPITS M.S. Thesis
Bradley S. Boyer Dec. 1994 62 p Limited Reproducibility: More than 20% of this document may be affected by microfiche quality
(AD-A289759; AFIT/CI/CIA-94-166) Avail: Issuing Activity (Defense Technical Information Center (DTIC))

The purpose of this study was to examine the effects of dimensionality and rotating frame of reference in a weather avoidance task. Forty student pilots, performed a 3-D route planning task to navigate around weather formations and arrive at a target within an airspace. The subjects were randomly blocked into four groups, each of which used all four of the display types (3-D rotating, 3-D fixed, 2-D rotating, and 2-D fixed) in varying orders. The subjects performed ten trials for each display type. The results indicated that the 2-D and rotating displays supported navigation through a shorter radial distance, and the 2-D displays also resulted in faster weather planning times. This additional distance and time is attributed to the ambiguity within the 3-D displays. There was no significant difference found between the displays in terms of vertical distance traveled, penetrations of the weather formations, number of vectors created, or the evaluation of situational awareness. DTIC

N95-28692 Air Force Inst. of Tech., Wright-Patterson AFB, OH.
CONCEPTUAL DESIGN OF A MAP INTERACTIVE SYSTEM FOR MILITARY AIRCRAFT COCKPITS M.S. Thesis
Craig J. Wenz Dec. 1994 103 p Limited Reproducibility: More than 20% of this document may be affected by microfiche quality
(AD-A289760; AFIT/CI/CIA-94-158) Avail: Issuing Activity (Defense Technical Information Center (DTIC))

As the complexity and sophistication of military aviation operations rise, the effective interaction and display of map information becomes increasingly important. The purpose of this thesis is to provide a background and directions for those developing new technology in the area of air navigation and to propose a conceptual design of a Map Interactive System (MIS) for military aircraft cockpits. The MIS is an air navigation system that will provide pilots with map displays both on the ground and in the cockpit. Map displays will allow a pilot to view the surrounding environment along the desired route of travel using multiple perspectives. The system will be designed so a pilot may interact with the display, and send and receive vital information while in flight. It will be an amalgamation of current and future technology. The primary purpose of the MIS is to verify a pilot's location and lead him/her to the mission target. DTIC

N95-29123* Tica Technologies, Inc., Cambridge, MA.
OPTIMIZING COCKPIT DISPLAY CONFIGURATIONS WITH A GENETIC ALGORITHM SYSTEM Final Report, 1 Jun. - 30 Nov. 1994

Lawrence Davis, Betsy Constantine, Stuart Shieber, Joe Marks, and Rebecca Hwa 1 Dec. 1994 134 p Limited Reproducibility: More than 20% of this document may be affected by microfiche quality
(Contract NAS2-14052)
(AD-A289799) Avail: Issuing Activity (Defense Technical Information Center (DTIC))

Our Phase I work resulted in a software prototype for MFD page organization, a technique for translating MFD page organizations into graph partitioning problems, and a genetic algorithm for carrying out the graph partitioning. We apply our system to a scenario taken from the Comanche attack helicopter task analysis. The system out-performs other published algorithms for graph partitioning. DTIC

N95-29950# Boeing Defense and Space Group, Seattle, WA.
INVESTIGATION AND CHARACTERIZATION OF SEU EFFECTS AND HARDENING STRATEGIES IN AVIONICS Technical Report, 1 Oct. 1990 - 30 Sep. 1992
Allen H. Taber and Eugene Normand 1 Feb. 1995 93 p Prepared in cooperation with Loral Federal Systems
(Contract DNA-MIPR-92-501)
(AD-A291058; DNA-TR-94-123) Avail: CASI HC A05/MF A01

Data from military/experimental flights and laboratory testing indicate that typical non-radiation-hardened 64k and 256k static random access memories (SRAM's) can experience a significant soft upset rate at aircraft altitudes due to energetic neutrons created by cosmic ray interactions in the atmosphere. It is suggested that error detection and correction (EDAC) circuitry be considered for all new avionics designs containing large amounts of semiconductor memory. DTIC

07 AIRCRAFT PROPULSION AND POWER

Includes prime propulsion systems and systems components, e.g., gas turbine engines and compressors; and onboard auxilliary power plants for aircraft.

For related information see also *20 Spacecraft Propulsion and Power, 28 Propellants and Fuels,* and *44 Energy Production and Conversion.*

N95-28908 Wright Lab., Wright-Patterson AFB, OH.
RECIRCULATING CAVITY CASING TREATMENT FAILURE Final Report, Apr. 1993 - Feb. 1994
Paul T. Kerney Aug. 1994 22 p Limited Reproducibility: More than 20% of this document may be affected by microfiche quality
(AD-A289330; WL-TR-94-2092) Avail: Issuing Activity (Defense Technical Information Center (DTIC))

As part of the Augmented Damping of Low Aspect Ratio Fans (ADLARF) program at the Compressor Research Facility (CRF), the Recirculating Cavity Casing Treatment was in test operation. The casing treatment was made of 6061-T6 aluminum alloy and was specially instrumented for the exploration of stall margin, performance data, and thermal effects. In addition to obtaining stall margin data, this casing treatment was part of a detailed test program to study the effects of five different casing treatments. After thermal cycling the casing treatment between ambient temperature and 650 F, the casing treatment failed after seven hours of test time. The casing treatment was removed and a failure analysis was performed. This paper will summarize the study findings and conclude with recommended actions. DTIC

N95-29115*# National Aeronautics and Space Administration. Lewis Research Center, Cleveland, OH.
LEADING EDGE FILM COOLING EFFECTS ON TURBINE BLADE HEAT TRANSFER
Vijay K. Garg (AYT Corp., Brook Park, OH.) and Raymond E. Gaugler Jun. 1995 19 p Presented at the 40th Gas Turbine and Aeroengine Congress and Exposition, Houston, TX, 5-8 Jun. 1995; sponsored by ASME Original contains color illustrations
(RTOP 505-62-52)
(NASA-TM-106955; E-9705; NAS 1.15:106955) Avail: CASI HC A03/MF A01; 3 functional color pages

An existing three dimensional Navier-Stokes code, modified to include film cooling considerations, has been used to study the effect of spanwise pitch of shower-head holes and coolant to mainstream mass flow ratio on the adiabatic effectiveness and heat transfer coefficient on a film-cooled turbine vane. The mainstream is akin to that under real engine conditions with stagnation temperature = 1900 K and stagnation pressure = 3 MPa. It is found that with the coolant to mainstream mass flow ratio fixed, reducing P, the spanwise pitch for shower-head holes, from 7.5 d to 3.0 d, where d is the hole diameter, increases the average effectiveness considerably over the blade surface. However, when P/d= 7.5, increasing the coolant mass flow increases the effectiveness on the pressure surface but reduces it on the suction surface due to coolant jet lift-off. For P/d = 4.5 or 3.0, such an anomaly does not occur within the range of coolant to mainstream mass flow ratios analyzed. In all cases, adiabatic effectiveness and heat transfer coefficient are highly three-dimensional. Author

N95-29244 Massachusetts Inst. of Tech., Cambridge, MA.
MODELING AND CONTROL OF ROTATING STALL IN HIGH SPEED MULTI-STAGE AXIAL COMPRESSORS Ph.D. Thesis
Matthew Roger Feulner 1994
Avail: Issuing Activity (MIT Libraries, Rm. 14-0551, Cambridge, MA 02139-4307)

Using a two-dimensional, compressible flow representation of axial compressor dynamics, a control-theoretic input-output model is derived which is of general utility in rotating stall and surge active control studies. Geometry of a three stage research compressor is used in this model to perform control configuration studies using operating range extension and mean-square costs in the comparisons. The derivation presented begins with a review of the fluid dynamic model, which is a 2D stage stacking technique that accounts for blade row pressure rise, loss and deviation as well as blade row and inter-blade row compressible flow. This model is extended to include the effects of the upstream and downstream geometry and boundary conditions, then manipulated into a transfer function form that dynamically relates actuator motion to sensor measurements. Transcendental functions in this input-output form are then approximated using rational polynomials. Further manipulations yield an approximate state-space model which is in standard form for studying active control of rotating stall and surge. Specifications on the control system are proposed which are standard restrictions in modern control theory. Cost functions are proposed to compare control configurations. Two control design methods are presented to design the compensators. The linear quadratic-Gaussian optimal control minimizes a mean-square cost function of the perturbations and the control activity. The H(sub infinity) optimal control minimizes the H(sub infinity)-norm related to the specifications. The control design methods are then applied to the geometry of a three stage research compressor. As examples of high current relevance, the transfer functions from an array of jet actuators to arrays of either static pressure, stagnation pressure, and velocity sensors are examined. It is found that using a jet actuator that reduces the momentum of the flow can be as good as a jet actuator which adds equivalent momentum. It is also found that velocity and stagnation pressure sensors are superior to static pressure sensors.
Dissert. Abstr.

N95-29496# Massachusetts Inst. of Tech., Cambridge, MA. Gas Turbine Lab.
INTELLIGENT TURBINE ENGINES FOR ARMY APPLICATIONS Final Report, 28 Feb. 1994 - 27 Aug. 1994
Alan H. Epstein Nov. 1994 165 p Workshop held in Cambridge, MA, 21-22 Mar. 1994; sponsored by the US Army Research Office
(Contract DAAH04-94-G-0038)
(AD-A290532; ARO-3305.1-EG-CF) Avail: CASI HC A08/MF A02

This report documents the proceedings of a workshop on Intelligent Turbine Engines for Army Applications held at the Massachusetts Institute of Technology on March 21-22, 1994. The workshop brought together experts from government, industry, and academia to explore ways in which advanced controls concepts can be used to significantly benefit Army gas turbine engines. Participants discussed Army control related requirements. Emphasis was placed on the integration of active control into helicopter and ground vehicle gas turbines. DTIC

N95-29679 Georgia Inst. of Tech., Atlanta, GA.
MODEL DEVELOPMENT FOR ACTIVE CONTROL OF STALL PHENOMENA IN AIRCRAFT GAS TURBINE ENGINES Ph.D. Thesis
Kevin Michael Eveker 1993 210 p
Avail: Univ. Microfilms Order No. DA9415634

This study addresses model development for active control of stall phenomena in aircraft gas turbine engines. The high-frequency nature of these phenomena requires a new approach for modelling aircraft gas turbine engines (and turbomachinery systems in general). Since the models developed using this approach are for use in control design, they must be control-oriented (i.e. suitable for use in control design). An approach for control-oriented high-frequency turbomachinery modelling based on quasi-1D flow equations is developed. The suitability of this approach for developing control-oriented high-frequency turbo machinery models is illustrated by developing models of generic systems of this type which are easily adapted to specific systems. Models are developed in detail for the case of calorically perfect single species gases, and extension of the approach to develop models to the case of thermally perfect multiple species gases is also discussed. Models of specific systems are given to demonstrate the ability of the models to predict 1D stall phenomena and the suitability of these models for use in the design of active control of these 1D phenomena. The specific systems mentioned are an axial compressor rig and a turbojet engine rig for which experimental data is available for use in model development and validation. In addition to the models which predict 1D stall phenomena, use of the approach based on quasi-ID flow equations to model 2D stall phenomena which involve circumferentially varying 1D flow is also discussed. Dissert. Abstr.

N95-29764# Georgia Tech Research Inst., Atlanta, GA.
MEASUREMENTS OF IONS FORMED IN JET ENGINE EXHAUST PLUMES
F. L. Eisele 23 Jun. 1994 20 p
(Contract F19628-93-K-0018)
(AD-A290940; PL-TR-94-2253; SR-1) Avail: CASI HC A03/MF A01

An atmospheric pressure chemical ionization mass spectrometer was modified to measure either ion or neutral effluents from a jet engine. The instrument was set up behind an F-15 aircraft at Eglin Air Force Base and measured the ions formed in both the positive and negative spectrum. Since the ion concentrations in the jet plume were quite small and measurement times relatively short, most of the measurements performed were of ions artificially produced in the exhaust using a corona ion source. The most obvious change in the ion spectrum after the jet engines were started was the dramatic increase in what appeared to be sulfuric acid. The spectra resulting from these measurements are shown and discussed. DTIC

N95-29934# Wright Research Development Center, Wright-Patterson AFB, OH. Aero Propulsion and Power Lab.
CHARACTERIZATION OF STALL INCEPTION IN HIGH-SPEED SINGLE-STAGE COMPRESSORS Final Report, 1 Aug. - 1 Dec. 1992
Keith Boyer Dec. 1994 166 p
(AF Proj. 2307)
(AD-A291275; WL-TR-93-2058) Avail: CASI HC A08/MF A02

All aircraft gas turbine engines currently compromise compression system performance at some point(s) in their operating envelope to obtain 'adequate' stall margin. This work pursues the concept of active stall control to minimize or eliminate this penalty, thereby improving the performance of any aircraft gas turbine engine. DTIC

N95-30007*# National Aeronautics and Space Administration. Lewis Research Center, Cleveland, OH.
INLET FLOW TEST CALIBRATION FOR A SMALL AXIAL COMPRESSOR RIG. PART 2: CFD COMPARED WITH EXPERIMENTAL RESULTS
D. P. Miller and P. S. Prahst (NYMA, Inc., Brook Park, OH.) Jul. 1995 16 p Presented at the 31st Joint Propulsion Conference and Exhibit, San Diego, CA, 10-12 Jul. 1995; sponsored by AIAA, ASME, SAE, and ASEE
(RTOP 505-62-10)
(NASA-TM-106999; E-9778; NAS 1.15:106999; AIAA Paper 95-3037)
Avail: CASI HC A03/MF A01

An axial compressor test rig has been designed for the operation of small turbomachines. A flow test was run to calibrate and determine the source and magnitudes of the loss mechanisms in the compressor inlet for a highly loaded two-stage axial compressor test. Several flow conditions and inlet guide vane (IGV) angle settings were established, for which detailed surveys were completed. Boundary layer bleed was also provided along the casing of the inlet behind the support struts and ahead of the IGV. Several computational fluid dynamics (CFD) calculations were made for selected flow conditions established during the test. Good agreement between the CFD and test data were obtained for these test conditions. Author

08 AIRCRAFT STABILITY AND CONTROL

Includes aircraft handling qualities; piloting; flight controls; and autopilots.

For related information see also *05 Aircraft Design, Testing and Performance.*

N95-29156 Kansas Univ. Center for Research, Inc., Lawrence, KS.
APPLICATION OF OPTIMIZATION TECHNIQUE TO CONTROL SYSTEM DESIGN FOR DEPARTURE PREVENTION AND AIRCRAFT MODEL ESTIMATION THROUGH DYNAMIC INVERSION Ph.D. Thesis
Fuying Ge 1993 222 p
Avail: Univ. Microfilms Order No. DA9425908

The numerical optimization technique allows one to formulate a nonlinear problem in an easily understandable manner. The objective of increasing the performance and maneuverability without departure/spin is established in a simple mathematical expression and by sets of constraints. The feedback gains in the control system and unknown coefficients present in aircraft models are defined as design variables. The maneuver boundaries for departure prevention are directly characterized by motion parameters, alpha, beta, p, q, and r, and inequality constraints. The optimizer automatically cycles through the combinations of design variables to determine the best design satisfying the objective without violating the maneuver boundaries. Both the processes of defining the system or models (the design process) and the process of determining the response of the specified system or models (the analysis process) are directly based on the six degree-of-freedom (6-DOF) dynamic simulation. Therefore the complex nature of the aerodynamics, and dynamics and interactions at high angles of attack addressed in the 6-DOF equations of motion are included in the control system design and/or aircraft model estimation. The design of an aileron-rudder-interconnect (ARI) and stability yaw damper using this method is demonstrated for a F-5A configuration. The design of an angle-of-attack limiter is demonstrated using an F-16 configuration to prevent coupled pitch and yaw departure. The mathematical model to be estimated is related to the nonlinear characteristics at high angles of attack flight conditions. Using the present optimization technique, a control system to provide good maneuverability and high departure/spin resistance can be designed simultaneously with aircraft model estimation. Dissert. Abstr.

N95-29680 Stanford Univ., CA.
LINEAR MATRIX INEQUALITIES FOR THE PROBLEM OF ABSOLUTE STABILITY OF CONTROL SYSTEMS Ph.D. Thesis
Eric Marie Feron 1994 102 p
Avail: Univ. Microfilms Order No. DA9414567

The problem of absolute stability of dynamic systems deals with the stability of linear systems perturbed by different classes of unknown elements. These elements are unsteady, nonlinear or simply unknown, constant gains. These systems, which encompass a broader class than linear time invariant systems, are able to better represent physical systems. Many techniques have been developed in the past to study them the famous Circle and Popov criteria, for example. They are graphical procedures and their practical use is limited to one element. In this thesis, we propose to show how advances in computer power and convex optimization allow us to extend these criteria to multiple elements. We also present an extension of these criteria that can be used to derive performance bounds. Dissert. Abstr.

N95-30254*# Kansas Univ. Center for Research, Inc., Lawrence, KS.
DESIGN, ANALYSIS AND CONTROL OF LARGE TRANSPORTS SO THAT CONTROL OF ENGINE THRUST CAN BE USED AS A BACK-UP OF THE PRIMARY FLIGHT CONTROLS Ph.D. Thesis
Jan Roskam, Deane E. Ackers, and Donna S. Gerren Apr. 1995 463 p
(Grant NAG2-789)
(NASA-CR-198958; NAS 1.26:198958) Avail: CASI HC A20/MF A04

A propulsion controlled aircraft (PCA) system has been developed at

NASA Dryden Flight Research Center at Edwards Air Force Base, California, to provide safe, emergency landing capability should the primary flight control system of the aircraft fail. As a result of the successful PCA work being done at NASA Dryden, this project investigated the possibility of incorporating the PCA system as a backup flight control system in the design of a large, ultra-high capacity megatransport in such a way that flight path control using only the engines is not only possible, but meets MIL-Spec Level 1 or Level 2 handling quality requirements. An 800 passenger megatransport aircraft was designed and programmed into the NASA Dryden simulator. Many different analysis methods were used to evaluate the flying qualities of the megatransport while using engine thrust for flight path control, including: (1) Bode and root locus plot analysis to evaluate the frequency and damping ratio response of the megatransport; (2) analysis of actual simulator strip chart recordings to evaluate the time history response of the megatransport; and (3) analysis of Cooper-Harper pilot ratings by two NaSA test pilots. Author

N95-30327*# National Aeronautics and Space Administration. Langley Research Center, Hampton, VA.
MANUAL FOR A WORKSTATION-BASED GENERIC FLIGHT SIMULATION PROGRAM (LaRCsim), VERSION 1.4
E. Bruce Jackson May 1995 142 p
(RTOP 505-64-52-01)
(NASA-TM-110164; NAS 1.15:110164) Avail: CASI HC A07/MF A02

LaRCsim is a set of ANSI C routines that implement a full set of equations of motion for a rigid-body aircraft in atmospheric and low-earth orbital flight, suitable for pilot-in-the-loop simulations on a workstation-class computer. All six rigid-body degrees of freedom are modeled. The modules provided include calculations of the typical aircraft rigid-body simulation variables, earth geodesy, gravity and atmospheric models, and support several data recording options. Features/limitations of the current version include English units of measure, a 1962 atmosphere model in cubic spline function lookup form, ranging from sea level to 75,000 feet, rotating oblate spheroidal earth model, with aircraft C.G. coordinates in both geocentric and geodetic axes. Angular integrations are done using quaternion state variables Vehicle X-Z symmetry is assumed. Author

09 RESEARCH AND SUPPORT FACILITIES (AIR)

Includes airports, hangars and runways; aircraft repair and overhaul facilities; wind tunnels; shock tubes; and aircraft engine test stands.

For related information see also *14 Ground Support Systems and Facilities (Space).*

N95-29468# Polytechnic Univ., Farmingdale, NY.
RESEARCH INSTRUMENTATION FOR POLYTECHNIC UNIVERSITY'S SUPERSONIC WIND TUNNEL FACILITY Final Report, 15 Sep. 1993 - 14 Sep. 1994
Iraj M. Kalkhoran and M. V. Otugen 8 Nov. 1994 20 p
(Contract F49620-93-1-0588)
(AD-A290232; POLY-AE-94-02; AFOSR-95-0048TR) Avail: CASI HC A03/MF A01

Modern instrumentation was acquired for use in Polytechnic University's Supersonic wind tunnel facility. The equipment is currently being incorporated in several on-going research projects dealing with development of non-intrusive measurement techniques, flow visualization, and pressure measurements in high speed unsteady flows. The major components of the research instrumentation include a Q-Switched ND:YAG laser, a CCD camera system with necessary hardware and software and a 16 channel data acquisition and control system with appropriate hardware and software. This report describes the basic function of the acquired equipment and the anticipated use of the equipment for conducting supersonic wind tunnel testing. DTIC

N95-29522# Naval Command, Control and Ocean Surveillance Center, San Diego, CA. Research, Development, Technology and Evaluation Div.
COMPACT SUBSTRATE HEATER FOR USE IN AN OXIDIZING ATMOSPHERE
T. E. Jones, W. C. McGinnis, and J. S. Briggs Dec. 1994 16 p
Submitted for publication in Review of Scientific Instruments
(NR Proj. ZW4-4)
(AD-A290860) Avail: CASI HC A03/MF A01

A compact heater, designed for the deposition of thin films at high temperatures in an oxidizing atmosphere or vacuum, is described. The heater, including an oxygen-resistant case and the attached substrate, can be loaded into a vacuum deposition chamber through a small-diameter load-lock system, and will operate in 0 to 1 atmosphere of oxygen at temperatures up to at least 800 C. Heat is generated resistively, and the substrates are heated directly by thermal conduction. The heater was built specifically to heat substrates during the growth of high-temperature superconducting thin films. DTIC

N95-29795 Stanford Univ., CA.
A METHOD FOR THE MODELLING OF POROUS AND SOLID WIND TUNNEL WALLS IN COMPUTATIONAL FLUID DYNAMICS CODES Ph.D. Thesis
Thomas John Beutner 1994 126 p
Avail: Univ. Microfilms Order No. DA9414538

Porous wall wind tunnels have been used for several decades and have proven effective in reducing wall interference effects in both low speed and transonic testing. They allow for testing through Mach 1, reduce blockage effects and reduce shock wave reflections in the test section. Their usefulness in developing computational fluid dynamics (CFD) codes has been limited, however, by the difficulties associated with modelling the effect of a porous wall in CFD codes. Previous approaches to modelling porous wall effects have depended either upon a simplified linear boundary condition, which has proven inadequate, or upon detailed measurements of the normal velocity near the wall, which require extensive wind tunnel time and instrumentation. The current work was initiated in an effort to find a simple, accurate method of modelling a porous wall boundary condition in CFD codes. The development of such a method would allow data from porous wall wind tunnels to be used more readily in validating CFD codes. This would be beneficial when transonic validations are desired, or when large models are used to achieve high Reynolds numbers in testing. A computational and experimental study was undertaken to investigate a new method of modelling solid and porous wall boundary conditions in CFD codes. The method utilizes experimental measurements at the walls to develop a flow field solution based on the method of singularities. This flow field solution was then imposed as a pressure boundary condition in a CFD simulation of the internal flow field. The effectiveness of this method in describing the effect of porosity changes on the wall was investigated. Also, the effectiveness of this method when only sparse experimental measurements were available has been investigated. The current work demonstrated this approach for low speed flows and compared the results with experimental data obtained from a heavily instrumented variable porosity test section. The approach developed was simple, computationally inexpensive, and does not require extensive or intrusive measurements of the boundary conditions during the wind tunnel test. It may be applied to both solid and porous wall wind tunnel tests. Dissert. Abstr.

N95-29967# Federal Aviation Administration, Atlantic City, NJ. Technical Center.
EVALUATION OF RETRO-REFLECTIVE BEADS IN AIRPORT PAVEMENT MARKINGS Final Report
Keith W. Bagot Dec. 1994 66 p
(AD-A291065; DOT/FAA/CT-94/120) Avail: CASI HC A04/MF A01

This report identifies the results of a 1-year comparative evaluation on the use of retro-reflective glass beads in airport surface pavement markings. Class beads meeting Federal Specification TT-B-1325B, Type 1 and 3 were tested at three airports for retro-reflectivity, effects on runway friction, conspicuity, and durability. The three test airports were Atlantic City, Greater Pittsburgh, and Phoenix Sky Harbor International airports. Data from this study show the use of beaded materials in airport markings increased the conspicuity and quality of the airport markings. Also discovered in this evaluation was the friction enhancement gained from the incorporation of beads and silica additives into the paint materials. As a result of the findings of this study, certain modifications are recommended for the two existing specifications regarding airport pavement markings, AC 150/5370-10A, Standards for Specifying Construction on Airports and AC 150/5340-1G Standards for Airport Markings. DTIC

N95-30067*# NYMA, Inc., Brook Park, OH.
A PC PROGRAM FOR ESTIMATING MEASUREMENT UNCERTAINTY FOR AERONAUTICS TEST INSTRUMENTATION Final Contractor Report
Philip Z. Blumenthal Cleveland, OH NASA Jul. 1995 16 p Presented at the 31st Joint Propulsion Conference, San Diego, CA, 10-12 Jul. 1995; sponsored by AIAA, ASME, SAE, and ASEE
(Contract NAS3-27186; RTOP 505-62-82)
(NASA-CR-198361; E-9759; NAS 1.26:198361; AIAA Paper 95-3072)
Avail: CASI HC A03/MF A01

A personal computer program was developed which provides aeronautics and operations engineers at Lewis Research Center with a uniform method to quickly provide values for the uncertainty in test measurements and research results. The software package used for performing the calculations is Mathcad 4.0, a Windows version of a program which provides an interactive user interface for entering values directly into equations with immediate display of results. The error contribution from each component of the system is identified individually in terms of the parameter measured. The final result is given in common units, SI units, and percent of full scale range. The program also lists the specifications for all instrumentation and calibration equipment used for the analysis. It provides a presentation-quality printed output which can be used directly for reports and documents.
Author

N95-30228*# National Aeronautics and Space Administration. Ames Research Center, Moffett Field, CA.
NUMERICAL SIMULATIONS OF THE FLOW IN THE HYPULSE EXPANSION TUBE
Gregory J. Wilson, Myles A. Sussman, and Robert J. Bakos (General Applied Science Labs., Inc., Ronkonkoma, NY.) Jun. 1995 53 p
(RTOP 505-70-62)
(NASA-TM-110357; A-950072; NAS 1.15:110357) Avail: CASI HC A04/MF A01

Axisymmetric numerical simulations with finite-rate chemistry are presented for two operating conditions in the HYPULSE expansion tube. The operating gas for these two cases is nitrogen and the computations are compared to experimental data. One test condition is at a total enthalpy of 15.2 MJ/Kg and a relatively low static pressure of 2 kPa. This case is characterized by a laminar boundary layer and significant chemical nonequilibrium in the acceleration gas. The second test condition is at a total enthalpy of 10.2 MJ/Kg and a static pressure of 38 kPa and is characterized by a turbulent boundary layer. For both cases, the time-varying test gas pressure predicted by the simulations is in good agreement with experimental data. The computations are also found to be in good agreement with Mirels' correlations for shock tube flow. It is shown that the nonuniformity of the test gas observed in the HYPULSE expansion tube is strongly linked to the boundary layer thickness. The turbulent flow investigated has a larger boundary layer and greater test gas nonuniformity. In order to investigate possibilities of improving expansion tube flow quality by reducing the boundary layer thickness, parametric studies showing the effect of density and turbulent transition point on the test conditions are also presented. Although an increase in the expansion tube operating pressure level would reduce the boundary layer thickness, the simulations indicate that the reduction would be less than what is predicted by flat plate boundary layer correlations.
Author

12 ASTRONAUTICS (GENERAL)

For extraterrestrial exploration see *91 Lunar and Planetary Exploration.*

N95-29351*# National Aeronautics and Space Administration. Ames Research Center, Moffett Field, CA.
BIBLIOGRAPHY OF DOCTOR CHUL PARK
Lawrence A. Gochberg (National Academy of Sciences - National Research Council, Moffett Field, CA.), Ethiraj Venkatapathy (Thermoscience Inst., Moffett Field, CA.), and Chul Park May 1995 180 p
(RTOP 242-10-80)
(NASA-TM-110353; A-950065; NAS 1.15:110353) Avail: CASI HC A09/MF A02

This document contains a comprehensive bibliography of the published works, and a short biography, of Dr. Chul Park. The contents of this bibliography were compiled primarily from the NASA RECON data base. The RECON citations have been modified to appear in a uniform format with all other listed citations . These other citations were located by computer searches in the INSPEC, NTIS, COMPENDEX, and Chemical Abstracts data bases, as well as through the cooperation of Dr. Chul Park, and his associates in the Reacting Flow Environments Branch at NASA Ames Research Center. All citations are presented in an approximate reverse chronological order from the present date. This work was created to honor the occasion of Dr. Chul Park's retirement on December 14, 1994, after 27 years of distinguished government service at the NASA Ames Research Center.
Author

N95-29407* National Aeronautics and Space Administration. Lyndon B. Johnson Space Center, Houston, TX.
APOLLO 11: FOR ALL MANKIND (Videotape)
[1969] Videotape: 34 min. playing time, in color, with sound
(NASA-TM-110622; NONP-NASA-VT-95-51757) Avail: CASI VHS A02/BETA A22

Historical film footage of Apollo 11 is shown. The pre-flight, launch, module docking, lunar orbit, lunar landing, ascent, and return-to-Earth flight is shown. There are lunar surface shots, Moon views, Earth views from Earth orbit, Earth views from the Moon, and footage of actual moon walk by astronauts. Mission control and space to ground control communication is heard.
CASI

13 ASTRODYNAMICS

Includes powered and free-flight trajectories; and orbital and launching dynamics.

N95-30347 Georgia Inst. of Tech., Atlanta, GA.
GUIDANCE LAW DEVELOPMENT FOR AEROASSISTED TRANSFER VEHICLES USING MATCHED ASYMPTOTIC EXPANSIONS Ph.D. Thesis
Nahum Melamed 1993 102 p
Avail: Univ. Microfilms Order No. DA9415656

This thesis addresses and clarifies a number of issues related to the Matched Asymptotic Expansion (MAE) analysis of skip trajectories, or any class of problems that give rise to inner layers that are not associated directly with satisfying boundary conditions. The procedure for matching inner and outer solutions, and using the composite solution to satisfy boundary conditions is developed and rigorously followed to obtain a set of algebraic equations for the problem of inclination change with minimum energy loss. A detailed evaluation of the zeroth order guidance algorithm for aeroassisted orbit transfer is performed. It is shown that by exploiting the structure of the MAE solution procedure, the original problem, which requires the solution of a set of 20 implicit algebraic equations, can be reduced to a problem of 6 implicit equations in 6 unknowns. A solution that is near optimal, requires a minimum of computation, and thus can be implemented in real time and on-board the vehicle, has been obtained. Guidance law implementation entails treating the current state as a new initial state and repetitively solving the zeroth order MAE problem to obtain the feedback controls. Finally, a general procedure is developed for constructing a MAE solution up to first order, of the Hamilton-Jacobi-Bellman equation based on the method of characteristics. The development is valid for a class of perturbation problems whose solution exhibits two-time-scale behavior. A regular expansion for problems of this type is shown to be inappropriate since it is not valid over a narrow range of the independent variable. That is, it is not uniformly valid. Of particular interest here is the manner in which matching and boundary conditions are enforced when the expansion is carried out to first order. Two cases are distinguished--one where the left boundary condition coincides with, or lies to the right of, the singular region, and another one where the left boundary condition lies to the left of the singular region. A simple example is used to illustrate the procedure where the obtained solution is uniformly valid to O(epsilon(exp 2)). The potential application of this procedure to aeroassisted plane change is also described and partially evaluated.
Dissert. Abstr.

14 GROUND SUPPORT SYSTEMS AND FACILITIES (SPACE)

Includes launch complexes, research and production facilities; ground support equipment, e.g., mobile transporters; and simulators.

For related information see also *09 Research and Support Facilities (Air).*

No abstracts in this category.

15 LAUNCH VEHICLES AND SPACE VEHICLES

Includes boosters; operating problems of launch/space vehicle systems; and reusable vehicles.

For related information see also *20 Spacecraft Propulsion and Power.*

N95-28680 Naval Postgraduate School, Monterey, CA.
DESIGN AND ANALYSIS OF THE LAUNCH VEHICLE ADAPTER FITTING FOR THE PETITE AMATEUR NAVY SATELLITE (PANSAT) M.S. Thesis
Brian B. Gannon Sep. 1994 54 p Limited Reproducibility: More than 20% of this document may be affected by microfiche quality
(AD-A289693) Avail: Issuing Activity (Defense Technical Information Center (DTIC))

The Petite Amateur Navy Satellite (PANSAT) is a small communications satellite being developed at the Naval Postgraduate School. This thesis provides a structural design and analysis for the adapter fitting which mates PANSAT to the space shuttle Get Away Special (GAS) cannister launching system. Launch vehicle loading and interface requirements were combined with PANS AT design priorities to determine design specifications. Structural Dynamics Research Corporation's 1-DEAS Masters Series software was utilized to model two adapter designs. The finite element solver in 1-DEAS was used to analyze the two designs for strength and natural frequency. Design and analysis of fasteners, used to attach the adapter fitting to PANSAT, were also conducted. The results showed that a titanium alloy adapter, which does not shadow the solar arrays, and stainless steel fasteners exceeded all design specifications. DTIC

N95-28718*# National Aeronautics and Space Administration. Marshall Space Flight Center, Huntsville, AL.
TEST LOAD VERIFICATION THROUGH STRAIN DATA ANALYSIS
V. Verderaime and F. Harrington Washington May 1995 23 p
(NASA-TP-3558; M-783; NAS 1.60:3558) Avail: CASI HC A03/MF A01

A traditional binding acceptance criterion on polycrystalline structures is the experimental verification of the ultimate factor of safety. At fracture, the induced strain is inelastic and about an order-of-magnitude greater than designed for maximum expected operational limit. At this extreme strained condition, the structure may rotate and displace at the applied verification load such as to unknowingly distort the load transfer into the static test article. Test may result in erroneously accepting a submarginal design or rejecting a reliable one. A technique was developed to identify, monitor, and assess the load transmission error through two back-to-back surface-measured strain data. The technique is programmed for expediency and convenience. Though the method was developed to support affordable aerostructures, the method is also applicable for most high-performance air and surface transportation structural systems. Author

N95-29339*# Georgia Inst. of Tech., Atlanta, GA. School of Aerospace Engineering.
ANALYTICAL INVESTIGATIONS IN AIRCRAFT AND SPACECRAFT TRAJECTORY OPTIMIZATION AND OPTIMAL GUIDANCE Final Report
Nikos Markopoulos and Anthony J. Calise May 1995 187 p
(Grants NAG1-922; NAG1-1257; RTOP 242-80-01-02)
(NASA-CR-4672; NAS 1.26:4672) Avail: CASI HC A09/MF A02

A collection of analytical studies is presented related to unconstrained and constrained aircraft (a/c) energy-state modeling and to spacecraft (s/c) motion under continuous thrust. With regard to a/c unconstrained energy-state modeling, the physical origin of the singular perturbation parameter that accounts for the observed 2-time-scale behavior of a/c during energy climbs is identified and explained. With regard to the constrained energy-state modeling, optimal control problems are studied involving active state-variable inequality constraints. Departing from the practical deficiencies of the control programs for such problems that result from the traditional formulations, a complete reformulation is proposed for these problems which, in contrast to the old formulation, will presumably lead to practically useful controllers that can track an inequality constraint boundary asymptotically, and even in the presence of 2-sided perturbations about it. Finally, with regard to s/c motion under continuous thrust, a thrust program is proposed for which the equations of 2-dimensional motion of a space vehicle in orbit, viewed as a point mass, afford an exact analytic solution. The thrust program arises under the assumption of tangential thrust from the costate system corresponding to minimum-fuel, power-limited, coplanar transfers between two arbitrary conics. The thrust program can be used not only with power-limited propulsion systems, but also with any propulsion system capable of generating continuous thrust of controllable magnitude, and, for propulsion types and classes of transfers for which it is sufficiently optimal the results of this report suggest a method of maneuvering during planetocentric or heliocentric orbital operations, requiring a minimum amount of computation; thus uniquely suitable for real-time feedback guidance implementations. Author

N95-29992# Aerospace Corp., El Segundo, CA. Technology Operations.
PERFORMANCE EVALUATION OF BOLT-CUTTER SYSTEM ON FIRST TAURUS LAUNCH
F. Baban, R. Williams, S. Amimoto, W. Hansen, and T. Bixler 15 Oct. 1994 34 p
(Contract F04701-93-C-0094)
(AD-A291237; TR-94(4508)-1; SMC-TR-95-3) Avail: CASI HC A03/MF A01

In rapid response to the request of the Space Test and Experimentation Directorate in Space Launch Operations, a launch-critical experimental investigation was conducted to evaluate the performance of a particular bolt-cutter system for separating stages on the first Taurus launch. The tests were to examine the variation of tension preloading on the bolt system and to demonstrate the tolerable margin on this parameter for such launches with the new types of bolts since the preloading was known to vary as much as 12% from a preset value before launch. We planned and carried out the experiment, designed and assembled the fixture to properly simulate flight application, and developed diagnostics. Four bolt cutters were purchased from the manufacturer for these tests, and one was provided by the contractor. In addition to the obvious requirement to demonstrate the successful severing of bolts under varying preloads, ignition-wire current and timing of chisel impact on the bolt were monitored. An optical diagnostic was designed to determine the flyout velocity and kinetic energy of the broken pieces. These latter measurements will be useful in anchoring performance codes simulating and assessing the structural dynamics of the bolt-cutter function for future missions. The tests were conducted successfully and the bolts were severed successfully in all five tests. The preloads were successively lowered from 2,500 lb to 2,250, 2,000, 1,500, and 1,000 lb These tests contributed in a timely manner to the STEP launch decision and to launch mission assurance. They demonstrated important margin to the nominally set 3,200 lb. preload. The entire complicated experimental program from inception to completion was accomplished in less than three weeks. DTIC

16 SPACE TRANSPORTATION

Includes passenger and cargo space transportation, e.g., shuttle operations; and space rescue techniques.

For related information see also *03 Air Transportation and Safety* and *18 Spacecraft Design, Testing and Performance.* For space suits see *54 Man/System Technology and Life Support.*

N95-28715* National Aeronautics and Space Administration. Lyndon B. Johnson Space Center, Houston, TX.
STS-67 MISSION HIGHLIGHTS RESOURCE TAPE (Videotape)
Chuck Welch, ed. 10 May 1995 Videotape: 57 min. playing time, in

color, with sound
(NASA-TM-110530; JSC-1478; NONP-NASA-VT-95-50092) Avail: CASI VHS A02/BETA A22

The Space Shuttle Mission, STS-67, is highlighted in this video. Flight crew (Stephen S. Oswald (Commander), William G. Gregory (Pilot), Tamara E. Jernigan, Wendy B. Lawrence, John M. Grunfeld (Mission Specialists), Samuel T. Durrance, and Ronald A. Parise (Payload Specialists)) prelaunch and launch activities, EVA activities with payload deployment and retrieval (ASTRO-2 and WUPPE (Wisconsin Ultraviolet Photo Polarimeter Experiment)), spaceborne experiments (astronomical observation and data collection, protein crystal growth, and human physiological processes), and pre-reentry activities are shown. There are astronomical telescopic observation from the two telescopes in the payload, the Hopkins Ultraviolet Telescope and the Ultraviolet Imaging Telescope, of Io and of globular clusters, and their emission spectra is collected via a spectrometer. Earth view film and photography is shown, which includes lightning on terrestrial surfaces, cyclone activity, and cloud cover. CASI

N95-29447*# Draper (Charles Stark) Lab., Inc., Cambridge, MA. EG/Aeroscience and Flight Mechanics Div.
A VEHICLE HEALTH MONITORING SYSTEM FOR THE SPACE SHUTTLE REACTION CONTROL SYSTEM DURING REENTRY M.S. Thesis - Massachusetts Inst. of Technology
Anthony David Rosello 22 May 1995 120 p
(Contract NAS9-18426)
(NASA-CR-188370; NAS 1.26:188370; CSDL-T-1250) Avail: CASI HC A06/MF A02

A general two tier framework for vehicle health monitoring of Guidance Navigation and Control (GN&C) system actuators, effectors, and propulsion devices is presented. In this context, a top level monitor that estimates jet thrust is designed for the Space Shuttle Reaction Control System (RCS) during the reentry phase of flight. Issues of importance for the use of estimation technologies in vehicle health monitoring are investigated and quantified for the Shuttle RCS demonstration application. These issues include rate of convergence, robustness to unmodeled dynamics, sensor quality, sensor data rates, and information recording objectives. Closed loop simulations indicate that a Kalman filter design is sensitive to modeling error and robust estimators may reduce this sensitivity. Jet plume interaction with the aerodynamic flowfield is shown to be a significant effect adversely impacting the ability to accurately estimate thrust. Author

N95-29954* National Aeronautics and Space Administration. Lyndon B. Johnson Space Center, Houston, TX.
STS-71 SHUTTLE/MIR FLIGHT: DAY 1 (Videotape)
30 Jun. 1995 Videotape: 15 min. 45 sec. playing time, in color, with sound
(NASA-TM-110744; BRF1343A; NONP-NASA-VT-95-56567) Avail: CASI VHS A02/BETA A22

The first day of the STS-71 flight of the Space Shuttle Atlantis is contained in this video. This mission highlights the first U.S. docking with the Mir Space Station. The scope of this part of the STS-71 mission is to drop off and pickup two cosmonauts, and to pickup one American astronaut who has been living aboard the Mir Station for several months. The STS-71 flight crew consists of: Atlantis Mission Specialist Gregory Harbaugh; Ellen Baker, Flight Commander Robert Gibson; Russian cosmonaut Anatoly Solovyen; Vladimir Dezhuroz; Gennady Strekalov; and Dr. Norman Thagard. Flight footage contains prelaunch activities. Author

N95-29955* National Aeronautics and Space Administration. Lyndon B. Johnson Space Center, Houston, TX.
STS-71 SHUTTLE/MIR FLIGHT: DAY 2 (Videotape)
30 Jun. 1995 Videotape: 20 min. 45 sec. playing time, in color, with sound
(NASA-TM-110745; BRF1343B; NONP-NASA-VT-95-56568) Avail: CASI VHS A02/BETA A22

The second day of the STS-71 flight of the Space Shuttle Atlantis is contained in this video. Flight footage contains launch, and orbital activities. Author

N95-29956* National Aeronautics and Space Administration. Lyndon B. Johnson Space Center, Houston, TX.
STS-71 SHUTTLE/MIR FLIGHT: DAY 3 (Videotape)
30 Jun. 1995 Videotape: 32 min. 30 sec. playing time, in color, with sound
(NASA-TM-110746; BRF1343C; NONP-NASA-VT-95-56569) Avail: CASI VHS A02/BETA A22

The third day of the STS-71 flight of the Space Shuttle Atlantis is contained in this video. Flight footage contains earth views from space, and views of Mir Space Station taken from various angles. Author

N95-29957* National Aeronautics and Space Administration. Lyndon B. Johnson Space Center, Houston, TX.
STS-71 SHUTTLE/MIR FLIGHT: DAY 4 (Videotape)
30 Jun. 1995 Videotape: 29 min. 30 sec. playing time, in color, with sound
(NASA-TM-110747; BRF1343D; NONP-NASA-VT-95-56570) Avail: CASI VHS A02/BETA A22

Day 4 of the STS-71 flight Space Shuttle Atlantis mission is highlighted in this video. During this segment of the mission the Space Station is docked with the Mir Space Station. There are interviews with the astronauts by Vice President Al Gore. Author

N95-29958* National Aeronautics and Space Administration. Lyndon B. Johnson Space Center, Houston, TX.
STS-71 SHUTTLE/MIR FLIGHT: DAY 5 (Videotape)
30 Jun. 1995 Videotape: 22 min. playing time, in color, with sound
(NASA-TM-110748; BRF1343E; NONP-NASA-VT-95-56571) Avail: CASI VHS A02/BETA A22

Day 5 of the STS-71 flight Space Shuttle Atlantis mission is highlighted in this video. During this segment of the mission the Space Station is docked with the Mir Space Station and they are orbiting the earth together. There is footage of the astronauts performing physiological tests inside the Shuttle. Author

N95-29959* National Aeronautics and Space Administration. Lyndon B. Johnson Space Center, Houston, TX.
STS-71 SHUTTLE/MIR FLIGHT: DAY 6 (Videotape)
30 Jun. 1995 Videotape: 27 min. 30 sec. playing time, in color, with sound
(NASA-TM-110749; BRF1343F; NONP-NASA-VT-95-56572) Avail: CASI VHS A02/BETA A22

Day 6 of the STS-71 flight Space Shuttle Atlantis mission is highlighted in this video. During this segment of the mission the Space Station is docked with the Mir Space Station and they are orbiting the earth together. Also contained are views of the orbiter docking system and brief views of earth. Author

N95-29960* National Aeronautics and Space Administration. Lyndon B. Johnson Space Center, Houston, TX.
STS-71 SHUTTLE/MIR FLIGHT: DAY 7 (Videotape)
3 Jul. 1995 Videotape: 29 min. 30 sec. playing time, in color, with sound
(NASA-TM-110750; BRF1343G; NONP-NASA-VT-95-56573) Avail: CASI VHS A02/BETA A22

Day 7 of the STS-71 mission are featured in this video, a continuation from day 1-6, this video includes live footage onboard the STS-71 Space Station Atlantis and the Mir Space Station. Astronaut, Dr. Norman Thagard, after living in space for 3 months onboard the Mir Space Station, joins the crew of Atlantis for his trip back to earth. Live interviews are conducted with the crew of Atlantis. Author

N95-29961* National Aeronautics and Space Administration. Lyndon B. Johnson Space Center, Houston, TX.
STS-71 SHUTTLE/MIR FLIGHT: DAY 8 (Videotape)
3 Jul. 1995 Videotape: 17 min. 45 sec. playing time, in color, with sound
(NASA-TM-110751; BRF1343H; NONP-NASA-VT-95-56574) Avail: CASI VHS A02/BETA A22

Day 8 of the STS-71 mission are featured in this video, a continuation from days 1-7, this video includes live footage onboard the STS-71 Space Shuttle Atlantis and the Mir Space Station. Live interviews are conducted with the crew of Atlantis. Views are shown of the Mir Space Station from various angles. Author

N95-29962* National Aeronautics and Space Administration. Lyndon B. Johnson Space Center, Houston, TX.
STS-71 SHUTTLE/MIR FLIGHT: DAY 9 (Videotape)
3 Jul. 1995 Videotape: 17 min. 30 sec. playing time, in color, with sound (NASA-TM-110752; BRF1343I; NONP-NASA-VT-95-56575) Avail: CASI VHS A02/BETA A22

Day 9 of the STS-71 mission are featured in this video, a continuation from days 1-8, this video includes live footage onboard the STS-71 Space Shuttle Atlantis and the Mir Space Station. Views are shown of the Mir Space Station from various angles and its earth orbit after disconnection from Atlantis. Author

N95-29963* National Aeronautics and Space Administration. Lyndon B. Johnson Space Center, Houston, TX.
STS-71 SHUTTLE/MIR FLIGHT: DAY 10 (Videotape)
6 Jul. 1995 Videotape: 22 min. playing time, in color, with sound (NASA-TM-110753; BRF1343J; NONP-NASA-VT-95-56623) Avail: CASI VHS A02/BETA A22

Day 10, the last day of the STS-71 Space Shuttle mission, is featured in this video. There is live footage from onboard the shuttle and interviews with the Shuttle's astronauts. Also, some earth view footage from the Shuttle is included. Author

17 SPACE COMM., SPACECRAFT COMM., COMMAND & TRACKING

Includes telemetry; space communications networks; astronavigation and guidance; and radio blackout.

For related information see also *04 Aircraft Communications and Navigation* and *32 Communications and Radar.*

N95-30090*# SRI International Corp., Menlo Park, CA.
ALTERNATIVE PACKET SWITCH ARCHITECTURES FOR A 30/20 GHz FDMA/TDMA GEOSTATIONARY COMMUNICATION SATELLITE NETWORK Final Contractor Report
Roy Stehle and Richard G. Ogier Cleveland, OH NASA Jun. 1995 26 p
(Contract NAS3-25934; RTOP 506-72-21)
(NASA-CR-195470; E-9656; NAS 1.26:195470) Avail: CASI HC A03/MF A01

This study has investigated alternatives for realizing a packet-based network switch for deployment on a communication satellite. The emphasis was on the avoidance of contention problems that can occur due to the simultaneous arrival of an excessive number of packets destined for the same downlink dwell. The study was to look ahead, beyond the current Advanced Communications Technology Satellite (ACTS) capability, to the next generation of satellites. The study has not been limited by currently available technology, but has used university and commercial research efforts as a basis for designs that can be readily constructed and launched within the next five years. Tradeoffs in memory requirement, power requirement, and architecture have been considered as a part of our study. Author

N95-30251*# National Aeronautics and Space Administration. Langley Research Center, Hampton, VA.
EMISSIVITY MEASUREMENTS IN THIN METALLIZED MEMBRANE REFLECTORS USED FOR MICROWAVE RADIOMETER SENSORS
Lyle C. Schroeder, Robin L. Cravey, Michael J. Scherner, Chase P. Hearn, and Hans-Juergen C. Blume Jun. 1995 42 p
(RTOP 233-01-03-06)
(NASA-TM-110179; NAS 1.15:110179) Avail: CASI HC A03/MF A01

This paper is concerned with electromagnetic losses in metallized films used for inflatable reflectors. An inflatable membrane is made of tough elastic material such as Kapton, and it is not electromagnetically reflective by design. A film of conducting metal is added to the membrane to enhance its reflective properties. Since the impetus for use of inflatables for spacecraft is the light weight and compact packaging, it is important that the metal film be as thin as possible. However, if the material is not conductive or thick enough, the radiation due to the emissivity of the reflector could be a significant part of the radiation gathered by the radiometer. The emissivity would be of little consequence to a radar or solar collector; but for a radiometer whose signal is composed of thermal radiation, this contribution could be severe. Bulk properties of the metal film cannot be used to predict its loss. For this reason, a program of analysis and measurement was undertaken to determine the emissivities of a number of candidate metallized film reflectors. This paper describes the three types of measurements which were performed on the metallized thin films: (1) a network analyzer system with an L-band waveguide; (2) an S-band radiometer; and (3) a network analyzer system with a C-band antenna free-space transmission system. Author

N95-29625# Army Medical Command (18th), (18th). Unit 15281.
REQUIREMENT FOR ONBOARD TELEMETRY EQUIPMENT
Mathew S. Granger and Craig L. Urbauer *In* AGARD, Recent Issues and Advances in Aeromedical Evacuation (MEDEVAC) Feb. 1995 5 p
(For primary document see N95-29604 10-66)
Copyright Avail: CASI HC A01/MF A02

18 SPACECRAFT DESIGN, TESTING AND PERFORMANCE

Includes satellites; space platforms; space stations; spacecraft systems and components such as thermal and environmental controls; and attitude controls.

For life support systems see *54 Man/System Technology and Life Support.* For related information see also *05 Aircraft Design, Testing and Performance, 39 Structural Mechanics,* and *16 Space Transportation.*

N95-28688 Naval Postgraduate School, Monterey, CA.
A PROCEDURE FOR ACCESSING DIGITAL SATELLITES CONTAINING AMATEUR PAYLOADS M.S. Thesis
Stephanie L. ONeal Sep. 1994 102 p Limited Reproducibility: More than 20% of this document may be affected by microfiche quality
(AD-A289748) Avail: Issuing Activity (Defense Technical Information Center (DTIC))

The Space Systems Academic Group's (SSAG's) Amateur Radio Station User's Guide and an embedded user-friendly menu interaction system comprise the scope and purpose of this thesis. The User's Guide was developed in an effort to identify the best procedures to use when accessing amateur radio frequencies. Although the Amateur Radio Station is capable of voice and continuous wave (CW) communications, these areas are not addressed within the context of this manual. This manual is dedicated to the processes involved in accessing digital satellites containing amateur payloads. Most of the information found in this user's manual was obtained from existing sources. This manual attempts to organize that information, and demonstrate how it applies specifically to the SSAG Amateur Radio Station. DTIC

N95-28700 Naval Postgraduate School, Monterey, CA.
A LAYMAN'S LOOK AT ORBITAL DEBRIS M.S. Thesis
Armando R. Sanchezcastellanos Sep. 1994 122 p Limited Reproducibility: More than 20% of this document may be affected by microfiche quality
(AD-A289801) Avail: Issuing Activity (Defense Technical Information Center (DTIC))

Artificial space debris is a new threatening reality. This thesis examines the requirement of acknowledging this threat as one of the major considerations in the design of Low Earth Orbit (LEO) satellites. The paper commences with a comprehensive view of the issue; the facts of the case are presented. It is necessary to understand the physical fundamentals of this multi-faceted problem in order to view it as a genuine threat to satellites. Following this introduction, an overview of how the problem is currently approached, from a political and technical standpoint, is discussed. Strategies for coping with the space debris issue are then presented. From these, the paper focuses on the most promising prospect for the future. It highlights the need for new and responsible satellite design philosophies in order to deal with the uncertainties of the LEO environment. The research effort concludes that space debris considerations must be incorporated at the

earliest phases of satellite's design efforts and must be a continuing commitment throughout the operational life of a satellite. DTIC

N95-28721*# National Aeronautics and Space Administration. Marshall Space Flight Center, Huntsville, AL.

A CONCEPTUAL DESIGN FOR THE ATTITUDE CONTROL AND DETERMINATION SYSTEM FOR THE MAGNETOSPHERE IMAGER SPACECRAFT

M. E. Polites and C. K. Carrington Washington May 1995 30 p
(NASA-TP-3560; M-784; NAS 1.60:3560) Avail: CASI HC A03/MF A01

This paper presents a conceptual design for the attitude control and determination (ACAD) system for the Magnetosphere Imager (MI) spacecraft. The MI is a small spin-stabilized spacecraft that has been proposed for launch on a Taurus-S expendable launch vehicle into a highly-ellipdcal polar Earth orbit. Presently, launch is projected for 1999. The paper describes the MI mission and ACAD requirements and then proposes an ACAD system for meeting these requirements. The proposed design is low-power, low-mass, very simple conceptually, highly passive, and consistent with the overall MI design philosophy, which is faster-better-cheaper. Still, the MI ACAD system is extremely robust and can handle a number of unexpected, adverse situations on orbit without impacting the mission as a whole. Simulation results are presented that support the soundness of the design approach. Author

N95-28852*# National Academy of Sciences - National Research Council, Washington, DC. Committee on Space Debris.

ORBITAL DEBRIS: A TECHNICAL ASSESSMENT

George Gleghorn (TRW Space Technology Labs., Rancho Palos Verdes, CA.), James Asay (Sandia National Labs., Albuquerque, NM.), Dale Atkinson (POD Associates, Inc., Albuquerque, NM.), Walter Flury (European Space Agency. European Space Operations Center, Darmstadt, Germany.), Nicholas Johnson (Kaman Sciences Corp., Albuquerque, NM.), Donald Kessler (National Aeronautics and Space Administration. Lyndon B. Johnson Space Center, Houston, TX.), Stephen Knowles (Naval Space Surveillance System, Dahlgren, VA.), Dietrich Rex (Technische Univ., Brunswick, Germany.), Susumu Toda (National Aerospace Lab., Tokyo, Japan.), and Stanislav Veniaminov (Space Research Center Kosmos, Moscow, Russia.) et al 1995 211 p
(Grant NAGw-3414)
(NASA-CR-198639; NAS 1.26:198639; ISBN-0-309-05125-8; LC-95-18686)
Copyright Avail: CASI HC A10/MF A03

To acquire an unbiased technical assessment of (1) the research needed to better understand the debris environment, (2) the necessity and means of protecting spacecraft against the debris environment, and (3) potential methods of reducing the future debris hazard, NASA asked the National Research Council to form an international committee to examine the orbital debris issue. The committee was asked to draw upon available data and analyses to: characterize the current debris environment, project how this environment might change in the absence of new measures to alleviate debris proliferation, examine ongoing alleviation activities, explore measures to address the problem, and develop recommendations on technical methods to address the problems of debris proliferation. Derived from text

N95-28867# Aerospace Corp., El Segundo, CA. Technology Operations.

OVERVIEW OF THE SPACE DEBRIS ENVIRONMENT

M. J. Meshishnek 15 Mar. 1995 34 p
(Contract F04701-93-C-0094)
(AD-A292302; TR-95(5231)-3; SMC-TR-95-9) Avail: CASI HC A03/MF A01

There is a component of the space environment that is man-made pollution, termed 'space debris' it exists at all inclinations and, primarily, at altitudes of roughly 350 km to 2000 km. The size of this debris ranges from several meters to a fraction of a micrometer in diameter, and the particle distribution follows an inverse power law, with the smaller size component far exceeding that of the larger. Debris is composed primarily of alumina from solid rocket motor exhausts, aluminum from spacecraft structures, and zinc and titanium oxides from thermal control coatings. The accepted model of the space debris environment is that of Kessler et al., a complex model that predicts the number of particles that will impact a surface as a function of altitude, inclination, solar cycle, and particle diameter, as well as their collision velocities. Recent data from LDEF has demonstrated both the accuracy and shortcomings of the Kessler model. Measured debris impactor fluxes are in good agreement with the model for ram surfaces. However, predictions of the model for other surfaces of a spacecraft are less accurate, most notably for the wake or trailing side. While the Kessler model is appropriate for long-term, average flux predictions, spatial-temporal impact fluxes measured on LDEF dramatically illustrated the presence of strong debris clouds that do not dissipate quickly in space and will encounter an orbiting spacecraft cyclically and repeatedly over its lifetime. LDEF data has also indicated the presence of debris in elliptical orbits, a fact not predicted by the Kessler model. This fact is responsible for the discrepancy between measured impact fluxes and predictions on trailing edge surfaces. DTIC

N95-29026# Radex, Inc., Bedford, MA.

FFT SPACE PROCESSING FOR THE ACF OF SPREE PARTICLE FLUX MEASUREMENTS

K. H. Bounar, W. J. McNeil, and N. A. Bonito 31 Aug. 1994 29 p
Limited Reproducibility: Document partially illegible
(Contract F19628-93-C-0091)
(AD-A290166; PL-TR-94-2230; SR-1) Avail: CASI HC A03/MF A01

This manuscript is intended to describe the processing and the X Window display of the Fourier transform of the autocorrelation measurement from the SPREE (Shuttle Potential and Return Electron Experiment) particle correlator experiment (SPACE). The SPREE was flown aboard the Space Shuttle Atlantis flight STS 46 as part of the Tethered Satellite System (TSS 1). SPACE is essentially a signal processing unit that analyzes the particle fluxes from the SPREE electrostatic analyzers (ESA) to identify wave-particle modulations. The SPACE outputs autocorrelation function (ACF) data containing information on the wave particle modulations. An efficient way to examine these modulations is by means of the Fourier transform techniques. The SPACE Fourier analysis and display tools, which are part of the SIDAT package, are presented. These tools use color raster graphics and text displays based on the X11 and XView X Window System libraries on Sun SPARC workstations. DTIC

N95-29332 Pennsylvania State Univ., University Park, PA.

TIME-OPTIMAL MULTI-AXIS ATTITUDE MANEUVERS OF RIGID SPACECRAFT USING COLLOCATION AND NONLINEAR PROGRAMMING Ph.D. Thesis

Sandra Lynn Scrivener 1993 175 p
Avail: Univ. Microfilms Order No. DA9414368

Spacecraft attitude control is an important aspect of satellite technology: in particular, time-optimal maneuvers are critical in military applications, communications satellites, and for scientific flyby missions. Although the problem is fairly easy to formulate, it has proved nearly impossible to solve, either numerically or analytically except in a few simplified cases. The thesis begins with a comprehensive survey of the literature of the last thirty years, from early attempts to solve the time-optimal reorientation problem to the latest approaches applied to flexible spacecraft. The background and details of a particular solution method, collocation and nonlinear programming, are discussed in detail. The discussion concludes with application and usage notes for using this method to solve time-optimal attitude maneuver problems. Applying the method of collocation and nonlinear programming to these maneuvers yields the solution of several classes of problems which have not been solvable by other means. This method has several advantages over traditional methods of solution: it is straightforward to formulate, it is easy to use and to modify, requires low computation times, and is extraordinarily robust with respect to the initial guess used to obtain a solution. The results obtained using this method are compared to known solutions, and show excellent agreement with them. Solutions for several additional spacecraft configurations and different maneuvers are presented, including rest-to-rest reorientations, detumble, and spin-up motions. The thesis concludes with a brief discussion of future developments for the method and the types of problems to which it might be applied. Dissert. Abstr.

N95-29377*# National Aeronautics and Space Administration. Langley Research Center, Hampton, VA.

ROBUST CONTROL OF NONLINEAR FLEXIBLE MULTIBODY SYSTEMS USING QUATERNION FEEDBACK AND DISSIPATIVE COMPENSATION

Atul G. Kelkar (Old Dominion Coll., Norfolk, VA.) and Suresh M. Joshi Apr. 1994 19 p

(RTOP 233-01-01-05)
(NASA-TM-109099; NAS 1.15:109099) Avail: CASI HC A03/MF A01

Global asymptotic stability of a class of nonlinear multibody flexible space-structures under dissipative compensation is established. Two cases are considered. The first case allows unlimited nonlinear motions of the entire system and uses quaternion feedback. The second case assumes that the central body motion is in the linear range although the other bodies can undergo unrestricted nonlinear motion. The stability is proved to be robust to the inherent modeling nonlinearities and uncertainties. Furthermore for the second case the stability is also shown to be robust to certain actuator and sensor nonlinearities. The stability proofs use the Lyapunov approach and exploit the inherent passivity of such systems. The results are applicable to a wide class of systems including flexible space-structures with articulated flexible appendages. Author

N95-29408 Texas Univ., Austin, TX.
SUBSTRUCTURE-BASED CONTROL OF FLEXIBLE STRUCTURES Ph.D. Thesis
Vit Babuska 1993 140 p
Avail: Univ. Microfilms Order No. DA9413430

The desire to build large space structures has motivated research into the problem of flexible structure control. In general, the controllers for these structures can be designed using a centralized strategy or a decentralized strategy. In the centralized approach, the controller is based on a model of the complete structure. In the decentralized approach, the structure model is decomposed into subsystems for which controllers are designed, and then these subsystem controllers are combined to control the complete structure. The subsystems can be mathematical constructs such as groups of modes, or physical subsystems like substructures. This dissertation examines substructure-based decentralized design of controllers for flexible structures. Three different, but related, topics are discussed in this work. First, a relationship is shown to exist between the substructural controller synthesis (SCS) method of designing active controllers for flexible structures and decentralized control using overlapping information sets. It is shown that, in the case of full-state feedback, the SCS method is a specific case of decentralized control using overlapping subsystems. In the case of dynamic output feedback (e.g., LQG controllers), the SCS method departs from standard decentralized control techniques. The controllers are 'assembled' by extending the concept of substructural assembly to general linear systems. Next, a new design method is proposed which combines the concept of component mode synthesis (CMS) with control theory in a decentralized method for the design of controllers for flexible structures. This method, called the augmented physical component synthesis (APCS) method, creates augmented substructural components. These components are substructures whose boundaries are loaded with some dynamics of the adjacent substructures. This allows global control objectives such as line-of-sight error minimization to be met with a substructure-based design strategy. Finally, the problem of building a substructure-based controller with a decentralized architecture is considered and a formal design strategy is proposed. The assembly of substructure models is viewed from the perspective of robust control theory, and robust control theory concepts are used to suggest a formal framework by which controllers can be designed to stabilize individual substructures that comprise a larger structure, as well as the larger structure itself. Dissert. Abstr.

N95-29410# Naval Postgraduate School, Monterey, CA.
SPACECRAFT ATTITUDE CONTROL SYSTEM PERFORMANCE USING PULSE-WIDTH PULSE-FREQUENCY MODULATED THRUSTERS M.S. Thesis
Robert S. McClelland Mar. 1994 101 p
(AD-A291803) Avail: CASI HC A06/MF A02

Many current satellites employ on-off thrusters to accomplish attitude control tasks which may include initial acquisition, rotational maneuvers, and on-orbit stabilization. This work shows that the use of pulse-width pulse-frequency (PWPF)-modulated thrusters provides several important advantages over conventional bang- bang thruster control methods, including less thruster activity and closer-to-linear actuation. The PWPF modulator is implemented in simulations using the Matrix/System build software package. Simulations assuming a rigid spacecraft are first performed to compare the performance of the PWPF-modulated thrust controller with that of conventional bang-bang and time-optimal bang-bang controllers. The discussion is then extended to the case of a spacecraft with structural flexibility, as is encountered quite often in three-axis stabilized vehicles with large fold-out solar arrays. Simulations for comparison of the controllers are performed using the flexible spacecraft dynamics model. The control loop design in the presence of flexibility and possible interaction with the PWPF modulator nonlinearity are addressed. Using a describing function model of the modulator, stability margin with respect to the structural mode limit cycle is predicted. Simulations are then conducted to verify the predicted stability margin. DTIC

N95-29464# Los Alamos National Lab., NM.
THE LOS ALAMOS PHOTON COUNTING DETECTOR DEBRIS DETECTION PROJECT: AN UPDATE
Cheng Ho, W. Priedhorsky, M. Baron, and D. Casperson 1995 9 p Presented at the 13th Space Surveilliance Workshop, Lexington, MA, 28-30 Mar. 1995
(Contract W-7405-eng-36)
(DE95-007883; LA-UR-95-554; CONF-9503107-1) Avail: CASI HC A02/MF A01

At Los Alamos, the authors have been pursuing a project for space debris detection using a photon counting detector with high spatial and time resolution. By exploiting the three dimensionality of the high quality data, they expect to be able to detect an orbiting object of size below 2 cm, using a moderate size telescope and state-of-the-art photon counting detector. A working tube has been used to collect skyward looking data during dusk. In this paper, they discuss the progress in the development of detector and data acquisition system. They also report on analysis and results of these data sets. DOE

N95-29633* Roland House, Arlington, VA.
HERNANDEZ ENGINEERING: NASA (Videotape)
22 Apr. 1992 Sponsored by NASA, Washington Videotape: 2 min. 54 sec. playing time, in color, with sound
(NASA-CR-197665; HQ-92-04-0371; NONP-NASA-VT-95-46019) Avail: CASI VHS A02/BETA A22

A short explanation of NASA's accomplishments and goals are discussed in this video. Space Station Freedom, lunar bases, manned Mars mission, and robotic spacecrafts to explore other worlds are briefly described. CASI

N95-30011*# National Aeronautics and Space Administration. Lewis Research Center, Cleveland, OH.
TEST RESULTS OF A 20 GHz, LOW NOISE DOWNCONVERTER FOR USAT APPLICATIONS
Gene Fujikawa and James S. Svoboda (NYMA, Inc., Brook Park, OH.) Jun. 1995 8 p
(RTOP 235-01-0E)
(NASA-TM-106892; E-9536; NAS 1.15:106892) Avail: CASI HC A02/MF A01

A key component in the development of the Advanced Communications Technology Satellite (ACTS) ultra small aperture terminal (USAT) earth station is the low noise downconverter (NLD). NASA Lewis Research Center (LeRC) has tested a version of an LND designed by Electrodyne Systems Corporation. A number of tests were conducted to characterize the radio frequency performance of the LND over temperature. The test results presented in this paper are frequency response, noise figure, gain, group delay, power transfer characteristics, image rejection, and spurious product suppression. The LND was one of several critical microwave subsystems developed and tested for the ACTS USAT earth stations. Author

N95-30036*# Draper (Charles Stark) Lab., Inc., Boston, MA.
PERFORMANCE ANALYSIS OF A GPS INTERFEROMETRIC ATTITUDE DETERMINATION SYSTEM FOR A GRAVITY GRADIENT STABILIZED SPACECRAFT M.S. Thesis
John C. Stoll May 1995 128 p
(Contract NAS9-18426)
(NASA-CR-188372; NAS 1.26:188372; CSDL-T-1253) Copyright Avail: CASI HC A07/MF A02

The performance of an unaided attitude determination system based on GPS interferometry is examined using linear covariance analysis. The modelled system includes four GPS antennae onboard a gravity gradient stabilized spacecraft, specifically the Air Force's RADCAL satellite. The principal error sources are identified and modelled. The optimal system's

sensitivities to these error sources are examined through an error budget and by varying system parameters. The effects of two satellite selection algorithms, Geometric and Attitude Dilution of Precision (GDOP and ADOP, respectively) are examined. The attitude performance of two optimal-suboptimal filters is also presented. Based on this analysis, the limiting factors in attitude accuracy are the knowledge of the relative antenna locations, the electrical path lengths from the antennae to the receiver, and the multipath environment. The performance of the system is found to be fairly insensitive to torque errors, orbital inclination, and the two satellite geometry figures-of-merit tested. Author

N95-30280 Stanford Univ., CA.
SPIN AUGMENTED DEPLOYMENT AND RETRIEVAL OF TETHERED ARTIFICIAL GRAVITY SPACECRAFT Ph.D. Thesis
Jeffrey Donald Stoen 1994 120 p
Avail: Univ. Microfilms Order No. DA9422120

The dynamics and control of a tethered centrifuge during constant spin deployment and retrieval of the tether is investigated. First, a simple two segment tether model is used to demonstrate that tangential thrusters on the end bodies can maintain a constant centrifuge spin rate and provide the control action necessary to damp lateral oscillations of the tether. An LQR controller is devised to create a balanced control scheme that provides such coordination between actuators as is required to produce a comfortable environment for occupants of the centrifuge. Next, the stability of motions of the tether end bodies is studied to assess effects of varying the body's mass properties and the position of the tether attachment joint. Finally, an improved, multi-segment model of the tether is employed to deal with limitations due to imperfect monitoring of the state of the system and difficulties in delivering accurate thrust levels. We construct a Kalman filter to furnish both estimates for the unknown states and smoothing of noisy measurements of sensed states. Dissert. Abstr.

N95-30316*# National Aeronautics and Space Administration. Langley Research Center, Hampton, VA.
A CONCEPTUAL THERMAL DESIGN STUDY OF AN ELECTRONICALLY SCANNED THINNED ARRAY RADIOMETER
D. C. Gould May 1995 13 p
(RTOP 233-01-06-01)
(NASA-TM-110173; NAS 1.15:110173) Avail: CASI HC A03/MF A01

This report describes conceptual thermal design study for an Electronically Scanned Thinned Array Radiometer (ESTAR). ESTAR is an instrument concept for the measurement of soil moisture from space using synthetic aperture radiometry. The thermal design goal is to minimize the orbital temperature variation of the radiometer receivers using established materials and techniques. Two design approaches have been investigated; the first uses the waveguide as a heat sink, and the second uses a nadir facing radiator on the receiver assembly. The second approach minimizes the receiver's impact on the waveguide temperatures. Predicted temperatures for all receivers are presented for the two cases indicating the transient thermal environments the receivers would experience during an orbit. In addition, the effects of the receiver heat dissipation on the waveguide temperatures are shown. Author

N95-30357*# Missouri Univ., Kansas City, MO. Dept. of Mechanical and Aerospace Engineering.
GUIDANCE, NAVIGATION, AND CONTROL STUDY FOR A SOLAR ELECTRIC PROPULSION SPACECRAFT Final Report
Craig A. Kluever [1995] 24 p
(Grant NAG3-1581)
(NASA-CR-198920; NAS 1.26:198920) Avail: CASI HC A03/MF A01

A preliminary investigation of a lunar-comet rendezvous mission using a solar electric propulsion (SEP) spacecraft was performed in two phases.The first phase involved exploration of the moon and the second involved rendezvous with a comet. The initial phase began with a chemical propulsion translunar injection and chemical insertion into a lunar orbit, followed by a low thrust SEP transfer to a circular, polar, low-lunar orbit. After collecting scientific data at the moon, the SEP spacecraft performed a spiral lunar escape maneuver to begin the interplanetary leg of the mission. After escape from the Earth-moon system, the SEP spacecraft maneuvered in interplanetary space and performed a rendezvous with a comet.The immediate goal of this study was to demonstrate the feasibility of using a low-thrust SEP spacecraft for orbit transfer to both the moon and a comet. Another primary goal was to develop a computer optimization code which would be robust enough to obtain minimum-fuel rendezvous trajectories for a wide range of comets. Derived from text

19 SPACECRAFT INSTRUMENTATION

For related information see also *06 Aircraft Instrumentation* and *35 Instrumentation and Photography.*

N95-29643*# National Aeronautics and Space Administration. Lewis Research Center, Cleveland, OH.
SUMMARY REPORT OF MISSION ACCELERATION MEASUREMENTS FOR STS-66. LAUNCHED NOVEMBER 3, 1994
Melissa J. B. Rogers (Tal-Cut Co., Beachwood, OH.) and Richard DeLombard May 1995 211 p Original contains color illustrations
(RTOP 963-60-OD)
(NASA-TM-106914; E-9622; NAS 1.15:106914) Avail: CASI HC A10/MF A03; 59 functional color pages

Experiments flown in the middeck of Atlantis during the STS-66 mission were supported by the Space Acceleration Measurement System (SAMS). In particular, the three triaxial SAMS sensor heads collected data in support of protein crystal growth experiments. Data collected during STS-66 are reviewed in this report. The STS-66 SAMS data represent the microgravity environment in the 0.01 Hz to 10 Hz range. Variations in the environment related to differing levels of crew activity are discussed in the report. A comparison is made among times when the crew was quiet during a public affairs conference, working quietly, and exercising. These levels of activity are also compared to levels recorded by a SAMS unit in the Spacelab on Columbia during the STS-65 mission. Author

N95-29794 Stanford Univ., CA.
DC ELECTROSTATIC GYRO SUSPENSION SYSTEM FOR THE GRAVITY PROBE B EXPERIMENT Ph.D. Thesis
Chang-Huei Wu 1994 149 p
Avail: Univ. Microfilms Order No. DA9414678

The Gravity Probe B experiment is a satellite-based experiment primarily designed to test two aspects of Einstein's General Theory of Relativity by observing the spin axis drift of near-perfect gyroscopes in a 650-km circular polar orbit. The goal of this experiment is to measure the drift angles to an accuracy of 0.3 milli-arcsec after one year in orbit. As a result, electrostatically suspended free-spinning gyroscopes operating at a very low temperature became the final choice for their ultra-low Newtonian torque-induced drift rate. The Conventional AC current-driven suspension system faces two fundamental difficulties for ground gyro testing. Field emission causes rotor charging and arcing with an imperfect electrode or rotor surfaces because the electric field intensity needed to support a solid rotor in the 1-g field is more than 107 V/m. The system not only becomes unstable at a high rotor charge, which can be more than 500 volts, but may also lose control in case of arcing. Both the high voltage AC suspension signal and the high frequency (1 MHz) signal for rotor position sensing interfere with the superconducting SQUID magnetometer for spin axis readout through inductive coupling. These problems were resolved by using DC voltage to generate a suspension force and a low frequency position sensor. In addition to the Input/Output linearization algorithm developed to remove the system nonlinearity for global stability and dynamic performance, we also minimized the electric field intensity to reduce rotor charging. Experimental results verified the desired global stability and satisfactory dynamic performance. The problem of rotor charging is virtually eliminated. More importantly, the DC system is compatible with the SQUID readout system in the Science Mission configuration. Consequently, experiments in low magnetic field at a sub-micro-gauss level for SQUID design verification and trapped flux distribution study were finally realizable in ground environment. The second part of the research focused on design issues for the Science Mission in a micro-g environment. The unique requirement of the GP-B experiment is to minimize suspension-induced torque and subsequent spin axis drift. A nonlinear control law which employs stiffened spring and stiffened damping coefficients was developed to achieve both low RMS noise in steady-state operation and quick response for situations like a micrometeoroid impact. Rotor voltage measurement and in-flight sensor bias correction schemes were developed to ensure system stability and absolute centering accuracy. Simulation results

verified the system performances and confirmed that a suspension system induced rotor spin axis drift lower than 0.1 milli arcsec/year can be reached. Dissert. Abstr.

20 SPACECRAFT PROPULSION AND POWER

Includes main propulsion systems and components, e.g., rocket engines; and spacecraft auxilliary power sources.

For related information see also *07 Aircraft Propulsion and Power, 28 Propellants and Fuels, 44 Energy Production and Conversion,* and *15 Launch Vehicles and Space Vehicles.*

N95-29114*# NYMA, Inc., Brook Park, OH. Engineering Services Div.
A TRANSIENT MODEL OF THE RL10A-3-3A ROCKET ENGINE
Michael P. Binder Cleveland, OH NASA Jun. 1995 22 p Presented at the 31st Joint Propulsion Conference and Exhibit, San Diego, CA, 10-12 Jul. 1995; cosponsored by AIAA, ASME, SAE, ASEE
(Contract NAS3-27186; RTOP 242-70-04)
(NASA-CR-195478; NAS 1.26:195478; E-9702; AIAA Paper 95-2968)
Avail: CASI HC A03/MF A01

RL10A-3-3A rocket engines have served as the main propulsion system for Centaur upper stage vehicles since the early 1980's. This hydrogen/oxygen expander cycle engine continues to play a major role in the American launch industry. The Space Propulsion Technology Division at the NASA Lewis Research Center has created a computer model of the RL10 engine, based on detailed component analyses and available test data. This RL10 engine model can predict the performance of the engine over a wide range of operating conditions. The model may also be used to predict the effects of any proposed design changes and anticipated failure scenarios. In this paper, the results of the component analyses are discussed. Simulation results from the new system model are compared with engine test and flight data, including the start and shut-down transient characteristics. Author

N95-29245 Massachusetts Inst. of Tech., Cambridge, MA.
MULTIFLUID NONEQUILIBRIUM SIMULATION OF ARCJET THRUSTERS S.D. Thesis
Scott Alan Miller 1994
Avail: Issuing Activity (MIT Libraries, Rm. 14-0551, Cambridge, MA 02139-4307)

A detailed numerical model has been developed to study the gas dynamic flow in an electrothermal arcjet thruster. This two-temperature, Navier-Stokes model consistently incorporates viscosity, heat conduction, ohmic dissipation, collisional energy transfer between electrons and heavy species, ambipolar diffusion, nonequilibrium dissociation and ionization, and radiation. The fluid equations are solved by Mac Cormack's method while an iterative procedure is used to relax an electric potential equation, from which the current distribution in the thruster is obtained. Using hydrogen propellant, solutions are achieved for a range of input parameters and the underlying physics and internal structures of these arcjet flows are revealed. In particular, a mechanism for self-sustaining anodic arc attachment is identified. It is found that ambipolar diffusion from the arc core coupled with enhanced nonequilibrium dissociation and ionization in the outer flow provide enough charge carriers for the current to pass self-consistently between the arc core and the anode wall. Numerical solutions are compared with experimental results from the German TT1 radiatively-cooled arcjet thruster. Calculated discharge voltage is within 1-2% to 10% of experimental measurements, and predicted specific impulse is within 5-10% agreement over a range of applied currents and mass flow rates. In addition, flow solutions are used to explain observed trends in performance as quantities such as the specific power and mass flow rate are varied. An anode thermal model is constructed which yields more accurate predictions of the inlet gas and electrode wall temperatures, and this model is coupled to the arcjet flow solver in order to obtain a more self-consistent solution. Finally, a simplified stability analysis of the near-anode arc attachment region is performed. It is found that a localized ionization instability may be initiated in this region, but that the system is stable under the flow conditions predicted by the arcjet simulation of this research. Dissert. Abstr.

N95-29284# Institute for Defense Analyses, Alexandria, VA.
ESTIMATES OF PROBABILITY OF A CLOUD-FREE LINE OF SIGHT FOR RAPTOR TALON Final Report, Mar. 1993 - Jan. 1994
Ernest Bauer Jul. 1994 32 p
(Contract DASW01-94-C-0054)
(AD-A291908; IDA-D-1442) Avail: CASI HC A03/MF A01

RAPTOR TALON is a concept that includes optical sensing of rocket plumes from low altitudes (2 km) through burnout from an air vehicle at 18-20 km, at a long range, i.e., R approx. 20-100 km. The presence of clouds can interfere with optical sensing, and thus it is important to establish the Probability of a Cloud-Free Line of Sight (PCFLOS) at locations and times of concern. Some previous estimates of PCFLOS were counter-intuitive and provided varying results; POET was asked to resolve the discrepancies. Here we ask for the PCFLOS for paths from 18 km altitude above all clouds to 2 km, at a slant range of about 20 - 100 km at two different locations (Baghdad, Iraq, and Seoul, Korea) for January and July at average cloudiness. There are very few clouds in Iraq during the summer, so for this case PCFLOS - 0.9 - 0.95. At the other locations and seasons the mean cloud cover ranges between 0.4 and 0.7, and the POFLOS values range between 0.6 and 0.7 at P = 20 km, and between 0.4 and 0.6 at P = 100 km. Estimates made by a variety of methods are generally consistent with this finding. DTIC

N95-29331 Georgia Inst. of Tech., Atlanta, GA.
INVESTIGATION OF THE FLOW TURNING LOSS IN UNSTABLE SOLID PROPELLANT ROCKET MOTORS Ph.D. Thesis
Lawrence Mark Matta 1993 182 p
Avail: Univ. Microfilms Order No. DA9415654

The goal of this study was to improve the understanding of the flow turning loss, which contributes to the damping of axial acoustic instabilities in solid propellant rocket motors. This understanding is needed to develop practical methods for designing motors that do not exhibit such instabilities. The flow turning loss results from the interaction of the flow of combustion products leaving the surface of the propellant with the acoustic field in an unstable motor. While state of the art solid rocket stability models generally account for the flow turning loss, its magnitude and characteristics have never been fully investigated. This thesis describes a combined theoretical, numerical, and experimental investigation of the flow turning loss and its dependence upon various motor design and operating parameters. First, a one dimensional acoustic stability equation that verifies the existence of the flow turning loss was derived for a chamber with constant mean pressure and temperature. The theoretical development was then extended to include the effects of mean temperature gradients to accommodate combustion systems in which mean temperature gradients and heat losses are significant. These analyses provided the background and expressions necessary to guide an experimental study. The relevant equations were then solved for the developed experimental setup to predict the behavior of the flow turning loss and the other terms of the developed acoustic stability equation. This was followed by and experimental study in which the flow turning region of an unstable solid propellant rocket motor was simulated. The setup was used, with and without combustion, to determine the dependence of the flow turning loss upon operating conditions. These studies showed that the flow turning loss strongly depends upon the gas velocity at the propellant surface and the location of the flow turning region relative to the standing acoustic wave. The flow turning loss measured in the experiment was found to be small relative to other mechanisms. This, however, was characteristic of the experimental setup and is not representative of actual rocket motors, in which the flow turning loss is often a significant part of the overall stability. Dissert. Abstr.

N95-29584*# Engineering Research and Consulting, Inc., Tullahoma, TN.
AUTOMATED PROPULSION DATA SCREENING DEMONSTRATION SYSTEM Final Report, 17 Dec. 1992 - 16 Dec. 1994
W. Andes Hoyt, Timothy D. Choate, and Bruce A. Whitehead (Tennessee Univ. Space Inst., Tullahoma, TN.) 8 May 1995 36 p
(Contracts NAS8-39782; NAS8-39184)
(NASA-CR-196636; NAS 1.26:196636; ERC-R-94-082; SBA-0474-93-2-00007) Avail: CASI HC A03/MF A01

A fully-instrumented firing of a propulsion system typically generates a very large quantity of data. In the case of the Space Shuttle Main Engine (SSME), data analysis from ground tests and flights is currently a labor-intensive process. Human experts spend a great deal of time examining

the large volume of sensor data generated by each engine firing. These experts look for any anomalies in the data which might indicate engine conditions warranting further investigation. The contract effort was to develop a 'first-cut' screening system for application to SSME engine firings that would identify the relatively small volume of data which is unusual or anomalous in some way. With such a system, limited and expensive human resources could focus on this small volume of unusual data for thorough analysis. The overall project objective was to develop a fully operational Automated Propulsion Data Screening (APDS) system with the capability of detecting significant trends and anomalies in transient and steady-state data. However, the effort limited screening of transient data to ground test data for throttle-down cases typical of the 3-g acceleration, and for engine throttling required to reach the maximum dynamic pressure limits imposed on the Space Shuttle. This APDS is based on neural networks designed to detect anomalies in propulsion system data that are not part of the data used for neural network training. The delivered system allows engineers to build their own screening sets for application to completed or planned firings of the SSME. ERC developers also built some generic screening sets that NASA engineers could apply immediately to their data analysis efforts. Derived from text

N95-29642*# National Aeronautics and Space Administration. Lewis Research Center, Cleveland, OH.

PREDICTION OF PRESSURANT MASS REQUIREMENTS FOR AXISYMMETRIC LIQUID HYDROGEN TANKS

N. T. VanDresar Jun. 1995 8 p Presented at the 31st Joint Propulsion Conference and Exhibit, San Diego, CA, 10-12 Jul. 1995; sponsored by AIAA, ASME, SAE, ASEE

(RTOP 242-70-04)

(NASA-TM-106973; E-9734; NAS 1.15:106973; AIAA Paper 95-2964)

Copyright Avail: CASI HC A02/MF A01

Experimental data from several test series are compared to an existing correlation that predicts the amount of pressurant gas mass required to expel liquid hydrogen from axisymmetric tanks. It was necessary to use an alternate definition of the tank equivalent diameter to accommodate thermal mass in the tank wall that is initially warm and to accommodate liquid residuals in the tank after expulsion is stopped. With this modification, the existing correlation predicted mass requirements to within 14 percent of experimental results. Revision of the correlation constants using a nonlinear least-squares fit of the current experimental data has a minor effect, thus supporting the validity of the original correlation's form, its fitted constants, and the alternate definition of the tank equivalent diameter. Author

N95-29784 Case Western Reserve Univ., Cleveland, OH.

A GENETIC ALGORITHM APPROACH TO SCHEDULING RESOURCSES FOR A SPACE POWER SYSTEM Ph.D. Thesis

Ted Wright 1994 120 p

Avail: Univ. Microfilms Order No. DA9425524

The scheduling of electrical power on NASA's space station is a difficult and interesting optimization problem. Electrical power is a scarce resource on the space station, and power consumption must be scheduled to avoid outages. Genetic algorithms offer great potential for solving computationally difficult optimization problems, such as scheduling. A new approach to space power system resource scheduling based on a genetic algorithm is presented. Results are presented using a genetic algorithm to calculate solutions to small, well-defined tiling problems. The tiling genetic algorithm directly calculates the position and orientation of tiles. Since the tiling problem shares many features with the space station scheduling problem, a genetic algorithm for scheduling is developed which operates in a manner similar to the tiling genetic algorithm. This scheduling genetic algorithm directly calculates starting times and alternatives for the resource consuming events to be scheduled, and uses a penalty method to enforce the scheduling constraints. This thesis explores this new method of solving the space station power scheduling problem. Dissert. Abstr.

N95-30012*# National Aeronautics and Space Administration. Lewis Research Center, Cleveland, OH.

ANALYSIS OF SHADOWING EFFECTS ON SPACECRAFT POWER SYSTEMS

H. J. Fincannon Jul. 1995 8 p Presented at the Fourth European Space Power Conference, Poitiers, France, 4-8 Sep. 1995; sponsored by ESA

(RTOP 478-12-10)

(NASA-TM-106994; E-9770; NAS 1.15:106994) Avail: CASI HC A02/MF A01

This paper describes the Orbiting Spacecraft Shadowing Analysis (OSSA) computer program that was developed at NASA Lewis Research Center in order to assess the shadowing effects on various power systems. The algorithms, inputs and outputs are discussed. Examples of typical shadowing analyses that have been performed for the International Space Station Freedom, International Space Station Alpha and the joint United States/Russian Mir Solar Dynamic Flight Experiment Project are covered. Effects of shadowing on power systems are demonstrated. Author

N95-28733*# National Aeronautics and Space Administration. Marshall Space Flight Center, Huntsville, AL.

MARSHALL SPACE FLIGHT CENTER SURFACE MODELING AND GRID GENERATION APPLICATIONS

Robert W. Williams, Theodore G. Benjamin, and Joni W. Cornelison *In* NASA. Lewis Research Center, Surface Modeling, Grid Generation, and Related Issues in Computational Fluid Dynamic (CFD) Solutions Mar. 1995 p 105-120 (For primary document see N95-28723 10-02)

Avail: CASI HC A03/MF A10

N95-30257*# National Aeronautics and Space Administration. Lewis Research Center, Cleveland, OH.

HIGH PERFORMANCE NICKEL ELECTRODES FOR SPACE POWER APPLICATIONS Abstract Only

Prosper K. Adanuvor (Auburn Univ., AL.), Johnnie A. Pearson (Auburn Univ., AL.), Brian Miller (Auburn Univ., AL.), Bruce Tatarchuk (Auburn Univ., AL.), and Doris L. Britton *In its* Space Electrochemical Research and Technology. Abstracts Apr. 1995 p 5 (For primary document see N95-30255 10-44)

Avail: CASI HC A01/MF A01

23 CHEMISTRY AND MATERIALS (GENERAL)

N95-28803 ESDU International Ltd., London (England).

THERMAL CONDUCTIVITY OF LIQUID HALOGENATED ALIPHATIC HYDROCARBONS. PART 4: HALOGENATED ALKENES AND DIENES (C1 TO C4)

Sep. 1994 22 p

(ISSN 0141-4062)

(ESDU-94024-Pt-4; ISBN-0-856-79911-4) Avail: ESDU

ESDU 94024 gives data for 7 haloethylenes, 4 halopropenes, 3 chlorobutenes, chloroprene and l-chlorobuta-1,3-diene. Experimental results drawn from the literature for each compound were fitted with a four-term polynomial equation in reduced temperature. The coefficients were also faired with changing molecular structure to ensure the best correlation not only for the individual compounds but also as members of their chemical series. The coefficient correlations also allowed values to be predicted for compounds for which no measured data exist. The equations were used to tabulate thermal conductivity values from the melting point to about 0.9 critical temperature in SI units at 10 K and 10 degree Celsius intervals. The critical point, coefficients and sources of the data are given for each compound. Conversion factors are provided for common British units, the effect of pressure is briefly considered and the likely accuracy of the tabulated values is discussed. ESDU

N95-28804 ESDU International Ltd., London (England).

THERMAL CONDUCTIVITY OF LIQUID HALOGENATED ALIPHATIC HYDROCARBONS. PART 1: HALOGENATED METHANES AND AZEOTROPIC MIXTURES

Sep. 1994 50 p

(ISSN 0141-4062)

(ESDU-94021-Pt-1; ISBN-0-85679-908-4) Avail: ESDU

ESDU 94021 gives data for all four monohalomethanes, 6 dihalo-, 11 trihalo-, and 11 tetrahalomethanes together with four azeotropic mixtures. Experimental results drawn from the literature for each compound were fitted with a four-term polynomial equation in reduced temperature. The coefficients were also faired with changing molecular structure to ensure

the best correlation not only for the individual compounds but also as members of their chemical series. The coefficient correlations also allowed values to be predicted for compounds for which no measured data exist. The equations were used to tabulate thermal conductivity values from the melting point to about 0.9 critical temperature in SI units at 10 K and 10 C intervals. The critical point, coefficients and sources of the data are given for each compound. Conversion factors are provided for common British units, the effect of pressure is briefly considered, and the likely accuracy of the tabulated values is discussed. Author

N95-29017 ESDU International Ltd., London (England).
THERMAL CONDUCTIVITY OF LIQUID HALOGENATED ALIPHATIC HYDROCARBONS. PART 2: HALOGENATED ETHANES
Sep. 1994 76 p
(ISSN 0141-4062)
(ESDU-94022; ISBN-0-85679-909-2) Avail: ESDU

ESDU 94022 gives data for all four monohaloethanes, 10 dihalo-, 10 trihalo-, 12 tetrahalo-, 13 hexahalo- and 12 pentahaloethanes. Experimental results drawn from the literature for each compound were fitted with a four-term polynomial equation in reduced temperature. The coefficients were also faired with changing molecular structure to ensure the best correlation not only for the individual compounds but also as members of their chemical series. The coefficient correlations also allowed values to be predicted for compounds for which no measured data exist. The equations were used to tabulate thermal conductivity values from the melting point to about 0.9 critical temperature in SI units at 10 K and 10 degree Celsius intervals. The critical point, coefficients and sources of the data are given for each compound. Conversion factors are provided for common British units, the effect of pressure is briefly considered and the likely accuracy of the tabulated values is discussed. ESDU

N95-29052 Office of Naval Research, Arlington, VA.
THE FLUORESCENT DETECTION OF HYDRAZINE, MONOMETHYLHYDRAZINE, AND 1,1-DIMETHYLHYDRAZINE BY DERIVATIZATION WITH AROMATIC DICARBOXALDEHYDES Patent Application
Gregory E. Collins, inventor (to Navy) and Susan Rose-Pehrsson, inventor (to Navy) 20 Oct. 1994 47 p Filed 20 Oct. 1994 Limited Reproducibility: More than 20% of this document may be affected by microfiche quality
(Navy-Case-75451; AD-A288877; US-Patent-Appl-SN-326518) Avail: Issuing Activity (Defense Technical Information Center (DTIC))

A method and apparatus for the detection of hydrazine, monomethylhydrazine, 1,1-dimethylhydrazine in air (or other gas medium) or in an aqueous solution is described. The detection is accomplished by introducing a stream of air, or other gas medium, or aqueous solution suspected of containing hydrazine, monomethylhydrazine, 1,1-dimethylhydrazine or mixtures thereof into a pH controlled reagent solution containing an aromatic dicarboxaldehyde to react with the hydrazine, monomethylhydrazine, 1,1-dimethylhydrazine or mixtures thereof, respectively, and by exposing the reacted reagent solution to an excitation wavelength range and monitoring an emission from the exposed reagent solution at an emission wavelength range to detect the presence of a hydrazine derivative, monomethylhydrazine derivative, 1,1-dimethylhydrazine derivative, or mixtures thereof (i.e. a derivative formed by the reaction between hydrazine, monomethylhydrazine, 1,1-dimethylhydrazine and the aromatic dicarboxal dehyde) indicating the presence of hydrazine, monomethylhydrazine, 1,1-dimethylhydrazine or mixtures thereof within the stream of air or other gas medium or aqueous solution. DTIC

N95-29168# Princeton Univ., NJ. Dept. of Civil Engineering.
SURFACTANT-ENHANCED IN SITU BIODEGRADATION OF STRONGLY SORBING ORGANIC SUBSTANCES IN SOIL ENVIRONMENTS Final Report, 30 Sep. 1991 - 15 Sep. 1994
Peter R. Jaffe 15 Sep. 1994 62 p
(Grant AF-AFOSR-0435-91)
(AD-A290253; AFOSR-95-0016TR) Avail: CASI HC A04/MF A01

Low-solubility Polycyclic Aromatic Hydrocarbons such as phenanthrene are easily biodegradable but due to sorption onto soil or/and their presence ina non-aqueous phase, their bioavailability is greatly reduced. In an aqueous environment where surfactants exist above their critical micelle concentration hydrophobic contaminant will partitioning into the hydrophobic core of the micelle. This enhances the apparent solubility of these hydrocarbons and therefore also their desorption from soils. Conceivably, in the absence of any inhibitory effects, such surfactants may enhance the biodegradation of the hydrocarbon. Through a set of screening experiments a group of non-ionic surfactants were identified which do not inhibit the bacterial degradation of the phenanthrene. A mathematical model was formulated to describe the interaction of the biomass-contaminant-water-surfactant system. The model assumes that the surfactant affects the solubility of phenanthrene and does not affect the biochemical characteristics of the biomass. An effective bioavailable concentration was defined. The model predicts experimental data well indicating that a part of the phenanthrene in the micelle phase can be degraded simultaneously with the phenanthrene in the aqueous phase. DTIC

N95-29373*# National Aeronautics and Space Administration. Lewis Research Center, Cleveland, OH.
A SIMULATION TECHNIQUE FOR PREDICTING THICKNESS OF THERMAL SPRAYED COATINGS
John G. Goedjen, Robert A. Miller, William J. Brindley, and George W. Leissler (NYMA, Inc., Brook Park, OH.) Jun. 1995 17 p
(Contract NAS3-27186; RTOP 505-63-52; DA Proj. 1L1-61102-AH-45)
(NASA-TM-106939; E-9667; NAS 1.15:106939; ARL-TR-762) Avail: CASI HC A03/MF A01

The complexity of many of the components being coated today using the thermal spray process makes the trial and error approach traditionally followed in depositing a uniform coating inadequate, thereby necessitating a more analytical approach to developing robotic trajectories. A two dimensional finite difference simulation model has been developed to predict the thickness of coatings deposited using the thermal spray process. The model couples robotic and component trajectories and thermal spraying parameters to predict coating thickness. Simulations and experimental verification were performed on a rotating disk to evaluate the predictive capabilities of the approach. Author

N95-29900 ESDU International Ltd., London (England).
THERMAL CONDUCTIVITY OF LIQUID HALOGENATED ALIPHATIC HYDROCARBONS. PART 3: HALOGENATED HIGHER HYDROCARBONS (C3 TO C16)
Sep. 1994 100 p
(ISSN 0141-4062)
(ESDU-94023-Pt-3; ISBN-0-85679-910-6) Avail: ESDU

ESDU 94023 gives data for 88 halogenated hydrocarbons from C3 to C10 and 6 chloroalkanes from C11 to C16. Experimental results drawn from the literature for each compound were fitted with a four-term polynomial equation in reduced temperature. The coefficients were also faired with changing molecular structure to ensure the best correlation not only for the individual compounds but also as members of their chemical series. The coefficient correlations also allowed values to be predicted for compounds for which no measured data exist. The equations were used to tabulate thermal conductivity values from the melting point to about 0.9 critical temperature in SI units at 10 K and 10 degree Celsius intervals. The critical point, coefficients and sources of the data are given for each compound. Conversion factors are provided for common British units, the effect of pressure is briefly considered and the likely accuracy of the tabulated values is discussed. ESDU

N95-30225*# Boeing Defense and Space Group, Seattle, WA.
EFFECTS OF SPACE EXPOSURE ON METALS FLOWN ON THE LONG DURATION EXPOSURE FACILITY
H. Gary Pippin and R. J. Bourassa Jun. 1995 343 p
(Contracts NAS1-18224; NAS1-19247; RTOP 506-43-61-01; RTOP 233-03-02-02)
(NASA-CR-4662; NAS 1.26:4662) Avail: CASI HC A15/MF A03

This report includes measurements on copper, aluminum, and stainless steel from the Long Duration Exposure Facility (LDEF). Summaries of the performance of a variety of metals flown on LDEF are presented. An extensive list of references directs the reader to other detailed investigations. The influence of contamination on a number of measurements is documented. Author

24 COMPOSITE MATERIALS

Includes physical, chemical, and mechanical properties of laminates and other composite materials.

For ceramic materials see *27 Nonmetallic Materials.*

N95-28809*# Texas A&M Univ., College Station, TX. Center for Mechanics of Composites

ANALYSIS OF STATIC CONTACT IN LAMINATED COMPOSITE PLATES USING DAMAGE MECHANICS Final Technical Report

David H. Allen May 1995 190 p

(Grant NAG1-1407)

(NASA-CR-198656; NAS 1.26:198656) Avail: CASI HC A09/MF A02

This document reports the research performed to construct a model capable of predicting the damage development caused by out-of-plane static loading in laminated graphite/epoxy composite plates.

Author (revised)

N95-28817*# West Virginia Univ., Morgantown, VA. Dept. of Mechanical and Aerospace Engineering.

EFFECT OF OPEN HOLE ON TENSILE FAILURE PROPERTIES OF 2D TRIAXIAL BRAIDED TEXTILE COMPOSITES AND TAPE EQUIVALENTS Final Report

Timothy L. Norman, Colin Anglin, David Gaskin, and Mike Patrick Jun. 1995 49 p

(Grant NAG1-1381; RTOP 510-02-11-07)

(NASA-CR-4676; NAS 1.26:4676) Avail: CASI HC A03/MF A01

The unnotched and notched (open hole) tensile strength and failure mechanisms of two-dimensional (2D) triaxial braided composites were examined. The effect of notch size and notch position were investigated. Damage initiation and propagation in notched and unnotched coupons were also examined. Theory developed to predict the normal stress distribution near an open hole and failure for tape laminated composites was evaluated for its applicability to triaxial braided textile composite materials. Four fiber architectures were considered with different combinations of braid angle, longitudinal and braider yam size, and percentage of longitudinal yarns. Tape laminates equivalent to textile composites were also constructed for comparison. Unnotched tape equivalents were stronger than braided textiles but exhibited greater notch sensitivity. Notched textiles and tape equivalents have roughly the same strength at large notch sizes. Two common damage mechanisms were found: braider yams cracking and near notch longitudinal yarn splitting. Cracking was found to initiate in braider yarns in unnotched and notched coupons, and propagate in the direction of the braider yarns until failure. Longitudinal yarn splitting occurred in three of four architectures that were longitudinally fiber dominated. Damage initiation stress decreased with increasing braid angle. No significant differences in prediction of near notch stress between measured and predicted stress were weak for textiles with large braid angle. Notch strength could not be predicted using existing anisotropic theory for braided textiles due to their insensitivity to notch.

Author

N95-28823*# National Aeronautics and Space Administration. Langley Research Center, Hampton, VA.

THIRD NASA ADVANCED COMPOSITES TECHNOLOGY CONFERENCE, VOLUME 1, PART 2

John G. Davis, Jr., comp. and Herman L. Bohon, comp. (Lockheed Engineering and Sciences Co., Hampton, VA.) Jan. 1993 495 p Conference held in Long Beach, CA, 8-11 Jun. 1992; sponsored by NASA, Washington, and DOD

(RTOP 510-02-13-01)

(NASA-CP-3178-Vol-1-Pt-2; L-17167B-Vol-1-Pt-2; NAS 1.55:3178-Vol-1-Pt-2) Avail: CASI HC A21/MF A04

This document is a compilation of papers presented at the Third NASA Advanced Composites Technology (ACT) Conference held at Long Beach, California, 8-11 June 1992. The ACT Program is a major multi-year research initiative to achieve a national goal of technology readiness before the end of the decade. Conference papers recorded results of research in the ACT Program in the specific areas of automated fiber placement, resin transfer molding, textile preforms, and stitching as these processes influence design, performance, and cost of composites in aircraft structures. Papers sponsored by the Department of Defense on the Design and Manufacturing of Low Cost Composites (DMLCC) are also included in Volume 2 of this document. For individual titles, see N95-28824 through N95-28849.

N95-28824*# BASF Structural Materials, Inc., Charlotte, NC.

CHARACTERIZATION AND DEVELOPMENT OF MATERIALS FOR ADVANCED TEXTILE COMPOSITES

J. Timothy Hartness, Timothy L. Greene, and Leo E. Taske *In* NASA. Langley Research Center, Third NASA Advanced Composites Technology Conference, Volume 1, Part 2 Jan. 1993 p 505-522 (For primary document see N95-28823 10-24)

Avail: CASI HC A03/MF A04

Work ongoing under the NASA Langley - Advanced Composite Technology (ACT) program is discussed. The primary emphasis of the work centers around the development and characterization of graphite fiber that has been impregnated with an epoxy powder. Four epoxies have been characterized in towpreg form as to their weaveability and braidability. Initial mechanical properties have been generated on each resin system. These include unidirectional as well as 8-harness satin cloth. Initial 2D and 3D weaving and braiding trials will be reported on as well as initial efforts to develop towpreg suitable for advanced tow placement.

Derived from text

N95-28825*# Lockheed Engineering and Sciences Co., Hampton, VA.

THE EFFECTS OF SPECIMEN WIDTH ON TENSILE PROPERTIES OF TRIAXIALLY BRAIDED TEXTILE COMPOSITES

John E. Masters, Peter G. Ifju (Virginia Polytechnic Inst. and State Univ., Blacksburg, VA.), Christopher M. Pastore (North Carolina State Univ., Raleigh, NC.), and Alexander E. Bogdanovich (North Carolina State Univ., Raleigh, NC.) *In* NASA. Langley Research Center, Third NASA Advanced Composites Technology Conference, Volume 1, Part 2 Jan. 1993 p 523-536 (For primary document see N95-28823 10-24)

Avail: CASI HC A03/MF A04

The objective of this study was to examine the effect of the unit cell architecture on the mechanical response of textile reinforced composite materials. Specifically, the study investigated the effect of unit cell size on the tensile properties of 2D triaxially braided graphite epoxy laminates. The figures contained in this paper reflect the presentation given at the conference. They may be divided into four sections: (1) a short definition of the material system tested; (2) a statement of the problem and a review of the experimental results; (3) experimental results consist of a Moire interferometry study of the strain distribution in the material plus modulus and strength measurements; and (4) a short summary and a description of future work will close the paper. Derived from text

N95-28826*# Sundstrand Aviation-Rockford, IL.

IN SITU PROCESSING METHODS FOR COMPOSITE FUSELAGE SANDWICH STRUCTURES

Hossein Saatchi, Bill Durako, Dick Reynolds, Ernest Dost (Boeing Co., Seattle, WA.), and Kurtis Willden (Boeing Co., Seattle, WA.) *In* NASA. Langley Research Center, Third NASA Advanced Composites Technology Conference, Volume 1, Part 2 Jan. 1993 p 537-546 (For primary document see N95-28823 10-24)

Avail: CASI HC A02/MF A04

Conventional sandwich structure fabrication methods are labor intensive and high in cost. A low cost method is needed to produce lightweight sandwich structures. Sundstrand has developed a series of in situ composite fabrication methods in which the raw materials (skin and core materials) are placed in a closed mold, and the component is produced in one heating cycle. Internal pressure is generated by chemical agents during the thermal cycles, which consolidates the skins and produces the foam core. The finished part is a net-shape composite sandwich structure with skins and a foamed core. The in situ process reduces cost by eliminating several secondary operations that are used in conventional fabrication methods. Further, a strong molecular bond is produced between the core and skin, which eliminates adhesive bonding and prevents a weak bond section in the sandwich structure. In this investigation, we evaluated the feasibility of the in situ process using thermoset materials currently under consideration for commercial airplane fuselage applications, such as keel sections. The materials used were Hercules 855340 toughened epoxy resin in both liquid and powder forms, and 3M Scotchply PR500 resin, manufactured by 3M Corporation, in powder form. We successfully foamed

these resins and produced experimental panels with AS-4/855340 Hercules prepreg skins. Chopped fibers were added to the core to increase performance of the foam. Mechanical property testing on these panels showed properties competitive with other foams. Additional experiments are required to optimize the in situ foam core sandwiches for specific properties and applications. Author

N95-28827*# Utah Univ., Salt Lake City, UT. Dept. of Material Science and Engineering.

THE EFFECT OF MIXED MODE PRECRACKING ON THE MODE 1 FRACTURE TOUGHNESS OF COMPOSITE LAMINATES

Prashanth Shankar, Williard D. Bascom, and John A. Nairn *In* NASA. Langley Research Center, Third NASA Advanced Composites Technology Conference, Volume 1, Part 2 Jan. 1993 p 547-555 (For primary document see N95-28823 10-24)

(Contract NAS1-18883)

Avail: CASI HC A02/MF A04

We subjected double cantilever beam specimens from four different composite materials to mixed-mode precracking. Three different precracking mode 1 to mode 2 ratios were used--1 to 4, 1 to 1, and 4 to 1. Following precracking the specimens were tested for mode I fracture toughness. The mixed-mode precracking often influenced the mode 1 toughness and its influence persisted for as much as 60 mm of mode 1 crack growth. We tested composites with untoughened matrices, composites with rubber-toughened matrices, and composites with interlayer toughening. Depending on material type and precracking mode ratio, the precracking could cause either a significant increase or a significant decrease in the mode 1 fracture toughness. Author

N95-28828*# Utah Univ., Salt Lake City, UT. Dept. of Material Science and Engineering.

MASTER PLOT ANALYSIS OF MICROCRACKING IN GRAPHITE/EPOXY AND GRAPHITE/PEEK LAMINATES

John A. Nairn, Shoufeng Hu, and Jong Song Bark *In* NASA. Langley Research Center, Third NASA Advanced Composites Technology Conference, Volume 1, Part 2 Jan. 1993 p 557-569 Sponsored in part by Du Pont de Nemours (E. I.) and Co. and ICI Composites (For primary document see N95-28823 10-24)

(Contract NAS1-18833)

Avail: CASI HC A03/MF A04

We used a variational stress analysis and an energy release rate failure criterion to construct a master plot analysis of matrix microcracking. In the master plot, the results for all laminates of a single material are predicted to fall on a single line whose slope gives the microcracking toughness of the material. Experimental results from 18 different layups of AS4/3501-6 laminates show that the master plot analysis can explain all observations. In particular, it can explain the differences between microcracking of central 90 deg plies and of free-surface 90 deg plies. Experimental results from two different AS4/PEEK laminates tested at different temperatures can be explained by a modified master plot that accounts for changes in the residual thermal stresses. Finally, we constructed similar master plot analyses for previous literature microcracking models. All microcracking theories that ignore the thickness dependence of the stresses gave poor results. Author

N95-28829*# Delaware Univ., Newark, DE. Dept. of Mechanical Engineering.

ESTABLISHING THE RELATIONSHIP BETWEEN MANUFACTURING AND COMPONENT PERFORMANCE IN STRETCH FORMED THERMOPLASTIC COMPOSITES

Michael H. Santare, R. Byron Pipes, A. J. Beaussart, D. W. Coffin, B. J. OToole, and S. F. Shuler *In* NASA. Langley Research Center, Third NASA Advanced Composites Technology Conference, Volume 1, Part 2 Jan. 1993 p 571-590 (For primary document see N95-28823 10-24)

Avail: CASI HC A03/MF A04

Flexible manufacturing methods are needed to reduce the cost of using advanced composites in structural applications. One method that allows for this is the stretch forming of long discontinuous fiber materials with thermoplastic matrices. In order to exploit this flexibility in an economical way, a thorough understanding of the relationship between manufacturing and component performance must be developed. This paper reviews some of the recent work geared toward establishing this understanding. Micromechanics models have been developed to predict the formability of the material during processing. The latest improvement of these models includes the viscoelastic nature of the matrix and comparison with experimental data. A finite element scheme is described which can be used to model the forming process. This model uses equivalent anisotropic viscosities from the micromechanics models and predicts the microstructure in the formed part. In addition, structural models have been built to account for the material property gradients that can result from the manufacturing procedures. Recent developments in this area include the analysis of stress concentrations and a failure model each accounting for the heterogeneous material fields. Author

N95-28830*# Grumman Aircraft Engineering Corp., Bethpage, NY.

NOVEL COST CONTROLLED MATERIALS AND PROCESSING FOR PRIMARY STRUCTURES

S. J. Dastin *In* NASA. Langley Research Center, Third NASA Advanced Composites Technology Conference, Volume 1, Part 2 Jan. 1993 p 591-599 (For primary document see N95-28823 10-24)

Avail: CASI HC A02/MF A04

Textile laminates, developed a number of years ago, have recently been shown to be applicable to primary aircraft structures for both small and large components. Such structures have the potential to reduce acquisition costs but require advanced automated processing to keep costs controlled while verifying product reliability and assuring structural integrity, durability and affordable life-cycle costs. Recently, resin systems and graphite-reinforced woven shapes have been developed that have the potential for improved RTM processes for aircraft structures. Ciba-Geigy, Brochier Division has registered an RTM prepreg reinforcement called 'Injectex' that has shown effectivity for aircraft components. Other novel approaches discussed are thermotropic resins producing components by injection molding and ceramic polymers for long-duration hot structures. The potential of such materials and processing will be reviewed along with initial information/data available to date. Author

N95-28831*# Boeing Commercial Airplane Co., Seattle, WA.

THE EFFECTS OF DESIGN DETAILS ON COST AND WEIGHT OF FUSELAGE STRUCTURES **c05**

G. D. Swanson, S. L. Metschan, M. R. Morris, and C. Kassapoglou (Sikorsky Aircraft, Stratford, CT.) *In* NASA. Langley Research Center, Third NASA Advanced Composites Technology Conference, Volume 1, Part 2 Jan. 1993 p 601-622 (For primary document see N95-28823 10-24)

(Contract NAS1-18889)

Avail: CASI HC A03/MF A04

Crown panel design studies showing the relationship between panel size, cost, weight, and aircraft configuration are compared to aluminum design configurations. The effects of a stiffened sandwich design concept are also discussed. This paper summarizes the effect of a design cost model in assessing the cost and weight relationships for fuselage crown panel designs. Studies were performed using data from existing aircraft to assess the effects of different design variables on the cost and weight of transport fuselage crown panel design. Results show a strong influence of load levels, panel size, and material choices on the cost and weight of specific designs. A design tool being developed under the NASA ACT program is used in the study to assess these issues. The effects of panel configuration comparing postbuckled and buckle resistant stiffened laminated structure is compared to a stiffened sandwich concept. Results suggest some potential economy with stiffened sandwich designs for compression dominated structure with relatively high load levels. Author

N95-28832*# Hercules Aerospace Co., Magna, UT. Composite Structures Group.

AUTOMATED FIBER PLACEMENT: EVOLUTION AND CURRENT DEMONSTRATIONS

Carroll G. Grant and Vernon M. Benson *In* NASA. Langley Research Center, Third NASA Advanced Composites Technology Conference, Volume 1, Part 2 Jan. 1993 p 625-648 (For primary document see N95-28823 10-24)

Avail: CASI HC A03/MF A04

The automated fiber placement process has been in development at Hercules since 1980. Fiber placement is being developed specifically for aircraft and other high performance structural applications. Several major milestones have been achieved during process development. These

milestones are discussed in this paper. The automated fiber placement process is currently being demonstrated on the NASA ACT program. All demonstration projects to date have focused on fiber placement of transport aircraft fuselage structures. Hercules has worked closely with Boeing and Douglas on these demonstration projects. This paper gives a description of demonstration projects and results achieved. Author

N95-28833*# Hercules Aerospace Co., Magna, UT. Composite Products Group.

RESPONSE OF AUTOMATED TOW PLACED LAMINATES TO STRESS CONCENTRATIONS

Douglas S. Cairns, Larry B. Ilcewicz (Boeing Commercial Airplane Co., Seattle, WA.), and Tom Walker (Boeing Commercial Airplane Co., Seattle, WA.) *In* NASA. Langley Research Center, Third NASA Advanced Composites Technology Conference, Volume 1, Part 2 Jan. 1993 p 649-663 (For primary document see N95-28823 10-24)

Avail: CASI HC A03/MF A04

In this study, the response of laminates with stress concentrations is explored. Automated Tow Placed (ATP, also known as Fiber Placement) laminates are compared to conventional tape layup manufacturing. Previous tensile fracture tests on fiber placed laminates show an improvement in tensile fracture of large notches over 20 percent compared to tape layup laminates. A hierarchial modeling scheme is presented. In this scheme, a global model is developed for laminates with notches. A local model is developed to study the influence of inhomogeneities at the notch tip, which are a consequence of the fiber placement manufacturing technique. In addition, a stacked membrane model was developed to study delaminations and splitting on a ply-by-ply basis. The results indicate that some benefit with respect to tensile fracture (up to 11 percent) can be gained from inhomogeneity alone, but that the most improvement may be obtained with splitting and delaminations which are more severe in the case of fiber placement compared to tape layup. Improvements up to 36 percent were found from the model for fiber placed laminates with damage at the notch tip compared to conventional tape layup. Author

N95-28834*# National Aeronautics and Space Administration. Langley Research Center, Hampton, VA.

MECHANICAL CHARACTERIZATION OF TWO THERMOPLASTIC COMPOSITES FABRICATED BY AUTOMATED TOW PLACEMENT

Larry C. Dickinson (Lockheed Engineering and Sciences Co., Hampton, VA.) and Jerry W. Deaton *In its* Third NASA Advanced Composites Technology Conference, Volume 1, Part 2 Jan. 1993 p 665-687 (For primary document see N95-28823 10-24)

Avail: CASI HC A03/MF A04

AS4/PEEK towpreg and IM7/Radel 8320 slit tape were used to make flat panels by automated tow placement. The panels were tested in notched and un-notched tension, notched and un-notched compression and compression after impact (CAI) at room temperature and under hot/wet conditions (notched and un-notched compression and CAI only). The properties were compared with AS4/PEEK tape laminate properties found in the literature. The tow placed AS4/PEEK material was stronger in tension but weaker in compression than the AS4/PEEK tape laminates. The tow placed AS4/PEEK was stronger but less stiff than the tow placed IM7/Radel 8320 in all compression tests. The IM7/Radel performed better in all other mechanical tests. The IM7/Radel outperformed the AS4/PEEK in all CAI tests. Author

N95-28835*# Boeing Commercial Airplane Co., Seattle, WA.

MANUFACTURING SCALE-UP OF COMPOSITE FUSELAGE CROWN PANELS

Kurtis Willden, M. Gessel, Carroll G. Grant (Hercules Aerospace Co., Magna, UT.), and T. Brown (Hercules Aerospace Co., Magna, UT.) *In* NASA. Langley Research Center, Third NASA Advanced Composites Technology Conference, Volume 1, Part 2 Jan. 1993 p 689-704 (For primary document see N95-28823 10-24)

(Contract NAS1-18889)

Avail: CASI HC A03/MF A04

The goal of the Boeing effort under the NASA ACT program is to reduce manufacturing costs of composite fuselage structure. Materials, fabrication of complex subcomponents and assembly issues are expected to drive the costs of composite fuselage structure. Several manufacturing concepts for the crown section of the fuselage were evaluated through the efforts of a Design Build Team (DBT). A skin-stringer-frame intricate bond design that required no fasteners for the panel assembly was selected for further manufacturing demonstrations. The manufacturing processes selected for the intricate bond design include Advanced Tow Placement (ATP) for multiple skin fabrication, resin transfer molding (RTM) of fuselage frames, innovative cure tooling, and utilization of low-cost material forms. Optimization of these processes for final design/manufacturing configuration was evaluated through the fabrication of several intricate bond panels. Panels up to 7 ft. by 10 ft. in size were fabricated to simulate half scale production parts. The qualitative and quantitative results of these manufacturing demonstrations were used to assess manufacturing risks and technology readiness for production. Author

N95-28836*# Boeing Commercial Airplane Co., Seattle, WA.

DIMENSIONAL STABILITY OF CURVED PANELS WITH COCURED STIFFENERS AND COBONDED FRAMES

G. E. Mabson, B. W. Flynn, G. D. Swanson, R. C. Lundquist (Boeing Aerospace Co., Seattle, WA.), and P. L. Rupp (Washington Univ., Seattle, WA.) *In* NASA. Langley Research Center, Third NASA Advanced Composites Technology Conference, Volume 1, Part 2 Jan. 1993 p 705-725 (For primary document see N95-28823 10-24)

(Contract NAS1-18889)

Avail: CASI HC A03/MF A04

Closed form and finite element analyses are presented for axial direction and transverse direction dimensional stability of skin/stringer panels. Several sensitivity studies are presented to illustrate the influence of various design parameters on the dimensional stability of these panels. Panel geometry, material properties (stiffness and coefficient of thermal expansion), restraint conditions and local details, such as resin fillets, all combine to influence dimensional stability, residual and assembly forces. Author

N95-28837*# National Aeronautics and Space Administration. Langley Research Center, Hampton, VA.

TENSION FRACTURE OF LAMINATES FOR TRANSPORT FUSELAGE. PART 2: LARGE NOTCHES

Tom H. Walker (Boeing Commercial Airplane Co., Seattle, WA.), Larry B. Ilcewicz (Boeing Commercial Airplane Co., Seattle, WA.), D. R. Polland (Boeing Defense and Space Group, Seattle, WA.), and C. C. Poe, Jr. *In its* Third NASA Advanced Composites Technology Conference, Volume 1, Part 2 Jan. 1993 p 727-758 (For primary document see N95-28823 10-24)

(Contract NAS1-18889)

Avail: CASI HC A03/MF A04

Tests were conducted on over 200 center-crack specimens to evaluate: (a) the tension-fracture performance of candidate materials and laminates for commercial fuselage applications; and (b) the accuracy of several failure criteria in predicting response. Crack lengths of up to 12 inches were considered. Other variables included fiber/matrix combination, layup, lamination manufacturing process, and intraply hybridization. Laminates fabricated using the automated tow-placement process provided significantly higher tension-fracture strengths than nominally identical tape laminates. This confirmed earlier findings for other layups, and possibly relates to a reduced stress concentration resulting from a larger scale of repeatable material inhomogeneity in the tow-placed laminates. Changes in material and layup result in a trade-off between small-notch and large-notch strengths. Toughened resins and 0 deg-dominate layups result in higher small-notch strengths but lower large-notch strengths than brittle resins, 90 deg and 45 deg dominated layups, and intraply S2-glass hybrid material forms. Test results indicate that strength-prediction methods that allow for a reduced order singularity of the crack-tip stress field are more successful at predicting failure over a range of notch sizes than those relying on the classical square-root singularity. The order of singularity required to accurately predict large-notch strength from small-notch data was affected by both material and layup. Measured crack-tip strain distributions were generally higher than those predicted using classical methods. Traditional methods of correcting for finite specimen width were found to be lacking, confirming earlier findings with other specimen geometries. Fracture tests of two stiffened panels, identical except for differing materials, with severed central stiffeners resulted in nearly identical damage progression and failure sequences. Strain-softening laws implemented within finite element models appear attractive to account for load redistribution in configured structure due to damage-induced crack tip softening Author

N95-28838*# Boeing Co., Seattle, WA.
IMPACT DAMAGE RESISTANCE OF COMPOSITE FUSELAGE STRUCTURE, PART 2
Ernest F. Dost, Scott R. Finn, Daniel P. Murphy, and Amy B. Huisken *In* NASA. Langley Research Center, Third NASA Advanced Composites Technology Conference, Volume 1, Part 2 Jan. 1993 p 759-787 (For primary document see N95-28823 10-24)
(Contract NAS1-18889)
Avail: CASI HC A03/MF A04

The strength of laminated composite materials may be significantly reduced by foreign object impact induced damage. An understanding of the damage state is required in order to predict the behavior of structure under operational loads or to optimize the structural configuration. Types of damage typically induced in laminated materials during an impact event include transverse matrix cracking, delamination, and/or fiber breakage. The details of the damage state and its influence on structural behavior depend on the location of the impact. Damage in the skin may act as a soft inclusion or affect panel stability, while damage occurring over a stiffener may include debonding of the stiffener flange from the skin. An experiment to characterize impact damage resistance of fuselage structure as a function of structural configuration and impact threat was performed. A wide range of variables associated with aircraft fuselage structure such as material type and stiffener geometry (termed, intrinsic variables) and variables related to the operating environment such as impactor mass and diameter (termed, extrinsic variables) were studied using a statistically based design-of-experiments technique. The experimental design resulted in thirty-two different 3-stiffener panels. These configured panels were impacted in various locations with a number of impactor configurations, weights, and energies. The results obtained from an examination of impacts in the skin midbay and hail simulation impacts are documented. The current discussion is a continuation of that work with a focus on nondiscrete characterization of the midbay hail simulation impacts and discrete characterization of impact damage for impacts over the stiffener. Author

N95-28839*# Boeing Commercial Airplane Co., Seattle, WA.
DESIGN, ANALYSIS, AND FABRICATION OF A PRESSURE BOX TEST FIXTURE FOR TENSION DAMAGE TOLERANCE TESTING OF CURVED FUSELAGE PANELS
P. J. Smith, J. B. Bodine, C. H. Preuss, and W. J. Koch (Boeing Computer Services Co., Seattle, WA.) *In* NASA. Langley Research Center, Third NASA Advanced Composites Technology Conference, Volume 1, Part 2 Jan. 1993 p 789-805 (For primary document see N95-28823 10-24)
(Contract NAS1-18889)
Avail: CASI HC A03/MF A04

A pressure box test fixture was designed and fabricated to evaluate the effects of internal pressure, biaxial tension loads, curvature, and damage on the fracture response of composite fuselage structure. Previous work in composite fuselage tension damage tolerance, performed during NASA contract NAS1-17740, evaluated the above effects on unstiffened panels only. This work extends the tension damage tolerance testing to curved stiffened fuselage crown structure that contains longitudinal stringers and circumferential frame elements. The pressure box fixture was designed to apply internal pressure up to 20 psi, and axial tension loads up to 5000 lb/in, either separately or simultaneously. A NASTRAN finite element model of the pressure box fixture and composite stiffened panel was used to help design the test fixture, and was compared to a finite element model of a full composite stiffened fuselage shell. This was done to ensure that the test panel was loaded in a similar way to a panel in the full fuselage shell, and that the fixture and its attachment plates did not adversely affect the panel. Author

N95-28840*# Boeing Commercial Airplane Co., Seattle, WA.
GLOBAL COST AND WEIGHT EVALUATION OF FUSELAGE KEEL DESIGN CONCEPTS **c05**
B. W. Flynn, M. R. Morris, S. L. Metschan, G. D. Swanson, P. J. Smith, K. H. Griess, M. R. Schramm, and R. J. Humphrey *In* NASA. Langley Research Center, Third NASA Advanced Composites Technology Conference, Volume 1, Part 2 Jan. 1993 p 807-836 (For primary document see N95-28823 10-24)
(Contract NAS1-18889)
Avail: CASI HC A03/MF A04

The Boeing program entitled Advanced Technology Composite Aircraft Structure (ATCAS) is focused on the application of affordable composite technology to pressurized fuselage structure of future aircraft. As part of this effort, a design study was conducted on the keel section of the aft fuselage. A design build team (DBT) approach was used to identify and evaluate several design concepts which incorporated different material systems, fabrication processes, structural configurations, and subassembly details. The design concepts were developed in sufficient detail to accurately assess their potential for cost and weight savings as compared with a metal baseline representing current wide body technology. The cost and weight results, along with an appraisal of performance and producibility risks, are used to identify a globally optimized keel design; one which offers the most promising cost and weight advantages over metal construction. Lastly, an assessment is given of the potential for further cost and weight reductions of the selected keel design during local optimization. Author

N95-28841*# National Aeronautics and Space Administration. Langley Research Center, Hampton, VA.
DESIGN AND EVALUATION OF A FOAM-FILLED HAT-STIFFENED PANEL CONCEPT FOR AIRCRAFT PRIMARY STRUCTURAL APPLICATIONS **c05**
Damodar R. Ambur *In its* Third NASA Advanced Composites Technology Conference, Volume 1, Part 2 Jan. 1993 p 839-857 (For primary document see N95-28823 10-24)
Avail: CASI HC A03/MF A04

Geodesically stiffened structures are very efficient in carrying combined bending, torsion, and pressure loading that is typical of primary aircraft structures. They are also very damage tolerant since there are multiple load paths available to redistribute loads compared to prismatically stiffened structures. Geodesically stiffened structures utilize continuous filament composite materials which make them amenable to automated manufacturing processes to reduce cost. The current practice for geodesically stiffened structures is to use a solid blade construction for the stiffener. This stiffener configuration is not an efficient concept and there is a need to identify other stiffener configurations that are more efficient but utilize the same manufacturing process as the solid blade. This paper describes a foam-filled stiffener cross section that is more efficient than a solid-blade stiffener in the load range corresponding to primary aircraft structures. A prismatic hat-stiffener panel design is then selected for structural evaluation in uni-axial compression with and without impact damage. Experimental results for both single stiffener specimens and multi-stiffener panel specimens are presented. Finite element analysis results are presented that predict the buckling and postbuckling response of the test specimens. Analytical results for both the element and panel specimens are compared with experimental results. Derived from text

N95-28842*# National Aeronautics and Space Administration. Langley Research Center, Hampton, VA.
A STUDY OF STRUCTURALLY EFFICIENT GRAPHITE-THERMOPLASTIC TRAPEZOIDAL-CORRUGATION SANDWICH AND SEMI-SANDWICH PANELS
Dawn C. Jegley *In its* Third NASA Advanced Composites Technology Conference, Volume 1, Part 2 Jan. 1993 p 859-878 (For primary document see N95-28823 10-24)
Avail: CASI HC A03/MF A04

The structural efficiency of compression-loaded trapezoidal-corrugation sandwich and semi-sandwich composite panels is studied to determine their weight savings potential. Sandwich panels with two identical face sheets and a trapezoidal corrugated core between them, and semi-sandwich panels with a corrugation attached to a single skin are considered. An optimization code is used to find the minimum weight designs for critical compressive load levels ranging from 3,000 to 24,000 lb/in. Graphite-thermoplastic panels based on the optimal minimum weight designs were fabricated and tested. A finite-element analysis of several test specimens was also conducted. The results of the optimization study, the finite-element analysis, and the experiments are presented. Author

N95-28843*# Northrop Corp., Hawthorne, CA. Aircraft Div.
A WEIGHT-EFFICIENT DESIGN STRATEGY FOR CUTOUTS IN COMPOSITE TRANSPORT STRUCTURES
S. G. Russell, J. Hangen, and T. E. Palm *In* NASA. Langley Research Center, Third NASA Advanced Composites Technology Conference, Volume

1, Part 2 Jan. 1993 p 879-897 (For primary document see N95-28823 10-24)
(Contract NAS1-18842)
Avail: CASI HC A03/MF A04

Two design procedures for composite panels with cutouts are described and illustrated by example applications. One of these procedures uses a specialized cutout analysis code to obtain preliminary sizing information for the panel laminate, cutout padup, and cutout stiffener reinforcements. The other procedure uses a finite element based structural optimization code to develop a minimum weight panel design. The best features of both procedures form the basis of a design strategy for weight-efficient cutout panels. Author

N95-28844*# National Aeronautics and Space Administration. Langley Research Center, Hampton, VA.
EFFECTS OF CUTOUTS ON THE BEHAVIOR OF SYMMETRIC COMPOSITE LAMINATES SUBJECTED TO BENDING AND TWISTING LOADS
C. B. Prasad (Analytical Services and Materials, Inc., Hampton, VA.), M. J. Shuart, N. J. Bains, and M. Rouse *In its* Third NASA Advanced Composites Technology Conference, Volume 1, Part 2 Jan. 1993 p 899-918 (For primary document see N95-28823 10-24)
Avail: CASI HC A03/MF A04

Composite structures are used for a wide variety of aerospace applications. Practical structures contain cutouts and these structures are subjected to in-plane and out-of-plane loading conditions. Structurally efficient designs for composite structures require a thorough understanding of the effects of cutouts on the response of composite plates subjected to inplane or out-of-plane loadings. Most investigations of the behavior of composite plates with cutouts have considered in-plane loadings only. Out-of-plane loadings suchas bending or twisting have received very limited attention. The response of homogeneous plates (e.g., isotropic or orthotropic plates) subjected to bending or twisting moments has been studied analytically. These analyses are for infinite plates and neglect finite-plate effects. Recently, analytical and experimental studies were conducted to determine the effects of cutouts on the response of laminated composite plates subjected to bending moments. No analytical or experimental results are currently available for the effects of cutouts on the response of composite laminates subjected to twisting moments. Author

N95-28845*# National Aeronautics and Space Administration. Langley Research Center, Hampton, VA.
BUCKLING ANALYSIS OF CURVED COMPOSITE SANDWICH PANELS SUBJECTED TO INPLANE LOADINGS
Juan R. Cruz *In its* Third NASA Advanced Composites Technology Conference, Volume 1, Part 2 Jan. 1993 p 919-932 (For primary document see N95-28823 10-24)
Avail: CASI HC A03/MF A04

Composite sandwich structures are being considered for primary structure in aircraft such as subsonic and high speed civil transports. The response of sandwich structures must be understood and predictable to use such structures effectively. Buckling is one of the most important response mechanisms of sandwich structures. A simple buckling analysis is derived for sandwich structures. This analysis is limited to flat, rectangular sandwich panels loaded by uniaxial compression (N(sub x)) and having simply supported edges. In most aerospace applications, however, the structure's geometry, boundary conditions, and loading are usually very complex. Thus, a general capability for analyzing the buckling behavior of sandwich structures is needed. The present paper describes and evaluates an improved buckling analysis for cylindrically curved composite sandwich panels. This analysis includes orthotropic facesheets and first-order transverse shearing effects. Both simple support and clamped boundary conditions are also included in the analysis. The panels can be subjected to linearly varying normal loads N(sub x) and N(sub y) in addition to a constant shear load N(sub xy). The analysis is based on the modified Donnell's equations for shallow shells. The governing equations are solved by direct application of Galerkin's method. The accuracy of the present analysis is verified by comparing results with those obtained from finite element analysis for a variety of geometries, loads, and boundary conditions. The limitations of the present analysis are investigated, in particular those related to the shallow shell assumptions in the governing equations. Finally, the computational efficiency of the present analysis is considered. Derived from text

N95-28846*# Lockheed Aeronautical Systems Co., Marietta, GA.
ISPAN (INTERACTIVE STIFFENED PANEL ANALYSIS): A TOOL FOR QUICK CONCEPT EVALUATION AND DESIGN TRADE STUDIES
John W. Hairr, William J. Dorris, J. Edward Ingram, and Bharat M. Shah *In* NASA. Langley Research Center, Third NASA Advanced Composites Technology Conference, Volume 1, Part 2 Jan. 1993 p 933-949 (For primary document see N95-28823 10-24)
Avail: CASI HC A03/MF A04

Interactive Stiffened Panel Analysis (ISPAN) modules, written in FORTRAN, were developed to provide an easy to use tool for creating finite element models of composite material stiffened panels. The modules allow the user to interactively construct, solve and post-process finite element models of four general types of structural panel configurations using only the panel dimensions and properties as input data. Linear, buckling and post-buckling solution capability is provided. This interactive input allows rapid model generation and solution by non finite element users. The results of a parametric study of a blade stiffened panel are presented to demonstrate the usefulness of the ISPAN modules. Also, a non-linear analysis of a test panel was conducted and the results compared to measured data and previous correlation analysis. Author

N95-28847*# National Aeronautics and Space Administration. Langley Research Center, Hampton, VA.
TECHNOLOGY INTEGRATION BOX BEAM FAILURE STUDY c39
M. J. Shuart, Damodar R. Ambur, D. D. Davis, Jr., R. C. Davis, G. L. Farley, C. G. Lotts, and J. T. Wang *In its* Third NASA Advanced Composites Technology Conference, Volume 1, Part 2 Jan. 1993 p 951-965 (For primary document see N95-28823 10-24)
Avail: CASI HC A03/MF A04

Composite structures have the potential to be cost-effective, structurally efficient primary aircraft structures. The Advanced Composites Technology (ACT) Program has the goal to develop the technology to exploit this potential for heavily loaded aircraft structures. As part of the ACT Program, Lockheed Aeronautical Systems Company completed the design and fabrication of the Technology Integration Box Beam (TIBB). The TIBB is an advanced composite prototype structure for the center wing section of the C-130 aircraft. Lockheed subjected the TIBB to downbending, upbending, torsion and combined upbending and torsion load conditions to verify the design. The TIBB failed at 83 percent of design ultimate load for the combined upbending and torsion load condition. The objective of this paper is to describe the mechanisms that led to the failure of the TIBB. The results of a comprehensive analytical and experimental study are presented. Analytical results include strain and deflection results from both a global analysis of the TIBB and a local analysis of the failure region. These analytical results are validated by experimental results from the TIBB tests. The analytical and experimental results from the TIBB tests are used to determine a sequence of events that resulted in failure of the TIBB. A potential cause of failure is high stresses in a stiffener runout region. Analytical and experimental results are also presented for a stiffener runout specimen that was used to simulate the TIBB failure mechanisms. Derived from text

N95-28848*# National Aeronautics and Space Administration. Langley Research Center, Hampton, VA.
A GLOBAL/LOCAL ANALYSIS METHOD FOR TREATING DETAILS IN STRUCTURAL DESIGN c39
Mohammad A. Aminpour (Analytical Services and Materials, Inc., Hampton, VA.), Susan L. McCleary (Lockheed Engineering and Sciences Co., Hampton, VA.), and Jonathan B. Ransom *In its* Third NASA Advanced Composites Technology Conference, Volume 1, Part 2 Jan. 1993 p 967-986 (For primary document see N95-28823 10-24)
(Contracts NAS1-19317; NAS1-19000)
Avail: CASI HC A03/MF A04

A method for analyzing global/local behavior of plate and shell structures is described. In this approach, a detailed finite element model of the local region is incorporated within a coarser global finite element model. The local model need not be nodally compatible (i.e., need not have a one-to-one nodal correspondence) with the global model at their common boundary; therefore, the two models may be constructed independently. The nodal incompatibility of the models is accounted for by introducing appropriate constraint conditions into the potential energy in a hybrid variational formulation. The primary advantage of this method is that the need for

transition modeling between global and local models is eliminated. Eliminating transition modeling has two benefits. First, modeling efforts are reduced since tedious and complex transitioning need not be performed. Second, errors due to the mesh distortion, often unavoidable in mesh transitioning, are minimized by avoiding distorted elements beyond what is needed to represent the geometry of the component. The method is applied reduced to a plate loaded in tension and transverse bending. The plate has a central hole, and various hole sixes and shapes are studied. The method is also applied to a composite laminated fuselage panel with a crack emanating from a window in the panel. While this method is applied herein to global/local problems, it is also applicable to the coupled analysis of independently modeled components as well as adaptive refinement.

Author

N95-28849*# National Aeronautics and Space Administration. Lewis Research Center, Cleveland, OH.

IPACS (INTEGRATED PROBABILISTIC ASSESSMENT OF COMPOSITE STRUCTURES): CODE DEVELOPMENT AND APPLICATIONS

C. C. Chamis and Michael C. Shiao (Sverdrup Technology, Inc., Brook Park, OH.) *In* NASA. Langley Research Center, Third NASA Advanced Composites Technology Conference, Volume 1, Part 2 Jan. 1993 p 987-999 (For primary document see N95-28823 10-24)

Avail: CASI HC A03/MF A04

A methodology and attendant computer code have been developed and are described to computationally simulate the uncertain behavior of composite structures. The uncertain behavior includes buckling loads, stress concentration factors, displacements, stress/strain etc., which are the consequences of the inherent uncertainties (scatter) in the primitive (independent random) variables (constituent, ply, laminate and structural) that describe the composite structures. The computer code, IPACS (Integrated Probabilistic Assessment of Composite Structures), can handle both composite mechanics and composite structures. Application to probabilistic composite mechanics is illustrated by its uses to evaluate the uncertainties in the major Poisson's ratio and in laminate stiffness and strength. IPACS application to probabilistic structural analysis is illustrated by its use to evaluate the uncertainties in the buckling of a composite plate, in the stress concentration factor in a composite panel and in the vertical displacement and ply stress in a composite aircraft wing segment.

Author

N95-28899 ESDU International Ltd., London (England).

THROUGH-THE-THICKNESS STRESSES AND FAILURE IN THE CORNER RADIUS OF A LAMINATED COMPOSITE SECTION

Nov. 1994 28 p

(ISSN 0141-4097)

(ESDU-94019; ISBN-0-85679-906-8) Avail: ESDU

ESDU 94019 introduces a Fortran program (ESDUpac A9419) that calculates the through-thickness radial and shear stresses in a specially-orthotropic section subjected to a bending moment, and radial and tangential forces. It provides a distribution of the stresses over a mesh throughout any part of the corner defined by the user. The corresponding moment and forces just to cause failure at any point in the corner are also calculated, that is in the same ratio to each other as those initially input. The transverse failure criterion applied is the quadratic stress equation due to Chang and Springer and it requires values for the ply material compressive, tensile and shear strengths in the through-thickness direction to test for material failure, and those same values at the ply interface to test for interface failure. The program is based on the theory of elasticity for a homogeneous anisotropic material and the appropriate equations are detailed. The program tests that the laminate analysed conforms to that assumption and provides a warning if it fails that test together with an assessment of the underestimate of the maximum stress that may then occur. Comparisons are made of results obtained using the program with other results derived from the literature for both experiments and finite element analyses. The input to and output from the program are explained and illustrated by a worked example. The program is provided on disc in the software volume both uncompiled and compiled within ESDUview, a user-friendly shell that prompts for input data on screen.

Author

N95-28906*# National Aeronautics and Space Administration. Lewis Research Center, Cleveland, OH.

EMI SHIELDS MADE FROM INTERCALATED GRAPHITE COMPOSITES

James R. Gaier and Jennifer Terry (Manchester Coll., North Manchester, IN.) Jun. 1995 15 p Presented at the Seventh International Materials and Processing Conference, Parsippany, NJ, 21-23 Jun. 1994; sponsored by Society for the Advancement of Materials and Processing

(Contract NCC3-317; RTOP 506-41-41)

(NASA-TM-106979; E-9743; NAS 1.15:106979) Avail: CASI HC A03/MF A01

Electromagnetic interference (EMI) shielding typically makes up about twenty percent of the mass of a spacecraft power system. Graphite fiber/polymer composites have significantly lower densities and higher strengths than aluminum, the present material of choice for EMI shields, but they lack the electrical conductivity that enables acceptable shielding effectiveness. Bromine intercalated pitch-based graphite/epoxy composites have conductivities fifty times higher than conventional structural graphite fibers. Calculations are presented which indicate that EMI shields made from such composites can have sufficient shielding at less than 20% of the mass of conventional aluminum shields. EMI shields provide many functions other than EMI shielding including physical protection, thermal management, and shielding from ionizing radiation. Intercalated graphite composites perform well in these areas also. Mechanically, they have much higher specific strength and modulus than aluminum. They also have shorter half thicknesses for x-rays and gamma radiation than aluminum. Thermally, they distribute infra-red radiation by absorbing and re-radiating it rather than concentrating it by reflection as aluminum does. The prospects for intercalated graphite fiber/polymer composites for EMI shielding are encouraging.

Author

N95-28951 Naval Surface Warfare Center, Bethesda, MD.

SORPTION AND DIFFUSION OF MOISTURE IN MULTILAYER COMPOSITE AEM/S SANDWICH MATERIALS

Joseph M. Augl 1 Oct. 1994 77 p Limited Reproducibility: More than 20% of this document may be affected by microfiche quality

(AD-A289807; CARDIVNSWC-TR-94/018) Avail: Issuing Activity (Defense Technical Information Center (DTIC))

The moisture diffusion coefficients and solubilities of Advanced Enclosed Mast/Sensor (AEM/S) sandwich constituent materials of interest have been determined at 22, 35, and 50 deg C and at 80 percent relative humidity. Expressions for calculating the diffusion coefficients and solubilities for any temperature of interest to marine environments are provided. The objective of this study was to provide input data for finite element moisture diffusion analyses that permits one to predict the moisture take-up and internal distributions a function of time for composite mast sandwich structures in specified marine environments. The following materials were included in this investigation: E-glass/SP Systems 3113 epoxy, E-glass/510A vinyl-ester (RTM3), E-glass/G10 epoxy, Balsa wood type D57, PVC foam (Klegecell), and Nomex honeycomb phenolic core material.

DTIC

N95-29029*# National Aeronautics and Space Administration. Langley Research Center, Hampton, VA.

THIRD NASA ADVANCED COMPOSITES TECHNOLOGY CONFERENCE, VOLUME 1, PART 1

John G. Davis, Jr., comp. and Herman L. Bohon, comp. (Lockheed Engineering and Sciences Co., Hampton, VA.) Jan. 1993 498 p Conference held in Long Beach, CA, 8-11 Jun. 1992; sponsored by NASA, Washington and DOD

(RTOP 510-02-13-01)

(NASA-CP-3178-Vol-1-Pt-1; L-17167A-Vol-1-Pt-1; NAS 1.55:3178-Vol-1-Pt-1) Avail: CASI HC A21/MF A04

This document is a compilation of papers presented at the Third NASA Advanced Composites Technology (ACT) Conference. The ACT Program is a major multi-year research initiative to achieve a national goal of technology readiness before the end of the decade. Conference papers recorded results of research in the ACT Program in the specific areas of automated fiber placement, resin transfer molding, textile preforms, and stitching as these processes influence design, performance, and cost of composites in aircraft structures. Papers sponsored by the Department of Defense on the Design and Manufacturing of Low Cost Composites (DMLCC) are also included in Volume 2 of this document. For individual titles, see N95-29030 through N95-29051.

N95-29030*# Douglas Aircraft Co., Inc., Long Beach, CA.
IMPACT OF COMPOSITES ON FUTURE TRANSPORT AIRCRAFT
Robert H. Kinder *In* NASA. Langley Research Center, Third NASA Advanced Composites Technology Conference, Volume 1, Part 1 Jan. 1993 p 3-24 (For primary document see N95-29029 10-24)
Avail: CASI HC A03/MF A04

In the current environment, new technology must be cost-effective in addition to improving operability. Various approaches have been used to determine the 'hurdle' or 'breakthrough' return that must be achieved to gain customer commitment for a new product or aircraft, or in this case, a new application of the technology. These approaches include return-on-investment, payback period, and addition to net worth. An easily understood figure-of-merit and one used by our airline customers is improvement in direct operating cost per seat-mile. Any new technology must buy its way onto the aircraft through reduction in direct operating cost (DOC). Derived from text

N95-29031*# Boeing Co., Seattle, WA.
CHALLENGES AND PAYOFF OF COMPOSITES IN TRANSPORT AIRCRAFT: 777 EMPENNAGE AND FUTURE APPLICATIONS
John Quinlivan *In* NASA. Langley Research Center, Third NASA Advanced Composites Technology Conference, Volume 1, Part 1 Jan. 1993 p 25-45 (For primary document see N95-29029 10-24)
Avail: CASI HC A03/MF A04

The Boeing 777 is the first of a new family of wide body airplanes. The new large twin is sized to accommodate 360 to 390 passengers in typical two-class configurations and planned growth beyond that. The 777 offers airlines three engine options, extremely attractive operating costs, and compatibility with existing airport gates and taxiways. The 777 has a wingspan of nearly 197 feet and is offered with a wing-tip folding mechanism that will reduce the span to 156 feet. Extensive use of advance composite is included in the 777. The application range from fiberglass fairing to primary structures. The 777 empennage includes vertical fin and a horizontal stabilizer. The material used for the empennage is a new, toughened epoxy materials. The material provides outstanding resistance to impact damage. Derived from text

N95-29032*# National Aeronautics and Space Administration. Langley Research Center, Hampton, VA.
ADVANCED COMPOSITES TECHNOLOGY PROGRAM
John G. Davis, Jr. *In its* Third NASA Advanced Composites Technology Conference, Volume 1, Part 1 Jan. 1993 p 49-78 (For primary document see N95-29029 10-24)
Avail: CASI HC A03/MF A04

This paper provides a brief overview of the NASA Advanced Composites Technology (ACT) Program. Critical technology issues that must be addressed and solved to develop composite primary structures for transport aircraft are delineated. The program schedule and milestones are included. Work completed in the first 3 years of the program indicates the potential for achieving composite structures that weigh less and are cost effective relative to conventional aluminum structure. Selected technical accomplishments are noted. Readers who are seeking more in-depth technical information should study the other papers included in these proceedings. Derived from text

N95-29033*# Lockheed Aeronautical Systems Co., Marietta, GA.
TEXTILE COMPOSITE FUSELAGE STRUCTURES DEVELOPMENT
Anthony C. Jackson, Ronald E. Barrie, and Robert L. Chu *In* NASA. Langley Research Center, Third NASA Advanced Composites Technology Conference, Volume 1, Part 1 Jan. 1993 p 79-96 (For primary document see N95-29029 10-24)
(Contract NAS1-18888)
Avail: CASI HC A03/MF A04

Phase 2 of the NASA ACT Contract (NAS1-18888), Advanced Composite Structural Concepts and Materials Technology for Transport Aircraft Structures, focuses on textile technology, with resin transfer molding or powder coated tows. The use of textiles has the potential for improving damage tolerance, reducing cost and saving weight. This program investigates resin transfer molding (RTM), as a maturing technology for high fiber volume primary structures and powder coated tows as an emerging technology with a high potential for significant cost savings and superior structural properties. Powder coated tow technology has promise for significantly improving the processibility of high temperature resins such as polyimides. Derived from text

N95-29034*# Boeing Commercial Airplane Co., Seattle, WA.
ADVANCED COMPOSITE FUSELAGE TECHNOLOGY
Larry B. Ilcewicz, Peter J. Smith, and Ray E. Horton *In* NASA. Langley Research Center, Third NASA Advanced Composites Technology Conference, Volume 1, Part 1 Jan. 1993 p 97-156 (For primary document see N95-29029 10-24)
(Contract NAS1-18889)
Avail: CASI HC A04/MF A04

Boeing's ATCAS program has completed its third year and continues to progress towards a goal to demonstrate composite fuselage technology with cost and weight advantages over aluminum. Work on this program is performed by an integrated team that includes several groups within The Boeing Company, industrial and university subcontractors, and technical support from NASA. During the course of the program, the ATCAS team has continued to perform a critical review of composite developments by recognizing advances in metal fuselage technology. Despite recent material, structural design, and manufacturing advancements for metals, polymeric matrix composite designs studied in ATCAS still project significant cost and weight advantages for future applications. A critical path to demonstrating technology readiness for composite transport fuselage structures was created to summarize ATCAS tasks for Phases A, B, and C. This includes a global schedule and list of technical issues which will be addressed throughout the course of studies. Work performed in ATCAS since the last ACT conference is also summarized. Most activities relate to crown quadrant manufacturing scaleup and performance verification. The former was highlighted by fabricating a curved, 7 ft. by 10 ft. panel, with cocured hat-stiffeners and cobonded J-frames. In building to this scale, process developments were achieved for tow-placed skins, drape formed stiffeners, braided/RTM frames, and panel cure tooling. Over 700 tests and supporting analyses have been performed for crown material and design evaluation, including structural tests that demonstrated limit load requirements for severed stiffener/skin failsafe damage conditions. Analysis of tests for tow-placed hybrid laminates with large damage indicates a tensile fracture toughness that is higher than that observed for advanced aluminum alloys. Additional recent ATCAS achievements include crown supporting technology, keel quadrant design evaluation, and sandwich process development. Author

N95-29035*# Lockheed Aeronautical Systems Co., Marietta, GA.
ADVANCED RESIN SYSTEMS AND 3D TEXTILE PREFORMS FOR LOW COST COMPOSITE STRUCTURES
J. G. Shukla and T. D. Bayha *In* NASA. Langley Research Center, Third NASA Advanced Composites Technology Conference, Volume 1, Part 1 Jan. 1993 p 159-173 (For primary document see N95-29029 10-24)
Avail: CASI HC A03/MF A04

Advanced resin systems and 3D textile preforms are being evaluated at Lockheed Aeronautical Systems Company (LASC) under NASA's Advanced Composites Technology (ACT) Program. This work is aimed towards the development of low-cost, damage-tolerant composite fuselage structures. Resin systems for resin transfer molding and powder epoxy towpreg materials are being evaluated for processability, performance and cost. Three developmental epoxy resin systems for resin transfer molding (RTM) and three resin systems for powder towpregging are being investigated. Various 3D textile preform architectures using advanced weaving and braiding processes are also being evaluated. Trials are being conducted with powdered towpreg, in 2D weaving and 3D braiding processes for their textile processability and their potential for fabrication in 'net shape' fuselage structures. The progress in advanced resin screening and textile preform development is reviewed here. Author

N95-29036*# National Aeronautics and Space Administration. Langley Research Center, Hampton, VA.
WEAVABILITY OF DRY POLYMER POWDER TOWPREG
Maylene K. Hugh (Old Dominion Univ., Norfolk, VA.), Joseph M. Marchello (Old Dominion Univ., Norfolk, VA.), Janice R. Maiden (Textile Technologies, Inc., Hatboro, PA.), and Norman J. Johnston *In its* Third NASA Advanced Composites Technology Conference, Volume 1, Part 1 Jan. 1993

p 175-189 (For primary document see N95-29029 10-24)
(Grant NAG1-1067)
Avail: CASI HC A03/MF A04

Carbon fiber yarns (3k, 6k, 12k) were impregnated with LARC (tm) thermoplastic polyimide dry powder. Parameters for weaving these yarns were established. Eight-harness satin fabrics were successfully woven from each of the three classes of yarns and consolidated into test specimens to determine mechanical properties. It was observed that for optimum results warp yarns should have flexural rigidities between 10,000 and 100,000 mg-cm. Tow handling minimization, low tensioning, and tow bundle twisting were used to reduce fiber breakage, the separation of filaments, and tow-to-tow abrasion. No apparent effect of tow size or twist was observed on either tension or compression modulus. However, fiber damage and processing costs favor the use of 12k yarn bundles versus 3k or 6k yarn bundles in the weaving of powder-coated towpreg. Author

N95-29037*# National Aeronautics and Space Administration. Langley Research Center, Hampton, VA.
EFFECTS OF TEMPERATURE AND HUMIDITY CYCLING ON THE STRENGTHS OF TEXTILE REINFORCED CARBON/EPOXY COMPOSITE MATERIALS
Roberto J. Cano and Keith W. Furrow (Virginia Polytechnic Inst. and State Univ., Blacksburg, VA.) *In its* Third NASA Advanced Composites Technology Conference, Volume 1, Part 1 Jan. 1993 p 191-208 (For primary document see N95-29029 10-24)
Avail: CASI HC A03/MF A04

Results are presented from an experimental evaluation of the combined effects of temperature and humidity cycling on AS4/3501-6 composites (unstitched, Kevlar 29 stitched, and S-2 glass stitched uniweave fabric) and AS4/E905L composites (2-D, S-2 glass stitched 2-D, and 3-D braided fabric). The AS4/3501-6 uniweave material had a quasi-isotropic layup, whereas the AS4/E905L materials were braided in a (+/-30 deg/0 deg)(sub s) orientation. Data presented include compression strengths and compression-compression fatigue results for uncycled composites and cycled composites (160, 480, 720, and 1280 cycles from 140 deg F at 95 percent relative humidity to -67 deg F). To observe the presence of microcracking within the laminates, photomicrographs were taken of each material type at the end of each cycling period. Microcracks were found to be more prevalent within stitched laminates, predominantly around individual stitches. The glass stitched laminates showed significant microcracking even before cycling. Less microcracking was evident in the Kevlar stitched materials, whereas the unstitched uniweave material developed microcracks only after cycling. The 3-D braid did not develop microcracks. The static compression strengths of the unstitched and Kevlar stitched uniweave materials were degraded by about 10 percent after 1280 temperature/humidity cycles, whereas the reduction in compression strength for the glass stitched uniweave was less than 3 percent. The reduction in compression strength for the glass stitched 2-D braid was less than 8 percent. The unstitched 2-D and 3-D braids did not lose strength from temperature/humidity cycling. The compression-compression fatigue properties of all six material types were not affected by temperature/humidity cycling. Author

N95-29038*# National Aeronautics and Space Administration. Langley Research Center, Hampton, VA.
MECHANICAL CHARACTERIZATION OF 2D, 2D STITCHED, AND 3D BRAIDED/RTM MATERIALS
Jerry W. Deaton, Susan M. Kullerd (Lockheed Engineering and Sciences Co., Hampton, VA.), and Marc A. Portanova (Lockheed Engineering and Sciences Co., Hampton, VA.) *In its* Third NASA Advanced Composites Technology Conference, Volume 1, Part 1 Jan. 1993 p 209-230 (For primary document see N95-29029 10-24)
Avail: CASI HC A03/MF A04

Braided composite materials have potential for application in aircraft structures. Fuselage frames, floor beams, wing spars, and stiffeners are examples where braided composites could find application if cost effective processing and damage tolerance requirements are met. Another important consideration for braided composites relates to their mechanical properties and how they compare to the properties of composites produced by other textile composite processes being proposed for these applications. Unfortunately, mechanical property data for braided composites do not appear extensively in the literature. Data are presented in this paper on the mechanical characterization of 2D triaxial braid, 2D triaxial braid plus stitching, and 3D (through-the-thickness) braid composite materials. The braided preforms all had the same graphite tow size and the same nominal braid architectures, (+/- 30 deg/0 deg), and were resin transfer molded (RTM) using the same mold for each of two different resin systems. Static data are presented for notched and unnotched tension, notched and unnotched compression, and compression after impact strengths at room temperature. In addition, some static results, after environmental conditioning, are included. Baseline tension and compression fatigue results are also presented, but only for the 3D braided composite material with one of the resin systems. Derived from text

N95-29039*# National Aeronautics and Space Administration. Langley Research Center, Hampton, VA.
PERFORMANCE OF RESIN TRANSFER MOLDED MULTIAXIAL WARP KNIT COMPOSITES
H. Benson Dexter and Gregory H. Hasko (Lockheed Engineering and Sciences Co., Hampton, VA.) *In its* Third NASA Advanced Composites Technology Conference, Volume 1, Part 1 Jan. 1993 p 231-261 (For primary document see N95-29029 10-24)
Avail: CASI HC A03/MF A04

Composite materials that are subjected to complex loads have traditionally been fabricated with multidirectionally oriented prepreg tape materials. Some of the problems associated with this type of construction include low delamination resistance, poor out-of-plane strength, and labor intensive fabrication processes. Textile reinforced composites with through-the-thickness reinforcement have the potential to solve some of these problems. Recently, a relatively new class of noncrimp fabrics designated as multiaxial warp knits have been developed to minimize some of the high cost and damage tolerance concerns. Multiple stacks of warp knit fabrics can be knitted or stitched together to reduce layup labor cost. The through-the-thickness reinforcement can provide significant improvements in damage tolerance and out-of-plane strength. Multilayer knitted/stitched preforms, in conjunction with resin transfer molding (RTM), offer potential for significant cost savings in fabrication of primary aircraft structures. The objectives of this investigation were to conduct RTM processing studies and to characterize the mechanical behavior of composites reinforced with three multiaxial warp knit fabrics. The three fabrics investigated were produced by Hexcel and Milliken in the United States, and Saerbeck in Germany. Two resin systems, British Petroleum E9O5L and 3M PR 500, were characterized for RTM processing. The performance of Hexcel and Milliken quasi-isotropic knitted fabrics are compared to conventional prepreg tape laminates. The performance of the Saerbeck fabric is compared to uniweave wing skin layups being investigated by Douglas Aircraft Company in the NASA Advanced Composites Technology (ACT) program. Tests conducted include tension, open hole tension, compression, open hole compression, and compression after impact. The effects of fabric defects, such as misaligned fibers and gaps between tows, on material performance are also discussed. Estimated material and labor cost savings are projected for the Saerbeck fabric as compared to uniweave fabric currently being used by Douglas in the NASA ACT wing development program. Derived from text

N95-29040*# Lockheed Engineering and Sciences Co., Hampton, VA.
EXPERIMENTAL AND ANALYTICAL CHARACTERIZATION OF TRIAXIALLY BRAIDED TEXTILE COMPOSITES
John E. Masters, Mark J. Fedro (Boeing Co., Seattle, WA.), and Peter G. Ifju (Virginia Polytechnic Inst. and State Univ., Blacksburg, VA.) *In* NASA. Langley Research Center, Third NASA Advanced Composites Technology Conference, Volume 1, Part 1 Jan. 1993 p 263-285 (For primary document see N95-29029 10-24)
Avail: CASI HC A03/MF A04

There were two components, experimental and analytical, to this investigation of triaxially braided textile composite materials. The experimental portion of the study centered on measuring the materials' longitudinal and transverse tensile moduli, Poisson's ratio, and strengths. The identification of the damage mechanisms exhibited by these materials was also a prime objective of the experimental investigation. The analytical portion of the investigation utilized the Textile Composites Analysis (TECA) model to predict modulus and strength. The analytical and experimental results were compared to assess the effectiveness of the analysis. The figures contained in this paper reflect the presentation made at the conference. They may be divided into four sections: a definition of the material system tested;

followed by a series of figures summarizing the experimental results (these figures contain results of a Moire interferometry study of the strain distribution in the material, examples and descriptions of the types of damage encountered in these materials, and a summary of the measured properties); a description of the TECA model follows the experimental results (this includes a series of predicted results and a comparison with measured values); and finally, a brief summary completes the paper.
Derived from text

N95-29041*# Grumman Aircraft Engineering Corp., Bethpage, NY.
CROSS-STIFFENED CONTINUOUS FIBER STRUCTURES
John R. Ewen and Jim A. Suarez *In* NASA. Langley Research Center, Third NASA Advanced Composites Technology Conference, Volume 1, Part 1 Jan. 1993 p 287-308 (For primary document see N95-29029 10-24)
Avail: CASI HC A03/MF A04

Under NASA's Novel Composites for Wing and Fuselage Applications (NCWFA) program, Contract NAS1-18784, Grumman is evaluating the structural efficiency of graphite/epoxy cross-stiffened panel elements fabricated using innovative textile preforms and cost effective Resin Transfer Molding (RTM) and Resin Film Infusion (RFI) processes. Two three-dimensional woven preform assembly concepts have been defined for application to a representative window belt design typically found in a commercial transport airframe. The 3D woven architecture for each of these concepts is different; one is vertically woven in the plane of the window belt geometry and the other is loom woven in a compressed state similar to an unfolded eggcrate. The feasibility of both designs has been demonstrated in the fabrication of small test element assemblies. These elements and the final window belt assemblies will be structurally tested, and results compared. Author

N95-29042*# Rockwell International Science Center, Thousand Oaks, CA.
AN ENGINEERING MODEL OF WOVEN COMPOSITES BASED ON MICROMECHANICS
W. C. Carter, B. N. Cox, M. S. Dadkhah, and W. L. Morris *In* NASA. Langley Research Center, Third NASA Advanced Composites Technology Conference, Volume 1, Part 1 Jan. 1993 p 309-322 (For primary document see N95-29029 10-24)
(Contract NAS1-18840)
Avail: CASI HC A03/MF A04

Composites with three-dimensional woven architectures exhibit large strains to failure when compared to composites made up of the same materials but not with three-dimensional interlocking tows. The fracture mechanics of such three-dimensional architectures is a subject requiring substantial investigation and experimental testing. Classical fracture mechanics concepts (for instance, an isolated defect in a homogeneous body) will not be applicable to the woven fracture test specimen. The use of an isolated singularity to characterize an entire specimen is inadequate when the density of defects is considerable and the material is heterogeneous. Modelling of such a complex system requires a great deal of insight and consideration as well as prudent choices of model sizes to make numerical schemes feasible. The purpose of this manuscript is to review our recently acquired knowledge of damage accumulation in woven composites and to describe a practicable model of the macroscopic behavior in these and other complex composite architectures based on such knowledge. In this manuscript, discussion will be limited to uniaxial compressive loading; considerations of general loading (monotonic and cyclic) will appear in a subsequent manuscript. Our modelling efforts may be briefly described as follows: the composite is subdivided into microstructural elements (microelements) in which the micromechanical modelling is either understood rigorously or can be represented adequately by statistical parameters. There can be microstructural elements for many different types of composite components, such as the various types of warp and weft and matrix for three-dimensional woven composites. The physical dimensions of microelements are made as large as possible while the response within the element can still be represented by a single micromechatlical calculation. The various elements are linked together(sometimes by associating distinct corners and edges, sometimes by superposition) in a pattern which resembles a particular weave architecture. The model can then be loaded in any manner and the linear and nonlinear elastic responses of representative weaves can be calculated. After the elastic regime, the fracture response is determined by monitoring the damage accumulation. Derived from text

N95-29043*# Boeing Commercial Airplane Co., Seattle, WA.
COST MODEL RELATIONSHIPS BETWEEN TEXTILE MANUFACTURING PROCESSES AND DESIGN DETAILS FOR TRANSPORT FUSELAGE ELEMENTS
Stephen L. Metschan, Kurtis S. Wilden, Garrett C. Sharpless (Fiber Innovations, Inc., Norwood, MA.), and Rich M. Andelman (Dow Chemical Co., Midland, MI.) *In* NASA. Langley Research Center, Third NASA Advanced Composites Technology Conference, Volume 1, Part 1 Jan. 1993 p 323-340 (For primary document see N95-29029 10-24)
(Contract NAS1-18889)
Avail: CASI HC A03/MF A04

Textile manufacturing processes offer potential cost and weight advantages over traditional composite materials and processes for transport fuselage elements. In the current study, design cost modeling relationships between textile processes and element design details were developed. Such relationships are expected to help future aircraft designers to make timely decisions on the effect of design details and overall configurations on textile fabrication costs. The fundamental advantage of a design cost model is to insure that the element design is cost effective for the intended process. Trade studies on the effects of processing parameters also help to optimize the manufacturing steps for a particular structural element. Two methods of analyzing design detail/process cost relationships developed for the design cost model were pursued in the current study. The first makes use of existing databases and alternative cost modeling methods (e.g. detailed estimating). The second compares design cost model predictions with data collected during the fabrication of seven foot circumferential frames for ATCAS crown test panels. The process used in this case involves 2D dry braiding and resin transfer molding of curved 'J' cross section frame members having design details characteristic of the baseline ATCAS crown design. Author

N95-29044*# Dow Chemical Co., Midland, MI.
DEVELOPMENT OF RTM AND POWDER PREPREG RESINS FOR SUBSONIC AIRCRAFT PRIMARY STRUCTURES
Edmund P. Woo, Michael R. Groleau, James L. Bertram (Dow Chemical Co., Freeport, TX.), Paul M. Puckett (Dow Chemical Co., Freeport, TX.), and Shawn J. Maynard (Dow Chemical Co., Freeport, TX.) *In* NASA. Langley Research Center, Third NASA Advanced Composites Technology Conference, Volume 1, Part 1 Jan. 1993 p 345-360 (For primary document see N95-29029 10-24)
(Contract NAS1-18841)
Avail: CASI HC A03/MF A04

Dow developed a thermoset resin which could be used to produce composites via the RTM process. The composites formed are useful at 200 F service temperatures after moisture saturation, and are tough systems that are suitable for subsonic aircraft primary structure. At NASA's request, Dow also developed a modified version of the RTM resin system which was suitable for use in producing powder prepreg. In the course of developing the RTM and powder versions of these resins, over 50 different new materials were produced and evaluated. Author

N95-29045*# Virginia Polytechnic Inst. and State Univ., Blacksburg, VA. Dept. of Engineering Science and Mechanics.
ANALYTICAL MODELING AND SENSOR MONITORING FOR OPTIMAL PROCESSING OF ADVANCED TEXTILE STRUCTURAL COMPOSITES BY RESIN TRANSFER MOLDING
Alfred C. Loos, John D. Macrae, Vincent H. Hammond, David E. Kranbuehl (College of William and Mary, Williamsburg, VA.), Sean M. Hart (College of William and Mary, Williamsburg, VA.), Gregory H. Hasko (Lockheed Engineering and Sciences Co., Hampton, VA.), and Alan M. Markus (Douglas Aircraft Co., Inc., Long Beach, CA.) *In* NASA. Langley Research Center, Third NASA Advanced Composites Technology Conference, Volume 1, Part 1 Jan. 1993 p 361-379 (For primary document see N95-29029 10-24)
(Grants NAG1-343; NAG1-237)
Avail: CASI HC A03/MF A04

A two-dimensional model of the resin transfer molding (RTM) process was developed which can be used to simulate the infiltration of resin into

an anisotropic fibrous preform. Frequency dependent electromagnetic sensing (FDEMS) has been developed for in situ monitoring of the RTM process. Flow visualization tests were performed to obtain data which can be used to verify the sensor measurements and the model predictions. Results of the tests showed that FDEMS can accurately detect the position of the resin flow-front during mold filling, and that the model predicted flow-front patterns agreed well with the measured flow-front patterns.
Author

N95-29046*# Lockheed Engineering and Sciences Co., Hampton, VA.
A DESIGNED EXPERIMENT IN STITCHED/RTM COMPOSITES
Larry C. Dickinson *In* NASA. Langley Research Center, Third NASA Advanced Composites Technology Conference, Volume 1, Part 1 Jan. 1993 p 381-397 (For primary document see N95-29029 10-24)
(Contract NAS1-19000)
Avail: CASI HC A03/MF A04

The damage tolerance of composite laminates can be significantly improved by the addition of through-the-thickness fibrous reinforcement such as stitching. However, there are numerous stitching parameters which can be independently varied, and their separate and combined effects on mechanical properties need to be determined. A statistically designed experiment (a 2(sup 5-1) fractional factorial, also known as a Taguchi L16 test matrix) used to evaluate five important parameters is described. The effects and interactions of stitch thread material, stitch thread strength, stitch row spacing and stitch pitch are examined for both thick (48 ply) and thin (16 ply) carbon/epoxy (AS4/E905L) composites. Tension, compression and compression after impact tests are described. Preliminary results of completed tension testing are discussed. Larger threads decreased tensile strength. Panel thickness was found not to be an important stitching parameter for tensile properties. Tensile modulus was unaffected by stitching.
Author

N95-29047*# National Aeronautics and Space Administration. Langley Research Center, Hampton, VA.
THE EFFECTS OF AIRCRAFT FUEL AND FLUIDS ON THE STRENGTH PROPERTIES OF RESIN TRANSFER MOLDED (RTM) COMPOSITES
Anthony Falcone (Boeing Defense and Space Group, Seattle, WA.) and Marvin B. Dow *In its* Third NASA Advanced Composites Technology Conference, Volume 1, Part 1 Jan. 1993 p 399-413 (For primary document see N95-29029 10-24)
(Contract NAS1-18954)
Avail: CASI HC A03/MF A04

The resin transfer molding (RTM) process offers important advantages for cost-effective composites manufacturing, and consequently has become the subject of intense research and development efforts. Several new matrix resins have been formulated specifically for RTM applications in aircraft and aerospace vehicles. For successful use on aircraft, composite materials must withstand exposure to the fluids in common use. The present study was conducted to obtain comparative screening data on several state-ofthe-art RTM resins after environmental exposures were performed on RTM composite specimens. Four graphite/epoxy composites and one graphite/bismaleimide composite were tested; testing of two additional graphite epoxy composites is in progress. Zero-deg tension tests were conducted on specimens machined from eight-ply (+45-deg, -45-deg) laminates, and interlaminar shear tests were conducted on 32-ply 0-deg laminate specimens. In these tests, the various RTM resins demonstrated widely different strengths, with 3501-6 epoxy being the strongest. As expected, all of the matrix resins suffered severe strength degradation from exposure to methylene chloride (paint stripper). The 3501-6 epoxy composites exhibited about a 30 percent drop in tensile strength in hot, wet tests. The E905-L epoxy exhibited little loss of tensile strength (less than 8 percent) after exposure to water. The CET-2 and 862 epoxies as well as the bismaleimide exhibited reduced strengths at elevated temperature after exposure to oils and fuel. In terms of the percentage strength reductions, all of the RTM matrix resins compared favorably with 3501-6 epoxy.
Author

N95-29048*# Douglas Aircraft Co., Inc., Long Beach, CA.
EFFECTS OF THERMAL AND MOISTURE CYCLING ON THE INTERNAL STRUCTURE OF STITCHED RTM LAMINATES
Jeff Walker, Lance Roundy (McDonnell Aircraft Co., Saint Louis, MO.), and Jon Goering (McDonnell Aircraft Co., Saint Louis, MO.) *In* NASA. Langley Research Center, Third NASA Advanced Composites Technology Conference, Volume 1, Part 1 Jan. 1993 p 415-432 (For primary document see N95-29029 10-24)
(Contract NAS1-18580)
Avail: CASI HC A03/MF A04

Conventional aerospace composites are strong and stiff in the directions parallel to the carbon fibers, but they are prone to delaminations and damage in the through-the-thickness directions. Recent research has shown that substantial improvements in damage tolerance are obtained from textile composites with Z-direction reinforcement provided by stitching, weaving, or braiding. Because of the mismatch in thermal and moisture expansion properties of the various material components, there is a potential for microcracks to develop in the resin matrix. These cracks can form to relieve the mechanical stresses that are generated during curing or in-service temperature cycles.
Author

N95-29049*# Lockheed Engineering and Sciences Co., Hampton, VA.
THE COMBINED EFFECT OF GLASS BUFFER STRIPS AND STITCHING ON THE DAMAGE TOLERANCE OF COMPOSITES
Susan M. Kullerd *In* NASA. Langley Research Center, Third NASA Advanced Composites Technology Conference, Volume 1, Part 1 Jan. 1993 p 433-451 (For primary document see N95-29029 10-24)
(Contract NAS1-19000)
Avail: CASI HC A03/MF A04

Recent research has demonstrated that through-the-thickness stitching provides major improvements in the damage tolerance of composite laminates loaded in compression. However, the brittle nature of polymer matrix composites makes them susceptible to damage propagation, requiring special material applications and designs to limit damage growth. Glass buffer strips, embedded within laminates, have shown the potential for improving the damage tolerance of unstitched composite laminates loaded in tension. The glass buffer strips, less stiff than the surrounding carbon fibers, arrest crack growth in composites under tensile loads. The present study investigates the damage tolerance characteristics of laminates that contain both stitching and glass buffer strips.
Derived from text

N95-29050*# Douglas Aircraft Co., Inc., Long Beach, CA.
PROGRESS IN MANUFACTURING LARGE PRIMARY AIRCRAFT STRUCTURES USING THE STITCHING/RTM PROCESS
Alan Markus, Patrick Thrash, and Kim Rohwer *In* NASA. Langley Research Center, Third NASA Advanced Composites Technology Conference, Volume 1, Part 1 Jan. 1993 p 453-479 (For primary document see N95-29029 10-24)
Avail: CASI HC A03/MF A04

The Douglas Aircraft/NASA Act contract has been focused over the past three years at developing a materials, manufacturing, and cost base for stitched/Resin Transfer Molded (RTM) composites. The goal of the program is to develop RTM and stitching technology to provide enabling technology for application of these materials in primary aircraft structure with a high degree of confidence. Presented in this paper will be the progress to date in the area of manufacturing and associated cost values of stitched/RTM composites.
Derived from text

N95-29051*# Douglas Aircraft Co., Inc., Long Beach, CA.
TEST RESULTS FROM LARGE WING AND FUSELAGE PANELS
Ram C. Madan and Mike Voldman *In* NASA. Langley Research Center, Third NASA Advanced Composites Technology Conference, Volume 1, Part 1 Jan. 1993 p 481-502 (For primary document see N95-29029 10-24)
Avail: CASI HC A03/MF A04

This paper presents the first results in an assessment of the strength, stiffness, and damage tolerance of stiffened wing and fuselage subcomponents. Under this NASA funded program, 10 large wing and fuselage panels, variously fabricated by automated tow placement and dry-stitched preform/resin transfer molding, are to be tested. The first test of an automated tow placement six-longeron fuselage panel under shear load was completed successfully. Using NASTRAN finite-element analysis the stiffness of the panel in the linear range prior to buckling was predicted within 3.5 percent. A nonlinear analysis predicted the buckling load within 10 percent and final failure load within 6 percent. The first test of a resin transfer molding six-stringer wing panel under compression was also completed. The panel failed unexpectedly in buckling because of inadequate

supporting structure. The average strain was 0.43 percent with a line load of 20.3 kips per inch of width. This strain still exceeds the design allowable strains. Also, the stringers did not debond before failure, which is in contrast to the general behavior of unstitched panels. Author

N95-29124# Stanford Univ., CA.
COMPOSITE MATERIAL STUDIES FOR LOW TEMPERATURE THERMIONIC EMISSION Final Report, 1 May 1992 - 31 Dec. 1993
Clayton W. Bates, Jr. 26 May 1994 3 p
(Contract F49620-92-J-0361)
(AD-A292159; AFOSR-95-0112TR) Avail: CASI HC A02/MF A01

The primary objectives of this project were to prepare and measure the photoemissive properties of metal-semiconductor inhomogeneous composite systems for use as low temperature thermionic emitters. The system investigated in this study was Au-CuInSe2 where the Au was in the form of particles 5-50 nm in size dispersed throughout p-type CuInSe2. Much like oxide-coated cathodes the surface of this composite must be treated in order to reduce the barrier to emission of electrons. If the electron affinity of the semiconductor is made close to zero or negative by appropriate surface treatments one has a system with an electron thermal energy barrier of 1 eV at room temperature. DTIC

N95-29133*# Battelle Memorial Inst., Columbus, OH.
IN-PHASE THERMOMECHANICAL FATIGUE MECHANISMS IN AN UNIDIRECTIONAL SCS-6/Ti 15-3 MMC Final Report
Golam M. Newaz and Bhaskar S. Majumdar (Universal Energy Systems, Inc., Dayton, OH.) Cleveland, OH NASA Jun. 1995 67 p
(Contract NAS3-26822; RTOP 505-63-12)
(NASA-CR-195482; E-9716; NAS 1.26:195482) Avail: CASI HC A04/MF A01

The objective of this investigation was to identify the inelastic deformation and damage mechanisms under in-phase (IP) thermomechanical fatigue (TMF) in a unidirectional SCS-6/Ti 15-3 metal matrix composite (MMC). Load-controlled IP TMF tests were conducted at 300-538 C at various stress ranges in high-purity argon. A major emphasis of this work was to identify damage mechanism well before final fracture of specimens, rather than to generate life diagrams, to aid development of a realistic deformation/damage and life model. Author

N95-29136# Army Research Lab., Watertown, MA. Materials Directorate.
FABRICATION AND CHARACTERIZATION OF BARIUM STRONTIUM TITANATE AND NON-FERROELECTRIC OXIDE COMPOSITES
E. Ngo, S. Stowell, L. C. Sengupta, M. E. ODay, and R. Lancto Dec. 1994 13 p
(AD-A289994; ARL-TR-657) Avail: CASI HC A03/MF A01

Various composites of BSTO combined with other nonelectrically active oxide ceramics have been formulated. In general, the composites have adjustable electronic properties which can be tailored for use in various electronic devices. Two applications which are of interest in regard to the composites being discussed here are phased array antennas and capacitor-varistor monolithic devices. For the phased array antennas, these properties include reduced dielectric constants, epsilon', where epsilon equals epsilon' - i epsilon'', and loss tangents, tan delta. The reduction of the dielectric constant and lowering of the loss tangents reduce the overall impedance mismatch and the insertion loss of the device. In addition, the overall tunability, change in the dielectric constant with applied voltage, is maintained at a sufficiently high level for all dielectric constants of interest. Another application (for one of the composite materials) is a combined capacitor-varistor device. In general, this would be used to protect against spurious voltage surges and voltage transients in electronic microcircuits. The microstructures including grain size and phase analysis have been examined using SEM and x-ray diffraction. DTIC

N95-29169# Johns Hopkins Univ., Baltimore, MD. Center for Nondestructive Evaluation.
ORIGINS OF IMPERFECTIONS IN COMPOSITE MATERIALS Final Report, 30 Sep. 1991 - 29 Sep. 1994
Robert E. Green, Jr. 29 Nov. 1994 55 p
(Grant AF-AFOSR-0437-91)
(AD-A290261; AFOSR-95-0050TR) Avail: CASI HC A04/MF A01

This research applied advanced ultrasonic techniques for detection of the origin of imperfections in composite materials used in aircraft and aerospace structures. Previous work supported by the U.S. Air Force Office of Scientific Research showed that ultrasonic attenuation monitoring proved to be superior to other nondestructive evaluation techniques for detection of early fatigue damage in aluminum alloys used in aircraft construction. In addition ultrasonics is the only technique which affords the possibility of detecting defects from one side of the material. In order to detect microscopic defects, an additional aspect of this work was to optimize acoustic microscopy techniques for detection of the origin of very small imperfections. Included in the techniques used were air-coupled ultrasound to detect the quality of composite prepregs. Because ultrasonic techniques are not capable of measuring residual stress in composite materials a novel micro-photoelastic system was developed for measurement of residual stress in optically translucent ceramic matrix composites. However, ultrasonics could detect manufacturing flaws and micro-porosity in ceramic composites. The overall goal was to identify the origin of imperfections in composite materials used in aircraft and aerospace structures and to optimize ultrasonic nondestructive evaluation techniques for detecting these imperfections. DTIC

N95-29185# Tennessee Univ., Knoxville, TN. Dept. of Engineering Science and Mechanics.
THREE DIMENSIONAL EFFECTS IN FIBER REINFORCED COMPOSITES UNDER COMPRESSION Technical Report, 1 Oct. 1992 - 2 Feb. 1995
S. Xu and Y. J. Weitsman 2 Feb. 1995 27 p
(Contract N00014-90-J-1556)
(AD-A292027; ESM95-2.0-CM) Avail: CASI HC A03/MF A01

This article demonstrates that the stress and displacement fields in composites reinforced by hexagonal fiber arrays differ both qualitatively and quantitatively from results obtained for fiber and matrix layers. The layered representation is a commonly used approximation for analyzing the compressive response of composites. Finite element computational results are presented for the mechanical fields in uni-axially reinforced fibrous composites subjected to compression parallel to the fiber direction. The fibers are assumed to deflect in a shearing mode deformation and both linear and non-linear responses are considered for the matrix material. The results exhibit a pronounced three dimensional character, with significant stress concentrations near the fiber/matrix interfaces and shear stresses(T sub yz) of magnitudes equivalent to those of T(sub xz). All these features are disregarded by the layered model and may account for its inadequacy in predicting compressive failure. DTIC

N95-29189# South Carolina Univ., Columbia, SC.
FIBER OPTIC RAMAN AND MICRO RAMAN MEASUREMENTS OF BONDING AGENTS AT INTERFACE DURING THE CURING PROCESS Final Report, 1992-1994
M. L. Myrick and S. M. Angel Dec. 1994 123 p
(Contract DAAL03-92-G-0316)
(AD-A292042; ARO-30450.5-MS-41P) Avail: CASI HC A06/MF A02

Curing of polymers has been studied with Raman, Surface-enhanced Raman, and Micro-Raman Spectroscopy. Ab initio calculations model compound and multivariate statistics were used to develop understanding of the cure kinetics of epoxies in bulk and interfacial processing. DTIC

N95-29277# Army Research Lab., Watertown, MA. Materials Directorate.
FIRE HARDENING ASSESSMENT (FHA) TECHNOLOGY FOR COMPOSITE SYSTEMS Final Report
Archibald Tewarson Nov. 1994 100 p
(Contract DAAL01-93-M-S403)
(AD-A289964; ARL-CR-178) Avail: CASI HC A05/MF A02

This report describes the application of a Fire Hardening Assessment (FHA) methodology to five composite materials. The results are compared to eight materials previously evaluated under Army contract and also materials examined for the U.S. Navy. The FHA Methodology consists for four tests: (1) ignition, (2) combustion, (3) fire propagation, and (4) flame extinction. The tests are performed in a Flammability Apparatus designed to perform such tests. The test data was used to establish the Critical Heat Flux, Thermal Response Parameter, Fire Propagation Index, Heat Release Rate, Product Generation Parameter, Smoke Damage Parameter, Corrosion Index and Flame Extinction using Halon. The application of these composite materials is primarily for Army armored combat vehicle. DTIC

N95-29326# Rhode Island Univ., Kingston, RI.
GORDON RESEARCH CONFERENCE ON PHYSICAL METALLURGY: MATERIALS BY DESIGN Final Report, 20 Jul. 1993 - 19 Jul. 1994
Jerome B. Cohen 19 Jul. 1994 4 p Held in Plymouth, NH, 2-6 Aug. 1993
(Contract DAAH04-93-G-0264)
(AD-A290519; ARO-31184.1-MS-CF) Avail: CASI HC A01/MF A01

The 1993 Physical Metallurgy Gordon Research Conference on 'Materials by Design' was held 2 - 6 Aug. 1993 at Plymouth State College South, Plymouth NH, with J.B. Cohen and G.B. Olson of Northwestern University as chairmen. Eleven of the twenty-six speakers were from foreign countries, and the nearly 100 total participants showed a similar distribution. Overall, there was a healthy mixture of scientists and engineers from universities, national laboratories, and private industry, including young researchers and graduate students as well as established scientists. The program explored a new relationship between science and engineering tuned to the new responsibilities of the science enterprise in the post-Cold War era. DTIC

N95-29329# Army Research Lab., Watertown, MA. Materials Directorate.
FABRICATION AND CHARACTERIZATION OF BSTO AND NONFERROELECTRIC OXIDE COMPOSITES FOR USE IN PHASED ARRAY ANTENNAS AND OTHER ELECTRONIC DEVICES
L. C. Sengupta, E. Ngo, M. E. ODay, S. Stowell, and R. Lancto Dec. 1994 18 p
(AD-A290070; ARL-TR-652) Avail: CASI HC A03/MF A01

A ceramic ferroelectric phase shifting device has been demonstrated using Ba(1-x)Sr(x)TiO3 (BSTO) ceramics. As a part of an effort to optimize the electronic device performance in the phase shifter, various composites of BSTO combined with other nonelectrically active oxide ceramics have been formulated. In general, the composites have reduced dielectric constants, epsilon', where epsilon = epsilon' = i(epsilon)', and loss tangents, tan delta. The low dielectric constant and low loss tangent reduce the overall impedance mismatch and the insertion loss of the device. In addition, the overall tunability, change in the dielectric constant with applied voltage, is maintained at a relatively high level. The combination of electronic properties of these materials offer substantially higher operating frequencies, 10 GHz and above. Another application for one of the composites is for use as a capacitor-varistor surge protector. The microstructures including grain size and phase analysis have been examined using SEM and X-ray diffraction. The analysis of the phase formation, compositional variations, and grain size will be related to the electronic properties of the materials. DTIC

N95-29337 Akron Univ., Akron, OH.
FIBER-MATRIX ADHESION IN SINGLE-FIBER MODEL COMPOSITES Ph.D. Thesis
Seunghee Yun 1994 148 p
Avail: Univ. Microfilms Order No. DA9425867

A single-fiber fragmentation test is a useful technique to provide a measure of fiber-matrix adhesion. A four-point bending test was used to determine the final fragmentation length for the glass fiber-polycarbonate system. Surface treatment of the glass fiber with a mold release agent decreased the interfacial adhesion and caused an increase in fragment length. Fragment lengths from the four-point bending test were compared with those from a tensile test. Good agreement was obtained from the two tests. The effect of fiber diameter on fragmentation length also was examined. The full fragment length increased linearly with the fiber diameter. Applied forces for a resin droplet adhering to a fiber were calculated in terms of the strain energy release rate G of the fiber-resin interface. Finite element analysis was performed using the ADINA code. Results for the displacement were compared with the experimental results for a silicone rubber sphere adhered to a steel rod. Good agreement was obtained. Force versus displacement relationship of the model fiber composite was non-linear. Therefore, a non-linear fracture mechanics approach was used. Two types of bonding, poor and good, were considered in the present study. The force required to propagate a crack was compared with the values predicted by theory and an empirical method. Good agreement was obtained. Further crack growth required a large force. Thus, in this system the crack propagates in a stable manner. Two different fracture modes were observed in the model. One is adhesive fracture along the interface for poor bonding. In the other fracture mode, for good bonding, both adhesive and cohesive failure occurred competitively along the interface. Calculated results for force versus displacement as a function of vise hole radius gave good agreement with the experimental results. Stiffness decreases as the vise gap increases from 2.1 mm to 3.8 mm. The force required to propagate a crack was predicted by an empirical method at all stages of crack growth and for a range of dimensions. By using the values of pull-out force from several fiber-epoxy microbond tests, values of fracture energy Gc were estimated from the empirical calculation. These values tend to be rather low, i.e., 10-20 J/m(exp 2). Dissert. Abstr.

N95-29374*# National Aeronautics and Space Administration. Marshall Space Flight Center, Huntsville, AL.
PROBABILITY OF DETECTION OF DEFECTS IN COATINGS WITH ELECTRONIC SHEAROGRAPHY
S. S. Russell, M. D. Lansing (Alabama Univ., Huntsville, AL.), C. M. Horton (Alabama Univ., Huntsville, AL.), and W. J. Gnacek (Alabama Univ., Huntsville, AL.) Washington Jun. 1995 22 p
(NASA-TM-108493; NAS 1.15:108493) Avail: CASI HC A03/MF A01

The goal of this research was to utilize statistical methods to evaluate the probability of detection (POD) of defects in coatings using electronic shearography. The coating system utilized in the POD studies was to be the paint system currently utilized on the external casings of the NASA space transportation system reusable solid rocket motor boosters. The population of samples was to be large enough to determine the minimum defect size for 90-percent POD of 95-percent confidence POD on these coatings. Also, the best methods to excite coatings on aerospace components to induce deformations for measurement by electronic shearography were to be determined. Author

N95-29409# Dartmouth Coll., Hanover, NH. Thayer School of Engineering.
MEASUREMENT OF INTERFACE STRENGTH, INTRINSIC TOUGHNESS AND THEIR DEPENDENCE ON INTERFACIAL SEGREGANTS Final Report, 31 Mar. 1991 - 15 Sep. 1994
Vijay Guptia 26 Dec. 1994 44 p
(Contract DAAL03-91-G-0059)
(AD-A291798; ARO-28480.17-MS) Avail: CASI HC A03/MF A01

This report discusses a novel laser spallation technique for measuring the tensile strength of planar thin film interfaces. In this technique, a laser-produced compressive stress pulse in the substrate, reflecting from the coating's free surface pulls the interface in tension and leads to its failure if the tensile amplitude is high enough. The interface stress is determined by recording the coating or substrate free-surface velocities using a Doppler interferometer. Interface strengths of several metal/ceramic, ceramic-ceramic and ceramic/polymer systems are summarized from our recent efforts. In addition, two breakthroughs, the first of a novel interferometer to record velocities from rough surfaces and the second of a technique to produce subnanosecond rise-time stress pulses with no asymptotic post-peak decay, are discussed which further allows the technique to be applied to rough thermal spray coatings and also to films as thin as 0.1 um. This technique is used to establish a fundamental strength-structure chemistry relationship for Nb/sapphire interfaces, with and without the interlayers of Cr and Sb. This allows the interface strengths to be controlled over a wide range, as required for realizing the strategy of deflecting impinging matrix cracks along the fiber/matrix interfaces so as to impart toughness in otherwise brittle composites. The required values of fiber/matrix interface toughness needed for crack deflection were obtained by using the method of dual singular integral equations. Finally, in a separate study, the short stress pulses are used to determine the dynamic response of laminates, and preliminary results are presented that show their potential in evaluating the damage in composites in a nondestructive mode. DTIC

N95-29411 Arizona State Univ., Tempe, AZ.
ANALYTICAL AND EXPERIMENTAL STUDIES OF THE ENERGY ABSORPTION BEHAVIOR OF COMPOSITE STRUCTURES Ph.D. Thesis
Akif Oksal Bolukbasi 1993 139 p
Avail: Univ. Microfilms Order No. DA9410941

Analytical and experimental investigations were performed to investigate the energy absorption behavior of composite structural elements. The experimental studies consisted of crush tests of flat plate and stiffener specimens. In addition to the crush tests, double cantilever beam (DCB) and end notched flexure (ENF) tests were also conducted to determine

the fracture toughness properties of the T650-35/F584 plain weave graphite/epoxy fabric material and to provide additional validation to the analysis models. All flat plate and stiffeners, except the stiffeners with the (45) sub 5 layup, crushed in a lamina bending mode. The specific sustained crushing stress (SSCS) for all stiffeners showed an increase with increasing number of zero-degree plies in the laminate. The SSCS for all stiffeners were also lower than the SSCS for flat plate specimens with identical layups. The failure initiator, in the form of a 0.010-in. chamfer machined at one end of all crush specimens was very effective. The nonlinear finite element analyses performed were able to predict the fundamental failure mechanisms during the sustained crushing phase of the energy absorption process as observed during the experimental studies. Friction between the sublaminates and the crush surface has been identified as a major contributor to the energy absorption process of composite structural elements. A parametric study conducted with different friction coefficients has identified up to fifty percent increase in the energy absorption capability when the specimen crushes on a rough rather than a smooth surface. A semi-empirical analysis methodology to predict the energy absorption capability of composite stiffeners was also developed. The predicted energy absorption capability was within three percent of the stiffener crush test results. Therefore, the semi-empirical analysis methodology along with flat plate crush test data can potentially be used to eliminate or reduce costly fabrication and crush testing of actual composite structural elements. Dissert. Abstr.

N95-29476# Asian Office of Aerospace Research and Development, APO San Francisco, CA. Air Force Office of Scientific Research.
CENTER FOR ADVANCED AEROSPACE MATERIALS (CAAM), SEOUL NATIONAL UNIVERSITY, 29 JUNE 1994
P. McQuay 29 Jun. 1994 5 p
(AD-A292344; AOARD-TR-94-27) Avail: CASI HC A01/MF A01

This report summarizes discussions held with eight members of the newly organized Center for Advanced Aerospace Materials, which is supported by the Korea Science and Engineering Foundation. Although the majority of projects at the center do fall under the broad category of aerospace materials, some of the work is also aimed at the application of traditional aerospace materials to automotive and other applications. The largest amount of research is based on Al alloys such as the 7000 series, Al-Li alloys, and Rs Al alloys. Of note among this work is a high strength and weldable Mn-modified Al-Zn-Mg alloy which is being developed for commercialization. Other work of interest includes elemental PM-based gamma Ti-Al alloys, AlN fibers, whiskers and foams produced by SHS, and theoretical advancements in SPF. DTIC

N95-29492# New York State Coll. of Ceramics, Alfred, NY.
BILATERAL US/RUSSIA WORKSHOP ON SELF-PROPAGATING HIGH-TEMPERATURE SYNTHESIS HELD IN HONOLULU, HAWAII ON 6-7 NOVEMBER 1993
Gregory C. Stangle and Richard M. Spriggs 15 Dec. 1994 20 p
(Contract DAAH04-93-G-0515)
(AD-A290466; ARO-32561.1-MS-CF) Avail: CASI HC A03/MF A01

This report summarizes the ARO- and NSF-sponsored 'Biiateral US/Russian Workshop on Self-Propagating High-Temperature Synthesis' that was held on November 6-7, 1993, in Honolulu, Hawaii. The workshop focused on the fundamental as well the applied aspects of the self-propagating high-temperature synthesis (SHS) process. The goal of the discussion of the fundamental topics was to identify-and suggest approaches to remedy-the generally acknowledged gaps that exist in our detailed, quantitative understanding of the essential chemistry and physics of the SHS process. The goal of the discussion of he applied topics was to focus on the rather more practical aspects of the SHS process, in order to help prioritize our fundamental studies in such a way that our enhanced understanding leads to improved SHS-based advanced materials fabrication methods. The two topic areas are of course interrelated: Fundamental studies can enhance commercialization potential, and technological, market-driven needs can suggest important fundamental, science-driven studies. The workshop also allowed many of the world's key, presently active SHS researchers to: (1) discuss the state-of-the-art, and remaining work, of SHS research; and (2) initiate meaningful collaborative research projects between US and Russian scientists. DTIC

N95-29512 Maryland Univ., College Park, MD.
A THREE DIMENSIONAL FINITE ELEMENT SCHEME FOR FIBER MICROBUCKLING IN THICK MULTIDIRECTIONAL LAMINATED COMPOSITES Ph.D. Thesis
Ming-Huei Chen 1993 175 p
Avail: Univ. Microfilms Order No. DA9425008

A three-dimensional finite element scheme with enhanced displacement functions has been established to analyze fiber microbuckling failures under compressive loads in thick unidirectional and multidirectional laminated composites. The purpose of this model is to overcome the deficiencies of existing two-dimensional closed-form analytical models. New displacement functions and constraint schemes are proposed for predictions of either the symmetric (or extensional) microbuckling mode found in composites with low fiber volume fraction, or the antisymmetric (or shear) mode which occurs at higher fiber volume fraction. From analytical considerations, microbuckling is considered only in the plane of the lamina. This model is utilized to examine the three-dimensional nature of fiber microbuckling deformations in thick, arbitrarily laminated composites. As expected, a critical wavelength and a corresponding minimum critical microbuckling strength are found for the symmetric mode in unidirectional laminates. Timoshenko beam theory is verified to lower the microbuckling strength only by 3 percent compared to Bernoulli-Euler beam theory. Parametric studies show a weaker dependence on fiber volume fraction than predicted by popular closed-form two dimensional models. Excellent agreement is found between the present model and experimental data for fiber volume fraction equal to 0.046. For the antisymmetric mode in unidirectional laminates, Timoshenko beam theory is chosen due to the influence of matrix shear deformation on the fiber deformation. The microbuckling strength monotonically decreases with increasing wavelength and is more strongly dependent on wavelength and on fiber volume fraction than predicted by two-dimensional models. Good agreement is found with experimental data for fiber volume fractions less than 0.6. Consideration of the antisymmetric mode in multidirectional laminates of 60 percent fiber volume fraction and lamination sequence ((alpha(sub 2)/0(sub n)) sub s) sub l shows ply thickness and lamination sequence to have a distinct influence on the critical buckling strength. Alpha indicates the fiber angle and l denotes that this unit is repeated many times in a thick laminate. The((45(sub 2)/0(sub 2)) sub s) sub l laminate provides the maximum buckling strength among the modeled laminates because this angle-ply lamina has the greatest in-plane shear modulus. In the eta-ply laminate with stacking sequence ((alpha (sub m)/0(sub n-m)) sub s) sub l the microbuckling strength is found to increase with increasing m. Dissert. Abstr.

N95-29513 Virginia Polytechnic Inst. and State Univ., Blacksburg, VA.
FIBER FRACTURE IN CONTINUOUS-FIBER REINFORCED COMPOSITE MATERIALS DURING CYCLIC LOADING Ph.D. Thesis
Ahmad Razvan 1992 116 p
Avail: Univ. Microfilms Order No. DA9425592

The final tensile fracture of any composite structure is primarily due to the failure of its constituents, namely fibers and matrix in the present case. To date, no experimental data exists, to the author's knowledge, to define the behavior of constitutive fibers of a composite structure throughout its life span. The prime candidate for a fiber based investigation is unidirectional zero-degree composite coupons. But unidirectional coupons do not demonstrate any significant loss of stiffness during fatigue cycling compared to other lay-ups. Even if stiffness degradation was significant, due to the nature of damage in this material system it would be impossible, practically, to monitor that change using conventional techniques (e.g. an extensometer) because the damage and failure process destroys the integrity of the contact between those devices and the material, under cyclic conditions. This investigation presents the findings of a fiber-based investigation of unidirectional composite material systems. In particular, a unidirectional graphite/epoxy system was studied, and the influence of applied load level on fiber fractures, and their influence on damage growth documented. A damage monitoring technique (patent pending) was developed to accurately record the state of damage in this material system without the usage or extensometers or strain gages. Following this method, two new damage norms were introduced, namely, 'percent phase damage' and 'percent gain damage'. Fiber fracture, strength degradation, and the life of unidirectional specimens were investigated and recorded as a function of various load levels. Fiber fracture, in general, showed no definitive

growth pattern during fatigue cycling. It appears that the majority of the broken fibers that occur over nearly 90 percent of the life are due to the initial applied load cycle. This is one of the key findings of this investigation. 'Proof testing' which is a common practice in industry for 'verifying' the integrity of a structure, could very well be causing significant subsequent reductions in life. With these findings as a base, it is now possible to postulate the first well-founded mechanistic model of fiber-dominated fatigue degradation under tensile loading. Dissert. Abstr.

N95-29533# Asian Office of Aerospace Research and Development, APO San Francisco, CA. Air Force Office of Scientific Research.

NIPPON STEEL RESEARCH LABORATORIES, FUTTSU, 28 FEBRUARY 1994. AND ADVANCED MATERIALS AND TECHNOLOGY RESEARCH LABORATORIES, KAWASAKI, 15 JUNE 1994

P. McQuay 15 Jun. 1994 8 p

(AD-A292346; AOARD-TR-94-16) Avail: CASI HC A02/MF A01

Visits were paid to two of Nippon Steel's premier research laboratories: Steel Research and Advance Materials and Technology Research. The main focus of the visits were titanium, titanium-aluminide, and carbon-based materials development at Nippon Steel, all areas in which Nippon Steel is trying to develop new products and markets. In particular, Nippon Steel has been somewhat successful in marketing Ti as a structural and functional material in new non-aerospace markets such as construction and consumer goods. They have also placed emphasis on the automotive markets, but so far have met only limited success. Their penetration into the high performance aerospace Ti alloys markets have been very limited. Research and development efforts in new self-lubricating materials and functionally gradient materials technologies are also reviewed. DTIC

N95-29549 Massachusetts Inst. of Tech., Cambridge, MA.

IMPACT RESISTANCE AND DAMAGE TOLERANCE OF COMPOSITE SANDWICH PANELS Ph.D. Thesis

Pui Ho Wilson Tsang 1994

Avail: Issuing Activity (MIT Libraries, Rm. 14-0551, Cambridge, MA 02139-4307)

Work was conducted to better understand the damage created in sandwich panels subjected to indentation/impact loading and the subsequent failure process under compressive loads. Three different damage states were created by indenting sandwich panels to a 3 mm indentation depth with indentors of three different diameters: 12.7 mm, 25.4 mm, and 38.1 mm. The sandwich panels were 89 mm wide and 356 mm long with (0/90) and (+/-45) facesheets made from AW193/3501-6 graphite/epoxy plain weave fabric. The Nomex honeycomb core has a density of 48 kg/m3, a thickness of 25.4 mm, and a cell size of 3.2 mm. The damage states were characterized by various techniques in terms of geometric facesheet damage (shape of permanent dimple as a result of indentation), material facesheet damage (fiber damage, delaminations, and matrix cracks), and core damage (buckled/crushed cell walls). Damage inspection shows that the permanent dimple is deeper, more localized, and contains more extensive material facesheet damage for the smaller indentor diameter. Based on the damage characterization results, specimens with simulated damage types were designed and manufactured to separately model the core damage and geometric facesheet damage (simulated core damage) and the material facesheet damage (simulated facesheet damage) observed in the indented specimen. Uniaxial compression tests were conducted to failure and monitored with the shadow moire method to obtain quantitative measurements of the out-of-plane deformation of the dimple. The failure mechanism of specimens with simulated core damage and those with static indentation damage is via dimple propagation primarily perpendicular to the loading direction, followed by catastrophic failure in the form of facesheet fracture across the width of the specimens. The dimple propagation is driven by load redistribution in the presence of out-of-plane eccentricity (i.e. the dimple), a combination which causes local bending of the facesheet and progressive core crushing perpendicular to the loading direction. Material facesheet damage and nonlinear stress-strain behavior of the (+/-45) facesheets cause a local reduction in facesheet stiffness which induces more severe load redistribution and, hence, greater rates of dimple propagation. Such local reduction in facesheet stiffness needs to be included in the dimple propagation model to improve the predictions for specimens with material facesheet damage and/or (+45) facesheets. The final failure in specimens with static indentation damage and simulated core damage is caused by high longitudinal stress due to load redistribution in the facesheet within the dimple. The applied stress levels at which the calculated peak longitudinal membrane stress along the centerline through the dimple and perpendicular to the loading direction reaches the compressive strength of the corresponding undamaged specimens correlates well with the residual strengths of specimens with (0/90) facesheets and simulated core damage. Dissert. Abstr.

N95-29561# Purdue Univ., West Lafayette, IN. School of Aeronautics and Astronautics.

HIGH VELOCITY IMPACT AND PENETRATION OF THICK COMPOSITE LAMINATES Final Report

C. T. Sun 26 Oct. 1994 10 p

(Contract DAAL03-91-G-0013)

(AD-A290642; ARO-28307.7-EG) Avail: CASI HC A02/MF A01

Ballistic impact of thick-section composites is an extremely complex technical problem. In this research project we have introduced a new approach in using the quasi-static punch curve to describe the mechanics of penetration. Using this punch curve, we are able to capture the mechanical characteristics of penetration and avoid modeling the untractable damage progression in the target during penetration. DTIC

N95-29597 Columbia Univ., New York, NY.

INTERLAMINAR FRACTURE MECHANICS AND MECHANISMS: LINEAR AND NONLINEAR ASPECTS Ph.D. Thesis

Kaspal Reddy Thumma 1994 163 p

Avail: Univ. Microfilms Order No. DA9421411

A lack of adequate understanding of the mechanics and mechanisms of the delamination fracture of laminated composites is a serious obstacle to the damage-tolerant design of components and structures using these materials. This investigation aims at extending this understanding by developing experimental methods to study interlaminar fracture toughness, G(IC) and nonlinear and time dependent behavior of interlaminar crack growth using graphite/epoxy laminated composite. Two major approaches were pursued to achieve this aim: (1) a comparative study of methods of determining G(IC) with attention to the rate of crack growth and to models for data reduction, using double cantilever beam (DCB) specimens; and (2) development of a novel experimental technique to excite high amplitude flexural vibrations of 22.5 kHz in the jaws of DCB specimen and to detect signals from the crack tip. In the first approach, the G(IC) values show crack length dependency at the initial stages of the crack growth, possibly due to variations in precracking processes. The values of G(IC) are only moderately affected by the choice of data reduction model or by specimen thickness. However lower strain rates yielded higher G(IC) values indicating time dependent behavior. The load-deflection plots of DCB tests show some nonlinearity and also slight hysteresis. In the second approach, at high amplitude of vibrations, nonlinear (amplitude dependent) damping in the system and harmonic generation with up to five harmonics in the strain signals on either side of the crack tip were observed. Possible models for explaining this behavior are discussed considering lattice anharmonicity, dislocations in graphite fibers, dispirations in epoxy matrix, crack as dislocation pileup, microcracks, stress field around graphite fibers and damage zone at crack tip. At amplitudes of vibration of sufficient magnitude to cause permanent change at the crack tip, spikes of acoustic emission were observed superimposed on the strain signals from ahead of the crack tip. Models of microcrack opening and closing and discontinuous microcrack growth are proposed to explain these spikes. The harmonic generation and the acoustic emission are a promising technique for the investigation of interlaminar fracture mechanisms and possibly for nondestructive testing. Dissert. Abstr.

N95-29598 Civil Engineering Research Foundation, Washington, DC.

MATERIALS FOR TOMORROW'S INFRASTRUCTURE: A TEN-YEAR PLAN FOR DEPLOYING HIGH-PERFORMANCE CONSTRUCTION MATERIALS AND SYSTEMS

Richard A. Belle and Kathleen H. Almand American Society of Civil Engineers 27 Dec. 1994 159 p Limited Reproducibility: More than 20% of this document may be affected by microfiche quality

(AD-A289782; CERF-94-5011; ISBN-0-7844-0059-8; LC-94-31335) Avail: Issuing Activity (Defense Technical Information Center (DTIC))

This report presents a detailed program to transform our nation's infrastructure. The Intended audience Is the Administration and Congress, other national policy makers, and government and industry leaders.

Descriptions of major high-performance research and commercialization projects are provided by working groups representing ten different materials: aluminum, coatings, fiber-reinforced polymer composites, concrete, hot mix asphalt, masonry, roofing materials, smart material devices and monitoring systems, steel, and wood. The report builds on the 1991 National Civil Engineering Research Needs Forum organized by the Civil Engineering Research Foundation (CERF) and the 1993 initial program plan as presented in High-Performonce Construction Materials and Systems: An Essential Program for America and its infrastructure. The high-performance CONstruction MATerials and systems program (CONMAT) will create significant improvements in the nation's infrastructure and U.S. competitiveness in the construction market. The report concludes by reviewing the strong support that the Administration has shown the CONMAT research effort to date and recommends continued support from government, industry, and academia to support this critical initiative. DTIC

N95-29638# Naval Surface Warfare Center, Silver Spring, MD.
USE OF FINITE ELEMENT ANALYSIS FOR TRANSIENT MOISTURE DIFFUSION STUDIES IN MULTILAYER COMPOSITE AEM/S SYSTEM SANDWICH MATERIALS
Joseph M. Augi 1 Nov. 1994 90 p
(AD-A291092; CARDIVNSWC/TR-94/019) Avail: CASI HC A05/MF A01

The NISA II finite element analysis transient heat transfer code was adapted to study the sorption and internal moisture distribution in two groups of sandwich panels being considered for use in Navy shipboard structures. Using a suitable conversion of the material input parameters and time units, this heat transfer code can be used for diffusion calculations. Analysis was performed on two groups of test panels. For the first group, a simple, one-dimensional finite element model was adequate for testing material panels proposed for the Advanced Enclosed Mast/Sensor (AEM/S) System. A second group of panels was analyzed to determine the best approach for accelerated moisture conditioning. One-, two- and three-dimensional diffusion models were used in the calculations. Results indicate only the three dimensional model is acceptable and that a substantial time saving for preparing such test panels is attained if panel components can be saturated before they are bonded together to form the final sandwich. In such cases, it would be desirable to use room temperature curing adhesives to prevent partial moisture desorption. DTIC

N95-29732# Texas Univ., Austin, TX.
SOLID FREEFORM FABRICATION SYMPOSIUM
Harris L. Marcus, Joseph J. Beaman, Joel W. Barlow, David L. Bourell, and Richard H. Crawford Sep. 1994 439 p Symposium held in Austin, TX, 8-10 Aug. 1994
(AD-A290949) Avail: CASI HC A19/MF A04

Solid freeform fabrication (SFF) as an important and totally integrated approach to design, materials processing, and manufacturing research results related to it is contained in this proceedings of the SFF Symposium. SFF topics covered in the symposium include: machine design; computer sectioning; reverse engineering; materials processing: metals, ceramics, polymers, waxes, and composites; and applications. DTIC

N95-29758# Air Force Inst. of Tech., Wright-Patterson AFB, OH.
INVESTIGATION OF TENSION-COMPRESSION FATIGUE BEHAVIOR OF A UNIDIRECTIONAL METAL MATRIX COMPOSITE AT ELEVATED TEMPERATURE M.S. Thesis
Darren L. Kraabel Dec. 1994 101 p
(AD-A289394; AFIT/GAE/ENY/94D-6) Avail: CASI HC A06/MF A02

This study investigated the fatigue behavior in a unidirectional metal matrix composite under tension-compression loading conditions. Stress-strain responses, modulus, and strain trends were monitored to characterize damage. Fractography and microscopy were used to characterize failure modes. Fatigue life curves were plotted base on different parameters such as stress and strain. Tension-compression fatigue life was shorter than that obtained under tension-tension fatigue cycling. Creep, observed in tension-tension fatigue cycling, and the effects of the compressive load on the plastic zone around the crack tip explain shorter life under tension-compression fatigue loading. DTIC

N95-29763# Illinois Univ., Chicago, IL. Dept. of Civil and Materials Engineering.
THE STROH FORMALISM FOR ANISOTROPIC ELASTICITY WITH APPLICATIONS TO COMPOSITE MATERIALS Final Report, 15 Jun. 1991 - 14 Jun. 1994
T. C. T. Ting 6 Oct. 1994 5 p
(Contract DAAL03-91-G-0082)
(AD-A290710; ARO-28606.9-MA) Avail: CASI HC A01/MF A01

Ten papers which have been published under this research project are listed and important findings are outlined. Potential applications to composite materials are indicated. Anisotropic elasticity has been an active research topic since the need of high strength, light weight composites in the aerospace industry became apparent. A composite material consists of two or more materials that are in general anisotropic. We have extended the Stroh formalism by presenting new identities and sum rules that allow one to convert a complex form expression into a real form. Using these identities and sum rules previously unsolved problems are solved and solutions that are available but are in a complex form are converted into a real form. Derived from text

N95-29770# Air Force Inst. of Tech., Wright-Patterson AFB, OH.
INVESTIGATION OF TENSION-COMPRESSION FATIGUE BEHAVIOR OF A NOTCHED CROSS-PLY METAL MATRIX COMPOSITE AT ELEVATED TEMPERATURE M.S. Thesis
Matthew W. Yocum Dec. 1994 148 p Limited Reproducibility: Document partially illegible
(AD-A291479; AFIT/GAE/ENY/94D-8) Avail: CASI HC A07/MF A02

This research extends the existing knowledge of MMC (metal matrix composite) fatigue damage mechanisms by studying the tension-compression fatigue behavior of a notched cross-ply laminate MMC at elevated temperature. A (0/90)25 SCS-6/Ti-15-3 laminate with a center hole was subjected to tension-compression fatigue at 427 C (800 F). Stress and strain data was taken to evaluate macro-mechanic behavior of the material. Microscopy and fractography were performed to characterize the damage on a micro-mechanical level. Crack initiation and progression was monitored using acetate face replicas. Four cracks were found to develop around the periphery of the hole, two of which became dominant and proceeded through to the end of the specimen. On a maximum applied stress basis, tension-compression notched specimens had shorter fatigue lives than tension-tension notched specimens. Also, tension-compression adds more damage due to the compressive portion of the loading, and tension-compression loading increased the time to crack initiation for a given maximum stress and increased the rate of crack propagation over tension-tension cases. DTIC

N95-29825*# National Aeronautics and Space Administration. Langley Research Center, Hampton, VA.
SIMPLIFIED DATA REDUCTION METHODS FOR THE ECT TEST FOR MODE 3 INTERLAMINAR FRACTURE TOUGHNESS
Jian Li and T. Kevin OBrien (Army Research Lab., Hampton, VA.) May 1995 22 p
(RTOP 505-63-50-04)
(NASA-TM-110176; NAS 1.15:110176; ARL-MR-234) Avail: CASI HC A03/MF A01

Simplified expressions for the parameter controlling the load point compliance and strain energy release rate were obtained for the Edge Crack Torsion (ECT) specimen for mode 3 interlaminar fracture toughness. Data reduction methods for mode 3 toughness based on the present analysis are proposed. The effect of the transverse shear modulus, G(sub 23), on mode 3 interlaminar fracture toughness characterization was evaluated. Parameters influenced by the transverse shear modulus were identified. Analytical results indicate that a higher value of G(sub 23) results in a low load point compliance and lower mode 3 toughness estimation. The effect of G(sub 23) on the mode 3 toughness using the ECT specimen is negligible when an appropriate initial delamination length is chosen. A conservative estimation of mode 3 toughness can be obtained by assuming G(sub 23) = G(sub 12) for any initial delamination length. Author

N95-29842# Florida Univ., Gainesville, FL. Dept. of Materials Science and Engineering.
INNOVATIVE PROCESSING OF COMPOSITES FOR ULTRA-HIGH TEMPERATURE APPLICATIONS, BOOK 1 Final Report

Reza Abbaschian Sep. 1994 78 p
(Contract N00014-91-J-4075)
(AD-A290889) Avail: CASI HC A05/MF A01

Processing and Properties of Silicon Carbide Fibers; Processing of Mullite Composite Fibers; Chemical Vapor Deposition (CVD) and Chemical Vapor Infiltration (CVI) are described is this report. DTIC

N95-29864# Kentucky Univ., Lexington, KY.
DEVELOPMENT OF 'SMART' PIEZOTHERMOELASTIC LAMINAE: THEORY AND APPLICATIONS Final Report, Mar. 1991 - Aug. 1994
H. S. Tzou, T. R. Tauchert, and G. E. Blandford 30 Oct. 1994 31 p
(Contract DAAL03-91-G-0065)
(AD-A290852; ARO-28754.30-EG-SM) Avail: CASI HC A03/MF A01

Active 'smart' structures with self-sensation, action and reaction capabilities can lead to a major technology breakthrough for the next-generation high-performance structures and mechanical systems. This new emerging area encompassing sensors, actuators, electromechanical systems, active materials, controls, and structural continual can be defined as the structure-electronics - StrucTronics. Among the commonly used sensor/actuator materials, piezoelectric materials possess unique electromechanical properties (the direct and converse piezoelectric effects which can be respectively applied to sensor and actuator applications. The main objective of this research is to study the multi-field piezothermoelastic phenomena of piezoelectric laminae and to investigate the thermal effects to the performance of distributed piezoelectric sensors and actuators. There are three research components: (1) to develop new generic piezothermoelastic shell lamination theories, (2) to formulate piezothermoelastic finite elements and associated sensing/control numerical capabilities, and (3) to validate analytical and/or finite element solutions via laboratory experiments. This report includes all three aspects of the piezothermoelastic research. As described in the standard ARO Report Instructions, this report begins with Statement of Problems Studied, and followed by Summary of Research Results. Lists of technical publications and participating personnel are also provided. DTIC

N95-29923# University of Southern California, University Park, CA. Dept. of Materials Science.
CHEMICALLY INDUCED PASSIVITY OF ALUMINUM ALLOYS AND Al-BASED METAL MATRIX COMPOSITES Final Report, 1 Oct. 1990 - 30 Sep. 1994
Florian Mansfeld and Y. Wang Jan. 1995 66 p
(Contract N00014-91-J-1041)
(AD-A290778) Avail: CASI HC A04/MF A01

The concept of surface modification has been applied for corrosion protection of commercial aluminum alloys such as Al 2024, Al 6013, Al 6061 and Al 7075. The goal of this project was to develop methods of corrosion protection which do not use toxic chemicals. The Ce-Mo process consisting of immersion in hot solutions of CeC13 and Ce(N03)3 followed by anodic polarization in a molybdate solution has produced surfaces with exceptional resistance to localized corrosion for Al 6013 and 6061. Surface modified samples did not pit during exposure to 0.5 M NaCl for 30 days. For Al 2024 and Al 7075 it was found that a copper removal pretreatment step was necessary for complete corrosion protection. For Al 2024 replacement of CeCl3 by Ce acetate produced optimum results. Surface analysis showed that both Ce and Mo are incorporated in the modified surface layers. For Al 7075 it was found that increase concentrations of Ce and Mo occur at sites where Cu-containing particles are located. It is assumed that the exceptional corrosion resistance is in part due to elimination of local cathodes during the Ce-Mo process. Anodic polarization curves for Al 2024 and Al 7075 showed that the pitting potential E(pit) was increased after surface modification, while the corrosion potential E(corr) remained constant. Apparently the amount of adsorbed Cl(-) at a given potential is reduced in the presence of negatively charged Mo species in the modified surface layers. DTIC

N95-30028*# National Aeronautics and Space Administration. Langley Research Center, Hampton, VA.
ANALYTICAL INVESTIGATION OF THE HYGROTHERMAL EFFECTS AND PARAMETRIC STUDY OF THE EDGE CRACK TORSION (ECT) MODE 3 TEST LAY-UPS
Jian Li and T. Kevin OBrien (Army Research Lab., Hampton, VA.) Jun. 1995 38 p
(RTOP 505-63-50-04)
(NASA-TM-110183; NAS 1.15:110183; ARL-TR-807) Avail: CASI HC A03/MF A01

A shear deformation theory including residual thermal and moisture effects is developed for the analysis of either symmetric or unsymmetric laminates with mid-plane edge delamination under torsion loading. The theory is based on an assumed displacement field which includes shear deformation. The governing equations and boundary conditions are obtained from the principle of virtual work. The analysis of the (90/(+/- 45)(n)/(-/+ 45)(n)/90)(s) ECT mode 3 test lay-up indicates that there are no hygrothermal effects on the mode 3 strain energy release rate because the laminate, and both sublaminates above and below the delamination, are symmetric lay-ups. A further parametric study reveals that some other lay-ups can have negligible hygrothermal effects even when the sublaminates above and below the delamination are not symmetric about their own mid-planes. However, these lay-ups may suffer from distortion after the curing process. Another interesting set of lay-ups investigated is a class of antisymmetric laminates with (+/-(theta/(theta -90)(2)/theta))(n) lay-ups. It is observed that when n takes on even numbers (2 and 4), both hygrothermal and mode 1 effects can be neglected. From this point of view, these lay-ups provide a way to determine the mode 3 toughness between two dissimilar layers. However, when n takes on odd numbers (1 and 3), both hygrothermal and mode 1 effects may be strong in these lay-ups. In particular, when theta equals 45 deg, the lay-ups are free from both hygrothermal and mode 1 effects irrespective of n. Author

N95-30037# Oak Ridge National Lab., TN.
PROCESSING AND PROPERTIES OF EXTRUDED TUNGSTEN-HAFNIUM AND TUNGSTEN-STEEL COMPOSITES
E. K. Ohriner, V. K. Sikka, and D. Kapoor (Army Armament Research, Development and Engineering Center, Picatinny Arsenal, NJ.) 1995 8 p Presented at the 1994 International Conference on Tungsten and Refractory Metals, McLean, VA, 17-19 Oct. 1994
(Contract DE-AC05-84OR-21400)
(DE95-007371; CONF-9410213-6) Avail: CASI HC A02/MF A01

The purpose of this study was to evaluate the processing behavior and properties of tungsten-hafnium (W-Hf) and W-steel composites produced by hot extrusion of canned powders. The W-Hf composite was consolidated by extrusion of blended powders with preheat temperatures over the temperature range of 1100 to 1400 C. All extrusions produced fully dense material which exhibits elongation of the tungsten phase within the hafnium matrix. The flow stress, as characterized by the extrusion constant, decreases with increasing temperature up to 1300 C and increases substantially at 1400 C as significant quantities of intermetallic phase are formed during preheating. The room-temperature (RT) hardness and compressive yield stress increase modestly with increased extrusion ratio and are not affected by extrusion temperature in the range 1100 to 1300 C. The microstructures are essentially fully recrystallized at the 1300 C preheat temperature and partially recrystallized at lower temperatures. Additionally, a mixture of tungsten and steel powder was consolidated to full density by hot extrusion at a 1000 C preheat temperature and a reduction ratio of 4.2. Increased reduction of the W-steel composite results in increased RT hardness. DOE

N95-30175# Oak Ridge National Lab., TN.
ELEVATED TEMPERATURE STATIC FATIGUE OF A NICALON FIBER-REINFORCED SiC COMPOSITE
H. T. Lin, P. F. Becher, and P. F. Tortorelli 1994 6 p Presented at the 1994 Fall Meeting of the Materials Research Society (MRS), Boston, MA, 28 Nov. - 2 Dec. 1994
(Contract DE-AC05-84OR-21400)
(DE95-008780; CONF-941144-95) Avail: CASI HC A02/MF A01

Static fatigue tests of a Nicalon fiber-reinforced SiC matrix composite were conducted in four-point bending over a temperature range of 425 to 1,150 C in air at selected stress levels. The composite consisted of a Nicalon cloth with a 0.3 micro m graphite interfacial coating and a Forced Chemical Vapor Infiltration (FCVI) SiC matrix composite; samples were tested with or without a final protective SiC seal coat. The results indicated that the fatigue life of the Nicalon-SiC composite decreased with an increase in either applied stresses or test temperatures. However, the composite exhibited a fatigue limit of approximately 100 MPa at temperatures less than 950 C which decreased to approximately 70 MPa at 1,150 C. Both

electron microscopy and thermogravimetric studies suggested that the lifetime of the composites was dictated by the oxidation of graphite interfacial layer at temperatures less than or equal 700 C and by oxidation of graphite coating accompanied by formation of silicate interfacial layer via oxidation of the Nicalon fiber (and the SiC matrix) at temperatures greater than or equal 950 C. Use of a SiC seal coat effectively retarded the oxidation reactions and increased the lifetime by at least one order of magnitude at 425 C. On the other hand, the SiC seal coat made little (if any) difference in fatigue life at 950 C. DOE

N95-30180# Utah Univ., Salt Lake City, UT. Dept. of Materials Science and Engineering.

ALUMINA REINFORCED TETRAGONAL ZIRCONIA (TZP) COMPOSITES Annual Progress Report, 16 Feb. 1994 - 15 Feb. 1995

D. K. Shetty 1995 15 p

(Contract DE-FG02-87ER-45312)

(DE95-008990; DOE/ER-45312/7) Avail: CASI HC A03/MF A01

Objective is to develop high-strength and high-toughness ceramic composites by combining mechanisms of platelet, whisker or fiber reinforcement with transformation toughening. The approach being used includes reinforcement of ceria or yttria-partially-stabilized zirconia (CE-TZP or Y-T-ZP) with platelets, whiskers or continuous filaments of alumina. Critical stresses for extension of filament-bridged matrix cracks were measured as a function of crack length in a model composite system, SiC (filament)-reinforced epoxy-alumina (matrix). The crack-length dependence of the crack extension stress at short crack lengths followed the prediction of a fracture-mechanics analysis that employed a new force-displacement law for the crack-bridging filaments developed in this study. At large crack lengths, the measured matrix-cracking stress was close to the prediction of the steady-state theory of Budiansky, Hutchinson and Evans. Optical fluorescence was employed to measure stresses in crack-bridging sapphire filaments and assess interfacial properties in a model sapphire-epoxy composite. Composites of yttria-partially-stabilized zirconia (Y-TZP) matrix dispersed with either single crystal Al2O3 platelets or particulars were fabricated by a hybrid suspension/powder processing route to densities greater than 99.0% of theoretical. Both transformation toughening and platelet reinforcement contribute to the high fracture toughness of the Al2O3 (platelet)-Y-TZP composites. DOE

N95-30276 California Univ., Los Angeles, CA.

MICROMECHANICS OF CRACK EXTENSION IN COMPOSITES Ph.D. Thesis

Jung Ki Lee 1994 123 p

Avail: Univ. Microfilms Order No. DA9420519

A volume integral equation method is introduced as a new numerical scheme for the solution of certain plane elastodynamic and elastostatic problems in unbounded solids containing multiple inclusions and voids or cracks. Multiple scattering problems in elastodynamics are considered first. The effectiveness of the method is compared with the boundary integral equation method for different problem geometries. For the single inclusion problem, both methods are found to work very well. For multiple inclusions, the volume integral equation method is shown to be much more convenient for numerical formulation and to give very accurate results. Next, elastostatic problems containing multiple inclusions, voids, and cracks are considered as a special case of the corresponding elastodynamic problem in the limiting case of zero frequency. The influence of fiber-matrix interphases and fiber-cores on the interfacial stresses in metal matrix composites subject to arbitrary loading is investigated. The stress intensity factors for microcracks in the matrix in presence of interacting fibers are calculated for a variety of model geometries. Finally, a combination of volume and boundary integral equation methods is introduced for the solution of elastodynamic and elastostatic problems in solids containing multiple inclusions and voids or cracks. Dissert. Abstr.

N95-30334*# National Aeronautics and Space Administration. Marshall Space Flight Center, Huntsville, AL.

COMPOSITE PROCESSING DEVELOPMENT TO IMPROVE INTERLAMINAR STRENGTH USING PLY INTERFACE PARTICLES Final Report

A. Nettles Jun. 1995 22 p

(NASA-TM-108495; NAS 1.15:108495) Avail: CASI HC A03/MF A01

The interlaminar shear strength of carbon-epoxy laminates was to be improved by placing particles of aluminum between plies of prepreg tape used for the layup. Difficulty in aligning the aluminum whiskers in the transverse direction prevented any gain in strength. A discussion of shear within a laminate is presented to better understand the results. Author

N95-30340*# National Aeronautics and Space Administration. Langley Research Center, Hampton, VA.

IMPACT DAMAGE RESISTANCE AND RESIDUAL PROPERTY ASSESSMENT OF (0/+/-45/90)s SCS-6/TIMETAL 21S

Jennifer L. Miller, Marc A. Portanova (Lockheed Martin Corp., Hampton, VA.), and W. Steven Johnson (Georgia Inst. of Tech., Atlanta, GA.) May 1995 38 p

(RTOP 505-63-50-04)

(NASA-TM-110178; NAS 1.15:110178) Avail: CASI HC A03/MF A01

The impact damage resistance and residual mechanical properties of (0/ +/- 45/90)s SCS-6/Timetal 21S composites were evaluated. Both quasi-static indentation and drop-weight impact tests were used to investigate the impact behavior at two nominal energy levels (5.5 and 8.4 J) and determine the onset of internal damage. Through x-ray inspection, the extent of internal damage was characterized non-destructively. The composite strength and constant amplitude fatigue response were evaluated to assess the effects of the sustained damage. Scanning electron microscopy was used to characterize internal damage from impact in comparison to damage that occurs during mechanical loading alone. The effect of stacking sequence was examined by using specimens with the long dimension of the specimen both parallel (longitudinal) and perpendicular (transverse) to the 0 deg fiber direction. Damage in the form of longitudinal and transverse cracking occurred in all longitudinal specimens tested at energies greater than 6.3 J. Similar results occurred in the transverse specimens tested above 5.4 J. Initial load drop, characteristic of the onset of damage, occurred on average at 6.3 J in longitudinal specimens and at 5.0 J in transverse specimens. X-ray analysis showed broken fibers in the impacted region in specimens tested at the higher impact energies. At low impact energies, visible matrix cracking may occur, but broken fibers may not. Matrix cracking was noted along fiber swims and it appeared to depend on the surface quality of composite. At low impact energies, little damage has been incurred by the composite and the residual strength and residual life is not greatly reduced as compared to an undamaged composite. At higher impact energies, more damage occurred and a greater effect of the impact damage was observed. Author

N95-30341*# National Aeronautics and Space Administration. Langley Research Center, Hampton, VA.

FORMULATION OF AN IMPROVED SMEARED STIFFENER THEORY FOR BUCKLING ANALYSIS OF GRID-STIFFENED COMPOSITE PANELS

Navin Jaunky (Old Dominion Univ., Norfolk, VA.), Norman F. Knight, Jr. (Old Dominion Univ., Norfolk, VA.), and Damodar R. Ambur Jun. 1995 16 p Presented at the 10th International Conference on Composite Materials, British Columbia, Canada, 14-18 Aug. 1995

(RTOP 510-02-12-01)

(NASA-TM-110162; NAS 1.15:110162) Avail: CASI HC A03/MF A01

A smeared stiffener theory for stiffened panels is presented that includes skin-stiffener interaction effects. The neutral surface profile of the skin-stiffener combination is developed analytically using the minimum potential energy principle and statics conditions. The skin-stiffener interaction is accounted for by computing the stiffness due to the stiffener and the skin in the skin-stiffener region about the neutral axis at the stiffener. Buckling load results for axially stiffened, orthogrid, and general grid-stiffened panels are obtained using the smeared stiffness combined with a Rayleigh-Ritz method and are compared with results from detailed finite element analyses. Author

25 INORGANIC AND PHYSICAL CHEMISTRY

Includes chemical analysis, e.g., chromatography; combustion theory; electrochemistry; and photochemistry.

For related information see also *77 Thermodynamics and Statistical Physics.*.

N95-28703 ESDU International Ltd., London (England).
ORTHOBARIC DENSITIES AND MOLAR VOLUMES OF LIQUIDS. GLYCOL ETHERS (CELLOSOLVES AND CARBITOLS, ETC.)
Jan. 1995 38 p
(ISSN 0141-4062)
(ESDU-95005; ISBN-0-85679-939-4) Avail: ESDU

ESDU 95005 tabulates density and molar volume for 10 C3 to C8 monoalkyl ethers (6 cellosolves and 4 carbitols) and 6 C4 to C10 dialkyl ethers (2 cellosolves, 2 carbitols, triglyme and tetraglyme) in units of kg/cu m at 5 degree C intervals and cu cm/mol at 5 K intervals from near the melting point to the critical point except for a few compounds for which the correlation is terminated at about 0.95 critical. A further table gives at specified Celsius temperatures the density, molar volume and their derivatives with respect to temperature. The critical density was calculated using the Rackett equation and values of critical pressure and temperature were adjusted until an optimum correlation was obtained for critical values from the vapor pressure data provided for these compounds in ESDU 95004 and the density data given here. The equation used relates log reduced density to a polynomial function of reduced temperature. Values for the coefficients in the equation are tabulated for each compound together with estimates of the accuracy of the predictions using them and a list of the sources of data used. Values at the critical point are also given together with normal boiling and melting points. ESDU

N95-28712 ESDU International Ltd., London (England).
VISCOSITY OF LIQUIDS: ALIPHATIC AND CYCLIC KETONES
Sep. 1994 50 p
(ISSN 0141-4062)
(ESDU-94025; ISBN-0-856-70912-2) Avail: ESDU

ESDU 94025 tabulates the viscosity of 34 alkanones and cyclopentanone, -hexanone, -heptanone and -octanone at saturation pressure for temperatures from just above the melting point to approximately 0.9 of the critical temperature. Experimental data extracted from the literature were fitted by an equation for the logarithm of dynamic viscosity as a function of reduced temperature. The equation contains four constants and the values determined for them from the correlation are tabulated for each compound. Viscosities are given at 10 K and 10 degree Celsius intervals, together with an assessment of the uncertainty in each value. The sources of the data for each compound are listed, and the critical temperature is given. It is noted that viscosity increases by 1 per cent for a pressure increase of 10 bar, and an equation is suggested for calculating the effect of pressure up to 500 bar. ESDU

N95-28776 Mississippi State Univ., Mississippi State, MS. Dept. of Physics and Astronomy.
NON-COINCIDENT MULTI-WAVELENGTH EMISSION ABSORPTION SPECTROSCOPY
Leslie E. Bauman 1995 10 p Presented at the 32nd Symposium on Engineering Aspects of Magnetohydrodynamics (SEAM-32), Pittsburgh, PA, 27-30 Jun. 1994 Limited Reproducibility: More than 20% of this document may be affected by microfiche quality
(Contract DE-AC02-80ET-15601)
(DE95-006480; CONF-9406163-3) Avail: CASI HC A02

An analysis is presented of the effect of noncoincident sampling on the measurement of atomic number density and temperature by multiwavelength emission absorption. The assumption is made that the two signals, emission and transmitted lamp, are time resolved but not coincident. The analysis demonstrates the validity of averages of such measurements despite fluctuations in temperature and optical depth. At potassium-seeded MHD conditions, the fluctuations introduce additional uncertainty into measurements of potassium atom number density and temperature but do not significantly bias the average results. Experimental measurements in the CFFF aerodynamic duct with coincident and noncoincident sampling support the analysis. DOE

N95-28802 ESDU International Ltd., London (England).
THERMOPHYSICAL PROPERTIES OF R-32 (DIFLUOROMETHANE)
Sep. 1994 17 p
(ISSN 0141-4062; ISSN 0141-4070)
(ESDU-94032; ISBN-0-85679-919-X) Avail: ESDU

ESDU 94032 gives equations obtained from a critical evaluation of experimental data in the literature for the variation along the saturation line with temperature, for both the liquid and the vapor, of: density, enthalpy, heat capacity at constant pressure, dynamic viscosity and thermal conductivity. Also given are equations for the variation with temperature along the saturation line of the vapor pressure, latent heat of vaporization and surface tension, together with equations for the variation with temperature for the ideal gas of specific heat capacity at constant pressure, enthalpy, dynamic viscosity and thermal conductivity. Results on the saturation line evaluated in SI units using the equations are tabulated at 5 K intervals and at 5 C intervals from the melting point to the critical point, or as close to it as possible for some properties. Results for the ideal gas evaluated also in SI units using the equations are also tabulated at 20 K and at 20 C intervals from the melting point to 620 K. In the absence of experimental values some of these results involve extrapolation and they are indicated in the tables. Conversion factors to facilitate use of the data in British units are included. Author

N95-28854 Office of Naval Research, Arlington, VA.
SELECTIVE ATTACHMENT OF NUCLEIC ACID MOLECULES TO PATTERNED SELF-ASSEMBLED SURFACES Patent Application
Linda A. Chrisey, inventor (to Navy), Walter J. Dressick, inventor (to Navy), and Jeffrey M. Calvert, inventor (to Navy) 1 Dec. 1994 46 p Filed 1 Dec. 1994 Limited Reproducibility: More than 20% of this document may be affected by microfiche quality
(AD-D017379; Navy-Case-76081; US-Patent-Appl-SN-352126) Avail: Issuing Activity (Defense Technical Information Center (DTIC))

Patterns of pre-formed hybridizable nucleic acid oligomers are formed upon a substrate. The substrate is coated with molecules, such as aminosilanes, whose reactivity with nucleic acid molecules can be transformed by irradiation. The coated substrate exposed to patterned irradiation then contacted with preformed nucleic acid oligomers. The binding of the preformed nucleic acid oligomers to the coating molecules may be covalent or non-covalent (for example, ionic bonding or hydrogen bonding). If desired, a heterobifunctional crosslinker may be employed, before or after irradiation, with the coating to promote covalent binding of the nucleic acid oligomers to the coating molecules. Also, the irradiation step may be performed with the assistance of a positive-tone or negative-tone photoresist. DTIC

N95-28876 Army Research Lab., Aberdeen Proving Ground, MD.
SPECTROMETRIC STUDIES OF SELECTED NITROCOMPOUNDS USING LASER-INDUCED PHOTOFRAGMENTATION/PHOTOIONIZATION AT 193 NM Final Report, Aug. 1993 - Feb. 1994
Rosario C. Sausa, Josef B. Simeonsson, and George W. Lemire Nov. 1994 35 p Limited Reproducibility: More than 20% of this document may be affected by microfiche quality
(DA Proj. 1L1-61102-AH-43)
(AD-A289947; ARL-TR-628) Avail: Issuing Activity (Defense Technical Information Center (DTIC))

A new method for detection trace vapors of NO2 containing compounds near atmospheric conditions has been demonstrated using one color laser photofragmentation/fragment ionization spectrometry. An ArF laser is employed to both photolytically fragment the target molecules in a collision-free environment and ionize the characteristic NO fragments. The production of NO is hypothesized to result from a combination of two NO2 unimolecular fragmentation pathways, one yielding NO in its X(2)Pi electronic ground state and the other in its A(2)Sigma+ excited state. Ionization of ground state NO molecules is accomplished by resonance-enhanced multiphoton ionization processes via their A(2)Sigma(+) yields(reverse) X(2)Pi (3,0), B(2)Pi yeilds (reverse) X(2)Pi (7,0), and/or D(2)Sigma(+) yields (reverse) X(2)Pi (0,1) bands at 193 nm. The analytical utility of this method is demonstrated in a molecular beam time-of-flight apparatus. Limits of detection range from the parts-per-million (ppm) to parts-per-billion (ppb) level for NO, NO2, CH3NO2, dimethylnitramine (DMNA), ortho- and meta-nitrotoluene, nitrobenzene, and trinitrotoluene (TNT). Under effusive beam experimental conditions, discrimination between structural isomers,

ortho-nitrotoluene and meta-nitrotoluene, has been demonstrated with the use of their characteristic photofragmentation/photoionization mass spectra. DTIC

N95-28895 ESDU International Ltd., London (England).
ORTHOBARIC DENSITIES AND MOLAR VOLUMES OF LIQUIDS. GLYCOLS AND CYCLIC DIOLS
Jan. 1995 50 p
(ISSN 0141-4062)
(ESDU-95003; ISBN-0-85679-937-8) Avail: ESDU

ESDU 95003 tabulates density and molar volume for 19 glycols and 3 cyclic diols (molecules from C2 to C6) in units of kg/cu m at 5 C intervals and cu cm/mol at 5 K intervals from near the melting point to the critical point. A further table gives at specified Celsius temperatures the density, molar volume and their derivatives with respect to temperature. The critical density was calculated using the Rackett equation and values of critical pressure and temperature were adjusted until an optimum correlation was obtained for critical values from the vapour pressure data provided for these compounds in ESDU 95002 and the density data given here. The equation used relates log reduced density to a polynomial function of reduced temperature. Values for the coefficients in the equation are tabulated for each compound together with estimates of the accuracy of the predictions using them and a list of the sources of data used. Values at the critical point are also given together with normal boiling and melting points. Author

N95-28916# Mississippi State Univ., Mississippi State, MS. Diagnostic Instrumentation and Analysis Lab.
DEVELOPMENT OF LASER OPTOGALVANIC SPECTROSCOPY AS A PROBE OF ALKALI ATOMS IN AN MHD ENVIRONMENT
D. L. Monts, S. Qian, R. L. Cook, and W. S. Shepard 1995 9 p Presented at the 32nd Symposium on Engineering Aspects of Magnetohydrodynamics (SEAM-32), Pittsburgh, PA, 27-30 Jun. 1994
(Contract DE-AC02-80ET-15601)
(DE95-006481; CONF-9406163-2) Avail: CASI HC A02/MF A01

Application of Laser Optogalvanic Spectroscopy (LOGS) to MHD combustion systems requires selection of an appropriate alkali atom electronic transition to monitor. These studies suggest that in MHD combustion systems, it is desirable to use cesium, which occurs as an impurity in potassium compounds, as a surrogate for potassium rather than to directly monitor potassium in order to obtain reliable determinations of seed concentration. Studies were also performed to investigate the effect of electrode corrosion on the normalized LOGS signal intensity at a fixed wavelength (578.238 nm). During six-hour experiments in a near-stoichiometric flame, the normalized LOGS signal intensity decreased by 40-50% for a -960 V rod electrode and by 10-20% for a -500 V rod electrode. These changes are attributed to buildup of an oxide coating on the electrode, reducing the collection efficiency of the electrode. DOE

N95-28942 Aerospace Corp., El Segundo, CA. Technology Operations.
THE EFFECTS OF PLATINUM ON NICKEL ELECTRODES IN THE NICKEL HYDROGEN CELL
Albert H. Zimmerman 1 Mar. 1995 32 p Limited Reproducibility: More than 20% of this document may be affected by microfiche quality
(Contract F04701-88-C-0089)
(AD-A291607; TR-009(6945-01)-1; SMC-TR-95-4) Avail: Issuing Activity (Defense Technical Information Center (DTIC))

Under conditions of nickel precharge in nickel hydrogen cells, it is possible for platinum complex ions to form at the platinum catalyst electrode when no hydrogen is present. Platinum complex ions have been shown to interact with the active material in the nickel electrode to catalyze the formation of a nickel-cobalt compound within the active material lattice. This compound is readily identified by its characteristic voltage signature. A mechanism for the formation of this compound is proposed, and the effects that this compound has on the performance of the nickel electrode in the nickel hydrogen cell are described. DTIC

N95-28945 Pennsylvania State Univ., University Park, PA. Dept. of Chemistry.
FORMATION OF STRIPED SURFACE PHASES BY SHORT-RANGE FORCES Technical Report, 1 Jun. 1993 - 31 May 1994
J. A. Meyers, S. J. Stranick, and P. S. Weiss 1 May 1994 19 p
(Contract N00014-91-J-1630)
(AD-A279962; TR-14) Avail: Issuing Activity (Defense Technical Information Center (DTIC))

Anisotropic Cu-0 islands form striped periodic supergratings upon annealing an oxygen-exposed Cu(110) surface. While the formation of these striped phases has been attributed to long-range repulsive forces between stripes, we show using the one-dimensional Ising model and Monte Carlo simulations that short range adsorbate-adsorbate interactions are capable of producing striped phases. In these systems there are (at least) two time scales of importance: the time required for the formation of Cu-0 strings and the time required for the formation of stripes. It is demonstrated that the latter process can be extremely slow at room temperature and that approximately evenly spaced stripes are formed upon annealing by employing only short range interactions. DTIC

N95-29246*# Alabama Univ., Huntsville, AL.
STUDY OF THE SPACE ENVIRONMENTAL EFFECTS ON SPACECRAFT ENGINEERING MATERIALS Final Report
Susan K. OBrien, Gary L. Workman, and Guy A. Smith 1 May 1995 71 p Original contains color illustrations
(Contract NAS8-38609)
(NASA-CR-196638; NAS 1.26:196638) Avail: CASI HC A04/MF A01; 8 functional color pages

The space environment in which the Space Station Freedom and other space platforms will orbit is truly a hostile environment. For example, the current estimates of the integral fluence for electrons above 1 Mev at 2000 nautical miles is above 2 x 10(exp 10) electrons/sq cm/day. and the proton integral fluence is above 1 x 109 protons/sq cm/day. At the 200 - 400 nautical miles, which is more representative of the altitude which will provide the environment for the Space Station, each of these fluences will be proportionately less; however, the data indicates that the radiation environment will obviously have an effect on structural materials exposed to the environment for long durations. The effects of this combined environment is the issue which needs to be understood for the long term exposure of structures in space. In order to better understand the effect of these hostile phenomena on spacecraft, several types of studies are worth performing in order to simulate at some level the effect of the environment. For example the effect of protons and electrons impacting structural materials are easily simulated through experiments using the Van de Graff and Pelletron accelerators currently housed in the Environmental Effects Facility at MSFC. Proton fluxes with energies of 700 Kev-2.5 Mev can be generated and used to impinge on sample targets to determine the effects of the particles. Also the Environmental Effects Facility has the capability to generate electron beams with energies from 700 Kev to 2.5 Mev. These facilities will be used in this research to simulate space environmental effects from energetic particles. Ultraviolet radiation, particularly in the ultraviolet (less than 400 nm wavelength) is less well characterized at this time. The Environmental Effects Facility has a vacuum system dedicated to studying the effects of ultraviolet radiation on specific surface materials. This particular system was assembled in a previous study (NAS8-38609) in order to perform a variety of experiments on materials proposed for the Space Station. That system has continued to function as planned and has been used in carrying out portions of the proposed study. Derived from text

N95-29248*# National Aeronautics and Space Administration. John F. Kennedy Space Center, Cocoa Beach, FL.
PRECISION CLEANING VERIFICATION OF FLUID COMPONENTS BY AIR/WATER IMPINGEMENT AND TOTAL CARBON ANALYSIS
Ronald G. Barile (I-NET, Inc., Cocoa Beach, FL.), Chris Fogarty (I-NET, Inc., Cocoa Beach, FL.), Chris Cantrell (I-NET, Inc., Cocoa Beach, FL.), and Gregory S. Melton [1994] 4 p Presented at the Joint Army, Navy, NASA, Air Force (JANNAF) Conference, San Diego, CA, 13-14 Jul. 1995
(Contract NAS10-11943)
(NASA-TM-110742; NAS 1.15:110742) Avail: CASI HC A01/MF A01

NASA personnel at Kennedy Space Center's Material Science Laboratory have developed new environmentally sound precision cleaning and verification techniques for systems and components found at the center. This technology is required to replace existing methods traditionally employing CFC-113. The new patent-pending technique of precision cleaning verification is for large components of cryogenic fluid systems. These are

stainless steel, sand cast valve bodies with internal surface areas ranging from 0.2 to 0.9 sq m. Extrapolation of this technique to components of even larger sizes (by orders of magnitude) is planned. Currently, the verification process is completely manual. In the new technique, a high velocity, low volume water stream impacts the part to be verified. This process is referred to as Breathing Air/Water Impingement and forms the basis for the Impingement Verification System (IVS). The system is unique in that a gas stream is used to accelerate the water droplets to high speeds. Water is injected into the gas stream in a small, continuous amount. The air/water mixture is then passed through a converging/diverging nozzle where the gas is accelerated to supersonic velocities. These droplets impart sufficient energy to the precision cleaned surface to place non-volatile residue (NVR) contaminants into suspension in the water. The sample water is collected and its NVR level is determined by total organic carbon (TOC) analysis at 880 C. The TOC, in ppm carbon, is used to establish the NVR level. A correlation between the present gravimetric CFC113 NVR and the IVS NVR is found from experimental sensitivity factors measured for various contaminants. The sensitivity has the units of ppm of carbon per mg/sq ft of contaminant. In this paper, the equipment is described and data are presented showing the development of the sensitivity factors from a test set including four NVRs impinged from witness plates of 0.05 to 0.75 sq m. Author

N95-29250*# Cleveland State Univ., OH. Dept. of Chemical Engineering.

IN-PLANT TESTING OF MEMBRANES TO TREAT ELECTROPLATING WASTEWATER Final Report

D. B. Shah and Orhan Talu 8 May 1995 31 p

(Contract NCC3-301)

(NASA-CR-198796; NAS 1.26:198796) Avail: CASI HC A03/MF A01

This is the final report submitted for the work performed under the NASA Cooperative Agreement NCC3-301 for the project entitled 'In-Plant Testing of Membranes To Treat Electroplating Waste water'. The main objective of the research project was to determine if the crosslinked polyacrylic acid salt films developed by NASA scientists could be used for heavy metal removal from the wastewater generated by the metals-finishing or electroplating industry. A variety of tasks identified in the original proposal were completed. These included: (1) analysis of our industrial partner Aetna Plating's zinc electroplating process and its wastewater treatment needs for zinc removal; (2) design and construction of a laboratory-scale unit to continuously supply and remove the ion exchange films from the zinc wastewater; (3) performance of a series of runs on such a unit to determine its operating characteristics; and (4) design of a prototype unit for use at the industrial site. In addition, there were a number of tasks that had not been identified in the original proposal but were later judged to be necessary for the successful completion of the project. These were: (1) batch equilibrium and kinetic experiments with analysis of the experimental results to accurately determine the equilibrium and kinetic parameters for the ion exchange films; (2) simulation studies for proper design of the prototype unit; and (3) preliminary runs to exchange the films from H form to Calcium form. Derived from text

N95-29273# Software and Engineering Associates, Inc., Carson City, NV.

SCAP SPRAY COMBUSTION ANALYSIS PROGRAM Final Report, 3 Jul. 1991 - 30 Sep. 1994

Curtis W. Johnson and Gary R. Nickerson Nov. 1994 113 p

(Contract F29601-91-C-0099)

(AD-A289946; PL-TR-94-3032) Avail: CASI HC A06/MF A02

A computer program (SCAP) has been developed which determines the state of a propellant combustion mixture at any point along the axis of a bipropellant rocket engine. The combustion model is based upon the work of Priem and Heidmann and has been extended to treat generalized propellant and gas property data. The primary assumption of this method is that the propellant vaporization is the rate governing mechanism of the combustion process and that the vaporization of the drops can be expressed by a Ranza and Marshall type correlation. The governing equations consider mass, momentum, and heat transfer between the gas and liquid phases, and cast in one dimension. The equations are represented by a set of ordinary differential equations and are solved simultaneously using the 4th order Runge-Kutta Adams-Moulton method. This report describes the program inputs and engineering methods for the SCAP computer code. DTIC

N95-29357# Iowa Univ., Iowa City, IA. Dept. of Mechanical Engineering.

A THERMOCHEMICAL TRANSPORT MODEL FOR ANALYSIS OF HOT-SPOT FORMATION IN ENERGETIC MATERIALS Final Report, 1 Jan. 1991 - 31 Aug. 1994

P. Barry Butler and David Bonnett 2 Dec. 1994 41 p

(Contract DAAL03-91-G-0020)

(AD-A290441; UIME-PBB-94-003; ARO-28310.3-EG) Avail: CASI HC A03/MF A01

The focus of this research is on the prediction of inadvertent ignition and detonation of condensed-phase, energetic materials. Specifically, the work focuses on hot spot formation in high-energy propellants and explosives. A viscoplastic pore collapse model is developed to analyze the potential for hot spot formation in porous, condensed-phase, energetic materials. This model treats the dynamics and thermodynamics of a collapsing spherical void that has been subjected to weak shock loading. An volume-averaged energy balance is used to track temporal variations of the pore gas temperature, and a finite-difference method is used to solve the complete condensed-phase energy equation in the vicinity of a material discontinuity. Results from sample calculations focus on the interfacial energy balance in predicting the rate of localized temperature increase during shock compression. DTIC

N95-29483# Missouri Univ., Columbia, MO. Dept. of Chemistry.

THE REDOX CHEMISTRY OF SOME PEROXO AND SUPEROXO METAL ION COMPLEXES Final Report, 15 Apr. 1991 - 14 Oct. 1994

Richard C. Thompson 18 Nov. 1994 5 p

(Contract DAAL03-91-G-0105)

(AD-A290761; ARO-28486.10-CH) Avail: CASI HC A01/MF A01

All mononuclear peroxomolybdales and peroxovanadates, which form rapidly over virtually the entire pH range in aqueous solution, have been fully characterized and their formation constants determined. The reactivities of the mono- and diperoxo complexes have been examined; the peroxo ligands are strongly activated by Mo(VI) and mildly so by V(V). Mo(VI) and W(VI) are highly effective and robust catalysts for oxidations by hydrogen peroxide, and should find a number of practical uses in the near future. The system Mo(VI), H2O2, and base is probably the most promising chemical means of producing singlet oxygen known. Substantial progress has been made in elucidating the mechanistic aspects of these systems. Incorporation of heteroligands in peroxometallates does not appear to significantly the redox reactivity of the peroxo ligand(s), but can profoundly affect the lability of the peroxo ligand and also render the peroxo complex soluble in nonaqueous media. Preliminary experiments have revealed that calorimetry is the method of choice to determine formation constants for polynuclear peroxometallates. These species are of importance when relatively high concentrations of catalyst are employed, as will probably be the case in some practical applications. The formation constants are prerequisite to meaningful reactivity studies of these polynuclear complexes. DTIC

N95-29487# Army Research Lab., Aberdeen Proving Ground, MD.

REACTION FIELD (RF) CALCULATION OF THE SPECTRAL SHIFTS OF INDOLE Final Report, Sep. 1991 - Mar. 1993

C. F. Chabalowski, D. R. Garmer, J. O. Jensen, and M. Krauss Feb. 1995 36 p

(DA Proj. 1L1-61102-AH-43)

(AD-A290449; ARL-TR-677) Avail: CASI HC A03/MF A01

The excitation energy of indole has been investigated at geometries relevant to both the absorption and emission spectra using first-order configuration interaction (FOCI) methods. The calculation focused on the shift in the relative energy between the two excited states, L(B) and L(a), and the excitation energies with geometry. A reaction field (RF) calculation also examined the shift in excitation energies when the molecule is dissolved in water. The excited states are found to be separated in vacuo by about 4,500/cm at both the ground state and an approximation to the equilibrium L(B) geometry, M, and by 2,500/cm at the optimized geometry of both the first triplet excited state, T, and the first excited singlet state represented by a singles-only configuration interaction (S1). In water, the excited states are essentially degenerate and axed at the ground-state geometry. However, at the excited-states geometries, M and T, the L(A) state is shifted lower in energy than the L(B) state due to the large L sub A excited-state RF.

At the S1 geometry, the electronic behavior of the two excited states is different from that at the other geometries. An approximation to the L(A) state is now the lower state both in vacuo and in the presence of the RF. There is a large calculated solvent fluorescent red shift in water at any geometry as well substantial Franck-Condon (FC) shift due to the steeper energy surface in the ground state compared to the excited states. The calculated energy shifts, dipole moments, and relative transition dipoles are in qualitative accord with experiment. However, the calculated fluorescent reaction dipoles are substantially larger than estimated in earlier studies. DTIC

N95-29556# Purdue Univ., West Lafayette, IN.
SUPER HYDRIDES Final Report, 31 Jul. 1991 - 31 Jul. 1994
Herbert C. Brown 31 Oct. 1994 28 p
(Contract DAAL03-91-G-0024)
(AD-A290594; ARO-28528.9-CH) Avail: CASI HC A03/MF A01

Beta-Chlorodiisopinocampheylborane (DIP-Chloride) introduced by us several years ago is an excellent reagent for the asymmetric reduction of aralkyl and alpha-hindered ketones. We have now shown that this reagent is extremely efficient for the reduction of aryl and alkyl perfluoroalkyl ketones, including alpha-perfluoroalkyl alpha-acetylenic ketones, generally providing (greater than or equal) 90% ee for the product alcohols. A systematic study of the electronic and steric influence in the reduction of fluoroalkyl ketones with DIP-Chloride and Beta-isopiocampheyl-9-borabicyclo onane (Alpine-Borane), and a comparison of the reduction of fluoroalkyl ketones with that of the corresponding chloroalkyl ketones have been made. The compatibility of DIP-Chloride with different functional groups substituted in the phenyl ring of acetophenone has been studied. The results show that most groups are compatible with the reagent. However, ortho-hydroxyl and carboxyl substitutions result in the opposite configuration for the product alcohol, probably due to a chelation followed by intramolecular reduction. DIP-Chloride reacts with o,o-disubstituted acetophenones with reduced rate and decreased ee for the product alcohols. The utility of DIP-Chloride in the syntheses of optically pure pharmaceuticals, such as an analog of BMS-181100 and eprozinol has been demonstrated. Studies to prepare new and improved asymmetric reducing reagents led to diiso-2-Beta-chloroethylapopinocampheylborane (Cleap2BC1). This reagent reduces representative ketones of 8 of the 10 classes to the corresponding sec-alcohols in excellent ee. DTIC

N95-29572# Army Tank-Automotive Systems Development Center, Warren, MI.
EVALUATION OF COMMERCIAL WATER-IN-FUEL TEST KITS Final Report
William R. Williams and Chris Keehan Dec. 1994 25 p
(AD-A292135; TARDEC-TR-13613) Avail: CASI HC A03/MF A01

This report describes evaluation tests on four commercial water-in-fuel test kits intended to measure the level of free water in aircraft fuels. Evaluations were conducted using water saturated fuel deliberately contaminated with predetermined levels of free water. The readings of the test kits were compared to determine the test kit that is most appropriate for Army use. DTIC

N95-29575# Purdue Univ., West Lafayette, IN. High Temperature Materials Information Analysis Center.
HTMIAC/CINDAS SILICON PROPERTIES DATABASE. USER'S GUIDE
C. Y. Ho 21 Mar. 1995 9 p
(Contract DLA900-93-D-5002)
(AD-A292602) Avail: CASI HC A02/MF A01

The Silicon Properties Database presents numerical data and technical information on the properties of pure and doped silicon. Materials comprise a variety of doped silicon materials, having both n-type and p-type conduction, as well as intrinsic silicon. Property coverage includes optical (absorption coefficient, refractive index, and band gap), thermoradiative (normal spectral reflectance, angular spectral reflectance, normal spectral emittance, and normal spectral transmittance), electrical (electrical conductivity and dielectric constant), thermophysical (thermal conductivity, specific heat, thermal expansion, and lattice parameters), damage threshold (rain erosion and laser irradiation), and mechanical (elastic constants, stress-strain, yield strength under tensile, compressive, and shear loading, flexural strength, fracture toughness, and hardness). Property data for silicon that are available in the literature are widely recognized to be sensitive to variations in material related factors. Many issues that are important in determining property behavior of these materials have been sought out in our database activity. Our objective is to bring them together into a single volume (database), and to document the data and supporting information that bear upon the behavior of silicon, in particular the temperature, wavelength, and composition (purity, dopants, carrier concentration) dependence of its properties. DTIC

N95-29581# Rockwell International Corp., Canoga Park, CA. Rocketdyne Div.
INORGANIC HALOGEN OXIDIZERS Final Report, 1 Jun. 1991 - 30 Nov. 1994
K. O. Christe and W. W. Wilson 23 Sep. 1994 302 p
(Contract DAAL03-91-C-0025)
(AD-A290747; RI/RD94-271; ARO-28655.24-CH) Avail: CASI HC A14/MF A03

A research program was carried out in novel energetic materials. This program was highly successful and resulted in 28 major publications. Highlights of this effort include: the characterization of the XeF5(-) anion which is the first example of a pentagonal planar XY5 structure, completion of our work on a quantitative oxidizer strength scale, the synthesis and characterization of new compounds at the limits of coordination and oxidation, such as XeOF5(-), TeOF6(2-), IOF6(-), IF8(-), TeF8(2-), TeF7(-), and XeF7(+), the study of fluxionality and steric repulsion effects in hexa- and hepta-coordinated species, such as W7, HPF5(-), HSF5, and IOF5, the controlled replacement of two fluorine ligands by one doubly bonded oxygen ligand, studies of the thermal instability of NF5 and the F3(-) anion, the characterization of the N2F(+) cation, N(CH3)4N3, H2N3(+) cation and the SF4(-) and SOF4(-) radical anions, the synthesis and characterization of a new Os(+VIII) compound, OsF4O2, theoretical studies on ONOF and a new family of polynitrogen compounds, the synthesis and characterization of the novel PF4(-) anion and its hydrolysis products, and the electrophilic fluorination of CH4 with F(+) equivalent N2F(+) and NF4(+) salts. DTIC

N95-29722# State Univ. of New York, Stony Brook, NY. Dept. of Chemistry.
A CLUSTER BEAM STUDY OF BORON, BORON OXIDE AND B(x)O(y)H CHEMISTRY WITH HYDROGEN FLUORIDE
Jason Smolanoff, Adam Lapicki, Scott L. Anderson, and Marianne Sowa-Resat 26 Dec. 1994 38 p
(Contract N00014-92-J-1202)
(AD-A290826; SBIL-C-94) Avail: CASI HC A03/MF A01

Using an improved version of the Cluster Beam technique, we have probed the chemistry of B(x)O(y)H(z)+ clusters with HF as a function of the B:O:H stoichiometry of the cluster reactant. Reactant compositions were varied from pure boron to stoichiometric oxide, with and without added hydrogen. Boron oxide clusters react with HF at about 50% efficiency and the collision energy dependence suggests that the reaction is sterically hindered, i.e. reaction occurs primarily at certain sites in the oxide network. The principle reaction is attack by the HF on a terminal BO group, followed by loss of fragments such as FBOH and FBO. Addition of a single hydrogen atom has a significant effect on the chemistry. The products of the reaction (and probably the mechanism) are similar to those for the pure oxides, but the reactivity is substantially reduced. We propose that the hydrogen atom blocks a reactive site on the cluster, thereby reducing the reactivity. Pure boron clusters react by addition of HF, followed by elimination of fragments such as BF and HBF. For small clusters the reaction is efficient, but we see activation barriers grow in for the larger clusters, suggesting that there may be activation barriers for boron surface-HF reactions as well. In contrast to the situation for the oxides, addition of hydrogen to the pure boron clusters generally increases the reactivity with HF. DTIC

N95-29870# Texas A&M Univ., College Station, TX.
DEVELOPMENT OF PRECIPITATED IRON FISCHER-TROPSCH CATALYSTS Quarterly Technical Progress Report, 1 Oct. 1994 - 31 Dec. 1994
Dragomir B. Bukur 1 Mar. 1995 15 p
(Contract DE-AC22-94PC-93069)
(DE95-009334; DOE/PC-93069/3) Avail: CASI HC A03/MF A01

The work on Task 3: Testing of Previously Synthesized Catalysts was initiated in early October as scheduled. Two initial tests were not successful (runs SB-2764 and SB-3064). It took us a great deal of time and effort to

overcome these problems, which included conducting a blank test (run SB-3184) and a test of commercial Ruhrchemie catalyst (run SB-3254). Finally, a successful test of catalyst with nominal composition 100 Fe/5 Cu/6 K/24 SiO2 (run SB-3354) was completed using a different slurry medium (Ethylflo 164 oil). Low activities in unsuccessful tests SB-2764 and SB-3064 may be due to catalyst poisoning by impurities in the initial slurry medium (purified n-octacosane). DOE

N95-29897 ESDU International Ltd., London (England).
VAPOUR PRESSURES AND CRITICAL POINTS OF LIQUIDS. GLYCOLS AND CYCLIC DIOLS
Jan. 1995 62 p
(ISSN 0141-4062)
(ESDU-95002; ISBN-0-85679-936-X) Avail: ESDU

ESDU 95002 presents vapor pressure data for 22 glycols and 6 cyclic diols (molecules from C2 to C6). The data were obtained by a critical evaluation of experimental results in the literature. The data available were limited but using a correlation previously developed relating the behaviour of the coefficients of the Wagner vapor pressure equation to the latent heat of vaporization and the compression factor it was possible to extrapolate the data. The Wagner equation was used over a temperature range from close to the melting point to about 0.9 of the critical temperature, although for the cyclic compounds it is extended to close to the critical point. The coefficients of the equation are given and two tables of vapor pressure calculated using them are included; in SI units at 5 K intervals and in mm of mercury or atmospheres (for the higher values) at 5 C intervals. A table also gives the saturation temperature at various specified pressures and indicates the possible uncertainty in the calculated values. Also given are values of acentric factor, normal melting point, normal boiling point and the slope of the saturation temperature v vapor pressure curve at the normal boiling point. The sources of data for each compound are listed. Density data for the compounds (except pentane-2,4-diol, hexane-1,2-diol, cyclohexane-1,3-diol, cyclohexane-1,4-diol and benzene-1,4-diol) appear in ESDU 95003, and the choice of critical point values gave the best correlations for both vapor pressure and density. ESDU

N95-29901 ESDU International Ltd., London (England).
VAPOUR PRESSURES AND CRITICAL POINTS OF LIQUIDS. GLYCOL ETHERS (ALKYL CELLOSOLVES AND CARBITOLS, ETC.)
Jan. 1995 38 p
(ISSN 0141-4062)
(ESDU-95004; ISBN-0-85679-938-6) Avail: ESDU

ESDU 95004 presents vapor pressure data for 10 C3 to C8 monoalkyl ethers (6 cellosolves and 4 carbitols) and 6 C4 to C10 dialkyl ethers (2 cellosolves, 2 carbitols, triglyme and tetraglyme). The data were obtained by a critical evaluation of experimental results in the literature. The data available were limited but using a correlation previously developed for the alkanes that relates the second differential of the Wagner vapor pressure equation to the difference between the ideal gas and liquid heat capacities, extrapolation was possible assuming the behavior of each monoalkyl ether to be like that of the homomorphic alkan-1-ol and the behaviour of each dialkyl ether to be like that of the homomorphic alkane. The Wagner equation was used over a temperature range from close to the melting point to about the critical temperature, although for some compounds it is terminated at around 0.9 critical point. The coefficients of the equation are given and two tables of vapor pressure calculated using them are included; in SI units at 5 K intervals and in mm of mercury or atmospheres (for the higher values) at 5 C intervals. A table also gives the saturation temperature at various specified pressures and indicates the possible uncertainty in the calculated values. Also given are values of acentric factor, normal melting point, normal boiling point and the slope of the saturation temperature v vapor pressure curve at the normal boiling point. The sources of data for each compound are listed. Density data for the compounds appear in ESDU 95005, and the choice of critical point values gave the best correlations for both vapor pressure and density. ESDU

N95-29922# Stanford Univ., CA. Dept. of Chemistry.
THEORY AND EXPERIMENTS ON CHEMICAL INSTABILITIES Final Report, 15 Mar. 1991 - 14 Sep. 1994
John Ross 14 Sep. 1994 25 p
(Grant AF-AFOSR-0215-91)
(AD-A290773; AFOSR-95-0066TR) Avail: CASI HC A03/MF A01

We are pleased to report extensive progress in a number of areas in thermodynamics kinetics, and stochastic theories in non-linear chemical reactions far from equilibrium. Research includes both theoretical and experimental studies. Specific areas of research include the following: (1) Thermodynamic and Stochastic Theory of Electrical Circuits; (2) Thermodynamic and Stochastic Theory for Non-equilibrium Systems with Multiple Reactive Intermediates: The Concept and Role of Excess Work; (3) The relation of Fluxes and forces to work in Nonequilibrium Systems; (4) Multiple Steady States in Coupled Flow Tank Reactors; (5) Thermodynamic and Stochastic Theory for Non-Ideal Systems Far from Equilibrium; (6) Thermodynamic and Stochastic Theory of Reaction Diffusion Systems with Multiple Stationary States; (7) Stationary Probability Distribution Near Stable Limit Cycles Far from Hopf Bifurcation Points; (8) Fluctuation-dissipation Relations for Chemical Systems; (9) Thermodynamic and Stochastic Theory of Nonequilibrium systems: Fluctuation Probabilities and excess Work; (10) Thermodynamic and Stochastic Theory of Non-equilibrium Systems: A Lagrangian Approach to Fluctuations and Relation to excess work. Experiments on Relative Stability in the Bistable Multivariable Bromate-Ferroin Reaction. DTIC

N95-29994# Army Research Lab., Aberdeen Proving Ground, MD.
ANALYTICAL POTENTIAL ENERGY SURFACE FOR METHYLENE NITRAMINE (CH2NNO2) Final Report, Sep. 1993 - Jun. 1994
Betsy M. Rice, George F. Adams, Michael Page, and Donald L. Thompson
Feb. 1995 38 p
(DA Proj. 1L1-61102-AH-43)
(AD-A291247; ARL-TR-680) Avail: CASI HC A03/MF A01

An analytic potential energy surface (PES) that accurately describes the reaction of CH2NNO2 was developed. The surface is based on MCSCF and MRCI calculations of Mowrey et al.. The two primary decomposition pathways that can be described by this PES are: (1) N-N bond scission to form H2CN and NO2; and (2) concerted dissociation via a five-center transition state to eliminate HONO + HCN. The classical barrier heights differ by 2 kcal/mol. Thermal rates, calculated with Variational Transition State Theory, were used to parameterize this function to agree with the Mowrey et al. results. This model can be used in molecular dynamics or Monte Carlo simulations for this chemical system. DTIC

N95-30078# New Orleans Univ., LA. Dept. of Chemistry.
ANALYSIS OF FACTORS AFFECTING CHEMICAL REACTIONS IN SUPERCRITICAL FLUIDS Final Report
Peter Politzer 3 Feb. 1995 20 p
(Contract N00014-91-J-1897)
(AD-A290905) Avail: CASI HC A03/MF A01

Our objectives in this project have been to achieve a better fundamental understanding of supercritical fluids, particularly their solvent powers and the mechanisms by which influence the rates and equilibria of chemical reactions, and to develop data and a predictive capability for the controlled oxidations in supercritical fluids of chemical defense agents. We have developed a General Interaction Properties Function (GIPF) based on molecular surface properties (primarily the surface electrostatic potential), which allows us to correlate and predict a variety of fluid phase properties, including supercritical solubilities and enhancement factors, critical constants, normal boiling points, pKa values and partition coefficients. We used our GIPF approach to carry out a similarity analysis of some toxic nerve agents and their suggested simulants, and have predicted supercritical solubilities for these. We investigated how homolytic and heterolytic bond-breaking energies of sulfur mustard bonds are affected by media of different dielectric constants. A number of theoretical approaches were used to understand the behavior of oxygen in supercritical water. The oxygen-water interactions are concluded to be weak. Molecular dynamics simulations show that O2 expands the volume of supercritical water and decreases the extent of clustering of the water molecules. DTIC

N95-30085# California Univ., San Diego, La Jolla, CA.
THE 5TH INTERNATIONAL MEETING ON CHOLINESTERASE
Palmer Taylor 1 Feb. 1995 126 p Meeting held in Madras, India, 24-28 Sep. 1994
(Contract DAMD17-94-J-4010)
(AD-A291253) Avail: CASI HC A07/MF A02

The principal role played by acetylcholinesterase in neurotransmission within the central and peripheral nervous systems commands the interest

of chemists, biochemists, cell biologists, pharmacologists, clinical scientists, neuroscientists, and toxicologists. The field has a very large, multidisciplinary, international following. Recent rapid advances in the understanding of molecular properties and structure of the cholinesterases, in genes encoding the enzymes, and pharmacological properties of cholinesterase inhibitors and reactivators provide an opportunity for an unparalleled account of our knowledge of this rapidly evolving field. These developments have arisen from the molecular cloning and characterization of the cholinesterase genes and the elucidation of the three-dimensional structure of acetylcholinesterase. DTIC

N95-30111# Energy International, Inc., Bellevue, WA.
INVESTIGATION OF LAMINAR METHANE FLAMES WITH EMPHASIS ON KINETICS ELUCIDATION AND NOx REDUCTION Final Report, Aug. 1993 - Nov. 1994
S. Arrigotti, B. Groten, P. Malte, D. Nicol, and K. Hase Feb. 1995 60 p Prepared in cooperation with Tokyo Gas Co.
(Contract GRI-5093-260-2657)
(PB95-200531; GRI-95/0009) Avail: CASI HC A04/MF A01

The report presents a truncation procedure for reducing full chemical kinetic mechanisms to reduced mechanisms for specified operating conditions. Three reduced mechanisms were developed for partially premixed, rich natural gas combustion. The reduced mechanisms include both Zedovich and prompt NOx formation pathways as well as methane oxidation. All three reduced mechanisms correlate well with the full mechanism and experimental results. The number of species and reaction steps have been significantly reduced from the full mechanism, allowing for multidimensional combustion modeling to be practical on conventional workstations. NTIS

N95-30113# Oak Ridge National Lab., TN.
THE MORPHOLOGY OF BLENDS OF LINEAR AND BRANCHED POLYETHYLENES IN SOLID STATE BY SANS
G. D. Wignall, J. D. Londono, R. G. Alamo (Florida State Univ., Tallahassee, FL.), and L. Mandelkern (Florida State Univ., Tallahassee, FL.) 1995 3 p Presented at the 209th American Chemical Society National Meeting, Anaheim, CA, 2-7 Apr. 1995
(Contract DE-AC05-84OR-21400)
(DE95-008675; CONF-950402-5) Avail: CASI HC A01/MF A01

In a previous paper, the authors have shown how small-angle neutron and x-ray scattering (SANS, SAXS) can be used to determine the melt compatibility of different polyolefins, including high-density (HD), low-density (LD), and linear low density (LLD) polyethylene. Such blends have attained widespread commercial applications, though the understanding of the mechanical and melt-flow properties of such blends has hitherto been handicapped by the absence of a consensus concerning the degree of mixing of the components, both in the melt and solid states. Recent SANS data indicate that for HDPE/LDPE blends, the melt is homogeneous for all compositions after proper accounting for H/D isotope effects. In this publication the authors use complementary SANS, DSC, and SAXS to examine the types of morphologies and the different degrees of phase separation which may arise via crystallization effects on cooling from a homogeneous melt. DOE

N95-30198# Gas Research Inst., Chicago, IL.
BIOLOGICAL METHANE ACTIVATION Final Report, Jun. 1993 - 1994
H. Dalton Jan. 1995 34 p
(Contract GRI-5089-260-1826)
(PB95-200705; GRI-94/0440) Avail: CASI HC A03/MF A01

The objective of the research was to utilize and expand on details of the structure and function of the active site of soluble methane monoxygenase (sMMO). Using chemical, physical and molecular biological techniques the authors have moved several stages closer to constructing a small stable mimic Crosslinking of sMMO increased the thermostability of both the native and trypsinised protein. Modification of native and proteolysed sMMO using polyethylene glycols derivatives resulted in an increase in solubility in organic solvents and is accompanied by an increase in thermostability. The occurrence of iso-enzymes of the hydroxylase component was suggested by both chromatographic and mass spectrometric techniques. NTIS

N95-30282# Technische Univ., Delft (Netherlands). Interfaculty Reactor Inst.
A Pr-141 MOESSBAUER STUDY OF PRASEODYMIUM COM POUNDS Ph.D. Thesis
Antoon Alfons Moolenaar Sep. 1994 200 p Sponsored by Nederlandse Organisatie voor Wetenschappelijk Onderzoek, The Hague
(PB95-192449; ISBN-90-73861-20-9) Avail: CASI HC A09/MF A03

In the thesis the authors have studied the Mossbauer effect in the Pr-141 nucleus in various compounds using the current integrating technique (CIT). Chapter 2 contains a survey of the theory relevant to Mossbauer spectroscopy and rare-earth compounds. Because a major part of the thesis deals with the development and testing of CIT and the measurements that were subsequently performed with Pr-141, they give in chapter 3 a rather extensive exposition of CIT. In chapter 4 the authors give a description of the experimental equipment besides that used for CIT, and of the sources and the source handling. They review in the chapter the spectra they have been obtained using CeO2 and CeF3 as source materials. In chapter 5 the authors will describe the procedures they apply in order to analyze the Pr-141 Mossbauer spectra. NTIS

26 METALLIC MATERIALS

Includes physical, chemical, and mechanical properties of metals, e.g., corrosion; and metallurgy.

N95-28701*# National Aeronautics and Space Administration. Lewis Research Center, Cleveland, OH.
MACROSEGREGATION AND NUCLEATION IN UNDERCOOLED Pb-Sn ALLOYS
Henry C. deGroh, III May 1989 36 p Revised
(RTOP 674-25-05)
(NASA-TM-102023-Rev; E-4759-Rev; NAS 1.15:102023-Rev) Avail: CASI HC A03/MF A01

A novel technique resulting in large undercoolings in bulk samples (23 g) of lead-tin alloys was developed. Samples of Pb-12.5 wt percent Sn, Pb-61.9 wt.% Sn, and Pb-77 wt.% Sn were processed with undercoolings ranging from 4 to 34 K and with cooling rates varying between 0.04 and 4 K/s. The nucleation behavior of the Pb-Sn system was found to be nonreciprocal. The solid Sn phase effectively nucleated the Pb phase of the eutectic; however, large undercoolings developed in Sn-rich eutectic liquid in the presence of the solid Pb phase. This phenomenon is believed to be mainly the result of differences in interfacial energies between solid Sn-eutectic liquid, and solid Pb-eutectic liquid rather than lattice misfit between Pb and Sn. Large amounts of segregation developed in the highly undercooled eutectic ingots. This macrosegregation was found to increase as undercooling increases. Macrosegregation in these undercooled eutectic alloys was found to be primarily due to a sink/float mechanism and the nucleation behavior of the alloy. Lead-rich dendrites are the primary phase in the undercooled eutectic system. These dendrites grow rapidly into the undercooled bath and soon break apart due to recalescence and Sn enrichment of the liquid. These fragmented Pb dendrites are then free to settle to the bottom portion of the ingot causing the macrosegregation observed in this study. A eutectic Pb-Sn alloy undercooled 20 K and cooled at 4 K/s had a composition of about Pb-72 wt.% Sn at the top and 55% Sn at the bottom. Author

N95-28889# Army Armament Research, Development and Engineering Center, Watervliet, NY. Benet Lab.
APPLICATION OF A RAPID QUENCH THERMOMAGNETIC ANALYZER TO AUSTEMPERED DUCTILE IRON Final Technical Report
P. J. Cote, T. Hickey, and M. D. Witherell Nov. 1994 20 p
(DA Proj. M02-B-2-FR-21-ABJ)
(AD-A292261; ARCCB-TR-94044) Avail: CASI HC A03/MF A01

A thermormagnetic analyzer was fabricated to provide in-situ monitoring of isothermal decompositions of austenite in steels and related alloys. The analyzer provides a convenient and rapid means for establishing time-temperature-transformation characteristics of a ferrous alloy by cycling a given specimen through a series of thermal treatments and monitoring the transformations magnetically. The present report describes the apparatus and gives results on the transformation characteristics of austempered

ductile iron (ADI). This analyzer was also used to investigate alternative processing procedures; the results indicate that an improved heat treatment is available for large ADI components. DTIC

N95-28959# Lockheed Idaho Technologies Co., Idaho Falls, ID.
ADVANCED MANUFACTURING BY SPRAY FORMING: ALUMINUM STRIP AND MICROELECTROMECHANICAL SYSTEMS
Kevin M. McHugh 1994 10 p Presented at the Technology 2004, Washington, DC, 8-10 Nov. 1994
(Contract DE-AC07-94ID-13223)
(DE95-008615; EGG-M-94157; CONF-9411151-3) Avail: CASI HC A02/MF A01

Spray forming is an advanced materials processing technology that converts a bulk liquid metal to a near-net-shape solid by depositing atomized droplets onto a suitably shaped substrate. By combining rapid solidification processing with product shape control, spray forming can reduce manufacturing costs while improving product quality. INEL is developing a unique spray-forming method based on de Laval (converging/diverging) nozzle designs to produce near-net-shape solids and coatings of metals, polymers, and composite materials. Properties of the spray-formed material are tailored by controlling the characteristics of the spray plume and substrate. Two examples are described: high-volume production of aluminum alloy strip, and the replication of micron-scale features in micropatterned polymers during the production of microelectromechanical systems. DOE

N95-29137# Army Research Lab., Watertown, MA. Materials Directorate.
CORROSION IN METHYLPHOSPHONIC DIFLUORIDE
Chester V. Zabielski and Milton Levy Dec. 1994 12 p
(AD-A289995; ARL-TR-651) Avail: CASI HC A03/MF A01

Electrochemical potentiodynamic polarization studies were conducted for a variety of ferrous and nonferrous metals in methylphosphonic difluoride. Studies were also made of the effects of organic inhibitors on the corrosion rates of 1020 steel (UNS G10200), type 316L (UNS S31603), and type 304 stainless steel (UNS S30400), and magnesium in methylphosphonic difluoride. DTIC

N95-29298# Pennsylvania State Univ., University Park, PA. Dept. of Materials Science and Engineering.
PREDICTION OF HYDROGEN ENTRY AND PERMEATION IN METALS AND ALLOYS Annual Report, 1 Oct. 1993 - 30 Sep. 1994
Howard W. Pickering Feb. 1995 45 p
(Contract N00014-94-I-0086)
(AD-A292047) Avail: CASI HC A03/MF A01

This report summarizes results of the past year on our continuing experiments directed to the problem of hydrogen entry and degradation of materials both of planar surfaces and for the more complicated recessed surface. For the planar surface the hydrogen permeation and scanning tunneling microscopy (STM) techniques were used, and for the recessed surface the study used the hydrogen permeation technique and a microscopy/electrochemical probe technique. Microstructural effects and the role of microbes are also under study. In aqueous solutions both IR drop and acidification within recesses in iron surfaces were found to enhance proton reduction and hydrogen absorption. In addition, it was found that flat, smooth surfaces can form or develop recesses as a result of corrosion or other reasons, e.g., grain boundary grooves that form during corrosion of Cr-depleted alloy in sensitized stainless steel. These recesses were found to be just as prone to proton discharge and hydrogen absorption as pre-existing recesses. Distributions of anodic and cathodic reaction sites were analyzed within a propagating crack under cathodic protection conditions using an IR based model. Results are presented of STM studies of hydrogen adsorption from the gas phase on silicon. DTIC

N95-29427# Dartmouth Coll., Hanover, NH. Dept. of Chemistry.
TRANSITION METAL COMPLEXES WITH PERFLUORINATED LIGANDS Final Report, 1 Apr. 1991 - 31 Mar. 1994
Russell P. Hughes 31 Mar. 1994 10 p
(Grant AF-AFOSR-0227-91)
(AD-A290250; AFOSR-95-0017TR) Avail: CASI HC A02/MF A01

We have continued to make progress in preparing transition metal complexes containing fluorinated ligands, and have completed several sub-projects. We have prepared the first examples of transition metal compounds containing tetrafluoroethylene ligands that rotate rapidly on the NMR time scale. This is a significant discovery en route to a transition metal catalyst that will promote the Ziegler-Natta polymerization of fluorinated olefins to give high polymers. The factors governing the barrier to fluoroolefin rotation have been identified. We have synthesized the first example of a transition metal complex containing the penta-fluoro-cyclopentadienyl ligand. This is an important ligand that may improve thethermal robustness of many transition metal compounds. DTIC

N95-29461 Texas Instruments, Inc., Dallas, TX. Defense Systems and Electronics Group.
LIQUEFIED METAL JET PROGRAM AUTOMATION AND ROBOTICS RESEARCH INSTITUTE (ARRI) Quarterly Status Report, 15 Oct. 1994 - 15 Jan. 1995
Nick Dringenburg, Charles Smith, Patrick DuBois, Elwin Whetsel, and John Priest 12 Jan. 1995 11 p Limited Reproducibility: More than 20% of this document may be affected by microfiche quality
(Contract MDA972-93-C-0035; ARPA Order 9328)
(AD-A289781) Avail: Issuing Activity (Defense Technical Information Center (DTIC))

This report covers the period from 15 Oct. 1994 - 15 Jan. 1995. Our program has initiated test and evaluation of the no lead system, pursued several risk reduction activities, and continued concept design efforts for the copper system. Progress during reporting period: produced primitive test coupons demonstrating line and single ball capability; identified and studied problem areas for no lead system reliability including the environmental chamber, nozzle, and material contamination; designed and installed a new environmental chamber to improve process reliability; started effort to resolve nozzle problems by working with the vendor concerning orifice surface finish and redesigning orifice holder (nozzle); implemented new material handling procedures to minimize contamination problems; continued testing copper melting and construction material compatibility; completed 60 percent of the conceptual design of the copper system and subsystems; added a contract engineer for three months to insure continued design progress. DTIC

N95-29467# Asian Office of Aerospace Research and Development, APO San Francisco, CA. Air Force Office of Scientific Research.
DAIDO STEEL'S SHIBUKAWA PLANT, SHIBUKAWA CITY, GUMMA PREFECTURE, JAPAN, 29 JUL. 1994
P. McQuay 29 Jul. 1994 11 p
(AD-A292343; AOARD-TR-94-31) Avail: CASI Hc A03/MF A01

Daido Steel is the largest specialty steel maker in the world, and therefore has a strong interest in aerospace materials, such as heat and corrosion resistant steels, and Ti and Ni-based alloys. Daido Steel features some of the most advanced melting and processing equipment and practices available, and appears to be constantly upgrading their facilities and capabilities. Daido Steel has recently designed and is now testing an in-house developed unique spin forming press, designated the SRH, for Spinning and Rolling - Hot. This unique press allows for complex case and ring production in a single work piece, with the ability to produce both variable diameter and thickness with good precision. Additionally, utilizing it's high speed rotary forge, the Shibukawa Plant has unique capabilities for producing very large turbine shafts economically. Several Ti alloy/part development programs currently underway are also reviewed. DTIC

N95-29473# Asian Office of Aerospace Research and Development, APO San Francisco, CA. Air Force Office of Scientific Research.
VISIT TO THE DEPARTMENT OF METALLURGICAL ENGINEERING, TOKYO INSTITUTE OF TECHNOLOGY, 22 SEP. 1994
P. McQuay 22 Sep. 1994 5 p
(AD-A292310; AOARD-TR-94-32) Avail: CASI HC A01/MF A01

This report summarizes a visit to TIT's Department of Metallurgical Engineering. A visitor was given a brief overview of TIT by Prof. Matsuo. Following that overview, the visitor gave a brief seminar on microstructure/property relationships in gamma TiAl alloys to several members of the faculty and a handful of graduate students. Prof. Takeyama arrived at TIT in 1992 from the Science and Technology Agency (S&TA) National Research Institute for Metals (NRIM) which is located in Tstikuba. While at NRIM Prof. Takeyama performed research on phase stability and transformations of several intermetallic alloy systems, including gamma TiAl. Since coming to TIT, Prof. Takeyama has broadened this research to

include microstructure/property effects, with the emphasis on fixed effect of static heat treatments on microstructure and properties, while continuing his research on the effect of ternary additions to the phase stability of near gamma alloys. The majority of the phase stability work in Ti-Al-X systems have been where X is Cr, Nb, V or Mo. Of potential commercial significance is Prof. Takeyamas work on air cooling and rapid quenching from the single phase alpha region, followed by tempering or aging. Prof. Takeyama hasdemonstrated it is possible to use quench and tempering treatments to refine the as-cast structure, thus improving the room temperature strength and ductility over typical coarse cast microstructures. DTIC

N95-29526# Michigan State Univ., East Lansing, MI. Dept. of Materials Science and Mechanics.

EXAMINATION OF DISLOCATION CORE STRUCTURES IN B2 INTERMETALLIC ALLOYS Final Technical Report

Martin A. Crimp 27 Feb. 1995 53 p

(Contract N00014-90-J-1910)

(AD-A291486) Avail: CASI HC A04/MF A01

In an effort to understand the detailed mechanisms involved in the plastic deformation of crystalline materials, the atomic level structure of dislocations has been studied in B2 ordered intermetallic alloys. High resolution electron microscopy (HREM) has been used to directly image dislocation cores in NiAl, CoAl and FeAl alloys. Alloys have been studied with stoichiometric and non-stoichiometric compositions. The observed structures have been related to the mechanical behavior observed in these alloys. The experimentally observed dislocation core structures have been compared to theoretical structures modeled (under ONR support) by Prof. D. Faikas. This has led to a critical analysis of the model structures and improvement in the modeling approaches, in particular for non-stoichiometric alloys. DTIC

N95-29724# North Carolina State Univ., Raleigh, NC. Dept. of Materials Science and Engineering.

INTEGRATED SYNTHESIS AND POST-PROCESSING OF SiC AND AlN Final Report, 15 Aug. 1989 - 15 May 1993

A. I. Kingon, R. F. Davis, and A. K. Singh 1994 15 p

(Contract DAAL03-89-K-0131)

(AD-A290853; ARO-26673.9-MS-A) Avail: CASI HC A03/MF A01

Synthesis of nanocrystalline powders of SiC, AlN, Si, Si3N4, TiN, TiC, TiO2 have been achieved by a non thermal microwave plasma reactor from vapor phase precursors. In the case of TiO2 the phase can be a metastable high pressure plasma (Beta-TiO2). Nanoparticles of Si and SiOx displayed strong red-orange photoluminescence. Two mechanisms for photoluminescence were identified one based on 3-D quantum confinement and a second based on natural surface oxides. Creep of fine grained (0.7 micrometers) AlN has been studied for the first time. The mechanism was identified as being diffusion-accommodated grain-boundary sliding. DTIC

N95-29759# Naval Surface Warfare Center, Bethesda, MD. Carderock Div.

THE EFFECTS OF ALLOYING ELEMENTS ON THE STRENGTH AND COOLING RATE SENSITIVITY OF ULTRA-LOW CARBON ALLOY STEEL WELD METALS

M. G. Vassilaros Mar. 1994 60 p

(AD-A290681; CARDIVNSWC-TR-61-93/12) Avail: CASI HC A04/MF A01

A study was conducted to evaluate the effect of weld cooling rate on the strength of autogenous gas-tungsten-arc welding (GTAW) deposited weld metal. The basic weld metal composition was based on a low carbon bainite metallurgical system. The weld metal yield strength goal was 130 ksi, needed to surpass the current HY-13O weld metal requirements. Vacuum induction melted (VIM) heats of steel were produced and processed into 3/4 inch thick plates. The autogenous gas tungsten are welds (GTAW) on the parent steel plates were produced under two different heat input conditions. Tensile specimens were produced from the weldments; specimens from certain heats were subjected to gleeble thermal simulations of multi-pass welding conditions using the Gleeble 1500. All specimens were then evaluated for yield and ultimate tensile strength. From the data presented, it was found that the experimental compositions studied were less sensitive to cooling rate than current HY-130 welding consumables. The compositions tested approached the target yield strength of 130 ksi. DTIC

N95-29835# Army Research Lab., Aberdeen Proving Ground, MD.

HOT EXPLOSIVE CONSOLIDATION OF W-Ti ALLOYS Final Report, Oct. 1991 - Apr. 1993

Laszlo J. Kecskes and Ian W. Hall (Delaware Univ., Wilmington, DE.) Jan. 1995 74 p

(AD-A290880; ARL-TR-669) Avail: CASI HC A04/MF A01

High density (98 percent T.D.) 95W-5Ti (wt. percentage) alloys have been fabricated by a hot explosive consolidation (HEC) technique. In the current procedure, a W+Ti powder compact is preheated by the heat released by a Ti+C exothermic combustion synthesis reaction and subsequently consolidated by pressure waves generated by the detonation of an explosive. The amount of explosive charge, sample configuration, and molar ratio of exothermic material to sample were found to affect the degree of consolidation. Auxiliary temperature measurements were performed to determine the precompaction thermal history of the sample to obtain the optimum delay time for consolidation. As observed with scanning electron microscopy, the HEC microcomposites consist of W particles surrounded by a partially discontinuous Ti-rich matrix. Transmission electron microscopy was also used to further characterize the W/Ti interfacial region. The pertinent features of the technique as well as those of the product microstructures are discussed. DTIC

N95-29869# Edgerton, Germeshausen and Grier, Inc., Idaho Falls, ID.

AUSTENITE TO FERRITE TRANSFORMATION KINETICS DURING CONTINUOUS COOLING

M. Militzer (British Columbia Univ., Vancouver, British Columbia.), R. Pandi (British Columbia Univ., Vancouver, British Columbia.), and E. B. Hawbolt (British Columbia Univ., Vancouver, British Columbia.) 1994 7 p Presented at the International Conference on Solid-to-solid Phase Transformations in Organic Materials, Pittsburgh, PA, 17-22 Jul. 1994 Sponsored in part by the American Iron and Steel Inst.

(Contract DE-FC07-93ID-13205)

(DE95-008582; EGG-M-94205; CONF-940704-5) Avail: CASI HC A02/MF A01

The austenite decomposition has been investigated in a hypo-eutectoid plain carbon steel under continuous cooling conditions using a dilatometer and a Gleeble 1500 thermomechanical simulator. The experimental results were used to verify model calculations based on a fundamental approach for the dilute ternary systems Fe-C-Mn. The austenite to ferrite transformation start temperature can be predicted from a nucleation model for slow cooling rates. The formation of ferrite nuclei takes place with equilibrium composition on austenite grain boundaries. The nuclei are assumed to have a pill box shape in accordance with minimal interfacial energy. For higher cooling rates, early growth has to be taken into account to describe the transformation start. In contrast to nucleation, growth of the ferrite is characterized by paraequilibrium; i.e. only carbon can redistribute, whereas the diffusion of Mn is too slow to allow full equilibrium in the ternary system. However, Mn segregation to the moving ferrite-austenite interface has to be considered. The latter, in turn, exerts a solute drag effect on the boundary movement. Thus, growth kinetics is controlled by carbon diffusion in austenite modified by interfacial segregation of Mn. Employing a phenomenological segregation model, good agreement has been achieved with the measurements. DOE

N95-30018# Argonne National Lab., IL.

MECHANICAL PROPERTIES OF NANOPHASE METALS

R. W. Siegel and G. E. Fougere (Northwestern Univ., Evanston, IL.) Nov. 1994 13 p Presented at the 2nd International Conference on Nanostructured Materials, Stuttgart, Germany, 3-7 Oct. 1994

(Contracts W-31-109-eng-38; DE-FG02-86ER-45229)

(DE95-005408; ANL/MSD/CP-83455; CONF-941039-4) Avail: CASI HC A03/MF A01

Nanophase metals have grain-size dependent mechanical properties that are significantly different than those of their coarse-grained counterparts. Pure metals are much stronger and apparently less ductile than conventional ones; intermetallics are also strengthened, but they tend toward increased ductility at the smallest grain sizes. These property changes are primarily related to grain size limitations, but they are also affected by the large percentage of atoms in grain boundaries and other microstructural features.

Strengthening appears to result from a limitation of dislocation activity, while increased ductility probably relates to grain boundary sliding. A brief overview of our present understanding of the mechanical properties of nanophase metals is presented. DOE

N95-30038# Oak Ridge National Lab., TN.
ANALYTICAL ELECTRON MICROSCOPY OF PRECIPITATES IN ION-IMPLANTED MgAl2O4 SPINEL
N. D. Evans (Oak Ridge Inst. for Science and Education, TN.), S. J. Zinkle, and J. Bentley 1994 6 p Presented at the 1994 Fall Meeting of the Materials Research Society (MRS), Boston, MA, 28 Nov. - 2 Dec. 1994 Prepared in cooperation with Oak Ridge Inst. for Science and Education, TN
(Contracts DE-AC05-84OR-21400; DE-AC05-76OR-00033)
(DE95-007406; CONF-941144-92) Avail: CASI HC A02/MF A01

Magnesium aluminate spinel (MgAl2O4) is being considered as an insulator material within proposed fusion reactors where considerable radiation fields are anticipated. Analytical electron microscopy (AEM) has been used to investigate precipitates within MgAl2O4 spinel following implantation of Al(+), Mg(+), or Fe(2+) ions. Combined diffraction experiments, energy dispersive x-ray spectrometry (EDS), electron energy-loss spectrometry (EELS), and energy-filtered imaging were employed to identify and characterize precipitates observed in the implanted ion region. Diffraction studies suggested these are metallic aluminum colloids, although EELS and energy-filtered images revealed this to be the case only for the Al(+) and Mg(+) implantations, and not for Fe(2+) ion implantations. Multiple-least-squares (MLS) fitting of EELS spectra was employed to quantify the volume fraction of metallic aluminum when present in the implanted ion region. Energy-filtered images of the implanted ion region clearly show the colloid distribution in the Al(+) and Mg(+) implanted spinel. Energy-filtered images from the Fe(2+) ion implanted spinel indicate that the features visible in diffraction contrast cannot be associated with either metallic aluminum or iron-rich precipitates. DOE

N95-30178# Sandia National Labs., Albuquerque, NM.
SIMULATION OF POWDER METAL FABRICATION WITH HIGH PRESSURE GAS ATOMIZATION
D. W. Kuntz and J. L. Payne 1994 15 p Presented at the International Conference on Powder Metallurgy and Particulate Materials, Seattle, WA, 14-17 May 1995
(Contract DE-AC04-94AL-85000)
(DE95-008820; SAND-95-0493C; CONF-950558-1) Avail: CASI HC A03/MF A01

A computational/analytical technique has been developed which models the physics of high pressure gas atomization. The technique uses an uncoupled approach, such that the gas flowfield is initially calculated with a commercially-available Navier-Stokes code. The liquid metal droplet breakup, dynamics, and thermodynamics, are then calculated using the pre-computed flowfield by a separate computer program written by the authors. The atomization code models the primary breakup of the liquid metal stream, tracks the droplets resulting from primary breakup through the flowfield until they undergo secondary breakup, and then tracks the subdroplets until they breakup, solidify, or leave the flowfield region of interest. The statistical properties of the metal powder produced are then computed from the characteristics of these droplets. Comparisons between experimental measurements and computations indicate that the Navier-Stokes code is predicting the gas flowfield well, and that the atomization code is properly modeling the physics of the droplet dynamics and breakup. DOE

N95-30179# Oak Ridge National Lab., TN.
INFLUENCE OF DISLOCATION-SOLUTE INTERACTIONS ON THE MECHANICAL PROPERTIES OF ZIRCONIUM-DOPED NiAl
R. Jayaram (Tennessee Univ., Knoxville, TN.) and M. K. Miller 1995 6 p Presented at the 1994 Fall Meeting of the Materials Research Society (MRS), Boston, MA, 28 Nov. - 2 Dec. 1994
(Contract DE-AC05-84OR-21400)
(DE95-008848; CONF-941144-101) Avail: CASI HC A02/MF A01

Atom probe field ion microscopy (APFIM) has been used to characterize NiAl microalloyed with molybdenum and zirconium. Field ion images and atom probe analyses revealed segregation of zirconium to dislocation strain fields and ribbon-like morphological features that are probably related to dislocations. These results provide direct experimental evidence in support of the suggestion that the tremendous increase in the ductile-to-brittle transition temperature (DBTI) in zirconium-doped NiAl is due to pinning of dislocations by zirconium atoms. Atom probe analyses also revealed segregation of zirconium to grain boundaries. This result is consistent with the change from an intergranular fracture mode in undoped NiAl to a mixture of intergranular and transgranular fracture mode in zirconium-doped NiAl. The NiAl matrix was severely depleted of the solutes molybdenum and zirconium. Small Mo-rich precipitates, detected in the matrix and grain boundaries, are likely to contribute to the significant increase in the room-temperature yield stress of microalloyed NiAl through a precipitation hardening mechanism. DOE

N95-30205# Technische Univ., Delft (Netherlands).
FORMATION AND PROPERTIES OF TITANIUM DISILICIDE: A STUDY ON THE DEVELOPMENT OF STRESS IN Ti-Si THIN FILMS Ph.D. Thesis
J. F. Jongste 6 Dec. 1994 146 p Sponsored by Nederlandse Organisatie voor Wetenschappelijk Ondersoek, The Hague, and Stichting voor Fundamenteel Onderzoek der Materie
(PB95-197315) Avail: CASI HC A07/MF A02

In this thesis the formation of titanium disilicide in thin films on silicon substrates is studied. During the formation process mechanical stresses can appear due to a number of phenomena: during deposition an intrinsic stress may occur due to insufficient mobility of the atoms to reach their equilibrium positions; the formation of a compound or a phase transformation can be accompanied by a change of the volume of the film; extrinsic thermal stresses may occur due to different thermal stresses may occur due to different thermal expansion coefficients of film and substrate. The aim of the research presented in this thesis is to measure and analyze the stress in thin Ti-Si films during the various stages of the titanium disilicide formation process. NTIS

N95-30216# Oak Ridge National Lab., TN. Metals and Ceramics Div.
TENSILE PROPERTIES OF AS-CAST IRON-ALUMINIDE ALLOYS
S. Viswanathan, C. G. McKamey, and P. J. Maziasz 1995 11 p Presented at the 8th Annual Conference on Fossil Energy Materials, Oak Ridge, TN, 10-12 May 1994
(Contract DE-AC05-84OR-21400)
(DE95-005396; CONF-9405143-10) Avail: CASI HC A03/MF A01

Room-temperature tensile properties of as-cast Fe3Al-based FA-129 alloy were investigated. Tensile properties were obtained in the as-cast condition in air, oxygen, and water-vapor environments, and after homogenization at 700, 900, and 1200 C. Transmission electron microscopy (TEM) was used to characterize ordered phases and dislocation structure, and optical metallography and scanning electron microscopy (SEM) were used to characterize the grain microstructure and fracture morphology. Tensile properties in the as-cast condition exhibited an environmental effect; tensile ductilities in oxygen atmosphere were greater than those obtained in laboratory air. Homogenized samples of FA-129 alloy exhibited almost twice the ductility found in the as-cast condition. Microstructural characterization of the homogenized samples and comparison of the as-cast and homogenized microstructures provided clues that helped to explain the poor ductility in the as-cast state. DOE

N95-30287# Technische Univ., Delft (Netherlands).
DECOMPOSITION OF HYPO-EUTECTOID IRON CARBON AUSTENITES Ph.D. Thesis [ONTLEDING VAN HYPO-EUTECTOIDISCHE IJZER-KOOLSTOF AUSTENIETEN]
Marcel Onink 13 Feb. 1995 174 p
(PB95-196945) Avail: CASI HC A08/MF A02

This thesis deals with the study of diffusional phase transformations in binary hypo-eutectoid iron-carbon alloys. These alloys are considered as model systems for the study of the transformation behavior of low-alloy, low-carbon steels. Nowadays steel is one of the most versatile materials in the world. The properties of these iron-based alloys can be modified by variations in the chemical composition and, in particular, the microstructure. The latter is achieved by means of thermal treatments, if necessary in combination with plastic deformation. It is the purpose of this thesis to contribute to the understanding of the phase transformation crucial for the control of the microstructure of many steels: the decomposition of austenite. NTIS

27 NONMETALLIC MATERIALS

Includes physical, chemical, and mechanical properties of plastics, elastomers, lubricants, polymers, textiles, adhesives, and ceramic materials.

For composite materials see *24 Composite Materials.*

N95-28784 Office of Naval Research, Arlington, VA.
EPOXY PIPELINING COMPOSITION AND METHOD OF MANUFACTURE Patent Application
James D. Adkins, inventor (to Navy) and Robert F. Brady, Jr., inventor (to Navy) 14 Dec. 1994 56 p Filed 14 Dec. 1994 Limited Reproducibility: More than 20% of this document may be affected by microfiche quality
(AD-D017380; Navy-Case-76105; US-Patent-Appl-SN-355581) Avail: Issuing Activity (Defense Technical Information Center (DTIC))

A cross-linked pipelining network polymer composition for the in situation of pipes is formed. The polymer composition comprises at least one liquid epoxy resin and an effective amount of a liquid curing agent blend comprising an aliphatic polyamine, an aliphatic imidazoline, and an aliphatic amidoamine. The polymer composition may further comprise a pigment, a diluent and/or a viscosity controlling agent. DTIC

N95-28850# Colorado State Univ., Fort Collins, CO. Dept. of Chemistry.
POLYMERIC MICROCAPSULE ARRAYS Interim Report
Charles R. Martin and Ranjani V. Parthasarathy 24 Mar. 1995 10 p Submitted for publication
(Contract N00014-82-K-0612)
(AD-A291937; CSU-TR-101) Avail: CASI HC A02/MF A01

Immobilized enzymes are used in bioreactors and biosensors. Current methods for immobilizing enzymes include adsorption or covalent attachment to a support, microencapsulation and entrapment within a membrane/film or gel. The ideal enzyme immobilization method would (1) employ mild chemical conditions; (2) allow for large quantities of enzyme to be immobilized; (3) provide a large surface area for enzyme/substrate contact within a small total volume; (4) minimize barriers to mass transport of substrate and product and (5) provide a chemically and mechanically robust system. This report describes a new method for enzyme immobilization that satisfies all of these criteria. We have developed a template-based synthetic method that yields hollow polymeric microcapsules of uniform diameter and length. These microcapsules are arranged in a high density array in which the individual capsules protrude from a surface like the bristles of a brush. We have developed procedures for filling these microcapsules with high concentrations of enzymes. The enzyme-loaded microcapsule arrays function as enzymatic bioreactors in both aqueous solution and organic solvents. DTIC

N95-28860# Rutgers - The State Univ., Piscataway, NJ.
FERROELECTRIC POLARIZATION MECHANISM OF THE ODD-NUMBERED NYLONS Technical Report, 1 Jun. 1993 - 31 May 1994
B. Z. Mei, J. I. Scheinbeim, and B. A. Newman Aug. 1994 26 p
(Contract N00014-91-J-1078)
(AD-A292276; TR-33) Avail: CASI HC A03/MF A01

Following studies of the ferroelectric behavior of the odd-numbered nylons, the ferroelectric switching mechanisms have been investigated in terms of the crystal orientation or reorientation using wide angle X-ray diffraction method. It has been found that the degree of double crystallite orientation resulting from uniaxial stretching below T(sub g) for the odd-numbered nylon films decreases with increasing amide content. The electric field poling results in a reorientation of unit cells without changing the crystal structure or chain packing in the nylon films. Moisture absorbed by the nylon samples can strongly affect the resultant reorientation of the crystal unit cell. With the presence of some level of moisture, a 90 deg reorientation of the unit cells is observed for all the nylons studied. A 72 deg unit cell reorientation is observed for nylon 11 samples when poled using a dry-air purge. This difference may be attributed to the increase in electric field applied to the crystalline phase when moisture is present in the amorphous region during poling. DTIC

N95-28864# Rutgers - The State Univ., Piscataway, NJ. Coll. of Engineering.
HIGH FIELD ELECTROSTRICTIVE RESPONSE OF POLYMERS Technical Report, 1 Jun. 1993 - 31 May 1994
Ma Zhenyi, Jerry I. Scheinbeim, Jar Wha Lee, and Brian A. Newman Aug. 1994 13 p
(Contract N00014-91-J-1078)
(AD-A292298; TR-32) Avail: CASI HC A02/MF A01

It is well known that electrostrictive strains are proportional to the square of the applied electric field. It therefore appeared reasonable to assume that for some polymeric materials, a large acoustic thickness response might be obtained by application of high dc bias fields, approx. 20 MV/m, to a film while driving the film with an ac signal to access the high slope region of the electrostrictive strain vs. applied field curve. Previous studies of crystallizing poly(vinylidene fluoride) (PVF2) from solution under high electric fields have demonstrated that gel-like samples of PVF2 with high content of the plasticizer tricresyl phosphate (TCP) could he subjected to electric fields as high as approx. 100 MV/m. Using this type of heavily plasticized PVF2, d sub T values approx. 4 Angstrom/V were obtained. Values of 9 Angstrom/V were obtained for a certain class of thermoplastic elastomer (i.e., a polyurethane). These d(sub T) values are considerably greater than those obtained from conventional piezoelectric ceramic materials. In addition, large elastic strains (greater than 3%) were observed as a function of applied dc field. DTIC

N95-28891# Rutgers - The State Univ., Piscataway, NJ.
FERROELECTRIC AND PIEZOELECTRIC PROPERTIES OF NYLON 11/POLY(VINYLIDENE FLUORIDE) BILAMINATE FILMS Technical Report, 1 Jun. 1993 - 31 May 1994
J. Su, Z. Ma, J. I. Scheinbeim, and B. A. Newman Aug. 1994 9 p
(Contract N00014-91-J-1078)
(AD-A292274; TR-31) Avail: CASI HC A02/MF A01

The ferroelectric and piezoelectric properties of a new class of polymer ferroelectric and piezoelectric materials, nylon 11/polyvinyl lidene fluoride (PVF2) bilaminate films, prepared by a co-melt-pressing method, is presented. The bilaminate films exhibit typical ferroelectric D-E hysteresis behavior with a remanent polarization, P(sub r), of about 75 mC/sq m, which is higher than the value of 52 mC/sq m observed for PVF2 or nylon 11 films measured under the same conditions. The coercive field, E(sub c), of the bilaminate films is approx. 78 Mv/m which is higher than that of either PVF2 or nylon 11 films. Measurements of the temperature dependence of the piezoelectric strain coefficient, d31, and the piezoelectric stress coefficient, e31, were also carried out. The bilaminate films exhibit a piezoelectric strain coefficient, d31, of 41 pC/N at room temperature, which is significantly higher than the PVF2 films (25 pC/N) and the nylon 11 films (3.1 pC/N). DTIC

N95-28898 ESDU International Ltd., London (England).
SELECTION OF SYNTHETIC OILS
Sep. 1994 36 p
(ISSN 0141-2590)
(ESDU-94020; ISBN-0-85679-907-6) Avail: ESDU

ESDU 94020 primarily applies when there is a continuous lubricant film as in hydrodynamic or hydrostatic bearings, but also has application in boundary lubrication. It does not treat greases. Classes of lubricants considered are mineral oils (for comparison), synthetic hydrocarbons, diesters, polyol esters, polyglycols, phosphate esters, silicones, silicate esters and disiloxanes, polyphenyl- and C-ethers, and perfluoropolyalkyl ethers (PFPAE). Graphs illustrate the comparative behaviour of them in terms of working temperature based on viscosity limits, pressure exponent of viscosity, thermal stability, oxidation limits, resistance to radiation, flash point, ignition temperature, and relative cost. A table also compares their density, thermal conductivity, thermal capacity, bulk modulus, toxicity, effect on environment, and biodegradability. A data sheet is given for each class of lubricant giving broad guidance on viscosity/temperature behaviour, volatility, fire resistance, boundary lubrication characteristics, and a table of advantages and disadvantages. The properties of typical members of each class are indicated. Author

N95-28900 ESDU International Ltd., London (England).
LUBRICANT FILM THICKNESS BETWEEN DISC CAMS AND FOLLOWERS

Jul. 1994 58 p
(ISSN 0141-4046)
(ESDU-94008; ISBN-0-85679-895-9) Avail: ESDU

ESDU 94008 introduces a Fortran program (ESDUpac A9408) that calculates at 1 degree rotation intervals, the film thickness in the contact region for cams with translating or swinging arm crowned flat-faced, domed or roller followers, and also the smallest value in the cycle and the rotation angle at which it occurs. Also output at those intervals are the sliding and entrainment velocities. The method involves calculation of the force acting at the cam/follower interface due to follower system inertia, externally applied load and action of the return spring. The program includes an option to determine suitable values for spring rate and preload to maintain contact between the cam and follower; alternatively, for given values of those quantities it will check that contact is maintained. A check to ensure that profile undercutting is avoided is included. Other inputs required are the geometry of the cam and follower, their materials properties, and the properties of the lubricant. A cam law must be used for each segment; six are provided or additional ones may be added by modifying the source code according to instructions provided. Alternatively, a file of follower displacement, velocity and acceleration at 1 degree rotation intervals may be input. A full description of the mathematical model used is included together with guidance on the use of the program to improve the design. The input to and output from the program are illustrated by three practical worked examples of its use and warning messages that may be output are detailed together with suggestions for appropriate corrective procedures. The program is available on disc in the software volume uncompiled and compiled in ESDUview, a user-friendly shell that prompts on screen for input data. Author

N95-28925# Hughes Aircraft Co., Tucson, AZ.
ZERO DISCHARGE ORGANIC COATINGS: POWDER PAINT. UV CURABLE PAINT. E-COAT Quarterly Technical Report, Oct. - Dec. 1994
James Leal, Stephen J. Spadafora (Naval Air Warfare Center, Warminster, PA.), Richard D. Granata (Lehigh Univ., Bethlehem, PA.), Steven R. Felstein, and Srini Raghavan (Arizona Univ., Tucson, AZ.) 1995 54 p
(Contract MDA972-93-C-0020; ARPA Order-9328)
(AD-A292180; ZDOC/9404) Avail: CASI HC A04/MF A01

The Zero Discharge Organic Coatings (ZDOC) R&D project will substantially advance coatings technology through the development of high performance zero-discharge coating systems. Development efforts are proceeding on three coating technologies, powder paint, ultraviolet (UV) curable paint, and electro-coating (E-coat) paint. These three paint technologies offer the potential of high performance coatings with no volatile organic compound (VOC) emissions or hazardous waste generation. These three technologies and their associated application processes will be applicable to a wide variety of military equipment and structures, thereby eliminating volatile organic compound (VOC's) and toxic heavy metals from coatings and painting operations. The ZDOC team of Hughes Aircraft Company, Lehigh University, University of Arizona, and the Naval Air Warfare Center Aircraft Division Warminster offers a blend of experience, expertise, and capabilities in all aspects of organic coatings technology. This quarterly report reviews the team's technical activities and results during the period October 1994 - December 1994. DTIC

N95-28953 Air Force Inst. of Tech., Wright-Patterson AFB, OH.
NEW TETRAARYLBORATE AND ETHYLDIBUTYLSTANNANE REAGENTS Ph.D. Thesis
Ronald C. Marks Dec. 1994 186 p Limited Reproducibility: More than 20% of this document may be affected by microfiche quality
(AD-A289813; AFIT/CI/CIA-94-044D) Avail: Issuing Activity (Defense Technical Information Center (DTIC))

The scope of this investigation focused on two separate goals. The first was to develop a synthesis for potential cation exchange resins containing tetraarylborate anions. The second was to investigate stereochemical aspects of the hydrostannation of alkynes using a polymer bound dibutyl2-(3- AND 4-ETHYLPHENYL)ETHYLtin reagent. A convenient synthesis of triphenylboron was achieved by covalently attaching the triarylboron to commercial macroreticular polystyrene beads (Amberlite XE-305). This new synthesis was achieved in fewer synthetic steps than previously reported synthetic schemes. Synthesis of a trithiophenylboron supported on commercial polystyrene was also achieved using the same method established for the tetraphenylborate species. The second area of research focused on organostannanes used for radiolabeling which had been previously investigated by Kabalka et al., who showed that terminal alkynes may be reacted with polymeric dibutyl2-(3-ETHENYLPHENYL)ETHYLtin hydrides to form a polymer bound alkenyldibutylstannane. This poly(dibutyl2-(3-AND 4-ETHENYLPHENYL)-ETHYLtin was reacted with radioactive iodine to yield radioiodinated alkenes for use in medical imaging. Both (E)- and (Z)-alkenes were synthesized by this method. This present work focus on the stereochemical aspects of the hydrostannation using a series of macroreticular polymers. The ratio of (E)- to (Z)-alkenes were comparable to solution chemistry reactions. DTIC

N95-28960# Lockheed Idaho Technologies Co., Idaho Falls, ID. Idaho National Engineering Lab.
CORROSION INVESTIGATION OF MULTILAYERED CERAMICS AND EXPERIMENTAL NICKEL ALLOYS IN SCWO PROCESS ENVIRONMENTS
Karen M. Garcia and Ron Mizia Feb. 1995 200 p
(Contract DE-AC07-94ID-13223)
(DE95-008666; INEL-94-0017) Avail: CASI HC A09/MF A03

A corrosion investigation was done at MODAR, Inc., using a supercritical water oxidation (SCWO) vessel reactor. Several types of multilayered ceramic rings and experimental nickel alloy coupons were exposed to a chlorinated cutting oil TrimSol, in the SCWO process. A corrosion casing was designed and mounted in the vessel reactor with precautions to minimize chances of degrading the integrity of the pressure vessel. Fifteen of the ceramic coated rings were stacked vertically in the casing at one time for each test. There was a total of 36 rings. The rings were in groupings of three rings that formed five sections. Each section saw a different SCWO environment, ranging from 650 to 300 C. The metal coupons were mounted on horizontal threaded holders welded to a vertical rod attached to the casing cover in order to hang down the middle of the casing. The experimental nickel alloys performed better than the baseline nickel alloys. A titania multilayered ceramic system sprayed onto a titanium ring remained intact after 120-180 hours of exposure. This is the longest time any coating system has withstood such an environment without significant loss. DOE

N95-28963# Army Research Lab., Watertown, MA. Materials Directorate.
INVESTIGATION OF THE CHARACTERISTICS OF FERROELECTRIC THIN FILMS DEPOSITED BY PULSED LASER ABLATION
S. Sengupta, N. Sonnenberg, D. P. Vijay, and S. B. Desu Dec. 1994 13 p
(AD-A292306; ARL-TR-682) Avail: CASI HC A02/MF A01

Ferroelectric thin films of barium strontium titanate (BSTO) have been deposited on bare and metallized substrates by the pulsed laser ablation method under different oxygen ambients (150 mT and 50 mT). Under an oxygen pressure of 150 mT, the film composition was similar to that of its ablation target composition, viz. Ba(0.6)Sr(0.4)TiO3. However, when the films were deposited under the lower oxygen pressure, x-ray diffraction studies showed the presence of a secondary phase. The electrical characteristics of the films were measured to examine the effect of the stoichiometry on the dielectric constant and tunability. DTIC

N95-29021# Colorado Univ., Boulder, CO. Dept. of Electrical and Computer Engineering.
STUDY OF UV BLEACHED CHANNEL WAVEGUIDE PERFORMANCE IN NLO POLYMER FILMS
Wei Feng, Sihan Lin, R. Hooker, and Alan R. Mickelson Oct. 1994 32 p
(Contract N00014-92-J-1190; DAAL-92-G-0289; NSF ECS-90-15752)
(AD-A292008; ECE/GWOL-63) Avail: CASI HC A03/MF A01

We report the studies on UV photo bleached optical channel waveguides in nonlinear optical polymer films. The nonlinear optical polymer used is PMMA/DR1 side chain polymer. Effective indices of the channel waveguides are measured with prism coupling technique along with the effective indices of the bleached and unbleached polymer films. The effective index method was used to predict the effective indices of the channel waveguides from measurements of the slab waveguides without detailed knowledge of the index distributions in the polymer films. Some local effects on the boundaries of the channel waveguides caused by the UV bleaching process are identified

with the comparison between direct channel measurement and prediction. It is found that the technique used in this paper can be employed to predict the performance of the channel waveguides processed with proper bleaching process. DTIC

N95-29055# Boeing Defense and Space Group, Seattle, WA.
PROCESSING, FABRICATION, CHARACTERIZATION AND DEVICE DEMONSTRATION OF HIGH TEMPERATURE SUPERCONDUCTING CERAMICS Annual Technical Report, 1 Sep. 1993 - 30 Nov. 1994
Thomas S. Luhman and Ilhan A. Aksay 30 Nov. 1994 291 p
(Contract F49620-90-C-0079; ARPA Order 7476; AF Proj. 7476)
(AD-A290183) Avail: CASI HC A13/MF A03

The goals of this program on YBa2Cu3O(7-x) superconductors are to (1) focus on engineering designs and demonstration of flux-trap magnets; (2) develop improved processing and fabrication methods to enhance current densities in strong magnetic fields; (3) optimize processes for grain alignment in bulk and tape samples; and (4) provide a technology base for utilization of flux-trap magnets. DTIC

N95-29071# Rensselaer Polytechnic Inst., Troy, NY. Dept. of Materials Engineering.
HIGH-TOUGHNESS GLASS-CERAMICS Final Report, 1 Jul. 1991 - 30 Jun. 1994
Minoru Tomozana 31 Aug. 1994 10 p
(Contract DAAL03-91-G-0211)
(AD-A290562; ARO-28577.10-MS) Avail: CASI HC A02/MF A01

Two different methods were used to prepare tough glass-ceramics containing ZrO2. One was to melt ZrO2-containing Li2O-Al2O3-SiO2 glasses and transform them by control led crystallization. The other was to sinter BaO-SiO2-Al2O3 glass powder together with ZrO2 powder. In both materials, some toughness improvement by the transformation of zirconia during fracture was observed. However, unexpectedly, the greater toughness improvement was realized when the zirconia particles in the glass-ceramics were transformed prior to the fracture by cooling to a lower temperature, e.g., liquid nitrogen temperature. This drastic increase of the fracture toughness was attributed to the deflection of the propagating crack by the large stress fields around the transformed (monoclinic) zirconia. The examination of the fracture surface demonstrated clearly that the crack deflection is taking place in the specimen with transformed zirconia. DTIC

N95-29120 California Inst. of Tech., Pasadena, CA.
DYNAMIC DECOHESION OF BIMATERIAL INTERFACES Ph.D. Thesis
John Lambros 1994 135 p
Avail: Univ. Microfilms Order No. DA9427304

In the present work, findings of an experimental study of dynamic decohesion of bimaterial systems composed of constituents with a large material property mismatch are presented. PMMA/steel or PMMA/aluminum bimaterial fracture specimens are used. Dynamic one point bend loading is accomplished with a drop weight tower device (for low and intermediate loading rates) or a high speed gas gun (for high loading rates). High speed interferometric measurements are made using the lateral shearing interferometer of Coherent Gradient Sensing in conjunction with high speed photography. Very high crack propagation speeds (terminal crack tip speeds up to 1.5c(PMMA)(sub s), where c(PMMA)(sub s) is the shear wave speed of PMMA) and high accelerations (approximately equals 10(exp 7) g where g is the acceleration of gravity) are observed and reported. Issues regarding data analysis of the high speed interferograms are discussed. The effects of near tip three dimensionality are also analyzed. In crack propagation regions governed by large crack tip accelerations it is found that for accurate analysis of the optical data use of a transient elastodynamic crack tip field is necessary. Otherwise use of a K(exp d)-dominant analysis is sufficient. Using the dynamic complex stress factor histories obtained by fitting the experimental data, a dynamic crack growth criterion is proposed. In the subsonic regime of crack growth it is seen that the opening and shearing displacements behind the propagating crack tip remain constant, i.e., the crack retains a self-similar profile during crack growth at any speed. This forms the basis of the proposed dynamic inter facial fracture criterion. It is also found that the process of dynamic inter facial fracture is highly unstable. This is corroborated by both the very large measured values of crack tip speed and acceleration and by the observation that the energy release rate at the propagating crack tip decreases with increasing crack tip speed. A mechanism of energy transfer from the metal to the PMMA side of the specimen is believed to be responsible for the high transient and transonic effects. An analysis and discussion of this phenomenon is also presented in this work. Dissert. Abstr.

N95-29135# Army Research Lab., Watertown, MA. Materials Directorate.
ELECTRICAL CHARACTERISTICS OF BARIUM STRONTIUM TITANATE-OXIDE COMPOSITE FILMS
S. Sengupta, L. C. Sengupta, S. Stowell, D. P. Vijay, and S. B. Desu Dec. 1994 11 p
(AD-A289991; ARL-TR-681) Avail: CASI HC A03/MF A01

In a previous work, composites of BSTO combined with other nonelectrically active oxide ceramics have been formulated and have demonstrated adjustable electronic properties which can be tailored for use in various electronic devices. One application has been for use in phased array antennas and insertion has been accomplished into several working antenna systems. To further accommodate the frequencies required by these phased array antennas, thin films of the composites have been fabricated using a krypton fluoride excimer laser as an ablation source. The electrical properties, including the dielectric constant and the tunability (change in the dielectric constant with applied voltage), have been measured. The results have been compared to those obtained for the bulk ceramic composites and other BSTO/oxide composite thin film structures. DTIC

N95-29138# Army Armament Research, Development and Engineering Center, Watervliet, NY. Benet Lab.
CHROMIUM PLATING AND ELECTROPOLISHING SOLUTION ANALYSES BY ONLINE X RAY FLUORESCENCE SPECTROSCOPY Final Report
Samuel Sopok Sep. 1994 32 p
(AD-A290023; ARCCB-TR-94037) Avail: CASI HC A03/MF A01

Two increasingly important issues for the chemical processing industry are product quality and productivity. Traditionally, offline chemical analysis has been used to monitor both. The main disadvantage of offline analysis is the loss of time due to sampling, bringing samples to a lab, and waiting for results. Obvious efficiencies can be realized by continuous online chemical monitoring. The initial investment is high, but the return on investment can be very efficient process performance. X-ray fluorescence spectroscopy (oniine and offline) is investigated and evaluated as a means to quantitatively analyze metal finishing solutions such as actual chromium plating and electroplating solutions for chromium, sulfur, phosphorus, and iron. The identical experiment was conducted at three different manufacturers of this type of instrument, and included calibration, standardization, and analysis. Although this work has a specific objective related to chromium plating and electropolishing liquid samples, much information is related to and provided for other types of samples. Chemical analysis by x-ray fluorescence spectroscopy is nondestructive, applicable to multiple process streams (liquid or solid), and requires no dilutions. In addition, calibration, standardization, and maintenance are minimal. For the specific metal finishing applications discussed, the resultant data do not suggest that this online monitoring technique is useful at this time, but future work may show this technique to be practical. DTIC

N95-29194 Office of Naval Research, Arlington, VA.
EPOXY SELF-PRIMING TOPCOATS Patent Application
Charles R. Hegedus, inventor (to Navy), Donald J. Hirst, inventor (to Navy), and Anthony T. Eng, inventor (to Navy) 7 Mar. 1994 21 p Filed 7 Mar. 1994 Limited Reproducibility: More than 20% of this document may be affected by microfiche quality
(AD-D017383; Navy-Case-75558; US-Patent-Appl-SN-207448) Avail: Issuing Activity (Defense Technical Information Center (DTIC))

A corrosion-resistant coating which can be applied directly to a surface as a self-priming topcoat comprising an epoxy resin binder and a combination of pigments consisting essentially of an aluminum triphosphate, zinc salts of benzoic acids, and an alkaline earth metal phosphate such as zinc-barium phosphate is described. In addition, the coating contains up to about 30 parts by weight of a titanium dioxide pigment, up to about 2.0 parts by weight of an oil soluble surface active agent, and up to about 50 parts by weight of at least one organic paint solvent. DTIC

N95-29195# Fraunhofer-Inst. fuer Kurzzeitdynamik, Weil am Rhein (Germany).
EXPERIMENTAL INVESTIGATIONS OF WAVE AND FRACTURE PHENOMENA IN IMPACTED CERAMICS AND GLASSES Final Report, Sep. 1990 - Jun. 1994
E. Strassburger and H. Senf Feb. 1995 154 p
(Contract DAJA45-90-C-0053)
(AD-A292142; ARL-CR-214) Avail: CASI HC A08/MF A02

Four types of glass which differ in their chemical composition, hardness and material density and tiles of SiC, TiB2, and Al2O3 were impacted edge-on with blunt steel projectiles at striking velocities between 20 m/s and 1000 m/s. The propagation of shock waves and primary and secondary cracks and crack systems and the growing of crack systems from nucleated centers were visualized by means of a Cranz-Schardin high-speed camera within the first 20 microseconds before the projectile penetrated the target more than a few millimeters. The concept of damage velocity was introduced to describe the different damage processes quantitatively. All four types of glass revealed a similar behavior. The damage velocity equaled terminal crack velocity at low loadings, rose to transversal wave velocity when nucleation occurred and approached longitudinal wave velocity with very high loadings. Unlike glass, the ceramics generated different types of cracks, and different fracture velocities were observed at one impact velocity in one specimen. One had to distinguish between the velocity of continuously growing cracks, including the secondary cracks with sharp edges, fuzzy crack traces and crack fronts. In each of the ceramics, the damage velocity increased with increasing striking velocity and approached the longitudinal wave velocity at high loadings. A terminal crack velocity was found for one type of fracture in SiC. Ceramographical investigations of TiB2 fragments have shown that cracks within large grains as well as intercrystalline cracks are generated by coalescence of voids. DTIC

N95-29230# Massachusetts Inst. of Tech., Cambridge, MA.
REAL-TIME X-RAY SCATTERING STUDY OF PROCESSING OF EIGHT PERFORMANCE THERMOPLASTICS Final Report, Jul. 1991 - Sep. 1994
Peggy Cebe 14 Nov. 1994 26 p
(Contract DAAL03-91-G-0132)
(AD-A290374; ARO-28369.5-MS) Avail: CASI HC A03/MF A01

The purpose of the research was to use real time X-ray scattering: (1) to assist in development of a model for the shrinkage of thermoplastic polymers during processing, and (2) to study the kinetics of crystal structure development. The principle tasks involved real-time X-ray scattering experiments. The secondary tasks involved characterization studies of the materials. We are using real time X ray scattering to study the shrinkage of crystallizable thermoplastic polymers during heat treatment. Most processing models in use today do not use data collected in situ. The matrix shrinkage is determined in real time, directly from x ray scattering. The evolution of cell structure that develops during crystallization can be detected by small angle and wide angle real time x ray scattering. DTIC

N95-29269# Naval Postgraduate School, Monterey, CA.
THE MEASUREMENT OF ADHESION AT FILM-SUBSTRATE INTERFACES USING A CONSTANT DEPTH SCRATCH TEST M.S. Thesis
John C. Campbell Dec. 1994 103 p
(AD-A289940) Avail: CASI HC A06/MF A02

By using a constant depth scratch test, the interfaces shear strength of various thin film/substrate interfaces can be determined. The ability to quantitatively ascertain when thin film debonding occurs has become especially important in the fields of electronics, optics, and protective coatings. A new model and experimental apparatus have been developed in order to more accurately determine thin film interfacial shear strength. While other tests are either qualitative in nature or experimentally difficult, the constant depth scratch test, which utilizes a Vickers microindenter for scratching a film/substrate system to debond the interface, produces quantitative results that are based upon a simple model. Since the depth is maintained constant during scratching, the complexity of the analytical formulation is reduced considerably, enabling the calculation of a numerical value for shear stress. Tests were conducted on chromium films on glass, gold thin films on aluminum nitride, and diamond films on aluminum nitride in order to determine and compare various interfacial shear strengths. DTIC

N95-29270# Cornell Univ., Ithaca, NY. Baker Lab.
PHOTOGENERATED AMINES IN THE DESIGN OF IMAGING MATERIALS: THE RADIATION-INDUCED IMIDIZATION OF FUNCTIONALIZED POLYSTYRENES BEARING AMIDE-ESTER SIDE CHAINS
Jean M. Frechet, Man-Kit Leung, and Edward J. Urankar 20 Jan. 1995 30 p
(Contract N00014-91-J-1338)
(AD-A289943; TR-2) Avail: CASI HC A03/MF A01

The use of photogenerated base in polymer modification processes has been investigated with the study of the amine catalyzed intramolecular imidization of reactive functional groups attached to a polystyrene matrix. The monomers are prepared by reaction of 4-hydroxystyrene with suitable anhydrides such as phthalic anhydride or the corresponding diacid chlorides, followed by amidation with hexamethyldisilazane. Following their free-radical polymerization, the functionalized polystyrenes have been tested in imaging experiments involving in situ photogeneration of amine from a photoactive carbamate precursor followed by low temperature imidization. The amine catalyzed imidization occurs as a much lower temperature than the uncatalyzed process thereby allowing photopatterning. Because the imidization process results in the formation of aqueous base soluble by-products, image development may be accomplished used standard water-based developers. While the new materials themselves can be used as resists, the concepts demonstrated in this study can be used to design novel photopatternable imaging and packaging materials for microelectronics. DTIC

N95-29272# Cornell Univ., Ithaca, NY.
PHOTOGENERATED AMINES IN POLYMER CURING AND IMAGING: DESIGN AND SYNTHESIS OF (3', 5'-DIMETHOXYBENZOINYL)OXYCARBONYL CARBAMATES AS NOVEL PHOTOPRECURSORS OF AMINES Technical Report No. 20
Jean M. Frechet, James F. Cameron, and C. G. Willson 20 Jan. 1995 14 p
(Contract N00014-91-J-1338)
(AD-A289945) Avail: CASI HC A03/MF A01

The design of novel compounds that can be used to photogenerate amines when subjected to UV irradiation is explored. These novel compounds are dimethoxybenzoinyl)oxy carbonyl carbamates that undergo a light induced photocyclization with release of a free primary or secondary amine. The novel photogenerators can be used with 250-350 nm light in a process that is essentially free of side-reactions. These carbamate photogenerators of base may be useful both in polymer curing and imaging processes, and as protecting groups in organic synthesis. DTIC

N95-29288# SRI International Corp., Menlo Park, CA.
CHARACTERIZING AND MODELING PENETRATION OF CERAMIC ARMOR Final Report, 17 Jun. 1992 - 16 Feb. 1995
Donald A. Shockey, Donald R. Curran, Richard W. Klopp, Lynn Seaman, Christine H. Kanazawa, and Joseph T. McGinn Feb. 1995 126 p
(Contract DAAL03-92-K-0004)
(AD-A292588; SRI-PYU-3673; ARO-30488.3-MS) Avail: CASI HC A07/MF A02

To assist in the design of ceramic armor, a micromechanical model of the penetration of a long tungsten alloy rod was developed. An understanding of ceramic comminution and fragment flow at the tip of the advancing penetrator was obtained by examining in detail the damage in ballistically tested ceramic targets and measuring the high-strain-rate behavior of ceramics in pressure-shear impact experiments and dynamic spherical cavity expansion experiments. A mathematical description of the results was constructed from the observations and measurements. The model was tested by implementing it into the DYNA code and performing computational simulations of ballistic tests. DTIC

N95-29314# PDA Engineering, Costa Mesa, CA.
THERMOREACTIVE AIRCRAFT COATINGS (TRAC) PROGRAM Technical Report, 1 Sep. 1989 - 15 Apr. 1994
Kurt E. Jechel and Deborah E. Bielecka 1 Mar. 1995 247 p
(Contract DNA001-89-C-0066; Proj. RA)
(AD-A292054; PDA-TR-94-1161-54-13; DNA-TR-94-59) Avail: CASI HC A11/MF A03

A Thermoreactive Aircraft Coatings (TRAC) system has been developed

which, when used in place of conventional paint, provides aircraft or other weapon systems with the thermal hardness benefits of a white coating while retaining a dark camouflage color under benign conditions. The TRAC system, which can be applied by conventional spray techniques, consists of a white, heat reflective primer top-coated with a passively reactive, thermally activated coating which reversibly changes from dark grey to white upon exposure to radiant thermal flux. The effectiveness of the TRAC system was demonstrated through tests of white, grey, black and TRAC coated test samples constructed from composite/honeycomb sandwich material, simulating aircraft skin, which were subjected to combined radiant thermal energy exposure and simultaneous mechanical loading. Test results indicated that, compared to comparably painted grey samples, TRAC provided up to a 443% improvement in thermal hardness, and was up to 98% as effective as gloss white paint in protecting the composite substrate from damage induced by radiant thermal energy exposure. DTIC

N95-29353# Army Research Lab., Watertown, MA. Materials Directorate.

ANALYSIS OF THE FERROELECTRIC THIN FILMS DEPOSITED BY PULSED LASER DEPOSITION ON OXIDE AND FLUORIDE SUBSTRATES

S. Sengupta, W. E. Kosik, J. D. Demaree, and L. C. Sengupta Dec. 1994 18 p

(AD-A290088; ARL-TR-655) Avail: CASI HC A03/MF A01

This work has been carried out as part of an ongoing investigation in which thin film ferroelectric phase shifters are being constructed, tested, and optimized. These phase shifters will be incorporated into multi-element phased array antennas where the beam steering material used was Ba(0.6)Sr(0.4)TiO3 (BSTO) and BSTO with 1 wt.% oxide additive. Thin films of BSTO have been deposited by pulsed laser deposition (PLD) onto various oxide and fluoride substrates. These include oxide substrates such as magnesium oxide (MgO), sapphire (Al2O3), lanthanum aluminate (LaAlO3), neodymium gallate (NdGaO3), and fluoride substrates such as rubidium manganese fluoride (RbMnF3). DTIC

N95-29355# Pennsylvania State Univ., University Park, PA.

SURFACE STUDIES OF POLY(ORGANOPHOSPHAZENES) CONTAINING DIMETHYLSILOXANE GRAFTS

Harry R. Allcock and Dawn E. Smith 6 Mar. 1995 35 p

(Contract N00014-91-J-1194)

(AD-A291909) Avail: CASI HC A03/MF A01

Poly(organophosphazenes) containing dimethylsiloxane grafts were synthesized by carrying out hydrosilylation reactions on polymer precursors that contained unsaturated side groups. The surface properties of the siloxane-containing polymers were studied by contact angle measurements and X-ray photoelectron spectroscopy. A cosubstituent poly(organophosphazene) containing both trifluro- ethoxy side groups and grafted dimethylsiloxane side groups was found to have a surface rich in -CF3 groups. A poly(organophosphazene) with siloxane grafts but Phenoxy groups as the second substituent showed surface enrichment of the siloxane species. Surface-specific hydrosilylation reactions were detected between an allyl-functional polymer and heptamethyltrisiloxane dissolved in non-solvents for the polymer. Polymer films showed the presence of silicon to depths of 25-60 micrometers as measured by energy dispersive X-ray spectroscopy. DTIC

N95-29358# Pennsylvania State Univ., University Park, PA.

THE SYNTHESIS OF LIQUID CRYSTALLINE PHOPHAZENES CONTAINING CHIRAL MESOGENS

Harry R. Allcock and Eric H. Klingenberg 6 Mar. 1995 41 p

(Contract N00014-91-J-1194)

(AD-A291911) Avail: CASI HC A03/MF A01

Phosphazene cyclic trimers and high polymers containing biphenyl side groups with (S)-2-methyl-l-butoxy as a terminal unit were synthesized. The chiral biphenyl units were linked to the skeletal phosphorus atoms of the small molecule phosphazene cyclic trimers and high polymers through spacer linkages. Single substituent high polymeric poly(organophosphazenes) were synthesized that contained the chiral biphenyl unit linked to the backbone through spacer units. Cosubstituent polymers were also synthesized which contained both the chiral biphenyl derivative linked to the backbone through varying spacer lengths and through non-mesogenic cosubstituents. All the polymers synthesized showed enantiotropic liquid crystallinity. DTIC

N95-29367*# Cleveland State Univ., OH.

CERAMIC MATERIAL LIFE PREDICTION: A PROGRAM TO TRANSLATE ANSYS RESULTS TO CARES/LIFE RELIABILITY ANALYSIS Final Report, 1 Mar. 1988 - 26 Apr. 1994

Pieter VonHermann and Adam Pintz 26 Apr. 1994 29 p

(Grant NAG3-879)

(NASA-CR-198795; NAS 1.26:198795) Avail: CASI HC A03/MF A01

This manual describes the use of the ANSCARES program to prepare a neutral file of FEM stress results taken from ANSYS Release 5.0, in the format needed by CARES/LIFE ceramics reliability program. It is intended for use by experienced users of ANSYS and CARES. Knowledge of compiling and linking FORTRAN programs is also required. Maximum use is made of existing routines (from other CARES interface programs and ANSYS routines) to extract the finite element results and prepare the neutral file for input to the reliability analysis. FORTRAN and machine language routines as described are used to read the ANSYS results file. Sub-element stresses are computed and written to a neutral file using FORTRAN subroutines which are nearly identical to those used in the NASCARES (MSC/NASTRAN to CARES) interface. Derived from text

N95-29436# Texas State Univ., Austin, TX.

PHASE COUPLING AND MORPHOLOGY GENERATION IN ENGINEERING POLYMER ALLOYS

D. R. Paul 1994 11 p

(Contract DAAL03-91-G-0128)

(AD-A291868; ARO-28525.12-CH) Avail: CASI HC A03/MF A01

Blending of polymers offers attractive opportunities for achieving unique property combinations and for improving mechanical toughness but requires knowing how to control interactions to achieve miscibility or phase separated blends with proper interfacial coupling. Without controlled interactions, blends do not perform as desired and some strategy for compatibilization is necessary. Preformed block or graft copolymers may be added to act as interfacial agents or these may be formed in situ by reaction of suitably chosen functionalized polymeric components for control of phase morphology and the interface between these phases to obtain useful mechanical properties. This paper reviews some of the strategies currently being used to couple the phases in multicomponent engineering polymer alloys. DTIC

N95-29465# Los Alamos National Lab., NM.

DEPOSITION AND SURFACE TREATMENT WITH INTENSE PULSED ION BEAMS

J. C. Olson, H. A. Davis, D. J. Rej, W. J. Waganaar (Sandia National Labs., Albuquerque, NM.), R. W. Stinnett (Sandia National Labs., Albuquerque, NM.), and D. C. McIntyre (Sandia National Labs., Albuquerque, NM.) Feb. 1995 18 p Presented at the Annual Meeting and Exhibition of the Minerals, Metals and Materials Society, Las Vegas, NV, 12-16 Feb. 1995

(Contract W-7405-eng-36)

(DE95-007885; LA-UR-95-570; CONF-950201-7) Avail: CASI HC A03/MF A01

Intense pulsed ion beams (500 keV, 30 kA, 0.5 microsecond) are being investigated for materials processing. Demonstrated and potential applications include film deposition, glazing and joining, alloying and mixing, cleaning and polishing, corrosion improvement, polymer surface treatments, and nanophase powder synthesis. Initial experiments at Los Alamos have emphasized thin-film formation by depositing beam ablated target material on substrates. We have deposited films with complex stoichiometry such as YBa2Cu3O(7-x), and formed diamond-like-carbon films. Instantaneous deposition rates of 1 mm/sec have been achieved because of the short ion range (typically 1 micron), excellent target coupling, and the inherently high energy of these beams. Currently the beams are produced in single shot uncomplicated diodes with good electrical efficiency. High-voltage modulator technology and diodes capable of repetitive firing, needed for commercial application, are being developed. DOE

N95-29482 Lockheed Aeronautical Systems Co., Marietta, GA.

THERMALLY STABLE ORGANIC POLYMERS Final Report, 1 Feb. 1993 - 30 Jun. 1994

R. S. Boschan, Matthew Marrocco, and James McGrath 30 Jun. 1994 21 p Prepared in cooperation with Maxdem, Inc., and Virginia Polytechnic Institute and State Univ Limited Reproducibility: More than 20% of this document may be affected by poor print

(Contract DAAL03-92-C-0021)
(AD-A290755; LG94ER0129; ARO-30357.2-MS) Avail: Issuing Activity (Defense Technical Information Center (DTIC))

Environmentally durable high temperature polymer matrix resins are critical in the design of near-term high performance supersonic aircraft. Currently available 6F based polymers are thermally stable, but are expensive and difficulty processable into void-free laminates. 3F polymers have demonstrated equivalent thermal stability and processability, but are amenable to more facile, environmentally acceptable synthetic procedures. In the current program, Semi-interpenetrating Polymer Network (SIPN) blends of ethynyl and phenylethynyl terminated 3F polymers have been formulated, synthesized, and scaled up to quantities amenable to prepregging. Solution prepregging techniques were used by YLA, Inc. to fabricate 12 inch unidirectional prepreg tape. A series of test panels was fabricated from the IM7 prepreg tape, using dielectric monitoring procedures, from a 1:1 3F SIPN blend of phthalic anhydride terminated thermoplastic 3F oligomer with a phenylethynyl terminated 3F oligomer. Solution prepregging techniques were used to prepare unidirectional IM7 fiber prepreg tape. The primary goals of the program, including conception, synthesis development, scaleup, prepregging and panel fabrication, were all met. The void content of the laminates was somewhat higher than acceptable, probably due to the high melt viscosity and solvent inclusion. A plan, using powder prepregging, was offered to alleviate the void problem. DTIC

N95-29484# Puerto Rico Univ., Mayaguez. Dept. of Physics.
PULSED LASER DEPOSITION OF THIN FILM MATERIAL FOR NONLINEAR WAVEGUIDES Final Report, 15 Oct. 1990 - 14 Aug. 1994
Felix E. Fernandez 9 Oct. 1994 19 p
(Contract DAAL03-90-G-0213)
(AD-A290789; ARO-28185.3-PH-SAH) Avail: CASI HC A03/MF A01

Pulsed Laser Deposition (PLO) was used in order to fabricate thin films of various classes or materials of interest for future nonlinear optical waveguide devices. Materials investigated included potassium niobate, potassium tantalate niobate (KTN), and aluminum nitride. SiU films were also grown and studied as a step in producing doped-glass films via PLD. The films were characterized with several techniques, including Rutherford backscattering spectroscopy, x-ray diffraction, optical microscopy, electron microscopy, and when feasible, ellipsometry, and UV-visible light transmission. In addition, a method was devised to enhance the thickness uniformity or PLU-fabricated thin films, which is notoriously poor. This method uses a comic optic or novel design in order to produce concentric annular sources at the target being ablated. In principle, uniform coverage within rew percent is achievable for substrate sizes or a few inches, using current technology. DTIC

N95-29494# Virginia Polytechnic Inst. and State Univ., Blacksburg, VA. Dept. of Chemical Engineering.
PROCESSING STUDIES ON IN SITU COMPOSITES BASED ON BLENDS OF THERMOTROPIC LIQUID CRYSTALLINE POLYMERS WITH THERMOPLASTICS Final Report
Donald G. Baird 22 Sep. 1994 12 p
(Contract DAAL03-91-G-0166)
(AD-A290526; ARO-28560.29-MS) Avail: CASI HC A03/MF A01

The purpose of this work was to optimize the reinforcing effect provided by liquid crystalline polymers (LCP) when combined with thermoplastics. The first phase of the research was concerned with the generation of in situ composites in which the LCP fibrils are directly generated during processing. Because the formation of in situ composites requires extensional deformation, the fibrils are highly oriented in one direction leading to materials with highly anisotropic mechanical properties. Methods for reducing the mechanical anisotropy of in situ composites were studied next. The desire to reduce the mechanical anisotropy lead to pregeneration of LCP fibrils using a novel dual extrusion technique developed in our laboratory. The materials containing the pregenerated microfibrils, referred to as micro composites, were then processed at temperatures where the LCP fibrils were not melted. The mechanical anisotropy of injection molded microcomposites were reduced. Further details of the work carried out in this research are given below. First, the research concerned with the in situ composites is discussed. This is followed by a discussion of the process for generating the microcomposites. Finally the processing studies on the microcomposites is presented. DTIC

N95-29505# California Inst. of Tech., Pasadena, CA.
CONJUGATED POLYMERS FROM CYCLOHEXADIENEDIOL MONOMERS Final Report, 1 Sep. 1992 - 30 Nov. 1994
Robert H. Grubbs 31 Jan. 1995 6 p
(Contract F49620-92-J-0483)
(AD-A290247; AFOSR-95-0004TR) Avail: CASI HC A02/MF A01

The ICI cyclohexadiene monomer has been used to prepare poly(arylenevinylene) derivatives through a precursor route. The polyarylene vinylenes show interesting properties and some derivatives have been used to fabricate photoemitting diodes. A general route to polynathphalene vinylenes has been developed that is now being expanded in to the synthesis of block polymers. A simple route to substituted benzyne precursors was developed and the resulting benzynes were added to the ICI monomer. It was found that these adducts would not ROMP (Ring Opening Metathesis Polymerization) with any of the available catalysts. DTIC

N95-29510# Massachusetts Inst. of Tech., Cambridge, MA. Dept. of Chemical Engineering.
SYNTHESIS MORPHOLOGY AND PROPERTIES OF SEMICRYSTALLINE BLOCK COPOLYMERS Final Report
Robert E. Cohen 10 Jan. 1995 11 p
(Contract N00014-91-J-1045)
(AD-A290475) Avail: CASI HC A03/MF A01

Three years of research on the synthesis, structure and properties of semicrystalline block copolymers are summarized. Novel aspects of this relatively unexplored category of microphase-separated materials include: strongly path-dependent morphologies, unusual gas transport characteristics, compositionally enriched surfaces and favorable mechanical properties. Two industrial and one academic collaboration are mentioned. DTIC

N95-29551# Minnesota Univ., Minneapolis, MN. Dept. of Chemical Engineering and Materials Science.
RECENT PROGRESS IN THE STUDY OF THE KINETICS OF SOL-GEL SiO2 SYNTHESIS REACTIONS
A. V. McCormick 19 Jan. 1995 25 p
(Contract N00014-91-J-1893)
(AD-A290570; TR-6) Avail: CASI HC A03/MF A01

Sol-gel ceramic synthesis has drawn much interest in recent years. 1-5 Organometallic molecules, usually metal alkoxides, are polymerized in an alcohol/water solution with dissolved acids or bases to form a ceramic or glass material with exquisite chemical and microstructural control. Since the chemistry and microstructure of the solid determine its properties, this technology can be used to design materials with specified mechanical, optical, electronic, and physicochemical properties. These materials may be monoliths, films, fibers, or powders. Sol-gel synthesis offers a degree of control of composition and structure at the molecular level unachievable with traditional sintering or precipitation methods. It also offers an economical alternative to layered vapor deposition manufacture of coatings and fibers. Owing to their controlled chemistry and microstructure, sol-gel ceramics can be densified at much lower temperatures than conventional sintering temperatures, thereby saving energy and protecting delicate structures in the material itself or in its substrates. The microstructure can also be controlled to produce optical films, catalyst supports monolithic ceramic bodies, etc. Since the precursor molecules are pure and dissolved, atomic placement and bonding can be controlled to tune mechanical optical. DTIC

N95-29554# Minnesota Univ., Minneapolis, MN. Dept. of Chemical Engineering and Materials Science.
CAGE-LIKE PRECURSOR FORMATION FROM EXTENSIVE CYCLIZATION IN SOL-GEL INORGANIC CONDENSATION POLYMERIZATION
L. V. Ng, P. Thompson, J. Sanchez, and A. V. McCormick 19 Jan. 1995 15 p
(Contract N00014-91-J-1893)
(AD-A290589; TR-4) Avail: CASI HC A03/MF A01

In the sol-gel synthesis of silica by the acid catalyzed hydrolysis and condensation of tetraethyl orthosilicate (TEOS), the fractal dimension, density and homogeneity of the gel depends strongly on the reaction conditions such as the pH and water concentration. However 29Si NMR results have shown that gelation occurs consistently at 80% conversion. The 80% gel conversion is very high compared to the 30% predicted by random branching

theory. These results suggest that cyclization is strongly favorable, forming, typically, the most compact three-dimensional cage-like precursor of expected diameter around 10A. DTIC

N95-29559# Minnesota Univ., Minneapolis, MN. Dept. of Chemical Engineering and Materials Science.
17O NMR OF THE STRUCTURAL EVOLUTION OF V2O5 GELS
G. A. Pozarnsky and A. V. McCormick 19 Jan. 1995 23 p
(Contract N00014-91-J-1893)
(AD-A290623; TR-9) Avail: CASI HC A03/MF A01

Recent studies of the synthesis of V2O5 gels by acidifying metavanadate salt solutions suggest that dioxovanadium cations polymerize into chains of vanadate octahedra. In this study we characterize the growth of vanadate polymers by both solution and MAS(17)O NMR. The spectra are consistent with the formation of a chain polymer with a repeat unit of V sub OHO2(OH)(OH2)2. The 170 NMR spectra also suggest that the chains might connect ot each other through the hydrogen bonding. DTIC

N95-29569# Office of Naval Research, Arlington, VA.
HIGH TEMPERATURE THERMOSETS AND CERAMICS DERIVED FROM LINEAR CARBORANE-(SILOXANE OR SILANE)-ACETYLENE COPOLYMERS Patent Application
David Y. Son, inventor (to Navy) and Teddy M. Keller, inventor (to Navy) 7 Nov. 1994 60 p Filed 7 Nov. 1994
(AD-D017400; Navy-Case-76338; US-Patent-Appl-SN-337013) Avail: CASI HC A04/MF A01

This invention relates to a new class of novel inorganic-organic hybrid thermosetting polymers and ceramics that are formed from novel linear polymers of varying molecular weight and varying carborane content. These novel organoboron thermoset polymers and ceramics contain an unsaturated cross-linked moiety. DTIC

N95-29586# University of Southern Illinois, Carbondale, IL. Dept. of Chemistry and Biochemistry.
PREPARATION AND STUDIES OF URAZOLE CONTAINING POLYMERS Final Report, 15 Jan. 1990 - 31 Dec. 1991
Mark J. Bausch 2 Sep. 1994 7 p
(Contract DAAL03-90-G-0046)
(AD-A290685; ARO-27445.6-CH) Avail: CASI HC A02/MF A01

The fact that the three nitrogen atoms present in urazole and appropriately substituted urazoles have been shown to possess substantial bond-making reactivities has prompted our investigations of (1) the stabilities of nitrogen-entered anions and radicals derived from substituted urazoles; (2)issues related to the syntheses of selected urazole monomers; and (3) the properties of a number of polymers that contain urazoles as monomeric subunits. Published discoveries from this project include (1) determinations of acidity constants for urazole and substituted urazoles in dimethyl sulfoxide as well as aqueous solutions; (2) evaluations of the N-H homolytic bond strengths in urazole, substituted urazoles, and related heterocycles; and (3) determinations of the reaction products that result when 1-phenylurazole is subjected to conditions that result in its methylation. Unpublished results from this project include (1) synthesis of various dinitro- and diaminourazoles (useful urazole monomers); (2) synthesis of polyurazole-ketones; (3) synthesis of polyurazole epoxies; (4) synthesis of polyurazole-imides; and (5) characterization of the aforementioned polymers. The newly-synthesized polyurazoles were shown to be insoluble in chlorinated organic solvents but were found to be sparingly soluble in DMSO. The polyurazole- ketones and polyurazole epoxies had Tg's of about 260 C. DTIC

N95-29635# Stanford Univ., CA. Dept. of Materials Science and Engineering.
SUPERPLASTIC CERAMICS Final Report, 15 Jun. 1991 - 14 Jun. 1994
Oleg D. Sherby and Woo-Jin Kim 1 Sep. 1994 10 p
(Contract DAAL03-91-G-0172)
(AD-A290817; ARO-28761.1-MS) Avail: CASI HC A02/MF A01

Superplasticity is a newly observed phenomenon in ceramics, with the first publication appearing in 1986. The current program has centered on an experimental study of superplasticity in polycrystalline iron carbide. This material has been made superplastic by utilization of two processing methods: powder processing and ingot-processing. In both cases the end microstructure is a continuous phase of ultra-fine grained iron carbide. The ultra-fine grained powder processed material was successfully gas-pressure blow-formed into a spherical shaped object, and its deformation followed the predicted behavior of a high strain-rate sensitive material that is controlled by grain-boundary sliding. Thermo-mechanical processing routes were developed to refine the coarse as-cast ingot microstructure. Structural refinement is a result of creation of strain-free regions by carbon dissolution from high strain energy subgrain boundaries and slip bands. It is proposed that thermomechanical processing of ingot-cast eutectic-composition oxide ceramics to achieve a superplastic structure is feasible. DTIC

N95-29772 Texas Univ., Austin, TX.
TOUGHENING MECHANISMS IN MIXED-MODE INTERFACIAL FRACTURE Ph.D. Thesis
Yue-Miin Liang 1993 147 p
Avail: Univ. Microfilms Order No. DA9413536

The purpose of this study was to examine the mechanisms of toughening in interfacial fracture under mixed-mode conditions. A combined experimental, numerical, and analytical approach was used to examine interfacial crack initiation between glass and epoxy using edge-cracked bimaterial strip specimens. The specimen was subjected to biaxial loads, and could generate mode-mixes ranging from minus 90 deg to 74 deg. The material behavior of the epoxy was examined using tensile, plane strain compression, and biaxial tests with combinations of tension/compression and shear. The parameters for elasticity, rate-independent plasticity, and rate-dependent plasticity, were determined, and were then used in modelling interfacial fracture experiments that followed. In the crack initiation experiments, measurements of applied displacements and reactive loads were complemented by measurements of normal crack opening displacements (NCOD) using optical interferometry. The latter measurements allowed three-dimensional effects to be examined. There was very little variation in NCOD along straight crack fronts. However, for curved crack fronts, the NCOD varied significantly throughout the thickness. Three-dimensional finite element analyses indicated that the NCOD were very similar to those obtained by considering plane stress conditions. The plane stress predictions were in good agreement with measured NCOD, except for locations very close to the crack front, where long range cohesive stress were active. The cohesive stress distributions were determined from the difference between NCOD obtained from rate-dependent plasticity and measured values. These distributions were very similar to those obtained from Coulomb's Law of electrostatic attraction. Interfacial fracture toughnesses obtained from the current set of experiments were larger and had a different distribution than those from earlier experiments. Various shielding mechanisms were examined, including plasticity, viscoelasticity, electrostatic stresses, and interfacial asperities. Among them, plasticity and electrostatic stress shielding had the strongest effect on the total toughness, but still did not explain adequately the noted increase in toughness with increasing shear. Dissert. Abstr.

N95-29799 Virginia Polytechnic Inst. and State Univ., Blacksburg, VA.
A STUDY OF BLISTER TESTS FOR FILM ADHESION MEASUREMENT AND FRACTURE EFFICIENCY OF TESTS FOR ADHESIVE BONDS Ph.D. Thesis
Yeh-Hung Lai 1994 193 p
Avail: Univ. Microfilms Order No. DA9425578

A novel concept, the fracture efficiency, is proposed in this dissertation as a performance index of fracture specimen designs for adhesive bonds. Evaluated based on a simple quantity, the fracture efficiency parameter, the fracture efficiency represents how much crack driving force a certain specimen design can produce along the bondline for a given maximum non-singular stress in the adherends. In this dissertation, a study of membrane peeling specimens shows that various existing test geometries have little difference in the fracture efficiency. Furthermore, the study shows that it is unlikely to develop new membrane peeling tests with high fracture efficiency. Therefore, gross inelastic energy dissipation in the film specimen may occur when using the membrane peeling tests, and may result in large errors in the film adhesion measurement when only elastic material response is considered in the analysis. As a result, the use of a backing material for film adhesion measurement is suggested because of the significant increase in the fracture efficiency when a proper backing material is used. Besides the use as one of the guidelines for fracture specimen designs, it is also demonstrated in this dissertation that the fracture efficiency parameter can also be used to help one determine the validity of a measured bond fracture strength. The study of fracture efficiency leads to

new analyses of several existing fracture test geometries, and contributes to a better understanding of the standard blister, island blister, peninsula blister, peel, and cracked lap shear tests. It is found that the island blister and peninsula blister tests can produce very high energy release rates at low pressures by using a small island radius or a small peninsula width. However, these so called high energy release rate tests also induce localized high stress concentrations near the debond front and therefore, yielding or rupturing may still be unavoidable in such specimens. The significant localized inelastic effect on the measurement of the bond fracture strength is also demonstrated in the peninsula blister experiment for an adhesive tape specimen subjected to a relatively low pressure load. Another important conclusion drawn from the analyses of various membrane peeling tests is that the existing membrane blister tests are special cases of the peel test if compared very near the debond front. Besides analyses for membrane peeling specimens, this dissertation also reports a new closet form solution for the cracked lap shear specimen using a geometrically nonlinear beam-column approach. Excellent agreement for energy release rates has been shown between the closet form solution and geometrically nonlinear finite element analyses. The study also discusses how to design a cracked lap shear specimen of constant energy release rate and high fracture efficiency. Dissert. Abstr.

N95-29822 Akron Univ., Akron, OH.
STRUCTURE AND ORIENTATION BEHAVIOR OF HIGHLY ORIENTED POLYMERS UNDER TENSILE AND COMPRESSIVE STRESSES Ph.D. Thesis
Rafael Garcia-Ramirez 1994 205 p
Avail: Univ. Microfilms Order No. DA9425865

The birefringence of Kevlar 49(R) fibers has been shown to decrease with compressive strain, suggesting that structure changes under compression involve decreasing crystallite orientation. This mechanism appears to be the inverse of that occurring under tension, for which increasing crystallite orientation has been reported to occur, leading to non-linear elasticity. A contrast between the effects of both stress modes on structure (orientation) response is presented. While birefringence presents itself as a technically convenient and economically attractive technique for this type of study, caution must be exercised when interpreting results from measurements under stress. For highly crystalline fibers, experiments have led to the attribution of the observed changes in birefringence almost entirely to crystallite orientation. This study presents an analysis of the different contributions to birefringence under stress. X-ray diffraction experiments have been performed for Kevlar 49(R) fibers under tensile stress. Results from crystal orientation cannot account for changes observed in birefringence. Moreover, they appear to account only for a small fraction of the total change. These observations suggest significant contributions from other sources. Theoretical calculations have been carried out under simulated stress conditions to quantify the effect of molecular deformation on the observed birefringence of Kevlar 49(R) fibers. The results have been obtained using semi-empirical molecular orbital calculations with the AM1 Hamiltonian in MOPAC. This analysis has been applied to poly(p-phenylene terephthalamide) (PPTA) and polyethylene (PE) chains. For PE, stress free computations were performed on segments of up to 50 -(CH2-CH2)- units. Strains up to 1 percent were applied on segments of up to 40 units. For PPTA, segments of up to 5 PTA units were analyzed. Strain-free results indicate a linear dependence of molecular polarizability on chain length. The treatment yields also a linear trend for the effect of strain on the polarizability of PE segments. Thus, the calculations predict a plane in 3-D space for the dependence of molecular polarizability on both chain size and strain. The predicted molecular polarizabilities are used to evaluate the effect of stress on birefringence of the idealized polymers, by applying existing internal-field theory. Results indicate significant effects from molecules deforming under the stress field. Author

N95-29926# Dartmouth Coll., Hanover, NH.
MEASUREMENT OF INTERFACE STRENGTH, INTRINSIC TOUGHNESS AND THEIR DEPENDENCE ON INTERFACIAL SEGREGANTS Final Report
Vijay Gupta 26 Dec. 1994 43 p
(Contract DAAL03-91-G-0059)
(AD-A291169) Avail: CASI HC A03/MF A01

This report discusses a novel laser spallation technique for measuring the tensile strength of planar thin film interfaces. In this technique, a laser-produced compressive stress pulse in the substrate, reflecting from the coating's free surface pulls the interface in tension and leads to its failure if the tensile amplitude is high enough. The interface stress is determined by recording the coating or substrate free-surface velocities using a Doppler interferometer. Interface strengths of several metal/ceramic, ceramic-ceramic and ceramic/polymer systems are summarized from our recent efforts. In addition, two breakthroughs, the first of a novel interferometer to record velocities from rough surfaces, and the second of a technique to produce subnanosecond rise-time stress pulses with no asymptotic post-peak decay, are discussed which further allows the technique to be applied to rough thermal spray coatings and also to films as thin as 0.1 micrometer. This technique is used to establish a fundamental strength-structure-chemistry relationship for Nb/sapphire interfaces, with and without the interlayers of Cr and Sb. This allows the interface strengths to be controlled over a wide range, as required for realizing the strategy of deflecting impinging matrix cracks along the fiber/matrix interfaces so as to impart toughness in otherwise brittle composites. The required values of fiber/matrix interface toughness needed for crack deflection were obtained by using the method of dual singular integral equations. Finally, in a separate study, the short stress pulses are used to determine the dynamic response of laminates, and preliminary results are presented that show their potential in evaluating the damage in composites in a non-destructive mode. DTIC

N95-29939# Massachusetts Inst. of Tech., Cambridge, MA. Dept. of Chemical Engineering.
NANOCRYSTALLINE PROCESSING AND INTERFACE ENGINEERING OF Si3N4-BASED CERAMICS Progress Report, 1 Jul. - 30 Sep. 1994
Jackie Y. Ying 30 Sep. 1994 2 p
(Contract N00014-94-1-0546)
(AD-A291302) Avail: CASI HC A01/MF A01

During the past three months, our efforts have been devoted to synthesizing nanocrystalline Si3N4 and Y2O3. For nanocrystalline Si3N4, a tubular reactor design has been adopted to produce nanoclusters by inert gas condensation in a forced flux flow. This reactor involves various features that allow us to control the synthesis conditions. Evaporation of Si takes place in a cruible located near one end of the reactor. A gas flow is established through the use of a booster pump to bring the nanoclusters generated quickly out of the hot growth zone to prevent particle agglomeration. The nanometer-sized particles are deposited on a liquid-nitrogen cooled flat plate at the other end of the reactor through thermophoresis. DTIC

N95-29983# Asian Office of Aerospace Research and Development, APO San Francisco, CA. Air Force Office of Scientific Research.
THE 2ND INTERNATIONAL CONFERENCE ON THIN FILM PHYSICS AND APPLICATIONS
S. J. Yakura 17 Apr. 1994 6 p Conference held in Shanghai, China, 15-17 Apr. 1994
(AD-A292353; AOARD-TR-94-12) Avail: CASI HC A02/MF A01

The Second International Conference on Thin Film Physics and Applications was held 15-17 Apr. 1994 at the Jin Sha Hotel in Shanghai, China. The level of Chinese research carried out in thin film technology was found to be still immature as compared with the U.S., Japan, and Europe. Selected conference papers, presented by Chinese scientists, are included in this report to show the extent of research being carried in China in this field. DTIC

N95-30030# Army Research Lab., Watertown, MA. Materials Directorate.
POLYETHYLENE-BASED POLYURETHANE COPOLYMERS AND BLOCK COPOLYMERS Final Report
C. A. Byrne, C. R. Desper, N. S. Schneider, B. Chu, and Y. J. Li Nov. 1994 34 p
(AD-A289996; ARL-TR-649) Avail: CASI HC A03/MF A01

Low molecular weight hydroxy terminated polyethylene (HTPE) containing on average an ethyl group every 16-18 carbon atoms, and a hydroxy functionality of 2.6, has been used to prepare polyurethane copolymers and block copolymers which have good solvent resistance. The polymers show somewhat complicated thermal behavior, including T sub g at around -40 C due to the HTPE and diffuse endotherms between 40 and 60 C. The simple copolymers, containing only the polyol and a diisocyanate, show infrared evidence for two phases in the case where CHDI

(trans-1,4-diisocyanatocyclohexane), was used, and poorer phase separation where other diisocyanates were used. Dynamic mechanical spectra show very broad tan delta transitions for the copolymers in the range of -9 to -23 C. All the polymers exhibit another transition in the G curve above room temperature. For the simple copolymers at 30 C, SAXS reveals a microphase separated structure which increases in spacing, then disappears in the 60-70 C range. With cooling, the microphase separated structure reappears readily for the CHDI-based copolymer, while its reappearance shows a hysteresis resulting from rate effects for the other copolymers. DTIC

N95-30071# Arizona Univ., Tucson, AZ.
CERAMICS DERIVED FROM ORGANO-METALLIC PRECURSORS Final Report, 1 May - 30 Sep. 1994
Donald R. Uhlmann 10 Feb. 1995 43 p
(Contract F49620-94-1-0099)
(AD-A291434; AFOSR-95-0105TR) Avail: CASI HC A03/MF A01

During the five months covered by this grant, our research on the program was principally focused on two areas: (1) use of silylated laser dyes in solid state hosts; and (2) optical properties and surface patterning of polyceram materials. Progress in each of these areas will be summarized in the following sections. DTIC

N95-30118# Army Research Lab., Watertown, MA. Materials Directorate.
FRACTOGRAPHY OF ADVANCED STRUCTURAL CERAMICS: RESULTS FROM THE VAMAS ROUND ROBIN EXERCISE Final Report, Feb. 1993 - Jun. 1994
Jeffrey J. Swab and George Quinn (National Inst. of Standards and Technology, Gaithersburg, MD.) Dec. 1994 154 p
(AD-A290930; ARL-TR-656; VAMAS-TR-19) Avail: CASI HC A08/MF A02

Fractography of ceramic specimens and components is critical to the design and future use of ceramic materials in commercial applications. In 1992 the US Department of Defense released Military Handbook 790 'Fractography and Characterization of Fracture Origins in Advanced Structural Ceramics' which furnished guidelines for the comprehensive interpretation of ceramic fractographic information. Even with the release of this handbook there were still some issues which warranted further study. A round robin exercise sponsored by the Versailles Project on Advanced Materials and Standards (VAMAS) was conducted to determine the applicability of the handbook and to attempt to clarify any ambiguous sections or issues. The exercise was divided into three topics. Topic #1 addressed the detection and interpretation of machining damage on photographs of ceramic specimens. Topic #2 dealt with the fractographic analysis of ceramic specimens. Topic #3 was optional, and asked the participants to perform fractography on a ceramic material of their choice. DTIC

N95-30120# Albany International Research Corp., Mansfield, MA.
DEVELOPMENT OF FLAME RESISTANT, HIGH EFFICIENCY THERMAL INSULATION Final Report, May 1992 - May 1994
James G. Donovan Jan. 1995 105 p
(Contract DAAK60-92-C-0035)
(AD-A291136; NATICK-TR-95/013) Avail: CASI HC A06/MF A02

The purpose of the program was to build upon an understanding of polymeric-fiber-based thermal insulation, gained through two previous Al Research Co./U.S. Army Natick RD&E Center contracts, to develop two new flame-resistant insulator configurations. They were to be lofty, water-repellent, durable and highly efficient on a thermal resistance/weight basis. One was to be based upon staple (cut) fiber, the other on continuous filament (endless fiber). Ten inherently flame-resistant fiber candidates that were predicted to be feasible bases for highly efficient insulation were selected for laboratory trials. Initial work with them showed that flame resistance would be the most difficult-to-attain performance objective. A low insulator density target and the need to include binder material to provide insulator durability exacerbated the flammability problem. An empirical approach that relied heavily upon laboratory-scale batt making trials and flammability testing, but also included many other types of tests, eventually lead to adoption of a satisfactory, three-component, bonded, staple-fiber insulator prototype. It met all program performance objectives. Continuous filament insulator development was hindered by the lack of an adequately flame resistant, continuous filament material, by the lack of a satisfactory bonding system, and by the need to conduct many experiments on production, rather than laboratory scale. Further pursuit of the flame resistant, continuous filament insulator approach is not recommended unless new materials become available. However, it appears that the performance, versatility and reasonable cost of the flame resistant, staple-based insulator prototype will diminish the need for an alternative configuration. DTIC

N95-30132# Department of the Navy, Washington, DC.
LINEAR CARBORANE-(SILOXANE OR SILANE)-ACETYLENE BASED COPOLYMERS Patent Application
David Y. Son, inventor (to Navy) and Teddy M. Keller, inventor (to Navy) 7 Nov. 1994 49 p
(AD-D017321; US-Patent-Appl-SN-337012) Avail: CASI HC A03/MF A01

A novel organoboron polymer and its method of preparation is claimed. The organoboron polymer has a backbone having a repeating unit comprising at least one carboranyl group, at least two acetylenic groups, and one or more silyl or siloxanyl groups. DTIC

N95-30174# Oak Ridge National Lab., TN.
NANOINDENTATION AND NANOSCRATCHING OF HARD COATING MATERIALS FOR MAGNETIC DISKS
T. Y. Tsui (Rice Univ., Houston, TX.), G. M. Pharr (Rice Univ., Houston, TX.), W. C. Oliver (Nano Instruments, Inc., Knoxville, TN.), Y. W. Chung (Northwestern Univ., Evanston, IL.), and E. C. Cutiongco (Northwestern Univ., Evanston, IL.) 1994 6 p Presented at the 1994 Fall Meeting of the Materials Research Society (MRS), Boston, MA, 28 Nov. - 2 Dec. 1994
(Contract DE-AC05-84OR-21400)
(DE95-008776; CONF-941144-90) Avail: CASI HC A02/MF A01

Nanoindentation and nanoscratching experiments have been performed to assess the mechanical and tribological behavior of three thin film materials with potential application as wear resistant coatings for magnetic disk storage: (1) hydrogenated-carbon (CHx); (2) nitrogenated-carbon (CNx); and (3) boron suboxide (BOx). The hardness and elastic modulus were measured using nanoindentation. Ultra-low load nanoscratching tests were performed to assess the relative scratch resistance of the films and measure their friction coefficients. The mechanical and tribological performance of the three materials are discussed and compared. DOE

N95-30190# Oak Ridge National Lab., TN.
DEPTH-INDEPENDENT HARDNESS IMPROVEMENTS IN ION IRRADIATED POLYSTYRENE
G. R. Rao, L. Riester, and E. H. Lee 1994 9 p Presented at the 1994 Fall Meeting of the Materials Research Society (MRS), Boston, MA, 28 Nov. - 2 Dec. 1994
(Contract DE-AC05-84OR-21400)
(DE95-008682; CONF-941144-93) Avail: CASI HC A02/MF A01

Polystyrene (PS) was irradiated with 2 MeV He(+) ions to a fluence of 3.3 x 10(exp 19) ions/sq m. Across-section of the irradiated layer was subjected to hardness measurements across the section using a nanoindentation technique. Results showed that hardness increased as a function of irradiation depth and showed a maximum value of 12 GPa at a depth of approximately 6.5 micro m, for a total ion penetration range of 9 micro m, as compared to a hardness of 0.45 GPa for unirradiated PS. The hardness variation with depth followed the trend for Linear Energy Transfer (LET) for ionization from the energetic ions to substrate atoms. This investigation showed for the first time how hardness varies as a function of depth for ion-irradiated polymers; this variation approximately follows the ionization LET profile, suggesting that cross-linking in the polymers could be proportional to ionization. DOE

N95-30201# Technische Univ., Delft (Netherlands).
IMPACT PROPERTIES OF COATED ENGINEERING PLASTICS Ph.D. Thesis
M. Bosma 14 Oct. 1994 169 p
(PB95-197281) Avail: CASI HC A08/MF A02

In this study the surface embrittlement of coated plastics was determined at various temperatures and strain rates as a function of the level of adhesion between coating and substrate, the coating thickness and the ductility of the coating. For this reason, coated plastic samples were used for which these parameters were varied systematically. To determine the

influence of the level of adhesion and the coating ductility on the mechanical properties of coated plastics, it was found necessary to develop new test methods for the quantitative measurement of these properties. A very ductile, rubber-modified polyamide-66/polyphenylene ether-blend (IM PA66/PPE) was used as a model substrate. NTIS

N95-30237*# Worcester Polytechnic Inst., MA. Dept. of Mechanical Engineering.
ENGINEERING DESIGN OF SUB-MICRON TOPOGRAPHIES FOR SIMULTANEOUSLY ADHERENT AND REFLECTIVE METAL-POLYMER INTERFACES Final Report
Christopher A. Brown 29 Oct. 1993 56 p
(Grant NAG1-1476)
(NASA-CR-198845; NAS 1.26:198845) Avail: CASI HC A04/MF A01

The approach of the project is to base the design of multi-function, reflective topographies on the theory that topographically dependent phenomena react with surfaces and interfaces at certain scales. The first phase of the project emphasizes the development of methods for understanding the sizes of topographic features which influence reflectivity. Subsequent phases, if necessary, will address the scales of interaction for adhesion and manufacturing processes. A simulation of the interaction of electromagnetic radiation, or light, with a reflective surface is performed using specialized software. Reflectivity of the surface as a function of scale is evaluated and the results from the simulation are compared with reflectivity measurements made on multi-function, reflective surfaces. Author

N95-30252*# IMITECH, Inc., Schenectady, NY.
DEVELOPMENT OF LaRC (TM): IA THERMOPLASTIC POLYIMIDE COATED AEROSPACE WIRING
Jack Keating Mar. 1995 55 p
(Contract NAS1-20121; RTOP 506-43-11-01)
(NASA-CR-195048; NAS 1.26:195048) Avail: CASI HC A04/MF A01

NASA Langley has invented LaRC(exp TM) IA and IAX which are thermoplastic polyimides with good melting, thermal and chemical resistance properties. It was the objective of this contract to prepare and extrude LaRC (exp TM) polyimide onto aircraft wire and evaluate the polymers performance in this critical application. Based on rheology and chemical resistance studies at Imitec, LaRC (exp TM) IAX melts readily in an extruder, facilitating the manufacture of thin wall coatings. The polyimide does not corode the extruder, develop gel particles nor advance in viscosity. The insulated wire was tested according to MiL-W-22759E test specifications. The resulting wire coated with LaRC (exp TM) IAX displayed exceptional properties: surface resistance, non blocking, non burning, hot fluid resistance, impulse dielectric, insulation resistance, low temperature flexibility, thermal aging, wire weight, dimensions, negligible high temperature shrinkage and stripability. The light weight and other properties merit its application in satellites, missiles and aircraft applications. The extruded IAX results in a polyimide aircraft insulation without seams, outstanding moisture resistance, continuous lengths and abrasion resistance. Author

28 PROPELLANTS AND FUELS

Includes rocket propellants, igniters, and oxidizers; their storage and handling procedures; and aircraft fuels.

For related information see also *07 Aircraft Propulsion and Power, 20 Spacecraft Propulsion and Power,* and *44 Energy Production and Conversion.*

N95-29019# Army Tank-Automotive Research and Development Command, Warren, MI. Fuels and Lubricants Div.
DEVELOPMENT OF THE TEST KIT FOR FUEL ACID CONTAMINATION Final Report, 1 Oct. 1990 - 31 Mar. 1991
Shing-Bong Chen and Bill Williams Feb. 1995 33 p
(AD-A291953; TARDEC-TR-13617) Avail: CASI HC A03/MF A01

This report describes efforts to develop a test method for determining the presence of a fuel acid contaminant used as a possible anti-materiel agent in military fuels. The test method must be usable in a field environment. After investigation of the properties of candidate agents and evaluation of a substitution reaction detection method, the use of pH indicator solutions following water extraction was determined to be the most appropriate for this application. The report also describes the fabrication of test models of the Test Kit for Fuel Acid Contamination for use by troops in the latter stages of Operation Desert Storm. A copy of a draft Purchase Description that can be used for possible future procurement is included. DTIC

N95-29280# Argonne National Lab., IL. Chemical Technology Div.
TECHNOLOGY DEVELOPMENT GOALS FOR AUTOMOTIVE FUEL CELL POWER SYSTEMS Final Report
Brian D. James, George N. Baum, and Ira F. Kuhn, Jr. Aug. 1994 178 p Prepared in cooperation with Directed Technologies, Inc., Arlington, VA
(Contract W-31-109-eng-38)
(DE95-008764; ANL-94/44) Avail: CASI HC A09/MF A02

This report determines cost and performance requirements for Proton Exchange Membrane (PEM) fuel cell vehicles carrying pure H2 fuel, to achieve parity with internal combustion engine (ICE) vehicles. A conceptual design of a near term FCEV (fuel cell electric vehicle) is presented. Complete power system weight and cost breakdowns are presented for baseline design. Near term FCEV power system weight is 6% higher than ICE system, mid-term FCEV projected weights are 29% lower than ICE's. There are no inherently high-cost components in FCE, and at automotive production volumes, near term FCEV cost viability is closer at hand than at first thought. PEM current vs voltage performance is presented for leading PEM manufacturers and researchers. 5 current and proposed onboard hydrogen storage techniques are critically compared: pressurized gas, cryogenic liquid, combined pressurized/cryogenic, rechargeable hydride, adsorption. Battery, capacitor, and motor/controller performance is summarized. Fuel cell power system component weight and cost densities (threshold and goal) are tabulated. DOE

N95-29498# Cornell Univ., Ithaca, NY. Dept. of Chemistry.
STATE RESOLVED DIFFERENTIAL CROSS SECTIONS FOR REACTIONS IMPORTANT TO THE DECOMPOSITION OF ENERGETIC MATERIALS Final Report, 1 Jun. 1991 - 31 May 1994
Paul L. Houston 1 Sep. 1994 10 p
(Contract DAAL03-91-G-0125)
(AD-A290718; ARO-28700.3-CH) Avail: CASI HC A02/MF A01

This final report describes the research whose goal was to develop a new technique for characterizing the velocity distributions of state-selected reaction products and to use this technique to study reactions of importance to the decomposition of energetic materials. In this technique, the three-dimensional product velocity distribution is determined by ionizing the appropriate species, waiting for a delay while the species separate along their trajectories, and then projecting the spatial distribution of ions onto a two-dimensional screen. The technique was developed and tested using photodissociation of molecules such as NO2 and CH3NHNO2. Further advances were made by investigating the crossed beam dynamics of the collision of argon with NO. Initial attempts were made at investigating the reactions of H with NO2, CH3NHNO2, and H2NNO2: an intense hydrogen atom source has been developed. DTIC

N95-29525# Princeton Univ., NJ. Dept. of Chemistry.
QUANTUM DYNAMICAL STUDIES OF THE DECOMPOSITION OF ENERGETIC MATERIALS CONTAINING DEFECT STRUCTURES Final Technical Report, 1 Dec. 1992 - 30 Nov. 1994
Herschel Rabitz 23 Feb. 1995 9 p
(Contract N00014-91-J-1209)
(AD-A291456; Rept-130-6601-RPT-1) Avail: CASI HC A02/MF A01

During the period of this project, fundamental research was carried out in the area of chemical reactivity at the surface of solid materials. Emphasis was also placed on the underlying energetic transfer processes to the bulk material due to atomic and molecular fragment impacts at the interface. A fully quantum multiple collision theory approach was developed to study energetic materials reactivity, and a discrete-continuum hybrid theory for energy transfer was formulated. A series of model studies were executed with the theoretical formulations. The results revealed many of the basic principles of reactivity and energy transfer operative at interfaces or found in the propagating fronts of energetic materials. The specific research carried out under this grant is summarized in the report. DTIC

N95-29550# Johns Hopkins Univ., Baltimore, MD. Dept. of Mechanical Engineering.
A THEORETICAL STUDY ON IGNITION MECHANISMS OF LIQUID PROPELLANTS Final Report, 15 Aug. 1993 - 14 Aug. 1994
Andrea Prosperetti and He Yuan 14 Sep. 1994 67 p
(Contract DAAH04-93-G-0409)
(AD-A290569; ARO-31572.1-EG) Avail: CASI HC A04/MF A01

Two possible mechanisms for the accidental ignition of liquid propellants are studied: (1) The heating of the liquid surrounding a strongly compressed gas bubble; and (2) The heating due to viscous dissipation in a rapidly compressed drop. For the first problem the heating of the gas is calculated precisely rather than estimated on the basis of an adiabatic model. For the second problem proper allowance is made for the temperature dependence of the liquid viscosity. In general, the results indicate that ignition is in principle possible, although marginally so. This finding is generally consistent with experiment, and it may explain why it is difficult to deduce definite conclusions from the available experimental evidence. DTIC

N95-30024# Oak Ridge National Lab., TN.
INTRODUCTION TO THE PROCEEDINGS OF THE SIXTEENTH SYMPOSIUM ON BIOTECHNOLOGY FOR FUELS AND CHEMICALS
B. H. Davison 1994 4 p Presented at the 16th Symposium on Biotechnology for Fuels and Chemicals, Gatlinburg, TN, 9-13 May 1994 Prepared in cooperation with National Renewable Energy Lab.
(Contracts DE-AC05-84OR-21400; DE-AC36-83CH-10093)
(DE95-007029; CONF-940526-Summ) Avail: CASI HC A01/MF A01

Biotechnology can be defined as the use of biologically derived materials and biocatalysts to carry out desired transformations from one material to another. These biocatalysts can be enzymes or microorganisms. The transformation may be of raw materials into useful compounds or for the destruction of industrial wastes. One use of biotechnology is for the production of fuels and chemicals. This has been the broad area focused on by this symposium for the past 16 years. The Symposium on Biotechnology for Fuels and Chemicals presents both applied and fundamental work in this area performed by universities, industries, and government institutions. The goal, whether near term or long term, is to find and demonstrate efficient, economical methods for the use of biotechnology to supply society's needs for fuels and chemicals. The symposium allows interactions among the researchers in an intimate setting to foster the interactions that will be necessary to commercialize and use these technologies. Efforts presented include all aspects of the process: the pretreatment and beneficiation of the raw material, the biological conversion in some reactor, the separation and recovery of the desired product, and the treatment of the waste streams from this and earlier legacy processes. There are also efforts of the sensing, monitoring, and control of the process as well as the economic analysis to estimate the overall utility and impact. The Sixteenth Symposium on Biotechnology for Fuels and Chemicals provided a forum for the exchange of ideas. There were 34 oral presentations and 81 poster presentations. These were organized into sessions of thermal, chemical, and biological processing; bioprocessing research; process economics and commercialization; and environmental biotechnology. DOE

N95-30345# Los Alamos National Lab., NM.
ASSAY OF POTENTIALLY CONTAMINATED PROPELLANT
J. E. Koster, H. E. Williams, III, and W. S. Scott (Savanna Army Depot Activity, IL.) 1995 9 p Presented at the Waste Management 1995 Conference, Tucson, AZ, 27 Feb. - 3 Mar. 1995
(Contract W-7405-eng-36)
(DE95-006330; LA-UR-95-176; CONF-950216-114) Avail: CASI HC A02/MF A01

One of the decontamination and decommissioning projects within DOD is demilitarization of an aging stockpile of munitions. A large portion of the stockpile contains depleted uranium (DU) as an armor piercing core and so these munitions must be assayed for the presence of uranium in other components. The assay method must be fast and preferably easy to implement. Presence of DU is indicated by its alpha decay. The alpha particles in turn produce ions in the ambient air. If a significant fraction of these ions can escape the quantity of propellant, the ions can be detected instead of the alpha particles. As a test of the feasibility of detecting alpha emissions from DU somewhere within a cartridge of propellant, the transmission of ions through layers of real propellant was measured. The propellant is in the form of graphite-coated cylindrical pellets. A 105mm cartridge was modified for use as a pellet chamber. A check source served as an ion source. The ion detector consisted of a grid held at 300V coupled to an ammeter. Results confirm that this is a promising technique for testing the propellant for the presence of DU quickly yet with sensitivity. DOE

29 MATERIALS PROCESSING

Includes space-based development of products and processes for commercial applications.

For biological materials see *55 Space Biology*.

N95-30014*# Alabama Univ., Huntsville, AL. Center for Automation and Robotics.
REDUCE FLUID EXPERIMENT SYSTEM: FLIGHT DATA FROM THE IML-1 MISSION Final Report
Gary L. Workman and Sabrina Harper 13 May 1995 38 p
(Contract NAS8-38609)
(NASA-CR-196639; NAS 1.26:196639) Avail: CASI HC A03/MF A01

Processing and data reduction of holographic images from the International Microgravity Laboratory 1 (IML-1) presents some interesting challenges in determining the effects of microgravity on crystal growth processes. Use of several processing techniques, including the Computerized Holographic Image Processing System and the Software Development Package (SDP-151) will provide fundamental information for holographic and schlieren analysis of the space flight data. Author

N95-30339*# National Aeronautics and Space Administration. Lewis Research Center, Cleveland, OH.
SUMMARY REPORT OF MISSION ACCELERATION MEASUREMENTS FOR STS-65, LAUNCHED 8 JULY 1994
Melissa J. B. Rogers (Tal-Cut Co., Beachwood, OH.) and Richard DeLombard Mar. 1995 270 p Original contains color illustrations
(RTOP 963-60-OD)
(NASA-TM-106871; E-9490; NAS 1.15:106871) Avail: CASI HC A12/MF A03; 81 functional color pages

The second flight of the International Microgravity Laboratory (IML-2) payload on board the STS-65 mission was supported by three accelerometer instruments: The Orbital Acceleration Research Experiment (OARE) located close to the orbiter center of mass; the Quasi-Steady Acceleration Measurement experiment, and the Space Acceleration Measurement System (SAMS), both in the Spacelab module. A fourth accelerometer, the Microgravity Measuring Device recorded data in the middeck in support of exercise isolation tests.Data collected by OARE and SAMS during IML-2 are displayed in this report. The OARE data represent the microgravity environment below 1 Hz. The SAMS data represent the environment in the 0.01 Hz to 100 Hz range. Variations in the environment caused by unique activities are presented. Specific events addressed are: crew activity, crew exercise, experiment component mixing activities, experiment centrifuge operations, refrigerator/freezer operations and circulation pump operations. The analyses included in this report complement analyses presented in other mission summary reports. Author (revised)

31 ENGINEERING (GENERAL)

Includes vacuum technology; control engineering; display engineering; cryogenics; and fire prevention.

N95-28686 Naval Facilities Engineering Service Center, Port Hueneme, CA.
LIQUID PRESSURE AMPLIFICATION AND LIQUID INJECTION IN AIR CONDITIONING AND REFRIGERATION SYSTEMS
Bradley Yee Jun. 1994 5 p Limited Reproducibility: More than 20% of this document may be affected by microfiche quality
(AD-A289738; NFESC-TDS-2005-ENG) Avail: Issuing Activity (Defense Technical Information Center (DTIC))

Liquid pressure amplification and liquid injection are two patented methods of decreasing compressor energy consumption and increasing condenser

capacity in an existing reciprocating vapor compression refrigeration system. Although this 6-year-old technology has been installed on thousands of existing systems, it continues to generate controversy in engineering and utility circles. DTIC

N95-28705 ESDU International Ltd., London (England).
SELECTION AND COSTING OF HEAT EXCHANGERS. AIR-COOLED TYPE
Dec. 1994 21 p
(ISSN 0141-402X)
(ESDU-94043; ISBN-0-856-79930-0) Avail: ESDU

ESDU 94043 extends the information in ESDU 92013 which, when an air-cooled exchanger is found appropriate and is costed, provides the results for a datum design 40 ft (12.2 m) long with G-fins and 1 in (25 mm) diameter tube operating at a noise level of 85 dBa. It provides factors derived from an analysis of manufacturer's data to be applied to the cost results from ESDU 92013 to account for variations in those parameters and features. Additional guidance on the configuration and use of air-cooled exchangers is given. The data are incorporated in ESDUpac A9213 which is a Fortran program that implements the selection and costing method of ESDU 92013. It is provided on disc in the software volume compiled to run under DOS with a user-friendly interface that prompts on screen for input data. ESDU

N95-28706 ESDU International Ltd., London (England).
SELECTION AND COSTING OF HEAT EXCHANGERS. SHELL-AND-TUBE TYPE
Dec. 1994 42 p
(ISSN 0141-402X)
(ESDU-94042; ISBN-0-856-79929-7) Avail: ESDU

ESDU 94042 extends the information in ESDU 92013 which, when a shell-and-tube exchanger is found appropriate and is costed, provides the results for a datum design with fixed average values of fluid pressure, tube diameter, shell length-to-diameter ratio, baffle pitch and for a particular shell type, and shell and tube materials. It provides factors derived from an analysis of manufacturer's data to be applied to the cost results from ESDU 92013 to account for variations in those parameters and features. Additional guidance on the configuration and use of shell-and-tube exchangers is given. The performance of the exchangers is calculated using the effectiveness-NTU method and graphs of those data are included for E-shells in series. The data are incorporated in ESDUpac A9213 which is a Fortran program that implements the selection and costing method of ESDU 92013. It is provided on disc in the software volume compiled to run under DOS with a user-friendly interface that prompts on screen for input data. ESDU

N95-29307# Army Construction Engineering Research Lab., Champaign, IL. Energy and Utilities Systems Div.
ALTERNATIVE REFRIGERANT PERFORMANCE: FIELD TEST OF A NONCHLOROFLUOROCARBON CHILLER AT FORT LEONARD WOOD, MO Final Report
Chang W. Sohn, John J. Tomlinson, Nancy C. Herring, and Brian E. Boughton Jan. 1995 36 p
(DA Proj. 4A1-62784-AT-45)
(AD-A292052; CERL-FE-95/09) Avail: CASI HC A03/MF A01

Production of chlorofluorocarbon (CFC) refrigerants will stop permanently by the end of 1995, and air-conditioning and refrigeration (AC/R) systems will have to use alternatives to CFC. The U.S. Army's AC/R systems have a total cooling capacity of more than 1 million tons; approximately 55 percent of these systems use CFC-based refrigerants. Chillers currently using CFC refrigerants must be replaced or converted to operate with non-CFC refrigerants. The U.S. Army Construction Engineering Research Laboratories (USACERL) and the U.S. Army Center for Public Works (USACPW) are doing research to find an efficient, alternative refrigerant for Army installations. The current project monitored the performance of a non-CFC (R-134a) centrifugal chiller at Fort Leonard Wood (FLW), MO. Performance of this chiller under field conditions was compared with the manufacturer's published ratings. Operational characteristics of the R-134a chiller were obtained by measuring electrical energy consumption, cooling delivered to the chiller cooling loop, and heat rejected by the condenser. Results indicated an average performance of approximately 0.68 kilowatts per ton (kW/ton) for the study period. The manufacturer's design projection was 0.73 kW/ton. The performance evaluation of the R-134a system shows that it is an efficient addition to the FLW facility. DTIC

N95-29537# Army Construction Engineering Research Lab., Champaign, IL. Energy and Utilities Systems Div.
USE OF CHLOROFLUOROCARBON-BASED REFRIGERANTS IN USARMY FACILITY AIR-CONDITIONING AND REFRIGERATION SYSTEMS: RECOMMENDATIONS FOR THE INTERIM PERIOD 1994-2000 Final Report
Chang W. Sohn, Kelly O. Homan, and Nancy Herring Nov. 1994 26 p
(DA Proj. 4A1-62784-AT-41)
(AD-A290432; USACERL-TR-FE-95/05) Avail: CASI HC A03/MF A01

Production of chlorofluorocarbons (CFC's) and hydrochlorofluorocarbons (HCFC's) has been scheduled for phaseout because of the contribution of these chemicals to the depletion of the stratospheric ozone layer. CFC production is scheduled for phaseout by January 1, 1996; HCFC production will halt by the year 2020. The next generation of refrigerants is expected to be tested and widely available by the turn of the century. As a large-scale end user of CFC-based refrigerants, the U.S. Army is faced with a significant challenge by the phaseout of these chemicals. This report makes recommendations for refrigerant use in U.S. Army facility air-conditioning and refrigeration applications for the interim period from the present to the year 2000. Only equipment using CFC refrigerants is addressed since the lifetime of equipment using CFC's will expire before HCFC refrigerants are phased out. Available options to run as-is, convert, or replace CFC-based machines should be examined in cooperation with reputable contractors representing the original equipment manufacturers (OEM's). Only refrigerants approved by the U.S. Environmental Protection Agency (USEPA) should be considered for use in retrofitted or replaced equipment. As a part of the equipment evaluation, opportunities to improve system efficiency and reliability should also be sought. DTIC

N95-29579# Strathclyde Univ., Glasgow (Scotland).
THE 2ND EUROPEAN CONFERENCE ON SMART STRUCTURES AND MATERIALS
Alaster McDonach, Peter T. Gardiner, Ron S. McEwen, and Brian Culshaw 14 Oct. 1994 390 p Conference held in Glasgow, Scotland, 12-14 Oct. 1994
(AD-A290723) Avail: CASI HC A17/MF A04

In this conference, we increase our exploration of the practical benefits which can be obtained by the application of the Smart Structures and Materials concept. Space scientists and engineers are used to waiting half their lives for the fulfillment of their plans. Their enthusiastic vibrations remain undamped. But the Smart Structures and Materials concept has many strings to its bow. Cunningly implemented, it can enhance safety and prolong performance and thereby save money! It is not surprising therefore that smart concepts are invading the more down-to-earth world of buildings and bags, medicine and manufacturing. Examples of these applications will be found in this conference, affirmation that the subject is moving along with a life of its own. DTIC

N95-29918# Institute for Defense Analyses, Alexandria, VA.
PROPOSED DEPARTMENT OF DEFENSE SOFTWARE METRICS IMPLEMENTATION PLAN Final Report
Dennis W. Fife, Judy M. Popelas, and Beth Springsteen Sep. 1994 51 p
(Contract MDA903-89-C-0003)
(AD-A291404; IDA-P-3019) Avail: CASI HC A04/MF A01

This report presents a proposed plan for DOD implementation of software metrics in support of acquisition reform and improved software risk management. The report documents the concluding phase of a one-year task to assess software metrics and to determine how to improve their use in software acquisition, particularly of weapon system software. An earlier effort surveyed the state of development and use of software metrics in industry and defense organizations. This survey found (1) that industry is strongly committed to using software metrics in a corporate-wide approach to gain marketplace advantages, and (2) that defense contractors exhibit a state of evolution in metrics use that is comparable to that of strictly commercial companies, if not more mature. The overall vision of the proposed plan is to establish a department-wide, bottom-to-top corporate approach for collecting and using software metrics to improve analysis and

decision-making in software acquisition and risk management. Acquisition reform and the need for improved risk management should provide more specific goals to address under this vision, comparable to industry's goals of marketplace benefits from using software metrics. The plan is framed as eight specific recommendations, including a list of future research and development work that would support their implementation. DTIC

N95-29924# Federal Aviation Administration, Atlantic City, NJ.
THE COMPARATIVE EXTINGUISHMENT PERFORMANCE AND THERMAL DECOMPOSITION PRODUCTS OF HALON ALTERNATIVE AGENTS Final Report
Robert A. Filipczak Dec. 1994 75 p
(AD-A291161; DOT/FAA/CT-94/59) Avail: CASI HC A04/MF A01

Halon 1301, Halon 1211, and eleven alternative fire-fighting agents were compared for extinguishment effectiveness and thermal decomposition product generation, using a laboratory-scale test apparatus having methane as the fuel. Chemical analysis was conducted using a magnetic sector mass spectrometer with simultaneous measurement of oxygen consumption and carbon dioxide, water, and acid gas production. Chemical mechanisms are advanced to explain how halogenated hydrocarbons extinguish fires. The major conclusion was that the alternative agents were not as effective at fighting fires as Halons and that greater amounts of acid gases were produced during extinguishment. Hydrogen fluoride was found to be the predominant thermal decomposition product for all agents. DTIC

N95-30182# Lawrence Livermore National Lab., Livermore, CA.
SI HANDBOOK FOR THE LAWRENCE LIVERMORE NATIONAL LABORATORY: COMMITTEE ON METRIC TRANSITION
1 Mar. 1995 30 p
(Contract W-7405-eng-48)
(DE95-009329; UCRL-ID-119971) Avail: CASI HC A03/MF A01

This Handbook is a guide to the use of the International System of Units (SI) at the Lawrence Livermore National Laboratory. It describes the reasons for the United States converting to the metric system, legislation related to metric conversion, why the Laboratory is converting to the metric system, how international standards are established, the structure of SI, rules for using SI units and symbols, allowable non-SI units, and other important information about SI units and international standards. This handbook also demonstrates techniques for converting between inch-pound and metric units, and it contains tables of conversion factors. This Handbook is intended for the person who needs a practical working knowledge of the units of the modernized metric system, SI. The text and figures will be useful also to those who have had some experience with the metric system and want to update their knowledge, as well as to all who are interested in overcoming the normal human tendency to dislike a new system that they do not understand. The material is presented with the intent to implant the awareness of the simplifications possible with the new units, to warn of potential pitfalls associated with their use, and to guide in the recognition of which metric units and practices are correct. The text and figures are organized for ease of orientation. The sequence of units follows the natural progression from the everyday topics to the specialized ones. DOE

N95-30296# Kentucky Univ., Lexington, KY. Dept. of Mechanical Engineering.
FUNDAMENTAL STUDIES IN CRYOGENIC COOLING OF POWER ELECTRONICS Interim Report, 1 Sep. 1993 - 1 Aug. 1994
L. C. Chow, M. S. Sehmbey, O. J. Hahm, and C. J. Chui Sep. 1994 65 p
(Contract F33615-91-C-2152)
(AD-A291150; UK-ME-94-01; WL-TR-94-2100) Avail: CASI HC A04/MF A01

This study details the results from experiments conducted to study the heat transfer characteristics during liquid nitrogen spray cooling and pool boiling from a heater array. Four different nozzles at various pressures were used to study the variation in spray cooling heat transfer at liquid nitrogen temperature. Effect of nozzle and flow rate on the critical heat flux and the heat transfer coefficient are presented. This study also provides empirical correlations for the spray cooling characteristics. The critical heat flux and the heat transfer coefficient have been correlated using nondimensional numbers. The study also shows the importance of surface roughness for spray cooling with liquid nitrogen. The rougher surfaces were shown to have significantly higher heat transfer rates and similar critical heat fluxes occurring at lower temperatures. The results from experiments conducted to study the pool boiling heat transfer from a vertical array with flush mounted heat sources are also presented. The lower heaters were found to enhance the heat transfer from the upper heaters due to bubble pumped convection. DTIC

N95-30299# Washington Univ., Seattle, WA.
FEASIBILITY OF A JET-STIRRED REACTOR FOR EVALUATING REPLACEMENTS FOR HALON FIRE RETARDANTS M.S. Thesis
Jon Cybulski 14 Dec. 1994 58 p
(AD-A291155) Avail: CASI HC A04/MF A01

The main objective was to conduct preliminary experiments which would lead the way in the development of a chemical kinetic database on the flame behavior of fluorinated halon extinguishing agent replacement compounds. This was accomplished through the analysis of the combustion of simple fuels with halon additives in a jet-stirred reactor. This analysis was compared with computer modeling. The experiments addressed the flame chemistry of simple retardant compounds (CF3Br and CF3H) operating against methane fuel (CH4). Two retardants were used so that the kinetic modeling for CF3H and CF3Br reactions could be studied. The kinetic model used for CF3Br included reactions for CF3H since Halon 1301 (CF3Br) generates both the CF3 and HBr radicals during combustion reactions. Therefore, by analyzing data using two separate retardants, the overall behavior of the kinetic model could be studied. Derived from text

32 COMMUNICATIONS AND RADAR

Includes radar; land and global communications; communications theory; and optical communications.

For related information see also *04 Aircraft Communications and Navigation* and *17 Space Communications, Spacecraft Communications, Command and Tracking.* For search and rescue see *03 Air Transportation and Safety,* and *16 Space Transportation.*

N95-28687 Army Research Lab., Adelphi, MD.
CHARACTERIZING THE ELECTROMAGNETIC ENVIRONMENT PRODUCED BY THE ARMY'S REPETITIVE ELECTROMAGNETIC PULSE SIMULATOR (REPS) Final Report, 1-31 Aug. 1988
Bruce T. Benwell Oct. 1994 224 p Limited Reproducibility: More than 20% of this document may be affected by microfiche quality
(AD-A289739; ARL-TR-306) Avail: Issuing Activity (Defense Technical Information Center (DTIC))

This report characterizes the time-domain electromagnetic field environment generated by the Army's Repetitive Electromagnetic Pulse Simulator (REPS). The REPS system is a free-field radiating 3OO-m 'longwire' dipole antenna that is driven at the center by a 1-MV pulse generator. The RF environment generated by REPS was characterized in terms of two heights (1 and 2 m), field uniformity, symmetry about the antenna, and wavefront planarity. Based on measured data, 'usable' and 'recommended' test volumes have been defined. DTIC

N95-28699 Edgewood Research Development and Engineering Center, Aberdeen Proving Ground, MD.
ELECTROMAGNETIC SCATTERING BY MAGNETIC SPHERES: THEORY AND ALGORITHMS Final Report, Jul. 1993 - Jan. 1994
Merill E. Milham Oct. 1994 58 p Limited Reproducibility: More than 20% of this document may be affected by microfiche quality
(DA Proj. 1O1-62622-A-552)
(AD-A289798; ERDEC-TR-207) Avail: Issuing Activity (Defense Technical Information Center (DTIC))

The theory for the scattering of magnetic spheres is developed by means of scaling functions. This theory leads in a natural way to the development of scattering algorithms which use exponential scaling to overcome computational overflow problems. The design and testing of the algorithm is described. Fortran codes which implement the algorithmic design are presented and examples of code use are given. Listings of the code are included. DTIC

N95-28936 Institute for Defense Analyses, Alexandria, VA.
AN ALGORITHM FUSION APPROACH TO IRST SIGNAL PROCESSING (ILL): NONGAUSSIAN-CORRECTED FILTER FUSION
Jeffrey F. Nicoll and Elizabeth L. Ayers Nov. 1994 43 p Sponsored by the Office of Naval Research Limited Reproducibility: More than 20% of this document may be affected by microfiche quality
(Contract DASW01-94-C-0054)
(AD-A291565; IDA-D-1619) Avail: Issuing Activity (Defense Technical Information Center (DTIC))

The reduction of background clutter in Infrared Search and Track (IRST) systems remains a challenging problem. False alarm inducing clutter is typically nonstationary and nongaussian and may not be adequately treated by linear matched filter techniques. Previously, we examined the simultaneous use of two filters, 'filter fusion', to reduce the false alarms. This method depends upon the assumption that the residuals of two sufficiently different filters will be uncorrelated. In the present work we make explicit use of the nongaussian character of the clutter, using a threshold that depends on the local nongaussian character. The introduction of a nongaussian correction often improves the performance of both linear and nonlinear filters, including the optimal linear filter constructed for the scene. Fusing the nongaussian adjusted filters gives a further increase in performance. The use of the nongaussian correction appears to increase the robustness of the filters and the filter fusion, i.e., the performance from frame to frame within a given scene and from scene to scene is consistenly improved and made more regular. DTIC

N95-28939 Naval Research Lab., Washington, DC. Spacecraft Engineering Div.
ANALYSIS OF TROPOSPHERIC PROPAGATION CHARACTERISTICS BASED ON REGIONAL METEOROLOGICAL DATA
Junho Choi, Mara Melton, John Donohue (Allied-Signal Technical Services Corp., Alexandria, VA.), and Albert Fryland (Allied-Signal Technical Services Corp., Alexandria, VA.) 14 Feb. 1995 102 p Prepared in cooperation with Allied Technical Services Corp., Alexandria, VA Limited Reproducibility: More than 20% of this document may be affected by microfiche quality
(AD-A291581; NRL/MR/8140-95-7654) Avail: Issuing Activity (Defense Technical Information Center (DTIC))

Meteorological data has been processed to investigate RF (radio frequency) propagation efforts of the tropospheric region from ground to 28 km in space. A data base has been developed to provide enough information for analyzing many different phenomena of the troposphere in terms of lapse rate, refractivity, range error, angle error, slant range, and interrelationships among these parameters. Based on preliminary analysis, the results are very distinguishable from the values arrived at through the application of conventional data for analysis of RF propagation patterns. This implies that the seasonal average value provides better indications of the current atmospheric variation than the annual global average value which most users have adopted for convenience. DTIC

N95-28943 Rome Lab., Griffiss AFB, NY.
STATISTICAL PROPERTIES OF BISTATIC CLUTTER ECHOES Report, Dec. 1992 - Dec. 1993
William G. Stevens and Muralidhar Rangaswamy Mar. 1994 86 p Limited Reproducibility: More than 20% of this document may be affected by microfiche quality
(AF Proj. 230-4)
(AD-A291688; RL-TR-94-42) Avail: Issuing Activity (Defense Technical Information Center (DTIC))

In this report we present statistical results of bistatic terrain reflectivity measurements. A new technique for estimating statistical properties from limited data sets was used to examine underlying temporal probability density functions (PDFs) and correlation properties of echoes from several clutter range resolution bins. The case of locally vertically incident-vertically received signal polarization is reported for a single bistatic geometry. The terrain in the experiment consisted primarily of early-development deciduous trees. 10-15 feet high and brush approximately 8 feet high. The measurement system was a high resolution instrumentation radar operating at 3.2 GHz. Results from the estimation algorithm showed that there were small groups of contiguous clutter cells where the members within the group could be described by the same family of PDFs. while other PDF families would best describe neighboring clutter cell groups. Algorithm results for all tested clutter cells showed that the high-resolution, bistatic echoes were non-Rayleigh distributed. DTIC

N95-28979# Matis, Inc., Decatur, GA.
DEVELOPMENT OF THE THEORY AND ALGORITHMS FOR SYNTHESIS OF REFLECTOR ANTENNA SYSTEMS Final Technical Report, 1 Dec. 1991 - 30 Nov. 1994
Vladimir Oliker 26 Jan. 1995 10 p
(Contract F49620-92-C-0009)
(AD-A292579; RAS-F; AFOSR-95-0180TR) Avail: CASI HC A02/MF A01

The main objective of this work was research and development of the theory and constructive computational algorithms for synthesis of single and dual reflector antenna systems in geometrical optics approximation. During the contracting period a variety of new analytic techniques and computational algorithms have been developed. In particular, for single and dual reflector antenna systems conditions for solvability of the synthesis equations have been established. Numerical algorithms for computing surface data of the reflectors have been developed and successfully tested. In addition, efficient techniques have been developed for computing radiation patterns produced by reflections/refractions off surfaces with arbitrary geometry. These techniques can be used for geometrical optics analysis of complex geometric structures such as aircrafts. They can also be applied to determine effectively the aperture excitations required to produce specified fields at given observation points. The results have a variety of applications in military, civilian, and commercial sectors. DTIC

N95-28984# Lockheed Missiles and Space Co., Palo Alto, CA.
WAVELETS IN SIGNAL DETECTION AND IDENTIFICATION COMPARATIVE SIGNAL PROCESSING TECHNOLOGY EVALUATION Final Report, 23 Sep. 1991 - 22 Aug. 1994
Raghu Raghaven 1994 53 p
(Contracts F49620-91-C-0097; ARPA Order 7933)
(AD-A291952; LMSC-P412291; AFOSR-95-0098TR) Avail: CASI HC A04/MF A01

The Wavelet in Signal Detection and Identification: Comparative Signal Processing Technology Evaluation Program has been conducted by Lockheed Missiles and Space Company to develop wavelet based signal detection and classification techniques and compare them to Fourier time-frequency methods. The problem domain is submarine detection and identification using transient passive sonar signals. These nontraditional signals are critical in solving current antisubmarine warfare (ASW) problems which include ultra-quiet nuclear submarines and third world diesel submarines operating on batteries in shallow water. DTIC

N95-28986# Science Applications International Corp., Stow, MA.
ELECTROMAGNETIC ANTENNA MODELING (EAM) SYSTEM Final Technical Report
Malcolm Packer, Robert Powers, and Paul Tsitsopoulos Dec. 1994 212 p
(Contract F30602-91-C-0098)
(AD-A292194; RL-TR-94-224) Avail: CASI HC A10/MF A03

The determination of foreign communications capabilities and intent is an important assessment function performed by the USAF National Air Intelligence Center (NAIC). In this context, Rome Laboratory became the NAIC engineering agent for the development of an NAIC requirement for the rapid analysis and evaluation of antenna structures based on often vague to sometimes detailed dimensional information. To this end, the Rome Laboratory sponsored development of the Electromagnetic Antenna Modeling (EAM) System, a state-of-the-art Pascal program with an MS Windows graphical user interface (GUI) pre- and post-processor. Users of NAIC capabilities initiate antenna analysis efforts that range from simple parametric studies to more complex, detailed antenna design and communication-system evaluations. Accordingly, EAM provides a modeling capability 'matched' to the sophistication of the individual analyst, with features appropriate for users ranging from nontechnical analysts to experienced antenna engineers. This capability is particularly valuable in the military-intelligence environment, in which high-speed assessments are required. In particular, EAM meets the specific antenna-analysis requirements of NAIC with a versatile graphical user interface. DTIC

N95-29002# Air Force Inst. of Tech., Wright-Patterson AFB, OH.
A FORMATIVE EVALUATION OF CU-SEEME M.S. Thesis
Michael Bibeau Feb. 1995 148 p
(AD-A292443; AFIT/CI/CIA-95-007) Avail: CASI HC A07/MF A02

CU-SeeMe is a video conferencing software package that was designed and programmed at Cornell University. The program works with the TCP/IP network protocol and allows two or more parties to conduct a real-time video conference with full audio support. In this paper we evaluate CU-SeeMe through the process of Formative Evaluation. We first perform a Critical Review of the software using a subset of the Smith and Mosier Guidelines for Human-Computer Interaction. Next, we empirically review the software interface through a series of benchmark tests that are derived directly from a set of scenarios. The scenarios attempt to model real world situations that might be encountered by an individual in the target user class. Designing benchmark tasks becomes a natural and straightforward process when they are derived from the scenario set. Empirical measures are taken for each task, including completion times and error counts. These measures are accompanied by critical incident analysis 2 7 13 which serves to identify problems with the interface and the cognitive roots of those problems. The critical incidents reported by participants are accompanied by explanations of what caused the problem and why This helps in the process of formulating solutions for observed usability problems. All the testing results are combined in the Appendix in an illustrated partial redesign of the CU-SeeMe Interface. DTIC

N95-29081# Illinois Univ., Chicago, IL.
EXPERIMENTAL STUDIES OF ELECTROMAGNETIC PROPAGATION AT ULTRAHIGH INTENSITIES Final Report, 10 Jun. 1991 - 31 Aug. 1994
Charles K. Rhodes, Keith Boyer, Armon McPherson, and Ting Shan Luk Oct. 1994 108 p
(Contract DAAL03-91-C-0174)
(AD-A290284; ARO-28499.19-PH) Avail: CASI HC A06/MF A02

The development of a unified picture of short-pulse high-intensity multiphoton processes, embracing atoms, molecules, and solids, appears possible through the study of clusters. Of particular significance are possible intercluster processes that can influence the mechanism of ionization and lead to the production of inner-shell vacancies. Inner-shell excitation leading to prompt x-ray emission is specifically considered and the treatment leads to the definition of a critical cluster size representing the achievement of maximal x-ray emission from the ensemble. These results suggest the possibility of designing a new class of molecular materials optimized for the efficient production and amplification of x-rays. Recent experiments, specifically designed to evaluate certain essential predictions of the cluster picture, have furnished considerable supporting evidence for the main features of the proposed model. These studies, which involved Kr and Xe, (1) established the crucial role of cluster formation in the generation of soft x-ray emission, (2) verified the scaling of this new phenomenon into the kilovolt region, (3) provided important insights concerning the dynamical character of the strong-field coupling to the clusters, and (4) combined the cluster excitation with a recently discovered mode of channeled propagation. These results strongly indicate that the predicted amplification can be achieved. DTIC

N95-29106 Georgia Inst. of Tech., Atlanta, GA.
COMMUNICATION PROTOCOLS IN MULTI-HOP RADIO NETWORKS Ph.D. Thesis
Chungki Lee 1993 164 p
Avail: Univ. Microfilms Order No. DA9415651

Packet radio networks provide a challenging environment in which to develop and deploy protocols. The challenges stem from the shared broadcast channel and from the possibility of conflicts. The problem becomes even more complex when nodes have no priori knowledge of the topology of the entire network. Furthermore in many applications in a radio network, the topology may change over time. For this reason, it is desirable for protocols of radio networks not to make strong assumptions about the network topology, or about the information that nodes have concerning the topology. This thesis considers several important communication tasks in a multi-hop radio network. The thesis first studies the problem of broadcast in multi-hop radio networks. In this study, it is assumed that none of the nodes have initially any topological information, except for the size of the network and its maximum degree. The thesis presents a suite of randomized single-source broadcast protocols, in which only a single broadcast is allowed at any moment. Simulations snow that the protocols improve upon the randomized single-source broadcast protocol by Bar-Yehuda et al. in most typical cases. The thesis then presents a suite of randomized multi-source broadcast protocols, in which a node can initiate a broadcast any time. The protocols are compared with each other in several typical cases. The thesis next considers the problem of electing a 'leader' among a set of nodes in a multi-hop radio network. An efficient randomized leader election protocol in arbitrary multi-hop radio network is presented. Simulations show that the protocol is asymptotically more efficient than previous leader election protocols for (almost) all networks. Finally, the thesis investigates the problem of collecting responses in arbitrary multi-hop radio networks. In this work, it is assumed that each node has a unique identifier (ID) and initially knows the ID's of its neighbors. The thesis presents a deterministic and a randomized protocol for the problem. The two protocols are analysed and their performance is compared. Conclusions are drawn about the suitability of our protocols in various network environments. Dissert. Abstr.

N95-29159# Naval Postgraduate School, Monterey, CA.
THE 10TH ANNUAL REVIEW OF PROGRESS IN APPLIED COMPUTATIONAL ELECTROMAGNETICS, VOLUME 1
Andy Terzuoli, Jeff Fath, Dennis Andersh, Rob Lee, and Dick Adler 1994 590 p Conference held in Monterey, CA, 21-26 Mar. 1994; sponsored by the Applied Computational Electromagnetics Society and DOD and DOE in cooperation with IEEE, URSI, ASEE, SIAM, and AMTA
(AD-A286796; LC-94-70636) Avail: CASI HC A25/MF A06

The proceedings of the 10th Annual Applied Computational Electromagnetics are reported. Technological areas covered in this volume includes: Recent impacts of mathematics on computational electromagnetics, Transmission line method (TLM), Multipole, Finite element method, Boundary conditions, Optimization, Validation, Antennas, Finite difference time domain, and Arrays. CASI

N95-29166# Naval Command, Control and Ocean Surveillance Center, San Diego, CA.
A SIMPLE METHOD FOR RANGE FINDING VIA LASER TRIANGULATION Final Report
Hoa G. Nguyen and Michael R. Blackburn Jan. 1995 12 p
(AD-A292529; NRAD-TD-2734) Avail: CASI HC A03/MF A01

We present the design and implementation of a simple range finder for robotic applications via laser triangulation. The technique does not require knowledge of baseline separation and angles from camera and laser to the target. The system has been successfully implemented on a mobile robot, providing range information for controlling a remote manipulator. DTIC

N95-29174* National Aeronautics and Space Administration, Washington, DC.
HIGH RESOLUTION MICROWAVE SURVEY (Videotape)
J. Scheibe, ed. 18 Sep. 1992 Videotape: 12 min. 45 sec. playing time, in color, with sound
(NASA-TM-110566; AAV-1432; NONP-NASA-VT-95-46001) Avail: CASI VHS A02/BETA A22

Research information on radar tracking systems, computer animation of star formation, footage of solar systems, and desert radar equipment and research facilities are contained in this video. Frank Drake, President of SETI (Search for Extraterrestrial Intelligence) Institute is interviewed along with Jill Tarter, NASA's High Resolution Microwave Survey Project Scientist. CASI

N95-29176# Cognitech, Inc., Santa Monica, CA.
ACCURATE FEATURE DETECTION AND ESTIMATION USING NONLINEAR AND MULTIRESOLUTION ANALYSIS Final Report, 8 Oct. 1990 - 7 Mar. 1994
Leonid Rudin and Stanley Osher 19 Nov. 1994 24 p
(Contract F49620-91-C-0004)
(AD-A290267; TR-38; AFOSR-95-0038TR) Avail: CASI HC A03/MF A01

A program for feature detection and estimation using nonlinear and multiscale analysis was completed. The state-of-the-art edge detection was combined with multiscale restoration (as suggested by the first author) and robust results in the presence of noise were obtained. Successful applications

to numerous images of interest to DOD were made. Also, a new market in the criminal justice field was developed, based in part, on this work. DTIC

N95-29186# Colorado Univ., Boulder, CO. Dept. of Electrical and Computer Engineering.
AN INVESTIGATION OF THE CHANNEL CROSSTALK IN OPTICAL HETERODYNE CONTROLLED PHASED ARRAY RADARS Final Progress Report, 1 Aug. 1994 - 28 Feb. 1995
Alan R. Mickelson 1 Mar. 1995 7 p
(Contract N00014-92-J-1190)
(AD-A292028) Avail: CASI HC A02/MF A01

The principal objective of this project is to investigate problems associated with achieving the drive/read-out system complexity necessary to control a phased array antenna with optical heterodyne techniques. In particular, this work has concentrated on multi-channel microwave optical conversion. The approach has been to study the problems associated with device arrays of single sideband modulators that would be necessary to control the amplitudes and phases of all signals delivered to a phased array front end. The incorporation of our available in-house developed tools into that of already existing tools (such as MDS-Microwave Design Software) has been undertaken to design a single side-band modulator (SSBM). It was found that MESFET oscillators and the associated control lasers can be modeled by simply changing a constant in the model to give their characteristics with and with out optical injection. This is useful for injection locking of active antennas for accurate and efficient phased array antenna design. DTIC

N95-29203# California Univ., San Diego, La Jolla, CA.
IMPROVED INTERCEPTION CAPABILITY THROUGH THE USE OF TRANSFORM DOMAIN PROCESSING Final Report, 22 Mar. 1991 - 21 Sep. 1994
L. B. Milstein Mar. 1995 183 p
(Contract DAAL03-91-G-0071)
(AD-A292231; ARO-27754.4-EL) Avail: CASI HC A09/MF A03

The research conducted during the course of this grant was devoted to two basic problems. The first was that of designing and analyzing an enhanced radiometer possessing the capability of intercepting a signal which is embedded in narrowband interference. The essence of the design was to precede the radiometer with a narrowband interference suppression filter; this allowed the receiver to null out most of the energy of the interference before it entered the radiometer, with the net result being an intercept receiver with much lower false alarm probability. The second major topic that was studied dealt with the design and performance analysis of code division multiple access (CDMA) systems for military communications. This topic was chosen because it complemented the former research area of interception, in the sense that the two together provided coverage of the essence of military communication needs (i.e., knowledge of the enemy's signaling, and security of one's own signaling). The research on CDMA included optimizing the chip rate of a direct sequence system when used over a frequency selective fading channel, and designing an enhanced coarse acquisition system to allow synchronization in the presence of narrowband interference. DTIC

N95-29231# Naval Research Lab., Washington, DC.
COMPARISON STUDY OF UNEQUAL ERROR PROTECTION METHODS FOR ONE-DIMENSIONAL SIGNAL CONSTELLATIONS
Christopher C. Yu and Daniel A. Newman 31 Jan. 1995 18 p
(AD-A290386; NRL/FR/8120-95-9736) Avail: CASI HC A03/MF A01

Unequal error protection is a method to improve bandwidth efficiency where the source data are characterized by having coded bits of varying sensitivity to channel errors. In this report, a framework for comparing the performance of two schemes for unequal error protection is developed. The first scheme (embedded) is based on a clever design of signal constellations with nonuniformly spaced signal points. The second scheme (time-sharing) is based on time-multiplexing concept. It is shown that in the presence of white Gaussian noise, the time-sharing scheme can achieve improved performance over the embedded scheme for one-dimensional signal constellations. This report also describes an application of unequal error protection for MPEG (Motion Pictures Experts Group) video transmission. Corruption in the visual quality of a single frame and the effect of propagatable errors for MPEG coding are both minimized by the use of unequal error protection. DTIC

N95-29235# Kentucky Univ., Lexington, KY.
HIGH PERFORMANCE ELECTROMAGNETIC SIMULATION TOOLS Final Report, 1 Sep. 1993 - 31 Aug. 1994
Stephen D. Gedney and Keith W. Whites 27 Oct. 1994 35 p
(Contract DAAH04-93-G-0453)
(AD-A290405; ARO-32378.1-EL-DPS) Avail: CASI HC A03/MF A01

Army Research Office Grant #DAAH04-93-G-0453 has supported the purchase of 24 additional compute nodes that were installed in the Intel iPsC/860 hypercube at the Univesity Of Kentucky (UK), rendering a 32-node multiprocessor. This facility has allowed the investigators to explore and extend the boundaries of electromagnetic simulation for important areas of defense concerns including microwave monolithic integrated circuit (MMIC) design/analysis and electromagnetic materials research and development. The iPSC/860 has also provided an ideal platform for MMIC circuit simulations. A number of parallel methods based on direct time-domain solutions of Maxwell's equations have been developed on the iPSC/860, including a parallel finite-difference time-domain (FDTD) algorithm, and a parallel planar generalized Yee-algorithm (PGY). The iPSC/860 has also provided an ideal platform on which to develop a 'virtual laboratory' to numerically analyze, scientifically study and develop new types of materials with beneficial electromagnetic properties. These materials simulations are capable of assembling hundreds of microscopic inclusions from which an electromagnetic full-wave solution will be obtained in toto. This powerful simulation tool has enabled research of the full-wave analysis of complex multicomponent MMIC devices and the electromagnetic properties of many types of materials to be performed numerically rather than strictly in the laboratory. DTIC

N95-29236 Office of Naval Research, Arlington, VA.
A METHOD AND APPARATUS FOR SIGNAL FILTERING Patent Application
Edward M. Alexander, inventor (to Navy) and Anthony E. Spezio, inventor (to Navy) 29 Aug. 1994 23 p Filed 29 Aug. 1994 Limited Reproducibility: More than 20% of this document may be affected by microfiche quality
(AD-D017268; Navy-Case-75667; US-Patent-Appl-SN-296883) Avail: Issuing Activity (Defense Technical Information Center (DTIC))

A signal filter, and method of signal filtering, in which an optical signal is spatially dispersed according to frequency, and undesired frequencies blocked out, is introduced. In an embodiment, a Bragg cell receives a (typically microwave) signal, and transduces it to an acoustic signal. A light source, e.g. a laser diode, directs light through the acoustic signal in a known manner so as to produce an optical output which is spatially dispersed according to frequency. A programmable spatial light modulator blocks out unwanted frequency components. Upon removal of the optical carrier, e.g. by heterodyning the spatial light modulator's output with a reference signal from the light source, the components can be recombined into a resultant filtered signal. The invention can be used as a repeater, a military electronic countermeasure, in environments which have large amounts of electromagnetic clutter but in which one does not want the clutter repeated. The spatial light modulator can be programmed to pass only frequency components in which one is interested, thus blocking the clutter from the repeated signal. DTIC

N95-29240# Stanford Univ., CA. Dept. of Materials Science and Engineering.
TAILORED MICROSTRUCTURES FOR BROADBAND OR SELECTIVE DETECTION OF RADIATION FROM THE VISIBLE TO THE INFRARED Final Technical Report, 1 Jan. 1986 - 31 Dec. 1992
Clayton W. Bates, Jr. 25 Aug. 1994 152 p
(Contract N00014-86-K-0509)
(AD-A292097) Avail: CASI HC A08/MF A02

The primary objectives of this project were to prepare and measure the optical and electrical transport properties of metal-semiconductor inhomogeneous composite systems for possible optoelectronic applications. The systems investigated were Ag-O-Cs, Ag-Si and Ag, Au-CuInSe2, where the metal particles were dispersed throughout the semiconductor matrices in sizes ranging from about 5nm to 1OOnm. The approach was to relate the microstructure, i.e., the metal size distribution, volume fraction and

optical properties of metal and matrix to the optical and electrical transport properties of the composite system. For this purpose a complete, self-consistent electromagnetic theory was developed which accounted very accurately for experimentally measured composite optical properties. It was found that the optical absorption of these systems could be varied in a known fashion suggested by the developed theory and that transport properties such as the mobility of carriers was not compromised by the large volume fraction of metal in these systems. The high absorption at wavelengths determined by their microstructures makes them attractive as ultrathin elements in a variety of optoelectronic schemes. DTIC

N95-29266# Science and Technology Corp., Hampton, VA.
BROADBAND INTEGRATED TRANSMITTANCES (BITS) Final Report
Roger E. Davis and Stephen W. Berrick Feb. 1995 141 p
(Contract DAAD07-89-C-0003)
(AD-A292176; ARL-TR-273-2) Avail: CASI HC A07/MF A02

Broadband Integrated Transmittances (BITS) is an EOSAEL module that calculates transmittance for systems with broad spectral response. Path-integrated concentration data from COMBIC, other EOSAEL modules, or user models are used as input for BITS. The primary function of BITS is to provide rigorous transmittance calculations for broadband systems, replacing the Beer-Lambert law used in most obscuration models. To use BITS, the system detector, filters, optics, and source spectral functions must be defined. The spectral transmittances of the atmosphere and mass extinction coefficient spectral data for the obscurant are also required. The output consists of transmittance as a function of concentration length for Beer's law and band-integrated computation methods. The theory of the model, a description of the module organization, and an operations guide that provides input and output in EOSAEL format are provided in this user's guide. Example uses for BITS are also included. DTIC

N95-29289# Naval Postgraduate School, Monterey, CA.
METHODS OF GENERATING LOW REDUNDANCY DIRECTION FINDING ARRAY CONFIGURATIONS M.S. Thesis
Dafer R. Al-Jalahma Dec. 1994 91 p
(AD-A292590) Avail: CASI HC A05/MF A01

Standard uniformly spaced arrays are used to obtain direction information about jammers and other interference signals. In conventional systems the number of sources that can be identified by an array of N elements is N-1. Minimum redundancy arrays have the ability to handle more than N-1 interferers (up to N(N-1)/2) with N elements or less. They require the use of nonuniformly spaced array elements. The existing method for finding the element locations for an optimum minimum redundancy array (MRA) is restricted by its processing time. For a 10 element array with an array length of 36d (d is the fundamental element spacing, typically one half wavelength), the number of possibilities is much greater than 6 x 10(exp 10). Thus, even with today's fast computers, finding the optimum MRA for a large arrays is not practical. A new element locations are obtained from simple module computations, and by varying the base of the number systems, different configurations are generated. The residue array does not achieve the minimum redundancy of the optimum array, but has significantly lower redundancy than the conventional periodic array. The advantages and disadvantages of both methods are investigated, and the array response of each is compared. DTIC

N95-29290# Mississippi Univ., University, MS. Dept. of Electrical Engineering.
FINITE DIFFERENCE ANALYSIS OF A CYLINDRICAL TWO CONDUCTOR MICROSTRIP TRANSMISSION LINE WITH TRUNCATED DIELECTRICS Technical Report, 1 Sep. - 31 Dec. 1994
Atef Elsherbeni, Ying Yuan, and Charles Smith 27 Jan. 1995 124 p
(Contract DAAH04-94-G-0355)
(AD-A292592; Rept-95-1; ARO-33869.1-EL-DPS) Avail: CASI HC A06/MF A02

The characteristics of the quasi-static TEM mode of a cylindrical microstrip transmission line are investigated using the finite difference technique. The transmission line consists of two perfectly conducting strips located between two different layers of dielectric materials, and a dielectric notch embedded in the substrate between two strips. The dielectric overlay and substrate are truncated for practical purposes. The formulation of the problem is based on the solution of Laplace's equation subject to appropriate boundary conditions and the use of Taylor's expansion to approximate the first and the second order derivatives in Laplace's equation. To truncate the finite difference mesh, three different kinds of artificial boundaries have been considered. It has been found that an efficient solution is obtained when the artificial boundary is separated from the conducting core at a distance of the order of the height of the substrate. The goal of this research is to study the effects of the parameters of the multi-layered cylindrical transmission line on the odd and even mode phase velocities, and on the electrical coupling. Another objective of this study is to present several techniques to minimize the coupling between the two conductors. Once the odd and even mode phase velocities are equalized, the design of a distortionless line is achievable. The line capacitances are found to vary linearly with the dielectric constants of the overlay and the substrate. DTIC

N95-29308# Naval Postgraduate School, Monterey, CA. Dept. of Electrical and Computer Engineering.
APPLIED COMPUTATIONAL ELECTROMAGNETICS SOCIETY JOURNAL, VOLUME 10, NUMBER 1, MARCH 1995
Mar. 1995 80 p
(ISSN 1054-4887)
(AD-A292069) Avail: CASI HC A05/MF A01

The Applied Computational Electromagnetics Society Journal hereinafter known as the ACES Journal is devoted to the exchange of information in computational electromagnetics, to the advancement of the state-of-the-art, and to the promotion of related technical activities. A primary objective of the information exchange is the elimination of the need to 're-invent the wheel' to solve a previously-solved computational problem in electrical engineering, physics, or related fields of study. The technical activities promoted by this publication include code validation, performance analysis, and input/output standardization; code or technique optimization and error minimization; innovations in solution technique or in data input/output; identification of new applications for electromagnetics modeling codes and techniques; integration of computational electromagnetics techniques with new computer architectures; and correlation of computational parameters with physical mechanisms. DTIC

N95-29313# Defence Research Establishment Ottawa, Ottawa (Ontario).
LONG RANGE AIRCRAFT DETECTION USING HIGH-FREQUENCY SURFACE-WAVE RADAR DREO Report
Hank Leong Dec. 1994 63 p
(AD-A290148; DREO-1245) Avail: CASI HC A04/MF A01

Experimental data from a high-frequency surface-wave radar (HFSWR) operating at 1.95 MHz at Cape Bonavista, Newfoundland are analyzed to assess the capability of the radar to detect aircraft over an ocean surface. The results of the analysis show that the HFSWR could easily detect and track a low-flying CP-140 Aurora aircraft at ranges between 11 and 56 km. The radar's coverage area coincides with a trans-Atlantic international flight route, and the radar was also able to detect and track some commercial aircraft in range as far as 280 km. DTIC

N95-29318# Naval Postgraduate School, Monterey, CA.
RADAR CROSS SECTION SYNTHESIS FOR PLANAR RESISTIVE SURFACES M.S. Thesis
Nikolaos I. Faros Dec. 1994 115 p
(AD-A290151) Avail: CASI HC A06/MF A02

Equations are developed for synthesizing the radar cross section (RCS) of a planar resistive sheet. The equations are verified by first calculating the RCS of the sheet for an assumed resistivity function. The computed RCS is used in the synthesis equations, and the resistivity distribution is shown to be in agreement with the original assumed distribution. Several synthesis parameters are examined and their effect on the accuracy and computing time are discussed. Results are shown for both monostatic and bistatic RCS with arbitrary incident wave polarization. DTIC

N95-29328# Defence Research Establishment Ottawa, Ottawa (Ontario).
A LEAST SQUARE REAL TIME QUALITY CONTROL ROUTINE FOR THE NORTH WARNING NETTED RADAR SYSTEM
Henry Leung and Martin Blanchette Dec. 1994 48 p
(AD-A290063; DREO-1251) Avail: CASI HC A03/MF A01

The ground surveillance radar group of the Radar and Space Division of DREO has a requirement to investigate the feasibility and propose a cost effective approach of correcting the Real Time Quality Control (RTQC)

registration error problem of the North Warning System (NWS). The U.S. developed RTQC algorithm works poorly in northern Canadian radar sites. This is mainly caused by the deficiency of the RTQC algorithm to calculate properly the radar position bias when there is low aircraft traffic in areas of overlapping radar coverage. This problem results in track ambiguity and in display of ghost tracks. In this report, a modification of the RTQC algorithm using least-square techniques is proposed. The proposed least-square RTQC (LS-RTQC) algorithm was tested with real recorded data from the NWS. The LS-RTQC algorithm was found to work efficiently on the NWS data in a sense that it works properly in a low aircraft traffic environment with low computational complexity. The algorithm has been sent to the NORAD software support unit at Tyndall Air Force Base for testing. DTIC

N95-29383# Texas Univ. at Dallas, Richardson, TX. Center for Applied Optics.

SPECTRAL INVERSE SCATTERING THEORY FOR DIELECTRIC MEDIA: APPLICATION TO OPTICAL DEVICES Final Report, 1991 - 1994

Lakshman S. Tamil 10 Dec. 1995 112 p

(Contract N00014-92-J-1030)

(AD-A292651; UTD/CAO/35) Avail: CASI HC A06/MF A02

Optical devices and circuits can be synthesized from specified transmission characteristics using the methods of inverse scattering. Both analytical and numerical inverse scattering techniques that have been developed to synthesize optical devices and circuits are discussed. Large-scale guided-wave structures such as optical logic gates and optical interconnects can be synthesized using the techniques discussed here. Finite difference based frequency domain analysis technique has been used to verify the results obtained by these inverse scattering techniques. DTIC

N95-29386 Naval Postgraduate School, Monterey, CA. Dept. of Electrical and Computer Engineering.

FEATURE EXTRACTION FROM DIGITAL COMMUNICATIONS SIGNALS USING WAVELET TRANSFORMS Final Report, Apr. - Dec. 1994

Ralph D. Hippenstiel and Monique P. Fargues 8 Feb. 1995 81 p Limited Reproducibility: More than 20% of this document may be affected by poor print

(AD-A292655; NPSEC-95-001) Avail: Issuing Activity (Defense Technical Information Center (DTIC))

Research was conducted to evaluate the feasibility of applying wavelet transforms and methods based on proportional bandwidth processing to transient feature extraction. Classical wavelets and signal related basis functions were used to extract the switching instants from BPSK, QPSK, FSK, ASK, and AMQPSK signals in the presence of additive Gaussian white noise. Results show that using the magnitude of one output scale, the transient times can be detected above a certain signal to noise ratio level. This level depends on the type of signal and wavelet, as well as on the acceptable number of mistakes. Additional work, using several scales and a properly trained neural network, should demonstrate automated selection of the modulation type. DTIC

N95-29441# Massachusetts Inst. of Tech., Cambridge, MA.

TOWARDS AN EXAMPLE-BASED IMAGE COMPRESSION ARCHITECTURE FOR VIDEO-CONFERENCING Memorandum Report

Sebastian Toelg and Tomas Poggio Jun. 1994 38 p

(Contracts N00014-92-J-1879; N00014-93-J-0385)

(AD-A290041; AI-M-1494; CBCL-M-100) Avail: CASI HC A03/MF A01

This paper consists of two major parts. First, we present the outline of a simple approach to very-low bandwidth video-conferencing system relying on an example-based hierarchical image compression scheme. In particular, we discuss the use of example images as a model, the number of required examples, faces as a class of semi-rigid objects, a hierarchical model based on decomposition into different time-scales, and the decomposition of face images into patches of interest. In the second part, we present several algorithms for image processing and animation as well as experimental evaluations. Among the original contributions of this paper is an automatic algorithm for pose estimation and normalization. We also review and compare different algorithms for finding the nearest neighbors in a database for a new input as well as a generalized algorithm for blending patches of interest in order to synthesize new images. Finally, we outline the possible integration of several algorithms to illustrate a simple model based video conference system. DTIC

N95-29459 Arnold Engineering Development Center, Arnold AFS, TN.

SPECTRAL ANALYSIS TECHNIQUES USING WAVELETS AS AN ALTERNATIVE TO FOURIER ANALYSIS FOR TRANSIENT DYNAMIC DATA Final Report, Oct. 1993 - Sep. 1994

Kenneth R. Kimble and Thomas F. Tibbals Jan. 1995 65 p Limited Reproducibility: More than 20% of this document may be affected by microfiche quality

(AD-A289776; AEDC-TR-94-17) Avail: Issuing Activity (Defense Technical Information Center (DTIC))

Various dynamic data analysis tools for one-dimensional time-domain signals are employed to determine the frequency content of a signal for mechanical analysis. When tied to the fundamental frequency of the various components comprising the machinery being evaluated, this information gives an indication of the state or health of the machine. Current techniques for evaluating dynamic data for potential mechanical problems are primarily centered around the Fast Fourier Transform (FFT) and the Shon Time Fourier Transform (STFT). However, the use of Fourier analysis for frequency component extraction is restricted to bandlimited stationary signals. Because of the stationary requirement, small transients may not be detected due to a smoothing effect of the FFT, or the FFT spectrum may be smeared due to frequency ramping and abrupt incidents or discontinuities in the signal. Various techniques have been employed to overcome the limitations of the FFT for non-stationary data. These techniques include windowed Fourier analysis (including the STFT) and a background in wavelet theory based upon the analyzing function basis approach so that wavelet theory may be contrasted against Fourier analysis. A model signal with stationary and transient characteristics is developed to permit comparisons of various analysis techniques based upon a known analytic signal which resembles a real vibration signal. Some applications of wavelets to other transient signals are also provided. DTIC

N95-29462# Allied-Signal Aerospace Co., Kansas City, MO.

DIGITAL VIDEO TECHNOLOGY, TODAY AND TOMORROW

J. Liberman Oct. 1994 7 p Presented at the 18th Annual TRADE Conference: Customer-driven Training on Line Management Expectations, Dallas, TX, 31 Oct. - 2 Nov. 1994

(Contract DE-AC04-76DP-00613)

(DE95-007689; KCP-613-5524; CONF-9410300-2) Avail: CASI HC A02/MF A01

Digital video is probably computing's fastest moving technology today. Just three years ago, the zenith of digital video technology on the PC was the successful marriage of digital text and graphics with analog audio and video by means of expensive analog laser disc players and video overlay boards. The state of the art involves two different approaches to fully digital video on computers: hardware-assisted and software-only solutions. DOE

N95-29472# Magnascreen Corp., Pittsburgh, PA.

LOW VOLTAGE, HIGH RESISTANCE, POLYMER DISPERSED LIQUID CRYSTAL Final Report, 1 Sep. 1992 - 1 Mar. 1994

Jan Bernkopf and Patrick Mullen Mar. 1994 112 p

(Contract F33615-92-C-1907)

(AD-A291946; WL-TR-94-1086) Avail: CASI HC A06/MF 02

This document presents the results of the development of a low voltage, high resistivity, dyed Polymer Dispersed Liquid Crystal (PDLC) for use in direct view displays. Several methods for improving various PDLC characteristics are described. The optimized PDLC formulation shows substantial improvement in all operational characteristics with the single exception of hysteresis, which remains unacceptably high. Alternative applications of developed PDLC materials are discussed. DTIC

N95-29474# Asian Office of Aerospace Research and Development, APO San Francisco, CA. Air Force Office of Scientific Research.

THE 1994 IEEE INTERNATIONAL WORKSHOP ON INTELLIGENT SIGNAL PROCESSING AND COMMUNICATION SYSTEMS (ISPACS94) Abstracts Only

T. Davis 1994 34 p Workshop held in Seoul, Korea, 5-7 Oct. 1994; co-sponsored by the IEEE Communications Society and the IEEE Korea

Council
(AD-A292312; AOARD-TR-94-39) Avail: CASI HC A03/MF A01

A summary of the 1994 IEEE International Workshop on Intelligent Signal Processing and Communication Systems (ISPAC94), conducted at Yonsei University, Seoul, Korea is presented. Abstracts of all persented papers are included. This report is based upon information collected via workshop attendance, review of the proceedings, and conversations with other attendees. DTIC

N95-29489 Naval Undersea Warfare Center, New London, CT.
ADAPTIVE BLOCK SEQUENTIAL DETECTION OF ABRUPT SIGNAL CHANGES Final Report
Douglas A. Abraham 12 Dec. 1994 145 p Limited Reproducibility: More than 20% of this document may be affected by poor print
(NR Proj. A60-070)
(AD-A290456; NUWC-NL-TD-10785) Avail: Issuing Activity (Defense Technical Information Center (DTIC))

Estimation of the time of change of a parameter governing an observed sequence of independent multivariate random data samples is considered when the magnitude of the change is unknown and there exist unknown nuisance parameters that may be nonstationary. The particular application considered is the detection of the onset of a narrowband signal with unknown amplitude and phase at an array of sensors for radar or sonar processing in the presence of unknown, nonstationary, spatially distinct interferences hindering detection. The solution proposed in this dissertation entails segmenting the multivariate data into nonoverlapping blocks, from which univariate statistics are formed that are invariant to the unknown interference parameters. The log likelihood ratio for a specific signal-to-interference ratio (SIR) and the locally optimal nonlinearities are applied to two level statistics formed by generalized likelihood ratio (GLR) methods for data compression prior to submission to Page's test for rapid detection of the change. Once Page's test has determined that a change has occurred at the block level, the estimate of the change time is improved by post block processing in the form of a maximum likelihood estimator for the change time. Application of the locally optimal nonlinearity to the block level statistic formed from a GLR for the unknown signal and interference parameters achieved the best asymptotic performance. DTIC

N95-29504# Naval Postgraduate School, Monterey, CA. Dept. of Electrical and Computer Engineering.
HIGH RESOLUTION DIRECT DIGITIZITATION AND OPTICAL TELEMETRY OF SHIPBOARD ANTENNA SIGNALS Interim Report, Oct. 1993 - Sep. 1994
Phillip E. Pace, Ronald J. Pieper, and John P. Powers 19 Dec. 1994 46 p
(AD-A290238; NPS-EC-94-016) Avail: CASI HC A03/MF A01

This report describes the past year's research efforts (Oct. 1993 - Sep. 1994) in the design, development and construction of an optical processing system to directly digitize and transport shipboard antenna signals to below deck. The electro-optical guided wave analog-to-digital converter directly digitizes the antenna signals and is based on preprocessing the signals with a symmetrical number system (SNS) to achieve both an 8-bit design and a 14-bit design. The status of the hardware construction is described (8-bit expected completion - Mar. 1995, 14-bit expected completion - Jul. 1995). Using time division multiplexing (TDM) techniques, an optical digital link transports the bits over fiber to the receiver below deck. DTIC

N95-29563 Illinois Univ., Urbana, IL.
SIGNAL PROCESSING FOR HIGH-RESOLUTION IMAGE FORMATION Final Report
Arun S. Karalamangala 28 Sep. 1994 39 p Limited Reproducibility: More than 20% of this document may be affected by poor print
(Contract DAAL03-91-G-0118)
(AD-A290648; ARO-28476.8-MA-SDI) Avail: Issuing Activity (Defense Technical Information Center (DTIC))

This research program investigated signal processing problems encountered in high- resolution image formation. Reliable imaging of scenes with high resolution and high speed is an important and key part of any defense system. In some imaging systems, the image has to be constructed from linear measurements and convex constraints (such as upper and lower bounds on image sample magnitude, and support limits). studied iterative, finite parameter reconstructions that lead to images that meet constraints, match the data to within a pre-specified tolerance, and come closest to a given nominal. We addressed three different aspects of signal/image reconstruction, namely, (1) Developing fast algorithms for high resolution signal/image reconstruction, (2) Resolutions Analysis of signal reconstruction algorithms, (3) Numerical and computational aspects of signal reconstruction viz: stability and regularization. DTIC

N95-29564# SRI International Corp., Menlo Park, CA.
HIGH-PERFORMANCE SPEECH RECOGNITION USING CONSISTENCY MODELING Final Report
Vassilios Digalakis, Hy Murveit, Peter Monaco, Leo Neumeyer, and Ananth Sankar Dec. 1994 149 p
(Contract N00014-92-C-0154)
(AD-A290655) Avail: CASI HC A07/MF A02

The goal of SRI's consistency modeling project is to improve the raw acoustic modeling component of SRI's DECIPHER speech recognition system and develop consistency modeling technology. Consistency modeling aims to reduce the number of improper independence assumptions used in traditional speech recognition algorithms so that the resulting speech recognition hypotheses are more self-consistent and, therefore, more accurate. At the initial stages of this effort, SRI focused on developing the appropriate base technologies for consistency modeling. We first developed the Progressive Search technology that allowed us to perform large-vocabulary continuous speech recognition (LVCSR) experiments. Since its conception and development at SRI, this technique has been adopted by most laboratories, including other ARPA contracting sites, doing research on LVSR. Another goal of the consistency modeling project is to attack difficult modeling problems, when there is a mismatch between the training and testing phases. Such mismatches may include outlier speakers, different microphones and additive noise. We were able to either develop new, or transfer and evaluate existing, technologies that adapted our baseline genonic HMM recognizer to such difficult conditions. DTIC

N95-29603# Statistical Signal Processing, Inc., Yountville, CA.
CYCLIC FEATURE ANALYSIS, DESIGN AND EXPLOITATION Final Report, 1 Apr. 1991 - 31 Jul. 1994
William A. Gardner and Chad M. Spooner 26 Sep. 1994 111 p
(Contract DAAL03-91-C-0018)
(AD-A290639; ARO-27917.21-EL-S) Avail: CASI HC A06/MF A02

In this research project, we characterized the n-th order cyclostationarity properties of general types of LPI signals and used the characterizations to investigate and develop methods for both secure communication and interception. For secure communication, this includes means for reduction of strength of' and elimination of, cyclic features that could be exploited by an interceptor. Signal design for LPI communication was considered from the viewpoints of both the communicator's reception task and the interceptor's reception task. For interception, the characterizations were used to propose feature sets and discrimination rules for signal classification and identification. The basic approach to characterizing n-th order cyclostationarity properties of signals was extended and generalized from the recently developed theory of 2nd-order cyclostationarity, in which spectral characterizations play a crucial role. DTIC

N95-29645# Stanford Univ., CA. Edward L Ginzton Lab. of Physics.
RESEARCH STUDIES IN ELECTROMAGNETICALLY INDUCED TRANSPARENCY Final Report, 15 Dec. 1991 - 14 Oct. 1994
S. E. Harris Dec. 1994 40 p
(Contract F49620-92-J-0066; ARO-MIPR-130-94)
(AD-A290796; ARO-28978.31-PH) Avail: CASI HC A03/MF A01

Over the last three years our work has centered in the areas of electromagnetically induced transparency and applications and the development of short wavelength lasers and radiation sources. DTIC

N95-29655# Rome Lab., Griffiss AFB, NY.
ADVANCED PRESORT PROCESS Report, Dec. 1991 - Sep. 1993
David Grucza Nov. 1994 33 p
(AD-A291010; RL-TR-94-186) Avail: CASI HC A03/MF A01

The purpose of the Presort Processor is to excise strong narrow band signals from a wideband radar return. It is an optical notch filter based on acoustooptics and fourier transform optics. This latest iteration of this project uses a narrow bandwidth doubled Nd:YAG laser as an optical carrier and

a TIR (total internal reflection) liquid crystal spatial light modulator to perform the frequency excision. DTIC

N95-29707 Massachusetts Univ., Amherst, MA.
SCHEDULING ALGORITHMS FOR MOBILE PACKET RADIO NETWORKS Ph.D. Thesis
Hyeyeon Ahn 1994 129 p
Avail: Univ. Microfilms Order No. DA9420592

This dissertation presents new scheduling algorithms for sharing the common radio channel in mobile packet ratio networks. The idea of sharing a common, multiple-access channel among many users was used in the past as the basis of many communication systems. However, the unique characteristics of the packet radio networks preclude the straight forward application of existing protocols that are tuned to other types of networks. For single hop packet ratio networks with arbitrary multiple reception capacity, the first nontrivial scheduling algorithm is developed with guaranteed, almost optimal efficiency, obtained without requiring the simultaneous transmission/reception capability. We propose a robust scheduling protocol for multihop networks, which is unique in providing a topology transparent solution to scheduled access in mobile radio networks with guaranteed packet delivery. Dissert. Abstr.

N95-29769# Federal Aviation Administration, Atlantic City, NJ.
UHF LOW DENSITY RADIO COMMUNICATIONS LINK (LDRCL) OPERATIONAL TEST AND EVALUATION (OT&E) INTEGRATION AND OT&E OPERATIONAL FINAL TEST REPORT
Michael R. Melillo Jan. 1995 39 p
(AD-A291447; DOT/FAA/CT-TN94/56) Avail: CASI HC A03/MF A01

This report contains the results of the Operational Test and Evaluation (OT&E) Integration and OT&E Operational Testing of the Commercial-Off-The-Shelf (COTS) Low Density Radio Communications Link's (LDRCL) Ultra-High Frequency (UHF) radio system. The OT&E testing was accomplished by first testing the LDRCL equipment against its equipment specification (FAA-E-2853A), and then performing OT&E testing at the key sites; Nina and Tonopah, Nevada. These tests prove that the UHF LDRCL equipment can fulfill its mission in the National Airspace System (NAS) and that it is suitable and effective. Based on the test results, it is concluded that the UHF LDRCL equipment is qualified for operational deployment. DTIC

N95-29847# Defence Research Establishment Ottawa, Ottawa (Ontario).
WIDEBAND I/Q DEMODULATORS: MEASUREMENT TECHNIQUE AND MATCHING CHARACTERISTICS
Jim J. Lee Nov. 1994 36 p Limited Reproducibility: Document partially illegible
(AD-A291505; DREO-1242) Avail: CASI HC A03/MF A01

A simple I/Q demodulator which can be used to measure the amplitude, phase and instantaneous frequency of radar signals over a large bandwidth is investigated for electronic warfare applications. Imbalance errors and DC offsets are minimized by the techniques of component matching and calibration. A DFT technique is used to characterize the imbalances and DC offsets and improved matching characteristics on practical wideband demodulators are also given. DTIC

N95-29862# Asian Office of Aerospace Research and Development, APO San Francisco, CA. Air Force Office of Scientific Research.
SUMMARY OF THE 1ST INTERNATIONAL WORKSHOP ON NETWORKED REALITY IN TELECOMMUNICATION
T. Davis 14 May 1994 22 p Workshop held in Tokyo, Japan, 13-14 May 1994
(AD-A292366; AOARD-TR-94-21) Avail: CASI HC A03/MF A01

Abstracts of workshop papers are presented. Networked reality refers to the array of technologies and services involved in collecting a representation of reality at one location and using it to reconstruct an artificial representation of that reality at a remote location. The term encompasses transmission of the required information between the sites, and also includes the psychological, cultural, and legal implications of introducing derived communication systems. Networked reality is clearly derived from the emerging virtual reality technology base but is intended to go beyond the latter to include its integration with the required telecommunication technologies. A noteworthy feature of the Networked Reality '94 technical program is the extent of emphasis on social (particularly medical) impacts of the technology. CASI

N95-29875# Massachusetts Inst. of Tech., Cambridge, MA. Dept. of Earth Atmospheric and Planetary Sciences.
DEVELOPMENT OF IMPROVED GEOPHYSICAL IMAGING TECHNIQUES FOR ENVIRONMENTAL SITE CHARACTERIZATION Scientific Report No. 1
Robert J. Greaves, Jung M. Lee, David P. Lesmes, and M. N. Toksoef 8 Oct. 1994 43 p
(Contract F19628-93-K-0027)
(AD-A291003; Rept-60458; PL-TR-94-2267) Avail: CASI HC A03/MF A01

The common midpoint (CMP) processing technique has been shown to be effective in improving the results of ground penetrating radar (GPR) profiling. When radar data are collected with the CMP multi-offset geometry, stacking increases the signal-to-noise ratio of subsurface radar reflections and the effective penetration depth. An important aspect of CMP processing is normal moveout velocity analysis. Most, if not all, GPR surveys are very limited in spatial extent and the common perception is that within the survey range, radar velocity in the shallow subsurface has very slow or no lateral variation. Therefore, a single velocity function might be considered adequate to describe the subsurface. In this study we show that, in fact, lateral variation in radar velocity can be quite significant and that the stacked profile improves as the number of velocity analysis locations is increased, up to some practical limit. Interval velocity can be calculated from the normal moveout velocities derived in the CMP velocity analysis. An approximate relationship between interval velocity and water content is derived. By collecting GPR data in the multi-offset CMP geometry, not only is the radar profile improved but it also allows for an interpretation of subsurface variation in water content. DTIC

N95-29904# Naval Postgraduate School, Monterey, CA.
THE 10TH ANNUAL REVIEW OF PROGRESS IN APPLIED COMPUTATIONAL ELECTROMAGNETICS, VOLUME 2
Andy Terzuoli, Jeff Fath, Dennis Andersh, Rob Lee, and Dick Adler 1994 624 p Conference held in Monterey, CA, 21-26 Mar. 1994; sponsored by the Applied Computational Electromagnetic Society and DOD and DOE in cooperation with IEEE, URSI, ASEE, SIAM, and AMTA
(AD-A286799; LC-94-70636) Avail: CASI HC A99/MF A06

The proceeding of the 10th Annual Review of Progress in Applied Computational Electromagnetics are reported. Subject areas covered include: finite difference time domain; gemacs; moment methods; EMI/EMP/EMC; hybrid; propagation and imaging; pre and post processing; high frequency; low frequency; education; microwave; and materials and simulation methods. CASI

N95-29919# Technische Univ., Eindhoven (Netherlands).
UMTS NETWORK ARCHITECTURE
J. P. Katoen, A. Saiedi, and I. Baccaro May 1994 15 p Prepared in cooperation with Alcatel Bell Research, and Alcatel FACE
(PB95-206744; Memo-INF-94-44) Avail: CASI HC A03/MF A01

This paper proposes a Functional Architecture and a corresponding Network Architecture for the Universal Mobile Telecommunication System (UMTS). Procedures like call handling, location management, and handover are considered. The architecture covers the domestic, business, and public environments. Integration with existing and forthcoming networks for fixed communications is anticipated and the Intelligent Network (IN) philosophy is applied. NTIS

N95-29928# Naval Air Warfare Center, China Lake, CA.
ELECTRICALLY SMALL ARCHIMEDIAN SPIRAL METHOD OF MOMENT ANALYSIS Interim Report, Oct. 1993 - Sep. 1994
Michael M. Neel Feb. 1995 49 p
(Contract N00014-94-WX-35177)
(AD-A291171; NAWC-WPNS-TP-8245) Avail: CASI HC A03/MF A01

This paper presents an analysis of an electrically small archimedean spiral. Method of moment calculations were performed to find the spiral arm current distribution, and optimum arm road impedance over a three-to-one bandwidth. DTIC

N95-29940# Federal Aviation Administration, Atlantic City, NJ.
OPERATIONAL TEST AND EVALUATION (OT&E) INTEGRATION AND OPERATIONAL TEST PLAN FOR FIXED GROUND ANTENNA RADOME (FGAR)
Leonard H. Baker Jan. 1995 51 p
(AD-A291310; DOT/FAA/CT-TN94/63) Avail: CASI HC A04/MF A01

The Federal Aviation Administration (FAA) Fixed Ground Antenna Radome (FCAR) Operational Test and Evaluation (OT&E) Integration and Operational Test Plan is prepared by the Associate Program Manager for Test (APMT). It defines the overall planning, test activities, and coordination associated with OT&E Integration and Operational testing required to ensure the project meets the requirements of the project specification and the system and subsystem requirements allocated to the project. The purpose of the FCAR project is to provide new, larger radomes for en route surveillance radars that require collocated Mode Select Beacon System (Mode S) installations. As a result of the FAA's program to implement Mode S, many existing en route surveillance radar radomes cannot accommodate the additional space required by the new Mode S antennas. The FGARs will provide an environmental enclosure for a variety of single or dual-face monopulse beacon phased array and en route surveillance radar installations. Installations will be comprised of an installation mix ranging from beacon-only-sites (BOS) to collocated beacon and en route surveillance radar sites. DTIC

N95-29975# Federal Aviation Administration, Atlantic City, NJ.
OPERATIONAL TEST AND EVALUATION (OT&E) INTEGRATION AND OPERATIONAL TEST PROCEDURES FOR FIXED GROUND ANTENNA RADOME (FGAR)
Leonard Baker Jan. 1995 64 p
(AD-A291203; DOT/FAA/CT-TN94/65) Avail: CASI HC A04/MF A01

This document defines the Fixed Ground Antenna Radome (FGAR) integration and operational test procedures that will be performed at the Federal Aviation Administration (FAA) Technical Center's En Route Beacon Test Facility (ERBTF) and field operational facilities. These test procedures will be performed following the Contractor's Acceptance Inspection (CAI). The test configurations and their associated interfaces will be required to operate in as near an operational environment as possible. The testing includes the use of a specially equipped Radio Frequency Interference Monitoring (RFIM) van to measure primary and secondary radar electromagnetic performance parameters and the En Route Mode Select Beacon System (Mode S) installed at the Technical Center's Elwood ERBTF. In addition, the FGAR operational characteristics will be evaluated from a user's standpoint. DTIC

N95-29982# Nebraska Univ., Lincoln, NE. Dept. of Electrical Engineering.
A FULL WAVE STUDY OF RADAR CROSS SECTIONS OF ROUGH TERRAIN Final Report, 24 Jun. 1991 - 31 Dec. 1994
Ezekiel Bahar 31 Aug. 1994 60 p
(Contract DAAL03-91-G-0204)
(AD-A291227) Avail: CASI HC A04/MF A01

Full wave solutions are derived for the like and cross polarized electromagnetic diffuse single scattered fields from two dimensional irregular stratified media. Scattering upon reflection and transmission across random rough surfaces is considered. The surface is characterized by its joint probability density function for the heights and slopes at two points. The full wave expressions involve the height/slope correlations. The full wave results are compared with the small perturbation physical/geometrical, numerical (based on Monte Carlo simulations) and experimental results. Full wave solutions for the double scatter fields and cross sections are also derived for rough surfaces that exhibit enhanced backscatter. The solutions are expressed as an interaction integral between two single scatter cross sections associated with quasi parallel and quasi antiparallel paths. The dependence of the angular width and level of the enhanced backscatter cross section on the mean square height and slope and on the mean width of a typical depression on the rough surface is determined. The results are compared with numerical and experimental data. DTIC

N95-29991# Army Missile Command, Redstone Arsenal, AL. Advanced Sensors Directorate.
HIGH-FREQUENCY RADAR TARGET MODELING Summary Report
Virginia C. Monk and Fred W. Sedenquist Jan. 1995 32 p
(AD-A290965; TR-RD-AS-95-2) Avail: CASI HC A03/MF A01

This report contains the theories behind the commonly accepted electromagnetic techniques used for radar cross section (RCS) prediction and enumerates the prevailing computer models which characterize RCS for high-frequency complex targets. DTIC

N95-30072# Federal Aviation Administration, Atlantic City, NJ.
OFFSHORE NEXT GENERATION WEATHER RADAR (NEXRAD) TEST AND EVALUATION MASTER PLAN (TEMP)
Radame Martinez, Robert Cranston, and John Porcello Jan. 1995 49 p
(AD-A291435; DOT/FAA/CT-TN94/48) Avail: CASI HC A03/MF A01

This document provides the test philosophy and approach for the Offshore Next Generation Weather Radar (NEXRAD) Test and Evaluation Master Plan (TEMP). The NEXRAD differs from the typical Federal Aviation Administration (FAA) weather radar acquisition in that it is jointly funded by the Department of Defense (DOD), the Department of Commerce (DOC), and the Department of Transportation (DOT). These three agencies chartered the Joint System Program Office (JSPO) to manage the NEXRAD development and subsequent test programs. JSPO has deployed 70 single-channel radar systems across the continental United States (CONUS). The FAA is deploying NEXRAD systems at non-CONUS (offshore) locations such as Alaska, Hawaii, and the Caribbean. The FAA Offshore NEXRAD will have a redundant configuration and a Remote Monitoring Subsystem (EMS). A total of 14 Offshore NEXRAD's will be procured under this acquisition: 3 in the Caribbean, 4 in Hawaii, and 7 in Alaska. Funding constraints will limit the acquisition to seven NEXRAD's in the 1994-1995 timeframe. DTIC

N95-30073# Environmental Research Inst. of Michigan, Ann Arbor, MI.
HI-RES SAR DATA PROCESSING REPORT Final Report
D. R. Lyzenga, N. P. Malinas, P. A. Pantalone, and C. C. Wackerman Jan. 1995 27 p
(Contract N00014-94-C-0137)
(AD-A291443; ERIM-265400-2-F) Avail: CASI HC A03/MF A01

This report summarizes the digital processing activities which have been carried out on the SAR data sets collected during the two ONR/NRL High Resolution field experiments held in September 1991 and June 1993. Features associated with the Gulf Stream boundary are observed in these data sets, with signatures that are dependent on the wind speed, radar frequency and polarization. Estimation of currents using the displacement of features observed on multiple passes appears to be possible. A simplified procedure for large-scale INSAR data processing has been developed and applied to one of the data sets collected in June 1993. Preliminary comparisons with OSCR measurements indicate that similar features are observed in both data sets. A capability was also developed during this contract to plot image locations on a Transverse Mercator map using the navigation data and radar operating parameters recorded on the P3 engineering data disks. DTIC

N95-30096# Technische Univ., Twente (Netherlands). Tele-Informatics and Open Systems Group.
PERFORMANCE EVALUATION OF ATM CELL SCHEDULING POLICIES USING STOCHASTIC PETRI NETS
B. R. Haverkort, H. P. Idzenga, and B. G. Kim May 1994 24 p
(PB95-197158; Memo-INF-94-61) Copyright Avail: CASI HC A03/MF A01

This paper addresses the modeling and evaluation of cell scheduling policies in asynchronous transfer mode (ATM) switches using stochastic Petri net models. In particular, we compare four cell scheduling policies: a first-in, first out (FIFO) policy with and without non-preemptive priorities, a threshold priority policy, and a modification thereof. The aim of this paper is twofold. First of all, we want to stress the suitability of stochastic Petri nets as a versatile tool for modeling and evaluating ATM-related performance issues. Secondly, we like to point out that under fairly realistic traffic conditions, i.e., a combination of Poisson nonreal-time (data) traffic and Markov modulated Poisson process (MMPP) real-time (video) traffic, our proposed modification of the threshold priority scheduling policy not only reduces the average delay for real-time traffic at the cost of only a slight increase of the average delay of nonreal-time traffic, but also reduces the delay jitter in the real-time traffic. NTIS

N95-30177# Sandia National Labs., Albuquerque, NM.
PATCH DIAMETER LIMITS FOR TIERED SUBAPERTURE SAR IMAGE FORMATION ALGORITHMS
A. W. Doerry 1994 12 p Presented at the SPIE International Symposium on Aerospace/defense Sensing and Dual-use Photonics, Orlando, FL, 17-21 Apr. 1995
(Contract DE-AC04-94AL-85000)
(DE95-008816; SAND-94-2451C; CONF-950472-3) Avail: CASI HC A03/MF A01

Synthetic Aperture Radar image formation algorithms typically use transform techniques that often requires trading between image resolution, algorithm efficiency, and focussed image scene size limits. This is due to assumptions for the data such as simplified (often straight-line) flight paths, simplified imaging geometry, and simplified models for phase functions. Many errors in such assumptions are typically untreatable due to their dependence on both data domain positions and image domain positions. The result is that large scenes often require inefficient multiple image formation iterations, followed by a mosaicking operation of the focussed image patches. One class of image formation algorithms that performs favorably divides the spatial and frequency apertures into subapertures, and perhaps those subapertures into sub-subapertures, and so on, in a tiered subaperture fashion. This allows a gradual shift from data domain into image domain that allows correcting many types of errors that limit other image formation algorithms, even in a dynamic motion environment, thereby allowing larger focussed image patches without mosaicking. This paper presents and compares focussed patch diameter limits for tiered subaperture (TSA) image formation algorithms, for various numbers of tiers of subapertures. Examples are given that show orders-of-magnitude improvement in non-mosaicked focussed image patch size over traditional polar format processing, and that patch size limits increase with the number of tiers of subapertures, although with diminishing returns. DOE

N95-30203# Technische Univ., Eindhoven (Netherlands).
DELAYED CHOICE: AN OPERATOR FOR JOINING MESSAGE SEQUENCE CHARTS
J. C. M. Baeten and S. Mauw Sep. 1994 24 p
(PB95-206710) Avail: CASI HC A03/MF A01

We study the extension of a simple process algebra with the delayed choice operator. It differs from the normal non-deterministic choice in that the moment of choice is delayed until all alternatives can be distinguished by their first action. An application is in joining Message Sequence Charts. NTIS

N95-30219# Technische Univ., Eindhoven (Netherlands).
DESCRIPTION OF THE TV DISTRIBUTION SERVICE USING MAGIC MODELLING METHODS
L. Staalhagen and X. Hou Feb. 1994 81 p
(PB95-206728; Memo-INF-94-45) Copyright Avail: CASI HC A05/MF A01

This report deals with aspects to define the TV-distribution service in Broadband Integrated Services Digital Network (B-ISDN), and uses parts of the MAGIC modeling method to describe and define such a service. In chapter 1, four different scenarios of providing a TV-distribution service are described and analyzed, and one scenario is chosen to be described and defined, using the MAGIC method. Chapter 2 contains a short description of the MAGIC modeling method. Chapter 3, 4 and 5 contain the three steps of stage 1 of the MAGIC modeling method, applied to the description of the TV-distribution service, selected in chapter 1. Chapter 6 describes some of the dynamic aspects of the TV-distribution service, using some of stage 2 of the MAGIC modeling methods. NTIS

N95-30336*# National Aeronautics and Space Administration. Langley Research Center, Hampton, VA.
DIELECTRIC PROPERTY MEASUREMENTS IN THE ELECTROMAGNETIC PROPERTIES MEASUREMENT LABORATORY
Robin L. Cravey, Pacita I. Tiemsin, Kerri Bussell (Old Dominion Univ., Norfolk, VA.), and Kenneth L. Dudley Apr. 1995 17 p
(RTOP 505-64-52-04)
(NASA-TM-110147; NAS 1.15:110147) Avail: CASI HC A03/MF A01

The capability to measure the dielectric properties of various materials has been developed in the Electromagnetic Properties Measurement Laboratory (EPML) of the Electromagnetics Research Branch (ERB). Two measurement techniques which have been implemented in the EPML to characterize materials are the dielectric probe and waveguide techniques. Several materials, including some for which the dielectric properties are well known, have been measured in an attempt to establish the capabilities of the EPML in determining dielectric properties. Brief descriptions of the two techniques are presented in this report, along with representative results obtained during these measurements. Author

33 ELECTRONICS AND ELECTRICAL ENGINEERING

Includes test equipment and maintainability; components, e.g., tunnel diodes and transistors; microminiaturization; and integrated circuitry.

For related information see also *60 Computer Operations and Hardware* and *76 Solid-State Physics.*

N95-28812# CryoPower Associates, Los Alamos, NM.
CHALCOGENIDE SUPERCONDUCTORS: A SEARCH Final Report, 1 Jul. 1993 - 31 Mar. 1994
Henry L. Laquer 22 Jul. 1994 9 p
(Contract F49620-93-C-0025)
(AD-A292523; CPA-94-02; AFOSR-95-0132TR) Avail: CASI HC A02/MF A01

Experimental and theoretical evidence and arguments are presented to justify a search for new superconductors, similar to the perovskite-based high temperature superconductors, but with the oxygen replaced by a chalcogen, that is sulfur, selenium, or tellurium. Candidate compositions are proposed, together with methods of achieving their chemical synthesis. Safety and environmental issues were also analyzed. DTIC

N95-28813# Arizona State Univ., Tempe, AZ.
STRAINED-BOND SEMICONDUCTORS Final Technical Report, 1 Sep. 1991 - 30 Nov. 1993
John D. Dow 18 May 1994 8 p
(Contract AF-AFOSR-0418-91)
(AD-A292524; AFOSR-95-0133TR) Avail: CASI HC A02/MF A01

Theories of strained-bond semiconductors and superconductors have been developed that promise to have significant impact on future electronic devices of interest to the Air Force. These include: (1) development of a theory of high-temperature superconductivity based on the idea of strained-layer superlattices, (2) elucidation of the physics of doping in Type-2 semiconductor superlattices, which is now central to the development of high-speed field-effect transistors, (3) a theory of dimerization and reconstruction on (001) semiconductor surfaces, (4) theory of Mobius transforms as applied to physics and remote sensing, (5) new understanding of how defects affect the vibrational properties of semiconductors, (6) new methods of efficiently computing the trajectories of atoms in semiconductors by a priori molecular dynamics, (7) elucidation of the criteria affecting quantum-well luminescence from Si, (8) models of the effects of vacancies in large-gap Al(x)Ga(1-x)N alloys, (9) physics of rare-earth-doped silicon, (10) models of Co adsorption to silicon surfaces, (11) theories of how defects affect the properties of large band-gap superlattices, and (12) models of the effects of electronic structure on the properties of semiconductors. DTIC

N95-28855 Department of the Navy, Washington, DC.
LIGHTWEIGHT BATTERY ELECTRODE AND METHOD OF MAKING IT Patent
William A. Ferrando, inventor (to Navy) and Amarnath P. Divecha, inventor (to Navy) 8 Nov. 1994 9 p Filed 7 Jul. 1993
(AD-D017389; US-Patent-5,362,580; US-Patent-Appl-SN-087002) Avail: US Patent and Trademark Office

A process is introduced for producing a lightweight electrode grid by exposing a compressed, heated mat of dense graphite fibers to Ni(CO)4 gas wherein the Ni(CO)4 decomposes upon contact with the graphite fibers depositing a nickel metal coating on the graphite fibers which strongly bonds the fibers together to form a compressed mat or grid of nickel metal coated fibers. DTIC

N95-28859# Rochester Univ., NY.
QUASIOPTICAL JOSEPHSON OSCILLATOR Final Report, 1 May 1990 - 30 Apr. 1994
Michael J. Wengler 22 Sep. 1994 3 p
(Contract AF-AFOSR-0233-90)
(AD-A292481; AFOSR-95-0120TR) Avail: CASI HC A01/MF A01

The Quasioptical Josephson Oscillator (QJO) is a 2-D array of between 100 and 1,000,000 Josephson junctions, each at the center of a small dipole antenna. HYPRES, Inc. of Elmsford, NY has fabricated test chips which have demonstrated 0.35 microwatts radiation at 190 CHz in one case, and 0.7 microwatts radiation at 345 GHz in another case. A significant understanding of the 2-D oscillators was developed through theoretical and numerical calculations. DTIC

N95-28911 Air Force Systems Command, Wright-Patterson AFB, OH. National Air Intelligence Center.
CONFERENCE REPORTS
Chen Dongpei and Ma Yulong 16 Dec. 1994 12 p Transl. into ENGLISH from Yingyong Shengxue, China, v. 10, no. 2, Mar. 1991 p 46-47 Limited Reproducibility: More than 20% of this document may be affected by microfiche quality
(AD-A289630; NAIC-ID(RS)T-0367-94) Avail: Issuing Activity (Defense Technical Information Center (DTIC))

The Ultrasonic Electronics Branch Society of the China Acoustics Society, and the Electronics Countermeasure Branch Society of the China Electronics Society held and All-China Applications Conference of Ultrasonic Electronics Devices in Electronic Countermeasures, Radar and Military Communication Technology. A total of 66 papers was received by the conference with contents relating to surface acoustic wave devices, high-frequency acoustic wave devices, acousto-optical devices, applications of devices in radar, applications of devices in electronic countermeasures, and applications of devices in military communication systems. Derived from text

N95-28950 Army Missile Command, Redstone Arsenal, AL. Systems Simulation and Development Directorate.
THIN-FILM RESISTOR ARRAY CHARACTERIZATION Final Report, Jan. - Jun. 1994
Vicki Sanderford and Scott Mobley Dec. 1994 72 p Limited Reproducibility: More than 20% of this document may be affected by microfiche quality
(AD-A289806; AMSMI-RD-SS-94-18) Avail: Issuing Activity (Defense Technical Information Center (DTIC))

This paper provides the results of thin-film resistor array testing which was recently performed at the System Simulation and Development Directorate (SS&DD), Research, Development, and Engineering Center (RDEC). The objective of these tests was to determine the suitability of the Australian thin-film resistor technology for use as a key component in an Infrared Scene Projector (IRSP) for Hardware-in-the-Loop (HWIL) simulations involving systems which utilize linear rows of detectors. The tests were configured to measure spatial uniformity, temporal response, dynamic range, and relative energy output as a function of power input. D65O funding was used to purchase the resistor arrays. DTIC

N95-28961# Oak Ridge National Lab., TN.
XPS STUDY OF Ni-Fe MANGANITE THERMISTOR MATERIAL
D. N. Braski, N. R. Osborne (Dayton Univ. Research Inst., OH.), and J. M. Zurbuchen (Yellow Springs Instruments, Inc., Yellow Springs, OH.) 1995 6 p Presented at the 1994 Fall Meeting of the Materials Research Society, Boston, MA, 28 Nov. - 2 Dec. 1994 Sponsored by Martin Marietta Energy Systems, Inc.
(Contract DE-AC05-84OR-21400)
(DE95-008778; CONF-941144-91) Avail: CASI HC A02/MF A01

The resistivity of the as-fabricated thermistor material, nickel-iron-manganite, changes during initial aging in the temperature range of 150-300 C before becoming stable. X-ray photoelectron spectroscopy (XPS) was used to determine if any valence change or chemical shift of the cations or oxygen occurred after aging. The goal of the study was to identify any ionic changes that might affect thermistor stability. The only observed changes in 2p(sub 3/2) peaks due to aging were those related to Ni ions; the same peaks for Mn, Fe, and O remained unchanged. The changes in the Ni 2p(sub 3/2) peak may be related to: (1) the migration of Ni(2+) ions from octahedral to tetrahedral sites; (2) subtle changes in the energy states of Ni(2+) which promoted a more stable ionic structure; and/or (3) the presence of Ni(3+) ions, some of which revert back to Ni(2+). DOE

N95-28971# Wright Lab., Wright-Patterson AFB, OH.
CORONA TESTS OF PROTOTYPE CONNECTOR Final Report, 15 May - 15 Jul. 1994
Gregory L. Rhoads, John Horwath, and Daniel Schweickart Dec. 1994 19 p
(DA Proj. NAV-P)
(AD-A292542; WL-TR-94-2120) Avail: CASI HC A03/MF A01

Seven prototype connector boards were tested at Wright Laboratory in the Aerospace Power Division High Power Lab. Each connector board incorporates two types of connectors: (1) ac/dc hybrid connector with six power feedthroughs, i.e. two for dc power and four for ac power, and (2) dc connector with two power feedthroughs. The 270 volt dc rated power feedthroughs were tested with 500 volts dc. The three phase, 208 volt ac (line-to-line) power feedthroughs were tested with 354 volts ac rms. The boards were tested at ground level and at simulated altitudes of 50,000 and 100,000 feet. Corona data acquisition was accomplished in accordance with ASTM 1868-81, using a multichannel analyzer for discharge magnitude characterization. The boards performed well with only insignificant corona activity above five picocoulombs. DTIC

N95-29005# Texas Univ., Austin, TX.
NANOFABRICATION OF ELECTRONIC DEVICES WITH THE SCANNING TUNNELING MICROSCOPE Final Technical Report, 1 Nov. 1992 - 31 Oct. 1994
Alejandro DeLozanne 31 Oct. 1994 4 p
(Contract F49620-93-1-0007)
(AD-A292463; AFOSR-95-0160TR) Avail: CASI HC A01/MF A01

This grant represents one year of funding plus a one-year, no-cost extension. The main achievements were: (1) development of a new technique for imaging rapidly with the STM; (2) the reproducibility of the writing process was improved dramatically. (3) Commercial STM electronics were adapted to our STM; (4) fabrication of the smallest continuous metallic lines to date: 24 nm wide; and (5) design and construction of a compact STM for nanofabrication. These main points are described briefly below and in more detail in the publications listed at the end. Other groups have followed our lead in using the STM to break down precursor gases to make nanoscale deposits, namely Matsui's group at NBC in Tsukuba, Japan, Kent's group at IBM Yorktown (now at New York University), Behm's group in Munchen, Germany, and Nayfeh's group at U. Illinois. This technique is therefore likely to become more important over the next decade. DTIC

N95-29010# California Univ., Berkeley, CA. Electronics Research Lab.
JOINT SERVICES ELECTRONICS PROGRAM Final Report, 6 Jun. 1993 - 5 Jun. 1994
J. Bokor and M. A. Lieberman 5 Aug. 1994 147 p
(Contract AF-AFOSR-93-C-0014)
(AD-A292469; AFOSR-95-0143TR) Avail: CASI HC A07/MF A02

This report summarizes the research activity supported by the Joint Services Electronics Program at the Electronics Research Laboratory for the period June 1993 to June 1994. The Berkeley JSEP effort was organized into three themes: Quantum and Opto-electronic Devices, Semiconductor Electronic Devices, and Artificial Neural Networks. Under Quantum and Opto-electronic Devices, a new femtosecond laser laboratory for ultrafast measurements of carrier dynamics in semiconductors was completed. In the Semiconductor Electronic Device area, a novel device design was invented that has made possible quantitative measurement of the saturation velocity in inversion layers. This key parameter directly relates to the ultimate speed of transistors making it practical to realize CMOS-like circuits that can operate at voltages as low as 0.6V, and still maintain excellent speed and turn-off characteristics. Under Artificial Neural Networks, the focus continued to be the development of connectionist algorithms that are directly applicable to real-world problems, with particular attention given to applications of specific DOD interest. This work on speech recognition and machine vision emphasizes robustness in the face of noise. DTIC

N95-29014# Wayne State Univ., Detroit, MI.
SYNTHESIS AND CHARACTERIZATION OF CuO SUPERCONDUCTORS WITH HIGH TRANSIENT TEMPERATURES Technical Report, 1 Jun. 1993 - 30 Nov. 1994
Lowell E. Wenger and J. T. Chen 31 Jan. 1995 48 p
(Contract AF-AFOSR-91-1-0334)
(AD-A292478; F49620-93-1-0334; AFOSR-95-0126TR) Avail: CASI HC A03/MF A01

This final technical report describes the continual superconductivity research on the materials and structural phases responsible for the above 200 K superconducting transitions, their synthesis conditions, and the study of the physical properties associated with these transitions. Resistive transitions having superconducting-like character have been observed in multi-phase ceramic YBaCu0 samples and on surfaces of nominal YBa2Cu3O7 single crystals in the temperature range of 260 K to 340 K. The appearance of these transitions appears to require certain experimental measuring conditions including and oxygen atmosphere during measurements. Magnetization studies on these materials show a flux-trapping hysteretic behavior at similar temperatures, i.e., a more diamagnetic behavior in the zero-field-cooled- magnetization than the field-cooled-magnetization, which is characteristic of a weak superconducting phase being present. The synthesis conditions and structural information on multi-phase YBaCuO samples exhibiting reproducible flux-trapping phenomenon at 336 K is also detailed. DTIC

N95-29018# California Inst. of Tech., Pasadena, CA.
THEORETICAL INVESTIGATION OF SUPERCONDUCTIVITY IN DOPED FULLERENES Final Report
Radi A. Jishi Mar. 1995 5 p
(Contract F49620-92-J-0401)
(AD-A291942; AFOSR-95-0111TR) Avail: CASI HC A01/MF A01

The aim of the research we are conducting is to understand the phenomenon of superconductivity in the fullerene system. Towards achieving this goal we have conducted a series of studies and have published several papers quite recently. We have developed a force-constant model for the C60 molecule which accounts for all measured frequencies in C60. The model employs four bond-stretching and four angle-bending force constants that were doped to reproduce the correct values of the frequencies of the Raman-active vibrational modes. The model was successfully applied to higher fullerenes, such as C70 and the effect of doping by alkali metal atoms on the phonon modes in C60 and in C70 was considered. The study of the phonon spectrum in doped C60 and doped C70 is an important step in view of the fact that while doped C60 is superconducting, doped C70 is not. The studies we have carried out, combined with studies on the electronic states in doped C70, could elucidate the difference in the electrical properties between these two materials. DTIC

N95-29061# Advanced Fuel Research, Inc., East Hartford, CT.
HTS JOSEPHSON TECHNOLOGY ON SILICON WITH APPLICATION TO HIGH SPEED DIGITAL MICROELECTRONICS Monthly Progress Report, 29 Nov. 1994 - 31 Dec. 1994
Peter Rosenthal 27 Jan. 1995 4 p
(Contract N00014-94-C-0261)
(AD-A290206) Avail: CASI HC A01/MF A01

A summary of progress on (1) Josephson junction fabrication and testing and (2) rapid single-flux-quantum (RSFQ) modeling and design is given. An attempt was made to fabricate a Josephson junction from a high temperature superconductor (HTS) film on a silicon substrate. The film had good superconducting qualities as determined by resistance versus temperature measurements. The film was etched into three bridges approximately four microns across and measured again for resistance versus temperature. Two of the junctions were highly resistive at all temperatures, and the third showed a partial transition at 90 K, but retained a residual resistance of 400 Ohms below the superconducting transition temperature of the film. It is expected that functional RSFQ logic elements will be possible even with films as thin as 60 nm. Derived from text

N95-29073# Westinghouse Science and Technology Center, Pittsburgh, PA.
PROCESSING, FABRICATION, AND DEMONSTRATION OF HTS INTEGRATED MICROWAVE CIRCUITS Status Report, 25 Oct. 1994 - 24 Jan. 1995
S. H. Talisa and J. Talvacchio 7 Mar. 1995 20 p
(Contract ARPA Order 7932)
(AD-A292480; Rept-95-9SL2-LAFIL-R1) Avail: CASI HC A03/MF A01

The following tasks involving integrated microwave circuits are discussed: comparative technology assessment; functional component and subsystem design, fabrication, and testing; PVD multilayer film fabrication; MOCVD multilayer film fabrication; RF characterization of film properties; and switched filterbank. Derived from text

N95-29075# Naval Research Lab., Washington, DC.
NANOSCIENCE AND NANOTECHNOLOGY IN EUROPE Final Report, Jan. - Dec. 1994
William A. Tolles 30 Dec. 1994 157 p
(AD-A290214; NRL/FR/1003-94-9755) Avail: CASI HC A08/MF A02

The subject of nanoscience and/or nanotechnology is of considerable interest as a rapidly expanding frontier of research. This report documents information gathered at 44 laboratories in Europe by the author over a six month period. Research activities in physics, electronics, materials, chemistry, and biotechnology are included. Fundamental advances in fabrication, characterization, and utilization of nanostructures are presented. Areas of greatest interest include nanostructures for electronic and optical materials and devices, sensors, and other applications envisioned. Research programs covered include lithography, materials, self-assembly, local probes, transport properties, quantum dots and wires, surface film behavior, some magnetic and optical behavior, including nonlinear spectroscopy, high frequency device behavior, and mechanical measurements at nanodimensions. A short description of the environment at each laboratory visited is included. DTIC

N95-29078# Westinghouse Science and Technology Center, Pittsburgh, PA.
PROCESSING, FABRICATION, AND DEMONSTRATION OF HTS INTEGRATED MICROWAVE CIRCUITS R/D Status Report, No. 13, 25 Jul. - 24 Oct. 1994
S. H. Talisa, J. Talvacchio, and G. R. Wagner 24 Oct. 1994 32 p
(Contract N00014-91-C-0112; ARPA Order 7932)
(AD-A290220; Rept-94-9SL2-LAFIL-R2) Avail: CASI HC A03/MF A01

The following tasks involving integrated microwave circuits are discussed: comparative technology assessment; functional component and subsystem design, fabrication, and testing; PVD multilayer film fabrication; MOCVD multilayer film fabrication; RF characterization of film properties; and switched filterbank. Derived from text

N95-29099# Nobeyema Solar Radio Observatory (Japan).
NOBEYAMA RADIO OBSERVATORY REPORT, NO. 381: PARALLEL CONNECTED TWIN SIS JUNCTIONS FOR MILLIMETER AND SUBMILLIMETER WAVE MIXERS: ANALYSIS AND EXPERIMENTAL VERIFICATION
Takashi Noguchi, Sheng-Cai Shi, and Junji Inatani 1995 24 p Submitted for publication
(ISSN 0911-5501)
Avail: CASI HC A03/MF A01

A Superconductor-Insulator-Superconductor (SIS) mixer using two junctions connected in parallel through a stripline inductance has been studied. The essential point of the two-junctions device is that the capacitance of the junctions was tuned out by the inductance to obtain a broad-band operation without mechanical tuning elements. It has been shown by theoretical analysis that the performance of this type of device is excellent and nearly quantum-limited performance of the mixer can be obtained. It has been demonstrated that the double sideband (DSB) noise temperature of a receiver employing this type of device was less than 40 K over the bandwidth of 90-120 GHz and that the lowest receiver noise temperature of approximately 18 K, which is only 3.2 time as large as the quantum limited photon noise was obtained around 118 GHz. Junctions used in the two-junctions device have significantly larger area, i.e. larger capacitance, and smaller normal resistance than conventional ones. In order to obtain a good impedance match between the source and the junctions, an impedance transformer made of a superconducting stripline was integrated with the junctions. This type of two-junctions device can easily be scaled to submillimeter frequency without using submicron-sized SIS junctions. Author

N95-29163# Southern Univ., Baton Rouge, LA. Dept. of Physics.
COMPUTER SIMULATION STUDY OF HIGH t(SUB c) SUPERCONDUCTOR STRUCTURE Final Technical Report, 1 Jul. 1991 - 31 Dec. 1994
J. D. Fan Feb. 1995 24 p
(Grant AF-AFOSR-0337-91)
(AD-A292513; AFOSR-95-0129TR) Avail: CASI HC A03/MF A01

The project funded by AFOSR under the grant 91-0337 for the past three and a half of years has reached a brilliant achievement in understanding the mechanism of high-temperature superconductivity (HTSC). A basic theory describing the mechanism and origin of HTSC has been established. It is not completely finished, but the outline and kernel of the theory have been done. This is a revolutionary breakthrough in seeking the mechanism of HTSC that is entirely different from the currently prevailing theories and models. The main point of this theory lies in the mechanism of superconductivity in high-temperature superconductors (HTSCt's) or the origin of the attractive interaction between two electrons in a Cooper pair. It is said in the theory developed in the present project that the origin of attraction between two electrons in HTSC's stems from the Coulomb-type interaction due to the electron correlation effects enhanced by the layered spatial structure. In other words, the superconductivity in HTSC's is induced by the electron-electron correlations. In contrast to the viewpoint of electron-phonon interaction mechanism of superconductivity, stemming from the BCS theory, the new viewpoint is that the electron-electron interaction mediated by electron-hole excitations governs behaviors of HTSC. DTIC

N95-29164# North Dakota State Univ., Fargo, ND.
POWER MEASUREMENT AND CURRENT FEEDBACK IN A RESONANT DC LINK INVERTER Final Report, Sep. 1993 - 31 Aug. 1994
Subbaraya Yuvarajan 19 Oct. 1994 5 p
(Contract F49620-93-1-0534)
(AD-A292518; AFOSR-95-0118TR) Avail: CASI HC A01/MF A01

Resonant DC (direct current) Link (RDCL) inverters employ zero-voltage switching to reduce switching loss in power converters and to improve their efficiency. The project uses current feedback to eliminate zero-crossing failure in RDCL inverters. The zero-crossing failure is corrected by sensing the load current and feeding it back to control the operation of the link-shorting switch. The operation of the control scheme is first established by simulating the converter using computer simulation. The current feedback is implemented on an experimental RDCL inverter. The inverter is built using current-sensing Power MOSFETs that provide signals proportional to the current. The control signals to the inverter switches and the outputs from the current sensing MOSFETs are fed back to control the frequency and the duty cycle of the input to the link-shorting switch. The addition of proper level of current feedback is found to reduce the minimum link voltage to zero. The waveforms of the link voltage with and without current feedback are recorded and studied using a digital storage oscilloscope. The power loss in the RDCL inverter is also computed using the oscilloscope and it is seen the addition of current feedback results in a higher efficiency for the converter. DTIC

N95-29191 American Inst. of Physics, New York, NY.
SEMICONDUCTOR SCIENCE AND TECHNOLOGY
G. Bauer, F. Kuchar, and H. Heinrich Nov. 1994 184 p Presented at the 8th Winterschool on New Developments in Solid State Physics, Mauterndorf, Austria, 14-18 Feb. 1994 Limited Reproducibility: More than 20% of this document may be affected by microfiche quality
(Contract N00014-94-1-0401) (ISSN 0268-1242)
(AD-A289143) Avail: Issuing Activity (Defense Technical Information Center (DTIC))

The Eighth International Winterschool on New Developments in Solid State Physics, entitled Interaction and Scattering Phenomena in Nanostructures, was held in Mauterndorf Castle, Salzburg, Austria on 14-18 Feb. 1994. A total of 69 papers (including posters) were presented at the meeting. 28 invited papers are printed in this volume. As usual, it was intended to have the most recent highlights in low dimensional physics presented at this meeting. The main topics were: Composite fermions and fractional quantum Hall effect; Mesoscopic transport and chaos; Low dimensional tunnelling; Wires: spectroscopy and lasing action; Bloch oscillations and ultrafast phenomena; Coupled quantum wells and superlattices; Si/SiGe heterostructures; Microcavities. The success of this conference series relies heavily on the invited speakers, who made real efforts to give lucid presentations of their work. The event's strong international tradition was maintained by a total of about 190 scientists attending from 20 countries. DTIC

N95-29239# Naval Postgraduate School, Monterey, CA.
NUMERICAL MODELING OF OPTO-ELECTRONIC INTEGRATED CIRCUITS M.S. Thesis
Christopher C. Foster Dec. 1994 118 p Limited Reproducibility: Document partially illegible
(AD-A292096) Avail: CASI HC A06/MF A02

This thesis develops an efficient and effective method for designing and analyzing the performance of various integrated optical waveguide structures using the beam propagation method of analysis. Modifications in the physical layout of an optical device through changes in coupling connection design, splitting angles and waveguide dimensions may have significant effects on device performance. The beam propagation method is initially developed for a symmetric Mach-Zehnder interferometer for baseline validation of the accuracy and applicability of the propagation scheme. A major validation is achieved through modeling an asymmetric device designed and built by the Naval Research Laboratory. The validated simulation model is used to analyze the performance and design characteristics of complex parallel configurations of interferometers. The beam propagation method allows quantitative analysis of the performance of these integrated optical devices. The propagation model developed implements a new global propagator scheme that substantially reduces computational requirements and introduces a design methodology that ensures compatibility between the discrete implementation and the physical structure. Also identified are areas in which continued research can provide a complete modeling system that may be implemented as a stand-alone design and analysis. DTIC

N95-29275# Defence Research Establishment Ottawa, Ottawa (Ontario).
SOSDOR: SOLID-STATE DEVICE SIMULATOR CODE
L. Varga Oct. 1994 25 p
(AD-A289954; DREO-1235) Avail: CASI HC A03/MF A01

A 3-D solid state device simulator code, developed at DREO, is presented. The code uses a seven-point finite difference scheme to discretize Poisson's and the continuity equations. The equations are then solved using the Newton-Raphson iteration method. Additional information pertaining to griding, carrier mobility and recombination models as well as boundary condition types incorporated into the code is also presented. The source files of the code and the graphical interfaces are also described. The code was tested by simulating a PIN diode under no bias and under a 20V reverse bias condition. The simulation results are in excellent agreement with the results of simulation of the same device by the industry standard PADRE code. DTIC

N95-29301# Naval Research Lab., Washington, DC.
THEORY OF COMPETITION BETWEEN SYNCHRONOUS AND NONSYNCHRONOUS MODES IN A MAGNICON OUTPUT CAVITY Interim Report
Arne W. Fliflet and Steven H. Gold 16 Mar. 1995 22 p
(AD-A292048; NRL/MR/6793-95-7639) Avail: CASI HC A03/MF A01

In the magnicon amplifier, a scanning electron beam drives a synchronous fast-wave interaction in a gyrotron-like output cavity. The output cavity is designed to support the synchronous TM210 operating mode. However, a number of other TE or TM modes can be excited in the cavity via a nonsynchronous, gyrotron-type interaction. To investigate the possibility of competition from these nonsynchronous modes, a multimode gyrotron simulation theory and code nave been adapted to the magnicon configuration. The gyrotron theory and corresponding code have been generalized to include a synchronous TM mode as well as nonsynchronous TE modes. Proper phase averaging between the modes, and between the modes and the beam electrons, is critical to accurate mode competition calculations. In nonsynchronous interactions this is achieved by averaging with respect to electron entrance time and the orbit guiding center angle. The synchronous mode interaction is invariant with respect to these two averages; however, it is affected by scanning angle spread which is included via a third average over scanning angles. Calculations have been carried out to model a second-harmonic X-Band magnicon experiment which is currently underway at the Naval Research Laboratory (NRL). The output cavity has been optimized for the TM210 mode at 11.4 GHz or twice the

drive frequency (wd= 5.7 GHz). The principal competing mode is the TE121 mode. The simulations show that nonsynchronous mode interactions are suppressed by the synchronous interaction if the scanning angle spread is sufficiently small. DTIC

N95-29384# Massachusetts Inst. of Tech., Lexington, MA.
NOVEL HIGH-POWER SOLID-STATE SOURCES FOR THE MILLIMETER-WAVE REGION Final Report, 1 Oct. 1992 - 30 Sep. 1994
E. R. Brown 6 Mar. 1995 105 p
(AF Proj. 2305)
(AD-A292653; AFOSR-95-0237TR) Avail: CASI HC A06/MF A02

The goal of this two-year program was to create two new sources for ultrafast electronic circuits. Two technical approaches were pursued. The first was a cw optoelectronic photomixer using low- temperature-grown (LTG) GaAs as the active material. Prior to this research, little work had been done on cw photomixers at millimeter-wave (i.e., f greater than 30 GHz) or higher frequencies. The primary limitation was the lack of a suitably fast photoconductive material. LTG GaAs is a promising material for this application because of its short photoconductive lifetime and robust electrical properties. Through the research carried out on this program, the photomixer was developed into a very useful source for frequencies above 1006Hz. The second approach was an electronic pulse generator using a resonant-tunneling diode (RTD) as the active device. The basis for this generator was the high switching speed of the (RTD) when connected to a low-impedance transmission line. Previous work had produced single high-speed switching events in RTDs, but the switching d not heen made self- induced and repetitive. In this effort self-generated pulse trains were produced having a pulse width of approximately 25ps, a repetition rate up to 36Hz, and a pulse amplitude of approximately 0.5 V. One attractive feature of the RTh pulse generator is that it can be modified to generate several useful types of pulse waveforms, such as the impulse function and square waves. DTIC

N95-29406*# Analex Corp., Brook Park, OH.
SIMULATED IMAGING PROPERTIES OF A SERIES OF MAGNETIC ELECTRON LENSES Final Contractor Report
Carol L. Kory Jun. 1995 6 p Presented at the 1995 International Magnetics Conference, San Antonio, TX, 18-21 Apr. 1995; sponsored by IEEE
(Contract NAS3-25776; RTOP 235-01-00)
(NASA-CR-195474; E-9678; NAS 1.26:195474) Avail: CASI HC A02/MF A01

The paraxial lens data were determined for a series of symmetrical magnetic lenses of equal lens diameter but variable air gap width for a wide range of lens excitations using the three-dimensional electrodynamic computer code MAFIA. The results are compared with a similar study done by Liebman and Grad wherein the field distributions within the lenses were measured experimentally with a resistance network analogue. Using these fields the lens data were obtained through numerical trajectory tracing. The utility of using MAFIA, instead of experimental methods for lens design is shown by the excellent agreement of the simulated results compared to experiment. Also demonstrated is the capability of using MAFIA to investigate aberration sources such as higher order off-axis magnetic field and space-charge effects. Author

N95-29417# Maryland Univ., College Park, MD. Dept. of Electrical Engineering.
HYBRID HARMONIC GYROTRON TRAVELING WAVE AMPLIFIER Final Report
V. L. Granatstein and H. Guo Feb. 1995 13 p
(Contract F49620-93-1-0162)
(AD-A292686; AFOSR-95-0128TR) Avail: CASI HC A03/MF A01

This progress report summarizes the work done on the project 'Hybrid Harmonic Gyrotron Traveling Wave Amplifier' covering the period from March 15, 1994 to October 31, 1994. In the past seven and a half months, we have designed a compact harmonic multiplying gyro- TWT amplifier. The device is a threestage tube with the output section running as an fourth harmonic gyro-TWT, the input section running as a fundamental gyro-TWT, and the middle section operating at the second harmonic of the cyclotron frequency. Radiation is suppressed by servers between the sections. The electron beam which drives the tube is produced by a magnetron injection gun. DTIC

N95-29430# Duke Univ., Durham, NC.
THE QUANTUM HYDRODYNAMIC MODEL FOR SEMICONDUCTOR DEVICES Final Report
Carl L. Gardner 6 Feb. 1995 11 p
(Contract DAAL03-91-G-0146)
(AD-A291809; ARO-28799.9) Avail: CASI HC A03/MF A01

Quantum semiconductor devices are playing an increasingly important role in advanced microelectronic applications, including multiple-state logic and memory devices. To model quantum devices, the classical hydrodynamic model for semiconductor devices can be extended to include O(h(2)) quantum corrections. This proposal focused on theoretical and computational investigations of the flow of electrons in semiconductor devices based on the quantum hydrodynamic model. The development of efficient, robots numerical methods for the QHD model in one and two spatial dimensions we also emphasized. DTIC

N95-29478# Massachusetts Inst. of Tech., Cambridge, MA.
ASYMPTOTICALLY ZERO ENERGY COMPUTING USING SPLIT-LEVEL CHARGE RECOVERY LOGIC Ph.D. Thesis
Saed G. Younis Jun. 1994 116 p
(Contracts DABT63-92-C-0039; N00014-91-J-1698)
(AD-A290054; AI-TR-1500) Avail: CASI HC A06/MF A02

The dynamic dissipation of CMOS (complementary metal oxide superconductor) circuits is becoming a major concern for designers of personal information systems and large computers. Here, we present new CMOS logic families, including Split-Level Charge Recovery Logic (SCRL), within which the transfer of charge between the nodes occurs quasistatically, thus having a power consumption that drops quadratically with operating frequency as opposed to the linear drop of conventional CMOS. The technique in these new families rely on explicitly reversible pipelined logic gates to provide the necessary information needed to recover most of the energy used in the computation. We report results of testing the first fully quasistatic 8 x 8 multiplier chip (SCRL-I). DTIC

N95-29511# Optical Society of America, Washington, DC.
SUMMARIES OF PAPERS PRESENTED AT THE ULTRAFAST PHENOMENA TOPICAL MEETING Final Report
David W. Hennage Nov. 1994 680 p
(Contract DAAH04-94-G-0104)
(AD-A290998; ARO-32824.1-EL-CF) Avail: CASI HC A99/MF A06

Topics discussed include: femtosecond solid-state lasers, reaction and dynamics in solution, ultrashort light pulses, nonlinear spectroscopy and solvent dynamics, ultrafast dynamics in solids, biology, surfaces, quantum-confined systems, high spatial and temporal resolution, dispersion, high intensity, gas phase clusters, high field atomic physics, reactions in solution, dynamics in solution, and biological spectroscopy and medical applications. CASI

N95-29568# Office of Naval Research, Arlington, VA.
INTERBAND LATERAL RESONANT TUNNELING TRANSISTOR Patent Application
J. R. Meyer, inventor (to Navy), C. A. Hoffman, inventor (to Navy), and F. J. Bartoli, inventor (to Navy) 14 Nov. 1994 26 p Filed 14 Nov. 1994
(AD-D017399; Navy-Case-74851; US-Patent-Appl-SN-338842) Avail: CASI HC A03/MF A01

This invention describes a nanometer scale interband lateral resonant tunneling transistor, and the method for producing the same, with lateral geometry, good fanout properties and suitable for incorporation into large-scale integrated circuits. The transistor is of a single gate design and operation is based on resonant tunneling processes in narrow-gap nanostructures which are highly responsive to quantum phenomena. Such quantum-effect devices can have very high density, operate at much higher temperatures and are capable of driving other devices. DTIC

N95-29570# Office of Naval Research, Arlington, VA.
ADAPTIVE INFINITE IMPULSE RESPONSE (IIR) FILTER SYSTEM Patent Application
James Herchen, inventor (to Navy) and Allen Lindgren, inventor (to Navy) 26 Apr. 1994 26 p Filed 26 Apr. 1994
(AD-D017403; Navy-Case-75498; US-Patent-Appl-SN-233562) Avail: CASI HC A03/MF A01

An adaptive filter system for use in connection with a reference system

that receives an input u(s) and generating in response thereto a reference output y(s) defined by a reference transfer function H(s) = c(sI-A)(-1)b + d, where 'I' is the identity matrix and matrix A, vectors b and c, and scalar d are reference parameters, and 's' is a variable for the input. The adaptive filter system comprises a system model module, a gradient filter module, an adjustable parameter module, and a parameter adjustment module. DTIC

N95-29601 Central Connecticut Engineering, Inc., Rocky Hill, CT.
HIGH POWER SWITCH DESIGN Final Report, 10 Jan. 1994 - 30 Jan. 1995
David V. Turnquist and Brian W. Wegner 30 Jan. 1995 162 p Limited Reproducibility: More than 20% of this document may be affected by microfiche quality
(Contract N60921-94-C-A345)
(AD-A291608) Avail: Issuing Activity (Defense Technical Information Center (DTIC))

The complete manufacturing design of a high-power, high-repetition-rate switch has been developed. The switch will be capable of continuous operation at 100,000 volts, 100 kilowatts of average power, 100 joules per pulse, and 1000 hertz pulse repetition rates into a low impedance load. The inductance is minimized, as far as consistent with the other requirements, and the switch is designed for long life. The switch is a trigatron type spark gap with a high-pressure hydrogen-gas fill. The design is based directly on previous development of such devices by NSWCDD. The design includes an integrated fluid cooling system and a 100 kV, 1000 Hz trigger system. The design is capable of scaling to higher voltages and power levels. The manufactured switch will be vacuum sealed, and is designed to meet both military and commercial shock, vibration, temperature, and other environmental conditions. DTIC

N95-29728 Detroit Univ., MI.
TARGET AIRCRAFT IDENTIFICATION, TRAJECTORY TRACKING AND PREDICTION USING REGRESSION-BASED KALMAN FILTER TECHNIQUES Ph.D. Thesis
Luis Carlos Cattani 1993 173 p
Avail: Univ. Microfilms Order No. DA9418287

Techniques are presented for improving methods of aircraft identification and trajectory prediction. This work represents an extension of the advanced trackers that use both translation and attitude data to improve accuracy of trajectory tracking and prediction. The novel extension in this work deals with the development of a new tracking algorithm based on a radius of curvature estimator, use of regression-based artificial measurements during the prediction interval, and development of aircraft identification techniques for vehicles being tracked based on remote trajectory measurements. The procedure was evaluated with actual position and attitude trajectory data for a F-14A, AV-8B, and A6 aircraft acquired during training flights. Dissert. Abstr.

N95-29925# Southampton Univ. (England).
FIBER COMPATIBLE ACOUSTO-OPTIC MODULATOR USING A GRADIENT INDEX LENS Final Technical Report, 9 Jan. 1993 - 31 Aug. 1994
B. Wacogne, M. P. Roe, T. J. Pattinson, and C. N. Pannell Nov. 1994 127 p
(Contract F49620-93-1-0494)
(AD-A291164; EOARD-TR-95-04) Avail: CASI HC A07/MF A02

We present the work carried out at the Optoelectronics Research Centre concerning acoustooptic modulators. The first part deals with theoretical studies concerning the design of fibre-compatible acoustooptic switcher- connectors. We explain how to build efficient AOM's according to the characteristics required for specific applications. The concept of modulators exhibiting a double curvature is proposed. The second part deals with the deposition and evaluation of sputtered ZnO thin films. This work highlights several new aspects concerning the sputtering of thin piezoelectric films. An in situ interferometric method used to measure both the film thickness and the depth resolved optical losses of the film is developed. We also investigate the real piezoelectric activity of sputtered ZnO films. In part 3, we present experimental results obtained with the acoustooptic modulators we built. The main results are: a diffraction efficiency in good agreement with the theoretical calculations, a broad frequency range of operation, low transduction losses, the ability to electrically match every type of transducer, and a phase modulation efficiency in optical fibres twice that which has already been published. We also propose new acoustooptic devices we will be able to build within the near future. DTIC

N95-29938# Army Research Lab., Aberdeen Proving Ground, MD.
A STUDY OF POWER DIODE FAILURE MECHANISMS IN THE US ARMY RESEARCH LABORATORY 30-mm SOLID PROPELLANT ELECTROTHERMAL-CHEMICAL (SPETC) GUN FACILITY Final Report, Apr. 1993 - Sep. 1994
Gary L. Katulka and Kevin J. White Feb. 1995 38 p
(AD-A291300; ARL-TR-698) Avail: CASI HC A03/MF A01

Experiments have been performed with a 100-kJ Pulse Forming Network (PFN) at the U.S. Army Research Laboratory (ARL) for the purpose of characterizing semiconductor diodes which serve as capacitor-protecting crowbar devices. These devices are viewed as critical electronic power components required for electric gun research that is currently in progress within the U.S. Army and elsewhere. As part of this study, computer techniques were used to refine and develop the understanding of the dynamic, or switching, behavior of PFN diodes. In combination with experimental results, the computer simulations helped to define particular conditions within a given electric gun system that can cause vulnerable or stressful situations for the semiconductor devices under test. It was determined from analyses of the various data collected, that when operated in a PFN under specific loading conditions (simulated here with fixed resistive loads), diodes are subject to transient or high frequency voltage peaks. In some experimental cases at the ARL, the magnitude of the rate of change in voltage (dV/dt) across the devices was such that catastrophic failure was observed. The details of the boundary conditions necessary for device failure are described and several solutions that will circumvent operational problems including device grouping, choice of diode reverse recovery time, and selection of capacitive and inductive circuit parameters are discussed in detail. Background information describing some fundamental physics of semiconductor diodes and their role in electrothermal-chemical (ETC) propulsion technology is provided first. DTIC

N95-29968*# Arizona Univ., Tucson, AZ. Dept. of Chemical Engineering.
THE ONSET OF ELECTROHYDRODYNAMIC INSTABILITY IN ISOELECTRIC FOCUSING Final Technical Report, 14 Apr. 1992 - 31 Dec. 1993
James C. Baygents 31 Dec. 1993 79 p
(Grant NAG8-909)
(NASA-CR-198805; NAS 1.26:198805) Avail: CASI HC A05/MF A01

The onset of electrohydrodynamic motion associated with the imposition of an electric field across a thin layer of liquid has been investigated for the case in which the electrical conductivity varies linearly over the depth of the layer. The variation of the conductivity is due to concentration gradients in the charge-carrying solutes and its spatio-temporal evolution is represented by a convective-diffusion equation. When the viscous relaxation time is long compared to the time for charge relaxation, the analysis reveals that the neutral stability curves for the layer can be characterized by three dimensionless parameters: Ra(sub e) is equivalent to d(epsilon)E(sup 2, sub 0) Delta sigma/mu K(sub eff) sigma(sub 0), an electrical Rayleigh number; delta sigma/sigma(sub 0), the relative conductivity increment; and alpha, the transverse wave number of the disturbance. Here d is the thickness, epsilon is the dielectric constant, and mu is the viscosity of layer, E(sub 0) is the applied field strength at the lower conductivity boundary, and K(sub eff) is an effective diffusivity associated with the Brownian motion of the charge-carrying solutes. With viscous-stress-free boundaries, at which the electrical conductivity and the normal component of the electric field are prescribed, the critical Ra(sub e) is 1.504 x 10(exp 4) at a critical transverse wave number of 1.97 when Delta sigma/sigma(sub 0) is 10. As Delta sigma/sigma(sub 0) increases, the critical Ra(sub e) increases and shifts to shorter wavelength disturbances; the critical imposed field strength, however, passes through a minimum because the lower-conductivity boundary exerts a considerable stabilizing influence in the presence of steep conductivity gradients. Similar trends were obtained for liquid layers with rigid boundaries. Author

N95-29998*# National Aeronautics and Space Administration. Lewis Research Center, Cleveland, OH.

THREE-DIMENSIONAL SIMULATION OF TRAVELING-WAVE TUBE COLD-TEST CHARACTERISTICS USING MAFIA

Carol L. Kory and Jeffrey D. Wilson May 1995 30 p Original contains color illustrations

(Contract NAS3-25776)

(NASA-TP-3513; E-9192; NAS 1.60:3513) Avail: CASI HC A03/MF A01; 4 functional color pages

The three-dimensional simulation code MAFIA was used to compute the cold-test parameters - frequency-phase dispersion, beam on-axis interaction impedance, and attenuation - for two types of traveling-wave tube (TWT) slow-wave circuits. The potential for this electromagnetic computer modeling code to reduce the time and cost of TWT development is demonstrated by the high degree of accuracy achieved in calculating these parameters. Generalized input files were developed for ferruled coupled-cavity and TunneLadder slow-wave circuits. These files make it easy to model circuits of arbitrary dimensions. The utility of these files was tested by applying each to a specific TWT slow-wave circuit and comparing the results with experimental data. Excellent agreement was obtained.

Author

N95-30025# Brookhaven National Lab., Upton, NY.

RADIATION EFFECTS ON FRONT-END ELECTRONICS FOR NOBLE LIQUID CALORIMETRY

M. Citterio, S. Rescia, and V. Radeka Dec. 1994 10 p Presented at the 5th International Conference on Calorimetry in High Energy Physics, Upton, NY, 25 Sep. - 1 Oct. 1994

(Contract DE-AC02-76CH-00016)

(DE95-007304; BNL-61327; CONF-9409268-8) Avail: CASI HC A02/MF A01

Front-end electronics for liquid ionization chamber calorimetry at hadron collider experiments may be exposed to substantial levels of ionizing radiation and neutron fluences in a cryogenic environment. Measurements of devices built with rad-hard technologies have shown that devices able to operate in these conditions exist. Si-JFET's and GaAs MESFET devices have been irradiated and tested at a stable cryogenic temperature up to doses of 55 Mrad of ionizing radiation and up to neutron fluences of 4 x 10(exp 14) n/cm(exp 2). Radiation effects on DC characteristics and on noise are presented.

DOE

N95-30052# Department of the Navy, Washington, DC.

BALANCED, DOUBLE-SIDED CALIBRATION CIRCUIT FOR SENSOR ELEMENT DIFFERENTIAL PRE-AMPLIFIER Patent Application

James J. Hagerty, inventor (to Navy) 7 Oct. 1994 18 p

(AD-D017326; US-Patent-Appl-SN-319709) Avail: CASI HC A03/MF A01

The balanced, bi-directional calibration circuit of the present invention is joined to a sensor and a differential preamplifier. The sensor has two outputs which are received by the differential preamplifier such that common-mode line noise is rejected. The calibration circuit includes a broadband signal generator which provides the calibration signal. The calibration circuit also includes a switching network that allows the calibration signal to be switched to either of the two sensor outputs or isolated from the sensor and preamplifier. A dual-state switching control signal is applied via a single control wire to the switching network to select which preamplifier input receives the calibration signal. The calibration signal generator control line is electrically isolated from the preamplifier by an opto-isolator. The electrical balance of the bi-directional calibration circuit and electrical isolation of the calibration signal generator preserve the common-mode noise rejection of the differential preamplifier.

DTIC

N95-30055# Department of the Navy, Washington, DC.

UNITARY TRANSDUCER WITH VARIABLE RESISTIVITY Patent Application

Manfred Kahn, inventor (to Navy), Carl Wu, inventor (to Navy), and Saado Zain, inventor (to Navy) 29 Aug. 1994 19 p

(AD-D017329; US-Patent-Appl-SN-296881) Avail: CASI HC A03/MF A01

An actuator including a unitary ceramic element capable of bending in response to an applied voltage is described. The ceramic has a first region of lower resistivity in contact with a second region of higher resistivity.There is no seal where said regions contact each other. The first region contains an additive in an amount needed to reduce resistivity thereof relative to said second region. The second region is devoid of additive or contains a different additive that raises resistivity thereof or contains the same additive in a different amount than in the first region.

DTIC

N95-30070# Battelle Memorial Inst., Columbus, OH.

HIGH RELIABILITY, MAINTENANCE-FREE INS BATTERY DEVELOPMENT, PHASE 2 Final Report, 28 Aug. 1992 - 31 Aug. 1994

David G. Vutetakis 30 Sep. 1994 72 p

(Contract F04606-89-D-0034)

(AD-A291412; WL-TR-94-2097) Avail: CASI HC A04/MF A01

This report documents the findings of a study undertaken to develop a high reliability, maintenance-free battery (HRMFB) for application in the Litton LTN-72 and Delco Carousel IV Inertial Navigation Systems (INS). The current phase of this program, Phase 2, comprised the procurement and qualification of preproduction INS batteries based on the specification requirements developed in Phase 1.

DTIC

N95-30075# Department of the Navy, Washington, DC.

A SYSTEM FOR CONVENIENTLY PROVIDING LOAD TESTING TERMINATION OF AN AC POWER SOURCE HAVING AT LEAST ONE BATTERY Patent Application

Wilbert J. Morrell, III, inventor (to Navy) 3 Oct. 1994 26 p

(AD-D017408; US-Patent-Appl-SN-331231) Avail: CASI HC A03/MF A01

An AC uninterruptible power source is disclosed that provides multi-phase power output signals for actual use and a selectable single phase power output signal for use in testing. The AC uninterruptible power source further comprises at least one battery. The single phase output signal is connected to a dummy load by means of a power switch of the break-before-make type. The invention further includes the dummy load as preferably having metering capabilities to measure the frequency, current, and voltage parameters of the single phase output signal. The arrangement of the present invention allows for the single phase output to be mated to the dummy load without the need of removing input power to the AC uninterruptible power source so as to reduce, or even eliminate, transient caused failures to the AC uninterruptible power source and to its sensitive load equipment which the power source services.

DTIC

N95-30079# Naval Surface Warfare Center, Panama City, FL. Research and Technology Dept.

COMPLETE ANALYSIS OF ELECTRODE-TERMINATED CABLES IN TWO-LAYER CONDUCTOR BOUNDED ABOVE BY AIR: CURRENT DENSITY, MAGNETIC FIELD, AND MAGNETIC FIELD GRADIENT

W. M. Wynn Dec. 1994 48 p

(AD-A290907; CSS/TR-94/32) Avail: CASI HC A03/MF A01

A complete analysis is given for the current density, magnetic field, and magnetic field gradient of a point current source located in the upper layer of a two-layer conductor that is bounded above by air. This problem has a long history, and treatments varying degrees of completeness and/or rigor are scattered throughout the older geophysical literature. The intent here is to do a complete, self-contained analysis based on potential theory and Ampere's Law; treat all possible cases for the relative conductivity media, including the special cases of a lower medium that is an insulator or a perfect conductor; and provide expressions the magnetic field vector, the current density vector, and the magnetic field gradient tensor in both conducting layers. The effect of performing gradient measurements within an enclosure also is discussed. The principle new results are the inclusion of expressions for the current density and magnetic field in the lower conducting layer, expressions for the magnetic field gradient tensor in both conducting layers, and the analysis of the case of a perfectly conducting lower layer. To complete the set of tools needed to describe a cable terminated by point electrodes, compact general expressions are given for the magnetic field vector and magnetic gradient tensor for a straight current element with arbitrary end points. These are based on the Biot-Savart Law and can be used to calculate the field and gradient contribution from an arbitrary cable joining two or more electrodes by means of superposition. The end results are applicable to such diverse problems as long-wire, electro-prospecting the current distribution around sheet piling protected by

active electrodes, and the distributed currents of grounded direct current power systems. DTIC

N95-30122# Naval Surface Warfare Center, Bethesda, MD.
175HP CONTRAROTATING HOMOPOLAR MOTOR DESIGN REPORT
Michael J. Cannell, John L. Drake, Richard A. McConnell, and William R. Martino Jun. 1994 143 p
(AD-A291138; CARDIVNSWC-TR-81-94/25) Avail: CASI HC A07/MF A01

A normally conducting contrarotating homopolar motor has been designed and constructed. The reaction torque, in the outer rotor, from the inner rotor is utilized to produce true contrarotation. The machine utilizes liquid cooled conductors, high performance liquid metal current collectors, and ferrous conductors in the active region. The basic machine output is 175 hp at + or - 1,200 rpm with an input of 4 volts and 35,000 amps. DTIC

N95-30124# California Univ., Santa Barbara, CA. Dept. of Electrical and Computer Engineering.
VACUUM MICROELECTRONIC EMITTERS AND THEIR APPLICATIONS USING COMPOUND SEMICONDUCTOR TECHNOLOGY Final Report, 1 Aug. 1991 - 31 May 1994
David Holcombe, Wei-Nan Jiang, and Umesh K. Mishra 16 Jul. 1994 29 p
(Contract DAAL03-91-G-0161)
(AD-A291142; ARO-28569.2-PH) Avail: CASI HC A03/MF A01

Vacuum microelectronic devices (VMD's) are a class of devices in which electron transport occurs both in semiconductors and in vacuum. They have the potential of combining the advantages of vacuum tube based devices with those of modern semiconductor devices. The key to the success of VMD's is fabricating reliable solid state electron emitters with high emission efficiency and high emission current density. This report will present the design, growth, fabrication and characterization of Planar-Doped-Barrier Electron Emitters (PDBEE's) made of compound semiconductor AlGaAs/GaAs. In PDBEE's, electrons, as majority carriers, are injected over a triangular barrier into a high field region accelerated towards the surface. Injected Electrons gain kinetic energy from the field and lose kinetic energy through scattering processes. Those electrons with enough energy to overcome the surface barrier upon reaching the surface could be emitted into vacuum. The surface work function of semiconductors (GaAs in this work) is lowered by cesiation. An emission efficiency of 4.2 percent and an emission current density of 5.8 A/cm(2) have been obtained from Al(0.3)Ga(0.7)As/GaAs PDBEE's. DTIC

N95-30165# Department of the Navy, Washington, DC.
THIN-FILM EDGE FIELD EMITTER DEVICE AND METHOD OF MANUFACTURE THEREFOR Patent Application
David S. Hsu, inventor (to Navy) 11 Oct. 1994 62 p Continuation of US-Patent-Appl-SN-040944, filed 31 Mar. 1993
(AD-D017323; Navy-Case-75894; US-Patent-Appl-SN-321642; US-Patent-Appl-SN-040944) Avail: CASI HC A04/MF A01

A thin-film edge field emitter device includes a substrate having a first portion and having a protuberance extending from the first portion, the protuberance defining at least one side-wall, the side-wall constituting a second portion. An emitter layer is disposed on the substrate including the second portion, the emitter layer being selected from the group consisting of semiconductors and conductors and is a thin-film including a portion extending beyond the second portion and defining an exposed emitter edge. A pair of supportive layers is disposed on opposite sides of the emitter layer, the pair of supportive layers each being selected from the group consisting of semiconductors and conductors and each having a higher work function than the emitter layer. DTIC

N95-30188# Sandia National Labs., Albuquerque, NM.
A CMOS-COMPATIBLE, SURFACE-MICROMACHINED PRESSURE SENSOR FOR AQUEOUS ULTRASONIC APPLICATION
W. P. Eaton (New Mexico Univ., Albuquerque, NM.) and J. H. Smith 1994 8 p Presented at the North American Conference on Smart Structures and Materials, San Diego, CA, 26 Feb. - 3 Mar. 1995
(Contract DE-AC04-94AL-85000)
(DE95-008538; SAND-94-2146C; CONF-950228-2) Avail: CASI HC A02/MF A01

A surface micromachined pressure sensor array is under development at the Integrated Micromechanics, Microsensors, and CMOS Technologies organization at Sandia National Laboratories. This array is designed to sense absolute pressures from ambient pressure to 650 psia with frequency responses from DC to 2 MHz. The sensor is based upon a sealed, deformable, circular LPCVD silicon nitride diaphragm. Absolute pressure is determined from diaphragm deflection, which is sensed with low-stress, micromechanical, LPCVD polysilicon piezoresistors. All materials and processes used for sensor fabrication are CMOS compatible, and are part of Sandia's ongoing effort of CMOS integration with micro-electromechanical systems (MEMS). Test results of individual sensors are presented along with process issues involving the release etch and metal step coverage. DOE

N95-30256*# National Aeronautics and Space Administration. Lewis Research Center, Cleveland, OH.
DEVELOPMENT OF A MICRO-FIBER NICKEL ELECTRODE FOR NICKEL-HYDROGEN CELL Abstract Only
Doris L. Britton *In its* Space Electrochemical Research and Technology. Abstracts Apr. 1995 p 3 (For primary document see N95-30255 10-44)
Avail: CASI HC A01/MF A01

N95-30258*# Eagle-Picher Industries, Inc., Colorado Springs, CO.
MAGNUM(R) NiCd ADVANCED NICKEL-CADMIUM BATTERY CELLS Abstract Only
Darren Scoles *In* NASA. Lewis Research Center, Space Electrochemical Research and Technology. Abstracts Apr. 1995 p 7 (For primary document see N95-30255 10-44)
Avail: CASI HC A01/MF A01

N95-30259*# National Aeronautics and Space Administration. Lewis Research Center, Cleveland, OH.
BENDING PROPERTIES OF NICKEL ELECTRODES FOR NICKEL-HYDROGEN BATTERIES Abstract Only
Bradley Lerch *In its* Space Electrochemical Research and Technology. Abstracts Apr. 1995 p 9 (For primary document see N95-30255 10-44)
Avail: CASI HC A01/MF A01

N95-30260*# National Aeronautics and Space Administration. Goddard Space Flight Center, Greenbelt, MD.
EFFECT OF KOH CONCENTRATION AND ANIONS ON THE PERFORMANCE OF Ni-H2 BATTERY POSITIVE PLATE Abstract Only
H. Vaidyanathan (Communications Satellite Corp., Clarksburg, MD.), Kathleen Robbins (Communications Satellite Corp., Clarksburg, MD.), and Rao M. Gopalakrishna *In* NASA. Lewis Research Center, Space Electrochemical Research and Technology. Abstracts Apr. 1995 p 11 (For primary document see N95-30255 10-44)
Avail: CASI HC A01/MF A01

N95-30261*# Eagle-Picher Industries, Inc., Joplin, MO. Advanced Systems Operation.
ADVANCED DEPENDENT PRESSURE VESSEL (DPV) NICKEL-HYDROGEN SPACECRAFT CELL AND BATTERY DESIGN Abstract Only
Dwaine Coates, Doug Wright, and Ron Repplinger *In* NASA. Lewis Research Center, Space Electrochemical Research and Technology. Abstracts Apr. 1995 p 13 (For primary document see N95-30255 10-44)
Avail: CASI HC A01/MF A01

N95-30262*# Aerospace Corp., Washington, DC.
ELECTROLYTE MANAGEMENT CONSIDERATIONS IN MODERN NICKEL HYDROGEN AND NICKEL CADMIUM CELL AND BATTERY DESIGNS Abstract Only
L. H. Thaller and A. H. Zimmerman *In* NASA. Lewis Research Center, Space Electrochemical Research and Technology. Abstracts Apr. 1995 p 17 (For primary document see N95-30255 10-44)
Avail: CASI HC A01/MF A01

N95-30268*# Boundary Technologies, Inc., Buffalo Grove, IL.
HERMETICALLY SEALED ALUMINUM ELECTROLYTIC CAPACITOR Abstract Only
Robert S. Alwitt, Yanming Liu, and William Elias (BACE Technologies, Pickens, SC.) *In* NASA. Lewis Research Center, Space Electrochemical Research and Technology. Abstracts Apr. 1995 p 35 (For primary document see N95-30255 10-44)
Avail: CASI HC A01/MF A01

N95-30270*# Giner, Inc., Waltham, MA.
DEVELOPMENT OF ELECTROCHEMICAL SUPER CAPACITORS FOR EMA APPLICATIONS Abstract Only
J. A. Kosek, T. Dunning, and A. B. LaConti *In* NASA. Lewis Research Center, Space Electrochemical Research and Technology. Abstracts Apr. 1995 p 39 (For primary document see N95-30255 10-44)
Avail: CASI HC A01/MF A01

N95-30271*# Evans Co., East Providence, RI.
HIGH ENERGY DENSITY ELECTROLYTIC CAPACITOR Abstract Only
David A. Evans *In* NASA. Lewis Research Center, Space Electrochemical Research and Technology. Abstracts Apr. 1995 p 41 (For primary document see N95-30255 10-44)
Avail; CASI HC A01/MF A01

34 FLUID MECHANICS AND HEAT TRANSFER

Includes boundary layers; hydrodynamics; fluidics; mass transfer; and ablation cooling.

For related information see also *02 Aerodynamics* and *77 Thermodynamics and Statistical Physics.*

N95-28696 Air Force Inst. of Tech., Wright-Patterson AFB, OH.
THE EFFECT OF VISCOUS ATTENUATION ON SHOCK TUBE PERFORMANCE M.S. Thesis
Nick R. McKenzie Dec. 1994 76 p Limited Reproducibility: More than 20% of this document may be affected by microfiche quality
(AD-A289793; AFIT/CI/CIA-94-168) Avail: Issuing Activity (Defense Technical Information Center (DTIC))

Shock wave attenuation affects experimental results by reducing results shock velocity as it travels down the shock tube. Until recently, attenuation has not been readily predictable with accuracy and was simply accepted during the experimental process. A mass loss theory was developed by Dr. Harold Mirels which accounted for the shock wave attenuation by considering the formed boundary layer due to the passage of a shock wave. The purpose of this thesis to develop a computer code, which would apply Mirels' theory to a prediction model, and validate the results with acoustic theory and Mirels' data. It will then be used to determine an accurate shock velocity for an additional shock tube. The computer results will be proven to match the experimental data well. However, additional corrections involving friction, heating, and real gas effects are needed to produce excellent results. It will also be discovered that mass loss correction results are a significant part of the total shock wave attenuation. DTIC

N95-28719*# National Aeronautics and Space Administration. Lewis Research Center, Cleveland, OH.
INFLUENCE OF TURBULENCE PARAMETERS, REYNOLDS NUMBER, AND BODY SHAPE ON STAGNATION-REGION HEAT TRANSFER
G. James VanFossen, Robert J. Simoneau, and Chan Y. Ching (Syracuse Univ., NY.) Dec. 1994 48 p
(RTOP 505-62-52)
(NASA-TP-3487; E-8882; NAS 1.60:3487) Avail: CASI HC A03/MF A01

The purpose of the present work was threefold: (1) to determine if a free-stream turbulence length scale existed that would cause the greatest augmentation in stagnation-region heat transfer over laminar levels; (2) to investigate the effect of velocity gradient on stagnation-region heat transfer augmentation by free-stream turbulence; and (3) to develop a prediction tool for stagnation heat transfer in the presence of free-stream turbulence. Heat transfer was measured in the stagnation region of four models with elliptical leading edges that had ratios of major to minor axes of 1:1, 1.5:1, 2.25:1, and 3:1. Five turbulence-generating grids were fabricated; four were square mesh, biplane grids made from square bars. The fifth grid was an array of fine parallel wires that were perpendicular to the model spanwise direction. Heat transfer data were taken at Reynolds numbers ranging from 37 000 to 228 000. Turbulence intensities were in the range of 1.1 to 15.9% while the ratio of integral length scale to leading-edge diameter ranged from 0.05 to 0.30. Stagnation-point velocity gradient was varied by nearly 50%. Stagnation-region heat transfer augmentation was found to increase with decreasing length scale but no optimum length scale was found. Heat transfer augmentation due to turbulence was found to be unaffected by the velocity gradient near the leading edge. A correlation was developed that fit heat transfer data for the square-bar grids to within +/- 4%. Author

N95-28902 ESDU International Ltd., London (England).
NACA 1-SERIES GEOMETRY REPRESENTATION FOR COMPUTATIONAL FLUID DYNAMICS
Jun. 1994 9 p
(ISSN 0141-4356)
(ESDU-94013; ISBN-0-85679-900-9) Avail: ESDU

ESDU 94013 presents the coordinates for the cowl external profile as originally defined and now taken as a 'standard', together with the lip radius. When second divided differences of the coordinates are taken they are found to lack smoothness which means that the curvatures are not smooth. As a result computed pressure distributions also contain irregularities. A simple curve fit to the profile is given but is not felt to model the profile closely enough for flow computations (it fits the profile to about 0.6% of Y, where Y is half the difference of the maximum and the highlight diameters). A more complex fitting equation is also provided that fits the profile to 0.15Y and is felt to meet the requirements for flow calculations; a comparison of pressure distribution results using the original profile and the fitted one illustrates the improvement found. Author

N95-28903 ESDU International Ltd., London (England).
WAVE DRAG COEFFICIENT FOR AXISYMMETRIC FORECOWLS AT ZERO INCIDENCE (M SUB INFINITY LESS THAN OR EQUAL TO 1.5)
Jun. 1994 89 p
(ISSN 0141-4356)
(ESDU-94014; ISBN-0-85679-901-7) Avail: ESDU

ESDU 94014 presents charts for 20 cowls of the coefficient computed from finite difference solutions to the Euler equations for inviscid compressible flow. Computed shock waves are smeared over a few mesh cells which should give correct shock pressure jumps and wave drag. Data are presented for ranges of values of mass flow ratio and freestream Mach number. Sixteen cowls have NACA 1-series external profile, with differing combinations of diameter ratio and fineness ratio. The remaining four have fixed diameter ratio and fineness ratio but external profiles that differ systematically from the NACA 1-series profile. Charts of computed forecowl pressure force coefficient and pre-entry force coefficient are also given for each cowl for conditions at which a non-zero wave drag is calculated. See ESDU 94013 for details of the NACA 1-series profile and ESDU 94015 for pressure distribution data for the same profiles as treated here. Author

N95-28948 Air Force Inst. of Tech., Wright-Patterson AFB, OH.
A NONINTRUSIVE METHOD OF QUANTIFYING FLOW VISUALIZATION DATA IN VORTEX FLOW FIELDS M.S. Thesis
Vincent J. Sei Dec. 1994 86 p Limited Reproducibility: More than 20% of this document may be affected by microfiche quality
(AD-A289802; AFIT/CI/CIA-94-170) Avail: Issuing Activity (Defense Technical Information Center (DTIC))

The High Angle of Attack Research Vehicle (HARV) as well as other similar flight test aircraft have been using smoke flow visualization techniques to characterize the vortex flow created by leading edge extensions and the forebody. With the advent of video measurement techniques, this type of flow visualization can not only provide a qualitative assessment of the flow but also a quantitative measure to be used to validate computational fluid dynamic codes and wind tunnel test. One of the major drawbacks to employing video imaging was the introduction of false motion due to camera movement in flight. A relative motion approach using fixed targets along with the flow visualization scheme was utilized to remove unwanted motion. The relative motion algorithm was tested using a laboratory test setup

where cameras underwent both translational and rotational motion to simulate both wing bending and torsion. The method was effective in removing both motions with only a slight loss of accuracy. DTIC

N95-28956# Los Alamos National Lab., NM.
BUBBLE FUSION: PRELIMINARY ESTIMATES OF SPHERICAL MICRO-IMPLOSIONS IN CAVITATING LIQUIDS
R. A. Krakowski 1995 7 p Presented at the DOE/EPRI Workshop on the Physics of Spherical Continuous Inertial Fusion, Santa Fe, NM, 12-14 Jan. 1995
(Contract W-7405-eng-36)
(DE95-006260; LA-UR-95-211; CONF-950170-1) Avail: CASI HC A02/MF A01

Liquids irradiated with intense ultrasonic waves can generate small cavities or bubbles. Upon nonlinear expansion to a state of disequilibrium, wherein the externally imposed hydrostatic pressure far exceeds that of entrapped non-condensable gas, these bubbles undergo a rapid and violent collapse. This collapse, if symmetric, can generate high pressures and temperatures through a number of possible mechanisms. The simplest and oldest explanation suggests a focusing of the kinetic energy of all the surrounding liquid onto the collapsing bubble and the subsequent heating of entrapped gases under either adiabatic or isothermal conditions. Although induced by externally imposed millisecond pressure oscillations, these collapses can occur on sub-microsecond timescales and are accompanied by picosecond light emissions; this combination of sound and light is called sonoluminescence. Recent explanations of observed high temperatures and picosecond radiation pulses accompanying such collapses are based on the interaction of multiple shock waves that are launched off the inward cavity wall. Other potential explanations invoke dipole emissions induced by intermolecular collisions or the release of Casimir energy when a dielectric hole is filled. Conjectures have been made that the processes responsible for sonoluminescence may be extended to generated conditions where thermonuclear fusion might occur. Such an achievement would extend scientific interest in sonoluminescence out of a purely chemical context to include the study of matter subjected to more extreme conditions. The main goal of this 'scoping' study is to understand better conditions where deuterium-tritium fusion might be observed in conjunction with micro-implosions in cavitating liquids; prognoses of fusion application at this point are unintended. DOE

N95-28990# Air Force Inst. of Tech., Wright-Patterson AFB, OH.
FLOW VISUALIZATION OF VORTICITY CANCELLATION OF JETS IN CROSSFLOW M.S. Thesis
Anthony G. Simpson Mar. 1995 110 p
(AD-A292414; AFIT/CI/CIA-94-004) Avail: CASI HC A06/MF A02

An experimental apparatus was designed and constructed for water tunnel flow visualization of multiple, staggered and in-line row jet injection in cross flow. Specifically, a physical explanation was sought for existing film cooling performance results from turbine test rigs. Experiments were conducted in the University of Washington low-speed, free surface water tunnel facility having a 3.0 x 0.7 x 0.7 meter test section and a speed capability of up to 0.7 rn/s. Jet injection was controlled for each row independently at blowing ratios from 0.5 to 2.5, with the jet development length to diameter ratio set at 6.0. Flow visualization using both colored dye and fluorescent laser sheeting was accomplished to track vortex structure and interaction in the flow. The results indicate that vorticity cancellation is a factor in improved cooling performance over single row injection through a reduction in both jet lift off from the surface and entrainment of the main flow toward the surface. DTIC

N95-29015 ESDU International Ltd., London (England).
CONDENSATION INSIDE TUBES: CONDENSATE FILM COEFFICIENT IN HORIZONTAL TUBES
Dec. 1994 23 p
(ISSN 0141-402X)
(ESDU-94041; ISBN-0-856-79928-9) Avail: ESDU

ESDU 94041 provides correlations in vapor shear-controlled annular and gravity-controlled stratified flows for the local heat transfer coefficient at a specified vapor mass flow fraction. A flow regime map defines the regions where those conditions occur as predicted from the available data. The range of data extracted from the literature that was used to develop the correlations is tabulated and the correlation achieved is illustrated with a sketch that shows most of the predicted values falling within 30% of the experimental values. A step-by-step calculation procedure is set out and illustrated with a worked example. The effect of sub-cooling is discussed and practical design details such as the use of multi-pass units, condensate drainage and venting are considered. ESDU

N95-29024# Stanford Univ., CA.
LINEAR STABILITY ANALYSIS OF HYPERSONIC BOUNDARY LAYERS Final Report, 1 Oct. 1992 - 30 Sep. 1994
Tadepalli, Srinivas. and Joel H. Ferziger 18 Nov. 1994 59 p
(Contract F49620-92-J-0005)
(AD-A290159; AFOSR-95-0056TR) Avail: CASI HC A04/MF A01

For linear stability analysis of high speed boundary layers, we use a direct method for its ability to yield eigenvalues without a priori knowledge and to capture all modes. Temporal linear stability analysis is performed for the 2D boundary layer on a flat plate using the local parallel flow assumption. An estimate of all the eigenvalues is obtained by solving the generalized eigenvalue problem; a local eigenvalue search is used to improve the accuracy of the most unstable eigenvalue. A compact fourth order accurate method is to compute both the mean flow and the most unstable eigenfunction. This method is more efficient than lower order methods. Local grid refinement based on error estimates is useful in providing the accuracy needed for initial conditions for direct numerical simulation of transition. Grid adaptation based on refinement yields better than power law convergence in the mean flow error. DTIC

N95-29058# Army Research Lab., Aberdeen Proving Ground, MD.
COMPUTATIONAL FLUID DYNAMICS (CFD) SIMULATION OF TEST CHAMBER AND SMOKE-GENERATING DEVICE Final Report, Dec. 1993 - Aug. 1994
Michael J. Nusca Jan. 1995 44 p
(AD-A290199; ARL-TR-663) Avail: CASI HC A03/MF A01

The U.S. Army Research Laboratory (ARL) has completed an initial investigation of the flow field within a typical U.S. Army Edgewood Research, Development, and Engineering Center (ERDEC) test chamber via numerical simulation. The ERDEC test chamber is designed to mix compressor-driven airflow with gas/solid effluent from a test article placed inside the chamber. An example of such a test article is a smoke generator, or smoke pot. Simulation of this flow utilized ARL computational fluid dynamics (CFD) codes that include multispecies chemical kinetics. Numerical solutions of the gas flow and effluent concentration distributions in the test chamber were generated for operating times up to 4.5 min. Numerical simulations reveal that certain values of chamber through-flow induce flow patterns within the chamber that are dominated by rotating vortices. This flow pattern increases the effluent residence time in the chamber as well as the mixing of gas/particulate from the test article with air. As a result, pockets of high effluent concentration can form in the chamber. Graphical results with discussion are presented. DTIC

N95-29060# Arizona State Univ., Tempe, AZ.
EXPERIMENTAL AND THEORETICAL STUDIES OF WAKES IN STRATIFIED FLOWS Final Report
Don L. Boyer and H. J. Fernando 20 Jan. 1995 6 p
(Contract N00014-90-J-4063)
(AD-A290203) Avail: CASI HC A02/MF A01

The long range goal was to obtain, by laboratory experimentation and associated theoretical/numerical analysis, an increased understanding of the dynamics of stratified flow past blunt obstacles including two-dimensional ones such as right circular cylinders and three-dimensional ones such as spheres. Emphasis was given to such phenomena as blocking, flow separation, vortex shedding, lee-wave generation, unsteady characteristics of the free stream, and lift and drag on the obstacles in question. DTIC

N95-29068# Central State Univ., Wilberforce, OH.
A NOVEL APPROACH TO THE NUMERICAL SIMULATION OF TURBULENT FLOWS Final Report, 30 Sep. 1993 - 30 Sep. 1994
James C. Turner, Jr. 7 Nov. 1994 4 p
(Contract DAAH04-83-G-0513)
(AD-A290352; ARO-32412.1-MA-H) Avail: CASI HC A01/MF A01

We have studied the global dynamics of incompressible, viscous fluid motion. This activity included a study of discrete dynamical systems generated by temporal and spatial discretizations of the Navier Stokes

equations. We investigated the existence of absorbing sets and attractors associated with the two dimensional Navier-Stokes equations. The dynamical properties of various finite difference and finite element schemes for these equations were also considered. Our goal was to investigate the existence of spurious steady state solutions. DTIC

N95-29069# Hampton Univ., VA.
COMPUTATIONAL METHODS FOR THE SIMULATION OF NON-NEWTONIAN FLOWS Final Report, 5 Aug. 1991 - 6 Aug. 1993
James C. Turner Dec. 1994 40 p
(Contract DAAL03-91-G-0237)
(AD-A290355; ARO-28709.5-MA-SAH) Avail: CASI HC A03/MF A01

The research included two projects: (1) Temperature Control In Polymer Extrusion Processes: here an optimization problem was formulated. This problem was motivated by the desire to obtain uniform extrudate temperature at the die exit in a polymer extrusion process. Control was effected by adjustments to the heat flux along the surface of the pipe. An optimality system of partial differential equations was derived from which optimal controls and states may be determined. Then, finite element discretizations of the optimality system were defined and error estimates were provided along with an efficient solution algorithm for the discreet. Finally, computational results were given for a model example with Oldroyd type fluid, demonstrating the effectiveness of our theory and methods, as well as their potential applicability to industrial problems. (2) Analysis and Finite Element Approximation of An Optimal Control Problem in Electrochemistry with Current Density Controls: here an optimal control problem for impressed cathodic systems in electrochemistry was studied. The control in this problem was the current density on the anode. A matching objective functional was considered. The existence of an optimal solution was proved. The use of Lagrange multiplier rules was justified and an optimality system of equations established. Finally, a finite element algorithm was defined and optimal error estimates were derived. DTIC

N95-29096 Texas Univ., Austin, TX.
PHYSICAL CAUSES OF SEPARATION SHOCK UNSTEADINESS IN SHOCK WAVE/TURBULENT BOUNDARY LAYER INTERACTIONS Ph.D. Thesis
Mehmet Erdal Erengil 1993 143 p
Avail: Univ. Microfilms Order No. DA9413480

The purpose of this study was first to determine the effects of sweep back on unsteady separation in compression ramp interactions, and second to examine separation shock unsteadiness in different interactions and determine whether a universal model describing the unsteadiness could be developed. In the first phase, wall pressure fluctuation measurements were different in interactions generated by unswept, and 10, 20, 25, 30, 40, and 50 deg swept compression ramp models in a high Reynolds number, Mach 5 turbulent boundary layer. The streamwise ramp angle was 28 deg in all cases. The results showed that: (1) In highly swept interactions the rms distributions of pressure fluctuations as well as the mean distributions are essentially quasi-conically symmetric. The rms levels decrease globally with increasing sweep as does the maximum rms generated by the translating separation shock. (2) The length of the intermittent region, over which the separation shock foot translates, decreases with increasing sweep. In a given interaction, the length of the intermittent region grows spanwise. (3) Dominant separation shock frequencies increase with increasing sweep, whereas in a given interaction, they decrease spanwise. (4) The higher frequencies are shown to be a direct result of the decrease in the intermittent region length. In the second phase, wall pressure fluctuation measurements were made in interactions generated by unswept and 25 deg swept compression ramp models, and by 8 and 30 deg swept blunt-fin models. Using conditional sampling algorithms, the separation shock unsteadiness was characterized in terms of its position and velocity histories. These quantities were then correlated with conditionally extracted static pressure ratio histories, and with wall pressure measurements made upstream and downstream of the region of shock motion in each of these interactions. Results show that separation shock unsteadiness can be caused by two different physical phenomena. The small-scale or jittery motion is caused by fluctuations in the ratio of static quantities across the shock foot. These perturbations induce fluctuations in the separation shock velocity and thus changes in separation shock position are an integral result of the velocity fluctuations. The large-scale or global motion of the separation shock is caused by a displacement mechanism related to the dynamics of the separated flow. Thus, an expansion of the separated flow, for example, displaces the separation shock to an upstream position, whereas a contraction of the separated flow results in a displacement in the downstream direction. In addition to experimental results, computations of an inviscid, unsteady, quasi one-dimensional flow have also been performed. Although this does not model the experimental conditions, the analysis provides computational support for the explanation offered for the small-scale jittery motion of the separation shock. Dissert. Abstr.

N95-29119 Concordia Univ., Montreal (Quebec).
FINITE ELEMENT VORTICITY-BASED METHODS FOR THE SOLUTION OF THE INCOMPRESSIBLE AND COMPRESSIBLE NAVIER-STOKES EQUATIONS Ph.D. Thesis
Grant Guevremont 1993 178 p
Avail: Univ. Microfilms Order No. DANN87265

Finite element vorticity-based methods are applied to the analysis of viscous flows. This is carried out in terms of a stream function-vorticity formulation for 2-D flows and a velocity-vorticity formulation for 2-D and 3-D flows. Second order equations are obtained for the variables and the discretization is based on the weak-Galerkin weighted residual method. The stream function-vorticity approach proposed in this thesis reverses the traditional imposition of wall boundary conditions. The finite element method is used to naturally impose the no-slip condition on the stream function equation accurate for complex geometries. This method is extended to two-dimensional subsonic external lifting flow. The unknown stream function value on the airfoil, for lifting flow, is obtained by enforcing a continuous pressure distribution over the entire airfoil. This is imposed naturally through the finite element discretized vorticity transport equation. The velocity-vorticity scheme proposed in this thesis was the first to use a finite element weak-Galerkin method. This method is extended beyond incompressible flow to two- and three-dimensional subsonic internal flow. A new accurate wall vorticity boundary condition is also proposed. The finite element is chosen to have equal order interpolation for the virtuosity and the first derivatives of velocity. The stream function and virtuosity or the velocity and virtuosity are solved simultaneously using a Newton method. At each iteration, the linear algebraic system is solved by either a direct or an iterative matrix solver. For subsonic flows, the iteration is completed by obtaining the pressure, temperature, density and viscosity. Although it was found necessary in some cases to obtain solutions at intermediary Reynolds numbers, no artificial viscosity was required to stabilize the iteration algorithm. The schemes demonstrate the advantages of the finite element method in providing natural boundary conditions for such problems. Dissert. Abstr.

N95-29127# Wright State Univ., Dayton, OH. Dept. of Mechanical and Materials Engineering.
MICRO/MINIATURE HEAT PIPE ANALYSIS Interim Report, Jun. 1992 - Dec. 1993
Amir Faghri and Dmitry Khrustalev Jul. 1994 175 p
(Contract F33615-92-C-2276)
(AD-A292232; WL-TR-94-2085) Avail: CASI HC A08/MF A01

Analysis presented in this report shows that longitudinal groove designs are crucial to increase the heat transport capacity of miniature heat pipes. Furthermore vapor continuum limitation for a micro heat pipe operation is also defined and presented. The steady-state mathematical models of a micro heat pipe operation and miniature axially-grooved heat pipe are developed where the importance of the interfacial phenomena at the surfaces of the ultra-thin films is emphasized. The predicted capillary and boiling limitations as well as the thermal resistances are compared to existing experimental data on micro, miniature and conventional axially-grooved heat pipes. It is found that flat miniature heat pipes are easily capable of withstanding heat fluxes on the order of 40 w/ sq cm on the evaporator wall. DTIC

N95-29131*# Cleveland State Univ., OH. Dept. of Engineering.
EFFECTS OF COOLING SYSTEM PARAMETERS ON HEAT TRANSFER IN PAFC STACK Ph.D. Thesis
Ali A. Abdul-Aziz Aug. 1985 179 p Sponsored by NASA. Lewis Research Center
(NASA-CR-198817; NAS 1.26:198817) Avail: CASI HC A09/MF A02

Analytical and experimental study for the effects of cooling system parameters on the heat transfer and temperature distribution in the electrode plates of a phosphoric acid fuel-cell has been conducted. An experimental

set-up that simulates the operating conditions prevailing in a phosphoric-acid fuel-cell stack was designed and constructed. The set-up was then used to measure the overall heat transfer coefficient, the thermal contact resistance, and the electrode temperature distribution for two different cooling plate configurations. Two types of cooling plate configurations, serpentine and straight, were tested. Air, water, and oil were used as coolants. Measurements for the heat transfer coefficient and the thermal contact resistance were made for various flow rates ranging from 16 to 88 Kg/hr, and stack clamping pressure ranging from O to 3448 Kpa. The experimental results for the overall heat transfer coefficient were utilized to derive mathematical relations for the overall heat transfer coefficient as a function of stack clamping pressure and Reynolds number for the three coolants. The empirically derived formulas were incorporated in a previously developed computer program to predict electrodes temperature distribution and the performance of the stack cooling system. The results obtained were then compared with those available in the literature. The comparison showed maximum deviation of +/- 11%. Author

N95-29145# Stanford Univ., CA. Dept. of Mechanical Engineering.
INTERACTION OF TURBULENCE WITH COMPLEX SHOCK WAVES Final Technical Report, 1 Jan. 1992 - 30 Jun. 1994
Parviz Moin and Sanjiva Lele 25 Oct. 1994 133 p
(Contract F49620-92-J-0128)
(AD-A290225; AFOSR-95-0054TR) Avail: CASI HC A07/MF A02

Linear analysis and direct numerical simulation (DNS) are used to study the interaction of a shock wave with a turbulent flow. Effects central to shock wave/boundary layer interaction are identified and explained. The quantitative importance of the turbulence anisotropy and the shock oblique angle is demonstrated. Drop in Reynolds shear stress across a normal shock is shown. The implication for Reynolds stress models is discussed. The role of dilatational turbulent fluctuations on turbulence amplification is studied in detail. An explanation is suggested for lower amplification reported in wind-tunnel studies. Linear analysis & DNS are used to demonstrate the considerable influence of entropic fluctuations on turbulence evolution across a shock. Positive correlation between u' and T ' suppress amplification while negative correlation enhances it. Invalidity of Morkovin's hypothesis is demonstrated. A high order scheme is developed to allow strong shock/turbulence interaction. Results are presented for isotropic turbulence/normal shock interaction. DTIC

N95-29181# Michigan State Univ., East Lansing, MI. Dept. of Mechanical Engineering.
MOLECULAR MIXING IN SHEAR LAYERS FORCED BY 2-D AND 3-D DISTURBANCES Final Technical Report
Manoochehr M. Koochesfahani 26 Oct. 1994 153 p
(Grant AF-AFOSR-0314-91)
(AD-A290272; AFOSR-95-0057TR) Avail: CASI HC A08/MF A02

Experiments on 2-D forcing of shear layers were completed. Analysis of data from two different forcing techniques have revealed that much of the global aspects of the scalar mixing field appear to exhibit a universal behavior in terms of the non-dimensional downstream distance x(sup *) = x(lambda)f /Uc where lambda = (U1 - U2)/(U1 + U2) and Uc = (U1 + U2)/2. This universal behavior suggests that the total amount of mixing per unit width of the layer is enhanced in regions where x(sup *) greater than 1.5. Work on 3-D forcing andcombined 2-D/3-D forcing has lead to new findings. Results show that high amplitude 2-D forcing of a low Reynolds number wake can lead to a dramatic increase in mixing due to 3-D interaction of the vorticity field with the test section side walls. The possible application of this finding to mixing enhancement at higher Reynolds numbers is being investigated. Experiments on shear layers forced by a localized 3-D perturbation at the splitter plate along with 2-D forcing have shown that it is possible to significantly alter not only the predominant mixed-fluid composition but also the actual pdf structure (e.g. non-marching and marching behavior). Preliminary results suggest that the behavior of the span-averaged total mixing is similar to the case of purely 2-D forcing. DTIC

N95-29187# Wright Lab., Wright-Patterson AFB, OH.
COMPUTATIONAL FLUID DYNAMICS (CFD) ANALYSIS OF A C-135 AIRCRAFT WITH A SIDE-MOUNTED SPLITTER PLATE (WITH COMPARISON TO WIND TUNNEL DATA) Final Report, Mar. - Jun. 1993
Howard T. Emsley Jun. 1994 114 p
(AF Proj. 2404)
(AD-A292029; WL-TR-94-3089) Avail: CASI HC A06/MF A02

A Computational Fluid Dynamics (CFD) analysis was performed on a C-135 aircraft with a side-mounted splitter plate at the request of the Airborne Laser SPO at Kirtland AFB, and the 4950 Test Wing at Wright-Patterson AFB. The data collected from the analysis was provided to the Test Wing to augment wind tunnel tests and to provide loading and stability information on the modified aircraft. This work was a precursor to a planned flight test program in which a splitter plate will be tested on a Test Wing aircraft. Four flight conditions were analyzed with a modified and unmodified C-135 aerodynamic model, and incremental stability and aerodynamic derivatives were determined. Additionally, pressure coefficient data were tabulated for use in a structural analysis by the Test Wing. DTIC

N95-29197 Stanford Univ., CA.
SOLUTION OF THE NAVIER-STOKES EQUATIONS ON LOCALLY REFINED CARTESIAN MESHES USING STATE-VECTOR SPLITTING Ph.D. Thesis
Carl Frederick Gooch 1994 162 p
Avail: Univ. Microfilms Order No. DA9414570

A large amount of user time and expertise is currently required to obtain accurate computational solutions to compressible flow problems, especially if the geometry or flow field is complex. This presents a barrier for the novice user and an inconvenience for the experienced user. This thesis explores several options for improving this situation. First, grid-independent solution schemes would relax the current astringent criteria on grid quality. Recent developments in the area of multi-dimensional upwind schemes show promise for reducing grid dependence significantly. In the present work, a multi-dimensional upwind scheme for the Euler equations has been extended in a natural way to solve the Navier-Stokes equations. This approach treats the viscous and inviscid terms together. Second, automatic grid generation would drastically reduce the amount of work required to obtain a solution -- of any quality -- for complex geometries. Grid generation for complex, multi-body geometries is presently a formidable task, especially for structured grids. If non-body-fitted Cartesian grids are used, however, grid generation becomes trivial. The primary difficulty in using non-body-fitted grids is the enforcement of the solid wall boundary condition. The present work uses Cartesian grids in conjunction with a boundary condition similar to the usual finite volume boundary condition. Finally, an automatic grid refinement scheme with the capability to produce and recognize a grid-converged solution would obviate the grid refinement studies currently required to ensure the accuracy of a solution. A refinement scheme has been developed which adds cells based on a measure of the local error in the steady-state solution rather than on derivatives of some flow variable. As such, the scheme can in principle continue to refine until the local error in the solution is everywhere less than some user-specified quantity. The Navier-Stokes solver and the new Cartesian mesh boundary conditions have been validated. Comparison has been made to several cases for which analytic solutions are known. Inviscid subsonic flow around a biplane configuration was calculated to demonstrate the generality of the grid generation and local refinement schemes. A separated laminar airfoil flow has also been calculated, in conjunction with the automatic grid refinement scheme. Dissert. Abstr.

N95-29211# McDonnell-Douglas Aerospace, Saint Louis, MO.
NUMERICAL INVESTIGATION OF SURFACE CURVATURE EFFECTS IN COMPRESSIBLE TURBULENT FLOWS Final Report, 1 Dec. 1991 - 30 Nov. 1993
Linda D. Kral and John F. Donovan 2 Dec. 1994 37 p
(Contract F49620-92-C-0012)
(AD-A290114; MDC-94X0041; AFOSR-95-0052TR) Avail: CASI HC A03/MF A01

The objective of this work has been to develop a direct numerical simulation capability for compressible, non-canonical wall-bounded flows which is directly applicable to actual flight vehicles. Data from the simulations is used to deduce information about the organized motion. In the flow and bow they are affected by the extra strain rates due to concave wall curvature. A second-order finite volume approach and both fourth-order and sixth-order compact differences are available for the spatial derivatives. The algorithm allows for generalized coordinates so that simulations about

complex geometries can be performed. Extensive testing was done for two subgrid-scale models, the compressible Smagoriusky and structure function models, for a supersonic boundary layer. As the subgrid-scale viscosity also behaves as an artificial viscosity for central differencing codes, the study reinforced the need for high-order dissipation models in the simulation code. Validation of the numerical method was performed for flow over a concave surface for subsonic flow in which streamwise vortices develop in the boundary-layer due to the Gortler instability. The geometry and flow conditions closely approximated the incompressible experiments of Swearingen and Blackwelder. The simulations captured the essential features of the experiments in which counter-rotating vortices developed near the wall. As these streamwise vortices develop, the laminar boundary layer on the concave wall rapidly becomes three-dimensional. Higher-momentum fluid is pulled towards the wall from the outer flow as vortices grow downstream. The low-speed fluid lying between the vortices induces low-momentum fluid away from the wall, leading to inflectional streamwise velocity profiles, in good agreement with the experiments. DTIC

N95-29219 California Univ., San Diego, CA.
COLLECTIVE PHENOMENA IN GRANULAR FLUIDS Ph.D. Thesis
Tina Maria Mello 1994 141 p
Avail: Univ. Microfilms Order No. DA9425255

This dissertation considers the consequences of a simple model of the constitutive properties of rapidly flowing grains. In particular the kinetic theory equations are examined, which describe completely fluidized grains. In this regime there may be long range collective phenomena, which are characterized by the hydrodynamic modes. The canonical rheometric flow is a laminar flow with a linear velocity profile. The modes for this particular solution are examined. Longitudinal disturbances perpendicular to the shear plane transmit a compression wave via intergrain collisions, and have propagation speeds which are orders of magnitude smaller than those of solid materials. Velocity disturbances within the shear plane are more complex: these interact with, and exchange energy with, the mean flow. The shearing of the mean flow couples longitudinal and transverse waves, and may lead to the transient growth of disturbances. The expected form of the maximum disturbances is mainly a density wave, and is confirmed in computer simulations. The growth of these disturbances is, however, not exponential, and the system is stabilized by viscous effects. The energy equations for the various modes are derived and discussed. An example of such waves is found in hopper flows, where estimates of the propagation speeds are made and compared in detail to experimental results. Major features of the waves are predicted: the change from upstream to downstream propagating waves as the flow becomes supersonic, and the bending of wave fronts due to the spatial variations of the sound speed. The conclusions drawn about collective phenomena are valid for all kinetic theories, as they have the same general form for the transport coefficients. Examples are illustrated using exact expressions for both spheres and disks. Dissert. Abstr.

N95-29228# Texas Univ., Austin, TX.
UNSTEADINESS OF SHOCK-INDUCED TURBULENT BOUNDARY LAYER SEPARATION. AN INHERENT FEATURE OF TURBULENT FLOW OR SOLELY A WIND TUNNEL PHENOMENON Final Report
D. S. Dolling and M. E. Erengil Aug. 1994 55 p
(Contract DAAL03-91-G-0023)
(AD-A290367; ARO-28293.4-EG) Avail: CASI HC A04/MF A01

The purpose of this work was to: (1) examine separation shock wave unsteadiness in different turbulent interactions and determine whether a universal model describing the unsteadiness could be developed, and (2) determine whether or not the observed unsteadiness is a feature of turbulent flow in general, or is specific to the wind tunnel environment. To this end, wall and pitot pressure fluctuation measurements were made in interactions generated by unswept and 25 deg swept compression ramp models, and by 8 deg and 30 deg swept blunt-fin models in a high Reynolds number, Mach 5 turbulent boundary layer. It is clear that the high-frequency, jittery motion of the separation shock is the result of the passage through the wave of individual large-scale turbulent structures. Thus, this component of the unsteadiness is an inherent feature of all turbulent flows. The primary outstanding question concerns the cause of the low-frequency expansion/contraction of the separated flow which is characterized by the large-scale, long-duration excursions of the separation shock wave. Preliminary experimental work to address this question has revealed two very interesting, complementary results. First, there is a distinct correlation between large-scale expansion or contraction of the separated flow and long duration (i.e., low-frequency) falls or rises in pitot pressure in the incoming turbulent boundary layer. Second, results from the same experiment show that the ensemble-averaged pitot pressure at a fixed location in the incoming undisturbed boundary layer correlates with separation shock wave position. DTIC

N95-29242 Georgia Inst. of Tech., Atlanta, GA.
A FOURTH ORDER EULER/NAVIER-STOKES PREDICTION METHOD FOR THE AERODYNAMICS AND AEROELASTICITY OF HOVERING ROTOR BLADES Ph.D. Thesis
Marilyn Jones Smith 1994 226 p
Avail: Univ. Microfilms Order No. DA9421065

Some of the computational issues relating to the development of a three-dimensional fourth-order compact Euler/Navier-Stokes methodology for rotary wing flows and its coupling with an elastic rotor blade beam structural model have been explored. The compact Euler/NavierStokes method is used to predict the aerodynamic loads on an isolated rotor blade. Because the scheme is fourth-order, fewer grid nodes are necessary to predict loads with the same accuracy as traditional second order methodologies on finer grids. Grid and numerical parameter optimizations were performed to examine the changes in the predictive capabilities of the higher-order scheme. Comparisons were made with experimental data for a rotor using NACA 0012 airfoil sections and a rectangular planform with no twist. Simulations for both lifting and non-lifting configurations at various tip Mach numbers were performed. This Euler/Navier-Stokes methodology can be applied to rotor blades with either rigid-blade or elastic-beam-structural models to determine the steady-state response in hovering flight. The blade is represented by a geometrically nonlinear beam model which accounts for coupled flap bending, lead-lag bending and torsion. Moderately large displacements and rotations due to structural deformations can be simulated. The analysis has been performed for blade configurations having uniform mass and stiffness, no twist, and no chordwise offsets of the elastic and tension axes, as well as the center of mass. The results are compared with a panel method coupled with the same structural dynamics model. Computations have been made to predict the aerodynamic deflections for the rotor in hover. A starting solution using initial deflections predicted by aeroelastic analyses with a two-dimensional aerodynamic model was investigated. The present Euler/Navier-Stokes method using a momentum wake and a contracting vortex wake shows the impact on the aeroelastic deflections of a three-dimensional aerodynamic module which includes rotational and viscous effects, particularly at higher collective pitch angles. The differences in the aeroelastic predictions using fully coupled and loosely coupled aerodynamic analyses are examined. The induced wake plays a critical role in determining the final equilibrium tip deflections. Dissert. Abstr.

N95-29249*# Cleveland State Univ., OH. Dept. of Engineering.
EFFECTS OF THE COOLING SYSTEM PARAMETERS ON HEAT TRANSFER AND PERFORMANCE OF THE PAFC STACK DURING TRANSIENT OPERATION Ph.D. Thesis
Rabi M. J. Ridha 1992 407 p
(Contract NCC3-17)
(NASA-CR-197654; NAS 1.26:197654) Avail: CASI HC A18/MF A04

An experimental investigation for the effects of transient operation of a phosphoric acid fuel-cell stack on heat transfer and temperature distribution in the electrodes has been conducted. The proposed work utilized the experimental setup with modifications, which was designed and constructed under NASA Contract No. NCC-3-17(5). The experimental results obtained from this investigation and the mathematical model obtained under NASA Contract No. NCC3-17(4) after modifications, were utilized to develop mathematical models for transient heat transfer coefficient and temperature distribution in the electrode and to evaluate the performance of the cooling - system under unsteady state conditions. The empirical formulas developed were then implemented to modifying the developed computer code. Two incompressible coolants were used to study experimentally the effect of the thermophysical properties of the cool-ants on the transient heat transfer coefficient and the thermal contact resistance during start-up and shut-down processes. Coolant mass flow rates were verified from 16 to 88.2 Kg/hr during the transient process when the electrical power supply was gradually

increased or decreased in the range (O to 3000 W/sq m). The effect of the thermal contact resistance with a range of stack pressure from O to 3500 KPa was studied. Author

N95-29268# Stanford Univ., CA. Thermosciences Div.
NUMERICAL EXPERIMENTS ON THE FLOW PAST A CIRCULAR CYLINDER AT SUB-CRITICAL REYNOLDS NUMBER
Patrick Beaudan and Parviz Moin Dec. 1994 262 p
(Contract N00014-91-J-4072)
(AD-A289937; TF-62) Avail: CASI HC A12/MF A03

The performance of the dynamic subgrid-scale eddy-viscosity model and the suitability of high-order accurate, upwind-biased numerical methods for large eddy simulations of complex flows are investigated in the case of the turbulent wake behind a circular cylinder at Reynolds number 3,900, based on freestream velocity and cylinder diameter. The numerical method consists of high-order upwind-biased finite difference techniques applied to the compressible Navier-Stokes equations written in generalized coordinates. Integration in time is done using a fully implicit, second-order accurate iterative technique. The results of three fifth-order accurate simulations performed on identical grids with the least-squares version of the dynamic model, the fixed-coefficient Smagorinsky model, and with no subgrid-scale model are compared in the first 10 diameters of the wake. The impact of three-dimensionality is also examined via two and three-dimensional calculations without a subgrid-scale model. The effect of numerical dissipation is investigated by comparing two simulations using upwind-biased schemes, the first being fifth-order, and the second seventh-order accurate. It is found that the near-wake is highly three-dimensional at this Reynolds number. It contains pairs of counter-rotating streamwise vortices, the effect of which cannot be reproduced in two-dimensional calculations. Three-dimensional computations are essential for predicting flow statistics of engineering interest. DTIC

N95-29271# Naval Postgraduate School, Monterey, CA.
VORTEX ELEMENT ANALYSIS OF SELECTED TIME-DEPENDENT FLOWS M.S. Thesis
Michael R. Maixxner Dec. 1994 292 p
(AD-A289944) Avail: CASI HC A13/MF A03

Previous investigations of oscillating (harmonic) flow past circular cylinders via the discrete vortex method have met with limited success due to a variety of reasons. These assumptions have proven to be too severe, and cannot allow the prediction of the kinematics and dynamics of the oscillating flow about bluff bodies in general and about a circular cylinder in particular. In the current analysis, the ambient velocity was given by U = Um sin wt, and the velocity distribution and the boundary layer were calculated about the cylinder at suitable time intervals. Several methods were implemented to predict separation, all of which required a minimum of arbitrary assumptions. Nascent vortices were placed at the separation points in such a manner that the Kutta condition was satisfied. Several functional forms of dissipation were investigated, but it was found not to be of overriding influence in the flow kinematics. Counter vortices were found to be a necessary aspect of the analysis, providing continuity from one half cycle to the next. Flow visualization experiments were conducted for a Keulegan-Carpenter number of 10 as a basis for comparison. The kinematics obtained from the numerical model produced a vortex shedding pattern which was typical of those observed experimentally for higher Keulegan-Carpenter numbers. Significant problems were encountered in the prediction of boundary layer separation. At this point, it was obvious that the interaction of a vortex with a boundary layer warranted analysis in a much simpler flow situation; the blade-vortex interaction (BVI) problem proved to be ideal. A boundary layer code which predicted separation on an infinite flat plate under the influence of a line vortex was adapted to the BVI problem, so that it could be used with a semi-infinite plate in a flow field comprised of a free stream and numerous discrete vortices. DTIC

N95-29324# Minnesota Univ., Minneapolis, MN. Dept. of Aerospace Engineering and Mechanics.
THREE PROBLEMS IN FLUID DYNAMICS Report, 15 Jun. 1991 - 14 Jun. 1994
Daniel D. Joseph 10 Nov. 1994 7 p
(Contract DAAL03-91-G-0181)
(AD-A290481; ARO-28797.1-MA) Avail: CASI HC A02/MF A01

Three problems were proposed for study. The first was to determine the fluid dynamics of spin-up of two fluids in a rotating container. The applications of these studies are the problem of stabilization of rotating liquid-filled artillery shells in free flight and the determination of the rheological properties of blends of polymers used to fabricate plastic composites with improved material properties. The second problem is to study the motion of solid particles in a flowing viscous fluid by direct numerical simulation of the Navier-Stokes equations and the particles equations of motion. The third problem was to identify correct physical mechanisms to regularize ill-posed problems which arise in the study of two-phase flows of bubbly mixture in spinoidal regions of phase change mixtures of vapour bubbles in liquids. DTIC

N95-29334 Clarkson Univ., Potsdam, NY.
RIGOROUS DRAG BOUNDS IN TURBULENT SHEAR FLOW Ph.D. Thesis
Mark Alexander Orwoll 1994 186 p
Avail: Univ. Microfilms Order No. DA9422821

Directly from the incompressible Navier-Stokes equations, Doering and Constantin have derived a rigorous upper bound on estimates of the energy dissipation rate, and its associated drag force, for the case of shear-driven turbulence in a viscous Newtonian fluid confined between rigid parallel plates. Their variational bound is the result of decomposing the fluid velocity field into a 'background flow' and a 'fluctuation flow' and thereby obtaining a functional integral to be minimized. This bound imposes upon the solution a condition called the 'spectral constraint': namely, that all eigenvalues of the associated self-adjoint operator must be non-negative definite. This dissertation reports the research results obtained by fully enforcing this spectral constraint in both two- and three-dimensional flows. This full enforcement of the spectral constraint leads to an eigenvalue system of coupled partial differential equations for the fluctuation velocity components. We have obtained the 2-d and 3-d solutions to this eigenvalue system for the special case of piece-wise linear background flow profiles. For a chosen value of the Reynolds number, our solutions enabled the determination of critical values of the 'boundary layer thickness' parameter at some particular critical value of the wave number. This critical value of the boundary layer thickness parameter allowed the calculation of the Doering and Constantin upper bound. Our results improved upon the Doering and Constantin upper bound by an order of magnitude in the two-dimensional case. We found our worst-case three-dimensional result to have improved the Doering and Constantin upper bound by a factor of five. The drag force was found to have a Reynolds number squared dependency. The solution we obtained thus did not result in the drag-force dependency well-known as the 'logarithmic friction law,' as had been hoped. The solution technique resulted in the derivation of an eigenfunction system that could serve as a natural basis set, already adapted to turbulence, in which to expand arbitrary functions of interest, or for use in turbulent data analysis. Dissert. Abstr.

N95-29335 Minnesota Univ., Minneapolis, MN.
DYNAMICS OF SIMPLE CHEMICALLY REACTIVE FLUIDS Ph.D. Thesis
Lihong Qin 1994 103 p
Avail: Univ. Microfilms Order No. DA9424329

A kinetic theory has been constructed for chemically reactive fluids. This theory is based on a simple but reasonably realistic model for chemically reactive collision processes, A + B reversibly yields C + D. The reactive cross sections are characterized by effective collision diameters and activation energies. The theory is an extension to reactive species of the highly successful 'generalized Enskog Theory' and as such, can be expected to produce reliable predictions over a broad range of physical conditions, extending from the dilute gas regions to high pressure gases and liquids. A procedure was then developed for linearizing the Enskog-like kinetic equations and transforming them into equations of motion for dynamic correlation functions, among which are the van Hove functions and their Fourier transforms, the dynamic scattering functions. Approximated solutions of these equations were constructed and comparison was made with the results of a variety of experiments. Of particular interest are the results found for the short wavelength propagating modes called 'fast sound' and for light scattering from chemically reactive gas mixtures. Dissert. Abstr.

N95-29371*# National Aeronautics and Space Administration. Lewis Research Center, Cleveland, OH.

GRID ORTHOGONALITY EFFECTS ON PREDICTED TURBINE MIDSPAN HEAT TRANSFER AND PERFORMANCE

R. J. Boyle and A. A. Ameri (Kansas Univ., Lawrence, KS.) Jun. 1995 13 p Presented at the 39th International Gas Turbine and Aeroengine Congress and Exposition, The Hague, NL, 13-16 Jun. 1994; sponsored by ASME

(RTOP 505-62-52)

(NASA-TM-106931; E-9652; NAS 1.15:106931) Avail: CASI HC A03/MF A01

The effect of five different C type grid geometries on the predicted heat transfer and aerodynamic performance of a turbine stator is examined. Predictions were obtained using two flow analysis codes. One was a finite difference analysis, and the other was a finite volume analysis. Differences among the grids in terms of heat transfer and overall performance were small. The most significant difference among the five grids occurred in the prediction of pitchwise variation in total pressure. There was consistency between results obtained with each of the flow analysis codes when the same grid was used. A grid generating procedure in which the viscous grid is embedded within an inviscid type grid resulted in the best overall performance. Author

N95-29372*# National Aeronautics and Space Administration. Lewis Research Center, Cleveland, OH.

APPLICATION OF THE SPACE-TIME CONSERVATION ELEMENT AND SOLUTION ELEMENT METHOD TO TWO-DIMENSIONAL ADVECTION-DIFFUSION PROBLEMS

Xiao-Yen Wang (Colorado Univ., Boulder, CO.), Chuen-Yen Chow (Colorado Univ., Boulder, CO.), and Sin-Chung Chang Jun. 1995 45 p

(Grant NAG3-1566; RTOP 505-62-52)

(NASA-TM-106946; E-9681; NAS 1.15:106946) Avail: CASI HC A03/MF A01

The existing 2-D alpha-mu scheme and alpha-epsilon scheme based on the method of space-time conservation element and solution element, which were constructed for solving the linear 2-D unsteady advection-diffusion equation and unsteady advection equation, respectively, are tested. Also, the alpha-epsilon scheme is modified to become the V-E scheme for solving the nonlinear 2-D inviscid Burgers equation. Numerical solutions of six test problems are presented in comparison with their exact solutions or numerical solutions obtained by traditional finite-difference or finite-element methods. It is demonstrated that the 2-D alpha-mu, alpha-epsilon, and nu-epsilon schemes can be used to obtain numerical results which are more accurate than those based on some of the traditional methods but without using any artificial tuning in the computation. Similar to the previous 1-D test problems, the high accuracy and simplicity features of the space-time conservation element and solution element method have been revealed again in the present 2-D test results. Author

N95-29380# Air Force Inst. of Tech., Wright-Patterson AFB, OH.

THE EFFECTS OF THE THERMAL BOUNDARY CONDITION AND TURBULENCE ON HEAT TRANSFER FROM A CYLINDER, FLAT PLATE, AND TURBINE BLADE USING THE TRANSIENT SHROUD AND HEATED-COATING TECHNIQUES Ph.D. Thesis

Robert J. Butler Mar. 1995 286 p

(AD-A292646; AFIT/CI/CIA-95-001D) Avail: CASI HC A13/MF A03

A new technique to measure local heat transfer is developed, it and other methods are used to study the effects of the thermal boundary condition on local heat transfer and turbulence level effects on turbine blade heat transfer. The new technique is called the shroud technique and is a variation on the transient method. It is designed for use on arbitrarily shaped models in a wind tunnel. The shroud acts as a protective covering during in-situ heating of the model. A transient is produced by sudden removal of the shroud. Measurements on a cylinder in cross-flow are used as one method for validation of this technique. These measurements showed that the shroud technique produced good results except in the wake region where the duration of the flow development sometimes created problems. The shroud technique and a gold-film heated-coating method are both used for measurements on a flat plate with a laminar boundary layer to investigate the effect of thermal boundary conditions. The results are compared to numerical solutions, done as part of this study, for uniform temperature, uniform heat flux, and transient thermal boundary conditions. The experimental results agreed well with theory with the uniform heat flux producing 36% higher heat transfer rates than those for uniform temperature. The transient results were highly dependent on the non-dimensional temperature used, producing heat transfer rates as low as the uniform temperature or higher than the uniform heat flux boundary conditions. DTIC

N95-29382# California Inst. of Tech., Pasadena, CA.

RESEARCH ON BLUFF-BODY VORTEX WAKES Final Technical Report, 1 Jan. 1990 - 30 Jun. 1994

Anatol Roshko 22 Feb. 1995 8 p

(Contract N00014-90-J-1589)

(AD-A292650) Avail: CASI HC A02/MF A01

Comparison of laboratory experiments and computational results for two dimensional flows showed that, in impulsively started flows, laboratory flows are two dimensional in the early stages and that three dimensional effects develop after acceleration is complete. In fully developed flow the mean and fluctuating forces are considerably lower (up to 50%) in the laboratory flows (ie with three dimensionality) than in the two dimensional numerical simulations. The experiments in tow tank and water tunnel also revealed the existence of long-time modulations of vortex shedding forces. These have the form of bursts with duration of order 10 vortex shedding periods. A novel method of introducing controlled spanwise components of velocity into otherwise two dimensional flow, at low Reynolds number was to give the cylinder an axial (spanwise) motion, either a steady translation or a periodic oscillation. For unsteady, periodic axial oscillation of the cylinder, the experiments showed how the ratio of the spanwise period to the vortex shedding period determines the patterns of vortex dislocation in the wake, how regimes of chaos are formed and how shedding frequency and wake spectra are affected. DTIC

N95-29387# Hampton Univ., VA.

DEVELOPMENT OF A ROTARY WING NAVIER-STOKES CFD CODE BASED ON TLNS3D CODE Final Report, 30 Sep. 1992 - 31 Aug. 1994

Hong Hu Sep. 1994 38 p

(Contract DAAL03-92-G-0416)

(AD-A290421; ARO-30697.1-EG-H) Avail: CASI HC A03/MF A01

This report documents the development of a multi-grid Navier-Stokes code for rotary wing calculations, TLNS3DR. The TLNS3DR is based on the fixed-wing TLNS3D code by adding a rotation term and making necessary modifications on boundary conditions. The TLNS3D code solves the thin-layer Navier-Stokes equations using an explicit multistage Runge-Kutta type of time stepping with multigrid method. The TLNS3DR code reformulates the TLNS3D code in the rotor blade-fixed moving frame of reference and solves relative motion of fluids. In this report, the formulation of the Navier-Stokes equations in the moving frame of reference in terms of relative velocity is given. Several numerical examples are then presented. The results of rotor blade in hover calculated by the new TLNS3DR code seems quantitatively correct. The computation also shows that this multigrid code is efficient. DTIC

N95-29405*# Institute for Computer Applications in Science and Engineering, Hampton, VA.

AN ASSESSMENT OF ARTIFICIAL DAMPING MODELS FOR AEROACOUSTIC CALCULATIONS

M. Ehtesham Hayder Jun. 1995 18 p Presented at the 26th Fluid Dynamics Conference, San Diego, CA, 19-22 Jun. 1995; sponsored by AIAA

(Contract NCC3-370; RTOP 505-90-5K)

(NASA-CR-198354; E-9728; NAS 1.26:198354; ICOMP-95-11; AIAA Paper 95-2167) Avail: CASI HC A03/MF A01

We present a study of the effect of artificial dissipation models on nonlinear wave computations using a few high order schemes. Our motivation is to assess the effectiveness of artificial dissipation models for their suitability for aeroacoustic computations. We solve three model problems in one dimension using the Euler equations. Initial conditions are chosen to generate nonlinear waves in the computational domain. We examine various dissipation models in central difference schemes such as the Dispersion Relation Preserving (DRP) scheme and the standard fourth and sixth order schemes. We also make a similar study with the fourth order MacCormack scheme due to Gottieb and Turkel. Author

N95-29421# Alabama Univ., Huntsville, AL. Dept. of Mechanical Engineering.
DIRECT NUMERICAL SIMULATION OF COMPRESSIBLE TURBULENT FLOWS, USING ADAPTIVE SPECTRAL ELEMENT METHOD Final Report, 1 Nov. 1993 - 31 Oct. 1994
T. J. Chung and K. T. Yoon Dec. 1994 40 p
(Contract F49620-93-1-0020)
(AD-A290115; AFOSR-95-0051TR) Avail: CASI HC A03/MF A01

In this final report covering the period 1993-1994, the preliminary results of the research on direct numerical simulation of compressible turbulent flows are presented. Specifically, the adaptive Legendre polynomial spectral element method with the mixed explicit-implicit (MEI) Taylor-Galericin formulation is used in order to capture detailed physics involved in three-dimensional shock wave turbulent boundary layer interactions. DTIC

N95-29469# Stanford Univ., CA. Dept. of Aeronautics and Astronautics.
INVESTIGATION OF BURNETT EQUATIONS FOR TWO-DIMENSIONAL HYPERSONIC FLOW Final Report, 1 Dec. 1993 - 30 Nov. 1994
Dean R. Chapman and Robert W. MacCormack Nov. 1994 14 p
(Contract F49620-94-1-0055)
(AD-A290233; AFOSR-95-0049TR) Avail: CASI HC A03/MF A01

Two separate investigations have been made: evaluation of various forms of Burnett equations for 2D flows including the frame dependent as well as frame independent forms; and exploration of the compatibility of Burnett equations with the second law of thermodynamics. Among eight different Burnett formulations investigated, six were found either to be impractical for 2D/3D computations, or to yield unphysical heat conduction. The remaining two forms yielded virtually identical numerical results, which led to an investigation that has revealed their previously unsuspected analytical identity. The frame dependence problem for Burnett equations is therefore not fully resolved. Detailed analysis of Burnett forms for the rate of irreversible production of entropy has demonstrated incompatibility with the second law of thermodynamics for certain flows. DTIC

N95-29637# Alabama A & M Univ., Normal, AL.
GRAPHICS SUPERCOMPUTER FOR COMPUTATIONAL FLUID DYNAMICS RESEARCH Final Report, 30 Sep. 1993 - 30 Sep. 1994
Goang S. Liaw 29 Nov. 1994 11 p
(Contract F49620-93-1-0601)
(AD-A291087; AFOSR-95-0088TR) Avail: CASI HC A03/MF A01

The objective of this project is to purchase a state-of-the-art graphics supercomputer to improve the Computational Fluid Dynamics (CFD) research capability at Alabama A & M University (AAMU) and to support the Air Force research projects. A cutting-edge graphics supercomputer system, Onyx VTX, from Silicon Graphics Computer Systems (SGI), was purchased and installed. Other equipment including a desktop personal computer, PC-486 DX2 with a built-in 10-BaseT Ethernet card, a 10-BaseT hub, an Apple Laser Printer Select 360, and a notebook computer from Zenith were also purchased. A reading room has been converted to a research computer lab by adding some furniture and an air conditioning unit in order to provide an appropriate working environments for researchers and the purchase equipment. All the purchased equipment were successfully installed and are fully functional. Several research projects, including two existing Air Force projects, are being performed using these facilities. DTIC

N95-29654# Imperial Coll. of Science and Technology, London (England).
THE EFFECTS OF THREE DIMENSIONAL IMPOSED DISTURBANCES ON BLUFF BODY NEAR WAKE FLOWS
Nicholas Tombazis and Peter Bearman Apr. 1994 208 p
(Contract N00014-90-J-4083)
(AD-A290824) Avail: CASI HC A10/MF A03

The three-dimensionality of the near wake of bluff bodies at high Reynolds numbers is studied experimentally. Measurements were carried out in a 0.91 m x 0.91m wind tunnel (for Re =20000 to 60000) and flow visualisation in a 0.6m x 0.6m water flume (for Re=2500). The main purpose is to identify inherent three-dimensional features that may also arise in nominally two-dimensional flows. In order to fix the three-dimensional effects in both time and space, a mild, periodic, geometrical disturbance was imposed on the otherwise two-dimensional geometry of a model with a blunt trailing edge. The trailing edge thus followed a sinusoidal pattern, but a straight edge model was also studied for comparison purposes. Quantitative measurements and flow visualisation revealed that a dual shedding frequency characteristic prevails in the wake of the sinusoidal model. Base drag shows a noticeable drop (in comparison to the straight edge model). Most of the activity seems to happen in the region of the peak, where the dual frequency characteristic is more apparent and also the base drag shows its largest variations. Flow visualisation showed different modes of vortex shedding to exist. Vortical structures in the x- and z-directions were observed for both models. WZ vortices are present in the near wake. It is believed that the observed vortices are responsible for the intense base pressure fluctuations and gradients, and also for thin 'wisps' appearing between Karman' vortices in flow visualisation. DTIC

N95-29712# Tokyo Univ. (Japan). Inst. of Space and Astronautical Science.
EXPERIMENTAL STUDIES ON BOUNDARY-LAYER TRANSITION ON A REENTRY VEHICLE AT TRANSONIC AND SUPERSONIC SPEEDS
Kojiro Suzuki and Takashi Abe Mar. 1995 20 p
(ISAS-659) Avail: CASI HC A03/MF A01

The boundary-layer transition on the EXPRESS reentry capsule at transonic and supersonic speeds is studied experimentally by the wind tunnel tests. For the diagnostic of the turbulent transition of the boundary layer, the China-clay method is used. The experimental results clarify that when the freestream Mach number increases, the transition point moves downstream on the body surface and the distance between the beginning of the transition and its completion to the fully turbulent flow becomes larger. The effects of the freestream Mach number on the location of the boundary-layer transition are described successfully in terms of two nondimensional quantities, that is, the transition Reynolds number and the local Mach number at the boundary-layer edge. The oil-flow pictures reveal that in the transonic regime, the separation bubble is formed at the junction between the blunt nose and the conical part of the body and therefore the transition begins behind the reattachment point of the separation bubble. The effects of the turbulent transition on the aerodynamic characteristics of the reentry body are investigated by using the technique of the boundary-layer trip and the experimental results show that the aerodynamic characteristics of the EXPRESS reentry vehicle are not sensitive to the boundary-layer transition. Author

N95-29718 University of Western Ontario, London (Ontario).
UNSTEADY ROTATIONAL SHEAR FLOW OF POWER LAW FLUIDS Ph.D. Thesis
Jean-Paul Pascal 1993 154 p
(ISBN-0-315-81287-7) Avail: Univ. Microfilms Order No. DANN81287

In this thesis we have investigated unsteady circular Couette flow for Non-Newtonian fluids of power law behavior. We considered two specific problems: (1) a solid cylinder rotating in a power law fluid of infinite extent and (2) a power law fluid filing the gap between two concentric rotating cylinders. Due to the nonlinearity of Non-Newtonian constitutive equations, velocity disturbances from a rotating cylinder propagate through the fluid with finite speed. The existence of this moving velocity disturbance front was observed in the analytic similarity solutions and numerical solutions. For the problem with one cylinder two numerical methods were used to determine the velocity and shear stress distributions: (1) the method of lines combined with the shooting method, and (2) a front fixing transformation was employed and the resulting problem solved via various implicit (including Crank-Nicolson) finite difference schemes. For the two cylinder problem the velocity distribution was obtained via the Method of Lines together with a variable step-size finite difference method. For both problems the temperature distribution was obtained numerically via an implicit finite difference method. The interaction effect between the angular velocity and the thermal field was addressed. The centrifugal stability of the flow was analyzed analytically and numerically. The supercritical flow (Taylor-vortex flow and wavy Taylor-vortex flow) was determined through nonlinear stability analysis. The results were compared with experimental ones and previous analytic investigations for newtonian fluids. The obtained results were analyzed and conclusions were drawn upon the rheo-logical effects and temperature distribution of the power law fluids. Dissert. Abstr.

N95-29719 Princeton Univ., NJ.
EFFECT OF REYNOLDS NUMBER ON THE STRUCTURE OF

TURBULENT BOUNDARY LAYERS Ph.D. Thesis
Randall William Smith 1994 384 p
Avail: Univ. Microfilms Order No. DA9415425

This dissertation presents an investigation of the Reynolds number dependence of the structure of turbulent boundary layers. Experiments were performed in an incompressible, constant property, turbulent boundary layer developing on a flat plate in zero pressure gradient. Measurements of the mean flow spanned a momentum thickness Reynolds number range 4,600 less than Re(sub theta) less than 13,200. Turbulence statistics and space-time correlations were measured at two Reynolds numbers, Re(sub theta) approximately equal to 5,000 and 13,000. The mean flow data is used to assess the validity of the traditional mean flow scaling laws. The present data favor an alternative defect law, recently revived by George et al., which results in a Reynolds number dependent power-law overlap region. Measurements of single-point turbulence statistics are compared with existing data in an effort to distinguish between true Reynolds number effects and experimental uncertainties, especially errors due to inadequate spatial resolution. The Reynolds normal and shear stresses exhibit definite Reynolds number variations, and follow a distinctive behavior in the overlap region. The shear correlation coefficient and shear rate suggest a change in the character of the near-wall turbulence as Reynolds number increases. However, the distribution of the shear stress among the quadrants of the u'-v' plane is independent of Reynolds number. The production term of the turbulence kinetic energy budget scales on mixed variables. Space-time correlation measurements are used to examine the Reynolds number dependence of the large scale outer layer structure. Convection velocities and decay distances are only weakly dependent on Reynolds number, but the structure angle increases with Reynolds number. The wavelet transform is used to filter the data and examine how these properties vary with the scale of the motions considered. Convection velocities and structure angles decrease with increasing scale, but decay distances increase. Isocorrelation contour maps reveal an increase in streamwise length scales with increasing Reynolds number. The present results are compared to results from a boundary layer in a supersonic (M approximately equal to 3) flow revealing that, as the flow becomes compressible, Reynolds number and Mach number effects are likely to either counteract each other or interact nonlinearly.
Dissert. Abstr.

N95-29729 Clemson Univ., SC.
EFFECTS OF ELEVATED FREE-STREAM TURBULENCE AND STREAMWISE ACCELERATION ON FLOW AND THERMAL STRUCTURES IN TRANSITIONAL BOUNDARY LAYERS Ph.D. Thesis
Dadong Zhou 1993 339 p
Avail: Univ. Microfilms Order No. DA9419670

The effects of elevated free-stream turbulence and streamwise accelerations on flow and thermal structures in transitional boundary layers were investigated experimentally on a heated flat plate with elevated free-stream turbulence (FSTI) levels ranged from 3 to 7 percent, and the acceleration strength, based on K (defined as (nu/U sub infinity squared) dU sub infinity/dx), ranged from 0.39 x 10(exp -6) to 4.1 x 10(exp -6). A case with low FSTI at 0.5 percent without streamwise acceleration was used as the baseline case for comparison. A miniature three-wire probe was used to measure detailed momentum and thermal boundary layer structures, including the streamwise and cross-steam velocity fluctuations, temperature fluctuations, Reynolds stresses, Reynolds heat fluxes, eddy viscosity, turbulent thermal diffusivity, and turbulent Prandtl numbers. Wall heat transfer measurements were made on the heated test wall. Onset and end of transition were inferred from the Stanton number distributions. A conditional sampling technique was utilized to separate the flow into the turbulent and nonturbulent portions. An analysis of flow and thermal structures was performed in each portion separately. Spectral analyses for turbulent energy and thermal energy were performed. Dissert. Abstr.

N95-29761# California Inst. of Tech., Pasadena, CA. Graduate Aeronautical Labs.
NEW PREDICTIVE METHODS IN CHAOTIC FLUID DYNAMICS WITH APPLICATION TO TURBULENT HEAT TRANSFER Final Report, 15 Apr. 1991 - 30 Jun. 1994
Anthony Leonard and Stephen Wiggins 28 Oct. 1994 8 p
(Grant AF-AFOSR-0241-91)
(AD-A290691; AFOSR-95-0075TR) Avail: CASI HC A02/MF A01

Dynamical systems techniques were being developed and applied to problems of transport in fluid flows, e.g., turbulent heat transfer. Earlier successful development for two-dimensional flows were extended to include the effect of diffusion in the presence of a wall, to investigate steady and unsteady three-dimensional effects, and to study interface dynamics.
DTIC

N95-29778 Wisconsin Univ., Madison, WI.
THE STUDY OF NON-NEWTONIAN CONTRACTION FLOWS WITH A PARALLEL FINITE ELEMENT METHOD Ph.D. Thesis
Tai-Ping Tsai 1994 114 p
Avail: Univ. Microfilms Order No. DA9418579

Planar contraction flows of both shear-thinning and non Newtonian integral models for non-Newtonian fluids are studied to investigate the problem of numerical breakdown when high WEissenberg or DEbroah, i.e., the WE or DE limit, is reached. Spurious shear stress extrema are found on the wall downstream of the corner for both sharp and rounded corner. Moreover, a nonmonotonic relation between shear stress and strain rate is found when DE limit is approached, and it correlates with these shear extrema. This strongly suggests that non-monotonicity between shear stress and strain rate is responsible for the DE limit problem for all contraction flows. This non-monotonicity is caused by the inaccuracy of the quadrature rather than by the constitutive equations. This conclusion agrees with recent analytical findings by others that inaccuracy of the integration along the streamlines -- either by numerical integration or asymptotic approximation -- makes the problem ill-conditioned and spurious growth occurs on the downstream wall. The goal of the second part of this thesis is to develop a parallel finite element code on Intel's i860 Hypercube to enhance the computing power of the original serial code, FLUCODE. This involves developing the load balancing method and parallelizing linear equation solver. The resulting code on 16 parallel computing nodes has about the same speed as a CRAY YMP. Dissert. Abstr.

N95-29811 California Univ., Los Angeles, CA.
EXPERIMENTAL AND ANALYTICAL STUDY OF HEAT TRANSFER AND TURBULENT FLOW FIELD IN TANGENTIALLY INJECTED SWIRL FLOW Ph.D. Thesis
Fengteng Chang 1994 194 p
Avail: Univ. Microfilms Order No. DA9420450

Enhancement of heat transfer in a tube has been experimentally studied when fluid is injected tangentially. The experiments were conducted with electrically heated tubes of different diameters and air as the test fluid. The effects of tube diameter, injector diameter, momentum flux ratio and Reynolds number were studied parametrically. The results show that with tangential injection, significant enhancement in heat transfer is possible. To obtain understanding of the mechanisms by which heat transfer is augmented and the rate at which swirl decays, additional experiments were conducted by injecting air through injectors placed on the periphery of an 88.9 mm inside diameter and 2.5 m long acrylic tube. Four injectors of 15.88 mm inside diameter and six injectors of 22.23 mm inside diameter were used in the two sets of experiments. Tangential to total momentum flux rate ratio of 7.84 and 2.67 respectively were obtained in the two sets of experiments. Using a single rotated straight hot wire and a single rotated slanted hot wire anemometer, profiles for mean velocities in the axial and tangential directions, as well as the Reynolds stresses were obtained. Axial velocity profile shows existence of flow reversal region in the central portion of the tube and an increased axial velocity near the wall. Tangential velocity profiles have a local maximum, the location of which moves radially inwards with distance. Reynolds stress data show an anisotropy in eddy viscosity. Furthermore, a separate set of experiments was conducted with the test section heated with a heating tape wrapped around the test section. No significant difference in mean velocities and Reynolds stresses was found between the adiabatic experiments and diabatic ones. Two major mechanisms for enhancement of heat transfer are identified: (1) high maximum axial velocity near the wall produces higher heat flux from the wall; (2) high turbulence level improves mixing and thus the rate of heat transfer. Furthermore, it is observed that both the kinetic energy of the mean flow and the turbulence level decrease as swirl decays. However, during decay process the high turbulence energy-production from Reynolds stresses is necessary to transfer the kinetic energy of the mean flow to the turbulence energy. This high turbulence-production, in turn, slows down the rate of decrease of the turbulence level. As a result, the swirl and the

heat transfer enhancement are preserved for several tens of hydraulic diameters downstream. Dissert. Abstr.

N95-29817 Southampton Univ. (England). Inst. of Sound and Vibration Research.

THE ONE-DIMENSIONAL BUBBLE: THEORY, EXPERIMENT, AND RELEVANCE TO EXPOSURE OF DIVERS TO LOW FREQUENCY SOUND, AND OF LUNG TO LITHOTRIPSY

T. G. Leighton, P. R. White, and M. A. Marsden May 1995 44 p
(ISVR-TR-246) Copyright Avail: Issuing Activity

In this paper the oscillation dynamics of a linear gas pocket in a liquid are analysed. These include several features of potential use at undergraduate level for illustrating characteristics beyond those normally encountered in expositions of simple harmonic oscillators (for example, the simple linear spring-bob system). The oscillator in question is unusual firstly in that, as with all gas bubbles in liquid, the inertia is invested primarily in the surrounding liquid, rather than in the pocket itself. In other words the radiation mass is far larger than the mass of the trapped gas. This is demonstrable even in the simplest analysis, that of linear undamped small-amplitude oscillations. Secondly, the oscillator is nonlinear. The equation of motion of a damped, forced, one-dimensional bubble is obtained, the nonlinearity arising through the dependence of the oscillator stiffness (or alternatively the gas compressibility) on the amplitude of oscillation. In reduced forms, this equation can be solved analytically for the natural frequency of undamped oscillations in the linear limit, and also in the nonlinear regime of finite-amplitude free oscillation, where the fundamental frequency is found to be amplitude-dependent. Whilst analytical solutions of the undamped, unforced form of the equation of motion can be obtained in phase space, the full nonlinear damped forced equation must be solved numerically. These solutions are compared with those of the linear undamped analysis. Experimental measurements of the phase and amplitude response of a laboratory one-dimensional bubble are made, and compared with theory. Viscous effects, which for three dimensional bubbles in water are second-order and often justifiably neglected in simple analyses based on the gas stiffness and liquid inertia, are in the case of one-dimensional water bubbles comparable with these other effects (i.e. stiffness and inertia), and cannot be neglected. The analysis is used to predict: (1) the response of air bubbles within the ear canals of divers to low frequency underwater sound (from several tens of hertz to several hundred, such as is being used increasingly in the ocean for climate monitoring); and (2) the theoretical potential of bubbles in blood to cause hemorrhage of blood vessels, particularly within the lung, when subjected to high-amplitude ultrasonic pulses. Author

N95-29913# DynaFlow, Inc., Columbus, OH.

CROSS FLOW INSTABILITY OF SUPERSONIC FLOW OVER A 4:1 ELLIPTIC CONE Final Report, 1 Jun. 1994 - 31 Jan. 1995

S. L. Huang, G. K. Stuckert, and T. Herbert 20 Jan. 1995 51 p
Limited Reproducibility: Document partially illegible
(Contract F49620-94-C-0053)
(AD-A291128; AFOSR-95-0077TR) Avail: CASI HC A04/MF A01

The cross flow-initiated transition process over the surface of a supersonic 4:1 elliptic cone with 17.5 degree half-angle has been investigated using state-of-the-art local and PSE stability analyses. The basic flow was computed using the AFWAL PNS code. The local stability analysis was performed in order to find the regions and parameter ranges in which the cross flow vortex is unstable. The PSE analyses were then carried out in order to study the nonparallel effects of the flow on the most dangerous vortices--those with the greatest growth. The PSE analyses predict much greater amplification of the cross flow vortices and transition near the apex of the cone compared to the local analysis. DTIC

N95-29920# Pennsylvania State Univ., University Park, PA. Dept. of Mechanical Engineering.

EXPERIMENTAL RESEARCH ON CROSSING SHOCK WAVE BOUNDARY LAYER INTERACTIONS Final Technical Report, 1 Apr. 1991 - 30 Sep. 1994

G. S. Settles and T. J. Garrison 30 Oct. 1994 42 p
(Grant AF-AFOSR-0315-89)
(AD-A290764; AFOSR-95-0073TR) Avail: CASI HC A03/MF A01

An experimental research effort of the Penn State Gas Dynamics Laboratory on the subject of crossing shock wave boundary layer interactions is reported. This three year study was supported by AFOSR Grant 89-0315. A variety of experimental techniques were employed to study the above phenomena including planar laser scattering flowfield visualization, kerosene lampblack surface flow visualization, laser-interferometer skin friction surveys, wall static pressure measurements, and flowfield five-hole probe surveys. For a model configuration producing two intersecting shock waves, measurements were made for a range of oblique shock strengths at freestream Mach numbers of 3.0 and 3.85. Additionally, measurements were made at Mach 3.85 for a configuration producing three intersecting waves. The combined experimental dataset was used to formulate the first detailed flowfield models of the crossing-shock and triple-shock wave/boundary layer interactions. The structure of these interactions was found to be similar over a broad range of interaction strengths and is dominated by a large, separated, viscous flow region. DTIC

N95-29948# Pennsylvania State Univ., University Park, PA. Dept. of Mechanical Engineering.

THE EFFECT OF TURBULENCE ON VAPORIZATION AND MIXING IN FUEL SPRAYS Final Report, 1 Jun. 1991 - 30 Nov. 1994

Domenic A. Santavicca 8 Feb. 1995 9 p
(Contract DAAL03-91-G-0137)
(AD-A291347; ARO-28427.1-EG) Avail: CASI HC A02/MF A01

An experimental study of droplet-turbulence interactions under simulated fuel spray conditions has been conducted. The behavior of individual droplets transversely injected into laminar and turbulent flows has been characterized by measuring droplet position, shape and size as a function of time. From these measurements new information has been obtained on the effects of vaporization and unsteady curvilinear motion on droplet drag and lift in laminar flows. These measurements have also provided new data which characterize the effects of turbulence on droplet drag, dispersion and secondary breakup. DTIC

N95-29988# Argonne National Lab., IL.

STATE-OF-THE-ART REVIEW OF COMPUTATIONAL FLUID DYNAMICS MODELING FOR FLUID-SOLIDS SYSTEMS

R. W. Lyczkowski, J. X. Bouillard, J. Ding, S. L. Chang, and S. W. Burge (Babcock and Wilcox Co., Alliance, OH.) 12 May 1994 15 p Presented at the American Society of Mechanical Engineers' Winter Annual Meeting, Chicago, IL, 6-11 Nov. 1994
(Contract W-31-109-eng-38)
(DE95-005866; ANL/ES/CP-82070; CONF-941142-32) Avail: CASI HC A03/MF A01

As the result of 15 years of research (50 staff years of effort) Argonne National Laboratory (ANL), through its involvement in fluidized-bed combustion, magnetohydrodynamics, and a variety of environmental programs, has produced extensive computational fluid dynamics (CFD) software and models to predict the multiphase hydrodynamic and reactive behavior of fluid-solids motions and interactions in complex fluidized-bed reactors (FBR's) and slurry systems. This has resulted in the FLUFIX, IRF, and SLUFIX computer programs. These programs are based on fluid-solids hydrodynamic models and can predict information important to the designer of atmospheric or pressurized bubbling and circulating FBR, fluid catalytic cracking (FCC) and slurry units to guarantee optimum efficiency with minimum release of pollutants into the environment. This latter issue will become of paramount importance with the enactment of the Clean Air Act Amendment (CAAA) of 1995. Solids motion is also the key to understanding erosion processes. Erosion rates in FBR's and pneumatic and slurry components are computed by ANL's EROSION code to predict the potential metal wastage of FBR walls, intervals, feed distributors, and cyclones. Only the FLUFIX and IRF codes will be reviewed in the paper together with highlights of the validations because of length limitations. It is envisioned that one day, these codes with user-friendly pre- and post-processor software and tailored for massively parallel multiprocessor shared memory computational platforms will be used by industry and researchers to assist in reducing and/or eliminating the environmental and economic barriers which limit full consideration of coal, shale, and biomass as energy sources; to retain energy security; and to remediate waste and ecological problems. DOE

N95-30027# Air Force Inst. of Tech., Wright-Patterson AFB, OH. National Air Intelligence Center.

THE APPLICATION OF ADAPTIVE MESH REFINEMENT TO THE NUMERICAL SIMULATION OF COMPRESSIBLE FLOW

Jianxiong Shen and Lanjie Huang 17 Nov. 1994 20 p Transl. into ENGLISH from Kongqidonglixue Xuebao (China), v. 9, no. 3, Sep. 1991 p 330-337
(AD-A289595; NAIC-ID(RS)T-0921-92) Avail: CASI HC A03/MF A01

This article is based on the adaptive mesh refinement calculation methods developed by M.J.Berger and J.Oliger. It opts for the use of the concept of numerous units formed into a grid, used in solving hyperbolic type equation sets. It combines finite difference forms, opts for the use of Richardson extrapolation techniques to automatically carry out local truncation error estimates, and, for regions with low accuracy, produces new fine mesh local refinements or eliminates old fine mesh refinements which are no longer needed, in order to reach, in the minimum amount of operations, the specified accuracy requirements. Grids are capable of going down into a layer on layer refinement. On the basis of the layered sequence of coverage, each individual grid is a rectangular uniform grid or mesh in any direction desired. This set of algorithms is independent of difference forms used in solutions, is very easy, and combines various types of forms. DTIC

N95-30034*# Pennsylvania State Univ., University Park, PA.
RELIABILITY ENHANCEMENT OF NAVIER-STOKES CODES THROUGH CONVERGENCE ACCELERATION Final Report
Charles L. Merkle and George S. Dulikravich Apr. 1995 223 p Sponsored in part by the Penn State NASA Propulsion Engineering Research Center
(Contract NAS8-38861; NAGw-1356)
(NASA-CR-196635; NAS 1.26:196635) Avail: CASI HC A10/MF A03

Methods for enhancing the reliability of Navier-Stokes computer codes through improving convergence characteristics are presented. The improving of these characteristics decreases the likelihood of code unreliability and user interventions in a design environment. The problem referred to as a 'stiffness' in the governing equations for propulsion-related flowfields is investigated, particularly in regard to common sources of equation stiffness that lead to convergence degradation of CFD algorithms. Von Neumann stability theory is employed as a tool to study the convergence difficulties involved. Based on the stability results, improved algorithms are devised to ensure efficient convergence in different situations. A number of test cases are considered to confirm a correlation between stability theory and numerical convergence. The examples of turbulent and reacting flow are presented, and a generalized form of the preconditioning matrix is derived to handle these problems, i.e., the problems involving additional differential equations for describing the transport of turbulent kinetic energy, dissipation rate and chemical species. Algorithms for unsteady computations are considered. The extension of the preconditioning techniques and algorithms derived for Navier-Stokes computations to three-dimensional flow problems is discussed. New methods to accelerate the convergence of iterative schemes for the numerical integration of systems of partial differential equtions are developed, with a special emphasis on the acceleration of convergence on highly clustered grids. CASI

N95-30039# Texas Univ. at Dallas, Richardson, TX. Dept. of Chemistry.
DEVELOPMENT AND APPLICATION OF FLUORESCENT DIAGNOSTICS TO FUNDAMENTAL DROPLET AND SPRAY PROBLEMS Final Report, 16 May 1991 - 15 May 1994
Lynn A. Melton 12 Sep. 1994 11 p
(Contract DAAL03-91-G-0033)
(AD-A290553; ARO-28250.3-EG) Avail: CASI HC A03/MF A01

This final report describes work carried out under ARO grant DAALO3-91-G-0033 for the development and application of fluorescent diagnostics to fundamental droplet problems. Particular emphasis has been placed on attempts to understand the heating, evaporation, and internal circulation processes of sub-millimeter droplets. At the University of Texas at Dallas, a new type of exciplex fluorescence thermometer, based on the temperature dependent shift of the exciplex band, has been developed and applied to thermometry of evaporating droplets and surface liquids. Algorithms and programs have been developed and disseminated for the correction of 'droplet slicing images' (DSI) for the effects of refraction by the front hemisphere of the droplet. At United Technologies Research Center, DSI techniques have been used to demonstrate unequivocally that aerodynamic shear can induce internal circulation in sub-millimeter droplets and to show that droplets rotate and interact with the surrounding gas phase flow field. DTIC

N95-30056*# National Aeronautics and Space Administration. Langley Research Center, Hampton, VA.
HYDROGEN FILM COOLING WITH INCIDENT AND SWEPT-SHOCK INTERACTIONS IN A MACH 6.4 NITROGEN FREE STREAM
George C. Olsen and Robert J. Nowak Jun. 1995 47 p
(RTOP 506-43-31-03)
(NASA-TM-4603; L-17367; NAS 1.15:4603) Avail: CASI HC A03/MF A01

The effectiveness of slot film cooling of a flat plate in a Mach 6.4 flow with and without incident and swept oblique shock interactions was experimentally investigated. Hydrogen was the primary coolant gas, although some tests were conducted using helium as the coolant. Tests were conducted in the Calspan 48-Inch Shock Tunnel with a nitrogen flow field to preclude combustion of the hydrogen coolant gas. A two-dimensional highly instrumented model developed in a previous test series was used. Parameters investigated included coolant mass flow rate, coolant gas, local free-stream Reynolds number, incident oblique shock strength, and a swept oblique shock. Both gases were highly effective coolants in undisturbed flow; however, both incident and swept shocks degraded that effectiveness. Author

N95-30087# Wright Lab., Wright-Patterson AFB, OH.
SURVEY OF CFD APPLICATIONS FOR HIGH SPEED INLETS Final Report, Aug. 1992 - Jul. 1994
Keith E. Numbers Jul. 1994 60 p
(AF Proj. 2404)
(AD-A291365; WL-TR-94-3131) Avail: CASI HC A04/MF A01

A comprehensive review of techniques and methods for applying computational fluid dynamics (CFD) analysis to high speed inlets and related flows is provided via an extensive literature survey of such applications. Topics covered include: governing equations, numerical integration schemes, boundary conditions, gridding requirements, and turbulence models. Results of applications from the literature survey shed light on the relative success of the techniques being used throughout the industry. DTIC

N95-30187# Argonne National Lab., IL.
NMR IMAGING AND HYDRODYNAMIC ANALYSIS OF NEUTRALLY BUOYANT NON-NEWTONIAN SLURRY FLOWS
J. X. Bouillard and S. W. Sinton (Lockheed Missiles and Space Co., Palo Alto, CA.) 1995 16 p
(Contract W-31-109-eng-38)
(DE95-005842; ANL/ES/PP-79002) Avail: CASI HC A03/MF A01

The flow of solids loaded suspension in cylindrical pipes has been the object of intense experimental and theoretical investigations in recent years. These types of flows are of great interest in chemical engineering because of their important use in many industrial manufacturing processes. Such flows are for example encountered in the manufacture of solid-rocket propellants, advanced ceramics, reinforced polymer composites, in heterogeneous catalytic reactors, and in the pipeline transport of liquid-solids suspensions. In most cases, the suspension microstructure and the degree of solids dispersion greatly affect the final performance of the manufactured product. For example, solid propellant pellets need to be extremely-well dispersed in gel matrices for use as rocket engine solid fuels. The homogeneity of pellet dispersion is critical to allow good uniformity of the burn rate, which in turn affects the final mechanical performance of the engine. Today's manufacturing of such fuels uses continuous flow processes rather than batch processes. Unfortunately, the hydrodynamics of such flow processes is poorly understood and is difficult to assess because it requires the simultaneous measurements of liquid/solids phase velocities and volume fractions. Due to the recent development in pulsed Fourier Transform NMR imaging, NMR imaging is now becoming a powerful technique for the non intrusive investigation of multi-phase flows. This paper reports and exposes a state-of-the-art experimental and theoretical methodology that can be used to study such flows. The hydrodynamic model developed for this study is a two-phase flow shear thinning model with standard constitutive fluid/solids interphase drag and solids compaction stresses. this model shows good agreement with experimental data and the limitations of this model are discussed. DOE

N95-30202# Technische Univ., Delft (Netherlands).
MULTI-DIMENSIONAL UPWIND DISCRETIZATION METHOD FOR THE

EULER EQUATIONS ON UNSTRUCTURED GRIDS Ph.D. Thesis
R. Struijs 24 Jun. 1994 222 p
(PB95-197307) Avail: CASI HC A10/MF A03

This thesis deals with the development of a multi-dimensional upwind solver for the Euler equations on unstructured grids. The method is constructed following the three concepts which constitute Roe's one-dimensional approximate Riemann solver: (1) an analytic eigenvector or wave decomposition of the flux derivative; (2) a discrete counterpart using a conservative linearization of the flux difference over a cell; (3) an upwind distribution of the decomposed parts over the meshpoints according to the sign of the corresponding eigenvalues. Each of these three elements is generalized for multi-dimensional flow, avoiding a dimension-by-dimension discretization. NTIS

N95-30224*# National Aeronautics and Space Administration. Ames Research Center, Moffett Field, CA.
BOUNDARY-LAYER TRANSITION AND GLOBAL SKIN FRICTION MEASUREMENT WITH AN OIL-FRINGE IMAGING TECHNIQUE
Daryl J. Monson, George G. Mateer, and Florian R. Menter 1993 15 p
(NASA-CR-198814; NAS 1.26:198814) Avail: CASI HC A03/MF A01

A new oil-fringe imaging system skin friction (FISF) technique to measure skin friction on wind tunnel models is presented. In the method used to demonstrate the technique, lines of oil are applied on surfaces that connect the intended sets of measurement points, and then a wind tunnel is run so that the oil thins and forms interference fringes that are spaced in proportion to local skin friction. After a run the fringe spacings are imaged with a CCD-array digital camera and measured on a computer. Skin friction and transition measurements on a two-dimensional wing are presented and compared with computational predictions. Author

N95-30233 Stanford Univ., CA.
NUMERICAL SOLUTION OF THE EQUATIONS GOVERNING NON-NEWTONIAN FLOW AT MODERATE REYNOLDS NUMBERS Ph.D. Thesis
Charles Dionisio Eggleton 1994 197 p
Avail: Univ. Microfilms Order No. DA9422079

A numerical method proven to be efficient for solving the Navier-Stokes equations is extended to solve the equations including the Oldroyd B model of viscoelasticity. The continuity equation is treated by the artificial compressibility method and the resulting set of equations are split into a hyperbolic set and one that contributes to the mixed character of the system. A flux difference splitting scheme is used to approximate the hyperbolic set and an implicit method is used to time march to steady state. The numerical method is used to solve channel entry and flat plate flow problems. Solutions are found first in the entry region of the channel and are then matched to solutions in the downstream region. The solutions in the downstream region of the channel are compared with the predictions of linear perturbation analysis. Very good agreement is found for the mode shapes of the velocities and viscoelastic stresses. The rates of development are in excellent agreement and increase with the elasticity of the fluid at fixed Reynolds number; thus the entrance length is smaller than for a Newtonian fluid. Hsu's boundary layer equations poorly predict the development rates while predictions from newly proposed boundary layer equations valid for larger elasticities produce very good agreement. The flow over a flat plate is studied in the leading edge and far downstream regions. Leading edge solutions are qualitatively compared with linear theory. Vorticity discontinuities propagate from the leading edge when the flow is supercritical, but are quickly dissipated in the nonlinear case. Velocity and viscoelastic stress oscillations are found in both the linear and nonlinear cases. Nonlinear solutions for perturbed uniform flow show vorticity waves propagating along characteristics as predicted by linear theory. Farther downstream of the leading edge, the elasticity of the flow decreases and the velocity profiles reduce to the Blasius profile to first order, in agreement with the predictions of Hsu's instantaneous boundary layer equations. Dissert. Abstr.

N95-30250*# Colorado Univ., Boulder, CO. Dept. of Aerospace Engineering Sciences.
NUMERICAL SIMULATION OF STABILITY AND STABILITY CONTROL OF HIGH SPEED COMPRESSIBLE ROTATING COUETTE FLOW Final Report
Sedat Biringen and Ferhat F. Hatay 1993 50 p
(Grant NAG1-1103)
(NASA-CR-198832; NAS 1.26:198832) Avail: CASI HC A03/MF A01

The nonlinear temporal evolution of disturbances in compressible flow between infinitely long, concentric cylinders is investigated through direct numerical simulations of the full, three-dimensional Navier-Stokes and energy equations. Counter-rotating cylinders separated by wide gaps are considered with supersonic velocities of the inner cylinder. Initially, the primary disturbance grows exponentially in accordance with linear stability theory. As the disturbances evolve, higher harmonics and subharmonics are generated in a cascading order eventually reaching a saturation state. Subsequent highly nonlinear stages of the evolution are governed by the interaction of the disturbance modes, particularly the axial subharmonics. Nonlinear evolution of the disturbance field is characterized by the formation of high-shear layers extending from the inner cylinder towards the center of the gap in the form of jets similar to the ejection events in transitional and turbulent wall-bounded shear flows. Author

N95-30275 California Univ., Los Angeles, CA.
CONTROL OF VORTEX DYNAMICS Ph.D. Thesis
Hsiao-Lung Chang 1994 120 p
Avail: Univ. Microfilms Order No. DA9420530

Discrete vortex methods are used to provide computationally efficient simulations of vortex dynamics in fluid flows. An adaptive LQG controller is applied to reduce the oscillations in the wake caused by the vortex dynamics. The controller design is based on a discrete-time input/output model rather than the nonlinear differential equations of the discrete vortex model. The control philosophy is to identify time-varying parameters in the input/output model adaptively and use the identified parameters to update the control law. For numerically stable identification, an adaptive algorithm based on inverse QR decomposition is introduced. The derivation shows that this algorithm is a square-root implementation of recursive least squares estimation. For a preliminary test of the control strategy, the adaptive LQG controller is applied to a vortex street model simulated by discrete vortices. The identification shows that the stability of the identified zeros depends on whether the sensor is upstream or downstream of the actuator. Flow past a flat plate is another important application of the discrete vortex method. A control problem is studied and simulated in which suction at the back face of the plate is used to trap vortices behind the plate. Qualitatively, the results obtained with the discrete-vortex method used here agree with earlier results for a substantially different vortex method involving a small number of differential equations. Dissert. Abstr.

N95-30284 Johns Hopkins Univ., Baltimore, MD.
ENSEMBLE PHASE AVERAGED EQUATIONS FOR MULTIPHASE FLOWS Ph.D. Thesis
Duan Zhong Zhang 1994 161 p
Avail: Univ. Microfilms Order No. DA9420049

An ensemble phase averaging method has been developed for the theoretical study of disperse two-phase flows. Applying this averaging method, a two-fluid model is developed directly from the microscopic equations for each phase. In the present averaging method, differential and averaging operators do not commute. The commutators connect the microscopic qualities to averaged quantities, and represent phase interactions. A new stress tensor is found. Correct to the first order in the particle volume fraction, the averaged equations are closed in the situation of potential flow, Stokes flow, and for the energy equation in the situations of low particle Reynolds and Peclet number flows. Effective properties, such as added mass, effective heat conductivity, and viscosity are found. It is noted that knowledge of these effective properties is not sufficient to close the averaged equations in general. Further terms arise from the detailed calculation. For linear flows with finite volume fraction, we use general principles of Continuum Mechanics to find the functional forms of the constitutive relations. This ensemble phase averaging method is rigorous, general and flexible, and hence can be used as a general tool to study suspensions of particles, and to establish the fundamental equations of suspension mechanics. Dissert. Abstr.

N95-30290 Iowa State Univ. of Science and Technology, Ames, IA.
AN INTERACTING BOUNDARY LAYER METHOD FOR UNSTEADY COMPRESSIBLE FLOWS Ph.D. Thesis

Robert Edwin Bartels 1994 199 p
Avail: Univ. Microfilms Order No. DA9424195

A time accurate compressible interactive boundary layer procedure for airfoils using the quasi-simultaneous method of Veldman is developed. It couples the high frequency transonic small disturbance equation with the complete set of unsteady compressible boundary equations in Levy-Lees variable form, using a pseudo-time derivative of displacement thickness for enhanced stability. Included is a simple procedure for time accurately updating the viscous wake location. The basis of the interaction is an extension of the asymptotic matching condition of Davis for unsteady compressible interaction. This analysis identifies several possible unsteady transonic separation structures and highlights the importance of the pseudo-time derivative in stabilizing the interaction. The method is applied to oscillating airfoils experiencing light shock-induced stall. Comparisons are made with several standard turbulence models. Shock-induced oscillatory flow about the 18 percent circular arc airfoil is investigated with this method and found to be modeled quite accurately. Dissert. Abstr.

N95-30301 California Univ., Los Angeles, CA.
THE PHYSICS OF THE COLLISIONLESS BOW SHOCK Ph.D. Thesis
Michael Howard Farris 1993 427 p
Avail: Univ. Microfilms Order No. DA9420461

The physical processes of the collisionless bow shock are examined using spacecraft data from the International Sun-Earth Explorer (ISEE) mission. These processes are analyzed as a function of the upstream parameters of the solar wind medium. The four main parameters which are important in determining the physical behavior of the shock are the ratio between the thermal and magnetic pressure of the solar wind, or the plasma beta, beta, the ratio between the oncoming solar wind velocity and the speed at which fast magnetosonic waves travel, or the magnetosonic Mach number, M(MS), the angle between the magnetic field and shock normal directions, theta(BN), and the ratio of specific heats, gamma. At low Mach numbers, the shock steepens out a precursor whistler mode wave, and the shock becomes decoupled from the precursor wave as the Mach number increases. There is a noncoplanar magnetic field component within the shock ramp which serves to differentially heat the electrons and ions in their passage through the shock layer. For higher Mach numbers, ion cyclotron waves remove ion temperature anisotropies downstream of the quasi-perpendicular shock and upstream magnetosonic waves are mode converted to Alfven mode wave downstream of the quasi-parallel shock. Mirror mode waves exist downstream of the quasi-perpendicular shock for conditions when the downstream plasma beta and solar wind helium content is high. The ratio of criticality, an upstream parameter which is highly correlated with the downstream plasma beta, can best order the wave behavior and structural changes of the shock. Dissert. Abstr.

N95-30303 Dartmouth Coll., Hanover, NH.
SUPERCRITICAL STATES OF TWO-DIMENSIONAL WALL-BOUNDED SHEAR FLOW Ph.D. Thesis
Wesley Berger Jones 1994 139 p
Avail: Univ. Microfilms Order No. DA9420581

The behavior of high Reynolds number two-dimensional incompressible viscous Navier-Stokes fluids confined to a channel with periodically identified ends is investigated numerically. Two-dimensional steady states, quasi-steady states and persistently temporally evolving states of plane Poiseuille flow are found by following the evolution of the fluid for very long times. Using the primitive variable formulation of the Navier-Stokes equations, a splitting method is implemented to enforce incompressibility and no-slip boundary conditions. The resulting equations are solved using a pseudo-spectral method with a Fourier series as the expansion basis in the streamwise direction and a Chebyshev polynomial expansion basis in the cross-stream direction. Steady states for Reynolds numbers up to 15000 are presented and characterized in the frame of reference where the vorticity is accurately time independent. In this frame of reference the vorticity and stream function display and interesting correlation, showing that the flow is divided into three spatially distinct regions. The simulation is motivated by the previous success of the mean-field statistical mechanics of large numbers of discrete line vortices in describing vortical structures found at late times in doubly-periodic two-dimensional turbulent decay calculations. The steady-states of channel flow are not globally well described by the mean-field theory nor were we able to formulate a similar theory to predict the form of the steady-states. Dissert. Abstr.

N95-30304 Connecticut Univ., Storrs, CT.
THE FLUID MECHANICS OF A HIGH ASPECT RATIO SLOT WITH AN IMPRESSED PRESSURE GRADIENT AND SECONDARY INJECTION Ph.D. Thesis
John Bertram Sobanik 1993 258 p
Avail: Univ. Microfilms Order No. DA9419439

A high aspect ratio slot flow (which emulates the gas leakage path in a gas turbine engine outer turbine air seal) is studied by use of a high aspect ratio slot using water as the working fluid. The cross section of the geometry is similar to a 'T', the slot being the vertical stroke and the main flow being the cross bar. A pressure gradient in the axial direction is created by blocking the main flow at a discreet location with an orifice plate (or blade tip simulator), located above the slot. Seven individually metered secondary flow injectors are located periodically along the bottom of the wall of the slot. Two slot widths, 1/8 and 1/4 inch, were investigated for length to width aspect ratios of 384 and 192 and height to width aspect ratios 33.2 and 16.6 respectively. Orifice plate pressure drops sufficient to give Reynolds numbers based upon half width of the slot, without secondary injection turned on, of 2350 and 4700 in the 1/8 inch slot and 4700 and 9400 in the 1/4 inch slot were run. Various secondary injection scenarios were added to the flow, the cases most studied being the no-injection and the all injectors flowing equal mass rates. Total injection rates for all seven injectors of 3.78 and 7.56 slot volumes per second were run. Laser velocimetry data and flow visualization pictures using fluorescein dye in the secondary flow are compared with computational results form the TEACH 3-D computer code. Major features and trends of the flow are captured by the computational model. Recommendations for further improvement of the numerical accuracy involves modification of the TEACH 3-D code to allow the 'slip condition' on all confining boundaries of the flow, or using a code which permits the 'slip condition' on all boundaries as a built-in option. Dissert. Abstr.

N95-28724*# McDonnell-Douglas Aerospace, Saint Louis, MO.
FUTURE REQUIREMENTS IN SURFACE MODELING AND GRID GENERATION
Raymond R. Cosner *In* NASA. Lewis Research Center, Surface Modeling, Grid Generation, and Related Issues in Computational Fluid Dynamic (CFD) Solutions Mar. 1995 p 3-13 (For primary document see N95-28723 10-02)
Avail: CASI HC A03/MF A10

N95-28725*# Lockheed Aeronautical Systems Co., Marietta, GA.
REQUIREMENTS FOR EFFECTIVE USE OF CFD IN AEROSPACE DESIGN
Pradeep Raj *In* NASA. Lewis Research Center, Surface Modeling, Grid Generation, and Related Issues in Computational Fluid Dynamic (CFD) Solutions Mar. 1995 p 15-28 (For primary document see N95-28723 10-02)
Avail: CASI HC A03/MF A10

N95-28726*# General Electric Co., Schenectady, NY. Research and Development Center.
GRID GENERATION AND SURFACE MODELING FOR CFD
Stuart D. Connell, Janet S. Sober, and Scott H. Lamson *In* NASA. Lewis Research Center, Surface Modeling, Grid Generation, and Related Issues in Computational Fluid Dynamic (CFD) Solutions Mar. 1995 p 29-43 (For primary document see N95-28723 10-02)
Avail: CASI HC A03/MF A10

N95-28727*# Pratt and Whitney Aircraft, East Hartford, CT.
GRID GENERATION: A VIEW FROM THE TRENCHES
David Ives, Robert Miller, William Siddons, and Kevin VanDyke (Pratt and Whitney Aircraft, West Palm Beach, FL.) *In* NASA. Lewis Research Center, Surface Modeling, Grid Generation, and Related Issues in Computational Fluid Dynamic (CFD) Solutions Mar. 1995 p 45-54 (For primary document see N95-28723 10-02)
Avail: CASI HC A02/MF A10

N95-28728*# National Aeronautics and Space Administration. Ames Research Center, Moffett Field, CA.
APPLICATION OF CFD IN AERONAUTICS AT NASA AMES RESEARCH CENTER

Catherine M. Maksymiuk, Francis Y. Enomoto, and William R. VanDalsem *In* NASA. Lewis Research Center, Surface Modeling, Grid Generation, and Related Issues in Computational Fluid Dynamic (CFD) Solutions Mar. 1995 p 57-67 (For primary document see N95-28723 10-02)
Avail: CASI HC A03/MF A10

N95-28732*# National Aeronautics and Space Administration. Lewis Research Center, Cleveland, OH.
SURFACE MODELING AND GRID GENERATION FOR AEROPROPULSION CFD
Yung K. Choo, John W. Slater, James Loellbach, and Jinho Lee (NYMA, Inc., Cleveland, OH.) *In its* Surface Modeling, Grid Generation, and Related Issues in Computational Fluid Dynamic (CFD) Solutions Mar. 1995 p 89-103 (For primary document see N95-28723 10-02)
Avail: CASI HC A03/MF A10

N95-28736*# National Aeronautics and Space Administration. Langley Research Center, Hampton, VA.
BLOCK-STRUCTURED GRIDS FOR COMPLEX AERODYNAMIC CONFIGURATIONS: CURRENT STATUS
Veer N. Vatsa, Mark D. Sanetrik (AS&M, Inc., Hampton, VA.), and Edward B. Parlette (Vigyan Research Associates, Inc., Hampton, VA.) *In* NASA. Lewis Research Center, Surface Modeling, Grid Generation, and Related Issues in Computational Fluid Dynamic (CFD) Solutions Mar. 1995 p 163-177 (For primary document see N95-28723 10-02)
Avail: CASI HC A03/MF A10

N95-28737*# National Aeronautics and Space Administration. Ames Research Center, Moffett Field, CA.
GRID RELATED ISSUES FOR STATIC AND DYNAMIC GEOMETRY PROBLEMS USING SYSTEMS OF OVERSET STRUCTURED GRIDS
Robert L. Meakin *In* NASA. Lewis Research Center, Surface Modeling, Grid Generation, and Related Issues in Computational Fluid Dynamic (CFD) Solutions Mar. 1995 p 181-192 (For primary document see N95-28723 10-02)
Avail: CASI HC A03/MF A10

N95-28738*# Wright Lab., Eglin AFB, FL.
THE ROLE OF OVERSET GRIDS IN THE DEVELOPMENT OF THE GENERAL PURPOSE CFD CODE
Davy M. Belk *In* NASA. Lewis Research Center, Surface Modeling, Grid Generation, and Related Issues in Computational Fluid Dynamic (CFD) Solutions Mar. 1995 p 193-204 (For primary document see N95-28723 10-02)
Avail: CASI HC A03/MF A10

N95-28739*# National Aeronautics and Space Administration. Lewis Research Center, Cleveland, OH.
A CARTESIAN, CELL-BASED APPROACH FOR ADAPTIVELY-REFINED SOLUTIONS OF THE EULER AND NAVIER-STOKES EQUATIONS
William J. Coirier and Kenneth G. Powell (Michigan Univ., Ann Arbor, MI.) *In its* Surface Modeling, Grid Generation, and Related Issues in Computational Fluid Dynamic (CFD) Solutions Mar. 1995 p 207-224 (For primary document see N95-28723 10-02)
Avail: CASI HC A03/MF A10

N95-28740*# National Aeronautics and Space Administration. Ames Research Center, Moffett Field, CA.
DEVELOPMENT AND APPLICATION OF A 3D CARTESIAN GRID EULER METHOD
John E. Melton, Michael J. Aftosmis (Wright Lab., Wright-Patterson AFB, OH.), Marsha J. Berger (New York Univ., New York, NY.), and Michael D. Wong (Sterling Software, Inc., Palo Alto, CA.) *In* NASA. Lewis Research Center, Surface Modeling, Grid Generation, and Related Issues in Computational Fluid Dynamic (CFD) Solutions Mar. 1995 p 225-249 (For primary document see N95-28723 10-02)
(Contracts DE-FG02-88ER-25053; F49620-94-1-0132)
Avail: CASI HC A03/MF A10

N95-28742*# Princeton Univ., NJ. Dept. of Mechanical and Aerospace Engineering.
PROSPECTS AND EXPECTATIONS FOR UNSTRUCTURED METHODS
Timothy J. Baker *In* NASA. Lewis Research Center, Surface Modeling, Grid Generation, and Related Issues in Computational Fluid Dynamic (CFD) Solutions Mar. 1995 p 273-287 (For primary document see N95-28723 10-02)
Avail: CASI HC A03/MF A10

N95-28744*# Texas Univ., Austin, TX. Dept. of Aerospace Engineering and Engineering Mechanics
ADAPTIVE HYBRID PRISMATIC-TETRAHEDRAL GRIDS FOR VISCOUS FLOWS
Yannis Kallinderis, Aly Khawaja, and Harlan McMorris *In* NASA. Lewis Research Center, Surface Modeling, Grid Generation, and Related Issues in Computational Fluid Dynamic (CFD) Solutions Mar. 1995 p 311-332 (For primary document see N95-28723 10-02)
(Grants NAG1-1459; NSF ASC-93-57677)
Avail: CASI HC A03/MF A10

N95-28746*# National Aeronautics and Space Administration. Ames Research Center, Moffett Field, CA.
EMERGING CFD TECHNOLOGIES AND AEROSPACE VEHICLE DESIGN
Michael J. Aftosmis *In* NASA. Lewis Research Center, Surface Modeling, Grid Generation, and Related Issues in Computational Fluid Dynamic (CFD) Solutions Mar. 1995 p 359-384 Prepared in cooperation with Wright Lab., Wright-Patterson AFB, OH (For primary document see N95-28723 10-02)
Avail: CASI HC A03/MF A10

N95-28747*# Lockheed Aeronautical Systems Co., Marietta, GA.
AN ASSESSMENT OF UNSTRUCTURED GRID TECHNOLOGY FOR TIMELY CFD ANALYSIS
Tom A. Kinard and Deanne M. Schabowski (Lockheed-Fort Worth Co., Fort Worth, TX.) *In* NASA. Lewis Research Center, Surface Modeling, Grid Generation, and Related Issues in Computational Fluid Dynamic (CFD) Solutions Mar. 1995 p 385-400 (For primary document see N95-28723 10-02)
Avail: CASI HC A03/MF A10

N95-28766*# National Aeronautics and Space Administration. Lewis Research Center, Cleveland, OH.
ADVANCED METHODOLOGY FOR SIMULATION OF COMPLEX FLOWS USING STRUCTURED GRID SYSTEMS
Erlendur Steinthorsson and David Modiano *In its* Surface Modeling, Grid Generation, and Related Issues in Computational Fluid Dynamic (CFD) Solutions Mar. 1995 p 697-710 (For primary document see N95-28723 10-02)
Avail: CASI HC A03/MF A10

N95-28767*# National Aerospace Lab., Amsterdam (Netherlands).
DEMONSTRATION OF AN AUTOMATED CFD SYSTEM FOR THREE-DIMENSIONAL FLOW SIMULATIONS
J. W. vanderBurg, J. E. J. Maseland, R. Hagmeijer, and K. M. J. deCock *In* NASA. Lewis Research Center, Surface Modeling, Grid Generation, and Related Issues in Computational Fluid Dynamic (CFD) Solutions Mar. 1995 p 713-730 Sponsored by Netherlands Agency for Aerospace Programs (For primary document see N95-28723 10-02)
Avail: CASI HC A03/MF A10

N95-28768*# National Aeronautics and Space Administration. Ames Research Center, Moffett Field, CA.
A PROCEDURE FOR AUTOMATING CFD SIMULATIONS OF AN INLET-BLEED PROBLEM
Wei J. Chyu, Mark J. Rimlinger (Carnegie-Mellon Univ., Pittsburgh, PA.), and Tom I.-P. Shih (Carnegie-Mellon Univ., Pittsburgh, PA.) *In* NASA. Lewis Research Center, Surface Modeling, Grid Generation, and Related Issues in Computational Fluid Dynamic (CFD) Solutions Mar. 1995 p 731-749 (For primary document see N95-28723 10-02)
Avail: CASI HC A03/MF A10

N95-28770*# National Aeronautics and Space Administration. Lewis Research Center, Cleveland, OH.
A COMBINED GEOMETRIC APPROACH FOR COMPUTATIONAL FLUID DYNAMICS ON DYNAMIC GRIDS

John W. Slater *In its* Surface Modeling, Grid Generation, and Related Issues in Computational Fluid Dynamic (CFD) Solutions Mar. 1995 p 763-780 (For primary document see N95-28723 10-02)
Avail: CASI HC A03/MF A10

N95-30142*# Electricite de France, Clamart (France). Dept. Acoustique et Mechanique Vibratoire.
COMPUTATION OF WAVE PROPAGATION IN A COMPLEX FLOW
Philippe Lafon *In* NASA. Langley Research Center, ICASE/LaRC Workshop on Benchmark Problems in Computational Aeroacoustics (CAA) May 1995 p 125-132 (For primary document see N95-30133 10-71)
Avail: CASI HC A02/MF A04

N95-30149*# Ohio Aerospace Inst., Cleveland, OH. Inst. for Computational Mechanics in Propulsion.
EVALUATION OF HIGH ORDER SCHEMES FOR NONLINEAR WAVE COMPUTATIONS
M. Ehtesham Hayder *In* NASA. Langley Research Center, ICASE/LaRC Workshop on Benchmark Problems in Computational Aeroacoustics (CAA) May 1995 p 203-207 (For primary document see N95-30133 10-71)
(Contract NCC3-233)
Avail: CASI HC A01/MF A04

N95-30151*# National Aeronautics and Space Administration. Langley Research Center, Hampton, VA.
NONLINEAR WAVE PROPAGATION USING THREE DIFFERENT FINITE DIFFERENCE SCHEMES (CATEGORY 2 APPLICATION)
D. Stuart Pope (Lockheed Engineering and Sciences Co., Hampton, VA.) and J. C. Hardin *In its* ICASE/LaRC Workshop on Benchmark Problems in Computational Aeroacoustics (CAA) May 1995 p 217-223 (For primary document see N95-30133 10-71)
(Contract NAS1-19000)
Avail: CASI HC A02/MF A04

N95-30161*# Notre Dame Univ., IN.
THE PRESSURE FIELD OF A GUST INTERACTING WITH A FLAT PLATE
Hafiz M. Atassi and Sheryl M. Patrick *In* NASA. Langley Research Center, ICASE/LaRC Workshop on Benchmark Problems in Computational Aeroacoustics (CAA) May 1995 p 291-296 (For primary document see N95-30133 10-71)
Avail: CASI HC A02/MF A04

35 INSTRUMENTATION AND PHOTOGRAPHY

Includes remote sensors; measuring instruments and gages; detectors; cameras and photographic supplies; and holography.

For aerial photography see *43 Earth Resources and Remote Sensing*. For related information see also *06 Aircraft Instrumentation*, and *19 Spacecraft Instrumentation*.

N95-28917 Los Alamos National Lab., NM.
SAO HMC PHOTODETECTOR/EVENT TIMER ENGINEERING MODEL TEST REPORT
Oct. 1994 95 p Limited Reproducibility: More than 20% of this document may be affected by poor print
(Contract W-7405-eng-36)
(DE95-007889; LA-UR-95-600) Avail: Issuing Activity (Department of Energy (DOE))

The test unit is a custom photodetector/event timer, PET, built for the Smithsonian Astrophysical Observatory, SAO, by Los Alamos which records elapsed time in 10 ps steps. The 1 Kg, 12 cm diameter PET unit uses 10 watts of electrical power and was tested to SAO's specified flight conditions. The event timer has two inputs -- a reference clock oscillator input and a stop signal. Like a stop watch with split timing capability, the event timer records the instant a stop signal arrives. At that sample instant, the number of elapsed clock cycles are stored and the sample instant position between two reference clock edges is interpolated and stored. Then that stored data can be shifted serially to an external computer. The photodetector part of the PET responds to an optical input and provides the electrical output signal to the event timer specifying the sample instant. This test report discusses the event timer test results. Test equipment is shown for most of the operational tests. The relay rack contains test pursers and clocks. The environmental chamber controls temperature. The computer reads and records the serial data from the PET. Reported testing topics include: Pulse shapes to be used as test inputs, test results obtained using the electrical source's input, optical test results which are the best simulation of specified operational conditions, heat sink operation in vacuum. Vibration tests performed to SAO's specification. DOE

N95-28966# Schofield (Andrew N.) and Associates Ltd., Cambridge (England).
COORDINATION OF OPERATIONS FOR CENTRIFUGE QUALITY CONTROL. PHASE 3C Final Technical Report
Andrew N. Schofield and R. S. Steedman 10 Jan. 1995 69 p
(Contract DAJA45-93-C-0021)
(AD-A292533; ANS/A-26-03-R-009; R/D-7100-EN-01) Avail: CASI HC A04/MF A01

ANS&A Associates have held extensive discussions with each of the participating laboratories during the period of research to start to define and to prepare for the initial research experimentation on the WES centrifuge. Briefings on the principles of centrifuge modelling have been given and round table discussions have led to the development of ideas for applications of the centrifuge which will benefit future research programmes. In all fields novel applications of physical modelling have been identified using the centrifuge and these are expected to lead to unique experiments and important new discoveries. In some fields the opportunities afforded by the ability to change gravity have been hard to identify. In other fields, applications and potential future sources of funding for experimental programmes have been easily identified. DTIC

N95-29004# Rensselaer Polytechnic Inst., Troy, NY. Dept. of Physics.
THE 1.3 MICROMETER FIBER PHOTODETECTOR Final Technical Report
X.-C. Zhang 1994 9 p
(Contract F49620-93-1-0161)
(AD-A292462; AFOSR-95-0159TR) Avail: CASI HC A02/MF A01

Under the support from AFOSR, we have studied ultrafast optoelectronics in two projects: (1) time-resolved optoelectronic measurements of nitrogen-implanted GaAs crystals and InGaAs; and (2) photoresponse of Si/Ge superlattice and its alloy materials. DTIC

N95-29113*# National Aeronautics and Space Administration. Lewis Research Center, Cleveland, OH.
DEMONSTRATION OF A STABILIZED ALUMINA/ETHANOL COLLOIDAL DISPERSION TECHNIQUE FOR SEEDING HIGH TEMPERATURE AIR FLOWS
Mark P. Wernet, Gary J. Skoch (Army Research Lab., Cleveland, OH.), and Judith H. Wernet (Case Western Reserve Univ., Cleveland, OH.) Jun. 1995 11 p Presented at the 16th International Congress on Instrumentation for Aerospace Simulation Facilities,Dayton, OH, 18-21 Jul. 1995; sponsored by IEEE
(RTOP 505-62-50)
(NASA-TM-106945; E-9680; NAS 1.15:106945; ARL-MR-233) Avail: CASI HC A03/MF A01

Laser anemometry enables the measurement of complex flow fields via the light scattered from small particles entrained in the flow. In the study of turbomachinery, refractory seed materials are required for seeding the flow due to the high temperatures encountered. In this work we present a pH stabilization technique commonly employed in ceramic processing to obtain stable dispersions for generating aerosols of refractory seed material. By adding submicron alumina particles to a preadjusted pH solution of ethanol, a stable dispersion is obtained which when atomized, produces a high quality aerosol. Commercial grade alumina powder is used with a moderate size distribution. Other metal oxide powders in various polar solvents could also be used once the point of zero charge (pH(pzc)) of the powder in the solvent has been determined. Laser anemometry measurements obtained using the new seeding technique are compared to measurements obtained using Polystyrene Latex (PSL) spheres as the seed material. Author

N95-29220 Office of Naval Research, Arlington, VA.
ADJUSTABLE TWO-AXIS INSTRUMENT MOUNT Patent Application

William H. Nedderman, inventor (to Navy) 5 Dec. 1994 14 p Filed 5 Dec. 1994 Limited Reproducibility: More than 20% of this document may be affected by microfiche quality
(AD-D017393; Navy-Case-76290; US-Patent-Appl-SN-349656) Avail: Issuing Activity (Defense Technical Information Center (DTIC))

A two-axis adjustable instrument mount having a fixed base plate, an intermediate plate, and an instrument mount plate is disclosed. The intermediate plate is attached to the base plate by a three-point mount in the shape of an isosceles triangle. The two mounting points corresponding to the base of the triangle include hinge flex plates fixed to the base plate by means of rigid stand-offs. The flex plates are also fixed to the edge of the intermediate plate. The third mounting point corresponding to the apex of the triangle has a resilient block between the intermediate plate and the base plate. A threaded fastener passes through the resilient block and secures the intermediate plate to the base plate. Tightening or loosening the threaded fastener causes the resilient block to compress or expand thus allowing adjustment of the angle of the intermediate plate about the axis of the hinge plates with respect to the base plate. The instrument mount plate is similarly attached to the intermediate plate with the axis of the isosceles triangle formed by the three-point mount of the instrument mount plate being rotated 90 degrees from that of the intermediate plate. DTIC

N95-29361# New Mexico State Univ., Las Cruces, NM.
THE (HMI9293) ACQUISITION OF A 200 MHz NUCLEAR MAGNETIC RESONANCE SPECTROMETER Final Report, 30 Sep. 1993 - 29 Sep. 1994
James H. Hageman 29 Sep. 1994 2 p
(Contract F49620-93-1-0582)
(AD-A291913; AFOSR-95-0095TR) Avail: CASI HC A01/MF A01

With the funds awarded from DOD-AFOSR and matching funds from New Mexico State a new Varian Gemini 200 MHz nmr was purchased and installed in the spring of 1994. This instrument is capable of 1H and 130 nmr, is very sensitive, and can also do Hetcor experiments to facilitate proton assignments. It is very easy to use and has proven thus far to be extremely reliable. The change in the research output in the department has been significant. Whereas previously students had to sometimes wait days to run routine nmr spectra because our high field instrument was otherwise occupied with longer experiments, now they can run spectra immediately (or with minimal wait). This speeds up structure assignments, and gives students instant gratification when experiments succeed and rapid feedback when they are not successful. DTIC

N95-29453*# National Aeronautics and Space Administration. Langley Research Center, Hampton, VA.
A HYBRID ELECTRONICALLY SCANNED PRESSURE MODULE FOR CRYOGENIC ENVIRONMENTS
J. J. Chapman, P. Hopson, Jr., and N. Kruse May 1995 12 p
(RTOP 505-59-54-02)
(NASA-TM-110146; NAS 1.15:110146) Avail: CASI HC A03/MF A01

Pressure is one of the most important parameters measured when testing models in wind tunnels. For models tested in the cryogenic environment of the National Transonic Facility at NASA Langley Research Center, the technique of utilizing commercially available multichannel pressure modules inside the models is difficult due to the small internal volume of the models and the requirement of keeping the pressure transducer modules within an acceptable temperature range well above the -173 degrees C tunnel temperature. A prototype multichannel pressure transducer module has been designed and fabricated with stable, repeatable sensors and materials optimized for reliable performance in the cryogenic environment. The module has 16 single crystal silicon piezoresistive pressure sensors electrostatically bonded to a metalized Pyrex substrate for sensing the wind tunnel model pressures. An integral temperature sensor mounted on each silicon micromachined pressure sensor senses real-time temperature fluctuations to within 0.1 degrees C to correct for thermally induced non-random sensor drift. The data presented here are from a prototype sensor module tested in the 0.3 M cryogenic tunnel and thermal equilibrium conditions in an environmental chamber which approximates the thermal environment (-173 degrees C to +60 degrees C) of the National Transonic Facility. Author

N95-29470# Naval Research Lab., Washington, DC.
GENAH USER'S GUIDE AND REFERENCE MANUAL VERSION 1.0 Memorandum Report, 1 Jul. - 26 Sep. 1994
Karl B. Washburn 17 Jan. 1995 127 p
(AD-A290236; NRL/MR/7130-95-7649) Avail: CASI HC A07/MF A02

This document is the User's Guide and Reference Manual for GENAH, the Generalized Nearfield Acoustical Holography processing program. The User's Guide provides instructions for operating the GENAH programs. This includes installing and running the code, choosing input parameters and a discussion of the input and output file structure. The Reference Manual contains material explaining the theory of cylindrical nearfield holography and how this theory is implemented in the GENAH code. Sufficient detail is provided to allow a user with an operating knowledge of FORTRAN-77 to diagnose and alter the code to suit local needs. Appendices are included detailing the file formats, the file header, a list of operator inputs to GENAH, a list of all routines needed to compile and run the GENAH code, and a discussion of wavenumber filtering in holography. DTIC

N95-29508 Michigan Univ., Ann Arbor, MI.
THE ROLE OF THE COHERENCE FUNCTION IN HOLOGRAPHIC IMAGING Ph.D. Thesis
Pang-Chen Sun 1994 123 p
Avail: Univ. Microfilms Order No. DA9423328

A holographic system illuminated with a temporally or spatially incoherent source can produce significant imaging characteristics. In this situation, the image from the hologram becomes localized with the consequence that different parts of the image can be seen only through different parts of the hologram. This distribution of the localized image on the hologram is determined by the coherence of the light source. The concept of coherence cell is introduced to model the holographic image formation with an incoherent source. Each coherence cell represents a localized area on the hologram for one object point where its image can be reconstructed and the integration of all coherence cells produces a motion picture of the optical field interacting with the object. The interaction can be a time or space function depending on the type of the incoherence of the sources. A light-in-flight image is produced by coherence cells if a temporally incoherent but spatially coherent source is used in holography. The source for producing such an image can be either a pulse laser or a CW broad spectrum laser, and in our case, a CW swept frequency dye laser. The first arriving light principle for image formation through highly diffusing media is demonstrated by light-in-flight holography. Conversely, if the source is spatially incoherent but temporally coherent, the holographic system can become a lensless image system in which the image is formed by the mutual intensity function. In this case, the coherence cells function like a bridge connecting the object plane with the hologram plane and by which the image can be transferred directly. A holographic counterpart of the confocal scanning microscope is found to be incoherent image plane holography. This holographic system has some interesting properties, such as depth discrimination and suppressing of noise from out of plane scatterers, that are also possessed by confocal scanning imaging; however, the holographic system requires no scanning. The property of depth discrimination enables us to build a non-scanning confocal ranging system based on incoherent image plane holography. The system can measure the 3D contour of an object by slicing one cross-section image at each depth and scanning through the entire depth of the object. Dissert. Abstr.

N95-29656# Air Force Systems Command, Wright-Patterson AFB, OH. National Air Intelligence Center.
MULTI-FOCAL LENGTH AND MULTI-CHANNEL HOLOGRAPHIC OPTICAL ELEMENT
Zhou Ge and Zhang Yimo 29 Dec. 1994 10 p Transl. into ENGLISH from Guangxue Xuebao, China, v. 11, no. 7, Jul. 1991 p 636-639
(AD-A291011; NAIC-ID(RS)T-0390-94) Avail: CASI HC A02/MF A01

A new holographic optical element (HOE) consisting of the hololenses with different focal lengths and diffractional channels is described. The object space axes of all hololenses in the HOE are the same, while each optical axis in the image space is different. By the aid of such HOE, the object planes at different distances can be imaged into the corresponding channels. Therefore, a 3-D object field may be displayed by many 2-D images. The primary experimental results for sampling 3-D particles field are presented. DTIC

N95-29664 Stanford Univ., CA.
A GYROSCOPE CLOCK FOR A NULL GRAVITATIONAL REDSHIFT EXPERIMENT Ph.D. Thesis
Todd Walter 1994 277 p
Avail: Univ. Microfilms Order No. DA9414674

This dissertation describes the analysis and experimental testing of the frequency stability of electrostatically-levitated, superconducting gyroscopes. The tests were conducted on the ground at cryogenic temperatures using a magnetic readout of the gyroscope rotor's spin phase. By achieving fractional frequency stabilities on the order of 3 x 10(exp -11) (or better) over one year it would be possible to perform a test of Local Position Invariance (LPI) to the 10 percent level. LPI states that in local freely falling frames, the outcome of any non-gravitational test is independent of where and when in the universe it is performed. This means that all clocks, independent of the physical principle on which they are based, should exhibit the same gravitational redshift. The experiment proposed in this thesis is intended to compare a gyroscope clock to an atomic clock as they both experience the same time-varying gravitational potential. Since there is expected to be no difference between the two types of clocks, this is a null gravitational redshift experiment. A unique opportunity to perform a gravitational redshift experiment exists in the Gravity Probe B (GPB) program. GPB is a satellite experiment whose purpose is to test two predictions of Einstein's General Theory of Relativity: the geodetic and frame-dragging effects. These effects will be measured by monitoring the precession rates of nearly perfect gyroscopes against the inertial stars. Navigation of the satellite is aided by means of the Global Positioning System (GPS). Thus GPB already has in place nearly all of the essential elements for the proposed clock experiment. These include nearly disturbance-free gyroscopes whose pointing and spin phase can be referenced to the inertial frame of the fixed stars and onboard access to Earth-bound atomic clocks through GPS. The varying gravitational potential is provided by the eccentricity of the Earth's orbit about the Sun. Therefore with very little change to GPB, the clock experiment can be performed using the same gyroscopes. I have performed extensive ground-based testing which indicates that it should be possible to achieve a spin frequency stability of 3 x 10(exp -12) or better in space.
Dissert. Abstr.

36 LASERS AND MASERS

Includes parametric amplifiers.
For related information see also *76 Solid-State Physics.*

N95-28678 Schwartz Electro-Optics, Inc., Concord, MA. Research Div.
ARPA SOLID STATE LASER AND NONLINEAR MATERIALS PROGRAM Final Report
Peter F. Moulton Jun. 1994 233 p Limited Reproducibility: More than 20% of this document may be affected by microfiche quality
(Contract N00014-90-C-0235)
(AD-A289657) Avail: Issuing Activity (Defense Technical Information Center (DTIC))

The Research Division of Schwartz Electro-Optics, as part of the ARPA Solid State Laser and Nonlinear Materials Program, conducted a three-year study 'Erbium-Laser-Based Infrared Sources.' The aim of the study was to improve the understanding of semiconductor-laser-pumped, infrared (IR) solid state lasers based on the trivalent rare-earth ion erbium (Er) doped into a variety of host crystals. The initial program plan emphasized operation of erbium-doped materials on the 2.8-3.0 micrometers laser transition. Pulsed, Q-switched sources using that transition, when employed as a pump source for parametric oscillators, can provide tunable mid-IR energy. The dynamics of erbium lasers are more complex than conventional neodymium (Nd)-doped lasers and we intended to use pump-probe techniques to measure the level and temporal behavior of gain in various materials. To do so we constructed a number of different cw Er-doped lasers as probe sources and employed the Cr:LiSAF(LiSrAlF6) laser as a pulsed pump source that would simulate pulsed diode arrays. We identified the 970-nm wavelength pump band of Er as the most efficient and were able to make use of recently developed cw and pulsed InGaAs strained-quantum-well diode lasers in the effort. At the conclusion of the program we demonstrated the first pulsed diode bar pumping of the most promising materials for pulsed operation, the oxide garnets YSGG and GGG and the fluoride BaY2F8. DTIC

N95-28679 Air Force Systems Command, Wright-Patterson AFB, OH. National Air Intelligence Center.
PROPAGATION AND TRANSFORMATION PROPERTIES OF AXICON OPTICAL SYSTEMS FOR LASER BEAMS
Bangwei Cai and Baida Lu 15 Dec. 1994 16 p Transl. into ENGLISH from Zhongguo Jiguang, China,vA21, no. 1, Jan. 1994 p 21-25 Limited Reproducibility: More than 20% of this document may be affected by microfiche quality
(AD-A289661; NAIC-ID(RS)T-0705-94) Avail: Issuing Activity (Defense Technical Information Center (DTIC))

Axicon optical systems can transform a gaussian beam into a diffraction-free Bessel beam. In addition mutual, transformation between solid beam and annular beam can also be realized. The paper details theoretical analyses and experimental studies on the axicon and its composite optical system; both results are in agreement. Axicon optical systems are shown to have wide applications in laser techniques. DTIC

N95-28808*# Johns Hopkins Univ., Baltimore, MD. Dept. of electrical and Computer Engineering.
RECEIVER DESIGN, PERFORMANCE ANALYSIS, AND EVALUATION FOR SPACE-BORNE LASER ALTIMETERS AND SPACE-TO-SPACE LASER RANGING SYSTEMS Interim Progress Report, 16 Oct. 1994 - 15 Apr. 1995
Frederic M. Davidson, Xiaoli Sun, and Christopher T. Field May 1995 45 p
(Grant NAG5-2232)
(NASA-CR-198655; NAS 1.26:198655) Avail: CASI HC A03/MF A01

Laser altimeters measure the time of flight of the laser pulses to determine the range of the target. The simplest altimeter receiver consists of a photodetector followed by a leading edge detector. A time interval unit (TIU) measures the time from the transmitted laser pulse to the leading edge of the received pulse as it crosses a preset threshold. However, the ranging error of this simple detection scheme depends on the received, pulse amplitude, pulse shape, and the threshold. In practice, the pulse shape and the amplitude are determined by the target target characteristics which has to be assumed unknown prior to the measurement. The ranging error can be improved if one also measures the pulse width and use the average of the leading and trailing edges (half pulse width) as the pulse arrival time. The ranging error becomes independent of the received pulse amplitude and the pulse width as long as the pulse shape is symmetric. The pulse width also gives the slope of the target. The ultimate detection scheme is to digitize the received waveform and calculate the centroid as the pulse arrival time. The centroid detection always gives unbiased measurement even for asymmetric pulses. In this report, we analyze the laser altimeter ranging errors for these three detection schemes using the Mars Orbital Laser Altimeter (MOLA) as an example. Author

N95-28892# Martin Marietta Labs., Baltimore, MD.
LASER SIMULATION OF SINGLE-EVENT EFFECTS: A STATE OF THE ART REVIEW Final Report, Aug. 1990 - Aug. 1993
Stephen Buchner Mar. 1995 56 p
(AD-A292308) Avail: CASI HC A04/MF A01

A pulsed laser system for simulating heavy-ion, single-event effects in semiconductor devices is described. The fundamentals of ion and laser interactions in silicon are compared. The results of several case studies demonstrate the utility of the laser technique for both hardness assurance and diagnostic purposes. DTIC

N95-29007# Deacon Research, Palo Alto, CA.
DOUBLED DIODE LASER. PHASE 1 Final Report, 15 May - 14 Nov. 1994
David A. Deacon 30 Dec. 1994 19 p
(Contract F49620-94-C-0039)
(AD-A292465; AFOSR-95-0155TR) Avail: CASI HC A03/MF A01

In this Phase 1 program, we have demonstrated that electric field poling is an advantageous technique for manufacturing frequency doublers. We demonstrated bulk periodic poling with 15 micron period lithium niobate samples, and showed that we can overcome the problems with electrical breakdown. From our other testing results, we can predict that our periodic

poled samples will perform near the theoretical optimum. While the poling process shows peculiarities such as a strong crystal axis dependence and a complicated voltage-time scaling, we conclude that the process is ready for development into a reliable manufacturing process. DTIC

N95-29025# Emory Univ., Atlanta, GA. School of Dentistry.
STUDIES OF ENERGY TRANSFER PROCESSES OF RELEVANCE TO CHEMICALLY AND OPTICALLY PUMPED LASERS Final Report, 1 Nov. 1991 - 31 Oct. 1994
Michael C. Heaven 27 Dec. 1994 36 p
(Contract F49620-92-J-0073)
(AD-A290164; AFOSR-95-0012TR) Avail: CASI HC A03/MF A01

The relaxation dynamics of vibrationally excited levels of I2(X) are of relevance to the chemical oxygen iodine laser (COIL). Rotational and vibrational energy transfer rate constants have been measured for selected levels with v'' greater than 20. The collision partners He, Ar, I2, Cl2, O2, and H2O were investigated. A numerical model that relates state-to-state energy transfer rate constants to I2+ deactivation processes in COIL has been developed. The results for H2O show that the true deactivation rate constant is about an order of magnitude smaller than the estimate used in current computer simulations of COIL systems. Energy transfer from O2(a1 delta) and I(2P(sub 1/2)) to I2(X) has been investigated. The nascent vibrational distribution resulting from I(2P(sub 1/2)) + I2(X) collisions was characterized, and improved spectroscopic constants for the D state of I2 are reported. Jet-cooling and emission spectroscopy techniques have been used to characterize the D'(2)-A'(2) and beta(1)-A(1) ion-pair to valence state transitions of iodine monobromide. DTIC

N95-29053# Arizona Univ., Tucson, AZ.
EXACT PHYSICAL MODELS AND METHODS FOR STABILIZATION AND CONTROL OF REFLECTION-INDUCED INSTABILITIES IN SEMICONDUCTOR LASERS Final Report
Moloney 9 May 1994 3 p
(Contract F49620-93-1-0306)
(AD-A292437; AFOSR-95-0116TR) Avail: CASI HC A01/MF A01

Microscopic many-body effects were incorporated into a full scale simulation code of a semiconductor laser (SCL). The latter includes counterpropagating optical waves in the Fabry-Perot structure, longitudinal carrier diffusion, and, importantly, gain and refractive index dispersion derived from a look-up table. Boundary conditions are applied at each end of the cavity and an additional feedback mirror is simple to incorporate allowing the study of the transition from weak to strong optical feedback. This approach enables investigation of mutli-longitudinal mode oscillations and discrimination of these from mode-hopping phenomena. The response function derived from the many-body theory can be 'engineered' to optimize the dynamic response of the SCL. In other words, the role of bulk versus quantum well and strained layer materials on lasing action can be systematically investigated. When mounted internally (relaxed oscillations, feedback instabilities) or externally (injection current), the dispersion can vary significantly as the carrier density varies. Derived from text

N95-29208# Army Research Lab., Watertown, MA. Materials Directorate.
PULSED LASER DEPOSITION OF FERROELECTRIC THIN FILMS IN CONJUNCTION WITH SUPERCONDUCTING OXIDES
S. Sengupta, L. C. Sengupta, J. D. Demaree, and W. Kosik Dec. 1994 18 p
(AD-A290101; ARL-TR-654) Avail: CASI HC A03/MF A01

The possibility of combining ferroelectrics and superconductors has been of interest for use in memory storage devices. Additionally, superconductors offer crystal structures compatible to the epitaxial growth of the ferroelectric, Ba(0.6)Sr(0.4)TiO3 (BSTO), which is cubic at this stoichiometry. BSTO has a lattice constant of 3.94 A as compared to the superconducting Pr(2 - x)Ce(x)CuO4 tetragonal single crystal which also has a lattice constant of a = 3.94 A. (minor variations with Cerium content). In this study, ferroelectric thin films of BSTO were deposited on single crystals of Pr2CuO4 and Pr(2 - x)Ce(x)CuO4. The optical constants of the substrates, single crystals of Pr2CuO4 and Pr(2 - x)Ce(x)CuO4, were determined using Variable Angle Spectroscopic Ellipsometry (VASE) and the composition and crystal structure were examined using Rutherford Backscattering Spectrometry (RBS) with ion beam channeling. The substrate/film interfaces and the compositional variation in the films were also studied with RBS and with SEM/EDS. Glancing angle x-ray diffraction was used to verify the epitaxial nature of the films. The effect of the deposition parameters (laser repetition rate, oxygen backfill pressure, and deposition geometry) on the quality of the films was experimented with previously and only the optimized parameters were used. DTIC

N95-29217 Office of Naval Research, Arlington, VA.
LASER OPTICS PROTECTIVE DEVICE Patent Application
Alan L. Huston, inventor (to Navy), Brian L. Justus, inventor (to Navy), Charles D. Merrit, inventor (to Navy), and Anthony J. Campillo, inventor (to Navy) 30 Nov. 1994 23 p Filed 30 Nov. 1994 Limited Reproducibility: More than 20% of this document may be affected by microfiche quality
(AD-D017384; Navy-Case-75785; US-Patent-Appl-SN-351070) Avail: Issuing Activity (Defense Technical Information Center (DTIC))

A broadband thermal optical limiter disposed between a laser oscillator and a laser amplifier system for protecting optical components in the laser oscillator from damage due to amplified optical feedback from the laser amplifier system at all near ultraviolet, visible, and near infrared wavelengths is disclosed. The thermal optical limiter comprises: a first lens for focusing the amplified optical feedback to a focal point on an optical axis; a flowing dye cell disposed near the focal point and being responsive to the focused amplified optical feedback for thermally defocusing and aberrating the focused amplified optical feedback into a plurality of rings about the optical axis; a second lens for passing only a small portion of the defocused amplified optical feedback; and a blocking aperture disposed around the second lens for blocking substantially all of the thermally defocused amplified optical feedback from the flowing dye cell and passing therethrough into the second lens only a small portion of the thermally defocused amplified optical feedback from the flowing dye cell. DTIC

N95-29247*# Alabama Univ., Huntsville, AL.
ANALYSIS OF MEASUREMENTS FOR SOLID STATE LASER REMOTE LIDAR SYSTEM Final Report, 1 Jun. 1993 - 31 Sep. 1994
Farzin Amzajerdian 7 Apr. 1995 58 p
(Contract NAS8-38609)
(NASA-CR-196640; NAS 1.26:196640) Avail: CASI HC A04/MF A01

The merits of using lidar systems for remote measurements of various atmospheric processes such as wind, turbulence, moisture, and aerosol concentration are widely recognized. Although the lidar technology has progressed considerably over the past two decades, significant research particularly in the area of solid state lidars remains to be conducted in order to fully exploit this technology. The work performed by the UAH (University of Alabama in Huntsville) personnel under this Delivery Order concentrated on analyses of measurements required in support of solid state laser remote sensing lidar systems which are to be designed, deployed, and used to measure atmospheric processes and constituents. UAH personnel has studied and recommended to NASA/MSFC the requirements of the optical systems needed to characterize the detection devices suitable for solid state wavelengths and to evaluate various heterodyne detection schemes. The 2-micron solid state laser technology was investigated and several preliminary laser designs were developed and their performance for remote sensing of atmospheric winds and clouds from a spaceborne platform were specified. In addition to the laser source and the detector, the other critical technologies necessary for global wind measurements by a spaceborne solid state coherent lidar systems were identified to be developed and demonstrated. As part of this work, an analysis was performed to determine the atmospheric wind velocity estimation accuracy using the line-of-sight measurements of a scanning coherent lidar. Under this delivery order, a computer database of materials related to the theory, development, testing, and operation of lidar systems was developed to serve as a source of information for lidar research and development.

Derived from text

N95-29274# Armstrong Lab., Brooks AFB, TX. Occupational and Environmental Health Directorate.
A COMPACT UNIVERSAL POWER SUPPLY FOR LASER DIODES Interim Report, Feb. 1993 - Jul. 1994
Gary D. Noojin, Daniel X. Hammer, Floyd Messick, William Robinson, and Jessica L. Josephson Sep. 1994 21 p
(AF Proj. 7757)
(AD-A289950; AL/OE-TR-1994-0079) Avail: CASI HC A03/MF A01

A compact universal power supply for laser diodes was designed and

built. The power source will supply current for laser diodes with forward operating current up to approximately 350 milliamps (mA). The power supply has a feedback stage, a slow start circuit, ac transient suppression, and digital optical power meter. The power supply is based upon a Toshiba design, with modifications in the feedback loop to provide utility for a wide range of laser diodes. The power supply was built into a compact unit and tested on: a Toshiba TOLD9200 visible laser diode with optical power of 3 milliwatts (mW) at an operating current of approximately 75 mA; an OKi OL308A-75 high power infrared laser diode with optical power of 80mW at an operating current of approximately 220 mA; and a Sharp near infrared laser diode with optical power of 3 mW at an operating current of approximately 57 mA. DTIC

N95-29292# Montana State Univ., Bozeman, MT. Dept. of Physics.
TUNABLE LASER FOR PERSISTENT SPECTRAL HOLE BURNING OPTICAL MEMORIES Final Report, 1 Oct. 1993 - 30 Sep. 1994
Rufus L. Cone 23 Dec. 1994 10 p
(Contract F49620-93-1-0530)
(AD-A292598; AFOSR-95-0144TR) Avail: CASI HC A02/MF A01

A tunable laser for infrared and visible operation was purchased to expand our work on optical memories based on persistent spectral hole burning. The Coherent 899-21 laser uses Ti:sapphire and dye media to cover the spectral regions required for semiconductor laser operation and for photon-gated memories. A large argon-ion pump laser for use with the tunable laser was purchased with local funds. Searching for new hole burning materials, evaluation of their properties, and studies of the limits on material performance were the goals of our research. Attention was focussed on rare earth or transition metal ion materials. DTIC

N95-29330# Defence Research Establishment Ottawa, Ottawa (Ontario).
CHARACTERIZATION AND CALIBRATION OF A PULSED LASER SYSTEM FOR SINGLE EVENT UPSET SIMULATION DREO Report
G. T. Pepper and A. Fechete Nov. 1994 44 p
(AD-A290075; DREO-1241) Avail: CASI HC A03/MF A01

A pulsed Nd:Glass laser facility that was developed at Defence Research Establishment Ottawa, for the simulation of single event upsets (SEUs) in electronics, is described in detail. The performance of the laser system, the associated instrumentation and data acquisition systems were extensively characterized during the process of studying the charge collected in a silicon p-i-n photodiode, due to laser and ion-induced SEU. Laser simulation of SEUs is demonstrated to be an accurate and convenient complementary method to ion accelerator-based SEU experimentation. DTIC

N95-29336 Maryland Univ., College Park, MD.
INHIBITION OF MODE COMPETITION IN FREE-ELECTRON LASER OSCILLATORS Ph.D. Thesis
Edward Rosemond Stanford 1993 134 p
Avail: Univ. Microfilms Order No. DA9425137

Free electron lasers generate short-wavelength high-power electromagnetic radiation by inducing coherent oscillations in an electron beam traversing a spatially sinusoidal magnetic field. The velocity of the electron beam and the wavelength of the magnetic field can be combined to give a resonant frequency. Radiation fields near that frequency which are present in the interaction region between the electron beam and the magnetic field can grow exponentially. Typically, many allowable radiation cavity frequencies fall within the FEL gain bandwidth near the resonance frequency. Mode competition refers to the tendency of many cavity modes to grow in an FEL. Since narrow spectral width is a highly desirable quality, it is preferable to prevent more than one such mode from extracting appreciable amounts of beam energy. When the beam current is low, one mode can often dominate the others, so the output is essentially monochromatic. As the current is increased, the amount of energy available to other modes increases, eventually causing radiation at other frequencies to grow exponentially and broaden the radiation spectral width. Numerical simulations are used to examine three methods of inhibiting mode competition. In the first, the possibility that competition will arise among the TE(ll') modes that describe the cross section of the radiation profile is examined in large aspect ratio cavities. A current threshold is found below which such competition is suppressed. In the second, low-loss dispersive elements are used to alter the frequency spacing between the longitudinal cavity modes that describe the axial profile so that undesired modes are prevented from coupling to one another and thus damp more quickly. This proves to be a highly flexible technique to narrow the observed spectral width of the output radiation and to hasten the formation of stable equilibria. In the third, the current, and thus the free energy, is increased until many modes grow large. The nonlinear dynamics of the time dependence of the resulting extremely complicated radiation fields is examined using the methods of chaos theory. A proposal to study the use of small beam perturbations to stabilize single-frequency equilibria in this operating regime is advanced. Dissert. Abstr.

N95-29425# Phillips Lab., Kirtland AFB, NM.
INVESTIGATION OF THE PASCHEN CURVE OF NITROGEN VIA THE APPLICATION OF NANOSECOND PULSED ELECTROMAGNETIC RADIATION Final Report, 1 Aug. 1990 - 1 Aug. 1993
David W. Scholfield Dec. 1994 123 p
(AF Proj. 3152)
(AD-A290129; PL-TR-94-1125) Avail: CASI HC A06/MF A02

In order to obtain lasing in microwave excited gases, a knowledge of the Paschen curve is required so that estimates can be made of the required intensity of the electromagnetic field for a given pulse duration. Data in the region below 10(exp -8) Torr-s with electromagnetic fields in excess of 10 kV/cm/Torr had been unobtainable due to technical limitations. The Paschen curve of nitrogen from pressures of 0.336 Torr via the application of nanosecond pulsed electromagnetic radiation has been investigated. Breakdown of the gas was achieved through pumping by short electromagnetic pulses and verified through the use of an optical multichannel analyzer. Previous investigations have utilized monofrequency electromagnetic signals. Adjustments for the short pulse nature of this investigation have been derived and are applied to the Paschen curve. Experiments have been conducted utilizing a pulser with machine parameters of 1 J delivered during 1.375 ns FWHM into a 50 omega coaxial line, at a peak power of 1 GW. DTIC

N95-29514# Georgia Tech Research Inst., Atlanta, GA.
DEVELOPMENT OF CONTINUOUS VISIBLE CHEMICAL LASER AMPLIFIERS AND OSCILLATORS FROM THE Na3-X(Cl, Br, I) REACTIONS AND THEIR ANALOGS AND ENERGY TRANSFER PUMPING FROM EFFICIENTLY PRODUCED METASTABLE STATES Final Report, 1 Jun. 1990 - 31 Oct. 1994
James L. Gole Dec. 1994 433 p Limited Reproducibility: Document partially illegible
(Grant AF-AFOSR-0285-90)
(AD-A290999; AFOSR-95-0064TR) Avail: CASI HC A19/MF A04

Visible chemical laser amplifiers have been generated employing the highly efficient and selective formation of sodium dimer electronically excited states from the sodium trimer-halogen atom (X = Cl, Br, I) reactions. Optical gain through stimulated emission has been demonstrated in select regions close to 527, 492, and 460 nm. With a focus to increasing amplifier gain length and amplifying medium concentration, a newly configured device creates intersecting alkali and halogen sheaths which form the basis for the creation of visible chemical laser oscillators. This device has now revealed the first Raman pumping due purely to chemical reaction in the absence of an external light source. Extrapolations on the Na3-X amplifier concept involving Group IIA metal - F,Cl reactions are considered. Very near resonant energy transfers from selectively formed metastable states of SiO and GeO to receptor alkali atoms form sodium or potassium atom laser amplifiers and a gain condition at lambda = 569, 616, 819, and 581 nm. These results form the basis for full cavity oscillation in the Na system at 569 nm. Silane based thermolysis - discharge and thermolysis - photolysis sources of SiO metastables are under development. The efficient energy transfer pumping of potential amplifying transitions in the lead (Pb), copper (Cu), and tin (Sn) systems is outlined. DTIC

N95-29631 Maryland Univ., College Park, MD.
DEVELOPMENT OF DISTRIBUTED FEEDBACK DYE LASERS FOR GENERATION OF HIGH-POWER 193 nm EXCIMER LASER SHORT PULSES Ph.D. Thesis
Yifeng Cui 1993 113 p
Avail: Univ. Microfilms Order No. DA9425015

The combination of picosecond dye lasers, nonlinear mixing in crystals, and excimer amplifiers offers an attractive way to generate intense diffraction-limited pulses throughout the ultraviolet region. However, it is difficult to generate 193 nm seed pulses because this wavelength cannot

be obtained by second harmonic generation method in any known crystals. The thesis will describe a laser system which efficiently generates short, relatively stable high power 193 nm pulses. A new type of distributed feedback dye laser which has a grating on a thin substrate was also developed. It is reliable and easy to use. Two such DFDL's are used in the laser system to generate 10 ps pulses at two selected wavelengths of 266 nm and 706 nm that are frequency up-converted in a BBO crystal to generate nearly transform-limited 193 nm seed pulse about 10 ps in duration. The entire cascading dye laser system is pumped by a 350 mJ, 15 ns pulse at 308 nm generated by a XeCl excimer laser. The 193 nm seed pulse from BBO crystal is amplified in an ArF* excimer laser amplifier to 10 mJ in a nearly diffraction-limited beam. The system routinely produces 193 nm pulses of about 10 picosecond duration which can be focused to intensities of 10(exp 14) W/cm(exp 2). One application of this system is investigation of the interaction of intense radiation fields with diatomic molecules. A DFDL model which included non-sinusoidal profile of the modulated gain was developed. The model is used to study theoretically the fluctuation in pulse duration due to the pump variation and intrinsic fluctuation in spontaneous emission which leads the laser pulse. A two-grating DFDL was also developed, tested experimentally, and analyzed theoretically. It allows wavelength tuning and generation of shorter pulses. This type of system should be able to reach the subpicosecond regime with comparable pulse energies and beam divergences by using two-grating DFDL and thin BBO crystal. Dissert. Abstr.

N95-29653 Optical Society of America, Washington, DC.
LASER APPLICATIONS TO CHEMICAL ANALYSIS: SUMMARIES OF PAPERS PRESENTED AT THE LASER APPLICATIONS TO CHEMICAL ANALYSIS TOPICAL MEETING Final Report, 7 Mar. 1994 - 6 Mar. 1995
David W. Hennage Dec. 1994 285 p Meeting held in Jackson Hole, WY, 8-11 Mar. 1994 Limited Reproducibility: More than 20% of this document may be affected by poor print
(Contract DAAH04-94-G-0046)
(AD-A290738; ARO-32826.1-PH-CF) Avail: Issuing Activity (Defense Technical Information Center (DTIC))

Summaries of papers presented at the Laser Applications to Chemical Analysis Topical Meeting, March 8-11, 1994, Jackson Hole, Wyoming. DTIC

N95-29660# Air Force Systems Command, Wright-Patterson AFB, OH. National Air Intelligence Center.
THE LASER RANGING OF ETALON SATELLITES
De-Tong Tan and Fu-Min Yang 4 Jan. 1995 14 p Transl. into ENGLISH from Tianwen Xuebao, China, v. 33, no. 3, Sep. 1992 p 246-250
(AD-A291019; NAIC-ID(RS)T-0556-94) Avail: CASI HC A03/MF A01

This paper presents a summary of the laser ranging of 2 geodynamics satellites Etalon launched by the USSR, observed by the Shanghai Astronomical Observatory. From April to December of 1990, data of laser ranging of totally 73 passes were obtained, among which a maximum of 4,256 ranging data have been recorded in each pass, and the ranging distances sometimes exceeded 20,000 km. DTIC

N95-29689 Princeton Univ., NJ.
COHERENT SOFT X-RAY GENERATION USING A POWERFUL SUBPICOSECOND LASER Ph.D. Thesis
Karl Michael Krushelnick 1994 264 p
Avail: Univ. Microfilms Order No. DA9415421

A powerful subpicosecond laser system is used to examine the interaction of high intensity ultraviolet laser radiation with plasmas. A final large aperture KrF* amplifier has been added to increase the output energy of the laser system to more than 300 mJ. The output parameters of the laser are measured and the pulse is found to be focusable to intensities of 2 x 10(exp 18) W/sq cm. Soft X-ray emission due to the interaction of intense laser light with solid targets of various materials is examined and plasmas having near solid densities (ne greater than 10(exp 23) cm(exp -3) are produced. The plateau structure of high harmonic emission from the interaction of very intense laser light with gases is verified and the emission of the 7th and 9th harmonics from aluminum plasmas is measured. X-ray laser experiments involving the creation of fast recombining plasmas using optical field ionization of preformed lithium fluoride plasmas are performed. A nonlinear increase in the intensity of the emitted 2-1 line of hydrogenic lithium (135 A) is observed for short target lengths in situations where the temperature of the performed plasma is low. Dissert. Abstr.

N95-29912# Spire Corp., Bedford, MA.
ION DOPED QUANTUM WELL LASERS Annual Report, 30 Sep. 1993 - 30 Sep. 1994
Anton C. Greenwald 6 Feb. 1995 31 p
(Contract F49620-93-C-0069)
(AD-A290937; AR-10154.01) Avail: CASI HC A03/MF A01

The objective of this research project is to fabricate erbium-doped light emitting diode lasers. Such lasers are expected to be temperature independent, frequency stable sources of 1538 nm light especially well suited for optical communications. During the first year of the project new volatile erbium-silylamide sources were synthesized for metalorganic chemical vapor deposition of doped III-V compound films, required for laser fabrication. Doping levels to 30 atomic percent were tested but the maximum substitutional dopant level was 0.02 percent. Carbon and nitrogen contaminant levels were minimized, while the amount of silicon left in the film was a function of deposition temperature. Narrow photo- and cathode-luminescence spectra were obtained from these films. Diffusion rates for erbium in gallium arsenide was higher than expected. Device studies are planned for the second year of the project. DTIC

N95-29914# Defence Science and Technology Organisation, Canberra (Australia).
CHARACTERISATION OF A LINE-TUNABLE He-Xe LASER OPERATING AT 2.026 AND 3.894 MICROMETERS
Kenneth J. Grant and Robert J. Rossiter Aug. 1994 20 p Limited Reproducibility: Document partially illegible
(AD-A291129; DSTO-GD-0022; DODA-AR-008-943) Avail: CASI HC A03/MF A01

A neutral rare gas laser has been built, and used to produce continuous wave output in the near- and mid-infra-red regions. The He-Xe mixture was excited by a hollow cathode discharge, and line-tunability was achieved by use of a diffraction grating as the rear optic. Two of these lines, viz. 2.026 and 3.894 micrometers, are of particular interest due to their location in the 2 and 4 micrometers atmospheric windows, respectively. A parametric study was conducted to determine the optimum working regimes (total pressure, partial pressure ratio, current, output coupler transmission, and grating). This General Document is a paper presented at the Australian Conference on Optics, Lasers and Spectroscopy (ACOLS), held at the University of Melbourne in December, 1993. DTIC

N95-29930# Dartmouth Coll., Hanover, NH. Dept. of Physics and Astronomy.
SEMICONDUCTOR FILM CHERENKOV LASERS Final Progress Report, 1 Jun. 1991 - 31 May 1994
John E. Walsh 28 Dec. 1994 62 p
(Contract DAAL03-91-G-0189)
(AD-A291177) Avail: CASI HC A04/MF A01

The technical achievements for the project 'Semiconductor Film Cherenkov Lasers' are summarized. Described in the fourteen appendices are the operation of a sapphire Cherenkov laser and various grating-coupled oscillators. These coherent radiation sources were operated over the spectral range extending from 3 mm down to 400 micrometers. The utility of various types of open, multi-grating resonators and mode-locked operation were also demonstrated. In addition to these experiments, which were carried out with a 10-100 kV pulse generator, a low-energy (3-3.6 MeV) Van de Graaff generator and a low-energy RF linac (2.8 MeV) were used to investigate the properties of continuum incoherent Smith-Purcell radiation. It was shown that levels of intensity comparable to the infrared beam lines on a synchrotron could be obtained and thus that grating-coupled sources are potentially an important new source for Fourier transform spectroscopy. Finally, a scanning electron microscope was adapted for investigating mu-electron-beam-driven far-infrared sources. At the close of the project, spontaneous emission over the 288-800 micrometers band had been observed. Intensity levels were in accord with expectations based on theory. One or more of the Appendices address these topics in detail. DTIC

N95-29931# Aerospace Corp., El Segundo, CA. Technology Operations.
HIGH-EFFICIENCY LONGITUDINAL DIODE BAR PUMPING OF SOLID-STATE LASERS

Todd S. Rose, James S. Swenson, and Renny A. Fields 15 Mar. 1994 9 p
(Contract F04701-88-C-0089)
(AD-A291180; TR-92(2925)-1; SMC-TR-95-5) Avail: CASI HC A02/MF A01

A longitudinal diode bar pumping scheme for a solid state laser has been conceived which can concentrate tens of watts of pump power into a 250 micrometers spot with nearly 100% efficiency. DTIC

N95-29937# Naval Research Lab., Washington, DC.
OBSERVATION OF X RAY GENERATION IN A PROOF-OF-PRINCIPLE LASER SYNCHROTRON SOURCE EXPERIMENT Interim Report
A. Ting, R. Fischer, A. Fisher, J. Krall, and E. Esarey 15 Feb. 1995 13 p
(AD-A291298; NRL/MR/6790-95-7647) Avail: CASI HC A03/MF A01

A Laser Synchrotron Source (LSS) was proposed to generate short-pulsed, tunable x-rays by Thomson scattering of laser photons from a relativistic electron beam. A proof-of-principle (p.o.p) experiment on this LSS configuration is performed. An intense laser pulse (Lambda(sub 0) = 1.053 micrometers) is Thomson backscattered from a focussed relativistic electron beam. Time integrated x-ray signals from a photocathode/electron multiplier, at an electron beam energy of 650 keV and an x-ray photon energy of 20 eV, indicate an increase in the x-ray signals above the baseline by an amount comparable to the theoretically predicted value. This is the first observation of x-rays in the ten's of eV range generated by the Thomson scattering of near infrared photons from a relativistic electron beam. DTIC

N95-29980# Heriot-Watt Univ., Edinburgh (Scotland).
DYNAMICAL INSTABILITIES, CHAOS AND SPATIAL COMPLEXITY IN FUNDAMENTAL NONLINEAR OPTICAL INTERACTIONS Final Report, 1 Jun. 1993 - 31 May 1994
Robert G. Harrison 31 May 1994 13 p
(Grant AF-AFOSR-0286-91)
(AD-A291223; PL-TR-95-07) Avail: CASI HC A03/MF A01

Experimental and theoretical investigations address nonlinear dynamics and complexity in basic nonlinear optical interactions. Notably contributions include: (1) first demonstration of chaotic dynamics of stimulated Brillouin scattering (SBS) confirmed through the latest dynamical measurement tools; (2) stochastic effects shown to dominate dynamics for cavityless operation but to be suppressed for SBS with feedback; (3) first generalised treatment of stimulated scattering in which deterministic dynamics and chaos are shown to be inherent features of behaviour consistent with experimental findings; (4) first evidence of patterns, singularities and turbularie in SBS through multi transverse mode interactions; (5) generalized analysis of transverse patterns and instabilities of diffraction-diffusion type systems in nonlinear optics - ongoing; (6) low frequency (MHz) dynamics and chaos in diode lasers with feedback and in NdYAG modulated lasers - ongoing; (7) control of chaos in diode lasers and development of new all optical control algorithms - ongoing; (8) lasing without inversion in V systems; and (9) new approach to the theory of radiation matter interactions for arbitrary field strength. DTIC

N95-30006# Sandia National Labs., Albuquerque, NM.
AUGER RATES IN MID-IR InAsSb LASER STRUCTURES
H. P. Hjalmarson and S. R. Kurtz 1995 10 p Presented at the International Conference on Narrow Gap Semiconductors, Santa Fe, NM, 9-12 Jan. 1995
(Contract DE-AC04-94AL-85000)
(DE95-006325; SAND-94-2784C; CONF-950167-4) Avail: CASI HC A02/MF A01

Auger rates are calculated for three InAsSb mid-infrared laser structures as a function of temperature. Compressive strain in the quantum wells reduces the mass of the holes; it is shown that this leads to a reduction in the Auger rate compared with an unstrained quantum well. The Auger rates for these structures are similar primarily due to their similar bandgap energies. DOE

N95-30045# Arizona Univ., Tucson, AZ. Optical Sciences Center.
A KILOHERTZ FEMTOSECOND Ti: SAPPHIRE REGENERATIE AMPLIFIER Final Report
N. Peyghamberian and B. McGinnis 3 Jan. 1995 3 p
(AD-A290591) Avail: CASI HC A01/MF A01

To have capabilities in the near-infrared, we proposed to develop a Ti:S regenerative amplifier operating at one kilohertz. This amplifier was developed to amplify the pulses from our femtosecond Ti:S laser oscillator to the 2-3 mu J/pulse energy level. This type of energy in a femtosecond pulse allowed us to generate a broadband (similar or equal 1000 A) in the near-infrared for spectroscopic studies of 3-5-based semiconductors. DTIC

N95-30050# Optical Concepts, Inc., Lompoc, CA.
VERTICAL CAVITY SURFACE EMITTING LASERS FOR OPTICAL SIGNAL PROCESSING AND OPTICAL COMPUTING APPLICATIONS Final Technical Report, 1 Jan. 1993 - 30 Nov. 1994
Frank H. Peters, Jeff W. Scott, M. K. Kilcoyne, and Gerald D. Robinson 23 Dec. 1994 136 p
(Contract DAAH04-93-C-0001)
(AD-A290626; ARO-30695-EL-SB2) Avail: CASI HC A07/MF A02

This final technical report outlines the development of Vertical-Cavity Surface-Emitting Lasers (VCSEL's) for use in high-speed parallel data links. During this contract, Optical Concepts has produced VCSEL's with greatly improved performance, and has developed packaging technologies for VCSEL's. VCSEL's have been developed that operate at greater than 5 GHz with sub-milliamp threshold currents. With low turn on delays, these devices have demonstrated GHz data rates with no pre-bias. VCSEL arrays have been incorporated into high-speed, parallel1 fiber coupled packages. Optical Concepts has demonstrated packages using both top and bottom emitting VCSEL's, and has developed an integrated microlens technology to ease packaging tolerances. DTIC

37 MECHANICAL ENGINEERING

Includes auxiliary systems (nonpower); machine elements and processes; and mechanical equipment.

N95-28702* National Aeronautics and Space Administration. Goddard Space Flight Center, Greenbelt, MD.
CARRIER-LESS, ANTI-BACKLASH PLANETARY DRIVE SYSTEM Patent
John M. Vranish, inventor (to NASA) 25 Apr. 1995 10 p Filed 2 Nov. 1993
(NASA-Case-GSC-13608-1; US-Patent-5,409,431;
US-Patent-Appl-SN-147276; US-Patent-Class-475-342;
US-Patent-Class-F16H-1/28) Avail: US Patent and Trademark Office

This invention relates to a carrier-less, anti-backlash planetary gear system that has an input sun gear, a force-balancing and planet-alignment 'speeder' gear above the sun gear, a split ring gear that has a fixed lower ring gear coaxial with the sun gear and a rotating upper ring gear also coaxial with the sun gear. A preload bolt is used for securing the split ring gears together. Within the split ring gear is an even number of planet gears between the split ring gear and the sun gear. Each planet gear consists of an upper planet gear, and lower planet gear with the upper and lower planet gears splined together and pushed apart by a spring which causes separation and relative twist between the upper and lower planet gears. The lower planet gear meshes with the input sun gear and the fixed ring gear while the upper planet gear is driven by the lower planet gear and meshes with the rotating ring gear.
Official Gazette of the U.S. Patent and Trademark Office

N95-28785 Office of Naval Research, Arlington, VA.
EXTERNAL COMBUSTION ENGINE HAVING AN ASYMMETRICAL CAM Patent Application
Anthony W. Duva, inventor (to Navy) 30 Nov. 1994 14 p Filed 30 Nov. 1994 Limited Reproducibility: More than 20% of this document may be affected by microfiche quality
(AD-D017382; Navy-Case-76289; US-Patent-Appl-SN-348688) Avail: Issuing Activity (Defense Technical Information Center (DTIC))

An external combustion engine having an asymmetrical cam is the focus of this patent. The engine includes a combustion chamber for generating a high-pressure, energized gas from a monopropellant fuel and an even number of cylinders for receiving sequentially the energized gas through the rotary valve, the gas performing work on a piston disposed

within each cylinder. The pistons transfer energy to a drive shaft through a connection to the asymmetrically shaped cam. The cam is shaped having two identical halves, each half having a power and an exhaust stroke. The identical halves provide that opposing cylinders are in thermodynamic balance, thus reducing rocking vibrations and torque pulsations. Having opposing pistons within the same thermodynamic cycle allows piston stroke to be reduced while maintaining displacement comparable to an engine having individual cycle positions. The reduced stroke diminishes gas flow velocity thus reducing flow induced noise. The power and exhaust strokes within each identical half of the cam are asymmetrical in that the power stroke is of greater duration than the exhaust stroke. The shape and length of the power stroke is optimized for increased efficiency. DTIC

N95-28791# Office of Naval Research, Arlington, VA.
AN ELECTRICAL AND FIBER-OPTIC CONNECTOR Patent Application
Gregory Ames, inventor (to Navy) and Roger L. Morency, inventor (to Navy) 25 Nov. 1994 27 p Filed 25 Nov. 1994
(AD-D017404; Navy-Case-75355; US-Patent-Appl-SN-345049) Avail: CASI HC A03/MF A01

There is presented a hybrid electrical and fiber-optic connector and a method of making the same. The connector comprises a plurality of bodies, the bodies including at least one fiber-optic ferrule having extending centrally therethrough a single optical fiber, and at least one electrical contact having an electrically conductive wire fixed thereto. The connector further includes structure exercising a radially compressive force on the bodies for urging the bodies into a configuration in which said bodies are coparallel and nested so as to form a stable bundle which in transverse section is substantially axisymmetrical, and retaining said bodies in the configuration. The connector still further includes alignment structure for angular positioning of said bodies in said connector in said transverse section about a nominal longitudinal axis of said bundle for registry of the connector with a second connector of complementary configuration. DTIC

N95-28901 ESDU International Ltd., London (England).
CONTACT STRESS IN DISC CAMS WITH DOMES OF FLAT-FACED FOLLOWERS
Nov. 1994 42 p
(ISSN 0141-4046)
(ESDU-94011; ISBN-0-85679-898-3) Avail: ESDU

ESDU 94011 introduces a Fortran program (ESDUpac A9411) that calculates at 1 degree rotation intervals the compressive stress in the contact region for cams with translating or swinging arm crowned flat-faced or domed followers, and also the peak value in the cycle and the rotation angle at which it occurs. Also output at those intervals are the contact dimensions and the reduction in separation of between the cam and follower. The method involves calculation of the force acting at the cam/follower interface due to follower system inertia, externally applied load and action of the return spring. The program includes an option to determine suitable values for spring rate and preload to maintain contact between the cam and follower; alternatively, for given values of those quantities it will check that contact is maintained. A check to ensure that profile undercutting is avoided is included. Other inputs required are the geometry of the cam and follower and their materials properties. A cam law must be used for each segment; six are provided or additional ones may be added by modifying the source code according to instructions provided. Alternatively, a file of follower displacement, velocity and acceleration at 1 degree rotation intervals may be input. A full description of the mathematical model used is included together with guidance on the use of the program to improve the design. It neglects any traction force and therefore applies only when the lubrication regime is mixed or elastohydrodynamic. The input to and output from the program are illustrated by a practical worked example of its use and warning messages that may be output are detailed together with suggestions for appropriate corrective procedures. The program is available on disc in the software volume uncompiled and compiled in ESDUview, a user-friendly shell that prompts on screen for input data.
Author

N95-28905 ESDU International Ltd., London (England).
SELECTION OF MATERIALS, MANUFACTURING METHODS AND LUBRICANTS FOR CAM MECHANISMS
Nov. 1994 38 p
(ISSN 0141-4046)
(ESDU-94017; ISBN-0-85679-904-1) Avail: ESDU

ESDU 94017 discusses the various causes of failure (pitting, scuffing, polishing and, for a roller follower, bearing fatigue) and provides pictures of the damage seen in the first three cases. The design procedure is discussed and set out in two flowcharts, one for sliding contact and one for rolling contact. Material selection is considered and tables provide guidance on appropriate properties for various types of materials. The choice of manufacturing method is then considered in relation to profile generation and also surface treatments for which a table summarises the features, advantages and limitations of those most used. The choice of lubricant is discussed and the use of ESDU 94008 to determine the film thickness in sliding contacts is explained. Contact stress is evaluated using ESDU 93001 for roller followers or ESDU 94011 for sliding contacts and allowable values are suggested for steel, and nodular or cast iron. Roller bearing fatigue life is calculated using ESDU 91026. Extensive notes on the interpretation of the data and a comprehensive series of suggestions for improving cam designs is also given. Two worked examples illustrate the use of the methods and the design guidance. Author

N95-28946 Japan Welding Society, Tokyo (Japan).
A 1993 REVIEW OF WELDING IN JAPAN
1 Jul. 1994 94 p In JAPANESE Limited Reproducibility: More than 20% of this document may be affected by poor print and microfiche quality
(DE95-758701; ETDE-JP-mf-95-758701) Avail: Issuing Activity (Department of Energy (DOE))

This paper describes a prospect on Japanese welding technologies available in 1993. Amid the increasing research publications on non-ferrous metals as structural materials, publications are also increasing on steel materials as to their fracture and welding mechanics, and structural control. Studies are being made on ceramics with respect to its bonding, interface reaction mechanisms, and mechanical characteristics. The paper describes the progress and improvement in conventional technologies in welding and cutting processes. Especially active is the study on solid face welding such as pressure welding and diffusion. A considerable decrease is seen in reports on thermal spraying. The paper also introduces surface processing and hydrostatic pressure processing as new processing techniques. In the area of welding devices, practical use of arc welding robots has come to near a completion stage. Technological development and cost reduction are indispensable to transfer to visual sensing with a higher intelligence level. With respect to the performance of joints, a large number of research has been reported on welding deformation and residual stress. The paper also dwells on corrosion resistance and welding cracks. Quality assurance, inspection, and related standards are described. Details are given on application of welding to different industrial fields. DOE

N95-29112*# National Aeronautics and Space Administration. Lewis Research Center, Cleveland, OH.
INFLUENCE OF TOOTH PROFILE MODIFICATION ON SPUR GEAR DYNAMIC TOOTH STRAIN
Fred B. Oswald and Dennis P. Townsend Jun. 1995 11 p Presented at the 31st Joint Propulsion Conference and Exhibit, San Diego, CA, 10-12 Jul. 1995; sponsored by AIAA, ASME, SAE, and ASEE
(RTOP 505-62-36; DA Proj. 1L1-62211-A-47-A)
(NASA-TM-106952; E-9691; NAS 1.15:106952; ARL-TR-778; AIAA Paper 95-3050) Avail: CASI HC A03/MF A01

This paper presents results of dynamic strain gage measurements performed on the NASA gear-noise rig. The experiments were part of a joint research program between NASA and the U.S. Army Research Laboratory to advance the technology of rotorcraft transmissions. Tests were performed on six sets of low contact ratio spur gears with different tooth profile modifications. Results presented include static and dynamic measurements of gear tooth strain taken over a matrix of operating conditions. The results demonstrate that a well-designed tooth profile modification can significantly reduce dynamic loads in spur gears, especially for gears which operate at high speed and under high torque. The two parabolic modifications tested were not as effective as linear modifications, possibly because the modification zone was too long. Author

N95-29184# Naval Postgraduate School, Monterey, CA.
CORRELATION OF INCLUSION SIZE AND CHEMISTRY WITH WELD METAL COMPOSITION AND MICROSTRUCTURE ARC WELDMENTS OF HIGH STRENGTH STEELS M.S. Thesis
Mark W. Eakes Dec. 1994 144 p
(AD-A292024) Avail: CASI HC A07/MF A02

Non-metallic inclusions are crucial to the development of acicular ferrite, the desired microstructure for optimal strength and toughness in weld metal. This study focused on obtaining correlation between the size and chemistry of inclusions and weld metal properties, especially the amount of acicular ferrite, in Gas Metal Arc (GMA) and Submerged Arc (SA) weldments in HY-100 and HSLA-100 steel. A strong correlation was found between the amount of acicular ferrite, flux basicity and inclusion composition and volume fraction in SAW weld metal samples. An index developed to consider the effect of chemistry and volume fraction of inclusions on acicular ferrite showed good correlation. The GMA weld samples were found to contain less acicular ferrite than the SAW samples, principally because of their lower oxygen content. However, it was again found possible to correlate inclusion chemistry and volume fraction with acicular ferrite formation. Unfortunately, the large amount of data scatter precluded the development of an index in this case. DTIC

N95-29369*# Lamar Univ., Beaumont, TX. Coll. of Engineering.
DAMAGE TOLERANCE IN FILAMENT-WOUND GRAPHITE/EPOXY PRESSURE VESSELS Final Report
William E. Simon, Vinh D. Ngueyen, and Ravi K. Chenna 1 Jul. 1995 97 p
(Grant NAG9-698)
(NASA-CR-198804; NAS 1.26:198804) Avail: CASI HC A05/MF A02

Graphite/epoxy composites are extensively used in the aerospace and sporting goods industries due to their superior engineering properties compared to those of metals. However, graphite/epoxy is extremely susceptible to impact damage which can cause considerable and sometimes undetected reduction in strength. An inelastic impact model was developed to predict damage due to low-velocity impact. A transient dynamic finite element formulation was used in conjunction with the 3D Tsai-Wu failure criterion to determine and incorporate failure in the materials during impact. Material degradation can be adjusted from no degradation to partial degradation to full degradation. The developed software is based on an object-oriented implementation framework called Extensible Implementation Framework for Finite Elements (EIFFE). Author

N95-29538*# Textron Bell Helicopter, Fort Worth, TX.
BELL HELICOPTER ADVANCED ROTOCRAFT TRANSMISSION (ART) PROGRAM Final Report
Zachary S. Henry Jun. 1995 221 p
(Contract NAS3-25455; RTOP 505-62-36; DA Proj. 1L1-6221-A-47-A)
(NASA-CR-195479; E-9708; NAS 1.26:195479; ARL-CR-238) Avail: CASI HC A10/MF A03

Future rotorcraft transmissions require key emerging material and component technologies using advanced and innovative design practices in order to meet the requirements for a reduced weight to power ratio, a decreased noise level, and a substantially increased reliability. The specific goals for the future rotorcraft transmission when compared with a current state-of-the-art transmission (SOAT) are: (1) a 25 percent weight reduction; (2) a 10 dB reduction in the transmitted noise level; and (3) a system reliability of 5000 hours mean-time-between-removal (MTBR) for the transmission. This report summarizes the work conducted by Bell Helicopter Textron, Inc. to achieve these goals under the Advanced Rotorcraft Transmission (ART) program from 1988 to 1995. The reference aircraft selected by BHTI for the ART program was the Tactical Tiltrotor which is a 17,000 lb gross weight aircraft. A tradeoff study was conducted comparing the ART with a Selected SOAT. The results showed the ART to be 29 percent lighter and up to 13 dB quieter with a calculated MTBR in excess of 5000 hours. The results of the following high risk component and material tests are also presented: (1) sequential meshing high contact ratio planetary with cantilevered support posts; (2) thin dense chrome plated M50 NiL double row spherical roller planetary bearings; (3) reduced kinematic error and increased bending strength spiral bevel gears; (4) high temperature WE43 magnesium housing evaluation and coupon corrosion tests; (5) flexure fatigue tests of precision forged coupons simulating precision forged gear teeth; and (6) flexure fatigue tests of plasma carburized coupons simulating plasma carburized gear teeth. Author

N95-29552# Maryland Univ., College Park, MD. Center for Automation Research.
ESTIMATION OF UNSTABILIZED COMPONENTS IN VEHICULAR MOTION
Yi-Sheng Yao and Rama Chellappa Sep. 1994 30 p
(Contract DAAH04-93-G-0419)
(AD-A290580; CAR-TR-735; CS-TR-3349; ARO-32365.3-MA) Avail: CASI HC A03/MF A01

This paper presents a kinetic-model based algorithm for estimating some unstabilized components in vehicular motion. In addition to smooth movement, there are unstabilized components such as bounce, pitch and roll in vehicular motion. To reliably accomplish other tasks like tracking and obstacle avoidance using visual inputs, it is essential to consider these disturbances. A two-wheel vehicle model available in the literature is used for this purpose. It takes into account the bouncing and pitching components. The dynamics of these unstabilized components are formulated using standard equations of motion. Assuming that depth information is known for some landmarks in the scene (e.g., obtained from a laser range finder) and additional information from inertial sensors such as accelerometers is available, a feature-based approach is proposed to estimate the unstabilized components. Simulation results for both deterministic and stochastic terrain profiles are presented. The robustness of the filter with respect to various parameter mismatches is also addressed. DTIC

N95-29807 Wisconsin Univ., Madison, WI.
AIR/FUEL RATIO VISUALIZATION IN A DIESEL SPRAY Ph.D. Thesis
Kevin David Carabell 1993 258 p
Avail: Univ. Microfilms Order No. DA9410596

To investigate some features of high pressure diesel spray ignition, we have applied a newly developed planar imaging system to a spray in an engine-fed combustion bomb. The bomb is designed to give flow characteristics similar to those in a direct injection diesel engine yet provide nearly unlimited optical access. A high pressure electronic unit injector system with on-line manually adjustable main and pilot injection features was used. The primary scalar of interest was the local air/fuel ratio, particularly near the spray plumes. To make this measurement quantitative, we have developed a calibration LIF technique. The development of this technique is the key contribution of this dissertation. The air/fuel ratio measurement was made using biacetyl as a seed in the air inlet to the engine. When probed by a tripled Nd:YAG laser the biacetyl fluoresces, with a signal proportional to the local biacetyl concentration. This feature of biacetyl enables the fluorescent signal to be used as as indicator of local fuel vapor concentration. The biacetyl partial pressure was carefully controlled, enabling estimates of the local concentration of air and the approximate local stoichiometry in the fuel spray. The results indicate that the image quality generated with this method is sufficient for generating air/fuel ratio contours. The processes during the ignition delay have a marked effect on ignition and the subsequent burn. These processes, vaporization and pre-flame kinetics, very much depend on the mixing of the air and fuel. This study has shown that poor mixing and over-mixing of the air and fuel will directly affect the type of ignition. An optimal mixing arrangement exists and depends on the swirl ratio in the engine, the number of holes in the fuel injector and the distribution of fuel into a pilot and main injection. If a short delay and a diffusion burn is desired, the best mixing parameters among those surveyed would be a high swirl ratio, a 4-hole nozzle and a small pilot. This arrangement provided the best combination of short ignition delay and diffusion burn for the majority of cases. Dissert. Abstr.

N95-29820# Wisconsin Univ., Madison, WI. Engine Research Center.
CYLINDER-AVERAGED HISTORIES OF NITROGEN OXIDE IN A DI DIESEL WITH SIMULATED TURBOCHARGING
Ronald J. Donahue, Gary L. Borman, and Glenn R. Bower 20 Oct. 1994 16 p
(Contract DAAL03-92-G-0122)
(AD-A290568; ARO-30340.25-EG-URI) Avail: CASI HC A03/MF A01

An experimental study was conducted using the dumping technique (total cylinder sampling) to produce cylinder mass-averaged nitric oxide

histories. Data were taken using a four stroke diesel research engine employing a quiescent chamber, high pressure direct injection fuel system, and simulated turbocharging. Two fuels were used to determine fuel cetane number effects. Two loads were run, one at an equivalence ratio of 0.5 and the other at a ratio of 0.3. The engine speed was held constant at 1500 rpm. Under the turbocharged and retarded timing conditions of this study, nitric oxide was produced up to the point of about 85% mass burned. Two different models were used to simulate the engine mn conditions: the phenomenological Hiroyasu spray-combustion model, and the three dimensional, U.W.-ERO modified KIVA-2 computational fluid dynamic code. Both of the models predicted the correct nitric oxide trend. Although the modified KIVA-2 combustion model using Zeldovich kinetics correctly predicted the shapes of the nitric oxide histories, it did not predict the exhaust concentrations without arbitrary adjustment based on experimental values. DTIC

N95-30110# Gas Research Inst., Chicago, IL.
EVALUATION OF WEAR RESISTANT CERAMIC VALVE SEATS IN GAS-FUELED POWER GENERATION ENGINES Topical Report, Dec. 1991 - Apr. 1994
R. W. Burrahm, R. J. Branecky, P. C. Sui, J. P. Latusek, and S. M. Hsu Dec. 1994 127 p Prepared in cooperation with National Inst.
(Contract GRI-5091-288-2319)
(PB95-200218; SWRI-4770; GRI-94/0411) Avail: CASI HC A07/MF A02

This project is directed at the reduction of valve recession in natural gas-fueled engines. Ceramic valve seat inserts have been procured, installed in a Caterpillar G3516 natural gas generator set, and tested for 1000 hours. Two different silicon nitride materials are being utilized for the valve seats in addition to stock Eatonite metallic inserts. Three valve face materials are being tested. These include stock Caterpillar stellite 1 faced, stellite 6 faced, and unfaced valves. A test matrix was used to allow comparison of all three valve face materials in combination with all three insert materials. The testing is scheduled to continue for an additional 7000 hours. No problems have been encountered with the test materials. In general, it has been shown that two types of silicon nitride materials have at least short term durability in engine operation. Neither material has exhibited any deficiencies thus far. An economic analysis spreadsheet has been created to calculate potential cost savings potential using ceramic valve seat inserts. Valve recession data for the first 1000 hours shows expected trends. Exhaust valve positions are wearing more than intake valve positions. If the intake positions and all positions with unfaced valve are ignored, then ceramic inserts paired with Stellite 1 valves show the most wear. NTIS

N95-30211# Lockheed Idaho Technologies Co., Idaho Falls, ID.
ELECTRIC AND HYBRID VEHICLE PROGRAM: SITE OPERATOR PROGRAM Quarterly Progress Report, Apr. - Jun. 1994
D. M. Kiser and H. L. Brown Oct. 1994 57 p
(Contract DE-AC07-94ID-13223)
(DE95-008620; INEL-94/0072-Qtr-3; EGG-EP-11237-Qtr-3) Avail: CASI HC A04/MF A01

The DOE Site Operator Program was initially established to meet the requirements of the Electric and Hybrid Vehicle Research, Development, and Demonstration Act of 1976. The program has since evolved in response to new legislation and interests. Its mission now includes three major activity categories: advancement of electric vehicle (EV) technologies, development of infrastructure elements needed to support significant EV use, and increasing public awareness and acceptance of EV's. The 13 program participants, their geographic locations, and the principal thrusts of their efforts are identified. The EV inventories of each participant are summarized. This third quarter report (FY-94) will include a summary of activities from the previous three quarters. The report section sequence has been revised to provide a more easily seen program overview, and specific operator activities are now included. DOE

N95-30273 Los Alamos National Lab., NM.
NUMERICAL IMPLEMENTATION OF A STATE VARIABLE MODEL FOR FRICTION
David A. Korzekwa and D. E. Boyce (Cornell Univ., Ithaca, NY.) 1995 8 p Presented at the 5th International Conference on Numerical Methods in Industrial Forming Processes, Ithaca, NY, 18-21 Jun. 1995 Submitted for publication Limited Reproducibility: More than 20% of this document may be affected by microfiche quality
(Contract W-7405-eng-36)
(DE95-007844; LA-UR-95-784; CONF-9506144-1) Avail: CASI HC A02

A general state variable model for friction has been incorporated into a finite element code for viscoplasticity. A contact area evolution model is used in a finite element model of a sheet forming friction test. The results show that a state variable model can be used to capture complex friction behavior in metal forming simulations. It is proposed that simulations can play an important role in the analysis of friction experiments and the development of friction models. DOE

N95-30277 Alabama Univ., Tuscaloosa, AL.
DYNAMIC MODELLING AND LINK MECHANISM DESIGN OF FOUR-LEGGED MOBILE ROBOT
Sung-Ho Park 1993 231 p
Avail: Univ. Microfilms Order No. DA9419851

In order to apply the advanced biological phenomena to the leg design of mobile robots, the structural and locomotive characteristics of several selected animals and insects are studied, and the four-legged mobile robot which can cover all existing leg arrangements and locomotion patterns is modeled by a rigid multibody system consisting of links and joints. The model is simulated to prove that the given structure or locomotive conditions satisfy the requirement of minimum energy expenditure. According to the first simulation, there exist ideal forward and backward stroke distances for each pair leg. Therefore, the walking volume and link lengths of existing legged mobile robots should be modified. Also, for other structural and locomotive characteristics which have been used by living creatures, the model is simulated to determine whether or not the actual or possible biological phenomena can be applied to the leg mechanism design of mobile robot. Dissert. Abstr.

N95-30285# Technische Univ., Delft (Netherlands).
NUMERICAL SIMULATION OF MECHANISMS AND MANIPULATOR ROBOTS WITH FLEXIBLE LINKS AND FLEXIBLE JOINTS Ph.D. Thesis
D. Gong 10 Jan. 1995 146 p
(PB95-196903; ISBN-90-370-0117-3) Copyright Avail: CASI HC A07/MF A02

This thesis deals with numerical simulation of mechanical systems like mechanisms and manipulator robots. The mechanical system may be considered in a two or three dimensional space, may have electrical machines, and may contain flexible links and flexible joints. Methods and algorithms to perform static analysis, kinematic analysis, dynamic analysis, linearization of nonlinear systems, periodic solution of periodically forced systems and control simulation of robots have been applied. A finite element method is used to get the mathematical model for a mechanical system. Friendly interfaces for pre- and post-processing have been designed by using X Window on Sun workstations. An integrated program network and data base has been applied in the software system SPACAR. For the simulation of robots with flexible links and flexible joints, two linearization methods have been studied: the variational linearization method and the feedback linearization method. Numerical examples for simulation of robots with flexible links and flexible joints have been presented to show the elegance and powerfulness of the introduced methods and the designed software system. NTIS

38 QUALITY ASSURANCE AND RELIABILITY

Includes product sampling procedures and techniques; and quality control.

N95-28682 Naval Facilities Engineering Service Center, Port Hueneme, CA.
CATHODIC PROTECTION SYSTEM INSPECTION 6
Jim Jenkins Feb. 1994 5 p Limited Reproducibility: More than 20% of this document may be affected by microfiche quality
(AD-A289720; NFESC-TDS-2003-SHR) Avail: Issuing Activity (Defense Technical Information Center (DTIC))

If the cathodic protection system is periodically inspected and maintained to provide continuous protection the condition of the protected structure can be inferred from the cathodic protection system records without the need for physical inspection of the protected structure. DTIC

N95-28684 Naval Facilities Engineering Service Center, Port Hueneme, CA.
CATHODIC PROTECTION SYSTEM INSPECTION 5
Jim Jenkins and Dan Polly Feb. 1994 6 p Limited Reproducibility: More than 20% of this document may be affected by microfiche quality
(AD-A289724; NFESC-TDS-2002-SHR) Avail: Issuing Activity (Defense Technical Information Center (DTIC))

The rectifier is the heart of an impressed current cathodic protection system. As it is subject to many adverse conditions including power surges, lightning strikes, vandalism, physical damage, and deterioration from atmospheric exposure, frequent inspections of rectifiers are vital to keeping an impressed current system operating so that it can provide nearly continuous protection of the underground, or submerged structures that are being protected. DTIC

N95-29012# Tristan Technologies, Inc., San Diego, CA.
FIVE-CHANNEL SQUID BASED NON-DESTRUCTIVE EVALUATION (NDE) INSTRUMENT Final Report
Douglas Paulson 1994 58 p
(Contract F49620-92-C-0026)
(AD-A292474; AFOSR-95-0142TR) Avail: CASI HC A04/MF A01

A 5-channel SQUID-based NDE instrument has been built and tested. A combination of first derivative axial and planar concentric gradiometers enable the simultaneous evaluation of magnetic signatures of surface and deep sources. Features of the system include: Liquid Helium dewar to cool the probe with 5 mm coil to external dewar surface distance, superconducting magnet assembly to provide both DC and AC applied fields, noise reduction circuitry to cancel signals generated by applied AC signals coupled to pick up coils, computerized data acquisition and control system, including customized software, to control system, to collect, analyze and display data. Testing includes studies of transformation induced plasticity in steel, defects in non-magnetic metals using AC magnetic fields, defects in metals by applied modulated currents, AC fields applied to magnetic systems, and magnetization changes induced by applied tension. These tests indicate this system can locate and identity defects and sources in a variety of different applications using a number of novel experimental techniques. DTIC

N95-29104 Virginia Polytechnic Inst. and State Univ., Blacksburg, VA.
THE DEVELOPMENT OF AN INTERPRETIVE METHODOLOGY FOR THE APPLICATION OF REAL-TIME ACOUSTO-ULTRASONIC NDE TECHNIQUE FOR MONITORING DAMAGE IN CERAMIC COMPOSITES UNDER DYNAMIC LOADS Ph.D. Thesis
Anil Tiwari 1993 227 p
Avail: Univ. Microfilms Order No. DA9414096

Research effort was directed towards developing a near real-time acousto-ultrasonic (AU), nondestructive evaluation (NDE) tool study the failure mechanisms of ceramic composites. Progression damage is monitored in real-time by observing the changes in the received AU signal during the actual test. During the real-time AU test the AU signals are generated and received by the AU transducers attached to the specimen while it is being subjected to increasing quasi static loads or cyclic loads (10 Hz, R = 0.1). The received AU signals for 64 successive pulses were gated in the time domain (T = 40.96) and then averaged every second over ten load cycles and store in a computer file during fatigue tests. These averaged gated signal are representative of the damage state of the specimen at that point c its fatigue life. This is also the first major attempt in the development and application of real-time AU for continuously monitoring damage accumulation during fatigue without interrupting the test. The present work has verified the capability of the AU technique to assess the damage state in silicon carbide/calcium aluminosilicatt (SiC/CAS) and silicon carbide/magnesium aluminosilicate (SiC/MAS) ceramic composites. Continuous monitoring of damage initiation and progression under quasi-static ramp loading in tension to failure of unidirectional and cross-ply SiC/CAS and quasi-isotropic SiC/MAS ceramic composite specimens at room temperature was accomplished using near real-time AU parameters. The AU technique was shown to be able to detect the stress levels for the onset and saturation of matrix cracks, respectively. The critical cracking stress level is used as a design stress for brittle matrix composites operating at elevated temperatures. The AU technique has found that the critical cracking stress level is 10-15 percent below the level presently obtained for design purposes from analytical models. An acousto-ultrasonic stress-strain response (AUSSR) model for unidirectional and cross-ply ceramic composites was formulated. The AUSSR model predicts the strain response to increasing stress levels using real-time AU data and classical laminated plate theory. The Weibull parameters of the AUSSR model are used to calculate the design stress for thermo-structural applications. Real-time AU together with the AUSSR model was used to study the failure mechanisms of SiC/CAS ceramic composites-under ceramic and fatigue loading. An S-N curve was generated for a cross-ply SiC/CAS ceramic composite material. The AU results are corroborated and complemented by other NDE techniques, namely, in-situ optical microscope video recordings and edge replication. Dissert. Abstr.

N95-29256 Iowa State Univ. of Science and Technology, Ames, IA.
EFFICIENT INVERSION OF FOURIER AND LAPLACE DOMAIN BOUNDARY ELEMENT SOLUTIONS FOR ELASTODYNAMIC SCATTERING Ph.D. Thesis
Joel Kevin Ness 1994 132 p
Avail: Univ. Microfilms Order No. DA9424245

In ultrasonic nondestructive testing, the actual time domain signature of a scattered wave due to a pulsed input is the common observable (via oscilloscope) quality. Numerically simulated solutions are thus desirable in the time domain. These can be obtained by working directly in the time domain or by inversions of integral transform solutions in the frequency (Fourier) or Laplace domains. Direct time solutions are suitable for short times but generally deteriorate for longer times. Alternately, the transform techniques generally require solutions over a wide spectrum in the transform variable to provide accurate inversions back to the time domain. However, without special provisions, numerical implementations like boundary or finite elements are limited to lower frequencies or Laplace parameter values. Hence, ways to minimize the number of transform variable solutions for canonical problems are important. In this dissertation the Fourier and Laplace transform methods are compared and investigations are made into ways of minimizing the solutions in the spectrum space in a boundary element setting. Three common scattering models--a spherical void and two spherical inclusions--are used in the analysis and the numerical results are compared to analytical solutions and to experimental results. Dissert. Abstr.

N95-29423# Florida State Univ., Tallahassee, FL. Dept. of Statistics.
CONTINUATION OF RESEARCH IN THE STATISTICAL ASPECTS OF RELIABILITY, AVAILABILITY, AND MAINTAINABILITY Final Summary Report, 1 Oct. 1990 - 30 Sep. 1994
Myles Hollander 23 Nov. 1994 8 p
(Grant AF-AFOSR-0048-91)
(AD-A290126; AFOSR-95-0046TR) Avail: CASI HC A02/MF A01

Research areas included standby redundancy policies, redundancy allocations in series and parallel systems, goodness-of-fit tests for censored data, autopsy models, nonparametric methods for imperfect repair, inference for systems operating in different environments, and dynamic reliability models. Twenty-nine technical reports were written in the period and twenty-six papers were published in the period. DTIC

N95-29786 Texas Univ., Austin, TX.
ROBUST FAULT DETECTION FILTER DESIGN Ph.D. Thesis
Randal Kirk Douglas 1993 280 p
Avail: Univ. Microfilms Order No. DA9413475

The detection filter is a specially tuned linear observer that forms the residual generation part of an analytical redundancy system designed for model-based fault detection and identification. The detection filter has an invariant state subspace structure that produces a residual with known and fixed directional characteristics in response to a known design fault direction. In addition to a parameterization of the detection filter gain, three methods are given for improving performance in the presence of system disturbances, sensor noise, model mismatch and sensitivity to small parameter variations. First, it is shown that by solving a modified algebraic Riccati equation, a stabilizing detection filter gain is found that bounds the H-infinity norm of the transfer matrix from system disturbances and sensor noise to the detection filter residual. Second, a specially chosen expanded-order detection filter is formed with fault detection properties identical to a set of independent reduced-order filters that have no structural constraints. This result is important to the practitioner because the difficult problem of finding a detection filter insensitive to disturbances and sensor noise is converted to the easier problem of finding a set of uncoupled noise insensitive filters.

Furthermore, the statistical properties of the reduced-order filter residuals are easier to find than the statistical properties of the structurally constrained detection filter residual. Third, an interpretation of the detection filter as a special case of the dual of the restricted decoupling problem leads to a new detection filter eigenstructure assignment algorithm. The new algorithm places detection filter left eigenvectors, which annihilate the detection spaces, rather than right eigenvectors, which span the detection spaces. This allows for a more flexible observer based fault detection system structure that could not be formulated as a detection filter. Furthermore, the link to the dual problem allows existing results relating supremal controllability subspaces and ill-conditioned eigenvector to be easily applied to the detection filter. The practitioner will find these results useful as they provide guidelines for desensitizing the detection filter to small parameter variations. Dissert. Abstr.

N95-29941# Conductus, Inc., Sunnyvale, CA.
THE mm-WAVE RESONANT METHODS FOR THE DETECTION OF CORROSION, PHASE 1 Final Report, 15 Jun. - 14 Dec. 1994
J. Martens and S. Sachtjen 10 Feb. 1995 38 p
(Contract F49620-94-C-0049)
(AD-A291315; Rept-95-C-SRA-001; AFOSR-95-0099TR) Avail: CASI HC A03/MF A01

In this program, a class of mm-wave resonant tools known as surface resistance analyzers were evaluated for their ability to detect corrosion and extract information on corrosion products. The study was performed primarily on aluminum alloys exposed to salt fog conditions although a high temperature material sand steel alloys were also measured. The results on detection were uniformly encouraging. Statistically significant deviations in surface resistance were reported prior to visible corrosion products appearing. Incipient stress-related cracks around rivet holes were also detected on length scales of 0.1 mm. Complex permittivity data was extracted for the corrosion products and was used to estimated thicknesses, impurity levels, and composition changes during different exposure conditions. Incipient corrosion was also detected underneath several varieties of paint. The results suggest that this may be a useful measurement tool for the detection and analysis of corrosion in an aircraft maintenance environment. DTIC

N95-29946# Eltron Research, Inc., Boulder, CO.
ELECTROCHEMICAL IMPEDANCE PATTERN RECOGNITION FOR DETECTION OF HIDDEN CHEMICAL CORROSION ON AIRCRAFT COMPONENTS, PHASE 1 Final Report, 15 Jun. - 15 Dec. 1994
A. F. Sammells and J. S. Bowers 8 Feb. 1995 87 p
(Contract F49620-94-C-0043)
(AD-A291345; AFOSR-95-0106TR) Avail: CASI HC A05/MF A01

This investigation addressed the need for diagnostic instrumentation compatible with performing the Nondestructive Evaluation (NDE) of hidden chemical corrosion with a high degree of accuracy, sensitivity and versatility on both titanium and aluminum alloys currently used in Air Force and commercial aircraft. The overall approach was directed towards development of pattern recognition schemes based upon the on-line data acquisition of Fast Fourier Transform Electrochemical Impedance Spectroscopy (FFTEIS) instrumentation from the suspect hidden chemical corrosion site. Resulting impedance patterns were then analyzed by application of a Neural Network pattern recognition scheme. The Neural Network Analysis (NNA) was then trained to both detect and grade the severity of hidden corrosion present on the aircraft metal substrate interface of interest. Nueral Net Analysis of FFTEIS data was verified as a powerful diagnostic strategy for in situ hidden corrosion process identification, quantitative analysis and severity grading. Correlations between impedance measurements and corrosion depth were verified by subsequent SEM and EDX examination of the metal interfacial regions. The approach will also be powerful for gaining fundamental information into the nature of corrosion processes and conditions leading to their inception at hidden sites. DTIC

39 STRUCTURAL MECHANICS

Includes structural element design and weight analysis; fatigue; and thermal stress.

For applications see *05 Aircraft Design, Testing and Performance* and *18 Spacecraft Design, Testing and Performance.*

N95-28711 ESDU International Ltd., London (England).
DIMENSIONS, DEFLECTIONS AND STRESSES FOR HERTZIAN CONTACTS UNDER COMBINED NORMAL AND TANGENTIAL LOADING. (GUIDE TO USE OF COMPUTER PROGRAM A9434.)
Dec. 1994 63 p
(ISSN 0141-2590)
(ESDU-94034; ISBN-0-956-79921-1) Avail: ESDU

ESDU 94034 introduces a Fortran program (ESDUpac A9434) to calculate stresses in point contacts that occur in rolling element bearings, gears, cams and other engineering components. Both normal and combined normal and tangential loading are allowed. Contact dimensions, orientation and gross deflection (normal closure) are calculated from specified radii and other properties of the contacting bodies. The surface velocities can also be specified and the program determines the directions of sliding and contact motion, although those directions and the contact dimensions can be input directly if already known. The maximum stress values and their locations are determined for use in criteria for brittle failure or failure due to yield or fatigue. Also stress distributions may be output over any plane or along any line through the volume of the components affected or around the perimeter of the contact area. Sets of worked examples illustrate the use of the program when the contact dimensions are known and in the more practical case when those dimensions and the directions of any friction or contact motion are unknown. The input to and the output from the program are explained and the program is provided on disc (uncompiled) in the software volume. ESDU

N95-28789# Army Armament Research, Development and Engineering Center, Watervliet, NY. Benet Lab.
STRESS CONCENTRATION, STRESS INTENSITY, AND FATIGUE CRACK GROWTH ALONG EVACUATORS OF PRESSURIZED, AUTOFRETTAGED TUBES Final Report
A. P. Parker (Northumbria Univ., Newcastle-upon-Tyne, England.) and J. H. Underwood Dec. 1994 30 p
(DA Proj. 1A1-1-Z-1-CANMBJ)
(AD-A291920; ARCCB-TR-94046) Avail: CASI HC A03/MF A01

A stress analysis has been conducted on a pressurized, fully or partially autofrettaged cylinder with a small diameter evacuator hole penetrating radially through the wall. Pressure was applied on the inside diameter (ID) of the tube, and all or part of this pressure was applied on the evacuator hole surfaces. Total hoop stress concentrations have been determined for a range of radial locations along the evacuator and stress intensity factors have been determined along a crack emanating from the evacuator hole. Fatigue crack growth rates. and hence crack profiles, were predicted at each of the radial locations. These predictions indicate that the critical location for the crack in a non-autofrettaged tube is at the ID, whereas in a fully autofrettaged tube, it is located approximately halfway through the wall thickness. Stress ratio has a significant influence on crack shape in autofrettaged tubes, however, it has a limited effect upon lifetime. The effect of axial residual stresses upon fatigue lifetime due to the autofrettage process has been described and an insignificant reduction in lifetime was a result of such stresses. Finally, the predicted profiles are compared with experimental observations of fatigue crack evacuators, and a limited comparison of predicted and actual lifetimes is presented. Good agreement has been observed in both comparisons. DTIC

N95-28801 ESDU International Ltd., London (England).
FLAT RECTANGULAR ISOTROPIC PLATES UNDER UNIFORMLY DISTRIBUTED NORMAL PRESSURE. ELASTIC DEFLECTIONS, STRESSES, AND STRAINS, MOMENTS AND FORCES, FOR VARIOUS FORMS OF EDGE RESTRAINT
Nov. 1994 27 p
(ISSN 0141-4089)
(ESDU-94033; ISBN-0-856-79920-3) Avail: ESDU

ESDU 94033 introduces a Fortran program which gives (1) the detailed distribution of deflection and either the moments and in-plane forces, or

the stresses, or the strains, throughout the plate for a given pressure load or (2) the maximum deflection and the peak values of moments, forces, stresses and strains and their location for a range of pressure loads. The differential equations formed in terms of stress and displacement functions apply to elastic, large deflection, moderate rotation, thin plate theory and are solved by a finite difference technique for edge conditions of elastic rotation, translation or shear restraint. The plate is rigidly restrained in its own plane. It is treated as symmetrical so behavior in one quarter only is considered with a grid chosen by the user of 4 x 4, 6 x 6, or 8 x 8 points. Output of the distributions can be chosen to be at every point or at alternate points. The program input and output are fully described, error messages that may be output are explained, and a worked example illustrates its use. The program is available on disc (uncompiled) in the software volume as ESDUpac A9433 and compiled within ESDUview, a user-friendly shell running under MS DOS that prompts on screen for input data.

ESDU

N95-28853# Purdue Univ., West Lafayette, IN. School of Mechanical Engineering.

MODAL INTERACTIONS AND COMPLEX RESPONSES IN WEAKLYNONLINEAR MULTI-DEGREE-OF-FREEDOM MECHANICAL SYSTEMS Final Report, 1 Nov. 1990 - 30 Apr. 1994

A. K. Bajaj and P. Davies 1 Dec. 1994 191 p

(Contract DAAL03-90-G-0220)

(AD-A292023; ARO-27300.10-EG) Avail: CASI HC A09/MF A02

The analysis of forced nonlinear response of mechanical and structural systems, subjected to harmonic excitations, is considered in this report. It is shown that the presence of internal resonances on the various linear modes of vibration of the structure can result in quite complex dynamical motions and the motion may not settle down to either a periodic or a sub/super-harmonic response. Internal resonances, which allow for the exchange of energy between the participating modes give rise to beat-like fluctuations in the amplitudes of vibration. The nonlinear amplitude variation is very slow and can be either periodic or chaotic, depending on the level of forcing, damping and the nonlinearity coefficients. The analytical and numerical results are derived for the nonlinear vibrations of a thin rectangular plate, the response of the pendulum vibration absorber, and a double pendulum. Some experimental results of the measured response for a harmonically forced rectangular plate are also presented and compared to analytical predictions.

DTIC

N95-28909 Army Engineer Waterways Experiment Station, Vicksburg, MS. Structures Lab.

SHEAR REINFORCEMENT IN DEEP SLABS Final Report

Stanley C. Woodson Nov. 1994 138 p Limited Reproducibility: More than 20% of this document may be affected by microfiche quality

(AD-A289528; WES/TR/SL-94-24) Avail: Issuing Activity (Defense Technical Information Center (DTIC))

A considerable amount of data is available in the literature regarding the behavior of normally proportioned slabs, those with span-to-effective-depth (L/d) ratios greater than approximately 8. However, guidance for shear design and response limits of deep slabs (L/d less than 6) used in protective construction is lacking. Thirteen one-way reinforced concrete deep slabs were statically loaded with uniform water pressure to gain a basic understanding of the behavior of deep slabs with reinforcing details typical of protective construction. The post-ultimate behavior of the slabs indicated that a substantial amount of reserve capacity is available in deep slabs with large quantities of principal reinforcement. Based on this series, the recommended response limit for deep slabs having a principal steel ratio near 0.01 and adequate shear reinforcement is approximately 12 deg. For deep slabs with relatively small quantities of principal steel, the response should probably be limited to approximately 8 deg for design purposes.

DTIC

N95-28949 Army Armament Research, Development and Engineering Center, Watervliet, NY. Benet Lab.

EXPERIMENTAL METHODS IN RESIDUAL STRESS MEASUREMENT USING A POSITION-SENSITIVE SINGLE-EXPOSURE SCINTILLATION DETECTION SYSTEM Final Report

S. L. Lee, M. Doxbeck, and G. P. Capsimalis Sep. 1994 33 p Limited Reproducibility: More than 20% of this document may be affected by microfiche quality

(AD-A289803; ARCCB-TR-94036) Avail: Issuing Activity (Defense Technical Information Center (DTIC))

In the Denver D-1000-A single-exposure position-sensitive scintillation detection (PSSD) system, surface residual stress measurement in any chosen direction is based on crystalline plane spacings determined in two directions normal to the surface made simultaneously in a single psi tilt. This technical allows fast, noncontacting, and nondestructive biaxial stress analysis. In this report, system performance is characterized by studying the noise, gain, and diffraction peak profiles as a function of diode array element. A four-point bend experiment was performed to determine the elastic constant of the 211 plane of body-centered cubic martensitic steel. Residual stress measurements were performed in several steel specimens and compared to measurements made on a similar system at Pennsylvania State University. Local software development allowed the single-exposure PSSD to run in a multiple-exposure mode for improved accuracy in biaxial stress analysis.

DTIC

N95-29063# Stanford Univ., CA. Div. of Applied Mechanics.

A NEW METHODOLOGY FOR THE NUMERICAL SIMULATION OF STRAIN SOFTENING IN INELASTIC SOLIDS Final Report, Oct. 1992 - Sep. 1994

Juan C. Simo Dec. 1994 31 p

(Contract N47408-91-C-1217)

(AD-A290295; NFESC-CR-95-002) Avail: CASI HC A03/MF A01

This document summarizes the work on a new approach to the analysis and simulation of localization arising in inelastic solids that exhibit strain-softening response. In addition, the document describes new results pertaining to the extension of these ideas to the finite deformation regime. The techniques described in this document lead to the systematic construction of numerical methods that completely eliminate the strong mesh dependence exhibited by conventional treatments of the problem.

DTIC

N95-29067# Stanford Univ., CA. Dept. of Aeronautics and Astronautics.

EFFECT OF NOSE SHAPE AND MASS OF THE IMPACTOR ON IMPACT DAMAGE OF LAMINATED COMPOSITES Final Report, 15 Mar. 1991 - 14 Mar. 1994

Fu-Kuo Chang 21 Nov. 1994 42 p

(Contract DAAL03-91-G-0087)

(AD-A290351; ARO-28253.1-EG) Avail: CASI HC A03/MF A01

The investigation studied impact damage resistance of laminated composites caused by a low-velocity foreign object. Effects of material interfacial strength and impactor's mass and nose size on damage resistance were the study's concern. An analytical model was developed for predicting the dynamic response of composites during impact. The model consists of damage accumulation prediction and material degradation modeling. Damage accumulation criteria were adopted for predicting failure and mode of failure due to impact. Appropriate material constitutive relations were also proposed to relate strains to stresses for material that was inflicted with impact damage. The Hertzian contact law was modified by taking into account material degradation during impact. The proposed model and modified Hertzian contact law were implemented in a transient dynamic finite element analysis designated 3DIMPACT. The code predicts force response and damage accumulation of a composite during impact. Composites with and without toughening interleaves were tested experimentally to verify the model and the computer code. The effect of the impactor's size and nose radius was considered in verifying the code, very useful for evaluating impact resistance and for screening materials.

DTIC

N95-29150# Princeton Univ., NJ. Dept. of Civil Engineering and Operations Research.

SENSITIVITY OF STRESS AND BOUNDARY IMPERFECTION OF DIELECTRIC RESONATOR DISKS Final Report, 1 Apr. 1993 - 31 Mar. 1994

Peter C. Lee Aug. 1994 5 p

(Contract DAAH04-93-G-0081)

(AD-A290488; ARO-30993.5-MA) Avail: CASI HC A01/MF A01

The objective of the research is to investigate (a) the sensitivity of the resonant frequencies of the dielectric disks under various applied forces and accelerations, and (b) the effect of the boundary imperfections of the dielectric disks on the resonances. The present research is a continuation

of an ARO-supported project (DAAL 03-90-G-0079, 26909 MA). The research is conducted in two aspects: for isotropic dielectrics and for anisotropic dielectrics. The results for the present period are listed as below. (1) The stress effect on the resonant frequencies of TE modes in isotropic circular disks were obtained by a perturbation method for three cases of loading conditions: a pair of diametral forces, steady vertical acceleration, and steady horizontal acceleration. (2) The above study has been extended to include both the TE and TM modes in circular disks. For anisotropic dielectrics-- (3) A system of 2-D governing equations for guided waves in anisotropic dielectric plates has been derived and dispersion relations computed from these 2-D equations are compared with those obtained from the 3-D Maxwell's equations. DTIC

N95-29192 Office of Naval Research, Arlington, VA.
CABLE LOAD TRANSDUCER Patent Application
Scott E. Hassan and David A. Abdow 13 Oct. 1994 17 p Filed 13 Oct. 1994 Limited Reproducibility: More than 20% of this document may be affected by microfiche quality
(AD-A289548; Navy-Case-73983; US-Patent-Appl-SN-322668) Avail: Issuing Activity (Defense Technical Information Center (DTIC))

An apparatus for measuring the loads, moments and torque at a constrained end of a cable created by the action of the cable in a fluid medium in which the cable is suspended. The cable is suspended in the medium by means of a strut. The apparatus connects the cable to the strut. The apparatus includes two flexure members, one rigidly connected to the strut, the other to the cable. A universal joint couples the two flexure members so that the flexure member connected to the strut can be fitted with strain gages to measure bending while the other flexure member has strain gages to measure axial force and torque. The universal joint enables the isolation of axial and torsional strains at the flexure member connected to the cable. DTIC

N95-29419 Stanford Univ., CA.
AN IMPACT LOAD IDENTIFICATION METHOD USING DISTRIBUTED SENSOR MEASUREMENTS Ph.D. Thesis
Keeyoung Choi 1994 124 p
Avail: Univ. Microfilms Order No. DA9414553

An investigation was performed to develop a method that could identify the location and history of an impact load applied to a structure with built-in piezoelectric sensors. The load identification method consists of two parts: a system model and an estimator. A piezoelectric sensor mechanism was studied as well as structural dynamic models as parts of the system model. Standing and propagating wave approaches were used to obtain dynamic models of a finite and an infinite beam respectively. A figure of merit was defined to measure the difference between the model prediction of the system response based on the estimates of the load parameters (the location and history) and sensor measurements. The estimator was designed to find the parameters by minimizing the figure of merit. This was a quadratic fitting problem with a two-stage minimization process. The inner minimization was done with respect to the force history for an estimated location. With a variation method, this was converted into a two-point boundary value problem and was solved using a smoothing algorithm. In this phase, the gradient of the figure of merit with respect to the location is calculated. The outer minimization was done to find the best estimate of the location. A Newton-Raphson method incorporating the gradient information calculated in the inner minimization process was implemented. This identification method was applied to both the finite and the infinite beams. After showing the process for specific problems, the reliability was verified for various cases. In the verification process, arbitrarily varying load conditions (load history and location) were used. To parameterize the load history, the energy transferred to the structure was used. In all cases studied, the identification system succeeded in estimating the location and the transferred energy. The predicted location was well within the specified criterion. Dissert. Abstr.

N95-29424 Georgia Inst. of Tech., Atlanta, GA.
COMPRESSIVE BEHAVIOR OF THICK COMPOSITE SHELLS: BENCHMARK SOLUTIONS FOR LOSS OF STABILITY AND HYGROSCOPIC EFFECTS Ph.D. Thesis
Chang-Bum Chung 1993 96 p
Avail: Univ. Microfilms Order No. DA9415630

First, a formulation based on the three dimensional theory of elasticity is employed to study the buckling of an orthotropic cylindrical shell under external pressure. The results from this elasticity solution are compared with the critical loads predicted by the orthotropic Donnell and Timoshenko nonshallow shell formulations. In all cases the elasticity approach predicts a lower critical load than the shell theories, the percentage reduction being larger with increasing thickness. Second, an exact elasticity solution is obtained for the stresses and displacements in an orthotropic cylindrical shell loaded by an external pressure under imposed constant moisture concentrations on the inner and outer surfaces. Since the moisture diffusion process is relatively slow, the hygroscopic stresses are confined for practical time values to a boundary-layer region near the surfaces. Illustrative results are presented for graphite-epoxy material regarding the boundary-layer hygroscopic effect on the stress field with respect to time and the coupling of mechanical loading (external pressure) and moisture diffusion. Finally, the influence of transient hygroscopic and thermal stresses on the critical point of a hollow orthotropic circular cylinder loaded by external pressure is examined. The effects of the size, time, moisture concentration, and temperature on the critical load are investigated. The hygroscopic boundary-layer stress is found to have a negligible influence on the critical load. Dissert. Abstr.

N95-29535# Michigan Technological Univ., Houghton, MI.
THEORETICAL, EXPERIMENTAL AND COMPUTATIONAL STUDIES IN PLASTICITY Final Report, 30 Jun. 1990 - 29 Jun. 1994
E. C. Aifantis and H. Zbib (Washington State Univ., Pullman, WA.) 4 Oct. 1994 7 p Prepared in cooperation with Washington State Univ
(Contract DAAL03-90-G-0151)
(AD-A290428; ARO-27409.12-EG) Avail: CASI HC A02/MF A01

The following main results were completed during the previous grant period. A photoelastic technique to measure plastic flow and instability has been developed and measurements for shear band characteristics have been obtained. An innovative biaxial experimental apparatus for determining the evolution of the yield loci with plate specimens has been designed and manufactured. Constitutive models incorporating the effects of anisotropy, texture, material rotation, and inhomogeneity have been developed and successfully used to interpret available experimental data such as axial effects in torsion. Numerical evaluations for shear band and plastic instability problems have been performed resulting in new information about the effects of anisotropy and texture on the stability of plastic deformation. DTIC

N95-29546 Illinois Univ., Urbana-Champaign, IL.
ENERGY THEOREMS AND BOUNDS IN LINEARIZED ELASTICITY WITH RESIDUAL STRESS Ph.D. Thesis
F. George Abatt 1994 65 p
Avail: Univ. Microfilms Order No. DA9416332

Residual stress is the stress present in a fixed reference placement in which the body is at rest in the absence of external forces. In this work, residual stress is viewed as constitutive information so as to develop nondestructive mechanical tests that provide information about the residual stress fields in bodies that respond in a linearly elastic manner to small deformations from the residually stressed state. In order to construct the necessary background, a number of results from classical linear elastostatics are modified to include the presence of residual stress. Among these results are the Principles of Minimum Potential Energy and Minimum Complementary Energy. These minimum principles are used to derive a bound on the residual stress in terms of experimental data plus solutions to classical problems which correspond to the experiment. Dissert. Abstr.

N95-29562# Virginia Univ., Charlottesville, VA. School of Engineering and Applied Science.
SEVERE EDGE EFFECTS AND SIMPLE COMPLIMENTARY INTERIOR SOLUTIONS FOR THIN-WALLED ANISOTROPIC AND COMPOSITE STRUCTURES Final Report, 1 Jan. 1991 - 31 Dec. 1994
C. O. Horgan and J. G. Simmonds 31 Dec. 1994 16 p
(Contract DAAL03-91-G-0022)
(AD-A290645; ARO-28399.15-EG) Avail: CASI HC A03/MF A01

Many useful thin-walled structures of interest to the U.S. Army, such as rifle barrels, automotive parts, rocket casings, helicopter blades, driveshafts, and containment vessels, are often constructed of layers of anisotropic, filament or fiber-reinforced materials. While many of these structures are subject to severe mechanical, inertial, or thermal loads, they

often must be designed to remain elastic. This means that it is particularly important to be able to compute accurately global characteristics, such as buckling loads and natural frequencies, as well as local information such as stresses near holes or edges. Two important, complementary regions of such structures, have been studied, namely, the interior where there are no steep stress gradients, and the edge zone(s) where stress gradients are high. For both regions, simplified, cost-effective asymptotic methods have been developed. These considerations are particularly important in layered, anisotropic structures because many investigators have (1) claimed that higher-order (and hence computationally expensive) beam, plate, or shell theories are needed for such structures and (2) not paid sufficient attention to the particularly severe end effects (breakdown of Saint-Venant's principle) such structures engender. DTIC

N95-29580# Pennsylvania State Univ., University Park, PA.
PROCEEDINGS OF THE 6TH INTERNATIONAL CONFERENCE ON NONDESTRUCTIVE CHARACTERIZATION OF MATERIALS Final Report, Apr. 1993 - Mar. 1994
Robert E. Green, Jr., Krzysztof J. Kozaczek, and Clayton O. Ruud Dec. 1994 823 p Conference held in Oahu, HI, 7-11 Jun. 1994
(Contract N00014-93-1-0553)
(AD-A290727) Avail: CASI HC A99/MF A10

The role of nondestructive testing has expanded far beyond its historical mission of detecting macroscopic defects in structures and devices which had already been constructed and most often had been in service for an extended period of time. Today, and ever increasingly in the future, using advanced sensors and modern measurement technology, along with signal/data processing techniques, information on the processing conditions and the properties and characteristics of the materials being processed can be continuously generated. Real-time process monitoring for more effective and efficient real-time process control and improved product quality and reliability will now become a practical reality. The optimization of the processing and properties of polymers, ceramics and composites, the development of synthetically structured materials, the characterization of surfaces and interfaces, the measurement and character-characterization of amorphous metals and semiconductors, the growth of perfect electronic and optical crystals and thin films, and in all cases, the structures, devices and systems made from these materials demand the innovative application of modern nondestructive materials characterization techniques to monitor and control as many stages of the production process as possible. Simply put, intelligent manufacturing is impossible without integrating modern nondestructive evaluation into the production system. DTIC

N95-29582 Missouri Univ., Rolla, MO.
ANALYSIS OF ADIABATIC SHEAR BANDS IN THERMOVISCOPLASTIC MATERIALS UNDER COMBINED LOADING
Romesh C. Batra Nov. 1994 13 p Limited Reproducibility: More than 20% of this document may be affected by poor print
(Contract DAAL03-92-G-0131)
(AD-A290666; ARO-29907.1-EG-AAS) Avail: Issuing Activity (Defense Technical Information Center (DTIC))

We study the initiation and growth of adiabatic shear bands in a thin-walled steel tube deformed first quasistatically either in simple compression or simple tension or by a pressure applied to the inner surface of the tube and then one end of the tube is kept fixed and the other end is twisted with a prescribed tangential speed. The objective is to see how prior quasistatic deformations of the tube affect the nominal shear strain at which a shear band initiates in the tube. The first set of numerical experiments simulates tests recently conducted by Murphy who found that the nominal strain at the initiation of the shear bands decreased with an increase in the axial static compressive stress induced in the tube. DTIC

N95-29929# Army Research Lab., Aberdeen Proving Ground, MD.
PENETRATION OF SEMI-INFINITE, BI-ELEMENT TARGETS BY LONG ROD PENETRATORS Final Report, 1 Oct. 1992 - 30 Sep. 1993
Nevin L. Rupert and Fred I. Grace Jan. 1995 46 p
(DA Proj. 1L1-62618-AH-80)
(AD-A291176; ARL-TR-666) Avail: CASI HC A03/MF A01

The use of semi-infinite, bielement targets arises from the previous development of the depth of penetration (DOP) testing for ranking ceramic materials. Performance is measured by the DOP of a long rod penetrator into a semi-infinite steel backplate after passing through a ceramic applique. Here, an additional step was taken before evaluating a ceramic applique. Metallic bi-element targets were tested to identify possible nonmaterial-related effects present in DOP testing. As a result, this work identifies and postulates a dynamic effect inherent in both metal/metal and ceramic/metal bielement targets, establishing a clear separation between kinematic effects and ceramic responses. DTIC

N95-30008*# National Aeronautics and Space Administration. Lewis Research Center, Cleveland, OH.
HIGH-TEMPERATURE OPTICAL WINDOW DESIGN
Norman Roeloffs (Aerospace Design and Fabrication, Inc., Brook Park, OH.) and Nick Taranto May 1995 13 p
(RTOP 537-02-20)
(NASA-TM-106783; E-9236; NAS 1.15:106783) Avail: CASI HC A03/MF A01

A high-temperature optical window is essential to the optical diagnostics of high-temperature combustion rigs. Laser Doppler velocimetry, schlieren photography, light sheet visualization, and laser-induced fluorescence spectroscopy are a few of the tests that require optically clear access to the combustor flow stream. A design was developed for a high-temperature window that could withstand the severe environment of the NASA Lewis 3200 F Lean Premixed Prevaporized (LPP) Flame Tube Test Rig. The development of this design was both time consuming and costly. This report documents the design process and the lessons learned, in an effort to reduce the cost of developing future designs for high-temperature optical windows. Author

N95-30049# Technische Univ., Delft (Netherlands).
GRADIENT-DEPENDENT PLASTICITY IN NUMERICAL SIMULATION OF LOCALIZATION PHENOMENA Ph.D. Thesis
J. Pamin 7 Nov. 1994 144 p
(PB95-197257; ISBN-90-407-1042-2) Copyright Avail: CASI HC A07/MF A02

In this thesis we focus our attention on the computational mechanics of frictional materials, in particular granular materials (soils) and quasi-brittle materials (concrete). They are characterized by highly nonlinear stress-strain and volume change relations and their failure usually involves strain localization in the form of shear bands or cracks. We use the framework of plasticity theory, which is a natural choice for the description of soil behavior but can also be adapted to give meaningful results for quasi-brittle materials like concrete and rock. However, the used theory of the rate-independent plastic flow is not classical: to preserve well-posedness of the governing equations we incorporate higher-order gradients of plastic strains in the definition of the yield function. The main objective of this work is thus a finite element implementation of an enhanced elasto-plastic continuum model for the analysis of localized deformation in softening materials. Our aim is not a formulation or verification of an accurate or general constitutive model for soil or concrete, but the development of a regularization methodology (localization limiter) that prevents the loss of well-posedness and its negative consequences in numerical analysis. NTIS

N95-30119# Army Armament Research, Development and Engineering Center, Watervliet, NY. Benet Lab.
FATIGUE LIFE ANALYSIS AND TESTS FOR THICK-WALLED CYLINDERS INCLUDING EFFECTS OF OVERSTRAIN AND AXIAL GROOVES Final Report
J. H. Underwood (Northumbria Univ., Newcastle-upon-Tyne, England.) and A. P. Parker (Northumbria Univ., Newcastle-upon-Tyne, England.) Sep. 1994 24 p Presented at the ASME Pressure Vessel Conference, Minneapolis, MN, 19-23 June 1994 Submitted for publication in ASME Journal of Pressure Vessel Technology
(AD-A290931; ARCCB-TR-94038) Avail: CASI HC A03/MF A01

A fracture mechanics-based fatigue life analysis was developed for pressurized thick-walled cylinders autofrettaged by overstrain and with one or several semi-elliptical-shaped axial grooves at the inner diameter. The fatigue life for a crack initiating at the root of the groove was calculated for various cylinder, groove, and crack configurations and for different material yielding condition. Comparisons were made with fatigue crack growth and laboratory life results from A723 thick-walled cylinders in which cannon firing tests were first performed to produce axial erosion grooves, followed

by cyclic hydraulic pressurization to failure in the laboratory. The life analysis, with an initial crack size based on the expected preexisting defects, gave a good description of the crack growth and fatigue life of the tests for cylinders with and without grooves. General fatigue life calculations summarized important and configurational effects on the fatigue life design of overstrained cylinders, including effects of material yield strength, cylinder diameter ratio, stress concentration-factor, and initial crack size. DTIC

N95-30123# Stanford Univ., CA. Dept. of Mechanical Engineering.
MATHEMATICAL MODELING AND NUMERICAL SIMULATION OF THE DYNAMICS OF FLEXIBLE STRUCTURES UNDERGOING LARGE OVERALL MOTIONS Final Report
J. C. Simo 1994 16 p
(Contract F49620-91-C-0048)
(AD-A291139; AFOSR-95-0079TR) Avail: CASI HC A03/MF A01

This document is a final report of the research sponsored by AFOSR under contract No. F49620-91-C-0048-P0002 with Stanford University. This research effort focused on the mathematical modeling and numerical simulation of the dynamics of flexible structures undergoing large overall motions. The results reported below fall within the following areas: (1) Enhanced numerical models for shell intersections, (2) Asymptotic methods for nonlinear shells, and (3) Conserving time-stepping algorithm s for nonlinear dynamics. DTIC

N95-30169# Technische Univ., Eindhoven (Netherlands). Dept. of Mathematics and Computing Science.
BOUNDARY ELEMENT ALGORITHMS FOR SOMIGLIANA'S IDENTITY
D. A. Overdijk Aug. 1994 15 p
(PB95-206959; MEMO-COSOR-94-25) Avail: CASI HC A03/MF A01

In this paper we present a method for the evaluation of the finite part or Cauchy principal value of singular surface integrals occurring in boundary element methods. In section 1 we briefly discuss Somigliana's identity. This identity is the starting point for the calculation of elastic deformation and stress in elastostatics by use of boundary element methods. In section 2 we describe the boundary element approximation of the geometry of the elastic solid under consideration. If the source point of the fundamental solution of the Navier-Cauchy equilibrium equation is a vertex of a triangular element of the boundary element mesh, then the integration over that triangle must be performed analytically. For the evaluation of the finite part or Cauchy principal value of singular integrals we use a two-dimensional version of the theorem of Gauss. In section 3 we present the formulas for these integrals for implementation in boundary element algorithms in elastostatics based on Somigliana's identity. NTIS

N95-30206 Technische Univ., Delft (Netherlands). Faculty of Aerospace Engineering.
ELASTOPLASTIC BUCKLING ANALYSIS OF CYLINDRICAL SHELLS USING A SEMI-ANALYTICAL FORMULATION Ph.D. Thesis
E. Deerenberg 31 Oct. 1994 184 p Limited Reproducibility: More than 20% of this document may be affected by poor print and microfiche quality
(PB95-197349; ISBN-90-9007614-X) Copyright Avail: Issuing Activity (National Technical Information Service (NTIS))

In this thesis, a semi-analytical formulation for the buckling analysis of circular cylindrical shells is described that takes into account the combined effects of initial geometric imperfections, elastoplastic material behavior and boundary conditions. The model is based on small strains-moderate rotations shell theory. The governing equations are formulated as a coupled set of first-order ordinary differential and algebraic equations. The basic variables in these equations are the variables that can be prescribed at the shell edges. The model described in this thesis is valid for cylinders with a multi-layer wall construction that may be loaded by axial compression, external pressure and/or torsion. The governing differential/algebraic equations are solved using Newton-type iteration methods. Separate equations are formulated for the bifurcation analysis of axisymmetric prebuckling states and an efficient solution method for the eigenvalue problem is described. The correctness of the formulation is checked by analyzing a number of elastic and elastoplastic buckling problems of perfect and imperfect shells. NTIS

N95-30210# Sandia National Labs., Albuquerque, NM.
HEALTH MONITORING OF OPERATIONAL STRUCTURES: INITIAL RESULTS
G. James, R. Mayes, T. Carne, T. Simmermacher (Houston Univ., TX.), and J. Goodding (CSA Engineering, Inc., Palo Alto, CA.) 1995 12 p Presented at the AIAA Adaptive Structures Conference, New Orleans, LA, 13-14 Apr. 1995
(Contract DE-AC04-94AL-85000)
(DE95-008551; SAND-95-0345C; CONF-950444-2) Avail: CASI HC A03/MF A01

Two techniques for damage localization (structural translational and rotational error checking - STRECH, and matrix completion - MAXCON) are described and applied to operational structures. The structures include a horizontal axis wind turbine (HAWT) blade undergoing a fatigue test and a highway bridge undergoing an induced damage test. STRECH is seen to provide a global damage indicator to assess the global damage state of a structure. STRECH is also seen to provide damage localization for static flexibility shapes or the first mode of simple structures. MAXCON is a robust damage localization tool using the higher order dynamics of a structure. Several options arc available to allow the procedure to be tailored to a variety of structures. DOE

N95-30293# Asian Office of Aerospace Research and Development, APO San Francisco, CA. Air Force Office of Scientific Research.
VISIT TO THE LABORATORY FOR EVALUATION AND FAILURE PREVENTION OF MATERIALS, TOYOHASHI UNIVERSITY OF TECHNOLOGY, 17 OCT 94
P. McQuay 17 Oct. 1994 3 p
(AD-A292340; AOARD-TR-94-33) Avail: CASI HC A01/MF A01

This report summarizes a visit to the Laboratory for Evaluation and Failure Prevention of Materials, Toyohashi University of Technology, on 17 Oct 94. Discussions were held regarding a research proposal from Professor Niinomi to compare the microstructure/property effects of several emerging low cost Ti alloys from Japan and the U.S. Prof Niinomi's laboratory is well equipped to conduct static and dynamic fracture studies on a wide range of engineering materials, from very tough and strong steel and Ti alloys, to very brittle glasses and ceramics. DTIC

N95-30328*# National Aeronautics and Space Administration. Marshall Space Flight Center, Huntsville, AL.
ANALYSIS OF STRESS CONCENTRATION IN THE DUTTON GROOVE REGIONS OF THE SUPER LIGHTWEIGHT EXTERNAL TANK
R. Ahmed Washington May 1995 36 p Original contains color illustrations
(NASA-TM-108490; NAS 1.15:108490) Avail: CASI HC A03/MF A01; 16 functional color pages

Because the 2195 aluminum-lithium material of the super lightweight external tank (SLWT ET) has a lower toughness than the 2219 aluminum used in previous ET's, careful attention must be paid to stress concentrations. This report details the analysis performed on some of the stress concentrations in the orthogrid panels of the liquid hydrogen tank. Author

N95-28847*# National Aeronautics and Space Administration. Langley Research Center, Hampton, VA.
TECHNOLOGY INTEGRATION BOX BEAM FAILURE STUDY
M. J. Shuart, Damodar R. Ambur, D. D. Davis, Jr., R. C. Davis, G. L. Farley, C. G. Lotts, and J. T. Wang *In its* Third NASA Advanced Composites Technology Conference, Volume 1, Part 2 Jan. 1993 p 951-965 (For primary document see N95-28823 10-24)
Avail: CASI HC A03/MF A04

N95-28848*# National Aeronautics and Space Administration. Langley Research Center, Hampton, VA.
A GLOBAL/LOCAL ANALYSIS METHOD FOR TREATING DETAILS IN STRUCTURAL DESIGN
Mohammad A. Aminpour (Analytical Services and Materials, Inc., Hampton, VA.), Susan L. McCleary (Lockheed Engineering and Sciences Co., Hampton, VA.), and Jonathan B. Ransom *In its* Third NASA Advanced Composites Technology Conference, Volume 1, Part 2 Jan. 1993 p 967-986 (For primary document see N95-28823 10-24)
(Contracts NAS1-19317; NAS1-19000)
Avail: CASI HC A03/MF A04

42 GEOSCIENCES (GENERAL)

No abstracts in this category.

43 EARTH RESOURCES AND REMOTE SENSING

Includes remote sensing of earth resources by aircraft and spacecraft; photogrammetry; and aerial photography.
For instrumentation see *35 Instrumentation and Photography.*

N95-28929# Instituto de Pesquisas Espaciais, Sao Jose dos Campos (Brazil).
MONITORING OF BURNING IN THE BRAZILIAN CERRADO REGION USING AVHRR/NOAA DATA CALIBRATED BY TM/LANDSAT DATA M.S. Thesis [MONITORAMENTO DE QUEIMADAS NA REGIAO DOS CERRADOS UTILIZANDO DADOS AVHRR/NOAA CORRIGIDOS POR DADOS TM/LANDSAT]
Alfredo DaCostaPereiraJunior Mar. 1992 230 p In PORTUGUESE Original contains color illustrations
(INPE-5490-TDI/507) Avail: CASI HC A11/MF A03

Images from AVHRR/NOAA sensor were used to detect burnings on the Brazilian cerrado region in the dry season of 1989. Data were tested against TM/Landsat high spatial resolution images in a calibration area. Active burnings were best detected with AVHRR band 3, while TM band 4 defined better the burned areas through the scars left by the fires; both sensors characterized the burnings as low grey level areas. Temporal behavior showed that most burnings happened during the second half of August, with frequency reaching 9 thousand points of burning per day. It was found that detection made by AVHRR underestimated by about 26 percent the number of burnings. Some regions concentrated higher number of burnings: (1) south of Maranhao; (2) central-east of Tocantins; (3) central-west of Bahia; (4) central-east and central-west of Mato Grosso; and (5) central-south of Goias. AVHRR datashowed that fire is used more intensively on wooded savanna unities, savanna parklands and anthropic activity areas, indicating that natural vegetation areas were transformed into farmlands during the 1980 decade. Linear regression between classified burnings by AVHRR/NOAA and TM/Landsat had a R(sup 2) of 0.63. From the regression equation, an estimate of the total area burned resulted in 196 thousand sq km, corresponding to 9 percent of the Brazilian cerrado region. Author

N95-28931 Naval Research Lab., Bay Saint Louis, MS.
A COMPREHENSIVE ANALYSIS OF NAVY AND MARINE CORPS DIGITAL MAPPING, CHARTING, AND GEODESY REQUIREMENTS FOR MODELING AND SIMULATION Final Report
Kevin B. Shaw, Steven Kuder, Susan V. Carter, Sharon D. Coughlan, and Julian P. Richard 9 Jan. 1995 84 p Limited Reproducibility: More than 20% of this document may be affected by microfiche quality
(AD-A291601; NRL/FR/7441-93-9435) Avail: Issuing Activity (Defense Technical Information Center (DTIC))

The Naval Research Laboratory conducted an extensive in-person survey of the Navy and Marine Corps modeling and simulation (M&S) community's digital Mapping, Charting, and Geodesy (dMC&G) and value-added data requirements during late 1992 and early 1993. Simultaneously, the Air Force, the Army, and the National Security Agency (NSA) conducted similar studies for their respective services/agencies. Over 100 programs responded to this Navy study. This report presents an analysis of the collected requirements and emphasizes identifying feature, attribute, and value-added information that the M&S community requires but that is currently not available. Attention is given to required modifications to existing DMA dMC&G products. This report seeks to identify modifications to emerging and existing DMA products needed for optimum use by the Navy M&S community, and focuses only on the changes and improvements. DTIC

N95-29175* National Aeronautics and Space Administration, Washington, DC.
NASA TO USE TELEPRESENCE TO EXPLORE ANTARCTIC LAKES (Videotape)
4 Sep. 1992 Videotape: 5 min. 30 sec. playing time, in color, with sound (NASA-TM-110567; AAV-1427; NONP-NASA-VT-95-46002) Avail: CASI HC A01/MF A01

Scenes of Antarctic lakes using telepresence are contained in this video. Dr. Carol Stroker, a scientist from Ames Research Center, explains how images from a camera on a remote vehicle are projected directly into your eyes so that your entire field of view is filled with the information from these images. She also states that Virtual Reality would help to expand the range of access we have to Mars and would allow robots to do scientific work. CASI

N95-29281 Massachusetts Inst. of Tech., Cambridge, MA. Lincoln Lab.
THE DETECTION OF OIL SLICKS AT NIGHT WITH AIRBORNE INFRARED IMAGERS Final Report, Oct. 1993 - Apr. 1994
G. M. Daniels and G. L. Hover Dec. 1994 84 p Limited Reproducibility: More than 20% of this document may be affected by microfiche quality
(Contract F19628-90-C-0002)
(AD-A289731; USCG-D-30-94) Avail: Issuing Activity (Defense Technical Information Center (DTIC))

The detection of oil slicks on the ocean is a Coast Guard priority. Daytime detection in clear weather is routine; but nighttime detection requires sophisticated imaging sensors. Infrared imagers have demonstrated some capability to detect oil slicks at night in the marine environment. Infrared imagers sense the thermal radiation, and its variations, in a scene rather than the reflected radiation. Gimbal-mounted thermal imagers operating in the 8-12 micron region are currently flown on Coast Guard aircraft. This study compared the performance of these imagers with hand-held imagers operating in the 3-5 micron region. The comparison was primarily theoretical with semi-quantitative support from an uncalibrated data base of infrared images taken with various sensors. It was found theoretically, and supported by image data, that the 8-12 micron instruments produced images with better water-oil contrast at night. This differential behavior was theoretically predicted to hold over a wide range of environmental conditions. The differential behavior was traced to the fact that the optical properties of water and oil are more different in the 8-12 than in the 3-5 micron bands. The utility of night-vision imagers or low-light level TV's was also assessed. Calculations indicated that typical water-oil contrasts would not be seen with current sensors. Image data appearing to contradict this conclusion was found to be defective in the sense that the conditions of the experiments were not representative of operational conditions. It is recommended that: the use of 8-12 micron imagers be continued for oil slick searches at night and the potential of new night-time imaging devices be assessed. DTIC

N95-29433# Instituto de Pesquisas Espaciais, Sao Jose dos Campos (Brazil).
OPTICAL (LANDSAT/TM) AND RADAR (ERS-1/SAR) IMAGERY SINERGISM STUDIES APPLIED TO LAND USE DISCRIMINATION M.S. Thesis, Jun. 1994 [ESTUDO DA COMPLEMENTARIDADE DE IMAGENS OTICAS (LANDSAT/TM) E DE RADAR (ERS-1/SAR) NA DISCRIMINACAOTEMATICA DE USO DA TERRA]
Tatianna Mora Kuplich Oct. 1994 124 p In PORTUGUESE Original contains color illustrations
(INPE-5608-TDI/554) Avail: CASI HC A06/MF A02

This work presents the results of a comparative analysis between products of two kinds of sensors used for target discrimination: SAR images of the ERS-1 satellite and TM images of the LANDSAT-5 satellite. The test area has 361 km(sup 2) and is located in the northwest of Campinas city, Sao Paulo state, Brazil. This area has several classes of land use, including urban, agricultural and forestal targets. The different images were registered, the SAR images were filtered with an average filter, and the Principal Components Transformation was applied. All the Principal Components (from SAR filtered, SAR, TM and coregistered TM+SAR and TM+SAR filtered images) were classified by Maximum Likelihood. Tests of goodness of fit were also made to assess the adequacy of the Maximum Likelihood technique and the statistical properties of the images. The results confirmed by Kappa statistics show a significant improvement of the classification when the Principal Components of coregistered filtered

SAR+TM images were used for urban, pasture and forest classes. The complementarity between SAR and TM images were observed, mainly on the strong radar returns coming from urban areas and produced by corner reflections. It should be emphasized that it is very important to filter SAR images in order to reduce the speckle noise (for this type of the analysis). Author

N95-29523# Princeton Univ., NJ. Dept. of Chemistry.
RETRIEVAL DISPLAY AND ANALYSIS SUPPORT TOOL REQUIREMENTS ANALYSIS Final Report
Gary A. Stahl Oct. 1994 69 p
(Contract DLA900-88-D-0392)
(AD-A291448; ERIM-253850-4-T) Avail: CASI HC A04/MF A01

This report establishes a methodology for assessing the information and data requirements of users of remote sensing within the U.S. Government. The parameters needed for characterizing data requirements are identified and related to the parameters of available sensors. In the course of performing the requirements analysis a sizable database of users, information requirements and sensors was developed. DTIC

N95-29539 Iowa Univ., Iowa City, IA.
HYDROLOGY OF THE CONTINENTAL UNITED STATES Ph.D. Thesis
Alexandre Kolodynski Guetter 1993 433 p
Avail: Univ. Microfilms Order No. DA9421133

Continental hydrologic processes are examined through a diagnostic study of the temporal and spatial scales of the response of U.S. aggregate streamflow to variations in the forcing atmospheric circulation, precipitation, and temperature. Ten independent regions of coherent streamflow variability are defined within the conterminous U.S. The seasonality and persistence characteristics of each region are identified using a rotated principal component analysis of the aggregate outflow over three-degree lat/lon segments along the US boundary for the period 1939-1988. The scaling properties of daily streamflow for the coherent regions and subregions establish the appropriate scales for studies of surface water balance, soil moisture inferences, and investigation of the association between streamflow and circulation. The average specific outflow for the U.S. is found to be 210 mm/year, with a strong seasonal cycle. Dominant modes of U.S. streamflow variability are identified at 10.7 and 3.6 years. High-frequency scaling invariance exists for periods shorter than 10-30 days, regardless of the size of the basin. The spectral properties of streamflow are examined through dimensional analysis, and they support the hypothesis that an equilibrium subrange exists in analogy to turbulence, with a variance cascade mechanism to transfer energy from large to smaller scales. Within the equilibrium subrange, the streamflow spectrum has a power-law exponent ranging from -5/3 to -11/3, with lower values corresponding to higher-dimensional anisotropy. For the southeastern coherent region identified, the exponent remains remarkably constant for drainage areas ranging from 10(exp 3) to 10(exp 6) sq km. Furthermore, for that coherent region, soil water content identified from water budget computations shows temporal anomalies that remain similar for scales ranging from 10(exp 4) to 10(exp 6) sq km. Composite-pattern analysis with seasonal resolution is used to diagnose low-frequency associations between the temporal variability of streamflow patterns and the forcing tropospheric circulation, precipitation, and temperature anomalies. Precipitation forcing anomalies resulting in high and low streamflow are of a mesoscale extent. Their location and size are substantially independent of the size of the associated drainage basin within a coherent region. Dissert. Abstr.

N95-29540 Boston Univ., MA.
MODELING THE DIRECT-BEAM INSTANTANEOUS SPECTRAL SURFACE ALBEDO OF A FOREST LANDSCAPE USING GEOMETRIC-OPTICS AND A DISTRIBUTED PARAMETER APPROACH Ph.D. Thesis
Crystal Lynn Barker Schaaf 1994 122 p
Avail: Univ. Microfilms Order No. DA9422509

Since realistic surface albedos are required to initialize a variety of climate, weather, and energy budget models, there is a great deal of interest in the ability of fairly simplistic physical models, such as the Li-Strahler geometric-optical model, to accurately simulate surface hemispherical reflectance. This model was originally formulated to determine the bidirectional reflectance distribution function (BRDF) of a canopied surface. Geometric-optics and Boolean set theory are used to determine the areal proportions of shadowed and sunlit canopy and background associated with a particular view angle and illumination condition. These areal proportions are then weighted by independently determined spectral signatures characteristic of each shadowed or sunlit component. By integrating over all view angles, the model has been extended to also provide a hemispherical reflectance or surface albedo of the canopy. In this study, while exploring the sensitivity of the modeled bidirectional and hemispherical reflectances to illumination angle, the importance of accurate and timely component signatures was highlighted. A need to intensify the sunlit component signature (due to crown mutual shadowing) was identified and incorporated. The model was then successfully validated with data of a spruce forest collected during the 1990 Forest Ecosystem Dynamics Multisensor Aircraft Campaign. Not only were the necessary forest shape parameters and component signatures available for model initialization, but there were directional radiances from Advanced Solid State Array Spectroradiometer overflights and pyranometer measurements from the site to serve as validation data. Once validated for level terrain, the geometric-optical model was then modified to accommodate a sloping surface by assuming that the model domain (simulating a sensor field of view) is smaller than the slope and then transforming the geometric relationships among the illumination angle, view angle, and tree shape into the coordinate system of the slope. With the incorporation of topography, it was possible to compute direct beam surface albedos for an entire landscape. Using realistic landcovers and topography, a section of the Sierra Nevada was simulated. Canopies on gentle to moderate slopes generated surface albedos sufficiently similar to those from flat surfaces to suggest that albedo values can be confidently scaled to coarser resolutions. Although most land remote sensing is currently performed at fine resolutions, future instruments, such as the Moderate Resolution Imaging Spectroradiometer, will operate at resolutions as coarse as 1 km. These results suggest that simple schemes, such as geometric-optical models, will be of use in simulating both directional and hemispherical reflectance at a variety of scales. Dissert. Abstr.

N95-29703 Missouri Univ., Columbia, MO.
MAIZE YIELD ESTIMATION THROUGH THE SIMULATION OF RADIATION PENETRATION INTO THE CANOPY Ph.D. Thesis
David Kasina Musembi 1993 126 p
Avail: Univ. Microfilms Order No. DA9423985

It is essential for planning purposes to be able to assess or predict the output of vital crops in order to develop strategies to cope with shortfalls or surpluses with sufficient lead time. This is usually done by developing yield prediction models based on well specified production factors. Crop yield results from the interaction among plant, physical and environmental factors. Radiation is a key environmental factor in this regard and the principal driver of the biological system. When all the other conditions are optimum, productivity is a function of the available energy and the size of the plant surface able to trap it. However, the distribution of radiation within the plant canopy is uncertain. The objectives of this study were to determine whether the light extinction coefficients of three maize hybrids of different morphological description are different; whether these coefficients change with time during the growing season; and attempt to establish the nature of the relationships between biomass accumulation and the observed morphological plant characters. The extinction coefficients of the three hybrids were not significantly different. They increased with vegetative growth to reach maxima at anthesis and decreased subsequently as the crops approached physiological maturity. These coefficients were used to fit Beer-Bougher type regressions for predicting light penetration into the various canopy levels. There were significant differences in light penetration, among the hybrids, during the growing season as well as within each day. The largest leaf area (index) and the highest light absorption occurred at the top layer of the canopies. Moreover, the highest light penetration into the canopies does not appear to take place at zenith but seems to occur when the solar elevation and leaf angles reach certain critical values. Leaf area index (LAI) had the greatest effect on light penetration during the growing season while the effect of leaf angle was secondary and more manifest after anthesis. Biomass and grain yields were not significantly different among the hybrids and a lower LAI seemed to favor a higher light use efficiency. No correlation was found between biomass and LAI. Consequently, no method was developed to predict biomass accumulation in the study. Growing conditions were sub-optimal in a few occasions

during the season which, together with inadequate instrumentation, made it difficult to isolate the effects of extraneous factors from those of the main factors. Recommendations are given for conducting the experiment to insure better results. Dissert. Abstr.

N95-29730 Colorado Univ., Boulder, CO.
DEPICTING DUST AND SAND STORM SIGNATURES THROUGH THE MEANS OF SATELLITE IMAGES AND GROUND-BASED OBSERVATIONS FOR SAUDI ARABIA Ph.D. Thesis
Sameer Abdulelah Bukhari 1993 141 p
Avail: Univ. Microfilms Order No. DA9423473

Dust/sand storms are serious hazards to human activities in Saudi Arabia. Visibility is greatly reduced for aviation operators, and the abrasive effects are very discomforting to personnel and detrimental to structures and equipment. The orientation of the Arabian Peninsula and the northwesterly prevailing surface wind over much of the area lends itself to a long fetch and to well-developed dust/sand storms that can continue for many days. Therefore, a requirement exists for the Saudi Arabian Meteorological and Environmental Protection Administration (MEPA) to develop the capability to detect, monitor, and predict the behavior of dust/sand storms. This in-depth research program, using a combination of satellite infrared and visual images and related ground-based climatological data, has increased our understanding of satellite sensor capabilities to detect weak signature phenomena such as dust/sand storms and has made it possible to better detect and monitor the evolution of these storms in the Kingdom. Different satellite data channel combinations were used to describe different aspects of these storms. Combined geostationary and polar orbiting satellite data were used to develop a capability to monitor and describe these storms. This thesis will enable MEPA to provide improved dust/sand storm detection and forecasting services to users and has provided data sets for additional research and forecaster training.
Dissert. Abstr.

N95-29754*# Hydex Corp., Vienna, VA.
REMOTE SENSING OF HYDROLOGIC VARIABLES IN BOREAL AREAS Final Report
Eugene L. Peck and Thomas R. Carroll (National Oceanic and Atmospheric Administration, Chanhassen, MN.) May 1995 28 p Original contains color illustrations
(Contract NAS5-32336)
(NASA-CR-189422; Rept-H355; NAS 1.26:189422) Avail: CASI HC A03/MF A01; 1 functional color page

During Phase 2 airborne Gamma Radiation measurements were conducted over 48 BOREAS flight lines. Ground measurements of the soil moisture (SM) of the mineral soil and of the depth and water content (WC) of the moss/humus layer were collected for calibration of the flight lines. Special attention has been given to the flight lines over and near the primary tower sites in the southern study area (SSA): Old Black Spruce (OBS), Old Jack Pine, Old Aspen, and Young Aspen. Multiple ground surveys (September 1993; July, August, and September 1994) show the variation of the water content of the moss/humus layers and changes in the amount of standing water near the SSA, OBS tower during the period September 1993 to September 1994. All ground data, airborne estimates and locations of flight lines and ground sampling points have been submitted to BORIS (Boreas Information System). On 8-10 September 1994 exceptionally high values of cosmic radiation were observed by the airborne gamma radiation system over the SSA. Follow-up investigation has not determined the source of, or what caused, the high cosmic count rates.
Author

N95-29815# Instituto de Pesquisas Espaciais, Sao Jose dos Campos (Brazil). Ministry of Science and Technology.
PROPOSAL FOR A FLEXIBLE SYSTEM OF PHYTOGEOGRAPHIC CLASSIFICATION: EMPHASIS ON THE USE OF MULTISTAGE REMOTE SENSORING [PROPOSTA DE UM SISTEMA FLEXIVEL DE CLASSIFICACAO FITOGEOGRAFICA: ENFASE NO USO DE SENSORIAMENTO REMOTO MULTIESTAGIO]
Vitor Celsode deCarvalho Jan. 1995 63 p In PORTUGUESE Presented at the Round Table Session: Phytogeographic Systems of Classification in Brazil, at the National Botany Congress, Ribeirao Preto, Brazil, 27 Jan. 1995
(INPE-5609-PRE/1821) Avail: CASI HC A04/MF A01

The threat of extinction of limited vegetal resources and their economic importance is becoming increasingly obvious in today's world. These facts, together with the process of ecological awareness which has been in evidence in the last decades, has led to an increase in efforts to carry out research and development into both the study and protection of the little remaining natural vegetation which covers the earth. The task of classifying and mapping the vegetation can be considered a basis for the guidance of these endeavors. In spite of pioneering attempts, according to Kuchler (1982), Brazil still possesses only vague knowledge of its natural vegetation. However, efforts made in the last few years have allowed the aforementioned author to conclude that the mapping of vegetation in Brazil could be rapidly expanded and could contribute significantly to the development of the country and to the knowledge of its vegetal resources. Mapping on a continental scale (Map of the Vegetation of South America - UNESCO, 1981) on a national scale (Map of the Vegetation of Brazil - IBGE/IBDF, 1988) and on a regional scale (Maps of the Vegetation from Leaves to the Millionth Part - RADAMBRASIL Project, 1973-1987) all reflect the strength of this resumption of effort to study Brazilian vegetation. Despite a long tradition of study on the subject reflected in a voluminous body of scientific works as mentioned by KUCHLER (1988), there is still no satisfactory system of classification for the general necessities of this area of research. A large part of this effort has been characterized by the collection of data in situ, and this data has concentrated on the description of the most important characteristics of the vegetation. In addition to being long overdue, these projects have been characterized both by their high cost and limitations in terms of the area and frequency of observations made.
Derived from text

N95-29821 Princeton Univ., NJ.
MICROWAVE REMOTE SENSING OF SURFACE SOIL MOISTURE AND ITS APPLICATION TO HYDROLOGIC MODELING Ph.D. Thesis
Dah-Syang Lin 1994 178 p
Avail: Univ. Microfilms Order No. DA9424711

This thesis addresses the problems associated with the retrieval of surface soil moisture distributions from microwave remote sensing measurements, and the application of this information to hydrologic simulations. A qualitative analysis of aircraft radar and radiometer data collected from two field campaigns is conducted to examine the sensors' behavior under various land surface conditions. For the Slapton Wood catchment in Devon, England, the analysis results indicate that existing soil moisture retrieval algorithms and theoretical scattering models often produce biased estimates; and there is a need to develop new algorithms for the NASA Jet Propulsion Laboratory airborne Synthetic Aperture Radar (AIRSAR) -- the sensor used in the experiments. A signal simulation procedure based on a calibrated coupled vegetation surface scattering model, is developed to enhance the limited experimental data set. Two different techniques (stepwise regressions and artificial neural networks) are employed to devise semi-empirical retrieval algorithms for grass covered areas. Results from a verification study based on 250 hypothetical conditions indicate that the average root mean square error of volumetric soil moisture estimates is approximately 3 to 7 percent when assuming no a priori information concerning the illuminated areas. For the Mahantango catchment in central Pennsylvania, linear regression models are developed to relate AIRSAR backscatters with soil moisture. The microwave derived soil moistures are compared with ground measurements and predictions from hydrologic models. The results suggest that both passive and active sensors correctly reflect the temporal variations of soil moisture. The model predictions based on the standard streamflow-derived initial condition significantly overestimate the surface soil moisture content. A two-layer process-based hydrologic model is developed to improve the simulations. This model uses remotely sensed soil moistures as a feedback to adjust the catchment average water table depth and obtains satisfactory results in good agreement with field measurements. The simulation results point out that for small areas such as the studied catchment, the advantage of finer spatial resolution soil moisture information upon hydrologic simulations is not decisive. Finally, a systematic framework is constructed to fully incorporate multi-temporal soil moisture data from future satellite Sensors into the developed hydrologic model. Dissert. Abstr.

N95-29866# Montana State Univ., Bozeman, MT. Dept. of Civil Engineering and Engineering Mechanics.

CHANGES IN MICROSTRUCTURAL PARAMETERS OF SNOW DURING DEFORMATION Final Report, Sep. 1991 - Aug. 1994

Robert L. Brown 24 Dec. 1994 10 p

(Contract DAAL03-91-G-0310)

(AD-A290887; ARO-28040.1-GS) Avail: CASI HC A02/MF A01

This study utilized quantitative and morphology theory to describe the microstructure of cohesive granular materials and to relate microstructure to mechanical and physical properties. Snow was used as the experimental material. A unique feature of the theory developed in this grant involved the description of the necked areas which are the intergranular restricted regions which tie the grains together to form a bonded granular material. Using a set of criteria to specify what would constitute a neck, the formulation was developed to automatically identify the necks and determine their geometry as they appeared in surface sections. For the three-dimensional properties, the necks were modeled as double truncated cones in order to provide an accurate description of the neck geometry and volume. Stereology theory was then used to calculate the three dimensional properties of the necks based on this model. In addition, other features such as pore size, grain size, coordination number and density were found. The final computer code consisted of approximately 150,000 lines of code and represents a very effective and automated means of describing cohesive granular materials. Finally an elastic-viscoplastic constitutive relation utilizing microstructure of the material was developed and validated against experimental data. DTIC

N95-29905# Asian Office of Aerospace Research and Development, APO San Francisco, CA. Air Force Office of Scientific Research.

JAPANESE REMOTE SENSING ORGANIZATIONS, RESEARCH, AND TECHNOLOGY

Franklin P. Mills 14 Jun. 1994 53 p

(AD-A292420; AOARD-TR-94-14) Avail: CASI HC A04/MF A01

Remote sensing research and satellite remote sensing technology have been selected by the Japanese government for government-sponsored commercial development. This report provides an overview of some of the remote sensing programs sponsored by the Ministry of International Trade and Industry (MITh), the National Space Development Agency (NASDA), and the Ministry of Education, Science, and Culture (Monbusho). It describes many of the key organizations, evaluates some of their research efforts, and assesses Japanese infrared remote sensing technology. Two Japanese organizations have good research programs in geophysics and remote sensing. The Center for Climate System Research (CCSR) is retrieving cloud properties from satellite data, modeling the effects of clouds on climate, and modeling the East Asian climate. The Meteorological Research Institute (RRI) is developing radiative transfer codes for an inhomogeneous surface beneath a multiply-scattering atmosphere for retrieving land surface characteristics from satellite measurements. Japanese commercial satellite remote sensing technology, currently, is roughly one to two generations behind US capabilities. However, Japan is developing a multispectral remote sensing instrument for a 1998 NASA satellite that will roughly match (or exceed) the capabilities of all existing commercial remote sensing satellite (from any country). It will have three bands in the 0.5 - 0.9 micrometer region with 15 meter pixel size, six bands in the 1.5 - 2.5 micrometer region with 30 meter pixel size, five bands in the 8.0 - 12.0 micrometer region with 90 meter pixel size, and same bit stereo imaging. DTIC

N95-29977# Naval Research Lab., Bay Saint Louis, MS.

DIGITAL MAPPING, CHARTING, AND GEODESY ANALYSIS PROGRAM TECHNICAL REVIEW OF VECTOR SMART MAP PROTOTYPES 1 AND 2 Final Report

H. V. Miller, Steve Kuder, Susan V. Carter, Hillary C. Mesick, and Julian P. Richa 19 Jan. 1995 49 p

(NR Proj. R19-87)

(AD-A291217; NRL/MR/7441-94-7516) Avail: CASI HC A03/MF A01

Currently under development by the Defense Mapping Agency (DMA), the Vector Smart Map (VMAP) represents a significant step forward in digital mapping. This Vector Product Format (VPF) relational database is intended to digitally represent map sheets (e.g., Joint Operational Graphics and Topographic Line Maps) at medium (Level 1) and high (Level 2) resolutions. In an effort to optimize Naval (meaning U.S. Navy and Marine Corps) usage of such data, the Digital Mapping, Charting, and Geodesy Analysis Program (DMAP) has evaluated VMAP Prototypes 1 and 2 and has suggested modifications. The review of Prototype 1 consists mainly of a comparison with a similar DMA product, namely Digital Feature Analysis Data, which contains features that are missing from the VMAP prototype. DMAP recommends the inclusion of these features in VMAP. In Prototype 2, DMAP discovered multiple quality control errors, which were found by viewing data around Texas and Bolivia. Comparisons with another VPF product, Interim Terrain Data, led to the discovery of even more VMAP inconsistencies. DMAP recommends that VMAP remain in the prototype stage until all errors are rectified. DTIC

N95-29999# Instituto de Pesquisas Espaciais, Sao Jose dos Campos (Brazil). Ministry of Science and Technology.

EVALUATION OF THE UTILIZATION OF SAR POLARIMETRIC IMAGES IN THE SURVEY OF LAND RESOURCES IN THE AMAZON AREA TAPAJOS FOREST RESERVE [AVALIACAO DO USO DE IMAGENS SAR POLARIMETRICAS PARA LEVANTAMENTO DE RECURSOS TERRESTRES NA AMAZONIA: RESERVA FLORESTAL DE TAPAJOS]

Luciano VieiraDutra, Alejandro C. Frery, Pedro HernandesFilho, Sidnei J. S. SantAnna, and Corina daCostaFreitasYanasse 1993 7 p In PORTUGUESE Presented at the 6th Brazilian Symposium on Computer Graphics and Image Processing, Recife, Brazil, 19-22 Oct. 1993

(INPE-5517-PRE/1792) Avail: CASI HC A02/MF A01

A growing tendency in using radar imagery has been noticed in the remote sensing community. Three radar satellites have already been launched (ERS-1, Almaz-II and JERS-1). Canada plans to launch another one (Radarsat) and has planned and conducted the SAREX mission in Brazil using airborne radar, in preparation to Radarsat. One of the SAREX sites -Tapajos- was selected to test the C-band polarimetric radar capabilities on discriminating forest types and other forest related problems like deforestation. In this paper some test procedures for radar images utilization for forest discrimination are defined and intrinsic characteristics of radar images, mainly its statistical properties are defined. Author

N95-30061# Environmental Research Inst. of Michigan, Ann Arbor, MI.

RETRIEVAL, DISPLAY, AND ANALYSIS SUPPORT TOOL FOR EARTH IMAGERY (RDAST) Final Report

R. C. Anderson, C. C. Chiesa, and W. A. Tyler Sep. 1994 68 p

(Contract DLA900-88-D-0392)

(AD-A291366; ERIM-253850-5-0) Avail: CASI HC A04/MF A01

The Retrieval, Display, and Analysis Support Tool (RDAST) is a system designed to facilitate access to the wide variety of available earth imagery. Using the ARC/INFO geographic information system, RDAST converts user requirements into specific sensor parameters and searches internal and external databases for the availability of suitable imagery. Sample imagery are displayed. The current implementation is based on public systems (LANDSAT, SPOT) and several airborne collections, but is not limited to this. This document contains viewgraphs from the final briefing for this program. DTIC

N95-30247*# Colorado Univ., Boulder, CO. Center for Astrodynamics Research.

SEA ICE MOTIONS IN THE CENTRAL ARCTIC PACK ICE AS INFERRED FROM AVHRR IMAGERY Final Progress Report

William Emery, James Maslanik, and Charles Fowler Mar. 1995 26 p

(Grant NAGw-2948)

(NASA-CR-198835; NAS 1.26:198835) Avail: CASI HC A03/MF A01

Synoptic observations of ice motion in the Arctic Basin are currently limited to those acquired by drifting buoys and, more recently, radar data from ERS-1. Buoys are not uniformly distributed throughout the Arctic, and SAR coverage is currently limited regionally and temporally due to the data volume, swath width, processing requirements, and power needs of the SAR. Additional ice-motion observations that can map ice responses simultaneously over large portions of the Arctic on daily to weekly time intervals are thus needed to augment the SAR and buoys data and to provide an intermediate-scale measure of ice drift suitable for climatological analyses and ice modeling. Principal objectives of this project were to: (1) demonstrate whether sufficient ice features and ice motion existed within the consolidated ice pack to permit motion tracking using AVHRR imagery; (2) determine the limits imposed on AVHRR mapping by cloud cover; and (3) test the applicability of AVHRR-derived motions in studies of ice-atmosphere interactions. Each of these main objectives was addressed.

We conclude that AVHRR data, particularly when blended with other available observations, provide a valuable data set for studying sea ice processes. In a follow-on project, we are now extending this work to cover larger areas and to address science questions in more detail. Author

44 ENERGY PRODUCTION AND CONVERSION

Includes specific energy conversion systems, e.g., fuel cells; global sources of energy; geophysical conversion; and windpower.

For related information see also *07 Aircraft Propulsion and Power, 20 Spacecraft Propulsion and Power,* and *28 Propellants and Fuels.*

N95-28858# Naval Facilities Engineering Service Center, Port Hueneme, CA.

GEOTHERMAL HEAT PUMPS FOR HEATING AND COOLING

Suresh C. Garg Mar. 1994 4 p

(AD-A292115; NFESC-TDS-2004-ENG) Avail: CASI HC A01/MF A01

Naval Facilities Engineering Service Center (NFESC) has been tasked by Naval Shore Facilities Energy Office to evaluate the NAS Patuxent River ground-source heat pump (GHP) installation. A large part of a building's energy consumption consists of heating and air conditioning for occupant comfort. The space heating requirements are normally met by fossil-fuel-fired equipment or electric resistance heating. Cooling is provided by either air conditioners or heat pumps, both using electricity as an energy source. DTIC

N95-29103 Colorado State Univ., Fort Collins, CO.

MULTI-DECADE TIME-DEPENDENT VOLTAGE OF POLYCRYSTALLINE THIN-FILM SOLAR CELLS Ph.D. Thesis

Richard Anthony Sasala 1993 86 p

Avail: Univ. Microfilms Order No. DA9415085

The open circuit voltage of CuInSe2 and CdTe solar cells continues to increase during the time range from 10(exp -3) to 10(exp 4) s after the cell is illuminated or otherwise placed in forward bias. The effect is qualitatively similar in all samples measured to date, however, the magnitude of the voltage shift varies from 4 to 40 mV. The shift increases with increasing light intensity. The voltage shift depends on the voltage history of the sample and not the illumination history. Application of an appropriate pre-measurement bias in the dark can significantly reduce the voltage shift. When the cells remains in the dark with a constant forward current, a nearly identical voltage shift is seen. The time required for the cell to relax back to the dark zero-bias steady-state condition is similar to the time the cell has been in forward bias. The voltage increase is caused physically by long-lived traps in the depletion region which depopulate in forward bias an effective-Fermi level is introduced. the depopulation of the traps results in a net localized positive charge in the depletion region which causes a dip in the bands and change in carrier concentration. This, in turn, lowers the forward recombination current which is observed as an increasing voltage when the cell is held at constant-current. The long-lived traps are located in an energy range of 200 meV near midgap and are more highly concentrated near the metallurgical junction. The density of the traps is of the same order of magnitude as the carrier density of the p-type material. Dissert. Abstr.

N95-29200# Massachusetts Inst. of Tech., Cambridge, MA. Space Power and Propulsion Lab.

ARCING MITIGATION AND PREDICTIONS FOR HIGH VOLTAGE SOLAR ARRAYS

Renee L. Mong, James D. Soldi, Jr., and Daniel E. Hastings 26 Jul. 1994 81 p

(Contract F19628-92-K-0016)

(AD-A292227; PL-TR-94-2233; SR-1) Avail: CASI HC A05/MF A01

Future solar arrays are being designed for much higher voltages in order to meet high power demands at low currents. Unfortunately, negatively biased high voltage solar cells have been observed to arc when exposed to the low earth orbit plasma environment. Analytical and numerical models of this arcing phenomenon on conventional solar cells have been developed which show excellent agreement with experimental data. With an understanding of a mechanism for arcing, it is possible to determine methods of arc rate mitigation and to predict arc rates for experiments. Of the various arc rate mitigation methods examined in this research, decreasing the ratio of coverglass/adhesive dielectric constants and overhanging the coverglass show the most promise in reducing or even eliminating arcing. In addition, arcing rates were predicted for the high voltage biased arrays of the Air Force's Photovoltaic Array Space Power Plus Diagnostics experiment (PASP Plus). These predictions provide both expectations for the mission and a means to test the numerical and analytical models in the space environment for different solar cell technologies. Finally, a numerical model of the arc initiation process was also developed for wrap-through-contact cells. DTIC

N95-29201# Massachusetts Inst. of Tech., Cambridge, MA. Space Power and Propulsion Lab.

ARCING PREDICTIONS FOR PASP PLUS SOLAR ARRAYS

James D. Soldi, Jr. and Daniel E. Hastings 2 Aug. 1994 49 p

(Contract F19628-92-K-0016)

(AD-A292230; PL-TR-94-2234; SR-2) Avail: CASI HC A03/MF A01

Future solar arrays are being designed for much higher voltages in order to meet high power demands at low currents. Unfortunately, negatively biased high voltage solar arrays have been observed to arc when exposed to the low earth orbit plasma environment. In previous work, analytical and numerical models of this arcing phenomenon on conventional solar cells have been developed which show excellent agreement with experimental data. The analytical model has been further developed to be more physically accurate and to be able to realistically model space experiments which will be operating in a widely changing environment. With this model, predictions were made for the solar array arcing on the upcoming Air Force Photovoltaic Array Space Power Plus Diagnostics (PASP Plus) experiment. These simulations predict arcing rates ranging from 0 to 4.3 arcs/second, depending on the array and the experimental and environmental conditions. It was found that the cell thickness plays a dominant role in relative arc rates between the various cells. The large simulated database generated was used to develop software that will he used to examine and analyze the flight data, extracting correlations between arc rate and the various material properties, environmental variables, and operational parameters. DTIC

N95-29463# Pacific Northwest Lab., Richland, WA.

THE TEES PROCESS CLEANS WASTE AND PRODUCES ENERGY

D. C. Elliott and L. J. Silva Feb. 1995 8 p Presented at the R 1995 Conference, Geneva, Switzerland, 1-3 Feb. 1995

(Contract DE-AC06-76RL-01830)

(DE95-007799; PNL-SA-25504; CONF-950279-1) Avail: CASI HC A02/MF A01

A gasification system is under development that can be used with most types of wet organic wastes. The system operates at 350 C and 205 atm using a liquid water phase as the processing medium. Since a pressurized system is used, the wet waste can be fed as a solution or slurry to the reactor without drying. Through the development of catalysts, a useful processing system has been produced. The system has utility both for direct conversion of high-moisture biomass to fuel gas or as a wastewater cleanup system for wet organic wastes including unconverted biomass from bioconversion processes. By the use of this system more than 99% conversions of organic waste to medium-Btu fuel gas can be achieved. DOE

N95-29949# Phillips Lab., Edwards AFB, CA.

HIGH TEMPERATURE SPECTROSCOPY OF ALKALI METAL VAPORS FOR SOLAR TO THERMAL ENERGY CONVERSION Interim Report, Jun. 1991 - Sep. 1992

Paul S. Erdman and William C. Stwalley Nov. 1994 13 p

(AD-A291355; PL-TR-94-3000) Avail: CASI HC A03/MF A01

Solar Plasma propulsion methods proposed by the Air Force have lead to the study of high temperature optical absorption of metal vapors. The Plasma Spectroscopy Cell in the Phillips Laboratory at Edwards AFB, CA has been used to obtain an abundance of absorption spectra at temperatures approaching 2000 K and pressures of one atmosphere for lithium and sodium metal vapors. Tentative assignments of molecular transitions are improved upon by use of modern computational techniques for generating intensities of molecular transitions which possibly have been observed. Identification of contributing molecular transitions to overall absorption of

radiant energy assists the efforts to develop propulsion methods which rely on the direct absorption of solar energy. DTIC

N95-29953# Aerospace Corp., El Segundo, CA. Technology Operations.
DESIGN OF A MORE ACCURATE, HIGHER FIDELITY, DUAL-SOURCE AIR MASS ZERO SOLAR SIMULATOR
L. C. Kilmer 15 Jan. 1995 14 p
(Contract F04701-93-C-0094)
(AD-A291364; TR-94(4524)-1; SMC-TR-95-6) Avail: CASI HC A03/MF A01

A dual-source solar simulator has been designed that provides a more accurate, higher fidelity spectral match to the Air Mass Zero (AMO) solar spectrum in comparison to presently available conventional and state-of-the-art solar simulators. The dual-source solar simulator design combines the ultraviolet (UV) light from a xenon arc lamp and the visible and infrared (IR) light from a tungsten lamp using standard wide-band hot and cold mirrors. However, additional filtering is required to match the dual source and AMO spectra. It was determined that the required transmission function cannot be met with a single filter, so separate filtering of the individual sources was necessary. A standard color glass filter has been chosen to both change the shape of the xenon UV spectrum and reduce the magnitude of the high-intensity spikes in the visible and IR wavelengths. A custom thin-film filter was designed to meet the required transmission function of the visible and IR portions of the tungsten light. The combined, filtered spectra provides a more accurate spectral distribution and integral energy match to the AMO spectrum over the entire wavelength range while completely removing the common high-intensity xenon arc lamp spikes. The design is presented by comparing conventional solar simulators, identifying the limitations posed by the presence of spikes in the xenon arc lamp spectrum, analyzing each of the separate components of the design and their system impacts, and concluding with additional options or variations that may improve the accuracy range of the dual-source solar simulator. DTIC

N95-30015*# Cleveland State Univ., OH.
TRANSIENT RESPONSES OF PHOSPHORIC ACID FUEL CELL POWER PLANT SYSTEM Ph.D. Thesis
Cheng-Yi Lu Nov. 1983 310 p
(Contract NCC3-17)
(NASA-CR-198948; NAS 1.26:198948) Avail: CASI HC A14/MF A03

An analytical and computerized study of the steady state and transient response of a phosphoric acid fuel cell (PAFC) system was completed. Parametric studies and sensitivity analyses of the PAFC system's operation were accomplished. Four non-linear dynamic models of the fuel cell stack, reformer, shift converters, and heat exchangers were developed based on nonhomogeneous non-linear partial differential equations, which include the material, component, energy balance, and electrochemical kinetic features. Due to a lack of experimental data for the dynamic response of the components only the steady state results were compared with data from other sources, indicating reasonably good agreement. A steady state simulation of the entire system was developed using, nonlinear ordinary differential equations. The finite difference method and trial-and-error procedures were used to obtain a solution. Using the model, a PAFC system, that was developed under NASA Grant, NCC3-17, was improved through the optimization of the heat exchanger network. Three types of cooling configurations for cell plates were evaluated to obtain the best current density and temperature distributions. The steady state solutions were used as the initial conditions in the dynamic model. The transient response of a simplified PAFC system, which included all of the major components, subjected to a load change was obtained. Due to the length of the computation time for the transient response calculations, analysis on a real-time computer was not possible. A simulation of the real-time calculations was developed on a batch type computer. The transient response characteristics are needed for the optimization of the design and control of the whole PAFC system. All of the models, procedures and simulations were programmed in Fortran and run on IBM 370 computers at Cleveland State University and the NASA Lewis Research Center.
Author

N95-30016# National Renewable Energy Lab., Golden, CO.
EXPERIMENTAL INVESTIGATION OF AERODYNAMIC DEVICES FOR WIND TURBINE ROTATIONAL SPEED CONTROL, PHASE 1
L. S. Miller (Wichita State Univ., Wichita, KS.) Feb. 1995 49 p
(Contract DE-AC36-83CH-10093)
(DE95-004034; NREL/TP-441-6913) Avail: CASI HC A03/MF A01

An investigation was undertaken to identify the aerodynamic performance of five separate trailing-edge control devices, and to evaluate their potential for wind turbine overspeed and power modulation applications. A modular two-dimensional wind tunnel model was constructed and evaluated during extensive wind tunnel testing. Aerodynamic lift, drag, suction, and pressure coefficient data were acquired and analyzed for various control configurations and angles of attack. To further interpret their potential performance, the controls were evaluated numerically using a generic wind turbine geometry and a performance analysis computer program. Results indicated that the Spoiler-Flap control configuration was best suited for turbine braking applications. It exhibited a large negative suction coefficient over a broad angle-of-attack range, and good turbine braking capabilities, especially at low tip-speed ratio. DOE

N95-30017# National Renewable Energy Lab., Golden, CO.
US PHOTOVOLTAIC PATENTS: 1991-1993
L. Pohle Mar. 1995 128 p
(Contract DE-AC36-83CH-10093)
(DE95-004051; NREL/SP-410-7689) Avail: CASI HC A07/MF A02

This document contains US patents on terrestrial photovoltaic (PV) power applications, including systems, components, and materials as well as manufacturing and support functions. The patent entries in this document were issued from 1991 to 1993. The entries were located by searching USPA, the database of the US Patent Office. The final search retrieved all patents under the class 'Batteries, Thermoelectric and Photoelectric' and the subclasses 'Photoelectric,' 'Testing,' and 'Applications.' The search also located patents that contained the words 'photovoltaic(s)' or 'solar cell(s)' and their derivatives. After the initial list was compiled, most of the patents on the following subjects were excluded: space photovoltaic technology, use of the photovoltaic effect for detectors, and subjects only peripherally concerned with photovoltaic. Some patents on these three subjects were included when it appeared that those inventions might be of use in terrestrial PV power technologies. DOE

N95-30127# National Renewable Energy Lab., Golden, CO.
SOLAR HEATING AND YOU
Aug. 1994 8 p
(Contract DE-AC36-83CH-10093)
(DE95-004012; DOE/CH-10093/272) Avail: CASI HC A02/MF A01

This fact sheet for use with primary school classes describes what solar collectors are and how they work, passive solar rooms, flat-plate collectors, and why one should use solar heating systems. Making a solar air heater is described step-by-step with illustrations. A resource list for both students and teachers is provided for further information. DOE

N95-30200# Technische Univ., Delft (Netherlands).
PREDICHAT: FIRST ORDER PERFORMANCE CALCULATIONS OF WINDTURBINE ROTORS USING THE METHOD OF THE ACCELERATION POTENTIAL
G. J. W. vanBussel Oct. 1993 240 p
(PB95-206454; IW-93069R) Avail: CASI HC A11/MF A03

A method is described for the calculation of aerodynamic loads on a horizontal axis wind turbine rotor. The method is based upon acceleration potential theory. An approximate solution of the boundary value problem has been obtained using a matched asymptotic expansion technique. Furthermore a numerical integration procedure has been applied for the integration of the pressure field gradient necessary for fulfillment of the final boundary condition. A partial delinearization of the method concerning the axial induction velocities turned out to be necessary. This is carried out in a numerical integration step. NTIS

N95-30213# Sandia National Labs., Albuquerque, NM.
FATIGUE CASE STUDY AND RELIABILITY ANALYSES FOR WIND TURBINES
Herbert J. Sutherland and Paul S. Veers 1994 7 p Presented at the American Society of Mechanical Engineers/Japanese Society of Mechanical Engineers/Japan Solar Energy Society International Solar Energy Conference, Lahaina, HI, 19-24 Mar. 1995

(Contract DE-AC04-94AL-85000)
(DE95-004770; SAND-94-2704C; CONF-950336-16) Avail: CASI HC A02/MF A01

Modern wind turbines are fatigue critical machines used to produce electrical power. To insure long term, reliable operation, their structure must be optimized if they are to be economically viable. The fatigue and reliability projects in Sandia's Wind Energy Program are developing the analysis tools required to accomplish these design requirements. The first section of the paper formulates the fatigue analysis of a wind turbine using a cumulative damage technique. The second section uses reliability analysis for quantifying the uncertainties and the inherent randomness associated with turbine performance and the prediction of service lifetimes. Both research areas are highlighted with typical results. DOE

N95-30217# Sandia National Labs., Albuquerque, NM.
HIGH-EFFICIENCY SOLAR CELLS USING HEM SILICON
C. P. Khattak (Crystal Systems, Inc., Salem, MA.), F. Schmid (Crystal Systems, Inc., Salem, MA.), and W. K. Schubert 1994 6 p Presented at the 1st World Conference on Photovoltaic Energy Conversion, Waikoloa, HI, 5-9 Dec. 1994
(Contract DE-AC04-94AL-85000)
(DE95-005424; SAND-94-1588C; CONF-941203-18) Avail: CASI HC A02/MF A01

Developments in Heat Exchanger Method (HEM) technology for production of multicrystalline silicon ingot production have led to growth of larger ingots (55 cm square cross section) with lower costs and reliability in production. A single reusable crucible has been used to produce 18 multicrystalline 33 cm square cross section 40 kg ingots, and capability to produce 44 cm ingots has been demonstrated. Large area solar cells of 16.3% (42 sq cm) and 15.3% (100 sq cm) efficiency have been produced without optimization of the material production and the solar cell processing. DOE

N95-30255*# National Aeronautics and Space Administration. Lewis Research Center, Cleveland, OH.
SPACE ELECTROCHEMICAL RESEARCH AND TECHNOLOGY. ABSTRACTS Abstracts Only
Apr. 1995 30 p Conference held in Cleveland, OH, 1-3 May 1995 (RTOP 506-41-21)
(NASA-CP-10172; E-9609; NAS 1.55:10172) Avail: CASI HC A03/MF A01

This document contains abstracts of the proceedings of NASA's fifth Space Electrochemical Research and Technology (SERT) Conference, held at the NASA Lewis Research Center on May 1-3, 1995. The objective of the conference was to assess the present status and general thrust of research and development in those areas of electrochemical technology required to enable NASA missions into the next century. The conference provided a forum for the exchange of ideas and opinions of those actively involved in the field, in order to define new opportunities for the application of electrochemical processes in future NASA missions. Papers were presented in three technical areas: (1) the electrochemical interface, (2) the next generation in aerospace batteries and fuel cells, and (3) electrochemistry for non-energy storage applications. This document contains the abstracts of the papers presented. For individual titles, see N95-30256 through N95-30271.

N95-30256*# National Aeronautics and Space Administration. Lewis Research Center, Cleveland, OH.
DEVELOPMENT OF A MICRO-FIBER NICKEL ELECTRODE FOR NICKEL-HYDROGEN CELL Abstract Only **c33**
Doris L. Britton *In its* Space Electrochemical Research and Technology. Abstracts Apr. 1995 p 3 (For primary document see N95-30255 10-44)
Avail: CASI HC A01/MF A01

Development of a high specific energy nickel electrode is the main goal of the lightweight nickel electrode program at the NASA Lewis Research Center. The approach has been to improve the nickel electrode by continuing combined in-house and contract efforts to develop a more efficient and lighter weight electrode for the nickel-hydrogen cell. Small fiber diameter nickel plaques are used as conductive supports for the nickel hydroxide active material. These plaques are commercial products and have an advantage of increased surface area available for the deposition of active material. Initial tests include activation and capacity measurements at different discharge levels followed by half-cell cycle testing at 80 percent depth-of-discharge in a low-Earth-orbit regime. The electrodes that pass the initial tests are life cycle-tested in a boiler plate nickel-hydrogen cell before flightweight designs are built and tested. Author

N95-30257*# National Aeronautics and Space Administration. Lewis Research Center, Cleveland, OH.
HIGH PERFORMANCE NICKEL ELECTRODES FOR SPACE POWER APPLICATIONS Abstract Only **c20**
Prosper K. Adanuvor (Auburn Univ., AL.), Johnnie A. Pearson (Auburn Univ., AL.), Brian Miller (Auburn Univ., AL.), Bruce Tatarchuk (Auburn Univ., AL.), and Doris L. Britton *In its* Space Electrochemical Research and Technology. Abstracts Apr. 1995 p 5 (For primary document see N95-30255 10-44)
Avail: CASI HC A01/MF A01

The specific energy density and the performance of nickel electrodes are generally limited by the electrode microstructure and the nature of the active material within the electrode matrix. Progress is being made in our laboratory in a collaborative effort with NASA-LEWIS Research Center to develop lighter weight, mechanically stable and highly efficient nickel electrodes for aerospace applications. Our approach is based on an electrode microstructure fabricated from a mixture of nickel fibers as small as 2 micro m diameter and cellulose fibers. Results will be presented to show the optimum conditions for impregnating this electrode microstructure with nickel hydroxide active material. Performance data in half-cell tests and cycle life data will also be presented. The flexibility of this electrode microstructure and the significant advantages it offers in terms of weight and performance will be demonstrated, in particular its ability to accept charge at high rates and to discharge at high rates. Author

N95-30258*# Eagle-Picher Industries, Inc., Colorado Springs, CO.
MAGNUM(R) NiCd ADVANCED NICKEL-CADMIUM BATTERY CELLS Abstract Only **c33**
Darren Scoles *In* NASA. Lewis Research Center, Space Electrochemical Research and Technology. Abstracts Apr. 1995 p 7 (For primary document see N95-30255 10-44)
Avail: CASI HC A01/MF A01

The Power Systems Department of Eagle-Picher Industries, Inc., located in Colorado Springs, Colorado, had developed a long-life advanced Nickel-Cadmium battery cell for aerospace applications. This battery cell, known as the MAGNUM NiCd cell, offers significant life expectancy increase over traditional NiCd battery cells. In addition, it offers significant cost reduction from the Super NiCd battery cell (developed by Hughes Aircraft Company and manufactured by the Power Systems Department of Eagle-Picher Industries, Inc.). Author

N95-30259*# National Aeronautics and Space Administration. Lewis Research Center, Cleveland, OH.
BENDING PROPERTIES OF NICKEL ELECTRODES FOR NICKEL-HYDROGEN BATTERIES Abstract Only **c33**
Bradley Lerch *In its* Space Electrochemical Research and Technology. Abstracts Apr. 1995 p 9 (For primary document see N95-30255 10-44)
Avail: CASI HC A01/MF A01

Recent changes in manufacturing have resulted in nickel-hydrogen batteries which fail prematurely by electrical shorting. This is believed to be a result of a blistering problem in the nickel electrodes. This study investigates the bending properties of nickel electrodes in an attempt to correlate the bending properties with the propensity of the electrode to blister. Nickel electrodes from three different batches of material were tested in both the as-received and impregnated forms. Effects of specimen curvature and position within the electrode on the bending strength were studied and within-electrode and batch-to-batch variation were addressed. Two color imaging techniques were employed which allowed differentiation of phases within the electrodes. These techniques aided in distinguishing the relative amounts of nickel hydroxide surface loading on each electrode, relating surface loading to bend strength. Bend strength was found to increase with the amount of surface loading. Author

N95-30260*# National Aeronautics and Space Administration. Goddard Space Flight Center, Greenbelt, MD.

EFFECT OF KOH CONCENTRATION AND ANIONS ON THE PERFORMANCE OF Ni-H2 BATTERY POSITIVE PLATE Abstract Only **c33**

H. Vaidyanathan (Communications Satellite Corp., Clarksburg, MD.), Kathleen Robbins (Communications Satellite Corp., Clarksburg, MD.), and Rao M. Gopalakrishna *In* NASA. Lewis Research Center, Space Electrochemical Research and Technology. Abstracts Apr. 1995 p 11 (For primary document see N95-30255 10-44)

Avail: CASI HC A01/MF A01

The capacity and voltage behavior of electrochemically impregnated sintered nickel positive plates was examined by galavanostatic charging; and discharging in a flooded electrolyte cell. Three different concentrations of KOH (40 percent, 31 percent, and 26 percent) and 31 percent KOH containing dissolved nitrate, sulfate or silicate were investigated. The end of charge voltage at C/10 charge and at 10 C showed the following order: 40 percent KOH is greater than 31 percent KOH alone and in the presence of the anions greater than 26 percent KOE. The middischarge voltage at C/2 discharge was higher in 26 percent KOH, almost the same for 31 percent KOH with and without the added contaminants and much lower for 40 percent KOH. The plate capacity was marginally affected by cycling in all cases except for 40 percent KOH where the capacity declined after 1000 cycles at 80 percent DOD. At the end of cycling the plate tested in the presence of sulfate and silicate experienced measurable weight loss as a result of active material extrusion. Cyclic voltammetry of miniature electrodes in 31 percent KOH showed that the second oxidation peak that corresponds to the formation of a different phase of oxidized Ni has a lower peak current at -5 C compared to 25 C and oxygen evolution occurs a higher potential at -5 C. The reduction peak (discharge reaction) is more polarized at 25 C compared to -5 C. The presence of silicate alters the potentials only marginally. The implications of these results in plate treatment and low temperature operation are discussed. Author

N95-30261*# Eagle-Picher Industries, Inc., Joplin, MO. Advanced Systems Operation.

ADVANCED DEPENDENT PRESSURE VESSEL (DPV) NICKEL-HYDROGEN SPACECRAFT CELL AND BATTERY DESIGN Abstract Only **c33**

Dwaine Coates, Doug Wright, and Ron Repplinger *In* NASA. Lewis Research Center, Space Electrochemical Research and Technology. Abstracts Apr. 1995 p 13 (For primary document see N95-30255 10-44)

Avail: CASI HC A01/MF A01

The dependent pressure vessel (DPV) nickel-hydrogen (NiH2) battery is being developed as a potential spacecraft battery design for both military and commercial satellites. Individual pressure vessel (IPV) NiH2 batteries are currently flying on more than 70 Earth orbital satellites and have accumulated more than 140,000,000 cell-hours in actual spacecraft operation. The limitations of standard NiH2 IPV flight battery technology are primarily related to the internal cell design and the battery packaging issues associated with grouping multiple cylindrical cells. The DPV cell design offers higher specific energy and reduced cost, while retaining the established IPV NiH2 technology flight heritage and database. The advanced cell design offers a more efficient mechanical, electrical and thermal cell configuration and a reduced parts count. The internal electrode stack is a prismatic flat-plate arrangement. The flat individual cell pressure vessel provides a maximum direct thermal path for removing heat from the electrode stack. The cell geometry also minimizes multiple-cell battery packaging constraints by using an established end-plateltie-rod battery design. A major design advantage is that the battery support structure is efficiently required to restrain only the force applied to a portion of the end cell. As the cells are stacked in series to achieve the desired system voltage, this increment of the total battery weight becomes small. The geometry of the DPV cell promotes compact, minimum volume packaging and places all cell terminals along the length of the battery. The resulting ability to minimize intercell wiring offers additional design simplicity and significant weight savings. The DPV battery design offers significant cost and weight savings advantages while providing minimal design risks. Cell and battery level design issues will be addressed including mechanical, electrical and thermal design aspects. A design performance analysis will be presented at both the cell and battery level. The DPV is capable of delivering up to 76 Watt-hours per kilogram (Wh/kg) at the cell level and 70 Wh/kg at the full battery level. This represents a 40 percent increase in specific energy at the cell level and a 60 percent increase in specific energy at the battery level compared to current IPV NiH2 technology. Author

N95-30262*# Aerospace Corp., Washington, DC.

ELECTROLYTE MANAGEMENT CONSIDERATIONS IN MODERN NICKEL HYDROGEN AND NICKEL CADMIUM CELL AND BATTERY DESIGNS Abstract Only **c33**

L. H. Thaller and A. H. Zimmerman *In* NASA. Lewis Research Center, Space Electrochemical Research and Technology. Abstracts Apr. 1995 p 17 (For primary document see N95-30255 10-44)

Avail: CASI HC A01/MF A01

In the early 1980's the NASA Lewis group addressed the topic of designing nickel hydrogen cells for LEO applications. As published in 1984, the design addressed the topics of gas management, liquid management, plate expansion, and the recombination of oxygen during overcharge. This design effort followed principles set forth in an earlier Lewis paper that addressed the topic of pore size engineering. At about that same time, the beneficial effect on cycle life of lower electrolyte concentrations was verified by Hughes Aircraft as part of a Lewis funded study. A succession of life cycle tests of these concepts have been carried out that essentially verified all of this earlier work. During these past two decades, some of the mysteries involved in the active material of the nickel electrode have been resolved by careful research efforts carried out at several laboratories. At The Aerospace Corporation, Dr. Zimmerman has been developing a sophisticated model of an operating nickel hydrogen cell which will be used to model certain mechanisms that have contributed to premature failures in nickel hydrogen and nickel cadmium cells. During the course of trying to understand and model abnormal nickel hydrogen cell behaviors, we have noted that not enough attention has been paid to the potassium ion content in these cells, and more recently batteries. Several of these phenomenon have been well known in the area of alkaline fuel cells, but only recently have they been examined as they might impact alkaline cell designs. This paper will review three general areas where the potassium ion content can impact the performance and life of nickel hydrogen and nickel cadmium devices, Once these phenomenon are understood conceptually, the impact of potassium content on a potential cell design can be evaluated with the aid of an accurate model of an operating cell or battery. All three of these areas are directly related to the volume tolerance and pore size engineering aspects of the components used in the cell or battery design: (1) The gamma phase uptake of potassium ion can result in a lowering of the electrolyte concentration. This leads to a higher electrolyte resistance as well as electrolyte diffusional limitations on the discharge rate. This phenomenon will also impact the response of the cell to a reconditioning cycle. (2) The impact of low level shunt currents in multi-cell con figurations will result in the movement of potassium ion from one part of the battery to another. This will impact the electrolyte volume/vapor pressure relationships within the cell or battery. (3) The transport of water vapor from place to place under the driving force of a tempetature gradient has already impacted cells for the case where water vapor is condensed on a colder cell wall. The paper will explore the convective and diffusive movement of gases saturated with water vapor from a warmer plate pack to a cooler one - both with and without liquid communication. Author

N95-30263*# Lynntech, Inc., College Station, TX.

A NOVEL UNITIZED REGENERATIVE PROTON EXCHANGE MEMBRANE FUEL CELL Abstract Only

O. J. Murphy, A. J. Cisar, A. Gonzalez-Martin, C. E. Salinas, and S. F. Simpson *In* NASA. Lewis Research Center, Space Electrochemical Research and Technology. Abstracts Apr. 1995 p 21 (For primary document see N95-30255 10-44)

Avail: CASI HC A01/MF A01

A difficulty encountered in designing a unitized regenerative proton exchange membrane (PEM) fuel cell lies in the incompatibility of electrode structures and electrocatalyst materials optimized for either of the two functions (fuel cell or electrolyzer) with the needs of the other function. This difficulty is compounded in previous regenerative fuel cell designs by the fact that water, which is needed for proton conduction in the PEM during both modes of operation, is the reactant supplied to the anode in

the electrolyzer mode of operation and the product formed at the cathode in the fuel cell mode. Drawbacks associated with existing regenerative fuel cells have been addressed in work performed at Lynntech. In a first innovation, electrodes function either as oxidation electrodes (hydrogen ionization or oxygen evolution) or as reduction electrodes (oxygen reduction or hydrogen evolution) in the fuel cell and electrolyzer modes, respectively. Control of liquid water within the regenerative fuel cell has been brought about by a second innovation. A novel PEM has been developed with internal channels that permit the direct access of water along the length of the membrane. Lateral diffusion of water along the polymer chains of the PEM provides the water needed at electrode/PEM interfaces. Fabrication of the novel unitized regenerative fuel cell and results obtained on testing it will be presented. Author

N95-30264*# Argonne National Lab., IL.
FUEL CELL SYSTEMS FOR FIRST LUNAR OUTPOST-REACTANT STORAGE OPTION Abstract Only
P. A. Nelson *In* NASA. Lewis Research Center, Space Electrochemical Research and Technology. Abstracts Apr. 1995 p 23 (For primary document see N95-30255 10-44)
(Contract W-31-109-eng-38)
Avail: CASI HC A01/MF A01

The office of Space, DOE, appointed a Lunar Surface Power Working Group to review candidate systems for the First Lunar Outpost habitat. The working group met for a total of five days in the fall of 1992 and concluded that the candidate involving a photovoltaic unit, a fuel cell, a regenerator to recycle the reactants, and storage of oxygen and hydrogen gases was the most attractive for this application. Most of the volume (97 percent) and weight (63 percent) are taken up by the reactants and their storage tanks. Therefore, in my work for the Group, and in this report, I have concentrated on finding ways to reduce these volumes and weights. Three options were considered: (1) the baseline case considered in the preliminary system design, that of separate high pressure (200 bar) storage tanks; (2) the use of two of the descent storage propellant tanks wrapped with graphite fibers to increase the pressure capability; and (3) the use of cryogenic storage of reactants in the propellant tanks. The first option results in high storage tank mass and volume. The second option saves 90 percent of the volume by making use of the propellant tanks, but it has little if any weight advantages; the weight saved by not providing extra tanks for reactant storage is nearly entirely added back by the weight of the additional material (graphite fibers) to strengthen the propellant tanks. Use of the descent storage propellant tanks for storage of the fuel cell reactants as cryogenic liquids requires a gas liquefaction system. The weight of this system is expected to be less than that of the storage tanks but it would require development and testing to prove its reliability. The solar array would have to be 40 percent larger and the heat projection range would be 170 percent larger than for storage of reactants as high pressure gases. For a high power system (greater than 20 kW) the larger energy storage requirement would probably favor the cryogenic storage option. Author

N95-30265*# Technology Management, Inc., Cleveland, OH.
THE TMI REGENERABLE SOLID OXIDE FUEL CELL Abstract Only
Thomas L. Cable *In* NASA. Lewis Research Center, Space Electrochemical Research and Technology. Abstracts Apr. 1995 p 25 (For primary document see N95-30255 10-44)
Avail: CASI HC A01/MF A01

Energy storage and production in space requires rugged, reliable hardware which minimizes weight, volume, and maintenance while maximizing power output and usable energy storage. These systems generally consist of photovoltaic solar arrays which operate during sunlight cycles to provide system power and regenerate fuel (hydrogen) via water electrolysis; during dark cycles, hydrogen is converted by the fuel cell into system. The currently preferred configuration uses two separate systems (fuel cell and electrolyzer) in conjunction with photovoltaic cells. Fuel cell/electrolyzer system simplicity, reliability, and power-to-weight and power-to-volume ratios could be greatly improved if both power production (fuel cell) and power storage (electrolysis) functions can be integrated into a single unit. The Technology Management, Inc. (TMI), solid oxide fuel cell-based system offers the opportunity to both integrate fuel cell and electrolyzer functions into one unit and potentially simplify system requirements. Based an the TMI solid oxide fuel cell (SOPC) technology, the TMI integrated fuel cell/electrolyzer utilizes innovative gas storage and operational concepts and operates like a rechargeable 'hydrogen-oxygen battery'. Preliminary research has been completed on improved H2/H2O electrode (SOFC anode/electrolyzer cathode) materials for solid oxide, regenerative fuel cells. Improved H2/H2O electrode materials showed improved cell performance in both fuel cell and electrolysis modes in reversible cell tests. In reversible fuel cell/electrolyzer mode, regenerative fuel cell efficiencies (ratio of power out (fuel cell mode) to power in (electrolyzer model)) improved from 50 percent (using conventional electrode materials) to over 80 percent. The new materials will allow the TMI SOFC system to operate as both the electrolyzer and fuel cell in a single unit. Preliminary system designs have also been developed which indicate the technical feasibility of using the TMI SOFC technology for space applications with high energy storage efficiencies and high specific energy. Development of small space systems would also have potential dual-use, terrestrial applications. Author

N95-30266*# Loral Defense Systems, Akron, OH.
ENGINEERING DEVELOPMENT PROGRAM OF A CLOSED ALUMINUM-OXYGEN SEMI-CELL SYSTEM FOR AN UNMANNED UNDERWATER VEHICLE: AN UPDATE Abstract Only
Dane W. Gregg and Susan E. Hall *In* NASA. Lewis Research Center, Space Electrochemical Research and Technology. Abstracts Apr. 1995 p 27 (For primary document see N95-30255 10-44)
(Contract NAS3-26715)
Avail: CASI HC A01/MF A01

Most emerging unmanned undersea vehicle (UUV) missions require significantly longer range and endurance than is achievable with existing battery technology. The Aluminum-Oxygen (Al-O2) semi-cell is a candidate technology capable of providing a significant improvement in endurance compared to the silver-zinc battery technology currently used in UUVs and compares favorably to other proposed UUV power systems not only in performance, but also in safety and logistics. An Al-O2 semi-cell system is under development by Loral Defense Systems-Akron (Loral) for the ARPA/Navy 44 in. diameter UUV test vehicle. The power plant consists of a cell stack, gas management, oxygen storage, electrolyte management, coolant and controller subsystems, designed to replace the existing silver-zinc battery and meet existing weight, volume, electrical and thermal requirements, therefore minimizing modifications to the UUV. A detailed system design is complete. A component and material endurance test to evaluate compatibility and reliability of various material arid components is complete. Sub scale (Short stack) system testing is completed. A full-scale demonstration unit is now under construction in the second half of 1995. The full scale demonstration test will simulate environmental conditions of the operational system. This paper summarizes the results of the extensive short stack and endurance test programs, describes the plan for full-scale testing, and concludes with a brief discussions of future directions for this technology. This program is sponsored by ARPA Maritime Systems Technology Office under NASA contract NAS3-26715. Author

N95-30267*# United Technologies Corp., Windsor Locks, CT. Hamilton Standard Div.
SPE(R)-OBOGS: ON-BOARD OXYGEN GENERATING SUSTEM Abstract Only **c54**
J. McElroy and W. Smith *In* NASA. Lewis Research Center, Space Electrochemical Research and Technology. Abstracts Apr. 1995 p 33 (For primary document see N95-30255 10-44)
Avail: CASI HC A01/MF A01

Regulations require oxygen usage by commercial airline flight crews during check out and during certain aircraft configurations. This oxygen is drawn from a high pressure onboard pressure cylinder storage system. In a typical aircraft oxygen cylinder removal for oxygen ground servicing is conducted every 4 to 6 weeks. An on board oxygen generating system has been developed to eliminate the need for oxygen ground servicing. The SPE-OBOGS supplies oxygen during flight in a 'trickle charge' mode to replenish the consumed oxygen at pressures up to 1850 psi. The Electrochemical cell stack is the fundamental SPE-OBOGS system component. The same basic proton exchange membrane technology, previously used for the Gemini program fuel cells and currently used in nuclear submarines as oxygen generators, is used in the SPE-OBOGS. An in-serivce evaluation of the SPE-OBOGS is in the planning stage and a zero gravity version is being promoted for on orbit space suit oxygen

system recharge. Summary results of the SPE-OBOGS development will be addressed. Author

N95-30268*# Boundary Technologies, Inc., Buffalo Grove, IL.
HERMETICALLY SEALED ALUMINUM ELECTROLYTIC CAPACITOR Abstract Only **c33**
Robert S. Alwitt, Yanming Liu, and William Elias (BACE Technologies, Pickens, SC.) *In* NASA. Lewis Research Center, Space Electrochemical Research and Technology. Abstracts Apr. 1995 p 35 (For primary document see N95-30255 10-44)
Avail: CASI HC A01/MF A01

Aluminum electrolytic capacitors are presently not allowed on NASA missions because they outgas water and organic vapors, as well as H2. As a consequence, much larger and heavier packages of tantalum capacitors are used. A hermetically sealed aluminum capacitor has been developed under NASA-MSFC SBIR contracts. This capacitor contains a nongassing electrolyte that was developed for this application so internal pressure would remain low. Capacitors rated at 250 to 540 V have been operated under full load for thousands of hours at 85 and 105 C with good electrical performance and low internal pressure. Electrolyte chemistry and seal engineering concepts will be discussed. Author

N95-30269*# Chemat Technology, Inc., Northridge, CA.
FABRICATION OF ADVANCED ELECTROCHEMICAL ENERGY MATERIALS USING SOL-GEL PROCESSING TECHNIQUES Abstract Only
C. T. Chu, Jay Chu, and Haixing Zheng *In* NASA. Lewis Research Center, Space Electrochemical Research and Technology. Abstracts Apr. 1995 p 37 (For primary document see N95-30255 10-44)
Avail: CASI HC A01/MF A01

Advanced materials play an important role in electrochemical energy devices such as batteries, fuel cells, and electrochemical capacitors. They are being used as both electrodes and electrolytes. Sol-gel processing is a versatile solution technique used in fabrication of ceramic materials with tailored stoichiometry, microstructure, and properties. The application of sol-gel processing in the fabrication of advanced electrochemical energy materials will be presented. The potentials of sol-gel derived materials for electrochemical energy applications will be discussed along with some examples of successful applications. Sol-gel derived metal oxide electrode materials such as V2O5 cathodes have been demonstrated in solid-state thin film batteries; solid electrolytes materials such as beta-alumina for advanced secondary batteries had been prepared by the sol-gel technique long time ago; and high surface area transition metal compounds for capacitive energy storage applications can also be synthesized with this method. Author

N95-30270*# Giner, Inc., Waltham, MA.
DEVELOPMENT OF ELECTROCHEMICAL SUPER CAPACITORS FOR EMA APPLICATIONS Abstract Only **c33**
J. A. Kosek, T. Dunning, and A. B. LaConti *In* NASA. Lewis Research Center, Space Electrochemical Research and Technology. Abstracts Apr. 1995 p 39 (For primary document see N95-30255 10-44)
Avail: CASI HC A01/MF A01

In a NASA SBIR Phase I program (Contract No. NAS8-40119), Giner, Inc. evaluated the feasibility of fabricating an all-solid-ionomer multicell electrochemical capacitor having a unit cell capacitance greater than 2 F/sq cm and a repeating element thickness of 6 mils. This capacitor can possibly be used by NASA as a high-rate energy source for electromechanical actuator (EMA) activation for advanced space missions. The high unit cell capacitance and low repeating element thickness will allow for the fabrication of a low-volume, low-weight device, favorable characteristics for space applications. These same characteristics also make the capacitor attractive for terrestrial applications, such as load-leveling batteries or fuel cells in electric vehicle applications. Although the projected energy densities for electrochemical capacitors are about two orders of magnitude lower than that of batteries, the high-power-density characteristics of these devices render them as potentially viable candidates for meeting pulse or peak electrical power requirements for some anticipated aerospace mission scenarios, especially those with discharge times on the millisecond to second time scale. On a volumetric or gravimetric basis, the advantages of utilizing electrochemical capacitors rather than batteries for meeting the peak power demands associated with a specific mission scenario will largely depend upon the total and pulse durations of the power peaks. The effect of preparation conditions on RuO(x), the active component in an all-solid-ionomer electrochemical capacitor, was evaluated during this program. Methods were identified to prepare RuO(x) having a surface areagreater than 180 sq m/g, and a capacitance of greater than 2 F/sq cm. Further efforts to reproducibly obtain these high-surface-area materials in scaled-up batches will be evaluated in Phase 2. During this Phase 1 program we identified a superior Nafion 105 membrane, having a film thickness of 5 mils, that showed excellent performance in our all-solid-ionomer capacitors and resulted in electrochemical capacitors with a repeating element thickness of 8 mils. We are currently working with membrane manufacturers to obtain a high performance membrane in less than 3 mil thickness to obtain a repeating element thickness of 6 mils or less. A 10-cell all-solid ionomer capacitor stack, with each cell having a 222 sq cm active area, was fabricated and evaluated as part of the Phase 1 program. Further Scale-up of a high-energy-density stack is plannedin Phase 2. Author

N95-30271*# Evans Co., East Providence, RI.
HIGH ENERGY DENSITY ELECTROLYTIC CAPACITOR Abstract Only **c33**
David A. Evans *In* NASA. Lewis Research Center, Space Electrochemical Research and Technology. Abstracts Apr. 1995 p 41 (For primary document see N95-30255 10-44)
Avail: CASI HC A01/MF A01

Recently a new type of electrolytic capacitor was developed. This capacitor, the Evans Hybrid, combines an electrolytic capacitor anode with an electrochemical capacitors cathode. The resulting capacitor has four times the energy density of other electrolytic capacitors, with comparable electrical performance. The prototype, a 480 micro F, 200 V device, had an energy density exceeding 4 J/cc. Now, a 680 micro F, 50 V, MIL-style all tantalum device has been constructed and is undergoing qualification testing. Pending a favorable outcome, work will begin on other ratings. Potential for commercially significant development exists in applying this technology to aluminum-based electrolytic capacitors. It is possible to at least double the energy density of aluminum electrolytics, while using existing manufacturing methods, and without adding material expense. Data presented include electrical characteristics and performance measurements of the 200 V and 50 V Hybrid capacitors and results of ongoing qualification status of the MJL-style tantalum. Author

N95-30278# Department of Energy, Morgantown, WV.
SOLID OXIDE FUEL CELL COMMERCIALIZATION IN THE UNITED STATES
Mark C. Williams 1995 12 p Presented at the 1995 Department of Energy/Agency of Industrial Science and Technology International Fuel Cell Symposium, Yokohama, Japan, 12-16 Jun. 1995
(DE95-008210; DOE/METC-C/95/7170; CONF-9506143-1) Avail: CASI HC A03/MF A01

This paper discusses aspects of solid oxide fuel cell (SOFC) technology commercialization in the US. It provides the status of the major SOFC developments occurring in the U.S. by addressing both intermediate- and high-temperature SOFC's, several SOFC designs, including both planar and tubular, and SOFC system configurations. This paper begins with general characteristics, proceeds with designs and system configurations, and finishes with a discussion of commercialization, funding, and policies. The U.S. Department of Energy's (DOE) Morgantown Energy Technology Center (METC) is the lead U.S. DOE center for the implementation of a Research, Development, and Demonstration Program to develop fuel cells for stationary power. METC's stakeholders include the electric power and gas industries, as well as fuel cell developers and others. This paper offers some new perspectives on SOFC development and commercialization which come from the broad consideration of the commercialization efforts of the entire fuel cell industry. DOE

N95-30281# Westinghouse Electric Corp., Pittsburgh, PA. Science and Technology Center.
ADVANCES IN TUBULAR SOLID OXIDE FUEL CELL TECHNOLOGY
S. C. Singhal 1995 14 p Presented at the 4th International Symposium on Solid Oxide Fuel Cells, Yokohama, Japan, 18-23 Jun. 1995
(Contract DE-FC21-91MC-28055)

(DE95-008361; DOE/MC-28055/95/C0447; CONF-950683-1) Avail: CASI HC A03/MF A01

This paper reviews the design and performance of tubular solid oxide fuel cells (SOFC's). A large number of tubular cells of the porous support tube type have been electrically tested, some to times over 50,000 hours; these cells show excellent performance and performance stability. Since 1984 successfully larger electrical generators utilizing these cells have been built and operated, a 20 kW integrated SOFC system operated for 7064 hours during 1993-94. Results of development efforts to reduce cost and increase power output of tubular cells by eliminating porous support tube and increasing active length are described, and plans to utilize such air electrode supported cells in the future SOFC systems are discussed. DOE

45 ENVIRONMENT POLLUTION

Includes atmospheric, noise, thermal, and water pollution.

N95-28717*# National Aeronautics and Space Administration. Langley Research Center, Hampton, VA.

COMPENDIUM OF NASA DATA BASE FOR THE GLOBAL TROPOSPHERIC EXPERIMENT'S TRANSPORT AND ATMOSPHERIC CHEMISTRY NEAR THE EQUATOR-ATLANTIC (TRACE-A)

Gerald L. Gregory and A. Donald Scott, Jr. Apr. 1995 144 p
(RTOP 464-54-03-70)
(NASA-TM-110151; NAS 1.15:110151) Avail: CASI HC A07/MF A02

This compendium describes aircraft data that are available from NASA's Transport and Atmospheric Chemistry near the Equator - Atlantic (TRACE-A) conducted in September/October 1992. The broad objectives of TRACE-A were to study chemical processes and long-range transport associated with South American and African continental outflow during periods of widespread vegetation burning, and to understand the ozone enhancements observed from satellite data measured over the southern tropical Atlantic Ocean during the September/October time period. Flight experiments were conducted from Brazil, South Africa, Namibia, and the Ascension Island. This document provides a representation of aircraft data that are available from NASA Langley's Distributed Active Archive Center (DAAC). The data format of time series and altitude profile plots is not intended to support original analyses, but to assist the reader in identifying data that are of interest. This compendium is for only the NASA aircraft data. The DAAC data base includes numerous supporting data-meteorological products, results from surface studies, satellite observations, and data from sonde releases. Author

N95-28787# Army Construction Engineering Research Lab., Champaign, IL.

THE ENVIRONMENTAL ASSESSMENT AND MANAGEMENT (TEAM) GUIDE Final Report

Diane K. Mann and Donna J. Schell Nov. 1994 1141 p
(Contract MIPR-PRJORD-94004)
(AD-A286748; CERL-SR-EC-95/05) Avail: CASI HC A99/MF A10

Environmental assessments help determine compliance with current environmental regulations. The U.S. Air Force, U.S. Army, Defense Logistic Agency, and Crops of Engineers (Civil Works) have programs that identify compliance problems before they are cited as violations by the U.S. Environmental Protection Agency (USEPA). Since 1984, the U.S. Army Construction Engineering Research Laboratories (USACERL), in cooperation with Department of Defense (DOD) components, has developed environmental compliance assessment checklist manuals. The Environmental Assessment and Management (TEAM) Guide was developed for use by all DOD components. Currently there are five participating components: the Air Force, Air Force National Guard, Army, Army National Guard, Army Reserves, Civil Works, and the Defense Logistics Agency (DLA). These agencies have agreed to share the development and maintenance of this guide. This guide combines Code of Federal Regulations (CFR's) and management practices (MP's) into checklists that show legal requirements and the specific operations or items to review. The TEAM Guide is supplemented by DOD component-specific manuals detailing regulations and policies. The TEAM Guide is an update, revision, and replacement of the current U.S. ECAMP, U.S. ECAS, and DLA compliance assessment checklist manuals and will be continually updated with new compliance laws and regulations. DTIC

N95-28920# Pacific Northwest Lab., Richland, WA.

MEASUREMENT OF THE SEASONAL AND ANNUAL VARIABILITY OF TOTAL COLUMN AEROSOL IN A NORTHEASTERN US NETWORK

J. J. Michalsky (Albany Univ., Albany, NY.), J. A. Schlemmer (Albany Univ., Albany, NY.), L. C. Harrison (Albany Univ., Albany, NY.), W. E. Berkheiser, III (Albany Univ., Albany, NY.), N. R. Larson, and N. S. Laulainen Sep. 1994 13 p Presented at the Conference on Aerosols and Atmospheric Optics: Radiation Balance and Visual Air Quality, Snowbird, UT, 25-30 Sep. 1994
(Contract DE-AC06-76RL-01830; DE-FG02-90ER-61072)
(DE95-007259; PNL-SA-25348; CONF-9409255-3) Avail: CASI HC A03/MF A01

A network of multi-filter rotating shadowband radiometers has operated since late 1991 in the northeastern U.S. The data acquired are simultaneous measurements of total and diffuse horizontal irradiances in six narrowband filtered detectors and one broadband shortwave detector. The direct normal irradiances are calculated from these measurements. These direct data are corrected for cosine response and used to calculate extraterrestrial irradiance (I(sub o)) using the Langley method of regressing the natural logarithm of direct irradiance versus air mass. With frequent determinations of I(sub o), changes in I(sub o) caused by soiling and filter degradation, for example, can be tracked. Using these I(sub o)'s, total optical depth is calculated for every clear 30-minute period in the record. Consequently, total optical depth may be obtained on a fair number of days throughout the year. Using daily average total optical depth the authors have calculated aerosol optical depths for five wavelengths by subtracting Rayleigh scattering optical depths and Chappuis ozone absorption optical depths at each wavelength. The aerosol pattern at nearly every site is an annual cycle superimposed on a decaying stratospheric loading associated with the Mount Pinatubo volcanic eruption. An attempt is made to remove the volcanic signal using data from another site. DOE

N95-28922# Mission Research Corp., Santa Barbara, CA.

STOCHASTIC MODELING AND GLOBAL WARMING TREND EXTRACTION FOR OCEAN ACOUSTIC TRAVEL TIMES Interim Technical Report

Steven Bottone, Henry L. Gray, and Wayne A. Woodward (Southern Methodist Univ., Dallas, TX.) 6 Jan. 1995 46 p
(Contract ARPA Order-9376; MDA972-93-C-0021)
(AD-A292114; MRC-R-1488) Avail: CASI HC A03/MF A01

A possible indication of the existence of global climate warming is a negative trend for the travel time of an acoustic pulse along a fixed long path, or paths, in the ocean over a period of many years. The goal of this report is the development of methods specifically for determining the presence of a long term trend for climate change from a temporal sequence of measurements of acoustic propagation times. Robust statistical methods for determining whether a significant trend is present in a given set of time series data have been developed and, for illustration, applied to some specific traveltime time series generated by the MASIG and GFDL ocean models. In this report we consider line + noise and ARIMA statistical models. We show that if the time series are long enough, somewhat over 20 years, then series such as those simulated by the MASIG and GFDL models can be classified reliably as line + noise when this is the case. However, it is shown that the results are considerably different for the two ocean models under consideration and that these models can not currently be relied upon by themselves to predict global warming. Experimental data is most certainly needed, not only to measure global warming itself, but to help improve the ocean model themselves. DTIC

N95-29213 Michigan Univ., Ann Arbor, MI.

DEVELOPMENT OF A MULTIPLEX FABRY-PEROT INTERFEROMETER AND MEASUREMENT OF ATMOSPHERIC HF AND HCl Ph.D Thesis

Hilary Edmund Snell 1994 225 p
Avail: Univ. Microfilms Order No. DA9423319

Remote sensing of major and minor constituents in the earth's atmosphere is of great importance to the study of climate and global change. Because much of remote sensing involves placing instrumentation in environments that are not easily accessible, such as balloons, spacecraft, or remote field stations, it is usually necessary that the instrumentation be

compact, lightweight, and rugged. This thesis describes the development of a new type of remote sensing instrument and measurements of trace gases in the earth's atmosphere. The Multiplex Fabry-Perot Interferometer (MFPI) consists of a Fabry-Perot interferometer in which the etalon plate separation is changed over a large optical distance. Fourier-transformation of the resultant interferogram allows one to treat the multiple reflections within the etalon cavity in a manner analogous to an array of Michelson-type interferometers. However, even for high spectral resolution measurements the scan distance required by the MFPI is much less than for the comparable Michelson. The MFPI will be ideal for remote sensing applications where weight, size, and mechanical reliability are primary considerations . Hydrofluoric acid (HF) and hydrochloric acid (HCl) are important fluorine and chlorine reservoir species in the atmosphere. We have measured the column density of HF and HCl using the techniques of solar absorption spectroscopy and their spectral lines at 4038.962 cm(exp -1) and 2925.897 cm(exp -1). Our measurements consistently show that the HCl line is asymmetric. While previously published measurements of HCl by other groups using this spectral line claim that the asymmetry is instrumental in nature, our measurements indicate that it is caused by spectral contamination. Dissert. Abstr.

N95-29450 Virginia Polytechnic Inst. and State Univ., Blacksburg, VA. Center for Environmental and Hazardous Materials Studies.

MEASURING VARIATION IN ECOSYSTEM SENSITIVITY TO STRESS Final Report, 1 Sep. 1991 - 31 Oct. 1994

John Cairns, Jr., Paul V. McCormick, Matthew Arnegard, and Eric P. Smith 28 Dec. 1994 96 p Limited Reproducibility: More than 20% of this document may be affected by poor print

(Grant AF-AFOSR-0379-91)

(AD-A290415; AFOSR-95-0002TR) Avail: Issuing Activity (Defense Technical Information Center (DTIC))

Chemical-releasing substrates that allow the effects of certain pollutants on attached algal communities to be studied under natural stream conditions without impacting the stream ecosystems were developed. Several investigations in both artificial streams and in the field were conducted with these substrates; in them algal communities were first allowed to colonize and develop on the diffusing surface of these substrates for several weeks, after which time toxicant solutions were added to the flasks and allowed to diffuse through the attached algal communities. Laboratory studies revealed that the responses of algal communities to substrate-released copper were not different from responses generated in traditional toxicity tests. The experimental substrates may be useful in validating the results of laboratory toxicity tests under natural environmental conditions, confirming the results of upstream-downstream pollution studies, which are flawed by the lack of rigorous controls, and measuring the variation in algal community sensitivity to stress. Field studies focusing on the last application failed to reject the null hypothesis that communities in polluted streams respond to copper differently from those in unpolluted streams, but they were flawed by unpredicted methodological problems. DTIC

N95-29721# Defense Systems Management School, Fort Belvoir, VA. Div. of Research, Consulting and Information.

ENVIRONMENTAL PRACTICE IN PROGAM MANAGEMENT OFFICES Research Report, Oct. 1993 - Jan. 1995

George P. Noble, III Jan. 1995 104 p

(AD-A290823; DSMC-TR-1-95) Avail: CASI HC A06/MF A02

A study of environmental practice in Department of Defense Program Management Offices produced data and analysis presented here. This information is relative to policy and guidance, organization, reference materials, documentation, funding, contracting actions, technology, training, audits/inspections, and impacts of environmental issues. Both a survey instrument and an interview process were used in the project. DTIC

N95-29804 Stanford Univ., CA.

A MODEL ANALYSIS OF THE SPATIAL DISTRIBUTION AND TEMPORAL TRENDS OF NITROUS OXIDE SOURCES AND SINKS Ph.D. Thesis

Cynthia Dale Nevison 1994 238 p

Avail: Univ. Microfilms Order No. DA9422111

Nitrous oxide (N2O), an atmospheric trace gas that contributes to both greenhouse warming and stratospheric ozone depletion, is increasing at an annual rate of about 0.25%/yr. By use of a global model of the changing terrestrial nitrogen cycle, the timing and magnitude of this increase are shown to be consistent with enhanced microbial N2O production due to fertilizer, land clearing, livestock manure, and human sewage. Fertilizer appears to be a particularly important source. Increasing emissions from additional anthropogenic N2O sources, including fossil fuel combustion and nylon production are also shown to coincide with and contribute to N2O's annual atmospheric increase. Collectively, these industrial, combustion-related, and enhanced microbial N2O emissions add up to a total anthropogenic source of about 5 Tg N/yr. Natural N2O emissions from microbial activity in soils and oceans and from natural fires are estimated to produce an annual source of about 11 Tg N/yr, of which the oceans contribute a substantially larger fraction than reported in most current budgets. In contrast to anthropogenic emissions, which are increasing rapidly, natural emissions are predicted to remain relatively constant from 1860 to 2050, although this prediction ignores possible enhancements in microbial N2O production due to global warming. Also in contrast to anthropogenic emissions, which are heavily dominated by the Northern Hemisphere, the natural source is fairly evenly distributed over the Earth. The predicted magnitude of the natural source is checked against an estimate of the N2O stratospheric sink, while the predicted present day distribution of natural and anthropogenic sources is tested in a 3-dimensional transport model run. This run reproduces the observed 1ppb interhemispheric gradient (higher in the north), and suggests that larger gradients may exist over strong continental source regions. Substantial increases in most anthropogenic N2O sources are projected for the future if current trends continue. In contrast to purely industrial greenhouse gases like the CFC's, which can be phased out fairly easily, attempts to control N2O emissions may conflict with efforts to reduce urban smog (i.e., NO(x) emissions) and to feed the world's growing human population. These conflicts could be mitigated, however, by improved energy efficiency, decreased dependence on synthetic fertilizer, reduced numbers of livestock, and a slowdown in the rate of human population growth. Dissert. Abstr.

N95-29878 Wisconsin Univ., Madison, WI.

SOIL WETNESS AND CLIMATE VARIABILITY Ph.D. Thesis

Thomas L. Delworth 1994 173 p

Avail: Univ. Microfilms Order No. DA9410602

The climate system is characterized by substantial amounts of variability at a wide range of spatial and temporal scales. A key issue in climate research is obtaining a better description of this variability and the physical mechanisms responsible for it. In this thesis the importance of land-surface processes for atmospheric variability on seasonal to interannual time scales is examined through detailed analyses of the output of a general circulation model (GCM) of the atmosphere coupled to a land-surface hydrology formulation. The GCM has horizontal resolution of approximately 4.5 deg latitude by 7.5 deg longitude, nine levels in the vertical, and incorporates subgrid scale parameterizations for precipitation and convection. The model has a seasonal cycle of insolation, but no diurnal cycle. A seasonal cycle of sea surface temperatures is prescribed from observations. It is shown that modelled interactions between the land surface and the atmosphere can make a substantial contribution to the spectrum of near-surface atmospheric variability, both increasing the total variability and lengthening the time scales of near-surface atmospheric fluctuations. Such effects are most pronounced in the tropics and summer hemisphere extratropics. The time scales of such variability in the model are shown to depend on both potential evaporation and the water-holding capacity of the soil. Observational evidence is presented supporting this analysis. The relevance of these results for the issue of droughts is also examined. An additional measure of the importance of land surface processes for climate is the degree of precipitation recycling. A water vapor tracer capability was implemented in the GCM such that water vapor could be traced from its evaporative source region to the area where it precipitates. The model is shown to have a high degree of precipitation recycling over continental interiors during summer. The month to month persistence of precipitation originating from continental evaporation is shown to be larger than that from oceanic evaporation. Model recycling estimates compare favorably to recent observed estimates. The sensitivity of the variability results to several key features of the land-surface formulation and of the atmospheric model is also evaluated. While the essential variability results are fairly robust, there is

some sensitivity of the results to aspects of the land surface formulation, particularly the total water-holding capacity. Dissert. Abstr.

N95-29885 Johns Hopkins Univ., Baltimore, MD.
INDUCED COMPTON SCATTERING BY RELATIVISTIC ELECTRONS IN MAGNETIZED ASTROPHYSICAL PLASMAS Ph.D. Thesis
Mark William Sincell 1994 118 p
Avail: Univ. Microfilms Order No. DA9420036

The effects of stimulated scattering on high brightness temperature radiation are studied in two important contexts. In the first case, we assume that the radiation is confined to a collimated beam traversing a relativistically streaming magnetized plasma. When the plasma is cold in the bulk frame, stimulated scattering is only significant if the angle between the photon motion and the plasma velocity is less than gamma(sup -1), where gamma is the bulk Lorentz factor. Under the assumption that the center of the photon beam is parallel to the bulk motion, we calculate the scattering rate as a function of the angular spread of the beam and gamma. Magnetization changes the photon recoil, without which stimulated scattering has no effect. It also introduces a strong dependence on frequency and polarization if the photon frequency matches the electron cyclotron frequency, the scattering rate of photons polarized perpendicular to the magnetic field can be substantially enhanced relative to Thomson, and if the photon frequency is much less than the cyclotron frequency the scattering is suppressed Applying these calculations to pulsars, we find that stimulated scattering of the radio beam in the magnetized wind believed to exist outside the light cylinder can substantially alter the spectrum and polarization state of the radio signal. We suggest that the scattering rate is so high in some pulsars that the ability of the radio signal to penetrate the pulsar magnetosphere requires modification of either the conventional model of the magnetosphere or assumptions about the effects of stimulated scattering upon a beam. In the second case, we present a model of the radio emission from synchrotron self-absorbed sources, including the effects of induced Compton scattering by the relativistic electrons in the source. Order of magnitude estimates show that stimulated scattering becomes the dominant absorption process when (kT(sub B)/m(sub e) c(sup 2)) tau(sub T) is approximately greater than 0.1. Numerical simulations demonstrate that relativistic induced Compton scattering limits the brightness temperature of a self-absorbed synchrotron source to T(sub B) approximately less than a few x 10(exp 11) K and can significantly flatten the radio spectrum. The radio spectrum of the core of 3C279 is well matched by a model in which stimulated scattering is important, and the additional constraint T(sub B) approximately less than 2 x 10(exp 11) K may be important to the interpretation of the broad band spectra in variable extra-galactic compact radio sources (Landau, et al 1986). Stimulated scattering reduces the amplitude of the radio frequency variability relative to the x-ray variability, an effect which can be detected by multi-wavelength variability studies. Data for a sample of resolved compact radio cores (Ghisellini, et al. 1993) indicate that it is inconsistent to neglect induced Compton scattering stratospheric (16 to 30 km) chlorine chemistry. The observations are compared to a photochemical model which incorporates hydrolysis of N2O5 on sulfate aerosols. This yields good agreement between calculation and measurement, except below 20 km where observed ClO is greater by up to a factor of four. In a model constrained to reproduce observed ClO below 20 km, the ozone loss rate is dominated by HO(x) and halogen oxide catalytic cycles, which may help to explain the observed negative ozone trends in the lower stratosphere. Data from the Airborne Arctic Stratospheric Expedition 2 are compared with measurements made at similar latitudes and seasons during earlier ER-2 flight series to assess the effects of the Mt. Pinatubo eruption on the partitioning of inorganic chlorine. While the comparisons show little enhancement in ClO poleward of 40 deg N, there is a substantial increase between 20 deg and 40 deg N. These results are indicative of volcanic perturbation to stratospheric chemistry via enhanced sulfate aerosol loading. Dissert. Abstr.

N95-30176# Argonne National Lab., IL.
LOAD-BALANCING ALGORITHMS FOR THE PARALLEL COMMUNITY CLIMATE MODEL
I. T. Foster and B. R. Toonen Jan. 1995 21 p
(Contract W-31-109-eng-38)
(DE95-008795; ANL/MCS-TM-190) Avail: CASI HC A03/MF A01

Implementations of climate models on scalable parallel computer systems can suffer from load imbalances resulting from temporal and spatial variations in the amount of computation required for physical parameterizations such as solar radiation and convective adjustment. We have developed specialized techniques for correcting such imbalances. These techniques are incorporated in a general-purpose, programmable load-balancing library that allows the mapping of computation to processors to be specified as a series of maps generated by a programmer-supplied load-balancing module. The communication required to move from one map to another is performed automatically by the library, without programmer intervention. In this paper, we describe the load-balancing problem and the techniques that we have developed to solve it. We also describe specific load-balancing algorithms that we have developed for PCCM2, a scalable parallel implementation of the Community Climate Model, and present experimental results that demonstrate the effectiveness of these algorithms on parallel computers. The load-balancing library developed in this work is available for use in other climate models. DOE

N95-30181# Colorado State Univ., Fort Collins, CO. Dept. of Atmospheric Science.
USE OF ARM DATA TO TEST AN IMPROVED PARAMETERIZATION OF UPPER TROPOSPHERIC CLOUDS FOR USE IN CLIMATE MODELS Final Report, 1 Dec. 1991 - - 30 May 1995
D. A. Randall and KuanMan Xu Mar. 1995 25 p
(Contract DE-FG02-92ER-61363)
(DE95-009324; DOE/ER-61363/3) Avail: CASI HC A03/MF A01

We have developed new cloud parameterizations, and tested them in an SCM, a CEM, and a full three-dimensional GCM. We have demonstrated the ability to drive the SCM and the CEM with observations similar to those that we are about to receive from ARM. We have used the three-dimensional GCM to investigate some aspects of the role of clouds in climate. The climate simulation, and especially the Earth's radiation budget, has been substantially improved through use of the new parameterizations. DOE

N95-30195# Central Research Inst. of Electric Power Industry, Tokyo (Japan).
ANALYSIS OF GLOBAL ECONOMIC INSTRUMENTS FOR CO2 EMISSION REDUCTION: EQUITY AND EFFICIENCY
T. Sugiyama, K. Yamaji, K. Okada, and H. Yamamoto Apr. 1994 48 p
(DE95-764057; CRIE-Y-93015) Avail: CASI HC A03/MF A01

The economic efficiency and the equity of economic burden are the most important things to choose a framework for global CO2 emission reduction. As one of the candidates for this framework, the global market of CO2 emission permit is studied. When it is assumed that the cost required for transactions of emission permit is ignored, the market of emission permit can be separated into the execution of uniform carbon tax to the whole area and the income transfer effect. By utilizing this assumption, various trial calculations for the market of emission permit are carried out. The relation between the price of emission permit (marginal cost of emission reduction) and the global reduction target is sought by using the Edmonds-Reilly model. Assuming that the reduction ratio in 2000 is 15%, the emission permit price becomes $54/t-C. The marginal costs in advanced countries are reduced more than those in the case where each country tries to achieve its reduction target. Trial calculations on the income transfer through trading of emission permit in the case where the initial quota of emission permit is proportional to population, GNP, or current emission amount, it is shown that the population-based quota is highly realizable. DOE

N95-30197# Gas Research Inst., Chicago, IL.
NITROGEN DIOXIDE MEASUREMENT METHOD CHARACTERIZATION AT THE GRI CONVENTIONAL RESEARCH HOUSE Topical Report, Aug. - Sep. 1989
R. L. Hedrick, F. Rasouli, E. K. Krug, and G. Pudlo Dec. 1994 64 p
(Contract GRI-5094-250-3084; Projs. GARD-A1-197)
(PB95-200549; GRI-95/0056) Avail: CASI HC A04/MF A01

Experiments were conducted to measure NO2 concentrations using three types of instruments: (1) Chemiluminescent NO/NOx analyzer (EPA reference method); (2) Chemiluminescent NO2 analyzer using luminol solution; and (3) Electrochemical NO2 analyzer. The electrochemical and luminol analyzers were evaluated in terms of their linearity, bias and correlation relative to the chemiluminescent analyzer, and interference by nitric oxide (NO) and nitrous acid (HONO). The chemiluminescent analyzer measured

concentrations in samples that included some that were passed through an acid denuder to remove HONO. The electrochemical analyzers were small and portable, but were not as accurate and precise as the other types. The luminol based analyzers had good accuracy at concentrations below about 120 ppb. The luminol analyzer was not sensitive to HONO. NTIS

N95-30212# Oak Ridge National Lab., TN.
INTERACTIONS BETWEEN ENERGY EFFICIENCY AND EMISSION TRADING UNDER THE 1990 CLEAN AIR ACT AMENDMENTS
E. L. Hillsman and D. R. Alvic (Tennessee Univ., Knoxville, TN.) Aug. 1994 43 p
(Contract DE-AC05-84OR-21400)
(DE95-008649; ORNL/CON-400) Avail: CASI HC A03/MF A01

The 1990 Clean Air Act Amendments affect electric utilities in numerous ways. The feature that probably has received the greatest attention is the provision to let utilities trade emissions of sulfur dioxide (SO2), while at the same time requiring them to reduce SO2 emissions in 2000 by an aggregate 43%. The emission trading system was welcomed by many as a way of reducing the cost of reducing emissions, by providing greater flexibility than past approaches. This report examines some of the potential interactions between trading emissions and increasing end-use energy efficiency. The analysis focuses on emission trading in the second phase of the trading program, which begins in 2000. The aggregate effects, calculated by an emission compliance and trading model, turn out to be rather small. Aggressive improvement of end-use efficiency by all utilities might reduce allowance prices by $22/ton (1990 dollars), which is small compared to the reduction that has occurred in the estimates of future allowance prices and when compared to the roughly $400/ton price we estimate as a base case. However, the changes in the allowance market that result are large enough to affect some compliance decisions. If utilities in only a few states improve end-use efficiency aggressively, their actions may not have a large effect on the price of an allowance, but they could alter the demand for allowances and thereby the compliance decisions of utilities in other states. The analysis shows how improving electricity end-use efficiency in some states can cause smaller emission reductions in other states, relative to what would have happened without the improvements. Such a result, while not surprising given the theory behind the emission trading system, is upsetting to people who view emissions, environmental protection, and energy efficiency in moral rather than strictly economic terms. DOE

N95-30300 Johns Hopkins Univ., Baltimore, MD.
THE EFFECTS OF CLOUDS AS A FEEDBACK MECHANISM ON THE EARTH'S CLIMATE IN THE TROPICAL PACIFIC Ph.D. Thesis
Daniel Charles Ziskin 1994 167 p
Avail: Univ. Microfilms Order No. DA9420057

The thesis investigates two aspects of the interactions involving clouds, the Earth's radiation budget, and surface temperature. The first is how clouds affect the radiative fluxes at the top of the atmosphere. The net effect of clouds in the Indinesian region is to increase the net heating of the column. Different cloud types segregated by height and optical depth, have distinct radiative properties. We calculate, via linear regression analysis, the sensitivity of the fluxes to cloud amount for each cloud type. The data is temporally resolved, so the influence of the diurnal circle is demonstrated. We compare the empirical cloud sensitivities to those calculated using a radiation model. There is overall agreement between the model-based and observational sensitivities. The second aspect of the thesis is to determine the role of clouds as a feedback mechanism on the radiation budget in response to climate change. In the tropical Pacific ocean clouds respond to warmer sea surface temperatures by becoming more numerous, higher and optically thicker. This increases both longwave and shortwave cloud radiative effects at the TOA. Our principal result is that the longwave effect, created by higher cloud tops, is the dominant feedback. So, the net effect is for clouds in the tropical Pacific to act as a positive feedback by intensifying the heating of the column in response to a warmer surface. A tnird portion, included as an appendix in a modeling project, designed to simulate the energetics of the atmosphere and surface, taking into account the radiation budget at the surface and top of the atmosphere, evaporation and the latent and sensible heat flux into the atmosphere. The model shows that clouds tend to have a cooling effect on the surface. This effect is stronger at tropical latitudes, where the solar insolation is a larger, than toward higher latitudes. A second experiment reveals that under doubled CO2, the clouds behave as a negative feedback, reducing the increase in surface temperature due to the greenhouse effect of the CO2. Dissert. Abstr.

N95-30348# Concord Science and Technology, Inc., Knoxville, TN.
NOVEL PHOTOELECTRIC SENSING TECHNOLOGY FOR ENVIRONMENTAL MONITORING, PHASE 1 Final Report, 19 Jul. 1994 - 18 Jan. 1995
Ida Lee 18 Jan. 1995 24 p Limited Reproducibility: Document partially illegible
(Contract DASG60-94-C-0102)
(AD-A292026) Avail: CASI HC A03/MF A01

We have proposed to develop and improve the function of a new environmental monitor using the Photoelectric Atmospheric Proportional Counter (PAPC) sensor technology. This is a simple, reliable, inexpensive, hand-held instrument for chlorinated contaminant measurements. The proposed objectives are to review and assess relevant pollutant monitoring technologies, to conduct concept analysis and design of PAPC sensor, to carry out bench-scale experiments for investigating the key properties of PAPC for environmental monitoring, to analyze data and delineate development needs, and to document results. DTIC

46 GEOPHYSICS

Includes aeronomy; upper and lower atmosphere studies; ionospheric and magnetospheric physics; and geomagnetism.
For space radiation see *93 Space Radiation.*

N95-28693 Naval Postgraduate School, Monterey, CA.
A GROUND SUPPORT ELECTRONIC INTERFACE FOR THE IONOSPHERIC SPECTROSCOPY AND ATMOSPHERIC CHEMISTRY (ISAAC) ULTRAVIOLET SPECTROGRAPH M.S. Thesis
Jeffrey A. MacQuarrie Dec. 1994 221 p Limited Reproducibility: More than 20% of this document may be affected by microfiche quality
(AD-A289761) Avail: Issuing Activity (Defense Technical Information Center (DTIC))

This thesis details the design and development of an electronic Ground Support Equipment (GSE) interface for the Naval Postgraduate School's (NPS) Ionospheric Spectroscopy and Atmospheric Chemistry (ISAAC) spectrograph. The ISAAC spectrograph, which was designed at NPS and built by Research Support Instruments, Inc., is intended to observe atmospheric airglow and auroral emissions in the ultraviolet (1800A to 3300A) wavelength region. It is to be included as one of several sensors flown onboard the Advanced Research and Global Observation Satellite (ARGOS), which is scheduled for an early 1996 launch. The GSE was developed in order to allow ground testing and calibration of the instrument prior to and during integration with the satellite bus. The GSE includes hardware to provide the connections between various components of the spectrograph and a Macintosh computer with an installed I/O card. The GSE also includes a user-friendly software interface written with LabVIEW 2.2 that provides the ability to view spectra obtained from the instrument and to remotely control mechanical functions of the spectrograph. An initial wavelength calibration of the spectrograph has been performed using the completed GSE. DTIC

N95-28697 Utah State Univ., Logan, UT. Space Dynamics Labs.
AN INVESTIGATION OF THUNDERSTORMS AS A SOURCE OF SHORT PERIOD MESOSPHERIC GRAVITY WAVES
M. J. Taylor, V. Taylor, and R. Edwards 6 Jan. 1995 10 p Prepared in cooperation with Southampton Univ., (United Kingdom). Presented at Chapman Conference, Limited Reproducibility: More than 20% of this document may be affected by microfiche quality
(Contract F19628-93-C-0165)
(AD-A289795; SDL/94-090; PL-TR-95-2001; SR-1) Avail: Issuing Activity (Defense Technical Information Center (DTIC))

For three months during the spring and early summer of 1988, low-light TV images showing wave structure in the near infrared hydroxyl (OH) nightglow emission (peak altitude approx. 87 km) were recorded from the Mountain Research Station near Nederland, Colorado (40.0 deg N, 105.6 deg W) as part of the AFOSR MAPSTAR'88 campaign. Well-defined,

coherent wave patterns associated with the passage of short period (less than 1 hour) gravity waves were observed on a total of 22 occasions. One potential source of these waves has been studied using radar summary charts to identify regions of strong convection associated with the existence or development of thunderstorms. Comparison of the 'storm' positions with the location and direction of motion of the OH patterns shows that there was always at least one disturbance suitably located in both space and time to have been the source. The analysis presented here is qualitative, but the large number of wave events associated with favorably located convective activity provide strong evidence for a relationship between the observed waves and storms. This result, although preliminary, suggests that thunderstorms are an important source of mesospheric gravity waves at this site and time of year. DTIC

N95-28871# Tel-Aviv Univ., Ramat-Aviv, Tel-Aviv (Israel).
CORRELATION AND GRADIENT CHARACTERISTICS OF IONOSPHERIC PARAMETERS IN EUROPE Interim Report, No. 2, 1 Dec. 1994 - 28 Feb. 1995
Ehud Heyman, Elene E. Tsedilina, and O. V. Weitsman 20 Feb. 1995 14 p
(Contract N68171-94-C-9119)
(AD-A292295; Rept-731/2; R/D-7216-EE-01) Avail: CASI HC A02/MF A01

The differences in critical frequencies of the ionosphere between measured values of the European continent and the model parameters of 'International Reference Ionosphere of 1990' were considered. In general, absolute relative differences of f(sub o)F2 are of the order of 10 percent. They increase for twilight and night periods up to 20 or 30 percent. Relative difference for f(sub o)E are less than 5 percent for day-time periods and usually are larger for twilight periods. DTIC

N95-28972# Southern Methodist Univ., Dallas, TX.
DESIGN, EVALUATION AND CONSTRUCTION OF TEXESS AND LUXESS, AND RESEARCH IN MINI-ARRAY TECHNOLOGY AND USE OF DATA FROM SINGLE STATIONS AND SPARSE NETWORKS
Eugene Herrin, Paul Golden, and Herbert Robertson Oct. 1994 72 p
(Contracts F19628-93-C-0057; ARPA ORDER-A128)
(AD-A292546; PL-TR-94-2258) Avail: CASI HC A04/MF A01

Objectives of the contract are twofold: (1)' to conduct research in seismic mini-array technology & use of data from single stations & sparse networks, and (2) to design, evaluate and construct 2 mini-array, TEXESS (Texas Experimental Seismic System) in s.w. Texas and LUXESS (Luxor Experimental Seismic System), which is NE of Luxor, Egypt. These two tasks are dubbed CLIN 1 & CLIN 2. The proposed design was along the lines of a GSE Alpha Station. TEXESS was installed by SMU personnel the week of Aug 22, 1993, & the 1st event was a local, recorded on 31 Aug. With de-installation on hold until diplomatic agreements are in place between the U.S. and Egypt for the installation of LUXESS, work has been directed to CLIN 1 research; array processing, Ms:mb studies, & the AR (3) discrimination method. Research on time-domain processing of array data has resulted in a significant decrease in the standard deviation of azimuths as compared with this statistic obtained using f-k processing. The Ms:mb method is an effective and transportable discriminant for shallow events with mb greater than 4.75. Autoregressive (AR) modeling on Lg data has resulted in the ability to discriminate small economic explosions from small earthquakes. DTIC

N95-28985# Scripps Institution of Oceanography, La Jolla, CA.
REGIONAL SEISMIC EVENT IDENTIFICATION AND IMPROVED LOCATIONS WITH SMALL ARRAYS
Frank L. Vernon, J. Bernard Minster, and John A. Orcutt 6 Jul. 1994 32 p
(Contract F19628-93-K-0021; ARPA Order 128)
(AD-A292188; PL-TR-94-2225; SR-1) Avail: CASI HC A03/MF A01

As part of our work in receiver site characterization we have written Kirchoff migration software that can be used to process small-aperture three-component array recordings of regional earthquakes and explosions to develop images of sub- and free-surface scatterers. Essentially, the software back-projects code energy from the recording stations into the crust from which it propagated after suppressing the primary energy. If the crustal volume contains scatterers that were excited by the primary events and these scattered phases were detected by the sensor array, this energy is collapsed in space by the migration onto the scattering loci. Although most sensor array's offer limited aperture, and thus limited spatial resolution, by considering a broadly distributed event array we can take advantage of the synthetic aperture and increase spatial resolution. We have applied this type of processing to synthetics to gauge imaging resolution. We have examined local events recorded by the Pinon Flat Broadband Array (PFBA) and used three-component backprojection to image a deeply buried scatterer in the vicinity of the San Andreas Fault at Moho depth. We are currently assessing the feasibility of using this software to refine regional shallow-source depth estimates. DTIC

N95-29140# Tel-Aviv Univ., Ramat-Aviv, Tel-Aviv (Israel).
CORRELATION AND GRADIENT CHARACTERISTICS OF IONOSPHERIC PARAMETERS IN EUROPE Interim Report No. 1, Sep. - Nov. 1994
Ehud Heyman and Elene E. Tsedilina 29 Nov. 1994 9 p
(Contract N68171-94-C-9119)
(AD-A290135; R/D-7216-EE-01) Avail: CASI HC A02/MF A01

The differences in critical frequencies of the ionosphere between measured values on the European continent and the model parameters of 'International Reference Ionosphere of 1990' were considered. In general, absolute relative differences of foF2 are of the order of 10 percent. They increase for twilight and night periods up to 20 or 30 percent. Relative differences for foE are less than 5 percent for day-time periods and usually are larger for twilight periods. DTIC

N95-29199 Arizona Univ., Tucson, AZ.
DIFFERENTIATION IN THE EARLY EARTH: AN EXPERIMENTAL INVESTIGATION Ph.D. Thesis
Elisabeth Ann McFarlane 1994 153 p
Avail: Univ. Microfilms Order No. DA9424944

The Earth may have been covered with a terrestrial magma ocean. Is there evidence for resulting extensive mineral fractionation? Agee and Walker, 1988, proposed that significant flotation and addition of olivine into the upper mantle can explain the elevated Mg/Si ratio of this region A number of element ratios were present in the primitive mantle of the Earth in approximately chondritic ratios (e.g., Jagoutz et al, 1979) providing constraints on amounts of mineral fractionation if appropriate partition coefficient values are known (e.g., Kato et al, 1988a) In addition, the V, Cr and Mn abundance pattern in the mantles of the Earth and moon are similar to one another, which could imply a related origin for these bodies (e.g., Ringwood, 1990). Previous attempts to explain the origin of this abundance pattern have been unsuccessful (e.g., Drake et al., 1989) High pressure and temperature mantle mineral/silicate melt partition coefficient values are experimentally determined in this work These values are used via equilibrium crystallization to examine the effect of mineral fractionation on the primitive mantle The effect of mineral fractionation on the abundance pattern of V, Cr and Mn in the upper mantle of the Earth is examined. Fractionation of majority garnet, magnesiowustite and Mg-perovskite yields a V, Cr and Mn abundance pattern that is different than inferred Thus, the pattern of V, Cr and Mn was not established by high pressure mantle mineral/dlicate melt fractionation Other mineral fractionation effects are also examined Significant addition of olivine to the upper mantle is disallowed based on the Ni/Co ratio Significant fractionation of majorite garnet, magnesiowustite and Mg-perovskite is precluded based on several element ratios (e.g., Mg/Al, Ca/Al for majorite garnet; e.g., Mg/Al, Ca/Al, Mg/Si, Mg/Ca for magnesiowustite; e.g., Ca/Al, Sc/Sm, Mg/Ca for Mg-perovskite) Thus, the primitive mantle does not show evidence of significant fractionation of volumetrically important liquidus phases The implication is that the Earth's Mg/Si ratio unique, ant that compositionally distinct reservoirs of material were largely preserved in the accretionary environment. Dissert. Abstr.

N95-29212 Princeton Univ., NJ.
PARAMETER STUDY OF THE STATISTICALLY STEADY STATE OF A MULTI-LAYER QUASI-GEOSTROPHIC MODEL Ph.D Thesis
Valentina Pavan 1994 192 p
Avail: Univ. Microfilms Order No. DA9423395

This work is a study of the sensitivity of the statistically steady solution of a baroclinically unstable quasi-geostrophic model of the atmosphere to changes in the values of its parameters. Using the two-layer version of our model we argue that it is useful to think of the lower layer potential vorticity as being diffused through the flow. The 'baroclinic adjustment' hypothesis is found to be invalid in this model. The sensitivity of the

statistically steady solution to the Ekman friction coefficient and to the ambient potential vorticity gradient is studied at various vertical resolutions. We note that the meridional structure of the fluxes plays a very important role in the stabilization process. Attention is also given to the sensitivity to changes in the vertical profile of the forcing, a question raised by global warming scenarios. The eddy potential vorticity flux in the lowest layer is found to be more sensitive to the lower than to the upper tropospheric temperature gradient both in the three and in the twenty-layer case. We argue that this difference in sensitivity is due to the fact that both shallow and deep eddies contribute to the eddy potential vorticity flux, but, while the lower tropospheric forcing affects both the deep and shallow eddies, the upper tropospheric forcing affects only deep eddies. In contrast the surface wind in the three-layer case is as sensitive to changes in the lower as in the upper tropospheric temperature gradient, while in the twenty-layer case it is more sensitive to the lower gradient. Finally we study the sensitivity of the statistically steady solution of a multi-layer, non-Boussinesq quasi-geostrophic model to changes in the intensity of the thermal forcing, describing the sensitivity of the vertical structure and amplitude of the eddy fluxes. We compare our result with the prediction of Held and find that this prediction is only partially verified by our model, possibly due to the coarse vertical resolution. Dissert. Abstr.

N95-29214 Michigan Univ., Ann Arbor, MI.
STUDIES OF THERMOSPHERIC NEUTRAL WINDS UTILIZING GROUND-BASED OPTICAL AND RADAR MEASUREMENTS Ph.D. Thesis
Youngin Won 1994 220 p
Avail: Univ. Microfilms Order No. DA9423347

The neutral dynamics of the F-region and the lower thermosphere have been investigated through extensive ground-based measurements. Ground-based Fabry-Perot interferometers at Thule Air Base (76.5 N, 68.4 W) and Sondre Stromfjord (67.0 N, 50.9 W), Greenland, are utilized to investigate high-latitude neutral dynamics in the F-region (approximately 250 km) by observing the (OI)6300 A emission line profiles. They are also used to study the lower thermospheric region (approximately 97 km) by observing the (OI)5577 A line profiles. The high-latitute mean neutral winds in the F-region thermosphere vary significantly with changes in the level of solar activity and geomagnetic condition due to the direct and indirect influence of high-latitute magnetospheric and ionospheric processes. Careful treatment is used in analyzing the (OI)5577 A measurements because of the possible contamination from auroral emission and weak F-region emission. The ambiguity in the altitude of the emission layer is removed by eliminating data with relatively high signal intensity, because the auroral emission contribution is always much greater than the nightglow. The contribution originating from the upper layer to the measured winds has been quantified by performing a computer simulation. The simulation results indicate that the measured winds at Thule may have a substantial diurnal oscillatory component from the F-region. The same simulation shows negligible F-region contamination for Sondre Stromfjord winds. Tidal information is extracted from the averaged winds and compared with radar measurements in similar locations and model output. The global structure of lower thermospheric dynamics is investigated utilizing a comprehensive data base of lower thermospheric wind measurements. Data are assembled from various radar systems. The data, together with FPI measurements, are used to develop an empirical model of global lower thermospheric diurnal and semidiurnal tidal oscillations. The amplitudes of tidal oscillations generally increase with height in the lower thermospheric region.
Dissert. Abstr.

N95-29253 Oregon State Univ., Corvallis, OR.
THE SPATIAL-SCALE DEPENDENCE OF THE OBSERVED ANISOTROPY OF REFLECTED AND EMITTED RADIATION Ph.D. Thesis
Qian Ye 1993 179 p
Avail: Univ. Microfilms Order No. DA9413763

The Earth Radiation Budget Experiment (ERBE) uses angular dependence models (ADM's) to convert satellite observed radiances to radiative fluxes at the top of the atmosphere. Owing to errors in scene identification and to the relationship between the spatial scales of cloud systems and the spatial resolution of the ERBE scanner, the anisotropy of the radiation fields determined from ERBE observations was suspected of exhibiting a field of view size dependence. In order to remove effects due to the spatial scale of cloud fields, ERBE scanner observations from the Earth Radiation Budget Satellite (ERBS) were averaged to construct observations having a constant size field of view for all scan angles. Comparing the anisotropy for constant size fields of view with that obtained using unaltered full-resolution scanner observations, it was found that there were significant and systematic differences of the order of 5-10 percent for all scene types. The frequencies of occurrence for clear, partly cloudy, mostly cloudy, and overcast cloud categories identified by the ERBE scene identification algorithm were calculated for the constant size field of view observations. It was found that the ERBE scene identification method failed to correctly identify scene types. A bispectral threshold method was developed for scene identification. In the determination of the thresholds, the ERBE scene identification method was assumed to be correct for nadir observations. The thresholds were then determined so that the population of scene types remained constant from nadir to limb for the constant size field of view observations. ADM's were developed using the threshold scene identification method. Results showed that the spatial-scale dependence of the ADM's was significantly reduced. The threshold ADM's satisfied the principle of reciprocity more closely than did the ERBE ADM's for all cloud categories. Using the threshold scene identification, the view zenith angle dependence of the global average albedo and the longwave flux were significantly reduced compared with those obtained using the ERBE scene identification. The estimated global average albedo increases from 0.282 for the ERBE algorithm to 0.299 for the threshold algorithm. There was no significant change for the value of the estimated longwave flux. Dissert. Abstr.

N95-29293# Radix Systems, Inc., Rockville, MD.
TWO-DIMENSIONAL SIGNAL PROCESSING FOR REGIONAL SEISMIC EVENT IDENTIFICATION Final Report, 3 Jun. 1993 - 31 Aug. 1994
Jay J. Pulli and Paul S. Dysart Sep. 1994 51 p
(Contract F19628-93-C-0060; ARPA Order 128)
(AD-A292601; PL-TR-94-2235) Avail: CASI HC A04/MF A01

The objective of this research was to develop a methodology for regional seismic event identification which utilizes 2-dimensional signal processing and treats the seismogram as an image. The motivation for this research comes from the observation that the spectral features which distinguish quarry explosions from earthquakes can be seen throughout the entire seismogram. These features, which include spectral banding, are apparent in the time-frequency (TF) representation of the seismogram. We parameterized the TF representation by computing the wavenumber spectrum of the image and fitting this to a stochastic surface model developed to characterize bathymetric surfaces. Five model parameters control image features such as lineations, spatial orientation, characteristics lengths, and roughness of the surface. DTIC

N95-29317# Spectral Sciences, Inc., Burlington, MA.
RESEARCH INTO ARTIFICIALLY INDUCED ATMOSPHERIC DISTURBANCES Scientific Report No. 1
James W. Duff and Fritz Bien Jun. 1994 27 p
(Contract F19628-93-C-0052)
(AD-A290150; SSI-TR-246; PL-TR-94-2206) Avail: CASI HC A03/MF A01

A detailed chemical kinetics model describing the interaction of an electron beam with the atmosphere is used to study the effects of the reaction of translationally hot N(4S) atoms with O2 on NO formation and emission during the EXCEDE 3 artificial auroral experiment. The rate constants and vibrational distributions for rotationally hot NO are obtained from extensive quasiclassical trajectory calculations for the N(4S) + O2 reaction using realistic ab initio potential energy surfaces. It is shown that a quantitative description of rotationally thermal and hot NO emission observed in EXCEDE 3 requires the inclusion of hyperthermal N atom chemistry in our chemical kinetics model. This analysis provides the first quantitative evidence of the importance of hyperthermal N(4S) and N(2D) atoms in the formation of vibrationally and rotationally excited NO. Excellent agreement between the chemical kinetics model developed for EXCEDE and the vibrational populations derived from the interferometer data is obtained under conditions of thermalization of nitrogen atoms (i.e., at 103 km under max dose conditions). Analysis of the vibrational populations from the interferometer under other conditions indicate that hyperthermal N(2D) atoms also play an important role in NO formation. DTIC

N95-29413# Oslo Univ. (Norway).
EURASIAN SEISMIC SURVEILLANCE - 2D FD SEISMIC SYNTHETICS AND EVENT DISCRIMINATION Final Report, 1 Oct. 1992 - 30 Sep. 1994
Bent O. Ruud and Eystein S. Husebye 23 Feb. 1995 67 p
(Contract F49620-92-J-0510)
(AD-A292659; AFOSR-95-0175TR) Avail: CASI HC A04/MF A01

Most efforts have been devotes to 2D FD synthetics for simulating seismic wave propagation in a complex lithosphere. The FD scheme used is tied to the numerical solution of the elastodynamic wave equation. We have demonstrated the usefulness of this approach by computing synthetic seismograms for a set of progressively complex lithosphere models. In practice, model set-up for FD computations have proved cumbersome so we have elaborated on automating structural model generation. The computed synthetics are SEG-Y formatted and thus are easily processed using standard software packages like the ProMAX. As part of the 2D FD studies, we have critically examined optimal design of boundary conditions in order to reduce edge reflection artifacts. Our synthetic wavefield scheme recently extended to 3D modelling can also handle surface topography.
DTIC

N95-29524 Texas Univ., Dallas, TX.
CHARACTERIZATION OF THE GEOMETRIES OF THE HIGH-LATITUDE IONOSPHERIC CONVECTION PATTERN Ph.D. Thesis
Christopher Francis Keating 1994 131 p
Avail: Univ. Microfilms Order No. DA9419484

An investigation of the geometries of the high-latitude convection pattern is conducted using spacecraft observations of the northern hemisphere during conditions when the z-component of the interplanetary magnetic field is negative. In the first part of this investigation we examine the specification of the polar cap boundary as a circle using data from nearly simultaneous satellites to investigate the variation in size and location of the circle and the means by which such variations may be specified. We also investigate the degree to which a circle departs from the instantaneous configuration of the boundary and the effect that such departures may have on the global potential distribution. The DMSP satellites F8 and F9 provide an opportunity to identify the polar cap boundary with four nearly simultaneous points that can be used in a least squares fitting procedure to derive a best fit circle describing the polar cap boundary. The results of this exercise confirmed that the polar cap boundary can be well represented by a circle with the center offset towards the midnight sector with a B(sub y) and seasonal dependence in the radius of the circle and the location of the center point. Our results indicated that departures from a nominally circular boundary occur most frequently on the dayside. These departures led us to conclude that the polar cap boundary can be best represented by two circular segments with a smaller segment on the dawnside for conditions of B(sub y) negative. We also identified localized bulges or depressions as departures from the circle that are consistent with the descriptions of suggested impulsive additions of magnetic flux to the polar cap. In the second part of this investigation we examine the latitude distribution of the potential at latitudes below the polar cap boundary to determine its sensitivity to interplanetary conditions, magnetic activity, and local time. We use a gaussian curve segment to best represent the distribution of the potential equatorward of the polar cap and find the gaussian halfwidth is dependent on the potential at the polar cap boundary with the halfwidth being larger on the duskside than on the dawnside. We also find this parameter is dependent on local time as well as Kp and IMF B(sub z). In all cases, the halfwidth shows a greater variability on the duskside than on the dawnside. Finally, we note that the potential distribution around the polar cap boundary shows significant departures from the sinusoidal distribution frequently assumed in model treatments. As a final exercise, we use our results to generate inputs into a mathematical model of the high-latitude convection pattern and compare the results to measured data and find the model results to be reasonable representations of the actual conditions. Dissert. Abstr.

N95-29585# Boston Univ., MA. Center for Space Physics.
THE EFFECTS OF MAGNETIC STORM PHASES ON F-LAYER IRREGULARITIES FROM AURORAL TO EQUATORIAL LATITUDES Quarterly Report, 1 Oct. - 31 Dec. 1994
Jules Aarons and Michael Mendillo 31 Dec. 1994 4 p
(Contract N00014-89-J-1754)
(AD-A290674) Avail: CASI HC A01/MF A01

During the past twenty years our understanding of Equatorial Scintillation Storms (ESS) has reached a considerable maturity. We understand the average occurrence pattern and underlying physics quite well. We also understand many of the processes which create the day to day variability and which are crucial to the development of forecasting techniques. Yet there remains a persistent, illusive quality in predicting degradation of signals propagating through the ionosphere because no one has created a synthesis of this understanding. The purpose of this joint study is to outline a three year program which brings together the capabilities of the three major ONR groups in the Northeast for a cooperative venture to predict ESS on time scales of 3-6 hours. DTIC

N95-29590 Alabama Univ., Huntsville, AL.
THERMAL N(+) IN THE INNER MAGNETOSPHERE Ph.D. Thesis
Paul D. Craven 1993 210 p
Avail: Univ. Microfilms Order No. DA9415101

In this study the statistical behavior of the minor ion N(+) in the plasmasphere is characterized in order to understand the causes for the changes seen in the concentration of this ion; this includes quantifying the response of N(+) to geophysical conditions (solar activity geomagnetic activity). The survey of the measurements is based mainly on measurements made with DE1/RIMS, although we also use measurements from the Atmospheric Explorer and the Orbiting Geophysical Observatory series of satellites. A numerical model, the Field Line Interhemispheric Plasma (FLIP) model, of the plasma is used to predict the response of the density of N(+) to geophysical conditions. The predicted behavior is compared with the measured responses; this last process is, in effect, a check of our knowledge of the processed and transport to which N(+) is subjected. The behavior of the density of N(+) and the other three ions in the ionosphere is examined for their behavior with solar activity seasons, local time, and geomagnetic activity levels. The occurrence frequency of N(+) for all the RIMS data and the ratio of N(+) to O(+) , both averaged over all seasons and solar and geomagnetic levels, is examined to determine the extent of N(+) in the inner magnetosphere. The model is used with the ionospheric data to examine the qualitative and quantitative behavior of the density calculated with FLIP in this region. The RIMS measurements, supported by FLIP, show that N(+) is a constant companion of O(+) . We find indications that on a statistical basis these two ions undergo similar, if not the same, dynamic processes at altitudes above the F region. The survey also shows that the density of N(+) is a significant fraction of the density of O(+) when averaged over space and time. The presence of N(+) in the thermal plasma is an important factor in the propagation of plasma plasma because the frequency and the propagation of these waves is affected by mass composition. We find that the ratio of N(+) to O(+) is, however, quite variable The FLIP model shows that the magnitude of the ratio depends on altitude, solar conditions, season, local time and geomagnetic conditions. Using the FLIP model, we show that the ratio above the ionosphere increases with altitude and inversely with ion temperature. The RIMS measurements qualitatively support the ratios calculated using FLIP densities in that most of the mean ratios above 1000 km altitude are between 0.1 and 1.0. However, temperature is not the only variable affecting the ratio. Processes that affect the density of N(+) in the ionosphere influence the density at higher altitudes. In the outer plasmasphere, the temperature of the light ions used to constrain the model parameters leads to ratios of the heavy ions at high altitudes that are not supported by any measurement. We suggest that this result indicates that the light ions and the heavy ions are not in thermal equilibrium on the edge of the plasmasphere. The comparison of the model and the measurements for the inner plasmasphere show that the model closely matches the measurements for almost all the conditions examined. Our results show that the FLIP model is an excellent model of the ionosphere and the plasmasphere. This model when combined with realistic constraints on the ion temperature is an excellent tool for studying the ionosphere and plasmasphere. Dissert. Abstr.

N95-29650 Texas Univ., Dallas, TX.
APPLICATION OF POYNTING FLUX MEASUREMENTS TO THE DETERMINATION OF ENERGY TRANSFER RATES IN THE HIGH-LATITUDE IONOSPHERE Ph.D. Thesis

James Bennett Gary 1994 119 p
Avail: Univ. Microfilms Order No. DA9419483

The use of Poynting flux measured from a polar orbiting satellite to determine energy transfer rates between the ionized and neutral constituents of the high latitude ionosphere has been examined in detail. Previous work on the topic suggested the applicability of the technique, but early derivations and examples lacked the refinement that a more in depth study could provide. The application of Poynting's theorem to satellite measurements is worked out with sufficient rigor to clearly identify the assumptions required for a sensible interpretation of the results. The errors inherent in the determination of the field-aligned Poynting flux are explored, which includes the errors from deriving the electric field from the drift velocity measurements and the errors involved in the perturbation magnetic field determination. The resulting relative error in the Poynting flux increases with decreasing field strengths, and the smallest relative error is shown to be about 15 percent. Several case studies are presented along with a detailed description of the analysis technique. These examples include a case where the magnetosphere dominates the electrodynamics in the ionosphere, a case where the thermospheric winds dominate the electrodynamics over a large region in the ionosphere, and a series of observations where stable conditions in the interplanetary environment allow a quasi-steady state to be achieved in the ionosphere. This variety of case studies highlights the use of Poynting flux observations to identify the relative strengths of the magnetospheric and neutral wind dynamos in driving the large scale energy flow into and out of the ionosphere. The work concludes with a statistical survey of the distribution of energy transfer rates in the high latitude ionosphere as inferred from Poynting flux observations. The average Poynting flux has been found to be directed into the ionosphere, indicating that the magnetosphere is dominantly in control of the plasma circulation in the ionosphere, as expected. The distributions for northward and southward interplanetary magnetic field conditions at high and low geomagnetic activity are given, and the results are shown to be compatible with the differences in the average circulation patterns of the ions and neutrals under those conditions. Upward Poynting flux occurrences have been examined independently, with the unexpected result of significant occurrences of upward Poynting flux in the post-midnight sector for southward IMF.

Dissert. Abstr.

N95-29666 California Univ., Los Angeles, CA.
NUMERICAL STUDIES OF THE STRATOSPHERIC AEROSOL LAYER UNDER BACKGROUND AND PERTURBED CONDITIONS Ph.D. Thesis
Jingxia Zhao 1993 240 p
Avail: Univ. Microfilms Order No. DA9420447

The stratospheric aerosol layer (referred to as the Junge layer) has been the subject of considerable research because of its potential effects on global climate and ozone abundance. To explain all of the observed details in the spatial patterns and microphysical features of the aerosol layer, and to study variations caused by natural and anthropogenic sources, a new comprehensive stratospheric sulfate aerosol model is described in this thesis. This model includes treatments of gas-phase sulfur chemistry, gas and particle interactions, aerosol microphysics and dynamical transport. An efficient method for calculating the nucleation rates of H2SO4/H2O aerosol droplets has been developed from classical nucleation theory, which leads to rapid new particle formation under a variety of conditions. The aerosol model has been employed to simulate the ambient Junge layer, as well as major perturbations to the layer caused by volcanic eruption clouds, aircraft sulfur emissions, and special meteorological conditions in the polar region during spring. In the first application, the nucleation model is used to calculate the homogeneous and heterogeneous nucleation rates of H2SO4/H2O aerosols in the exhaust stream of a supersonic aircraft flying in the stratosphere. Background sulfate aerosol concentrations may increase substantially in the vicinity of stratospheric aircraft corridors. These simulations clearly demonstrate that homogeneous nucleation of H2SO4/H2O droplets is an important mechanism leading to the increase in aerosol concentrations. Model results are consistent with a serendipitous balloon measurement taken in the exhaust plume of a stratospheric aircraft. With a one-dimensional version of the aerosol model, the principal features of a layer of small particles (condensation nuclei, or CN) observed in the springtime polar stratosphere have been successfully simulated for the first time. The photochemical reactions associated with lower temperature lead to heteromolecular homogeneous nucleation and production of large numbers of H2SO4/H2O droplets. The descending air originating from the mesosphere inside the polar vortex provides a sulfur source for the formation of CN layers. The main focus of this work is to simulate volcanic eruption clouds, which represent the most important perturbation of the Junge layer. Simulations have been performed using a 1-D version of a volcanic aerosol model It is demonstrated that homogeneous nucleation plays an essential role in the formation of the volcanic aerosols. The predicted volcanic cloud parameters agree well with measurements in terms of the distribution and duration of the volcanic aerosols, their basic microphysical properties including size distribution, concentration, modal radius, mass mixing ratio and surface area, and radiative properties. The persistent volcanic aerosols can produce significant anomalies in the radiation field, which have important climate consequences. The large enhancement in aerosol surface area can result in measurable global stratospheric ozone depletion.

Dissert. Abstr.

N95-29687 Minnesota Univ., Minneapolis, MN.
TURBULENT COUPLING OF THE MAGNETOSPHERE-IONOSPHERE THROUGH SHEAR-MODE ALFVEN WAVES Ph.D. Thesis
John Clarence Grieger 1993 188 p
Avail: Univ. Microfilms Order No. DA9413004

Alfven waves have been observed at various altitudes along magnetospheric field lines, and may be used to account for a host of auroral phenomena. Other electromagnetic plasma mechanisms, common on aurora field lines, such as electrostatic ion cyclotron waves, double layers, ion beams and electrostatic shock structures, although important, are generally confined to a limited altitude range, therefore restricting their domain of influence. The purpose of this work is to investigate the coupling of electromagnetic and kinetic energy from the outer magnetosphere to the ionosphere along a magnetospheric, auroral flux tube via shear-mode Alfven waves. A MHD approach is taken, and the nonlinearities of the equations are fully modeled. In this manner, the development of structure in the auroral fields are followed as the waves reflect from inhomogeneities along the flux tube and from the ionospheric boundary. The question which is used is the following: how are small scale (1 km and less) auroral features formed from large scale (order of an earth radius) structures in the outer regions of the magnetosphere? Alfven wave propagation along a flux tube is modeled through the Strauss equations, a set of reduced, three dimensional MHD equations. The turbulent 2-D planes perpendicular to the background magnetic field are coupled by Alfven waves traveling parallel to this field. Two MHD instabilities are studied as a means of generating auroral flux tube turbulence, the Kelvin-Helmholtz instability and the collisionless tearing mode instability. The effects of ionospheric conductivity and a finite k(parallel) associated with Alfven waves on the evolution of the K-H instability are investigated. The effects of a topside ionospheric Alfven resonator cavity on the tearing mode instability is numerically studied. An inhomogeneous, dynamic ionosphere is modeled, in which Hall and Pedersen conductivities are time dependent. The effects of secondary waves launched upward from Hall conductivity gradients are studied. In addition, a generalized conjugate-gradient scheme of solving the coupled equations at the ionospheric boundary is developed, and this work is illustrated in the appendix. Dissert. Abstr.

N95-29693 Texas Univ. at Dallas, Richardson, TX.
THE HIGH LATITUDE IONOSPHERIC CONVECTION PATTERN DURING NORTHWARD INTERPLANETARY MAGNETIC FIELD Ph.D. Thesis
Judy Anne Cumnock 1994 129 p
Avail: Univ. Microfilms Order No. DA9422833

An investigation of the earth's magnetospheric convection signature in the high latitude ionosphere is conducted using spacecraft observations. In particular we examine the ionospheric convection pattern under various interplanetary magnetic field conditions. The DMSP F8 satellite's coverage of the earth's polar regions provides horizontal ion drift velocities along the dawn-dusk meridian at about 835 km altitude in each hemisphere during the approximately 100 minute orbital period. We first consider five passes over the southern summer hemisphere during a time when the z component of the interplanetary magnetic field was stable and positive and the y component changed slowly from positive to negative. Large-scale regions of sunward flow are observed at very high latitudes consistent with a strong z component. When B(sub y) and B(sub z) are positive, but B(sub y) is greater in magnitude than B(sub z), strong evidence exists for dayside merging in a manner similar to that expected when B(sub z) is

negative. This signature is diminished as B(sub y) decreases and becomes smaller than B(sub z) resulting in a four-cell convection pattern displaced toward the sunward side of the dawn-dusk meridian. In this case the sign of B(sub y) affects the relative sizes of the two highest-latitude cells. In the southern hemisphere the duskside high latitude cell is dominant for B(sub y) positive and the dawnside high-latitude cell is dominant for B(sub y) negative. The relative importance of possible electric field sources in the low-latitude boundary layer, the dayside cusp, and the lobe all need to be considered to adequately explain the observed evolution of the convection pattern. We next examine the ionospheric convection signatures observed by DMSP F8 in the summer and winter hemispheres during periods when the IMF is directed northward for at least 45 minutes prior to the satellite entering the polar region and remains northward throughout the polar pass. These convection signatures can be readily categorized by the number of sunward and antisunward flow regions and by their potential distributions. Here we describe the most frequently identifiable and reproducible features of the convection pattern that exist during steady northward IMF conditions. In addition to IMF B(sub z) the influences on the convection pattern of the IMF B(sub z)/(absolute value of B(sub y)) ratio, season, latitude, and solar wind velocity are all considered. These parameters cannot be used to reliably predict a specific convection pattern; however, B(sub z)/(absolute value of B(sub y)) provides a first order selection for those signatures that occur on the dayside of the dawn-dusk meridian. Sunward flow at highest latitudes on the dayside of the dawn-dusk meridian is the dominant feature seen in the large-scale convection signature during steady northward IMF; however sunward flow at highest latitudes does not imply the existence of a particular number of convection cells. Dissert. Abstr.

N95-29696 Michigan Univ., Ann Arbor, MI.
HIGH-LATITUDE ELECTRODYNAMICS: ELECTROMAGNETIC ENERGY DISSIPATION AND NEUTRAL WIND FEEDBACK EFFECTS Ph.D. Thesis
Wei Deng 1994 186 p
Avail: Univ. Microfilms Order No. DA9423175

Results of an experimental and theoretical investigation into the electromagnetic energy budget and the effects of the time dependent neutral wind flywheel on high-latitude electrodynamics are presented. Thin investigation is carried out using measurements obtained from the DE-2 satellite and numerical simulations from the National Center for Atmospheric Research Thermosphere Ionosphere General Circulation Model (NCAR-TIGCM). A one-dimendonal hybrid satellite-track model has been developed to map the DE-2 satellite measurements into the low-altitude dynamo region. A validation study, made using measurements taken from an Incoherent Scatter Radar site during a DE-2 overflight, indicates that the model is able to determine the electric conductivities and Joule heating rate in the dynamo region to a reasonable accuracy. The model is then used to study the conversion of electromagnetic energy in the lower thermosphere. The electromagnetic energy input into the thermosphere is measured by the downward Poynting Flux at DE-2 satellite orbit. Good agreement was found between the amount of energy dissipated by Joule heating and that transferred into the thermosphere by Poynting flux during a southward IMF B(sub z) condition. A relatively small part (approximately 10 percent) of this electromagnetic energy is converted into the neutral mechanical energy. The mechanical energy stored in the neutral gas may maintain the high-latitude electric fields and/or drive the reversed currents during decaying magnetic activity. This has been called 'fly wheel effect'. A numerical experiment has been conducted to simulate this effect using the NCAR-TIGCM and its diagnostic package. The results of this simulation indicate that the height-integrated Hall currents, Poynting flux and field-aligned currents are dominated by neutral-wind-driven components for several hours after the end of main phase of the storm, if the magnetosphere is assumed to act as a perfect conductor with respect to the thermospheric dynamo. The direction of these currents and fluxes reverse from their normal direction. On the other hand, if it is assumed that magnetosphere acts as an insulator, this study indicates that the high-latitude neutral wind dynamo can generate about 20-30 KV polarization electric fields in the period immediately following the geomagnetic storm. Data from the DE-2 satellite have provided a demonstration of existences of the local flywheel effect and are in good agreement with model calculations. Dissert. Abstr.

N95-29698 North Carolina State Univ., Raleigh, NC.
THE INTERACTIVE ROLE OF CLOUDS AND RADIATIVE TRANSFER IN MAINTAINING ATMOSPHERIC CIRCULATION Ph.D Thesis
Martin John Leach 1994 178 p
Avail: Univ. Microfilms Order No. DA9425475

Radiative flux divergence is one of the principal physical forces for atmospheric circulation. It affects the temperature, winds, cloud evolution and structure, and the water budget on all time and space scales. In this study, numerical models are used to study the effects of radiative transfers on a variety of atmospheric circulation systems on time scales from several hours to several days, and on space scales of about 10 kilometers to 10 thousand kilometers. Shortwave and longwave radiative transfer are added to a mesoscale model which includes detailed microphysics and turbulence closure schemes. This model is used to study three cases where radiative transfer plays a role in the structure of the atmosphere. The first is stratocumulus clouds that form in the wake of thunderstorms. Longwave radiative flux divergence at the top of the boundary layer maintains the cloud layer by cooling at cloud top, enhancing the inversion strength. Eventually, shortwave energy reaching the surface creates sufficient buoyancy to overcome the longwave forcing of the cloud layer, and the cloud dissipates. The same longwave forcing is responsible for the formation of boundary layer clouds in the second case studied, the coastal front. In that case, the presence of clouds also affects the horizontal heating of the atmosphere, as clouds effectively trap longwave energy below clouds, but also reflect shortwave energy, so that surface heating over land is less. The differences in radiative forcing changes the relative intensity of the thermal circulations that form over the Gulf Stream and at the coastline, with further feedback to the clouds, winds, temperature, and atmospheric water vapor. Finally, the third case was an examination of the effects of radiative transfer on low level cyclogenesis. Again, the longwave flux divergence at the top of the clouds maintained a cloud layer against the destructive force of mixing from below and entrainment from above. Once clouds form, horizontal thermal gradients lead to increased vorticity generation and a more intense circulation. A stronger circulation feedback to the cloud formation processes and water budget results. Finally, radiative transfer was added to a numerical weather prediction model to study the Indian summer monsoon. The length and time scales in this study were much longer, covering a 180 degree longitude by 90 degree latitude domain for 10 day forecasts. The conclusions however were remarkably similar to those from the smaller model. Radiative transfer maintains the strength and structure of the components of the monsoon circulation system with feedback to cloud and precipitation processes. Dissert. Abstr.

N95-29716 Alabama Univ., Huntsville, AL.
EQUATORIAL HEATING EFFECTS ON OUTER PLASMASPHERE EVOLUTION Ph.D. Thesis
Fengchiao Joyce Lin 1993 186 p
Avail: Univ. Microfilms Order No. DA9415105

This dissertation is an investigation of core plasma evolution on closed magnetic field lines in the inner part of the Earth's magnetosphere. The study incorporates both new plasma modeling methods and analysis of core ion data measured from spacecraft. The semikinetic model utilized incorporates both large-scale ion kinetic effects and plasma microprocesses, allowing direct calculation of the ion distribution functions and investigation of effects such as velocity dispersion, Coulomb collisions, and wave-particle interactions. The ions are treated as kinetic gyrocenters while electrons are treated both with a modified Boltzmann relation and with a generalized fluid description. In this dissertation, the effects of equatorial ion and electron heating on the overall evolution of ionospheric plasma flows onto initially empty magnetic flux tubes are emphasized. This model predicts several observed features in core ion measurements analyzed by Olsen et al. (1987) and Olsen (1992). In the corresponding analysis of DE-1/RIMS core ion data, we have characterized the interface between trapped and field-aligned ion distribution regions obvserved during the unique 'field-line skimming' orbits of the Dynamics Explorer-1 spacecraft. We may interpret the features of this interface in terms of Liouville mapping of equatorially trapped ions and the reflection of the incoming ionospheric ion streams from the equatorial potential peaks associated with such trapped ions.
Dissert. Abstr.

N95-29737# RDP, Inc., Waltham, MA.
DATA RE-FORMATTER PROGRAM FOR THE TOPSIDE THERMAL PLASMA MONITOR (PLIESPP)
Andrew J. Mazzella, Jr. and J. R. Cornelius 20 Oct. 1994 63 p

(Contract F19628-89-C-0079)
(AD-A290960; RDP-TR-9403; PL-TR-94-2278; SR-5) Avail: CASI HC A04/MF A01

The data reformatting program (PLIESPP) for the SSIES thermal plasma monitor allows data from the Phillips Laboratory, Geophysics Directorate (PL/GP) Time History Data Base (THIDB) format to be used by the Space Forecast Center (SFC) analysis program (APGA). This version of the PLIESPP program was designed to process data for the SSIES-2 telemetry formats, with provisions for adaptation to processing the older SSIES format or the SSIES-3 format, planned for future instruments. DTIC

N95-29765# RDP, Inc., Waltham, MA.
THE TOPSIDE IONOSPHERIC PLASMA MONITOR (SSIES, SSIES-2 AND SSIES-3) ON THE SPACECRAFT OF THE DEFENSE METEOROLOGICAL SATELLITE PROGRAM (DMSP), USER'S GUIDE. VOLUME 3: PROGRAM MAINTENANCE MANUAL
J. R. Cornelius and Andrew J. Mazzella, Jr. 11 Oct. 1994 310 p
(Contract F19628-89-C-0079)
(AD-A290941; RDP-TR-9402-Vol-3; PL-TR-94-2271; SR-4) Avail: CASI HC A14/MF A03

The objective of the Program Maintenance Manual for the DMSP SSIES flight data processing software is to provide AFSFC programming personnel with the information necessary to understand and maintain the various components of the system. This software has been specifically developed to process the SSIES-2 and SSIES-2A data formats, with provisions for retroactive adaptation to the original SSIES format and future adaptation to the SSIES-3 format. This Program Maintenance Manual describes the three programs which constitute the AFSFC SSIES processing system: BNBA, LDCON02, and APGA. The BNBA program performs data format conversions for the various SSIES telemetry data formats to generate a common file format for subsequent processing by the APGA program. The LDCON02 program generates the reference parameter file of satellite and instrument conversion constants and processing options for use by the APGA program. The APGA program performs quality evaluations and analyses of the SSIES telemetry data to create database files and reports of quantities which characterize the ionosphere. DTIC

N95-29773 Arizona Univ., Tucson, AZ.
THE GRAVITATIONAL POTENTIAL ENERGY OF THE EARTH'S LITHOSPHERE Ph.D. Thesis
David Dwight Coblentz 1994 217 p
Avail: Univ. Microfilms Order No. DA9424935

This dissertation explores the tectonic implications of lateral potential-energy variations within the Earth's lithosphere. The central hypothesis of this study is that much of the observed intraplate-stress field is explainable in terms of these variations. The study develops the concept of a tectonic reference state (TRS), defined here as the mean potential energy of the lithosphere, U(l). A simple, first-order lithospheric density model is used to calculate U(l), which was found to correspond to both near-sealevel continental lithosphere and cooling oceanic lithosphere at a depth of 4.3 km. Although the potential energy of the continental lithosphere with elevated topography is sensitive to the assumed crustal density, rho(c), both global- and plate-scale TRS values were found to be robust. A finite element analysis of the intraplate stress field in the African, South American and Indo-Australian plates was used to demonstrate that many of the long-wavelength features in the intraplate stress fields of these plates can be explained in terms of lateral variations in the lithospheric potential energy. Constraints for the numerical modeling were provided by an analysis of the long-wavelength trends in the intraplate stress field and a study of the intraplate stress magnitude in the South American plate. It was found that the value of U(t) changes significantly in response to the aging of oceanic lithosphere such that continental regions become increasingly susceptible to extensional collapse as the plate ages. In the case of the African and Antarctic plates, the aging of the ocean lithosphere since the late Jurassic has contributed a mean stress difference of about 5 MPa and 7.5 MPa (averaged over a 125km-thick lithosphere) in the respective continents. This extensional stress may contribute as much as 50 percent of cumulative force needed to deform continental lithosphere. One important implication of this calculation is that rifting in present-day continents and the breakup of supercontinents may be explained in terms of the time-evolution of the potential-energy distribution. Dissert. Abstr.

N95-29777 Colorado Univ., Boulder, CO.
HEAT AND MOMENTUM FLUX MEASUREMENTS IN THE PLANETARY BOUNDARY LAYER WITH A WIND PROFILING RADAR/RADIO ACOUSTIC SOUNDING SYSTEM Ph.D. Thesis
Wayne Merrill Angevine 1993 136 p
Avail: Univ. Microfilms Order No. DA9423460

The planetary or atmospheric boundary layer is the lowest 100-2000 m of the atmosphere, and contains the sources of most energy and pollutants that affect the entire atmosphere. Boundary-layer structure and dynamics are key to understanding, modeling, and predicting climate, weather, and pollution. New and improved techniques for measuring the dynamics of the boundary layer are needed. One of the most important needs is for improved methods of measuring the turbulent fluxes of heat and momentum. Existing methods involving towers, surface measurements, or aircraft have limited flexibility or are expensive. This dissertation describes methods for measuring heat flux (virtual temperature flux) and momentum flux in convective boundary layers. The instrument used is the 916 MHz boundary-layer radar wind profiler radio acoustic sounding system (profiler/RASS). As the name suggests, the profiler was developed to make wind measurements, and this work is an expansion of its capabilities. The radio acoustic sounding system uses the profiler and attachments to measure virtual temperature. Before the profiler/RASS could be used to make flux measurements, the ability to make simultaneous measurements of wind velocity and temperature had to be developed. A feasibility study was conducted at Platteville, Colorado, in June 1991 to determine if flux measurements were a practical application of the profiler, with encouraging results. The Rural Oxidants in the Southern Environment II (ROSE II) experiment in Alabama in June 1992 provided the opportunity to compare flux measurements from the profiler/RASS to those made by a surface sonic anemometer and an aircraft, the National Center for Atmospheric Research (NCAR) King Air. The results indicate that the profiler/RASS is capable of making heat flux measurements that compare well with aircraft and surface measurements. The primary limitation on the precision of the measurements is the sampling uncertainty of the turbulence, a limitation that is the same for any fixed instrument. The feasibility of making momentum flux measurements needs to be explored further in more favorable conditions. In the course of analyzing the flux measurements, methods of determining the mixing depth (boundary layer height) and improved data quality control techniques were developed. Dissert. Abstr.

N95-29796 California Univ., Santa Barbara, CA.
LARGE SCALE FLUCTUATIONS OF THE GEOMAGNETIC FIELD Ph.D. Thesis
Joanna Dimitrios Eva Athanassopoulos 1993 736 p
Avail: Univ. Microfilms Order No. DA9419051

The present controversy over the reversal records centers on the distribution of Virtual Geomagnetic Pole (VGP) paths and on the fidelity with which rocks record the directions and intensities of the reversing geomagnetic field. This dissertation focuses on three main objectives. The Atlas of the Reversal Records is a documentation of 115 reversal records that have been published. Each reversal record is presented in a standard form consisting of a listing of the site, rock type, age, reference, and magnetization data, declination, inclination, intensity plots, and VGP plots in both Lambert and Hammer projections. The Atlas has been compiled to enable comparisons of the available reversal records that help model the nature of the transitional field and its behavior. Statistical analysis indicated that most VGP paths lie in the Western Hemisphere, and that if plotted with respect to site longitude they exhibit a near-sided nature. To help establish the character of the intensities of the transitional fields, independent evidence of the field intensity decrease, associated with the Matuyama-Brunhes (R-N) reversal (0.73 MY), has been obtained from measurements of the abundance of 10 Be in marine sedimentary cores. Previous paleomagnetic work suggested that the dipole field oscillated strongly in intensity before the reversal and that the polarity change was rapid. Results show that the abundance of the cosmogenic radionuclide 10 Be increased by a factor of at least three for transitional samples, apparently as a result of the reduced field intensity. Further, 10 Be abundances accurately reflect magnetic intensity oscillations implying that they are global in character, indicating that the transitional fields are dominated by low order harmonics. A high resolution record of the Matuyama-Brunhes polarity transition from a Northern Hemisphere deep

sea sediment core (ODP site 883B; 51.2 deg N, 167.75 deg E) is also presented. This record was obtained using thermal and alternating field demagnetization. The VGP is neither near- nor far-sided, nor confined over the Americas, but tracks in longitude moving from 250 deg South to 0 deg North, crossing the equator approximately 140 deg East of the site.
Dissert. Abstr.

N95-29830 Harvard Univ., Cambridge, MA.
IN SITU MEASUREMENTS OF ClO AND IMPLICATIONS FOR THE CHEMISTRY OF INORGANIC CHLORINE IN THE LOWER STRATOSPHERE Ph.D. Thesis
Linnea Marie Avallone 1993 278 p
Avail: Univ. Microfilms Order No. DA9421935

The role of anthropogenic chlorine compounds in wintertime polar ozone loss has been extensively examined. However, the causes of smaller, yet geographically more pervasive, declines in ozone over mid-latitudes are unknown. Measurements of chlorine oxide (ClO) from the NASA ER-2 aircraft and balloon platforms are analyzed to assess the contribution of chlorine to lower stratospheric ozone loss and the effects of heterogeneous chemistry on sulfate aerosols on the observed distributions of ClO. We employ the technique of chemical conversion/resonance fluorescence, in which nitric oxide converts ClO to chlorine atoms, which are detected by resonant scattering at 118.9 nm. The results of experiments that gauge the purity of resonance lamps, the kinetics of the conversion process, the flow characteristics within the instrument and the low-pressure chlorine atom calibration are presented. The effect of the equilibrium process Cl + O2 reversibly yields ClOO is investigated over the range of stratospheric temperatures and pressures. Each of these tests provides important data for determining the overall uncertainty of ClO measurements. In situ measurements of ClO obtained with a new balloon-borne instrument provide a test for our understanding of mid-latitude lower atmosphere chemistry.
Dissert. Abstr.

N95-29970# California Inst. of Tech., Pasadena, CA. Seismological Lab.
MAPPING CRUST AND UPPER MANTLE STRUCTURE BENEATH SOUTHERN EURASIA Final Technical Report, 1 Sep. 1992 - 31 Aug. 1994
Donald V. Helmberger 9 Jan. 1995 70 p
(Contract F49620-92-J-0470)
(AD-A291074; AFOSR-95-0090TR) Avail: CASI HC A04/MF A01

Travel-time tomography was used to obtain the lateral variations in P(n) velocities and P(n) velocity azimuthal anisotropy beneath the Basin and Range Province. We used 1226 P(n) arrivals from 184 earthquakes recorded by 113 stations. The tomographic image shows the lateral variation in P(n) velocity from 7.9 km/s in the northern Province to 7.6 km/s in the southern Province. Azimuthal variations in P(n) velocities are less than one percent as determined from the travel time residuals after taking out the contribution of the lateral velocity variations of the P(n) tomography. Although the standard errors of the azimuthal variations are about two percent, there is no reason to believe the existence of the P(n) azimuthal anisotropy in the uppermost mantle beneath the Basin and Range Province. Beghoul and Barazangi's (1990) suggestion of more than three percent azimuthal anisotropy is the result of the lateral heterogeneity and mantle velocity gradient Before tomographic inversion, we refined the P(n) travel times by considering the lateral variations in the crustal thickness and velocities in the region based on the numerical experiment and theoretical development given in this paper. These refinements are crucial in obtaining an accurate velocity image.
DTIC

N95-29976# Army Research Lab., White Sands Missle Range, NM.
THE SCANNING FAST FIELD PROGRAM (SCAFFIP) GENERAL VERSION 1.0 USER'S MANUAL
John M. Noble and Dave Marlin Jan. 1995 128 p
(AD-A291209; ARL-TR-545) Avail: CASI HC A07/MF A02

The Scanning Fast Field Program (SCAFFIP) is an atmospheric acoustic propagation model incorporating many of the effects on the environment on the sound field such as geometrical spreading, refraction, diffraction, molecular absorption, and complex ground impedance. SCAFFIP provides attenuation levels with range and azimuth or sound pressure levels in dB (re: 20 mu Pa) with range and azimuth for a given geometry, frequency, and meteorological profile. The meteorological profile and the geometry provides the model the ability to calculate the sound speed profile. The geometry profile is required because the angular dependence of the sound speed on the wind direction is relative to the direction of propagation. This model works over a flat-earth and a non-turbulent atmosphere. Even with these restrictions, the model performs very well for many scenarios. The model contains a friendly user interface requiring a minimum amount of information to run the model. There are also flags that can be set to obtain more detailed information.
DTIC

N95-29981# Massachusetts Inst. of Tech., Cambridge, MA. Dept. of Earth Atmospheric and Planetary Sciences.
CRUSTAL DEFORMATION MEASUREMENTS IN THE VICINITY OF VANDENBERG AIR FORCE BASE Final Technical Report, 1 Sep. 1990 - 15 Jul. 1994
R. W. King, B. H. Hager, T. A. Herring, A. Cooray, and S. McClusky 20 Dec. 1994 52 p Limited Reproducibility: Document partially illegible
(Grant AF-AFOSR-0339-90)
(AD-A291224; AFOSR-95-0083TR) Avail: CASI HC A04/MF A01

Recent geological and geodetic studies have suggested that the region surrounding Vandenberg Air Force Base, CA, is undergoing active crustal deformation, with important implications for both the geodetic stability and the seismogenic potential of the Western Test Range. In 1989, funding was received (AFOSR 89-0400) for the purchase of several GPS receivers. Beginning in 1990, a series of measurements was funded (AFOSR 90-0339) to determine the magnitude and spatial distribution of deformation in the Santa Maria Fold and Thrust Belt and subsequently to install continuously operating GPS stations at Vandenberg and the China Lake Naval Center. GPS measurements in the thrust belt and surrounding area reveal a zone of both strike slip and compressive deformation not readily identifiable with known faults. Experience with the Landers and Northridge earthquakes underscores findings here that 'blind' thrust faults likely serve as the principal architects of the topography in the thrust belt and the basin areas. Annual or biennial GPS measurements into the future will allow refinement of the estimates of deformation and the geodynamic motions in southern California.
DTIC

N95-30082# RDP, Inc., Waltham, MA.
THE TOPSIDE IONOSPHERIC PLASMA MONITOR (SSIES, SSIES-2 AND SSIES-3) ON THE SPACECRAFT OF THE DEFENSE METEOROLOGICAL SATELLITE PROGRAM (DMSP), USER'S GUIDE. VOLUME 2: PROGRAMMER'S GUIDE FOR SOFTWARE AT AFSFC Scientific Report No. 4
J. R. Cornelius and Andrew J. Mazzella, Jr. 11 Oct. 1994 79 p
(Contract F19628-89-C-0079; AF Proj. 7659)
(AD-A290913; RDP-TR-9401-Vol-2; PL-TR-94-2270) Avail: CASI HC A05/MF A01

The objective of the Programmer's Guide for the DMSP SSIES flight data processing software is to provide AFSFC personnel with the information necessary to understand and use the various components of the system. This software has been specifically developed to process the SSIES-2 and SSIES-2A data formats, with provisions for retroactive adaptation to the original SSIES format and future adaptation to the SSIES-3 format. This Programmer's Guide describes the three programs which constitute the AFSFC SSIES processing system: BNBA, LDCONO2 and APGA. The BNBA program performs data format conversions for the various SSIES telemetry data formats to generate a common file format for subsequent processing by the APGA program. The LDCONO2 program generates the reference parameter file of satellite and instrument conversion constants and processing options for use by the APGA program. The APGA program performs quality evaluations and analyses of the SSIES telemetry data to create database files and reports of quantities which characterize the ionosphere.
DTIC

N95-30129# Los Alamos National Lab., NM.
EXTREME NONLINEARITY IN ROCKS: AN INVESTIGATION USING ELASTIC PULSE WAVE PROPAGATION
Koen E.-A. VanDenAbeele 1995 6 p Presented at the 15th International Congress on Acoustics (ICA), Trondheim, Norway, 26-30 Jun. 1995
(Contract W-7405-eng-36)
(DE95-007879; LA-UR-95-511; CONF-9506141-1) Avail: CASI HC A02/MF A01

Because of the presence of structural defects such as microcracks and grain boundaries, the effective moduli in a highly disordered material

change dramatically as a function of stress. Earth materials (rocks) are an important example of this type of disordered media and are of practical interest in geophysics and seismology. At the laboratory scale, static stress-strain theory and elastic resonance experiments on rocks suggest that the ratio of third order elastic constants to second-order elastic constants in such materials is several orders of magnitude higher than in the case of ordinary uncracked materials. We report a model that describes the nonlinear interaction of frequency components in arbitrary pulsed elastic waves during one-dimensional propagation in an infinite medium. The model is based on the use of one dimensional Green's function theory in combination with a perturbation method. A polynomial expansion is used for the stress-strain relation in which we account for four orders of nonlinearity. The perturbation expression corresponds to a higher order equivalent of the Burgers' equation solution for velocity fields in solids. It has conceptual clarity and is easy to implement numerically, even with the inclusion of an arbitrary attenuation function. A comparison with experimental data on Berea sandstone is given to illustrate the model when used in an iterative procedure, and good agreement is obtained limiting model parameters up to cubic anharmonicity. The resulting values for the nonlinear parameters are several orders of magnitude larger than those for uncracked materials. Finally we discuss the values obtained for the dynamic nonlinearity parameters in comparison with static and resonance results. DOE

N95-30351 Alaska Univ., Fairbanks, AK.
STUDIES OF GRAVITY-WAVE FILTERING AND TIDAL INTERACTION IN THE MIDDLE ATMOSPHERE Ph.D. Thesis
Wentong Lu 1993 153 p
Avail: Univ. Microfilms Order No. DA9419756

Based on the spectral character of the observed gravity wave field, a parameterization scheme for gravity wave propagation and effects in the lower and middle atmosphere has been proposed. This effort begins with spectral expressions for gravity wave energy and momentum fluxes and prescribes the manner in which such idealized spectra respond to variations in the gravity wave environment. Means of specifying spectral amplitudes in response to specific wave sources at lower levels and the spread of wave influences horizontally as the spectrum propagates vertically through the lower and middle atmosphere are suggested. The parameterization scheme relies on a separable and invariant spectral form that is consistent with observations throughout the atmosphere. By choosing representative gravity wave parameters, the scheme yields predictions of mean fluxes of momentum for winter and summer CIRA 1986 model atmosphere profiles that agree well with mean flux observation in the lower and middle atmosphere. In the troposphere and lower stratosphere, both winter and summer profiles imply a negative zonal mean flux of approximately 0.2 sq m/sq s, consistent with airborne and radar measurements and the needs of large-scale GCM models. In the mesosphere, mean fluxes tend to oppose the zonal mean wind with flux maxima above the wind maxima and vertical profiles in general agreement with radar estimates at these heights. To assess the importance of gravity wave-tidal interactions in the middle atmosphere, the parameterization scheme is further applied to a static mean wind plus a typical tidal wind structure. The results suggest that the gravity wave-tidal interaction is likely to be strong where tidal amplitudes become large, yielding a significant modulation in the anisotropy of the gravity wave field due to differential filtering and saturation processes. Consistent with observations, this filtering leads to wave momentum fluxes that are approximately anti-correlated with the tidal wind field and which may far exceed mean values in magnitude. Dissert. Abstr.

47 METEOROLOGY AND CLIMATOLOGY

Includes weather forecasting and modification.

N95-28872# Scripps Institution of Oceanography, La Jolla, CA. Marine Physical Lab.
UPGRADING THE DAY/NIGHT WHOLE SKY IMAGER FROM MANUAL/INTERACTIVE TO FULL AUTOMATIC CONTROL Final Report, 1 Jan. 1991 - 31 May 1993
Janet E. Shields, Richard W. Johnson, and Monette E. Karr Dec. 1994 7 p
(Contract N00014-89-D-0142)
(AD-A292296; MPL-U-140/94) Avail: CASI HC A02/MF A01

The Whole Sky Imager (WSI) is a ground-based system for assessment of cloud cover over the full upper hemisphere. Using a fish-eye lens and a slow scan CCD sensor, it acquires imagery through daylight, into moonlight and starlight conditions. At the start of this contract, the new Day/Night WSI was in brassboard configuration. This contract funding enabled MPL to complete assembly of the system, acquire system calibrations for measuring system characteristics, and develop algorithms for control of the system. The WSI was fielded and cloud decision algorithms were developed based on the acquired test data. DTIC

N95-28938 Naval Research Lab., Monterey, CA.
QUALITY CONTROL OF METEOROLOGICAL OBSERVATIONS AT FLEET NUMERICAL METEOROLOGY AND OCEANOGRAPHY CENTER Final Report
Nancy L. Baker Dec. 1994 26 p Limited Reproducibility: More than 20% of this document may be affected by microfiche quality
(NRL Proj. R03-5-E-72)
(AD-A291577; NRL/FR/7531-94-9451) Avail: Issuing Activity (Defense Technical Information Center (DTIC))

Meteorological observations are subjected to extensive objective quality control (QC) before they are stored in the operational atmospheric data base at Fleet Numerical Meteorology and Oceanography Center (FNMOC, Monterey, CA). This QC identifies erroneous observations that could adversely affect the quality of operational products produced by the Navy's global and regional atmospheric prediction models and stratospheric analysis. These QC procedures have recently been substantially modified and improved. This report describes the QC system currently in use operationally with the Navy Operational Global/Regional Atmospheric Prediction Systems (NOGAPS/NORAPS) on the FNMOC supercomputers. A primary change was the inclusion of the Complex QC developed at the National Meteorological Center; other QC procedures were updated to reflect those in use at the European Center for Medium range Weather Forecasts. DTIC

N95-28975# Wisconsin Univ., Madison, WI. Space Science and Engineering Center.
TYPHOON MONITORING USING PASSIVE MICROWAVE OBSERVATIONS Final Report, Sep. 1992 - Oct. 1994
Robert T. Merrill Oct. 1994 27 p
(Contract MIPR-FY7121-91-00003; DA Proj. 402-6)
(AD-A292567; PL-TR-95-2012) Avail: CASI HC A03/MF A01

Tropical cyclones are amenable to monitoring using passive microwave radiometers in the 55 GHz (Oxygen) band because they have warm cores. However, such radiometers currently have horizontal resolution of 100 km or more, which is significantly larger than the eye of most tropical cyclones. The warm anomaly directly observable in the brightness temperature distribution is therefore an underestimate of the actual warm anomaly strength. The subject of this contract is an algorithm to correct for this underestimate. Passive microwave observations are modeled as an interaction between the radiometer antenna pattern and an analytic function approximating the thermal structure of a tropical cyclone. Solution of the inverse of this model using a maximum likelihood method yields an estimate of the amplitude of the warm anomaly. Application of this technique to observations from two different radiometers (MSU and SSM/T) indicates that it is relatively successful at correcting for horizontal resolution differences. However, the warm anomalies so obtained are little better than the raw observations themselves as estimators of tropical cyclone intensity. Reasons for this are examined and some potential avenues of research are suggested. DTIC

N95-28989# Air Force Inst. of Tech., Wright-Patterson AFB, OH.
ANALYSIS OF THE STRUCTURAL CHARACTERISTICS AND INTENSITY EVOLUTION OF SUPER TYPHOON FLO (1990) IN SPECIAL SENSOR MICROWAVE/IMAGER (SSM/I) DATA M.S. Thesis
Edward C. Melton, III. Dec. 1994 127 p
(AD-A292413; AFIT/CI/CIA-94-173) Avail: CASI HC A07/MF A02

The purpose of this research has been to observe and analyze the structural details and intensity evolution of Super Typhoon Flo (1990) using SSM/I data. Flo's structural characteristics were observed with SSM/I imagery and then compared with conventional, infrared and visible satellite data to illustrate qualitative distinctions between the two types of data. High resolution 85-0hz imagery showed more convective detail than

operational line scan (OLS) data while low resolution 19-0Hz data afforded more realistic analysis of the active tropical cyclone region when compared with 0MS data. Center locations determined in horizontally polarized 85-0hz imagery offered improvement over the OLS fixes obtained from corresponding DMSP passes. However, the SSM/I derived 85 and 19-0Hz retrieval statistics, employed as intensity indicators in previous tropical cyclone research, were poorly correlated with changes in Flo' 5 intensity. Two over ocean SSM/I rainfall rate retrieval algorithms were compared for accuracy. The more accurate algorithm employing the 85-0Hz frequency was used to characterize Super Typhoon Flo's rainfall rate distribution and intensity evolution. Results are generally similar to previous studies. Maximum rainfall rates were usually confined to the eyewall and inner-core region. Furthermore, changes in Flo's average inner-core rainfall rate correlated reasonably well with intensity changes. DTIC

N95-29110 Minnesota Univ., Minneapolis, MN.
EXPERIMENTS ON MICROBURSTS Ph.D. Thesis
Jie Yao 1994 166 p
Avail: Univ. Microfilms Order No. DA9420114

An isolated dynamic microburst is modelled in our laboratory by releasing a volume of salt water solution which is slightly heavier than ambient fresh water, allowing it to fall onto a horizontal plate and develop into a turbulent microburst vortex ring. Several visualization methods are used to observe the event and a high resolution video camera is used to record it. Quantitative results are achieved in two ways. The descending rates and wind front positions of the modelled microburst are measured from the video record by means of a digitizing cursor on a monitor. A cross wire type hot film anemometer is utilized to detect the transient wind velocity induced by the vortex ring at different radial positions near the impact center. Ensemble averaging methods are applied to get an average velocity time traces. An inviscid scaling law is derived from the Boussinesq approximation and is used to present the experimental results in an appropriate dimensionless form. This model exhibits many of the features of naturally occurring microbursts which are known to be a hazard to aviation. Experimental results are in good agreement with the real microburst DL191, which occurred at Dallas Fort-Worth airport in August 1985, and with an 'average' microburst abstracted from field investigations. Dissert. Abstr.

N95-29193 Army Cold Regions Research and Engineering Lab., Hanover, NH.
UPPER-AIR DATA COLLECTED ON ICE STATION WEDDELL Report, Feb. - Jun. 1993
Kerry J. Claffey, Edgar L. Andreas, and Aleksandr P. Makshtas Aug. 1994 67 p Limited Reproducibility: More than 20% of this document may be affected by microfiche quality
(AD-A289707; CRREL-SR-94-25) Avail: Issuing Activity (Defense Technical Information Center (DTIC))

From Feb. to Jun. 1992, as Ice Station Weddell (ISW) drifted through the uncharted western Weddell Sea, we launched radiosondes, typically twice a day, to study the structure of the lower atmosphere. Here, we describe the 15W radiosounding program, report on the availability of the data, and offer preliminary analyses of some of the atmospheric features we observed. For 10 days in late May and early June, as the Russian icebreaker Akademik Fedorov approached ISW from the northeast to help remove the ice camp, we made simultaneous soundings four times a day from 15W and from the Fedorov. We, therefore, also describe here the radiosounding system on the Fedorov, report on the availability of these data, and present preliminary comparisons of the simultaneous 15W and Fedorov soundings. Our soundings showed that temperature inversions were very common in this part of the Weddell Sea in fall and winter. Over 95 percent of the 15W soundings and 100 percent of the Fedorov soundings showed low-level temperature inversions. Of these, over 40 percent of the 15W soundings and over 67 percent of the Fedorov soundings were surface-based. A low-level jet in the wind speed profile was also common. We found such a jet in almost 80 percent of the 15W soundings for which we had wind information. The jet core was usually between 25 and 175 m above the surface, and speeds in the core were commonly between 4 and 10 m/s. DTIC

N95-29206 Princeton Univ., NJ.
SENSITIVITY OF THE SIMULATED GLOBAL CLIMATE TO PERTURBATIONS IN LOW CLOUD MICROPHYSICAL PROPERTIES Ph.D Thesis
Cheng-Ta Chen 1994 295 p
Avail: Univ. Microfilms Order No. DA9423397

The sensitivity of the solar radiative fluxes and global climate to perturbations in the microphysical properties of low clouds is investigated. First, a broadband parameterization of the solar radiative characteristics of low-lying water clouds is obtained. The parameterization is a function of cloud liquid water path (LWP), effective radius of water drops, and in-cloud water vapor amount. The parameterization overcomes the technical deficiencies in some of the earlier treatments and is, in general, more accurate than the older formulations. It is found that differences in the solar radiative fluxes due to inaccurate parameterizations can lead to biases in surface heat and moisture budgets. Perturbations in cloud microphysics, even if they are uniform on a global and annual basis, yield a zonally-and-seasonally dependent solar radiative forcing. While the variation of insolation is the major contributor to the forcing, the effect due to surface albedo at the high latitudes and the zenith angle-dependent cloud reflectivity at low latitudes are also important factors. The zonal mean dependence of this forcing is different from that due to increases in carbon dioxide. The climate response is investigated using a general circulation model (GCM) coupled to a mixed-layer ocean, with fixed cloud distributions and incorporating the new broadband. A series of GCM experiments involving globally uniform or spatially localized (20-70N) perturbations in cloud microphysical properties, along with one for a doubling of carbon dioxide, lead to the following results: (1) the model's climate sensitivity (ratio of global mean surface temperature response to the global mean radiative forcing) is virtually independent of the sign, magnitude, and the domain of the applied forcing; (2) although the total feedback is very similar in the different experiments, the strength of the individual feedback mechanisms (water vapor, albedo, lapse rate) is not the same; (3) besides the radiative forcing, physical processes such as the weak interhemispheric heat exchange and the high latitude sea ice formation in each hemisphere govern the spatial and seasonal pattern of the temperature response; (4) the zonal climate response is different for experiments leading to a warmer or colder climate, and tends to be more spatially confined for localized perturbations; (5) the localized perturbation experiments induce significant changes in the mean meridional circulation and precipitation near the equator, which is not obtained in the global perturbation experiments. Dissert. Abstr.

N95-29254# Colorado State Univ., Fort Collins, CO. Dept. of Atmospheric Science.
FORECAST OF ATLANTIC SEASONAL HURRICANE ACTIVITY FOR 1995
William M. Gray, Christopher W. Landsea, Paul W. Mielke, Jr., and Kenneth J. Berry 7 Jun. 1995 23 p Sponsored by the National Science Foundation and the National Atmospheric and Oceanic Administration National Weather Service and Climate Control Center
Avail: CASI HC A03/MF A01

This paper presents details of the authors' forecast for the amount of tropical cyclone activity expected to occur in the Atlantic Ocean region including the Caribbean Sea and the Gulf of Mexico during 1995. This forecast is based on the authors' ongoing research relating the amount of seasonal Atlantic tropical cyclone activity to five basic physical parameters. These are: (1) the Quasi-Biennial Oscillation (QBO) of equatorial stratospheric winds; (2) the El Nino-Southern Oscillation (ENSO); (3) West African Rainfall (AR) anomalies during the previous year; (4) anomalous west to east gradients of surface pressure and surface temperature (delta PT) in West Africa during February through May; and (5) Caribbean Basin Sea Level Pressure and Upper Level Zonal Wind Anomalies (SLPA and ZWA, respectively). Information received by the authors up to 6 June 1995 indicates that the overall 1995 hurricane season should be an above average season with about 8 hurricanes (average is 5.7), 12 named storms (average is 9.3) of at least tropical storm intensity, a total of about 35 hurricane days (average is 23), 65 named storm days (average is 46) and total Hurricane Destruction Potential (HDP) of 110 (average is 68). It is also expected that there should be 3 intense or major hurricanes of Saffir/Simpson intensity category 3, 4 or 5 this season (average is 2.1) and about 6 major hurricane days (average is 4.5). These parameters represent an overall measure of

total hurricane and tropical cyclone activity which is about 140 percent of the last 45-year average. The amount of hurricane activity in this forecast has been increased somewhat from that in the first author's 30 November 1994 forecast and is above the 13 April 1995 assessment given at the Atlantic City National Hurricane Conference. This early June enhancement of the hurricane forecast is due to the dissipation of the long running El Nino event and the observed return of cold water conditions in the equatorial East Pacific, to new estimates of African Western Sahel rainfall (+0.27 S.D.), and to warm eastern Atlantic sea surface temperature conditions which have become established the last two months. This is favorable for hurricane activity. This forecast will again be updated on 4 August 1995, at the beginning of what is climatologically the most active part of the hurricane season. The updated August forecast will make use of June and July data and should provide a more reliable forecast, particularly with regard to the African rainfall as it relates to prospects for intense hurricane activity during the most active part of the season. The updated August forecast will also provide a much better gage on the extent of expected development of a (cold water) La Nina event in the equatorial east Pacific. Author

N95-29333# Massachusetts Inst. of Tech., Cambridge, MA.
FORECASTING GLOBAL TEMPERATURE VARIATIONS BY NEURAL NETWORKS
Takaya Miyano and Federico Girosi Aug. 1994 12 p
(Contracts N00014-92-J-1879; N00014-93-1-0385)
(AD-A290081; AIM-1447; CBCL-101) Avail: CASI HC A03/MF A01

Global temperature variations between 1861 and 1984 are forecast using regularization networks, multilayer perceptrons and linear autoregression. The regularization network, optimized by stochastic gradient descent associated with colored noise, gives the best forecasts. For all the models, prediction errors noticeably increase after 1965. These results are consistent with the hypothesis that the climate dynamics is characterized by low-dimensional chaos and that it may have changed at some point after 1965, which is also consistent with the recent idea of climate change. DTIC

N95-29416# Naval Postgraduate School, Monterey, CA.
CONTINENTAL AEROSOL EFFECTS ON STRATOCUMULUS MICROPHYSICS DURING MAST 1994 M.S. Thesis
Joseph R. Brenner Dec. 1994 68 p
(AD-A292674) Avail: CASI HC A04/MF A01

Variations in marine stratocumulus clouds during the MAST (Monterey Area Ship Tracks) Experiment of June 1994 are observed and analyzed through the use of NOAA-9/10/11/12 AVHRR satellite data. The relationship between channel 3 reflectance and cloud microphysical properties is examined through direct observation of pixel brightness and aerosol trajectories based on a pollutant transport and dispersion model. Satellite observations show significant regions of continental influence over the ocean through higher channel 3 reflectance values as a result of the injection of anthropogenic aerosols. Forward and backward aerosol trajectories are used to show correlation of cloud albedo enhanced regions and the probable routes of continental aerosol injection in the marine environment. This technique may prove useful for determining climatic implications of cloud reflectance changes due to the influence of natural and man-made aerosol sources, and a means for predicting enhanced cloudiness in littoral regions. DTIC

N95-29497# Oregon Graduate Inst. of Science and Technology, Beaverton, OR.
PATH RESOLVED OPTICAL SENSING OF ATMOSPHERIC WINDS UTILIZING SPECKLE-TURBULENCE INTERACTION AND PSEUDORANDUM CODE MODULATION Final Report, 15 Feb. 1991 - 1 Sep. 1994
J. F. Holmes 28 Oct. 1994 4 p
(Contract DAAL03-91-G-0060)
(AD-A290800; ARO-28102.1-GS) Avail: CASI HC A01/MF A01

An innovative new technique for path resolved laser doppler velocimetry is being developed that uses a continuous wave (CW) source. The use of a CW rather than the conventional pulsed laser should result in a light, compact, rugged and more reliable LDV system suitable for use in both spacecraft and aircraft. In addition, the use of multiple CW beams and complimentary pseudo random codes should allow the vector wind to be measured without scanning the beams. Potential applications are global remote sensing of atmospheric winds, wind shear and turbulence detection and primary air instrumentation. In order to obtain range resolved wind and develop the required signal to noise ratio, pseudo random, diphase modulation of the laser and a novel detection scheme has been used. Additional applications for this lidar system are path resolved optical remote sensing of chemical species (DIAL), temperature and pressure. DTIC

N95-29507# New Mexico State Univ., Las Cruces, NM. Physical Science Lab.
COMPARISON OF BOUNDARY-LAYER WIND AND TEMPERATURE MEASUREMENTS WITH MODEL ESTIMATIONS Final Report
Richard Okrasinski and Robert Olsen Nov. 1994 158 p
(AD-A290471; ARL-CR-112) Avail: CASI HC A08/MF A02

Five simple models that estimate vertical profiles of wind speed or temperature in the boundary layer were evaluated by comparing the predictions with measured data. The models evaluated consist of three Monin-Obukhov similarity algorithms for predicting wind speed and temperature, a p-profile algorithm for estimating wind speed, and an inversion algorithm for estimating temperature. The data for the study was collected by towers, sodars, and radiosondes at four field experiments in 1990 and 1991. Using one or two levels of the tower measurements, wind speed, and temperatures were predicted at several measurement heights. The predicted and measured data were statistically compared. The results are presented in this report showing the comparability of the model predictions as a function of height above the surface and time of day. DTIC

N95-29595 Columbia Univ., New York, NY.
THE EFFECT OF CLIMATE PERTURBATIONS ON EXTRATROPICAL CYCLOGENESIS ALONG THE EAST COAST OF NORTH AMERICA Ph.D. Thesis
Judah Levi Cohen 1994 256 p
Avail: Univ. Microfilms Order No. DA9421331

Large scale snow cover anomalies cause significant changes in the diabatic heating of the earth's surface. It is thought that changes in the diabatic heating can significantly alter both surface temperatures and the storm dynamics of a region. This theory was tested using the GISS 3-D GCM (General Circulation Model). The results of the GCM experiment showed that snow cover caused only a short term local decrease in the surface temperature. The results emphasized the negative feedback which limits the impact of snow cover anomalies over longer time scales. In addition, four East Coast storms were run with varying snow cover and it was found that the snow cover had little impact on the outcome of the storm's intensity and the storm's track. Other boundary conditions were varied as a comparison to snow cover such as sea surface temperatures and topography. All boundary conditions were found to have little impact on the dynamics of all four storms, although sea surface temperatures had the largest effect. The experiment was then expanded to study the impact of varying boundary conditions over much longer time scales. Storm dynamics were compared among different climate change boundary conditions for an entire winter (December-March). Possibly significant changes were found in the storm track) and storm intensity of the North Atlantic as boundary conditions varied from a cold climate to a warm climate. As temperatures warmed overall storm intensity increased and the main storm track shifted north and west from an over ocean track to a more inland track. The thesis paper is divided into four chapters. The first chapter discusses modelling work done to determine the effect of anomalous snow cover on surface temperatures, which was published in the Journal of Climate. The remaining three chapters discuss the experiments involving extratropical storm dynamics along the East Coast. The second chapter gives background information on cyclogenesis along the east coast of North America, with special emphasis on explosive cyclogenesis The chapter then goes on to explain how the experiment was set up and what modifications were necessary in the GCM to better study storm dynamics. The third chapter describes the four real world storms used in the experiment, the four model storms and the various altered boundary condition runs. The storms are described in terms of the synoptic conditions, energy and vorticity quantities. Finally, chapter four compares storm track and storm intensity along the east coast of North America for three different climates: the current climate, an Ice Age climate and a doubled CO2 climate. The chapter concludes by describing one storm from each climate in terms of synoptic conditions, energy and vorticity quantities. Dissert. Abstr.

N95-29662# Air Force Systems Command, Wright-Patterson AFB, OH. National Air Intelligence Center.

ON THE LARGE SCALE CIRCULATION OF THE EAST ASIA MEI-YU FRONTS AND SECONDARY WEATHER DIMENSION DISTURBANCES

Gongwang Si 16 Dec. 1994 37 p Transl. into ENGLISH from unidentified Chinese Language article, p 312-323.

(AD-A291036; NAIC-ID(RS)T-0372-93) Avail: CASI HC A03/MF A01

This article discusses the large scale circulation of the East Asian Mei-Yu fronts as well as their secondary weather dimension or subsynoptic disturbances. It brings out the following points. The East Asian Mei-Yu is a phenomenon produced in the transition belt between Indian monsoon systems and the north Pacific Hadley (or tradewind) systems. Mei-Yu fronts are semi-tropical and semi-extratropical weather systems by nature. There is a relationship between the development of Mei-Yu front torrential rains and previous mei-yu front weather dimension or subsynoptic disturbances. DTIC

N95-29676 North Carolina Univ., Chapel Hill, NC.

NUMERICAL STUDIES OF ABLATIVE MASS LOSS FROM WIND ACCELERATED CLOUDS Ph.D. Thesis

Jeffrey Matthew Knerr 1993 138 p

Avail: Univ. Microfilms Order No. DA9415341

We have used numerical hydrodynamics to study the acceleration of dense gas clouds via wind ram pressure. Our goal has been to examine a model for the explanation of broad absorption lines (BAL's) seen in the spectra of certain fraction of observed QSO's. This model postulates cool dense clouds moving at very high speeds as the source of the BAL's. Furthermore, it invokes simple wind ram pressure as the acceleration mechanism for the clouds. A crucial question is whether the clouds can survive potentially disruptive fluid instabilities, allowing time for acceleration to speeds comparable to the wind velocity. Linear stability arguments imply Rayleigh-Taylor (RT) instability growth occurs on time scales much shorter than the acceleration time scale. These arguments conclude acceleration via ram pressure cannot produce bulk cloud velocities in excess of the cloud's internal sound speed. Our simulations show this is simply not true. We present two-dimensional slab-symmetric simulations where clouds are accelerated to speeds close to an order of magnitude greater than their internal sound speed. Ablative mass loss by the flow of shocked wind gas around the periphery of the clouds acts to limit the growth of potentially disruptive instabilities. Simulations run at different computational grid resolutions clearly show the stabilizing effect ablation has on the evolution of the clouds. Simplified models for line profiles have been developed using mass-velocity histograms generated from the numerical simulations. There is good qualitative agreement between the simulated line profiles and observed BAL profiles. Dissert. Abstr.

N95-29688 Alabama Univ., Huntsville, AL.

THE HIGH-ALTITUDE POLAR WIND: SIMULATION AND OBSERVATION Ph.D. Thesis

Chi Wing Ho 1993 226 p

Avail: Univ. Microfilms Order No. DA9415106

In comparing the transport and semikinetic descriptions of the expansion of the polar wind, it is found that the transport model produces shocks in the profiles of all moments, while a generalized semikinetic (GSK) model produces smooth profiles. The inadequacy of the transport model to deal with velocity dispersion, phase mixing and multi-streams is clearly demonstrated. In the study of the effects of hot magnetospheric electrons on polar outflow, it is found that by imposing a large increase in electron temperature (T(sub e)) over a short altitude range, a potential barrier is formed at which H(+) is partially reflected. For cases in which the T(sub e) profile is established by thermal conduction from a high upper boundary T(sub e), the upward flux of H(+) decreases with increasing upper boundary T(sub e), while O(+) shows a peak in the upward flux. The polar cap O(+) data collected by the DE1/RIMS are analyzed by fitting drifting Maxwellian distributions to the retarding potential curves, so that the O(+) characteristics in terms of its density, velocity and temperature are determined. The results show that these observed data can be matched by the GSK model which includes the effect of centrifugal acceleration due to E x B convection. The model results also match other observed low- and mid-altitude polar wind density profiles. The matching with satellite data is obtained by using the GSK model which uses observed low-altitude O(+) polar wind data as lower boundary conditions. Model polar wind density profiles that match mid-altitude satellite data, as well as the newly analyzed O(+) velocity and temperature, can be obtained when an electron temperature and base ion temperature of 9000 K and an ionospheric convection electric field of 70 mV/m are assumed. Dissert. Abstr.

N95-29697 Michigan Univ., Ann Arbor, MI.

A STUDY OF BOUNDARY LAYER AEROSOL AND WIND PROFILES USING INCOHERENT DOPPLER LIDAR Ph.D. Thesis

Kenneth Wayne Fischer 1994 223 p

Avail: Univ. Microfilms Order No. DA9423180

Light detection and ranging (lidar) systems in use today measure a variety of atmospheric parameters including profiles of aerosol backscatter, wind, and limited trace chemical species. Lidar systems are particularly useful tools for field studies because of their portability, flexibility, and wealth of data they provide. A lidar system has been built at the University of Michigan capable of measuring wind speed and direction as well as aerosol/molecular scattering profiles using an incoherent (direct detection) technique. This mobile lidar instrument was used in the field for the first time during the 1992 Southern Oxidants Research Program on Ozone Non-Attainment (SORP-ONA) field intensive in Atlanta, Georgia. The technical portion of the dissertation begins with descriptions of the lidar instrument components and derivations of the analytical equations which describe instrument throughput. The equations have been parameterized into a computer model to predict instrument performance under a variety of atmospheric conditions. The model predicts lidar wind measurements with 2 m/s accuracy or better with integration times of 2 minutes or less. New algorithms to process wind velocity and aerosol/molecular scattering information from the data are developed and discussed. Lidar data taken in Ann Arbor, Michigan and during the SORP-ONA Atlanta Field Intensive are presented as proof of concept and for scientific analysis. Wind field data are compared with a co-located rawinsonde for accuracy. An RMS difference of 3.1 m/s in measured wind speed was seen with mean winds of 8-10 m/s. Aerosol data are used to study boundary layer aerosol morphology, including testing of the uniform mixing hypothesis, estimation of mixing height, and calculation of total boundary layer column aerosol. Strong layering and structure was seen in the aerosol data indicating the uniform mixing assumption was not always valid, even on relatively hot summer days. Constrained mixing height estimates from the lidar showed a 0.85 correlation with rawinsonde-derived mixing height estimates. Based on these findings, it was concluded that the incoherent Doppler lidar technique is extremely useful for both wind profile measurements and aerosol loading determination. Dissert. Abstr.

N95-29701 Arizona Univ., Tucson, AZ.

LEE VORTICITY PRODUCTION BY TROPICAL MOUNTAIN RANGES Ph.D. Thesis

Joel Barney Mozer 1994 125 p

Avail: Univ. Microfilms Order No. DA9424934

Numerical simulations using the Penn State University/NCAR MM4 model are performed to examine a stably stratified, zonal easterly flow past large scale three-dimensional mountain ranges in a rotating, initially barotropic, atmosphere. Upstream blocking by the mountain range diverts the flow primarily to the south and around the mountain. Conservation of potential vorticity results in the formation of a horizontal jet at low levels south of the mountain. This jet is barotropically unstable and leads to a continuous production of synoptic scale vorticity maxima which separate from the mountain and propagate downstream. Numerical simulations using topography representative of the Sierra Madre in Mexico imply that this mechanism may be important in providing some of the initial disturbances which grow into tropical cyclones in the eastern North Pacific Ocean. The wave train produced in the simulations corresponds to waves with 3-7 day periods which have been identified observationally in the eastern North Pacific region. The sensitivity of this effect to the stability of the basic state and the upstream wind speed is investigated. Simulations are also performed which show that the Hoggar and Atlas mountains of west-central Africa block the low-level easterlies resulting in a barotropically unstable jet and a train of vorticity maxima which separate from the mountain and propagate downstream. The spacing of these disturbances is roughly 1600 km and they propagate to the east with a period of about 2.5 days. These characteristics correspond to those of observed waves in the Africa/Atlantic region. It will also be shown that the unique topography of north-central Africa results in a mid-tropospheric easterly jet which has a maximum

between 0-10 deg E and 15-20 deg N. The location and magnitude of this jet correspond to the so-called African easterly jet which is usually attributed to the strong surface temperature gradients over the continent of Africa. The numerical simulations presented in this work suggest that the mechanical effect of the topography may provide a constant source of energy for the maintenance of the African easterly jet. Dissert. Abstr.

N95-29713 Pennsylvania State Univ., University Park, PA.
ENERGY BUDGET IN THE ASIAN MONSOON REGION Ph.D. Thesis
Pui King Chan 1993 168 p
Avail: Univ. Microfilms Order No. DA9414255

The energy distribution is an important facet of the monsoons. Using a radiative transfer model with temperature, humidity, and cloud amount data from synoptic observations and the Cloud Radiation Consistency Method (CRCM), we derive the radiative flux convergences in the atmosphere (ATM) and at the surface (SFC) for winter, spring, and summer. In the CRCM, uncertainties in cloud parameters are constrained by the satellite observed OLR and albedo. The SFC (ATM) computed using the CRCM is quite reliable as uncertainties in cloud levels, cloud optical depth, cloud overlap, cirrus amount, and surface albedo cause small errors. The radiative heating profile in the atmosphere, SFC, and ATM derived from the new technique (CRCM) are believed to be the best currently available. By restricting the cloud particle radius to certain values, computations can be fast. Based on the SFC and ATM and using precipitation data, estimates of sensible heating over ocean and evaporation, other energy terms such as sensible heating over land, oceanic heat storage and transport, heat source, and moisture source are also derived. Many signals in the monsoon region are strong and cannot be masked by the large uncertainties in the estimates of precipitation over ocean and evaporation. The spatial and temporal distributions of these energy terms help to elucidate the significance of various monsoon processes. The energy budget, radiation and temperature fields indicate that the winter and summer monsoons are very different in nature. The winter monsoon is baroclinic which results from the rapid latitudinal decrease of the SFC due to the strong meridional gradients of solar insolation and albedo and the land-sea distribution in Asia. Strong baroclinicity causes development of baroclinic disturbances. The winter monsoon circulation is probably driven by the meridional sensible heating gradient and is much enhanced by the strong baroclinicity. The winter monsoon region is a moisture source and a heat sink. In contrast, the summer monsoon is quite barotropic which results from the rather uniform distributions of solar insolation and the SFC. The summer monsoon circulation is probably driven by sensible heating and latent heating of precipitation gradients. Moist processes are very important; latent heating of precipitation is often much larger than sensible heating and atmospheric cooling. The greatest difference in the energy budget between a strong and a weak summer monsoon is in the latent heat flux of precipitation. The summer monsoon region is a strong moisture sink and a strong heat source. The transition from winter to summer monsoon flow is related to diabatic heating and Rossby adjustment processes, which change the temperature field and consequently the wind field. Dissert. Abstr.

N95-29714 Drexel Univ., Philadelphia, PA.
AN AIR STREAM ANALYSIS OF THE OCCLUDED CYCLONE Ph.D. Thesis
Robert Alan Cohen 1993 230 p
Avail: Univ. Microfilms Order No. DA9411510

The structural evolution of the occluded cyclone is studied within an air stream conceptual framework. This framework utilizes a scheme that places the various air streams within four classifications (occidental, warm-sector, oriental and in-situ) and four types (A, D, C and W). It is argued that this perspective allows the structural evolution to be easily visualized and comprehended. Three wintertime, oceanic cyclones of varying intensity are simulated and analyzed. To carry out the analysis, a technique is introduced that derives the air stream boundaries from the numerical output. The technique is shown to be relatively insensitive to the spatial and temporal resolution of the model output and can be performed with modest computational burden. The occluded cyclone evolves as the occidental air streams (cold air topped by descending air) spiral in toward the circulation center from the west, impinging upon the oriental air streams (cloudy or cold airstreams that encircle the north side of the cyclone) east of the circulation center. In the process, the warm-sector air streams are occluded from the circulation center and a 'trailing region', consisting of clouds associated with the occidental/oriental boundary, is left behind as the crest of the warm-sector air moves east of the surface cyclone. This boundary is associated with the occluded front or bent-back front east of the circulation center and with the secondary cold front west of the center. The trailing region can also exist during the incipient stage of the cyclone when in-situ cloudy air northwest of the low borders the occidental air streams. In some cases, a core of warm air develops near the circulation center that is associated with a portion of the oriental air streams at low levels and with a tongue of descended occidental air aloft. These findings not only reproduce and extend many earlier findings but show that the perspective and objective technique allows the structures to be easily visualized and comprehended. As more details are examined, higher order subdivisions of airstreams can be made. Dissert. Abstr.

N95-29715 Colorado State Univ., Fort Collins, CO.
MICROWAVE REMOTE SENSING ALGORITHMS FOR CIRRUS CLOUDS AND PRECIPITATION Ph.D. Thesis
K. Franklin Evans 1993 243 p
Avail: Univ. Microfilms Order No. DA9415054

The global distribution of ice mass in cirrus clouds is very poorly known, but important for validating climate models that predict cirrus ice content. In this work theoretical modeling is carried out to investigate the feasibility of and possible techniques for high frequency microwave sensing of cirrus clouds from satellite. The discrete dipole approximation is used to compute the scattering properties for horizontally oriented ice crystals at frequencies of 85, 157, 220, and 340 GHz. Five particle shapes (solid columns, hollow columns, plates, planar rosettes, and spheres) and 18 gamma size distributions are considered. Upwelling brightness temperatures are computed with a polarized radiative transfer model. The brightness temperature depression (delta T(sub b)) relative to clear sky, is proportional to the ice water path (IWP), but the relationship depends strongly on the characteristic particle size and also on the crystal shape (typical range is a factor of two). Multiple frequencies and polarizations are shown to be useful for determining particle size and shape. Moderate IWP is detectable, e.g. 30 g/m(exp 2) produces delta T(sub b) = 3 K at 340 GHz for a typical distribution. A multichannel passive microwave precipitation retrieval algorithm is also developed in this work. Bayes theorem is used to combine statistical information from numerical cloud models with forward radiative transfer modeling. A multivariate log-normal prior probability distribution contains the covariance information about hydrometer distributions that resolves the nonuniqueness inherent in the inversion process. Hydrometer profiles are retrieved by maximizing the posterior probability density for each vector of observations. Theoretical tests with brightness temperatures simulated from cloud model data show that a five layer structure with variable rain, graupel, and cloud water is as effective as more complex structures. The hydrometer profile retrieval method is tested with four channel (10 to 85 GHz) aircraft based microwave radiometer data from convection over ocean and land in Florida. Multiparameter radar data is used to verify the retrieved profiles. The results show that the method generally works, but that more research needs to be done to improve the use of cloud model information. Dissert. Abstr.

N95-29725 Colorado State Univ., Fort Collins, CO.
THE DYNAMICS OF CIRCULATIONS WITHIN THE STRATIFORM REGIONS OF SQUALL LINES Ph.D. Thesis
William Andrew Gallus, Jr. 1993 305 p
Avail: Univ. Microfilms Order No. DA9415058

A dynamic version of the 2D kinematic cloud model of Rutledge and Houze (1987) has been developed to investigate the effect of microphysics in the stratiform region on circulations there. The design of the model allows for specified inputs of hydrometeors, vapor and heat from the convective region. The 10-11 June 1985 PRE-STORM squall line is simulated well, with a stratiform rain area and transition zone broadening over time. Significant ascent is simulated with peak intensities agreeing with observations. In-situ condensate production within the updraft contributes increasingly to the surface rainfall. Simulated horizontal flows agree qualitatively with observations, and include a sloping rear-inflow jet. Surface rainfall is underestimated, possibly implying the importance of 3D convergent forcing of strong anvil ascent. Although peak ascent agrees with observations, cloud top ascent is underestimated, perhaps indicating the importance of radiative effects. Strong rear-inflow is restricted to within 100 km of the convective line; rear-inflow at high levels farther rearward

may require large-scale baroclinicity. Convective heating alone generates significant ascent in the anvil; however, rainfall is scarce without hydrometeor advection from the convective line. Hydrometeor advection alone only induces weak anvil ascent, implying the importance of both heat and hydrometeor advection in generating a stratiform region. Vertical motion in the stratiform region depends strongly on stability; 3D variations in stratiform regions may be due to variations in stability. The amount of stratiform rainfall depends significantly on the intensity of hydrometeor advection. Finer resolution simulations of the 3-4 June PRE-STORM MCS find a delicate balance between microphysical cooling and adiabatic warming. Small changes in temperature, moisture, or precipitation rate, greatly affect surface wake low intensity. Heavier precipitation produces stronger descent, but microphysical cooling opposes adiabatic warming so that pressure falls are minimal. A collapsing precipitation core strengthens the wake low toward observed values. Microphysical processes alone may therefore be sufficient to explain intense descent and strong wake lows near the back of the stratiform region. A GATE system is also realistically significantly simulated in a moister environment with significantly different convective line hydrometeor contents. Although more moist conditions reduce evaporation from individual hydrometeors, greater hydrometeor input from the convective line is sufficient to produce net evaporation rates similar to those in the mid-latitude cases. Dissert. Abstr.

N95-29726 Pennsylvania State Univ., University Park, PA.
A THEORETICAL MODEL OF MULTIPLE REGIMES IN A STRATOCUMULUS-TOPPED BOUNDARY LAYER Ph.D. Thesis
Mark John Laufersweiler 1993 78 p
Avail: Univ. Microfilms Order No. DA9414323

The possible effects on stratocumulus circulations caused by drizzle and radiative cooling or heating are investigated theoretically using a simple Nonlinear Dynamical System (NDS). These effects are incorporated implicitly via the background temperature profile, and are expressed as departures from neutral conditions. These neutral conditions are assumed to be dry adiabatic in the surface, sub-cloud and inversion regions, and moist adiabatic in the cloud region. The NDS domain is divided into six distinct regions that represent those commonly observed in the planetary boundary layer: (1) the surface layer, (2) the sub-cloud layer, (3) the cloud base layer, (4) the cloud layer, (5) the cloud top layer, and (6) the capping inversion. The NDS successfully represented the effects of the capping inversion. Circulations were limited in their upward extent by the inversion, and would only penetrate into it when surface forcing rates were quite large. Surprisingly, when there are identical forcing rates but different initial conditions for the dynamic and thermodynamic fields, the NDS yielded two solutions throughout a wide range of cloud base stabilities. This range covers the transition from a stable to an unstable cloud base layer (layer 3 above). The first solution is a steady one having a decoupled form, with separate circulations in the sub-cloud region and the cloud region. The second solution is a temporally varying one exhibiting intermittent coupling. The circulation in this case starts as a shallow eddy near the surface. This eddy grows into a deeper plume that penetrates into the inversion before finally dying and beginning the process again. The simultaneous existence of these two solutions, or multiple regime, suggests that the planetary boundary layer (PBL) response to a particular forcing rate may depend on a large range for the initial conditions of dynamic and thermodynamic fields. As a consequence, future modeling efforts of the PBL should consider numerous initial fields. Dissert. Abstr.

N95-29727 Pennsylvania State Univ., University Park, PA.
OBSERVATIONS OF MESOSCALE CELLULAR CONVECTION FROM THE MARINE STRATOCUMULUS PHASE OF FIRE Ph.D. Thesis
Kerry Allen Moyer 1993 106 p
Avail: Univ. Microfilms Order No. DA9414344

A common mode of convection within the atmospheric boundary layer, mesoscale cellular convection (MCC) assumes the form of an organized array of three-dimensional polygonal cells. These cells not only have a profound impact upon the radiation budget of their environment, but also play a key role in governing the exchange of heat, moisture, and momentum between the atmosphere and the surface. Realistic parameterization of MCC within numerical models of both weather and climate is necessary in order to improve the accuracy of their simulations. This investigation focuses exclusively on the closed variety of marine MCC and employs aircraft data collected off the coast of California in association with the marine stratocumulus phase of the First ISCCP (International Satellite Cloud Climatology Project) Regional Experiment (FIRE). Forty-five transections of closed mesoscale convective cells are employed in this study. Data from these transections are used to calculate first-order and scale-dependent second-order kinematic, thermodynamic, and radiation statistics. From these statistics, an observational model of closed MCC is constructed which details the horizontal and vertical structure of the cells in coupled as well as decoupled boundary layer environments. The observed structure of the cells is explained in terms of physical processes operating within the marine stratocumulus-topped boundary layer. Dissert. Abstr.

N95-29797 Toronto Univ. (Ontario).
HAILSTONE HEAT AND MASS TRANSFER MEASUREMENTS Ph.D. Thesis
Blair John William Greenan 1993 128 p
(ISBN-0-315-86304-8) Avail: Univ. Microfilms Order No. DANN86304

Results of experiments performed in an icing tunnel demonstrate, for the first time, that existing theory accurately describes the heat and mass transfer of individual hailstones growing in a supercooled cloud. The experiments were carried out using spheroidal ice models with a major axis diameter of 2 cm and aspect ratio of 0.67. In previous hail growth studies in the University of Toronto icing tunnel, air speed, pressure, temperature, and hailstone size were coupled to atmospheric free fall conditions. In the present study, the four controllable icing parameters are varied independently over the following ranges: air temperature: 21 C less than or equal to t(sub a) less than or equal to 3 C; air speed: 9 m/s less than or equal to V(sub a) less than or equal to 24m/s; air pressure: 40 kPa less than or equal to P(sub a) less than or equal to 100 kPa; and cloud liquid water content: 1 g m(exp -3) less than or equal to W(sub f) less than or equal to 5 g m(exp -3). Icing time, ice and water mass of the hailstone deposit, and major and minor axis diameters are measured to determine the rate of mass transfer by accretion of supercooled droplets from the air flow. An infrared imaging system is used to measure local and mean hailstone surface temperature, thereby allowing closure of the heat and mass transfer equation. Experiment results are used to calculate two unknown in the heat and mass balance equations: the Nusselt number, Nu, and the net collection efficiency, E(sub net). For experiments with no shedding of accreted water, the net collection efficiency is best described by E(sub net) = 0.59 K(exp 0.15) over the Stokes parameter range 6 less than K less than 18. This result is not inconsistent with the analytic solutions of Langmuir and Blodgett (1946) for potential flow over a sphere. Heat transfer measurements indicate that a relationship of Nu = 0.15 Re(exp 0.69) is appropriate for the Reynolds number range 13000 less than or equal to Re less than or equal to 50,000. This Re range is representative of small (approximately 1 cm) to medium-sized (approximately 3 cm) hailstones in free-fall. The Nusselt number results are 60 percent larger than those compiled by Whitaker (1972) for smooth spheres. Approximately 30 percent of this enhancement can be attributed to hailstone surface roughness. The present study provides a substantial improvement over the parameterizations of hailstone heat transfer currently used in computer models of severe convective storms. Dissert. Abstr.

N95-29800 California Univ., Los Angeles, CA.
DEVELOPMENT OF AN IMPROVED CLOUD MODEL FOR USE IN CUMULUS PARAMETERIZATION Ph.D. Thesis
Chichung Lin 1994 287 p
Avail: Univ. Microfilms Order No. DA9420534

A cloud model is a very important component of cumulus parameterization. It can be considered as a part of the closures necessary for parameterization of cumulus convection. There remain many uncertainties, however, about the basic assumptions underlying the cloud model. A numerical cumulus ensemble model (CEM) is used as a tool for better understanding the moist-convective processes, with special emphasis on cumulus entrainment. The goal of this study is to provide a basis for further improvement of the cloud model in cumulus parameterization. We find that moist static energy is dramatically diluted along updraft trajectories, but is approximately conserved along downdraft trajectories. It is suggested that turbulent entrainment can be neglected for downdrafts in a cumulus parameterization scheme, while a formulation of turbulent entrainment process for updrafts is essential, especially at lower levels. The Paluch (1979) diagram is studied using simulated data. It is found that the CEM we are using is successful in producing typical observed distribution of

thermodynamical properties inside clouds, and the backward trajectories calculated for the in-cloud data suggest that the entrained environmental air parcel typically originate from levels below. With simulated data, we calculate the fractional rate of entrainment for each cloud type. It is found that the fractional rate of entrainment at lower levels is relatively large and has comparable magnitudes between different types of clouds. A branching of the fractional rate of entrainment can be identified near the 1.5-km level. The branching of the profiles of fractional rate of entrainment of the simulated clouds indicates that different types of clouds cannot be recognized in a transition layer below a certain level. We show that a spectral cloud model based on a specified fractional rate of entrainment within the transition layer and a spectrum of the fractional rate of entrainment above that layer can produce reasonable profiles of moist static energy for different types of clouds. However, some important questions remain to be answered, including how to treat the shallow clouds whose tops are within the transition layer and how to formulate the e&cts of horizontal inhomogenety of the SCL properties on cumulus clouds. Dissert. Abstr.

N95-29805 Purdue Univ., West Lafayette, IN.
RADIATIVE COOLING PROFILES CALCULATED FROM ECMWF ANALYSES AND ISCCP C1 DATA, AND THEIR APPLICATION TO DETERMINATION OF DISTRIBUTIONS OF APPARENT CONVECTIVE HEATING IN THE EQUATORIAL PACIFIC Ph.D. Thesis
Perry G. Ramsey 1993 179 p
Avail: Univ. Microfilms Order No. DA9420888

A meteorologically important quantity whose magnitude has not been thoroughly examined is vertical distribution of heating in the tropics. The details of the vertical distribution of heating have a significant impact on a number of phenomena, including the 30-60 day oscillation, sometimes known as the Intra-Seasonal Oscillation (ISO). Prior attempts to establish the structure of the heating relied on limited field data or assimilated data, coupled with climatological radiative heating parameters. The availability of high-quality global-scale data sets has made it possible to make more accurate calculations than were possible a few years ago. The longwave heating distribution is found using the ECMWF/ WCRP/TOGA (European Center for Medium Weather Forecasts/World Climate Research Program/Tropical Ocean and Global Atmosphere) Archive II and ISCCP (International Satellite Cloud Climatology Project) C1 datasets. A method is developed that can be used to estimate the low cloud amounts, and the results are used with a wideband longwave parameterization (Harshvardhan et al., 1987) to produce longwave cooling rates over the tropical Pacific Ocean. The ECMWF data are used to calculate apparent heat source (Q(1)) and the results are combined to produce profiles of convective heating. Also, the precipitation rates were found using methods similar to prior work (e.g., Vincent et al., 1991). Outgoing Longwave Radiation (OLR) and Clear-sky OLR were calculated and compared to ERBE results. The calculated values were generally higher than ERBE; this discrepancy was attributed to the longwave model lacking trace gases and insufficient upper tropospheric water vapor in the ECMWF archive. Spatially, the results agree quite well with available observations of longwave radiation. Q(1) budget derived precipitation rates agree with rain gauge data only in a general way, but this is likely due to the problems inherent in island rain gauge data. The vertical structure of the convective heating is similar to that found in most prior studies, with the level of maximum heating near 400 mb in areas with deep convection. Its shape is strongly affected by the radiative profile, confirming that longwave radiation is highly important in calculating these values. Dissert. Abstr.

N95-29806 Oklahoma Univ., Norman, OK.
NUMERICAL SIMULATION OF THE GENESIS OF TORNADO-LIKE VORTICES Ph.D. Thesis
Robert Jeffrey Trapp 1994 213 p
Avail: Univ. Microfilms Order No. DA9421093

Two novel approaches to tornadogenesis modeling have been developed, and are used to articulate the full sequence of events which leads to tornadogenesis. The 'pseudo-storm' and the 'sans-storm' are idealized thunderstorm representations, and emulate the storm-relative flow, into an updraft, of the horizontal streamwise vorticity that is baroclinically-generated in the cold-air outflow. These simplified models allow us to isolate and 'control' thunderstorm features hypothesized to have a role in tornadogenesis, and therefore allow us to transcend many of the experimental limitations encountered by cloud modelers. Intense, near-ground, cyclonic vortices, which we classify as 'tornado-like', form in both models. In the pseudo-storm, we represent and can control a thunderstorm updraft and its propagation, as well as a downdraft with an associated source of baroclinically-generated horizontal vorticity. The specified propagation of the updraft is such that the horizontal vorticity always has a large streamwise component in the coordinate framework of the updraft. Sensitivity experiments reveal that vortex formation is inhibited for certain updraft propagation rates (and thus storm-relative flow strengths), and downdraft intensities. Regardless of the lower boundary condition, none of the pseudo-storm vortices exceed the thermodynamic speed limit based on the vertically-integrated buoyancy (or CAPE). The sans-storm approach accounts only for the updraft and horizontal streamwise vorticity. The configuration of this model allows us to look more closely at the actual genesis of the consultant vortex. In particular, we find that the vortexgenesis is not 'triggered', but is instead the outcome of a continuous process of amplification of vertical vorticity generated initially through tilting. Experiments show that the subsequent intensification of the vertical vorticity proceeds with a large degree of uniformity, owing to the dynamics of the columnar vortex itself. Such a dynamical balance obviates the need for a mechanism like the 'dynamic pipe effect' to essentially advance, towards the ground, the incipient tornado-like vortex. Dissert. Abstr.

N95-29832 Wisconsin Univ., Madison, WI.
SHORT-RANGE PRECIPITATION FORECASTS USING ASSIMILATION OF SIMULATED SATELLITE WATER VAPOR PROFILES AND CLOUD LIQUID WATER Ph.D. Thesis
Xiaohua Wu 1993 200 p
Avail: Univ. Microfilms Order No. DA9410634

The principal emphasis of this study is on the assimilation of satellite-observed water vapor and cloud liquid water data in the initialization of a limited-area primitive equation model in order to improve short-range precipitation forecasts. The assimilation procedure presented includes two critical aspects: specification of an initial cloud liquid water distribution and diabatic initialization. A diagnostic method to specify an initial cloud water distribution is presented, based on satellite-observed cloud-top height and total column cloud liquid water amount. This method diagnoses the existing clouds, modifies the initial moisture distribution in cloudy areas and specifies the cloud water distribution. Using this diagnostic cloud water method in conjunction with diabatic initialization, latent heating profiles are then directly assimilated into the numerical model. The estimate of diabatic heating rates are obtained by time averaging the latent heat release from convective and large-scale condensation during the early forecast stage after insertion of satellite-observed temperature, water vapor and cloud water information. The dynamic balance induced by the diabatic initialization reafirms the conclusion that adiabatic initialization is unable to generate divergent circulations which are diabatically driven. With large-scale latent heating rates, diabatic initialization can generate divergent circulations which are consistent with the cloud field's latent heating sources. The experimental forecasts emphasis that the short range precipitation problem cannot be solved by diabatic initialization alone; improvement of the initial moisture distribution by incorporating new data is critical. The assimilation of satellite-observed moisture and cloud water together with diabatic initializations significantly reduces the precipitation spinup problem, especially in the earliest three hours, because of the ability to improve the initial moisture distribution and diagnose the existing clouds and specify associated circulations. The experimental forecasts indicate that the impact of satellite-observed temperature, water vapor and cloud water alone shortens the spinup time of precipitation rates by 1 to 2 hours and of areal coverage by 3 hours. Diabatic initialization together with cloud water initialization further reduces the precipitation spinup time (compared to adiabatic initialization) by 1 hour. Dissert. Abstr.

N95-29833 California Univ., Los Angeles, CA.
THE TROPICAL ATMOSPHERE UNDER CONVECTION ADJUSTMENT Ph.D. Thesis
Jia-Yuh Yu 1993 230 p
Avail: Univ. Microfilms Order No. DA9420550

A linear primitive-equation model on the equatorial beta-plane, under a Betts-Miller moist convective adjustment (MCA) scheme, is used to study the characteristics and maintenance of the large-scale tropical variability. The Betts-Miller MCA scheme employs a relaxation time scale, which is typical of the finite cumulus life cycle, in smoothly adjusting the temperature

and moisture toward the selected reference profiles. Both analytical and numerical techniques are employed to examine the modes arising through the interaction between collective effect of cumulus convection and the large-scale dynamics, and to study the steady-state characteristics of the atmospheric response to sea surface temperature (SST) anomalies. Our results indicate that all eigenmodes are stable for homogeneous basic states in presence of damping effects. Thus there is no 'CISK' (conditional instability of the second kind) at any scale under MCA. However, convective interaction with dynamics (CID) singles out one vertical mode with vertical structure and phase speed highly suggestive of the tropical Madden-Julian oscillation (MJO). The phase speed of the MJO is dictated by an internally-defined 'gross moist stability', while the MJO can be maintained either through instability due to the evaporation-wind feedback or through excitation by stochastic forcing from sub-grid scale thermal processes. Scale selectivity, favoring planetary wavenumbers, occurs through both vertical radiation of shorter waves and finite, cumulus adjustment time. Our results also indicate that, under convective, quasi-equilibrium assumptions, CID dominates the atmospheric response to SST anomalies at zeroth order as implied by the strong thermodynamic constraints under the MCA scheme. Different mechanisms proposed in simpler models, such as modified versions of the Neelin-Held and Lindren-Nigam theories, are reconcilable for linear perturbations about a slowly-varying basic state. Representations of momentum damping have significant impact on steady-state characteristics of the CID dominated circulation. Splitting of the ITCZ (Intertropical Convergence Zone) can occur through dynamical modulation by Ekman effects. A preliminary result in Chapter 7 also suggests that the impact of shallow convection on the CID-dominated circulation is very modest. However, we recognize that non-precipitating shallow convection may play an important role in regions with little climatological precipitation. To what extent the shallow convection can modify the steady-state circulation is an interesting question to be clarified in the near future. Dissert. Abstr.

N95-29834 Wisconsin Univ., Madison, WI.
THE ROLE OF DIABATIC HEATING, TORQUES AND STABILITY IN FORCING THE MERIDIONAL CIRCULATION WITHIN CYCLONES Ph.D. Thesis
Zhuojian Yuan 1993 225 p
Avail: Univ. Microfilms Order No. DA9410636

Simulations of meridional motion within cyclones are carried out based on a linear diagnostic equation of azimuthally-averaged mass weighted meridional circulation within translating cyclones. The consistency between transport processes and physical processes, and the contribution of various physical processes to the forcing of the meridional circulation are investigated. With the use of the linear diagnostic equation, the relative importance of several physical processes is discussed for different cyclones and different stages of development. Three extratropical cyclones and one typhoon were selected for the diagnostic study. The results show that intensification of these four cyclones is accompanied by strengthening of the meridional mass circulation. The development of cyclones requires: (1) mass and mean angular momentum transport forced by torques and inward eddy angular momentum transport; and (2) vertical transport of angular momentum associated with diabatic heating and/or angular momentum transfer across inclined isentropic surfaces through pressure and inertial torques. The dominant factors for forcing the meridional circulation within the extratropical cyclones are those associated with the baroclinic/barotropic structure within the vortex and its environment, and the effect of topography. The relative importance of these factors vary from cyclone to cyclone, particularly in the early stages. For the typhoon over the South China Sea, the main factors are associated with latent heat release and weak hydrodynamic stability. This investigation confirms results from previous studies of cyclone development and demonstrates the importance of cyclone translation on forcing the meridional motion within cyclones. The results for these four cyclones show that the simulation of meridional motion within cyclones agrees quite well with the observed meridional circulation. The excellent agreement indicates that the diagnostic equation, simplified under the assumptions of hydrostatic and gradient balances, provides: (1) a systematic assessment of the distinct physical processes responsible for the meridional motion which is related to cyclone development; and (2) an unique unified approach for investigating the forcing of the systematic meridional circulation within both extratropical and tropical cyclones.
Dissert. Abstr.

N95-29849# Meteorological Satellite Center, Tokyo (Japan).
METEOROLOGICAL SATELLITE CENTER TECHNICAL NOTE, NO. 28, 1994 [KISHO EISEI SENTA GIJUTSU HOKOKU, DAI 28 GO]
Yoshinobu Shimizu, ed., Seiichiro Kigawa, ed., Shuzo Matsuda, ed., Sachio Takata, ed., Jiro Yamanouchi, ed., Kazuo Yamamoto, ed., Toshiharu Tanaka, ed., Yosuke Nishimoto, ed., Shigeo Uchida, ed., and Tadashi Kikuchi, ed. et al 31 Mar. 1994 69 p In JAPANESE Original contains color illustrations
(ISSN 0388-9653)
(JTN-95-80926) Avail: CASI HC A04/MF A01

The following topics were discussed: (1) the survey of cloud band and dense cloud overcast of tropical cyclones at the genesis stage; (2) application software to supply image data; and (3) sea surface temperature grid point value from AVHRR (Advanced Very High Resolution Radiometer) data by using the cloud filtering technique and the multi-channel sea surface temperature retrieval algorithm. These studies were carried out using data from meteorological satellites, and aim at putting accurate meteorological information to practical use. For individual titles, see N95-29850 through N95-29852.

N95-29868 EG and G Rocky Flats, Inc., Golden, CO.
MANAGEMENT OF METEOROLOGICAL DATA AT A FORMER NUCLEAR WEAPONS FACILITY
Carey L. Dickerman and David R. Maxwell 1995 10 p Presented at the Air and Waste Management Association Meeting, San Antonio, TX, 18-23 Jun. 1995 Limited Reproducibility: More than 20% of this document may be affected by microfiche quality
(Contract DE-AC34-90DP-62349)
(DE95-007619; CONF-950646-5) Avail: CASI HC A02

The purposes of the Climatological Data Management and Meteorological Monitoring programs at the Rocky Flats Environmental Technology Site are to support emergency response (ER) programs at the site for use in assessing the transport, diffusion, and deposition of effluents actually or potentially released into the atmosphere by site operations, to provide information for on-site and off-site projects concerned with the design of environmental monitoring networks for impact assessments, environmental surveillance activities, and remediation activities. Also, maintenance of a meteorological monitoring network, which includes measuring, archiving, analyzing, interpreting, and summarizing resulting data, is required for successfully generating monthly and annual environmental monitoring reports and for providing assistance for on-site and off-site projects. Finally, the Meteorological Monitoring Program provides information for site-specific weather forecasting, which supports site operations, employee safety, and emergency response operations. DOE

N95-29876 Purdue Univ., West Lafayette, IN.
AN AIR-SEA INTERACTION MODEL FOR STRESS, SENSIBLE HEAT, LATENT HEAT, AND SEA STATE, APPLICABLE TO THE FULL RANGE OF WIND SPEEDS Ph.D. Thesis
Mark Allan Bourassa 1993 108 p
Avail: Univ. Microfilms Order No. DA9420787

An improved air-sea interface model has been developed. The model differs from others in that it is applicable to low wind speeds, as well as moderate and high wind speeds. Most interface models are not accurate at low wind speeds and, consequently, they underestimate fluxes in low wind speed regions, such as the tropical oceans. Results include a wave age parameterization that is valid for wind tunnels, as well as the open ocean. The model's improvements were achieved through the development of a capillary wave roughness length parameterization and an improved sea state model. The theory behind these improvements is described. The flux model results are contrasted with surface fluxes obtained from the popular LKB model and from the 1988-1992 ECMWF parameterization. Data from a pre-TOGA-COARE IOP cruise were used to evaluate the accuracy of the models. At low wind speeds the ECMWF model was found to strongly underestimate fluxes of latent and sensible heat. The low wind speed results of the model discussed herein are similar to the LKB results; however, the high wind speed results of the new model more closely resemble those of the ECMWF parameterization. A comparison is made among bulk fluxes from the tropical Pacific ocean (30 deg N to 30 deg N and 140 deg E to 90 deg W). The surface data used for input into the models came from the ECMWF surface fields on the TOGA CD ROM data archive. For low wind speeds, the fluxes estimated by the new model

are of greater magnitude than fluxes predicted by the ECMWF and LKB models. A strong dependence upon atmospheric stability is evident in the bulk fluxes. The important influence of atmospheric stability is confirmed in a sensitivity study of the new model. Dissert. Abstr.

N95-29877 Clemson Univ., SC.
A STUDY OF PRECIPITATION USING DUAL-FREQUENCY AND INTERFEROMETRIC DOPPLER RADARS Ph.D. Thesis
Phillip Bruce Chilson 1993 124 p
Avail: Univ. Microfilms Order No. DA9419682

The primary focus of this dissertation involves the investigation of precipitation using Doppler radar but using distinctly different methods. Each method will be treated separately. The first part describes an investigation of a tropical thunderstorm that occurred in the summer of 1991 over the National Astronomy and Ionosphere Center in Arecibo, Puerto Rico. Observations were made using a vertically pointing, dual wavelength, collinear beam Doppler radar which permits virtually simultaneous observations of the same pulse volume using transmission and reception of coherent UHF and VHF signals on alternate pulses. This made it possible to measure directly the vertical wind within the sampling volume using the VHF signal while using the UHF signal to study the nature of the precipitation. The observed storm showed strong similarities with systems observed in the Global Atmospheric Research Program's (GARP) Atlantic Tropical Experiment (GATE) study. The experiment provided a means of determining various parameters associated with the storm, such as the vertical air velocity, the mean fall speeds of the precipitation, and the reflectivity. Rogers proposed a means of deducing the mean fall speed of precipitation particles using the radar reflectivity factor. Using the data from our experiment, the mean precipitation fall speeds were calculated and compared with those that would be inferred from Rogers' method. The results suggest the Rogers method of estimating mean precipitation fall speeds to be unreliable in turbulent environments. The second part reports observations made with the 50 MHz Middle and Upper Atmosphere (MU) radar located at Shigaraki, Japan during May of 1992. The facility was operated in a spatial interferometry (SI) mode while observing frontal precipitation. The data suggest that the presence of precipitation can produce a bias in the SI cross-spectral phase that in turn creates an overestimation of the horizontal wind. The process is likened to turbulent fading which produces a temporal decorrelation in the time history of the complex radar voltages. In the case of precipitation, it is proposed that the size distribution of the hydrometeors produces a similar effect. This work examines the supposition by creating mathematical and computer simulations to test for any biases introduced by an exponential form of the drop-size distribution. The simulations were run for both the cases of Bragg scatter from turbulent variations in the refractive index and Rayleigh scatter from precipitation particles. Finally the simulation results were compared with actual radar data. It is shown that particle size distributions do indeed influence the cross-spectral phase which in turn leads to erroneous horizontal wind estimates. Dissert. Abstr.

N95-29944# Yankee Environmental Systems, Inc., Turners Falls, MA.
RESEARCH RESULTS ON AN IMPROVED IN-SITU TROPOSPHERIC HUMIDITY SENSOR Final Report, 6 Jun. - 6 Dec. 1994
Arthur F. Bisberg, James F. Morrissey, and David J. Beaubien 6 Jan. 1995 22 p
(Contract F19628-94-C-0064)
(AD-A291339; FR-950106) Avail: CASI HC A03/MF A01

There is a requirement to obtain improved upper air humidity data from radiosondes, as they are the only available vehicle to obtain the quantity of data and vertical resolution needed. The radiosonde uses the carbon humidity element which has several salient features; it is inexpensive, very repeatable, fast responding at temperatures above 0 C, with good sensitivity above 20 RH. However, it is unable to satisfy the current requirements due to several undesirable characteristics; specifically, it is very sensitive to temperature differences between the element and the ambient air, it has poor sensitivity at low RH, and has slow response below -20 C. To eliminate these shortcomings, we have integrated the carbon element with a force balance system wherein the element is kept at a constant RH. This eliminates the temperature sensitivity and significantly improves its poor sensitivity at low RH. It also greatly improves its temperature response time. This report reviews the results of a development program designed to demonstrate tie operational suitability of the technique. Initial laboratory tests designed to define the performance characteristics of the new sensor are reported. This development should provide the meteorological community with a low cost, reference grade radiosonde humidity sensor. DTIC

N95-29993# Pennsylvania State Univ., University Park, PA. Dept. of Meteorology.
DEVELOPMENT AND TESTING OF IMPROVED TECHNIQUES FOR MODELING THE HYDROLOGIC CYCLE IN A MESOSCALE WEATHER PREDICTION SYSTEM Final Report, 16 Dec. 1991 - 14 Dec. 1994
Toby N. Carlson, Thomas T. Warner, and J. M. Fritsch Dec. 1994 26 p
(Contract F49620-92-J-0118)
(AD-A291243; AFOSR-95-0086TR) Avail: CASI HC A03/MF A01

This project addresses the need to improve the surface hydrology component in mesoscale atmospheric prediction models and specifically the temperature and humidity forecasts. One way we did this was to initialize the mesoscale model with continuously updated and reasonable values of soil moisture content. To accomplish this task two approaches were taken one in which a soil hydrology model (SHM): Capehart and Carlson, 1994a, was used to update the initial values of soil water content in the BATS land surface component of the Penn State/NCAR mesoscale model (MM), specifically its most recent, non-hydrostatic version. The other approach was to use two remote sensing techniques to make better estimates of initial conditions. One of these techniques involved using radar reflectivity data to initialize the humidity field on the basis of existing convection ion which is specified from radar observations during a pre-forecast period. The other technique is to estimate the surface soil moisture availability using remote measurement of surface radiant temperature and vegetation index obtained via satellite and then to nudge the values of initial soil water content determined from the hydrology toward those values of initial soil water content determined from the hydrology toward those values estimated from the satellite measurements. DTIC

N95-30044# Naval Research Lab., Monterey, CA.
A REGRESSION MODEL FOR THE WESTERN NORTH PACIFIC TROPICAL CYCLONE INTENSITY FORECAST Final Report
Jan-Hwa Chu Nov. 1994 36 p
(AD-A290588; NRL/MR/7541-94-7215) Avail: CASI HC A03/MF A01

Tropical cyclone forecasting is an important but difficult task. The term 'intensity' refers to the maximum surface or low-level wind speed associated with a tropical cyclone. A regression model for forecasting this wind intensity in the western North Pacific was derived by using the 19-year (1971-89) post-determined best-track data, which include the date, time and location of the tropical cyclone's circulation (cyclonic) center, and the estimated maximum sustained surface wind speed (one-minute average at 10-meter elevation). This model provides intensity forecasts out to 72 hours for 12-hour intervals, and is designed for the intensity of all classes of tropical cyclones in the western North Pacific. To establish characteristics of this regression model, intensity forecasts from the model are compared with official forecasts from the Joint Typhoon Warning Center at Guam and with forecasts from a persistence method, for the year 1990, in terms of relative statistics. DTIC

N95-30048# Naval Air Weapons Station, China Lake, CA.
COSO MONITORING PROGRAM Annual Report, 1 Oct. 1993 - 30 Sep. 1994
S. C. Bjornstad, J. H. Monahan, and J. K. Sprouse Jan. 1995 110 p
(AD-A290604; NAWS-CL-TP-006) Avail: CASI HC A06/MF A02

The Coso Monitoring Program is a continuing effort in support of the Navy's geothermal resources within the Known Geothermal Resource Area (KGRA). Data are presented on the monitoring of steam flow rates and temperatures, water levels in ponds and wells, water chemistry, and rainfall in the Coso Hot Springs Resort Area. A monthly photographic essay of the mudfields and pools shows the variation of the surface water levels throughout the year. DTIC

N95-30066# Army Engineer Waterways Experiment Station, Vicksburg, MS.
TROPICAL STORM DATABASE: EAST AND GULF OF MEXICO

COASTS OF THE UNITED STATES
Sep. 1994 14 p
(AD-A291406; WES-TN-DRP-1-17) Avail: CASI HC A03/MF A01

This technical note describes the availability of a database of tropical storm surge elevations and currents produced from the numerical simulation of 134 historically based events that impacted the east and Gulf of Mexico coasts of the United States. The database consists of surge data hydrographs recorded at 486 discrete locations along the east and Gulf coasts and Puerto Rico. Also described are a summary atlas and cross reference tables of storm track and maximum storm surge corresponding to a 246 station nearshore subset of the 486-location database. DTIC

N95-30272*# METSAT, Inc., Fort Collins, CO.
PRODUCTION OF A LONG-TERM GLOBAL WATER VAPOR AND LIQUID WATER DATA SET USING ULTRA-FAST METHODS TO ASSIMILATE MULTI-SATELLITE AND RADIOSONDE OBSERVATIONS Final Report, Jul. 1992 - Jul. 1995
Thomas H. VonderHaar, David L. Randel, Donald L. Reinke, Graeme L. Stephens, Mark A. Ringerud, Cynthia L. Combs, Thomas J. Greenwald, and Ian L. Wittmeyer Hampton, VA Jul. 1995 33 p Original contains color illustrations
(Contract NASw-4715)
(NASA-CR-198955; NAS 1.26:198955; STC-TR-2927) Avail: CASI HC A03/MF A01; 6 functional color pages

There is a well-documented requirement for a comprehensive and accurate global moisture data set to assist many important studies in atmospheric science. Currently, atmospheric water vapor measurements are made from a variety of sources including radiosondes, aircraft and surface observations, and in recent years, by various satellite instruments. Creating a global data set from a single measuring system produces results that are useful and accurate only in specific situations and/or areas. Therefore, an accurate global moisture data set has been derived from a combination of these measurement systems. Under a NASA peer-reviewed contract, STC-METSAT produced two 5-yr (1988-1992) global data sets. One is the total column (integrated) water vapor data set and the other, a global layered water vapor data set using a combination of radiosonde observations, Television and Infrared Observation Satellite (TIROS) Operational Satellite (TOVS), and Special Sensor Microwave/Imager (SSM/I) data sets. STC-METSAT also produced a companion, global, integrated liquid water data set. The complete data set (all three products) has been named NVAP, an anachronym for NASA Water Vapor Project. STC-METSAT developed methods to process the data at a daily time scale and 1 x 1 deg spatial resolution. Author

N95-30343*# Jet Propulsion Lab., California Inst. of Tech., Pasadena, CA.
AN ATLAS OF MONTHLY MEAN DISTRIBUTIONS OF SSMI SURFACE WIND SPEED, AVHRR/2 SEA SURFACE TEMPERATURE, AMI SURFACE WIND VELOCITY, TOPEX/POSEIDON SEA SURFACE HEIGHT, AND ECMWF SURFACE WIND VELOCITY DURING 1993
D. Halpern, L. Fu, W. Knauss, G. Pihos, O. Brown (Miami Univ., FL.), M. Freilich (Oregon State Univ., Corvallis, OR.), and F. Wentz (Remote Sensing Systems, Inc., Santa Rosa, CA.) Jan. 1995 95 p Original contains color illustrations
(Contract NAS7-1260)
(NASA-CR-198880; JPL-Publ-95-3; NAS 1.26:198880) Avail: CASI HC A05/MF A01; 58 functional color pages

The following monthly mean global distributions for 1993 are presented with a common color scale and geographical map: 10-m height wind speed estimated from the Special Sensor Microwave Imager (SSMI) on a United States (U.S.) Air Force Defense Meteorological Satellite Program (DMSP) spacecraft; sea surface temperature estimated from the Advanced Very High Resolution Radiometer (AVHRR/2) on a U.S. National Oceanic and Atmospheric Administration (NOAA) satellite; 10-m height wind speed and direction estimated from the Active Microwave Instrument (AMI) on the European Space Agency (ESA) European Remote Sensing (ERS-1) satellite; sea surface height estimated from the joint U.S.-France Topography Experiment (TOPEX)/POSEIDON spacecraft; and 10-m height wind speed and direction produced by the European Center for Medium-Range Weather Forecasting (ECMWF). Charts of annual mean, monthly mean, and sampling distributions are displayed. Author

N95-30356*# Pennsylvania State Univ., University Park, PA. Dept. of Meteorology.
EXTENDED FIELD OBSERVATIONS OF CIRRUS CLOUDS USING A GROUND-BASED CLOUD OBSERVING SYSTEM Final Report, 1 Feb. 1990 - 31 Jul. 1994
Thomas P. Ackerman 31 Jul. 1994 78 p
(Grant NAG1-1095)
(NASA-CR-198855; NAS 1.26:198855) Avail: CASI HC A05/MF A01

The evolution of synoptic-scale dynamics associated with a middle and upper tropospheric cloud event that occurred on 26 November 1991 is examined. The case under consideration occurred during the FIRE CIRRUS-II Intensive Field Observing Period held in Coffeyville, KS during Nov. and Dec., 1991. Using data from the wind profiler demonstration network and a temporally and spatially augmented radiosonde array, emphasis is given to explaining the evolution of the kinematically-derived ageostrophic vertical circulations and correlating the circulation with the forcing of an extensively sampled cloud field. This is facilitated by decomposing the horizontal divergence into its component parts through a natural coordinate representation of the flow. Ageostrophic vertical circulations are inferred and compared to the circulation forcing arising from geostrophic confluence and shearing deformation derived from the Sawyer-Eliassen Equation. It is found that a thermodynamically indirect vertical circulation existed in association with a jet streak exit region. The circulation was displaced to the cyclonic side of the jet axis due to the orientation of the jet exit between a deepening diffluent trough and building ridge. The cloud line formed in the ascending branch of the vertical circulation with the most concentrated cloud development occurring in conjunction with the maximum large-scale vertical motion. The relationship between the large scale dynamics and the parameterization of middle and upper tropospheric clouds in large-scale models is discussed and an example of ice water contents derived from a parameterization forced by the diagnosed vertical motions and observed water vapor contents is presented. Author

48 OCEANOGRAPHY

Includes biological, dynamic, and physical oceanography; and marine resources.

For related information see also *43 Earth Resources and Remote Sensing.*

N95-28796# Scripps Institution of Oceanography, La Jolla, CA. Marine Physical Lab.
BACKSCATTER DATA ACQUISITION FOR HYDROSWEEP DS ABOARD RV EWING Final Report
Christian DeMoustier Dec. 1994 6 p
(Contract N00014-90-J-1781)
(AD-A292332; MPL-U-141/94) Avail: CASI HC A02/MF A01

The long term objectives of this work are to establish efficient and accurate signal processing techniques for seafloor remote sensing operations aimed at characterizing the bottom by acoustic methods. This work focuses on acoustic measurements made with a Hydrosweep DS multibeam echo-sounding system installed aboard R.V.M. Ewing. The objectives are to design and implement a data acquisition scheme that preserves base-banded quadrature samples of the output of individual hydrophone staves. DTIC

N95-28865# Scripps Institution of Oceanography, La Jolla, CA. Marine Physical Lab.
MULTI-SCALE STUDIES OF SEAFLOOR TOPOGRAPHY Final Report, 1 Oct. 1990 - 30 Sep. 1994
Fred N. Spiess and Christian DeMoustier Jan. 1995 7 p
(Contract N00014-91-J-1095)
(AD-A292301; MPL-U-17/95) Avail: CASI HC A02/MF A01

The long term goals of this research were to acquire and use spatially overlapping swath bathymetry data sets at different scales using multibeam echo-sounders, for use in characterizing the statistical nature of the deep sea floor in the contexts of marine geology and ocean acoustics. The work included construction of a deeply towed multibeam swath mapping sounding system that can be operated as a part of our Deep Tow system (Spiess and Lonsdale, 1982), seagoing work to validate system capability,

an initial expedition to use the system in the Pacific Natural Laboratory site (9 deg N, 104 deg-30' W) and subsequent data reduction and dissemination. DTIC

N95-28873# Naval Command, Control and Ocean Surveillance Center, San Diego, CA.
ANALYSIS OF HISTORICAL OCEANOGRAPHIC DATA ON A MINICOMPUTER: PROGRAM WAHOO Final Report
Alvan Fisher, Jr. Dec. 1994 50 p
(AD-A292530; NRAD-TR-2727) Avail: CASI HC A03/MF A01

Program WAHOO uses a Sun SPARC 10 minicomputer to process and analyze temperature, salinity, and sound speed data in various formats. The data, extracted from the Master Oceanographic Observation Data Set (MOODS) files maintained by the Naval Oceanographic Office, must be reformatted into regional files prior to analysis. This document provides guidelines required to process and analyze the MOODS data, thus providing valuable information required to characterize the oceanic and acoustic properties of an area. DTIC

N95-28982 Naval Postgraduate School, Monterey, CA. Dept. of Oceanography.
A NUMERICAL STUDY OF THE EFFECTS OF WIND FORCING ON THE CHILE CURRENT SYSTEM M.S. Thesis
Chih-Ping Hu Dec. 1994 50 p Limited Reproducibility: More than 20% of this document may be affected by microfiche quality
(AD-A289808; NPS-OC-94-007) Avail: Issuing Activity (Defense Technical Information Center (DTIC))

A high-resolution, multi-level, primitive equation ocean model is used to examine the response of the coastal region from 22.50 degree south to 350 degree south of the Chile Current System to both equatorward and climatological wind forcing. The results from both types of forcing show that an equatorward surface current, a poleward undercurrent, upwelling, meanders, filaments and eddies develop in response to the predominant equatorward wind forcing. When climatological wind forcing is used, an offshore branch of the equatorward surface current is also generated. These features are consistent with available observations of the Chile Current System. The model results support the hypothesis that wind forcing is an important mechanism for generating currents, eddies and filaments in the Chile eastern boundary current system and in other eastern boundary current regions which have predominantly equatorward wind forcing. DTIC

N95-28991# Naval Research Lab., Bay Saint Louis, MS.
HINDCASTING CHANGES IN THERMAL STRUCTURE AND ACOUSTIC TRANSMISSION LOSS IN THE UPPER OCEAN ON SHORT TIME SCALES WITH DATA FROM MILE AND FROM OCEAN WEATHER STATION PAPA Final Report
Paul J. Martin 18 Jan. 1995 28 p
(AD-A292419; NRL/FR/7322-93-9429) Avail: CASI HC A03/MF A01

The skill of mixed-layer hindcasts of short (less than 5 d) duration was investigated using data from Ocean Weather Station Papa for the years 1960 to 1968, and with data from the Mixed-Layer Experiment (MILE), which was conducted about 40 km southwest of Papa in late summer of 1977. The hindcasts were initialized and validated with observed temperature profiles and forced with surface wind stresses and heat fluxes calculated from meteorological observations. Mean and rms hindcast errors for sea-surface temperature (SST) mixed-layer depth (MILD), surface sound-channel depth (SCD), and acoustic-detection range (ADR) were compared with errors for persistence and climatology. Hindcast skill was calculated as the percent improvement of the hindcast rms error over the persistence rms error. The hindcast skill was significantly higher for the MILE data than for the Papa data, and hindcast skill with the Papa data was generally higher in spring and summer than in fall and winter. The range of hindcast skill for hindcasts of 12- and 36-h duration was 39 to 48% for SST, 28 to 37% for MLD, and 38 to 43% for SCD for the MILE data versus 14 to 19% for SST, 22 to 33% for MLI), and 8 to 31% for SCD for the Papa data for the spring and summer. Smoothing the MILE temperature observations with a 2-h running mean resulted in an increase in hindcast skill of about 3% due to the reduction in small-scale noise. DTIC

N95-29023# Naval Postgraduate School, Monterey, CA. Dept. of Oceanography.
MODELING STUDIES OF THE LEEUWIN CURRENT OFF WESTERN AND SOUTHERN AUSTRALIA M.S. Thesis
Christopher L. Butler Dec. 1994 158 p
(AD-A290158; NPS-OC-94-009) Avail: CASI HC A08/MF A03

A high-resolution, multilevel, primitive equation ocean model is used to examine the response of an eastern boundary oceanic regime to thermal and wind forcing. The focus of this study is the anomalous Leeuwin Current System off western and southern Australia. Three types of experiments are conducted. The first type forces the model from rest with the Indian Ocean climatological temperature gradient as an initial condition only, while the second type repeats the first experiment with the added contribution of the North West Shelf water temperature profile. The role of irregular coastline geometry on the generation of currents and eddies is also examined by comparing these cases with and without an irregular (realistic) coastline. The third type, with an irregular coastline, forces the model from rest with constant thermal and wind forcing. A one-time application of the North West Shelf water is added during the model run. In all experiments, surface currents, undercurrents, meanders, and eddies are generated. The results from experiments with an irregular, rather than an idealized, coastline show preferred eddy generation locations. The results from the third type of experiment, which has the most realistic features, agree well with available observations off western and southern Australia. These results support the hypothesis that both thermal and wind forcing are important mechanisms for the generation of many of the observed features in the Leeuwin Current System. DTIC

N95-29054# Naval Postgraduate School, Monterey, CA.
AIRY FUNCTIONS AND THE RECURSIVE RAY ACOUSTICS ALGORITHM M.S. Thesis
Robert S. House Dec. 1994 74 p
(AD-A290182) Avail: CASI HC A04/MF A01

Two main problems are analyzed and discussed. First, a detailed derivation of the exact solution for the inhomogeneous Helmholtz equation for a free-space propagation problem when the square of the index of refraction is a linear function of depth and the input is an omnidirectional point source is performed and discussed. The exact solution is in terms of Airy and Bairy functions. Second, the accuracy of the recursive ray acoustics (RRA) algorithm was tested by generating test cases using a sound-speed profile with the square of the index of refraction a linear function of depth. The acoustic pressure (amplitude and phase) calculations obtained from the RRA algorithm were then compared to the exact Airy functional solution. Computer simulation results indicate that both solutions are in good agreement. DTIC

N95-29085# Washington Univ., Seattle, WA.
REVISIONS AND NOTES ON A MODEL FOR BUBBLE ATTENUATION IN NEAR-SURFACE PROPAGATION
Peter H. Dahl Nov. 1994 26 p
(Contract N00039-91-C-0072)
(AD-A290312; APL-UW-TR-9411) Avail: CASI HC A03/MF A01

A revised model for predicting surface bubble loss (SBL) as a function of wind speed, surface grazing angle, and frequency is discussed. SBL is defined as the residual loss (i.e., the loss in excess of that due to spreading and chemical absorption) in acoustic energy propagating near the sea surface that is attributable to attenuation by near-surface bubbles. This loss is a key input parameter for predicting bubble attenuation in simulations of weapon-system performance in near-surface environments. The original SBL model was introduced by the Applied Physics Laboratory, University of Washington, in 1993. The revision consists of a new wind-speed threshold for breaking waves and the subsequent onset of bubble production, and an alternative formulation capable of handling more general ray geometries such as a ray vertexing near the surface. Model/data comparisons and examples of the model applied to a linear sound-speed profile are presented. DTIC

N95-29160# Army Cold Regions Research and Engineering Lab., Hanover, NH.
ANALYZING THE STABILITY OF FLOATING ICE FLOES
Barry Coutermarsh and Randy McGilvary Dec. 1994 27 p
(AD-A292149; CRREL-94-13) Avail: CASI HC A03/MF A01

This report describes an experimental study to measure the pressure caused by fluid acceleration beneath a floating parallelepiped block. Dynamic fluid pressure was measured at discrete points beneath the block for several flow velocities, flow depths, block angles of attack and block-thickness-to-depth ratios. The measured pressures were used to calculate block underturning moments, and a hydrostatic analysis was used to calculate a block righting moment. From this, a densimetric Froude undertuning criterion is presented. The measured hydrodynamic pressure distribution on the bottom of a single model ice floe is used to estimate the dynamic stability at three thickness-to-depth ratios. The energy-based analysis details the conditions required for instability, metastability and stability. At three thickness-to-depth ratios, block rotational inertia has the effect of reducing the Froude stability number by 5 to 10% over a completely static stability criterion. DTIC

N95-29198# Army Engineer Waterways Experiment Station, Vicksburg, MS.

TIDAL CONSTITUENT DATABASE: WEST COAST OF THE UNITED STATES AND EASTERN NORTH PACIFIC OCEAN

Jan. 1995 12 p

(AD-A292224; WES/TN/DRP-1-19) Avail: CASI HC A03/MF A01

This technical note describes a database of tidal elevation boundary condition information generated in support of the 'Long-Term Fate of Dredged Material Disposed in Open Water' research of the Dredging Research Program (DRP), being conducted at the U.S. Army Engineer Waterways Experiment Station. The database, described in detail by Hench and others (1994), allows the user to manually generate time series of tidal elevations or to use a program to access the full database to generate time series of both tidal elevations and currents for any location along the West Coast of the United States and Eastern North Pacific Ocean, extending from Seal Cape on Unimak Island, Alaska, in the North to Punta Parada, Peru, in the South. The land boundary includes the Pacific shorelines of Alaska, Canada, mainland United States, Mexico, Guatemala, El Salvador, Nicaragua, Costa Rica, Panama, Columbia, and Northern Peru. Although the capability to generate these time series was developed to provide input to the Long-Term Fate and Stability Model (LTFATE), the generated time series can be used for any application requiring tidal forcing data. DTIC

N95-29237*# Mississippi State Univ., Mississippi State, MS. Dept. of Computer Science.

CONVERSION OF AN OCEANOGRAPHIC EXPERT SYSTEM TO A C-BASED LANGUAGE Final Report

Susan Bridges and Liang-Chun Chen 1 Feb. 1995 35 p

(Contract NAS13-330; Proj. X15-98)

(NASA-CR-198695; NAS 1.26:198695; AD-A292076; NRL-FR/7240-94-9449) Avail: CASI HC A03/MF A01

The objectives of this project were to convert the NRL oceanographic expert system from the computer language OPS83 into the C language and CLIPS (C Language Integrated Production System), to redesign the control structure and the user interface and to improve the readability, understandability, and maintainability of the code. The eddy prediction component of an oceanographic expert system that was originally implemented in OPS83 has been translated to the CLIPS expert system shell. Portions of the system that were originally implemented in OPS83 procedural code have been translated to C. These changes will allow the system to be incorporated into the Semi-Automated Mesoscale Analysis System 1.2 (SAMAS 1.2). SAMAS 1.2 will eventually be incorporated in to the third generation of the Navy's Tactical Environmental Support System, TESS(3), which does not support OPS83 code. In addition to the translation tasks, the main control structure of the expert system was redesigned to achieve increased modularity and thus to improve the understandability of the code. An explanation component that was recently added to the system was also revised to improve maintainability. The revised and translated code was tested using several data sets that had previously been used to test the original system. The functionality of the revised system was exactly the same as that of the original system using all of the test data. DTIC

N95-29418 Woods Hole Oceanographic Inst., MA.

MAPTOOL VERSION 2. USER'S MANUAL

Peter Lemmond May 1994 76 p Limited Reproducibility: More than 20% of this document may be affected by poor print

(Contract N00014-90-J-1621)

(AD-A289470; WHOI-94-17) Avail: Issuing Activity (Defense Technical Information Center (DTIC))

MapTool is an interactive computer program for the display of common marine geophysical data. At present, the program displays isolines, color-filled contours, navigation tracklines, and navigated scalar values in a variety of styles. A variety of map projections are supported. This document describes the basic requirements for running the Map Tool program, for creating various displays, and generating hard copy output. The supported data file formats are described. All of the options, displays, menus, and windows are documented. DTIC

N95-29520 Delaware Univ., Newark, DE.

A STUDY OF DYNAMICS IN THE TROPICAL PACIFIC USING SATELLITE DATA Ph.D. Thesis

Chung-Ru Ho 1994 169 p

Avail: Univ. Microfilms Order No. DA9419535

A 10-year time series of satellite infrared data and a 4.5-year time series of satellite altimeter data were used to investigate the dynamics of the tropical Pacific Ocean (30 deg N to 30 deg S, 120 deg E to 90 deg W). Spatial integration filtering, pattern matching, fast Fourier transform, short time Fourier transform, and some statistical methods were applied in this research. The studies were focused on the evolution of the western Pacific warm pool (WPWP) from 1982 to 1991, the variation in frequency of the equatorial Kelvin waves, and the theoretical analysis of the equatorially long waves with a wavelength of 1000 km and a phase speed of about 45 cm/s which are observed in the eastern equatorial Pacific Ocean. During the duration of the data used in this research, there were two El Nino events (1982-1983, 1986-1987) and one La Nina event (1988). The results show that the dynamics in the tropical Pacific Ocean are strongly related to El Nino events. The evolution of the WPWP is affected by the solar cycle, the equatorial current system, and the El Nino event. The centroid of the WPWP normally moved counterclockwise except during the years prior to the El Nino onsets, when it moved clockwise. The time-frequency planes of the sea surface elevation anomaly show that the frequency spectra split during an El Nino event and then joined together after an El Nino event. The mean phase speed of the Kelvin waves during the 1986-1987 El Nino was higher than that in the period before the El Nino event. The theoretical analyses show that the long waves are a type of Rossby waves which are shear-trapped by the equatorial current system. The waves vanish or even reverse their propagation direction during the El Nino onset because the equatorial current system changes at that time. Dissert. Abstr.

N95-29528 California Univ., Santa Cruz, CA.

THE NATURE OF WAVEFRONT FLUCTUATIONS INDUCED BY INTERNAL GRAVITY WAVES IN LONG-RANGE OCEANIC ACOUSTIC PULSE TRANSMISSIONS Ph.D. Thesis

John Anthony Colosi 1993 127 p

Avail: Univ. Microfilms Order No. DA9419762

A recent 1000-km acoustic pulse transmission experiment in the Pacific obtained high resolution wavefront measurements and revealed several unexpected wavefront fluctuations. These fluctuations include a dominant rapid variation, called the broadband fluctuation, with time scales less than 10 minutes and spatial scales of less than 60 m; a distinct break-down of the geometrical optics wavefront pattern and broadening of the wavefront near the transmission finale; and a coherent wavefront motion with a time scale near the semi-diurnal tidal period. Parabolic-equation numerical simulations have been carried out which utilize environmental data and which take into account internal-wave-induced sound-speed perturbations obeying the Garrett-Munk (GM) spectral model. It is shown that the effects of internal waves can account for the broadband fluctuations, the breakdown of the geometrical optics pattern, and the wavefront broadening. The sensitivity of these fluctuations to internal-wave energy and modal content is examined. The spectral energy in the GM model at tidal periods proves insufficient to explain the tidal period coherent fluctuations. This result strongly suggests the influence of an internal tide during the experiment. The simulations allow for the estimation of the average travel-time bias caused by internal waves. The simulation results for travel-time wander and bias are compared with analytic calculations based on the path-integral technique. Dissert. Abstr.

N95-29541 New Hampshire Univ., Durham, NH.
THE STRUCTURE OF WATER MASS, SALT, AND TEMPERATURE TRANSPORTS WITHIN INTERMEDIATE DEPTHS OF THE WESTERN TROPICAL ATLANTIC OCEAN Ph.D. Thesis
Frank Lee Bub 1993 235 p
Avail: Univ. Microfilms Order No. DA9420570

Water mass flow patterns within the 150-1300 m intermediate layer of the western tropical Atlantic were determined from observations during four 1990-1991 Pegasus velocity and CTD hydrographic surveys. Non-divergent flows were analyzed to determine transports. A survey-average 29 Sverdrups (1 Sv = 10(exp 6) m(exp 3)/s) of southern hemisphere water masses flowed northwestward across 44 deg W near the equator as part of the subsurface South Equatorial Current (SEC). Twenty-one Sv retroflected anticyclonically around the Amazon Eddy (2 deg N 45 deg W) and flowed eastward toward the North Equatorial Undercurrent (NEUC). The other 8 Sv moved northwestward within a series of anticyclonic retroflection eddies which periodically separate from the Amazon Eddy. 61 Sv of a northern/southern water mass mixture flowed southeastward across 9 deg N as part of the North Equatorial Current (NEC) and bifurcated: 32 Sv turned anticyclonically northwestward, and 29 Sv turned cyclonically around a low (6 deg N 44 deg W), merged with the southern water, and flowed toward the NEUC. The 50 Sv NEUC, a mixture of mostly southern water, flowed eastward into the interior. The remaining NEC and SEC branches blended to form a 40 Sv northwestward transport across 53 deg W. These observed transports were generally about three times larger than the wind-driven equatorial and tropical gyre return transports, suggesting the existence of subgyre-scale recirculation eddies in the western tropics. One of the retroflection eddies was measured during September 1990. Its structure was approximated by a 300 km diameter cylinder which extended vertically through the surface and intermediate layers to 1300 m. During two other surveys, retroflection eddies were identified at the region's northwestern corner. Instantaneous transport associated with an eddy which translated at 10 cm/s was about 30 Sv. Assuming three were generated each year, retroflection eddy translation could account for the 8 Sv alongshore flow through the region. According to water mass budgets, 21 Sv of northern water masses were transformed by mixing within the region. Temperature-salinity relationships indicated this mixing effectively transports the cool, low salinity Antarctic Intermediate Water into the North Atlantic by as yet unknown pathways. Dissert. Abstr.

N95-29856# Naval Research Lab., Bay Saint Louis, MS.
FINITE DIFFERENCE OCEAN ACOUSTIC MODEL USERS GUIDE Final Report
R. A. Zingarelli 23 Dec. 1994 16 p
(AD-A291544; NRL/MR/7181-94-7533) Avail: CASI HC A03/MF A01

The computer program FIDO (Finite Difference Ocean acoustic model) computes the real acoustic pressure via a finite- difference approximation to the undamped wave equation, with attenuation implemented by the insertion of an additional radiation condition term in sediment regions of the computation grid. The program is implemented in FORTRAN and is well suited to most supercomputer architectures. Both time-domain and continuous-wave versions are described. Input file formats are given along with two sample input files. Test cast solutions for standard benchmarks and other problems are presented and compared to analytic and coupled-mode solutions. DTIC

N95-30069# Oregon State Univ., Corvallis, OR.
NUMERICAL MODELING OF SYNOPTIC SCALE OCEAN DYNAMICS Final Technical Report
Robert N. Miller 1994 2 p
(Contract N00014-90-J-1125)
(AD-A291411) Avail: CASI HC A01/MF A01

Research continued on theory and practice of data assimilation. Results of a study of the application of optimal interpolation (OI), the data assimilation method most commonly used in numerical weather prediction, to a regional data set were published. In that study, hydrographic data from the California Current were assimilated into the Harvard quasigeostrophic open ocean model. Good results were obtained. A study of the application of advanced data assimilation methods to simple highly nonlinear systems which exhibit strongly nonlinear behavior such as bimodality and chaos was completed. Most data assimilation methods were derived under assumptions of linearity, and therefore could be expected to fail when applied to systems which exhibit multiple equilibria or chaos. A finite element quasigeostrophic model of the Kuroshio near the coast of Japan was implemented and tested, and found to exhibit multiple stable equilibria in parameter ranges of physical interest. These multiple equilibria correspond to the observed formation and decay of the large meander inshore of the main current off the coast of Honshu. We plan to apply our newly-developed data assimilation methods for nonlinear systems to this model. Theoretical results pertaining to application of adjoint data assimilation methods to regional and large-scale models were obtained. Appearance of high-wavenumber noise which had been noted in a number of published data assimilation studies was found to be the result of omission of necessary constraints in the original formulation of the methods. DTIC

N95-30231*# Jet Propulsion Lab., California Inst. of Tech., Pasadena, CA.
DATA CATALOG FOR JPL PHYSICAL OCEANOGRAPHY DISTRIBUTED ACTIVE ARCHIVE CENTER (PO.DAAC)
Susan Digby 1 Nov. 1995 64 p
(Contract NAS7-1260)
(NASA-CR-198872; JPL-Publ-90-49-Rev-6; NAS 1.26:198872) Avail: CASI HC A04/MF A01

The Physical Oceanography Distributed Active Archive Center (PO.DAAC) archive at the Jet Propulsion Laboratory contains satellite data sets and ancillary in-situ data for the ocean sciences and global-change research to facilitate multidisciplinary use of satellite ocean data. Geophysical parameters available from the archive include sea-surface height, surface-wind vector, surface-wind speed, surface-wind stress vector, sea-surface temperature, atmospheric liquid water, integrated water vapor, phytoplankton pigment concentration, heat flux, and in-situ data. PO.DAAC is an element of the Earth Observing System Data and Information System and is the United States distribution site for TOPEX/POSEIDON data and metadata. Author

N95-30236*# National Aeronautics and Space Administration. Goddard Space Flight Center, Greenbelt, MD.
SeaWiFS TECHNICAL REPORT SERIES. VOLUME 24: SeaWiFS TECHNICAL REPORT SERIES CUMULATIVE INDEX, VOLUMES 1-23
Elaine R. Firestone, ed. (General Sciences Corp., Laurel, MD.) and Stanford B. Hooker, ed. Jun. 1995 39 p
(NASA-TM-104556; Rept-95B00092; NAS 1.15:104556) Avail: CASI HC A03/MF A01

The Sea-viewing Wide Field-of-view Sensor (SeaWiFS) is the follow-on ocean color instrument to the Coastal Zone Color Scanner (CZCS), which ceased operations in 1986, after an eight-year mission. SeaWiFS is expected to be launched in 1995, on the SeaStar satellite, being built by Orbital Sciences Corporation (OSC). The SeaWiFS Project at the National Aeronautics and Space Administration's (NASA) Goddard Space Flight Center (GSFC), has undertaken the responsibility of documenting all aspects of this mission, which is critical to the ocean color and marine science communities. This documentation, entitled the SeaWiFS Technical Report Series, is in the form of NASA Technical Memorandum Number 104566. All reports published are volumes within the series. This particular volume serves as a reference, or guidebook, to the previous 23 volumes and consists of 6 sections including: an errata, an addendum (summaries of various SeaWiFS Working Group Bio-optical Algorithm and Protocols Subgroups Workshops, and other auxiliary information), an index to key words and phrases, a list of all references cited, and lists of acronyms and symbols used. It is the editors' intention to publish a cumulative index of this type after every five volumes in the series. Each index covers the topics published in all previous editions, that is, each new index will include all of the information contained in the preceding indices. Author

51 LIFE SCIENCES (GENERAL)

N95-28685 Woods Hole Oceanographic Inst., MA. Dept. of Biology.
AUTOMATED ANALYSIS OF ZOOPLANKTON SIZE AND TAXONOMIC COMPOSITION USING THE VIDEO PLANKTON RECORDER Final Report, 1 Jan. 1993 - 31 Dec. 1994
Cabell S. Davis and Scott M. Gallager 31 Dec. 1994 6 p Limited Reproducibility: More than 20% of this document may be affected by

microfiche quality
(Contract N00014-93-1-0602)
(AD-A289725; WHOI-7800-35/8687-1) Avail: Issuing Activity (Defense Technical Information Center (DTIC))

The goal of this project was to develop methods for automated analysis of zooplankton size and taxonomic composition using images from the Video Plankton Recorder (VPR). Our three main objectives are to: (1) use our existing hardware to develop methods for detecting, in real time (60 fields per second, fps), the presence of in-focus organisms on the video and storing the images to disk; (2) develop pattern recognition software for classification of organisms into major taxonomic groupings (copepods, chaetognaths, doliolids, etc.); and (3) develop specifications for transferring the software routines to hardware to enable real-time sorting of zooplankton according to major taxa. The first objective was accomplished in year 1 and significant progress was made on the second two objectives in year 2. Our new 3-year grant which begins 1/1/95 will allow us to complete objectives 2 and 3 and develop a system for real-time visualization of planktonic taxa distributions while at sea. DTIC

N95-28947# Society of Instrument and Control Engineers, Tokyo (Japan).
PROCEEDINGS OF THE 33D SICE (THE SOCIETY OF INSTRUMENT AND CONTROL ENGINEERS) ANNUAL CONFERENCE, PART 1
1994 374 p Conference held in Tokyo, Japan, 26-28 Jul. 1994
(DE95-758947; CONF-9407173-Pt-1) Avail: CASI HC A16/MF A03

This is proceedings of the English papers presented to the 33rd SICE Annual Conference. As for vision control, reports are made on image recognition, visual servo, obstacle detection, and artificial intelligence. As to neuro and fuzzy, reported are learning rule in control, artificial intelligence traffic signal lights using fuzzy logic, and fuzzy petri net scheme for fuzzy production rule expression. With respect to robot, discussed are intelligent manipulator, and navigation control by robot system. With respect to measurements, described are measurement of internal resistivity distribution by tomography technique, minute drag measurement of the fluid, precision measurement, etc. As to bio-system, studies are made on muscle activation pattern and arterial tree, and as biomedical measurement, on heart behavior, and Alzheimer's disease. Reports are further made on control system, signal processing, robust control, industrial application of control technology, etc. The paper on estimation and identification is presented. DOE

N95-29088# Massachusetts Inst. of Tech., Cambridge, MA.
PROCEEDINGS OF THE 11TH CONGRESS OF THE INTERNATIONAL SOCIETY FOR ARTIFICIAL CELLS, BLOOD SUBSTITUTES AND IMMOBILIZATION BIOTECHNOLOGY
Robert S. Langer 1 Nov. 1994 213 p Meeting held in Boston, MA, 24-27 Jul. 1994
(Contract DAMD17-94-J-4017)
(AD-A290342) Avail: CASI HC A10/MF A01

This journal covers artificial cells, blood substitutes, and immobilization biotechnology. The emphasis of this journal is to allow for interdisciplinary interactions. Therefore, approaches based on biotechnology, chemical engineering, medicine, surgery, biomedical engineering, basic medical sciences, chemistry, and others were welcomed. DTIC

N95-29155# Michigan State Univ., East Lansing, MI. Dept. of Psychology.
ELECTRICAL AND ELECTRONIC PROPERTIES OF SELF-ASSEMBLED LIPID BILAYERS Final Report, Apr. 1991 - Jul. 1994
H. T. Tien 12 Oct. 1994 7 p
(Contract DAAL03-91-G-0062)
(AD-A290507; ARO-28750.1-LS-SM) Avail: CASI HC A02/MF A01

Cell membranes play a pivotal role in signal transduction and information processing. This is owing to the fact that most physiological activities involve some kind of lipid bilayer-based receptor-ligand contact interactions. There are many outstanding examples such as ion sensing, antigen-antibody binding, and ligand-gated channels, to name a few. One approach to study these interactions in vitro is facilitated by employing artificial bilayer lipid membranes (BLMs). We have focused the efforts on ion and/or molecular selectivity and specificity using newly available self-assembled BLMs on solid support (i.e. s-BLMs), whose enhanced stability greatly aid in research areas of membrane biochemistry, biophysics and cell biology as well as in biosensor designs and molecular devices development. In this report, our current work along with the experiments done in collaboration with others on s-BLMs will be presented. DTIC

N95-29263 Air Force Systems Command, Wright-Patterson AFB, OH. National Air Intelligence Center.
RESEARCH ON PGI2 AND TXA2 EFFECTS AT TIMES OF HYPERBARIC OXYGENATION OF DOMESTIC RABBITS WITH ACUTE CEREBRAL ISCHEMIA REIRRIGATION DAMAGE
Teng Yansheng and Gao Guangkai 15 Dec. 1994 16 p Transl. into ENGLISH from Shung-Hua Shen Ching Ching Shen Ko Tsa Chih, China, v. 25, no. 1, Feb. 1992 p 31-34 Limited Reproducibility: More than 20% of this document may be affected by microfiche quality
(AD-A289606; NAIC-ID(RS)T-0310-93) Avail: Issuing Activity (Defense Technical Information Center (DTIC))

There were 33 New Zealand white rabbits taken and randomly divided into a control group, a hyperbaric air group, and a hyperbaric oxygenation (HBO) group. All were reirrigated types following the creation of acute, incomplete cerebral ischemia. Respective measurements were taken of the overall carotid artery and interior jugular vein blood gases as well as cortical brain tissue homogenate amounts of 6-Keto-PGF1 and TXB2 contained. In conjunction with this, pathological investigations were made. The results were that: the amounts of 6-Keto-PGF1 contained for the HBO group were clearly greatly increased (P less than 0.01). TXB2 clearly dropped (P less than 0.05). Blood P02 in the HB0 group clearly went up (P less than 0.0l). Pathological investigations showed that the HBO groups brain tissue damage was relatively light. Conclusion: there were clear effects on PGI2 and TXA2 with HBO when there was reirrigation after acute cerebral ischemia in the domestic rabbits. This is possibly one mechanism of HBO therapy for acute cerebral ischemia. DTIC

N95-29320# New Mexico State Univ., Las Cruces, NM. Dept. of Civil Engineering.
MODELING JOINT EFFECTS OF MIXTURES OF CHEMICALS ON MICROORGANISMS USING QUANTITATIVE STRUCTURE ACTIVITY RELATIONSHIP TECHNIQUES, PHASE 3 Final Report, 23 Oct. 1991 - 22 Oct. 1994
N. Nirmalakhandan, V. R. Arulgnanendran, J. Prakash, B. Sun, and J. Peace 22 Oct. 1994 90 p
(Grant AF-AFOSR-0394-91)
(AD-A290153; AFOSR-95-0015TR) Avail: CASI HC A05/MF A01

A laboratory procedure was developed to measure the toxicity of 35 organic chemicals in the soil medium using the respirometric technique. These toxicity assays were carried out using a commercially available surrogate test culture of microorganisms. Reproducibility tests were done on 12 of the chemicals yielding an average standard deviation of 0.034 and a coefficient of variation of 0.08. These tests were also repeated at different moisture holding capacities of 33%, 50%, 80%, and 100% for six chemicals yielding an average standard deviation of 0.20 and coefficient of variation of 0.27. Using a part of the experimental IC50 results as a training set, quantitative structure activity relationship (QSAR) models were developed to predict the toxicity of 12 chemicals in the testing set. Joint toxicity of 35 different combinations of mixtures in the soil were also measured at equitoxic ratios. The joint effects in there mixtures were analyzed for simple additivity. Results indicate that the test chemicals exhibited simple additivity when acting jointly in a uniform mixture. A QSAR approach is proposed to predict mixture toxicity based on single chemical QSAR models. DTIC

N95-29375*# National Aeronautics and Space Administration. John F. Kennedy Space Center, Cocoa Beach, FL.
EFFECT OF IRRADIANCE, SUCROSE, AND CO2 CONCENTRATION ON THE GROWTH OF POTATO (SOLANUM TUBEROSUM L.) IN VITRO
Neil C. Yorio (Dynamac Corp., Rockville, MD.), Raymond M. Wheeler, and Russell C. Weigel (Florida Inst. of Tech., Melbourne, FL.) Jun. 1995 27 p
(NASA-TM-110654; NAS 1.15:110654) Avail: CASI HC A03/MF A01

Growth measurements were taken of potato plantlets (Solanum tuberosum L.) cvs. Norland (NL), Denali (DN), and Kennebec (KN), grown in vitro. Studies were conducted in a growth chamber, with nodal explants grown for 21 days on Murashige and Skoog salts with either 0, 1, 2, or 3% sucrose and capped with loose-fitted Magenta 2-way caps that allowed

approximately 2.25 air exchanges/hour. Plantlets were exposed to either 100 or 300 micro mol/sq m/s photosynthetic photon flux (PPF), and the growth chamber was maintained at either 400 or 4000 micro mol/mol CO2. Regardless of PPF, all cvs. that were grown at 4000 micro mol/mol CO2 showed significant increases in total plantlet dry weight (TDW) and shoot length (SL) when sucrose was omitted from the media, indicating an autotrophic response. At 400 micro mol/mol CO2, all cvs. showed an increase in TDW and SL with increasing sucrose under both PPF levels. Within any sucrose treatment, the highest TDW for all cvs. resulted from 300 micro mol/sq m/s PPF and 4000 micro mol/mol CO2 At 4000 micro mol/mol CO2, TDW showed no further increase with sucrose levels above 1% for cvs. NL and DN at both PPF levels, suggesting that sucrose levels greater than 1% may hinder growth when CO2 enrichment is used.

Author

N95-29471# Genetics Society of America, Bethesda, MD.

GENETICS AND THE UNITY OF BIOLOGY [GENETIQUE ET UNITE EN BIOLOGIE]

1995 305 p Presented at the 16th International Congress of Genetics, Toronto, Canada, 20-27 Aug. 1988; sponsored by the Genetics Society of Canada, the National Research Council Canada, The Royal Society of Canada, and the Biological Council of Canada

(Contract DE-FG05-88ER-60672)

(DE95-006484; CONF-8808142-Pt-3) Avail: CASI HC A14/MF A03

International Congresses of Genetics, convened just once every five years, provide a rare opportunity for overview in the field of genetic engineering. The Congress, held August 20-27, 1988 in Toronto, Canada focused on the theme Genetics and the Unity of Biology, which was chosen because the concepts of modern genetics have provided biology with a unifying theoretical structure. This program guide contains a schedule of all Congress activities and a listing of all Symposia, Workshops and Poster Sessions held. DOE

N95-30114# Argonne National Lab., IL.

PARALLEL CONTINUATION-BASED GLOBAL OPTIMIZATION FOR MOLECULAR CONFORMATION AND PROTEIN FOLDING

Thomas F. Coleman and Zhijun Wu (Cornell Univ., Ithaca, NY.) 1994 22 p Presented at the Supercomputing '94 Meeting, Washington, DC, 14-18 Nov. 1994

(Contract W-31-109-eng-38)

(DE95-005860; ANL/MCS/CP-83621; CONF-941118-10) Avail: CASI HC A03/MF A01

This paper presents the authors' recent work on developing parallel algorithms and software for solving the global minimization problem for molecular conformation, especially protein folding. Global minimization problems are difficult to solve when the objective functions have many local minimizers, such as the energy functions for protein folding. In their approach, to avoid directly minimizing a 'difficult' function, a special integral transformation is introduced to transform the function into a class of gradually deformed, but 'smoother' or 'easier' functions. An optimization procedure is then applied to the new functions successively, to trace their solutions back to the original function. The method can be applied to a large class of nonlinear partially separable functions including energy functions for molecular conformation and protein folding. Mathematical theory for the method, as a special continuation approach to global optimization, is established. Algorithms with different solution tracing strategies are developed. Different levels of parallelism are exploited for the implementation of the algorithms on massively parallel architectures. DOE

N95-30292* Interface Video Systems, Inc., Washington, DC.

LIFE SCIENCES PROGRAM (Videotape)

1995 Videotape: 17 min. 45 sec. playing time, in color, with sound

(NASA-CR-197658; NONP-NASA-VT-95-46006) Avail: CASI VHS A02/BETA A22

This Life Science Program video examines the variety of projects that study both the physiological and psychological impacts on astronauts due to extended space missions. The hazards of space radiation and microgravity effects on the human body are described, along with these effects on plant growth, and the performance of medical procedures in space. One research technique, which is hoped to provide help for future space travel, is the study of aquanauts and their life habits underwater. CASI

52 AEROSPACE MEDICINE

Includes physiological factors; biological effects of radiation; and effects of weightlessness on man and animals.

N95-28793# Armstrong Lab., Brooks AFB, TX. Aerospace Medicine Directorate.

A DISCRETE-EVENT SIMULATION MODEL OF MYOCARDIAL ELECTRICAL ACTIVITY: MATHEMATICAL ELECTROPHYSIOLOGY Final Report

R. B. Howe Dec. 1994 26 p

(DA Proj. 775-5)

(AD-A292323; AL/AO-TP-1994-0014) Avail: CASI HC A03/MF A01

This work unit was opened to provide a channel for in-house work on mathematical modeling and computer simulation of the electrocardiogram (ECG) and its underlying electrophysiology. This work was intended to complement work being done in contracted efforts aimed at model-based enhancement of ECG diagnostic criteria for detection of coronary artery disease in USAF aircrew members. Both the contract and in-house efforts have been terminated due to funding constraints and organizational shifts in research focus. In this technical paper, we report on the development of a simulation model of the depolarization and repolarization processes in the ventricles which was to be used as a cardiac electrical source model in simulations of the ECG, as well as attempt to provide some commentary regarding the relation of these efforts to broader contexts. DTIC

N95-28866# Texas Univ. Health Science Center, San Antonio, TX. Dept. of Radiology.

CELLULAR AND MOLECULAR LEVEL RESPONSES AFTER RADIOFREQUENCY RADIATION EXPOSURE, ALONE OR IN COMBINATION WITH X RAYS OR CHEMICALS Final Report, 1 Apr. 1991 - 30 Sep. 1994

Martin L. Meltz, Mohan Natarajan, and Adapa V. Prasad 21 Feb. 1995 101 p

(Contract AF-AFOSR-0206-91)

(AD-A292488; AFOSR-94-0206TR) Avail: CASI HC A06/MF A02

This project was initiated to explore the potential bioeffects of microwave radiation, alone or in combination with ionizing radiation and chemicals. Over the time period of the project, an automated thermal control system, to be used for maintaining the temperature in tissue culture medium during microwave exposures, was designed, constructed, and software was created. While this was underway during the project period, numerous positive control biological experiments were performed on two different cell types, the Epstein Barr Virus transformed 244B human lymphoblastoid cell, and the freshly isolated peripheral human lymphocyte. The 244B cells were used to address the question of whether a physical agent, ionizing radiation, at low doses where cells would predominantly remain viable, would induce the DNA binding protein NF-kB, and/or four immediate early genes (IEG) (protooncogenes). DTIC

N95-28875*# Baylor Coll. of Medicine, Houston, TX.

THE INFLUENCE OF SPACE FLIGHT ON ERYTHROKINETICS IN MAN. SPACE LIFE SCIENCES MISSIONS 1 AND 2. EXPERIMENT E261 Final Report

Clarence P. Alfrey 1995 100 p

(Contract NAS9-18024)

(NASA-CR-188368; NAS 1.26:188368) Avail: CASI HC A05/MF A02

The purpose of this contract was to design and conduct experiments that would increase our understanding of the influence of space flight on erythrokinetics and the rapid change that occurs in the red blood cell mass during spaceflight. The experiment designated E261, was flown on Space Life Science missions SLS-1 and SLS-2 (STS 40 and STS 58). Unique features of this experiment included radionuclide tracer studies during flight and frequent in-flight blood samples specifically for the first three or four days of the mission. Plasma volume measurements were made early and late in the missions. Radioactive iron kinetics studies were initiated after one or three days in microgravity since the magnitude of the red blood cell mass decrease dictated that bone marrow production must be decreased very early in the flight. The schedule was designed to study the time course of the changes that occur during spaceflight and to possibly define a mechanism for the rapid reduction in red blood cell mass.

Derived from text

N95-28915 Pittsburgh Univ., Pittsburgh, PA. Dept. of Psychiatry.
ORGANIZATION OF THE HUMAN CIRCADIAN SYSTEM Annual Report, 1 Jun. 1993 - 31 May 1994
Robert Y. Moore 31 May 1994 4 p Limited Reproducibility: More than 20% of this document may be affected by microfiche quality
(Contract F49620-93-1-0244)
(AD-A288223; AFOSR-94-0682TR) Avail: Issuing Activity (Defense Technical Information Center (DTIC))

The overall objective of this project is a detailed description of the primate circadian timing system with special attention to the human. The specific objectives for this year were as follows: (1) characterization of the chemical neuroanatomy of the human suprachiasmatic nucleus (SCN); (2) characterization of a putative retinohypothalasic tract in the human; (3) characterization of the projections of the human SCN using antisera to vasoactive intestinal polypeptide (VIP). DTIC

N95-28940 Army Aeromedical Research Lab., Fort Rucker, AL. Aircrew Protection Div.
MILITARY FLYING AND AEROMEDICAL EVALUATION OF CARDIAC ARRHYTHMIAS Final Report
Kevin T. Mason Dec. 1994 19 p Limited Reproducibility: More than 20% of this document may be affected by microfiche quality
(AD-A291595; USAARL-95-7) Avail: Issuing Activity (Defense Technical Information Center (DTIC))

The evaluation and management of cardiac arrhythmias in military aircrew members are complex, and perhaps, more aggressive than clinical cardiologists, internists, and family physicians expect. However, these policies are based on the needs of the services, mission completion requirements, public safety, and an extensive, ongoing, observational epidemiology research program of the military flying population. This paper summarizes the general considerations of the flying environment as they relate to cardiac arrhythmias. A discussion of the screening principles and epidemiologic confounders is followed by a summary of the joint U.S. Air Force and U.S. Army waiver policy on cardiac arrhythmias and flying duties. DTIC

N95-28941 Army Aeromedical Research Lab., Fort Rucker, AL.
ACTUAL EFFECTIVENESS OF HEARING PROTECTION IN HIGH LEVEL IMPULSE NOISE
James H. Patterson, Jr. and Daniel L. Johnson Aug. 1994 19 p Limited Reproducibility: More than 20% of this document may be affected by microfiche quality
(AD-A291604; USAARL-94-48) Avail: Issuing Activity (Defense Technical Information Center (DTIC))

Current exposure limits for high intensity impulse noise contain factors for hearing protection which are based on very limited data. Recent studies in the U.S. and in France have provided new insights into the protection afforded by hearing protective devices. For impulses with an A-duration of approximately 3.0 microseconds, protection was found to be adequate for peak pressures up to 190 dB SPL for 6 impulses and 187 dB for 100 impulses. Protection was found to be adequate for 6 impulses with an A-duration of approximately 0.8 microsecond up to 196 dB SPL. For this A-duration, protection was adequate for 12 impulses up to 190 dB SPL and for 50 and 100 impulses at 187 dB SPL. The hearing protectors used in these studies were earmuffs with perforations in the cushions which provided essentially attenuation below 500 Hz. In a series of French studies, hearing protection was found be adequate for impulses produced by a variety of weapons with peak pressures ranging from 165 dB SPL to 180 dB SPL. These included small arms with A-durations less than 1.0 artillery with A-durations of approximately 3.0 microseconds and other weapons with durations between these extremes. A variety of insert hearing protectors (earplugs) was used in these studies. DTIC

N95-29022# California Univ., Berkeley, CA.
COMPUTER MODELS OF RETINAL FUNCTION Final Report, 1 Feb. 1991 - 30 Jun. 1994
Frank Werblin 30 Jun. 1994 9 p
(Contract AF-AFOSR-0196-91)
(AD-A290156; AFOSR-95-0013TR) Avail: CASI HC A02/MF A01

The vertebrate retina consists of a series of sheets of neurons each containing a patterned representation, or neural image, corresponding to the incoming visual scene. Most of the operations can be described as convolutions implementing small kernels involving local neighborhoods. These patterns become more complex as the visual signal passes through the retina as each new convolution builds upon previous ones. Because we have access only to single cells, these patterns of activity have never been recorded. As a first step in visualizing these patterns we have attempted to simulate them using modern image processors operating in real time, that like the retina invoke local convolutions, in an effort to understand the mechanisms, and the physiological roles of each of these biological image processing operations. In addition, we have now developed methods for measuring these patterns in living retinas. The comparison between the modeled and measured patterns will show us what components of retinal function have not yet been incorporated into our understanding, as expressed by the models. These studies will help us to understand biological image processing by forcing us to assemble the retina using well-defined physiological functional building blocks, derived from retinal function. A long-term objective of this research is the implementation of biological image processing algorithms for man made systems such as tracking, target identification, guidance, and navigation. DTIC

N95-29059# California Inst. of Tech., Pasadena, CA.
LARGE-SCALE NEURONAL THEORIES OF THE BRAIN
Christof Koch and Joel L. Davis 1994 348 p
(AD-A290200) Avail: CASI HC A15/MF A03

This book originated at a small and informal workshop held in December of 1992 in Idyllwild, CA, where eighteen colleagues from a broad range of disciplines, including biophysics, electrophysiology, neuroanatomy, psychophysics, clinical studies, mathematics, and computer vision, discussed 'Large Scale Models of the Brain,' that is, theories and models that cover a broad range of phenomena, including early and late vision, various memory systems, selective attention, and the neuronal code underlying figure-ground segregation and awareness. The bias in the selection of the speakers toward researchers in the area of visual perception reflects both the academic background of one of the organizers as well as the (relative) more mature status of vision compared with other modalities. This should not be surprising given the emphasis we humans place on 'seeing' for orienting ourselves, as well as the intense scrutiny visual processes have received due to their obvious usefullness in military, industrial, and robotic applications. DTIC

N95-29086# Army Medical Center, Aurora, CO.
ANALYSIS OF WOUNDS BY EVAPORATIVE WATER LOSS IN MAN Final Report, 1 Jun. 1992 - 31 Jul. 1994
Sharon L. Hammond, Henry C. Jefferson, and Samuel Cucinell 21 Sep. 1994 7 p
(Contract MIPR-92MM2583)
(AD-A290327) Avail: CASI HC A02/MF A01

Cytokine growth factors are known to increase wound healing in animals and may be found to soon have an impact on human wounds, wound infections, and debridements. In order to assess the impact of these factors one must first establish a quantitative method of measurement for wound healing. This protocol's intent was to devise such a method using evaporative water loss otherwise referred to as transcutaneous water evaporative loss (TWEL). We attempted to apply an evapormeter to assist in the measurement of TWEL. Patients entered into the study were those who had undergone recent breast biopsies with TWEL readings taken immediately after the biopsy and approximately five additional readings at clinic visits once a week. Data thus far, however, has been noncontributory to the analysis due to multiple difficulties with the evapormeter and establishing a method for using the evapormeter in this type of a wound healing process. DTIC

N95-29139 Massachusetts Univ. Medical Center, Worcester, MA.
STUDIES OF ALTERED RESPONSE TO INFECTION INDUCED BY SEVERE INJURY Midterm Report, 14 Apr. 1992 - 14 Oct. 1994
Carol L. Miller-Graziano 15 Nov. 1994 46 p Limited Reproducibility: More than 20% of this document may be affected by microfiche quality
(Contract DAMD17-92-C-2033)
(AD-A288907) Avail: Issuing Activity (Defense Technical Information Center (DTIC))

The Systemic Inflammatory Response Syndrome (SIRS) that frequently occurs post-injury, is a major cause of post-trauma mortality and is characterized by both immunosuppression and cytokine aberrations. This research focuses on identifying the relative contributions of T cell and monocyte (MO) aberrations to SIRS. In the first half of the contract, we

have shown that MO TNF(alpha) production (a major contributor to SIRS) is aberrantly increased in trauma patients by: (1) failure to rapidly degrade TNF(alpha) mRNA leading to prolonged TNF(alpha) protein production; (2) insensitivity to normal downregulation by prostaglandin E(sub 2) and TGF(beta) ; (3) increased sensitivity of MO to TNF(alpha) induction by LTB(sub 4) ; (4) increased MO autocrine stimulation by TNF(alpha) due to stimulation through unshed TNFR; (5) decreased production of the TNF(alpha) immunoregulatory cytokine IL-1O by patients MO and T lymphocytes; and (6) decreased T lymphocyte production of IF. DTIC

N95-29141# Army Aeromedical Research Lab., Fort Rucker, AL.
A COMPARISON OF THE AEROMEDICAL ADMINISTRATION REQUIREMENTS FOR US AIR FORCES AND MAJOR ALLIES Final Report
Kevin T. Mason Dec. 1994 28 p
(DA Proj. 301-62787-A-878)
(AD-A290137; USAARL-95-5) Avail: CASI HC A03/MF A01

Although numerous international agreements provide for interchangeability of aircrew medical categories for the medical examination of aircrew visiting or jointly serving with sister air forces or allied air forces, the basic administrative processes remain unique between air forces. Publication of information regarding aeromedical administration would facilitate an understanding of regulatory references, requirements, and terminology between air forces. A better understanding and sharing of information might provide for further standardization of basic administrative terms and processes for aircrew medical examination. The Air Standardization Coordinating Committee tasked the U.S. Army Aeromedical Research Laboratory to develop such a publication. DTIC

N95-29153# Minnesota Univ., Minneapolis, MN. Office of Research and Technoogy Transfer Administration.
COUPLING OF BRAIN MUSCARINIC RECEPTORS TO SECOND MESSENGERS Final Report, 1 Oct. 1991 - 30 Sep. 1994
Esam E. El-Fakahany 28 Oct. 1994 5 p
(Contract DAAL03-91-G-0337)
(AD-A290498; ARO-29594.1-LS) Avail: CASI HC A01/MF A01

Stimulating muscarinic acetylcholine receptors results in activation of various signal transduction pathways. The goal of the research was to investigate the selectivity of coupling of the currently known 5 subtypes of muscarinic receptors to these different second messenger pathways. Results indicate that m1, m3 and m5 muscarinic receptors are coupled to enhanced phosphoinositide hydrolysis, while m2 and m4 receptors are coupled to a decrease in cyclic AMP formation. Results also demonstrate efficient coupling of m5 muscarinic receptors to generation of nitric oxide. DTIC

N95-29158*# Pennsylvania Univ. Medical Center, Philadelphia, PA. Inst. for Environmental Medicine.
CO2-O2 INTERACTIONS IN EXTENSION OF TOLERANCE TO ACUTE HYPOXIA Final Report, 1 Apr. 1992 - 31 Mar. 1995
C. J. Lambertsen 20 Apr. 1995 72 p
(Grant NAG9-597)
(NASA-CR-198575; NAS 1.26:198575; Rept-4-20-95) Avail: CASI HC A04/MF A01

Objectives and results of experimental projects a re summarized. The scope of information desired included (1) physiological and performance consequences of exposures to simulated microgravity, in rest and graded physical activity, (2) separate influences of graded degrees of atmospheric hypercapnia and hypoxia, and (3) composite effects of hypoxia and hypercapnia. The research objectives were selected for close relevance to existing quantitative information concerning interactions of hypercapnia and hypoxia on respiratory and brain circulatory control. They include: (1) to determine influences of normoxic immersion on interrelations of pulmonary ventilation, arterial PCO2 and PO2, and brain blood flow, in rest and physical work; (2) to determine influence of normoxic immersion on respiratory reactivity to atmospheric hypercapnia at rest; (3) to determine influence of atmospheric hypoxia on respiratory reactivity to hypercapnia at rest and in work; and (4) to provide physiological baselines of data concerning adaptations in acute exposures to aid in investigation of rates of adaptation or deteriorations in physiological or performance capability during subsequent multi-day exposures. A list of publications related to the present grant period is included along with an appendix describing the Performance Measurement System (human perceptual, cognitive and psychomotor functions). Derived from text

N95-29161# Armstrong Lab., Brooks AFB, TX. Aerospace Medicine Directorate.
FLYING WAIVERS FOR HISTORY OF ANGIOPLASTY AND MYOCARDIAL INFRACTION
Jeb S. Pickard and Joe E. Burton 18 Nov. 1994 4 p
(AF Proj. 7755)
(AD-A292505; AL/AO-TM-1995-0001) Avail: CASI HC A01/MF A01

Angioplasty has become common for the treatment of significant coronary disease (SCAD). In many cases an aeromedically significant lesion (50% or greater stenosis) may be dilated to less than 50%, raising the question of whether these patients could be considered under minimal coronary artery disease (MCAD) criteria, and allowed to fly. Suitability of MCAD to fly is based on a study of ACS patients with 20-40% lesions, who had an annual cardiac event rate of 0.6%. An extensive literature review by AOC presented at ASMA in May 1994 showed that the lowest cardiac event rate, after one year following successful angioplasty, was 2.4% per year with no subsequent decline. A lesion classified as SCAD which is subsequently dilated to less than 50% cannot be considered to be equivalent to MCAD. The Aeromedical Consult Service recommends that aviators who require angioplasty be permanently disqualified from all classes of flying duties. DTIC

N95-29173# Madigan Army Medical Center, Takoma, WA.
REFRACTIVE CHANGES DURING PROLONGED EXPOSURE TO ALTITUDE FOLLOWING REFRACTIVE SURGERY Final Report
Thomas Mader and Christopher L. Blanton 24 Oct. 1994 12 p
(AD-A290263) Avail: CASI HC A03/MF A01

This document reports corneal changes in patients exposed to altitude after radial Keratotomy and photorefractive Keratectomy. Refractive parameters were measured during the exposure. The results ofthese measurements are discussed. Radialkeratotomy patients (11 eyes), 6 photorefractive keratectomy patients (12 eyes) and 9 control myopes (17 eyes) had the following measured at sea level: cycloplegic and manifest refraction, kerntometry, and pachymetry both central and peripheral. Patients also had videokeratography performed prior to being taken to altitude. Subjects then had these same parameters measured daily at 14,110 feet on Pike's Peak, CO for 3 days. Radial keratotomy patients demonstrated a significant hyperopic shift and corneal flattening during exposure to altitude when compared to control myopic eyes. Patients who had undergone photorefractive kerntectometry did not demonstrate a statistically significant shift in refraction or keratometry when compared with control myopes. Significance: Anecdotal reports have shown hyperopic shifts in radial kerntotomy patients after exposure to altitude. We confirmed this in a study population. Photorefractive keratectomy patients do not appear to be susceptible to this refractive shift. DTIC

N95-29188# Lovelace Biomedical and Environmental Research Inst., Albuquerque, NM. Inhalation Toxicology Research Inst.
INHALATION TOXICOLOGY RESEARCH INSTITUTE Annual Report, 1 Oct. 1993 - 30 Sep. 1994
Steven A. Belinsky, Joe L. Mauderly, Mark D. Hoover, and Paula L. Bradley Nov. 1994 227 p
(Contract DE-AC04-76EV-10103)
(AD-A292037; ITRI-144) Avail: CASI HC A11/MF A03

The Inhalation Toxicology Research Institute (ITRI) is a Federally Funded Research and Development Center operated for the U.S. Department of Energy (DOE) by The lovelace Biomedical and Environmental Research Institute, a nonprofit subsidiary of The lovelace Institutes. fifil is designated as a 'Specific Mission laboratory' within the DOE Office of Health and Environmental Research, Office of Energy Research. Approximately 80% of the Institute's research is funded by DOE; the remainder is funded by a variety of governmental, trade association, and industry sources. The mission of ITRI is to conduct basic and applied research to improve our understanding of the nature and magnitude of the human health impacts of inhaling airborne materials in the home, workplace, and general environment Institute research programs have a strong basic science orientation with emphasis on the nature and behavior of airborne materials, the fundamental biology of the respiratory tract, the fate of inhaled materials and the mechanisms by which they cause disease, and the means by which data produced in

the laboratory can be used to estimate risks to human health. Disorders of the respiratory tract continue to be a major health concern, and inhaled toxicants are thought to contribute substantially to respiratory morbidity. As the largest laboratory dedicated to the study of basic inhalation toxicology, ITRI provides a national resource of specialized facilities, personnel, and educational activities serving the needs of government, academia, and industry. DTIC

N95-29190* National Aeronautics and Space Administration, Washington, DC.
AEROSPACE MEDICINE AND BIOLOGY: A CONTINUING BIBLIOGRAPHY WITH INDEXES (SUPPLEMENT 403)
Jul. 1995 101 p
(NASA-SP-7011(403); NAS 1.21:7011(403)) Avail: CASI HC A06

This bibliography lists 217 reports, articles and other documents introduced into the NASA Scientific and Technical Information System during July 1995. Subject coverage includes: aerospace medicine and physiology, life support systems and man/system technology, protective clothing, exobiology and extraterrestrial life, planetary biology, and flight crew behavior and performance. Author

N95-29224# Federal Aviation Administration, Oklahoma City, OK.
THE POTENTIAL FOR PULMONARY HEAT INJURY RESULTING FROM THE ACTIVATION OF A CABIN WATER SPRAY SYSTEM TO FIGHT AIRCRAFT CABIN FIRES Final Report
Robert P. Garner May 1995 11 p
(DOT/FAA/AM-95/17) Avail: CASI HC A03/MF A01

A cabin water spray system (CWSS) has been suggested as a means of attenuating the severity of smoke and fire commonly associated with aircraft accidents. All aspects of passenger and cabin safety must be considered when evaluating a new safety system or concept. The purposes of this report are to briefly review the pathophysiological changes occurring in the respiratory system as a result of thermal injury and to quantitatively estimate the risk of creating a more hazardous cabin environment by activation of CWSS. Changes in the heat content of the cabin atmosphere resulting from CWSS activation were calculated using parameters consistent with current aircraft and proposals for CWSS design. The results suggest that only a very small volume of the aircraft cabin would have an increase in heat content that could result in thermal injury. Author

N95-29238# Naval Health Research Center, San Diego, CA.
EFFECTS OF CHROMIUM PICOLINATE ON BODY COMPOSITION IN A REMEDIAL CONDITIONING PROGRAM Interim Report
L. K. Trent and D. Thieding-Cancel 6 Dec. 1994 20 p
(AD-A292079; NHRC-94-20) Avail: CASI HC A03/MF A01

Recent evidence suggests that nutritional supplementation with chromium picolinate might help reduce excess body fat and increase lean muscle mass. This study explored the efficiency of chromium picolinate as a weight-reduction aid for obese personnel enrolled in the Navy's mandatory remedial conditioning program (Level 1). Participants were 95 active-duty Navy members (79 men, 16 women) enrolled in several remedial programs, which met a minimum of three times per week for at least 30 minutes of aerobic exercise. The study employed a double- blind, placebo-controlled protocol. Percent body fat was computed from body circumference measurements obtained at baseline and again after 16 weeks. Participants also completed a pre-post questionnaire concerning their lifestyle habits. Half of the participants received a daily capsule containing 400 micrograms of chromium picolinate; the other half received a placebo. At the end of 16 weeks, the group as a whole had lost a small amount of weight and body fat; however, the Chromium group failed to show a significantly greater reduction in either percent body fat or body weight, or a greater increase in lean body mass, than did the Placebo group. It was concluded that chromium picolinate was ineffective in enhancing body fat reduction in this group. DTIC

N95-29360# Systems Research Labs., Inc., Dayton, OH.
PULSE WAVEFORM AND PULSE AMPLITUDE ANALYSIS DURING LOWER BODY NEGATIVE PRESSURE Final Report, Dec. 1993 - Mar. 1994
Rainer K. Effenhauser and Lloyd D. Tripp, Jr. Apr. 1994 41 p
(Contract F33615-89-C-0574)
(AD-A290521; AL/CF-TR-1994-0091) Avail: CASI HC A03/MF A01

The use of lower body negative pressure (LENP) as an acceleration pre-conditioning technique for space applications was investigated. The purpose of this study was to evaluate changes in cephalic blood flow during LBNP. The intent was to see if detection or warning of impending syncope was possible, and to simulate effects which occur under exposure to + Gz. Ten subjects underwent the following LBNP profile while in a standing position: Five minutes of baseline at ambient pressure, followed by increments of -10 mm Hg every three minutes to a minimum of -50 mm Hg. They remained at -50 mm Hg for a maximum of twenty minutes or until presyncopal symptoms occurred. An additional five minutes of post-LBNP baseline data were collected. The analog pulse waveform signals were obtained from a pulse oximeter sensor located approximately at eye level on the subject's ear lobe. The pulse waveform analysis included pulse area, amplitude, and duration. Six of the ten subjects experienced presyncopal symptoms during the LBNP profile. Significant changes were observed in several variables at the presyncopal endpoint and included: pulse waveform area ($P=0.0048$), pulse waveform amplitude ($P=0.0236$). In the non-presyncopal group, pulse waveform area ($P=0.0208$), amplitude ($P=0.0070$), and duration ($P=0.0030$) demonstrated significant changes compared to baseline values after exposure to LBNP. DTIC

N95-29557# Hebrew Univ., Jerusalem (Israel).
MEMBRANE FLUIDITY AND SHAPE OF HUMAN RED BLOOD CELLS ARE ALTERED BY PHYSIOLOGICAL LEVELS OF HYDROSTATIC PRESSURE
Gregory Barshtein, Lev Bergelson, Arie Dagan, Enrico Grafton, and Saul Yedgar 1994 22 p
(AD-A290595) Avail: CASI HC A03/MF A01

The effect of hydrostatic pressure at physiological levels, such as that applied to humans in diving or hyperbaric chamber, on human red blood cell (RBC) membrane fluidity and morphology was studied. Membrane fluidity was determined by fluorescence anisotropy (FA) of lipid probes (mainly diphenyl hexatriene (DPH), and of tryptophan), as well as by energy transfer from the tryptophan to the lipid probes, in ghosts prepared prior to or after application of pressure to intact RBC. The morphology of intact RBC, prior to or after application of pressure, was evaluated by scanning electron microscopy. It was found that: (1) The FA of DPH, which resides in different apolar membrane regions, was increased as a function of the pressure applied and the duration of the treatment. At 15 atm the FA increased by 50%, reaching a plateau after 60 min of application of pressure; (2) Increased FA, to various extents, was observed also with the lipid probes which reside in the membrane lipid core, but not with probes which monitor the polar/apolar phospholipid interface, or the cell surface; (3) The same treatment increased tryptophan anisotropy by about 20%. (4) Tryptophan energy transfer to the lipid probes which resides in the lipid core was increased to various degrees which were related to the increase of the FA of these probes; and (5) Following application of 15 atm for 1 hour, at least 60% of the RBC change their shape from discocytes to stomatocytes. These results demonstrate that hydrostatic pressure at physiological levels, might induce reduction of the membrane fluidity of RBC, which affects the physical state of protein environment, and might alter RBC morphology. DTIC

N95-29757# Army Medical Research and Development Command, Fort Detrick, MD.
HUMAN FLUID BALANCE AND DEHYDRATION DURING COLD WEATHER MILITARY OPERATIONS
Beau J. Freund and Michael N. Sawka Dec. 1994 40 p
(AD-A289192; USAMRMC-T95-4) Avail: CASI HC A03/MF A01

Not unlike exposure to hot environments, exposure to the cold can disrupt body fluid balance. While the mechanisms responsible for cold-induced dehydration (i.e., cold diuresis, increased respiratory water loses, fluid losses associated with wearing bulky winter clothing, poor fluid availability/delivery, inadequate thirst sensation, etc.) are somewhat different than those for hot environments, the impact of the fluid imbalance is often quite similar. For example, cold-induced dehydration can negatively influence both physical and cognitive performance as well as disrupt normal thermoregulation. It is also thought that dehydration may increase the susceptibility to peripheral cold injuries. This paper reviews the literature regarding factors influencing body fluid balance in the cold as well as the impact of the fluid imbalance on soldier performance and mission

accomplishment. Described are potential countermeasures for preventing or delaying body fluid imbalances in the cold, including recent advances in hyperhydration techniques. DTIC

N95-29846# Naval Health Research Center, San Diego, CA.
ADAPTATIONS TO THREE WEEKS OF AEROBIC/ANAEROBIC TRAINING IN WEST COAST U.S: NAVY SEA-AIR-LAND PERSONNEL (SEAL'S) Final Report, Jun. - Aug. 1991
I. Jacobs, W. K. Prusaczyk, and H. W. Goforth, Jr. Dec. 1994 25 p
(AD-A291500; NHRC-94-28) Avail: CASI HC A03/MF A01

SEAL's must optimize physical training 'efficiency' i.e., adaptation per unit training time. This study was designed to determine if a single training program could simultaneously elicit aerobic and anaerobic adaptations. SEAL's were assigned to groups matched for initial aerobic and anaerobic fitness. Each group trained on cycle ergometers for 30 min 3 times per week as follows: continuous (CNT; n=8) at 70 percent VO(sub 2peak); intermittent (TNT; n=6) at an average of 70 percent VO(sub 2peak) (10 x (2 min x 50 percent VO(sub 2peak) + 1 min x 110 percent V0(sub 2peak))); supramaximal (SMX; n =6) (3-5 x 30 sec maximal effort sprints spaced over 30 min). Before and after 3 weeks of training, measurement of time to exhaustion (TE), VO(sub 2peak), and blood lactate concentration (LA) during submaximal exercise were used to assess aerobic fitness, and maximal O2 deficit to evaluate anaerobic capacity. After training, VO(sub 2peak) did not change significantly for any group. Mean TE increased (p less than 0.05) for all groups, averaging 18.1 to 19.3 min. LA at 180 w decreased (p less than 0.05) for all groups, with pre to post changes of 3.3 to 2.1 mmol(dot)/L. Maximal O2 deficit increased (p less than 0.05) for TNT and SMX averaging 38 to 46 mLO2(dot)/kg, but did not increase (p more than 0.05) for CNT. There were no other significant differences across training groups for any training adaptations. The results indicate that TNT or SMX training can induce rapid improvements in both aerobic and anaerobic fitness using a single 30-min bout. DTIC

N95-29872# Hebrew Univ., Jerusalem (Israel).
EFFECT OF MILD HYDROSTATIC PRESSURE ON RED BLOOD CELLS Final Report, Aug. 1991 - Oct. 1994
Saul Yedgar 26 Dec. 1994 5 p
(Contract N00014-91-J-1880)
(AD-A290520) Avail: CASI HC A01/MF A01

We studied the effect of physiological levels of hydrostatic pressure, such as that applied in diving or hyperbaric treatment, on (1) flow (rheological) properties and (2) membrane fluidity and morphology of red blood cells (RBC). It was found that application of such pressure (1) enhances the aggregability of RBC (studied by a computerized image analysis which was developed for this purpose), and higher than normal flow rate was required to disperse the cells; and (2) reduces RBC membrane fluidity (studied by fluorescence anisotropy of lipid probes and tryptophan), and changes the cell morphology (studied by scanning electron microscopy) from normal discocytes to stomatocytes. Physical and rheological properties of RBO, as well as their shape, play a major role in blood flow and in their cellular-biochemical functions. Thus, the alterations in RBC reported here may be pertinent to the microcirculatory and physiological disorders observed among humans subjected to elevated pressure. DTIC

N95-29927# California Univ., San Francisco, CA.
MOLECULAR PROBES OF GATING AND OPEN CHANNEL CONFORMATIONAL TRANSITIONS OF MECHANOSENSITIVE ION CHANNELS Final Report
Jeffry B. Lansman 14 Nov. 1994 7 p
(Contract DAAL03-91-G-0329)
(AD-A291170) Avail: CASI HC A02/MF A01

The objective of this project was to elucidate the molecular mechanisms which control the gating behavior and ion transport properties of mechanosensitive ion channels in skeletal muscle. The project utilized recordings of single-channel activity to address two general questions: (1) How does an absence of the cytoskeletal protein, dystrophin, influence the mechanosensitive gating of single channels? (2) What is the mechanism by which positively charged aminoglycoside antibiotics inhibit the flow of current through these channels. DTIC

N95-29933# Wright State Univ., Dayton, OH.
PATTERN-ANALYSIS BASED MODELS OF MASKING BY SPATIALLY SEPARATED SOUNDS Final Report, 15 May 1991 - 30 Sep. 1994
Robert H. Gilkey 9 Feb. 1995 25 p
(Grant AF-AFOSR-0289-91)
(AD-A291270; AFOSR-95-0104TR) Avail: CASI HC A03/MF A01

Work is presented on masked detection, sound localization, neural networks, and the sense of presence. Both free-field and headphone-based studies of masking indicate that traditional models of binaural interaction may be inadequate to explain the reductions in masking that often occur with dichotic, as opposed to diotic, stimulation. The accuracy of localization judgments in the presence of a masker is determined by both the signal-to-noise ratio and the spatial location of the masker. Localization judgments for speech stimuli are in general less accurate than those for some nonspeech stimuli. Neural - network models of sound localization can achieve performance similar to human observers based on monaural information alone or based on interaural information alone. The reports of suddenly-deafened adults suggest that realistic auditory stimulation may be critical for determining the sense of presence in virtual environments. DTIC

N95-29995# Naval Health Research Center, San Diego, CA.
THE EFFECT OF BRIGHT LIGHT AND LEET ON SLEEP AFTER A 10-HOUR PHASE DELAY Final Report, 1 Oct. 1991 - 30 Sep. 1994
Tamsin L. Kelly, Roza Hyduk, and David Ryman Nov. 1994 22 p
(AD-A291264; NHRC-94-23) Avail: CASI HC A03/MF A01

Shift work and jet lag can cause circadian desynchronosis. Bright light and Low Energy Emission Therapy (LEET), separately and together, were tested as interventions to improve sleep after a 10-hr phase delay of the work/rest cycle. Both interventions decreased awakenings during the first daytime sleep period after the phase shift. After 3 nights of bright light administration from 2200-0200 each night, the subjects who received bright light had greater total sleep time, better sleep efficiency, and less wake time during the sleep period as compared to subjects who were exposed to dim light. Three days of LEET treatment for 20-min prior to each daytime sleep period showed a non-significant trend for similar additive benefits, with the group who received both bright light and LEET showing greater total sleep time than the group who received only light, and the group that received only LEET showing greater total sleep time than the control group who received neither intervention. DTIC

N95-30083# Naval Health Research Center, San Diego, CA.
SLEEP DURING SEAL DELIVERY VEHICLE (SDV)/DRY DOCK SHELTER EXERCISES ANALYZED BY A GRAPHIC APPROACH Final Report
P. Naitoh, T. L. Kelly, P. Hunt, and H. W. Goforth, Jr. Nov. 1994 28 p
(AD-A290916; NHRC-94-30) Avail: CASI HC A03/MF A01

Naval Special Warfare (NSW) personnel frequently participate in missions involving extended work hours and nocturnal waking periods. This can have a negative effect on sleep patterns, which in turn could have detrimental impact on cognitive performance. Environmental factors aboard submarines that degrade quantity and quality of sleep and increase fatigue of NSW Sea-Air-Land (SEAL) personnel have been previously evaluated by Phil Hunt, CDR, MC, USN, a submarine medical officer (unpublished memorandum). Such factors include (1) persistent light, noise, crowding and activity in the berthing area, and (2) conflicts between the work/rest schedules of the submarine crew and SEAL Delivery Vehicle (SDV)/Dry Deck Shelter (DDS) personnel. Hunt recommended that the berthing area be made more conducive to quality sleep. He also recommended regular use of an aerobic exercise machine which, in addition to physiological benefits, may improve quality and quantity of sleep. Sleep surveys are an important tool to assist in the development of an appropriate work/rest schedule for a given mission scenario. These techniques have been used previously in relation to many different occupations, both in the military and the civilian sectors (e.g., Investigation of the Navy Workweek at Sea, 1975, by the Navy Personnel Research and Development Center, San Diego, and The Standard ShiftWork Index, 1991, by the Shiftwork Research Team at the University of Sheffield, England). A guide to optimizing sleep during special warfare operations has been published (Naitoh & Kelly, 1992); however, the sleep log/sleep questionnaire analysis techniques necessary to assess wake/sleep patterns were not explained in that report. DTIC

N95-29627# Institute of Aviation Medicine, Oslo (Norway).
EFFECT OF HYPOXIA ON ARTERIAL BLOOD GASES IN SUBJECTS WITH LUNG DYSFUNCTION
Morten Ryg and Carl C. Christensen *In* AGARD, Recent Issues and Advances in Aeromedical Evacuation (MEDEVAC) Feb. 1995 14 p
(For primary document see N95-29604 10-66)
Copyright Avail: CASI HC A03/MF A02

N95-29629# Hellenic Air Force General Hospital, Athens (Greece).
FLIGHT NURSE SCHOOL IN THE HELLENIC AIR FORCE
Kal. Papastogiannidou and Alex. Katsika *In* AGARD, Recent Issues and Advances in Aeromedical Evacuation (MEDEVAC) Feb. 1995 5 p
(For primary document see N95-29604 10-66)
Copyright Avail: CASI HC A01/MF A02

53 BEHAVIORAL SCIENCES

Includes psychological factors; individual and group behavior; crew training and evaluation; and psychiatric research.

N95-28918# Minnesota Univ., Minneapolis, MN. Dept. of Phychology.
IMPROVING PROBLEM-SOLVING AND DECISION-MAKING SKILLS UNDER STRESS: PREDICTION AND TRAINING Final Report, Sep. 1991 - Jul. 1994
Phillip L. Ackeerman and Ruth Kanfer 10 Sep. 1994 81 p
(Contract N00014-91-J-4159)
(AD-A292104; Rept-94-01) Avail: CASI HC A05/MF A01

This investigation draws on a theoretical framework developed by Kanfer & Ackerman to: (1) assess individual differences in reactivity to stress, particularly from information processing; and (2) to develop a battery of cognitive ability tests/self-regulation measures for predicting performance under stress. Three studies were conducted. Two studies used a dynamic Target/Threat Identification Task under time-pressure. The remaining study used a complex air traffic controller task (TRACON) over extended practice. Personality, motivation, and self-regulatory activity measures are often significantly associated with performance under task load. However, the mixture of cognitive ability influences and stress-reactions associated with performance on cognitive and perceptual speed abilities account for the major amount of individual differences in performance, and also account for variance that is common to the non-ability predictors and task performance. The Dial Reading and Directional Headings Tests are promising predictors of performance in stressful information processing activities. We conclude that such measures have definite advantages to self-reports in predicting individual differences in performance under stress. DTIC

N95-28937 Harvard Univ., Cambridge, MA. Dept. of Psychology.
INTERMEDIATE LEVELS OF VISUAL PROCESSING Final Report, 1 Oct. 1991 - 30 Sep. 1994
Ken Nakayama 30 Sep. 1994 4 p Limited Reproducibility: More than 20% of this document may be affected by microfiche quality
(Contract F49620-92-J-0016)
(AD-A291569; AFOSR-95-0110TR) Avail: Issuing Activity (Defense Technical Information Center (DTIC))

We completed a comprehensive theoretical account of visual surface representation based on a new understanding of many of our recently reported perceptual phenomena. In particular, we determined the degree to which the 'generic view principle' can explain these new findings and also extended its domain to a large number of perceptual phenomena (Shimojo and Nakayama, 1992). We apply the generic sampling principle which indicates that the visual system acts as if it were viewing surface layouts from generic, not accidental vantage points. Through the observer's experience of optical sampling, which can be characterize geometrically, the visual system makes associative connections between images and surfaces, passively internalizing the conditional probabilities of image sampling from surfaces. In turn, this enables the visual system to determine which surface a given image most strongly predicts. Thus, visual surface perception can be considered as inverse ecological optics based on learning through ecological optics. Because of its neglect of prior probabilities and higher level knowledge, visual surface perception deviates from strict Bayesian notions of inference. DTIC

N95-29090# Human Resources Research Organization, Alexandria, VA.
COPING AND ADAPTATION: THEORETICAL AND APPLIED PERSPECTIVES Interim Report, Sep. - Dec. 1980
Rosamary Dawson, Sharon Batia, Kathy Brooks, and Wendy J. McGuire Nov. 1994 146 p
(Contract MDA903-78-C-2042)
(AD-A290513; ARI-RN-95-06) Avail: CASI HC A07/MF A02

Soldiers who have limited skills and affective attributes from which to draw to cope with the barrage of requirements from assignment in Germany are less likely to adapt successfully to that environment. At the level of the individual soldier, actions could be taken to assist in acquisition of vital life coping skills that, in turn, would facilitate successful adaptation to life in Europe and reduce problems with retention and performance. This report describes the theoretical framework for the Life Coping Skills in USAREUR project, develops a model of the coping process, summarizes studies that have identified needed life coping skills, reviews literature related to adaptation to the military and to foreign countries, and makes recommendations concerning directions and procedures for project tasks. DTIC

N95-29162# Armstrong Lab., Brooks AFB, TX. Aerospace Medicine Directorate.
ASTRONAUT SELECTION (NASA-MIPR) Technical Note
John C. Patterson Jan. 1995 3 p
(AD-A292512; AL-AO-TN-1995-0001) Avail: CASI HC A01/MF A01

Since the last technical note, one selection cycle has been run: 26 June - 2 September 1994. A selection cycle had been planned for fall, 1993 but was cancelled by NASA. During the June - September cycle a total of 122 applicants were screened, about 20 applicants for each of the 6 weeks. From these applicants 10 pilots and 9 mission specialist candidates were selected. Among those selected 6 were rated as Exceptionally Well Qualified (EWQ) by the panel, 3 were Qualified+ (Q+), 10 were Qualified (Q), and no selectees were rated Qualified with Reservations (Q-R) nor Disqualified (DQ). Among the entire applicant pool 23 candidates were rated as EWQ. 84 were rated as Q, 15 were rated as Q-R and none were found DQ. Three USAF psychiatrists and two USN psychiatrists served as evaluators; three USAF psychologists, one USA psychologist, and one USN psychologist were evaluators. As in the past briefing and testing began on Sunday at 1200, tests were scored Sunday evening to prepare for the interviews beginning on Monday and lasting through Thursday; out briefs were available for volunteers (as in the past, nearly 100%) on Friday. Staffing occurred each day of interviews at noon and day's end which consisted of a case presentation by the interviewer, testing review by the psychologists observer, group discussion and consensus recommendation. The psychologists divided the applicants tests among them, interpreted the tests and sat in with the psychiatrist as an observer to better integrate the test findings. The psychiatrists dictated reports based on the structured interviews and recommendations. DTIC

N95-29261# Federal Aviation Administration, Oklahoma City, OK. Office of Avaiation Medicine.
SHIFT WORK, AGE, AND PERFORMANCE: INVESTIGATION OF THE 2-2-1 SHIFT SCHEDULE USED IN AIR TRAFFIC CONTROL FACILITIES I. THE SLEEP/WAKE CYCLE Final Report
Pamela S. Della Rocco and Crystal E. Cruz May 1995 29 p
(DOT/FAA/AM-95/19) Avail: CASI HC A03/MF A01

Air Traffic Control Specialists (ATCS) work rotating shift schedules for most of their careers. Specifically, many work a counterclockwise rotating shift schedule, called the 2-2-1, or some variation of the schedule. The 2-2-1 involves rotating from two afternoon shifts to two mornings and, finally, to a midnight shift over the course of one work week. The purpose of the present study was to investigate sleep patterns during this type of rotating shift and the potential cumulative partial sleep loss in a laboratory-based synthetic work environment. Four groups of five male subjects between the ages of 30 to 35 (n-10) and 50 to 55 (n = 10) participated in the four week study. Subjects were screened on medical and cognitive criteria. The Multiple Task Performance Battery (MTPB) was utilized to provide a motivating synthetic work environment. Subjects were asked to work three 2-hour sessions on the MTPB per eight hour day for the last three weeks of the protocol. During the second and fourth weeks, subjects worked day shift (0800-1630). During the third week, subjects worked the 2-2-1 schedule. Sleep duration and quality, as well as mood,

sleepiness and fatigue ratings were reported in log books. Wrist activity monitors were used to verify sleep duration. Average sleep durations decreased over the week of the 2-2-1 from an average of 7.6 hours, on Sunday night prior to the first afternoon shift, to 3.0 hours just prior to the midnight shift. Comparison of sleep duration for the first week of day shifts (excluding weekends) to the 2-2-1 week revealed that total sleep time was significantly less for the 2-2-1 week (p is less than .01). No differences were found between age groups. Data suggest that sleep management interventions could improve adaptation to the quick-rotating shift schedules. This study was the first report from a laboratory-based study of the 2-2-1. It was part of a research program designed to develop fatigue countermeasures for implementation with Air Traffic Control Specialists in the field. Author

N95-29422# Rochester Univ., NY. Center for Visual Science.
REFERENCE FRAMES IN VISION Final Report, 15 Jan. 1991 - 30 Jul. 1994
Mary M. Hayhoe 9 Jan. 1995 9 p
(Grant AF-AFOSR-0332-91)
(AD-A290117; Rept-5-27959; AFOSR-95-0021TR) Avail: CASI HC A02/MF A01

The goal of this project is to examine the consequences of observer motion for visual function. The research has focussed on two issues: One issue is how a grossly time-varying retinal input (because of eye, head, and body notion) results in the perception of a continuous and directionally stable visual world. A second issue concerns how the information in successive views is related, and the nature of the visual information retained from previous views. Understanding these processes is important for a wide variety of visuo-motor tasks. Progress has been made on the following projects: (1) The role of the visual scene and eye position signals in visual stability; (2) The role of attention in integrating across saccades; (3) Reference frames for spatial memory; (4) Hand-eye coordination during complex tasks; (5) Detectability of changes during saccades; and (6) Short term visual memory of complex scenes. DTIC

N95-29432# Educational Testing Service, Princeton, NJ.
TEST THEORY RECONCEIVED
Robert J. Mislevy Jan. 1995 59 p
(Contract N00014-91-J-4101; NR Proj. 042-04)
(AD-A291836; RR-94-2-ONR) Avail: CASI HC A04/MF A01

Educational test theory consists of statistical and methodological tools to support inference about examinees' knowledge, skills, and accomplishments. The evolution of test theory has been shaped by the nature of users' inferences, which until recently, have been framed almost exclusively in terms of trait and behavioral psychology. Progress in the methodology of test theory enabled users to extend the range of inference, sharpen the logic, and ground their interpretations more solidly within these psychological paradigms. In particular, the focus remained on student's over-all tendency to perform in prespecified ways in prespecified domains of tasks; for example, to make correct answers to mixed-number subtraction problems. Developments in cognitive and developmental psychology broaden the range of desired inferences, especially to conjectures about the nature and acquisition of students' knowledge. Commensurately broader ranges of data-types and student models are entertained. The same underlying principles of inference that led to standard test theory can be applied to support inference in this broader universe of discourse. Familiar models and methods - sometimes extended, sometimes reinterpreted, sometimes applied to problems wholly different from those for which they were first devised - can play a useful role to this end. DTIC

N95-29434# Army Aeromedical Research Lab., Fort Rucker, AL.
US ARMY AVIATION EPIDEMIOLOGY DATA REGISTER: GENDER-SPECIFIC ATTRITION AMONG THE US ARMY STUDENT AVIATOR CLASS OF 1987 Final Report
Kevin T. Mason and Samuel G. Shannon Jan. 1995 22 p
(DA Proj. 301-62787-A-878)
(AD-A291856; USAARL-95-12) Avail: CASI HC A03/MF A01

Graduated aviators from the U.S. Army student aviator cohort of the Class of 1987 were followed in the Aviation Epidemiology Data Register for 6 years to determine if there was a gender-specific difference in attrition from aviation service. Overall, 30 percent attrition was found in 6 years of observation following initial aviator training. There was no significant gender-specific difference in attrition (p greater than 0.05, life table analysis). Pregnancy was the most common identified cause of female aviator attrition. However, there was no significant increase risk for attrition among all pregnant aviators after delivery (relative risk = 0.545, CI0.95 = 0.144, 2.06). Among male aviators, flying evaluation boards with nonmedical termination of aviation service, death due to aircraft mishaps, and alcohol abuse were common identified causes of attrition. These three conditions accounted for 47 percent of known causes for male aviator attrition. DTIC

N95-29439# Wright State Univ., Dayton, OH.
VISUALIZATION OF CAD OBJECTS USING A STEREOSCOPIC DISPLAY Technical Report
Michael E. Brown and Jennie J. Gallimore 15 Jan. 1995 3 p
(Contract N00014-92-J-4096)
(AD-A290034) Avail: CASI HC A01/MF A01

Subjects memorized the shape of a static 3-D object displayed on a stereoscopic CRT (cathode ray tube). In each of a series of trials that followed, single static objects were presented. The angular orientation of each trial object was one of six 36-deg increments relative to the angle of the memorized stimulus. The subject's task was to determine, as quickly and accurately as possible, whether the trial object was the same shape as the memorized object or its mirrored image. One of the two cases was always true. Disparity and interposition were manipulated in a within-subject manner during the initial memorization period and the trials that followed. Subject response time and error rate were evaluated. The experimental objective was to determine the extent to which stereopsis and hidden surface affect subjects' ability to: (1) transfer to and retrieve from long-term memory spatial information about a 3-D object; and (2) visualize spatial characteristics in a quick and direct manner. Improved performance due to hidden surface is the most convincing experimental finding. The study also found a significant but limited stereopsis effect. DTIC

N95-29443# Massachusetts Inst. of Tech., Cambridge, MA.
INTERACTION AND INTELLIGENT BEHAVIOR
Maja J. Mataric Aug. 1994 191 p
(Contract N00014-91-J-4038)
(AD-A290049; AI-TR-1495) Avail: CASI HC A09/MF A02

We introduce basic behaviors as primitives for control and learning in situated, embodied agents interacting in complex domains. We propose methods for selecting, formally specifying, algorithmically implementing, empirically evaluating, and combining behaviors from a basic set. We also introduce a general methodology for automatically constructing higher--level behaviors by learning to select from this set. Based on a formulation of reinforcement learning using conditions, behaviors, and shaped reinforcement, out approach makes behavior selection learnable in noisy, uncertain environments with stochastic dynamics. All described ideas are validated with groups of up to 20 mobile robots performing safe--wandering, following, aggregation, dispersion, homing, flocking, foraging, and learning to forage. DTIC

N95-29458 National Biomedical Research Foundation, Washington, DC.
GEORGETOWN INSTITUTE FOR COGNITIVE AND COMPUTATIONAL SCIENCES Annual Report, 1 Oct. 1993 - 30 Sep. 1994
Robert S. Ledley and Alan I. Faden 4 Nov. 1994 11 p Limited Reproducibility: More than 20% of this document may be affected by microfiche quality
(Contract DAMD17-93-V-3018)
(AD-A289775) Avail: Issuing Activity (Defense Technical Information Center (DTIC))

Georgetown Institute for Cognitive and Computational Sciences Georgetown University Medical Center has established a Department of Neuroscience to provide the optimal academic structure to support the Georgetown Institute for Cognitive and Computational Science (GICCS). Several experts in the field were invited to participate in the planning, organization and recruitment of the chair and faculty for the Department of Neuroscience. The chair of this department is being actively recruited; final candidates have been identified and this process is entering its final stages. In addition, we have advertised for faculty positions for GICCS; 42 applications have been received to dat. An administrator of the Institute has been hired. The scientific project entitled 'Texture Analysis for Scene

Segmentation' led by Dr. Robert S. Ledley has begun. This study will provide an important tool to explore various aspects of biological pattern recognition. DTIC

54 MAN/SYSTEM TECHNOLOGY AND LIFE SUPPORT

Includes human engineering; biotechnology; and space suits and protective clothing.

For related information see also *16 Space Transportation.*

N95-28683 Systems Research Labs., Inc., Dayton, OH.
GENERATOR OF BODY DATA (GEBOD) MANUAL Final Report, Apr. 1991 - Mar. 1994
Huaining Cheng, Louise Obergefell, and Annette Rizer Mar. 1994 71 p Limited Reproducibility: More than 20% of this document may be affected by microfiche quality
(AD-A289721; AL/CF-TE-1994-0051) Avail: Issuing Activity (Defense Technical Information Center (DTIC))

The Generator of Body Data (GEBOD) program is an interactive computer program that produces the human and dummy body description data used by the Articulated Total Body (ATB) model. GEBOD computes the body segments' geometric and mass properties, and the joints' locations and mechanical properties. These data may be computed for children, adult human males, adult human females, or anthropomorphic dummies. This report is a comprehensive manual that covers the applicable material from earlier reports and the most recent upgrades to the GEBOD program, including improved height calculations. The user's guide section of the report describes how to run the program and what options are available. A more detailed description of how the data is generated and on what studies the calculations are based is included in the program description section. Also included are a brief history of GEBOD's development, a detailed description of GEBOD program subroutines, and example output files. DTIC

N95-28792# Armstrong Lab., Brooks AFB, TX. Crew Systems Directorate.
TEST AND EVALUATION OF THE IMPACT INSTRUMENTATIONS, INC. UNI-VENT MODEL 750M VENTILATOR Interim Report, Oct. 1993 - Jun. 1994
Mary L. Thomas Nov. 1994 23 p
(DA Proj. 793-0)
(AD-A292321; AL/CF-TR-1994-0112) Avail: CASI HC A03/MF A01

The Aeromedical Research Function tested and evaluated the Uni-Vent 750M ventilator for use on aeromedical evacuation aircraft in response to a request from the Director, Aeromedical Evacuation and Medical Plans and Requirements, Human Systems Center at Brooks AFB. A collaborative evaluation was conducted with the U.S. Army Aeromedical Research Laboratory, Ft. Rucker, Alabama. The Impact Instrumentations, Inc. Uni-Vert Model 750M ventilator was found acceptable for use on cargo aircraft used for USAF aeromedical evacuation. DTIC

N95-28794# Army Natick Research and Development Command, MA.
AN ANALYSIS OF ANTHROPOMETRIC DIFFERENCES AMONG OCCUPATIONAL GROUPS IN THE US ARMY Final Report, Dec. 1991 - Jul. 1992
Thomas M. Greiner, Claire C. Gordon, and Elizabeth A. Carson Jan. 1995 73 p
(AD-A292326; NATICK/TR-95/016) Avail: CASI HC A04/MF A01

This report addresses the design relevance of anthropometric differences among occupation groups in the U.S. Army. The analysis is based upon the examination of 15 body dimensions of Army enlisted men and women within 10 broadly defined occupation groups (Career Management Fields or CMF's). The membership of each occupation group comprises unique age, race, and sex proportions. Statistical analyses (ANOVA) show that observed differences among CMF's were most strongly associated with these demographic proportions. Still, observable anthropometric differences among groups were very small. Clothing and equipment designs would have to be extremely sensitive to be influences by these differences. These findings suggest that the anthropometric relationships among CMF's may change as the demographic proportions of the Army population change. Thus, it appears that clothing and equipment designers should be more concerned with the impact of anthropometric differences due to race and sex than to the differences among occupation groups. DTIC

N95-28935 Naval Biodynamics Lab., New Orleans, LA.
OPERATING PROCEDURES FOR ANTHROPOMETRY AND INITIAL CONDITIONS PHOTOGRAMMETRIC PROGRAM Final Report
Dorothy A. Francis Mar. 1994 188 p Limited Reproducibility: More than 20% of this document may be affected by microfiche quality (MR00-97)
(AD-A291553; NBDL-93R010) Avail: Issuing Activity (Defense Technical Information Center (DTIC))

This publication provides documentation of the Anthropometry and Initial Conditions Photogrammetric Program used on an IBM-compatible 486 personal computer at the Naval Biodynamics Laboratory in New Orleans, LA. DTIC

N95-28969# Naval Air Warfare Center, Warminster, PA. Air Vehicle and Crew Systems Technology Dept.
TASK-DEPENDENT EFFECTS OF AUTOMATION: THE ROLE OF INTERNAL MODELS IN PERFORMANCE, WORKLOAD, AND SITUATIONAL AWARENESS IN A SEMI-AUTOMATED COCKPIT Final Report, Dec. 1991 - Dec. 1993
Meghan A. Carmody 1 Mar. 1994 462 p
(AD-A292538; NAWCADWAR-94140-60) Avail: CASI HC A20/MF A04

The present study investigated the effects of automating different aviation tasks on a pilot's ability to regain manual control following automation failure. The investigation employed a version of the Multi-Attribute Task (MAT) battery (Comstock and Arnegard, 1990) which presents subjects three aviation-relevant tasks: A Tracking task, a System Monitoring task, and a Fuel Management task. Specifically, this study examined task-specific effects on performance, workload, and situational awareness of removing the human operator from the control loop for long periods of time and then requiring him/her to suddenly reenter that loop. A hypothesized task distinction was formulated on the basis of the dynamic versus stable qualities of the internal cognitive model guiding the decision-making process within a particular task. This distinction is presented within the context of a theoretical model of human decision-making in complex, semi-automated cockpits. Results indicated task-specific effects of automation on human performance. Furthermore, data regarding task-specific effects of automation on situational awareness were strongly indicative of the hypothesized distinctions. DTIC

N95-28970# Naval Air Warfare Center, Warminster, PA. Air Vehicle and Crew Systems Technology Dept.
CURRENT ISSUES IN THE MEASUREMENT OF MILITARY AIRCREW PERFORMANCE: A CONSIDERATION OF THE RELATIONSHIP BETWEEN AVAILABLE METRICS AND OPERATIONAL CONCERNS Final Report, Oct. - Dec. 1993
Meghan A. Carmody 1 Mar. 1994 67 p
(AD-A292539; NAWCADWAR-94139-60) Avail: CASI HC A04/MF A01

This report discusses the primary categories of metrics used by DoD researchers to assess human performance in the aviation domain. In addition to outlining the categories and several representative metrics, various approaches are evaluated on the basis of pre-defined measurement criteria as well as the specific considerations and limitations of the particular testing environment. DTIC

N95-29020# Boeing Defense and Space Group, Seattle, WA.
INTERACTIVE MULTIMEDIA PRESENTATION FOR APPLIED COMPUTER TOMOGRAPHY: IMPACT Interim Report, 1 Jan. 1993 - 1 Jun. 1994
Richard H. Bossi and Robert J. Kruse Jun. 1994 29 p
(Contract F33615-88-C-5404)
(AD-A291955; WL-TR-94-4099) Avail: CASI HC A03/MF A01

An interactive multimedia presentation has been developed for viewing on a Macintosh workstation that summarizes the results of the 'Advanced Development of X-ray Computed Tomography Applications' demonstration (CTAD) program. The Interactive Multimedia Presentation for Applied Computed Tomography (IMPACT) package includes the following areas: (1) conclusions and recommendations; (2) X-ray computed tomography; (3)

CT application stories; (4) interactive imaging program; and (5) for more information. The 'Advanced Development of X-ray Computed Tomography Applications' demonstration (CTAD) program, sponsored by Wright Laboratory, generated significant amounts of data and conclusions on the application of X-ray computed tomography (CT) to aircraft structures, materials and components. Over 18 formal technical reports have been written for WL publication. The approach for summarizing the data has been to create a presentation package for use on a Macintosh computer containing the major conclusions of the CTAD program with a number of specific examples. The package can be used by an individual to review information or can be used by a presenter to an audience with an LCD screen and overhead projector. The interactive multimedia allows the users to move through the material at their pace, entering deeper levels of detail as desired. The presentation contains the summary conclusions of the CTAD program, background material on basic X Ray CT, examples of the applications of computed tomography that were demonstrated in the CTAD program, an image processing program for demonstrating CT image analysis, and references for more information. The CD presentation package is available from Wright Laboratory. DTIC

N95-29180* Lockheed Engineering and Sciences Co., Washington, DC.
LOCKHEED STABILIZER SYSTEM FOR SPACE EXERCISE EQUIPMENT (Videotape)
25 Feb. 1992 Sponsored by NASA, Washington Videotape: 5 min. playing time, in color, without sound
(NASA-CR-197657; HQ-91-03N; NONP-NASA-VT-95-46004) Avail: CASI VHS A02/BETA A22

Through the use of computer animation, the Lockheed Stabilizer System for spaceborne exercise equipment is shown. A bicycle mounted onto a shuttle floor demonstrates the range of vibrations that occur without the Lockheed Stabilizer. There is animation of the stabilizer system's tests and normal protein crystal growth in microgravity environments. Actual short clips of astronauts exercising in space are also presented. CASI

N95-29359# Naval Command, Control and Ocean Surveillance Center, San Diego, CA.
IMPROVED OPERATOR AWARENESS OF TELEOPERATED LAND VEHICLE ATTITUDE Final Report, Jun. 1990 - Jun. 1992
Tracy Heath Pastore Jun. 1994 34 p
(AD-A290443; NRAD-TR-1659) Avail: CASI HC A03/MF A01

The operator of a teleoperated land vehicle must have a sufficient understanding of the attitude of a remote vehicle to successfully operate it in an unstructured outdoor environment. The goal of this effort was to develop a human-machine interface that provides sufficient remote vehicle attitude information while minimally impacting operator workload. Referencing the remote video sensors to the earth's gravitational field was proposed as a means of providing vehicle attitude information to the operator. The hood of the remote vehicle appeared in the video image and served as a two-dimensional artificial horizon, providing the operator with vehicle pitch and roll information in a natural, nonintrusive manner. The effectiveness of gravity-referencing the sensors was experimentally tested and compared with vehicle-referencing the sensors on the same teleoperator system. Experimental results confirmed that gravity-referencing the sensors provided the operator with improved vehicle attitude information. In addition, results showed a significantly higher level of operator confidence in vehicle attitude awareness with the gravity-referencing method. A minimal increase in operator workload was also documented for the method of gravity-referencing. DTIC

N95-29365# Federal Aviation Administration, Oklahoma City, OK. Human Resources Research Div.
A HUMAN FACTORS EVALUATION OF THE OPERATIONAL DEMONSTRATION FLIGHT INSPECTION AIRCRAFT Final Report
M. D. Rodgers, ed. May 1995 25 p
(DOT/FAA/AM-95/18) Avail: CASI HC A03/MF A01

These reports describe the data collection and analysis efforts performed by the Civil Aeromedical Institute's Human Factors Research Laboratory to assist the Office of Aviation System Standards (AVN) in the human factors evaluation of the Operational Demonstration (Ops Demo) candidate flight inspection aircraft (FIA). Although there was not sufficient time to conduct an exhaustive human factors evaluation of the Ops Demo FIA, several efforts were undertaken to assist in the determination of the suitability of the proposed aircraft for integration of flight inspection equipment and performance of the flight inspection mission. These efforts included an evaluation of flight inspection pilot and technician preferences for certain aircraft characteristics, an evaluation of aircraft cabin noise levels, an anthropometric familiarization for flight inspection pilots and technicians participating in the Ops Demo, and an evaluation of the proposed flight inspection workstation design for the medium-size, medium-range (MSR) aircraft. Author

N95-29378# Army Tank-Automotive Command, Warren, MI.
RIDE MOTION SIMULATOR (RMS) TESTING USING HUMAN OCCUPANTS Final Report, 17 Oct. - 4 Nov. 1994
AnnMarie Berger Dec. 1994 16 p
(AD-A292641; TARDEC-TR-13660) Avail: CASI HC A03/MF A01

The objective of this report is to summarize the results of using human occupants in the RMS during the Crewmans Associate Job. This report does not address the subjective data obtained on the helmet mounted displays and controllers preferobility and usability. This report will be submitted to the Human Use Committee and describes the tests conducted. DTIC

N95-29600 Office of Naval Research, Arlington, VA.
INFLATABLE LIFE VEST Patent Application
Cleveland A. Heath, inventor (to Navy) and Maurice W. Roy, inventor (to Navy) 30 Sep. 1994 17 p Filed 30 Sep. 1994 Limited Reproducibility: More than 20% of this document may be affected by microfiche quality
(AD-D017273; Navy-Case-75646; US-Patent-Appl-SN-316709) Avail: Issuing Activity (Defense Technical Information Center (DTIC))

An inflatable life vest comprises two sheets of polymeric material. The edges of these sheets are sealed to form an inner cavity with a plurality of discrete, inflatable chambers disposed in a U-shaped pattern to define collar and chest portions of the life vest. A manifold connects to an inflation source and has a plurality of openings. A check valve connects each manifold opening with one of the chambers to permit inflation medium flow into the chamber and to block inflation medium flow outwardly from a chamber into the manifold. This construction isolates the chambers from one another so the rupture of one chamber does not affect the ability of the other chambers to be buoyant. DTIC

N95-29908# Computer Technology Associates, Inc., McKee City, NJ.
VISUAL AND AUDITORY SYMBOLS: A LITERATURE REVIEW
James P. Duncanson Oct. 1994 69 p
(AD-A290222; DOT/FAA/CT-TN-94/37) Avail: CASI HC A04/MF A01

This report is a review of the human factors literature on visual and auditory symbols. The review is the first step in an effort to develop a set of standard symbols for use throughout Airway Facilities. The topics included in the review are: general principles, experimental findings, and standard guidelines. The report also includes an annotated bibliography and a list of possible research topics suggested by gaps in the experimental findings. DTIC

N95-29943# Dayton Univ., OH. Research Inst.
DISTANCE ESTIMATION TRAINING WITH NIGHT VISION GOGGLES UNDER LOW ILLUMINATION Interim Report, Oct. - Dec. 1993
Jack D. Reising and Elizabeth L. Martin Jan. 1995 27 p
(Contract F33615-90-C-0005)
(AD-A291338; AL/HR-TR-1994-0138) Avail: CASI HC A03/MF A01

Aircrews have reported significant problems in depth perception and distance estimation with night vision goggles (NVG's). The purpose of this experiment was to examine the value of a simple training procedure as a means of reducing errors. A pre/post-test design was used in which distance estimates for a training group and control group were compared. The results revealed significant reductions in errors and variability following exposure to the training procedure. No significant reduction in errors and variability occurred with the control group. These results are consistent with a preliminary experiment using NVG's and earlier research using unaided vision. Issues for future research are also addressed. DTIC

N95-29624# Department of the Air Force, Brooks AFB, TX. Armstrong Lab.
AEROMEDICAL IMPACT OF THE TRANSPORTABLE PRESSURE VENTILATOR IN WARTIME AEROMEDICAL EVACUATION

L. Richardson and R. Munson *In* AGARD, Recent Issues and Advances in Aeromedical Evacuation (MEDEVAC) Feb. 1995 5 p (For primary document see N95-29604 10-66)
Copyright Avail: CASI HC A01/MF A02

N95-29626# Department of the Air Force, Scott AFB, IL.
CARE IN THE AIR: A SYSTEM ANALYSIS OF CLINICAL OUTCOMES IN AEROMEDICAL EVACUATION
Arleen M. Saenger *In* AGARD, Recent Issues and Advances in Aeromedical Evacuation (MEDEVAC) Feb. 1995 7 p (For primary document see N95-29604 10-66)
Copyright Avail: CASI HC A02/MF A02

N95-30267*# United Technologies Corp., Windsor Locks, CT. Hamilton Standard Div.
SPE(R)-OBOGS: ON-BOARD OXYGEN GENERATING SUSTEM Abstract Only
J. McElroy and W. Smith *In* NASA. Lewis Research Center, Space Electrochemical Research and Technology. Abstracts Apr. 1995 p 33 (For primary document see N95-30255 10-44)
Avail: CASI HC A01/MF A01

55 SPACE BIOLOGY

Includes exobiology; planetary biology; and extraterrestrial life.

N95-28722*# National Aeronautics and Space Administration. Ames Research Center, Moffett Field, CA.
EXPERIMENT KITS FOR PROCESSING BIOLOGICAL SAMPLES INFLIGHT ON SLS-2
P. D. Savage, W. E. Hinds, R. Jaquez (Lockheed Engineering and Sciences Co., Moffett Field, CA.), J. Evans (Lockheed Engineering and Sciences Co., Moffett Field, CA.), and L. Dubrovin (Lockheed Engineering and Sciences Co., Moffett Field, CA.) May 1995 9 p
(RTOP 106-30-02)
(NASA-TM-4685; A-950016; NAS 1.15:4685) Avail: CASI HC A02/MF A01

This paper describes development of an innovative, modular approach to packaging the instruments used to obtain and preserve the inflight rodent tissue and blood samples associated with hematology experiments on the Spacelab Life Sciences-2 (SLS-2) mission. The design approach organized the multitude of instruments into twelve 5- x 6- x 1-in. kits which were each used for a particular experiment. Each kit contained the syringes, vials, microscope slides, etc., necessary for processing and storing blood and tissue samples for one rat on a particular day. A total of 1245 components, packaged into 128 kits and stowed in 17 Zero(registered trademark) boxes, were required. Crewmembers found the design easy to use and laid out in a logical, simple configuration which minimized chances for error during the complex procedures in flight. This paper also summarizes inflight performance of the kits on SLS-2. Author

N95-28818*# National Aeronautics and Space Administration. Ames Research Center, Moffett Field, CA.
AN INFLIGHT REFILL UNIT FOR REPLENISHING RESEARCH ANIMAL DRINKING WATER
P. D. Savage, M. L. Hines, and R. Barnes (Lockheed Engineering and Sciences Co., Moffett Field, CA.) May 1995 11 p
(RTOP 106-30-02)
(NASA-TM-4684; A-950015; NAS 1.15:4684) Avail: CASI HC A03/MF A01

This paper presents the design process and development approach for a method of maintaining sufficient quantities of water for research animals during a Shuttle mission of long duration. An inflight refill unit (IRU) consisting of two major subsystems, a fluid pumping unit (FPU) and a collapsible water reservoir (CWR), were developed. The FPU provides the system measurement and controls, pump, water lines, and plumbing necessary to collect water coming into the unit from the potable water system and pump it out into the RAHF drinking water tanks. The CWR is a Kevlar (TM) reinforced storage bladder connected to the FPU, which has a capacity of 6 liters in its expanded volume and functions to store the water collected from the potable water system, allowing for transport of the water back to the Spacelab where it is pumped into each of two research animal holding facilities. Additional components of the IRU system include the inlet and outlet fluid hoses, a power cable for providing 29V direct current spacecraft electrical power to the pump within the FPU, a tether system for the unit when in use in Spacelab, and an adapter for mating the unit to the orbiter waste collection system in order to dump excess water after use in Spacelab. Author

59 MATHEMATICAL AND COMPUTER SCIENCES (GENERAL)

No abstracts in this category.

60 COMPUTER OPERATIONS AND HARDWARE

Includes hardware for computer graphics, firmware, and data processing.

For components see *33 Electronics and Electrical Engineering.*

N95-28974# Nonvolatile Electronics, Inc., Edina, MN.
LOW COST WRITABLE RFID TAG WITH MRAM MEMORY Final Report
Jay L. Brown 1 Mar. 1995 139 p
(Contract DAAH04-94-C-0032)
(AD-A292553; ARO-33571.1-EL-SBI) Avail: CASI HC A07/MF A02

The objective of this work was to show proof of concept for a writable RFID tag that used an integrated antenna and MRAM nonvolatile memory to store data. Circuit designs for the reader/writer unit and the tag IC were completed during the work, and showed that the design concept was feasible. MRAM memory cells specifically designed for this low energy application were constructed and tested, and are clearly suitable for use in this application. These memory cells offer bipolar signals for easier sensing during the read cycle, and are denser than the ROMs normally used in read-only RFID tags, leading to a lower IC cost. Four different integrated antennas, using two IC processes developed specifically for this work, were constructed during the course of the program. The processes were developed to be used on top of existing circuitry, so the antennas would pose no area penalty on the IC. Problems with the new processes prevented successful fabrication of any of the antenna designs; however, extensive failure analysis was performed on the completed parts, and the processing problems have been conclusively identified. Good parts are expected with a mask modification and several minor process modifications. NVE considers the program a major success, and will submit a Phase II proposal. DTIC

N95-28976# Rome Lab., Griffiss AFB, NY.
N4 PROCESSOR Report, for Oct. - Dec. 1991
David R. Christie and Richard J. Michalak Dec. 1994 18 p
(DA Proj. 460-0)
(AD-A292571; RL-TR-94-219) Avail: CASI HC A02/MF A01

The purpose of the effort was to build and demonstrate a highly interconnected optical processing stage using a novel architecture which makes possible high throughput, exceedingly low power operation. Basic interconnect feasibility was shown, but the effort ended without demonstrating a working processing subsystem due to technical problems. DTIC

N95-29146# Carnegie-Mellon Univ., Pittsburgh, PA. School of Computer Science.
AN ARCHITECTURAL DESIGN OF A TOOLKIT FOR SYNCHRONOUS GROUPWARE APPLICATIONS
Nobuhisa Yoda and Brad A. Myers 16 Dec. 1994 39 p
(Contract N66001-94-C-6037)
(AD-A290226; CMU-CS-94-226) Avail: CASI HC A03/MF A01

The central question studied in this thesis is how to design high-level reusable components for developing synchronous groupware applications. A modern user interface requires the separation of applications into two components namely application and graphical user interface. An effective

architecture for synchronous, multiple-user groupware applications requires a separation of one more component from the application: the management of the session and shared data. This component provides a framework that manages the collaborative user session, shared data in an abstraction form, and floor control. This thesis calls this separation 'coordination independence.' This thesis demonstrates the feasibility of the architecture by describing an experimental system, called TALISMAN, using Garnet. TALISMAN is implemented as a single-process, centralized system with multiple remote graphical displays. The system which features this separation relies upon object inheritance and the constraint satisfaction mechanism in the underlying object system. The architecture also makes the conversion of a single-user application into a multiple-user application relatively easy. DTIC

N95-29381 Michigan Univ., Ann Arbor, MI.
RESEARCH AND DEVELOPMENT OF A HIGH PERFORMANCE GaAs MICROCOMPUTER SYSTEM Final Report, 1 Aug. 1990 - 30 Sep. 1994
Richard B. Brown 25 Jan. 1995 31 p Limited Reproducibility: More than 20% of this document may be affected by poor print
(Contract DAAL03-90-C-0028; ARPA Order 7509)
(AD-A292647; ARO-28325.50-EL) Avail: Issuing Activity (Defense Technical Information Center (DTIC))

The object of this research was to achieve an order of magnitude increase in RISC microprocessor computing power over the duration of the project. This was to result in a processor capable of executing MIPS instructions at a sustained rate of 150 million instructions per second, and a peak rate of 250 million instructions per second. We proposed implementing the machine in gallium arsenide direct-coupled FET logic (DCFL) from Vitesse Semiconductor, which showed promise as a high-performance technology. To achieve this goal, the GaAs process would have to be increased substantially over their levels at the beginning of the project. Circuits would have to be designed to take advantage of the inherent speed in GaAs devices while overcoming the limitations of DCFL. Microarchitectures would have to be developed to be appropriate for a processor with this high clock rate. We also proposed developing a comprehensive suite of CAD tools to support the design of such processors.This would include architectural, logic, and circuit simulators; it would build on the technology-independent physical design software of Cascade Design Automation to realize a GaAs circuit compiler. DTIC

N95-29921# Maine Univ., Orono, ME. Dept. of Electrical Engineering.
ADC TEST SUPPORT PROGRAM Technical Report, 1 Nov. 1993 - 31 Oct. 1994
Fred H. Irons and Donald M. Hummels 31 Oct. 1994 31 p
(Contract N00014-93-1-1007)
(AD-A289445) Avail: CASI HC A03/MF A01

This report summarizes accomplishments made under Grant No.: N00014-93-1-1007 for providing ADC Test Support to the ARPA HBT/ADC technology development program during the period of 1 Nov. through 31 Oct. 94. The following were accomplishments for this period: (1) recruited and trained one graduate assistant to study ADC architectures and error modeling procedures; (2) participated in the ARPA HBT/ADC design review on 26 Apr. 94 and presented initial results relating ADC error basis functions to specific error phenomena. These results represent new procedures and ways to characterize ADCs based upon architectural error models; (3) recruited an advanced graduate student in Jun. 94 to begin implementation of orthogonal search procedures to facilitate ADC error modeling with the use of many-element basis sets. This student has recently started to develop simulation procedures for Delta-Sigma ADC architectures and their error effects; (4) visited Lincoln Laboratory on 28 Jul. 94 to review status of probe testing hardware development and prototype testing and evaluation plans; (5) obtained and evaluated raw data samples obtained from Lincoln Laboratory for a 4-bit TRW prototype sampled at 1 GHz; and (6) wrote and submitted two papers for the 1995 IEEE International Symposium on Circuits and Systems dealing with ADC error modeling procedures developed under this program. DTIC

N95-30108# Gesellschaft fuer Mathematik und Datenverarbeitung, Saint Augustin (Germany).
SPEEDLOG: THE KEY ARCHITECTURAL ELEMENT TO PROVIDE EFFICIENT LOG MANAGEMENT
E. Nett and B. Weiler Dec. 1994 41 p
(PB95-198453; GMD-248) Copyright Avail: CASI HC A03/MF A01

Logging is an indispensable mechanism to provide fault tolerance in computer based systems. Our approach on logging focuses on providing a general-purpose logging tool to support various kinds of applications and system level services. Flexible logging mechanisms usually decrease the performance in log management. In contrast, our generic log-service allows us to realize log management very efficiently while satisfying the requirements of different applications. Our approach is based on exploiting application-specific semantics which is interpreted and evaluated within the log-service very efficiently. The main idea behind it is to support fast recovery after a node crash by minimizing the amount of log information to be retrieved during restart. To achieve this, we periodically discard obsolete log information in a very effective manner without consulting the log user. NTIS

N95-30109# Technische Univ., Delft (Netherlands).
TRANSFORMATIONAL DESIGN OF A DIRECTION DETECTOR FOR THE PROGRESSIVE SCAN CONVERSION PROCESSOR
P. F. A. Middelhoek Oct. 1994 32 p
(PB95-198487; Memo-INF-94-64) Copyright Avail: CASI HC A03/MF A01

This document discusses the transformational design of a direction detector used in the progressive scan conversion processor. The purpose is to show the feasibility of transformational design for real life designs and in particular the use of transformational design for the synthesis of processing units for the PHIDEO silicon compilation system. The processor design is used to reduce screen flicker by doubling the screen frequency by means of interpolating intermediate lines of a field of an interlaced frame. The interpolation algorithm takes the presence of edges in a field into account. This report shows in detail the design of the Abs-Diff function which is extensively used in the algorithm. The design of the complete direction detector is shown in less detail. Based on the experience gained, a first attempt towards developing a systematic approach to transformational design is made. NTIS

61 COMPUTER PROGRAMMING AND SOFTWARE

Includes computer programs, routines, alogorithms, and specific applications, e.g., CAD/CAM.

N95-28690 Air Force Inst. of Tech., Wright-Patterson AFB, OH.
AUTOMATED TESTING OF APPLICATION DOMAINS Ph.D. Thesis
Richard T. Mraz Dec. 1994 208 p Limited Reproducibility: More than 20% of this document may be affected by microfiche quality
(AD-A289753; AFIT/CI/CIA-94-042D) Avail: Issuing Activity (Defense Technical Information Center (DTIC))

Test data generation is a difficult, time consuming, costly phase in the software life cycle. Software engineers address this problem by decomposing it into three phases: unit test, integration test, and system test. For each phase, testers use abstract representations of the software product to define test objectives, specify test case design strategies, and generate tests. At the system test level, we find few general purpose test data generation methods, little use of abstract representations of the system under test, and application specific test generation schemes. This research shows one way to generalize system level tests by viewing an application through its user interface. We focus on command-based system or command language user interfaces. A test case for a command-based system is a list of fully parameterized commands. Each command in the test case in issued to the system under test and the system is examined for its response. We capture command language syntax and semantics in a domain model. The result is a test data generation method called Domain Based Testing (DBT). Testers guide test generation by defining test criteria, and map the test criteria to the domain model. The result is a test subdomain from which the test generator creates tests. To evaluate DBT and the quality of its test cases, this research uses a neural network classifier to assess test case effectiveness. DTIC

N95-28694 Naval Postgraduate School, Monterey, CA.
ANALYSIS OF MULTIGRID TECHNIQUES FOR SYSTEM MODELING WITH TOEPLITZ APPROXIMATION M.S. Thesis
John S. Volk, III Sep. 1994 165 p Limited Reproducibility: More than 20% of this document may be affected by microfiche quality
(AD-A289784) Avail: Issuing Activity (Defense Technical Information Center (DTIC))

An empirical analysis on the applicability of multigrid techniques to system modeling using system identification techniques is presented. Multigrid with the Toeplitz approximation algorithm is used to model an infinite impulse response (FIR) system with a finite impulse response (FIR) model. Matrix analysis experiments are conducted on the Toeplitz iteration matrix. A comparison of alternative multigrid operators for solving the system modeling problem is presented. The extension of multigrid techniques to system modeling of odd order filters is explored. Computer simulations are developed for analyzing the effectiveness of multigrid techniques in system modeling. DTIC

N95-28713*# National Aeronautics and Space Administration. Goddard Space Flight Center, Greenbelt, MD.
COLLECTED SOFTWARE ENGINEERING PAPERS, VOLUME 12
Nov. 1994 117 p
(NASA-CR-189409; SEL-94-004; NAS 1.26:189409) Avail: CASI HC A06/MF A02

This document is a collection of selected technical papers produced by participants in the Software Engineering Laboratory (SEL) from November 1993 through October 1994. The purpose of the document is to make available, in one reference, some results of SEL research that originally appeared in a number of different forums. This is the 12th such volume of technical papers produced by the SEL. Although these papers cover several topics related to software engineering, they do not encompass the entire scope of SEL activities and interests. Additional information about the SEL and its research efforts may be obtained from the sources listed in the bibliography at the end of this document. Author

N95-28714*# National Aeronautics and Space Administration. Goddard Space Flight Center, Greenbelt, MD.
AN OVERVIEW OF THE SOFTWARE ENGINEERING LABORATORY
Dec. 1994 64 p
(NASA-CR-189410; SEL-94-005; NAS 1.26:189410) Avail: CASI HC A04/MF A01

This report describes the background and structure of the SEL organization, the SEL process improvement approach, and its experimentation and data collection process. Results of some sample SEL studies are included. It includes a discussion of the overall implication of trends observed over 17 years of process improvement efforts and looks at the return on investment based on a comparison of total investment in process improvement with the measurable improvements seen in the organization's software product. Author

N95-28777# Oak Ridge Inst. for Science and Education, TN.
SUMMARY REPORT FOR COOPERATIVE RESEARCH AND DEVELOPMENT AGREEMENT BETWEEN OAK RIDGE ASSOCIATED UNIVERSITIES AND INTERACTIVE PRESENTATION SYSTEMS
T. McKinley 1994 3 p
(DE95-006874; ORISE-95006874) Avail: CASI HC A01/MF A01

The status of the cooperative research and development agreement between Oak Ridge Associated Universities (ORAU) and Interactive Presentation Systems, Inc. (IPS) is reported. The cooperation involves ORAU's training and course development expertise with IPS's interactive presentation projects. DOE

N95-28782 Oregon Graduate Inst. of Science and Technology, Beaverton, OR.
SOFTWARE DESIGN FOR RELIABILITY AND REUSE PROOF OF CONCEPT PROJECT. PHASE 1 Final Report, Jun. 1993 - Jan. 1995
Richard Kieburtz and James Hook 28 Feb. 1995 233 p Limited Reproducibility: More than 20% of this document may be affected by microfiche quality
(Contract F19628-93-C-0069)
(AD-A291690) Avail: Issuing Activity (Defense Technical Information Center (DTIC))

The Pacific Software Research Center was sponsored by the Air Materiel Command to develop a new method to support reuse and introduce reliability into software. The method is based on design capture in domain-specific design languages and automatic program generation using a reusable suite of program transformation tools. The transformation tools, and a domain-specific component generator incorporating them, were implemented as part of a proof-of-concept project at the Oregon Graduate Institute of Science and Technology. A software engineering experiment was performed on the generator to assess its usability and flexibility. This final report documents the Software Design for Reliability and Reuse (SDRR) Method, the Algebraic Design Language, system design, a survey of tools used and developed, baseline performance measures on instances produced by the generator, analysis of experiment results, final measurement report, and an SDRR implementation plan. DTIC

N95-28805*# National Aeronautics and Space Administration. Goddard Space Flight Center, Greenbelt, MD.
ANNOTATED BIBLIOGRAPHY OF SOFTWARE ENGINEERING LABORATORY LITERATURE
David Kistler (Computer Sciences Corp., Greenbelt, MD.), John Bristow, and Don Smith Jul. 1994 200 p
(NASA-CR-189406; SEL-82-1306; NAS 1.26:189406) Avail: CASI HC A09/MF A03

This document is an annotated bibliography of technical papers, documents, and memorandums produced by or related to the Software Engineering Laboratory. Nearly 200 publications are summarized. These publications cover many areas of software engineering and range from research reports to software documentation. This document has been updated and reorganized substantially since the original version (SEL-82-006, November 1982). All materials have been grouped into eight general subject areas for easy reference: (1) The Software Engineering Laboratory; (2) The Software Engineering Laboratory: Software Development Documents; (3) Software Tools; (4) Software Models; (5) Software Measurement; (6) Technology Evaluations; (7) Ada Technology; and (8) Data Collection. This document contains an index of these publications classified by individual author. Author

N95-28806*# National Aeronautics and Space Administration. Goddard Space Flight Center, Greenbelt, MD.
SOFTWARE MEASUREMENT GUIDEBOOK
Mitchell J. Bassman (Computer Sciences Corp., Greenbelt, MD.), Frank McGarry, and Rose Pajerski Jul. 1994 153 p
(NASA-CR-189407; SEL-94-002; NAS 1.26:189407) Avail: CASI HC A08/MF A02

This software Measurement Guidebook presents information on the purpose and importance of measurement. It discusses the specific procedures and activities of a measurement program and the roles of the people involved. The guidebook also clarifies the roles that measurement can and must play in the goal of continual, sustained improvement for all software production and maintenance efforts. Author

N95-28807*# National Aeronautics and Space Administration. Goddard Space Flight Center, Greenbelt, MD.
IMPACT OF Ada AND OBJECT-ORIENTED DESIGN IN THE FLIGHT DYNAMICS DIVISION AT GODDARD SPACE FLIGHT CENTER
Sharon Waligora (Computer Sciences Corp., Greenbelt, MD.), John Bailey (Software Metrics, Inc., Haymarket, VA.), and Mike Stark Mar. 1995 92 p
(NASA-CR-189412; SEL-95-001; NAS 1.26:189412) Avail: CASI HC A05/MF A01

The Software Engineering Laboratory (SEL) is an organization sponsored by NASA/GSFC and created to investigate the effectiveness of software engineering technologies when applied to the development of applications software. The goals of the SEL are (1) to understand the software development process in the GSFC environment; (2) to measure the effects of various methodologies, tools, and models on this process; and (3) to identify and then to apply successful development practices. The activities, findings, and recommendations of the SEL are recorded in the Software Engineering Laboratory Series, a continuing series of reports that includes this document. Author

N95-28814# Martin Marietta Corp., Moorestown, NJ.
R&M DESIGN EXPERT SYSTEM Final Technical Report, Sep. 1991 - Sep. 1994
Angela M. Kitchen, Jeff Steelhammer, Doug Doskocil, Eric Freeman, and Glenn Elias Dec. 1994 119 p
(Contract F30602-91-C-0159)
(AD-A292525; RL-TR-94-232) Avail: CASI HC A06/MF A01

This effort investigated and developed a proof-of-concept software system that combines reliability, testability, and maintainability analysis capabilities into a single tool. The system recommends tests and testpoints based on potential faults (associated with a component within the design) and a functional-block description of the design. The system directs the user in injecting faults into a simulation model. The tests and testpoints are then used to perform fault isolation using the results of the simulation. Case-based reasoning techniques were used as a basis for the testability and test coverage aspects of the program. The casebase is a repository of 'past knowledge' gained from expert designers and testability experts. The system adds to this repository if an unfamiliar situation occurs, allowing the system to 'learn' over time. The expert knowledge was encoded into a fault mode map that represents how the experts relate faulty behavior of the circuits to actual failures. Rome Laboratory Oracle (a reliability prediction tool), Mentor Graphics Design Architect (a schematic capture tool), and Analogy Saber (a circuit simulation tool) were integrated to allow the user to exercise all system capabilities from a single user perspective. The system was tested against Martin Marietta power supply design. DTIC

N95-28821*# National Aeronautics and Space Administration. Goddard Space Flight Center, Greenbelt, MD.
C STYLE GUIDE
Jerry Doland (Computer Sciences Corp., Greenbelt, MD.) and Jon Valett Aug. 1994 106 p
(NASA-CR-189408; SEL-94-003; NAS 1.26:189408) Avail: CASI HC A06/MF A02

This document discusses recommended practices and style for programmers using the C language in the Flight Dynamics Division environment. Guidelines are based on generally recommended software engineering techniques, industry resources, and local convention. The Guide offers preferred solutions to common C programming issues and illustrates through examples of C Code. Author

N95-28878# Carnegie-Mellon Univ., Pittsburgh, PA. Dept. of Computer Science.
COMPETITIVE ANALYSIS OF CALL ADMISSION ALGORITHMS THAT ALLOW DELAY
Anja Feldmann, Bruce Maggs, Jiri Sgall, Daniel D. Sleator, and Andrew Tomkins 13 Jan. 1995 35 p
(Contract F33615-93-1-1330; NSF CCR-94-57766)
(AD-A292242; CMU-CS-95-102) Avail: CASI HC A03/MF A01

This paper presents an analysis of several simple on-line algorithms for processing requests for connections in distributed networks. These algorithms are called call admission algorithms. Each request comes with a source, a destination, and a bandwidth requirement. The call admission algorithm decides whether to accept a request, and if so, when to schedule it and which path the connection should use through the network. The duration of the request is unknown to the algorithm when the request is made. We analyze the performance of the algorithms on simple networks such as linear arrays, trees, and networks with small separators. We use three measures to quantify their performance: makespan, maximum response time, and data-admission ratio. Our results include a proof that greedy algorithms are Theta(log n)-competitive with respect to makespanon n-node trees for arbitrary durations and bandwidth, a proof that on an n-node tree no algorithm can be better than Omega (log log n/log log log n)- competitive with respect to makespan, and a proof that no algorithm can be better than Omega(log n)-competitive with respect to call-admission and data-admission ratio on a linear array, if each request can be delayed for at most some constant times its (known) duration. DTIC

N95-28881# Carnegie-Mellon Univ., Pittsburgh, PA. Dept. of Computer Science.
PROBLEM DECOMPOSITION FOR REUSE
Daniel Jackson and Michael Jackson Jan. 1995 37 p
(Contracts F33615-93-1-1330; NSF-CCR93-08726)
(AD-A292245; CMU-CS-95-108) Avail: CASI HC A03/MF A01

An approach to software development problems is presented, and illustrated by an example. The approach is based on the ideas of problem frames and structuring specifications by views. It is claimed that decomposition obtained by this approach result in a more effective separation of concerns, and that the resulting components are more likely to be reusable than those obtained by more conventional approaches. The characteristics of desirable integration mechanisms are discussed, together with some other considerations arising out of the approach presented. DTIC

N95-28883# Carnegie-Mellon Univ., Pittsburgh, PA. Dept. of Computer Science.
MODELING FORESHORTENING IN STEREO VISION USING LOCAL SPATIAL FREQUENCY
Mark W. Maimone and Steven A. Shafer Jan. 1995 35 p
(Contract DAAH04-94-G-0008)
(AD-A292246; CMU-CS-95-104) Avail: CASI HC A03/MF A01

Many aspects of the real world continue to plague stereo matching systems. One of these is perspective foreshortening, an effect that occurs when a surface is viewed at a sharp angle. Because each stereo camera has a slightly different view, the image of the surface is more compressed and occupies a smaller area in one view. These effects cause problems because most stereo methods compare similarly-sized regions (using the same-sized windows in both images), tacitly assuming that objects occupy the same extents in both images. Clearly this condition is violated by perspective foreshortening. We show how to overcome this problem using a Local Spatial Frequency representation. A simple geometric analysis leads to an elegant solution in the frequency domain which, when applied to a Gabor filter-based stereo system, increases the system's maximum matchable surface angle from 30 degrees to over 75 degrees. DTIC

N95-28886# Carnegie-Mellon Univ., Pittsburgh, PA. School of Computer Science.
STRUCTURAL CUT ELIMINATION IN LINEAR LOGIC
Frank Pfenning Dec. 1994 64 p
(Grant NSF CCR-93-03383)
(AD-A292248; CMU-CS-94-222) Avail: CASI HC A04/MF A01

We present a new proof of cut elimination for linear logic which proceeds by three nested structural inductions, avoiding the explicit use of multi-sets and termination measures on sequent derivations. The computational content of this proof is a non-deterministic algorithm for cut elimination which is amenable to an elegant implementation in Elf. We show this implementation in detail. DTIC

N95-28894# Carnegie-Mellon Univ., Pittsburgh, PA. Dept. of Computer Science.
FORMALIZING STYLE TO UNDERSTAND DESCRIPTIONS OF SOFTWARE ARCHITECTURE
Gregory Abowd, Robert Allen, and David Garlan Jan. 1995 33 p
(Contracts F33615-93-1-1330; NSF-CCR91-09469)
(AD-A292237; CMU-CS-95-111) Avail: CASI HC A03/MF A01

The software architecture of most systems is usually described informally and diagrammatically by means of boxes and lines. In order for these descriptions to be meaningful, the diagrams are understood by interpreting the boxes and lines in specific, conventionalized ways. The informal, imprecise nature of these interpretations has a number of limitations. In this paper we consider these conventionalized interpretations as architectural styles and provide a formal framework for their uniform definition. In addition to providing a template for precisely defining new architectural styles, this framework allows for analysis within and between different architectural styles. DTIC

N95-28934 Naval Health Research Center, San Diego, CA.
WINCD: COMPLEX DEMODULATION TIME-SERIES ANALYSIS FOR WINDOWS Interim Report, 1 Oct. 1993 - 30 Sep. 1994
Timothy F. Elsmore (Walter Reed Army Inst. of Research, Washington, DC.), P. Naitoh, and F. W. Hegge (Walter Reed Army Inst. of Research, Washington, DC.) 3 Nov. 1994 31 p Sponsored by the Department of the Navy, Navy Medical Research and Development Command, Bethesda, MD; and by the US Army Medical Research and Material Command Limited

Reproducibility: More than 20% of this document may be affected by microfiche quality
(MR04101)
(AD-A291550; NHRC-TD-94-4D) Avail: Issuing Activity (Defense Technical Information Center (DTIC))

This document describes WinCD, a program for extracting quantitative information about periodicity in time-series data using the method of Complex Demodulation (CD). The method is particularly well-suited for the analysis of variables that may produce changes in biological rhythms, such as sleep deprivation, adaptation to changes in work schedules, time-zone displacements, and various sorts of pathology (e.g., sleep disorders). WinCD enables exploratory analysis of time-series data by providing graphical displays of raw and processed time series, as well as numerous options for viewing and saving quantitative data. This document presents detailed descriptions of WinCD operations, examples of the use of the program, a discussion of CD theory and background, and a glossary of CD terms. The program and documentation are available for free distribution to interested parties. DTIC

N95-28964# Adaptive Solutions, Inc., Beaverton, OR.
HIGH PERFORMANCE HARDWARE AND SOFTWARE FOR PATTERN RECOGNITION AND IMAGE PROCESSING Status Report, 1 Dec. 1994 - 28 Feb. 1995
Wendell A. Henry 15 Mar. 1995 5 p
(Contract N00014-93-C-0234)
(AD-A292307) Avail: CASI HC A01/MF A01

The CNAPS Development Environment consists of several software tools required by the software developer. These are: CNAPS application program interface CNAPS-C compiler & assembler CNAPS source-level debugger (command-line interface) & (graphical interface) CNAPS Backpropagation Neural Network function library The CNAPS compiler, assembler, application program interface, and Backpropagation Neural Network function library have been ported to the Windows 3.x environment and CNAPS/PC hardware and integrated with the source-level debugger. These tools are now in Beta test. The port of the graphical interface for the source-level debugger is still in progress. DTIC

N95-28968# University of Southern Mississippi, Bay Saint Louis, MS.
GLENDA SOFTWARE DESIGN Technical Report
Benjamin R. Seyfarth, Jerry L. Bickham, and Germana Peggion Feb. 1995 24 p
(Contract N00014-92-J-4112)
(AD-A292537; TR-3-95) Avail: CASI HC A03/MF A01

Glenda is an environment for parallel processing which is modeled after the Linda language and utilizes the PVM software system to provide underlying communications. The resulting software maintains the friendly parallel programming, typical of Linda, and the PVM efficiency in message-passing operations. This document describes the functions, data structure, and algorithms of the Glenda software architecture. DTIC

N95-28995# Naval Surface Warfare Center, Dahlgren, VA.
PROCEEDINGS OF THE COMPLEX SYSTEMS ENGINEERING SYNTHESIS AND ASSESSMENT TECHNOLOGY WORKSHOP (CSESAW 1994)
Steven Howell 12 Jan. 1995 268 p Workshop held in Beltsville, MD, 19-20 Jul. 1994
(AD-A292433; NSWCDD/MP-94-122) Avail: CASI HC A12/MF A03

CSESAW '94 is exploring system level design synthesis and assessment capabilities for large, complex systems. These capabilities will facilitate the development of such systems from informal system requirements, through the design phase prototyping, and into implementation and post deployment. Component products produced by these capabilities are specifications that subenvironments will receive. The focus of the workshop is the development and integration of these multiple technologies and the exploration of the creation of a system level engineering discipline with support technologies to provide potential high payoff solutions to the difficult problems encountered by designers, developers, and maintainers of real-time systems. Further emphasis is on resolving system level technology issues that cut across component boundaries, such as those associated with system behavior requirements of real-time, fault tolerance, cost, and security. Specifically, the theme of this year's workshop is system engineering synthesis for evolutionary systems. Issues addressed within the workshop include requirements specification, requirements traceability, design capture, design evaluation, design optimization, security engineering, and dependability engineering. Panel discussions will emphasize essential domain models for long-life evolutionary systems, new paradigms in system engineering, and early evaluation metrics of system developments. DTIC

N95-29008# Naval Postgraduate School, Monterey, CA.
NPSNETIV: AN OBJECT-ORIENTED INTERFACE FOR A THREE-DIMENSIONAL VIRTUAL WORLD M.S. Thesis
Christopher B. McMahan Dec. 1994 72 p
(AD-A292467) Avail: CASI HC A04/MF A01

All simulations require some type of user interface to be functional. The problem is that this interface is sometimes written as a tightly coupled part of the simulation itself, buried in the main body of code. This makes the interface very difficult to create, and once created, more difficult to alter. Thus these tightly coupled simulations do not support a simple way to prototype new interface models and incorporate them into the application. The solution is to segregate the interface from the main simulation in a loosely coupled system. Communication with the application is through a well-defined interface. By separating the two, changes can easily be incorporated into either module without significant impact on the other. The approach taken was to create the interface as a separate program. Communication with the main simulation is through data structures passed over a socket communications link. The resulting application displays a control panel on a separate monitor. Using object-oriented techniques, components are defined, incorporated, rearranged, and deleted from the panel as needed. The loose coupling to NPSNET means that changes made to one application have little effect on the other. New interfaces can now be quickly and easily created without effecting the core NPSNET application to any significant degree. DTIC

N95-29056# Naval Postgraduate School, Monterey, CA.
VISUALIZATION OF IMPROVED TARGET ACQUISITION ALGORITHM FOR JANUS (A) M.S. Thesis
Mark R. Whitney Dec. 1994 171 p
(AD-A290191) Avail: CASI HC A08/MF A01

This thesis successfully demonstrates the ability to apply realistic visualization to a training application with a commercially available software program. It is increasingly important with the trend of decreasing military spending to maintain force readiness through quality training. Utilization of realistic visualization in simulations of realtime scenarios is essential to achieving this quality training. This thesis utilizes the Improved Target Acquisition Algorithm for Janus (A) in the visualization of sensor to moving target lines of sight. This visualization takes place in an obstruction constrained terrain using a representation of the higher resolution one meter style Pegasus database numbers. DTIC

N95-29066# David Sarnoff Research Center, Princeton, NJ.
OEIC ULTRA. A NEW APPROACH TO OEIC CAD Final Report, 1 Jun. 1993 - 31 Aug. 1994
R. Amantea Oct. 1994 144 p
(Contract DAAH04-93-C-0019)
(AD-A290349; ARO-31500.2-EL) Avail: CASI HC A07/MF A02

Integrated optoelectronics will lead to advances in ultra-fast computing that go beyond the functionality that conventional electronics can reach through size reduction. Optoelectronic integrated circuit (OEIC) design is currently hampered by the lack of a unified computer-aided design (CAD) tool that aids in managing the complex data implicit in component, subsystem, and system-level modeling. To address the advanced CAD requirements of ULTRA, the David Sarnoff Research Center (Sarnoff) has created a hierarchical OEIC design system built using a platform-independent simulation and visualization environment supported by commercial off-the-shelf software. Sarnoff has demonstrated integration of existing modules by graphically 'wiring' them up on-screen to represent the complete design problem. Sarnoff has demonstrated how integrated visualization tools can support the design process by allowing automatic exploration of the effects of parameters and structural features on lasers and OEIC devices while the system automatically manages data flow among modules. This CAD environment will enable the ARPA ULTRA program to exploit optoelectronics at a faster place than achievable by the stand-alone design approaches in use today. DTIC

N95-29125# Carnegie-Mellon Univ., Pittsburgh, PA. Dept. of Computer Science.

A DIFFERENTIAL APPROACH TO GRAPHICAL INTERACTION Ph.D. Thesis

Michael L. Gleicher 18 Nov. 1994 264 p

(AD-A292165; CMU-CS-94-217) Avail: CASI HC A12/MF A01

Direct manipulation has become the preferred interface for controlling graphical objects. Despite its success, the ad hoc manner with which such interfaces have been designed and implemented restricts the types of interactive controls. This dissertation presents a new approach that provides a systematic method for implementing flexible, combinable interactive controls. This differential approach to graphical interaction uses constrained optimization to couple user controls to graphical objects in a manner that permits a variety of controls to be freely combined. The differential approach provides a new set of abstractions that enable new types of interaction techniques and new ways of modularizing applications. DTIC

N95-29143# Carnegie-Mellon Univ., Pittsburgh, PA. School of Computer Science.

STABLE FUNCTION APPROXIMATION IN DYNAMIC PROGRAMMING

Geoffrey J. Gordon Jan. 1995 24 p

(Grant NSF BES-94-02439)

(AD-A290224; CMU-CS-95-103) Avail: CASI HC A02/MF A01

The success of reinforcement learning in practical problems depends on the ability to combine function approximation with temporal difference methods such as value iteration. Experiments in this area have produced mixed results; there have been both notable successes and notable disappointments. Theory has been scarce, mostly due to the difficulty of reasoning about function approximators that generalize beyond the observed data. We provide a proof of convergence for a wide class of temporal difference methods involving function approximators such as k-nearest-neighbor, and show experimentally that these methods can be useful. The proof is based on a view of function approximators as expansion or contraction mappings. In addition, we present a novel view of approximate value iteration: an approximate algorithm for one environment turns out to be an exact algorithm for a different environment. DTIC

N95-29147# Carnegie-Mellon Univ., Pittsburgh, PA. School of Computer Science.

PORTING A VECTOR LIBRARY: A COMPARISON OF MPI, PARIS, CMMD AND PVM (OR, 'I'LL NEVER HAVE TO PORT CVL AGAIN')

Jonathan C. Hardwick Nov. 1994 18 p

(Contract F33615-93-1-1330)

(AD-A290231; CMU-CS-94-200) Avail: CASI HC A03/MF A01

This paper describes the design and implementation in MPI of the parallel vector library CVL, which is used as the basis for implementing nested data-parallel languages such as NEsL and Proteus. We compare the ease of writing and debugging the portable MPI implementation of CVL with our experiences writing previous versions in CM-2 Paris, CM-5 CMMD, and PVM, and give initial performance results for MPI CVL running on an IBM SP-1, Intel Paragon, and TMC CM-5. DTIC

N95-29179# Massachusetts Inst. of Tech., Cambridge, MA.

COMPUTING 3-D MOTION IN CUSTOM ANALOG AND DIGITAL VLSI Ph.D. Thesis

Lisa Dron 9 Aug. 1994 308 p

(Contract N00014-85-K-0124; NSF MIP-91-17724)

(AD-A290270; AI-TR-1498) Avail: CASI HC A14/MF A03

This thesis examines a complete design framework for a real-time, autonomous system with specialized VLSI hardware for computing 3-D camera motion. In the proposed architecture, the first step is to determine point correspondences between two images. Two processors, a CCD array edge detector and a mixed analog/digital binary block correlator, are proposed for this task. The report is divided into three parts. Part 1 covers the algorithmic analysis; part 2 describes the design and test of a 32 times 32 CCD edge detector fabricated through MOSIS; and part 3 compares the design of the mixed analog/digital correlator to a fully digital implementation. DTIC

N95-29223# Carnegie-Mellon Univ., Pittsburgh, PA. School of Computer Science.

EXPLOITING SYMMETRY IN THE MODEL CHECKING OF RELATIONAL SPECIFICATIONS

Daniel Jackson Dec. 1994 23 p

(Contract F33615-93-1-1330)

(AD-A290230; CMU-CS-94-219) Avail: CASI HC A03/MF A01

Errors in a software design can be detected early on by analyzing a formal model expressed in a specification language such as Z. Since software designs tend to involve infinite (or at least very big) state spaces, it has been assumed that this analysis cannot be automated. Consequently, few formal specifications have been extensively analyzed, and the potential for early detection of errors has not been realized. This paper argues that, while proving properties of designs may be intractable, detecting errors may not be. State transitions of an operation can be enumerated exhaustively, within a 'scope' defined by the user that places a bound on the size of the state components. Symmetry can then be exploited to reduce this finite state space. A state can be shown to be symmetrical, in the context of this analysis, to a state already examined, and thus guaranteed not to reveal an error. Preliminary experiments with a prototype are promising. A small scope often seems sufficient to catch errors, and exhibits enough symmetry to reduce search by a factor of 10 or more. DTIC

N95-29226# West Virginia Univ., Morgantown, VA.

AN INTRODUCTION TO THE PRINCIPLES OF COMPUTER SCIENCE: A REUSE-ORIENTED PHILOSOPHY Final Report, 28 Sep. 1992 - 31 May 1994

Murali Sitaraman and Douglas E. Harms 27 Oct. 1994 10 p

(Contract DAAL03-92-G-0412)

(AD-A290364; ARO-30998.4-MA) Avail: CASI HC A02/MF A01

The long-term goal of our project is to redesign the software development courses in computer science around a philosophy of software reuse, where new components are constructed largely from assembling existing ones. The emphasis is on formal specification, design, and development of 'high quality' reusable components. Ada, when augmented with the RESOLVE technology for component-based software development, facilities introduction this approach. This result has been successfully demonstrated in principle and in practice for the second course in computer science under this project. DTIC

N95-29276# Army Research Lab., Aberdeen Proving Ground, MD.

XMAP: A GENERAL PURPOSE MAPPING PROGRAM Final Report, Jan. - Jun. 1993

Holly A. Ingham Jan. 1995 26 p

(AD-A289958; ARL-TR-671) Avail: CASI HC A03/MF A01

The Military Computer Science Branch (MCSB) of the Advanced Computational and Information Sciences Directorate, Army Research Laboratory, has been developing concepts to provide enhanced information exchange on the battlefield as part of an on-going, long-term research effort known as the Information Distribution Technology (IDT). Application programs were developed to test, evaluate, and demonstrate information distribution research concepts. As the IDT matured, new application programs were needed that could more readily address the information distribution concepts. Hence, a new suite of demonstration application programs was developed. Among these applications is the program XMap, a general purpose program for displaying topographical map information and other military symbols used in planning. This report focuses on the development and execution of XMap. DTIC

N95-29278# Defense Information Systems Agency, Arlington, VA.

SOFTWARE SYSTEMS REENGINEERING PROCESS MODEL, VERSION 2.0

Tamra Moore Sep. 1994 87 p

(AD-A289968) Avail: CASI HC A05/MF A01

This document describes the Software Systems Reengineering Process Model, Version 2.0. The activities described in the Model compose the software reengineering process, including Define Project, Reverse Engineer, and Forward Engineer The Model is represented using the IDEFO Activity Modeling technique. The intended audience for the Model is any organization within DoD tasked to reengineer an automated information system (AIS). The Model can be obtained from the Defense Technical Information Center, (703) 274-7633. DTIC

N95-29285# Florida Agricultural and Mechanical Univ., Tallahassee, FL.
ADA IN INTRODUCTORY COURSES Final Report, 1 Jan. 1993 - 24 Nov. 1994
Sara Stoecklin and Marion Harmon 1 Dec. 1994 26 p
(Contract DAAL03-92-G-0415)
(AD-A292219; ARO-30999.1-MA) Avail: CASI HC A03/MF A01

This project at Florida A & M University sponsored development of a new sequence of two lecture courses entitled (1) Fundamentals of Programming with Ada and (2) Program, File and Data Structures with Ada with two innovative supporting laboratory courses.These four courses replaced a sequence of courses previously taught with Pascal. The laboratory courses were developed to support the theory that reading programs and experimenting with those programs prior to writing original programs would be helpful iii teaching complex programming languages such as Ada. The intent of this project was to allow students to learn a usable language during their first courses in programming and for these same students to develop projects using the ADA language during project courses. Additionally, there are several industries who needed programmers in ADA and these students were targeted for those types of industries. DTIC

N95-29297# Stanford Univ., CA. Dept. of Computer Science.
RESEARCH IN GRAPH ALGORITHMS AND COMBINATORIAL OPTIMIZATION Final Report, 15 Apr. 1991 - 15 Apr. 1994
Serge Plotkin 6 Mar. 1995 9 p
(Contract DAAL03-91-G-0102)
(AD-A292630; ARO-28143.6-MA) Avail: CASI HC A02/MF A01

This project focused on designing fast algorithms for basic combinational optimization problems, including maximum flow, matching, multicommodity flow, and generalized flow. Many important applications are naturally stated as variants of these problems, and hence improved algorithms for these problems immediately lead to improved algorithms for a wide variety of applications. Our goal was to improve both sequential and parallel complexity. In many applications, solving a multicommodity or a generalized flow problem is only a first step in approximately solving an NP-complete problem; in the majority of such cases there is no need to have an exact solution of the problem. One of the focuses of the project was design of efficient approximation algorithms. DTIC

N95-29304# Naval Postgraduate School, Monterey, CA. Dept. of Mathematics.
THE (IN)COMPLETE COMPENDIUM OF COMPUTATIONAL CURIOSITIES: GIVENS' ROTATIONS Technical Report, Jan. - Feb. 1995
Carlos F. Borges 15 Feb. 1995 11 p
(AD-A292050; NPS-MA-95-001) Avail: CASI HC A03/MF A01

We look at the properties of Givens' rotations computed and performed in floating point arithmetic that conforms to the IEEE 754 standard. We describe an algorithm for constructing computationally orthogonal Givens' rotations. DTIC

N95-29310# Illinois Univ., Urbana, IL. Coordinated Science Lab.
PERFORMANCE AND ROBUSTNESS OF SELF-TUNING AND ADAPTATION ALGORITHMS FOR IDENTIFICATION, FILTERING AND CONTROL Final Report, 1 Jan. 1991 - 20 Nov. 1994
P. R. Kumar 18 Jan. 1995 6 p
(Contract DAAL03-91-G-0182)
(AD-A292070; ARO-28718.25-MA) Avail: CASI HC A02/MF A01

We present the main results obtained by us on the topics of: (1) design of adaptive systems; (2) analysis of identification, adaptive filtering and adaptive control algorithms; (3) design and analysis of robustness modifications for adaptive algorithms; (4) development of simulation software; (5) analysis of simulated annealing; (6) design and analysis of learning algorithms; and (7) design and analysis of queueing networks and scheduling policies. DTIC

N95-29319# Naval Research Lab., Washington, DC.
THE GENERALIZED RAILROAD CROSSING: A CASE STUDY IN FORMAL VERIFICATION OF REAL-TIME SYSTEMS Memorandum Report, Oct. 1992 - Sep. 1994
Constance Heitmeyer and Nancy Lynch 31 Dec. 1994 47 p
(AD-A290152; NRL/MR/5540-94-7619) Avail: CASI HC A03/MF A01

A new solution to the Generalized Railroad Crossing problem, based on timed automata, invariants, and simulation mappings, is presented and evaluated. The solution shows formally the correspondence between four system descriptions: an axiomatic specification, an operational specification, a discrete system implementation, and a system implementation that works with a continuous gate model. DTIC

N95-29321# Naval Postgraduate School, Monterey, CA.
A FRIENDLY EDITING ENVIRONMENT FOR COMPUTER-AIDED RAPID PROTOTYPING OF HARD REAL-TIME SYSTEMS M.S. Thesis
Mehdi E. Rowshanaee Dec. 1994 341 p
(AD-A290154) Avail: CASI HC A15/MF A03

The Computer Aided Prototyping System (CAPS) was created to make the software development cycle more efficient. CAPS provides a graphics editor and a syntax-directed editor (SDE) for users to enter prototypes' specifications. The major problem: the user must have a good knowledge of the Prototyping Systems Description Language (PSDL) program syntax in order to use the SDE. Such a requirement imposes a very steep learning curve on a new CAPS user. The challenge was to minimize the time a user needs to spend in order to complete a development without extensive knowledge of other tools like PSDL and SDE. The solution is to redesign and implement a new graphics editor to allow the user to enter all PSDL specifications via the graphics editor with hierarchical pulldown menus. The approach taken was to first determine where to start and what type of language and graphic tools should be used in combination to give the ultimate results. The choices were TAEplus, Motif, and the Idraw from Stanford University. Idraw was chosen because of its design, capabilities, and user friendliness. The major contribution of this thesis is a powerful and user friendly graphics editor to rapidly construct a prototype of a large real-time system. The new CAPS graphic editor has been evaluated by members of the CAPS user group and early feedback shows that the new editor is a truly usable tool. SDE can now take advantage of this graphics editor to enhance the protyping capabilities of CAPS. DTIC

N95-29325# City Coll. of the City Univ. of New York, NY.
MACROPROCESSES AND ADAPTIVE INSTRUCTION Final Report, Sep. 1982 - Sep. 1986
Sigmund Tobias Nov. 1994 206 p
(Contract MDA903-82-C-0353)
(AD-A290483; ARI-RN-95-08) Avail: CASI HC A10/MF A03

A paradigm for the unobtrusive monitoring of students' cognitive processing of instruction (macroprocessing) by microcomputer was developed for this project. The paradigni was used in four experiments that examined the types of processing students use during their reading of expository texts. The results indicated that students' voluntary use of macroprocesses and review was highly variable and ineffective. However, when the instructional system prescribed or prompted use of review if there was evidence of poor comprehension, or when an explanation of the value of review was provided, learning generally improved, especially for students with limited prior knowledge of the content. The implications of these results for further research are discussed. The findings also suggest that the paradigm can be used to deliver cost-effective instruction to improve students' cognitive processing of reading and ultimately their comprehension. This project solved some of the programming, procedural, and technical problems encountered in developing a computer-based delivery system for such instruction. DTIC

N95-29356# Army Missile Command, Redstone Arsenal, AL. Systems Simulation and Development Directorate.
COMPUTATIONAL COMPLEXITY AND ENCRYPTION Final Report
John R. Coward Feb. 1995 15 p
(AD-A291910; AMSMI/RD-SE-95-2) Avail: CASI HC A02/MF A01

Complexity theory has had a major impact on the design of encryption algorithms. Number theory has also made important contributions and is now the focus of much research in the cryptographic community. Work in theoretical computer science has lead to the development of a polynomial hierarchy used to classify the computational complexity of problems which are difficult to solve. NP-Complete problems have proven to be an excellent vehicle for the development of encryption algorithms. Asymmetrical (Public Key) encryption uses complexity theory for the design of algorithms that provide information security and integrity. Encryption algorithms based on complexity theory are relatively new, and questions remain about the security and integrity of these algorithms. Complexity theory has proven to this

point to be a powerful ally in the design of encryption algorithms, but only time will tell if the polynomial hierarchy is real, or if advances in mathematics and computer science will render these algorithms insecure. DTIC

N95-29376# Carnegie-Mellon Univ., Pittsburgh, PA. Dept. of Computer Science.

CHARACTERISTICS OF HIGHER-LEVEL LANGUAGES FOR SOFTWARE ARCHITECTURE Research Report

Mary Shaw and David Garlan Dec. 1994 19 p Sponsored in part by Siemens Corp.

(Contracts F33615-93-1-1330; NSF CCR-91-09469; NSF CCR-91-12880; F19628-90-C-0003)

(AD-A292215; CMU-CS-94-210) Avail: CASI HC A02/MF A01

As the size and complexity of software systems increases, the design and specification of overall system structure-or software architecture-emerges as a central concern. Architectural issues include the gross organization of the system, protocols for communication and data access, assignment of functionality to design elements, and selection among design alternatives. Currently system designers have at their disposal two primary ways of defining software architecture: they can use the modularization facilities of existing programming languages and module interconnection languages; or they can describe their designs using informal diagrams and idiomatic phrases (such as 'client-server organization'). In this paper we explain why neither alternative is adequate. We consider the nature of architectural description as it is performed informally by systems designers. Then we show that regularities in these descriptions can form the basis for architectural description languages. Next we identify specific properties that such languages should have. Finally, we illustrate how current notations fail to satisfy those properties. DTIC

N95-29404*# Institute for Computer Applications in Science and Engineering, Hampton, VA.

ROPES: SUPPORT FOR COLLECTIVE OPERTIONS AMONG DISTRIBUTED THREADS Final Report

Matthew Haines, Piyush Mehrotra, and David Cronk May 1995 20 p Submitted for publication

(Contract NAS1-19480; RTOP 505-90-52-01)

(NASA-CR-198157; NAS 1.26:198157; ICASE-95-36) Avail: CASI HC A03/MF A01

Lightweight threads are becoming increasingly useful in supporting parallelism and asynchronous control structures in applications and language implementations. Recently, systems have been designed and implemented to support interprocessor communication between lightweight threads so that threads can be exploited in a distributed memory system. Their use, in this setting, has been largely restricted to supporting latency hiding techniques and functional parallelism within a single application. However, to execute data parallel codes independent of other threads in the system, collective operations and relative indexing among threads are required. This paper describes the design of ropes: a scoping mechanism for collective operations and relative indexing among threads. We present the design of ropes in the context of the Chant system, and provide performance results evaluating our initial design decisions. Author

N95-29429# State Univ. of New York, Buffalo, NY.

PROGRAMMABLE MATERIALS AND STRUCTURES Final Report

Daniel J. Inman 16 Jan. 1995 11 p

(Contract DAAL03-91-G-0063)

(AD-A291807; ARO-28755.3-EG-SM) Avail: CASI HC A03/MF A01

This summarizes the findings of our effort to exploit the concept of programmable structures and related topics. Results indicate that modeling and control methods are extremely significant in the performance of such integrated structures. In addition results on model updating, eigenstructure assignment, smart rotor shaft control of critical speeds and a new nonlinear model control algorithm have been developed. DTIC

N95-29435# Naval Postgraduate School, Monterey, CA.

SOFTWARE TESTING TOOLKIT FOR DISTRIBUTED SIMULATIONS M.S. Thesis

Mitchell K. Turner Sep. 1994 81 p

(AD-A291867) Avail: CASI HC A05/MF A01

This thesis discusses the need for and design of a software toolkit to monitor Distributed Interactive Simulation (DIS) network performance. Plans to merge virtual environment and wargaming simulations into combined exercises will have significant performance effects on existing networks, but the tools to quantify the impact are lacking. Given the need for performance measurement tools, the network environment is described and two software development methods, Motif and Tc1/Tk, are considered. The merits of Tc1/Tk, including extensibility to access DIS networks and ease of application development, resulted in a programming environment well-suited for this requirement. The network toolkit design is presented, including the required modifications to Tc1/Tk. Areas for future research include using the PDU Monitor and the Tc1/Tk application, and expanding their capabilities. DTIC

N95-29442# Naval Postgraduate School, Monterey, CA.

THE DESIGN OF PROGRAMMABLE CONVOLUTIONAL ENCODER USING VHDL AND AN FPGA M.S. Thesis

Andrew H. Snelgrove Dec. 1994 121 p

(AD-A290048) Avail: CASI HC A06/MF A02

Convolutional encoding is a Forward Error Correction (FEC) technique used in continuous one-way and real time communication links. It can provide substantial improvement in bit error rates so that small, low power, inexpensive transmitters can be used in such applications as satellites and hand-held communication devices. This thesis documents the development of a programmable convolutional encoder implemented in a Field Programmable Gate Array (FPGA) from Xilinx, Inc., called the XC3064 Logic Cell Array (LCA). The encoder is capable of coding a digital data stream with any one of 39 convolutional codes. Because the LCA is used for the hardware implementation, the design can be changed or expanded conveniently in the lab. In particularly flexible systems, several encoder designs can be stored in the system RAM, each one being downloaded into the LCA under different circumstances. The encoder has a simple microprocessor interface, a register file for storage of code parameters, a test circuit, and a maximum bit rate of about 15 Mbits/s. Special design techniques like one-hot state assignment, pipelining, and the use of redundant states are employed to tailor the hardware to the LCA architecture Other ways to improve the output bit rate are suggested. The VHSIC Hardware Description Language (VFIDL) is used to model abstract behavior and to define relationships between building blocks before the hardware implementation phase. DTIC

N95-29455*# Institute for Computer Applications in Science and Engineering, Hampton, VA.

ON THE UTILITY OF THREADS FOR DATA PARALLEL PROGRAMMING Final Report

Thomas Fahringer (Wien Univ., Austria.), Matthew Haines (Wien Univ., Austria.), and Piyush Mehrotra (Wien Univ., Austria.) May 1995 15 p

(Contract NAS1-19480; RTOP 505-90-52-01)

(NASA-CR-198155; ICASE-95-35; NAS 1.26:198155) Avail: CASI HC A03/MF A01

Threads provide a useful programming model for asynchronous behavior because of their ability to encapsulate units of work that can then be scheduled for execution at runtime, based on the dynamic state of a system. Recently, the threaded model has been applied to the domain of data parallel scientific codes, and initial reports indicate that the threaded model can produce performance gains over non-threaded approaches, primarily through the use of overlapping useful computation with communication latency. However, overlapping computation with communication is possible without the benefit of threads if the communication system supports asynchronous primitives, and this comparison has not been made in previous papers. This paper provides a critical look at the utility of lightweight threads as applied to data parallel scientific programming. Author

N95-29456 Institute for the Study of Learning and Expertise, Palo Alto, CA.

WORKSHOP ON FIELDED APPLICATIONS OF MACHINE LEARNING Final Report, 1 Apr. - 30 Sep. 1993

Pat Langley 11 May 1994 6 p Workshop held in CA

(Contract N00014-93-I-0209)

(AD-A280168) Avail: Issuing Activity (Defense Technical Information Center (DTIC))

This report summaries the talks presented at the Workshop on Fielded

Applications of Machine Learning, and draws some initial conclusions about the state of machine learning and its potential for solving real-world problems. DTIC

N95-29480# Rensselaer Polytechnic Inst., Troy, NY.
SCALABLE SOFTWARE TOOLS FOR ADAPTIVE SCIENTIFIC COMPUTATION
Boleslaw K. Szymanski, Can Oztura, and Joseph E. Flaherty 1994 15 p
(Contract DAAL03-91-G-0215; NSF CCR-89-20694)
(AD-A290446; ARO-29167.10-MA) Avail: CASI HC A03/MF A01

With a constant need to solve scientific and engineering problems of ever growing complexity, there is a corresponding need for software tools that assist in generating solutions with minimal user involvement. Parallel computation is becoming indispensable in solving the large-scale problems that arise in science and engineering applications. Adaptivity is at the center of efficient methods for solving partial differential equations often used in such applications. Yet the use of parallel computation and adaptive techniques is limited by the high cost of developing the needed software. To overcome this difficulty, we advocate a comprehensive approach to the development of scalable architecture-independent software for adaptive solutions of partial differential equations. DTIC

N95-29509# Stanford Univ., CA. Dept. of Computer Science.
DESIGN AND IMPLEMENTATION OF LOGICAL DATABASE LANGUAGES Final Report, 1 Jul. 1991 - 30 Jun. 1994
Jeffrey D. Ullman 15 Aug. 1994 6 p
(Contract DAAL03-91-G-0177)
(AD-A290474; ARO-28354.5-MA) Avail: CASI HC A02/MF A01

Studies were made of the prototype GLUE/NAIL system which is a deductive database system, techniques for optimizing constraint maintenance in a distributed environment, approaches to nonmonotonic reasoning in databases, efficient main-memory algorithms for essential database operations, especially join, multiway join and transitive closure, the problem of maintaining an instantiated view of data, magic-sets implementation techniques, theory of logic programs, and object-oriented versus deductive database approaches. DTIC

N95-29515# Naval Postgraduate School, Monterey, CA. Dept. of Computer Science.
AUTOMATICALLY COMBINING CHANGES TO SOFTWARE SYSTEMS Final Report
Valdis Berzins Jan. 1995 8 p
(AD-A290628; ARO-117-93) Avail: CASI HC A02/MF A01

This project has been working to establish a theoretically sound approach to managing changes to software systems via automated methods for combining changes with provable guarantees of correctness. Given a base version of a software system and two different enhanced versions we are seeking to automatically construct a combined version that incorporates both of the enhancements to the base version. Combining changes to a system is a central problem in many software development and maintenance activities, particularly in contexts where several enhancements are developed concurrently. DTIC

N95-29517# Missouri Univ., Rolla, MO.
ROBUST ALGORITHMS FOR PENETRATION MECHANICS PROBLEMS Final Report
Romesh C. Batra Oct. 1994 28 p
(Contract DAAL03-92-G-0315)
(AD-A290650; ARO-30284.7-EG) Avail: CASI HC A03/MF A01

We have studied the punching of a circular cylindrical hole in a steel plate impacted by a long rigid cylindrical rod. The material of the plate has been modeled by the Litonski-Batra constitutive relation, the effect of heat conduction is considered, the contacting surfaces are taken to be smooth, and the mesh is refined adaptively. Subsequent to the initial shock phase of impact during which the deformed plate material protrudes backwards, a plug ahead of the punch extrudes through the plate and a thin shear layer, characterized by the sharp transition of the axial velocity of plate particles, develops. In an attempt to delineate the susceptibility of tungsten and depleted uranium penetrators to adiabatic shear banding, we have investigated the development of shear bands in a rectangular block of these materials deformed in plane strain compression at a nominal strain-rate of 5000/s. Deformations of a quarter of the domain are analyzed. The undeformed region is divided into 10(exp 4) uniform rectangular elements and the yield strength of 300 randomly located elements is lowered by 5%. The numbers and orientations of shear bands are different in these two materials. The shear bands are found to initiate in tungsten at a lower value of the average strain than that in depleted uranium. DTIC

N95-29534# Asian Office of Aerospace Research and Development, APO San Francisco, CA. Air Force Office of Scientific Research.
THE INSTITUTE FOR MATERIAL SCIENCE AND DEPARTMENT OF MATERIAL SCIENCE, TOHOKU UNIVERSITY, SENDAI JAPAN, 2-3 JUNE 1994
P. McQuay 3 Jun. 1994 10 p
(AD-A292348; AOARD-TR-94-13) Avail: CASI HC A02/MF A01

Two labs were visited at the University of Tohoku: the Materials Design by Computer Simulation Laboratory of Professor Yoshiyuki Kawazoe, in the Institute of Materials Research; and the Structural Materials Laboratory of Professor Hiroshi Oikawa, of the Department of Material Science. The Computer Simulation Lab, recently armed with arguably the most powerful supercomputer CPU in the world, and specifically configured to work material science and design problems, is attempting to position itself for a future leadership role in the field of computational material science. Professor Oikawa's Structural Materials Group continues to explore the high temperature deformation behavior of titanium alloys, with most of his current work aimed at understanding the high temperature deformation of the intermetallic compound, gamma TiAl. His results on the constitutive effect of microstructural features offer insight into improving the high temperature performance of this emerging class of structural materials. DTIC

N95-29536# Carnegie-Mellon Univ., Pittsburgh, PA. School of Computer Science.
CLIENT-SERVER INTERACTIONS IN MULTI-SERVER OPERATING SYSTEMS: THE MACH-US APPROACH
J. Mark Stevenson and Daniel P. Julin Sep. 1994 18 p
(Contract DABT63-93-C-0054)
(AD-A290431; CMU-CS-94-191) Avail: CASI HC A03/MF A01

This paper describes requirements placed upon client-server interaction in a multi-server operating system and how to answer those requirements. Addressed are the problems of binding maintenance in the face of: remote method invocation, forking, binding transfer, authentication, asynchronous interruption, and client crashes. Design and implementation choices are analyzed. The solutions, used by the CMU Mach-US multi-server UNIX 4.313 SD emulation on the Mach3.O kernel, are described. The lessons learned are applicable to multi-server Os design and should be applicable to object based systems that must resolve these binding problems in a 'micro' kernel environment. DTIC

N95-29576# Institute for the Study of Learning and Expertise, Palo Alto, CA.
LEARNING OBJECT MODELS FROM VISUAL OBSERVATION AND BACKGROUND KNOWLEDGE Interim Report, 1 Aug. - 1 Nov. 1994
Pat Langley, Thomas O. Binford (Stanford Univ., CA.), and Tod S. Levitt (Stanford Univ., CA.) 15 Nov. 1994 11 p Submitted for publication in Proceedings of the ARPA Image Understanding Workshop
(Contract N00014-94-1-0746)
(AD-A292606; ISLE-TR-94-4) Avail: CASI HC A03/MF A01

This research project aims to use machine learning techniques to improve the performance of three dimensional vision systems. Building on our earlier work, our approach represents and organizes models of object classes in a hierarchy of probabilistic concepts, and it uses Bayesian inference methods to focus attention, recognize objects in images, and make predictions about occluded parts. The learning process involves not only updating of the probabilistic descriptions in the concept hierarchy but also involves changes in the structure of memory, including the creation of novel categories, the merging of similar classes, and the elimination of unnecessary ones. An evaluation metric based on probability theory guides decisions about such structural changes, and background knowledge about function and generic object classes further constrains the learning process. We plan to carry out systematic experiments to determine the ability of this approach to improve both classification accuracy and predictive ability on novel images. DTIC

N95-29639# Sterling Software, Inc., Bellevue, NE. Information Technology Div.

AFGWC DIAL-IN SUBSYSTEM (AFDIS) SOFTWARE USERS MANUAL, VERSION 3.1 Technical Note

Jan. 1995 197 p

(Contract F11623-92-D-0003)

(AD-A291103; AFGWC/TN-95-001) Avail: CASI HC A09/MF A03

This technical note describes the Air Force Global Weather Central's (AFGWC's) Dial-In Subsystem (AFDIS) Remote User Software (AFRUS) that allows remote access (by small computer and modem) to certain applications of AFGWC's Satellite Data Handling System (SDHS). It provides step-by-step instructions for installing and using the software required for access to SDHS. DTIC

N95-29644# Norfolk State Univ., VA.

PROCEEDINGS OF THE 12TH ANNUAL NATIONAL CONFERENCE ON Ada TECHNOLOGY

24 Mar. 1994 349 p Conference held in Williamsburg, VA, 21-24 Mar. 1994; sponsored by ANCOST, Inc.

(Contract F33615-91-C-1758)

(AD-A290693) Avail: CASI HC A15/MF A03

Partial contents include the following: OOP/Groupware; Software Engineering; Comparison of Design Diversity Techniques for Fault Tolerant Ada Software Development; An Overview of the Ada Semantic Interface Specification; Ada's Role in Preventing Data Corruption; Theory Vs. Reality in a large Avionics Software Project; Metrics; Ada Language Issues; Education - The Undergraduate Student and Ada; Object Oriented Development; and Integrating Ada into Reuseable Software. DTIC

N95-29735# RAND Corp., Santa Monica, CA.

DEFENSE MODELING AND SIMULATION OFFICE INFORMATION/DATA BASE TECHNOLOGY WORKING GROUP (I/DBTWG) MEETINGS

Iris M. Kameny 15 Jul. 1994 860 p Meeting held in Santa Monica, CA, 11-15 Jul. 1994 Limited Reproducibility: Document partially illegible

(Contract MDA903-90-C-0004)

(AD-A290953) Avail: CASI HC A99/MF A10

Because data is critical to modeling and simulation (M&S), the main and continuing objective of the I/DBTWG is to provide the M&S community, at low cost and with efficiency, timely, verified, and valid data to promote reuse and sharing of data, interoperability of models and simulations, and improved credibility of modeling and simulation results. To accomplish this goal requires data administration policies, procedures, standards, and supporting tools compatible with those of DOD Corporate Information Management (CIM) and the Services. It also requires access to information throughout the M&S community about what is happening as well as information about the existence and availability of models and simulations and the data they need. Of critical concern to the community is the quality of the models and simulations as well as the data they use and generate. DTIC

N95-29736# RAND Corp., Santa Monica, CA.

SEMINT: SEAMLESS MODEL INTEGRATION Research Report

Jed Marti, Phyllis Kantar, William Sollfrey, and Keith Brendley 1994 30 p

(Contracts MDA903-91-C-0006; MDA903-90-C-0004)

(AD-A290956; RAND/MR-403-OSD/A) Avail: CASI HC A03/MF A01

This report details the design of the Seamless Model Integration program (SEMINT), a software connection system that connects engineering and simulation models without significant reprogramming. We used SEMINT to augment the JANUS combat simulation with improved target acquisition models, surface-to-air combat models, and flight planners. The approach is less expensive than combining these models into a single, monolithic entity. Since recoding is not particularly intrusive, the models can still run in their original stand-alone form. The advantage of our approach is the reuse of existing models, simultaneous use of multiple processors, use of otherwise incompatible programming languages and systems, and ease of implementation and maintenance. Its drawbacks are limited scale-up potential and a central failure point. We used SEMINT to complete a number of analyses that require special intervisibility computations of low-observable vehicles and high-resolution, ground-air combat involving helicopters. This report discusses the approach, the models integrated to date, and the lessons learned during implementation. DTIC

N95-29762# Carnegie-Mellon Univ., Pittsburgh, PA. Software Engineering Inst.

A COMPARISON OF ISO 9001 AND THE CAPABILITY MATURITY MODEL FOR SOFTWARE

Mark C. Paulk Aug. 1994 78 p

(AD-A290697; CMU/SEI-94-TR-12; ESC-TR-94-12) Avail: CASI HC A05/MF A01

The Capability Maturity Model for Software (CMM), developed by the Software Engineering Institute, and the ISO 9000 series of standards, developed by the International Standards Organization, share a common concern with quality and process management. The two are driven by similar concerns and intuitively correlated. The purpose of this report is to contrast the CMM and ISO 9001, showing both their differences and their similarities. The results of the analysis indicate that, although an ISO 9001-compliant organization would not necessarily satisfy all of the level 2 key process areas, it would satisfy most of the level 2 goals and many level 3 goals. Because there are practices in the CMM that are not addressed in ISO 9000, it is possible for a level 1 organization to receive 9001 station; similarly, there are areas addressed by ISO 9001 that are not addressed in the CMM. A level 3 organization would have little difficulty in obtaining ISO 9001 certification, and a level 2 organization would have significant advantages in obtaining certification. DTIC

N95-29861# Commissariat a l'Energie Atomique, Villeneuve-Saint-Georges (France). Centre d'Etudes de Limeil.

THE 2D EUROGRAPHICS WORKSHOP ON VIRTUAL ENVIRONMENTS

Martin Goebel, ed. 1 Feb. 1995 161 p Workshop was held in Monte Carlo, Monaco, 1 Jan. - 1 Feb. 1995

(AD-A292015) Avail: CASI HC A08/MF A02

Papers are presented in the following sessions: experiments and experience; systems and platforms; interaction; metaphors and legibility; algorithms; facial expression; application; and scientific visualization application. Topics include: Is VR better than a workstation? A report on human performance experiments in progress; the influence of dynamic shadows on presence in immersive environments; an object oriented graphics system on the way to VR; dynamic rendering system - a fuzzy logic controlled system using LoD technology optimized with genetic algorithms; VIPER (virtuality programming environment); fine object manipulation in virtual environments; virtual and real multisensor grasping; interaction models for speech interfaces to VEs; modern holy grail - the metaphor towards a methodology of choice; and improving the legibility of virtual environments. CASI

N95-29871# Sandia National Labs., Albuquerque, NM.

ENCRYPTION AND NETWORKING APPLICATIONS

John P. Long 1995 4 p Presented at the 17th Department of Energy Computer Security Group Training Conference, Milwaukee, WI, 1-4 May 1995

(Contract DE-AC04-94AL-85000)

(DE95-009587; SAND-95-0590C; CONF-9505191-2) Avail: CASI HC A01/MF A01

The DOE requires that sensitive unclassified data be protected while being transmitted electronically. On most large networks it is difficult and expensive to provide the required level of physical protection. At Sandia National Laboratories, we are assembling the structure necessary to protect sensitive unclassified data using software-based encryption. This approach has the advantage that the data can be protected after arrival at its destination without additional investment. While Sandia has expertise in cryptography, we had not used cryptography in this field. This discussion deals with the client-server model of file-based data exchange and interactive access to on-line data bases using Unix workstations, Macs, and PC's. DOE

N95-29932# RDP, Inc., Waltham, MA.

SETA/ADS SOFTWARE DEVELOPMENT Scientific Report No. 6

Andrew J. Mazzella, Jr. and Kevin P. Larson 3 Nov. 1994 160 p

(Contract F19628-89-C-0079)

(AD-A291181; RDP-TR-9404; PL-TR-94-2279) Avail: CASI HC A08/MF A02

Requirements for increased accuracy in the measurement of thermospheric densities and winds prompted the development of the STEP-1 mission, which employed a complement of instruments to measure local

densities, compositions and relative velocity components. The triaxial accelerometer (SETA) for this mission could be utilized individually or in conjunction with other instruments to determine local density and wind values, which could then be correlated with geophysical parameters and other geophysical measurements to develop and evaluate thermospheric density and circulation models. This document describes the data processing flow and software developed to support this mission. DTIC

N95-29989# Los Alamos National Lab., NM.
POLYNOMIAL APPROXIMATIONS FOR MATERIALS SIMULATIONS
R. N. Silver, A. F. Voter, J. D. Kress, and H. Roeder (Bayreuth Univ., Germany.) 1995 7 p Presented at the SMS Simulation Multiconference: Simulation As A Critical Technology, Phoenix, AZ, 9-13 Apr. 1995
(Contract W-7405-eng-36)
(DE95-006168; LA-UR-95-437; CONF-950439-9) Avail: CASI HC A02/MF A01

Chebyshev polynomial approximations are an efficient and numerically stable way to calculate properties of the very large Hamiltonians important in computational materials science. The authors describe kernel polynomial methods (KPM) producing estimates for densities-of-states (DOS) which are strictly positive and simple convolutions of known broadening functions, or kernels, with true DOS. The methods are demonstrated for tight binding electronic structure calculations of Si, yielding rapid convergence of cohesive and vacancy formation energies. KPM are also applicable to dynamical spectral functions, statistical mechanics, and density matrices. DOE

N95-29996# TRW Systems Group, Redondo Beach, CA.
PSEE ARCHITECTURE REPORT: ARCHITECTURES AND MODELS FOR NEXT GENERATION PROCESS-BASED SOFTWARE ENGINEERING ENVIRONMENTS Interim Report
Maria H. Penedo Feb. 1995 107 p
(Contract N00039-95-C-0017; ARPA Order B343)
(AD-A291268) Avail: CASI HC A06/MF A02

This Architecture Report documents investigations towards the definition of a process-based Software Engineering Environment (PSEE) Reference Architecture. Those investigations are in support of the definition of a component-based architectural approach for the rapid construction of PSEE's. It represents work in progress. These investigations were conducted within the 'Architectures and Models for Next Generation process-based SEE's project; they also revise and enhance prior related work. This document is to be the first in a series of Architecture Reports to be delivered by this contract (pending continuous funding). This document actually consists of eleven (11) reports and four (4) references which provide technical data related to the current state (art and practice) of SEE's including architectural recommendations, requirements, and lessons learned; the data was gathered from national and international efforts and systems, and includes recent developments in the commercial sector and research programs. A key underlying assumption of this work is community participation and community consensus; therefore, some of the documents have been jointly developed with members of the community. DTIC

N95-30013*# Alabama Univ., Huntsville, AL. Dept. of Mechanical and Aerospace Engineering.
IMPACT OF UNCERTAINTY ON MODELING AND TESTING Final Report, 10 Jan. 1994 - 30 Apr. 1995
Hugh W. Coleman and Kendall K. Brown Apr. 1995 118 p
(Contract NAS8-38609)
(NASA-CR-196637; NAS 1.26:196637) Avail: CASI HC A06/MF A02

A thorough understanding of the uncertainties associated with the modeling and testing of the Space Shuttle Main Engine (SSME) Engine will greatly aid decisions concerning hardware performance and future development efforts. This report will describe the determination of the uncertainties in the modeling and testing of the Space Shuttle Main Engine test program at the Technology Test Bed facility at Marshall Space Flight Center. Section 2 will present a summary of the uncertainty analysis methodology used and discuss the specific applications to the TTB SSME test program. Section 3 will discuss the application of the uncertainty analysis to the test program and the results obtained. Section 4 presents the results of the analysis of the SSME modeling effort from an uncertainty analysis point of view. The appendices at the end of the report contain a significant amount of information relative to the analysis, including discussions of venturi flowmeter data reduction and uncertainty propagation, bias uncertainty documentations, technical papers published, the computer code generated to determine the venturi uncertainties, and the venturi data and results used in the analysis. Author

N95-30020# Argonne National Lab., IL.
W-MATRICES, NONORTHOGONAL MULTIRESOLUTION ANALYSIS, AND FINITE SIGNALS OF ARBITRARY LENGTH
M. K. Kwong and P. T. P. Tang 1994 24 p Presented at the Gigabyte Image Processing Workshop, Argonne, IL, 8-9 Jul. 1994
(Contract W-31-109-eng-38)
(DE95-005846; ANL/MCS/CP-84114; CONF-9407170-1) Avail: CASI HC A03/MF A01

Wavelet theory and discrete wavelet transforms have had great impact on the field of signal and image processing. In this paper the authors propose a new class of discrete transforms. It 'includes' the classical Haar and Daubechies transforms. These transforms treat the endpoints of a signal in a different manner from that of conventional techniques. This new approach allows the authors to efficiently handle signals of any length; thus, one is not restricted to work with signal or image sizes that are multiples of a power of 2. Their method does not lengthen the output signal and does not require an additional bookkeeping vector. An exciting result is the uncovering of a new and simple transform that performs very well for compression purposes. It has compact support of length 4, and so is its inverse. The coefficients are symmetrical, and the associated scaling function is fairly smooth The Associated dual wavelet has vanishing moments up to order 2. Numerical results comparing the performance of this transform with that of the Daubechies D(sub 4) transform are given. The multiresolution decomposition, however, is not orthogonal. They will see why this apparent defect is not a real problem in practice. Furthermore, they will give a method to compute an orthogonal compensation that gives them the best approximation possible with the given scaling space. The transform can be described completely within the context of matrix theory and linear algebra. Thus, even without prior knowledge of wavelet theory, one can easily grasp the concrete algorithm and apply it to specific problems within a very short time, without having to master complex functional analysis. At the end of the paper, they shall make the connection to wavelet theory. DOE

N95-30042# Delaware Univ., Newark, DE. Dept. of Computer and Information Sciences.
FORMAL DESIGN OF COMMUNICATION PROTOCOLS USING ESTELLE Final Report, 1 Apr. 1991 - 30 Jul. 1994
Paul D. Amer 21 Oct. 1994 7 p
(Contract DAAL03-91-G-0086)
(AD-A290584; ARO-28506.7-EL) Avail: CASI HC A02/MF A01

In 1989, Estelle was approved as one of two ISO International Standard Formal Description Techniques (FDT) for the formal specification of computer communication protocols. Based on communicating extended finite state machines (CEFSM), Estelle has a formal, mathematical, implementation-independent semantics. It is an expressive, well-defined, well-structured language that is capable of specifying distributed, concurrent information processing systems in a complete, consistent, concise and unambiguous manner. Over the past 3 years with the support of ARO and US Army CECOM, the PI has derived a number of results in the areas: Extensions and enhancements of Estelle; Protocol Visualization, and Automatic Test Case Generation. These results are described herein. DTIC

N95-30047# Carnegie-Mellon Univ., Pittsburgh, PA. Software Engineering Inst.
SOFTWARE RISK EVALUATION METHOD VERSION 1.0 Final Report
Frank J. Sisti and Sujoe Joseph Dec. 1994 160 p
(Contract F19628-90-C-0003)
(AD-A290597; CMU/SEI-94-TR-19; ESC-TR-94-019) Avail: CASI HC A08/MF A02

The Software Risk Evaluation (SRE) method is used for identifying, analyzing, communicating, and mitigating software risks. The SRE method is intended to be used by decision-makers for managing the software risks of software-intensive programs and projects. The SRE method facilitates the mitigation of software risks for managers. This document reports on the Software Risk Evaluation method version 1.0 and provides a high-level description of the method. The report is intended to provide the reader

with an overview of the functional components and the implementation aspects of the method. The current version of the SRE method evolved from two earlier versions. The first version was developed under a technical collaboration agreement with the Director of Defense Research and Engineering for mitigating the risks inherent in software acquisitions. The latter version was developed to improve and enhance the capabilities of the method for users in software intensive programs and projects. DTIC

N95-30063# George Mason Univ., Fairfax, VA. Center for Computational Statistics.

HUGE DATA SETS AND THE FRONTIERS OF COMPUTATIONAL FEASIBILITY

Edward J. Wegman Nov. 1994 23 p

(Contracts DAAH04-94-G-0267; DAAL03-91-G-0039)

(AD-A291384; GMU-TR-110) Avail: CASI HC A03/MF A01

Recently, Huber offered a taxonomy of data set sizes ranging from tiny (100 bytes) to huge (10 to the 10th power bytes). This taxonomy is particularly appealing because it quantifies the meaning of tiny, small, medium, large and huge. Indeed, some investigators consider 300 small and 10,000 large while others consider 10,000 small. In Huber's taxonomy, most statistical and visualization techniques are computationally feasible with tiny data sets. However with larger data sets computers run out of computational horsepower and graphics displays run out of resolution fairly quickly. In this paper, we discuss aspects of data set size and computational feasibility for general classes of algorithms in the context of CPU performance, memory size, hard disk capacity, screen resolution and massively parallel architectures. We discuss some strategies such as recursive formulations which mitigate the impact of size. We also discuss the potential for scalable parallelization which will mitigate the effects of computational complexity. DTIC

N95-30080# Air Force Inst. of Tech., Wright-Patterson AFB, OH. Dept. of Electrical and Computer Engineering.

A FORMAL EXTENSION TO OBJECT ORIENTED ANALYSIS USING Z

Thomas C. Hartrum and Paul Bailor 7 Oct. 1994 93 p

(AD-A290911; AFIT/EN/TR-94-07) Avail: CASI HC A05/MF A01

This report describes extending an informal object oriented analysis model with formal constructs. In particular, the object modeling technique (OMT) of Rumbaugh et. al. is integrated with the formal specification language Z. The result is a software analysis process that is easy to understand and apply, while resulting in a formal specification. DTIC

N95-30094# Technische Univ., Twente (Netherlands). Dept. of Computer Science.

DESCRIPTION AND MANIPULATION OF METHOD FRAGMENTS FOR THE ASSEMBLY OF SITUATIONAL METHODS

F. Harmsen and S. Brinkkemper Oct. 1994 22 p

(PB95-197133; Memo-INF-94-52) Copyright Avail: CASI HC A03/MF A01

This paper deals with the issue of assembly of project-specific or situational methods out of proven parts of existing information system (IS) development methods, so-called method fragments. The need to employ situational methods stems from the observation that standard IS development methods cannot anticipate adequately to new developments and are difficult to tune to specific situations. An overview of the entire process of situational method engineering is given, along with an architecture for the required computerized support tool. In assembling situational methods, we adopt a product-oriented viewpoint, taking the products to be delivered as a starting point for the processes required. After an introduction to the method fragment description language MEL, we describe a classification of method fragments, a layering, and a model containing the elementary building blocks of method fragments. A procedure for assembling method fragments is described. NTIS

N95-30095# Technische Univ., Twente (Netherlands). Dept. of Computer Scienec.

STATIC ANALYSIS OF FUNCTIONAL PROGRAMS

K. G. vandenBerg and P. M. vandenBroek Oct. 1994 36 p

(PB95-197141; Memo-INF-94-53) Copyright Avail: CASI HC A03/MF A01

In this paper, the static analysis of programs in the functional programming language Miranda is described based on two graph models. A new control-flow graph model of Miranda definitions is presented, and a model of four classes of callgraphs. Standard software metrics are applicable to these models. A Miranda front end for Prometrix, a tool for the automated analysis of flowgraphs and callgraphs, has been developed. This front end produces the flowgraph and callgraph representations of Miranda programs. Some features of the metric analyzer are illustrated with an example program. The tool provides a promising access to standard metrics on functional programs. NTIS

N95-30098# Technische Univ., Twente (Netherlands). Tele-Informatics and Open Systems Group.

FAST SIMULATION OF THE LEAKY BUCKET ALGORITHM

V. F. Nicola, G. A. Hagesteijn, and B. G. Kim 1994 13 p

(PB95-197174; Memo-INF-94-65) Copyright Avail: CASI HC A03/MF A01

In this paper we use fast simulation methods, based on importance sampling, to efficiently estimate cell loss probability in queuing models of the Leaky Bucket algorithm. One of these models was introduced by Berger, in which the rare event of a cell loss is related to the rare event of an empty finite buffer in an 'overloaded' queue. In particular, we propose a heuristic change of measure for importance sampling to efficiently estimate the probability of the rare empty-buffer event in an asymptotically unstable GI/GI/1/k queue. This change of measure is, in a way, 'dual' to that proposed by Parekh and Walrand to estimate the probability of a rare buffer overflow event. We present empirical results to demonstrate the effectiveness of our fast simulation method. NTIS

N95-30099# Technische Univ., Twente (Netherlands). Tele-Informatics and Open Systems Group.

CHECKPOINTING AND THE MODELING OF PROGRAM EXECUTION TIME

V. F. Nicola 3 Nov. 1994 31 p

(PB95-197182; Memo-INF-94-66) Copyright Avail: CASI HC A03/MF A01

Checkpointing is a commonly used technique for reducing the execution time of long-running programs in the presence of failures. With checkpointing, the status of the program under execution is saved intermittently. Upon the occurrence of a failure, the program execution is restarted from the most recent checkpoint rather than from the beginning. Due to its overhead, checkpointing may not always be beneficial, and, if it is, an optimal checkpointing strategy may be determined so as to minimize the expected execution time or to maximize the probability of the execution time not exceeding a critical limit. The paper considers several models of checkpointing and recovery in a program in order to derive the distribution of program execution time or its expectation. It makes important extensions to some existing results as well as introduces and analyzes new models. It is shown that the expected execution time increases linearly (exponentially) with the processing requirement in the presence (absence) of checkpointing. Furthermore, these models can be used to compare different checkpointing strategies and to determine an optimal interval between checkpoints. NTIS

N95-30105# Technische Univ., Twente (Netherlands). Dept. of Computer Science.

REALISATION OF AN INTEGRATED SOFTWARE ENGINEERING ENVIRONMENT THROUGH HETEROGENEOUS CASE-TOOL INTEGRATION

R. Bosua (South Africa Univ., Pretoria.) and S. Brinkkemper Dec. 1994 18 p

(PB95-197646; Memo-INF-94-73) Copyright Avail: CASI HC A03/MF A01

The development of large software systems needs appropriate automated support in the form of an integrated software engineering environment (ISEE) to support the system development process. This paper describes an approach, the CUBE approach, to integrate heterogeneous CASE tools and system development perspectives, in order to realize an ISEE. Heterogeneous refers to the Conventional system development paradigm as opposed to the Object-oriented system development paradigm. Integration between these paradigms and also its supporting tools can be realized by employing meta-models. Hence, a method link as well as a tool link can be realized. An example outlines the integration of the data perspective of

the methods Structured Analysis and Object-oriented Modeling Technique (OMT), by using meta-models. NTIS

N95-30107# Technische Univ., Eindhoven (Netherlands).
BOYER-MOORE TYPE ALGORITHM FOR REGULAR EXPRESSION PATTERN MATCHING
B. W. Watson and R. E. Watson 15 Aug. 1994 34 p Prepared in cooperation with Simon Fraser Univ.
(PB95-198131) Avail: CASI HC A03/MF A01

This paper presents a Boyer-Moore type algorithm for regular expression pattern matching. The new algorithm handles patterns specified by regular expression - a generalization of the Boyer-Moore and Commentz-Walter algorithms (which deal with patterns that are single keywords and finite sets of keywords, respectively). Like the Boyer-Moore and Commentz-Walter algorithms, the new algorithm makes use of shift functions which can be precomputed and tabulated. The precomputation algorithms are derived, and it is shown that the required shift functions can be precomputed from Commentz-Walter's shift functions known as d1 and d2. In certain cases, the Boyer-Moore (Commentz-Walter) algorithm has greatly outperformed the Knuth-Morris-Pratt (Aho-Corasick) algorithm. In testing, the algorithm presented in this paper also frequently outperforms the regular expression generalization of the Aho-Corasick algorithm. NTIS

N95-30115 Allied-Signal Aerospace Co., Kansas City, MO. Kansas City Div.
THE TELEMETRY AGILE MANUFACTURING EFFORT
K. D. Brown Jan. 1995 19 p Presented at the Agile Manufacturing Enterprise Forum, Atlanta, GA, 7-8 Mar. 1995 Limited Reproducibility: More than 20% of this document may be affected by microfiche quality
(Contract DE-AC04-76DP-00613)
(DE95-006177; KCP-613-5542; CONF-9503109-1) Avail: CASI HC A03

The Telemetry Agile Manufacturing Effort (TAME) is an agile enterprising demonstration sponsored by the US Department of Energy (DOE). The project experimented with new approaches to product realization and assessed their impacts on performance, cost, flow time, and agility. The purpose of the project was to design the electrical and mechanical features of an integrated telemetry processor, establish the manufacturing processes, and produce an initial production lot of two to six units. This paper outlines the major methodologies utilized by the TAME, describes the accomplishments that can be attributed to each methodology, and finally, examines the lessons learned and explores the opportunities for improvement associated with the overall effort. The areas for improvement are discussed relative to an ideal vision of the future for agile enterprises. By the end of the experiment, the TAME reduced production flow time by approximately 50% and life cycle cost by more than 30%. Product performance was improved compared with conventional DOE production approaches. DOE

N95-30121# Software Productivity Consortium, Herndon, VA.
SOFTWARE ESTIMATION PROGRAM (SWEEP) USER MANUAL
Sep. 1994 94 p
(Contract MDA972-92-J-1018)
(AD-A291137; SPC-92017-CMC) Avail: CASI HC A05/MF A01

The Software Error Estimate Program (SWEEP) aids you in the management and prediction of errors and defects in software intensive systems. It will support you in establishing goals for error detection during software development and can help to track progress against those goals. You can also use SWEEP to monitor and help control the quality of software products by predicting the number of defects remaining in your software system, or latent error content. You use the latent error content to estimate the amount of testing and repair effort needed to reach different quality levels and to understand the quality of a delivered product. SWEEP can also help you project software outages due to software related defects in software intensive systems. SWEEP supports a variety of different organizational approaches to monitoring defects during software development. Organizations that measure and track defects during the software implementation phase can iterate through development and test intervals, suing SWEEP to predict the latent error content. Organizations that measure and track in one phase based upon the data collected in previous phases. SWEEP can also assist you in the planning of software projects. You enter the number of defects (per code unit) and the estimated latent error content to derive a profile pattern for error discovery that will project the number of remaining errors on a phase-by-phase basis. DTIC

N95-30125# Logicon Technical Services, Inc., Dayton, OH.
TOOLS FOR AUTOMATED KNOWLEDGE ENGINEERING (TAKE) SYSTEM EVALUATION METHODOLOGY Interim Report, Dec. 1993 - Jun. 1994
John J. Spravka, Marie E. Gomes, and Stephanie Lind Jun. 1994 39 p
(Contract F41624-94-D-6000)
(AD-A291145; AL/CF-TR-1994-0113) Avail: CASI HC A03/MF A01

This paper describes the methodology in which the Tools for Automated Knowledge Engineering (TAKE) software application has been used to conduct various military human-system interface evaluations. The TAKE methodology involves collecting relevant information through a knowledge elicitation technique known as 'Concept Mapping.' Concept Mapping is more user-oriented than other techniques such as written questionnaires or oral interviews. The information is more useful because its medium of communication ensures an accurate portrayal of the system, as viewed by the user, unbiased by any preconceived notions of the questionnaire author or interviewer. TAKE consists of several knowledge engineering tools. These include the capability to draw, copy, edit, save and print concept maps for user-specified information. Armstrong Laboratory has used TAKE within the context of the described methodology for the evaluation and/or design/redesign of various military human-system interfaces. DTIC

N95-30183# California Univ., Berkeley. Lawrence Berkeley Lab, CA.
NEAREST NEIGHBOR ANALYSIS IN ONE DIMENSION
M. Weingart and S. Selvin Feb. 1995 66 p
(Contract DE-AC03-76SF-00098)
(DE95-009378; LBL-36888) Avail: CASI HC A04/MF A01

Since its initial presentation by Clark and Evans, nearest neighbor analysis for spatial randomness has gained considerable popularity in fields as diverse as geography, ecology, archaeology, cell biology, forestry, meteorology, and epidemiology. Epidemiologists are often interested in determining whether disease cases are clustered, dispersed, or randomly distributed, since different patterns of disease incidence over time or space can provide dues to the etiology of the disease. An environmental hazard or a transmissable agent can produce a cluster of disease events, i.e. a set of events occurring unusually dose to each other in time, space, or both time and space. In spite of its wide applicability, few attempts have been made to adapt the nearest neighbor method to the analysis of points distributed along a line. This report outlines the theoretical derivation of the moments of the mean nearest neighbor distance in the one dimension case and the correction of its expected value in order to overcome the boundary problem. It presents the derivation of the moments of order statistics, for specific sample sizes and for the general case. These results are then used for the derivation of the moments of nearest neighbor distances, and for the derivation of the moments of the mean nearest neighbor distance. Then the boundary problem and an examination of five alternative ways to compensate for it in the calculation of the expected value of the mean nearest neighbor distance are discussed. Finally, the results from a large scale computer simulation which compares the various correction methods are presented. DOE

N95-30189# Oak Ridge National Lab., TN.
SIMULATION OF ROBOT MANIPULATORS
R. L. Kress, S. M. Babcock, K. C. Bills, D. S. Kwon, and D. A. Schoenwald 1995 7 p Presented at the 6th American Nuclear Society Meeting on Robotics and Remote Systems, Monterey, CA, 5-10 Feb. 1995
(Contract DE-AC05-84OR-21400)
(DE95-008680; CONF-950232-26) Avail: CASI HC A02/MF A01

This paper describes Oak Ridge National Laboratory's development of an environment for the simulation of robotic manipulators. Simulation includes the modeling of kinematics, dynamics, sensors, actuators, control systems, operators, and environments. Models will be used for manipulator design, proposal evaluation, control system design and analysis, graphical preview of proposed motions, safety system development, and training. Of particular interest is the development of models for robotic manipulators having at least one flexible link. As a first application, models have been developed for the Pacific Northwest Laboratories' Flexible Beam Testbed which is a one-Degree-Of-Freedom, flexible arm with a hydraulic base actuator. Initial results show good agreement between model and experiment. DOE

N95-30209# Sandia National Labs., Albuquerque, NM.
PASSIVE DAMPING TO ENHANCE ACTIVE POSITIONING OF A PROTOTYPE LITHOGRAPHY PLATEN
D. J. Segalman, R. L. Kipp, and D. L. Gregory 1994 9 p Presented at the North American Conference on Smart Structures and Materials, San Diego, CA, 26 Feb. - 3 Mar. 1995
(Contract DE-AC04-94AL-85000)
(DE95-008539; SAND-94-2407C; CONF-950228-3) Avail: CASI HC A02/MF A01

A viscoelastic tuned-mass damper was used to suppress specific structural modes of a prototype lithography platen. The platen is magnetically levitated and it is repositioned and held in position by a closed-loop feedback control system. Important capabilities of the platen control system are precise positioning and rapid repositioning, which tend to require high frequency bandwidth. The high bandwidth excites structural vibration modes which are disruptive to the control system. The present work was to develop and demonstrate a means to suppress these modes using passive vibration damping techniques. The motivation is to increase the robustness of the platen positioning and control system by reducing unwanted modal accelerations excited by high control system bandwidth. Activities performed and discussed include the analytical design of viscoelastic tuned-mass dampers and the demonstration/testing of their effectiveness on the platen while levitated and controlled. DOE

N95-30218# Technische Univ., Twente (Netherlands). Dept. of Computer Science.
STRUCTURED APPROACH FOR THE METHODICAL AND TECHNICAL INTEGRATION OF HETEROGENEOUS CASE TOOLS
R. Bosua (South Africa Univ., Pretoria.) and S. Brinkkemper Dec. 1994 22 p
(PB95-197653; Memo-INF-94-74) Copyright Avail: CASI HC A03/MF A01

Heterogeneous Computer Aided Software Engineering (CASE) tools, meaning CASE tools that support the conventional system development paradigm on the one hand and tools that support the object-oriented paradigm on the other hand, need to be integrated to support system development either in both system development paradigms, or to enable a change over from one system development paradigm to the other. Although standards and frameworks for tool integration are emerging, a structured method or approach to integrate tools is required. This paper proposes the CUBE approach, especially the creation of a technical link, to integrate heterogeneous CASE tools. It outlines the unique problems associated with heterogeneous workbench integration. Two modes are described that may be applied to realize the technical link between heterogeneous tool repositories. NTIS

N95-30220# Technische Univ., Eindhoven (Netherlands).
CORRECTNESS OF REAL-TIME SYSTEMS BY CONSTRUCTION
J. Hooman Jul. 1994 35 p
(PB95-206827) Avail: CASI HC A03/MF A01

To design distributed real-time systems in a top-down way, we present a mixed formalism in which programs and assertional specifications are combined. Specifications consist of an assumption-commitment pair, extending Hoare logic to real-time and progress properties. By defining the theory in the Prototype Verification System (PVS) specification language, the interactive proof checker of PVS can be used to reason in this framework. We show how this tool can be used during the design of real-time systems to derive programs that are correct by construction. NTIS

N95-30248* National Aeronautics and Space Administration. Ames Research Center, Moffett Field, CA.
TELEPRESENCE MEDIA RESOURCE TAPE (Videotape)
31 Jan. 1992 Sponsored by NASA, Washington Videotape: 9 min. playing time, in color, with sound
(NASA-TM-110648; NASA-AAV-1387; NONP-NASA-VT-95-57872) Avail: CASI VHS A02/BETA A22

Dr. Michael McGreevey (NASA's Ames Research Center) explains what virtual reality is and how NASA uses this concept. Computer animation of different planets using virtual reality is shown. One Ames research tool, the Virtual Wind Tunnel allows air flow to be studied inside the tunnel from any conceivable location. Dr. Carol Stoker (NASA's Ames Research Center) comments on Telepresence, one form of virtual reality. CASI

N95-30283# Helsinki Univ. of Technology, Espoo (Finland). Dept. of Computer Science.
PRODUCT CONFIGURATIONS: AN APPLICATION FOR PROTOTYPE OBJECT APPROACH
Hannu Peltonen, Tomi Maennistoe, Kari Alho, and Reijo Sulonen 1995 24 p Supersedes PB94-179140
(PB95-192589; TKO-B118) Avail: CASI HC A03/MF A01

Product configuration management is presented as a practical application for a prototype-based object model. Data model requirements for a configuration system are first introduced using a realistic example from industry. Problems with the traditional type-instance model in this application domain are then identified and given as motivation for the prototype approach. A prototype-based object model with inheritance tree transformations, constraints and component relationships is presented as a tool for expressing dynamic configuration data. Finally, a sample configuration process is described using the prototype object model. NTIS

N95-30306*# Institute for Computer Applications in Science and Engineering, Hampton, VA.
PARALLEL RENDERING Final Report
Thomas W. Crockett Apr. 1995 51 p Submitted for publication in The Encyclopedia of Computer Science and Technology
(Contract NAS1-19480; RTOP 505-90-52-01)
(NASA-CR-195080; NAS 1.26:195080; ICASE-95-31) Avail: CASI HC A04/MF A01

This article provides a broad introduction to the subject of parallel rendering, encompassing both hardware and software systems. The focus is on the underlying concepts and the issues which arise in the design of parallel rendering algorithms and systems. We examine the different types of parallelism and how they can be applied in rendering applications. Concepts from parallel computing, such as data decomposition, task granularity, scalability, and load balancing, are considered in relation to the rendering problem. We also explore concepts from computer graphics, such as coherence and projection, which have a significant impact on the structure of parallel rendering algorithms. Our survey covers a number of practical considerations as well, including the choice of architectural platform, communication and memory requirements, and the problem of image assembly and display. We illustrate the discussion with numerous examples from the parallel rendering literature, representing most of the principal rendering methods currently used in computer graphics. Author

N95-30307*# NASA Center for AeroSpace Information, Linthicum Heights, MD.
CD-ROM PREPARATION: AN OVERVIEW AND GUIDE
Ralph E. Daniel (RMS Associates, Linthicum Heights, MD.), Mark W. Jeschke (RMS Associates, Linthicum Heights, MD.), and James A. Schroer (RMS Associates, Linthicum Heights, MD.) Jun. 1995 123 p Sponsored by NASA, Washington
(Contract NASw-4584)
(NASA-CR-198756; NAS 1.26:198756) Avail: CASI HC A06/MF A02

A primer on the options and procedures involved in producing CD-ROM products in a small to medium sized business operation is presented in language that persons with a minimal technical background can easily understand. The capabilities, limitations, and standards of CD-ROM technology are surveyed. Emphasis is placed on CD-ROM production, especially upon design, data conversion to an electronic medium, data file preparation, the use of vendors, and the steps for in-house production of CD-ROM products. Author

N95-28729*# National Aeronautics and Space Administration. Langley Research Center, Hampton, VA.
GEOMETRY LABORATORY (GEOLAB) SURFACE MODELING AND GRID GENERATION TECHNOLOGY AND SERVICES
Patricia A. Kerr, Robert E. Smith, and Mary-Anne K. Posenau *In* NASA. Lewis Research Center, Surface Modeling, Grid Generation, and Related Issues in Computational Fluid Dynamic (CFD) Solutions Mar. 1995 p 69-86 (For primary document see N95-28723 10-02)
Avail: CASI HC A03/MF A10

N95-28734*# United Technologies Research Center, East Hartford, CT.
AUTOMATIC BLOCKING FOR COMPLEX THREE-DIMENSIONAL CONFIGURATIONS

John F. Dannenhoffer, III *In* NASA. Lewis Research Center, Surface Modeling, Grid Generation, and Related Issues in Computational Fluid Dynamic (CFD) Solutions Mar. 1995 p 123-142 (For primary document see N95-28723 10-02)
Avail: CASI HC A03/MF A10

N95-28735*# Program Development Corp., White Plains, NY.
MULTIBLOCK GRID GENERATION WITH AUTOMATIC ZONING
Peter R. Eiseman *In* NASA. Lewis Research Center, Surface Modeling, Grid Generation, and Related Issues in Computational Fluid Dynamic (CFD) Solutions Mar. 1995 p 143-162 (For primary document see N95-28723 10-02)
Avail: CASI HC A03/MF A10

N95-28741*# Lockheed-Fort Worth Co., Fort Worth, TX. Engineering Group.
UNSTRUCTURED CARTESIAN/PRISMATIC GRID GENERATION FOR COMPLEX GEOMETRIES
Steve L. Karman, Jr. *In* NASA. Lewis Research Center, Surface Modeling, Grid Generation, and Related Issues in Computational Fluid Dynamic (CFD) Solutions Mar. 1995 p 251-270 (For primary document see N95-28723 10-02)
Avail: CASI HC A03/MF A10

N95-28745*# MDA Engineering, Inc., Arlington, TX.
THREE-DIMENSIONAL HYBRID GRID GENERATION USING ADVANCING FRONT TECHNIQUES
John P. Steinbrenner and Ralph W. Noack *In* NASA. Lewis Research Center, Surface Modeling, Grid Generation, and Related Issues in Computational Fluid Dynamic (CFD) Solutions Mar. 1995 p 333-356 (For primary document see N95-28723 10-02)
(Contract F08630-93-C-0074)
Avail: CASI HC A03/MF A10

N95-28748*# CFD Research Corp., Huntsville, AL.
EVALUATION OF GRID GENERATION TECHNOLOGIES FROM AN APPLIED PERSPECTIVE
Gary S. Hufford, Vincent J. Harrand, Bhavin C. Patel, and Curtis R. Mitchell *In* NASA. Lewis Research Center, Surface Modeling, Grid Generation, and Related Issues in Computational Fluid Dynamic (CFD) Solutions Mar. 1995 p 401-420 (For primary document see N95-28723 10-02)
Avail: CASI HC A03/MF A10

N95-28749*# Mississippi State Univ., Mississippi State, MS.
THE NATIONAL GRID PROJECT: A SYSTEM OVERVIEW
Adam Gaither, Kelly Gaither, Brian Jean, Michael Remotigue, John Whitmire, Bharat Soni, Joe Thompson, Dannenhoffer, John (United Technologies Research Center, East Hartford, CT.), and Nigel Weatherill (Wales Univ., Swansea, United Kingdom.) *In* NASA. Lewis Research Center, Surface Modeling, Grid Generation, and Related Issues in Computational Fluid Dynamic (CFD) Solutions Mar. 1995 p 423-446 (For primary document see N95-28723 10-02)
Avail: CASI HC A03/MF A10

N95-28750*# National Aeronautics and Space Administration. Ames Research Center, Moffett Field, CA.
A 3DGRAPE/AL: THE AMES/LANGLEY TECHNOLOGY UPGRADE
Reese L. Sorenson and Stephen J. Alter (Lockheed Engineering and Sciences Co., Hampton, VA.) *In* NASA. Lewis Research Center, Surface Modeling, Grid Generation, and Related Issues in Computational Fluid Dynamic (CFD) Solutions Mar. 1995 p 447-462 (For primary document see N95-28723 10-02)
(Contract NAS1-19000)
Avail: CASI HC A03/MF A10

N95-28751*# Pointwise, Inc., Bedford, TX.
AUTOMATIC STRUCTURED GRID GENERATION USING GRIDGEN (SOME RESTRICTIONS APPLY)
John R. Chawner and John P. Steinbrenner *In* NASA. Lewis Research Center, Surface Modeling, Grid Generation, and Related Issues in Computational Fluid Dynamic (CFD) Solutions Mar. 1995 p 463-476 (For primary document see N95-28723 10-02)
Avail: CASI HC A03/MF A10

N95-28752*# ICEM CFD Engineering, Berkeley, CA.
TUNED GRID GENERATION WITH ICEM CFD
Armin Wulf and Vedat Akdag *In* NASA. Lewis Research Center, Surface Modeling, Grid Generation, and Related Issues in Computational Fluid Dynamic (CFD) Solutions Mar. 1995 p 477-488 (For primary document see N95-28723 10-02)
Avail: CASI HC A03/MF A10

N95-28753*# Mississippi State Univ., Mississippi State, MS. Engineering Research Center for Computational Field Simulation.
GEOMETRY MODELING AND GRID GENERATION USING 3D NURBS CONTROL VOLUME
Tzu-Yi Yu, Bharat K. Soni, and Ming-Hsin Shih *In* NASA. Lewis Research Center, Surface Modeling, Grid Generation, and Related Issues in Computational Fluid Dynamic (CFD) Solutions Mar. 1995 p 491-503 Sponsored by NASA. Marshall Space Flight Center (For primary document see N95-28723 10-02)
Avail: CASI HC A03/MF A10

N95-28754*# McDonnell-Douglas Corp., Saint Louis, MO. Computational Fluid Dynamics Project.
GENERATING GRIDS DIRECTLY ON CAD DATABASE SURFACES USING A PARAMETRIC EVALUATOR APPROACH
Timothy D. Gatzhe and Thomas G. Melson *In* NASA. Lewis Research Center, Surface Modeling, Grid Generation, and Related Issues in Computational Fluid Dynamic (CFD) Solutions Mar. 1995 p 505-515 (For primary document see N95-28723 10-02)
Avail: CASI HC A03/MF A10

N95-28755*# Rockwell International Corp., Seal Beach, CA. North American Aircraft Div.
GRID GENERATION ON TRIMMED BEZIER AND NURBS QUILTED SURFACES
Chung-Jin Woan, Willard C. Clever, and Clement K. Tam *In* NASA. Lewis Research Center, Surface Modeling, Grid Generation, and Related Issues in Computational Fluid Dynamic (CFD) Solutions Mar. 1995 p 517-534 (For primary document see N95-28723 10-02)
Avail: CASI HC A03/MF A10

N95-28756*# Pratt and Whitney Aircraft, East Hartford, CT.
GEOMETRIC GRID GENERATION
David Ives *In* NASA. Lewis Research Center, Surface Modeling, Grid Generation, and Related Issues in Computational Fluid Dynamic (CFD) Solutions Mar. 1995 p 535-557 (For primary document see N95-28723 10-02)
Avail: CASI HC A03/MF A10

N95-28757*# Centre Europeen Recherche et de Formation Advance en Calcul Scientific, Toulouse (France).
ALGORITHMS FOR THE AUTOMATIC GENERATION OF 2-D STRUCTURED MULTI-BLOCK GRIDS
Thilo Schoenfeld, Per Weinerfelt (Linkoeping Univ., Sweden.), and Carl B. Jenssen (Selskapet for Industriell og Teknisk Forskning, Trondheim, Norway.) *In* NASA. Lewis Research Center, Surface Modeling, Grid Generation, and Related Issues in Computational Fluid Dynamic (CFD) Solutions Mar. 1995 p 561-580 (For primary document see N95-28723 10-02)
Avail: CASI HC A03/MF A10

N95-28758*# Rutgers - The State Univ., New Brunswick, NJ. Dept. of Computer Science.
INTELLIGENT AUTOMATED SURFACE GRID GENERATION
Ke-Thia Yao and Andrew Gelsey *In* NASA. Lewis Research Center, Surface Modeling, Grid Generation, and Related Issues in Computational Fluid Dynamic (CFD) Solutions Mar. 1995 p 581-595 (For primary document see N95-28723 10-02)
(Contract NAG2-645; ARPA-63-93-C-0064; NSF CCR-92-09793)
Avail: CASI HC A03/MF A10

N95-28759*# Korea Air Force Academy, Cheong-Ju (Korea). Dept. of Aerospace Engineering.
OPTIMAL DOMAIN DECOMPOSITION STRATEGIES
Yonghyun Yoon and Bharat K. Soni (Mississippi State Univ., Mississippi State, MS.) *In* NASA. Lewis Research Center, Surface Modeling, Grid Generation, and Related Issues in Computational Fluid Dynamic (CFD) Solutions Mar. 1995 p 597-613 (For primary document see N95-28723 10-02)
Avail: CASI HC A03/MF A10

N95-28760*# National Aerospace Lab., Amsterdam (Netherlands).
ELLIPTIC SURFACE GRID GENERATION ON MINIMAL AND PARMETRIZED SURFACES
S. P. Spekreijse, G. H. Nijhuis, and J. W. Boerstoel *In* NASA. Lewis Research Center, Surface Modeling, Grid Generation, and Related Issues in Computational Fluid Dynamic (CFD) Solutions Mar. 1995 p 617-636 (For primary document see N95-28723 10-02)
Avail: CASI HC A03/MF A10

N95-28761*# Boeing Co., Seattle, WA. Aerodynamics Configuration Computing.
COOPERATIVE SOLUTIONS COUPLING A GEOMETRY ENGINE AND ADAPTIVE SOLVER CODES
Thomas P. Dickens *In* NASA. Lewis Research Center, Surface Modeling, Grid Generation, and Related Issues in Computational Fluid Dynamic (CFD) Solutions Mar. 1995 p 637-646 (For primary document see N95-28723 10-02)
Avail: CASI HC A02/MF A10

N95-28762*# Rockwell International Corp., Canoga Park, CA. Rocketdyne Div.
AUTOMATION OF THREE-DIMENSIONAL STRUCTURED MESH GENERATION FOR TURBOMACHINERY BLADE PASSAGES
Edward P. Ascoli and George H. Prueger *In* NASA. Lewis Research Center, Surface Modeling, Grid Generation, and Related Issues in Computational Fluid Dynamic (CFD) Solutions Mar. 1995 p 647-655 (For primary document see N95-28723 10-02)
Avail: CASI HC A02/MF A10

N95-28763*# Computer Sciences Corp., Hampton, VA.
A GRID GENERATION SYSTEM FOR MULTI-DISCIPLINARY DESIGN OPTIMIZATION
William T. Jones and Jamshid Samareh-Abolhassani *In* NASA. Lewis Research Center, Surface Modeling, Grid Generation, and Related Issues in Computational Fluid Dynamic (CFD) Solutions Mar. 1995 p 657-667 (For primary document see N95-28723 10-02)
Avail: CASI HC A03/MF A10

N95-28764*# Washington Univ., Seattle, WA. Dept. of Aeronautics and Astronautics.
AUTOMATIC MULTI-BLOCK GRID GENERATION FOR HIGH-LIFT CONFIGURATION WINGS
Byoungsoo Kim and Scott Eberhardt *In* NASA. Lewis Research Center, Surface Modeling, Grid Generation, and Related Issues in Computational Fluid Dynamic (CFD) Solutions Mar. 1995 p 671-688 Sponsored by NASA. Ames Research Center (For primary document see N95-28723 10-02)
Avail: CASI HC A03/MF A10

N95-28765*# National Aeronautics and Space Administration. Langley Research Center, Hampton, VA.
MULTILEVEL ELLIPTIC SMOOTHING OF LARGE THREE-DIMENSIONAL GRIDS
C. Wayne Mastin *In* NASA. Lewis Research Center, Surface Modeling, Grid Generation, and Related Issues in Computational Fluid Dynamic (CFD) Solutions Mar. 1995 p 689-696 (For primary document see N95-28723 10-02)
Avail: CASI HC A02/MF A10

N95-28769*# United Technologies Research Center, East Hartford, CT.
A TECHNIQUE FOR OPTIMIZING GRID BLOCKS
John F. Dannenhoffer, III *In* NASA. Lewis Research Center, Surface Modeling, Grid Generation, and Related Issues in Computational Fluid Dynamic (CFD) Solutions Mar. 1995 p 751-762 (For primary document see N95-28723 10-02)
Avail: CASI HC A03/MF A10

N95-28771*# AeroHydro, Inc., Southwest Harbor, ME.
PARAMETRIC DESIGN AND GRIDDING THROUGH RELATIONAL GEOMETRY
John S. Letcher, Jr. and D. Michael Shook *In* NASA. Lewis Research Center, Surface Modeling, Grid Generation, and Related Issues in Computational Fluid Dynamic (CFD) Solutions Mar. 1995 p 783-800 (For primary document see N95-28723 10-02)
(Contract N00167-95-C-0003)
Avail: CASI HC A03/MF A10

N95-28772*# Program Development Corp., White Plains, NY.
EXAMPLES OF GRID GENERATION WITH IMPLICITLY SPECIFIED SURFACES USING GridPro (TM)/az3000. 1: FILLETED MULTI-TUBE CONFIGURATIONS
Zheming Cheng and Peter R. Eiseman *In* NASA. Lewis Research Center, Surface Modeling, Grid Generation, and Related Issues in Computational Fluid Dynamic (CFD) Solutions Mar. 1995 p 801-819 (For primary document see N95-28723 10-02)
Avail: CASI HC A03/MF A10

N95-28773*# Computer Sciences Corp., Hampton, VA.
GridTool: A SURFACE MODELING AND GRID GENERATION TOOL
Jamshid Samareh-Abolhassani *In* NASA. Lewis Research Center, Surface Modeling, Grid Generation, and Related Issues in Computational Fluid Dynamic (CFD) Solutions Mar. 1995 p 821-831 (For primary document see N95-28723 10-02)
Avail: CASI HC A03/MF A10

N95-28774*# Program Development Corp., White Plains, NY.
INTERACTIVE HIGH QUALITY GRID GENERATION
Ning Lu and Peter R. Eiseman *In* NASA. Lewis Research Center, Surface Modeling, Grid Generation, and Related Issues in Computational Fluid Dynamic (CFD) Solutions Mar. 1995 p 833-843 (For primary document see N95-28723 10-02)
Avail: CASI HC A03/MF A10

N95-28775*# Computer Sciences Corp., Moffett Field, CA.
NASA-IGES TRANSLATOR AND VIEWER
Jin J. Chou and Michael A. Logan *In* NASA. Lewis Research Center, Surface Modeling, Grid Generation, and Related Issues in Computational Fluid Dynamic (CFD) Solutions Mar. 1995 p 845-855 (For primary document see N95-28723 10-02)
Avail: CASI HC A03/MF A10

N95-30157*# National Aeronautics and Space Administration. Lewis Research Center, Cleveland, OH.
CATEGORY 5 PROBLEM SOLUTION USING AN UNSTRUCTURED FINITE VOLUME ALGORITHM
Trong T. Bui and Reda R. Mankbadi *In* NASA. Langley Research Center, ICASE/LaRC Workshop on Benchmark Problems in Computational Aeroacoustics (CAA) May 1995 p 267-272 (For primary document see N95-30133 10-71)
Avail: CASI HC A02/MF A04

62 COMPUTER SYSTEMS

Includes computer networks and special application computer systems.

N95-28689 Naval Postgraduate School, Monterey, CA.
ANALYSIS OF THE NAVAL POSTGRADUATE SCHOOL COMPUTER NETWORK ARCHITECTURE M.S. Thesis
Paul E. Wiedenhoeft Sep. 1994 181 p Limited Reproducibility: More than 20% of this document may be affected by microfiche quality
(AD-A289749) Avail: Issuing Activity (Defense Technical Information Center (DTIC))

The computer network on the Naval Postgraduate School campus has become an integral part of the operations of the Naval Postgraduate School organization. An analysis of the network architecture will help formulate strategic plans that will support the network and the Naval Postgraduate School to the end of the century. This study describes the Naval Postgraduate School computer network architecture, driving forces, imitations, and possible measures of network benefits. It considers network alternatives and reasonable transition strategies. The study offers recommendations for improvements to the existing network architecture.
DTIC

N95-28879# Carnegie-Mellon Univ., Pittsburgh, PA. Dept. of Computer Science.
THE SCOTCH PARALLEL STORAGE SYSTEMS
Garth A. Gibson, Daniel Stodolsky, Fay W. Chang, Willliam V. Courtright, II., and Chris G. Demetriou 12 Jan. 1995 12 p
(Contracts DABT63-93-C-0054; NSF-ECD89-07068)
(AD-A292243; CMU-CS-95-107) Avail: CASI HC A03/MF A01

To meet the bandwidth needs of modern computer systems, parallel storage systems are evolving beyond RAID levels 1 through 5. The Parallel Data Lab at Carnegie Mellon University has constructed three Scotch parallel storage testbeds to explore and evaluate five directions in RAID evolution: first, the development of new RAID architectures to reduce the cost/performance penalty of maintaining redundant data; second, an extensible software framework for rapid prototyping of new architectures; third, mechanisms to reduce the complexity of and automate error-handling in RAID subsystems; fourth, a file system extension that allows serial programs to exploit parallel storage; and lastly, a parallel file system that extends the RAID advantages to distributed, parallel computing environments. This paper describes these five RAID evolutions and the testbeds in which they are being implemented and evaluated. DTIC

N95-28884# Carnegie-Mellon Univ., Pittsburgh, PA. Dept. of Computer Science.
WAX: A WIDE-AREA COMPUTATION SYSTEM Ph.D. Thesis
Peter D. Stout Dec. 1994 113 p
(Contract DABT63-93-C-0054)
(AD-A292247; CMU-CS-94-230) Avail: CASI HC A06/MF A01

This dissertation explores the use of machines connected to wide-area networks to provide the parallelism needed to work on large coarse-grain parallel applications. Large applications, such as circuit simulations, integer factoring, graphics applications, and NP-complete approximations, have potential coarse-grain parallelism that exceeds the parallel processing facilities at any single site. At the same time, the machines connected to wide-area networks represent a large and growing source of under-utilized computing power. However, in order to transform the idle machines on a wide-area network into a large scale, wide-area distributed computing system, a number of problems need to be addressed: latency, failure, security, process management, scale, and system administration. This dissertation describes a prototype wide-area distributed computation system, called Wax, that has been built and used to explore solutions to these problems. Wax implements a programming model that takes into consideration the problems that exist in distributed computing environments, particularly wide-area ones. The key differences from traditional parallel programming models are a reduced global consistency guarantee, the explicit incorporation of failure into the model, and reduced access to the local execution machine. The first two differences allow Wax to expose the effects of some these wide-area problems (failure, latency, scale) to the application programmer. The most appropriate solutions to these problems often require application-specific knowledge. The third difference allows Wax to incorporate mechanisms to protect the resources used to process applications from abuse by those applications. DTIC

N95-28955 Naval Air Warfare Center, China Lake, CA.
MULTILAYER PIECEWISE LINEAR NETWORKS. REVISION 1 Final Report, 1993 - 1994
W. O. Alltop Nov. 1994 57 p Limited Reproducibility: More than 20% of this document may be affected by microfiche quality
(AD-A289885; NAWC-WPNS-TP-8217-REV-1) Avail: Issuing Activity (Defense Technical Information Center (DTIC))

Feed-forward layered networks are the simplest neural computers. These networks provide fast compact devices for computing discriminant functions and other mappings applicable to pattern recognition problems. This report treats the problem of weight initialization/assignment for feed-forward networks with piecewise linear neuron transfer function. Specific transformations are shown to be impossible with a single hidden layer. Techniques are presented for constructing such transformations with two hidden layers. DTIC

N95-28965# Syracuse Univ., NY. Northeast Parallel Architectures Center.
ROME LABORATORY SOFTWARE ENGINEERING COOPERATIVE VIRTUAL MACHINE Final Technical Report
Geoffrey C. Fox, Salim Hariri, H. J. Siegel, and H. G. Dietz Dec. 1994 73 p
(Contract F30602-92-C-0150)
(AD-A292396; RL-TR-94-221) Avail: CASI HC A04/MF A01

This final technical report summarizes research accomplished by Syracuse University, Purdue University, and the University of California at Berkeley under the Expert Science and Engineering Program. The research accomplished a high-level analysis and feasibility study for building a virtual machine model for parallel software development. The report summarizes the three approaches (components, compiler techniques, and client-server) recommended by the researchers. DTIC

N95-29074# Stanford Univ., CA.
A STUDY OF FLUID PROBLEMS REQUIRING A DIRECT PARTICLE SIMULATION Final Report, 1 Apr. 1993 - 30 Sep. 1994
Donald Baganoff 28 Nov. 1994 30 p
(Contract F49620-93-1-0143)
(AD-A290212; AFOSR-95-0055TR) Avail: CASI HC A03/MF A01

The principal objective was to make use of a parallel computer code recently developed by our group, for Bird's direct simulation Monte Carlo (DSMC) method, and to gain experience in simulating various rarefied three-dimensional flows about bodies having reasonably complex geometries, for example, bodies based on geometries associated with current practical applications. DTIC

N95-29079# Carnegie-Mellon Univ., Pittsburgh, PA. Graduate School of Industrial Administrati On.
SOLVING LINEAR PROGRAMS USING DISTRIBUTED PARALLEL COMPUTING
N. R. Natraj, G. L. Thompson, and F. Harche Nov. 1994 25 p
Prepared in cooperation with Stern School of Business
(Contract N00014-85-K-0198)
(AD-A290221) Avail: CASI HC A03/MF A01

Parallel and distributed computing has attracted a lot of attention from researchers over the past few years. It is a promising new approach for solving large problems that were hitherto considered very difficult to solve using traditional serial computers. The advancement of technology and the introduction of fiber-optic networks for high speed data transmission has made distributed computing on a network of computers very attractive. We address the problem of solving linear programs using distributed computing. We present a two-phase parallel standard simplex algorithm for solving linear programs with single upper bounded variables. The parallel simplex algorithm was implemented on NECTAR (NEtwork CompuTer ARchitecture) a collection of SUN4/33O workstations on a fiber-optic network and evaluated using randomly generated problems and those available from the netlib database. DTIC

N95-29196# Carnegie-Mellon Univ., Pittsburgh, PA. School of Computer Science.
IMPLEMENTING DISTRIBUTED SERVER GROUPS FOR THE WORLD WIDE WEB
Michael Garland, Sebastian Grassia, Robert Monroe, and Siddhartha Puri 25 Jan. 1995 13 p
(Contracts F33615-93-1-1330; F19628-93-C-0171)
(AD-A292221; CMU-CS-95-114) Avail: CASI HC A03/MF A01

The World Wide Web (WWW) has recently become a very popular facility for the dissemination of information. As a result of this popularity, it is experiencing rapidly increasing traffic load. Single machine servers cannot keep pace with the ever greater load being placed upon them. To alleviate this problem, we have implemented a distributed Web server group. The server group can effectively balance request load amongst its members

(within about 10% of optimal), and client response time is no worse than in the single server case. Client response time was not improved because the measured client traffic consumed all available network throughput. The distributed operation of the server groups is completely transparent to standard Web clients. DTIC

N95-29225# Pennsylvania Univ., Philadelphia, PA.
EFFICIENT COMPILATION OF HIGH-LEVEL DATA PARALLEL ALGORITHMS
Dan Suciu and Val Tannen Apr. 1994 17 p
(Contract DAAL03-89-C-0031)
(AD-A290362; MS-CIS-94-17; ARO-26779.37-MA-AI) Avail: CASI HC A03/MF A01

We present a high-level parallel calculus for nested sequences, NSC, offered as a possible theoretical 'core' of an entire class of collection-oriented parallel languages. NSC is based on while-loops as opposed to general recursion. A formal, machine independent definition of the parallel time complexity and the work complexity of programs in NSC is given. Our main results are: (1) we give a translation method for a particular form of recursion, called map-recursion, into NSC, that preserves the time complexity and adds an arbitrarily small overhead to the work complexity, and (2) we give a compilation method for NSC into a very simple vector parallel machine, which preserves the time complexity and again adds an arbitrarily small overhead to the work complexity. DTIC

N95-29420# Massachusetts Inst. of Tech., Lexington, MA.
THE MESH SYNCHRONOUS PROCESSOR MeshSP (TRADEMARK)
I. H. Gilbert and W. S. Farmer 14 Dec. 1994 99 p
(Contract F19628-95-C-0002)
(AD-A289875; TR-1004) Avail: CASI HC A05/MF A02

The Mesh Synchronous Processor (MeshSP) is a parallel computer architecture, primarily SIMD, combining high throughput with modest size, weight, power, and cost. Each MeshSP processor node consists of a single DSP chip: the ADSP-21060 (SIIARC) chip of Analog Devices Inc. The MeshSP-1 processor, a hardware realization of the MeshSP, incorporates an 8 X 8 array of ADSP-21060 chips, providing a peak throughput of 7 GFlops. The processor is programmed in ANSI C or C++ with no parallel extensions. A combination of on-chip DMA hardware and system software makes data I/O and interprocessor communication uniquely simple. The MeshSP is easily programmed to solve a wide variety of computationally demanding signal-processing problems. A functional Simulator enables MeshSP algorithms to be coded and tested on a personal computer. Some example applications are described. DTIC

N95-29454*# National Aeronautics and Space Administration. Langley Research Center, Hampton, VA.
TRANSPORT DELAYS ASSOCIATED WITH NASA LANGLEY FLIGHT SIMULATION FACILITY
R. Marshall Smith, Victoria I. Chung, and Debbie Martinez Feb. 1995 10 p
(RTOP 505-90-53-02)
(NASA-TM-110150; NAS 1.15:110150) Avail: CASI HC A02/MF A01

This paper describes the transport delays associated with flight simulation programs currently operating at the NASA Langley Research Center (LaRC). Formulas are presented for calculating a rough estimate of the transport delay for a particular simulation. Various simulation programs that used the Flight Simulation Facility at LaRC, during the period of October 1993 to March 1994, were tested to determine the transport delays associated with the simulation program and any associated hardware. Several simulators were tested, including the Differential Maneuvering Simulator (DMS), the Visual Motion Simulator (VMS), and the Transport System Research Vehicle (TSRV). Author

N95-29566# Kent State Univ., OH. Inst. for Computational Mathematics.
HIGH-LEVEL PARALLEL PROGRAMMING TOOLS FOR FINITE ELEMENT ANALYSIS Final Report, 1 May 1991 - 31 Jul. 1994
Paul S. Wang 17 Oct. 1994 4 p
(Contract DAAL03-91-G-0149)
(AD-A290566; ARO-28908.4-MA) Avail: CASI HC A01/MF A01

Automatic generation of sequential and parallel programs can bring the power of modern computers to more engineers and scientists. The project investigated parallel code generation and automatic derivation of parallel finite element routines. Software packages GENCRAY, a code translator producing Cray Fortran, and PIER, a finite element code derivation system, have been constructed as research tools. DTIC

N95-29760# Air Force Inst. of Tech., Wright-Patterson AFB, OH. School of Engineering.
PARALLELIZATION OF THE 2D ROE SCHEME ON THE INTEL PARAGON M.S. Thesis
John R. Graham, III Dec. 1994 100 p
(AD-A290690; AFIT/GCS/ENG/94D-04) Avail: CASI HC A05/MF A02

This study presented a methodology for determining the general performance characteristics of a computational fluid dynamics (CFD) algorithm on the Intel Paragon. By performing a rigorous time complexity analysis of a parallel CFD algorithm, the general performance could be characterized before the code was actually parallelized. This was shown by implementing a serial version of the 2-D Roe Scheme on the Paragon. This explicit code was parallelized by the addition of generic yet efficient routines that decomposed the domain, automatically adjusted partition indices, and performed 2-D and 3-D buffer exchanges. Additionally, efficient global routines available for the Paragon were used in order to reduce the overall complexity of the parallel implementation. Comparison of the predicted performance and the measured performance showed that for the Roe Scheme, the general performance characteristics on the Intel Paragon could be accurately predicted. While a complexity analysis of the Beam-Warming algorithm was performed, a working parallel implementation on the Paragon was not completed. DTIC

N95-29823*# National Aeronautics and Space Administration. Langley Research Center, Hampton, VA.
DEFINING THE IEEE-854 FLOATING-POINT STANDARD IN PVS
Paul S. Miner Jun. 1995 24 p
(RTOP 505-64-10-13)
(NASA-TM-110167; NAS 1.15:110167) Avail: CASI HC A03/MF A01

A significant portion of the ANSI/IEEE-854 Standard for Radix-Independent Floating-Point Arithmetic is defined in PVS (Prototype Verification System). Since IEEE-854 is a generalization of the ANSI/IEEE-754 Standard for Binary Floating-Point Arithmetic, the definition of IEEE-854 in PVS also formally defines much of IEEE-754. This collection of PVS theories provides a basis for machine checked verification of floating-point systems. This formal definition illustrates that formal specification techniques are sufficiently advanced that is is reasonable to consider their use in the development of future standards. Author

N95-29915# Georgia Inst. of Tech., Atlanta, GA.
DPARTS. A DYNAMIC PARALLEL ADAPTIVE MULTIPROCESS OR REAL-TIME SCHEDULER Progress Report No. 1, 1 Jul. 1993 - 30 Jun. 1994
Byron Jeff and Karsten Schwan 12 Jan. 1995 7 p
(Contract N00014-93-1-0783)
(AD-A291160) Avail: CASI HC A02/MF A01

The research questions addressed in this work focus on the development of fast heuristic algorithms, on experimentation with those algorithms, and on the use of such algorithms within the music applications. We are not developing optimal algorithms since all of the scheduling and assignment problems we are addressing have been shown NP-hard. Some specific questions we are addressing include: When should DPARTS be invoked? What is the required frequency of DPARTS invocation with respect to the latency of scheduling decisions and the overheads incurred by scheduling? Should DPARTS have the option of rescheduling existing tasks if such rescheduling can result in the successful scheduling of otherwise unschedulable process sequences? Deadline semantics. In our sample music application, precise deadlines are usually not necessary in order to produce acceptable results. As such we are evaluating what type of semantics are appropriate for addressing the application we are scheduling. DTIC

N95-29985# Argonne National Lab., IL.
COMPUTATIONAL RESULTS FOR PARALLEL UNSTRUCTURED MESH COMPUTATIONS
M. T. Jones (Tennessee Univ., Knoxville, TN.) and P. E. Plassmann 1994 20 p Presented at the 3rd National Symposium on Large-scale Structural Analysis for High-performance Computers and Workstations, Norfolk, VA, 8-11 Nov. 1994

(Contract W-31-109-eng-38)
(DE95-005856; ANL/MCS/CP-84514; CONF-9411205-1) Avail: CASI HC A03/MF A01

The majority of finite element models in structural engineering are composed of unstructured meshes. These unstructured meshes are often very large and require significant computational resources; hence they are excellent candidates for massively parallel computation. Parallel solution of the sparse matrices that arise from such meshes has been studied heavily, and many good algorithms have been developed. Unfortunately, many of the other aspects of parallel unstructured mesh computation have gone largely ignored. The authors present a set of algorithms that allow the entire unstructured mesh computation process to execute in parallel - including adaptive mesh refinement, equation reordering, mesh partitioning, and sparse linear system solution. They briefly describe these algorithms and state results regarding their running-time and performance. They then give results from the 512-processor Intel DELTA for a large-scale structural analysis problem. These results demonstrate that the new algorithms are scalable and efficient. The algorithms are able to achieve up to 2.2 gigaflops for this unstructured mesh problem. DOE

N95-30102# Technische Univ., Twente (Netherlands). Tele-Informatics and Open Systems Group.
CAUSAL BEHAVIOURS AND NETS
J. P. Katoen 22 Nov. 1994 33 p
(PB95-197612; Memo-INF-94-70) Copyright Avail: CASI HC A03/MF A01

In this paper we consider a specification formalism in which causal relations between actions play a central role and provide a semantics in terms of (an extension of) labeled place/transition nets. The formalism belongs to the category of true concurrency approaches, allowing the expression of interleaving of actions at a syntactical level. The behavior of nets is defined by families of labeled partially ordered sets. Based on this partial-order semantics two expansion theorems are defined that enable composed specifications to be rewritten into equivalent monolithic ones. NTIS

N95-30104 Technische Univ., Twente (Netherlands). Dept. of Computer Science.
LAYERS AS KNOWLEDGE TRANSITIONS IN THE DESIGN OF DISTRIBUTED SYSTEMS
W. Janssen Dec. 1994 30 p Limited Reproducibility: More than 20% of this document may be affected by poor print and microfiche quality
(PB95-197638; Memo-INF-94-71) Copyright Avail: Issuing Activity (National Technical Information Service (NTIS))

Knowledge based logics allow one to give specifications of classes of network protocols. This genericity is combined with methods to derive sequentially structured or layered implementations of distributed algorithms. Knowledge based logic is used to specify layers in such algorithms as knowledge transitions. The resulting layered implementations are transformed to distributed algorithms by means of a transformation rule based on the principle of communication closed layers. This design technique for distributed algorithms is applied to a class of Two-Phase Commit protocols and an algorithm to compute minimal distances in networks. NTIS

N95-30116# Sandia National Labs., Albuquerque, NM.
DISTRIBUTED MULTITASKING ITS WITH PVM
Wesley C. Fan and John A. Halbleib, Sr. 1995 5 p Presented at the Annual Meeting of the American Nuclear Society, Philadelphia, PA, 25-29 Jun. 1995
(Contract DE-AC04-94AL-85000)
(DE95-006821; SAND-95-0140C; CONF-950601-3) Avail: CASI HC A01/MF A01

Advances of computer hardware and communication software have made it possible to perform parallel-processing computing on a collection of desktop workstations. For many applications, multitasking on a cluster of high-performance workstations has achieved performance comparable or better than that on a traditional supercomputer. From the point of view of cost-effectiveness, it also allows users to exploit available but unused computational resources, and thus achieve a higher performance-to-cost ratio. Monte Carlo calculations are inherently parallelizable because the individual particle trajectories can be generated independently with minimum need for interprocessor communication. Furthermore, the number of particle histories that can be generated in a given amount of wall-clock time is nearly proportional to the number of processors in the cluster. This is an important fact because the inherent statistical uncertainty in any Monte Carlo result decreases as the number of histories increases. For these reasons, researchers have expended considerable effort to take advantage of different parallel architectures for a variety of Monte Carlo radiation transport codes, often with excellent results. The initial interest in this work was sparked by the multitasking capability of MCNP on a cluster of workstations using the Parallel Virtual Machine (PVM) software. On a 16-machine IBM RS/6000 cluster, it has been demonstrated that MCNP runs ten times as fast as on a single-processor CRAY YMP. In this paper, we summarize the implementation of a similar multitasking capability for the coupled electron/photon transport code system, the Integrated TIGER Series (ITS), and the evaluation of two load balancing schemes for homogeneous and heterogeneous networks. DOE

N95-30128# Los Alamos National Lab., NM.
HIPPI - GIGABIT LANS ARE HERE TODAY
D. E. Tolmie and S. C. Tenbrink 1995 4 p Presented at the NetWorld and Interop 1995, Las Vegas, NV, 29 Mar. 1995
(Contract W-7405-eng-36)
(DE95-007877; LA-UR-95-476; CONF-9503103-1) Avail: CASI HC A01/MF A01

The need for higher speed data transmission led to the development of the High-Performance Parallel Interface (HIPPI) ANSI standards supporting data rates of 800 Mbit/s and 1.6 Gbit/s. HIPPI-based equipment first appeared in 1988, and HIPPI is currently the interface of choice in the gigabit-per-second range. While HIPPI has limitations, it is expected to be heavily used until equipment based on the emerging ATM and Fibre Channel standards mature. This paper covers the development of the HIPPI standards, some HIPPI-based devices, and the advantages and shortcomings of HIPPI. DOE

N95-30192# Lawrence Livermore National Lab., Livermore, CA.
REQUIREMENTS FOR A PORTABLE PARALLEL I/O LIBRARY FOR SCIENTIFIC COMPUTATION
R. K. Yates 1 Dec. 1994 6 p
(Contract W-7405-eng-48)
(DE95-009383; UCRL-ID-119527) Avail: CASI HC A02/MF A01

We outline the requirements for a potable parallel I/O library to serve developers of parallel programs for scientific applications on massively parallel processors. DOE

N95-30193# Lawrence Livermore National Lab., Livermore, CA.
MASSIVELY PARALLEL FAST ELLIPTIC EQUATION SOLVER FOR THREE DIMENSIONAL HYDRODYNAMICS AND RELATIVITY
P. L. Sholl, J. R. Wilson, G. J. Mathews, and J. H. Avila (San Jose State Univ., CA.) Jan. 1995 17 p
(Contract W-7405-eng-48)
(DE95-009385; UCRL-ID-119803) Avail: CASI HC A03/MF A01

Through the work proposed in this document we expect to advance the forefront of large scale computational efforts on massively parallel distributed-memory multiprocessors. We will develop tools for effective conversion to a parallel implementation of sequential numerical methods used to solve large systems of partial differential equations. The research supported by this work will involve conversion of a program which does state of the art modeling of multi-dimensional hydrodynamics, general relativity and particle transport in energetic astrophysical environments. The proposed parallel algorithm development, particularly the study and development of fast elliptic equation solvers, could significantly benefit this program and other applications involving solutions to systems of differential equations. We shall develop a data communication manager for distributed memory computers as an aid in program conversions to a parallel environment and implement it in the three dimensional relativistic hydrodynamics program discussed below; develop a concurrent system/concurrent subgrid multigrid method. Currently, five systems are approximated sequentially using multigrid successive overrelaxation. Results from an iteration cycle of one multigrid system are used in following multigrid systems iterations. We shall develop a multigrid algorithm for simultaneous computation of the sets of equations. In addition, we shall implement a method for concurrent processing of the subgrids in each of the multigrid computations. The conditions for convergence of the method will be

examined. We'll compare this technique to other parallel multigrid techniques, such as distributed data/sequential subgrids and the Parallel Superconvergent Multigrid of Frederickson and McBryan. We expect the results of these studies to offer insight and tools both for the selection of new algorithms as well as for conversion of existing large codes for massively parallel architectures. DOE

N95-30215# Los Alamos National Lab., NM.
BICRITERIA NETWORK DESIGN PROBLEMS
M. V. Marathe, R. Ravi, R. Sundaram, S. S. Ravi, D. J. Rosenkrantz, and H. B. Hunt, III 1994 16 p Presented at the Conference on Functional Programming Languages and Computer Architectures, La Jolla, CA, 26-28 Jun. 1995
(Contract W-7405-eng-36)
(DE95-005261; LA-UR-94-4088; CONF-950644-1) Avail: CASI HC A03/MF A01

We study several bicriteria network design problems phrased as follows: given an undirected graph and two minimization objectives with a budget specified on one objective, find a subgraph satisfying certain connectivity requirements that minimizes the second objective subject to the budget on the first. Define an (alpha, beta)-approximation algorithm as a polynomial-time algorithm that produces a solution in which the first objective value is at most alpha times the budget, and the second objective value is at most alpha times the minimum cost of a network obeying the budget oil the first objective. We present the first approximation algorithms for bicriteria problems obtained by combining classical minimization objectives such as the total edge cost of the network, the diameter of the network and a weighted generalization of the maximum degree of any node in the network. We first develop some formalism related to bicriteria problems that leads to a clean way to state bicriteria approximation results. Secondly, when the two objectives are similar but only differ based on the cost function under which they are computed we present a general parametric search technique that yields approximation algorithms by reducing the problem to one of minimizing a single objective of the same type. Thirdly, we present an O(log n, log n)-approximation algorithm for finding a diameter-constrained minimum cost spanning tree of an undirected graph on n nodes generalizing the notion of shallow, light trees and light approximate shortest-path trees that have been studied before. Finally, for the class of treewidth-bounded graphs, we provide pseudopolynomial-time algorithms for a number of bicriteria problems using dynamic programming. These pseudo-polynomial-time algorithms can be converted to fully polynomial-time approximation schemes using a scaling technique. DOE

N95-30295# Stanford Univ., CA.
PARALLEL ADAPTIVE FINITE ELEMENT: SOFTWARE FOR SEMICONDUCTOR DEVICE SIMULATION
Robert W. Dutton, Kincho H. Law, Peter M. Pinsky, Narayana R. Aluru, and Bruce P. Herndon 12 Jan. 1995 240 p
(AD-A291149) Avail: CASI HC A11/MF A03

Parallel algorithms and fully functional application codes for 2D and 3D device analysis of semiconductor devices have been demonstrated. Advanced modeling based on a hydrodynamic formulation (HD) of the semiconductor transport equations and using a Galerkin Least Squares Finite Element Method (GLS-FEM) has demonstrated nearly ideal parallel performance for 2D MOS and bipolar transistor applications across Intel and IBM machines. Parallelization of conventional drift-diffusion (DD) based device solvers has broken new ground in both direct and iterative solvers. A well-known application code, PISCES, has been parallelized and ported across Intel, TMC, and IBM architectures with best results to date that now approach 6.5 GFlops sustained performance on a 128 node IBM SP/2. A prototype 3D code (STRIDE) which uses iterative methods has parallelized preconditioners for ILU(O), ILU(1), and ILUV and achieved excellent benchmarks on both the Intel and IBM machines. A 4.9 million grid problem run on the Intel Delta machine achieved 20% efficiency using 512 nodes and convergent solutions for a highly nonlinear bipolar transistor problem in 20 minutes per bias point. In support of both 2D and 3D TCAD applications, a new geometry-based structure generator called VIP3D was created. Quad- and oct-tree utilities were developed and used to support the gridding of complex IC structures benchmarked in this work. Results of industrial impact and collaborative interactions are also discussed. DTIC

N95-30150*# Pennsylvania State Univ., University Park, PA. Dept. of Aerospace Engineering.
TIME ACCURATE APPLICATION OF THE MACCORMACK 2-4 SCHEME ON MASSIVELY PARALLEL COMPUTERS
Dale A. Hudson and Lyle N. Long *In* NASA. Langley Research Center, ICASE/LaRC Workshop on Benchmark Problems in Computational Aeroacoustics (CAA) May 1995 p 209-215 (For primary document see N95-30133 10-71)
(Grant NAG1-1479)
Avail: CASI HC A02/MF A04

N95-30156*# Pennsylvania State Univ., University Park, PA. Dept. of Aerospace Engineering.
COMPUTATIONAL AEROACOUSTICS ON MASSIVELY PARALLEL COMPUTERS
Yusuf Oezyoeruek and Lyle N. Long *In* NASA. Langley Research Center, ICASE/LaRC Workshop on Benchmark Problems in Computational Aeroacoustics (CAA) May 1995 p 261-265 (For primary document see N95-30133 10-71)
(Grant NAG1-1367)
Avail: CASI HC A01/MF A04

63 CYBERNETICS

Includes feedback and control theory, artificial intelligence, robotics and expert systems.

For related information see also *54 Man/System Technology and Life Support.*

N95-28788 North Carolina Univ., Chapel Hill, NC.
INTERNATIONAL WORKSHOP ON STOCHASTIC FILTERING THEORY Final Report, 1 Apr. - 31 Dec. 1994 Abstracts Only
G. Kallianpur Jan. 1995 31 p Workshop held in Chapel Hill, NC, 26-28 Jun. 1994 Limited Reproducibility: More than 20% of this document may be affected by microfiche quality
(Contract DAAH04-94-G-0077)
(AD-A291670; ARO-32357.1-MA-CF) Avail: Issuing Activity (Defense Technical Information Center (DTIC))

A total of 39 participants registered and attended this workshop held on the campus of the University of North Carolina in Chapel Hill, to review the most recent advances in major new areas of filtering theory. They came from 17 foreign countries and the United States. There were major talks by 20 distinguished mathematicians and shorter talks by three young researchers in the field. DTIC

N95-28926# Stottler Henke Associates, Inc., Belmont, CA.
ARTIFICIAL INTELLIGENCE TECHNIQUES FOR PARTS OBSOLESCENCE PREDICTION Final Report
Andrea L. Henke and Timothy P. Maher 14 Mar. 1995 99 p
(Contract N00600-94-C-1827)
(AD-A292185) Avail: CASI HC A05/MF A01

The primary objective of our Phase 1 effort was to explore the feasibility of a Navy-wide diminishing manufacturing sources and material shortages (DMSMS) prediction system and develop improved methods of obsolescence prediction. In pursuit of this goal we investigated the DMSMS process at various Navy sites and identified and evaluated tools or processes currently in use. We decided to focus our efforts on micro circuit obsolescence prediction, because our study revealed that other types of parts are not nearly as significant a DMSMS problem. Furthermore, we concentrated on automating the largely manual obsolescence prediction currently performed by the Microcircuit Obsolescence Management (MOM) program. We used the artificial intelligence techniques of knowledge engineering, case-based reasoning, knowledge base development, and object oriented programming to devise a solution to the obsolescence prediction problem. We also developed a preliminary design and functional description for a proactive Navy-wide DMSMS intelligent system which will be developed in a Phase 2 effort. We implemented both these solutions in a prototype to prove their feasibility beyond a doubt. There is great potential for use of the Phase 2 system throughout the Navy, other branches of the military, and in the commercial sector. DTIC

N95-28978# AI WARE, Inc., Cleveland, OH.
PROCESS OPTIMIZATION THROUGH DISCOVERY AND INTEGRATION OF MATERIALS AND PROCESSING PROPERTIES. PHASE 1 Final Report, 1 Jul. - 31 Dec. 1994
Percy Yip Jan. 1995 22 p
(Contract F33615-94-C-5805)
(AD-A292576; WL-TR-95-4019) Avail: CASI HC A03/MF A01

The research objective is to examine process discovery methods for increasing the productivity of materials research with use of computational intelligence paradigms Phase 1 work focused on the study of procedures and enabling technologies to achieve the ultimate goal. The overall work consists of four important tasks. Task 1 was related to process modeling and monitoring. Once this task has been achieved, appropriate control actions can be generated based on an estimation of the current state of a process. In task 2, we focused our study on a feedforward/feedback optimal control methodology with use of neural networks and evolutionary programming. Task 3 was an illustration how a pattern of film thickness estimated from task 1 could be used to formulate an objective function. With such an objective function, appropriate control actions can be generated via an optimal control software. Task 4 was concerned with development of an intelligent visualization display enabling users to understand and discover the process behavior. DTIC

N95-28988# Carnegie-Mellon Univ., Pittsburgh, PA. Dept. of Computer Science.
MANAGEMENT OF SPEEDUP MECHANISMS IN LEARNING ARCHITECTURES Ph.D. Thesis
John Cheng Jan. 1995 167 p Prepared in cooperation with the Advanced Research Projects Agency
(Contract F33615-93-1-1330)
(AD-A292206; CMU-CS-95-112) Avail: CASI HC A08/MF A02

Learning architectures typically operate rather inefficiently. To increase performance, two strategies are commonly used: speedup mechanisms are incorporated into the architecture, and architecture operation is simplified. Unfortunately, both these strategies have drawbacks. Because of the utility problem, inappropriate use of speedup mechanisms can actually decrease system efficiency. Hence, good speedup mechanism management - deciding when, where, and which speedup mechanism to use - is important if the mechanisms are to be effective. Typically, however, good management strategies are not available. Architecture-provided strategies are usually very simple, and cannot use the mechanisms appropriately all the time. Good user-provided strategies are also difficult to develop - under a complex system or domain, it can be difficult to understand system behavior well enough to specify a good management strategy. Furthermore, user or architecture-provided management techniques are usually fixed, and cannot adapt to environment dynamics. Hence, lack of good management strategies limit the effectiveness of speedup mechanisms. DTIC

N95-29095 Stanford Univ., CA.
EXPERIMENTS IN COOPERATIVE MANIPULATION OF OBJECTS BY FREE-FLYING ROBOT TEAMS Ph.D. Thesis
William Charles Dickson 1994 236 p
Avail: Univ. Microfilms Order No. DA9414558

This dissertation makes several contributions to the control of objects using a team of robots. To verify these contributions, laboratory experiments have demonstrated a team of free-flying robots capturing, transporting, and docking a large, freely moving object. In these experiments, the object and robots float on a thin cushion of air over a granite surface plate, simulating in two dimensions the drag-free, zero-gravity conditions of space. A human user commands the object location and orientation through a graphical user interface. The robots then capture and so position the object, with no additional input required from the user. On command, the robots dock the captured object with a second stationary object. This dissertation presents the AUTOMAN (AUtonomous robot Team Object MANipulation) hierarchy developed in this research as a framework for providing object-based task-level control of a system that uses a team of independently operating robots. The AUTOMAN hierarchy implements a carefully chosen set of interfaces between the various elements of the distributed-computation system that maximizes the autonomy of the robots -- under the constraint that the robots must provide cooperative control of a common object. A Decentralized Object-Impedance Controller was developed to allow a team of independently operating robots to work as a team to cooperatively manipulate a common object. The communication interface between a central coordinating processor and the robots is a low-bandwidth specification of a desired object trajectory and a programmable impedance relationship between the object's motion and external forces. Addressing the low-level control of the robots themselves, this dissertation presents the Hybrid-Dynamics controller that uses a novel control approach to assimilated both discrete-valued actuators (such as the on-off thrusters used by the experimental robots) and continuous valued actuators (such as motors) in system applications requiring precise control. The Subsystem-Merging dynamic modelling method has been developed for producing a system model directly from subsystem descriptions. This method takes advantage of simple kinematic relationships to merge subsystem descriptions into a full system model with no need for decomposing the subsystems. The resulting system model is expressed in terms of the subsystem descriptions; thus the model can be interpreted symbolically as well as numerically. Dissert. Abstr.

N95-29109 Ohio State Univ., Columbus, OH.
ON-LINE DAMAGE IDENTIFICATION AND MOTION CONTROL OF ADAPTIVE STRUCTURES: AN INTELLIGENT CONTROL APPROACH Ph.D. Thesis
Po-Yu Tsou 1994 135 p
Avail: Univ. Microfilms Order No. DA9421027

In this dissertation, an on-line damage identification technique and a motion controller for the adaptive structure are developed under the scope of an intelligent control framework. The computational intelligence techniques, especially neural networks and fuzzy logic control, are studied as applied to the adaptive truss structure. The adaptive structure has the ability to change the configuration and/or physical properties amenable to the varying environment or to accomplish various mission requirements. This dissertation first overviews an intelligent control framework specified for the adaptive structures. The intelligent control system consists of three hierarchical levels, from up to down, Management and Organization level, Coordination level, and Execution level. The elementary classification of the levels and the responsibilities of major functions in each level are described in this study. The work then investigates two major functions in the Execution level: structural damage detection and identification, and motion control. A neural-network-based damage identification technique which is able to detect the damage location accurately and then to identify the damage severity with reasonable precision is proposed. The new architecture of a neural network provides several advantages over conventional approaches: first, this technique only needs as few as possible modal data, i.e. eigenvalues and normalized mode shape, to identify structural damages; second, it can detect the multiple damages case; third, the process can be realized on-line, moreover, the damage location detection can be done in real-time. Next, a fuzzy logic controller is used for the motion control of the adaptive truss structure. A systematic procedure to design a fuzzy controller is proposed. The fuzzy rules can be constructed by referring the kinematics of the structure, thus omitting the conventional trial-and-error approach. The controller was tested on several different tasks such as rendezvous/docking, target pursuing, and trajectory tracking. The results show the control scheme is effective and reliable. The effects on the performance by varying design parameters are also investigated. The general guidelines for selecting the design parameters are addressed. Dissert. Abstr.

N95-29144# Society of Instrument and Control Engineers, Tokyo (Japan).
PROCEEDING OF THE 33RD SICE ANNUAL CONFERENCE
1994 708 p Presented at the 33rd SICE (Society of Instrument and Control Engineers) Annual Conference, Tokyo, Japan, 26-28 Jul. 1994
(DE95-758943; CONF-9407173-Pt-2) Avail: CASI HC A99/MF A06

This is proceedings of the Japanese papers presented in the 33rd SICE (the Society of Instrument and Control Engineers) Annual Conference. As for programming, reports are made relating to genetic algorithm and neural network. Also discussed are neural learning, fuzzy control, and adaptation and learning for intelligent control. As to robot, a variety of reports are made such as robotic vision, positioning system, motion control, force control and actuator, and mobile robot. As human engineering approach, discussions are made on human interface and decision making/virtual reality/cooperative control. About sensing, reports are made on biomedical measurement, remote sensing, force sensor, and gas sensing.

Papers are presented on image processing, temperature/acoustical measurement, optical measurement, signal processing, pattern recognition, etc. As to control system, reported are system design, digital control, process control, adaptive control/robust control, control theory, etc. DOE

N95-29183# North Carolina State Univ., Raleigh, NC. Precision Engineering Center.

DESIGN OF A FAST-TOOL SERVO SYSTEM USING MAGNETIC SERVO LEVITATION Progress Report

Paul I. Ro 15 Jan. 1995 33 p

(AD-A290273) Avail: CASI HC A03/MF A01

Magnetic Servo Levitation is proposed as a method to drive a Fast Tool Servo System, in order to compensate for errors resulting from mechanical misalignment, slide vibration, tool wear, and cutting dynamics on a Diamond Turning Machine. Theoretical magnetic equations have provided a basis for electromagnet design. Further analyses have used finite element models to find trends in magnetic properties, as well as assisting in structural design. A T-shaped, state-of-the-art composite structure has been proposed to transfer the electromagnet armature motion to the cutting tool. Flexural bearings are used to guide the T-structure as well as assist motion with their restoring force. Design of these are critical for the success of the servo. A static test fixture has been designed to investigate static forces as a function of coil current and separation gap of the electromagnet and armature. Results show very good correlation with theoretical values. A dynamic test fixture has been designed as well to determine limits in bandwidth, range, and positioning accuracy. Dynamics of the proposed system are discussed, along with simulation issues. Preliminary experimental data from the dynamic fixture are also presented. DTIC

N95-29241 Arizona Univ., Tucson, AZ.

CLOSED LOOP CONTROL OF GUIDED MISSILES USING NEURAL NETWORKS Ph.D. Thesis

Seyed Hossein Sadati 1993 187 p

Avail: Univ. Microfilms Order No. DA9421739

An optimal guidance law for a missile flight is one which determines appropriate controls to produce a flight path such that some mission objective will be achieved in the most efficient manner. Optimal Control Theory is often used to accomplish this task. One must bear in mind, however, that the usefulness of optimal control is sharply divided between two distinct classes of dynamical systems, namely, linear systems and nonlinear systems. For linear systems, the theory is complete in the sense that given a quadratic cost, a closed-loop feedback guidance law may be determined. For nonlinear systems, generally the best one can do is to determine an open-loop guidance law numerically using a software package such as MISER. (Some notable exceptions exist where a complete analytical synthesis of the closed-loop control may be obtained for nonlinear systems. Although open-loop optimal guidance laws for nonlinear systems can now be computed quite efficiently with the advances of sophisticated numerical techniques along with high-speed digital computers, the highly-nonlinear and complex dynamics of missiles precludes the possibility of on-line implementation of open-loop optimal control. It has always been realized that if optimal closed-loop solutions could be obtained for comprehensive nonlinear systems such as missiles, then guidance laws based on such results would be superior to any other guidance laws available today. This superiority is due to, among other things, the elimination of some of the restrictive, and in many cases unrealistic assumptions made in the derivation of most current guidance laws in use such as, for instance, 'tail-chase', unbounded control, simplified dynamics and/or aerodynamics, and non-maneuvering target, to name a few. In this study, an optimal closed-loop control law is obtained off-line by means of a Neural Network which is then used as an on-line controller for a generic missile. In the nonlinear case, the missile/target scenario is set up as a mathematical model using realistic dynamics. Then, given a Performance Index, the open-loop control is obtained by solving the problem using the optimal control software MISER for a number of different initial configurations. These open-loop solutions are then used to 'teach' a neural network via backpropagation. Through simulation, it is then demonstrated how well the neural network performs as a feedback controller. The miss distance as well as the value of the Performance Index are used as measures of performance to be compared under the original open-loop control and the neural network closed-loop control. This problem is further extended to include a time lag in the missile dynamics. The effect of this time delay in the overall performance of the optimal controller is then examined. Dissert. Abstr.

N95-29251 Purdue Univ., West Lafayette, IN.

LINEAR AND NONLINEAR DISCRETE-TIME STATE-SPACE MODELING OF DYNAMIC SYSTEMS FOR CONTROL APPLICATIONS Ph.D. Thesis

Eduardo Alves Rodrigues 1993 170 p

Avail: Univ. Microfilms Order No. DA9420895

This research proposes a methodology to model a class of nonlinear dynamic systems, known as linear-analytic systems, by discrete-time state-space models. The method is based on a series of deterministic simulations of the differential equations of motion using well designed step-like input functions. The simulation results are processed to generate a vector series characterizing the selected discrete-time state-space model. A realizations algorithm developed in this research is then applied to the computed vector series in order to obtain the matrices describing the state-space model. It is shown that the vector series obtained from the simulation results are discrete-time triangular Volterra kernels. Therefore, the designed simulations can be viewed as a new method to identify discrete-time Volterra kernels. Nevertheless, the emphasis here is in generating state-space models, since they are more attractive for design and analysis of control systems than the Volterra system representation. The novelty of the methodology being proposed is the fact it does not require continuous-time state-space modeling of the system as an intermediate step in the process: it goes from nonlinear differential equations directly to discrete-time state-space models. Such a philosophy seems attractive in the modeling of dynamic systems immersed in air flow fields, with aerodynamic forces being computed through the use of CFD codes. The main disadvantage in the methodology is that the number of simulations grows exponentially with the discrete-time model order, a direct consequence of the number of parameters needed to be fed into the nonlinear realizations algorithm. Nevertheless, since each simulation is independent of the others, the simulations could be carried out by parallel processing in modern computers, reducing the total time necessary to obtain the simulations by a factor equal to the number of processors available in the parallel processing. Applications are first made to the modeling of simple dynamic systems containing nonlinearities caused by the presence of trigonometric functions on the differential equations of motion. Subsequently, the methodology is applied to an aeroservoelastic system containing nonlinear phenomena caused by transonic unsteady aerodynamics. Dissert. Abstr.

N95-29477# Massachusetts Inst. of Tech., Cambridge, MA.

AUTOMATED REASONING ABOUT CLASSICAL MECHANICS

Leon Wong May 1994 108 p

(Contract N00014-91-J-4038)

(AD-A290052; MIT-AI-TR-1488) Avail: CASI HC A06/MF A02

In recent years, researchers in artificial intelligence have become interested in replicating human physical reasoning talents in computers. One of the most important skills in this area is predicting how physical systems will behave. This thesis discusses an implemented program that generates algebraic descriptions of how systems of rigid bodies evolve over time. Discussion about the design of this program identifies a physical reasoning paradigm and knowledge representation approach based on mathematical model construction and algebraic reasoning. This paradigm offers several advantages over methods that have become popular in the field, and seems promising for reasoning about a wide variety of classical mechanics problems. DTIC

N95-29479# Massachusetts Inst. of Tech., Cambridge, MA.

NEURAL NETWORK EXPLORATION USING OPTIONAL EXPERIMENT DESIGN

David Cohn Jun. 1994 13 p

(AD-A290058; AIM-1491; CBCL-99) Avail: CASI HC A03/MF A01

We consider the question 'How should one act when the only goal is to learn as much as possible?' Building on the theoretical results of Fedorov (1972) and MacKay (1992), we apply techniques from Optimal Experiment Design (OED) to guide the query/action selection of a neural network learner. We demonstrate that these techniques allow the learner to minimize its generalization error by exploring its domain efficiently and completely. We conclude that, while not a panacea, OED-based query/action has

much to offer, especially in domains where its high computational costs can be tolerated. DTIC

N95-29499# Naval Command, Control and Ocean Surveillance Center, San Diego, CA.
DEVELOPMENT OF AN ARTIFICIAL NEURAL NETWORK FOR REAL-TIME CLASSIFICATION OF CONE PENETROMETER STRAIN GAUGE DATA Final Report
John M. Andrews and Stephen H. Lieberman Oct. 1994 29 p
(AD-A290719; NRAD-TR-1682) Avail: CASI HC A03/MF A01

This document describes the development of an artificial neural-network-based algorithm for classifying soil behavior type from cone penetrometer strain gauge data. The network input consists of the two standard cone penetration test parameters: the logarithm of cone pressure and the percentage of sleeve friction to cone pressure (friction ratio). Network output is a one-of-n coding of 12 soil classifications. Three- and four-layer backpropagation networks are trained to associate 11,000 data points with the appropriate soil type. The best recall performance is obtained from a four-layer, 2 x 15 x 15 x 12 network with a tested accuracy rate of 98.2%. All classification errors occur at the decision boundaries between class regions. The network was incorporated into the data collection software of the prototype SCAPS vehicle in October 1993. The C source code is included as appendix A. DTIC

N95-29544 Cincinnati Univ., OH.
PERIODIC AND NONSMOOTH OPTIMAL CONTROL PROBLEMS GOVERNED BY PARTIAL DIFFERENTIAL EQUATIONS Ph.D. Thesis
Feiyue He 1993 115 p
Avail: Univ. Microfilms Order No. DA9416787

This thesis considers four different optimal control problems. In chapter 2, we studied the optimal harvesting control of a biological species, whose growth is governed by the parabolic diffusive Volterra-Lotka equation. We proved that such equation with L(infinity) periodic coefficients has a unique positive solution. We show the existence and uniqueness of an optimal control, and under certain conditions we characterize the optimal control in terms of a parabolic optimal system. A monotone sequence which converges to the optimal control is constructed. In chapter 3, we considered the competing case for the same optimal control problem discussed in chapter 2 and similar results have been obtained. In chapter 4, an optimal control problem governed by a class of delay semi linear differential equations have been studied. The maximum principle and approximating schemes have been found. As applications, three examples have been discussed. Finally, in chapter 5, an optimal control problem, when the state equation is an elliptic equation with a distribution on the right hand side, is considered. The associated functional is not differentiable. We prove existence and compute the multi-valued generalized gradient. Dissert. Abstr.

N95-29548 Massachusetts Inst. of Tech., Cambridge, MA.
BROADBAND CONTROL OF STRUCTURAL VIBRATION USING SIMULTANEOUS SENSING AND ACTUATION WITH NONLINEAR PIEZOELECTRIC ELEMENTS Ph.D. Thesis
Ronald L. Spangler, Jr. 1994
Avail: Issuing Activity (MIT Libraries, Rm. 14-0551, Cambridge, MA 02139-4307)

This thesis describes the design of a broadband structural vibration control system, in which piezoelectric materials are used simultaneously as sensor and actuator in a truly collocated feedback architecture. Collocation allows the use of positive real compensation to guarantee stability. A new non-reverberant positive real compensator design is presented. Application of positive real techniques to the design of passive electrical shunting networks for the piezoelectric element is explored. The stability guarantee is absolute in this case. Broadband performance is shown to be limited by the relatively large piezoelectric capacitance. Alternatively, an active approach is considered, in which the piezoelectric element is placed in a capacitive bridge. The transfer function from bridge driving voltage to output is free of any limitations imposed by the piezoelectric capacitance, provided the circuit parameters are properly chosen. A comprehensive treatment of this bridge tuning is presented, and simple modification by integration or differentiation of the output is shown to create a positive real plant. Preliminary experiments show that nonlinearities in the piezoelectric material limit the precision of bridge tuning, thus limiting the resolution of structural modes, and also the closed-loop performance. This nonlinearity is investigated, and is found to be effectively separable into phase and gain effects in the bridge transfer function. The phase difficulty is eliminated by modifying the bridge design to include local charge feedback. Closed-loop experiments on the SERC interferometer testbed, using several piezoelectric struts and the modified bridge circuit, show much improved performance. Results of a further series of tests illustrate the limitation imposed on the modified system by the gain nonlinearity. Dissert. Abstr.

N95-29574# Institute for the Study of Learning and Expertise, Palo Alto, CA.
OBLIVIOUS DECISION TREES AND ABSTRACT CASES Interim Report, 1 Mar. - 31 Jul. 1994
Pat Langley and Stephanie Sage 1 Aug. 1994 7 p Submitted for publication in Working Notes of the AAAI Workshop on Case-Based Reasoning
(Contract N00014-94-1-0505)
(AD-A292577; ISLE-TR-94-1) Avail: CASI HC A02/MF A01

In this paper, we address the problem of case-based learning in the presence of irrelevant features. We review previous work on attribute selection and present a new algorithm, OBLIVION, that carries out greedy pruning of oblivious decision trees, which effectively store a set of abstract cases in memory. We hypothesize that this approach will efficiently identify relevant features even when they interact, as in parity concepts. We report experimental results on artificial domains that support this hypothesis, and experiments with natural domains that show improvement in some cases but not others. In closing, we discuss the implications of our experiments, consider additional work on irrelevant features, and outline some directions for future research. DTIC

N95-29577# Institute for the Study of Learning and Expertise, Palo Alto, CA.
APPLICATIONS OF MACHINE LEARNING AND RULE INDUCTION Interim Report, 1 Aug. 1994 - 1 Feb. 1995
Pat Langley and Herbert A. Simon (Carnegie-Mellon Univ., Pittsburgh, PA.) 15 Feb. 1995 20 p Submitted for publication in Communications of the Association for Computing Machinery Prepared in cooperation with Stanford Univ., and Carnegie Mellon Univ.
(Contracts N00014-94-1-0505; N00014-94-1-0746; F49620-94-1-0118)
(AD-A292607; ISLE-TR-95-1) Avail: CASI HC A03/MF A01

An important area of application for machine learning is in automating the acquisition of knowledge bases required for expert systems. In this paper, we review the major paradigms for machine learning, including neural networks, instance-based methods, genetic learning, rule induction, and analytic approaches. We consider rule induction in greater detail and review some of its recent applications, in each case stating the problem, how rule induction was used, and the status of the resulting expert system. In closing, we identify the main stages in fielding an applied learning system and draw some lessons from successful applications. DTIC

N95-29636# Massachusetts Inst. of Tech., Cambridge, MA. Dept. of Electrical Engineering and Computer Science.
FUNDAMENTAL LIMITATIONS AND CAPABILITIES OF ROBUST IDENTIFICATION AND ADAPTIVE CONTROL Final Report
M. A. Dahleh and J. N. Tsitsiklis 17 Jan. 1995 167 p
(Grant AF-AFOSR-0368-91)
(AD-A291085; AFOSR-95-0101TR) Avail: CASI HC A08/MF A02

In the past decade, a powerful theory for designing robust control systems has emerged. Starting with a model, and a description of the uncertainty (structured, parametric etc.), a controller can be designed to meet a variety of performance specifications. This development, however, has not been accompanied by parallel development in system identification methods by which a plant model and a description of uncertainty is provided. In an attempt to bridge this gap, a new area of research in robust identification has emerged in the last few years. DTIC

N95-29657# Lockheed Missiles and Space Co., Albuquerque, NM.
PRECISION POINTING EXPERIMENT Final Report, 23 Feb. 1989 - 30 Sep. 1994
Richard C. Smith, Ross Blankinship, Marshall Edwards, Ed Weston, and Brian Hamilton Oct. 1994 193 p
(Contract F29601-89-C-0015)
(AD-A291015; PL-TR-94-1014) Avail: CASI HC A09/MF A03

The objective of the Spice Program was to demonstrate improvement in precision pointing, tracking, and retargeting by integration of active isolation, active and passive structural control, advanced materials, active optics, and adaptive control. Experiments were carried out on a full-size and well- characterized precision test-bed that represented a space laser structure. In the Precision Pointing Experiment, an active control system that combined low authority local rate feedback and high authority global control was designed with the goal of achieving 50:1 attenuation of line-of-sight jitter in the 5- to 500-Hz band. The jitter was due to disturbances input at the base of the structure and at the simulated secondary mirror. A custom suite of optical sensors allowed determination of the line of sight of the structure. Proof mass actuators of unprecedented force and linearity were developed during this and preceding subtasks. A series of tests culminated with the attainment of repeatable attenuation of line-of-sight jitter by 75:1 in the band 5 to 500 Hz with little spillover into unmodeled structural modes or unregulated degrees of freedom. The control system proved to be robust, with gain margin greater than 1.75 demonstrated. Comparison of measure transfer functions with those calculated from the structural model used in the control system design showed that high controller performance does not require unreasonable structural model accuracy. DTIC

N95-29720 Pennsylvania State Univ., University Park, PA.
NEURAL NETWORK-BASED DECISION SUPPORT FOR INCOMPLETE DATABASES Ph.D. Thesis
Bo Jin 1993 272 p
Avail: Univ. Microfilms Order No. DA4914306

The idea of applying neural network techniques to handling large databases containing incomplete information is presented. In an incomplete relational database model, maybe algebra operations are introduced to provide the user the opportunity to investigate the potential set of data values in order to draw his/her own conclusions. While such a set of operations allows a better information utilization it can be the source of problems which should be taken into consideration. In a large database system, the data generated by maybe algebra operations can be enormous in size, erroneous in semantics, and less informative. To allow the maybe algebra operations to be practical, it is desired to develop a mechanism to increase the quality and integrity of the results, i.e., to filter out the erroneous and less informative data. A neural network-based decision support system is proposed to improve database performance in the presence of missing/incomplete information, provide intelligent assistance to the end-user, and explore the learning capability of a neural network-based system. The proposed system has a strong learning capability and adjusts itself according to the specific characteristics of the underlying database and the user special requirements. To support the automated training pair generation, the fuzzy logic technique is incorporated into the knowledge acquisition module to oversee, guide, and update the quality status of each training pattern. By approximate reasoning, the fuzzy controller works in a fashion that automatically incorporates the intrinsic ambiguities, imprecision, and undecidabilities associated with the quality status of each training pattern. Issues of enhancing the functionality of the decision support system are studied with a concentration on data representation for the decision-making network and multi-network configurations. Dissert. Abstr.

N95-29831# Naval Command, Control and Ocean Surveillance Center, San Diego, CA. Research, Development, Technology and Evaluation Div.
NEURAL NETWORK CONSTRUCTION USING EVOLUTIONARY SEARCH
J. R. McDonnell, W. C. Page, and D. E. Waagen (TRW Systems Integration Group, Ogden, UT.) Dec. 1994 10 p
(NR Proj. ZW6-7)
(AD-A290862) Avail: CASI HC A02/MF A01

This work investigates the application of evolutionary search for training candidate hidden units in cascade-correlation learning architectures. A hybrid evolutionary search algorithm which implements techniques from evolutionary programming and evolution strategies is proposed. This approach is evaluated on selected low-dimensional examples which are non-linearly separable. DTIC

N95-29863# David Sarnoff Research Center, Princeton, NJ.
HYBRID PYRAMID/NEURAL NETWORK VISION SYSTEM Research and Development Status Report, 1 Sep. - 30 Nov. 1994
John Pearson, Paul Sajda, and Clay Spence 30 Nov. 1994 5 p
(Contract N00014-93-C-0202)
(AD-A290565) Avail: CASI HC A01/MF A01

As part of the goal for automating pattern tree learning, the authors have tested whether a neural network can be trained to discover a single salient component which discriminates targets from non-targets. For the building-detection problem, a second network has been trained to find a different salient component than the first. The neural network/pyramid architecture has been applied to the detection of microcalcifications in mammograms. A curious side-issue of the microcalcification problem is that the coordinates for the microcalcifications frequently did not match their apparent positions in the mammograms. Two possible objective functions for training a network in such circumstances were developed, with the usual argument for the cross-entropy error function as a model. CASI

N95-29874# Air Force Systems Command, Wright-Patterson AFB, OH. National Air Intelligence Center.
PROGRESS AND TRENDS OF MULTI-VALUED LOGIC RESEARCH
Mu Hou 6 Jan. 1995 19 p Transl. into ENGLISH from Jisuanji Xuebao, China, v. 15, no. 1, 1992 p 55-60
(AD-A290997; NAIC-ID(RS)T-0399-94) Avail: CASI HC A03/MF A01

This paper summarizes the progress made in the multivalued logic research during recent years in China, with emphasis on introducing some representative results. Analyses are made on the recent trend in the multivalued logic research in the world, with emphasis given to the relationship between multivalued logic research with respect to molecular computers, optical computers, and artificial intelligence, etc. DTIC

N95-29971# Washington Univ., Saint Louis, MO. Dept. of Systems Science and Mathematics.
NONLINEAR CONTROL SYSTEMS Final Report, 15 Aug. 1991 - 14 Oct. 1994
C. I. Byrnes 13 Dec. 1994 36 p
(Grant AF-AFOSR-0226-91)
(AD-A291083; SSM-94-06; AFOSR-95-0080TR) Avail: CASI HC A03/MF A01

The ability to systematically control dominant nonlinear effects in the evolution of complex dynamical systems is an important research goal, with applications in several existing and emerging DOD research and development programs. The research we describe here is aimed at the development of a control methodology for lumped and distributed parameter systems, similar in scope and applicability to classical automatic control design for lumped linear systems. This program is aimed at the systematic development of feedback design methodologies for shaping, or at least influencing, the response of a broad class of nonlinear systems. DTIC

N95-29979# Texas A&M Univ., College Station, TX.
ROBUST TESTING OF CELLULAR NEURAL NETWORKS
Jose PinedadeGyvez 1 Feb. 1995 19 p
(Contract N00014-94-1-0516)
(AD-A291219; Rept-93-549/4) Avail: CASI HC A03/MF A01

A method for detecting circuit faults within two dimensional Cellular Neural Network (CNN) arrays is presented. The need to develop robust methods for detecting faults is driven by the lack of visibility of the internal nodes in VLSI implementations of CNN arrays. The method is composed of both behavioral and parametric tests and detects faults independent of the size or topology of the CNN array. The behavioral tests reveal nodes that exhibit opened, shorted, or stuck-at a supply voltage faults. The parametric tests reveal excessive time constant mismatches, impedance mismatches and voltage offsets. Seven fault cases are introduced into a macromodel of a voltage mode CNN array to provide insight to the usefulness of the proposed testing methodology. DTIC

N95-29987# Argonne National Lab., IL.
MAGNETIC DAMPING FOR MAGLEV
S. S. Chen, S. Zhu, Y. Cai, and D. M. Rote 1994 28 p Presented at the American Society of Mechanical Energy (ASME) Annual Winter Meeting, Atlanta, GA, 14-16 Nov. 1994
(Contract W-31-109-eng-38)
(DE95-005861; ANL/ET/CP-82419; CONF-9411194-2) Avail: CASI HC A03/MF A01

Magnetic damping is one of the important parameters to control the response and stability of Maglev systems. An experimental study is presented to measure the magnetic damping using a direct method. A plate attached to a permanent magnet levitated on a rotating drum was tested to investigate the effect of various parameters on magnetic damping such as conductivity, gap, excitation frequency, and oscillation amplitude. The experimental technique is capable of measuring all magnetic damping coefficients, some of which can not be measured by an indirect method. DOE

N95-30026# Case Western Reserve Univ., Cleveland, OH.
A BIOLOGICALLY-INSPIRED AUTONOMOUS ROBOT Performance Report
Randall D. Beer 27 Dec. 1994 4 p
(Contract N00014-90-J-1545)
(AD-A289446) Avail: CASI HC A01/MF A01

The distributed nature of the stick insect leg coordination mechanisms permitted a straightforward implementation of reflexes for the negotiation of rough terrain in our second robot. Using a searching behavior based the work of Pearson and Franklin with the locust, the robot can also walk over slatted surfaces. Horizontal compliance was added to allow legs to comply with external disturbances by actively reducing the stiffness. In response to a sufficiently large horizontal disturbance, the legs exhibit a stepping behavior reminiscent of the stepping strategy reported by Zill in locust. In addition, when one leg of a walking robot is placed on a substrate that is stationary relative to the moving robot (so that it does not step), the remaining legs continue to step due to the distributed nature of the controller. This experiment is analogous to one performed on the stick insect by Cruse and colleagues. DTIC

N95-30040# Princeton Univ., NJ.
WORKSHOP ON COMPUTING AND INTELLIGENT SYSTEMS Final Report, 1 Dec. 1993 - 31 May 1994
Sanjeev R. Kulkarni Sep. 1994 5 p
(Contract DAAH04-94-G-0009)
(AD-A290581; ARO-32361.1-MA-CF) Avail: CASI HC A01/MF A01

This grant provided block international travel funds to help enable researchers to attend an international workshop on 'Computing and Intelligent Systems' held in Bangalore, India from December 20-23, 1993. The conference venue was the Indian Institute of Science, Bangalore, a Premier Research Institute in India. This conference was organized by the Indian Institute of Science in cooperation with the Jawaharlal Nehru Centre for Advanced Scientific Research, Bangalore. The occasion also commemorated the SILVER JUBILEE of the department of Computer Science & Automation. The Workshop was comprised of a series of invited presentations by frontline researchers in the areas of Computer Science and Intelligence Systems, and included talks by several Indian faculty and graduate students. One of the primary objectives of the workshop was to bring together leading researchers and distinguished alumni in these areas, and to discuss and exchange ideas on frontier topics of research. The conference attracted scientific workers in the area from all over the world thus provided a forum for global technical interaction. The requested funds were instrumental in guaranteeing the technical success of the meeting by enabling participation of a sufficient number of key U.S. researchers. DTIC

N95-30041# Technische Univ., Delft (Netherlands).
DIGITAL CONTROL OF DISTRIBUTED PARAMETER SYSTEMS: A STATE-SPACE APPROACH Ph.D. Thesis
F. D. Barb 7 Dec. 1994 231 p
(PB95-197216) Avail: CASI HC A11/MF A03

Two modern discrete-time control theories represent the theoretical framework for this thesis where we have approached the problem of digital control of infinite-dimensional systems with possible unbounded input and/or output operators. We have outlined the main Popov theory based results on the discrete-time H-infinity control problem and we have given a full extension to discrete-time infinite-systems of the classical results of discrete Hyland-Bernstein theory known in the literature. Having available the framework offered by these two discrete control theories, we have approached the problem of digital control of linear infinite-dimensional systems with unbounded input and/or output operators. The type of unboundedness considered here was the one commonly accepted for systems that fall in the so-called Pritchard-Salamon class. Another feature that has been captured in the picture offered by this dissertation is represented by the fact that the two discrete control theories we have applied are suitable for coping with so-called singular control problems. The last part of this thesis was concerned with the applications. Two special Pritchard-Salamon systems, a parabolic system and a hyperbolic one were considered. NTIS

N95-30101# Technische Univ., Eindhoven (Netherlands). Dept. of Mathematics and Computing Science.
APPLICABILITY OF NEURAL NETWORKS FOR PRODUCTION PLANNING UNDER UNCERTAINTY
H. P. Stehouwer, E. H. L. Aarts (Philips Research Labs., Eindhoven, Netherlands.), and J. Wessels (International Inst. for Applied Systems Analysis, Laxenburg, Austria.) Aug. 1994 24 p
(PB95-197406; MEMO-COSOR-94-32) Avail: CASI HC A03/MF A01

The report begins with an introduction on multi-layered perceptrons (MLP's) and supervised learning. It discusses the applicability of MLP's for production planning using a well-known taxonomy. It divides the problem area with potential possibilities for the use of MLP's into two subareas: forecasting and decision making. Finally, an example is given of how MLP's can be used in a lot sizing situation with incomplete demand information. NTIS

N95-30112 Oak Ridge National Lab., TN.
ALLIANCE: AN ARCHITECTURE FOR FAULT TOLERANT MULTI-ROBOT COOPERATION
L. E. Parker Feb. 1995 43 p Limited Reproducibility: More than 20% of this document may be affected by microfiche quality
(Contract DE-AC05-84OR-21400)
(DE95-008658; ORNL/TM-12920) Avail: Issuing Activity (Department of Energy (DOE))

ALLIANCE is a software architecture that facilitates the fault tolerant cooperative control of teams of heterogeneous mobile robots performing missions composed of loosely coupled, largely independent subtasks. ALLIANCE allows teams of robots, each of which possesses a variety of high-level functions that it can perform during a mission, to individually select appropriate actions throughout the mission based on the requirements of the mission, the activities of other robots, the current environmental conditions, and the robot's own internal states. ALLIANCE is a fully distributed, behavior-based architecture that incorporates the use of mathematically modeled motivations (such as impatience and acquiescence) within each robot to achieve adaptive action selection. Since cooperative robotic teams usually work in dynamic and unpredictable environments, this software architecture allows the robot team members to respond robustly, reliably, flexibly, and coherently to unexpected environmental changes and modifications in the robot team that may occur due to mechanical failure, the learning of new skills, or the addition or removal of robots from the team by human intervention. The feasibility of this architecture is demonstrated in an implementation on a team of mobile robots performing a laboratory version of hazardous waste cleanup. DOE

N95-30117# Springer-Verlag G.m.b.H. and Co. K.G., New York, NY.
METHODOLOGIES FOR INTELLIGENT SYSTEMS
Zbigniew W. Ras, ed. and Maria Zemankova, ed. 19 Oct. 1994 627 p Presented at the 8th International Symposium, Charlotte, NC, 16-19 Oct. 1994
(Contract N00014-94-1-0799)
(AD-A290901) Avail: CASI HC A99/MF A06

This volume contains the papers selected for presentation at the Eight International Symposium on Methodologies for Intelligent Systems - ISMIS'94, held in Charlotte, North Carolina, October 16-19, 1994. The symposium was hosted by the University of North Carolina at Charlotte and sponsored by Office of Naval Research, Oak Ridge National Laboratory, MITRE Corporation, UNC-Charlotte, and IBM-Charlotte. DTIC

N95-30167# Technische Univ., Eindhoven (Netherlands). Dept. of Mathematics and Computing Science.
INFINITE DIVISIBILITY AND THE WAITING-TIME PARADOX
K. vanHarn and F. W. Steutel Aug. 1994 17 p
(PB95-206934; MEMO-COSOR-94-24) Avail: CASI HC A03/MF A01

It is shown that the interarrival time Z covering the point zero in a stationary renewal process generated by X has the form Z is equal in distribution to X + Y and Y nonnegative and independent of X, if and

only if X is infinitely divisible. In the special case that X has a compound-exponential distribution there is a similar decomposition of the stationary waiting time. These results shed some new light on the waiting-time paradox. NTIS

N95-30168# Technische Univ., Eindhoven (Netherlands). Dept. of Mathematics and Computing Science.
H(SUB 2) ALMOST DISTURBANCE DECOUPLING PROBLEM WITH INTERNAL STABILITY
A. Saberi, Z. Lin, and A. A. Stoorvogel Aug. 1994 21 p Prepared in cooperation with Washington State Univ., Pullman, School of Electrical Engineering and Computer Science, and State Univ. of New York at Stony Brook
(PB95-206942; MEMO-COSOR-94-23) Avail: CASI HC A03/MF A01

For both continuous-time and discrete-time systems, we establish the necessary and sufficient conditions under which an H(sub 2) almost disturbance decoupling problem with internal stability is solvable by proper controllers and/or strictly proper controllers. NTIS

N95-30171# Technische Univ., Eindhoven (Netherlands). Dept. of Mathematics and Computing Science.
FACTORIZATION AND INPUT-OUTPUT DECOUPLING BY STATIC OUTPUT FEEDBACK FOR NONLINEAR CONTROL SYSTEMS
H. J. C. Huijberts, L. Colpier, and P. Moreau Aug. 1994 36 p Prepared in cooperation with Nantes Univ.
(PB95-206975; MEMO-COSOR-94-28) Avail: CASI HC A03/MF A01

In this paper we study the strong input-output decoupling problem via regular static output feedback for nonlinear control systems (SIODPof). It turns out that the solvability of the problem is equivalent to the solvability of a factorization problem for a set of functions with respect to certain codistributions. Checkable conditions for the solvability of this factorization problem are given. NTIS

N95-30207# Technische Univ., Delft (Netherlands).
FRAMEWORK FOR COMPARING AND CONTROLLING NUMBER-BASED DESIGN REASONING SYSTEMS Ph.D. Thesis
L. Yu 12 Dec. 1994 276 p
(PB95-197364; ISBN-90-5269-164-9) Copyright Avail: CASI HC A13/MF A03

The thesis presents an attempt to search for a systematic way of interpreting design reasoning in a cross-cultural context. The present approach towards the problem of discourse-based communication is based on a comparative case study of two culturally distinct architectural documents, an ancient Chinese house manual and a modern western architecture treatise, by examining how they are applied to similar design problems. A System of Identifying Patterns of Design Argumentation (SIPDA) is developed and discussed with respect to architectural discourse analysis and its computerization. In addition to cross-cultural communication, SIPDA may be used to support decision making processes in design practice, through the education of architectural students, by providing a framework for controlling design reasoning. NTIS

N95-30221# Technische Univ., Eindhoven (Netherlands).
PRECEDENCE RELATION METHOD FOR DERIVING FLEXIBLE BOUND MODELS FOR QUEUEING SYSTEMS
G. J. vanHoutum, I. J. B. F. Adan, J. Wessels, and W. H. M. Zijm Aug. 1994 14 p
(PB95-206835; MEMO-COSOR-94-27) Avail: CASI HC A03/MF A01

In this paper, we describe the so-called precedence relation method. This method may be used to derive truncation models which produce bounds for the relevant performance measures of a given Markovian queueing system. The truncation models may be defined such that the size of the state space is flexible in the sense that it depends on the choice of certain truncation parameters. The models which we obtain in this way are called flexible bound models, and they may lead to efficient procedures for the determination of the performance measures of interest. The precedence relation method will be demonstrated for the symmetric shortest queue system. NTIS

N95-30222# Technische Univ., Eindhoven (Netherlands).
NEURAL NETWORKS FOR COMBINATORIAL OPTIMIZATION
E. H. L. Aarts, P. H. P. Stehouwer, J. Wessels, and P. J. Zwietering Aug. 1994 24 p Prepared in cooperation with Philips Research Labs., and International Inst. for Applied Systems Analysis
(PB95-206843; MEMO-COSOR-94-29) Avail: CASI HC A03/MF A01

In most applications of neural network models to combinatorial optimization problems reproduction is used. In this paper we concentrate on reproduction approaches that apply to combinatorial optimization problems in general. In that context we deal with Boltzmann machines, Hopfield networks, and multi-layered perceptrons. In Section 2, we introduce our formulation of combinatorial optimization problems. Selection 3 discusses Boltzmann machines and Hopfield networks and their relation with combinatorial optimization. The emphasis in this section is on Boltzmann machines. In Section 4 we show how combinatorial optimization problems can be reformulated as classification problems and how they can be solved by multi-layered perceptrons. Section 5 presents a discussion and some concluding remarks. NTIS

N95-30234 Purdue Univ., West Lafayette, IN.
A UNIFIED MATRIX INEQUALITY APPROACH TO LINEAR CONTROL DESIGN Ph.D. Thesis
Tetsuya Iwasaki 1993 166 p
Avail: Univ. Microfilms Order No. DA9420848

The objective of this research is to develop a simple unifying methodology for designing linear controllers which meet different specifications. Contributions of this unifying methodology include alleviation of the gap between practical applications and control theories, in the following two ways. Firstly, the single elementary framework allows practicing engineers and students to learn many modern control design methods efficiently and thoroughly. Secondly, our unifying methodology is naturally suited for computer-aided controller design since it requires only one computer software package supported by powerful convex programming techniques for designing controllers with different specifications. Thus, our result provides control engineers with reliable design tools. Our approach is purely algebraic and based on matrix inequalities. System analysis results are first developed as preliminary materials or cited from the literature to characterize certain control specifications in terms of matrix inequalities. Then, it is shown that many control design problems with stability, performance, and robustness specifications can be reduced to a single algebraic problem of solving a matrix inequality. The solution to this problem is derived by using only elementary algebra. With this approach, necessary and sufficient conditions for the existence of a controller which meets a given set of specifications are obtained in terms of linear matrix inequalities (LMI's), and all such controllers are parameterized explicitly in the state space using solutions to the LMI's. If the controller order is not specified a priori, then matrices satisfying the LMI existence condition form a convex set, and can be computed by efficient algorithms. In this case, the resulting controller order can always be chosen to be equal to or less than the plant order. If the controller order is fixed, then we have an additional nonconvex coupling constraint for the existence condition, and the computational problem becomes much harder. We shall propose an algorithm to address this nonconvex problem, and numerical examples will illustrate the idea and demonstrate the applicability of our matrix inequality based method for fixed order controller design. Dissert. Abstr.

N95-30238# Columbia Univ., New York, NY.
LEARNING CONTROL IN LINEAR AND NONLINEAR SYSTEMS Ph.D. Thesis
Chikuang Chang 1994 133 p
Avail: Univ. Microfilms Order No. DA9421327

In many applications, control systems are asked to perform the same task repeatedly. Learning control laws have been developed over the last few years that allow the controller to improve its performance each repetition. In this dissertation, a series of new learning control laws are developed, aimed at obtaining improved performance by comparison to the standard learning control methods. The first portion of the dissertation generates a new type of learning control law that learns to minimize a quadratic cost function for tracking a desired trajectory. Besides being of interest in its own right, this objective alleviates the need to specify a desired trajectory that can actually be performed by the system. The approach used here is to adapt appropriate methods from numerical optimization theory in order to produce learning control algorithms that adjust the system command from repetition to repetition in order to converge to the quadratic cost optimal trajectory. The second portion of the dissertation studies the transient

behavior of the learning process, when the basic integral-control based learning control is used. Then, a series of new learning control schemes are developed that very significantly improve the error transients. These include a new method using an alternating sign on the learning gain which is very effective in limiting peak transients, and also very important in practical applications for multiple-input, multiple-output systems. Another law developed directly controls the error produced during the learning process. In the third portion of the dissertation, methods are developed for single-input, single-output nonlinear dynamic systems. Conditions for convergence of integral-control based learning are given, and shown to be satisfied by a large class of nonlinear problems. Improved algorithms are developed that eliminate restrictions on the size of the learning gain, and on knowledge of the appropriate sign of the learning gain, for convergence to zero tracking error. Then, the behavior of learning control in the presence of an extreme type of nonlinearity is examined, coulomb friction with stiction. Dissert. Abstr.

N95-30279# Brookhaven National Lab., Upton, NY. Dept. of Physics.
SELF-ORGANIZATION IN A SIMPLE BRAIN MODEL
Dimitris Stassinopoulos, Per Bak, and Preben Alstroem (Niels Bohr Inst., Copenhagen, Denmark.) 10 Mar. 1994 23 p Presented at the World Congress on Neural Networks, San Diego, CA, 4-9 Jun. 1994
(Contract DE-AC02-76CH-00016)
(DE95-008312; BNL-61443; CONF-9406191-2) Avail: CASI HC A03/MF A01

Simulations on a simple model of the brain are presented. The model consists of a set of randomly connected neurons. Inputs and outputs are also connected randomly to a subset of neurons. For each input there is a set of output neurons which must fire in order to achieve success. A signal giving information as to whether or not the action was successful is fed back to the brain from the environment. The connections between firing neurons are strengthened or weakened according to whether or not the action was successful. The system learns, through a self-organization process, to react intelligently to input signals, i.e. it learns to quickly select the correct output for each input. If part of the network is damaged, the system relearns the correct response after a training period. DOE

N95-30288# Technische Univ., Eindhoven (Netherlands). Dept. of Mathematics and Computing Science.
H INFINITY CONTROL PROBLEM WITH ZEROS ON THE BOUNDARY OF THE STABILITY DOMAIN
A. A. Stoorvogel 2 Dec. 1994 34 p
(PB95-197042; MEMO-COSOR-94-39) Avail: CASI HC A03/MF A01

In this paper we study the discrete and continuous time H-infinity control problems without any assumptions on the system parameters. Our approach yields necessary and sufficient conditions for the existence of a suitable controller. NTIS

64 NUMERICAL ANALYSIS

Includes iteration, difference equations, and numerical approximation.

N95-28861# Pittsburgh Univ., Pittsburgh, PA. Dept. of Mathematics and Statistics.
DISCONTINUOUS SOLUTIONS OF SEMILINEAR DIFFERENTIAL-ALGEBRAIC EQUATIONS. PART 2: RHO-CONSISTENCY Technical Report
Patrick J. Rabier and Werner C. Rheinboldt Aug. 1994 35 p
(Contracts N00014-90-J-1025; NSF-CCR92-03488)
(AD-A292285; ICMA-94-191) Avail: CASI HC A03/MF A01

Part 1 of this paper presented a theory of distribution solutions of semilinear differential-algebraic equations (DAE's). In particular, it was shown that uniqueness of solutions of initial value problems breaks down completely in the class of discontinuous solutions. Here a mathematical procedure is introduced for selecting physically acceptable solutions which satisfy some new consistency condition relative to admissible perturbations of the original DAE. Several nonlinear circuit examples are given to support the theory. DTIC

N95-28863# Pittsburgh Univ., Pittsburgh, PA. Dept. of Mathematics and Statistics.
DISCONTINUOUS SOLUTIONS OF SEMILINEAR DIFFERENTIAL-ALGEBRAIC EQUATIONS. PART 1: DISTRIBUTION SOLUTIONS
Patrick J. Rabier and Werner C. Rheinboldt Aug. 1994 25 p
(Contracts N00014-90-J-1025; NSF-CCR92-03488)
(AD-A292286; ICMA-94-190) Avail: CASI HC A02/MF A01

There is strong physical evidence that a full treatment of differential-algebraic equations SHOULD INCORPORATE SOLUTIONS WITH JUMP discontinuities. It is shown here that for semilinear problems the setting of distributions allows for the development of a theory where indeed such discontinuities may occur. This approach also settles the problem of inconsistent initial conditions in a very simple way. On the other hand, new issues arise as not only uniqueness. but even countability of the number of solutions of initial value problems may now be lost. A physically motivated but purely mathematical selection procedure to overcome this difficulty is discussed in part 2 of this paper. DTIC

N95-28890# Army Armament Research, Development and Engineering Center, Watervliet, NY. Benet Lab.
AN HP-ADAPTIVE METHOD IN SPACE AND TIME FOR PARABOLIC SYSTEMS Final Report
Joseph E. Flaherty and Peter K. Moore Dec. 1994 43 p
(AD-A292262; ARCCB-TR-94045) Avail: CASI HC A03/MF A01

We describe an adaptive method-of-lines hp-refinement algorithm in space and time for one-dimensional vector systems of parabolic partial differential equations. Solutions are calculated using Galerkin's method with a piecewise-polynomial hierarchical basis in space and singly-implicit Runge-Kutta (SIRK) methods in time. A posteriori estimates of the local spatial and temporal discretization error are used with a priori error estimates to control spatial and temporal enrichment. Computational results are used to compare and verify the utility of several variants of the basic hp-refinement procedure. DTIC

N95-29064# Maryland Univ., College Park, MD.
DISPERSION ANALYSIS AND ERROR ESTIMATION OF GALERKIN FINITE ELEMENT METHODS FOR THE NUMERICAL COMPUTATION OF WAVES Final Technical Note
Frank Ihlenburg and Ivo Babuska 26 Jul. 1994 51 p
(Contract N00014-93-I-0131)
(AD-A290296; BN-1174) Avail: CASI HC A04/MF A01

The recent result on the phase difference for one-dimensional problems is numerically evaluated and discussed in the context of other work directed to this topic. It is shown that previous error estimates in integral norm are of nondispersive character but hold for medium or high wavenumber on extremely refined mesh only. On the other hand, recently proven error estimates on normalized mesh contain a pollution term. With certain assumptions on the exact solution, this term is of the order of the phase difference. Thus a link is established between the results of dispersion analysis and the results of numerical analysis. DTIC

N95-29065# Maryland Univ., College Park, MD.
POLLUTION ERROR IN THE h-VERSION OF THE FINITE ELEMENT METHOD AND THE LOCAL QUALITY OF THE RECOVERED DERIVATIVES Final Report
I. Babuska, T. Strouboulis, S. K. Gangaraj, and C. S. Upadhyay Jan. 1995 61 p
(Contract N00014-90-J-1030; NSF CCR-88-20279)
(AD-A290297; TR-BN-1180) Avail: CASI HC A04/MF A01

We previously showed that the error in the finite-element solution has two parts, namely, the local-error and the pollution-error, and we gave methods for estimating and controlling the pollution-error in any region of interest. In this paper we show that the control of the pollution-error is essential in order to guarantee that the derivatives obtained from local recoveries have higher accuracy than the derivatives computed directly from the finite-element solution and that this control must be more stringent than the one needed to guarantee the reliability of local a-posteriori error estimation. We give an algorithm for controlling the local and the pollution-error simultaneously, in any region of interest. We show that, when one is interested in obtaining high accuracy only in some parts of

the domain, the proposed algorithm gives meshes which are much more economical than the ones obtained from the classical adaptive algorithms which control the global energy-norm of the error. DTIC

N95-29070# Maryland Univ., College Park, MD.
NONLINEAR MECHANICS AND APPLIED ANALYSIS Final Report, 1 Feb. 1992 - 31 Oct. 1994
John Maddocks 31 Oct. 1994 6 p
(Contracts F49620-92-J-0093; F49620-93-1-0323)
(AD-A290356; AFOSR-95-0011) Avail: CASI HC A02/MF A01

The general objective of this research program is the development and application of new methods of analysis, numerical analysis, and scientific computation visualization techniques within the context of specific nonlinear mechanics problems that model significant physical phenomena. In general mathematical terms the analysis and numerics can be classified as dealing with problems of continuation, bifurcation, and stability exchange as they arise in the variational principles of mechanics, and especially within the context of Hamiltonian systems. The fields of application all have these themes as common mathematical underpinnings, but specific models are as diverse as describing gravity-gradient effects on the attitude dynamics of large satellites, or the supercoiling and molecular dynamics of long-chain macro-molecules such as DNA. The guiding philosophy of the research is that substantial progress can be made by simultaneously considering context-specific modeling issues along with the development of new and generally applicable analytical and numerical techniques. Within the project there is a particular emphasis on the exploitation of computation combined with interactive visualization to provide understanding of data, and to generate insight and conjectures that lead to analytical conclusions. DTIC

N95-29080# Maryland Univ., College Park, MD.
A GENERALIZED FINITE ELEMENT METHOD FOR SOLVING THE HELMHOLTZ EQUATION IN TWO DIMENSIONS WITH MINIMAL POLLUTION Final Report
Ivo M. Babuska, Frank Ihlenburg, Ellen T. Paik, and Stefan A. Sauter Sep. 1994 50 p
(Contract N00014-93-I-0131)
(AD-A290280; BN-1179) Avail: CASI HC A03/MF A01

When using the Galerkin FEM for solving the Helmholtz equation in two dimensions, the error of the corresponding solution differs substantially from the error of the best approximation, and this effect increases with higher wave number k. In this paper we design a generalized finite element method (GFEM) for the Helmholtz equation such that the pollution effect is minimal. DTIC

N95-29083# North Carolina Univ., Raleigh, NC. Dept. of Mathematics.
SYSTEMS OF HYPERBOLIC PARTIAL DIFFERENTIAL EQUATIONS Final Report, 1 May 1991 - 31 Oct. 1994
Michael Shearer 2 Dec. 1994 5 p
(Contract DAAL03-91-G-0122)
(AD-A290287; ARO-28702.5-MA) Avail: CASI HC A01/MF A01

This description of results covers research in two areas: (1) wave propagation for equations describing elastoplastic deformations of granular materials and (2) hyperbolic conservation laws. DTIC

N95-29084# Maryland Univ., College Park, MD.
FINITE ELEMENT SOLUTION TO THE HELMHOLTZ EQUATION WITH HIGH WAVE NUMBER. PART 2. THE H-P VERSION OF THE FEM Final Report
Frank Ihlenburg and Ivo M. Babuska Jun. 1994 63 p
(Contract N00014-93-I-0131)
(AD-A290289; TN-BN-1173) Avail: CASI HC A04/MF A01

The investigation of the Galerkin finite element solution to the Helmholtz equation is continued. While part 1 contained results on the h-version with piecewise linear approximation, the present part deals with approximation spaces of order p greater than or equal 1. The method is assumed to be uniform both with respect to h and p. The results are presented on a one-dimensional model problem with Dirichlet/Robin boundary conditions. In particular there are proven stability estimates, both with respect to data of higher regularity and data that is bounded in lower norms. DTIC

N95-29105 Iowa State Univ. of Science and Technology, Ames, IA.
SOLUTION OF SECOND ORDER NONLINEAR BOUNDARY VALUE PROBLEMS BY THE BOUNDARY ELEMENT METHOD Ph.D. Thesis
V. Ravichandran 1993 166 p
Avail: Univ. Microfilms Order No. DA9414028

In this work a procedure has been developed which makes it possible to use the boundary element method to solve non-linear partial differential equations of the second order in two variables. The problems solved are boundary value problems, and the non-linearity can be of any kind. A mathematical formulation is given which makes it unnecessary to have a knowledge of the fundamental solution for every type of non-linear equation. For second order partial differential equations, the use of Green's function for the Laplace equation as the fundamental solution has proved adequate to solve a wide variety of non-linear problems. Newton Raphson method was used to solve the algebraic non-linear equations resulting from a discretization of the boundary integral equation. A method is also presented to improve the grid once the solution has been found on an existing grid. This method has proved to be very efficient in the solution of nonlinear problems. The method uses some of the features unique to the boundary element method to calculate the local errors. The problem is solved on the refined grid, and, if necessary, the grid is refined repeatedly until some convergence criterion is satisfied. A grid generation algorithm which borrows heavily from the grid optimization process has been developed. Using an initial coarse grid, the elements are broken up into smaller elements until a grid of desired fineness is obtained. The algorithm developed can handle regions enclosed by curved boundaries, the only stipulation being that the curved boundaries have a parametric representation. The grid generation algorithm also generates boundary elements by using a procedure similar to the boundary optimization scheme developed earlier. Dissert. Abstr.

N95-29128# Carnegie-Mellon Univ., Pittsburgh, PA. Dept. of Computer Science.
INDUCTIVE BOOLEAN FUNCTION MANIPULATION: A HARDWARE VERIFICATION METHODOLOGY FOR AUTOMATIC INDUCTION Ph.D. Thesis
Aarti Gupta 31 Oct. 1994 227 p
(Contract F33615-93-1-1330)
(AD-A292236; CMU-CS-94-108) Avail: CASI HC A11/MF A03

The high level of complexity of current hardware systems has led to an interest in formal methods for proving their correctness. This thesis presents a methodology for formal verification of inductively-defined hardware, based on automatic symbolic manipulation of classes of inductive Boolean functions (IBFs). It combines reasoning by induction and symbolic tautology-checking in a way that incorporates the advantages of both, where the key idea is that by building an inductive argument into the IBF representations, explicit proofs by induction can be avoided. The methodology consists of identifying classes of inductive Boolean functions that are useful for representation of hardware and specifications, associating a schema with each class (consisting of a canonical representation and symbolic manipulation algorithms), and appropriately manipulating these representations for performing formal verification. DTIC

N95-29229# Tufts Univ., Medford, MA.
STOCHASTIC HYPERBOLIC AND PARABOLIC PARTIAL DIFFERENTIAL EQUATIONS Final Report
Robert C. Dalang and N. Frangos 31 Jul. 1994 10 p
(Contract DAAL03-92-G-0333)
(AD-A290372; ARO-30072.9-MA) Avail: CASI HC A02/MF A01

The primary objective was to understand fundamental properties of stochastic partial differential equations. The main results obtained concern properties of level sets of the solution of the one-dimensional wave equation, and regularity properties of the two-dimensional wave equation driven by non-white Gaussian noise. Additional results were obtained in the areas of stochastic optimization and stability of random matrix models. DTIC

N95-29233# Old Dominion Univ., Norfolk, VA.
LARGE DEVIATION LIMIT THEOREMS, WITH APPLICATIONS Final Report, 15 May 1991 - 30 Dec. 1994
Narasinga R. Chaganty 20 Dec. 1994 11 p
(Contract DAAL03-91-G-0179)
(AD-A290392; ARO-29053.8-MA-SDI) Avail: CASI HC A03/MF A01

In this research project we have established several landmark results

in large deviation theory, invariant properties of common statistical tests, Bahadur efficiency computations and the study of standby redundant systems. These results have numerous applications to Statistical methodology, Monte Carlo simulations, bootstrap methods and Bayesian statistics and in the study of reliability of systems. DTIC

N95-29296# Edgewood Research Development and Engineering Center, Aberdeen Proving Ground, MD.
SOME NEW SATURATED TWO-LEVEL DESIGNS Final Report, Apr. - Oct. 1994
Ronald B. Crosier Jan. 1995 19 p
(DA Proj. 1O1-61102-A-71-A)
(AD-A292627; ERDEC-TR-225) Avail: CASI HC A03/MF A01

First-order saturated designs can have the two desirable properties of being an orthogonal design and having two levels only if n=O mod 4, where n is the number of design points. For other cases, researchers have developed D-optimal two level designs. Recently, two-level saturated designs that are efficient for submodels containing only a few of the factors were developed. These p-efficient designs (p is the number of parameters in a submodel) have two properties not possessed by the D-optimal designs: (near) equal-occurrence of -1's and 1's in each column and near orthogonality of each pair of columns. In this report saturated, two-level designs that estimate the effects of all factors with equal precision are developed. These equal-precision designs are generally better than the p-efficient designs by the three criteria D-effidency, G-efficiency, and maximum variance inflation factor. Equal-precision designs are given for n=3-30, 38, 42, and 50. DTIC

N95-29311# California Univ., Davis, CA. Dept. of Civil Engineering.
INVESTIGATION OF AN ALTERNATIVE FINITE ELEMENT PROCEDURE: A ONE-STEP, STEADY-STATE ANALYSIS Final Report, Sep. 1993 - Sep. 1994
Leonard R. Herrmann and Joe Mello Dec. 1994 39 p
(AD-A290030; CR-95.001) Avail: CASI HC A03/MF A01

A one-step, steady-state finite element analysis procedure that is applicable to the problem of determining stresses and the driving force to pass a plane through soil at constant velocity is developed. This type of analysis is shown to be an alternative to doing a multi-step analysis using a commercial finite element code if it becomes computationally expensive. A steady-state problem allows the time dependence to be expressed as a space dependence and thus solved in one step. The feasibility of this type of analysis is demonstrated but more investigation is needed in soil failure at the plow tip and an associated soil plasticity model before any attempt is made to produce a production three-dimensional one-step code or to do a multi-step transient analysis using existing code. DTIC

N95-29312# Connecticut Univ., Storrs, CT. Dept. of Mathematics.
MULTIVARIATE WAVELET REPRESENTATIONS AND APPROXIMATIONS Final Technical Report, 1 Jun. 1990 - 31 May 1994
Wolodymyr Madych and K. Grochenig Oct. 1994 84 p
(Grant DARPA Order 9806; AF-AFOSR-0311-90)
(AD-A290147; TR-8; AFOSR-95-0006TR) Avail: CASI HC A05/MF A01

The following work has been completed: (1) The recovery of irregularly sampled band-limited functions via tempered spline - Band limited functions can be recovered from their values on certain irregularly distributed discrete sampling sets as the limits of the piecewise polynomial spline interpolants when the order of the splines goes to infinity. This significant extension of the classical case when the sampling set is a lattice was considered by L. Collatz, W. Quade, I. J. Schoenberg, and others. (2) Orthogonality criteria for compactly supported scaling functions - The question of whether the integer translates of the scaling function constructed from a prescribed scaling sequence in the standard way are mutually orthogonal is quite subtle. The various conditions and the supporting arguments which are currently in the literature are very complicated. DTIC

N95-29352# Massachusetts Inst. of Tech., Cambridge, MA.
RELATIVE AFFINE STRUCTURE: CANONICAL MODEL FOR 3D FROM 2D GEOMETRY AND APPLICATIONS
Amnon Shashua and Nassir Navab Jun. 1994 15 p
(Contracts N00014-92-J-1879; N00014-93-1-0385)
(AD-A290085; AI-M-1489; CBCL-97) Avail: CASI HC A02/MF A01

We propose an affine framework for perspective views, captured by a single extremely simple equation based on a viewer-centered invariant we call relative affine structure. Via a number of corollaries of our main results we show that our framework unifies previous work - including Euclidean, projective and affine - in a natural and simple way, and introduces new, extremely simple, algorithms for the tasks of reconstruction from multiple views, recognition by alignment, and certain image coding applications. DTIC

N95-29385# Colorado Univ., Boulder, CO. Boulder Dept. of Computer Science.
NEW METHODS FOR NONLINEAR OPTIMIZATION Final Report, 15 May 1991 - 30 Jun. 1994
Robert B. Schnabel and Richard H. Byrd 30 Aug. 1994 10 p
(Contract DAAL03-91-G-0151)
(AD-A290522; ARO-28701.10-MA) Avail: CASI HC A02/MF A01

Over the course of this research grant, considerable progress was made in all the areas discussed in the proposal, namely limited memory methods for problems with constraints, tensor methods for large sparse nonlinear problems and for constrained optimization, and trust regions methods for nonlinearly constrained optimization. In addition, substantial progress was made in the development of large scale global optimization methods for molecular configuration problems. A topic supported in part by other agencies but one in which ARO has expressed considerable interest as well. We summarize the work in these areas in Sections 1-4. In addition, we have worked on several other topics, including symmetric-rank one update methods for unconstrained optimization, implementations of the linear algebraic operations of the BFGS method on sequential and parallel computers, and parallel methods for solving block bordered systems of nonlinear equations. We summarize this work very briefly in Section 5. Section 6 contains a listing of publications and reports supported by this grant, and Section 7 contains a list of research personnel supported by this grant. DTIC

N95-29403*# Institute for Computer Applications in Science and Engineering, Hampton, VA.
THE LARGE DISCRETIZATION STEP METHOD FOR TIME-DEPENDENT PARTIAL DIFFERENTIAL EQUATIONS Final Report
Zigo Haras (Weizmann Inst. of Science, Rehovot, Israel.) and Shlomo Taasan (Weizmann Inst. of Science, Rehovot, Israel.) Apr. 1995 55 p
Submitted for publication
(Contract NAS1-19480; RTOP 505-90-52-01)
(NASA-CR-195068; NAS 1.26:198068; ICASE-95-25) Avail: CASI HC A04/MF A01

A new method for the acceleration of linear and nonlinear time dependent calculations is presented. It is based on the Large Discretization Step (LDS) approximation, defined in this work, which employs an extended system of low accuracy schemes to approximate a high accuracy discrete approximation to a time dependent differential operator. Error bounds on such approximations are derived. These approximations are efficiently implemented in the LDS methods for linear and nonlinear hyperbolic equations, presented here. In these algorithms the high and low accuracy schemes are interpreted as the same discretization of a time dependent operator on fine and coarse grids, respectively. Thus, a system of correction terms and corresponding equations are derived and solved on the coarse grid to yield the fine grid accuracy. These terms are initialized by visiting the fine grid once in many coarse grid time steps. The resulting methods are very general, simple to implement and may be used to accelerate many existing time marching schemes. Author

N95-29440# Massachusetts Inst. of Tech., Cambridge, MA.
TRAJECTORY MAPPING (TM): A NEW NON-METRIC SCALING TECHNIQUE Memorandum Report
Whitman Richards and Jan J. Koenderink May 1994 17 p
(Contracts N00014-91-J-4038; N00014-93-J-0385)
(AD-A290036; AI-M-1468; CBCL-98) Avail: CASI HC A03/MF A01

Trajectory Mapping 'TM' is a new scaling technique designed to recover the parameterizations, axes, and paths used to traverse a feature space. Unlike Multidimensional Scaling (MDS), there is no assumption that the space is homogeneous or metric. Although some metric ordering information is obtained with TM, the main output is the feature parameterizations that partition the given domain of object samples into different categories.

Following an introductory example, the technique is further illustrated using first a set of colors and then a collection of textures taken from Brodatz (1966). DTIC

N95-29446*# National Aeronautics and Space Administration. Lyndon B. Johnson Space Center, Houston, TX. Structures and Mechanics Div.
METHOD FOR THE CALCULATION OF SPACECRAFT UMBRA AND PENUMBRA SHADOW TERMINATOR POINTS
Carlos R. OrtizLongo and Steven L. Rickman Apr. 1995 37 p
(NASA-TP-3547; S-800; NAS 1.60:3547) Avail: CASI HC A03/MF A01

A method for calculating orbital shadow terminator points is presented. The current method employs the use of an iterative process which is used for an accurate determination of shadow points. This calculation methodology is required since orbital perturbation effects can introduce large errors when a spacecraft orbits a planet in a high altitude and/or highly elliptical orbit. To compensate for the required iteration methodology, all reference frame change definitions and calculations are performed with quaternions. Quaternion algebra significantly reduces the computational time required for the accurate determination of shadow terminator points. Author

N95-29451*# Institute for Computer Applications in Science and Engineering, Hampton, VA.
IMPLICIT SCHEMES AND PARALLEL COMPUTING IN UNSTRUCTURED GRID CFD Final Report
V. Venkatakrishnam May 1995 63 p Presented at the 26th Computational Fluid Dynamics Lecture Series Program of the von Karman Institute (VKI) for Fluid Dynamics, Rhode-Saint-Genese, Belgium, 13-17 Mar. 1995
(Contract NAS1-19480; RTOP 505-90-52-01)
(NASA-CR-195071; ICASE-95-28; NAS 1.26:195071) Avail: CASI HC A04/MF A01

The development of implicit schemes for obtaining steady state solutions to the Euler and Navier-Stokes equations on unstructured grids is outlined. Applications are presented that compare the convergence characteristics of various implicit methods. Next, the development of explicit and implicit schemes to compute unsteady flows on unstructured grids is discussed. Next, the issues involved in parallelizing finite volume schemes on unstructured meshes in an MIMD (multiple instruction/multiple data stream) fashion are outlined. Techniques for partitioning unstructured grids among processors and for extracting parallelism in explicit and implicit solvers are discussed. Finally, some dynamic load balancing ideas, which are useful in adaptive transient computations, are presented. Author

N95-29485# Northeastern Univ., Boston, MA.
OBJECT ORIENTED SEGMENTATION OF IMAGES Final Report, Mar. 1991 - Oct. 1994
Jayant Shah 21 Dec. 1994 19 p
(Contract DAAL03-91-G-0041)
(AD-A290792; ARO-27790.6-MA) Avail: CASI HC A03/MF A01

The central theme of this research project is recovery of object shapes from noisy images. The main mathematical techniques are energy functionals and gradient descent. The goal is to construct vertically integrated models capable of incorporating constraints imposed by various objectives such as noise suppression, boundary detection, shape description and object recognition. The difficulty with this approach is that these functionals are very hard to implement on account of their nonlinerity and the need to find discontinuous solutions. Therefore, the main emphasis of this research project has been on the formulation of approximate models. The key ingredient is representation of the discontinuity locus by a continuous variable which is then used to control processes at hand such as noise suppression or stereo matching. Specific formulations are developed for nonlinear smoothing of images, stereo matching which takes into account half-occlusions, recovery of surface shapes from shading data in the presence of noise and discontinuities and finally, curve evolution for locating and smoothing object boundaries. DTIC

N95-29488 Rensselaer Polytechnic Inst., Troy, NY. Scientific Computation Research Center.
LOAD BALANCING FOR THE PARALLEL ADAPTIVE SOLUTION OF PARTIAL DIFFERENTIAL EQUATIONS
H. L. deCougny, K. D. Devine, J. E. Flaherty, R. M. Loy, and C. Ozturan Apr. 1994 36 p Limited Reproducibility: More than 20% of this document may be affected by poor print
(Contract DAAL03-91-G-0215)
(AD-A290450; RPI-94-8; ARO-29167.25-MA) Avail: Issuing Activity (Defense Technical Information Center (DTIC))

An adaptive technique for a partial differential system automatically adjusts a computational mesh or varies the order of a numerical procedure with a goal of obtaining a solution satisfying prescribed accuracy criteria in an optimal fashion. Processor load imbalances will, therefore, be introduced at adaptive enrichment steps during the course of a parallel computation. We develop and describe three procedures for retaining and restoring load balance that have low unit cost and are appropriate for use in an adaptive solution environment. Tiling balances loading by using local optimality criteria within overlapping processor neighborhoods. Elemental data are migrated between processors within the same neighborhoods to restore balance. Tiling can potentially be improved by creating a dynamic partition graph connecting processors and their neighboring regions. After coloring the edges of the graph, elemental data are transferred between processors by pairwise exchange. Octree decomposition of a spatial domain is a successful three-dimensional mesh generation strategy. By performing tree traversals that: (1) appraise subtree costs; and (2) partition spatial regions accordingly, we show that octree structures may also be used to balance processor loading. Computational results are reported for two- and three-dimensional systems using nCUBE/2 hypercube, MasPar MP-2, and Thinking Machines CM-5 computers. DTIC

N95-29516# Northwestern Univ., Evanston, IL. Dept. of Mechanical Engineering.
FINITE ELEMENT TECHNOLOGY FOR PENETRATION PROBLEMS Final Report, 1 Jan. 1991 - 30 Sep. 1994
Ted Belytschko and Wing Kam Liu 22 Dec. 1994 10 p
(Contract DAAL03-91-G-0016)
(AD-A290644; ARO-28320.8-MA) Avail: CASI HC A02/MF A01

Finite element methods for penetration mechanics are developed. A pinball contact-impact algorithm which is easily vectorizable has been implemented on partitioned memory SIMD computers. The pinball algorithm is further extended to problems with friction and erosion; Lagrange and augmented Lagrange multiplier methods and their convergence have also been studied. Multiple-quadrature elements with hourglass control and physical stabilization and multi-time step integration have also been studied. Numerical results of the multiple-quadrature elements with stabilization showed that simple stabilization forces can be obtained which are convergent and based on physical parameters. The implementation of this algorithm on massively parallel machines has also been investigated. DTIC

N95-29558# Yale Univ., New Haven, CT. Dept. of Computer Science.
LINEAR ALGEBRAIC COMPUTATION ON DISTRIBUTED MEMORY PARALLEL MACHINES Final Report, 1 Feb. 1991 - 30 Jun. 1994
Stanley C. Eisenstat Sep. 1994 4 p
(Contract DAAL03-91-G-0032)
(AD-A290615; ARO-28007.13-MA) Avail: CASI HC A01/MF A01

The project entailed investigating several problems in the parallel solution of sparse systems of linear equations and eigenproblems, including: algorithms for factoring sparse matrices; techniques for the solution of sparse triangular systems; iterative methods for sparse systems, focusing mainly on preconditioning techniques for conjugate-direction methods; the solution of the symmetric tridiagonal eigenproblem. While this may seem to be an eclectic group of topics, there are, in fact, close relationships among them. As one example, a common technique for preconditioning iterative methods depends crucially on efficient solution of triangular systems. As another, it should be possible to construct an effective Lanczos-type algorithm for sparse, symmetric eigenproblems by combining the techniques required for conjugate-direction iterations for linear systems with those required for the solution of symmetric tridiagonal eigenproblems. DTIC

N95-29578# Wisconsin Univ., Madison, WI.
BOOTSTRAP AND PARTITIONING METHODS Final Report, 1 Jun. 1991 - 30 Sep. 1994
Wei-Yin Loh 15 Nov. 1994 6 p
(Contract DAAL03-91-G-0111)
(AD-A290662; ARO-28679.15-MA) Avail: CASI HC A02/MF A01

The following problems are studied and their solutions found. Bootstrap methods for confidence interval estimation of a binomial parameter and for model selection in linear regression. Tree-structured algorithms for

classification, piecewise-linear regression and generalized linear models, and proportional hazards regression for censored observations. Asymptotic efficiency of tests following data transformations. Identification of significant effects from unreplicated two-level factorial designed experiments. Bounds on the asymptotic size of the likelihood ratio test of independence in a cross-classified table. DTIC

N95-29647# Mathematical Association of America, Inc., Washington, DC.
MATHEMATICAL OLYMPIAD SUMMER PROGRAM (MOSP) 1994 Report, 1 Feb. 1994 - 31 Jan. 1995
Marcia P. Sward and Anne Hudson 31 Jan. 1995 10 p
(Contract N00014-94-1-0383)
(AD-A290801; MAA-1994-MOSP) Avail: CASI HC A02/MF A01

The objective is to prepare a team of U.S. high school students to compete in the International Mathematical Olympiad (IMO) held in Hong Kong, July 8-20, 1994. Those selected are introduced to a wide range of mathematical problems and theory at the Mathematical Olympiad Summer Program (MOSP) held at the U.S. Naval Academy June 7 - July 6, 1994. The U.S. Team placed first among all competing nations in Hong Kong, with 6 perfect scores. DTIC

N95-29824*# National Aeronautics and Space Administration. Marshall Space Flight Center, Huntsville, AL.
ANSYS DUPLICATE FINITE-ELEMENT CHECKER ROUTINE
R. Ortega Washington May 1995 20 p
(NASA-TM-108492; NAS 1.15:108492) Avail: CASI HC A03/MF A01

An ANSYS finite-element code routine to check for duplicated elements within the volume of a three-dimensional (3D) finite-element mesh was developed. The routine developed is used for checking floating elements within a mesh, identically duplicated elements, and intersecting elements with a common face. A space shuttle main engine alternate turbopump development high pressure oxidizer turbopump finite-element model check using the developed subroutine is discussed. Finally, recommendations are provided for duplicate element checking of 3D finite-element models. Author

N95-30029# Massachusetts Inst. of Tech., Cambridge, MA. Lab. for Information and Decision Systems.
PROBABILISTIC MODELING AND STATISTICAL INFERENCE FOR RANDOM FIELDS AND SPACE-TIME PROCESSES Final Report
15 Jan. 1995 14 p
(Contract N00014-91-J-1004)
(AD-A289956; LIDS-FR-2285) Avail: CASI HC A03/MF A01

In this report we summarize the research effort, funded under ONR Grant N00014-91-J-1004, on probabilistic modeling and statistical inference for random fields and space-time processes. The research we have pursued in this project consists of the investigation of a set of interrelated topics involving the development of new mathematical methods for the challenging problems of random field analysis and inference and the application of these methods to problems of practical significance. In particular, the problems of interest in this work were motivated by and directly address issues that are central both to the challenging large-scale data assimilation and estimation problems arising in physical oceanography and to a number of other remote sensing and imaging problems of direct interest to the Navy. DTIC

N95-30046# Technische Univ., Eindhoven (Netherlands).
OPTIMAL HANKEL NORM IDENTIFICATION OF DYNAMICAL SYSTEMS
S. Weiland and A. A. Stoorvogel Nov. 1994 26 p
(PB95-197232; Memo-COSOR-94-38) Avail: CASI HC A03/MF A01

The problem of optimal approximate system identification is addressed with a newly defined measure of misfit between observed time series and linear time-invariant models. The behavioral framework is used as a suitable axiomatic setting for a non-parametric introduction of system complexity and a notion of misfit of dynamical systems which is independent of system representations. The misfit function introduced here is characterized in terms of the induced norm of a Hankel operator associated with the data and a co-inner kernel representation of a model. Two optimal approximate identification problems are considered in this framework. New conceptual algorithms are proposed for optimal approximate identification of time series. NTIS

N95-30086*# Institute for Computer Applications in Science and Engineering, Hampton, VA.
EXPERIMENTAL CONFIRMATION OF A PDE-BASED APPROACH TO DESIGN OF FEEDBACK CONTROLS Final Report
H. T. Banks (North Carolina State Univ., Raleigh, NC.), Ralph C. Smith (Iowa State Univ. of Science and Technology, Ames, IA.), D. E. Brown (National Aeronautics and Space Administration. Langley Research Center, Hampton, VA.), R. J. Silcox (National Aeronautics and Space Administration. Langley Research Center, Hampton, VA.), and Vern L. Metcalf (National Aeronautics and Space Administration. Langley Research Center, Hampton, VA.) May 1995 43 p Submitted for publication in SIAM Journal of Control and Optimization
(Contracts NAS1-198167; NAS1-19480; NAG1-1600; RTOP 505-90-52-01; F49620-93-1-0198)
(NASA-CR-198167; NAS 1.26:198167; ICASE-95-42) Avail: CASI HC A03/MF A01

Issues regarding the experimental implementation of partial differential equation based controllers are discussed in this work. While the motivating application involves the reduction of vibration levels for a circular plate through excitation of surface-mounted piezoceramic patches, the general techniques described here will extend to a variety of applications. The initial step is the development of a PDE model which accurately captures the physics of the underlying process. This model is then discretized to yield a vector-valued initial value problem. Optimal control theory is used to determine continuous-time voltages to the patches, and the approximations needed to facilitate discrete time implementation are addressed. Finally, experimental results demonstrating the control of both transient and steady state vibrations through these techniques are presented. Author

N95-30088# Technische Univ., Eindhoven (Netherlands).
COMPARISON OF THE LOCAL DEFECT CORRECTION ITERATION AND THE FAST ADAPTIVE COMPOSITE GRID ITERATION
P. J. J. Ferket and A. A. Reusken Aug. 1994 29 p
(PB95-206769; RANA-94-12) Avail: CASI HC A03/MF A01

The local defect correction method by Hackbusch and the fast adaptive composite grid method by McCormick are presented for a model situation. The main differences and similarities between both methods are discussed. It is shown that for suitable choices of the components the iterates in the local defect correction iteration and in the fast adaptive composite grid iteration are the same. NTIS

N95-30089# Technische Univ., Eindhoven (Netherlands).
FISCHER'S PROTOCOL IN TIMED PROCESS ALGEBRA
J. J. Vereijken 15 Aug. 1994 47 p
(PB95-206777) Avail: CASI HC A03/MF A01

Timed algebraic process theories can be developed with quite different purposes in mind. One can aim for theoretical results about the theory itself (completeness, expressiveness, decidability), or one can aim for practical applicability to non-trivial protocols. Unfortunately, these aims do not go well together. In this paper we take two theories, which are probably of the first kind, and try to find out how well suited they are for practical verifications. We verify Fischer's protocol for mutual exclusion in the settings of discrete-time process algebra and real-time process algebra. We do this by transforming the recursive specification into an equivalent linear specification, and then dividing out the maximal bisimulation relation. The required mutual exclusion result can then be found by reasoning about the obtained process graph. Finally, we consider the ease of the verification, and ways to adapt the theory to make it more practical. It will turn out that the theories investigated are quite unsatisfactory when verifying real-life protocols. NTIS

N95-30092# Technische Univ., Eindhoven (Netherlands). Dept. of Mathematics and Computing Science.
TRANSLATION INVARIANT OPERATORS ON LP-TYPE SPACES
S. J. L. vanEijndhoven Oct. 1994 20 p
(PB95-197117; RANA-94-18) Avail: CASI HC A03/MF A01

The continuous, translation invariant, linear operators from L(sub loc, sup p)(R) into L(sub loc, sup p)(R) and from L(sub comp, sup p)(R) into L(sub comp, sup p)(R), 1 = or less than p = or less than infinity are characterized. This characterization is in terms of the convolution ring ba(sub c)(R) consisting of all compactly varying, right continuous functions

of bounded variation. It turns out that for p = 1 and p = infinity, each translation invariant operator on L(sub loc, sup p)(R) leaves invariant the space C(R) of continuous functions on R. NTIS

N95-30093# Technische Univ., Eindhoven (Netherlands). Dept. of Mathematics and Computing Science.
THEOREM ON THE EXISTENCE OF SOLUTIONS OF QUASI-STATIC MOVING BOUNDARY PROBLEMS
B. K. Obbink Oct. 1994 15 p
(PB95-197125; RANA-94-20) Avail: CASI HC A03/MF A01

Using the theory of conformal mappings, we show that two-dimensional quasi-static moving boundary problems can be described by a non-linear Lowner-Kufarev-equation and a functional relation F between the shape of the boundary and the velocity at the boundary. Together with the initial data, this leads to an initial value problem (i.v.p.). Assuming that F satisfies certain conditions, we prove a theorem stating that this i.v.p. has a local solution in time. The proof is based on some straightforward estimates on solutions of Lowner-Kufarev-equations and an iteration technique. NTIS

N95-30097# Technische Univ., Twente (Netherlands). Tele-Informatics and Open Systems Group.
EFFICIENT SOLUTION OF A CLASS OF INFINITE STOCHASTIC PETRI NETS: THEORY AND APPLICATIONS
B. R. Haverkort 13 Oct. 1994 26 p
(PB95-197166; Memo-INF-94-60) Copyright Avail: CASI HC A03/MF A01

In this paper we characterize, at the stochastic Petri net level, a class of stochastic Petri nets that can be solved using matrix geometric techniques. Advantages of such an approach are that very efficient mathematical techniques become available for practical usage, as well as that the problem of large state spaces can be circumvented. We first characterize the class of stochastic Petri nets of interest by formally defining a number of constraints that have to be fulfilled (these constraints apply at the Petri net level directly). We then discuss the matrix geometric solution technique that can be employed and present some boundary conditions on tool support. We illustrate the practical usage of the class of stochastic Petri nets with two examples: a queueing system with delayed service and a model of connection management in asynchronous transfer mode (ATM) networks. NTIS

N95-30103# Technische Univ., Twente (Netherlands). Dept. of Computer Science.
PROVING THE GENERICITY LEMMA BY LEFTMOST REDUCTION IS SIMPLE
J. Kuper Nov. 1994 12 p
(PB95-197620; Memo-INF-94-69) Copyright Avail: CASI HC A03/MF A01

In this report we present an elementary and general proof of the Genericity Lemma, which says (in the untyped lambda calculus): Suppose M is an unsolvable term, and let N be a normal form. If FM = N, then for each term X we have FX = N. The informal meaning of this lemma is that if a term M is meaningless (undefined), and if a context containing M is convertible to a well-defined answer, then M did not have any influence on the computation of this answer and so M may be replaced by any term. In fact, the Genericity Lemma is one of the most important motivations to take in the untyped lambda calculus the notion of solvability as a formal representation of the informal notion of undefinedness. In this report we prove the Genericity Lemma for a more general situation than just untyped lambda calculus. Therefore, we first generalize the notion of solvability towards typed lambda calculi. We call this generalization usability, and we show that the Genericity Lemma holds for un-usable terms. We prove the lemma by concentrating on the leftmost reduction of FM. This strongly simplifies the proofs that are known from the literature. NTIS

N95-30106# Technische Univ., Eindhoven (Netherlands).
PROCESS ALGEBRA WITH FEEDBACK
J. C. M. Baeten, J. A. Bergstra, and G. Stefanescu Jul. 1994 35 p Prepared in cooperation with Amsterdam Univ.
(PB95-206819) Avail: CASI HC A03/MF A01

We consider process graphs over a set of pins, i.e. with multiple entries and exits. On process graphs modulo bisimulation, we can define all standard process algebra operators plus the feedback operator from flowchart theory. We provide a complete axiomatization for finite processes. Considering the one-point pin structure, we get back standard process algebra. NTIS

N95-30126# George Mason Univ., Fairfax, VA. Center for Computational Statistics.
A NEW VISUALIZATION TECHNIQUE TO STUDY THE TIME EVOLUTION OF FINITE AND ADAPTIVE MIXTURE ESTIMATORS
Jeffrey L. Solka (Naval Surface Warfare Center, Dahlgren, VA.), Wendy L. Poston (Naval Surface Warfare Center, Dahlgren, VA.), and Edward J. Wegman Dec. 1994 31 p
(Contracts DAAH04-94-G-0267; DAAL03-91-G-0039)
(AD-A291147; TR-114) Avail: CASI HC A03/MF A01

This paper focuses on recent work which analyzes the expectation maximization (EM) evolution of mixtures based estimators. The goal of this research is the development of effective visualization techniques to portray the mixture model parameters as they change in time. This is an inherently high dimensional process. Techniques are presented which portray the time evolution of univariate, bivariate, and trivariate finite and adaptive mixtures estimators. Adaptive mixtures is a recently developed variable bandwidth kernel estimator where each of the kernels is not constrained to reside at a sample location. The future role of these techniques in developing new versions of the adaptive mixtures procedure are also discussed. DTIC

N95-30172# Helsinki Univ. of Technology, Espoo (Finland). Electromagnetics Lab.
STATIC FIELD SOLUTIONS AND IMAGE THEORY FOR A CONDUCTING SPHERE WITH RADIAL ANISOTROPY
J. C. E. Sten Jul. 1994 15 p
(PB95-207171; ISBN-951-22-2217-5) Avail: CASI HC A03/MF A01

Static problems involving a conducting sphere with radial anisotropy (radial and tangential conductivity, denoted alpha and eta) are considered. Conditions for alpha, eta and the external isotropic conductivity sigma(0) are given, for which the sphere becomes transparent in a homogeneous current flow, i.e., the dipole moment totally vanishes. Also problems involving external and internal point sources of current are examined, and simple interpretations in terms of image sources are presented for cases where alpha much greater than eta and alpha approx. = eta. Image expressions for radial and tangential dipole sources are finally elaborated. NTIS

N95-30195# Technische Univ., Twente (Netherlands). Dept. of Computer Science.
USABILITY: FORMALISING (UN)DEFINEDNESS IN TYPED LAMBDA CALCULUS
J. Kuper Nov. 1994 23 p
(PB95-197190; Memo-INF-94-67) Copyright Avail: CASI HC A03/MF A01

In this paper we discuss usability, and propose to take that notion as a formalization of (un)definedness in typed lambda calculus. Usability can be considered as a generalization of the notion of solvability, which is widely recognized as an adequate formalization of (un)definedness in the untyped lambda calculus. Some important properties that make usability attractive as a formalization of (un)definedness, are: it has a good conceptual motivation; restricting its definition to the untyped case yields solvability; for closed terms of ground type, the unusable terms are precisely the terms without a normal form; the Genericity Lemma holds for unusable terms; and all unusable terms (of the same type, of course) can be consistently identified. This identification is maximal in the sense that additionally identifying a usable term to the unusable terms makes the calculus inconsistent. There is a remarkable difference between usability and solvability: in the untyped lambda calculus the solvable terms are precisely the terms with a head normal form, whereas in typed lambda calculus the usable terms are 'between' the terms with a normal form and the terms with a head normal form. NTIS

N95-30204# Technische Univ., Eindhoven (Netherlands).
SPECTRAL ESTIMATES FOR POSITIVE ROCKLAND OPERATORS
A. F. M. terElst and D. W. Robinson Aug. 1994 22 p Prepared in cooperation with Australian National Univ.
(PB95-206751; RANA-94-13) Avail: CASI HC A03/MF A01

Let (H, G, U) be an irreducible unitary representation of a homogeneous Lie group G and H a self-adjoint operator on H associated with a positive

Rockland operator. We derive upper and lower bounds on the eigenvalue distribution of H in terms of volume estimates on the coadjoint orbit corresponding to the representation U. Hence we deduce bounds on the partition function beta maps to Tr(sub H)(exp (-(beta)H)). An application is given to the spectrum and eigenfunctions of the general anharmonic oscillator. NTIS

N95-30227*# National Aeronautics and Space Administration. Langley Research Center, Hampton, VA.
COARSENING STRATEGIES FOR UNSTRUCTURED MULTIGRID TECHNIQUES WITH APPLICATION TO ANISOTROPIC PROBLEMS Final Report
E. Morano, D. J. Mavriplis, and V. Venkatakrishnan May 1995 20 p
Submitted for publication in SIAM Journal of Scientific Computing
(Contract NAS1-19480; RTOP 505-90-52-01)
(NASA-CR-198154; NAS 1.26:198154; ICASE-95-34) Avail: CASI HC A03/MF A01

Over the years, multigrid has been demonstrated as an efficient technique for solving inviscid flow problems. However, for viscous flows, convergence rates often degrade. This is generally due to the required use of stretched meshes (i.e., the aspect-ratio AR = delta y/delta x is much less than 1) in order to capture the boundary layer near the body. Usual techniques for generating a sequence of grids that produce proper convergence rates on isotopic meshes are not adequate for stretched meshes. This work focuses on the solution of Laplace's equation, discretized through a Galerkin finite-element formulation on unstructured stretched triangular meshes. A coarsening strategy is proposed and results are discussed. Author

N95-30291# Technische Univ., Twente (Netherlands). Dept. of Computer Science.
ESSENTIAL STRUCTURE OF THE JACOPINI TECHNIQUE
J. Kuper Nov. 1994 19 p
(PB95-197208; Memo-INF-94-68) Copyright Avail: CASI HC A03/MF A01

The general concern of the Jacopini technique (introduced by Jacopini in 1975 in his proof of the easiness of Omega in the untyped lambda calculus) is the following question: Is it consistent to add an equation P = Q to the lambda calculus. The paper introduces the notion of proof-replaceability which makes the essential structure of the technique more explicit and easier to understand. A second notion which is needed to make the Jacopini technique better understandable is genericity. The paper defines this notion and then formulates the technique in a general way such that it also works for other terms than Omega. Furthermore, it works for untyped and typed lambda calculus alike. It gives some examples of the use of the Jacopini technique. The generality of the approach is illustrated by an example from a lambda calculus which is extended with a mu abstractor. NTIS

N95-30353*# Institute for Computer Applications in Science and Engineering, Hampton, VA.
PRESSURE UPDATING METHODS FOR THE STEADY-STATE FLUID EQUATIONS
A. Fiterman (Weizmann Inst. of Science, Rehovot, Israel.), E. Turkel (Tel-Aviv Univ., Ramat-Aviv, Tel-Aviv, Israel.), and V. Vatsa May 1995 16 p
(Contract NAS1-19480; RTOP 505-90-52-01)
(NASA-CR-198163; NAS 1.26:198163; ICASE-95-40) Avail: CASI HC A03/MF A01

We consider the steady state equations for a compressible fluid. Since we wish to solve for a range of speeds we must consider the equations in conservation form. For transonic speeds these equations are of mixed type. Hence, the usual approach is to add time derivatives to the steady state equations and then march these equations in time. One then adds a time derivative of the density to the continuity equation, a derivative of the momentum to the momentum equation and a derivative of the total energy to the energy equation. This choice is dictated by the time consistent equations. However, since we are only interested in the steady state this is not necessary. Thus we shall consider the possibility of adding a time derivative of the pressure to the continuity equation and similar modifications for the energy equation. This can then be generalized to adding combinations of time derivatives to each equation since these vanish in the steady state. When using acceleration techniques such as residual smoothing, multigrid, etc. these are applied to the pressure rather than the density. Hence, the code duplicates the behavior of the incompressible equations for low speeds. Author

N95-30143*# National Aeronautics and Space Administration. Langley Research Center, Hampton, VA.
SECOND-ORDER NUMERICAL SOLUTION OF TIME-DEPENDENT, FIRST-ORDER HYPERBOLIC EQUATIONS
Patricia L. Shah (Boston Univ., MA.) and Jay Hardin *In its* ICASE/LaRC Workshop on Benchmark Problems in Computational Aeroacoustics (CAA) May 1995 p 133-141 (For primary document see N95-30133 10-71)
(Contract NAS1-19480)
Avail: CASI HC A02/MF A04

N95-30145*# Florida State Univ., Tallahassee, FL. Dept. of Mathematics.
SOLUTIONS OF THE BENCHMARK PROBLEMS BY THE DISPERSION-RELATION-PRESERVING SCHEME
Christopher K. W. Tam, H. Shen, K. A. Kurbatskii, and L. Auriault *In* NASA. Langley Research Center, ICASE/LaRC Workshop on Benchmark Problems in Computational Aeroacoustics (CAA) May 1995 p 149-171 (For primary document see N95-30133 10-71)
(Grant NAG3-1267)
Avail: CASI HC A03/MF A04

65 STATISTICS AND PROBABILITY

Includes data sampling and smoothing; Monte Carlo method; and stochastic processes.

N95-29490# Rensselaer Polytechnic Inst., Troy, NY. Scientific Computation Research Center.
PARALLEL ADAPTIVE TECHNIQUES FOR TRANSIENT PARTIAL DIFFERENTIAL EQUATIONS Final Report, 1 Jul. 1991 - 30 Jun. 1994
Joseph E. Flaherty and Mark S. Shephard 10 Nov. 1994 19 p
(Contract DAAL03-91-G-0215)
(AD-A290460; ARO-29167.19-MA) Avail: CASI HC A03/MF A01

As scientific and engineering problems increase in complexity, there is a corresponding need to automate a greater portion of the solution process. Adaptive methods are capable of providing many of the decisions - that arise when solving problems involving partial differential equations. When automatic mesh generation, refinement and coarsening is combined with method-order variation, it is possible to construct methods having spectral convergence rates. Accuracy and solution reliability are verified by asymptotically correct estimates of discretization errors. With parallel computation becoming more widespread and necessary, it is important to consider parallel adaptive strategies. Much more difficult to parallelize than traditional algorithms, adaptive strategies necessarily require dynamic processor scheduling because of load changes introduced by periodic solution enrichment. DTIC

N95-29491# Stanford Univ., CA. Dept. of Operations Research.
SIMULATION METHODOLOGY Final Report, 15 Apr. 1991 - 14 Apr. 1994
Peter W. Glynn and Donald L. Iglehart Aug. 1994 8 p
(Contract DAAL03-91-G-0101)
(AD-A290461; ARO-28809.18-MA-SDI) Avail: CASI HC A02/MF A01

This contract covered the period April 15, 1991 through April 14, 1994. The participating personnel included two faculty members and nine Ph.D. students. The research carried out under this contract involved both work on simulation methodology and stochastic models/processes. The simulation work involved the use of simulation to carry out stochastic system optimization, a variety of variance reduction ideas to improve simulation efficiency, and methods for improving output analysis for a single stochastic process. Stochastic models studied involved a network of water reservoirs, the general single-server queue, and a financial model for trading securities. Stochastic processes studied were cumulative processes, counting process, and sampling of a general stochastic press. DTIC

N95-29587# Wisconsin Univ., Madison, WI. Dept. of Statistics.
OPTIMAL UNIVERSAL CODING AND DENSITY ESTIMATION Final Report, 1 Jun. 1991 - 30 Sep. 1994
Bin Yu 28 Nov. 1994 5 p
(Contract DAAL03-91-G-0107)
(AD-A290694; ARO-28722.17-MA) Avail: CASI HC A01/MF A01

Research progress has been made in the areas of empirical processes for mixing sequences, information theory, minimax estimation theory in source coding and nonparametric statistics, and Markov chain Monte Carlo (MCMC) methods. Rates of convergence and Central Limit Theorems results have been obtained for empirical processes of dependent data, and they are very useful for studying statistical models with dependence structure. On the important MCMC convergence diagnostic problem, regeneration points have been introduced into the Markov chain using the split-chain technique; so has been a global approach based on the the estimated L1 error and the Cusum path plot. Making connections between information theory and statistics, we obtained an information-theoretic result on the rate of convergence of a D-semifaithful code, and we also introduced non-parametric minimax lower bound techniques into bounding from below the redundancy in source coding. DTIC

N95-29634# Chicago Univ., Chicago, IL. Dept. of Statistics.
RANDOMIZED INQUIRIES ABOUT SHAPE: AN APPLICATION TO HANDWRITTEN DIGIT RECOGNITION
Yali Amit and Donald Geman (Massachusetts Univ., Amherst, MA.) Nov. 1994 29 p
(Contracts DAAL03-92-G-0322; MDA972-93-1-0012; N00014-91-J-1021; NSF DMS-92-17655)
(AD-A290812; TR-401; ARO-30167.6-MA) Avail: CASI HC A03/MF A01

We describe an approach to shape recognition based on asking relational questions about the arrangement of landmarks, basically localized and oriented boundary segments. The questions are grouped into highly structured inquiries in the form of a tree. There are, in fact, many trees, each constructed from training data based on entropy reduction. The outcome of each tree is not a classification but rather a distribution over shape classes. The final classification is based on an aggregate distribution. The framework is non-Euclidean and there is no feature vector in the standard sense. Instead, the representation of the image data is graphical and each question is associated with a labeled subgraph. The ordering of the questions is highly constrained in order to maintain computational feasibility, and dependence among the trees is reduced by randomly sub-sampling from the available pool of questions. Experiments are reported on the recognition of handwritten digits. Although the amount of training data is modest by today's standards, the rates we achieve are competitive with those reported elsewhere using neural network, nearest-neighbor and other nonparametric classifiers. DTIC

N95-29768# Maryland Univ., Baltimore, MD.
STATISTICAL INFERENCE PROBLEMS IN SOME MULTIVARIATE LINEAR MODELS WITH APPLICATIONS TO MULTIVARIATE CALIBRATION AND META-ANALYSIS Final Technical Report, Oct. 1992 - Sep. 1994
Thomas Mathew Nov. 1994 5 p
(Contract F49620-93-1-0001)
(AD-A291125; AFOSR-95-0078TR) Avail: CASI HC A01/MF A01

The proposal addressed some statistical inference problems in the areas of multivariate calibration and meta-analysis. Multivariate calibration deals with using the statistical relationship between a response variable and an explanatory variable for statistical inference concerning an unknown value of the explanatory variable using available data. The problems that have been solved deal with the construction of confidence regions for the unknown value of the explanatory variable. Satisfactory solutions to some open problems in this area have been obtained. Meta-analysis deals with combining several independent tests concerning a common parameter. Five papers have been written based on the proposal, of which three are already published. In addition, two papers are currently under preparation. DTIC

N95-29819 George Mason Univ., Fairfax, VA. Center for Computational Statistics.
A CONTRIBUTION TO THE THEORY OF ROBUST ESTIMATION OF MULTIVARIATE LOCATION AND SHAPE: EID
Wendy L. Poston (Naval Surface Warfare Center, Dahlgren, VA.), Edward J. Wegman (George Mason Univ., Fairfax, VA.), Carey E. Priebe (Johns Hopkins Univ., Baltimore, MD.), and Jeffrey L. Solka (Naval Surface Warfare Center, Dahlgren, VA.) Oct. 1994 26 p Limited Reproducibility: More than 20% of this document may be affected by poor print
(Contracts N00014-92-J-1303; N00014-93-1-0527)
(AD-A290435; TR-106) Avail: Issuing Activity (Defense Technical Information Center (DTIC))

The existence of outliers in a data set and how to deal with them is an important problem in statistics. The Minimum Volume Ellipsoid (MVE) estimator is a robust estimator of location and shape; however its use has been limited because few computationally attractive methods exist to calculate it. Determining the MVE consists of two parts: finding the subset of points to be used in the estimate and finding the ellipse that covers this set. This paper will address the first problem. The proposed method of subset selection is called the Effective Independence Distribution (EID) method which chooses the subset by minimizing determinants of matrices containing the data. This method is deterministic yielding reproducible estimates of location and scatter for a given data set. The EID method of finding the MVE is applied to several regression data sets where the true estimate is known. Results show that the EID method produces the subset of data in less than a second and that there is less than 6% relative error in the estimates. DTIC

N95-29906# Institute for the Study of Learning and Expertise, Palo Alto, CA.
INDUCTION OF SELECTIVE BAYESIAN CLASSIFIERS Interim Report, 1 Mar. 1994 - 31 Jul. 1994
Pat Langley and Stephanie Sage 15 Aug. 1994 11 p Submitted for publication in Proceedings of the 10th Conference on Uncertainty in Artificial Intelligence
(Contract N00014-94-1-0746)
(AD-A292690; ISLE-TR-94-2) Avail: CASI HC A03/MF A01

In this paper, we examine previous work on the naive Bayesian classifier and review its limitations, which include a sensitivity to correlated features. We respond to this problem by embedding the naive Bayesian induction scheme within an algorithm that carries out a greedy search through the space of features. We hypothesize that this approach will improve asymptotic accuracy in domains that involve correlated features without reducing the rate of learning in ones that do not. We report experimental results on six natural domains, including comparisons with decision-tree induction, that support these hypotheses. In closing, we discuss other approaches to extending naive Bayesian classifiers and outline some directions for future research. DTIC

N95-30170# Technische Univ., Eindhoven (Netherlands). Dept. of Mathematics and Computing Science.
SHORT AND ELEMENTARY PROOF OF THE MAIN BAHADUR-KIEFER THEOREM
J. H. J. Einmahl Aug. 1994 13 p
(PB95-206967; MEMO-COSOR-94-26) Avail: CASI HC A03/MF A01

A short proof of the lower bound in the strong version of the famous Theorem 1A on the Bahadur-Kiefer process is presented. The proof is elementary and does, in particular, not use strong approximations. NTIS

N95-30297# Chicago Univ., Chicago, IL.
IMPROVEMENT OF INTER-EVENT DISTANCE TESTS OF RANDOMNESS IN SPATIAL POINT PROCESSES
Linda Brant Collins, Anna Pluzhnikov, and Michael L. Stein 21 Oct. 1994 22 p
(Contract DAAL03-92-G-0322)
(AD-A291151; TR-384; ARO-30167.7-MA) Avail: CASI HC A02/MF A01

A natural test of complete spatial randomness (CSR) for spatial point patterns based on the inter-event distance distribution has poor power against even obvious departures. We propose two modifications of the test statistic to improve its power. The first is a reweighting to put more emphasis on deviations from CSR at shorter distances. The second is to apply the theory of the projection of U-statistics to lower the variance of the test statistic under the null hypothesis. In examples where previous methods based on inter-event distances failed to detect alternatives, we show that these modifications to the test statistic allow the detection of departures from CSR. Simulations of stationary and near stationary

alternatives to CSR further illustrate the improvement in inter-event distance tests of CSR gained from weighting and projection. In addition, we propose two simple modifications to the graphical presentation of the empirical inter-event distance distribution to elucidate alternatives. DTIC

66 SYSTEMS ANALYSIS

Includes mathematical modeling; network analysis; and operations research.

N95-29604# Advisory Group for Aerospace Research and Development, Neuilly-Sur-Seine (France). Aerospace Medical Panel.
RECENT ISSUES AND ADVANCES IN AEROMEDICAL EVACUATION (MEDEVAC) [LES PROGRES RECENTS ET LES QUESTIONS POSEES DANS LE DOMAINE DE L'EVACUATION AEROMEDICALE (MEDEVAC)]
Feb. 1995 132 p Symposium held in Athens, Greece, 3-7 Oct. 1994 (AGARD-CP-554; ISBN-92-836-1012-1) Copyright Avail: CASI HC A07/MF A02

Recent experience has demonstrated NATO's difficulty in planning and coordinating International Aeromedical Evacuation of acutely sick, injured and wounded patients. There is much discussion which seeks to clarify and define NATO's role in medical air evacuation. Papers in this Symposium updated available data in medicine research and development and provided a focal point for discussion of specialized equipment and techniques required to care for patients in the NATO Medevac System. The Symposium covered also the role, training, procedures as well as command and control in the management of casualties in the aeromedical evacuation system. There is a clear operational need to provide medical planners within NATO and Alliance Nations with a generic concept of integrated aeromedical evacuation to improve the effectiveness of NATO forces. For individual titles, see N95-29605 through N95-29629.

N95-29605# Department of the Air Force, Scott AFB, IL. Transportation Command.
USE OF QUALITY TOOLS TO RE-ENGINEER THE AEROMEDICAL EVACUATION (AE) SYSTEM
Carroll R. Bloomquist *In* AGARD, Recent Issues and Advances in Aeromedical Evacuation (MEDEVAC) Feb. 1995 4 p (For primary document see N95-29604 10-66)
Copyright Avail: CASI HC A01/MF A02

The element of change pervades each of our activities; defining change should be accomplished in a logical fashion using definitive tools. A number of quality tools are available to produce rational, well-defined change in a large complex system. One of these methods, the Theory of Constraints (TOC) will be the focus of this paper with regard to designing and implementing change for the United States (U.S.) Department of Defense (DOD) aeromedical evacuation (AE) system. Improvements in the U.S. AE system may provide a systemic benefit to multinational operations. Author

N95-29606# Canadian Forces Air Command, Winnipeg (Manitoba).
THE CANADIAN EXPERIENCE IN UN AIREVAC SARAJEVO AIRLIFT: APRIL 1993-OCTOBER 1994
Julia M. Read *In* AGARD, Recent Issues and Advances in Aeromedical Evacuation (MEDEVAC) Feb. 1995 6 p (For primary document see N95-29604 10-66)
Copyright Avail: CASI HC A02/MF A02

For the first time since the Korean Conflict, Canadian aeromedical evacuation (airevac) crews have been deployed to a theater of war. While certainly not of the same magnitude as the Korean operation, this deployment has helped us re-learn some of the lessons forgotten in the intervening 40 years, and has reinforced the readiness posture for which we have trained. The vagaries of emergency airlift have brought our airevac mission very clearly into focus. Author

N95-29607# Department of the Air Force, Shaw AFB, SC.
UNITED NATIONS AEROMEDICAL EVACUATION OPERATIONS IN THE FORMER YUGOSLAVIA
W. P. Thornton and J. C. Neubauer (Department of the Air Force, Pope AFB, NC.) *In* AGARD, Recent Issues and Advances in Aeromedical Evacuation (MEDEVAC) Feb. 1995 8 p (For primary document see N95-29604 10-66)
Copyright Avail: CASI HC A02/MF A02

This paper examines intratheater aeromedical evacuation of United Nations Protection Force (UNPROFOR) casualties during peacekeeping operations in the republics of Croatia, Bosnia-Hercegovina, and the Former Yugoslav Republic of Macedonia. Its purpose is to inform NATO countries that participate in future UN operations of the inherent deficiencies of the force medical support for such multinational missions. UNPROFOR consists of over 40,000 personnel representing 36 nations organized into at least 37 battalion size units in a widely dispersed deployment. The paper is a summary of observations from the HQ, UNPROFOR Medical Branch compiled from reports, liaison visits to units, and direct participation in planning and training activities for aeromedical evacuation. Effective aeromedical evacuation in this mission was complicated by many factors: lack of dedicated aeromedical evacuation units; difficult weather and terrain; restrictions of flight imposed by warring factions; lack of standardized communications and medical equipment; wide variation in the level of proficiency, training, and experience of various contingents; and lack of standardized international procedures and policies. There is no medical unit in theater to bridge the gap between first level medical units in the field and the level three field hospitals. Accordingly, most NATO member contingents have elected to place field surgical teams at the battalion level. Discussion includes capabilities provided by military and civilian utility helicopter and fixed-wing aircraft. Efforts in training and simplification of procedures for evacuation are also summarized. The limitations of the current system are described, and existing shortfalls are defined with recommendations for future improvements. Author

N95-29608# Royal Netherlands Air Force, The Hague (Netherlands).
CIVIL MILITARY CO-OPERATION: A TEN YEAR EXPERIENCE OF AN AFFILIATIVE AEROMEDICAL EVACUATION PROGRAMME OF THE NETHERLANDS ARMED FORCES AND A CIVILIAN REPATRIATION ORGANIZATION
A. J. vanLousden and F. Rutten (University Hospital, Rotterdam, Netherlands.) *In* AGARD, Recent Issues and Advances in Aeromedical Evacuation (MEDEVAC) Feb. 1995 3 p (For primary document see N95-29604 10-66)
Copyright Avail: CASI HC A01/MF A02

The increase in the number of peace-keeping activities of the armed forces, and the continuing pressure on national defense budgets, are making a demand for maximum efficiency. Triservice co-operation between army, navy and airforce is being pushed in all areas (not just in the medical area), as well as international co-operation between services and civil-military co-operation. Derived from text

N95-29609# Royal Netherlands Air Force, The Hague (Netherlands).
AEROMEDICAL EVACUATION BY RNLAF - WORK ACCORDING TO PROTOCOL
Robert P. vanderMeulen *In* AGARD, Recent Issues and Advances in Aeromedical Evacuation (MEDEVAC) Feb. 1995 2 p (For primary document see N95-29604 10-66)
Copyright Avail: CASI HC A01/MF A02

In this presentation the benefit of using a protocol will be clarified. For some two years now the Royal Netherlands Air Force uses a protocol with respect to the following three items: Requesting a Medevac, Selecting the Medical Equipment and Medical crew and Evaluation Rapportation. The protocol enhances the simplicity and flexibility of aeromedical evacuation. Derived from text

N95-29610# Hospital del Aire, Madrid (Spain).
CRITICAL EVALUATION OF AEROMEDICAL EVACUATION IN A MULTINATIONAL FORCES SCENARIO
V. Navarro-Ruiz, J. I. Peralba-Vano, Z. G. Sanchez-Sanchez, F. Rios-Tejada, P. Miles, and C. Alonso-Rodriguez *In* AGARD, Recent Issues and Advances in Aeromedical Evacuation (MEDEVAC) Feb. 1995 3 p (For primary document see N95-29604 10-66)
Copyright Avail: CASI HC A01/MF A02

A little more than hundred years ago, the injured soldiers were left behind in the battlefield and it was not extraordinary to see wounded still being picked up days after the battle, and then to receive, if they were lucky, only some degree of wound care and lifesaving amputations. Everyone

is aware of the changes that have occurred in our society following the scientific achievements of the last century. These technical advances have changed the view of our planet. For the first time we realize not only that we are in the same boat, but that we can change its course. Medicine has not turned its back to these changes. Today's therapeutic possibilities are far beyond the expectations present just a few decades ago. Those can be made available to any wounded or sick, thanks the progress in transportation, mainly air transportation and medical airevacuation. However, two facts have to be taken into account: (1) Warfare, with its everchanging situation and hi-tech weapon systems has developed an enormous destruction potential; (2) Medicine, has become more complex and has to face limited health resources in the military and civilian environment. Medical care and treatment are expensive, complicated and this applies also to med-evac media, especially the ones involved in aeromedical evacuation. Bearing all this in mind, we describe problems encountered with airevacuations during our involvement in multinational forces and make recommendations after their analysis. Derived from text

N95-29611# SEU-061, Madrid (Spain).
EXPERIENCE IN HELICOPTER AEROEVACUATION IN THE COMMUNITY OF MADRID, SPAIN
J. Cepas, C. DelPozo, C. Hernandez, J. Aparicio, J. A. Lopez, and M. Romero *In* AGARD, Recent Issues and Advances in Aeromedical Evacuation (MEDEVAC) Feb. 1995 4 p (For primary document see N95-29604 10-66)
Copyright Avail: CASI HC A01/MF A02

It's now well-known the fact that in the last few years a new concept of trauma patient medical assistance is imposing itself in the field of emergency medicine. This is helicopter aeroevacuation, and this together with the appropriate coordination between pre-hospital medical care and intensive care units, is making important changes in the disease and death toll of this kind of patients. The objective of this talk is to transmit the experience of this pre-hospital care service and to evaluate its results and evolution in its first three years of life. Author

N95-29612# Human Systems Div., Brooks AFB, TX.
AEROMEDICAL EVACUATION IN COMBINED OPERATIONS
Robert P. Belihar and Robert H. Brannon *In* AGARD, Recent Issues and Advances in Aeromedical Evacuation (MEDEVAC) Feb. 1995 2 p (For primary document see N95-29604 10-66)
Copyright Avail: CASI HC A01/MF A02

The Gulf War (Desert Shield/Desert Storm) was a military effort involving multinational participation on a scale unparalleled in the history of modern warfare. Numerous countries were involved in the operation--many providing combatants. The nature and scope of the allied involvement led to numerous interoperability issues in many areas, including medical. United States forces were deployed in accordance with an existing operational plan (OPLAN) which had been developed to counter an Iraqi threat to Kuwait and Saudi Arabia. That OPLAN included the development of a theater medical system (TMS) to support all components of the U.S. military. The details of the relationship between U.S. forces and its allies were not part of that OPLAN and evolved as deployment of forces took place. In order to resolve interoperability issues, Friendly Force Medical Conferences were conducted during the course of the war. Senior medical officers from the allied forces gathered together to resolve areas of concern. There was considerable variation in the medical capabilities of the deployed allied forces--particularly related to aeromedical evacuation. Derived from text

N95-29613# Vaerloese Air Base, Vaerloese (Denmark). Medical Squadron 590.
DANISH AEROMEDICAL EVACUATION EFFORTS DURING THE GULF WAR
S. Lyduch, J. Nybo Nielsen, and F. K. Larsen *In* AGARD, Recent Issues and Advances in Aeromedical Evacuation (MEDEVAC) Feb. 1995 3 p (For primary document see N95-29604 10-66)
Copyright Avail: CASI HC A01/MF A02

During the Gulf War 1990/1991 a Boeing 737-300 was leased from a civilian airline company and prepared for aeromedical evacuation of injured allied soldiers from U.S. bases in Saudi Arabia, or from staging facilities in West Germany or England, to Holstebro Military Hospital in Denmark. Additional fuel tanks and military communication, navigational and identification systems were installed. The original interior was replaced with stretcher racks placed along the cabin wall on both sides together with intensive care medical monitoring equipment. Object was to operate 24 hours a day, and three medical crews were established. Patient selection, categorization, prioritization and loading plans would be decided by a Senior Flight Surgeon in a forward position. After 3 weeks, on February 8, 1991 the system was declared operational, and a test flight to Rhein Main AB, Germany was accomplished. Though the system was never activated due to the limited number of casualties, valuable experience was gained, and the system should be considered in connection with future international military operations. Author

N95-29614# Hospital del Aire, Madrid (Spain).
EXPERIENCES LEARNED FROM THE SPANISH ARMED FORCES AEROMEDICAL EVACUATION SYSTEM IN THE FORMER YUGOSLAVIA
Z. G. Sanchez-Sanchez, J. I. Peralba-Vano, P. Miles, F. Rios-Tejada, and V. Navarro-Ruiz *In* AGARD, Recent Issues and Advances in Aeromedical Evacuation (MEDEVAC) Feb. 1995 4 p (For primary document see N95-29604 10-66)
Copyright Avail: CASI HC A01/MF A02

During the last two years, Spain has participated as a part of the United Nations Forces in the former Yugoslavia. The Spanish Forces bore a major responsibility for maintaining the access of relief personnel and supplies to the areas designated to them, especially around Mostar and the Neretva valley. Medical personnel from the Army accompanied these forces establishing certain sanitary objectives and implementing their medical deployment plans. These plans consisted of a small classification post in Dracevo with an ICU with surgical Unit (1 Surgeon, 1 Orthopedist, 1 Anesthesiologist, 1 Intensivist, etc.) a few hospital beds and 4 ambulance teams, each with a doctor and a nurse on board. As the first casualties occurred, the aeromedical evacuation plan was activated (this task was 'commended' to the Air Force Med-Evac Teams). These teams had had some relatively recent experience drawn from operations in Namibia and south-west Asia in the last years. But the real scenario, taught new lessons which had to be assimilated, and the conclusions drawn implemented to improve our operational activity. Author

N95-29615# Department of the Air Force, Scott AFB, IL. Office of the Command Surgeon.
RE-ENGINEERING SUPPORT TO THE PATIENT MOVEMENT PROCESS
John D. Power, William P. Frank, Phillip Mahlum, and Jack Simpson, II *In* AGARD, Recent Issues and Advances in Aeromedical Evacuation (MEDEVAC) Feb. 1995 3 p (For primary document see N95-29604 10-66)
Copyright Avail: CASI HC A01/MF A02

The complexity and dynamics of medical evacuation planning - for peacetime, wartime, and disaster scenarios - require decision support aids that provide much more than data base access and spreadsheet solutions. This paper presents an overview of the development and early user operational and technical assessment of a Decision Support System (DSS) that incorporates innovative object-oriented data bases, state-of-the-art mapping capability, and constraint-directed planning technology. Author

N95-29616# Royal Norwegian Inst. of Aviation Medicine, Oslo (Norway).
THE IMPACT OF OCCUPATIONAL CULTURES ON COORDINATION OF EMERGENCY MEDICAL SERVICE CREW
V. M. Fonne and G. Myhre *In* AGARD, Recent Issues and Advances in Aeromedical Evacuation (MEDEVAC) Feb. 1995 7 p (For primary document see N95-29604 10-66)
Copyright Avail: CASI HC A02/MF A02

The purpose of the study was to see whether one can observe different occupational cultures in the Emergency Medical Service and whether these differences in orientation among the crewmembers may have an impact on effective crew coordination. The number of crew members is usually limited to pilot, paramedic rescuer and medical doctors or registered nurse. Due to their different professional training, each crew member joins the Emergency Medical Service (EMS) with different backgrounds, interests and expectations. The operational stresses of this kind of service, however, demand team work and expose the crew's ability to coordinate their actions to work as a team. The initial study consisted of 60 operational crewmembers from the Norwegian Air Ambulance Service. They represent 65 percent of the company's flying personnel. Hofstede's Values Survey Module was administered for an evaluation of occupational culture. The analysis reveals

group differences at the occupational level in the perception of power distribution, team orientation and achievement preferences. The results are further discussed in relation to the crewmembers' different task demands and areas of responsibility, and emphasis is put on organizational responsibility for enhancing safety and effectiveness in the service.

Author

N95-29617# Army Medical Command (18th), (18th). Unit 15281.

MEDICAL EVACUATION: A TRAINING PRIORITY

Craig L. Urbauer and Mathew S. Granger *In* AGARD, Recent Issues and Advances in Aeromedical Evacuation (MEDEVAC) Feb. 1995 2 p (For primary document see N95-29604 10-66)

Copyright Avail: CASI HC A01/MF A02

Medical evacuation is a comprehensive process which includes selecting the patients to be evacuated, determining the means of evacuation, and providing enroute medical care and intervention. The military medical community continues to stress the fact that medical evacuation is a medical process, not a logistic one. The 'chain of medical responsibility' is an important principle, but it does not relieve the ground maneuver commander of responsibility for the treatment and evacuation of casualties from the battlefield. Medical treatment and evacuation is a sustainment function as critical to the ground commander's success as arming, fueling, fixing, or moving. If the chain of medical responsibility is to have the proper means to succeed on the battlefield, the ground maneuver commander must establish medical evacuation as a training priority equal to the other sustainment functions.

Author

N95-29618# Vaerloese Air Base, Vaerloese (Denmark). Medical Squadron 590.

FLYING AMBULANCES: THE APPROACH OF A SMALL AIR FORCE TO LONG DISTANCE AEROMEDICAL EVACUATION OF CRITICALLY INJURED PATIENTS

J. Nybo Nielsen, S. Lyduch, and F. K. Larsen *In* AGARD, Recent Issues and Advances in Aeromedical Evacuation (MEDEVAC) Feb. 1995 3 p (For primary document see N95-29604 10-66)

Copyright Avail: CASI HC A01/MF A02

The Danish Air Force has developed a system for Aeromedical Evacuation of injured soldiers, based on flying ambulances inside a C-130. The ambulances function as mobile intensive care units, and provide a quiet, well lit and air-conditioned environment for observation and treatment of the patients. The system has a limited capacity, but it has so far proved sufficient to support the Danish participation in the UN-peacekeeping missions in the former Yugoslavia. A number of missions have been successfully carried out, three of them with two ambulances in the C-130. The system has the added advantage of providing door to door transport, without the need for moving the patient from ambulance to aircraft, and again from the aircraft to another ambulance on arrival in Denmark. To increase the capacity in the future, a system using specially equipped containers to be carried in the cargo bay of a C-130 is under consideration, and 2 such containers will probably be ordered this year. For the future AIREVAC support of a Danish battalion as part of NATO's Rapid Reaction Forces, we suggest a system based on chartered Boeing 737's or similar aircraft, and reservist personnel which should be identified and trained for the mission. The readiness of the system should be insured through planning, including contracts with airlines and personnel, training of medical personnel and procurement of stretcher support system and medical supplies.

Author

N95-29619# Department of the Air Force, Brooks AFB, TX. Nurse Corps.

CIVIL RESERVE AIR FLEET-AEROMEDICAL EVACUATION SHIPSET (CRAF-AESS)

Candy Jean Nistler *In* AGARD, Recent Issues and Advances in Aeromedical Evacuation (MEDEVAC) Feb. 1995 2 p (For primary document see N95-29604 10-66)

Copyright Avail: CASI HC A01/MF A02

In 1985, the USAF/SG, AMC/SG, and CINCAMC agreed in time of war there would not be enough C-141's and C-9's that could be dedicated to Aeromedical Evacuation (AE). It was decided to design a kit that could re-configure Civil Reserve Air Fleet aircraft, specifically the Boeing 767, into AE aircraft to perform strategic and CONUS missions. A formal acquisition program was planned and executed by the Human Systems Program Office, Brooks AFB, TX, to design, develop, and produce the conversion kit for the Boeing 767. Developmental and Operational Test Evaluation Flights were flown in March 1991. The FAA issued flying certificates for two configurations of the Boeing 767 conversion kit; one to carry 111 litter patients and one to carry 87 litter patients. The CRAF-AESS has three subsystems. The Patient Transport Subsystem (PTS) consists of the litter stanchions and litter support arms for up to 111 litter patients. The Medical Oxygen Subsystem (MOS) consists of six 75 liter Dewars, which supply therapeutic oxygen outlets located at each potential litter position. The Aeromedical Operations Subsystem (AOS) consists of six 35 amp electrical converters to convert aircraft power to regular hospital current for medical equipment use. Electrical outlets are located at each potential litter position. This subsystem also includes two nurse workstations and seats. The airlines signed a contract with the USAF to be a CRAF-AESS supporter. Civilian airline pilots will fly the CRAF-AESS aircraft, airline flight attendants will be in charge of emergency egress, and the Systems Program Office is currently in full production for 44 shipsets. There are 17 complete shipsets delivered to date. CRAF-AESS will expand the USAF AE capabilities during war and allows medical personnel to provide excellent medical care.

Author

N95-29620# Army Aeromedical Research Lab., Fort Rucker, AL. Aircrew Protection Div.

FIRST MEDICAL TEST OF THE UH-60Q AND EQUIPMENT FOR USE IN US ARMY MEDEVAC HELICOPTERS

J. E. Bruckart, J. R. Licina, and M. D. Quattlebaum *In* AGARD, Recent Issues and Advances in Aeromedical Evacuation (MEDEVAC) Feb. 1995 5 p (For primary document see N95-29604 10-66)

Copyright Avail: CASI HC A01/MF A02

The U.S. Army operates helicopters worldwide, including over 500 designated for medical evacuation (MEDEVAC). Advanced avionics and a commercial medical interior have been installed in a Black Hawk helicopter, designated the UH-60Q. MEDEVAC aircraft also carry commercial medical devices that can fail from stresses of in-flight use or interfere with critical rotary-wing aircraft systems. The U.S. Army Aeromedical Research Laboratory (USAARL) performed the first flight tests evaluating the medical interior in the UH-60Q and tested commercial medical devices to determine their compatibility with MEDEVAC aircraft. Flight tests in the UH-60Q validated the enhanced capability provided by the new avionics systems, external rescue hoist, oxygen generator, built-in suction, litter lifts, and improved crew seating. The new litter lift system provided inadequate vertical clearance and several components of the restraint hardware were not sufficiently durable. From January 1989 to January 1994, 40 medical devices, including monitor/defibrillators, infusion pumps, vital sign monitors, ventilators, oxygen generators, and infant transport incubators, were tested under extreme conditions of temperature, humidity, altitude, and vibration (MIL-STD 810). Electromagnetic emissions and susceptibility were measured (MIL-STD 461 & 462). Thirty-two percent of the medical devices failed at least one environmental test and 92 percent of the devices failed to meet electromagnetic interference standards. Eighteen percent of the commercial medical devices were judged unsuitable for use in the UH-60 MEDEVAC helicopter. Testing is critical to discover the ability of a new aircraft system or medical device to perform in the harsh rotary-wing MEDEVAC environment. Failure of a device or interference with aircraft systems can result in loss of a patient or aircrew.

Author

N95-29621# Army Aviation Brigade, Mendig (Germany).

THE LARGE-CAPACITY RESCUE-HELICOPTER CH-53 G

Christoph Schroedl *In* AGARD, Recent Issues and Advances in Aeromedical Evacuation (MEDEVAC) Feb. 1995 3 p (For primary document see N95-29604 10-66)

Copyright Avail: CASI HC A01/MF A02

A new concept has been developed: (1) for handling great numbers of casualties during disasters and events entailing major damage; (2) for providing quick support of medical treatment facilities employed by crisis reaction forces during out-of-area operations; and (3) for accomplishing medical evacuation and combat rescue missions. In view of current planning conducted by the German armed forces in conjunction with the crisis reaction forces this concept takes on an increased tactical significance in the context of studies concerning medical support of medical treatment facilities and also when it comes to missions related to combat rescue

and medical evacuation. During several real-time operations and numerous exercises the 'large rescue helicopter CH- 53 G' concept has proved to be efficient. Author

N95-29622# Department of the Air Force, Brooks AFB, TX. Armstrong Lab.

INTERNATIONAL ACCESS TO AEROMEDICAL EVACUATION MEDICAL EQUIPMENT ASSESSMENT DATA

Jacqueline Hale *In* AGARD, Recent Issues and Advances in Aeromedical Evacuation (MEDEVAC) Feb. 1995 3 p (For primary document see N95-29604 10-66)

Copyright Avail: CASI HC A01/MF A02

Aeromedical evacuation medical equipment development using evaluation and often times modification by the manufacturer to achieve compatibility in the airborne environment began over 25 years ago at Brooks AFB in support of Military Airlift Commands (now Air Mobility Command) medical evacuation mission. This approach was adopted because sometimes standard research and development methods were not responsive to Command requirements. In the course of those years simple items such as securing devices to those as complicated as an Extracorporeal Membrane Oxygenation System have been extensively evaluated using a battery of tests to verify adapt ability to altitude and compatibility with aircraft systems. Because technology in aircraft systems and in medical equipment has advanced, so has the importance of testing for situational compatibility. Medical devices may produce electromagnetic interference with aircraft navigation or communication systems and aircraft systems can interfere with the operation of medical devices. Results of tests conducted at Armstrong Laboratory Brooks AFB are published as individual detailed Technical Reports and later compiled into a comprehensive document entitled 'Status Report on Medical Material Items Tested And Evaluated For Use In The USAF Aeromedical Evacuation System'. This publication was available for public release and met customer access needs of the day. However, with the advent of independent air ambulance services and increase in countries actively engaged in aeromedical evacuation, a need to better communicate results of testing emerged. Researchers at Armstrong Laboratory developed a database program for rapid dissemination of medical equipment airworthiness evaluation results and are exploring electronic delivery avenues to meet the need for worldwide accessibility. Author

N95-29623# Princess Alexandra Hospital, Swindon (England).

A GENERIC SPECIFICATION FOR SPECIAL PURPOSE AEROMEDICAL EQUIPMENT **c05**

I. Spencer *In* AGARD, Recent Issues and Advances in Aeromedical Evacuation (MEDEVAC) Feb. 1995 5 p (For primary document see N95-29604 10-66)

Copyright Avail: CASI HC A01/MF A02

A generic specification for Special Purpose Aeromedical Equipment (SPAME) has been prepared which, if met, would largely overcome the problems faced by medical operators seeking clearance for the use of such equipment in aircraft. It is suggested that this specification might be used by NATO medical forces as a base for future standardization and thus perhaps increased interoperability of aeromedical resources and equipment. Author

N95-29624# Department of the Air Force, Brooks AFB, TX. Armstrong Lab.

AEROMEDICAL IMPACT OF THE TRANSPORTABLE PRESSURE VENTILATOR IN WARTIME AEROMEDICAL EVACUATION **c54**

L. Richardson and R. Munson *In* AGARD, Recent Issues and Advances in Aeromedical Evacuation (MEDEVAC) Feb. 1995 5 p (For primary document see N95-29604 10-66)

Copyright Avail: CASI HC A01/MF A02

Mechanical ventilation permits the early air transport of patients in respiratory failure. Ventilator-dependent patients have been successfully air transported since the 1970's in the United States Air Force (U.S.A.F.) peacetime aeromedical evacuation system. The selection of suitable ventilation equipment, patient management and related safety issues, such as ventilator performance characteristics during rapid decompression, have been previously reviewed. During peacetime aeromedical operations, space is not usually an issue and volume ventilators are generally used. During wartime operations the bulky volume ventilator and the 100 volt AC (VAC) at 60 Hz electrical power converter are not readily available and take up too much space to be used on the C-130 and C-141 aircraft opportunely diverted from cargo missions to perform aeromedical evacuation. Each litter station in these cargo aircraft can hold up to ten litter patients. When a volume ventilator-dependent patient requires air transport, the litter station is typically reduced to only one or two litters. Recent conflicts such as Operations Just Cause and Desert Storm have refocused the need to provide acute care while enroute to definitive care. The projected large numbers of litter casualties and the potential increased demand for ventilator support for biological chemical or burn injuries during Desert Storm resulted in the distribution of the TXP ventilator to U.S.A.F. Aeromedical Staging Facilities. Use of the TXP ventilator has the potential of reclaiming the eight or nine litter positions lost during the air transport of a volume ventilator-dependent patient due to its ability to be attached to the patient's litter. Derived from text

N95-29625# Army Medical Command (18th), (18th). Unit 15281.

REQUIREMENT FOR ONBOARD TELEMETRY EQUIPMENT **c17**

Mathew S. Granger and Craig L. Urbauer *In* AGARD, Recent Issues and Advances in Aeromedical Evacuation (MEDEVAC) Feb. 1995 5 p (For primary document see N95-29604 10-66)

Copyright Avail: CASI HC A01/MF A02

The use of onboard telemetry equipment in EMS ground and air ambulances has made significant inroads in the civilian sector. This article reviews data from 661 patients evacuated by UH-60A helicopters in the Republic of Korea from June 1993 through May 1994. Patient categories, enroute care provided, and patient outcomes are analyzed to determine if onboard telemetry equipment would have improved enroute care provided or patient outcome. The data indicates onboard telemetry would have been of marginal utility and would not have affected patient outcomes. It is the conclusion of the authors that onboard telemetry equipment would be of limited value in military aeromedical evacuation operations. Author

N95-29626# Department of the Air Force, Scott AFB, IL.

CARE IN THE AIR: A SYSTEM ANALYSIS OF CLINICAL OUTCOMES IN AEROMEDICAL EVACUATION **c54**

Arleen M. Saenger *In* AGARD, Recent Issues and Advances in Aeromedical Evacuation (MEDEVAC) Feb. 1995 7 p (For primary document see N95-29604 10-66)

Copyright Avail: CASI HC A02/MF A02

In 1993 a clinical outcomes study of the Continental United States (CONUS) Aeromedical Evacuation (AE) system was undertaken. Between 15 Feb. and 31 Oct. 1993, AE patients were screened for a series of adverse clinical outcome indicators and process discrepancy indicators. Rates were determined for each of the indicators. Defense Medical Regulating Information System (DMRIS) records were reviewed to obtain patients' demographic data. Correlations between diagnoses and adverse clinical outcomes were evaluated. During AE missions the adverse clinical outcome rate was 0.9 per 1000 patients. Unanticipated need for O2 and development of chest pain in flight accounted for 73 percent of the in-flight adverse outcomes and occurred primarily in cardiac patients. The process discrepancy rate was 10 per 1000 patients - 10 times the adverse outcome rate. For patients remaining over night in Aeromedical Staging Facilities the adverse outcome rate was 2.9 per 1000 patients. ENT barotrauma accounted for 66 percent of these patients. The adverse clinical outcome rate for peacetime AE patients is very low. Patients with limited cardiopulmonary reserve are at higher risk during AE. During wartime and military operations other than war, AE patients are more likely to have limited cardiopulmonary reserve and be at higher risk due to injuries, malnutrition, or limited medical care prior to flight. Special attention to oxygen requirements, altitude restrictions, complete documentation of care required en route, and proper selection of medical attendants are crucial for good outcomes in AE. Author

N95-29627# Institute of Aviation Medicine, Oslo (Norway).

EFFECT OF HYPOXIA ON ARTERIAL BLOOD GASES IN SUBJECTS WITH LUNG DYSFUNCTION **c52**

Morten Ryg and Carl C. Christensen *In* AGARD, Recent Issues and Advances in Aeromedical Evacuation (MEDEVAC) Feb. 1995 14 p (For primary document see N95-29604 10-66)

Copyright Avail: CASI HC A03/MF A02

Although air transportation is an efficient way of evacuating casualties out of combat zones, even the mild hypoxia in a pressure cabin may

adversely affect the oxygen supply of subjects whose lung function is compromised. Obviously, the wounded are difficult to study systematically. It is, however, possible to evaluate pulmonary limitations of oxygen transport by investigating persons with various lung diseases. This paper presents the effects of very light physical work in hypoxia on subjects with chronic obstructive lung disease (COPD). These patients are characterized by obstruction of the airways, resulting in low expiratory air flow rates, and low maximal ventilation rates (Cotes 1993). We analyze the consequences of inadequate alveolar ventilation and increased resistance to diffusion in the lung for oxygen partial pressures in alveoli and arterial blood, and on arterial oxygen saturation. We also try to evaluate the usefulness of standard clinical tests in predicting susceptibility of lung patients to hypoxia.
Derived from text

N95-29628# United States Air Forces in Europe, APO New York, NY.
CHANGES IN THE MEDEVAC MISSION RESULT IN AN INCREASED ROLE FOR THE FLIGHT SURGEON
T. J. Lyons and S. B. Connor *In* AGARD, Recent Issues and Advances in Aeromedical Evacuation (MEDEVAC) Feb. 1995 10 p (For primary document see N95-29604 10-66)
Copyright Avail: CASI HC A02/MF A02

Historically physicians were involved in the development of aeromedical evacuation (medevac) and flight surgeons flew as crewmembers on the first US military medevac flights. However, since World War II flight surgeons have not been routinely assigned to operational medevac units. The aeromedical literature addressing the role of physicians in medevac is controversial. Recent contingencies involving the U.S. Air Force (USAF) have required the augmentation of medevac units with flight surgeons. Since 2 February 1993, USAFE has moved 221 patients on 27 missions out of the former Yugoslavia -- most of these missions had a flight surgeon on the crew. Because advanced medical information on the status of these patients is often non-existent, the presence of a physician on the crew proved lifesaving in some instances. In peacetime operations, there has been a recent trend in the European theater for the USAF to move more unstable patients. Beginning in 1993, USAFE assigned three flight surgeons to the medevac squadron. Dedicated medevac flight surgeons have proven to have the specific experience and training to perform effectively in the role of in-flight medical attendant. Their understanding of the system also makes them more effective in medical validation than non-medevac flight surgeons. In addition, they are effective in negotiating with referring physicians about the urgency of movement, required equipment, the need for medical attendants, etc. These flight surgeons provide medical coverage of transiting patients in the Aeromedical Staging Flight (ASF), thus providing needed continuity in the medevac system. In conclusion, dedicated medevac flight surgeons fill a unique and valuable role. Recommend that agencies with medevac units consider assigning flight surgeons to these units. Author

N95-29629# Hellenic Air Force General Hospital, Athens (Greece).
FLIGHT NURSE SCHOOL IN THE HELLENIC AIR FORCE **c52**
Kal. Papastogiannidou and Alex. Katsika *In* AGARD, Recent Issues and Advances in Aeromedical Evacuation (MEDEVAC) Feb. 1995 5 p (For primary document see N95-29604 10-66)
Copyright Avail: CASI HC A01/MF A02

The necessity of specialized nursing personnel for air evacuated patients in peace and war time led Medical Service of the Hellenic Air Force (HAF) to train officer nurses in the USA F.N. School in order to create a similar school in our country. This School was established in 1988 and the first FN's graduated the same year. At this moment, the training courses are for officers with a near future schedule for petty officers. The structure and performance of school conducted in accordance to US FN School in Brooks AFB San Antonio TEXAS, corresponded to the needs and abilities of our country. The ultimate purposes concerning the foundation of the school are: (1) to advance the quality of nursing care; (2) to install the minimum demands - standards of care for FN; 3) to access FN nursing enlightment to all levels of medical personnel; (4) the readiness to respond in every emergency condition involving air evacuation demands in agreement with an appropriate program; (5) the attachment of education to all FN; and (6) to advance assurance quality with a predetermined procedure. Course is mandatory and operates on a theoretical base with a minimum of practical application. The experiences gained from FN during the involvement in three (3) scheduled air drills were fewer than expected. Flight nursing offers a unique and broad field to professional nursing with an opportunity to serve patients, community, integrating nursing as a basic part of aerospace medicine. Author

67 THEORETICAL MATHEMATICS

Includes topology and number theory.

N95-29072# Texas Univ., Austin, TX.
THE DEVELOPMENT OF METHODS AND TECHNIQUES TO DETECT AND MODEL THE UNDERLYING STRUCTURE OF CHAOTIC SYSTEMS M.S. Thesis
James R. Bookhart, Jr. May 1995 132 p
(AD-A292435; Rept-95-005) Avail: CASI HC A07/MF A02

This analysis begins by generating data sets from at least three models known to exhibit chaotic behavior. The data sets are then treated as though the generating functions are unknown and several tests for randomness are applied to determine if the data may be the result of a chaotic system. Next, a model is built in an attempt to recreate the original model from the data. In addition, a statistical model is built using standard multiple regression and time series techniques. The traditional method uses a Box-Jenkins autoregressive integrated moving average (ARIMA) model. The predictive power of the two models, chaotic and stochastic, is then compared to determine the effectiveness of the chaos approach. Data sets studied are from the logistic equation, the Henon equations, and the Rossler equations. The results demonstrate that it is possible to recover, or at least effectively approximate, the functions which generated a series of random looking data. Derived from text

70 PHYSICS (GENERAL)

For precision time and time interval (PTTI) see *35 Instrumentation and Photography;* for geophysics, astrophysics or solar physics see *46 Geophysics, 90 Astrophysics,* or *92 Solar Physics.*

N95-28810# Princeton Univ., NJ. Dept. of Physics.
THE PHYSICS OF SPIN POLARIZED GASES Final Technical Report, 1 Apr. 1992 - 31 Aug. 1994
Gordon D. Cates 15 Jan. 1995 8 p
(Contract F49620-92-J-0211)
(AD-A292511; AFOSR-95-0164TR) Avail: CASI HC A02/MF A01

Most of our research was connected either directly or indirectly to the study of spin polarized atoms and nuclei, and their applications. In most cases we used lasers to optically pump, and hence polarize, alkali-metal vapors. Spin-exchange collisions were used to transfer the angular momentum to other systems. Of particular interest was our continuing study of the polarization of noble gas nuclei, which are characterized by extremely long spin relaxation times of minutes to many days. During this past research period we have demonstrated several applications of polarized noble gas nuclei that may have important implications for such diverse areas as nondestructive testing and medical diagnostics, as well as many areas in fundamental research. Of particular note is the use of spin-exchange polarized He-3 and Xe-129 for magnetic resonance imaging. At present, our imaging work has focused on the lungs of small animals such as mice and guinea pigs. We believe, however, that our technique would also be useful for nondestructive testing. We have also continued our study of Xe that is polarized in the gaseous state, and subsequently frozen. This novel technique for producing a highly polarized solid has received considerable attention in the NMR community. DTIC

N95-28893*# National Aeronautics and Space Administration. Lewis Research Center, Cleveland, OH.
EXPERIMENTAL RESULTS OF HOOPER'S GRAVITY-ELECTROMAGNETIC COUPLING CONCEPT
Marc G. Millis and Gary Scott Williamson Jun. 1995 12 p Presented at the 31st Joint Propulsion Conference and Exhibit, San Diego, CA, 10-12 Jul. 1995; sponsored by AIAA, ASME, SAE, and ASEE
(RTOP 307-51-00)
(NASA-TM-106963; E-9719; NAS 1.15:106963; AIAA Paper 95-2601)
Avail: CASI HC A03/MF A01

Experiments were conducted to test assertions from Patent 3,610,971, by W.J. Hooper that self-canceling electromagnetic coils can reduce the weight of objects placed underneath. No weight changes were observed within the detectability of the instrumentation. More careful examination of the patent and other reports from Hooper led to the conclusion that Hooper may have misinterpreted thermal effects as his 'Motional Field' effects. There is a possibility that the claimed effects are below the detection thresholds of the instrumentation used for these tests. Author

N95-28923# American Inst. of Physics, New York, NY.
PROCEEDINGS OF THE 6TH JOINT MAGNETISM AND MAGNETIC MATERIALS INTERMAG CONFERENCE
W. B. Yelon, ed., F. E. Pinkerton, ed., Y. Idzerda, ed., and W. Y. Ching, ed. 23 Jun. 1994 1186 p Repr. from the Journal of Applied Physics (New York, NY), v. 76, no. 10, Nov. 1994 Conference held in Albuquerque, NM, 20-23 Jun. 1994; sponsored by the American Inst. of Physics and the Magnetics Society of the IEEE
(Grant NSF DMR-92-22976) (ISSN 0021-8979)
(AD-A286752; LC-94-79021; ISBN-1-56396-403-1; CONF-940629-Vol-1)
Avail: CASI HC A09/MF A01

This year's topic was 'Magnetic multilayers: fundamental issues to applications.' In addition to the usual invited papers, there were eight invited symposia; there were three on topics relating to magnetic and magneto-optic recording, and one each on magnetic microscopy, magnetic aftereffect, giant magnetoresistance, magneto-impedance, and neutron scattering studies of vortex structures in superconductors. There was also an evening panel discussion on units in magnetism. The Journal of Applied Physics volume includes 280 contributed papers and 47 invited papers. CASI

N95-28924# American Inst. of Physics, New York, NY.
PROCEEDINGS OF THE 38TH ANNUAL CONFERENCE ON MAGNETISM AND MAGNETIC MATERIALS
W. B. Yelon, ed., J. L. Nix, ed., F. E. Pinkerton, ed., W. M. Saslow, ed., and R. H. Victora, ed. 15 May 1994 792 p Repr. from the Journal of Applied Physics (New York, NY), v. 75, no. 10, 1994 Conference held in Minneapolis, MN, 15-18 Nov. 1993; sponsored by the American Inst. of Physics and the Magnetics Society of the IEEE
(ISSN 0021-8979)
(AD-A286753; LC-94-70649; ISBN-1-56396-337-X; CONF-931133-Vol-1)
Avail: CASI HC A99/MF A02

The conference proceedings is subdivided into 59 sections and contains 30 invited papers, 479 contributed papers, and 153 abstracts. The meeting began with a tutorial on magnetism, magnetic measurements, magnetic force microscopy and other imaging techniques, and materials science (deposition and characterization). There were symposia on magnetic circular dichroism, novel time-resolved probes of dynamical magnetism, perpendicular transport in layered structures, environmental magnetism, and national user facilities. Studies relating to the magnetic properties of surfaces and artificially structured magnetic materials were especially prominent. Derived from text

N95-28962# American Inst. of Physics, New York, NY.
PROCEEDINGS OF THE 38TH ANNUAL CONFERENCE ON MAGNETISM AND MAGNETIC MATERIALS
W. B. Yelon, ed., J. L. Nix, ed., F. E. Pinkerton, ed., W. M. Saslow, ed., and R. H. Victora, ed. New York, NY American Institute of Physics 15 May 1994 1009 p Repr. from the Journal of Applied Physics (New York, New York, American Inst. of Physics), v. 75, no. 10, May 1994 Conference held at Minneapolis, MN, 15-18 Nov. 1993
(ISSN 0021-8979)
(AD-A286751; LC-94-70649; ISBN-1-563-96337-X; CONF-931133) Avail: CASI HC A99/MF A10

The proceeding of the 38th Annual Conference on Magnetism and Magnetic Materials are reported. Technological areas covered includes: magnetic materials and applications, magnetic properties (tunneling), magnetoelastic behavior of films and crystals, thin and ultrathin films, micromagnetics and hysteresis, magnetic semiconductors, magnetic circular dichroism, critical phenomena and disordered systems, new instrumentations and measurement techniques, environmental magnetism, field computations, magnetic bubble and VBL memories, novel time-resolved probes of dynamical magnetism, magnetic ordering and magnetic structure, high temperature superconductivity, and magneto-optics CASI

N95-28987# Wright Lab., Wright-Patterson AFB, OH. Solid State Electronics Directorate.
HIGH RESOLUTION, LARGE SCALE MEASUREMENT PROCESSES Final Report, 1 May 1991 - 30 Jun. 1993
Jeff L. Brown Jul. 1994 34 p
(AD-A292200; WL-TR-94-5045) Avail: CASI HC A03/MF A01

As spatial resolution of any measurement process increases, the amount of data per unit area (or volume) increases, leading to huge amounts of data and/or long measurement times when attempting to map small spatial variations in material properties over large spatial dimensions. It is therefore desirable to develop techniques in which high resolution information can be obtained, while maintaining the ability to cover large areas without being overwhelmed by measurement time or data. This report discusses the issues involved and seeks to formulate and advocate strategies that could guide such endeavors. DTIC

N95-29000# Air Force Inst. of Tech., Wright-Patterson AFB, OH.
HYBRID FUZZY LOGIC CONTROL TO STABILIZE AN INVERTED PENDULUM FROM ARBITRARY INITIAL CONDITIONS M.S. Thesis
Michael J. DeSylva Dec. 1994 83 p
(AD-A292441; AFIT/CI/CIA-94-174) Avail: CASI HC A05/MF A01

The purpose of this work was to develop a controller that could perform the highly discontinuous and nonlinear task of balancing the inverted pendulum from an arbitrary set of initial conditions. Fuzzy logic was chosen as the control technique because of its ability to deal with nonlinear systems, as well as its intuitive nature. The rule base depends on intuition and logic, rather than an exact mathematical model. This makes it more robust to changes in the model, and also gets rid of the need to solve nonlinear differential equations or optimality conditions. Using a set of fuzzy logic controllers, linked in the right way, the primary research objectives were accomplished. In addition, the adjustable desired energy allows for different tip masses and arm lengths to be controlled equally as well with a simple number adjustment on the interactive animation window. This makes the controller very robust. There are many options for future research on the inverted pendulum using fuzzy logic. The current controller could be improved by further adjustment of the membership functions. This adjustment could be performed manually by experimenting and checking the results. An optimization routine using Genetic Algorithms could also be used. This would involve letting the computer run simulations and compare results automatically. DTIC

N95-29062# Kansas State Univ., Manhattan, KS.
RADIATIVE LIFETIME AND QUENCHING RATE CONSTANTS OF PF(B(1) SIGMA+) AND TESTS FOR AN ELECTRONIC TO VIBRATIONAL ENERGY TRANSFER QUENCHING MECHANISM Final Report, 15 May 1992 - 14 Aug. 1994
D. W. Setser 22 Dec. 1994 15 p
(Contract F49620-92-J-0275)
(AD-A290294; AFOSR-95-0044TR) Avail: CASI HC A03/MF A01

Methods were developed to generate and isolate the PF(X(3)Sigma-, a(1)Delta, b(1)Sigma+, A(3)Pi, and d(1)Pi) states in a flow reactor. Radiative lifetimes and total removal constants at 300 K have been measured. Except for halogens, the PF(b(1)Sigma+) state is stable to chemical reaction. The other PF states seem to participate in chemical reactions at 300 K. Preliminary experiments were done with PCl(b(1)Sigma+) and NCl(b(1)Sigma+) to establish their radiative lifetimes. The reactions of excess H atoms with PF2Cl and PF2Br were explored as a chemical source for the generation of PF(a(1)Delta) from the H + PF2 secondary reaction. DTIC

N95-29481# Carnegie-Mellon Univ., Pittsburgh, PA. Dept. of Materials Science and Engineering.
STUDIES DIRECTED TOWARD NEW AND IMPROVED PERMANENT MAGNET MATERIALS Final Report, 1 Apr. 1991 - 31 Aug. 1994
W. E. Wallace 28 Sep. 1994 22 p
(Contract DAAL03-91-G-0027)
(AD-A290749; ARO-28146.17-MS) Avail: CASI HC A03/MF A01

The utility or a permanent magnet is in many applications determined by its maximum energy product, (BH)(sub max). This is the maximum

value of the product of B and H in the 2nd quadrant of the hysteresis loop. The amount of magnetic material to meet a certain need is inversely related to (BH)(sub max). If size of a device is controlled by the volume of magnetic material needed, it is clear that on may downsize the device by using a higher energy product material. High energy permanent magnets find utility in many devices - TWT's, klystrons, linear induction accelerators, etc., as well as electric motors and generators. At present there are only 3 permanent magnet materials in widespread use - SmCo5, Nd2Fe14B and SmCo5-Sm2Co17. Each has weakness. The present study sought to find new and better materials. The findings in this work are described in detail in 33 journal publications. About a third of the effort has been devoted to effecting improvements in existing materials which occur in the SmCo5 or Nd2Fe14B structures. Materials forming in the ThMn12 and LaCo13 structures were also studied. About half of the effort was devoted to developing a preparation scheme to form Fe16N2, which is reported to have a theoretical energy product of approximately 200 MGOe. Fe16N2 has been formed but in the presence of large amounts of alpha Fe and gamma Fe-N alloy. The enlarged B value reported for Fe16N2 has been confirmed in the present study. DTIC

N95-29588# North Carolina State Univ., Raleigh, NC. Dept. of Civil Engineering.
SHORT TERM VISITS FOR COLLABORATIVE RESEARCH Final Report
Yasuyuki Horie 16 Dec. 1994 8 p
(Contract DAAH04-93-G-0255)
(AD-A290704; ARO-32156.1-MS) Avail: CASI HC A02/MF A01

Two Russian scientists were invited to spend six months at North Carolina State University, Raleigh, NC, to develop and promote individual research interactions that are of mutual benefits in the field of shock compression chemistry. The principal results of their visits are: (1) up-to-date reviews and evaluations not only of their own research activities, but also of Russian publications since 1986; (2) a comparative study of U.S. and Russian approaches to the modeling of heterogeneous continual; and (3) the development of a new computational technique to analyze and interpret the mesoscale response of heterogeneous media to shock loading. A further extension of the third project will be continued at one of the home institutions in Russia under the auspices of the program titled 'Industrial Partnering with the New Independent States of the Former Soviet Union.' DTIC

N95-29952# Air Force Systems Command, Wright-Patterson AFB, OH. National Air Intelligence Center.
BRIEF INTRODUCTION TO STATE KEY PHYSICS LABORATORIES AND DIVISION OPEN LABORATORIES
22 Dec. 1994 16 p Transl. into ENGLISH from Wuli, China, v. 20, no. 1, Jan. 1991 p 53-56
(AD-A291064; NAIC-ID(RS)T-0413-94) Avail: CASI HC A03/MF A01

This is a brief introduction of some of the State Key Physics Laboratories and divisional open laboratories. The laboratories to be discussed are those whose operations have been evaluated in 1990 by The Committee of the National Science Foundation, division of mathematics and physics. The evaluation was authorized by The National Science & Technology Committee. Since the evaluation reports were not submitted in an unified format, the style of this article also varies from place to place. Table 1 lists the labs to be discussed. DTIC

N95-30051# Department of the Navy, Washington, DC.
PERMANENT MAGNET TORQUE/FORCE TRANSFER APPARATUS Patent Application
Chahee P. Cho, inventor (to Navy) and Ralph A. Bidingfield, inventor (to Navy) 11 Oct. 1994 15 p
(AD-D017325; US-Patent-Appl-SN-322655) Avail: CASI HC A03/MF A01

There is presented a torque/force transfer apparatus including an annular ring having therein permanent first magnets side by side about the interior of the ring. The first magnets are arranged so as to alternate in polar orientation to present an inside circumference of alternating north and south magnetic poles. The apparatus further comprises a cylindrical central member having therein permanent second magnets side by side about the exterior of the central member. The second magnets are arranged so as to alternate in polar orientation to present an outside circumference of alternating north and south magnetic poles. The apparatus is provided with a strut assembly pivotally attached to a center of a side of the central member and having arms extending radially outwardly from the central member center and is provided with planetary members rotatably connected each to one of the arms. DTIC

N95-30131# Battelle Columbus Labs., OH.
FLUX PINNING AND STABILIZER STUDIES Final Report
E. W. Collings 29 Nov. 1994 10 p
(Contract DE-AC02-86ER-40296)
(DE95-008131; DOE/ER-40296/T3) Avail: CASI HC A02/MF A01

A synopsis of the results of the flux-pinning and stabilizer studies that form the central theme of the subject contract is followed by a list of papers that were published during the period August 28, 1986 to November 31, 1992. Topics discussed include physical and superconducting properties of NbTi and NbTiMn; filament surface effects; position and amplitude of proximity effect peaks; advanced strand design; and magnetically compensated strands. DOE

N95-30232 Johns Hopkins Univ., Baltimore, MD.
PHYSICAL MODELING AND DESIGN OF SEMICONDUCTOR HETEROSTRUCTURES FOR OPTICAL AND ELECTRONICAL APPLICATIONS Ph.D. Thesis
Shaozhong Li 1994 201 p
Avail: Univ. Microfilms Order No. DA9420007

The optical and electrical properties of semiconductor heterostructures are studied theoretically. The dissertation is divided into three main parts: electroabsorption properties, nonlinear optical properties, and electrical properties. In Chapter Two, the electroabsorption properties of semiconductor heterostructures are described for various structures. Excitonic enhancement of electroabsorption, especially longitudinal effects, is extensively examined. It is found that excitonic effects greatly improve the electroabsorption properties. Asymmetric structures and type II superlattices are also investigated as candidates for low insertion loss devices. The results showed that large blue shifts of the absorption edge can be achieved. In Chapter Three, nonlinear optical properties of semiconductor heterostructures are studied. Second and third order nonlinearities, due to intersubband transitions, are calculated. Large values of nonlinear susceptibilities, compatible to the values of most bulk nonlinear optical materials, are obtained. In the last section of the chapter, the Coulomb enhancement of nonlinearity is investigated for different structures and transitions. It is found that third order nonlinearities can be enhanced by Coulomb effects up to about 10 times. In Chapter Four, electrical properties are studied for various semiconductor heterostructures. A method of reducing the base current of bipolar transistors with type II superlattices is proposed. A few feasible schemes, in which a large transconductance can be achieved, are also suggested. Dissert. Abstr.

71 ACOUSTICS

Includes sound generation, transmission and attenuation.
For noise pollution see *45 Environmental Pollution.*

N95-28709 ESDU International Ltd., London (England).
THE PREDICTION OF SOUND ATTENUATION AS A RESULT OF PROPAGATION CLOSE TO THE GROUND
Nov. 1994 17 p
(ISSN 0307-0115)
(ESDU-94036; ISBN-0-856-79923-8) Avail: ESDU

ESDU 94036 introduces a Fortran program for calculating either a difference spectrum between a source and a point close to the ground or, knowing the spectrum at one point, the spectrum at another point, both at discrete frequency noise levels at constant intervals or at one-third octave band levels of broad-band noise. The effects of spherical spreading, atmospheric attenuation, and ground reflection may be treated separately or in any combination. For reflection a two-parameter ground impedance model is used and atmospheric turbulence is treated through consideration of its effect on the coherence between the direct and reflected rays. Guidance on quantities required to define the ground impedance model and the turbulence level is provided. The input to and the output from the program, ESDUpac A9436, are illustrated by a worked example, and the

program is provided on disc in the software volume both uncompiled and compiled in ESDUview, a user-friendly shell that prompts for input data on screen. ESDU

N95-28710 ESDU International Ltd., London (England).
THE CORRECTION OF MEASURED NOISE SPECTRA FOR THE EFFECTS OF GROUND REFLECTION
Nov. 1994 30 p
(ISSN 0307-0115)
(ESDU-94035; ISBN-0-856-79922-X) Avail: ESDU

ESDU 94035 introduces a Fortran program to calculate a difference spectrum between the measured and free-field spectra either at discrete frequency noise levels at constant intervals or at one-third band levels of broad-band noise. The method takes into account both ground impedance through a two-parameter model and atmospheric turbulence by considering its effect on the coherence between the direct and reflected rays, and guidance is included on values for the parameters required to define the impedance model and the turbulence level. The program may also be used to correct a measured spectrum, automatically adjusting for any discrepancy between the cancellation frequencies of the predicted and measured spectra arising from such effects as atmospheric turbulence, errors in source location, or timing errors. An allowance may be made for the characteristics of the filters used to analyse measured data. The method applies to a discrete, stationary source but techniques for taking account of source velocity and distributed source effects are discussed. The minimization of reflection effects by suitable choice of microphone height is considered. The input to and output from the program are illustrated by a worked example and the program, ESDUpac A9435, is provided in the software volume uncompiled and compiled in ESDUview, a user-friendly shell that prompts on screen for input data. ESDU

N95-28783 Office of Naval Research, Arlington, VA.
SYSTEM AND METHOD FOR RAPIDLY TRACKING VEHICLES OF SPECIAL UTILITY IN LOW SIGNAL-TO-NOISE ENVIRONMENTS Patent Application
John S. Davis, inventor (to Navy), Kai F. Gong, inventor (to Navy), and Sherry E. Hammel, inventor (to Navy) 18 Oct. 1994 24 p Filed 18 Oct. 1994 Limited Reproducibility: More than 20% of this document may be affected by microfiche quality
(AD-D017378; Navy-Case-76256; US-Patent-Appl-SN-324639) Avail: Issuing Activity (Defense Technical Information Center (DTIC))

This document discloses a system for facilitating the tracking of a target vehicle in connection with successively-received acoustic sensor signal data items. A fast Fourier transform operation is performed in connection with each successive acoustic sensor signal data item to generate a phase and amplitude beam map reflecting spectral signal energy in the received acoustic sensor signal data item. If the beam map for an acoustic sensor signal data item indicates that the item represents a signal having a signal-to-noise ratio above a first predetermined threshold value, a beam map generated for a previous acoustic sensor signal data item is used to generate a bounded beam map, a determination is made as to whether the bounded beam map represents a signal having a second predetermined signal-to-noise ratio. In response to a positive determination for the latter signal-to-noise determination, both the beam maps are used to generate tracking information for the target vehicle. DTIC

N95-28973# Mississippi Univ., University, MS.
PHYSICAL ACOUSTICS SUMMER SCHOOL, 1994. VOLUME 1. TRANSCRIPT Final Report, 1 Feb. 1994 - 15 Mar. 1995
H. Bass, O. Anderson, S. Putterman, S. Garrett, and G. Swift 15 Mar. 1995 436 p
(Contract N00014-94-1-0468)
(AD-A292552) Avail: CASI HC A19/MF A04

This is the verbatim transcript of the 1994 Physical Acoustics Summer School. It has been edited by the authors and includes in volume 2 a copy of the viewgraphs presented by the lecturers. DTIC

N95-28999# Army Armament Research, Development and Engineering Center, Watervliet, NY. Benet Lab.
SPECTRAL CHARACTERIZATION OF PULSED ULTRASOUND USING NEURAL NETWORKS Final Technical Report
Mark A. Johnson, Michael A. Cipollo, and R. D. Scanlon Dec. 1994 17 p
(AD-A292440; ARCCB-TR-94048) AVAIL: CASI HC A03/MF A01

A novel nondestructive evaluation technique that uses the spectral signature of a pulsed ultrasound signal to identify metals had recently been abandoned because of the difficulty in interpreting the results. Traditional analysis is inconvenient to apply to this type of problem because of the complicated, noisy and incomplete nature of the data. Neural networks provide a radically different approach to computation. These massively parallel systems provide a mechanism to extract pertinent information from input data while maintaining a high degree of fault tolerance. This report discusses design of a neural network system capable of accepting data from nondestructive test equipment and producing output relative to the quality of the sample being tested. DTIC

N95-29077# Army Construction Engineering Research Lab., Champaign, IL.
ESTIMATING ATTENUATION AND PROPAGATION OF NOISE BANDS FROM A DISTANT SOURCE USING THE LOOKUP PROGRAM AND DATA BASE Final Report
Michael J. White Oct. 1994 42 p
(DA Proj. 4A1-62720-A-896)
(AD-A290218; CERL-94/12) Avail: CASI HC A03/MF A01

Unavoidable noise generated by military activities can disturb the surrounding community and become a source of complaint. Military planners must quickly and accurately predict noise levels at distant points from various sound sources to manage noisy operations on a daily basis. This study developed the Lookup computer program and data base to provide rapid estimates of outdoor noise levels from a variety of sound sources. Lookup accesses a data base of archived results (requiring about 5 MB disk space) from typical situations rather than performing fresh calculations for each consultation. Initial timing tests show that Lookup can predict the sound levels from a noise source at distances up to 20 km in 1 second on a DOS-compatible personal computer (PC). This report includes the Lookup program source code, and describes the required input for the program, the contents of the archival data base, and the program output. Lookup was written to compile with MS-Fortran, and will run under DOS on any IBM compatible with 640k random access memory. Lookup also conforms to ANSI 1978 standard Fortran and will run under the Unix operating system. DTIC

N95-29232# Naval Postgraduate School, Monterey, CA.
ACOUSTIC IMAGING OF ULTRASONIC WAVE PROPAGATION M.S. Thesis
Benito E. Baylosis Dec. 1994 113 p
(AD-A290390) Avail: CASI HC A06/MF A02

A pulsed ultrasonic collection facility was used to study the accuracy of a previous program which models pulsed ultrasonic wave propagation. The previous program modeling was initially reviewed for its validity and found to have a scaling factor error. This error was corrected before a comparison of the theoretical and the experimental pulsed response was conducted. The excitation studied was a circular piston impulse input. For proper comparison, the acoustic potential produced by the program modeling (at a given distance from the acoustic source) was expressed in terms of acoustic pressure. Two separation distances were used to compare the output produced by the theoretical modeling and the measured experimental response. A general comparison of the experimental and the theoretical pulsed response appears to be in good agreement. The MATLAB program was used to perform all necessary mathematical computations and manipulations to produce a graphical representation of the collected data. The graphics program, AXUM, was used to compare the results graphically. DTIC

N95-29401*# National Aeronautics and Space Administration. Lewis Research Center, Cleveland, OH.
ACOUSTIC SCATTERING FROM ELLIPSES BY THE MODAL ELEMENT METHOD
Kevin L. Kreider (Akron Univ., Akron, OH.) and Kenneth J. Baumeister Jun. 1995 15 p
(RTOP 505-62-52)
(NASA-TM-106935; E-9663; NAS 1.15:106935) Avail: CASI HC A03/MF A01

The modal element method is used to study acoustic scattering from ellipses, which may be acoustically soft (absorbing) or hard (reflecting). Because exact solutions are available, the results provide a benchmark for algorithm performance for scattering from airfoils and similar shapes. Numerical results for scattering from rigid ellipses are presented for a wide variety of eccentricities at moderate frequencies. These results indicate that the method is practical. Author

N95-29415 Florida State Univ., Tallahassee, FL.
THE SPECTRUM AND DIRECTIVITY OF TURBULENT MIXING NOISE FROM SUPERSONIC JETS Ph.D. Thesis
Ping Chen 1993 132 p
Avail: Univ. Microfilms Order No. DA9413275

There is now a substantial body of theoretical and experimental evidence that the dominant part of the turbulent mixing noise of supersonic jets is generated directly by the large turbulence structures/instability waves of the jet flow. The relationship between the instability waves and noise of hot jets at moderate supersonic Mach number is examined in Chapters 1 and 2. It is found that the highest sound pressure level of the far-field noise occurs at a direction and frequency that closely match the Mach wave radiation direction and frequency of the most amplified instability wave of the jet. The calculations show that for jet Mach number up to 2.0 and jet total temperature to ambient temperature ratio up to 2.5, the Kelvin-Helmholtz instability waves always grow to a higher amplitude than the supersonic instability wave. Numerical results indicate that for hot jets the most amplified wave invariably belongs to the helical mode Kelvin-Helmholtz instability wave. For lower speed hot jets with jet static temperature higher than or equal to the ambient temperature there is also a fair correlation between the Strouhal number at the peak sound-pressure level of the far-field noise and that of the most amplified instability wave. In Chapters 3, 4, 5, and 6, a broadband jet noise theory is constructed. In this theory, the compressible flow equations with eddy viscosity are used to calculate the wave propagation characteristics of the instability waves. These equations are solved by the method of matched asymptotic expansions. The inner solution is the instability wave solution. The outer solution gives the associated acoustic field. The amplitudes of the instability waves are assumed to be stochastic random functions. The statistical properties of the random amplitude function are determined by the requirement that the wave spectrum at the nozzle exit has no intrinsic length and time scales. The present theory can predict the dominant part of jet mixing noise from first principles up to a single multiplicative constant. The spectra and directivities of a Mach 2 jet at total temperatures of 500 K and 1114 K are calculated. The numerical results agree favorably with experimental measurements. Dissert. Abstr.

N95-29452*# National Aeronautics and Space Administration. Langley Research Center, Hampton, VA.
AN EXTENSION OF THE LIGHTHILL THEORY OF JET NOISE TO ENCOMPASS REFRACTION AND SHIELDING
Herbert S. Ribner May 1995 45 p
(RTOP 505-59-52-01)
(NASA-TM-110163; NAS 1.15:110163) Avail: CASI HC A03/MF A01

A formalism for jet noise prediction is derived that includes the refractive 'cone of silence' and other effects; outside the cone it approximates the simple Lighthill format. A key step is deferral of the simplifying assumption of uniform density in the dominant 'source' term. The result is conversion to a convected wave equation retaining the basic Lighthill source term. The main effect is to amend the Lighthill solution to allow for refraction by mean flow gradients, achieved via a frequency-dependent directional factor. A general formula for power spectral density emitted from unit volume is developed as the Lighthill-based value multiplied by a squared 'normalized' Green's function (the directional factor), referred to a stationary point source. The convective motion of the sources, with its powerful amplifying effect, also directional, is already accounted for in the Lighthill format: wave convection and source convection are decoupled. The normalized Green's function appears to be near unity outside the refraction dominated 'cone of silence', this validates our long term practice of using Lighthill-based approaches outside the cone, with extension inside via the Green's function. The function is obtained either experimentally (injected 'point' source) or numerically (computational aeroacoustics). Approximation by unity seems adequate except near the cone and except when there are shrouding jets: in that case the difference from unity quantifies the shielding effect. Further extension yields dipole and monopole source terms (cf. Morfey, Mani, and others) when the mean flow possesses density gradients (e.g., hot jets). Author

N95-29502 California Univ., Los Angeles, CA.
TURBULENT AIRFLOW NOISE PRODUCTION AND PROPAGATION PATTERNS OF A SUBSONIC JET IMPINGING ON A FLAT PLATE Ph.D. Thesis
Stephen Allen Martin 1993 171 p
Avail: Univ. Microfilms Order No. DA9420452

A four inch diameter jet impinging on a flat plate with plate-jet distances of 12, 20, 24, and 28 inches is studied. The analysis utilizes cross-correlation techniques to investigate the far field sound pressure relationship to turbulent sources produced near the plate surface. The variables studied include the effects of jet axis speed, the angle of the plate with respect to the jet axis, the location of the turbulent source from the center of the plate, the location of the far field microphone, and the plate-jet distance. The cross-correlation techniques allow discrimination of the far field sound pressure related to the turbulent noise source located near the surface of the plate. By rotating the far field microphones, directivity patterns are obtained for a source located a particular distance from the center of the plate. The resulting directivity patterns were cloverleaf shaped, indicating a quadrupole source, verifying Powell's developments on Lighthill's theory on jet noise. The variations of the parameters of the experiment allow a comparison of the directivity patterns for each condition The results of the study provoked questions, resulting in providing a fluid flow model as an explanation. The large turbulence at 6 centimeters from the center of the plate, along with the disappearance of the cross-correlation with far field microphones at this position, indicated a singular point in the fluid flow. The model utilizes the jet and surface vortices as an explanation of the phenomena. Dissert. Abstr.

N95-29641*# General Electric Co., Cincinnati, OH. Aircraft Engines.
UHB ENGINE FAN BROADBAND NOISE REDUCTION STUDY Final Report
Philip R. Gliebe, Patrick Y. Ho, and Ramani Mani (General Electric Co., Schenectady, NY.) Jun. 1995 48 p
(Contract NAS3-26617; RTOP 538-03-11)
(NASA-CR-198357; E-9740; NAS 1.26:198357) Avail: CASI HC A03/MF A01

A study has been completed to quantify the contribution of fan broadband noise to advanced high bypass turbofan engine system noise levels. The result suggests that reducing fan broadband noise can produce 3 to 4 EPNdB in engine system noise reduction, once the fan tones are eliminated. Further, in conjunction with the elimination of fan tones and an increase in bypass ratio, a potential reduction of 7 to 10 EPNdB in system noise can be achieved. In addition, an initial assessment of engine broadband noise source mechanisms has been made, concluding that the dominant source of fan broadband noise is the interaction of incident inlet boundary layer turbulence with the fan rotor. This source has two contributors, i.e., unsteady life dipole response and steady loading quadrupole response. The quadrupole contribution was found to be the most important component, suggesting that broadband noise reduction can be achieved by the reduction of steady loading field-turbulence field quadrupole interaction. Finally, for a controlled experimental quantification and verification, the study recommends that further broadband noise tests be done on a simulated engine rig, such as the GE Aircraft Engine Universal Propulsion Simulator, rather than testing on an engine statically in an outdoor arena The rig should be capable of generating forward and aft propagating fan noise, and it needs to be tested in a large freejet or a wind tunnel. Author

N95-29659# Air Force Systems Command, Wright-Patterson AFB, OH. National Air Intelligence Center.
THE ANGULAR SPREAD OF THE DEFLECTED ACOUSTIC BEAM DIFFRACTED BY A BRAGG GRATING OUT OF A SURFACE ACOUSTIC WAVE
Zuoqing Wang and Chenghao Wang 3 Jan. 1995 19 p Transl. into ENGLISH from Shengxue Xuebao, China, v. 14, no. 1, Jan. 1989 p 51-57
(AD-A291018; NAIC-ID(RS)T-0368-94) Avail: CASI HC A03/MF A01

In this paper, basing on the equations of the deflection angle and of the deflection efficiency, the relation between the angular spread of the deflected SAW beam on the Bragg grating denoted by Delta-Theta sub 1

and the parameters of the grating is analyzed. A parameter referred to as 'Bragg width of the angular spectrum' of the acoustic grating is defined and it is designated with Delta-Theta sub B. The meaning of the parameter Delta-Theta sub B for distinguishing the angular spread range of the deflection beam is discussed as well. It is concluded from the analysis that if the spread angle of the incident beam (labelled with Delta-Theta sub 1me) is larger than the Bragg width of the angular spectrum: of the grating, the spread angle of the deflection beam Delta-Theta sub 1 will equal to Delta-Theta sub m; On the contrary, if the angular divergency of the incident beam is less than Delta-Theta sub B, then, Delta-Theta sub 1 = Delta-Theta sub 1me. DTIC

N95-29681# Air Force Systems Command, Wright-Patterson AFB, OH. National Air Intelligence Center.

MULTIPLE DIMENSIONAL ACOUSTO-OPTIC DIFFRACTION AND MULTIPLE DIMENSIONAL ACOUSTO-OPTIC DEVICE

Qida Zhao, Taiyi Hu, Fengyi Cai, Xiaoyi Dong, and Qiuqin Sheng 3 Jan. 1995 20 p Transl. into ENGLISH from Shengxue Xuebao, China, v. 16, no. 6, Nov. 1991 p 450-457

(AD-A291037; NAIC-ID(RS)T-0397-94) Avail: CASI HC A03/MF A01

A set of coupled wave equations for multiple dimensional acoustooptic diffraction with multiple acoustic waves along different directions is put forward and its solutions are derived. The characteristics of the diffraction efficiency, compression, cross modulation, and intermodulation intensities are analyzed theoretically. The theoretical results are supported by experimental measurements through our new multiple dimensional acoustooptic devices. DTIC

N95-29826 Colorado Univ., Boulder, CO.

ULTRASONIC GUIDED WAVES IN CYLINDERS: THEORY AND EXPERIMENT Ph.D. Thesis

Thomas W. Kohl 1993 193 p

Avail: Univ. Microfilms Order No. DA9423509

The dispersive propagation of ultrasonic guided wave pulses in cylinders has been investigated analytically and experimentally, primarily for use in nondestructive evaluation of pipes and tubes. Guided waves are particularly attractive for the inspection of fiber reinforced advanced composite structures because low frequency ultrasound can be utilized. More traditional ultrasonic testing methods use higher frequency elastic waves which can be excessively attenuating in these materials. A model of axially symmetric guided wave dispersion and pulse propagation in hollow and solid cylinders with stress free lateral surface has been formulated. The model applies to radially inhomogeneous and cylindrically anisotropic tubes, such as those made from filament wound composite lamina. The numerical solution allows for computation of any of the elastic fields, given the elastic properties of the material, the geometry of the waveguide, and boundary conditions applied at tube end which generate the pulse. The capability of modeling the dispersion and pulse propagation in cylinders was used in developing guided wave experimental techniques for material property characterization of metallic cylinders and graphite/epoxy filament wound composite tubes. Measurement of phase velocities of guided waves and curve fitting with theoretical velocities was used to determine elastic properties. The boundary value problem examined was an incident pressure pulse and vanishing shear stress acting on the cylinder end. The modeling reflected the experimental method, where the pulse was generated using contact with the cylinder end of an electrically excited longitudinal wave piezoelectric transducer. Comparisons between measured pulses and predictions of the propagation based on the derived elastic properties were employed to gauge the accuracy of the material property characterization. Detection of localized defects in composite tubes using a low frequency guided wave contact transducer technique was also examined. Spatially scanned phase measurements of low frequency narrowband pulses exhibited anomalous wave propagation features which could be used to locate and image defects in the structure. Defect detection and, to a lesser extent, imaging capabilities were demonstrated. Modeling of the pulse propagation in a filament wound cylindrical structure with an idealized delamination defect indicated that guided wave mode conversion and backscatter due to the defect were the mechanisms affecting the measured phase. Dissert. Abstr.

N95-29942# Washington Univ., Seattle, WA.

100 Hz-10 kHz BOTTOM BACKSCATTERING MODEL: GENERALIZED TREATMENT OF SEDIMENT SOUND PROPAGATION, SEDIMENT VOLUME SCATTERING AND INTERFACE-ROUGHNESS SCATTERING

Darrell R. Jackson, Paul D. Ingalis, and Kou-Ying Moravan Apr. 1994 35 p

(Contract N00039-91-C-0072)

(AD-A291323; APL-UW-TM-1-94) Avail: CASI HC A03/MF A01

A model for bottom backscattering strength in the frequency range 100 Hz to 10 kHz is presented. This model generalizes an earlier low-frequency model intended for the smaller frequency range 100-1000 Hz. The new model matches the predictions of an existing high-frequency model (10-100 kHz) but offers new insights into the effect of fine-scale layering. Scattering from both sediment volume inhomogeneity and interface roughness is included in the model. For silt and clay sediments, sediment volume scattering is usually the dominant process. The model requires profile functions for average sound speed, mass density, sound absorption, and volume scattering strength in the sediment. In addition, two parameters describing the spectrum of interface roughness are required. Use of the small-roughness perturbation approximation prevents application of the model to extremely rough bottoms (e.g., gravel and rock). Preliminary comparisons with data show that the model can reproduce an interesting frequency dependence often seen in bottom backscattering. This includes a decrease in scattering strength with increasing frequency in the 100-1000 Hz range, an increase as frequency approaches 10 kHz, and approximate constancy or a slow rise above 10 kHz. The increase in sound speed with depth typically observed in sediments causes upward refraction which, in some cases, leads to enhancements of scattering by 6-8 dB. DTIC

N95-29945# Naval Research Lab., Bay Saint Louis, MS.

A BIBLIOGRAPHY, WITH ABSTRACTS AND ANNOTATIONS, OF PUBLICATIONS ON AND RELATED TO UNDERWATER ACOUSTIC FLUCTUATIONS Final Report

Craig A. Fisher 6 Jan. 1995 67 p

(NR Proj. RJ3-5-C-51)

(AD-A291342; NRL/MR/7176-94-7563) Avail: CASI HC A04/MF A01

A bibliography of publications on and related to underwater acoustic fluctuation phenomena is given. The bibliography is annotated with up to three items: the abstract of each publication, a list of keywords characterizing the publication's subject matter, and one or more comments describing the publication's subject matter in more detail. DTIC

N95-29951# Air Force Systems Command, Wright-Patterson AFB, OH. National Air Intelligence Center.

THEORY AND EXPERIMENT ANALYSIS OF TWO-DIMENSIONAL ACOUSTO-OPTIC INTERACTION

Ren Zhanxiang, Dong Xiaoyi, Zhang Jianzhong, Sheng Qinqin, and Zhao Qida 3 Jan. 1995 13 p Transl. into ENGLISH from Guangxue Xuebao, China, v. 10, no. 11, Nov. 1990 p 1047-1051

(AD-A291059; NAIC-ID(RS)T-0371-94) Avail: CASI HC A03/MF A01

The universal coupled wave equation of two dimensional acousto optic effect has been deduced and the solution of normal Raman-Hath acousto optic diffraction was derived from it. The theory was compared with the experimental results of a two dimensional acousto optic device consisting of two one dimensional modulators. The experiment results agree with the theory. DTIC

N95-30084# Mississippi Univ., University, MS.

PROCEEDINGS OF THE SIXTH INTERNATIONAL SYMPOSIUM ON LONG-RANGE SOUND PROPAGATION Final Report, 1 May - 31 Oct. 1994

David H. Havelock, comp. (National Research Council of Canada, Ottawa, Ontario.), Michael R. Stinson, comp. (National Research Council of Canada, Ottawa, Ontario.), Gilles A. Daigle (National Research Council of Canada, Ottawa, Ontario.), and Keith Attenborough (Open Univ., Milton Keynes, England.) Dec. 1994 526 p Symposium held in Ottawa, Ontario, 12-14 Jun. 1994 Sponsored by National Research Council of Canada, Mississippi Univ. and ARO

(Contract DAAH04-94-G-0039)

(AD-A290920; ARO-32664.1-GS-CF) Avail: CASI HC A23/MF A04

Papers at presented at the Sixth International Symposium on Long-Range

Sound Propagation, 12-14 June 1994, at Chateau Laurier Hotel, Ottawa, Canada. DTIC

N95-30133*# National Aeronautics and Space Administration. Langley Research Center, Hampton, VA.

ICASE/LaRC WORKSHOP ON BENCHMARK PROBLEMS IN COMPUTATIONAL AEROACOUSTICS (CAA)

Jay C. Hardin, ed., J. Ray Ristorcelli, ed. (Institute for Computer Applications in Science and Engineering, Hampton, VA.), and Christopher K. W. Tam, ed. (Florida State Univ., Tallahassee, FL.) May 1995 389 p Workshop held in Hampton, VA, 24-26 Oct. 1994; sponsored by NASA, Washington and Inst. for Computer Applications in Science and Engineering
(RTOP 505-90-52-01)
(NASA-CP-3300; L-17497; NAS 1.55:3300) Avail: CASI HC A17/MF A04

The proceedings of the Benchmark Problems in Computational Aeroacoustics Workshop held at NASA Langley Research Center are the subject of this report. The purpose of the Workshop was to assess the utility of a number of numerical schemes in the context of the unusual requirements of aeroacoustical calculations. The schemes were assessed from the viewpoint of dispersion and dissipation -- issues important to long time integration and long distance propagation in aeroacoustics. Also investigated were the effect of implementation of different boundary conditions. The Workshop included a forum in which practical engineering problems related to computational aeroacoustics were discussed. This discussion took the form of a dialogue between an industrial panel and the workshop participants and was an effort to suggest the direction of evolution of this field in the context of current engineering needs. For individual titles, see N95-30134 through N95-30163.

N95-30134*# Florida State Univ., Tallahassee, FL. Dept. of Mathematics.

BENCHMARK PROBLEMS AND SOLUTIONS

Christopher K. W. Tam *In* NASA. Langley Research Center, ICASE/LaRC Workshop on Benchmark Problems in Computational Aeroacoustics (CAA) May 1995 p 1-13 (For primary document see N95-30133 10-71)
Avail: CASI HC A03/MF A04

The scientific committee, after careful consideration, adopted six categories of benchmark problems for the workshop. These problems do not cover all the important computational issues relevant to Computational Aeroacoustics (CAA). The deciding factor to limit the number of categories to six was the amount of effort needed to solve these problems. For reference purpose, the benchmark problems are provided here. They are followed by the exact or approximate analytical solutions. At present, an exact solution for the Category 6 problem is not available. Author

N95-30135*# National Aeronautics and Space Administration. Langley Research Center, Hampton, VA.

APPLICATION OF ESSENTIALLY NONOSCILLATORY METHODS TO AEROACOUSTIC FLOW PROBLEMS

Harold L. Atkins *In its* ICASE/LaRC Workshop on Benchmark Problems in Computational Aeroacoustics (CAA) May 1995 p 15-26 (For primary document see N95-30133 10-71)
Avail: CASI HC A03/MF A04

A finite-difference essentially nonoscillatory (ENO) method has been applied to several of the problems prescribed for the workshop sponsored jointly by the Institute for Computer Applications in Science and Engineering and by NASA Langley Research Center entitled 'Benchmark Problems in Computational Aeroacoustics'. The workshop focused on computational challenges specific to aeroacoustics. Among these are long-distance propagation of a short-wavelength disturbance, propagation of small-amplitude disturbances, and nonreflective boundary conditions. The shock capturing-capability inherent to the ENO method effectively eliminates oscillations near shock waves without the need to add and tune dissipation or filter terms. The method-of-lines approach allows the temporal and spatial operators to be chosen separately in accordance with the demands of a particular problem. The ENO method was robust and accurate for all problems in which the propagating wave was resolved with 8 or more points per wavelength. The finite-wave-model boundary condition, a local nonlinear acoustic boundary condition, performed well for the one-dimensional problems. The buffer-domain approach performed well for the two-dimensional test problem. The amplitude of nonphysical reflections were less than 1 percent of the exiting wave's amplitude. Author

N95-30136*# National Aeronautics and Space Administration. Ames Research Center, Moffett Field, CA.

COMPUTATIONAL AEROACOUSTICS USING HYPERBOLIC WAVE PRIMITIVES

Sanford S. Davis *In* NASA. Langley Research Center,Hampton, VA. ICASE/LaRC Workshop on Benchmark Problems in Computational Aeroacoustics (CAA) May 1995 p 27-45 (For primary document see N95-30133 10-71)
Avail: CASI HC A03/MF A04

A compact high order three-spatial point, two-time level dissipationless scheme is derived by matching amplification factors from differential and difference forms hyperbolic systems of partial differential equations. This approach has the advantage of allowing large time steps (Courant numbers of one) and imposing boundary conditions that are globally compatible with the wave operators. Solutions are presented for planar and spherical one dimensional acoustic waves and more complex wave patterns in two dimensions. Author

N95-30137*# Korea Advanced Inst. of Science and Technology, Taejon (Republic of Korea). Dept. of Aerospace Engineering.

COMPARATIVE STUDY OF NUMERICAL SCHEMES OF TVD3, UNO3-ACM AND OPTIMIZED COMPACT SCHEME

Duck-Joo Lee, Chang-Jeon Hwang, Duck-Kon Ko, and Jae-Wook Kim *In* NASA. Langley Research Center, ICASE/LaRC Workshop on Benchmark Problems in Computational Aeroacoustics (CAA) May 1995 p 47-57 (For primary document see N95-30133 10-71)
Avail: CASI HC A03/MF A04

Three different schemes are employed to solve the benchmark problem. The first one is a conventional TVD-MUSCL (Monotone Upwind Schemes for Conservation Laws) scheme. The second scheme is a UNO3-ACM (Uniformly Non-Oscillatory Artificial Compression Method) scheme. The third scheme is an optimized compact finite difference scheme modified by us: the 4th order Runge Kutta time stepping, the 4th order pentadiagonal compact spatial discretization with the maximum resolution characteristics. The problems of category 1 are solved by using the second (UNO3-ACM) and third (Optimized Compact) schemes. The problems of category 2 are solved by using the first (TVD3) and second (UNO3-ACM) schemes. The problem of category 5 is solved by using the first (TVD3) scheme. It can be concluded from the present calculations that the Optimized Compact scheme and the UNO3-ACM show good resolutions for category 1 and category 2 respectively. Author

N95-30138*# National Aeronautics and Space Administration. Ames Research Center, Moffett Field, CA.

A COMPACT SOLUTION TO COMPUTATIONAL ACOUSTICS

K.-Y. Fung (Miami Univ., Coral Gables, FL.), Raymond S. O. Man (Arizona Univ., Tucson, AZ.), and Sanford Davis *In* NASA. Langley Research Center, ICASE/LaRC Workshop on Benchmark Problems in Computational Aeroacoustics (CAA) May 1995 p 59-72 (For primary document see N95-30133 10-71)
(Contract NCA2-707)
Avail: CASI HC A03/MF A04

This paper demonstrates that the linearized, dimensional Euler equations for acoustic computation can be accurately solved as a set of decoupled first-order wave equations, and that if ordered properly, this system of simple waves has unambiguous, easily implemented boundary conditions, allowing waves of same group speeds to pass through numerical boundaries or comply with wall conditions. Thus, the task of designing a complex multi-dimensional scheme with approximate far-field boundary conditions reduces to the design of higher order schemes for the one-dimensional simple wave equation. A compact finite-difference scheme and a characteristically exact but numerically n(th) order accurate boundary condition are introduced for solving the first order wave equation. Spanning a three-point two-level stencil, this low-dispersion implicit scheme has a third order spatial accuracy when used on nonuniform meshes, fourth order accurate on uniform meshes, and a temporal accuracy of second order due to the choice of trapezoidal integration for algorithmic simplicity. The robustness and accuracy of the scheme are demonstrated through a series of numerical experiments and comparisons with published results.

When tested on the one-dimensional wave equation on a uniform grid, this scheme allows a Gaussian wave packet to pass through any finite domain with low numerical dispersion characteristic of a spatially fourth-order scheme and reflections at numerical boundaries maintained below truncation error. On highly stretched and irregular grids, only mild dispersions are found in the solution while solutions by other methods fail or are severely distorted. Yet, this scheme is no more sophisticated to solve or implement than the Crank-Nicolson scheme. This scheme has been tested on four categories of the ICASE/LaRC benchmark problems, which include propagation of acoustic and convective waves in Cartesian and cylindrical domains, reflection of acoustic wave at stationary/moving boundaries, and sound generation by gust-blade interaction. Author

N95-30139*# Old Dominion Univ., Norfolk, VA. Dept. of Mathematics and Statistics.

APPLICATION OF LOW DISSIPATION AND DISPERSION RUNGE-KUTTA SCHEMES TO BENCHMARK PROBLEMS IN COMPUTATIONAL AEROACOUSTICS

F. Q. Hu, M. Y. Hussaini (Institute for Computer Applications in Science and Engineering, Hampton, VA.), and J. Manthey *In* NASA. Langley Research Center, ICASE/LaRC Workshop on Benchmark Problems in Computational Aeroacoustics (CAA) May 1995 p 73-98 (For primary document see N95-30133 10-71)

(Contract NAS1-19480)

Avail: CASI HC A03/MF A04

We investigate accurate and efficient time advancing methods for computational aeroacoustics, where non-dissipative and non-dispersive properties are of critical importance. Our analysis pertains to the application of Runge-Kutta methods to high-order finite difference discretization. In many CFD applications, multi-stage Runge-Kutta schemes have often been favored for their low storage requirements and relatively large stability limits. For computing acoustic waves, however, the stability consideration alone is not sufficient, since the Runge-Kutta schemes entail both dissipation and dispersion errors. The time step is now limited by the tolerable dissipation and dispersion errors in the computation. In the present paper, it is shown that if the traditional Runge-Kutta schemes are used for time advancing in acoustic problems, time steps greatly smaller than that allowed by the stability limit are necessary. Low Dissipation and Dispersion Runge-Kutta (LDDRK) schemes are proposed, based on an optimization that minimizes the dissipation and dispersion errors for wave propagation. Optimizations of both single-step and two-step alternating schemes are considered. The proposed LDDRK schemes are remarkably more efficient than the classical Runge-Kutta schemes for acoustic computations. Numerical results of each Category of the Benchmark Problems are presented. Moreover, low storage implementations of the optimized schemes are discussed. Special issues of implementing numerical boundary conditions in the LDDRK schemes are also addressed. Author

N95-30140*# National Aeronautics and Space Administration. Lewis Research Center, Cleveland, OH.

RESULTS OF TWO NEW METHODS FOR AEROACOUSTICS BENCHMARK PROBLEMS

H. T. Huynh *In* NASA. Langley Research Center, ICASE/LaRC Workshop on Benchmark Problems in Computational Aeroacoustics (CAA)p 99-116 (SEE N95-30133 10-71) May 1995 (For primary document see N95-30133 10-71)

Avail: CASI HC A03/MF A04

Two new methods for the numerical solution of conservation laws (the Euler equations in particular) are presented: a uniformly second-order accurate upwind scheme and a third-order accurate centered scheme. Results of these schemes are shown for problems 1, 2, and 5 of this workshop's benchmark problems. Author

N95-30141*# Florida State Univ., Tallahassee, FL. Supercomputer Computations Research Inst.

SOLUTION OF ACOUSTIC WORKSHOP PROBLEMS BY A SPECTRAL MULTIDOMAIN METHOD

Davis A. Kopriva and John H. Kolias *In* NASA. Langley Research Center, ICASE/LaRC Workshop on Benchmark Problems in Computational Aeroacoustics (CAA) May 1995 p 117-124 (For primary document see N95-30133 10-71)

(Contract DE-FC05-85ER-25000; NSF DMS-94-04322)

Avail: CASI HC A02/MF A04

We use a new staggered grid Chebyshev spectral multidomain method to solve three of the Workshop benchmark problems. The method defines solution unknowns at the nodes of the Chebyshev Gauss quadrature, and the fluxes at the nodes of the Chebyshev Gauss-Lobatto quadrature. The Chebyshev spectral method gives exponentially convergent phase and dissipation errors. The multidomain approximation gives the method flexibility. Using the method, we solve problems in Categories 1 and 5 of the benchmark problems. Author

N95-30142*# Electricite de France, Clamart (France). Dept. Acoustique et Mechanique Vibratoire.

COMPUTATION OF WAVE PROPAGATION IN A COMPLEX FLOW c34

Philippe Lafon *In* NASA. Langley Research Center, ICASE/LaRC Workshop on Benchmark Problems in Computational Aeroacoustics (CAA) May 1995 p 125-132 (For primary document see N95-30133 10-71)

Avail: CASI HC A02/MF A04

A numerical method has been developed in order to address aeroacoustic problems modeled by the linearized Euler equations. A weak formulation of the equations leads to a time-dependent equation for the test functions. The basic solver being one dimensional, two dimensional problems are handled by directional splitting. This method shows low dissipation and dispersion errors. Author

N95-30143*# National Aeronautics and Space Administration. Langley Research Center, Hampton, VA.

SECOND-ORDER NUMERICAL SOLUTION OF TIME-DEPENDENT, FIRST-ORDER HYPERBOLIC EQUATIONS c64

Patricia L. Shah (Boston Univ., MA.) and Jay Hardin *In its* ICASE/LaRC Workshop on Benchmark Problems in Computational Aeroacoustics (CAA) May 1995 p 133-141 (For primary document see N95-30133 10-71)

(Contract NAS1-19480)

Avail: CASI HC A02/MF A04

A finite difference scheme is developed to find an approximate solution of two similar hyperbolic equations, namely a first-order plane wave and spherical wave problem. Finite difference approximations are made for both the space and time derivatives. The result is a conditionally stable equation yielding an exact solution when the Courant number is set to one. Author

N95-30144*# Pennsylvania State Univ., University Park, PA. Graduate Program in Acoustics.

LATTICE GAS METHODS FOR COMPUTATIONAL AEROACOUSTICS

Victor W. Sparrow *In* NASA. Langley Research Center, ICASE/LaRC Workshop on Benchmark Problems in Computational Aeroacoustics (CAA) May 1995 p 143-147 (For primary document see N95-30133 10-71)

Avail: CASI HC A01/MF A04

This paper presents the lattice gas solution to the category 1 problems of the ICASE/LaRC Workshop on Benchmark Problems in Computational Aeroacoustics. The first and second problems were solved for Delta t = Delta x = 1, and additionally the second problem was solved for Delta t = 1/4 and Delta x = 1/2. The results are striking: even for these large time and space grids the lattice gas numerical solutions are almost indistinguishable from the analytical solutions. A simple bug in the Mathematica code was found in the solutions submitted for comparison, and the comparison plots shown at the end of this volume show the bug. An Appendix to the present paper shows an example lattice gas solution with and without the bug. Author

N95-30145*# Florida State Univ., Tallahassee, FL. Dept. of Mathematics.

SOLUTIONS OF THE BENCHMARK PROBLEMS BY THE DISPERSION-RELATION-PRESERVING SCHEME c64

Christopher K. W. Tam, H. Shen, K. A. Kurbatskii, and L. Auriault *In* NASA. Langley Research Center, ICASE/LaRC Workshop on Benchmark Problems in Computational Aeroacoustics (CAA) May 1995 p 149-171 (For primary document see N95-30133 10-71)

(Grant NAG3-1267)

Avail: CASI HC A03/MF A04

The 7-point stencil Dispersion-Relation-Preserving scheme of Tam and Webb is used to solve all the six categories of the CAA benchmark

problems. The purpose is to show that the scheme is capable of solving linear, as well as nonlinear aeroacoustics problems accurately. Nonlinearities, inevitably, lead to the generation of spurious short wave length numerical waves. Often, these spurious waves would overwhelm the entire numerical solution. In this work, the spurious waves are removed by the addition of artificial selective damping terms to the discretized equations. Category 3 problems are for testing radiation and outflow boundary conditions. In solving these problems, the radiation and outflow boundary conditions of Tam and Webb are used. These conditions are derived from the asymptotic solutions of the linearized Euler equations. Category 4 problems involved solid walls. Here, the wall boundary conditions for high-order schemes of Tam and Dong are employed. These conditions require the use of one ghost value per boundary point per physical boundary condition. In the second problem of this category, the governing equations, when written in cylindrical coordinates, are singular along the axis of the radial coordinate. The proper boundary conditions at the axis are derived by applying the limiting process of r approaches 0 to the governing equations. The Category 5 problem deals with the numerical noise issue. In the present approach, the time-independent mean flow solution is computed first. Once the residual drops to the machine noise level, the incident sound wave is turned on gradually. The solution is marched in time until a time-periodic state is reached. No exact solution is known for the Category 6 problem. Because of this, the problem is formulated in two totally different ways, first as a scattering problem then as a direct simulation problem. There is good agreement between the two numerical solutions. This offers confidence in the computed results. Both formulations are solved as initial value problems. As such, no Kutta condition is required at the trailing edge of the airfoil.

Author

N95-30146*# Maryland Univ., College Park, MD.

THE CONSTRUCTION OF HIGH-ACCURACY SCHEMES FOR ACOUSTIC EQUATIONS

Lei Tang and James D. Baeder *In* NASA. Langley Research Center, ICASE/LaRC Workshop on Benchmark Problems in Computational Aeroacoustics (CAA) May 1995 p 173-183 (For primary document see N95-30133 10-71)

Avail: CASI HC A03/MF A04

An accuracy analysis of various high order schemes is performed from an interpolation point of view. The analysis indicates that classical high order finite difference schemes, which use polynomial interpolation, hold high accuracy only at nodes and are therefore not suitable for time-dependent problems. Thus, some schemes improve their numerical accuracy within grid cells by the near-minimax approximation method, but their practical significance is degraded by maintaining the same stencil as classical schemes. One-step methods in space discretization, which use piecewise polynomial interpolation and involve data at only two points, can generate a uniform accuracy over the whole grid cell and avoid spurious roots. As a result, they are more accurate and efficient than multistep methods. In particular, the Cubic-Interpolated Psuedoparticle (CIP) scheme is recommended for computational acoustics. Author

N95-30147*# Lockheed Aeronautical Systems Co., Marietta, GA.

A COMPARATIVE STUDY OF UPWIND AND MACCORMACK SCHEMES FOR CAA BENCHMARK PROBLEMS

K. Viswanathan and L. N. Sankar (Georgia Inst. of Tech., Atlanta, GA.) *In* NASA. Langley Research Center, ICASE/LaRC Workshop on Benchmark Problems in Computational Aeroacoustics (CAA) May 1995 p 185-195 (For primary document see N95-30133 10-71)

(Contract NAS1-20102)

Avail: CASI HC A03/MF A04

In this study, upwind schemes and MacCormack schemes are evaluated as to their suitability for aeroacoustic applications. The governing equations are cast in a curvilinear coordinate system and discretized using finite volume concepts. A flux splitting procedure is used for the upwind schemes, where the signals crossing the cell faces are grouped into two categories: signals that bring information from outside into the cell, and signals that leave the cell. These signals may be computed in several ways, with the desired spatial and temporal accuracy achieved by choosing appropriate interpolating polynomials. The classical MacCormack schemes employed here are fourth order accurate in time and space. Results for categories 1, 4, and 6 of the workshop's benchmark problems are presented. Comparisons are also made with the exact solutions, where available. The main conclusions of this study are finally presented. Author (revised)

N95-30148*# Pennsylvania State Univ., University Park, PA. Dept. of Aerospace Engineering.

APPLICATION OF TRADITIONAL CFD METHODS TO NONLINEAR COMPUTATIONAL AEROACOUSTICS PROBLEMS

Thomas S. Chyczewski and Lyle N. Long *In* NASA. Langley Research Center, ICASE/LaRC Workshop on Benchmark Problems in Computational Aeroacoustics (CAA) May 1995 p 197-201 (For primary document see N95-30133 10-71)

(Grant NGT-51118)

Avail: CASI HC A01/MF A04

This paper describes an implementation of a high order finite difference technique and its application to the category 2 problems of the ICASE/LaRC Workshop on Computational Aeroacoustics (CAA). Essentially, a popular Computational Fluid Dynamics (CFD) approach (central differencing, Runge-Kutta time integration and artificial dissipation) is modified to handle aeroacoustic problems. The changes include increasing the order of the spatial differencing to sixth order and modifying the artificial dissipation so that it does not significantly contaminate the wave solution. All of the results were obtained from the CM5 located at the Numerical Aerodynamic Simulation Laboratory. It was coded in CMFortran (very similar to HPF), using programming techniques developed for communication intensive large stencils, and ran very efficiently. Author

N95-30149*# Ohio Aerospace Inst., Cleveland, OH. Inst. for Computational Mechanics in Propulsion.

EVALUATION OF HIGH ORDER SCHEMES FOR NONLINEAR WAVE COMPUTATIONS c34

M. Ehtesham Hayder *In* NASA. Langley Research Center, ICASE/LaRC Workshop on Benchmark Problems in Computational Aeroacoustics (CAA) May 1995 p 203-207 (For primary document see N95-30133 10-71)

(Contract NCC3-233)

Avail: CASI HC A01/MF A04

We present results of the workshop's benchmark problems of the category 2. This category of problems is designed to test the nonlinear wave propagation properties of a computational scheme. We chose three high order spatially accurate algorithms for our computations. These are the Dispersion- Relation- Preserving (DRP) scheme proposed by Tam and his colleagues, a fourth order extension of the MacCormack scheme proposed by Gottlieb and Turkel and an Essentially Non Oscillatory (ENO) scheme proposed by Shu and Osher. Author (revised)

N95-30150*# Pennsylvania State Univ., University Park, PA. Dept. of Aerospace Engineering.

TIME ACCURATE APPLICATION OF THE MACCORMACK 2-4 SCHEME ON MASSIVELY PARALLEL COMPUTERS c62

Dale A. Hudson and Lyle N. Long *In* NASA. Langley Research Center, ICASE/LaRC Workshop on Benchmark Problems in Computational Aeroacoustics (CAA) May 1995 p 209-215 (For primary document see N95-30133 10-71)

(Grant NAG1-1479)

Avail: CASI HC A02/MF A04

Many recent computational efforts in turbulence and acoustics research have used higher order numerical algorithms. One popular method has been the explicit MacCormack 2-4 scheme. The MacCormack 2-4 scheme is second order accurate in time and fourth order accurate in space, and is stable for CFL's below 2/3. Current research has shown that the method can give accurate results but does exhibit significant Gibbs phenomena at sharp discontinuities. The impact of adding Jameson type second, third, and fourth order artificial viscosity was examined here. Category 2 problems, the nonlinear traveling wave and the Riemann problem, were computed using a CFL number of 0.25. This research has found that dispersion errors can be significantly reduced or nearly eliminated by using a combination of second and third order terms in the damping. Use of second and fourth order terms reduced the magnitude of dispersion errors but not as effectively as the second and third order combination. The program was coded using Thinking Machine's CM Fortran, a variant of Fortran 90/High Performance Fortran, and was executed on a 2K CM-200. Simple extrapolation boundary conditions were used for both problems.

Author

N95-30151*# National Aeronautics and Space Administration. Langley Research Center, Hampton, VA.
NONLINEAR WAVE PROPAGATION USING THREE DIFFERENT FINITE DIFFERENCE SCHEMES (CATEGORY 2 APPLICATION) **c34**
D. Stuart Pope (Lockheed Engineering and Sciences Co., Hampton, VA.) and J. C. Hardin *In its* ICASE/LaRC Workshop on Benchmark Problems in Computational Aeroacoustics (CAA) May 1995 p 217-223 (For primary document see N95-30133 10-71)
(Contract NAS1-19000)
Avail: CASI HC A02/MF A04

Three common finite difference schemes are used to examine the computation of one-dimensional nonlinear wave propagation. The schemes are studied for their responses to numerical parameters such as time step selection, boundary condition implementation, and discretization of governing equations. The performance of the schemes is compared and various numerical phenomena peculiar to each is discussed. Author

N95-30152*# Pennsylvania State Univ., University Park, PA. Dept. of Aerospace Engineering.
WAVE PROPAGATION AND SCATTERING IN COMPUTATIONAL AEROACOUSTICS
Cathy Chung and Philip J. Morris *In* NASA. Langley Research Center, ICASE/LaRC Workshop on Benchmark Problems in Computational Aeroacoustics (CAA) May 1995 p 225-232 (For primary document see N95-30133 10-71)
(Grant NAG1-1479)
Avail: CASI HC A02/MF A04

This paper describes predictions of model problems in computational aeroacoustics. Two problem classes are considered: The first (Workshop Category 3, Problem 1 and 2) considers two-dimensional wave propagation and non-reflecting boundary conditions in the presence of a mean flow. The second (Workshop Category 4, Problem 1) examines wall boundary conditions. For the last problem we introduce the Impedance Mismatch Method (IMM) to treat the solid wall boundaries. In this method the solid wall is simulated using a wall region in which the characteristic impedance is set to a different value to that in the fluid region. This method has advantages over traditional solid wall boundary conditions including simplicity of coding, speed of computations, and the ability to treat curved boundaries efficiently. Several numerical examples are given in addition to the Workshop Problems. The discretization of the Euler equations is performed in all cases with a Dispersion-Relation-Preserving (DRP) algorithm. The numerical results are compared with either analytical solutions or solutions obtained using traditional solid wall boundary conditions. Author

N95-30153*# Joint Inst. for Advancement of Flight Sciences, Hampton, VA.
THE USE OF STAGGERED SCHEME AND AN ABSORBING BUFFER ZONE FOR COMPUTATIONAL AEROACOUSTICS
Douglas M. Nark *In* NASA. Langley Research Center, ICASE/LaRC Workshop on Benchmark Problems in Computational Aeroacoustics (CAA) May 1995 p 233-244 (For primary document see N95-30133 10-71)
Avail: CASI HC A03/MF A04

Various problems from those proposed for the Computational Aeroacoustics (CAA) workshop were studied using second and fourth order staggered spatial discretizations in conjunction with fourth order Runge-Kutta time integration. In addition, an absorbing buffer zone was used at the outflow boundaries. Promising results were obtained and provide a basis for application of these techniques to a wider variety of problems. Author

N95-30154*# Tennessee Univ. Space Inst., Tullahoma, TN.
A NUMERICAL SOLUTION METHOD FOR ACOUSTIC RADIATION FROM AXISYMMETRIC BODIES
John E. Caruthers and G. K. Raviprakash *In* NASA. Langley Research Center, ICASE/LaRC Workshop on Benchmark Problems in Computational Aeroacoustics (CAA) May 1995 p 245-254 (For primary document see N95-30133 10-71)
(Grant NAG3-1516)
Avail: CASI HC A02/MF A04

A new and very efficient numerical method for solving equations of the Helmholtz type is specialized for problems having axisymmetric geometry. It is then demonstrated by application to the classical problem of acoustic radiation from a vibrating piston set in a stationary infinite plane. The method utilizes 'Green's Function Discretization', to obtain an accurate resolution of the waves using only 2-3 points per wave. Locally valid free space Green's functions, used in the discretization step, are obtained by quadrature. Results are computed for a range of grid spacing/piston radius ratios at a frequency parameter, omega R/c(sub 0), of 2 pi. In this case, the minimum required grid resolution appears to be fixed by the need to resolve a step boundary condition at the piston edge rather than by the length scale imposed by the wave length of the acoustic radiation. It is also demonstrated that a local near-field radiation boundary procedure allows the domain to be truncated very near the radiating source with little effect on the solution. Author

N95-30155*# National Aeronautics and Space Administration. Lewis Research Center, Cleveland, OH.
APPLICATION OF A NEW FINITE DIFFERENCE ALGORITHM FOR COMPUTATIONAL AEROACOUSTICS
John W. Goodrich *In* NASA. Langley Research Center, ICASE/LaRC Workshop on Benchmark Problems in Computational Aeroacoustics (CAA) May 1995 p 255-259 (For primary document see N95-30133 10-71)
Avail: CASI HC A01/MF A04

Acoustic problems have become extremely important in recent years because of research efforts such as the High Speed Civil Transport program. Computational aeroacoustics (CAA) requires a faithful representation of wave propagation over long distances, and needs algorithms that are accurate and boundary conditions that are unobtrusive. This paper applies a new finite difference method and boundary algorithm to the Linearized Euler Equations (LEE). The results demonstrate the ability of a new fourth order propagation algorithm to accurately simulate the genuinely multidimensional wave dynamics of acoustic propagation in two space dimensions with the LEE. The results also show the ability of a new outflow boundary condition and fourth order algorithm to pass the evolving solution from the computational domain with no perceptible degradation of the solution remaining within the domain. Derived from text

N95-30156*# Pennsylvania State Univ., University Park, PA. Dept. of Aerospace Engineering.
COMPUTATIONAL AEROACOUSTICS ON MASSIVELY PARALLEL COMPUTERS **c62**
Yusuf Oezyoeruek and Lyle N. Long *In* NASA. Langley Research Center, ICASE/LaRC Workshop on Benchmark Problems in Computational Aeroacoustics (CAA) May 1995 p 261-265 (For primary document see N95-30133 10-71)
(Grant NAG1-1367)
Avail: CASI HC A01/MF A04

A computational fluid dynamics (CFD) technique is employed to solve aeroacoustics problems on massively parallel computers. The algorithm is based on a 4th order accurate central finite difference and 4th order accurate 4-stage Runge-Kutta time integration method that solves the 3-D full Navier-Stokes/Euler equations on a curvilinear coordinate system. The code has been developed to predict noise radiation from ducted fans. A specific application of this code is made here to the oscillating circular piston problem (Workshop Category 4, Problem 2) by solving the full Euler equations with nonreflecting boundary conditions in the axisymmetric mode. The features of the code that apply to this particular problem are described in this paper. Author

N95-30157*# National Aeronautics and Space Administration. Lewis Research Center, Cleveland, OH.
CATEGORY 5 PROBLEM SOLUTION USING AN UNSTRUCTURED FINITE VOLUME ALGORITHM **c61**
Trong T. Bui and Reda R. Mankbadi *In* NASA. Langley Research Center, ICASE/LaRC Workshop on Benchmark Problems in Computational Aeroacoustics (CAA) May 1995 p 267-272 (For primary document see N95-30133 10-71)
Avail: CASI HC A02/MF A04

For the simulation of flows with complex geometries, unstructured finite volume methods have proven to be very popular, and simulations of a large number of flows have been done with good results using this approach. Since most of the simulations to date were done for steady flows, it is not clear that present unstructured finite volume algorithms can accurately track the unsteady propagation of acoustic waves in a computation. Therefore, there is a need to assess the accuracy of these

methods for acoustic calculations. In this paper, we perform the numerical simulation of a very small amplitude acoustic wave incident on the non-uniform steady flow in a quasi- 1 D convergent-divergent nozzle using an unstructured finite volume algorithm with piece-wise linear, least square reconstruction, Roe flux difference splitting, and second-order MacCormack time marching. First, the spatial accuracy of the algorithm is evaluated for the steady flow by running the simulation with a sequence of successively finer meshes. Then the unsteady numerical solution with the acoustic perturbation is presented. Author

N95-30158*# McDonnell-Douglas Corp., Saint Louis, MO.
COMPARISON OF SPATIAL NUMERICAL OPERATORS FOR DUCT-NOZZLE ACOUSTICS
A. B. Cain and W. W. Bower *In* NASA. Langley Research Center, ICASE/LaRC Workshop on Benchmark Problems in Computational Aeroacoustics (CAA) May 1995 p 273-278 (For primary document see N95-30133 10-71)
Avail: CASI HC A02/MF A04

A production Navier-Stokes/Euler CFD code, NASTD, developed for aircraft flowfield analysis has been modified to analyze acoustic fields associated with propulsion exhaust systems. The modified code has been applied to the Category 5 nozzle problem using six different spatial discretization schemes combined with a third-order, compact storage Runge-Kutta time integration. NASTD was found capable of tracking pressure disturbances normalized by the freestream value of order 10(exp -6), even with lower-order schemes, for the benchmark problem. Author

N95-30159*# Vigyan Research Associates, Inc., Hampton, VA.
HIGH-ORDER ESSENTIALLY NON-OSCILLATORY METHODS FOR COMPUTATIONAL AEROACOUSTICS
Jay Casper *In* NASA. Langley Research Center, ICASE/LaRC Workshop on Benchmark Problems in Computational Aeroacoustics (CAA) May 1995 p 279-283 (For primary document see N95-30133 10-71)
(Contract NAS1-19672)
Avail: CASI HC A01/MF A04

The desire to obtain acoustic information from the numerical solution of a nonlinear system of equations is a demanding proposition for a computational algorithm. High-order accuracy is required for the propagation of high-frequency, low-amplitude waves. In addition, it is desirable to highly resolve discontinuities that can develop in the solutions of the Euler or Navier-Stokes equations. The class of essentially non-oscillatory (ENO) shock-capturing schemes has been designed to have both of these properties. The dual capacity of ENO schemes for high-order accuracy and non-oscillatory shock-capturing is achieved through the use of adaptive stenciling, which makes these schemes highly nonlinear. These schemes are briefly described and referenced herein. A fourth-order algorithm is then applied to the solution of an acoustic wave in a quasi-one-dimensional converging-diverging nozzle. Author

N95-30160*# National Aeronautics and Space Administration. Lewis Research Center, Cleveland, OH.
NUMERICAL SIMULATIONS OF SMALL AMPLITUDE ACOUSTIC WAVE PROPAGATION IN A CONVERGING-DIVERGING NOZZLE
Thomas Z. Dong and Reda R. Mankbadi *In* NASA. Langley Research Center, ICASE/LaRC Workshop on Benchmark Problems in Computational Aeroacoustics (CAA) May 1995 p 285-290 (For primary document see N95-30133 10-71)
Avail: CASI HC A02/MF A04

Numerical simulations of the small amplitude acoustic wave propagation in a converging-diverging nozzle proposed in Category 5 are performed and presented here. The quasi 1-D unsteady flow equations in conservative form are discretized by the DRP scheme with the artificial damping developed by Tam and Webb. Characteristic boundary conditions are used at both the inlet and outlet of the nozzle. The effect of different numerical implementations of the subsonic inflow boundary conditions on the convergence of the solution to the steady state is studied. In the case of a subsonic outflow in which a shock is formed in the nozzle, the interaction between acoustics and the shock is also investigated. Author

N95-30161*# Notre Dame Univ., IN.
THE PRESSURE FIELD OF A GUST INTERACTING WITH A FLAT PLATE c34
Hafiz M. Atassi and Sheryl M. Patrick *In* NASA. Langley Research Center, ICASE/LaRC Workshop on Benchmark Problems in Computational Aeroacoustics (CAA) May 1995 p 291-296 (For primary document see N95-30133 10-71)
Avail: CASI HC A02/MF A04

A semianalytical solution is presented for the unsteady pressure field of a vortical gust interacting with a flat-plate airfoil in subsonic flow. The solution will serve as a benchmark for evaluating the accuracy and efficiency of time dependent numerical schemes. The specific case considered corresponds to the ICASE benchmark problem number 6. The results are compared with those of asymptotic theories for high frequency and show excellent agreement. Author

N95-30162*# Christopher Newport Coll., Newport News, VA. Dept. of Mathematics.
AEROACOUSTIC COMPUTATION OF A GUST-PLATE INTERACTION VIA MACCORMACK SCHEMES
James E. Martin *In* NASA. Langley Research Center, ICASE/LaRC Workshop on Benchmark Problems in Computational Aeroacoustics (CAA) May 1995 p 297-301 (For primary document see N95-30133 10-71)
Avail: CASI HC A01/MF A04

We apply second, fourth, and sixth order spatially accurate variations of the MacCormack scheme to calculate the noise radiated by the interaction of a flat plate with an oncoming gust. For the given gust wavelength and numerical discretization, the fourth and sixth order schemes each are effective in capturing the occurring acoustic waves. However, for the case of the sixth order scheme, the high order of extrapolation applied at the far field boundaries necessitates an extension of the computational boundaries from their prescribed location. Author

N95-30163*# National Aeronautics and Space Administration. Lewis Research Center, Cleveland, OH.
EVALUATION OF NUMERICAL SCHEMES FOR THE ANALYSIS OF SOUND GENERATION BY BLADE-GUST INTERACTION
J. N. Scott (Ohio Univ., Columbus, OH.), S. I. Hariharan (Akron Univ., Akron, OH.), and R. Mankbadi *In* NASA. Langley Research Center, ICASE/LaRC Workshop on Benchmark Problems in Computational Aeroacoustics (CAA) May 1995 p 303-312 (For primary document see N95-30133 10-71)
Avail: CASI HC A02/MF A04

In this investigation three different numerical algorithms have been utilized to compute the flow about a flat plate in the presence of a transverse gust described by a sinusoidal disturbance. The three schemes include the MacCormack explicit finite difference scheme which is second order accurate in both time and space, the Gottlieb and Turkel modification of MacCormack's scheme which is fourth order accurate in space and second order accurate in time, (referred to as the 2-4 scheme), and a two step scheme developed by Bayliss et al. which has second order temporal accuracy and sixth order spatial accuracy (a 2-6 scheme). The flow field results are obtained with these schemes by using the same code with the only difference being the implementation of the respective solution algorithms. The problem is set up so that the sinusoidal disturbance is imposed at the surface of the flat plate as a surface boundary condition. Thus the problem is treated as scattering problem. The computed results include the time average of the acoustic pressure squared along grid lines five points away from the boundaries; distribution throughout the computational domain is monitored at various times. The numerical results are compared with an exact solution obtained by Atassi, Dusey, and Davis. Author

72 ATOMIC AND MOLECULAR PHYSICS

Includes atomic structure, electron properties, and molecular spectra.

N95-28779# California Univ., Berkeley. Lawrence Berkeley Lab, CA. Theoretical Physics Group.
TABLES OF SU3 ISOSCALAR FACTORS
Thomas A. Kaeding 16 Feb. 1995 49 p
(Contract DE-AC03-76SF-00098)

(DE95-009375; LBL-36659; UCB-PTH-95/01) Avail: CASI HC A03/MF A01

The Clebsch-Gordan coefficients of SU(3) are useful in calculations involving baryons and mesons, as well as in calculations involving arbitrary numbers of quarks. For the latter case, one needs the coupling constants between states of nonintegral hypercharges. The existing published tables are insufficient for many such applications, and therefore we have compiled this collection. This report supplies the isoscalar factors required to reconstruct the Clebsch-Gordan coefficients for a large set of products of representations. DOE

N95-28856*# Lockheed Missiles and Space Co., Huntsville, AL.
SURFACE CONVERSION TECHNIQUES FOR LOW ENERGY NEUTRAL ATOM IMAGERS Final Report
J. M. Quinn 14 Mar. 1995 48 p
(Contract NAS8-39950)
(NASA-CR-196604; NAS 1.26:196604) Avail: CASI HC A03/MF A01

This investigation has focused on development of key technology elements for low energy neutral atom imaging. More specifically, we have investigated the conversion of low energy neutral atoms to negatively charged ions upon reflection from specially prepared surfaces. This 'surface conversion' technique appears to offer a unique capability of detecting, and thus imaging, neutral atoms at energies of 0.01 - 1 keV with high enough efficiencies to make practical its application to low energy neutral atom imaging in space. Such imaging offers the opportunity to obtain the first instantaneous global maps of macroscopic plasma features and their temporal variation. Through previous in situ plasma measurements, we have a statistical picture of large scale morphology and local measurements of dynamic processes. However, with in situ techniques it is impossible to characterize or understand many of the global plasma transport and energization processes. A series of global plasma images would greatly advance our understanding of these processes and would provide the context for interpreting previous and future in situ measurements. Fast neutral atoms, created from ions that are neutralized in collisions with exospheric neutrals, offer the means for remotely imaging plasma populations. Energy and mass analysis of these neutrals provides critical information about the source plasma distribution. The flux of neutral atoms available for imaging depends upon a convolution of the ambient plasma distribution with the charge exchange cross section for the background neutral population. Some of the highest signals are at relatively low energies (well below 1 keV). This energy range also includes some of the most important plasma populations to be imaged, for example the base of the cleft ion fountain. Author

N95-28868# New Orleans Univ., LA. Dept. of Chemistry.
COMPUTATIONAL INVESTIGATION OF THE STABILITIES OF SOME N, O, F IONS
M. E. Grice and Peter Politzer 16 Mar. 1995 4 p
(Contract N00014-95-1-0028)
(AD-A292305; TR-79) Avail: CASI HC A02/MF A01

In response to the suggestion of Jeff Bottaro, we have investigated the potential stabilities of four N, 0, F ions, 1 - 4. All four molecular geometries were optimized using a non-local density functional (DF) procedure (Gaussian 92/DEF; BLYP6/-31+G**) and also at the ab initio MP2/6-31+G** (frozen core) level. For 1, the MP optimization was carried out as well without the frozen-core approximation. All calculations were for spin-restricted singlet states; however the DF results were checked for stability relative to allowing them to become spin-unrestricted and/or complex and were determined to be stable in this respect. In order to ascertain whether the optimized structures correspond to true energy minima, vibration frequencies were computed for all four systems at the DF level and for 1 and 2 at the MP2; for the anions 3 and 4, the number of basis functions being used precluded MP2 frequency calculations. No imaginary vibration frequencies were found. This confirms that the optimized structures of all four systems do correspond to true energy minima, and that these ions should be able to exist. DTIC

N95-28888# International Business Machines Corp., San Jose, CA.
PUBLICATIONS/PATENTS/PRESENTATIONS/HONORS REPORT: FORCE AND TUNNELING MICROSCOPY STUDIES OF ATOMIC LEVEL MECHANICAL PROPERTIES OF SOLIDS Final Report, 15 Jul. 1988 - 14 Jan. 1992
Gary M. McClelland Dec. 1994 6 p
(Contract N00014-88-C-0419)
(AD-A292254) Avail: CASI HC A02/MF A01

We are using atomic force microscopy (AFM) to characterize the tribological properties of materials on an atomic scale. For these experiments we employ an ultrahigh vacuum instrument which measures the lateral and normal forces and current through a tip in contact with a surface which can be positioned with sub-Angstrom resolution. Friction of a sharp tip on a surface is investigated by profiling the surface, sliding the tip across the surface while measuring the normal and parallel forces and contact resistance, and profiling the surface after sliding. DTIC

N95-28913 Rutherford Appleton Lab., Oxford (England).
PHOTOPRODUCTION OF HYBRID MESONS FROM CEBAF TO HERA
F. E. Close and P. R. Page Dec. 1994 11 p Prepared in cooperation with Oxford Univ.
(PB95-196218; RAL-94-122) Avail: Issuing Activity (National Technical Information Service (NTIS))

Decay widths, branching ratios and production dynamics of some recently discovered J(PC) = 1(-+), 0(-+), 1(--) and 2(-+) mesons are found to be in remarkable agreement with the predicted properties of hybrid mesons. We propose tests for this new dynamics, emphasize the critical role of pi b(1) or pi h(1) decay channels in discriminating hybrids from conventional states, and suggest that photoproduction may offer special opportunities for isolation and confirmation of hybrids. NTIS

N95-28919# New Orleans Univ., LA. Dept. of Chemistry.
MOLECULAR DYNAMICS SIMULATION OF LIQUID NITROMETHANE SHOCKED TO 143 kbar
Jorge M. Seminario, Monica C. Concha, and Peter Politzer 20 Mar. 1994 10 p
(Contract N00014-95-1-0028)
(AD-A292107; TR-83) Avail: CASI HC A02/MF A01

A molecular dynamics simulation, using a force field established by density functional calculations, has been used to investigate structural and vibrational frequency shifts that accompany a compression from 1 bar, 300 K to 143 kbar, 600 K. Under the latter conditions, most pairs of nitromethane molecules are found to be linked by two hydrogen bonds, instead of the one that is observed at 1 bar, 300 K. The computed shifts in the CN and NO2 stretching frequencies are in good agreement with experimental results. DTIC

N95-28944# Princeton Univ., NJ. Dept. of Chemistry.
OPTIMAL CONTROL OF MOLECULAR MOTION Final Technical Report, 1 Nov. 1991 - 31 Oct. 1994
Herschel Rabitz 13 Jan. 1995 8 p
(Contract F49620-92-J-0076)
(AD-A291919; AFOSR-95-0097TR) Avail: CASI HC A02/MF A01

The overall objective of this research is to establish the physical principles for achieving control over molecular motion through the introduction of tailor-made optical fields. During the past year, this effort has involved both basic theoretical developments, as well as selected applications. Particular emphasis was given to establishing the robustness of laser field designs to various inevitable uncertainties and errors that may arise. In addition, an entirely new algorithm based on quantum mechanical tracking was introduced as a basis for a comprehensive treatment for both molecular control, as well as the inversion of controlled dynamics, to learn about the underlying Hamiltonians. The application of these various theoretical efforts was made to high quality ro-vibronic population inversion and the selective dissociation of HCN. Finally, a fundamental controllability algorithm was established, with the capability of assessing whether it is feasible to reach acceptable degrees of control in any particular molecule. DTIC

N95-28952 SRI International Corp., Menlo Park, CA.
MOLECULAR DYNAMICS STUDY OF ELECTROMIGRATION Final Report, Jul. 1993 - Dec. 1994
Herbert F. Helbig Nov. 1994 23 p Limited Reproducibility: More than 20% of this document may be affected by microfiche quality
(Contract F30602-91-D-0001)
(AD-A289811; RL-TR-94-210) Avail: Issuing Activity (Defense Technical Information Center (DTIC))

A software package has been assembled (written and adapted from

commercial sources) that allows three dimensional atomic level modeling, simulation and visualization of polycrystalline samples subjected to various stresses. Sample preparation, is accomplished with a commercial software package, ADESH, that allows initial atomic coordinates to be prepared conveniently for submission to the dynamics portion of the code. The code, mdem. exe, that traces the atom motions was written in the C programming language for convenient portability across computing platforms. On an Intel 486/66 class machine, it can provide 10 ps of history for a system containing 1896 atoms in approximately 62 hours of computing time. Temperature control is provided by a thermostat function known to preserve the statistical integrity of the dynamic variables. Several techniques have been developed for visualization of the output data. Preliminary results demonstrating thermal expansion, specific heat, self-diffusion and annealing behavior have been published. DTIC

N95-28981# Florida Agricultural and Mechanical Univ., Tallahassee, FL.
AB INITIO STUDIES OF ELECTRON AND POSITRON SCATTERING FROM NON-LINEAR MOLECULES Final Report, 1 Jul. 1989 - 30 Sep. 1992
Charles A. Weatherford Mar. 1995 6 p
(Contract DAAL03-89-G-0111)
(AD-A292586; ARO-27256.4-PH-SAH) Avail: CASI HC A02/MF A01

During a period of three years, several important developments and calculations were made on the electron-molecule scattering. We presented rotationally elastic, inelastic and summed cross sections for electron scattering with several polyatomic molecules (CH4, SiH4, GeH4, H2O, H2S and NH3) in a highly sophisticated close-coupling non-empirical theory. Exchange effects were included exactly, while polarization corrections were considered approximately but without involving any fitting parameter. Results were compared with measurements where such data were available. No previous theoretical investigation is available on these molecules in such detail and energy range. DTIC

N95-28994# Pennsylvania State Univ., University Park, PA.
[ACTIVITIES UPDATE] Final Report, 15 Jun. 1992 - 14 Jun. 1994
Gerald A. Smith 18 Jul. 1994 69 p
(Contract F49620-92-J-0374)
(AD-A292431; PSU-LEPS-94-15; AFOSR-95-01154TR) Avail: CASI HC A04/MF A01

The present report is an update on activities for the second year of funding. Research leading to a detailed characterization of antiproton annihilation in nuclei has resulted in a published analysis of fast deuteron production from carbon and uranium targets. This follows previously reported work and publications by our group on gamma-ray, neutral and charged pion, proton, and neutron production. The deuteron measurements are important to our SHIVA Star antiproton- catalyzed microfission experiment at the Phillips Laboratory, Kirtland AFB, in that they help constrain theoretical models of light nuclei production and subsequent energy deposition in the target. Work continues at SHIVA Star on working fluid formation and target compression for the microfission experiment. Excellent progress has been made, both theoretically and experimentally, on these important aspects of the experiment. The Penn State group, working in collaboration with Los Alamos National Laboratory physicists, trapped and held up to 721,000 antiprotons per beam injection pulse from the LEAR accelerator during July, 1993. This was a crucial step to the ultimate goal of transferring large numbers of antiprotons to the Phillips Laboratory for the antiproton-catalyzed microfission experiment. DTIC

N95-29076# Naval Postgraduate School, Monterey, CA.
THICKNESS MEASUREMENT OF AMMONIA TARGETS USED IN SLAC E143 EXPERIMENT M.S. Thesis
David R. Garvey Dec. 1994 47 p
(AD-A290215) Avail: CASI HC A03/MF A01

One of the primary research tools in high energy physics is the collision of beams of particles with stationary targets. The useful information that may be extracted from such experiments is proportional to knowledge of the thickness of the target. This determines how many point constituents were available for the particles in the beam to interact with. It is possible to determine the thickness of a target with statistical errors of the order of one percent by the use of x-ray attenuation measurements. Six target samples from the Stanford Linear Accelerator Center Experiment #143, 'Nucleon Spin Structure at 30 GeV,' were measured using this method. The targets were frozen ammonia crystals. A 40 mCurie americium 241 source was used to pass a colimated beam of known intensity x-rays through the samples. The x-ray intensity on the other side was measured by a silicon cell detector. The ammonia material was removed and the process repeated. By comparing the intensities with and without the material to the tabulated attenuation coefficients, the thickness of material is calculated. (AN) DTIC

N95-29082# Johns Hopkins Univ., Baltimore, MD. Dept. of Chemistry.
THE INTERACTION OF GROUP 3A ATOMS WITH SMALL MOLECULES Final Report, 1 Sep. 1991 - 30 Nov. 1994
Paul J. Dagdigian and Millard H. Alexander 6 Jan. 1995 24 p
(Contract AF-AFOSR-0363-91)
(AD-A290285; AFOSR-95-0043TR) Avail: CASI HC A03/MF A01

A collaborative theoretical and experimental investigation of the nonbonding interactions of the boron atom with the hydrogen molecule and other species has been carried out. Additionally, bimolecular collisions of electronically excited boron atoms and nonbonding interactions of other boron-containing species, namely BH and the isovalent AlH radical, were investigated. The main advances from the experimental component of this program has been in the spectroscopy of weakly bound complexes of atomic boron, while those from the concurrent theoretical work has involved the elucidation of potential energy surfaces of weakly bound complexes of open-shell species. DTIC

N95-29092# New Mexico Univ., Albuquerque, NM. Dept. of Chemistry.
CHARACTERIZATION OF EXCITED STATE OXYGEN-ORGANIC MOLECULE COMPLEXES Final Report, 1 Sep. 1991 - 31 Aug. 1994
Peter R. Ogilby 28 Nov. 1994 7 p
(Contract DAAL03-91-G-0321)
(AD-A290548; ARO-28628.5-CH) Avail: CASI HC A02/MF A01

Spectroscopic experiments designed to better characterize excited-state interactions between oxygen and organic molecules (M) were performed. Data were recorded in both liquids and solid organic polymers. Problems of interest included: (1) the effect of an applied magnetic field on the kinetics and yields of processes in the M-O2 photosystem; (2) the effect of changes in the M and O2 diffusion coefficients on both physical and chemical processes in the M-O2 photosystem; and (3) the effect of stabilizers used to inhibit polymer photodegradation on processes in the M-O2 photosystem. DTIC

N95-29227# Georgia Univ., Athens, GA.
ANALYTICAL THEORY OF CONTINUED FRACTIONS AND TIME EVOLUTION IN MANY-PARTICLE SYSTEMS Final Report, 10 Apr. 1991 - 30 Sep. 1994
M. H. Lee 15 Nov. 1994 4 p
(Contract DAAL03-91-G-0108)
(AD-A290365; ARO-27580.7-MA) Avail: CASI HC A01/MF A01

The analytical theory of continued fractions plays a key role in the time evolution behavior in many-particle systems. The aim of this study was to understand and to develop properties of relevant continued fractions for physical applications. Substantial progress has been made and reported in eleven (11) journal articles and several other conference proceedings also published. DTIC

N95-29388# California Inst. of Tech., Pasadena, CA.
SYMPOSIUM ON METAL-MEDIATED MOLECULAR ARCHITECTURES Final Report, 14 Apr. 1994 - 15 Apr. 1995
Frances H. Arnold 18 Jan. 1995 6 p Symposium held in Washington, DC, 24 Aug. 1994
(Contract N00014-94-1-0813)
(AD-A290427) Avail: CASI HC A02/MF A01

The symposium 'Metal-Mediated Molecular Architectures' was held in the Division of Biological Chemistry at the American Chemical Society meeting, Aug. 24, 1994 in Washington, D.C. It was co-chaired by Professor Frances Arnold, Caltech, and Dr. Harold Bright, ONR. The desire was to bring to the Division (and to the general ACS audience) some ideas and faces from other disciplines, with a particular emphasis on multidisciplinary research with potential applications. The goal of this particular symposium thus was to (1) introduce the Biological Chemistry Division to the interdisciplinary research in this emerging area; (2) attract researchers from the other Divisions that will also be represented at the ACS meeting

(Polymer Chemistry, Organic Chemistry, Inorganic Chemistry, etc.); and (3) to stimulate discussion among researchers from these different disciplines. DTIC

N95-29431# Colorado Univ., Boulder, CO.
SEMICONDUCTOR DEPOSITION AND ETCHING INTERACTIONS OF LASER-GENERATED TRANSLATIONALLY HOT ATOMS AND RADICALS Final Report, 1 Jun. 1991 - 31 Dec. 1994
Stephen R. Leone 31 Dec. 1994 32 p
(Contract DAAL03-91-G-0191)
(AD-A291824; ARO-28561.7-PH) Avail: CASI HC A03/MF A01

Laser vaporization of cryogenic films is employed to produce translationally fast atoms and radicals, and these kinetic-energy-enhanced species are used for studies of semiconductor etching; the results are important for the basic physics of electronics materials processing. Recent accomplishments include: (1) production of a novel source of kinetic-energy-enhanced beams of Cl2, Cl, and F atoms by laser vaporization; (2) observation of substantial enhancement of the etching rate and sustained etching of room temperature Si(100) by chlorine molecules with energies greater than or equal to 3 eV; (3) scattering studies of translationally fast Cl2 and Cl with Si(100); (4) velocity selection of the translationally fast beams for energy-resolved studies of dry etching processes; and (5) measurements of SiCl(x) product distributions as a function of substrate temperature. DTIC

N95-29460 Florida Univ., Gainesville, FL.
MOLECULAR SPECTRA AND DYNAMICS AT INTERFACES Final Report
N. Y. Ohrn and David A. Micha 15 Dec. 1994 7 p Limited Reproducibility: More than 20% of this document may be affected by microfiche quality
(Contract N00014-93-1-0122)
(AD-A289779) Avail: Issuing Activity (Defense Technical Information Center (DTIC))

The purpose of the project is to develop a theory of molecular spectra and dynamics of species adsorbed at solid interfaces, in order to provide insight into the properties of interfaces starting from their molecular structure. An additional goal is to develop computational tools to do quantitative calculations of spectroscopic and dynamical quantities. The theoretical and computational tools are developed recognizing that advanced light sources such as tunable lasers, and synchrotron radiation and pulsed lasers provide important tools in the study of solid surfaces to excite adsorbed molecules and to dissociate bonds of adsorbates. Photoelectron spectroscopy (PBS) probes the electronic structure of adsorbed species and also, by comparison to free molecules, provides information on the electronic structure of the solid substrate. Photoinduced desorption (PID) provides information on the strengths of chemical bonds and of Van der Waals forces at surfaces. DTIC

N95-29521# Colorado Univ., Boulder, CO.
THE 14TH INTERNATIONAL CONFERENCE ON ATOMIC PHYSICS
D. J. Wineland, ed. (National Inst. of Standards and Technology, Rockville, MD.), C. E. Wieman, ed., and S. J. Smith, ed. 24 Jan. 1995 489 p Conference held in Boulder, CO, 31 Jul. - 5 Aug. 1994
(Contract N00014-94-1-0333)
(AD-A290726; Rept-153-1072; LC-94-73219; ISBN-1-56396-348-5) Avail: CASI HC A21/MF A04

The program for this conference consisted primarily of 28 invited papers, all presented in plenary session, each authored by a scientist at the forefront of this development. In this volume the written texts submitted by these plenary speakers are presented. These proceedings provide a comprehensive and authoritative overview of the state of the field of atomic physics. Papers are presented in the following categories: atomic tests of fundamental theories, atomic structure and high resolution spectroscopy, precise measurements of atomic masses, advances in laser cooling and trapping of atoms, atom optics, quantum optics and coherence, collisional and optical properties of ultracold atoms, atoms in intense fields, and impacts of atomic physics in other disciplines. Derived from text

N95-29555# Oregon Univ., Eugene, OR.
EXPERIMENTAL STUDIES OF FUNDAMENTAL ONE- AND TWO-PHOTON LASING PROCESSES Final Report
Thomas W. Mossberg 15 Sep. 1994 6 p
(Contract DAAL03-91-G-0316)
(AD-A290593; ARO-29015.5-PH) Avail: CASI HC A02/MF A01

Theoretical and experimental investigations of two-photon lasing and inversionless lasing have been completed. Continuous-wave two-photon lasing has been demonstrated for the first time and its predicted bistable character verified. The role of pump bandwidth in the production of inversionless gain has been studied and the maximal efficacy of narrow bandwidth of pumps identified. Continuous-wave lasing in a Cascade-type three-level atomic system has been observed. DTIC

N95-29583# California Univ., Berkeley. Lawrence Berkeley Lab, CA. Physics Div.
FROM THE (PSI) TO CHARMED MESONS
Gerson Goldhaber Nov. 1994 40 p Presented at the International Conference on the History of Original Ideas and Basic Discoveries in Particle Physics, Erice (Italy), 29 Jul. - 4 Aug. 1994
(Contract DE-AC03-76SF-00098; NSF ADT-88-09616)
(DE95-006564; LBL-36431; CONF-9407157-4) Avail: CASI HC A03/MF A01

This talk deals with the author's recollections about the discoveries of the J/(psi) the (psi)(prime) as well as psion spectroscopy and charmed mesons. He gives a chronology for the (psi) and (psi)(prime) discoveries. He also discusses the events which led to the charmed meson discovery as well as detailed discussions on the proof that the resonance observed in the K(sup -) (pi)(sup +) system, at 1,865 MeV, was indeed the predicted charmed meson. DOE

N95-29723# Clark Univ., Worcester, MA.
MOLECULAR LEVEL CHARACTERIZATION BY NMR OF THE TRANSPORT AND STRUCTURAL ENVIRONMENT OF GASES AND CONDENSED PENETRANTE Final Technical Report, Jun. 1991 - Sep. 1994
Paul T. Inglefield 25 Sep. 1994 146 p
(Contract DAAL03-91-G-0207)
(AD-A290831; ARO-26840.9-CH) Avail: CASI HC A07/MF A02

NMR measurements have been made on polyisobutylene containing gaseous and condensed penetrants (CO2 and toluene respectively). Both NMR relaxation and pulse field gradient measurements have been made to characterize both penetrant diffusion and polymer segmental motion simultaneously. The relaxation data are analyzed using conventional models for polymer chain dynamics and the diffusion constants are expressed using free volume theories. It is found that there is a correlation between penetrant diffusion and polymer segmental reorientation. This correlation can be quantified both in terms of timescale and free volume requirements. The unusual slow permeability of polyisobutylene to various penetrants can be rationalized. The data provides a very comprehensive base for critical discussion of segmental chain dynamic descriptions and free volume theories in systems of this type. DTIC

N95-29748# Fukui Inst. of Tech. (Japan).
TRAPPED ELECTRON INSTABILITIES DUE TO ELECTRON TEMPERATURE GRADIENT AND ANOMALOUS TRANSPORT
T. Yamagishi Nagoya, Japan National Inst. for Fusion Science Oct. 1993 22 p
(ISSN 0915-633X)
(AD-B179859L; NIFS-247) Avail: CASI HC A03/MF A01

The electrostatic trapped electron instabilities have been investigated by numerically solving the local single energy integral form dispersion relation. With the electron temperature gradient, the electron collision effect destabilizes the dissipative trapped electron mode (DTEM). For collisionless electrons, the energy dependent curvature drift effect strongly destabilizes the collisionless trapped electron mode. The growth rate is, however, reduced by a small collision effect. The anomalous transport due to these trapped electron modes is discussed. Author

N95-29865# Georgia Univ., Athens, GA. Research Foundation.
FUNDAMENTAL STUDIES OF OXYGEN RINGS AND OTHER HIGH ENERGY DENSITY MOLECULAR SYSTEMS Final Report, 1 Nov. 1991 - 31 Oct. 1994
Henry F. Schaefer, III 15 Nov. 1994 225 p

(Contract F49620-92-J-0047)
(AD-A290875; AFOSR-95-0019TR) Avail: CASI HC A10/MF A03

The object of this research is to characterize the energetics, spectroscopic properties, and elementary chemical reactions (including unimolecular reactions) of the oxygen ring molecules O4 and O12 and related species. The approach used will exploit recent developments in ab initio molecular quantum mechanics. In a collaborative effort with ongoing experimental research to identify and synthesize high energy density molecules, excited electronic states and positive ions of these species will be studied. DTIC

N95-29886# Universidad Nacional Autonoma de Mexico, Mexico City (Mexico).
CALCULATION OF SHIELDING PARAMETERS Ph.D. Thesis
Zeferino Jorge Montoya 1994 123 p
(DE95-608735; INIS-mf-14395) Avail: CASI HC A06/MF A02 (US Sales Only)

Within the nuclear reaction exists three types of energy producing reactions: (1) radioactive disintegration; (2) fission; and (3) fusion. Besides the radiation produced in these reactions there are radioactive emissions of a different type, and in some of these cases they are of great penetration power and scope. The radiation produces great damage when interacted with materials, in particular the most dangerous are neutrons and gamma photons. For this reason it is necessary to protect people who work in places which operate with radioactive sources from the radiation, in addition to reducing the radiation doses to the most reasonably possible, considering the circumstances of the installations. The three determining factors in the proposition of reducing exposure to radiation are: (1) to maintain control over the reduced exposure in the time of the permanence in the irradiated areas; (2) to increase the distance between the source and the operating personnel as much as possible; and (3) to place an armor-plate between the source and the receptor. The work described in this paper has its objective a calculation of the parameters of an armor-plate in radioactive sources, with the goal of estimating the doses of radiation in protecting people and other biological systems from exposure to radiation produced during the nuclear reactions. The parameters to be principally considered are: (1) characteristics of the source; (2) geometry of the source at the point of exposure; and (3) material and thickness of the armor-plate. DOE

N95-30019# Argonne National Lab., IL.
PROSPECTS FOR HERMES-SPIN STRUCTURE STUDIES AT HERA
H. E. Jackson 1994 16 p Presented at the International Symposia on High Energy Spin Physics and Polarization Phenomena in Nuclear Physics, Bloomington, IN, 15-22 Sep. 1994
(Contract W-31-109-eng-38)
(DE95-005845; ANL/PHY/CP-84488; CONF-9409103-15) Avail: CASI HC A03/MF A01

HERMES (HERA Measurement of Spin), is a second generation experiment to study the spin structure of the nucleon by using polarized internal gas targets in the HERA 35-GeV electron storage ring. Scattered electrons and coincident hadrons will be detected in an open geometry spectrometer which will include particle identification. Measurements are planned for each of the inclusive structure functions, g(sub 1),(x), g(sub 2)(x), b(sub 1)(x) and A(x), as well as the study of semi-inclusive pion and kaon asymmetries. Targets of hydrogen, deuterium and He-3 will be studied. The accuracy of data for the inclusive structure functions will equal or exceed that of current experiments. The semi-inclusive asymmetries will provide a unique and sensitive probe of the flavor dependence of quark helicity distributions and properties of the quark sea. Monte Carlo simulations of HERMES data for experiment asymmetries and polarized structure functions are discussed. DOE

N95-30059# Los Alamos National Lab., NM.
APPLICATIONS OF LANGEVIN AND MOLECULAR DYNAMICS METHODS
P. S. Lomdahl 1994 11 p Presented at the Summer School Verano on Nonlinearity and Disorder, Madrid, Spain, 15-19 Aug. 1994
(Contract W-7405-eng-36)
(DE95-007875; LA-UR-95-438; CONF-9408218-2) Avail: CASI HC A03/MF A01

Computer simulation of complex nonlinear and disordered phenomena from materials science is rapidly becoming an active and new area serving as a guide for experiments and for testing of theoretical concepts. This is especially true when novel massively parallel computer systems and techniques are used on these problems. In particular the Langevin dynamics simulation technique has proven useful in situations where the time evolution of a system in contact with a heat bath is to be studied. The traditional way to study systems in contact with a heat bath has been via the Monte Carlo method. While this method has indeed been used successfully in many applications, it has difficulty addressing true dynamical questions. Large systems of coupled stochastic ODE's (or Langevin equations) are commonly the end result of a theoretical description of higher dimensional nonlinear systems in contact with a heat bath. The coupling is often local in nature, because it reflects local interactions formulated on a lattice, the lattice for example represents the underlying discreteness of a substrate of atoms or discrete k-values in Fourier space. The fundamental unit of parallelism thus has a direct analog in the physical system the authors are interested in. In these lecture notes the authors illustrate the use of Langevin stochastic simulation techniques on a number of nonlinear problems from materials science and condensed matter physics that have attracted attention in recent years. First, the authors review the idea behind the fluctuation-dissipation theorem which forms that basis for the numerical Langevin stochastic simulation scheme. The authors then show applications of the technique to various problems from condensed matter and materials science. DOE

N95-30060# Missouri Univ., Kansas City, MO.
SAM1-A NEW SEMIEMPIRICAL METHOD INCLUDING d-ORBITALS Final Report, Feb. 1993 - Jan. 1995
Andrew J. Holder 17 Jan. 1995 12 p
(Contract F49620-93-1-0142)
(AD-A290903; AFOSR-95-0072TR) Avail: CASI HC A03/MF A01

Elemental parameter sets have been completely developed and validated for sulfur (S), silicon (Si), and phosphorous (P). Results are much superior to those older semiempirical treatments. Extensive work has been completed on SAM1 parameters for iron (Fe), although final results are not available. Substantial obstacles have been overcome in the work and a clear route to the objective has been established. The theoretical framework is in place and all that is required is completion of the parameterization process. The experience we have gained will allow us to parameterize SAM1 for other transition metals very quickly. Iron parameters are currently in beta testing in a number of labs. DTIC

N95-30065# Manchester Univ. (England). Inst. of Science and Technology.
PROCEEDINGS OF THE 18TH INTERNATIONAL WORKSHOP ON CONDENSED MATTER THEORIES
R. F. Bishop 10 Jun. 1994 185 p Conference held in Valencia, Spain, Jun. 1994
(Contract N68171-94-M-5711)
(AD-A291396; R/D-7342-PH-03) Avail: CASI HC A09/MF A02

This workshop covered various techniques in nuclear many-body problems as well as various theoretical techniques, ranging through the coupled cluster method, variational Jastrow-like approaches, parquet theory etc. Particular emphasis was placed on the technique of density functional theory (plus a little on density matrices), a wide range of applications including atomic cluster theory, inhomogeneous liquids and especially He-4, simple metals and metal surfaces. In this context, there was a special session, with two papers related to the density-functional technique; one on time-dependent theory and the other on the many-body construction of density functionals with illustrative applications. Other especially notable contributions applied information turning from (mainly) techniques to physical areas in condensed matter, there was considerable emphasis on the quantal liquid He-4, with discussion not only of bulk properties but of wetting, surface tension and H-3 and He-4 mixtures. Contact with new neutron scattering experiments was highlighted in connection with bulk He-4. Some papers on high Tc materials, plus a discussion of recent progress, both experiment and theory, on electron solids, reflected important growth areas in condensed matter. In the latter area, the equilibrium between Laughlin electron liquid and electron solid was considered, the electron liquid being treated in a number of papers, including a study by quantal hypernetted chain methods. DTIC

N95-30185# Argonne National Lab., IL. High Energy Physics Div.
SEA AND GLUON SPIN STRUCTURE FUNCTION MEASUREMENTS AT RHIC
A. Yokosawa 1995 8 p Presented at the International Symposia on High Energy Spin Physics and Polarization Phenomena in Nuclear Physics, Bloomington, IN, 15-22 Sep. 1994
(Contract W-31-109-eng-38)
(DE95-005823; ANL-HEP-CP-94-70; CONF-9409103-17) Avail: CASI HC A02/MF A01

The first polarized collider where one collides 250-GeV/c beams of 70% polarized protons at high luminosity is under construction. This will allow a determination of the nucleon spin-dependent structure functions over a large range in x and a collection of sufficient W and Z events to investigate extremely interesting spin-related phenomena. DOE

N95-30186# Argonne National Lab., IL. High Energy Physics Div.
MEASUREMENTS OF (DELTA)(SIGMA)(SUB L)(PP) AND (DELTA)(SIGMA)(SUB L)((BAR P)P) AT 200 GeV/c
D. P. Grosnick 1995 5 p Presented at the International Symposia on High Energy Spin Physics and Polarization Phenomena in Nuclear Physics, Bloomington, IN, 15-22 Sep. 1994
(Contract W-31-109-eng-38)
(DE95-005837; ANL-HEP-CP-94-63; CONF-9409103-18) Avail: CASI HC A01/MF A01

A measurement was made at Fermilab of the difference in the total cross sections between states with beam and target polarizations aligned antiparallel and parallel, Delta(sigma)(sub L) = Delta(sigma)(antiparallel)) - (Delta)(sigma)(parallel), using 200-GeV/c, polarized proton and antiproton beams and a polarized proton target. This measurement explores the spin dependence of particle interactions and the constituent dynamics. A difference in the spin-dependent total cross sections has been observed in previous experiments at lower energies, and this experiment was the first to explore possible spin effects in (Delta)(sigma)(sub L) at much higher energies. The polarized proton beam is produced from parity-nonconserving decays of the (Lambda)(sup 0) hyperon, where protons emitted from these decays have their spins aligned along the direction of their momenta. The Lambda hyperons are produced, along with other particles, when unpolarized, 800-GeV/c protons strike a beryllium target. A virtual source of protons is produced at the target from these decays and the proton polarization is correlated to the transverse distance from the target. A beam of polarized antiprotons can be produced in an analogous manner using (bar Lambda(sup 0)) decays. The beam transport system goal was to produce no net spin precession and to preserve the correlation between the beam particle polarization and the transverse position at the virtual source. The beam transport used four sets of quadrupole magnets to focus the beam at intermediate and final focal points. An electronic, particle-tagging system was located at the intermediate focus, while the polarized target was near the final focus. DOE

N95-30191# Texas Univ., Austin, TX. Center for Particle Physics.
INCLUSIVE HADRONIC PRODUCTION OF THE B(SUB c) MESON VIA HEAVY QUARK FRAGMENTATION
K. Cheung Mar. 1995 7 p
(Contract DE-FG03-93ER-40757)
(DE95-008739; DOE/ER-40757/065) Avail: CASI HC A02/MF A01

The author summarizes the studies on the hadronic production of S- and P-wave ((bar-b)c) mesons via direct fragmentation of the bottom antiquark as well as the Altarelli-Parisi induced gluon fragmentation. DOE

N95-30302 California Univ., San Diego, CA.
EXPERIMENTS ON NONLINEAR WAVE-PARTICLE INTERACTIONS Ph.D. Thesis
Dirk Albrecht Hartmann 1994 193 p
Avail: Univ. Microfilms Order No. DA9420719

Experiments on nonlinear wave-particle interactions using a traveling wave tube (TWT) are described. There, one or more waves modify the motions of energetic beam particles, and these beam perturbations affect the wave evolution. At large amplitudes, mode-coupling is observed and forms the focus of this study. The wave-particle interactions are very similar to those in beam-plasma systems. However, the slow wave structure of the TWT stays linear for all wave amplitudes reached and does not introduce noise. The precise wave evolution can thus be obtained by launching a specified waveform, allowing it to interact with the beam, and analyzing the received waveform. Two cases are considered. To study the 'weak warm beam instability', a broad spectrum of waves on a warm beam is launched. At saturation, significant mode-coupling results in wave correlations smaller than 0.5 with their launch values. Experimentally each wave is separated into two components: one component proportional to the launch amplitude and the other due to mode-coupling. The mode-coupling component growth rate is about three times larger than the ensemble-averaged wave growth rate, which is in agreement with a four-wave coupling model. Strongest coupling occurs between waves whose wavelengths match within about a turbulent trapping length. In the linear regime, the measured ensemble-averaged wave growth rates and beam velocity diffusion rates agree reasonably with quasilinear and resonance-broadening theory; in the nonlinear regime up to saturation, the discrepancies are larger. To study the 'sideband instability', both a large amplitude wave that traps a cold electron beam and two small amplitude sidebands are launched. For a range of sideband frequencies, mode-coupling results in phase-locking between the side-bands, characterized by the 'modulational phase'. These two growing sidebands can be interpreted as a single normal mode of the Kruer, Dawson, Sudan macro-particle model. The measured sideband growth rates, wavenumber shifts, modulational phase and amplitude ratio qualitatively agree with the model. However, quantitative agreement is found only with computer simulations that follow the full phase-space distribution of the particles. Therefore the discrepancies are due to the simplicity of the model. Dissert. Abstr.

73 NUCLEAR AND HIGH-ENERGY PHYSICS

Includes elementary and nuclear particles; and reactor theory. For space radiation see *93 Space Radiation.*

N95-28930# Massachusetts Inst. of Tech., Cambridge, MA.
DESIGN OF AN ELECTRONIC CHARGED PARTICLE SPECTROMETER TO MEASURE (RHO R), YIELD, AND IMPLOSION SYMMETRY ON THE OMEGA UPGRADE
D. G. Hicks, C. K. Li, R. D. Petrasso, K. W. Wenzel, and J. P. Knauer (Rochester Univ., NY.) Nov. 1994 34 p
(Contract DE-FG02-91ER-54109)
(DE95-006088; DOE/ER-54109/T4; PFC/RR-94-11) Avail: CASI HC A03/MF A01

The preliminary design for a state-of-the-art diagnostic that will measure a broad energy spectrum of charged particles generated in the OMEGA Upgrade facility is investigated. Using a set of photodiodes approximately 10 and a 0.8 Tesla permanent magnet, the diagnostic will uniquely determine particle energies and identities from 0.2 MeV up to the maximum charged particle energies (10.6 MeV tritons, 12.5 MeV deuterons and 17.4 MeV protons). With its high density picture elements, each photodiode has 10(exp 6) single-hit detectors, giving the spectrometer a dynamic range of 1 - 10(exp 5) particles/shot. For example, in the case of a DT yield of 10(exp 9) neutrons, about 100 knock-on charged particles will be detected when the spectrometer aperture is 60 cm from the implosion. Furthermore, the measurement of knock-on D and T spectra will allow rho R's up to 0.15 g/sq cm to be measured (for a 1 keV plasma), or 0.3 g/sq cm if hydrogen doping is used. In addition, the yield and slowing down of secondary protons may be used to determine rho R up to 0.3 g/sq cm. Significantly, this diagnostic will also directly measure the DD fusion yield and energy degradation of nascent 3 MeV protons. By using two such compact spectrometers to measure the yield and spectra on widely separated ports around the OMEGA Upgrade target chamber, the implosion and burn symmetry can be determined. Furthermore, the ion temperature, and, in principle, even the electron temperature can be measured. The diagnostic and its development will be fully tested at several critical steps, utilizing 0.2-16 MeV protons (and several other charged particles and neutrons) from our absolutely calibrated Cockcroft-Walton facility. DOE

N95-28957# Oak Ridge National Lab., TN.
MOLTEN FLUORIDE FUEL SALT CHEMISTRY
L. M. Toth, G. D. DelCul, S. Dai, and D. H. Metcalf 1995 5 p Presented at the Conference on Accelerator-driven Transmutation Technologies and Applications (A-DTTA), Albuquerque, NM, 8-12 Jan.

1995
(Contract DE-AC05-84OR-21400)
(DE95-007025; CONF-950145-3) Avail: CASI HC A01/MF A01

The chemistry of molten fluorides is traced from their development as fuels in the Molten Salt Reactor Experiment with important factors in their selection being discussed. Key chemical characteristics such as solubility, redox behavior, and chemical activity are explained as they relate to the behavior of molten fluoride fuel systems. Development requirements for fitting the current state of the chemistry to modern nuclear fuel system are described. It is concluded that while much is known about molten fluoride behavior which can be used effectively to reduce the amount of development required for future systems, some significant molten salt chemical questions must still be addressed. DOE

N95-29142# Oak Ridge National Lab., TN.
THE INTERNATIONAL FUSION MATERIALS IRRADIATION FACILITY
T. E. Shannon, F. Cozzani (European Union-Commission, Brussels, Belgium.), D. H. Crandall, F. W. Wiffen, and K. Ehrlich (Kernforschungszentrum G.m.b.H., Karlsruhe, Germany.) 1994 7 p Presented at the 15th International Conference on Plasma Physics and Controlled Nuclear Fusion Research, Madrid, Spain, 26 Sep. - 1 Oct. 1994
(Contract DE-AC05-84OR-21400)
(DE95-006536; CONF-940933-35; IAEA-CN-60/F-2-II-5) Avail: CASI HC A02/MF A01

It is widely agreed that the development of materials for fusion systems requires a high flux, 14 MeV neutron source. The European Union, Japan, Russia and the U.S. have initiated the conceptual design of such a facility. This activity, under the International Energy Agency (IEA) Fusion Materials Agreement, will develop the design for an accelerator-based D-Li system. The first organizational meeting was held in June 1994. This paper describes the system to be studied and the approach to be followed to complete the conceptual design by early 1997. DOE

N95-29495# Oregon State Univ., Corvallis, OR.
HOT ELECTRON PHYSICS OF ALTERNATING-CURRENT THIN-FILM ELECTROLUMINESCENT DEVICES Final Report, Jul. 1991 - Sep. 1994
J. F. Wager and S. M. Goodnick 30 Sep. 1994 11 p
(Contract DAAL03-91-G-0242)
(AD-A290528; ARO-28852.25-PH) Avail: CASI HC A03/MF A01

The goal of this research program was to elucidate the hot electron physics of ACTFEL devices with particular emphasis on: (1) hot electron transport; (2) defect state hot electron sourcing and trapping; and (3) hot electron-induced ACTFEL aging. Highlights of our research accomplishments are summarized in terms of these three topical categories. DTIC

N95-30009# Brookhaven National Lab., Upton, NY.
A PRACTICAL HIGH-ENERGY HIGH-LUMINOSITY MU(+)-MU(-) COLLIDER
R. B. Palmer (Stanford Linear Accelerator Center, Menlo Park, CA), J. Gallardo (Stanford Linear Accelerator Center, Menlo Park, CA), D. V. Neuffer (Continuous Electron Beam Accelerator Facility, Newport New, VA.), and J. Gallardo Jun. 1994 11 p Presented at the Advanced Accelerator Concepts Workshop, Lake Geneva, WI, 13-18 Jun. 1994
(Contract DE-AC02-76CH-00016)
(DE95-006769; BNL-61266; CONF-940681-13; CAP-110-MUON-94C)
Avail: CASI HC A03/MF A01

We present a candidate design for a high-energy high-luminosity mu(+)-mu(-) collider, with E(sub cm) = 4 TeV, L = 3 x 10(exp 4) cm(exp -2) s(exp -1), using only existing technology. The design uses a rapid-cycling medium-energy proton synchrotron, which produces proton beam pulses which are focused onto two pi-producing targets, with two pi-decay transport lines producing mu(+)'s and mu(-)'s. The mu's are collected, rf-rotated, cooled and compressed into a recirculating linac for acceleration, and then transferred into a storage ring collider. The keys to high luminosity are maximal mu collection and cooling; innovations with these goals are presented, and future plans for collider development are discussed. This example demonstrates a novel high-energy collider type, which will permit exploration of elementary particle physics at energy frontiers beyond the reach of currently existing and proposed electron and hadron colliders. DOE

N95-30021# Brookhaven National Lab., Upton, NY.
LATTICE/BEAM DYNAMICS WORKING GROUP Summary Report
M. Syphers 1994 7 p Presented at the Workshop on Future Hadron Facilities in the United States, Bloomington, IN, 6-10 Jul. 1994
(Contract DE-AC02-76CH-00016)
(DE95-006774; BNL-61287; CONF-9407128-Pt-1) Avail: CASI HC A02/MF A01

The Lattice/Beam Dynamics Working Group was charged with reviewing and identifying technical issues and their potential solutions for (1) a 2 x 2 TeV high luminosity p p-bar collider, and (2) a 30 x 30 TeV high luminosity pp collider. Rather than attempting to solve very specific problems for these devices in the relatively short time scale of a workshop, the group attempted to look at more general questions to try to indicate in which directions future work in these areas should proceed. The emphasis of the group tended toward lattice issues and general accelerator design issues for the above two cases, with more specific questions being addressed as directed by the needs seen by the workshop synthesizers. DOE

N95-30057# Los Alamos National Lab., NM.
TESTING OF THE ENDF/B-VI NEUTRON DATA LIBRARY ENDF60 FOR USE WITH MCNP(TRADEMARK)
R. E. MacFarlane and S. C. Frankle 1995 5 p Presented at the Nuclear Criticality Technology and Safety Project (NCTSP) Annual Meeting, San Diego, CA, 17 May 1995
(Contract W-7405-eng-36)
(DE95-007858; LA-UR-95-627; CONF-9505195-1) Avail: CASI HC A01/MF A01

This report presents information detailing the continuous-energy neutron data library ENDF60, for use with the Monte Carlo N-particle radiation transport code MCNP4A, released fall of 1994. DOE

N95-30337*# National Aeronautics and Space Administration. Langley Research Center, Hampton, VA.
PARAMETERIZED SPECTRAL DISTRIBUTIONS FOR MESON PRODUCTION IN PROTON-PROTON COLLISIONS
John P. Schneider (Wisconsin State Univ., La Crosse, WI.), John W. Norbury (Wisconsin State Univ., La Crosse, WI.), and Francis A. Cucinotta Jun. 1995 20 p
(Grant NAG1-1154; RTOP 199-45-16-12)
(NASA-TM-4675; L-17464; NAS 1.15:4675) Avail: CASI HC A03/MF A01

Accurate semiempirical parameterizations of the energy-differential cross sections for charged pion and kaon production from proton-proton collisions are presented at energies relevant to cosmic rays. The parameterizations, which depend on both the outgoing meson parallel momentum and the incident proton kinetic energy, are able to be reduced to very simple analytical formulas suitable for cosmic ray transport through spacecraft walls, interstellar space, the atmosphere, and meteorites. Author

74 OPTICS

Includes light phenomena; and optical devices.
For lasers see *36 Lasers and Masers.*

N95-28695 Tennessee State Univ., Nashville, TN.
PREDICTING POLARIZED LIGHT SCATTERING BY MARINE MICRO-ORGANISM Report for 1 Mar. 1992 - 28 Feb. 1994
Patricia G. Hull 28 Feb. 1994 9 p Limited Reproducibility: More than 20% of this document may be affected by microfiche quality
(Contract N00014-92-J-1284)
(AD-A289790) Avail: Issuing Activity (Defense Technical Information Center (DTIC))

To understand and quantify light scattering from ensembles of irregularly-shaped objects. To characterize the effect of ensembles of micro-organisms on the propagation of polarized light through sea water. To determine the feasibility of detecting particle orientation and to assess the importance of scattering to underwater imaging techniques and irradiance calculations. To develop a numerical or analytical model that predicts angle-dependent scattering of polarized light from ensembles of non-spherical marine organisms and marine detritus. To verify and examine the validity and range of applications of the model by comparison with exact calculations

and/or experimental results as appropriate. To apply the model to investigate the effects caused by the orientation of ensembles of non-spherical particles, and to determine the feasibility of detecting orientation by measuring scattering matrix elements that are normally zero. DTIC

N95-28698 Tennessee State Univ., Nashville, TN.
PREDICTING POLARIZED LIGHT SCATTERING BY MARINE MICRO-ORGANISMS Annual Report
Patricia G. Hull 1995 11 p Limited Reproducibility: More than 20% of this document may be affected by microfiche quality
(Contract N00014-92-J-1284)
(AD-A289796) Avail: Issuing Activity (Defense Technical Information Center (DTIC))

The objectives of this research is to develop a numerical or analytical model that predicts angle-dependent scattering of polarized light from ensembles of non-spherical marine organisms and marine detritus and to verify and examine the validity and range of applications of the model by comparison with exact calculations and/or experimental results as appropriate. Specific tasks toward the objectives are: (1) to develop an artificial neural network to recognize features in the scattering matrix elements associated with the irregular shape of oceanic scatterers; and (2) to refine and enhance the coupled-dipole approximation method. DTIC

N95-28778 Army Cold Regions Research and Engineering Lab., Hanover, NH.
VARIATION IN VISUAL AND NEAR-INFRARED CONTRAST WITH A SNOW BACKGROUND
Lindamae Peck Aug. 1994 31 p Limited Reproducibility: More than 20% of this document may be affected by microfiche quality
(AD-A289710; CRREL-SR-94-28) Avail: Issuing Activity (Defense Technical Information Center (DTIC))

Visual and near-infrared concealment against a snow cover are considered in terms of the daily and longer-term variation in albedo of a shallow (less than or = 26 cm) snow cover. Examples of albedo of a Vermont snow cover demonstrate the influence of time of day (solar angle), incident solar radiation, snow depth, and snow wetness. Most albedos felt within the range 0.75-0.98. The most consistent variation was a decrease in albedo during the morning as the sun angle increased and a corresponding increase with decreasing sun angle in the afternoon. Albedo was low when the snow surface temperature indicated melting was occurring or when an increase in temperature of the soil beneath the snow cover indicated solar radiation was being absorbed by the soil. Examples of the diurnal variation in sun angle and the seasonal variation in maximum potential solar radiation, as calculated from site latitude and longitude and calendar date, are presented. DTIC

N95-28795# GTE Labs., Inc., Waltham, MA.
METHODS AND COMPONENTS FOR OPTICAL CONTENTION RESOLUTION IN HIGH SPEED NETWORKS Interim Report, 23 Nov. 1994 - 23 Feb. 1995
Paul Melman and Han Kim 23 Feb. 1995 8 p
(Contract MDA972-93-C-0057; ARPA Order 9339)
(AD-A292331) Avail: CASI HC A02/MF A01

During the sixth quarter of the CORD project, Stanford University has continued experimental investigation of the CORD testbed. The transmission and reception of the 2.488 GHz payload data clock and its affect on the payload data and control channels were investigated. The electronic multiplexer and demultiplexer circuits were tested and measured. The payload data pseudo random data generator and bit error rate measurement logic were designed, components selected, and the CR0 controller was designed. DTIC

N95-28798# Florida Inst. of Tech., Melbourne, FL.
AUTOMATED OPTICAL TARGET RECOGNITION Final Report, Dec. 1993 - Sep. 1994
Samuel P. Kozaitis Dec. 1994 33 p
(Contract F30602-94-C-0008)
(AD-A292397; RL-TR-94-228) Avail: CASI HC A03/MF A01

This report presents an overview of continuous and discrete wavelet transforms. Both digital and optical implementations of the discrete wavelet transform are discussed. Examples of typical wavelet basis functions are compared and the constraints imposed by optical implementations are discussed. A multi-resolution signal processing approach to object recognition is presented using an optical correlator for generating a wavelet transform. The practicality of using an optical correlator to perform target recognition with a wavelet representation approach is considered. DTIC

N95-28799# Massachusetts Inst. of Tech., Cambridge, MA. Research Lab. of Electronics.
INTERFEROMETRIC MEASUREMENT WITH SQUEEZED LIGHT Annual Technical Report, 1 Feb. 1994 - 31 Jan. 1995
Hermann A. Haus, Karen Bergman, and Luc Boivin 14 Mar. 1995 5 p
(Contract N00014-92-J-1302)
(AD-A292402) Avail: CASI HC A01/MF A01

The goal of the project is to develop interferometric measurement methods, using squeezed light, with noise levels below the 'standard quantum limit'. The 'standard quantum limit' is the shot noise level. If squeezed radiation is injected into the, normally, unexcited port of a Mach-Zehuder interferometer, the phase shift of the interferometer can be measured in a noise background that is below the shot noise level. In past experiments performed at 1.3 microns wavelength using a nonlinear Sagnac loop, we have demonstrated shot noise reduction of -5.1 dB. In a phase measurement with a Mach-Zehnder interferometer we have achieved a noise level 3 dB below the shot noise level. In this measurement the losses of the bulk- (rather than fiber-) interferometer prevented the full utilization of the 5.1 dB shot noise reduction. It is our present goal to achieve improved noise performance by increased noise reduction below the shot noise level. DTIC

N95-28870# Donmar Ltd., Newport Beach, CA.
COST EFFECTIVE, DUAL-PURPOSE MACHINE VISION-BASED DETECTORS FOR (1) SMOKE AND FLAME DETECTION, AND (2) ENGINE OVERHEAD/BURN-THROUGH AND FLAME DETECTION Final Report
A. D. Goedeke, B. Drda, C. Fitzpatrick, and G. Healey 8 Mar. 1995 87 p
(Contract F33615-94-C-3402)
(AD-A292284) Avail: CASI HC A05/MF A01

Three major accomplishments resulted from this effort: (1) It was determined that the Machine Vision Fire Detection System (MVFDS) could be augmented with a near-infrared imaging FPA/CCD, 4-8 IR transmitting optic waveguides, and modified algorithms to measure small changes in temperature of small areas on the engine casing and therefore determine overheat condition and/or possible burn-through condition. The IR-MVFDS would also detect small burn-through torch-like fires as well as nacelle fires associated with munitions and leaking/broken fuel and hydraulic lines. (2) Tests verified the ability of the visible MVFDS flame detector to simultaneously detect smoke and measure its transmissivity. This dual function, in addition to possibly as many as 16 or more separate fields-of-view using small fiber optic cables, makes the Smoke/Flame-MVFDS cost effective in aircraft and in commercial applications. (3) The potential benefits and cost savings of both the IR-MVFDS and Smoke/Flame-MVFDS were demonstrated. The technical basis was proven feasible with minimum risk for development of both the IR-MVFDS and the Flame/Smoke-MVFDS in Phase II. DTIC

N95-28912# EG and G Energy Measurements, Inc., Pleasanton, CA.
AN IMAGE CANCELLATION APPROACH TO DEPTH-FROM-FOCUS
Shin-yee Lu (Lawrence Livermore National Lab., Livermore, CA.) and M. Graser 1995 10 p Presented at the SPIE Annual Conference of the Optical Society of America and Exhibit, Boston, MA, 30 Oct. - 4 Nov. 1994
(Contract DE-AC08-93NV-11265)
(DE95-007625; EGG-11265-4012; CONF-941006-4) Avail: CASI HC A02/MF A01

Depth calculation of an object allows computer reconstruction of the surface of the object in three dimensions. Such information provides human operators 3D measurements for visualization, diagnostic and manipulation. It can also provide the necessary coordinates for semi or fully automated operations. This paper describes a microscopic imaging system with computer vision algorithms that can obtain the depth information by making use of the shallow depth of field of microscopic lenses. DOE

N95-28914# Physical Optics Corp., Torrance, CA.
FOURIER SYNTHESIS LITHOGRAPHIC MACHINE FOR LARGE PANEL DISPLAY FABRICATION Final Report, 1 Aug. 1994 - 31 Jan. 1995
Lev Sadovnik 31 Jan. 1995 52 p
(Contract DAAH04-94-C-00029)
(AD-A291921; ARO-33577.1-EL-SBI) Avail: CASI HC A04/MF A01

This report addresses the development of a substitute for conventional lithographic technologies used to fabricate flat panel displays. Conventional technology has several weaknesses: an image field less than 50 mm x 50 mm, a need for expensive projection equipment and precision stepper machines with a positioning accuracy of -0.25 microns and depth of focus of -1 micron; and the necessity to use complicated mask technologies which pollute the environment. Physical Optics Corporation (POC) is developing a new Fourier synthesis lithography technology which will provide a field size of 500 mm x 500 mm without optical distortion or aberration. During Phase I, POC completed an optimization procedure to find the exact harmonic exposure to create the highest edge gradient in a synthetic lithographic pattern. We produced a comprehensive computer model of photoresist multiple exposure, and confirmed it experimentally. We also experimentally confirmed our simulation of the lateral propagation of the development process in photoresist. We completely designed the proposed Fourier synthesis lithographic machine (FSLM). We anticipate that development of this new technology will lead to the construction of a full scale FSLM. DTIC

N95-28932 Southampton Univ. (England).
FIBRE-COUPLED REMOTE OPTICAL VIBROMETRY Final Technical Report, 30 Sep. 1993 - 29 Sep. 1994
Alex Lawrow, Mark Johnson, Henry O. Edwards, and Christopher N. Pannell Oct. 1994 69 p Limited Reproducibility: More than 20% of this document may be affected by microfiche quality
(Grant AF-AFOSR-0406-91)
(AD-A291606; EOARD-TR-95-08) Avail: Issuing Activity (Defense Technical Information Center (DTIC))

This report covers the work performed at the Southampton Optoelectronics Research Center into fibre optic remote vibrometry in the period 1991-1994. A number of instruments have been constructed including a passive homodyne scheme based on 3 x 3 coupler with digital signal processing, a simple lead insensitive heterodyne system employing a single birefringent fibre connecting the probe bead with the processing optics and a scheme using a single frequency fiber laser operating at a wavelength of 1.5 microns as an optical source. In addition we have investigated the effects of noise in the detector circuits and of laser linewidth on the fundamental sensitivity of such vibrometers and have presented the results in terms of effects on minimum detectable phase. The usage of erbium-doped fiber amplifiers (EDFA's) in interferometric sensors of the type used in vibrometry has been considered theoretically. The conclusions are that provided an ASE filter of modest width (of the order of 1 GHz) is used at the output, the use of an EDFA in the signal arm of the interferometer is highly desirable as the low levels of received light will in general make it difficult to get close to shot noise limited detector performance. DTIC

N95-28980# Naval Postgraduate School, Monterey, CA.
DESIGN, DEVELOPMENT AND TESTING OF A PROTOTYPE PRECISION ANGULAR POSITIONING CONTROL SYSTEM FOR A NEXT GENERATION MULTIPLEXED IMAGER M.S. Thesis
Mark E. Middleton Dec. 1994 59 p
(AD-A292585) Avail: CASI HC A04/MF A01

This thesis presents a design for a precision angular position control system for use in a proposed multiplexed imager. The control system is designed to rapidly position a disk to within a tolerance of 2.5 microrad. Evaluation during the design phase shows an inherent trade-off between precision angular positioning and allowed angular velocities. Recommendations are provided for improving the time response of the control system. No testing was performed to determine the actual positioning tolerance. In theory, the control system should have a tolerance of 0.65 microrad with a limiting angular velocity of 37 rpm. DTIC

N95-28983# Sandia National Labs., Livermore, CA.
MEASUREMENT OF ULTRASHORT PULSES WITH A NON-INSTANTANEOUS NONLINEARITY
Kenneth W. DeLong, Celso L. Ladera, Rick Trebino, Bern Kohler (California Univ., San Diego, CA.), and Kent R. Wilson (California Univ., San Diego, CA.) 1995 9 p Presented at the 15th Conference on Lasers and Electro-optics and 5th Quantum Electronics and Laser Science Conference, Baltimore, MD, 21-26 May 1995
(Contract DE-AC04-94AL-85000)
(DE95-006500; SAND-95-8460C; CONF-950540-7) Avail: CASI HC A02/MF A01

We show how non-instantaneous nonlinearities can be used to characterize an ultrashort pulse in an extension of the Frequency-Resolved Optical Gating technique. We demonstrate this principle using the Raman effect in fused silica. DOE

N95-28992# Stanford Univ., CA. Dept. of Electrical Engineering.
LINEWIDTH-INSENSITIVE COHERENT ANALOG OPTICAL LINKS Final Report, Oct. 1991 - Sep. 1994
L. G. Kazovsky, J. Pan, T. K. Fong, R. F. Kalman, and D. J. Sabido Dec. 1994 245 p
(Contract F30602-91-C-0141)
(AD-A292422; RL-TR-94-222) Avail: CASI HC A11/MF A03

This program has analyzed the performance of four classes of links as quantified by spurious-free dynamic range (SFDR), RF power transfer ratio and noise figure, and compared them to conventional detection links. The four classes analyzed were coherent links, optically amplified links, angle modulated links, and combinations of these. Experimental validation of the analysis was accomplished at 2 GHz and is described. The linewidth-insensitive operation in all cases using both semiconductor laser and solid-state Nd:YAG lasers has been demonstrated. DTIC

N95-28996# Naval Surface Warfare Center, Dahlgren, VA.
NONLINEAR CALIBRATION OF AN INFRARED RADIOMETER Final Report
Peter O. Cervenka and Lou Massa Dec. 1994 34 p
(AD-A292436; CARDIVNSWC-TR-94/024) Avail: CASI HC A03/MF A01

At best, the calibration of an infrared radiometer, also known as a Forward Looking Infrared (FLIR) system, is a complex procedure. Effective calibration must (1) be tailored to the actual radiometer being studied; (2) be carried out to each of the many subsystems involved; (3) relate internal system parameters to physical quantities familiar to the infrared community; and (4) be revisited at some interval to ensure that it is still valid. The details of some of the ideas that form the basis for a valid calibration of the GEC Avionics Ltd Dual Waveband Imaging Radiometer FUR are discussed. The need for the removal of a systematic error due to magnification optics emission, as described by Braim, is emphasized. Another systematic error, associated with an analysis of FLIR gray scale response based upon linear interpolation from reference temperatures, is examined. A novel method of nonlinear interpolation is presented that is aimed at the reduction of systematic calibration errors. DTIC

N95-28997# Institute of Electrical and Electronics Engineers, Piscataway, NJ.
CONFERENCE PROCEEDINGS: IEEE NONLINEAR OPTICS, MATERIALS, FUNDAMENTALS, AND APPLICATIONS
29 Jul. 1994 482 p Conference held in Waikoloa, HI, 25-29 Jul. 1994
(AD-A292438) Avail: CASI HC A21/MF A04

Some major topics discussed at this conference include the following: (1) nonlinear organic materials; (2) novel NLO effects; (3) nonlinear frequency conversion; (4) quantum wells and semiconductors; (5) ultrafast spectroscopy; (6) photorefractive applications; and (7) holographic optical storage. DTIC

N95-28998# Washington Univ., Saint Louis, MO.
(DEPSCOR-92) ACQUISITION OF A METALLURGICAL OPTICAL MICROSCOPE Final Report
Dr. Krchnavek 24 Feb. 1995 3 p
(Contract F49620-93-1-0591)
(AD-A292439; AFOSR-95-0115TR) Avail: CASI HC A01/MF A01

This DEPSCoR awards was an equipment grant to acquire a high performance metallurgical microscope with optical imaging analysis capability. The system assembled includes a high-power optical microscope, a visible and infrared (lambda less than 1.6 micrometer)imaging system, computerized analysis of video images, and Michelson and Abbe refractometer components for characterizing optical materials. DTIC

N95-29006# California Univ., Los Angeles, CA. Dept. of Electrical Engineering.
OPTOELECTRONICS BASED ON SiGe/Si HETEROSTRUCTURES Final Technical Report, 15 Jul. 1991 - 14 Oct. 1994
Kang L. Wang 17 Feb. 1995 35 p
(Contract AF-AFOSR-0313-91)
(AD-A292464; AFOSR-95-0153TR) Avail: CASI HC A03/MF A01

The overall objective of the research was to explore SiGe/Si heterostructures for optoelectronics applications. We have extensively investigated intersubband transitions of Si/Ge quantum structures including p-type Si quantum well, n-type Si(110) quantum wells, and n-type Ge(001) quantum wells. We have also studied many-body effects on the intersubband transitions. The application of these transitions for the fabrication of tunable normal incidence infrared detectors has been demonstrated. In the area of optical properties, we have also demonstrated a large Stark shift in type 2 SiGe/Si multiple quantum wells and luminescence from Si(sub m)Ge(sub n) superlattices. In the area of transport properties, we have studied the in-plane mobility of coupled delta doped quantum wells as a function of spacing between the wells. An enhancement of hole mobility above that of the Si was found due to the penetration of wavefunctions into the spacer where the impurity scattering is minimal. In addition to exploration of new devices, alternative growth techniques for achieving the layer thickness to the monolayer scale and doping control were also investigated. In the area of the growth control of SiGe epitaxial layers, we have constructed a gas source molecular beam epitaxy 5 stem. We have investigated the orientation dependence of as beam epitaxy. Selective epitaxy growth on SiO2-masked substrates has been demonstrated. We have also studied the role of surfactants for obtaining high quality coherently strained SiGe epitaxial layers and for providing doping control in quantum wells an superlattices. DTIC

N95-29148# Louisville Univ., KY.
TESTBED FOR PRECISION CHARACTERIZATION OF SPATIAL LIGHT MODULATORS AND OPTICAL PROCESSORS Final Report, 1 Sep. 1993 - 31 Aug. 1994
Robert W. Cohn 30 Sep. 1994 10 p
(Contract DAAH04-93-G-0467)
(AD-A290484; ARO-32402.1-PH-DPS) Avail: CASI HC A02/MF A01

The purpose of this award is to construct a dedicated testbed for the characterization of phase and amplitude modulating properties of spatial light modulators (SLM). The system is specifically a phase shift interferometer configured around a 2000 x 2000 CCD imager to precisely measure the SLM transmittance and diffraction pattern with a resolution in excess of current SLMs. The testbed will be used in current and pending studies. It also has application to a new optical correlation architecture described in a recent patent and journal paper. DTIC

N95-29177# Cognitech, Inc., Santa Monica, CA.
FEATURE-ORIENTED IMAGE RECONSTRUCTION AND AERO-OPTIC METROLOGY IN TURBULENCE Final Report, 1 Jun. - 30 Sep. 1994
Stanley Osher and Leonid Rudin 28 Nov. 1994 9 p
(Contract F49620-94-C-0054)
(AD-A290269; Rept-39; AFOSR-95-0041TR) Avail: CASI HC A02/MF A01

Cognitech researchers have worked with Dr. Brent Ellerbroek of Philips Laboratory on the task of restoring noisy, blurry images which arise in aero-optic metrology. Cognitech's TV and MTV (recently developed by Dr. Rudin) algorithms were applied to Philips supplied data using experimentally obtained point spread functions and various nonlinear noise models. The algorithms were speeded up using an implicit method which allowed the constraints to be enforced for large time marching steps. The results, successfully applied to real images, are displayed. DTIC

N95-29222 Arizona Univ., Tucson, AZ.
DECONVOLUTION OF LATERAL SHEAR INTERFEROGRAMS Ph.D. Thesis
Joseph George Ambrose 1994 126 p
Avail: Univ. Microfilms Order No. DA9424943

This dissertation develops and presents an existing but little known method to provide an exact solution to the wavefront difference equation routinely encountered in the reduction of lateral shear interferograms (LSI). The method first suggested by Dr. Roland Shack treats LSI as a convolution of the wavefront with an odd impulse pair. This representation casts the lateral shear problem in terms of Fourier optics operators and filters with a simplified treatment of the reduction of the LSI possible. This work extends the original proposal applied to line scans of wavefronts to full two-dimensional recovery of the wavefront along with developing the associated mathematical theory and computer code to efficiently execute the wavefront reduction. Further, a number of applications of the wavefront reduction technique presented here are developed. The applications of the filtering technique developed here include optical imaging systems exhibiting the primary aberrations, a model of residual tool marks after fabrication, and propagation of an optical probe through atmospheric turbulence. The computer program developed resides on a PC and produces accurate results to a 1/500 wave when compared to ray traced input wavefronts. The combination of the relatively simple concept providing the basis of the reduction technique with the highly accurate results over a wide range of input wavefronts makes this a timely effort. Finally, the reduction technique can be applied to the accurate testing of aspheric optical components. Dissert. Abstr.

N95-29283 Department of the Navy, Washington, DC.
IN-LINE FIBER ETALON STRAIN SENSOR Patent Application
Jim Sirkis, inventor (to Navy), Marty Putman, inventor (to Navy), Tim Berkoff, inventor (to Navy), Alan Kersey, inventor (to Navy), and Joseph Friebele, inventor (to Navy) 9 Sep. 1994 20 p Limited Reproducibility: More than 20% of this document may be affected by microfiche quality
(AD-D017266; US-Patent-Appl-SN-302013) Avail: Issuing Activity (Defense Technical Information Center (DTIC))

An in-line fiber etalon strain sensor, and method for making the sensor, is disclosed. The in-line fiber etalon strain sensor uses a short segment of silica hollow-core fiber spliced between two cleaved sections of single-mode fiber to form a mechanically robust in-line cavity. In making the sensor, a portion of a protective coating is removed from one end of each of the two cleaved sections of the single-mode fiber to form a bare portion adjacent to a partially reflective end face on each fiber section. The silica hollow core fiber is fabricated to have the same outside diameter as each of the bare portions of the fiber sections. One end of the silica hollow core fiber is then fusion spliced in-line with the partially reflective end face of one of the fiber sections, before the other end of the silica core fiber is fusion spliced in line with the partially reflective end face of the other fiber section to form a cavity within the silica hollow core fiber that is bounded by the two partially reflective end faces. Operation of the in-line fiber etalon is based on interference between the Fresnel reflections from the two glass/air interfaces formed by the cleaved surfaces of the single mode fibers at each end of the hollow core fiber. Strain induced changes result in a concomitant change between the two optical paths. The phase changes can then be demodulated and related to the input strain stimuli. DTIC

N95-29295# Rockwell International Corp., Huntsville, AL. Rocketdyne Div.
PHOTON-COUNTING SPATIAL LIGHT MODULATOR TECHNOLOGY DEVELOPMENT Final Report, Sep. 1992 - Sep. 1994
Richard B. Holmes and Jeffrey H. Hunt 30 Oct. 1994 76 p
(Contract F49620-92-C-0064; DARPA Order 8961)
(AD-A292619; RI/RD95-106; AFOSR-95-0149TR) Avail: CASI HC A05/MF A01

The goal of this program is to measure and improve the performance of photon-counting spatial light modulators operating in an optically-addressed reflection mode. Experimental results are obtained for silicon devices. These device consists of an avalanche photodiode (APD) operated in the Geiger mode with the front and back surface of the diode forming an asymmetric Fabry-Perot cavity. The phase delay within the cavity is modified directly by the avalanche via the free-carrier refractive index or by Joule heating. Experiments were conducted first with the write laser beam at 1064 nm and the read beam at the same wavelength and second with the write beam at 850 nm and the read beam at 1300 nm. The device differs qualitatively from other approaches such as smart pixels by virtue of its photon-counting sensitivity its low cost and its ability to form a spatially-coherent read-out wavefront. DTIC

N95-29354# Defence Research Establishment Ottawa, Ottawa (Ontario).
A COMPARISON OF THREE PEDESTAL REMOVAL TECHNIQUES FOR AN OPTICAL TIME-INTEGRATING CORRELATOR
N. Brousseau and J. W. Salt Dec. 1994 26 p
(AD-A290092; DREO-TN-94-16) Avail: CASI HC A03/MF A01

The correlation peak produced by a time-integrating optical correlator appears on a pedestal. It is advantageous to remove this pedestal to allow the detection of the peak by a simple thresholding operation. This technical note presents two new techniques developed and tested at DREO to remove the pedestal. The new methods are compared for speed and accuracy with the conventional method and experimental results are presented. DTIC

N95-29366*# Louisiana State Univ., Baton Rouge, LA. Dept. of Mechanical Engineering.
AN INTEGRATED OPTICAL CO2 SENSOR. PHASE 0: DESIGN AND FABRICATION OF CRITICAL ELEMENTS Final Report
Michael C. Murphy, Kevin W. Kelly, B. Q. Li, En Ma, Wanjun Wang, Yuli Vladimirsky, and Olga Vladimirsky Dec. 1994 18 p
(Contract NCC2-5055)
(NASA-CR-198792; NAS 1.26:198792) Avail: CASI HC A03/MF A01

Significant progress has been made toward all of the goals for the first phase of the project short of actual fabrication of a light path. Two alternative approaches to fabricating gold mirrors using the basic LIGA process were developed, one using electroplated solid gold mirrors and the second using gold plated over a nickel base. A new method of fabrication, the transfer mask process, was developed and demonstrated. Analysis of the projected surface roughness and beam divergence effects was completed. With gold surface with low surface roughness scattering losses are expected to be insignificant. Beam divergence due to diffraction will require a modification of the original design, but should be eliminated by fabricating mirrors 1000 mu m in height by 1000 mu m in width and using a source with an initial beam radius greater than 300 mu m. This may eliminate any need for focusing optics. Since the modified design does not affect the mask layout, ordering of the mask and fabrication of the test structures can begin immediately at the start of Phase 1.
Derived from text

N95-29379# Rochester Univ., NY. Lab. for Laser Energetics.
OPTICALLY TRIGGERED, SUPERCONDUCTING OPENING SWITCH Final Report
William R. Donaldson and Alan M. Kadin 1994 28 p
(Contract N00014-92-J-1993)
(AD-A292642) Avail: CASI HC A03/MF A01

The advent of high-temperature superconductors (HTS) introduced the possibility of a new class of opening switches. The switches exploit the dramatic change in material properties at the critical temperature, Tc, in the HTS materials. The transition to the normal state can form the basis of an opening switch. Since this phase transition is fully reversibie, the switch can be operated repetitively. Such devices could switch currents in the range of a few kA with switching time of the order of nanoseconds. We have developed and tested two types of opening switches based on HTS materials: a photoresistive switch and an inductively coupled switch. Each switch was demonstrated at low power levels and subsequently scaled up to power levels corresponding to tens of amperes current interruption. DTIC

N95-29412# Silicon Mountain Design, Inc., Colorado Springs, CO.
AN ULTRA-HIGH SPEED INCOHERENT-TO-COHERENT CONVERTER FOR OPTICAL COMPUTING Monthly Status Report, 1-31 Dec. 1994
David W. Gardner 28 Dec. 1994 5 p
(Contract N00014-94-C-0241)
(AD-A292658) Avail: CASI HC A01/MF A01

Many optical computing problems are centered around the processing of incoherent images. These images may be conventional visible light such a's those taken with a CCD imager or camcorder. They may also take the form of infrared images in the case of missile seekers or x-ray images from medical or other sources. For optical processing, these images must be converted to either phase or amplitude modulated coherent light. This is typically accomplished by electronically feeding the originally captured image into a spatial light modulator (e.g., liquid crystal or deformable mirror array) and modulating a coherent reference beam with the 2 dimensional data pattern. DTIC

N95-29543 Colorado Univ., Boulder, CO.
PASSIVE RANGING WITH AN INCOHERENT OPTICAL SYSTEM Ph.D. Thesis
Edward Raymond Dowski, Jr. 1993 168 p
Avail: Univ. Microfilms Order No. DA9423480

This work introduces a new system for single-lens, incoherent, passive ranging. The only a priori object information this system requires is that the object to be ranged must possess at least a low-pass spatial frequency profile. Physically, this system for passive ranging is a standard optical imaging system that has been customized with a special-purpose optical mask or filter. Analytically, this optical mask customizes the optical system in such a way that objects will form images that contain range-dependent information that can be extracted after sampling of the image. The optical mask codes complex electromagnetic range information, available at the lens, into spatial information, available at the image. This spatial range-dependent information can then be decoded by processing the image. In theory, this type of passive ranging system can yield estimated object ranges over a system-dependent spatial grid, essentially forming a three-dimensional image. This ranging system requires only a single-lens, incoherent optical system, as well as only a single image. We derive a formulation for this ranging system and show examples of masks that can be used for passive ranging. Range detection and estimation algorithms are given, and the theoretical range accuracy obtainable is described. In addition, we give results of our proof-of-concept passive ranging experiments that validate our theories. We finish with an outline of future directions for research in passive ranging system. Dissert. Abstr.

N95-29553# North Carolina Agricultural and Technical State Univ., Greensboro, NC.
HIGH GAIN, LOW NOISE AND BROADBAND RAMAN AND BRILLOUIN FIBER-OPTIC AMPLIFIERS, CHANNEL SELECTORS AND SWITCHES Interim Technical Report, 15 Jul. 1993 - 14 Jul. 1994
Chung Yu 12 Sep. 1994 29 p
(Contract DAAL03-91-G-0301)
(AD-A290585; ARO-28653.1-EL-SAH) Avail: CASI HC A03/MF A01

Stimulated Brillouin and Raman scattering has been studied at 10.6 micrometers wavelength in fibers without much success due to the lack of low-loss, single-mode fibers and lasers with sufficiently narrow linewidth. The Brillouin based technology has advanced significantly with the advent of low-loss, single-mode fibers at 1.55 and 1.310 micrometers wavelengths. Conclusive experimental evidence points to the narrowband nature of Brillouin amplifiers, and redirects interest in their application to sensor and switching applications. Both stimulated Brillouin backscattering and guided acoustic wave forward scattering have been observed in fibers and are being explored for practical application as sensors to be bonded to or embedded in structures to monitor structural integrity. The stimulated Brillouin fiber ring laser is also being studied for its optical switching capabilities. The capability of this unique sensing mechanism is demonstrated in this report. DTIC

N95-29560# Ohio State Univ., Columbus, OH. Dept. of Physics.
THEORIES OF THE NONLINEAR OPTICAL PROPERTIES OF COMPOSITE MEDIA: APPLICATIONS TO PHTHALOCYANINE DYES Final Report, 1 Jun. 1992 - 31 Jan. 1994
David G. Stroud 18 Oct. 1994 9 p
(Contract DAAL03-92-G-0263)
(AD-A290640; ARO-30108.1-MS) Avail: CASI HC A02/MF A01

This report describes the results of a theoretical investigation into the nonlinear optical response of granular composites. In particular, we have investigated the degree to which the cubic nonlinear response can be enhanced in such composites, relative to the same response in pure materials. Cubic nonlinear response is potentially of great practical importance in developing novel materials with a strongly intensity-dependent transmission coefficient, index of refraction, etc. We find that there are many types of composite geometries which give rise to such strong enhancements. These include composites near the percolation threshold, composites in which one of the components is arranged in the form of a fractal cluster, and nonlinear coatings (such as dyes) adsorbed onto the surface of particles which have a resonant optical response at an appropriate

frequency. We have carried out this investigation using both analytical approximations and a variety of approximate numerical techniques, including large-scale computer simulations. Finally, we briefly describe some work in progress, in which a composite composed of materials with a purely guardratic response can exhibit an enhanced curbic response. DTIC

N95-29571# Department of the Air Force, Wright-Patterson AFB, OH. National Air Intelligence Center.

APPLIED OPTICS LABORATORY

Guoguang Tian and Daheng Wang 22 Dec. 1994 9 p Transl. into ENGLISH from Zhongguo Kexueyuan Yuoukan (China), v. 3, no. 4, 1988 p 367-368

(AD-A292006; NAIC-ID(RS)T-0409-94) Avail: CASI HC A02/MF A01

The major directions of research of this lab will be transport, transformation, processing, receiving and display of information in modern optics, optical calculation and optical processing of non-optical signals. Main research contents include the following: (1) Optical design and image quality evaluation; (2) Optical super-fine processing and measurement technology; (3) Optical calculation technology; (4) Imaging spectral technology; (5) Color vision and robot vision; (6) Optical information processing and holographic interference technology; and (7) Short wave optical technology. DTIC

N95-29602 Office of Naval Research, Arlington, VA.

VARIABLE RATE OPTICAL ITERATIVE PROCESSING OF OPTICAL INFORMATION Patent Application

Sonlink N. Ohuvan, inventor (to Navy) and Nicholas P. Caviris, inventor (to Navy) 20 Dec. 1994 10 p Filed 20 Dec. 1994 Limited Reproducibility: More than 20% of this document may be affected by microfiche quality

(AD-D017397; Navy-Case-73922; US-Patent-Appl-SN-359757) Avail: Issuing Activity (Defense Technical Information Center (DTIC))

Two-dimensional image data is transferred by a delay module through an optical ring to a subsequent optical data processor at a controlled cyclic processing rate varied to operationally match such data processor. Cyclic processing of the input image data is performed within-the optical ring by rotational reorientation or scaling of the image data. DTIC

N95-29630 Maryland Univ., College Park, MD.

PHOTOTHERMAL DEFLECTION IN A SUPERCRITICAL FLUID Ph.D. Thesis

Matthew E. Briggs 1993 208 p

Avail: Univ. Microfilms Order No. DA9425002

We have measured and calculated the response of supercritical xenon in a collinear photothermal deflection apparatus. Such an apparatus uses optical methods to measure the thermal energy dissipated by optical absorption in a sample. The diverging coefficient of thermal expansion of a supercritical fluid is found to provide a means for a dramatic increase in the sensitivity of this technique. By using a supercritical fluid close to the critical point as the sensing fluid in a calibrated surface-absorption measurement, we find that a signal-to-noise of one in our apparatus corresponds to an absorptance of 10(exp -10). Previously, the most sensitive photothermal techniques had noise-floors of about 2 x 10(exp -7). The response of a supercritical sensing fluid is also measured in a bulk-absorption measurement, and again the increase in sensitivity is dramatic, with a noise-floor corresponding to 10(exp -13) cm(exp -1), compared with 10(exp -8) cm(exp -1) for work with normal fluids. We take advantage of the increased surface-absorption sensitivity to measure the smallest absorption yet reported from a surface, approximately 10(exp -5) for super-polished surfaces of sapphire and fused silica, and similar levels for the best available antireflection coatings deposited on these surfaces. Bulk-absorption levels in xenon are measured to be approximately 2 x 10(exp -6) cm(exp -1), putting it among the most transparent of fluids. We provide an understanding of the physics of the fluid response, and a formalism from which to calculate expected signal levels, by adapting the existing theory for the response of a collinear photothermal deflection apparatus to accommodate the thermal properties of a supercritical fluid. A no adjustable-parameter calculation of the expected signal-levels is made with the resulting expressions, and is found to agree with the data to within the uncertainty of +/- 50 percent, tracking the changing fluid properties as the critical point is approached. Dissert. Abstr.

N95-29646# RGB Associates, Inc., Wayland, MA.

UNCONVENTIONAL IMAGE RECOVERY TECHNIQUES Final Report, 1 Aug. 1992 - 31 Jul. 1994

Richard Barakat 20 Sep. 1994 34 p

(Contract DAAL03-92-C-0045)

(AD-A290799; ARO-30606.1-MA-SDI) Avail: CASI HC A03/MF A01

The main theme of this contract is the development of unconventional imaging techniques. The imaging methods advocated result in complicated nonlinear relations between the object and its image, inversion techniques are required to translate the measured data into a meaningful estimate of the object. Although these methods require a large amount of computation, they are relatively cheap compared to the costs of large aperture optical systems. The technical approach is two-fold: first, development of the theory of the unconventional imaging scenario in question; second, adaption of the latest techniques from numerical analysis to carry out the inversion from measured data to reconstructed object. One problem was completed and written up for publication: Inversion of the modulus and phase of a coherently illuminated object from its measured diffraction image. This constitutes the main body of the report along with representative numerical calculations. The inversion techniques developed here should be of great use in various biomedical imaging techniques and could result in replacing phase contract microscopy. DTIC

N95-29661# Air Force Systems Command, Wright-Patterson AFB, OH. National Air Intelligence Center.

INTENSITY OPTICAL CORRELATION THROUGH OPTICAL DIFFERENTIATION PREPROCESSING

Wenshang Chen, Zhaoqi Wang, and Gouguang Mu 22 Dec. 1994 13 p Transl. into ENGLISH from Zhongguo Jiguang, China, v. 18, no. 9, Sep. 1991 p 697-701

(AD-A291020; NAIC-ID(RS)T-0391-94) Avail: CASI HC A03/MF A01

A high discrimination intensity optical correlation system is presented in this article. By using a lenseless special differentiation filter to achieve edge enhancement for the input images, the discrimination of the intensity optical correlator with the Fresnel holographic filter is improved. Theoretical analysis and experimental demonstration are given. DTIC

N95-29706 Arizona Univ., Tucson, AZ.

ATMOSPHERIC WAVEFRONT SENSING AND CORRECTION INCLUDING THE STELLAR PHASE SHIFTING INTERFEROMETER Ph.D. Thesis

Dnardo Colucci 1993 190 p

Avail: Univ. Microfilms Order No. DA9421776

Because atmospheric turbulence causes distortions in stellar wavefronts, passive ground based telescopes, no matter how large, are limited to the resolution limit of a 0.1-0.2 m aperture when imaging in the visible. If the new class of large aperture (10 m) telescopes is to reach its resolution potential, adaptive optics must be employed to compensate for the atmospheric wavefront distortions. Vital to an adaptive optics system is the ability to accurately sense the distorted wavefront. Two new methods for wavefront sensing show great promise for the field of adaptive optics. A reflective hybrid of the traditional Shack-Hartmann wavefront sensor has produced near diffraction limited imaging with the Multiple Mirror Telescope, a hexagonal array of six, 1.83 m mirrors. It is also directly applicable to filled aperture telescopes. Another wavefront sensor, the stellar phase shifting interferometer, has produced for the first time ever direct phase map measurements of atmospherically distorted wavefronts. The ability to directly measure the phase of the wavefront at each detector pixel paves the way for a new generation of light efficient and accurate wavefront sensors for adaptive optics. Dissert. Abstr.

N95-29766# Imperial Coll. of Science and Technology, London (England).

LOW ORDER ADAPTIVE OPTICAL SYSTEMS Final Report, 1 Sep. 1993 - 31 Aug. 1994

J. C. Dainty and A. Koryabin 4 Jan. 1995 37 p

(AD-A291121; EOARD-TR-95-03) Avail: CASI HC A03/MF A01

This report presents the evaluation results of the performance of a bimorph piezoelectric mirror supplied by the International Laser Center. The first part describes the spatial modes of the mirror, their linearity, hysteresis and their temperature dependence. The next part describes the dynamic behavior. The final part of the report presents results of the

performance of a simple adaptive optical system for imaging through laboratory generated turbulence. The mirror and system might be suitable for low order correction in a 1m-class telescope. DTIC

N95-29867# Optical Society of America, Washington, DC.
DIFFRACTIVE OPTICS: DESIGN, FABRICATION, AND APPLICATIONS Final Report
David W. Hennage Dec. 1994 369 p
(Contract DAAH04-94-G-0080)
(AD-A290942; ARO-32828.1-PH-CF) Avail: CASI HC A16/MF A03

This document contains summaries of papers presented at the Topical Meeting, Diffractive Optics: Design, Fabrication, and Applications , June 6-9, 1994, at Rochester, New York. DTIC

N95-29910# International Society for Optical Engineering, Bellingham, WA.
OCEAN OPTICS XII
Jules S. Jaffe, ed. 15 Jun. 1994 1024 p Presented at SPIE, Bergen, Norway, 13-15 Jun. 1994
(AD-A286734) Avail: CASI HC A99/MF A10

Partial contents include the following: (1) fiber optics; (2) optical instrumentation; (3) biooptical variability; (4) optical properties of water; (5) coastal regions; and (6) light detection and ranging (LIDAR). DTIC

N95-29969# Air Force Systems Command, Wright-Patterson AFB, OH. National Air Intelligence Center.
PHOTOREFRACTIVE Bi12SiO20 SPATIAL LIGHT MODULATOR
Mingjun Zhao, Yulin Li, and Zhao Wang 29 Dec. 1994 12 p Transl. into ENGLISH from Guangxue Xuebao, China, v. 11, no. 9, Sep. 1991 p 810-814
(AD-A291070; NAIC-ID(RS)T-0389-94) Avail: CASI HC A03/MF A01

We used home-made photorefractive crystal Bi12SiO20 as a real-time non-degenerate and degenerate four-wave mixing medium to accomplish conversion from incoherent to coherent, wave length conversion, and image subtraction between coherent and incoherent image. The experimental results are presented in this paper. DTIC

N95-29973# Oklahoma State Univ., Stillwater, OK.
SENSOR PROTECTION PORTION OF THE DEVELOPMENT OF NONLINEAR OPTICAL MATERIALS AND PROCESSES FOR LASER HARDENING OF SENSORS Final Report, 1 Jan. 1992 - 31 Mar. 1993
Jin-Joo Song 31 Oct. 1994 66 p
(Contract DAAB07-88-C-F407; ARPA Order 6324)
(AD-A291200; NV-94-C11) Avail: CASI HC A04/MF A01

Nonlinear optical properties of several lead galliate glasses, CdMnTe and CdMnSe semiconductors, and SBN photorefractive crystals were studied in nanosecond and picosecond time regimes. Optical limiting characteristics of lead galliates were investigated as a function of the material properties, device geometries and incident wavelengths. Broad band clamping was observed under nanosecond illumination. Nonlinear absorption and refraction in semiconductors were studied in the picosecond time regimes. A saturation in the nonlinear refraction at high input intensities were observed which may hinder applicability of these materials as picosecond optical limiters. Picosecond and subpicosecond photorefractive properties of SBN crystals revealed that in addition to the photorefractive behavior, this material exhibited induced absorption by retrapped pump generated carriers. DTIC

N95-29974# Rockwell International Corp., Canoga Park, CA. Rocketdyne Div.
INORGANIC HALOGEN OXIDIZERS Final Report, 1 Jun. 1991 - 31 Aug. 1994
K. O. Christe and W. W. Wilson 23 Sep. 1994 305 p
(Contract DAAL03-91-C-0025)
(AD-A291201; RI/RD94-271) Avail: CASI HC A14/MF A03

A research program was carried out in novel energetic materials. This program was highly successful and resulted in 28 major publications. Highlights of this effort include: the characterization of the XeF5(-) anion which is the first example of a pentagonal planar XY5 structure, completion of our work on a quantitative oxidizer strength scale, the synthesis and characterization of new compounds at the limits of coordination and oxidation, such as XeOF5(-), TeOF6(2-), IOF6(-), IF8(-), TeF8(2-), TeF7(-), and XeF7(+), the study of fluxionality and steric repulsion effects in hexa- and hepta-coordinated species, such as IF7, HPF5(-), HSF5, and IOF5, the controlled replacement of two fluorine ligands by one doubly bonded oxygen ligand, studies of the thermal instability of NF5 and the F3(-) anion, the characterization of the N2F(+) cation N(CH3)4N3, H2N3(+) cation and the SF4(-) and SOF4(-) radical anions, the synthesis and characterization of a new Os(+VIII) compound, OsF4O2, theoretical studies on ONOF and a new family of polynitrogen compounds, the synthesis and characterization of the novel PF4(-) anion and it hydrolysis products, and the electrophilic fluorination of CH4 with F(+) equivalent N2F(+) and NF4(+) salts. DTIC

N95-29978# SRI International Corp., Menlo Park, CA.
InTISb AS A LONG-WAVE INFRARED (LWIR) MATERIAL: DEFECTS AND TRANSPORTATION PROPERTIES Final Report, 19 Apr. 1993 - 14 Jan. 1995
S. Krishnamurthy, M. VanSchilfgaarde, M. A. Berding, and A. Sher Feb. 1995 67 p
(Contract N00014-93-C-0091)
(AD-A291218) Avail: CASI HC A04/MF A01

We have evaluated three 3-5 semiconductor alloys as possible candidates for future long-wave infrared (LWIR) detector materials. The cohesive energies, elastic constants, band structures, electron mobilities, and phase diagrams are calculated and are compared to those of Hg(1-x)Cd(x)Te (MCT) alloys. All three of these 3-5 alloys have their band gap change from negative to positive values as the alloy composition x decreases from 1 to 0. The x values for the 0.1-eV gap are estimated to be 0.67,0.15, and 0.08, respectively, for ITP, ITA, and ITS. While ITP and ITA form stable zincblende solid solutions for all alloy compositions, zincblende ITS is stable only for a range of x less than 0.15. ITP and ITA have considerably larger cohesive energies and elastic constants than does MCT, indicating that they are structurally robust. At a 0.1 -eV gap, the band structures near the gap and the electron mobilities in ITP, ITA, and ITS are also found to be comparable to those of MCT. Because the lattice constants of ITP and ITA are less than 2% larger than the respective values in InP and InAs, the latter should provide natural substrates for the growth of active LWIR alloys. DTIC

N95-30035*# District of Columbia Univ., Washington, DC. Dept. of Engineering and Technology.
HIGH Tc SUPERCONDUCTING BOLOMETRIC AND NONBOLOMETRIC INFRARED (IR) DETECTORS Annual Report, 1994-1995
Samuel Lakeou 1995 26 p
(Grant NAG5-2348)
(NASA-CR-198789; NAS 1.26:198789) Avail: CASI HC A03/MF A01

Activities carried out during the reporting period are summarized. The workplan for the period August 1994 to August 1995 included the following: (1) expansion of the Applied Superconductivity Laboratory to include stand-alone optical response and noise measurement setups; (2) study the low frequency excess electrical noise in YBCO films; and (3) enhancement of the academic support component of the project through increased student and faculty participation. Abstracts of papers submitted for publication during this reporting period are included as attachments. CASI

N95-30053# Department of the Navy, Washington, DC.
SHOCK RESISTANT OPTIC FIBER ROTARY SLICE HOLDING DEVICE Patent Application
Daniel D. Thomas, inventor (to Navy), Sara M. Leite, inventor (to Navy), Gair D. Brown, inventor (to Navy), and Alan Schwarting, inventor (to Navy) 22 Nov. 1994 9 p
(AD-D017327; US-Patent-Appl-SN-345716) Avail: CASI HC A02/MF A01

Rotary mechanical splices between axially aligned optic fibers are seated in axial confinement within bays indented into the shock absorbing body of a holding tray. A retention lid, positioned on the tray covers the splice seating bays and guide slots extending therefrom within which the optic fibers are received to provide cushioned confinement for the splices and resist relative bending of the fibers. DTIC

N95-30054# Technische Univ., Delft (Netherlands).
MODAL ANALYSIS OF STRAIGHT AND CURVED INTEGRATED OPTICAL WAVEGUIDES: AN INTEGRAL EQUATION APPROACH Ph.D. Thesis
H. J. M. Bastiaansen 20 Dec. 1994 236 p Prepared in cooperation

with PTT Research
(PB95-197265; ISBN-90-72125-41-X) Copyright Avail: CASI HC A11/MF A03

In this thesis, a mathematically rigorous method is presented for the determination of the light-guiding properties of the elementary building blocks of integrated optical components: the straight and circularly curved, planar and channel waveguides. The thesis consists of six chapters. Chapter 1 contains a general introduction into the world of optical communications, followed by the presentation of the mathematical equations describing the propagation of electromagnetic waves. Furthermore, the aim of this thesis is outlined in more detail. The source-type integral equation method is considered in Chapter 2 to Chapter 5. In each chapter, a mathematical derivation of the method is given, the numerical implementation is described and numerous numerical examples are presented. Each of these chapters considers a specific waveguide configuration. The complexity of the configuration to which the source-type integral equation analysis is applied, increases through the successive chapters. Finally, a number of conclusions for the source-type integral equation method are presented in Chapter 6. NTIS

N95-30062# Kent Univ., Canterbury (England).
INVESTIGATION OF OPTICAL DAMAGE, ENERGY PARTITIONING AND SCALING LAWS AT EXTREMELY HIGH VELOCITIES Contract Report, Aug. 1993 - Aug. 1994
J. A. McDonnell, P. R. Ratcliff, L. Kay, D. H. Niblett, and M. J. Burchell Oct. 1994 115 p
(Contract F49620-93-1-0487)
(AD-A291368; AFOSR-95-05TR) Avail: CASI HC A06/MF A02

Optical damage assessment is presented from analysis of retrieved space damaged material (solar cell arrays); results, show a peak in the space environment damage effects in millimetre region and a dominance by meteoroids in this region. Impact damage features on glass will be folded with the results of the energy partitioning which derive from the unique 2 MV Van de Graaff facility achieving (in this report) velocities of up to 42 km/sec. Results from experimental campaigns incorporating simultaneous measurement of impact plasma, impact light flash and momentum enhancement provide new data on the fundamental features of energy partitioning in hypervelocity impacts phenomena such as ejecta momentum and kinetic energy, plasma and vapour production, and light flash energies. Hydrocode simulations are also described, which give insight into energy partitioning. Results from a study of the impact light flash are presented which have proven principles of the prototype chamber design. Results which complement the energy partitioning data obtained from the plasma studies show readily the sensitivity of this technique as a study tool on the Van de Graaff facility. DTIC

N95-30064# Air Force Systems Command, Wright-Patterson AFB, OH. National Air Intelligence Center.
DISTORTION-INVARIANT OPTICAL PATTERN RECOGNITION BY CORRELATIVE MATRIX FEATURE CRITERION
Yang Baotang and Lan Zhengping 29 Dec. 1994 12 p Transl. into ENGLISH from Guangxue Xuebano, v. 12, no. 1, Jan. 1992 p 52-56
(AD-A291389; NAIC-ID(RS)T-0387-94) Avail: CASI HC A03/MF A01

In this paper, we used correlative matrix as a feature criterion in K-L transformation for feature compression, and then the synthetic matched filter (SMF) was prepared by means of the synthetic discriminant function (SDF). This method can effectively reduce the size of feature image. By this fiber, the shift, scale and rotation in variant optical pattern recognition was realized with a high signal noise ratio of correlation output. DTIC

N95-30076# Department of the Navy, Washington, DC.
SELECTIVE MULTI-CHEMICAL FIBER OPTIC SENSOR Patent Application
Jasbinder Sanghera, inventor (to Navy), Pablo C. Pureza, inventor (to Navy), Ishwar D. Aggarwal, inventor (to Navy), and Gregory Nau, inventor (to Navy) 31 Oct. 1994 26 p
(AD-D017409; US-Patent-Appl-SN-332294) Avail: CASI HC A03/MF A01

A fiber optic sensor for detecting at least one chemical by evanescent wave spectroscopy comprises a generator of a light signal, a mirror for introducing the light signal into a fiber, a clad optical chalcogenide glass fiber, a mirror for directing the light signal from the fiber into a detector, and a detector for detecting chemicals by the fiber. The fiber comprises a core and a clad having lower refractive index than the core enveloping and being in continuous contact with the core, at least one region on the fiber completely or partially devoid of the clad, and a polymer disposed in the region having affinity for the chemical(s). There being a different polymer in each region if there is more than one region. DTIC

N95-30081# Kings Coll., London (England). Dept. of Physics.
DIFFRACTION LIMITED IMAGING USING ABERRATED OPTICS Final Report, 2 Jul. 1992 - 30 Jun. 1994
D. A. Fish and E. R. Pike Sep. 1994 44 p
(Contract DAAL03-92-G-0142)
(AD-A290912; ARO-30390.1-MA-SDI) Avail: CASI HC A03/MF A01

Researchers have introduced a scanning method for SVD reconstruction of images. This method removes the blocking effects that would normally be associated with a reconstruction by parts. It is also vastly superior in terms of computation speed as compared with conventional SVD. The method is also applicable to the case of spatially varying blurs. The results have shown that the blocking effects are removed to a tolerable level with the scanning technique, and good constructions can be obtained with large complex images containing noise. To show the potential for the reconstruction of images formed with a spatially variant PSF and approximate method using Fourier transforms was shown. This introduced artifacts into the reconstruction which were controlled by use of a regularization parameter. An example reconstruction has been shown for an SVD reconstruction which is more accurate than the Fourier method, but far slower in computational speed. DTIC

N95-30166 Department of the Navy, Washington, DC.
METHOD OF MEASURING LIQUID LEVEL WITH A THERMAL INTERFACE DETECTION Patent
Lloyd C. Bobb, inventor (to Navy) 22 Nov. 1994 10 p Filed 24 Nov. 1993
(AD-D017341; US-Patent-5,367,175; US-Patent-Appl-SN-159962; US-Patent-Class-250-577) Avail: US Patent and Trademark Office

A method of measuring the position of a liquid surface within a vessel is described. An optical fiber is provided which has first and second ends and has an energy-absorbing element of a predetermined length disposed upon a portion of the cladding thereof such that there is a thermal interface between the energy-absorbing element and the cladding. The optical fiber is then positioned in the vessel that the energy-absorbing element disposed thereon extends a known distance into the vessel along a known depth gradient of the vessel and so that the energy-absorbing element will intersect the liquid surface over the anticipated range of positions thereof. DTIC

75 PLASMA PHYSICS

Includes magnetohydrodynamics and plasma fusion.

For ionospheric plasmas see *46 Geophysics*. For space plasmas see *90 Astrophysics*.

N95-29001# California Univ., Irvine, CA.
HIGH POWER, HIGH FREQUENCY RADIATION FROM BEAM-PLASMA INTERACTIONS Final Progress Report
Gregory Benford 26 May 1994 30 p
(Contract AF-AFOSR-0255-90)
(AD-A292442; AFOSR-95-0117TR) Avail: CASI HC A03/MF A01

The attached papers sum up our program's research for the last inclusive funding period. This is the final report. DTIC

N95-29003# New Mexico Univ., Albuquerque, NM.
HBCU/MI INSTRUMENTATION FOR THE PULSED POWER PLASMA SCIENCES LABORATORY AT THE UNIVERSITY OF NEW MEXICO, FY92-93 Final Technical Report
Edi Schamiloglu, Charles Fledderman, John Gahl, and Donald Shiffler 30 Nov. 1994 14 p
(Contract F49620-93-1-0585)
(AD-A292444; AFOSR-95-0165TR) Avail: CASI HC A01/MF A01

The Pulsed Power & Plasma Science Laboratory at the University of New Mexico (UNM) is pleased to have equipped its laboratory with modern instrumentation in support of its AFOSR-funded program on high power

microwave sources. The instrumentation acquired can be broken broadly into three categories: (1) microwave measurement/calibration (network analyzer and components); (2) data acquisition (digital oscilloscopes, computers, LabView); and (3) high vacuum capabilities (turbo pumps, residual gas analyzer). This report describes the instrumentation and how it is used in support of the research program. DTIC

N95-29011# Washington Univ., Seattle, WA. Aerospace and Energetics Research Program.
DEVELOPMENT OF A TRANSIENT INTERNAL PROBE DIAGNOSTIC Final Report, 15 Oct. 1992 - 14 Oct. 1994
Thomas R. Jarboe and Arthur T. Mattick 16 Dec. 1994 42 p
(Contract F49620-93-1-0025)
(AD-A292470; AFOSR-95-0126TR) Avail: CASI HC A03/MF A01

A research effort was carried out to develop and test key components of the transient internal probe, a diagnostic tool for measuring internal magnetic fields in a plasma. A gasdynamic sabot separation method was developed for discarding the sabot upstream of the plasma. Separation is effected in a vented 50-caliber gun barrel, and the sabot is deflected upstream of the plasma, reliably removing the sabot without disrupting the probe trajectory. A vacuum interface was constructed to isolate the plasma from gun gases, which uses a very fast trap-door valve to prevent gas from entering the plasma chamber. A full-up test of the diagnostic was made using a 2.2 km/sec probe to measure a static field in a vacuum. This yielded excellent agreement with Hall probe measurements, with a resolution of 20 Gauss, and the gun gas entering the measurement chamber is to be acceptably small for application to plasma devices. DTIC

N95-29130*# Iowa Univ., Iowa City, IA. Dept. of Physics and Astronomy.
SOLAR SYSTEM PLASMA WAVES
Donald A. Gurnett 1995 42 p
(Contracts NAS9-59193; NAS9-58779)
(NASA-CR-198767; NAS 1.26:198767) Avail: CASI HC A03/MF A01

An overview is given of spacecraft observations of plasma waves in the solar system. In situ measurements of plasma phenomena have now been obtained at all of the planets except Mercury and Pluto, and in the interplanetary medium at heliocentric radial distances ranging from 0.29 to 58 AU. To illustrate the range of phenomena involved, we discuss plasma waves in three regions of physical interest: (1) planetary radiation belts, (2) planetary auroral acceleration regions and (3) the solar wind. In each region we describe examples of plasma waves that are of some importance, either due to the role they play in determining the physical properties of the plasma, or to the unique mechanism involved in their generation.
Author

N95-29205 Utah State Univ., Logan, UT.
A MONTE CARLO SIMULATION OF COULOMB COLLISIONS AND WAVE-PARTICLE INTERACTIONS IN SPACE PLASMA AT HIGH LATITUDES Ph.D. Thesis
Imad Ahmad Barghouthi 1994 161 p
Avail: Univ. Microfilms Order No. DA9423091

In study 1, a Monte Carlo simulation was used to investigate the behavior of O(+) ions that are E x B-drifting through a background of neutral O, with the effect of O(+) (Coulomb) self-collisions included. Wide ranges of the ion-to-neutral density ratio n(sub i)/n(sub n) and electrostatic field E were considered in order to investigate the change of ion behavior with respect to the solar cycle and altitude. For low altitudes and/or solar minimum (n(sub i)/n(sub n) less than or equal to 10(exp -5)), the effect of self-collisions is negligible. For higher values of n(sub i)/n(sub n), the effect of self-collisions becomes significant and, hence, the non-Maxwellian features of the O(+) distributions are reduced. In study 2, the steady-state flow of the polar wind protons through a background of O(+) ions was studied. The Fokker-Planck expression was used to represent H(+)-O(+) Coulomb collisions. The transition layer between the collision-dominated and the collisionless regions plays a pivotal role in the behavior of the H(+) flow. In the transition region, the shape of H(+) distribution changes in a complicated manner from Maxwellian to 'kidney bean.' The flow also changes from subsonic to supersonic within the transition region. The heat fluxes of parallel and perpendicular energies change rapidly from their maximum (positive) to their minimum (negative) values within the same transition region. In study 3, a Monte Carlo simulation was developed in order to study the effect of the wave-particle interactions (WPI) on O(+) and H(+) ions outflow in the polar wind. The simulation also considered the other mechanisms included in the classical polar wind studies such as gravity, polarization electrostatic field, and divergence of geomagnetic field lines. Also, an altitude dependent wave spectral density was adopted. The main conclusions are (1) the O(+) velocity distribution develops conic features at high altitudes; (2) the O(+) ions are preferentially energized; (3) the escape flux of O(+) increased by a factor of 40, while the escape flux of H(+) remained constant; (4) including the effect of a finite ion Larmor radius produced toroidal features for O(+) and H(+) distributions at higher altitudes. In study 4, a comparison between the effect of WPI on H(+) and O(+) ion outflow in the polar wind and in the auroral regions was studied. It was concluded that (1) O(+) is preferentially energized in both regions; (2) both ions (H(+) and O(+)) are more energetic in the auroral region at most altitudes; (3) in the auroral region, the ion conics formed at lower altitudes, at 1.6 Re, for O(+) and 2.5 Re for H(+), while in the polar wind H(+) did not form conics and O(+) formed conics at high altitudes; (4) the effects of body forces are more important in the polar wind than in the auroral region, and for O(+) than H(+).
Dissert. Abstr.

N95-29215 California Univ., Los Angeles, CA.
A STUDY OF PLASMA WAVES ARISING FROM THE SOLAR WIND INTERACTION WITH VENUS Ph.D. Thesis
Gregory Kim Crawford 1993 348 p
Avail: Univ. Microfilms Order No. DA9423071

We examine the plasma wave emissions which are generated due to the solar wind interaction with Venus. The analysis of these plasma waves provides a useful diagnostic of the underlying physical processes in the plasma allowing us to infer information about the particle distributions and instabilities. We use the measured wave emissions to construct statistical 'images' of the Venus foreshock. This analysis method allows us to develop a macroscopic picture of the wave properties, the inferred particle distributions, and their evolution as a function of position within the foreshock. The electron foreshock emissions are parallel polarized Langmuir mode waves with the same intensity at the foreshock boundary as the terrestrial emissions (10 mV/m). However, the wave characteristics differ markedly between the upstream and downstream foreshocks for Parker spiral IMF orientations. Additionally there is a dramatic decrease in intensity for distances beyond approximately 15 R(sub v) from the point of tangency along the foreshock boundary. Our observations provide conclusive evidence that reflection and energization of solar wind electrons at the shock provide the upstream source for the upstream electrons, not leakage. In the ion foreshock the wave emissions are parallel polarized ion acoustic like waves with similar intensities and spectral characteristics to terrestrial emissions. However, these waves are situated much deeper in the foreshock than expected from terrestrial observations. No emissions are observed in regions where field aligned ion distributions are expected. Rather the emissions are found in a region where diffuse ion distributions are expected. Lastly, we have evaluated the characteristics of the enhanced wave emissions at the dayside Venus ionopause. Previous theories had focused almost exclusively on wave measurements made in the 100 Hz OEFD channel and had suggested that these waves provided heat flux into the ionosphere. Rather we find that these broadband emissions are a different wave mode than hypothesized and probably not important in carrying heat flux into the ionosphere.
Dissert. Abstr.

N95-29218 Michigan Univ., Ann Arbor, MI.
TOPICS IN HIGH-PEAK INTENSITY, ULTRASHORT PULSE LASER-PLASMA INTERACTIONS Ph.D. Thesis
Xinbing Liu 1994 177 p
Avail: Univ. Microfilms Order No. DA9423250

The interactions of ultrashort (less than 1 ps), high intensity laser pulses with matter - a gas or a solid target - are studied. For a gas target, the propagation of high intensity laser pulses through a low pressure gas undergoing ionization is shown to produce multiple foci experimentally. Results of numerical modeling of the propagation, taking into consideration both self-focusing by atomic nonlinear susceptibility and defocusing by the laser-produced plasma, are presented. The numerical results are in qualitative agreement with the experimental observation when higher than 'normal' values of nonlinear susceptibility which is responsible for self-focusing are used. We attribute the increase in nonlinearity at high laser intensities to

the excited state susceptibility. Aspects of solid-density laser-plasma hydrodynamics are studied both experimentally and numerically. Particularly, the effect of the high laser pressure on the plasma expansion and the scale length is investigated. Experimental and numerical results show that the laser pressure competes with thermal pressure in determining plasma expansion and density profiles. Dissert. Abstr.

N95-29466# Lawrence Livermore National Lab., Livermore, CA.
INSIGHTS ON THE LOCAL DENSITY APPROXIMATION PLASMA POLARIZATION SHIFT AS PROVIDED BY THE OPTIMUM POTENTIAL METHOD
B. Wilson and D. A. Liberman 18 Jan. 1995 18 p Presented at the 6th International Workshop on Radiative Properties of Hot Dense Matter, Sarasota, FL, 31 Oct. - 4 Nov. 1994
(Contract W-7405-eng-48)
(DE95-008078; UCRL-JC-119340; CONF-9410314-1) Avail: CASI HC A03/MF A01

The plasma poiarization shift computed with a Local Density Functional model of an ion-sphere model is compared with results calculated using an optimum central field effective exchange potential. Indications are that the bulk of the shift is an artifact of the approximate exchange functional describing the interaction between bound and continuum orbitals in the LDA. DOE

N95-29519# Boston Coll., Chestnut Hill, MA. Dept. of Physics.
NEW RADIATION SOURCES THROUGH GENERATION AND RESONANT ENHANCEMENT OF CURRENT DRIVEN PLASMA INSTABILITIES IN LOWER DIMENSIONAL SOLID STATE SYSTEMS Final Report, Jul. 1993 - Jun. 1994
P. Bakshi and K. Kempa Sep. 1994 8 p
(Contract DAAH04-93-G-0259)
(AD-A290669; ARO-30935.1-PH) Avail: CASI HC A02/MF A01

We have identified theoretically the most promising candidates for current driven plasma instabilities (CDPI) in semiconductor based systems: the modulated quantum wires and lateral surface superlattices (LSSL). Feasibility of CDPI at much lower driving fields, as compared to the corresponding uniform systems, was established. Investigation of CDPI in a superconducting system was continued in close collaboration with an experimental group. We have also developed contacts with a number of experimental groups to stimulate parallel efforts for verification of CDPI in layered semiconductor systems. A workshop was arranged with ARO sponsorship, held at Boston College in August 1994, to discuss future efforts and collaborations. DTIC

N95-29547 Massachusetts Inst. of Tech., Cambridge, MA.
IONIZATIONAL NONEQUILIBRIUM AND IGNITION IN PLASMA ACCELERATORS S.D. Thesis
Eric James Sheppard 1994
Avail: Issuing Activity (MIT Libraries, Rm. 14-0551, Cambridge, MA 02139-4307)

The focus of this work is on identifying the processes behind the sustained initiation of ionization, or 'ignition', at the inlet of a self-field magnetoplasma-dynamic thruster (MPDT). Atomic or ionic species are modeled by their electronically excited state structure for detailed finite-rate analysis of multi-step ionization processes, including both inelastic collisions and radiation (in a parametric form). The time scales for the excited states are found to be small enough compared to the ground state's to make the quasi-steadystate-solution assumption, which allows the excited state population distribution relative to the ground state to be determined by a modified mass balance law. Neglecting radiative effects, which are shown to be small in MPDT's, the overall rate coefficients for electron-neutral ionization collisions and electron-electron-ion recombination collisions are calculated for the hydrogen atom, and the argon atom and first ion. These rate models are applied to the problem of ignition in a self field MPDT, where the propellant is injected into the thruster neutral, but the plasma must be at least partially ionized at the inlet for effective electromagnetic thrust. Back-diffusion is assumed to be responsible for transporting electron-ion pairs back to the inlet wall (which is ion-attracting), and sustaining the initiation of ionization there. If the propellant is injected at a speed less than the blowoff speed, then back-diffusion is sufficient to supply the inlet wall with enough electrons to initiate ionization. If the propellant is injected at a speed greater than the blowoff speed, then diffusion cannot supply the inlet with electrons, and the ionization front gets 'blown' downstream. For atomic injection, the blowoff speed depends on the ambipolar coefficient, and the ionization rate constant of the propellant. Therefore, propellants of high diffusivity and low ionization potential will ignite more readily at a given temperature. Although temperature variation in the ionizing region is found to have little effect on the ignition of a constant speed plasma, the ionization rate coefficient is a strong function of the electron temperature, which is set by an overall energy balance in the channel. In the accelerating plasma ignition model, both momentum and energy are accounted for self-consistently. The resulting inlet speeds were generally small enough to avoid 'blowoff', and the ionizing length scales were on the order of mm and were shorter than the magnetic diffusion scale length under typical self-field MPDT conditions. It was found that increasing the contraction ratio in the thruster channel lowered the electron temperature, which tended to quench ionization and stretch out the ionizing region. This work has shown that the initiation of ionization at the inlet of an MPDT may be explained by convective, diffusive, and collisional ionization processes alone. Dissert. Abstr.

N95-29567# National Inst. for Fusion Science, Nagoya (Japan).
DEVELOPMENT OF AN INTENSE NEGATIVE HYDROGEN ION SOURCE WITH A WIDE-RANGE OF EXTERNAL MAGNETIC FILTER FIELD
Y. Takeiri, A. Ando, O. Kaneko, Y. Oka, K. Tsumori, and R. Akiyama Sep. 1994 24 p
(ISSN 0915-633X)
(AD-B195514L; NIFS-307) Avail: CASI HC A03/MF A01

An intense negative hydrogen ion source has been developed, which has a strong external magnetic filter field in the wide area of 35 cm x 62 cm produced by a pair of permanent magnet rows located with 35.4 cm separation. The filter strength is 70 G in the center and the line-integrated filter strength is 850 G cm, which keeps the low electron temperature in the extraction region. Strong cusp magnetic field, 1.8 kG on the chamber surface, is generated for improvement of the plasma confinement. These resulted in the high arc efficiency at the low operational gas pressure. A 16.2 A of the H ion current with the energy of 47 keV was obtained at the arc efficiency of 0.1 A/kW at the gas pressure of 3.8 mTorr in the cesium-mode operation. The magnetic field in the extraction gap is also strong, 450 G, for the electron suppression. The ratio of the extraction to the negative ion currents was less than 2.2 at the gas pressure of 3 mTorr. The two-stage acceleration was tried, and a 13.6 A of the H ion beam was accelerated to 125 keV. DTIC

N95-29632 Arizona Univ., Tucson, AZ.
HIGH-DENSITY PLASMA DYNAMICS IN SEMICONDUCTORS Ph.D. Thesis
Kenith Erwin Meissner, II 1994 94 p
Avail: Univ. Microfilms Order No. DA9424962

This dissertation presents a study of high density plasma dynamics in semiconductors. Chapter 1 serves as an introduction and presents the basics of how we will use optical nonlinearities in the study of a high density plasma. Chapter 2 develops the necessary femtosecond laser system and techniques utilized in this investigation. The basics of our colliding pulse modelocked femtosecond laser system are presented. A variety of data acquisition systems are also outlined and discussed. A detailed description of our method of chirp measurement and correction rounds out the chapter. Chapter 3 presents a study of plasma dynamics in type I and type II GaAs multiple quantum well samples. First, the samples are compared in the quasi-equilibrium regime. The transfer of carriers from the wells to the barriers in the type II sample is found to profoundly affect the optical nonlinearities. A many-body theory calculation of these nonlinearities is then presented. We also utilize the unique properties of the type II structure to study the picosecond dynamics of a one component (hole) plasma. Finally, the possibility of transient gain in the type II structure is explored and discussed. Chapter 4 describes an investigation into the gain dynamics in an optically inverted semiconductor. Spectral hole burning is observed throughout the gain region, and the dynamics of the hole burning are shown. Since this system is highly inhomogeneously broadened, these results are first modeled by a group of noninteracting, inhomogeneously broadened, two level transitions. This model permits simple insight into the dynamics, but does not do a complete job of modeling the results. So, a full many-body treatment is included to more completely describe the experiment. Chapter 5 presents a study of the dephasing time through the gain region and into the absorption region of an optically excited GaAs

multiple quantum well sample. Both spectral and temporal methods for measuring the dephasing time are utilized. A distinct maximum of the dephasing time is observed at the transparency point. A many-body theory calculating the carrier-carrier scattering rate is presented to explain this maximum. Dissert. Abstr.

N95-29668 Iowa Univ., Iowa City, IA.
SOLITONS IN NEGATIVE ION PLASMAS Ph.D. Thesis
Jamie Cooney 1993 172 p
Avail: Univ. Microfilms Order No. DA9421113

Properties of ion acoustic solitons are studied in a plasma consisting of positive ions, electrons and negative ions -- a negative ion plasma. In one dimension these solitons are perturbations described by either the Korteweg-deVries (KdV) or modified Korteweg-deVries equation. In two dimensions, they are planar solitons described by the Kadomtsev-Petviashvili equation or cylindrical and spherical solitons described by a geometric KdV equation. Solitons in a negative ion plasma can be easily launched from metal surfaces or from grids using small excitation voltages. These methods of excitation are demonstrated in this thesis. The soliton phenomena investigated include overtaking collisions in one dimension, oblique collisions in two dimensions that result in a soliton resonance and the reflection of KdV solitons by the sheath of a conductor. Many properties of positive ion-electron plasmas change when the electrons are replaced with much heavier negative ions. The changes discussed include modifications to the Langmuir curve, to the dispersion characteristics and phase velocity of ion acoustic perturbations and to the Bohm drift velocity. Negative ions also alter sheath dimensions in a plasma. Changes of the Debye, Langmuir and ion-matrix sheaths are examined. A pseudopotential method presented also shows that positive excitation produces shocks and solitary waves in negative ion plasmas for only a limited range of negative ion concentrations. Dissert. Abstr.

N95-29686# Alabama Univ., Huntsville, AL.
A GENERALIZED SEMIKINETIC (GSK) MODEL FOR MESOSCALE AURORAL PLASMA TRANSPORT Ph.D. Thesis
David Gillespie Brown 1993 215 p
Avail: Univ. Microfilms Order No. DA9415108

The auroral region of the Earth's ionosphere-magnetosphere system is a complex and active part of the Earth's environment. In order to study the transport of ionospheric plasma in this region, we have developed a generalized semikinetic (GSK) model which combines the tracking of ionospheric ion gyrocenters (between stochastic impulses from waves), with a generalized fluid treatment of ionospheric electrons and Liouville mapping of magnetospheric plasma components. This model has been used to simulate the effects of 'self-consistent' heating ('self consistent' in the sense that heating occurs only where the modelled plasma is unstable) due to the current-driven ion cyclotron instability in the return current regions. Our results include generation of 'conics' whose wings are drawn in towards the upsilon(parallel)-axis at higher energies (such distributions were subsequently found in recent studies of DE-1 data for this region) and an alternative formation mechanism for toroidal (or 'ring'-shaped) ion velocity-space distributions. We also present results illustrating the effects of combining large scale electric fields (generated by anisotropic magnetospheric plasma distributions) with wave heating by a presumed distribution of wave spectra. In the presence of an upwards electric field the addition of wave heating increases the density of the O(sup +) 'beam' ('ion feeder' effect), while a downwards hot plasma-induced electric field increases the time which ions spend within the heating region ('pressure cooker' effect), resulting in greater ion energization. Dissert. Abstr.

N95-29717 Stanford Univ., CA.
MODELING THE BOUNDARY LAYER INTERACTIONS BETWEEN WEAKLY IONIZED PLASMAS AND COOLED, PLANAR ELECTRODES IN STAGNATION-POINT FLOWS Ph.D. Thesis
Ellen Meeks 1994 159 p
Avail: Univ. Microfilms Order No. DA9414617

This thesis presents a two-temperature multifluid model of weakly ionized, near-thermal plasmas in stagnation-flow against cooled, electrically biased surfaces. The model includes coupling between bulk fluid motion; species drift, diffusion and convection; electron- and bulk energy transport; and finite-rate chemistry including net ionization. In addition, the model includes Poisson's equation for determination of the electric field and for resolution of the space-charge sheath. Application of the model to high-temperature argon flow reveals important interactions between thermal, hydrodynamic, chemical, and electrical boundary layers, with implications to current-limiting regimes. The analyses include results using a quasineutral approximation results from the full formulation, and a detailed comparison between the two approaches. The model employs a global, finite, electron-ion recombination rate at the stagnation surface together with a specified current density. These boundary conditions determine the electron and ion fluxes at the surface consistent with mass and charge conservation The derivation of this surface-recombination formulation is discussed, as well as the sensitivity of model predictions to the assumed heterogeneous rate coefficient. Results from the quasineutral approximation demonstrate the importance of considering net convection, electrode cooling, and thermal non-equilibnum in the evaluation of plasma properties in the presheath region. The effects of net fluid flow, neutral thermal gradients, and finite-rate chemistry are determined through parametric variation of specified conditions and model assumptions. Inclusion of Poisson's equation and resolution of the ion-rich, collisional sheath allows investigation into the effects of specified conditions on the sheath structure. The analysis examines the response of a planar electrostatic probe in contact with a collisional, flowing plasma. Determinations of current-voltage behavior compare well to simple theory including dependence on freestream conditions. Departures from this theory arise from boundary-layer perturbations near the electrode surface. The model also correlates current-saturation and breakdown phenomena with changes in the sheath structure and ionization due to Joule heating for large cathode current densities. More quantitative comparisons of current-voltage conditions to experimental data for both cathode and anode reveal good agreement between the model predictions and the experimental measurements. Dissert. Abstr.

N95-29731# National Inst. for Fusion Science, Nagoya (Japan).
ANOMALOUS TRANSPORT THEORY FOR TOROIDAL HELICAL PLASMAS
K. Itoh, M. Yagi, S.-I. Itoh, and A. Fukuyama Aug. 1994 16 p Presented at the 15th International Conference on Plasma Physics and Controlled Nuclear Fusion Research, Seville, Spain, 26 Sep. - 1 Oct. 1994
(ISSN 0915-633X)
(AD-B192000L; NIFS-296; IAEA-CN-60/D-3-3) Avail: CASI HC A03/MF A01

Anomalous transport coefficients in toroidal helical plasmas are studied, based on the innovative theoretical method. The self-sustained turbulence is analyzed by balancing the nonlinear growth due to the current diffusivity with the nonlinear damping by the ion viscosity and thermal conductivity. Interchange and ballooning mode turbulence is investigated, and the geometrical dependence of the anomalous transport coefficient is clarified. Variation of transport owing to the geometrical difference in toroidal helical plasmas is illustrated. The mechanism for confinement improvement is searched for. To verify the nonlinear destabilization and the self-sustained state, the nonlinear simulation of the interchange mode turbulence is performed in a sheared slab. It is demonstrated that the nonlinear enhancement of the growth rate occurs when the fluctuation amplitude exceeds the critical level. In the saturation stage, the fluctuation level becomes higher associated with the enhanced nonlinear growth. Author

N95-29734# National Inst. for Fusion Science, Nagoya (Japan).
SELF-SUSTAINED MAGNETIC BRAIDING IN TOROIDAL PLASMAS
K. Itoh, A. Fukuyama (Okayama Univ., Japan.), S.-I. Itoh (Kyushu Univ., Kasuga, Japan), M. Yagi (Japan Atomic Energy Research Inst., Ibaraki, Japan.), and M. Azumi (Japan Atomic Energy Research Inst., Ibaraki, Japan.) Jul. 1994 19 p
(ISSN 0915-633X)
(AD-B191998L; NIFS-288) Avail: CASI HC A03/MF A01

Theory for the magnetic braiding in toroidal plasmas, which is caused by microscopic pressure-gradient-driven turbulence, is developed. When the pressure gradient exceeds a threshold, the self-sustaining of the magnetic braiding and enhanced anomalous transport occur. The balance between the nonlinear destabilization and nonlinear stabilization, which determines the stationary turbulence, is solved analytically for the case of interchange mode. The enhanced thermal conductivity and magnetic perturbation amplitude as well as the threshold pressure gradient are obtained. Cusp-type catastrophe is predicted, allowing the abrupt burst of magnetic perturbations. Author

N95-29738# Tsukuba Univ. (Japan).
INTERCHANGE STABILITY CRITERIA FOR ANISOTROPIC CENTRAL-CELL PLASMAS IN THE TANDEM MIRROR GAMMA 10
Hitoshi Hojo, Masaaki Inutake, Makoto Ichimura, Ryota Katsumata, and Tsuguhiro Watanabe (National Inst. for Fusion Science, Nagoya, Japan.) Nagoya, Japan National Inst. for Fusion Science May 1993 17 p Sponsored by Ministry of Education, Science and Culture
(ISSN 0915-633X)
(AD-B176253L; NIFS-222) Avail: CASI HC A03/MF A01

Flute interchange stability of anisotropic central-cell plasmas in the tandem mirror GAMMA 10 is studied numerically. The stability criteria on the beta value is obtained as a function of axial localization length of the pressure in both central and anchor cells. The temperature anisotropy of the plasma is also discussed. Author

N95-29739# National Inst. for Fusion Science, Nagoya (Japan).
HIDENEK: AN IMPLICIT PARTICLE SIMULATION OF KINETIC-MHD PHENOMENA IN THREE-DIMENSIONAL PLASMAS
Motohiko Tanaka May 1993 39 p
(ISSN 0915-633X)
(AD-B176255L; NIFS-224) Avail: CASI HC A03/MF A01

An advanced 'kinetic-MHD' simulation method and its applications to plasma physics are given in this lecture. This method is quite stable for studying strong nonlinear, kinetic processes associated with large space-scale, low-frequency electromagnetic phenomena of plasmas. A full set of the Maxwell equations, and the Newton-Lorentz equations of motion for particle ions and guiding-center electrons are adopted. In order to retain only the low-frquency waves and instabilities, implicit particle-field equations are derived. The present implicit-particle method is proved to reproduce the MHD eigenmodes such as Alfven, magnetosonic and kinetic Alfven waves in a thermally near-equilibrium plasma. In the second part of the lecture, several physics applications are shown. These include not only the growth of the instabilities of beam ions against the background plasmas and helical link of the current, but they also demonstrate nonlinear results such as pitch-angle scattering of the ions. Recent progress in the simulation of the Kelvin-Helmholtz instability is also presented with a special emphasis on the mixing of the plasma particles. Author

N95-29740# Nagoya Univ., Nagoya (Japan).
EFFECTIVE EMISSION AND IONIZATION RATE COEFFICIENTS OF ATOMIC CARBONS IN PLASMAS
Y. Ohkouchi, S. Sasaki, S. Takamura, and T. Kato (National Inst. for Fusion Science, Nagoya, Japan.) National Inst. for Fusion Science Jun. 1993 57 p Sponsored by Japan Ministry of Education, Science and Culture
(ISSN 0915-633X)
(AD-B175932L; NIFS-228) Avail: CASI HC A04/MF A01

Effective emission and ionization rate coefficients of carbon atoms taking into account the density effects in plasmas are studied using a collisional radiative model including 31 sub-levels up to the principal quantum number n = 4. Atomic processes such as electron impact ionization, excitation, de-excitation and spontaneous emission, which are the dominant processes for carbon atoms generated from the wall material in fusion devices, are considered in our calculations. In a relatively high density plasma with electron density above 10(exp 13) cm(exp -3), the effective ionization rate coefficient increases by a factor of four compared with that in a low density plasma at low temperatures of approx. 10 eV because of the increase of ionization from the excited states. Effective emission rate coefficients for several lines, which are useful for plasma diagnostics, are also presented. Author

N95-29741# National Inst. for Fusion Science, Nagoya (Japan).
COMMENT ON A MEAN FIELD OHM'S LAW FOR COLLISIONLESS PLASMAS
K. Itoh, M. Yagi (Japan Atomic Energy Research Inst., Naka, Japan.), A. Fukuyama (Okayama Univ., Japan.), S.-I. Itoh (Kyushu Univ., Kasuga, Japan), and M. Azumi (Japan Atomic Energy Research Inst., Naka, Japan.) Jun. 1993 13 p Sponsored by Ministry of Education
(ISSN 0915-633X)
(AD-B176252L; NIFS-229) Avail: CASI HC A03/MF A01

Recently, kinetic calculation of the current diffusivity (lambda) was made and it was commented that the fluid model of anomalous transport, in which the self-sustained turbulence and L-mode transport has been obtained, has overestimated lambda. This comment was misled by the improper evaluation of the wave number. The kinetic estimate of lambda is in the same order as the one in the fluid model. This would be one of the reasons that the transport theory, which was derived by using the fluid equations, explains well the present experimental results. Author

N95-29742# National Inst. for Fusion Science, Nagoya (Japan).
TRANSITION OF RADIAL ELECTRIC FIELD BY ELECTRON CYCLOTRON HEATING IN THE STELLARATOR PLASMAS
H. Idei, K. Ida, H. Sanuki, H. Yamada, H. Iguchi, S. Kubo, R. Akiyama, H. Arimoto, M. Fujiwara, and M. Hosokawa et al Jun. 1993 21 p Sponsored by Ministry of Education
(ISSN 0915-633X)
(AD-B176254L; NIFS-230) Avail: CASI HC A03/MF A01

The transition of a radial electric field from a negative to a positive value is observed in the Compact Helical System when the electron loss is sufficiently enhanced by the superposition of the off-axis second harmonic electron cyclotron heating on the neutral beam heated plasmas. The observed threshold for the enhanced particle flux required to cause the transition is compared with a theoretical prediction. Author

N95-29743# National Inst. for Fusion Science, Nagoya (Japan).
FREE-BOUNDARY EQUILIBRIUM STUDIES FOR THE LARGE HELICAL DEVICE
H. J. Gardner and K. Ichiguchi Jun. 1993 29 p Sponsored by Japanese Ministry of Science, Education and Culture
(ISSN 0915-633X)
(AD-B175931L; NIFS-231) Avail: CASI HC A03/MF A01

A free-boundary version of the VMEC three-dimensional equilibrium code, together with a code, DIAGNO, to determine the response to a set of magnetic diagnostic coils has been applied to the Large Helical Device. Two sequences of equilibria were considered: one where an external vertical field was used to keep the plasma centered and another where the outwardly shifting plasma was truncated by a limiter. The predictions of a simple cylindrical model have been verified for a diamagnetic loop. A set of simple response curves has been obtained which should be useful for the analysis and control of the finite (beta) plasma. The ideal Mercier criterion suggests that the centered plasma might be more stable. Author

N95-29744# National Inst. for Fusion Science, Nagoya (Japan).
PRANDTL NUMBER OF TOROIDAL PLASMAS
K. Itoh, S.-I. Itoh (Kyushu Univ., Kasuga, Japan), A. Fukuyama (Okayama Univ., Japan.), M. Yagi (Japan Atomic Energy Research Inst., Naka, Japan.), and M. Azumi (Japan Atomic Energy Research Inst., Naka, Japan.) Jun. 1993 30 p
(ISSN 0915-633X)
(AD-B179181L; NIFS-234) Avail: CASI HC A03/MF A01

Theory of the L-mode confinement in toroidal plasmas is developed. The Prandtl number, the ratio between the ion viscosity and the thermal conductivity is obtained for the anomalous transport process which is caused by the self-sustained turbulence in the toroidal plasma. It is found that the Prandtl number is of order unity both for the ballooning mode turbulence in tokamaks and for the interchange mode turbulence in a helical system. The influence on the anomalous transport and fluctuation level is evaluated. Hartmann number and magnetic Prandtl number are also discussed.
Author

N95-29745# National Inst. for Fusion Science, Nagoya (Japan).
THEORETICAL STUDY OF CYLINDRICAL ENERGY ANALYZERS FOR MeV RANGE HEAVY ION BEAM PROBES
A. Fujisawa and Y. Hamada Jul. 1993 43 p
(ISSN 0915-633X)
(AD-B17200L; NIFS-236) Avail: CASI HC A03/MF A01

A cylindrical energy analyzer with drift spaces is shown to have a second order focusing for beam incident angle when the deflection angle is properly chosen. The analyzer could possibly be applied to MeV range heavy ion beam probes, and will also be available for accurate particle energy measurements in many other fields. Author

N95-29746# Max-Planck-Inst. fuer Plasmaphysik, Garching (Germany).
DISCRIMINANT ANALYSIS TO PREDICT THE OCCURRENCE OF ELMS IN H-MODE DISCHARGES
O. J. W. F. Kardaun, S.-I. Itoh (Kyushu Univ., Kasuga, Japan), K. Itoh (National Inst. for Fusion Science, Nagoya, Japan.), and J. W. P. F. Kardaun (Central Bureau of Statistics, Voorburg, Netherlands.) Nagoya, Japan National Inst. for Fusion Science Aug. 1993 59 p
(ISSN 0915-633X)
(AD-B179183L; NIFS-242) Avail: CASI HC A04/MF A01

After an exposition of its theoretical background, discriminant analysis is applied to the H-mode confinement database to find the region in plasma parameter space in which H-mode with small ELM's (Edge Localized Modes) is likely to occur. The boundary of this region is determined by the condition that the probability of appearance of such a type of H-mode, as a function of the plasma parameters, should be larger than some threshold value and larger than the corresponding probability for other types of H-mode (i.e., H-mode without ELM's or with giant ELM's). In practice, the discrimination has been performed for the ASDEX, JET and JFT-2M tokamaks using four instantaneous plasma parameters (injected power Pinj, magnetic field Bt, plasma current Ip and line averaged electron density ne) and taking also memory effects of the plasma and the distance between the plasma and the wall into account, while using variables that are normalized with respect to machine size. Generally speaking, it is found that there is a substantial overlap between the region of H-mode with small ELM's and the region of the two other types of H-mode. However, the ELM-free and the giant ELM H-modes relatively rarely appear in the region, that, according to the analysis, is allocated to small ELM's. A reliable production of H-mode with only small ELM's seems well possible by choosing this regime in parameter space. In the present study, it was not attempted to arrive at a unified discrimination across the machines. So, projection from one machine to another remains difficult, and a reliable determination of the region where small ELM's occur still requires a training sample from the device under consideration. Author (revised)

N95-29747# National Inst. for Fusion Science, Nagoya (Japan).
MODELLING OF TRANSPORT PHENOMENA
Kimitaka Itoh, Sanae-I. Itoh (Kyushu Univ., Kasuga, Japan), and Atsushi Fukuyama (Okayama Univ., Japan.) Sep. 1993 40 p Presented at the Workshop on Local Transportation Studies in Fusion Plasmas, Varenna, Italy, 30 Aug. - 3 Sep. 1993
(ISSN 0915-633X)
(AD-B179223L; NIFS-243) Avail: CASI HC A03/MF A01

In this review article, we discuss key features of the transport phenomena and theoretical modeling to understand them. Experimental observations have revealed the nature of anomalous transport, i.e., the enhancement of the transport coefficients by the gradients of the plasma profiles, the pinch phenomena, the radial profile of the anomalous transport coefficients, the variation of the transport among the Bohm diffusion, Pseudo-classical confinement, L-mode and a variety of improved confinement modes, and the sudden jumps such as L-H transition. Starting from the formalism of the transport matrix, the modeling based on the low frequency instabilities are reviewed. Theoretical results in the range of drift wave frequency are examined. Problems in theories based on the quasilinear and mixing-length estimates lead to the renewal of the turbulence theory, and the physics picture of the self-sustained turbulence is discussed. The theory of transport using the fluid equation of plasma is developed, showing that the new approach is very promising in explaining above mentioned characteristics of anomalous transport in both L-mode and improved confinement plasmas. The interference of the fluxes is the key to construct the physics basis of the bifurcation theory for the L-H transition. The present status of theories on the mechanisms of improved confinement is discussed. Modeling on the nonlocal nature of transport is briefly discussed. Finally, the impact of the anomalous transport on disruptive phenomena is also described.
Author

N95-29749# National Inst. for Fusion Science, Nagoya (Japan).
MONTE CARLO SIMULATION STUDY OF THE ICRF MINORITY HEATING IN THE LARGE HELICAL DEVICE
S. Murakami, M. Okamoto, N. Nakajima, M. Ohnishi (Kyoto Univ., Uji, Japan.), and H. Okada (Kyoto Univ., Uji, Japan.) Oct. 1993 39 p
(ISSN 0915-633X)
(AD-B179858L; NIFS-249) Avail: CASI HC A03/MF A01

A Monte Carlo simulation code is developed for the ICRF (ion cyclotron range of frequencies) heating in helical systems, which takes into account finite beta effects, complicated orbits of high energetic particles, Coulomb collisions, and interactions between the particles and the applied waves. The code is used to investigate the ICRF minority heating in the Large Helical Device. The configuration of the magnetic fields changes significantly due to finite beta effects in the Large Helical Device. The resonance layer position is found to be crucial to the heating efficiency as the plasma beta increases. When the strength of the resonance magnetic field is set to the value at the magnetic axis, the higher heat efficiency is obtained and no clear difference of the heat efficiency due to the finite beta effects is found at the high ICRF wave power region. However the radial profile of the transferred power to majority ions and electrons from minority ions changes by the deformation of the trapped particle orbits due to the finite beta effects. The heat efficiency is improved if the radial electric field, E(r), is positive (E(r) is directed radially outward) and it is also improved by supplying He-3 minority ions rather than proton minority ions. Author

N95-29755# National Inst. for Fusion Science, Nagoya (Japan).
INTERMITTENT ENERGY BURSTS AND RECURRENT TOPOLOGICAL CHANGE OF A TWISTING MAGNETIC FLUX TUBE
Hiroyoshi Amo (Graduate Univ. for Advanced Studies, Japan.), Tetsuya Sato (Graduate Univ. for Advanced Studies, Japan.), and Akira Kageyama Sep. 1994 21 p Sponsored by Ministry of Education, Science and Culture; and Graduate Univ. for Advanced Studies
(ISSN 0915-633X)
(AD-B195513L; NIFS-309) Avail: CASI HC A03/MF A01

When continuously twisted, a magnetic flux tube suffers a large kink distortion in the middle part of the tube, like a knot-of-tension instability of a bundle of twisted rubber strings; reconnection is triggered starting with the twisted field lines and quickly proceeding to the untwisted field lines at the twist-untwist boundary, whereby a giant burst-like energy release takes place. Subsequently, bursts occur intermittently and reconnection advances deeper into the untwisted region. Then, a companion pair of the linked twist-untwist flux tubes reconnect with each other to return to the original axisymmetric tube. The process is thus repeatable. Author

N95-29783 Boston Univ., MA.
CHEMICAL RELEASE EXPERIMENTS TO INDUCE F REGION IONOSPHERIC PLASMA IRREGULARITIES AT THE MAGNETIC EQUATOR Ph.D. Thesis
Peter Jared Sultan 1994 242 p
Avail: Univ. Microfilms Order No. DA9422513

The largest-scale plasma instability that occurs naturally in the Earth's ionosphere is a turbulent upwelling of the equatorial F region known as equatorial spread-F (ESF). During an ESF event, high plasma density magnetic fluxtubes at the bottomside of the F region are thought to change places with lower plasma density flux-tubes from below in a Rayleigh-Taylor type (heavy fluid over light fluid) instability. This interchange creates a large-scale (10's of km) density perturbation locally, which rapidly penetrates through to the topside of the F region, creating a plume of cascading smaller-scale (meter to centimeter scale) irregularities from the sharp density gradients at the edges of the rising plasma 'bubble'. In a theoretical test of this overall scenario for ESF, a linear instability growth rate is derived following the magnetic fluxtube formalism of Haerendel. Using realistic atmospheric and ionospheric density model inputs, growth rates are calculated for a range of geophysical conditions. Time/altitude domains having positive growth rates are found to coincide with observed time/altitude patterns of ESF occurrence, thus supporting the fluxtube model. The physics also are tested experimentally by the deliberate creation of plasma bubbles in ambient ionospheres that the fluxtube model predicts are susceptible to the Rayleigh-Taylor instability. Two such artificial seed perturbations were generated during the 1990 NASA/Boston University CRRES-at-Kwajalein campaign, when clouds of sulfur hexafluoride (SF6) were released by sounding rockets to initiate plasma recombinations near the bottomside of the equatorial ionosphere. Multiple diagnostics (incoherent scatter radar, high frequency radar, optics, and satellite polarimeters at several sites) were used to monitor the prelaunch status of the ionosphere and the electron depleted regions that resulted from the chemical releases. Small ESF plumes were observed to form in the region of the artificial perturbation during both experiments. The successes in being able to model the natural occurrence of ESF, as well as being able to initiate it artificially, lend

support to the physical model adopted for the equatorial ionosphere, and open up new avenues of research into ESF predictability on a night-to-night, and even an hour-to-hour, basis. Dissert. Abstr.

N95-29789# National Inst. for Fusion Science, Nagoya (Japan).
DYNAMICAL MODEL OF PRESSURE-GRADIENT-DRIVEN TURBULENCE AND SHEAR FLOW GENERATION IN L-H TRANSITION
H. Sugama and W. Horton (Texas Univ., Austin, TX.) Aug. 1994 19 p Presented at the 15th International Conference on Plasma Physics and Controlled Nuclear Fusion Research, Seville, Spain, 26 Sep. - 1 Oct. 1994
(ISSN 0915-633X)
(AD-B195511L; NIFS-300; IAEA-CN-60/D-P-I-11) Avail: CASI HC A03/MF A01

We present a dynamical model for the L-H transition consisting of three ordinary differential equations. This model describes temporal evolutions of three characteristic variables, i.e., the free energy contained in the pressure gradient, the turbulent kinetic energy and the shear flow energy in the resistive pressure-gradient-driven turbulence. The model equations have stationary solutions corresponding to the L- and H-modes and their stabilities depend on the energy input to the peripheral region. Changing the energy input parameter yields the L to H and H to L transitions. We also find the parameter region in which the H-mode stationary solution becomes unstable and bifurcate to the limit cycle which shows periodic oscillations like ELM. It depends on the viscosity for the shear flow which the type of the L-H transition is, a first-order or second-order transition. Author

N95-29801# National Inst. for Fusion Science, Nagoya (Japan).
EXPERIMENTAL STUDY ON SCALING LAW OF OUTGASSING RATE WITH A PUMPING PARAMETER
Kenya Akaishi, Yusuke Kubota, Kazuhiro Ezaki, and Osamu Motojima Aug. 1994 19 p
(ISSN 0915-633X)
(AD-B191999L; NIFS-294) Avail: CASI HC A03/MF A01

The outgassing rate of a small test chamber made of 304 type stainless steel has been measured as a function of pumping speed in a range from 0.3 to 200 l/s. In the experiment the chamber has been first exposed to the air and then pumped with different pumping speeds for 3 days at room temperature of 20 C without baking. The typical outgassing rates of the chamber are determined from the measurement of steady pressures at the pumping time of 72 h. As a result of experiment, it is found that measured outgassing rates q obey a set of power laws of 1(1)=c(1)(S/A)(exp m)1 and q(2)=c(2)(S/A)(exp m)2 where S/A is the ratio of pumping speed S to surface area A of the chamber, c(1) and c(2) are constants, exponents of m(1) and m(2) are 0.8282 for S/A greater than or equal to 10(exp -3) l/sq scm and 0.4655 for S/A less than or equal to 10(exp -3) l/sq scm, respectively. Technical application of the obtained scaling law is discussed in connection with the design of pumping system for a large vacuum device. Author

N95-29802# National Inst. for Fusion Science, Nagoya (Japan).
FORMATION OF POSITIVE RADIAL ELECTRIC FIELD BY ELECTRON CYCLOTRON HEATING IN COMPACT HELICAL SYSTEM
H. Idei, K. Ida, H. Sanuki, S. Kubo, H. Yamada, H. Iguchi, S. Morita, S. Okamura, R. Akiyama, and H. Arimoto (Nagoya Univ., Nagoya, Japan.) et al Jul. 1994 40 p
(ISSN 0915-633X)
(AD-B191994L; NIFS-291) Avail: CASI HC A03/MF A01

The radial electric field is driven to positive value by off-axis second harmonic electron cyclotron heating (ECH) in the Compact Helical System. The observed positive electric field is associated with the outward particle flux enhanced with ECH. The enhanced particle flux triggered by the production of the electrons accelerated perpendicularly to the magnetic field with ECH results in the change of the electric field. Author

N95-29803# Osaka Univ., Suita (Japan). Faculty of Engineering.
EFFECTS OF IMPURITIES RELEASED FROM HIGH Z TEST LIMITER ON PLASMA PERFORMANCE IN TEXTOR
Y. Ueda, T. Tanabe (Forschungszentrum Juelich G.m.b.H., Juelich, Germany.), V. Philipps (Forschungszentrum Juelich G.m.b.H., Juelich, Germany.), L. Koenen (Forschungszentrum Juelich G.m.b.H., Juelich, Germany.), A. Pospieszczyk (Forschungszentrum Juelich G.m.b.H., Juelich, Germany.), U. Samm (Forschungszentrum Juelich G.m.b.H., Juelich, Germany.), B. Schweer (Forschungszentrum Juelich G.m.b.H., Juelich, Germany.), B. Unterberg (Forschungszentrum Juelich G.m.b.H., Juelich, Germany.), M. Wada (Doshisha Univ., Kyoto, Japan.), and N. Hawkes (United Kingdom Atomic Energy Authority, Abingdon, England.) et al Nagoya, Japan National Inst. for Fusion Science Aug. 1994 22 p Presented at the 11th International Conference on Plasma Surface Interactions on controlled Fusion Devices, Mito, Japan, 23-27 May 1994 Submitted for publication in Journal of Nuclear Materials
(ISSN 0915-633X)
(AD-B191995L; NIFS-293) Avail: CASI HC A03/MF A01

To investigate the feasibility of high Z metals as plasma facing materials, a Mo test limiter was inserted into the TEXTOR edge plasma and the Mo content in the core plasma and its flux from the limiter have been observed. In OH plasma the additional radiation due to Mo impurities increased with line averaged density n(e). Beyond n(e) of about 3 x 10(exp 19)/cu m, the central radiation increased strongly with time and a hollow temperature profile appeared. In contrast, Mo impurity radiation decreased with n(e) in NBI (co-injection) plasma and no clear Mo accumulation in the plasma center was observed. However, when the edge plasma was cooled by neon injection in NBI plasma, the Mo concentration in the plasma center substantially increased. The Mo flux from the limiter showed no remarkable change during the OH and NBI density scan or with neon cooling. The possible reasons for the Mo behavior in the core plasma are discussed. Author

N95-29808# National Inst. for Fusion Science, Nagoya (Japan).
BORONIZATION STUDY FOR APPLICATION TO LARGE HELICAL DEVICE
N. Noda, A. Sagara, H. Yamada, Y. Kubota, N. Inoue, K. Akaishi, O. Motojima, K. Iwamoto (Hokkaido Univ., Sapporo, Japan.), M. Hashiba (Hokkaido Univ., Sapporo, Japan.), and I. Fujita (Hokkaido Univ., Sapporo, Japan.) et al Jul. 1994 21 p
(ISSN 0915-633X)
(AD-B191996L; NIFS-292) Avail: CASI HC A03/MF A01

An experimental device named SUT (SUrface modification Teststand) was constructed for a boronization study. An ultra high vacuum (UHV) condition, a changeable high temperature liner and in-situ AES (Auger Electron Spectroscopy) are three distinctive feature of the SUT device. Saturation density of oxygen atoms was as large as 1.2 x 10(exp 17)/sq cm on a boronized surface, whereas 1.5 x 10(exp 16)/sq cm on a bare stainless steel surface. It is found by AES analysis that the oxygen-contained layer was as thick as 50 nm from the top surface of the boron film. From such a large oxygen-saturation density, we expect that the oxygen-gettering ability of the boronized surface is likely to be maintained during one-day experiment of LHD. The oxygen-saturation behavior was quite similar between the boronized surfaces obtained with decaborane and diborane, which indicates that, as a working gas of the boronization, the decaborane works well compared with diborane, as far as oxygen gettering is concerned. Author

N95-29809# National Inst. for Fusion Science, Nagoya (Japan).
THEORY OF PSEUDO-CLASSICAL CONFINEMENT AND TRANSMUTATION TO L-MODE
K. Itoh, S.-I. Itoh (Kyushu Univ., Kasuga, Japan), M. Yagi (Japan Atomic Energy Research Inst., Naka, Japan.), A. Fukuyama (Okayama Univ., Japan.), and M. Azumi (Japan Atomic Energy Research Inst., Naka, Japan.) May 1993 25 p Sponsored by Ministry of Education
(ISSN 0915-633X)
(AD-B175957L; NIFS-231) Avail: CASI HC A03/MF A01

Theory of the self-sustained turbulence is developed for resistive plasma in toroidal devices. Pseudo-classical confinement is obtained in the low temperature limit. As temperature increases, the current-diffusivity prevails upon resistivity, and the turbulence nature changes so as to recover the L-mode transport. Comparison with experimental observation on this transition is made. Hartmann number is also given. Author

N95-29810# National Inst. for Fusion Science, Nagoya (Japan).
COLLISIONLESS DRIVEN MAGNETIC RECONNECTION
Ritoku Horiuchi and Tetsuya Sato Jun. 1993 21 p
(ISSN 0915-633X)
(AD-B178946L; NIFS-233) Avail: CASI HC A03/MF A01

Driven magnetic reconnection in a collisionless plasma is investigated by means of a two-and-one-half dimensional particle simulation. The dynamical compression by plasma inflow forms a peaked profile of current density in the neutral sheet. When the width of current layer is compressed as thin as the ion Larmor radius, the charge separation becomes distinct abruptly at the center of the current layer due to the finite ion Larmor radius effect. The charge separation in the central current region and the subsequent spatial modification of the current profile result in excitation of collisionless driven magnetic reconnection. In the case of collisionless driven magnetic reconnection an efficient energy conversion from field energy to particle energy is observed. Author

N95-29812# National Inst. for Fusion Science, Nagoya (Japan).
CARBON SHEET PUMPING
N. Ohyabu, A. Sagara, T. Ono (Nagoya Univ., Nagoya, Japan.), T. Kawamura, and O. Motojima Jul. 1993 14 p
(ISSN 0915-633X)
(AD-B179443L; NIFS-237) Avail: CASI HC A03/MF A01

A new hydrogen pumping scheme has been proposed which controls recycling of the particles for significant improvements of the energy confinement in toroidal magnetic fusion devices. In this scheme, a part of the vacuum vessel surface near the divertor is covered with carbon sheets of a large surface area. Before discharge initiation, the sheets are baked up to 700 to approximately 1000 C to remove the previously trapped hydrogen atoms. After being cooled down to below approximately 200 C, the unsaturated carbon sheets trap high energy charge exchange hydrogen atoms effectively during a discharge and overall pumping efficiency can be as high as approximately 50 percent. Author

N95-29813# National Inst. for Fusion Science, Nagoya (Japan).
THE ORIGIN OF COLLISIONLESS DISSIPATION IN MAGNETIC RECONNECTION
Motohiko Tanaka Sep. 1993 20 p
(ISSN 0915-633X)
(AD-B178949L; NIFS-245) Avail: CASI HC A03/MF A01

The mechanism of collisionless reconnection in magnetized plasmas is studied in terms of coalescence of two flux tubes using implicit particle simulation. The motional electric field resulting from magnetic attraction generates the non-MHD (magneto-hydrodynamic), scalar electrical potential of a quadrupole configuration across the x-point. This electric field transports the plasma and magnetic flux into and out of the diffusion layer, and also accelerates the finite mass electrons to produce the current J(sub parallel) along the helical magnetic field. These processes provide equivalent dissipation which makes magnetic reconnection possible in collisionless magnetized plasmas. Author

N95-29841# Hachinohe Inst. of Tech. (Japan).
RELATIVISTIC EFFECTS ON LARGE AMPLITUDE NONLINEAR LANGMUIR WAVES IN A TWO-FLUID PLASMA
Yasunori Nejoh (National Inst. for Fusion Science, Nagoya, Japan.) Nagoya, Japan National Inst. for Fusion Science Jul. 1994 28 p
(ISSN 0915-633X)
(AD-B191960L; NIFS-289) Avail: CASI HC A03/MF A01

Large amplitude relativistic nonlinear Langmuir waves are analyzed by the pseudo-potential method. The existence conditions for nonlinear langmuir waves are confirmed by considering relativistic high-speed electrons in a two-fluid plasma. The significant feature of this investigation is that the propagation of nonlinear Langmuir waves depends on the ratio of the electron streaming velocity to the velocity of light, the normalized potential and the ion mass to electron mass ratio. The constant energy is determined by the specific range of the relativistic effect. In the non-relativistic limit, large amplitude relativistic Langmuir waves do not exist. The present investigation predicts new findings of large amplitude nonlinear Langmuir waves in space plasma phenomena in which relativistic electrons are important. Author

N95-29843# Nagaoka Technological Univ. (Japan).
SCREENING CONSTANTS FOR PLASMA
Shigeo Kawata, Shigeru Kato, and Syuji Kiyokawa (Nara Women's Univ., Japan.) Nagoya, Japan National Inst. for Fusion Science Jun. 1993 28 p Sponsored by Ministry of Education, Science and Culture
(ISSN 0915-633X)
(AD-B179442L; NIFS-235) Avail: CASI HC A03/MF A01

We present the improved screening constants, with which the atomic energy levels for the finite temperature materials are obtained by the screened-Hydrogen model. The improved screening constants are obtained for each of 34 materials. Each screening constant has the temperature dependence in order to realize the better reproducibility of the Hartree-Fock-Slater (HFS) energy levels. The improved screening constants provide the better results compared with More's screening constants: the improvement from the results by More's screening constants is about 40 percent for n = 1 and about 20 percent for n = 2, in average over 34 materials. Here n is the principal quantum number. Author

N95-29844# Gunma Univ., Kiryu (Japan). Dept. of Electronic Engineering.
ATTRACTORS OF DISSIPATIVE STRUCTURE IN THREE DISSIPATIVE FLUIDS
Yoshiomi Kondoh Nagoya, Japan Natonal Inst. for Fusion Science Oct. 1993 35 p
(ISSN 0915-633X)
(AD-B180030L; NIFS-248) Avail: CASI HC A03/MF A01

A general theory with use of auto-correlations for distributions is presented to derive that realization of coherent structures in general dissipative dynamic systems is equivalent to that of self-organized states with a minimum dissipation rate for instantaneously contained energy. Attractors of dissipative structure are shown to be given by eigenfunctions for dissipative dynamic operators of the dynamic system and to constitute the self-organized and self-similar decay phase. Three typical examples related to incompressible viscous fluids, incompressible viscous and resistive magnetohydrodynamic (MHD) fluids, and compressible resistive MHD plasmas are presented to lead to attractors in the three dissipative fluids and to describe a common physical picture of self-organization and bifurcation of the dissipative structure. Author

N95-29857# National Inst. for Fusion Science, Nagoya (Japan).
HYDROGEN PRODUCTION IN FUSION REACTORS
S. Sudo, Y. Tomita, S. Yamaguchi, A. Iiyoshi, H. Momota, O. Motojima, M. Okamoto, M. Ohnishi (Kyoto Univ., Uji, Japan.), M. Onozuka (Mitsubishi Heavy Industries Ltd., Tokyo, Japan.), and C. Uenosono (Kansai Electric Power Co., Inc., Osaka, Japan.) Nov. 1993 18 p
(ISSN 0915-633X)
(AD-B180028L; NIFS-253) Avail: CASI HC A03/MF A01

As one of the methods of innovative energy production in fusion reactors (that do not include a conventional turbine-type generator), the efficient use of fusion-reactor radiation and semiconductors to supply clean fuel in the form of hydrogen gas is studied. Taking the reactor candidates such as a toroidal system and an open system for application of the new concepts, the expected efficiency and a plant system concept are investigated. Author

N95-29909 Oak Ridge National Lab., TN. Engineering Div.
REMOTE MAINTENANCE CHALLENGES PRESENTED IN THE ITER ENGINEERING DESIGN
T. W. Burgess, J. N. Herndon, S. L. Schrock, and D. C. Lousteau 1995 8 p Presented at the 6th American Nuclear Society Meeting on Robotics and Remote Systems, Monterey, CA, 5-10 Feb. 1995 Limited Reproducibility: More than 20% of this document may be affected by microfiche quality
(Contract DE-AC05-84OR-21400)
(DE95-006392; CONF-950232-30) Avail: CASI HC A02

Leading fusion energy research institutions are currently engaged in the Engineering Design Activity for the International Thermonuclear Experimental Reactor (ITER). A tokamak reactor design is evolving which emphasizes high system performance in a minimum overall reactor and building size. The resulting high component density dictates careful attention to ITER remote maintenance considerations in the development of the configuration. The complexity and scale of ITER remote maintenance tasks are well beyond the scope of today's experience and technology. This paper discusses the remote maintenance philosophy, describes the basic configuration as it relates to maintenance, and describes the basic procedures and equipment required. Key enabling technology research and development needs are also addressed. DOE

N95-29966# National Inst. for Fusion Science, Nagoya (Japan). Graduate Univ. for Advanced Studies.
LECTURE NOTE ON THE BASES OF PLASMA PHYSICS
Masao Oxamoto Feb. 1994 172 p In JAPANESE Submitted for publication
(ISSN 0915-6348)
(NIFS-PROC-15) Avail: CASI HC A08/MF A02

The lecture on the 'Bases of Plasma Physics' was given from April to June, 1993 to the students of the Fusion Science Course, Department of Mathematical and Physical Science of the Graduate University for Advanced Studies and to other graduate students at the National Institute for Fusion Science. A transcript of the lecture is presented in Japanese. Author

N95-30023# Oak Ridge National Lab., TN.
MAGNETIC FUSION COMMERCIAL POWER PLANTS
J. Sheffield 1994 7 p Presented at the Fusion Power Associates Annual Meeting and Symposium, San Diego, CA, 8-9 Sep. 1994
(Contract DE-AC05-84OR-21400)
(DE95-007027; CONF-9409308-1) Avail: CASI HC A02/MF A01

Toroidal magnetic systems present the best opportunity to make a commercial fusion power plant. They offer potential solutions to the main requirements that confront a power plant designer. An ideal system may be postulated in which the coils are a very small part of the cost, and the cost stems primarily from the inescapable components: minimal plasma heating (and sustaining system), tritium breeding blanket, shield, particle input, removal and treatment system, heat transfer system, generators, buildings, and balance of plant. No present system meets the ideal standards; however, toroidal systems contain among them the elements required. Consequently, a logical program may be based upon an evolutionary development, building on the contributions of the tokamak, which has been the mainline of research for a number of years. DOE

N95-30032# National Inst. for Fusion Science, Nagoya (Japan).
INNOVATIVE DIVERTOR CONCEPTS FOR LHD
N. Ohyabu, A. Komori, K. Akaishi, N. Inoue, Y. Kubota, A. I. Livshit (Bonch-Bruyevich Electrotechnical Inst. of Communication, Saint Petersburg, Russia.), N. Noda, A. Sagara, H. Suzuki, and T. Watanabe et al Jul. 1994 18 p
(ISSN 0915-633X)
(AD-B191997L; NIFS-290) Avail: CASI HC A03/MF A01

We are developing various innovative divertor concepts which improve the Large Helical Device (LHD) plasma performance. These are two divertor magnetic geometries (helical and local island divertors), three operational scenarios (radiative cooling in the high density, cold boundary; confinement improvement by generating high temperature divertor plasma; and simultaneous achievement of radiative cooling and H-mode like confinement improvement) and technological development of new efficient hydrogen pumping schemes. Author

N95-30033# National Inst. for Fusion Science, Nagoya (Japan).
AVERAGED RESISTIVE MHD EQUATIONS
Jiro Todoroki Sep. 1993 19 p
(ISSN 0915-633X)
(AD-B178947L; NIFS-244) Avail: CASI HC A03/MF A01

Averaged resistive MHD equations are derived by using the Lagrangian formalism. The assumption is that the perturbation is of single toroidal harmonics on the special magnetic coordinates Jacobian which is independent of the toroidal angle. The metrics contained in the obtained resistive equations are those appearing in the averaged equilibrium equations. The local stability conditions are also derived. Author

N95-30130# Lawrence Livermore National Lab., Livermore, CA.
TECHNIQUES AND RESULTS OF TOKAMAK-EDGE SIMULATION
G. R. Smith, P. N. Brown, M. E. Rensink, T. D. Rognlien, R. B. Campbell (Sandia National Labs., Albuquerque, NM.), D. A. Knoll (Idaho National Engineering Lab., Idaho Falls, ID.), and P. R. McHugh (Idaho National Engineering Lab., Idaho Falls, ID.) 20 May 1994 13 p Presented at the 11th International Conference on Plasma Surface Interactions in Controlled Fusion Devices, Mito, Japan, 23-27 May 1994
(DE95-008075; UCRL-JC-115909; CONF-940580-24) Avail: CASI HC A03/MF A01

This paper describes recent development of the UEDGE code in three important areas. (1) Nonorthogonal grids allow accurate treatment of experimental geometries in which divertor plates intersect flux surfaces at oblique angles. (2) Radiating impurities are included by means of one or more continuity equations that describe transport and sources, and sinks due to ionization and recombination processes. (3) Advanced iterative methods that reduce storage and execution time allow us to find fully converged solutions of larger problems (i.e., finer grids). Sample calculations are presented to illustrate these development. DOE

N95-30173# Texas Univ., Austin, TX. Inst. for Fusion Studies.
HEAVY LIGHT BULLETS IN ELECTRON-POSITRON PLASMA
V. I. Berezhiani (International Centre for Theoretical Physics, Trieste, Italy.) and S. M. Mahajan Mar. 1995 42 p
(Contract DE-FG05-80ET-53088)
(DE95-008751; DOE/ET-53088/696; IFSR-696) Avail: CASI HC A03/MF A01

The nonlinear propagation of circularly polarized electromagnetic waves with relativistically strong amplitudes in an unmagnetized hot electron-positron plasma with a small fraction of ions is investigated. The possibility of finding localized solutions in such a plasma is explored. It is shown that these plasmas support the propagation of 'heavy light bullets'; nondiffracting and nondispersive electromagnetic (EM) pulses with large density bunching. DOE

N95-30274# Rochester Univ., NY. Lab. for Laser Energetics.
INERTIAL FUSION PROGRAM AND NATIONAL LASER USERS FACILITY PROGRAM Annual Report, Oct. 1993 - Sep. 1994
Jan. 1995 171 p
(Contract DE-FC03-92SF-19460)
(DE95-008202; DOE/SF-19460/52) Avail: CASI HC A08/MF A02

This is the 1994 annual report for the University of Rochester, Laboratory for Laser Energetics. The report is presented as a series of research type reports. The titles emphasize the breadth of work carried out. They are: stability analysis of unsteady ablation fronts; characterization of laser-produced plasma density profiles using grid image refractometry; transport and sound waves in plasmas with light and heavy ions; three-halves-harmonic radiation from long-scale-length plasmas revisited; OMEGA upgrade status report; target imaging and backlighting diagnosis; effect of electron collisions on ion-acoustic waves and heat flow; particle-in-cell code simulations of the interaction of gaussian ultrashort laser pulses with targets of varying initial scale lengths; characterization of thick cryogenic fuel layers: compensation for the lens effect using convergent beam interferometry; compact, multijoule-output, Nd:Glass, large-aperture ring amplifier; atomic force microscopy observation of water-induced morphological changes in Y2O3 monolayer coatings; observation of longitudinal acceleration of electrons born in a high-intensity laser focus; spatial intensity nonuniformities of an OMEGA beam due to nonlinear beam propagation; calculated X-ray backlighting images of mixed imploded targets; evaluation of cosmic rays for use in the monitoring of the MEDUSA scintillator-photomultiplier diagnostic array; highly efficient second-harmonic generation of ultra-intense Nd:Glass laser pulses multiple cutoff wave numbers of the ablative Rayleigh-Taylor instability; ultrafast, all-silicon light modulator; angular dependence of the stimulated Brillouin scattering in homogeneous plasma; and femtosecond excited-state dynamics of a conjugated ladder polymer. DOE

N95-30338*# National Aeronautics and Space Administration. Marshall Space Flight Center, Huntsville, AL.
ON THE AZIMUTHAL VARIATION OF THE EQUATORIAL PLASMAPAUSE
D. L. Gallagher, P. D. Craven, R. H. Comfort (Alabama Univ., Huntsville, AL.), and T. E. Moore [1994] 33 p
(Grants NAGw-1630; NAG8-239)
(NASA-CR-198929; NAS 1.26:198929) Avail: CASI HC A03/MF A01

Previous results of plasmapause position surveys have been synthesized into a comprehensive description of the plasmapause, taken to represent the boundary between diurnal near-corotation and large-scale circulation streamlines that traverse the entire magnetosphere. The result indicates a plasmapause that has a pronounced bulge in the dusk sector, that rotates sunward and shrinks markedly as geomagnetic activity (and presumably magnetospheric convection) increase. The shape of the plasmapause so determined is significantly different from that associated with the simple

superposition of sunward flow and corotation, both in its detailed shape and in its varying orientation. The results imply that the magnetospheric circulation departs from a uniform flow field, having a radial dependence with respect to the Earth that is qualitatively consistent with electrostatic shielding of the convection electric field. Also, the results imply the the inner magnetospheric flow field rotates from duskward to dawnward as its intensity increases. Author

76 SOLID-STATE PHYSICS

Includes superconductivity.

For related information, see also *33 Electronics and Electrical Engineering* and *36 Lasers and Masers.*

N95-28681 Arizona State Univ., Tempe, AZ.
CORRELATIONS BETWEEN MICROMAGNETIC, MICROSTRUCTURAL AND MICROCHEMICAL PROPERTIES IN ULTRATHIN EPITAXIAL MAGNETIC STRUCTURES Annual Report, 1 Jan. - 31 Dec. 1994
Michael R. Scheinfein and G. G. Hembree 31 Dec. 1994 109 p Limited Reproducibility: More than 20% of this document may be affected by microfiche quality
(Contract N00014-93-1-0099)
(AD-A289705) Avail: Issuing Activity (Defense Technical Information Center (DTIC))

The proposed goal of this project is to obtain quantitative measurements of the microstructural, microchemical and micromagnetic properties of surfaces and interfaces of ultrathin films composed of magnetic materials deposited on non-magnetic, antiferromagnetic (metal) and insulating substrates. Surface microanalytic methods based on a unique ultrahigh-vacuum scanning transmission electron microscope/scanning electron microscope (UHV-STEM/SEM) equipped with in-situ thin film preparation and characterization tools are being used. Magnetic characterization is performed in-situ using the surface magneto-optical Kerr effect (SMOKE). Additional magnetic microstructure measurements are being conducted in a novel STEM based electron holography system where absolutely calibrated nanometer resolution magnetometry is possible. The measurements are designed to clarify the relationship between observed real-space micro-structure of interfaces, ultrathin magnetic films and superlattices with magnetic properties, such as surface anisotropy. The dependence of magnetic properties on film morphology, which may be a function of the deposition parameters during the initial stages of growth, and on structural properties such as strain and interface roughness is being studied. We are exploring the electron beam modification of CaF2 and CoF2, both as an electron beam resist and as a damagable material for preferential nucleation, as a means of defining one and two dimensional nanometer sized epitaxial magnetic devices. Here, we report on our progress in year 2 of this 3 year project. DTIC

N95-28815# State Univ. of New York, Stony Brook, NY.
MATERIALS SCIENCE AND FABRICATION OF YBCO-SrTi(1-x)Nb(x)O3-YBCO DEVICE STRUCTURES Final Report
Shang Hou 1995 6 p
(Contract F49620-92-J-0111)
(AD-A292527; AFOSR-95-0137TR) Avail: CASI HC A02/MF A01

As described in our proposal for making YBCO/SrTiNbO/YBCO junctions, the success of this project relies on work in three different thrusts: growth of high quality, ultra-thin high-quality YBCO films; acquisition of metallically doped SrTiO3 substrates with high structural quality; and the fabrication and characterization of S-N-S Josephson structure based on YBCO/SrTiNbO heteroepitaxy. While there has been encouraging progress in the thin film growth part, problems were found in obtaining metallically doped SrTiO3 substrates with the desired electrical/structural properties. A better alternative for the doped SrTiO3 will be the growth of YBCO films on top of a metallic oxide thin film SrRuO3. DTIC

N95-28862# Physical Optics Corp., Torrance, CA.
LOW THRESHOLD ALL-OPTICAL CROSSBAR SWITCH ON GaAs-GaAlAs CHANNEL WAVEGUIDE ARRAYS Final Report, 15 Jul. 1992 - 14 Jul. 1994
Tomasz Jannson and Andrew Kostrzewski 14 Sep. 1994 73 p
(Contract F49620-92-C-0047)
(AD-A292483; Rept-3176; AFOSR-95-0147TR) Avail: CASI HC A04/MF A01

During the Phase 2 project entitled 'Low Threshold All-Optical Crossbar Switch on GaAs - GaAlAs Channel Waveguide Array,' Physical Optics Corporation (POC) developed the basic principles for the fabrication of all-optical crossbar switches. Based on this development. POC fabricated a 2 x 2 GaAs/GaAlAs switch that changes the direction of incident light with minimum insertion loss and nonlinear distortion. This unique technology can be used in both analog and digital networks. The applications of this technology are widespread. Because the all-optical network does not have any speed limitations (RC time constant), POC's approach will be beneficial to SONET networks, phased array radar networks, very high speed oscilloscopes, all-optical networks, IR countermeasure systems, BER equipment, and the fast growing video conferencing network market. The novel all-optical crossbar switch developed in this program will solve interconnect problems. and will be a key component in the widely proposed all-optical 200 Gb/s SONET/ATM networks. DTIC

N95-28869# Nebraska Univ., Lincoln, NE.
DRIFT MOBILITY MEASUREMENTS IN THIN FILM BORON CARBIDE Final Report
Philip Dowben 1995 8 p
(Contract F49620-94-1-0018)
(AD-A292510; AFOSR-95-0121TR) Avail: CASI HC A02/MF A01

Improvements in electronic device technology can occur through incremental changes and improvements in current and existing technologies or by the introduction of new techniques. This research program has developed a new technique for manufacturing nanoscale silicon compatible devices in a single step fabrication process leaping beyond existing technologies. Using chemical vapor techniques in combination with carefully designed source molecules, it has now become possible to fabricate thin materials by selective area processing - the 'direct writing' of material. Our general approach to device fabrication requires the use of novel source molecules for chemical vapor deposition (CVD). Synchrotron (x-ray) radiation has been employed to selectively deposit each active layer of a semiconductor device in a single step process. There is the potential that each step in fabricating a diode or thin film transistor can deposit material with submicron feature resolution. These processes are a form of projection lithography which requires far fewer steps than conventional lithography and can be employed to fabricate devices from novel semiconductors with abrupt, well characterized interfaces. DTIC

N95-28874# Michigan Univ., Ann Arbor, MI. Dept. of Electrical Engineering and Computer Science.
EPITAXIAL GROWTH AND CHARACTERIZATION OF Si(1-x)Ge(x) MATERIALS AND DEVICES Final Report
P. Bhattacharya and J. Singh Oct. 1994 24 p
(Contract AF-AFOSR-0349-91)
(AD-A292528; AFOSR-95-0141TR) Avail: CASI HC A03/MF A01

The current program of research was aimed at understanding the issues related to growth and doping of SiGe/Si heterostructures by gas-source MBE, studying the transport properties of the alloys, determining the fundamental material parameters, and designing and demonstrating electronic and optoelectronic devices. The specific electronic device is the HBT with high Ge-containing base layers, and the optoelectronic devices are detectors, photoreceivers, and electro-optic modulators. The overall objective is to demonstrate, reliably and reproducibly, the feasibility of integrating SeGe-based optoelectronics with Si-based VLSI technology. We summarize some of the highlights of the program related to work done in the last year. DTIC

N95-28910 North Carolina State Univ., Raleigh, NC.
NITRIDE SEMICONDUCTORS FOR ULTRAVIOLET DETECTION Semiannual Technical Report, 1 Jul. 1994 - 31 Dec. 1994
R. F. Davis, K. Linthicum, B. Perry, L. Smith, and W. Weeks 31 Dec. 1994 43 p Limited Reproducibility: More than 20% of this document may be affected by microfiche quality
(Contract N00014-92-J-1720)
(AD-A289546) Avail: Issuing Activity (Defense Technical Information Center (DTIC))

Monocrystalline, undoped, high resistivity GaN thin films have been

grown on (6H)-SiC(0001) wafers via organometallic vapor phase epitaxy (OMVPE) employing a high-temperature monocrystalline AlN buffer layer using a cold-wall, vertical pancake-style reactor with triethylgallium (TEG), triethylaluminum (TEA) and ammonia. The surface morphologies of films deposited on both vicinal and on-axis, Si- and C-polar planes of SiC(0001) are described. Controlled n-type Si-doping in GaN has been achieved with carrier concentrations from 10(exp 17) to 10(exp 20)/cu cm. SEM and TEM of the latter films revealed high microstructural quality Photoluminescence (PL) of the undoped GaN revealed a sharp donor-bound exciton peak at 357.2 nm with a FWHM of 4 meV. The defect peaks in these samples were very weak. The Si-doped GaN exhibited a strong PL emission at 358 nm due to donor-to-valence band transitions. Mg-doped GaN emitted strong blue light with a peak wavelength of 426 nm. Cathodoluminescence measurements of Al(x)Ga(1 - x)N were also successful, with strong emission at the band-edge. An ammonia cracker cell, has also been designed and installed in the gas source MBE to replace the ECR plasma source to minimize film damage and to enhance film quality and growth rate. Low resistivity Al, Cu3Ge, and TiN ohmic contacts have been achieved on Si-doped, n-type GaN. Au and a Au/Mg/Au layered structure exhibited ohmic behavior on p-GaN when annealed at high temperature or in the as-deposited condition, respectively. As-deposited Pt formed ohmic contacts to Mg:GaN. Microstructural characterization of the Al/n-GaN and Au/p-GaN contact systems revealed that interfacial reactions occurred during annealing and markedly affected contact performance. DTIC

N95-28933# CoreTek, Inc., Waltham, MA.
COMMERCIAL PHOTOREFRACTIVE DEVICE USING NONSTOICHIOMETRIC 3-5 SEMICONDUCTORS Final Report, 15 Jul. - 15 Dec. 1994
Parviz Tayebati 15 Dec. 1994 22 p
(Contract F49620-94-C-0037)
(AD-A292494; AFOSR-95-0127TR) Avail: CASI HC A03/MF A01

Non-stoichiometric (NS) III-V materials offer a unique opportunity to technologies such as optoelectronic based photorefractive devices that require both short carrier diffusion length and enhanced electrooptic properties. With the ability to process 2D data at rates two orders of magnitude higher than the capability of digital electronics, these devices will facilitate commercialization of enormously marketable technologies such as ultra high speed object recognition, defect and parts recognition in assembly lines and supermarkets, etc. DTIC

N95-28954 North Carolina State Univ., Raleigh, NC.
INTERFACE PROPERTIES OF WIDE BANDGAP SEMICONDUCTOR STRUCTURES Semiannual Technical Report, 1 Jul. - 31 Dec. 1994
Robert F. Davis, R. J. Nemanich, Salah Bedair, Jerry Bernholc, and Jeffrey T. Glass Dec. 1994 205 p Limited Reproducibility: More than 20% of this document may be affected by microfiche quality
(Contract N00014-92-J-1477)
(AD-A289817) Avail: Issuing Activity (Defense Technical Information Center (DTIC))

The initial stages of epitaxial growth of SiC on 6H-SiC substrates were studied by UHV STM. The results showed single bilayer undulating steps and stepped structures that were related to the annealing temperature. A new method of cleaning SiC based on silane exposure was developed, and the surfaces examined by UV photoemission showed the presence of surface electronic states. Gas source MBE growth of SiC on 2H-A1N indicated the potential of the formation of 2H-SiC, and doped 3C- and 6H-SiC have been grown on 6H-SiC. Pt films on 6H-SiC exhibited 1.26eV Schottky barrier with nearly ideal electrical properties. A planar RF system was developed for large area diamond deposition. Bias-enhanced nucleation of diamond on TiC(111) has been demonstrated. Theoretical studies of F-based ALE of diamond indicated that HF desorption is a crucial step. The negative electron affinity of H-terminated diamond was verified with combined theoretical and experimental studies. Future studies of NEA diamond surfaces will involve a new plasma system integrated into the UHV transfer line. A system for measuring electron emission has been designed. High purity GaN powder has been synthesized. ALE of GaN and InGaN has been analyzed to address several growth related difficulties. A1N and SiC/AlN pseudomorphic heterostructures have been grown by plasma assisted GSMBE. A computer controlled CVD system has been constructed for the growth of A1N, GaN and InN. OMVPE techniques have been used to prepare doped GaN monocrystalline thin films. A system has been designed for ECR deposition of the nitrides. DTIC

N95-28967# California Univ., Berkeley, CA.
STUDIES OF LATTICE-MISMATCHED AND LOW-TEMPERATURE-GROWN SEMICONDUCTOR MULTIPLE-PHASE SYSTEMS Final Report, 1 Jul. 1993 - 30 Jun. 1994
J. S. Smith and E. Weber 18 Nov. 1994 14 p
(Contract AF-AFOSR-0327-91)
(AD-A292536; Rept-442427-22518; AFOSR-95-0124TR) Avail: CASI HC A03/MF A01

The research efforts for this project were aimed at implementing novel concepts in the integration of GaAs and Si structures for optoelectronic applications. A major breakthrough in the area of nanofabrication of foreign microstructures on host substrates was achieved. DTIC

N95-28993# Duke Univ., Durham, NC. Dept. of Chemistry.
SYNTHESIS AND COMPLETE CHARACTERIZATION OF A GALLIUM-MIXED-PNICOGEN FOUR-MEMBERED RING COMPOUND: I2GaAs(SiMe3)(SUB 2)Ga(I)2P(SiMe3)(SUB 2)
Richard L. Wells, Steven R. Aubuchon, Michael S. Lube, and Peter S. White 11 Mar. 1995 19 p
(Contracts N00014-89-J-1545; N00014-95-1-0194)
(AD-A292423; DU/DC/TR-49) Avail: CASI HC A03/MF A01

The quest for single-source precursors to binary 13-15 compound semiconductors has led to the discovery of many novel compounds of varying structures and compositions. This search has been recently expanded to include precursors to ternary 13-15 compound semiconductors, although few successful accounts of such species have been recorded to date. Cowley, et al, have reported NMR evidence for a mixed-metal complex of formula Me2GaP(tBu)2InMe2P(tBu)2, however no detailed structural information was reported for this complex. Previous attempts to prepare ternary 13-15 compounds in our laboratory have proven difficult, as direct syntheses of such compounds from binary 13-15 precursors often yielded binary ligand rearrangement products instead of the desired ternary compound. DTIC

N95-29013# Army Research Lab., Aberdeen Proving Ground, MD.
BALLISTIC PENETRATION PHENOMENOLOGY OF HIGH SYMMETRY SINGLE CRYSTALS Final Report, Mar. 1989 - Mar. 1990
Pat W. Kingman and Rodney A. Herring Feb. 1995 32 p
(AD-A292476; ARL-TR-700) Avail: CASI HC A03/MF A01

The ballistic performance of tungsten single crystal penetrators is known to be a function of crystallographic symmetry. The macroscopic deformation geometry of both single crystal and polycrystal tungsten penetrators is a continuous eversion of the rod into a hollow tube. The differences in energy partitioning leading to these variations in ballistic performance must therefore be accounted for by detailed material deformation processes governed by crystallographic orientation. Inferences about these processes have been drawn from microstructural characterization of recovered penetrators. Residual penetrators of both 011 and 111 orientations were found to have repeatedly deformed and recrystalized, but the actual operative processes led to quite different macrostructures, microstructures, and penetration depths. The 001 orientation deformed by a unique process which allowed very efficient deformation, resulting in maximum penetration depth. These single crystal experiments demonstrate the critical role of detailed deformation processes in determining the final penetration depths even when similar macroscopic material flow geometry occurs. DTIC

N95-29087# California Inst. of Tech., Pasadena, CA.
GROWTH, CHARACTERIZATION AND APPLICATION OF KTN FAMILY NONLINEAR OPTICAL CRYSTALS Final Report, 12 Aug. 1992 - 30 Jun. 1994
Amnon Yariv, Anthony Kewitsch, and Rudy Hofmeister 8 Nov. 1994 7 p
(Contract DAAL03-91-G-0305)
(AD-A290330; ARO-29321.3-PH) Avail: CASI HC A02/MF A01

We have recently grown KLTN:(Cu, Ni, Ni/Ti) and strontium barium titanate (SBT) crystals and characterized their nonlinear-optical properties. The growth of these high quality crystals is a result of recent improvements

in the crystal growth system; namely, improved flux uniformity and higher operating temperature. These and other materials have been characterized for application to holographic data storage and quasi-phase matched second harmonic generation. In particular, the paraelectric KLTN materials doped with Ni exhibit an enhanced long wavelength sensitivity (greater than 600 nm), which is desirable for recording holograms with ubiquitous He-Ne or semiconductor lasers. Furthermore, we have discovered that dynamic ferroelectric domain gratings in addition to the more common electrooptic gratings are present in strontium barium niobate (SBN), a close relative of SBT. This has important applications to permanent fixing of volume holograms and tunable quasi-phase matching. To complement this experimental work, we have also derived analytical expressions for the two beam coupling process which allows us to deduce photorefractive material parameters for these crystals. This balance of experimental and theoretical work has enabled us to continually develop new materials whose properties are optimized for nonlinear optical applications. DTIC

N95-29089# Florida Univ., Gainesville, FL.
DEVELOPMENT OF ULTRA-LOW DARK CURRENT, HIGH PERFORMANCE 3-5 QUANTUM WELL INFRARED PHOTODETECTORS (QWIPS) FOR FOCAL PLANE ARRAYS STARING IMAGING SENSOR SYSTEMS Final Technical Report, 1 Aug. 1991 - 31 Jan. 1995
Sheng S. Li 1 Feb. 1995 209 p
(Contract N00014-91-J-1976)
(AD-A290343) Avail: CASI HC A10/MF A03

Specific achievements include: (1) development of the first bound-to-miniband (BTM) transition GaAs/GaAlAs QWIP for 8-12 micrometers detection - large area (128x128, 256x256, and 512x512) focal plane arrays (FPAs) based on the BTM QWIP structure have been demonstrated by Martin Marietta with excellent imagery; (2) development of a normal incidence type-II AlAs/AlGaAs QWIP grown on (110) GaAs substrate for multicolor detection in the 3-5 and 8-14 micrometers spectral windows; (3) design of 2-D metal grating couplers for efficient coupling of normal incidence IR radiation in n-type QWIPs; and (4) development of two new normal incidence p-type strained-layer III-V QWIPs for 3-5 and 8-12 micrometers detection. An ultra-low dark current p-type tensile strained-layer (PTSL) In(0.3)Ga(0.7)As/In(0.52)Al(0.48)As QWIP grown on InP by MBE for 8-12 micrometers detection has been developed with BLIP condition for T less than 100 K. The BLIP detectivity for this PTSL-QWIP was found to be 5.9 x 10(exp 10) Jones at 8.1 micrometers, V(sub b) = 2 V, and T = 77 K. A new p-type compressive strained-layer (PCSL) In(0.4)Ga(0.6)As/GaAs QWIP grown on GaAs substrate for 3-5 and 8-14 micrometers was demonstrated for the first time. Detectivity for this PCSL-QWIP was found to be 4.0 x 10(exp 9) Jones at 8.9 micrometers, V(sub b) = 0.3 V, and T = 75 K. DTIC

N95-29134# Argonne National Lab., IL.
CRYSTAL FIELD AND EXCHANGE INTERACTIONS IN DyT4Al8 (T = Fe AND Mn)
M. Loewenhaupt, P. Tils, W. Hahn, and C. K. Loong 1994 6 p Presented at the 1994 Fall Meeting of the Materials Research Society, Boston, MA, 28 Nov. - 2 Dec. 1994
(Contract W-31-109-eng-38)
(DE95-007131; ANL/IPNS/CP-83322; CONF-941144-80) Avail: CASI HC A02/MF A01

The authors investigated the magnetic excitations in polycrystalline samples of hard magnet related compounds DyFe4Al8 and DyMn4Al8 by neutron spectroscopy. For both compounds the magnetic spectra at energies below 40 meV are dominated by the response of the Dy(3+) ions. In DyMn4Al8 they observed pure crystal-field transitions within the Dy(3+) J = 15/2 ground multiplet ID which is split into 8 doublets under the low point-group symmetry of 4/mmm. In DyFe4Al8 the Dy crystal-field-split states are perturbed by the molecular fields of the ordered Fe sublattice. DOE

N95-29152# Wayne State Univ., Detroit, MI.
TRANSPORT PHENOMENA AND NOISE IN REAL QUANTUM WIRES Final Report, 30 Mar. 1992 - 1 Sep. 1994
Vladimir Mitin Dec. 1994 10 p
(Contract DAAL03-92-G-0044)
(AD-A290493; ARO-29541.13-EL) Avail: CASI HC A02/MF A01

We have calculated electron scattering by confined LO, localized SO, and bulk-like acoustic phonons in quantum wires (QWIs). We have demonstrated that the role of LO phonon scattering is dominant in a wide range of parameters. The elasticity of acoustic phonon scattering has been a commonly used approximation. Our results demonstrate that electron scattering by acoustic phonons in QWIs becomes essentially inelastic and is an effective mechanism of energy dissipation. We have obtained superlinear electron transport in QWIs at low temperatures. This superlinearity stems from reduction of acoustic phonon scattering efficiency when the electron system is heated. We have discovered a novel effect of negative absolute photoconductivity in QWIs. This effect is caused by strong asymmetry of the electron distribution function due to resonant scattering by optical phonons. We have investigated the role of different phonons on electron transport in and have found that a square cross-section is optimum for high mobilities. We have calculated nonequilibrium electron noise in QWIs. Our results show that a major noise source in QWIs is electron scattering by acoustic (low field) and optical (high field) phonons. In general, noise in QWIs is essentially suppressed. DTIC

N95-29157# Sandia National Labs., Albuquerque, NM.
SELF-STRESSING STRUCTURES FOR WAFER-LEVEL OXIDE BREAKDOWN TO 200 MHz
E. S. Snyder, D. M. Tanner, M. R. Bowles, S. E. Swanson, C. H. Anderson (Philips Semiconductors, Albuqerque, NM.), and J. P. Perry (Philips Semiconductors, Albuqerque, NM.) 1995 6 p Presented at the 1994 Integrated Reliability Workshop, Lake Tahoe, CA, 16-19 Oct. 1994
(Contract DE-AC04-94AL-85000)
(DE95-006818; SAND-95-0146C; CONF-9410311-1) Avail: CASI HC A02/MF A01

We have demonstrated for the first time high frequency (210 MHz) oxide breakdown at the wafer-level using on-chip, self-stressing test structures. This is the highest frequency oxide breakdown that has been reported. We used these structures to characterize the variation in oxide breakdown with frequency (from 1 Hz to over 200 MHz) and duty cycle (from 10% to 90%). Since the stress frequency, duty cycle and temperature are controlled by DC signals in these structures, we used conventional DC wafer-level equipment without any special modifications (such as high frequency cabling). This self-stressing structure significantly reduces the cost of performing realistic high frequency oxide breakdown experiments necessary for developing reliability models and building-in-reliability. DOE

N95-29165# California Univ., Berkeley, CA.
ELECTRONIC PROPERTIES OF LOW-TEMPERATURE GROWN III/V THIN FILMS Final Technical Report, 1 Jul. 1991 - 30 Jun. 1994
Eicke Weber 5 Dec. 1994 17 p
(Grant AF-AFOSR-0321-91)
(AD-A292521; AFOSR-95-0135TR) Avail: CASI HC A03/MF A01

Our study of LT GaAs in the previous contract is furthered by: (1) employing several novel techniques to investigate the defects present and the transport mechanism in LT GaAs; (2) expanding to other LT-III/V compounds; and (3) exploring the unique properties of these LT semiconductors for device applications. Photocurrent spectroscopy of annealed LT GaAs gives clear evidence of substantial presence of As(sub Ga) defects in the material. The 'internal photoemission' spectrum is actually found to be due to photoexcitation from As(sub Ga) defects. Magnetic circular dichroism and near-infrared absorption provide sensitive and quantitative measurements of the concentration of the As(sub Ga) defects in both neutral and positively charged states. A systematical study of materials grown and annealed at different temperatures shows that As(sub Ga) defects can account for the pinning of Fermi energy and play a dominant role in the materials. Nuclear magnetic resonance has started to be used to study LT GaAs. Although the study is in its early stage, it has been demonstrated that by using a spin echo technique it is possible to obtain characteristic responses from As in perfect sites and defective sites. in contrast to LT GaAs. LT InP was found to be highly conductive. DTIC

N95-29209# Gordon Research Conferences, Inc., Kingston, RI.
GORDON RESEARCH CONFERENCE ON POINT DEFECTS, LINE DEFECTS, AND INTERFACES IN SEMICONDUCTORS Final Report
Michael Stavola 5 Aug. 1994 18 p Conference held in Plymouth, NH, 31 Jul. - 5 Aug. 1994
(Contract N00014-94-1-0578)
(AD-A290103) Avail: CASI HC A03/MF A01

The technical program has continued to evolve and to deal with the hottest new issues, the field of defects. There were two sessions on defects in wide bandgap semiconductors like the group III nitrides and II-VI materials that are receiving much recent attention because of renewed interest in visible optical devices. The presentation of very fundamental research was mixed with device-related defect problems which led to well balanced sessions which should help the community to focus on important issues. Heteroepitaxy and related defect issues continue to play an important role. Talks on strain relief in SiGe epitaxial layers and on the interactions of defects with surfaces and interfaces were especially exciting and well received. Studies of point defects continue to generate exciting results. The talks by Johnson and Estreicher on hydrogen in semiconductors raised several controversial issues which were vigorously discussed. DTIC

N95-29234# Missouri Univ., Rolla, MO.
CONSIDERATION OF MICROSTRUCTURAL CHANGES IN THE STUDY OF ADIABATIC SHEAR BANDS Final Report, 10 Mar. 1991 - 9 Sep. 1994
Romesh C. Batra Sep. 1994 159 p
(Contract DAAL03-91-G-0084)
(AD-A290398; ARO-28283.22-EG) Avail: CASI HC A08/MF A02

We have analyzed the effect of microstructural changes on the initiation and growth of shear bands. These have been studied by developing an adaptive mesh refinement technique to decipher adiabatic shear bands in two-dimensional problems, formulating a three-dimensional finite-deformation theory for dipolar thermoviscoplastic materials and using it to examine the initiation and growth of shear bands in plane strain thermomechanical deformations of dipolar materials, employing an internal variable theory of Brown, Kim and Anand to study the shear band problem, investigating the possibility of phase transformations during the development of adiabatic shear bands in a steel specimen, ascertaining the speed of propagation of a shear band in a steel tube, assessing the effect of frictional forces between the loading device and the cylinder ends, and, analyzing the development of a shear band in a FCC single crystal. Principal results obtained during these investigations are summarized in the report. DTIC

N95-29267# Oregon Graduate Inst. of Science and Technology, Portland, OR. Dept. of Electrical Engineering and Applied Physics.
LOW TEMPERATURE MATERIALS GROWTH AND PROCESSING DEVELOPMENT FOR FLAT PANEL DISPLAY TECHNOLOGY APPLICATIONS Quarterly Technical Report, 15 Nov. 1994 - 14 Feb. 1995
C. Neil Berglund 14 Feb. 1995 13 p
(Contract N00014-93-1-0312)
(AD-A292177) Avail: CASI HC A03/MF A01

The project goal is to make DC, AC, transient measurements on the TFT's, fabricated by Professor Sigmon and his group at Arizona State University using low temperature processing techniques. From these measurements, SPICE parameters will be extracted and these results will be used for process monitoring and device and process optimization for display applications. The devices from ASU are expected to be ready during the later part of 1995. Meanwhile, previously obtained measurements on TET's fabricated at Tektronix Inc. are being used to establish a reliable extraction methodology. DTIC

N95-29438# Northwestern Univ., Evanston, IL. Dept. of Physics and Astronomy.
STRUCTURAL AND ELECTRONIC PROPERTIES OF ADSORBATES ON SEMICONDUCTORS, METAL-SEMICONDUCTOR INTERFACES AND SEMICONDUCTOR HETEROJUNCTIONS Report, 1 Nov. 1991 - 31 Oct. 1994
A. J. Freeman 7 Mar. 1995 10 p
(Contract N00014-89-J-1290)
(AD-A291917) Avail: CASI HC A02/MF A01

Studies of the electronic structure of adsorbates on metal-semiconductor and semiconductor-semiconductor interfaces and semiconductor surfaces were carried out using the molecular cluster LCAO-DVM method (as developed into the DMo1 program) also in a full potential local (spin) density approach. The new capability of DMo1 to calculate atomic forces allows automatic geometry optimization; and allowed us to study atomic relaxation and reconstruction at the surfaces and interfaces with and without adsorbates. The method calculated variationally self-consistent highly precise solutions of the local density equations with which to determine the structural and electronic properties of the system. Specific problems addressed included studies of: (1) semiconductor heterojunctions (and their bulk constituents) such as Sn/Ge; and (2) adsorbates on silicon and germanium. The research led to the development of general concepts and simpler theoretical models with which to understand the electronic structure and the relevant parameters governing the interaction between the adsorbate and the substrate. Predictions of theory were compared with experiment. Accurate total energy investigations were undertaken to determine from first principles, equilibrium, internuclear distances, vibrational frequencies, separations and positional (geometric) bonding configurations. DTIC

N95-29444# Duke Univ., Durham, NC. Dept. of Chemistry.
SYNTHESIS AND CHARACTERIZATION OF (Me3SiCH2)3M(DOT)E(SiMe3)3 (M = Ga, E = P OR As; M = In, E = P). X-RAY CRYSTAL STRUCTURES OF (Me3SiCH2)3Ga(DOT)P(SiMe3)3 AND (Me3SiCH2)3In(DOT)P(SiMe3)3
Richard L. Wells, Ryan A. Baldwin, and Peter S. White 6 Mar. 1995 22 p
(Contract N00014-89-J-1545)
(AD-A291907; DU/DC/TR-47) Avail: CASI HC A03/MF A01

Recent investigations in our laboratory have centered on the facile formation of the 13-15 bond by reactions of organo-group 13 reagents with either the silylpnicogen compounds E(SiMe3)3 (E=P or As) or their monolithium salts in solution. As a result of our efforts, we have isolated several new compounds containing the 13-15 covalent bond. Included in our results are compounds which exhibit dimeric structures in the solid-state and those in which two group 13 centers are bridged by a halogen atom and a group 15 atom. In addition, adducts of the type R3M(dot)E(SiMe3)3 (R = Me3SiCH2, M = In, E = As(3); R = Ph(3) or C6F5(4), M = Ga, E = As or P) have been isolated in our laboratory. Adducts of this type may find utility as potential single source precursors to binary 13-15 semiconductors; however, a review of the literature finds limited structural and thermal analysis data for adducts of this type. We report herein the synthesis, characterization, and thermal analysis of three new main group adducts, (Me3SiCH2)Ga(dot)P(SiMe3)3; (Me3SiCH2)3Ga(dot)As(SiMe3)3; and (Me3SiCH2)3In(dot)e3)3. DTIC

N95-29486# Duke Univ., Durham, NC. Dept. of Chemistry.
SYNTHESIS OF NANOCRYSTALLINE INDIUM ARSENIDE AND INDIUM PHOSPHIDE FROM INDIUM(III) HALIDES AND TRIS(TRIMETHYLSILYL)PNICOGENS; SYNTHESIS, CHARACTERIZATION, AND DECOMPOSITION BEHAVIOR OF I3In(DOT)P(SiMe3)3
Richard L. Wells, Steven R. Aubuchon, Shreyas S. Kher, Michael S. Lube, and Peter S. White 6 Mar. 1995 39 p
(Contract N00014-89-J-1545)
(AD-A291905; DU/DC/TR-48) Avail: CASI HC A03/MF A01

Nanocrystalline indium arsenide and indium phosphide were synthesized by heating the products of the independent 1:1 mole ratio reactions of InX3 (X = Cl, Br, I) with As(SiMe3)3 and P(SiMe3)3, respectively, and the 2:1 mole ratio reaction of InCl3 with As(SiMe3)3. The 1:1 mole ratio reaction of As(SiMe3)3 with InCl3 produced a black powder, which after annealing at 400 C afforded InAs crystallites of up to 99.96% purity with an average domain size of 9 nm. InAs obtained from the separate 1:1 mole ratio reactions of InBr3 and InI3 with As(SiMe3)3 and the 2:1 mole ratio reaction of InCl3 with As(SiMe3)3 consisted of crystallites with average domain sizes of 10, 12, and 16 nm, and purities of 99.65%, 85.95%, and 87.90%, respectively. The independent 1:1 mole ratio reactions of InCl3 and InBr3 with P(SiMe3)3 both produced colored powders, which after annealing afforded nanocrystalline InP particles with respective purities of 91.53% and 93.08% and average domain size of approximately 4 nm for both samples. The 1:1 mole reaction of InI3 with P(SiMe3)3 afforded the 1:1 adduct I3In.P(SiMe3)3 (I). Compound 1 crystallizes in the monoclinic system, space group P 2(1)/c, with a = 16.074(7), b = 9.730(3), C = 16.454(6) A, V = 2362.1(15) cu A, D(calc) = 2.098 g/cu cm for Z = 4; the In-P bond length is 2.537(3) A. Decomposition of 1 affords nanocrystalline InP of 84.06% purity with an approximate average domain size of 2.5 nm.
DTIC

N95-29493# Illinois Univ., Urbana, IL. Dept. of Chemistry.
TRANSITIONS IN LIQUID CRYSTALS INITIATED WITH CIRCULARLY POLARIZED LIGHT Final Report, 1 Jun. 1991 - 31 May 1994
Gary B. Schuster Sep. 1994 13 p
(Contract ARO-MIPR-111-94)
(AD-A290525; ARO-28319.4-CH) Avail: CASI HC A03/MF A01

The fundamental goal of this research is the discovery of new means to control the physical and optical properties of liquid crystals with light. In work on this project we focused on the development of chiroptical triggers designed to induce a reversible nematic to cholesteric transition in a liquid crystal under the influence of circularly polarized light. Three classes of systems were investigated -- biaryl chromophores, axially symmetric benzylidene cyclohexanes, and chiral cycloheptatrienes. None of these compounds meet all of the requirements for a chiroptical trigger, but the knowledge gained enables a clearer definition of the properties a successful trigger must possess. DTIC

N95-29506# Missouri Univ., Columbia, MO. Dept. of Physics and Astronomy.
RAMAN AND PHOTO-MODULATED REFLECTIVITY STUDIES OF ZnTe/InAs SEMICONDUCTOR HETEROSTRUCTURE UNDER HYDROSTATIC PRESSURE
Robert J. Thomas, Mark S. Boley, H. R. Chandrasekhar, Meera Chandrasekhar, and C. Parks 1994 5 p
(Contract DAAL03-92-G-0381)
(AD-A290467; ARO-29682.4-PH) Avail: CASI HC A01/MF A01

The photo-modulated reflectivity spectrum of a biaxially-strained pseudomorphic ZnTe epilayer, grown on an InAs epilayer by molecular beam epitaxy is studied as a function of applied hydrostatic pressure at 80 K. With increasing hydrostatic compression, the biaxially compressive strain is progressively compensated by the pressure induced tensile strain. At approximately 55 kbars the epilayer becomes strain free, and is under a biaxial tension at higher pressures. The separation between the heavy hole and light hole signatures is superlinear in pressure, suggestive of a pressure dependent shear deformation potential constant for the valence and conduction bands. We also compare the pressure dependence of the Raman LO phonon of the ZnTe epilayer on InAs with that of a bulk ZnTe sample at 13 K. The pressure dependent strain is found to be linear. Accurate values of the first order strain derivatives of the LO-phonons and mode Gruneisen constants are obtained. DTIC

N95-29658# SRI International Corp., Menlo Park, CA.
HIGH T(SUB c) SUPERCONDUCTOR/FERROELECTRIC HETEROSTRUCTURES Final Report
Daniel F. Ryder, Jr. Dec. 1994 8 p
(Contract F30602-91-D-0001)
(AD-A291016; RL-TR-94-231) Avail: CASI HC A02/MF A01

Thin films of the ferroelectric perovskite, Ba(x) Sr(1-x) TiO3 (BST), were deposited on superconducting (100)YBa2Cu3O(x)(YBCO)/(100)Yttria-stabilized zirconia(YSZ) substrates and (100)Si by ion-beam sputtering. Microstructural and compositional features of the ceramic bilayer were assessed by a combination of x-ray diffraction (XRD) and scanning electron microscopy. The films were smooth and featureless, and energy dispersive x-ray spectroscopy (EDX) data indicated that film composition closely matched target composition. XRD analysis showed that films deposited on YBCO substrates were highly c-axis textured, while the films deposited on (100)Si did not exhibit any preferred growth morphology. The superconducting properties of the YBCO substrate layer were maintained throughout the processing stages and, as such, it was demonstrated that ion beam sputtering is a viable method for the deposition of Ferroelectric/YBCO heterostructures. DTIC

N95-29767# Brown Univ., Providence, RI. Div. of Engineering.
THE NUCLEATION OF CRYSTALLINE FILMS FROM VAPOR PHASE REACTANTS Final Report, 1 Sep. 1991 - 31 Oct. 1994
Brian W. Sheldon 6 Jan. 1995 13 p
(Grant AF-AFOSR-0357-91)
(AD-A291122; AFOSR-95-0085TR) Avail: CASI HC A03/MF A01

Understanding and controlling the nucleation of diamond, silicon nitride, and silicon oxynitride was the primary objective of this research program, This work has made it possible to form the desired phase under more favorable processing conditions, and has also led to better control of the resultant film microstructures and properties. In this research we have focused on the use of thin interlayers to control and enhance nucleation. In the case of silicon oxynitride, we have also demonstrated the potential for using thin interlayers to enhance materials properties (i.e., oxidation resistance). DTIC

N95-29785# Florida Univ., Fort Lauderdale, FL.
INVESTIGATION OF A NORMAL INCIDENT HIGH PERFORMANCE P-TYPE STRAINED LAYER In(0.3)Ga(0.7)As/In(0.52)Al(0 48)As QUANTUM WELL INFRARED PHOTODETECTOR Semiannual Progress Report No. 3, 16 Jul. 1994 - 15 Feb. 1995
Jerome T. Chu and Sheng S. Li 15 Feb. 1995 44 p
(Contract N00014-93-1-0827)
(AD-A290946) Avail: CASI HC A03/MF A01

A significant achievement was made in the development of a new compressionally strained p-type GaAs/InGaAs quantum well infrared photodetector (QWIP) grown on GaAs by MBE. This new QWIP achieved two color detection with detective peaks at 8.9 and 8.4 microns in the LWIR band and 5.5 microns in the MWIR band. This detector is under background limited performance (BLIP) at temperatures up to 70 K. The measured responsivity were found to be 24 and 45 mA/W for the two LWIR peaks respectively, while a responsivity of 13 mA/W was found for the MWIR peak, all at T = 75 K. In addition, a new InGaAs/AlGaAs on GaAs compressionally strained p-QWIP was developed which exhibits extremely low dark currents and comparable responsivities when compared with the previous PCSL-QWIP. The measured responsivity was found to be 38 and 8 mA/W at T = 77 K, with the detective peaks at 7 A and 5.5 microns, respectively. The detector is under BLIP conditions at T = 63 K with applied biases from -3 to +3 V. DTIC

N95-29814# Sandia National Labs., Albuquerque, NM. Dept. of Electrical and Computer Engineering.
ELECTRONIC STATES IN Cd(1-x)Zn(x)Te/CdTe STRAINED LAYER COUPLED DOUBLE QUANTUM WELLS AND THEIR PHOTOLUMINESCENCE
Tiesheng Li (Ohio Univ., Athens, OH.), H. J. Lozykowski (Ohio Univ., Athens, OH.), and J. Reno 1994 6 p Presented at the 1994 Fall Meeting of the Materials Research Society, Boston, MA, 28 Nov. - 2 Dec. 1994
(Contracts DE-AC04-94AL-85000; F49620-94-1-0024)
(DE95-006806; SAND-95-0168C; CONF-941144-81) Avail: CASI HC A02/MF A01

Experimental and theoretical investigation of electronic states in a strained-layer CdTe/CdZnTe coupled double quantum well structure are presented. The optical properties of this lattice-mismatched heterostructure were characterized with photoluminescence (PL), PL excitation and polarization spectroscopies. Influence of electrical field on exciton states in the strained-layer CdTe/CdZnTe coupled double quantum well structure is experimentally studied. The confined electronic states were calculated in the framework of the envelope function approach, taking into account the strain effect induced by the lattice-mismatch. Experimental results are compared with the calculated transition energies. DOE

N95-29984# Argonne National Lab., IL.
PROCESSING AND PROPERTIES OF LONG-LENGTHS OF Ag-clad BSCCO SUPERCONDUCTORS AND HIGH-(Tc) MAGNETS
U. Balachandran, A. N. Iyer, R. Jammy, P. Haldar (Intermagnetics General Corp., Latham, NY.), J. G. Hoehn, Jr. (Intermagnetics General Corp., Latham, NY.), and M. Suenaga (Brookhaven National Lab., Upton, NY.) Oct. 1994 9 p Presented at the 7th International Symposium on Superconductivity, Kita Kiyushu, Japan, 8-11 Nov. 1994
(Contract W-31-109-eng-38)
(DE95-005855; ANL/ET/CP-83565; CONF-941176-3) Avail: CASI HC A02/MF A01

Long lengths of Ag-clad mono and multicore BSCCO tapes were fabricated by the powder-in-tube technique. The critical current density (J(sub c)) of 125-m-long monocore tapes was approximately 12,000 A/cm(exp 2) (critical current, I(sub c) approximately equal to 20 A) at 77 K. A 230-m-long 37-filament tape carried an I(sub c) of 14 A (corresponding to a J(sub c) of approximately 10,000 A/cm(exp 2)). Pancake-shaped coils were formed from long-length conductors by the wind-and-react approach. High-T(sub c) magnets were then assembled by stacking the pancake coils and connecting them in series. The magnets were tested as a function

of applied magnetic fields at 4.2, 27, 64, and 77 K. A magnet containing 480 m of high-T(sub c) tape generated a record-high field of 2.6 T at 4.2 K. Another magnet assembled with approximately 770 m of tape generated a field of approximately 1 T at 4.2 K and approximately 0.6 T at 27 K, both in an applied background field of approximately 20 T. Strain tolerance of high-T(sub c) tapes was evaluated by measuring J(sub c) retention as a function of applied strain in an 0.5 T applied field at 77 K. DOE

N95-29986# Argonne National Lab., IL.
WHAT DO WE REALLY KNOW ABOUT THE ATOMIC SCALE STRUCTURES OF NANOPHASE MATERIALS?
R. W. Siegel Jun. 1994 23 p Presented at the Fall Meeting of the Materials Research Society (MRS), Boston, MA, 29 Nov. - 3 Dec. 1993
(Contract W-31-109-eng-38)
(DE95-005858; ANL/MSD/CP-79956; CONF-931108-114) Avail: CASI HC A03/MF A01

Robert W. Balluffi has spent a lifetime critically investigating and elucidating the atomic scale defect structures of materials. Now, a new class of ultrafine-grained materials has been created in which such defects exercise a dominant role. The structures of these new nanophase materials, both metals and ceramics, have been investigated over the past several years by a wide range of experimental methods. These studies have included observations by x-ray and neutron scattering; transmission and scanning electron microscopy; Moessbauer, Raman, and positron annihilation spectroscopy; and most recently scanning tunneling and atomic force microscopy and nuclear magnetic resonance. While the experiments have yielded considerable useful information about the structures of nanophase materials on a variety of length scales, much about the local atomic arrangements in the grains and interfaces of these materials remains to be elucidated. The present status of the author's knowledge of these structures is reviewed and some future research needs and opportunities are considered. DOE

N95-29990# Sandia National Labs., Albuquerque, NM.
INTERFACES IN InAsSb/InGaAs STRAINED-LAYER SUPERLATTICES GROWN BY MOCVD FOR USE IN INFRARED EMITTERS
R. M. Biefeld, D. M. Follstaedt, S. R. Kurtz, and K. C. Baucom 1995 6 p Presented at the International Conference on Narrow Gap Semiconductors, Santa Fe, NM, 9-12 Jan. 1995
(Contract DE-AC04-94AL-85000)
(DE95-006323; SAND-94-2292C; CONF-950167-3) Avail: CASI HC A02/MF A01

The authors have prepared InAsSb/InGaAs strained-layer superlattices (SLS's) using metal-organic chemical vapor deposition (MOCVD). X-ray diffraction was used to determine lattice matching as well as composition and structure of the SLS's. The presence of an InGaAsSb interface layer was indicated by x-ray diffraction for samples grown under nonoptimized conditions. Interfacial layers were also identified with transmission electron microscopy (TEM). Two types of interfaces were observed by TEM. The different contrasts observed by TEM could be due to a difference in composition at the interfaces. The width of the x-ray peaks can be explained by a variation of the layer thickness. DOE

N95-30005# Sandia National Labs., Albuquerque, NM.
ORDERING AND BANDGAP REDUCTION IN InAs(1-x)Sb(x) ALLOYS
D. M. Follstaedt, R. M. Biefeld, S. R. Kurtz, L. R. Dawson, and K. C. Baucom 1995 6 p Presented at the International Conference on Narrow Gap Semiconductors, Santa Fe, NM, 9-12 Jan. 1995
(Contract DE-AC04-94AL-85000)
(DE95-006324; SAND-94-2288C; CONF-950167-2) Avail: CASI HC A02/MF A01

InAs(1-x)Sb(x) alloys grown by MBE and MOCVD are found to have reduced emission energies due to CuPt-type order, even for Sb concentrations as low as x = 0.07 (Delta E = 25-65 meV). Cross-section TEM examination of such alloys shows the two /111/(sub B) variants are separated into regions 1-2 microns across with platelet domains 10-40 nm thick on habit planes tilted approximately 30 deg from the (001) growth surface. Nomarski optical images show a cross-hatched surface pattern expected for lattice-mismatched layers. The local tilt of the surface correlates with the dominant variant in each region. InAs(1-x)Sb(x)/In(1-y)Ga(y)As strained-layer superlattices with low Sb content and flat surfaces also show CuPt ordering. DOE

N95-30022# Sandia National Labs., Albuquerque, NM.
ION BEAM MODIFICATION OF Tl-Ba-Ca-Cu-O TYPE HIGH TEMPERATURE SUPERCONDUCTORS DURING IRRADIATION
P. P. Newcomer, B. Morosin, and L. M. Wang (New Mexico Univ., Albuquerque, NM.) 1994 6 p Presented at the 1994 Fall Meeting of the Materials Research Society (MRS), Boston, MA, 28 Nov. - 2 Dec. 1994
(Contract DE-AC04-94AL-85000)
(DE95-006807; SAND-94-1731C; CONF-941144-82) Avail: CASI HC A02/MF A01

Microstructural modification of high temperature superconductor (HTS) single-crystal plates of Tl-1212 and Tl-2212 (numbers designate the Tl/Ba/Ca/Cu cation ratio) was studied during 1.5 MeV Kr(+) and Xe(+) ion irradiation with in-situ electron diffraction and after ion irradiation with high resolution TEM (HRTEM). Similar in-situ temperature dependence effects are seen for both phases. During irradiations from 22 K to 673 K, an amorphous halo develops after very low ion dose or fluence (1.7 x 10(exp 12) ions/cm(exp 2)). During irradiation at 100 and 300 K, complete amorphization is obtained, while at 22 and greater than or equal to 533 K, the halo fades slightly and a polycrystalline ring pattern develops, indicating ion irradiation induced crystallization occurred. After a low ion dose (8.5 x 10(exp 12) ions/cm(exp 2)) at 100 and 300 K, HRTEM reveals amorphous regions 5-20 nm in size which are not columnar and do not all penetrate the entire sample thickness. At 22 and greater than or equal to 533 K, Moire fringes and misoriented crystallites of cascade size are observed. The 4-6 nm crystallites are thallium-rich. DOE

N95-30068# Advanced Fuel Research, Inc., East Hartford, CT.
EPITAXIAL GROWTH OF HIGH QUALITY SiC OF PULSED LASER DEPOSITION, PHASE 1 Final Report, 21 Jul. 1994 - 21 Jan. 1995
David G. Hamblen, David B. Fenner, Peter A. Rosenthal, Joseph Cosgrove, and Pang-Jen Kung 20 Feb. 1995 44 p
(Contract F33615-94-C-5417)
(AD-A291410; Rept-526033) Avail: CASI HC A03/MF A01

The goal of this research program is to develop Pulsed Laser Deposition (PLD) as a method for depositing device quality, single crystal silicon carbide (SiC) thin films. Phase 1 has demonstrated the ability to deposit single crystal 3C-SiC thin films on Si(100) and 6H-SiC(0001) substrates. An existing PLD facility was improved for SiC depositions. Prior to PLD, all substrates were prepared using a novel spin etch technique. Numerous experiments explored the effect of substrate temperature and laser fluence on the resulting SiC films. Composition of the films was measured by Rutherford backscattering spectrometry and Scanning Auger Microprobe. The films were slightly carbon-rich although the excess carbon component was attributed to background contaminants in our vacuum system. Optical analyses included Fourier Transform infrared (FT-IR) spectroscopy. Epitaxy of the 3C-SiC films was confirmed by x-ray diffraction, transmission electron microscopy, and electron diffraction. Epitaxial SiC films were grown on Si(100) at temperatures as low as 930 C, although the crystallinity of the films improved with increasing temperature. The best films result at laser fluences of 1.5 - 2 J/sq cm. Single crystal films were obtained on 6H-SiC(0001) and vicinal 6H-SiC(0001) oriented 3.5 towards (1120) at 1200 C. DTIC

N95-30077# Argonne National Lab., IL.
NEUTRON SCATTERING FROM AMORPHOUS, DISORDERED AND NANOCRYSTALLINE MATERIALS
D. L. Price Oct. 1994 18 p Presented at the Workshop on Neutron Applications in Materials Science and Engineering, Chalk River, Canada, 17 Aug. 1994
(Contract W-31-109-eng-38)
(DE95-005848; ANL/MSD/CP-84502; CONF-9408211-2) Avail: CASI HC A03/MF A01

The author has described the power of neutron diffraction and inelastic scattering techniques for determining the structure and dynamics of disordered systems, using the archetypal glass SiO2 as a detailed example. Of course the field of amorphous and disordered systems contains a much greater variety of types of materials exhibiting a wide range of possible types of disorder. The author gives a brief review of the varieties of order and disorder exhibited by condensed matter. DOE

N95-30164# Department of the Navy, Washington, DC.
APPARATUS AND METHOD FOR ACHIEVING GROWTH-ETCH DEPOSITION OF DIAMOND USING A CHOPPED OXYGEN-ACETYLENE FLAME Patent Application
Thomas P. Thorpe, inventor (to Navy) and Ronald A. Weimer, inventor (to Navy) 4 Nov. 1994 29 p
(AD-D017322; US-Patent-Appl-SN-334088) Avail: CASI HC A03/MF A01

A novel apparatus and method for the cyclic growth-etch deposition of diamond on a substrate by flame chemical vapor deposition (CVD) is developed. The cyclic growth-etch diamond deposition is accomplished by placing a suitable substrate to be coated under a CVD flame and providing a disk or face plate or other shapes having one or more teeth (or holes) wherein upon rotation of the disk, or face plate, or other shape, the teeth attached to the disk, or face plate, or other shape obstruct the path of the CVD flame from contacting the substrate at a desired time scale of T(growth) and t(cycle) to produce high quality FWHM of 1-3.5/cm diamond. DTIC

N95-30184# Argonne National Lab., IL. Experimental Facilities Div.
A FINITE ELEMENT ANALYSIS OF ROOM TEMPERATURE SILICON CRYSTALS FOR THE ADVANCED PHOTON SOURCE BENDING-MAGNET AND INSERTION-DEVICE BEAMS
Lahsen Assoufid, Wah-Keat Lee, and Dennis M. Mills Oct. 1994 23 p Presented at the International Meeting on Synchrotron Radiation Instrumentation, Stony Brook, NY, 18-22 Jul. 1994
(Contract W-31-109-eng-38)
(DE95-005822; ANL/XFD/CP-82848; CONF-940714-52) Avail: CASI HC A03/MF A01

In this paper, we give the results of a series of thermal and distortion finite element analyses performed on room temperature silicon for the three standard APS sources, namely, the bending magnet, Wiggler A, and Undulator A. The modeling was performed with the silicon cooled directly with water or liquid gallium through rectangular channels. DOE

N95-30214# Sandia National Labs., Albuquerque, NM.
DEFECT CENTERS IN CHEMICAL-MECHANICAL POLISHED MOS OXIDES
M. R. Shaneyfelt, W. L. Warren, D. L. Hetherington, R. P. Timon, P. J. Resnick, and P. S. Winokur 1994 5 p Presented at the INFOS '95 Conference: Insulating Films on Semiconductors, Grenoble, France, 7-10 J un. 1995
(Contract DE-AC04-94AL-85000)
(DE95-004777; SAND-94-2619C; CONF-9506105-1) Avail: CASI HC A01/MF A01

Defect centers generated in vacuum-ultraviolet irradiated chemical-mechanical polished oxides have been characterized using electron paramagnetic resonance and C-V analysis. Both oxide trap E(sub (gamma)) and interface trap P(sub b0) centers were detected in unpolished and polished oxides. In addition, another interface defect center known as the P(sub b1) center was only identified in the polished oxides, suggesting that the polishing process altered the SiO2/Si interface. DOE

N95-30298# Rensselaer Polytechnic Inst., Troy, NY.
PHOTONIC BAND STRUCTURES FOR OPTOELECTRONICS Final Report, 20 Aug. 1993 - 19 Aug. 1994
Joseph W. Haus and H. Sami Sozuer 29 Dec. 1994 9 p
(Contract DAAH04-93-G-0416)
(AD-A291154) Avail: CASI HC A02/MF A01

The grant partially funded an examination of photonic band structures. We report a new geometry based on stacking layers of dielectric rods; the dispersion curves reveal a large direct band gap. A collaborative experiment-theory effort was developed to characterize new two-dimensional structures with a band gap in the infrared. The lattice constant is three orders of magnitude smaller than all previous reports. Finally, a novel real-space numerical method was applied to one-dimensional structures; the technique can be extended to higher dimensions and it is useful for finite-sized systems and pulse propagation. DTIC

77 THERMODYNAMICS AND STATISTICAL PHYSICS

Includes quantum mechanics; theoretical physics; and Bose and Fermi statistics.

For related information see also *25 Inorganic and Physical Chemistry* and *34 Fluid Mechanics and Heat Transfer.*

N95-28857# IBM Watson Research Center, Yorktown Heights, NY.
NOVEL ELECTRIC-FIELD EFFECTS IN QUANTUM WELLS AND SUPERLATTICES Final Report, Jul. - Dec. 1994
Emilio E. Mendez 16 Mar. 1995 5 p
(Contract DAAH04-94-C-0007)
(AD-A292317; ARO-32287.1-PH) Avail: CASI HC A02/MF A01

This report summarizes the most important result obtained during the short span of this grant, namely, the (theoretical) possibility of electric-field induced TE to TM mode switching in semiconductor quantum well lasers under moderate tensile strain. DTIC

N95-28927# Weizmann Inst. of Science, Rehovot (Israel). Dept. of Chemical Physics.
SELF-INDUCED TRANSPARENCY IN PHOTONIC BAND STRUCTURES: GAP SOLITONS NEAR ABSORPTION RESONANCES 3rd Interim Report, Dec. 1994 - Feb. 1995
Gershon Kurizki Feb. 1995 4 p
(Contract N68171-94-C-9081)
(AD-A292187; R/D-7345-PH-01) Avail: CASI HC A01/MF A01

Pulse propagation in a nonuniform resonant medium, e.g., a periodic array of resonant films, can destroy self-induced transparency (SIT), because the pulse area is then split between the forward and backward (reflected) coupled waves, and is no longer conserved. Should we then anticipate severely hampered transmission through a medium whose resonance lies in a reflective spectral domain (photonic band gap) of a periodically-layered structure (a Bragg reflector)? We have shown analytically that it is possible for the pulse to overcome the band-gap reflection and produce SIT in a near-resonant medium embedded in a Bragg reflector. The predicted SIT propagation is a principally new type of a gap soliton, which does not obey any of the familiar soliton equations, such as the nonlinear Schroedinger equation (NLSE) or the sine-Gordon equation. Its spatio-temporal form and intensity dependence are shown here to be distinct from the extensively-studied gap solitons in Kerr-nonlinear Bragg reflectors, which are described by the NLSE. In treatments of bidirectional field propagation in media with arbitrary spatial distribution of near-resonant atoms the Bloch equations for the population inversion and polarization are entangled in a fashion which leads to an infinite hierarchy of equations for successive spatial harmonics. DTIC

N95-29009# Missouri Univ., Saint Louis, MO. Dept. of Physics.
THE 6TH VAN DER ZIEL SYMPOSIUM ON QUANTUM 1/F NOISE AND OTHER LOW FREQUENCY FLUCTUATIONS IN ELECTRONIC DEVICES Final Report, 15 Apr. - 14 Oct. 1994
Peter H. Handel 7 Dec. 1994 18 p Symposium held in St. Louis, MO, 27-28 May 1994
(Contract F49620-94-1-0230)
(AD-A292468; AFOSR-95-0154TR) Avail: CASI HC A03/MF A01

This report acknowledges funding for the 6th van der Ziel Symposium on Quantum 1/f Noise and Other Low Frequency Fluctuations in Electronic Devices, which was organized by the author at the University of Missouri - St. Louis, on May 27-28, 1994. Like the previous symposia organized by us in October 1985, October 1986, April 1988, May 1990 and May 1992, this event brought together 24 researchers from universities, industrial and governmental research laboratories, and the industry, working in the field of Quantum 1/f Noise and other low frequency fluctuations in high - technology devices. A total of 21 papers was presented, including 6 invited papers. They mark important progress in the field, both in theory and experiment. The proceedings are still in print, and 6 copies will be appended as soon as they come out. DTIC

N95-29149# Illinois Univ. at Urbana-Champaign, Savoy, IL. Urbana Coordinated Science Lab.
TRANSPORT SIMULATION IN SPATIALLY MODULATED LOW DIMENSIONALITY SYSTEMS Final Report, 1 Apr. 1991 - 30 Sep. 1994

J. P. LeBurton 16 Nov. 1994 6 p
(Contract DAAL03-91-G-0052)
(AD-A290486; ARO-28406.11-EL) Avail: CASI HC A02/MF A01

The research effort addresses several issues related to nonlinear transport in quantum wire systems characterized by spatially nonuniform confinement. We have successively investigated quantum transport through a variety of quantum cavities by using a Recursive Green Function Technique with emphasis on the effect of disorder on the conductance of the structure, one-dimensional transport in coupled quantum boxes structures with emphasis on the effect of suppression of optic phonon scattering on the transport properties, and finally the detailed influence of confined optic phonon modes on the scattering processes in quantum wires. DTIC

N95-29216 Maryland Univ., College Park, MD.
EFFECTS OF CRITICAL FLUCTUATIONS ON THE THERMODYNAMIC PROPERTIES OF FLUIDS AND FLUID MIXTURES Ph.D. Thesis
Guo-Xiong Jin 1993 217 p
Avail: Univ. Microfilms Order No. DA9425055

In fluids and fluid mixtures, the effects of critical fluctuations remain significant in a very large region of temperatures and densities. Asymptotically close to the critical point, these effects can be described by the scaling theory. However, the asymptotic region is usually extremely small. This thesis presents a crossover formalism to deal with the complete effects of the critical fluctuations on the thermodynamic properties of fluids and fluid mixtures. Continuing the work of Nicoll and Albright and Chen et al., we propose an approximate crossover solution of the renormalization-group equation, which accounts for the critical fluctuations. This solution provides us with a procedure to construct a thermodynamic free energy that reproduces the singular behavior near the critical point and incorporates the crossover from singular critical behavior to regular mean-field behavior of one-component fluids. This procedure is then extended to binary fluid mixtures near the vapor-liquid critical line. The resulting thermodynamic free energy for mixtures yields an accurate description of the thermodynamic properties of mixtures of carbon dioxide and ethane. The renormalization of the critical exponents in these mixtures is also analyzed in detail. Finally, a crossover theory in closed form is constructed, which connects the universal critical behavior with the universal ideal-gas behavior at low densities. Dissert. Abstr.

N95-29501 Massachusetts Univ., Amherst, MA.
A SEARCH FOR A COMPOSITION-DEPENDENT GRAVITATIONAL FORCE Ph.D. Thesis
Paul Andrew Nakroshis 1994 165 p
Avail: Univ. Microfilms Order No. DA9420667

The weak equivalence principle (WEP) maintains that all objects in a uniform gravitational field fall at the same rate, and this rate is independent of composition. I have used the Northfield Mountain Pumped Storage Reservoir as a modulated source of gravitational mass and measured the acceleration of copper and polyethylene test masses towards the reservoir with a sensitive torsion pendulum. The geometry of the pendulum is such that any differential acceleration would manifest itself as a shift in the pendulum period. Therefore, the signature of a WEP-violating force would be a period shift that correlates with the rise and fall of the mass in the Northfield Mountain reservoir. I have looked for such a correlation and find that if there is a difference in the accelerations of copper and polyethylene toward the water in the reservoir, it is less that 6.0 x 10(exp -9) cm/s. We report the limits this places on the possible coupling strength of a possible composition dependent fifth force. Dissert. Abstr.

N95-29527 Tufts Univ., Medford, MA.
QUANTUM FLUCTUATIONS AND SEMICLASSICAL GRAVITY THEORY Ph.D. Thesis
Chung-I. Kuo 1994 119 p
Avail: Univ. Microfilms Order No. DA9419336

Semiclassical gravity theory should serve as a working model before the final theory of quantized gravity is known, or as an approximation for manageable calculations even when the final theory is known. We deal with the important issue of the applicability of the semiclassical theory of gravity, specifically considering the effects of quantum fluctuations of the matter fields and the induced metric perturbations. The quantum fields with negative energy densities are proposed to be the cases where the semiclassical theory is no longer valid. We start with a discussion of the basic notions and developments of semiclassical gravity theory, and continue with a discussion of the establishment of a meaningful measurement of the deviation from semiclassical theory. The measure is a normalized dispersion of the energy density. The non-positive-definiteness of the energy density of quantum fields is derived and discussed. Important cases, like squeezed states and the Casimir effect, which exhibit negative energy densities, are discussed and the deviations from semiclassical theory are checked. A test particle method using a generalized Langevin equation is formulated for the physical description of systems for which the semiclassical theory can not be used. Quantum fields around straight infinite cosmic string is another example of where the negative energy densities may arise. We examine the validity of semiclassical theory for this case. The Casimir force due to the zero-point fluctuations of the electromagnetic fields in the presence of a conducting plate is another case where the quantum fluctuations are large and naive classical consideration should be modified. Using the test particle method, we are able to show that it is a relaxation phenomenon and that a notion of effective temperature can be associated with it. Dissert. Abstr.

N95-29677 McMaster Univ., Hamilton (Ontario).
QUANTUM MECHANICAL PROBLEMS IN ONE, TWO, AND THREE DIMENSIONS Ph.D. Thesis
Shuxi Li 1993 163 p
(ISBN-0-315-84931-2) Avail: Univ. Microfilms Order No. DANN84931

The underlying theme of this thesis is to solve mathematical models related to physical problems in one, two and three spatial dimensions. In some cases, particularly in one spatial dimension, the equations could be solved exactly, while for models in higher dimensions, the solutions were approximate. Although the four separate chapters of the thesis are largely independent, quantum statistics played an important role in the models considered. An exactly solvable field theoretical model in one spatial dimension and its classical bound state solution (including the zero mode) are presented in chapter one. The related bosonization and vacuum charge are discussed. In chapter two, a many-anyon system in two dimensional space with a confining potential is solved using the Thomas-Fermi mean-field method. The ground-state energy and spatial distribution are obtained as functions of the statistical parameter. In chapter three, Chern-Simions coupling to fermions in two dimensions is considered. A zero-mode soliton solution is obtained. Classical vortices in fluid mechanics are shown to be mathematically analogous to anons. Some new results are derived using this analogy. Finally, in three-dimensional space, the vacuum properties of the Nambu-Jona-Lasinio model are studied at both zero and finite temperatures. The vacuum condensation energy per unit volume is calculated and is identified as the MIT bag constant. Some other thermodynamic properties are also calculated, showing striking similarity to the BCS superconductor. A scaling law of the chiral condensation energy density in a nuclear medium is suggested. Dissert. Abstr.

N95-29756# West Virginia Univ., Morgantown, VA.
EQUIPMENT RESOURCE FOR MCM TECHNOLOGY AND SYSTEM PROTOTYPING Final Report
L. A. Hornak and S. K. Tewksbury May 1994 11 p
(AF Proj. 3484)
(AD-A292492; F49620-93-1-0543; AFOSR-95-0138TR) Avail: CASI HC A03/MF A01

Activation in the early summer of 1994 of the awarded Reactive Ion Etch (RIE) and magnetron sputtering systems, coupled with major corporate donations of other critical equipment, has put in place the first microfabrication laboratory at West Virginia University. The System Microfabrication Laboratory is one of three major labs within the Microelectronic Systems Research Center of the Department of Electrical and Computer Engineering, and has been chartered with two important roles. The first to support prototyping of advanced packaged MCM-based systems and the microfabrication of system-level technologies (e.g. optical interconnections) and devices for insertion in these systems. The second role which has emerged for the System Microfabrication Laboratory is to be a catalyst for interdepartmental collaboration on interdisciplinary research at West Virginia University enabling faculty teams to effectively compete in a wider range of research than was possible previous to the award of the equipment and activation of the lab. The two pieces of processing equipment purchased under this award were: (1) an Oxford Instruments RIE systems;

and (2) a CVC 610 Magnetron Sputtering System. A description of the equipment, the current research, and the pending research proposals for the equipment are reviewed. Derived from text

N95-29879# Asian Office of Aerospace Research and Development, APO San Francisco, CA. Air Force Office of Scientific Research.
THE 41ST JAPAN SOCIETY OF APPLIED PHYSICS SPRING MEETING
S. J. Yakura 31 Mar. 1994 8 p Meeting held in Kawasaki, Japan, 28-31 Mar. 1994
(AD-A292333; AOARD-TR-94-10) Avail: CASI HC A02/MF A01

The 41st Japan Society of Applied Physics Spring Meeting attracted a thousands of Japanese scientists and a few non-Japanese scientists coming mostly from Japanese universities, Japanese industrial research laboratories, and Japanese federally funded research centers. During a four day meeting, there were more than fifty simultaneous sessions in progress, covering most of the applied physics disciplines such as radiation and plasmas, measurements, optics, quantum electronics, optoelectronics, thin film physics, beam physics, applied materials, superconductivity, bioelectronics, semiconductors, crystal formations, and non-metallic formations. Presented here is an overview of papers presented in three topical sessions which covered the future and prospects of new light emitting materials, nanostructure control and single-electron electronics, and recent progress in silicon carbide and nitride related wide bandgap material research. Mr. S. Nakamura, Nichia Chemical industries, Inc., presented the latest data on InGaN/AlGaN double heterostructure light emitting diodes, which showed a luminescence value of 1.2 candelas, corresponding to an increase in brightness by a factor of 100 as compared to the existing SiC diodes. DTIC

N95-29936# Army Research Lab., Aberdeen Proving Ground, MD.
AB INITIO CALCULATION OF VIBRATIONAL ABSORPTION AND CIRCULAR DICHROISM SPECTRA USING DENSITY FUNCTIONAL FORCE FIELDS Final Report, Jan. 1993 - Aug. 1994
P. J. Stephens, F. J. Devlin, C. F. Chabalowski, and M. J. Frisch Feb. 1995 33 p
(AD-A291297; ARL-TR-695) Avail: CASI HC A03/MF A01

The unpolarized absorption and circular dichroism spectra of the fundamental vibrational transitions of the chiral molecule, 4-methyl-2-oxetanone, are calculated ab initio. Harmonic force fields are obtained using Density Functional Theory (DFT), MP2, and SCF methodologies and a 5S4P2D/3S2P (TZ2P) basis set. DFT calculations use the Local Spin Density Approximation (LSDA), BLYP, and Becke3LYP (B3LYP) density functionals. Mid-IR spectra predicted using LSDA, BLYP, and B3LYP force fields are of significantly different quality, the B3LYP force field yielding spectra in clearly superior, and overall excellent, agreement with experiment. The MP2 force field yields spectra in slightly worse agreement with experiment than the B3LYP force field. The SCF force field yields spectra in poor agreement with experiment.The basis set dependence of B3LYP force fields is also explored: the 6-31G and TZ2P basis sets give very similar results while the 3-21G basis set yields spectra in substantially worse agreements with experiment. DTIC

80 SOCIAL SCIENCES (GENERAL)

Includes educational matters.

N95-30223* National Aeronautics and Space Administration. Marshall Space Flight Center, Huntsville, AL.
INTERNATIONAL SPACE UNIVERSITY (Videotape)
Maggie Kassler, ed. 9 Aug. 1993 Videotape: 16 min. 16 sec. playing time, in color, with sound
(NASA-TM-110646; NONP-NASA-VT-95-57868) Avail: CASI VHS A02/BETA A22

The International Space University (ISU) is described in this video, hosted by Marina Sirtis from the 'Star Trek' television show's Starship Enterprise. A complete explanation of what ISU is, how the university functions, and the benefits that the university provides are described. Included are brief comments from former ISU graduates. CASI

81 ADMINISTRATION AND MANAGEMENT

Includes management planning and research.

N95-29170* National Aeronautics and Space Administration, Washington, DC.
NASA: THE STATE OF THE AGENCY (Videotape)
7 Oct. 1992 Videotape: 19 min. 37 sec. playing time, in color, with sound
(NASA-TM-110563; NONP-NASA-VT-95-45998) Avail: CASI VHS A02/BETA A22

NASA's challenges, accomplishments, and goals are described in this video. Historical footage of man's first lunar walk are shown and there are brief descriptions covering several of NASA's major projects, such as: Skylab; Viking Voyager; Coby; and the 1990 Hubble Space Telescope. CASI

N95-29171* National Aeronautics and Space Administration, Washington, DC.
AN ANNOUNCEMENT BY DAN GOLDIN (Videotape)
15 Oct. 1992 Videotape: 15 min. 45 sec. playing time, in color, with sound
(NASA-TM-110739; NONP-NASA-VT-95-45999) Avail: CASI VHS A02/BETA A22

Daniel S. Goldin (NASA Administrator) announces the reconstruction of several NASA programs and management structural changes. The upcoming developments for Space Station Freedom, the Office of Space Science Applications (OSSA), and the field of Aeronautics are discussed. CASI

N95-29935# NATO Defence Research Group, Brussels (Belgium).
COADE: A FRAMEWORK FOR COGNITIVE ANALYSIS, DESIGN, AND EVALUATION Final Report
P. Essens, J. Fallesen, C. McCann, J. Cannon-Bowers, and G. Dorfel 23 Jan. 1995 220 p
(AD-A291282; NATO-AC/243(PANEL 8)TR/17) Avail: CASI HC A10/MF A03

The development of support of decision making processes in complex systems requires a systematic approach based upon knowledge of the human's role, capabilities, and the tasks to be performed. Results from a survey and a workshop show that there is a need for methodologies that systematically address the cognitive factors of complex task situations. COADE provides the developer and cognitive specialist with an approach to the development of cognitively-centered systems. The COADE framework comprises a set of activities for cognitive analysis, design and evaluation. Analysis activities result in the specification of cognitive requirements; design activities translate those into design requirements; evaluation activities control the quality of the intermediate and final products of the development process. DTIC

82 DOCUMENTATION AND INFORMATION SCIENCE

Includes information management; information storage and retrieval technology; technical writing; graphic arts; and micrography.

For computer documentation see *61 Computer Programming and Software.*

N95-28797# Logistics Management Inst., Bethesda, MD.
DOD ELECTRONIC DATA INTERCHANGE (EDI) CONVENTION: TDCC/EDIA TRANSACTION SET 210 MOTOR CARRIER INVOICE (VERSION 003020). REVISION 1 Final Report
W. M. Bridges and Harold L. Frohman May 1994 95 p
(Contract MDA903-90-C-0006)
(AD-A292375; LMI-DF301LN2) Avail: CASI HC A05/MF A01

This is an electronic data interchange (EDI) systems design document that describes the standard or convention the Department of Defense (DOD) will use to accept a transaction invoice using the ASC X12.104 Transaction Set 210 Motor Carrier Invoice (003020). DTIC

N95-28877# Carnegie-Mellon Univ., Pittsburgh, PA. Dept. of Computer Science.

ABSTRACT MODELS OF MEMORY MANAGEMENT

Greg Morrisett, Mattias Felleisen, and Robert Harper Jan. 1995 37 p
(Contract F19628-91-C-0168; ARPA Order-8313)
(AD-A292238; CMU-CS-95-110) Avail: CASI HC A03/MF A01

Most specifications of garbage collectors concentrate on the low-level algorithmic details of how to find and preserve accessible objects. Often, they focus on bit-level manipulations such as 'scanning stack frames,' 'marking objects,' 'tagging data,' etc. While these details are important in some contexts, they often obscure the more fundamental aspects of memory management: what objects are garbage and why? We develop a series of calculi that are just low-level enough that we can express allocation and garbage collection, yet are sufficiently abstract that we may formally prove the correctness of various memory management strategies. By making the heap of a program syntactically apparent, we can specify memory actions as rewriting rules that allocate values on the heap and automatically dereference pointers to such objects when needed. This formulation permits the specification of garbage collection as a relation that removes portions of the heap without affecting the outcome of the evaluation. DTIC

N95-28880# Carnegie-Mellon Univ., Pittsburgh, PA. Dept. of Computer Science.

USING ORDERED BINARY-DECISION DIAGRAMS FOR COMPRESSING IMAGES AND IMAGE SEQUENCES

Mike Starkey and Randy Bryant Jan. 1995 13 p
(Contract F33615-93-1-1330)
(AD-A292244; CMU-CS-95-105) Avail: CASI HC A03/MF A01

The Ordered Binary-Decision Diagram (OBDD) has been used to reduce the amount of space and computation required for verifying digital circuits by removing redundant copies of subfunctions. Similarly, image compression algorithms attempt to reduce their space requirements by finding replicated patterns or features in images. OBDDs would therefore appear to be a good candidate as a data structure for representing images. We show how images can be encoded using Ordered Binary-Decision Diagrams and compare our results to quadtrees. We also show how using this method extends naturally to compressing sequences of related images such those that comprise movies. DTIC

N95-28907 Air Force Inst. of Tech., Wright-Patterson AFB, OH. School of Engineering.

USING OBJECT-ORIENTED DATABASE TECHNOLOGY TO DEVELOP A MULTIPLE DOMAIN CAPABILITY FOR DOMAIN-ORIENTED APPLICATION COMPOSITION SYSTEMS M.S. Thesis

Alfred W. Harris, Jr. Dec. 1994 118 p Limited Reproducibility: More than 20% of this document may be affected by microfiche quality
(AD-A289244; AFIT/GCS/ENG-94D-07) Avail: Issuing Activity (Defense Technical Information Center (DTIC))

This thesis describes the design and implementation of a multiple domain capability for a domain-oriented application composition system, named Architect. The research goal was to show how object-oriented database management system (OODBMS) technology can be used to provide simultaneous access to multiple domain-oriented knowledge bases. Since the Architect system was originally designed using the object-oriented paradigm, insertion of OODBMS technology was relatively simple and many of the object-oriented concepts, such as inheritance and aggregation, proved beneficial. Inheritance was used to encapsulate domain knowledge by defining each domain as a subclass of Architect's software architecture. Aggregation was used to allow applications to cross domain boundaries by nesting components from multiple domains in an application. To validate this approach, domain extensions to two existing domain models were implemented to make the domains compatible in a multiple domain environment, and applications containing objects from both the logic circuits and digital signal processing domains were successfully developed. One of the primary benefits of this research is the potential for greater reuse of objects. To satisfy new requirements, domain engineers can now search for and access objects from other domains as an alternative to implementing them in their own domains. DTIC

N95-28958# Westinghouse Hanford Co., Richland, WA.

QUEST2: SYSTEM ARCHITECTURE DELIVERABLE SET

F. D. Braaten 27 Feb. 1995 150 p
(Contract DE-AC06-87RL-10930)
(DE95-008427; WHC-SD-GN-CSWD-20010) Avail: CASI HC A07/MF A02

This document contains the system architecture and related documents which were developed during the Preliminary Analysis/System Architecture phase of the Quality, Environmental, Safety Tracking System redesign (QUEST2) project. Each discreet document in this deliverable set applies to a analytic effort supporting the architectural model of QUEST2. The P+ methodology cites a list of P+ documents normally included in a 'typical' system architecture. Some of these were deferred to the release development phase of the project. The documents included in this deliverable set represent the system architecture itself. Related to that architecture are some decision support documents which provided needed information for management reviews that occurred during April. Consequently, the deliverables in this set were logically grouped and provided to support customer requirements. The remaining System Architecture Phase deliverables will be provided as a 'Supporting Documents' deliverable set for the first release. DOE

N95-29028*# National Aeronautics and Space Administration. Langley Research Center, Hampton, VA.

NASA/DOD AEROSPACE KNOWLEDGE DIFFUSION RESEARCH PROJECT. PAPER 49: BECOMING AN AEROSPACE ENGINEER: A CROSS-GENDER COMPARISON

Laura M. Hecht (Indiana Univ., Bloomington, IN.), Thomas E. Pinelli, Rebecca O. Barclay (Electronic Information Age, Inc., Portsmouth, VA.), and John M. Kennedy (Indiana Univ., Bloomington, IN.) Jul. 1995 9 p Repr. from Journal of Engineering Education, v. 84, no. 3, Jul. 1995 p 263-270 Sponsored in cooperation with the Council on Library Resources
(NASA-TM-110731; NAS 1.15:110731) Avail: CASI HC A02/MF A01

We conducted a mail (self-reported) survey of 4300 student members of the American Institute of Aeronautics and Astronautics (AIAA) during the spring of 1993 as a Phase 3 activity of the NASA/DoD Aerospace Knowledge Diffusion Research Project. The survey was designed to explore students' career goals and aspirations, communications skills training, and their use of information sources, products, and services. We received 1723 completed questionnaires for an adjusted response rate of 42%. In this article, we compare the responses of female and male aerospace engineering students in the context of two general aspects of their educational experience. First, we explore the extent to which women and men differ in regard to factors that lead to the choice to study aerospace engineering, their current level of satisfaction with that choice, and their career-related goals and aspirations. Second, we examine students' responses to questions about communications skills training and the helpfulness of that training, and their use of and the importance to them of selected information sources, products, and services. The cross-gender comparison revealed more similarities than differences. Female students appear to be more satisfied than their male counterparts with the decision to major in aerospace engineering. Both female and male student respondents consider communications skills important for professional success, but females place a higher value than males do on oral communications skills. Women students also place a higher value than men do on the roles of other students and faculty members in satisfying their needs for information. Author

N95-29093 Illinois Inst. of Tech., Chicago, IL.

DATA MIGRATION POLICIES FOR DISTRIBUTED DATABASE SYSTEMS Ph.D. Thesis

Peijone Wu 1993 154 p
Avail: Univ. Microfilms Order No. DA9415463

Data migration is a technique which transfers a data item from one site to another to enhance system performance. In conventional distributed databases, a request is executed either locally or remotely. Compared to these approaches, data migration increases communication cost for the current request. However, the system can benefit from the change of data locations in some cases, e.g., when the system load is highly unbalanced, or when the next requests have a high locality of reference. Therefore, data migration provides a distributed database system an alternative approach for reducing average response time. In this thesis, we present two novel approaches to data migration: load-sharing data migration and hot spot data migration. Load-sharing data migration integrates load sharing and data migration and transfers a data item according to system load indices, while hot spot data migration determines data transfer according

to the probability of data access from each site. The simulation results show that load-sharing data migration improves system performance dramatically under heavy system loads, and hot spot data migration considerably reduces average response time under light system loads. Combining these two approaches results in a comprehensive approach for improving system performance in distributed database systems.
Dissert. Abstr.

N95-29116 Universitaire Instelling Antwerpen, Wilrijk (Belgium).
FORMAL ASPECTS OF OBJECT IDENTITY IN DATABASE MANIPULATION Ph.D. Thesis
Jan Gilbert VandenBussche 1993 123 p
Avail: Univ. Microfilms Order No. DA9415262

This thesis contains a study of the impact of object identity on the manipulation of object-oriented databases In particular due to the possibility for object creation, i.e., the presence of identifiers of new objects in the result of a query or update, various new questions have arisen which have not been considered in the study of conventional database queries and updates. First, we consider the representation of complex values by typed network a of abstract objects Two different objects in such a network may represent the same complex value, i.e., duplicates can occur We consider various means for the elimination of such duplicates, and establish the connections that exist between these different operations We also study the notion of object creation from the most general point of view, and pursue the following question in great depth when can a data manipulation language supporting object creation be called computationally complete? Finally, we study a new form of non-determinism in database queries, called semi-determinism,inspired by the problem of copy elimination put forward by Abiteboul and Kanellakis. Semi-determinism arises naturally in the context of object creation, but has also unexpected applications in more efficiently expressing deterministic queries using non-determinism.
Dissert. Abstr.

N95-29154# North Carolina State Univ., Raleigh, NC. Dept. of Electrical and Computer Engineering.
MOTION PLANNING AND SENSORY PROCESSING IN A DYNAMIC ENVIRONMENT Final Report
Ren C. Luo and David W. Hislop 31 Mar. 1994 34 p
(Contract DAAL03-89-D-0003)
(AD-A290504; ARO-27567.3-MA) Avail: CASI HC A03/MF A01

The objective of this research is to develop a sensor controlled intelligent mobile robot system for operating in a dynamic environment. In contrast to approaches for operating in a static environment, the proposed method is designed explicitly for navigation in dynamic environments and is able to immediately modify its control strategies in response to unexpected changes in the environment. The research herein is divided into two major areas: motion planning and sensory processing. The motion planning research introduces the concept of traversability vectors which can be used to represent a dynamic environment, and uses a temporal reasoning scheme to plan the robot motion. The primary research in sensory processing being the control or integration of multiple sensors on the mobile robot so as to allow for their coordinated use for the detection and avoidance of objects and obstacles in the environment. DTIC

N95-29182# Florida International Univ., Miami, FL. School of Computer Science.
A PIPELINE CASE TOOL FOR DATABASE DESIGN
Naphtali Rishe and Wei Sun 12 Dec. 1994 10 p
(Contract DAAH04-94-G-0024)
(AD-A292017; ARO-32427.1-MA-SDI) Avail: CASI HC A02/MF A01

We have developed a tool for design of relational databases, including schemas, integrity constraints, reports, and data entry forms, using semantic binary schemas. The tool is based on a top-down methodology. In this methodology, a conceptual description of an enterprise is designed using a semantic binary model. Then, this description is converted into the relational database design. The tool automates virtually all the busy work of design. With respect to the intelligent design decisions, the tool accepts instructions from its user, who is a database designer, or, when the user defaults, makes decisions itself based on rule-of-thumb principles guided by the knowledge of the database's semantics. The tool creates a turn-key database application and its documentation with graphically-illustrated design reports, manuals, application glossaries, and data dictionaries, as well as an application-customized report generator. Changes in the semantic description or designer's instructions are propagated into the products. DTIC

N95-29207# Massachusetts Inst. of Tech., Cambridge, MA.
GARBAGE COLLECTION IS FAST, BUT A STACK IS FASTER
James S. Miller and Guillermo J. Rozas Mar. 1994 38 p
(Contract N00014-89-J-32022)
(AD-A290099; AIM-1462) Avail: CASI HC A03/MF A01

Prompted by claims that garbage collection can outperform stack allocation when sufficient physical memory is available, we present a careful analysis and set of cross-architecture measurements comparing these two approaches for the implementation of continuation (procedure call) frames. When the frames are allocated on a heap they require additional space, increase the amount of data transferred between memory and registers, and, on current architectures, require more instructions. We find that stack allocation of continuation frames outperforms heap allocation in some cases by almost a factor of three. Thus, stacks remain an important implementation technique for procedure calls, even in the presence of an efficient, compacting garbage collector and large amounts of memory. DTIC

N95-29221# Defence Research Establishment Ottawa, Ottawa (Ontario).
DESCRIPTION OF THE OHGR DATABASE
Anastasios Drosopoulos Dec. 1994 42 p
(AD-A290146; DREO-TN-94-14) Avail: CASI HC A03/MF A01

This technical note describes the Osborne Head database, collected at Osborne Head Gunnery Range (OHGR) in November 1993, with the McMaster University IPIX radar. Representative examples are worked out for the different operational modes of the radar (staring, scanning, alternate/single polarization, single/multi-frequency). Strengths and weaknesses of the database are pointed out as well. The purpose of this technical note is to serve as a guide to the database, presenting enough information to allow the extraction of individual datasets from the raw data. These can subsequently be used for sea clutter, target model validation, and/or testing of signal processing techniques, leading to enhanced target detection in sea clutter. DTIC

N95-29287 Logistics Management Inst., Bethesda, MD.
DOD ELECTRONIC DATA INTERCHANGE (EDI) CONVENTION: ASC X12 TRANSACTION SET 410 RAIL CARRIER INVOICE, VERSION 003020 Final Report
W. M. Bridges and Harold L. Frohman Sep. 1994 93 p Limited Reproducibility: More than 20% of this document may be affected by poor print
(Contract MDA903-90-C-0006)
(AD-A292495; LMI-DF301LN4) Avail: Issuing Activity (Defense Technical Information Center (DTIC))

This is an electronic data interchange (EDI) systems design document that describes the standard or 'convention' the Department of Defense (DOD) will use to accept a transaction invoice using the ASC X12.139 Transaction Set 410 Rail Carrier Invoice (003020). DTIC

N95-29363# Instituto de Pesquisas Espaciais, Sao Jose dos Campos (Brazil).
INTERFACE FOR THE TRANSLATION OF SENTENCES IN A NATURAL LANGUAGE INTO A GEOMETRICAL REPRESENTATION LANGUAGE [INTERFACE PARA TRADUCAO DE FRASES EM LINGUAGEM NATURAL PARA UMA LINGUAGEM DE REPRESENTACAO GEOMETRICA]
Carlos AlbertodeOliveira 1993 17 p In PORTUGUESE Presented at the 9th Symposium Brasileiro de Inteligencia Artificial, Rio de Janeiro,—Brazil, 5-8 Oct. 1992; and the 3rd Intercambio de Pesquisas, SaoPaulo, Brazil,—26-27 Nov. 1992
(INPE-5467-PRE/1775) Avail: CASI HC A03/MF A01

Due to the need for natural language (NL) interfaces in situation where other interactive methods perform inadequately, a NL command translation system for a Geometric representation language is introduced. For use in the 2D Computer Graphics domain, this system has a blackboard architecture and a frame-based knowledge representation, interacting in free Portuguese language and acquiring knowledge during the interactive sessions. Author

N95-29449# Department of Energy, Washington, DC. Office of Scientific and Technical Information.
SCIENTIFIC AND TECHNICAL INFORMATION POLICY IMPLEMENTATION UNDER OMB CIRCULAR A-130. REPORT OF AGENCY FINDINGS AND RECOMMENDATIONS Final Report
Elizabeth V. Buffman, Barbara T. Bauldock, Mark D. Fornwall, Judy C. Gilmore, and Bonnie C. Carroll May 1995 63 p
(DE-95-11601; DOE/OSTI-11686) Avail: CASI HC A04/MF A01

A six-month study of the implementation of OMB Circular A-130 in the Federal scientific and technical information community was conducted by a team of information managers and experts from 15 Federal information organizations. The study showed that A-130 has been a useful tool in assisting these Federal managers with the responsibility of managing scientific and technical information. The report offers six recommendations to the Office of Information and Regulatory Affairs, OMB, for clarifying the Circular's guidance to facilitate more effective information management: clarify 'life-cycle planning' for information usability; develop guidelines to ensure information integrity for the public good; clarify guidance concerning public access to agency information; resolve conflicts between A-130 objectives and those of other Government initiatives; sponsor an effort to develop a selected mode of operation for Government information services; and institutionalize interagency cooperative efforts for information sharing. The report also includes a summary of agency practices and a template which Federal agencies can use to measure their progress toward the objectives of the Circular. Author

N95-29518 Syracuse Univ., NY.
THE IDENTIFICATION OF USER CRITERIA OF RELEVANCE AND DOCUMENT CHARACTERISTICS: BEYOND THE TOPICAL APPROACH TO INFORMATION RETRIEVAL Ph.D. Thesis
Carol Lee Barry 1993 255 p
Avail: Univ. Microfilms Order No. DA9422230

The objective of this study was twofold: first, to describe the criteria mentioned by users evaluating the information within documents as it related to the users' information need situations; and second, to describe the characteristics of documents that allowed users to predict the presence or absence of criteria within documents. This research was intended to provide a better understanding of the notion of relevance, which is a fundamental concept in the design and evaluation of information retrieval systems. This study was an exploratory effort to examine these issues by eliciting mentions of criteria and document characteristics directly from motivated users in actual information seeking and use situations. Data were collected by asking users in an academic environment (e.g. undergraduate students, graduate students and faculty) to evaluate representations of documents that had been retrieved specifically for each user's information need situation. Users were asked to mark the portions of the document representations that indicated to the users whether they would or would not pursue the information within documents. An open-ended interview technique was then employed to discuss each marked portion of the documents with users. The interviews were audiotaped, the tapes transcribed, and the transcriptions were content analyzed in order to identify and describe evaluation criteria and document characteristics. The major results consisted of descriptions of document characteristics (e.g., authors, publication dates) and criteria (e.g., recency, accuracy) mentioned by users. The results indicated that the criteria employed by users included tangible characteristics of documents (e.g., the information content of the document, the provision of references to other sources of information), subjective qualities (e.g., agreement with the information provided by the document) and situational factors (e.g., the time constraints under which the user was working). The results also examined the co-occurrence of document characteristics and criteria, in an attempt to determine where users were finding clues to the presence or absence of criteria. The implications of this research for the design and evaluation of information retrieval systems, as well as directions for future research, are discussed. Dissert. Abstr.

N95-29573# Institute for the Study of Learning and Expertise, Palo Alto, CA.
ACQUISITION OF PLACE KNOWLEDGE THROUGH CASE-BASED LEARNING Annual Report, 1 Mar. 1994 - 28 Feb. 1995
Pat Langley and Karl Pfleger (Stanford Univ., CA.) 15 Mar. 1995 20 p Submitted for publication
(Contract N00014-94-1-0505)
(AD-A292574; ISLE-TR-95-2) Avail: CASI HC A03/MF A01

In this paper we define the task of place learning and describe one approach to this problem. The framework represents distinct places as evidence grids, a probabilistic description of occupancy. Place recognition relies on case-based classification, augmented by a registration process to correct for translations. The learning mechanism is also similar to that in case-based system's, involving the simple storage of inferred evidence grids. Experimental studies with physical and simulated robots suggest that this approach improves place recognition with experience, that it can handle significant sensor noise, that it benefits from improved quality in stored cases, and that it scales well to environments with many distinct places. Previous researchers have studied evidence grids and place learning, but they have not combined these two powerful concepts, nor have they used the experimental methods of machine learning to evaluate their methods' abilities. DTIC

N95-29589 Maryland Univ. Baltimore County, Catonsville, MD.
A STUDY OF THE CONCEPTUAL SYMBOLICS OF INFORMATION SYSTEM DEVELOPMENT LANGUAGES Ph.D. Thesis
William R. Eddins 1994 207 p
Avail: Univ. Microfilms Order No. DA9416011

The notation of languages used in Information Systems (IS) development is examined. This is a study of conceptual symbolics. It explores the impact of graphical and textual forms of notation and cognitive task upon the performance of novice and experienced computer users. The following fields in Management Information Systems (MIS) are reviewed: Computer Aided Software Engineering (CASE), program design, data base modeling, structured methodologies, and visual languages. Two experiments were conducted. Experiment One examined the impact that Data Flow Diagram (DFD) notation (graphical or textual) and complexity have on a perceptual task performed by novice computer users. Novices using the graphical notations responded faster than with the textual notations. However, at the medium level of complexity, subjects viewing a well designed textual notation performed as well as subjects viewing the graphical notations. Novice computer users preferred graphical notations over textual notations in most cases. Experiment Two examined the impact that DFD notation and cognitive task have upon perceptual tasks performed by experienced computer users. Experienced computer users using the graphical notation perceived faster than when using the textual notation. An experienced user performing a taxonomizing task completed a perceptual task sooner than when performing a sequencing task. Experienced computer users did not favor graphical notations over textual notations in four out of six tasks. Conclusions are that novice and experienced users alike perform faster with graphical notations, novice users tend to prefer graphical notations more than experienced users, subjects viewing a well designed textual notation may perform as well as subjects viewing graphical notations at the medium level of complexity, and a sequencing cognitive task requires more time to complete than a taxonomizing task. Dissert. Abstr.

N95-29690 University of North Texas, Denton, TX.
INFORMATION MANAGEMENT IN LOCAL AREA NETWORKS: IMPACT ON USERS' PERCEPTIONS Ph.D. Thesis
Melanie J. Norton 1994 70 p
Avail: Univ. Microfilms Order No. DA9424393

In this study, computer human interaction factors are examined as a possible source of information to aid in the operation and management of local area computer networks. Users' perceptions of computer performance and response time are evaluated in relation to specific modifications in the information organization of a file server in a local area network configuration running in Novell 3.11. Investigating network users' perceptions provides data relative to the file server's information organization affect on users. Understanding whether users can detect changes made to the file server information organization structures, such as modifications in mapping or minimization of duplicate files, provides data that will improve local area network management. Recognizing what users actually perceive provides a framework for evaluating use of system management time, equipment and software. This study uses two treatment groups and a control group. The dependent variables are the subjects' perceptions of the computer performance as indicated by their perception of response time and common interface features including menu usability. The independent variables are

the drive mapping levels, a network file management parameter, and the file collection status. Dissert. Abstr.

N95-29798 Oklahoma Univ., Norman, OK.
ON THE TOPOLOGICAL COMPLEXITY OF THE COST FUNCTION IN VARIATIONAL DATA ASSIMILATION Ph.D. Thesis
Yong Li 1994 178 p
Avail: Univ. Microfilms Order No. DA9421091

We investigate here the causes and implications of topological complexity in the cost function in the context of the variational data of similation. This complexity, which can take many forms from multiple minima to very flat regions with almost no curvature, causes severe problems for minimization algorithms and can lead to a retrieved state that is strongly related to the initial guess, i.e., non-uniqueness. To determine the origin of multiple minima, we first utilize guess, simple dynamical systems: the chaotic logistic equation, Duffing's equation, and Burgers equation. We demonstrate that multiple minima are associated with nonlinear dynamics, and that the length of the assimilation window and data availability also exert a strong influence over the topology of the cost function. This finding is validated for the somewhat more complicated resonant Rossby wave model. Having established the principal causes of topological complexity in the cost function, we extend our work to the corrective regime by per forming retrievals using simulated data from a 3-D Boussinesq model and its adjoint. We find that the complexity of the cost function is not as serious a problem as shown in the simple nonlinear system. Only in an extreme case, where the first guess is chosen to differ substantially from the true solution, does the retrieved state depart from the control, and even then it does so only superficially. This result could be due to the high dimensionality (i.e., greater degrees of freedom) of the Boussinesq flow. By including a penalty term, consisting of second-order temporal derivatives of the model state variables, the cost function is regularized and an improved retrieval is obtained. Such a penalty term can also improve the conditioning of the Hessian and thus the efficiency of the minimizations process. The role of diffusion in data retrieval is also examined, and a linear analysis based on the one-dimensional diffusion equation shows that the retrieved initial state will be amplified (smoothed) if the diffusion in the prediction model is larger (smaller) than that of the observations. This amplification (smoothing) increases dramatically as the length scale of the features under consideration decreases. From a topological point of view, errors in the diffusion processes essentially shift the locations of minima in the cost function. Further, because of the irreversible loss of information associated with diffusion, our analysis suggests that diffusive processes place a limit on the length of the assimilation window. The 3-D convection model and its adjoint are again used to extend and verify our suppositions in a more physically relevant context. Dissert. Abstr.

N95-29818 Carnegie-Mellon Univ., Pittsburgh, PA. School of Computer Science.
HIGH-LEVEL FAULT TOLERANCE IN DISTRIBUTED PROGRAMS
Erik Seligman and Adam Beguelin Dec. 1994 12 p Limited Reproducibility: More than 20% of this document may be affected by poor print
(Contract DABT63-93-C-0054; NSF NCR-89-19038)
(AD-A290430; CMU-CS-94-223) Avail: Issuing Activity (Defense Technical Information Center (DTIC))

We have been developing high-level checkpoint and restart methods for Dome (Distributed Object Migration Environment), a C++ library of data-parallel objects that are automatically distributed using PVM. There are several levels of programming abstraction at which fault tolerance mechanisms can be designed: high-level, where the checkpoint and restart are built into our C++ objects, but the program structure is severely constrained; high-level with preprocessing, where a preprocessor inserts extra C++ statements into the code to facilitate checkpoint and restart; and low-level, where periodically an interrupt causes a memory image to be written out. Because we consider portability (both of our libraries and of the checkpoints they produce) to be an important goal, we focus on the higher-level checkpointing methods. In addition, we describe an implementation of high-level checkpointing, demonstrate it on multiple architectures, and show that it is efficient enough to provide good expected run times with low overhead, even in the case of frequent failures. DTIC

N95-29828 Syracuse Univ., NY.
A STUDY OF PROBLEMATIC SITUATIONS AND INFORMATION NEEDS OF SOFTWARE MANAGERS IN THE UNITED STATES AND JAPAN Ph.D. Thesis
Lorraine Mary Duvall 1993 253 p
Avail: Univ. Microfilms Order No. DA9422248

The purpose of this dissertation research was to increase our understanding of the problems in managing software development, the situations in which these problems occurred, and the information needed and used in these situations - all from the perspective of software managers. The qualitative research method utilized during this study was based upon Grounded Theory, a user-based approach from the social sciences that facilitates the discovery and definition of generalizations and themes about a complex subject, such as software development. Thirty-two managers from 14 companies in the United States and Japan were interviewed. The results of the analysis of the data collected suggest that there are many interacting technical and non-technical factors that came into play. Managers spoke about problems with requirements, people (developers and customers), constraints placed upon the development efforts, performance, and change. They spoke of the source of their problems and the entity influenced by the situations they considered problematic. The actions taken by managers and/or their people were activity driven. That is, what managers did was dependent upon the situation in which the problem, or potential problem, occurred. The roles managers played also depended upon the situation. Managers spoke of the context in which they used information including why they needed or used the information, the source of the information or the vehicle that supplied the information, the form and content of the information, and the problems they had getting or using the information. Two major differences between the development contexts of the managers in the United States and Japan were related to development personnel and constraints placed upon the projects. Similar hardware, software tools, and software processes were applied to their development efforts. Examining the technological aspects of software development, there appears to be few distinguishing characteristics between the practices of the two countries. In contrast, the examination of management and sociological issues provides insight into the differences, specifically related to roles managers played with their people, subcontractors, and customer. Dissert. Abstr.

N95-29829 California Univ., Los Angeles, CA.
TRAINING END-USERS ON DATABASE QUERIES: THE EFFECTIVENESS OF EXAMPLE FORMAT AND SPATIAL ABILITY ON LEARING OUTCOMES Ph.D. Thesis
Anita Rose White 1993 167 p
Avail: Univ. Microfilms Order No. DA9420497

Despite vendors' claims of user friendliness, people continue to have difficulties using software packages. Are our training manuals as effective as they could be? Previous studies in software training manuals emphasized the manual's content. While content is important, recent studies on training in mathematics, physics, and numerical control programming indicate that format can influence the effectiveness of examples used in training manuals. This study examined the effect of different training formats (split attention vs. integrated examples), learning outcomes (near transfer vs. far transfer tasks), and spatial ability (high and low) in an experiment where subjects received training in the execution of queries using the database application package Paradox. Sixty-five subjects were assigned to conditions with different training manuals on the basis of their spatial ability. Subjects were tested on both near and far transfer of learning tasks. The results indicated that on near transfer tasks subjects trained with integrated examples obtained higher accuracy scores than those trained with split attention examples. However, on far transfer tasks, spatial ability rather than type of example was associated with better performance. Subjects with high spatial ability obtained higher accuracy scores and spent less time on the training manual and on the task than did subjects with low spatial ability. Dissert. Abstr.

N95-29947# Department of Defense, Washington, DC. Directorate for Information Operations and Reports.
DOD LISTING OF APPROVED RECURRING INFORMATION REQUIREMENTS
1 Jan. 1995 97 p Supersedes AD-A287049 and AD-A267934
(AD-A291346; DOD-8910.1-L) Avail: CASI HC A05/MF A02

This listing is issued under the authority of DOD Directive 8910.1,

'Management and Control of Information Requirements,' June 11, 1993, and supersedes DOD 8910.1-L 'Listing of Approved Recurring Information Requirements,' dated July 1, 1994. Its purpose of DOD internal information requirements approved by (OSD), interagency reporting requirements approved by (GSA), and DOD public-use reports approved by the Office of Management and Budget (OMB). DOD 8910.1-L is divided into the following parts: List of Recurring and One-Time DOD Internal Reports; List of Recurring and One-Time DOD Internal Reports Cancelled; List of Recurring and One-Time DOD Internal Expired Reports and List of Recurring and One-Time Interagency Reports. DTIC

N95-30043# Boston Coll., Chestnut Hill, MA. Inst. for Space Research.
PASP PLUS TIME HISTORY DATA BASE FILE STRUCTURES Technical Report
Dennis E. Delorey 19 Sep. 1994 68 p
(Contract F19628-93-K-0019)
(AD-A290587; BC-ISR-94-04; PL-TR-94-2242; SR-1) Avail: CASI HC A04/MF A01

A Time History Data Base (THDB) is to be developed for the Photovoltaic Array and Space Power Experiment - Plus Diagnostics (PASP+) sensor package flown aboard the APEX satellite. A THDB system has been developed for the generation and display of the THDB data. DTIC

N95-30100# Commission of the European Communities, Brussels (Belgium).
FUNCTIONALLY SPECIFIED DISTRIBUTED TRANSACTIONS IN CO-OPERATIVE SCENARIOS
R. A. deBy, S. J. Evan, and P. A. C. Verkoulen Dec. 1994 24 p
(PB95-197380; Memo-INF-94-72) Copyright Avail: CASI HC A03/MF A01

In this paper, we address the problem of specifying co-operative, distributed transactions as a form of database interoperability, i.e., we show how to obtain a clear and formal protocol for distributed database transactions meant to describe co-operation scenarios, that can be subject to verification and testing. We argue that a separation of concerns, namely interaction of database applications on the one hand and data modeling on the other hand, results in a practical approach that is formally well-founded. To this end, we discuss the combination of the process-algebraic language LOTOS and the object-oriented database modeling language TM, and show how the two can be combined. We are especially interested in modular designs and discuss how we may vary over transaction models to support the language combination. Our ideas are presented in the context of a small, but real life example. We identify a primitive for distributed transaction specification and object base dynamics, and give its semantics. We also discuss key questions and issues that we hope to resolve in the near future within the ESPRIT basic research action TransCoop. NTIS

N95-30194# Oak Ridge K-25 Site, TN.
ENGINEERING DESIGN INFORMATION SYSTEM (EDIS), INFORMATION MANAGEMENT SERVICES (IMS), INDEX FUNCTION, USER'S MANUAL: REVISION 1
R. K. Schwarz, ed. Feb. 1995 86 p
(Contract DE-AC05-84OR-21400)
(DE95-009538; K/CSD/TM-101-Rev-1) Avail: CASI HC A05/MF A01

The Engineering Design Information System (EDIS) Information Management Services (IMS) Index Function is an interactive system developed for IMS personnel to perform indexing, maintenance, and retrieval of information about engineering documents. This manual gives an overview of the system structure, data, and functionality, as well as the hardware and security environment within which the system operates. It gives a detailed description of the interactive menus, screens, and prompts that provide access to the system functions and the requirements for data entry. Appendixes are included to display data definitions, modification rules, help screen formats, explanation of system help and informational messages, code translations, and a report format. DOE

N95-30208# Technische Univ., Twente (Netherlands). Dept. of Computer Science.
ENHANCING THE SEMANTICS OF FEDERATED SCHEMATA BY TRANSLATING SQ1-QUERIES INTO OBJECT METHODS
M. W. W. Vermeer and P. M. G. Apers Dec. 1994 38 p
(PB95-197372; Memo-INF-94-82) Copyright Avail: CASI HC A03/MF A01

The paper argues the feasibility of equipping object-oriented federated schemata with methods reflecting operations on the component schemata extracted from the applications. An algorithm to obtain object methods in an object-oriented DML from SQL-queries is described, based on the matching of query join graphs with object structures. It is shown that the navigational structure provided by the object model can be exploited to present joins and nesting constructs contained in an SQL-query. It is also shown that with such a translation, considerable gain in the intuitive meaning of the query can be achieved. When applied to queries from applications on the underlying data bases in a federated data base system, both the subsequent schema integration phase and the development on new, federated, applications benefit from this additional insight in the semantics of the underlying schema. NTIS

N95-30286 Princeton Univ., NJ.
DISTRIBUTED QUERIES AND INCREMENTAL UPDATES IN INFORMATION RETRIEVAL SYSTEMS Ph.D. Thesis
Anthony Slavko Tomasic 1994 157 p
Avail: Univ. Microfilms Order No. DA9424705

The proliferation of the world's 'information highways' has renewed interest in efficient document indexing techniques. This thesis considers the architecture of information retrieval systems. Distributed queries are studied with analytical and trace-driven simulations. We focus on physical index design, inverted index caching, and database scaling in a distributed shared-nothing system. All three issues are shown to have a strong effect on response time and throughput. Incremental updates of inverted lists are studied using a new dual-structure index data structure. The index dynamically separates long and short inverted lists and optimizes the retrieval, update, and storage of each type of list. To study the behavior of the index, a space of engineering trade-offs which range from optimizing update time to optimizing query performance is described. We quantitatively explore this space by using actual data and hardware in combination with a simulation of an information retrieval system. The best algorithm for a variety of criteria is determined. Finally, implementation of our incremental update algorithms is compared to an existing information retrieval system. Dissert. Abstr.

N95-30289 Universitaire Instelling Antwerpen, Wilrijk (Belgium).
DATA MODELING FROM A CATEGORICAL PERSPECTIVE Ph.D. Thesis
Chris Tuijn 1994 118 p
Avail: Univ. Microfilms Order No. DA9424425

The last decades, a lot of effort has been spent in defining formalisms to model data storage and retrieval. This is in particular true for the more recently introduced object-oriented systems. Some models were based on logic, other models were more graphically inspired, yet others were based on more complicated mathematical structures such as abstract data types, semantic networks, or Petri nets. The diversity of the techniques and formalisms used to model the systems referred to above asks for a more unifying approach. The approach we propose is based on category theory, a formalism that is especially useful for data modeling purposes because of its generic and fundamental character. This thesis can roughly be divided in two parts. In the first part, we study complex-object and object-oriented systems from a fundamental perspective. Therefore, we first introduce the so-called typegraph model. In this model, the scheme is represented by a small category (generated by the typegraph) and the instances as functors from this category to an instance category. Although this model is structurally equivalent with well-known models such as IQL, the query-language is entirely defined using so-called universal constructions. The functional nature of the typegraph model suggested to investigate another approach which considers instances as mappings from an instance to the scheme. This approach is taken with the introduction of the CGOOD model, a categorical graph-based data model. The second part of this thesis fully exploits the abstraction power of category theory. In this part we use category theory as a framework to study classes of data models and investigate in particular some important object-oriented properties such as object-identify and inheritance. Dissert. Abstr.

83 ECONOMICS AND COST ANALYSIS

Includes cost effectiveness studies.

No abstracts in this category.

84 LAW, POLITICAL SCIENCE AND SPACE POLICY

Includes NASA appropriation hearings; aviation law; space law and policy; international law; international cooperation; and patent policy.

No abstracts in this category.

85 URBAN TECHNOLOGY AND TRANSPORTATION

Includes applications of space technology to urban problems; technology transfer; technology assessment; and surface and mass transportation.

For related information see also *03 Air Transportation and Safety, 16 Space Transportation,* and *44 Energy Production and Conversion.*

No abstracts in this category.

88 SPACE SCIENCES (GENERAL)

No abstracts in this category.

89 ASTRONOMY

Includes radio, gamma-ray, and infrared astronomy, and astrometry.

N95-28822*# Applied Research Corp., Landover, MD.
X-RAY OBSERVATIONS OF RAPIDLY ROTATING O STARS Final Report
Wayne L. Waldron and Derck Massa 31 May 1995 13 p
(NASA Order S-14626-F)
(NASA-CR-189423; NAS 1.26:189423; ARC-1272; ARC-R95-236) Avail: CASI HC A03/MF A01

HEAO-2 results suggest that high vsini O stars appear to be significantly fainter x-ray sources. We proposed to observe additional high vsini O stars to test this hypothesis. Unfortunately, the PSPC was shot down during our scheduled observation time, and the observation was not re-scheduled. The contract work was modified to carry out other related x-ray tasks. Author

N95-29101# Nobeyema Solar Radio Observatory (Japan).
NOBEYAMA RADIO OBSERVATORY REPORT, NO. 380: DETECTION OF THE (29)SIO v=1, J=1-0 MASER FROM TX CAMELOPARDALIS
Se-Hyung Cho and Nobuharu Ukita 1995 11 p
(ISSN 0911-5501)
Avail: CASI HC A03/MF A01

The maser emission from the v=1, J=1-0 transition of (29)SiO has been detected for the first time toward the Mira variable star TX Cam among 54 surveyed late-type stars. The line was fairly narrower than the SiO-29 v=0, J=1-0 transition, and slightly redshifted compared to the v=0 line. In addition, the SiO-28 v=2, J=2-1 transition has also been newly detected in this star. Based on the line intensity, the pumping mechanism for the SiO-29 v=1, J=1-0 maser is discussed. The simple large velocity-gradient model and the line overlap of H2O can not be adopted for this maser. Author

N95-29172* Tokyo Univ. (Japan). Inst. for Space and Astronautical Science.
YOHKOH SOFT X-RAY TELESCOPE (Videotape)
21 Apr. 1992 Sponsored by NASA, Washington Videotape: 6 min. playing time, in color, with sound
(NASA-CR-197655; HQ-92-03L; NONP-NASA-VT-95-46000) Avail: CASI VHS A02/BETA A22

This video describes the Soft X-Ray Telescope (SXT), Yohkoh. This is a cooperative program between NASA and the Institute for Space and Astronautical Science of Japan. Images of the Suns rotation were obtained with the SXT. CASI

N95-29204 Arizona Univ., Tucson, AZ.
LOW-BACKGROUND BALLOON-BORNE DIRECT SEARCH FOR IONIZING MASSIVE PARTICLES AS A COMPONENT OF THE DARK GALACTIC HALO MATTER Ph.D. Thesis
Patrick Charles McGuire 1994 185 p
Avail: Univ. Microfilms Order No. DA9424987

A dark matter (DM) search experiment was flown on the IMAX balloon payload, which tested the hypothesis that a minor component of the dark matter in the Galactic halo is composed of ionizing (dE/dx greater than 1 MeV/g/cm(exp 2) or sigma greater than 2 x 10(exp -20) sq cm supermassive particles (m(sub x) is an element of (10(exp 4), 10(exp 12))GeV/c(exp 2) that cannot penetrate the atmosphere due to their low velocities (beta belongs to (0.0003, 0.00025)). The DM search experiment consisted of a delayed coincidence between four approximately 2400 cm(exp 2) plastic scintillation detectors, with a total acceptance of approximately 100 cm(exp 2) sr. In order to search for ultra-slow particles which do not slow down in the IMAX telescope, the experiment contained TDCs which measured the time-delays T(sub i,i+1)is an element of (0.3, 14.0)microseconds between hits in a successive counters to approximately 1 percent precision. Using the first 5 hours of data at float altitude (5 g/sq cm residual atmosphere), we observed approximately 5 candidate nonslowing dark matter events, consistent with the background from accidental coincidences of 4 events. This implies that the DM flux is less than 6.5 x 10(exp -6) cm(exp -2)s(exp -1)sr(exp -1) (95 percent C.L.). Similar results were also obtained for particles which slow down in the counter telescope. This experiment effectively closes much of a previously unconstrained 'window' in the mass/cross-section joint parameter space for massive particles as the dominant halo DM, and implies that for certain regions of this parameter space massive particles cannot be more than one part in 10(exp 5) by mass of all the DM. These results can also directly constrain 'light' magnetic monopoles and neutra CHAMPs in a previously unconstrained mass region m(sub x) belongs to (10(exp 6), 10(exp 9)) GeV. Dissert. Abstr.

N95-29370*# Computer Sciences Corp., Calverton, MD. System Science Div.
SIMULTANEOUS UV AND OPTICAL STUDY OF O STAR WINDS AND UV AND OPTICAL COVARIABILITY OF O STAR WINDS Final Report
Joy S. Nichols Apr. 1995 36 p Sponsored in part by the Netherlands Organization for Scientific Research
(Contract NAS5-32473)
(NASA-CR-189424; NAS 1.26:189424) Avail: CASI HC A03/MF A01

Simultaneous ultraviolet and optical observations of 10 bright O stars were organized in several observing campaigns lasting 3-6 days each. The observing campaigns included 12 observatories in the Northern hemisphere obtaining high resolution spectroscopy, photometry, and polarimetry, as well as 24-hour coverage with the IUE (International Ultraviolet Explorer) observatory. Over 600 high dispersion SWP spectra were acquired with IUE at both NASA and VILSPA for the completion of this work. The

massive amount of data from these observing campaigns, both from IUE and the ground-based instruments, has been reduced and analyzed. The accompanying paper describes the data acquisition, analysis, and conclusions of the study performed. The most important results of this study are the strong confirmation of the ubiquitous variability of winds of O stars, and the critical correlation between rotation of the star and the wind variability as seen in the ultraviolet and optical spectral lines. Author

N95-29529 Stanford Univ., CA.
FIRST FLIGHT OF THE MULTI-SPECTRAL SOLAR TELESCOPE ARRAY: CALIBRATION, RESULTS AND FUTURE PLANS Ph.D. Thesis
Max J. Allen 1994 186 p
Avail: Univ. Microfilms Order No. DA9422066

The Multi-Spectral Solar Telescope Array (MSSTA) is a comprehensive solar rocket-borne observatory which utilizes multilayer coated optics to achieve high resolution thermally resolved images of the sun at FUV, EUV, and soft x-ray wavelengths. The MSSTA was successfully flown on May 13, 1991, obtaining high resolution images of chromospheric and coronal structures, including loops, filaments, polar plumes, and bright points. These images were obtained in six emission bandpasses (C IV lambda approximately 1550 A, H Lyman-alpha lambda approximately 1216 A, Fe XIV lambda approximately 211 A, Fe XII/XIII lambda approximately 193 A, Fe IX/X lambda approximately 173 A, and Si XII lambda approximately 44.1 A) and represent a unique combination of high spatial resolution and spectral differentiation. Four chapters are contained in this thesis. Chapter one reviews the scientific objectives, configuration, and initial flight results from the 1991 MSSTA launch. Chapter two discusses the pre-flight and post-flight calibration of the MSSTA instruments. Chapter three uses the May 13, 1991 image data to present an analysis of polar plumes and their possible role in the generation of the solar wind. The final chapter details a complete redesign of the payload control electronics undertaken to significantly enhance the capabilities and reliability of the MSSTA for future flights. Dissert. Abstr.

N95-29532 Harvard Univ., Cambridge, MA.
A SEARCH FOR CATACLYSMIC VARIABLES IN GLOBULAR CLUSTERS Ph.D. Thesis
Adrienne Margaret Cool 1994 185 p
Avail: Univ. Microfilms Order No. DA9421432

This thesis is a multiwavelength search for cataclysmic variables (CVs) in globular star clusters. Its aim is to test models which predict that significant numbers of these binary-stars should form via tidal capture or exchange collisions in clusters with dense cores. Its principal focus is on two nearby clusters, NGC 6397 and NGC 6752, which are so-called 'post-core-collapse' clusters with highly dense cores. Complementary observing programs were carried out at optical and x-ray wavelengths, using the Hubble Space Telescope (HST), ground-based optical telescopes, and the ROSAT x-ray satellite. The optical studies, aimed at detecting CVs in quiescence, are photometric studies whose primary selection criterion is for objects with H alpha emission lines. Two x-ray sources toward omega Cen (NGC 5139) at radii of greater than 10 arcminutes, which had previously been considered potential cluster CVs, are identified as foreground dMe stars, reinforcing the view that a significant fraction of x-ray sources at large radii are not cluster members. Candidate CVs are identified in both NGC 6397 and NGC 6752. ROSAT High Resolution Imager observations reveal 3-5 faint x-ray sources less than 1.5 arcminutes from the centers of each cluster, whose luminosities are typical of galactic CVs. HST Planetary Camera studies, coupled with analyses of archival HST Faint Object Camera images, yielded three candidates within 10 arcseconds of the center of NGC 6397 which are both H alpha bright and UV-bright. Associating these optical candidates with x-ray sources found with ROSAT produces a self-consistent picture of these stars as CVs with properties similar to those of CVs known elsewhere in the galaxy. Ground-based observations yielded two CV candidates in NGC 6752 at radii of 2-3 arcminutes. If the x-ray sources identified near the centers of NGC 6397 and NGC 6752 are CVs, the total CV population in the two clusters is likely to be greater than 10-20 and greater than 20-30, respectively. The total number of CVs in NGC 6397 inferred from the optical candidates agrees to within a factor of two. These inferred total populations are in reasonable agreement with theoretical predictions of CV formation rates. Dissert. Abstr.

N95-29545 Georgia Inst. of Tech., Atlanta, GA.
THE USE OF CHARGE COUPLED DEVICES IN ASTRONOMICAL SPECKLE IMAGING Ph.D. Thesis
Jerome A. Zadnik 1993 162 p
Avail: Univ. Microfilms Order No. DA9415677

This research consists of a theoretical and experimental evaluation of charge coupled devices (CCD's) for use in astronomical speckle imaging. Speckle imaging is a technique for removing atmospheric blurring from ground based telescope images. Imaging performance was quantified by deriving the signal to noise ratio (SNR), including CCD readout noise, of the power spectrum and Knox-Thompson product. To verify theoretical SNR calculations, an advanced CCD camera system was built and characterized. With noise of 7.2 electrons/pixel rms at 1 Mpixel/sec, this is presently the lowest noise, high speed CCD camera for astronomical imaging. Ground based telescope observations at various light levels were obtained with the newly developed system. The telescope data validated theoretical predictions and CCD's were found to be effective speckle imaging detectors over a wide range of observational conditions. Comparisons were made between CCD's and photon counting cameras based on SNR calculations, quantum efficiency and maximum count rate. Appropriate operating regions were defined graphically for each camera. Dissert. Abstr.

N95-29591 Colorado Univ., Boulder, CO.
THE X-RAY SCATTERING HALO AROUND SCO-X1 Ph.D. Thesis
Dennis Joseph Gallagher 1993 111 p
Avail: Univ. Microfilms Order No. DA9423488

This study describes the results of an x-ray observation (0.25 less than E less than 2.5 keV) of Sco X-1 designed to detect the presence of x-ray scattering off of interstellar dust grains in the form of a halo around Sco X-1. The data for this thesis were collected from a NASA sounding rocket, flight (36.077UH). The fabrication process and imaging analysis of the Wolter Type-I grazing incidence telescope built for this experiment are presented. A unique method of imaging x-rays from the telescope, out of the plane of incidence was used to reduce the amount of scattering from the x-ray optics. I discuss how I analyze the data for detecting the presence of x-ray scattering around the image of Sco-X1. The results of this work suggest that the interstellar reddening estimates to Sco-X1 using the 2200 Angstroms interstellar absorption feature, which indicate reddening of E(B - V) approximately equals 0.3, have possibly overestimated the reddening to Sco-X1. The results presented here favor a lower reddening estimate of E(B - V) approximately equals 0.1 for Sco-X1. The lower estimate was derived by using an interstellar extinction curve particular for the area near the Sco-X1 direction. This suggests that the higher reddening estimates could be due to absorption intrinsic to Sco-X1. Dissert. Abstr.

N95-29648 California Univ., Los Angeles, CA.
AN INVESTIGATION INTO THE EXISTENCE OF ASTEROIDS AT SATURN'S TRIANGULAR LAGRANGIAN POINTS Ph.D. Thesis
Colette Marie delaBarre 1993 320 p
Avail: Univ. Microfilms Order No. DA9420493

Many asteroids have been observed around the triangular Lagrangian points (L4 and L5) of Jupiter, but none around Saturn's where they are difficult to observe. Hence, a study of their orbital stability would focus future searches, or place constraints on the last phases of solar system formation. I numerically integrated orbits around the L4 and L5 points of Jupiter (Trojans) and Saturn ('Bruins'): 40 Trojans and 360 Bruins, all of inclination less than 12 deg. Four Bruins remained stable until the integration was stopped at 412 Myrs. Properties of these stable orbits were: (1) proper eccentricities less than 0.028; (2) librations in true longitude about L4 and L5 of more than 80 deg; (3) longitudes of perihelion that librated relative to a libration center 45 deg from Saturn's longitude of perihelion, such that the perihelia were never close when the forced eccentricity was near 0.08; (4) longitudes of perihelion that were never close to Jupiter's longitude of aphelion when their eccentricities were near maximum; and (5) maximum eccentricities that never occur at the same time as Jupiter's maximum eccentricity. These properties of a stable Bruin's orbit reduce the perturbations by Jupiter and Saturn. Orbits with librations in true longitude less than 80 deg were unstable, the time to instability being correlated with libration angle. While Bruins of small libration angle went unstable, no unstable region was found around Jupiter's triangular Lagrangian points, and stable Trojans may have longitudes of perihelion that either circulate

or librate with respect to Jupiter's, with proper eccentricities as much as an order of magnitude larger than those for the Bruins. A major contributor to Bruins going unstable near L4 and L5 is the presence of three separatrices of motion caused, in part, by the Great Inequality (GI) between Jupiter and Saturn. The GI separatrices drive up the eccentricity of Bruins on small tadpole orbits, but have much less effect on large tadpole orbits (like the four long-lived Bruins). Dissert. Abstr.

N95-29651 Johns Hopkins Univ., Baltimore, MD.
CORONAGRAPHIC IMAGING OF PROTOPLANETARY-DISK CANDIDATE STARS USING ADAPTIVE OPTICS Ph.D. Thesis
David Andrew Golimowski 1994 139 p
Avail: Univ. Microfilms Order No. DA9419974

A coronagraph has been equipped with adaptive optics to provide high-resolution ground-based images of the circumstellar environments of bright stars at optical wavelengths. The Adaptive Optics Coronagraph presently contains an image-motion compensation system for stabilization of the telescope field. By stopping the telescope aperture D to approximately 4 r(sub 0), where r(sub 0) is Fried's parameter, the maximum attainable resolution gain factor of 2.2 has been achieved. Gains measured for D/r(sub 0) greater than 14 are below theoretical expectation and are indicative of centroid anisoplanatism, a small spatial-coherence outer scale, or both. A comparison of stabilized and unstabilized images shows that this coronagraph may detect circumstellar objects 2 magnitudes fainter than those detectable with a conventional coronagraph. Coronagraphic observations of two protoplanetary-disk candidate stars are described. R-band images of the beta Pictoris circumstellar disk obtained in 1991 provide the first reliable optical photometry of the disk 40-100 AU from the star. At 100 AU, the radial power-law dependence of the disk-midplane surface brightness changes abruptly; the brightness gradient becomes less steep within 100 AU. Further, the brightness gradients of the two disk extensions are asymmetric. The geometric thickness of the disk appears nearly constant within approximately 115 AU and increases proportionally with radius beyond approximately 115 AU. These changes in brightness gradient and disk thickness at approximately 100 AU may mark the boundary of rapid ice sublimation within which only refractory grains exist, but may also reflect a flattened grain distribution associated with planetary formation within 40 AU. Images of epsilon Sagittarii obtained in 1990 and 1992 reveal a pointlike source, presumably a star, approximately 2".1 from epsilon Sgr. Although the star appears partially occulted by the coronagraphic mask in the V- and R-band images, it is clearly resolved in the I-band image obtained with a smaller mask. Large photometric uncertainties preclude an accurate assessment of the star's spectral type. Although the proximity of the star to epsilon Sgr supports the hypothesis that previously reported optical and UV spectra of epsilon Sgr are composite, the star appears too faint to account for the noted spectral anomalies. However, a K- or M-type companion to epsilon Sgr may explain the observed infrared excess.
Dissert. Abstr.

N95-29652 Stanford Univ., CA.
SPECKLE IMAGING WITH THE MULTI-ANODE MICROCHANNEL ARRAY DETECTOR Ph.D. Thesis
Elliott Pierce Horch 1994 242 p
Avail: Univ. Microfilms Order No. DA9422091

This dissertation combines an instrument and a technique that have been studied separately for several years. The instrument is the multi-anode microchannel array (MAMA) detector. This is a photon-counting imaging system which has the ability to record the arrival time of every detected photon and which can distinguish events that arrive only 140 nanoseconds apart. The technique is speckle imaging. In conventional astronomy, fluctuations in the atmosphere above the telescope blur images so that the resolution is typically 1 to 2 arcseconds, much worse than the theoretical diffraction-limited resolution of large telescopes. Speckle imaging allows for reconstruction of image features on a much smaller scale by taking many short exposure images of an object, where over the exposure time the atmospheric fluctuations are effectively frozen. Speckle imaging cameras must therefore have the ability to read out images much faster than most astronomical imaging devices. Since the MAMA detector offers outstanding timing abilities as well as good spatial linearity and is available in a visible light version, it is an excellent choice for the imaging device in a speckle imaging system. A new MAMA-based speckle system has been built at Stanford University and a study of its performance forms a principle part of this work. Under certain conditions, the phenomenon of channel saturation of the MAMA detector can have significant effects on the signal-to-noise ratio of the speckle imaging results. Channel saturation also leads to a systematic error in the determination of the irradiance ratios of interferometric binary stars. A correction algorithm is described which leads to better estimates of these ratios in simulated data. Four methods of computing correlation functions necessary for producing high resolution reconstructed images are compared wing MAMA speckle data; two of these explicitly make use of the time-tagging ability of the detector. The highest signal-to-noise ratio in power spectra and bispectra is obtained with a weighted running-window method. Reconstructed images of several objects are presented. The MAMA-based speckle imaging system is shown to determine accurate position angles and separations of sub-arcsecond separation binary stars. Dissert. Abstr.

N95-29665 Boston Univ., MA.
MULTIWAVEBAND OBSERVATIONS OF QUASARS Ph.D. Thesis
Steven David Bloom 1994 165 p
Avail: Univ. Microfilms Order No. DA9415012

Multiwaveband observations of thirty quasars and active galaxies with flat radio spectra (referred to here as FRSQ's) have been conducted to determine their radio to infrared and X-ray to gamma-ray properties and the relationships between them. Specifically, the synchrotron self-Compton (SSC) process is examined as a likely common radiation mechanism. Very Long Baseline Interferometry is used in conjunction with radio to submillimeter-wave observations to determine the parameters of the synchrotron spectrum. These parameters are used to predict the SSC X-ray flux densities. Seven of thirty sources have predicted Compton X-ray flux densities well above the observed flux densities obtained with the ROSAT satellite. It is concluded that these sources experience internal relativistic motion directed toward the ovserver's line of sight, which lowers the predicted Compton X-ray flux. Three of these seven sources are detected at gamma-ray frequencies. Model spectra show that the X-rays are consistent with the first order SSC process. The gamma-rays are not produced via second order self-Compton scattering, but are rather produced either by first order self-Compton scattering or by another process. A comparison of the ROSAT X-ray flux densities and those obtained earlier with the Einstein Observatory show that many FRSQ's are X-ray variables, with a factor of 2-3 between minimum and maximum brightness. Sources that were observed more than once with ROSAT also show variability over this shorter timescale. In several sources (e.g., 4C 39.25 and NRAO 140) the X-ray variability is associated with millimeter variability. Gamma-ray detections are also related to increases in the radio to millimeter-wave spectrum. Model spectra show that the relationship between the predicted high energy and radio to infrared spectra is sensitive to whether magnetic field or electron energy density dominates the variations. Implications for the SSC model and models that include scattering of external photons are discussed. Statistical analysis shows that the millimeter-wave and X-ray luminosities for the sample are strongly correlated, with a linear regression slope of approximately 0.6. The peak in the distribution of X-ray to millimeter spectral indices also indicates a strong connection between millimeter-wave and X-ray emission.
Dissert. Abstr.

N95-29667 Pennsylvania State Univ., University Park, PA.
MODELS OF ACCRETION-POWERED X-RAY PULSARS Ph.D. Thesis
Tomasz Wojciech Bulik 1993 148 p
Avail: Univ. Microfilms Order No. DA9414249

Accretion powered X-ray pulsars are investigated in detail. Models of emission region are developed based on the self-consistent solution of the radiative transfer together with the hydrostatic and radiative equilibrium equations. The dominant opacity is due to electron scattering in a strong magnetic field, and free-free absorption is included, the cross sections being calculated with first order relativistic corrections. Radiation pressure effects are taken into account in detail. Estimates of the critical luminosity in the magnetic case are found to be lower than the gray Eddington luminosity. The dependence of the outgoing spectrum on the energy deposition mechanism is discussed. X-ray pulsar light curves are simulated taking into account the effects of gravitational bending, general geometry, and a parametrized accretion cap structure. The model spectra as a function of time are compared with observations of two X-ray pulsars, 4U1538-52 and Vela X-1, and satisfactory fits are obtained. The fits suggest some anomalies in the geometry of the objects, e.g. the magnetic axes seem to

be off-center, and a quite complex magnetic field structure on the caps is indicated. The accretion cap sizes are found to differ for a given pulsar, being generally compatible with theoretical models of accretion. General relativistic effects are found to be important in the formation of the spectra. The fluxes found in the fits indicate that the effects of radiation pressure cannot be neglected. The work presented here is the first analysis of X-ray pulsar spectra as a function of phase based on a detailed physical model. Dissert. Abstr.

N95-29678 Cornell Univ., Ithaca, NY.
A MULTI-WAVELENGTH STUDY OF ROTATION-DRIVEN PULSARS Ph.D. Thesis
Scott Campbell Lundgren 1994 273 p
Avail: Univ. Microfilms Order No. DA9416706

The Crab pulsar emits bursts of radio emission as high as 2000 times the average flux density amplitude. We undertook concurrent radio and gamma-ray observations of these giant pulses. A two component model fits the pulse flux density distribution--a sharply peaked distribution of low intensity pulses and a steep power law for giant pulses with a low end cutoff that is 33 times the mean of the low intensity pulses. The absence of pulses at flux densities between the low intensity and giant pulses suggest two entirely different emission mechanisms. Lack of time delay between giant and average pulses (Delta t = 6 +/- 12 micro seconds) suggests that all radiation eminates from a single region. Long-term apparent changes in the flux density of the giant pulses are caused by propagation effects in the interstellar medium. Correlating radio and gamma-ray emission constrains the radio coherence mechanism and the steadiness of particle outflow. We have found that gamma-ray flux increases by less than a factor of 2.5 concurrent with radio bursts. We have conducted several searches for rotation driven pulsars at radio and infrared wavelengths. A piggyback search at Arecibo Observatory was designed to maximize sky coverage and to exploit signal variability due to scintillations by cross comparing multiple observations of the same sky position. To handle the large data rate we developed a coarsely parallel algorithm for processing data simultaneously on multiple workstations. In another radio search targeted at unidentified gamma-ray sources we found a new binary millisecond pulsar J0751+18. We explore the possibility of association of the high energy emmission with the pulsar. To find distant pulsars whose pulsed radio emission is quenched by scattering in the interstellar plasma, we have conducted a targeted infrared search. Targets included the Galactic Center, globular clusters, supernova remnants, and known pulsars. A rebinning method of acceleration searching was developed to increase sensitivity to binary systems. All fields yielded only upper limits on infrared pulsations ranging from 40 to 150 micro Jy. The 35 micro Jy upper limit on emission from Geminga is used to constrain models for magnetospheric and surface thermal emission. Dissert. Abstr.

N95-29709 Stanford Univ., CA.
OBSERVATIONAL SIGNATURES OF ROTATING BLACK HOLES Ph.D. Thesis
Christopher Antonio Perez 1994 153 p
Avail: Univ. Microfilms Order No. DA9414636

Accretion disks provide an excellent medium for studying the strong-field structure of rotating black holes. We examine two potentially observable relativistic effects. In the first part, we explore the effects of the gravitational field of a rotating black hole on the propagation of light from the accretion disk. In the second part, we investigate adiabatic oscillations trapped near the inner edge of the accretion disk. To obtain an accurate depiction of an accretion disk at the image plane, we solve the photon orbit equations analytically in the kerr metric to determine the point of origin on a thin accretion disk of a photon which intersects a specified point on the image plane. We employ simple models for the spectral intensity emitted by the disk. Using this solution, we generate grayscale computer images of intensity of accretion disks with various angles of inclination around black and other relativistic effects on the light propagation. For the observational relevance of these effects, we also obtain light curves produced by gravitational lensing by much smaller intervening masses passing in front of our model accretion disk (acting as a gravitational microscope to reveal the structure of the disk). We extend our studies by examining trapped adiabatic oscillations in accretion disks around Kerr black holes. We analyze the normal modes of oscillations (which are analogous to the p- and g-modes of stars) within thin accretion disks which are terminated by an innermost stable orbit. We develop a general formalism for investigating the adiabatic oscillations of arbitrary unperturbed disk models. We obtain the lowest eignenfrequencies and eigenfunctions of various modes. Each of these modes will be obtained for various angular momenta of the black hole. These trapped modes do not exist in Newtonian gravity, and thus provide a probe of the strong-field structure of rotating black holes. Our predictions are related to past and future observations which could detect modulation in the X-rays from stellar mass black holes and in the optical and UV from supermassive AGN black holes. Dissert. Abstr.

N95-29710 Columbia Univ., New York, NY.
FAR-ULTRAVIOLET HIGH-RESOLUTION EMISSION LINE SPECTROSCOPY OF THE CYGNUS LOOP SUPERNOVA REMNANT Ph.D. Thesis
Andrew Peter Rasmussen 1993 161 p
Avail: Univ. Microfilms Order No. DA9412836

A new picture of the Cygnus Loop supernova remnant is presented in the light of the far ultraviolet resonance transition 2S(sub 1/2) - 2P(sup O, sub 1/2,3/2) of O VI (O(sup 5+)). The data was obtained from the first flight of the rocket borne, High Resolution Emission Line Spectrometer (HIRES). The O VI lines were much broader than the instrument's spectral resolution, and were readily measurable. The motion of the O VI emitters is in excess by a factor of approximately 100 over the most likely thermal velocity, but has a velocity distribution consistent with that of an expanding shell. Model fits to the O VI line profiles indicate a blast wave velocity within the range 210-250 km s(exp -1). In contrast, radiative shock observations of filaments in the Cygnus Loop derive much lower shock velocities through line ratio diagnostics. The O VI Cygnus Loop probably represents, therefore, nonradiative shocks that will cool at a later stage of the remnant's evolution, and will be seen in other wavebands at that time. If a nonradiative blast wave is responsible for the observed global emission, emissivity models require that it have a substantial covering factor over the Cygnus Loop, probably as much as 26 percent. This notion is encouraged by the spatial distribution of the O VI Cygnus Loop, because its distribution appears like that of a limb brightened shell, and similar to soft X-ray maps. Dissert. Abstr.

N95-29774 Maryland Univ., College Park, MD.
A STUDY OF ONE-ARMED SPIRAL GALAXIES Ph.D. Thesis
Bikram Phookun 1993 155 p
Avail: Univ. Microfilms Order No. DA9425113

We present VLA HI observations of the one-armed spiral galaxies, NGC 4027, NGC 4654, NGC 4254, NGC 5713, and NGC 3162, and H-alpha observations of the last three. With the help of these and existing observations, we study the properties of these galaxies. One-armed galaxies are uncommon and not well understood; they are important not only because of their exceptional spiral structure but also for two other reasons: (1) according to swing-amplification theory the one-armed mode is most likely when there is little or no dark matter around the disk of the galaxy; and (2) a trailing one-armed mode has no inner Lindblad resonance (ILR), and through repeated amplification can grow very large, possibly disrupting the galaxy. The HI observations reveal that all of the galaxies in our sample are interacting, NGC 4027, NGC 5713, and NGC 3162 with companion galaxies, NGC 4254 with a cloud of gas that is disintegrating and falling into it, and NGC 4654 with the intergalactic medium. The H-alpha data on NGC 4027, NGC 4254, NGC 5713, and NGC 3162 provide kinematic data of high spatial resolution in the inner parts. In all but NGC 4654 the direct effects of interaction are limited to the fragile outer parts of the galaxies; but their indirect effects are profound--they are the likely cause of the one-armed structure in these galaxies. In none of the galaxies is there strong evidence that an exceptional deficiency of dark matter is the primary cause of the one-armed structure. We propose the following scenario for all the galaxies except NGC 4654: gravitational interaction induces weak leading spiral waves, which are unwound by shear and swing amplified into the observed structure; the one-armed mode dominates as a result of the repeated amplification expected when the ILR is absent. In NGC 4254 and NGC 4027 the one-armed structure is exceptionally strong, so much so in the latter that the galaxy may be on the way to becoming an irregular. In NGC 4654 an offset bar is the likely cause of the spiral structure. Dissert. Abstr.

N95-29776 Maryland Univ., College Park, MD.
THE COMPLEX BROADBAND X-RAY SPECTRA OF SEYFERT GALAXIES Ph.D. Thesis
Kimberly Ann Weaver 1993 329 p
Avail: Univ. Microfilms Order No. DA9425154

The Broadband X-ray Telescope (BBXRT) and HEAO-1 A2 data presented in this thesis provide strong evidence for, and confirmation of, a multitude of complexities in the X-ray spectra of Seyfert galaxies. The HEAO-1 data confirm spectral flattening at greater than 9 keV that was recently discovered with Ginga, while the BBXRT data suggest that soft X-ray excesses as well as Fe K lines may be complex features in at least some Seyfert galaxies. From the small but representative BBXRT sample, it is clear that there is no 'universal' soft X-ray excess shape. The variety of soft excess shapes suggest that many soft X-ray production mechanisms are operating in Seyfert galaxies, and that the resulting spectra depend on: (1) the distribution of the X-ray emitting gas, (2) the geometry of the central regions of the galaxy, and (3) whether the nuclear X-ray source is affected by absorption. A combination of spectral, spatial, and variability information indicates that the soft excesses in the Seyfert galaxies NGC 2110 and NGC 4151 are not nuclear in origin. This implies that other, similar, soft excesses that were previously thought to be due to soft X-ray 'leakage' may prove to have a large contribution from an extended component. One of the goals of this thesis was to test ideas for the origin of Fe K alpha lines in Seyfert galaxies. In contrast to the general belief that most Fe K alpha lines arise in accretion disks, we have found evidence that at least strong Fe K alpha lines are not produced in accretion disks. In the HEAO-1 sample, strong lines are detected in sources that show no evidence of Compton reflection from a disk while sources with evidence for reflection do not possess strong Fe K alpha lines. This, along with the strong, narrow (less than 7,500 km s(exp -1) FWHM) Fe K alpha line observed in the BBXRT spectrum of NGC 4151, suggests that strong Fe K alpha lines are not associated with accretion disks, but are produced somewhere else, perhaps in the broad line region. Alternatively, strong Fe K alpha lines may prove to be complex features when we are able to fully resolve their line profiles. Dissert. Abstr.

N95-29781 Rutgers - The State Univ., New Brunswick, NJ.
THE SEARCH FOR MASS SEGREGATION IN STAR CLUSTERS OF THE MAGELLANIC CLOUDS Ph.D. Thesis
Paul Stephen Papenhausen 1994 397 p
Avail: Univ. Microfilms Order No. DA9421822

The goal of this thesis is to determine the amount of mass segregation in star clusters as a function of their age-to-(relaxation time) ratios. We obtained B and V CCD images of five star clusters in the Magellanic Clouds using the four meter telescope at Cerro Tololo Inter-American Observatory. The clusters are: NGC 458, NGC 2249, NGC 2097, IC 2146, and 121SCO3. These clusters are rich in stars and span a broad range in age (approximately 300 million to 10 billion years). Stellar positions and magnitudes are determined using the DAOPHOT computer package. The ages, metallicities, distant moduli, and reddenings of the clusters are determined by fitting theoretical isochrones to their color-magnitude diagrams. Individual stars cannot be detected within one core radius of the center because of crowding. We derive numerical correction factors to the star count densities as a function of magnitude and radius. We then present a model for the completeness correction factors. Structural parameters are determined by fitting King models to the surface brightness profiles. Using these, we estimate the cluster masses and the two-body relaxation timescales and find that three clusters are unrelaxed (NGC 458, NGC 2097, and IC 2146) and two are relaxed (NGC 2249 and 121SCO3). We search for mass segregation by two different methods. The first is a pairwise comparison of the luminosity functions in different regions using K-S tests. We find significant differences in NGC 2249 and IC 2146, but not in the other clusters. The second method fits both multimass and single-mass King models to the joint combination of stellar number density profiles and surface brightness profiles. We are unsuccessful in detecting mass segregation because the data is fitted equally well by both types of models. The lack of significant differences in the second test is probably due to the inclusion of systematic uncertainties associated with the correction factors. We find a color gradient in the cores of NGC 2249 and 121SCO3 (both are centrally blue), which is consistent with these clusters being relaxed. We suggest that future studies should be conducted with the use of the Hubble Space Telescope. Dissert. Abstr.

N95-29782 Iowa Univ., Iowa City, IA.
RADIOASTRONOMICAL MEASUREMENTS OF PLASMA CHARACTERISTICS OF THE SOLAR CORONA AND THE SOLAR WIND Ph.D. Thesis
Takayuki Sakurai 1993 209 p
Avail: Univ. Microfilms Order No. DA9421194

The plasma characteristics of the solar wind and the solar corona were studied with radio remote sensing techniques using the Very Large Array and the U.S. Very Long Baseline Interferometer network. Ten extragalactic radio sources were observed with VLBI in September 1989 at 4.99 GHz when several sources were close to the Sun. Angular broadening was detected in five sources with elongations less than 61 solar radii. The broadening sizes were consistent with those estimated from the electron density power spectrum model of Coles and Harmon, which consists of a Kolmogorov spectrum at large scale sizes comparable to the VLBI baselines, but with an enhancement in power at small spatial scales near the ion inertial length. No measurable anisotropy in the scattering was detected. The phase structure function was also obtained from the same set of observations, and it also was shown to be consistent with the spectrum of Coles and Harmon. Faraday rotation through the solar corona was measured with the VLA using the polarization position angles of extragalactic radio sources in March 1990 at 1464 and 1636 MHz. The source closest to the Sun showed an excess rotation measure, which is consistent with a coronal magnetic field of -12.5 +/- 2.3 mG at an elongation of 9 solar radii. A time series consisting of hourly measurement of the rotation measure were filtered for the background plasma contribution to extract the component which could be attributed to coronal Alfven waves. The data were corrected for second order polarimeter errors to removed the instrumental errors as well as ionospheric Faraday rotation errors. From the corrected data, an upper limit to the amplitude of coronal Alfven waves was estimated to be less than or equal to approximately 4.2 mG at a solar distance of 10.5 solar radii. This gives an upper limit to the Alfven wave energy flux of less than or equal to approximately 3.4 x 10(exp 4) ergs/cm(exp 2)/s at the coronal base, which is lower than what is believed to be the necessary amount for heating and accelerating the solar wind. Our estimate of delta B/B is roughly 0.5-0.7, indicating that Alfven waves at this solar distance are highly nonlinear. Dissert. Abstr.

N95-29827 California Univ., Santa Cruz, CA.
THE PROPERTIES OF LOCAL POOR ABELL CLUSTERS AND INSTRUMENTATION FOR THE STUDY OF CLUSTERED OBJECTS Ph.D. Thesis
R. Hank Donnelly 1994 193 p
Avail: Univ. Microfilms Order No. DA9423559

Since the identification of the Abell galaxy cluster sample in the 1950's observational cosmologists have been interested in the characteristics of these systems. However, until recently little more than their most basic properties, such as morphology and distance (from a small sample of member velocities), has been known. Some fundamental questions still remain unanswered. Do clusters form from field galaxies? Have they evolved significantly since their formation? Is their morphological type an indicator of their age? With the advent of wide-field imaging CCD's and multiplexing spectroscopic instruments, considerably more information has been accumulated for the richer clusters (those with memberships greater than 50). However, the poorer clusters, which potentially represent a transitional phase from field to the richer clusters, have received relatively little attention. This thesis represents a two element study of these objects. The first half discusses the issues involved in the construction of a multiplexing spectrographic system, specifically the Lick/LLNL Automated Multiobject Spectrograph (AMOS). Issues of systemic efficiency are examined with computer modeling and laboratory trials. The second half presents the results of a deep photometric survey of three poor clusters of galaxies out to 0.5 Abell radii. Data were taken in both V and I bands from the Johnson-Kron-Cousins system and are complete to a limiting magnitude of V = 19.5. The three clusters are located at essentially the same redshift (z = 0.07) and span the full range of Rood-Sastry morphological types. While surface distributions support the morphological typing, comparison of the three luminosity functions shows no indication of an evolutionary

sequence. A composite luminosity function is presented for comparison with samples at other redshifts and richness classes. Dissert. Abstr.

N95-29916# Arizona Univ., Tucson, AZ. Lunar and Planetary Lab.
ADVANCED RESEARCH IN SKY SURVEILLANCE: A SEARCH FOR LOW-LUMINOSITY OBJECTS Final Report, 1 Nov. 1991 - 31 Oct. 1994
Tom Gehrels Oct. 1994 12 p
(Contract F49620-92-J-0051)
(AD-A291184; AFOSR-95-0081TR) Avail: CASI HC A03/MF A01

Regarding astrophysical research, an increasing number of moving objects in the solar system is formed per year, positions are distributed electronically to others. Our own usage of the discoveries is to study magnitude-frequency relations for a variety of populations in the solar system, such as comets, Centaurs, main-belt asteroids, and objects that can come into the Earth's vicinity. For the near-Earth objects, the discovery rate now is about 25 percent per year, and expected to increase. These are followed up as much as possible in order to obtain the best possible orbits. The origin of 10-in objects, we call Arjunas is being studied, as is the chaotic behavior of large Centaurs in the outer parts of the solar system. Regarding the new techniques in sky surveillance, there still is lively progress and improvement for the old 0.9-m Spacewatch Telescope with the development of new scanning techniques computer programs and optical devices The construction of the 1.8-m Spacewatch Telescope is well under way. It is a device of great research interest, even for future generations of planetary scientists. It is of importance as a prototype for future instruments in sky surveillance. It has a compact and stiff design. DTIC

N95-30004*# National Aeronautics and Space Administration. Goddard Space Flight Center, Greenbelt, MD.
TOTAL SOLAR ECLIPSE OF 1997 MARCH 9
Fred Espenak and Jay Anderson (Environment Canada, Winnipeg, Manitoba.) Jul. 1995 66 p
(NASA-RP-1173; Rept-95B00100; NAS 1.61:1369) Avail: CASI HC A04/MF A01

A total eclipse of the Sun will be visible from Asia and the Pacific Ocean on 1997 March 9. The path of the Moon's umbral shadow begins in eastern Kazakhstan and travels through Mongolia and eastern Siberia, where it swings northward to end at sunset in the Arctic Ocean. A partial eclipse will be seen within the much broader path of the Moon's penumbral shadow, which includes eastern Asia, the northern Pacific, and the northwest corner of North America. Detailed predictions for this event are presented and include besselian elements, geographic coordinates of the path of totality, physical ephemeris of the umbra, topocentric limb profile corrections, local circumstances for 280 cities, maps of the eclipse path, weather prospects, the lunar limb profile, and the sky during totality. Tips and suggestions are also given on how to safely view and photograph the eclipse. Author

N95-30230*# Jet Propulsion Lab., California Inst. of Tech., Pasadena, CA.
OPTIMIZATION OF 100-METER GREEN BANK TELESCOPE
Douglas Strain Mar. 1994 26 p
(Contract NAS7-1260; RTOP 973-22-60-54-90)
(NASA-CR-198868; JPL-94-6; NAS 1.26:198868) Avail: CASI HC A03/MF A01

Candidate designs for NRAO's 100-m clear-aperture radio telescope were evaluated and optimized by JPL using JPL-developed structural optimization and analysis software. The weight of a non-optimum design was reduced from 9.4 million pounds to 9.2 million pounds. The half-pathlength error due to gravity deformations was reduced from 0.041-inch rms to 0.034-inch rms. Author

N95-30317* National Aeronautics and Space Administration, Washington, DC.
SPACE ASTRONOMY UPDATE (Videotape)
6 Jun. 1995 Videotape: 38 min. playing time, in color, with sound
(NASA-TM-110754; NONP-NASA-VT-95-56622) Avail: CASI VHS A02/BETA A22

A discussion of the images obtained by NASA's Hubble Space Telescope (HST) is featured on this video. The discussion panel consists of Dr. Jeff Hester (Arizona State Univ.), Dr. Jon Morse (Space Telescope Science Inst.), Dr. Chris Burrows (European Space Agency), Dr. Bruce Margon (Univ. of Washington), and host Don Savage (Goddard Space Flight Center). A variety of graphics and explanations are provided for the images of star formations and other astronomical features that were viewed by the HST. Author

90 ASTROPHYSICS

Includes cosmology; celestial mechanics; space plasmas; and interstellar and interplanetary gases and dust.

For related information see also *75 Plasma Physics*.

N95-29097# Nobeyema Solar Radio Observatory (Japan).
NOBEYAMA RADIO OBSERVATORY REPORT, NO. 378: THE POLAR RING SPIRAL GALAXY NGC 660
W. vanDriel (Tokyo Univ., Mitake, Japan.), F. Combes (Observatoire de Paris, France.), F. Cusoli (Observatoire de Paris, France.), M. Gerin (Ecole Normale Superieure, Paris, France.), N. Nakia, T. Miyaji, M. Hamabe (Tokyo Univ., Mitake, Japan.), Y. Sofue (Tokyo Univ., Mitake, Japan.), T. Ichikawa (Tokyo Univ., Mitake, Japan.), and S. Yoshida (Tokyo Univ., Mitake, Japan.) et al 1995 31 p Submitted for publication
(ISSN 0911-5501)
Avail: CASI HC A03/MF A01

NGC 660 is a unique, nearby, peculiar polar ring spiral LINER galaxy with two distinct morphological and kinematic components: a spiral disk, seen almost edge-on (i approximately 70 deg), with a major axis position angle of 45 deg and a diameter of approximately 11 kpc (D=13 Mpc, H(sub o) = 75 kms(exp -1) Mpc(exp -1)), and an outer polar ring (p.a. 170 deg) with a diameter of 31 kpc, inclined on average 55 deg with respect to the disk major axis. It was mapped in the 21 cm H(sub I) line with a resolution of 13 inches x 60 inches and in the CO(1-0) and CO(2-1) lines with a 12 inches -22 inches beam. B, V, R, I, J, H, K prime-band images, and a long-slit H(alpah) spectrum along the disk major axis were obtained as well. It has been morphologically classified as SBa, but our data show it has the global characteristics of a later-type (Sc?), gas-rich disk. The disk and the polar ring both have an exponential luminosity profile, with scalelengths of 1 3 and 3.9 kpc, respectively. The polar ring is blue (V-I approximately 1.0), indicating a stellar population age of a few billion years, according to our stellar population synthesis model and the nucleus is red (V-I approximately 1.8). H(alpha) images show H(sub II) regions throughout the polar ring. The near-infrared images show a boxy/X-shape of the bulge and 1.4 kpc long linear features along the disk major axis on both sides of the bulge. The disk was detected in radio continuum at 21 cm. It has a compact 300 mJy nuclear source and an extended (7.5 kpc diameter) component of 80 mJy. The central source has a very high radio power for a spiral galaxy, while the disk has a normal radio power. The radio spectral index is -0.57, indicating an important contribution from thermal radiation. Author

N95-29100# Nobeyema Solar Radio Observatory (Japan).
NOBEYAMA RADIO OBSERVATORY REPORT, NO. 382: THE MASS OF A STAR FORMED IN A CLOUD CORE: THEORY AND ITS APPLICATION TO THE ORION A CLOUD
Takenori Nakano, Tetsuo Hasegawa (Tokyo Univ., Mitake, Japan.), and Colin Norman (Johns Hopkins Univ., Baltimore, MD.) 1995 33 p Submitted for publication
(ISSN 0911-5501)
Avail: CASI HC A03/MF A01

We have investigated the mechanisms of determining the stellar mass in the process of star formation. Because the stellar core grows by the inflow of matter from the parent cloud core, the mass of the growing star is fixed when supply of matter from the cloud core is stopped. Because the cloud core matter falls onto the stellar core mostly through an accretion disk, a significant fraction of the mass outflow from the stellar vicinity and the stellar radiation escapes from the inner region without interacting with the infalling matter. A considerable fraction of the cloud core matter which has not yet contracted much is blown off by the mass outflow and the HII region developed by the stellar ultraviolet radiation. Although some cloud core matter may remain at this stage, it disperses soon because it is no longer gravitationally bound. Consequently supply of matter to the accretion disk and then to the stellar core stops. The stellar mass M(sub *) determined in this way is a function of the density of the cloud core, n(sub c), the

mass inflow rate from the cloud core, M(sub I), the mass outflow rate relative to the inflow rate, M(sub O)/M(sub I), and the cloud core mass relative to the generalized Jeans mass, M(sub c)/M(sub J), and can also be represented as a function of n(sub c), M(sub c), M(sub O)/M(sub I), and M(sub c)/M(sub J). When the mass outflow is dominant in blowing off the cloud core matter, we have M(sub *) varies as (M(sub c)(exp 7/6)) (n(sub c)(exp 1/12)) with the proportionality coefficient dependent on M(sub O)/M(sub I), and thus the stellar mass is almost independent of n(sub c). The star formation efficiency M(sub *)/M(sub c) is therefore mainly determined by M(sub O)/M(sub I) and is only weakly dependent on the core parameters M(sub c) and n(sub c); for a typical value M(sub O)/M(sub I) = 0.1 we obtain M(sub *)/M(sub c) approximately equal to 0.04 around M(sub c) approximately 100 solar mass. Applying this method to the observed cloud cores in the Orion A molecular cloud by assuming that each core does not contain subclumps we estimate the stellar mass and the initial mass function of stars (IMF) expected in this cloud. As long as M(sub O)/M(sub I) greater than 0.02, the mass outflow is more efficient than the HII region in determining the stellar mass for all the Orion A cores. The IMF at M(sub *) approximately greater than 4 solar mass can be approximated by a power law dN(sub *)/dlogM(sub *) varies as (M(sub *)(exp -1.7)) for M(sub O)/M(sub I) = 0.1, which is in reasonable agreement with the IMF of field stars varies as (M(sub *)(exp -1.5)) at M(sub *) approximately greater than 3 solar mass. We also discuss star formation in the cloud core which contains many subclumps. Author

N95-29252 Texas Univ., Austin, TX.
CONTINUUM SPECTRA OF SUPERMASSIVE ACCRETION DISKS Ph.D. Thesis
Homer Howard Coleman, Jr. 1993 117 p
Avail: Univ. Microfilms Order No. DA9413467

The lack of recognizable hydrogen Lyman edge features in the ultraviolet continua of active galactic nuclei (AGN) has been cited as evidence against the most popular model for the source of AGN continua: thermal emission from thin accretion disks. Disk models have also had difficulty in reproducing observed soft x-ray luminosities. It is shown here that disk atmospheres are characterized by low effective gravities which lead to small photospheric densities and small bound-free absorption opacities. For high temperature disks around rotating black holes, such atmospheres produce continuum emission characterized by weak Lyman edges and soft x-ray luminosities consistent with those observed. Further, weak Lyman edges from face-on disks, distorted by relativistic effects, resemble observed continuum features, suggesting that hitherto unrecognized Lyman edges may be present in AGN spectra. Dissert. Abstr.

N95-29255 Arizona Univ., Tucson, AZ.
DELIVERY OF METEORITES FROM THE ASTEROID BELT Ph.D. Thesis
Michael Craig Nolan 1994 212 p
Avail: Univ. Microfilms Order No. DA9424977

The process of the delivery of meteorites to the surface of the Earth from plausible source regions such as the asteroid belt is currently understood in general terms, but important uncertainties and conflicts remain to be resolved. Stochastic effects of the rare disruptions of large asteroids on the population of meteorite-sized Earth-crossing asteroids can change the flux and the proportions of compositional types in the infalling meteorite population. These changes can be significant in magnitude over timescales of 10(exp 8) years. Changes of the order of 1 percent can be expected on timescales of 10(exp 5)-10(exp 6) y, consistent with small differences between the Antarctic meteorites and modern falls. The magnitude of changes depends strongly on poorly-understood details of collisions. Asteroids 951 Gaspra and 243 Ida were recently imaged by the Galileo spacecraft. I use a numerical hydrocode model to examine the outcomes of various sire impacts into targets the sizes of these asteroids. A shock wave fractures the asteroid in advance of crater excavation flow; thus, for impactors larger than 100 m, impacting at 5.3 km s(exp -1), tensile strength is unimportant in these bodies, whether they are initially intact or are 'rubble piles'. Because of the shock-induced fracture, impact results are controlled by gravity. Therefore these asteroids are much more resistant to catastrophic disruption than predicted by previous estimates, which had assumed that strength was controlling these processes for rock targets. Fracture of km-size asteroids is different from fracture in terrestrial experiments using few-cm targets. The composition distribution of delivered meteorites depends on the outcomes of such asteroid impacts. Dissert. Abstr.

N95-29530 California Univ., Santa Cruz, CA.
THE DYNAMICS OF FU ORIONIS OUTBURSTS: TIME-DEPENDENT ACCRETION THROUGH PROTOSTELLAR DISKS Ph.D. Thesis
Katherine Robbins Bell 1993 128 p
Avail: Univ. Microfilms Order No. DA9419760

Although active accretion disks are thought to be ubiquitous among low mass young stellar objects (YSO's), few constraints are imposed on physical conditions in these disks. Time scales of FU Orionis events (dramatic outbursts thought to occur in all YSO's) are used to estimate the magnitude of the disk's viscosity. We propose that disks which receive steady infall, M(sub in)-dot, at a rate greater than the critical value: M(sub crit)-dot = 5 x 10(exp -7) solar mass/yr for which hydrogen ionizes in the disk, will be subject to thermally triggered, repetitive accretion outbursts. Results from one dimensional convective vertical structure and radial time dependent diffusion calculations create a self-consistent picture in which FU Orionis outbursts occur due to self-regulated ionization fronts propagating radially out to several tenths of an AU. With viscous efficiency alpha between 10(exp -3) and 10(exp -4), disk models with one solar mass central objects accreting (1-10) x 10(exp -6) solar mass/yr (consistent with estimates of molecular cloud core collapse rates) display FU Orionis outburst behavior and time scales. Beyond 1/4 AU modeled disks transport mass steadily inward at the input rate: M(sub in)-dot, while inner regions are regulated by the thermal instability such that long intervals (approximately 1000 yrs) of low mass flux: (1-30) x 10(exp -8) solar mass/yr, are punctuated by short intervals (approximately 100 yrs) of high mass flux: (1-30) x 10(exp -5) solar mass/yr. The model is substantiated by black body fits to time dependent models which display spectral features characteristic of observed objects. The rise time of Fuor V1515 Cyg is matched by a self-regulated outburst model. The rapid rise times of FU Ori and V1057 Cyg require the application of modest perturbations. That after peak light in V1057 Cyg short wavelength radiation decayed more rapidly than 2-5 micron radiation is naturally explained if mass flux drops in the inner disk (r less than 1/4 AU) while remaining steady in the outer disk. The decrease in line width seen after peak light in V1057 Cyg may be accounted for by the decreasing Keplerian velocity encountered by the outward propagating ionization front. We suggest that FU Orionis outbursts primarily occur to systems during the embedded phase with ages less than several x10(exp 5) yrs. Evidence is reviewed which suggests that HL Tau is a system subject to FU Orionis type outbursts which is currently quiescent. Dissert. Abstr.

N95-29592 Arizona State Univ., Tempe, AZ.
CARBON ISOTOPE ABUNDANCE RATIOS IN COMETS Ph.D. Thesis
Marvin Leroy Kleine, Jr. 1994 146 p
Avail: Univ. Microfilms Order No. DA9424117

Fluorescence spectra of the R-branch of the B(sup 2)Sigma(sup +) - X(sup 2)Sigma(sup +) (0-0) band of CN observed in the coma of comets P/Halley, C/Levy, C/Austin and C/Okazaki-Levy-Rudenko were analyzed to determine the C-12/C-13 abundance ratios. Long slit high resolution spectroscopic observations were obtained using the Mt Stromlo coude echelle spectrograph and a photon counting array detector. Computed rotational line fluorescence efficiencies for the stable isotopes of cyanogen (CN) were used to convert observed emission line intensities to carbon isotopic abundance ratios. Rotational lines belonging to the C-13/N-14 molecule were identified in each of the cometary spectra. The carbon isotope abundance ratios determined for P/Halley, C/Levy, C/Austin, and C/Okazaki-Levy-Rudenko were 95 +/- 12, 90 +/- 10, 85 +/- 20, and 93 +/- 20 respectively. No lines of C-12/N-15 were detected in any of the four cometary spectra. The carbon isotope ratios determined from the observations agree with the solar system ratio, C-12/C-13 = 90, established at least 4.6 billion years ago prior to the time the solar system formed. The results for these four comets provide evidence that comets coevolved with the other members of the solar system, and that they represent pristine samples of the protosolar nebula. The consistency of the carbon isotope ratios among the four comets with the bulk solar system value indicates homogeneity in the solar nebula, and makes the capture hypothesis for the origin of the Oort comet cloud implausible. Dissert. Abstr.

N95-29599 Naval Air Warfare Center, Point Mugo, CA. Weapons Div.
TIDAL AND LUNAR DATA FOR POINT MUGU, SAN NICOLAS ISLAND, AND THE BARKING SANDS AREA DURING 1995
Charles J. Fisk and Bernard C. Cohenour Dec. 1994 41 p Limited Reproducibility: More than 20% of this document may be affected by microfiche quality
(AD-A289877; NAWC-WPNS-TP-8065) Avail: Issuing Activity (Defense Technical Information Center (DTIC))

Basic lunar and tidal data for Point Mugu, San Nicolas Island and the Barking Sands area during 1995 are provided. The data presented are: (1) Tidal data; (2) times of moonrise and moonset; (3) times of lunar phases; and (4) times of sunrise and sunset. DTIC

N95-29649 Rensselaer Polytechnic Inst., Troy, NY.
DUST FORMATION IN STELLAR OUTFLOWS: A TIME-DEPENDENT MODEL Ph.D. Thesis
Michael P. Egan 1993 158 p
Avail: Univ. Microfilms Order No. DA9420316

Asymptotic Giant Branch (AGB) stars are sites of dust formation and undergo significant mass loss, at rates ranging from 10(exp -7) to 10(exp -4) solar mass/yr. Observations of CO lines indicate that outflow velocities of 5 to 25 km/s exist. The outflow is believed to be driven by radiation pressure on grains and momentum coupling between the grains and gas. While the physics of shell dynamics and dust grain formation are strongly coupled, most previous models of circumstellar shells have treated the problems separately. Studies of shell dynamics typically assume the existence of grains needed to drive the outflow. Most grain formation models assume a constant velocity wind, at observed outflow velocities, in which grains form. In addition, models of grain formation have relied primarily on classical nucleation theory to determine grain formation rates as opposed to a more realistic chemical kinetics approach. To model grain formation in carbon-rich AGB stars, I have coupled the kinetic equations governing small cluster growth to moment equations which determine the growth of large particles. Stationary outflow models are presented to demonstrate the differences between the classical nucleation approach and the kinetic equation method. It is found that classical nucleation theory predicts nucleation at a lower supersaturation ratio than is predicted by the kinetic equations, resulting in significant differences in grain properties. For a more complete physical model, the hydrodynamics equations of an outflow modified to include grain formation are solved. The time-dependent model results indicate that grain formation is a two-stage process, with large grains forming close to the stellar photosphere (within about 1 stellar radius), and evaporating to smaller sizes as they are accelerated by radiation pressure into lower density regions. As the expanding gas cools, formation of additional small grains occurs. The location of the dust formation zone is consistent with recent interferometric observations of IRC +/- 10216. The velocity structure of the circumstellar shell consists of a number of shocks corresponding to bursts of grain formation of addition. In addition, it is seen that the density distribution of gas in the outflow is dragged by the grains into a flat, power law like distribution. The effect of different (C)/(O) ratios, stellar temperature, and stellar luminosity are investigated. The models demonstrate that higher values of (C)/(O) result in higher mass loss rates. An order of magnitude enhancement in carbon abundance results in up to a factor of 5 increase in mass loss rate. This is due to the formation of larger grains which cause higher outflow velocities. Increasing stellar temperature also results in higher mass loss rates. However, when holding other quantities equal, models with higher stellar luminosities yield lower mass loss rates, due to the smaller grains formed around high luminosity sources. Observations of IRC + 10216 at minimum and maximum luminosity confirm that this is a real effect. Dissert. Abstr.

N95-29663 Columbia Univ., New York, NY.
THE EVOLUTION OF BINARY MILLISECOND PULSARS AND THE FORMATION OF PLANETS AROUND THEM Ph.D. Thesis
Menashe Banit 1993 82 p
Avail: Univ. Microfilms Order No. DA9412728

We show that the formation of planets around a millisecond pulsar may occur in a very late phase of Low-Mass X-Ray Binary (LMXB) or Binary-Millisecond-Pulsar (BMP) evolution. We propose a new mechanism in which the companion winds in these phases form through the combined action of the radiation heat on the companion's atmosphere and the radiation force on the slowly lifting wind. This mechanism can produce relatively high mass flow rates, and provided the companion is bloated, it explains the observed rapid angular momentum loss of the binary millisecond pulsar 1957 + 20. With such wind the evaporated matter can be supplied to a circumbinary 'excretion' disk in which the physical conditions, similar to those appropriate for the BMP1957 + 20 system, may allow the formation of planets like those observed in PSR1257 + 12. This model connects the conventional evolutionary scenario for the formation of a millisecond pulsar with the formation of planets around it. Dissert. Abstr.

N95-29669 Yale Univ., New Haven, CT.
EFFECTS OF MICROSCOPIC DIFFUSION AND ROTATIONAL MIXING ON STELLAR MODELS Ph.D. Thesis
Brian Charles Chaboyer 1993 200 p
Avail: Univ. Microfilms Order No. DA9415850

We have calculated evolutionary tracks for halo stars and constructed isochrones with alpha-enhanced compositions which cover the entire globular cluster metallicity range and include the effects of the diffusion of He-4. We find that including the effects of helium diffusion has a negligible effect (less than 0.5 Gyr) on the derived ages of globular clusters. Regardless of the inclusion of helium diffusion, we find a significant age spread of 5 Gyr among the globular clusters. The oldest globular cluster studied was M92 with an age of 17 +/- 2 Gyr old. The stellar models may be tested by comparing the Li-7 depletion and surface rotation rates to observations in young clusters stars. The observed Li-7 abundances clearly indicate that standard or diffusive models do not deplete enough Li-7. Instabilities induced by rotation provide an additional mixing mechanism. For this reason the stellar evolution code was modified to include the combined effects of diffusion and rotational mixing of H-1, He-4 and the trace elements He-3, Li-7 and Be-9. The calibrated solar models have a convection zone depth of 0.709-0.714 solar radius, in excellent agreement with the observed depth of (0.713 +/- 0.003) solar radius. The rotational mixing inhibits the diffusion in the outer parts of the models, leading to a decrease in the envelope diffusion by 50-80 percent. These models are able to reproduce the Li-7 abundances and rotation velocities observed in young cluster stars. Observations of Li-7 abundances in extremely metal poor halo stars provide another test of the stellar models. Standard models do a good job of fitting the observed Li-7 abundances and predict a primordial Li-7 abundance of log N(Li) = 2.24 +/- 0.03. Models of hot stars which include microscopic diffusion, but not rotational mixing, deplete too much Li-7. The (Fe/H) = 2.28 stellar models which include both diffusion and rotational mixing provide an excellent match to the observations, and predict a primordial Li-7 abundance of log N(Li) = 3.13 +/- 0.1. However, the (Fe/H) = -3.28 Li-7 destruction isochrones reveal severe problems with the combined models. These low metallicity isochrones predict a tend of decreasing log N(Li) with increasing T(sub eff) which is clearly not present in the observations. Dissert. Abstr.

N95-29672 Hawaii Univ., Honolulu, HI.
SPECTRAL REFLECTANCE STUDIES AND OPTICAL SURFACE ALTERATION IN THE SEARCH FOR LINKS BETWEEN METEORITES AND ASTEROIDS Ph.D. Thesis
Beth Ellen Clark 1993 336 p
Avail: Univ. Microfilms Order No. DA9416041

The ordinary chondrites (OC's) are the most numerous and most ancient of meteorites, but as yet their Solar System source region has not been identified. Meteoriticists have scrutinized these meteorites for clues as to the origin and evolution of the Solar System. They are among the most chemically primitive meteorites known, having been relatively unprocessed since their formation 4.6 billion years ago. The textures they preserve are records of prevailing conditions during the formation of the planets. There is a long history to the search for the ordinary chondrite parent bodies. Dynamical modelling indicates that they are most likely to be from the main asteroid belt at 2.5 AU. This happens to be where the S-type asteroids are located, and hence the 'OC meteorite-S Type asteroid controversy' arises. S-type asteroid reflectance spectra indicate surface compositions of olivine, pyroxene, and Fe,Ni metal. These are also the minerals that compose the ordinary chondrites, and so a genetic link is indicated. The subject of this dissertation is the connection, or lack thereof, between the ordinary chondrites and the S-type asteroids. To begin the investigations, Chapter two is a report on laboratory experiments which were performed in an attempt to simulate the optical surfaces or ordinary chondrite patent bodies to see if the optical properties of the S-type

asteroids could be manufactured. The next chapter is a three-parameter analysis of the main spectral features which were found to be most altered by the experiments in Chapter two. Chapter four is an examination of the first spacecraft images of an S-type asteroid, 951 Gaspra, with possible mineralogic implications. Chapter five is a presentation of a new infrared telescopic survey of the S-type asteroids. Specifically, we investigate the suggestion that the OC parent-bodies may be found among the smaller main-belt asteroids. Finally, in Chapter six, an analysis of the compositions of S-type asteroids is performed using the Hapke spectral reflectance theory. In the concluding pages we recount the evidence presented and summarize our current knowledge before closing this book on the S-type asteroid-ordinary chondrite mystery. Dissert. Abstr.

N95-29673 Yale Univ., New Haven, CT.
THE EFFECTS OF ROTATION ON THE EVOLUTION OF 15 TO 30 SOLAR MASS STARS Ph.D. Thesis
Jamie Michael Howard 1993 174 p
Avail: Univ. Microfilms Order No. DA9415861

The Yale Rotating Evolution Code has been modified to allow for the computation of models of massive stars. Theoretical evolutionary sequences have been generated for a 15 M solar magnitude star from the ZAMS to core helium exhaustion with a variety of physical assumptions: (1) no convective overshoot, mass loss, or rotation, (2) convective overshoot only, by amounts 0.1, 0.2, and 0.35 Hp, (3) mass loss only, for log T(sub eff) greater than 4.1 at rates given by the parameterization of Waldon and for log T(sub eff) less than 4.1 at rates given by Reimers' formulation, (4) mass loss and overshoot by 0.1 Hp, (5) no overshoot of mass loss, but rotation without instabilities, and (6) no overshoot or mass loss, but full rotation. An additional sequence, (7) mass loss and full rotation, was run to just past core helium ignition. Models were also run for 20, 25, and 20 M solar magnitude stars using the same physical assumptions, but all of these sequences were terminated just after core helium ignition due to time constraints. The non-rotating models agree qualitatively with other models found in the literature. The addition of only rotational distortion has little discernable effect on the models, while the full treatment of rotation results in additional mixing and theoretical tracks that are similar to models with small amounts of convective overshoot. Models which include only rotation have fair agreement with the observed main sequence surface rotation velocities, but rotate too rapidly during the post-main sequence phases. The addition of mass loss at the given rates helps this problem somewhat but does not appear to completely resolve it. Neither the non-rotating models nor the rotating models provide full agreement with the terminal-age main sequence band used by Maeder and Meynet: this may be indicative that additional mixing processes are necessary or that a more recent TAMS, such as that of Stothers, should be used.
Dissert. Abstr.

N95-29675 Princeton Univ., NJ.
APPLICATIONS OF PULSAR TIMING Ph.D. Thesis
Victoria Michelle Kaspi 1994 187 p
Avail: Univ. Microfilms Order No. DA9415420

Timing observations of radio pulsars have long been known to yield a wealth of information for a wide variety of applications. In this thesis, we describe an assortment of results obtained using this powerful technique. We have made timing observations of 106 southern-hemisphere pulsars at the 64-m radio telescope at Parkes, New South Wales. These observations were motivated by the launch of NASA's Compton Gamma Ray Observatory, and have resulted in improved parameters for most sources and the discovery of two new gamma-ray emitting pulsars. Serendipitously discovered in the Parkes data in the unusual binary pulsar PSR J0045-7314, the only known pulsar in the Small Magellanic Cloud. We show that the pulsar is in orbit around a approximately 10M solar magnitude main-sequence B star, and that the absence of eclipses and variations in the observed dispersion of the radio signal at periastron imply the companion has a surprisingly tenuous wind. We also describe Parkes timing observations of four young pulsars, and draw conclusions about their possible associations with nearby supernova remnants. We find two of the associations to be compelling, one plausible, and one doubtful. Our timing data confirm that young pulsars have frequent period discontinuities known as 'glitches,' and we obtain a new confirmation of the fundamental equation of neutron star spin-down. Finally, we describe long-term, high-precision timing observations of two millisecond pulsars using the 305-m telescope at Arecibo. We use the data for a variety of applications including cosmology, general relativity, high-precision astrometry, physics of the interstellar medium, and time-keeping metrology. For the first time, we compare the timing data for the two millisecond pulsars, and suggest that the most straight-forward explanation for the low-frequency, unmodeled signal in the PSR B1937+21 residuals is that it is intrinsic to the pulsar itself. Dissert. Abstr.

N95-29775 California Univ., Santa Barbara, CA.
EXPERIMENTAL COSMOLOGY USING FAST PARALLEL N-BODY METHODS Ph.D. Thesis
Michael S. Warren 1994 227 p
Avail: Univ. Microfilms Order No. DA9423886

This dissertation describes a parallel treecode N-body algorithm and a number of simulations which have been performed on massively parallel computers. We use the results of these simulations (which use between 1 and 17 million particles each) to investigate the structure, kinematics, shapes, masses, spatial correlations, and relative pairwise velocity dispersions of dark matter halos. Using cold dark matter (CDM) initial conditions normalized to the anisotropies detected by the COBE satellite, we show that the mass function and spatial distribution of halos is compatible with the observations. We also show the value of the relative pair-wise velocity dispersion sigma(nu), used as evidence against COBE-normalized CDM models, is significantly lower for halos than for individual particles. When the observational methods of extracting sigma(nu) are applied to catalogs obtained from the numerical experiments, estimates differ significantly between different observation-sized samples, and overlap observational estimates. We also study smaller systems which form by gravitational collapse from scale-free and more general Gaussian initial density perturbations. We analyze the structure and kinematics of the approximately 10(exp 2) largest relaxed halos in a number of simulations. A typical halo is a triaxial spheroid which tends to be more often prolate than oblate. These shapes are maintained by anisotropic velocity dispersion rather than by angular momentum (spin parameter lambda approximately 0.05). Nevertheless, there is a significant tendency for the total angular momentum vector to be aligned with the minor axis of the density distribution. In addition, we report on an efficient adaptive parallel N-body method which we have designed and implemented. The algorithm computes the forces on an arbitrary distribution of bodies in a time which scales as N log N with the particle number. The accuracy of the force calculations is analytically bounded, and can be adjusted via a user defined parameter between a few percent relative accuracy down to machine arithmetic accuracy. Instead of using pointers to indicate the topology of the tree, we identify each possible cell with a key. The mapping of keys into memory locations is achieved via a hash table. This allows the program to access data in an efficient manner across multiple processors. Dissert. Abstr.

N95-29780 Johns Hopkins Univ., Baltimore, MD.
STATISTICS AND LARGE-SCALE STRUCTURE Ph.D. Thesis
Stephen Daniel Landy 1994 139 p
Avail: Univ. Microfilms Order No. DA9419998

Various statistical measures are derived and applied to analyze the large scale structure of the Universe. First, the unique methodological role of statistics in astrophysics is discussed and illustrated through an example of fitting and applying the Tully-Fisher relation to galaxy velocity data. The subtleties of fitting an observed bivariate probability distribution to the relation are discussed as well as the consequences of a lack of knowledge of the source of scatter in the distribution, with regard to systematic bias effects. Next, a general solution to the problem of Malmquist Bias in galaxy velocity fields is presented and applied to elliptical galaxy data. Results indicate that much of the infall signal seen in the Centarus region, the Great Attractor, may be an artifact due to inadequate Malmquist Bias correction. A method using the radial velocity correlation functions of galaxies is derived as a test of whether the large scale mass distribution can be considered a Gaussian random field. This is a prediction of canonical theories of inflation. Present data show consistency with a Gaussian field. A new estimator for the angular correction function is presented with reduced variance and no bias. Heretofore common estimators are shown to have significantly greater variance than the Poisson variance generally assumed. This estimator is then applied to faint galaxy data as a measure of the angular correction function of faint galaxies as a function of color. Results show that both the extreme red and blue galaxy subsets have a marked increase in correlation amplitude. This is expected for the red

galaxies as they can be identified as the cluster ellipticals. However, the cross correlation of these subsets show that they are uncorrelated with each other. For the faint blue galaxies, this is indicative of a disparate population of galaxies with a tight distribution in redshift space. It is summarized that these galaxies are either a faint population found relatively nearby or tightly clustered such as in sheets. Dissert. Abstr.

N95-29836# Nobeyema Solar Radio Observatory (Japan).
NOBEYAMA RADIO OBSERVATORY REPORT, NO. 379
1994 9 p
(ISSN 0911-5501)
Avail: CASI HC A02/MF A01

Four presentations from four different symposiums are included in this report of the Nobeyama Radio Observatory. The papers are: 'SIO Maser Survey of the IRAS Bulge Sources'; 'Observational Properties of SiO Masers in the Galactic Bulge IRAS Sources'; 'Aperture Synthesis Observations of HCN J = 1-0 Emission from Y Canum Venaticorum'; and 'Extended Dust Shells Around carbon Stars Resolved by 'HIRAS'.' For individual titles, see N95-29837 through N95-29840.

N95-29837# Space Research Organization Netherlands, Groningen (Netherlands).
SIO MASER SURVEY OF THE IRAS BULGE SOURCES
Hideyuki Izumiura, I. Yamamura (Tokyo Univ., Japan.), S. Deguchi (Nobeyema Solar Radio Observatory, Japan.), N. Ukita (Nobeyema Solar Radio Observatory, Japan.), O. Hashimoto (Seikei Univ., Tokyo, Japan.), T. Onaka (Tokyo Univ., Japan.), and Y. Nakada (Tokyo Univ., Japan.) *In* Nobeyema Solar Radio Observatory, Nobeyama Radio Observatory Report, No. 379 1994 2 p Presented at the Formation of the Milky Way, Ganada, Spain, 5-10 Sep. 1994 (For primary document see N95-29836 10-90)
Avail: CASI HC A01/MF A01

We searched for SiO maser emission from the J = 1-0, v = 1 and 2 transitions toward color-selected IRAS sources in the Galactic Bulge. The detection rate exceeds 80 percent for the brighter sources. The line of sight velocities of the SiO masers agree within 3 km/sec with the center velocities of the OH masers. The completeness of our survey is discussed. Kinematics of the Bulge is examined in terms of the longitude versus radial velocity diagram. There is possibly a hole (a zone of avoidance) in the diagram, which might be related to the bar structure in the Bulge.
Author

N95-29838# Space Research Organization Netherlands, Groningen (Netherlands). Lab. for Space Research.
OBSERVATIONAL PROPERTIES OF SIO MASERS IN THE GALACTIC BULGE IRAS SOURCES
Hideyuki Izumiura *In* Nobeyema Solar Radio Observatory, Nobeyama Radio Observatory Report, No. 379 1994 2 p Presented at the IAU Symposium 169: Unsolved Problems of the Milky Way, Hague, Netherlands, 23-27 Aug. 1994 (For primary document see N95-29836 10-90)
Avail: CASI HC A01/MF A01

We surveyed 313 color-selected IRAS sources in the Bulge in the SiO J = 1-0 (v = 1,2) lines with the Nobeyama 45m telescope, which resulted in 222 detections. The detection rates exceeded 80 percent for the brighter samples. We discuss the observed SiO maser characteristics and the implications of the obtained I-v diagram. We examined the integrated SiO intensity against the 12 mu m flux density. On average, our sample stars show much stronger SiO intensities for a particular 12 mu m flux than found by Jewell et al. (1991) for stars in the solar neighborhood. The highest observed value of the SiO intensity for a fixed 12 mu m flux is 10 times as high as theirs. This large discrepancy should be confirmed with future observations of the nearby stars with the 45m telescope. In terms of 12 mu m flux, our survey is almost complete down to F(sub 12) approximately 1.5 Jy in the absolute value of b = 7-8 deg strips. According to Whitelock et al. (1991) our survey reached the far side of the Bulge, as far as 4 kpc away from the galactic center. Our sample, however, may be biased to the intrinsically brighter objects in the far-side. In the absolute value of b = 4-5 deg strips the sampling is complete down to F(sub 12) = 3 Jy, which means that our survey is almost complete in the near side of the Bulge. The far side has also been substantially sampled as far as 10 kpc from the Sun. In addition, these arguments are valid for the region of l greater than -8 deg due to the declination limit at Nobeyama.
Derived from text

N95-29839# Tokyo Gakugei Univ., Koganei (Japan). Dept. of Astronomy and Earth Sciences.
APERTURE SYNTHESIS OBSERVATION OF HCN J = 1-0 EMISSION FROM Y CANUM VENATICORUM
Hideyuki Izumiura, A. Fujiyoshi, and N. Ukita (Nobeyema Solar Radio Observatory, Japan.) *In* Nobeyema Solar Radio Observatory, Nobeyama Radio Observatory Report, No. 379 1994 2 p Presented at the Circumstellar Matter 1994, Edinburgh, Scotland, 29 Aug. - 2 Sep. 1994 (For primary document see N95-29836 10-90)
Avail: CASI HC A01/MF A01

We have made high resolution observations of HCN (hydrogen cyanide) (1-0) emission from the carbon star Y Canum Venaticorum using the Nobeyama Millimeter Array. We find that the emission region is not well resolved by the synthesized beam of 3.7' x 4.6' over the entire velocity range V(sub LSR) = 10 to 35 km/s. We find that the true brightness temperature probably exceeds 200 K at many velocity channels as well as at the 26 km/s maser spike. The broad emission component may be the result of superimposed maser spikes. The high brightness requires an unreasonably high HCN fractional abundance if LTE is assumed. It is likely that the HCN abundance previously reported for the star is considerably affected by the maser action. A new maser spike has been found at V(sub LSR) = 29 km/s.
Author

N95-29840# Space Research Organization Netherlands, Groningen (Netherlands). Lab. for Space Research.
EXTENDED DUST SHELLS AROUND CARBON STARS RESOLVED BY HIRAS
Hideyuki Izumiura, D. J. M. Kester, T. DeJong, C. Loup (Institut d'Astrophysique, Paris, France.), L. B. F. M. Waters (Amsterdam Univ., Netherlands.), and Tj. R. Bontekoe (Bontekoe Data Consultancy, Katwijk, Netherlands.) *In* Nobeyema Solar Radio Observatory, Nobeyama Radio Observatory Report, No. 379 1994 2 p Presented at the Circumstellar Matter 1994, Edinburgh, Scotland, 29 Aug. - 2 Sep. 1994 (For primary document see N95-29836 10-90)
Avail: CASI HC A01/MF A01

We have examined forty-two carbon stars which show an excess emission at 60 and/or 100 mu m by applying maximum entropy image reconstruction techniques to the IRAS 60 mu m survey data. Thirteen stars are found to be extended in the reconstructed images. Four of them show a detached ring centered on the stellar position. In particular, U Ant may have a double detached dust shell. The implications of our results are discussed concerning the variation of mass loss on the AGB evolution.
Author

N95-29917# Virginia Univ., Charlottesville, VA. Dept. of Astronomy.
THE 12 UM CONTRIBUTION OF NEARBY GALAXIES TO THE INFRARED BACKGROUND Final Report, 1 Aug. 1989 - 30 Sep. 1994
Trinh X. Thuan 30 Sep. 1994 5 p
(Grant AF-AFOSR-0467-89)
(AD-A291185; AFOSR-95-0103TR) Avail: CASI HC A01/MF A01

There were twelve publications in the final with the emphasis on the study of blue compact galaxies. The blue compact dwarf galaxy He 2-10 has been observed in the mid-IR. The central regions contained two resolved components which have the same mid-IR properties but different H-alpha fluxes. The energy sources for the mid-IR to far-IR emission were studied and showed that the mid-IR emission unambiguously is associated with the young massive stars, but that the far-IR emissions requires the heating contribution from a slightly more evolved stellar population. The primordial helium abundance of low-metallicity blue compact galaxies was determined with high-quality spectrophotometric observations. The results were consistent with those obtained from chemical evolution models with differential galactic winds. The hot gas outflow in the blue compact dwarf galaxy VIIZw4O3 was observed. The X-ray morphology from ROSAT is interpreted as hot gas outflow from the core of the galaxy powered by the present starburst activity. The spatial distribution of blue compact galaxies is the Second Byurakan Survey were studied. The large deficiency of blue compact galaxies support the hypothesis that the majority of dwarf galaxies. High quality spectrophotometric observations of 15 supergiant HII regions in 14 new low-metallicity blue compact galaxies were made. It was concluded that all these heavy elements have a primary origin and were produced by the same massive stars.
DTIC

91 LUNAR AND PLANETARY EXPLORATION

Includes planetology; and manned and unmanned flights.

For spacecraft design or space stations see *18 Spacecraft Design, Testing and Performance.*

N95-29117 Michigan Technological Univ., Houghton, MI.
A GEOTECHNICAL CHARACTERIZATION OF LUNAR SOILS AND LUNAR SOIL SIMULANTS Ph.D. Thesis
John Carl Graf 1994 166 p
Avail: Univ. Microfilms Order No. DA9425340

Many of the essential materials needed for the construction of a lunar base can be produced from the resources found on the lunar surface. Processing natural resources on the moon into useful products will reduce the need, and the cost, to bring everything from earth. The lunar regolith has been intensely studied with respect to understanding the formation of the moon and the earth, but as a construction material, the regolith is poorly characterized and poorly understood. To better understand how to 'work' with the lunar regolith, four loosely related research projects were conducted. Two projects relate to characterizing and understanding the geotechnical properties of regolith, two projects relate to manipulating and processing granular materials in the lunar environment. The shapes of lunar soil grains are characterized using fractals - results directly and quantitatively describe the rugged reentrant nature of the large scale structure and the relatively smooth surface texture of lunar soil grains. The nature of lunar soil cohesion is considered using tensile strength measurements of lunar soil simulant. It is likely that mechanical interlocking of irregular grains is the primary cause of lunar soil cohesion. This mechanism is highly sensitive to grain shape, but relatively insensitive to particle packing density. A series of experiments are conducted to try to understand how granular particles might sort by size in a vacuum. Even in a vacuum, fine particle subjected to shear strain segregate by a mechanism called the random fluctuating sieve The random fluctuating sieve also controls particle motion that determines the structure of wind-blown sand ripples. Hybrid microwave heating was used to sinter large structural bricks from lunar soil stimulant. While heating was prone to thermal runaway, microwave heating holds great promise as a simple, direct method of making sintered structural bricks. Dissert. Abstr.

N95-29178* Jet Propulsion Lab., California Inst. of Tech., Pasadena, CA.
COLLECTION OF MAGELLAN VENUS RADAR MAPPING RESULTS (Videotape)
8 Mar. 1991 Videotape: 6 min. playing time, in color, with sound
(NASA-CR-197656; AVC-91-091; NONP-NASA-VT-95-46003) Avail: CASI VHS A02/BETA A22

Through computer animation several geological features of Venus are presented in this video. The Sif Mons, a 1.2 mile high volcano and the Gula Mons, a 1.8 mile high volcano are shown. Also, radar images of a rift valley, several impact craters, and a corona can be seen. The video ends with a northeast view of Eistla Regio. CASI

N95-29593 Arizona Univ., Tucson, AZ.
CHANNELS AND VALLEYS ON VENUS Ph.D. Thesis
Goro Komatsu 1993 121 p
Avail: Univ. Microfilms Order No. DA9421744

Venusian channel meanders properties generally follow terrestrial river trends of wavelength (L) to width (W) ratios, suggesting an equilibrium adjustment of channel form. The unusually low L/W values for some sinuous rilles probably indicate modification of original meander patterns by lava-erodonal channel widening. A drainage channel constructed by typical basaltic lavas can be significantly deepened and widened by highly fluid and hot superheated tholeiitic basalt or ultramafic lava to form sinuous rilles. Canali-type channels are unique because of their great lengths (up to 6800 km) and nearly constant channel cross sectional shapes along their paths. Common terrestrial-type tholeiite lava cannot sustain a superheated and turbulent state for the long distances required for thermal erosion of canali within allowable discharge rates. If canali formed mainly by constructional processes, sustained discharge rates might travel the observed distances. An exotic low-temperature, low-viscosity lava like carbonatite or sulfur seems to be required for the erosional genesis of canali. The 'Outflow Channel' has a morphology similar to that of terrestrial catastrophic flood channels and Martian outflow channels. Calculated discharge rates and power/unit area imply that the channel was carved by very energetic lava flows. Valley network formation seems to require sapping processes which may be caused by low-viscosity lavas moving through a relatively permeable, fractured, medium. The close associations of many sinuous rilles with coronae leads to the hypothesis that mantle-plume volcanism caused the high-effusion and sustained lava eruptions essential for sinuous rill formation. Canali lengths exceed the lengths of other common volcanic channel types on Venus, implying a large volume of lava and long duration of the eruption. An hypothesized global resurfacing event late in history may be responsible for canali formation. Longitudinal profiles of canali-type channels show clear evidence of deformation by plains tectonism. Deformation occurred at multiple scales as evidenced in the profiles. The range of lava channel morphology on Venus is wider than for other terrestrial planets and the Moon. This is probably attributed to the volcanological conditions unique to Venus and to a lack of intense erosional processes. Dissert. Abstr.

N95-29594 Hawaii Univ., Honolulu, HI.
SOME ASPECTS OF LUNAR AND MARTIAN VOLCANISM AS EXAMINED WITH SPECTRAL, TOPOGRAPHIC, AND MORPHOLOGIC DATA DERIVED FROM SPACECRAFT IMAGES Ph.D. Thesis
Mark Southwick Robinson 1993 257 p
Avail: Univ. Microfilms Order No. DA9416071

Utilizing newly calibrated Mariner 10 color images, the titanium abundances of lunar mare soils on the eastern limb and farside are examined. These maria are found to have TiO2 contents in the range of less than 2 to 5%. The existence of cryptomare deposits northeast of Mare Marginis is confirmed. This leads to the prediction that no high TiO2 (greater than 8 wt%) mare basalt soils will be found in regions with thickened crust (most of the lunar farside) that are yet to be examine with spectrometers, due to the greater density of high titanium magma. Utilizing Viking Orbiter and Mariner 9 data, the martian volcanoes Biblis Patera, Ceraunius Tholus, Jovis Tholus, Ulysses Patera Uranius Patera, and Uranius Tholus are analyzed. Specifically, morphologic and topographic features indicative of the eruption style (effusive vs. explosive) that formed each edifice are examined. From new digital mosaics of these volcanoes, both effusive and explosive deposits are found. It is proposed that the initial period of activity for some martian volcanoes was dominantly explosive (driven by juvenile gases), whereas later activity was mostly effusive. In support a this hypothesis, an analysis of the martian volcano Apollinaris Patera is presented. Using digital images, thermal inertia data and a new topographic model, the chronology of Apollinaris Patera is determined to have been dominated early on by explosive activity, followed by later effusive eruption. From the topographic data, its volume is estimated to be approximately 10(exp 5)/cu km. The volcano may have been active for approximately 10(exp 7) yrs, based on its volume and an inferred rate of eruption of 1.5 x 10(exp -2)/cu km/yr. It is proposed that at least 2 x 10(exp 16) kg of juvenile water was added to the martian atmosphere as a consequence of these eruptions. Detailed examination of a multi-temporal series of Viking Orbiter color images of the Apollinaris Patera region shows, that, for a given area on the surface, the red over violet ratio varies from 2.9 to 3.4, and the albedo ranges from 21 to 16%. These changes are interpreted to be predominately due to variations in the amount of atmospheric condensates. Dissert. Abstr.

N95-29964* Interface Video Systems, Inc., Washington, DC.
ROVER STORY (Videotape)
9 Jul. 1990 Sponsored by NASA, Washington Videotape: 6 min. playing time, in color, with sound
(NASA-CR-198757; JB-0-06-0272; NONP-NASA-VT-95-56825) Avail: CASI VHS A02/BETA A22

Future Mars exploration missions and operations are discussed using computer animation along with proposed vehicles and equipment, for example, a Mars surface land rover. There is a Presidential Address by President George Bush where he discusses future goals for space exploration. This video also outlines the Outreach Program, which offers the public the chance to suggest new ideas for space research and exploration. Author

N95-30058*# National Aeronautics and Space Administration. Ames Research Center, Moffett Field, CA.

PIONEER VENUS 12.5 KM ANOMALY WORKSHOP REPORT, VOLUME 1

A. Seiff (San Jose State Univ., Moffett Field, CA.), L. Sromovsky (Wisconsin Univ., Madison, WI.), W. Borucki, R. Craig (MCAT Inst., Moffett Field, CA.), D. Juergens (Jet Propulsion Lab., California Inst. of Tech., Pasadena, CA.), R. E. Young, and B. Ragent (San Jose State Univ., Moffett Field, CA.) Jun. 1995 27 p Workshop held in Moffet Field, CA, 28-29 Sep. 1993 (RTOP 370-24-01)

(NASA-CP-3303; A-950043; NAS 1.55:3303) Avail: CASI HC A03/MF A01

A workshop was convened at Ames Research Center on September 28 and 29, 1993, to address the unexplained electrical anomalies experienced in December 1978 by the four Pioneer Venus probes below a Venus altitude of 12.5 km. These anomalies caused the loss of valuable data in the deep atmosphere, and, if their cause were to remain unexplained, could reoccur on future Venus missions. The workshop participants reviewed the evidence and studied all identified mechanisms that could consistently account for all observed anomalies. Both hardware problems and atmospheric interactions were considered. Based on a workshop recommendation, subsequent testing identified the cause as being an insulation failure of the external harness. All anomalous events are now explained. Author

N95-30249* National Aeronautics and Space Administration. Lyndon B. Johnson Space Center, Houston, TX.

LUNAR/MARS EXPLORATION FOR SYNTHESIS GROUP (Videotape)

12 Aug. 1992 Videotape: 10 min. 21 sec. playing time, in color, with sound

(NASA-TM-110647; NONP-NASA-VT-95-57873) Avail: CASI VHS A02/BETA A22

Computer animation of future expeditions, research projects, and equipment (satellites, telescopes, etc.,) are contained on this video. President George Bush, in a Presidential Address, speaks on future plans for NASA emphasizing Space Station Freedom and a manned mission to Mars. CASI

N95-30318* National Aeronautics and Space Administration. Lyndon B. Johnson Space Center, Houston, TX.

APOLLO 14: SHEPARD HITTING GOLF BALL ON MOON (Videotape)

[1970] Videotape: 3 min. playing time, in color, with sound

(NASA-TM-110638; VJSC-1207; NONP-NASA-VT-95-56871) Avail: CASI VHS A02/BETA A22

Live footage of astronaut Alan Shepard hitting a golf ball on the Moon is featured on this video. Author

N95-30344*# Jet Propulsion Lab., California Inst. of Tech., Pasadena, CA.

THE JPL MARS GRAVITY FIELD, Mars50c, BASED UPON VIKING AND MARINER 9 DOPPLER TRACKING DATA

Alexander S. Konopliv and William L. Sjogren Feb. 1995 83 p

(Contract NAS7-1260)

(NASA-CR-198881; JPL-Publ-95-5; NAS 1.26:198881) Avail: CASI HC A05/MF A01

This report summarizes the current JPL efforts of generating a Mars gravity field from Viking 1 and 2 and Mariner 9 Doppler tracking data. The Mars 50c solution is a complete gravity field to degree and order 50 with solutions as well for the gravitational mass of Mars, Phobos, and Deimos. The constants and models used to obtain the solution are given and the method for determining the gravity field is presented. The gravity field is compared to the best current gravity GMM1 of Goddard Space Flight Center. Author

92 SOLAR PHYSICS

Includes solar activity, solar flares, solar radiation and sunspots. For related information see *93 Space Radiation.*

N95-28780 National Geophysical Data Center, Boulder, CO.

SOLAR-GEOPHYSICAL DATA NUMBER 605, JANUARY 1995. PART 2 (COMPREHENSIVE REPORTS): DATA FOR JULY 1994 AND MISCELLANEOUS

H. E. Coffey Jan. 1995 37 p Limited Reproducibility: More than 20% of this document may be affected by microfiche quality

(PB95-190997; SDG-605-Pt-2) Avail: CASI HC A03

This report contains an index of solar-geophysical data for July 1994. The following are included: SolarFlares, Solar Radio Bursts at Fixed Frequencies, Solar X-ray Radiation from GOES Satellite, Active Prominences and Filaments. NTIS

N95-28781 National Geophysical Data Center, Boulder, CO.

SOLAR-GEOPHYSICAL DATA NUMBER 605, JANUARY 1995. PART 1 (PROMPT REPORTS): DATA FOR DECEMBER, NOVEMBER 1994 AND LATE DATA

H. E. Coffey Jan. 1995 130 p Limited Reproducibility: More than 20% of this document may be affected by microfiche quality

(PB95-191003; SDG-605-Pt-1) Avail: CASI HC A07

This document contains a detailed Index data for 1994. The December (1994) data includes the following: Solar Terrestrial Environment, IUWDS Alert Periods (Advance and Worldwide), Solar Active Indices, Solar Flares, Solar Radio Emission, Stanford Mean Solar Magnetic Field, GOES-7 Daily Electron Fluence. November's (1994) data focused on the following: Solar Active Regions, Sudden Ionospheric Disturbances, Solar Radio Spectral Observations, Solar Radioheliograph-164 MHz-Nancay, Cosmic Ray Measurements by Neutron Monitor, Geomagnetic Indices, Principal Magnetic Storms, Sudden Commencements/Solar Flare Effects, Plot of SC and Sunspot Number, Plus Chart of Three-hourly Indices aa. Late Data--Geomagnetic Indices--Provisional values of Hourly Equatorial DST is given in January-July 1994. NTIS

N95-29098# Nobeyema Solar Radio Observatory (Japan).

NOBEYAMA RADIO OBSERVATORY REPORT, NO. 361: THE RADIO PROPERTIES OF SOLAR ACTIVE REGION SOFT X-RAY TRANSIENT BRIGHTENINGS

S. M. White (Maryland Univ., College Park, MD.), M. R. Kundu (Maryland Univ., College Park, MD.), T. Shimizu (Tokyo Univ., Mitake, Japan.), K. Shibasaki, and S. Enome 1995 22 p Submitted for publication Its Radioheliograph Series No. 7

(ISSN 0911-5501)

Avail: CASI HC A03/MF A01

We present the results of a search for radio emission from active-region transient brightenings identified in Yohkoh Soft X-ray Telescope observations of active region AR 7260. We present detailed observations of four events in which 17 GHz radio emission is clearly detected in observations by the Nobeyama Radioheliograph. The time profiles of the 17 GHz data are very similar to those of the soft X-ray fluxes, and the 17 GHz flux is very close to that expected from plasma with the temperature and emission measure derived for the soft X-ray-emitting material from filter ratios. No impulsive nonthermal radio emission was detected from any of the 4 events, although each was at least GOES class B1 in soft X-rays. Weak hard X-rays may have been detected by GRO/BATSE from the strongest of the events, but not from two others. These negative results leave open the possibility that there is a difference between active region transient brightenings and solar flares, in that the former do not convert a significant amount of the released energy into accelerated electrons. However, confirmation of this hypothesis will require a larger sample of events. Author

N95-29151 Carnegie-Mellon Univ., Pittsburgh, PA. School of Computer Science.

REFLECTANCE ANALYSIS UNDER SOLAR ILLUMINATION

Yoichi Sato and Katsushi Ikeuchi 7 Dec. 1994 40 p Limited Reproducibility: More than 20% of this document may be affected by poor print

(Contract DAAH04-94-G-0006)

(AD-A290489; CMU-CS-94-221) Avail: Issuing Activity (Defense Technical Information Center (DTIC))

The paper describes reflectance analysis of real images taken in an outdoor environment. This is one of the first attempts for analyzing reflection in outdoor images. In the past, the fundamental difficulties involved in analyzing outdoor images have prevented the use of traditional techniques for reflectance analysis such as shape from shading and photometric stereo. Those difficulties include: (1) multiple reflection components due to two light sources of different spectral and spatial distributions, namely the sunlight and the skylight; (2) ambiguity in surface normal determination caused by the sun's restricted motion on the ecliptic, and (3) non-uniform surface albedo of object surfaces. In order to overcome those difficulties, we developed a reflectance model under solar illumination. Based on this model, we proposed solutions for each of these problems. We have successfully tested our algorithms using real color images taken both in a laboratory setup simulating sunlight, and in an outdoor environment under solar illumination. DTIC

N95-29202 Colorado Univ., Boulder, CO.
OBSERVATIONS AND ANALYSIS OF SOLAR FLARES AT RADIO AND OTHER WAVELENGTHS Ph.D. Thesis
Therese Ann Kucera 1993 186 p
Avail: Univ. Microfilms Order No. DA9423514

This thesis concerns observations and modeling of two flares observed by the Very Large Array (VLA) and other instruments on 20 June 1989. We investigate the events to determine the emission mechanism of the observed radiation, the structure of the magnetic fields, and the spectra and locations of the accelerated electron populations. The event of 1454 UT consisted of an eruptive prominence accompanied by a flare. The event was observed with an unusual number of instruments in radio, H(alpha), and X-ray wavelengths. These data are used to construct a new, advanced model of a source observed at 1.4 GHz as gyrosynchrotron radiation emitted from a high coronal loop. Our results indicate that the initial acceleration occurred in smaller, denser loops which also produced the flare's hard X-ray emission. We also present evidence that other sources observed at 1.4 GHz later in the event were due to second harmonic plasma radiation emitted from the prominence. Microwave observations of erupting prominences are very rare, and we are the first to observe and analyze plasma emission from such an event. Finally, we investigate a source of microwaves and soft X-rays occurring later in the flare and calculate a lower limit to the density of the source. The flare of 2155 UT was observed by the VLA and Owens Valley Radio Observatory. We develop a second gyrosynchrotron model to analyze the sources observed at flare peak. This model differs from the previous one in that it has a different radio source structure. It uses a new gyrosynchrotron approximation which is valid at very low harmonics of the gyrofrequency. For the first time we find that the cause of the change of microwave source size with frequency in the event studied was variation in the accelerated electron density. This is contrary to the common assumptions that the variation in size is due to a nonuniform magnetic field. Dissert. Abstr.

N95-29279# Aerospace Corp., El Segundo, CA. Technology Operations.
Si 13 EMISSION LINES IN SOLAR FLARE X RAY SPECTRA OBTAINED WITH THE P78-1 SATELLITE
F. P. Keenan, E. S. Conlon, D. L. McKenzie, and K. J. Phillips 1 Nov. 1994 9 p Prepared in cooperation with The Queen's Univ. of Belfast, and Rutherford Appleton Lab.
(Contract F04701-88-C-0089)
(AD-A290000; TR-93(3940)-14; SMC-TR-94-47) Avail: CASI HC A02/MF A01

Theoretical Si 13 electron-temperature-sensitive emission-line ratios, which include satellite-line contributions to the intensities of the forbidden (f) 1s2 (1)S-1s2s(3)S, intercombination (i) 1s2 (1)S-1s2p(3)P sub 2, and resonance (r) 1s2 (1)S-1s2p (1)p transitions, are presented for G = (I(f) + I(i))/I(r), R = I(f)/I(i), R1 = I(1s 2 (1)S-1s3p(1)p)/I(r), and R2 = I(1s2 (1)S-1s4p(1)P)/I(r). These ratios are significantly different from those calculated assuming that satellites do not contribute to f, i, and r, and, in addition, are more temperature-sensitive over the range log T sub e = 6.4-7.4. Electron temperatures deduced using the new diagnostics in conjunction with observed values of G, R1, and R2 from solar-flare spectra obtained by the SOLEX spectrometers aboard the P78-1 satellite are found to be generally consistent. This provides support for the validity of the theoretical R1 and R2 diagnostics and also resolves discrepancies noted previously when the line ratios were compared with observation from the Solar Maximum Mission spectrometers. The R ratio, which is in the low-density limit under solar flare conditions, is found not to be a useful T sub e diagnostic when satellite contributions to f and i are included in the theoretical line ratios. However, the observed values of R from the SOLEX spectra are in good agreement with theoretical predictions, which provides additional support for the accuracy of the line-ratio calculations. DTIC

N95-29327# Naval Research Lab., Washington, DC.
YOHKOH BRAGG CRYSTAL SPECTROMETER LIGHT CURVES FOR Ca 29(3.1633 - 3.1933 A): 1 OCTOBER 1993 - 30 SEPTEMBER 1994
John T. Mariska, R. D. Bentley, and C. D. Pike 30 Dec. 1994 370 p
(AD-A290027; NRL/MR/7673-94-7642) Avail: CASI HC A16/MF A01

This memorandum report summarizes the data produced during the third year of operation by the Bragg Crystal Spectrometer (BCS) on the Yohkoh spacecraft. Each page shows the total count rate in the Ca XIX channel of the BCS for a single day. This channel nominally observes the Sun in the wavelength range from 3.1633 to 3.1933 A. These plots are useful for identifying flare data for further analysis and for determining the data file name and tape name that contains the data. DTIC

N95-29475# Asian Office of Aerospace Research and Development, APO San Francisco, CA. Air Force Office of Scientific Research.
A TURBULENT MODEL OF THE SOLAR GRANULATION
Vinod Krishan (Indian Inst. of Astrophysics, Bangalore.) 1994 5 p Presented at the XV NSO/Sac Peak Solar Workshop, Sunspot, NM, 19-23 Sep. 1994
(AD-A292318; AOARD-TR-94-37) Avail: CASI HC A01/MF A01

The paper dealt with a new model for the development of convective velocity fields at various spatial scales in order to understand the differential rotation of the sun which affects the solar dynamo responsible for the magnetic activity as seen in its myriad forms. The new model is based on inverse cascading of energy to take into account the granulation phenomenon in its entirety. DTIC

N95-29704 Maryland Univ., College Park, MD.
ONE AND TWO FLUID NUMERICAL INVESTIGATIONS OF SOLAR WIND GAS RELEASES Ph.D. Thesis
James Benedict Harold 1993 173 p
Avail: Univ. Microfilms Order No. DA9425045

The dynamics of gas releases into high Mach number flowing plasmas are investigated. Emphasis is placed on systems of intermediate magnetization for which the scale size of the release lies between the ion and electron Larmor radii. The study is motivated by the December 1984 AMPTE (Active Magnetospheric Particle Tracer Explorer) solar wind barium release in which, contrary to the predictions of MHD theory, the barium cloud shifted transverse to the solar wind (in the u(sub wind) x B(sub 0) direction) before eventually turning downstream. Particular emphasis is given to identifying mechanisms responsible for this lateral motion. A modified MHD cold fluid approach that takes advantage of the supersonic nature of the problem forms the basis of this work. Two specific models are developed which incorporate large effective ion Larmor radius effects. The first is for a single ion species, the second for two ion species. Two physical effects are identified which are not present in the conventional MHD system: the Hall effect, based on a Hall magnetic drift wave, and a hybrid electrostatic ion cyclotron mode. Linear analysis shows that the effect of the Hall term is to propagate the upwind magnetic field compression azimuthally to the downwind side of the cloud, leading to a quasi-steady state field compression on the -u(sub wind) x B(sub O) side of the cloud. The cyclotron mode can lead to a similar compression through deflection of the solar wind ions into the u(sub wind) x B(sub O) direction. In each case the resulting compression leads to a transverse acceleration of the cloud. The relative importance of these two mechanisms is shown to depend on delta(sub c) / r(sub c), the ratio of the collisionless skin depth to the cloud size. Nonlinear, two-dimensional simulations are performed for each model. These simulations produce the expected field compressions and the resultant lateral acceleration, in general qualitative agreement with the AMPTE experiment. The dependence of these mechanisms on the ratio delta(sub c) / r(sub c) is demonstrated. While no simulations are performed that precisely duplicate the parameters of the AMPTE release, the results suggest

that the Hall effect, and possibly deflection of the solar wind by the cyclotron mode, constitute plausible mechanisms for the AMPTE shift.
Dissert. Abstr.

N95-30074# Asian Office of Aerospace Research and Development, APO San Francisco, CA. Air Force Office of Scientific Research.
15TH NSO/SAC PEAK SOLAR WORKSHOP
G. C. Joshi (Uttar Pradesh State Observatory, Naini Tal, India.) 23 Sep. 1994 5 p Workshop held in Sunspot, NM, 19-23 Sep. 1994
(AD-A292297; AOARD-TR-94-36) Avail: CASI HC A01/MF A01

A review of the 15th NSO/Sac Peak Solar Workshop is presented. The workshop emphasized the need for new experimental/observational facilites for the theoretical and observational understanding of the corona because there has been on real up-to-date corona spectra measurements done since 1970. The workshop also discussed how infrared obsorvations can contribute to the understanding of corona, chromosphere, and photosphere as well as night time objects. CASI

N95-30199# National Center for Atmospheric Research, Boulder, CO.
INTERACTION OF ACOUSTIC OSCILLATIONS WITH MAGNETIC FLUX TUBES IN THE SOLAR PHOTOSPHERE Cooperative Thesis No. 155
R. Keppens 1994 245 p Prepared in cooperation with Katholieke Univ.
(PB95-201810; NCAR/CT-155) Avail: CASI HC A11/MF A03

This thesis touches upon some outstanding puzzles concerning the Sun and its visible surface layers, the solar photosphere. The solar photosphere is permeated by all kinds of magnetic features. In chapter one we summarize their overall surface characteristics and introduce the equations of magnetohydrodynamics to discuss the magnetic features in a theoretical perspective. In chapter 2 we introduce the basic mathematical theory to treat multiple scattering and absorption of acoustic waves. We start from general solutions to the wave equation, to develop the T-matrix theory for sound wave interactions. In chapter 3 we linearize the ideal MHD equations, and use these linearized equations to calculate T-matrices and U-matrices for simple (magnetized) scatters. Subsequently, we extend the discussion to linear, resistive MHD, to incorporate resonant absorption. Chapter 4 deals with multiple scattering and resonant absorption in flux tube bundles. NTIS

93 SPACE RADIATION

Includes cosmic radiation; and inner and outer earth's radiation belts.

For biological effects of radiation see *52 Aerospace Medicine*. For theory see *73 Nuclear and High-Energy Physics*.

N95-29265# Stanford Linear Accelerator Center, Menlo Park, CA
GLAST
E. D. Bloom 1995 13 p Presented at the Workshop on TeV Gamma Ray Astrophysics, Heidelberg, Germany, 3-7 Oct. 1994
(Contract DE-AC03-76SF-00515)
(DE95-008596; SU-SLAC-PUB-95-6738; CONF-9410308-1) Avail: CASI HC A03/MF A01

Recent results from the Energetic Gamma-Ray Experiment Telescope (EGRET) aboard the Compton Observatory have generated strong interest in space based high-energy (E(sub gamma) greater than 10 MeV) gamma ray astronomy. This science has wetted the authors' curiosity of what might be observed with an instrument having considerably more capability than EGRET, if such a device were practical in these fiscally difficult times. Advances in silicon technology over the past decade, and the resulting rapid drop in costs, encourage the development of a dramatically new type of high-energy gamma ray space telescope based on silicon strip technology. The GLAST team (GLAST stands for Gamma-ray Large Area Space Telescope) has been working for the past two years on the design of such an instrument, and the development of the silicon strip hardware and readout electronics needed to realize this design. As in previous high-energy instruments, GLAST is a pair spectrometer backed by a total absorption electro-magnetic shower counter. Measurement of the energy and direction of the induced electro-magnetic shower provides information about the energy and direction of the incident gamma-ray. However, due to the flexibility and relatively low cost of the silicon strip technology, the telescope has about a factor of 10 increase in effective area over EGRET, and about a factor of 5 increase in field of view. At the same time, the GLAST design is calculated to have much better point source sensitivity, and to have an energy range of 10 MeV less than E(sub gamma) less than 300 GeV. Due to the economics of silicon technology, along with weight, and size savings compared to gas based detector technology, the authors estimate that this instrument can be built and flown as a Delta II mission. Thus, GLAST would easily fit into the NASA intermediate category with an estimated total cost of about $200 million. DOE

N95-29531 Chicago Univ., Chicago, IL.
FLUXES AND RELATIVE ABUNDANCES OF LIGHT COSMIC RAY NUCLEI AT ENERGIES ABOVE 40 GeV/n Ph.D. Thesis
James Henry Buckley 1994 175 p
Avail: Univ. Microfilms Order No. DA9419822

The first results from the September 1991 balloon flight of the University of Chicago's Ring Imaging Cerenkov (RICH) detector are presented. A detailed description of the RICH detector and the data analysis procedures are given. Also reported here are new measurements of the absolute flux and differential energy spectra of the primary cosmic ray species helium, carbon, and oxygen between 40 and 320 GeV/n as well as the spectra of the secondary species lithium, beryllium, and boron above 40 GeV/n. A comparison with results from previous measurements of heavier nuclei (Z greater than or equal to 4) from HEAO-3 and Spacelab-2 indicates good agreement between these experiments. The entire data set is compared with the results of a leaky box propagation model with the same parameters that had been deduced from the analysis of the results of the Spacelab-2 experiment. Given this new data, it now appears that helium as well as carbon and oxygen are in good agreement with this model if the source spectrum is taken to be a power law in energy proportional to E(exp -2.15). It appears that our results also strengthen the case for an anticorrelation of the abundance of cosmic ray nuclei with the first ionization potential, but are inconsistent with a step function form for this trend.
Dissert. Abstr.

N95-29671 Stanford Univ., CA.
GAMMA RADIATION FROM ROTATION POWERED PULSARS AND RESULTS FROM THE ENERGETIC GAMMA-RAY EXPERIMENT TELESCOPE Ph.D. Thesis
James Chiang 1994 207 p
Avail: Univ. Microfilms Order No. DA9414551

The Polar Cap and Outer Gap models of gamma-ray emission from rotation-powered pulsars are examined. In the Polar Cap model, a detailed Monte Carlo calculation is performed. Electrons and positrons are accelerated in vacuum gaps near the magnetic polar cap of a rotating neutron star. The curvature radiation they emit interacts with the strong magnetic field of the pulsar and produces e(sup +/-) pairs via the Sturrock process. These pairs in turn emit synchrotron radiation which also interacts with the strong magnetic field. An electromagnetic cascade results, and the gamma-ray flux seen at the Earth consists of the escaping curvature and synchrotron radiation. In the Outer Gap model, a much refined calculation of high energy emission from the outer gap region is performed. In this case, vacuum gaps form in the outer regions of the pulsar magnetosphere along the boundary between the 'closed' and 'open' field line zones. The large potential drops which are postulated to form in the outer gaps accelerate counter-streaming beams of electrons and positrons to highly relativistic energies (E(sub e) equivalent to 10(exp 13) eV). The curvature and inverse-Compton radiation emitted by these particle beams interact with lower energy radiation to produce secondary pairs of electrons and positrons. These secondary particles produce the synchrotron and inverse-Compton radiation which provides the required photon-photon opacity for the counter-streaming very high energy radiation. Improvements over previous outer gap calculations include a more detailed treatment of the high energy emission processes in the pulsar magnetosphere and the incorporation of particle and photon transport to and from different emitting regions. For both the Polar Cap and Outer Gap calculations, predictions of light curve shapes and spectral variation as a function of pulse phase are made using standard assumptions about the geometry of the pulsar magnetosphere. A description of the EGRET instrument and the various data analysis methods is presented. Maximum likelihood techniques are used with calibration information including instrument efficiency, energy, and angular resolution to determine fluxes, spectra and time variability for

a variety of gamma-ray sources. Analyses of the high energy emission from the X-ray binary Cygnus X-3 and from the Crab Pulsar and Nebula are presented. A detailed study of the new source class of gamma-ray loud Active Galactic Nuclei (AGN) is performed in the context of the 'unified picture'. Source spectra, variability and source luminosity evolution are examined and related to the prevailing theoretical models.
Dissert. Abstr.

N95-29705 Chicago Univ., Chicago, IL.
THE ENERGY SPECTRUM AND FLUX OF COSMIC RAY HELIUM AT HIGH ENERGY Ph.D. Thesis
Joseph Richard Dwyer 1994 114 p
Avail: Univ. Microfilms Order No. DA9419814

I describe a new measurement of the absolute flux and differential energy spectrum of the primary cosmic ray species helium between 40 and 320 GeV/n. This measurement was made by a new cosmic ray detector, flown from Fort Sumner, NM in September 1991, that utilized a ring imaging Cherenkov (RICH) counter to determine the energy of light cosmic ray nuclei. The design and performance of the instrument is described, and the data analysis procedures used for the energy determination are discussed. The results are compared with the results of the standard leaky box model. A good agreement is found if the source spectrum is assumed to follow a power law in energy proportional to E(exp -2.15).
Dissert. Abstr.

N95-29779 Chicago Univ., Chicago, IL.
X-RAY EMISSION FROM HYBRID STARS Ph.D. Thesis
Vinay L. Kashyap 1994 64 p
Avail: Univ. Microfilms Order No. DA9419845

We report on deep ROSAT observations of two Hybrid atmosphere stars, alpha TrA and iota Aur, and our analysis of these observations. We detect high energy transient phenomena on alpha TrA, and consider the implications of this discovery to the atmospheres of Hybrid stars. We detect iota Aur in the high energy passband of ROSAT, implying the existence of multi-million degree plasma on the star. Our major results include: The discovery of two large flare events, detected during pointed observations of alpha TrA; the demonstration that the flare emission most likely comes from the giant itself, rather than from a previously-unseen low-mass companion star; the demonstration that the plasma characteristics associated with the flares and with the 'quiescent' component are essentially indistinguishable; and that the geometric dimensions of the emitting plasma are considerably smaller than the critical dimension characterizing stable 'hot' coronal loop structures. Our results suggest that alpha TrA does not have any steady x-ray emission, consistent with theoretical expectations, and support the argument that Hybrid stars constitute a transitional type of object in which large-scale magnetic dynamo activity ceases, and the dominant spatial scales characterizing coronal structure rapidly decline as such stars evolve across the x-ray 'dividing line' in the H-R diagram.
Dissert. Abstr.

99 GENERAL

N95-28786*# National Aeronautics and Space Administration. John F. Kennedy Space Center, Cocoa Beach, FL.
RESEARCH AND TECHNOLOGY: 1994 ANNUAL REPORT OF THE JOHN F. KENNEDY SPACE CENTER
Dec. 1994 142 p
(NASA-TM-110143; NAS 1.15:110143) Avail: CASI HC A07/MF A02

As the NASA Center responsible for assembly, checkout, servicing, launch, recovery, and operational support of Space Transportation System elements and payloads, the John F. Kennedy Space Center is placing increasing emphasis on its advanced technology development program. This program encompasses the efforts of the Engineering Development Directorate laboratories, most of the KSC operations contractors, academia, and selected commercial industries - all working in a team effort within their own areas of expertise. This edition of the Kennedy Space Center Research and Technology 1994 Annual Report covers efforts of all these contributors to the KSC advanced technology development program, as well as our technology transfer activities. The Technology Programs and Commercialization Office (DE-TPO), (407) 867-3017, is responsible for publication of this report and should be contacted for any desired information regarding the advanced technology program.
Author

N95-28882*# National Aeronautics and Space Administration. Goddard Space Flight Center, Greenbelt, MD.
THE 1994 RESEARCH AND TECHNOLOGY REPORT AT THE GODDARD SPACE FLIGHT CENTER
Gerald Soffen, ed., Milton Halem, ed., James Green, ed., Kenneth Frost, ed., Stephen Maran, ed., Charles Boyle, ed., Walter Truszlowski, ed., Walter Sullivan, ed., and Howard Ottenstein, ed. 1994 260 p Original contains color illustrations
(NASA-TM-110623; NAS 1.15:110623) Avail: CASI HC A12/MF A03; 41 functional color pages

The breadth of subject material in this 1994 edition of the Research and Technology Report illustrates the broad scope of activities at the Goddard Space Flight Center. The numerous entries dealing with data processing and visualization show the strong emphasis on data and its interpretation. Reports are presented in the following sections: data processing and visualization; space sciences - high energy astronomy, solar system, and new techniques; earth system science - atmospheres, oceans and ice, solid earth, and soils and vegetation; networks, planning, and information systems - mission scheduling and operations, spacecraft operation and status, software engineering, and infrastructure support; engineering and materials - spacecraft subsystems, launch vehicles, thermal control, new mechanisms, and testing and evaluation; and flight projects.
CASI

N95-29816*# National Aeronautics and Space Administration. Lyndon B. Johnson Space Center, Houston, TX.
THE JSC RESEARCH AND DEVELOPMENT ANNUAL REPORT 1993
Aug. 1994 208 p
(NASA-TM-104787; S-757; NAS 1.15:104787) Avail: CASI HC A10/MF A03

Issued as a companion to Johnson Space Center's Research and Technology Annual Report, which reports JSC accomplishments under NASA Research and Technology Operating Plan (RTOP) funding, this report describes 47 additional projects that are funded through sources other than the RTOP. Emerging technologies in four major disciplines are summarized: space systems technology, medical and life sciences, mission operations, and computer systems. Although these projects focus on support of human spacecraft design, development, and safety, most have wide civil and commercial applications in areas such as advanced materials, superconductors, advanced semiconductors, digital imaging, high density data storage, high performance computers, optoelectronics, artificial intelligence, robotics and automation, sensors, biotechnology, medical devices and diagnosis, and human factors engineering.
Author

Typical Subject Index Listing

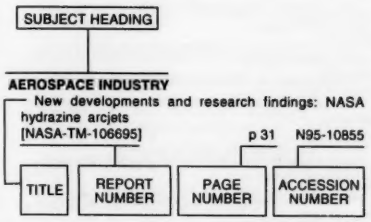

The subject heading is a key to the subject content of the document. Titles, report numbers, and accession numbers of pertinent documents are provided under each subject heading. When the title is insufficiently descriptive of the document content, a title extension is added, separated from the title by three hyphens. The report number helps to indicate the type of document cited (e.g., NASA report, NASA translation, NASA contractor report). The accession number is the number by which the document abstracts are arranged in this journal and by which the document is sold or requested. The page number helps you locate the citation in the abstract section. The titles, with title extensions if present, are arranged under each subject heading in ascending accession number order. The subject headings have been selected from the latest revision of the *NASA Thesaurus*.

A

ABLATION
Numerical studies of ablative mass loss from wind accelerated clouds p 2622 N95-29676

ABRASION RESISTANCE
Nanoindentation and nanoscratching of hard coating materials for magnetic disks
[DE95-008776] p 2547 N95-30174

ABSORPTION SPECTRA
Reaction field (RF) calculation of the spectral shifts of indole
[AD-A290449] p 2532 N95-29487
Numerical studies of ablative mass loss from wind accelerated clouds p 2622 N95-29676
Ab initio calculation of vibrational absorption and circular dichroism spectra using density functional force fields
[AD-A291297] p 2720 N95-29936
High temperature spectroscopy of alkali metal vapors for solar to thermal energy conversion
[AD-A291355] p 2602 N95-29949

ABSORPTION SPECTROSCOPY
Non-coincident multi-wavelength emission absorption spectroscopy
[DE95-006480] p 2530 N95-28776

ABSORPTIVITY
HTMIAC/CINDAS silicon properties database. User's guide
[AD-A292602] p 2533 N95-29575

ABSTRACTS
Bibliography of Doctor Chul Park
[NASA-TM-110353] p 2503 N95-29351
A bibliography, with abstracts and annotations, of publications on and related to underwater acoustic fluctuations
[AD-A291342] p 2685 N95-29945

ABUNDANCE
Carbon isotope abundance ratios in comets p 2732 N95-29592
Large scale fluctuations of the geomagnetic field p 2617 N95-29796
Aperture synthesis observation of HCN J = 1-0 emission from Y Canum Venaticorum p 2735 N95-29839

ACCELERATION (PHYSICS)
A search for a composition-dependent gravitational force p 2719 N95-29501
Summary Report of mission acceleration measurements for STS-66. Launched November 3, 1994
[NASA-TM-106914] p 2509 N95-29643

ACCELERATORS
The international fusion materials irradiation facility
[DE95-006536] p 2696 N95-29142

ACCELEROMETERS
Summary report of mission acceleration measurements for STS-65, launched 8 July 1994
[NASA-TM-106871] p 2549 N95-30339

ACCESS TIME
Geometric grid generation p 2483 N95-28756

ACCIDENTS
A theoretical study on ignition mechanisms of liquid propellants
[AD-A290569] p 2549 N95-29550

ACCRETION DISKS
Continuum spectra of supermassive accretion disks p 2732 N95-29252
The dynamics of FU Orionis outbursts: Time-dependent accretion through protostellar disks p 2732 N95-29530
Observational signatures of rotating black holes p 2729 N95-29709

ACCUMULATORS
Garbage collection is fast, but a stack is faster
[AD-A290099] p 2722 N95-29207
175Hp contrarotating homopolar motor design report
[AD-A291138] p 2567 N95-30122

ACETATES
Investigation of tension-compression fatigue behavior of a notched cross-ply metal matrix composite at elevated temperature
[AD-A291479] p 2527 N95-29770

ACETYL COMPOUNDS
Coupling of brain muscarinic receptors to second messengers
[AD-A290498] p 2635 N95-29153
The 5th International Meeting on Cholinesterase
[AD-A291253] p 2534 N95-30085

ACETYLENE
Linear carborane-(siloxane or silane)-acetylene based copolymers
[AD-D017321] p 2547 N95-30132

ACIDITY
Prediction of hydrogen entry and permeation in metals and alloys
[AD-A292047] p 2536 N95-29298
Preparation and studies of urazole containing polymers
[AD-A290685] p 2545 N95-29586

ACIDS
Photogenerated amines in the design of imaging materials: The radiation-induced imidization of functionalized polystyrenes bearing amide-ester side chains
[AD-A289943] p 2542 N95-29270

ACOUSTIC ATTENUATION
The prediction of sound attenuation as a result of propagation close to the ground
[ESDU-94036] p 2682 N95-28709
Actual effectiveness of hearing protection in high level impulse noise
[AD-A291604] p 2634 N95-28941
Revisions and notes on a model for bubble attenuation in near-surface propagation
[AD-A290312] p 2629 N95-29085
100 Hz-10 kHz bottom backscattering model: Generalized treatment of sediment sound propagation, sediment volume scattering and interface-roughness scattering
[AD-A291323] p 2685 N95-29942

ACOUSTIC COUPLING
The acoustic characteristics of turbomachinery cavities
[NASA-CR-4671] p 2478 N95-28720

ACOUSTIC EMISSION
The angular spread of the deflected acoustic beam diffracted by a Bragg grating out of a surface acoustic wave
[AD-A291018] p 2684 N95-29659

ACOUSTIC IMAGING
Acoustic imaging of ultrasonic wave propagation
[AD-A290390] p 2683 N95-29232

ACOUSTIC IMPEDANCE
The prediction of sound attenuation as a result of propagation close to the ground
[ESDU-94036] p 2682 N95-28709
Proceedings of the Sixth International Symposium on Long-Range Sound Propagation
[AD-A290920] p 2685 N95-30084

ACOUSTIC INSTABILITY
Investigation of the flow turning loss in unstable solid propellant rocket motors p 2510 N95-29331

ACOUSTIC MEASUREMENT
Backscatter data acquisition for Hydrosweep DS aboard RV Ewing
[AD-A292332] p 2628 N95-28796

ACOUSTIC PROPAGATION
Hindcasting changes in thermal structure and acoustic transmission loss in the upper ocean on short time scales with data from MILE and from ocean weather station papa
[AD-A292419] p 2629 N95-28991
Airy functions and the recursive ray acoustics algorithm
[AD-A290182] p 2629 N95-29054
Revisions and notes on a model for bubble attenuation in near-surface propagation
[AD-A290312] p 2629 N95-29085
The nature of wavefront fluctuations induced by internal gravity waves in long-range oceanic acoustic pulse transmissions p 2630 N95-29528
Finite difference ocean acoustic model users guide
[AD-A291544] p 2631 N95-29856
The Scanning Fast Field Program (SCAFFIP) general version 1.0 user's manual
[AD-A291209] p 2618 N95-29976
ICASE/LaRC Workshop on Benchmark Problems in Computational Aeroacoustics (CAA)
[NASA-CP-3300] p 2686 N95-30133
Benchmark problems and solutions p 2686 N95-30134
Solution of acoustic workshop problems by a spectral multidomain method p 2687 N95-30141
Evaluation of high order schemes for nonlinear wave computations p 2582 N95-30149
Nonlinear wave propagation using three different finite difference schemes (category 2 application) p 2582 N95-30151
Wave propagation and scattering in computational aeroacoustics p 2689 N95-30152
Application of a new finite difference algorithm for computational aeroacoustics p 2689 N95-30155
Computational aeroacoustics on massively parallel computers p 2661 N95-30156
Category 5 problem solution using an unstructured finite volume algorithm p 2657 N95-30157
High-order essentially non-oscillatory methods for computational aeroacoustics p 2690 N95-30159
Numerical simulations of small amplitude acoustic wave propagation in a converging-diverging nozzle p 2690 N95-30160
Aeroacoustic computation of a gust-plate interaction via MacCormack schemes p 2690 N95-30162

ACOUSTIC PROPERTIES
The effect of viscous attenuation on shock tube performance
[AD-A289793] p 2568 N95-28696
Physical acoustics summer school, 1994. volume 1. transcript
[AD-A292552] p 2683 N95-28973

ACOUSTIC SCATTERING
Physical acoustics summer school, 1994. volume 1. transcript
[AD-A292552] p 2683 N95-28973
Transport phenomena and noise in real quantum wires
[AD-A290493] p 2714 N95-29152
Acoustic scattering from ellipses by the modal element method
[NASA-TM-106935] p 2683 N95-29401
High gain, low noise and broadband Raman and Brillouin fiber-optic amplifiers, channel selectors and switches
[AD-A290585] p 2700 N95-29553
Wave propagation and scattering in computational aeroacoustics p 2689 N95-30152
Evaluation of numerical schemes for the analysis of sound generation by blade-gust interaction p 2690 N95-30163

ACOUSTIC VELOCITY
Analysis of historical oceanographic data on a minicomputer: Program WAHOO
[AD-A292530] p 2629 N95-28873
Stochastic modeling and global warming trend extraction for ocean acoustic travel times
[AD-A292114] p 2608 N95-28922
Physical acoustics summer school, 1994. volume 1. transcript
[AD-A292552] p 2683 N95-28973
Numerical studies of ablative mass loss from wind accelerated clouds p 2622 N95-29676
100 Hz-10 kHz bottom backscattering model: Generalized treatment of sediment sound propagation, sediment volume scattering and interface-roughness scattering
[AD-A291323] p 2685 N95-29942

ACOUSTICAL HOLOGRAPHY
GENAH user's guide and reference manual version 1.0
[AD-A290236] p 2583 N95-29470

ACOUSTICS
The acoustic characteristics of turbomachinery cavities
[NASA-CR-4671] p 2478 N95-28720
Physical acoustics summer school, 1994. volume 1. transcript
[AD-A292552] p 2683 N95-28973
The development of an interpretive methodology for the application of real-time acousto-ultrasonic NDE technique for monitoring damage in ceramic composites under dynamic loads p 2592 N95-29104
A human factors evaluation of the operational demonstration flight inspection aircraft
[DOT/FAA/AM-95/18] p 2641 N95-29365
A compact solution to computational acoustics p 2686 N95-30138
Time accurate application of the MacCormack 2-4 scheme on massively parallel computers p 2661 N95-30150

ACOUSTO-OPTICS
Conference reports
[AD-A289630] p 2561 N95-28911
A method and apparatus for signal filtering
[AD-D017268] p 2554 N95-29236
A comparison of three pedestal removal techniques for an optical time-integrating correlator
[AD-A290092] p 2700 N95-29354
Advanced presort process
[AD-A291010] p 2557 N95-29655
Multiple dimensional acousto-optic diffraction and multiple dimensional acousto-optic device
[AD-A291037] p 2685 N95-29681
Fiber compatible acousto-optic modulator using a gradient index lens
[AD-A291164] p 2565 N95-29925
Theory and experiment analysis of two-dimensional acousto-optic interaction
[AD-A291059] p 2685 N95-29951

ACQUISITION
The (HMI9293) acquisition of a 200 MHz nuclear magnetic resonance spectrometer
[AD-A291913] p 2583 N95-29361

ACRYLIC ACID
In-plant testing of membranes to treat electroplating wastewater
[NASA-CR-198796] p 2532 N95-29250

ACTIVE CONTROL
Modeling and control of rotating stall in high speed multi-stage axial compressors p 2500 N95-29244
Precision pointing experiment
[AD-A291015] p 2664 N95-29657
Model development for active control of stall phenomena in aircraft gas turbine enginas p 2500 N95-29679
Development of 'smart' piezothermoelastic laminae: Theory and applications
[AD-A290852] p 2528 N95-29864
Characterization of stall inception in high-speed single-stage compressors
[AD-A291275] p 2501 N95-29934

ACTIVE GALACTIC NUCLEI
Continuum spectra of supermassive accretion disks p 2732 N95-29252

ACTIVE GALAXIES
Multiwaveband observations of quasars p 2728 N95-29665

ACTS
Test results of a 20 GHz, low noise downconverter for USAT applications
[NASA-TM-106892] p 2508 N95-30011

ACTUATORS
Modeling and control of rotating stall in high speed multi-stage axial compressors p 2500 N95-29244
Robust control of nonlinear flexible multibody systems using quaternion feedback and dissipative compensation
[NASA-TM-109099] p 2507 N95-29377
Transitions in liquid crystals initiated with circularly polarized light
[AD-A290525] p 2716 N95-29493
Broadband control of structural vibration using simultaneous sensing and actuation with nonlinear piezoelectric elements p 2664 N95-29548
Unitary transducer with variable resistivity
[AD-D017329] p 2566 N95-30055
Development of electrochemical super capacitors for EMA applications p 2568 N95-30270

ADA (PROGRAMMING LANGUAGE)
Collected software engineering papers, volume 12
[NASA-CR-189409] p 2644 N95-28713
Impact of Ada and object-oriented design in the flight dynamics division at Goddard Space Flight Center
[NASA-CR-189412] p 2644 N95-28807
An introduction to the principles of computer science: A reuse-oriented philosophy
[AD-A290364] p 2647 N95-29226
ADA in introductory courses
[AD-A292219] p 2648 N95-29285
Proceedings of the 12th Annual National Conference on Ada Technology
[AD-A290693] p 2651 N95-29644

ADAPTATION
Coping and adaptation: Theoretical and applied perspectives
[AD-A290513] p 2638 N95-29090
Performance and robustness of self-tuning and adaptation algorithms for identification, filtering and control
[AD-A292070] p 2648 N95-29310

ADAPTERS
Design and analysis of the launch vehicle adapter fitting for the petite amateur navy satellite (PANSAT)
[AD-A289693] p 2504 N95-28680

ADAPTIVE CONTROL
Grid related issues for static and dynamic geometry problems using systems of overset structured grids p 2480 N95-28737
A Cartesian, cell-based approach for adaptively-refined solutions of the Euler and Navier-Stokes equations p 2480 N95-28739
Adaptive hybrid prismatic-tetrahedral grids for viscous flows p 2481 N95-28744
On-line damage identification and motion control of adaptive structures: An intelligent control approach p 2662 N95-29109
Performance and robustness of self-tuning and adaptation algorithms for identification, filtering and control
[AD-A292070] p 2648 N95-29310
Scalable software tools for adaptive scientific computation
[AD-A290446] p 2650 N95-29480
Load balancing for the parallel adaptive solution of partial differential equations
[AD-A290450] p 2671 N95-29488
Adaptive block sequential detection of abrupt signal changes
[AD-A290456] p 2557 N95-29489
Parallel adaptive techniques for transient partial differential equations
[AD-A290460] p 2674 N95-29490
Fundamental limitations and capabilities of robust identification and adaptive control
[AD-A291085] p 2664 N95-29636
Precision pointing experiment
[AD-A291015] p 2664 N95-29657
Methodologies for intelligent systems
[AD-A290901] p 2666 N95-30117
Learning control in linear and nonlinear systems p 2667 N95-30238
Control of vortex dynamics p 2579 N95-30275

ADAPTIVE FILTERS
Performance and robustness of self-tuning and adaptation algorithms for identification, filtering and control
[AD-A292070] p 2648 N95-29310
Adaptive Infinite Impulse Response (IIR) filter system
[AD-D017403] p 2564 N95-29570

ADAPTIVE OPTICS
Coronagraphic imaging of protoplanetary-disk candidate stars using adaptive optics p 2728 N95-29651
Atmospheric wavefront sensing and correction including the stellar phase shifting interferometer p 2701 N95-29706
Low order adaptive optical systems
[AD-A291121] p 2701 N95-29766
15th NSO/Sac Peak Solar Workshop
[AD-A292297] p 2739 N95-30074

ADDITIVES
Theoretical investigation of superconductivity in doped fullerenes
[AD-A291942] p 2562 N95-29018
High-performance speech recognition using consistency modeling
[AD-A290655] p 2557 N95-29564
Unitary transducer with variable resistivity
[AD-D017329] p 2566 N95-30055

ADDRESSING
Photon-counting spatial light modulator technology development
[AD-A292619] p 2699 N95-29295

ADHESION
The measurement of adhesion at film-substrate interfaces using a constant depth scratch test
[AD-A289940] p 2542 N95-29269
Impact properties of coated engineering plastics
[PB95-197281] p 2547 N95-30201

ADHESION TESTS
A study of blister tests for film adhesion measurement and fracture efficiency of tests for adhesive bonds p 2545 N95-29799

ADHESIVE BONDING
Fiber-matrix adhesion in single-fiber model composites p 2524 N95-29337
A study of blister tests for film adhesion measurement and fracture efficiency of tests for adhesive bonds p 2545 N95-29799

ADIABATIC CONDITIONS
Consideration of microstructural changes in the study of adiabatic shear bands
[AD-A290398] p 2715 N95-29234

ADIPOSE TISSUES
Effects of chromium picolinate on body composition in a remedial conditioning program
[AD-A292079] p 2636 N95-29238

ADJUSTING
Adjustable two-axis instrument mount
[AD-D017393] p 2582 N95-29220

ADSORBENTS
Structural and electronic properties of adsorbates on semiconductors, metal-semiconductor interfaces and semiconductor heterojunctions
[AD-A291917] p 2715 N95-29438

ADVANCED VERY HIGH RESOLUTION RADIOMETER
Monitoring of burning in the Brazilian cerrado region using AVHRR/NOAA data calibrated by TM/Landsat data
[INPE-5490-TDI/507] p 2598 N95-28929
Continental aerosol effects on stratocumulus microphysics during MAST 1994
[AD-A292674] p 2621 N95-29416
Sea ice motions in the Central Arctic pack ice as inferred from AVHRR imagery
[NASA-CR-198835] p 2601 N95-30247
An atlas of monthly mean distributions of SSMI surface wind speed, AVHRR/2 sea surface temperature, AMI surface wind velocity, TOPEX/POSEIDON sea surface height, and ECMWF surface wind velocity during 1993
[NASA-CR-198880] p 2628 N95-30343

ADVECTION
Application of the space-time conservation element and solution element method to two-dimensional advection-diffusion problems
[NASA-TM-106946] p 2574 N95-29372

AEROACOUSTICS
Interaction of turbulence with complex shock waves
[AD-A290225] p 2571 N95-29145
An assessment of artificial damping models for aeroacoustic calculations
[NASA-CR-198354] p 2574 N95-29405
The spectrum and directivity of turbulent mixing noise from supersonic jets p 2684 N95-29415
An extension of the Lighthill theory of jet noise to encompass refraction and shielding
[NASA-TM-110163] p 2684 N95-29452

ICASE/LaRC Workshop on Benchmark Problems in Computational Aeroacoustics (CAA)
[NASA-CP-3300] p 2686 N95-30133
Benchmark problems and solutions
p 2686 N95-30134
Application of essentially nonoscillatory methods to aeroacoustic flow problems p 2686 N95-30135
Computational aeroacoustics using hyperbolic wave primitives p 2686 N95-30136
Comparative study of numerical schemes of TVD3, UNO3-ACM and optimized compact scheme
p 2686 N95-30137
Application of low dissipation and dispersion Runge-Kutta schemes to benchmark problems in computational aeroacoustics p 2687 N95-30139
Results of two new methods for aeroacoustics benchmark problems p 2687 N95-30140
Computation of wave propagation in a complex flow
p 2582 N95-30142
Lattice gas methods for computational aeroacoustics
p 2687 N95-30144
Solutions of the benchmark problems by the dispersion-relation-preserving scheme
p 2674 N95-30145
The construction of high-accuracy schemes for acoustic equations p 2688 N95-30146
A comparative study of upwind and MacCormack schemes for CAA benchmark problems
p 2688 N95-30147
Application of traditional CFD methods to nonlinear computational aeroacoustics problems
p 2688 N95-30148
Nonlinear wave propagation using three different finite difference schemes (category 2 application)
p 2582 N95-30151
Wave propagation and scattering in computational aeroacoustics p 2689 N95-30152
The use of staggered scheme and an absorbing buffer zone for computational aeroacoustics
p 2689 N95-30153
Application of a new finite difference algorithm for computational aeroacoustics p 2689 N95-30155
Computational aeroacoustics on massively parallel computers p 2661 N95-30156
Comparison of spatial numerical operators for duct-nozzle acoustics p 2690 N95-30158
High-order essentially non-oscillatory methods for computational aeroacoustics p 2690 N95-30159
Numerical simulations of small amplitude acoustic wave propagation in a converging-diverging nozzle
p 2690 N95-30160
The pressure field of a gust interacting with a flat plate p 2582 N95-30161
Aeroacoustic computation of a gust-plate interaction via MacCormack schemes p 2690 N95-30162
Evaluation of numerical schemes for the analysis of sound generation by blade-gust interaction
p 2690 N95-30163

AEROASSIST
Guidance law development for aeroassisted transfer vehicles using Matched Asymptotic Expansions
p 2503 N95-30347

AEROBES
Adaptations to three weeks of aerobic/anaerobic training in west coast U.S: Navy Sea-Air-Land personnel (SEAL's)
[AD-A291500] p 2637 N95-29846

AERODYNAMIC BALANCE
High-and low-frequency dynamics of isolated blades and rotors with dynamic stall and wake
[AD-A290358] p 2497 N95-29322

AERODYNAMIC CHARACTERISTICS
Computational Fluid Dynamics (CFD) analysis of a C-135 aircraft with a side-mounted splitter plate (with comparison to wind tunnel data)
[AD-A292029] p 2571 N95-29187
Transonic, supersonic and hypersonic wind-tunnel tests on aerodynamic characteristics of reentry body with blunted cone configuration
[ISAS-658] p 2490 N95-29640
Experimental studies on boundary-layer transition on a reentry vehicle at transonic and supersonic speeds
[ISAS-659] p 2575 N95-29712
Computational algorithms for aerodynamic analysis and design
[AD-A291084] p 2491 N95-29972
Experimental investigation of aerodynamic devices for wind turbine rotational speed control, phase 1
[DE95-004034] p 2603 N95-30016

AERODYNAMIC COEFFICIENTS
increments in aerofoil lift coefficient at zero angle of attack and in maximum lift coefficient due to deployment of a plain trailing-edge flap, with or without a leading-edge high-lift device, at low speeds
[ESDU-94028] p 2486 N95-28885
Wave drag coefficient for axisymmetric forecowls at zero incidence (M sub infinity less than or equal to 1.5)
[ESDU-94014] p 2568 N95-28903
Increments in aerofoil lift coefficient at zero angle of attack and in maximum lift coefficient due to deployment of a trailing-edge split flap, with or without a leading-edge high-lift device, at low speeds
[ESDU-94029] p 2488 N95-29129
Increments in aerofoil lift coefficient at zero angle of attack and in maximum lift coefficient due to deployment of various leading-edge high-lift devices at low speeds
[ESDU-94027] p 2490 N95-29898
Introduction to the estimation of the lift coefficients at zero angle of attack and at maximum lift for aerofoils with high-lift devices at low speeds
[ESDU-94026] p 2491 N95-29899

AERODYNAMIC CONFIGURATIONS
Rapid Airplane Parametric Input Design (RAPID)
p 2479 N95-28730
Automatic blocking for complex three-dimensional configurations p 2480 N95-28734
Block-structured grids for complex aerodynamic configurations: Current status p 2480 N95-28736
A two element laminar flow airfoil optimized for cruise
[NASA-CR-198580] p 2489 N95-29338
An experimental investigation of the time-dependent separation of tangent bodies in supersonic flow
[AD-A290720] p 2489 N95-29500
Transonic, supersonic and hypersonic wind-tunnel tests on aerodynamic characteristics of reentry body with blunted cone configuration
[ISAS-658] p 2490 N95-29640
The 1995 version of the NSWC aeroprediction code. Part 1: Summary of new theoretical methodology
[AD-A291518] p 2490 N95-29853
Computational algorithms for aerodynamic analysis and design
[AD-A291084] p 2491 N95-29972

AERODYNAMIC DRAG
Excrescence drag levels on aircraft
[ESDU-94044] p 2487 N95-28897
Wave drag coefficient for axisymmetric forecowls at zero incidence (M sub infinity less than or equal to 1.5)
[ESDU-94014] p 2568 N95-28903
High-and low-frequency dynamics of isolated blades and rotors with dynamic stall and wake
[AD-A290358] p 2497 N95-29322
A two element laminar flow airfoil optimized for cruise
[NASA-CR-198580] p 2489 N95-29338

AERODYNAMIC INTERFERENCE
A method for the modelling of porous and solid wind tunnel walls in computational fluid dynamics codes
p 2502 N95-29795

AERODYNAMIC LOADS
Estimation of aerodynamic load distributions on the F/A-18 aircraft using a CFD panel code
[DSTO-TR-0147] p 2498 N95-29445
PREDICHAT: First order performance calculations of windturbine rotors using the method of the acceleration potential
[PB95-206454] p 2603 N95-30200

AERODYNAMIC NOISE
The spectrum and directivity of turbulent mixing noise from supersonic jets p 2684 N95-29415
Turbulent airflow noise production and propagation patterns of a subsonic jet impinging on a flat plate
p 2684 N95-29502

AERODYNAMIC STABILITY
An aerodynamic and static-stability analysis of the Hypersonic Applied Research Technology (HART) missile
[DA9426923] p 2491 N95-29965
Low-speed wind-tunnel investigation of the stability and control characteristics of a series of flying wings with sweep angles of 50 deg
[NASA-TM-4640] p 2498 N95-30226

AERODYNAMIC STALLING
Interactions of spanwise and chordwise vorticity associated with three-dimensional dynamic stall over an oscillating wing
[AD-A290546] p 2487 N95-29091
PIV investigation of compressibility effects on dynamic stall p 2487 N95-29102
Dynamic stall of a NACA 0012 airfoil in laminar flow
p 2489 N95-29243
Pressure based high order TVD methodology for dynamic stall control
[AD-A290149] p 2489 N95-29316
High-and low-frequency dynamics of isolated blades and rotors with dynamic stall and wake
[AD-A290358] p 2497 N95-29322

AERODYNAMICS
A fourth order Euler/Navier-Stokes prediction method for the aerodynamics and aeroelasticity of hovering rotor blades p 2572 N95-29242

AEROELASTICITY
A fourth order Euler/Navier-Stokes prediction method for the aerodynamics and aeroelasticity of hovering rotor blades p 2572 N95-29242

AEROSOLS
Measurement of the seasonal and annual variability of total column aerosol in a northeastern US network
[DE95-007259] p 2608 N95-28920
Demonstration of a stabilized alumina/ethanol colloidal dispersion technique for seeding high temperature air flows
[NASA-TM-108945] p 2582 N95-29113
Continental aerosol effects on stratocumulus microphysics during MAST 1994
[AD-A292674] p 2621 N95-29416
Numerical studies of the stratospheric aerosol layer under background and perturbed conditions
p 2615 N95-29666
A study of boundary layer aerosol and wind profiles using incoherent Doppler lidar p 2622 N95-29697

AEROSPACE ENGINEERING
A conceptual design for the attitude control and determination system for the Magnetosphere Imager spacecraft
[NASA-TP-3560] p 2507 N95-28721
Surface Modeling, Grid Generation, and Related Issues in Computational Fluid Dynamic (CFD) Solutions
[NASA-CP-3291] p 2478 N95-28723
Future requirements in surface modeling and grid generation p 2478 N95-28724
Requirements for effective use of CFD in aerospace design p 2478 N95-28725
Grid generation: A view from the trenches
p 2478 N95-28727
Application of CFD in aeronautics at NASA Ames Research Center p 2478 N95-28728
Block-structured grids for complex aerodynamic configurations: Current status p 2480 N95-28736
Prospects and expectations for unstructured methods
p 2481 N95-28742
An unstructured-grid software system for solving complex aerodynamic problems p 2481 N95-28743
Emerging CFD technologies and aerospace vehicle design p 2482 N95-28746
An assessment of unstructured grid technology for timely CFD analysis p 2482 N95-28747
Evaluation of grid generation technologies from an applied perspective p 2482 N95-28748
A 3DGRAPE/AL: The Ames/Langley technology upgrade p 2482 N95-28750
The 1994 research and technology report at the Goddard Space Flight Center
[NASA-TM-110623] p 2740 N95-28882
NASA/DOD Aerospace Knowledge Diffusion Research Project. Paper 49: Becoming an aerospace engineer: A cross-gender comparison
[NASA-TM-110731] p 2721 N95-29028
A transient model of the RL10A-3-3A rocket engine
[NASA-CR-195478] p 2510 N95-29114
Study of the space environmental effects on spacecraft engineering materials
[NASA-CR-196638] p 2531 N95-29246
Hernandez Engineering: NASA
[NASA-CR-197665] p 2508 N95-29633
The JSC research and development annual report 1993
[NASA-TM-104787] p 2740 N95-29816
US photovoltaic patents: 1991-1993
[DE95-004051] p 2603 N95-30017
Design, analysis and control of large transports so that control of engine thrust can be used as a back-up of the primary flight controls
[NASA-CR-198958] p 2501 N95-30254
Manual for a workstation-based generic flight simulation program (LaRCsim), version 1.4
[NASA-TM-110164] p 2502 N95-30327
Developing a workstation-based, real-time simulation for rapid handling qualities evaluations during design
[NASA-CR-198831] p 2499 N95-30335
Formulation of an improved smeared stiffener theory for buckling analysis of grid-stiffened composite panels
[NASA-TM-110162] p 2529 N95-30341

AEROSPACE ENVIRONMENTS
A layman's look at orbital debris
[AD-A289801] p 2506 N95-28700
Overview of the space debris environment
[AD-A292302] p 2507 N95-28867
Study of the space environmental effects on spacecraft engineering materials
[NASA-CR-196638] p 2531 N95-29246
Investigation of optical damage, energy partitioning and scaling laws at extremely high velocities
[AD-A291368] p 2703 N95-30062

AEROSPACE INDUSTRY
Surface Modeling, Grid Generation, and Related Issues in Computational Fluid Dynamic (CFD) Solutions
[NASA-CP-3291] p 2478 N95-28723
Grid generation: A view from the trenches
p 2478 N95-28727
An announcement by Dan Goldin
[NASA-TM-110739] p 2720 N95-29171

AEROSPACE MEDICINE
Experiment kits for processing biological samples inflight on SLS-2
[NASA-TM-4685] p 2642 N95-28722
Test and evaluation of the Impact Instrumentations, Inc. Uni-Vent model 750M ventilator
[AD-A292321] p 2640 N95-28792
Cellular and molecular level responses after radiofrequency radiation exposure, alone or in combination with x rays or chemicals
[AD-A292488] p 2633 N95-28866
The influence of space flight on erythrokinetics in man. Space Life Sciences Missions 1 and 2. Experiment E261
[NASA-CR-188368] p 2633 N95-28875
Military flying and aeromedical evaluation of cardiac arrhythmias
[AD-A291595] p 2634 N95-28940
A comparison of the aeromedical administration requirements for US Air Forces and major allies
[AD-A290137] p 2635 N95-29141
CO2-O2 interactions in extension of tolerance to acute hypoxia
[NASA-CR-198575] p 2635 N95-29158
Flying waivers for history of angioplasty and myocardial infraction
[AD-A292505] p 2635 N95-29161
Astronaut selection (NASA-MIPR)
[AD-A292512] p 2638 N95-29162
Aerospace medicine and biology: A continuing bibliography with indexes (supplement 403)
[NASA-SP-7011(403)] p 2636 N95-29190
A human factors evaluation of the operational demonstration flight inspection aircraft
[DOT/FAA/AM-95/18] p 2641 N95-29365
A generic specification for Special Purpose Aeromedical Equipment p 2499 N95-29623
Aeromedical impact of the transportable pressure ventilator in wartime aeromedical evacuation
p 2641 N95-29624
Care in the air: A system analysis of clinical outcomes in aeromedical evacuation p 2642 N95-29626
The one-dimensional bubble: Theory, experiment, and relevance to exposure of divers to low frequency sound, and of lung to lithotripsy
[ISVR-TR-246] p 2577 N95-29817
Life sciences program
[NASA-CR-197658] p 2633 N95-30292

AEROSPACE PLANES
Computation of the integrated aerodynamic and propulsive flowfields of a generic hypersonic space plane p 2490 N95-29788

AEROSPACE SCIENCES
The 1994 research and technology report at the Goddard Space Flight Center
[NASA-TM-110623] p 2740 N95-28882
The JSC research and development annual report 1993
[NASA-TM-104787] p 2740 N95-29816

AEROSPACE SYSTEMS
A procedure for accessing digital satellites containing amateur payloads
[AD-A289748] p 2506 N95-28688
Design and evaluation of a LQR controller for the bluebird unmanned air vehicle
[AD-A289769] p 2498 N95-29457

AEROSPACE VEHICLES
Emerging CFD technologies and aerospace vehicle design p 2482 N95-28746

AEROTHERMOCHEMISTRY
Surface modeling and grid generation for aeropropulsion CFD p 2479 N95-28732

AEROTHERMODYNAMICS
Bibliography of Doctor Chul Park
[NASA-TM-110353] p 2503 N95-29351
The 1995 version of the NSWC aeroprediction code. Part 1: Summary of new theoretical methodology
[AD-A291518] p 2490 N95-29853

AGE FACTOR
An analysis of anthropometric differences among occupational groups in the US Army
[AD-A292326] p 2640 N95-28794

AGGLOMERATION
Nanocrystalline processing and interface engineering of Si3N4-based ceramics
[AD-A291302] p 2546 N95-29939

AIR BAG RESTRAINT DEVICES
Biodynamic simulation of pilot interaction with a helicopter multiairbag restraint system
[AD-A290196] p 2492 N95-29057

AIR CONDITIONING
Liquid pressure amplification and liquid injection in air conditioning and refrigeration systems
[AD-A289738] p 2549 N95-28686
Geothermal heat pumps for heating and cooling
[AD-A292115] p 2602 N95-28858

AIR CONDITIONING EQUIPMENT
Alternative refrigerant performance: Field test of a nonchlorofluorocarbon chiller at Fort Leonard Wood, MO
[AD-A292052] p 2550 N95-29307
Use of chlorofluorocarbon-based refrigerants in USArmy facility air-conditioning and refrigeration systems: Recommendations for the interim period 1994-2000
[AD-A290432] p 2550 N95-29537

AIR COOLING
Selection and costing of heat exchangers. Air-cooled type
[ESDU-94043] p 2550 N95-28705
Condensation inside tubes: Condensate film coefficient in horizontal tubes
[ESDU-94041] p 2569 N95-29015

AIR CURRENTS
An air stream analysis of the occluded cyclone
p 2623 N95-29714
The tropical atmosphere under convection adjustment
p 2625 N95-29833

AIR FLOW
Computational fluid dynamics (CFD) simulation of test chamber and smoke-generating device
[AD-A290199] p 2569 N95-29058
Demonstration of a stabilized alumina/ethanol colloidal dispersion technique for seeding high temperature air flows
[NASA-TM-106945] p 2582 N95-29113
Linear and nonlinear discrete-time state-space modeling of dynamic systems for control applications
p 2663 N95-29251
Turbulent airflow noise production and propagation patterns of a subsonic jet impinging on a flat plate
p 2684 N95-29502
On the large scale circulation of the East Asia Mei-Yu fronts and secondary weather dimension disturbances
[AD-A291036] p 2622 N95-29662

AIR INTAKES
Air/fuel ratio visualization in a diesel spray
p 2590 N95-29807

AIR JETS
An analysis of B-1B exterior jet blast windshield anti-icing performance using pre-cooled compressor bleed air
[AD-A292522] p 2492 N95-28811

AIR LAND INTERACTIONS
Lee vorticity production by tropical mountain ranges
p 2622 N95-29701
A theoretical model of multiple regimes in a stratocumulus-topped boundary layer
p 2624 N95-29726
Soil wetness and climate variability
p 2609 N95-29878

AIR MASSES
Design of a more accurate, higher fidelity, dual-source air mass zero solar simulator
[AD-A291364] p 2603 N95-29953

AIR NAVIGATION
Conceptual design of a map interactive system for military aircraft cockpits
[AD-A289760] p 2499 N95-28692

AIR POLLUTION
The Environmental Assessment and Management (TEAM) guide
[AD-A286748] p 2608 N95-28787
Overview of the space debris environment
[AD-A292302] p 2507 N95-28867
Environmental practice in progam management offices
[AD-A290823] p 2609 N95-29721
Analysis of global economic instruments for CO2 emission reduction: Equity and efficiency
[DE95-764057] p 2610 N95-30195
Interactions between energy efficiency and emission trading under the 1990 Clean Air Act Amendments
[DE95-008649] p 2611 N95-30212

AIR SEA ICE INTERACTIONS
Sea ice motions in the Central Arctic pack ice as inferred from AVHRR imagery
[NASA-CR-198835] p 2601 N95-30247

AIR TRAFFIC
Federal aviation administration plan for research, engineering and development
[AD-A290952] p 2494 N95-29733

AIR TRAFFIC CONTROL
Automation and cognition in air traffic control: An empirical investigation
[AD-A291932] p 2493 N95-28790
Conversion of the TRACON operations concepts database into a formal sentence outline job task taxonomy
[DOT/FAA/AM-95/16] p 2493 N95-28819
MATSurv multisensor air traffic surveillance
[AD-A292253] p 2494 N95-28887
Shift work, age, and performance: Investigation of the 2-2-1 shift schedule used in Air Traffic Control facilities I. The sleep/wake cycle
[DOT/FAA/AM-95/19] p 2638 N95-29261
Terminal area forecasts-fiscal years 1993-2010
[AD-A290835] p 2495 N95-29880
Offshore next generation weather radar (NEXRAD) test and evaluation master plan (TEMP)
[AD-A291435] p 2559 N95-30072

AIR TRAFFIC CONTROLLERS (PERSONNEL)
Shift work, age, and performance: Investigation of the 2-2-1 shift schedule used in Air Traffic Control facilities I. The sleep/wake cycle
[DOT/FAA/AM-95/19] p 2638 N95-29261

AIR TRANSPORTATION
Test and evaluation of the Impact Instrumentations, Inc. Uni-Vent model 750M ventilator
[AD-A292321] p 2640 N95-28792
Recent Issues and Advances in Aeromedical Evacuation (MEDEVAC)
[AGARD-CP-554] p 2676 N95-29604
Use of quality tools to re-engineer the Aeromedical Evacuation (AE) system p 2676 N95-29605
The Canadian experience in UN airevac Sarajevo airlift: April 1993-October 1994 p 2676 N95-29606
United Nations aeromedical evacuation operations in the former Yugoslavia p 2676 N95-29607
Civil military co-operation: A ten year experience of an affiliative aeromedical evacuation programme of the Netherlands Armed Forces and a civilian repatriation organization p 2676 N95-29608
Aeromedical evacuation by RNLAF - work according to protocol p 2676 N95-29609
Critical evaluation of aeromedical evacuation in a multinational forces scenario p 2676 N95-29610
Experience in helicopter aeroevacuation in the community of Madrid, Spain p 2677 N95-29611
Aeromedical evacuation in combined operations
p 2677 N95-29612
Danish aeromedical evacuation efforts during the Gulf War p 2677 N95-29613
Experiences learned from the Spanish armed forces aeromedical evacuation system in the former Yugoslavia
p 2677 N95-29614
Flying ambulances: The approach of a small air force to long distance aeromedical evacuation of critically injured patients p 2678 N95-29618
Civil Reserve Air Fleet-Aeromedical Evacuation Shipset (CRAF-AESS) p 2678 N95-29619
The large-capacity rescue-helicopter CH-53 G
p 2678 N95-29621
International access to aeromedical evacuation medical equipment assessment data p 2679 N95-29622
A generic specification for Special Purpose Aeromedical Equipment p 2499 N95-29623
Aeromedical impact of the transportable pressure ventilator in wartime aeromedical evacuation
p 2641 N95-29624
Requirement for onboard telemetry equipment
p 2506 N95-29625
Care in the air: A system analysis of clinical outcomes in aeromedical evacuation p 2642 N95-29626
Effect of hypoxia on arterial blood gases in subjects with lung dysfunction p 2638 N95-29627
Changes in the medevac mission result in an increased role for the flight surgeon p 2680 N95-29628
Federal aviation administration plan for research, engineering and development
[AD-A290952] p 2494 N95-29733

AIR WATER INTERACTIONS
Modeling studies of the Leeuwin current off western and southern Australia
[AD-A290158] p 2629 N95-29023
Observations of mesoscale cellular convection from the marine stratocumulus phase of FIRE
p 2624 N95-29727
Radiative cooling profiles calculated from ECMWF analyses and ISCCP C1 data, and their application to determination of distributions of apparent convective heating in the equatorial Pacific p 2625 N95-29805
An air-sea interaction model for stress, sensible heat, latent heat, and sea state, applicable to the full range of wind speeds p 2626 N95-29876

AIRBORNE EQUIPMENT
Remote sensing of hydrologic variables in boreal areas
[NASA-CR-189422] p 2600 N95-29754

AIRBORNE LASERS
Computational Fluid Dynamics (CFD) analysis of a C-135 aircraft with a side-mounted splitter plate (with comparison to wind tunnel data)
[AD-A292029] p 2571 N95-29187
AIRBORNE RADAR
Evaluation of the utilization of SAR polarimetric images in the survey of land resources in the Amazon area Tapajos Forest Reserve
[INPE-5517-PRE/1792] p 2601 N95-29999
AIRCRAFT ACCIDENTS
Mode of human image representation and error checking strategies in complex visual displays
[AD-A290107] p 2492 N95-29210
US Army aviation epidemiology data register: Gender-specific attrition among the US Army student aviator class of 1987
[AD-A291856] p 2639 N95-29434
AIRCRAFT COMPARTMENTS
The potential for pulmonary heat injury resulting from the activation of a cabin water spray system to fight aircraft cabin fires
[DOT/FAA/AM-95/17] p 2636 N95-29224
A human factors evaluation of the operational demonstration flight inspection aircraft
[DOT/FAA/AM-95/18] p 2641 N95-29365
AIRCRAFT CONFIGURATIONS
The effects of design details on cost and weight of fuselage structures p 2499 N95-28831
AIRCRAFT CONSTRUCTION MATERIALS
Third NASA Advanced Composites Technology Conference, volume 1, part 2
[NASA-CP-3178-VOL-1-PT-2] p 2513 N95-28823
In situ processing methods for composite fuselage sandwich structures p 2513 N95-28826
Novel cost controlled materials and processing for primary structures p 2514 N95-28830
A weight-efficient design strategy for cutouts in composite transport structures p 2516 N95-28843
Technology integration box beam failure study p 2517 N95-28847
Third NASA Advanced Composites Technology Conference, volume 1, part 1
[NASA-CP-3178-VOL-1-PT-1] p 2518 N95-29029
Challenges and payoff of composites in transport aircraft: 777 empennage and future applications p 2519 N95-29031
Advanced composite fuselage technology p 2519 N95-29034
Cross-stiffened continuous fiber structures p 2521 N95-29041
Development of RTM and powder prepreg resins for subsonic aircraft primary structures p 2521 N95-29044
The effects of aircraft fuel and fluids on the strength properties of Resin Transfer Molded (RTM) composites p 2522 N95-29047
Progress in manufacturing large primary aircraft structures using the stitching/RTM process p 2522 N95-29050
Origins of imperfections in composite materials
[AD-A290261] p 2523 N95-29169
Thermally stable organic polymers
[AD-A290755] p 2543 N95-29482
AIRCRAFT DESIGN
Rapid Airplane Parametric Input Design (RAPID) p 2479 N95-28730
A grid generation system for multi-disciplinary design optimization p 2484 N95-28763
The effects of design details on cost and weight of fuselage structures p 2499 N95-28831
Global cost and weight evaluation of fuselage keel design concepts p 2499 N95-28840
Cost model relationships between textile manufacturing processes and design details for transport fuselage elements p 2521 N95-29043
A two element laminar flow airfoil optimized for cruise
[NASA-CR-198580] p 2489 N95-29338
Design, analysis and control of large transports so that control of engine thrust can be used as a back-up of the primary flight controls
[NASA-CR-198958] p 2501 N95-30254
Developing a workstation-based, real-time simulation for rapid handling qualities evaluations during design
[NASA-CR-198831] p 2499 N95-30335
AIRCRAFT DETECTION
Long range aircraft detection using high-frequency surface-wave radar
[AD-A290148] p 2555 N95-29313
A least square real time quality control routine for the North Warning Netted Radar System
[AD-A290063] p 2555 N95-29328
Target aircraft identification, trajectory tracking and prediction using regression-based Kalman filter techniques p 2565 N95-29728
AIRCRAFT ENGINES
Surface modeling and grid generation for aeropropulsion CFD p 2479 N95-28732
Model development for active control of stall phenomena in aircraft gas turbine engines p 2500 N95-29679
Characterization of stall inception in high-speed single-stage compressors
[AD-A291275] p 2501 N95-29934
AIRCRAFT EQUIPMENT
Helicopter life substantiation: Review of some USA and UK initiatives
[AD-A290045] p 2495 N95-28851
Development of LaRC (TM): IA thermoplastic polyimide coated aerospace wiring
[NASA-CR-195048] p 2548 N95-30252
SPE(R)-OBOGS: On-board oxygen generating system p 2606 N95-30267
AIRCRAFT FUELS
The effects of aircraft fuel and fluids on the strength properties of Resin Transfer Molded (RTM) composites p 2522 N95-29047
Evaluation of commercial water-in-fuel test kits
[AD-A292135] p 2533 N95-29572
AIRCRAFT GUIDANCE
Wide Area Differential GPS (WADGPS) p 2494 N95-29107
Analytical investigations in aircraft and spacecraft trajectory optimization and optimal guidance
[NASA-CR-4672] p 2504 N95-29339
An investigation into the use of satellite-based positioning systems for flight reference/autoland operations p 2494 N95-29542
AIRCRAFT ICING
An analysis of B-1B exterior jet blast windshield anti-icing performance using pre-cooled compressor bleed air
[AD-A292522] p 2492 N95-28811
Users manual for the improved NASA Lewis ice accretion code LEWICE 1.6
[NASA-CR-198355] p 2492 N95-29132
AIRCRAFT LANDING
An investigation into the use of satellite-based positioning systems for flight reference/autoland operations p 2494 N95-29542
AIRCRAFT MAINTENANCE
The use of electrochemistry and ellipsometry for identifying and evaluating corrosion on aircraft
[AD-A290249] p 2497 N95-29426
AGARD flight test techniques series. Volume 13: Reliability and maintainability
[AGARD-AG-300-VOL-13] p 2498 N95-29503
AIRCRAFT MANEUVERS
Evaluation of proposed agility metrics using X-31 vs. F/A-18 flight data
[AD-A292573] p 2496 N95-28977
AIRCRAFT MODELS
Application of optimization technique to control system design for departure prevention and aircraft model estimation through dynamic inversion p 2501 N95-29156
Design and evaluation of a LQR controller for the bluebird unmanned air vehicle
[AD-A289769] p 2498 N95-29457
AIRCRAFT NOISE
Influence of tooth profile modification on spur gear dynamic tooth strain
[NASA-TM-106952] p 2589 N95-29112
A human factors evaluation of the operational demonstration flight inspection aircraft
[DOT/FAA/AM-95/18] p 2641 N95-29365
AIRCRAFT PERFORMANCE
Evaluation of proposed agility metrics using X-31 vs. F/A-18 flight data
[AD-A292573] p 2496 N95-28977
AIRCRAFT PILOTS
Biodynamic simulation of pilot interaction with a helicopter multiairbag restraint system
[AD-A290196] p 2492 N95-29057
Flying waivers for history of angioplasty and myocardial infraction
[AD-A292505] p 2635 N95-29161
US Army aviation epidemiology data register: Gender-specific attrition among the US Army student aviator class of 1987
[AD-A291856] p 2639 N95-29434
AIRCRAFT RELIABILITY
AGARD flight test techniques series. Volume 13: Reliability and maintainability
[AGARD-AG-300-VOL-13] p 2498 N95-29503
International access to aeromedical evacuation medical equipment assessment data p 2679 N95-29622
AIRCRAFT SAFETY
Biodynamic simulation of pilot interaction with a helicopter multiairbag restraint system
[AD-A290196] p 2492 N95-29057
The effect of wear on fire-blocking layer material effectiveness
[AD-A291520] p 2493 N95-29855
Development of an intervention program to encourage shoulder harness use and aircraft retrofit in general aviation aircraft: Phases 1 and 2
[AD-A290966] p 2493 N95-29873
AIRCRAFT STRUCTURES
Third NASA Advanced Composites Technology Conference, volume 1, part 2
[NASA-CP-3178-VOL-1-PT-2] p 2513 N95-28823
Novel cost controlled materials and processing for primary structures p 2514 N95-28830
Automated fiber placement: Evolution and current demonstrations p 2514 N95-28832
Dimensional stability of curved panels with cocured stiffeners and cobonded frames p 2515 N95-28836
Design and evaluation of a foam-filled hat-stiffened panel concept for aircraft primary structural applications p 2499 N95-28841
A weight-efficient design strategy for cutouts in composite transport structures p 2516 N95-28843
Buckling analysis of curved composite sandwich panels subjected to inplane loadings p 2517 N95-28845
Technology integration box beam failure study p 2517 N95-28847
Advanced composite structural concepts and materials technologies for primary aircraft structures: Advanced material concepts
[NASA-CR-4485] p 2496 N95-29027
Third NASA Advanced Composites Technology Conference, volume 1, part 1
[NASA-CP-3178-VOL-1-PT-1] p 2518 N95-29029
Impact of composites on future transport aircraft p 2519 N95-29030
Challenges and payoff of composites in transport aircraft: 777 empennage and future applications p 2519 N95-29031
Weavability of dry polymer powder towpreg p 2519 N95-29036
Mechanical characterization of 2D, 2D stitched, and 3D braided/RTM materials p 2520 N95-29038
Performance of resin transfer molded multiaxial warp knit composites p 2520 N95-29039
Cost model relationships between textile manufacturing processes and design details for transport fuselage elements p 2521 N95-29043
Development of RTM and powder prepreg resins for subsonic aircraft primary structures p 2521 N95-29044
Progress in manufacturing large primary aircraft structures using the stitching/RTM process p 2522 N95-29050
Innovative processing of composites for ultra-high temperature applications, book 1
[AD-A290889] p 2527 N95-29842
AIRCRAFT WAKES
A numerical method for modelling wings with sharp edges maneuvering at high angles of attack p 2496 N95-29122
AIRFOIL OSCILLATIONS
Dynamic stall of a NACA 0012 airfoil in laminar flow p 2489 N95-29243
Compressibility effects on and control of dynamic stall of oscillating airfoil
[AD-A291804] p 2489 N95-29428
AIRFOIL PROFILES
A fourth order Euler/Navier-Stokes prediction method for the aerodynamics and aeroelasticity of hovering rotor blades p 2572 N95-29242
Introduction to the estimation of the lift coefficients at zero angle of attack and at maximum lift for aerofoils with high-lift devices at low speeds
[ESDU-94026] p 2491 N95-29899
AIRFOILS
Increments in aerofoil lift coefficient at zero angle of attack and in maximum lift coefficient due to deployment of a plain trailing-edge flap, with or without a leading-edge high-lift device, at low speeds
[ESDU-94028] p 2486 N95-28885
PIV investigation of compressibility effects on dynamic stall p 2487 N95-29102
Finite element vorticity-based methods for the solution of the incompressible and compressible Navier-Stokes equations p 2570 N95-29119
Increments in aerofoil lift coefficient at zero angle of attack and in maximum lift coefficient due to deployment of a trailing-edge split flap, with or without a leading-edge high-lift device, at low speeds
[ESDU-94029] p 2488 N95-29129
Dynamic stall of a NACA 0012 airfoil in laminar flow p 2489 N95-29243
Acoustic scattering from ellipses by the modal element method
[NASA-TM-106935] p 2683 N95-29401

The decay of longitudinal vortices shed from airfoil vortex generators
[NASA-CR-198356] p 2489 N95-29402
Compressibility effects on and control of dynamic stall of oscillating airfoil
[AD-A291804] p 2489 N95-29428
Increments in aerofoil lift coefficient at zero angle of attack and in maximum lift coefficient due to deployment of various leading-edge high-lift devices at low speeds
[ESDU-94027] p 2490 N95-29898
Introduction to the estimation of the lift coefficients at zero angle of attack and at maximum lift for aerofoils with high-lift devices at low speeds
[ESDU-94026] p 2491 N95-29899
An interacting boundary layer method for unsteady compressible flows p 2579 N95-30290
Growth and development of roughness-induced stationary crossflow vortices p 2492 N95-30294

AIRFRAMES
Cross-stiffened continuous fiber structures p 2521 N95-29041

AIRGLOW
A ground support electronic interface for the ionospheric spectroscopy and atmospheric chemistry (ISAAC) ultraviolet spectrograph
[AD-A289761] p 2611 N95-28693

AIRPORT TOWERS
Terminal area forecasts-fiscal years 1993-2010
[AD-A290835] p 2495 N95-29880

AIRPORTS
Terminal area forecasts-fiscal years 1993-2010
[AD-A290835] p 2495 N95-29880
Evaluation of retro-reflective beads in airport pavement markings
[AD-A291065] p 2502 N95-29967
Prototype stop bar system evaluation at Seattle-Tacoma International Airport
[AD-A290136] p 2495 N95-30031

AIRSPACE
Three-D weather displays for aircraft cockpits
[AD-A289759] p 2499 N95-28691

AIRY FUNCTION
Airy functions and the recursive ray acoustics algorithm
[AD-A290182] p 2629 N95-29054

ALBEDO
Variation in visual and near-infrared contrast with a snow background
[AD-A289710] p 2697 N95-28778
Energy budget in the Asian monsoon region p 2623 N95-29713

ALCOHOLS
Super hydrides
[AD-A290594] p 2533 N95-29556

ALGAE
Measuring variation in ecosystem sensitivity to stress
[AD-A290415] p 2609 N95-29450

ALGEBRA
Discontinuous solutions of semilinear differential-algebraic equations. part 2: Rho-consistency
[AD-A292285] p 2668 N95-28861
New methods for nonlinear optimization
[AD-A290522] p 2670 N95-29385
Linear algebraic computation on distributed memory parallel machines
[AD-A290615] p 2671 N95-29558
Fischer's protocol in timed process algebra
[PB95-206777] p 2672 N95-30089
Process algebra with feedback
[PB95-206819] p 2673 N95-30106

ALGORITHMS
Analysis of multigrid techniques for system modeling with toeplitz approximation
[AD-A289784] p 2644 N95-28694
Electromagnetic scattering by magnetic spheres: Theory and algorithms
[AD-A289798] p 2551 N95-28699
Algorithms for high aspect ratio oriented triangulations p 2479 N95-28731
Development and application of a 3D Cartesian grid Euler method p 2481 N95-28740
Emerging CFD technologies and aerospace vehicle design p 2482 N95-28746
Algorithms for the automatic generation of 2-D structured multi-block grids p 2483 N95-28757
Abstract models of memory management
[AD-A292238] p 2721 N95-28877
Competitive analysis of call admission algorithms that allow delay
[AD-A292242] p 2645 N95-28878
Structural cut elimination in linear logic
[AD-A292248] p 2645 N95-28886
An HP-Adaptive method in space and time for parabolic systems
[AD-A292262] p 2668 N95-28890
An algorithm fusion approach to IRST signal processing (III): Nongaussian-corrected filter fusion
[AD-A291565] p 2552 N95-28936
Optimal control of molecular motion
[AD-A291919] p 2691 N95-28944
Glenda software design
[AD-A292537] p 2646 N95-28968
Development of the theory and algorithms for synthesis of reflector antenna systems
[AD-A292579] p 2552 N95-28979
Airy functions and the recursive ray acoustics algorithm
[AD-A290182] p 2629 N95-29054
Visualization of improved target acquisition algorithm for Janus (A)
[AD-A290191] p 2646 N95-29056
Optimizing cockpit display configurations with a genetic algorithm system
[AD-A289799] p 2499 N95-29123
Inductive boolean function manipulation: A hardware verification methodology for automatic induction
[AD-A292236] p 2669 N95-29128
Stable function approximation in dynamic programming
[AD-A290224] p 2647 N95-29143
Proceeding of the 33rd SICE Annual Conference
[DE95-758943] p 2662 N95-29144
Efficient compilation of high-level data parallel algorithms
[AD-A290362] p 2659 N95-29225
High performance electromagnetic simulation tools
[AD-A290405] p 2554 N95-29235
Research in graph algorithms and combinatorial optimization
[AD-A292630] p 2648 N95-29297
The (in)complete compendium of computational curiosities: Givens' rotations
[AD-A292050] p 2648 N95-29304
Performance and robustness of self-tuning and adaptation algorithms for identification, filtering and control
[AD-A292070] p 2648 N95-29310
Computational complexity and encryption
[AD-A291910] p 2648 N95-29356
Acoustic scattering from ellipses by the modal element method
[NASA-TM-106935] p 2683 N95-29401
The large discretization step method for time-dependent partial differential equations
[NASA-CR-195068] p 2670 N95-29403
Parallel adaptive techniques for transient partial differential equations
[AD-A290460] p 2674 N95-29490
Robust algorithms for penetration mechanics problems
[AD-A290650] p 2650 N95-29517
Estimation of unstabilized components in vehicular motion
[AD-A290580] p 2590 N95-29552
Linear algebraic computation on distributed memory parallel machines
[AD-A290615] p 2671 N95-29558
Signal processing for high-resolution image formation
[AD-A290648] p 2557 N95-29563
High-performance speech recognition using consistency modeling
[AD-A290655] p 2557 N95-29564
Oblivious decision trees and abstract cases
[AD-A292577] p 2664 N95-29574
Bootstrap and partitioning methods
[AD-A290662] p 2671 N95-29578
Scheduling algorithms for mobile packet radio networks p 2558 N95-29707
Microwave remote sensing algorithms for cirrus clouds and precipitation p 2623 N95-29715
Neural network construction using evolutionary search
[AD-A290862] p 2665 N95-29831
Computational algorithms for aerodynamic analysis and design
[AD-A291084] p 2491 N95-29972
Computational results for parallel unstructured mesh computations
[DE95-005856] p 2659 N95-29985
Reliability enhancement of Navier-Stokes codes through convergence acceleration
[NASA-CR-196635] p 2578 N95-30034
Optimal hankel norm identification of dynamical systems
[PB95-197232] p 2672 N95-30046
Huge data sets and the frontiers of computational feasibility
[AD-A291384] p 2653 N95-30063
Efficient solution of a class of infinite stochastic petri nets: Theory and applications
[PB95-197166] p 2673 N95-30097
Fast simulation of the leaky bucket algorithm
[PB95-197174] p 2653 N95-30098
Layers as knowledge transitions in the design of distributed systems
[PB95-197638] p 2660 N95-30104
Boyer-moore type algorithm for regular expression pattern matching
[PB95-198131] p 2654 N95-30107
Application of traditional CFD methods to nonlinear computational aeroacoustics problems p 2688 N95-30148
Application of a new finite difference algorithm for computational aeroacoustics p 2689 N95-30155
Category 5 problem solution using an unstructured finite volume algorithm p 2657 N95-30157
Load-balancing algorithms for the parallel community climate model
[DE95-008795] p 2610 N95-30176
Patch diameter limits for tiered subaperture SAR image formation algorithms
[DE95-008816] p 2560 N95-30177
Enhancing the semantics of federated schemata by translating SQ1-queries into object methods
[PB95-197372] p 2725 N95-30208

ALIGNMENT
An electrical and fiber-optic connector
[AD-D017404] p 2589 N95-28791

ALIPHATIC HYDROCARBONS
Viscosity of liquids: Aliphatic and cyclic ketones
[ESDU-94025] p 2530 N95-28712
Thermal conductivity of liquid halogenated aliphatic hydrocarbons. Part 4: Halogenated alkenes and dienes (C1 to C4)
[ESDU-94024-PT-4] p 2511 N95-28803
Thermal conductivity of liquid halogenated aliphatic hydrocarbons. Part 1: Halogenated methanes and azeotropic mixtures
[ESDU-94021-PT-1] p 2511 N95-28804
Thermal conductivity of liquid halogenated aliphatic hydrocarbons. Part 2: Halogenated ethanes
[ESDU-94022] p 2512 N95-29017
Thermal conductivity of liquid halogenated aliphatic hydrocarbons. Part 3: Halogenated higher hydrocarbons (C3 to C16)
[ESDU-94023-PT-3] p 2512 N95-29900

ALKALI METALS
The physics of spin polarized gases
[AD-A292511] p 2680 N95-28810
Theoretical investigation of superconductivity in doped fullerenes
[AD-A291942] p 2562 N95-29018
High temperature spectroscopy of alkali metal vapors for solar to thermal energy conversion
[AD-A291355] p 2602 N95-29949

ALKALIES
Development of Laser Optogalvanic Spectroscopy as a probe of alkali atoms in an MHD environment
[DE95-006481] p 2531 N95-28916

ALKENES
Thermal conductivity of liquid halogenated aliphatic hydrocarbons. Part 4: Halogenated alkenes and dienes (C1 to C4)
[ESDU-94024-PT-4] p 2511 N95-28803
Transition metal complexes with perfluorinated ligands
[AD-A290250] p 2536 N95-29427

ALKOXIDES
Recent progress in the study of the kinetics of sol-gel SiO2 synthesis reactions
[AD-A290570] p 2544 N95-29551

ALKYL COMPOUNDS
Super hydrides
[AD-A290594] p 2533 N95-29556
Vapour pressures and critical points of liquids. Glycol ethers (alkyl cellosolves and carbitols, etc.)
[ESDU-95004] p 2534 N95-29901

ALKYNES
New tetraarylborate and ethyldibutylstannane reagents
[AD-A289813] p 2540 N95-28953

ALLOYING
The effects of alloying elements on the strength and cooling rate sensitivity of ultra-low carbon alloy steel weld metals
[AD-A290681] p 2537 N95-29759

ALLOYS
Gordon research conference on physical metallurgy: Materials by design
[AD-A290519] p 2524 N95-29326

ALTERNATING CURRENT
Corona tests of prototype connector
[AD-A292542] p 2561 N95-28971
Five-channel SQUID based non-destructive evaluation (NDE) instrument
[AD-A292474] p 2592 N95-29012
Hot electron physics of alternating-current thin-film electroluminescent devices
[AD-A290528] p 2696 N95-29495

A system for conveniently providing load testing termination of an AC power source having at least one battery
[AD-D017408] p 2566 N95-30075

ALTERNATIVES
QUEST2: System architecture deliverable set
[DE95-008427] p 2721 N95-28958
Alternative refrigerant performance: Field test of a nonchlorofluorocarbon chiller at Fort Leonard Wood, MO
[AD-A292052] p 2550 N95-29307
Use of chlorofluorocarbon-based refrigerants in USArmy facility air-conditioning and refrigeration systems: Recommendations for the interim period 1994-2000
[AD-A290432] p 2550 N95-29537

ALTITUDE
Investigation and characterization of SEU effects and hardening strategies in avionics
[AD-A291058] p 2500 N95-29950

ALUMINATES
Analytical electron microscopy of precipitates in ion-implanted MgAl2O4 spinel
[DE95-007406] p 2538 N95-30038

ALUMINUM
Nitride semiconductors for ultraviolet detection
[AD-A289546] p 2712 N95-28910
Advanced manufacturing by spray forming: Aluminum strip and microelectromechanical systems
[DE95-008615] p 2536 N95-28959
Effects of space exposure on metals flown on the Long Duration Exposure Facility
[NASA-CR-4662] p 2512 N95-30225
Engineering development program of a closed aluminum-oxygen semi-cell system for an unmanned underwater vehicle: An update p 2606 N95-30266
Hermetically sealed aluminum electrolytic capacitor p 2568 N95-30268
Analysis of stress concentration in the Dutton groove regions of the Super Lightweight External Tank
[NASA-TM-108490] p 2597 N95-30328
Composite processing development to improve interlaminar strength using ply interface particles
[NASA-TM-108495] p 2529 N95-30334

ALUMINUM ALLOYS
Crystal field and exchange interactions in DyT4Al8 (T = Fe and Mn)
[DE95-007131] p 2714 N95-29134
Origins of imperfections in composite materials
[AD-A290261] p 2523 N95-29169
The use of electrochemistry and ellipsometry for identifying and evaluating corrosion on aircraft
[AD-A290249] p 2497 N95-29426
Visit to the Department of Metallurgical Engineering, Tokyo Institute of Technology, 22 Sep. 1994
[AD-A292310] p 2536 N95-29473
Center for Advanced Aerospace Materials (CAAM), Seoul National University, 29 June 1994
[AD-A292344] p 2525 N95-29476
Examination of dislocation core structures in B2 intermetallic alloys
[AD-A291486] p 2537 N95-29526
Chemically induced passivity of aluminum alloys and Al-based metal matrix composites
[AD-A290778] p 2528 N95-29923
The mm-wave resonant methods for the detection of corrosion, phase 1
[AD-A291315] p 2593 N95-29941
Electrochemical impedance pattern recognition for detection of hidden chemical corrosion on aircraft components, phase 1
[AD-A291345] p 2593 N95-29946
Influence of dislocation-solute interactions on the mechanical properties of zirconium-doped NiAl
[DE95-008848] p 2538 N95-30179
Tensile properties of as-cast iron-aluminide alloys
[DE95-005396] p 2538 N95-30216

ALUMINUM ARSENIDES
Development of ultra-low dark current, high performance 3-5 quantum well infrared photodetectors (QWIPs) for focal plane arrays staring imaging sensor systems
[AD-A290343] p 2714 N95-29089

ALUMINUM COATINGS
Materials for tomorrow's infrastructure: A ten-year plan for deploying high-performance construction materials and systems
[AD-A289782] p 2526 N95-29598

ALUMINUM COMPOUNDS
Dynamic decohesion of bimaterial interfaces p 2541 N95-29120

ALUMINUM GALLIUM ARSENIDES
Low threshold all-optical crossbar switch on GaAs-GaAlAs channel waveguide arrays
[AD-A292483] p 2712 N95-28862
Investigation of a normal incident high performance P-type strained layer In(0.3)Ga(0.7)As/In(0.52)Al(0.48)As quantum well infrared photodetector
[AD-A290946] p 2716 N95-29785
Ion doped quantum well lasers
[AD-A290937] p 2587 N95-29912
Vacuum microelectronic emitters and their applications using compound semiconductor technology
[AD-A291142] p 2567 N95-30124

ALUMINUM NITRIDES
Integrated synthesis and post-processing of SiC and AlN
[AD-A290853] p 2537 N95-29724

ALUMINUM OXIDES
Overview of the space debris environment
[AD-A292302] p 2507 N95-28867
Demonstration of a stabilized alumina/ethanol colloidal dispersion technique for seeding high temperature air flows
[NASA-TM-106945] p 2582 N95-29113
Experimental investigations of wave and fracture phenomena in impacted ceramics and glasses
[AD-A292142] p 2542 N95-29195
Analytical electron microscopy of precipitates in ion-implanted MgAl2O4 spinel
[DE95-007406] p 2538 N95-30038
Alumina reinforced Tetragonal Zirconia (TZP) composites
[DE95-008990] p 2529 N95-30180

AMBERLITE (TRADEMARK)
New tetraarylborate and ethyldibutylstannane reagents
[AD-A289813] p 2540 N95-28953

AMBULANCES
Flying ambulances: The approach of a small air force to long distance aeromedical evacuation of critically injured patients p 2678 N95-29618

AMINES
Photogenerated amines in the design of imaging materials: The radiation-induced imidization of functionalized polystyrenes bearing amide-ester side chains
[AD-A289943] p 2542 N95-29270
Photogenerated amines in polymer curing and imaging: Design and synthesis of (3', 5'-dimethoxybenzoinyl)oxycarbonyl carbamates as novel photoprecursors of amines
[AD-A289945] p 2542 N95-29272

AMMONIA
Thickness measurement of ammonia targets used in SLAC e143 experiment
[AD-A290215] p 2692 N95-29076

AMORPHOUS MATERIALS
Ferroelectric polarization mechanism of the odd-numbered nylons
[AD-A292276] p 2539 N95-28860
Neutron scattering from amorphous, disordered and nanocrystalline materials
[DE95-005848] p 2717 N95-30077

AMPLIFICATION
Liquid pressure amplification and liquid injection in air conditioning and refrigeration systems
[AD-A289738] p 2549 N95-28686

AMPLIFIERS
A kilohertz femtosecond Ti: Sapphire regeneratie amplifier
[AD-A290591] p 2588 N95-30045

AMPLITUDE MODULATION
An ultra-high speed incoherent-to-coherent converter for optical computing
[AD-A292658] p 2700 N95-29412

ANAEROBES
Adaptations to three weeks of aerobic/anaerobic training in west coast U.S: Navy Sea-Air-Land personnel (SEAL's)
[AD-A291500] p 2637 N95-29846

ANALOG COMPUTERS
A comparison of three pedestal removal techniques for an optical time-integrating correlator
[AD-A290092] p 2700 N95-29354

ANALOG DATA
Computing 3-D motion in custom analog and digital VLSI
[AD-A290270] p 2647 N95-29179

ANALOG SIMULATION
Simulated imaging properties of a series of magnetic electron lenses
[NASA-CR-195474] p 2564 N95-29406

ANALOG TO DIGITAL CONVERTERS
High resolution direct digitization and optical telemetry of shipboard antenna signals
[AD-A290238] p 2557 N95-29504
Wideband I/Q demodulators: Measurement technique and matching characteristics
[AD-A291505] p 2558 N95-29847

ANALYTICAL CHEMISTRY
The redox chemistry of some peroxo and superoxo metal ion complexes
[AD-A290761] p 2532 N95-29483

ANGLE OF ATTACK
A nonintrusive method of quantifying flow visualization data in vortex flow fields
[AD-A289802] p 2568 N95-28948
A numerical method for modelling wings with sharp edges maneuvering at high angles of attack p 2496 N95-29122
The 1995 version of the NSWC aeroprediction code. Part 1: Summary of new theoretical methodology
[AD-A291518] p 2490 N95-29853
Low-speed wind-tunnel investigation of the stability and control characteristics of a series of flying wings with sweep angles of 50 deg
[NASA-TM-4640] p 2498 N95-30226

ANGULAR MOMENTUM
The role of diabatic heating, torques and stability in forcing the meridional circulation within cyclones p 2626 N95-29834

ANHYDRIDES
Photogenerated amines in the design of imaging materials: The radiation-induced imidization of functionalized polystyrenes bearing amide-ester side chains
[AD-A289943] p 2542 N95-29270

ANIONS
New tetraarylborate and ethyldibutylstannane reagents
[AD-A289813] p 2540 N95-28953
Inorganic halogen oxidizers
[AD-A290747] p 2533 N95-29581
Preparation and studies of urazole containing polymers
[AD-A290685] p 2545 N95-29586
Inorganic halogen oxidizers
[AD-A291201] p 2702 N95-29974
Effect of KOH concentration and anions on the performance of Ni-H2 battery positive plate p 2567 N95-30260

ANISOTROPIC MEDIA
The Stroh formalism for anisotropic elasticity with applications to composite materials
[AD-A290710] p 2527 N95-29763
Static field solutions and image theory for a conducting sphere with radial anisotropy
[PB95-207171] p 2673 N95-30172

ANISOTROPIC PLATES
Sensitivity of stress and boundary imperfection of dielectric resonator disks
[AD-A290488] p 2594 N95-29150

ANISOTROPY
Interaction of turbulence with complex shock waves
[AD-A290225] p 2571 N95-29145
The spatial-scale dependence of the observed anisotropy of reflected and emitted radiation p 2613 N95-29253
Theoretical, experimental and computational studies in plasticity
[AD-A290428] p 2595 N95-29535
Membrane fluidity and shape of human red blood cells are altered by physiological levels of hydrostatic pressure
[AD-A290595] p 2636 N95-29557
Severe edge effects and simple complimentary interior solutions for thin-walled anisotropic and composite structures
[AD-A290645] p 2595 N95-29562
Mapping crust and upper mantle structure beneath southern Eurasia
[AD-A291074] p 2618 N95-29970
Static field solutions and image theory for a conducting sphere with radial anisotropy
[PB95-207171] p 2673 N95-30172

ANNEALING
Formation of striped surface phases by short-range forces
[AD-A279962] p 2531 N95-28945
Interface properties of wide bandgap semiconductor structures
[AD-A289817] p 2713 N95-28954

ANNIHILATION REACTIONS
Activities update
[AD-A292431] p 2692 N95-28994
Lattice/beam dynamics working group
[DE95-006774] p 2696 N95-30021

ANNOTATIONS
Annotated bibliography of software engineering laboratory literature
[NASA-CR-189406] p 2644 N95-28805
Visual and auditory symbols: A literature review
[AD-A290222] p 2641 N95-29908
A bibliography, with abstracts and annotations, of publications on and related to underwater acoustic fluctuations
[AD-A291342] p 2685 N95-29945

ANNUAL VARIATIONS
Measurement of the seasonal and annual variability of total column aerosol in a northeastern US network
[DE95-007259] p 2608 N95-28920
Analysis of tropospheric propagation characteristics based on regional meteorological data
[AD-A291581] p 2552 N95-28939
Hydrology of the continental United States
p 2599 N95-29539
The high latitude ionospheric convection pattern during northward interplanetary magnetic field
p 2615 N95-29693
Energy budget in the Asian monsoon region
p 2623 N95-29713

ANNULAR FLOW
Condensation inside tubes: Condensate film coefficient in horizontal tubes
[ESDU-94041] p 2569 N95-29015

ANOMALIES
Forecast of Atlantic seasonal hurricane activity for 1995 p 2620 N95-29254
Automated Propulsion Data Screening demonstration system
[NASA-CR-196636] p 2510 N95-29584

ANTARCTIC REGIONS
NASA to use telepresence to explore Antarctic Lakes
[NASA-TM-110567] p 2598 N95-29175
Upper-air data collected on Ice Station Weddell
[AD-A289707] p 2620 N95-29193

ANTENNA ARRAYS
An investigation of the channel crosstalk in optical heterodyne controlled phased array radars
[AD-A292028] p 2554 N95-29186
Fabrication and characterization of BSTO and nonferroelectric oxide composites for use in phased array antennas and other electronic devices
[AD-A290070] p 2524 N95-29329

ANTENNA DESIGN
Low cost writable RFID tag with MRAM memory
[AD-A292553] p 2642 N95-28974
Development of the theory and algorithms for synthesis of reflector antenna systems
[AD-A292579] p 2552 N95-28979
Electromagnetic antenna modeling (EAM) system
[AD-A292194] p 2552 N95-28986
High resolution direct digitization and optical telemetry of shipboard antenna signals
[AD-A290238] p 2557 N95-29504

ANTENNA RADIATION PATTERNS
Development of the theory and algorithms for synthesis of reflector antenna systems
[AD-A292579] p 2552 N95-28979

ANTENNAS
The 10th Annual Review of Progress in Applied Computational Electromagnetics, volume 1
[AD-A286796] p 2553 N95-29159

ANTHROPOMETRY
An analysis of anthropometric differences among occupational groups in the US Army
[AD-A292326] p 2640 N95-28794
Operating procedures for Anthropometry and Initial Conditions Photogrammetric Program
[AD-A291553] p 2640 N95-28935
A human factors evaluation of the operational demonstration flight inspection aircraft
[DOT/FAA/AM-95/18] p 2641 N95-29365

ANTIFERROMAGNETISM
Correlations between micromagnetic, microstructural and microchemical properties in ultrathin epitaxial magnetic structures
[AD-A289705] p 2712 N95-28681

ANTIGRAVITY
Experimental results of Hooper's gravity-electromagnetic coupling concept
[NASA-TM-106963] p 2680 N95-28893

ANTIPROTONS
Activities update
[AD-A292431] p 2692 N95-28994
Measurements of (Delta)(sigma)(sub L)(pp) and (Delta)(sigma)(sub L)((bar p)p) at 200 GeV/c
[DE95-005837] p 2695 N95-30186

ANTIREFLECTION COATINGS
Diffractive optics: Design, fabrication, and applications
[AD-A290942] p 2702 N95-29867

ANTISUBMARINE WARFARE
Wavelets in signal detection and identification comparative signal processing technology evaluation
[AD-A291952] p 2552 N95-28984

APOLLO 11 FLIGHT
Apollo 11: For all mankind
[NASA-TM-110622] p 2503 N95-29407

APOLLO 14 FLIGHT
Apollo 14: Shepard hitting golf ball on Moon
[NASA-TM-110638] p 2737 N95-30318

APPLICATIONS OF MATHEMATICS
Nearest neighbor analysis in one dimension
[DE95-009376] p 2654 N95-30183

APPLICATIONS PROGRAMS (COMPUTERS)
Ejectors and jet pumps: Computer program for design and performance for steam/gas flow
[ESDU-94046] p 2495 N95-28704
Computer program for estimation of leading-edge suction distribution for plane thin wings at subsonic speeds
[ESDU-94038] p 2477 N95-28708
The prediction of sound attenuation as a result of propagation close to the ground
[ESDU-94036] p 2682 N95-28709
The correction of measured noise spectra for the effects of ground reflection
[ESDU-94035] p 2683 N95-28710
Dimensions, deflections and stresses for Hertzian contacts under combined normal and tangential loading. (Guide to use of computer program A9434.)
[ESDU-94034] p 2593 N95-28711
Cooperative solutions coupling a geometry engine and adaptive solver codes p 2484 N95-28761
Automation of three-dimensional structured mesh generation for turbomachinery blade passages
p 2484 N95-28762
Advanced methodology for simulation of complex flows using structured grid systems p 2485 N95-28766
A procedure for automating CFD simulations of an inlet-bleed problem p 2485 N95-28768
GridTool: A surface modeling and grid generation tool
p 2486 N95-28773
NASA-IGES Translator and Viewer
p 2486 N95-28775
Flat rectangular isotropic plates under uniformly distributed normal pressure. Elastic deflections, stresses, and strains, moments and forces, for various forms of edge restraint
[ESDU-94033] p 2593 N95-28801
Impact of Ada and object-oriented design in the flight dynamics division at Goddard Space Flight Center
[NASA-CR-189412] p 2644 N95-28807
ISPAN (Interactive Stiffened Panel Analysis): A tool for quick concept evaluation and design trade studies
p 2517 N95-28846
Analysis of historical oceanographic data on a minicomputer: Program WAHOO
[AD-A292530] p 2629 N95-28873
MATSurv multisensor air traffic surveillance
[AD-A292253] p 2494 N95-28887
Through-the-thickness stresses and failure in the corner radius of a laminated composite section
[ESDU-94019] p 2518 N95-28899
Lubricant film thickness between disc cams and followers
[ESDU-94008] p 2539 N95-28900
Contact stress in disc cams with domes of flat-faced followers
[ESDU-94011] p 2589 N95-28901
Application of parallel processing technology in complex helicopter analysis. Phase 1
[NASA-CR-197850] p 2496 N95-28928
WinCD: Complex demodulation time-series analysis for windows
[AD-A291550] p 2645 N95-28934
Molecular dynamics study of electromigration
[AD-A289811] p 2691 N95-28952
Electromagnetic antenna modeling (EAM) system
[AD-A292194] p 2552 N95-28986
A formative evaluation of CU-SeeMe
[AD-A292443] p 2553 N95-29002
Estimating attenuation and propagation of noise bands from a distant source using the lookup program and data base
[AD-A290218] p 2683 N95-29077
Closed loop control of guided missiles using neural networks p 2663 N95-29241
Macroprocesses and adaptive instruction
[AD-A290483] p 2648 N95-29325
Gordon research conference on physical metallurgy: Materials by design
[AD-A290519] p 2524 N95-29326
Fiber-matrix adhesion in single-fiber model composites
p 2524 N95-29337
Ceramic material life prediction: A program to translate ANSYS results to CARES/LIFE reliability analysis
[NASA-CR-198795] p 2543 N95-29367
Development of a rotary wing Navier-Stokes CFD code based on TLNS3D code
[AD-A290421] p 2574 N95-29387
Design and evaluation of a LQR controller for the bluebird unmanned air vehicle
[AD-A289769] p 2498 N95-29457
GENAH user's guide and reference manual version 1.0
[AD-A290236] p 2583 N95-29470
Linear matrix inequalities for the problem of absolute stability of control systems p 2501 N95-29680
SEMINT: Seamless model integration
[AD-A290956] p 2651 N95-29736
The study of non-Newtonian contraction flows with a parallel finite element method p 2576 N95-29778
ANSYS duplicate finite-element checker routine
[NASA-TM-108492] p 2672 N95-29824
Training end-users on database queries: The effectiveness of example format and spatial ability on learing outcomes p 2724 N95-29829
Meteorological Satellite Center technical note, no. 28, 1994
[JTN-95-80926] p 2626 N95-29849
The 1995 version of the NSWC aeroprediction code. Part 1: Summary of new theoretical methodology
[AD-A291518] p 2490 N95-29853
Finite difference ocean acoustic model users guide
[AD-A291544] p 2631 N95-29856
State-of-the-art review of computational fluid dynamics modeling for fluid-solids systems
[DE95-005866] p 2577 N95-29988
High-frequency radar target modeling
[AD-A290965] p 2559 N95-29991
Analysis of shadowing effects on spacecraft power systems
[NASA-TM-106994] p 2511 N95-30012
Testing of the ENDF/B-VI neutron data library ENDF60 for use with MCNP(trademark)
[DE95-007858] p 2696 N95-30057
A PC program for estimating measurement uncertainty for aeronautics test instrumentation
[NASA-CR-198361] p 2503 N95-30067
The topside ionospheric plasma monitor (SSIES, SSIES-2 and SSIES-3) on the spacecraft of the Defense Meteorological Satellite Program (DMSP), user's guide. Volume 2: Programmer's guide for software at AFSFC
[AD-A290913] p 2618 N95-30082
Description and manipulation of method fragments for the assembly of situational methods
[PB95-197133] p 2653 N95-30094
Checkpointing and the modeling of program execution time
[PB95-197182] p 2653 N95-30099
Framework for comparing and controlling number-based design reasoning systems
[PB95-197364] p 2667 N95-30207

APPROXIMATION
Analysis of multigrid techniques for system modeling with toeplitz approximation
[AD-A289784] p 2644 N95-28694
International Workshop on Stochastic Filtering Theory
[AD-A291670] p 2661 N95-28788
Stable function approximation in dynamic programming
[AD-A290224] p 2647 N95-29143
Research in graph algorithms and combinatorial optimization
[AD-A292630] p 2648 N95-29297
Multivariate wavelet representations and approximations
[AD-A290147] p 2670 N95-29312
Three problems in fluid dynamics
[AD-A290481] p 2573 N95-29324
New methods for nonlinear optimization
[AD-A290522] p 2670 N95-29385
The large discretization step method for time-dependent partial differential equations
[NASA-CR-195068] p 2670 N95-29403
Modeling the boundary layer interactions between weakly ionized plasmas and cooled, planar electrodes in stagnation-point flows p 2706 N95-29717
Optimal hankel norm identification of dynamical systems
[PB95-197232] p 2672 N95-30046
PREDICHAT: First order performance calculations of windturbine rotors using the method of the acceleration potential
[PB95-206454] p 2603 N95-30200
Emissivity measurements in thin metallized membrane reflectors used for microwave radiometer sensors
[NASA-TM-110179] p 2506 N95-30251

AQUEOUS SOLUTIONS
Polymeric microcapsule arrays
[AD-A291937] p 2539 N95-28850
The fluorescent detection of hydrazine, monomethylhydrazine, and 1,1-dimethylhydrazine by derivatization with aromatic dicarboxaldehydes
[NAVY-CASE-75451] p 2512 N95-29052
Prediction of hydrogen entry and permeation in metals and alloys
[AD-A292047] p 2536 N95-29298
The redox chemistry of some peroxo and superoxo metal ion complexes
[AD-A290761] p 2532 N95-29483

Preparation and studies of urazole containing polymers
[AD-A290685] p 2545 N95-29586

ARC JET ENGINES
Multifluid nonequilibrium simulation of arcjet thrusters
p 2510 N95-29245

ARC LAMPS
Design of a more accurate, higher fidelity, dual-source air mass zero solar simulator
[AD-A291364] p 2603 N95-29953

ARCHITECTURE
UMTS network architecture
[PB95-206744] p 2558 N95-29919
Framework for comparing and controlling number-based design reasoning systems
[PB95-197364] p 2667 N95-30207

ARCHITECTURE (COMPUTERS)
Analysis of the naval postgraduate school computer network architecture
[AD-A289749] p 2657 N95-28689
Abstract models of memory management
[AD-A292238] p 2721 N95-28877
The scotch parallel storage systems
[AD-A292243] p 2658 N95-28879
Formalizing style to understand descriptions of software architecture
[AD-A292237] p 2645 N95-28894
Using object-oriented database technology to develop a multiple domain capability for domain-oriented application composition systems
[AD-A289244] p 2721 N95-28907
QUEST2: System architecture deliverable set
[DE95-008427] p 2721 N95-28958
N4 processor
[AD-A292571] p 2642 N95-28976
An architectural design of a toolkit for synchronous groupware applications
[AD-A290226] p 2642 N95-29146
Porting a vector library: A comparison of MPI, paris, CMMD and PVM (or, 'I'll never have to port CVL again')
[AD-A290231] p 2647 N95-29147
Implementing distributed server groups for the World Wide Web
[AD-A292221] p 2658 N95-29196
Interface for the translation of sentences in a natural language into a geometrical representation language
[INPE-5467-PRE/1775] p 2722 N95-29363
Characteristics of higher-level languages for software architecture
[AD-A292215] p 2649 N95-29376
The mesh synchronous processor MeshSP (trademark)
[AD-A289875] p 2659 N95-29420
Towards an example-based image compression architecture for video-conferencing
[AD-A290041] p 2556 N95-29441
The design of programmable convolutional encoder using VHDL and an FPGA
[AD-A290048] p 2649 N95-29442
High-level fault tolerance in distributed programs
[AD-A290430] p 2724 N95-29818
Neural network construction using evolutionary search
[AD-A290862] p 2665 N95-29831
PSEE architecture report: Architectures and models for next generation process-based software engineering environments
[AD-A291268] p 2652 N95-29996
Workshop on computing and intelligent systems
[AD-A290581] p 2666 N95-30040
Requirements for a portable parallel I/O library for scientific computation
[DE95-009383] p 2660 N95-30192

ARCTIC OCEAN
Sea ice motions in the Central Arctic pack ice as inferred from AVHRR imagery
[NASA-CR-198835] p 2601 N95-30247

ARCTIC REGIONS
Studies of thermospheric neutral winds utilizing ground-based optical and radar measurements
p 2613 N95-29214
Characterization of the geometries of the high-latitude ionospheric convection pattern p 2614 N95-29524
Sea ice motions in the Central Arctic pack ice as inferred from AVHRR imagery
[NASA-CR-198835] p 2601 N95-30247

ARGON
Modeling the boundary layer interactions between weakly ionized plasmas and cooled, planar electrodes in stagnation-point flows p 2706 N95-29717

ARMED FORCES
The Environmental Assessment and Management (TEAM) guide
[AD-A286748] p 2608 N95-28787

ARMED FORCES (FOREIGN)
Experiences learned from the Spanish armed forces aeromedical evacuation system in the former Yugoslavia
p 2677 N95-29614

ARMED FORCES (UNITED STATES)
US Army aviation epidemiology data register: Gender-specific attrition among the US Army student aviator class of 1987
[AD-A291856] p 2639 N95-29434

ARMOR
Characterizing and modeling penetration of ceramic armor
[AD-A292588] p 2542 N95-29288
Penetration of semi-infinite, bi-element targets by long rod penetrators
[AD-A291176] p 2596 N95-29929

ARPA COMPUTER NETWORK
ARPA solid state laser and nonlinear materials program
[AD-A289657] p 2584 N95-28678
High-performance speech recognition using consistency modeling
[AD-A290655] p 2557 N95-29564
ADC test support program
[AD-A289445] p 2643 N95-29921

ARRAYS
Design, evaluation and construction of TEXESS and LUXESS, and research in mini-array technology and use of data from single stations and sparse networks
[AD-A292546] p 2612 N95-28972
Regional seismic event identification and improved locations with small arrays
[AD-A292188] p 2612 N95-28985

ARRHYTHMIA
Military flying and aeromedical evaluation of cardiac arrhythmias
[AD-A291595] p 2634 N95-28940

ARTIFICIAL INTELLIGENCE
Electromagnetic scattering by magnetic spheres: Theory and algorithms
[AD-A289798] p 2551 N95-28699
Artificial intelligence techniques for parts obsolescence prediction
[AD-A292185] p 2661 N95-28926
Proceedings of the 33d SICE (the Society of Instrument and Control Engineers) Annual Conference, part 1
[DE95-758947] p 2632 N95-28947
Process optimization through discovery and integration of materials and processing properties. phase 1
[AD-A292576] p 2662 N95-28978
Management of speedup mechanisms in learning architectures
[AD-A292206] p 2662 N95-28988
Interface for the translation of sentences in a natural language into a geometrical representation language
[INPE-5467-PRE/1775] p 2722 N95-29363
Interaction and intelligent behavior
[AD-A290049] p 2639 N95-29443
Workshop on Fielded Applications of Machine Learning
[AD-A290168] p 2649 N95-29456
Automated reasoning about classical mechanics
[AD-A290052] p 2663 N95-29477
Neural network exploration using optional experiment design
[AD-A290058] p 2663 N95-29479
Scalable software tools for adaptive scientific computation
[AD-A290446] p 2650 N95-29480
Oblivious decision trees and abstract cases
[AD-A292577] p 2664 N95-29574
Neural network-based decision support for incomplete databases p 2665 N95-29720
Methodologies for intelligent systems*
[AD-A290901] p 2666 N95-30117
Self-organization in a simple brain model
[DE95-008312] p 2668 N95-30279

ARTIFICIAL SATELLITES
Design and analysis of the launch vehicle adapter fitting for the petite amateur navy satellite (PANSAT)
[AD-A289693] p 2504 N95-28680
Spacecraft attitude control system performance using pulse-width pulse-frequency modulated thrusters
[AD-A291803] p 2508 N95-29410

ASCENT TRAJECTORIES
Effects of small changes on rate of climb
[ESDU-94039] p 2495 N95-28707

ASIA
Mapping crust and upper mantle structure beneath southern Eurasia
[AD-A291074] p 2618 N95-29970

ASPECT RATIO
Low-speed wind-tunnel investigation of the stability and control characteristics of a series of flying wings with sweep angles of 50 deg
[NASA-TM-4640] p 2498 N95-30226

ASPHALT
Materials for tomorrow's infrastructure: A ten-year plan for deploying high-performance construction materials and systems
[AD-A289782] p 2526 N95-29598

ASSESSMENTS
US Army aviation epidemiology data register: Gender-specific attrition among the US Army student aviator class of 1987
[AD-A291856] p 2639 N95-29434

ASSIMILATION
On the topological complexity of the cost function in variational data assimilation p 2724 N95-29798
Short-range precipitation forecasts using assimilation of simulated satellite water vapor profiles and cloud liquid water p 2625 N95-29832
Probabilistic modeling and statistical inference for random fields and space-time processes
[AD-A289956] p 2672 N95-30029

ASTEROID BELTS
Delivery of meteorites from the asteroid belt
p 2732 N95-29255

ASTEROID CAPTURE
An investigation into the existence of asteroids at Saturn's triangular Lagrangian points
p 2727 N95-29648

ASTEROIDS
An investigation into the existence of asteroids at Saturn's triangular Lagrangian points
p 2727 N95-29648
Spectral reflectance studies and optical surface alteration in the search for links between meteorites and asteroids p 2733 N95-29672

ASTRONAUTS
Astronaut selection (NASA-MIPR)
[AD-A292512] p 2638 N95-29162
Apollo 14: Shepard hitting golf ball on Moon
[NASA-TM-110638] p 2737 N95-30318

ASTRONOMICAL MODELS
Observations and analysis of solar flares at radio and other wavelengths p 2738 N95-29202
A turbulent model of the solar granulation
[AD-A292318] p 2738 N95-29475

ASTRONOMICAL OBSERVATORIES
X-ray observations of rapidly rotating O stars
[NASA-CR-189423] p 2726 N95-28822
Nobeyama Radio Observatory report, no. 378: The polar ring spiral galaxy NGC 660 p 2731 N95-29097
Nobeyama Radio Observatory report, no. 361: The radio properties of solar active region soft x-ray transient brightenings p 2737 N95-29098
Observations and analysis of solar flares at radio and other wavelengths p 2738 N95-29202
The laser ranging of etalon satellites
[AD-A291019] p 2587 N95-29660

ASTRONOMICAL PHOTOGRAPHY
Space astronomy update
[NASA-TM-110754] p 2731 N95-30317

ASTRONOMICAL PHOTOMETRY
A search for cataclysmic variables in globular clusters
p 2727 N95-29532
The properties of local poor Abell clusters and instrumentation for the study of clustered objects
p 2730 N95-29827

ASTRONOMICAL POLARIMETRY
STS-67 mission highlights resource tape
[NASA-TM-110530] p 2504 N95-28715

ASTRONOMICAL SPECTROSCOPY
STS-67 mission highlights resource tape
[NASA-TM-110530] p 2504 N95-28715
Carbon isotope abundance ratios in comets
p 2732 N95-29592
The properties of local poor Abell clusters and instrumentation for the study of clustered objects
p 2730 N95-29827

ASTROPHYSICS
Nobeyama Radio Observatory report, no. 382: The mass of a star formed in a cloud core: Theory and its application to the Orion A cloud p 2731 N95-29100
Low-background balloon-borne direct search for ionizing massive particles as a component of the dark galactic halo matter p 2726 N95-29204
Statistics and large-scale structure
p 2734 N95-29780
Advanced research in sky surveillance: A search for low-luminosity objects
[AD-A291184] p 2731 N95-29916
Heavy light bullets in electron-positron plasma
[DE95-008751] p 2711 N95-30173
Massively parallel fast elliptic equation solver for three dimensional hydrodynamics and relativity
[DE95-009385] p 2660 N95-30193

ASYMMETRY
External combustion engine having an asymmetrical CAM
[AD-D017382] p 2588 N95-28785

Numerical modeling of opto-electronic integrated circuits
[AD-A292096] p 2563 N95-29239
Photon-counting spatial light modulator technology development
[AD-A292619] p 2699 N95-29295
Computational complexity and encryption
[AD-A291910] p 2648 N95-29356
Super hydrides
[AD-A290594] p 2533 N95-29556
Prospects for HERMES-spin structure studies at HERA
[DE95-005845] p 2694 N95-30019

ASYMPTOTIC GIANT BRANCH STARS
Dust formation in stellar outflows: A time-dependent model p 2733 N95-29649

ASYMPTOTIC METHODS
Examples of grid generation with implicitly specified surfaces using GridPro (TM)/az3000. 1: Filleted multi-tube configurations p 2486 N95-28772
Severe edge effects and simple complimentary interior solutions for thin-walled anisotropic and composite structures
[AD-A290645] p 2595 N95-29562
Mathematical modeling and numerical simulation of the dynamics of flexible structures undergoing large overall motions
[AD-A291139] p 2597 N95-30123

ASYMPTOTIC SERIES
PREDICHAT: First order performance calculations of windturbine rotors using the method of the acceleration potential
[PB95-206454] p 2603 N95-30200
Guidance law development for aeroassisted transfer vehicles using Matched Asymptotic Expansions p 2503 N95-30347

ATLANTIC OCEAN
The structure of water mass, salt, and temperature transports within intermediate depths of the western tropical Atlantic Ocean p 2631 N95-29541

ATMOSPHERIC & OCEANOGRAPHIC INFORM SYS
Meteorological Satellite Center technical note, no. 28, 1994
[JTN-95-80926] p 2626 N95-29849

ATMOSPHERIC ATTENUATION
Broadband Integrated Transmittances (BITS)
[AD-A292176] p 2555 N95-29266

ATMOSPHERIC BOUNDARY LAYER
Comparison of boundary-layer wind and temperature measurements with model estimations
[AD-A290471] p 2621 N95-29507
A theoretical model of multiple regimes in a stratocumulus-topped boundary layer p 2624 N95-29726
Observations of mesoscale cellular convection from the marine stratocumulus phase of FIRE p 2624 N95-29727
Heat and momentum flux measurements in the planetary boundary layer with a wind profiling radar/radio acoustic sounding system p 2617 N95-29777

ATMOSPHERIC CHEMISTRY
A ground support electronic interface for the ionospheric spectroscopy and atmospheric chemistry (ISAAC) ultraviolet spectrograph
[AD-A289761] p 2611 N95-28693
Compendium of NASA data base for the global tropospheric experiment's Transport and Atmospheric Chemistry Near the Equator-Atlantic (TRACE-A)
[NASA-TM-110151] p 2608 N95-28717
Research into artificially induced atmospheric disturbances
[AD-A290150] p 2613 N95-29317
In situ measurements of ClO and implications for the chemistry of inorganic chlorine in the lower stratosphere p 2618 N95-29830
Production of a long-term global water vapor and liquid water data set using ultra-fast methods to assimilate multi-satellite and radiosonde observations
[NASA-CR-198955] p 2628 N95-30272

ATMOSPHERIC CIRCULATION
Parameter study of the statistically steady state of a multi-layer quasi-geostrophic model p 2612 N95-29212
Studies of thermospheric neutral winds utilizing ground-based optical and radar measurements p 2613 N95-29214
Path resolved optical sensing of atmospheric winds utilizing speckle-turbulence interaction and pseudorandum code modulation
[AD-A290800] p 2621 N95-29497
The interactive role of clouds and radiative transfer in maintaining atmospheric circulation p 2616 N95-29699
Lee vorticity production by tropical mountain ranges p 2622 N95-29701
An air stream analysis of the occluded cyclone p 2623 N95-29714
The dynamics of circulations within the stratiform regions of squall lines p 2623 N95-29725
The tropical atmosphere under convection adjustment p 2625 N95-29833
The role of diabatic heating, torques and stability in forcing the meridional circulation within cyclones p 2626 N95-29834
Load-balancing algorithms for the parallel community climate model
[DE95-008795] p 2610 N95-30176
On the azimuthal variation of the equatorial plasmapause
[NASA-CR-198929] p 2711 N95-30338
Extended field observations of cirrus clouds using a ground-based cloud observing system
[NASA-CR-198855] p 2628 N95-30356

ATMOSPHERIC COMPOSITION
Compendium of NASA data base for the global tropospheric experiment's Transport and Atmospheric Chemistry Near the Equator-Atlantic (TRACE-A)
[NASA-TM-110151] p 2608 N95-28717
Development of a multiplex Fabry-Perot interferometer and measurement of atmospheric HF and HCl p 2608 N95-29213
A model analysis of the spatial distribution and temporal trends of nitrous oxide sources and sinks p 2609 N95-29804
In situ measurements of ClO and implications for the chemistry of inorganic chlorine in the lower stratosphere p 2618 N95-29830

ATMOSPHERIC CORRECTION
The use of charge coupled devices in astronomical speckle imaging p 2727 N95-29545

ATMOSPHERIC DENSITY
SETA/ADS software development
[AD-A291181] p 2651 N95-29932

ATMOSPHERIC ENTRY
Pioneer Venus 12.5 km Anomaly Workshop Report, volume 1
[NASA-CP-3303] p 2737 N95-30058

ATMOSPHERIC GENERAL CIRCULATION MODELS
Sensitivity of the simulated global climate to perturbations in low cloud microphysical properties p 2620 N95-29206
The effect of climate perturbations on extratropical cyclogenesis along the east coast of North America p 2621 N95-29595
Soil wetness and climate variability p 2609 N95-29878
Use of ARM data to test an improved parameterization of upper tropospheric clouds for use in climate models
[DE95-009324] p 2610 N95-30181
Studies of gravity-wave filtering and tidal interaction in the middle atmosphere p 2619 N95-30351
Extended field observations of cirrus clouds using a ground-based cloud observing system
[NASA-CR-198855] p 2628 N95-30356

ATMOSPHERIC HEATING
The effect of climate perturbations on extratropical cyclogenesis along the east coast of North America p 2621 N95-29595
A model analysis of the spatial distribution and temporal trends of nitrous oxide sources and sinks p 2609 N95-29804
Radiative cooling profiles calculated from ECMWF analyses and ISCCP C1 data, and their application to determination of distributions of apparent convective heating in the equatorial Pacific p 2625 N95-29805
The tropical atmosphere under convection adjustment p 2625 N95-29833
The effects of clouds as a feedback mechanism on the Earth's climate in the tropical Pacific p 2611 N95-30300

ATMOSPHERIC IONIZATION
Equatorial heating effects on outer plasmasphere evolution p 2616 N95-29716
Heavy light bullets in electron-positron plasma
[DE95-008751] p 2711 N95-30173

ATMOSPHERIC MODELS
Correlation and gradient characteristics of ionospheric parameters in Europe
[AD-A290135] p 2612 N95-29140
Parameter study of the statistically steady state of a multi-layer quasi-geostrophic model p 2612 N95-29212
Numerical studies of the stratospheric aerosol layer under background and perturbed conditions p 2615 N95-29666
A generalized semikinetic (GSK) model for mesoscale auroral plasma transport p 2706 N95-29686
Turbulent coupling of the magnetosphere-ionosphere through shear-mode Alfven waves p 2615 N95-29687
The high-altitude polar wind: Simulation and observation p 2622 N95-29688
An air stream analysis of the occluded cyclone p 2623 N95-29714
Microwave remote sensing algorithms for cirrus clouds and precipitation p 2623 N95-29715
The dynamics of circulations within the stratiform regions of squall lines p 2623 N95-29725
A theoretical model of multiple regimes in a stratocumulus-topped boundary layer p 2624 N95-29726
Observations of mesoscale cellular convection from the marine stratocumulus phase of FIRE p 2624 N95-29727
Chemical release experiments to induce F region ionospheric plasma irregularities at the magnetic equator p 2708 N95-29783
Development of an improved cloud model for use in cumulus parameterization p 2624 N95-29800
A model analysis of the spatial distribution and temporal trends of nitrous oxide sources and sinks p 2609 N95-29804
Short-range precipitation forecasts using assimilation of simulated satellite water vapor profiles and cloud liquid water p 2625 N95-29832
The tropical atmosphere under convection adjustment p 2625 N95-29833
The role of diabatic heating, torques and stability in forcing the meridional circulation within cyclones p 2626 N95-29834
Manual for a workstation-based generic flight simulation program (LaRCsim), version 1.4
[NASA-TM-110164] p 2502 N95-30327

ATMOSPHERIC MOISTURE
Observations of mesoscale cellular convection from the marine stratocumulus phase of FIRE p 2624 N95-29727
Short-range precipitation forecasts using assimilation of simulated satellite water vapor profiles and cloud liquid water p 2625 N95-29832
Production of a long-term global water vapor and liquid water data set using ultra-fast methods to assimilate multi-satellite and radiosonde observations
[NASA-CR-198955] p 2628 N95-30272

ATMOSPHERIC OPTICS
Atmospheric wavefront sensing and correction including the stellar phase shifting interferometer p 2701 N95-29706

ATMOSPHERIC PHYSICS
Numerical studies of the stratospheric aerosol layer under background and perturbed conditions p 2615 N95-29666
Production of a long-term global water vapor and liquid water data set using ultra-fast methods to assimilate multi-satellite and radiosonde observations
[NASA-CR-198955] p 2628 N95-30272

ATMOSPHERIC RADIATION
Measurement of the seasonal and annual variability of total column aerosol in a northeastern US network
[DE95-007259] p 2608 N95-28920
Energy budget in the Asian monsoon region p 2623 N95-29713
The effects of clouds as a feedback mechanism on the Earth's climate in the tropical Pacific p 2611 N95-30300

ATMOSPHERIC REFRACTION
Analysis of tropospheric propagation characteristics based on regional meteorological data
[AD-A291581] p 2552 N95-28939

ATMOSPHERIC SOUNDING
Upper-air data collected on Ice Station Weddell
[AD-A289707] p 2620 N95-29193
Development of a multiplex Fabry-Perot interferometer and measurement of atmospheric HF and HCl p 2608 N95-29213
Comparison of boundary-layer wind and temperature measurements with model estimations
[AD-A290471] p 2621 N95-29507
Heat and momentum flux measurements in the planetary boundary layer with a wind profiling radar/radio acoustic sounding system p 2617 N95-29777
Production of a long-term global water vapor and liquid water data set using ultra-fast methods to assimilate multi-satellite and radiosonde observations
[NASA-CR-198955] p 2628 N95-30272

ATMOSPHERIC TEMPERATURE
Effects of temperature and humidity cycling on the strengths of textile reinforced carbon/epoxy composite materials p 2520 N95-29037
Forecasting global temperature variations by neural networks
[AD-A290081] p 2621 N95-29333
Comparison of boundary-layer wind and temperature measurements with model estimations
[AD-A290471] p 2621 N95-29507
Heat and momentum flux measurements in the planetary boundary layer with a wind profiling radar/radio acoustic sounding system p 2617 N95-29777

Radiative cooling profiles calculated from ECMWF analyses and ISCCP C1 data, and their application to determination of distributions of apparent convective heating in the equatorial Pacific p 2625 N95-29805
Development and testing of improved techniques for modeling the hydrologic cycle in a mesoscale weather prediction system
[AD-A291243] p 2627 N95-29993

ATMOSPHERIC TIDES
Studies of gravity-wave filtering and tidal interaction in the middle atmosphere p 2619 N95-30351

ATMOSPHERIC TURBULENCE
Influence of turbulence parameters, Reynolds number, and body shape on stagnation-region heat transfer
[NASA-TP-3487] p 2568 N95-28719
Path resolved optical sensing of atmospheric winds utilizing speckle-turbulence interaction and pseudorandum code modulation
[AD-A290800] p 2621 N95-29497
Atmospheric wavefront sensing and correction including the stellar phase shifting interferometer p 2701 N95-29706
Development of an improved cloud model for use in cumulus parameterization p 2624 N95-29800

ATOMIC CLUSTERS
Experimental studies of electromagnetic propagation at ultrahigh intensities
[AD-A290284] p 2553 N95-29081
Proceedings of the 18th International Workshop on Condensed Matter Theories
[AD-A291396] p 2694 N95-30065

ATOMIC COLLISIONS
Multifluid nonequilibrium simulation of arcjet thrusters p 2510 N95-29245
Semiconductor deposition and etching interactions of laser-generated translationally hot atoms and radicals
[AD-A291824] p 2693 N95-29431
Parameterized spectral distributions for meson production in proton-proton collisions
[NASA-TM-4675] p 2696 N95-30337

ATOMIC ENERGY LEVELS
Reaction field (RF) calculation of the spectral shifts of indole
[AD-A290449] p 2532 N95-29487
Screening constants for plasma
[AD-B179442L] p 2710 N95-29843

ATOMIC EXCITATIONS
Reaction field (RF) calculation of the spectral shifts of indole
[AD-A290449] p 2532 N95-29487
Ionizational nonequilibrium and ignition in plasma accelerators p 2705 N95-29547

ATOMIC FORCE MICROSCOPY
Publications/Patents/Presentations/Honors report: Force and tunneling microscopy studies of atomic level mechanical properties of solids
[AD-A292254] p 2691 N95-28888

ATOMIC INTERACTIONS
The interaction of group 3A atoms with small molecules
[AD-A290285] p 2692 N95-29082

ATOMIC PHYSICS
Publications/Patents/Presentations/Honors report: Force and tunneling microscopy studies of atomic level mechanical properties of solids
[AD-A292254] p 2691 N95-28888
The 14th International Conference on Atomic Physics
[AD-A290726] p 2693 N95-29521

ATOMIC SPECTRA
A Pr-141 Moessbauer study of praseodymium com pounds
[PB95-192449] p 2535 N95-30282
Parameterized spectral distributions for meson production in proton-proton collisions
[NASA-TM-4675] p 2696 N95-30337

ATOMIC STRUCTURE
Structural and electronic properties of adsorbates on semiconductors, metal-semiconductor interfaces and semiconductor heterojunctions
[AD-A291917] p 2715 N95-29438
The 14th International Conference on Atomic Physics
[AD-A290726] p 2693 N95-29521
Examination of dislocation core structures in B2 intermetallic alloys
[AD-A291486] p 2537 N95-29526
What do we really know about the atomic scale structures of nanophase materials?
[DE95-005858] p 2717 N95-29986
Polynomial approximations for materials simulations
[DE95-006168] p 2652 N95-29989

ATOMS
Publications/Patents/Presentations/Honors report: Force and tunneling microscopy studies of atomic level mechanical properties of solids
[AD-A292254] p 2691 N95-28888
Molecular dynamics study of electromigration
[AD-A289811] p 2691 N95-28952
Ionizational nonequilibrium and ignition in plasma accelerators p 2705 N95-29547

ATTITUDE (INCLINATION)
Experimental methods in residual stress measurement using a position-sensitive single-exposure scintillation detection system
[AD-A289803] p 2594 N95-28949
Improved operator awareness of teleoperated land vehicle attitude
[AD-A290443] p 2641 N95-29359

ATTITUDE CONTROL
A conceptual design for the attitude control and determination system for the Magnetosphere Imager spacecraft
[NASA-TP-3560] p 2507 N95-28721
Time-optimal multi-axis attitude maneuvers of rigid spacecraft using collocation and nonlinear programming p 2507 N95-29332
Spacecraft attitude control system performance using pulse-width pulse-frequency modulated thrusters
[AD-A291803] p 2508 N95-29410

ATTITUDE INDICATORS
A conceptual design for the attitude control and determination system for the Magnetosphere Imager spacecraft
[NASA-TP-3560] p 2507 N95-28721

AUDITORY SIGNALS
Visual and auditory symbols: A literature review
[AD-A290222] p 2641 N95-29908
DPARTS. A dynamic parallel adaptive multiprocess or real-time scheduler
[AD-A291160] p 2659 N95-29915

AUGER EFFECT
Auger rates in mid-IR InAsSb laser structures
[DE95-006325] p 2588 N95-30006

AUGMENTATION
A discrete-event simulation model of myocardial electrical activity: Mathematical electrophysiology
[AD-A292323] p 2633 N95-28793
Theories of the nonlinear optical properties of composite media: Applications to phthalocyanine dyes
[AD-A290640] p 2700 N95-29560
Intensity optical correlation through optical differentiation preprocessing
[AD-A291020] p 2701 N95-29661
Evaluation of retro-reflective beads in airport pavement markings
[AD-A291065] p 2502 N95-29967
Analysis of factors affecting chemical reactions in supercritical fluids
[AD-A290905] p 2534 N95-30078

AURORAL ZONES
Solar system plasma waves
[NASA-CR-198767] p 2704 N95-29130
The effects of magnetic storm phases on F-layer irregularities from auroral to equatorial latitudes
[AD-A290674] p 2614 N95-29585
A generalized semikinetic (GSK) model for mesoscale auroral plasma transport p 2706 N95-29686
Turbulent coupling of the magnetosphere-ionosphere through shear-mode Alfven waves p 2615 N95-29687

AURORAS
A ground support electronic interface for the ionospheric spectroscopy and atmospheric chemistry (ISAAC) ultraviolet spectrograph
[AD-A289761] p 2611 N95-28693
A Monte Carlo simulation of Coulomb collisions and wave-particle interactions in space plasma at high latitudes p 2704 N95-29205
A generalized semikinetic (GSK) model for mesoscale auroral plasma transport p 2706 N95-29686

AUSTENITE
Application of a rapid quench thermomagnetic analyzer to austempered ductile iron
[AD-A292261] p 2535 N95-28889
Austenite to ferrite transformation kinetics during continuous cooling
[DE95-008582] p 2537 N95-29869
Decomposition of hypo-eutectoid iron carbon austenites
[PB95-196945] p 2538 N95-30287

AUSTRALIA
Modeling studies of the Leeuwin current off western and southern Australia
[AD-A290158] p 2629 N95-29023

AUTOCORRELATION
FFT space processing for the ACF of SPREE particle flux measurements
[AD-A290166] p 2507 N95-29026

AUTOMATA THEORY
Grid generation and surface modeling for CFD p 2478 N95-28726
The generalized railroad crossing: A case study in formal verification of real-time systems
[AD-A290152] p 2648 N95-29319

AUTOMATIC CONTROL
Multiblock grid generation with automatic zoning p 2480 N95-28735
Automatic structured grid generation using Gridgen (some restrictions apply) p 2483 N95-28751
A technique for optimizing grid blocks p 2485 N95-28769
Upgrading the Day/Night whole sky imager from Manual/Interactive to full automatic control
[AD-A292296] p 2619 N95-28872
Automated reasoning about classical mechanics
[AD-A290052] p 2663 N95-29477
Automatically combining changes to software systems
[AD-A290628] p 2650 N95-29515
Automated Propulsion Data Screening demonstration system
[NASA-CR-196636] p 2510 N95-29584

AUTOMATIC FLIGHT CONTROL
Design and evaluation of a LQR controller for the bluebird unmanned air vehicle
[AD-A289769] p 2498 N95-29457

AUTOMATION
Automatic blocking for complex three-dimensional configurations p 2480 N95-28734
Automation of three-dimensional structured mesh generation for turbomachinery blade passages p 2484 N95-28762
Upgrading the Day/Night whole sky imager from Manual/Interactive to full automatic control
[AD-A292296] p 2619 N95-28872
Task-dependent effects of automation: The role of internal models in performance, workload, and situational awareness in a semi-automated cockpit
[AD-A292538] p 2640 N95-28969
Workshop on Fielded Applications of Machine Learning
[AD-A280168] p 2649 N95-29456

AUTOMOBILE FUELS
Technology development goals for automotive fuel cell power systems
[DE95-008764] p 2548 N95-29280

AUTOMOBILES
Severe edge effects and simple complimentary interior solutions for thin-walled anisotropic and composite structures
[AD-A290845] p 2595 N95-29562

AUTONOMOUS NAVIGATION
Motion planning and sensory processing in a dynamic environment
[AD-A290504] p 2722 N95-29154

AUTONOMY
Experiments in cooperative manipulation of objects by free-flying robot teams p 2662 N95-29095
Computing 3-D motion in custom analog and digital VLSI
[AD-A290270] p 2647 N95-29179
A biologically-inspired autonomous robot
[AD-A289446] p 2666 N95-30026

AUTOPSIES
Continuation of research in the statistical aspects of reliability, availability, and maintainability
[AD-A290126] p 2592 N95-29423

AUXILIARY PROPULSION
A vehicle health monitoring system for the Space Shuttle Reaction Control System during reentry
[NASA-CR-188370] p 2505 N95-29447

AVALANCHES
Photon-counting spatial light modulator technology development
[AD-A292619] p 2699 N95-29295

AVIATION PSYCHOLOGY
Astronaut selection (NASA-MIPR)
[AD-A292512] p 2638 N95-29162

AVIONICS
Nonlinear calibration of an infrared radiometer
[AD-A292436] p 2698 N95-28996
Investigation and characterization of SEU effects and hardening strategies in avionics
[AD-A291058] p 2500 N95-29950

AXIAL FLOW
Unsteady pressure and inflow velocity on a pitching rotor blade in hover p 2490 N95-29771
Laser doppler velocimeter system for subsonic jet mixer nozzle testing at the NASA Lewis Aeroacoustic Propulsion Lab
[NASA-TM-106984] p 2477 N95-30229

AXIAL LOADS
Cable load transducer
[AD-A289548] p 2595 N95-29192
Toughening mechanisms in mixed-mode interfacial fracture p 2545 N95-29772

AXIAL STRESS
Experimental methods in residual stress measurement using a position-sensitive single-exposure scintillation detection system
[AD-A289803] p 2594 N95-28949
Raman and photo-modulated reflectivity studies of ZnTe/InAs semiconductor heterostructure under hydrostatic pressure
[AD-A290467] p 2716 N95-29506
Analysis of adiabatic shear bands in thermoviscoplastic materials under combined loading
[AD-A290666] p 2596 N95-29582

AXISYMMETRIC BODIES
A numerical solution method for acoustic radiation from axisymmetric bodies p 2689 N95-30154

AXISYMMETRIC FLOW
A combined geometric approach for computational fluid dynamics on dynamic grids p 2485 N95-28770
Transitions in liquid crystals initiated with circularly polarized light
[AD-A290525] p 2716 N95-29493
Prediction of pressurant mass requirements for axisymmetric liquid hydrogen tanks
[NASA-TM-106973] p 2511 N95-29642
Inlet flow test calibration for a small axial compressor rig. Part 2: CFD compared with experimental results
[NASA-TM-106999] p 2501 N95-30007
Numerical simulations of the flow in the HYPULSE expansion tube
[NASA-TM-110357] p 2503 N95-30228

AZEOTROPES
Thermal conductivity of liquid halogenated aliphatic hydrocarbons. Part 1: Halogenated methanes and azeotropic mixtures
[ESDU-94021-PT-1] p 2511 N95-28804

AZIMUTH
Mapping crust and upper mantle structure beneath southern Eurasia
[AD-A291074] p 2618 N95-29970
On the azimuthal variation of the equatorial plasmapause
[NASA-CR-198929] p 2711 N95-30338

B

B-1 AIRCRAFT
An analysis of B-1B exterior jet blast windshield anti-icing performance using pre-cooled compressor bleed air
[AD-A292522] p 2492 N95-28811

BACKGROUND NOISE
An algorithm fusion approach to IRST signal processing (III): Nongaussian-corrected filter fusion
[AD-A291565] p 2552 N95-28936
Visual and auditory symbols: A literature review
[AD-A290222] p 2641 N95-29908

BACKGROUND RADIATION
The 12 UM contribution of nearby galaxies to the infrared background
[AD-A291185] p 2735 N95-29917

BACKSCATTERING
Backscatter data acquisition for Hydrosweep DS aboard RV Ewing
[AD-A292332] p 2628 N95-28796
High gain, low noise and broadband Raman and Brillouin fiber-optic amplifiers, channel selectors and switches
[AD-A290585] p 2700 N95-29553
Observation of x ray generation in a proof-of-principle laser synchrotron source experiment
[AD-A291298] p 2588 N95-29937
100 Hz-10 kHz bottom backscattering model: Generalized treatment of sediment sound propagation, sediment volume scattering and interface-roughness scattering
[AD-A291323] p 2685 N95-29942

BACKUPS
Design, analysis and control of large transports so that control of engine thrust can be used as a back-up of the primary flight controls
[NASA-CR-198958] p 2501 N95-30254

BACTERIAL DISEASES
Studies of altered response to infection induced by severe injury
[AD-A288907] p 2634 N95-29139

BAGS
The 2nd European Conference on Smart Structures and Materials
[AD-A290723] p 2550 N95-29579

BAINITIC STEEL
The effects of alloying elements on the strength and cooling rate sensitivity of ultra-low carbon alloy steel weld metals
[AD-A290681] p 2537 N95-29759

BALANCING
Hybrid fuzzy logic control to stabilize an inverted pendulum from arbitrary initial conditions
[AD-A292441] p 2681 N95-29000
Load balancing for the parallel adaptive solution of partial differential equations
[AD-A290450] p 2671 N95-29488

BALLISTICS
Ballistic penetration phenomenology of high symmetry single crystals
[AD-A292476] p 2713 N95-29013

BALLOON SOUNDING
Upper-air data collected on Ice Station Weddell
[AD-A289707] p 2620 N95-29193
Low-background balloon-borne direct search for ionizing massive particles as a component of the dark galactic halo matter p 2726 N95-29204

BALLOON-BORNE INSTRUMENTS
Low-background balloon-borne direct search for ionizing massive particles as a component of the dark galactic halo matter p 2726 N95-29204
Fluxes and relative abundances of light cosmic ray nuclei at energies above 40 GeV/n p 2739 N95-29531

BAND STRUCTURE OF SOLIDS
Photonic band structures for optoelectronics
[AD-A291154] p 2718 N95-30298

BANDWIDTH
Feature extraction from digital communications signals using wavelet transforms
[AD-A292655] p 2556 N95-29386
Advanced presort process
[AD-A291010] p 2557 N95-29655

BARIUM OXIDES
Pulsed laser deposition of ferroelectric thin films in conjunction with superconducting oxides
[AD-A290101] p 2585 N95-29208
Deposition and surface treatment with intense pulsed ion beams
[DE95-007885] p 2543 N95-29465
Ion beam modification of Tl-Ba-Ca-Cu-O type high temperature superconductors during irradiation
[DE95-006807] p 2717 N95-30022

BARIUM TITANATES
Investigation of the characteristics of ferroelectric thin films deposited by pulsed laser ablation
[AD-A292306] p 2540 N95-28963
Growth, characterization and application of KTN family nonlinear optical crystals
[AD-A290330] p 2713 N95-29087
Electrical characteristics of barium strontium titanate-oxide composite films
[AD-A289991] p 2541 N95-29135
Fabrication and characterization of barium strontium titanate and non-ferroelectric oxide composites
[AD-A289994] p 2523 N95-29136
Fabrication and characterization of BSTO and nonferroelectric oxide composites for use in phased array antennas and other electronic devices
[AD-A290070] p 2524 N95-29329
Analysis of the ferroelectric thin films deposited by pulsed laser deposition on oxide and fluoride substrates
[AD-A290088] p 2543 N95-29353

BAROCLINIC WAVES
The role of diabatic heating, torques and stability in forcing the meridional circulation within cyclones p 2626 N95-29834

BAROCLINITY
Parameter study of the statistically steady state of a multi-layer quasi-geostrophic model p 2612 N95-29212

BARRIER LAYERS
The effect of wear on fire-blocking layer material effectiveness
[AD-A291520] p 2493 N95-29855

BARYONS
Tables of SU3 isoscalar factors
[DE95-009375] p 2690 N95-28779

BASE FLOW
Navier-Stokes solution of wing wake structure and its perturbation p 2488 N95-29121
The effects of three dimensional imposed disturbances on bluff body near wake flows
[AD-A290824] p 2575 N95-29654

BAYES THEOREM
Large deviation limit theorems, with applications
[AD-A290392] p 2669 N95-29233
Test theory reconceived
[AD-A291836] p 2639 N95-29432
Learning object models from visual observation and background knowledge
[AD-A292606] p 2650 N95-29576
Induction of selective Bayesian classifiers
[AD-A292690] p 2675 N95-29906

BEACONS
Operational test and evaluation (OT&E) integration and operational test plan for fixed ground antenna radome (FGAR)
[AD-A291310] p 2559 N95-29940
Operational test and evaluation (OT&E) integration and operational test procedures for Fixed Ground Antenna Radome (FGAR)
[AD-A291203] p 2559 N95-29975

BEADS
New tetraarylborate and ethyldibutylstannane reagents
[AD-A289813] p 2540 N95-28953
Evaluation of retro-reflective beads in airport pavement markings
[AD-A291065] p 2502 N95-29967

BEAM INTERACTIONS
Lattice/beam dynamics working group
[DE95-006774] p 2696 N95-30021
Sea and gluon spin structure function measurements at RHIC
[DE95-005823] p 2695 N95-30185
Measurements of (Delta)(sigma)(sub L)(pp) and (Delta)(sigma)(sub L)((bar p)p) at 200 GeV/c
[DE95-005837] p 2695 N95-30186

BEAMS (RADIATION)
The angular spread of the deflected acoustic beam diffracted by a Bragg grating out of a surface acoustic wave
[AD-A291018] p 2684 N95-29659

BEAMS (SUPPORTS)
Continental aerosol effects on stratocumulus microphysics during MAST 1994
[AD-A292674] p 2621 N95-29416

BEARINGS
Dimensions, deflections and stresses for Hertzian contacts under combined normal and tangential loading. (Guide to use of computer program A9434.)
[ESDU-94034] p 2593 N95-28711

BEHAVIOR
Interaction and intelligent behavior
[AD-A290049] p 2639 N95-29443
Causal behaviours and nets
[PB95-197612] p 2660 N95-30102

BELL AIRCRAFT
Bell Helicopter Advanced Rotocraft Transmission (ART) program
[NASA-CR-195479] p 2590 N95-29538

BENDING
Design and evaluation of a foam-filled hat-stiffened panel concept for aircraft primary structural applications p 2499 N95-28841
Effects of cutouts on the behavior of symmetric composite laminates subjected to bending and twisting loads p 2517 N95-28844
Technology integration box beam failure study p 2517 N95-28847
Fiber-matrix adhesion in single-fiber model composites p 2524 N95-29337
A finite element analysis of room temperature silicon crystals for the Advanced Photon Source bending-magnet and insertion-device beams
[DE95-005822] p 2718 N95-30184
Bending properties of nickel electrodes for nickel-hydrogen batteries p 2567 N95-30259

BENDING MOMENTS
Shear force, bending moment and torque of rigid aircraft in symmetric steady maneuvering flight
[ESDU-94045] p 2495 N95-28896
Through-the-thickness stresses and failure in the corner radius of a laminated composite section
[ESDU-94019] p 2518 N95-28899
Cable load transducer
[AD-A289548] p 2595 N95-29192
Unitary transducer with variable resistivity
[AD-D017329] p 2566 N95-30055

BERYLLIUM
Fluxes and relative abundances of light cosmic ray nuclei at energies above 40 GeV/n p 2739 N95-29531

BIAS
Nitrogen dioxide measurement method characterization at the GRI conventional research house
[PB95-200549] p 2610 N95-30197

BIBLIOGRAPHIES
Collected software engineering papers, volume 12
[NASA-CR-189409] p 2644 N95-28713
Annotated bibliography of software engineering laboratory literature
[NASA-CR-189406] p 2644 N95-28805
Aerospace medicine and biology: A continuing bibliography with indexes (supplement 403)
[NASA-SP-7011(403)] p 2636 N95-29190
Bibliography of Doctor Chul Park
[NASA-TM-110353] p 2503 N95-29351
Visual and auditory symbols: A literature review
[AD-A290222] p 2641 N95-29908

A bibliography, with abstracts and annotations, of publications on and related to underwater acoustic fluctuations
[AD-A291342] p 2685 N95-29945

BINARY DATA
Synthesis and complete characterization of a Gallium-Mixed-Pnicogen four-membered ring compound: I2GaAs(SiMe3)(sub 2)Ga(I)2P(SiMe3)(sub 2)
[AD-A292423] p 2713 N95-28993
A pipeline case tool for database design
[AD-A292017] p 2722 N95-29182

BINARY FLUIDS
Effects of critical fluctuations on the thermodynamic properties of fluids and fluid mixtures
p 2719 N95-29216

BINARY PHASE SHIFT KEYING
Feature extraction from digital communications signals using wavelet transforms
[AD-A292655] p 2556 N95-29386

BINARY STARS
A pipeline case tool for database design
[AD-A292017] p 2722 N95-29182
Applications of pulsar timing p 2734 N95-29675

BINARY SYSTEMS (MATERIALS)
Synthesis and complete characterization of a Gallium-Mixed-Pnicogen four-membered ring compound: I2GaAs(SiMe3)(sub 2)Ga(I)2P(SiMe3)(sub 2)
[AD-A292423] p 2713 N95-28993
Dynamic decohesion of bimaterial interfaces
p 2541 N95-29120

BINAURAL HEARING
Pattern-analysis based models of masking by spatially separated sounds
[AD-A291270] p 2637 N95-29933

BINDERS (MATERIALS)
Epoxy self-priming topcoats
[AD-D017383] p 2541 N95-29194
Development of flame resistant, high efficiency thermal insulation
[AD-A291136] p 2547 N95-30120

BINOMIALS
Bootstrap and partitioning methods
[AD-A290662] p 2671 N95-29578

BIOCHEMISTRY
Electrical and electronic properties of self-assembled lipid bilayers
[AD-A290507] p 2632 N95-29155
Surfactant-enhanced in situ biodegradation of strongly sorbing organic substances in soil environments
[AD-A290253] p 2512 N95-29168
Symposium on Metal-Mediated Molecular Architectures
[AD-A290427] p 2692 N95-29388

BIOCONVERSION
The TEES process cleans waste and produces energy
[DE95-007799] p 2602 N95-29463
Introduction to the proceedings of the sixteenth symposium on biotechnology for fuels and chemicals
[DE95-007029] p 2549 N95-30024

BIODEGRADABILITY
Surfactant-enhanced in situ biodegradation of strongly sorbing organic substances in soil environments
[AD-A290253] p 2512 N95-29168

BIODEGRADATION
Surfactant-enhanced in situ biodegradation of strongly sorbing organic substances in soil environments
[AD-A290253] p 2512 N95-29168

BIODYNAMICS
Operating procedures for Anthropometry and Initial Conditions Photogrammetric Program
[AD-A291553] p 2640 N95-29935
Biodynamic simulation of pilot interaction with a helicopter multiairbag restraint system
[AD-A290196] p 2492 N95-29057
Dynamic modelling and link mechanism design of four-legged mobile robot p 2591 N95-30277

BIOINSTRUMENTATION
Polymeric microcapsule arrays
[AD-A291937] p 2539 N95-28850

BIOLOGICAL EFFECTS
Cellular and molecular level responses after radiofrequency radiation exposure, alone or in combination with x rays or chemicals
[AD-A292488] p 2633 N95-28866
Aerospace medicine and biology: A continuing bibliography with indexes (supplement 403)
[NASA-SP-7011(403)] p 2636 N95-29190
Modeling joint effects of mixtures of chemicals on microorganisms using quantitative structure activity relationship techniques, phase 3
[AD-A290153] p 2632 N95-29320
Effect of irradiance, sucrose, and CO2 concentration on the growth of potato (Solanum tuberosum L.) in vitro
[NASA-TM-110854] p 2632 N95-29375

BIOLOGICAL MODELS (MATHEMATICS)
Computer models of retinal function
[AD-A290156] p 2634 N95-29022

BIOLOGY
Genetics and the unity of biology
[DE95-006484] p 2633 N95-29471

BIOMASS
Maize yield estimation through the simulation of radiation penetration into the canopy p 2599 N95-29703

BIOMASS ENERGY PRODUCTION
The TEES process cleans waste and produces energy
[DE95-007799] p 2602 N95-29463

BIOMETRICS
Analysis of wounds by evaporative water loss in man
[AD-A290327] p 2634 N95-29086

BIOTECHNOLOGY
Proceedings of the 11th congress of the international society for artificial cells, blood substitutes and immobilization biotechnology
[AD-A290342] p 2632 N95-29088
Introduction to the proceedings of the sixteenth symposium on biotechnology for fuels and chemicals
[DE95-007029] p 2549 N95-30024

BIPOLAR TRANSISTORS
Epitaxial growth and characterization of Si(1-x)Ge(x) materials and devices
[AD-A292528] p 2712 N95-28874

BIPOLARITY
The 6th Van der Ziel symposium on quantum 1/f noise and other low frequency fluctuations in electronic devices
[AD-A292468] p 2718 N95-29009

BIREFRINGENCE
Fibre-coupled remote optical vibrometry
[AD-A291606] p 2698 N95-28932
Structure and orientation behavior of highly oriented polymers under tensile and compressive stresses
p 2546 N95-29822

BISTATIC REFLECTIVITY
Statistical properties of bistatic clutter echoes
[AD-A291688] p 2552 N95-28943

BIVARIATE ANALYSIS
Statistics and large-scale structure
p 2734 N95-29780

BLACK HOLES (ASTRONOMY)
Continuum spectra of supermassive accretion disks
p 2732 N95-29252
Observational signatures of rotating black holes
p 2729 N95-29709

BLADE SLAP NOISE
UHB engine fan broadband noise reduction study
[NASA-CR-198357] p 2684 N95-29641

BLADE-VORTEX INTERACTION
Development of a rotary wing Navier-Stokes CFD code based on TLNS3D code
[AD-A290421] p 2574 N95-29387
Evaluation of numerical schemes for the analysis of sound generation by blade-gust interaction
p 2690 N95-30163

BLOCK COPOLYMERS
Phase coupling and morphology generation in engineering polymer alloys
[AD-A291868] p 2543 N95-29436
Conjugated polymers from cyclohexadienediol monomers
[AD-A290247] p 2544 N95-29505
Synthesis morphology and properties of semicrystalline block copolymers
[AD-A290475] p 2544 N95-29510
Polyethylene-based polyurethane copolymers and block copolymers
[AD-A289996] p 2546 N95-30030

BLOCKING
Grid generation and surface modeling for CFD
p 2478 N95-28726
Automatic blocking for complex three-dimensional configurations p 2480 N95-28734
Block-structured grids for complex aerodynamic configurations: Current status p 2480 N95-28736
Adaptive block sequential detection of abrupt signal changes
[AD-A290456] p 2557 N95-29489
Diffraction limited imaging using aberrated optics
[AD-A290912] p 2703 N95-30081

BLOOD
Experiment kits for processing biological samples inflight on SLS-2
[NASA-TM-4685] p 2642 N95-28722
Proceedings of the 11th congress of the international society for artificial cells, blood substitutes and immobilization biotechnology
[AD-A290342] p 2632 N95-29088
Research on PGI2 and TXA2 effects at times of hyperbaric oxygenation of domestic rabbits with acute cerebral ischemia reirrigation damage
[AD-A289606] p 2632 N95-29263
Effect of hypoxia on arterial blood gases in subjects with lung dysfunction p 2638 N95-29627

BLOOD CELLS
Proceedings of the 11th congress of the international society for artificial cells, blood substitutes and immobilization biotechnology
[AD-A290342] p 2632 N95-29088

BLOOD FLOW
Pulse waveform and pulse amplitude analysis during Lower Body Negative Pressure
[AD-A290521] p 2636 N95-29360
Effect of mild hydrostatic pressure on red blood cells
[AD-A290520] p 2637 N95-29872

BLOOD PLASMA
The influence of space flight on erythrokinetics in man. Space Life Sciences Missions 1 and 2. Experiment E261
[NASA-CR-188368] p 2633 N95-28875

BLOOD PRESSURE
The influence of space flight on erythrokinetics in man. Space Life Sciences Missions 1 and 2. Experiment E261
[NASA-CR-188368] p 2633 N95-28875

BLOOD VOLUME
The influence of space flight on erythrokinetics in man. Space Life Sciences Missions 1 and 2. Experiment E261
[NASA-CR-188368] p 2633 N95-28875

BLOWING
Pressure based high order TVD methodology for dynamic stall control
[AD-A290149] p 2489 N95-29316

BLUFF BODIES
The effects of three-dimensional imposed disturbances on bluff body near wake flows: Effects of taper and splitter plates on the near wake characteristics of a circular cylinder in uniform and shear flow
[AD-A292113] p 2487 N95-28921
Vortex element analysis of selected time-dependent flows
[AD-A289944] p 2573 N95-29271
Research on bluff-body vortex wakes
[AD-A292650] p 2574 N95-29382

BLUNT BODIES
Experimental and theoretical studies of wakes in stratified flows
[AD-A290203] p 2569 N95-29060
Transonic, supersonic and hypersonic wind-tunnel tests on aerodynamic characteristics of reentry body with blunted cone configuration
[ISAS-658] p 2490 N95-29640

BLUNT TRAILING EDGES
The effects of three dimensional imposed disturbances on bluff body near wake flows
[AD-A290824] p 2575 N95-29654

BODY FLUIDS
Human fluid balance and dehydration during cold weather military operations
[AD-A289192] p 2636 N95-29757

BODY-WING AND TAIL CONFIGURATIONS
Shear force, bending moment and torque of rigid aircraft in symmetric steady maneuvering flight
[ESDU-94045] p 2495 N95-28896

BODY-WING CONFIGURATIONS
Demonstration of an automated CFD system for three-dimensional flow simulations p 2485 N95-28767
The 1995 version of the NSWC aeroprediction code. Part 1: Summary of new theoretical methodology
[AD-A291518] p 2490 N95-29853
A numerical study of the small scale wing-body junction problem p 2491 N95-30235

BOEING 737 AIRCRAFT
Danish aeromedical evacuation efforts during the Gulf War p 2677 N95-29613

BOEING 767 AIRCRAFT
Civil Reserve Air Fleet-Aeromedical Evacuation Shipset (CRAF-AESS) p 2678 N95-29619

BOEING 777 AIRCRAFT
Challenges and payoff of composites in transport aircraft: 777 empennage and future applications
p 2519 N95-29031

BOLTS
Performance evaluation of bolt-cutter system on first Taurus launch
[AD-A291237] p 2504 N95-29992

BONDED JOINTS
Aircraft advanced materials research and development program plan
[AD-A290542] p 2498 N95-29565
A study of blister tests for film adhesion measurement and fracture efficiency of tests for adhesive bonds
p 2545 N95-29799

BONDING
Lightweight battery electrode and method of making it
[AD-D017389] p 2560 N95-28855
A 1993 review of welding in Japan
[DE95-758701] p 2589 N95-28946

Fiber optic Raman and micro Raman measurements of bonding agents at interface during the curing process
[AD-A292042] p 2523 N95-29189
BOOLEAN FUNCTIONS
Inductive boolean function manipulation: A hardware verification methodology for automatic induction
[AD-A292236] p 2669 N95-29128
BORON
The interaction of group 3A atoms with small molecules
[AD-A290285] p 2692 N95-29082
Fluxes and relative abundances of light cosmic ray nuclei at energies above 40 GeV/n p 2739 N95-29531
A cluster beam study of boron, boron oxide and B(x)O(y)H chemistry with hydrogen fluoride
[AD-A290826] p 2533 N95-29722
Boronization study for application to large helical device
[AD-B191996L] p 2709 N95-29808
BORON CARBIDES
Drift mobility measurements in thin film boron carbide
[AD-A292510] p 2712 N95-28869
BORON OXIDES
A cluster beam study of boron, boron oxide and B(x)O(y)H chemistry with hydrogen fluoride
[AD-A290826] p 2533 N95-29722
BOSONS
Sea and gluon spin structure function measurements at RHIC
[DE95-005823] p 2695 N95-30185
BOTANY
Effect of irradiance, sucrose, and CO2 concentration on the growth of potato (Solanum tuberosum L.) in vitro
[NASA-TM-110654] p 2632 N95-29375
BOUNDARIES
Multiblock grid generation with automatic zoning
p 2480 N95-28735
Sensitivity of stress and boundary imperfection of dielectric resonator disks
[AD-A290488] p 2594 N95-29150
Theorem on the existence of solutions of quasi-static moving boundary problems
[PB95-197125] p 2673 N95-30093
BOUNDARY CONDITIONS
Elliptic surface grid generation on minimal and parmetrized surfaces p 2484 N95-28760
Solution of the Navier-Stokes equations on locally refined Cartesian meshes using state-vector splitting
p 2571 N95-29197
SOSDOR: Solid-state device simulator code
[AD-A289954] p 2563 N95-29275
The effects of the thermal boundary condition and turbulence on heat transfer from a cylinder, flat plate, and turbine blade using the transient shroud and heated-coating techniques
[AD-A292646] p 2574 N95-29380
Development of a rotary wing Navier-Stokes CFD code based on TLNS3D code
[AD-A290421] p 2574 N95-29387
Efficient solution of a class of infinite stochastic petri nets: Theory and applications
[PB95-197166] p 2673 N95-30097
Benchmark problems and solutions
p 2686 N95-30134
Application of essentially nonoscillatory methods to aeroacoustic flow problems p 2686 N95-30135
Computational aeroacoustics using hyperbolic wave primitives p 2686 N95-30136
A compact solution to computational acoustics
p 2686 N95-30138
Solutions of the benchmark problems by the dispersion-relation-preserving scheme
p 2674 N95-30145
A comparative study of upwind and MacCormack schemes for CAA benchmark problems
p 2686 N95-30147
Wave propagation and scattering in computational aeroacoustics p 2689 N95-30152
The use of staggered scheme and an absorbing buffer zone for computational aeroacoustics
p 2689 N95-30153
A numerical solution method for acoustic radiation from axisymmetric bodies p 2689 N95-30154
Application of a new finite difference algorithm for computational aeroacoustics p 2689 N95-30155
Numerical simulations of small amplitude acoustic wave propagation in a converging-diverging nozzle
p 2690 N95-30160
Elastoplastic buckling analysis of cylindrical shells using a semi-analytical formulation
[PB95-197349] p 2597 N95-30206
Grid resolution and turbulent inflow boundary condition recommendations for NPARC calculations
[NASA-TM-106959] p 2492 N95-30253
Guidance law development for aeroassisted transfer vehicles using Matched Asymptotic Expansions
p 2503 N95-30347
BOUNDARY ELEMENT METHOD
Solution of second order nonlinear boundary value problems by the boundary element method
p 2669 N95-29105
Efficient inversion of Fourier and Laplace domain boundary element solutions for elastodynamic scattering
p 2592 N95-29256
Boundary element algorithms for Somigliana's identity
[PB95-206959] p 2597 N95-30169
BOUNDARY INTEGRAL METHOD
Boundary element algorithms for Somigliana's identity
[PB95-206959] p 2597 N95-30169
BOUNDARY LAYER CONTROL
A procedure for automating CFD simulations of an inlet-bleed problem p 2485 N95-28768
Pressure based high order TVD methodology for dynamic stall control
[AD-A290149] p 2489 N95-29316
BOUNDARY LAYER EQUATIONS
Modeling the boundary layer interactions between weakly ionized plasmas and cooled, planar electrodes in stagnation-point flows p 2706 N95-29717
BOUNDARY LAYER FLOW
The effects of three-dimensional imposed disturbances on bluff body near wake flows: Effects of taper and splitter plates on the near wake characteristics of a circular cylinder in uniform and shear flow
[AD-A292113] p 2487 N95-28921
Linear stability analysis of hypersonic boundary layers
[AD-A290159] p 2569 N95-29024
Effects of elevated free-stream turbulence and streamwise acceleration on flow and thermal structures in transitional boundary layers p 2576 N95-29729
Numerical simulations of the flow in the HYPULSE expansion tube
[NASA-TM-110357] p 2503 N95-30228
A numerical study of the small scale wing-body junction problem p 2491 N95-30235
An interacting boundary layer method for unsteady compressible flows p 2579 N95-30290
BOUNDARY LAYER PLASMAS
On the azimuthal variation of the equatorial plasmapause
[NASA-CR-198929] p 2711 N95-30338
BOUNDARY LAYER SEPARATION
A procedure for automating CFD simulations of an inlet-bleed problem p 2485 N95-28768
Physical causes of separation shock unsteadiness in shock wave/turbulent boundary layer interactions
p 2570 N95-29096
Unsteadiness of shock-induced turbulent boundary layer separation. An inherent feature of turbulent flow or solely a wind tunnel phenomenon
[AD-A290367] p 2572 N95-29228
BOUNDARY LAYER STABILITY
Linear stability analysis of hypersonic boundary layers
[AD-A290159] p 2569 N95-29024
Unsteadiness of shock-induced turbulent boundary layer separation. An inherent feature of turbulent flow or solely a wind tunnel phenomenon
[AD-A290367] p 2572 N95-29228
BOUNDARY LAYER TRANSITION
Linear stability analysis of hypersonic boundary layers
[AD-A290159] p 2569 N95-29024
Experimental studies on boundary-layer transition on a reentry vehicle at transonic and supersonic speeds
[ISAS-659] p 2575 N95-29712
Effects of elevated free-stream turbulence and streamwise acceleration on flow and thermal structures in transitional boundary layers p 2576 N95-29729
Development of an improved cloud model for use in cumulus parameterization p 2624 N95-29800
Boundary-layer transition and global skin friction measurement with an oil-fringe imaging technique
[NASA-CR-198814] p 2579 N95-30224
BOUNDARY LAYERS
The effect of viscous attenuation on shock tube performance
[AD-A289793] p 2568 N95-28696
Dynamic stall of a NACA 0012 airfoil in laminar flow
p 2489 N95-29243
Vortex element analysis of selected time-dependent flows
[AD-A289944] p 2573 N95-29271
Modeling the boundary layer interactions between weakly ionized plasmas and cooled, planar electrodes in stagnation-point flows p 2706 N95-29717
Grid resolution and turbulent inflow boundary condition recommendations for NPARC calculations
[NASA-TM-106959] p 2492 N95-30253
BOUNDARY LUBRICATION
Selection of synthetic oils
[ESDU-94020] p 2539 N95-28898
BOUNDARY VALUE PROBLEMS
International Workshop on Stochastic Filtering Theory
[AD-A291670] p 2661 N95-28788
Discontinuous solutions of semilinear differential-algebraic equations. part 2: Rho-consistency
[AD-A292285] p 2668 N95-28861
A generalized finite element method for solving the Helmholtz equation in two dimensions with minimal pollution
[AD-A290280] p 2669 N95-29080
Finite element solution to the Helmholtz equation with high wave number. Part 2. The h-p version of the FEM
[AD-A290289] p 2669 N95-29084
Solution of second order nonlinear boundary value problems by the boundary element method
p 2669 N95-29105
The Stroh formalism for anisotropic elasticity with applications to composite materials
[AD-A290710] p 2527 N95-29763
Comparison of the local defect correction iteration and the fast adaptive composite grid iteration
[PB95-206769] p 2672 N95-30088
Theorem on the existence of solutions of quasi-static moving boundary problems
[PB95-197125] p 2673 N95-30093
Computational aeroacoustics using hyperbolic wave primitives p 2686 N95-30136
Solutions of the benchmark problems by the dispersion-relation-preserving scheme
p 2674 N95-30145
PREDICHAT: First order performance calculations of windturbine rotors using the method of the acceleration potential
[PB95-206454] p 2603 N95-30200
BOW WAVES
An extension of the continuum model by Grad's thirteen moment equations for hypersonic rarefied flows
p 2488 N95-29118
The physics of the collisionless bow shock
p 2580 N95-30301
BOX BEAMS
Technology integration box beam failure study
p 2517 N95-28847
BRAGG ANGLE
The angular spread of the deflected acoustic beam diffracted by a Bragg grating out of a surface acoustic wave
[AD-A291018] p 2684 N95-29659
BRAGG CELLS
A method and apparatus for signal filtering
[AD-D017268] p 2554 N95-29236
BRAIDED COMPOSITES
Effect of open hole on tensile failure properties of 2D triaxial braided textile composites and tape equivalents
[NASA-CR-4676] p 2513 N95-28817
Characterization and development of materials for advanced textile composites p 2513 N95-28824
The effects of specimen width on tensile properties of triaxially braided textile composites
p 2513 N95-28825
Effects of temperature and humidity cycling on the strengths of textile reinforced carbon/epoxy composite materials p 2520 N95-29037
Mechanical characterization of 2D, 2D stitched, and 3D braided/RTM materials p 2520 N95-29038
Experimental and analytical characterization of triaxially braided textile composites p 2520 N95-29040
Effects of thermal and moisture cycling on the internal structure of stitched RTM laminates
p 2522 N95-29048
BRAIN
Large-scale neuronal theories of the brain
[AD-A290200] p 2634 N95-29059
Coupling of brain muscarinic receptors to second messengers
[AD-A290498] p 2635 N95-29153
Self-organization in a simple brain model
[DE95-008312] p 2668 N95-30279
BRAIN CIRCULATION
CO2-O2 interactions in extension of tolerance to acute hypoxia
[NASA-CR-198575] p 2635 N95-29158
BRAIN DAMAGE
Research on PGI2 and TXA2 effects at times of hyperbaric oxygenation of domestic rabbits with acute cerebral ischemia reirrigation damage
[AD-A289606] p 2632 N95-29263
BRAZIL
Proposal for a flexible system of phytogeographic classification: Emphasis on the use of multistage remote sensoring
[INPE-5609-PRE/1821] p 2600 N95-29815
BRIGHTNESS
Aperture synthesis observation of HCN J = 1-0 emission from Y Canum Venaticorum p 2735 N95-29839

BRIGHTNESS TEMPERATURE
Microwave remote sensing algorithms for cirrus clouds and precipitation p 2623 N95-29715
BRILLOUIN EFFECT
High gain, low noise and broadband Raman and Brillouin fiber-optic amplifiers, channel selectors and switches [AD-A290585] p 2700 N95-29553
Dynamical instabilities, chaos and spatial complexity in fundamental nonlinear optical interactions [AD-A291223] p 2588 N95-29980
BROADBAND
Tailored microstructures for broadband or selective detection of radiation from the visible to the infrared [AD-A292097] p 2554 N95-29240
Broadband Integrated Transmittances (BITS) [AD-A292176] p 2555 N95-29266
Broadband control of structural vibration using simultaneous sensing and actuation with nonlinear piezoelectric elements p 2664 N95-29548
High gain, low noise and broadband Raman and Brillouin fiber-optic amplifiers, channel selectors and switches [AD-A290585] p 2700 N95-29553
UHB engine fan broadband noise reduction study [NASA-CR-198357] p 2684 N95-29641
Advanced presort process [AD-A291010] p 2557 N95-29655
Description of the TV distribution service using MAGIC modelling methods [PB95-206728] p 2560 N95-30219
BROADCASTING
Communication protocols in multi-hop radio networks p 2553 N95-29106
BSCCO SUPERCONDUCTORS
Processing and properties of long-lengths of Ag-clad BSCCO superconductors and high-(Tc) magnets [DE95-005855] p 2716 N95-29984
BUBBLES
Bubble fusion: Preliminary estimates of spherical micro-implosions in cavitating liquids [DE95-006260] p 2569 N95-28956
Revisions and notes on a model for bubble attenuation in near-surface propagation [AD-A290312] p 2629 N95-29085
Three problems in fluid dynamics [AD-A290481] p 2573 N95-29324
A theoretical study on ignition mechanisms of liquid propellants [AD-A290569] p 2549 N95-29550
The one-dimensional bubble: Theory, experiment, and relevance to exposure of divers to low frequency sound, and of lung to lithotripsy [ISVR-TR-246] p 2577 N95-29817
BUCKLING
Buckling analysis of curved composite sandwich panels subjected to inplane loadings p 2517 N95-28845
ISPAN (Interactive Stiffened Panel Analysis): A tool for quick concept evaluation and design trade studies p 2517 N95-28846
A three dimensional finite element scheme for fiber microbuckling in thick multidirectional laminated composites p 2525 N95-29512
Severe edge effects and simple complimentary interior solutions for thin-walled anisotropic and composite structures [AD-A290645] p 2595 N95-29562
Elastoplastic buckling analysis of cylindrical shells using a semi-analytical formulation [PB95-197349] p 2597 N95-30206
Formulation of an improved smeared stiffener theory for buckling analysis of grid-stiffened composite panels [NASA-TM-110162] p 2529 N95-30341
BUFFER STORAGE
Garbage collection is fast, but a stack is faster [AD-A290099] p 2722 N95-29207
BUILDINGS
The 2nd European Conference on Smart Structures and Materials [AD-A290723] p 2550 N95-29579
BULK MODULUS
Experimental and analytical characterization of triaxially braided textile composites p 2520 N95-29040
BUOYANCY
Inflatable life vest [AD-D017273] p 2641 N95-29600

C

C (PROGRAMMING LANGUAGE)
C style guide [NASA-CR-189408] p 2645 N95-28821
Conversion of an oceanographic expert system to a C-based language [NASA-CR-198695] p 2630 N95-29237
C++ (PROGRAMMING LANGUAGE)
The mesh synchronous processor MeshSP (trademark) [AD-A289875] p 2659 N95-29420
High-level fault tolerance in distributed programs [AD-A290430] p 2724 N95-29818
C-130 AIRCRAFT
Technology integration box beam failure study p 2517 N95-28847
Flying ambulances: The approach of a small air force to long distance aeromedical evacuation of critically injured patients p 2678 N95-29618
C-135 AIRCRAFT
Computational Fluid Dynamics (CFD) analysis of a C-135 aircraft with a side-mounted splitter plate (with comparison to wind tunnel data) [AD-A292029] p 2571 N95-29187
CABLES (ROPES)
Cable load transducer [AD-A289548] p 2595 N95-29192
CADMIUM TELLURIDES
Multi-decade time-dependent voltage of polycrystalline thin-film solar cells p 2602 N95-29103
Electronic states in Cd(1-x)Zn(x)Te/CdTe strained layer coupled double quantum wells and their photoluminescence [DE95-006806] p 2716 N95-29814
CALCIUM OXIDES
Ion beam modification of Tl-Ba-Ca-Cu-O type high temperature superconductors during irradiation [DE95-006807] p 2717 N95-30022
CALCULUS
Proving the genericity lemma by leftmost reduction is simple [PB95-197620] p 2673 N95-30103
Usability: Formalising (un)definedness in typed lambda calculus [PB95-197190] p 2673 N95-30196
Essential structure of the jacopini technique [PB95-197208] p 2674 N95-30291
CALDERAS
Some aspects of lunar and martian volcanism as examined with spectral, topographic, and morphologic data derived from spacecraft images p 2736 N95-29594
CALIBRATING
Nonlinear calibration of an infrared radiometer [AD-A292436] p 2698 N95-28996
Characterization and calibration of a pulsed laser system for single event upset simulation [AD-A290075] p 2586 N95-29330
A hybrid electronically scanned pressure module for cryogenic environments [NASA-TM-110146] p 2583 N95-29453
Wideband I/Q demodulators: Measurement technique and matching characteristics [AD-A291505] p 2558 N95-29847
Inlet flow test calibration for a small axial compressor rig. Part 2: CFD compared with experimental results [NASA-TM-106999] p 2501 N95-30007
Balanced, double-sided calibration circuit for sensor element differential pre-amplifier [AD-D017326] p 2566 N95-30052
CAMERAS
Modeling foreshortening in stereo vision using local spatial frequency [AD-A292246] p 2645 N95-28883
NASA to use telepresence to explore Antarctic Lakes [NASA-TM-110567] p 2598 N95-29175
Computing 3-D motion in custom analog and digital VLSI [AD-A290270] p 2647 N95-29179
CAMOUFLAGE
Thermoreactive aircraft coatings (TRAC) program [AD-A292054] p 2542 N95-29314
CAMS
Dimensions, deflections and stresses for Hertzian contacts under combined normal and tangential loading. (Guide to use of computer program A9434.) [ESDU-94034] p 2593 N95-28711
Lubricant film thickness between disc cams and followers [ESDU-94008] p 2539 N95-28900
Contact stress in disc cams with domes of flat-faced followers [ESDU-94011] p 2589 N95-28901
Selection of materials, manufacturing methods and lubricants for cam mechanisms [ESDU-94017] p 2589 N95-28905
CANADA
The Canadian experience in UN airevac Sarajevo airlift: April 1993-October 1994 p 2676 N95-29606
CANALS
Channels and valleys on Venus p 2736 N95-29593
CANCELLATION
Flow visualization of vorticity cancellation of jets in crossflow [AD-A292414] p 2569 N95-28990
CANTILEVER BEAMS
The effect of mixed mode precracking on the mode 1 fracture toughness of composite laminates p 2514 N95-28827
CAPACITANCE
Development of electrochemical super capacitors for EMA applications p 2568 N95-30270
CAPACITANCE-VOLTAGE CHARACTERISTICS
Electrical characteristics of barium strontium titanate-oxide composite films [AD-A289991] p 2541 N95-29135
CAPACITORS
Hermetically sealed aluminum electrolytic capacitor p 2568 N95-30268
Development of electrochemical super capacitors for EMA applications p 2568 N95-30270
High energy density electrolytic capacitor p 2568 N95-30271
CARBAMATES (TRADENAME)
Photogenerated amines in polymer curing and imaging: Design and synthesis of (3', 5'-dimethoxybenzoinyl)oxycarbonyl carbamates as novel photoprecursors of amines [AD-A289945] p 2542 N95-29272
CARBIDES
Superplastic ceramics [AD-A290817] p 2545 N95-29635
CARBON
Activities update [AD-A292431] p 2692 N95-28994
Precision cleaning verification of fluid components by air/water impingement and total carbon analysis [NASA-TM-110742] p 2531 N95-29248
Deposition and surface treatment with intense pulsed ion beams [DE95-007885] p 2543 N95-29465
Fluxes and relative abundances of light cosmic ray nuclei at energies above 40 GeV/n p 2739 N95-29531
Effective emission and ionization rate coefficients of atomic carbons in plasmas [AD-B175932L] p 2707 N95-29740
Carbon sheet pumping [AD-B179443L] p 2710 N95-29812
Research results on an improved in-situ tropospheric humidity sensor [AD-A291339] p 2627 N95-29944
CARBON DIOXIDE
CO2-O2 interactions in extension of tolerance to acute hypoxia [NASA-CR-198575] p 2635 N95-29158
An integrated optical CO2 sensor. Phase 0: Design and fabrication of critical elements [NASA-CR-198792] p 2700 N95-29366
Analysis of global economic instruments for CO2 emission reduction: Equity and efficiency [DE95-764057] p 2610 N95-30195
CARBON DIOXIDE CONCENTRATION
Effect of irradiance, sucrose, and CO2 concentration on the growth of potato (Solanum tuberosum L.) in vitro [NASA-TM-110654] p 2632 N95-29375
CARBON DIOXIDE LASERS
Propagation and transformation properties of axicon optical systems for laser beams [AD-A289661] p 2584 N95-28679
CARBON FIBER REINFORCED PLASTICS
A study of structurally efficient graphite-thermoplastic trapezoidal-corrugation sandwich and semi-sandwich panels p 2516 N95-28842
Effects of cutouts on the behavior of symmetric composite laminates subjected to bending and twisting loads p 2517 N95-28844
Weavability of dry polymer powder towpreg p 2519 N95-29036
CARBON FIBERS
Lightweight battery electrode and method of making it [AD-D017389] p 2560 N95-28855
Effects of temperature and humidity cycling on the strengths of textile reinforced carbon/epoxy composite materials p 2520 N95-29037
A designed experiment in stitched/RTM composites p 2522 N95-29046
Effects of thermal and moisture cycling on the internal structure of stitched RTM laminates p 2522 N95-29048
The combined effect of glass buffer strips and stitching on the damage tolerance of composites p 2522 N95-29049
CARBON ISOTOPES
Carbon isotope abundance ratios in comets p 2732 N95-29592

CARBON STARS
Aperture synthesis observation of HCN J = 1-0 emission from Y Canum Venaticorum p 2735 N95-29839
Extended dust shells around carbon stars resolved by HIRAS p 2735 N95-29840
CARBONYL COMPOUNDS
Photogenerated amines in polymer curing and imaging: Design and synthesis of (3', 5'-dimethoxybenzoinyl)oxycarbonyl carbamates as novel photoprecursors of amines
[AD-A289945] p 2542 N95-29272
CARBORANE
Linear carborane-(siloxane or silane)-acetylene based copolymers
[AD-D017321] p 2547 N95-30132
CARDIOLOGY
Military flying and aeromedical evaluation of cardiac arrhythmias
[AD-A291595] p 2634 N95-28940
CARGO AIRCRAFT
Test and evaluation of the Impact Instrumentations, Inc. Uni-Vent model 750M ventilator
[AD-A292321] p 2640 N95-28792
CARRIER MOBILITY
SOSDOR: Solid-state device simulator code
[AD-A289954] p 2563 N95-29275
CARTESIAN COORDINATES
Surface Modeling, Grid Generation, and Related Issues in Computational Fluid Dynamic (CFD) Solutions
[NASA-CP-3291] p 2478 N95-28723
Marshall Space Flight Center surface modeling and grid generation applications p 2480 N95-28733
A Cartesian, cell-based approach for adaptively-refined solutions of the Euler and Navier-Stokes equations p 2480 N95-28739
Development and application of a 3D Cartesian grid Euler method p 2481 N95-28740
Unstructured Cartesian/prismatic grid generation for complex geometries p 2481 N95-28741
An assessment of unstructured grid technology for timely CFD analysis p 2482 N95-28747
Solution of the Navier-Stokes equations on locally refined Cartesian meshes using state-vector splitting p 2571 N95-29197
CAST ALLOYS
Tensile properties of as-cast iron-aluminide alloys
[DE95-005396] p 2538 N95-30216
CASTINGS
Tensile properties of as-cast iron-aluminide alloys
[DE95-005396] p 2538 N95-30216
CASUALTIES
Recent Issues and Advances in Aeromedical Evacuation (MEDEVAC)
[AGARD-CP-554] p 2676 N95-29604
Critical evaluation of aeromedical evacuation in a multinational forces scenario p 2676 N95-29610
Effect of hypoxia on arterial blood gases in subjects with lung dysfunction p 2638 N95-29627
CATACLYSMIC VARIABLES
A search for cataclysmic variables in globular clusters p 2727 N95-29532
CATALOGS (PUBLICATIONS)
Data catalog for JPL Physical Oceanography Distributed Active Archive Center (PO.DAAC)
[NASA-CR-198872] p 2631 N95-30231
CATALYSIS
Photogenerated amines in the design of imaging materials: The radiation-induced imidization of functionalized polystyrenes bearing amide-ester side chains
[AD-A289943] p 2542 N95-29270
Cage-like precursor formation from extensive cyclization in sol-gel inorganic condensation polymerization
[AD-A290589] p 2544 N95-29554
CATALYSTS
The TEES process cleans waste and produces energy
[DE95-007799] p 2602 N95-29463
The redox chemistry of some peroxo and superoxo metal ion complexes
[AD-A290761] p 2532 N95-29483
Conjugated polymers from cyclohexadienediol monomers
[AD-A290247] p 2544 N95-29505
Development of precipitated iron Fischer-Tropsch catalysts
[DE95-009334] p 2533 N95-29870
CATALYTIC ACTIVITY
Development of precipitated iron Fischer-Tropsch catalysts
[DE95-009334] p 2533 N95-29870
CATHODIC COATINGS
Cathodic protection system inspection 6
[AD-A289720] p 2591 N95-28682
Cathodic protection system inspection 5
[AD-A289724] p 2592 N95-28684
CATIONS
New tetraarylborate and ethyldibutylstannane reagents
[AD-A289813] p 2540 N95-28953
XPS study of Ni-Fe manganite thermistor material
[DE95-008778] p 2561 N95-28961
17O NMR of the structural evolution of V2O5 gels
[AD-A290623] p 2545 N95-29559
CAUCHY PROBLEM
Boundary element algorithms for Somigliana's identity
[PB95-206959] p 2597 N95-30169
CAVITATION FLOW
Bubble fusion: Preliminary estimates of spherical micro-implosions in cavitating liquids
[DE95-006260] p 2569 N95-28956
CAVITIES
The acoustic characteristics of turbomachinery cavities
[NASA-CR-4671] p 2478 N95-28720
Recirculating cavity casing treatment failure
[AD-A289330] p 2500 N95-28908
In-line fiber etalon strain sensor
[AD-D017266] p 2699 N95-29283
Theory of competition between synchronous and nonsynchronous modes in a magnicon output cavity
[AD-A292048] p 2563 N95-29301
Inflatable life vest
[AD-D017273] p 2641 N95-29600
CAVITY FLOW
The acoustic characteristics of turbomachinery cavities
[NASA-CR-4671] p 2478 N95-28720
CAVITY RESONATORS
Inhibition of mode competition in free-electron laser oscillators p 2586 N95-29336
CD-ROM
CD-ROM preparation: An overview and guide
[NASA-CR-198756] p 2655 N95-30307
CELESTIAL BODIES
Space astronomy update
[NASA-TM-110754] p 2731 N95-30317
CELESTIAL MECHANICS
An investigation into the existence of asteroids at Saturn's triangular Lagrangian points p 2727 N95-29648
Total solar eclipse of 1997 March 9
[NASA-RP-1173] p 2731 N95-30004
CELL MEMBRANES (BIOLOGY)
Electrical and electronic properties of self-assembled lipid bilayers
[AD-A290507] p 2632 N95-29155
CELLS (BIOLOGY)
Cellular and molecular level responses after radiofrequency radiation exposure, alone or in combination with x rays or chemicals
[AD-A292488] p 2633 N95-28866
Electrical and electronic properties of self-assembled lipid bilayers
[AD-A290507] p 2632 N95-29155
CENTAUR LAUNCH VEHICLE
A transient model of the RL10A-3-3A rocket engine
[NASA-CR-195478] p 2510 N95-29114
CENTER OF MASS
Summary report of mission acceleration measurements for STS-65, launched 8 July 1994
[NASA-TM-106871] p 2549 N95-30339
CENTRAL NERVOUS SYSTEM
The 5th International Meeting on Cholinesterase
[AD-A291253] p 2534 N95-30085
CENTRAL PROCESSING UNITS
N4 processor
[AD-A292571] p 2642 N95-28976
The Institute for Material Science and Department of Material Science, Tohoku University, Sendai Japan, 2-3 June 1994
[AD-A292348] p 2650 N95-29534
CENTRIFUGAL FORCE
Numerical simulation of stability and stability control of high speed compressible rotating couette flow
[NASA-CR-198832] p 2579 N95-30250
CENTRIFUGES
Coordination of operations for centrifuge quality control. phase 3C
[AD-A292533] p 2582 N95-28966
Spin augmented deployment and retrieval of tethered artificial gravity spacecraft p 2509 N95-30280
Summary report of mission acceleration measurements for STS-65, launched 8 July 1994
[NASA-TM-106871] p 2549 N95-30339
CERAMIC COATINGS
Corrosion investigation of multilayered ceramics and experimental nickel alloys in SCWO process environments
[DE95-008666] p 2540 N95-28960
CERAMIC FIBERS
Innovative processing of composites for ultra-high temperature applications, book 1
[AD-A290889] p 2527 N95-29842
CERAMIC MATRIX COMPOSITES
The development of an interpretive methodology for the application of real-time acousto-ultrasonic NDE technique for monitoring damage in ceramic composites under dynamic loads p 2592 N95-29104
Origins of imperfections in composite materials
[AD-A290261] p 2523 N95-29169
Innovative processing of composites for ultra-high temperature applications, book 1
[AD-A290889] p 2527 N95-29842
Alumina reinforced Tetragonal Zirconia (TZP) composites
[DE95-008990] p 2529 N95-30180
CERAMICS
A 1993 review of welding in Japan
[DE95-758701] p 2589 N95-28946
Corrosion investigation of multilayered ceramics and experimental nickel alloys in SCWO process environments
[DE95-008666] p 2540 N95-28960
Synthesis and characterization of CuO superconductors with high transient temperatures
[AD-A292478] p 2562 N95-29014
Processing, fabrication, characterization and device demonstration of high temperature superconducting ceramics
[AD-A290183] p 2541 N95-29055
High-toughness glass-ceramics
[AD-A290562] p 2541 N95-29071
Fabrication and characterization of barium strontium titanate and non-ferroelectric oxide composites
[AD-A289994] p 2523 N95-29136
Experimental investigations of wave and fracture phenomena in impacted ceramics and glasses
[AD-A292142] p 2542 N95-29195
Characterizing and modeling penetration of ceramic armor
[AD-A292588] p 2542 N95-29288
Fabrication and characterization of BSTO and nonferroelectric oxide composites for use in phased array antennas and other electronic devices
[AD-A290070] p 2524 N95-29329
Ceramic material life prediction: A program to translate ANSYS results to CARES/LIFE reliability analysis
[NASA-CR-198795] p 2543 N95-29367
Measurement of interface strength, intrinsic toughness and their dependence on interfacial segregants
[AD-A291798] p 2524 N95-29409
Recent progress in the study of the kinetics of sol-gel SiO2 synthesis reactions
[AD-A290570] p 2544 N95-29551
High temperature thermosets and ceramics derived from linear carborane-(siloxane or silane)-acetylene copolymers
[AD-D017400] p 2545 N95-29569
Proceedings of the 6th International Conference on Nondestructive Characterization of Materials
[AD-A290727] p 2596 N95-29580
Superplastic ceramics
[AD-A290817] p 2545 N95-29635
Integrated synthesis and post-processing of SiC and AlN
[AD-A290853] p 2537 N95-29724
Solid freeform fabrication symposium
[AD-A290949] p 2527 N95-29732
Measurement of interface strength, intrinsic toughness and their dependence on interfacial segregants
[AD-A291169] p 2546 N95-29926
Penetration of semi-infinite, bi-element targets by long rod penetrators
[AD-A291176] p 2596 N95-29929
Nanocrystalline processing and interface engineering of Si3N4-based ceramics
[AD-A291302] p 2546 N95-29939
What do we really know about the atomic scale structures of nanophase materials?
[DE95-005858] p 2717 N95-29986
Ceramics derived from organo-metallic precursors
[AD-A291434] p 2547 N95-30071
Evaluation of wear resistant ceramic valve seats in gas-fueled power generation engines
[PB95-200218] p 2591 N95-30110
Fractography of advanced structural ceramics: Results from the VAMAS round robin exercise
[AD-A290930] p 2547 N95-30118
Fabrication of advanced electrochemical energy materials using sol-gel processing techniques p 2607 N95-30269

CEREBRUM
Research on PGI2 and TXA2 effects at times of hyperbaric oxygenation of domestic rabbits with acute cerebral ischemia reirrigation damage
[AD-A289606] p 2632 N95-29263
CERENKOV COUNTERS
Fluxes and relative abundances of light cosmic ray nuclei at energies above 40 GeV/n p 2739 N95-29531
CERIUM OXIDES
Pulsed laser deposition of ferroelectric thin films in conjunction with superconducting oxides
[AD-A290101] p 2585 N95-29208
A Pr-141 Moessbauer study of praseodymium com pounds
[PB95-192449] p 2535 N95-30282
CESIUM
Development of Laser Optogalvanic Spectroscopy as a probe of alkali atoms in an MHD environment
[DE95-006481] p 2531 N95-28916
Chemically induced passivity of aluminum alloys and Al-based metal matrix composites
[AD-A290778] p 2528 N95-29923
CETANE
Cylinder-averaged histories of nitrogen oxide in a DI diesel with simulated turbocharging
[AD-A290568] p 2590 N95-29820
CH-46 HELICOPTER
An operational comparison of the CH-46E and HH-60H as Navy combat support helicopter replacement options using the Simulated Mobility Modeling and Analysis Toolbox (SMMAT)
[AD-A288494] p 2498 N95-29911
CHAINS
Photogenerated amines in the design of imaging materials: The radiation-induced imidization of functionalized polystyrenes bearing amide-ester side chains
[AD-A289943] p 2542 N95-29270
17O NMR of the structural evolution of V2O5 gels
[AD-A290623] p 2545 N95-29559
CHALCOGENIDES
Chalcogenide superconductors: A search
[AD-A292523] p 2560 N95-28812
CHANGE DETECTION
Experimental results of Hooper's gravity-electromagnetic coupling concept
[NASA-TM-106963] p 2680 N95-28893
CHANNEL FLOW
Numerical solution of the equations governing non-Newtonian flow at moderate Reynolds numbers p 2579 N95-30233
Supercritical states of two-dimensional wall-bounded shear flow p 2580 N95-30303
CHANNELS (DATA TRANSMISSION)
Methods and components for optical contention resolution in high speed networks
[AD-A292331] p 2697 N95-28795
Study of UV bleached channel waveguide performance in NLO polymer films
[AD-A292008] p 2540 N95-29021
CHAOS
The development of methods and techniques to detect and model the underlying structure of chaotic systems
[AD-A292435] p 2680 N95-29072
New predictive methods in chaotic fluid dynamics with application to turbulent heat transfer
[AD-A290691] p 2576 N95-29761
Dynamical instabilities, chaos and spatial complexity in fundamental nonlinear optical interactions
[AD-A291223] p 2588 N95-29980
CHARACTER RECOGNITION
Visualization of CAD objects using a stereoscopic display
[AD-A290034] p 2639 N95-29439
CHARACTERIZATION
Thin-film resistor array characterization
[AD-A289806] p 2561 N95-28950
Simplified data reduction methods for the ECT test for mode 3 interlaminar fracture toughness
[NASA-TM-110176] p 2527 N95-29825
Nitrogen dioxide measurement method characterization at the GRI conventional research house
[PB95-200549] p 2610 N95-30197
CHARGE CARRIERS
Nitride semiconductors for ultraviolet detection
[AD-A289546] p 2712 N95-28910
CHARGE COUPLED DEVICES
Upgrading the Day/Night whole sky imager from Manual/Interactive to full automatic control
[AD-A292296] p 2619 N95-28872
Testbed for precision characterization of spatial light modulators and optical processors
[AD-A290484] p 2699 N95-29148
Computing 3-D motion in custom analog and digital VLSI
[AD-A290270] p 2647 N95-29179
An ultra-high speed incoherent-to-coherent converter for optical computing
[AD-A292658] p 2700 N95-29412
Research instrumentation for polytechnic university's supersonic wind tunnel facility
[AD-A290232] p 2502 N95-29468
The use of charge coupled devices in astronomical speckle imaging p 2727 N95-29545
CHARGED PARTICLES
Design of an electronic charged particle spectrometer to measure (rho R), yield, and implosion symmetry on the OMEGA Upgrade
[DE95-006088] p 2695 N95-28930
CHARTS
Digital mapping, charting, and geodesy analysis program technical review of vector smart map prototypes 1 and 2
[AD-A291217] p 2601 N95-29977
Delayed choice: An operator for joining message sequence charts
[PB95-206710] p 2560 N95-30203
CHEBYSHEV APPROXIMATION
Polynomial approximations for materials simulations
[DE95-006188] p 2652 N95-29989
Solution of acoustic workshop problems by a spectral multidomain method p 2687 N95-30141
CHEMICAL ANALYSIS
XPS study of Ni-Fe manganite thermistor material
[DE95-008778] p 2561 N95-28961
Chromium plating and electropolishing solution analyses by online x ray fluorescence spectroscopy
[AD-A290023] p 2541 N95-29138
Precision cleaning verification of fluid components by air/water impingement and total carbon analysis
[NASA-TM-110742] p 2531 N95-29248
In-plant testing of membranes to treat electroplating wastewater
[NASA-CR-198796] p 2532 N95-29250
Laser applications to chemical analysis: Summaries of papers presented at the laser applications to chemical analysis topical meeting
[AD-A290738] p 2587 N95-29653
The effect of wear on fire-blocking layer material effectiveness
[AD-A291520] p 2493 N95-29855
The comparative extinguishment performance and thermal decomposition products of halon alternative agents
[AD-A291161] p 2551 N95-29924
CHEMICAL BONDS
Structural and electronic properties of adsorbates on semiconductors, metal-semiconductor interfaces and semiconductor heterojunctions
[AD-A291917] p 2715 N95-29438
CHEMICAL CLOUDS
One and two fluid numerical investigations of solar wind gas releases p 2738 N95-29704
CHEMICAL COMPOSITION
Synthesis and complete characterization of a Gallium-Mixed-Pnicogen four-membered ring compound: I2GaAs(SiMe3)(sub 2)Ga(I)2P(SiMe3)(sub 2)
[AD-A292423] p 2713 N95-28993
Electrochemical impedance pattern recognition for detection of hidden chemical corrosion on aircraft components, phase 1
[AD-A291345] p 2593 N95-29946
CHEMICAL COMPOUNDS
Commercial photorefractive device using nonstoichiometric 3-5 semiconductors
[AD-A292494] p 2713 N95-28933
CHEMICAL DEFENSE
Analysis of factors affecting chemical reactions in supercritical fluids
[AD-A290905] p 2534 N95-30078
CHEMICAL EFFECTS
Molten fluoride fuel salt chemistry
[DE95-007025] p 2695 N95-28957
Modeling joint effects of mixtures of chemicals on microorganisms using quantitative structure activity relationship techniques, phase 3
[AD-A290153] p 2632 N95-29320
Effect of irradiance, sucrose, and CO2 concentration on the growth of potato (Solanum tuberosum L.) in vitro
[NASA-TM-110654] p 2632 N95-29375
CHEMICAL ENGINEERING
Phase coupling and morphology generation in engineering polymer alloys
[AD-A291868] p 2543 N95-29436
Introduction to the proceedings of the sixteenth symposium on biotechnology for fuels and chemicals
[DE95-007029] p 2549 N95-30024
CHEMICAL EQUILIBRIUM
XPS study of Ni-Fe manganite thermistor material
[DE95-008778] p 2561 N95-28961
Theory and experiments on chemical instabilities
[AD-A290773] p 2534 N95-29922
CHEMICAL LASERS
Studies of energy transfer processes of relevance to chemically and optically pumped lasers
[AD-A290164] p 2585 N95-29025
Development of continuous visible chemical laser amplifiers and oscillators from the Na3-X(Cl, Br, I) reactions and their analogs and energy transfer pumping from efficiently produced metastable states
[AD-A290999] p 2586 N95-29514
CHEMICAL PROPULSION
Guidance, navigation, and control study for a solar electric propulsion spacecraft
[NASA-CR-198920] p 2509 N95-30357
CHEMICAL REACTIONS
Compendium of NASA data base for the global tropospheric experiment's Transport and Atmospheric Chemistry Near the Equator-Atlantic (TRACE-A)
[NASA-TM-110151] p 2608 N95-28717
Characterization of excited state oxygen-organic molecule complexes
[AD-A290548] p 2692 N95-29092
Dynamics of simple chemically reactive fluids p 2573 N95-29335
Reaction field (RF) calculation of the spectral shifts of indole
[AD-A290449] p 2532 N95-29487
Quantum dynamical studies of the decomposition of energetic materials containing defect structures
[AD-A291456] p 2548 N95-29525
Boronization study for application to large helical device
[AD-B191996L] p 2709 N95-29808
Analysis of factors affecting chemical reactions in supercritical fluids
[AD-A290905] p 2534 N95-30078
CHEMICAL REACTORS
Feasibility of a jet-stirred reactor for evaluating replacements for halon fire retardants
[AD-A291155] p 2551 N95-30299
CHEMICAL VAPOR INFILTRATION
Innovative processing of composites for ultra-high temperature applications, book 1
[AD-A290889] p 2527 N95-29842
Elevated temperature static fatigue of a Nicalon fiber-reinforced SiC composite
[DE95-008780] p 2528 N95-30175
CHEMICALS
Selective multi-chemical fiber optic sensor
[AD-D017409] p 2703 N95-30076
CHEMILUMINESCENCE
Nitrogen dioxide measurement method characterization at the GRI conventional research house
[PB95-200549] p 2610 N95-30197
CHEMISORPTION
Molecular spectra and dynamics at interfaces
[AD-A289779] p 2693 N95-29460
CHEST
Inflatable life vest
[AD-D017273] p 2641 N95-29600
CHILE
A numerical study of the effects of wind forcing on the Chile Current System
[AD-A289808] p 2629 N95-28982
CHINA
The 2nd International Conference on Thin Film Physics and Applications
[AD-A292353] p 2546 N95-29983
CHIPS
The mesh synchronous processor MeshSP (trademark)
[AD-A289875] p 2659 N95-29420
CHIPS (ELECTRONICS)
Improved interception capability through the use of transform domain processing
[AD-A292231] p 2554 N95-29203
Asymptotically zero energy computing using split-level charge recovery logic
[AD-A290054] p 2564 N95-29478
CHLORINATION
Corrosion investigation of multilayered ceramics and experimental nickel alloys in SCWO process environments
[DE95-008666] p 2540 N95-28960
Novel photoelectric sensing technology for environmental monitoring, phase 1
[AD-A292026] p 2611 N95-30348
CHLORINE
Semiconductor deposition and etching interactions of laser-generated translationally hot atoms and radicals
[AD-A291824] p 2693 N95-29431
CHLORINE OXIDES
In situ measurements of ClO and implications for the chemistry of inorganic chlorine in the lower stratosphere p 2618 N95-29830

CHLOROCARBONS
Alternative refrigerant performance: Field test of a nonchlorofluorocarbon chiller at Fort Leonard Wood, MO
[AD-A292052] p 2550 N95-29307
CHLOROFLUOROCARBONS
Use of chlorofluorocarbon-based refrigerants in USArmy facility air-conditioning and refrigeration systems: Recommendations for the interim period 1994-2000
[AD-A290432] p 2550 N95-29537
CHOLESTEROL
Transitions in liquid crystals initiated with circularly polarized light
[AD-A290525] p 2716 N95-29493
CHOLINE
Coupling of brain muscarinic receptors to second messengers
[AD-A290498] p 2635 N95-29153
CHOLINESTERASE
The 5th International Meeting on Cholinesterase
[AD-A291253] p 2534 N95-30085
CHONDRITES
Spectral reflectance studies and optical surface alteration in the search for links between meteorites and asteroids p 2733 N95-29672
CHROMIUM
Chromium plating and electropolishing solution analyses by online x ray fluorescence spectroscopy
[AD-A290023] p 2541 N95-29138
Effects of chromium picolinate on body composition in a remedial conditioning program
[AD-A292079] p 2636 N95-29238
Effects of space exposure on metals flown on the Long Duration Exposure Facility
[NASA-CR-4662] p 2512 N95-30225
CHROMOPHORES
Transitions in liquid crystals initiated with circularly polarized light
[AD-A290525] p 2716 N95-29493
CHROMOSPHERE
First flight of the Multi-Spectral Solar Telescope Array: Calibration, results and future plans
p 2727 N95-29529
15th NSO/Sac Peak Solar Workshop
[AD-A292297] p 2739 N95-30074
CHRONOLOGY
From the (psi) to charmed mesons
[DE95-006564] p 2693 N95-29583
CIRCADIAN RHYTHMS
Organization of the human circadian system
[AD-A288223] p 2634 N95-28915
Shift work, age, and performance: Investigation of the 2-2-1 shift schedule used in Air Traffic Control facilities I. The sleep/wake cycle
[DOT/FAA/AM-95/19] p 2638 N95-29261
The effect of bright light and LEET on sleep after a 10-hour phase delay
[AD-A291264] p 2637 N95-29995
CIRCUIT RELIABILITY
R&M design expert system
[AD-A292525] p 2645 N95-28814
CIRCUITS
Inductive boolean function manipulation: A hardware verification methodology for automatic induction
[AD-A292236] p 2669 N95-29128
A compact universal power supply for laser diodes
[AD-A289950] p 2585 N95-29274
Research and development of a high performance GaAs microcomputer system
[AD-A292647] p 2643 N95-29381
Spectral inverse scattering theory for dielectric media: Application to optical devices
[AD-A292651] p 2556 N95-29383
Novel high-power solid-state sources for the millimeter-wave region
[AD-A292653] p 2564 N95-29384
Robust testing of cellular neural networks
[AD-A291219] p 2665 N95-29979
CIRCULAR CYLINDERS
The effects of three-dimensional imposed disturbances on bluff body near wake flows: Effects of taper and splitter plates on the near wake characteristics of a circular cylinder in uniform and shear flow
[AD-A292113] p 2487 N95-28921
Numerical experiments on the flow past a circular cylinder at sub-critical Reynolds number
[AD-A289937] p 2573 N95-29268
Vortex element analysis of selected time-dependent flows
[AD-A289944] p 2573 N95-29271
Elastoplastic buckling analysis of cylindrical shells using a semi-analytical formulation
[PB95-197349] p 2597 N95-30206
CIRCULATION
Recirculating cavity casing treatment failure
[AD-A289330] p 2500 N95-28908
CIRRUS CLOUDS
Microwave remote sensing algorithms for cirrus clouds and precipitation p 2623 N95-29715
Extended field observations of cirrus clouds using a ground-based cloud observing system
[NASA-CR-198855] p 2628 N95-30356
CIVIL AVIATION
Effects of cabin pressure on climb and descent rates
[ESDU-94040] p 2496 N95-29016
The effect of wear on fire-blocking layer material effectiveness
[AD-A291520] p 2493 N95-29855
CLASSICAL MECHANICS
Automated reasoning about classical mechanics
[AD-A290052] p 2663 N95-29477
CLASSIFICATIONS
Development of an artificial neural network for real-time classification of cone penetrometer strain gauge data
[AD-A290719] p 2664 N95-29499
Acquisition of place knowledge through case-based learning
[AD-A292574] p 2723 N95-29573
Bootstrap and partitioning methods
[AD-A290662] p 2671 N95-29578
Cyclic feature analysis, design and exploitation
[AD-A290639] p 2557 N95-29603
Description and manipulation of method fragments for the assembly of situational methods
[PB95-197133] p 2653 N95-30094
Neural networks for combinatorial optimization
[PB95-206843] p 2667 N95-30222
CLASSIFIERS
Induction of selective Bayesian classifiers
[AD-A292690] p 2675 N95-29906
CLEAN FUELS
Hydrogen production in fusion reactors
[AD-B180028L] p 2710 N95-29857
CLEANING
Precision cleaning verification of fluid components by air/water impingement and total carbon analysis
[NASA-TM-110742] p 2531 N95-29248
Boronization study for application to large helical device
[AD-B191996L] p 2709 N95-29808
CLEAVAGE
Analytical potential energy surface for methylene nitramine (CH2NNO2)
[AD-A291247] p 2534 N95-29994
CLEBSCH-GORDAN COEFFICIENTS
Tables of SU3 isoscalar factors
[DE95-009375] p 2690 N95-28779
CLIMATE
Observations of mesoscale cellular convection from the marine stratocumulus phase of FIRE
p 2624 N95-29727
Soil wetness and climate variability
p 2609 N95-29878
CLIMATE CHANGE
Measurement of the seasonal and annual variability of total column aerosol in a northeastern US network
[DE95-007259] p 2608 N95-28920
Stochastic modeling and global warming trend extraction for ocean acoustic travel times
[AD-A292114] p 2608 N95-28922
Forecasting global temperature variations by neural networks
[AD-A290081] p 2621 N95-29333
The effect of climate perturbations on extratropical cyclogenesis along the east coast of North America
p 2621 N95-29595
Use of ARM data to test an improved parameterization of upper tropospheric clouds for use in climate models
[DE95-009324] p 2610 N95-30181
The effects of clouds as a feedback mechanism on the Earth's climate in the tropical Pacific
p 2611 N95-30300
CLIMATE MODELS
Load-balancing algorithms for the parallel community climate model
[DE95-008795] p 2610 N95-30176
Use of ARM data to test an improved parameterization of upper tropospheric clouds for use in climate models
[DE95-009324] p 2610 N95-30181
CLIMATOLOGY
Stochastic modeling and global warming trend extraction for ocean acoustic travel times
[AD-A292114] p 2608 N95-28922
A numerical study of the effects of wind forcing on the Chile Current System
[AD-A289808] p 2629 N95-28982
Sensitivity of the simulated global climate to perturbations in low cloud microphysical properties
p 2620 N95-29206
Numerical studies of the stratospheric aerosol layer under background and perturbed conditions
p 2615 N95-29666
Production of a long-term global water vapor and liquid water data set using ultra-fast methods to assimilate multi-satellite and radiosonde observations
[NASA-CR-198955] p 2628 N95-30272
CLIMBING FLIGHT
Effects of small changes on rate of climb
[ESDU-94039] p 2495 N95-28707
Effects of cabin pressure on climb and descent rates
[ESDU-94040] p 2496 N95-29016
CLINICAL MEDICINE
Military flying and aeromedical evaluation of cardiac arrhythmias
[AD-A291595] p 2634 N95-28940
Flying waivers for history of angioplasty and myocardial infraction
[AD-A292505] p 2635 N95-29161
CLIPS
Conversion of an oceanographic expert system to a C-based language
[NASA-CR-198695] p 2630 N95-29237
CLOCKS
Methods and components for optical contention resolution in high speed networks
[AD-A292331] p 2697 N95-28795
A gyroscope clock for a null gravitational redshift experiment p 2584 N95-29664
CLOUD COVER
Upgrading the Day/Night whole sky imager from Manual/Interactive to full automatic control
[AD-A292296] p 2619 N95-28872
The spatial-scale dependence of the observed anisotropy of reflected and emitted radiation
p 2613 N95-29253
Estimates of probability of a cloud-free line of sight for RAPTOR TALON
[AD-A291908] p 2510 N95-29284
The interactive role of clouds and radiative transfer in maintaining atmospheric circulation
p 2616 N95-29699
A theoretical model of multiple regimes in a stratocumulus-topped boundary layer
p 2624 N95-29726
Use of ARM data to test an improved parameterization of upper tropospheric clouds for use in climate models
[DE95-009324] p 2610 N95-30181
CLOUD PHYSICS
Sensitivity of the simulated global climate to perturbations in low cloud microphysical properties
p 2620 N95-29206
Continental aerosol effects on stratocumulus microphysics during MAST 1994
[AD-A292674] p 2621 N95-29416
The interactive role of clouds and radiative transfer in maintaining atmospheric circulation
p 2616 N95-29699
CLOUDS (METEOROLOGY)
Sensitivity of the simulated global climate to perturbations in low cloud microphysical properties
p 2620 N95-29206
The dynamics of circulations within the stratiform regions of squall lines p 2623 N95-29725
Short-range precipitation forecasts using assimilation of simulated satellite water vapor profiles and cloud liquid water p 2625 N95-29832
Use of ARM data to test an improved parameterization of upper tropospheric clouds for use in climate models
[DE95-009324] p 2610 N95-30181
The effects of clouds as a feedback mechanism on the Earth's climate in the tropical Pacific
p 2611 N95-30300
CLUTTER
An algorithm fusion approach to IRST signal processing (III): Nongaussian-corrected filter fusion
[AD-A291565] p 2552 N95-28936
Statistical properties of bistatic clutter echoes
[AD-A291688] p 2552 N95-28943
Description of the OHGR database
[AD-A290146] p 2722 N95-29221
CMOS
Asymptotically zero energy computing using split-level charge recovery logic
[AD-A290054] p 2564 N95-29478
CN EMISSION
Aperture synthesis observation of HCN J = 1-0 emission from Y Canum Venaticorum p 2735 N95-29839
COARSENESS
Mechanical properties of nanophase metals
[DE95-005408] p 2537 N95-30018
COASTAL ZONE COLOR SCANNER
SeaWiFS technical report series. Volume 24: SeaWiFS technical report series cumulative index, volumes 1-23
[NASA-TM-104556] p 2631 N95-30236
COASTS
Tidal constituent database: West coast of the United States and eastern North Pacific Ocean
[AD-A292224] p 2630 N95-29198

The detection of oil slicks at night with airborne infrared imagers
[AD-A289731] p 2598 N95-29281

COATING
Zero Discharge Organic Coatings: Powder paint. UV curable paint. E-coat
[AD-A292180] p 2540 N95-28925
Thermoreactive aircraft coatings (TRAC) program
[AD-A292054] p 2542 N95-29314
Impact properties of coated engineering plastics
[PB95-197281] p 2547 N95-30201

COATINGS
Impact properties of coated engineering plastics
[PB95-197281] p 2547 N95-30201

COCKPITS
Three-D weather displays for aircraft cockpits
[AD-A289759] p 2499 N95-28691
Conceptual design of a map interactive system for military aircraft cockpits
[AD-A289760] p 2499 N95-28692
Task-dependent effects of automation: The role of internal models in performance, workload, and situational awareness in a semi-automated cockpit
[AD-A292538] p 2640 N95-28969
Optimizing cockpit display configurations with a genetic algorithm system
[AD-A289799] p 2499 N95-29123

CODE DIVISION MULTIPLE ACCESS
Improved interception capability through the use of transform domain processing
[AD-A292231] p 2554 N95-29203

CODERS
The design of programmable convolutional encoder using VHDL and an FPGA
[AD-A290048] p 2649 N95-29442

CODING
Optimal universal coding and density estimation
[AD-A290694] p 2675 N95-29587
The 5th International Meeting on Cholinesterase
[AD-A291253] p 2534 N95-30085

COEFFICIENTS
W-matrices, nonorthogonal multiresolution analysis, and finite signals of arbitrary length
[DE95-005846] p 2652 N95-30020

COGNITION
Automation and cognition in air traffic control: An empirical investigation
[AD-A291932] p 2493 N95-28790
Macroprocesses and adaptive instruction
[AD-A290483] p 2648 N95-29325
Visualization of CAD objects using a stereoscopic display
[AD-A290034] p 2639 N95-29439
Georgetown Institute for Cognitive and Computational Sciences
[AD-A289775] p 2639 N95-29458
COADE: A framework for cognitive analysis, design, and evaluation
[AD-A291282] p 2720 N95-29935

COGNITIVE PSYCHOLOGY
Automation and cognition in air traffic control: An empirical investigation
[AD-A291932] p 2493 N95-28790
Test theory reconceived
[AD-A291836] p 2639 N95-29432

COHERENT LIGHT
An ultra-high speed incoherent-to-coherent converter for optical computing
[AD-A292658] p 2700 N95-29412

COHERENT RADIATION
Semiconductor film Cherenkov lasers
[AD-A291177] p 2587 N95-29930

COHESION
InTlSb as a long-wave infrared (LWIR) material: Defects and transportation properties
[AD-A291218] p 2702 N95-29978

COLD FLOW TESTS
Hydrogen film cooling with incident and swept-shock interactions in a Mach 6.4 nitrogen free stream
[NASA-TM-4603] p 2578 N95-30056

COLD FRONTS
An air stream analysis of the occluded cyclone
p 2623 N95-29714

COLD WEATHER
Human fluid balance and dehydration during cold weather military operations
[AD-A289192] p 2636 N95-29757

COLLAPSE
A thermochemical transport model for analysis of hot-spot formation in energetic materials
[AD-A290441] p 2532 N95-29357

COLLECTION
Tools for Automated Knowledge Engineering (TAKE) system evaluation methodology
[AD-A291145] p 2654 N95-30125

COLLISION PARAMETERS
Measurements of (Delta)(sigma)(sub L)(pp) and (Delta)(sigma)(sub L)((bar p)p) at 200 GeV/c
[DE95-005837] p 2695 N95-30186

COLLISIONAL PLASMAS
Modeling the boundary layer interactions between weakly ionized plasmas and cooled, planar electrodes in stagnation-point flows p 2706 N95-29717
Monte Carlo simulation study of the ICRF minority heating in the large helical device
[AD-B179858L] p 2708 N95-29749

COLLISIONLESS PLASMAS
Comment on a mean field Ohm's law for collisionless plasmas
[AD-B176252L] p 2707 N95-29741
Collisionless driven magnetic reconnection
[AD-B178946L] p 2709 N95-29810
The origin of collisionless dissipation in magnetic reconnection
[AD-B178949L] p 2710 N95-29813
Relativistic effects on large amplitude nonlinear langmuir waves in a two-fluid plasma
[AD-B191980L] p 2710 N95-29841
The physics of the collisionless bow shock
p 2580 N95-30301

COLLISIONS
Delivery of meteorites from the asteroid belt
p 2732 N95-29255

COLLOCATION
Time-optimal multi-axis attitude maneuvers of rigid spacecraft using collocation and nonlinear programming
p 2507 N95-29332

COLLOIDS
Demonstration of a stabilized alumina/ethanol colloidal dispersion technique for seeding high temperature air flows
[NASA-TM-106945] p 2582 N95-29113

COLOR
Thermoreactive aircraft coatings (TRAC) program
[AD-A292054] p 2542 N95-29314

COLOR-MAGNITUDE DIAGRAM
The search for mass segregation in star clusters of the Magellanic Clouds p 2730 N95-29781

COMBAT
An operational comparison of the CH-46E and HH-60H as Navy combat support helicopter replacement options using the Simulated Mobility Modeling and Analysis Toolbox (SMMAT)
[AD-A288494] p 2498 N95-29911

COMBINATORIAL ANALYSIS
Research in graph algorithms and combinatorial optimization
[AD-A292630] p 2648 N95-29297
Neural networks for combinatorial optimization
[PB95-206843] p 2667 N95-30222

COMBUSTION
SCAP spray combustion analysis program
[AD-A289946] p 2532 N95-29273
Fire hardening assessment (FHA) technology for composite systems
[AD-A289964] p 2523 N95-29277

COMBUSTION CHAMBERS
External combustion engine having an asymmetrical CAM
[AD-D017382] p 2588 N95-28785
High-temperature optical window design
[NASA-TM-106783] p 2596 N95-30008

COMBUSTION PHYSICS
Compendium of NASA data base for the global tropospheric experiment's Transport and Atmospheric Chemistry Near the Equator-Atlantic (TRACE-A)
[NASA-TM-110151] p 2608 N95-28717
SCAP spray combustion analysis program
[AD-A289946] p 2532 N95-29273

COMBUSTION PRODUCTS
Investigation of the flow turning loss in unstable solid propellant rocket motors p 2510 N95-29331
Measurements of ions formed in jet engine exhaust plumes
[AD-A290940] p 2501 N95-29764

COMBUSTION SYNTHESIS
Hot explosive consolidation of W-Ti alloys
[AD-A290880] p 2537 N95-29835

COMETS
Carbon isotope abundance ratios in comets
p 2732 N95-29592
Guidance, navigation, and control study for a solar electric propulsion spacecraft
[NASA-CR-198920] p 2509 N95-30357

COMMAND GUIDANCE
Closed loop control of guided missiles using neural networks p 2663 N95-29241

COMMAND LANGUAGES
Automated testing of application domains
[AD-A289753] p 2643 N95-28690

COMMERCE
Solid Oxide Fuel Cell commercialization in the United States
[DE95-008210] p 2607 N95-30278
CD-ROM preparation: An overview and guide
[NASA-CR-198756] p 2655 N95-30307

COMMERCIAL AIRCRAFT
In situ processing methods for composite fuselage sandwich structures p 2513 N95-28826
The effect of wear on fire-blocking layer material effectiveness
[AD-A291520] p 2493 N95-29855
Electrochemical impedance pattern recognition for detection of hidden chemical corrosion on aircraft components, phase 1
[AD-A291345] p 2593 N95-29946
SPE(R)-OBOGS: On-board oxygen generating sustem
p 2606 N95-30267

COMMINUTION
Characterizing and modeling penetration of ceramic armor
[AD-A292588] p 2542 N95-29288

COMMUNICATING
Formal design of communication protocols using Estelle
[AD-A290584] p 2652 N95-30042
Software risk evaluation method version 1.0
[AD-A290597] p 2652 N95-30047

COMMUNICATION EQUIPMENT
Conference reports
[AD-A289630] p 2561 N95-28911
Test results of a 20 GHz, low noise downconverter for USAT applications
[NASA-TM-106892] p 2508 N95-30011

COMMUNICATION NETWORKS
Wax: A wide-area computation system
[AD-A292247] p 2658 N95-28884
NPSNETIV: An object-oriented interface for a three-dimensional virtual world
[AD-A292467] p 2646 N95-29008
Communication protocols in multi-hop radio networks
p 2553 N95-29106
Towards an example-based image compression architecture for video-conferencing
[AD-A290041] p 2556 N95-29441
The design of programmable convolutional encoder using VHDL and an FPGA
[AD-A290048] p 2649 N95-29442
Scheduling algorithms for mobile packet radio networks p 2558 N95-29707
UHF Low Density Radio Communications Link (LDRCL) Operational Test and Evaluation (OT&E) integration and OT&E operational final test report
[AD-A291447] p 2558 N95-29769
UMTS network architecture
[PB95-206744] p 2558 N95-29919
Formal design of communication protocols using Estelle
[AD-A290584] p 2652 N95-30042
Description of the TV distribution service using MAGIC modelling methods
[PB95-206728] p 2560 N95-30219

COMMUNICATION SATELLITES
Design and analysis of the launch vehicle adapter fitting for the petite amateur navy satellite (PANSAT)
[AD-A289693] p 2504 N95-28680
Alternative packet switch architectures for a 30/20 GHz FDMA/TDMA geostationary communication satellite network
[NASA-CR-195470] p 2506 N95-30090

COMPACT GALAXIES
The 12 UM contribution of nearby galaxies to the infrared background
[AD-A291185] p 2735 N95-29917

COMPATIBILITY
Super hydrides
[AD-A290594] p 2533 N95-29556

COMPENSATORS
Modeling and control of rotating stall in high speed multi-stage axial compressors p 2500 N95-29244

COMPETITION
Theory of competition between synchronous and nonsynchronous modes in a magnicon output cavity
[AD-A292048] p 2563 N95-29301

COMPLETENESS
Delayed choice: An operator for joining message sequence charts
[PB95-206710] p 2560 N95-30203

COMPLEX COMPOUNDS
The interaction of group 3A atoms with small molecules
[AD-A290285] p 2692 N95-29082
Characterization of excited state oxygen-organic molecule complexes
[AD-A290548] p 2692 N95-29092

Transition metal complexes with perfluorinated ligands
[AD-A290250] p 2536 N95-29427

COMPLEX SYSTEMS

Proceedings of the Complex Systems Engineering Synthesis and Assessment Technology Workshop (CSESAW 1994)
[AD-A292433] p 2646 N95-28995

COADE: A framework for cognitive analysis, design, and evaluation
[AD-A291282] p 2720 N95-29935

Nonlinear control systems
[AD-A291083] p 2665 N95-29971

COMPOSITE MATERIALS

The effects of design details on cost and weight of fuselage structures p 2499 N95-28831

Mechanical characterization of two thermoplastic composites fabricated by automated tow placement p 2515 N95-28834

Impact damage resistance of composite fuselage structure, part 2 p 2516 N95-28838

ISPAN (Interactive Stiffened Panel Analysis): A tool for quick concept evaluation and design trade studies p 2517 N95-28846

Technology integration box beam failure study p 2517 N95-28847

IPACS (Integrated Probabilistic Assessment of Composite Structures): Code development and applications p 2518 N95-28849

Ferroelectric and piezoelectric properties of nylon 11/Poly(Vinylidene fluoride) bilaminate films
[AD-A292274] p 2539 N95-28891

Through-the-thickness stresses and failure in the corner radius of a laminated composite section
[ESDU-94019] p 2518 N95-28899

Shear reinforcement in deep slabs
[AD-A289528] p 2594 N95-28909

Third NASA Advanced Composites Technology Conference, volume 1, part 1
[NASA-CP-3178-VOL-1-PT-1] p 2518 N95-29029

Advanced composites technology program p 2519 N95-29032

Textile composite fuselage structures development p 2519 N95-29033

Advanced composite fuselage technology p 2519 N95-29034

Performance of resin transfer molded multiaxial warp knit composites p 2520 N95-29039

Composite material studies for low temperature thermionic emission
[AD-A292159] p 2523 N95-29124

Fabrication and characterization of barium strontium titanate and non-ferroelectric oxide composites
[AD-A289994] p 2523 N95-29136

Gordon research conference on point defects, line defects, and interfaces in semiconductors
[AD-A290103] p 2714 N95-29209

Gordon research conference on physical metallurgy: Materials by design
[AD-A290519] p 2524 N95-29326

Center for Advanced Aerospace Materials (CAAM), Seoul National University, 29 June 1994
[AD-A292344] p 2525 N95-29476

Studies directed toward new and improved permanent magnet materials
[AD-A290749] p 2681 N95-29481

Processing studies on in situ composites based on blends of thermotropic Liquid Crystalline Polymers with thermoplastics
[AD-A290526] p 2544 N95-29494

Quantum dynamical studies of the decomposition of energetic materials containing defect structures
[AD-A291456] p 2548 N95-29525

Aircraft advanced materials research and development program plan
[AD-A290542] p 2498 N95-29565

Interlaminar fracture mechanics and mechanisms: Linear and nonlinear aspects p 2526 N95-29597

Laser applications to chemical analysis: Summaries of papers presented at the laser applications to chemical analysis topical meeting
[AD-A290738] p 2587 N95-29653

Solid freeform fabrication symposium
[AD-A290949] p 2527 N95-29732

The Stroh formalism for anisotropic elasticity with applications to composite materials
[AD-A290710] p 2527 N95-29763

Simplified data reduction methods for the ECT test for mode 3 interlaminar fracture toughness
[NASA-TM-110176] p 2527 N95-29825

Measurement of interface strength, intrinsic toughness and their dependence on interfacial segregants
[AD-A291169] p 2546 N95-29926

Penetration of semi-infinite, bi-element targets by long rod penetrators
[AD-A291176] p 2596 N95-29929

Micromechanics of crack extension in composites p 2529 N95-30276

Visit to the Laboratory For Evaluation and Failure Prevention of Materials, Toyohashi University of Technology, 17 Oct 94
[AD-A292340] p 2597 N95-30293

COMPOSITE STRUCTURES

Analysis of static contact in laminated composite plates using damage mechanics
[NASA-CR-198656] p 2513 N95-28809

Third NASA Advanced Composites Technology Conference, volume 1, part 2
[NASA-CP-3178-VOL-1-PT-2] p 2513 N95-28823

Characterization and development of materials for advanced textile composites p 2513 N95-28824

In situ processing methods for composite fuselage sandwich structures p 2513 N95-28826

Establishing the relationship between manufacturing and component performance in stretch formed thermoplastic composites p 2514 N95-28829

The effects of design details on cost and weight of fuselage structures p 2499 N95-28831

Automated fiber placement: Evolution and current demonstrations p 2514 N95-28832

Manufacturing scale-up of composite fuselage crown panels p 2515 N95-28835

Design, analysis, and fabrication of a pressure box test fixture for tension damage tolerance testing of curved fuselage panels p 2516 N95-28839

Global cost and weight evaluation of fuselage keel design concepts p 2499 N95-28840

A study of structurally efficient graphite-thermoplastic trapezoidal-corrugation sandwich and semi-sandwich panels p 2516 N95-28842

A weight-efficient design strategy for cutouts in composite transport structures p 2516 N95-28843

Effects of cutouts on the behavior of symmetric composite laminates subjected to bending and twisting loads p 2517 N95-28844

Buckling analysis of curved composite sandwich panels subjected to inplane loadings p 2517 N95-28845

ISPAN (Interactive Stiffened Panel Analysis): A tool for quick concept evaluation and design trade studies p 2517 N95-28846

Technology integration box beam failure study p 2517 N95-28847

A global/local analysis method for treating details in structural design p 2517 N95-28848

IPACS (Integrated Probabilistic Assessment of Composite Structures): Code development and applications p 2518 N95-28849

Sorption and diffusion of moisture in multilayer composite AEM/S sandwich materials
[AD-A289807] p 2518 N95-28951

Advanced composite structural concepts and materials technologies for primary aircraft structures: Advanced material concepts
[NASA-CR-4485] p 2496 N95-29027

Third NASA Advanced Composites Technology Conference, volume 1, part 1
[NASA-CP-3178-VOL-1-PT-1] p 2518 N95-29029

Impact of composites on future transport aircraft p 2519 N95-29030

Challenges and payoff of composites in transport aircraft: 777 empennage and future applications p 2519 N95-29031

Advanced composites technology program p 2519 N95-29032

Textile composite fuselage structures development p 2519 N95-29033

Advanced composite fuselage technology p 2519 N95-29034

Advanced resin systems and 3D textile preforms for low cost composite structures p 2519 N95-29035

Performance of resin transfer molded multiaxial warp knit composites p 2520 N95-29039

Experimental and analytical characterization of triaxially braided textile composites p 2520 N95-29040

Cost model relationships between textile manufacturing processes and design details for transport fuselage elements p 2521 N95-29043

Development of RTM and powder prepreg resins for subsonic aircraft primary structures p 2521 N95-29044

Analytical modeling and sensor monitoring for optimal processing of advanced textile structural composites by resin transfer molding p 2521 N95-29045

Progress in manufacturing large primary aircraft structures using the stitching/RTM process p 2522 N95-29050

Test results from large wing and fuselage panels p 2522 N95-29051

Design of a fast-tool servo system using magnetic servo levitation
[AD-A290273] p 2663 N95-29183

Compressive behavior of thick composite shells: Benchmark solutions for loss of stability and hygroscopic effects p 2595 N95-29424

Fiber fracture in continuous-fiber reinforced composite materials during cyclic loading p 2525 N95-29513

Severe edge effects and simple complimentary interior solutions for thin-walled anisotropic and composite structures
[AD-A290645] p 2595 N95-29562

Use of finite element analysis for transient moisture diffusion studies in multilayer composite AEM/S system sandwich materials
[AD-A291092] p 2527 N95-29638

Ultrasonic guided waves in cylinders: Theory and experiment p 2685 N95-29826

Development of 'smart' piezothermoelastic laminae: Theory and applications
[AD-A290852] p 2528 N95-29864

Formulation of an improved smeared stiffener theory for buckling analysis of grid-stiffened composite panels
[NASA-TM-110162] p 2529 N95-30341

COMPRESSED GAS

External combustion engine having an asymmetrical CAM
[AD-D017382] p 2588 N95-28785

A theoretical study on ignition mechanisms of liquid propellants
[AD-A290569] p 2549 N95-29550

Experimental study on scaling law of outgassing rate with a pumping parameter
[AD-B191999L] p 2709 N95-29801

COMPRESSIBILITY

Three dimensional effects in fiber reinforced composites under compression
[AD-A292027] p 2523 N95-29185

Raman and photo-modulated reflectivity studies of ZnTe/InAs semiconductor heterostructure under hydrostatic pressure
[AD-A290467] p 2716 N95-29506

Structure and orientation behavior of highly oriented polymers under tensile and compressive stresses p 2546 N95-29822

Crustal deformation measurements in the vicinity of Vandenberg Air Force Base
[AD-A291224] p 2618 N95-29981

COMPRESSIBILITY EFFECTS

PIV investigation of compressibility effects on dynamic stall p 2487 N95-29102

Compressibility effects on and control of dynamic stall of oscillating airfoil
[AD-A291504] p 2489 N95-29428

Numerical simulation and analysis of the hypersonic turbulent flow past a blunt-fin/ramp configuration
[DLR-FB-94-19] p 2492 N95-30349

COMPRESSIBLE BOUNDARY LAYER

Interaction of turbulence with complex shock waves
[AD-A290225] p 2571 N95-29145

An interacting boundary layer method for unsteady compressible flows p 2579 N95-30290

COMPRESSIBLE FLOW

Wave drag coefficient for axisymmetric forecowls at zero incidence (M sub infinity less than or equal to 1.5)
[ESDU-94014] p 2568 N95-28903

Surface pressure coefficient distributions for axisymmetric forecowls at zero incidence (M sub infinity less than or equal to 1.5)
[ESDU-94015] p 2487 N95-28904

Interaction of turbulence with complex shock waves
[AD-A290225] p 2571 N95-29145

Solution of the Navier-Stokes equations on locally refined Cartesian meshes using state-vector splitting p 2571 N95-29197

Numerical investigation of surface curvature effects in compressible turbulent flows
[AD-A290114] p 2571 N95-29211

Modeling and control of rotating stall in high speed multi-stage axial compressors p 2500 N95-29244

Direct numerical simulation of compressible turbulent flows, using adaptive spectral element method
[AD-A290115] p 2575 N95-29421

Experimental research on crossing shock wave boundary layer interactions
[AD-A290764] p 2577 N95-29920

Survey of CFD applications for high speed inlets
[AD-A291365] p 2578 N95-30087

Numerical simulation of stability and stability control of high speed compressible rotating couette flow
[NASA-CR-198832] p 2579 N95-30250

COMPRESSIBLE FLUIDS

Pressure updating methods for the steady-state fluid equations
[NASA-CR-198163] p 2674 N95-30353

COMPRESSING

Experimental study on scaling law of outgassing rate with a pumping parameter
[AD-B191999L] p 2709 N95-29801

COMPRESSION LOADS
Test load verification through strain data analysis
[NASA-TP-3558] p 2504 N95-28718
Contact stress in disc cams with domes of flat-faced followers
[ESDU-94011] p 2589 N95-28901
Shear reinforcement in deep slabs
[AD-A289528] p 2594 N95-28909
Molecular dynamics simulation of liquid nitromethane shocked to 143 kbar
[AD-A292107] p 2691 N95-28919
Measurement of interface strength, intrinsic toughness and their dependence on interfacial segregants
[AD-A291798] p 2524 N95-29409
Impact resistance and damage tolerance of composite sandwich panels p 2526 N95-29549
Investigation of tension-compression fatigue behavior of a notched cross-ply metal matrix composite at elevated temperature
[AD-A291479] p 2527 N95-29770

COMPRESSION TESTS
Shear reinforcement in deep slabs
[AD-A289528] p 2594 N95-28909
Molecular dynamics simulation of liquid nitromethane shocked to 143 kbar
[AD-A292107] p 2691 N95-28919
A designed experiment in stitched/RTM composites p 2522 N95-29046
Analytical and experimental studies of the energy absorption behavior of composite structures p 2524 N95-29411
Investigation of tension-compression fatigue behavior of a notched cross-ply metal matrix composite at elevated temperature
[AD-A291479] p 2527 N95-29770
Structure and orientation behavior of highly oriented polymers under tensile and compressive stresses p 2546 N95-29822

COMPRESSION WAVES
Collective phenomena in granular fluids p 2572 N95-29219

COMPRESSIVE STRENGTH
Effects of temperature and humidity cycling on the strengths of textile reinforced carbon/epoxy composite materials p 2520 N95-29037

COMPRESSORS
Liquid pressure amplification and liquid injection in air conditioning and refrigeration systems
[AD-A289738] p 2549 N95-28686
Recirculating cavity casing treatment failure
[AD-A289330] p 2500 N95-28908

COMPTON EFFECT
Multiwaveband observations of quasars p 2728 N95-29665
Induced Compton scattering by relativistic electrons in magnetized astrophysical plasmas p 2610 N95-29885

COMPUTATION
Spectral characterization of pulsed ultrasound using neural networks
[AD-A292440] p 2683 N95-28999
On the utility of threads for data parallel programming
[NASA-CR-198155] p 2649 N95-29455
Scalable software tools for adaptive scientific computation
[AD-A290446] p 2650 N95-29480
Linear algebraic computation on distributed memory parallel machines
[AD-A290615] p 2671 N95-29558
Proving the genericity lemma by leftmost reduction is simple
[PB95-197620] p 2673 N95-30103

COMPUTATIONAL CHEMISTRY
Fundamental studies of oxygen rings and other high energy density molecular systems
[AD-A290875] p 2693 N95-29865

COMPUTATIONAL ELECTROMAGNETICS
Electromagnetic antenna modeling (EAM) system
[AD-A292194] p 2552 N95-28986
The 10th Annual Review of Progress in Applied Computational Electromagnetics, volume 1
[AD-A286796] p 2553 N95-29159
Applied Computational Electromagnetics Society Journal, volume 10, number 1, March 1995
[AD-A292069] p 2555 N95-29308
The 10th Annual Review of Progress in Applied Computational Electromagnetics, volume 2
[AD-A286799] p 2558 N95-29904
High-frequency radar target modeling
[AD-A290965] p 2559 N95-29991

COMPUTATIONAL FLUID DYNAMICS
Surface Modeling, Grid Generation, and Related Issues in Computational Fluid Dynamic (CFD) Solutions
[NASA-CP-3291] p 2478 N95-28723
Requirements for effective use of CFD in aerospace design p 2478 N95-28725
Grid generation and surface modeling for CFD p 2478 N95-28726
Grid generation: A view from the trenches p 2478 N95-28727
Application of CFD in aeronautics at NASA Ames Research Center p 2478 N95-28728
Rapid Airplane Parametric Input Design (RAPID) p 2479 N95-28730
Algorithms for high aspect ratio oriented triangulations p 2479 N95-28731
Surface modeling and grid generation for aeropropulsion CFD p 2479 N95-28732
Grid related issues for static and dynamic geometry problems using systems of overset structured grids p 2480 N95-28737
The role of overset grids in the development of the general purpose CFD code p 2480 N95-28738
A Cartesian, cell-based approach for adaptively-refined solutions of the Euler and Navier-Stokes equations p 2480 N95-28739
Development and application of a 3D Cartesian grid Euler method p 2481 N95-28740
Unstructured Cartesian/prismatic grid generation for complex geometries p 2481 N95-28741
Prospects and expectations for unstructured methods p 2481 N95-28742
An unstructured-grid software system for solving complex aerodynamic problems p 2481 N95-28743
Adaptive hybrid prismatic-tetrahedral grids for viscous flows p 2481 N95-28744
Three-dimensional hybrid grid generation using advancing front techniques p 2481 N95-28745
An assessment of unstructured grid technology for timely CFD analysis p 2482 N95-28747
The National Grid Project: A system overview p 2482 N95-28749
A 3DGRAPE/AL: The Ames/Langley technology upgrade p 2482 N95-28750
Automatic structured grid generation using Gridgen (some restrictions apply) p 2483 N95-28751
Tuned grid generation with ICEM CFD p 2483 N95-28752
Geometry modeling and grid generation using 3D NURBS control volume p 2483 N95-28753
Intelligent automated surface grid generation p 2484 N95-28758
Advanced methodology for simulation of complex flows using structured grid systems p 2485 N95-28766
Demonstration of an automated CFD system for three-dimensional flow simulations p 2485 N95-28767
A procedure for automating CFD simulations of an inlet-bleed problem p 2485 N95-28768
A technique for optimizing grid blocks p 2485 N95-28769
A combined geometric approach for computational fluid dynamics on dynamic grids p 2485 N95-28770
GridTool: A surface modeling and grid generation tool p 2486 N95-28773
NACA 1-series geometry representation for computational fluid dynamics
[ESDU-94013] p 2568 N95-28902
A nonintrusive method of quantifying flow visualization data in vortex flow fields
[AD-A289802] p 2568 N95-28948
A novel approach to the numerical simulation of turbulent flows
[AD-A290352] p 2569 N95-29068
Computational methods for the simulation of non-Newtonian flows
[AD-A290355] p 2570 N95-29069
A study of fluid problems requiring a direct particle simulation
[AD-A290212] p 2658 N95-29074
A vorticity-velocity approach for three-dimensional unsteady viscous flow over wings p 2488 N95-29108
An extension of the continuum model by Grad's thirteen moment equations for hypersonic rarefied flows p 2488 N95-29118
A numerical method for modelling wings with sharp edges maneuvering at high angles of attack p 2496 N95-29122
Interaction of turbulence with complex shock waves
[AD-A290225] p 2571 N95-29145
Molecular mixing in shear layers forced by 2-D and 3-D disturbances
[AD-A290272] p 2571 N95-29181
Computational Fluid Dynamics (CFD) analysis of a C-135 aircraft with a side-mounted splitter plate (with comparison to wind tunnel data)
[AD-A292029] p 2571 N95-29187
Solution of the Navier-Stokes equations on locally refined Cartesian meshes using state-vector splitting p 2571 N95-29197
A fourth order Euler/Navier-Stokes prediction method for the aerodynamics and aeroelasticity of hovering rotor blades p 2572 N95-29242
High-and low-frequency dynamics of isolated blades and rotors with dynamic stall and wake
[AD-A290358] p 2497 N95-29322
Rigorous drag bounds in turbulent shear flow p 2573 N95-29334
Application of the space-time conservation element and solution element method to two-dimensional advection-diffusion problems
[NASA-TM-106946] p 2574 N95-29372
Development of a rotary wing Navier-Stokes CFD code based on TLNS3D code
[AD-A290421] p 2574 N95-29387
An assessment of artificial damping models for aeroacoustic calculations
[NASA-CR-198354] p 2574 N95-29405
Direct numerical simulation of compressible turbulent flows, using adaptive spectral element method
[AD-A290115] p 2575 N95-29421
Estimation of aerodynamic load distributions on the F/A-18 aircraft using a CFD panel code
[DSTO-TR-0147] p 2498 N95-29445
Implicit schemes and parallel computing in unstructured grid CFD
[NASA-CR-195071] p 2671 N95-29451
Investigation of Burnett equations for two-dimensional hypersonic flow
[AD-A290233] p 2575 N95-29469
Graphics supercomputer for computational fluid dynamics research
[AD-A291087] p 2575 N95-29637
Parallelization of the 2D Roe Scheme on the Intel Paragon
[AD-A290690] p 2659 N95-29760
Computation of the integrated aerodynamic and propulsive flowfields of a generic hypersonic space plane p 2490 N95-29788
A method for the modelling of porous and solid wind tunnel walls in computational fluid dynamics codes p 2502 N95-29795
Cross flow instability of supersonic flow over a 4:1 elliptic cone
[AD-A291128] p 2577 N95-29913
Computational algorithms for aerodynamic analysis and design
[AD-A291084] p 2491 N95-29972
State-of-the-art review of computational fluid dynamics modeling for fluid-solids systems
[DE95-005866] p 2577 N95-29988
Inlet flow test calibration for a small axial compressor rig. Part 2: CFD compared with experimental results
[NASA-TM-106999] p 2501 N95-30007
Reliability enhancement of Navier-Stokes codes through convergence acceleration
[NASA-CR-196635] p 2578 N95-30034
Survey of CFD applications for high speed inlets
[AD-A291365] p 2578 N95-30087
Use of the PARC code to estimate the off-design transonic performance of an over/under turboramjet nozzle
[NASA-TM-106924] p 2491 N95-30091
ICASE/LaRC Workshop on Benchmark Problems in Computational Aeroacoustics (CAA)
[NASA-CP-3300] p 2686 N95-30133
Benchmark problems and solutions p 2686 N95-30134
Application of essentially nonoscillatory methods to aeroacoustic flow problems p 2686 N95-30135
Computational aeroacoustics using hyperbolic wave primitives p 2686 N95-30136
Comparative study of numerical schemes of TVD3, UNO3-ACM and optimized compact scheme p 2686 N95-30137
A compact solution to computational acoustics p 2686 N95-30138
The construction of high-accuracy schemes for acoustic equations p 2688 N95-30146
A comparative study of upwind and MacCormack schemes for CAA benchmark problems p 2688 N95-30147
Application of traditional CFD methods to nonlinear computational aeroacoustics problems p 2688 N95-30148
Time accurate application of the MacCormack 2-4 scheme on massively parallel computers p 2661 N95-30150
Computational aeroacoustics on massively parallel computers p 2661 N95-30156
Comparison of spatial numerical operators for duct-nozzle acoustics p 2690 N95-30158
High-order essentially non-oscillatory methods for computational aeroacoustics p 2690 N95-30159
Aeroacoustic computation of a gust-plate interaction via MacCormack schemes p 2690 N95-30162
Coarsening strategies for unstructured multigrid techniques with application to anisotropic problems
[NASA-CR-198154] p 2674 N95-30227

Numerical solution of the equations governing non-Newtonian flow at moderate Reynolds numbers p 2579 N95-30233
A numerical study of the small scale wing-body junction problem p 2491 N95-30235
Pressure updating methods for the steady-state fluid equations [NASA-CR-198163] p 2674 N95-30353

COMPUTATIONAL GEOMETRY
Grid related issues for static and dynamic geometry problems using systems of overset structured grids p 2480 N95-28737
Unstructured Cartesian/prismatic grid generation for complex geometries p 2481 N95-28741
Adaptive hybrid prismatic-tetrahedral grids for viscous flows p 2481 N95-28744
Three-dimensional hybrid grid generation using advancing front techniques p 2481 N95-28745
Emerging CFD technologies and aerospace vehicle design p 2482 N95-28746
Evaluation of grid generation technologies from an applied perspective p 2482 N95-28748
Tuned grid generation with ICEM CFD p 2483 N95-28752
A combined geometric approach for computational fluid dynamics on dynamic grids p 2485 N95-28770
Parametric design and gridding through relational geometry p 2486 N95-28771
Examples of grid generation with implicitly specified surfaces using GridPro (TM)/az3000. 1: Filleted multi-tube configurations p 2486 N95-28772
Interactive high quality grid generation p 2486 N95-28774
NASA-IGES Translator and Viewer p 2486 N95-28775
Multilayer piecewise linear networks. Revision 1 [AD-A289885] p 2658 N95-28955
Users manual for the improved NASA Lewis ice accretion code LEWICE 1.6 [NASA-CR-198355] p 2492 N95-29132
Grid orthogonality effects on predicted turbine midspan heat transfer and performance [NASA-TM-106931] p 2574 N95-29371
Acoustic scattering from ellipses by the modal element method [NASA-TM-106935] p 2683 N95-29401

COMPUTATIONAL GRIDS
Marshall Space Flight Center surface modeling and grid generation applications p 2480 N95-28733
Multiblock grid generation with automatic zoning p 2480 N95-28735
Grid related issues for static and dynamic geometry problems using systems of overset structured grids p 2480 N95-28737
The role of overset grids in the development of the general purpose CFD code p 2480 N95-28738
Development and application of a 3D Cartesian grid Euler method p 2481 N95-28740
Adaptive hybrid prismatic-tetrahedral grids for viscous flows p 2481 N95-28744
An assessment of unstructured grid technology for timely CFD analysis p 2482 N95-28747
A 3DGRAPE/AL: The Ames/Langley technology upgrade p 2482 N95-28750
Geometry modeling and grid generation using 3D NURBS control volume p 2483 N95-28753
Generating grids directly on CAD database surfaces using a parametric evaluator approach p 2483 N95-28754
Grid generation on trimmed Bezier and NURBS quilted surfaces p 2483 N95-28755
Geometric grid generation p 2483 N95-28756
Intelligent automated surface grid generation p 2484 N95-28758
Cooperative solutions coupling a geometry engine and adaptive solver codes p 2484 N95-28761
A grid generation system for multi-disciplinary design optimization p 2484 N95-28763
Multilevel elliptic smoothing of large three-dimensional grids p 2485 N95-28765
A global/local analysis method for treating details in structural design p 2517 N95-28848
An HP-Adaptive method in space and time for parabolic systems [AD-A292262] p 2668 N95-28890
A new methodology for the numerical simulation of strain softening in inelastic solids [AD-A290295] p 2594 N95-29063
Pollution error in the h-version of the finite element method and the local quality of the recovered derivatives [AD-A290297] p 2668 N95-29065
Solution of second order nonlinear boundary value problems by the boundary element method p 2669 N95-29105
Navier-Stokes solution of wing wake structure and its perturbation p 2488 N95-29121
Solution of the Navier-Stokes equations on locally refined Cartesian meshes using state-vector splitting p 2571 N95-29197
Consideration of microstructural changes in the study of adiabatic shear bands [AD-A290398] p 2715 N95-29234
Grid orthogonality effects on predicted turbine midspan heat transfer and performance [NASA-TM-106931] p 2574 N95-29371
ANSYS duplicate finite-element checker routine [NASA-TM-108492] p 2672 N95-29824
Finite difference ocean acoustic model users guide [AD-A291544] p 2631 N95-29856
The application of adaptive mesh refinement to the numerical simulation of compressible flow [AD-A289595] p 2577 N95-30027
Reliability enhancement of Navier-Stokes codes through convergence acceleration [NASA-CR-196635] p 2578 N95-30034
Survey of CFD applications for high speed inlets [AD-A291365] p 2578 N95-30087
Comparison of the local defect correction iteration and the fast adaptive composite grid iteration [PB95-206769] p 2672 N95-30088
Solution of acoustic workshop problems by a spectral multidomain method p 2687 N95-30141
Evaluation of numerical schemes for the analysis of sound generation by blade-gust interaction p 2690 N95-30163
Grid resolution and turbulent inflow boundary condition recommendations for NPARC calculations [NASA-TM-106959] p 2492 N95-30253

COMPUTER AIDED DESIGN
A conceptual design for the attitude control and determination system for the Magnetosphere Imager spacecraft [NASA-TP-3560] p 2507 N95-28721
Surface Modeling, Grid Generation, and Related Issues in Computational Fluid Dynamic (CFD) Solutions [NASA-CP-3291] p 2478 N95-28723
Future requirements in surface modeling and grid generation p 2478 N95-28724
Requirements for effective use of CFD in aerospace design p 2478 N95-28725
Grid generation and surface modeling for CFD p 2478 N95-28726
Grid generation: A view from the trenches p 2478 N95-28727
Application of CFD in aeronautics at NASA Ames Research Center p 2478 N95-28728
Rapid Airplane Parametric Input Design (RAPID) p 2479 N95-28730
Surface modeling and grid generation for aeropropulsion CFD p 2479 N95-28732
Marshall Space Flight Center surface modeling and grid generation applications p 2480 N95-28733
Automatic blocking for complex three-dimensional configurations p 2480 N95-28734
Multiblock grid generation with automatic zoning p 2480 N95-28735
Block-structured grids for complex aerodynamic configurations: Current status p 2480 N95-28736
Prospects and expectations for unstructured methods p 2481 N95-28742
An unstructured-grid software system for solving complex aerodynamic problems p 2481 N95-28743
Adaptive hybrid prismatic-tetrahedral grids for viscous flows p 2481 N95-28744
Three-dimensional hybrid grid generation using advancing front techniques p 2481 N95-28745
Emerging CFD technologies and aerospace vehicle design p 2482 N95-28746
An assessment of unstructured grid technology for timely CFD analysis p 2482 N95-28747
Evaluation of grid generation technologies from an applied perspective p 2482 N95-28748
The National Grid Project: A system overview p 2482 N95-28749
A 3DGRAPE/AL: The Ames/Langley technology upgrade p 2482 N95-28750
Automatic structured grid generation using Gridgen (some restrictions apply) p 2483 N95-28751
Tuned grid generation with ICEM CFD p 2483 N95-28752
Geometry modeling and grid generation using 3D NURBS control volume p 2483 N95-28753
Generating grids directly on CAD database surfaces using a parametric evaluator approach p 2483 N95-28754
Grid generation on trimmed Bezier and NURBS quilted surfaces p 2483 N95-28755
Geometric grid generation p 2483 N95-28756
Intelligent automated surface grid generation p 2484 N95-28758
Optimal domain decomposition strategies p 2484 N95-28759
Automation of three-dimensional structured mesh generation for turbomachinery blade passages p 2484 N95-28762
GridTool: A surface modeling and grid generation tool p 2486 N95-28773
Interactive high quality grid generation p 2486 N95-28774
NASA-IGES Translator and Viewer p 2486 N95-28775
R&M design expert system [AD-A292525] p 2645 N95-28814
Operating procedures for Anthropometry and Initial Conditions Photogrammetric Program [AD-A291553] p 2640 N95-28935
Electromagnetic antenna modeling (EAM) system [AD-A292194] p 2552 N95-28986
OEIC ultra. A new approach to OEIC CAD [AD-A290349] p 2646 N95-29066
A transient model of the RL10A-3-3A rocket engine [NASA-CR-195478] p 2510 N95-29114
Inductive boolean function manipulation: A hardware verification methodology for automatic induction [AD-A292236] p 2669 N95-29128
A friendly editing environment for computer-aided rapid prototyping of hard real-time systems [AD-A290154] p 2648 N95-29321
Simulated imaging properties of a series of magnetic electron lenses [NASA-CR-195474] p 2564 N95-29406
The Institute for Material Science and Department of Material Science, Tohoku University, Sendai Japan, 2-3 June 1994 [AD-A292348] p 2650 N95-29534
Graphics supercomputer for computational fluid dynamics research [AD-A291087] p 2575 N95-29637
Three-dimensional simulation of traveling-wave tube cold-test characteristics using MAFIA [NASA-TP-3513] p 2566 N95-29998
The Telemetry Agile Manufacturing Effort [DE95-006177] p 2654 N95-30115
Simulation of robot manipulators [DE95-008680] p 2654 N95-30189
Developing a workstation-based, real-time simulation for rapid handling qualities evaluations during design [NASA-CR-198831] p 2499 N95-30335

COMPUTER AIDED MANUFACTURING
Process optimization through discovery and integration of materials and processing properties. phase 1 [AD-A292576] p 2662 N95-28978
The Telemetry Agile Manufacturing Effort [DE95-006177] p 2654 N95-30115

COMPUTER AIDED MAPPING
A comprehensive analysis of Navy and Marine corps digital mapping, charting, and geodesy requirements for modeling and simulation [AD-A291601] p 2598 N95-28931
Collection of Magellan Venus radar mapping results [NASA-CR-197656] p 2736 N95-29178
Trajectory mapping (TM): A new non-metric scaling technique [AD-A290036] p 2670 N95-29440
Digital mapping, charting, and geodesy analysis program technical review of vector smart map prototypes 1 and 2 [AD-A291217] p 2601 N95-29977

COMPUTER AIDED TOMOGRAPHY
Interactive multimedia presentation for applied computer tomography: Impact [AD-A291955] p 2640 N95-29020

COMPUTER ANIMATION
High resolution microwave survey [NASA-TM-110566] p 2553 N95-29174
Lockheed Stabilizer System for space exercise equipment [NASA-CR-197657] p 2641 N95-29180

COMPUTER ASSISTED INSTRUCTION
Visualization of improved target acquisition algorithm for Janus (A) [AD-A290191] p 2646 N95-29056
Macroprocesses and adaptive instruction [AD-A290463] p 2648 N95-29325
Operational test and evaluation (OT&E) integration and operational test procedures for Fixed Ground Antenna Radome (FGAR) [AD-A291203] p 2559 N95-29975

COMPUTER CONFERENCING
Summary of the 1st International Workshop on Networked Reality in Telecommunication [AD-A292366] p 2558 N95-29862

COMPUTER DESIGN
OEIC ultra. A new approach to OEIC CAD [AD-A290349] p 2646 N95-29066

COMPUTER GRAPHICS
The National Grid Project: A system overview p 2482 N95-28749

A 3DGRAPE/AL: The Ames/Langley technology upgrade p 2482 N95-28750
Automatic structured grid generation using Gridgen (some restrictions apply) p 2483 N95-28751
Interactive high quality grid generation p 2486 N95-28774
NASA-IGES Translator and Viewer p 2486 N95-28775
Summary report for cooperative research and development agreement between Oak Ridge Associated Universities and Interactive Presentation Systems [DE95-006874] p 2644 N95-28777
WinCD: Complex demodulation time-series analysis for windows [AD-A291550] p 2645 N95-28934
Operating procedures for Anthropometry and Initial Conditions Photogrammetric Program [AD-A291553] p 2640 N95-28935
High performance hardware and software for pattern recognition and image processing [AD-A292307] p 2646 N95-28964
A differential approach to graphical interaction [AD-A292165] p 2647 N95-29125
An architectural design of a toolkit for synchronous groupware applications [AD-A290226] p 2642 N95-29146
XMap: A general purpose mapping program [AD-A289958] p 2647 N95-29276
A friendly editing environment for computer-aided rapid prototyping of hard real-time systems [AD-A290154] p 2648 N95-29321
Software testing toolkit for distributed simulations [AD-A291867] p 2649 N95-29435
Design and evaluation of a LQR controller for the bluebird unmanned air vehicle [AD-A289769] p 2498 N95-29457
Digital video technology, today and tomorrow [DE95-007689] p 2556 N95-29462
A study of the conceptual symbolics of information system development languages p 2723 N95-29589
Graphics supercomputer for computational fluid dynamics research [AD-A291087] p 2575 N95-29637
The 2d Eurographics Workshop on Virtual Environments [AD-A292015] p 2651 N95-29861
A new visualization technique to study the time evolution of finite and adaptive mixture estimators [AD-A291147] p 2673 N95-30126
Parallel rendering [NASA-CR-195080] p 2655 N95-30306

COMPUTER INFORMATION SECURITY

Encryption and networking applications [DE95-009587] p 2651 N95-29871

COMPUTER NETWORKS

Analysis of the naval postgraduate school computer network architecture [AD-A289749] p 2657 N95-28689
Competitive analysis of call admission algorithms that allow delay [AD-A292242] p 2645 N95-28878
Wax: A wide-area computation system [AD-A292247] p 2658 N95-28884
Multilayer piecewise linear networks. Revision 1 [AD-A289885] p 2658 N95-28955
Solving linear programs using distributed parallel computing [AD-A290221] p 2658 N95-29079
Implementing distributed server groups for the World Wide Web [AD-A292221] p 2658 N95-29196
Simulation methodology [AD-A290461] p 2674 N95-29491
Encryption and networking applications [DE95-009587] p 2651 N95-29871
Functionally specified distributed transactions in co-operative scenarios [PB95-197380] p 2725 N95-30100
Bicriteria network design problems [DE95-005261] p 2661 N95-30215

COMPUTER PROGRAM INTEGRITY

Proceedings of the 12th Annual National Conference on Ada Technology [AD-A290693] p 2651 N95-29644

COMPUTER PROGRAMMING

Automated testing of application domains [AD-A289753] p 2643 N95-28690
Collected software engineering papers, volume 12 [NASA-CR-189409] p 2644 N95-28713
An overview of the Software Engineering Laboratory [NASA-CR-189410] p 2644 N95-28714
Annotated bibliography of software engineering laboratory literature [NASA-CR-189406] p 2644 N95-28805
Software measurement guidebook [NASA-CR-189407] p 2644 N95-28806
C style guide [NASA-CR-189408] p 2645 N95-28821
Abstract models of memory management [AD-A292238] p 2721 N95-28877
Problem decomposition for reuse [AD-A292245] p 2645 N95-28881
Wax: A wide-area computation system [AD-A292247] p 2658 N95-28884
Rome laboratory software engineering cooperative virtual machine [AD-A292396] p 2658 N95-28965
Process optimization through discovery and integration of materials and processing properties. phase 1 [AD-A292576] p 2662 N95-28978
An architectural design of a toolkit for synchronous groupware applications [AD-A290226] p 2642 N95-29146
Performance and robustness of self-tuning and adaptation algorithms for identification, filtering and control [AD-A292070] p 2648 N95-29310
Macroprocesses and adaptive instruction [AD-A290483] p 2648 N95-29325
Programmable materials and structures [AD-A291807] p 2649 N95-29429
Software testing toolkit for distributed simulations [AD-A291867] p 2649 N95-29435
Scalable software tools for adaptive scientific computation [AD-A290446] p 2650 N95-29480
High-level parallel programming tools for finite element analysis [AD-A290566] p 2659 N95-29566
Proceedings of the 12th Annual National Conference on Ada Technology [AD-A290693] p 2651 N95-29644
Neural network construction using evolutionary search [AD-A290862] p 2665 N95-29831
Proposed Department of Defense software metrics implementation plan [AD-A291404] p 2550 N95-29918
Software risk evaluation method version 1.0 [AD-A290597] p 2652 N95-30047
A formal extension to object oriented analysis using Z [AD-A290911] p 2653 N95-30080
The topside ionospheric plasma monitor (SSIES, SSIES-2 and SSIES-3) on the spacecraft of the Defense Meteorological Satellite Program (DMSP), user's guide. Volume 2: Programmer's guide for software at AFSFC [AD-A290913] p 2618 N95-30082
Static analysis of functional programs [PB95-197141] p 2653 N95-30095
Realisation of an integrated software engineering environment through heterogeneous CASE-tool integration [PB95-197646] p 2653 N95-30105
Software Estimation Program (SWEEP) user manual [AD-A291137] p 2654 N95-30121
Essential structure of the jacopini technique [PB95-197208] p 2674 N95-30291

COMPUTER PROGRAMS

Generator of body data (GEBOD) manual [AD-A289721] p 2640 N95-28683
The effect of viscous attenuation on shock tube performance [AD-A289793] p 2568 N95-28696
Collected software engineering papers, volume 12 [NASA-CR-189409] p 2644 N95-28713
Rapid Airplane Parametric Input Design (RAPID) p 2479 N95-28730
Multiblock grid generation with automatic zoning p 2480 N95-28735
Block-structured grids for complex aerodynamic configurations: Current status p 2480 N95-28736
The role of overset grids in the development of the general purpose CFD code p 2480 N95-28738
An unstructured-grid software system for solving complex aerodynamic problems p 2481 N95-28743
An assessment of unstructured grid technology for timely CFD analysis p 2482 N95-28747
A 3DGRAPE/AL: The Ames/Langley technology upgrade p 2482 N95-28750
Automatic structured grid generation using Gridgen (some restrictions apply) p 2483 N95-28751
Tuned grid generation with ICEM CFD p 2483 N95-28752
Geometry modeling and grid generation using 3D NURBS control volume p 2483 N95-28753
Examples of grid generation with implicitly specified surfaces using GridPro (TM)/az3000. 1: Filleted multi-tube configurations p 2486 N95-28772
Software Design for Reliability and Reuse proof of concept project. Phase 1 [AD-A291690] p 2644 N95-28782
Leading-edge suction distribution for plane thin wings at subsonic speeds [ESDU-94037] p 2486 N95-28800
Software measurement guidebook [NASA-CR-189407] p 2644 N95-28806
IPACS (Integrated Probabilistic Assessment of Composite Structures): Code development and applications p 2518 N95-28849
Correlation and gradient characteristics of ionospheric parameters in europe [AD-A292295] p 2612 N95-28871
Using object-oriented database technology to develop a multiple domain capability for domain-oriented application composition systems [AD-A289244] p 2721 N95-28907
Operating procedures for Anthropometry and Initial Conditions Photogrammetric Program [AD-A291553] p 2640 N95-28935
High performance hardware and software for pattern recognition and image processing [AD-A292307] p 2646 N95-28964
Glenda software design [AD-A292537] p 2646 N95-28968
Leading edge film cooling effects on turbine blade heat transfer [NASA-TM-106955] p 2500 N95-29115
Optimizing cockpit display configurations with a genetic algorithm system [AD-A289799] p 2499 N95-29123
Porting a vector library: A comparison of MPI, paris, CMMD and PVM (or, 'I'll never have to port CVL again') [AD-A290231] p 2647 N95-29147
Arcing predictions for PASP PLUS solar arrays [AD-A292230] p 2602 N95-29201
Mode of human image representation and error checking strategies in complex visual displays [AD-A290107] p 2492 N95-29210
Exploiting symmetry in the model checking of relational specifications [AD-A290230] p 2647 N95-29223
An introduction to the principles of computer science: A reuse-oriented philosophy [AD-A290364] p 2647 N95-29226
Acoustic imaging of ultrasonic wave propagation [AD-A290390] p 2683 N95-29232
SCAP spray combustion analysis program [AD-A289946] p 2532 N95-29273
Software systems reengineering process model, version 2.0 [AD-A289968] p 2647 N95-29278
Grid orthogonality effects on predicted turbine midspan heat transfer and performance [NASA-TM-106931] p 2574 N95-29371
Simulated imaging properties of a series of magnetic electron lenses [NASA-CR-195474] p 2564 N95-29406
MapTool version 2. User's manual [AD-A289470] p 2630 N95-29418
The mesh synchronous processor MeshSP (trademark) [AD-A289875] p 2659 N95-29420
Research instrumentation for polytechnic university's supersonic wind tunnel facility [AD-A290232] p 2502 N95-29468
Scalable software tools for adaptive scientific computation [AD-A290446] p 2650 N95-29480
Parallel adaptive techniques for transient partial differential equations [AD-A290460] p 2674 N95-29490
Automatically combining changes to software systems [AD-A290628] p 2650 N95-29515
AFGWC dial-in subsystem (AFDIS) software users manual, version 3.1 [AD-A291103] p 2651 N95-29639
Proposed Department of Defense software metrics implementation plan [AD-A291404] p 2550 N95-29918
Electrically small archimedian spiral method of moment analysis [AD-A291171] p 2558 N95-29928
SETA/ADS software development [AD-A291181] p 2651 N95-29932
A formal extension to object oriented analysis using Z [AD-A290911] p 2653 N95-30080
Static analysis of functional programs [PB95-197141] p 2653 N95-30095
Checkpointing and the modeling of program execution time [PB95-197182] p 2653 N95-30099
Distributed multitasking ITS with PVM [DE95-006821] p 2660 N95-30116
Software Estimation Program (SWEEP) user manual [AD-A291137] p 2654 N95-30121

Tools for Automated Knowledge Engineering (TAKE) system evaluation methodology
[AD-A291145] p 2654 N95-30125
Techniques and results of tokamak-edge simulation
[DE95-008075] p 2711 N95-30130
Lattice gas methods for computational aeroacoustics
p 2687 N95-30144
Application of traditional CFD methods to nonlinear computational aeroacoustics problems
p 2688 N95-30148
Computational aeroacoustics on massively parallel computers p 2661 N95-30156
Simulation of powder metal fabrication with high pressure gas atomization
[DE95-008820] p 2538 N95-30178
Grid resolution and turbulent inflow boundary condition recommendations for NPARC calculations
[NASA-TM-106959] p 2492 N95-30253
Parallel rendering
[NASA-CR-195080] p 2655 N95-30306
Developing a workstation-based, real-time simulation for rapid handling qualities evaluations during design
[NASA-CR-198831] p 2499 N95-30335
Formulation of an improved smeared stiffener theory for buckling analysis of grid-stiffened composite panels
[NASA-TM-110162] p 2529 N95-30341

COMPUTER STORAGE DEVICES
The scotch parallel storage systems
[AD-A292243] p 2658 N95-28879
Low cost writable RFID tag with MRAM memory
[AD-A292553] p 2642 N95-28974
The quantum hydrodynamic model for semiconductor devices
[AD-A291809] p 2564 N95-29430

COMPUTER SYSTEMS DESIGN
The National Grid Project: A system overview
p 2482 N95-28749
Automatic structured grid generation using Gridgen (some restrictions apply) p 2483 N95-28751
QUEST2: System architecture deliverable set
[DE95-008427] p 2721 N95-28958
Data migration policies for distributed database systems p 2721 N95-29093
An architectural design of a toolkit for synchronous groupware applications
[AD-A290226] p 2642 N95-29146
Implementing distributed server groups for the World Wide Web
[AD-A292221] p 2658 N95-29196
Ropes: Support for collective opertions among distributed threads
[NASA-CR-198157] p 2649 N95-29404
The design of programmable convolutional encoder using VHDL and an FPGA
[AD-A290048] p 2649 N95-29442
Design and implementation of logical database languages
[AD-A290474] p 2650 N95-29509
Graphics supercomputer for computational fluid dynamics research
[AD-A291087] p 2575 N95-29637
High-level fault tolerance in distributed programs
[AD-A290430] p 2724 N95-29818

COMPUTER SYSTEMS PERFORMANCE
An architectural design of a toolkit for synchronous groupware applications
[AD-A290226] p 2642 N95-29146
Modeling spatio-temporal databases to measure the performance of the GPS satellite constellation
p 2494 N95-29596
Information management in local area networks: Impact on users' perceptions p 2723 N95-29690
Parallelization of the 2D Roe Scheme on the Intel Paragon
[AD-A290690] p 2659 N95-29760

COMPUTER SYSTEMS PROGRAMS
Causal behaviours and nets
[PB95-197612] p 2660 N95-30102
Layers as knowledge transitions in the design of distributed systems
[PB95-197636] p 2660 N95-30104

COMPUTER TECHNIQUES
High performance hardware and software for pattern recognition and image processing
[AD-A292307] p 2646 N95-28964
Observational signatures of rotating black holes
p 2729 N95-29709
A study of power diode failure mechanisms in the US Army research laboratory 30-mm solid propellant electrothermal-chemical (SPETC) gun facility
[AD-A291300] p 2565 N95-29938
Parallel continuation-based global optimization for molecular conformation and protein folding
[DE95-005860] p 2633 N95-30114
Distributed multitasking ITS with PVM
[DE95-006821] p 2660 N95-30116
Time accurate application of the MacCormack 2-4 scheme on massively parallel computers
p 2661 N95-30150
Optimization of 100-meter Green Bank Telescope
[NASA-CR-198868] p 2731 N95-30230

COMPUTER VISION
Cost effective, dual-purpose machine vision-based detectors for (1) smoke and flame detection, and (2) engine overhead/burn-through and flame detection
[AD-A292284] p 2697 N95-28870
Modeling foreshortening in stereo vision using local spatial frequency
[AD-A292246] p 2645 N95-28883
An image cancellation approach to depth-from-focus
[DE95-007625] p 2697 N95-28912
Proceeding of the 33rd SICE Annual Conference
[DE95-758943] p 2662 N95-29144
NASA to use telepresence to explore Antarctic Lakes
[NASA-TM-110567] p 2598 N95-29175
Computing 3-D motion in custom analog and digital VLSI
[AD-A290270] p 2647 N95-29179
Relative affine structure: Canonical model for 3D from 2D geometry and applications
[AD-A290085] p 2670 N95-29352
Hybrid pyramid/neural network vision system
[AD-A290565] p 2665 N95-29863

COMPUTERIZED SIMULATION
Surface Modeling, Grid Generation, and Related Issues in Computational Fluid Dynamic (CFD) Solutions
[NASA-CP-3291] p 2478 N95-28723
Rapid Airplane Parametric Input Design (RAPID)
p 2479 N95-28730
Adaptive hybrid prismatic-tetrahedral grids for viscous flows p 2481 N95-28744
Emerging CFD technologies and aerospace vehicle design p 2482 N95-28746
The National Grid Project: A system overview
p 2482 N95-28749
Advanced methodology for simulation of complex flows using structured grid systems p 2485 N95-28766
Demonstration of an automated CFD system for three-dimensional flow simulations p 2485 N95-28767
A discrete-event simulation model of myocardial electrical activity: Mathematical electrophysiology
[AD-A292323] p 2633 N95-28793
Fourier Synthesis Lithographic Machine for large panel display fabrication
[AD-A291921] p 2698 N95-28914
Molecular dynamics simulation of liquid nitromethane shocked to 143 kbar
[AD-A292107] p 2691 N95-28919
A comprehensive analysis of Navy and Marine corps digital mapping, charting, and geodesy requirements for modeling and simulation
[AD-A291601] p 2598 N95-28931
Electromagnetic antenna modeling (EAM) system
[AD-A292194] p 2552 N95-28986
Exact physical models and methods for stabilization and control of reflection-induced instabilities in semiconductor lasers
[AD-A292437] p 2585 N95-29053
Visualization of improved target acquisition algorithm for Janus (A)
[AD-A290191] p 2646 N95-29056
Experiments in cooperative manipulation of objects by free-flying robot teams p 2662 N95-29095
Users manual for the improved NASA Lewis ice accretion code LEWICE 1.6
[NASA-CR-198355] p 2492 N95-29132
Interaction of turbulence with complex shock waves
[AD-A290225] p 2571 N95-29145
Computer simulation study of high t(sub c) superconductor structure
[AD-A292513] p 2563 N95-29163
High performance electromagnetic simulation tools
[AD-A290405] p 2554 N95-29235
A fourth order Euler/Navier-Stokes prediction method for the aerodynamics and aeroelasticity of hovering rotor blades p 2572 N95-29242
Multifluid nonequilibrium simulation of arcjet thrusters
p 2510 N95-29245
Software systems reengineering process model, version 2.0
[AD-A289968] p 2647 N95-29278
Theory of competition between synchronous and nonsynchronous modes in a magnicon output cavity
[AD-A292048] p 2563 N95-29301
Three problems in fluid dynamics
[AD-A290481] p 2573 N95-29324
Gordon research conference on physical metallurgy: Materials by design
[AD-A290519] p 2524 N95-29326
Investigation of the flow turning loss in unstable solid propellant rocket motors p 2510 N95-29331
A simulation technique for predicting thickness of thermal sprayed coatings
[NASA-TM-106939] p 2512 N95-29373
Software testing toolkit for distributed simulations
[AD-A291867] p 2649 N95-29435
Applications of digital video and synthetic environments to unmanned aerial vehicles
[AD-A291875] p 2497 N95-29437
Transport delays associated with NASA Langley Flight Simulation Facility
[NASA-TM-110150] p 2659 N95-29454
Design and evaluation of a LQR controller for the bluebird unmanned air vehicle
[AD-A289769] p 2498 N95-29457
Simulation methodology
[AD-A290461] p 2674 N95-29491
Thermal N(+) in the inner magnetosphere
p 2614 N95-29590
Graphics supercomputer for computational fluid dynamics research
[AD-A291087] p 2575 N95-29637
The high-altitude polar wind: Simulation and observation p 2622 N95-29688
A study of boundary layer aerosol and wind profiles using incoherent Doppler lidar p 2622 N95-29697
Defense Modeling and Simulation Office information/data base technology working group (I/DBTWG) meetings
[AD-A290953] p 2651 N95-29735
SEMINT: Seamless model integration
[AD-A290956] p 2651 N95-29736
Monte Carlo simulation study of the ICRF minority heating in the large helical device
[AD-B179858L] p 2708 N95-29749
Experimental cosmology using fast parallel N-body methods p 2734 N95-29775
Numerical simulation of the genesis of tornado-like vortices p 2625 N95-29806
Collisionless driven magnetic reconnection
[AD-B178946L] p 2709 N95-29810
The 2d Eurographics Workshop on Virtual Environments
[AD-A292015] p 2651 N95-29861
The 10th Annual Review of Progress in Applied Computational Electromagnetics, volume 2
[AD-A286799] p 2558 N95-29904
A study of power diode failure mechanisms in the US Army research laboratory 30-mm solid propellant electrothermal-chemical (SPETC) gun facility
[AD-A291300] p 2565 N95-29938
Three-dimensional simulation of traveling-wave tube cold-test characteristics using MAFIA
[NASA-TP-3513] p 2566 N95-29998
Performance analysis of a GPS Interferometric attitude determination system for a gravity gradient stabilized spacecraft
[NASA-CR-188372] p 2508 N95-30036
Distortion-invariant optical pattern recognition by correlative matrix feature criterion
[AD-A291389] p 2703 N95-30064
Tropical storm database: East and Gulf of Mexico coasts of the United States
[AD-A291406] p 2627 N95-30066
A formal extension to object oriented analysis using Z
[AD-A290911] p 2653 N95-30080
Techniques and results of tokamak-edge simulation
[DE95-008075] p 2711 N95-30130
Lattice gas methods for computational aeroacoustics
p 2687 N95-30144
Application of traditional CFD methods to nonlinear computational aeroacoustics problems
p 2688 N95-30148
Category 5 problem solution using an unstructured finite volume algorithm p 2657 N95-30157
Simulation of powder metal fabrication with high pressure gas atomization
[DE95-008820] p 2538 N95-30178
Nearest neighbor analysis in one dimension
[DE95-009378] p 2654 N95-30183
Numerical simulations of the flow in the HYPULSE expansion tube
[NASA-TM-110357] p 2503 N95-30228
Telepresence media resource tape
[NASA-TM-110648] p 2655 N95-30248
Parallel adaptive finite element: Software for semiconductor device simulation
[AD-A291149] p 2661 N95-30295
Manual for a workstation-based generic flight simulation program (LaRCsim), version 1.4
[NASA-TM-110164] p 2502 N95-30327
Numerical simulation and analysis of the hypersonic turbulent flow past a blunt-fin/ramp configuration
[DLR-FB-94-19] p 2492 N95-30349

COMPUTERS
Methods of generating low redundancy direction finding array configurations
[AD-A292590] p 2555 N95-29289
High-level parallel programming tools for finite element analysis
[AD-A290566] p 2659 N95-29566
Workshop on computing and intelligent systems
[AD-A290581] p 2666 N95-30040
CONCENTRATION (COMPOSITION)
The redox chemistry of some peroxo and superoxo metal ion complexes
[AD-A290761] p 2532 N95-29483
Effect of KOH concentration and anions on the performance of Ni-H2 battery positive plate
p 2567 N95-30260
CONCENTRIC CYLINDERS
Numerical simulation of stability and stability control of high speed compressible rotating couette flow
[NASA-CR-198832] p 2579 N95-30250
CONCRETES
Shear reinforcement in deep slabs
[AD-A289528] p 2594 N95-28909
Materials for tomorrow's infrastructure: A ten-year plan for deploying high-performance construction materials and systems
[AD-A289782] p 2526 N95-29598
Gradient-dependent plasticity in numerical simulation of localization phenomena
[PB95-197257] p 2596 N95-30049
CONDENSATES
Condensation inside tubes: Condensate film coefficient in horizontal tubes
[ESDU-94041] p 2569 N95-29015
The dynamics of circulations within the stratiform regions of squall lines p 2623 N95-29725
CONDENSED MATTER PHYSICS
Proceedings of the 18th International Workshop on Condensed Matter Theories
[AD-A291396] p 2694 N95-30065
CONDITIONS
Cathodic protection system inspection 5
[AD-A289724] p 2592 N95-28684
CONDUCTIVE HEAT TRANSFER
Compact substrate heater for use in an oxidizing atmosphere
[AD-A290860] p 2502 N95-29522
CONDUCTORS
Finite difference analysis of a cylindrical two conductor microstrip transmission line with truncated dielectrics
[AD-A292592] p 2555 N95-29290
Complete analysis of electrode-terminated cables in two-layer conductor bounded above by air: Current density, magnetic field, and magnetic field gradient
[AD-A290907] p 2566 N95-30079
CONFERENCES
Surface Modeling, Grid Generation, and Related Issues in Computational Fluid Dynamic (CFD) Solutions
[NASA-CP-3291] p 2478 N95-28723
Third NASA Advanced Composites Technology Conference, volume 1, part 2
[NASA-CP-3178-VOL-1-PT-2] p 2513 N95-28823
Conference reports
[AD-A289630] p 2561 N95-28911
Proceedings of the 6th Joint Magnetism and Magnetic Materials Intermag Conference
[AD-A286752] p 2681 N95-28923
Proceedings of the 38th Annual Conference on Magnetism and Magnetic Materials
[AD-A286753] p 2681 N95-28924
Proceedings of the 33d SICE (the Society of Instrument and Control Engineers) Annual Conference, part 1
[DE95-758947] p 2632 N95-28947
Proceedings of the 38th Annual Conference on Magnetism and Magnetic Materials
[AD-A286751] p 2681 N95-28962
Proceedings of the Complex Systems Engineering Synthesis and Assessment Technology Workshop (CSESAW 1994)
[AD-A292433] p 2646 N95-28995
Conference proceedings: IEEE Nonlinear Optics, Materials, Fundamentals, and Applications
[AD-A292438] p 2698 N95-28997
A formative evaluation of CU-SeeMe
[AD-A292443] p 2553 N95-29002
The 6th Van der Ziel symposium on quantum 1/f noise and other low frequency fluctuations in electronic devices
[AD-A292468] p 2718 N95-29009
Third NASA Advanced Composites Technology Conference, volume 1, part 1
[NASA-CP-3178-VOL-1-PT-1] p 2518 N95-29029
Proceedings of the 11th congress of the international society for artificial cells, blood substitutes and immobilization biotechnology
[AD-A290342] p 2632 N95-29088
Proceeding of the 33rd SICE Annual Conference
[DE95-758943] p 2662 N95-29144
The 10th Annual Review of Progress in Applied Computational Electromagnetics, volume 1
[AD-A286796] p 2553 N95-29159
Semiconductor science and technology
[AD-A289143] p 2563 N95-29191
Gordon research conference on point defects, line defects, and interfaces in semiconductors
[AD-A290103] p 2714 N95-29209
Gordon research conference on physical metallurgy: Materials by design
[AD-A290519] p 2524 N95-29326
Symposium on Metal-Mediated Molecular Architectures
[AD-A290427] p 2692 N95-29388
Workshop on Fielded Applications of Machine Learning
[AD-A280168] p 2649 N95-29456
Genetics and the unity of biology
[DE95-006484] p 2633 N95-29471
Bilateral US/Russia Workshop on Self-Propagating High-Temperature Synthesis held in Honolulu, Hawaii on 6-7 November 1993
[AD-A290466] p 2525 N95-29492
Intelligent turbine engines for Army applications
[AD-A290532] p 2500 N95-29496
Summaries of papers presented at the ultrafast phenomena topical meeting
[AD-A290998] p 2564 N95-29511
The 14th International Conference on Atomic Physics
[AD-A290726] p 2693 N95-29521
The 2nd European Conference on Smart Structures and Materials
[AD-A290723] p 2550 N95-29579
Proceedings of the 6th International Conference on Nondestructive Characterization of Materials
[AD-A290727] p 2596 N95-29580
Recent Issues and Advances in Aeromedical Evacuation (MEDEVAC)
[AGARD-CP-554] p 2676 N95-29604
Proceedings of the 12th Annual National Conference on Ada Technology
[AD-A290693] p 2651 N95-29644
Solid freeform fabrication symposium
[AD-A290949] p 2527 N95-29732
Defense Modeling and Simulation Office information/data base technology working group (I/DBTWG) meetings
[AD-A290953] p 2651 N95-29735
Summary of the 1st International Workshop on Networked Reality in Telecommunication
[AD-A292366] p 2558 N95-29862
The 2nd International Conference on Thin Film Physics and Applications
[AD-A292353] p 2546 N95-29983
Workshop on computing and intelligent systems
[AD-A290581] p 2666 N95-30040
Pioneer Venus 12.5 km Anomaly Workshop Report, volume 1
[NASA-CP-3303] p 2737 N95-30058
Proceedings of the 18th International Workshop on Condensed Matter Theories
[AD-A291396] p 2694 N95-30065
Proceedings of the Sixth International Symposium on Long-Range Sound Propagation
[AD-A290920] p 2685 N95-30084
Methodologies for intelligent systems
[AD-A290901] p 2666 N95-30117
ICASE/LaRC Workshop on Benchmark Problems in Computational Aeroacoustics (CAA)
[NASA-CP-3300] p 2686 N95-30133
CONFIDENCE LIMITS
Statistical inference problems in some multivariate linear models with applications to multivariate calibration and meta-analysis
[AD-A291125] p 2675 N95-29768
CONFIGURATION INTERACTION
Reaction field (RF) calculation of the spectral shifts of indole
[AD-A290449] p 2532 N95-29487
CONFIGURATION MANAGEMENT
Automatically combining changes to software systems
[AD-A290628] p 2650 N95-29515
Product configurations: An application for prototype object approach
[PB95-192589] p 2655 N95-30283
CONFINEMENT
Theory of pseudo-classical confinement and transmutation to L-mode
[AD-B175957L] p 2709 N95-29809
Electronic states in Cd(1-x)Zn(x)Te/CdTe strained layer coupled double quantum wells and their photoluminescence
[DE95-006806] p 2716 N95-29814
CONICAL BODIES
Cross flow instability of supersonic flow over a 4:1 elliptic cone
[AD-A291128] p 2577 N95-29913
CONJUGATION
Conjugated polymers from cyclohexadienediol monomers
[AD-A290247] p 2544 N95-29505
CONNECTORS
Load balancing for the parallel adaptive solution of partial differential equations
[AD-A290450] p 2671 N95-29488
Fiber compatible acousto-optic modulator using a gradient index lens
[AD-A291164] p 2565 N95-29925
CONSERVATION EQUATIONS
Application of the space-time conservation element and solution element method to two-dimensional advection-diffusion problems
[NASA-TM-106946] p 2574 N95-29372
CONSERVATION LAWS
Systems of hyperbolic partial differential equations
[AD-A290287] p 2689 N95-29083
Comparative study of numerical schemes of TVD3, UNO3-ACM and optimized compact scheme
p 2686 N95-30137
Results of two new methods for aeroacoustics benchmark problems p 2687 N95-30140
CONSISTENCY
High-performance speech recognition using consistency modeling
[AD-A290655] p 2557 N95-29564
CONSOLIDATION
Hot explosive consolidation of W-Ti alloys
[AD-A290880] p 2537 N95-29635
CONSTANTS
Screening constants for plasma
[AD-B179442L] p 2710 N95-29843
CONSTELLATIONS
Comparison study of unequal error protection methods for one-dimensional signal constellations
[AD-A290386] p 2554 N95-29231
CONSTRUCTION
Correctness of real-time systems by construction
[PB95-206827] p 2655 N95-30220
CONSTRUCTION MATERIALS
Shear reinforcement in deep slabs
[AD-A289528] p 2594 N95-28909
Liquefied metal jet program Automation and Robotics Research Institute (ARRI)
[AD-A289781] p 2536 N95-29461
Nippon Steel Research Laboratories, Futtsu, 28 February 1994. and Advanced Materials and Technology Research Laboratories, Kawasaki, 15 June 1994
[AD-A292346] p 2526 N95-29533
The Institute for Material Science and Department of Material Science, Tohoku University, Sendai Japan, 2-3 June 1994
[AD-A292348] p 2650 N95-29534
CONTACT LOADS
Dimensions, deflections and stresses for Hertzian contacts under combined normal and tangential loading. (Guide to use of computer program A9434.)
[ESDU-94034] p 2593 N95-28711
Contact stress in disc cams with domes of flat-faced followers
[ESDU-94011] p 2589 N95-28901
CONTACT RESISTANCE
Effects of the cooling system parameters on heat transfer and performance of the PAFC stack during transient operation
[NASA-CR-197654] p 2572 N95-29249
CONTAINERS
Polymeric microcapsule arrays
[AD-A291937] p 2539 N95-28850
CONTAINMENT
Severe edge effects and simple complimentary interior solutions for thin-walled anisotropic and composite structures
[AD-A290645] p 2595 N95-29562
CONTAMINANTS
Development of the test kit for fuel acid contamination
[AD-A291953] p 2548 N95-29019
Surfactant-enhanced in situ biodegradation of strongly sorbing organic substances in soil environments
[AD-A290253] p 2512 N95-29168
Measuring variation in ecosystem sensitivity to stress
[AD-A290415] p 2609 N95-29450
Effect of KOH concentration and anions on the performance of Ni-H2 battery positive plate
p 2567 N95-30260
CONTAMINATION
Modeling joint effects of mixtures of chemicals on microorganisms using quantitative structure activity relationship techniques, phase 3
[AD-A290153] p 2632 N95-29320

Evaluation of commercial water-in-fuel test kits
[AD-A292135] p 2533 N95-29572
Boronization study for application to large helical device
[AD-B191996L] p 2709 N95-29808

CONTINENTS
The gravitational potential energy of the Earth's lithosphere p 2617 N95-29773

CONTINUITY EQUATION
SOSDOR: Solid-state device simulator code
[AD-A289954] p 2563 N95-29275
Numerical solution of the equations governing non-Newtonian flow at moderate Reynolds numbers p 2579 N95-30233

CONTINUOUS RADIATION
A procedure for accessing digital satellites containing amateur payloads
[AD-A289748] p 2506 N95-28688
Novel high-power solid-state sources for the millimeter-wave region
[AD-A292653] p 2564 N95-29384
Experimental studies of fundamental one- and two-photon lasing processes
[AD-A290593] p 2693 N95-29555
Finite difference ocean acoustic model users guide
[AD-A291544] p 2631 N95-29856
Characterisation of a line-tunable He-Xe laser operating at 2.026 and 3.894 micrometers
[AD-A291129] p 2587 N95-29914

CONTINUOUS SPECTRA
Continuum spectra of supermassive accretion disks p 2732 N95-29252

CONTINUOUS WAVE LASERS
Path resolved optical sensing of atmospheric winds utilizing speckle-turbulence interaction and pseudorandum code modulation
[AD-A290800] p 2621 N95-29497
Development of continuous visible chemical laser amplifiers and oscillators from the Na3-X(Cl, Br, I) reactions and their analogs and energy transfer pumping from efficiently produced metastable states
[AD-A290999] p 2586 N95-29514

CONTINUUM MODELING
An extension of the continuum model by Grad's thirteen moment equations for hypersonic rarefied flows p 2488 N95-29118

CONTRACTION
The study of non-Newtonian contraction flows with a parallel finite element method p 2576 N95-29778

CONTRACTORS
Operational test and evaluation (OT&E) integration and operational test procedures for Fixed Ground Antenna Radome (FGAR)
[AD-A291203] p 2559 N95-29975
Performance evaluation of bolt-cutter system on first Taurus launch
[AD-A291237] p 2504 N95-29992

CONTROL EQUIPMENT
Experimental investigation of aerodynamic devices for wind turbine rotational speed control, phase 1
[DE95-004034] p 2603 N95-30016

CONTROL ROCKETS
A vehicle health monitoring system for the Space Shuttle Reaction Control System during reentry
[NASA-CR-188370] p 2505 N95-29447

CONTROL SIMULATION
Numerical simulation of mechanisms and manipulator robots with flexible links and flexible joints
[PB95-196903] p 2591 N95-30285

CONTROL STABILITY
Lockheed Stabilizer System for space exercise equipment
[NASA-CR-197657] p 2641 N95-29180
H(sub 2) almost disturbance decoupling problem with internal stability
[PB95-206942] p 2667 N95-30168

CONTROL SYSTEMS DESIGN
A conceptual design for the attitude control and determination system for the Magnetosphere Imager spacecraft
[NASA-TP-3560] p 2507 N95-28721
Design, development and testing of a prototype precision angular positioning control system for a next generation multiplexed imager
[AD-A292585] p 2698 N95-28980
Application of optimization technique to control system design for departure prevention and aircraft model estimation through dynamic inversion p 2501 N95-29156
Lockheed Stabilizer System for space exercise equipment
[NASA-CR-197657] p 2641 N95-29180
Conversion of an oceanographic expert system to a C-based language
[NASA-CR-198695] p 2630 N95-29237
Substructure-based control of flexible structures p 2508 N95-29408
Spacecraft attitude control system performance using pulse-width pulse-frequency modulated thrusters
[AD-A291803] p 2508 N95-29410
Design and evaluation of a LQR controller for the bluebird unmanned air vehicle
[AD-A289769] p 2498 N95-29457
Broadband control of structural vibration using simultaneous sensing and actuation with nonlinear piezoelectric elements p 2664 N95-29548
Fundamental limitations and capabilities of robust identification and adaptive control
[AD-A291085] p 2664 N95-29636
Linear matrix inequalities for the problem of absolute stability of control systems p 2501 N95-29680
Experimental confirmation of a PDE-based approach to design of feedback controls
[NASA-CR-198167] p 2672 N95-30086
A unified matrix inequality approach to linear control design p 2667 N95-30234
Design, analysis and control of large transports so that control of engine thrust can be used as a back-up of the primary flight controls
[NASA-CR-198958] p 2501 N95-30254
H infinity control problem with zeros on the boundary of the stability domain
[PB95-197042] p 2668 N95-30288

CONTROL THEORY
Geometry modeling and grid generation using 3D NURBS control volume p 2483 N95-28753
International Workshop on Stochastic Filtering Theory
[AD-A291670] p 2661 N95-28788
A differential approach to graphical interaction
[AD-A292165] p 2647 N95-29125
Proceeding of the 33rd SICE Annual Conference
[DE95-758943] p 2662 N95-29144
Substructure-based control of flexible structures p 2508 N95-29408
Interaction and intelligent behavior
[AD-A290049] p 2639 N95-29443
Fundamental limitations and capabilities of robust identification and adaptive control
[AD-A291085] p 2664 N95-29636
Computational algorithms for aerodynamic analysis and design
[AD-A291084] p 2491 N95-29972
Digital control of distributed parameter systems: A state-space approach
[PB95-197216] p 2666 N95-30041
H(sub 2) almost disturbance decoupling problem with internal stability
[PB95-206942] p 2667 N95-30168
Factorization and input-output decoupling by static output feedback for nonlinear control systems
[PB95-206975] p 2667 N95-30171
A unified matrix inequality approach to linear control design p 2667 N95-30234
Learning control in linear and nonlinear systems p 2667 N95-30238
Control of vortex dynamics p 2579 N95-30275
H infinity control problem with zeros on the boundary of the stability domain
[PB95-197042] p 2668 N95-30288

CONTROLLED FUSION
Carbon sheet pumping
[AD-B179443L] p 2710 N95-29812

CONTROLLERS
Conversion of the TRACON operations concepts database into a formal sentence outline job task taxonomy
[DOT/FAA/AM-95/16] p 2493 N95-28819
Hybrid fuzzy logic control to stabilize an inverted pendulum from arbitrary initial conditions
[AD-A292441] p 2681 N95-29000
On-line damage identification and motion control of adaptive structures: An intelligent control approach p 2662 N95-29109
Conversion of an oceanographic expert system to a C-based language
[NASA-CR-198695] p 2630 N95-29237
Closed loop control of guided missiles using neural networks p 2663 N95-29241
Analytical investigations in aircraft and spacecraft trajectory optimization and optimal guidance
[NASA-CR-4672] p 2504 N95-29339
Ride motion simulator (RMS) testing using human occupants
[AD-A292641] p 2641 N95-29378
Spacecraft attitude control system performance using pulse-width pulse-frequency modulated thrusters
[AD-A291803] p 2508 N95-29410
Design and evaluation of a LQR controller for the bluebird unmanned air vehicle
[AD-A289769] p 2498 N95-29457
Fundamental limitations and capabilities of robust identification and adaptive control
[AD-A291085] p 2664 N95-29636
Experimental confirmation of a PDE-based approach to design of feedback controls
[NASA-CR-198167] p 2672 N95-30086
H(sub 2) almost disturbance decoupling problem with internal stability
[PB95-206942] p 2667 N95-30168
A unified matrix inequality approach to linear control design p 2667 N95-30234
H infinity control problem with zeros on the boundary of the stability domain
[PB95-197042] p 2668 N95-30288

CONVECTION
Analysis of the structural characteristics and intensity evolution of super typhoon flo (1990) in special sensor Microwave/Imager (SSM/I) data
[AD-A292413] p 2619 N95-28989
Characterization of the geometries of the high-latitude ionospheric convection pattern p 2614 N95-29524
The high latitude ionospheric convection pattern during northward interplanetary magnetic field p 2615 N95-29693
Observations of mesoscale cellular convection from the marine stratocumulus phase of FIRE p 2624 N95-29727

CONVECTION CURRENTS
The tropical atmosphere under convection adjustment p 2625 N95-29833

CONVECTIVE HEAT TRANSFER
Radiative cooling profiles calculated from ECMWF analyses and ISCCP C1 data, and their application to determination of distributions of apparent convective heating in the equatorial Pacific p 2625 N95-29805
The tropical atmosphere under convection adjustment p 2625 N95-29833

CONVENTIONS
DOD electronic data interchange (EDI) convention: TDCC/EDIA transaction set 210 motor carrier invoice (version 003020). Revision 1
[AD-A292375] p 2720 N95-28797
DOD electronic data interchange (EDI) convention: ASC X12 transaction set 410 Rail Carrier Invoice, version 003020
[AD-A292495] p 2722 N95-29287

CONVERGENCE
Stable function approximation in dynamic programming
[AD-A290224] p 2647 N95-29143
Optimal universal coding and density estimation
[AD-A290694] p 2675 N95-29587
Reliability enhancement of Navier-Stokes codes through convergence acceleration
[NASA-CR-196635] p 2578 N95-30034

CONVERGENT-DIVERGENT NOZZLES
Category 5 problem solution using an unstructured finite volume algorithm p 2657 N95-30157
High-order essentially non-oscillatory methods for computational aeroacoustics p 2690 N95-30159

CONVEXITY
Signal processing for high-resolution image formation
[AD-A290648] p 2557 N95-29563

COOLANTS
Effects of cooling system parameters on heat transfer in PAFC stack
[NASA-CR-198817] p 2570 N95-29131
Effects of the cooling system parameters on heat transfer and performance of the PAFC stack during transient operation
[NASA-CR-197654] p 2572 N95-29249
Hydrogen film cooling with incident and swept-shock interactions in a Mach 6.4 nitrogen free stream
[NASA-TM-4603] p 2578 N95-30056

COOLING
Micro/Miniature heat pipe analysis
[AD-A292232] p 2570 N95-29127
Alternative refrigerant performance: Field test of a nonchlorofluorocarbon chiller at Fort Leonard Wood, MO
[AD-A292052] p 2550 N95-29307
The effects of alloying elements on the strength and cooling rate sensitivity of ultra-low carbon alloy steel weld metals
[AD-A290681] p 2537 N95-29759
Austenite to ferrite transformation kinetics during continuous cooling
[DE95-008582] p 2537 N95-29869

COOLING SYSTEMS
Geothermal heat pumps for heating and cooling
[AD-A292115] p 2602 N95-28858
Effects of cooling system parameters on heat transfer in PAFC stack
[NASA-CR-198817] p 2570 N95-29131

Effects of the cooling system parameters on heat transfer and performance of the PAFC stack during transient operation
[NASA-CR-197654] p 2572 N95-29249
COORDINATION
Inorganic halogen oxidizers
[AD-A290747] p 2533 N95-29581
Operational test and evaluation (OT&E) integration and operational test plan for fixed ground antenna radome (FGAR)
[AD-A291310] p 2559 N95-29940
Inorganic halogen oxidizers
[AD-A291201] p 2702 N95-29974
A biologically-inspired autonomous robot
[AD-A289446] p 2666 N95-30026
COPOLYMERS
High temperature thermosets and ceramics derived from linear carborane-(siloxane or silane)-acetylene copolymers
[AD-D017400] p 2545 N95-29569
Polyethylene-based polyurethane copolymers and block copolymers
[AD-A289996] p 2546 N95-30030
Linear carborane-(siloxane or silane)-acetylene based copolymers
[AD-D017321] p 2547 N95-30132
COPPER
Formation of striped surface phases by short-range forces
[AD-A279962] p 2531 N95-28945
Liquefied metal jet program Automation and Robotics Research Institute (ARRI)
[AD-A289781] p 2536 N95-29461
A search for a composition-dependent gravitational force p 2719 N95-29501
Effects of space exposure on metals flown on the Long Duration Exposure Facility
[NASA-CR-4662] p 2512 N95-30225
COPPER ALLOYS
Examination of dislocation core structures in B2 intermetallic alloys
[AD-A291486] p 2537 N95-29526
COPPER COMPOUNDS
Composite material studies for low temperature thermionic emission
[AD-A292159] p 2523 N95-29124
COPPER OXIDES
Synthesis and characterization of CuO superconductors with high transient temperatures
[AD-A292478] p 2562 N95-29014
Pulsed laser deposition of ferroelectric thin films in conjunction with superconducting oxides
[AD-A290101] p 2585 N95-29208
Deposition and surface treatment with intense pulsed ion beams
[DE95-007885] p 2543 N95-29465
Ion beam modification of Tl-Ba-Ca-Cu-O type high temperature superconductors during irradiation
[DE95-006807] p 2717 N95-30022
COPPER SELENIDES
Multi-decade time-dependent voltage of polycrystalline thin-film solar cells p 2602 N95-29103
CORDAGE
Methods and components for optical contention resolution in high speed networks
[AD-A292331] p 2697 N95-28795
CORES
Examination of dislocation core structures in B2 intermetallic alloys
[AD-A291486] p 2537 N95-29526
CORNERS
Through-the-thickness stresses and failure in the corner radius of a laminated composite section
[ESDU-94019] p 2518 N95-28899
CORONAGRAPHS
Coronagraphic imaging of protoplanetary-disk candidate stars using adaptive optics p 2728 N95-29651
CORONARY ARTERY DISEASE
A discrete-event simulation model of myocardial electrical activity: Mathematical electrophysiology
[AD-A292323] p 2633 N95-28793
Flying waivers for history of angioplasty and myocardial infraction
[AD-A292505] p 2635 N95-29161
CORRECTION
The effect of viscous attenuation on shock tube performance
[AD-A289793] p 2568 N95-28696
The correction of measured noise spectra for the effects of ground reflection
[ESDU-94035] p 2683 N95-28710
CORRELATION
Correlations between micromagnetic, microstructural and microchemical properties in ultrathin epitaxial magnetic structures
[AD-A289705] p 2712 N95-28681
Correlation of inclusion size and chemistry with weld metal composition and microstructure arc weldments of high strength steels
[AD-A292024] p 2590 N95-29184
Intensity optical correlation through optical differentiation preprocessing
[AD-A291020] p 2701 N95-29661
A full wave study of radar cross sections of rough terrain
[AD-A291227] p 2559 N95-29982
CORROSION
Corrosion investigation of multilayered ceramics and experimental nickel alloys in SCWO process environments
[DE95-008666] p 2540 N95-28960
The mm-wave resonant methods for the detection of corrosion, phase 1
[AD-A291315] p 2593 N95-29941
Electrochemical impedance pattern recognition for detection of hidden chemical corrosion on aircraft components, phase 1
[AD-A291345] p 2593 N95-29946
CORROSION PREVENTION
Zero Discharge Organic Coatings: Powder paint. UV curable paint. E-coat
[AD-A292180] p 2540 N95-28925
Corrosion in methylphosphonic difluoride
[AD-A289995] p 2536 N95-29137
Epoxy self-priming topcoats
[AD-D017383] p 2541 N95-29194
Chemically induced passivity of aluminum alloys and Al-based metal matrix composites
[AD-A290778] p 2528 N95-29923
CORROSION RESISTANCE
Epoxy self-priming topcoats
[AD-D017383] p 2541 N95-29194
Chemically induced passivity of aluminum alloys and Al-based metal matrix composites
[AD-A290778] p 2528 N95-29923
CORROSION TESTS
The use of electrochemistry and ellipsometry for identifying and evaluating corrosion on aircraft
[AD-A290249] p 2497 N95-29426
Bell Helicopter Advanced Rotocraft Transmission (ART) program
[NASA-CR-195479] p 2590 N95-29538
CORRUGATED PLATES
A study of structurally efficient graphite-thermoplastic trapezoidal-corrugation sandwich and semi-sandwich panels p 2516 N95-28842
COSMIC DUST
The x-ray scattering halo around Sco-X1 p 2727 N95-29591
Dust formation in stellar outflows: A time-dependent model p 2733 N95-29649
Extended dust shells around carbon stars resolved by HIRAS p 2735 N95-29840
COSMIC RAYS
The energy spectrum and flux of cosmic ray helium at high energy p 2740 N95-29705
Investigation and characterization of SEU effects and hardening strategies in avionics
[AD-A291058] p 2500 N95-29950
COSMOLOGY
Experimental cosmology using fast parallel N-body methods p 2734 N95-29775
Statistics and large-scale structure p 2734 N95-29780
COST ANALYSIS
Selection and costing of heat exchangers. Air-cooled type
[ESDU-94043] p 2550 N95-28705
Selection and costing of heat exchangers. Shell-and-tube type
[ESDU-94042] p 2550 N95-28706
Future requirements in surface modeling and grid generation p 2478 N95-28724
Global cost and weight evaluation of fuselage keel design concepts p 2499 N95-28840
Cost model relationships between textile manufacturing processes and design details for transport fuselage elements p 2521 N95-29043
The Telemetry Agile Manufacturing Effort
[DE95-006177] p 2654 N95-30115
COST REDUCTION
Impact of composites on future transport aircraft p 2519 N95-29030
Magnum(R) NiCd advanced nickel-cadmium battery cells p 2567 N95-30258
Advanced Dependent Pressure Vessel (DPV) nickel-hydrogen spacecraft cell and battery design p 2567 N95-30261
COSTS
Technology development goals for automotive fuel cell power systems
[DE95-006764] p 2548 N95-29280
An analysis of the impact of ASPA on organizational and depot level maintenance
[AD-A292670] p 2477 N95-29414
The mesh synchronous processor MeshSP (trademark)
[AD-A289875] p 2659 N95-29420
On the topological complexity of the cost function in variational data assimilation p 2724 N95-29798
COUETTE FLOW
Studies in drag reduction p 2487 N95-29094
Unsteady rotational shear flow of power law fluids
[ISBN-0-315-81287-7] p 2575 N95-29718
Numerical simulation of stability and stability control of high speed compressible rotating couette flow
[NASA-CR-198832] p 2579 N95-30250
COULOMB COLLISIONS
A Monte Carlo simulation of Coulomb collisions and wave-particle interactions in space plasma at high latitudes p 2704 N95-29205
Monte Carlo simulation study of the ICRF minority heating in the large helical device
[AD-B179858L] p 2708 N95-29749
COUNTER ROTATION
Numerical simulation of stability and stability control of high speed compressible rotating couette flow
[NASA-CR-198832] p 2579 N95-30250
COUNTERS
GLAST
[DE95-008596] p 2739 N95-29265
COUNTING
The Los Alamos Photon Counting Detector Debris Detection Project: An update
[DE95-007883] p 2508 N95-29464
COUPLED MODES
Experiments on nonlinear wave-particle interactions p 2695 N95-30302
COVARIANCE
Performance analysis of a GPS Interferometric attitude determination system for a gravity gradient stabilized spacecraft
[NASA-CR-188372] p 2508 N95-30036
COWLINGS
NACA 1-series geometry representation for computational fluid dynamics
[ESDU-94013] p 2568 N95-28902
Wave drag coefficient for axisymmetric forecowls at zero incidence (M sub infinity less than or equal to 1.5)
[ESDU-94014] p 2568 N95-28903
Surface pressure coefficient distributions for axisymmetric forecowls at zero incidence (M sub infinity less than or equal to 1.5)
[ESDU-94015] p 2487 N95-28904
CRACK BRIDGING
The effect of mixed mode precracking on the mode 1 fracture toughness of composite laminates p 2514 N95-28827
Alumina reinforced Tetragonal Zirconia (TZP) composites
[DE95-008990] p 2529 N95-30180
CRACK INITIATION
Effect of open hole on tensile failure properties of 2D triaxial braided textile composites and tape equivalents
[NASA-CR-4676] p 2513 N95-28817
The effect of mixed mode precracking on the mode 1 fracture toughness of composite laminates p 2514 N95-28827
Experimental investigations of wave and fracture phenomena in impacted ceramics and glasses
[AD-A292142] p 2542 N95-29195
Interlaminar fracture mechanics and mechanisms: Linear and nonlinear aspects p 2526 N95-29597
Toughening mechanisms in mixed-mode interfacial fracture p 2545 N95-29772
CRACK OPENING DISPLACEMENT
Toughening mechanisms in mixed-mode interfacial fracture p 2545 N95-29772
Analytical investigation of the hygrothermal effects and parametric study of the Edge Crack Torsion (ECT) mode 3 test lay-ups
[NASA-TM-110183] p 2528 N95-30028
CRACK PROPAGATION
Stress concentration, stress intensity, and fatigue crack growth along evacuators of pressurized, autofrettaged tubes
[AD-A291920] p 2593 N95-28789
Effect of open hole on tensile failure properties of 2D triaxial braided textile composites and tape equivalents
[NASA-CR-4676] p 2513 N95-28817
Tension fracture of laminates for transport fuselage. Part 2: Large notches p 2515 N95-28837
The combined effect of glass buffer strips and stitching on the damage tolerance of composites p 2522 N95-29049
Dynamic decohesion of bimaterial interfaces p 2541 N95-29120

Fiber-matrix adhesion in single-fiber model composites p 2524 N95-29337
Interlaminar fracture mechanics and mechanisms: Linear and nonlinear aspects p 2526 N95-29597
Micromechanics of crack extension in composites p 2529 N95-30276

CRACK TIPS
Tension fracture of laminates for transport fuselage. Part 2: Large notches p 2515 N95-28837
Dynamic decohesion of bimaterial interfaces p 2541 N95-29120
Interlaminar fracture mechanics and mechanisms: Linear and nonlinear aspects p 2526 N95-29597

CRACKING (FRACTURING)
Shear reinforcement in deep slabs
[AD-A289528] p 2594 N95-28909
Dynamic decohesion of bimaterial interfaces p 2541 N95-29120
Experimental investigations of wave and fracture phenomena in impacted ceramics and glasses
[AD-A292142] p 2542 N95-29195
Interlaminar fracture mechanics and mechanisms: Linear and nonlinear aspects p 2526 N95-29597
Fatigue life analysis and tests for thick-walled cylinders including effects of overstrain and axial grooves
[AD-A290931] p 2596 N95-30119

CRACKS
Stress concentration, stress intensity, and fatigue crack growth along evacuators of pressurized, autofrettaged tubes
[AD-A291920] p 2593 N95-28789
Dynamic decohesion of bimaterial interfaces p 2541 N95-29120
Experimental investigations of wave and fracture phenomena in impacted ceramics and glasses
[AD-A292142] p 2542 N95-29195
Investigation of tension-compression fatigue behavior of a notched cross-ply metal matrix composite at elevated temperature
[AD-A291479] p 2527 N95-29770
A study of blister tests for film adhesion measurement and fracture efficiency of tests for adhesive bonds p 2545 N95-29799
The mm-wave resonant methods for the detection of corrosion, phase 1
[AD-A291315] p 2593 N95-29941
Analytical investigation of the hygrothermal effects and parametric study of the Edge Crack Torsion (ECT) mode 3 test lay-ups
[NASA-TM-110183] p 2528 N95-30028

CRASH INJURIES
Biodynamic simulation of pilot interaction with a helicopter multiairbag restraint system
[AD-A290196] p 2492 N95-29057

CRASHWORTHINESS
Biodynamic simulation of pilot interaction with a helicopter multiairbag restraint system
[AD-A290196] p 2492 N95-29057

CREW EXPERIMENT STATIONS
Summary Report of mission acceleration measurements for STS-66. Launched November 3, 1994
[NASA-TM-106914] p 2509 N95-29643

CRITERIA
Test load verification through strain data analysis
[NASA-TP-3558] p 2504 N95-28718
The identification of user criteria of relevance and document characteristics: Beyond the topical approach to information retrieval p 2723 N95-29518

CRITICAL FREQUENCIES
Correlation and gradient characteristics of ionospheric parameters in Europe
[AD-A290135] p 2612 N95-29140

CRITICAL LOADING
Compressive behavior of thick composite shells: Benchmark solutions for loss of stability and hygroscopic effects p 2595 N95-29424

CRITICAL POINT
Thermophysical properties of R-32 (difluoromethane)
[ESDU-94032] p 2530 N95-28802
Thermal conductivity of liquid halogenated aliphatic hydrocarbons. Part 1: Halogenated methanes and azeotropic mixtures
[ESDU-94021-PT-1] p 2511 N95-28804
Effects of critical fluctuations on the thermodynamic properties of fluids and fluid mixtures p 2719 N95-29216
Photothermal deflection in a supercritical fluid p 2701 N95-29630
Vapour pressures and critical points of liquids. Glycols and cyclic diols
[ESDU-95002] p 2534 N95-29897
Vapour pressures and critical points of liquids. Glycol ethers (alkyl cellosolves and carbitols, etc.)
[ESDU-95004] p 2534 N95-29901
Analysis of factors affecting chemical reactions in supercritical fluids
[AD-A290905] p 2534 N95-30078

CRITICAL TEMPERATURE
Thermal conductivity of liquid halogenated aliphatic hydrocarbons. Part 1: Halogenated methanes and azeotropic mixtures
[ESDU-94021-PT-1] p 2511 N95-28804
Optically triggered, superconducting opening switch
[AD-A292642] p 2700 N95-29379
Vapour pressures and critical points of liquids. Glycols and cyclic diols
[ESDU-95002] p 2534 N95-29897
Vapour pressures and critical points of liquids. Glycol ethers (alkyl cellosolves and carbitols, etc.)
[ESDU-95004] p 2534 N95-29901

CRITICAL VELOCITY
Transonic, supersonic and hypersonic wind-tunnel tests on aerodynamic characteristics of reentry body with blunted cone configuration
[ISAS-658] p 2490 N95-29640

CROSS CORRELATION
Correlation and gradient characteristics of ionospheric parameters in Europe
[AD-A290135] p 2612 N95-29140

CROSS FLOW
Flow visualization of vorticity cancellation of jets in crossflow
[AD-A292414] p 2569 N95-28990
The effects of the thermal boundary condition and turbulence on heat transfer from a cylinder, flat plate, and turbine blade using the transient shroud and heated-coating techniques
[AD-A292646] p 2574 N95-29380
The decay of longitudinal vortices shed from airfoil vortex generators
[NASA-CR-198356] p 2489 N95-29402
Cross flow instability of supersonic flow over a 4:1 elliptic cone
[AD-A291128] p 2577 N95-29913
Growth and development of roughness-induced stationary crossflow vortices p 2492 N95-30294

CROSS POLARIZATION
A full wave study of radar cross sections of rough terrain
[AD-A291227] p 2559 N95-29982

CROSS SECTIONS
Parameterized spectral distributions for meson production in proton-proton collisions
[NASA-TM-4675] p 2696 N95-30337

CROSSLINKING
Biological methane activation
[PB95-200705] p 2535 N95-30198

CROSSTALK
An investigation of the channel crosstalk in optical heterodyne controlled phased array radars
[AD-A292028] p 2554 N95-29186

CRUISING FLIGHT
A two element laminar flow airfoil optimized for cruise
[NASA-CR-198580] p 2489 N95-29338

CRUSHING
Analytical and experimental studies of the energy absorption behavior of composite structures p 2524 N95-29411

CRUSTAL FRACTURES
Crustal deformation measurements in the vicinity of Vandenberg Air Force Base
[AD-A291224] p 2618 N95-29981

CRUSTS
Mapping crust and upper mantle structure beneath southern Eurasia
[AD-A291074] p 2618 N95-29970

CRYOGENIC COOLING
Fundamental studies in cryogenic cooling of power electronics
[AD-A291150] p 2551 N95-30296

CRYOGENIC EQUIPMENT
Five-channel SQUID based non-destructive evaluation (NDE) instrument
[AD-A292474] p 2592 N95-29012
A hybrid electronically scanned pressure module for cryogenic environments
[NASA-TM-110146] p 2583 N95-29453

CRYOGENIC FLUID STORAGE
Fuel cell systems for First Lunar Outpost-reactant storage option p 2606 N95-30264

CRYOGENIC FLUIDS
Precision cleaning verification of fluid components by air/water impingement and total carbon analysis
[NASA-TM-110742] p 2531 N95-29248
Fuel cell systems for First Lunar Outpost-reactant storage option p 2606 N95-30264

CRYOGENIC TEMPERATURE
A hybrid electronically scanned pressure module for cryogenic environments
[NASA-TM-110146] p 2583 N95-29453
A gyroscope clock for a null gravitational redshift experiment p 2584 N95-29664
Radiation effects on front-end electronics for noble liquid calorimetry
[DE95-007304] p 2566 N95-30025

CRYOGENIC WIND TUNNELS
A hybrid electronically scanned pressure module for cryogenic environments
[NASA-TM-110146] p 2583 N95-29453

CRYOGENICS
Technology development goals for automotive fuel cell power systems
[DE95-008764] p 2548 N95-29280
Semiconductor deposition and etching interactions of laser-generated translationally hot atoms and radicals
[AD-A291824] p 2693 N95-29431
Inertial fusion program and national laser users facility program
[DE95-008202] p 2711 N95-30274

CRYPTOGRAPHY
Computational complexity and encryption
[AD-A291910] p 2648 N95-29356
Encryption and networking applications
[DE95-009587] p 2651 N95-29871

CRYSTAL DEFECTS
Nitride semiconductors for ultraviolet detection
[AD-A289546] p 2712 N95-28910
What do we really know about the atomic scale structures of nanophase materials?
[DE95-005858] p 2717 N95-29986
Defect centers in chemical-mechanical polished MOS oxides
[DE95-004777] p 2718 N95-30214

CRYSTAL FIELD THEORY
Crystal field and exchange interactions in DyT4Al8 (T = Fe and Mn)
[DE95-007131] p 2714 N95-29134

CRYSTAL GROWTH
Processing, fabrication, characterization and device demonstration of high temperature superconducting ceramics
[AD-A290183] p 2541 N95-29055
Growth, characterization and application of KTN family nonlinear optical crystals
[AD-A290330] p 2713 N95-29087
Electronic properties of low-temperature grown III/V thin films
[AD-A292521] p 2714 N95-29165
Low temperature materials growth and processing development for flat panel display technology applications
[AD-A292177] p 2715 N95-29267
Pulsed laser deposition of thin film material for nonlinear waveguides
[AD-A290789] p 2544 N95-29484
Reduce Fluid Experiment System: Flight data from the IML-1 Mission
[NASA-CR-196639] p 2549 N95-30014
High-efficiency solar cells using HEM silicon
[DE95-005424] p 2604 N95-30217

CRYSTAL LATTICES
Studies of lattice-mismatched and Low-Temperature-Grown semiconductor multiple-phase systems
[AD-A292536] p 2713 N95-28967
Brief introduction to state key physics laboratories and division open laboratories
[AD-A291064] p 2682 N95-29952

CRYSTAL STRUCTURE
Ferroelectric polarization mechanism of the odd-numbered nylons
[AD-A292276] p 2539 N95-28860
Synthesis and complete characterization of a Gallium-Mixed-Pnicogen four-membered ring compound: I2GaAs(SiMe3)(sub 2)Ga(I)2P(SiMe3)(sub 2)
[AD-A292423] p 2713 N95-28993
Crystal field and exchange interactions in DyT4Al8 (T = Fe and Mn)
[DE95-007131] p 2714 N95-29134
Pulsed laser deposition of ferroelectric thin films in conjunction with superconducting oxides
[AD-A290101] p 2585 N95-29208
Real-time x-ray scattering study of processing of eight performance thermoplastics
[AD-A290374] p 2542 N95-29230
Synthesis and characterization of (Me3SiCH2)3M(dot)E(SiMe3)3 (M = Ga, E = P or As; M = In, E = P). X-ray crystal structures of (Me3SiCH2)3Ga(dot)P(SiMe3)3 and (Me3SiCH2)3In(dot)P(SiMe3)3
[AD-A291907] p 2715 N95-29444
Pulsed laser deposition of thin film material for nonlinear waveguides
[AD-A290789] p 2544 N95-29484

Synthesis morphology and properties of semicrystalline block copolymers
[AD-A290475] p 2544 N95-29510
Structure and orientation behavior of highly oriented polymers under tensile and compressive stresses
p 2546 N95-29822
Ordering and bandgap reduction in InAs(1-x)Sb(x) alloys
[DE95-006324] p 2717 N95-30005
Neutron scattering from amorphous, disordered and nanocrystalline materials
[DE95-005848] p 2717 N95-30077

CRYSTALLINITY
Experimental methods in residual stress measurement using a position-sensitive single-exposure scintillation detection system
[AD-A289803] p 2594 N95-28949
The synthesis of liquid crystalline phophazenes containing chiral mesogens
[AD-A291911] p 2543 N95-29358
Processing studies on in situ composites based on blends of thermotropic Liquid Crystalline Polymers with thermoplastics
[AD-A290526] p 2544 N95-29494
Structure and orientation behavior of highly oriented polymers under tensile and compressive stresses
p 2546 N95-29822

CRYSTALLITES
Synthesis of nanocrystalline indium arsenide and indium phosphide from Indium(III) halides and tris(trimethylsilyl)pnicogens; synthesis, characterization, and decomposition behavior of I3In(dot)P(SiMe3)3
[AD-A291905] p 2715 N95-29486

CRYSTALLIZATION
High-toughness glass-ceramics
[AD-A290562] p 2541 N95-29071

CRYSTALLOGRAPHY
Synthesis and characterization of (Me3SiCH2)3M(dot)E(SiMe3)3 (M = Ga, E = P or As; M = In, E = P). X-ray crystal structures of (Me3SiCH2)3Ga(dot)P(SiMe3)3 and (Me3SiCH2)3In(dot)P(SiMe3)3
[AD-A291907] p 2715 N95-29444

CRYSTALS
Ferroelectric polarization mechanism of the odd-numbered nylons
[AD-A292276] p 2539 N95-28860
The 1.3 micrometer fiber photodetector
[AD-A292462] p 2582 N95-29004
Synthesis morphology and properties of semicrystalline block copolymers
[AD-A290475] p 2544 N95-29510
Photorefractive Bi12SiO20 spatial light modulator
[AD-A291070] p 2702 N95-29969
Sensor protection portion of the development of nonlinear optical materials and processes for laser hardening of sensors
[AD-A291200] p 2702 N95-29973

CULTURE (SOCIAL SCIENCES)
Framework for comparing and controlling number-based design reasoning systems
[PB95-197364] p 2667 N95-30207

CUMULUS CLOUDS
Development of an improved cloud model for use in cumulus parameterization p 2624 N95-29800

CURING
Fiber optic Raman and micro Raman measurements of bonding agents at interface during the curing process
[AD-A292042] p 2523 N95-29189
Photogenerated amines in polymer curing and imaging: Design and synthesis of (3', 5'-dimethoxybenzoinyl)oxycarbonyl carbamates as novel photoprecursors of amines
[AD-A289945] p 2542 N95-29272

CURRENT DENSITY
Processing, fabrication, characterization and device demonstration of high temperature superconducting ceramics
[AD-A290183] p 2541 N95-29055
Computational methods for the simulation of non-Newtonian flows
[AD-A290355] p 2570 N95-29069
Processing and properties of long-lengths of Ag-clad BSCCO superconductors and high-(Tc) magnets
[DE95-005855] p 2716 N95-29984
Complete analysis of electrode-terminated cables in two-layer conductor bounded above by air: Current density, magnetic field, and magnetic field gradient
[AD-A290907] p 2566 N95-30079
Vacuum microelectronic emitters and their applications using compound semiconductor technology
[AD-A291142] p 2567 N95-30124

CURRENT DISTRIBUTION
Multifluid nonequilibrium simulation of arcjet thrusters
p 2510 N95-29245

CURVATURE
Numerical investigation of surface curvature effects in compressible turbulent flows
[AD-A290114] p 2571 N95-29211

CURVE FITTING
NACA 1-series geometry representation for computational fluid dynamics
[ESDU-94013] p 2568 N95-28902

CURVED PANELS
Dimensional stability of curved panels with cocured stiffeners and cobonded frames p 2515 N95-28836
Design, analysis, and fabrication of a pressure box test fixture for tension damage tolerance testing of curved fuselage panels p 2516 N95-28839
Buckling analysis of curved composite sandwich panels subjected to inplane loadings p 2517 N95-28845

CURVES (GEOMETRY)
Parametric design and gridding through relational geometry p 2486 N95-28771

CUSHIONS
Alternative methods for flotation seat cushion use
[DOT/FAA/AM-95/20] p 2493 N95-29448
The effect of wear on fire-blocking layer material effectiveness
[AD-A291520] p 2493 N95-29855

CUTTERS
Design of a fast-tool servo system using magnetic servo levitation
[AD-A290273] p 2663 N95-29183
Performance evaluation of bolt-cutter system on first Taurus launch
[AD-A291237] p 2504 N95-29992

CUTTING
Development of flame resistant, high efficiency thermal insulation
[AD-A291136] p 2547 N95-30120

CYCLIC COMPOUNDS
Viscosity of liquids: Aliphatic and cyclic ketones
[ESDU-94025] p 2530 N95-28712
Conjugated polymers from cyclohexadienediol monomers
[AD-A290247] p 2544 N95-29505
Vapour pressures and critical points of liquids. Glycols and cyclic diols
[ESDU-95002] p 2534 N95-29897

CYCLIC LOADS
Effects of temperature and humidity cycling on the strengths of textile reinforced carbon/epoxy composite materials p 2520 N95-29037
Fiber fracture in continuous-fiber reinforced composite materials during cyclic loading p 2525 N95-29513
Investigation of tension-compression fatigue behavior of a notched cross-ply metal matrix composite at elevated temperature
[AD-A291479] p 2527 N95-29770

CYCLOGENESIS
The effect of climate perturbations on extratropical cyclogenesis along the east coast of North America
p 2621 N95-29595

CYCLONES
Typhoon monitoring using passive microwave observations
[AD-A292567] p 2619 N95-28975
Analysis of the structural characteristics and intensity evolution of super typhoon flo (1990) in special sensor Microwave/Imager (SSM/I) data
[AD-A292413] p 2619 N95-28989
Forecast of Atlantic seasonal hurricane activity for 1995 p 2620 N95-29254
An air stream analysis of the occluded cyclone
p 2623 N95-29714
The role of diabatic heating, torques and stability in forcing the meridional circulation within cyclones
p 2626 N95-29834
A regression model for the western north pacific tropical cyclone intensity forecast
[AD-A290588] p 2627 N95-30044
Tropical storm database: East and Gulf of Mexico coasts of the United States
[AD-A291406] p 2627 N95-30066

CYCLOTRON FREQUENCY
Hybrid harmonic gyrotron traveling wave amplifier
[AD-A292686] p 2564 N95-29417

CYCLOTRON RESONANCE DEVICES
Theory of competition between synchronous and nonsynchronous modes in a magnicon output cavity
[AD-A292048] p 2563 N95-29301
Hybrid harmonic gyrotron traveling wave amplifier
[AD-A292686] p 2564 N95-29417
Monte Carlo simulation study of the ICRF minority heating in the large helical device
[AD-B179858L] p 2708 N95-29749

CYLINDRICAL BODIES
Stress concentration, stress intensity, and fatigue crack growth along evacuators of pressurized, autofrettaged tubes
[AD-A291920] p 2593 N95-28789
Experimental and theoretical studies of wakes in stratified flows
[AD-A290203] p 2569 N95-29060
Finite difference analysis of a cylindrical two conductor microstrip transmission line with truncated dielectrics
[AD-A292592] p 2555 N95-29290
Permanent magnet torque/force transfer apparatus
[AD-D017325] p 2682 N95-30051

CYLINDRICAL SHELLS
Compressive behavior of thick composite shells: Benchmark solutions for loss of stability and hygroscopic effects p 2595 N95-29424
Fatigue life analysis and tests for thick-walled cylinders including effects of overstrain and axial grooves
[AD-A290931] p 2596 N95-30119
Elastoplastic buckling analysis of cylindrical shells using a semi-analytical formulation
[PB95-197349] p 2597 N95-30206

D

DAMAGE
Test results from large wing and fuselage panels
p 2522 N95-29051
The development of an interpretive methodology for the application of real-time acousto-ultrasonic NDE technique for monitoring damage in ceramic composites under dynamic loads p 2592 N95-29104
On-line damage identification and motion control of adaptive structures: An intelligent control approach
p 2662 N95-29109
High velocity impact and penetration of thick composite laminates
[AD-A290642] p 2526 N95-29561

DAMAGE ASSESSMENT
Effect of nose shape and mass of the impactor on impact damage of laminated composites
[AD-A290351] p 2594 N95-29067
The potential for pulmonary heat injury resulting from the activation of a cabin water spray system to fight aircraft cabin fires
[DOT/FAA/AM-95/17] p 2636 N95-29224
Damage tolerance in filament-wound graphite/epoxy pressure vessels
[NASA-CR-198804] p 2590 N95-29369
Impact resistance and damage tolerance of composite sandwich panels p 2526 N95-29549
Investigation of tension-compression fatigue behavior of a notched cross-ply metal matrix composite at elevated temperature
[AD-A291479] p 2527 N95-29770
Investigation of optical damage, energy partitioning and scaling laws at extremely high velocities
[AD-A291368] p 2703 N95-30062
Fractography of advanced structural ceramics: Results from the VAMAS round robin exercise
[AD-A290930] p 2547 N95-30118
Health monitoring of operational structures: Initial results
[DE95-008551] p 2597 N95-30210

DAMPING
Recirculating cavity casing treatment failure
[AD-A289330] p 2500 N95-28908
High-and low-frequency dynamics of isolated blades and rotors with dynamic stall and wake
[AD-A290358] p 2497 N95-29322
An assessment of artificial damping models for aeroacoustic calculations
[NASA-CR-198354] p 2574 N95-29405
Magnetic damping for Maglev
[DE95-005861] p 2665 N95-29987
Solutions of the benchmark problems by the dispersion-relation-preserving scheme
p 2674 N95-30145
Time accurate application of the MacCormack 2-4 scheme on massively parallel computers
p 2661 N95-30150
Nonlinear wave propagation using three different finite difference schemes (category 2 application)
p 2582 N95-30151

DARK MATTER
Low-background balloon-borne direct search for ionizing massive particles as a component of the dark galactic halo matter p 2726 N95-29204
Experimental cosmology using fast parallel N-body methods p 2734 N95-29775

DATA ACQUISITION
An overview of the Software Engineering Laboratory
[NASA-CR-189410] p 2644 N95-28714

Backscatter data acquisition for Hydrosweep DS aboard RV Ewing
[AD-A292332] p 2628 N95-28796
Quality Control of meteorological observations at Fleet Numerical Meteorology and Oceanography Center
[AD-A291577] p 2619 N95-28938
QUEST2: System architecture deliverable set
[DE95-008427] p 2721 N95-28958
HBCU/MI instrumentation for the Pulsed Power Plasma Sciences Laboratory at the University of New Mexico, FY92-93
[AD-A292444] p 2703 N95-29003
Upper-air data collected on Ice Station Weddell
[AD-A289707] p 2620 N95-29193
The Los Alamos Photon Counting Detector Debris Detection Project: An update
[DE95-007883] p 2508 N95-29464
Research instrumentation for polytechnic university's supersonic wind tunnel facility
[AD-A290232] p 2502 N95-29468
Acquisition of place knowledge through case-based learning
[AD-A292574] p 2723 N95-29573
Remote sensing of hydrologic variables in boreal areas
[NASA-CR-189422] p 2600 N95-29754
On the topological complexity of the cost function in variational data assimilation p 2724 N95-29798
Electrochemical impedance pattern recognition for detection of hidden chemical corrosion on aircraft components, phase 1
[AD-A291345] p 2593 N95-29946
Retrieval, display, and analysis support tool for earth imagery (RDAST)
[AD-A291366] p 2601 N95-30061

DATA BASE MANAGEMENT SYSTEMS
Using object-oriented database technology to develop a multiple domain capability for domain-oriented application composition systems
[AD-A289244] p 2721 N95-28907
Functionally specified distributed transactions in co-operative scenarios
[PB95-197380] p 2725 N95-30100

DATA BASES
Compendium of NASA data base for the global tropospheric experiment's Transport and Atmospheric Chemistry Near the Equator-Atlantic (TRACE-A)
[NASA-TM-110151] p 2608 N95-28717
Conversion of the TRACON operations concepts database into a formal sentence outline job task taxonomy
[DOT/FAA/AM-95/16] p 2493 N95-28819
Using ordered binary-decision diagrams for compressing images and image sequences
[AD-A292244] p 2721 N95-28880
Using object-oriented database technology to develop a multiple domain capability for domain-oriented application composition systems
[AD-A289244] p 2721 N95-28907
Quality Control of meteorological observations at Fleet Numerical Meteorology and Oceanography Center
[AD-A291577] p 2619 N95-28938
Estimating attenuation and propagation of noise bands from a distant source using the lookup program and data base
[AD-A290218] p 2683 N95-29077
Formal aspects of object identity in database manipulation p 2722 N95-29116
A pipeline case tool for database design
[AD-A292017] p 2722 N95-29182
Tidal constituent database: West coast of the United States and eastern North Pacific Ocean
[AD-A292224] p 2630 N95-29198
Description of the OHGR database
[AD-A290146] p 2722 N95-29221
Analysis of measurements for solid state laser remote lidar system
[NASA-CR-196640] p 2585 N95-29247
The detection of oil slicks at night with airborne infrared imagers
[AD-A289731] p 2596 N95-29281
Design and implementation of logical database languages
[AD-A290474] p 2650 N95-29509
Retrieval display and analysis support tool requirements analysis
[AD-A291448] p 2599 N95-29523
HTMIAC/CINDAS silicon properties database. User's guide
[AD-A292602] p 2533 N95-29575
Modeling spatio-temporal databases to measure the performance of the GPS satellite constellation p 2494 N95-29596
International access to aeromedical evacuation medical equipment assessment data p 2679 N95-29622
Neural network-based decision support for incomplete databases p 2665 N95-29720
Digital mapping, charting, and geodesy analysis program technical review of vector smart map prototypes 1 and 2
[AD-A291217] p 2601 N95-29977
US photovoltaic patents: 1991-1993
[DE95-004051] p 2603 N95-30017
PASP plus time history data base file structures
[AD-A290587] p 2725 N95-30043
Testing of the ENDF/B-VI neutron data library ENDF60 for use with MCNP(trademark)
[DE95-007858] p 2696 N95-30057
Huge data sets and the frontiers of computational feasibility
[AD-A291384] p 2653 N95-30063
Tropical storm database: East and Gulf of Mexico coasts of the United States
[AD-A291406] p 2627 N95-30066
Hi-res SAR data processing report
[AD-A291443] p 2559 N95-30073
The topside ionospheric plasma monitor (SSIES, SSIES-2 and SSIES-3) on the spacecraft of the Defense Meteorological Satellite Program (DMSP), user's guide. Volume 2: Programmer's guide for software at AFSFC
[AD-A290913] p 2618 N95-30082
Functionally specified distributed transactions in co-operative scenarios
[PB95-197380] p 2725 N95-30100
Enhancing the semantics of federated schemata by translating SQ1-queries into object methods
[PB95-197372] p 2725 N95-30208
Production of a long-term global water vapor and liquid water data set using ultra-fast methods to assimilate multi-satellite and radiosonde observations
[NASA-CR-198955] p 2628 N95-30272

DATA COMPRESSION
Using ordered binary-decision diagrams for compressing images and image sequences
[AD-A292244] p 2721 N95-28880

DATA CONVERSION ROUTINES
Ceramic material life prediction: A program to translate ANSYS results to CARES/LIFE reliability analysis
[NASA-CR-198795] p 2543 N95-29367
Data re-formatter program for the topside thermal plasma monitor (PLIESPP)
[AD-A290960] p 2616 N95-29737
The topside ionospheric plasma monitor (SSIES, SSIES-2 and SSIES-3) on the spacecraft of the Defense Meteorological Satellite Program (DMSP), user's guide. Volume 3: Program maintenance manual
[AD-A290941] p 2617 N95-29765

DATA FLOW ANALYSIS
Simulation methodology
[AD-A290461] p 2674 N95-29491

DATA INTEGRATION
MATSurv multisensor air traffic surveillance
[AD-A292253] p 2494 N95-28887

DATA LINKS
UHF Low Density Radio Communications Link (LDRCL) Operational Test and Evaluation (OT&E) integration and OT&E operational final test report
[AD-A291447] p 2558 N95-29769

DATA MANAGEMENT
Abstract models of memory management
[AD-A292238] p 2721 N95-28877
Competitive analysis of call admission algorithms that allow delay
[AD-A292242] p 2645 N95-28878
Problem decomposition for reuse
[AD-A292245] p 2645 N95-28881
Design, evaluation and construction of TEXESS and LUXESS, and research in mini-array technology and use of data from single stations and sparse networks
[AD-A292546] p 2612 N95-28972
Garbage collection is fast, but a stack is faster
[AD-A290099] p 2722 N95-29207
Load balancing for the parallel adaptive solution of partial differential equations
[AD-A290450] p 2671 N95-29488
Defense Modeling and Simulation Office information/data base technology working group (I/DBTWG) meetings
[AD-A290953] p 2651 N95-29735
Management of meteorological data at a former nuclear weapons facility
[DE95-007619] p 2626 N95-29868
Retrieval, display, and analysis support tool for earth imagery (RDAST)
[AD-A291366] p 2601 N95-30061
Huge data sets and the frontiers of computational feasibility
[AD-A291384] p 2653 N95-30063
Enhancing the semantics of federated schemata by translating SQ1-queries into object methods
[PB95-197372] p 2725 N95-30208
Data catalog for JPL Physical Oceanography Distributed Active Archive Center (PO.DAAC)
[NASA-CR-198872] p 2631 N95-30231
Product configurations: An application for prototype object approach
[PB95-192589] p 2655 N95-30283

DATA PROCESSING
The 1994 research and technology report at the Goddard Space Flight Center
[NASA-TM-110623] p 2740 N95-28882
Operating procedures for Anthropometry and Initial Conditions Photogrammetric Program
[AD-A291553] p 2640 N95-28935
Quality Control of meteorological observations at Fleet Numerical Meteorology and Oceanography Center
[AD-A291577] p 2619 N95-28938
Formal aspects of object identity in database manipulation p 2722 N95-29116
Macroprocesses and adaptive instruction
[AD-A290483] p 2648 N95-29325
A comparison of three pedestal removal techniques for an optical time-integrating correlator
[AD-A290092] p 2700 N95-29354
GENAH user's guide and reference manual version 1.0
[AD-A290236] p 2583 N95-29470
Retrieval display and analysis support tool requirements analysis
[AD-A291448] p 2599 N95-29523
Automated Propulsion Data Screening demonstration system
[NASA-CR-196636] p 2510 N95-29584
Data re-formatter program for the topside thermal plasma monitor (PLIESPP)
[AD-A290960] p 2616 N95-29737
The topside ionospheric plasma monitor (SSIES, SSIES-2 and SSIES-3) on the spacecraft of the Defense Meteorological Satellite Program (DMSP), user's guide. Volume 3: Program maintenance manual
[AD-A290941] p 2617 N95-29765
SETA/ADS software development
[AD-A291161] p 2651 N95-29932
Hi-res SAR data processing report
[AD-A291443] p 2559 N95-30073
The topside ionospheric plasma monitor (SSIES, SSIES-2 and SSIES-3) on the spacecraft of the Defense Meteorological Satellite Program (DMSP), user's guide. Volume 2: Programmer's guide for software at AFSFC
[AD-A290913] p 2618 N95-30082
CD-ROM preparation: An overview and guide
[NASA-CR-198756] p 2655 N95-30307

DATA PROCESSING EQUIPMENT
Variable rate optical iterative processing of optical information
[AD-D017397] p 2701 N95-29602

DATA REDUCTION
Analysis of historical oceanographic data on a minicomputer: Program WAHOO
[AD-A292530] p 2629 N95-28873
Simplified data reduction methods for the ECT test for mode 3 interlaminar fracture toughness
[NASA-TM-110176] p 2527 N95-29825
Impact of uncertainty on modeling and testing
[NASA-CR-196637] p 2652 N95-30013

DATA RETRIEVAL
Data modeling from a categorical perspective p 2725 N95-30289

DATA SAMPLING
Multivariate wavelet representations and approximations
[AD-A290147] p 2670 N95-29312

DATA STORAGE
The scotch parallel storage systems
[AD-A292243] p 2658 N95-28879
Garbage collection is fast, but a stack is faster
[AD-A290099] p 2722 N95-29207
Data modeling from a categorical perspective p 2725 N95-30289

DATA STRUCTURES
Parametric design and gridding through relational geometry p 2486 N95-28771
GridTool: A surface modeling and grid generation tool p 2486 N95-28773
Glenda software design
[AD-A292537] p 2646 N95-28968
NPSNETIV: An object-oriented interface for a three-dimensional virtual world
[AD-A292467] p 2646 N95-29008
ADA in introductory courses
[AD-A292219] p 2648 N95-29285
Data modeling from a categorical perspective p 2725 N95-30289

DATA SYSTEMS
DOD electronic data interchange (EDI) convention: TDCC/EDIA transaction set 210 motor carrier invoice (version 003020). Revision 1
[AD-A292375] p 2720 N95-28797
Data migration policies for distributed database systems p 2721 N95-29093
DOD electronic data interchange (EDI) convention: ASC X12 transaction set 410 Rail Carrier Invoice, version 003020
[AD-A292495] p 2722 N95-29287
Automated Propulsion Data Screening demonstration system
[NASA-CR-196636] p 2510 N95-29584
DATA TRANSFER (COMPUTERS)
Data migration policies for distributed database systems p 2721 N95-29093
HIPPI - Gigabit LANS are here today
[DE95-007877] p 2660 N95-30128
DATA TRANSMISSION
The mesh synchronous processor MeshSP (trademark)
[AD-A289875] p 2659 N95-29420
Encryption and networking applications
[DE95-009587] p 2651 N95-29871
A bibliography, with abstracts and annotations, of publications on and related to underwater acoustic fluctuations
[AD-A291342] p 2685 N95-29945
The Telemetry Agile Manufacturing Effort
[DE95-006177] p 2654 N95-30115
HIPPI - Gigabit LANS are here today
[DE95-007877] p 2660 N95-30128
Requirements for a portable parallel I/O library for scientific computation
[DE95-009383] p 2660 N95-30192
Bicriteria network design problems
[DE95-005261] p 2661 N95-30215
DAYTIME
The effect of bright light and LEET on sleep after a 10-hour phase delay
[AD-A291264] p 2637 N95-29995
DC 8 AIRCRAFT
Investigation of wing upper surface flow-field disturbance due to NASA DC-8-72 in-flight inboard thrust-reverser deployment
[NASA-TM-110351] p 2477 N95-28816
DEBONDING (MATERIALS)
The measurement of adhesion at film-substrate interfaces using a constant depth scratch test
[AD-A289940] p 2542 N95-29269
Probability of detection of defects in coatings with electronic shearography
[NASA-TM-108493] p 2524 N95-29374
DECISION MAKING
Improving problem-solving and decision-making skills under stress: Prediction and training
[AD-A292104] p 2638 N95-28918
Interaction and intelligent behavior
[AD-A290049] p 2639 N95-29443
Automated reasoning about classical mechanics
[AD-A290052] p 2663 N95-29477
Re-engineering support to the patient movement process p 2677 N95-29615
Neural network-based decision support for incomplete databases p 2665 N95-29720
Induction of selective Bayesian classifiers
[AD-A292690] p 2675 N95-29906
COADE: A framework for cognitive analysis, design, and evaluation
[AD-A291282] p 2720 N95-29935
Applicability of neural networks for production planning under uncertainty
[PB95-197406] p 2666 N95-30101
DECISION THEORY
Oblivious decision trees and abstract cases
[AD-A292577] p 2664 N95-29574
DECOMMISSIONING
Assay of potentially contaminated propellant
[DE95-006330] p 2549 N95-30345
DECOMPOSITION
Automated testing of application domains
[AD-A289753] p 2643 N95-28690
Problem decomposition for reuse
[AD-A292245] p 2645 N95-28881
Quantum dynamical studies of the decomposition of energetic materials containing defect structures
[AD-A291456] p 2548 N95-29525
Analytical potential energy surface for methylene nitramine (CH2NNO2)
[AD-A291247] p 2534 N95-29994
W-matrices, nonorthogonal multiresolution analysis, and finite signals of arbitrary length
[DE95-005846] p 2652 N95-30020
Multi-dimensional upwind discretization method for the Euler equations on unstructured grids
[PB95-197307] p 2578 N95-30202
Decomposition of hypo-eutectoid iron carbon austenites
[PB95-196945] p 2538 N95-30287
DECONTAMINATION
Assay of potentially contaminated propellant
[DE95-006330] p 2549 N95-30345
DECOUPLING
H(sub 2) almost disturbance decoupling problem with internal stability
[PB95-206942] p 2667 N95-30168
Factorization and input-output decoupling by static output feedback for nonlinear control systems
[PB95-206975] p 2667 N95-30171
DEFECTS
Sensitivity of stress and boundary imperfection of dielectric resonator disks
[AD-A290488] p 2594 N95-29150
Electronic properties of low-temperature grown III/V thin films
[AD-A292521] p 2714 N95-29165
Origins of imperfections in composite materials
[AD-A290261] p 2523 N95-29169
Quantum dynamical studies of the decomposition of energetic materials containing defect structures
[AD-A291456] p 2548 N95-29525
Proceedings of the 6th International Conference on Nondestructive Characterization of Materials
[AD-A290727] p 2596 N95-29580
InTlSb as a long-wave infrared (LWIR) material: Defects and transportation properties
[AD-A291218] p 2702 N95-29978
W-matrices, nonorthogonal multiresolution analysis, and finite signals of arbitrary length
[DE95-005846] p 2652 N95-30020
Comparison of the local defect correction iteration and the fast adaptive composite grid iteration
[PB95-206769] p 2672 N95-30088
Software Estimation Program (SWEEP) user manual
[AD-A291137] p 2654 N95-30121
Elastoplastic buckling analysis of cylindrical shells using a semi-analytical formulation
[PB95-197349] p 2597 N95-30206
DEFENSE PROGRAM
DOD electronic data interchange (EDI) convention: TDCC/EDIA transaction set 210 motor carrier invoice (version 003020). Revision 1
[AD-A292375] p 2720 N95-28797
Mode of human image representation and error checking strategies in complex visual displays
[AD-A290107] p 2492 N95-29210
DOD electronic data interchange (EDI) convention: ASC X12 transaction set 410 Rail Carrier Invoice, version 003020
[AD-A292495] p 2722 N95-29287
Defense Modeling and Simulation Office information/data base technology working group (I/DBTWG) meetings
[AD-A290953] p 2651 N95-29735
Proposed Department of Defense software metrics implementation plan
[AD-A291404] p 2550 N95-29918
The topside ionospheric plasma monitor (SSIES, SSIES-2 and SSIES-3) on the spacecraft of the Defense Meteorological Satellite Program (DMSP), user's guide. Volume 2: Programmer's guide for software at AFSFC
[AD-A290913] p 2618 N95-30082
DEFLECTION
Dimensions, deflections and stresses for Hertzian contacts under combined normal and tangential loading. (Guide to use of computer program A9434.)
[ESDU-94034] p 2593 N95-28711
Flat rectangular isotropic plates under uniformly distributed normal pressure. Elastic deflections, stresses, and strains, moments and forces, for various forms of edge restraint
[ESDU-94033] p 2593 N95-28801
Development of a transient internal probe diagnostic
[AD-A292470] p 2704 N95-29011
The angular spread of the deflected acoustic beam diffracted by a Bragg grating out of a surface acoustic wave
[AD-A291018] p 2684 N95-29659
DEFORMATION
Three dimensional effects in fiber reinforced composites under compression
[AD-A292027] p 2523 N95-29185
Analysis of adiabatic shear bands in thermoviscoplastic materials under combined loading
[AD-A290666] p 2596 N95-29582
Changes in microstructural parameters of snow during deformation
[AD-A290887] p 2601 N95-29866
Crustal deformation measurements in the vicinity of Vandenberg Air Force Base
[AD-A291224] p 2618 N95-29981
Analytical investigation of the hygrothermal effects and parametric study of the Edge Crack Torsion (ECT) mode 3 test lay-ups
[NASA-TM-110183] p 2528 N95-30028
DEGENERATION
Photorefractive Bi12SiO20 spatial light modulator
[AD-A291070] p 2702 N95-29969
DEGRADATION
Prediction of hydrogen entry and permeation in metals and alloys
[AD-A292047] p 2536 N95-29298
DEGREES OF FREEDOM
Precision pointing experiment
[AD-A291015] p 2664 N95-29657
DEHYDRATION
Human fluid balance and dehydration during cold weather military operations
[AD-A289192] p 2636 N95-29757
DEICERS
An analysis of B-1B exterior jet blast windshield anti-icing performance using pre-cooled compressor bleed air
[AD-A292522] p 2492 N95-28811
DEICING
An analysis of B-1B exterior jet blast windshield anti-icing performance using pre-cooled compressor bleed air
[AD-A292522] p 2492 N95-28811
Users manual for the improved NASA Lewis ice accretion code LEWICE 1.6
[NASA-CR-198355] p 2492 N95-29132
DELAMINATING
Interlaminar fracture mechanics and mechanisms: Linear and nonlinear aspects p 2526 N95-29597
Simplified data reduction methods for the ECT test for mode 3 interlaminar fracture toughness
[NASA-TM-110176] p 2527 N95-29825
DELAY
Transport delays associated with NASA Langley Flight Simulation Facility
[NASA-TM-110150] p 2659 N95-29454
Efficient solution of a class of infinite stochastic petri nets: Theory and applications
[PB95-197166] p 2673 N95-30097
Delayed choice: An operator for joining message sequence charts
[PB95-206710] p 2560 N95-30203
DELTA WINGS
Navier-Stokes solution of wing wake structure and its perturbation p 2488 N95-29121
A numerical method for modelling wings with sharp edges maneuvering at high angles of attack p 2496 N95-29122
DEMODULATION
WinCD: Complex demodulation time-series analysis for windows
[AD-A291550] p 2645 N95-28934
In-line fiber etalon strain sensor
[AD-D017266] p 2699 N95-29283
DEMODULATORS
Wideband I/Q demodulators: Measurement technique and matching characteristics
[AD-A291505] p 2558 N95-29647
DEMOGRAPHY
An analysis of anthropometric differences among occupational groups in the US Army
[AD-A292326] p 2640 N95-28794
DENDRITIC CRYSTALS
Macrosegregation and nucleation in undercooled Pb-Sn alloys
[NASA-TM-102023-REV] p 2535 N95-28701
DENSE PLASMAS
High-density plasma dynamics in semiconductors p 2705 N95-29632
DENSITY (MASS/VOLUME)
Orthobaric densities and molar volumes of liquids. Glycol ethers (cellosolves and carbitols, etc.)
[ESDU-95005] p 2530 N95-28703
Orthobaric densities and molar volumes of liquids. Glycols and cyclic diols
[ESDU-95003] p 2531 N95-28895
DENSITY (NUMBER/VOLUME)
Fundamental studies of oxygen rings and other high energy density molecular systems
[AD-A290875] p 2693 N95-29865
DENSITY DISTRIBUTION
A multi-wavelength study of rotation-driven pulsars p 2729 N95-29678
DENSITY MEASUREMENT
Non-coincident multi-wavelength emission absorption spectroscopy
[DE95-006480] p 2530 N95-28776
SETA/ADS software development
[AD-A291181] p 2651 N95-29932

DEOXYRIBONUCLEIC ACID
Cellular and molecular level responses after radiofrequency radiation exposure, alone or in combination with x rays or chemicals
[AD-A292488] p 2633 N95-28866
DEPLOYMENT
Proceedings of the Complex Systems Engineering Synthesis and Assessment Technology Workshop (CSESAW 1994)
[AD-A292433] p 2646 N95-28995
Materials for tomorrow's infrastructure: A ten-year plan for deploying high-performance construction materials and systems
[AD-A289782] p 2526 N95-29598
DEPOSITION
Deposition and surface treatment with intense pulsed ion beams
[DE95-007885] p 2543 N95-29465
Apparatus and method for achieving growth-etch deposition of diamond using a chopped oxygen-acetylene flame
[AD-D017322] p 2718 N95-30164
Formation and properties of titanium disilicide: A study on the development of stress in Ti-Si thin films
[PB95-197315] p 2538 N95-30205
DEPTH
An image cancellation approach to depth-from-focus
[DE95-007625] p 2697 N95-28912
The measurement of adhesion at film-substrate interfaces using a constant depth scratch test
[AD-A289940] p 2542 N95-29269
Estimation of unstabilized components in vehicular motion
[AD-A290580] p 2590 N95-29552
The onset of electrohydrodynamic instability in isoelectric focusing
[NASA-CR-198805] p 2565 N95-29968
DERIVATION
Five-channel SQUID based non-destructive evaluation (NDE) instrument
[AD-A292474] p 2592 N95-29012
US photovoltaic patents: 1991-1993
[DE95-004051] p 2603 N95-30017
Biological methane activation
[PB95-200705] p 2535 N95-30198
Multi-dimensional upwind discretization method for the Euler equations on unstructured grids
[PB95-197307] p 2578 N95-30202
DESCENT
Effects of cabin pressure on climb and descent rates
[ESDU-94040] p 2496 N95-29016
DESIGN ANALYSIS
Design and analysis of the launch vehicle adapter fitting for the petite amateur navy satellite (PANSAT)
[AD-A289693] p 2504 N95-28680
Grid generation and surface modeling for CFD p 2478 N95-28726
Rapid Airplane Parametric Input Design (RAPID) p 2479 N95-28730
A grid generation system for multi-disciplinary design optimization p 2484 N95-28763
Receiver design, performance analysis, and evaluation for space-borne laser altimeters and space-to-space laser ranging systems
[NASA-CR-198655] p 2584 N95-28808
An efficiency study of the simultaneous analysis and design of structures
[NASA-TM-110166] p 2495 N95-28820
Dimensional stability of curved panels with cocured stiffeners and cobonded frames p 2515 N95-28836
Design, analysis, and fabrication of a pressure box test fixture for tension damage tolerance testing of curved fuselage panels p 2516 N95-28839
Global cost and weight evaluation of fuselage keel design concepts p 2499 N95-28840
Design and evaluation of a foam-filled hat-stiffened panel concept for aircraft primary structural applications p 2499 N95-28841
Selection of materials, manufacturing methods and lubricants for cam mechanisms
[ESDU-94017] p 2589 N95-28905
Low cost writable RFID tag with MRAM memory
[AD-A292553] p 2642 N95-28974
Influence of tooth profile modification on spur gear dynamic tooth strain
[NASA-TM-106952] p 2589 N95-29112
The international fusion materials irradiation facility
[DE95-006536] p 2696 N95-29142
Application of optimization technique to control system design for departure prevention and aircraft model estimation through dynamic inversion p 2501 N95-29156
GLAST
[DE95-008596] p 2739 N95-29265
Gordon research conference on physical metallurgy: Materials by design
[AD-A290519] p 2524 N95-29326
Applied optics laboratory
[AD-A292006] p 2701 N95-29571
ADC test support program
[AD-A289445] p 2643 N95-29921
Computational algorithms for aerodynamic analysis and design
[AD-A291084] p 2491 N95-29972
Framework for comparing and controlling number-based design reasoning systems
[PB95-197364] p 2667 N95-30207
Bicriteria network design problems
[DE95-005261] p 2661 N95-30215
Optimization of 100-meter Green Bank Telescope
[NASA-CR-198868] p 2731 N95-30230
Design, analysis and control of large transports so that control of engine thrust can be used as a back-up of the primary flight controls
[NASA-CR-198958] p 2501 N95-30254
Advanced Dependent Pressure Vessel (DPV) nickel-hydrogen spacecraft cell and battery design p 2567 N95-30261
Electrolyte management considerations in modern nickel hydrogen and nickel cadmium cell and battery designs p 2567 N95-30262
Advances in tubular solid oxide fuel cell technology
[DE95-008361] p 2607 N95-30281
A conceptual thermal design study of an electronically scanned thinned array radiometer
[NASA-TM-110173] p 2509 N95-30316
DESIGN TO COST
The effects of design details on cost and weight of fuselage structures p 2499 N95-28831
DESTABILIZATION
Self-sustained magnetic braiding in toroidal plasmas
[AD-B191998L] p 2706 N95-29734
DESTRUCTIVE TESTS
Analysis of static contact in laminated composite plates using damage mechanics
[NASA-CR-198656] p 2513 N95-28809
Analytical and experimental studies of the energy absorption behavior of composite structures p 2524 N95-29411
DETECTION
Automated analysis of zooplankton size and taxonomic composition using the video plankton recorder
[AD-A289725] p 2631 N95-28685
Predicting polarized light scattering by marine micro-organism
[AD-A289790] p 2696 N95-28695
Spectrometric studies of selected nitrocompounds using laser-induced photofragmentation/photoionization at 193 nm
[AD-A289947] p 2530 N95-28876
Experimental methods in residual stress measurement using a position-sensitive single-exposure scintillation detection system
[AD-A289803] p 2594 N95-28949
Development of the test kit for fuel acid contamination
[AD-A291953] p 2548 N95-29019
The fluorescent detection of hydrazine, monomethylhydrazine, and 1,1-dimethylhydrazine by derivatization with aromatic dicarboxaldehydes
[NAVY-CASE-75451] p 2512 N95-29052
Tailored microstructures for broadband or selective detection of radiation from the visible to the infrared
[AD-A292097] p 2554 N95-29240
Estimates of probability of a cloud-free line of sight for RAPTOR TALON
[AD-A291908] p 2510 N95-29284
The use of electrochemistry and ellipsometry for identifying and evaluating corrosion on aircraft
[AD-A290249] p 2497 N95-29426
The Los Alamos Photon Counting Detector Debris Detection Project: An update
[DE95-007883] p 2508 N95-29464
Broadband control of structural vibration using simultaneous sensing and actuation with nonlinear piezoelectric elements p 2664 N95-29548
Proceedings of the 6th International Conference on Nondestructive Characterization of Materials
[AD-A290727] p 2596 N95-29580
Investigation and characterization of SEU effects and hardening strategies in avionics
[AD-A291058] p 2500 N95-29950
Robust testing of cellular neural networks
[AD-A291219] p 2665 N95-29979
Selective multi-chemical fiber optic sensor
[AD-D017409] p 2703 N95-30076
Software Estimation Program (SWEEP) user manual
[AD-A291137] p 2654 N95-30121
Novel photoelectric sensing technology for environmental monitoring, phase 1
[AD-A292026] p 2611 N95-30348
DETERIORATION
An analysis of the impact of ASPA on organizational and depot level maintenance
[AD-A292670] p 2477 N95-29414
DETONATION
A thermochemical transport model for analysis of hot-spot formation in energetic materials
[AD-A290441] p 2532 N95-29357
DETONATION WAVES
Molecular dynamics simulation of liquid nitromethane shocked to 143 kbar
[AD-A292107] p 2691 N95-28919
DEUTERIUM
Bubble fusion: Preliminary estimates of spherical micro-implosions in cavitating liquids
[DE95-006260] p 2569 N95-28956
Effects of impurities released from high Z test limiter on plasma performance in TEXTOR
[AD-B191995L] p 2709 N95-29803
DEUTERONS
Activities update
[AD-A292431] p 2692 N95-28994
DIAGNOSIS
(DEPSCOR-92) acquisition of a metallurgical optical microscope
[AD-A292439] p 2698 N95-28998
Care in the air: A system analysis of clinical outcomes in aeromedical evacuation p 2642 N95-29626
Performance evaluation of bolt-cutter system on first Taurus launch
[AD-A291237] p 2504 N95-29992
Development and application of fluorescent diagnostics to fundamental droplet and spray problems
[AD-A290553] p 2578 N95-30039
PASP plus time history data base file structures
[AD-A290587] p 2725 N95-30043
DIAMOND FILMS
Deposition and surface treatment with intense pulsed ion beams
[DE95-007885] p 2543 N95-29465
The nucleation of crystalline films from vapor phase reactants
[AD-A291122] p 2716 N95-29767
The 2nd International Conference on Thin Film Physics and Applications
[AD-A292353] p 2546 N95-29983
DIAMONDS
Apparatus and method for achieving growth-etch deposition of diamond using a chopped oxygen-acetylene flame
[AD-D017322] p 2718 N95-30164
DIAPHRAGMS (MECHANICS)
A CMOS-compatible, surface-micromachined pressure sensor for aqueous ultrasonic application
[DE95-008538] p 2567 N95-30188
DICHOTOMIES
Proposal for a flexible system of phytogeographic classification: Emphasis on the use of multistage remote sensoring
[INPE-5609-PRE/1821] p 2600 N95-29815
DICHROISM
Proceedings of the 38th Annual Conference on Magnetism and Magnetic Materials
[AD-A286751] p 2681 N95-28962
Ab initio calculation of vibrational absorption and circular dichroism spectra using density functional force fields
[AD-A291297] p 2720 N95-29936
DIELECTRICS
Sensitivity of stress and boundary imperfection of dielectric resonator disks
[AD-A290488] p 2594 N95-29150
Finite difference analysis of a cylindrical two conductor microstrip transmission line with truncated dielectrics
[AD-A292592] p 2555 N95-29290
Spectral inverse scattering theory for dielectric media: Application to optical devices
[AD-A292651] p 2556 N95-29383
Development of LaRC (TM): IA thermoplastic polyimide coated aerospace wiring
[NASA-CR-195048] p 2548 N95-30252
Photonic band structures for optoelectronics
[AD-A291154] p 2718 N95-30298
Dielectric property measurements in the Electromagnetic Properties Measurement Laboratory
[NASA-TM-110147] p 2560 N95-30336
DIENES
Thermal conductivity of liquid halogenated aliphatic hydrocarbons. Part 4: Halogenated alkenes and dienes (C1 to C4)
[ESDU-94024-PT-4] p 2511 N95-28803
DIESEL ENGINES
Air/fuel ratio visualization in a diesel spray p 2590 N95-29607
Cylinder-averaged histories of nitrogen oxide in a DI diesel with simulated turbocharging
[AD-A290568] p 2590 N95-29820

DIESEL FUELS
Air/fuel ratio visualization in a diesel spray
p 2590 N95-29807
DIFFERENCE EQUATIONS
Deconvolution of lateral shear interferograms
p 2699 N95-29222
SOSDOR: Solid-state device simulator code
[AD-A289954] p 2563 N95-29275
DIFFERENTIAL AMPLIFIERS
Balanced, double-sided calibration circuit for sensor element differential pre-amplifier
[AD-D017326] p 2566 N95-30052
DIFFERENTIAL EQUATIONS
Discontinuous solutions of semilinear differential-algebraic equations. part 2: Rho-consistency
[AD-A292285] p 2668 N95-28861
Discontinuous solutions of semilinear differential-algebraic equations. part 1: Distribution solutions
[AD-A292286] p 2668 N95-28863
Dynamical model of pressure-gradient-driven turbulence and shear flow generation in L-H transition
[AD-B195511L] p 2709 N95-29789
Applications of Langevin and Molecular Dynamics methods
[DE95-007875] p 2694 N95-30059
Multi-dimensional upwind discretization method for the Euler equations on unstructured grids
[PB95-197307] p 2578 N95-30202
Spectral estimates for positive Rockland operators
[PB95-206751] p 2673 N95-30204
Elastoplastic buckling analysis of cylindrical shells using a semi-analytical formulation
[PB95-197349] p 2597 N95-30206
Ensemble phase averaged equations for multiphase flows p 2579 N95-30284
DIFFERENTIAL PRESSURE
Effects of cabin pressure on climb and descent rates
[ESDU-94040] p 2496 N95-29016
DIFFRACTION
Experimental methods in residual stress measurement using a position-sensitive single-exposure scintillation detection system
[AD-A289803] p 2594 N95-28949
Acoustic imaging of ultrasonic wave propagation
[AD-A290390] p 2683 N95-29232
Compressibility effects on and control of dynamic stall of oscillating airfoil
[AD-A291804] p 2489 N95-29428
The angular spread of the deflected acoustic beam diffracted by a Bragg grating out of a surface acoustic wave
[AD-A291018] p 2684 N95-29659
Multiple dimensional acousto-optic diffraction and multiple dimensional acousto-optic device
[AD-A291037] p 2685 N95-29681
Diffractive optics: Design, fabrication, and applications
[AD-A290942] p 2702 N95-29867
Theory and experiment analysis of two-dimensional acousto-optic interaction
[AD-A291059] p 2685 N95-29951
The Scanning Fast Field Program (SCAFFIP) general version 1.0 user's manual
[AD-A291209] p 2618 N95-29976
Diffraction limited imaging using aberrated optics
[AD-A290912] p 2703 N95-30081
DIFFUSION
Sorption and diffusion of moisture in multilayer composite AEM/S sandwich materials
[AD-A289807] p 2518 N95-28951
Application of the space-time conservation element and solution element method to two-dimensional advection-diffusion problems
[NASA-TM-106946] p 2574 N95-29372
Effects of microscopic diffusion and rotational mixing on stellar models p 2733 N95-29669
Decomposition of hypo-eutectoid iron carbon austenites
[PB95-196945] p 2538 N95-30287
DIFFUSION COEFFICIENT
Sorption and diffusion of moisture in multilayer composite AEM/S sandwich materials
[AD-A289807] p 2518 N95-28951
DIFFUSION LENGTH
Commercial photorefractive device using nonstoichiometric 3-5 semiconductors
[AD-A292494] p 2713 N95-28933
DIFFUSIVITY
Effects of microscopic diffusion and rotational mixing on stellar models p 2733 N95-29669
Theory of pseudo-classical confinement and transmutation to L-mode
[AD-B175957L] p 2709 N95-29809
DIFLUORIDES
Corrosion in methylphosphonic difluoride
[AD-A289995] p 2536 N95-29137
DIFLUORO COMPOUNDS
Thermophysical properties of R-32 (difluoromethane)
[ESDU-94032] p 2530 N95-28802
DIGITAL COMPUTERS
HBCU/MI instrumentation for the Pulsed Power Plasma Sciences Laboratory at the University of New Mexico, FY92-93
[AD-A292444] p 2703 N95-29003
DIGITAL DATA
A comprehensive analysis of Navy and Marine corps digital mapping, charting, and geodesy requirements for modeling and simulation
[AD-A291601] p 2598 N95-28931
Computing 3-D motion in custom analog and digital VLSI
[AD-A290270] p 2647 N95-29179
The design of programmable convolutional encoder using VHDL and an FPGA
[AD-A290048] p 2649 N95-29442
Digital mapping, charting, and geodesy analysis program technical review of vector smart map prototypes 1 and 2
[AD-A291217] p 2601 N95-29977
DIGITAL ELECTRONICS
Commercial photorefractive device using nonstoichiometric 3-5 semiconductors
[AD-A292494] p 2713 N95-28933
DIGITAL SYSTEMS
Using ordered binary-decision diagrams for compressing images and image sequences
[AD-A292244] p 2721 N95-28880
Fibre-coupled remote optical vibrometry
[AD-A291606] p 2698 N95-28932
N4 processor
[AD-A292571] p 2642 N95-28976
Nonlinear calibration of an infrared radiometer
[AD-A292436] p 2698 N95-28996
Accurate feature detection and estimation using nonlinear and multiresolution analysis
[AD-A290267] p 2553 N95-29176
Computing 3-D motion in custom analog and digital VLSI
[AD-A290270] p 2647 N95-29179
Design and evaluation of a LQR controller for the bluebird unmanned air vehicle
[AD-A289769] p 2498 N95-29457
High resolution direct digitization and optical telemetry of shipboard antenna signals
[AD-A290238] p 2557 N95-29504
Digital control of distributed parameter systems: A state-space approach
[PB95-197216] p 2666 N95-30041
DIGITAL TECHNIQUES
Wideband I/Q demodulators: Measurement technique and matching characteristics
[AD-A291505] p 2558 N95-29847
DIGITAL TELEVISION
Applications of digital video and synthetic environments to unmanned aerial vehicles
[AD-A291875] p 2497 N95-29437
Digital video technology, today and tomorrow
[DE95-007689] p 2556 N95-29462
DIISOCYANATES
Polyethylene-based polyurethane copolymers and block copolymers
[AD-A289996] p 2546 N95-30030
DIMENSIONAL MEASUREMENT
Thickness measurement of ammonia targets used in SLAC e143 experiment
[AD-A290215] p 2692 N95-29076
DIMENSIONAL STABILITY
Dimensional stability of curved panels with cocured stiffeners and cobonded frames p 2515 N95-28836
Investigation of the flow turning loss in unstable solid propellant rocket motors p 2510 N95-29331
DIMENSIONLESS NUMBERS
Second-order numerical solution of time-dependent, first-order hyperbolic equations p 2674 N95-30143
DIMETHYL COMPOUNDS
The effects of aircraft fuel and fluids on the strength properties of Resin Transfer Molded (RTM) composites
p 2522 N95-29047
DIMETHYLHYDRAZINES
The fluorescent detection of hydrazine, monomethylhydrazine, and 1,1-dimethylhydrazine by derivatization with aromatic dicarboxaldehydes
[NAVY-CASE-75451] p 2512 N95-29052
DIODES
Doubled diode laser. phase 1
[AD-A292465] p 2584 N95-29007
High-efficiency longitudinal diode bar pumping of solid-state lasers
[AD-A291180] p 2587 N95-29931
A study of power diode failure mechanisms in the US Army research laboratory 30-mm solid propellant electrothermal-chemical (SPETC) gun facility
[AD-A291300] p 2565 N95-29938
DIPOLE ANTENNAS
Characterizing the electromagnetic environment produced by the army's repetitive electromagnetic pulse simulator (REPS)
[AD-A289739] p 2551 N95-28687
Quasioptical Josephson Oscillator
[AD-A292481] p 2561 N95-28859
DIPOLE MOMENTS
Static field solutions and image theory for a conducting sphere with radial anisotropy
[PB95-207171] p 2673 N95-30172
DIRECT CURRENT
Corona tests of prototype connector
[AD-A292542] p 2561 N95-28971
Five-channel SQUID based non-destructive evaluation (NDE) instrument
[AD-A292474] p 2592 N95-29012
Power measurement and current feedback in a resonant DC link inverter
[AD-A292518] p 2563 N95-29164
DC electrostatic gyro suspension system for the Gravity Probe B experiment p 2509 N95-29794
DIRECTION FINDING
Methods of generating low redundancy direction finding array configurations
[AD-A292590] p 2555 N95-29269
DIRECTIONAL CONTROL
A vehicle health monitoring system for the Space Shuttle Reaction Control System during reentry
[NASA-CR-188370] p 2505 N95-29447
DIRECTIVITY
The spectrum and directivity of turbulent mixing noise from supersonic jets p 2684 N95-29415
DIRICHLET PROBLEM
Object oriented segmentation of images
[AD-A290792] p 2671 N95-29485
DISCONTINUITY
Discontinuous solutions of semilinear differential-algebraic equations. part 1: Distribution solutions
[AD-A292286] p 2668 N95-28863
DISCRETE FUNCTIONS
Unstructured Cartesian/prismatic grid generation for complex geometries p 2481 N95-28741
Linear and nonlinear discrete-time state-space modeling of dynamic systems for control applications
p 2663 N95-29251
The large discretization step method for time-dependent partial differential equations
[NASA-CR-195068] p 2670 N95-29403
DISCRIMINANT ANALYSIS (STATISTICS)
Multilayer piecewise linear networks. Revision 1
[AD-A289885] p 2658 N95-28955
Design, evaluation and construction of TEXESS and LUXESS, and research in mini-array technology and use of data from single stations and sparse networks
[AD-A292546] p 2612 N95-28972
Discriminant analysis to predict the occurrence of ELMS in H-mode discharges
[AD-B179183L] p 2708 N95-29746
DISILICIDES
Formation and properties of titanium disilicide: A study on the development of stress in Ti-Si thin films
[PB95-197315] p 2538 N95-30205
DISLOCATIONS (MATERIALS)
Examination of dislocation core structures in B2 intermetallic alloys
[AD-A291486] p 2537 N95-29526
Influence of dislocation-solute interactions on the mechanical properties of zirconium-doped NiAl
[DE95-008848] p 2538 N95-30179
DISPLACEMENT
Flat rectangular isotropic plates under uniformly distributed normal pressure. Elastic deflections, stresses, and strains, moments and forces, for various forms of edge restraint
[ESDU-94033] p 2593 N95-28801
Three dimensional effects in fiber reinforced composites under compression
[AD-A292027] p 2523 N95-29185
DISPLAY DEVICES
Three-D weather displays for aircraft cockpits
[AD-A289759] p 2499 N95-28691
Conceptual design of a map interactive system for military aircraft cockpits
[AD-A289760] p 2499 N95-28692
Summary report for cooperative research and development agreement between Oak Ridge Associated Universities and Interactive Presentation Systems
[DE95-006874] p 2644 N95-28777
WinCD: Complex demodulation time-series analysis for windows
[AD-A291550] p 2645 N95-28934
Optimizing cockpit display configurations with a genetic algorithm system
[AD-A289799] p 2499 N95-29123

An architectural design of a toolkit for synchronous groupware applications
[AD-A290226] p 2642 N95-29146
Mode of human image representation and error checking strategies in complex visual displays
[AD-A290107] p 2492 N95-29210
MapTool version 2. User's manual
[AD-A289470] p 2630 N95-29418
Visualization of CAD objects using a stereoscopic display
[AD-A290034] p 2639 N95-29439
Low voltage, high resistance, Polymer Dispersed Liquid Crystal
[AD-A291946] p 2556 N95-29472
Retrieval display and analysis support tool requirements analysis
[AD-A291448] p 2599 N95-29523

DISRUPTING
Development of a transient internal probe diagnostic
[AD-A292470] p 2704 N95-29011

DISSIPATION
Vortex element analysis of selected time-dependent flows
[AD-A289944] p 2573 N95-29271
The origin of collisionless dissipation in magnetic reconnection
[AD-B178949L] p 2710 N95-29813
Attractors of dissipative structure in three dissipative fluids
[AD-B180030L] p 2710 N95-29844
Application of low dissipation and dispersion Runge-Kutta schemes to benchmark problems in computational aeroacoustics p 2687 N95-30139

DISSOCIATION
Optimal control of molecular motion
[AD-A291919] p 2691 N95-28944
Analytical potential energy surface for methylene nitramine (CH2NNO2)
[AD-A291247] p 2534 N95-29994

DISTRIBUTED FEEDBACK LASERS
Development of distributed feedback dye lasers for generation of high-power 193 nm excimer laser short pulses p 2586 N95-29631

DISTRIBUTED PARAMETER SYSTEMS
Nonlinear control systems
[AD-A291083] p 2665 N95-29971
Digital control of distributed parameter systems: A state-space approach
[PB95-197216] p 2666 N95-30041
Layers as knowledge transitions in the design of distributed systems
[PB95-197638] p 2660 N95-30104
Speedlog: The key architectural element to provide efficient log management
[PB95-198453] p 2643 N95-30108

DISTRIBUTED PROCESSING
Competitive analysis of call admission algorithms that allow delay
[AD-A292242] p 2645 N95-28878
Wax: A wide-area computation system
[AD-A292247] p 2658 N95-28884
Application of parallel processing technology in complex helicopter analysis. Phase 1
[NASA-CR-197850] p 2496 N95-28928
Solving linear programs using distributed parallel computing
[AD-A290221] p 2658 N95-29079
Data migration policies for distributed database systems p 2721 N95-29093
Implementing distributed server groups for the World Wide Web
[AD-A292221] p 2658 N95-29196
Garbage collection is fast, but a stack is faster
[AD-A290099] p 2722 N95-29207
Ropes: Support for collective opertions among distributed threads
[NASA-CR-198157] p 2649 N95-29404
Design and implementation of logical database languages
[AD-A290474] p 2650 N95-29509
High-level fault tolerance in distributed programs
[AD-A290430] p 2724 N95-29818
Neural network construction using evolutionary search
[AD-A290662] p 2665 N95-29831
DPARTS. A dynamic parallel adaptive multiprocess or real-time scheduler
[AD-A291160] p 2659 N95-29915
Formal design of communication protocols using Estelle
[AD-A290584] p 2652 N95-30042
Huge data sets and the frontiers of computational feasibility
[AD-A291384] p 2653 N95-30063

DISTRIBUTION
Description of the TV distribution service using MAGIC modelling methods
[PB95-206728] p 2560 N95-30219

DISTRIBUTION FUNCTIONS
Short and elementary proof of the main Bahadur-Kiefer theorem
[PB95-206967] p 2675 N95-30170
Parameterized spectral distributions for meson production in proton-proton collisions
[NASA-TM-4675] p 2696 N95-30337

DIURNAL VARIATIONS
On the azimuthal variation of the equatorial plasmapause
[NASA-CR-198929] p 2711 N95-30338

DIVERTERS
Carbon sheet pumping
[AD-B179443L] p 2710 N95-29812

DIVERTORS (FUSION REACTORS)
Innovative divertor concepts for LHD
[AD-B191997L] p 2711 N95-30032
Techniques and results of tokamak-edge simulation
[DE95-008075] p 2711 N95-30130

DIVING (UNDERWATER)
Membrane fluidity and shape of human red blood cells are altered by physiological levels of hydrostatic pressure
[AD-A290595] p 2636 N95-29557
The one-dimensional bubble: Theory, experiment, and relevance to exposure of divers to low frequency sound, and of lung to lithotripsy
[ISVR-TR-246] p 2577 N95-29817

DMSP SATELLITES
Data re-formatter program for the topside thermal plasma monitor (PLIESPP)
[AD-A290960] p 2616 N95-29737
The topside ionospheric plasma monitor (SSIES, SSIES-2 and SSIES-3) on the spacecraft of the Defense Meteorological Satellite Program (DMSP), user's guide. Volume 3: Program maintenance manual
[AD-A290941] p 2617 N95-29765
The topside ionospheric plasma monitor (SSIES, SSIES-2 and SSIES-3) on the spacecraft of the Defense Meteorological Satellite Program (DMSP), user's guide. Volume 2: Programmer's guide for software at AFSFC
[AD-A290913] p 2618 N95-30082

DOMAINS
Automated testing of application domains
[AD-A289753] p 2643 N95-28690

DOPED CRYSTALS
ARPA solid state laser and nonlinear materials program
[AD-A289657] p 2584 N95-28678
Materials science and fabrication of YBCO-SrTi(1-x)Nb(x)O3-YBCO device structures
[AD-A292527] p 2712 N95-28815
Nitride semiconductors for ultraviolet detection
[AD-A289546] p 2712 N95-28910
Interface properties of wide bandgap semiconductor structures
[AD-A289817] p 2713 N95-28954
Optoelectronics based on SiGe/Si heterostructures
[AD-A292464] p 2699 N95-29006
Theoretical investigation of superconductivity in doped fullerenes
[AD-A291942] p 2562 N95-29018
Growth, characterization and application of KTN family nonlinear optical crystals
[AD-A290330] p 2713 N95-29087
Pulsed laser deposition of thin film material for nonlinear waveguides
[AD-A290789] p 2544 N95-29484
HTMIAC/CINDAS silicon properties database. User's guide
[AD-A292602] p 2533 N95-29575
Ion doped quantum well lasers
[AD-A290937] p 2587 N95-29912
Influence of dislocation-solute interactions on the mechanical properties of zirconium-doped NiAl
[DE95-008848] p 2538 N95-30179

DOPPLER RADAR
A study of boundary layer aerosol and wind profiles using incoherent Doppler lidar p 2622 N95-29697
A study of precipitation using dual-frequency and interferometric Doppler radars p 2627 N95-29877
Offshore next generation weather radar (NEXRAD) test and evaluation master plan (TEMP)
[AD-A291435] p 2559 N95-30072
The JPL Mars gravity field, Mars50c, based upon Viking and Mariner 9 Doppler tracking data
[NASA-CR-198881] p 2737 N95-30344

DOWN-CONVERTERS
Test results of a 20 GHz, low noise downconverter for USAT applications
[NASA-TM-106692] p 2508 N95-30011

DRAG
Rigorous drag bounds in turbulent shear flow p 2573 N95-29334

DRAG MEASUREMENT
Excrescence drag levels on aircraft
[ESDU-94044] p 2487 N95-28397

DRAG REDUCTION
Studies in drag reduction p 2487 N95-29094

DRAINAGE
Hydrology of the continental United States p 2599 N95-29539

DREDGED MATERIALS
Tidal constituent database: West coast of the United States and eastern North Pacific Ocean
[AD-A292224] p 2630 N95-29198

DRIFT RATE
DC electrostatic gyro suspension system for the Gravity Probe B experiment p 2509 N95-29794

DROP SIZE
The effect of turbulence on vaporization and mixing in fuel sprays
[AD-A291347] p 2577 N95-29948

DROPS (LIQUIDS)
Advanced manufacturing by spray forming: Aluminum strip and microelectromechanical systems
[DE95-008615] p 2536 N95-28959
The effect of turbulence on vaporization and mixing in fuel sprays
[AD-A291347] p 2577 N95-29948
Development and application of fluorescent diagnostics to fundamental droplet and spray problems
[AD-A290553] p 2578 N95-30039
Simulation of powder metal fabrication with high pressure gas atomization
[DE95-008820] p 2538 N95-30178

DRYDOCKS
Sleep during SEAL Delivery Vehicle (SDV)/Dry dock shelter exercises analyzed by a graphic approach
[AD-A290916] p 2637 N95-30083

DUCT GEOMETRY
Marshall Space Flight Center surface modeling and grid generation applications p 2480 N95-28733

DUCTED FLOW
Optimal domain decomposition strategies p 2484 N95-28759
Comparison of spatial numerical operators for duct-nozzle acoustics p 2690 N95-30158

DUCTILITY
Application of a rapid quench thermomagnetic analyzer to austempered ductile iron
[AD-A292261] p 2535 N95-28889
Mechanical properties of nanophase metals
[DE95-005408] p 2537 N95-30018
Tensile properties of as-cast iron-aluminide alloys
[DE95-005396] p 2538 N95-30216

DUCTS
The acoustic characteristics of turbomachinery cavities
[NASA-CR-4671] p 2478 N95-28720
The decay of longitudinal vortices shed from airfoil vortex generators
[NASA-CR-198356] p 2489 N95-29402

DUMPING
Cylinder-averaged histories of nitrogen oxide in a DI diesel with simulated turbocharging
[AD-A290568] p 2590 N95-29820

DURABILITY
Advanced composite structural concepts and materials technologies for primary aircraft structures: Advanced material concepts
[NASA-CR-4485] p 2496 N95-29027
Evaluation of retro-reflective beads in airport pavement markings
[AD-A291065] p 2502 N95-29967
Development of flame resistant, high efficiency thermal insulation
[AD-A291136] p 2547 N95-30120

DUST STORMS
Depicting dust and sand storm signatures through the means of satellite images and ground-based observations for Saudi Arabia p 2600 N95-29730

DWARF GALAXIES
The 12 UM contribution of nearby galaxies to the infrared background
[AD-A291185] p 2735 N95-29917

DYE LASERS
Development of distributed feedback dye lasers for generation of high-power 193 nm excimer laser short pulses p 2586 N95-29631
Ceramics derived from organo-metallic precursors
[AD-A291434] p 2547 N95-30071

DYES
Tunable laser for persistent spectral hole burning optical memories
[AD-A292598] p 2586 N95-29292

Theories of the nonlinear optical properties of composite media: Applications to phthalocyanine dyes
[AD-A290640] p 2700 N95-29560

DYNAMIC CHARACTERISTICS
A study of power diode failure mechanisms in the US Army research laboratory 30-mm solid propellant electrothermal-chemical (SPETC) gun facility
[AD-A291300] p 2585 N95-29938

DYNAMIC CONTROL
On-line damage identification and motion control of adaptive structures: An intelligent control approach
p 2662 N95-29109
Linear and nonlinear discrete-time state-space modeling of dynamic systems for control applications
p 2663 N95-29251
Computational algorithms for aerodynamic analysis and design
[AD-A291084] p 2491 N95-29972

DYNAMIC LOADS
The development of an interpretive methodology for the application of real-time acousto-ultrasonic NDE technique for monitoring damage in ceramic composites under dynamic loads p 2592 N95-29104
Influence of tooth profile modification on spur gear dynamic tooth strain
[NASA-TM-106952] p 2589 N95-29112
Consideration of microstructural changes in the study of adiabatic shear bands
[AD-A290398] p 2715 N95-29234

DYNAMIC MODELS
Modeling and control of rotating stall in high speed multi-stage axial compressors p 2500 N95-29244
Linear and nonlinear discrete-time state-space modeling of dynamic systems for control applications
p 2663 N95-29251
Numerical experiments on the flow past a circular cylinder at sub-critical Reynolds number
[AD-A289937] p 2573 N95-29268
Continuation of research in the statistical aspects of reliability, availability, and maintainability
[AD-A290126] p 2592 N95-29423
Model development for active control of stall phenomena in aircraft gas turbine engines p 2500 N95-29679
The dynamics of circulations within the stratiform regions of squall lines p 2623 N95-29725
An analytic modeling and system identification study of helicopter dynamics p 2498 N95-29787
Dynamical model of pressure-gradient-driven turbulence and shear flow generation in L-H transition
[AD-B195511L] p 2709 N95-29789
Transient responses of phosphoric acid fuel cell power plant system
[NASA-CR-198948] p 2603 N95-30015

DYNAMIC PROGRAMMING
Stable function approximation in dynamic programming
[AD-A290224] p 2647 N95-29143
Parallel adaptive techniques for transient partial differential equations
[AD-A290460] p 2674 N95-29490
Bicriteria network design problems
[DE95-005261] p 2661 N95-30215

DYNAMIC RANGE
Linewidth-insensitive coherent analog optical links
[AD-A292422] p 2698 N95-28992

DYNAMIC RESPONSE
Design and analysis of the launch vehicle adapter fitting for the petite amateur navy satellite (PANSAT)
[AD-A289693] p 2504 N95-28680
Modal interactions and complex responses in weaklyNONLINEAR MULTI-DEGREE-OF-FREEDOM MECHANICAL SYSTEMS
[AD-A292023] p 2594 N95-28853
Exact physical models and methods for stabilization and control of reflection-induced instabilities in semiconductor lasers
[AD-A292437] p 2585 N95-29053
Analytical theory of continued fractions and time evolution in many-particle systems
[AD-A290365] p 2692 N95-29227
High-and low-frequency dynamics of isolated blades and rotors with dynamic stall and wake
[AD-A290358] p 2497 N95-29322
Measurement of interface strength, intrinsic toughness and their dependence on interfacial segregants
[AD-A291798] p 2524 N95-29409
An impact load identification method using distributed sensor measurements p 2595 N95-29419
Spectral analysis techniques using wavelets as an alternative to Fourier analysis for transient dynamic data
[AD-A289776] p 2556 N95-29459
Mathematical modeling and numerical simulation of the dynamics of flexible structures undergoing large overall motions
[AD-A291139] p 2597 N95-30123

DYNAMIC STABILITY
Analyzing the stability of floating ice floes
[AD-A292149] p 2629 N95-29160
Design and evaluation of a LQR controller for the bluebird unmanned air vehicle
[AD-A289769] p 2498 N95-29457
Theory and experiments on chemical instabilities
[AD-A290773] p 2534 N95-29922

DYNAMIC STRUCTURAL ANALYSIS
Design and analysis of the launch vehicle adapter fitting for the petite amateur navy satellite (PANSAT)
[AD-A289693] p 2504 N95-28680
An analytic modeling and system identification study of helicopter dynamics p 2498 N95-29787
Mathematical modeling and numerical simulation of the dynamics of flexible structures undergoing large overall motions
[AD-A291139] p 2597 N95-30123

DYNAMIC TESTS
Photoproduction of hybrid mesons from CEBAF to HERA
[PB95-196218] p 2691 N95-28913

DYNAMICAL SYSTEMS
The development of methods and techniques to detect and model the underlying structure of chaotic systems
[AD-A292435] p 2680 N95-29072
Closed loop control of guided missiles using neural networks p 2663 N95-29241
New predictive methods in chaotic fluid dynamics with application to turbulent heat transfer
[AD-A290691] p 2576 N95-29761
On the topological complexity of the cost function in variational data assimilation p 2724 N95-29798
Attractors of dissipative structure in three dissipative fluids
[AD-B180030L] p 2710 N95-29844
Nonlinear control systems
[AD-A291083] p 2665 N95-29971
Optimal hankel norm identification of dynamical systems
[PB95-197232] p 2672 N95-30046

DYSPROSIUM COMPOUNDS
Crystal field and exchange interactions in DyT4Al8 (T = Fe and Mn)
[DE95-007131] p 2714 N95-29134

E

E REGION
Correlation and gradient characteristics of ionospheric parameters in europe
[AD-A292295] p 2612 N95-28871

EAR PROTECTORS
Actual effectiveness of hearing protection in high level impulse noise
[AD-A291604] p 2634 N95-28941

EARTH ALBEDO
Modeling the direct-beam instantaneous spectral surface albedo of a forest landscape using geometric-optics and a distributed parameter approach
p 2599 N95-29540

EARTH CORE
Large scale fluctuations of the geomagnetic field
p 2617 N95-29796

EARTH IONOSPHERE
Correlation and gradient characteristics of ionospheric parameters in Europe
[AD-A290135] p 2612 N95-29140
Characterization of the geometries of the high-latitude ionospheric convection pattern p 2614 N95-29524
Thermal N(+) in the inner magnetosphere
p 2614 N95-29590
Application of Poynting flux measurements to the determination of energy transfer rates in the high-latitude ionosphere p 2614 N95-29650
A generalized semikinetic (GSK) model for mesoscale auroral plasma transport p 2706 N95-29686
Turbulent coupling of the magnetosphere-ionosphere through shear-mode Alfven waves p 2615 N95-29687
The high latitude ionospheric convection pattern during northward interplanetary magnetic field
p 2615 N95-29693
Data re-formatter program for the topside thermal plasma monitor (PLIESPP)
[AD-A290960] p 2616 N95-29737
The topside ionospheric plasma monitor (SSIES, SSIES-2 and SSIES-3) on the spacecraft of the Defense Meteorological Satellite Program (DMSP), user's guide. Volume 3: Program maintenance manual
[AD-A290941] p 2617 N95-29765

EARTH MAGNETOSPHERE
Surface conversion techniques for low energy neutral atom imagers
[NASA-CR-196604] p 2691 N95-28856
Thermal N(+) in the inner magnetosphere
p 2614 N95-29590
A generalized semikinetic (GSK) model for mesoscale auroral plasma transport p 2706 N95-29686
Turbulent coupling of the magnetosphere-ionosphere through shear-mode Alfven waves p 2615 N95-29687
The high-altitude polar wind: Simulation and observation p 2622 N95-29688
Equatorial heating effects on outer plasmasphere evolution p 2616 N95-29716
On the azimuthal variation of the equatorial plasmapause
[NASA-CR-198929] p 2711 N95-30338

EARTH MANTLE
Differentiation in the early Earth: An experimental investigation p 2612 N95-29199

EARTH OBSERVATIONS (FROM SPACE)
STS-67 mission highlights resource tape
[NASA-TM-110530] p 2504 N95-28715
Apollo 11: For all mankind
[NASA-TM-110622] p 2503 N95-29407
Depicting dust and sand storm signatures through the means of satellite images and ground-based observations for Saudi Arabia p 2600 N95-29730
STS-71 Shuttle/Mir flight: Day 3
[NASA-TM-110746] p 2505 N95-29956
STS-71 Shuttle/Mir flight: Day 6
[NASA-TM-110749] p 2505 N95-29959
Sea ice motions in the Central Arctic pack ice as inferred from AVHRR imagery
[NASA-CR-198835] p 2601 N95-30247
A conceptual thermal design study of an electronically scanned thinned array radiometer
[NASA-TM-110173] p 2509 N95-30316

EARTH OBSERVING SYSTEM (EOS)
Data catalog for JPL Physical Oceanography Distributed Active Archive Center (PO.DAAC)
[NASA-CR-198872] p 2631 N95-30231

EARTH ORBITAL ENVIRONMENTS
A layman's look at orbital debris
[AD-A289801] p 2506 N95-28700
Orbital debris: A technical assessment
[NASA-CR-198639] p 2507 N95-28852
Summary report of mission acceleration measurements for STS-65, launched 8 July 1994
[NASA-TM-106871] p 2549 N95-30339

EARTH ORBITS
STS-71 Shuttle/Mir flight: Day 3
[NASA-TM-110746] p 2505 N95-29956
STS-71 Shuttle/Mir flight: Day 5
[NASA-TM-110748] p 2505 N95-29958
STS-71 Shuttle/Mir flight: Day 6
[NASA-TM-110749] p 2505 N95-29959
STS-71 Shuttle/Mir flight: Day 7
[NASA-TM-110750] p 2505 N95-29960
STS-71 Shuttle/Mir flight: Day 8
[NASA-TM-110751] p 2505 N95-29961
STS-71 Shuttle/Mir flight: Day 10
[NASA-TM-110753] p 2506 N95-29963

EARTH RADIATION BUDGET
The effects of clouds as a feedback mechanism on the Earth's climate in the tropical Pacific
p 2611 N95-30300

EARTH RADIATION BUDGET EXPERIMENT
The spatial-scale dependence of the observed anisotropy of reflected and emitted radiation
p 2613 N95-29253

EARTH RESOURCES
A geotechnical characterization of lunar soils and lunar soil simulants p 2736 N95-29117

EARTH SCIENCES
The 1994 research and technology report at the Goddard Space Flight Center
[NASA-TM-110623] p 2740 N95-28882

EARTH SURFACE
Differentiation in the early Earth: An experimental investigation p 2612 N95-29199

EARTH TERMINALS
Test results of a 20 GHz, low noise downconverter for USAT applications
[NASA-TM-106892] p 2508 N95-30011

EARTH TIDES
Tidal constituent database: West coast of the United States and eastern North Pacific Ocean
[AD-A292224] p 2630 N95-29198

EARTH-MOON SYSTEM
Guidance, navigation, and control study for a solar electric propulsion spacecraft
[NASA-CR-198920] p 2509 N95-30357

EARTHQUAKES
Two-dimensional signal processing for regional seismic event identification
[AD-A292601] p 2613 N95-29293
Mapping crust and upper mantle structure beneath southern Eurasia
[AD-A291074] p 2618 N95-29970

Crustal deformation measurements in the vicinity of Vandenberg Air Force Base
[AD-A291224] p 2618 N95-29981

ECCENTRICITY
Acoustic scattering from ellipses by the modal element method
[NASA-TM-106935] p 2683 N95-29401

ECONOMIC ANALYSIS
Analysis of global economic instruments for CO2 emission reduction: Equity and efficiency
[DE95-764057] p 2610 N95-30195
Interactions between energy efficiency and emission trading under the 1990 Clean Air Act Amendments
[DE95-008649] p 2611 N95-30212

ECONOMIC IMPACT
Environmental practice in progam management offices
[AD-A290823] p 2609 N95-29721

ECOSYSTEMS
Measuring variation in ecosystem sensitivity to stress
[AD-A290415] p 2609 N95-29450

EDDY CURRENTS
Numerical investigation of surface curvature effects in compressible turbulent flows
[AD-A290114] p 2571 N95-29211

EDDY VISCOSITY
Numerical experiments on the flow past a circular cylinder at sub-critical Reynolds number
[AD-A289937] p 2573 N95-29268
Experimental and analytical study of heat transfer and turbulent flow field in tangentially injected swirl flow
p 2576 N95-29811

EDGE DETECTION
Accurate feature detection and estimation using nonlinear and multiresolution analysis
[AD-A290267] p 2553 N95-29176
Object oriented segmentation of images
[AD-A290792] p 2671 N95-29485

EDGE DISLOCATIONS
Superplastic ceramics
[AD-A290817] p 2545 N95-29635

EDGE LOADING
Analytical investigation of the hygrothermal effects and parametric study of the Edge Crack Torsion (ECT) mode 3 test lay-ups
[NASA-TM-110183] p 2528 N95-30028

EDGES
Inflatable life vest
[AD-D017273] p 2641 N95-29600

EDITING ROUTINES (COMPUTERS)
A friendly editing environment for computer-aided rapid prototyping of hard real-time systems
[AD-A290154] p 2648 N95-29321

EDUCATION
Improving problem-solving and decision-making skills under stress: Prediction and training
[AD-A292104] p 2638 N95-28918
Physical acoustics summer school, 1994. volume 1. transcript
[AD-A292552] p 2683 N95-28973
Macroprocesses and adaptive instruction
[AD-A290483] p 2648 N95-29325
Test theory reconceived
[AD-A291836] p 2639 N95-29432
US Army aviation epidemiology data register: Gender-specific attrition among the US Army student aviator class of 1987
[AD-A291856] p 2639 N95-29434
High-performance speech recognition using consistency modeling
[AD-A290655] p 2557 N95-29564
Medical evacuation: A training priority
p 2676 N95-29617
Flight nurse school in the Hellenic Air Force
p 2638 N95-29629
Mathematical olympiad summer program (MOSP) 1994
[AD-A290801] p 2672 N95-29647
Adaptations to three weeks of aerobic/anaerobic training in west coast U.S: Navy Sea-Air-Land personnel (SEAL's)
[AD-A291500] p 2637 N95-29846
Distance estimation training with night vision goggles under low illumination
[AD-A291338] p 2641 N95-29943
Solar heating and you
[DE95-004012] p 2603 N95-30127

EFFLUENTS
Computational fluid dynamics (CFD) simulation of test chamber and smoke-generating device
[AD-A290199] p 2569 N95-29058
Measurements of ions formed in jet engine exhaust plumes
[AD-A290940] p 2501 N95-29764

EFFUSIVES
Numerical studies of the stratospheric aerosol layer under background and perturbed conditions
p 2615 N95-29666

EIGENVALUES
Multi-dimensional upwind discretization method for the Euler equations on unstructured grids
[PB95-197307] p 2578 N95-30202

EIGENVECTORS
Multi-dimensional upwind discretization method for the Euler equations on unstructured grids
[PB95-197307] p 2578 N95-30202

EJECTORS
Ejectors and jet pumps: Computer program for design and performance for steam/gas flow
[ESDU-94046] p 2495 N95-28704

EL NINO
Forecast of Atlantic seasonal hurricane activity for 1995 p 2620 N95-29254
A study of dynamics in the tropical Pacific using satellite data p 2630 N95-29520

ELASTIC BENDING
Test load verification through strain data analysis
[NASA-TP-3558] p 2504 N95-28718

ELASTIC BODIES
Boundary element algorithms for Somigliana's identity
[PB95-206959] p 2597 N95-30169

ELASTIC BUCKLING
Compressive behavior of thick composite shells: Benchmark solutions for loss of stability and hygroscopic effects p 2595 N95-29424

ELASTIC DEFORMATION
Flat rectangular isotropic plates under uniformly distributed normal pressure. Elastic deflections, stresses, and strains, moments and forces, for various forms of edge restraint
[ESDU-94033] p 2593 N95-28801
The Stroh formalism for anisotropic elasticity with applications to composite materials
[AD-A290710] p 2527 N95-29763
The study of non-Newtonian contraction flows with a parallel finite element method p 2576 N95-29778

ELASTIC PROPERTIES
Experimental methods in residual stress measurement using a position-sensitive single-exposure scintillation detection system
[AD-A289803] p 2594 N95-28949
Energy theorems and bounds in linearized elasticity with residual stress p 2595 N95-29546
The Stroh formalism for anisotropic elasticity with applications to composite materials
[AD-A290710] p 2527 N95-29763
Structure and orientation behavior of highly oriented polymers under tensile and compressive stresses
p 2546 N95-29822
Ultrasonic guided waves in cylinders: Theory and experiment p 2685 N95-29826
InTlSb as a long-wave infrared (LWIR) material: Defects and transportation properties
[AD-A291218] p 2702 N95-29978
Extreme nonlinearity in rocks: An investigation using elastic pulse wave propagation
[DE95-007879] p 2618 N95-30129

ELASTIC SHELLS
Compressive behavior of thick composite shells: Benchmark solutions for loss of stability and hygroscopic effects p 2595 N95-29424

ELASTIC WAVES
Ultrasonic guided waves in cylinders: Theory and experiment p 2685 N95-29826
Extreme nonlinearity in rocks: An investigation using elastic pulse wave propagation
[DE95-007879] p 2618 N95-30129

ELASTODYNAMICS
Dynamic decohesion of bimaterial interfaces
p 2541 N95-29120
Efficient inversion of Fourier and Laplace domain boundary element solutions for elastodynamic scattering
p 2592 N95-29256
Eurasian seismic surveillance - 2D FD seismic synthetics and event discrimination
[AD-A292659] p 2614 N95-29413
Micromechanics of crack extension in composites
p 2529 N95-30276

ELASTOHYDRODYNAMICS
Contact stress in disc cams with domes of flat-faced followers
[ESDU-94011] p 2589 N95-28901

ELASTOMERS
High field electrostrictive response of polymers
[AD-A292298] p 2539 N95-28864

ELASTOPLASTICITY
Systems of hyperbolic partial differential equations
[AD-A290287] p 2669 N95-29083
Elastoplastic buckling analysis of cylindrical shells using a semi-analytical formulation
[PB95-197349] p 2597 N95-30206

ELASTOSTATICS
Energy theorems and bounds in linearized elasticity with residual stress p 2595 N95-29546
Boundary element algorithms for Somigliana's identity
[PB95-206959] p 2597 N95-30169
Micromechanics of crack extension in composites
p 2529 N95-30276

ELECTRIC ARCS
Arcing mitigation and predictions for high voltage solar arrays
[AD-A292227] p 2602 N95-29200
Arcing predictions for PASP PLUS solar arrays
[AD-A292230] p 2602 N95-29201

ELECTRIC BATTERIES
US photovoltaic patents: 1991-1993
[DE95-004051] p 2603 N95-30017
Engineering development program of a closed aluminum-oxygen semi-cell system for an unmanned underwater vehicle: An update p 2606 N95-30266

ELECTRIC CONDUCTORS
Radar cross section synthesis for planar resistive surfaces
[AD-A290151] p 2555 N95-29318
Processing and properties of long-lengths of Ag-clad BSCCO superconductors and high-(Tc) magnets
[DE95-005855] p 2716 N95-29984
175Hp contrarotating homopolar motor design report
[AD-A291138] p 2567 N95-30122

ELECTRIC CONNECTORS
An electrical and fiber-optic connector
[AD-D017404] p 2589 N95-28791
Corona tests of prototype connector
[AD-A292542] p 2561 N95-28971
Diffractive optics: Design, fabrication, and applications
[AD-A290942] p 2702 N95-29867

ELECTRIC CONTACTS
Nitride semiconductors for ultraviolet detection
[AD-A289546] p 2712 N95-28910

ELECTRIC CORONA
Corona tests of prototype connector
[AD-A292542] p 2561 N95-28971

ELECTRIC CURRENT
Static field solutions and image theory for a conducting sphere with radial anisotropy
[PB95-207171] p 2673 N95-30172

ELECTRIC FIELDS
Novel electric-field effects in quantum wells and superlattices
[AD-A292317] p 2718 N95-28857
High field electrostrictive response of polymers
[AD-A292298] p 2539 N95-28864
Corona tests of prototype connector
[AD-A292542] p 2561 N95-28971
Doubled diode laser. phase 1
[AD-A292465] p 2584 N95-29007
Five-channel SQUID based non-destructive evaluation (NDE) instrument
[AD-A292474] p 2592 N95-29012
A generalized semikinetic (GSK) model for mesoscale auroral plasma transport p 2706 N95-29686
Transition of radial electric field by electron cyclotron heating in the stellarator plasmas
[AD-B176254L] p 2707 N95-29742
Formation of positive radial electric field by Electron Cyclotron Heating in Compact Helical System
[AD-B191994L] p 2709 N95-29802
Electronic states in Cd(1-x)Zn(x)Te/CdTe strained layer coupled double quantum wells and their photoluminescence
[DE95-006806] p 2716 N95-29814
The onset of electrohydrodynamic instability in isoelectric focusing
[NASA-CR-198805] p 2565 N95-29968
Unitary transducer with variable resistivity
[AD-D017329] p 2566 N95-30055

ELECTRIC GENERATORS
175Hp contrarotating homopolar motor design report
[AD-A291138] p 2567 N95-30122

ELECTRIC HYBRID VEHICLES
Electric and hybrid vehicle program: Site operator program
[DE95-008620] p 2591 N95-30211

ELECTRIC MOTOR VEHICLES
Technology development goals for automotive fuel cell power systems
[DE95-008764] p 2548 N95-29280
Electric and hybrid vehicle program: Site operator program
[DE95-008620] p 2591 N95-30211

ELECTRIC NETWORKS
R&M design expert system
[AD-A292525] p 2645 N95-28814

Electrically small archimedian spiral method of moment analysis
[AD-A291171] p 2558 N95-29928

ELECTRIC POTENTIAL
Arcing predictions for PASP PLUS solar arrays
[AD-A292230] p 2602 N95-29201
Multifluid nonequilibrium simulation of arcjet thrusters
p 2510 N95-29245
Technology development goals for automotive fuel cell power systems
[DE95-008764] p 2548 N95-29280
A study of power diode failure mechanisms in the US Army research laboratory 30-mm solid propellant electrothermal-chemical (SPETC) gun facility
[AD-A291300] p 2565 N95-29938
Unitary transducer with variable resistivity
[AD-D017329] p 2566 N95-30055
175Hp contrarotating homopolar motor design report
[AD-A291138] p 2567 N95-30122
Effect of KOH concentration and anions on the performance of Ni-H2 battery positive plate
p 2567 N95-30260

ELECTRIC POWER
A system for conveniently providing load testing termination of an AC power source having at least one battery
[AD-D017408] p 2566 N95-30075

ELECTRIC WIRE
Development of LaRC (TM): IA thermoplastic polyimide coated aerospace wiring
[NASA-CR-195048] p 2548 N95-30252

ELECTRICAL ENGINEERING
Applied Computational Electromagnetics Society Journal, volume 10, number 1, March 1995
[AD-A292069] p 2555 N95-29308
Equipment resource for MCM technology and system prototyping
[AD-A292492] p 2719 N95-29756

ELECTRICAL FAULTS
R&M design expert system
[AD-A292525] p 2645 N95-28814

ELECTRICAL IMPEDANCE
Electrically small archimedian spiral method of moment analysis
[AD-A291171] p 2558 N95-29928
A system for conveniently providing load testing termination of an AC power source having at least one battery
[AD-D017408] p 2566 N95-30075

ELECTRICAL INSULATION
Development of LaRC (TM): IA thermoplastic polyimide coated aerospace wiring
[NASA-CR-195048] p 2548 N95-30252

ELECTRICAL MEASUREMENT
Effects of cooling system parameters on heat transfer in PAFC stack
[NASA-CR-198817] p 2570 N95-29131
Dielectric property measurements in the Electromagnetic Properties Measurement Laboratory
[NASA-TM-110147] p 2560 N95-30336

ELECTRICAL PROPERTIES
Interface properties of wide bandgap semiconductor structures
[AD-A289817] p 2713 N95-28954
Electrical and electronic properties of self-assembled lipid bilayers
[AD-A290507] p 2632 N95-29155
Tailored microstructures for broadband or selective detection of radiation from the visible to the infrared
[AD-A292097] p 2554 N95-29240
Fabrication and characterization of BSTO and nonferroelectric oxide composites for use in phased array antennas and other electronic devices
[AD-A290070] p 2524 N95-29329
Novel high-power solid-state sources for the millimeter-wave region
[AD-A292653] p 2564 N95-29384
Physical modeling and design of semiconductor heterostructures for optical and electronical applications
p 2682 N95-30232

ELECTRICAL RESISTIVITY
XPS study of Ni-Fe manganite thermistor material
[DE95-008778] p 2561 N95-28961
Radar cross section synthesis for planar resistive surfaces
[AD-A290151] p 2555 N95-29318
HTMIAC/CINDAS silicon properties database. User's guide
[AD-A292602] p 2533 N95-29575
The onset of electrohydrodynamic instability in isoelectric focusing
[NASA-CR-198805] p 2565 N95-29968
Unitary transducer with variable resistivity
[AD-D017329] p 2566 N95-30055
Static field solutions and image theory for a conducting sphere with radial anisotropy
[PB95-207171] p 2673 N95-30172

ELECTRO-OPTICS
ARPA solid state laser and nonlinear materials program
[AD-A289657] p 2584 N95-28678
Fibre-coupled remote optical vibrometry
[AD-A291606] p 2698 N95-28932
Commercial photorefractive device using nonstoichiometric 3-5 semiconductors
[AD-A292494] p 2713 N95-28933
Studies of lattice-mismatched and Low-Temperature-Grown semiconductor multiple-phase systems
[AD-A292536] p 2713 N95-28967
The 1.3 micrometer fiber photodetector
[AD-A292462] p 2582 N95-29004
Optoelectronics based on SiGe/Si heterostructures
[AD-A292464] p 2699 N95-29006
High resolution direct digitization and optical telemetry of shipboard antenna signals
[AD-A290238] p 2557 N95-29504
Equipment resource for MCM technology and system prototyping
[AD-A292492] p 2719 N95-29756
The 41st Japan Society of Applied Physics Spring Meeting
[AD-A292333] p 2720 N95-29879
Photorefractive Bi12SiO20 spatial light modulator
[AD-A291070] p 2702 N95-29969
Photonic band structures for optoelectronics
[AD-A291154] p 2718 N95-30298

ELECTROCARDIOGRAPHY
A discrete-event simulation model of myocardial electrical activity: Mathematical electrophysiology
[AD-A292323] p 2633 N95-28793

ELECTROCATALYSTS
A novel unitized regenerative proton exchange membrane fuel cell p 2605 N95-30263

ELECTROCHEMICAL CELLS
Space Electrochemical Research and Technology. Abstracts
[NASA-CP-10172] p 2604 N95-30255

ELECTROCHEMICAL CORROSION
Corrosion in methylphosphonic difluoride
[AD-A289995] p 2536 N95-29137
The use of electrochemistry and ellipsometry for identifying and evaluating corrosion on aircraft
[AD-A290249] p 2497 N95-29426

ELECTROCHEMISTRY
The effects of platinum on nickel electrodes in the nickel hydrogen cell
[AD-A291607] p 2531 N95-28942
Computational methods for the simulation of non-Newtonian flows
[AD-A290355] p 2570 N95-29069
The use of electrochemistry and ellipsometry for identifying and evaluating corrosion on aircraft
[AD-A290249] p 2497 N95-29426
Space Electrochemical Research and Technology. Abstracts
[NASA-CP-10172] p 2604 N95-30255
High energy density electrolytic capacitor
p 2568 N95-30271

ELECTRODE MATERIALS
Bending properties of nickel electrodes for nickel-hydrogen batteries p 2567 N95-30259
A novel unitized regenerative proton exchange membrane fuel cell p 2605 N95-30263
The TMI regenerable solid oxide fuel cell
p 2606 N95-30265
Fabrication of advanced electrochemical energy materials using sol-gel processing techniques
p 2607 N95-30269

ELECTRODES
Lightweight battery electrode and method of making it
[AD-D017389] p 2560 N95-28855
Development of Laser Optogalvanic Spectroscopy as a probe of alkali atoms in an MHD environment
[DE95-006481] p 2531 N95-28916
The effects of platinum on nickel electrodes in the nickel hydrogen cell
[AD-A291607] p 2531 N95-28942
Effects of cooling system parameters on heat transfer in PAFC stack
[NASA-CR-198817] p 2570 N95-29131
Effects of the cooling system parameters on heat transfer and performance of the PAFC stack during transient operation
[NASA-CR-197654] p 2572 N95-29249
Development of a micro-fiber nickel electrode for nickel-hydrogen cell p 2567 N95-30256
High performance nickel electrodes for space power applications p 2511 N95-30257
Bending properties of nickel electrodes for nickel-hydrogen batteries p 2567 N95-30259
Effect of KOH concentration and anions on the performance of Ni-H2 battery positive plate
p 2567 N95-30260
Electrolyte management considerations in modern nickel hydrogen and nickel cadmium cell and battery designs p 2567 N95-30262
A novel unitized regenerative proton exchange membrane fuel cell p 2605 N95-30263
High energy density electrolytic capacitor
p 2568 N95-30271

ELECTRODYNAMICS
High-latitude electrodynamics: Electromagnetic energy dissipation and neutral wind feedback effects
p 2616 N95-29696

ELECTROHYDRODYNAMICS
The onset of electrohydrodynamic instability in isoelectric focusing
[NASA-CR-198805] p 2565 N95-29968

ELECTROLUMINESCENCE
Hot electron physics of alternating-current thin-film electroluminescent devices
[AD-A290528] p 2696 N95-29495

ELECTROLYTES
Electrolyte management considerations in modern nickel hydrogen and nickel cadmium cell and battery designs p 2567 N95-30262
Hermetically sealed aluminum electrolytic capacitor
p 2568 N95-30268
High energy density electrolytic capacitor
p 2568 N95-30271

ELECTROMAGNETIC ABSORPTION
HTMIAC/CINDAS silicon properties database. User's guide
[AD-A292602] p 2533 N95-29575
Photothermal deflection in a supercritical fluid
p 2701 N95-29630
Maize yield estimation through the simulation of radiation penetration into the canopy p 2599 N95-29703
High temperature spectroscopy of alkali metal vapors for solar to thermal energy conversion
[AD-A291355] p 2602 N95-29949
Physical modeling and design of semiconductor heterostructures for optical and electronical applications
p 2682 N95-30232

ELECTROMAGNETIC COUPLING
Experimental results of Hooper's gravity-electromagnetic coupling concept
[NASA-TM-106963] p 2680 N95-28893

ELECTROMAGNETIC FIELDS
Characterizing the electromagnetic environment produced by the army's repetitive electromagnetic pulse simulator (REPS)
[AD-A289739] p 2551 N95-28687
Research studies in electromagnetically induced transparency
[AD-A290796] p 2557 N95-29645
A full wave study of radar cross sections of rough terrain
[AD-A291227] p 2559 N95-29982

ELECTROMAGNETIC INTERACTIONS
Laser simulation of single-event effects: A state of the art review
[AD-A292308] p 2584 N95-28892

ELECTROMAGNETIC INTERFERENCE
EMI Shields made from intercalated graphite composites
[NASA-TM-106979] p 2518 N95-28906
Multiple dimensional acousto-optic diffraction and multiple dimensional acousto-optic device
[AD-A291037] p 2685 N95-29681

ELECTROMAGNETIC PROPERTIES
High performance electromagnetic simulation tools
[AD-A290405] p 2554 N95-29235

ELECTROMAGNETIC PULSES
Characterizing the electromagnetic environment produced by the army's repetitive electromagnetic pulse simulator (REPS)
[AD-A289739] p 2551 N95-28687
Experimental studies of electromagnetic propagation at ultrahigh intensities
[AD-A290284] p 2553 N95-29081
Investigation of the Paschen curve of nitrogen via the application of nanosecond pulsed electromagnetic radiation
[AD-A290129] p 2586 N95-29425
Heavy light bullets in electron-positron plasma
[DE95-008751] p 2711 N95-30173

ELECTROMAGNETIC RADIATION
Analysis of tropospheric propagation characteristics based on regional meteorological data
[AD-A291581] p 2552 N95-28939

Investigation of the Paschen curve of nitrogen via the application of nanosecond pulsed electromagnetic radiation
[AD-A290129] p 2586 N95-29425
Multi-focal length and multi-channel holographic optical element
[AD-A291011] p 2583 N95-29656
Modal analysis of straight and curved integrated optical waveguides: An integral equation approach
[PB95-197265] p 2702 N95-30054
Heavy light bullets in electron-positron plasma
[DE95-008751] p 2711 N95-30173

ELECTROMAGNETIC SCATTERING
Electromagnetic scattering by magnetic spheres: Theory and algorithms
[AD-A289798] p 2551 N95-28699
Induced Compton scattering by relativistic electrons in magnetized astrophysical plasmas p 2610 N95-29885
The 10th Annual Review of Progress in Applied Computational Electromagnetics, volume 2
[AD-A286799] p 2558 N95-29904

ELECTROMAGNETIC SHIELDING
EMI Shields made from intercalated graphite composites
[NASA-TM-106979] p 2518 N95-28906

ELECTROMAGNETIC WAVE FILTERS
A method and apparatus for signal filtering
[AD-D017268] p 2554 N95-29236

ELECTROMAGNETIC WAVE TRANSMISSION
Experimental studies of electromagnetic propagation at ultrahigh intensities
[AD-A290284] p 2553 N95-29081
The 10th Annual Review of Progress in Applied Computational Electromagnetics, volume 1
[AD-A286796] p 2553 N95-29159
Broadband Integrated Transmittances (BITS)
[AD-A292176] p 2555 N95-29266
Emissivity measurements in thin metallized membrane reflectors used for microwave radiometer sensors
[NASA-TM-110179] p 2506 N95-30251
Photonic band structures for optoelectronics
[AD-A291154] p 2718 N95-30298
Dielectric property measurements in the Electromagnetic Properties Measurement Laboratory
[NASA-TM-110147] p 2560 N95-30336

ELECTROMAGNETS
Design of a fast-tool servo system using magnetic servo levitation
[AD-A290273] p 2663 N95-29183

ELECTROMECHANICAL DEVICES
Development of electrochemical super capacitors for EMA applications p 2568 N95-30270

ELECTROMIGRATION
Molecular dynamics study of electromigration
[AD-A289811] p 2691 N95-28952

ELECTRON BEAMS
Theory of competition between synchronous and nonsynchronous modes in a magnicon output cavity
[AD-A292048] p 2563 N95-29301
Research into artificially induced atmospheric disturbances
[AD-A290150] p 2613 N95-29317
Hybrid harmonic gyrotron traveling wave amplifier
[AD-A292686] p 2564 N95-29417
Experiments on nonlinear wave-particle interactions p 2695 N95-30302

ELECTRON CYCLOTRON HEATING
Transition of radial electric field by electron cyclotron heating in the stellarator plasmas
[AD-B176254L] p 2707 N95-29742
Monte Carlo simulation study of the ICRF minority heating in the large helical device
[AD-B179858L] p 2708 N95-29749
Formation of positive radial electric field by Electron Cyclotron Heating in Compact Helical System
[AD-B191994L] p 2709 N95-29802

ELECTRON DENSITY (CONCENTRATION)
Non-coincident multi-wavelength emission absorption spectroscopy
[DE95-006480] p 2530 N95-28776
High power, high frequency radiation from beam-plasma interactions
[AD-A292442] p 2703 N95-29001

ELECTRON DIFFUSION
Trapped electron instabilities due to electron temperature gradient and anomalous transport
[AD-B179859L] p 2693 N95-29748

ELECTRON ENERGY
Si 13 emission lines in solar flare x ray spectra obtained with the P78-1 satellite
[AD-A290000] p 2738 N95-29279
Trapped electron instabilities due to electron temperature gradient and anomalous transport
[AD-B179859L] p 2693 N95-29748

ELECTRON MICROSCOPES
Correlations between micromagnetic, microstructural and microchemical properties in ultrathin epitaxial magnetic structures
[AD-A289705] p 2712 N95-28681
Nanofabrication of electronic devices with the scanning tunneling microscope
[AD-A292463] p 2561 N95-29005

ELECTRON MICROSCOPY
Analytical electron microscopy of precipitates in ion-implanted MgAl2O4 spinel
[DE95-007406] p 2538 N95-30038

ELECTRON MOBILITY
InTlSb as a long-wave infrared (LWIR) material: Defects and transportation properties
[AD-A291218] p 2702 N95-29978

ELECTRON OPTICS
Simulated imaging properties of a series of magnetic electron lenses
[NASA-CR-195474] p 2564 N95-29406

ELECTRON PHONON INTERACTIONS
Computer simulation study of high t(sub c) superconductor structure
[AD-A292513] p 2563 N95-29163

ELECTRON PLASMA
Discriminant analysis to predict the occurrence of ELMS in H-mode discharges
[AD-B179183L] p 2708 N95-29746
Formation of positive radial electric field by Electron Cyclotron Heating in Compact Helical System
[AD-B191994L] p 2709 N95-29802

ELECTRON SCATTERING
AB initio studies of electron and positron scattering from non-linear molecules
[AD-A292586] p 2692 N95-28981
Transport phenomena and noise in real quantum wires
[AD-A290493] p 2714 N95-29152
Computer simulation study of high t(sub c) superconductor structure
[AD-A292513] p 2563 N95-29163
Semiconductor science and technology
[AD-A289143] p 2563 N95-29191
Models of accretion-powered x-ray pulsars p 2728 N95-29667

ELECTRON STATES
Interface properties of wide bandgap semiconductor structures
[AD-A289817] p 2713 N95-28954
Radiative lifetime and quenching rate constants of PF(b(1) Sigma+) and tests for an electronic to vibrational energy transfer quenching mechanism
[AD-A290294] p 2681 N95-29062
Electronic states in Cd(1-x)Zn(x)Te/CdTe strained layer coupled double quantum wells and their photoluminescence
[DE95-006806] p 2716 N95-29814

ELECTRON TRANSFER
Transport phenomena and noise in real quantum wires
[AD-A290493] p 2714 N95-29152
Vacuum microelectronic emitters and their applications using compound semiconductor technology
[AD-A291142] p 2567 N95-30124

ELECTRON TRANSITIONS
Development of Laser Optogalvanic Spectroscopy as a probe of alkali atoms in an MHD environment
[DE95-006481] p 2531 N95-28916

ELECTRON TUNNELING
Nanofabrication of electronic devices with the scanning tunneling microscope
[AD-A292463] p 2561 N95-29005
Semiconductor science and technology
[AD-A289143] p 2563 N95-29191

ELECTRON-ION RECOMBINATION
Modeling the boundary layer interactions between weakly ionized plasmas and cooled, planar electrodes in stagnation-point flows p 2706 N95-29717

ELECTRON-POSITRON PLASMAS
Heavy light bullets in electron-positron plasma
[DE95-008751] p 2711 N95-30173

ELECTRONIC COUNTERMEASURES
Conference reports
[AD-A289630] p 2561 N95-28911
A method and apparatus for signal filtering
[AD-D017268] p 2554 N95-29236

ELECTRONIC EQUIPMENT
A ground support electronic interface for the ionospheric spectroscopy and atmospheric chemistry (ISAAC) ultraviolet spectrograph
[AD-A289761] p 2611 N95-28693
Conference reports
[AD-A289630] p 2561 N95-28911
Micro/Miniature heat pipe analysis
[AD-A292232] p 2570 N95-29127
Hot electron physics of alternating-current thin-film electroluminescent devices
[AD-A290528] p 2696 N95-29495

ELECTRONIC EQUIPMENT TESTS
Geothermal heat pumps for heating and cooling
[AD-A292115] p 2602 N95-28858
Improved interception capability through the use of transform domain processing
[AD-A292231] p 2554 N95-29203
UHF Low Density Radio Communications Link (LDRCL) Operational Test and Evaluation (OT&E) integration and OT&E operational final test report
[AD-A291447] p 2558 N95-29769
Radiation effects on front-end electronics for noble liquid calorimetry
[DE95-007304] p 2566 N95-30025

ELECTRONIC MODULES
Equipment resource for MCM technology and system prototyping
[AD-A292492] p 2719 N95-29756

ELECTRONIC WARFARE
Wideband I/Q demodulators: Measurement technique and matching characteristics
[AD-A291505] p 2558 N95-29847

ELECTRONS
AB initio studies of electron and positron scattering from non-linear molecules
[AD-A292586] p 2692 N95-28981
Composite material studies for low temperature thermionic emission
[AD-A292159] p 2523 N95-29124
Prospects for HERMES-spin structure studies at HERA
[DE95-005845] p 2694 N95-30019

ELECTROPHORESIS
The onset of electrohydrodynamic instability in isoelectric focusing
[NASA-CR-198805] p 2565 N95-29968

ELECTROPHYSIOLOGY
A discrete-event simulation model of myocardial electrical activity: Mathematical electrophysiology
[AD-A292323] p 2633 N95-28793

ELECTROPLATING
Chromium plating and electropolishing solution analyses by online x ray fluorescence spectroscopy
[AD-A290023] p 2541 N95-29138
In-plant testing of membranes to treat electroplating wastewater
[NASA-CR-198796] p 2532 N95-29250
An integrated optical CO2 sensor. Phase 0: Design and fabrication of critical elements
[NASA-CR-198792] p 2700 N95-29366

ELECTROPOLISHING
Chromium plating and electropolishing solution analyses by online x ray fluorescence spectroscopy
[AD-A290023] p 2541 N95-29138

ELECTROSTATIC PROBES
Modeling the boundary layer interactions between weakly ionized plasmas and cooled, planar electrodes in stagnation-point flows p 2706 N95-29717

ELECTROSTATICS
Analysis of factors affecting chemical reactions in supercritical fluids
[AD-A290905] p 2534 N95-30078
Static field solutions and image theory for a conducting sphere with radial anisotropy
[PB95-207171] p 2673 N95-30172

ELECTROSTRICTION
High field electrostrictive response of polymers
[AD-A292298] p 2539 N95-28864

ELEMENTARY PARTICLES
Quantum dynamical studies of the decomposition of energetic materials containing defect structures
[AD-A291456] p 2548 N95-29525

ELLIPSES
Acoustic scattering from ellipses by the modal element method
[NASA-TM-106935] p 2683 N95-29401

ELLIPSOIDS
A contribution to the theory of robust estimation of multivariate location and shape: EID
[AD-A290435] p 2675 N95-29819

ELLIPSOMETRY
The use of electrochemistry and ellipsometry for identifying and evaluating corrosion on aircraft
[AD-A290249] p 2497 N95-29426

ELLIPTIC DIFFERENTIAL EQUATIONS
Automatic multi-block grid generation for high-lift configuration wings p 2485 N95-28764
Massively parallel fast elliptic equation solver for three dimensional hydrodynamics and relativity
[DE95-009385] p 2660 N95-30193

ELLIPTICITY
Elliptic surface grid generation on minimal and parmetrized surfaces p 2484 N95-28760
Multilevel elliptic smoothing of large three-dimensional grids p 2485 N95-28765

EMBEDDING
A procedure for accessing digital satellites containing amateur payloads
[AD-A289748] p 2506 N95-28688
Finite difference analysis of a cylindrical two conductor microstrip transmission line with truncated dielectrics
[AD-A292592] p 2555 N95-29290
EMBRITTLEMENT
Impact properties of coated engineering plastics
[PB95-197281] p 2547 N95-30201
EMERGENCIES
The impact of occupational cultures on coordination of emergency medical service crew p 2677 N95-29616
EMISSION
Observations and analysis of solar flares at radio and other wavelengths p 2738 N95-29202
EMISSION SPECTRA
Non-coincident multi-wavelength emission absorption spectroscopy
[DE95-006480] p 2530 N95-28776
Si 13 emission lines in solar flare x ray spectra obtained with the P78-1 satellite
[AD-A290000] p 2738 N95-29279
Yohkoh Bragg Crystal Spectrometer light curves for Ca 29(3.1633 - 3.1933 A): 1 October 1993 - 30 September 1994
[AD-A290027] p 2738 N95-29327
Reaction field (RF) calculation of the spectral shifts of indole
[AD-A290449] p 2532 N95-29487
Some aspects of lunar and martian volcanism as examined with spectral, topographic, and morphologic data derived from spacecraft images p 2736 N95-29594
Far-ultraviolet high-resolution emission line spectroscopy of the Cygnus Loop supernova remnant p 2729 N95-29710
EMISSIVITY
Far-ultraviolet high-resolution emission line spectroscopy of the Cygnus Loop supernova remnant p 2729 N95-29710
Emissivity measurements in thin metallized membrane reflectors used for microwave radiometer sensors
[NASA-TM-110179] p 2506 N95-30251
EMITTANCE
The spatial-scale dependence of the observed anisotropy of reflected and emitted radiation p 2613 N95-29253
EMITTERS
Vacuum microelectronic emitters and their applications using compound semiconductor technology
[AD-A291142] p 2567 N95-30124
Thin-film edge field emitter device and method of manufacture therefor
[AD-D017323] p 2567 N95-30165
ENERGETIC PARTICLES
Experiments on nonlinear wave-particle interactions p 2695 N95-30302
ENERGY ABSORPTION
Analytical and experimental studies of the energy absorption behavior of composite structures p 2524 N95-29411
ENERGY BUDGETS
A thermochemical transport model for analysis of hot-spot formation in energetic materials
[AD-A290441] p 2532 N95-29357
Energy budget in the Asian monsoon region p 2623 N95-29713
ENERGY CONSERVATION
Interactions between energy efficiency and emission trading under the 1990 Clean Air Act Amendments
[DE95-008649] p 2611 N95-30212
ENERGY CONSUMPTION
Liquid pressure amplification and liquid injection in air conditioning and refrigeration systems
[AD-A289738] p 2549 N95-28686
Geothermal heat pumps for heating and cooling
[AD-A292115] p 2602 N95-28858
A genetic algorithm approach to scheduling resources for a space power system p 2511 N95-29784
ENERGY CONVERSION
Collisionless driven magnetic reconnection
[AD-B178946L] p 2709 N95-29810
High temperature spectroscopy of alkali metal vapors for solar to thermal energy conversion
[AD-A291355] p 2602 N95-29949
ENERGY DISSIPATION
Rigorous drag bounds in turbulent shear flow p 2573 N95-29334
Robust control of nonlinear flexible multibody systems using quaternion feedback and dissipative compensation
[NASA-TM-109099] p 2507 N95-29377
Asymptotically zero energy computing using split-level charge recovery logic
[AD-A290054] p 2564 N95-29478
High-latitude electrodynamics: Electromagnetic energy dissipation and neutral wind feedback effects p 2616 N95-29696
A study of blister tests for film adhesion measurement and fracture efficiency of tests for adhesive bonds p 2545 N95-29799
ENERGY GAPS (SOLID STATE)
Self-Induced Transparency in photonic band structures: Gap solitons near absorption resonances
[AD-A292187] p 2718 N95-28927
Interface properties of wide bandgap semiconductor structures
[AD-A289817] p 2713 N95-28954
Ordering and bandgap reduction in InAs(1-x)Sb(x) alloys
[DE95-006324] p 2717 N95-30005
ENERGY LEVELS
Insights on the local density approximation plasma polarization shift as provided by the optimum potential method
[DE95-008078] p 2705 N95-29466
ENERGY SPECTRA
Fluxes and relative abundances of light cosmic ray nuclei at energies above 40 GeV/n p 2739 N95-29531
The energy spectrum and flux of cosmic ray helium at high energy p 2740 N95-29705
ENERGY STORAGE
Radiative lifetime and quenching rate constants of PF(b(1) Sigma+) and tests for an electronic to vibrational energy transfer quenching mechanism
[AD-A290294] p 2681 N95-29062
The TMI regenerable solid oxide fuel cell p 2606 N95-30265
ENERGY TECHNOLOGY
Inhalation Toxicology Research Institute
[AD-A292037] p 2635 N95-29188
Solid Oxide Fuel Cell commercialization in the United States
[DE95-008210] p 2607 N95-30278
ENERGY TRANSFER
Physical acoustics summer school, 1994. volume 1. transcript
[AD-A292552] p 2683 N95-28973
Studies of energy transfer processes of relevance to chemically and optically pumped lasers
[AD-A290164] p 2585 N95-29025
Radiative lifetime and quenching rate constants of PF(b(1) Sigma+) and tests for an electronic to vibrational energy transfer quenching mechanism
[AD-A290294] p 2681 N95-29062
Application of Poynting flux measurements to the determination of energy transfer rates in the high-latitude ionosphere p 2614 N95-29650
Models of accretion-powered x-ray pulsars p 2728 N95-29667
Permanent magnet torque/force transfer apparatus
[AD-D017325] p 2682 N95-30051
ENGINE DESIGN
Surface modeling and grid generation for aeropropulsion CFD p 2479 N95-28732
Marshall Space Flight Center surface modeling and grid generation applications p 2480 N95-28733
A transient model of the RL10A-3-3A rocket engine
[NASA-CR-195478] p 2510 N95-29114
ENGINE INLETS
A procedure for automating CFD simulations of an inlet-bleed problem p 2485 N95-28768
ENGINE MONITORING INSTRUMENTS
Cost effective, dual-purpose machine vision-based detectors for (1) smoke and flame detection, and (2) engine overhead/burn-through and flame detection
[AD-A292284] p 2697 N95-28870
ENGINE NOISE
UHB engine fan broadband noise reduction study
[NASA-CR-198357] p 2684 N95-29641
ENGINE TESTING LABORATORIES
Inlet flow test calibration for a small axial compressor rig. Part 2: CFD compared with experimental results
[NASA-TM-106999] p 2501 N95-30007
ENGINE TESTS
A transient model of the RL10A-3-3A rocket engine
[NASA-CR-195478] p 2510 N95-29114
UHB engine fan broadband noise reduction study
[NASA-CR-198357] p 2684 N95-29641
Impact of uncertainty on modeling and testing
[NASA-CR-196637] p 2652 N95-30013
ENGINEERING MANAGEMENT
Federal aviation administration plan for research, engineering and development
[AD-A290952] p 2494 N95-29733
ENGINEERS
Automated testing of application domains
[AD-A289753] p 2643 N95-28690
The 2nd European Conference on Smart Structures and Materials
[AD-A290723] p 2550 N95-29579
ENRICHMENT
Surface studies of Poly(organophosphazenes) containing dimethylsiloxane grafts
[AD-A291909] p 2543 N95-29355
ENTRAPMENT
Polymeric microcapsule arrays
[AD-A291937] p 2539 N95-28850
ENTROPY
Investigation of Burnett equations for two-dimensional hypersonic flow
[AD-A290233] p 2575 N95-29469
ENVIRONMENT EFFECTS
Overview of the space debris environment
[AD-A292302] p 2507 N95-28867
Study of the space environmental effects on spacecraft engineering materials
[NASA-CR-196638] p 2531 N95-29246
The Scanning Fast Field Program (SCAFFIP) general version 1.0 user's manual
[AD-A291209] p 2618 N95-29976
ENVIRONMENT MANAGEMENT
The Environmental Assessment and Management (TEAM) guide
[AD-A286748] p 2608 N95-28787
Environmental practice in progam management offices
[AD-A290823] p 2609 N95-29721
ENVIRONMENT PROTECTION
The Environmental Assessment and Management (TEAM) guide
[AD-A286748] p 2608 N95-28787
The TEES process cleans waste and produces energy
[DE95-007799] p 2602 N95-29463
Proposal for a flexible system of phytogeographic classification: Emphasis on the use of multistage remote sensoring
[INPE-5609-PRE/1821] p 2600 N95-29815
Interactions between energy efficiency and emission trading under the 1990 Clean Air Act Amendments
[DE95-008649] p 2611 N95-30212
ENVIRONMENT SIMULATION
Experiments in cooperative manipulation of objects by free-flying robot teams p 2662 N95-29095
Software testing toolkit for distributed simulations
[AD-A291867] p 2649 N95-29435
Applications of digital video and synthetic environments to unmanned aerial vehicles
[AD-A291875] p 2497 N95-29437
Liquefied metal jet program Automation and Robotics Research Institute (ARRI)
[AD-A289781] p 2536 N95-29461
The 2d Eurographics Workshop on Virtual Environments
[AD-A292015] p 2651 N95-29861
ENVIRONMENTAL MONITORING
Environmental practice in progam management offices
[AD-A290823] p 2609 N95-29721
Depicting dust and sand storm signatures through the means of satellite images and ground-based observations for Saudi Arabia p 2600 N95-29730
Proposal for a flexible system of phytogeographic classification: Emphasis on the use of multistage remote sensoring
[INPE-5609-PRE/1821] p 2600 N95-29815
Management of meteorological data at a former nuclear weapons facility
[DE95-007619] p 2626 N95-29868
Novel photoelectric sensing technology for environmental monitoring, phase 1
[AD-A292026] p 2611 N95-30348
ENVIRONMENTAL TESTS
Study of the space environmental effects on spacecraft engineering materials
[NASA-CR-196638] p 2531 N95-29246
Characterization and calibration of a pulsed laser system for single event upset simulation
[AD-A290075] p 2586 N95-29330
Effects of space exposure on metals flown on the Long Duration Exposure Facility
[NASA-CR-4662] p 2512 N95-30225
ENZYMES
Polymeric microcapsule arrays
[AD-A291937] p 2539 N95-28850
EOS DATA AND INFORMATION SYSTEM
Retrieval, display, and analysis support tool for earth imagery (RDAST)
[AD-A291366] p 2601 N95-30061
EPHEMERIDES
Total solar eclipse of 1997 March 9
[NASA-RP-1173] p 2731 N95-30004
EPIDEMIOLOGY
Military flying and aeromedical evaluation of cardiac arrhythmias
[AD-A291595] p 2634 N95-28940

US Army aviation epidemiology data register: Gender-specific attrition among the US Army student aviator class of 1987
[AD-A291856] p 2639 N95-29434
Nearest neighbor analysis in one dimension
[DE95-009378] p 2654 N95-30183

EPITAXY
Correlations between micromagnetic, microstructural and microchemical properties in ultrathin epitaxial magnetic structures
[AD-A289705] p 2712 N95-28681
Interface properties of wide bandgap semiconductor structures
[AD-A289817] p 2713 N95-28954
Process optimization through discovery and integration of materials and processing properties. phase 1
[AD-A292576] p 2662 N95-28978
Pulsed laser deposition of ferroelectric thin films in conjunction with superconducting oxides
[AD-A290101] p 2585 N95-29208
Epitaxial growth of high quality SiC of pulsed laser deposition, phase 1
[AD-A291410] p 2717 N95-30068

EPOXY MATRIX COMPOSITES
Epoxy pipelining composition and method of manufacture
[AD-D017380] p 2539 N95-28784
Challenges and payoff of composites in transport aircraft: 777 empennage and future applications p 2519 N95-29031
Effects of temperature and humidity cycling on the strengths of textile reinforced carbon/epoxy composite materials p 2520 N95-29037
A designed experiment in stitched/RTM composites p 2522 N95-29046
Interlaminar fracture mechanics and mechanisms: Linear and nonlinear aspects p 2526 N95-29597
Composite processing development to improve interlaminar strength using ply interface particles
[NASA-TM-108495] p 2529 N95-30334

EPOXY RESINS
In situ processing methods for composite fuselage sandwich structures p 2513 N95-28826
Sorption and diffusion of moisture in multilayer composite AEM/S sandwich materials
[AD-A289807] p 2518 N95-28951
Advanced resin systems and 3D textile preforms for low cost composite structures p 2519 N95-29035
Epoxy self-priming topcoats
[AD-D017383] p 2541 N95-29194
Toughening mechanisms in mixed-mode interfacial fracture p 2545 N95-29772

EQUALIZERS (CIRCUITS)
The 1994 IEEE International Workshop on Intelligent Signal Processing and Communication Systems (ISPACS94)
[AD-A292312] p 2556 N95-29474

EQUATIONS OF MOTION
Linear and nonlinear discrete-time state-space modeling of dynamic systems for control applications p 2663 N95-29251
Three problems in fluid dynamics
[AD-A290481] p 2573 N95-29324
Programmable materials and structures
[AD-A291807] p 2649 N95-29429
Estimation of unstabilized components in vehicular motion
[AD-A290580] p 2590 N95-29552
Averaged resistive MHD equations
[AD-B178947L] p 2711 N95-30033

EQUATIONS OF STATE
Linear and nonlinear discrete-time state-space modeling of dynamic systems for control applications p 2663 N95-29251
Investigation of Burnett equations for two-dimensional hypersonic flow
[AD-A290233] p 2575 N95-29469
Pressure updating methods for the steady-state fluid equations
[NASA-CR-198163] p 2674 N95-30353

EQUATORIAL REGIONS
Compendium of NASA data base for the global tropospheric experiment's Transport and Atmospheric Chemistry Near the Equator-Atlantic (TRACE-A)
[NASA-TM-110151] p 2608 N95-28717
Radiative cooling profiles calculated from ECMWF analyses and ISCCP C1 data, and their application to determination of distributions of apparent convective heating in the equatorial Pacific p 2625 N95-29805
On the azimuthal variation of the equatorial plasmapause
[NASA-CR-198929] p 2711 N95-30338

EQUILIBRIUM EQUATIONS
Averaged resistive MHD equations
[AD-B178947L] p 2711 N95-30033
Boundary element algorithms for Somigliana's identity
[PB95-206959] p 2597 N95-30169

EQUIPMENT SPECIFICATIONS
A generic specification for Special Purpose Aeromedical Equipment p 2499 N95-29623

ERBIUM
Ion doped quantum well lasers
[AD-A290937] p 2587 N95-29912

ERROR ANALYSIS
Error modeling for differential GPS
[NASA-CR-188367] p 2493 N95-28716
An HP-Adaptive method in space and time for parabolic systems
[AD-A292262] p 2668 N95-28890
Dispersion analysis and error estimation of Galerkin finite element methods for the numerical computation of waves
[AD-A290296] p 2668 N95-29064
Pollution error in the h-version of the finite element method and the local quality of the recovered derivatives
[AD-A290297] p 2668 N95-29065
A generalized finite element method for solving the Helmholtz equation in two dimensions with minimal pollution
[AD-A290280] p 2669 N95-29080
Mode of human image representation and error checking strategies in complex visual displays
[AD-A290107] p 2492 N95-29210
A contribution to the theory of robust estimation of multivariate location and shape: EID
[AD-A290435] p 2675 N95-29819
ADC test support program
[AD-A289445] p 2643 N95-29921
Performance analysis of a GPS Interferometric attitude determination system for a gravity gradient stabilized spacecraft
[NASA-CR-188372] p 2508 N95-30036
A PC program for estimating measurement uncertainty for aeronautics test instrumentation
[NASA-CR-198361] p 2503 N95-30067
Software Estimation Program (SWEEP) user manual
[AD-A291137] p 2654 N95-30121
Time accurate application of the MacCormack 2-4 scheme on massively parallel computers p 2661 N95-30150

ERROR CORRECTING CODES
Quality Control of meteorological observations at Fleet Numerical Meteorology and Oceanography Center
[AD-A291577] p 2619 N95-28938
Comparison study of unequal error protection methods for one-dimensional signal constellations
[AD-A290386] p 2554 N95-29231
The design of programmable convolutional encoder using VHDL and an FPGA
[AD-A290048] p 2649 N95-29442

ERROR DETECTION CODES
Exploiting symmetry in the model checking of relational specifications
[AD-A290230] p 2647 N95-29223

ERRORS
Pollution error in the h-version of the finite element method and the local quality of the recovered derivatives
[AD-A290297] p 2668 N95-29065
Design of a fast-tool servo system using magnetic servo levitation
[AD-A290273] p 2663 N95-29183
Exploiting symmetry in the model checking of relational specifications
[AD-A290230] p 2647 N95-29223
Comparison study of unequal error protection methods for one-dimensional signal constellations
[AD-A290386] p 2554 N95-29231
Applied Computational Electromagnetics Society Journal, volume 10, number 1, March 1995
[AD-A292069] p 2555 N95-29308
ADC test support program
[AD-A289445] p 2643 N95-29921
Distance estimation training with night vision goggles under low illumination
[AD-A291338] p 2641 N95-29943
Mapping crust and upper mantle structure beneath southern Eurasia
[AD-A291074] p 2618 N95-29970
Software Estimation Program (SWEEP) user manual
[AD-A291137] p 2654 N95-30121

ERYTHROCYTES
The influence of space flight on erythrokinetics in man. Space Life Sciences Missions 1 and 2. Experiment E261
[NASA-CR-188368] p 2633 N95-28875
Membrane fluidity and shape of human red blood cells are altered by physiological levels of hydrostatic pressure
[AD-A290595] p 2636 N95-29557
Effect of mild hydrostatic pressure on red blood cells
[AD-A290520] p 2637 N95-29672

ESSENTIALLY NON-OSCILLATORY SCHEMES
Application of essentially nonoscillatory methods to aeroacoustic flow problems p 2686 N95-30135
Comparative study of numerical schemes of TVD3, UNO3-ACM and optimized compact scheme p 2686 N95-30137
Evaluation of high order schemes for nonlinear wave computations p 2582 N95-30149
High-order essentially non-oscillatory methods for computational aeroacoustics p 2690 N95-30159

ESTIMATES
Bubble fusion: Preliminary estimates of spherical micro-implosions in cavitating liquids
[DE95-006260] p 2569 N95-28956
Estimates of probability of a cloud-free line of sight for RAPTOR TALON
[AD-A291908] p 2510 N95-29284
Comparison of boundary-layer wind and temperature measurements with model estimations
[AD-A290471] p 2621 N95-29507
Studies of gravity-wave filtering and tidal interaction in the middle atmosphere p 2619 N95-30351

ESTIMATING
Excrescence drag levels on aircraft
[ESDU-94044] p 2487 N95-28897
Estimation of unstabilized components in vehicular motion
[AD-A290580] p 2590 N95-29552
Optimal universal coding and density estimation
[AD-A290694] p 2675 N95-29587
A model analysis of the spatial distribution and temporal trends of nitrous oxide sources and sinks p 2609 N95-29804
A contribution to the theory of robust estimation of multivariate location and shape: EID
[AD-A290435] p 2675 N95-29819
A PC program for estimating measurement uncertainty for aeronautics test instrumentation
[NASA-CR-198361] p 2503 N95-30067

ETALONS
In-line fiber etalon strain sensor
[AD-D017266] p 2699 N95-29283
The laser ranging of etalon satellites
[AD-A291019] p 2587 N95-29660

ETCHING
Epitaxial growth of high quality SiC of pulsed laser deposition, phase 1
[AD-A291410] p 2717 N95-30068

ETHANE
Thermal conductivity of liquid halogenated aliphatic hydrocarbons. Part 2: Halogenated ethanes
[ESDU-94022] p 2512 N95-29017

ETHERS
Orthobaric densities and molar volumes of liquids. Glycol ethers (cellosolves and carbitols, etc.)
[ESDU-95005] p 2530 N95-28703
Vapour pressures and critical points of liquids. Glycol ethers (alkyl cellosolves and carbitols, etc.)
[ESDU-95004] p 2534 N95-29901

ETHYL ALCOHOL
Demonstration of a stabilized alumina/ethanol colloidal dispersion technique for seeding high temperature air flows
[NASA-TM-106945] p 2582 N95-29113

ETHYL COMPOUNDS
Polyethylene-based polyurethane copolymers and block copolymers
[AD-A289996] p 2546 N95-30030

ETIOLOGY
Nearest neighbor analysis in one dimension
[DE95-009378] p 2654 N95-30183

EULER EQUATIONS OF MOTION
A Cartesian, cell-based approach for adaptively-refined solutions of the Euler and Navier-Stokes equations p 2480 N95-28739
Development and application of a 3D Cartesian grid Euler method p 2481 N95-28740
A differential approach to graphical interaction
[AD-A292165] p 2647 N95-29125
A fourth order Euler/Navier-Stokes prediction method for the aerodynamics and aeroelasticity of hovering rotor blades p 2572 N95-29242
Implicit schemes and parallel computing in unstructured grid CFD
[NASA-CR-195071] p 2671 N95-29451
Benchmark problems and solutions p 2686 N95-30134
Results of two new methods for aeroacoustics benchmark problems p 2687 N95-30140
Computation of wave propagation in a complex flow p 2582 N95-30142
Application of a new finite difference algorithm for computational aeroacoustics p 2689 N95-30155
Pressure updating methods for the steady-state fluid equations
[NASA-CR-198163] p 2674 N95-30353

EUROPE
Nanoscience and nanotechnology in Europe
[AD-A290214] p 2562 N95-29075
Correlation and gradient characteristics of ionospheric parameters in Europe
[AD-A290135] p 2612 N95-29140
Mapping crust and upper mantle structure beneath southern Eurasia
[AD-A291074] p 2618 N95-29970
EUTECTIC ALLOYS
Macrosegregation and nucleation in undercooled Pb-Sn alloys
[NASA-TM-102023-REV] p 2535 N95-28701
EUTECTICS
Macrosegregation and nucleation in undercooled Pb-Sn alloys
[NASA-TM-102023-REV] p 2535 N95-28701
EVACUATING (TRANSPORTATION)
Test and evaluation of the Impact Instrumentations, Inc. Uni-Vent model 750M ventilator
[AD-A292321] p 2640 N95-28792
Recent Issues and Advances in Aeromedical Evacuation (MEDEVAC)
[AGARD-CP-554] p 2676 N95-29604
Use of quality tools to re-engineer the Aeromedical Evacuation (AE) system p 2676 N95-29605
The Canadian experience in UN airevac Sarajevo airlift: April 1993-October 1994 p 2676 N95-29606
United Nations aeromedical evacuation operations in the former Yugoslavia p 2676 N95-29607
Civil military co-operation: A ten year experience of an affiliative aeromedical evacuation programme of the Netherlands Armed Forces and a civilian repatriation organization p 2676 N95-29608
Aeromedical evacuation by RNLAF - work according to protocol p 2676 N95-29609
Critical evaluation of aeromedical evacuation in a multinational forces scenario p 2676 N95-29610
Experience in helicopter aeroevacuation in the community of Madrid, Spain p 2677 N95-29611
Aeromedical evacuation in combined operations p 2677 N95-29612
Danish aeromedical evacuation efforts during the Gulf War p 2677 N95-29613
Experiences learned from the Spanish armed forces aeromedical evacuation system in the former Yugoslavia p 2677 N95-29614
Re-engineering support to the patient movement process p 2677 N95-29615
Medical evacuation: A training priority p 2678 N95-29617
Flying ambulances: The approach of a small air force to long distance aeromedical evacuation of critically injured patients p 2678 N95-29618
Civil Reserve Air Fleet-Aeromedical Evacuation Shipset (CRAF-AESS) p 2678 N95-29619
First medical test of the UH-60Q and equipment for use in US Army medevac helicopters p 2678 N95-29620
The large-capacity rescue-helicopter CH-53 G p 2678 N95-29621
International access to aeromedical evacuation medical equipment assessment data p 2679 N95-29622
A generic specification for Special Purpose Aeromedical Equipment p 2499 N95-29623
Aeromedical impact of the transportable pressure ventilator in wartime aeromedical evacuation p 2641 N95-29624
Requirement for onboard telemetry equipment p 2506 N95-29625
Care in the air: A system analysis of clinical outcomes in aeromedical evacuation p 2642 N95-29626
Effect of hypoxia on arterial blood gases in subjects with lung dysfunction p 2638 N95-29627
Changes in the medevac mission result in an increased role for the flight surgeon p 2680 N95-29628
Flight nurse school in the Hellenic Air Force p 2638 N95-29629
EVALUATION
Performance evaluation of bolt-cutter system on first Taurus launch
[AD-A291237] p 2504 N95-29992
Performance evaluation of ATM cell scheduling policies using stochastic petri nets
[PB95-197158] p 2559 N95-30096
EVAPORATION
Analysis of wounds by evaporative water loss in man
[AD-A290327] p 2634 N95-29086
Nanocrystalline processing and interface engineering of Si3N4-based ceramics
[AD-A291302] p 2546 N95-29939
Development and application of fluorescent diagnostics to fundamental droplet and spray problems
[AD-A290553] p 2578 N95-30039
EVOLUTION (DEVELOPMENT)
Test theory reconceived
[AD-A291836] p 2639 N95-29432
Numerical simulation of the genesis of tornado-like vortices p 2625 N95-29806
EXCITATION
Characterization of excited state oxygen-organic molecule complexes
[AD-A290548] p 2692 N95-29092
Nobeyama Radio Observatory report, no. 380: Detection of the (29)SiO v=1, J=1-0 maser from TX Camelopardalis p 2726 N95-29101
Crystal field and exchange interactions in DyT4Al8 (T = Fe and Mn)
[DE95-007131] p 2714 N95-29134
Electronic states in Cd(1-x)Zn(x)Te/CdTe strained layer coupled double quantum wells and their photoluminescence
[DE95-006806] p 2716 N95-29814
EXCITONS
Electronic states in Cd(1-x)Zn(x)Te/CdTe strained layer coupled double quantum wells and their photoluminescence
[DE95-006806] p 2716 N95-29814
EXERCISE PHYSIOLOGY
Adaptations to three weeks of aerobic/anaerobic training in west coast U.S: Navy Sea-Air-Land personnel (SEAL's)
[AD-A291500] p 2637 N95-29846
EXHAUST EMISSION
Interactions between energy efficiency and emission trading under the 1990 Clean Air Act Amendments
[DE95-008649] p 2611 N95-30212
EXHAUST GASES
Estimates of probability of a cloud-free line of sight for RAPTOR TALON
[AD-A291908] p 2510 N95-29284
Measurements of ions formed in jet engine exhaust plumes
[AD-A290940] p 2501 N95-29764
Laser doppler velocimeter system for subsonic jet mixer nozzle testing at the NASA Lewis Aeroacoustic Propulsion Lab
[NASA-TM-106984] p 2477 N95-30229
EXOBIOLOGY
Aerospace medicine and biology: A continuing bibliography with indexes (supplement 403)
[NASA-SP-7011(403)] p 2636 N95-29190
EXOTHERMIC REACTIONS
Hot explosive consolidation of W-Ti alloys
[AD-A290880] p 2537 N95-29835
EXPANDABLE STRUCTURES
An inflight refill unit for replenishing research animal drinking water
[NASA-TM-4684] p 2642 N95-28818
EXPERIMENT DESIGN
Coordination of operations for centrifuge quality control. phase 3C
[AD-A292533] p 2582 N95-28966
Some new saturated two-level designs
[AD-A292627] p 2670 N95-29296
Neural network exploration using optional experiment design
[AD-A290058] p 2663 N95-29479
Numerical simulation of the genesis of tornado-like vortices p 2625 N95-29806
EXPERIMENTATION
ADA in introductory courses
[AD-A292219] p 2648 N95-29285
EXPERT SYSTEMS
Intelligent automated surface grid generation p 2484 N95-28758
R&M design expert system
[AD-A292525] p 2645 N95-28814
Conversion of an oceanographic expert system to a C-based language
[NASA-CR-198695] p 2630 N95-29237
Applications of machine learning and rule induction
[AD-A292607] p 2664 N95-29577
Automated Propulsion Data Screening demonstration system
[NASA-CR-196636] p 2510 N95-29584
Tools for Automated Knowledge Engineering (TAKE) system evaluation methodology
[AD-A291145] p 2654 N95-30125
EXPLOITATION
Cyclic feature analysis, design and exploitation
[AD-A290639] p 2557 N95-29603
EXPLOSIONS
Two-dimensional signal processing for regional seismic event identification
[AD-A292601] p 2613 N95-29293
EXPLOSIVES
A thermochemical transport model for analysis of hot-spot formation in energetic materials
[AD-A290441] p 2532 N95-29357
Hot explosive consolidation of W-Ti alloys
[AD-A290880] p 2537 N95-29835
EXPOSURE
Thermoreactive aircraft coatings (TRAC) program
[AD-A292054] p 2542 N95-29314
Pulse waveform and pulse amplitude analysis during Lower Body Negative Pressure
[AD-A290521] p 2636 N95-29360
The one-dimensional bubble: Theory, experiment, and relevance to exposure of divers to low frequency sound, and of lung to lithotripsy
[ISVR-TR-246] p 2577 N95-29817
EXPULSION
Prediction of pressurant mass requirements for axisymmetric liquid hydrogen tanks
[NASA-TM-106973] p 2511 N95-29642
EXTERNAL COMBUSTION ENGINES
External combustion engine having an asymmetrical CAM
[AD-D017382] p 2588 N95-28785
EXTERNAL STORE SEPARATION
An experimental investigation of the time-dependent separation of tangent bodies in supersonic flow
[AD-A290720] p 2489 N95-29500
EXTERNAL SURFACE CURRENTS
Dynamic stall of a NACA 0012 airfoil in laminar flow p 2489 N95-29243
EXTERNAL TANKS
Analysis of stress concentration in the Dutton groove regions of the Super Lightweight External Tank
[NASA-TM-108490] p 2597 N95-30328
EXTINGUISHING
Fire hardening assessment (FHA) technology for composite systems
[AD-A289964] p 2523 N95-29277
The comparative extinguishment performance and thermal decomposition products of halon alternative agents
[AD-A291161] p 2551 N95-29924
Feasibility of a jet-stirred reactor for evaluating replacements for halon fire retardants
[AD-A291155] p 2551 N95-30299
EXTRACTION
Stochastic modeling and global warming trend extraction for ocean acoustic travel times
[AD-A292114] p 2608 N95-28922
Feature extraction from digital communications signals using wavelet transforms
[AD-A292655] p 2556 N95-29386
The mm-wave resonant methods for the detection of corrosion, phase 1
[AD-A291315] p 2593 N95-29941
EXTRAPOLATION
The application of adaptive mesh refinement to the numerical simulation of compressible flow
[AD-A289595] p 2577 N95-30027
EXTRATERRESTRIAL RADIATION
Effects of space exposure on metals flown on the Long Duration Exposure Facility
[NASA-CR-4662] p 2512 N95-30225
EXTRUDING
Computational methods for the simulation of non-Newtonian flows
[AD-A290355] p 2570 N95-29069
Processing studies on in situ composites based on blends of thermotropic Liquid Crystalline Polymers with thermoplastics
[AD-A290526] p 2544 N95-29494
Processing and properties of extruded tungsten-hafnium and tungsten-steel composites
[DE95-007371] p 2528 N95-30037
EYE (ANATOMY)
Refractive changes during prolonged exposure to altitude following refractive surgery
[AD-A290263] p 2635 N95-29173
Reference frames in vision
[AD-A290117] p 2639 N95-29422

F

F REGION
Studies of thermospheric neutral winds utilizing ground-based optical and radar measurements p 2613 N95-29214
The effects of magnetic storm phases on F-layer irregularities from auroral to equatorial latitudes
[AD-A290674] p 2614 N95-29585
Thermal N(+) in the inner magnetosphere p 2614 N95-29590
Chemical release experiments to induce F region ionospheric plasma irregularities at the magnetic equator p 2708 N95-29783
F 2 REGION
Correlation and gradient characteristics of ionospheric parameters in europe
[AD-A292295] p 2612 N95-28871

Correlation and gradient characteristics of ionospheric parameters in Europe
[AD-A290135] p 2612 N95-29140

F-15 AIRCRAFT
Measurements of ions formed in jet engine exhaust plumes
[AD-A290940] p 2501 N95-29764

F-16 AIRCRAFT
Application of optimization technique to control system design for departure prevention and aircraft model estimation through dynamic inversion
p 2501 N95-29156

F-18 AIRCRAFT
Evaluation of proposed agility metrics using X-31 vs. F/A-18 flight data
[AD-A292573] p 2496 N95-28977
Estimation of aerodynamic load distributions on the F/A-18 aircraft using a CFD panel code
[DSTO-TR-0147] p 2498 N95-29445

FABRICATION
In situ processing methods for composite fuselage sandwich structures p 2513 N95-28826
Design, analysis, and fabrication of a pressure box test fixture for tension damage tolerance testing of curved fuselage panels p 2516 N95-28839
Drift mobility measurements in thin film boron carbide
[AD-A292510] p 2712 N95-28869
Low cost writable RFID tag with MRAM memory
[AD-A292553] p 2642 N95-28974
Cost model relationships between textile manufacturing processes and design details for transport fuselage elements p 2521 N95-29043
HTS Josephson technology on silicon with application to high speed digital microelectronics
[AD-A290206] p 2562 N95-29061
High-toughness glass-ceramics
[AD-A290562] p 2541 N95-29071
Processing, fabrication, and demonstration of HTS integrated microwave circuits
[AD-A292480] p 2562 N95-29073
Nanoscience and nanotechnology in Europe
[AD-A290214] p 2562 N95-29075
Processing, fabrication, and demonstration of HTS integrated microwave circuits
[AD-A290220] p 2562 N95-29078
In-line fiber etalon strain sensor
[AD-D017266] p 2699 N95-29283
Solid freeform fabrication symposium
[AD-A290949] p 2527 N95-29732
Diffractive optics: Design, fabrication, and applications
[AD-A290942] p 2702 N95-29867
Ion doped quantum well lasers
[AD-A290937] p 2587 N95-29912
High performance nickel electrodes for space power applications p 2511 N95-30257
A novel unitized regenerative proton exchange membrane fuel cell p 2605 N95-30263
Fabrication of advanced electrochemical energy materials using sol-gel processing techniques
p 2607 N95-30269
Development of electrochemical super capacitors for EMA applications p 2568 N95-30270
Solid Oxide Fuel Cell commercialization in the United States
[DE95-008210] p 2607 N95-30278

FABRY-PEROT INTERFEROMETERS
Development of a multiplex Fabry-Perot interferometer and measurement of atmospheric HF and HCl
p 2608 N95-29213
Studies of thermospheric neutral winds utilizing ground-based optical and radar measurements
p 2613 N95-29214

FACTORIALS
Bootstrap and partitioning methods
[AD-A290662] p 2671 N95-29578

FACTORIZATION
Factorization and input-output decoupling by static output feedback for nonlinear control systems
[PB95-206975] p 2667 N95-30171

FAILURE
The measurement of adhesion at film-substrate interfaces using a constant depth scratch test
[AD-A289940] p 2542 N95-29269
A study of power diode failure mechanisms in the US Army research laboratory 30-mm solid propellant electrothermal-chemical (SPETC) gun facility
[AD-A291300] p 2565 N95-29938
Checkpointing and the modeling of program execution time
[PB95-197182] p 2653 N95-30099
Visit to the Laboratory For Evaluation and Failure Prevention of Materials, Toyohashi University of Technology, 17 Oct 94
[AD-A292340] p 2597 N95-30293

FAILURE ANALYSIS
Effect of open hole on tensile failure properties of 2D triaxial braided textile composites and tape equivalents
[NASA-CR-4676] p 2513 N95-28817
Tension fracture of laminates for transport fuselage. Part 2: Large notches p 2515 N95-28837
Technology integration box beam failure study
p 2517 N95-28847
Through-the-thickness stresses and failure in the corner radius of a laminated composite section
[ESDU-94019] p 2518 N95-28899
Selection of materials, manufacturing methods and lubricants for cam mechanisms
[ESDU-94017] p 2589 N95-28905
Recirculating cavity casing treatment failure
[AD-A289330] p 2500 N95-28908
An engineering model of woven composites based on micromechanics p 2521 N95-29042
Test results from large wing and fuselage panels
p 2522 N95-29051
Effect of nose shape and mass of the impactor on impact damage of laminated composites
[AD-A290351] p 2594 N95-29067
The development of an interpretive methodology for the application of real-time acousto-ultrasonic NDE technique for monitoring damage in ceramic composites under dynamic loads p 2592 N95-29104
Damage tolerance in filament-wound graphite/epoxy pressure vessels
[NASA-CR-198804] p 2590 N95-29369
A three dimensional finite element scheme for fiber microbuckling in thick multidirectional laminated composites p 2525 N95-29512
Pioneer Venus 12.5 km Anomaly Workshop Report, volume 1
[NASA-CP-3303] p 2737 N95-30058
Bending properties of nickel electrodes for nickel-hydrogen batteries p 2567 N95-30259

FAILURE MODES
Investigation of tension-compression fatigue behavior of a unidirectional metal matrix composite at elevated temperature
[AD-A289394] p 2527 N95-29758

FALSE ALARMS
An algorithm fusion approach to IRST signal processing (III): Nongaussian-corrected filter fusion
[AD-A291565] p 2552 N95-28936

FAN BLADES
UHB engine fan broadband noise reduction study
[NASA-CR-198357] p 2684 N95-29641

FAR INFRARED RADIATION
15th NSO/Sac Peak Solar Workshop
[AD-A292297] p 2739 N95-30074

FAR ULTRAVIOLET RADIATION
Far-ultraviolet high-resolution emission line spectroscopy of the Cygnus Loop supernova remnant
p 2729 N95-29710

FARM CROPS
Maize yield estimation through the simulation of radiation penetration into the canopy p 2599 N95-29703

FAST FOURIER TRANSFORMATIONS
FFT space processing for the ACF of SPREE particle flux measurements
[AD-A290166] p 2507 N95-29026

FATIGUE (BIOLOGY)
Shift work, age, and performance: Investigation of the 2-2-1 shift schedule used in Air Traffic Control facilities I. The sleep/wake cycle
[DOT/FAA/AM-95/19] p 2638 N95-29261

FATIGUE (MATERIALS)
Stress concentration, stress intensity, and fatigue crack growth along evacuators of pressurized, autofrettaged tubes
[AD-A291920] p 2593 N95-28789
Shear reinforcement in deep slabs
[AD-A289528] p 2594 N95-28909
Experimental investigations of wave and fracture phenomena in impacted ceramics and glasses
[AD-A292142] p 2542 N95-29195
Fiber fracture in continuous-fiber reinforced composite materials during cyclic loading p 2525 N95-29513
Fatigue case study and reliability analyses for wind turbines
[DE95-004770] p 2603 N95-30213
Analysis of stress concentration in the Dutton groove regions of the Super Lightweight External Tank
[NASA-TM-108490] p 2597 N95-30328
Composite processing development to improve interlaminar strength using ply interface particles
[NASA-TM-108495] p 2529 N95-30334

FATIGUE LIFE
Helicopter life substantiation: Review of some USA and UK initiatives
[AD-A290045] p 2495 N95-28851
Selection of materials, manufacturing methods and lubricants for cam mechanisms
[ESDU-94017] p 2589 N95-28905
Ceramic material life prediction: A program to translate ANSYS results to CARES/LIFE reliability analysis
[NASA-CR-198795] p 2543 N95-29367
Investigation of tension-compression fatigue behavior of a unidirectional metal matrix composite at elevated temperature
[AD-A289394] p 2527 N95-29758
Fatigue life analysis and tests for thick-walled cylinders including effects of overstrain and axial grooves
[AD-A290931] p 2596 N95-30119
Elevated temperature static fatigue of a Nicalon fiber-reinforced SiC composite
[DE95-008780] p 2528 N95-30175
Fatigue case study and reliability analyses for wind turbines
[DE95-004770] p 2603 N95-30213

FATIGUE TESTS
Analysis of static contact in laminated composite plates using damage mechanics
[NASA-CR-198656] p 2513 N95-28809
Bell Helicopter Advanced Rotocraft Transmission (ART) program
[NASA-CR-195479] p 2590 N95-29538
Investigation of tension-compression fatigue behavior of a unidirectional metal matrix composite at elevated temperature
[AD-A289394] p 2527 N95-29758
Fatigue life analysis and tests for thick-walled cylinders including effects of overstrain and axial grooves
[AD-A290931] p 2596 N95-30119
Elevated temperature static fatigue of a Nicalon fiber-reinforced SiC composite
[DE95-008780] p 2528 N95-30175
Health monitoring of operational structures: Initial results
[DE95-008551] p 2597 N95-30210
Fatigue case study and reliability analyses for wind turbines
[DE95-004770] p 2603 N95-30213

FAULT DETECTION
Automated Propulsion Data Screening demonstration system
[NASA-CR-196636] p 2510 N95-29584
Robust fault detection filter design
p 2592 N95-29786
Health monitoring of operational structures: Initial results
[DE95-008551] p 2597 N95-30210

FAULT TOLERANCE
Proceedings of the Complex Systems Engineering Synthesis and Assessment Technology Workshop (CSESAW 1994)
[AD-A292433] p 2646 N95-28995
High-level fault tolerance in distributed programs
[AD-A290430] p 2724 N95-29818
Speedlog: The key architectural element to provide efficient log management
[PB95-198453] p 2643 N95-30108
ALLIANCE: An architecture for fault tolerant multi-robot cooperation
[DE95-008658] p 2666 N95-30112

FEASIBILITY
Rome laboratory software engineering cooperative virtual machine
[AD-A292396] p 2658 N95-28965

FEASIBILITY ANALYSIS
Sea ice motions in the Central Arctic pack ice as inferred from AVHRR imagery
[NASA-CR-198835] p 2601 N95-30247

FEEDBACK
A compact universal power supply for laser diodes
[AD-A289950] p 2585 N95-29274
The (HMI9293) acquisition of a 200 MHz nuclear magnetic resonance spectrometer
[AD-A291913] p 2583 N95-29361
Dynamical instabilities, chaos and spatial complexity in fundamental nonlinear optical interactions
[AD-A291223] p 2588 N95-29980
Process algebra with feedback
[PB95-206819] p 2673 N95-30106

FEEDBACK AMPLIFIERS
Laser optics protective device
[AD-D017384] p 2585 N95-29217

FEEDBACK CONTROL
Application of optimization technique to control system design for departure prevention and aircraft model estimation through dynamic inversion
p 2501 N95-29156
Power measurement and current feedback in a resonant DC link inverter
[AD-A292518] p 2563 N95-29164
Closed loop control of guided missiles using neural networks p 2663 N95-29241

Robust control of nonlinear flexible multibody systems using quaternion feedback and dissipative compensation
[NASA-TM-109099] p 2507 N95-29377
Broadband control of structural vibration using simultaneous sensing and actuation with nonlinear piezoelectric elements p 2664 N95-29548
Experimental confirmation of a PDE-based approach to design of feedback controls
[NASA-CR-198167] p 2672 N95-30086
H(sub 2) almost disturbance decoupling problem with internal stability
[PB95-206942] p 2667 N95-30168
Factorization and input-output decoupling by static output feedback for nonlinear control systems
[PB95-206975] p 2667 N95-30171
H infinity control problem with zeros on the boundary of the stability domain
[PB95-197042] p 2668 N95-30288

FEMALES
An analysis of anthropometric differences among occupational groups in the US Army
[AD-A292326] p 2640 N95-28794
NASA/DOD Aerospace Knowledge Diffusion Research Project. Paper 49: Becoming an aerospace engineer: A cross-gender comparison
[NASA-TM-110731] p 2721 N95-29028

FERRITES
Application of a rapid quench thermomagnetic analyzer to austempered ductile iron
[AD-A292261] p 2535 N95-28889
Correlation of inclusion size and chemistry with weld metal composition and microstructure arc weldments of high strength steels
[AD-A292024] p 2590 N95-29184
Austenite to ferrite transformation kinetics during continuous cooling
[DE95-008582] p 2537 N95-29869

FERROELECTRICITY
Ferroelectric polarization mechanism of the odd-numbered nylons
[AD-A292276] p 2539 N95-28860
Ferroelectric and piezoelectric properties of nylon 11/Poly(Vinylidene fluoride) bilaminate films
[AD-A292274] p 2539 N95-28891
Investigation of the characteristics of ferroelectric thin films deposited by pulsed laser ablation
[AD-A292306] p 2540 N95-28963
Pulsed laser deposition of ferroelectric thin films in conjunction with superconducting oxides
[AD-A290101] p 2585 N95-29208
Analysis of the ferroelectric thin films deposited by pulsed laser deposition on oxide and fluoride substrates
[AD-A290088] p 2543 N95-29353
High T(sub c) superconductor/ferroelectric heterostructures
[AD-A291016] p 2716 N95-29658
The 2nd International Conference on Thin Film Physics and Applications
[AD-A292353] p 2546 N95-29983

FERROUS METALS
Corrosion in methylphosphonic difluoride
[AD-A289995] p 2536 N95-29137

FIBER COMPOSITES
Third NASA Advanced Composites Technology Conference, volume 1, part 2
[NASA-CP-3178-VOL-1-PT-2] p 2513 N95-28823
The effect of mixed mode precracking on the mode 1 fracture toughness of composite laminates
p 2514 N95-28827
Automated fiber placement: Evolution and current demonstrations p 2514 N95-28832
Response of automated tow placed laminates to stress concentrations p 2515 N95-28833
The combined effect of glass buffer strips and stitching on the damage tolerance of composites
p 2522 N95-29049
In-phase thermomechanical fatigue mechanisms in an unidirectional SCS-6/Ti 15-3 MMC
[NASA-CR-195482] p 2523 N95-29133
Three dimensional effects in fiber reinforced composites under compression
[AD-A292027] p 2523 N95-29185
Fire hardening assessment (FHA) technology for composite systems
[AD-A289964] p 2523 N95-29277
Fiber-matrix adhesion in single-fiber model composites
p 2524 N95-29337
Phase coupling and morphology generation in engineering polymer alloys
[AD-A291868] p 2543 N95-29436
A three dimensional finite element scheme for fiber microbuckling in thick multidirectional laminated composites p 2525 N95-29512
Fiber fracture in continuous-fiber reinforced composite materials during cyclic loading p 2525 N95-29513
Severe edge effects and simple complimentary interior solutions for thin-walled anisotropic and composite structures
[AD-A290645] p 2595 N95-29562
Materials for tomorrow's infrastructure: A ten-year plan for deploying high-performance construction materials and systems
[AD-A289782] p 2526 N95-29598
Investigation of tension-compression fatigue behavior of a unidirectional metal matrix composite at elevated temperature
[AD-A289394] p 2527 N95-29758
Ultrasonic guided waves in cylinders: Theory and experiment p 2685 N95-29826
Elevated temperature static fatigue of a Nicalon fiber-reinforced SiC composite
[DE95-008780] p 2528 N95-30175

FIBER OPTICS
An electrical and fiber-optic connector
[AD-D017404] p 2589 N95-28791
Cost effective, dual-purpose machine vision-based detectors for (1) smoke and flame detection, and (2) engine overhead/burn-through and flame detection
[AD-A292284] p 2697 N95-28870
Fibre-coupled remote optical vibrometry
[AD-A291606] p 2698 N95-28932
Linewidth-insensitive coherent analog optical links
[AD-A292422] p 2698 N95-28992
Solving linear programs using distributed parallel computing
[AD-A290221] p 2658 N95-29079
Fiber optic Raman and micro Raman measurements of bonding agents at interface during the curing process
[AD-A292042] p 2523 N95-29189
High gain, low noise and broadband Raman and Brillouin fiber-optic amplifiers, channel selectors and switches
[AD-A290585] p 2700 N95-29553
Ocean Optics XII
[AD-A286734] p 2702 N95-29910
Fiber compatible acousto-optic modulator using a gradient index lens
[AD-A291164] p 2565 N95-29925
Shock resistant optic fiber rotary slice holding device
[AD-D017327] p 2702 N95-30053
Selective multi-chemical fiber optic sensor
[AD-D017409] p 2703 N95-30076
Method of measuring liquid level with a thermal interface detection
[AD-D017341] p 2703 N95-30166

FIBER ORIENTATION
Automated fiber placement: Evolution and current demonstrations p 2514 N95-28832
Response of automated tow placed laminates to stress concentrations p 2515 N95-28833
Mechanical characterization of two thermoplastic composites fabricated by automated tow placement
p 2515 N95-28834
Three dimensional effects in fiber reinforced composites under compression
[AD-A292027] p 2523 N95-29185
Impact damage resistance and residual property assessment of (0/+/-45/90)s SCS-6/Timetal 21S
[NASA-TM-110178] p 2529 N95-30340

FIBER VOLUME FRACTION
A three dimensional finite element scheme for fiber microbuckling in thick multidirectional laminated composites p 2525 N95-29512

FIELD EFFECT TRANSISTORS
Power measurement and current feedback in a resonant DC link inverter
[AD-A292518] p 2563 N95-29164
An investigation of the channel crosstalk in optical heterodyne controlled phased array radars
[AD-A292028] p 2554 N95-29186
Research and development of a high performance GaAs microcomputer system
[AD-A292647] p 2643 N95-29381
Radiation effects on front-end electronics for noble liquid calorimetry
[DE95-007304] p 2566 N95-30025

FIELD OF VIEW
SeaWiFS technical report series. Volume 24: SeaWiFS technical report series cumulative index, volumes 1-23
[NASA-TM-104556] p 2631 N95-30236

FIELD THEORY (PHYSICS)
Molecular dynamics simulation of liquid nitromethane shocked to 143 kbar
[AD-A292107] p 2691 N95-28919
Ab initio calculation of vibrational absorption and circular dichroism spectra using density functional force fields
[AD-A291297] p 2720 N95-29936

FILAMENT WINDING
Response of automated tow placed laminates to stress concentrations p 2515 N95-28833
Damage tolerance in filament-wound graphite/epoxy pressure vessels
[NASA-CR-198804] p 2590 N95-29369

FILE MAINTENANCE (COMPUTERS)
Implementing distributed server groups for the World Wide Web
[AD-A292221] p 2658 N95-29196
Automatically combining changes to software systems
[AD-A290628] p 2650 N95-29515
Speedlog: The key architectural element to provide efficient log management
[PB95-198453] p 2643 N95-30108

FILLERS
Design and evaluation of a foam-filled hat-stiffened panel concept for aircraft primary structural applications
p 2499 N95-28841

FILM COOLING
Flow visualization of vorticity cancellation of jets in crossflow
[AD-A292414] p 2569 N95-28990
Leading edge film cooling effects on turbine blade heat transfer
[NASA-TM-106955] p 2500 N95-29115
Hydrogen film cooling with incident and swept-shock interactions in a Mach 6.4 nitrogen free stream
[NASA-TM-4603] p 2578 N95-30056

FILM THICKNESS
Lubricant film thickness between disc cams and followers
[ESDU-94008] p 2539 N95-28900
Pulsed laser deposition of ferroelectric thin films in conjunction with superconducting oxides
[AD-A290101] p 2585 N95-29208
Pulsed laser deposition of thin film material for nonlinear waveguides
[AD-A290789] p 2544 N95-29484

FILTERS
Robust fault detection filter design
p 2592 N95-29786

FILTRATION
Optical (LANDSAT/TM) and radar (ERS-1/SAR) imagery sinergism studies applied to land use discrimination
[INPE-5608-TDI/554] p 2598 N95-29433

FINITE DIFFERENCE THEORY
Wave drag coefficient for axisymmetric forecowls at zero incidence (M sub infinity less than or equal to 1.5)
[ESDU-94014] p 2568 N95-28903
Surface pressure coefficient distributions for axisymmetric forecowls at zero incidence (M sub infinity less than or equal to 1.5)
[ESDU-94015] p 2487 N95-28904
The 10th Annual Review of Progress in Applied Computational Electromagnetics, volume 1
[AD-A286796] p 2553 N95-29159
High performance electromagnetic simulation tools
[AD-A290405] p 2554 N95-29235
Numerical experiments on the flow past a circular cylinder at sub-critical Reynolds number
[AD-A289937] p 2573 N95-29268
SOSDOR: Solid-state device simulator code
[AD-A289954] p 2563 N95-29275
Finite difference analysis of a cylindrical two conductor microstrip transmission line with truncated dielectrics
[AD-A292592] p 2555 N95-29290
Grid orthogonality effects on predicted turbine midspan heat transfer and performance
[NASA-TM-106931] p 2574 N95-29371
Direct numerical simulation of compressible turbulent flows, using adaptive spectral element method
[AD-A290115] p 2575 N95-29421
Finite difference ocean acoustic model users guide
[AD-A291544] p 2631 N95-29856
The 10th Annual Review of Progress in Applied Computational Electromagnetics, volume 2
[AD-A286799] p 2558 N95-29904
The application of adaptive mesh refinement to the numerical simulation of compressible flow
[AD-A289595] p 2577 N95-30027
Comparison of the local defect correction iteration and the fast adaptive composite grid iteration
[PB95-206769] p 2672 N95-30088
Application of essentially nonoscillatory methods to aeroacoustic flow problems p 2686 N95-30135
Computational aeroacoustics using hyperbolic wave primitives p 2686 N95-30136
Comparative study of numerical schemes of TVD3, UNO3-ACM and optimized compact scheme
p 2686 N95-30137
A compact solution to computational acoustics
p 2686 N95-30138
Application of low dissipation and dispersion Runge-Kutta schemes to benchmark problems in computational aeroacoustics p 2687 N95-30139
Second-order numerical solution of time-dependent, first-order hyperbolic equations p 2674 N95-30143

The construction of high-accuracy schemes for acoustic equations p 2688 N95-30146
Application of traditional CFD methods to nonlinear computational aeroacoustics problems p 2688 N95-30148
Nonlinear wave propagation using three different finite difference schemes (category 2 application) p 2582 N95-30151
Application of a new finite difference algorithm for computational aeroacoustics p 2689 N95-30155
Computational aeroacoustics on massively parallel computers p 2661 N95-30156
Evaluation of numerical schemes for the analysis of sound generation by blade-gust interaction p 2690 N95-30163
Numerical simulation and analysis of the hypersonic turbulent flow past a blunt-fin/ramp configuration [DLR-FB-94-19] p 2492 N95-30349

FINITE ELEMENT METHOD
Establishing the relationship between manufacturing and component performance in stretch formed thermoplastic composites p 2514 N95-28829
Dimensional stability of curved panels with cocured stiffeners and cobonded frames p 2515 N95-28836
A study of structurally efficient graphite-thermoplastic trapezoidal-corrugation sandwich and semi-sandwich panels p 2516 N95-28842
A weight-efficient design strategy for cutouts in composite transport structures p 2516 N95-28843
Buckling analysis of curved composite sandwich panels subjected to inplane loadings p 2517 N95-28845
ISPAN (Interactive Stiffened Panel Analysis): A tool for quick concept evaluation and design trade studies p 2517 N95-28846
A global/local analysis method for treating details in structural design p 2517 N95-28848
An HP-Adaptive method in space and time for parabolic systems [AD-A292262] p 2668 N95-28890
Sorption and diffusion of moisture in multilayer composite AEM/S sandwich materials [AD-A289807] p 2518 N95-28951
Analytical modeling and sensor monitoring for optimal processing of advanced textile structural composites by resin transfer molding p 2521 N95-29045
Test results from large wing and fuselage panels p 2522 N95-29051
A new methodology for the numerical simulation of strain softening in inelastic solids [AD-A290295] p 2594 N95-29063
Dispersion analysis and error estimation of Galerkin finite element methods for the numerical computation of waves [AD-A290296] p 2668 N95-29064
Pollution error in the h-version of the finite element method and the local quality of the recovered derivatives [AD-A290297] p 2668 N95-29065
A generalized finite element method for solving the Helmholtz equation in two dimensions with minimal pollution [AD-A290280] p 2669 N95-29080
Finite element solution to the Helmholtz equation with high wave number. Part 2. The h-p version of the FEM [AD-A290289] p 2669 N95-29084
Finite element vorticity-based methods for the solution of the incompressible and compressible Navier-Stokes equations p 2570 N95-29119
The 10th Annual Review of Progress in Applied Computational Electromagnetics, volume 1 [AD-A286796] p 2553 N95-29159
Design of a fast-tool servo system using magnetic servo levitation [AD-A290273] p 2663 N95-29183
Three dimensional effects in fiber reinforced composites under compression [AD-A292027] p 2523 N95-29185
Investigation of an alternative finite element procedure: A one-step, steady-state analysis [AD-A290030] p 2670 N95-29311
Fiber-matrix adhesion in single-fiber model composites p 2524 N95-29337
Ceramic material life prediction: A program to translate ANSYS results to CARES/LIFE reliability analysis [NASA-CR-198795] p 2543 N95-29367
Acoustic scattering from ellipses by the modal element method [NASA-TM-106935] p 2683 N95-29401
Load balancing for the parallel adaptive solution of partial differential equations [AD-A290450] p 2671 N95-29488
A three dimensional finite element scheme for fiber microbuckling in thick multidirectional laminated composites p 2525 N95-29512
Finite element technology for penetration problems [AD-A290644] p 2671 N95-29516
Theoretical, experimental and computational studies in plasticity [AD-A290428] p 2595 N95-29535
High-level parallel programming tools for finite element analysis [AD-A290566] p 2659 N95-29566
Use of finite element analysis for transient moisture diffusion studies in multilayer composite AEM/S system sandwich materials [AD-A291092] p 2527 N95-29638
Toughening mechanisms in mixed-mode interfacial fracture p 2545 N95-29772
The study of non-Newtonian contraction flows with a parallel finite element method p 2576 N95-29778
ANSYS duplicate finite-element checker routine [NASA-TM-108492] p 2672 N95-29824
Computational results for parallel unstructured mesh computations [DE95-005856] p 2659 N95-29985
Tropical storm database: East and Gulf of Mexico coasts of the United States [AD-A291406] p 2627 N95-30066
Numerical modeling of synoptic scale ocean dynamics [AD-A291411] p 2631 N95-30069
A finite element analysis of room temperature silicon crystals for the Advanced Photon Source bending-magnet and insertion-device beams [DE95-005822] p 2718 N95-30184
Numerical implementation of a state variable model for friction [DE95-007844] p 2591 N95-30273
Numerical simulation of mechanisms and manipulator robots with flexible links and flexible joints [PB95-196903] p 2591 N95-30285
Parallel adaptive finite element: Software for semiconductor device simulation [AD-A291149] p 2661 N95-30295
Formulation of an improved smeared stiffener theory for buckling analysis of grid-stiffened composite panels [NASA-TM-110162] p 2529 N95-30341

FINITE VOLUME METHOD
Leading edge film cooling effects on turbine blade heat transfer [NASA-TM-106955] p 2500 N95-29115
Solution of the Navier-Stokes equations on locally refined Cartesian meshes using state-vector splitting p 2571 N95-29197
Grid orthogonality effects on predicted turbine midspan heat transfer and performance [NASA-TM-106931] p 2574 N95-29371
Implicit schemes and parallel computing in unstructured grid CFD [NASA-CR-195071] p 2671 N95-29451
A comparative study of upwind and MacCormack schemes for CAA benchmark problems p 2688 N95-30147
Category 5 problem solution using an unstructured finite volume algorithm p 2657 N95-30157

FINS
Estimation of aerodynamic load distributions on the F/A-18 aircraft using a CFD panel code [DSTO-TR-0147] p 2498 N95-29445

FIRE CONTROL
Fire hardening assessment (FHA) technology for composite systems [AD-A289964] p 2523 N95-29277

FIRE DAMAGE
Fire hardening assessment (FHA) technology for composite systems [AD-A289964] p 2523 N95-29277

FIRE FIGHTING
The comparative extinguishment performance and thermal decomposition products of halon alternative agents [AD-A291161] p 2551 N95-29924
Feasibility of a jet-stirred reactor for evaluating replacements for halon fire retardants [AD-A291155] p 2551 N95-30299

FIREPROOFING
The effect of wear on fire-blocking layer material effectiveness [AD-A291520] p 2493 N95-29855

FIRES
Cost effective, dual-purpose machine vision-based detectors for (1) smoke and flame detection, and (2) engine overhead/burn-through and flame detection [AD-A292284] p 2697 N95-28870
The potential for pulmonary heat injury resulting from the activation of a cabin water spray system to fight aircraft cabin fires [DOT/FAA/AM-95/17] p 2636 N95-29224
Fire hardening assessment (FHA) technology for composite systems [AD-A289964] p 2523 N95-29277

FISCHER-TROPSCH PROCESS
Development of precipitated iron Fischer-Tropsch catalysts [DE95-009334] p 2533 N95-29870

FITTING
Design and analysis of the launch vehicle adapter fitting for the petite amateur navy satellite (PANSAT) [AD-A289693] p 2504 N95-28680

FIXTURES
Performance evaluation of bolt-cutter system on first Taurus launch [AD-A291237] p 2504 N95-29992
Prototype stop bar system evaluation at Seattle-Tacoma International Airport [AD-A290136] p 2495 N95-30031

FLAME PROPAGATION
Fire hardening assessment (FHA) technology for composite systems [AD-A289964] p 2523 N95-29277

FLAME RETARDANTS
Feasibility of a jet-stirred reactor for evaluating replacements for halon fire retardants [AD-A291155] p 2551 N95-30299

FLAMES
Cost effective, dual-purpose machine vision-based detectors for (1) smoke and flame detection, and (2) engine overhead/burn-through and flame detection [AD-A292284] p 2697 N95-28870
Investigation of laminar methane flames with emphasis on kinetics elucidation and NOx reduction [PB95-200531] p 2535 N95-30111
Development of flame resistant, high efficiency thermal insulation [AD-A291136] p 2547 N95-30120
Apparatus and method for achieving growth-etch deposition of diamond using a chopped oxygen-acetylene flame [AD-D017322] p 2718 N95-30164

FLAMMABILITY
Fire hardening assessment (FHA) technology for composite systems [AD-A289964] p 2523 N95-29277
The effect of wear on fire-blocking layer material effectiveness [AD-A291520] p 2493 N95-29855

FLAPS (CONTROL SURFACES)
High-and low-frequency dynamics of isolated blades and rotors with dynamic stall and wake [AD-A290358] p 2497 N95-29322

FLAT PANEL DISPLAYS
Fourier Synthesis Lithographic Machine for large panel display fabrication [AD-A291921] p 2698 N95-28914
Low temperature materials growth and processing development for flat panel display technology applications [AD-A292177] p 2715 N95-29267

FLAT PLATES
A procedure for automating CFD simulations of an inlet-bleed problem p 2485 N95-28768
Flat rectangular isotropic plates under uniformly distributed normal pressure. Elastic deflections, stresses, and strains, moments and forces, for various forms of edge restraint [ESDU-94033] p 2593 N95-28801
The effects of the thermal boundary condition and turbulence on heat transfer from a cylinder, flat plate, and turbine blade using the transient shroud and heated-coating techniques [AD-A292646] p 2574 N95-29380
Analytical and experimental studies of the energy absorption behavior of composite structures p 2524 N95-29411
Investigation of Burnett equations for two-dimensional hypersonic flow [AD-A290233] p 2575 N95-29469
Turbulent airflow noise production and propagation patterns of a subsonic jet impinging on a flat plate p 2684 N95-29502
Effects of elevated free-stream turbulence and streamwise acceleration on flow and thermal structures in transitional boundary layers p 2576 N95-29729
The pressure field of a gust interacting with a flat plate p 2582 N95-30161
Aeroacoustic computation of a gust-plate interaction via MacCormack schemes p 2690 N95-30162
Evaluation of numerical schemes for the analysis of sound generation by blade-gust interaction p 2690 N95-30163
Numerical solution of the equations governing non-Newtonian flow at moderate Reynolds numbers p 2579 N95-30233

FLAT SURFACES
Prediction of hydrogen entry and permeation in metals and alloys [AD-A292047] p 2536 N95-29298

FLEXIBLE BODIES
Robust control of nonlinear flexible multibody systems using quaternion feedback and dissipative compensation
[NASA-TM-109099] p 2507 N95-29377
Mathematical modeling and numerical simulation of the dynamics of flexible structures undergoing large overall motions
[AD-A291139] p 2597 N95-30123
FLEXIBLE SPACECRAFT
Substructure-based control of flexible structures p 2508 N95-29408
Spacecraft attitude control system performance using pulse-width pulse-frequency modulated thrusters
[AD-A291803] p 2508 N95-29410
FLEXING
Cable load transducer
[AD-A289548] p 2595 N95-29192
FLICKER
Transformational design of a direction detector for the progressive scan conversion processor
[PB95-198487] p 2643 N95-30109
FLIGHT CHARACTERISTICS
Manual for a workstation-based generic flight simulation program (LaRCsim), version 1.4
[NASA-TM-110164] p 2502 N95-30327
FLIGHT CONDITIONS
Computational Fluid Dynamics (CFD) analysis of a C-135 aircraft with a side-mounted splitter plate (with comparison to wind tunnel data)
[AD-A292029] p 2571 N95-29187
FLIGHT CONTROL
An investigation into the use of satellite-based positioning systems for flight reference/autoland operations p 2494 N95-29542
The topside ionospheric plasma monitor (SSIES, SSIES-2 and SSIES-3) on the spacecraft of the Defense Meteorological Satellite Program (DMSP), user's guide. Volume 2: Programmer's guide for software at AFSFC
[AD-A290913] p 2618 N95-30082
Low-speed wind-tunnel investigation of the stability and control characteristics of a series of flying wings with sweep angles of 50 deg
[NASA-TM-4640] p 2498 N95-30226
Design, analysis and control of large transports so that control of engine thrust can be used as a back-up of the primary flight controls
[NASA-CR-198958] p 2501 N95-30254
Developing a workstation-based, real-time simulation for rapid handling qualities evaluations during design
[NASA-CR-198831] p 2499 N95-30335
FLIGHT CREWS
Military flying and aeromedical evaluation of cardiac arrhythmias
[AD-A291595] p 2634 N95-28940
Current issues in the measurement of military aircrew performance: A consideration of the relationship between available metrics and operational concerns
[AD-A292539] p 2640 N95-28970
A comparison of the aeromedical administration requirements for US Air Forces and major allies
[AD-A290137] p 2635 N95-29141
A human factors evaluation of the operational demonstration flight inspection aircraft
[DOT/FAA/AM-95/18] p 2641 N95-29365
Changes in the medevac mission result in an increased role for the flight surgeon p 2680 N95-29628
Distance estimation training with night vision goggles under low illumination
[AD-A291338] p 2641 N95-29943
FLIGHT HAZARDS
Orbital debris: A technical assessment
[NASA-CR-198639] p 2507 N95-28852
Experiments on microbursts p 2620 N95-29110
The potential for pulmonary heat injury resulting from the activation of a cabin water spray system to fight aircraft cabin fires
[DOT/FAA/AM-95/17] p 2636 N95-29224
FLIGHT NURSES
Flight nurse school in the Hellenic Air Force p 2638 N95-29629
FLIGHT OPERATIONS
STS-71 Shuttle/Mir flight: Day 9
[NASA-TM-110752] p 2506 N95-29962
STS-71 Shuttle/Mir flight: Day 10
[NASA-TM-110753] p 2506 N95-29963
FLIGHT PATHS
Analytical investigations in aircraft and spacecraft trajectory optimization and optimal guidance
[NASA-CR-4672] p 2504 N95-29339
FLIGHT SIMULATION
Transport delays associated with NASA Langley Flight Simulation Facility
[NASA-TM-110150] p 2659 N95-29454
Manual for a workstation-based generic flight simulation program (LaRCsim), version 1.4
[NASA-TM-110164] p 2502 N95-30327
Developing a workstation-based, real-time simulation for rapid handling qualities evaluations during design
[NASA-CR-198831] p 2499 N95-30335
FLIGHT SIMULATORS
Applications of digital video and synthetic environments to unmanned aerial vehicles
[AD-A291875] p 2497 N95-29437
Transport delays associated with NASA Langley Flight Simulation Facility
[NASA-TM-110150] p 2659 N95-29454
UHB engine fan broadband noise reduction study
[NASA-CR-198357] p 2684 N95-29641
FLIGHT STABILITY TESTS
Low-speed wind-tunnel investigation of the stability and control characteristics of a series of flying wings with sweep angles of 50 deg
[NASA-TM-4640] p 2498 N95-30226
FLIGHT SURGEONS
Changes in the medevac mission result in an increased role for the flight surgeon p 2680 N95-29628
FLIGHT TESTS
Investigation of wing upper surface flow-field disturbance due to NASA DC-8-72 in-flight inboard thrust-reverser deployment
[NASA-TM-110351] p 2477 N95-28816
A nonintrusive method of quantifying flow visualization data in vortex flow fields
[AD-A289802] p 2568 N95-28948
Evaluation of proposed agility metrics using X-31 vs. F/A-18 flight data
[AD-A292573] p 2496 N95-28977
Computational Fluid Dynamics (CFD) analysis of a C-135 aircraft with a side-mounted splitter plate (with comparison to wind tunnel data)
[AD-A292029] p 2571 N95-29187
AGARD flight test techniques series. Volume 13: Reliability and maintainability
[AGARD-AG-300-VOL-13] p 2498 N95-29503
FLIGHT TIME
An analysis of the impact of ASPA on organizational and depot level maintenance
[AD-A292670] p 2477 N95-29414
FLIR DETECTORS
Nonlinear calibration of an infrared radiometer
[AD-A292436] p 2698 N95-28996
FLOATING
Analyzing the stability of floating ice floes
[AD-A292149] p 2629 N95-29160
FLOATING POINT ARITHMETIC
The (in)complete compendium of computational curiosities: Givens' rotations
[AD-A292050] p 2648 N95-29304
Defining the IEEE-854 floating-point standard in PVS
[NASA-TM-110167] p 2659 N95-29823
FLOATS
Alternative methods for flotation seat cushion use
[DOT/FAA/AM-95/20] p 2493 N95-29448
FLOQUET THEOREM
High-and low-frequency dynamics of isolated blades and rotors with dynamic stall and wake
[AD-A290358] p 2497 N95-29322
FLOW CHARACTERISTICS
The effects of three-dimensional imposed disturbances on bluff body near wake flows: Effects of taper and splitter plates on the near wake characteristics of a circular cylinder in uniform and shear flow
[AD-A292113] p 2487 N95-28921
Air/fuel ratio visualization in a diesel spray p 2590 N95-29807
FLOW DISTRIBUTION
Surface modeling and grid generation for aeropropulsion CFD p 2479 N95-28732
Marshall Space Flight Center surface modeling and grid generation applications p 2480 N95-28733
Optimal domain decomposition strategies p 2484 N95-28759
Investigation of wing upper surface flow-field disturbance due to NASA DC-8-72 in-flight inboard thrust-reverser deployment
[NASA-TM-110351] p 2477 N95-28816
A nonintrusive method of quantifying flow visualization data in vortex flow fields
[AD-A289802] p 2568 N95-28948
Computational fluid dynamics (CFD) simulation of test chamber and smoke-generating device
[AD-A290199] p 2569 N95-29058
Development of a rotary wing Navier-Stokes CFD code based on TLNS3D code
[AD-A290421] p 2574 N95-29387
Investigation of Burnett equations for two-dimensional hypersonic flow
[AD-A290233] p 2575 N95-29469
Effects of elevated free-stream turbulence and streamwise acceleration on flow and thermal structures in transitional boundary layers p 2576 N95-29729
Computation of the integrated aerodynamic and propulsive flowfields of a generic hypersonic space plane p 2490 N95-29788
Experimental and analytical study of heat transfer and turbulent flow field in tangentially injected swirl flow p 2576 N95-29811
Reliability enhancement of Navier-Stokes codes through convergence acceleration
[NASA-CR-196635] p 2578 N95-30034
Comparison of spatial numerical operators for duct-nozzle acoustics p 2690 N95-30158
Numerical simulations of the flow in the HYPULSE expansion tube
[NASA-TM-110357] p 2503 N95-30228
FLOW EQUATIONS
Investigation of the flow turning loss in unstable solid propellant rocket motors p 2510 N95-29331
Application of the space-time conservation element and solution element method to two-dimensional advection-diffusion problems
[NASA-TM-106946] p 2574 N95-29372
Model development for active control of stall phenomena in aircraft gas turbine engines p 2500 N95-29679
Numerical solution of the equations governing non-Newtonian flow at moderate Reynolds numbers p 2579 N95-30233
Ensemble phase averaged equations for multiphase flows p 2579 N95-30284
FLOW GEOMETRY
Ballistic penetration phenomenology of high symmetry single crystals
[AD-A292476] p 2713 N95-29013
FLOW GRAPHS
Static analysis of functional programs
[PB95-197141] p 2653 N95-30095
FLOW MEASUREMENT
Experiments on microbursts p 2620 N95-29110
Laser doppler velocimeter system for subsonic jet mixer nozzle testing at the NASA Lewis Aeroacoustic Propulsion Lab
[NASA-TM-106984] p 2477 N95-30229
FLOW STABILITY
Cross flow instability of supersonic flow over a 4:1 elliptic cone
[AD-A291128] p 2577 N95-29913
The onset of electrohydrodynamic instability in isoelectric focusing
[NASA-CR-198805] p 2565 N95-29968
Numerical simulation of stability and stability control of high speed compressible rotating couette flow
[NASA-CR-198832] p 2579 N95-30250
Growth and development of roughness-induced stationary crossflow vortices p 2492 N95-30294
FLOW VELOCITY
Demonstration of a stabilized alumina/ethanol colloidal dispersion technique for seeding high temperature air flows
[NASA-TM-106945] p 2582 N95-29113
Navier-Stokes solution of wing wake structure and its perturbation p 2488 N95-29121
Investigation of the flow turning loss in unstable solid propellant rocket motors p 2510 N95-29331
The decay of longitudinal vortices shed from airfoil vortex generators
[NASA-CR-198356] p 2489 N95-29402
Unsteady pressure and inflow velocity on a pitching rotor blade in hover p 2490 N95-29771
Experimental study on scaling law of outgassing rate with a pumping parameter
[AD-B191999L] p 2709 N95-29801
Experimental and analytical study of heat transfer and turbulent flow field in tangentially injected swirl flow p 2576 N95-29811
Coso monitoring program
[AD-A290604] p 2627 N95-30048
Sea ice motions in the Central Arctic pack ice as inferred from AVHRR imagery
[NASA-CR-198835] p 2601 N95-30247
FLOW VISUALIZATION
Cooperative solutions coupling a geometry engine and adaptive solver codes p 2484 N95-28761
Automation of three-dimensional structured mesh generation for turbomachinery blade passages p 2484 N95-28762
Advanced methodology for simulation of complex flows using structured grid systems p 2485 N95-28766
Demonstration of an automated CFD system for three-dimensional flow simulations p 2485 N95-28767
Investigation of wing upper surface flow-field disturbance due to NASA DC-8-72 in-flight inboard thrust-reverser deployment
[NASA-TM-110351] p 2477 N95-28816
A nonintrusive method of quantifying flow visualization data in vortex flow fields
[AD-A289802] p 2568 N95-28948

Flow visualization of vorticity cancellation of jets in crossflow
[AD-A292414] p 2569 N95-28990
Experiments on microbursts p 2620 N95-29110
Vortex element analysis of selected time-dependent flows
[AD-A289944] p 2573 N95-29271
Research instrumentation for polytechnic university's supersonic wind tunnel facility
[AD-A290232] p 2502 N95-29468
Air/fuel ratio visualization in a diesel spray p 2590 N95-29807

FLOWMETERS
Impact of uncertainty on modeling and testing
[NASA-CR-196637] p 2652 N95-30013

FLUID DYNAMICS
Analyzing the stability of floating ice floes
[AD-A292149] p 2629 N95-29160
Three problems in fluid dynamics
[AD-A290481] p 2573 N95-29324
New predictive methods in chaotic fluid dynamics with application to turbulent heat transfer
[AD-A290691] p 2576 N95-29761

FLUID FLOW
The acoustic characteristics of turbomachinery cavities
[NASA-CR-4671] p 2478 N95-28720
A Cartesian, cell-based approach for adaptively-refined solutions of the Euler and Navier-Stokes equations p 2480 N95-28739
Prospects and expectations for unstructured methods p 2481 N95-28742
An unstructured-grid software system for solving complex aerodynamic problems p 2481 N95-28743
Epoxy pipelining composition and method of manufacture
[AD-D017380] p 2539 N95-28784
An inflight refill unit for replenishing research animal drinking water
[NASA-TM-4684] p 2642 N95-28818
Multifluid nonequilibrium simulation of arcjet thrusters p 2510 N95-29245
Channels and valleys on Venus p 2736 N95-29593
Prediction of pressurant mass requirements for axisymmetric liquid hydrogen tanks
[NASA-TM-106973] p 2511 N95-29642
The study of non-Newtonian contraction flows with a parallel finite element method p 2576 N95-29778
Air/fuel ratio visualization in a diesel spray p 2590 N95-29807
Experimental and analytical study of heat transfer and turbulent flow field in tangentially injected swirl flow p 2576 N95-29811
Application of essentially nonoscillatory methods to aeroacoustic flow problems p 2686 N95-30135

FLUID INJECTION
Experimental and analytical study of heat transfer and turbulent flow field in tangentially injected swirl flow p 2576 N95-29811

FLUID PRESSURE
Analyzing the stability of floating ice floes
[AD-A292149] p 2629 N95-29160

FLUID-SOLID INTERACTIONS
State-of-the-art review of computational fluid dynamics modeling for fluid-solids systems
[DE95-005866] p 2577 N95-29988

FLUORESCENCE
The fluorescent detection of hydrazine, monomethylhydrazine, and 1,1-dimethylhydrazine by derivatization with aromatic dicarboxaldehydes
[NAVY-CASE-75451] p 2512 N95-29052
Membrane fluidity and shape of human red blood cells are altered by physiological levels of hydrostatic pressure
[AD-A290595] p 2636 N95-29557
Carbon isotope abundance ratios in comets p 2732 N95-29592
Development and application of fluorescent diagnostics to fundamental droplet and spray problems
[AD-A290553] p 2578 N95-30039

FLUORIDES
Molten fluoride fuel salt chemistry
[DE95-007025] p 2695 N95-28957

FLUORINATION
Transition metal complexes with perfluorinated ligands
[AD-A290250] p 2536 N95-29427

FLUORINE
Computational investigation of the stabilities of some N, O, F ions
[AD-A292305] p 2691 N95-28868
Inorganic halogen oxidizers
[AD-A290747] p 2533 N95-29581
Inorganic halogen oxidizers
[AD-A291201] p 2702 N95-29974

FLUORINE COMPOUNDS
Radiative lifetime and quenching rate constants of PF(b(1) Sigma+) and tests for an electronic to vibrational energy transfer quenching mechanism
[AD-A290294] p 2681 N95-29062

FLUOROCARBONS
Alternative refrigerant performance: Field test of a nonchlorofluorocarbon chiller at Fort Leonard Wood, MO
[AD-A292052] p 2550 N95-29307

FLUX (RATE)
FFT space processing for the ACF of SPREE particle flux measurements
[AD-A290166] p 2507 N95-29026

FLUX DENSITY
The energy spectrum and flux of cosmic ray helium at high energy p 2740 N95-29705

FLUX DIFFERENCE SPLITTING
Parallelization of the 2D Roe Scheme on the Intel Paragon
[AD-A290690] p 2659 N95-29760
An aerodynamic and static-stability analysis of the Hypersonic Applied Research Technology (HART) missile
[DA9426923] p 2491 N95-29865

FLUX PINNING
Flux pinning and stabilizer studies
[DE95-008131] p 2682 N95-30131

FOAMS
The effect of wear on fire-blocking layer material effectiveness
[AD-A291520] p 2493 N95-29855

FOCAL PLANE DEVICES
Development of ultra-low dark current, high performance 3-5 quantum well infrared photodetectors (QWIPs) for focal plane arrays staring imaging sensor systems
[AD-A290343] p 2714 N95-29089

FOCUSING
An image cancellation approach to depth-from-focus
[DE95-007625] p 2697 N95-28912
Linear algebraic computation on distributed memory parallel machines
[AD-A290615] p 2671 N95-29558

FOG
The mm-wave resonant methods for the detection of corrosion, phase 1
[AD-A291315] p 2593 N95-29941

FORECASTING
Forecasting global temperature variations by neural networks
[AD-A290081] p 2621 N95-29333
Development and testing of improved techniques for modeling the hydrologic cycle in a mesoscale weather prediction system
[AD-A291243] p 2627 N95-29993
A regression model for the western north pacific tropical cyclone intensity forecast
[AD-A290588] p 2627 N95-30044
Applicability of neural networks for production planning under uncertainty
[PB95-197406] p 2666 N95-30101

FOREST FIRES
Monitoring of burning in the Brazilian cerrado region using AVHRR/NOAA data calibrated by TM/Landsat data
[INPE-5490-TDI/507] p 2598 N95-28929

FORESTS
Modeling the direct-beam instantaneous spectral surface albedo of a forest landscape using geometric-optics and a distributed parameter approach p 2599 N95-29540
Remote sensing of hydrologic variables in boreal areas
[NASA-CR-189422] p 2600 N95-29754
Evaluation of the utilization of SAR polarimetric images in the survey of land resources in the Amazon area Tapajos Forest Reserve
[INPE-5517-PRE/1792] p 2601 N95-29999

FORMALISM
The Stroh formalism for anisotropic elasticity with applications to composite materials
[AD-A290710] p 2527 N95-29763
Defining the IEEE-854 floating-point standard in PVS
[NASA-TM-110167] p 2659 N95-29823
Causal behaviours and nets
[PB95-197612] p 2660 N95-30102
Correctness of real-time systems by construction
[PB95-206827] p 2655 N95-30220

FORTRAN
Electromagnetic scattering by magnetic spheres: Theory and algorithms
[AD-A289798] p 2551 N95-28699
WinCD: Complex demodulation time-series analysis for windows
[AD-A291550] p 2645 N95-28934

FOUR-WAVE MIXING
Photorefractive Bi12SiO20 spatial light modulator
[AD-A291070] p 2702 N95-29969

FOURIER ANALYSIS
FFT space processing for the ACF of SPREE particle flux measurements
[AD-A290166] p 2507 N95-29026
Deconvolution of lateral shear interferograms p 2699 N95-29222
Spectral analysis techniques using wavelets as an alternative to Fourier analysis for transient dynamic data
[AD-A289776] p 2556 N95-29459

FOURIER TRANSFORMATION
System and method for rapidly tracking vehicles of special utility in low signal-to-noise environments
[AD-D017378] p 2683 N95-28783
Fourier Synthesis Lithographic Machine for large panel display fabrication
[AD-A291921] p 2698 N95-28914
Efficient inversion of Fourier and Laplace domain boundary element solutions for elastodynamic scattering p 2592 N95-29256
Spectral analysis techniques using wavelets as an alternative to Fourier analysis for transient dynamic data
[AD-A289776] p 2556 N95-29459
Advanced presort process
[AD-A291010] p 2557 N95-29655
Electrochemical impedance pattern recognition for detection of hidden chemical corrosion on aircraft components, phase 1
[AD-A291345] p 2593 N95-29946
Diffraction limited imaging using aberrated optics
[AD-A290912] p 2703 N95-30081

FRACTALS
Cage-like precursor formation from extensive cyclization in sol-gel inorganic condensation polymerization
[AD-A290589] p 2544 N95-29554
Theories of the nonlinear optical properties of composite media: Applications to phthalocyanine dyes
[AD-A290640] p 2700 N95-29560

FRACTOGRAPHY
Fractography of advanced structural ceramics: Results from the VAMAS round robin exercise
[AD-A290930] p 2547 N95-30118

FRACTURE MECHANICS
Stress concentration, stress intensity, and fatigue crack growth along evacuators of pressurized, autofrettaged tubes
[AD-A291920] p 2593 N95-28789
The effect of mixed mode precracking on the mode 1 fracture toughness of composite laminates p 2514 N95-28827
Response of automated tow placed laminates to stress concentrations p 2515 N95-28833
Tension fracture of laminates for transport fuselage. Part 2: Large notches p 2515 N95-28837
An engineering model of woven composites based on micromechanics p 2521 N95-29042
In-phase thermomechanical fatigue mechanisms in an unidirectional SCS-6/Ti 15-3 MMC
[NASA-CR-195482] p 2523 N95-29133
Fiber-matrix adhesion in single-fiber model composites p 2524 N95-29337
Phase coupling and morphology generation in engineering polymer alloys
[AD-A291868] p 2543 N95-29436
Interlaminar fracture mechanics and mechanisms: Linear and nonlinear aspects p 2526 N95-29597
Simplified data reduction methods for the ECT test for mode 3 interlaminar fracture toughness
[NASA-TM-110176] p 2527 N95-29825
Fatigue life analysis and tests for thick-walled cylinders including effects of overstrain and axial grooves
[AD-A290931] p 2596 N95-30119
Alumina reinforced Tetragonal Zirconia (TZP) composites
[DE95-008990] p 2529 N95-30180
Visit to the Laboratory For Evaluation and Failure Prevention of Materials, Toyohashi University of Technology, 17 Oct 94
[AD-A292340] p 2597 N95-30293

FRACTURE STRENGTH
The effect of mixed mode precracking on the mode 1 fracture toughness of composite laminates p 2514 N95-28827
Response of automated tow placed laminates to stress concentrations p 2515 N95-28833
High-toughness glass-ceramics
[AD-A290562] p 2541 N95-29071
Toughening mechanisms in mixed-mode interfacial fracture p 2545 N95-29772
A study of blister tests for film adhesion measurement and fracture efficiency of tests for adhesive bonds p 2545 N95-29799

Analytical investigation of the hygrothermal effects and parametric study of the Edge Crack Torsion (ECT) mode 3 test lay-ups
[NASA-TM-110183] p 2528 N95-30028

FRACTURING
Test load verification through strain data analysis
[NASA-TP-3558] p 2504 N95-28718
Design, analysis, and fabrication of a pressure box test fixture for tension damage tolerance testing of curved fuselage panels p 2516 N95-28839
A 1993 review of welding in Japan
[DE95-758701] p 2589 N95-28946
Delivery of meteorites from the asteroid belt p 2732 N95-29255
Fiber fracture in continuous-fiber reinforced composite materials during cyclic loading p 2525 N95-29513
A study of blister tests for film adhesion measurement and fracture efficiency of tests for adhesive bonds p 2545 N95-29799
Fractography of advanced structural ceramics: Results from the VAMAS round robin exercise
[AD-A290930] p 2547 N95-30118

FRAGMENTATION
Spectrometric studies of selected nitrocompounds using laser-induced photofragmentation/photoionization at 193 nm
[AD-A289947] p 2530 N95-28876
Fiber-matrix adhesion in single-fiber model composites p 2524 N95-29337
Inclusive hadronic production of the B(sub c) meson via heavy quark fragmentation
[DE95-008739] p 2695 N95-30191

FRAGMENTS
Characterizing and modeling penetration of ceramic armor
[AD-A292588] p 2542 N95-29288
Description and manipulation of method fragments for the assembly of situational methods
[PB95-197133] p 2653 N95-30094

FREE BOUNDARIES
Free-boundary equilibrium studies for the Large Helical Device
[AD-B175931L] p 2707 N95-29743

FREE CONVECTION
Development of an improved cloud model for use in cumulus parameterization p 2624 N95-29800

FREE ELECTRON LASERS
Inhibition of mode competition in free-electron laser oscillators p 2586 N95-29336

FREE ENERGY
Effects of critical fluctuations on the thermodynamic properties of fluids and fluid mixtures p 2719 N95-29216

FREE FALL
Hailstone heat and mass transfer measurements
[ISBN-0-315-86304-8] p 2624 N95-29797

FREE FLOW
Influence of turbulence parameters, Reynolds number, and body shape on stagnation-region heat transfer
[NASA-TP-3487] p 2568 N95-28719
Numerical experiments on the flow past a circular cylinder at sub-critical Reynolds number
[AD-A289937] p 2573 N95-29268
Experimental research on crossing shock wave boundary layer interactions
[AD-A290764] p 2577 N95-29920
Hydrogen film cooling with incident and swept-shock interactions in a Mach 6.4 nitrogen free stream
[NASA-TM-4603] p 2578 N95-30056
Comparison of spatial numerical operators for duct-nozzle acoustics p 2690 N95-30158

FREQUENCIES
Doubled diode laser. phase 1
[AD-A292465] p 2584 N95-29007
Spectral analysis techniques using wavelets as an alternative to Fourier analysis for transient dynamic data
[AD-A289776] p 2556 N95-29459
Transformational design of a direction detector for the progressive scan conversion processor
[PB95-198487] p 2643 N95-30109

FREQUENCY CONVERTERS
Conference proceedings: IEEE Nonlinear Optics, Materials, Fundamentals, and Applications
[AD-A292438] p 2698 N95-28997

FREQUENCY DIVISION MULTIPLE ACCESS
Alternative packet switch architectures for a 30/20 GHz FDMA/TDMA geostationary communication satellite network
[NASA-CR-195470] p 2506 N95-30090

FREQUENCY RANGES
100 Hz-10 kHz bottom backscattering model: Generalized treatment of sediment sound propagation, sediment volume scattering and interface-roughness scattering
[AD-A291323] p 2685 N95-29942

FREQUENCY STABILITY
A gyroscope clock for a null gravitational redshift experiment p 2584 N95-29664
Application of low dissipation and dispersion Runge-Kutta schemes to benchmark problems in computational aeroacoustics p 2687 N95-30139

FRICTION
Evaluation of retro-reflective beads in airport pavement markings
[AD-A291065] p 2502 N95-29967
Numerical implementation of a state variable model for friction
[DE95-007844] p 2591 N95-30273

FRICTION DRAG
Studies in drag reduction p 2487 N95-29094

FRICTION FACTOR
Studies in drag reduction p 2487 N95-29094
Gradient-dependent plasticity in numerical simulation of localization phenomena
[PB95-197257] p 2596 N95-30049

FRICTION MEASUREMENT
Boundary-layer transition and global skin friction measurement with an oil-fringe imaging technique
[NASA-CR-198814] p 2579 N95-30224

FRONTS (METEOROLOGY)
Forecast of Atlantic seasonal hurricane activity for 1995 p 2620 N95-29254
On the large scale circulation of the East Asia Mei-Yu fronts and secondary weather dimension disturbances
[AD-A291036] p 2622 N95-29662

FUEL CELLS
Effects of cooling system parameters on heat transfer in PAFC stack
[NASA-CR-198817] p 2570 N95-29131
Effects of the cooling system parameters on heat transfer and performance of the PAFC stack during transient operation
[NASA-CR-197654] p 2572 N95-29249
Technology development goals for automotive fuel cell power systems
[DE95-008764] p 2548 N95-29280
Transient responses of phosphoric acid fuel cell power plant system
[NASA-CR-198948] p 2603 N95-30015
Space Electrochemical Research and Technology. Abstracts
[NASA-CP-10172] p 2604 N95-30255
Fuel cell systems for First Lunar Outpost-reactant storage option p 2606 N95-30264
Solid Oxide Fuel Cell commercialization in the United States
[DE95-008210] p 2607 N95-30278
Advances in tubular solid oxide fuel cell technology
[DE95-008361] p 2607 N95-30281

FUEL COMBUSTION
Air/fuel ratio visualization in a diesel spray p 2590 N95-29807

FUEL CONTAMINATION
Development of the test kit for fuel acid contamination
[AD-A291953] p 2548 N95-29019

FUEL INJECTION
Air/fuel ratio visualization in a diesel spray p 2590 N95-29807

FUEL PRODUCTION
Hydrogen production in fusion reactors
[AD-B180028L] p 2710 N95-29857
Introduction to the proceedings of the sixteenth symposium on biotechnology for fuels and chemicals
[DE95-007029] p 2549 N95-30024

FUEL SPRAYS
Air/fuel ratio visualization in a diesel spray p 2590 N95-29807
The effect of turbulence on vaporization and mixing in fuel sprays
[AD-A291347] p 2577 N95-29948

FUEL SYSTEMS
Molten fluoride fuel salt chemistry
[DE95-007025] p 2695 N95-28957
Cylinder-averaged histories of nitrogen oxide in a DI diesel with simulated turbocharging
[AD-A290568] p 2590 N95-29820

FUEL TANK PRESSURIZATION
Prediction of pressurant mass requirements for axisymmetric liquid hydrogen tanks
[NASA-TM-106973] p 2511 N95-29642

FUEL TANKS
Analysis of stress concentration in the Dutton groove regions of the Super Lightweight External Tank
[NASA-TM-108490] p 2597 N95-30328

FUEL-AIR RATIO
Air/fuel ratio visualization in a diesel spray p 2590 N95-29807

FUELS
Development of the test kit for fuel acid contamination
[AD-A291953] p 2548 N95-29019

FULLERENES
Theoretical investigation of superconductivity in doped fullerenes
[AD-A291942] p 2562 N95-29018

FUNCTIONAL ANALYSIS
Trajectory mapping (TM): A new non-metric scaling technique
[AD-A290036] p 2670 N95-29440

FUNCTIONAL DESIGN SPECIFICATIONS
Fundamental limitations and capabilities of robust identification and adaptive control
[AD-A291085] p 2664 N95-29636

FUNCTIONS (MATHEMATICS)
Stable function approximation in dynamic programming
[AD-A290224] p 2647 N95-29143
On the topological complexity of the cost function in variational data assimilation p 2724 N95-29798

FUSELAGES
In situ processing methods for composite fuselage sandwich structures p 2513 N95-28826
The effects of design details on cost and weight of fuselage structures p 2499 N95-28831
Manufacturing scale-up of composite fuselage crown panels p 2515 N95-28835
Tension fracture of laminates for transport fuselage. Part 2: Large notches p 2515 N95-28837
Impact damage resistance of composite fuselage structure, part 2 p 2516 N95-28838
Design, analysis, and fabrication of a pressure box test fixture for tension damage tolerance testing of curved fuselage panels p 2516 N95-28839
Global cost and weight evaluation of fuselage keel design concepts p 2499 N95-28840
Advanced composites technology program p 2519 N95-29032
Textile composite fuselage structures development p 2519 N95-29033
Advanced composite fuselage technology p 2519 N95-29034
Advanced resin systems and 3D textile preforms for low cost composite structures p 2519 N95-29035
Cross-stiffened continuous fiber structures p 2521 N95-29041
Cost model relationships between textile manufacturing processes and design details for transport fuselage elements p 2521 N95-29043
Test results from large wing and fuselage panels p 2522 N95-29051
Estimation of aerodynamic load distributions on the F/A-18 aircraft using a CFD panel code
[DSTO-TR-0147] p 2498 N95-29445

FUSION REACTORS
The international fusion materials irradiation facility
[DE95-006536] p 2696 N95-29142
Hydrogen production in fusion reactors
[AD-B180028L] p 2710 N95-29857

FUZZY SYSTEMS
Proceedings of the 33d SICE (the Society of Instrument and Control Engineers) Annual Conference, part 1
[DE95-758947] p 2632 N95-28947
Hybrid fuzzy logic control to stabilize an inverted pendulum from arbitrary initial conditions
[AD-A292441] p 2681 N95-29000
On-line damage identification and motion control of adaptive structures: An intelligent control approach p 2662 N95-29109

G

GALACTIC BULGE
SiO maser survey of the IRAS bulge sources p 2735 N95-29837
Observational properties of SiO masers in the galactic bulge IRAS sources p 2735 N95-29838

GALACTIC CLUSTERS
The properties of local poor Abell clusters and instrumentation for the study of clustered objects p 2730 N95-29827

GALACTIC COSMIC RAYS
Parameterized spectral distributions for meson production in proton-proton collisions
[NASA-TM-4675] p 2696 N95-30337

GALACTIC EVOLUTION
Low-background balloon-borne direct search for ionizing massive particles as a component of the dark galactic halo matter p 2726 N95-29204
The properties of local poor Abell clusters and instrumentation for the study of clustered objects p 2730 N95-29827

GALACTIC RADIATION
The complex broadband x-ray spectra of Seyfert galaxies p 2730 N95-29776

GALACTIC STRUCTURE
Low-background balloon-borne direct search for ionizing massive particles as a component of the dark galactic halo matter p 2726 N95-29204
A study of one-armed spiral galaxies p 2729 N95-29774

GALAXIES
Statistics and large-scale structure p 2734 N95-29780

GALERKIN METHOD
An HP-Adaptive method in space and time for parabolic systems
[AD-A292262] p 2668 N95-28890
Dispersion analysis and error estimation of Galerkin finite element methods for the numerical computation of waves
[AD-A290296] p 2668 N95-29064
A generalized finite element method for solving the Helmholtz equation in two dimensions with minimal pollution
[AD-A290280] p 2669 N95-29080
Finite element solution to the Helmholtz equation with high wave number. Part 2. The h-p version of the FEM
[AD-A290289] p 2669 N95-29084
Finite element vorticity-based methods for the solution of the incompressible and compressible Navier-Stokes equations p 2570 N95-29119

GALLIUM ARSENIDES
Low threshold all-optical crossbar switch on GaAs-GaAlAs channel waveguide arrays
[AD-A292483] p 2712 N95-28862
Studies of lattice-mismatched and Low-Temperature-Grown semiconductor multiple-phase systems
[AD-A292536] p 2713 N95-28967
Synthesis and complete characterization of a Gallium-Mixed-Pnicogen four-membered ring compound: I2GaAs(SiMe3)(sub 2)Ga(I)2P(SiMe3)(sub 2)
[AD-A292423] p 2713 N95-28993
The 1.3 micrometer fiber photodetector
[AD-A292462] p 2582 N95-29004
Development of ultra-low dark current, high performance 3-5 quantum well infrared photodetectors (QWIPs) for focal plane arrays staring imaging sensor systems
[AD-A290343] p 2714 N95-29089
Electronic properties of low-temperature grown III/V thin films
[AD-A292521] p 2714 N95-29165
Research and development of a high performance GaAs microcomputer system
[AD-A292647] p 2643 N95-29381
Novel high-power solid-state sources for the millimeter-wave region
[AD-A292653] p 2564 N95-29384
High-density plasma dynamics in semiconductors p 2705 N95-29632
Investigation of a normal incident high performance P-type strained layer In(0.3)Ga(0.7)As/In(0.52)Al(0.48)As quantum well infrared photodetector
[AD-A290946] p 2716 N95-29785
Ion doped quantum well lasers
[AD-A290937] p 2587 N95-29912

GALLIUM NITRIDES
Nitride semiconductors for ultraviolet detection
[AD-A289546] p 2712 N95-28910

GAMMA RAY ASTRONOMY
GLAST
[DE95-008596] p 2739 N95-29265

GAMMA RAY BURSTS
GLAST
[DE95-008596] p 2739 N95-29265

GAMMA RAY TELESCOPES
GLAST
[DE95-008596] p 2739 N95-29265

GAMMA RAYS
Activities update
[AD-A292431] p 2692 N95-28994
Gamma radiation from rotation powered pulsars and results from the Energetic Gamma-Ray Experiment Telescope p 2739 N95-29671
Applications of pulsar timing p 2734 N95-29675
A multi-wavelength study of rotation-driven pulsars p 2729 N95-29678
Remote sensing of hydrologic variables in boreal areas
[NASA-CR-189422] p 2600 N95-29754

GAS ANALYSIS
The fluorescent detection of hydrazine, monomethylhydrazine, and 1,1-dimethylhydrazine by derivatization with aromatic dicarboxaldehydes
[NAVY-CASE-75451] p 2512 N95-29052
Development of a multiplex Fabry-Perot interferometer and measurement of atmospheric HF and HCl p 2608 N95-29213

GAS ATOMIZATION
Simulation of powder metal fabrication with high pressure gas atomization
[DE95-008820] p 2538 N95-30178

GAS DETECTORS
The fluorescent detection of hydrazine, monomethylhydrazine, and 1,1-dimethylhydrazine by derivatization with aromatic dicarboxaldehydes
[NAVY-CASE-75451] p 2512 N95-29052
An integrated optical CO2 sensor. Phase 0: Design and fabrication of critical elements
[NASA-CR-198792] p 2700 N95-29366

GAS DYNAMICS
Acoustic scattering from ellipses by the modal element method
[NASA-TM-106935] p 2683 N95-29401
Synthesis morphology and properties of semicrystalline block copolymers
[AD-A290475] p 2544 N95-29510
The one-dimensional bubble: Theory, experiment, and relevance to exposure of divers to low frequency sound, and of lung to lithotripsy
[ISVR-TR-246] p 2577 N95-29817

GAS EXPANSION
Numerical simulations of the flow in the HYPULSE expansion tube
[NASA-TM-110357] p 2503 N95-30228

GAS FLOW
External combustion engine having an asymmetrical CAM
[AD-D017382] p 2588 N95-28785
Investigation of the flow turning loss in unstable solid propellant rocket motors p 2510 N95-29331
Modeling the boundary layer interactions between weakly ionized plasmas and cooled, planar electrodes in stagnation-point flows p 2706 N95-29717
Experimental study on scaling law of outgassing rate with a pumping parameter
[AD-B191999L] p 2709 N95-29801
Nanocrystalline processing and interface engineering of Si3N4-based ceramics
[AD-A291302] p 2546 N95-29939
Hydrogen film cooling with incident and swept-shock interactions in a Mach 6.4 nitrogen free stream
[NASA-TM-4603] p 2578 N95-30056

GAS GENERATORS
Evaluation of wear resistant ceramic valve seats in gas-fueled power generation engines
[PB95-200218] p 2591 N95-30110

GAS HEATING
A theoretical study on ignition mechanisms of liquid propellants
[AD-A290569] p 2549 N95-29550

GAS INJECTION
Prediction of pressurant mass requirements for axisymmetric liquid hydrogen tanks
[NASA-TM-106973] p 2511 N95-29642

GAS IONIZATION
Coherent soft x-ray generation using a powerful subpicosecond laser p 2587 N95-29689

GAS JETS
The spectrum and directivity of turbulent mixing noise from supersonic jets p 2684 N95-29415
Turbulent airflow noise production and propagation patterns of a subsonic jet impinging on a flat plate p 2684 N95-29502
Laser doppler velocimeter system for subsonic jet mixer nozzle testing at the NASA Lewis Aeroacoustic Propulsion Lab
[NASA-TM-106984] p 2477 N95-30229

GAS LASERS
Characterisation of a line-tunable He-Xe laser operating at 2.026 and 3.894 micrometers
[AD-A291129] p 2587 N95-29914

GAS MIXTURES
Dynamics of simple chemically reactive fluids p 2573 N95-29335

GAS POCKETS
The one-dimensional bubble: Theory, experiment, and relevance to exposure of divers to low frequency sound, and of lung to lithotripsy
[ISVR-TR-246] p 2577 N95-29817

GAS PRESSURE
Prediction of pressurant mass requirements for axisymmetric liquid hydrogen tanks
[NASA-TM-106973] p 2511 N95-29642
Experimental study on scaling law of outgassing rate with a pumping parameter
[AD-B191999L] p 2709 N95-29801

GAS STREAMS
Precision cleaning verification of fluid components by air/water impingement and total carbon analysis
[NASA-TM-110742] p 2531 N95-29248

GAS TUNGSTEN ARC WELDING
The effects of alloying elements on the strength and cooling rate sensitivity of ultra-low carbon alloy steel weld metals
[AD-A290681] p 2537 N95-29759

GAS TURBINE ENGINES
Intelligent turbine engines for Army applications
[AD-A290532] p 2500 N95-29496
Model development for active control of stall phenomena in aircraft gas turbine engines p 2500 N95-29679
Characterization of stall inception in high-speed single-stage compressors
[AD-A291275] p 2501 N95-29934
The fluid mechanics of a high aspect ratio slot with an impressed pressure gradient and secondary injection p 2580 N95-30304

GAS TURBINES
Intelligent turbine engines for Army applications
[AD-A290532] p 2500 N95-29496

GAS VALVES
External combustion engine having an asymmetrical CAM
[AD-D017382] p 2588 N95-28785

GAS-SOLID INTERFACES
Structural and electronic properties of adsorbates on semiconductors, metal-semiconductor interfaces and semiconductor heterojunctions
[AD-A291917] p 2715 N95-29438

GASEOUS DIFFUSION
Characterization of excited state oxygen-organic molecule complexes
[AD-A290548] p 2692 N95-29092

GASIFICATION
The TEES process cleans waste and produces energy
[DE95-007799] p 2602 N95-29463

GATES (CIRCUITS)
Asymptotically zero energy computing using split-level charge recovery logic
[AD-A290054] p 2564 N95-29478

GEAR TEETH
Influence of tooth profile modification on spur gear dynamic tooth strain
[NASA-TM-106952] p 2589 N95-29112

GEARS
Carrier-less, anti-backlash planetary drive system
[NASA-CASE-GSC-13608-1] p 2588 N95-28702
Dimensions, deflections and stresses for Hertzian contacts under combined normal and tangential loading. (Guide to use of computer program A9434.)
[ESDU-94034] p 2593 N95-28711
Influence of tooth profile modification on spur gear dynamic tooth strain
[NASA-TM-106952] p 2589 N95-29112

GELATION
Cage-like precursor formation from extensive cyclization in sol-gel inorganic condensation polymerization
[AD-A290589] p 2544 N95-29554

GELS
17O NMR of the structural evolution of V2O5 gels
[AD-A290623] p 2545 N95-29559

GENERAL AVIATION AIRCRAFT
Development of an intervention program to encourage shoulder harness use and aircraft retrofit in general aviation aircraft: Phases 1 and 2
[AD-A290966] p 2493 N95-29873
Terminal area forecasts-fiscal years 1993-2010
[AD-A290835] p 2495 N95-29880

GENERAL OVERVIEWS
Progress and trends of multi-valued logic research
[AD-A290997] p 2665 N95-29874

GENES
The 5th International Meeting on Cholinesterase
[AD-A291253] p 2534 N95-30085

GENETIC ALGORITHMS
A genetic algorithm approach to scheduling resources for a space power system p 2511 N95-29784

GENETIC ENGINEERING
Genetics and the unity of biology
[DE95-006484] p 2633 N95-29471

GENETICS
Proceeding of the 33rd SICE Annual Conference
[DE95-758943] p 2662 N95-29144
Genetics and the unity of biology
[DE95-006484] p 2633 N95-29471
Applications of machine learning and rule induction
[AD-A292607] p 2664 N95-29577

GEOCHEMISTRY
Differentiation in the early Earth: An experimental investigation p 2612 N95-29199

GEOCHRONOLOGY
Some aspects of lunar and martian volcanism as examined with spectral, topographic, and morphologic data derived from spacecraft images p 2736 N95-29594
Large scale fluctuations of the geomagnetic field p 2617 N95-29796

GEODESY
A comprehensive analysis of Navy and Marine corps digital mapping, charting, and geodesy requirements for modeling and simulation
[AD-A291601] p 2598 N95-28931
Digital mapping, charting, and geodesy analysis program technical review of vector smart map prototypes 1 and 2
[AD-A291217] p 2601 N95-29977
Crustal deformation measurements in the vicinity of Vandenberg Air Force Base
[AD-A291224] p 2618 N95-29981
GEODYNAMICS
The laser ranging of etalon satellites
[AD-A291019] p 2587 N95-29660
GEOGRAPHIC INFORMATION SYSTEMS
Retrieval, display, and analysis support tool for earth imagery (RDAST)
[AD-A291366] p 2601 N95-30061
GEOLOGY
Multi-scale studies of seafloor topography
[AD-A292301] p 2628 N95-28865
Crustal deformation measurements in the vicinity of Vandenberg Air Force Base
[AD-A291224] p 2618 N95-29981
GEOMAGNETIC LATITUDE
The effects of magnetic storm phases on F-layer irregularities from auroral to equatorial latitudes
[AD-A290674] p 2614 N95-29585
GEOMAGNETISM
Solar-geophysical data number 605, January 1995. Part 1 (prompt reports): Data for December, November 1994 and late data
[PB95-191003] p 2737 N95-28781
Thermal N(+) in the inner magnetosphere
p 2614 N95-29590
Application of Poynting flux measurements to the determination of energy transfer rates in the high-latitude ionosphere p 2614 N95-29650
Large scale fluctuations of the geomagnetic field
p 2617 N95-29796
On the azimuthal variation of the equatorial plasmapause
[NASA-CR-198929] p 2711 N95-30338
GEOMETRICAL ACOUSTICS
Airy functions and the recursive ray acoustics algorithm
[AD-A290182] p 2629 N95-29054
GEOMETRICAL OPTICS
Development of the theory and algorithms for synthesis of reflector antenna systems
[AD-A292579] p 2552 N95-28979
Modeling the direct-beam instantaneous spectral surface albedo of a forest landscape using geometric-optics and a distributed parameter approach
p 2599 N95-29540
High-frequency radar target modeling
[AD-A290965] p 2559 N95-29991
GEOMETRICAL THEORY OF DIFFRACTION
High-frequency radar target modeling
[AD-A290965] p 2559 N95-29991
GEOMETRY
Generating grids directly on CAD database surfaces using a parametric evaluator approach
p 2483 N95-28754
Grid generation on trimmed Bezier and NURBS quilted surfaces p 2483 N95-28755
Cooperative solutions coupling a geometry engine and adaptive solver codes p 2484 N95-28761
NACA 1-series geometry representation for computational fluid dynamics
[ESDU-94013] p 2568 N95-28902
Interface for the translation of sentences in a natural language into a geometrical representation language
[INPE-5467-PRE/1775] p 2722 N95-29363
GEOMORPHOLOGY
A comprehensive analysis of Navy and Marine corps digital mapping, charting, and geodesy requirements for modeling and simulation
[AD-A291601] p 2598 N95-28931
GEOPHYSICS
Solar-geophysical data number 605, January 1995. Part 2 (comprehensive reports): Data for July 1994 and miscellaneous
[PB95-190997] p 2737 N95-28780
Solar-geophysical data number 605, January 1995. Part 1 (prompt reports): Data for December, November 1994 and late data
[PB95-191003] p 2737 N95-28781
MapTool version 2. User's manual
[AD-A289470] p 2630 N95-29418
SETA/ADS software development
[AD-A291181] p 2651 N95-29932
Complete analysis of electrode-terminated cables in two-layer conductor bounded above by air: Current density, magnetic field, and magnetic field gradient
[AD-A290907] p 2566 N95-30079
GEOSTROPHIC WIND
Parameter study of the statistically steady state of a multi-layer quasi-geostrophic model
p 2612 N95-29212
GEOTECHNICAL ENGINEERING
A geotechnical characterization of lunar soils and lunar soil simulants p 2736 N95-29117
GEOTHERMAL ENERGY CONVERSION
Geothermal heat pumps for heating and cooling
[AD-A292115] p 2602 N95-28858
GEOTHERMAL RESOURCES
Coso monitoring program
[AD-A290604] p 2627 N95-30048
GEOTHERMAL TECHNOLOGY
Geothermal heat pumps for heating and cooling
[AD-A292115] p 2602 N95-28858
GERMANIUM ALLOYS
Epitaxial growth and characterization of Si(1-x)Ge(x) materials and devices
[AD-A292528] p 2712 N95-28874
GET AWAY SPECIALS (STS)
Design and analysis of the launch vehicle adapter fitting for the petite amateur navy satellite (PANSAT)
[AD-A289693] p 2504 N95-28680
GIANT STARS
X-ray emission from Hybrid stars
p 2740 N95-29779
GLASS
High-toughness glass-ceramics
[AD-A290562] p 2541 N95-29071
Experimental investigations of wave and fracture phenomena in impacted ceramics and glasses
[AD-A292142] p 2542 N95-29195
Toughening mechanisms in mixed-mode interfacial fracture p 2545 N95-29772
Evaluation of retro-reflective beads in airport pavement markings
[AD-A291065] p 2502 N95-29967
Sensor protection portion of the development of nonlinear optical materials and processes for laser hardening of sensors
[AD-A291200] p 2702 N95-29973
Neutron scattering from amorphous, disordered and nanocrystalline materials
[DE95-005848] p 2717 N95-30077
GLASS COATINGS
Pulsed laser deposition of thin film material for nonlinear waveguides
[AD-A290789] p 2544 N95-29484
GLASS FIBERS
The combined effect of glass buffer strips and stitching on the damage tolerance of composites
p 2522 N95-29049
Fiber-matrix adhesion in single-fiber model composites
p 2524 N95-29337
GLOBAL POSITIONING SYSTEM
Error modeling for differential GPS
[NASA-CR-188367] p 2493 N95-28716
Wide Area Differential GPS (WADGPS)
p 2494 N95-29107
An investigation into the use of satellite-based positioning systems for flight reference/autoland operations p 2494 N95-29542
Modeling spatio-temporal databases to measure the performance of the GPS satellite constellation
p 2494 N95-29596
Crustal deformation measurements in the vicinity of Vandenberg Air Force Base
[AD-A291224] p 2618 N95-29981
Performance analysis of a GPS interferometric attitude determination system for a gravity gradient stabilized spacecraft
[NASA-CR-188372] p 2508 N95-30036
GLOBAL WARMING
Stochastic modeling and global warming trend extraction for ocean acoustic travel times
[AD-A292114] p 2608 N95-28922
GLOBULAR CLUSTERS
STS-67 mission highlights resource tape
[NASA-TM-110530] p 2504 N95-28715
A search for cataclysmic variables in globular clusters
p 2727 N95-29532
Effects of microscopic diffusion and rotational mixing on stellar models p 2733 N95-29669
GLYCOLS
Orthobaric densities and molar volumes of liquids. Glycol ethers (cellosolves and carbitols, etc.)
[ESDU-95005] p 2530 N95-28703
Orthobaric densities and molar volumes of liquids. Glycols and cyclic diols
[ESDU-95003] p 2531 N95-28895
Vapour pressures and critical points of liquids. Glycols and cyclic diols
[ESDU-95002] p 2534 N95-29897
Vapour pressures and critical points of liquids. Glycol ethers (alkyl cellosolves and carbitols, etc.)
[ESDU-95004] p 2534 N95-29901
Biological methane activation
[PB95-200705] p 2535 N95-30198
GOGGLES
Distance estimation training with night vision goggles under low illumination
[AD-A291338] p 2641 N95-29943
GOLD
Nitride semiconductors for ultraviolet detection
[AD-A289546] p 2712 N95-28910
Effects of space exposure on metals flown on the Long Duration Exposure Facility
[NASA-CR-4662] p 2512 N95-30225
GOLD COATINGS
An integrated optical CO2 sensor. Phase 0: Design and fabrication of critical elements
[NASA-CR-198792] p 2700 N95-29366
GOODNESS OF FIT
Continuation of research in the statistical aspects of reliability, availability, and maintainability
[AD-A290126] p 2592 N95-29423
GRADIENTS
Correlation and gradient characteristics of ionospheric parameters in Europe
[AD-A290135] p 2612 N95-29140
Complete analysis of electrode-terminated cables in two-layer conductor bounded above by air: Current density, magnetic field, and magnetic field gradient
[AD-A290907] p 2566 N95-30079
GRAIN SIZE
Dust formation in stellar outflows: A time-dependent model p 2733 N95-29649
Mechanical properties of nanophase metals
[DE95-005408] p 2537 N95-30018
GRANULAR MATERIALS
Systems of hyperbolic partial differential equations
[AD-A290287] p 2669 N95-29083
A geotechnical characterization of lunar soils and lunar soil simulants p 2736 N95-29117
Collective phenomena in granular fluids
p 2572 N95-29219
Changes in microstructural parameters of snow during deformation
[AD-A290887] p 2601 N95-29866
Gradient-dependent plasticity in numerical simulation of localization phenomena
[PB95-197257] p 2596 N95-30049
GRAPH THEORY
Research in graph algorithms and combinatorial optimization
[AD-A292630] p 2648 N95-29297
GRAPHICAL USER INTERFACE
An architectural design of a toolkit for synchronous groupware applications
[AD-A290226] p 2642 N95-29146
SOSDOR: Solid-state device simulator code
[AD-A289954] p 2563 N95-29275
A friendly editing environment for computer-aided rapid prototyping of hard real-time systems
[AD-A290154] p 2648 N95-29321
A study of the conceptual symbolics of information system development languages p 2723 N95-29589
GRAPHITE
Lightweight battery electrode and method of making it
[AD-D017389] p 2560 N95-28855
Mechanical characterization of 2D, 2D stitched, and 3D braided/RTM materials p 2520 N95-29036
Elevated temperature static fatigue of a Nicalon fiber-reinforced SiC composite
[DE95-008780] p 2528 N95-30175
GRAPHITE-EPOXY COMPOSITES
Analysis of static contact in laminated composite plates using damage mechanics
[NASA-CR-198656] p 2513 N95-28809
Characterization and development of materials for advanced textile composites p 2513 N95-28824
The effects of specimen width on tensile properties of triaxially braided textile composites
p 2513 N95-28825
Master plot analysis of microcracking in graphite/epoxy and graphite/PEEK laminates p 2514 N95-28828
Novel cost controlled materials and processing for primary structures p 2514 N95-28830
EMI Shields made from intercalated graphite composites
[NASA-TM-106979] p 2518 N95-28906
Cross-stiffened continuous fiber structures
p 2521 N95-29041
The effects of aircraft fuel and fluids on the strength properties of Resin Transfer Molded (RTM) composites
p 2522 N95-29047
Origins of imperfections in composite materials
[AD-A290261] p 2523 N95-29169

Damage tolerance in filament-wound graphite/epoxy pressure vessels
[NASA-CR-198804] p 2590 N95-29369
Analytical and experimental studies of the energy absorption behavior of composite structures
p 2524 N95-29411
Fiber fracture in continuous-fiber reinforced composite materials during cyclic loading p 2525 N95-29513
Impact resistance and damage tolerance of composite sandwich panels p 2526 N95-29549
Interlaminar fracture mechanics and mechanisms: Linear and nonlinear aspects p 2526 N95-29597

GRAPHS (CHARTS)
Sleep during SEAL Delivery Vehicle (SDV)/Dry dock shelter exercises analyzed by a graphic approach
[AD-A290916] p 2637 N95-30083
Process algebra with feedback
[PB95-206819] p 2673 N95-30106

GRATINGS (SPECTRA)
Diffractive optics: Design, fabrication, and applications
[AD-A290942] p 2702 N95-29867

GRAVITATION
Experimental results of Hooper's gravity-electromagnetic coupling concept
[NASA-TM-106963] p 2680 N95-28893
A search for a composition-dependent gravitational force p 2719 N95-29501
Quantum fluctuations and semiclassical gravity theory
p 2719 N95-29527

GRAVITATION THEORY
Quantum fluctuations and semiclassical gravity theory
p 2719 N95-29527

GRAVITATIONAL EFFECTS
Observational signatures of rotating black holes
p 2729 N95-29709
Life sciences program
[NASA-CR-197658] p 2633 N95-30292

GRAVITATIONAL FIELDS
Improved operator awareness of teleoperated land vehicle attitude
[AD-A290443] p 2641 N95-29359
A search for a composition-dependent gravitational force p 2719 N95-29501
Quantum fluctuations and semiclassical gravity theory
p 2719 N95-29527
The gravitational potential energy of the Earth's lithosphere p 2617 N95-29773
The JPL Mars gravity field, Mars50c, based upon Viking and Mariner 9 Doppler tracking data
[NASA-CR-198881] p 2737 N95-30344

GRAVITATIONAL PHYSIOLOGY
The influence of space flight on erythrokinetics in man. Space Life Sciences Missions 1 and 2. Experiment E261
[NASA-CR-188368] p 2633 N95-28875
Life sciences program
[NASA-CR-197658] p 2633 N95-30292

GRAVITY PROBE B
DC electrostatic gyro suspension system for the Gravity Probe B experiment p 2509 N95-29794

GRAVITY WAVES
An investigation of thunderstorms as a source of short period mesospheric gravity waves
[AD-A289795] p 2611 N95-28697
The nature of wavefront fluctuations induced by internal gravity waves in long-range oceanic acoustic pulse transmissions p 2630 N95-29528
Studies of gravity-wave filtering and tidal interaction in the middle atmosphere p 2619 N95-30351

GRAZING INCIDENCE TELESCOPES
The x-ray scattering halo around Sco-X1
p 2727 N95-29591

GREEN'S FUNCTIONS
Solution of second order nonlinear boundary value problems by the boundary element method
p 2669 N95-29105
Transport simulation in spatially modulated low dimensionality systems
[AD-A290486] p 2718 N95-29149
Acoustic imaging of ultrasonic wave propagation
[AD-A290390] p 2683 N95-29232
Extreme nonlinearity in rocks: An investigation using elastic pulse wave propagation
[DE95-007879] p 2618 N95-30129
A numerical solution method for acoustic radiation from axisymmetric bodies p 2689 N95-30154

GRID GENERATION (MATHEMATICS)
Surface Modeling, Grid Generation, and Related Issues in Computational Fluid Dynamic (CFD) Solutions
[NASA-CP-3291] p 2478 N95-28723
Future requirements in surface modeling and grid generation p 2478 N95-28724
Grid generation and surface modeling for CFD
p 2478 N95-28726
Grid generation: A view from the trenches
p 2478 N95-28727
Application of CFD in aeronautics at NASA Ames Research Center p 2478 N95-28728
Geometry Laboratory (GEOLAB) surface modeling and grid generation technology and services
p 2479 N95-28729
Rapid Airplane Parametric Input Design (RAPID)
p 2479 N95-28730
Algorithms for high aspect ratio oriented triangulations
p 2479 N95-28731
Surface modeling and grid generation for aeropropulsion CFD p 2479 N95-28732
Marshall Space Flight Center surface modeling and grid generation applications p 2480 N95-28733
Multiblock grid generation with automatic zoning
p 2480 N95-28735
Block-structured grids for complex aerodynamic configurations: Current status p 2480 N95-28736
Grid related issues for static and dynamic geometry problems using systems of overset structured grids
p 2480 N95-28737
The role of overset grids in the development of the general purpose CFD code p 2480 N95-28738
A Cartesian, cell-based approach for adaptively-refined solutions of the Euler and Navier-Stokes equations
p 2480 N95-28739
Development and application of a 3D Cartesian grid Euler method p 2481 N95-28740
Unstructured Cartesian/prismatic grid generation for complex geometries p 2481 N95-28741
Prospects and expectations for unstructured methods
p 2481 N95-28742
An unstructured-grid software system for solving complex aerodynamic problems p 2481 N95-28743
Adaptive hybrid prismatic-tetrahedral grids for viscous flows p 2481 N95-28744
Three-dimensional hybrid grid generation using advancing front techniques p 2481 N95-28745
Emerging CFD technologies and aerospace vehicle design p 2482 N95-28746
Evaluation of grid generation technologies from an applied perspective p 2482 N95-28748
The National Grid Project: A system overview
p 2482 N95-28749
A 3DGRAPE/AL: The Ames/Langley technology upgrade p 2482 N95-28750
Automatic structured grid generation using Gridgen (some restrictions apply) p 2483 N95-28751
Tuned grid generation with ICEM CFD
p 2483 N95-28752
Geometry modeling and grid generation using 3D NURBS control volume p 2483 N95-28753
Generating grids directly on CAD database surfaces using a parametric evaluator approach
p 2483 N95-28754
Grid generation on trimmed Bezier and NURBS quilted surfaces p 2483 N95-28755
Geometric grid generation p 2483 N95-28756
Algorithms for the automatic generation of 2-D structured multi-block grids p 2483 N95-28757
Intelligent automated surface grid generation
p 2484 N95-28758
Optimal domain decomposition strategies
p 2484 N95-28759
Elliptic surface grid generation on minimal and parmetrized surfaces p 2484 N95-28760
Automation of three-dimensional structured mesh generation for turbomachinery blade passages
p 2484 N95-28762
A grid generation system for multi-disciplinary design optimization p 2484 N95-28763
Automatic multi-block grid generation for high-lift configuration wings p 2485 N95-28764
Multilevel elliptic smoothing of large three-dimensional grids p 2485 N95-28765
Advanced methodology for simulation of complex flows using structured grid systems p 2485 N95-28766
Demonstration of an automated CFD system for three-dimensional flow simulations p 2485 N95-28767
A technique for optimizing grid blocks
p 2485 N95-28769
A combined geometric approach for computational fluid dynamics on dynamic grids p 2485 N95-28770
Examples of grid generation with implicitly specified surfaces using GridPro (TM)/az3000. 1: Filleted multi-tube configurations p 2486 N95-28772
GridTool: A surface modeling and grid generation tool
p 2486 N95-28773
Interactive high quality grid generation
p 2486 N95-28774
NASA-IGES Translator and Viewer
p 2486 N95-28775
Pollution error in the h-version of the finite element method and the local quality of the recovered derivatives
[AD-A290297] p 2668 N95-29065
Solution of second order nonlinear boundary value problems by the boundary element method
p 2669 N95-29105
Solution of the Navier-Stokes equations on locally refined Cartesian meshes using state-vector splitting
p 2571 N95-29197
Consideration of microstructural changes in the study of adiabatic shear bands
[AD-A290398] p 2715 N95-29234
Grid orthogonality effects on predicted turbine midspan heat transfer and performance
[NASA-TM-106931] p 2574 N95-29371
Computational results for parallel unstructured mesh computations
[DE95-005856] p 2659 N95-29985
The application of adaptive mesh refinement to the numerical simulation of compressible flow
[AD-A289595] p 2577 N95-30027
Comparison of the local defect correction iteration and the fast adaptive composite grid iteration
[PB95-206769] p 2672 N95-30088
Coarsening strategies for unstructured multigrid techniques with application to anisotropic problems
[NASA-CR-198154] p 2674 N95-30227
Grid resolution and turbulent inflow boundary condition recommendations for NPARC calculations
[NASA-TM-106959] p 2492 N95-30253
Parallel adaptive finite element: Software for semiconductor device simulation
[AD-A291149] p 2661 N95-30295

GROOVES
Micro/Miniature heat pipe analysis
[AD-A292232] p 2570 N95-29127
Analysis of stress concentration in the Dutton groove regions of the Super Lightweight External Tank
[NASA-TM-108490] p 2597 N95-30328

GROUND EFFECT (COMMUNICATIONS)
The correction of measured noise spectra for the effects of ground reflection
[ESDU-94035] p 2683 N95-28710

GROUND STATIONS
Wide Area Differential GPS (WADGPS)
p 2494 N95-29107

GROUND SUPPORT EQUIPMENT
A ground support electronic interface for the ionospheric spectroscopy and atmospheric chemistry (ISAAC) ultraviolet spectrograph
[AD-A289761] p 2611 N95-28693

GROUND SUPPORT SYSTEMS
SPE(R)-OBOGS: On-board oxygen generating system
p 2606 N95-30267

GROUND WIND
Hindcasting changes in thermal structure and acoustic transmission loss in the upper ocean on short time scales with data from MILE and from ocean weather station papa
[AD-A292419] p 2629 N95-28991
A regression model for the western north pacific tropical cyclone intensity forecast
[AD-A290588] p 2627 N95-30044

GROUND-AIR-GROUND COMMUNICATION
STS-71 Shuttle/Mir flight: Day 4
[NASA-TM-110747] p 2505 N95-29957
STS-71 Shuttle/Mir flight: Day 7
[NASA-TM-110750] p 2505 N95-29960
STS-71 Shuttle/Mir flight: Day 8
[NASA-TM-110751] p 2505 N95-29961

GROUP THEORY
Tables of SU3 isoscalar factors
[DE95-009375] p 2690 N95-28779
Spectral estimates for positive Rockland operators
[PB95-206751] p 2673 N95-30204

GROWTH
Analysis of adiabatic shear bands in thermoviscoplastic materials under combined loading
[AD-A290666] p 2596 N95-29582

GULF STREAM
Hi-res SAR data processing report
[AD-A291443] p 2559 N95-30073

GULFS
Role of unmanned aerial vehicles in future armed conflict scenarios
[AD-A289777] p 2497 N95-29282

GUNS (ORDNANCE)
Fatigue life analysis and tests for thick-walled cylinders including effects of overstrain and axial grooves
[AD-A290931] p 2596 N95-30119

GUSTS
The pressure field of a gust interacting with a flat plate p 2582 N95-30161
Aeroacoustic computation of a gust-plate interaction via MacCormack schemes p 2690 N95-30162
Evaluation of numerical schemes for the analysis of sound generation by blade-gust interaction
p 2690 N95-30163

GYROSCOPES
A gyroscope clock for a null gravitational redshift experiment p 2584 N95-29664
DC electrostatic gyro suspension system for the Gravity Probe B experiment p 2509 N95-29794
GYROSCOPIC STABILITY
DC electrostatic gyro suspension system for the Gravity Probe B experiment p 2509 N95-29794

H

H ALPHA LINE
A search for cataclysmic variables in globular clusters p 2727 N95-29532
The 12 UM contribution of nearby galaxies to the infrared background
[AD-A291185] p 2735 N95-29917
H II REGIONS
Nobeyama Radio Observatory report, no. 382: The mass of a star formed in a cloud core: Theory and its application to the Orion A cloud p 2731 N95-29100
H-INFINITY CONTROL
Digital control of distributed parameter systems: A state-space approach
[PB95-197216] p 2666 N95-30041
H infinity control problem with zeros on the boundary of the stability domain
[PB95-197042] p 2668 N95-30288
H-53 HELICOPTER
The large-capacity rescue-helicopter CH-53 G p 2678 N95-29621
HABITATS
Experiment kits for processing biological samples inflight on SLS-2
[NASA-TM-4685] p 2642 N95-28722
An inflight refill unit for replenishing research animal drinking water
[NASA-TM-4684] p 2642 N95-28818
HADRONS
Prospects for HERMES-spin structure studies at HERA
[DE95-005845] p 2694 N95-30019
HAFNIUM ALLOYS
Processing and properties of extruded tungsten-hafnium and tungsten-steel composites
[DE95-007371] p 2528 N95-30037
HAIL
Hailstone heat and mass transfer measurements
[ISBN-0-315-86304-8] p 2624 N95-29797
HALIDES
Synthesis of nanocrystalline indium arsenide and indium phosphide from Indium(III) halides and tris(trimethylsilyl)pnicogens; synthesis, characterization, and decomposition behavior of I3In(dot)P(SiMe3)3
[AD-A291905] p 2715 N95-29486
HALL EFFECT
Semiconductor science and technology
[AD-A289143] p 2563 N95-29191
HALOCARBONS
Thermal conductivity of liquid halogenated aliphatic hydrocarbons. Part 2: Halogenated ethanes
[ESDU-94022] p 2512 N95-29017
Thermal conductivity of liquid halogenated aliphatic hydrocarbons. Part 3: Halogenated higher hydrocarbons (C3 to C16)
[ESDU-94023-PT-3] p 2512 N95-29900
The comparative extinguishment performance and thermal decomposition products of halon alternative agents
[AD-A291161] p 2551 N95-29924
Feasibility of a jet-stirred reactor for evaluating replacements for halon fire retardants
[AD-A291155] p 2551 N95-30299
HALOGEN COMPOUNDS
Thermal conductivity of liquid halogenated aliphatic hydrocarbons. Part 4: Halogenated alkenes and dienes (C1 to C4)
[ESDU-94024-PT-4] p 2511 N95-28803
Thermal conductivity of liquid halogenated aliphatic hydrocarbons. Part 1: Halogenated methanes and azeotropic mixtures
[ESDU-94021-PT-1] p 2511 N95-28804
HALOGENS
Inorganic halogen oxidizers
[AD-A290747] p 2533 N95-29581
Inorganic halogen oxidizers
[AD-A291201] p 2702 N95-29974
HALOS
The x-ray scattering halo around Sco-X1 p 2727 N95-29591
Effects of microscopic diffusion and rotational mixing on stellar models p 2733 N95-29669
Experimental cosmology using fast parallel N-body methods p 2734 N95-29775
HAMILTONIAN FUNCTIONS
Nonlinear mechanics and applied analysis
[AD-A290356] p 2669 N95-29070
Polynomial approximations for materials simulations
[DE95-006168] p 2652 N95-29989
HANDBOOKS
SI Handbook for the Lawrence Livermore National Laboratory: Committee on metric transition
[DE95-009329] p 2551 N95-30182
CD-ROM preparation: An overview and guide
[NASA-CR-198756] p 2655 N95-30307
HANDLES
Boyer-moore type algorithm for regular expression pattern matching
[PB95-198131] p 2654 N95-30107
HARDNESS
Thermoreactive aircraft coatings (TRAC) program
[AD-A292054] p 2542 N95-29314
Depth-independent hardness improvements in ion irradiated polystyrene
[DE95-008682] p 2547 N95-30190
HARDWARE
Digital video technology, today and tomorrow
[DE95-007689] p 2556 N95-29462
ADC test support program
[AD-A289445] p 2643 N95-29921
Impact of uncertainty on modeling and testing
[NASA-CR-196637] p 2652 N95-30013
HARDWARE DESCRIPTION LANGUAGES
The design of programmable convolutional encoder using VHDL and an FPGA
[AD-A290048] p 2649 N95-29442
HARMONIC ANALYSIS
Modal interactions and complex responses in weaklyNONLINEAR MULTI-DEGREE-OF-FREEDOM MECHANICAL SYSTEMS
[AD-A292023] p 2594 N95-28853
HARMONIC EXCITATION
Coherent soft x-ray generation using a powerful subpicosecond laser p 2587 N95-29689
HARMONIC OSCILLATORS
The one-dimensional bubble: Theory, experiment, and relevance to exposure of divers to low frequency sound, and of lung to lithotripsy
[ISVR-TR-246] p 2577 N95-29817
Spectral estimates for positive Rockland operators
[PB95-206751] p 2673 N95-30204
HARMONICS
Numerical simulation of stability and stability control of high speed compressible rotating couette flow
[NASA-CR-198832] p 2579 N95-30250
HARNESSES
Development of an intervention program to encourage shoulder harness use and aircraft retrofit in general aviation aircraft: Phases 1 and 2
[AD-A290966] p 2493 N95-29873
HARTMANN NUMBER
Theory of pseudo-classical confinement and transmutation to L-mode
[AD-B175957L] p 2709 N95-29809
HARTREE-FOCK-SLATER METHOD
Screening constants for plasma
[AD-B179442L] p 2710 N95-29843
HAZARDS
Cathodic protection system inspection 5
[AD-A289724] p 2592 N95-28684
Bootstrap and partitioning methods
[AD-A290662] p 2671 N95-29578
Environmental practice in progam management offices
[AD-A290823] p 2609 N95-29721
HEAD (ANATOMY)
Pulse waveform and pulse amplitude analysis during Lower Body Negative Pressure
[AD-A290521] p 2636 N95-29360
HEALTH
Inhalation Toxicology Research Institute
[AD-A292037] p 2635 N95-29188
HEARING
Actual effectiveness of hearing protection in high level impulse noise
[AD-A291604] p 2634 N95-28941
HEART
Cathodic protection system inspection 5
[AD-A289724] p 2592 N95-28684
HEART FUNCTION
Military flying and aeromedical evaluation of cardiac arrhythmias
[AD-A291595] p 2634 N95-28940
HEAT EXCHANGERS
Selection and costing of heat exchangers. Air-cooled type
[ESDU-94043] p 2550 N95-28705
Selection and costing of heat exchangers. Shell-and-tube type
[ESDU-94042] p 2550 N95-28706
Transient responses of phosphoric acid fuel cell power plant system
[NASA-CR-198948] p 2603 N95-30015
High-efficiency solar cells using HEM silicon
[DE95-005424] p 2604 N95-30217
HEAT FLUX
Influence of turbulence parameters, Reynolds number, and body shape on stagnation-region heat transfer
[NASA-TP-3487] p 2568 N95-28719
Hindcasting changes in thermal structure and acoustic transmission loss in the upper ocean on short time scales with data from MILE and from ocean weather station papa
[AD-A292419] p 2629 N95-28991
Experimental and analytical study of heat transfer and turbulent flow field in tangentially injected swirl flow p 2576 N95-29811
HEAT OF VAPORIZATION
Thermophysical properties of R-32 (difluoromethane)
[ESDU-94032] p 2530 N95-28802
HEAT PIPES
Micro/Miniature heat pipe analysis
[AD-A292232] p 2570 N95-29127
HEAT PUMPS
Geothermal heat pumps for heating and cooling
[AD-A292115] p 2602 N95-28858
HEAT SHIELDING
EMI Shields made from intercalated graphite composites
[NASA-TM-106979] p 2518 N95-28906
HEAT SINKS
A model analysis of the spatial distribution and temporal trends of nitrous oxide sources and sinks p 2609 N95-29804
HEAT TRANSFER
Condensation inside tubes: Condensate film coefficient in horizontal tubes
[ESDU-94041] p 2569 N95-29015
Leading edge film cooling effects on turbine blade heat transfer
[NASA-TM-106955] p 2500 N95-29115
Micro/Miniature heat pipe analysis
[AD-A292232] p 2570 N95-29127
Effects of cooling system parameters on heat transfer in PAFC stack
[NASA-CR-198817] p 2570 N95-29131
Effects of the cooling system parameters on heat transfer and performance of the PAFC stack during transient operation
[NASA-CR-197654] p 2572 N95-29249
Grid orthogonality effects on predicted turbine midspan heat transfer and performance
[NASA-TM-106931] p 2574 N95-29371
The effects of the thermal boundary condition and turbulence on heat transfer from a cylinder, flat plate, and turbine blade using the transient shroud and heated-coating techniques
[AD-A292646] p 2574 N95-29380
Use of finite element analysis for transient moisture diffusion studies in multilayer composite AEM/S system sandwich materials
[AD-A291092] p 2527 N95-29638
Hailstone heat and mass transfer measurements
[ISBN-0-315-86304-8] p 2624 N95-29797
Experimental and analytical study of heat transfer and turbulent flow field in tangentially injected swirl flow p 2576 N95-29811
The role of diabatic heating, torques and stability in forcing the meridional circulation within cyclones p 2626 N95-29834
Fundamental studies in cryogenic cooling of power electronics
[AD-A291150] p 2551 N95-30296
HEAT TRANSFER COEFFICIENTS
Condensation inside tubes: Condensate film coefficient in horizontal tubes
[ESDU-94041] p 2569 N95-29015
HEAT TREATMENT
Visit to the Department of Metallurgical Engineering, Tokyo Institute of Technology, 22 Sep. 1994
[AD-A292310] p 2536 N95-29473
HEATING
A theoretical study on ignition mechanisms of liquid propellants
[AD-A290569] p 2549 N95-29550
Development and application of fluorescent diagnostics to fundamental droplet and spray problems
[AD-A290553] p 2578 N95-30039
HEATING EQUIPMENT
Geothermal heat pumps for heating and cooling
[AD-A292115] p 2602 N95-28858
Compact substrate heater for use in an oxidizing atmosphere
[AD-A290860] p 2502 N95-29522

HEAVY IONS
Laser simulation of single-event effects: A state of the art review
[AD-A292308] p 2584 N95-28892
Sea and gluon spin structure function measurements at RHIC
[DE95-005823] p 2695 N95-30185
HEAVY NUCLEI
Fluxes and relative abundances of light cosmic ray nuclei at energies above 40 GeV/n p 2739 N95-29531
HEIGHT
A full wave study of radar cross sections of rough terrain
[AD-A291227] p 2559 N95-29982
HELICAL FLOW
Monte Carlo simulation study of the ICRF minority heating in the large helical device
[AD-B179858L] p 2708 N95-29749
HELICOPTER PERFORMANCE
An analytic modeling and system identification study of helicopter dynamics p 2498 N95-29787
HELICOPTER PROPELLER DRIVE
Bell Helicopter Advanced Rotocraft Transmission (ART) program
[NASA-CR-195479] p 2590 N95-29538
HELICOPTER WAKES
High-and low-frequency dynamics of isolated blades and rotors with dynamic stall and wake
[AD-A290358] p 2497 N95-29322
HELICOPTERS
Application of parallel processing technology in complex helicopter analysis. Phase 1
[NASA-CR-197850] p 2496 N95-28928
Biodynamic simulation of pilot interaction with a helicopter multiairbag restraint system
[AD-A290196] p 2492 N95-29057
Bell Helicopter Advanced Rotocraft Transmission (ART) program
[NASA-CR-195479] p 2590 N95-29538
Severe edge effects and simple complimentary interior solutions for thin-walled anisotropic and composite structures
[AD-A290645] p 2595 N95-29562
Experience in helicopter aeroevacuation in the community of Madrid, Spain p 2677 N95-29611
First medical test of the UH-60Q and equipment for use in US Army medevac helicopters p 2678 N95-29620
An operational comparison of the CH-46E and HH-60H as Navy combat support helicopter replacement options using the Simulated Mobility Modeling and Analysis Toolbox (SMMAT)
[AD-A288494] p 2498 N95-29911
HELIOTRONS
Transition of radial electric field by electron cyclotron heating in the stellarator plasmas
[AD-B176254L] p 2707 N95-29742
Free-boundary equilibrium studies for the Large Helical Device
[AD-B175931L] p 2707 N95-29743
Formation of positive radial electric field by Electron Cyclotron Heating in Compact Helical System
[AD-B191994L] p 2709 N95-29802
Boronization study for application to large helical device
[AD-B191996L] p 2709 N95-29808
Innovative divertor concepts for LHD
[AD-B191997L] p 2711 N95-30032
HELIUM
Fluxes and relative abundances of light cosmic ray nuclei at energies above 40 GeV/n p 2739 N95-29531
The energy spectrum and flux of cosmic ray helium at high energy p 2740 N95-29705
Characterisation of a line-tunable He-Xe laser operating at 2.026 and 3.894 micrometers
[AD-A291129] p 2587 N95-29914
HELIUM IONS
Depth-independent hardness improvements in ion irradiated polystyrene
[DE95-006682] p 2547 N95-30190
HELIUM ISOTOPES
Proceedings of the 18th International Workshop on Condensed Matter Theories
[AD-A291396] p 2694 N95-30065
HELMET MOUNTED DISPLAYS
Ride motion simulator (RMS) testing using human occupants
[AD-A292641] p 2641 N95-29378
HELMETS
Biodynamic simulation of pilot interaction with a helicopter multiairbag restraint system
[AD-A290196] p 2492 N95-29057
HELMHOLTZ EQUATIONS
Airy functions and the recursive ray acoustics algorithm
[AD-A290182] p 2629 N95-29054
Dispersion analysis and error estimation of Galerkin finite element methods for the numerical computation of waves
[AD-A290296] p 2668 N95-29064
A generalized finite element method for solving the Helmholtz equation in two dimensions with minimal pollution
[AD-A290280] p 2669 N95-29080
Finite element solution to the Helmholtz equation with high wave number. Part 2. The h-p version of the FEM
[AD-A290289] p 2669 N95-29084
HEMATOPOIETIC SYSTEM
The influence of space flight on erythrokinetics in man. Space Life Sciences Missions 1 and 2. Experiment E261
[NASA-CR-188368] p 2633 N95-28875
HERMETIC SEALS
Hermetically sealed aluminum electrolytic capacitor p 2568 N95-30268
HETEROGENEITY
Short term visits for collaborative research
[AD-A290704] p 2682 N95-29588
Realisation of an integrated software engineering environment through heterogeneous CASE-tool integration
[PB95-197646] p 2653 N95-30105
Structured approach for the methodical and technical integration of heterogeneous CASE tools
[PB95-197653] p 2655 N95-30218
HETEROJUNCTION DEVICES
Novel electric-field effects in quantum wells and superlattices
[AD-A292317] p 2718 N95-28857
Epitaxial growth and characterization of Si(1-x)Ge(x) materials and devices
[AD-A292528] p 2712 N95-28874
The 41st Japan Society of Applied Physics Spring Meeting
[AD-A292333] p 2720 N95-29879
HETEROJUNCTIONS
Structural and electronic properties of adsorbates on semiconductors, metal-semiconductor interfaces and semiconductor heterojunctions
[AD-A291917] p 2715 N95-29438
Physical modeling and design of semiconductor heterostructures for optical and electronical applications p 2682 N95-30232
HEURISTIC METHODS
Fast simulation of the leaky bucket algorithm
[PB95-197174] p 2653 N95-30098
HEXADIENE
Conjugated polymers from cyclohexadienediol monomers
[AD-A290247] p 2544 N95-29505
HIERARCHIES
Computational complexity and encryption
[AD-A291910] p 2648 N95-29356
Learning object models from visual observation and background knowledge
[AD-A292606] p 2650 N95-29576
HIGH ALTITUDE
Refractive changes during prolonged exposure to altitude following refractive surgery
[AD-A290263] p 2635 N95-29173
The high-altitude polar wind: Simulation and observation p 2622 N95-29688
HIGH ASPECT RATIO
Algorithms for high aspect ratio oriented triangulations p 2479 N95-28731
The fluid mechanics of a high aspect ratio slot with an impressed pressure gradient and secondary injection p 2580 N95-30304
HIGH CURRENT
Vacuum microelectronic emitters and their applications using compound semiconductor technology
[AD-A291142] p 2567 N95-30124
HIGH ENERGY ELECTRONS
Relativistic effects on large amplitude nonlinear langmuir waves in a two-fluid plasma
[AD-B191980L] p 2710 N95-29841
Induced Compton scattering by relativistic electrons in magnetized astrophysical plasmas p 2610 N95-29885
HIGH ENERGY INTERACTIONS
Thickness measurement of ammonia targets used in SLAC e143 experiment
[AD-A290215] p 2692 N95-29076
A practical high-energy high-luminosity mu(+)-mu(-) collider
[DE95-006769] p 2696 N95-30009
Lattice/beam dynamics working group
[DE95-006774] p 2696 N95-30021
Sea and gluon spin structure function measurements at RHIC
[DE95-005823] p 2695 N95-30185
Measurements of (Delta)(sigma)(sub L)(pp) and (Delta)(sigma)(sub L)((bar p)p) at 200 GeV/c
[DE95-005837] p 2695 N95-30186
HIGH FIELD MAGNETS
Studies directed toward new and improved permanent magnet materials
[AD-A290749] p 2681 N95-29481
HIGH FREQUENCIES
A study of power diode failure mechanisms in the US Army research laboratory 30-mm solid propellant electrothermal-chemical (SPETC) gun facility
[AD-A291300] p 2585 N95-29938
HIGH GAIN
High gain, low noise and broadband Raman and Brillouin fiber-optic amplifiers, channel selectors and switches
[AD-A290585] p 2700 N95-29553
HIGH LEVEL LANGUAGES
Efficient compilation of high-level data parallel algorithms
[AD-A290362] p 2659 N95-29225
HIGH POLYMERS
The synthesis of liquid crystalline phophazenes containing chiral mesogens
[AD-A291911] p 2543 N95-29358
HIGH POWER LASERS
Topics in high-peak intensity, ultrashort pulse laser-plasma interactions p 2704 N95-29218
A compact universal power supply for laser diodes
[AD-A289950] p 2585 N95-29274
Development of distributed feedback dye lasers for generation of high-power 193 nm excimer laser short pulses p 2586 N95-29631
HIGH PRESSURE
High power switch design
[AD-A291608] p 2565 N95-29601
Cylinder-averaged histories of nitrogen oxide in a DI diesel with simulated turbocharging
[AD-A290568] p 2590 N95-29820
HIGH RESOLUTION
Statistical properties of bistatic clutter echoes
[AD-A291688] p 2552 N95-28943
A numerical study of the effects of wind forcing on the Chile Current System
[AD-A289808] p 2629 N95-28982
High resolution, large scale measurement processes
[AD-A292200] p 2681 N95-28987
Analysis of the structural characteristics and intensity evolution of super typhoon flo (1990) in special sensor Microwave/Imager (SSM/I) data
[AD-A292413] p 2619 N95-28989
High resolution microwave survey
[NASA-TM-110566] p 2553 N95-29174
The Los Alamos Photon Counting Detector Debris Detection Project: An update
[DE95-007883] p 2508 N95-29464
High resolution direct digitizitation and optical telemetry of shipboard antenna signals
[AD-A290238] p 2557 N95-29504
Signal processing for high-resolution image formation
[AD-A290648] p 2557 N95-29563
Computational algorithms for aerodynamic analysis and design
[AD-A291084] p 2491 N95-29972
HIGH REYNOLDS NUMBER
Supercritical states of two-dimensional wall-bounded shear flow p 2580 N95-30303
HIGH SPEED
Methods and components for optical contention resolution in high speed networks
[AD-A292331] p 2697 N95-28795
Low threshold all-optical crossbar switch on GaAs-GaAlAs channel waveguide arrays
[AD-A292483] p 2712 N95-28862
Modeling and control of rotating stall in high speed multi-stage axial compressors p 2500 N95-29244
Compressibility effects on and control of dynamic stall of oscillating airfoil
[AD-A291804] p 2489 N95-29428
Signal processing for high-resolution image formation
[AD-A290648] p 2557 N95-29563
Relativistic effects on large amplitude nonlinear langmuir waves in a two-fluid plasma
[AD-B191980L] p 2710 N95-29841
Characterization of stall inception in high-speed single-stage compressors
[AD-A291275] p 2501 N95-29934
Vertical cavity surface emitting lasers for optical signal processing and optical computing applications
[AD-A290626] p 2588 N95-30050
Numerical simulation of stability and stability control of high speed compressible rotating couette flow
[NASA-CR-198832] p 2579 N95-30250
HIGH SPEED CAMERAS
The use of charge coupled devices in astronomical speckle imaging p 2727 N95-29545
HIGH STRENGTH
EMI Shields made from intercalated graphite composites
[NASA-TM-106979] p 2518 N95-28906

Bilateral US/Russia Workshop on Self-Propagating High-Temperature Synthesis held in Honolulu, Hawaii on 6-7 November 1993
[AD-A290466] p 2525 N95-29492

HIGH STRENGTH STEELS
Correlation of inclusion size and chemistry with weld metal composition and microstructure arc weldments of high strength steels
[AD-A292024] p 2590 N95-29184

HIGH TEMPERATURE
Synthesis and characterization of CuO superconductors with high transient temperatures
[AD-A292478] p 2562 N95-29014
High temperature thermosets and ceramics derived from linear carborane-(siloxane or silane)-acetylene copolymers
[AD-D017400] p 2545 N95-29569
Modeling the boundary layer interactions between weakly ionized plasmas and cooled, planar electrodes in stagnation-point flows p 2706 N95-29717
Innovative processing of composites for ultra-high temperature applications, book 1
[AD-A290889] p 2527 N95-29842
High temperature spectroscopy of alkali metal vapors for solar to thermal energy conversion
[AD-A291355] p 2602 N95-29949

HIGH TEMPERATURE AIR
Demonstration of a stabilized alumina/ethanol colloidal dispersion technique for seeding high temperature air flows
[NASA-TM-106945] p 2582 N95-29113

HIGH TEMPERATURE ENVIRONMENTS
Non-coincident multi-wavelength emission absorption spectroscopy
[DE95-006480] p 2530 N95-28776
Advanced composite structural concepts and materials technologies for primary aircraft structures: Advanced material concepts
[NASA-CR-4485] p 2496 N95-29027
High-temperature optical window design
[NASA-TM-106783] p 2596 N95-30008

HIGH TEMPERATURE PLASMAS
Insights on the local density approximation plasma polarization shift as provided by the optimum potential method
[DE95-008078] p 2705 N95-29466
Heavy light bullets in electron-positron plasma
[DE95-008751] p 2711 N95-30173

HIGH TEMPERATURE RESEARCH
Bilateral US/Russia Workshop on Self-Propagating High-Temperature Synthesis held in Honolulu, Hawaii on 6-7 November 1993
[AD-A290466] p 2525 N95-29492

HIGH TEMPERATURE SUPERCONDUCTORS
Chalcogenide superconductors: A search
[AD-A292523] p 2560 N95-28812
Proceedings of the 38th Annual Conference on Magnetism and Magnetic Materials
[AD-A286751] p 2681 N95-28962
Computer simulation study of high t(sub c) superconductor structure
[AD-A292513] p 2563 N95-29163
Optically triggered, superconducting opening switch
[AD-A292642] p 2700 N95-29379
Deposition and surface treatment with intense pulsed ion beams
[DE95-007885] p 2543 N95-29465
Compact substrate heater for use in an oxidizing atmosphere
[AD-A290860] p 2502 N95-29522
Ion beam modification of Tl-Ba-Ca-Cu-O type high temperature superconductors during irradiation
[DE95-006807] p 2717 N95-30022
High Tc superconducting bolometric and nonbolometric infrared (IR) detectors
[NASA-CR-198789] p 2702 N95-30035

HIGH TEMPERATURE TESTS
Demonstration of a stabilized alumina/ethanol colloidal dispersion technique for seeding high temperature air flows
[NASA-TM-106945] p 2582 N95-29113
Computer simulation study of high t(sub c) superconductor structure
[AD-A292513] p 2563 N95-29163
Thermally stable organic polymers
[AD-A290755] p 2543 N95-29482
Bell Helicopter Advanced Rotocraft Transmission (ART) program
[NASA-CR-195479] p 2590 N95-29538
Investigation of tension-compression fatigue behavior of a notched cross-ply metal matrix composite at elevated temperature
[AD-A291479] p 2527 N95-29770

HIGH VOLTAGES
Arcing mitigation and predictions for high voltage solar arrays
[AD-A292227] p 2602 N95-29200
Arcing predictions for PASP PLUS solar arrays
[AD-A292230] p 2602 N95-29201

HISTORIES
NASA: The state of the agency
[NASA-TM-110563] p 2720 N95-29170
Apollo 11: For all mankind
[NASA-TM-110622] p 2503 N95-29407
Proceedings of the 6th International Conference on Nondestructive Characterization of Materials
[AD-A290727] p 2596 N95-29580

HOLDERS
Shock resistant optic fiber rotary slice holding device
[AD-D017327] p 2702 N95-30053

HOLE BURNING
Tunable laser for persistent spectral hole burning optical memories
[AD-A292598] p 2586 N95-29292
High-density plasma dynamics in semiconductors p 2705 N95-29632

HOLE MOBILITY
Optoelectronics based on SiGe/Si heterostructures
[AD-A292464] p 2699 N95-29006

HOLES (MECHANICS)
Leading edge film cooling effects on turbine blade heat transfer
[NASA-TM-106955] p 2500 N95-29115

HOLOGRAPHIC OPTICAL ELEMENTS
N4 processor
[AD-A292571] p 2642 N95-28976
Growth, characterization and application of KTN family nonlinear optical crystals
[AD-A290330] p 2713 N95-29087
Multi-focal length and multi-channel holographic optical element
[AD-A291011] p 2583 N95-29656

HOLOGRAPHY
The role of the coherence function in holographic imaging p 2583 N95-29508
Intensity optical correlation through optical differentiation preprocessing
[AD-A291020] p 2701 N95-29661
Reduce Fluid Experiment System: Flight data from the IML-1 Mission
[NASA-CR-196639] p 2549 N95-30014

HOMING DEVICES
An ultra-high speed incoherent-to-coherent converter for optical computing
[AD-A292658] p 2700 N95-29412

HOMOGENEITY
Cage-like precursor formation from extensive cyclization in sol-gel inorganic condensation polymerization
[AD-A290589] p 2544 N95-29554
Static field solutions and image theory for a conducting sphere with radial anisotropy
[PB95-207171] p 2673 N95-30172

HONEYCOMB STRUCTURES
Impact resistance and damage tolerance of composite sandwich panels p 2526 N95-29549

HORIZON SCANNERS
A conceptual design for the attitude control and determination system for the Magnetosphere Imager spacecraft
[NASA-TP-3560] p 2507 N95-28721

HOT ATOMS
Research into artificially induced atmospheric disturbances
[AD-A290150] p 2613 N95-29317
Semiconductor deposition and etching interactions of laser-generated translationally hot atoms and radicals
[AD-A291824] p 2693 N95-29431

HOT ELECTRONS
Computer simulation study of high t(sub c) superconductor structure
[AD-A292513] p 2563 N95-29163
Hot electron physics of alternating-current thin-film electroluminescent devices
[AD-A290528] p 2696 N95-29495
The high-altitude polar wind: Simulation and observation p 2622 N95-29688
Relativistic effects on large amplitude nonlinear langmuir waves in a two-fluid plasma
[AD-B191980L] p 2710 N95-29841

HOT PRESSING
Daido Steel's Shibukawa Plant, Shibukawa City, Gumma Prefecture, Japan, 29 Jul. 1994
[AD-A292343] p 2536 N95-29467

HOVERING
A fourth order Euler/Navier-Stokes prediction method for the aerodynamics and aeroelasticity of hovering rotor blades p 2572 N95-29242
Development of a rotary wing Navier-Stokes CFD code based on TLNS3D code
[AD-A290421] p 2574 N95-29387
Unsteady pressure and inflow velocity on a pitching rotor blade in hover p 2490 N95-29771
An analytic modeling and system identification study of helicopter dynamics p 2498 N95-29787

HUBBLE SPACE TELESCOPE
Space astronomy update
[NASA-TM-110754] p 2731 N95-30317

HUMAN BEINGS
Organization of the human circadian system
[AD-A288223] p 2634 N95-28915
Analysis of wounds by evaporative water loss in man
[AD-A290327] p 2634 N95-29086
Effects of chromium picolinate on body composition in a remedial conditioning program
[AD-A292079] p 2636 N95-29238

HUMAN BODY
Generator of body data (GEBOD) manual
[AD-A289721] p 2640 N95-28683

HUMAN FACTORS ENGINEERING
Conversion of the TRACON operations concepts database into a formal sentence outline job task taxonomy
[DOT/FAA/AM-95/16] p 2493 N95-28819
WinCD: Complex demodulation time-series analysis for windows
[AD-A291550] p 2645 N95-28934
Operating procedures for Anthropometry and Initial Conditions Photogrammetric Program
[AD-A291553] p 2640 N95-28935
Proceeding of the 33rd SICE Annual Conference
[DE95-758943] p 2662 N95-29144
A human factors evaluation of the operational demonstration flight inspection aircraft
[DOT/FAA/AM-95/18] p 2641 N95-29365
Visual and auditory symbols: A literature review
[AD-A290222] p 2641 N95-29908

HUMAN PERFORMANCE
Conversion of the TRACON operations concepts database into a formal sentence outline job task taxonomy
[DOT/FAA/AM-95/16] p 2493 N95-28819
Task-dependent effects of automation: The role of internal models in performance, workload, and situational awareness in a semi-automated cockpit
[AD-A292536] p 2640 N95-28969
Current issues in the measurement of military aircrew performance: A consideration of the relationship between available metrics and operational concerns
[AD-A292539] p 2640 N95-28970
Astronaut selection (NASA-MIPR)
[AD-A292512] p 2636 N95-29162
Mode of human image representation and error checking strategies in complex visual displays
[AD-A290107] p 2492 N95-29210
Shift work, age, and performance: Investigation of the 2-2-1 shift schedule used in Air Traffic Control facilities I. The sleep/wake cycle
[DOT/FAA/AM-95/19] p 2638 N95-29261
Human fluid balance and dehydration during cold weather military operations
[AD-A289192] p 2636 N95-29757
Adaptations to three weeks of aerobic/anaerobic training in west coast U.S: Navy Sea-Air-Land personnel (SEAL's)
[AD-A291500] p 2637 N95-29846

HUMAN TOLERANCES
CO2-O2 interactions in extension of tolerance to acute hypoxia
[NASA-CR-198575] p 2635 N95-29158

HUMAN-COMPUTER INTERFACE
Summary report for cooperative research and development agreement between Oak Ridge Associated Universities and Interactive Presentation Systems
[DE95-006874] p 2644 N95-28777
A formative evaluation of CU-SeeMe
[AD-A292443] p 2553 N95-29002
A differential approach to graphical interaction
[AD-A292165] p 2647 N95-29125
Georgetown Institute for Cognitive and Computational Sciences
[AD-A289775] p 2639 N95-29458
Client-server interactions in multi-server operating systems: The Mach-US approach
[AD-A290431] p 2650 N95-29536
A study of the conceptual symbolics of information system development languages p 2723 N95-29589
Information management in local area networks: Impact on users' perceptions p 2723 N95-29690
The 2d Eurographics Workshop on Virtual Environments
[AD-A292015] p 2651 N95-29861

HUMIDITY
Effects of temperature and humidity cycling on the strengths of textile reinforced carbon/epoxy composite materials p 2520 N95-29037
Energy budget in the Asian monsoon region p 2623 N95-29713
Research results on an improved in-situ tropospheric humidity sensor
[AD-A291339] p 2627 N95-29944
Development and testing of improved techniques for modeling the hydrologic cycle in a mesoscale weather prediction system
[AD-A291243] p 2627 N95-29993
Extended field observations of cirrus clouds using a ground-based cloud observing system
[NASA-CR-198855] p 2628 N95-30356
HURRICANES
Forecast of Atlantic seasonal hurricane activity for 1995 p 2620 N95-29254
HYBRID STRUCTURES
Adaptive hybrid prismatic-tetrahedral grids for viscous flows p 2481 N95-28744
Three-dimensional hybrid grid generation using advancing front techniques p 2481 N95-28745
Photoproduction of hybrid mesons from CEBAF to HERA
[PB95-196218] p 2691 N95-28913
HYDRAULIC FLUIDS
The effects of aircraft fuel and fluids on the strength properties of Resin Transfer Molded (RTM) composites p 2522 N95-29047
HYDRAULIC JETS
Precision cleaning verification of fluid components by air/water impingement and total carbon analysis
[NASA-TM-110742] p 2531 N95-29248
HYDRAZINES
The fluorescent detection of hydrazine, monomethylhydrazine, and 1,1-dimethylhydrazine by derivatization with aromatic dicarboxaldehydes
[NAVY-CASE-75451] p 2512 N95-29052
HYDRIDES
New tetraarylborate and ethyldibutylstannane reagents
[AD-A289813] p 2540 N95-28953
Super hydrides
[AD-A290594] p 2533 N95-29556
HYDROCARBON COMBUSTION
Feasibility of a jet-stirred reactor for evaluating replacements for halon fire retardants
[AD-A291155] p 2551 N95-30299
HYDROCARBONS
Super hydrides
[AD-A290594] p 2533 N95-29556
Thermal conductivity of liquid halogenated aliphatic hydrocarbons. Part 3: Halogenated higher hydrocarbons (C3 to C16)
[ESDU-94023-PT-3] p 2512 N95-29900
HYDROCHLORIC ACID
Development of a multiplex Fabry-Perot interferometer and measurement of atmospheric HF and HCl p 2608 N95-29213
HYDROCLIMATOLOGY
Hydrology of the continental United States p 2599 N95-29539
HYDROCYANIC ACID
Aperture synthesis observation of HCN J = 1-0 emission from Y Canum Venaticorum p 2735 N95-29839
Analytical potential energy surface for methylene nitramine (CH2NNO2)
[AD-A291247] p 2534 N95-29994
HYDRODYNAMICS
The acoustic characteristics of turbomachinery cavities
[NASA-CR-4671] p 2478 N95-28720
Analyzing the stability of floating ice floes
[AD-A292149] p 2629 N95-29160
Numerical investigation of surface curvature effects in compressible turbulent flows
[AD-A290114] p 2571 N95-29211
Collective phenomena in granular fluids p 2572 N95-29219
The quantum hydrodynamic model for semiconductor devices
[AD-A291809] p 2564 N95-29430
Modeling the boundary layer interactions between weakly ionized plasmas and cooled, planar electrodes in stagnation-point flows p 2706 N95-29717
State-of-the-art review of computational fluid dynamics modeling for fluid-solids systems
[DE95-005866] p 2577 N95-29988
NMR imaging and hydrodynamic analysis of neutrally buoyant non-Newtonian slurry flows
[DE95-005842] p 2578 N95-30187
Massively parallel fast elliptic equation solver for three dimensional hydrodynamics and relativity
[DE95-009385] p 2660 N95-30193
HYDROFLUORIC ACID
Development of a multiplex Fabry-Perot interferometer and measurement of atmospheric HF and HCl p 2608 N95-29213
A cluster beam study of boron, boron oxide and B(x)O(y)H chemistry with hydrogen fluoride
[AD-A290826] p 2533 N95-29722
HYDROGEN
The effects of platinum on nickel electrodes in the nickel hydrogen cell
[AD-A291607] p 2531 N95-28942
The interaction of group 3A atoms with small molecules
[AD-A290285] p 2692 N95-29082
Technology development goals for automotive fuel cell power systems
[DE95-008764] p 2548 N95-29280
Prediction of hydrogen entry and permeation in metals and alloys
[AD-A292047] p 2536 N95-29298
Hydrogen film cooling with incident and swept-shock interactions in a Mach 6.4 nitrogen free stream
[NASA-TM-4603] p 2578 N95-30056
The TMI regenerable solid oxide fuel cell p 2606 N95-30265
HYDROGEN ATOMS
State resolved differential cross sections for reactions important to the decomposition of energetic materials
[AD-A290718] p 2548 N95-29498
Carbon sheet pumping
[AD-B179443L] p 2710 N95-29812
HYDROGEN BONDS
17O NMR of the structural evolution of V2O5 gels
[AD-A290623] p 2545 N95-29559
HYDROGEN IONS
Development of an intense negative hydrogen ion source with a wide-range of external magnetic filter field
[AD-B195514L] p 2705 N95-29567
HYDROGEN OXYGEN ENGINES
A transient model of the RL10A-3-3A rocket engine
[NASA-CR-195478] p 2510 N95-29114
HYDROGEN PLASMA
Effects of impurities released from high Z test limiter on plasma performance in TEXTOR
[AD-B191995L] p 2709 N95-29803
HYDROGEN PRODUCTION
Hydrogen production in fusion reactors
[AD-B180028L] p 2710 N95-29857
HYDROGRAPHY
The structure of water mass, salt, and temperature transports within intermediate depths of the western tropical Atlantic Ocean p 2631 N95-29541
HYDROLOGICAL CYCLE
Soil wetness and climate variability p 2609 N95-29878
Development and testing of improved techniques for modeling the hydrologic cycle in a mesoscale weather prediction system
[AD-A291243] p 2627 N95-29993
HYDROLOGY
Hydrology of the continental United States p 2599 N95-29539
Development and testing of improved techniques for modeling the hydrologic cycle in a mesoscale weather prediction system
[AD-A291243] p 2627 N95-29993
HYDROLOGY MODELS
Microwave remote sensing of surface soil moisture and its application to hydrologic modeling p 2600 N95-29821
HYDROLYSIS
Coupling of brain muscarinic receptors to second messengers
[AD-A290498] p 2635 N95-29153
Cage-like precursor formation from extensive cyclization in sol-gel inorganic condensation polymerization
[AD-A290589] p 2544 N95-29554
HYDROMETEOROLOGY
The dynamics of circulations within the stratiform regions of squall lines p 2623 N95-29725
HYDROMETEORS
A study of precipitation using dual-frequency and interferometric Doppler radars p 2627 N95-29877
HYDROPHONES
Balanced, double-sided calibration circuit for sensor element differential pre-amplifier
[AD-D017326] p 2566 N95-30052
HYDROSTATIC PRESSURE
Raman and photo-modulated reflectivity studies of ZnTe/InAs semiconductor heterostructure under hydrostatic pressure
[AD-A290467] p 2716 N95-29506
Membrane fluidity and shape of human red blood cells are altered by physiological levels of hydrostatic pressure
[AD-A290595] p 2636 N95-29557
Effect of mild hydrostatic pressure on red blood cells
[AD-A290520] p 2637 N95-29872
HYDROXYL EMISSION
An investigation of thunderstorms as a source of short period mesospheric gravity waves
[AD-A289795] p 2611 N95-28697
HYGRAL PROPERTIES
Analytical investigation of the hygrothermal effects and parametric study of the Edge Crack Torsion (ECT) mode 3 test lay-ups
[NASA-TM-110183] p 2528 N95-30028
HYGROSCOPICITY
Compressive behavior of thick composite shells: Benchmark solutions for loss of stability and hygroscopic effects p 2595 N95-29424
HYPERBARIC CHAMBERS
Membrane fluidity and shape of human red blood cells are altered by physiological levels of hydrostatic pressure
[AD-A290595] p 2636 N95-29557
HYPERBOLIC DIFFERENTIAL EQUATIONS
Systems of hyperbolic partial differential equations
[AD-A290287] p 2669 N95-29083
Stochastic hyperbolic and parabolic partial differential equations
[AD-A290372] p 2669 N95-29229
The large discretization step method for time-dependent partial differential equations
[NASA-CR-195068] p 2670 N95-29403
The application of adaptive mesh refinement to the numerical simulation of compressible flow
[AD-A289595] p 2577 N95-30027
Second-order numerical solution of time-dependent, first-order hyperbolic equations p 2674 N95-30143
HYPERBOLIC FUNCTIONS
Computational aeroacoustics using hyperbolic wave primitives p 2686 N95-30136
HYPERCAPNIA
CO2-O2 interactions in extension of tolerance to acute hypoxia
[NASA-CR-198575] p 2635 N95-29158
HYPERCUBE MULTIPROCESSORS
High performance electromagnetic simulation tools
[AD-A290405] p 2554 N95-29235
The study of non-Newtonian contraction flows with a parallel finite element method p 2576 N95-29778
HYPERGOLIC ROCKET PROPELLANTS
The fluorescent detection of hydrazine, monomethylhydrazine, and 1,1-dimethylhydrazine by derivatization with aromatic dicarboxaldehydes
[NAVY-CASE-75451] p 2512 N95-29052
HYPERSONIC BOUNDARY LAYER
Linear stability analysis of hypersonic boundary layers
[AD-A290159] p 2569 N95-29024
HYPERSONIC FLOW
Linear stability analysis of hypersonic boundary layers
[AD-A290159] p 2569 N95-29024
A study of fluid problems requiring a direct particle simulation
[AD-A290212] p 2658 N95-29074
An extension of the continuum model by Grad's thirteen moment equations for hypersonic rarefied flows p 2488 N95-29118
Interaction of turbulence with complex shock waves
[AD-A290225] p 2571 N95-29145
Investigation of Burnett equations for two-dimensional hypersonic flow
[AD-A290233] p 2575 N95-29469
Hydrogen film cooling with incident and swept-shock interactions in a Mach 6.4 nitrogen free stream
[NASA-TM-4603] p 2578 N95-30056
Numerical simulation and analysis of the hypersonic turbulent flow past a blunt-fin/ramp configuration
[DLR-FB-94-19] p 2492 N95-30349
HYPERSONIC NOZZLES
Use of the PARC code to estimate the off-design transonic performance of an over/under turboramjet nozzle
[NASA-TM-106924] p 2491 N95-30091
HYPERSONIC SHOCK
Investigation of Burnett equations for two-dimensional hypersonic flow
[AD-A290233] p 2575 N95-29469
HYPERSONIC SPEED
Unsteadiness of shock-induced turbulent boundary layer separation. An inherent feature of turbulent flow or solely a wind tunnel phenomenon
[AD-A290367] p 2572 N95-29228
Transonic, supersonic and hypersonic wind-tunnel tests on aerodynamic characteristics of reentry body with blunted cone configuration
[ISAS-658] p 2490 N95-29640
HYPERSONICS
Computation of the integrated aerodynamic and propulsive flowfields of a generic hypersonic space plane p 2490 N95-29788

An aerodynamic and static-stability analysis of the Hypersonic Applied Research Technology (HART) missile
[DA9426923] p 2491 N95-29965

HYPERVELOCITY IMPACT
A layman's look at orbital debris
[AD-A289801] p 2506 N95-28700
Investigation of optical damage, energy partitioning and scaling laws at extremely high velocities
[AD-A291368] p 2703 N95-30062

HYPOTHESES
High-performance speech recognition using consistency modeling
[AD-A290655] p 2557 N95-29564

HYPOXIA
CO2-O2 interactions in extension of tolerance to acute hypoxia
[NASA-CR-198575] p 2635 N95-29158
Effect of hypoxia on arterial blood gases in subjects with lung dysfunction p 2638 N95-29627

HYSTERESIS
Proceedings of the 38th Annual Conference on Magnetism and Magnetic Materials
[AD-A286751] p 2681 N95-28962

I

ICE
Microwave remote sensing algorithms for cirrus clouds and precipitation p 2623 N95-29715
Sea ice motions in the Central Arctic pack ice as inferred from AVHRR imagery
[NASA-CR-198835] p 2601 N95-30247

ICE CLOUDS
Microwave remote sensing algorithms for cirrus clouds and precipitation p 2623 N95-29715

ICE FLOES
Analyzing the stability of floating ice floes
[AD-A292149] p 2629 N95-29160

ICE FORMATION
Users manual for the improved NASA Lewis ice accretion code LEWICE 1.6
[NASA-CR-198355] p 2492 N95-29132
Hailstone heat and mass transfer measurements
[ISBN-0-315-86304-8] p 2624 N95-29797

ICE MAPPING
Sea ice motions in the Central Arctic pack ice as inferred from AVHRR imagery
[NASA-CR-198835] p 2601 N95-30247

ICE PREVENTION
An analysis of B-1B exterior jet blast windshield anti-icing performance using pre-cooled compressor bleed air
[AD-A292522] p 2492 N95-28811

IDEAL GAS
Thermophysical properties of R-32 (difluoromethane)
[ESDU-94032] p 2530 N95-28802
Numerical simulation and analysis of the hypersonic turbulent flow past a blunt-fin/ramp configuration
[DLR-FB-94-19] p 2492 N95-30349

IDENTIFYING
Visualization of CAD objects using a stereoscopic display
[AD-A290034] p 2639 N95-29439
Software risk evaluation method version 1.0
[AD-A290597] p 2652 N95-30047

IDENTITIES
Formal aspects of object identity in database manipulation p 2722 N95-29116
Adaptive Infinite Impulse Response (IIR) filter system
[AD-D017403] p 2564 N95-29570

IGNITION
Fire hardening assessment (FHA) technology for composite systems
[AD-A289964] p 2523 N95-29277
A thermochemical transport model for analysis of hot-spot formation in energetic materials
[AD-A290441] p 2532 N95-29357
Ionizational nonequilibrium and ignition in plasma accelerators p 2705 N95-29547
A theoretical study on ignition mechanisms of liquid propellants
[AD-A290589] p 2549 N95-29550
Cylinder-averaged histories of nitrogen oxide in a DI diesel with simulated turbocharging
[AD-A290568] p 2590 N95-29820

IMAGE ANALYSIS
Reflectance analysis under solar illumination
[AD-A290489] p 2737 N95-29151

IMAGE CLASSIFICATION
Optical (LANDSAT/TM) and radar (ERS-1/SAR) imagery sinergism studies applied to land use discrimination
[INPE-5608-TDI/554] p 2598 N95-29433

IMAGE ENHANCEMENT
An image cancellation approach to depth-from-focus
[DE95-007625] p 2697 N95-28912

IMAGE PROCESSING
Using ordered binary-decision diagrams for compressing images and image sequences
[AD-A292244] p 2721 N95-28880
Modeling foreshortening in stereo vision using local spatial frequency
[AD-A292246] p 2645 N95-28883
An image cancellation approach to depth-from-focus
[DE95-007625] p 2697 N95-28912
Monitoring of burning in the Brazilian cerrado region using AVHRR/NOAA data calibrated by TM/Landsat data
[INPE-5490-TDI/507] p 2598 N95-28929
Operating procedures for Anthropometry and Initial Conditions Photogrammetric Program
[AD-A291553] p 2640 N95-28935
Intermediate levels of visual processing
[AD-A291569] p 2638 N95-28937
Multilayer piecewise linear networks. Revision 1
[AD-A289885] p 2658 N95-28955
High performance hardware and software for pattern recognition and image processing
[AD-A292307] p 2646 N95-28964
Design, development and testing of a prototype precision angular positioning control system for a next generation multiplexed imager
[AD-A292585] p 2698 N95-28980
Computer models of retinal function
[AD-A290156] p 2634 N95-29022
A differential approach to graphical interaction
[AD-A292165] p 2647 N95-29125
Accurate feature detection and estimation using nonlinear and multiresolution analysis
[AD-A290267] p 2553 N95-29176
Feature-oriented image reconstruction and aero-optic metrology in turbulence
[AD-A290269] p 2699 N95-29177
Relative affine structure: Canonical model for 3D from 2D geometry and applications
[AD-A290085] p 2670 N95-29352
Optical (LANDSAT/TM) and radar (ERS-1/SAR) imagery sinergism studies applied to land use discrimination
[INPE-5608-TDI/554] p 2598 N95-29433
Towards an example-based image compression architecture for video-conferencing
[AD-A290041] p 2556 N95-29441
Object oriented segmentation of images
[AD-A290792] p 2671 N95-29485
Randomized inquiries about shape: An application to handwritten digit recognition
[AD-A290812] p 2675 N95-29634
Unconventional image recovery techniques
[AD-A290799] p 2701 N95-29646
Intensity optical correlation through optical differentiation preprocessing
[AD-A291020] p 2701 N95-29661
Photorefractive Bi12SiO20 spatial light modulator
[AD-A291070] p 2702 N95-29969
Reduce Fluid Experiment System: Flight data from the IML-1 Mission
[NASA-CR-196639] p 2549 N95-30014
W-matrices, nonorthogonal multiresolution analysis, and finite signals of arbitrary length
[DE95-005846] p 2652 N95-30020
Retrieval, display, and analysis support tool for earth imagery (RDAST)
[AD-A291366] p 2601 N95-30061
Distortion-invariant optical pattern recognition by correlative matrix feature criterion
[AD-A291389] p 2703 N95-30064
Patch diameter limits for tiered subaperture SAR image formation algorithms
[DE95-008816] p 2560 N95-30177
Parallel rendering
[NASA-CR-195080] p 2655 N95-30306

IMAGE RECONSTRUCTION
Feature-oriented image reconstruction and aero-optic metrology in turbulence
[AD-A290269] p 2699 N95-29177
Unconventional image recovery techniques
[AD-A290799] p 2701 N95-29646
Speckle imaging with the multi-anode microchannel array detector p 2728 N95-29652
Extended dust shells around carbon stars resolved by HIRAS p 2735 N95-29840

IMAGE RESOLUTION
(DEPSCOR-92) acquisition of a metallurgical optical microscope
[AD-A292439] p 2698 N95-28998
Accurate feature detection and estimation using nonlinear and multiresolution analysis
[AD-A290267] p 2553 N95-29176
Applied optics laboratory
[AD-A292006] p 2701 N95-29571
W-matrices, nonorthogonal multiresolution analysis, and finite signals of arbitrary length
[DE95-005846] p 2652 N95-30020

IMAGERY
Upgrading the Day/Night whole sky imager from Manual/Interactive to full automatic control
[AD-A292296] p 2619 N95-28872
Towards an example-based image compression architecture for video-conferencing
[AD-A290041] p 2556 N95-29441
Object oriented segmentation of images
[AD-A290792] p 2671 N95-29485

IMAGES
Design, development and testing of a prototype precision angular positioning control system for a next generation multiplexed imager
[AD-A292585] p 2698 N95-28980
Feature-oriented image reconstruction and aero-optic metrology in turbulence
[AD-A290269] p 2699 N95-29177
Applied optics laboratory
[AD-A292006] p 2701 N95-29571
Multi-focal length and multi-channel holographic optical element
[AD-A291011] p 2583 N95-29656
Distortion-invariant optical pattern recognition by correlative matrix feature criterion
[AD-A291389] p 2703 N95-30064
Patch diameter limits for tiered subaperture SAR image formation algorithms
[DE95-008816] p 2560 N95-30177

IMAGING TECHNIQUES
STS-67 mission highlights resource tape
[NASA-TM-110530] p 2504 N95-28715
The physics of spin polarized gases
[AD-A292511] p 2680 N95-28810
Surface conversion techniques for low energy neutral atom imagers
[NASA-CR-196604] p 2691 N95-28856
Modeling foreshortening in stereo vision using local spatial frequency
[AD-A292246] p 2645 N95-28883
An image cancellation approach to depth-from-focus
[DE95-007625] p 2697 N95-28912
Fourier Synthesis Lithographic Machine for large panel display fabrication
[AD-A291921] p 2698 N95-28914
A nonintrusive method of quantifying flow visualization data in vortex flow fields
[AD-A289802] p 2568 N95-28948
Regional seismic event identification and improved locations with small arrays
[AD-A292188] p 2612 N95-28985
Nonlinear calibration of an infrared radiometer
[AD-A292436] p 2698 N95-28996
Nanofabrication of electronic devices with the scanning tunneling microscope
[AD-A292463] p 2581 N95-29005
Interactive multimedia presentation for applied computer tomography: Impact
[AD-A291955] p 2640 N95-29020
Photogenerated amines in the design of imaging materials: The radiation-induced imidization of functionalized polystyrenes bearing amide-ester side chains
[AD-A289943] p 2542 N95-29270
Photogenerated amines in polymer curing and imaging: Design and synthesis of (3', 5'-dimethoxybenzoinyl)oxycarbonyl carbamates as novel photoprecursors of amines
[AD-A289945] p 2542 N95-29272
The detection of oil slicks at night with airborne infrared imagers
[AD-A289731] p 2598 N95-29281
Simulated imaging properties of a series of magnetic electron lenses
[NASA-CR-195474] p 2564 N95-29406
Compressibility effects on and control of dynamic stall of oscillating airfoil
[AD-A291804] p 2489 N95-29428
Optical (LANDSAT/TM) and radar (ERS-1/SAR) imagery sinergism studies applied to land use discrimination
[INPE-5608-TDI/554] p 2598 N95-29433
The 1994 IEEE International Workshop on Intelligent Signal Processing and Communication Systems (ISPACS94)
[AD-A292312] p 2556 N95-29474
The role of the coherence function in holographic imaging p 2583 N95-29508
Passive ranging with an incoherent optical system p 2700 N95-29543
The use of charge coupled devices in astronomical speckle imaging p 2727 N95-29545

Signal processing for high-resolution image formation
[AD-A290648] p 2557 N95-29563
Applied optics laboratory
[AD-A292006] p 2701 N95-29571
The x-ray scattering halo around Sco-X1
p 2727 N95-29591
Unconventional image recovery techniques
[AD-A290799] p 2701 N95-29646
Coronagraphic imaging of protoplanetary-disk candidate stars using adaptive optics p 2728 N95-29651
Speckle imaging with the multi-anode microchannel array detector p 2728 N95-29652
The properties of local poor Abell clusters and instrumentation for the study of clustered objects
p 2730 N95-29827
Development of improved geophysical imaging techniques for environmental site characterization
[AD-A291003] p 2558 N95-29875
Probabilistic modeling and statistical inference for random fields and space-time processes
[AD-A289956] p 2672 N95-30029
Diffraction limited imaging using aberrated optics
[AD-A290912] p 2703 N95-30081
Patch diameter limits for tiered subaperture SAR image formation algorithms
[DE95-008816] p 2560 N95-30177
NMR imaging and hydrodynamic analysis of neutrally buoyant non-Newtonian slurry flows
[DE95-005842] p 2578 N95-30187
Boundary-layer transition and global skin friction measurement with an oil-fringe imaging technique
[NASA-CR-198814] p 2579 N95-30224

IMMOBILIZATION
Polymeric microcapsule arrays
[AD-A291937] p 2539 N95-28850
Proceedings of the 11th congress of the international society for artificial cells, blood substitutes and immobilization biotechnology
[AD-A290342] p 2632 N95-29088

IMMUNE SYSTEMS
Studies of altered response to infection induced by severe injury
[AD-A288907] p 2634 N95-29139

IMPACT
Finite element technology for penetration problems
[AD-A290644] p 2671 N95-29516
High velocity impact and penetration of thick composite laminates
[AD-A290642] p 2526 N95-29561

IMPACT DAMAGE
Analysis of static contact in laminated composite plates using damage mechanics
[NASA-CR-198656] p 2513 N95-28809
Impact damage resistance of composite fuselage structure, part 2 p 2516 N95-28838
A designed experiment in stitched/RTM composites
p 2522 N95-29046
The combined effect of glass buffer strips and stitching on the damage tolerance of composites
p 2522 N95-29049
Effect of nose shape and mass of the impactor on impact damage of laminated composites
[AD-A290351] p 2594 N95-29067
Experimental investigations of wave and fracture phenomena in impacted ceramics and glasses
[AD-A292142] p 2542 N95-29195
Damage tolerance in filament-wound graphite/epoxy pressure vessels
[NASA-CR-198804] p 2590 N95-29369
Investigation of optical damage, energy partitioning and scaling laws at extremely high velocities
[AD-A291368] p 2703 N95-30062
Impact damage resistance and residual property assessment of (0/+/-45/90)s SCS-6/Timetal 21S
[NASA-TM-110178] p 2529 N95-30340

IMPACT LOADS
An impact load identification method using distributed sensor measurements p 2595 N95-29419
Finite element technology for penetration problems
[AD-A290644] p 2671 N95-29516
Robust algorithms for penetration mechanics problems
[AD-A290650] p 2650 N95-29517

IMPACT RESISTANCE
Effect of nose shape and mass of the impactor on impact damage of laminated composites
[AD-A290351] p 2594 N95-29067
Impact resistance and damage tolerance of composite sandwich panels p 2526 N95-29549
Impact properties of coated engineering plastics
[PB95-197281] p 2547 N95-30201
Impact damage resistance and residual property assessment of (0/+/-45/90)s SCS-6/Timetal 21S
[NASA-TM-110178] p 2529 N95-30340

IMPACT STRENGTH
Impact properties of coated engineering plastics
[PB95-197281] p 2547 N95-30201

IMPACT TESTS
A designed experiment in stitched/RTM composites
p 2522 N95-29046
Composite processing development to improve interlaminar strength using ply interface particles
[NASA-TM-108495] p 2529 N95-30334
Impact damage resistance and residual property assessment of (0/+/-45/90)s SCS-6/Timetal 21S
[NASA-TM-110178] p 2529 N95-30340

IMPACT TOLERANCES
Impact damage resistance of composite fuselage structure, part 2 p 2516 N95-28838
The combined effect of glass buffer strips and stitching on the damage tolerance of composites
p 2522 N95-29049
Damage tolerance in filament-wound graphite/epoxy pressure vessels
[NASA-CR-198804] p 2590 N95-29369

IMPACTORS
Effect of nose shape and mass of the impactor on impact damage of laminated composites
[AD-A290351] p 2594 N95-29067
Robust algorithms for penetration mechanics problems
[AD-A290650] p 2650 N95-29517

IMPEDANCE
The use of electrochemistry and ellipsometry for identifying and evaluating corrosion on aircraft
[AD-A290249] p 2497 N95-29426
High power switch design
[AD-A291608] p 2565 N95-29601
Electrochemical impedance pattern recognition for detection of hidden chemical corrosion on aircraft components, phase 1
[AD-A291345] p 2593 N95-29946
The Scanning Fast Field Program (SCAFFIP) general version 1.0 user's manual
[AD-A291209] p 2618 N95-29976
Robust testing of cellular neural networks
[AD-A291219] p 2665 N95-29979

IMPLOSIONS
Bubble fusion: Preliminary estimates of spherical micro-implosions in cavitating liquids
[DE95-006260] p 2569 N95-28956

IMPULSES
Analysis of multigrid techniques for system modeling with toeplitz approximation
[AD-A289784] p 2644 N95-28694
Adaptive Infinite Impulse Response (IIR) filter system
[AD-D017403] p 2564 N95-29570

IMPURITIES
Effective emission and ionization rate coefficients of atomic carbons in plasmas
[AD-B175932L] p 2707 N95-29740
Effects of impurities released from high Z test limiter on plasma performance in TEXTOR
[AD-B191995L] p 2709 N95-29803

IN SITU MEASUREMENT
In-plant testing of membranes to treat electroplating wastewater
[NASA-CR-198796] p 2532 N95-29250
In situ measurements of ClO and implications for the chemistry of inorganic chlorine in the lower stratosphere
p 2618 N95-29830

INCLUSIONS
Correlation of inclusion size and chemistry with weld metal composition and microstructure arc weldments of high strength steels
[AD-A292024] p 2590 N95-29184
Micromechanics of crack extension in composites
p 2529 N95-30276

INCOHERENCE
The role of the coherence function in holographic imaging p 2583 N95-29508

INCOMPRESSIBLE FLOW
Finite element vorticity-based methods for the solution of the incompressible and compressible Navier-Stokes equations p 2570 N95-29119
Dynamic stall of a NACA 0012 airfoil in laminar flow
p 2489 N95-29243
Rigorous drag bounds in turbulent shear flow
p 2573 N95-29334
Supercritical states of two-dimensional wall-bounded shear flow p 2580 N95-30303
Pressure updating methods for the steady-state fluid equations
[NASA-CR-198163] p 2674 N95-30353

INCOMPRESSIBLE FLUIDS
A novel approach to the numerical simulation of turbulent flows
[AD-A290352] p 2569 N95-29068
Attractors of dissipative structure in three dissipative fluids
[AD-B180030L] p 2710 N95-29844

INDENTATION
Impact resistance and damage tolerance of composite sandwich panels p 2526 N95-29549

INDEXES
Annotated bibliography of software engineering laboratory literature
[NASA-CR-189406] p 2644 N95-28805

INDEXES (DOCUMENTATION)
Aerospace medicine and biology: A continuing bibliography with indexes (supplement 403)
[NASA-SP-7011(403)] p 2636 N95-29190
SeaWiFS technical report series. Volume 24: SeaWiFS technical report series cumulative index, volumes 1-23
[NASA-TM-104556] p 2631 N95-30236
Distributed queries and incremental updates in information retrieval systems p 2725 N95-30286

INDIUM
Synthesis of nanocrystalline indium arsenide and indium phosphide from Indium(III) halides and tris(trimethylsilyl)pnicogens; synthesis, characterization, and decomposition behavior of I3In(dot)P(SiMe3)3
[AD-A291905] p 2715 N95-29486

INDIUM ANTIMONIDES
Interfaces in InAsSb/InGaAs strained-layer superlattices grown by MOCVD for use in infrared emitters
[DE95-006323] p 2717 N95-29990
Ordering and bandgap reduction in InAs(1-x)Sb(x) alloys
[DE95-006324] p 2717 N95-30005
Auger rates in mid-IR InAsSb laser structures
[DE95-006325] p 2588 N95-30006

INDIUM ARSENIDES
Development of ultra-low dark current, high performance 3-5 quantum well infrared photodetectors (QWIPs) for focal plane arrays staring imaging sensor systems
[AD-A290343] p 2714 N95-29089
Synthesis of nanocrystalline indium arsenide and indium phosphide from Indium(III) halides and tris(trimethylsilyl)pnicogens; synthesis, characterization, and decomposition behavior of I3In(dot)P(SiMe3)3
[AD-A291905] p 2715 N95-29486
Raman and photo-modulated reflectivity studies of ZnTe/InAs semiconductor heterostructure under hydrostatic pressure
[AD-A290467] p 2716 N95-29506
Interfaces in InAsSb/InGaAs strained-layer superlattices grown by MOCVD for use in infrared emitters
[DE95-006323] p 2717 N95-29990
Ordering and bandgap reduction in InAs(1-x)Sb(x) alloys
[DE95-006324] p 2717 N95-30005
Auger rates in mid-IR InAsSb laser structures
[DE95-006325] p 2588 N95-30006

INDIUM COMPOUNDS
Multi-decade time-dependent voltage of polycrystalline thin-film solar cells p 2602 N95-29103

INDIUM GALLIUM ARSENIDES
The 1.3 micrometer fiber photodetector
[AD-A292462] p 2582 N95-29004
Investigation of a normal incident high performance P-type strained layer In(0.3)Ga(0.7)As/In(0.52)Al(0.48)As quantum well infrared photodetector
[AD-A290946] p 2716 N95-29785
Interfaces in InAsSb/InGaAs strained-layer superlattices grown by MOCVD for use in infrared emitters
[DE95-006323] p 2717 N95-29990

INDIUM PHOSPHIDES
Electronic properties of low-temperature grown III/V thin films
[AD-A292521] p 2714 N95-29165
Synthesis of nanocrystalline indium arsenide and indium phosphide from Indium(III) halides and tris(trimethylsilyl)pnicogens; synthesis, characterization, and decomposition behavior of I3In(dot)P(SiMe3)3
[AD-A291905] p 2715 N95-29486

INDOLES
Reaction field (RF) calculation of the spectral shifts of indole
[AD-A290449] p 2532 N95-29487

INDUCTANCE
High power switch design
[AD-A291608] p 2565 N95-29601

INDUSTRIAL WASTES
In-plant testing of membranes to treat electroplating wastewater
[NASA-CR-198796] p 2532 N95-29250

INDUSTRIES
The 6th Van der Ziel symposium on quantum 1/f noise and other low frequency fluctuations in electronic devices
[AD-A292468] p 2718 N95-29009
Inhalation Toxicology Research Institute
[AD-A292037] p 2635 N95-29188

Materials for tomorrow's infrastructure: A ten-year plan for deploying high-performance construction materials and systems
[AD-A289782] p 2526 N95-29598

INELASTIC SCATTERING
AB initio studies of electron and positron scattering from non-linear molecules
[AD-A292586] p 2692 N95-28981
Neutron scattering from amorphous, disordered and nanocrystalline materials
[DE95-005848] p 2717 N95-30077

INELASTIC STRESS
Test load verification through strain data analysis
[NASA-TP-3558] p 2504 N95-28718
In-phase thermomechanical fatigue mechanisms in an unidirectional SCS-6/Ti 15-3 MMC
[NASA-CR-195482] p 2523 N95-29133

INEQUALITIES
Linear matrix inequalities for the problem of absolute stability of control systems p 2501 N95-29680

INERTIAL CONFINEMENT FUSION
Design of an electronic charged particle spectrometer to measure (rho R), yield, and implosion symmetry on the OMEGA Upgrade
[DE95-006088] p 2695 N95-28930
Inertial fusion program and national laser users facility program
[DE95-008202] p 2711 N95-30274

INERTIAL FUSION (REACTOR)
The international fusion materials irradiation facility
[DE95-006536] p 2696 N95-29142

INERTIAL NAVIGATION
High reliability, maintenance-free INS battery development, phase 2
[AD-A291412] p 2566 N95-30070

INFECTIOUS DISEASES
Studies of altered response to infection induced by severe injury
[AD-A288907] p 2634 N95-29139
Nearest neighbor analysis in one dimension
[DE95-009378] p 2654 N95-30183

INFERENCE
Learning object models from visual observation and background knowledge
[AD-A292606] p 2650 N95-29576
Statistical inference problems in some multivariate linear models with applications to multivariate calibration and meta-analysis
[AD-A291125] p 2675 N95-29768
Induction of selective Bayesian classifiers
[AD-A292690] p 2675 N95-29906
Probabilistic modeling and statistical inference for random fields and space-time processes
[AD-A289956] p 2672 N95-30029

INFLATABLE STRUCTURES
Emissivity measurements in thin metallized membrane reflectors used for microwave radiometer sensors
[NASA-TM-110179] p 2506 N95-30251

INFORMATION
DOD listing of approved recurring information requirements
[AD-A291346] p 2724 N95-29947

INFORMATION DISSEMINATION
A comprehensive analysis of Navy and Marine corps digital mapping, charting, and geodesy requirements for modeling and simulation
[AD-A291601] p 2598 N95-28931
Scientific and technical information policy implementation under OMB Circular A-130. Report of agency findings and recommendations
[DE-95-11601] p 2723 N95-29449

INFORMATION FLOW
A nonintrusive method of quantifying flow visualization data in vortex flow fields
[AD-A289802] p 2568 N95-28948
A study of the conceptual symbolics of information system development languages p 2723 N95-29589

INFORMATION MANAGEMENT
Scientific and technical information policy implementation under OMB Circular A-130. Report of agency findings and recommendations
[DE-95-11601] p 2723 N95-29449
Design and implementation of logical database languages
[AD-A290474] p 2650 N95-29509
Retrieval display and analysis support tool requirements analysis
[AD-A291448] p 2599 N95-29523
Information management in local area networks: Impact on users' perceptions p 2723 N95-29690
DOD listing of approved recurring information requirements
[AD-A291346] p 2724 N95-29947
CD-ROM preparation: An overview and guide
[NASA-CR-198756] p 2655 N95-30307

INFORMATION PROCESSING (BIOLOGY)
Automation and cognition in air traffic control: An empirical investigation
[AD-A291932] p 2493 N95-28790
Improving problem-solving and decision-making skills under stress: Prediction and training
[AD-A292104] p 2638 N95-28918
Computer models of retinal function
[AD-A290156] p 2634 N95-29022
Large-scale neuronal theories of the brain
[AD-A290200] p 2634 N95-29059
Reference frames in vision
[AD-A290117] p 2639 N95-29422
Visualization of CAD objects using a stereoscopic display
[AD-A290034] p 2639 N95-29439
Georgetown Institute for Cognitive and Computational Sciences
[AD-A289775] p 2639 N95-29458

INFORMATION RETRIEVAL
The identification of user criteria of relevance and document characteristics: Beyond the topical approach to information retrieval p 2723 N95-29518
Retrieval display and analysis support tool requirements analysis
[AD-A291448] p 2599 N95-29523
Retrieval, display, and analysis support tool for earth imagery (RDAST)
[AD-A291366] p 2601 N95-30061
Engineering Design Information System (EDIS), Information Management Services (IMS), Index Function, User's manual: Revision 1
[DE95-009538] p 2725 N95-30194
Distributed queries and incremental updates in information retrieval systems p 2725 N95-30286

INFORMATION SYSTEMS
XMap: A general purpose mapping program
[AD-A289958] p 2647 N95-29276
The identification of user criteria of relevance and document characteristics: Beyond the topical approach to information retrieval p 2723 N95-29518
AFGWC dial-in subsystem (AFDIS) software users manual, version 3.1
[AD-A291103] p 2651 N95-29639
Description and manipulation of method fragments for the assembly of situational methods
[PB95-197133] p 2653 N95-30094
Engineering Design Information System (EDIS), Information Management Services (IMS), Index Function, User's manual: Revision 1
[DE95-009538] p 2725 N95-30194
Data catalog for JPL Physical Oceanography Distributed Active Archive Center (PO.DAAC)
[NASA-CR-198872] p 2631 N95-30231
Distributed queries and incremental updates in information retrieval systems p 2725 N95-30286
CD-ROM preparation: An overview and guide
[NASA-CR-198756] p 2655 N95-30307

INFORMATION THEORY
Optimal universal coding and density estimation
[AD-A290694] p 2675 N95-29587
Applicability of neural networks for production planning under uncertainty
[PB95-197406] p 2666 N95-30101

INFORMATION TRANSFER
Problem decomposition for reuse
[AD-A292245] p 2645 N95-28881
Scientific and technical information policy implementation under OMB Circular A-130. Report of agency findings and recommendations
[DE-95-11601] p 2723 N95-29449
Huge data sets and the frontiers of computational feasibility
[AD-A291384] p 2653 N95-30063

INFRARED ASTRONOMY
Observational properties of SiO masers in the galactic bulge IRAS sources p 2735 N95-29838

INFRARED ASTRONOMY SATELLITE
Nobeyama Radio Observatory report, no. 379
p 2735 N95-29836

INFRARED DETECTORS
Cost effective, dual-purpose machine vision-based detectors for (1) smoke and flame detection, and (2) engine overhead/burn-through and flame detection
[AD-A292284] p 2697 N95-28870
Design, development and testing of a prototype precision angular positioning control system for a next generation multiplexed imager
[AD-A292585] p 2698 N95-28980
Optoelectronics based on SiGe/Si heterostructures
[AD-A292464] p 2699 N95-29006
Development of ultra-low dark current, high performance 3-5 quantum well infrared photodetectors (QWIPs) for focal plane arrays staring imaging sensor systems
[AD-A290343] p 2714 N95-29089
Investigation of a normal incident high performance P-type strained layer In(0.3)Ga(0.7)As/In(0.52)Al(0.48)As quantum well infrared photodetector
[AD-A290946] p 2716 N95-29785
Japanese remote sensing organizations, research, and technology
[AD-A292420] p 2601 N95-29905
InTlSb as a long-wave infrared (LWIR) material: Defects and transportation properties
[AD-A291218] p 2702 N95-29978
High Tc superconducting bolometric and nonbolometric infrared (IR) detectors
[NASA-CR-198789] p 2702 N95-30035

INFRARED IMAGERY
Nobeyama Radio Observatory report, no. 378: The polar ring spiral galaxy NGC 660 p 2731 N95-29097
The detection of oil slicks at night with airborne infrared imagers
[AD-A289731] p 2598 N95-29281
An ultra-high speed incoherent-to-coherent converter for optical computing
[AD-A292658] p 2700 N95-29412
Hailstone heat and mass transfer measurements
[ISBN-0-315-86304-8] p 2624 N95-29797
Extended dust shells around carbon stars resolved by HIRAS p 2735 N95-29840
Meteorological Satellite Center technical note, no. 28, 1994
[JTN-95-80926] p 2626 N95-29849
Retrieval, display, and analysis support tool for earth imagery (RDAST)
[AD-A291366] p 2601 N95-30061

INFRARED INSTRUMENTS
Nonlinear calibration of an infrared radiometer
[AD-A292436] p 2698 N95-28996
(DEPSCOR-92) acquisition of a metallurgical optical microscope
[AD-A292439] p 2698 N95-28998

INFRARED LASERS
ARPA solid state laser and nonlinear materials program
[AD-A289657] p 2584 N95-28678
A compact universal power supply for laser diodes
[AD-A289950] p 2585 N95-29274
Auger rates in mid-IR InAsSb laser structures
[DE95-006325] p 2588 N95-30006

INFRARED RADIATION
ARPA solid state laser and nonlinear materials program
[AD-A289657] p 2584 N95-28678
Thin-film resistor array characterization
[AD-A289806] p 2561 N95-28950
Analysis of the structural characteristics and intensity evolution of super typhoon flo (1990) in special sensor Microwave/Imager (SSM/I) data
[AD-A292413] p 2619 N95-28989
Nonlinear calibration of an infrared radiometer
[AD-A292436] p 2698 N95-28996
Tailored microstructures for broadband or selective detection of radiation from the visible to the infrared
[AD-A292097] p 2554 N95-29240
The detection of oil slicks at night with airborne infrared imagers
[AD-A289731] p 2598 N95-29281
Tunable laser for persistent spectral hole burning optical memories
[AD-A292598] p 2586 N95-29292
On the large scale circulation of the East Asia Mei-Yu fronts and secondary weather dimension disturbances
[AD-A291036] p 2622 N95-29662
Multiwaveband observations of quasars
p 2728 N95-29665
The 12 UM contribution of nearby galaxies to the infrared background
[AD-A291185] p 2735 N95-29917
Design of a more accurate, higher fidelity, dual-source air mass zero solar simulator
[AD-A291364] p 2603 N95-29953
InTlSb as a long-wave infrared (LWIR) material: Defects and transportation properties
[AD-A291218] p 2702 N95-29978
Polyethylene-based polyurethane copolymers and block copolymers
[AD-A289996] p 2546 N95-30030

INFRARED RADIOMETERS
Nonlinear calibration of an infrared radiometer
[AD-A292436] p 2698 N95-28996

INFRARED SOURCES (ASTRONOMY)
SiO maser survey of the IRAS bulge sources
p 2735 N95-29837
Observational properties of SiO masers in the galactic bulge IRAS sources p 2735 N95-29838

INFRARED SPECTROSCOPY
15th NSO/Sac Peak Solar Workshop
[AD-A292297] p 2739 N95-30074

INFRARED TELESCOPES
Summary Report of mission acceleration measurements for STS-66. Launched November 3, 1994
[NASA-TM-106914] p 2509 N95-29643
INFRARED TRACKING
An algorithm fusion approach to IRST signal processing (III): Nongaussian-corrected filter fusion
[AD-A291565] p 2552 N95-28936
INGOTS
High-efficiency solar cells using HEM silicon
[DE95-005424] p 2604 N95-30217
INHOMOGENEITY
100 Hz-10 kHz bottom backscattering model: Generalized treatment of sediment sound propagation, sediment volume scattering and interface-roughness scattering
[AD-A291323] p 2685 N95-29942
INITIATION
Analysis of adiabatic shear bands in thermoviscoplastic materials under combined loading
[AD-A290666] p 2596 N95-29582
INJECTION
Flow visualization of vorticity cancellation of jets in crossflow
[AD-A292414] p 2569 N95-28990
INJECTION MOLDING
Processing studies on in situ composites based on blends of thermotropic Liquid Crystalline Polymers with thermoplastics
[AD-A290526] p 2544 N95-29494
INJURIES
Analysis of wounds by evaporative water loss in man
[AD-A290327] p 2634 N95-29086
Studies of altered response to infection induced by severe injury
[AD-A288907] p 2634 N95-29139
The potential for pulmonary heat injury resulting from the activation of a cabin water spray system to fight aircraft cabin fires
[DOT/FAA/AM-95/17] p 2636 N95-29224
INLET FLOW
Demonstration of an automated CFD system for three-dimensional flow simulations p 2485 N95-28767
A procedure for automating CFD simulations of an inlet-bleed problem p 2485 N95-28768
Unsteady pressure and inflow velocity on a pitching rotor blade in hover p 2490 N95-29771
Inlet flow test calibration for a small axial compressor rig. Part 2: CFD compared with experimental results
[NASA-TM-106999] p 2501 N95-30007
Survey of CFD applications for high speed inlets
[AD-A291365] p 2578 N95-30087
INOCULATION
Demonstration of a stabilized alumina/ethanol colloidal dispersion technique for seeding high temperature air flows
[NASA-TM-106945] p 2582 N95-29113
INPUT/OUTPUT ROUTINES
Parallel adaptive techniques for transient partial differential equations
[AD-A290460] p 2674 N95-29490
INSECTS
A biologically-inspired autonomous robot
[AD-A289446] p 2666 N95-30026
INSERTS
Evaluation of wear resistant ceramic valve seats in gas-fueled power generation engines
[PB95-200218] p 2591 N95-30110
INSOLATION
Analysis of shadowing effects on spacecraft power systems
[NASA-TM-106994] p 2511 N95-30012
The effects of clouds as a feedback mechanism on the Earth's climate in the tropical Pacific
p 2611 N95-30300
INSPECTION
Cathodic protection system inspection 6
[AD-A289720] p 2591 N95-28682
Cathodic protection system inspection 5
[AD-A289724] p 2592 N95-28684
A human factors evaluation of the operational demonstration flight inspection aircraft
[DOT/FAA/AM-95/18] p 2641 N95-29365
Ultrasonic guided waves in cylinders: Theory and experiment p 2685 N95-29826
Operational test and evaluation (OT&E) integration and operational test procedures for Fixed Ground Antenna Radome (FGAR)
[AD-A291203] p 2559 N95-29975
INSTRUMENT ORIENTATION
Adjustable two-axis instrument mount
[AD-D017393] p 2582 N95-29220
INSULATION
Self-stressing structures for wafer-level oxide breakdown to 200 MHz
[DE95-006815] p 2714 N95-29157
Finite difference analysis of a cylindrical two conductor microstrip transmission line with truncated dielectrics
[AD-A292592] p 2555 N95-29290
Development of flame resistant, high efficiency thermal insulation
[AD-A291136] p 2547 N95-30120
INSULATORS
Complete analysis of electrode-terminated cables in two-layer conductor bounded above by air: Current density, magnetic field, and magnetic field gradient
[AD-A290907] p 2566 N95-30079
Development of flame resistant, high efficiency thermal insulation
[AD-A291136] p 2547 N95-30120
INTEGRAL EQUATIONS
Modal analysis of straight and curved integrated optical waveguides: An integral equation approach
[PB95-197265] p 2702 N95-30054
INTEGRATED CIRCUITS
Low cost writable RFID tag with MRAM memory
[AD-A292553] p 2642 N95-28974
OEIC ultra. A new approach to OEIC CAD
[AD-A290349] p 2646 N95-29066
Processing, fabrication, and demonstration of HTS integrated microwave circuits
[AD-A292480] p 2562 N95-29073
Processing, fabrication, and demonstration of HTS integrated microwave circuits
[AD-A290220] p 2562 N95-29078
Self-stressing structures for wafer-level oxide breakdown to 200 MHz
[DE95-006818] p 2714 N95-29157
High performance electromagnetic simulation tools
[AD-A290405] p 2554 N95-29235
Numerical modeling of opto-electronic integrated circuits
[AD-A292096] p 2563 N95-29239
Interband lateral resonant tunneling transistor
[AD-D017399] p 2564 N95-29568
UHF Low Density Radio Communications Link (LDRCL) Operational Test and Evaluation (OT&E) integration and OT&E operational final test report
[AD-A291447] p 2558 N95-29769
INTEGRATED MISSION CONTROL CENTER
Shift work, age, and performance: Investigation of the 2-2-1 shift schedule used in Air Traffic Control facilities I. The sleep/wake cycle
[DOT/FAA/AM-95/19] p 2638 N95-29261
INTEGRATED OPTICS
Epitaxial growth and characterization of Si(1-x)Ge(x) materials and devices
[AD-A292528] p 2712 N95-28874
OEIC ultra. A new approach to OEIC CAD
[AD-A290349] p 2646 N95-29066
An integrated optical CO2 sensor. Phase 0: Design and fabrication of critical elements
[NASA-CR-198792] p 2700 N95-29366
High resolution direct digitization and optical telemetry of shipboard antenna signals
[AD-A290238] p 2557 N95-29504
INTELLIGENCE
Coping and adaptation: Theoretical and applied perspectives
[AD-A290513] p 2638 N95-29090
INTERACTING GALAXIES
A study of one-armed spiral galaxies
p 2729 N95-29774
INTERACTIONAL AERODYNAMICS
An interacting boundary layer method for unsteady compressible flows p 2579 N95-30290
INTERCEPTION
Cyclic feature analysis, design and exploitation
[AD-A290639] p 2557 N95-29603
INTERFACES
Gordon research conference on point defects, line defects, and interfaces in semiconductors
[AD-A290103] p 2714 N95-29209
Measurement of interface strength, intrinsic toughness and their dependence on interfacial segregants
[AD-A291169] p 2546 N95-29926
INTERFACIAL TENSION
Measurement of interface strength, intrinsic toughness and their dependence on interfacial segregants
[AD-A291169] p 2546 N95-29926
INTERFEROMETERS
Linewidth-insensitive coherent analog optical links
[AD-A292422] p 2698 N95-28992
Testbed for precision characterization of spatial light modulators and optical processors
[AD-A290484] p 2699 N95-29148
Atmospheric wavefront sensing and correction including the stellar phase shifting interferometer
p 2701 N95-29706
Measurement of interface strength, intrinsic toughness and their dependence on interfacial segregants
[AD-A291169] p 2546 N95-29926
INTERFEROMETRY
Interferometric measurement with squeezed light
[AD-A292402] p 2697 N95-28799
Development of a multiplex Fabry-Perot interferometer and measurement of atmospheric HF and HCl
p 2608 N95-29213
Deconvolution of lateral shear interferograms
p 2699 N95-29222
Compressibility effects on and control of dynamic stall of oscillating airfoil
[AD-A291804] p 2489 N95-29428
An investigation into the use of satellite-based positioning systems for flight reference/autoland operations p 2494 N95-29542
A study of precipitation using dual-frequency and interferometric Doppler radars p 2627 N95-29877
Performance analysis of a GPS interferometric attitude determination system for a gravity gradient stabilized spacecraft
[NASA-CR-188372] p 2508 N95-30036
Inertial fusion program and national laser users facility program
[DE95-008202] p 2711 N95-30274
INTERLAMINAR STRESS
Composite processing development to improve interlaminar strength using ply interface particles
[NASA-TM-108495] p 2529 N95-30334
INTERLAYERS
Measurement of interface strength, intrinsic toughness and their dependence on interfacial segregants
[AD-A291798] p 2524 N95-29409
Measurement of interface strength, intrinsic toughness and their dependence on interfacial segregants
[AD-A291169] p 2546 N95-29926
INTERMETALLICS
Crystal field and exchange interactions in DyT4Al8 (T = Fe and Mn)
[DE95-007131] p 2714 N95-29134
Visit to the Department of Metallurgical Engineering, Tokyo Institute of Technology, 22 Sep. 1994
[AD-A292310] p 2536 N95-29473
Examination of dislocation core structures in B2 intermetallic alloys
[AD-A291486] p 2537 N95-29526
The Institute for Material Science and Department of Material Science, Tohoku University, Sendai Japan, 2-3 June 1994
[AD-A292348] p 2650 N95-29534
Mechanical properties of nanophase metals
[DE95-005408] p 2537 N95-30018
INTERMODULATION
Multiple dimensional acousto-optic diffraction and multiple dimensional acousto-optic device
[AD-A291037] p 2685 N95-29681
INTERNAL COMBUSTION ENGINES
Technology development goals for automotive fuel cell power systems
[DE95-008764] p 2548 N95-29280
INTERNAL FLOW
Ejectors and jet pumps: Computer program for design and performance for steam/gas flow
[ESDU-94046] p 2495 N95-28704
The acoustic characteristics of turbomachinery cavities
[NASA-CR-4671] p 2478 N95-28720
Finite element vorticity-based methods for the solution of the incompressible and compressible Navier-Stokes equations p 2570 N95-29119
Laser doppler velocimeter system for subsonic jet mixer nozzle testing at the NASA Lewis Aeroacoustic Propulsion Lab
[NASA-TM-106984] p 2477 N95-30229
INTERNAL PRESSURE
Design, analysis, and fabrication of a pressure box test fixture for tension damage tolerance testing of curved fuselage panels p 2516 N95-28839
INTERNAL WAVES
The nature of wavefront fluctuations induced by internal gravity waves in long-range oceanic acoustic pulse transmissions p 2630 N95-29528
INTERNATIONAL COOPERATION
A comparison of the aeromedical administration requirements for US Air Forces and major allies
[AD-A290137] p 2635 N95-29141
Yohkoh Soft X-ray Telescope
[NASA-CR-197655] p 2726 N95-29172
Bilateral US/Russia Workshop on Self-Propagating High-Temperature Synthesis held in Honolulu, Hawaii on 6-7 November 1993
[AD-A290466] p 2525 N95-29492
INTERNATIONAL SUN EARTH EXPLORERS
Realisation of an integrated software engineering environment through heterogeneous CASE-tool integration
[PB95-197646] p 2653 N95-30105

INTERNATIONAL SYSTEM OF UNITS
SI Handbook for the Lawrence Livermore National Laboratory: Committee on metric transition
[DE95-009329] p 2551 N95-30182
INTERPLANETARY GAS
One and two fluid numerical investigations of solar wind gas releases p 2736 N95-29704
INTERPLANETARY MAGNETIC FIELDS
Characterization of the geometries of the high-latitude ionospheric convection pattern p 2614 N95-29524
Application of Poynting flux measurements to the determination of energy transfer rates in the high-latitude ionosphere p 2614 N95-29650
The high latitude ionospheric convection pattern during northward interplanetary magnetic field p 2615 N95-29693
INTERPLANETARY MEDIUM
Solar system plasma waves
[NASA-CR-198767] p 2704 N95-29130
INTERPOLATION
Multilevel elliptic smoothing of large three-dimensional grids p 2485 N95-28765
Leading-edge suction distribution for plane thin wings at subsonic speeds
[ESDU-94037] p 2486 N95-28800
Transformational design of a direction detector for the progressive scan conversion processor
[PB95-198487] p 2643 N95-30109
The construction of high-accuracy schemes for acoustic equations p 2688 N95-30146
INTERPROCESSOR COMMUNICATION
Implementing distributed server groups for the World Wide Web
[AD-A292221] p 2658 N95-29196
Ropes: Support for collective opertions among distributed threads
[NASA-CR-198157] p 2649 N95-29404
The mesh synchronous processor MeshSP (trademark)
[AD-A289875] p 2659 N95-29420
On the utility of threads for data parallel programming
[NASA-CR-198155] p 2649 N95-29455
Formal design of communication protocols using Estelle
[AD-A290584] p 2652 N95-30042
INTERRUPTION
Optically triggered, superconducting opening switch
[AD-A292642] p 2700 N95-29379
INTERSECTIONS
Mathematical modeling and numerical simulation of the dynamics of flexible structures undergoing large overall motions
[AD-A291139] p 2597 N95-30123
INTERSTELLAR MASERS
Nobeyama Radio Observatory report, no. 379 p 2735 N95-29836
SiO maser survey of the IRAS bulge sources p 2735 N95-29837
Observational properties of SiO masers in the galactic bulge IRAS sources p 2735 N95-29838
INTERSTELLAR MATTER
The x-ray scattering halo around Sco-X1 p 2727 N95-29591
INVARIANCE
A gyroscope clock for a null gravitational redshift experiment p 2584 N95-29664
INVENTIONS
Interband lateral resonant tunneling transistor
[AD-D017398] p 2564 N95-29568
High temperature thermosets and ceramics derived from linear carborane-(siloxane or silane)-acetylene copolymers
[AD-D017400] p 2545 N95-29569
INVENTORY MANAGEMENT
Artificial intelligence techniques for parts obsolescence prediction
[AD-A292185] p 2661 N95-28926
INVERSE SCATTERING
Spectral inverse scattering theory for dielectric media: Application to optical devices
[AD-A292651] p 2556 N95-29383
INVERSIONS
Joint services electronics program
[AD-A292469] p 2561 N95-29010
Application of optimization technique to control system design for departure prevention and aircraft model estimation through dynamic inversion p 2501 N95-29156
A theoretical model of multiple regimes in a stratocumulus-topped boundary layer p 2624 N95-29726
INVERTERS
Power measurement and current feedback in a resonant DC link inverter
[AD-A292518] p 2563 N95-29164
INVISCID FLOW
An unstructured-grid software system for solving complex aerodynamic problems p 2481 N95-28743
A combined geometric approach for computational fluid dynamics on dynamic grids p 2485 N95-28770
Wave drag coefficient for axisymmetric forecowls at zero incidence (M sub infinity less than or equal to 1.5)
[ESDU-94014] p 2568 N95-28903
Surface pressure coefficient distributions for axisymmetric forecowls at zero incidence (M sub infinity less than or equal to 1.5)
[ESDU-94015] p 2487 N95-28904
Solution of the Navier-Stokes equations on locally refined Cartesian meshes using state-vector splitting p 2571 N95-29197
Dynamic stall of a NACA 0012 airfoil in laminar flow p 2489 N95-29243
Experimental research on crossing shock wave boundary layer interactions
[AD-A290764] p 2577 N95-29920
Survey of CFD applications for high speed inlets
[AD-A291365] p 2578 N95-30087
Pressure updating methods for the steady-state fluid equations
[NASA-CR-198163] p 2674 N95-30353
IO
STS-67 mission highlights resource tape
[NASA-TM-110530] p 2504 N95-28715
IODINE LASERS
Studies of energy transfer processes of relevance to chemically and optically pumped lasers
[AD-A290164] p 2585 N95-29025
ION ACOUSTIC WAVES
Solitons in negative ion plasmas p 2706 N95-29668
Inertial fusion program and national laser users facility program
[DE95-008202] p 2711 N95-30274
ION BEAMS
Deposition and surface treatment with intense pulsed ion beams
[DE95-007885] p 2543 N95-29465
High T(sub c) superconductor/ferroelectric heterostructures
[AD-A291016] p 2716 N95-29658
Theoretical study of cylindrical energy analyzers for MeV range heavy ion beam probes
[AD-B17200L] p 2707 N95-29745
ION CONCENTRATION
Measurements of ions formed in jet engine exhaust plumes
[AD-A290940] p 2501 N95-29764
ION CYCLOTRON RADIATION
Monte Carlo simulation study of the ICRF minority heating in the large helical device
[AD-B179858L] p 2708 N95-29749
The physics of the collisionless bow shock p 2580 N95-30301
ION DISTRIBUTION
State resolved differential cross sections for reactions important to the decomposition of energetic materials
[AD-A290718] p 2548 N95-29498
ION EXCHANGE MEMBRANE ELECTROLYTES
In-plant testing of membranes to treat electroplating wastewater
[NASA-CR-198796] p 2532 N95-29250
ION EXCHANGING
In-plant testing of membranes to treat electroplating wastewater
[NASA-CR-198796] p 2532 N95-29250
Molecular probes of gating and open channel conformational transitions of mechanosensitive ion channels
[AD-A291170] p 2637 N95-29927
ION IMPLANTATION
Analytical electron microscopy of precipitates in ion-implanted MgAl2O4 spinel
[DE95-007406] p 2538 N95-30038
ION IRRADIATION
Ion beam modification of Tl-Ba-Ca-Cu-O type high temperature superconductors during irradiation
[DE95-006807] p 2717 N95-30022
Depth-independent hardness improvements in ion irradiated polystyrene
[DE95-008682] p 2547 N95-30190
ION SOURCES
Development of an intense negative hydrogen ion source with a wide-range of external magnetic filter field
[AD-B195514L] p 2705 N95-29567
ION TEMPERATURE
Thermal N(+) in the inner magnetosphere p 2614 N95-29590
IONIC WAVES
A generalized semikinetic (GSK) model for mesoscale auroral plasma transport p 2706 N95-29686
IONIZATION
Experimental studies of electromagnetic propagation at ultrahigh intensities
[AD-A290284] p 2553 N95-29081
Low-background balloon-borne direct search for ionizing massive particles as a component of the dark galactic halo matter p 2726 N95-29204
IONIZATION CHAMBERS
Radiation effects on front-end electronics for noble liquid calorimetry
[DE95-007304] p 2566 N95-30025
IONIZATION COEFFICIENTS
Effective emission and ionization rate coefficients of atomic carbons in plasmas
[AD-B175932L] p 2707 N95-29740
IONIZING RADIATION
Cellular and molecular level responses after radiofrequency radiation exposure, alone or in combination with x rays or chemicals
[AD-A292488] p 2633 N95-28866
Radiation effects on front-end electronics for noble liquid calorimetry
[DE95-007304] p 2566 N95-30025
IONOGRAMS
Correlation and gradient characteristics of ionospheric parameters in europe
[AD-A292295] p 2612 N95-28871
IONOPAUSE
A study of plasma waves arising from the solar wind interaction with Venus p 2704 N95-29215
IONOSPHERIC DISTURBANCES
Correlation and gradient characteristics of ionospheric parameters in Europe
[AD-A290135] p 2612 N95-29140
Chemical release experiments to induce F region ionospheric plasma irregularities at the magnetic equator p 2708 N95-29783
IONOSPHERIC ELECTRON DENSITY
A generalized semikinetic (GSK) model for mesoscale auroral plasma transport p 2706 N95-29686
IONOSPHERIC HEATING
A generalized semikinetic (GSK) model for mesoscale auroral plasma transport p 2706 N95-29686
IONOSPHERIC PROPAGATION
Analysis of tropospheric propagation characteristics based on regional meteorological data
[AD-A291581] p 2552 N95-28939
Correlation and gradient characteristics of ionospheric parameters in Europe
[AD-A290135] p 2612 N95-29140
IONOSPHERIC SOUNDING
Correlation and gradient characteristics of ionospheric parameters in europe
[AD-A292295] p 2612 N95-28871
Correlation and gradient characteristics of ionospheric parameters in Europe
[AD-A290135] p 2612 N95-29140
The topside ionospheric plasma monitor (SSIES, SSIES-2 and SSIES-3) on the spacecraft of the Defense Meteorological Satellite Program (DMSP), user's guide. Volume 3: Program maintenance manual
[AD-A290941] p 2617 N95-29765
IONS
Computational investigation of the stabilities of some N, O, F ions
[AD-A292305] p 2691 N95-28868
Crystal field and exchange interactions in DyT4Al8 (T = Fe and Mn)
[DE95-007131] p 2714 N95-29134
Electrical and electronic properties of self-assembled lipid bilayers
[AD-A290507] p 2632 N95-29155
IRON
Application of a rapid quench thermomagnetic analyzer to austempered ductile iron
[AD-A292261] p 2535 N95-28889
SAM1-A new semiempirical method including d-orbitals
[AD-A290903] p 2694 N95-30060
IRON ALLOYS
XPS study of Ni-Fe manganite thermistor material
[DE95-008778] p 2561 N95-28961
Crystal field and exchange interactions in DyT4Al8 (T = Fe and Mn)
[DE95-007131] p 2714 N95-29134
Examination of dislocation core structures in B2 intermetallic alloys
[AD-A291486] p 2537 N95-29526
Tensile properties of as-cast iron-aluminide alloys
[DE95-005396] p 2538 N95-30216
IRON COMPOUNDS
Superplastic ceramics
[AD-A290817] p 2545 N95-29635
Development of precipitated iron Fischer-Tropsch catalysts
[DE95-009334] p 2533 N95-29870

IRRADIANCE
Measurement of the seasonal and annual variability of total column aerosol in a northeastern US network
[DE95-007259] p 2608 N95-28920
Effect of irradiance, sucrose, and CO2 concentration on the growth of potato (Solanum tuberosum L.) in vitro
[NASA-TM-110654] p 2632 N95-29375
IRRADIATION
Selective attachment of nucleic acid molecules to patterned self-assembled surfaces
[AD-D017379] p 2530 N95-28854
The international fusion materials irradiation facility
[DE95-006536] p 2696 N95-29142
Photogenerated amines in polymer curing and imaging: Design and synthesis of (3', 5'-dimethoxybenzoinyl)oxycarbonyl carbamates as novel photoprecursors of amines
[AD-A289945] p 2542 N95-29272
IRREGULARITIES
The effects of magnetic storm phases on F-layer irregularities from auroral to equatorial latitudes
[AD-A290674] p 2614 N95-29585
IRREVERSIBLE PROCESSES
Investigation of Burnett equations for two-dimensional hypersonic flow
[AD-A290233] p 2575 N95-29469
ISCHEMIA
Research on PGI2 and TXA2 effects at times of hyperbaric oxygenation of domestic rabbits with acute cerebral ischemia reirrigation damage
[AD-A289606] p 2632 N95-29263
ISING MODEL
Formation of striped surface phases by short-range forces
[AD-A279962] p 2531 N95-28945
ISOLATION
Precision pointing experiment
[AD-A291015] p 2664 N95-29657
ISOTOPES
Nobeyama Radio Observatory report, no. 380: Detection of the (29)SiO v=1, J=1-0 maser from TX Camelopardalis p 2726 N95-29101
ISOTOPIC SPIN
Tables of SU3 isoscalar factors
[DE95-009375] p 2690 N95-28779
ISOTROPIC TURBULENCE
Interaction of turbulence with complex shock waves
[AD-A290225] p 2571 N95-29145
ITERATION
A 3DGRAPE/AL: The Ames/Langley technology upgrade p 2482 N95-28750
Multifluid nonequilibrium simulation of arcjet thrusters p 2510 N95-29245
Advanced presort process
[AD-A291010] p 2557 N95-29655
Comparison of the local defect correction iteration and the fast adaptive composite grid iteration
[PB95-206769] p 2672 N95-30088
ITERATIVE SOLUTION
Linear algebraic computation on distributed memory parallel machines
[AD-A290615] p 2671 N95-29558
Techniques and results of tokamak-edge simulation
[DE95-008075] p 2711 N95-30130

J

JAMMERS
Methods of generating low redundancy direction finding array configurations
[AD-A292590] p 2555 N95-29289
JAPAN
A 1993 review of welding in Japan
[DE95-758701] p 2589 N95-28946
A study of problematic situations and information needs of software managers in the United States and Japan p 2724 N95-29828
Japanese remote sensing organizations, research, and technology
[AD-A292420] p 2601 N95-29905
Visit to the Laboratory For Evaluation and Failure Prevention of Materials, Toyohashi University of Technology, 17 Oct 94
[AD-A292340] p 2597 N95-30293
JAPANESE SPACE PROGRAM
Yohkoh Soft X-ray Telescope
[NASA-CR-197655] p 2726 N95-29172
JET AIRCRAFT NOISE
The spectrum and directivity of turbulent mixing noise from supersonic jets p 2684 N95-29415
JET EXHAUST
Measurements of ions formed in jet engine exhaust plumes
[AD-A290840] p 2501 N95-29764
JET FLOW
Flow visualization of vorticity cancellation of jets in crossflow
[AD-A292414] p 2569 N95-28990
An extension of the Lighthill theory of jet noise to encompass refraction and shielding
[NASA-TM-110163] p 2684 N95-29452
JET IMPINGEMENT
Precision cleaning verification of fluid components by air/water impingement and total carbon analysis
[NASA-TM-110742] p 2531 N95-29248
Turbulent airflow noise production and propagation patterns of a subsonic jet impinging on a flat plate p 2684 N95-29502
JET LAG
The effect of bright light and LEET on sleep after a 10-hour phase delay
[AD-A291264] p 2637 N95-29995
JET MIXING FLOW
Molecular mixing in shear layers forced by 2-D and 3-D disturbances
[AD-A290272] p 2571 N95-29181
The spectrum and directivity of turbulent mixing noise from supersonic jets p 2684 N95-29415
JET NOZZLES
Laser doppler velocimeter system for subsonic jet mixer nozzle testing at the NASA Lewis Aeroacoustic Propulsion Lab
[NASA-TM-106984] p 2477 N95-30229
JET PROPULSION
Laser doppler velocimeter system for subsonic jet mixer nozzle testing at the NASA Lewis Aeroacoustic Propulsion Lab
[NASA-TM-106984] p 2477 N95-30229
JET PUMPS
Ejectors and jet pumps: Computer program for design and performance for steam/gas flow
[ESDU-94046] p 2495 N95-28704
JET STREAMS (METEOROLOGY)
Forecast of Atlantic seasonal hurricane activity for 1995 p 2620 N95-29254
Extended field observations of cirrus clouds using a ground-based cloud observing system
[NASA-CR-198855] p 2628 N95-30356
JET THRUST
A vehicle health monitoring system for the Space Shuttle Reaction Control System during reentry
[NASA-CR-188370] p 2505 N95-29447
Design, analysis and control of large transports so that control of engine thrust can be used as a back-up of the primary flight controls
[NASA-CR-198958] p 2501 N95-30254
JFET
Radiation effects on front-end electronics for noble liquid calorimetry
[DE95-007304] p 2566 N95-30025
JOINTS (JUNCTIONS)
NPSNETIV: An object-oriented interface for a three-dimensional virtual world
[AD-A292467] p 2646 N95-29008
Preparation and studies of urazole containing polymers
[AD-A290685] p 2545 N95-29586
Analytical potential energy surface for methylene nitramine (CH2NNO2)
[AD-A291247] p 2534 N95-29994
A numerical study of the small scale wing-body junction problem p 2491 N95-30235
JOSEPHSON JUNCTIONS
Materials science and fabrication of YBCO-SrTi(1-x)Nb(x)O3-YBCO device structures
[AD-A292527] p 2712 N95-28815
Quasioptical Josephson Oscillator
[AD-A292481] p 2561 N95-28859
HTS Josephson technology on silicon with application to high speed digital microelectronics
[AD-A290206] p 2562 N95-29061
Nobeyama Radio Observatory report, no. 381: Parallel connected twin SIS junctions for millimeter and submillimeter wave mixers: Analysis and experimental verification p 2562 N95-29099
JUPITER (PLANET)
An investigation into the existence of asteroids at Saturn's triangular Lagrangian points p 2727 N95-29648

K

K-EPSILON TURBULENCE MODEL
Grid resolution and turbulent inflow boundary condition recommendations for NPARC calculations
[NASA-TM-106959] p 2492 N95-30253
KALMAN FILTERS
A vehicle health monitoring system for the Space Shuttle Reaction Control System during reentry
[NASA-CR-188370] p 2505 N95-29447
Target aircraft identification, trajectory tracking and prediction using regression-based Kalman filter techniques p 2565 N95-29728
Performance analysis of a GPS interferometric attitude determination system for a gravity gradient stabilized spacecraft
[NASA-CR-188372] p 2508 N95-30036
Spin augmented deployment and retrieval of tethered artificial gravity spacecraft p 2509 N95-30280
KAON PRODUCTION
Parameterized spectral distributions for meson production in proton-proton collisions
[NASA-TM-4675] p 2696 N95-30337
KAONS
From the (psi) to charmed mesons
[DE95-006564] p 2693 N95-29583
Prospects for HERMES-spin structure studies at HERA
[DE95-005845] p 2694 N95-30019
KAPTON (TRADEMARK)
Emissivity measurements in thin metallized membrane reflectors used for microwave radiometer sensors
[NASA-TM-110179] p 2506 N95-30251
KEELS
Global cost and weight evaluation of fuselage keel design concepts p 2499 N95-28840
KELVIN WAVES
A study of dynamics in the tropical Pacific using satellite data p 2630 N95-29520
KERNEL FUNCTIONS
Polynomial approximations for materials simulations
[DE95-006168] p 2652 N95-29989
Optimal hankel norm identification of dynamical systems
[PB95-197232] p 2672 N95-30046
KETONES
Viscosity of liquids: Aliphatic and cyclic ketones
[ESDU-94025] p 2530 N95-28712
Super hydrides
[AD-A290594] p 2533 N95-29556
KEVLAR (TRADEMARK)
Structure and orientation behavior of highly oriented polymers under tensile and compressive stresses p 2546 N95-29822
KINEMATICS
Nobeyama Radio Observatory report, no. 378: The polar ring spiral galaxy NGC 660 p 2731 N95-29097
Vortex element analysis of selected time-dependent flows
[AD-A289944] p 2573 N95-29271
Numerical simulation of mechanisms and manipulator robots with flexible links and flexible joints
[PB95-196903] p 2591 N95-30285
KINETIC ENERGY
Turbulent coupling of the magnetosphere-ionosphere through shear-mode Alfven waves p 2615 N95-29687
KINETIC EQUATIONS
Dust formation in stellar outflows: A time-dependent model p 2733 N95-29649
KINETIC HEATING
Experimental and analytical study of heat transfer and turbulent flow field in tangentially injected swirl flow p 2576 N95-29811
KINETIC THEORY
Collective phenomena in granular fluids p 2572 N95-29219
Dynamics of simple chemically reactive fluids p 2573 N95-29335
KINETICS
Recent progress in the study of the kinetics of sol-gel SiO2 synthesis reactions
[AD-A290570] p 2544 N95-29551
Investigation of laminar methane flames with emphasis on kinetics elucidation and NOx reduction
[PB95-200531] p 2535 N95-30111
KITS
Experiment kits for processing biological samples inflight on SLS-2
[NASA-TM-4685] p 2642 N95-28722
Development of the test kit for fuel acid contamination
[AD-A291953] p 2548 N95-29019
Evaluation of commercial water-in-fuel test kits
[AD-A292135] p 2533 N95-29572
KLYSTRONS
Studies directed toward new and improved permanent magnet materials
[AD-A290749] p 2681 N95-29481
KNOWLEDGE BASED SYSTEMS
Artificial intelligence techniques for parts obsolescence prediction
[AD-A292185] p 2661 N95-28926

Interaction and intelligent behavior
[AD-A290049] p 2639 N95-29443
Workshop on Fielded Applications of Machine Learning
[AD-A280168] p 2649 N95-29456
Automated reasoning about classical mechanics
[AD-A290052] p 2663 N95-29477
COADE: A framework for cognitive analysis, design, and evaluation
[AD-A291282] p 2720 N95-29935

KNOWLEDGE BASES (ARTIFICIAL INTELLIGENCE)
Layers as knowledge transitions in the design of distributed systems
[PB95-197638] p 2660 N95-30104

KNOWLEDGE REPRESENTATION
Interface for the translation of sentences in a natural language into a geometrical representation language
[INPE-5467-PRE/1775] p 2722 N95-29363
Test theory reconceived
[AD-A291836] p 2639 N95-29432
Automated reasoning about classical mechanics
[AD-A290052] p 2663 N95-29477
Tools for Automated Knowledge Engineering (TAKE) system evaluation methodology
[AD-A291145] p 2654 N95-30125

KNUDSEN FLOW
Investigation of Burnett equations for two-dimensional hypersonic flow
[AD-A290233] p 2575 N95-29469

KORTEWEG-DEVRIES EQUATION
Solitons in negative ion plasmas p 2706 N95-29668

KRYPTON
Experimental studies of electromagnetic propagation at ultrahigh intensities
[AD-A290284] p 2553 N95-29081

KUTTA-JOUKOWSKI CONDITION
Vortex element analysis of selected time-dependent flows
[AD-A289944] p 2573 N95-29271

L

LABORATORIES
Annotated bibliography of software engineering laboratory literature
[NASA-CR-189406] p 2644 N95-28805
Brief introduction to state key physics laboratories and division open laboratories
[AD-A291064] p 2682 N95-29952
Visit to the Laboratory For Evaluation and Failure Prevention of Materials, Toyohashi University of Technology, 17 Oct 94
[AD-A292340] p 2597 N95-30293

LABORATORY EQUIPMENT
Coordination of operations for centrifuge quality control. phase 3C
[AD-A292533] p 2582 N95-28966

LAGRANGIAN EQUILIBRIUM POINTS
An investigation into the existence of asteroids at Saturn's triangular Lagrangian points
p 2727 N95-29648

LAGRANGIAN FUNCTION
Averaged resistive MHD equations
[AD-B178947L] p 2711 N95-30033

LAKES
NASA to use telepresence to explore Antarctic Lakes
[NASA-TM-110567] p 2598 N95-29175

LAMINAR BOUNDARY LAYER
Numerical investigation of surface curvature effects in compressible turbulent flows
[AD-A290114] p 2571 N95-29211
The effects of the thermal boundary condition and turbulence on heat transfer from a cylinder, flat plate, and turbine blade using the transient shroud and heated-coating techniques
[AD-A292646] p 2574 N95-29380
Numerical simulations of the flow in the HYPULSE expansion tube
[NASA-TM-110357] p 2503 N95-30228

LAMINAR FLOW
A combined geometric approach for computational fluid dynamics on dynamic grids p 2485 N95-28770
Collective phenomena in granular fluids
p 2572 N95-29219
Dynamic stall of a NACA 0012 airfoil in laminar flow
p 2489 N95-29243
Investigation of laminar methane flames with emphasis on kinetics elucidation and NOx reduction
[PB95-200531] p 2535 N95-30111
Numerical simulations of the flow in the HYPULSE expansion tube
[NASA-TM-110357] p 2503 N95-30228
Supercritical states of two-dimensional wall-bounded shear flow p 2580 N95-30303

LAMINAR FLOW AIRFOILS
A two element laminar flow airfoil optimized for cruise
[NASA-CR-198580] p 2489 N95-29338

LAMINAR HEAT TRANSFER
Influence of turbulence parameters, Reynolds number, and body shape on stagnation-region heat transfer
[NASA-TP-3487] p 2568 N95-28719

LAMINATES
Analysis of static contact in laminated composite plates using damage mechanics
[NASA-CR-198656] p 2513 N95-28809
The effects of specimen width on tensile properties of triaxially braided textile composites
p 2513 N95-28825
The effect of mixed mode precracking on the mode 1 fracture toughness of composite laminates
p 2514 N95-28827
Master plot analysis of microcracking in graphite/epoxy and graphite/PEEK laminates p 2514 N95-28828
Novel cost controlled materials and processing for primary structures p 2514 N95-28830
Response of automated tow placed laminates to stress concentrations p 2515 N95-28833
Mechanical characterization of two thermoplastic composites fabricated by automated tow placement
p 2515 N95-28834
Dimensional stability of curved panels with cocured stiffeners and cobonded frames p 2515 N95-28836
Tension fracture of laminates for transport fuselage. Part 2: Large notches p 2515 N95-28837
Impact damage resistance of composite fuselage structure, part 2 p 2516 N95-28838
A weight-efficient design strategy for cutouts in composite transport structures p 2516 N95-28843
Effects of cutouts on the behavior of symmetric composite laminates subjected to bending and twisting loads p 2517 N95-28844
A global/local analysis method for treating details in structural design p 2517 N95-28848
IPACS (Integrated Probabilistic Assessment of Composite Structures): Code development and applications p 2518 N95-28849
Through-the-thickness stresses and failure in the corner radius of a laminated composite section
[ESDU-94019] p 2518 N95-28899
A designed experiment in stitched/RTM composites
p 2522 N95-29046
Effects of thermal and moisture cycling on the internal structure of stitched RTM laminates
p 2522 N95-29048
The combined effect of glass buffer strips and stitching on the damage tolerance of composites
p 2522 N95-29049
Effect of nose shape and mass of the impactor on impact damage of laminated composites
[AD-A290351] p 2594 N95-29067
Finite difference analysis of a cylindrical two conductor microstrip transmission line with truncated dielectrics
[AD-A292592] p 2555 N95-29290
Measurement of interface strength, intrinsic toughness and their dependence on interfacial segregants
[AD-A291798] p 2524 N95-29409
Analytical and experimental studies of the energy absorption behavior of composite structures
p 2524 N95-29411
Thermally stable organic polymers
[AD-A290755] p 2543 N95-29482
A three dimensional finite element scheme for fiber microbuckling in thick multidirectional laminated composites p 2525 N95-29512
High velocity impact and penetration of thick composite laminates
[AD-A290642] p 2526 N95-29561
Interlaminar fracture mechanics and mechanisms: Linear and nonlinear aspects p 2526 N95-29597
Investigation of tension-compression fatigue behavior of a notched cross-ply metal matrix composite at elevated temperature
[AD-A291479] p 2527 N95-29770
Development of 'smart' piezothermoelastic laminae: Theory and applications
[AD-A290852] p 2528 N95-29864
Analytical investigation of the hygrothermal effects and parametric study of the Edge Crack Torsion (ECT) mode 3 test lay-ups
[NASA-TM-110183] p 2528 N95-30028
Composite processing development to improve interlaminar strength using ply interface particles
[NASA-TM-108495] p 2529 N95-30334

LAND USE
Optical (LANDSAT/TM) and radar (ERS-1/SAR) imagery sinergism studies applied to land use discrimination
[INPE-5608-TDI/554] p 2598 N95-29433

LANDMARKS
Estimation of unstabilized components in vehicular motion
[AD-A290580] p 2590 N95-29552

LANGEVIN FORMULA
Applications of Langevin and Molecular Dynamics methods
[DE95-007875] p 2694 N95-30059

LANGMUIR TURBULENCE
Relativistic effects on large amplitude nonlinear langmuir waves in a two-fluid plasma
[AD-B191980L] p 2710 N95-29841

LANGUAGE PROGRAMMING
NASA-IGES Translator and Viewer
p 2486 N95-28775

LANGUAGES
Characteristics of higher-level languages for software architecture
[AD-A292215] p 2649 N95-29376

LAPLACE EQUATION
Solution of second order nonlinear boundary value problems by the boundary element method
p 2669 N95-29105
Static field solutions and image theory for a conducting sphere with radial anisotropy
[PB95-207171] p 2673 N95-30172
Coarsening strategies for unstructured multigrid techniques with application to anisotropic problems
[NASA-CR-198154] p 2674 N95-30227

LAPLACE TRANSFORMATION
Efficient inversion of Fourier and Laplace domain boundary element solutions for elastodynamic scattering
p 2592 N95-29256

LARGE SPACE STRUCTURES
Substructure-based control of flexible structures
p 2508 N95-29408

LARMOR RADIUS
One and two fluid numerical investigations of solar wind gas releases p 2738 N95-29704
Collisionless driven magnetic reconnection
[AD-B178946L] p 2709 N95-29810

LASER ABLATION
Investigation of the characteristics of ferroelectric thin films deposited by pulsed laser ablation
[AD-A292306] p 2540 N95-28963
Inertial fusion program and national laser users facility program
[DE95-008202] p 2711 N95-30274

LASER ALTIMETERS
Receiver design, performance analysis, and evaluation for space-borne laser altimeters and space-to-space laser ranging systems
[NASA-CR-198655] p 2584 N95-28808

LASER APPLICATIONS
Joint services electronics program
[AD-A292469] p 2561 N95-29010
A simple method for range finding via laser triangulation
[AD-A292529] p 2553 N95-29166
Analysis of measurements for solid state laser remote lidar system
[NASA-CR-196640] p 2585 N95-29247
The role of the coherence function in holographic imaging p 2583 N95-29508
Research studies in electromagnetically induced transparency
[AD-A290796] p 2557 N95-29645
Laser applications to chemical analysis: Summaries of papers presented at the laser applications to chemical analysis topical meeting
[AD-A290738] p 2587 N95-29653
Brief introduction to state key physics laboratories and division open laboratories
[AD-A291064] p 2682 N95-29952

LASER BEAMS
Propagation and transformation properties of axicon optical systems for laser beams
[AD-A289661] p 2584 N95-28679
Fibre-coupled remote optical vibrometry
[AD-A291606] p 2698 N95-29932
Testbed for precision characterization of spatial light modulators and optical processors
[AD-A290484] p 2699 N95-29148
Topics in high-peak intensity, ultrashort pulse laser-plasma interactions p 2704 N95-29218
Photon-counting spatial light modulator technology development
[AD-A292619] p 2699 N95-29295
Semiconductor deposition and etching interactions of laser-generated translationally hot atoms and radicals
[AD-A291824] p 2693 N95-29431
The role of the coherence function in holographic imaging p 2583 N95-29508
Coherent soft x-ray generation using a powerful subpicosecond laser p 2587 N95-29689

LASER CAVITIES
Exact physical models and methods for stabilization and control of reflection-induced instabilities in semiconductor lasers
[AD-A292437] p 2585 N95-29053
Inhibition of mode competition in free-electron laser oscillators p 2586 N95-29336
Vertical cavity surface emitting lasers for optical signal processing and optical computing applications
[AD-A290626] p 2588 N95-30050

LASER DEPOSITION
Semiconductor deposition and etching interactions of laser-generated translationally hot atoms and radicals
[AD-A291824] p 2693 N95-29431

LASER DOPPLER VELOCIMETERS
Laser doppler velocimeter system for subsonic jet mixer nozzle testing at the NASA Lewis Aeroacoustic Propulsion Lab
[NASA-TM-106984] p 2477 N95-30229

LASER MATERIALS
ARPA solid state laser and nonlinear materials program
[AD-A289657] p 2584 N95-28678
Auger rates in mid-IR InAsSb laser structures
[DE95-006325] p 2588 N95-30006

LASER MODE LOCKING
Semiconductor film Cherenkov lasers
[AD-A291177] p 2587 N95-29930

LASER MODES
Exact physical models and methods for stabilization and control of reflection-induced instabilities in semiconductor lasers
[AD-A292437] p 2585 N95-29053

LASER OUTPUTS
Inhibition of mode competition in free-electron laser oscillators p 2586 N95-29336
Coherent soft x-ray generation using a powerful subpicosecond laser p 2587 N95-29689
Observation of x ray generation in a proof-of-principle laser synchrotron source experiment
[AD-A291298] p 2588 N95-29937

LASER PLASMA INTERACTIONS
Topics in high-peak intensity, ultrashort pulse laser-plasma interactions p 2704 N95-29218
Coherent soft x-ray generation using a powerful subpicosecond laser p 2587 N95-29689

LASER PUMPING
Optimal control of molecular motion
[AD-A291919] p 2691 N95-28944
Studies of energy transfer processes of relevance to chemically and optically pumped lasers
[AD-A290164] p 2585 N95-29025
Development of distributed feedback dye lasers for generation of high-power 193 nm excimer laser short pulses p 2586 N95-29631
High-efficiency longitudinal diode bar pumping of solid-state lasers
[AD-A291180] p 2587 N95-29931

LASER RANGE FINDERS
Receiver design, performance analysis, and evaluation for space-borne laser altimeters and space-to-space laser ranging systems
[NASA-CR-198655] p 2584 N95-28808
A simple method for range finding via laser triangulation
[AD-A292529] p 2553 N95-29166
Estimation of unstabilized components in vehicular motion
[AD-A290580] p 2590 N95-29552
The laser ranging of etalon satellites
[AD-A291019] p 2587 N95-29660

LASER SPECTROSCOPY
Summaries of papers presented at the ultrafast phenomena topical meeting
[AD-A290998] p 2564 N95-29511

LASER STABILITY
Exact physical models and methods for stabilization and control of reflection-induced instabilities in semiconductor lasers
[AD-A292437] p 2585 N95-29053

LASER TARGET INTERACTIONS
Topics in high-peak intensity, ultrashort pulse laser-plasma interactions p 2704 N95-29218
Measurement of interface strength, intrinsic toughness and their dependence on interfacial segregants
[AD-A291798] p 2524 N95-29409
Coherent soft x-ray generation using a powerful subpicosecond laser p 2587 N95-29689

LASER TARGETS
Coherent soft x-ray generation using a powerful subpicosecond laser p 2587 N95-29689

LASERS
Doubled diode laser, phase 1
[AD-A292465] p 2584 N95-29007
Tunable laser for persistent spectral hole burning optical memories
[AD-A292598] p 2586 N95-29292
Observation of x ray generation in a proof-of-principle laser synchrotron source experiment
[AD-A291298] p 2588 N95-29937
Sensor protection portion of the development of nonlinear optical materials and processes for laser hardening of sensors
[AD-A291200] p 2702 N95-29973
Inertial fusion program and national laser users facility program
[DE95-008202] p 2711 N95-30274

LASING
Investigation of the Paschen curve of nitrogen via the application of nanosecond pulsed electromagnetic radiation
[AD-A290129] p 2586 N95-29425
Experimental studies of fundamental one- and two-photon lasing processes
[AD-A290593] p 2693 N95-29555

LATENT HEAT
Thermophysical properties of R-32 (difluoromethane)
[ESDU-94032] p 2530 N95-28802
Short-range precipitation forecasts using assimilation of simulated satellite water vapor profiles and cloud liquid water p 2625 N95-29832
An air-sea interaction model for stress, sensible heat, latent heat, and sea state, applicable to the full range of wind speeds p 2626 N95-29876

LATTICES (MATHEMATICS)
Lattice gas methods for computational aeroacoustics p 2687 N95-30144

LAUNCH VEHICLES
Design and analysis of the launch vehicle adapter fitting for the petite amateur navy satellite (PANSAT)
[AD-A289693] p 2504 N95-28680

LAUNCHING
Performance evaluation of bolt-cutter system on first Taurus launch
[AD-A291237] p 2504 N95-29992

LAVA
Channels and valleys on Venus p 2736 N95-29593

LAY-UP
Analytical investigation of the hygrothermal effects and parametric study of the Edge Crack Torsion (ECT) mode 3 test lay-ups
[NASA-TM-110183] p 2528 N95-30028

LAYOUTS
Numerical modeling of opto-electronic integrated circuits
[AD-A292096] p 2563 N95-29239

LEAD (METAL)
Macrosegregation and nucleation in undercooled Pb-Sn alloys
[NASA-TM-102023-REV] p 2535 N95-28701

LEADING EDGE FLAPS
Increments in aerofoil lift coefficient at zero angle of attack and in maximum lift coefficient due to deployment of a plain trailing-edge flap, with or without a leading-edge high-lift device, at low speeds
[ESDU-94028] p 2486 N95-28885
Pressure based high order TVD methodology for dynamic stall control
[AD-A290149] p 2489 N95-29316
Increments in aerofoil lift coefficient at zero angle of attack and in maximum lift coefficient due to deployment of various leading-edge high-lift devices at low speeds
[ESDU-94027] p 2490 N95-29898
Low-speed wind-tunnel investigation of the stability and control characteristics of a series of flying wings with sweep angles of 50 deg
[NASA-TM-4640] p 2498 N95-30226

LEADING EDGES
Computer program for estimation of leading-edge suction distribution for plane thin wings at subsonic speeds
[ESDU-94038] p 2477 N95-28708
Leading-edge suction distribution for plane thin wings at subsonic speeds
[ESDU-94037] p 2486 N95-28800
A nonintrusive method of quantifying flow visualization data in vortex flow fields
[AD-A289802] p 2568 N95-28948
Leading edge film cooling effects on turbine blade heat transfer
[NASA-TM-106955] p 2500 N95-29115
Navier-Stokes solution of wing wake structure and its perturbation p 2488 N95-29121
A numerical method for modelling wings with sharp edges maneuvering at high angles of attack p 2496 N95-29122

LEAF AREA INDEX
Maize yield estimation through the simulation of radiation penetration into the canopy p 2599 N95-29703

LEAKAGE
The fluid mechanics of a high aspect ratio slot with an impressed pressure gradient and secondary injection p 2580 N95-30304

LEARNING
Training end-users on database queries: The effectiveness of example format and spatial ability on learing outcomes p 2724 N95-29829

LECTURES
ADA in introductory courses
[AD-A292219] p 2648 N95-29285
Lecture note on the bases of plasma physics
[NIFS-PROC-15] p 2711 N95-29966

LENS DESIGN
Simulated imaging properties of a series of magnetic electron lenses
[NASA-CR-195474] p 2564 N95-29406

LENSES
Laser optics protective device
[AD-D017384] p 2585 N95-29217
Fiber compatible acousto-optic modulator using a gradient index lens
[AD-A291164] p 2585 N95-29925

LESIONS
Flying waivers for history of angioplasty and myocardial infraction
[AD-A292505] p 2635 N95-29161

LIBRARIES
Porting a vector library: A comparison of MPI, paris, CMMD and PVM (or, 'I'll never have to port CVL again')
[AD-A290231] p 2647 N95-29147

LIE GROUPS
Spectral estimates for positive Rockland operators
[PB95-206751] p 2673 N95-30204

LIFE (DURABILITY)
High performance nickel electrodes for space power applications p 2511 N95-30257
Magnum(R) NiCd advanced nickel-cadmium battery cells p 2567 N95-30258
Electrolyte management considerations in modern nickel hydrogen and nickel cadmium cell and battery designs p 2567 N95-30262

LIFE CYCLE COSTS
Novel cost controlled materials and processing for primary structures p 2514 N95-28830

LIFE SCIENCES
Experiment kits for processing biological samples inflight on SLS-2
[NASA-TM-4685] p 2642 N95-28722
An inflight refill unit for replenishing research animal drinking water
[NASA-TM-4684] p 2642 N95-28818
Life sciences program
[NASA-CR-197658] p 2633 N95-30292

LIFE SUPPORT SYSTEMS
Aerospace medicine and biology: A continuing bibliography with indexes (supplement 403)
[NASA-SP-7011(403)] p 2636 N95-29190

LIFT
Increments in aerofoil lift coefficient at zero angle of attack and in maximum lift coefficient due to deployment of a plain trailing-edge flap, with or without a leading-edge high-lift device, at low speeds
[ESDU-94028] p 2486 N95-28885
Increments in aerofoil lift coefficient at zero angle of attack and in maximum lift coefficient due to deployment of a trailing-edge split flap, with or without a leading-edge high-lift device, at low speeds
[ESDU-94029] p 2488 N95-29129
A two element laminar flow airfoil optimized for cruise
[NASA-CR-198580] p 2489 N95-29338
Increments in aerofoil lift coefficient at zero angle of attack and in maximum lift coefficient due to deployment of various leading-edge high-lift devices at low speeds
[ESDU-94027] p 2490 N95-29898
Introduction to the estimation of the lift coefficients at zero angle of attack and at maximum lift for aerofoils with high-lift devices at low speeds
[ESDU-94026] p 2491 N95-29899

LIFT DEVICES
Increments in aerofoil lift coefficient at zero angle of attack and in maximum lift coefficient due to deployment of a plain trailing-edge flap, with or without a leading-edge high-lift device, at low speeds
[ESDU-94028] p 2486 N95-28885
Increments in aerofoil lift coefficient at zero angle of attack and in maximum lift coefficient due to deployment of various leading-edge high-lift devices at low speeds
[ESDU-94027] p 2490 N95-29898
Introduction to the estimation of the lift coefficients at zero angle of attack and at maximum lift for aerofoils with high-lift devices at low speeds
[ESDU-94026] p 2491 N95-29899

LIFT DRAG RATIO
A two element laminar flow airfoil optimized for cruise
[NASA-CR-198580] p 2489 N95-29338

LIGANDS
Transition metal complexes with perfluorinated ligands
[AD-A290250] p 2536 N95-29427
The redox chemistry of some peroxo and superoxo metal ion complexes
[AD-A290761] p 2532 N95-29483
Inorganic halogen oxidizers
[AD-A291201] p 2702 N95-29974
LIGHT AMPLIFIERS
Fibre-coupled remote optical vibrometry
[AD-A291606] p 2698 N95-28932
Development of continuous visible chemical laser amplifiers and oscillators from the Na3-X(Cl, Br, I) reactions and their analogs and energy transfer pumping from efficiently produced metastable states
[AD-A290999] p 2586 N95-29514
LIGHT CURVE
Yohkoh Bragg Crystal Spectrometer light curves for Ca 29(3.1633 - 3.1933 A): 1 October 1993 - 30 September 1994
[AD-A290027] p 2738 N95-29327
Gamma radiation from rotation powered pulsars and results from the Energetic Gamma-Ray Experiment Telescope p 2739 N95-29671
LIGHT EMISSION
The effect of bright light and LEET on sleep after a 10-hour phase delay
[AD-A291264] p 2637 N95-29995
LIGHT EMITTING DIODES
The 41st Japan Society of Applied Physics Spring Meeting
[AD-A292333] p 2720 N95-29879
Ion doped quantum well lasers
[AD-A290937] p 2587 N95-29912
Interfaces in InAsSb/InGaAs strained-layer superlattices grown by MOCVD for use in infrared emitters
[DE95-006323] p 2717 N95-29990
LIGHT MODULATION
Testbed for precision characterization of spatial light modulators and optical processors
[AD-A290484] p 2699 N95-29148
A method and apparatus for signal filtering
[AD-D017268] p 2554 N95-29236
Photon-counting spatial light modulator technology development
[AD-A292619] p 2699 N95-29295
Raman and photo-modulated reflectivity studies of ZnTe/InAs semiconductor heterostructure under hydrostatic pressure
[AD-A290467] p 2716 N95-29506
Theory and experiment analysis of two-dimensional acousto-optic interaction
[AD-A291059] p 2685 N95-29951
Photorefractive Bi12SiO20 spatial light modulator
[AD-A291070] p 2702 N95-29969
LIGHT SCATTERING
Predicting polarized light scattering by marine micro-organism
[AD-A289790] p 2696 N95-28695
Predicting polarized light scattering by marine micro-organisms
[AD-A289796] p 2697 N95-28698
High power, high frequency radiation from beam-plasma interactions
[AD-A292442] p 2703 N95-29001
Engineering design of sub-micron topographies for simultaneously adherent and reflective metal-polymer interfaces
[NASA-CR-198845] p 2548 N95-30237
LIGHT SOURCES
Propagation and transformation properties of axicon optical systems for laser beams
[AD-A289661] p 2584 N95-28679
Reflectance analysis under solar illumination
[AD-A290489] p 2737 N95-29151
A method and apparatus for signal filtering
[AD-D017268] p 2554 N95-29236
Molecular spectra and dynamics at interfaces
[AD-A289779] p 2693 N95-29460
The role of the coherence function in holographic imaging p 2583 N95-29508
LIGHT TRANSMISSION
Propagation and transformation properties of axicon optical systems for laser beams
[AD-A289661] p 2584 N95-28679
Self-Induced Transparency in photonic band structures: Gap solitons near absorption resonances
[AD-A292187] p 2718 N95-28927
Topics in high-peak intensity, ultrashort pulse laser-plasma interactions p 2704 N95-29218
Pulsed laser deposition of thin film material for nonlinear waveguides
[AD-A290789] p 2544 N95-29484
HTMIAC/CINDAS silicon properties database. User's guide
[AD-A292602] p 2533 N95-29575
Diffractive optics: Design, fabrication, and applications
[AD-A290942] p 2702 N95-29867
High temperature spectroscopy of alkali metal vapors for solar to thermal energy conversion
[AD-A291355] p 2602 N95-29949
LIGHTNING
Cathodic protection system inspection 5
[AD-A289724] p 2592 N95-28684
LIKELIHOOD RATIO
Bootstrap and partitioning methods
[AD-A290662] p 2671 N95-29578
LIMITERS (FUSION REACTORS)
Effects of impurities released from high Z test limiter on plasma performance in TEXTOR
[AD-B191995L] p 2709 N95-29803
LINE OF SIGHT
Visualization of improved target acquisition algorithm for Janus (A)
[AD-A290191] p 2646 N95-29056
Estimates of probability of a cloud-free line of sight for RAPTOR TALON
[AD-A291908] p 2510 N95-29284
Precision pointing experiment
[AD-A291015] p 2664 N95-29657
LINE SPECTRA
Simultaneous UV and optical study of O star winds and UV and optical covariability of O star winds
[NASA-CR-189424] p 2726 N95-29370
Numerical studies of ablative mass loss from wind accelerated clouds p 2622 N95-29676
Observational properties of SiO masers in the galactic bulge IRAS sources p 2735 N95-29838
15th NSO/Sac Peak Solar Workshop
[AD-A292297] p 2739 N95-30074
LINEAR ACCELERATORS
Semiconductor film Cherenkov lasers
[AD-A291177] p 2587 N95-29930
A practical high-energy high-luminosity mu(+)-mu(-) collider
[DE95-006769] p 2696 N95-30009
LINEAR ARRAYS
Competitive analysis of call admission algorithms that allow delay
[AD-A292242] p 2645 N95-28878
LINEAR EQUATIONS
Discontinuous solutions of semilinear differential-algebraic equations. part 2: Rho-consistency
[AD-A292285] p 2668 N95-28861
Discontinuous solutions of semilinear differential-algebraic equations. part 1: Distribution solutions
[AD-A292286] p 2668 N95-28863
Linear and nonlinear discrete-time state-space modeling of dynamic systems for control applications p 2663 N95-29251
Linear algebraic computation on distributed memory parallel machines
[AD-A290615] p 2671 N95-29558
The study of non-Newtonian contraction flows with a parallel finite element method p 2576 N95-29778
Benchmark problems and solutions p 2686 N95-30134
LINEAR OPERATORS
Translation Invariant Operators on Lp-Type Spaces
[PB95-197117] p 2672 N95-30092
LINEAR PROGRAMMING
Solving linear programs using distributed parallel computing
[AD-A290221] p 2658 N95-29079
LINEAR QUADRATIC GAUSSIAN CONTROL
Design and evaluation of a LQR controller for the bluebird unmanned air vehicle
[AD-A289769] p 2498 N95-29457
Control of vortex dynamics p 2579 N95-30275
LINEAR QUADRATIC REGULATOR
Spin augmented deployment and retrieval of tethered artificial gravity spacecraft p 2509 N95-30280
LINEAR SYSTEMS
Closed loop control of guided missiles using neural networks p 2663 N95-29241
Linear and nonlinear discrete-time state-space modeling of dynamic systems for control applications p 2663 N95-29251
Design and evaluation of a LQR controller for the bluebird unmanned air vehicle
[AD-A289769] p 2498 N95-29457
Interlaminar fracture mechanics and mechanisms: Linear and nonlinear aspects p 2526 N95-29597
Linear matrix inequalities for the problem of absolute stability of control systems p 2501 N95-29680
Digital control of distributed parameter systems: A state-space approach
[PB95-197216] p 2666 N95-30041
Fischer's protocol in timed process algebra
[PB95-206777] p 2672 N95-30089
Linear carborane-(siloxane or silane)-acetylene based copolymers
[AD-D017321] p 2547 N95-30132
Learning control in linear and nonlinear systems p 2667 N95-30238
LINEAR TRANSFORMATIONS
Multilayer piecewise linear networks. Revision 1
[AD-A289885] p 2658 N95-28955
LINEAR VIBRATION
Modal interactions and complex responses in weaklyNONLINEAR MULTI-DEGREE-OF-FREEDOM MECHANICAL SYSTEMS
[AD-A292023] p 2594 N95-28853
LINEARITY
Precision pointing experiment
[AD-A291015] p 2664 N95-29657
Nitrogen dioxide measurement method characterization at the GRI conventional research house
[PB95-200549] p 2610 N95-30197
LINEARIZATION
Fischer's protocol in timed process algebra
[PB95-206777] p 2672 N95-30089
Multi-dimensional upwind discretization method for the Euler equations on unstructured grids
[PB95-197307] p 2578 N95-30202
Numerical simulation of mechanisms and manipulator robots with flexible links and flexible joints
[PB95-196903] p 2591 N95-30285
LINGUISTICS
Interface for the translation of sentences in a natural language into a geometrical representation language
[INPE-5467-PRE/1775] p 2722 N95-29383
LIPIDS
Electrical and electronic properties of self-assembled lipid bilayers
[AD-A290507] p 2632 N95-29155
LIQUID COOLING
Effects of cooling system parameters on heat transfer in PAFC stack
[NASA-CR-198817] p 2570 N95-29131
175Hp contrarotating homopolar motor design report
[AD-A291138] p 2567 N95-30122
Fundamental studies in cryogenic cooling of power electronics
[AD-A291150] p 2551 N95-30296
LIQUID CRYSTALS
Summary report for cooperative research and development agreement between Oak Ridge Associated Universities and Interactive Presentation Systems
[DE95-006874] p 2644 N95-28777
Low voltage, high resistance, Polymer Dispersed Liquid Crystal
[AD-A291946] p 2556 N95-29472
Transitions in liquid crystals initiated with circularly polarized light
[AD-A290525] p 2716 N95-29493
Neutron scattering from amorphous, disordered and nanocrystalline materials
[DE95-005848] p 2717 N95-30077
LIQUID HELIUM
Five-channel SQUID based non-destructive evaluation (NDE) instrument
[AD-A292474] p 2592 N95-29012
LIQUID HYDROGEN
Prediction of pressurant mass requirements for axisymmetric liquid hydrogen tanks
[NASA-TM-106973] p 2511 N95-29642
Analysis of stress concentration in the Dutton groove regions of the Super Lightweight External Tank
[NASA-TM-108490] p 2597 N95-30328
LIQUID INJECTION
Liquid pressure amplification and liquid injection in air conditioning and refrigeration systems
[AD-A289738] p 2549 N95-28686
LIQUID LEVELS
Method of measuring liquid level with a thermal interface detection
[AD-D017341] p 2703 N95-30166
LIQUID METALS
Advanced manufacturing by spray forming: Aluminum strip and microelectromechanical systems
[DE95-008615] p 2536 N95-28959
Liquefied metal jet program Automation and Robotics Research Institute (ARRI)
[AD-A289781] p 2536 N95-29461
Simulation of powder metal fabrication with high pressure gas atomization
[DE95-008820] p 2538 N95-30178
LIQUID NITROGEN
Fundamental studies in cryogenic cooling of power electronics
[AD-A291150] p 2551 N95-30296

LIQUID PHASES
Thermal conductivity of liquid halogenated aliphatic hydrocarbons. Part 1: Halogenated methanes and azeotropic mixtures
[ESDU-94021-PT-1] p 2511 N95-28804
Molecular dynamics simulation of liquid nitromethane shocked to 143 kbar
[AD-A292107] p 2691 N95-28919
SCAP spray combustion analysis program
[AD-A289946] p 2532 N95-29273
The TEES process cleans waste and produces energy
[DE95-007799] p 2602 N95-29463

LIQUID ROCKET PROPELLANTS
SCAP spray combustion analysis program
[AD-A289946] p 2532 N95-29273
A theoretical study on ignition mechanisms of liquid propellants
[AD-A290569] p 2549 N95-29550

LIQUID SURFACES
The onset of electrohydrodynamic instability in isoelectric focusing
[NASA-CR-198805] p 2565 N95-29968
Method of measuring liquid level with a thermal interface detection
[AD-D017341] p 2703 N95-30166

LIQUIDS
Orthobaric densities and molar volumes of liquids. Glycols and cyclic diols
[ESDU-95003] p 2531 N95-28895
Bubble fusion: Preliminary estimates of spherical micro-implosions in cavitating liquids
[DE95-006260] p 2569 N95-28956
Dynamics of simple chemically reactive fluids
p 2573 N95-29335
Vapour pressures and critical points of liquids. Glycols and cyclic diols
[ESDU-95002] p 2534 N95-29897
Vapour pressures and critical points of liquids. Glycol ethers (alkyl celiosolves and carbitols, etc.)
[ESDU-95004] p 2534 N95-29901

LITHIUM
Fluxes and relative abundances of light cosmic ray nuclei at energies above 40 GeV/n p 2739 N95-29531

LITHIUM NIOBATES
Growth, characterization and application of KTN family nonlinear optical crystals
[AD-A290330] p 2713 N95-29087

LITHOGRAPHY
Drift mobility measurements in thin film boron carbide
[AD-A292510] p 2712 N95-28869
Fourier Synthesis Lithographic Machine for large panel display fabrication
[AD-A291921] p 2698 N95-28914
An integrated optical CO2 sensor. Phase 0: Design and fabrication of critical elements
[NASA-CR-198792] p 2700 N95-29366
Solid freeform fabrication symposium
[AD-A290949] p 2527 N95-29732
Passive damping to enhance active positioning of a prototype lithography platen
[DE95-008539] p 2655 N95-30209

LITHOSPHERE
Eurasian seismic surveillance - 2D FD seismic synthetics and event discrimination
[AD-A292659] p 2614 N95-29413
The gravitational potential energy of the Earth's lithosphere p 2617 N95-29773

LOAD DISTRIBUTION (FORCES)
An impact load identification method using distributed sensor measurements p 2595 N95-29419
Estimation of aerodynamic load distributions on the F/A-18 aircraft using a CFD panel code
[DSTO-TR-0147] p 2498 N95-29445

LOAD TESTS
Dynamic decohesion of bimaterial interfaces
p 2541 N95-29120
In-phase thermomechanical fatigue mechanisms in an unidirectional SCS-6/Ti 15-3 MMC
[NASA-CR-195482] p 2523 N95-29133
Experimental investigations of wave and fracture phenomena in impacted ceramics and glasses
[AD-A292142] p 2542 N95-29195
Fiber-matrix adhesion in single-fiber model composites
p 2524 N95-29337
Toughening mechanisms in mixed-mode interfacial fracture p 2545 N95-29772
Analytical investigation of the hygrothermal effects and parametric study of the Edge Crack Torsion (ECT) mode 3 test lay-ups
[NASA-TM-110183] p 2528 N95-30028
A system for conveniently providing load testing termination of an AC power source having at least one battery
[AD-D017408] p 2566 N95-30075

LOADS (FORCES)
Carrier-less, anti-backlash planetary drive system
[NASA-CASE-GSC-13608-1] p 2588 N95-28702
Investigation of an alternative finite element procedure: A one-step, steady-state analysis
[AD-A290030] p 2670 N95-29311
Severe edge effects and simple complimentary interior solutions for thin-walled anisotropic and composite structures
[AD-A290645] p 2595 N95-29562
High power switch design
[AD-A291608] p 2565 N95-29601
A study of blister tests for film adhesion measurement and fracture efficiency of tests for adhesive bonds
p 2545 N95-29799
Permanent magnet torque/force transfer apparatus
[AD-D017325] p 2682 N95-30051
Load-balancing algorithms for the parallel community climate model
[DE95-008795] p 2610 N95-30176

LOCAL AREA NETWORKS
Applications of digital video and synthetic environments to unmanned aerial vehicles
[AD-A291875] p 2497 N95-29437
Information management in local area networks: Impact on users' perceptions p 2723 N95-29690
HIPPI - Gigabit LANS are here today
[DE95-007877] p 2660 N95-30128

LOCAL GROUP (ASTRONOMY)
The 12 UM contribution of nearby galaxies to the infrared background
[AD-A291185] p 2735 N95-29917

LOCUSTS
A biologically-inspired autonomous robot
[AD-A289446] p 2666 N95-30026

LOGIC CIRCUITS
Using ordered binary-decision diagrams for compressing images and image sequences
[AD-A292244] p 2721 N95-28880
Asymptotically zero energy computing using split-level charge recovery logic
[AD-A290054] p 2564 N95-29478

LOGIC DESIGN
Progress and trends of multi-valued logic research
[AD-A290997] p 2665 N95-29874

LOGIC PROGRAMMING
Design ,and implementation of logical database languages
[AD-A290474] p 2650 N95-29509

LONG DURATION EXPOSURE FACILITY
Effects of space exposure on metals flown on the Long Duration Exposure Facility
[NASA-CR-4662] p 2512 N95-30225

LONG DURATION SPACE FLIGHT
Life sciences program
[NASA-CR-197658] p 2633 N95-30292

LONG TERM EFFECTS
Study of the space environmental effects on spacecraft engineering materials
[NASA-CR-196638] p 2531 N95-29246

LONGITUDINAL WAVES
Experimental investigations of wave and fracture phenomena in impacted ceramics and glasses
[AD-A292142] p 2542 N95-29195
Collective phenomena in granular fluids
p 2572 N95-29219
The decay of longitudinal vortices shed from airfoil vortex generators
[NASA-CR-198356] p 2489 N95-29402

LOSSES
The effect of viscous attenuation on shock tube performance
[AD-A289793] p 2568 N95-28696
Numerical studies of ablative mass loss from wind accelerated clouds p 2622 N95-29676

LOSSY MEDIA
Dielectric property measurements in the Electromagnetic Properties Measurement Laboratory
[NASA-TM-110147] p 2560 N95-30336

LOW ALTITUDE
Estimates of probability of a cloud-free line of sight for RAPTOR TALON
[AD-A291908] p 2510 N95-29284

LOW CARBON STEELS
The effects of alloying elements on the strength and cooling rate sensitivity of ultra-low carbon alloy steel weld metals
[AD-A290681] p 2537 N95-29759
Austenite to ferrite transformation kinetics during continuous cooling
[DE95-008582] p 2537 N95-29869

LOW COST
Low cost writable RFID tag with MRAM memory
[AD-A292553] p 2642 N95-28974
Research results on an improved in-situ tropospheric humidity sensor
[AD-A291339] p 2627 N95-29944

LOW CURRENTS
Arcing mitigation and predictions for high voltage solar arrays
[AD-A292227] p 2602 N95-29200
Arcing predictions for PASP PLUS solar arrays
[AD-A292230] p 2602 N95-29201

LOW EARTH ORBITS
A layman's look at orbital debris
[AD-A289801] p 2506 N95-28700

LOW FREQUENCIES
The 6th Van der Ziel symposium on quantum 1/f noise and other low frequency fluctuations in electronic devices
[AD-A292468] p 2718 N95-29009
100 Hz-10 kHz bottom backscattering model: Generalized treatment of sediment sound propagation, sediment volume scattering and interface-roughness scattering
[AD-A291323] p 2685 N95-29942
Dynamical instabilities, chaos and spatial complexity in fundamental nonlinear optical interactions
[AD-A291223] p 2588 N95-29980

LOW MOLECULAR WEIGHTS
Polyethylene-based polyurethane copolymers and block copolymers
[AD-A289996] p 2546 N95-30030

LOW NOISE
High gain, low noise and broadband Raman and Brillouin fiber-optic amplifiers, channel selectors and switches
[AD-A290585] p 2700 N95-29553
Test results of a 20 GHz, low noise downconverter for USAT applications
[NASA-TM-106892] p 2508 N95-30011
Balanced, double-sided calibration circuit for sensor element differential pre-amplifier
[AD-D017326] p 2566 N95-30052

LOW REYNOLDS NUMBER
Research on bluff-body vortex wakes
[AD-A292650] p 2574 N95-29382

LOW SPEED
Numerical investigation of surface curvature effects in compressible turbulent flows
[AD-A290114] p 2571 N95-29211
Low-speed wind-tunnel investigation of the stability and control characteristics of a series of flying wings with sweep angles of 50 deg
[NASA-TM-4640] p 2498 N95-30226

LOW TEMPERATURE
Composite material studies for low temperature thermionic emission
[AD-A292159] p 2523 N95-29124

LOW THRUST PROPULSION
Guidance, navigation, and control study for a solar electric propulsion spacecraft
[NASA-CR-198920] p 2509 N95-30357

LOW VOLTAGE
Low voltage, high resistance, Polymer Dispersed Liquid Crystal
[AD-A291946] p 2556 N95-29472

LOWER ATMOSPHERE
Upper-air data collected on Ice Station Weddell
[AD-A289707] p 2620 N95-29193
Studies of gravity-wave filtering and tidal interaction in the middle atmosphere p 2619 N95-30351

LOWER BODY NEGATIVE PRESSURE
Pulse waveform and pulse amplitude analysis during Lower Body Negative Pressure
[AD-A290521] p 2636 N95-29360

LUBRICANT TESTS
Selection of synthetic oils
[ESDU-94020] p 2539 N95-28898

LUBRICANTS
Selection of synthetic oils
[ESDU-94020] p 2539 N95-28898
Lubricant film thickness between disc cams and followers
[ESDU-94008] p 2539 N95-28900
Selection of materials, manufacturing methods and lubricants for cam mechanisms
[ESDU-94017] p 2589 N95-28905

LUBRICATING OILS
Selection of synthetic oils
[ESDU-94020] p 2539 N95-28898

LUBRICATION
Contact stress in disc cams with domes of flat-faced followers
[ESDU-94011] p 2589 N95-28901

LUMINAIRES
Prototype stop bar system evaluation at Seattle-Tacoma International Airport
[AD-A290136] p 2495 N95-30031

LUMINESCENCE
Optoelectronics based on SiGe/Si heterostructures
[AD-A292464] p 2699 N95-29006
LUMINOSITY
Nobeyama Radio Observatory report, no. 378: The polar ring spiral galaxy NGC 660 p 2731 N95-29097
Advanced research in sky surveillance: A search for low-luminosity objects
[AD-A291184] p 2731 N95-29916
LUMPED PARAMETER SYSTEMS
Nonlinear control systems
[AD-A291083] p 2665 N95-29971
LUNAR BASED EQUIPMENT
Fuel cell systems for First Lunar Outpost-reactant storage option p 2606 N95-30264
LUNAR EXPLORATION
Apollo 11: For all mankind
[NASA-TM-110622] p 2503 N95-29407
Lunar/Mars exploration for synthesis group
[NASA-TM-110647] p 2737 N95-30249
Apollo 14: Shepard hitting golf ball on Moon
[NASA-TM-110638] p 2737 N95-30318
LUNAR GEOLOGY
A geotechnical characterization of lunar soils and lunar soil simulants p 2736 N95-29117
Some aspects of lunar and martian volcanism as examined with spectral, topographic, and morphologic data derived from spacecraft images p 2736 N95-29594
LUNAR LANDING
Apollo 11: For all mankind
[NASA-TM-110622] p 2503 N95-29407
LUNAR LIMB
Total solar eclipse of 1997 March 9
[NASA-RP-1173] p 2731 N95-30004
LUNAR MARIA
Some aspects of lunar and martian volcanism as examined with spectral, topographic, and morphologic data derived from spacecraft images p 2736 N95-29594
LUNAR ORBITS
Apollo 11: For all mankind
[NASA-TM-110622] p 2503 N95-29407
Guidance, navigation, and control study for a solar electric propulsion spacecraft
[NASA-CR-198920] p 2509 N95-30357
LUNAR PHASES
Tidal and lunar data for Point Mugu, San Nicolas Island, and the Barking Sands area during 1995
[AD-A289877] p 2733 N95-29599
LUNAR PROGRAMS
Lunar/Mars exploration for synthesis group
[NASA-TM-110647] p 2737 N95-30249
LUNAR ROCKS
A geotechnical characterization of lunar soils and lunar soil simulants p 2736 N95-29117
LUNAR SHADOW
Total solar eclipse of 1997 March 9
[NASA-RP-1173] p 2731 N95-30004
LUNAR SOIL
A geotechnical characterization of lunar soils and lunar soil simulants p 2736 N95-29117
LUNAR SURFACE
A geotechnical characterization of lunar soils and lunar soil simulants p 2736 N95-29117
Apollo 11: For all mankind
[NASA-TM-110622] p 2503 N95-29407
Some aspects of lunar and martian volcanism as examined with spectral, topographic, and morphologic data derived from spacecraft images p 2736 N95-29594
Apollo 14: Shepard hitting golf ball on Moon
[NASA-TM-110638] p 2737 N95-30318
LUNGS
Effect of hypoxia on arterial blood gases in subjects with lung dysfunction p 2638 N95-29627
LYMAN SPECTRA
Continuum spectra of supermassive accretion disks p 2732 N95-29252
LYMPHOCYTES
Cellular and molecular level responses after radiofrequency radiation exposure, alone or in combination with x rays or chemicals
[AD-A292488] p 2633 N95-28866
Studies of altered response to infection induced by severe injury
[AD-A288907] p 2634 N95-29139

M

MACH NUMBER
An experimental investigation of the time-dependent separation of tangent bodies in supersonic flow
[AD-A290720] p 2489 N95-29500
Transonic, supersonic and hypersonic wind-tunnel tests on aerodynamic characteristics of reentry body with blunted cone configuration
[ISAS-658] p 2490 N95-29640
The 1995 version of the NSWC aeroprediction code. Part 1: Summary of new theoretical methodology
[AD-A291518] p 2490 N95-29853
An aerodynamic and static-stability analysis of the Hypersonic Applied Research Technology (HART) missile
[DA9426923] p 2491 N95-29965
MACH-ZEHNDER INTERFEROMETERS
Interferometric measurement with squeezed light
[AD-A292402] p 2697 N95-28799
Numerical modeling of opto-electronic integrated circuits
[AD-A292096] p 2563 N95-29239
MACHINE LEARNING
Management of speedup mechanisms in learning architectures
[AD-A292206] p 2662 N95-28988
Interface for the translation of sentences in a natural language into a geometrical representation language
[INPE-5467-PRE/1775] p 2722 N95-29363
Interaction and intelligent behavior
[AD-A290049] p 2639 N95-29443
Workshop on Fielded Applications of Machine Learning
[AD-A280168] p 2649 N95-29456
Automated reasoning about classical mechanics
[AD-A290052] p 2663 N95-29477
Neural network exploration using optional experiment design
[AD-A290058] p 2663 N95-29479
Acquisition of place knowledge through case-based learning
[AD-A292574] p 2723 N95-29573
Learning object models from visual observation and background knowledge
[AD-A292606] p 2650 N95-29576
Applications of machine learning and rule induction
[AD-A292607] p 2664 N95-29577
Neural network construction using evolutionary search
[AD-A290862] p 2665 N95-29831
Hybrid pyramid-neural network vision system
[AD-A290565] p 2665 N95-29863
Induction of selective Bayesian classifiers
[AD-A292690] p 2675 N95-29906
Learning control in linear and nonlinear systems p 2667 N95-30238
Self-organization in a simple brain model
[DE95-008312] p 2668 N95-30279
MAGELLANIC CLOUDS
The search for mass segregation in star clusters of the Magellanic Clouds p 2730 N95-29781
MAGNESIUM OXIDES
Analytical electron microscopy of precipitates in ion-implanted MgAl2O4 spinel
[DE95-007406] p 2538 N95-30038
MAGNETIC COILS
Experimental results of Hooper's gravity-electromagnetic coupling concept
[NASA-TM-106963] p 2680 N95-28893
MAGNETIC CONTROL
A conceptual design for the attitude control and determination system for the Magnetosphere Imager spacecraft
[NASA-TP-3560] p 2507 N95-28721
MAGNETIC DISKS
Nanoindentation and nanoscratching of hard coating materials for magnetic disks
[DE95-008776] p 2547 N95-30174
MAGNETIC EFFECTS
Gamma radiation from rotation powered pulsars and results from the Energetic Gamma-Ray Experiment Telescope p 2739 N95-29671
MAGNETIC EQUATOR
Chemical release experiments to induce F region ionospheric plasma irregularities at the magnetic equator p 2708 N95-29783
MAGNETIC FIELD CONFIGURATIONS
Correlations between micromagnetic, microstructural and microchemical properties in ultrathin epitaxial magnetic structures
[AD-A289705] p 2712 N95-28681
MAGNETIC FIELD RECONNECTION
Intermittent energy bursts and recurrent topological change of a twisting magnetic flux tube
[AD-B195513L] p 2708 N95-29755
Collisionless driven magnetic reconnection
[AD-B178946L] p 2709 N95-29810
The origin of collisionless dissipation in magnetic reconnection
[AD-B178949L] p 2710 N95-29813
MAGNETIC FIELDS
Development of a transient internal probe diagnostic
[AD-A292470] p 2704 N95-29011
Processing, fabrication, characterization and device demonstration of high temperature superconducting ceramics
[AD-A290183] p 2541 N95-29055
Observations and analysis of solar flares at radio and other wavelengths p 2738 N95-29202
Studies directed toward new and improved permanent magnet materials
[AD-A290749] p 2681 N95-29481
Development of an intense negative hydrogen ion source with a wide-range of external magnetic filter field
[AD-B195514L] p 2705 N95-29567
Equatorial heating effects on outer plasmasphere evolution p 2616 N95-29716
The origin of collisionless dissipation in magnetic reconnection
[AD-B178949L] p 2710 N95-29813
Properties and properties of long-lengths of Ag-clad BSCCO superconductors and high-(Tc) magnets
[DE95-005855] p 2716 N95-29984
Complete analysis of electrode-terminated cables in two-layer conductor bounded above by air: Current density, magnetic field, and magnetic field gradient
[AD-A290907] p 2566 N95-30079
MAGNETIC FILMS
Proceedings of the 6th Joint Magnetism and Magnetic Materials Intermag Conference
[AD-A286752] p 2681 N95-28923
Proceedings of the 38th Annual Conference on Magnetism and Magnetic Materials
[AD-A286753] p 2681 N95-28924
MAGNETIC FLUX
Intermittent energy bursts and recurrent topological change of a twisting magnetic flux tube
[AD-B195513L] p 2708 N95-29755
Large scale fluctuations of the geomagnetic field p 2617 N95-29796
Flux pinning and stabilizer studies
[DE95-008131] p 2682 N95-30131
Interaction of acoustic oscillations with magnetic flux tubes in the solar photosphere
[PB95-201810] p 2739 N95-30199
MAGNETIC LENSES
Simulated imaging properties of a series of magnetic electron lenses
[NASA-CR-195474] p 2564 N95-29406
MAGNETIC LEVITATION VEHICLES
Magnetic damping for Maglev
[DE95-005861] p 2665 N95-29987
MAGNETIC MATERIALS
Correlations between micromagnetic, microstructural and microchemical properties in ultrathin epitaxial magnetic structures
[AD-A289705] p 2712 N95-28681
Proceedings of the 6th Joint Magnetism and Magnetic Materials Intermag Conference
[AD-A286752] p 2681 N95-28923
Proceedings of the 38th Annual Conference on Magnetism and Magnetic Materials
[AD-A286753] p 2681 N95-28924
Proceedings of the 38th Annual Conference on Magnetism and Magnetic Materials
[AD-A286751] p 2681 N95-28962
Studies directed toward new and improved permanent magnet materials
[AD-A290749] p 2681 N95-29481
MAGNETIC MEASUREMENT
Magnetic damping for Maglev
[DE95-005861] p 2665 N95-29987
MAGNETIC POLES
Large scale fluctuations of the geomagnetic field p 2617 N95-29796
Permanent magnet torque/force transfer apparatus
[AD-D017325] p 2682 N95-30051
MAGNETIC PROPERTIES
Application of a rapid quench thermomagnetic analyzer to austempered ductile iron
[AD-A292261] p 2535 N95-28689
Proceedings of the 6th Joint Magnetism and Magnetic Materials Intermag Conference
[AD-A286752] p 2681 N95-28923
Proceedings of the 38th Annual Conference on Magnetism and Magnetic Materials
[AD-A286753] p 2681 N95-28924
Proceedings of the 38th Annual Conference on Magnetism and Magnetic Materials
[AD-A286751] p 2681 N95-28962
MAGNETIC RECORDING
Proceedings of the 38th Annual Conference on Magnetism and Magnetic Materials
[AD-A286753] p 2681 N95-28924
MAGNETIC RESONANCE
The physics of spin polarized gases
[AD-A292511] p 2680 N95-28810

MAGNETIC SIGNATURES
Five-channel SQUID based non-destructive evaluation (NDE) instrument
[AD-A292474] p 2592 N95-29012
MAGNETIC SPECTROSCOPY
Design of an electronic charged particle spectrometer to measure (rho R), yield, and implosion symmetry on the OMEGA Upgrade
[DE95-006068] p 2695 N95-28930
MAGNETIC STORMS
The effects of magnetic storm phases on F-layer irregularities from auroral to equatorial latitudes
[AD-A290674] p 2614 N95-29585
MAGNETIC SUSPENSION
Design of a fast-tool servo system using magnetic servo levitation
[AD-A290273] p 2663 N95-29183
Magnetic damping for Maglev
[DE95-005861] p 2665 N95-29987
MAGNETIC TRANSDUCERS
A conceptual design for the attitude control and determination system for the Magnetosphere Imager spacecraft
[NASA-TP-3560] p 2507 N95-28721
MAGNETIC VARIATIONS
Characterization of the geometries of the high-latitude ionospheric convection pattern p 2614 N95-29524
MAGNETIZATION
One and two fluid numerical investigations of solar wind gas releases p 2738 N95-29704
MAGNETO-OPTICS
Correlations between micromagnetic, microstructural and microchemical properties in ultrathin epitaxial magnetic structures
[AD-A289705] p 2712 N95-28681
Proceedings of the 38th Annual Conference on Magnetism and Magnetic Materials
[AD-A286753] p 2681 N95-28924
MAGNETOACOUSTIC WAVES
The physics of the collisionless bow shock p 2580 N95-30301
MAGNETOHYDRODYNAMIC GENERATORS
Non-coincident multi-wavelength emission absorption spectroscopy
[DE95-006480] p 2530 N95-28776
Development of Laser Optogalvanic Spectroscopy as a probe of alkali atoms in an MHD environment
[DE95-006481] p 2531 N95-28916
MAGNETOHYDRODYNAMIC STABILITY
New radiation sources through generation and resonant enhancement of Current Driven Plasma Instabilities in lower dimensional solid state systems
[AD-A290669] p 2705 N95-29519
Self-sustained magnetic braiding in toroidal plasmas
[AD-B191998L] p 2706 N95-29734
Interchange stability criteria for anisotropic central-cell plasmas in the tandem mirror GAMMA 10
[AD-B176253L] p 2707 N95-29738
HIDENEK: An implicit particle simulation of kinetic-MHD phenomena in three-dimensional plasmas
[AD-B176255L] p 2707 N95-29739
Modelling of transport phenomena
[AD-B179223L] p 2708 N95-29747
Trapped electron instabilities due to electron temperature gradient and anomalous transport
[AD-B179859L] p 2693 N95-29748
Chemical release experiments to induce F region ionospheric plasma irregularities at the magnetic equator p 2708 N95-29783
Theory of pseudo-classical confinement and transmutation to L-mode
[AD-B175957L] p 2709 N95-29809
Averaged resistive MHD equations
[AD-B178947L] p 2711 N95-30033
MAGNETOHYDRODYNAMIC TURBULENCE
Turbulent coupling of the magnetosphere-ionosphere through shear-mode Alfven waves p 2615 N95-29687
MAGNETOHYDRODYNAMIC WAVES
Solitons in negative ion plasmas p 2706 N95-29668
Turbulent coupling of the magnetosphere-ionosphere through shear-mode Alfven waves p 2615 N95-29687
Radioastronomical measurements of plasma characteristics of the solar corona and the solar wind p 2730 N95-29782
The physics of the collisionless bow shock p 2580 N95-30301
MAGNETOHYDRODYNAMICS
Development of Laser Optogalvanic Spectroscopy as a probe of alkali atoms in an MHD environment
[DE95-006481] p 2531 N95-28916
One and two fluid numerical investigations of solar wind gas releases p 2738 N95-29704
HIDENEK: An implicit particle simulation of kinetic-MHD phenomena in three-dimensional plasmas
[AD-B176255L] p 2707 N95-29739
The origin of collisionless dissipation in magnetic reconnection
[AD-B178949L] p 2710 N95-29813
Lecture note on the bases of plasma physics
[NIFS-PROC-15] p 2711 N95-29966
Techniques and results of tokamak-edge simulation
[DE95-008075] p 2711 N95-30130
Interaction of acoustic oscillations with magnetic flux tubes in the solar photosphere
[PB95-201810] p 2739 N95-30199
MAGNETOMETERS
A conceptual design for the attitude control and determination system for the Magnetosphere Imager spacecraft
[NASA-TP-3560] p 2507 N95-28721
MAGNETOSPHERE-IONOSPHERE COUPLING
Thermal N(+) in the inner magnetosphere p 2614 N95-29590
Application of Poynting flux measurements to the determination of energy transfer rates in the high-latitude ionosphere p 2614 N95-29650
A generalized semikinetic (GSK) model for mesoscale auroral plasma transport p 2706 N95-29686
Turbulent coupling of the magnetosphere-ionosphere through shear-mode Alfven waves p 2615 N95-29687
MAGNETOSPHERIC ELECTRON DENSITY
The high-altitude polar wind: Simulation and observation p 2622 N95-29688
MAGNETOSPHERIC ION DENSITY
Thermal N(+) in the inner magnetosphere p 2614 N95-29590
MAGNETS
Proceedings of the 6th Joint Magnetism and Magnetic Materials Intermag Conference
[AD-A286752] p 2681 N95-28923
Proceedings of the 38th Annual Conference on Magnetism and Magnetic Materials
[AD-A286753] p 2681 N95-28924
Processing, fabrication, characterization and device demonstration of high temperature superconducting ceramics
[AD-A290183] p 2541 N95-29055
MAINTAINABILITY
Conversion of an oceanographic expert system to a C-based language
[NASA-CR-198695] p 2630 N95-29237
Continuation of research in the statistical aspects of reliability, availability, and maintainability
[AD-A290126] p 2592 N95-29423
MAINTENANCE
Software systems reengineering process model, version 2.0
[AD-A289966] p 2647 N95-29278
An analysis of the impact of ASPA on organizational and depot level maintenance
[AD-A292670] p 2477 N95-29414
Remote maintenance challenges presented in the ITER engineering design
[DE95-006392] p 2710 N95-29909
MALES
NASA/DOD Aerospace Knowledge Diffusion Research Project. Paper 49: Becoming an aerospace engineer: A cross-gender comparison
[NASA-TM-110731] p 2721 N95-29028
MAN MACHINE SYSTEMS
Proceeding of the 33rd SICE Annual Conference
[DE95-758943] p 2662 N95-29144
NASA to use telepresence to explore Antarctic Lakes
[NASA-TM-110567] p 2598 N95-29175
Aerospace medicine and biology: A continuing bibliography with indexes (supplement 403)
[NASA-SP-7011(403)] p 2636 N95-29190
Improved operator awareness of teleoperated land vehicle attitude
[AD-A290443] p 2641 N95-29359
Telepresence media resource tape
[NASA-TM-110648] p 2655 N95-30248
MANAGEMENT INFORMATION SYSTEMS
QUEST2: System architecture deliverable set
[DE95-008427] p 2721 N95-28958
A study of the conceptual symbolics of information system development languages p 2723 N95-29589
MANAGEMENT METHODS
Management of speedup mechanisms in learning architectures
[AD-A292206] p 2662 N95-28988
Re-engineering support to the patient movement process p 2677 N95-29615
A study of problematic situations and information needs of software managers in the United States and Japan p 2724 N95-29628
MANAGEMENT PLANNING
An announcement by Dan Goldin
[NASA-TM-110739] p 2720 N95-29171
Federal aviation administration plan for research, engineering and development
[AD-A290952] p 2494 N95-29733
MANAGEMENT SYSTEMS
Artificial intelligence techniques for parts obsolescence prediction
[AD-A292185] p 2661 N95-28926
MANIPULATORS
Experiments in cooperative manipulation of objects by free-flying robot teams p 2662 N95-29095
Simulation of robot manipulators
[DE95-008680] p 2654 N95-30189
Numerical simulation of mechanisms and manipulator robots with flexible links and flexible joints
[PB95-196903] p 2591 N95-30285
MANNED MARS MISSIONS
Lunar/Mars exploration for synthesis group
[NASA-TM-110647] p 2737 N95-30249
MANNED SPACE FLIGHT
The influence of space flight on erythrokinetics in man. Space Life Sciences Missions 1 and 2. Experiment E261
[NASA-CR-188368] p 2633 N95-28875
MANNED SPACECRAFT
Apollo 11: For all mankind
[NASA-TM-110622] p 2503 N95-29407
MANUAL CONTROL
Task-dependent effects of automation: The role of internal models in performance, workload, and situational awareness in a semi-automated cockpit
[AD-A292538] p 2640 N95-28969
MANUALS
The topside ionospheric plasma monitor (SSIES, SSIES-2 and SSIES-3) on the spacecraft of the Defense Meteorological Satellite Program (DMSP), user's guide. Volume 2: Programmer's guide for software at AFSFC
[AD-A290913] p 2618 N95-30082
MANUFACTURING
Epoxy pipelining composition and method of manufacture
[AD-D017380] p 2539 N95-28784
Third NASA Advanced Composites Technology Conference, volume 1, part 2
[NASA-CP-3178-VOL-1-PT-2] p 2513 N95-28823
Establishing the relationship between manufacturing and component performance in stretch formed thermoplastic composites p 2514 N95-28829
Manufacturing scale-up of composite fuselage crown panels p 2515 N95-28835
Selection of materials, manufacturing methods and lubricants for cam mechanisms
[ESDU-94017] p 2589 N95-28905
Advanced manufacturing by spray forming: Aluminum strip and microelectromechanical systems
[DE95-008615] p 2536 N95-28959
Doubled diode laser. phase 1
[AD-A292465] p 2584 N95-29007
Advanced composite fuselage technology p 2519 N95-29034
Progress in manufacturing large primary aircraft structures using the stitching/RTM process p 2522 N95-29050
Daido Steel's Shibukawa Plant, Shibukawa City, Gumma Prefecture, Japan, 29 Jul. 1994
[AD-A292343] p 2536 N95-29467
High power switch design
[AD-A291608] p 2565 N95-29601
US photovoltaic patents: 1991-1993
[DE95-004051] p 2603 N95-30017
High energy density electrolytic capacitor p 2568 N95-30271
MANY BODY PROBLEM
Optoelectronics based on SiGe/Si heterostructures
[AD-A292464] p 2699 N95-29006
Analytical theory of continued fractions and time evolution in many-particle systems
[AD-A290365] p 2692 N95-29227
Experimental cosmology using fast parallel N-body methods p 2734 N95-29775
Proceedings of the 18th International Workshop on Condensed Matter Theories
[AD-A291396] p 2694 N95-30065
MAPPING
Multi-scale studies of seafloor topography
[AD-A292301] p 2628 N95-28865
MARINE BIOLOGY
Predicting polarized light scattering by marine micro-organisms
[AD-A289796] p 2697 N95-28698
Electromagnetic scattering by magnetic spheres: Theory and algorithms
[AD-A289798] p 2551 N95-28699
MARINE ENVIRONMENTS
Sorption and diffusion of moisture in multilayer composite AEM/S sandwich materials
[AD-A289807] p 2518 N95-28951

The detection of oil slicks at night with airborne infrared imagers
[AD-A289731] p 2598 N95-29281

MARINE METEOROLOGY
Hindcasting changes in thermal structure and acoustic transmission loss in the upper ocean on short time scales with data from MILE and from ocean weather station papa
[AD-A292419] p 2629 N95-28991
Upper-air data collected on Ice Station Weddell
[AD-A289707] p 2620 N95-29193
Continental aerosol effects on stratocumulus microphysics during MAST 1994
[AD-A292674] p 2621 N95-29416
Radiative cooling profiles calculated from ECMWF analyses and ISCCP C1 data, and their application to determination of distributions of apparent convective heating in the equatorial Pacific p 2625 N95-29805

MARINER 9 SPACE PROBE
The JPL Mars gravity field, Mars50c, based upon Viking and Mariner 9 Doppler tracking data
[NASA-CR-198881] p 2737 N95-30344

MARKOV CHAINS
Optimal universal coding and density estimation
[AD-A290694] p 2675 N95-29587

MARKOV PROCESSES
Stable function approximation in dynamic programming
[AD-A290224] p 2647 N95-29143
Precedence relation method for deriving flexible bound models for queueing systems
[PB95-206835] p 2667 N95-30221

MARS (PLANET)
The JPL Mars gravity field, Mars50c, based upon Viking and Mariner 9 Doppler tracking data
[NASA-CR-198881] p 2737 N95-30344

MARS EXPLORATION
Rover story
[NASA-CR-198757] p 2736 N95-29964
Lunar/Mars exploration for synthesis group
[NASA-TM-110647] p 2737 N95-30249

MARS SAMPLE RETURN MISSIONS
Rover story
[NASA-CR-198757] p 2736 N95-29964

MARS SURFACE
Some aspects of lunar and martian volcanism as examined with spectral, topographic, and morphologic data derived from spacecraft images p 2735 N95-29594
Rover story
[NASA-CR-198757] p 2736 N95-29964

MARTENSITE
Experimental methods in residual stress measurement using a position-sensitive single-exposure scintillation detection system
[AD-A289803] p 2594 N95-28949

MASERS
Propagation and transformation properties of axicon optical systems for laser beams
[AD-A289661] p 2584 N95-28679

MASKING
Pattern-analysis based models of masking by spatially separated sounds
[AD-A291270] p 2637 N95-29933

MASONRY
Materials for tomorrow's infrastructure: A ten-year plan for deploying high-performance construction materials and systems
[AD-A289782] p 2526 N95-29598

MASS DISTRIBUTION
Microwave remote sensing algorithms for cirrus clouds and precipitation p 2623 N95-29715
Experimental cosmology using fast parallel N-body methods p 2734 N95-29775
Statistics and large-scale structure p 2734 N95-29780
The search for mass segregation in star clusters of the Magellanic Clouds p 2730 N95-29781

MASS FLOW
Condensation inside tubes: Condensate film coefficient in horizontal tubes
[ESDU-94041] p 2569 N95-29015
Leading edge film cooling effects on turbine blade heat transfer
[NASA-TM-106955] p 2500 N95-29115
The structure of water mass, salt, and temperature transports within intermediate depths of the western tropical Atlantic Ocean p 2631 N95-29541
Prediction of pressurant mass requirements for axisymmetric liquid hydrogen tanks
[NASA-TM-106973] p 2511 N95-29642

MASS FLOW RATE
Multifluid nonequilibrium simulation of arcjet thrusters p 2510 N95-29245
Hydrogen film cooling with incident and swept-shock interactions in a Mach 6.4 nitrogen free stream
[NASA-TM-4603] p 2578 N95-30056

MASS SPECTRA
Design of a more accurate, higher fidelity, dual-source air mass zero solar simulator
[AD-A291364] p 2603 N95-29953

MASS TRANSFER
Hailstone heat and mass transfer measurements
[ISBN-0-315-86304-8] p 2624 N95-29797
The role of diabatic heating, torques and stability in forcing the meridional circulation within cyclones p 2626 N95-29834

MASSIVE STARS
The effects of rotation on the evolution of 15 to 30 solar mass stars p 2734 N95-29673
The 12 UM contribution of nearby galaxies to the infrared background
[AD-A291185] p 2735 N95-29917

MASSIVELY PARALLEL PROCESSORS
Efficient compilation of high-level data parallel algorithms
[AD-A290362] p 2659 N95-29225
Huge data sets and the frontiers of computational feasibility
[AD-A291384] p 2653 N95-30063
Requirements for a portable parallel I/O library for scientific computation
[DE95-009383] p 2660 N95-30192
Massively parallel fast elliptic equation solver for three dimensional hydrodynamics and relativity
[DE95-009385] p 2660 N95-30193

MATCHED FILTERS
Distortion-invariant optical pattern recognition by correlative matrix feature criterion
[AD-A291389] p 2703 N95-30064

MATCHING
Wideband I/Q demodulators: Measurement technique and matching characteristics
[AD-A291505] p 2558 N95-29847

MATERIALS HANDLING
Liquefied metal jet program Automation and Robotics Research Institute (ARRI)
[AD-A289781] p 2536 N95-29461

MATERIALS SCIENCE
Programmable materials and structures
[AD-A291807] p 2649 N95-29429

MATERIALS TESTS
Demonstration of a stabilized alumina/ethanol colloidal dispersion technique for seeding high temperature air flows
[NASA-TM-106945] p 2582 N95-29113
In-phase thermomechanical fatigue mechanisms in an unidirectional SCS-6/Ti 15-3 MMC
[NASA-CR-195482] p 2523 N95-29133
Experimental investigations of wave and fracture phenomena in impacted ceramics and glasses
[AD-A292142] p 2542 N95-29195
Study of the space environmental effects on spacecraft engineering materials
[NASA-CR-196638] p 2531 N95-29246
Liquefied metal jet program Automation and Robotics Research Institute (ARRI)
[AD-A289781] p 2536 N95-29461
Thermally stable organic polymers
[AD-A290755] p 2543 N95-29482
Effects of impurities released from high Z test limiter on plasma performance in TEXTOR
[AD-B191995L] p 2709 N95-29803
The effect of wear on fire-blocking layer material effectiveness
[AD-A291520] p 2493 N95-29855
Emissivity measurements in thin metallized membrane reflectors used for microwave radiometer sensors
[NASA-TM-110179] p 2506 N95-30251
Dielectric property measurements in the Electromagnetic Properties Measurement Laboratory
[NASA-TM-110147] p 2560 N95-30336

MATHEMATICAL LOGIC
Structural cut elimination in linear logic
[AD-A292248] p 2645 N95-28886
Progress and trends of multi-valued logic research
[AD-A290997] p 2665 N95-29874

MATHEMATICAL MODELS
The effect of viscous attenuation on shock tube performance
[AD-A289793] p 2568 N95-28696
Predicting polarized light scattering by marine micro-organisms
[AD-A289796] p 2697 N95-28698
Ejectors and jet pumps: Computer program for design and performance for steam/gas flow
[ESDU-94046] p 2495 N95-28704
Effects of small changes on rate of climb
[ESDU-94039] p 2495 N95-28707
Influence of turbulence parameters, Reynolds number, and body shape on stagnation-region heat transfer
[NASA-TP-3487] p 2568 N95-28719
Future requirements in surface modeling and grid generation p 2478 N95-28724
Geometry Laboratory (GEOLAB) surface modeling and grid generation technology and services p 2479 N95-28729
Rapid Airplane Parametric Input Design (RAPID) p 2479 N95-28730
Surface modeling and grid generation for aeropropulsion CFD p 2479 N95-28732
Marshall Space Flight Center surface modeling and grid generation applications p 2480 N95-28733
Automatic blocking for complex three-dimensional configurations p 2480 N95-28734
A Cartesian, cell-based approach for adaptively-refined solutions of the Euler and Navier-Stokes equations p 2480 N95-28739
Development and application of a 3D Cartesian grid Euler method p 2481 N95-28740
Unstructured Cartesian/prismatic grid generation for complex geometries p 2481 N95-28741
Emerging CFD technologies and aerospace vehicle design p 2482 N95-28746
Evaluation of grid generation technologies from an applied perspective p 2482 N95-28748
The National Grid Project: A system overview p 2482 N95-28749
Geometry modeling and grid generation using 3D NURBS control volume p 2483 N95-28753
Geometric grid generation p 2483 N95-28756
Algorithms for the automatic generation of 2-D structured multi-block grids p 2483 N95-28757
Elliptic surface grid generation on minimal and parmetrized surfaces p 2484 N95-28760
Automatic multi-block grid generation for high-lift configuration wings p 2485 N95-28764
Parametric design and gridding through relational geometry p 2486 N95-28771
GridTool: A surface modeling and grid generation tool p 2486 N95-28773
A discrete-event simulation model of myocardial electrical activity: Mathematical electrophysiology
[AD-A292323] p 2633 N95-28793
Analysis of static contact in laminated composite plates using damage mechanics
[NASA-CR-198656] p 2513 N95-28809
A global/local analysis method for treating details in structural design p 2517 N95-28848
Modal interactions and complex responses in weaklyNONLINEAR MULTI-DEGREE-OF-FREEDOM MECHANICAL SYSTEMS
[AD-A292023] p 2594 N95-28853
Stochastic modeling and global warming trend extraction for ocean acoustic travel times
[AD-A292114] p 2608 N95-28922
A numerical study of the effects of wind forcing on the Chile Current System
[AD-A289808] p 2629 N95-28982
Hybrid fuzzy logic control to stabilize an inverted pendulum from arbitrary initial conditions
[AD-A292441] p 2681 N95-29000
Modeling studies of the Leeuwin current off western and southern Australia
[AD-A290158] p 2629 N95-29023
An engineering model of woven composites based on micromechanics p 2521 N95-29042
Cost model relationships between textile manufacturing processes and design details for transport fuselage elements p 2521 N95-29043
Analytical modeling and sensor monitoring for optimal processing of advanced textile structural composites by resin transfer molding p 2521 N95-29045
The development of methods and techniques to detect and model the underlying structure of chaotic systems
[AD-A292435] p 2680 N95-29072
A transient model of the RL10A-3-3A rocket engine
[NASA-CR-195478] p 2510 N95-29114
A numerical method for modelling wings with sharp edges maneuvering at high angles of attack p 2496 N95-29122
A differential approach to graphical interaction
[AD-A292165] p 2647 N95-29125
Micro/Miniature heat pipe analysis
[AD-A292232] p 2570 N95-29127
Users manual for the improved NASA Lewis ice accretion code LEWICE 1.6
[NASA-CR-198355] p 2492 N95-29132
Application of optimization technique to control system design for departure prevention and aircraft model estimation through dynamic inversion p 2501 N95-29156
Computer simulation study of high t(sub c) superconductor structure
[AD-A292513] p 2563 N95-29163
Analytical theory of continued fractions and time evolution in many-particle systems
[AD-A290365] p 2692 N95-29227

Stochastic hyperbolic and parabolic partial differential equations
[AD-A290372] p 2669 N95-29229
Real-time x-ray scattering study of processing of eight performance thermoplastics
[AD-A290374] p 2542 N95-29230
Numerical modeling of opto-electronic integrated circuits
[AD-A292096] p 2563 N95-29239
A fourth order Euler/Navier-Stokes prediction method for the aerodynamics and aeroelasticity of hovering rotor blades p 2572 N95-29242
Modeling and control of rotating stall in high speed multi-stage axial compressors p 2500 N95-29244
Multifluid nonequilibrium simulation of arcjet thrusters p 2510 N95-29245
Linear and nonlinear discrete-time state-space modeling of dynamic systems for control applications p 2663 N95-29251
Software systems reengineering process model, version 2.0
[AD-A289968] p 2647 N95-29278
Investigation of an alternative finite element procedure: A one-step, steady-state analysis
[AD-A290030] p 2670 N95-29311
A simulation technique for predicting thickness of thermal sprayed coatings
[NASA-TM-106939] p 2512 N95-29373
Robust control of nonlinear flexible multibody systems using quaternion feedback and dissipative compensation
[NASA-TM-109099] p 2507 N95-29377
New methods for nonlinear optimization
[AD-A290522] p 2670 N95-29385
Acoustic scattering from ellipses by the modal element method
[NASA-TM-106935] p 2683 N95-29401
The large discretization step method for time-dependent partial differential equations
[NASA-CR-195068] p 2670 N95-29403
An assessment of artificial damping models for aeroacoustic calculations
[NASA-CR-198354] p 2574 N95-29405
Simulated imaging properties of a series of magnetic electron lenses
[NASA-CR-195474] p 2564 N95-29406
Continuation of research in the statistical aspects of reliability, availability, and maintainability
[AD-A290126] p 2592 N95-29423
Programmable materials and structures
[AD-A291807] p 2649 N95-29429
The quantum hydrodynamic model for semiconductor devices
[AD-A291809] p 2564 N95-29430
The 1994 IEEE International Workshop on Intelligent Signal Processing and Communication Systems (ISPACS94)
[AD-A292312] p 2556 N95-29474
A turbulent model of the solar granulation
[AD-A292318] p 2738 N95-29475
Object oriented segmentation of images
[AD-A290792] p 2671 N95-29485
Load balancing for the parallel adaptive solution of partial differential equations
[AD-A290450] p 2671 N95-29488
Simulation methodology
[AD-A290461] p 2674 N95-29491
Comparison of boundary-layer wind and temperature measurements with model estimations
[AD-A290471] p 2621 N95-29507
Theoretical, experimental and computational studies in plasticity
[AD-A290428] p 2595 N95-29535
Modeling the direct-beam instantaneous spectral surface albedo of a forest landscape using geometric-optics and a distributed parameter approach p 2599 N95-29540
Modeling spatio-temporal databases to measure the performance of the GPS satellite constellation p 2494 N95-29596
Interlaminar fracture mechanics and mechanisms: Linear and nonlinear aspects p 2526 N95-29597
Mathematical olympiad summer program (MOSP) 1994
[AD-A290801] p 2672 N95-29647
Quantum mechanical problems in one, two, and three dimensions
[ISBN-0-315-84931-2] p 2719 N95-29677
Turbulent coupling of the magnetosphere-ionosphere through shear-mode Alfven waves p 2615 N95-29687
The high-altitude polar wind: Simulation and observation p 2622 N95-29688
Maize yield estimation through the simulation of radiation penetration into the canopy p 2599 N95-29703
Modeling the boundary layer interactions between weakly ionized plasmas and cooled, planar electrodes in stagnation-point flows p 2706 N95-29717
Observations of mesoscale cellular convection from the marine stratocumulus phase of FIRE p 2624 N95-29727
Modelling of transport phenomena
[AD-B179223L] p 2708 N95-29747
Experimental cosmology using fast parallel N-body methods p 2734 N95-29775
The study of non-Newtonian contraction flows with a parallel finite element method p 2576 N95-29778
An analytic modeling and system identification study of helicopter dynamics p 2498 N95-29787
Dynamical model of pressure-gradient-driven turbulence and shear flow generation in L-H transition
[AD-B195511L] p 2709 N95-29789
On the topological complexity of the cost function in variational data assimilation p 2724 N95-29798
Development of an improved cloud model for use in cumulus parameterization p 2624 N95-29800
A model analysis of the spatial distribution and temporal trends of nitrous oxide sources and sinks p 2609 N95-29804
Numerical simulation of the genesis of tornado-like vortices p 2625 N95-29806
The one-dimensional bubble: Theory, experiment, and relevance to exposure of divers to low frequency sound, and of lung to lithotripsy
[ISVR-TR-246] p 2577 N95-29817
Microwave remote sensing of surface soil moisture and its application to hydrologic modeling p 2600 N95-29821
ANSYS duplicate finite-element checker routine
[NASA-TM-108492] p 2672 N95-29824
Relativistic effects on large amplitude nonlinear langmuir waves in a two-fluid plasma
[AD-B191980L] p 2710 N95-29841
The 10th Annual Review of Progress in Applied Computational Electromagnetics, volume 2
[AD-A286799] p 2558 N95-29904
Theory and experiments on chemical instabilities
[AD-A290773] p 2534 N95-29922
High-frequency radar target modeling
[AD-A290965] p 2559 N95-29991
Development and testing of improved techniques for modeling the hydrologic cycle in a mesoscale weather prediction system
[AD-A291243] p 2627 N95-29993
Probabilistic modeling and statistical inference for random fields and space-time processes
[AD-A289956] p 2672 N95-30029
A regression model for the western north pacific tropical cyclone intensity forecast
[AD-A290586] p 2627 N95-30044
Numerical modeling of synoptic scale ocean dynamics
[AD-A291411] p 2631 N95-30069
A formal extension to object oriented analysis using Z
[AD-A290911] p 2653 N95-30080
Comparison of the local defect correction iteration and the fast adaptive composite grid iteration
[PB95-206769] p 2672 N95-30088
Fast simulation of the leaky bucket algorithm
[PB95-197174] p 2653 N95-30098
Mathematical modeling and numerical simulation of the dynamics of flexible structures undergoing large overall motions
[AD-A291139] p 2597 N95-30123
Extreme nonlinearity in rocks: An investigation using elastic pulse wave propagation
[DE95-007879] p 2618 N95-30129
Simulation of robot manipulators
[DE95-008680] p 2654 N95-30189
Precedence relation method for deriving flexible bound models for queueing systems
[PB95-206835] p 2667 N95-30221
Physical modeling and design of semiconductor heterostructures for optical and electronical applications p 2682 N95-30232
Engineering design of sub-micron topographies for simultaneously adherent and reflective metal-polymer interfaces
[NASA-CR-198845] p 2548 N95-30237
Numerical implementation of a state variable model for friction
[DE95-007844] p 2591 N95-30273
Self-organization in a simple brain model
[DE95-008312] p 2668 N95-30279
Manual for a workstation-based generic flight simulation program (LaRCsim), version 1.4
[NASA-TM-110164] p 2502 N95-30327

MATHEMATICAL PROGRAMMING
An HP-Adaptive method in space and time for parabolic systems
[AD-A292262] p 2668 N95-28890
Interface for the translation of sentences in a natural language into a geometrical representation language
[INPE-5467-PRE/1775] p 2722 N95-29363

MATRICES (MATHEMATICS)
Analysis of multigrid techniques for system modeling with toeplitz approximation
[AD-A289784] p 2644 N95-28694
The (in)complete compendium of computational curiosities: Givens' rotations
[AD-A292050] p 2648 N95-29304
Linear algebraic computation on distributed memory parallel machines
[AD-A290615] p 2671 N95-29558
Linear matrix inequalities for the problem of absolute stability of control systems p 2501 N95-29680
Efficient solution of a class of infinite stochastic petri nets: Theory and applications
[PB95-197166] p 2673 N95-30097
Interaction of acoustic oscillations with magnetic flux tubes in the solar photosphere
[PB95-201810] p 2739 N95-30199
A unified matrix inequality approach to linear control design p 2667 N95-30234

MATRIX MATERIALS
Advanced composite structural concepts and materials technologies for primary aircraft structures: Advanced material concepts
[NASA-CR-4485] p 2496 N95-29027
Thermally stable organic polymers
[AD-A290755] p 2543 N95-29482
Use of finite element analysis for transient moisture diffusion studies in multilayer composite AEM/S system sandwich materials
[AD-A291092] p 2527 N95-29638

MATRIX THEORY
W-matrices, nonorthogonal multiresolution analysis, and finite signals of arbitrary length
[DE95-005846] p 2652 N95-30020

MAXIMUM ENTROPY METHOD
Extended dust shells around carbon stars resolved by HIRAS p 2735 N95-29840

MAXIMUM LIKELIHOOD ESTIMATES
Optical (LANDSAT/TM) and radar (ERS-1/SAR) imagery sinergism studies applied to land use discrimination
[INPE-5608-TDI/554] p 2598 N95-29433
An analytic modeling and system identification study of helicopter dynamics p 2498 N95-29787
A new visualization technique to study the time evolution of finite and adaptive mixture estimators
[AD-A291147] p 2673 N95-30126

MAXWELL EQUATION
The 10th Annual Review of Progress in Applied Computational Electromagnetics, volume 2
[AD-A286799] p 2558 N95-29904

MEASURING INSTRUMENTS
Proceedings of the 33d SICE (the Society of Instrument and Control Engineers) Annual Conference, part 1
[DE95-758947] p 2632 N95-28947
Research instrumentation for polytechnic university's supersonic wind tunnel facility
[AD-A290232] p 2502 N95-29468
Boronization study for application to large helical device
[AD-B191996L] p 2709 N95-29808

MECHANICAL DEVICES
Adjustable two-axis instrument mount
[AD-D017393] p 2582 N95-29220
Numerical simulation of mechanisms and manipulator robots with flexible links and flexible joints
[PB95-196903] p 2591 N95-30285

MECHANICAL DRIVES
Carrier-less, anti-backlash planetary drive system
[NASA-CASE-GSC-13608-1] p 2588 N95-28702
External combustion engine having an asymmetrical CAM
[AD-D017382] p 2588 N95-28785

MECHANICAL ENGINEERING
Influence of tooth profile modification on spur gear dynamic tooth strain
[NASA-TM-106952] p 2589 N95-29112

MECHANICAL PROPERTIES
Generator of body data (GEBOD) manual
[AD-A289721] p 2640 N95-28683
Characterization and development of materials for advanced textile composites p 2513 N95-28824
Mechanical characterization of two thermoplastic composites fabricated by automated tow placement p 2515 N95-28834
Publications/Patents/Presentations/Honors report: Force and tunneling microscopy studies of atomic level mechanical properties of solids
[AD-A292254] p 2691 N95-28888
Shear force, bending moment and torque of rigid aircraft in symmetric steady maneuvering flight
[ESDU-94045] p 2495 N95-28896
A 1993 review of welding in Japan
[DE95-758701] p 2589 N95-28946

Mechanical characterization of 2D, 2D stitched, and 3D braided/RTM materials p 2520 N95-29038
Daido Steel's Shibukawa Plant, Shibukawa City, Gumma Prefecture, Japan, 29 Jul. 1994
[AD-A292343] p 2536 N95-29467
Center for Advanced Aerospace Materials (CAAM), Seoul National University, 29 June 1994
[AD-A292344] p 2525 N95-29476
High velocity impact and penetration of thick composite laminates
[AD-A290642] p 2526 N95-29561
Changes in microstructural parameters of snow during deformation
[AD-A290887] p 2601 N95-29866
Mechanical properties of nanophase metals
[DE95-005408] p 2537 N95-30018
Nanoindentation and nanoscratching of hard coating materials for magnetic disks
[DE95-008776] p 2547 N95-30174
Influence of dislocation-solute interactions on the mechanical properties of zirconium-doped NiAl
[DE95-008848] p 2538 N95-30179

MECHANICS (PHYSICS)
Nonlinear mechanics and applied analysis
[AD-A290356] p 2669 N95-29070

MEDICAL EQUIPMENT
Use of quality tools to re-engineer the Aeromedical Evacuation (AE) system p 2676 N95-29605
Danish aeromedical evacuation efforts during the Gulf War p 2677 N95-29613
Experiences learned from the Spanish armed forces aeromedical evacuation system in the former Yugoslavia p 2677 N95-29614
Flying ambulances: The approach of a small air force to long distance aeromedical evacuation of critically injured patients p 2678 N95-29618
Civil Reserve Air Fleet-Aeromedical Evacuation Shipset (CRAF-AESS) p 2678 N95-29619
First medical test of the UH-60Q and equipment for use in US Army medevac helicopters p 2678 N95-29620
The large-capacity rescue-helicopter CH-53 G p 2678 N95-29621
International access to aeromedical evacuation medical equipment assessment data p 2679 N95-29622
A generic specification for Special Purpose Aeromedical Equipment p 2499 N95-29623
Aeromedical impact of the transportable pressure ventilator in wartime aeromedical evacuation p 2641 N95-29624
Requirement for onboard telemetry equipment p 2506 N95-29625

MEDICAL PERSONNEL
Military flying and aeromedical evaluation of cardiac arrhythmias
[AD-A291595] p 2634 N95-28940
The Canadian experience in UN airevac Sarajevo airlift: April 1993-October 1994 p 2676 N95-29606
Danish aeromedical evacuation efforts during the Gulf War p 2677 N95-29613
The impact of occupational cultures on coordination of emergency medical service crew p 2677 N95-29616
Flight nurse school in the Hellenic Air Force p 2638 N95-29629

MEDICAL SCIENCE
Georgetown Institute for Cognitive and Computational Sciences
[AD-A289775] p 2639 N95-29458

MEDICAL SERVICES
Test and evaluation of the Impact Instrumentations, Inc. Uni-Vent model 750M ventilator
[AD-A292321] p 2640 N95-28792
A comparison of the aeromedical administration requirements for US Air Forces and major allies
[AD-A290137] p 2635 N95-29141
Recent Issues and Advances in Aeromedical Evacuation (MEDEVAC)
[AGARD-CP-554] p 2676 N95-29604
Use of quality tools to re-engineer the Aeromedical Evacuation (AE) system p 2676 N95-29605
The Canadian experience in UN airevac Sarajevo airlift: April 1993-October 1994 p 2676 N95-29606
United Nations aeromedical evacuation operations in the former Yugoslavia p 2676 N95-29607
Civil military co-operation: A ten year experience of an affiliative aeromedical evacuation programme of the Netherlands Armed Forces and a civilian repatriation organization p 2676 N95-29608
Aeromedical evacuation by RNLAF - work according to protocol p 2676 N95-29609
Critical evaluation of aeromedical evacuation in a multinational forces scenario p 2676 N95-29610
Experience in helicopter aeroevacuation in the community of Madrid, Spain p 2677 N95-29611
Aeromedical evacuation in combined operations p 2677 N95-29612
Danish aeromedical evacuation efforts during the Gulf War p 2677 N95-29613
Experiences learned from the Spanish armed forces aeromedical evacuation system in the former Yugoslavia p 2677 N95-29614
Re-engineering support to the patient movement process p 2677 N95-29615
The impact of occupational cultures on coordination of emergency medical service crew p 2677 N95-29616
Medical evacuation: A training priority p 2678 N95-29617
Flying ambulances: The approach of a small air force to long distance aeromedical evacuation of critically injured patients p 2678 N95-29618
Civil Reserve Air Fleet-Aeromedical Evacuation Shipset (CRAF-AESS) p 2678 N95-29619
First medical test of the UH-60Q and equipment for use in US Army medevac helicopters p 2678 N95-29620
The large-capacity rescue-helicopter CH-53 G p 2678 N95-29621
International access to aeromedical evacuation medical equipment assessment data p 2679 N95-29622
Aeromedical impact of the transportable pressure ventilator in wartime aeromedical evacuation p 2641 N95-29624
Requirement for onboard telemetry equipment p 2506 N95-29625
Care in the air: A system analysis of clinical outcomes in aeromedical evacuation p 2642 N95-29626
Changes in the medevac mission result in an increased role for the flight surgeon p 2680 N95-29628
Flight nurse school in the Hellenic Air Force p 2638 N95-29629

MELTING
Differentiation in the early Earth: An experimental investigation p 2612 N95-29199

MELTING POINTS
Thermophysical properties of R-32 (difluoromethane)
[ESDU-94032] p 2530 N95-28802
Thermal conductivity of liquid halogenated aliphatic hydrocarbons. Part 1: Halogenated methanes and azeotropic mixtures
[ESDU-94021-PT-1] p 2511 N95-28804
Vapour pressures and critical points of liquids. Glycols and cyclic diols
[ESDU-95002] p 2534 N95-29897
Vapour pressures and critical points of liquids. Glycol ethers (alkyl cellosolves and carbitols, etc.)
[ESDU-95004] p 2534 N95-29901

MELTS (CRYSTAL GROWTH)
The morphology of blends of linear and branched polyethylenes in solid state by SANS
[DE95-008675] p 2535 N95-30113

MEMBRANE STRUCTURES
Emissivity measurements in thin metallized membrane reflectors used for microwave radiometer sensors
[NASA-TM-110179] p 2506 N95-30251

MEMBRANES
Membrane fluidity and shape of human red blood cells are altered by physiological levels of hydrostatic pressure
[AD-A290595] p 2636 N95-29557
A study of blister tests for film adhesion measurement and fracture efficiency of tests for adhesive bonds p 2545 N95-29799
A novel unitized regenerative proton exchange membrane fuel cell p 2605 N95-30263

MEMORY
Automation and cognition in air traffic control: An empirical investigation
[AD-A291932] p 2493 N95-28790
Reference frames in vision
[AD-A290117] p 2639 N95-29422
Visualization of CAD objects using a stereoscopic display
[AD-A290034] p 2639 N95-29439

MEMORY (COMPUTERS)
Abstract models of memory management
[AD-A292238] p 2721 N95-28877
Low cost writable RFID tag with MRAM memory
[AD-A292553] p 2642 N95-28974
Garbage collection is fast, but a stack is faster
[AD-A290099] p 2722 N95-29207
Ropes: Support for collective opertions among distributed threads
[NASA-CR-198157] p 2649 N95-29404
Linear algebraic computation on distributed memory parallel machines
[AD-A290615] p 2671 N95-29558

MENTAL PERFORMANCE
Improving problem-solving and decision-making skills under stress: Prediction and training
[AD-A292104] p 2638 N95-28918
Current issues in the measurement of military aircrew performance: A consideration of the relationship between available metrics and operational concerns
[AD-A292539] p 2640 N95-28970
Coping and adaptation: Theoretical and applied perspectives
[AD-A290513] p 2638 N95-29090
CO2-O2 interactions in extension of tolerance to acute hypoxia
[NASA-CR-198575] p 2635 N95-29158
Sleep during SEAL Delivery Vehicle (SDV)/Dry dock shelter exercises analyzed by a graphic approach
[AD-A290916] p 2637 N95-30083

MERCURY CADMIUM TELLURIDES
InTlSb as a long-wave infrared (LWIR) material: Defects and transportation properties
[AD-A291218] p 2702 N95-29978

MERIDIONAL FLOW
The role of diabatic heating, torques and stability in forcing the meridional circulation within cyclones p 2626 N95-29834

MESOMETEOROLOGY
Development and testing of improved techniques for modeling the hydrologic cycle in a mesoscale weather prediction system
[AD-A291243] p 2627 N95-29993

MESON RESONANCE
Photoproduction of hybrid mesons from CEBAF to HERA
[PB95-196218] p 2691 N95-28913

MESONS
Tables of SU3 isoscalar factors
[DE95-009375] p 2690 N95-28779
Photoproduction of hybrid mesons from CEBAF to HERA
[PB95-196218] p 2691 N95-28913
From the (psi) to charmed mesons
[DE95-006564] p 2693 N95-29583
Inclusive hadronic production of the B(sub c) meson via heavy quark fragmentation
[DE95-008739] p 2695 N95-30191
Parameterized spectral distributions for meson production in proton-proton collisions
[NASA-TM-4675] p 2696 N95-30337

MESOSCALE PHENOMENA
Short term visits for collaborative research
[AD-A290704] p 2682 N95-29588
A generalized semikinetic (GSK) model for mesoscale auroral plasma transport p 2706 N95-29686
The interactive role of clouds and radiative transfer in maintaining atmospheric circulation p 2616 N95-29699
Observations of mesoscale cellular convection from the marine stratocumulus phase of FIRE p 2624 N95-29727
Development and testing of improved techniques for modeling the hydrologic cycle in a mesoscale weather prediction system
[AD-A291243] p 2627 N95-29993

MESOSPHERE
An investigation of thunderstorms as a source of short period mesospheric gravity waves
[AD-A289795] p 2611 N95-28697
Studies of gravity-wave filtering and tidal interaction in the middle atmosphere p 2619 N95-30351

MESSAGE PROCESSING
Delayed choice: An operator for joining message sequence charts
[PB95-206710] p 2560 N95-30203

MESSAGES
Delayed choice: An operator for joining message sequence charts
[PB95-206710] p 2560 N95-30203

METAL CRYSTALS
Pulsed laser deposition of thin film material for nonlinear waveguides
[AD-A290789] p 2544 N95-29484

METAL FATIGUE
In-phase thermomechanical fatigue mechanisms in an unidirectional SCS-6/Ti 15-3 MMC
[NASA-CR-195482] p 2523 N95-29133
Investigation of tension-compression fatigue behavior of a notched cross-ply metal matrix composite at elevated temperature
[AD-A291479] p 2527 N95-29770
Fatigue life analysis and tests for thick-walled cylinders including effects of overstrain and axial grooves
[AD-A290931] p 2596 N95-30119

METAL FILMS
Boronization study for application to large helical device
[AD-B191996L] p 2709 N95-29808
Formation and properties of titanium disilicide: A study on the development of stress in Ti-Si thin films
[PB95-197315] p 2538 N95-30205

Emissivity measurements in thin metallized membrane reflectors used for microwave radiometer sensors
[NASA-TM-110179] p 2506 N95-30251

METAL IONS
ARPA solid state laser and nonlinear materials program
[AD-A289657] p 2584 N95-28678
The effects of platinum on nickel electrodes in the nickel hydrogen cell
[AD-A291607] p 2531 N95-28942
The redox chemistry of some peroxo and superoxo metal ion complexes
[AD-A290761] p 2532 N95-29483

METAL MATRIX COMPOSITES
In-phase thermomechanical fatigue mechanisms in an unidirectional SCS-6/Ti 15-3 MMC
[NASA-CR-195482] p 2523 N95-29133
Aircraft advanced materials research and development program plan
[AD-A290542] p 2498 N95-29565
Investigation of tension-compression fatigue behavior of a unidirectional metal matrix composite at elevated temperature
[AD-A289394] p 2527 N95-29758
Investigation of tension-compression fatigue behavior of a notched cross-ply metal matrix composite at elevated temperature
[AD-A291479] p 2527 N95-29770
Innovative processing of composites for ultra-high temperature applications, book 1
[AD-A290889] p 2527 N95-29842
Chemically induced passivity of aluminum alloys and Al-based metal matrix composites
[AD-A290778] p 2528 N95-29923
Processing and properties of extruded tungsten-hafnium and tungsten-steel composites
[DE95-007371] p 2528 N95-30037
Impact damage resistance and residual property assessment of (0/+/-45/90)s SCS-6/Timetal 21S
[NASA-TM-110178] p 2529 N95-30340

METAL OXIDE SEMICONDUCTORS
Power measurement and current feedback in a resonant DC link inverter
[AD-A292518] p 2563 N95-29164
Defect centers in chemical-mechanical polished MOS oxides
[DE95-004777] p 2718 N95-30214

METAL OXIDES
Fabrication of advanced electrochemical energy materials using sol-gel processing techniques
p 2607 N95-30269

METAL PARTICLES
Tailored microstructures for broadband or selective detection of radiation from the visible to the infrared
[AD-A292097] p 2554 N95-29240

METAL PLATES
Robust algorithms for penetration mechanics problems
[AD-A290650] p 2650 N95-29517

METAL POLISHING
Defect centers in chemical-mechanical polished MOS oxides
[DE95-004777] p 2718 N95-30214

METAL POWDER
Demonstration of a stabilized alumina/ethanol colloidal dispersion technique for seeding high temperature air flows
[NASA-TM-106945] p 2582 N95-29113
Hot explosive consolidation of W-Ti alloys
[AD-A290880] p 2537 N95-29635
Simulation of powder metal fabrication with high pressure gas atomization
[DE95-008820] p 2538 N95-30178

METAL SPINNING
Daido Steel's Shibukawa Plant, Shibukawa City, Gumma Prefecture, Japan, 29 Jul. 1994
[AD-A292343] p 2536 N95-29467

METAL STRIPS
Advanced manufacturing by spray forming: Aluminum strip and microelectromechanical systems
[DE95-008615] p 2536 N95-28959

METAL SURFACES
Prediction of hydrogen entry and permeation in metals and alloys
[AD-A292047] p 2536 N95-29298
Boronization study for application to large helical device
[AD-B191996L] p 2709 N95-29808

METAL VAPORS
The physics of spin polarized gases
[AD-A292511] p 2680 N95-28810
High temperature spectroscopy of alkali metal vapors for solar to thermal energy conversion
[AD-A291355] p 2602 N95-29949

METAL WORKING
Numerical implementation of a state variable model for friction
[DE95-007844] p 2591 N95-30273

METALLIC PLASMAS
Coherent soft x-ray generation using a powerful subpicosecond laser p 2587 N95-29689

METALLIZING
Investigation of the characteristics of ferroelectric thin films deposited by pulsed laser ablation
[AD-A292306] p 2540 N95-28963

METALLURGY
Gordon research conference on physical metallurgy: Materials by design
[AD-A290519] p 2524 N95-29326
Visit to the Department of Metallurgical Engineering, Tokyo Institute of Technology, 22 Sep. 1994
[AD-A292310] p 2536 N95-29473

METALORGANIC CHEMICAL VAPOR DEPOSITION
Ion doped quantum well lasers
[AD-A290937] p 2587 N95-29912
Interfaces in InAsSb/InGaAs strained-layer superlattices grown by MOCVD for use in infrared emitters
[DE95-006323] p 2717 N95-29990
Ordering and bandgap reduction in InAs(1-x)Sb(x) alloys
[DE95-006324] p 2717 N95-30005

METALS
Spectral characterization of pulsed ultrasound using neural networks
[AD-A292440] p 2683 N95-28999
In-plant testing of membranes to treat electroplating wastewater
[NASA-CR-198796] p 2532 N95-29250
Prediction of hydrogen entry and permeation in metals and alloys
[AD-A292047] p 2536 N95-29298
Symposium on Metal-Mediated Molecular Architectures
[AD-A290427] p 2692 N95-29388
Solid freeform fabrication symposium
[AD-A290949] p 2527 N95-29732
What do we really know about the atomic scale structures of nanophase materials?
[DE95-005858] p 2717 N95-29986
Mechanical properties of nanophase metals
[DE95-005408] p 2537 N95-30018
Proceedings of the 18th International Workshop on Condensed Matter Theories
[AD-A291396] p 2694 N95-30065
Engineering design of sub-micron topographies for simultaneously adherent and reflective metal-polymer interfaces
[NASA-CR-198845] p 2548 N95-30237
Numerical implementation of a state variable model for friction
[DE95-007844] p 2591 N95-30273

METEORITES
Delivery of meteorites from the asteroid belt
p 2732 N95-29255

METEORITIC COMPOSITION
Spectral reflectance studies and optical surface alteration in the search for links between meteorites and asteroids p 2733 N95-29672

METEOROLOGICAL INSTRUMENTS
Typhoon monitoring using passive microwave observations
[AD-A292567] p 2619 N95-28975

METEOROLOGICAL PARAMETERS
Quality Control of meteorological observations at Fleet Numerical Meteorology and Oceanography Center
[AD-A291577] p 2619 N95-28938
Analysis of tropospheric propagation characteristics based on regional meteorological data
[AD-A291581] p 2552 N95-28939
Hindcasting changes in thermal structure and acoustic transmission loss in the upper ocean on short time scales with data from MILE and from ocean weather station papa
[AD-A292419] p 2629 N95-28991
Correlation and gradient characteristics of ionospheric parameters in Europe
[AD-A290135] p 2612 N95-29140
Upper-air data collected on Ice Station Weddell
[AD-A289707] p 2620 N95-29193
Meteorological Satellite Center technical note, no. 28, 1994
[JTN-95-80926] p 2626 N95-29849
Management of meteorological data at a former nuclear weapons facility
[DE95-007619] p 2626 N95-29868
Extended field observations of cirrus clouds using a ground-based cloud observing system
[NASA-CR-198855] p 2628 N95-30356

METEOROLOGICAL RADAR
A study of boundary layer aerosol and wind profiles using incoherent Doppler lidar p 2622 N95-29697
Heat and momentum flux measurements in the planetary boundary layer with a wind profiling radar/radio acoustic sounding system p 2617 N95-29777
A study of precipitation using dual-frequency and interferometric Doppler radars p 2627 N95-29877
Offshore next generation weather radar (NEXRAD) test and evaluation master plan (TEMP)
[AD-A291435] p 2559 N95-30072

METEOROLOGICAL SATELLITES
Typhoon monitoring using passive microwave observations
[AD-A292567] p 2619 N95-28975

METEOROLOGICAL SERVICES
Management of meteorological data at a former nuclear weapons facility
[DE95-007619] p 2626 N95-29868

METEOROLOGY
Spectrometric studies of selected nitrocompounds using laser-induced photofragmentation/photoionization at 193 nm
[AD-A289947] p 2530 N95-28876

METHANE
Thermophysical properties of R-32 (difluoromethane)
[ESDU-94032] p 2530 N95-28802
Thermal conductivity of liquid halogenated aliphatic hydrocarbons. Part 1: Halogenated methanes and azeotropic mixtures
[ESDU-94021-PT-1] p 2511 N95-28804
Investigation of laminar methane flames with emphasis on kinetics elucidation and NOx reduction
[PB95-200531] p 2535 N95-30111
Biological methane activation
[PB95-200705] p 2535 N95-30198

METHOD OF CHARACTERISTICS
Guidance law development for aeroassisted transfer vehicles using Matched Asymptotic Expansions
p 2503 N95-30347

METHOD OF MOMENTS
The 10th Annual Review of Progress in Applied Computational Electromagnetics, volume 2
[AD-A286799] p 2558 N95-29904
Electrically small archimedian spiral method of moment analysis
[AD-A291171] p 2558 N95-29928

METHODOLOGY
Test theory reconceived
[AD-A291836] p 2639 N95-29432
Methodologies for intelligent systems
[AD-A290901] p 2666 N95-30117

METHYL COMPOUNDS
Corrosion in methylphosphonic difluoride
[AD-A289995] p 2536 N95-29137
Preparation and studies of urazole containing polymers
[AD-A290685] p 2545 N95-29586

METHYLENE
Analytical potential energy surface for methylene nitramine (CH2NNO2)
[AD-A291247] p 2534 N95-29994

METHYLHYDRAZINE
The fluorescent detection of hydrazine, monomethylhydrazine, and 1,1-dimethylhydrazine by derivatization with aromatic dicarboxaldehydes
[NAVY-CASE-75451] p 2512 N95-29052

METRICATION
SI Handbook for the Lawrence Livermore National Laboratory: Committee on metric transition
[DE95-009329] p 2551 N95-30182

METROLOGY
High resolution, large scale measurement processes
[AD-A292200] p 2681 N95-28987
Feature-oriented image reconstruction and aero-optic metrology in turbulence
[AD-A290269] p 2699 N95-29177

MICROANALYSIS
Correlations between micromagnetic, microstructural and microchemical properties in ultrathin epitaxial magnetic structures
[AD-A289705] p 2712 N95-28681

MICROBURSTS (METEOROLOGY)
Experiments on microbursts p 2620 N95-29110

MICROCOMPUTERS
Macroprocesses and adaptive instruction
[AD-A290483] p 2648 N95-29325
Research and development of a high performance GaAs microcomputer system
[AD-A292647] p 2643 N95-29381

MICROCRACKS
Master plot analysis of microcracking in graphite/epoxy and graphite/PEEK laminates p 2514 N95-28828
Interlaminar fracture mechanics and mechanisms: Linear and nonlinear aspects p 2526 N95-29597

Micromechanics of crack extension in composites
p 2529 N95-30276

MICROCRYSTALS
Synthesis of nanocrystalline indium arsenide and indium phosphide from Indium(III) halides and tris(trimethylsilyl)pnicogens; synthesis, characterization, and decomposition behavior of I3In(dot)P(SiMe3)3
[AD-A291905] p 2715 N95-29486

MICROELECTRONICS
Artificial intelligence techniques for parts obsolescence prediction
[AD-A292185] p 2661 N95-28926
HTS Josephson technology on silicon with application to high speed digital microelectronics
[AD-A290206] p 2562 N95-29061
Nanoscience and nanotechnology in Europe
[AD-A290214] p 2562 N95-29075
The quantum hydrodynamic model for semiconductor devices
[AD-A291809] p 2564 N95-29430
Equipment resource for MCM technology and system prototyping
[AD-A292492] p 2719 N95-29756
Semiconductor film Cherenkov lasers
[AD-A291177] p 2587 N95-29930
Vacuum microelectronic emitters and their applications using compound semiconductor technology
[AD-A291142] p 2567 N95-30124

MICROFIBERS
Development of a micro-fiber nickel electrode for nickel-hydrogen cell p 2567 N95-30256

MICROGRAVITY
Experimental results of Hooper's gravity-electromagnetic coupling concept
[NASA-TM-106963] p 2680 N95-28893
Lockheed Stabilizer System for space exercise equipment
[NASA-CR-197657] p 2641 N95-29180
Summary Report of mission acceleration measurements for STS-66. Launched November 3, 1994
[NASA-TM-106914] p 2509 N95-29643
Reduce Fluid Experiment System: Flight data from the IML-1 Mission
[NASA-CR-196639] p 2549 N95-30014
Summary report of mission acceleration measurements for STS-65, launched 8 July 1094
[NASA-TM-106871] p 2549 N95-30339

MICROINSTRUMENTATION
Equipment resource for MCM technology and system prototyping
[AD-A292492] p 2719 N95-29756

MICROMACHINING
A CMOS-compatible, surface-micromachined pressure sensor for aqueous ultrasonic application
[DE95-008538] p 2567 N95-30188

MICROMECHANICS
An engineering model of woven composites based on micromechanics p 2521 N95-29042
Characterizing and modeling penetration of ceramic armor
[AD-A292588] p 2542 N95-29288
A three dimensional finite element scheme for fiber microbuckling in thick multidirectional laminated composites p 2525 N95-29512
Micromechanics of crack extension in composites
p 2529 N95-30276

MICROMETEOROLOGY
Sensitivity of the simulated global climate to perturbations in low cloud microphysical properties
p 2620 N95-29206

MICROMINIATURIZATION
A CMOS-compatible, surface-micromachined pressure sensor for aqueous ultrasonic application
[DE95-008538] p 2567 N95-30188

MICROORGANISMS
Predicting polarized light scattering by marine micro-organism
[AD-A289790] p 2696 N95-28695
Predicting polarized light scattering by marine micro-organisms
[AD-A289796] p 2697 N95-28698
Prediction of hydrogen entry and permeation in metals and alloys
[AD-A292047] p 2536 N95-29298
Modeling joint effects of mixtures of chemicals on microorganisms using quantitative structure activity relationship techniques, phase 3
[AD-A290153] p 2632 N95-29320

MICROPHONES
High-performance speech recognition using consistency modeling
[AD-A290655] p 2557 N95-29564

MICROPROCESSORS
Research and development of a high performance GaAs microcomputer system
[AD-A292647] p 2643 N95-29381

MICROSCOPY
An image cancellation approach to depth-from-focus
[DE95-007625] p 2697 N95-28912
High resolution, large scale measurament processes
[AD-A292200] p 2681 N95-28987

MICROSTRIP TRANSMISSION LINES
Processing, fabrication, and demonstration of HTS integrated microwave circuits
[AD-A292480] p 2562 N95-29073
Processing, fabrication, and demonstration of HTS integrated microwave circuits
[AD-A290220] p 2562 N95-29078
Finite difference analysis of a cylindrical two conductor microstrip transmission line with truncated dielectrics
[AD-A292592] p 2555 N95-29290

MICROSTRUCTURE
Correlations between micromagnetic, microstructural and microchemical properties in ultrathin epitaxial magnetic structures
[AD-A289705] p 2712 N95-28681
Nitride semiconductors for ultraviolet detection
[AD-A289546] p 2712 N95-28910
Studies of lattice-mismatched and Low-Temperature-Grown semiconductor multiple-phase systems
[AD-A292536] p 2713 N95-28967
Correlation of inclusion size and chemistry with weld metal composition and microstructure arc weldments of high strength steels
[AD-A292024] p 2590 N95-29184
Consideration of microstructural changes in the study of adiabatic shear bands
[AD-A290398] p 2715 N95-29234
Tailored microstructures for broadband or selective detection of radiation from the visible to the infrared
[AD-A292097] p 2554 N95-29240
Prediction of hydrogen entry and permeation in metals and alloys
[AD-A292047] p 2536 N95-29298
Gordon research conference on physical metallurgy: Materials by design
[AD-A290519] p 2524 N95-29326
Visit to the Department of Metallurgical Engineering, Tokyo Institute of Technology, 22 Sep. 1994
[AD-A292310] p 2536 N95-29473
Pulsed laser deposition of thin film material for nonlinear waveguides
[AD-A290789] p 2544 N95-29484
Synthesis morphology and properties of semicrystalline block copolymers
[AD-A290475] p 2544 N95-29510
Recent progress in the study of the kinetics of sol-gel SiO2 synthesis reactions
[AD-A290570] p 2544 N95-29551
High T(sub c) superconductor/ferroelectric heterostructures
[AD-A291016] p 2716 N95-29658
Investigation of tension-compression fatigue behavior of a notched cross-ply metal matrix composite at elevated temperature
[AD-A291479] p 2527 N95-29770
Hot explosive consolidation of W-Ti alloys
[AD-A290880] p 2537 N95-29835
Changes in microstructural parameters of snow during deformation
[AD-A290887] p 2601 N95-29866
Chemically induced passivity of aluminum alloys and Al-based metal matrix composites
[AD-A290778] p 2528 N95-29923
What do we really know about the atomic scale structures of nanophase materials?
[DE95-005858] p 2717 N95-29986
Ion beam modification of Tl-Ba-Ca-Cu-O type high temperature superconductors during irradiation
[DE95-006807] p 2717 N95-30022
Fractography of advanced structural ceramics: Results from the VAMAS round robin exercise
[AD-A290930] p 2547 N95-30118
Tensile properties of as-cast iron-aluminide alloys
[DE95-005396] p 2538 N95-30216
High performance nickel electrodes for space power applications p 2511 N95-30257
Decomposition of hypo-eutectoid iron carbon austenites
[PB95-196945] p 2538 N95-30287
Visit to the Laboratory For Evaluation and Failure Prevention of Materials, Toyohashi University of Technology, 17 Oct 94
[AD-A292340] p 2597 N95-30293

MICROWAVE ANTENNAS
Quasioptical Josephson Oscillator
[AD-A292481] p 2561 N95-28859

MICROWAVE CIRCUITS
Processing, fabrication, and demonstration of HTS integrated microwave circuits
[AD-A292480] p 2562 N95-29073
Processing, fabrication, and demonstration of HTS integrated microwave circuits
[AD-A290220] p 2562 N95-29078
High performance electromagnetic simulation tools
[AD-A290405] p 2554 N95-29235

MICROWAVE FILTERS
Processing, fabrication, and demonstration of HTS integrated microwave circuits
[AD-A292480] p 2562 N95-29073
Processing, fabrication, and demonstration of HTS integrated microwave circuits
[AD-A290220] p 2562 N95-29078

MICROWAVE FREQUENCIES
Novel high-power solid-state sources for the millimeter-wave region
[AD-A292653] p 2564 N95-29384

MICROWAVE IMAGERY
Analysis of the structural characteristics and intensity evolution of super typhoon flo (1990) in special sensor Microwave/Imager (SSM/I) data
[AD-A292413] p 2619 N95-28989
Microwave remote sensing algorithms for cirrus clouds and precipitation p 2623 N95-29715
Microwave remote sensing of surface soil moisture and its application to hydrologic modeling
p 2600 N95-29821
An atlas of monthly mean distributions of SSMI surface wind speed, AVHRR/2 sea surface temperature, AMI surface wind velocity, TOPEX/POSEIDON sea surface height, and ECMWF surface wind velocity during 1993
[NASA-CR-198880] p 2628 N95-30343

MICROWAVE OSCILLATORS
Quasioptical Josephson Oscillator
[AD-A292481] p 2561 N95-28859
A kilohertz femtosecond Ti: Sapphire regeneratie amplifier
[AD-A290591] p 2588 N95-30045

MICROWAVE RADIOMETERS
Typhoon monitoring using passive microwave observations
[AD-A292567] p 2619 N95-28975
Emissivity measurements in thin metallized membrane reflectors used for microwave radiometer sensors
[NASA-TM-110179] p 2506 N95-30251
A conceptual thermal design study of an electronically scanned thinned array radiometer
[NASA-TM-110173] p 2509 N95-30316

MICROWAVE SENSORS
An atlas of monthly mean distributions of SSMI surface wind speed, AVHRR/2 sea surface temperature, AMI surface wind velocity, TOPEX/POSEIDON sea surface height, and ECMWF surface wind velocity during 1993
[NASA-CR-198880] p 2628 N95-30343

MICROWAVES
Cellular and molecular level responses after radiofrequency radiation exposure, alone or in combination with x rays or chemicals
[AD-A292488] p 2633 N95-28866
Typhoon monitoring using passive microwave observations
[AD-A292567] p 2619 N95-28975
HBCU/MI instrumentation for the Pulsed Power Plasma Sciences Laboratory at the University of New Mexico, FY92-93
[AD-A292444] p 2703 N95-29003
High resolution microwave survey
[NASA-TM-110566] p 2553 N95-29174
An investigation of the channel crosstalk in optical heterodyne controlled phased array radars
[AD-A292028] p 2554 N95-29186
Investigation of the Paschen curve of nitrogen via the application of nanosecond pulsed electromagnetic radiation
[AD-A290129] p 2586 N95-29425

MILITARY AIRCRAFT
Role of unmanned aerial vehicles in future armed conflict scenarios
[AD-A289777] p 2497 N95-29282

MILITARY HELICOPTERS
Helicopter life substantiation: Review of some USA and UK initiatives
[AD-A290045] p 2495 N95-28851
Optimizing cockpit display configurations with a genetic algorithm system
[AD-A289799] p 2499 N95-29123

MILITARY OPERATIONS
Estimating attenuation and propagation of noise bands from a distant source using the lookup program and data base
[AD-A290218] p 2683 N95-29077
Software testing toolkit for distributed simulations
[AD-A291867] p 2649 N95-29435
Applications of digital video and synthetic environments to unmanned aerial vehicles
[AD-A291875] p 2497 N95-29437

Human fluid balance and dehydration during cold weather military operations
[AD-A289192] p 2636 N95-29757
MILITARY TECHNOLOGY
Conference reports
[AD-A289630] p 2561 N95-28911
DOD listing of approved recurring information requirements
[AD-A291346] p 2724 N95-29947
MILLIMETER WAVES
Nobeyama Radio Observatory report, no. 381: Parallel connected twin SIS junctions for millimeter and submillimeter wave mixers: Analysis and experimental verification p 2562 N95-29099
Novel high-power solid-state sources for the millimeter-wave region
[AD-A292653] p 2564 N95-29384
Aperture synthesis observation of HCN J = 1-0 emission from Y Canum Venaticorum p 2735 N95-29839
The mm-wave resonant methods for the detection of corrosion, phase 1
[AD-A291315] p 2593 N95-29941
Investigation of optical damage, energy partitioning and scaling laws at extremely high velocities
[AD-A291368] p 2703 N95-30062
MINERALS
Differentiation in the early Earth: An experimental investigation p 2612 N95-29199
MINES (EXCAVATIONS)
Two-dimensional signal processing for regional seismic event identification
[AD-A292601] p 2613 N95-29293
MINIMAL SURFACES
Elliptic surface grid generation on minimal and parmetrized surfaces p 2484 N95-28760
MINIMAX TECHNIQUE
Optimal universal coding and density estimation
[AD-A290694] p 2675 N95-29587
MINORITY CARRIERS
Monte Carlo simulation study of the ICRF minority heating in the large helical device
[AD-B179858L] p 2708 N95-29749
MIR SPACE STATION
STS-71 Shuttle/Mir flight: Day 1
[NASA-TM-110744] p 2505 N95-29954
STS-71 Shuttle/Mir flight: Day 2
[NASA-TM-110745] p 2505 N95-29955
STS-71 Shuttle/Mir flight: Day 3
[NASA-TM-110746] p 2505 N95-29956
STS-71 Shuttle/Mir flight: Day 4
[NASA-TM-110747] p 2505 N95-29957
STS-71 Shuttle/Mir flight: Day 5
[NASA-TM-110748] p 2505 N95-29958
STS-71 Shuttle/Mir flight: Day 6
[NASA-TM-110749] p 2505 N95-29959
STS-71 Shuttle/Mir flight: Day 7
[NASA-TM-110750] p 2505 N95-29960
STS-71 Shuttle/Mir flight: Day 8
[NASA-TM-110751] p 2505 N95-29961
STS-71 Shuttle/Mir flight: Day 9
[NASA-TM-110752] p 2506 N95-29962
STS-71 Shuttle/Mir flight: Day 10
[NASA-TM-110753] p 2506 N95-29963
MIRA VARIABLES
Nobeyama Radio Observatory report, no. 380: Detection of the (29)SiO v=1, J=1-0 maser from TX Camelopardalis p 2726 N95-29101
MIRRORS
An integrated optical CO2 sensor. Phase 0: Design and fabrication of critical elements
[NASA-CR-196792] p 2700 N95-29366
Low order adaptive optical systems
[AD-A291121] p 2701 N95-29766
MISSILE COMPONENTS
The 1995 version of the NSWC aeroprediction code. Part 1: Summary of new theoretical methodology
[AD-A291518] p 2490 N95-29853
MISSILE CONFIGURATIONS
The 1995 version of the NSWC aeroprediction code. Part 1: Summary of new theoretical methodology
[AD-A291518] p 2490 N95-29853
An aerodynamic and static-stability analysis of the Hypersonic Applied Research Technology (HART) missile
[DA9426923] p 2491 N95-29965
MISSILE CONTROL
Closed loop control of guided missiles using neural networks p 2663 N95-29241
MISSILES
An ultra-high speed incoherent-to-coherent converter for optical computing
[AD-A292658] p 2700 N95-29412
The 1995 version of the NSWC aeroprediction code. Part 1: Summary of new theoretical methodology
[AD-A291518] p 2490 N95-29853
An aerodynamic and static-stability analysis of the Hypersonic Applied Research Technology (HART) missile
[DA9426923] p 2491 N95-29965
MISSION PLANNING
A conceptual design for the attitude control and determination system for the Magnetosphere Imager spacecraft
[NASA-TP-3560] p 2507 N95-28721
MIXERS
Laser doppler velocimeter system for subsonic jet mixer nozzle testing at the NASA Lewis Aeroacoustic Propulsion Lab
[NASA-TM-106984] p 2477 N95-30229
MIXING CIRCUITS
Nobeyama Radio Observatory report, no. 381: Parallel connected twin SIS junctions for millimeter and submillimeter wave mixers: Analysis and experimental verification p 2562 N95-29099
MIXING LAYERS (FLUIDS)
Grid resolution and turbulent inflow boundary condition recommendations for NPARC calculations
[NASA-TM-106959] p 2492 N95-30253
MIXTURES
Modeling joint effects of mixtures of chemicals on microorganisms using quantitative structure activity relationship techniques, phase 3
[AD-A290153] p 2632 N95-29320
Processing studies on in situ composites based on blends of thermotropic Liquid Crystalline Polymers with thermoplastics
[AD-A290526] p 2544 N95-29494
MOBILE COMMUNICATION SYSTEMS
Scheduling algorithms for mobile packet radio networks p 2558 N95-29707
UMTS network architecture
[PB95-206744] p 2558 N95-29919
MOBILITY
Drift mobility measurements in thin film boron carbide
[AD-A292510] p 2712 N95-28869
Formation and properties of titanium disilicide: A study on the development of stress in Ti-Si thin films
[PB95-197315] p 2538 N95-30205
MODAL RESPONSE
Modal interactions and complex responses in weaklyNONLINEAR MULTI-DEGREE-OF-FREEDOM MECHANICAL SYSTEMS
[AD-A292023] p 2594 N95-28853
MODELS
Description of the TV distribution service using MAGIC modelling methods
[PB95-206728] p 2560 N95-30219
Product configurations: An application for prototype object approach
[PB95-192589] p 2655 N95-30283
MODES
Inhibition of mode competition in free-electron laser oscillators p 2586 N95-29336
MODULATION
Path resolved optical sensing of atmospheric winds utilizing speckle-turbulence interaction and pseudorandum code modulation
[AD-A290800] p 2621 N95-29497
Experimental investigation of aerodynamic devices for wind turbine rotational speed control, phase 1
[DE95-004034] p 2603 N95-30016
MODULATORS
An investigation of the channel crosstalk in optical heterodyne controlled phased array radars
[AD-A292028] p 2554 N95-29186
Fiber compatible acousto-optic modulator using a gradient index lens
[AD-A291164] p 2565 N95-29925
Theory and experiment analysis of two-dimensional acousto-optic interaction
[AD-A291059] p 2685 N95-29951
MODULUS OF ELASTICITY
Simplified data reduction methods for the ECT test for mode 3 interlaminar fracture toughness
[NASA-TM-110176] p 2527 N95-29825
MOISTURE
Sorption and diffusion of moisture in multilayer composite AEM/S sandwich materials
[AD-A289807] p 2518 N95-28951
Effects of thermal and moisture cycling on the internal structure of stitched RTM laminates p 2522 N95-29048
Use of finite element analysis for transient moisture diffusion studies in multilayer composite AEM/S system sandwich materials
[AD-A291092] p 2527 N95-29638
MOISTURE CONTENT
The TEES process cleans waste and produces energy
[DE95-007799] p 2602 N95-29463
Remote sensing of hydrologic variables in boreal areas
[NASA-CR-189422] p 2600 N95-29754
Development and testing of improved techniques for modeling the hydrologic cycle in a mesoscale weather prediction system
[AD-A291243] p 2627 N95-29993
MOLECULAR ABSORPTION
The Scanning Fast Field Program (SCAFFIP) general version 1.0 user's manual
[AD-A291209] p 2618 N95-29976
MOLECULAR BEAM EPITAXY
Epitaxial growth and characterization of Si(1-x)Ge(x) materials and devices
[AD-A292528] p 2712 N95-28874
Interface properties of wide bandgap semiconductor structures
[AD-A289817] p 2713 N95-28954
Raman and photo-modulated reflectivity studies of ZnTe/InAs semiconductor heterostructure under hydrostatic pressure
[AD-A290467] p 2716 N95-29506
Ordering and bandgap reduction in InAs(1-x)Sb(x) alloys
[DE95-006324] p 2717 N95-30005
MOLECULAR CLOUDS
Nobeyama Radio Observatory report, no. 382: The mass of a star formed in a cloud core: Theory and its application to the Orion A cloud p 2731 N95-29100
MOLECULAR CLUSTERS
Experimental studies of electromagnetic propagation at ultrahigh intensities
[AD-A290284] p 2553 N95-29081
Structural and electronic properties of adsorbates on semiconductors, metal-semiconductor interfaces and semiconductor heterojunctions
[AD-A291917] p 2715 N95-29438
A cluster beam study of boron, boron oxide and B(x)O(y)H chemistry with hydrogen fluoride
[AD-A290826] p 2533 N95-29722
MOLECULAR COLLISIONS
Bubble fusion: Preliminary estimates of spherical micro-implosions in cavitating liquids
[DE95-006260] p 2569 N95-28956
AB initio studies of electron and positron scattering from non-linear molecules
[AD-A292586] p 2692 N95-28981
MOLECULAR DYNAMICS
Molecular dynamics simulation of liquid nitromethane shocked to 143 kbar
[AD-A292107] p 2691 N95-28919
Molecular dynamics study of electromigration
[AD-A289811] p 2691 N95-28952
Molecular spectra and dynamics at interfaces
[AD-A289779] p 2693 N95-29460
Molecular level characterization by NMR of the transport and structural environment of gases and condensed penetrante
[AD-A290831] p 2693 N95-29723
Applications of Langevin and Molecular Dynamics methods
[DE95-007875] p 2694 N95-30059
MOLECULAR ELECTRONICS
Nanoscience and nanotechnology in Europe
[AD-A290214] p 2562 N95-29075
MOLECULAR ENERGY LEVELS
Computational investigation of the stabilities of some N, O, F ions
[AD-A292305] p 2691 N95-28868
MOLECULAR EXCITATION
Molecular dynamics simulation of liquid nitromethane shocked to 143 kbar
[AD-A292107] p 2691 N95-28919
MOLECULAR INTERACTIONS
The interaction of group 3A atoms with small molecules
[AD-A290285] p 2692 N95-29082
Proceedings of the 18th International Workshop on Condensed Matter Theories
[AD-A291396] p 2694 N95-30065
MOLECULAR ORBITALS
SAM1-A new semiempirical method including d-orbitals
[AD-A290903] p 2694 N95-30060
MOLECULAR RELAXATION
Molecular level characterization by NMR of the transport and structural environment of gases and condensed penetrante
[AD-A290831] p 2693 N95-29723
MOLECULAR ROTATION
Optimal control of molecular motion
[AD-A291919] p 2691 N95-28944
MOLECULAR SPECTRA
Molecular spectra and dynamics at interfaces
[AD-A289779] p 2693 N95-29460

MOLECULAR SPECTROSCOPY
Physical acoustics summer school, 1994. volume 1. transcript
[AD-A292552] p 2683 N95-28973
MOLECULAR STRUCTURE
Computer simulation study of high t(sub c) superconductor structure
[AD-A292513] p 2583 N95-29163
Symposium on Metal-Mediated Molecular Architectures
[AD-A290427] p 2692 N95-29388
Molecular spectra and dynamics at interfaces
[AD-A289779] p 2693 N95-29460
Brief introduction to state key physics laboratories and division open laboratories
[AD-A291064] p 2682 N95-29952
The 5th International Meeting on Cholinesterase
[AD-A291253] p 2534 N95-30085
Parallel continuation-based global optimization for molecular conformation and protein folding
[DE95-005860] p 2633 N95-30114
MOLECULAR WEIGHT
High temperature thermosets and ceramics derived from linear carborane-(siloxane or silane)-acetylene copolymers
[AD-D017400] p 2545 N95-29569
MOLECULES
Orthobaric densities and molar volumes of liquids. Glycols and cyclic diols
[ESDU-95003] p 2531 N95-28895
Molecular dynamics simulation of liquid nitromethane shocked to 143 kbar
[AD-A292107] p 2691 N95-28919
AB initio studies of electron and positron scattering from non-linear molecules
[AD-A292586] p 2692 N95-28981
Characterization of excited state oxygen-organic molecule complexes
[AD-A290548] p 2692 N95-29092
Electrical and electronic properties of self-assembled lipid bilayers
[AD-A290507] p 2632 N95-29155
Recent progress in the study of the kinetics of sol-gel SiO2 synthesis reactions
[AD-A290570] p 2544 N95-29551
Fundamental studies of oxygen rings and other high energy density molecular systems
[AD-A290875] p 2693 N95-29865
Molecular probes of gating and open channel conformational transitions of mechanosensitive ion channels
[AD-A291170] p 2637 N95-29927
MOLTEN SALT NUCLEAR REACTORS
Molten fluoride fuel salt chemistry
[DE95-007025] p 2695 N95-28957
MOLTEN SALTS
Molten fluoride fuel salt chemistry
[DE95-007025] p 2695 N95-28957
MOLYBDATES
Chemically induced passivity of aluminum alloys and Al-based metal matrix composites
[AD-A290778] p 2528 N95-29923
MOLYBDENUM
Effects of impurities released from high Z test limiter on plasma performance in TEXTOR
[AD-B191995L] p 2709 N95-29803
Influence of dislocation-solute interactions on the mechanical properties of zirconium-doped NiAl
[DE95-008848] p 2538 N95-30179
MOMENTUM
Heat and momentum flux measurements in the planetary boundary layer with a wind profiling radar/radio acoustic sounding system p 2617 N95-29777
MOMENTUM TRANSFER
The role of diabatic heating, torques and stability in forcing the meridional circulation within cyclones p 2626 N95-29834
MONOCHROMATORS
A finite element analysis of room temperature silicon crystals for the Advanced Photon Source bending-magnet and insertion-device beams
[DE95-005822] p 2718 N95-30184
MONOMERS
Photogenerated amines in the design of imaging materials: The radiation-induced imidization of functionalized polystyrenes bearing amide-ester side chains
[AD-A289943] p 2542 N95-29270
Conjugated polymers from cyclohexadienediol monomers
[AD-A290247] p 2544 N95-29505
Preparation and studies of urazole containing polymers
[AD-A290685] p 2545 N95-29586
MONSOONS
On the large scale circulation of the East Asia Mei-Yu fronts and secondary weather dimension disturbances
[AD-A291036] p 2622 N95-29662
Energy budget in the Asian monsoon region p 2623 N95-29713
MONTE CARLO METHOD
Formation of striped surface phases by short-range forces
[AD-A279962] p 2531 N95-28945
A Monte Carlo simulation of Coulomb collisions and wave-particle interactions in space plasma at high latitudes p 2704 N95-29205
Large deviation limit theorems, with applications
[AD-A290392] p 2669 N95-29233
Optimal universal coding and density estimation
[AD-A290694] p 2675 N95-29587
Monte Carlo simulation study of the ICRF minority heating in the large helical device
[AD-B179858L] p 2708 N95-29749
Distributed multitasking ITS with PVM
[DE95-006821] p 2660 N95-30116
MOON
A geotechnical characterization of lunar soils and lunar soil simulants p 2736 N95-29117
Apollo 11: For all mankind
[NASA-TM-110622] p 2503 N95-29407
Total solar eclipse of 1997 March 9
[NASA-RP-1173] p 2731 N95-30004
Apollo 14: Shepard hitting golf ball on Moon
[NASA-TM-110638] p 2737 N95-30318
MORPHOLOGY
Nobeyama Radio Observatory report, no. 378: The polar ring spiral galaxy NGC 660 p 2731 N95-29097
Phase coupling and morphology generation in engineering polymer alloys
[AD-A291868] p 2543 N95-29436
Synthesis morphology and properties of semicrystalline block copolymers
[AD-A290475] p 2544 N95-29510
Membrane fluidity and shape of human red blood cells are altered by physiological levels of hydrostatic pressure
[AD-A290595] p 2636 N95-29557
Changes in microstructural parameters of snow during deformation
[AD-A290887] p 2601 N95-29866
Influence of dislocation-solute interactions on the mechanical properties of zirconium-doped NiAl
[DE95-008848] p 2538 N95-30179
Inertial fusion program and national laser users facility program
[DE95-008202] p 2711 N95-30274
MOSSBAUER EFFECT
A Pr-141 Moessbauer study of praseodymium compounds
[PB95-192449] p 2535 N95-30282
MOTION SIMULATION
Telepresence media resource tape
[NASA-TM-110648] p 2655 N95-30248
MOTION SIMULATORS
Ride motion simulator (RMS) testing using human occupants
[AD-A292641] p 2641 N95-29378
MOTION STABILITY
An investigation into the existence of asteroids at Saturn's triangular Lagrangian points p 2727 N95-29648
MOTIVATION
Two-dimensional signal processing for regional seismic event identification
[AD-A292601] p 2613 N95-29293
MOUNTAINS
Lee vorticity production by tropical mountain ranges p 2622 N95-29701
MOUNTING
Adjustable two-axis instrument mount
[AD-D017393] p 2582 N95-29220
MULLITES
Innovative processing of composites for ultra-high temperature applications, book 1
[AD-A290889] p 2527 N95-29842
MULTI-ANODE MICROCHANNEL ARRAYS
Speckle imaging with the multi-anode microchannel array detector p 2728 N95-29652
MULTIBLOCK GRIDS
Multiblock grid generation with automatic zoning p 2480 N95-28735
Algorithms for the automatic generation of 2-D structured multi-block grids p 2483 N95-28757
Optimal domain decomposition strategies p 2484 N95-28759
Automatic multi-block grid generation for high-lift configuration wings p 2485 N95-28764
MULTIDISCIPLINARY DESIGN OPTIMIZATION
Surface Modeling, Grid Generation, and Related Issues in Computational Fluid Dynamic (CFD) Solutions
[NASA-CP-3291] p 2478 N95-28723
Future requirements in surface modeling and grid generation p 2478 N95-28724
A grid generation system for multi-disciplinary design optimization p 2484 N95-28763
GridTool: A surface modeling and grid generation tool p 2486 N95-28773
MULTIDISCIPLINARY RESEARCH
Symposium on Metal-Mediated Molecular Architectures
[AD-A290427] p 2692 N95-29388
MULTIGRID METHODS
Surface Modeling, Grid Generation, and Related Issues in Computational Fluid Dynamic (CFD) Solutions
[NASA-CP-3291] p 2478 N95-28723
Block-structured grids for complex aerodynamic configurations: Current status p 2480 N95-28736
Three-dimensional hybrid grid generation using advancing front techniques p 2481 N95-28745
A 3DGRAPE/AL: The Ames/Langley technology upgrade p 2482 N95-28750
Automatic structured grid generation using Gridgen (some restrictions apply) p 2483 N95-28751
Tuned grid generation with ICEM CFD p 2483 N95-28752
Interactive high quality grid generation p 2486 N95-28774
Leading edge film cooling effects on turbine blade heat transfer
[NASA-TM-106955] p 2500 N95-29115
Development of a rotary wing Navier-Stokes CFD code based on TLNS3D code
[AD-A290421] p 2574 N95-29387
The large discretization step method for time-dependent partial differential equations
[NASA-CR-195068] p 2670 N95-29403
Coarsening strategies for unstructured multigrid techniques with application to anisotropic problems
[NASA-CR-198154] p 2674 N95-30227
Pressure updating methods for the steady-state fluid equations
[NASA-CR-198163] p 2674 N95-30353
MULTIMEDIA
Interactive multimedia presentation for applied computer tomography: Impact
[AD-A291955] p 2640 N95-29020
MULTIPHASE FLOW
Computational fluid dynamics (CFD) simulation of test chamber and smoke-generating device
[AD-A290199] p 2569 N95-29058
State-of-the-art review of computational fluid dynamics modeling for fluid-solids systems
[DE95-005866] p 2577 N95-29988
Ensemble phase averaged equations for multiphase flows p 2579 N95-30284
MULTIPHOTON ABSORPTION
Spectrometric studies of selected nitrocompounds using laser-induced photofragmentation/photoionization at 193 nm
[AD-A289947] p 2530 N95-28876
MULTIPLE ACCESS
Scheduling algorithms for mobile packet radio networks p 2558 N95-29707
MULTIPLE DOCKING ADAPTERS
STS-71 Shuttle/Mir flight: Day 6
[NASA-TM-110749] p 2505 N95-29959
MULTIPLEXING
Methods and components for optical contention resolution in high speed networks
[AD-A292331] p 2697 N95-28795
Design, development and testing of a prototype precision angular positioning control system for a next generation multiplexed imager
[AD-A292585] p 2698 N95-28980
The properties of local poor Abell clusters and instrumentation for the study of clustered objects p 2730 N95-29827
MULTIPLICATION
Hybrid harmonic gyrotron traveling wave amplifier
[AD-A292686] p 2564 N95-29417
MULTIPROCESSING (COMPUTERS)
Massively parallel fast elliptic equation solver for three dimensional hydrodynamics and relativity
[DE95-009385] p 2660 N95-30193
Neural networks for combinatorial optimization
[PB95-206843] p 2667 N95-30222
MULTISENSOR FUSION
MATSurv multisensor air traffic surveillance
[AD-A292253] p 2494 N95-28887
MULTIVARIATE STATISTICAL ANALYSIS
Multivariate wavelet representations and approximations
[AD-A290147] p 2670 N95-29312

Continuation of research in the statistical aspects of reliability, availability, and maintainability
[AD-A290126] p 2592 N95-29423
Adaptive block sequential detection of abrupt signal changes
[AD-A290456] p 2557 N95-29489
Statistical inference problems in some multivariate linear models with applications to multivariate calibration and meta-analysis
[AD-A291125] p 2675 N95-29768
A contribution to the theory of robust estimation of multivariate location and shape: EID
[AD-A290435] p 2675 N95-29819
A new visualization technique to study the time evolution of finite and adaptive mixture estimators
[AD-A291147] p 2673 N95-30126

MUONS
A practical high-energy high-luminosity mu(+)-mu(-) collider
[DE95-006769] p 2696 N95-30009

MUSCLES
Effects of chromium picolinate on body composition in a remedial conditioning program
[AD-A292079] p 2636 N95-29238

MUSCULOSKELETAL SYSTEM
The synthesis of liquid crystalline phophazenes containing chiral mesogens
[AD-A291911] p 2543 N95-29358
Molecular probes of gating and open channel conformational transitions of mechanosensitive ion channels
[AD-A291170] p 2637 N95-29927

MUSIC
DPARTS. A dynamic parallel adaptive multiprocess or real-time scheduler
[AD-A291160] p 2659 N95-29915

MYOCARDIAL INFARCTION
Flying waivers for history of angioplasty and myocardial infraction
[AD-A292505] p 2635 N95-29161

MYOCARDIUM
A discrete-event simulation model of myocardial electrical activity: Mathematical electrophysiology
[AD-A292323] p 2633 N95-28793
Flying waivers for history of angioplasty and myocardial infraction
[AD-A292505] p 2635 N95-29161

MYOPIA
Refractive changes during prolonged exposure to altitude following refractive surgery
[AD-A290263] p 2635 N95-29173

N

N-TYPE SEMICONDUCTORS
Epitaxial growth and characterization of Si(1-x)Ge(x) materials and devices
[AD-A292528] p 2712 N95-28874
Nitride semiconductors for ultraviolet detection
[AD-A289546] p 2712 N95-28910

NARROWBAND
High gain, low noise and broadband Raman and Brillouin fiber-optic amplifiers, channel selectors and switches
[AD-A290585] p 2700 N95-29553
Advanced presort process
[AD-A291010] p 2557 N95-29655

NASA PROGRAMS
Research and technology: 1994 annual report of the John F. Kennedy Space Center
[NASA-TM-110143] p 2740 N95-28786
NASA/DOD Aerospace Knowledge Diffusion Research Project. Paper 49: Becoming an aerospace engineer: A cross-gender comparison
[NASA-TM-110731] p 2721 N95-29028
NASA: The state of the agency
[NASA-TM-110563] p 2720 N95-29170
An announcement by Dan Goldin
[NASA-TM-110739] p 2720 N95-29171
The JSC research and development annual report 1993
[NASA-TM-104787] p 2740 N95-29816
SeaWiFS technical report series. Volume 24: SeaWiFS technical report series cumulative index, volumes 1-23
[NASA-TM-104556] p 2631 N95-30236

NASA SPACE PROGRAMS
Yohkoh Soft X-ray Telescope
[NASA-CR-197655] p 2726 N95-29172
Hernandez Engineering: NASA
[NASA-CR-197665] p 2508 N95-29633
Life sciences program
[NASA-CR-197658] p 2633 N95-30292

NATIONAL AIRSPACE SYSTEM
Federal aviation administration plan for research, engineering and development
[AD-A290952] p 2494 N95-29733

NATURAL GAS
Evaluation of wear resistant ceramic valve seats in gas-fueled power generation engines
[PB95-200218] p 2591 N95-30110
Investigation of laminar methane flames with emphasis on kinetics elucidation and NOx reduction
[PB95-200531] p 2535 N95-30111

NATURAL LANGUAGE (COMPUTERS)
Interface for the translation of sentences in a natural language into a geometrical representation language
[INPE-5467-PRE/1775] p 2722 N95-29363

NATURAL LANGUAGE PROCESSING
Interface for the translation of sentences in a natural language into a geometrical representation language
[INPE-5467-PRE/1775] p 2722 N95-29363
Boyer-moore type algorithm for regular expression pattern matching
[PB95-198131] p 2654 N95-30107

NAVIER-STOKES EQUATION
A Cartesian, cell-based approach for adaptively-refined solutions of the Euler and Navier-Stokes equations
p 2480 N95-28739
An unstructured-grid software system for solving complex aerodynamic problems p 2481 N95-28743
A vorticity-velocity approach for three-dimensional unsteady viscous flow over wings p 2488 N95-29108
Leading edge film cooling effects on turbine blade heat transfer
[NASA-TM-106955] p 2500 N95-29115
An extension of the continuum model by Grad's thirteen moment equations for hypersonic rarefied flows
p 2488 N95-29118
Finite element vorticity-based methods for the solution of the incompressible and compressible Navier-Stokes equations p 2570 N95-29119
Navier-Stokes solution of wing wake structure and its perturbation p 2488 N95-29121
Solution of the Navier-Stokes equations on locally refined Cartesian meshes using state-vector splitting
p 2571 N95-29197
A fourth order Euler/Navier-Stokes prediction method for the aerodynamics and aeroelasticity of hovering rotor blades p 2572 N95-29242
Multifluid nonequilibrium simulation of arcjet thrusters
p 2510 N95-29245
Numerical experiments on the flow past a circular cylinder at sub-critical Reynolds number
[AD-A289937] p 2573 N95-29268
Three problems in fluid dynamics
[AD-A290481] p 2573 N95-29324
Rigorous drag bounds in turbulent shear flow
p 2573 N95-29334
Grid orthogonality effects on predicted turbine midspan heat transfer and performance
[NASA-TM-106931] p 2574 N95-29371
Development of a rotary wing Navier-Stokes CFD code based on TLNS3D code
[AD-A290421] p 2574 N95-29387
Direct numerical simulation of compressible turbulent flows, using adaptive spectral element method
[AD-A290115] p 2575 N95-29421
Implicit schemes and parallel computing in unstructured grid CFD
[NASA-CR-195071] p 2671 N95-29451
Computation of the integrated aerodynamic and propulsive flowfields of a generic hypersonic space plane p 2490 N95-29788
Cross flow instability of supersonic flow over a 4:1 elliptic cone
[AD-A291128] p 2577 N95-29913
Reliability enhancement of Navier-Stokes codes through convergence acceleration
[NASA-CR-196635] p 2578 N95-30034
Survey of CFD applications for high speed inlets
[AD-A291365] p 2578 N95-30087
Use of the PARC code to estimate the off-design transonic performance of an over/under turboramjet nozzle
[NASA-TM-106924] p 2491 N95-30091
Simulation of powder metal fabrication with high pressure gas atomization
[DE95-008820] p 2538 N95-30178
Supercritical states of two-dimensional wall-bounded shear flow p 2580 N95-30303

NAVIGATION
Guidance, navigation, and control study for a solar electric propulsion spacecraft
[NASA-CR-198920] p 2509 N95-30357

NAVIGATION AIDS
Conceptual design of a map interactive system for military aircraft cockpits
[AD-A289760] p 2499 N95-28692
MapTool version 2. User's manual
[AD-A289470] p 2630 N95-29418

NAVSTAR SATELLITES
Modeling spatio-temporal databases to measure the performance of the GPS satellite constellation
p 2494 N95-29596

NAVY
Design and analysis of the launch vehicle adapter fitting for the petite amateur navy satellite (PANSAT)
[AD-A289693] p 2504 N95-28680
Adaptations to three weeks of aerobic/anaerobic training in west coast U.S: Navy Sea-Air-Land personnel (SEAL's)
[AD-A291500] p 2637 N95-29846
Digital mapping, charting, and geodesy analysis program technical review of vector smart map prototypes 1 and 2
[AD-A291217] p 2601 N95-29977

NEAR FIELDS
GENAH user's guide and reference manual version 1.0
[AD-A290236] p 2583 N95-29470
Unsteady pressure and inflow velocity on a pitching rotor blade in hover p 2490 N95-29771

NEAR INFRARED RADIATION
An investigation of thunderstorms as a source of short period mesospheric gravity waves
[AD-A289795] p 2611 N95-28697
Variation in visual and near-infrared contrast with a snow background
[AD-A289710] p 2697 N95-28778
A compact universal power supply for laser diodes
[AD-A289950] p 2585 N95-29274
Characterisation of a line-tunable He-Xe laser operating at 2.026 and 3.894 micrometers
[AD-A291129] p 2587 N95-29914

NEAR WAKES
The effects of three-dimensional imposed disturbances on bluff body near wake flows: Effects of taper and splitter plates on the near wake characteristics of a circular cylinder in uniform and shear flow
[AD-A292113] p 2487 N95-28921
Navier-Stokes solution of wing wake structure and its perturbation p 2488 N95-29121

NEGATIVE FEEDBACK
The effects of clouds as a feedback mechanism on the Earth's climate in the tropical Pacific
p 2611 N95-30300

NEGATIVE IONS
Surface conversion techniques for low energy neutral atom imagers
[NASA-CR-196604] p 2691 N95-28856
Development of an intense negative hydrogen ion source with a wide-range of external magnetic filter field
[AD-B195514L] p 2705 N95-29567
Solitons in negative ion plasmas p 2706 N95-29668

NETHERLANDS
Civil military co-operation: A ten year experience of an affiliative aeromedical evacuation programme of the Netherlands Armed Forces and a civilian repatriation organization p 2676 N95-29608
Aeromedical evacuation by RNLAF - work according to protocol p 2676 N95-29609

NETS
Causal behaviours and nets
[PB95-197612] p 2660 N95-30102

NETWORK ANALYSIS
Analysis of the naval postgraduate school computer network architecture
[AD-A289749] p 2657 N95-28689
R&M design expert system
[AD-A292525] p 2645 N95-28814
Communication protocols in multi-hop radio networks
p 2553 N95-29106
Bicriteria network design problems
[DE95-005261] p 2661 N95-30215

NEURAL NETS
Predicting polarized light scattering by marine micro-organisms
[AD-A289796] p 2697 N95-28698
Multilayer piecewise linear networks. Revision 1
[AD-A289885] p 2658 N95-28955
Process optimization through discovery and integration of materials and processing properties. phase 1
[AD-A292576] p 2662 N95-28978
Spectral characterization of pulsed ultrasound using neural networks
[AD-A292440] p 2683 N95-28999
Joint services electronics program
[AD-A292469] p 2561 N95-29010
On-line damage identification and motion control of adaptive structures: An intelligent control approach
p 2662 N95-29109
Proceeding of the 33rd SICE Annual Conference
[DE95-758943] p 2662 N95-29144
Closed loop control of guided missiles using neural networks p 2663 N95-29241

Forecasting global temperature variations by neural networks
[AD-A290081] p 2621 N95-29333
Neural network exploration using optional experiment design
[AD-A290058] p 2663 N95-29479
Development of an artificial neural network for real-time classification of cone penetrometer strain gauge data
[AD-A290719] p 2664 N95-29499
Applications of machine learning and rule induction
[AD-A292607] p 2664 N95-29577
Automated Propulsion Data Screening demonstration system
[NASA-CR-196636] p 2510 N95-29584
Neural network-based decision support for incomplete databases p 2665 N95-29720
Neural network construction using evolutionary search
[AD-A290862] p 2665 N95-29831
Hybrid pyramid/neural network vision system
[AD-A290565] p 2665 N95-29863
Induction of selective Bayesian classifiers
[AD-A292690] p 2675 N95-29906
Pattern-analysis based models of masking by spatially separated sounds
[AD-A291270] p 2637 N95-29933
Robust testing of cellular neural networks
[AD-A291219] p 2665 N95-29979
Workshop on computing and intelligent systems
[AD-A290581] p 2666 N95-30040
Applicability of neural networks for production planning under uncertainty
[PB95-197406] p 2666 N95-30101
Neural networks for combinatorial optimization
[PB95-206843] p 2667 N95-30222
Self-organization in a simple brain model
[DE95-008312] p 2668 N95-30279

NEUROLOGY
Organization of the human circadian system
[AD-A288223] p 2634 N95-28915
Large-scale neuronal theories of the brain
[AD-A290200] p 2634 N95-29059
Georgetown Institute for Cognitive and Computational Sciences
[AD-A289775] p 2639 N95-29458

NEURONS
Computer models of retinal function
[AD-A290156] p 2634 N95-29022
Large-scale neuronal theories of the brain
[AD-A290200] p 2634 N95-29059

NEUROPHYSIOLOGY
Large-scale neuronal theories of the brain
[AD-A290200] p 2634 N95-29059
Coupling of brain muscarinic receptors to second messengers
[AD-A290498] p 2635 N95-29153

NEUTRAL ATMOSPHERES
High-latitude electrodynamics: Electromagnetic energy dissipation and neutral wind feedback effects
p 2616 N95-29696

NEUTRAL ATOMS
Surface conversion techniques for low energy neutral atom imagers
[NASA-CR-196604] p 2691 N95-28856

NEUTRAL GASES
Characterisation of a line-tunable He-Xe laser operating at 2.026 and 3.894 micrometers
[AD-A291129] p 2587 N95-29914

NEUTRON DIFFRACTION
Neutron scattering from amorphous, disordered and nanocrystalline materials
[DE95-005848] p 2717 N95-30077

NEUTRON IRRADIATION
Calculation of shielding parameters
[DE95-608735] p 2694 N95-29886
Radiation effects on front-end electronics for noble liquid calorimetry
[DE95-007304] p 2566 N95-30025

NEUTRON SCATTERING
Neutron scattering from amorphous, disordered and nanocrystalline materials
[DE95-005848] p 2717 N95-30077

NEUTRONS
Activities update
[AD-A292431] p 2692 N95-28994
Investigation and characterization of SEU effects and hardening strategies in avionics
[AD-A291058] p 2500 N95-29950
Testing of the ENDF/B-VI neutron data library ENDF60 for use with MCNP(trademark)
[DE95-007858] p 2696 N95-30057
Neutron scattering from amorphous, disordered and nanocrystalline materials
[DE95-005848] p 2717 N95-30077

NEWTON-RAPHSON METHOD
Solution of second order nonlinear boundary value problems by the boundary element method
p 2669 N95-29105
SOSDOR: Solid-state device simulator code
[AD-A289954] p 2563 N95-29275

NICKEL
The effects of platinum on nickel electrodes in the nickel hydrogen cell
[AD-A291607] p 2531 N95-28942
Effects of space exposure on metals flown on the Long Duration Exposure Facility
[NASA-CR-4662] p 2512 N95-30225
Development of a micro-fiber nickel electrode for nickel-hydrogen cell p 2567 N95-30256
High performance nickel electrodes for space power applications p 2511 N95-30257
Bending properties of nickel electrodes for nickel-hydrogen batteries p 2567 N95-30259
Effect of KOH concentration and anions on the performance of Ni-H2 battery positive plate
p 2567 N95-30260

NICKEL ALLOYS
Corrosion investigation of multilayered ceramics and experimental nickel alloys in SCWO process environments
[DE95-008666] p 2540 N95-28960
XPS study of Ni-Fe manganite thermistor material
[DE95-008778] p 2561 N95-28961
Daido Steel's Shibukawa Plant, Shibukawa City, Gumma Prefecture, Japan, 29 Jul. 1994
[AD-A292343] p 2536 N95-29467
Examination of dislocation core structures in B2 intermetallic alloys
[AD-A291486] p 2537 N95-29526
Influence of dislocation-solute interactions on the mechanical properties of zirconium-doped NiAl
[DE95-008848] p 2538 N95-30179

NICKEL CADMIUM BATTERIES
Magnum(R) NiCd advanced nickel-cadmium battery cells p 2567 N95-30258
Electrolyte management considerations in modern nickel hydrogen and nickel cadmium cell and battery designs p 2567 N95-30262

NICKEL COATINGS
Lightweight battery electrode and method of making it
[AD-D017389] p 2560 N95-28855

NICKEL HYDROGEN BATTERIES
The effects of platinum on nickel electrodes in the nickel hydrogen cell
[AD-A291607] p 2531 N95-28942
Development of a micro-fiber nickel electrode for nickel-hydrogen cell p 2567 N95-30256
Bending properties of nickel electrodes for nickel-hydrogen batteries p 2567 N95-30259
Effect of KOH concentration and anions on the performance of Ni-H2 battery positive plate
p 2567 N95-30260
Advanced Dependent Pressure Vessel (DPV) nickel-hydrogen spacecraft cell and battery design
p 2567 N95-30261
Electrolyte management considerations in modern nickel hydrogen and nickel cadmium cell and battery designs p 2567 N95-30262

NICKEL OXIDES
Lightweight battery electrode and method of making it
[AD-D017389] p 2560 N95-28855

NIGHT
The detection of oil slicks at night with airborne infrared imagers
[AD-A289731] p 2598 N95-29281

NIGHT VISION
Distance estimation training with night vision goggles under low illumination
[AD-A291338] p 2641 N95-29943

NITRAMINE PROPELLANTS
Analytical potential energy surface for methylene nitramine (CH2NNO2)
[AD-A291247] p 2534 N95-29994

NITRIC OXIDE
Research into artificially induced atmospheric disturbances
[AD-A290150] p 2613 N95-29317
Cylinder-averaged histories of nitrogen oxide in a DI diesel with simulated turbocharging
[AD-A290568] p 2590 N95-29820
Nitrogen dioxide measurement method characterization at the GRI conventional research house
[PB95-200549] p 2610 N95-30197

NITROGEN
Computational investigation of the stabilities of some N, O, F ions
[AD-A292305] p 2691 N95-28868
Investigation of the Paschen curve of nitrogen via the application of nanosecond pulsed electromagnetic radiation
[AD-A290129] p 2586 N95-29425
Numerical simulations of the flow in the HYPULSE expansion tube
[NASA-TM-110357] p 2503 N95-30228

NITROGEN ATOMS
Research into artificially induced atmospheric disturbances
[AD-A290150] p 2613 N95-29317
Preparation and studies of urazole containing polymers
[AD-A290685] p 2545 N95-29586

NITROGEN COMPOUNDS
Spectrometric studies of selected nitrocompounds using laser-induced photofragmentation/photoionization at 193 nm
[AD-A289947] p 2530 N95-28876

NITROGEN DIOXIDE
State resolved differential cross sections for reactions important to the decomposition of energetic materials
[AD-A290718] p 2548 N95-29498
Nitrogen dioxide measurement method characterization at the GRI conventional research house
[PB95-200549] p 2610 N95-30197

NITROGEN IONS
Thermal N(+) in the inner magnetosphere
p 2614 N95-29590

NITROGEN OXIDES
Cylinder-averaged histories of nitrogen oxide in a DI diesel with simulated turbocharging
[AD-A290568] p 2590 N95-29820
Investigation of laminar methane flames with emphasis on kinetics elucidation and NOx reduction
[PB95-200531] p 2535 N95-30111

NITROMETHANE
Molecular dynamics simulation of liquid nitromethane shocked to 143 kbar
[AD-A292107] p 2691 N95-28919

NITROUS OXIDES
A model analysis of the spatial distribution and temporal trends of nitrous oxide sources and sinks
p 2609 N95-29804

NOAA SATELLITES
Meteorological Satellite Center technical note, no. 28, 1994
[JTN-95-80926] p 2626 N95-29849

NOISE GENERATORS
Turbulent airflow noise production and propagation patterns of a subsonic jet impinging on a flat plate
p 2684 N95-29502
UHB engine fan broadband noise reduction study
[NASA-CR-198357] p 2684 N95-29641

NOISE INJURIES
Actual effectiveness of hearing protection in high level impulse noise
[AD-A291604] p 2634 N95-28941

NOISE INTENSITY
Interferometric measurement with squeezed light
[AD-A292402] p 2697 N95-28799
Actual effectiveness of hearing protection in high level impulse noise
[AD-A291604] p 2634 N95-28941
Estimating attenuation and propagation of noise bands from a distant source using the lookup program and data base
[AD-A290218] p 2683 N95-29077
Bell Helicopter Advanced Rotocraft Transmission (ART) program
[NASA-CR-195479] p 2590 N95-29538
Solutions of the benchmark problems by the dispersion-relation-preserving scheme
p 2674 N95-30145

NOISE POLLUTION
Estimating attenuation and propagation of noise bands from a distant source using the lookup program and data base
[AD-A290218] p 2683 N95-29077

NOISE PREDICTION
The prediction of sound attenuation as a result of propagation close to the ground
[ESDU-94036] p 2682 N95-28709
Estimating attenuation and propagation of noise bands from a distant source using the lookup program and data base
[AD-A290218] p 2683 N95-29077
An extension of the Lighthill theory of jet noise to encompass refraction and shielding
[NASA-TM-110163] p 2684 N95-29452

NOISE PROPAGATION
The prediction of sound attenuation as a result of propagation close to the ground
[ESDU-94036] p 2682 N95-28709

The correction of measured noise spectra for the effects of ground reflection
[ESDU-94035] p 2683 N95-28710
Turbulent airflow noise production and propagation patterns of a subsonic jet impinging on a flat plate
p 2684 N95-29502

NOISE REDUCTION
Interferometric measurement with squeezed light
[AD-A292402] p 2697 N95-28799
An algorithm fusion approach to IRST signal processing (III): Nongaussian-corrected filter fusion
[AD-A291565] p 2552 N95-28936
Object oriented segmentation of images
[AD-A290792] p 2671 N95-29485
Bell Helicopter Advanced Rotocraft Transmission (ART) program
[NASA-CR-195479] p 2590 N95-29538
UHB engine fan broadband noise reduction study
[NASA-CR-198357] p 2684 N95-29641

NOISE SPECTRA
The prediction of sound attenuation as a result of propagation close to the ground
[ESDU-94036] p 2682 N95-28709
The correction of measured noise spectra for the effects of ground reflection
[ESDU-94035] p 2683 N95-28710
The spectrum and directivity of turbulent mixing noise from supersonic jets p 2684 N95-29415

NONDESTRUCTIVE TESTS
The physics of spin polarized gases
[AD-A292511] p 2680 N95-28810
Spectral characterization of pulsed ultrasound using neural networks
[AD-A292440] p 2683 N95-28999
Five-channel SQUID based non-destructive evaluation (NDE) instrument
[AD-A292474] p 2592 N95-29012
The development of an interpretive methodology for the application of real-time acousto-ultrasonic NDE technique for monitoring damage in ceramic composites under dynamic loads p 2592 N95-29104
Origins of imperfections in composite materials
[AD-A290261] p 2523 N95-29169
Efficient inversion of Fourier and Laplace domain boundary element solutions for elastodynamic scattering
p 2592 N95-29256
Probability of detection of defects in coatings with electronic shearography
[NASA-TM-108493] p 2524 N95-29374
Measurement of interface strength, intrinsic toughness and their dependence on interfacial segregants
[AD-A291798] p 2524 N95-29409
The use of electrochemistry and ellipsometry for identifying and evaluating corrosion on aircraft
[AD-A290249] p 2497 N95-29426
Proceedings of the 6th International Conference on Nondestructive Characterization of Materials
[AD-A290727] p 2596 N95-29580
Ultrasonic guided waves in cylinders: Theory and experiment p 2685 N95-29826
Electrochemical impedance pattern recognition for detection of hidden chemical corrosion on aircraft components, phase 1
[AD-A291345] p 2593 N95-29946
Health monitoring of operational structures: Initial results
[DE95-008551] p 2597 N95-30210
Dielectric property measurements in the Electromagnetic Properties Measurement Laboratory
[NASA-TM-110147] p 2560 N95-30336

NONEQUILIBRIUM FLOW
Theory and experiments on chemical instabilities
[AD-A290773] p 2534 N95-29922

NONEQUILIBRIUM IONIZATION
Multifluid nonequilibrium simulation of arcjet thrusters
p 2510 N95-29245
Ionizational nonequilibrium and ignition in plasma accelerators p 2705 N95-29547

NONEQUILIBRIUM THERMODYNAMICS
Theory and experiments on chemical instabilities
[AD-A290773] p 2534 N95-29922

NONFERROUS METALS
Corrosion in methylphosphonic difluoride
[AD-A289995] p 2536 N95-29137

NONFLAMMABLE MATERIALS
The effect of wear on fire-blocking layer material effectiveness
[AD-A291520] p 2493 N95-29855

NONINTRUSIVE MEASUREMENT
Research instrumentation for polytechnic university's supersonic wind tunnel facility
[AD-A290232] p 2502 N95-29468

NONLINEAR EQUATIONS
Hybrid fuzzy logic control to stabilize an inverted pendulum from arbitrary initial conditions
[AD-A292441] p 2681 N95-29000
Linear and nonlinear discrete-time state-space modeling of dynamic systems for control applications
p 2663 N95-29251
New methods for nonlinear optimization
[AD-A290522] p 2670 N95-29385
Transient responses of phosphoric acid fuel cell power plant system
[NASA-CR-198948] p 2603 N95-30015
Applications of Langevin and Molecular Dynamics methods
[DE95-007875] p 2694 N95-30059
Benchmark problems and solutions
p 2686 N95-30134

NONLINEAR OPTICS
Conference proceedings: IEEE Nonlinear Optics, Materials, Fundamentals, and Applications
[AD-A292438] p 2698 N95-28997
Growth, characterization and application of KTN family nonlinear optical crystals
[AD-A290330] p 2713 N95-29087
High-density plasma dynamics in semiconductors
p 2705 N95-29632
Unconventional image recovery techniques
[AD-A290799] p 2701 N95-29646
Laser applications to chemical analysis: Summaries of papers presented at the laser applications to chemical analysis topical meeting
[AD-A290738] p 2587 N95-29653
Equipment resource for MCM technology and system prototyping
[AD-A292492] p 2719 N95-29756
Dynamical instabilities, chaos and spatial complexity in fundamental nonlinear optical interactions
[AD-A291223] p 2588 N95-29980
Physical modeling and design of semiconductor heterostructures for optical and electronical applications
p 2682 N95-30232

NONLINEAR PROGRAMMING
Time-optimal multi-axis attitude maneuvers of rigid spacecraft using collocation and nonlinear programming
p 2507 N95-29332

NONLINEAR SYSTEMS
Modal interactions and complex responses in weaklyNONLINEAR MULTI-DEGREE-OF-FREEDOM MECHANICAL SYSTEMS
[AD-A292023] p 2594 N95-28853
Low threshold all-optical crossbar switch on GaAs-GaAlAs channel waveguide arrays
[AD-A292483] p 2712 N95-28862
Hybrid fuzzy logic control to stabilize an inverted pendulum from arbitrary initial conditions
[AD-A292441] p 2681 N95-29000
Nonlinear mechanics and applied analysis
[AD-A290356] p 2669 N95-29070
The development of methods and techniques to detect and model the underlying structure of chaotic systems
[AD-A292435] p 2680 N95-29072
Transport simulation in spatially modulated low dimensionality systems
[AD-A290486] p 2718 N95-29149
Closed loop control of guided missiles using neural networks p 2663 N95-29241
Linear and nonlinear discrete-time state-space modeling of dynamic systems for control applications
p 2663 N95-29251
Investigation of an alternative finite element procedure: A one-step, steady-state analysis
[AD-A290030] p 2670 N95-29311
Robust control of nonlihear flexible multibody systems using quaternion feedback and dissipative compensation
[NASA-TM-109099] p 2507 N95-29377
Pulsed laser deposition of thin film material for nonlinear waveguides
[AD-A290789] p 2544 N95-29484
Interlaminar fracture mechanics and mechanisms: Linear and nonlinear aspects p 2526 N95-29597
On the topological complexity of the cost function in variational data assimilation p 2724 N95-29798
Relativistic effects on large amplitude nonlinear langmuir waves in a two-fluid plasma
[AD-B191980L] p 2710 N95-29841
Attractors of dissipative structure in three dissipative fluids
[AD-B180030L] p 2710 N95-29844
Nonlinear control systems
[AD-A291083] p 2665 N95-29971
Factorization and input-output decoupling by static output feedback for nonlinear control systems
[PB95-206975] p 2667 N95-30171
Learning control in linear and nonlinear systems
p 2667 N95-30238
Experiments on nonlinear wave-particle interactions
p 2695 N95-30302

NONLINEARITY
ARPA solid state laser and nonlinear materials program
[AD-A289657] p 2584 N95-28678
International Workshop on Stochastic Filtering Theory
[AD-A291670] p 2661 N95-28788
Modal interactions and complex responses in weaklyNONLINEAR MULTI-DEGREE-OF-FREEDOM MECHANICAL SYSTEMS
[AD-A292023] p 2594 N95-28853
Measurement of ultrashort pulses with a non-instantaneous nonlinearity
[DE95-006500] p 2698 N95-28983
Nonlinear calibration of an infrared radiometer
[AD-A292436] p 2698 N95-28996
Conference proceedings: IEEE Nonlinear Optics, Materials, Fundamentals, and Applications
[AD-A292438] p 2698 N95-28997
Hybrid fuzzy logic control to stabilize an inverted pendulum from arbitrary initial conditions
[AD-A292441] p 2681 N95-29000
Study of UV bleached channel waveguide performance in NLO polymer films
[AD-A292008] p 2540 N95-29021
Three dimensional effects in fiber reinforced composites under compression
[AD-A292027] p 2523 N95-29185
Fiber-matrix adhesion in single-fiber model composites
p 2524 N95-29337
New methods for nonlinear optimization
[AD-A290522] p 2670 N95-29385
Broadband control of structural vibration using simultaneous sensing and actuation with nonlinear piezoelectric elements p 2664 N95-29548
Theories of the nonlinear optical properties of composite media: Applications to phthalocyanine dyes
[AD-A290640] p 2700 N95-29560
Self-sustained magnetic braiding in toroidal plasmas
[AD-B191998L] p 2706 N95-29734
The 1995 version of the NSWC aeroprediction code. Part 1: Summary of new theoretical methodology
[AD-A291518] p 2490 N95-29853
Nonlinear control systems
[AD-A291083] p 2665 N95-29971
Sensor protection portion of the development of nonlinear optical materials and processes for laser hardening of sensors
[AD-A291200] p 2702 N95-29973
Dynamical instabilities, chaos and spatial complexity in fundamental nonlinear optical interactions
[AD-A291223] p 2588 N95-29980
Transient responses of phosphoric acid fuel cell power plant system
[NASA-CR-198948] p 2603 N95-30015
Gradient-dependent plasticity in numerical simulation of localization phenomena
[PB95-197257] p 2596 N95-30049
Theorem on the existence of solutions of quasi-static moving boundary problems
[PB95-197125] p 2673 N95-30093
Application of traditional CFD methods to nonlinear computational aeroacoustics problems
p 2688 N95-30148
Evaluation of high order schemes for nonlinear wave computations p 2582 N95-30149
Time accurate application of the MacCormack 2-4 scheme on massively parallel computers
p 2661 N95-30150
Nonlinear wave propagation using three different finite difference schemes (category 2 application)
p 2582 N95-30151
High-order essentially non-oscillatory methods for computational aeroacoustics p 2690 N95-30159

NONNEWTONIAN FLOW
Computational methods for the simulation of non-Newtonian flows
[AD-A290355] p 2570 N95-29069
Numerical solution of the equations governing non-Newtonian flow at moderate Reynolds numbers
p 2579 N95-30233

NONNEWTONIAN FLUIDS
The study of non-Newtonian contraction flows with a parallel finite element method p 2576 N95-29778

NONPARAMETRIC STATISTICS
Continuation of research in the statistical aspects of reliability, availability, and maintainability
[AD-A290126] p 2592 N95-29423
Optimal universal coding and density estimation
[AD-A290694] p 2675 N95-29587

NORTH AMERICA
The effect of climate perturbations on extratropical cyclogenesis along the east coast of North America
p 2621 N95-29595

NORTH ATLANTIC TREATY ORGANIZATION (NATO)
Recent Issues and Advances in Aeromedical Evacuation (MEDEVAC)
[AGARD-CP-554] p 2676 N95-29604
NORTHERN HEMISPHERE
Simultaneous UV and optical study of O star winds and UV and optical covariability of O star winds
[NASA-CR-189424] p 2726 N95-29370
Large scale fluctuations of the geomagnetic field
p 2617 N95-29796
A model analysis of the spatial distribution and temporal trends of nitrous oxide sources and sinks
p 2609 N95-29804
NOSE CONES
Transonic, supersonic and hypersonic wind-tunnel tests on aerodynamic characteristics of reentry body with blunted cone configuration
[ISAS-658] p 2490 N95-29640
NOSES (FOREBODIES)
Effect of nose shape and mass of the impactor on impact damage of laminated composites
[AD-A290351] p 2594 N95-29067
NOTCH SENSITIVITY
Effect of open hole on tensile failure properties of 2D triaxial braided textile composites and tape equivalents
[NASA-CR-4676] p 2513 N95-28817
NOTCH STRENGTH
Effect of open hole on tensile failure properties of 2D triaxial braided textile composites and tape equivalents
[NASA-CR-4676] p 2513 N95-28817
NOTCH TESTS
Mechanical characterization of two thermoplastic composites fabricated by automated tow placement
p 2515 N95-28834
Investigation of tension-compression fatigue behavior of a notched cross-ply metal matrix composite at elevated temperature
[AD-A291479] p 2527 N95-29770
NOTCHES
Effect of open hole on tensile failure properties of 2D triaxial braided textile composites and tape equivalents
[NASA-CR-4676] p 2513 N95-28817
Tension fracture of laminates for transport fuselage. Part 2: Large notches p 2515 N95-28837
Finite difference analysis of a cylindrical two conductor microstrip transmission line with truncated dielectrics
[AD-A292592] p 2555 N95-29290
Advanced presort process
[AD-A291010] p 2557 N95-29655
NOZZLE DESIGN
Marshall Space Flight Center surface modeling and grid generation applications p 2480 N95-28733
Liquefied metal jet program Automation and Robotics Research Institute (ARRI)
[AD-A289781] p 2536 N95-29461
Use of the PARC code to estimate the off-design transonic performance of an over/under turboramjet nozzle
[NASA-TM-106924] p 2491 N95-30091
Laser doppler velocimeter system for subsonic jet mixer nozzle testing at the NASA Lewis Aeroacoustic Propulsion Lab
[NASA-TM-106984] p 2477 N95-30229
NOZZLE EFFICIENCY
Use of the PARC code to estimate the off-design transonic performance of an over/under turboramjet nozzle
[NASA-TM-106924] p 2491 N95-30091
NOZZLE FLOW
Ejectors and jet pumps: Computer program for design and performance for steam/gas flow
[ESDU-94046] p 2495 N95-28704
Use of the PARC code to estimate the off-design transonic performance of an over/under turboramjet nozzle
[NASA-TM-106924] p 2491 N95-30091
Solution of acoustic workshop problems by a spectral multidomain method p 2687 N95-30141
Category 5 problem solution using an unstructured finite volume algorithm p 2657 N95-30157
Comparison of spatial numerical operators for duct-nozzle acoustics p 2690 N95-30158
High-order essentially non-oscillatory methods for computational aeroacoustics p 2690 N95-30159
Numerical simulations of small amplitude acoustic wave propagation in a converging-diverging nozzle
p 2690 N95-30160
NOZZLE GEOMETRY
Use of the PARC code to estimate the off-design transonic performance of an over/under turboramjet nozzle
[NASA-TM-106924] p 2491 N95-30091
NUCLEAR CHEMISTRY
Molten fluoride fuel salt chemistry
[DE95-007025] p 2695 N95-28957
NUCLEAR FUELS
Design of an electronic charged particle spectrometer to measure (rho R), yield, and implosion symmetry on the OMEGA Upgrade
[DE95-006088] p 2695 N95-28930
Molten fluoride fuel salt chemistry
[DE95-007025] p 2695 N95-28957
NUCLEAR FUSION
Bubble fusion: Preliminary estimates of spherical micro-implosions in cavitating liquids
[DE95-006260] p 2569 N95-28956
Magnetic fusion commercial power plants
[DE95-007027] p 2711 N95-30023
NUCLEAR INTERACTIONS
Measurements of (Delta)(sigma)(sub L)(pp) and (Delta)(sigma)(sub L)((bar p)p) at 200 GeV/c
[DE95-005837] p 2695 N95-30186
NUCLEAR MAGNETIC RESONANCE
Synthesis and complete characterization of a Gallium-Mixed-Pnicogen four-membered ring compound: I2GaAs(SiMe3)(sub 2)Ga(I)2P(SiMe3)(sub 2)
[AD-A292423] p 2713 N95-28993
The (HMI9293) acquisition of a 200 MHz nuclear magnetic resonance spectrometer
[AD-A291913] p 2583 N95-29361
Transition metal complexes with perfluorinated ligands
[AD-A290250] p 2536 N95-29427
Cage-like precursor formation from extensive cyclization in sol-gel inorganic condensation polymerization
[AD-A290589] p 2544 N95-29554
17O NMR of the structural evolution of V2O5 gels
[AD-A290623] p 2545 N95-29559
Molecular level characterization by NMR of the transport and structural environment of gases and condensed penetrante
[AD-A290831] p 2693 N95-29723
NMR imaging and hydrodynamic analysis of neutrally buoyant non-Newtonian slurry flows
[DE95-005842] p 2578 N95-30187
NUCLEAR POWER PLANTS
Magnetic fusion commercial power plants
[DE95-007027] p 2711 N95-30023
NUCLEAR RADIATION SPECTROSCOPY
The (HMI9293) acquisition of a 200 MHz nuclear magnetic resonance spectrometer
[AD-A291913] p 2583 N95-29361
NUCLEAR REACTIONS
Calculation of shielding parameters
[DE95-608735] p 2694 N95-29886
NUCLEAR RESEARCH
Management of meteorological data at a former nuclear weapons facility
[DE95-007619] p 2626 N95-29868
NUCLEAR SPIN
Sea and gluon spin structure function measurements at RHIC
[DE95-005823] p 2695 N95-30185
NUCLEATION
Macrosegregation and nucleation in undercooled Pb-Sn alloys
[NASA-TM-102023-REV] p 2535 N95-28701
Dust formation in stellar outflows: A time-dependent model p 2733 N95-29649
Numerical studies of the stratospheric aerosol layer under background and perturbed conditions
p 2615 N95-29666
The nucleation of crystalline films from vapor phase reactants
[AD-A291122] p 2716 N95-29767
NUCLEIC ACIDS
Selective attachment of nucleic acid molecules to patterned self-assembled surfaces
[AD-D017379] p 2530 N95-28854
NUCLEONS
Prospects for HERMES-spin structure studies at HERA
[DE95-005845] p 2694 N95-30019
Sea and gluon spin structure function measurements at RHIC
[DE95-005823] p 2695 N95-30185
NULL HYPOTHESIS
Improvement of inter-event distance tests of randomness in spatial point processes
[AD-A291151] p 2675 N95-30297
NUMBER THEORY
Computational complexity and encryption
[AD-A291910] p 2648 N95-29356
NUMERICAL ANALYSIS
Nonlinear mechanics and applied analysis
[AD-A290356] p 2669 N95-29070
Numerical experiments on the flow past a circular cylinder at sub-critical Reynolds number
[AD-A289937] p 2573 N95-29268
The quantum hydrodynamic model for semiconductor devices
[AD-A291809] p 2564 N95-29430
NUMERICAL CONTROL
Ropes: Support for collective opertions among distributed threads
[NASA-CR-198157] p 2649 N95-29404
ALLIANCE: An architecture for fault tolerant multi-robot cooperation
[DE95-008658] p 2666 N95-30112
NUMERICAL INTEGRATION
The study of non-Newtonian contraction flows with a parallel finite element method p 2576 N95-29778
NUMERICAL WEATHER FORECASTING
The interactive role of clouds and radiative transfer in maintaining atmospheric circulation
p 2616 N95-29699
Short-range precipitation forecasts using assimilation of simulated satellite water vapor profiles and cloud liquid water p 2625 N95-29832
NYLON (TRADEMARK)
Ferroelectric polarization mechanism of the odd-numbered nylons
[AD-A292276] p 2539 N95-28860
Ferroelectric and piezoelectric properties of nylon 11/Poly(Vinylidene fluoride) bilaminate films
[AD-A292274] p 2539 N95-28891

O

O STARS
X-ray observations of rapidly rotating O stars
[NASA-CR-189423] p 2726 N95-28822
Simultaneous UV and optical study of O star winds and UV and optical covariability of O star winds
[NASA-CR-189424] p 2726 N95-29370
OBJECT-ORIENTED PROGRAMMING
Tuned grid generation with ICEM CFD
p 2483 N95-28752
Impact of Ada and object-oriented design in the flight dynamics division at Goddard Space Flight Center
[NASA-CR-189412] p 2644 N95-28807
Using object-oriented database technology to develop a multiple domain capability for domain-oriented application composition systems
[AD-A289244] p 2721 N95-28907
Formal aspects of object identity in database manipulation p 2722 N95-29116
Object oriented segmentation of images
[AD-A290792] p 2671 N95-29485
Design and implementation of logical database languages
[AD-A290474] p 2650 N95-29509
Data modeling from a categorical perspective
p 2725 N95-30289
OBLIQUE SHOCK WAVES
Experimental research on crossing shock wave boundary layer interactions
[AD-A290764] p 2577 N95-29920
Hydrogen film cooling with incident and swept-shock interactions in a Mach 6.4 nitrogen free stream
[NASA-TM-4603] p 2578 N95-30056
Grid resolution and turbulent inflow boundary condition recommendations for NPARC calculations
[NASA-TM-106959] p 2492 N95-30253
OBSERVATORIES
Nobeyama Radio Observatory report, no. 379
p 2735 N95-29836
OBSTACLE AVOIDANCE
Estimation of unstabilized components in vehicular motion
[AD-A290580] p 2590 N95-29552
OCCUPATION
An analysis of anthropometric differences among occupational groups in the US Army
[AD-A292326] p 2640 N95-28794
OCCURRENCES
The effects of magnetic storm phases on F-layer irregularities from auroral to equatorial latitudes
[AD-A290674] p 2614 N95-29585
OCEAN BOTTOM
Backscatter data acquisition for Hydrosweep DS aboard RV Ewing
[AD-A292332] p 2628 N95-28796
Multi-scale studies of seafloor topography
[AD-A292301] p 2628 N95-28865
Tidal constituent database: West coast of the United States and eastern North Pacific Ocean
[AD-A292224] p 2630 N95-29198
Large scale fluctuations of the geomagnetic field
p 2617 N95-29796
OCEAN COLOR SCANNER
An atlas of monthly mean distributions of SSMI surface wind speed, AVHRR/2 sea surface temperature, AMI surface wind velocity, TOPEX/POSEIDON sea surface height, and ECMWF surface wind velocity during 1993
[NASA-CR-198880] p 2628 N95-30343

OCEAN CURRENTS
Stochastic modeling and global warming trend extraction for ocean acoustic travel times
[AD-A292114] p 2608 N95-28922
Glenda software design
[AD-A292537] p 2646 N95-28968
Modeling studies of the Leeuwin current off western and southern Australia
[AD-A290158] p 2629 N95-29023
Tidal constituent database: West coast of the United States and eastern North Pacific Ocean
[AD-A292224] p 2630 N95-29198
The structure of water mass, salt, and temperature transports within intermediate depths of the western tropical Atlantic Ocean p 2631 N95-29541
Numerical modeling of synoptic scale ocean dynamics
[AD-A291411] p 2631 N95-30069

OCEAN DATA ACQUISITIONS SYSTEMS
An atlas of monthly mean distributions of SSMI surface wind speed, AVHRR/2 sea surface temperature, AMI surface wind velocity, TOPEX/POSEIDON sea surface height, and ECMWF surface wind velocity during 1993
[NASA-CR-198880] p 2628 N95-30343

OCEAN DYNAMICS
A study of dynamics in the tropical Pacific using satellite data p 2630 N95-29520
Probabilistic modeling and statistical inference for random fields and space-time processes
[AD-A289956] p 2672 N95-30029
Numerical modeling of synoptic scale ocean dynamics
[AD-A291411] p 2631 N95-30069
Data catalog for JPL Physical Oceanography Distributed Active Archive Center (PO.DAAC)
[NASA-CR-198872] p 2631 N95-30231

OCEAN MODELS
Stochastic modeling and global warming trend extraction for ocean acoustic travel times
[AD-A292114] p 2608 N95-28922
Glenda software design
[AD-A292537] p 2646 N95-28968
A numerical study of the effects of wind forcing on the Chile Current System
[AD-A289808] p 2629 N95-28982
Modeling studies of the Leeuwin current off western and southern Australia
[AD-A290158] p 2629 N95-29023
Revisions and notes on a model for bubble attenuation in near-surface propagation
[AD-A290312] p 2629 N95-29085
Finite difference ocean acoustic model users guide
[AD-A291544] p 2631 N95-29856
An air-sea interaction model for stress, sensible heat, latent heat, and sea state, applicable to the full range of wind speeds p 2626 N95-29876
Numerical modeling of synoptic scale ocean dynamics
[AD-A291411] p 2631 N95-30069

OCEAN SURFACE
Revisions and notes on a model for bubble attenuation in near-surface propagation
[AD-A290312] p 2629 N95-29085
Description of the OHGR database
[AD-A290146] p 2722 N95-29221
Long range aircraft detection using high-frequency surface-wave radar
[AD-A290148] p 2555 N95-29313
Continental aerosol effects on stratocumulus microphysics during MAST 1994
[AD-A292674] p 2621 N95-29416
A study of dynamics in the tropical Pacific using satellite data p 2630 N95-29520
An air-sea interaction model for stress, sensible heat, latent heat, and sea state, applicable to the full range of wind speeds p 2626 N95-29876
Data catalog for JPL Physical Oceanography Distributed Active Archive Center (PO.DAAC)
[NASA-CR-198872] p 2631 N95-30231

OCEAN TEMPERATURE
Analysis of historical oceanographic data on a minicomputer: Program WAHOO
[AD-A292530] p 2629 N95-28873
Modeling studies of the Leeuwin current off western and southern Australia
[AD-A290158] p 2629 N95-29023
An air-sea interaction model for stress, sensible heat, latent heat, and sea state, applicable to the full range of wind speeds p 2626 N95-29876

OCEANOGRAPHIC PARAMETERS
Analysis of historical oceanographic data on a minicomputer: Program WAHOO
[AD-A292530] p 2629 N95-28873
Quality Control of meteorological observations at Fleet Numerical Meteorology and Oceanography Center
[AD-A291577] p 2619 N95-28938

OCEANOGRAPHY
Multi-scale studies of seafloor topography
[AD-A292301] p 2628 N95-28865
A comprehensive analysis of Navy and Marine corps digital mapping, charting, and geodesy requirements for modeling and simulation
[AD-A291601] p 2598 N95-28931
Tidal constituent database: West coast of the United States and eastern North Pacific Ocean
[AD-A292224] p 2630 N95-29198
Conversion of an oceanographic expert system to a C-based language
[NASA-CR-198695] p 2630 N95-29237
Numerical modeling of synoptic scale ocean dynamics
[AD-A291411] p 2631 N95-30069
Data catalog for JPL Physical Oceanography Distributed Active Archive Center (PO.DAAC)
[NASA-CR-198872] p 2631 N95-30231
SeaWiFS technical report series. Volume 24: SeaWiFS technical report series cumulative index, volumes 1-23
[NASA-TM-104556] p 2631 N95-30236

OCEANS
Multi-scale studies of seafloor topography
[AD-A292301] p 2628 N95-28865
Hindcasting changes in thermal structure and acoustic transmission loss in the upper ocean on short time scales with data from MILE and from ocean weather station papa
[AD-A292419] p 2629 N95-28991
Tidal constituent database: West coast of the United States and eastern North Pacific Ocean
[AD-A292224] p 2630 N95-29198
The detection of oil slicks at night with airborne infrared imagers
[AD-A289731] p 2598 N95-29281
Ocean Optics XII
[AD-A286734] p 2702 N95-29910

OHMIC DISSIPATION
Photon-counting spatial light modulator technology development
[AD-A292619] p 2699 N95-29295

OHMS LAW
Comment on a mean field Ohm's law for collisionless plasmas
[AD-B176252L] p 2707 N95-29741

OIL SLICKS
The detection of oil slicks at night with airborne infrared imagers
[AD-A289731] p 2598 N95-29281

OILS
Effects of cooling system parameters on heat transfer in PAFC stack
[NASA-CR-198817] p 2570 N95-29131
Boundary-layer transition and global skin friction measurement with an oil-fringe imaging technique
[NASA-CR-198814] p 2579 N95-30224

OLIGOMERS
Selective attachment of nucleic acid molecules to patterned self-assembled surfaces
[AD-D017379] p 2530 N95-28854

ON-LINE SYSTEMS
On-line damage identification and motion control of adaptive structures: An intelligent control approach p 2662 N95-29109
DPARTS. A dynamic parallel adaptive multiprocess or real-time scheduler
[AD-A291160] p 2659 N95-29915
Electrochemical impedance pattern recognition for detection of hidden chemical corrosion on aircraft components, phase 1
[AD-A291345] p 2593 N95-29946

ONBOARD EQUIPMENT
High resolution direct digitization and optical telemetry of shipboard antenna signals
[AD-A290238] p 2557 N95-29504
Requirement for onboard telemetry equipment p 2506 N95-29625

ONE DIMENSIONAL FLOW
Model development for active control of stall phenomena in aircraft gas turbine engines p 2500 N95-29679
The one-dimensional bubble: Theory, experiment, and relevance to exposure of divers to low frequency sound, and of lung to lithotripsy
[ISVR-TR-246] p 2577 N95-29817

OPEN CIRCUIT VOLTAGE
Multi-decade time-dependent voltage of polycrystalline thin-film solar cells p 2602 N95-29103

OPENINGS
Inflatable life vest
[AD-D017273] p 2641 N95-29600

OPERATING COSTS
Impact of composites on future transport aircraft p 2519 N95-29030

OPERATING SYSTEMS (COMPUTERS)
Implementing distributed server groups for the World Wide Web
[AD-A292221] p 2658 N95-29196
Client-server interactions in multi-server operating systems: The Mach-US approach
[AD-A290431] p 2650 N95-29536

OPERATOR PERFORMANCE
Improving problem-solving and decision-making skills under stress: Prediction and training
[AD-A292104] p 2638 N95-28918

OPERATORS (MATHEMATICS)
Process algebra with feedback
[PB95-206819] p 2673 N95-30106

OPTICAL COMMUNICATION
High resolution direct digitization and optical telemetry of shipboard antenna signals
[AD-A290238] p 2557 N95-29504
Ion doped quantum well lasers
[AD-A290937] p 2587 N95-29912
Modal analysis of straight and curved integrated optical waveguides: An integral equation approach
[PB95-197265] p 2702 N95-30054

OPTICAL COMPUTERS
N4 processor
[AD-A292571] p 2642 N95-28976
Testbed for precision characterization of spatial light modulators and optical processors
[AD-A290484] p 2699 N95-29148
An ultra-high speed incoherent-to-coherent converter for optical computing
[AD-A292658] p 2700 N95-29412
Vertical cavity surface emitting lasers for optical signal processing and optical computing applications
[AD-A290626] p 2588 N95-30050

OPTICAL CORRECTION PROCEDURE
Atmospheric wavefront sensing and correction including the stellar phase shifting interferometer p 2701 N95-29706

OPTICAL CORRELATORS
Testbed for precision characterization of spatial light modulators and optical processors
[AD-A290484] p 2699 N95-29148
A comparison of three pedestal removal techniques for an optical time-integrating correlator
[AD-A290092] p 2700 N95-29354
Intensity optical correlation through optical differentiation preprocessing
[AD-A291020] p 2701 N95-29661

OPTICAL DATA PROCESSING
Testbed for precision characterization of spatial light modulators and optical processors
[AD-A290484] p 2699 N95-29148
Feature-oriented image reconstruction and aero-optic metrology in turbulence
[AD-A290269] p 2699 N95-29177
Photon-counting spatial light modulator technology development
[AD-A292619] p 2699 N95-29295
An ultra-high speed incoherent-to-coherent converter for optical computing
[AD-A292658] p 2700 N95-29412
Variable rate optical iterative processing of optical information
[AD-D017397] p 2701 N95-29602
Vertical cavity surface emitting lasers for optical signal processing and optical computing applications
[AD-A290626] p 2588 N95-30050
Distortion-invariant optical pattern recognition by correlative matrix feature criterion
[AD-A291389] p 2703 N95-30064

OPTICAL EQUIPMENT
Gordon research conference on point defects, line defects, and interfaces in semiconductors
[AD-A290103] p 2714 N95-29209
Laser optics protective device
[AD-D017384] p 2585 N95-29217
Numerical modeling of opto-electronic integrated circuits
[AD-A292096] p 2563 N95-29239
Spectral inverse scattering theory for dielectric media: Application to optical devices
[AD-A292651] p 2556 N95-29383
Investigation of the Paschen curve of nitrogen via the application of nanosecond pulsed electromagnetic radiation
[AD-A290129] p 2586 N95-29425
High resolution direct digitization and optical telemetry of shipboard antenna signals
[AD-A290238] p 2557 N95-29504
Applied optics laboratory
[AD-A292006] p 2701 N95-29571
Low order adaptive optical systems
[AD-A291121] p 2701 N95-29766
High-temperature optical window design
[NASA-TM-106783] p 2596 N95-30008
Shock resistant optic fiber rotary slice holding device
[AD-D017327] p 2702 N95-30053

Modal analysis of straight and curved integrated optical waveguides: An integral equation approach
[PB95-197265] p 2702 N95-30054
Investigation of optical damage, energy partitioning and scaling laws at extremely high velocities
[AD-A291368] p 2703 N95-30062

OPTICAL FIBERS
An electrical and fiber-optic connector
[AD-D017404] p 2589 N95-28791
Shock resistant optic fiber rotary slice holding device
[AD-D017327] p 2702 N95-30053
Selective multi-chemical fiber optic sensor
[AD-D017409] p 2703 N95-30076
Method of measuring liquid level with a thermal interface detection
[AD-D017341] p 2703 N95-30166

OPTICAL FILTERS
Deconvolution of lateral shear interferograms
p 2699 N95-29222
Passive ranging with an incoherent optical system
p 2700 N95-29543
Advanced presort process
[AD-A291010] p 2557 N95-29655
Japanese remote sensing organizations, research, and technology
[AD-A292420] p 2601 N95-29905

OPTICAL HETERODYNING
Fibre-coupled remote optical vibrometry
[AD-A291606] p 2698 N95-28932
An investigation of the channel crosstalk in optical heterodyne controlled phased array radars
[AD-A292028] p 2554 N95-29186

OPTICAL MATERIALS
Study of UV bleached channel waveguide performance in NLO polymer films
[AD-A292008] p 2540 N95-29021
Growth, characterization and application of KTN family nonlinear optical crystals
[AD-A290330] p 2713 N95-29087
Multi-focal length and multi-channel holographic optical element
[AD-A291011] p 2583 N95-29656
Fiber compatible acousto-optic modulator using a gradient index lens
[AD-A291164] p 2585 N95-29925
Sensor protection portion of the development of nonlinear optical materials and processes for laser hardening of sensors
[AD-A291200] p 2702 N95-29973
High-temperature optical window design
[NASA-TM-106783] p 2596 N95-30008

OPTICAL MEASUREMENT
Propagation and transformation properties of axicon optical systems for laser beams
[AD-A289661] p 2584 N95-28679
Analysis of measurements for solid state laser remote lidar system
[NASA-CR-196640] p 2585 N95-29247
Applied optics laboratory
[AD-A292006] p 2701 N95-29571
Photothermal deflection in a supercritical fluid
p 2701 N95-29630

OPTICAL MEASURING INSTRUMENTS
Passive ranging with an incoherent optical system
p 2700 N95-29543
Precision pointing experiment
[AD-A291015] p 2664 N95-29657
Method of measuring liquid level with a thermal interface detection
[AD-D017341] p 2703 N95-30166

OPTICAL MICROSCOPES
(DEPSCOR-92) acquisition of a metallurgical optical microscope
[AD-A292439] p 2698 N95-28998

OPTICAL PATHS
In-line fiber etalon strain sensor
[AD-D017266] p 2699 N95-29283

OPTICAL PROPERTIES
Intermediate levels of visual processing
[AD-A291569] p 2638 N95-28937
Optimal control of molecular motion
[AD-A291919] p 2691 N95-28944
Optoelectronics based on SiGe/Si heterostructures
[AD-A292464] p 2699 N95-29006
Growth, characterization and application of KTN family nonlinear optical crystals
[AD-A290330] p 2713 N95-29087
Tailored microstructures for broadband or selective detection of radiation from the visible to the infrared
[AD-A292097] p 2554 N95-29240
The detection of oil slicks at night with airborne infrared imagers
[AD-A289731] p 2598 N95-29281
Transitions in liquid crystals initiated with circularly polarized light
[AD-A290525] p 2716 N95-29493
The 14th International Conference on Atomic Physics
[AD-A290726] p 2693 N95-29521
Recent progress in the study of the kinetics of sol-gel SiO2 synthesis reactions
[AD-A290570] p 2544 N95-29551
Theories of the nonlinear optical properties of composite media: Applications to phthalocyanine dyes
[AD-A290640] p 2700 N95-29560
Electronic states in Cd(1-x)Zn(x)Te/CdTe strained layer. coupled double quantum wells and their photoluminescence
[DE95-006806] p 2716 N95-29814
Ocean Optics XII
[AD-A286734] p 2702 N95-29910
A bibliography, with abstracts and annotations, of publications on and related to underwater acoustic fluctuations
[AD-A291342] p 2685 N95-29945
Sensor protection portion of the development of nonlinear optical materials and processes for laser hardening of sensors
[AD-A291200] p 2702 N95-29973
Ceramics derived from organo-metallic precursors
[AD-A291434] p 2547 N95-30071
Physical modeling and design of semiconductor heterostructures for optical and electronical applications
p 2682 N95-30232

OPTICAL PUMPING
Development of continuous visible chemical laser amplifiers and oscillators from the Na3-X(Cl, Br, I) reactions and their analogs and energy transfer pumping from efficiently produced metastable states
[AD-A290999] p 2586 N95-29514
Coherent soft x-ray generation using a powerful subpicosecond laser p 2587 N95-29689

OPTICAL RADAR
Analysis of measurements for solid state laser remote lidar system
[NASA-CR-196640] p 2585 N95-29247
Path resolved optical sensing of atmospheric winds utilizing speckle-turbulence interaction and pseudorandum code modulation
[AD-A290800] p 2621 N95-29497
A study of boundary layer aerosol and wind profiles using incoherent Doppler lidar p 2622 N95-29697

OPTICAL RESONANCE
Self-Induced Transparency in photonic band structures: Gap solitons near absorption resonances
[AD-A292187] p 2718 N95-28927

OPTICAL WAVEGUIDES
Low threshold all-optical crossbar switch on GaAs-GaAlAs channel waveguide arrays
[AD-A292483] p 2712 N95-28862
Numerical modeling of opto-electronic integrated circuits
[AD-A292096] p 2563 N95-29239
Pulsed laser deposition of thin film material for nonlinear waveguides
[AD-A290789] p 2544 N95-29484
Modal analysis of straight and curved integrated optical waveguides: An integral equation approach
[PB95-197265] p 2702 N95-30054
A conceptual thermal design study of an electronically scanned thinned array radiometer
[NASA-TM-110173] p 2509 N95-30316

OPTICS
N4 processor
[AD-A292571] p 2642 N95-28976

OPTIMAL CONTROL
Optimal control of molecular motion
[AD-A291919] p 2691 N95-28944
Process optimization through discovery and integration of materials and processing properties. phase 1
[AD-A292576] p 2662 N95-28978
Computational methods for the simulation of non-Newtonian flows
[AD-A290355] p 2570 N95-29069
Closed loop control of guided missiles using neural networks p 2663 N95-29241
Modeling and control of rotating stall in high speed multi-stage axial compressors p 2500 N95-29244
Analytical investigations in aircraft and spacecraft trajectory optimization and optimal guidance
[NASA-CR-4672] p 2504 N95-29339
Neural network exploration using optional experiment design
[AD-A290058] p 2663 N95-29479
Periodic and nonsmooth optimal control problems governed by partial differential equations
p 2664 N95-29544
Linear matrix inequalities for the problem of absolute stability of control systems p 2501 N95-29680
H(sub 2) almost disturbance decoupling problem with internal stability
[PB95-206942] p 2667 N95-30168
Learning control in linear and nonlinear systems
p 2667 N95-30238

OPTIMIZATION
A technique for optimizing grid blocks
p 2485 N95-28769
Interactive high quality grid generation
p 2486 N95-28774
An efficiency study of the simultaneous analysis and design of structures
[NASA-TM-110168] p 2495 N95-28820
Users manual for the improved NASA Lewis ice accretion code LEWICE 1.6
[NASA-CR-198355] p 2492 N95-29132
Research in graph algorithms and combinatorial optimization
[AD-A292630] p 2648 N95-29297
New methods for nonlinear optimization
[AD-A290522] p 2670 N95-29385
A genetic algorithm approach to scheduling resources for a space power system p 2511 N95-29784
Neural networks for combinatorial optimization
[PB95-206843] p 2667 N95-30222
Optimization of 100-meter Green Bank Telescope
[NASA-CR-198868] p 2731 N95-30230

OPTOELECTRONIC DEVICES
Epitaxial growth and characterization of Si(1-x)Ge(x) materials and devices
[AD-A292528] p 2712 N95-28874
Commercial photorefractive device using nonstoichiometric 3-5 semiconductors
[AD-A292494] p 2713 N95-28933
OEIC ultra. A new approach to OEIC CAD
[AD-A290349] p 2646 N95-29066
Testbed for precision characterization of spatial light modulators and optical processors
[AD-A290484] p 2699 N95-29148
Photonic band structures for optoelectronics
[AD-A291154] p 2718 N95-30298

OPTOGALVANIC SPECTROSCOPY
Development of Laser Optogalvanic Spectroscopy as a probe of alkali atoms in an MHD environment
[DE95-006481] p 2531 N95-28916

ORBITAL ELEMENTS
Applications of pulsar timing p 2734 N95-29675

ORBITAL MECHANICS
An investigation into the existence of asteroids at Saturn's triangular Lagrangian points
p 2727 N95-29648

ORGANIC COMPOUNDS
Zero Discharge Organic Coatings: Powder paint. UV curable paint. E-coat
[AD-A292180] p 2540 N95-28925
Characterization of excited state oxygen-organic molecule complexes
[AD-A290548] p 2692 N95-29092
Modeling joint effects of mixtures of chemicals on microorganisms using quantitative structure activity relationship techniques, phase 3
[AD-A290153] p 2632 N95-29320

ORGANIC LIQUIDS
Orthobaric densities and molar volumes of liquids. Glycol ethers (cellosolves and carbitols, etc.)
[ESDU-95005] p 2530 N95-28703
Viscosity of liquids: Aliphatic and cyclic ketones
[ESDU-94025] p 2530 N95-28712
Thermal conductivity of liquid halogenated aliphatic hydrocarbons. Part 3: Halogenated higher hydrocarbons (C3 to C16)
[ESDU-94023-PT-3] p 2512 N95-29900

ORGANIC MATERIALS
Conference proceedings: IEEE Nonlinear Optics, Materials, Fundamentals, and Applications
[AD-A292438] p 2698 N95-28997

ORGANIC WASTES (FUEL CONVERSION)
The TEES process cleans waste and produces energy
[DE95-007799] p 2602 N95-29463

ORGANISMS
Automated analysis of zooplankton size and taxonomic composition using the video plankton recorder
[AD-A289725] p 2631 N95-28685

ORGANIZATIONS
An overview of the Software Engineering Laboratory
[NASA-CR-189410] p 2644 N95-28714

ORGANOMETALLIC COMPOUNDS
Synthesis and characterization of (Me3SiCH2)3M(dot)E(SiMe3)3 (M = Ga, E = P or As; M = In, E = P). X-ray crystal structures of (Me3SiCH2)3Ga(dot)P(SiMe3)3 and (Me3SiCH2)3In(dot)P(SiMe3)3
[AD-A291907] p 2715 N95-29444
Recent progress in the study of the kinetics of sol-gel SiO2 synthesis reactions
[AD-A290570] p 2544 N95-29551
Ceramics derived from organo-metallic precursors
[AD-A291434] p 2547 N95-30071

ORTHOGONALITY
Some new saturated two-level designs
[AD-A292627] p 2670 N95-29296
Grid orthogonality effects on predicted turbine midspan heat transfer and performance
[NASA-TM-106931] p 2574 N95-29371
ORTHOTROPIC SHELLS
Compressive behavior of thick composite shells: Benchmark solutions for loss of stability and hygroscopic effects p 2595 N95-29424
OSCILLATING FLOW
Interactions of spanwise and chordwise vorticity associated with three-dimensional dynamic stall over an oscillating wing
[AD-A290546] p 2487 N95-29091
Vortex element analysis of selected time-dependent flows
[AD-A289944] p 2573 N95-29271
OSCILLATIONS
Interaction of acoustic oscillations with magnetic flux tubes in the solar photosphere
[PB95-201810] p 2739 N95-30199
OSCILLATORS
An investigation of the channel crosstalk in optical heterodyne controlled phased array radars
[AD-A292028] p 2554 N95-29186
Inhibition of mode competition in free-electron laser oscillators p 2586 N95-29336
Development of continuous visible chemical laser amplifiers and oscillators from the Na3-X(Cl, Br, I) reactions and their analogs and energy transfer pumping from efficiently produced metastable states
[AD-A290999] p 2586 N95-29514
OSCILLOSCOPES
HBCU/MI instrumentation for the Pulsed Power Plasma Sciences Laboratory at the University of New Mexico, FY92-93
[AD-A292444] p 2703 N95-29003
OSMIUM
Effects of space exposure on metals flown on the Long Duration Exposure Facility
[NASA-CR-4662] p 2512 N95-30225
OUTGASSING
Experimental study on scaling law of outgassing rate with a pumping parameter
[AD-B191999L] p 2709 N95-29801
OVER-THE-HORIZON RADAR
Long range aircraft detection using high-frequency surface-wave radar
[AD-A290148] p 2555 N95-29313
OXIDATION
Corrosion investigation of multilayered ceramics and experimental nickel alloys in SCWO process environments
[DE95-008666] p 2540 N95-28960
Compact substrate heater for use in an oxidizing atmosphere
[AD-A290860] p 2502 N95-29522
Inorganic halogen oxidizers
[AD-A290747] p 2533 N95-29581
Innovative processing of composites for ultra-high temperature applications, book 1
[AD-A290889] p 2527 N95-29842
Inorganic halogen oxidizers
[AD-A291201] p 2702 N95-29974
OXIDATION RESISTANCE
The nucleation of crystalline films from vapor phase reactants
[AD-A291122] p 2716 N95-29767
OXIDATION-REDUCTION REACTIONS
The redox chemistry of some peroxo and superoxo metal ion complexes
[AD-A290761] p 2532 N95-29483
OXIDE FILMS
Materials science and fabrication of YBCO-SrTi(1-x)Nb(x)O3-YBCO device structures
[AD-A292527] p 2712 N95-28815
Electrical characteristics of barium strontium titanate-oxide composite films
[AD-A289991] p 2541 N95-29135
OXIDES
Fabrication and characterization of barium strontium titanate and non-ferroelectric oxide composites
[AD-A289994] p 2523 N95-29136
Self-stressing structures for wafer-level oxide breakdown to 200 MHz
[DE95-006818] p 2714 N95-29157
Solid Oxide Fuel Cell commercialization in the United States
[DE95-008210] p 2607 N95-30278
Advances in tubular solid oxide fuel cell technology
[DE95-008361] p 2607 N95-30281
OXIDIZERS
Inorganic halogen oxidizers
[AD-A290747] p 2533 N95-29581
ANSYS duplicate finite-element checker routine
[NASA-TM-108492] p 2672 N95-29824
Inorganic halogen oxidizers
[AD-A291201] p 2702 N95-29974
OXYGEN
Computational investigation of the stabilities of some N, O, F ions
[AD-A292305] p 2691 N95-28868
Formation of striped surface phases by short-range forces
[AD-A279962] p 2531 N95-28945
Characterization of excited state oxygen-organic molecule complexes
[AD-A290548] p 2692 N95-29092
Fluxes and relative abundances of light cosmic ray nuclei at energies above 40 GeV/n p 2739 N95-29531
Fundamental studies of oxygen rings and other high energy density molecular systems
[AD-A290875] p 2693 N95-29865
Engineering development program of a closed aluminum-oxygen semi-cell system for an unmanned underwater vehicle: An update p 2606 N95-30266
OXYGEN ATOMS
Boronization study for application to large helical device
[AD-B191996L] p 2709 N95-29808
OXYGEN CONSUMPTION
CO2-O2 interactions in extension of tolerance to acute hypoxia
[NASA-CR-198575] p 2635 N95-29158
Adaptations to three weeks of aerobic/anaerobic training in west coast U.S: Navy Sea-Air-Land personnel (SEAL's)
[AD-A291500] p 2637 N95-29846
OXYGEN IONS
A Monte Carlo simulation of Coulomb collisions and wave-particle interactions in space plasma at high latitudes p 2704 N95-29205
Thermal N(+) in the inner magnetosphere p 2614 N95-29590
OXYGEN SUPPLY EQUIPMENT
SPE(R)-OBOGS: On-board oxygen generating sustem p 2606 N95-30267
OXYGENATION
Research on PGI2 and TXA2 effects at times of hyperbaric oxygenation of domestic rabbits with acute cerebral ischemia reirrigation damage
[AD-A289606] p 2632 N95-29263
OXYNITRIDES
The nucleation of crystalline films from vapor phase reactants
[AD-A291122] p 2716 N95-29767
OZONE
Compendium of NASA data base for the global tropospheric experiment's Transport and Atmospheric Chemistry Near the Equator-Atlantic (TRACE-A)
[NASA-TM-110151] p 2608 N95-28717
A model analysis of the spatial distribution and temporal trends of nitrous oxide sources and sinks p 2609 N95-29804
OZONE DEPLETION
In situ measurements of ClO and implications for the chemistry of inorganic chlorine in the lower stratosphere p 2618 N95-29830

P

P WAVES
Inclusive hadronic production of the B(sub c) meson via heavy quark fragmentation
[DE95-008739] p 2695 N95-30191
P-TYPE SEMICONDUCTORS
Nitride semiconductors for ultraviolet detection
[AD-A289546] p 2712 N95-28910
Composite material studies for low temperature thermionic emission
[AD-A292159] p 2523 N95-29124
Investigation of a normal incident high performance P-type strained layer In(0.3)Ga(0.7)As/In(0.52)Al(0.48)As quantum well infrared photodetector
[AD-A290946] p 2716 N95-29785
PACIFIC OCEAN
Tidal constituent database: West coast of the United States and eastern North Pacific Ocean
[AD-A292224] p 2630 N95-29198
A study of dynamics in the tropical Pacific using satellite data p 2630 N95-29520
Radiative cooling profiles calculated from ECMWF analyses and ISCCP C1 data, and their application to determination of distributions of apparent convective heating in the equatorial Pacific p 2625 N95-29805
The effects of clouds as a feedback mechanism on the Earth's climate in the tropical Pacific p 2611 N95-30300
PACKET SWITCHING
Alternative packet switch architectures for a 30/20 GHz FDMA/TDMA geostationary communication satellite network
[NASA-CR-195470] p 2506 N95-30090
PACKET TRANSMISSION
Communication protocols in multi-hop radio networks p 2553 N95-29106
Scheduling algorithms for mobile packet radio networks p 2558 N95-29707
PAINTS
Zero Discharge Organic Coatings: Powder paint. UV curable paint. E-coat
[AD-A292180] p 2540 N95-28925
Thermoreactive aircraft coatings (TRAC) program
[AD-A292054] p 2542 N95-29314
Probability of detection of defects in coatings with electronic shearography
[NASA-TM-108493] p 2524 N95-29374
PALEOMAGNETISM
Large scale fluctuations of the geomagnetic field p 2617 N95-29796
PANEL METHOD (FLUID DYNAMICS)
Cooperative solutions coupling a geometry engine and adaptive solver codes p 2484 N95-28761
A numerical method for modelling wings with sharp edges maneuvering at high angles of attack p 2496 N95-29122
Estimation of aerodynamic load distributions on the F/A-18 aircraft using a CFD panel code
[DSTO-TR-0147] p 2498 N95-29445
PANELS
Mechanical characterization of two thermoplastic composites fabricated by automated tow placement p 2515 N95-28834
Manufacturing scale-up of composite fuselage crown panels p 2515 N95-28835
Design and evaluation of a foam-filled hat-stiffened panel concept for aircraft primary structural applications p 2499 N95-28841
A study of structurally efficient graphite-thermoplastic trapezoidal-corrugation sandwich and semi-sandwich panels p 2516 N95-28842
A weight-efficient design strategy for cutouts in composite transport structures p 2516 N95-28843
ISPAN (Interactive Stiffened Panel Analysis): A tool for quick concept evaluation and design trade studies p 2517 N95-28846
Analysis of stress concentration in the Dutton groove regions of the Super Lightweight External Tank
[NASA-TM-108490] p 2597 N95-30328
PARABOLIC DIFFERENTIAL EQUATIONS
Stochastic hyperbolic and parabolic partial differential equations
[AD-A290372] p 2669 N95-29229
PARALLEL COMPUTERS
New methods for nonlinear optimization
[AD-A290522] p 2670 N95-29385
The mesh synchronous processor MeshSP (trademark)
[AD-A289875] p 2659 N95-29420
Load-balancing algorithms for the parallel community climate model
[DE95-008795] p 2610 N95-30176
Parallel rendering
[NASA-CR-195080] p 2655 N95-30306
PARALLEL PROCESSING (COMPUTERS)
The scotch parallel storage systems
[AD-A292243] p 2658 N95-28879
Wax: A wide-area computation system
[AD-A292247] p 2658 N95-28884
Application of parallel processing technology in complex helicopter analysis. Phase 1
[NASA-CR-197850] p 2496 N95-28928
Glenda software design
[AD-A292537] p 2646 N95-28968
A study of fluid problems requiring a direct particle simulation
[AD-A290212] p 2658 N95-29074
Solving linear programs using distributed parallel computing
[AD-A290221] p 2658 N95-29079
Porting a vector library: A comparison of MPI, paris, CMMD and PVM (or, 'I'll never have to port CVL again')
[AD-A290231] p 2647 N95-29147
Efficient compilation of high-level data parallel algorithms
[AD-A290362] p 2659 N95-29225
Implicit schemes and parallel computing in unstructured grid CFD
[NASA-CR-195071] p 2671 N95-29451
Scalable software tools for adaptive scientific computation
[AD-A290446] p 2650 N95-29480

Load balancing for the parallel adaptive solution of partial differential equations
[AD-A290450] p 2671 N95-29488
Parallel adaptive techniques for transient partial differential equations
[AD-A290460] p 2674 N95-29490
Parallelization of the 2D Roe Scheme on the Intel Paragon
[AD-A290690] p 2659 N95-29760
Experimental cosmology using fast parallel N-body methods p 2734 N95-29775
The study of non-Newtonian contraction flows with a parallel finite element method p 2576 N95-29778
DPARTS. A dynamic parallel adaptive multiprocess or real-time scheduler
[AD-A291160] p 2659 N95-29915
Computational results for parallel unstructured mesh computations
[DE95-005856] p 2659 N95-29985
Huge data sets and the frontiers of computational feasibility
[AD-A291384] p 2653 N95-30063
Parallel continuation-based global optimization for molecular conformation and protein folding
[DE95-005860] p 2633 N95-30114
Distributed multitasking ITS with PVM
[DE95-006821] p 2660 N95-30116
Time accurate application of the MacCormack 2-4 scheme on massively parallel computers p 2661 N95-30150
Computational aeroacoustics on massively parallel computers p 2661 N95-30156
Requirements for a portable parallel I/O library for scientific computation
[DE95-009383] p 2660 N95-30192
Massively parallel fast elliptic equation solver for three dimensional hydrodynamics and relativity
[DE95-009385] p 2660 N95-30193
Parallel adaptive finite element: Software for semiconductor device simulation
[AD-A291149] p 2661 N95-30295
Parallel rendering
[NASA-CR-195080] p 2655 N95-30306

PARALLEL PROGRAMMING
Glenda software design
[AD-A292537] p 2646 N95-28968
Ropes: Support for collective opertions among distributed threads
[NASA-CR-198157] p 2649 N95-29404
On the utility of threads for data parallel programming
[NASA-CR-198155] p 2649 N95-29455
High-level parallel programming tools for finite element analysis
[AD-A290566] p 2659 N95-29566
Parallelization of the 2D Roe Scheme on the Intel Paragon
[AD-A290690] p 2659 N95-29760

PARALLELEPIPEDS
Analyzing the stability of floating ice floes
[AD-A292149] p 2629 N95-29160

PARAMETER IDENTIFICATION
An analytic modeling and system identification study of helicopter dynamics p 2498 N95-29787
Calculation of shielding parameters
[DE95-608735] p 2694 N95-29886

PARAMETERIZATION
Parametric design and gridding through relational geometry p 2486 N95-28771
Trajectory mapping (TM): A new non-metric scaling technique
[AD-A290036] p 2670 N95-29440
Development of an improved cloud model for use in cumulus parameterization p 2624 N95-29800
Parameterized spectral distributions for meson production in proton-proton collisions
[NASA-TM-4675] p 2696 N95-30337

PARITY
Oblivious decision trees and abstract cases
[AD-A292577] p 2664 N95-29574

PARTIAL DIFFERENTIAL EQUATIONS
Stochastic hyperbolic and parabolic partial differential equations
[AD-A290372] p 2669 N95-29229
The large discretization step method for time-dependent partial differential equations
[NASA-CR-195068] p 2670 N95-29403
Load balancing for the parallel adaptive solution of partial differential equations
[AD-A290450] p 2671 N95-29488
Parallel adaptive techniques for transient partial differential equations
[AD-A290460] p 2674 N95-29490
Periodic and nonsmooth optimal control problems governed by partial differential equations p 2664 N95-29544
Experimental confirmation of a PDE-based approach to design of feedback controls
[NASA-CR-198167] p 2672 N95-30086

PARTICLE ACCELERATOR TARGETS
Measurements of (Delta)(sigma)(sub L)(pp) and (Delta)(sigma)(sub L)((bar p)p) at 200 GeV/c
[DE95-005837] p 2695 N95-30186

PARTICLE ACCELERATORS
Lattice/beam dynamics working group
[DE95-006774] p 2696 N95-30021
Sea and gluon spin structure function measurements at RHIC
[DE95-005823] p 2695 N95-30185

PARTICLE COLLISIONS
Collisionless driven magnetic reconnection
[AD-B178946L] p 2709 N95-29810

PARTICLE DECAY
Photoproduction of hybrid mesons from CEBAF to HERA
[PB95-196218] p 2691 N95-28913

PARTICLE EMISSION
Effective emission and ionization rate coefficients of atomic carbons in plasmas
[AD-B175932L] p 2707 N95-29740

PARTICLE ENERGY
Theoretical study of cylindrical energy analyzers for MeV range heavy ion beam probes
[AD-B17200L] p 2707 N95-29745
Collisionless driven magnetic reconnection
[AD-B178946L] p 2709 N95-29810

PARTICLE IMAGE VELOCIMETRY
PIV investigation of compressibility effects on dynamic stall p 2487 N95-29102

PARTICLE IN CELL TECHNIQUE
On the utility of threads for data parallel programming
[NASA-CR-198155] p 2649 N95-29455

PARTICLE INTERACTIONS
Numerical studies of the stratospheric aerosol layer under background and perturbed conditions p 2615 N95-29666
Measurements of (Delta)(sigma)(sub L)(pp) and (Delta)(sigma)(sub L)((bar p)p) at 200 GeV/c
[DE95-005837] p 2695 N95-30186

PARTICLE PRODUCTION
Photoproduction of hybrid mesons from CEBAF to HERA
[PB95-196218] p 2691 N95-28913
From the (psi) to charmed mesons
[DE95-006564] p 2693 N95-29583
Inclusive hadronic production of the B(sub c) meson via heavy quark fragmentation
[DE95-008739] p 2695 N95-30191

PARTICLE SIZE DISTRIBUTION
Three problems in fluid dynamics
[AD-A290481] p 2573 N95-29324
A study of precipitation using dual-frequency and interferometric Doppler radars p 2627 N95-29877

PARTICLE TRAJECTORIES
Simulated imaging properties of a series of magnetic electron lenses
[NASA-CR-195474] p 2564 N95-29406

PARTITIONS (MATHEMATICS)
Spectral estimates for positive Rockland operators
[PB95-206751] p 2673 N95-30204

PASCAL (PROGRAMMING LANGUAGE)
ADA in introductory courses
[AD-A292219] p 2648 N95-29285

PASCHEN SERIES
Investigation of the Paschen curve of nitrogen via the application of nanosecond pulsed electromagnetic radiation
[AD-A290129] p 2586 N95-29425

PASSENGER AIRCRAFT
Design, analysis and control of large transports so that control of engine thrust can be used as a back-up of the primary flight controls
[NASA-CR-198958] p 2501 N95-30254

PASSIVITY
Chemically induced passivity of aluminum alloys and Al-based metal matrix composites
[AD-A290778] p 2528 N95-29923

PATENTS
US photovoltaic patents: 1991-1993
[DE95-004051] p 2603 N95-30017

PATIENTS
Flying waivers for history of angioplasty and myocardial infraction
[AD-A292505] p 2635 N95-29161
Experience in helicopter aeroevacuation in the community of Madrid, Spain p 2677 N95-29611
Re-engineering support to the patient movement process p 2677 N95-29615
Care in the air: A system analysis of clinical outcomes in aeromedical evacuation p 2642 N95-29626
Effect of hypoxia on arterial blood gases in subjects with lung dysfunction p 2638 N95-29627

PATTERN RECOGNITION
Electromagnetic scattering by magnetic spheres: Theory and algorithms
[AD-A289798] p 2551 N95-28699
Automated optical target recognition
[AD-A292397] p 2697 N95-28798
Multilayer piecewise linear networks. Revision 1
[AD-A289885] p 2658 N95-28955
High performance hardware and software for pattern recognition and image processing
[AD-A292307] p 2646 N95-28964
Wavelets in signal detection and identification comparative signal processing technology evaluation
[AD-A291952] p 2552 N95-28984
Feature extraction from digital communications signals using wavelet transforms
[AD-A292655] p 2556 N95-29386
Georgetown Institute for Cognitive and Computational Sciences
[AD-A289775] p 2639 N95-29458
Object oriented segmentation of images
[AD-A290792] p 2671 N95-29485
Randomized inquiries about shape: An application to handwritten digit recognition
[AD-A290812] p 2675 N95-29634
Intensity optical correlation through optical differentiation preprocessing
[AD-A291020] p 2701 N95-29661
Neural network construction using evolutionary search
[AD-A290862] p 2665 N95-29831
Hybrid pyramid/neural network vision system
[AD-A290565] p 2665 N95-29863
Electrochemical impedance pattern recognition for detection of hidden chemical corrosion on aircraft components, phase 1
[AD-A291345] p 2593 N95-29946
Probabilistic modeling and statistical inference for random fields and space-time processes
[AD-A289956] p 2672 N95-30029
Distortion-invariant optical pattern recognition by correlative matrix feature criterion
[AD-A291389] p 2703 N95-30064
Boyer-moore type algorithm for regular expression pattern matching
[PB95-198131] p 2654 N95-30107

PAVEMENTS
Evaluation of retro-reflective beads in airport pavement markings
[AD-A291065] p 2502 N95-29967

PAYLOAD CONTROL
Methods and components for optical contention resolution in high speed networks
[AD-A292331] p 2697 N95-28795

PAYLOADS
A procedure for accessing digital satellites containing amateur payloads
[AD-A289748] p 2506 N95-28688
Methods and components for optical contention resolution in high speed networks
[AD-A292331] p 2697 N95-28795

PEELING
A study of blister tests for film adhesion measurement and fracture efficiency of tests for adhesive bonds p 2545 N95-29799

PENDULUMS
Hybrid fuzzy logic control to stabilize an inverted pendulum from arbitrary initial conditions
[AD-A292441] p 2681 N95-29000

PENETRANTS
Molecular level characterization by NMR of the transport and structural environment of gases and condensed penetrante
[AD-A290831] p 2693 N95-29723

PENETRATION
Ballistic penetration phenomenology of high symmetry single crystals
[AD-A292476] p 2713 N95-29013
Characterizing and modeling penetration of ceramic armor
[AD-A292588] p 2542 N95-29288
Finite element technology for penetration problems
[AD-A290644] p 2671 N95-29516
Robust algorithms for penetration mechanics problems
[AD-A290650] p 2650 N95-29517
High velocity impact and penetration of thick composite laminates
[AD-A290642] p 2526 N95-29561
Penetration of semi-infinite, bi-element targets by long rod penetrators
[AD-A291176] p 2596 N95-29929

PENETROMETERS
Development of an artificial neural network for real-time classification of cone penetrometer strain gauge data
[AD-A290719] p 2664 N95-29499

PENUMBRAS
Method for the calculation of spacecraft umbra and penumbra shadow terminator points
[NASA-TP-3547] p 2671 N95-29446
Total solar eclipse of 1997 March 9
[NASA-RP-1173] p 2731 N95-30004
PERCOLATION
Theories of the nonlinear optical properties of composite media: Applications to phthalocyanine dyes
[AD-A290640] p 2700 N95-29560
PERFORATED PLATES
Effects of cutouts on the behavior of symmetric composite laminates subjected to bending and twisting loads p 2517 N95-28844
A global/local analysis method for treating details in structural design p 2517 N95-28848
PERFORMANCE PREDICTION
Improving problem-solving and decision-making skills under stress: Prediction and training
[AD-A292104] p 2638 N95-28918
Electromagnetic antenna modeling (EAM) system
[AD-A292194] p 2552 N95-28986
Arcing mitigation and predictions for high voltage solar arrays
[AD-A292227] p 2602 N95-29200
Effects of the cooling system parameters on heat transfer and performance of the PAFC stack during transient operation
[NASA-CR-197654] p 2572 N95-29249
Spacecraft attitude control system performance using pulse-width pulse-frequency modulated thrusters
[AD-A291803] p 2508 N95-29410
Automated reasoning about classical mechanics
[AD-A290052] p 2663 N95-29477
AGARD flight test techniques series. Volume 13: Reliability and maintainability
[AGARD-AG-300-VOL-13] p 2498 N95-29503
Modeling spatio-temporal databases to measure the performance of the GPS satellite constellation p 2494 N95-29596
Transonic, supersonic and hypersonic wind-tunnel tests on aerodynamic characteristics of reentry body with blunted cone configuration
[ISAS-658] p 2490 N95-29640
A study of boundary layer aerosol and wind profiles using incoherent Doppler lidar p 2622 N95-29697
Parallelization of the 2D Roe Scheme on the Intel Paragon
[AD-A290690] p 2659 N95-29760
Performance analysis of a GPS Interferometric attitude determination system for a gravity gradient stabilized spacecraft
[NASA-CR-188372] p 2508 N95-30036
PREDICHAT: First order performance calculations of windturbine rotors using the method of the acceleration potential
[PB95-206454] p 2603 N95-30200
PERFORMANCE TESTS
Receiver design, performance analysis, and evaluation for space-borne laser altimeters and space-to-space laser ranging systems
[NASA-CR-198655] p 2584 N95-28808
Influence of tooth profile modification on spur gear dynamic tooth strain
[NASA-TM-106952] p 2589 N95-29112
Improved interception capability through the use of transform domain processing
[AD-A292231] p 2554 N95-29203
Fire hardening assessment (FHA) technology for composite systems
[AD-A289964] p 2523 N95-29277
Deposition and surface treatment with intense pulsed ion beams
[DE95-007885] p 2543 N95-29465
UHF Low Density Radio Communications Link (LDRCL) Operational Test and Evaluation (OT&E) integration and OT&E operational final test report
[AD-A291447] p 2558 N95-29769
Effects of impurities released from high Z test limiter on plasma performance in TEXTOR
[AD-B191995L] p 2709 N95-29803
An operational comparison of the CH-46E and HH-60H as Navy combat support helicopter replacement options using the Simulated Mobility Modeling and Analysis Toolbox (SMMAT)
[AD-A288494] p 2498 N95-29911
Penetration of semi-infinite, bi-element targets by long rod penetrators
[AD-A291176] p 2596 N95-29929
Performance evaluation of bolt-cutter system on first Taurus launch
[AD-A291237] p 2504 N95-29992
Test results of a 20 GHz, low noise downconverter for USAT applications
[NASA-TM-106892] p 2508 N95-30011
Offshore next generation weather radar (NEXRAD) test and evaluation master plan (TEMP)
[AD-A291435] p 2559 N95-30072
Performance evaluation of ATM cell scheduling policies using stochastic petri nets
[PB95-197158] p 2559 N95-30096
Development of LaRC (TM): IA thermoplastic polyimide coated aerospace wiring
[NASA-CR-195048] p 2548 N95-30252
Hermetically sealed aluminum electrolytic capacitor p 2568 N95-30268
High energy density electrolytic capacitor p 2568 N95-30271
Advances in tubular solid oxide fuel cell technology
[DE95-008361] p 2607 N95-30281
PERIODIC VARIATIONS
WinCD: Complex demodulation time-series analysis for windows
[AD-A291550] p 2645 N95-28934
Forecast of Atlantic seasonal hurricane activity for 1995 p 2620 N95-29254
Simultaneous UV and optical study of O star winds and UV and optical covariability of O star winds
[NASA-CR-189424] p 2726 N95-29370
Tidal and lunar data for Point Mugu, San Nicolas Island, and the Barking Sands area during 1995
[AD-A289877] p 2733 N95-29599
PERMANENT MAGNETS
Studies directed toward new and improved permanent magnet materials
[AD-A290749] p 2681 N95-29481
Development of an intense negative hydrogen ion source with a wide-range of external magnetic filter field
[AD-B195514L] p 2705 N95-29567
Permanent magnet torque/force transfer apparatus
[AD-D017325] p 2682 N95-30051
PERMEABILITY
Molecular level characterization by NMR of the transport and structural environment of gases and condensed penetrante
[AD-A290831] p 2693 N95-29723
Dielectric property measurements in the Electromagnetic Properties Measurement Laboratory
[NASA-TM-110147] p 2560 N95-30336
PERMEATING
Prediction of hydrogen entry and permeation in metals and alloys
[AD-A292047] p 2536 N95-29298
PERMITTIVITY
Electrical characteristics of barium strontium titanate-oxide composite films
[AD-A289991] p 2541 N95-29135
The mm-wave resonant methods for the detection of corrosion, phase 1
[AD-A291315] p 2593 N95-29941
Dielectric property measurements in the Electromagnetic Properties Measurement Laboratory
[NASA-TM-110147] p 2560 N95-30336
PEROVSKITES
High T(sub c) superconductor/ferroelectric heterostructures
[AD-A291016] p 2716 N95-29658
A Pr-141 Moessbauer study of praseodymium com pounds
[PB95-192449] p 2535 N95-30282
PERSONAL COMPUTERS
Digital video technology, today and tomorrow
[DE95-007689] p 2556 N95-29462
PERSONNEL
Effects of chromium picolinate on body composition in a remedial conditioning program
[AD-A292079] p 2636 N95-29238
New methods for nonlinear optimization
[AD-A290522] p 2670 N95-29385
Adaptations to three weeks of aerobic/anaerobic training in west coast U.S: Navy Sea-Air-Land personnel (SEAL's)
[AD-A291500] p 2637 N95-29846
Calculation of shielding parameters
[DE95-608735] p 2694 N95-29886
Sleep during SEAL Delivery Vehicle (SDV)/Dry dock shelter exercises analyzed by a graphic approach
[AD-A290916] p 2637 N95-30083
PERSONNEL DEVELOPMENT
An analysis of anthropometric differences among occupational groups in the US Army
[AD-A292326] p 2640 N95-28794
PERSONNEL MANAGEMENT
An announcement by Dan Goldin
[NASA-TM-110739] p 2720 N95-29171
PERSONNEL SELECTION
Astronaut selection (NASA-MIPR)
[AD-A292512] p 2638 N95-29162
PERTURBATION
Navier-Stokes solution of wing wake structure and its perturbation p 2488 N95-29121
Sensitivity of the simulated global climate to perturbations in low cloud microphysical properties p 2620 N95-29206
Quantum fluctuations and semiclassical gravity theory p 2719 N95-29527
The effect of climate perturbations on extratropical cyclogenesis along the east coast of North America p 2621 N95-29595
Experiments on nonlinear wave-particle interactions p 2695 N95-30302
PETRI NETS
Proceedings of the 33d SICE (the Society of Instrument and Control Engineers) Annual Conference, part 1
[DE95-758947] p 2632 N95-28947
Performance evaluation of ATM cell scheduling policies using stochastic petri nets
[PB95-197158] p 2559 N95-30096
Efficient solution of a class of infinite stochastic petri nets: Theory and applications
[PB95-197166] p 2673 N95-30097
PH
Demonstration of a stabilized alumina/ethanol colloidal dispersion technique for seeding high temperature air flows
[NASA-TM-106945] p 2582 N95-29113
Cage-like precursor formation from extensive cyclization in sol-gel inorganic condensation polymerization
[AD-A290589] p 2544 N95-29554
PHASE CHANGE MATERIALS
Three problems in fluid dynamics
[AD-A290481] p 2573 N95-29324
PHASE DIAGRAMS
InTlSb as a long-wave infrared (LWIR) material: Defects and transportation properties
[AD-A291218] p 2702 N95-29978
PHASE LOCKED SYSTEMS
Experiments on nonlinear wave-particle interactions p 2695 N95-30302
PHASE MODULATION
An ultra-high speed incoherent-to-coherent converter for optical computing
[AD-A292658] p 2700 N95-29412
PHASE SEPARATION (MATERIALS)
Macrosegregation and nucleation in undercooled Pb-Sn alloys
[NASA-TM-102023-REV] p 2535 N95-28701
The morphology of blends of linear and branched polyethylenes in solid state by SANS
[DE95-008675] p 2535 N95-30113
PHASE SHIFT
Interferometric measurement with squeezed light
[AD-A292402] p 2697 N95-28799
Testbed for precision characterization of spatial light modulators and optical processors
[AD-A290484] p 2699 N95-29148
The effect of bright light and LEET on sleep after a 10-hour phase delay
[AD-A291264] p 2637 N95-29995
PHASE SHIFT KEYING
Feature extraction from digital communications signals using wavelet transforms
[AD-A292655] p 2556 N95-29386
PHASE TRANSFORMATIONS
Consideration of microstructural changes in the study of adiabatic shear bands
[AD-A290398] p 2715 N95-29234
Austenite to ferrite transformation kinetics during continuous cooling
[DE95-008582] p 2537 N95-29869
Decomposition of hypo-eutectoid iron carbon austenites
[PB95-196945] p 2538 N95-30287
PHASE VELOCITY
A study of dynamics in the tropical Pacific using satellite data p 2630 N95-29520
PHASED ARRAYS
Low threshold all-optical crossbar switch on GaAs-GaAlAs channel waveguide arrays
[AD-A292483] p 2712 N95-28862
An investigation of the channel crosstalk in optical heterodyne controlled phased array radars
[AD-A292028] p 2554 N95-29186
Fabrication and characterization of BSTO and nonferroelectric oxide composites for use in phased array antennas and other electronic devices
[AD-A290070] p 2524 N95-29329
Adaptive block sequential detection of abrupt signal changes
[AD-A290456] p 2557 N95-29489
PHENANTHRENE
Surfactant-enhanced in situ biodegradation of strongly sorbing organic substances in soil environments
[AD-A290253] p 2512 N95-29168

PHENOMENOLOGY
Ballistic penetration phenomenology of high symmetry single crystals
[AD-A292476] p 2713 N95-29013
PHENYLS
Super hydrides
[AD-A290594] p 2533 N95-29556
PHONONS
Transport phenomena and noise in real quantum wires
[AD-A290493] p 2714 N95-29152
PHOSPHAZENE
The synthesis of liquid crystalline phophazenes containing chiral mesogens
[AD-A291911] p 2543 N95-29358
PHOSPHORIC ACID
Effects of cooling system parameters on heat transfer in PAFC stack
[NASA-CR-198817] p 2570 N95-29131
Effects of the cooling system parameters on heat transfer and performance of the PAFC stack during transient operation
[NASA-CR-197654] p 2572 N95-29249
PHOSPHORIC ACID FUEL CELLS
Transient responses of phosphoric acid fuel cell power plant system
[NASA-CR-198948] p 2603 N95-30015
PHOSPHORUS
SAM1-A new semiempirical method including d-orbitals
[AD-A290903] p 2694 N95-30060
PHOSPHORUS COMPOUNDS
Radiative lifetime and quenching rate constants of PF(b(1) Sigma+) and tests for an electronic to vibrational energy transfer quenching mechanism
[AD-A290294] p 2681 N95-29062
PHOTOCHEMICAL REACTIONS
Ceramics derived from organo-metallic precursors
[AD-A291434] p 2547 N95-30071
PHOTOCONDUCTIVITY
Transport phenomena and noise in real quantum wires
[AD-A290493] p 2714 N95-29152
Novel high-power solid-state sources for the millimeter-wave region
[AD-A292653] p 2564 N95-29384
PHOTOCONDUCTORS
Fourier Synthesis Lithographic Machine for large panel display fabrication
[AD-A291921] p 2698 N95-28914
PHOTODECOMPOSITION
Characterization of excited state oxygen-organic molecule complexes
[AD-A290548] p 2692 N95-29092
PHOTODIODES
Design of an electronic charged particle spectrometer to measure (rho R), yield, and implosion symmetry on the OMEGA Upgrade
[DE95-006088] p 2695 N95-28930
Photon-counting spatial light modulator technology development
[AD-A292619] p 2699 N95-29295
PHOTODISSOCIATION
State resolved differential cross sections for reactions important to the decomposition of energetic materials
[AD-A290718] p 2548 N95-29498
PHOTOELECTRIC EMISSION
Interface properties of wide bandgap semiconductor structures
[AD-A289817] p 2713 N95-28954
Composite material studies for low temperature thermionic emission
[AD-A292159] p 2523 N95-29124
PHOTOELECTRICITY
Novel photoelectric sensing technology for environmental monitoring, phase 1
[AD-A292026] p 2611 N95-30348
PHOTOELECTRON SPECTROSCOPY
XPS study of Ni-Fe manganite thermistor material
[DE95-008778] p 2561 N95-28961
Surface studies of Poly(organophosphazenes) containing dimethylsiloxane grafts
[AD-A291909] p 2543 N95-29355
PHOTOELECTRONS
Molecular spectra and dynamics at interfaces
[AD-A289779] p 2693 N95-29460
PHOTOGRAMMETRY
Operating procedures for Anthropometry and Initial Conditions Photogrammetric Program
[AD-A291553] p 2640 N95-28935
PHOTOGRAPHIC MEASUREMENT
Experiments on microbursts p 2620 N95-29110
PHOTOIONIZATION
Spectrometric studies of selected nitrocompounds using laser-induced photofragmentation/photoionization at 193 nm
[AD-A289947] p 2530 N95-28876
PHOTOLUMINESCENCE
Integrated synthesis and post-processing of SiC and AlN
[AD-A290853] p 2537 N95-29724
Electronic states in Cd(1-x)Zn(x)Te/CdTe strained layer coupled double quantum wells and their photoluminescence
[DE95-006806] p 2716 N95-29814
PHOTOMETERS
SAO HMC photodetector/event timer engineering model test report
[DE95-007889] p 2582 N95-28917
The 1.3 micrometer fiber photodetector
[AD-A292462] p 2582 N95-29004
Development of ultra-low dark current, high performance 3-5 quantum well infrared photodetectors (QWIPs) for focal plane arrays staring imaging sensor systems
[AD-A290343] p 2714 N95-29089
Investigation of a normal incident high performance P-type strained layer In(0.3)Ga(0.7)As/In(0.52)Al(0.48)As quantum well infrared photodetector
[AD-A290946] p 2716 N95-29785
PHOTOMETRY
Nobeyama Radio Observatory report, no. 378: The polar ring spiral galaxy NGC 660 p 2731 N95-29097
Reflectance analysis under solar illumination
[AD-A290489] p 2737 N95-29151
PHOTON BEAMS
A finite element analysis of room temperature silicon crystals for the Advanced Photon Source bending-magnet and insertion-device beams
[DE95-005822] p 2718 N95-30184
PHOTONICS
Self-Induced Transparency in photonic band structures: Gap solitons near absorption resonances
[AD-A292187] p 2718 N95-28927
PHOTONS
Photon-counting spatial light modulator technology development
[AD-A292619] p 2699 N95-29295
The Los Alamos Photon Counting Detector Debris Detection Project: An update
[DE95-007883] p 2508 N95-29464
Observation of x ray generation in a proof-of-principle laser synchrotron source experiment
[AD-A291298] p 2588 N95-29937
PHOTOPRODUCTION
Photoproduction of hybrid mesons from CEBAF to HERA
[PB95-196218] p 2691 N95-28913
PHOTOSPHERE
Interaction of acoustic oscillations with magnetic flux tubes in the solar photosphere
[PB95-201810] p 2739 N95-30199
PHOTOVOLTAIC CELLS
PASP plus time history data base file structures
[AD-A290587] p 2725 N95-30043
Fuel cell systems for First Lunar Outpost-reactant storage option p 2606 N95-30264
The TMI regenerable solid oxide fuel cell p 2606 N95-30265
PHOTOVOLTAIC EFFECT
Arcing mitigation and predictions for high voltage solar arrays
[AD-A292227] p 2602 N95-29200
Arcing predictions for PASP PLUS solar arrays
[AD-A292230] p 2602 N95-29201
PHTHALOCYANIN
Theories of the nonlinear optical properties of composite media: Applications to phthalocyanine dyes
[AD-A290640] p 2700 N95-29560
PHYSICAL EXAMINATIONS
A comparison of the aeromedical administration requirements for US Air Forces and major allies
[AD-A290137] p 2635 N95-29141
PHYSICAL EXERCISE
Lockheed Stabilizer System for space exercise equipment
[NASA-CR-197657] p 2641 N95-29180
Adaptations to three weeks of aerobic/anaerobic training in west coast U.S: Navy Sea-Air-Land personnel (SEAL's)
[AD-A291500] p 2637 N95-29846
Summary report of mission acceleration measurements for STS-65, launched 8 July 1994
[NASA-TM-106871] p 2549 N95-30339
PHYSICAL FITNESS
Adaptations to three weeks of aerobic/anaerobic training in west coast U.S: Navy Sea-Air-Land personnel (SEAL's)
[AD-A291500] p 2637 N95-29846
PHYSICAL OPTICS
Low threshold all-optical crossbar switch on GaAs-GaAlAs channel waveguide arrays
[AD-A292483] p 2712 N95-28862
Fourier Synthesis Lithographic Machine for large panel display fabrication
[AD-A291921] p 2698 N95-28914
High-frequency radar target modeling
[AD-A290965] p 2559 N95-29991
PHYSICIANS
Military flying and aeromedical evaluation of cardiac arrhythmias
[AD-A291595] p 2634 N95-28940
PHYSICS
Brief introduction to state key physics laboratories and division open laboratories
[AD-A291064] p 2682 N95-29952
PHYSIOLOGICAL EFFECTS
Cellular and molecular level responses after radiofrequency radiation exposure, alone or in combination with x rays or chemicals
[AD-A292488] p 2633 N95-28866
Effects of cabin pressure on climb and descent rates
[ESDU-94040] p 2496 N95-29016
CO2-O2 interactions in extension of tolerance to acute hypoxia
[NASA-CR-198575] p 2635 N95-29158
Research on PGI2 and TXA2 effects at times of hyperbaric oxygenation of domestic rabbits with acute cerebral ischemia reirrigation damage
[AD-A289606] p 2632 N95-29263
Effect of mild hydrostatic pressure on red blood cells
[AD-A290520] p 2637 N95-29872
PHYSIOLOGICAL RESPONSES
Shift work, age, and performance: Investigation of the 2-2-1 shift schedule used in Air Traffic Control facilities I. The sleep/wake cycle
[DOT/FAA/AM-95/19] p 2638 N95-29261
A human factors evaluation of the operational demonstration flight inspection aircraft
[DOT/FAA/AM-95/18] p 2641 N95-29365
Effect of irradiance, sucrose, and CO2 concentration on the growth of potato (Solanum tuberosum L.) in vitro
[NASA-TM-110654] p 2632 N95-29375
The one-dimensional bubble: Theory, experiment, and relevance to exposure of divers to low frequency sound, and of lung to lithotripsy
[ISVR-TR-246] p 2577 N95-29817
PHYSIOLOGICAL TESTS
The influence of space flight on erythrokinetics in man. Space Life Sciences Missions 1 and 2. Experiment E261
[NASA-CR-188368] p 2633 N95-28875
PHYSIOLOGY
Membrane fluidity and shape of human red blood cells are altered by physiological levels of hydrostatic pressure
[AD-A290595] p 2636 N95-29557
PIEZOELECTRIC CERAMICS
High field electrostrictive response of polymers
[AD-A292298] p 2539 N95-28864
Low order adaptive optical systems
[AD-A291121] p 2701 N95-29766
Unitary transducer with variable resistivity
[AD-D017329] p 2566 N95-30055
PIEZOELECTRIC CRYSTALS
Development of 'smart' piezothermoelastic laminae: Theory and applications
[AD-A290852] p 2528 N95-29864
PIEZOELECTRIC TRANSDUCERS
An impact load identification method using distributed sensor measurements p 2595 N95-29419
A hybrid electronically scanned pressure module for cryogenic environments
[NASA-TM-110146] p 2583 N95-29453
Experimental confirmation of a PDE-based approach to design of feedback controls
[NASA-CR-198167] p 2672 N95-30086
PIEZOELECTRICITY
Ferroelectric and piezoelectric properties of nylon 11/Poly(Vinylidene fluoride) bilaminate films
[AD-A292274] p 2539 N95-28891
Sensitivity of stress and boundary imperfection of dielectric resonator disks
[AD-A290488] p 2594 N95-29150
Broadband control of structural vibration using simultaneous sensing and actuation with nonlinear piezoelectric elements p 2664 N95-29548
Development of 'smart' piezothermoelastic laminae: Theory and applications
[AD-A290852] p 2528 N95-29864
Fiber compatible acousto-optic modulator using a gradient index lens
[AD-A291164] p 2565 N95-29925
PILOTLESS AIRCRAFT
Unmanned aerial vehicles: No more Hunter systems should be bought until problems are fixed
[AD-A292172] p 2497 N95-29126
Role of unmanned aerial vehicles in future armed conflict scenarios
[AD-A289777] p 2497 N95-29282

Unmanned Aerial Vehicle technology
[DSTO-GD-0044] p 2497 N95-29362
Applications of digital video and synthetic environments to unmanned aerial vehicles
[AD-A291875] p 2497 N95-29437
Design and evaluation of a LQR controller for the bluebird unmanned air vehicle
[AD-A289769] p 2498 N95-29457

PILOTS
Task-dependent effects of automation: The role of internal models in performance, workload, and situational awareness in a semi-automated cockpit
[AD-A292538] p 2640 N95-28969

PINS
Process algebra with feedback
[PB95-206819] p 2673 N95-30106

PIONEER VENUS SPACECRAFT
Pioneer Venus 12.5 km Anomaly Workshop Report, volume 1
[NASA-CP-3303] p 2737 N95-30058

PIONS
Activities update
[AD-A292431] p 2692 N95-28994
From the (psi) to charmed mesons
[DE95-006564] p 2693 N95-29583
Prospects for HERMES-spin structure studies at HERA
[DE95-005845] p 2694 N95-30019
Parameterized spectral distributions for meson production in proton-proton collisions
[NASA-TM-4675] p 2696 N95-30337

PIPE FLOW
Condensation inside tubes: Condensate film coefficient in horizontal tubes
[ESDU-94041] p 2569 N95-29015
Studies in drag reduction p 2487 N95-29094
NMR imaging and hydrodynamic analysis of neutrally buoyant non-Newtonian slurry flows
[DE95-005842] p 2578 N95-30187

PIPELINES
Epoxy pipelining composition and method of manufacture
[AD-D017380] p 2539 N95-28784
A pipeline case tool for database design
[AD-A292017] p 2722 N95-29182

PIPELINING (COMPUTERS)
Asymptotically zero energy computing using split-level charge recovery logic
[AD-A290054] p 2564 N95-29478

PIPES (TUBES)
Condensation inside tubes: Condensate film coefficient in horizontal tubes
[ESDU-94041] p 2569 N95-29015
Intermittent energy bursts and recurrent topological change of a twisting magnetic flux tube
[AD-B195513L] p 2708 N95-29755
Ultrasonic guided waves in cylinders: Theory and experiment p 2685 N95-29826

PISTONS
External combustion engine having an asymmetrical CAM
[AD-D017382] p 2588 N95-28785

PITCH (INCLINATION)
PIV investigation of compressibility effects on dynamic stall p 2487 N95-29102
Unsteady pressure and inflow velocity on a pitching rotor blade in hover p 2490 N95-29771

PLANAR STRUCTURES
Radar cross section synthesis for planar resistive surfaces
[AD-A290151] p 2555 N95-29318
Inorganic halogen oxidizers
[AD-A290747] p 2533 N95-29581
Inorganic halogen oxidizers
[AD-A291201] p 2702 N95-29974

PLANE STRAIN
Robust algorithms for penetration mechanics problems
[AD-A290650] p 2650 N95-29517

PLANE STRESS
Toughening mechanisms in mixed-mode interfacial fracture p 2545 N95-29772

PLANE WAVES
Acoustic scattering from ellipses by the modal element method
[NASA-TM-106935] p 2683 N95-29401
Second-order numerical solution of time-dependent, first-order hyperbolic equations p 2674 N95-30143

PLANETARY BOUNDARY LAYER
Heat and momentum flux measurements in the planetary boundary layer with a wind profiling radar/radio acoustic sounding system p 2617 N95-29777

PLANETARY COMPOSITION
Differentiation in the early Earth: An experimental investigation p 2612 N95-29199

PLANETARY CRUSTS
Some aspects of lunar and martian volcanism as examined with spectral, topographic, and morphologic data derived from spacecraft images p 2736 N95-29594

PLANETARY EVOLUTION
Channels and valleys on Venus p 2736 N95-29593
The evolution of binary millisecond pulsars and the formation of planets around them p 2733 N95-29663

PLANETARY GEOLOGY
Collection of Magellan Venus radar mapping results
[NASA-CR-197656] p 2736 N95-29178
Channels and valleys on Venus p 2736 N95-29593
Some aspects of lunar and martian volcanism as examined with spectral, topographic, and morphologic data derived from spacecraft images p 2736 N95-29594

PLANETARY GRAVITATION
The JPL Mars gravity field, Mars50c, based upon Viking and Mariner 9 Doppler tracking data
[NASA-CR-198681] p 2737 N95-30344

PLANETARY IONOSPHERES
A study of plasma waves arising from the solar wind interaction with Venus p 2704 N95-29215

PLANETARY MAPPING
Collection of Magellan Venus radar mapping results
[NASA-CR-197656] p 2736 N95-29178

PLANETARY STRUCTURE
Channels and valleys on Venus p 2736 N95-29593

PLANETARY WAVES
A study of dynamics in the tropical Pacific using satellite data p 2630 N95-29520

PLANFORMS
Leading-edge suction distribution for plane thin wings at subsonic speeds
[ESDU-94037] p 2486 N95-28800
Low-speed wind-tunnel investigation of the stability and control characteristics of a series of flying wings with sweep angles of 50 deg
[NASA-TM-4640] p 2498 N95-30226

PLANKTON
Automated analysis of zooplankton size and taxonomic composition using the video plankton recorder
[AD-A289725] p 2631 N95-28685

PLANT ROOTS
Effect of irradiance, sucrose, and CO2 concentration on the growth of potato (Solanum tuberosum L.) in vitro
[NASA-TM-110654] p 2632 N95-29375

PLANTS (BOTANY)
Proposal for a flexible system of phytogeographic classification: Emphasis on the use of multistage remote sensoring
[INPE-5609-PRE/1821] p 2600 N95-29815

PLASMA ACCELERATORS
Ionizational nonequilibrium and ignition in plasma accelerators p 2705 N95-29547

PLASMA BUBBLES
Chemical release experiments to induce F region ionospheric plasma irregularities at the magnetic equator p 2708 N95-29783

PLASMA COMPOSITION
Techniques and results of tokamak-edge simulation
[DE95-008075] p 2711 N95-30130

PLASMA CONDUCTIVITY
Anomalous transport theory for toroidal helical plasmas
[AD-B192000L] p 2706 N95-29731

PLASMA CONTROL
Development of an intense negative hydrogen ion source with a wide-range of external magnetic filter field
[AD-B195514L] p 2705 N95-29567
Anomalous transport theory for toroidal helical plasmas
[AD-B192000L] p 2706 N95-29731
Interchange stability criteria for anisotropic central-cell plasmas in the tandem mirror GAMMA 10
[AD-B176253L] p 2707 N95-29738
Transition of radial electric field by electron cyclotron heating in the stellarator plasmas
[AD-B176254L] p 2707 N95-29742
Free-boundary equilibrium studies for the Large Helical Device
[AD-B175931L] p 2707 N95-29743
Prandtl number of toroidal plasmas
[AD-B179181L] p 2707 N95-29744
Discriminant analysis to predict the occurrence of ELMS in H-mode discharges
[AD-B179183L] p 2708 N95-29746
Modelling of transport phenomena
[AD-B179223L] p 2708 N95-29747
Formation of positive radial electric field by Electron Cyclotron Heating in Compact Helical System
[AD-B191994L] p 2709 N95-29802
Theory of pseudo-classical confinement and transmutation to L-mode
[AD-B175957L] p 2709 N95-29809
Carbon sheet pumping
[AD-B179443L] p 2710 N95-29812
Innovative divertor concepts for LHD
[AD-B191997L] p 2711 N95-30032

PLASMA CURRENTS
Comment on a mean field Ohm's law for collisionless plasmas
[AD-B176252L] p 2707 N95-29741
Discriminant analysis to predict the occurrence of ELMS in H-mode discharges
[AD-B179183L] p 2708 N95-29746
Theory of pseudo-classical confinement and transmutation to L-mode
[AD-B175957L] p 2709 N95-29809

PLASMA DENSITY
Effective emission and ionization rate coefficients of atomic carbons in plasmas
[AD-B175932L] p 2707 N95-29740
Chemical release experiments to induce F region ionospheric plasma irregularities at the magnetic equator p 2708 N95-29783

PLASMA DIAGNOSTICS
Solitons in negative ion plasmas p 2706 N95-29668
Theoretical study of cylindrical energy analyzers for MeV range heavy ion beam probes
[AD-B17200L] p 2707 N95-29745
Inertial fusion program and national laser users facility program
[DE95-008202] p 2711 N95-30274

PLASMA DIFFUSION
Modelling of transport phenomena
[AD-B179223L] p 2708 N95-29747

PLASMA DYNAMICS
High-density plasma dynamics in semiconductors p 2705 N95-29632
Lecture note on the bases of plasma physics
[NIFS-PROC-15] p 2711 N95-29966

PLASMA EQUILIBRIUM
Free-boundary equilibrium studies for the Large Helical Device
[AD-B175931L] p 2707 N95-29743
Averaged resistive MHD equations
[AD-B178947L] p 2711 N95-30033

PLASMA HEATING
Equatorial heating effects on outer plasmasphere evolution p 2616 N95-29716
Interchange stability criteria for anisotropic central-cell plasmas in the tandem mirror GAMMA 10
[AD-B176253L] p 2707 N95-29738
Transition of radial electric field by electron cyclotron heating in the stellarator plasmas
[AD-B176254L] p 2707 N95-29742

PLASMA INTERACTIONS
A Monte Carlo simulation of Coulomb collisions and wave-particle interactions in space plasma at high latitudes p 2704 N95-29205
A study of plasma waves arising from the solar wind interaction with Venus p 2704 N95-29215
Solitons in negative ion plasmas p 2706 N95-29668
The physics of the collisionless bow shock p 2580 N95-30301

PLASMA JETS
Discriminant analysis to predict the occurrence of ELMS in H-mode discharges
[AD-B179183L] p 2708 N95-29746
On the azimuthal variation of the equatorial plasmapause
[NASA-CR-198929] p 2711 N95-30338

PLASMA OSCILLATIONS
Dynamical model of pressure-gradient-driven turbulence and shear flow generation in L-H transition
[AD-B195511L] p 2709 N95-29789

PLASMA PHYSICS
HIDENEK: An implicit particle simulation of kinetic-MHD phenomena in three-dimensional plasmas
[AD-B176255L] p 2707 N95-29739
Screening constants for plasma
[AD-B179442L] p 2710 N95-29843
Attractors of dissipative structure in three dissipative fluids
[AD-B180030L] p 2710 N95-29844
Lecture note on the bases of plasma physics
[NIFS-PROC-15] p 2711 N95-29966
The physics of the collisionless bow shock p 2580 N95-30301
On the azimuthal variation of the equatorial plasmapause
[NASA-CR-198929] p 2711 N95-30338

PLASMA PINCH
Modelling of transport phenomena
[AD-B179223L] p 2708 N95-29747

PLASMA PRESSURE
Self-sustained magnetic braiding in toroidal plasmas
[AD-B191998L] p 2706 N95-29734

PLASMA PROBES
Theoretical study of cylindrical energy analyzers for MeV range heavy ion beam probes
[AD-B17200L] p 2707 N95-29745

PLASMA PROPULSION
High temperature spectroscopy of alkali metal vapors for solar to thermal energy conversion
[AD-A291355] p 2602 N95-29949
PLASMA PUMPING
Carbon sheet pumping
[AD-B179443L] p 2710 N95-29812
PLASMA RADIATION
Observations and analysis of solar flares at radio and other wavelengths p 2738 N95-29202
PLASMA SPECTRA
Insights on the local density approximation plasma polarization shift as provided by the optimum potential method
[DE95-008078] p 2705 N95-29466
PLASMA TEMPERATURE
Carbon sheet pumping
[AD-B179443L] p 2710 N95-29812
PLASMA TURBULENCE
Anomalous transport theory for toroidal helical plasmas
[AD-B192000L] p 2706 N95-29731
Self-sustained magnetic braiding in toroidal plasmas
[AD-B191998L] p 2706 N95-29734
Comment on a mean field Ohm's law for collisionless plasmas
[AD-B176252L] p 2707 N95-29741
Prandtl number of toroidal plasmas
[AD-B179181L] p 2707 N95-29744
Theory of pseudo-classical confinement and transmutation to L-mode
[AD-B175957L] p 2709 N95-29809
PLASMA WAVES
Solar system plasma waves
[NASA-CR-198767] p 2704 N95-29130
A study of plasma waves arising from the solar wind interaction with Venus p 2704 N95-29215
Relativistic effects on large amplitude nonlinear langmuir waves in a two-fluid plasma
[AD-B191980L] p 2710 N95-29841
PLASMA-PARTICLE INTERACTIONS
Deposition and surface treatment with intense pulsed ion beams
[DE95-007885] p 2543 N95-29465
Effective emission and ionization rate coefficients of atomic carbons in plasmas
[AD-B175932L] p 2707 N95-29740
PLASMAPAUSE
On the azimuthal variation of the equatorial plasmapause
[NASA-CR-198929] p 2711 N95-30338
PLASMAS (PHYSICS)
Surface conversion techniques for low energy neutral atom imagers
[NASA-CR-196604] p 2691 N95-28856
High power, high frequency radiation from beam-plasma interactions
[AD-A292442] p 2703 N95-29001
HBCU/MI instrumentation for the Pulsed Power Plasma Sciences Laboratory at the University of New Mexico, FY92-93
[AD-A292444] p 2703 N95-29003
Development of a transient internal probe diagnostic
[AD-A292470] p 2704 N95-29011
Ionizational nonequilibrium and ignition in plasma accelerators p 2705 N95-29547
Equatorial heating effects on outer plasmasphere evolution p 2616 N95-29716
Modelling of transport phenomena
[AD-B179223L] p 2708 N95-29747
High temperature spectroscopy of alkali metal vapors for solar to thermal energy conversion
[AD-A291355] p 2602 N95-29949
The topside ionospheric plasma monitor (SSIES, SSIES-2 and SSIES-3) on the spacecraft of the Defense Meteorological Satellite Program (DMSP), user's guide. Volume 2: Programmer's guide for software at AFSFC
[AD-A290913] p 2618 N95-30082
Heavy light bullets in electron-positron plasma
[DE95-008751] p 2711 N95-30173
PLASMASPHERE
Thermal N(+) in the inner magnetosphere p 2614 N95-29590
Equatorial heating effects on outer plasmasphere evolution p 2616 N95-29716
PLASTIC BODIES
A new methodology for the numerical simulation of strain softening in inelastic solids
[AD-A290295] p 2594 N95-29063
PLASTIC DEFORMATION
A new methodology for the numerical simulation of strain softening in inelastic solids
[AD-A290295] p 2594 N95-29063
Consideration of microstructural changes in the study of adiabatic shear bands
[AD-A290398] p 2715 N95-29234
Examination of dislocation core structures in B2 intermetallic alloys
[AD-A291486] p 2537 N95-29526
Theoretical, experimental and computational studies in plasticity
[AD-A290428] p 2595 N95-29535
Decomposition of hypo-eutectoid iron carbon austenites
[PB95-196945] p 2538 N95-30287
PLASTIC FLOW
Theoretical, experimental and computational studies in plasticity
[AD-A290428] p 2595 N95-29535
PLASTIC PROPERTIES
Five-channel SQUID based non-destructive evaluation (NDE) instrument
[AD-A292474] p 2592 N95-29012
Theoretical, experimental and computational studies in plasticity
[AD-A290428] p 2595 N95-29535
Toughening mechanisms in mixed-mode interfacial fracture p 2545 N95-29772
Gradient-dependent plasticity in numerical simulation of localization phenomena
[PB95-197257] p 2596 N95-30049
PLASTICS
Impact properties of coated engineering plastics
[PB95-197281] p 2547 N95-30201
PLATENS
Passive damping to enhance active positioning of a prototype lithography platen
[DE95-008539] p 2655 N95-30209
PLATES (STRUCTURAL MEMBERS)
Analysis of static contact in laminated composite plates using damage mechanics
[NASA-CR-198656] p 2513 N95-28809
The effects of three-dimensional imposed disturbances on bluff body near wake flows: Effects of taper and splitter plates on the near wake characteristics of a circular cylinder in uniform and shear flow
[AD-A292113] p 2487 N95-28921
Effects of cooling system parameters on heat transfer in PAFC stack
[NASA-CR-198817] p 2570 N95-29131
Adjustable two-axis instrument mount
[AD-D017393] p 2582 N95-29220
PLATES (TECTONICS)
The gravitational potential energy of the Earth's lithosphere p 2617 N95-29773
PLATINUM
The effects of platinum on nickel electrodes in the nickel hydrogen cell
[AD-A291607] p 2531 N95-28942
Effects of space exposure on metals flown on the Long Duration Exposure Facility
[NASA-CR-4662] p 2512 N95-30225
PLOWS
Investigation of an alternative finite element procedure: A one-step, steady-state analysis
[AD-A290030] p 2670 N95-29311
PLUMES
Estimates of probability of a cloud-free line of sight for RAPTOR TALON
[AD-A291908] p 2510 N95-29284
Measurements of ions formed in jet engine exhaust plumes
[AD-A290940] p 2501 N95-29764
POINT DEFECTS
Gordon research conference on point defects, line defects, and interfaces in semiconductors
[AD-A290103] p 2714 N95-29209
POINT SOURCES
Complete analysis of electrode-terminated cables in two-layer conductor bounded above by air: Current density, magnetic field, and magnetic field gradient
[AD-A290907] p 2566 N95-30079
Static field solutions and image theory for a conducting sphere with radial anisotropy
[PB95-207171] p 2673 N95-30172
POINTING CONTROL SYSTEMS
Precision pointing experiment
[AD-A291015] p 2664 N95-29657
POINTS
Parametric design and gridding through relational geometry p 2486 N95-28771
POISSON EQUATION
A 3DGRAPE/AL: The Ames/Langley technology upgrade p 2482 N95-28750
Modeling the boundary layer interactions between weakly ionized plasmas and cooled, planar electrodes in stagnation-point flows p 2706 N95-29717
POISSON RATIO
Experimental and analytical characterization of triaxially braided textile composites p 2520 N95-29040
POLAR CAPS
Characterization of the geometries of the high-latitude ionospheric convection pattern p 2614 N95-29524
Gamma radiation from rotation powered pulsars and results from the Energetic Gamma-Ray Experiment Telescope p 2739 N95-29671
The high-altitude polar wind: Simulation and observation p 2622 N95-29688
POLAR REGIONS
A Monte Carlo simulation of Coulomb collisions and wave-particle interactions in space plasma at high latitudes p 2704 N95-29205
The effects of magnetic storm phases on F-layer irregularities from auroral to equatorial latitudes
[AD-A290674] p 2614 N95-29585
Application of Poynting flux measurements to the determination of energy transfer rates in the high-latitude ionosphere p 2614 N95-29650
POLARIMETRY
Evaluation of the utilization of SAR polarimetric images in the survey of land resources in the Amazon area Tapajos Forest Reserve
[INPE-5517-PRE/1792] p 2601 N95-29999
POLARIZATION
Insights on the local density approximation plasma polarization shift as provided by the optimum potential method
[DE95-008078] p 2705 N95-29466
POLARIZATION (CHARGE SEPARATION)
Ferroelectric polarization mechanism of the odd-numbered nylons
[AD-A292276] p 2539 N95-28860
Collisionless driven magnetic reconnection
[AD-B178946L] p 2709 N95-29810
POLARIZATION (SPIN ALIGNMENT)
The physics of spin polarized gases
[AD-A292511] p 2680 N95-28810
POLARIZED LIGHT
Predicting polarized light scattering by marine micro-organism
[AD-A289790] p 2696 N95-28695
Predicting polarized light scattering by marine micro-organisms
[AD-A289796] p 2697 N95-28698
Transitions in liquid crystals initiated with circularly polarized light
[AD-A290525] p 2716 N95-29493
POLARIZED RADIATION
Sea and gluon spin structure function measurements at RHIC
[DE95-005823] p 2695 N95-30185
Measurements of (Delta)(sigma)(sub L)(pp) and (Delta)(sigma)(sub L)((bar p)p) at 200 GeV/c
[DE95-005837] p 2695 N95-30186
POLICIES
Scientific and technical information policy implementation under OMB Circular A-130. Report of agency findings and recommendations
[DE-95-11601] p 2723 N95-29449
Materials for tomorrow's infrastructure: A ten-year plan for deploying high-performance construction materials and systems
[AD-A289782] p 2526 N95-29598
Environmental practice in progam management offices
[AD-A290823] p 2609 N95-29721
Performance evaluation of ATM cell scheduling policies using stochastic petri nets
[PB95-197158] p 2559 N95-30096
POLLUTION CONTROL
Zero Discharge Organic Coatings: Powder paint. UV curable paint. E-coat
[AD-A292180] p 2540 N95-28925
POLLUTION TRANSPORT
Continental aerosol effects on stratocumulus microphysics during MAST 1994
[AD-A292674] p 2621 N95-29416
Management of meteorological data at a former nuclear weapons facility
[DE95-007619] p 2626 N95-29868
POLYATOMIC MOLECULES
AB initio studies of electron and positron scattering from non-linear molecules
[AD-A292586] p 2692 N95-28981
POLYCARBONATES
Fiber-matrix adhesion in single-fiber model composites p 2524 N95-29337
POLYCRYSTALS
Test load verification through strain data analysis
[NASA-TP-3558] p 2504 N95-28718
Molecular dynamics study of electromigration
[AD-A289811] p 2691 N95-28952
Multi-decade time-dependent voltage of polycrystalline thin-film solar cells p 2602 N95-29103
Crystal field and exchange interactions in DyT4Al8 (T = Fe and Mn)
[DE95-007131] p 2714 N95-29134

POLYCYCLIC AROMATIC HYDROCARBONS
Surfactant-enhanced in situ biodegradation of strongly sorbing organic substances in soil environments
[AD-A290253] p 2512 N95-29168
POLYETHYLENES
A search for a composition-dependent gravitational force p 2719 N95-29501
Polyethylene-based polyurethane copolymers and block copolymers
[AD-A289996] p 2546 N95-30030
The morphology of blends of linear and branched polyethylenes in solid state by SANS
[DE95-008675] p 2535 N95-30113
Biological methane activation
[PB95-200705] p 2535 N95-30198
POLYIMIDES
Advanced composite structural concepts and materials technologies for primary aircraft structures: Advanced material concepts
[NASA-CR-4485] p 2496 N95-29027
Weavability of dry polymer powder towpreg p 2519 N95-29036
Development of LaRC (TM): IA thermoplastic polyimide coated aerospace wiring
[NASA-CR-195048] p 2548 N95-30252
POLYISOBUTYLENE
Molecular level characterization by NMR of the transport and structural environment of gases and condensed penetrante
[AD-A290831] p 2693 N95-29723
POLYMER BLENDS
Phase coupling and morphology generation in engineering polymer alloys
[AD-A291868] p 2543 N95-29436
Thermally stable organic polymers
[AD-A290755] p 2543 N95-29482
The morphology of blends of linear and branched polyethylenes in solid state by SANS
[DE95-008675] p 2535 N95-30113
POLYMER CHEMISTRY
Selective attachment of nucleic acid molecules to patterned self-assembled surfaces
[AD-D017379] p 2530 N95-28854
Phase coupling and morphology generation in engineering polymer alloys
[AD-A291868] p 2543 N95-29436
Thermally stable organic polymers
[AD-A290755] p 2543 N95-29482
Conjugated polymers from cyclohexadienediol monomers
[AD-A290247] p 2544 N95-29505
Synthesis morphology and properties of semicrystalline block copolymers
[AD-A290475] p 2544 N95-29510
POLYMER MATRIX COMPOSITES
Effects of cutouts on the behavior of symmetric composite laminates subjected to bending and twisting loads p 2517 N95-28844
Advanced composite structural concepts and materials technologies for primary aircraft structures: Advanced material concepts
[NASA-CR-4485] p 2496 N95-29027
Advanced composite fuselage technology p 2519 N95-29034
The combined effect of glass buffer strips and stitching on the damage tolerance of composites p 2522 N95-29049
POLYMERIC FILMS
Ferroelectric and piezoelectric properties of nylon 11/Poly(Vinylidene fluoride) bilaminate films
[AD-A292274] p 2539 N95-28891
In-plant testing of membranes to treat electroplating wastewater
[NASA-CR-198796] p 2532 N95-29250
The 2nd International Conference on Thin Film Physics and Applications
[AD-A292353] p 2546 N95-29983
Development of LaRC (TM): IA thermoplastic polyimide coated aerospace wiring
[NASA-CR-195048] p 2548 N95-30252
POLYMERIZATION
Transition metal complexes with perfluorinated ligands
[AD-A290250] p 2536 N95-29427
Thermally stable organic polymers
[AD-A290755] p 2543 N95-29482
Recent progress in the study of the kinetics of sol-gel SiO2 synthesis reactions
[AD-A290570] p 2544 N95-29551
Cage-like precursor formation from extensive cyclization in sol-gel inorganic condensation polymerization
[AD-A290589] p 2544 N95-29554
17O NMR of the structural evolution of V2O5 gels
[AD-A290623] p 2545 N95-29559
POLYMERS
Photogenerated amines in polymer curing and imaging: Design and synthesis of (3', 5'-dimethoxybenzoinyl)oxycarbonyl carbamates as novel photoprecursors of amines
[AD-A289945] p 2542 N95-29272
Low voltage, high resistance, Polymer Dispersed Liquid Crystal
[AD-A291946] p 2556 N95-29472
Engineering design of sub-micron topographies for simultaneously adherent and reflective metal-polymer interfaces
[NASA-CR-198845] p 2548 N95-30237
POLYMETHYL METHACRYLATE
Dynamic decohesion of bimaterial interfaces p 2541 N95-29120
POLYNOMIALS
Some new saturated two-level designs
[AD-A292627] p 2670 N95-29296
Multivariate wavelet representations and approximations
[AD-A290147] p 2670 N95-29312
Computational complexity and encryption
[AD-A291910] p 2648 N95-29356
Polynomial approximations for materials simulations
[DE95-006168] p 2652 N95-29989
POLYPEPTIDES
Organization of the human circadian system
[AD-A288223] p 2634 N95-28915
POLYPHENYLS
The synthesis of liquid crystalline phophazenes containing chiral mesogens
[AD-A291911] p 2543 N95-29358
POLYSTYRENE
New tetraarylborate and ethyldibutylstannane reagents
[AD-A289813] p 2540 N95-28953
Photogenerated amines in the design of imaging materials: The radiation-induced imidization of functionalized polystyrenes bearing amide-ester side chains
[AD-A289943] p 2542 N95-29270
Depth-independent hardness improvements in ion irradiated polystyrene
[DE95-008682] p 2547 N95-30190
POLYURETHANE RESINS
High field electrostrictive response of polymers
[AD-A292298] p 2539 N95-28864
Polyethylene-based polyurethane copolymers and block copolymers
[AD-A289996] p 2546 N95-30030
PONDS
Coso monitoring program
[AD-A290604] p 2627 N95-30048
POPULATION INVERSION
Optimal control of molecular motion
[AD-A291919] p 2691 N95-28944
POROUS MATERIALS
A thermochemical transport model for analysis of hot-spot formation in energetic materials
[AD-A290441] p 2532 N95-29357
POROUS WALLS
A method for the modelling of porous and solid wind tunnel walls in computational fluid dynamics codes p 2502 N95-29795
POSEIDON SATELLITE
Data catalog for JPL Physical Oceanography Distributed Active Archive Center (PO.DAAC)
[NASA-CR-198872] p 2631 N95-30231
POSITION (LOCATION)
Generator of body data (GEBOD) manual
[AD-A289721] p 2640 N95-28683
Conceptual design of a map interactive system for military aircraft cockpits
[AD-A289760] p 2499 N95-28692
Methods of generating low redundancy direction finding array configurations
[AD-A292590] p 2555 N95-29289
Pattern-analysis based models of masking by spatially separated sounds
[AD-A291270] p 2637 N95-29933
A regression model for the western north pacific tropical cyclone intensity forecast
[AD-A290588] p 2627 N95-30044
Gradient-dependent plasticity in numerical simulation of localization phenomena
[PB95-197257] p 2596 N95-30049
POSITION ERRORS
Error modeling for differential GPS
[NASA-CR-188367] p 2493 N95-28716
Wide Area Differential GPS (WADGPS) p 2494 N95-29107
A least square real time quality control routine for the North Warning Netted Radar System
[AD-A290063] p 2555 N95-29328
Performance analysis of a GPS Interferometric attitude determination system for a gravity gradient stabilized spacecraft
[NASA-CR-188372] p 2508 N95-30036
POSITION INDICATORS
A conceptual design for the attitude control and determination system for the Magnetosphere Imager spacecraft
[NASA-TP-3560] p 2507 N95-28721
Design, development and testing of a prototype precision angular positioning control system for a next generation multiplexed imager
[AD-A292585] p 2698 N95-28980
POSITION SENSING
DC electrostatic gyro suspension system for the Gravity Probe B experiment p 2509 N95-29794
POSITIONING
An investigation into the use of satellite-based positioning systems for flight reference/autoland operations p 2494 N95-29542
POSITIONING DEVICES (MACHINERY)
Passive damping to enhance active positioning of a prototype lithography platen
[DE95-008539] p 2655 N95-30209
POSITIVE FEEDBACK
The effects of clouds as a feedback mechanism on the Earth's climate in the tropical Pacific p 2611 N95-30300
POSITRONS
AB initio studies of electron and positron scattering from non-linear molecules
[AD-A292586] p 2692 N95-28981
POSTFLIGHT ANALYSIS
Summary Report of mission acceleration measurements for STS-66. Launched November 3, 1994
[NASA-TM-106914] p 2509 N95-29643
POTABLE WATER
An inflight refill unit for replenishing research animal drinking water
[NASA-TM-4684] p 2642 N95-28818
POTASSIUM HYDROXIDES
Effect of KOH concentration and anions on the performance of Ni-H2 battery positive plate p 2567 N95-30260
POTATOES
Effect of irradiance, sucrose, and CO2 concentration on the growth of potato (Solanum tuberosum L.) in vitro
[NASA-TM-110654] p 2632 N95-29375
POTENTIAL ENERGY
The gravitational potential energy of the Earth's lithosphere p 2617 N95-29773
Analytical potential energy surface for methylene nitramine (CH2NNO2)
[AD-A291247] p 2534 N95-29994
POTENTIAL FLOW
Computational algorithms for aerodynamic analysis and design
[AD-A291084] p 2491 N95-29972
POTENTIAL THEORY
Relativistic effects on large amplitude nonlinear langmuir waves in a two-fluid plasma
[AD-B191980L] p 2710 N95-29841
Complete analysis of electrode-terminated cables in two-layer conductor bounded above by air: Current density, magnetic field, and magnetic field gradient
[AD-A290907] p 2566 N95-30079
PREDICHAT: First order performance calculations of windturbine rotors using the method of the acceleration potential
[PB95-206454] p 2603 N95-30200
POWDER (PARTICLES)
Weavability of dry polymer powder towpreg p 2519 N95-29036
Thermally stable organic polymers
[AD-A290755] p 2543 N95-29482
POWDER METALLURGY
Processing and properties of extruded tungsten-hafnium and tungsten-steel composites
[DE95-007371] p 2528 N95-30037
Simulation of powder metal fabrication with high pressure gas atomization
[DE95-008820] p 2538 N95-30178
POWER CONVERTERS
Power measurement and current feedback in a resonant DC link inverter
[AD-A292518] p 2563 N95-29164
POWER EFFICIENCY
Power measurement and current feedback in a resonant DC link inverter
[AD-A292518] p 2563 N95-29164
POWER SUPPLY CIRCUITS
Fundamental studies in cryogenic cooling of power electronics
[AD-A291150] p 2551 N95-30296

POYNTING THEOREM
Application of Poynting flux measurements to the determination of energy transfer rates in the high-latitude ionosphere p 2614 N95-29650
PRANDTL NUMBER
Prandtl number of toroidal plasmas
[AD-B179181L] p 2707 N95-29744
PRASEODYMIUM COMPOUNDS
Pulsed laser deposition of ferroelectric thin films in conjunction with superconducting oxides
[AD-A290101] p 2585 N95-29208
A Pr-141 Moessbauer study of praseodymium com pounds
[PB95-192449] p 2535 N95-30282
PRASEODYMIUM ISOTOPES
A Pr-141 Moessbauer study of praseodymium com pounds
[PB95-192449] p 2535 N95-30282
PREAMPLIFIERS
Balanced, double-sided calibration circuit for sensor element differential pre-amplifier
[AD-D017326] p 2566 N95-30052
PRECIPITATES
Analytical electron microscopy of precipitates in ion-implanted MgAl2O4 spinel
[DE95-007406] p 2538 N95-30038
PRECIPITATION (METEOROLOGY)
Forecast of Atlantic seasonal hurricane activity for 1995 p 2620 N95-29254
A study of precipitation using dual-frequency and interferometric Doppler radars p 2627 N95-29877
PRECISION
Precision cleaning verification of fluid components by air/water impingement and total carbon analysis
[NASA-TM-110742] p 2531 N95-29248
PRECONDITIONING
Reliability enhancement of Navier-Stokes codes through convergence acceleration
[NASA-CR-196635] p 2578 N95-30034
PREDICTION ANALYSIS TECHNIQUES
Artificial intelligence techniques for parts obsolescence prediction
[AD-A292185] p 2661 N95-28926
Quality Control of meteorological observations at Fleet Numerical Meteorology and Oceanography Center
[AD-A291577] p 2619 N95-28938
Arcing mitigation and predictions for high voltage solar arrays
[AD-A292227] p 2602 N95-29200
A fourth order Euler/Navier-Stokes prediction method for the aerodynamics and aeroelasticity of hovering rotor blades p 2572 N95-29242
A simulation technique for predicting thickness of thermal sprayed coatings
[NASA-TM-106939] p 2512 N95-29373
Prediction of pressurant mass requirements for axisymmetric liquid hydrogen tanks
[NASA-TM-106973] p 2511 N95-29642
Maize yield estimation through the simulation of radiation penetration into the canopy p 2599 N95-29703
Discriminant analysis to predict the occurrence of ELMS in H-mode discharges
[AD-B179183L] p 2708 N95-29746
Development and testing of improved techniques for modeling the hydrologic cycle in a mesoscale weather prediction system
[AD-A291243] p 2627 N95-29993
Analysis of factors affecting chemical reactions in supercritical fluids
[AD-A290905] p 2534 N95-30078
PREDICTIONS
Predicting polarized light scattering by marine micro-organism
[AD-A289790] p 2696 N95-28695
Predicting polarized light scattering by marine micro-organisms
[AD-A289796] p 2697 N95-28698
Total solar eclipse of 1997 March 9
[NASA-RP-1173] p 2731 N95-30004
PREDICTOR-CORRECTOR METHODS
Automatic multi-block grid generation for high-lift configuration wings p 2485 N95-28764
PREFORMS
Analytical modeling and sensor monitoring for optimal processing of advanced textile structural composites by resin transfer molding p 2521 N95-29045
PREMIXING
Investigation of laminar methane flames with emphasis on kinetics elucidation and NOx reduction
[PB95-200531] p 2535 N95-30111
PREPREGS
Advanced resin systems and 3D textile preforms for low cost composite structures p 2519 N95-29035
Weavability of dry polymer powder towpreg p 2519 N95-29036
Performance of resin transfer molded multiaxial warp knit composites p 2520 N95-29039
Development of RTM and powder prepreg resins for subsonic aircraft primary structures p 2521 N95-29044
Origins of imperfections in composite materials
[AD-A290261] p 2523 N95-29169
Thermally stable organic polymers
[AD-A290755] p 2543 N95-29482
Composite processing development to improve interlaminar strength using ply interface particles
[NASA-TM-108495] p 2529 N95-30334
PREPROCESSING
Intensity optical correlation through optical differentiation preprocessing
[AD-A291020] p 2701 N95-29661
PRESIDENTIAL REPORTS
Rover story
[NASA-CR-198757] p 2736 N95-29964
PRESSURE
Surface pressure coefficient distributions for axisymmetric forecowls at zero incidence (M sub infinity less than or equal to 1.5)
[ESDU-94015] p 2487 N95-28904
PRESSURE DISTRIBUTION
Computer program for estimation of leading-edge suction distribution for plane thin wings at subsonic speeds
[ESDU-94038] p 2477 N95-28708
The pressure field of a gust interacting with a flat plate p 2582 N95-30161
PRESSURE EFFECTS
Effects of cabin pressure on climb and descent rates
[ESDU-94040] p 2496 N95-29016
Research on PGI2 and TXA2 effects at times of hyperbaric oxygenation of domestic rabbits with acute cerebral ischemia reirrigation damage
[AD-A289606] p 2632 N95-29263
Membrane fluidity and shape of human red blood cells are altered by physiological levels of hydrostatic pressure
[AD-A290595] p 2636 N95-29557
Models of accretion-powered x-ray pulsars p 2728 N95-29667
Self-sustained magnetic braiding in toroidal plasmas
[AD-B191998L] p 2706 N95-29734
Effect of mild hydrostatic pressure on red blood cells
[AD-A290520] p 2637 N95-29872
Pressure updating methods for the steady-state fluid equations
[NASA-CR-198163] p 2674 N95-30353
PRESSURE GAGES
A CMOS-compatible, surface-micromachined pressure sensor for aqueous ultrasonic application
[DE95-008538] p 2567 N95-30188
PRESSURE GRADIENTS
Dynamical model of pressure-gradient-driven turbulence and shear flow generation in L-H transition
[AD-B195511L] p 2709 N95-29789
The fluid mechanics of a high aspect ratio slot with an impressed pressure gradient and secondary injection p 2580 N95-30304
PRESSURE MEASUREMENT
Interactions of spanwise and chordwise vorticity associated with three-dimensional dynamic stall over an oscillating wing
[AD-A290546] p 2487 N95-29091
Analyzing the stability of floating ice floes
[AD-A292149] p 2629 N95-29160
A hybrid electronically scanned pressure module for cryogenic environments
[NASA-TM-110146] p 2583 N95-29453
Research instrumentation for polytechnic university's supersonic wind tunnel facility
[AD-A290232] p 2502 N95-29468
Unsteady pressure and inflow velocity on a pitching rotor blade in hover p 2490 N95-29771
A CMOS-compatible, surface-micromachined pressure sensor for aqueous ultrasonic application
[DE95-008538] p 2567 N95-30188
PRESSURE OSCILLATIONS
The acoustic characteristics of turbomachinery cavities
[NASA-CR-4671] p 2478 N95-28720
Physical causes of separation shock unsteadiness in shock wave/turbulent boundary layer interactions p 2570 N95-29096
Unsteady pressure and inflow velocity on a pitching rotor blade in hover p 2490 N95-29771
Dynamical model of pressure-gradient-driven turbulence and shear flow generation in L-H transition
[AD-B195511L] p 2709 N95-29789
Radiative cooling profiles calculated from ECMWF analyses and ISCCP C1 data, and their application to determination of distributions of apparent convective heating in the equatorial Pacific p 2625 N95-29805
PRESSURE RATIO
Physical causes of separation shock unsteadiness in shock wave/turbulent boundary layer interactions p 2570 N95-29096
PRESSURE SENSORS
A hybrid electronically scanned pressure module for cryogenic environments
[NASA-TM-110146] p 2583 N95-29453
A CMOS-compatible, surface-micromachined pressure sensor for aqueous ultrasonic application
[DE95-008538] p 2567 N95-30188
PRESSURE VESSELS
Corrosion investigation of multilayered ceramics and experimental nickel alloys in SCWO process environments
[DE95-008666] p 2540 N95-28960
Damage tolerance in filament-wound graphite/epoxy pressure vessels
[NASA-CR-198804] p 2590 N95-29369
Advanced Dependent Pressure Vessel (DPV) nickel-hydrogen spacecraft cell and battery design p 2567 N95-30261
PRESSURIZED CABINS
Global cost and weight evaluation of fuselage keel design concepts p 2499 N95-28840
Effects of cabin pressure on climb and descent rates
[ESDU-94040] p 2496 N95-29016
Effect of hypoxia on arterial blood gases in subjects with lung dysfunction p 2638 N95-29627
PRESTRESSING
Performance evaluation of bolt-cutter system on first Taurus launch
[AD-A291237] p 2504 N95-29992
PREVENTION
Visit to the Laboratory For Evaluation and Failure Prevention of Materials, Toyohashi University of Technology, 17 Oct 94
[AD-A292340] p 2597 N95-30293
PRIMARY COSMIC RAYS
Fluxes and relative abundances of light cosmic ray nuclei at energies above 40 GeV/n p 2739 N95-29531
PRIMERS (COATINGS)
Epoxy self-priming topcoats
[AD-D017383] p 2541 N95-29194
PRIMITIVE EQUATIONS
A numerical study of the effects of wind forcing on the Chile Current System
[AD-A289808] p 2629 N95-28982
PRINCIPAL COMPONENTS ANALYSIS
Optical (LANDSAT/TM) and radar (ERS-1/SAR) imagery sinergism studies applied to land use discrimination
[INPE-5608-TDI/554] p 2598 N95-29433
PRINTED CIRCUITS
Theory and experiments on chemical instabilities
[AD-A290773] p 2534 N95-29922
PRIORITIES
NASA/DOD Aerospace Knowledge Diffusion Research Project. Paper 49: Becoming an aerospace engineer: A cross-gender comparison
[NASA-TM-110731] p 2721 N95-29028
PRISMS
Unstructured Cartesian/prismatic grid generation for complex geometries p 2481 N95-28741
Adaptive hybrid prismatic-tetrahedral grids for viscous flows p 2481 N95-28744
PROBABILITY DENSITY FUNCTIONS
Statistical properties of bistatic clutter echoes
[AD-A291688] p 2552 N95-28943
Induction of selective Bayesian classifiers
[AD-A292690] p 2675 N95-29906
PROBABILITY DISTRIBUTION FUNCTIONS
Infinite divisibility and the waiting-time paradox
[PB95-206934] p 2666 N95-30167
PROBABILITY THEORY
XMap: A general purpose mapping program
[AD-A289958] p 2647 N95-29276
Estimates of probability of a cloud-free line of sight for RAPTOR TALON
[AD-A291908] p 2510 N95-29284
Learning object models from visual observation and background knowledge
[AD-A292606] p 2650 N95-29576
Theory and experiments on chemical instabilities
[AD-A290773] p 2534 N95-29922
A full wave study of radar cross sections of rough terrain
[AD-A291227] p 2559 N95-29962
Fast simulation of the leaky bucket algorithm
[PB95-197174] p 2653 N95-30096
Checkpointing and the modeling of program execution time
[PB95-197182] p 2653 N95-30099
Infinite divisibility and the waiting-time paradox
[PB95-206934] p 2666 N95-30167

Short and elementary proof of the main Bahadur-Kiefer theorem
[PB95-206967] p 2675 N95-30170

PROBLEM SOLVING
An unstructured-grid software system for solving complex aerodynamic problems p 2481 N95-28743
A procedure for automating CFD simulations of an inlet-bleed problem p 2485 N95-28768
Discontinuous solutions of semilinear differential-algebraic equations. part 2: Rho-consistency
[AD-A292285] p 2668 N95-28861
Discontinuous solutions of semilinear differential-algebraic equations. part 1: Distribution solutions
[AD-A292286] p 2668 N95-28863
Improving problem-solving and decision-making skills under stress: Prediction and training
[AD-A292104] p 2638 N95-28918
An algorithm fusion approach to IRST signal processing (III): Nongaussian-corrected filter fusion
[AD-A291565] p 2552 N95-28936
An assessment of artificial damping models for aeroacoustic calculations
[NASA-CR-198354] p 2574 N95-29405
Automated reasoning about classical mechanics
[AD-A290052] p 2663 N95-29477
Parallel adaptive techniques for transient partial differential equations
[AD-A290460] p 2674 N95-29490
Mathematical olympiad summer program (MOSP) 1994
[AD-A290801] p 2672 N95-29647
Solutions of the benchmark problems by the dispersion-relation-preserving scheme
p 2674 N95-30145
Massively parallel fast elliptic equation solver for three dimensional hydrodynamics and relativity
[DE95-009385] p 2660 N95-30193

PROCESSING
Process optimization through discovery and integration of materials and processing properties. phase 1
[AD-A292576] p 2662 N95-28978

PRODUCT DEVELOPMENT
Requirements for effective use of CFD in aerospace design p 2478 N95-28725
High reliability, maintenance-free INS battery development, phase 2
[AD-A291412] p 2586 N95-30070
Engineering development program of a closed aluminum-oxygen semi-cell system for an unmanned underwater vehicle: An update p 2606 N95-30266
Hermetically sealed aluminum electrolytic capacitor p 2568 N95-30268
High energy density electrolytic capacitor p 2568 N95-30271
Product configurations: An application for prototype object approach
[PB95-192589] p 2655 N95-30283

PRODUCTION COSTS
Impact of composites on future transport aircraft p 2519 N95-29030
Challenges and payoff of composites in transport aircraft: 777 empennage and future applications p 2519 N95-29031

PRODUCTION MANAGEMENT
CD-ROM preparation: An overview and guide
[NASA-CR-198756] p 2655 N95-30307

PRODUCTION PLANNING
Geometric grid generation p 2483 N95-28756
Applicability of neural networks for production planning under uncertainty
[PB95-197406] p 2666 N95-30101

PRODUCTIVITY
Process optimization through discovery and integration of materials and processing properties. phase 1
[AD-A292576] p 2662 N95-28978
The Telemetry Agile Manufacturing Effort
[DE95-006177] p 2654 N95-30115

PROGRAM VERIFICATION (COMPUTERS)
An unstructured-grid software system for solving complex aerodynamic problems p 2481 N95-28743
Inductive boolean function manipulation: A hardware verification methodology for automatic induction
[AD-A292236] p 2669 N95-29128
Porting a vector library: A comparison of MPI, paris, CMMD and PVM (or, 'I'll never have to port CVL again')
[AD-A290231] p 2647 N95-29147
The 10th Annual Review of Progress in Applied Computational Electromagnetics, volume 1
[AD-A286796] p 2553 N95-29159
The generalized railroad crossing: A case study in formal verification of real-time systems
[AD-A290152] p 2648 N95-29319
Software testing toolkit for distributed simulations
[AD-A291867] p 2649 N95-29435
Grid resolution and turbulent inflow boundary condition recommendations for NPARC calculations
[NASA-TM-106959] p 2492 N95-30253

PROGRAMMING ENVIRONMENTS
A friendly editing environment for computer-aided rapid prototyping of hard real-time systems
[AD-A290154] p 2648 N95-29321
PSEE architecture report: Architectures and models for next generation process-based software engineering environments
[AD-A291268] p 2652 N95-29996
Realisation of an integrated software engineering environment through heterogeneous CASE-tool integration
[PB95-197646] p 2653 N95-30105

PROGRAMMING LANGUAGES
Structural cut elimination in linear logic
[AD-A292248] p 2645 N95-28886
Porting a vector library: A comparison of MPI, paris, CMMD and PVM (or, 'I'll never have to port CVL again')
[AD-A290231] p 2647 N95-29147
Conversion of an oceanographic expert system to a C-based language
[NASA-CR-198695] p 2630 N95-29237
Characteristics of higher-level languages for software architecture
[AD-A292215] p 2649 N95-29376
Design and implementation of logical database languages
[AD-A290474] p 2650 N95-29509
Workshop on computing and intelligent systems
[AD-A290581] p 2666 N95-30040
A formal extension to object oriented analysis using Z
[AD-A290911] p 2653 N95-30080
Static analysis of functional programs
[PB95-197141] p 2653 N95-30095

PROGRESS
The 6th Van der Ziel symposium on quantum 1/f noise and other low frequency fluctuations in electronic devices
[AD-A292468] p 2718 N95-29009

PROJECT MANAGEMENT
Electric and hybrid vehicle program: Site operator program
[DE95-008620] p 2591 N95-30211

PROJECT PLANNING
ARPA solid state laser and nonlinear materials program
[AD-A289657] p 2584 N95-28678
Aircraft advanced materials research and development program plan
[AD-A290542] p 2498 N95-29565

PROJECTIVE GEOMETRY
Relative affine structure: Canonical model for 3D from 2D geometry and applications
[AD-A290085] p 2670 N95-29352

PROPAGATION MODES
Discriminant analysis to predict the occurrence of ELMS in H-mode discharges
[AD-B179183L] p 2708 N95-29746

PROPELLANT COMBUSTION
SCAP spray combustion analysis program
[AD-A289946] p 2532 N95-29273

PROPELLANT PROPERTIES
SCAP spray combustion analysis program
[AD-A289946] p 2532 N95-29273

PROPELLANT TANKS
Fuel cell systems for First Lunar Outpost-reactant storage option p 2606 N95-30264

PROPELLANTS
A thermochemical transport model for analysis of hot-spot formation in energetic materials
[AD-A290441] p 2532 N95-29357
Fundamental studies of oxygen rings and other high energy density molecular systems
[AD-A290875] p 2693 N95-29865
Assay of potentially contaminated propellant
[DE95-006330] p 2549 N95-30345

PROPORTIONAL COUNTERS
Novel photoelectric sensing technology for environmental monitoring, phase 1
[AD-A292026] p 2611 N95-30348

PROPULSION SYSTEM CONFIGURATIONS
Surface modeling and grid generation for aeropropulsion CFD p 2479 N95-28732
External combustion engine having an asymmetrical CAM
[AD-D017382] p 2588 N95-28785
A transient model of the RL10A-3-3A rocket engine
[NASA-CR-195478] p 2510 N95-29114
Design, analysis and control of large transports so that control of engine thrust can be used as a back-up of the primary flight controls
[NASA-CR-198958] p 2501 N95-30254

PROTECTION
Cathodic protection system inspection 6
[AD-A289720] p 2591 N95-28682
Sensor protection portion of the development of nonlinear optical materials and processes for laser hardening of sensors
[AD-A291200] p 2702 N95-29973

PROTECTIVE COATINGS
Zero Discharge Organic Coatings: Powder paint. UV curable paint. E-coat
[AD-A292180] p 2540 N95-28925
Epoxy self-priming topcoats
[AD-D017383] p 2541 N95-29194
The measurement of adhesion at film-substrate interfaces using a constant depth scratch test
[AD-A289940] p 2542 N95-29269
In-line fiber etalon strain sensor
[AD-D017266] p 2699 N95-29283
Nanoindentation and nanoscratching of hard coating materials for magnetic disks
[DE95-008776] p 2547 N95-30174

PROTECTORS
Shock resistant optic fiber rotary slice holding device
[AD-D017327] p 2702 N95-30053

PROTEIN CRYSTAL GROWTH
Summary Report of mission acceleration measurements for STS-66. Launched November 3, 1994
[NASA-TM-106914] p 2509 N95-29643

PROTEINS
Cellular and molecular level responses after radiofrequency radiation exposure, alone or in combination with x rays or chemicals
[AD-A292488] p 2633 N95-28866
Parallel continuation-based global optimization for molecular conformation and protein folding
[DE95-005860] p 2633 N95-30114
Biological methane activation
[PB95-200705] p 2535 N95-30198

PROTOCOL (COMPUTERS)
A formative evaluation of CU-SeeMe
[AD-A292443] p 2553 N95-29002
Communication protocols in multi-hop radio networks p 2553 N95-29106
Mode of human image representation and error checking strategies in complex visual displays
[AD-A290107] p 2492 N95-29210
Characteristics of higher-level languages for software architecture
[AD-A292215] p 2649 N95-29376
Formal design of communication protocols using Estelle
[AD-A290584] p 2652 N95-30042
Fischer's protocol in timed process algebra
[PB95-206777] p 2672 N95-30089
Functionally specified distributed transactions in co-operative scenarios
[PB95-197380] p 2725 N95-30100
Layers as knowledge transitions in the design of distributed systems
[PB95-197638] p 2660 N95-30104

PROTON BEAMS
A practical high-energy high-luminosity mu(+)-mu(-) collider
[DE95-006769] p 2696 N95-30009
Sea and gluon spin structure function measurements at RHIC
[DE95-005823] p 2695 N95-30185
Measurements of (Delta)(sigma)(sub L)(pp) and (Delta)(sigma)(sub L)((bar p)p) at 200 GeV/c
[DE95-005837] p 2695 N95-30186

PROTON-PROTON REACTIONS
Lattice/beam dynamics working group
[DE95-006774] p 2696 N95-30021
Parameterized spectral distributions for meson production in proton-proton collisions
[NASA-TM-4675] p 2696 N95-30337

PROTONS
Activities update
[AD-A292431] p 2692 N95-28994
A Monte Carlo simulation of Coulomb collisions and wave-particle interactions in space plasma at high latitudes p 2704 N95-29205
Technology development goals for automotive fuel cell power systems
[DE95-008764] p 2548 N95-29280
A novel unitized regenerative proton exchange membrane fuel cell p 2605 N95-30263

PROTOPLANETS
Coronagraphic imaging of protoplanetary-disk candidate stars using adaptive optics p 2728 N95-29651

PROTOSTARS
The dynamics of FU Orionis outbursts: Time-dependent accretion through protostellar disks p 2732 N95-29530

PROTOTYPES
Proceedings of the Complex Systems Engineering Synthesis and Assessment Technology Workshop (CSESAW 1994)
[AD-A292433] p 2646 N95-28995
NPSNETIV: An object-oriented interface for a three-dimensional virtual world
[AD-A292467] p 2646 N95-29008
Design and implementation of logical database languages
[AD-A290474] p 2650 N95-29509
Solid freeform fabrication symposium
[AD-A290949] p 2527 N95-29732
Equipment resource for MCM technology and system prototyping
[AD-A292492] p 2719 N95-29756
Defining the IEEE-854 floating-point standard in PVS
[NASA-TM-110167] p 2659 N95-29823
Digital mapping, charting, and geodesy analysis program technical review of vector smart map prototypes 1 and 2
[AD-A291217] p 2601 N95-29977
Prototype stop bar system evaluation at Seattle-Tacoma International Airport
[AD-A290136] p 2495 N95-30031
Correctness of real-time systems by construction
[PB95-206827] p 2655 N95-30220
Product configurations: An application for prototype object approach
[PB95-192589] p 2655 N95-30283

PROTUBERANCES
Thin-film edge field emitter device and method of manufacture therefor
[AD-D017323] p 2567 N95-30165

PROVING
Test load verification through strain data analysis
[NASA-TP-3558] p 2504 N95-28718
Software Design for Reliability and Reuse proof of concept project. Phase 1
[AD-A291690] p 2644 N95-28782
Stable function approximation in dynamic programming
[AD-A290224] p 2647 N95-29143
Precision cleaning verification of fluid components by air/water impingement and total carbon analysis
[NASA-TM-110742] p 2531 N95-29248
From the (psi) to charmed mesons
[DE95-006564] p 2693 N95-29583
Defining the IEEE-854 floating-point standard in PVS
[NASA-TM-110167] p 2659 N95-29823
ANSYS duplicate finite-element checker routine
[NASA-TM-108492] p 2672 N95-29824
Proving the genericity lemma by leftmost reduction is simple
[PB95-197620] p 2673 N95-30103
Correctness of real-time systems by construction
[PB95-206827] p 2655 N95-30220

PSYCHOLOGICAL FACTORS
Life sciences program
[NASA-CR-197658] p 2633 N95-30292

PSYCHOLOGICAL TESTS
Visualization of CAD objects using a stereoscopic display
[AD-A290034] p 2639 N95-29439

PSYCHOMOTOR PERFORMANCE
CO2-O2 interactions in extension of tolerance to acute hypoxia
[NASA-CR-198575] p 2635 N95-29158

PUBLIC RELATIONS
Estimating attenuation and propagation of noise bands from a distant source using the lookup program and data base
[AD-A290218] p 2683 N95-29077

PULSAR MAGNETOSPHERES
Gamma radiation from rotation powered pulsars and results from the Energetic Gamma-Ray Experiment Telescope p 2739 N95-29671

PULSARS
The evolution of binary millisecond pulsars and the formation of planets around them p 2733 N95-29663
Models of accretion-powered x-ray pulsars p 2728 N95-29667
Gamma radiation from rotation powered pulsars and results from the Energetic Gamma-Ray Experiment Telescope p 2739 N95-29671
Applications of pulsar timing p 2734 N95-29675
A multi-wavelength study of rotation-driven pulsars p 2729 N95-29678

PULSE AMPLITUDE
Pulse waveform and pulse amplitude analysis during Lower Body Negative Pressure
[AD-A290521] p 2636 N95-29360
Relativistic effects on large amplitude nonlinear langmuir waves in a two-fluid plasma
[AD-B191980L] p 2710 N95-29841

PULSE COMMUNICATION
Feature extraction from digital communications signals using wavelet transforms
[AD-A292655] p 2556 N95-29386

PULSE DURATION
Novel high-power solid-state sources for the millimeter-wave region
[AD-A292653] p 2564 N95-29384

PULSE FREQUENCY MODULATION
Spacecraft attitude control system performance using pulse-width pulse-frequency modulated thrusters
[AD-A291803] p 2508 N95-29410

PULSE GENERATORS
Characterizing the electromagnetic environment produced by the army's repetitive electromagnetic pulse simulator (REPS)
[AD-A289739] p 2551 N95-28687
Novel high-power solid-state sources for the millimeter-wave region
[AD-A292653] p 2564 N95-29384
Semiconductor film Cherenkov lasers
[AD-A291177] p 2587 N95-29930

PULSED LASER DEPOSITION
Investigation of the characteristics of ferroelectric thin films deposited by pulsed laser ablation
[AD-A292306] p 2540 N95-28963
Electrical characteristics of barium strontium titanate-oxide composite films
[AD-A289991] p 2541 N95-29135
Pulsed laser deposition of ferroelectric thin films in conjunction with superconducting oxides
[AD-A290101] p 2585 N95-29208
Analysis of the ferroelectric thin films deposited by pulsed laser deposition on oxide and fluoride substrates
[AD-A290088] p 2543 N95-29353
Pulsed laser deposition of thin film material for nonlinear waveguides
[AD-A290789] p 2544 N95-29484
Epitaxial growth of high quality SiC of pulsed laser deposition, phase 1
[AD-A291410] p 2717 N95-30068

PULSED LASERS
Laser simulation of single-event effects: A state of the art review
[AD-A292308] p 2584 N95-28892
Investigation of the characteristics of ferroelectric thin films deposited by pulsed laser ablation
[AD-A292306] p 2540 N95-28963
Characterization and calibration of a pulsed laser system for single event upset simulation
[AD-A290075] p 2586 N95-29330
Measurement of interface strength, intrinsic toughness and their dependence on interfacial segregants
[AD-A291798] p 2524 N95-29409
Molecular spectra and dynamics at interfaces
[AD-A289779] p 2693 N95-29460
Development of distributed feedback dye lasers for generation of high-power 193 nm excimer laser short pulses p 2586 N95-29631
Research studies in electromagnetically induced transparency
[AD-A290796] p 2557 N95-29645
Observation of x ray generation in a proof-of-principle laser synchrotron source experiment
[AD-A291298] p 2588 N95-29937

PULSED RADIATION
Self-Induced Transparency in photonic band structures: Gap solitons near absorption resonances
[AD-A292187] p 2718 N95-28927

PULSES
Measurement of ultrashort pulses with a non-instantaneous nonlinearity
[DE95-006500] p 2698 N95-28983

PUMPS
Experimental studies of fundamental one- and two-photon lasing processes
[AD-A290593] p 2693 N95-29555

Q

QUADRATURES
Wideband I/Q demodulators: Measurement technique and matching characteristics
[AD-A291505] p 2558 N95-29847

QUALITY CONTROL
Conversion of the TRACON operations concepts database into a formal sentence outline job task taxonomy
[DOT/FAA/AM-95/16] p 2493 N95-28819
Quality Control of meteorological observations at Fleet Numerical Meteorology and Oceanography Center
[AD-A291577] p 2619 N95-28938
Coordination of operations for centrifuge quality control. phase 3C
[AD-A292533] p 2582 N95-28966
A least square real time quality control routine for the North Warning Netted Radar System
[AD-A290063] p 2555 N95-29328
AGARD flight test techniques series. Volume 13: Reliability and maintainability
[AGARD-AG-300-VOL-13] p 2498 N95-29503
A comparison of ISO 9001 and the Capability Maturity Model for Software
[AD-A290697] p 2651 N95-29762

QUANTILES
Short and elementary proof of the main Bahadur-Kiefer theorem
[PB95-206967] p 2675 N95-30170

QUANTUM CHEMISTRY
Optimal control of molecular motion
[AD-A291919] p 2691 N95-28944
Structural and electronic properties of adsorbates on semiconductors, metal-semiconductor interfaces and semiconductor heterojunctions
[AD-A291917] p 2715 N95-29438
Fundamental studies of oxygen rings and other high energy density molecular systems
[AD-A290875] p 2693 N95-29865

QUANTUM ELECTRONICS
The 6th Van der Ziel symposium on quantum 1/f noise and other low frequency fluctuations in electronic devices
[AD-A292468] p 2718 N95-29009
Nanoscience and nanotechnology in Europe
[AD-A290214] p 2562 N95-29075
Transport simulation in spatially modulated low dimensionality systems
[AD-A290486] p 2718 N95-29149
Transport phenomena and noise in real quantum wires
[AD-A290493] p 2714 N95-29152
The quantum hydrodynamic model for semiconductor devices
[AD-A291809] p 2564 N95-29430
Structural and electronic properties of adsorbates on semiconductors, metal-semiconductor interfaces and semiconductor heterojunctions
[AD-A291917] p 2715 N95-29438
New radiation sources through generation and resonant enhancement of Current Driven Plasma Instabilities in lower dimensional solid state systems
[AD-A290669] p 2705 N95-29519
Equipment resource for MCM technology and system prototyping
[AD-A292492] p 2719 N95-29756
The 41st Japan Society of Applied Physics Spring Meeting
[AD-A292333] p 2720 N95-29879

QUANTUM MECHANICS
Molecular spectra and dynamics at interfaces
[AD-A289779] p 2693 N95-29460
Quantum dynamical studies of the decomposition of energetic materials containing defect structures
[AD-A291456] p 2548 N95-29525
Quantum mechanical problems in one, two, and three dimensions
[ISBN-0-315-84931-2] p 2719 N95-29677
Fundamental studies of oxygen rings and other high energy density molecular systems
[AD-A290875] p 2693 N95-29865

QUANTUM NUMBERS
Screening constants for plasma
[AD-B179442L] p 2710 N95-29843

QUANTUM OPTICS
Self-Induced Transparency in photonic band structures: Gap solitons near absorption resonances
[AD-A292187] p 2718 N95-28927

QUANTUM THEORY
Transport simulation in spatially modulated low dimensionality systems
[AD-A290486] p 2718 N95-29149
Semiconductor science and technology
[AD-A289143] p 2563 N95-29191
Quantum fluctuations and semiclassical gravity theory p 2719 N95-29527
Fundamental studies of oxygen rings and other high energy density molecular systems
[AD-A290875] p 2693 N95-29865

QUANTUM WELL LASERS
Novel electric-field effects in quantum wells and superlattices
[AD-A292317] p 2718 N95-28857
Ion doped quantum well lasers
[AD-A290937] p 2587 N95-29912

QUANTUM WELLS
Novel electric-field effects in quantum wells and superlattices
[AD-A292317] p 2718 N95-28857
Conference proceedings: IEEE Nonlinear Optics, Materials, Fundamentals, and Applications
[AD-A292438] p 2698 N95-28997

Optoelectronics based on SiGe/Si heterostructures
[AD-A292464] p 2699 N95-29006
Development of ultra-low dark current, high performance 3-5 quantum well infrared photodetectors (QWIPs) for focal plane arrays staring imaging sensor systems
[AD-A290343] p 2714 N95-29089
Semiconductor science and technology
[AD-A289143] p 2563 N95-29191
High-density plasma dynamics in semiconductors
p 2705 N95-29632
Investigation of a normal incident high performance P-type strained layer In(0.3)Ga(0.7)As/In(0.52)Al(0.48)As quantum well infrared photodetector
[AD-A290946] p 2716 N95-29785
Electronic states in Cd(1-x)Zn(x)Te/CdTe strained layer coupled double quantum wells and their photoluminescence
[DE95-006806] p 2716 N95-29814
The 2nd International Conference on Thin Film Physics and Applications
[AD-A292353] p 2546 N95-29983
Auger rates in mid-IR InAsSb laser structures
[DE95-006325] p 2588 N95-30006

QUARKS
Inclusive hadronic production of the B(sub c) meson via heavy quark fragmentation
[DE95-008739] p 2695 N95-30191

QUASARS
Multiwaveband observations of quasars
p 2728 N95-29665
Numerical studies of ablative mass loss from wind accelerated clouds p 2622 N95-29676

QUATERNIONS
Robust control of nonlinear flexible multibody systems using quaternion feedback and dissipative compensation
[NASA-TM-109099] p 2507 N95-29377
Method for the calculation of spacecraft umbra and penumbra shadow terminator points
[NASA-TP-3547] p 2671 N95-29446

QUENCHING
Application of a rapid quench thermomagnetic analyzer to austempered ductile iron
[AD-A292261] p 2535 N95-28889

QUENCHING (ATOMIC PHYSICS)
Radiative lifetime and quenching rate constants of PF(b(1) Sigma+) and tests for an electronic to vibrational energy transfer quenching mechanism
[AD-A290294] p 2681 N95-29062

QUERY LANGUAGES
Formal aspects of object identity in database manipulation p 2722 N95-29116
Distributed queries and incremental updates in information retrieval systems p 2725 N95-30286

QUEUEING THEORY
Simulation methodology
[AD-A290461] p 2674 N95-29491
Fast simulation of the leaky bucket algorithm
[PB95-197174] p 2653 N95-30098
Infinite divisibility and the waiting-time paradox
[PB95-205934] p 2666 N95-30167
Precedence relation method for deriving flexible bound models for queueing systems
[PB95-206835] p 2667 N95-30221

R

RADAR
Adaptive block sequential detection of abrupt signal changes
[AD-A290456] p 2557 N95-29489

RADAR APPROACH CONTROL
Terminal area forecasts-fiscal years 1993-2010
[AD-A290635] p 2495 N95-29880

RADAR CROSS SECTIONS
Radar cross section synthesis for planar resistive surfaces
[AD-A290151] p 2555 N95-29318
A full wave study of radar cross sections of rough terrain
[AD-A291227] p 2559 N95-29982
High-frequency radar target modeling
[AD-A290965] p 2559 N95-29991

RADAR DATA
Microwave remote sensing of surface soil moisture and its application to hydrologic modeling
p 2600 N95-29821
Wideband I/Q demodulators: Measurement technique and matching characteristics
[AD-A291505] p 2558 N95-29847
Hi-res SAR data processing report
[AD-A291443] p 2559 N95-30073

RADAR DETECTION
Description of the OHGR database
[AD-A290146] p 2722 N95-29221
Long range aircraft detection using high-frequency surface-wave radar
[AD-A290148] p 2555 N95-29313
A least square real time quality control routine for the North Warning Netted Radar System
[AD-A290063] p 2555 N95-29328
Path resolved optical sensing of atmospheric winds utilizing speckle-turbulence interaction and pseudorandum code modulation
[AD-A290800] p 2621 N95-29497

RADAR ECHOES
Statistical properties of bistatic clutter echoes
[AD-A291688] p 2552 N95-28943
Development of improved geophysical imaging techniques for environmental site characterization
[AD-A291003] p 2558 N95-29875

RADAR EQUIPMENT
Conference reports
[AD-A289630] p 2561 N95-28911
Offshore next generation weather radar (NEXRAD) test and evaluation master plan (TEMP)
[AD-A291435] p 2559 N95-30072

RADAR IMAGERY
Collection of Magellan Venus radar mapping results
[NASA-CR-197656] p 2736 N95-29178
Optical (LANDSAT/TM) and radar (ERS-1/SAR) imagery sinergism studies applied to land use discrimination
[INPE-5608-TDI/554] p 2598 N95-29433
Development of improved geophysical imaging techniques for environmental site characterization
[AD-A291003] p 2558 N95-29875
Evaluation of the utilization of SAR polarimetric images in the survey of land resources in the Amazon area Tapajos Forest Reserve
[INPE-5517-PRE/1792] p 2601 N95-29999
Patch diameter limits for tiered subaperture SAR image formation algorithms
[DE95-008816] p 2560 N95-30177
Sea ice motions in the Central Arctic pack ice as inferred from AVHRR imagery
[NASA-CR-198835] p 2601 N95-30247

RADAR MAPS
Collection of Magellan Venus radar mapping results
[NASA-CR-197656] p 2736 N95-29178

RADAR MEASUREMENT
Studies of thermospheric neutral winds utilizing ground-based optical and radar measurements
p 2613 N95-29214
Heat and momentum flux measurements in the planetary boundary layer with a wind profiling radar/radio acoustic sounding system p 2617 N95-29777
Development of improved geophysical imaging techniques for environmental site characterization
[AD-A291003] p 2558 N95-29875

RADAR NETWORKS
Low threshold all-optical crossbar switch on GaAs-GaAlAs channel waveguide arrays
[AD-A292483] p 2712 N95-28862

RADAR REFLECTORS
Emissivity measurements in thin metallized membrane reflectors used for microwave radiometer sensors
[NASA-TM-110179] p 2506 N95-30251

RADAR SCATTERING
High-frequency radar target modeling
[AD-A290965] p 2559 N95-29991

RADAR TARGETS
High-frequency radar target modeling
[AD-A290965] p 2559 N95-29991

RADAR TRACKING
High resolution microwave survey
[NASA-TM-110566] p 2553 N95-29174
Long range aircraft detection using high-frequency surface-wave radar
[AD-A290148] p 2555 N95-29313
Sea ice motions in the Central Arctic pack ice as inferred from AVHRR imagery
[NASA-CR-198835] p 2601 N95-30247
The JPL Mars gravity field, Mars50c, based upon Viking and Mariner 9 Doppler tracking data
[NASA-CR-198881] p 2737 N95-30344

RADIAL DISTRIBUTION
Formation of positive radial electric field by Electron Cyclotron Heating in Compact Helical System
[AD-B191994L] p 2709 N95-29802

RADIAL VELOCITY
Statistics and large-scale structure
p 2734 N95-29780

RADIANT COOLING
Radiative cooling profiles calculated from ECMWF analyses and ISCCP C1 data, and their application to determination of distributions of apparent convective heating in the equatorial Pacific p 2625 N95-29805

RADIANT HEATING
The evolution of binary millisecond pulsars and the formation of planets around them p 2733 N95-29663

RADIATION
Upgrading the Day/Night whole sky imager from Manual/Interactive to full automatic control
[AD-A292296] p 2619 N95-28872

RADIATION BELTS
Solar system plasma waves
[NASA-CR-198767] p 2704 N95-29130

RADIATION DAMAGE
Calculation of shielding parameters
[DE95-608735] p 2694 N95-29886

RADIATION DETECTORS
Speckle imaging with the multi-anode microchannel array detector p 2728 N95-29652

RADIATION DISTRIBUTION
The spatial-scale dependence of the observed anisotropy of reflected and emitted radiation
p 2613 N95-29253

RADIATION DOSAGE
Calculation of shielding parameters
[DE95-608735] p 2694 N95-29886
Effects of space exposure on metals flown on the Long Duration Exposure Facility
[NASA-CR-4662] p 2512 N95-30225

RADIATION EFFECTS
Study of the space environmental effects on spacecraft engineering materials
[NASA-CR-196638] p 2531 N95-29246
Characterization and calibration of a pulsed laser system for single event upset simulation
[AD-A290075] p 2586 N95-29330
Ion beam modification of Tl-Ba-Ca-Cu-O type high temperature superconductors during irradiation
[DE95-006807] p 2717 N95-30022
Radiation effects on front-end electronics for noble liquid calorimetry
[DE95-007304] p 2566 N95-30025
Effects of space exposure on metals flown on the Long Duration Exposure Facility
[NASA-CR-4662] p 2512 N95-30225
Life sciences program
[NASA-CR-197658] p 2633 N95-30292

RADIATION HARDENING
Radiation effects on front-end electronics for noble liquid calorimetry
[DE95-007304] p 2566 N95-30025
Depth-independent hardness improvements in ion irradiated polystyrene
[DE95-008682] p 2547 N95-30190

RADIATION MEASUREMENT
The energy spectrum and flux of cosmic ray helium at high energy p 2740 N95-29705

RADIATION PRESSURE
Models of accretion-powered x-ray pulsars
p 2728 N95-29667

RADIATION PROTECTION
Laser optics protective device
[AD-D017384] p 2585 N95-29217
Calculation of shielding parameters
[DE95-608735] p 2694 N95-29886

RADIATION SHIELDING
Calculation of shielding parameters
[DE95-608735] p 2694 N95-29886

RADIATION SOURCES
HBCU/MI instrumentation for the Pulsed Power Plasma Sciences Laboratory at the University of New Mexico, FY92-93
[AD-A292444] p 2703 N95-29003
New radiation sources through generation and resonant enhancement of Current Driven Plasma Instabilities in lower dimensional solid state systems
[AD-A290669] p 2705 N95-29519
Research studies in electromagnetically induced transparency
[AD-A290796] p 2557 N95-29645
A multi-wavelength study of rotation-driven pulsars
p 2729 N95-29678

RADIATION TRANSPORT
Testing of the ENDF/B-VI neutron data library ENDF60 for use with MCNP(trademark)
[DE95-007858] p 2696 N95-30057
Distributed multitasking ITS with PVM
[DE95-006821] p 2660 N95-30116

RADIATIVE HEAT TRANSFER
Energy budget in the Asian monsoon region
p 2623 N95-29713

RADIATIVE LIFETIME
Radiative lifetime and quenching rate constants of PF(b(1) Sigma+) and tests for an electronic to vibrational energy transfer quenching mechanism
[AD-A290294] p 2681 N95-29062

RADIATIVE TRANSFER
Broadband Integrated Transmittances (BITS)
[AD-A292176] p 2555 N95-29266
Models of accretion-powered x-ray pulsars
p 2728 N95-29667

The interactive role of clouds and radiative transfer in maintaining atmospheric circulation
p 2616 N95-29699

RADICALS
Semiconductor deposition and etching interactions of laser-generated translationally hot atoms and radicals
[AD-A291824] p 2693 N95-29431
Preparation and studies of urazole containing polymers
[AD-A290685] p 2545 N95-29586

RADIO ANTENNAS
Electromagnetic antenna modeling (EAM) system
[AD-A292194] p 2552 N95-28986
Performance analysis of a GPS interferometric attitude determination system for a gravity gradient stabilized spacecraft
[NASA-CR-188372] p 2508 N95-30036

RADIO ASTRONOMY
High resolution microwave survey
[NASA-TM-110566] p 2553 N95-29174
Radioastronomical measurements of plasma characteristics of the solar corona and the solar wind
p 2730 N95-29782
Nobeyama Radio Observatory report, no. 379
p 2735 N95-29836
Optimization of 100-meter Green Bank Telescope
[NASA-CR-198868] p 2731 N95-30230

RADIO BURSTS
A multi-wavelength study of rotation-driven pulsars
p 2729 N95-29678

RADIO COMMUNICATION
Analysis of tropospheric propagation characteristics based on regional meteorological data
[AD-A291581] p 2552 N95-28939
Communication protocols in multi-hop radio networks
p 2553 N95-29106
High resolution microwave survey
[NASA-TM-110566] p 2553 N95-29174
Improved interception capability through the use of transform domain processing
[AD-A292231] p 2554 N95-29203
UHF Low Density Radio Communications Link (LDRCL) Operational Test and Evaluation (OT&E) integration and OT&E operational final test report
[AD-A291447] p 2558 N95-29769

RADIO ELECTRONICS
A conceptual thermal design study of an electronically scanned thinned array radiometer
[NASA-TM-110173] p 2509 N95-30316

RADIO EMISSION
Nobeyama Radio Observatory report, no. 361: The radio properties of solar active region soft x-ray transient brightenings p 2737 N95-29098
Induced Compton scattering by relativistic electrons in magnetized astrophysical plasmas p 2610 N95-29885

RADIO FREQUENCIES
Characterizing the electromagnetic environment produced by the army's repetitive electromagnetic pulse simulator (REPS)
[AD-A289739] p 2551 N95-28687
A procedure for accessing digital satellites containing amateur payloads
[AD-A289748] p 2506 N95-28688
Cellular and molecular level responses after radiofrequency radiation exposure, alone or in combination with x rays or chemicals
[AD-A292488] p 2633 N95-28866
Analysis of tropospheric propagation characteristics based on regional meteorological data
[AD-A291581] p 2552 N95-28939
Interface properties of wide bandgap semiconductor structures
[AD-A289817] p 2713 N95-28954
Improved interception capability through the use of transform domain processing
[AD-A292231] p 2554 N95-29203

RADIO FREQUENCY HEATING
Interchange stability criteria for anisotropic central-cell plasmas in the tandem mirror GAMMA 10
[AD-B176253L] p 2707 N95-29738
Monte Carlo simulation study of the ICRF minority heating in the large helical device
[AD-B179858L] p 2708 N95-29749

RADIO NAVIGATION
Wide Area Differential GPS (WADGPS)
p 2494 N95-29107

RADIO OBSERVATION
A multi-wavelength study of rotation-driven pulsars
p 2729 N95-29678

RADIO RECEIVERS
Improved interception capability through the use of transform domain processing
[AD-A292231] p 2554 N95-29203
A conceptual thermal design study of an electronically scanned thinned array radiometer
[NASA-TM-110173] p 2509 N95-30316

RADIO SIGNALS
Improved interception capability through the use of transform domain processing
[AD-A292231] p 2554 N95-29203

RADIO SOURCES (ASTRONOMY)
Aperture synthesis observation of HCN J = 1-0 emission from Y Canum Venaticorum p 2735 N95-29839

RADIO SPECTRA
Multiwaveband observations of quasars
p 2728 N95-29665
Induced Compton scattering by relativistic electrons in magnetized astrophysical plasmas p 2610 N95-29885

RADIO TELESCOPES
Optimization of 100-meter Green Bank Telescope
[NASA-CR-198868] p 2731 N95-30230

RADIO WAVES
Analysis of tropospheric propagation characteristics based on regional meteorological data
[AD-A291581] p 2552 N95-28939

RADIOACTIVE ISOTOPES
Large scale fluctuations of the geomagnetic field
p 2617 N95-29796

RADIOACTIVE WASTES
Assay of potentially contaminated propellant
[DE95-006330] p 2549 N95-30345

RADIOACTIVITY
New tetraarylborate and ethyldibutylstannane reagents
[AD-A289813] p 2540 N95-28953

RADIOMETERS
Measurement of the seasonal and annual variability of total column aerosol in a northeastern US network
[DE95-007259] p 2608 N95-28920
Nonlinear calibration of an infrared radiometer
[AD-A292436] p 2698 N95-28996
Improved interception capability through the use of transform domain processing
[AD-A292231] p 2554 N95-29203

RADIOSONDES
Upper-air data collected on Ice Station Weddell
[AD-A289707] p 2620 N95-29193
Research results on an improved in-situ tropospheric humidity sensor
[AD-A291339] p 2627 N95-29944
Production of a long-term global water vapor and liquid water data set using ultra-fast methods to assimilate multi-satellite and radiosonde observations
[NASA-CR-198955] p 2628 N95-30272

RADOMES
Operational test and evaluation (OT&E) integration and operational test plan for fixed ground antenna radome (FGAR)
[AD-A291310] p 2559 N95-29940
Operational test and evaluation (OT&E) integration and operational test procedures for Fixed Ground Antenna Radome (FGAR)
[AD-A291203] p 2559 N95-29975

RAILS
DOD electronic data interchange (EDI) convention: ASC X12 transaction set 410 Rail Carrier Invoice, version 003020
[AD-A292495] p 2722 N95-29287

RAIN
Analysis of the structural characteristics and intensity evolution of super typhoon flo (1990) in special sensor Microwave/Imager (SSM/I) data
[AD-A292413] p 2619 N95-28989
The dynamics of circulations within the stratiform regions of squall lines p 2623 N95-29725

RAINDROPS
Short-range precipitation forecasts using assimilation of simulated satellite water vapor profiles and cloud liquid water p 2625 N95-29832

RAMAN SPECTRA
Measurement of ultrashort pulses with a non-instantaneous nonlinearity
[DE95-006500] p 2698 N95-28983
Raman and photo-modulated reflectivity studies of ZnTe/InAs semiconductor heterostructure under hydrostatic pressure
[AD-A290467] p 2716 N95-29506
High gain, low noise and broadband Raman and Brillouin fiber-optic amplifiers, channel selectors and switches
[AD-A290585] p 2700 N95-29553

RAMAN SPECTROSCOPY
Fiber optic Raman and micro Raman measurements of bonding agents at interface during the curing process
[AD-A292042] p 2523 N95-29189

RANDOM ACCESS MEMORY
Investigation and characterization of SEU effects and hardening strategies in avionics
[AD-A291058] p 2500 N95-29950

RANDOM PROCESSES
The development of methods and techniques to detect and model the underlying structure of chaotic systems
[AD-A292435] p 2680 N95-29072
Probabilistic modeling and statistical inference for random fields and space-time processes
[AD-A289956] p 2672 N95-30029

RANDOM VARIABLES
A contribution to the theory of robust estimation of multivariate location and shape: EID
[AD-A290435] p 2675 N95-29819
Infinite divisibility and the waiting-time paradox
[PB95-206934] p 2666 N95-30167
Short and elementary proof of the main Bahadur-Kiefer theorem
[PB95-206967] p 2675 N95-30170

RANDOM WALK
Improvement of inter-event distance tests of randomness in spatial point processes
[AD-A291151] p 2675 N95-30297

RANGEFINDING
Receiver design, performance analysis, and evaluation for space-borne laser altimeters and space-to-space laser ranging systems
[NASA-CR-198655] p 2584 N95-28908
A simple method for range finding via laser triangulation
[AD-A292529] p 2553 N95-29186
Passive ranging with an incoherent optical system
p 2700 N95-29543
The laser ranging of etalon satellites
[AD-A291019] p 2587 N95-29660

RAPID QUENCHING (METALLURGY)
Advanced manufacturing by spray forming: Aluminum strip and microelectromechanical systems
[DE95-008615] p 2536 N95-28959

RARE EARTH ELEMENTS
ARPA solid state laser and nonlinear materials program
[AD-A289657] p 2584 N95-28678
A Pr-141 Moessbauer study of praseodymium compounds
[PB95-192449] p 2535 N95-30282

RARE GAS-HALIDE LASERS
Spectrometric studies of selected nitrocompounds using laser-induced photofragmentation/photoionization at 193 nm
[AD-A289947] p 2530 N95-28876

RARE GASES
The physics of spin polarized gases
[AD-A292511] p 2680 N95-28810
Nanocrystalline processing and interface engineering of Si3N4-based ceramics
[AD-A291302] p 2546 N95-29939

RAREFIED GAS DYNAMICS
A study of fluid problems requiring a direct particle simulation
[AD-A290212] p 2658 N95-29074
An extension of the continuum model by Grad's thirteen moment equations for hypersonic rarefied flows
p 2488 N95-29118

RATES (PER TIME)
Variable rate optical iterative processing of optical information
[AD-D017397] p 2701 N95-29602

RATIOS
Mechanical properties of nanophase metals
[DE95-005408] p 2537 N95-30018

RATS
Experiment kits for processing biological samples inflight on SLS-2
[NASA-TM-4685] p 2642 N95-28722

RAYLEIGH NUMBER
The onset of electrohydrodynamic instability in isoelectric focusing
[NASA-CR-198805] p 2565 N95-29968

RAYLEIGH-RITZ METHOD
Formulation of an improved smeared stiffener theory for buckling analysis of grid-stiffened composite panels
[NASA-TM-110162] p 2529 N95-30341

REACTING FLOW
Dynamics of simple chemically reactive fluids
p 2573 N95-29335
Bibliography of Doctor Chul Park
[NASA-TM-110353] p 2503 N95-29351
Computation of the integrated aerodynamic and propulsive flowfields of a generic hypersonic space plane p 2490 N95-29788
State-of-the-art review of computational fluid dynamics modeling for fluid-solids systems
[DE95-005866] p 2577 N95-29988
Reliability enhancement of Navier-Stokes codes through convergence acceleration
[NASA-CR-196635] p 2578 N95-30034

REACTION KINETICS
The influence of space flight on erythrokinetics in man. Space Life Sciences Missions 1 and 2. Experiment E261
[NASA-CR-188368] p 2633 N95-28875

Radiative lifetime and quenching rate constants of PF(b(1) Sigma+) and tests for an electronic to vibrational energy transfer quenching mechanism
[AD-A290294] p 2681 N95-29062
Research into artificially induced atmospheric disturbances
[AD-A290150] p 2613 N95-29317
Dynamics of simple chemically reactive fluids
p 2573 N95-29335
The redox chemistry of some peroxo and superoxo metal ion complexes
[AD-A290761] p 2532 N95-29483
Reaction field (RF) calculation of the spectral shifts of indole
[AD-A290449] p 2532 N95-29487
Preparation and studies of urazole containing polymers
[AD-A290685] p 2545 N95-29586
Short term visits for collaborative research
[AD-A290704] p 2682 N95-29588
Dust formation in stellar outflows: A time-dependent model p 2733 N95-29649
Austenite to ferrite transformation kinetics during continuous cooling
[DE95-008582] p 2537 N95-29869
Theory and experiments on chemical instabilities
[AD-A290773] p 2534 N95-29922
Investigation of laminar methane flames with emphasis on kinetics elucidation and NOx reduction
[PB95-200531] p 2535 N95-30111
Feasibility of a jet-stirred reactor for evaluating replacements for halon fire retardants
[AD-A291155] p 2551 N95-30299

REACTION PRODUCTS
State resolved differential cross sections for reactions important to the decomposition of energetic materials
[AD-A290718] p 2548 N95-29498

REACTIVITY
Selective attachment of nucleic acid molecules to patterned self-assembled surfaces
[AD-D017379] p 2530 N95-28854
Photogenerated amines in the design of imaging materials: The radiation-induced imidization of functionalized polystyrenes bearing amide-ester side chains
[AD-A289943] p 2542 N95-29270
Thermoreactive aircraft coatings (TRAC) program
[AD-A292054] p 2542 N95-29314
A cluster beam study of boron, boron oxide and B(x)O(y)H chemistry with hydrogen fluoride
[AD-A290826] p 2533 N95-29722

REACTOR DESIGN
Remote maintenance challenges presented in the ITER engineering design
[DE95-006392] p 2710 N95-29909
Nanocrystalline processing and interface engineering of Si3N4-based ceramics
[AD-A291302] p 2546 N95-29939

REACTOR MATERIALS
The international fusion materials irradiation facility
[DE95-006536] p 2696 N95-29142
Effects of impurities released from high Z test limiter on plasma performance in TEXTOR
[AD-B191995L] p 2709 N95-29803
Analytical electron microscopy of precipitates in ion-implanted MgAl2O4 spinel
[DE95-007406] p 2538 N95-30038

REACTOR SAFETY
Calculation of shielding parameters
[DE95-608735] p 2694 N95-29886

READING
ADA in introductory courses
[AD-A292219] p 2648 N95-29285

REAGENTS
New tetraarylborate and ethyldibutylstannane reagents
[AD-A289813] p 2540 N95-28953

REAL TIME OPERATION
Automated analysis of zooplankton size and taxonomic composition using the video plankton recorder
[AD-A289725] p 2631 N95-28685
Proceedings of the Complex Systems Engineering Synthesis and Assessment Technology Workshop (CSESAW 1994)
[AD-A292433] p 2646 N95-28995
A formative evaluation of CU-SeeMe
[AD-A292443] p 2553 N95-29002
The development of an interpretive methodology for the application of real-time acousto-ultrasonic NDE technique for monitoring damage in ceramic composites under dynamic loads p 2592 N95-29104
Real-time x-ray scattering study of processing of eight performance thermoplastics
[AD-A290374] p 2542 N95-29230
The generalized railroad crossing: A case study in formal verification of real-time systems
[AD-A290152] p 2648 N95-29319
A least square real time quality control routine for the North Warning Netted Radar System
[AD-A290063] p 2555 N95-29328
Transport delays associated with NASA Langley Flight Simulation Facility
[NASA-TM-110150] p 2659 N95-29454
Development of an artificial neural network for real-time classification of cone penetrometer strain gauge data
[AD-A290719] p 2664 N95-29499
Proceedings of the 6th International Conference on Nondestructive Characterization of Materials
[AD-A290727] p 2596 N95-29580
Photorefractive Bi12SiO20 spatial light modulator
[AD-A291070] p 2702 N95-29969
Fischer's protocol in timed process algebra
[PB95-206777] p 2672 N95-30089
Correctness of real-time systems by construction
[PB95-206827] p 2655 N95-30220
Manual for a workstation-based generic flight simulation program (LaRCsim), version 1.4
[NASA-TM-110164] p 2502 N95-30327
Developing a workstation-based, real-time simulation for rapid handling qualities evaluations during design
[NASA-CR-198831] p 2499 N95-30335

RECEIVERS
Receiver design, performance analysis, and evaluation for space-borne laser altimeters and space-to-space laser ranging systems
[NASA-CR-198655] p 2584 N95-28808

RECEPTORS (PHYSIOLOGY)
Coupling of brain muscarinic receptors to second messengers
[AD-A290498] p 2635 N95-29153

RECESSION
Evaluation of wear resistant ceramic valve seats in gas-fueled power generation engines
[PB95-200218] p 2591 N95-30110

RECOMMENDATIONS
Orbital debris: A technical assessment
[NASA-CR-198639] p 2507 N95-28852

RECONNAISSANCE
Unmanned aerial vehicles: No more Hunter systems should be bought until problems are fixed
[AD-A292172] p 2497 N95-29126

RECONSTRUCTION
Signal processing for high-resolution image formation
[AD-A290648] p 2557 N95-29563

RECOVERABILITY
Asymptotically zero energy computing using split-level charge recovery logic
[AD-A290054] p 2564 N95-29478

RECTANGULAR PLANFORMS
A fourth order Euler/Navier-Stokes prediction method for the aerodynamics and aeroelasticity of hovering rotor blades p 2572 N95-29242

RECTANGULAR PLATES
Flat rectangular isotropic plates under uniformly distributed normal pressure. Elastic deflections, stresses, and strains, moments and forces, for various forms of edge restraint
[ESDU-94033] p 2593 N95-28801

RECTANGULAR WINGS
Navier-Stokes solution of wing wake structure and its perturbation p 2488 N95-29121

RECTIFIERS
Cathodic protection system inspection 5
[AD-A289724] p 2592 N95-28684

RECURSIVE FUNCTIONS
Airy functions and the recursive ray acoustics algorithm
[AD-A290182] p 2629 N95-29054
Transport simulation in spatially modulated low dimensionality systems
[AD-A290486] p 2718 N95-29149

RECYCLING
Carbon sheet pumping
[AD-B179443L] p 2710 N95-29812

RED SHIFT
A gyroscope clock for a null gravitational redshift experiment p 2584 N95-29664

REDUNDANCY
Methods of generating low redundancy direction finding array configurations
[AD-A292590] p 2555 N95-29289
An analysis of the impact of ASPA on organizational and depot level maintenance
[AD-A292670] p 2477 N95-29414
Continuation of research in the statistical aspects of reliability, availability, and maintainability
[AD-A290126] p 2592 N95-29423
Robust fault detection filter design
p 2592 N95-29786

REENTRY VEHICLES
Transonic, supersonic and hypersonic wind-tunnel tests on aerodynamic characteristics of reentry body with blunted cone configuration
[ISAS-658] p 2490 N95-29640
Experimental studies on boundary-layer transition on a reentry vehicle at transonic and supersonic speeds
[ISAS-659] p 2575 N95-29712

REFLECTANCE
Reflectance analysis under solar illumination
[AD-A290489] p 2737 N95-29151
Continental aerosol effects on stratocumulus microphysics during MAST 1994
[AD-A292674] p 2621 N95-29416
Engineering design of sub-micron topographies for simultaneously adherent and reflective metal-polymer interfaces
[NASA-CR-198845] p 2548 N95-30237

REFLECTED WAVES
The spatial-scale dependence of the observed anisotropy of reflected and emitted radiation
p 2613 N95-29253
The detection of oil slicks at night with airborne infrared imagers
[AD-A289731] p 2598 N95-29281

REFLECTOR ANTENNAS
Development of the theory and algorithms for synthesis of reflector antenna systems
[AD-A292579] p 2552 N95-28979

REFLEXES
A biologically-inspired autonomous robot
[AD-A289446] p 2666 N95-30026

REFRACTION
Refractive changes during prolonged exposure to altitude following refractive surgery
[AD-A290263] p 2635 N95-29173
An extension of the Lighthill theory of jet noise to encompass refraction and shielding
[NASA-TM-110163] p 2684 N95-29452
The Scanning Fast Field Program (SCAFFIP) general version 1.0 user's manual
[AD-A291209] p 2618 N95-29976

REFRACTIVITY
Airy functions and the recursive ray acoustics algorithm
[AD-A290182] p 2629 N95-29054
Refractive changes during prolonged exposure to altitude following refractive surgery
[AD-A290263] p 2635 N95-29173
Photon-counting spatial light modulator technology development
[AD-A292619] p 2699 N95-29295
Theories of the nonlinear optical properties of composite media: Applications to phthalocyanine dyes
[AD-A290640] p 2700 N95-29560
HTMIAC/CINDAS silicon properties database. User's guide
[AD-A292602] p 2533 N95-29575
Selective multi-chemical fiber optic sensor
[AD-D017409] p 2703 N95-30076

REFRACTORY MATERIALS
Demonstration of a stabilized alumina/ethanol colloidal dispersion technique for seeding high temperature air flows
[NASA-TM-106945] p 2582 N95-29113
Semiconductor deposition and etching interactions of laser-generated translationally hot atoms and radicals
[AD-A291824] p 2693 N95-29431
Bilateral US/Russia Workshop on Self-Propagating High-Temperature Synthesis held in Honolulu, Hawaii on 6-7 November 1993
[AD-A290466] p 2525 N95-29492
Innovative processing of composites for ultra-high temperature applications, book 1
[AD-A290889] p 2527 N95-29842
The mm-wave resonant methods for the detection of corrosion, phase 1
[AD-A291315] p 2593 N95-29941

REFRIGERANTS
Alternative refrigerant performance: Field test of a nonchlorofluorocarbon chiller at Fort Leonard Wood, MO
[AD-A292052] p 2550 N95-29307
Use of chlorofluorocarbon-based refrigerants in USArmy facility air-conditioning and refrigeration systems: Recommendations for the interim period 1994-2000
[AD-A290432] p 2550 N95-29537

REFRIGERATING
Liquid pressure amplification and liquid injection in air conditioning and refrigeration systems
[AD-A289738] p 2549 N95-28686
Alternative refrigerant performance: Field test of a nonchlorofluorocarbon chiller at Fort Leonard Wood, MO
[AD-A292052] p 2550 N95-29307

Use of chlorofluorocarbon-based refrigerants in USArmy facility air-conditioning and refrigeration systems: Recommendations for the interim period 1994-2000
[AD-A290432] p 2550 N95-29537

REGENERATIVE FUEL CELLS
A novel unitized regenerative proton exchange membrane fuel cell p 2605 N95-30263
The TMI regenerable solid oxide fuel cell
p 2606 N95-30265

REGOLITH
A geotechnical characterization of lunar soils and lunar soil simulants p 2736 N95-29117

REGRESSION ANALYSIS
Stochastic modeling and global warming trend extraction for ocean acoustic travel times
[AD-A292114] p 2608 N95-28922
A contribution to the theory of robust estimation of multivariate location and shape: EID
[AD-A290435] p 2675 N95-29819
A regression model for the western north pacific tropical cyclone intensity forecast
[AD-A290588] p 2627 N95-30044

REGULATIONS
The Environmental Assessment and Management (TEAM) guide
[AD-A286748] p 2608 N95-28787

REINFORCED PLATES
Analytical and experimental studies of the energy absorption behavior of composite structures
p 2524 N95-29411
Formulation of an improved smeared stiffener theory for buckling analysis of grid-stiffened composite panels
[NASA-TM-110162] p 2529 N95-30341

REINFORCEMENT (STRUCTURES)
Shear reinforcement in deep slabs
[AD-A289528] p 2594 N95-28909

REINFORCING FIBERS
Phase coupling and morphology generation in engineering polymer alloys
[AD-A291868] p 2543 N95-29436
Investigation of tension-compression fatigue behavior of a notched cross-ply metal matrix composite at elevated temperature
[AD-A291479] p 2527 N95-29770
Alumina reinforced Tetragonal Zirconia (TZP) composites
[DE95-008990] p 2529 N95-30180
Composite processing development to improve interlaminar strength using ply interface particles
[NASA-TM-108495] p 2529 N95-30334

REINFORCING MATERIALS
Shear reinforcement in deep slabs
[AD-A289528] p 2594 N95-28909

RELATIVISTIC EFFECTS
Observational signatures of rotating black holes
p 2729 N95-29709
Relativistic effects on large amplitude nonlinear langmuir waves in a two-fluid plasma
[AD-B191980L] p 2710 N95-29841

RELATIVISTIC ELECTRON BEAMS
High power, high frequency radiation from beam-plasma interactions
[AD-A292442] p 2703 N95-29001
Relativistic effects on large amplitude nonlinear langmuir waves in a two-fluid plasma
[AD-B191980L] p 2710 N95-29841
Observation of x ray generation in a proof-of-principle laser synchrotron source experiment
[AD-A291298] p 2588 N95-29937

RELATIVISTIC PARTICLES
Induced Compton scattering by relativistic electrons in magnetized astrophysical plasmas p 2610 N95-29885

RELATIVITY
Massively parallel fast elliptic equation solver for three dimensional hydrodynamics and relativity
[DE95-009385] p 2660 N95-30193

RELAXATION METHOD (MATHEMATICS)
On the utility of threads for data parallel programming
[NASA-CR-198155] p 2649 N95-29455

RELIABILITY
Software Design for Reliability and Reuse proof of concept project. Phase 1
[AD-A291690] p 2644 N95-28782
Continuation of research in the statistical aspects of reliability, availability, and maintainability
[AD-A290126] p 2592 N95-29423
Liquefied metal jet program Automation and Robotics Research Institute (ARRI)
[AD-A289781] p 2536 N95-29461
Proceedings of the 6th International Conference on Nondestructive Characterization of Materials
[AD-A290727] p 2596 N95-29580
Prototype stop bar system evaluation at Seattle-Tacoma International Airport
[AD-A290136] p 2495 N95-30031
High reliability, maintenance-free INS battery development, phase 2
[AD-A291412] p 2566 N95-30070
Fatigue case study and reliability analyses for wind turbines
[DE95-004770] p 2603 N95-30213

RELIABILITY ANALYSIS
Software measurement guidebook
[NASA-CR-189407] p 2644 N95-28806
R&M design expert system
[AD-A292525] p 2645 N95-28814
Improved interception capability through the use of transform domain processing
[AD-A292231] p 2554 N95-29203
Applied Computational Electromagnetics Society Journal, volume 10, number 1, March 1995
[AD-A292069] p 2555 N95-29308
Ceramic material life prediction: A program to translate ANSYS results to CARES/LIFE reliability analysis
[NASA-CR-198795] p 2543 N95-29367
Continuation of research in the statistical aspects of reliability, availability, and maintainability
[AD-A290126] p 2592 N95-29423
Proceedings of the 12th Annual National Conference on Ada Technology
[AD-A290693] p 2651 N95-29644
A PC program for estimating measurement uncertainty for aeronautics test instrumentation
[NASA-CR-198361] p 2503 N95-30067
Fatigue case study and reliability analyses for wind turbines
[DE95-004770] p 2603 N95-30213

RELIABILITY ENGINEERING
Parallel adaptive techniques for transient partial differential equations
[AD-A290460] p 2674 N95-29490

RELIEF MAPS
Digital mapping, charting, and geodesy analysis program technical review of vector smart map prototypes 1 and 2
[AD-A291217] p 2601 N95-29977

REMOTE CONSOLES
AFGWC dial-in subsystem (AFDIS) software users manual, version 3.1
[AD-A291103] p 2651 N95-29639

REMOTE CONTROL
Experiments in cooperative manipulation of objects by free-flying robot teams p 2662 N95-29095
Analysis of measurements for solid state laser remote lidar system
[NASA-CR-196640] p 2585 N95-29247

REMOTE HANDLING
Remote maintenance challenges presented in the ITER engineering design
[DE95-006392] p 2710 N95-29909
Simulation of robot manipulators
[DE95-008680] p 2654 N95-30189

REMOTE SENSING
Backscatter data acquisition for Hydrosweep DS aboard RV Ewing
[AD-A292332] p 2628 N95-28796
Monitoring of burning in the Brazilian cerrado region using AVHRR/NOAA data calibrated by TM/Landsat data
[INPE-5490-TDI/507] p 2598 N95-28929
Typhoon monitoring using passive microwave observations
[AD-A292567] p 2619 N95-28975
Analysis of the structural characteristics and intensity evolution of super typhoon flo (1990) in special sensor Microwave/Imager (SSM/I) data
[AD-A292413] p 2619 N95-28989
NASA to use telepresence to explore Antarctic Lakes
[NASA-TM-110567] p 2598 N95-29175
Analysis of measurements for solid state laser remote lidar system
[NASA-CR-196640] p 2585 N95-29247
Optical (LANDSAT/TM) and radar (ERS-1/SAR) imagery sinergism studies applied to land use discrimination
[INPE-5608-TDI/554] p 2598 N95-29433
Path resolved optical sensing of atmospheric winds utilizing speckle-turbulence interaction and pseudorandum code modulation
[AD-A290800] p 2621 N95-29497
Microwave remote sensing algorithms for cirrus clouds and precipitation p 2623 N95-29715
Remote sensing of hydrologic variables in boreal areas
[NASA-CR-189422] p 2600 N95-29754
Proposal for a flexible system of phytogeographic classification: Emphasis on the use of multistage remote sensoring
[INPE-5609-PRE/1821] p 2600 N95-29815
Microwave remote sensing of surface soil moisture and its application to hydrologic modeling
p 2600 N95-29821
Japanese remote sensing organizations, research, and technology
[AD-A292420] p 2601 N95-29905
Evaluation of the utilization of SAR polarimetric images in the survey of land resources in the Amazon area Tapajos Forest Reserve
[INPE-5517-PRE/1792] p 2601 N95-29999
Probabilistic modeling and statistical inference for random fields and space-time processes
[AD-A289956] p 2672 N95-30029
Production of a long-term global water vapor and liquid water data set using ultra-fast methods to assimilate multi-satellite and radiosonde observations
[NASA-CR-198955] p 2628 N95-30272
A conceptual thermal design study of an electronically scanned thinned array radiometer
[NASA-TM-110173] p 2509 N95-30316
An atlas of monthly mean distributions of SSMI surface wind speed, AVHRR/2 sea surface temperature, AMI surface wind velocity, TOPEX/POSEIDON sea surface height, and ECMWF surface wind velocity during 1993
[NASA-CR-198880] p 2628 N95-30343

REMOTE SENSORS
Improved operator awareness of teleoperated land vehicle attitude
[AD-A290443] p 2641 N95-29359
Retrieval display and analysis support tool requirements analysis
[AD-A291448] p 2599 N95-29523

REMOTELY PILOTED VEHICLES
Unmanned aerial vehicles: No more Hunter systems should be bought until problems are fixed
[AD-A292172] p 2497 N95-29126
Role of unmanned aerial vehicles in future armed conflict scenarios
[AD-A289777] p 2497 N95-29282
Improved operator awareness of teleoperated land vehicle attitude
[AD-A290443] p 2641 N95-29359
Unmanned Aerial Vehicle technology
[DSTO-GD-0044] p 2497 N95-29362

RENDEZVOUS TRAJECTORIES
Guidance, navigation, and control study for a solar electric propulsion spacecraft
[NASA-CR-198920] p 2509 N95-30357

REPLACING
Inorganic halogen oxidizers
[AD-A290747] p 2533 N95-29581
Inorganic halogen oxidizers
[AD-A291201] p 2702 N95-29974

REPRODUCTION (COPYING)
An analysis of the impact of ASPA on organizational and depot level maintenance
[AD-A292670] p 2477 N95-29414

RESCUE OPERATIONS
The large-capacity rescue-helicopter CH-53 G
p 2678 N95-29621

RESEARCH
Genetics and the unity of biology
[DE95-006484] p 2633 N95-29471
Progress and trends of multi-valued logic research
[AD-A290997] p 2665 N95-29874

RESEARCH AND DEVELOPMENT
Research and technology: 1994 annual report of the John F. Kennedy Space Center
[NASA-TM-110143] p 2740 N95-28786
The 1994 research and technology report at the Goddard Space Flight Center
[NASA-TM-110623] p 2740 N95-28882
NASA/DOD Aerospace Knowledge Diffusion Research Project. Paper 49: Becoming an aerospace engineer: A cross-gender comparison
[NASA-TM-110731] p 2721 N95-29028
Daido Steel's Shibukawa Plant, Shibukawa City, Gumma Prefecture, Japan, 29 Jul. 1994
[AD-A292343] p 2536 N95-29467
Center for Advanced Aerospace Materials (CAAM), Seoul National University, 29 June 1994
[AD-A292344] p 2525 N95-29476
Nippon Steel Research Laboratories, Futtsu, 28 February 1994. and Advanced Materials and Technology Research Laboratories, Kawasaki, 15 June 1994
[AD-A292346] p 2526 N95-29533
The Institute for Material Science and Department of Material Science, Tohoku University, Sendai Japan, 2-3 June 1994
[AD-A292348] p 2650 N95-29534
Aircraft advanced materials research and development program plan
[AD-A290542] p 2498 N95-29565
Federal aviation administration plan for research, engineering and development
[AD-A290952] p 2494 N95-29733
The JSC research and development annual report 1993
[NASA-TM-104787] p 2740 N95-29816

Nonlinear control systems
[AD-A291083] p 2665 N95-29971
Magnum(R) NiCd advanced nickel-cadmium battery cells p 2567 N95-30258

RESEARCH FACILITIES
Management of meteorological data at a former nuclear weapons facility
[DE95-007619] p 2626 N95-29868
Visit to the Laboratory For Evaluation and Failure Prevention of Materials, Toyohashi University of Technology, 17 Oct 94
[AD-A292340] p 2597 N95-30293

RESEARCH MANAGEMENT
Federal aviation administration plan for research, engineering and development
[AD-A290952] p 2494 N95-29733
PSEE architecture report: Architectures and models for next generation process-based software engineering environments
[AD-A291268] p 2652 N95-29996

RESEARCH PROJECTS
The National Grid Project: A system overview p 2482 N95-28749
Rome laboratory software engineering cooperative virtual machine
[AD-A292396] p 2658 N95-28965
NASA: The state of the agency
[NASA-TM-110563] p 2720 N95-29170
Bilateral US/Russia Workshop on Self-Propagating High-Temperature Synthesis held in Honolulu, Hawaii on 6-7 November 1993
[AD-A290466] p 2525 N95-29492
Hernandez Engineering: NASA
[NASA-CR-197665] p 2508 N95-29633
Theory and experiments on chemical instabilities
[AD-A290773] p 2534 N95-29922

RESEARCH VEHICLES
A nonintrusive method of quantifying flow visualization data in vortex flow fields
[AD-A289802] p 2568 N95-28948

RESIDUAL STRENGTH
Damage tolerance in filament-wound graphite/epoxy pressure vessels
[NASA-CR-198804] p 2590 N95-29389
Impact damage resistance and residual property assessment of (0/+/-45/90)s SCS-6/Timetal 21S
[NASA-TM-110178] p 2529 N95-30340

RESIDUAL STRESS
Stress concentration, stress intensity, and fatigue crack growth along evacuators of pressurized, autofrettaged tubes
[AD-A291920] p 2593 N95-28789
Experimental methods in residual stress measurement using a position-sensitive single-exposure scintillation detection system
[AD-A289803] p 2594 N95-28949
Energy theorems and bounds in linearized elasticity with residual stress p 2595 N95-29546

RESIDUES
Methods of generating low redundancy direction finding array configurations
[AD-A292590] p 2555 N95-29289

RESIN MATRIX COMPOSITES
Master plot analysis of microcracking in graphite/epoxy and graphite/PEEK laminates p 2514 N95-28828
Establishing the relationship between manufacturing and component performance in stretch formed thermoplastic composites p 2514 N95-28829
A study of structurally efficient graphite-thermoplastic trapezoidal-corrugation sandwich and semi-sandwich panels p 2516 N95-28842
Advanced resin systems and 3D textile preforms for low cost composite structures p 2519 N95-29035
Mechanical characterization of 2D, 2D stitched, and 3D braided/RTM materials p 2520 N95-29038
Development of RTM and powder prepreg resins for subsonic aircraft primary structures p 2521 N95-29044
Analytical modeling and sensor monitoring for optimal processing of advanced textile structural composites by resin transfer molding p 2521 N95-29045
Effects of thermal and moisture cycling on the internal structure of stitched RTM laminates p 2522 N95-29048
Progress in manufacturing large primary aircraft structures using the stitching/RTM process p 2522 N95-29050
Test results from large wing and fuselage panels p 2522 N95-29051
Thermally stable organic polymers
[AD-A290755] p 2543 N95-29482

RESIN TRANSFER MOLDING
Manufacturing scale-up of composite fuselage crown panels p 2515 N95-28835
Third NASA Advanced Composites Technology Conference, volume 1, part 1
[NASA-CP-3178-VOL-1-PT-1] p 2518 N95-29029
Textile composite fuselage structures development p 2519 N95-29033
Advanced resin systems and 3D textile preforms for low cost composite structures p 2519 N95-29035
Performance of resin transfer molded multiaxial warp knit composites p 2520 N95-29039
Cross-stiffened continuous fiber structures p 2521 N95-29041
Cost model relationships between textile manufacturing processes and design details for transport fuselage elements p 2521 N95-29043
Development of RTM and powder prepreg resins for subsonic aircraft primary structures p 2521 N95-29044
Analytical modeling and sensor monitoring for optimal processing of advanced textile structural composites by resin transfer molding p 2521 N95-29045
A designed experiment in stitched/RTM composites p 2522 N95-29046
The effects of aircraft fuel and fluids on the strength properties of Resin Transfer Molded (RTM) composites p 2522 N95-29047
Effects of thermal and moisture cycling on the internal structure of stitched RTM laminates p 2522 N95-29048
Progress in manufacturing large primary aircraft structures using the stitching/RTM process p 2522 N95-29050
Test results from large wing and fuselage panels p 2522 N95-29051

RESINS
New tetraarylborate and ethyldibutylstannane reagents
[AD-A289813] p 2540 N95-28953
Performance of resin transfer molded multiaxial warp knit composites p 2520 N95-29039
Fiber-matrix adhesion in single-fiber model composites p 2524 N95-29337

RESISTANCE HEATING
Geothermal heat pumps for heating and cooling
[AD-A292115] p 2602 N95-28858
Photon-counting spatial light modulator technology development
[AD-A292619] p 2699 N95-29295

RESISTORS
Thin-film resistor array characterization
[AD-A289806] p 2561 N95-28950

RESOLUTION
Proceedings of the Complex Systems Engineering Synthesis and Assessment Technology Workshop (CSESAW 1994)
[AD-A292433] p 2646 N95-28995
Grid resolution and turbulent inflow boundary condition recommendations for NPARC calculations
[NASA-TM-106959] p 2492 N95-30253

RESONANCE
Modal interactions and complex responses in weaklyNONLINEAR MULTI-DEGREE-OF-FREEDOM MECHANICAL SYSTEMS
[AD-A292023] p 2594 N95-28853
Physical acoustics summer school, 1994. volume 1. transcript
[AD-A292552] p 2683 N95-28973
Si 13 emission lines in solar flare x ray spectra obtained with the P78-1 satellite
[AD-A290000] p 2738 N95-29279
From the (psi) to charmed mesons
[DE95-006564] p 2693 N95-29583
Far-ultraviolet high-resolution emission line spectroscopy of the Cygnus Loop supernova remnant p 2729 N95-29710

RESONANT FREQUENCIES
Power measurement and current feedback in a resonant DC link inverter
[AD-A292518] p 2563 N95-29164
Inhibition of mode competition in free-electron laser oscillators p 2586 N95-29336
The one-dimensional bubble: Theory, experiment, and relevance to exposure of divers to low frequency sound, and of lung to lithotripsy
[ISVR-TR-246] p 2577 N95-29817

RESONANT TUNNELING
Novel high-power solid-state sources for the millimeter-wave region
[AD-A292653] p 2564 N95-29384
Interband lateral resonant tunneling transistor
[AD-D017399] p 2564 N95-29568

RESONANT VIBRATION
Optimal control of molecular motion
[AD-A291919] p 2691 N95-28944

RESONATORS
Sensitivity of stress and boundary imperfection of dielectric resonator disks
[AD-A290488] p 2594 N95-29150

RESOURCES MANAGEMENT
A genetic algorithm approach to scheduling resources for a space power system p 2511 N95-29784

RESPIRATION
Inhalation Toxicology Research Institute
[AD-A292037] p 2635 N95-29188

RESPIRATORY PHYSIOLOGY
CO2-O2 interactions in extension of tolerance to acute hypoxia
[NASA-CR-198575] p 2635 N95-29158

RESPIRATORY SYSTEM
The potential for pulmonary heat injury resulting from the activation of a cabin water spray system to fight aircraft cabin fires
[DOT/FAA/AM-95/17] p 2636 N95-29224

RESPONSE TIME (COMPUTERS)
Modeling spatio-temporal databases to measure the performance of the GPS satellite constellation p 2494 N95-29596

RESTORATION
Accurate feature detection and estimation using nonlinear and multiresolution analysis
[AD-A290267] p 2553 N95-29176
Feature-oriented image reconstruction and aero-optic metrology in turbulence
[AD-A290269] p 2699 N95-29177

RETENTION (PSYCHOLOGY)
Visualization of CAD objects using a stereoscopic display
[AD-A290034] p 2639 N95-29439

RETINA
Computer models of retinal function
[AD-A290156] p 2634 N95-29022

RETROFITTING
Development of an intervention program to encourage shoulder harness use and aircraft retrofit in general aviation aircraft: Phases 1 and 2
[AD-A290966] p 2493 N95-29873

REUSE
Software Design for Reliability and Reuse proof of concept project. Phase 1
[AD-A291690] p 2644 N95-28782

REVERSE ENGINEERING
Software systems reengineering process model, version 2.0
[AD-A289968] p 2647 N95-29278

REVERSED FLOW
PIV investigation of compressibility effects on dynamic stall p 2487 N95-29102

REVERSING
Large scale fluctuations of the geomagnetic field p 2617 N95-29796

REYNOLDS NUMBER
Influence of turbulence parameters, Reynolds number, and body shape on stagnation-region heat transfer
[NASA-TP-3487] p 2568 N95-28719
The effects of three-dimensional imposed disturbances on bluff body near wake flows: Effects of taper and splitter plates on the near wake characteristics of a circular cylinder in uniform and shear flow
[AD-A292113] p 2487 N95-28921
Studies in drag reduction p 2487 N95-29094
Finite element vorticity-based methods for the solution of the incompressible and compressible Navier-Stokes equations p 2570 N95-29119
Numerical experiments on the flow past a circular cylinder at sub-critical Reynolds number
[AD-A289937] p 2573 N95-29268
Effect of Reynolds number on the structure of turbulent boundary layers p 2575 N95-29719
Experimental and analytical study of heat transfer and turbulent flow field in tangentially injected swirl flow p 2576 N95-29811

REYNOLDS STRESS
Interaction of turbulence with complex shock waves
[AD-A290225] p 2571 N95-29145

RHEOLOGY
Three problems in fluid dynamics
[AD-A290481] p 2573 N95-29324
Development of LaRC (TM): IA thermoplastic polyimide coated aerospace wiring
[NASA-CR-195048] p 2548 N95-30252

RIBLETS
Studies in drag reduction p 2487 N95-29094

RICCATI EQUATION
H infinity control problem with zeros on the boundary of the stability domain
[PB95-197042] p 2668 N95-30288

RIFLES
Severe edge effects and simple complimentary interior solutions for thin-walled anisotropic and composite structures
[AD-A290645] p 2595 N95-29562

RIGID ROTORS
High-and low-frequency dynamics of isolated blades and rotors with dynamic stall and wake
[AD-A290358] p 2497 N95-29322
RIGID STRUCTURES
Time-optimal multi-axis attitude maneuvers of rigid spacecraft using collocation and nonlinear programming
p 2507 N95-29332
Automated reasoning about classical mechanics
[AD-A290052] p 2663 N95-29477
RING GALAXIES
Nobeyama Radio Observatory report, no. 378: The polar ring spiral galaxy NGC 660 p 2731 N95-29097
RING STRUCTURES
Permanent magnet torque/force transfer apparatus
[AD-D017325] p 2682 N95-30051
RISC PROCESSORS
Research and development of a high performance GaAs microcomputer system
[AD-A292647] p 2643 N95-29381
RISK
The potential for pulmonary heat injury resulting from the activation of a cabin water spray system to fight aircraft cabin fires
[DOT/FAA/AM-95/17] p 2636 N95-29224
US Army aviation epidemiology data register: Gender-specific attrition among the US Army student aviator class of 1987
[AD-A291856] p 2639 N95-29434
Software risk evaluation method version 1.0
[AD-A290597] p 2652 N95-30047
RIVETS
The mm-wave resonant methods for the detection of corrosion, phase 1
[AD-A291315] p 2593 N95-29941
ROBOT ARMS
Simulation of robot manipulators
[DE95-008680] p 2654 N95-30189
ROBOT CONTROL
Experiments in cooperative manipulation of objects by free-flying robot teams p 2662 N95-29095
A simulation technique for predicting thickness of thermal sprayed coatings
[NASA-TM-106939] p 2512 N95-29373
Robust control of nonlinear flexible multibody systems using quaternion feedback and dissipative compensation
[NASA-TM-109099] p 2507 N95-29377
ALLIANCE: An architecture for fault tolerant multi-robot cooperation
[DE95-008658] p 2666 N95-30112
ROBOT DYNAMICS
Motion planning and sensory processing in a dynamic environment
[AD-A290504] p 2722 N95-29154
ROBOT SENSORS
Motion planning and sensory processing in a dynamic environment
[AD-A290504] p 2722 N95-29154
A simple method for range finding via laser triangulation
[AD-A292529] p 2553 N95-29166
ROBOTICS
Motion planning and sensory processing in a dynamic environment
[AD-A290504] p 2722 N95-29154
A simple method for range finding via laser triangulation
[AD-A292529] p 2553 N95-29166
Robust control of nonlinear flexible multibody systems using quaternion feedback and dissipative compensation
[NASA-TM-109099] p 2507 N95-29377
Interaction and intelligent behavior
[AD-A290049] p 2639 N95-29443
Liquefied metal jet program Automation and Robotics Research Institute (ARRI)
[AD-A289781] p 2536 N95-29461
Simulation of robot manipulators
[DE95-008680] p 2654 N95-30189
Numerical simulation of mechanisms and manipulator robots with flexible links and flexible joints
[PB95-196903] p 2591 N95-30285
ROBOTS
Proceedings of the 33d SICE (the Society of Instrument and Control Engineers) Annual Conference, part 1
[DE95-758947] p 2632 N95-28947
Experiments in cooperative manipulation of objects by free-flying robot teams p 2662 N95-29095
Proceeding of the 33rd SICE Annual Conference
[DE95-758943] p 2662 N95-29144
Motion planning and sensory processing in a dynamic environment
[AD-A290504] p 2722 N95-29154
Interaction and intelligent behavior
[AD-A290049] p 2639 N95-29443
Acquisition of place knowledge through case-based learning
[AD-A292574] p 2723 N95-29573
A biologically-inspired autonomous robot
[AD-A289446] p 2666 N95-30026
Dynamic modelling and link mechanism design of four-legged mobile robot p 2591 N95-30277
Self-organization in a simple brain model
[DE95-008312] p 2668 N95-30279
Numerical simulation of mechanisms and manipulator robots with flexible links and flexible joints
[PB95-196903] p 2591 N95-30285
ROBUSTNESS (MATHEMATICS)
Joint services electronics program
[AD-A292469] p 2561 N95-29010
Performance and robustness of self-tuning and adaptation algorithms for identification, filtering and control
[AD-A292070] p 2648 N95-29310
Time-optimal multi-axis attitude maneuvers of rigid spacecraft using collocation and nonlinear programming
p 2507 N95-29332
Robust control of nonlinear flexible multibody systems using quaternion feedback and dissipative compensation
[NASA-TM-109099] p 2507 N95-29377
Fundamental limitations and capabilities of robust identification and adaptive control
[AD-A291085] p 2664 N95-29636
Reliability enhancement of Navier-Stokes codes through convergence acceleration
[NASA-CR-196635] p 2578 N95-30034
ROCK MECHANICS
Extreme nonlinearity in rocks: An investigation using elastic pulse wave propagation
[DE95-007879] p 2618 N95-30129
ROCKET ENGINE DESIGN
A transient model of the RL10A-3-3A rocket engine
[NASA-CR-195478] p 2510 N95-29114
Investigation of the flow turning loss in unstable solid propellant rocket motors p 2510 N95-29331
ROCKET ENGINES
SCAP spray combustion analysis program
[AD-A289946] p 2532 N95-29273
Spacecraft attitude control system performance using pulse-width pulse-frequency modulated thrusters
[AD-A291803] p 2508 N95-29410
ROCKET EXHAUST
Estimates of probability of a cloud-free line of sight for RAPTOR TALON
[AD-A291908] p 2510 N95-29284
ROCKET FIRING
Automated Propulsion Data Screening demonstration system
[NASA-CR-196636] p 2510 N95-29584
ROCKET LAUNCHING
A transient model of the RL10A-3-3A rocket engine
[NASA-CR-195478] p 2510 N95-29114
ROCKET SOUNDING
Chemical release experiments to induce F region ionospheric plasma irregularities at the magnetic equator
p 2708 N95-29783
ROCKET-BORNE INSTRUMENTS
First flight of the Multi-Spectral Solar Telescope Array: Calibration, results and future plans
p 2727 N95-29529
ROCKS
Gradient-dependent plasticity in numerical simulation of localization phenomena
[PB95-197257] p 2596 N95-30049
ROLL
Estimation of unstabilized components in vehicular motion
[AD-A290580] p 2590 N95-29552
ROLLING CONTACT LOADS
Dimensions, deflections and stresses for Hertzian contacts under combined normal and tangential loading. (Guide to use of computer program A9434.)
[ESDU-94034] p 2593 N95-28711
ROOM TEMPERATURE
Experimental study on scaling law of outgassing rate with a pumping parameter
[AD-B191999L] p 2709 N95-29801
ROTARY WINGS
Interactions of spanwise and chordwise vorticity associated with three-dimensional dynamic stall over an oscillating wing
[AD-A290546] p 2487 N95-29091
A fourth order Euler/Navier-Stokes prediction method for the aerodynamics and aeroelasticity of hovering rotor blades p 2572 N95-29242
High-and low-frequency dynamics of isolated blades and rotors with dynamic stall and wake
[AD-A290358] p 2497 N95-29322
Development of a rotary wing Navier-Stokes CFD code based on TLNS3D code
[AD-A290421] p 2574 N95-29387
Unsteady pressure and inflow velocity on a pitching rotor blade in hover p 2490 N95-29771
ROTATING CYLINDERS
Unsteady rotational shear flow of power law fluids
[ISBN-0-315-81287-7] p 2575 N95-29718
ROTATING DISKS
Observational signatures of rotating black holes
p 2729 N95-29709
ROTATING FLUIDS
Three problems in fluid dynamics
[AD-A290481] p 2573 N95-29324
Numerical simulation of stability and stability control of high speed compressible rotating couette flow
[NASA-CR-198832] p 2579 N95-30250
ROTATING STALLS
Modeling and control of rotating stall in high speed multi-stage axial compressors p 2500 N95-29244
Model development for active control of stall phenomena in aircraft gas turbine engines p 2500 N95-29679
ROTATION
Three-D weather displays for aircraft cockpits
[AD-A289759] p 2499 N95-28691
Shift work, age, and performance: Investigation of the 2-2-1 shift schedule used in Air Traffic Control facilities I. The sleep/wake cycle
[DOT/FAA/AM-95/19] p 2638 N95-29261
The (in)complete compendium of computational curiosities: Givens' rotations
[AD-A292050] p 2648 N95-29304
A turbulent model of the solar granulation
[AD-A292318] p 2738 N95-29475
Shock resistant optic fiber rotary slice holding device
[AD-D017327] p 2702 N95-30053
ROTATIONAL STATES
Studies of energy transfer processes of relevance to chemically and optically pumped lasers
[AD-A290164] p 2585 N95-29025
ROTOR BLADES
A fourth order Euler/Navier-Stokes prediction method for the aerodynamics and aeroelasticity of hovering rotor blades p 2572 N95-29242
Unsteady pressure and inflow velocity on a pitching rotor blade in hover p 2490 N95-29771
ROTOR BODY INTERACTIONS
An analytic modeling and system identification study of helicopter dynamics p 2498 N95-29787
ROTOR DYNAMICS
An analytic modeling and system identification study of helicopter dynamics p 2498 N95-29787
ROTORS
PREDICHAT: First order performance calculations of windturbine rotors using the method of the acceleration potential
[PB95-206454] p 2603 N95-30200
ROUTES
Three-D weather displays for aircraft cockpits
[AD-A289759] p 2499 N95-28691
Conceptual design of a map interactive system for military aircraft cockpits
[AD-A289760] p 2499 N95-28692
Operational test and evaluation (OT&E) integration and operational test plan for fixed ground antenna radome (FGAR)
[AD-A291310] p 2559 N95-29940
Operational test and evaluation (OT&E) integration and operational test procedures for Fixed Ground Antenna Radome (FGAR)
[AD-A291203] p 2559 N95-29975
RUN TIME (COMPUTERS)
Checkpointing and the modeling of program execution time
[PB95-197182] p 2653 N95-30099
RUNGE-KUTTA METHOD
An HP-Adaptive method in space and time for parabolic systems
[AD-A292262] p 2668 N95-28890
A differential approach to graphical interaction
[AD-A292165] p 2647 N95-29125
Development of a rotary wing Navier-Stokes CFD code based on TLNS3D code
[AD-A290421] p 2574 N95-29387
Reliability enhancement of Navier-Stokes codes through convergence acceleration
[NASA-CR-196635] p 2578 N95-30034
Comparative study of numerical schemes of TVD3, UNO3-ACM and optimized compact scheme
p 2686 N95-30137
Application of low dissipation and dispersion Runge-Kutta schemes to benchmark problems in computational aeroacoustics p 2687 N95-30139
Solution of acoustic workshop problems by a spectral multidomain method p 2687 N95-30141
The use of staggered scheme and an absorbing buffer zone for computational aeroacoustics
p 2689 N95-30153

Computational aeroacoustics on massively parallel computers p 2661 N95-30156
Comparison of spatial numerical operators for duct-nozzle acoustics p 2690 N95-30158

RUNWAYS
Evaluation of retro-reflective beads in airport pavement markings
[AD-A291065] p 2502 N95-29967
Prototype stop bar system evaluation at Seattle-Tacoma International Airport
[AD-A290136] p 2495 N95-30031

RUSSIAN FEDERATION
Bilateral US/Russia Workshop on Self-Propagating High-Temperature Synthesis held in Honolulu, Hawaii on 6-7 November 1993
[AD-A290466] p 2525 N95-29492
Short term visits for collaborative research
[AD-A290704] p 2682 N95-29588

RUTHENIUM COMPOUNDS
Development of electrochemical super capacitors for EMA applications p 2568 N95-30270

S

S WAVES
Dynamic decohesion of bimaterial interfaces p 2541 N95-29120
Inclusive hadronic production of the B(sub c) meson via heavy quark fragmentation
[DE95-008739] p 2695 N95-30191

SABOT PROJECTILES
Development of a transient internal probe diagnostic
[AD-A292470] p 2704 N95-29011

SAFETY DEVICES
Alternative methods for flotation seat cushion use
[DOT/FAA/AM-95/20] p 2493 N95-29448
Calculation of shielding parameters
[DE95-008735] p 2694 N95-29886

SAFETY FACTORS
Test load verification through strain data analysis
[NASA-TP-3558] p 2504 N95-28718

SALINITY
Analysis of historical oceanographic data on a minicomputer: Program WAHOO
[AD-A292530] p 2629 N95-28873

SAMPLING
Intermediate levels of visual processing
[AD-A291569] p 2638 N95-28937
High resolution, large scale measurement processes
[AD-A292200] p 2681 N95-28987
Cylinder-averaged histories of nitrogen oxide in a DI diesel with simulated turbocharging
[AD-A290568] p 2590 N95-29820

SANDS
A geotechnical characterization of lunar soils and lunar soil simulants p 2736 N95-29117
Tidal and lunar data for Point Mugu, San Nicolas Island, and the Barking Sands area during 1995
[AD-A289877] p 2733 N95-29599

SANDWICH STRUCTURES
In situ processing methods for composite fuselage sandwich structures p 2513 N95-28826
The effects of design details on cost and weight of fuselage structures p 2499 N95-28831
A study of structurally efficient graphite-thermoplastic trapezoidal-corrugation sandwich and semi-sandwich panels p 2516 N95-28842
Buckling analysis of curved composite sandwich panels subjected to inplane loadings p 2517 N95-28845
Sorption and diffusion of moisture in multilayer composite AEM/S sandwich materials
[AD-A289807] p 2518 N95-28951
Impact resistance and damage tolerance of composite sandwich panels p 2526 N95-29549
Use of finite element analysis for transient moisture diffusion studies in multilayer composite AEM/S system sandwich materials
[AD-A291092] p 2527 N95-29638

SAPPHIRE
Semiconductor film Cherenkov lasers
[AD-A291177] p 2587 N95-29930
A kilohertz femtosecond Ti: Sapphire regeneratie amplifier
[AD-A290591] p 2588 N95-30045

SATELLITE ALTIMETRY
A study of dynamics in the tropical Pacific using satellite data p 2630 N95-29520

SATELLITE ANTENNAS
Performance analysis of a GPS Interferometric attitude determination system for a gravity gradient stabilized spacecraft
[NASA-CR-188372] p 2508 N95-30036

SATELLITE ATTITUDE CONTROL
Performance analysis of a GPS Interferometric attitude determination system for a gravity gradient stabilized spacecraft
[NASA-CR-188372] p 2508 N95-30036

SATELLITE CONSTELLATIONS
Modeling spatio-temporal databases to measure the performance of the GPS satellite constellation p 2494 N95-29596

SATELLITE DESIGN
A layman's look at orbital debris
[AD-A289801] p 2506 N95-28700
Study of the space environmental effects on spacecraft engineering materials
[NASA-CR-196638] p 2531 N95-29246

SATELLITE IMAGERY
Monitoring of burning in the Brazilian cerrado region using AVHRR/NOAA data calibrated by TM/Landsat data
[INPE-5490-TDI/507] p 2598 N95-28929
Optical (LANDSAT/TM) and radar (ERS-1/SAR) imagery sinergism studies applied to land use discrimination
[INPE-5608-TDI/554] p 2598 N95-29433
A study of dynamics in the tropical Pacific using satellite data p 2630 N95-29520
Some aspects of lunar and martian volcanism as examined with spectral, topographic, and morphologic data derived from spacecraft images p 2736 N95-29594
Depicting dust and sand storm signatures through the means of satellite images and ground-based observations for Saudi Arabia p 2600 N95-29730
Extended dust shells around carbon stars resolved by HIRAS p 2735 N95-29840

SATELLITE INSTRUMENTS
Microwave remote sensing of surface soil moisture and its application to hydrologic modeling p 2600 N95-29821

SATELLITE NAVIGATION SYSTEMS
An investigation into the use of satellite-based positioning systems for flight reference/autoland operations p 2494 N95-29542

SATELLITE NETWORKS
Alternative packet switch architectures for a 30/20 GHz FDMA/TDMA geostationary communication satellite network
[NASA-CR-195470] p 2506 N95-30090

SATELLITE OBSERVATION
A ground support electronic interface for the ionospheric spectroscopy and atmospheric chemistry (ISAAC) ultraviolet spectrograph
[AD-A289761] p 2611 N95-28693
Simultaneous UV and optical study of O star winds and UV and optical covariability of O star winds
[NASA-CR-189424] p 2726 N95-29370
Continental aerosol effects on stratocumulus microphysics during MAST 1994
[AD-A292674] p 2621 N95-29416
Characterization of the geometries of the high-latitude ionospheric convection pattern p 2614 N95-29524
The high-altitude polar wind: Simulation and observation p 2622 N95-29688
The high latitude ionospheric convection pattern during northward interplanetary magnetic field p 2615 N95-29693
Microwave remote sensing of surface soil moisture and its application to hydrologic modeling p 2600 N95-29821
Short-range precipitation forecasts using assimilation of simulated satellite water vapor profiles and cloud liquid water p 2625 N95-29832
Meteorological Satellite Center technical note, no. 28, 1994
[JTN-95-80926] p 2626 N95-29849
Japanese remote sensing organizations, research, and technology
[AD-A292420] p 2601 N95-29905

SATELLITE ORIENTATION
A conceptual design for the attitude control and determination system for the Magnetosphere Imager spacecraft
[NASA-TP-3560] p 2507 N95-28721

SATELLITE SOUNDING
Production of a long-term global water vapor and liquid water data set using ultra-fast methods to assimilate multi-satellite and radiosonde observations
[NASA-CR-198955] p 2628 N95-30272

SATELLITE-BORNE INSTRUMENTS
Japanese remote sensing organizations, research, and technology
[AD-A292420] p 2601 N95-29905
A conceptual thermal design study of an electronically scanned thinned array radiometer
[NASA-TM-110173] p 2509 N95-30316

SATURN (PLANET)
An investigation into the existence of asteroids at Saturn's triangular Lagrangian points p 2727 N95-29648

SAUDI ARABIA
Depicting dust and sand storm signatures through the means of satellite images and ground-based observations for Saudi Arabia p 2600 N95-29730

SCALARS
Adaptive Infinite Impulse Response (IIR) filter system
[AD-D017403] p 2564 N95-29570

SCALE MODELS
Transonic, supersonic and hypersonic wind-tunnel tests on aerodynamic characteristics of reentry body with blunted cone configuration
[ISAS-658] p 2490 N95-29640

SCALING
Trajectory mapping (TM): A new non-metric scaling technique
[AD-A290036] p 2670 N95-29440

SCALING LAWS
Experimental study on scaling law of outgassing rate with a pumping parameter
[AD-B191999L] p 2709 N95-29801
Investigation of optical damage, energy partitioning and scaling laws at extremely high velocities
[AD-A291368] p 2703 N95-30062

SCANNERS
Upgrading the Day/Night whole sky imager from Manual/Interactive to full automatic control
[AD-A292296] p 2619 N95-28872
Transformational design of a direction detector for the progressive scan conversion processor
[PB95-198487] p 2643 N95-30109

SCANNING
Diffraction limited imaging using aberrated optics
[AD-A290912] p 2703 N95-30081

SCANNING ELECTRON MICROSCOPY
Nanofabrication of electronic devices with the scanning tunneling microscope
[AD-A292463] p 2561 N95-29005
High T(sub c) superconductor/ferroelectric heterostructures
[AD-A291016] p 2716 N95-29658
Hot explosive consolidation of W-Ti alloys
[AD-A290880] p 2537 N95-29835

SCANNING TUNNELING MICROSCOPY
Prediction of hydrogen entry and permeation in metals and alloys
[AD-A292047] p 2536 N95-29298

SCATTER PROPAGATION
Analysis of tropospheric propagation characteristics based on regional meteorological data
[AD-A291581] p 2552 N95-28939

SCATTERING
Predicting polarized light scattering by marine micro-organism
[AD-A289790] p 2696 N95-28695
Electromagnetic scattering by magnetic spheres: Theory and algorithms
[AD-A289798] p 2551 N95-28699
100 Hz-10 kHz bottom backscattering model: Generalized treatment of sediment sound propagation, sediment volume scattering and interface-roughness scattering
[AD-A291323] p 2685 N95-29942
Dynamical instabilities, chaos and spatial complexity in fundamental nonlinear optical interactions
[AD-A291223] p 2588 N95-29980
A full wave study of radar cross sections of rough terrain
[AD-A291227] p 2559 N95-29982

SCATTERING CROSS SECTIONS
Analytical theory of continued fractions and time evolution in many-particle systems
[AD-A290365] p 2692 N95-29227

SCATTEROMETERS
Engineering design of sub-micron topographies for simultaneously adherent and reflective metal-polymer interfaces
[NASA-CR-198845] p 2548 N95-30237

SCENE ANALYSIS
Accurate feature detection and estimation using nonlinear and multiresolution analysis
[AD-A290267] p 2553 N95-29176

SCHEDULES
Shift work, age, and performance: Investigation of the 2-2-1 shift schedule used in Air Traffic Control facilities I. The sleep/wake cycle
[DOT/FAA/AM-95/19] p 2638 N95-29261

SCHEDULING
An analysis of the impact of ASPA on organizational and depot level maintenance
[AD-A292670] p 2477 N95-29414
Scheduling algorithms for mobile packet radio networks p 2558 N95-29707

A genetic algorithm approach to scheduling resources for a space power system p 2511 N95-29784
Performance evaluation of ATM cell scheduling policies using stochastic petri nets
[PB95-197158] p 2559 N95-30096

SCHLIEREN PHOTOGRAPHY
Reduce Fluid Experiment System: Flight data from the IML-1 Mission
[NASA-CR-196639] p 2549 N95-30014

SCHOOLS
Analysis of the naval postgraduate school computer network architecture
[AD-A289749] p 2657 N95-28689
Flight nurse school in the Hellenic Air Force p 2638 N95-29629

SCIENTIFIC VISUALIZATION
The 1994 research and technology report at the Goddard Space Flight Center
[NASA-TM-110623] p 2740 N95-28882
Visualization of improved target acquisition algorithm for Janus (A)
[AD-A290191] p 2646 N95-29056
Scalable software tools for adaptive scientific computation
[AD-A290446] p 2650 N95-29480
A new visualization technique to study the time evolution of finite and adaptive mixture estimators
[AD-A291147] p 2673 N95-30126

SCIENTISTS
The 2nd European Conference on Smart Structures and Materials
[AD-A290723] p 2550 N95-29579
The 5th International Meeting on Cholinesterase
[AD-A291253] p 2534 N95-30085

SCINTILLATION
Experimental methods in residual stress measurement using a position-sensitive single-exposure scintillation detection system
[AD-A289803] p 2594 N95-28949
The effects of magnetic storm phases on F-layer irregularities from auroral to equatorial latitudes
[AD-A290674] p 2614 N95-29585

SCINTILLATION COUNTERS
Low-background balloon-borne direct search for ionizing massive particles as a component of the dark galactic halo matter p 2726 N95-29204

SEA ICE
Sea ice motions in the Central Arctic pack ice as inferred from AVHRR imagery
[NASA-CR-198835] p 2601 N95-30247

SEA STATES
An air-sea interaction model for stress, sensible heat, latent heat, and sea state, applicable to the full range of wind speeds p 2626 N95-29876
An atlas of monthly mean distributions of SSMI surface wind speed, AVHRR/2 sea surface temperature, AMI surface wind velocity, TOPEX/POSEIDON sea surface height, and ECMWF surface wind velocity during 1993
[NASA-CR-198880] p 2628 N95-30343

SEA SURFACE TEMPERATURE
The tropical atmosphere under convection adjustment p 2625 N95-29833
Meteorological Satellite Center technical note, no. 28, 1994
[JTN-95-80926] p 2626 N95-29849
An atlas of monthly mean distributions of SSMI surface wind speed, AVHRR/2 sea surface temperature, AMI surface wind velocity, TOPEX/POSEIDON sea surface height, and ECMWF surface wind velocity during 1993
[NASA-CR-198880] p 2628 N95-30343

SEA WATER
Predicting polarized light scattering by marine micro-organism
[AD-A289790] p 2696 N95-28695
SeaWiFS technical report series. Volume 24: SeaWiFS technical report series cumulative index, volumes 1-23
[NASA-TM-104556] p 2631 N95-30236

SEALS (STOPPERS)
The fluid mechanics of a high aspect ratio slot with an impressed pressure gradient and secondary injection p 2580 N95-30304

SEARCH PROFILES
The identification of user criteria of relevance and document characteristics: Beyond the topical approach to information retrieval p 2723 N95-29518
Distributed queries and incremental updates in information retrieval systems p 2725 N95-30286

SEAS
Prototype stop bar system evaluation at Seattle-Tacoma International Airport
[AD-A290136] p 2495 N95-30031

SEAT BELTS
Development of an intervention program to encourage shoulder harness use and aircraft retrofit in general aviation aircraft: Phases 1 and 2
[AD-A290966] p 2493 N95-29873

SEATS
Alternative methods for flotation seat cushion use
[DOT/FAA/AM-95/20] p 2493 N95-29448
The effect of wear on fire-blocking layer material effectiveness
[AD-A291520] p 2493 N95-29855
Evaluation of wear resistant ceramic valve seats in gas-fueled power generation engines
[PB95-200218] p 2591 N95-30110

SECONDARY INJECTION
The fluid mechanics of a high aspect ratio slot with an impressed pressure gradient and secondary injection p 2580 N95-30304

SECURITY
Computational complexity and encryption
[AD-A291910] p 2648 N95-29356

SEDIMENT TRANSPORT
Tidal constituent database: West coast of the United States and eastern North Pacific Ocean
[AD-A292224] p 2630 N95-29198

SEDIMENTS
100 Hz-10 kHz bottom backscattering model: Generalized treatment of sediment sound propagation, sediment volume scattering and interface-roughness scattering
[AD-A291323] p 2685 N95-29942

SEGMENTS
Object oriented segmentation of images
[AD-A290792] p 2671 N95-29485

SEISMIC WAVES
Regional seismic event identification and improved locations with small arrays
[AD-A292188] p 2612 N95-28985
Eurasian seismic surveillance - 2D FD seismic synthetics and event discrimination
[AD-A292659] p 2614 N95-29413

SEISMOGRAMS
Two-dimensional signal processing for regional seismic event identification
[AD-A292601] p 2613 N95-29293

SEISMOGRAPHS
Regional seismic event identification and improved locations with small arrays
[AD-A292188] p 2612 N95-28985

SEISMOLOGY
Design, evaluation and construction of TEXESS and LUXESS, and research in mini-array technology and use of data from single stations and sparse networks
[AD-A292546] p 2612 N95-28972
Regional seismic event identification and improved locations with small arrays
[AD-A292188] p 2612 N95-28985
Two-dimensional signal processing for regional seismic event identification
[AD-A292601] p 2613 N95-29293
Eurasian seismic surveillance - 2D FD seismic synthetics and event discrimination
[AD-A292659] p 2614 N95-29413

SELECTION
Selection and costing of heat exchangers. Air-cooled type
[ESDU-94043] p 2550 N95-28705
Selection and costing of heat exchangers. Shell-and-tube type
[ESDU-94042] p 2550 N95-28706
Delayed choice: An operator for joining message sequence charts
[PB95-206710] p 2560 N95-30203
Precedence relation method for deriving flexible bound models for queueing systems
[PB95-206835] p 2667 N95-30221

SELECTORS
High gain, low noise and broadband Raman and Brillouin fiber-optic amplifiers, channel selectors and switches
[AD-A290585] p 2700 N95-29553

SELENIUM
Chalcogenide superconductors: A search
[AD-A292523] p 2560 N95-28812

SELF CONSISTENT FIELDS
Ab initio calculation of vibrational absorption and circular dichroism spectra using density functional force fields
[AD-A291297] p 2720 N95-29936

SELF LUBRICATING MATERIALS
Nippon Steel Research Laboratories, Futtsu, 28 February 1994. and Advanced Materials and Technology Research Laboratories, Kawasaki, 15 June 1994
[AD-A292346] p 2526 N95-29533

SELF ORGANIZING SYSTEMS
Attractors of dissipative structure in three dissipative fluids
[AD-B180030L] p 2710 N95-29844

SELF PROPAGATION
Bilateral US/Russia Workshop on Self-Propagating High-Temperature Synthesis held in Honolulu, Hawaii on 6-7 November 1993
[AD-A290466] p 2525 N95-29492

SEMANTICS
A pipeline case tool for database design
[AD-A292017] p 2722 N95-29182
Formal design of communication protocols using Estelle
[AD-A290584] p 2652 N95-30042
Functionally specified distributed transactions in co-operative scenarios
[PB95-197380] p 2725 N95-30100
Causal behaviours and nets
[PB95-197612] p 2660 N95-30102
Layers as knowledge transitions in the design of distributed systems
[PB95-197638] p 2660 N95-30104
Speedlog: The key architectural element to provide efficient log management
[PB95-198453] p 2643 N95-30108
Enhancing the semantics of federated schemata by translating SQ1-queries into object methods
[PB95-197372] p 2725 N95-30208

SEMICONDUCTING FILMS
Semiconductor deposition and etching interactions of laser-generated translationally hot atoms and radicals
[AD-A291824] p 2693 N95-29431
The 2nd International Conference on Thin Film Physics and Applications
[AD-A292353] p 2546 N95-29983

SEMICONDUCTOR DEVICES
Drift mobility measurements in thin film boron carbide
[AD-A292510] p 2712 N95-28869
Laser simulation of single-event effects: A state of the art review
[AD-A292308] p 2584 N95-28892
Interface properties of wide bandgap semiconductor structures
[AD-A289817] p 2713 N95-28954
Joint services electronics program
[AD-A292469] p 2561 N95-29010
Semiconductor science and technology
[AD-A289143] p 2563 N95-29191
Low temperature materials growth and processing development for flat panel display technology applications
[AD-A292177] p 2715 N95-29267
Characterization and calibration of a pulsed laser system for single event upset simulation
[AD-A290075] p 2586 N95-29330
The quantum hydrodynamic model for semiconductor devices
[AD-A291809] p 2564 N95-29430
A study of power diode failure mechanisms in the US Army research laboratory 30-mm solid propellant electrothermal-chemical (SPETC) gun facility
[AD-A291300] p 2565 N95-29938
Vacuum microelectronic emitters and their applications using compound semiconductor technology
[AD-A291142] p 2567 N95-30124
Parallel adaptive finite element: Software for semiconductor device simulation
[AD-A291149] p 2661 N95-30295

SEMICONDUCTOR DIODES
A study of power diode failure mechanisms in the US Army research laboratory 30-mm solid propellant electrothermal-chemical (SPETC) gun facility
[AD-A291300] p 2565 N95-29938

SEMICONDUCTOR LASERS
Novel electric-field effects in quantum wells and superlattices
[AD-A292317] p 2718 N95-28857
Linewidth-insensitive coherent analog optical links
[AD-A292422] p 2698 N95-28992
Exact physical models and methods for stabilization and control of reflection-induced instabilities in semiconductor lasers
[AD-A292437] p 2585 N95-29053
A compact universal power supply for laser diodes
[AD-A289950] p 2585 N95-29274
Semiconductor film Cherenkov lasers
[AD-A291177] p 2587 N95-29930
Dynamical instabilities, chaos and spatial complexity in fundamental nonlinear optical interactions
[AD-A291223] p 2588 N95-29980
Auger rates in mid-IR InAsSb laser structures
[DE95-006325] p 2588 N95-30006

SEMICONDUCTORS (MATERIALS)
Strained-bond semiconductors
[AD-A292524] p 2560 N95-28813
Commercial photorefractive device using nonstoichiometric 3-5 semiconductors
[AD-A292494] p 2713 N95-28933
Proceedings of the 38th Annual Conference on Magnetism and Magnetic Materials
[AD-A286751] p 2681 N95-28962

Studies of lattice-mismatched and Low-Temperature-Grown semiconductor multiple-phase systems
[AD-A292536] p 2713 N95-28967
Synthesis and complete characterization of a Gallium-Mixed-Pnicogen four-membered ring compound: I2GaAs(SiMe3)(sub 2)Ga(I)2P(SiMe3)(sub 2)
[AD-A292423] p 2713 N95-28993
Conference proceedings: IEEE Nonlinear Optics, Materials, Fundamentals, and Applications
[AD-A292438] p 2698 N95-28997
Joint services electronics program
[AD-A292469] p 2561 N95-29010
Development of ultra-low dark current, high performance 3-5 quantum well infrared photodetectors (QWIPs) for focal plane arrays staring imaging sensor systems
[AD-A290343] p 2714 N95-29089
Electronic properties of low-temperature grown III/V thin films
[AD-A292521] p 2714 N95-29165
Gordon research conference on point defects, line defects, and interfaces in semiconductors
[AD-A290103] p 2714 N95-29209
Tailored microstructures for broadband or selective detection of radiation from the visible to the infrared
[AD-A292097] p 2554 N95-29240
Research and development of a high performance GaAs microcomputer system
[AD-A292647] p 2643 N95-29381
Semiconductor deposition and etching interactions of laser-generated translationally hot atoms and radicals
[AD-A291824] p 2693 N95-29431
Structural and electronic properties of adsorbates on semiconductors, metal-semiconductor interfaces and semiconductor heterojunctions
[AD-A291917] p 2715 N95-29438
Synthesis and characterization of (Me3SiCH2)3M(dot)E(SiMe3)3 (M = Ga, E = P or As; M = In, E = P). X-ray crystal structures of (Me3SiCH2)3Ga(dot)P(SiMe3)3 and (Me3SiCH2)3In(dot)P(SiMe3)3
[AD-A291907] p 2715 N95-29444
Raman and photo-modulated reflectivity studies of ZnTe/InAs semiconductor heterostructure under hydrostatic pressure
[AD-A290467] p 2716 N95-29506
High-density plasma dynamics in semiconductors
p 2705 N95-29632
The 41st Japan Society of Applied Physics Spring Meeting
[AD-A292333] p 2720 N95-29879
Sensor protection portion of the development of nonlinear optical materials and processes for laser hardening of sensors
[AD-A291200] p 2702 N95-29973
InTlSb as a long-wave infrared (LWIR) material: Defects and transportation properties
[AD-A291218] p 2702 N95-29978
A kilohertz femtosecond Ti: Sapphire regeneratie amplifier
[AD-A290591] p 2588 N95-30045
Vacuum microelectronic emitters and their applications using compound semiconductor technology
[AD-A291142] p 2567 N95-30124
Thin-film edge field emitter device and method of manufacture therefor
[AD-D017323] p 2567 N95-30165
Physical modeling and design of semiconductor heterostructures for optical and electronical applications
p 2682 N95-30232

SENSITIVITY
Measuring variation in ecosystem sensitivity to stress
[AD-A290415] p 2609 N95-29450

SENTENCES
Conversion of the TRACON operations concepts database into a formal sentence outline job task taxonomy
[DOT/FAA/AM-95/16] p 2493 N95-28819
Interface for the translation of sentences in a natural language into a geometrical representation language
[INPE-5467-PRE/1775] p 2722 N95-29363

SEPARATED FLOW
Unsteadiness of shock-induced turbulent boundary layer separation. An inherent feature of turbulent flow or solely a wind tunnel phenomenon
[AD-A290367] p 2572 N95-29228
Dynamic stall of a NACA 0012 airfoil in laminar flow
p 2489 N95-29243
Experimental research on crossing shock wave boundary layer interactions
[AD-A290764] p 2577 N95-29920

SEQUENCING
Optimal universal coding and density estimation
[AD-A290694] p 2675 N95-29587

SEQUENTIAL ANALYSIS
An efficiency study of the simultaneous analysis and design of structures
[NASA-TM-110168] p 2495 N95-28820

SEQUENTIAL COMPUTERS
New methods for nonlinear optimization
[AD-A290522] p 2670 N95-29385

SEQUENTIAL CONTROL
Garbage collection is fast, but a stack is faster
[AD-A290099] p 2722 N95-29207

SERIES EXPANSION
Guidance law development for aeroassisted transfer vehicles using Matched Asymptotic Expansions
p 2503 N95-30347

SERUMS
Organization of the human circadian system
[AD-A288223] p 2634 N95-28915

SERVICE LIFE
A layman's look at orbital debris
[AD-A289801] p 2506 N95-28700
Helicopter life substantiation: Review of some USA and UK initiatives
[AD-A290045] p 2495 N95-28851
Advanced composite structural concepts and materials technologies for primary aircraft structures: Advanced material concepts
[NASA-CR-4485] p 2496 N95-29027

SERVOMECHANISMS
Proceedings of the 33d SICE (the Society of Instrument and Control Engineers) Annual Conference, part 1
[DE95-758947] p 2632 N95-28947
Design of a fast-tool servo system using magnetic servo levitation
[AD-A290273] p 2663 N95-29183

SEX FACTOR
An analysis of anthropometric differences among occupational groups in the US Army
[AD-A292326] p 2640 N95-28794

SEYFERT GALAXIES
The complex broadband x-ray spectra of Seyfert galaxies p 2730 N95-29776

SHADOWS
Method for the calculation of spacecraft umbra and penumbra shadow terminator points
[NASA-TP-3547] p 2671 N95-29446
Analysis of shadowing effects on spacecraft power systems
[NASA-TM-106994] p 2511 N95-30012

SHAFTS (MACHINE ELEMENTS)
External combustion engine having an asymmetrical CAM
[AD-D017382] p 2588 N95-28785

SHAPE CONTROL
Advanced manufacturing by spray forming: Aluminum strip and microelectromechanical systems
[DE95-008615] p 2536 N95-28959
Computational algorithms for aerodynamic analysis and design
[AD-A291084] p 2491 N95-29972

SHAPES
Influence of turbulence parameters, Reynolds number, and body shape on stagnation-region heat transfer
[NASA-TP-3487] p 2568 N95-28719
Visualization of CAD objects using a stereoscopic display
[AD-A290034] p 2639 N95-29439
Object oriented segmentation of images
[AD-A290792] p 2671 N95-29485
Membrane fluidity and shape of human red blood cells are altered by physiological levels of hydrostatic pressure
[AD-A290595] p 2636 N95-29557
Randomized inquiries about shape: An application to handwritten digit recognition
[AD-A290812] p 2675 N95-29634
Computational algorithms for aerodynamic analysis and design
[AD-A291084] p 2491 N95-29972
Theorem on the existence of solutions of quasi-static moving boundary problems
[PB95-197125] p 2673 N95-30093

SHEAR FLOW
The effects of three-dimensional imposed disturbances on bluff body near wake flows: Effects of taper and splitter plates on the near wake characteristics of a circular cylinder in uniform and shear flow
[AD-A292113] p 2487 N95-28921
Condensation inside tubes: Condensate film coefficient in horizontal tubes
[ESDU-94041] p 2569 N95-29015
Interaction of turbulence with complex shock waves
[AD-A290225] p 2571 N95-29145
Rigorous drag bounds in turbulent shear flow
p 2573 N95-29334
Unsteady rotational shear flow of power law fluids
[ISBN-0-315-81287-7] p 2575 N95-29718
Dynamical model of pressure-gradient-driven turbulence and shear flow generation in L-H transition
[AD-B195511L] p 2709 N95-29789
Supercritical states of two-dimensional wall-bounded shear flow p 2580 N95-30303

SHEAR LAYERS
Navier-Stokes solution of wing wake structure and its perturbation p 2488 N95-29121
Molecular mixing in shear layers forced by 2-D and 3-D disturbances
[AD-A290272] p 2571 N95-29181
Dynamic stall of a NACA 0012 airfoil in laminar flow
p 2489 N95-29243
Grid resolution and turbulent inflow boundary condition recommendations for NPARC calculations
[NASA-TM-106959] p 2492 N95-30253

SHEAR STRAIN
Effects of cutouts on the behavior of symmetric composite laminates subjected to bending and twisting loads p 2517 N95-28844
Consideration of microstructural changes in the study of adiabatic shear bands
[AD-A290398] p 2715 N95-29234
Analysis of adiabatic shear bands in thermoviscoplastic materials under combined loading
[AD-A290666] p 2596 N95-29582
The study of non-Newtonian contraction flows with a parallel finite element method p 2576 N95-29778

SHEAR STRENGTH
Shear reinforcement in deep slabs
[AD-A289528] p 2594 N95-28909
The measurement of adhesion at film-substrate interfaces using a constant depth scratch test
[AD-A289940] p 2542 N95-29269
Simplified data reduction methods for the ECT test for mode 3 interlaminar fracture toughness
[NASA-TM-110176] p 2527 N95-29825
Composite processing development to improve interlaminar strength using ply interface particles
[NASA-TM-108495] p 2529 N95-30334

SHEAR STRESS
Buckling analysis of curved composite sandwich panels subjected to inplane loadings p 2517 N95-28845
Shear force, bending moment and torque of rigid aircraft in symmetric steady maneuvering flight
[ESDU-94045] p 2495 N95-28896
Through-the-thickness stresses and failure in the corner radius of a laminated composite section
[ESDU-94019] p 2518 N95-28899
Unsteady rotational shear flow of power law fluids
[ISBN-0-315-81287-7] p 2575 N95-29718
The study of non-Newtonian contraction flows with a parallel finite element method p 2576 N95-29778
Analytical investigation of the hygrothermal effects and parametric study of the Edge Crack Torsion (ECT) mode 3 test lay-ups
[NASA-TM-110163] p 2528 N95-30028

SHEARING
Three dimensional effects in fiber reinforced composites under compression
[AD-A292027] p 2523 N95-29185

SHEETS
Carbon sheet pumping
[AD-B179443L] p 2710 N95-29812

SHELL STABILITY
Compressive behavior of thick composite shells: Benchmark solutions for loss of stability and hygroscopic effects p 2595 N95-29424

SHELL THEORY
Elastoplastic buckling analysis of cylindrical shells using a semi-analytical formulation
[PB95-197349] p 2597 N95-30206

SHELLS (STRUCTURAL FORMS)
A global/local analysis method for treating details in structural design p 2517 N95-28848

SHELTERS
Sleep during SEAL Delivery Vehicle (SDV)/Dry dock shelter exercises analyzed by a graphic approach
[AD-A290916] p 2637 N95-30083

SHIELDING
An extension of the Lighthill theory of jet noise to encompass refraction and shielding
[NASA-TM-110163] p 2684 N95-29452

SHIP TERMINALS
Sleep during SEAL Delivery Vehicle (SDV)/Dry dock shelter exercises analyzed by a graphic approach
[AD-A290916] p 2637 N95-30083

SHIPS
High resolution direct digitizitation and optical telemetry of shipboard antenna signals
[AD-A290238] p 2557 N95-29504

SHOCK ABSORBERS
Shock resistant optic fiber rotary slice holding device
[AD-D017327] p 2702 N95-30053

SHOCK LAYERS
Physical causes of separation shock unsteadiness in shock wave/turbulent boundary layer interactions
p 2570 N95-29096
SHOCK LOADS
Short term visits for collaborative research
[AD-A290704] p 2682 N95-29588
SHOCK RESISTANCE
Shock resistant optic fiber rotary slice holding device
[AD-D017327] p 2702 N95-30053
SHOCK TUBES
The effect of viscous attenuation on shock tube performance
[AD-A289793] p 2568 N95-28696
Numerical simulations of the flow in the HYPULSE expansion tube
[NASA-TM-110357] p 2503 N95-30228
SHOCK WAVE ATTENUATION
The effect of viscous attenuation on shock tube performance
[AD-A289793] p 2568 N95-28696
SHOCK WAVE INTERACTION
A procedure for automating CFD simulations of an inlet-bleed problem p 2485 N95-28768
Physical causes of separation shock unsteadiness in shock wave/turbulent boundary layer interactions
p 2570 N95-29096
Interaction of turbulence with complex shock waves
[AD-A290225] p 2571 N95-29145
Direct numerical simulation of compressible turbulent flows, using adaptive spectral element method
[AD-A290115] p 2575 N95-29421
Investigation of Burnett equations for two-dimensional hypersonic flow
[AD-A290233] p 2575 N95-29469
The 1995 version of the NSWC aeroprediction code. Part 1: Summary of new theoretical methodology
[AD-A291518] p 2490 N95-29853
Experimental research on crossing shock wave boundary layer interactions
[AD-A290764] p 2577 N95-29920
Hydrogen film cooling with incident and swept-shock interactions in a Mach 6.4 nitrogen free stream
[NASA-TM-4603] p 2578 N95-30056
Numerical simulations of small amplitude acoustic wave propagation in a converging-diverging nozzle
p 2690 N95-30160
SHOCK WAVES
The effect of viscous attenuation on shock tube performance
[AD-A289793] p 2568 N95-28696
Wave drag coefficient for axisymmetric forecowls at zero incidence (M sub infinity less than or equal to 1.5)
[ESDU-94014] p 2568 N95-28903
Surface pressure coefficient distributions for axisymmetric forecowls at zero incidence (M sub infinity less than or equal to 1.5)
[ESDU-94015] p 2487 N95-28904
Physical acoustics summer school, 1994. volume 1. transcript
[AD-A292552] p 2683 N95-28973
An extension of the continuum model by Grad's thirteen moment equations for hypersonic rarefied flows
p 2488 N95-29118
Interaction of turbulence with complex shock waves
[AD-A290225] p 2571 N95-29145
Experimental investigations of wave and fracture phenomena in impacted ceramics and glasses
[AD-A292142] p 2542 N95-29195
Unsteadiness of shock-induced turbulent boundary layer separation. An inherent feature of turbulent flow or solely a wind tunnel phenomenon
[AD-A290367] p 2572 N95-29228
An experimental investigation of the time-dependent separation of tangent bodies in supersonic flow
[AD-A290720] p 2489 N95-29500
Far-ultraviolet high-resolution emission line spectroscopy of the Cygnus Loop supernova remnant
p 2729 N95-29710
Survey of CFD applications for high speed inlets
[AD-A291365] p 2578 N95-30087
The physics of the collisionless bow shock
p 2580 N95-30301
SHORT WAVE RADIATION
High power, high frequency radiation from beam-plasma interactions
[AD-A292442] p 2703 N95-29001
SIDEBANDS
An investigation of the channel crosstalk in optical heterodyne controlled phased array radars
[AD-A292028] p 2554 N95-29186
SIGNAL ANALYSIS
Spectral analysis techniques using wavelets as an alternative to Fourier analysis for transient dynamic data
[AD-A289776] p 2556 N95-29459
SIGNAL DETECTION
Wavelets in signal detection and identification comparative signal processing technology evaluation
[AD-A291952] p 2552 N95-28984
Power measurement and current feedback in a resonant DC link inverter
[AD-A292518] p 2563 N95-29164
Adaptive block sequential detection of abrupt signal changes
[AD-A290456] p 2557 N95-29489
Neural network construction using evolutionary search
[AD-A290862] p 2665 N95-29831
SIGNAL DISTORTION
Adaptive block sequential detection of abrupt signal changes
[AD-A290456] p 2557 N95-29489
SIGNAL ENCODING
The design of programmable convolutional encoder using VHDL and an FPGA
[AD-A290048] p 2649 N95-29442
SIGNAL GENERATORS
Cyclic feature analysis, design and exploitation
[AD-A290639] p 2557 N95-29603
Balanced, double-sided calibration circuit for sensor element differential pre-amplifier
[AD-D017326] p 2566 N95-30052
SIGNAL MEASUREMENT
Wideband I/Q demodulators: Measurement technique and matching characteristics
[AD-A291505] p 2558 N95-29847
SIGNAL PROCESSING
Backscatter data acquisition for Hydrosweep DS aboard RV Ewing
[AD-A292332] p 2628 N95-28796
Automated optical target recognition
[AD-A292397] p 2697 N95-28798
Using object-oriented database technology to develop a multiple domain capability for domain-oriented application composition systems
[AD-A289244] p 2721 N95-28907
Fibre-coupled remote optical vibrometry
[AD-A291606] p 2698 N95-28932
An algorithm fusion approach to IRST signal processing (III): Nongaussian-corrected filter fusion
[AD-A291565] p 2552 N95-28936
Wavelets in signal detection and identification comparative signal processing technology evaluation
[AD-A291952] p 2552 N95-28984
Proceeding of the 33rd SICE Annual Conference
[DE95-758943] p 2662 N95-29144
Comparison study of unequal error protection methods for one-dimensional signal constellations
[AD-A290386] p 2554 N95-29231
A method and apparatus for signal filtering
[AD-D017268] p 2554 N95-29236
Two-dimensional signal processing for regional seismic event identification
[AD-A292601] p 2613 N95-29293
A comparison of three pedestal removal techniques for an optical time-integrating correlator
[AD-A290092] p 2700 N95-29354
Spectral analysis techniques using wavelets as an alternative to Fourier analysis for transient dynamic data
[AD-A289776] p 2556 N95-29459
The 1994 IEEE International Workshop on Intelligent Signal Processing and Communication Systems (ISPACS94)
[AD-A292312] p 2556 N95-29474
Adaptive block sequential detection of abrupt signal changes
[AD-A290456] p 2557 N95-29489
High resolution direct digitization and optical telemetry of shipboard antenna signals
[AD-A290238] p 2557 N95-29504
Signal processing for high-resolution image formation
[AD-A290648] p 2557 N95-29563
Applied optics laboratory
[AD-A292006] p 2701 N95-29571
Wideband I/Q demodulators: Measurement technique and matching characteristics
[AD-A291505] p 2558 N95-29847
DPARTS. A dynamic parallel adaptive multiprocess or real-time scheduler
[AD-A291160] p 2659 N95-29915
W-matrices, nonorthogonal multiresolution analysis, and finite signals of arbitrary length
[DE95-005846] p 2652 N95-30020
SIGNAL RECEPTION
Improved interception capability through the use of transform domain processing
[AD-A292231] p 2554 N95-29203
SIGNAL TO NOISE RATIOS
System and method for rapidly tracking vehicles of special utility in low signal-to-noise environments
[AD-D017378] p 2683 N95-28783
International Workshop on Stochastic Filtering Theory
[AD-A291670] p 2661 N95-28788
A comparison of three pedestal removal techniques for an optical time-integrating correlator
[AD-A290092] p 2700 N95-29354
The use of charge coupled devices in astronomical speckle imaging p 2727 N95-29545
SIGNATURES
Observational signatures of rotating black holes
p 2729 N95-29709
SILANES
Interface properties of wide bandgap semiconductor structures
[AD-A289817] p 2713 N95-28954
SILICA GLASS
Measurement of ultrashort pulses with a non-instantaneous nonlinearity
[DE95-006500] p 2698 N95-28983
SILICATES
Differentiation in the early Earth: An experimental investigation p 2612 N95-29199
SILICON
Laser simulation of single-event effects: A state of the art review
[AD-A292308] p 2584 N95-28892
Synthesis and complete characterization of a Gallium-Mixed-Pnicogen four-membered ring compound: I2GaAs(SiMe3)(sub 2)Ga(I)2P(SiMe3)(sub 2)
[AD-A292423] p 2713 N95-28993
GLAST
[DE95-008596] p 2739 N95-29265
Photon-counting spatial light modulator technology development
[AD-A292619] p 2699 N95-29295
Surface studies of Poly(organophosphazenes) containing dimethylsiloxane grafts
[AD-A291909] p 2543 N95-29355
HTMIAC/CINDAS silicon properties database. User's guide
[AD-A292602] p 2533 N95-29575
SAM1-A new semiempirical method including d-orbitals
[AD-A290903] p 2694 N95-30060
Transformational design of a direction detector for the progressive scan conversion processor
[PB95-198487] p 2643 N95-30109
A finite element analysis of room temperature silicon crystals for the Advanced Photon Source bending-magnet and insertion-device beams
[DE95-005822] p 2718 N95-30184
Formation and properties of titanium disilicide: A study on the development of stress in Ti-Si thin films
[PB95-197315] p 2538 N95-30205
SILICON ALLOYS
Epitaxial growth and characterization of Si(1-x)Ge(x) materials and devices
[AD-A292528] p 2712 N95-28874
SILICON CARBIDES
Nitride semiconductors for ultraviolet detection
[AD-A289546] p 2712 N95-28910
In-phase thermomechanical fatigue mechanisms in an unidirectional SCS-6/Ti 15-3 MMC
[NASA-CR-195482] p 2523 N95-29133
Integrated synthesis and post-processing of SiC and AlN
[AD-A290853] p 2537 N95-29724
Innovative processing of composites for ultra-high temperature applications, book 1
[AD-A290889] p 2527 N95-29842
The 41st Japan Society of Applied Physics Spring Meeting
[AD-A292333] p 2720 N95-29879
Epitaxial growth of high quality SiC of pulsed laser deposition, phase 1
[AD-A291410] p 2717 N95-30068
Elevated temperature static fatigue of a Nicalon fiber-reinforced SiC composite
[DE95-008780] p 2528 N95-30175
SILICON COMPOUNDS
The development of an interpretive methodology for the application of real-time acousto-ultrasonic NDE technique for monitoring damage in ceramic composites under dynamic loads p 2592 N95-29104
SILICON DIOXIDE
In-line fiber etalon strain sensor
[AD-D017266] p 2699 N95-29283
Recent progress in the study of the kinetics of sol-gel SiO2 synthesis reactions
[AD-A290570] p 2544 N95-29551
Cage-like precursor formation from extensive cyclization in sol-gel inorganic condensation polymerization
[AD-A290589] p 2544 N95-29554
Evaluation of retro-reflective beads in airport pavement markings
[AD-A291065] p 2502 N95-29967

SILICON FILMS
The 2nd International Conference on Thin Film Physics and Applications
[AD-A292353] p 2546 N95-29983
SILICON NITRIDES
The nucleation of crystalline films from vapor phase reactants
[AD-A291122] p 2716 N95-29767
Nanocrystalline processing and interface engineering of Si3N4-based ceramics
[AD-A291302] p 2546 N95-29939
Evaluation of wear resistant ceramic valve seats in gas-fueled power generation engines
[PB95-200218] p 2591 N95-30110
A CMOS-compatible, surface-micromachined pressure sensor for aqueous ultrasonic application
[DE95-008538] p 2567 N95-30188
SILICON OXIDES
Nobeyama Radio Observatory report, no. 380: Detection of the (29)SiO v=1, J=1-0 maser from TX Camelopardalis p 2726 N95-29101
SILOXANES
Surface studies of Poly(organophosphazenes) containing dimethylsiloxane grafts
[AD-A291909] p 2543 N95-29355
SILVER
Effects of space exposure on metals flown on the Long Duration Exposure Facility
[NASA-CR-4662] p 2512 N95-30225
SIMD (COMPUTERS)
The mesh synchronous processor MeshSP (trademark)
[AD-A289875] p 2659 N95-29420
SIMULATED ANNEALING
A technique for optimizing grid blocks p 2485 N95-28769
SIMULATION
Laser simulation of single-event effects: A state of the art review
[AD-A292308] p 2584 N95-28892
Thin-film resistor array characterization
[AD-A289806] p 2561 N95-28950
Molecular dynamics study of electromigration
[AD-A289811] p 2691 N95-28952
NPSNETIV: An object-oriented interface for a three-dimensional virtual world
[AD-A292467] p 2646 N95-29008
Characterization and calibration of a pulsed laser system for single event upset simulation
[AD-A290075] p 2586 N95-29330
Eurasian seismic surveillance - 2D FD seismic synthetics and event discrimination
[AD-A292659] p 2614 N95-29413
HIDENEK: An implicit particle simulation of kinetic-MHD phenomena in three-dimensional plasmas
[AD-B176255L] p 2707 N95-29739
The origin of collisionless dissipation in magnetic reconnection
[AD-B178949L] p 2710 N95-29813
An operational comparison of the CH-46E and HH-60H as Navy combat support helicopter replacement options using the Simulated Mobility Modeling and Analysis Toolbox (SMMAT)
[AD-A288494] p 2498 N95-29911
ADC test support program
[AD-A289445] p 2643 N95-29921
Fast simulation of the leaky bucket algorithm
[PB95-197174] p 2653 N95-30098
Simulation of robot manipulators
[DE95-008680] p 2654 N95-30189
SIMULATORS
Characterizing the electromagnetic environment produced by the army's repetitive electromagnetic pulse simulator (REPS)
[AD-A289739] p 2551 N95-28687
SOSDOR: Solid-state device simulator code
[AD-A289954] p 2563 N95-29275
SIMULTANEOUS EQUATIONS
An efficiency study of the simultaneous analysis and design of structures
[NASA-TM-110168] p 2495 N95-28820
SINE WAVES
Dynamic stall of a NACA 0012 airfoil in laminar flow p 2489 N95-29243
SINGLE CRYSTALS
Nitride semiconductors for ultraviolet detection
[AD-A289546] p 2712 N95-28910
Ballistic penetration phenomenology of high symmetry single crystals
[AD-A292476] p 2713 N95-29013
Synthesis and characterization of CuO superconductors with high transient temperatures
[AD-A292478] p 2562 N95-29014
Pulsed laser deposition of ferroelectric thin films in conjunction with superconducting oxides
[AD-A290101] p 2585 N95-29208
Ion beam modification of Tl-Ba-Ca-Cu-O type high temperature superconductors during irradiation
[DE95-006807] p 2717 N95-30022
Epitaxial growth of high quality SiC of pulsed laser deposition, phase 1
[AD-A291410] p 2717 N95-30068
SINGLE EVENT UPSETS
Laser simulation of single-event effects: A state of the art review
[AD-A292308] p 2584 N95-28892
Characterization and calibration of a pulsed laser system for single event upset simulation
[AD-A290075] p 2586 N95-29330
Investigation and characterization of SEU effects and hardening strategies in avionics
[AD-A291058] p 2500 N95-29950
SINGULARITY (MATHEMATICS)
Dynamical instabilities, chaos and spatial complexity in fundamental nonlinear optical interactions
[AD-A291223] p 2588 N95-29980
SINTERING
High-toughness glass-ceramics
[AD-A290562] p 2541 N95-29071
Solid freeform fabrication symposium
[AD-A290949] p 2527 N95-29732
SIS (SUPERCONDUCTORS)
Nobeyama Radio Observatory report, no. 381: Parallel connected twin SIS junctions for millimeter and submillimeter wave mixers: Analysis and experimental verification p 2562 N95-29099
SKIN FRICTION
Boundary-layer transition and global skin friction measurement with an oil-fringe imaging technique
[NASA-CR-198814] p 2579 N95-30224
SKY BRIGHTNESS
Reflectance analysis under solar illumination
[AD-A290489] p 2737 N95-29151
SKY SURVEYS (ASTRONOMY)
A multi-wavelength study of rotation-driven pulsars p 2729 N95-29678
The properties of local poor Abell clusters and instrumentation for the study of clustered objects p 2730 N95-29827
SiO maser survey of the IRAS bulge sources p 2735 N95-29837
Observational properties of SiO masers in the galactic bulge IRAS sources p 2735 N95-29838
SLABS
Shear reinforcement in deep slabs
[AD-A289528] p 2594 N95-28909
SLEEP
Shift work, age, and performance: Investigation of the 2-2-1 shift schedule used in Air Traffic Control facilities I. The sleep/wake cycle
[DOT/FAA/AM-95/19] p 2638 N95-29261
The effect of bright light and LEET on sleep after a 10-hour phase delay
[AD-A291264] p 2637 N95-29995
Sleep during SEAL Delivery Vehicle (SDV)/Dry dock shelter exercises analyzed by a graphic approach
[AD-A290916] p 2637 N95-30083
SLEEP DEPRIVATION
Shift work, age, and performance: Investigation of the 2-2-1 shift schedule used in Air Traffic Control facilities I. The sleep/wake cycle
[DOT/FAA/AM-95/19] p 2638 N95-29261
SLOPES
A full wave study of radar cross sections of rough terrain
[AD-A291227] p 2559 N95-29982
SLOTS
The fluid mechanics of a high aspect ratio slot with an impressed pressure gradient and secondary injection p 2580 N95-30304
SLURRIES
NMR imaging and hydrodynamic analysis of neutrally buoyant non-Newtonian slurry flows
[DE95-005842] p 2578 N95-30187
SMART STRUCTURES
On-line damage identification and motion control of adaptive structures: An intelligent control approach p 2662 N95-29109
The 2nd European Conference on Smart Structures and Materials
[AD-A290723] p 2550 N95-29579
Development of 'smart' piezothermoelastic laminae: Theory and applications
[AD-A290852] p 2528 N95-29864
Experimental confirmation of a PDE-based approach to design of feedback controls
[NASA-CR-198167] p 2672 N95-30086
SMOKE
Computational fluid dynamics (CFD) simulation of test chamber and smoke-generating device
[AD-A290199] p 2569 N95-29058
The potential for pulmonary heat injury resulting from the activation of a cabin water spray system to fight aircraft cabin fires
[DOT/FAA/AM-95/17] p 2636 N95-29224
SMOKE DETECTORS
Cost effective, dual-purpose machine vision-based detectors for (1) smoke and flame detection, and (2) engine overhead/burn-through and flame detection
[AD-A292284] p 2697 N95-28870
SMOOTHING
Grid generation and surface modeling for CFD p 2478 N95-28726
Multilevel elliptic smoothing of large three-dimensional grids p 2485 N95-28765
SNOW
Changes in microstructural parameters of snow during deformation
[AD-A290887] p 2601 N95-29866
SNOW COVER
Variation in visual and near-infrared contrast with a snow background
[AD-A289710] p 2697 N95-28778
The effect of climate perturbations on extratropical cyclogenesis along the east coast of North America p 2621 N95-29595
SNOWSTORMS
The effect of climate perturbations on extratropical cyclogenesis along the east coast of North America p 2621 N95-29595
SODIUM
Development of continuous visible chemical laser amplifiers and oscillators from the Na3-X(Cl, Br, I) reactions and their analogs and energy transfer pumping from efficiently produced metastable states
[AD-A290999] p 2586 N95-29514
SOFTWARE DEVELOPMENT TOOLS
Evaluation of grid generation technologies from an applied perspective p 2482 N95-28748
Software testing toolkit for distributed simulations
[AD-A291867] p 2649 N95-29435
Scalable software tools for adaptive scientific computation
[AD-A290446] p 2650 N95-29480
High-level parallel programming tools for finite element analysis
[AD-A290566] p 2659 N95-29566
Description and manipulation of method fragments for the assembly of situational methods
[PB95-197133] p 2653 N95-30094
Static analysis of functional programs
[PB95-197141] p 2653 N95-30095
Realisation of an integrated software engineering environment through heterogeneous CASE-tool integration
[PB95-197646] p 2653 N95-30105
Speedlog: The key architectural element to provide efficient log management
[PB95-198453] p 2643 N95-30108
Tools for Automated Knowledge Engineering (TAKE) system evaluation methodology
[AD-A291145] p 2654 N95-30125
Structured approach for the methodical and technical integration of heterogeneous CASE tools
[PB95-197653] p 2655 N95-30218
Developing a workstation-based, real-time simulation for rapid handling qualities evaluations during design
[NASA-CR-198831] p 2499 N95-30335
SOFTWARE ENGINEERING
Automated testing of application domains
[AD-A289753] p 2643 N95-28690
Collected software engineering papers, volume 12
[NASA-CR-189409] p 2644 N95-28713
An overview of the Software Engineering Laboratory
[NASA-CR-189410] p 2644 N95-28714
Surface Modeling, Grid Generation, and Related Issues in Computational Fluid Dynamic (CFD) Solutions
[NASA-CP-3291] p 2478 N95-28723
Requirements for effective use of CFD in aerospace design p 2478 N95-28725
Application of CFD in aeronautics at NASA Ames Research Center p 2478 N95-28726
Geometry Laboratory (GEOLAB) surface modeling and grid generation technology and services p 2479 N95-28729
Rapid Airplane Parametric Input Design (RAPID) p 2479 N95-28730
Algorithms for high aspect ratio oriented triangulations p 2479 N95-28731
Surface modeling and grid generation for aeropropulsion CFD p 2479 N95-28732
Automatic blocking for complex three-dimensional configurations p 2480 N95-28734
Multiblock grid generation with automatic zoning p 2480 N95-28735
Block-structured grids for complex aerodynamic configurations: Current status p 2480 N95-28736

Grid related issues for static and dynamic geometry problems using systems of overset structured grids p 2480 N95-28737
The role of overset grids in the development of the general purpose CFD code p 2480 N95-28738
An unstructured-grid software system for solving complex aerodynamic problems p 2481 N95-28743
Three-dimensional hybrid grid generation using advancing front techniques p 2481 N95-28745
Emerging CFD technologies and aerospace vehicle design p 2482 N95-28746
An assessment of unstructured grid technology for timely CFD analysis p 2482 N95-28747
The National Grid Project: A system overview p 2482 N95-28749
A 3DGRAPE/AL: The Ames/Langley technology upgrade p 2482 N95-28750
Automatic structured grid generation using Gridgen (some restrictions apply) p 2483 N95-28751
Tuned grid generation with ICEM CFD p 2483 N95-28752
Geometry modeling and grid generation using 3D NURBS control volume p 2483 N95-28753
Software Design for Reliability and Reuse proof of concept project. Phase 1
[AD-A291690] p 2644 N95-28782
DOD electronic data interchange (EDI) convention: TDCC/EDIA transaction set 210 motor carrier invoice (version 003020). Revision 1
[AD-A292375] p 2720 N95-28797
Annotated bibliography of software engineering laboratory literature
[NASA-CR-189406] p 2644 N95-28805
Software measurement guidebook
[NASA-CR-189407] p 2644 N95-28806
Impact of Ada and object-oriented design in the flight dynamics division at Goddard Space Flight Center
[NASA-CR-189412] p 2644 N95-28807
C style guide
[NASA-CR-189408] p 2645 N95-28821
Upgrading the Day/Night whole sky imager from Manual/Interactive to full automatic control
[AD-A292296] p 2619 N95-28872
Problem decomposition for reuse
[AD-A292245] p 2645 N95-28881
Formalizing style to understand descriptions of software architecture
[AD-A292237] p 2645 N95-28894
Using object-oriented database technology to develop a multiple domain capability for domain-oriented application composition systems
[AD-A289244] p 2721 N95-28907
Operating procedures for Anthropometry and Initial Conditions Photogrammetric Program
[AD-A291553] p 2640 N95-28935
Analysis of tropospheric propagation characteristics based on regional meteorological data
[AD-A291581] p 2552 N95-28939
High performance hardware and software for pattern recognition and image processing
[AD-A292307] p 2646 N95-28964
Rome laboratory software engineering cooperative virtual machine
[AD-A292396] p 2658 N95-28965
Glenda software design
[AD-A292537] p 2646 N95-28968
Exploiting symmetry in the model checking of relational specifications
[AD-A290230] p 2647 N95-29223
An introduction to the principles of computer science: A reuse-oriented philosophy
[AD-A290364] p 2647 N95-29226
Software systems reengineering process model, version 2.0
[AD-A289968] p 2647 N95-29278
DOD electronic data interchange (EDI) convention: ASC X12 transaction set 410 Rail Carrier Invoice, version 003020
[AD-A292495] p 2722 N95-29287
A friendly editing environment for computer-aided rapid prototyping of hard real-time systems
[AD-A290154] p 2648 N95-29321
Characteristics of higher-level languages for software architecture
[AD-A292215] p 2649 N95-29376
Programmable materials and structures
[AD-A291807] p 2649 N95-29429
Software testing toolkit for distributed simulations
[AD-A291867] p 2649 N95-29435
Digital video technology, today and tomorrow
[DE95-007689] p 2556 N95-29462
Automated reasoning about classical mechanics
[AD-A290052] p 2663 N95-29477
Neural network exploration using optional experiment design
[AD-A290058] p 2663 N95-29479
Scalable software tools for adaptive scientific computation
[AD-A290446] p 2650 N95-29480
Parallel adaptive techniques for transient partial differential equations
[AD-A290460] p 2674 N95-29490
Automatically combining changes to software systems
[AD-A290628] p 2650 N95-29515
A study of the conceptual symbolics of information system development languages p 2723 N95-29589
Modeling spatio-temporal databases to measure the performance of the GPS satellite constellation p 2494 N95-29596
Fundamental limitations and capabilities of robust identification and adaptive control
[AD-A291085] p 2664 N95-29636
Graphics supercomputer for computational fluid dynamics research
[AD-A291087] p 2575 N95-29637
AFGWC dial-in subsystem (AFDIS) software users manual, version 3.1
[AD-A291103] p 2651 N95-29639
Proceedings of the 12th Annual National Conference on Ada Technology
[AD-A290693] p 2651 N95-29644
A comparison of ISO 9001 and the Capability Maturity Model for Software
[AD-A290697] p 2651 N95-29762
A study of problematic situations and information needs of software managers in the United States and Japan p 2724 N95-29828
PSEE architecture report: Architectures and models for next generation process-based software engineering environments
[AD-A291268] p 2652 N95-29996
Workshop on computing and intelligent systems
[AD-A290581] p 2666 N95-30040
A formal extension to object oriented analysis using Z
[AD-A290911] p 2653 N95-30080
Layers as knowledge transitions in the design of distributed systems
[PB95-197638] p 2660 N95-30104
Realisation of an integrated software engineering environment through heterogeneous CASE-tool integration
[PB95-197646] p 2653 N95-30105
ALLIANCE: An architecture for fault tolerant multi-robot cooperation
[DE95-008658] p 2666 N95-30112
Software Estimation Program (SWEEP) user manual
[AD-A291137] p 2654 N95-30121
Tools for Automated Knowledge Engineering (TAKE) system evaluation methodology
[AD-A291145] p 2654 N95-30125
Structured approach for the methodical and technical integration of heterogeneous CASE tools
[PB95-197653] p 2655 N95-30218
Correctness of real-time systems by construction
[PB95-206827] p 2655 N95-30220
Parallel rendering
[NASA-CR-195080] p 2655 N95-30306
Manual for a workstation-based generic flight simulation program (LaRCsim), version 1.4
[NASA-TM-110164] p 2502 N95-30327
Developing a workstation-based, real-time simulation for rapid handling qualities evaluations during design
[NASA-CR-198831] p 2499 N95-30335

SOFTWARE RELIABILITY
Software measurement guidebook
[NASA-CR-189407] p 2644 N95-28806
Proposed Department of Defense software metrics implementation plan
[AD-A291404] p 2550 N95-29918

SOFTWARE REUSE
An introduction to the principles of computer science: A reuse-oriented philosophy
[AD-A290364] p 2647 N95-29226
SEMINT: Seamless model integration
[AD-A290956] p 2651 N95-29736

SOIL EROSION
Tidal constituent database: West coast of the United States and eastern North Pacific Ocean
[AD-A292224] p 2630 N95-29198

SOIL MAPPING
Development of improved geophysical imaging techniques for environmental site characterization
[AD-A291003] p 2558 N95-29875

SOIL MOISTURE
Remote sensing of hydrologic variables in boreal areas
[NASA-CR-189422] p 2600 N95-29754
Microwave remote sensing of surface soil moisture and its application to hydrologic modeling p 2600 N95-29821
Development of improved geophysical imaging techniques for environmental site characterization
[AD-A291003] p 2558 N95-29875
Soil wetness and climate variability p 2609 N95-29878
Development and testing of improved techniques for modeling the hydrologic cycle in a mesoscale weather prediction system
[AD-A291243] p 2627 N95-29993
A conceptual thermal design study of an electronically scanned thinned array radiometer
[NASA-TM-110173] p 2509 N95-30316

SOIL SCIENCE
Modeling joint effects of mixtures of chemicals on microorganisms using quantitative structure activity relationship techniques, phase 3
[AD-A290153] p 2632 N95-29320
Development of an artificial neural network for real-time classification of cone penetrometer strain gauge data
[AD-A290719] p 2664 N95-29499

SOILS
Surfactant-enhanced in situ biodegradation of strongly sorbing organic substances in soil environments
[AD-A290253] p 2512 N95-29168
Tidal constituent database: West coast of the United States and eastern North Pacific Ocean
[AD-A292224] p 2630 N95-29198
Investigation of an alternative finite element procedure: A one-step, steady-state analysis
[AD-A290030] p 2670 N95-29311
Gradient-dependent plasticity in numerical simulation of localization phenomena
[PB95-197257] p 2596 N95-30049

SOL-GEL PROCESSES
Recent progress in the study of the kinetics of sol-gel SiO2 synthesis reactions
[AD-A290570] p 2544 N95-29551
Cage-like precursor formation from extensive cyclization in sol-gel inorganic condensation polymerization
[AD-A290589] p 2544 N95-29554
Fabrication of advanced electrochemical energy materials using sol-gel processing techniques p 2607 N95-30269

SOLAR ACTIVITY
Solar-geophysical data number 605, January 1995. Part 2 (comprehensive reports): Data for July 1994 and miscellaneous
[PB95-190997] p 2737 N95-28780
Solar-geophysical data number 605, January 1995. Part 1 (prompt reports): Data for December, November 1994 and late data
[PB95-191003] p 2737 N95-28781
Nobeyama Radio Observatory report, no. 361: The radio properties of solar active region soft x-ray transient brightenings p 2737 N95-29098
Thermal N(+) in the inner magnetosphere p 2614 N95-29590

SOLAR ARRAYS
Arcing mitigation and predictions for high voltage solar arrays
[AD-A292227] p 2602 N95-29200
Arcing predictions for PASP PLUS solar arrays
[AD-A292230] p 2602 N95-29201
Analysis of shadowing effects on spacecraft power systems
[NASA-TM-106994] p 2511 N95-30012
PASP plus time history data base file structures
[AD-A290587] p 2725 N95-30043
The TMI regenerable solid oxide fuel cell p 2606 N95-30265

SOLAR CELLS
Multi-decade time-dependent voltage of polycrystalline thin-film solar cells p 2602 N95-29103
Arcing mitigation and predictions for high voltage solar arrays
[AD-A292227] p 2602 N95-29200
Arcing predictions for PASP PLUS solar arrays
[AD-A292230] p 2602 N95-29201
Investigation of optical damage, energy partitioning and scaling laws at extremely high velocities
[AD-A291368] p 2703 N95-30062
High-efficiency solar cells using HEM silicon
[DE95-005424] p 2604 N95-30217

SOLAR COLLECTORS
Solar heating and you
[DE95-004012] p 2603 N95-30127

SOLAR CORONA
First flight of the Multi-Spectral Solar Telescope Array: Calibration, results and future plans p 2727 N95-29529
Radioastronomical measurements of plasma characteristics of the solar corona and the solar wind p 2730 N95-29782
15th NSO/Sac Peak Solar Workshop
[AD-A292297] p 2739 N95-30074

SOLAR CYCLES
A turbulent model of the solar granulation
[AD-A292318] p 2738 N95-29475
SOLAR DYNAMIC POWER SYSTEMS
Analysis of shadowing effects on spacecraft power systems
[NASA-TM-106994] p 2511 N95-30012
SOLAR ECLIPSES
Total solar eclipse of 1997 March 9
[NASA-RP-1173] p 2731 N95-30004
SOLAR ELECTRIC PROPULSION
Guidance, navigation, and control study for a solar electric propulsion spacecraft
[NASA-CR-198920] p 2509 N95-30357
SOLAR ENERGY
A turbulent model of the solar granulation
[AD-A292318] p 2738 N95-29475
High temperature spectroscopy of alkali metal vapors for solar to thermal energy conversion
[AD-A291355] p 2602 N95-29949
SOLAR ENERGY CONVERSION
Solar heating and you
[DE95-004012] p 2603 N95-30127
SOLAR FLARES
Solar-geophysical data number 605, January 1995. Part 2 (comprehensive reports): Data for July 1994 and miscellaneous
[PB95-190997] p 2737 N95-28780
Solar-geophysical data number 605, January 1995. Part 1 (prompt reports): Data for December, November 1994 and late data
[PB95-191003] p 2737 N95-28781
Observations and analysis of solar flares at radio and other wavelengths p 2738 N95-29202
Si 13 emission lines in solar flare x ray spectra obtained with the P78-1 satellite
[AD-A290000] p 2738 N95-29279
Yohkoh Bragg Crystal Spectrometer light curves for Ca 29(3.1633 - 3.1933 A): 1 October 1993 - 30 September 1994
[AD-A290027] p 2738 N95-29327
First flight of the Multi-Spectral Solar Telescope Array: Calibration, results and future plans
p 2727 N95-29529
SOLAR GRANULATION
A turbulent model of the solar granulation
[AD-A292318] p 2738 N95-29475
SOLAR HEATING
Solar heating and you
[DE95-004012] p 2603 N95-30127
The effects of clouds as a feedback mechanism on the Earth's climate in the tropical Pacific
p 2611 N95-30300
SOLAR INSTRUMENTS
First flight of the Multi-Spectral Solar Telescope Array: Calibration, results and future plans
p 2727 N95-29529
SOLAR MAGNETIC FIELD
Solar-geophysical data number 605, January 1995. Part 1 (prompt reports): Data for December, November 1994 and late data
[PB95-191003] p 2737 N95-28781
Radioastronomical measurements of plasma characteristics of the solar corona and the solar wind
p 2730 N95-29782
SOLAR OBSERVATORIES
First flight of the Multi-Spectral Solar Telescope Array: Calibration, results and future plans
p 2727 N95-29529
SOLAR PHYSICS
Solar-geophysical data number 605, January 1995. Part 2 (comprehensive reports): Data for July 1994 and miscellaneous
[PB95-190997] p 2737 N95-28780
Solar-geophysical data number 605, January 1995. Part 1 (prompt reports): Data for December, November 1994 and late data
[PB95-191003] p 2737 N95-28781
SOLAR PLANETARY INTERACTIONS
A study of plasma waves arising from the solar wind interaction with Venus p 2704 N95-29215
The physics of the collisionless bow shock
p 2580 N95-30301
SOLAR RADIATION
Reflectance analysis under solar illumination
[AD-A290489] p 2737 N95-29151
Sensitivity of the simulated global climate to perturbations in low cloud microphysical properties
p 2620 N95-29206
SOLAR RADIATION SHIELDING
EMI Shields made from intercalated graphite composites
[NASA-TM-106979] p 2518 N95-28906
SOLAR RADIO BURSTS
Solar-geophysical data number 605, January 1995. Part 2 (comprehensive reports): Data for July 1994 and miscellaneous
[PB95-190997] p 2737 N95-28780
SOLAR RADIO EMISSION
Solar-geophysical data number 605, January 1995. Part 1 (prompt reports): Data for December, November 1994 and late data
[PB95-191003] p 2737 N95-28781
SOLAR SIMULATORS
Design of a more accurate, higher fidelity, dual-source air mass zero solar simulator
[AD-A291364] p 2603 N95-29953
SOLAR SPECTRA
Design of a more accurate, higher fidelity, dual-source air mass zero solar simulator
[AD-A291364] p 2603 N95-29953
SOLAR SYSTEM
Solar system plasma waves
[NASA-CR-198767] p 2704 N95-29130
Advanced research in sky surveillance: A search for low-luminosity objects
[AD-A291184] p 2731 N95-29916
SOLAR WIND
Solar system plasma waves
[NASA-CR-198767] p 2704 N95-29130
Arcing mitigation and predictions for high voltage solar arrays
[AD-A292227] p 2602 N95-29200
Arcing predictions for PASP PLUS solar arrays
[AD-A292230] p 2602 N95-29201
A Monte Carlo simulation of Coulomb collisions and wave-particle interactions in space plasma at high latitudes p 2704 N95-29205
A study of plasma waves arising from the solar wind interaction with Venus p 2704 N95-29215
One and two fluid numerical investigations of solar wind gas releases p 2738 N95-29704
Radioastronomical measurements of plasma characteristics of the solar corona and the solar wind
p 2730 N95-29782
The physics of the collisionless bow shock
p 2580 N95-30301
SOLAR X-RAYS
Solar-geophysical data number 605, January 1995. Part 2 (comprehensive reports): Data for July 1994 and miscellaneous
[PB95-190997] p 2737 N95-28780
Nobeyama Radio Observatory report, no. 361: The radio properties of solar active region soft x-ray transient brightenings p 2737 N95-29098
Yohkoh Bragg Crystal Spectrometer light curves for Ca 29(3.1633 - 3.1933 A): 1 October 1993 - 30 September 1994
[AD-A290027] p 2738 N95-29327
SOLID ELECTROLYTES
Fabrication of advanced electrochemical energy materials using sol-gel processing techniques
p 2607 N95-30269
Advances in tubular solid oxide fuel cell technology
[DE95-008361] p 2607 N95-30281
SOLID PHASES
Macrosegregation and nucleation in undercooled Pb-Sn alloys
[NASA-TM-102023-REV] p 2535 N95-28701
SOLID PROPELLANT ROCKET ENGINES
Investigation of the flow turning loss in unstable solid propellant rocket motors p 2510 N95-29331
SOLID PROPELLANTS
A study of power diode failure mechanisms in the US Army research laboratory 30-mm solid propellant electrothermal-chemical (SPETC) gun facility
[AD-A291300] p 2565 N95-29938
SOLID STATE
Novel high-power solid-state sources for the millimeter-wave region
[AD-A292653] p 2564 N95-29384
Vacuum microelectronic emitters and their applications using compound semiconductor technology
[AD-A291142] p 2567 N95-30124
SOLID STATE DEVICES
SOSDOR: Solid-state device simulator code
[AD-A289954] p 2563 N95-29275
New radiation sources through generation and resonant enhancement of Current Driven Plasma Instabilities in lower dimensional solid state systems
[AD-A290669] p 2705 N95-29519
SOLID STATE LASERS
ARPA solid state laser and nonlinear materials program
[AD-A289657] p 2584 N95-28678
Linewidth-insensitive coherent analog optical links
[AD-A292422] p 2698 N95-28992
Analysis of measurements for solid state laser remote lidar system
[NASA-CR-196640] p 2585 N95-29247
Summaries of papers presented at the ultrafast phenomena topical meeting
[AD-A290998] p 2564 N95-29511
Laser applications to chemical analysis: Summaries of papers presented at the laser applications to chemical analysis topical meeting
[AD-A290738] p 2587 N95-29653
High-efficiency longitudinal diode bar pumping of solid-state lasers
[AD-A291180] p 2587 N95-29931
A kilohertz femtosecond Ti: Sapphire regeneratie amplifier
[AD-A290591] p 2588 N95-30045
SOLID STATE PHYSICS
Semiconductor science and technology
[AD-A289143] p 2563 N95-29191
Brief introduction to state key physics laboratories and division open laboratories
[AD-A291064] p 2682 N95-29952
SOLID SURFACES
Surface Modeling, Grid Generation, and Related Issues in Computational Fluid Dynamic (CFD) Solutions
[NASA-CP-3291] p 2478 N95-28723
Future requirements in surface modeling and grid generation p 2478 N95-28724
Grid generation and surface modeling for CFD
p 2478 N95-28726
Geometry Laboratory (GEOLAB) surface modeling and grid generation technology and services
p 2479 N95-28729
Surface modeling and grid generation for aeropropulsion CFD p 2479 N95-28732
Marshall Space Flight Center surface modeling and grid generation applications p 2480 N95-28733
Molecular spectra and dynamics at interfaces
[AD-A289779] p 2693 N95-29460
SOLID-SOLID INTERFACES
Toughening mechanisms in mixed-mode interfacial fracture p 2545 N95-29772
Interfaces in InAsSb/InGaAs strained-layer superlattices grown by MOCVD for use in infrared emitters
[DE95-006323] p 2717 N95-29990
Engineering design of sub-micron topographies for simultaneously adherent and reflective metal-polymer interfaces
[NASA-CR-198845] p 2548 N95-30237
SOLIDIFICATION
Advanced manufacturing by spray forming: Aluminum strip and microelectromechanical systems
[DE95-008615] p 2536 N95-28959
SOLIDS
Parametric design and gridding through relational geometry p 2486 N95-28771
Publications/Patents/Presentations/Honors report: Force and tunneling microscopy studies of atomic level mechanical properties of solids
[AD-A292254] p 2691 N95-28888
Three problems in fluid dynamics
[AD-A290481] p 2573 N95-29324
SOLITARY WAVES
Self-Induced Transparency in photonic band structures: Gap solitons near absorption resonances
[AD-A292187] p 2718 N95-28927
Solitons in negative ion plasmas p 2706 N95-29668
SOLVENTS
Polymeric microcapsule arrays
[AD-A291937] p 2539 N95-28850
Analysis of factors affecting chemical reactions in supercritical fluids
[AD-A290905] p 2534 N95-30078
SONAR
Adaptive block sequential detection of abrupt signal changes
[AD-A290456] p 2557 N95-29489
SONDES
Compendium of NASA data base for the global tropospheric experiment's Transport and Atmospheric Chemistry Near the Equator-Atlantic (TRACE-A)
[NASA-TM-110151] p 2608 N95-28717
SONOLUMINESCENCE
Bubble fusion: Preliminary estimates of spherical micro-implosions in cavitating liquids
[DE95-006260] p 2569 N95-28956
SORPTION
Sorption and diffusion of moisture in multilayer composite AEM/S sandwich materials
[AD-A289807] p 2518 N95-28951
Use of finite element analysis for transient moisture diffusion studies in multilayer composite AEM/S system sandwich materials
[AD-A291092] p 2527 N95-29638

SOUND DETECTING AND RANGING
System and method for rapidly tracking vehicles of special utility in low signal-to-noise environments
[AD-D017378] p 2683 N95-28783
SOUND FIELDS
Investigation of the flow turning loss in unstable solid propellant rocket motors p 2510 N95-29331
The Scanning Fast Field Program (SCAFFIP) general version 1.0 user's manual
[AD-A291209] p 2618 N95-29976
ICASE/LaRC Workshop on Benchmark Problems in Computational Aeroacoustics (CAA)
[NASA-CP-3300] p 2686 N95-30133
SOUND GENERATORS
Acoustic imaging of ultrasonic wave propagation
[AD-A290390] p 2683 N95-29232
Evaluation of numerical schemes for the analysis of sound generation by blade-gust interaction
p 2690 N95-30163
SOUND LOCALIZATION
Pattern-analysis based models of masking by spatially separated sounds
[AD-A291270] p 2637 N95-29933
SOUND PRESSURE
Turbulent airflow noise production and propagation patterns of a subsonic jet impinging on a flat plate
p 2684 N95-29502
Finite difference ocean acoustic model users guide
[AD-A291544] p 2631 N95-29856
Evaluation of numerical schemes for the analysis of sound generation by blade-gust interaction
p 2690 N95-30163
SOUND PROPAGATION
The prediction of sound attenuation as a result of propagation close to the ground
[ESDU-94036] p 2682 N95-28709
100 Hz-10 kHz bottom backscattering model: Generalized treatment of sediment sound propagation, sediment volume scattering and interface-roughness scattering
[AD-A291323] p 2685 N95-29942
Proceedings of the Sixth International Symposium on Long-Range Sound Propagation
[AD-A290920] p 2685 N95-30084
SOUND TRANSMISSION
Hindcasting changes in thermal structure and acoustic transmission loss in the upper ocean on short time scales with data from MILE and from ocean weather station papa
[AD-A292419] p 2629 N95-28991
Proceedings of the Sixth International Symposium on Long-Range Sound Propagation
[AD-A290920] p 2685 N95-30084
SOUND WAVES
The acoustic characteristics of turbomachinery cavities
[NASA-CR-4671] p 2478 N95-28720
System and method for rapidly tracking vehicles of special utility in low signal-to-noise environments
[AD-D017378] p 2683 N95-28783
Stochastic modeling and global warming trend extraction for ocean acoustic travel times
[AD-A292114] p 2608 N95-28922
Physical acoustics summer school, 1994. volume 1. transcript
[AD-A292552] p 2683 N95-28973
Revisions and notes on a model for bubble attenuation in near-surface propagation
[AD-A290312] p 2629 N95-29085
Acoustic imaging of ultrasonic wave propagation
[AD-A290390] p 2683 N95-29232
A method and apparatus for signal filtering
[AD-D017268] p 2554 N95-29236
The nature of wavefront fluctuations induced by internal gravity waves in long-range oceanic acoustic pulse transmissions p 2630 N95-29528
Multiple dimensional acousto-optic diffraction and multiple dimensional acousto-optic device
[AD-A291037] p 2685 N95-29681
The one-dimensional bubble: Theory, experiment, and relevance to exposure of divers to low frequency sound, and of lung to lithotripsy
[ISVR-TR-246] p 2577 N95-29817
ICASE/LaRC Workshop on Benchmark Problems in Computational Aeroacoustics (CAA)
[NASA-CP-3300] p 2686 N95-30133
Benchmark problems and solutions
p 2686 N95-30134
Application of essentially nonoscillatory methods to aeroacoustic flow problems p 2686 N95-30135
Computational aeroacoustics using hyperbolic wave primitives p 2686 N95-30136
Application of low dissipation and dispersion Runge-Kutta schemes to benchmark problems in computational aeroacoustics p 2687 N95-30139
Computation of wave propagation in a complex flow
p 2582 N95-30142
Solutions of the benchmark problems by the dispersion-relation-preserving scheme
p 2674 N95-30145
A comparative study of upwind and MacCormack schemes for CAA benchmark problems
p 2688 N95-30147
Evaluation of high order schemes for nonlinear wave computations p 2582 N95-30149
Time accurate application of the MacCormack 2-4 scheme on massively parallel computers
p 2661 N95-30150
The use of staggered scheme and an absorbing buffer zone for computational aeroacoustics
p 2689 N95-30153
A numerical solution method for acoustic radiation from axisymmetric bodies p 2689 N95-30154
Computational aeroacoustics on massively parallel computers p 2661 N95-30156
Category 5 problem solution using an unstructured finite volume algorithm p 2657 N95-30157
Numerical simulations of small amplitude acoustic wave propagation in a converging-diverging nozzle
p 2690 N95-30160
Aeroacoustic computation of a gust-plate interaction via MacCormack schemes p 2690 N95-30162
Interaction of acoustic oscillations with magnetic flux tubes in the solar photosphere
[PB95-201810] p 2739 N95-30199
SOUTHERN OSCILLATION
Forecast of Atlantic seasonal hurricane activity for 1995 p 2620 N95-29254
SPACE DEBRIS
A layman's look at orbital debris
[AD-A289801] p 2506 N95-28700
Orbital debris: A technical assessment
[NASA-CR-198639] p 2507 N95-28852
Overview of the space debris environment
[AD-A292302] p 2507 N95-28867
The Los Alamos Photon Counting Detector Debris Detection Project: An update
[DE95-007883] p 2508 N95-29464
SPACE HABITATS
Fuel cell systems for First Lunar Outpost-reactant storage option p 2606 N95-30264
SPACE HEATING (BUILDINGS)
Geothermal heat pumps for heating and cooling
[AD-A292115] p 2602 N95-28858
SPACE MISSIONS
Life sciences program
[NASA-CR-197658] p 2633 N95-30292
SPACE OBSERVATIONS (FROM EARTH)
The use of charge coupled devices in astronomical speckle imaging p 2727 N95-29545
Coronagraphic imaging of protoplanetary-disk candidate stars using adaptive optics p 2728 N95-29651
Speckle imaging with the multi-anode microchannel array detector p 2728 N95-29652
SPACE PERCEPTION
Distance estimation training with night vision goggles under low illumination
[AD-A291338] p 2641 N95-29943
SPACE PLASMAS
Surface conversion techniques for low energy neutral atom imagers
[NASA-CR-196604] p 2691 N95-28856
Solar system plasma waves
[NASA-CR-198767] p 2704 N95-29130
A generalized semikinetic (GSK) model for mesoscale auroral plasma transport p 2706 N95-29686
One and two fluid numerical investigations of solar wind gas releases p 2738 N95-29704
X-ray emission from Hybrid stars
p 2740 N95-29779
Induced Compton scattering by relativistic electrons in magnetized astrophysical plasmas p 2610 N95-29885
SPACE PLATFORMS
Analysis of measurements for solid state laser remote lidar system
[NASA-CR-196640] p 2585 N95-29247
SPACE PROCESSING
Reduce Fluid Experiment System: Flight data from the IML-1 Mission
[NASA-CR-196639] p 2549 N95-30014
SPACE PROGRAMS
International Space University
[NASA-TM-110646] p 2720 N95-30223
SPACE SHUTTLE BOOSTERS
Probability of detection of defects in coatings with electronic shearography
[NASA-TM-108493] p 2524 N95-29374
SPACE SHUTTLE MAIN ENGINE
ANSYS duplicate finite-element checker routine
[NASA-TM-108492] p 2672 N95-29824
Impact of uncertainty on modeling and testing
[NASA-CR-196637] p 2652 N95-30013
SPACE SHUTTLE MISSIONS
STS-67 mission highlights resource tape
[NASA-TM-110530] p 2504 N95-28715
Summary Report of mission acceleration measurements for STS-66. Launched November 3, 1994
[NASA-TM-106914] p 2509 N95-29643
STS-71 Shuttle/Mir flight: Day 1
[NASA-TM-110744] p 2505 N95-29954
STS-71 Shuttle/Mir flight: Day 2
[NASA-TM-110745] p 2505 N95-29955
STS-71 Shuttle/Mir flight: Day 3
[NASA-TM-110746] p 2505 N95-29956
STS-71 Shuttle/Mir flight: Day 4
[NASA-TM-110747] p 2505 N95-29957
STS-71 Shuttle/Mir flight: Day 5
[NASA-TM-110748] p 2505 N95-29958
STS-71 Shuttle/Mir flight: Day 6
[NASA-TM-110749] p 2505 N95-29959
STS-71 Shuttle/Mir flight: Day 7
[NASA-TM-110750] p 2505 N95-29960
STS-71 Shuttle/Mir flight: Day 8
[NASA-TM-110751] p 2505 N95-29961
STS-71 Shuttle/Mir flight: Day 9
[NASA-TM-110752] p 2506 N95-29962
STS-71 Shuttle/Mir flight: Day 10
[NASA-TM-110753] p 2506 N95-29963
SPACE SHUTTLE ORBITERS
A vehicle health monitoring system for the Space Shuttle Reaction Control System during reentry
[NASA-CR-188370] p 2505 N95-29447
SPACE SHUTTLE PAYLOADS
STS-67 mission highlights resource tape
[NASA-TM-110530] p 2504 N95-28715
Summary Report of mission acceleration measurements for STS-66. Launched November 3, 1994
[NASA-TM-106914] p 2509 N95-29643
STS-71 Shuttle/Mir flight: Day 1
[NASA-TM-110744] p 2505 N95-29954
SPACE SHUTTLES
Design and analysis of the launch vehicle adapter fitting for the petite amateur navy satellite (PANSAT)
[AD-A289693] p 2504 N95-28680
STS-71 Shuttle/Mir flight: Day 1
[NASA-TM-110744] p 2505 N95-29954
STS-71 Shuttle/Mir flight: Day 2
[NASA-TM-110745] p 2505 N95-29955
STS-71 Shuttle/Mir flight: Day 3
[NASA-TM-110746] p 2505 N95-29956
STS-71 Shuttle/Mir flight: Day 5
[NASA-TM-110748] p 2505 N95-29958
STS-71 Shuttle/Mir flight: Day 6
[NASA-TM-110749] p 2505 N95-29959
STS-71 Shuttle/Mir flight: Day 7
[NASA-TM-110750] p 2505 N95-29960
STS-71 Shuttle/Mir flight: Day 8
[NASA-TM-110751] p 2505 N95-29961
STS-71 Shuttle/Mir flight: Day 9
[NASA-TM-110752] p 2506 N95-29962
STS-71 Shuttle/Mir flight: Day 10
[NASA-TM-110753] p 2506 N95-29963
SPACE STATION FREEDOM
Study of the space environmental effects on spacecraft engineering materials
[NASA-CR-196636] p 2531 N95-29246
Lunar/Mars exploration for synthesis group
[NASA-TM-110647] p 2737 N95-30249
SPACE STATION POWER SUPPLIES
A genetic algorithm approach to scheduling resources for a space power system p 2511 N95-29784
Analysis of shadowing effects on spacecraft power systems
[NASA-TM-106994] p 2511 N95-30012
High performance nickel electrodes for space power applications p 2511 N95-30257
SPACE STATIONS
STS-71 Shuttle/Mir flight: Day 4
[NASA-TM-110747] p 2505 N95-29957
SPACE SURVEILLANCE (GROUND BASED)
Advanced research in sky surveillance: A search for low-luminosity objects
[AD-A291184] p 2731 N95-29916
SPACE TRANSPORTATION SYSTEM
Research and technology: 1994 annual report of the John F. Kennedy Space Center
[NASA-TM-110143] p 2740 N95-28788
STS-71 Shuttle/Mir flight: Day 2
[NASA-TM-110745] p 2505 N95-29955
STS-71 Shuttle/Mir flight: Day 10
[NASA-TM-110753] p 2506 N95-29963
SPACE TRANSPORTATION SYSTEM FLIGHTS
STS-67 mission highlights resource tape
[NASA-TM-110530] p 2504 N95-28715

The influence of space flight on erythrokinetics in man. Space Life Sciences Missions 1 and 2. Experiment E261
[NASA-CR-188368] p 2633 N95-28875
Summary Report of mission acceleration measurements for STS-66. Launched November 3, 1994
[NASA-TM-106914] p 2509 N95-29643
STS-71 Shuttle/Mir flight: Day 1
[NASA-TM-110744] p 2505 N95-29954
STS-71 Shuttle/Mir flight: Day 2
[NASA-TM-110745] p 2505 N95-29955
STS-71 Shuttle/Mir flight: Day 3
[NASA-TM-110746] p 2505 N95-29956
STS-71 Shuttle/Mir flight: Day 4
[NASA-TM-110747] p 2505 N95-29957
STS-71 Shuttle/Mir flight: Day 5
[NASA-TM-110748] p 2505 N95-29958
STS-71 Shuttle/Mir flight: Day 6
[NASA-TM-110749] p 2505 N95-29959
STS-71 Shuttle/Mir flight: Day 7
[NASA-TM-110750] p 2505 N95-29960
STS-71 Shuttle/Mir flight: Day 8
[NASA-TM-110751] p 2505 N95-29961
STS-71 Shuttle/Mir flight: Day 9
[NASA-TM-110752] p 2506 N95-29962
STS-71 Shuttle/Mir flight: Day 10
[NASA-TM-110753] p 2506 N95-29963

SPACE-TIME FUNCTIONS
Linear and nonlinear discrete-time state-space modeling of dynamic systems for control applications
p 2663 N95-29251
Effect of Reynolds number on the structure of turbulent boundary layers p 2575 N95-29719

SPACEBORNE ASTRONOMY
STS-67 mission highlights resource tape
[NASA-TM-110530] p 2504 N95-28715
Simultaneous UV and optical study of O star winds and UV and optical covariability of O star winds
[NASA-CR-189424] p 2726 N95-29370
Space astronomy update
[NASA-TM-110754] p 2731 N95-30317

SPACEBORNE EXPERIMENTS
STS-67 mission highlights resource tape
[NASA-TM-110530] p 2504 N95-28715
Experiment kits for processing biological samples inflight on SLS-2
[NASA-TM-4685] p 2642 N95-28722
The influence of space flight on erythrokinetics in man. Space Life Sciences Missions 1 and 2. Experiment E261
[NASA-CR-188368] p 2633 N95-28875
FFT space processing for the ACF of SPREE particle flux measurements
[AD-A290166] p 2507 N95-29026
Arcing predictions for PASP PLUS solar arrays
[AD-A292230] p 2602 N95-29201
Summary Report of mission acceleration measurements for STS-66. Launched November 3, 1994
[NASA-TM-106914] p 2509 N95-29643
Reduce Fluid Experiment System: Flight data from the IML-1 Mission
[NASA-CR-196639] p 2549 N95-30014
Effects of space exposure on metals flown on the Long Duration Exposure Facility
[NASA-CR-4662] p 2512 N95-30225

SPACEBORNE LASERS
Precision pointing experiment
[AD-A291015] p 2664 N95-29657

SPACECRAFT COMMUNICATION
STS-71 Shuttle/Mir flight: Day 4
[NASA-TM-110747] p 2505 N95-29957
STS-71 Shuttle/Mir flight: Day 7
[NASA-TM-110750] p 2505 N95-29960
STS-71 Shuttle/Mir flight: Day 8
[NASA-TM-110751] p 2505 N95-29961

SPACECRAFT COMPONENTS
Overview of the space debris environment
[AD-A292302] p 2507 N95-28867

SPACECRAFT CONFIGURATIONS
Time-optimal multi-axis attitude maneuvers of rigid spacecraft using collocation and nonlinear programming
p 2507 N95-29332

SPACECRAFT CONSTRUCTION MATERIALS
Study of the space environmental effects on spacecraft engineering materials
[NASA-CR-196638] p 2531 N95-29246
Center for Advanced Aerospace Materials (CAAM), Seoul National University, 29 June 1994
[AD-A292344] p 2525 N95-29476

SPACECRAFT CONTROL
Time-optimal multi-axis attitude maneuvers of rigid spacecraft using collocation and nonlinear programming
p 2507 N95-29332
Spacecraft attitude control system performance using pulse-width pulse-frequency modulated thrusters
[AD-A291803] p 2508 N95-29410
A vehicle health monitoring system for the Space Shuttle Reaction Control System during reentry
[NASA-CR-188370] p 2505 N95-29447
Spin augmented deployment and retrieval of tethered artificial gravity spacecraft p 2509 N95-30280
Guidance, navigation, and control study for a solar electric propulsion spacecraft
[NASA-CR-198920] p 2509 N95-30357

SPACECRAFT DEFENSE
The topside ionospheric plasma monitor (SSIES, SSIES-2 and SSIES-3) on the spacecraft of the Defense Meteorological Satellite Program (DMSP), user's guide. Volume 2: Programmer's guide for software at AFSFC
[AD-A290913] p 2618 N95-30082

SPACECRAFT DESIGN
Orbital debris: A technical assessment
[NASA-CR-198639] p 2507 N95-28852

SPACECRAFT DOCKING
STS-71 Shuttle/Mir flight: Day 1
[NASA-TM-110744] p 2505 N95-29954
STS-71 Shuttle/Mir flight: Day 4
[NASA-TM-110747] p 2505 N95-29957
STS-71 Shuttle/Mir flight: Day 5
[NASA-TM-110748] p 2505 N95-29958
STS-71 Shuttle/Mir flight: Day 6
[NASA-TM-110749] p 2505 N95-29959
STS-71 Shuttle/Mir flight: Day 7
[NASA-TM-110750] p 2505 N95-29960
STS-71 Shuttle/Mir flight: Day 8
[NASA-TM-110751] p 2505 N95-29961

SPACECRAFT GUIDANCE
Analytical investigations in aircraft and spacecraft trajectory optimization and optimal guidance
[NASA-CR-4672] p 2504 N95-29339
A vehicle health monitoring system for the Space Shuttle Reaction Control System during reentry
[NASA-CR-188370] p 2505 N95-29447
Guidance, navigation, and control study for a solar electric propulsion spacecraft
[NASA-CR-198920] p 2509 N95-30357

SPACECRAFT INSTRUMENTS
Pioneer Venus 12.5 km Anomaly Workshop Report, volume 1
[NASA-CP-3303] p 2737 N95-30058

SPACECRAFT LANDING
STS-71 Shuttle/Mir flight: Day 10
[NASA-TM-110753] p 2506 N95-29963

SPACECRAFT LAUNCHING
STS-71 Shuttle/Mir flight: Day 1
[NASA-TM-110744] p 2505 N95-29954
Performance evaluation of bolt-cutter system on first Taurus launch
[AD-A291237] p 2504 N95-29992

SPACECRAFT MANEUVERS
Time-optimal multi-axis attitude maneuvers of rigid spacecraft using collocation and nonlinear programming
p 2507 N95-29332

SPACECRAFT MODELS
Spacecraft attitude control system performance using pulse-width pulse-frequency modulated thrusters
[AD-A291803] p 2508 N95-29410

SPACECRAFT MOTION
Analytical investigations in aircraft and spacecraft trajectory optimization and optimal guidance
[NASA-CR-4672] p 2504 N95-29339

SPACECRAFT ORBITS
Method for the calculation of spacecraft umbra and penumbra shadow terminator points
[NASA-TP-3547] p 2671 N95-29446

SPACECRAFT POWER SUPPLIES
EMI Shields made from intercalated graphite composites
[NASA-TM-106979] p 2518 N95-28906
Analysis of shadowing effects on spacecraft power systems
[NASA-TM-106994] p 2511 N95-30012
Advanced Dependent Pressure Vessel (DPV) nickel-hydrogen spacecraft cell and battery design
p 2567 N95-30261

SPACECRAFT PROPULSION
Experimental results of Hooper's gravity-electromagnetic coupling concept
[NASA-TM-106963] p 2680 N95-28893
A vehicle health monitoring system for the Space Shuttle Reaction Control System during reentry
[NASA-CR-188370] p 2505 N95-29447
Automated Propulsion Data Screening demonstration system
[NASA-CR-196636] p 2510 N95-29584

SPACECRAFT REENTRY
A vehicle health monitoring system for the Space Shuttle Reaction Control System during reentry
[NASA-CR-188370] p 2505 N95-29447

SPACECRAFT STABILITY
Spin augmented deployment and retrieval of tethered artificial gravity spacecraft p 2509 N95-30280

SPACECRAFT STRUCTURES
Substructure-based control of flexible structures
p 2508 N95-29408

SPACECRAFT TRAJECTORIES
Analytical investigations in aircraft and spacecraft trajectory optimization and optimal guidance
[NASA-CR-4672] p 2504 N95-29339

SPACELAB
Experiment kits for processing biological samples inflight on SLS-2
[NASA-TM-4685] p 2642 N95-28722
An inflight refill unit for replenishing research animal drinking water
[NASA-TM-4684] p 2642 N95-28818

SPACING
Methods of generating low redundancy direction finding array configurations
[AD-A292590] p 2555 N95-29289

SPAIN
Experience in helicopter aeroevacuation in the community of Madrid, Spain p 2677 N95-29611

SPALLATION
Measurement of interface strength, intrinsic toughness and their dependence on interfacial segregants
[AD-A291798] p 2524 N95-29409
Measurement of interface strength, intrinsic toughness and their dependence on interfacial segregants
[AD-A291169] p 2546 N95-29926

SPANWISE BLOWING
Pressure based high order TVD methodology for dynamic stall control
[AD-A290149] p 2489 N95-29316

SPARE PARTS
Artificial intelligence techniques for parts obsolescence prediction
[AD-A292185] p 2661 N95-28926

SPARK GAPS
High power switch design
[AD-A291608] p 2565 N95-29601

SPATIAL DISTRIBUTION
Reflectance analysis under solar illumination
[AD-A290489] p 2737 N95-29151
The spatial-scale dependence of the observed anisotropy of reflected and emitted radiation
p 2613 N95-29253
Load balancing for the parallel adaptive solution of partial differential equations
[AD-A290450] p 2671 N95-29488
Hydrology of the continental United States
p 2599 N95-29539
Modeling spatio-temporal databases to measure the performance of the GPS satellite constellation
p 2494 N95-29596
Experimental cosmology using fast parallel N-body methods p 2734 N95-29775
A model analysis of the spatial distribution and temporal trends of nitrous oxide sources and sinks
p 2609 N95-29804
Crustal deformation measurements in the vicinity of Vandenberg Air Force Base
[AD-A291224] p 2618 N95-29981
Improvement of inter-event distance tests of randomness in spatial point processes
[AD-A291151] p 2675 N95-30297

SPATIAL RESOLUTION
Monitoring of burning in the Brazilian cerrado region using AVHRR/NOAA data calibrated by TM/Landsat data
[INPE-5490-TDI/507] p 2598 N95-28929
High resolution, large scale measurement processes
[AD-A292200] p 2681 N95-28987
The Los Alamos Photon Counting Detector Debris Detection Project: An update
[DE95-007883] p 2508 N95-29464
A comparative study of upwind and MacCormack schemes for CAA benchmark problems
p 2688 N95-30147

SPECIFIC HEAT
Thermophysical properties of R-32 (difluoromethane)
[ESDU-94032] p 2530 N95-28802
HTMIAC/CINDAS silicon properties database. User's guide
[AD-A292602] p 2533 N95-29575

SPECIFICATIONS
Analysis of measurements for solid state laser remote lidar system
[NASA-CR-196640] p 2585 N95-29247
The generalized railroad crossing: A case study in formal verification of real-time systems
[AD-A290152] p 2648 N95-29319
A formal extension to object oriented analysis using Z
[AD-A290911] p 2653 N95-30080
Correctness of real-time systems by construction
[PB95-206827] p 2655 N95-30220

SPECKLE PATTERNS
Path resolved optical sensing of atmospheric winds utilizing speckle-turbulence interaction and pseudorandum code modulation
[AD-A290800] p 2621 N95-29497
Speckle imaging with the multi-anode microchannel array detector p 2728 N95-29652
SPECTRA
Spectral characterization of pulsed ultrasound using neural networks
[AD-A292440] p 2683 N95-28999
Tunable laser for persistent spectral hole burning optical memories
[AD-A292598] p 2586 N95-29292
Two-dimensional signal processing for regional seismic event identification
[AD-A292601] p 2613 N95-29293
Cyclic feature analysis, design and exploitation
[AD-A290639] p 2557 N95-29603
The angular spread of the deflected acoustic beam diffracted by a Bragg grating out of a surface acoustic wave
[AD-A291018] p 2684 N95-29659
Design of a more accurate, higher fidelity, dual-source air mass zero solar simulator
[AD-A291364] p 2603 N95-29953
SPECTRAL BANDS
Tunable laser for persistent spectral hole burning optical memories
[AD-A292598] p 2586 N95-29292
SPECTRAL METHODS
Solution of acoustic workshop problems by a spectral multidomain method p 2687 N95-30141
Parameterized spectral distributions for meson production in proton-proton collisions
[NASA-TM-4675] p 2696 N95-30337
SPECTRAL REFLECTANCE
Raman and photo-modulated reflectivity studies of ZnTe/InAs semiconductor heterostructure under hydrostatic pressure
[AD-A290467] p 2716 N95-29506
Modeling the direct-beam instantaneous spectral surface albedo of a forest landscape using geometric-optics and a distributed parameter approach p 2599 N95-29540
HTMIAC/CINDAS silicon properties database. User's guide
[AD-A292602] p 2533 N95-29575
Spectral reflectance studies and optical surface alteration in the search for links between meteorites and asteroids p 2733 N95-29672
SPECTRAL SIGNATURES
Spectral characterization of pulsed ultrasound using neural networks
[AD-A292440] p 2683 N95-28999
SPECTRAL THEORY
Spectral inverse scattering theory for dielectric media: Application to optical devices
[AD-A292651] p 2556 N95-29383
SPECTROGRAPHS
A ground support electronic interface for the ionospheric spectroscopy and atmospheric chemistry (ISAAC) ultraviolet spectrograph
[AD-A289761] p 2611 N95-28693
The properties of local poor Abell clusters and instrumentation for the study of clustered objects p 2730 N95-29827
SPECTROMETERS
Spectrometric studies of selected nitrocompounds using laser-induced photofragmentation/photoionization at 193 nm
[AD-A289947] p 2530 N95-28876
Design of an electronic charged particle spectrometer to measure (rho R), yield, and implosion symmetry on the OMEGA Upgrade
[DE95-006088] p 2695 N95-28930
The (HMI9293) acquisition of a 200 MHz nuclear magnetic resonance spectrometer
[AD-A291913] p 2583 N95-29361
Prospects for HERMES-spin structure studies at HERA
[DE95-005845] p 2694 N95-30019
SPECTROSCOPIC ANALYSIS
Measurements of ions formed in jet engine exhaust plumes
[AD-A290940] p 2501 N95-29764
The properties of local poor Abell clusters and instrumentation for the study of clustered objects p 2730 N95-29827
The comparative extinguishment performance and thermal decomposition products of halon alternative agents
[AD-A291161] p 2551 N95-29924
SPECTROSCOPY
A ground support electronic interface for the ionospheric spectroscopy and atmospheric chemistry (ISAAC) ultraviolet spectrograph
[AD-A289761] p 2611 N95-28693
The 14th International Conference on Atomic Physics
[AD-A290726] p 2693 N95-29521
From the (psi) to charmed mesons
[DE95-006564] p 2693 N95-29583
High temperature spectroscopy of alkali metal vapors for solar to thermal energy conversion
[AD-A291355] p 2602 N95-29949
A kilohertz femtosecond Ti: Sapphire regeneratie amplifier
[AD-A290591] p 2588 N95-30045
SPECTRUM ANALYSIS
Spectral analysis techniques using wavelets as an alternative to Fourier analysis for transient dynamic data
[AD-A289776] p 2556 N95-29459
Spectral reflectance studies and optical surface alteration in the search for links between meteorites and asteroids p 2733 N95-29672
Observational properties of SiO masers in the galactic bulge IRAS sources p 2735 N95-29838
SPEECH RECOGNITION
High-performance speech recognition using consistency modeling
[AD-A290655] p 2557 N95-29564
SPEED CONTROL
Experimental investigation of aerodynamic devices for wind turbine rotational speed control, phase 1
[DE95-004034] p 2603 N95-30016
SPHERES
Electromagnetic scattering by magnetic spheres: Theory and algorithms
[AD-A289798] p 2551 N95-28699
Experimental and theoretical studies of wakes in stratified flows
[AD-A290203] p 2569 N95-29060
Static field solutions and image theory for a conducting sphere with radial anisotropy
[PB95-207171] p 2673 N95-30172
SPHERICAL WAVES
Second-order numerical solution of time-dependent, first-order hyperbolic equations p 2674 N95-30143
SPIN DYNAMICS
Three problems in fluid dynamics
[AD-A290481] p 2573 N95-29324
SPIN STABILIZATION
Spacecraft attitude control system performance using pulse-width pulse-frequency modulated thrusters
[AD-A291803] p 2508 N95-29410
Spin augmented deployment and retrieval of tethered artificial gravity spacecraft p 2509 N95-30280
SPINEL
Analytical electron microscopy of precipitates in ion-implanted MgAl2O4 spinel
[DE95-007406] p 2538 N95-30038
SPIRAL ANTENNAS
Electrically small archimedian spiral method of moment analysis
[AD-A291171] p 2558 N95-29928
SPIRAL GALAXIES
Nobeyama Radio Observatory report, no. 378: The polar ring spiral galaxy NGC 660 p 2731 N95-29097
A study of one-armed spiral galaxies p 2729 N95-29774
SPLICING
Shock resistant optic fiber rotary slice holding device
[AD-D017327] p 2702 N95-30053
SPLINE FUNCTIONS
Generating grids directly on CAD database surfaces using a parametric evaluator approach p 2483 N95-28754
Multivariate wavelet representations and approximations
[AD-A290147] p 2670 N95-29312
SPLIT FLAPS
Increments in aerofoil lift coefficient at zero angle of attack and in maximum lift coefficient due to deployment of a trailing-edge split flap, with or without a leading-edge high-lift device, at low speeds
[ESDU-94029] p 2488 N95-29129
SPLITTING
Solution of the Navier-Stokes equations on locally refined Cartesian meshes using state-vector splitting p 2571 N95-29197
SPONTANEOUS EMISSION
Effective emission and ionization rate coefficients of atomic carbons in plasmas
[AD-B175932L] p 2707 N95-29740
SPRAY CHARACTERISTICS
Fundamental studies in cryogenic cooling of power electronics
[AD-A291150] p 2551 N95-30296
SPRAYED COATINGS
A simulation technique for predicting thickness of thermal sprayed coatings
[NASA-TM-106939] p 2512 N95-29373
SPRAYERS
Advanced manufacturing by spray forming: Aluminum strip and microelectromechanical systems
[DE95-008615] p 2536 N95-28959
The potential for pulmonary heat injury resulting from the activation of a cabin water spray system to fight aircraft cabin fires
[DOT/FAA/AM-95/17] p 2636 N95-29224
SCAP spray combustion analysis program
[AD-A289946] p 2532 N95-29273
Thermoreactive aircraft coatings (TRAC) program
[AD-A292054] p 2542 N95-29314
Air/fuel ratio visualization in a diesel spray p 2590 N95-29807
Development and application of fluorescent diagnostics to fundamental droplet and spray problems
[AD-A290553] p 2578 N95-30039
SPREADING
The Scanning Fast Field Program (SCAFFIP) general version 1.0 user's manual
[AD-A291209] p 2618 N95-29976
SPRINGS (ELASTIC)
Carrier-less, anti-backlash planetary drive system
[NASA-CASE-GSC-13608-1] p 2588 N95-28702
SPUTTERING
High T(sub c) superconductor/ferroelectric heterostructures
[AD-A291016] p 2716 N95-29658
SQUALLS
The dynamics of circulations within the stratiform regions of squall lines p 2623 N95-29725
STABILITY
Computational investigation of the stabilities of some N, O, F ions
[AD-A292305] p 2691 N95-28868
Experimental studies of fundamental one- and two-photon lasing processes
[AD-A290593] p 2693 N95-29555
Preparation and studies of urazole containing polymers
[AD-A290685] p 2545 N95-29586
Trapped electron instabilities due to electron temperature gradient and anomalous transport
[AD-B179859L] p 2693 N95-29748
Dynamical instabilities, chaos and spatial complexity in fundamental nonlinear optical interactions
[AD-A291223] p 2588 N95-29980
Crustal deformation measurements in the vicinity of Vandenberg Air Force Base
[AD-A291224] p 2618 N95-29981
Biological methane activation
[PB95-200705] p 2535 N95-30198
STABILITY TESTS
The effects of three-dimensional imposed disturbances on bluff body near wake flows: Effects of taper and splitter plates on the near wake characteristics of a circular cylinder in uniform and shear flow
[AD-A292113] p 2487 N95-28921
Multifluid nonequilibrium simulation of arcjet thrusters p 2510 N95-29245
STABILIZATION
Exact physical models and methods for stabilization and control of reflection-induced instabilities in semiconductor lasers
[AD-A292437] p 2585 N95-29053
Demonstration of a stabilized alumina/ethanol colloidal dispersion technique for seeding high temperature air flows
[NASA-TM-106945] p 2582 N95-29113
STABILIZED PLATFORMS
Lockheed Stabilizer System for space exercise equipment
[NASA-CR-197657] p 2641 N95-29180
STABILIZERS (FLUID DYNAMICS)
Estimation of aerodynamic load distributions on the F/A-18 aircraft using a CFD panel code
[DSTO-TR-0147] p 2498 N95-29445
Low-speed wind-tunnel investigation of the stability and control characteristics of a series of flying wings with sweep angles of 50 deg
[NASA-TM-4640] p 2498 N95-30226
STACKS
Garbage collection is fast, but a stack is faster
[AD-A290099] p 2722 N95-29207
STAGNATION FLOW
Influence of turbulence parameters, Reynolds number, and body shape on stagnation-region heat transfer
[NASA-TP-3487] p 2568 N95-28719
STAGNATION PRESSURE
Leading edge film cooling effects on turbine blade heat transfer
[NASA-TM-106955] p 2500 N95-29115

Modeling and control of rotating stall in high speed multi-stage axial compressors p 2500 N95-29244

STAGNATION TEMPERATURE
Leading edge film cooling effects on turbine blade heat transfer
[NASA-TM-106955] p 2500 N95-29115

STAINLESS STEELS
Precision cleaning verification of fluid components by air/water impingement and total carbon analysis
[NASA-TM-110742] p 2531 N95-29248
Effects of space exposure on metals flown on the Long Duration Exposure Facility
[NASA-CR-4662] p 2512 N95-30225

STALLING
Characterization of stall inception in high-speed single-stage compressors
[AD-A291275] p 2501 N95-29934

STANDARD DEVIATION
Design, evaluation and construction of TEXESS and LUXESS, and research in mini-array technology and use of data from single stations and sparse networks
[AD-A292546] p 2612 N95-28972

STANDARDIZATION
A comparison of the aeromedical administration requirements for US Air Forces and major allies
[AD-A290137] p 2635 N95-29141
Applied Computational Electromagnetics Society Journal, volume 10, number 1, March 1995
[AD-A292069] p 2555 N95-29308

STANDARDS
A comparison of ISO 9001 and the Capability Maturity Model for Software
[AD-A290697] p 2651 N95-29762

STAR CLUSTERS
The search for mass segregation in star clusters of the Magellanic Clouds p 2730 N95-29781

STAR DISTRIBUTION
A search for cataclysmic variables in globular clusters p 2727 N95-29532

STAR FORMATION
Nobeyama Radio Observatory report, no. 382: The mass of a star formed in a cloud core: Theory and its application to the Orion A cloud p 2731 N95-29100
Space astronomy update
[NASA-TM-110754] p 2731 N95-30317

STARS
Nobeyama Radio Observatory report, no. 378: The polar ring spiral galaxy NGC 660 p 2731 N95-29097
Nobeyama Radio Observatory report, no. 382: The mass of a star formed in a cloud core: Theory and its application to the Orion A cloud p 2731 N95-29100

STATE VECTORS
Solution of the Navier-Stokes equations on locally refined Cartesian meshes using state-vector splitting p 2571 N95-29197

STATIC LOADS
Analysis of static contact in laminated composite plates using damage mechanics
[NASA-CR-198656] p 2513 N95-28809
Shear reinforcement in deep slabs
[AD-A289528] p 2594 N95-28909
Formulation of an improved smeared stiffener theory for buckling analysis of grid-stiffened composite panels
[NASA-TM-110162] p 2529 N95-30341

STATIC PRESSURE
Modeling and control of rotating stall in high speed multi-stage axial compressors p 2500 N95-29244
Development of an improved cloud model for use in cumulus parameterization p 2624 N95-29800
Experimental research on crossing shock wave boundary layer interactions
[AD-A290764] p 2577 N95-29920

STATIC STABILITY
An aerodynamic and static-stability analysis of the Hypersonic Applied Research Technology (HART) missile
[DA9426923] p 2491 N95-29965

STATIC TESTS
Test load verification through strain data analysis
[NASA-TP-3558] p 2504 N95-28718

STATISTICAL ANALYSIS
An analysis of anthropometric differences among occupational groups in the US Army
[AD-A292326] p 2640 N95-28794
Intermediate levels of visual processing
[AD-A291569] p 2638 N95-28937
Statistical properties of bistatic clutter echoes
[AD-A291686] p 2552 N95-28943
Probability of detection of defects in coatings with electronic shearography
[NASA-TM-108493] p 2524 N95-29374
Test theory reconceived
[AD-A291836] p 2639 N95-29432
Prediction of pressurant mass requirements for axisymmetric liquid hydrogen tanks
[NASA-TM-106973] p 2511 N95-29642
Nearest neighbor analysis in one dimension
[DE95-009378] p 2654 N95-30183

STATISTICAL CORRELATION
Statistical inference problems in some multivariate linear models with applications to multivariate calibration and meta-analysis
[AD-A291125] p 2675 N95-29768

STATISTICAL DISTRIBUTIONS
Short and elementary proof of the main Bahadur-Kiefer theorem
[PB95-206967] p 2675 N95-30170

STATISTICAL TESTS
Large deviation limit theorems, with applications
[AD-A290392] p 2669 N95-29233
Continuation of research in the statistical aspects of reliability, availability, and maintainability
[AD-A290126] p 2592 N95-29423
Improvement of inter-event distance tests of randomness in spatial point processes
[AD-A291151] p 2675 N95-30297

STEADY STATE
Parameter study of the statistically steady state of a multi-layer quasi-geostrophic model p 2612 N95-29212
Investigation of an alternative finite element procedure: A one-step, steady-state analysis
[AD-A290030] p 2670 N95-29311
The tropical atmosphere under convection adjustment p 2625 N95-29833
Theory and experiments on chemical instabilities
[AD-A290773] p 2534 N95-29922
Transient responses of phosphoric acid fuel cell power plant system
[NASA-CR-198948] p 2603 N95-30015
Pressure updating methods for the steady-state fluid equations
[NASA-CR-198163] p 2674 N95-30353

STEAM
Ejectors and jet pumps: Computer program for design and performance for steam/gas flow
[ESDU-94046] p 2495 N95-28704

STEAM FLOW
Coso monitoring program
[AD-A290604] p 2627 N95-30048

STEELS
A 1993 review of welding in Japan
[DE95-758701] p 2589 N95-28946
Dynamic decohesion of bimaterial interfaces p 2541 N95-29120
Correlation of inclusion size and chemistry with weld metal composition and microstructure arc weldments of high strength steels
[AD-A292024] p 2590 N95-29184
Experimental investigations of wave and fracture phenomena in impacted ceramics and glasses
[AD-A292142] p 2542 N95-29195
Consideration of microstructural changes in the study of adiabatic shear bands
[AD-A290398] p 2715 N95-29234
Daido Steel's Shibukawa Plant, Shibukawa City, Gumma Prefecture, Japan, 29 Jul. 1994
[AD-A292343] p 2536 N95-29467
Analysis of adiabatic shear bands in thermoviscoplastic materials under combined loading
[AD-A290666] p 2596 N95-29582
Materials for tomorrow's infrastructure: A ten-year plan for deploying high-performance construction materials and systems
[AD-A289782] p 2526 N95-29598
Penetration of semi-infinite, bi-element targets by long rod penetrators
[AD-A291176] p 2596 N95-29929
The mm-wave resonant methods for the detection of corrosion, phase 1
[AD-A291315] p 2593 N95-29941
Processing and properties of extruded tungsten-hafnium and tungsten-steel composites
[DE95-007371] p 2528 N95-30037
Decomposition of hypo-eutectoid iron carbon austenites
[PB95-196945] p 2538 N95-30287

STELLAR ATMOSPHERES
X-ray emission from Hybrid stars p 2740 N95-29779

STELLAR COMPOSITION
Nobeyama Radio Observatory report, no. 380: Detection of the (29)SiO v=1, J=1-0 maser from TX Camelopardalis p 2726 N95-29101

STELLAR CORONAS
Nobeyama Radio Observatory report, no. 361: The radio properties of solar active region soft x-ray transient brightenings p 2737 N95-29096
X-ray emission from Hybrid stars p 2740 N95-29779

STELLAR ENVELOPES
Dust formation in stellar outflows: A time-dependent model p 2733 N95-29649
Coronagraphic imaging of protoplanetary-disk candidate stars using adaptive optics p 2728 N95-29651
Extended dust shells around carbon stars resolved by HIRAS p 2735 N95-29840

STELLAR EVOLUTION
The evolution of binary millisecond pulsars and the formation of planets around them p 2733 N95-29663
The effects of rotation on the evolution of 15 to 30 solar mass stars p 2734 N95-29673

STELLAR FLARES
X-ray emission from Hybrid stars p 2740 N95-29779

STELLAR LUMINOSITY
The search for mass segregation in star clusters of the Magellanic Clouds p 2730 N95-29781

STELLAR MAGNETIC FIELDS
Models of accretion-powered x-ray pulsars p 2728 N95-29667
Gamma radiation from rotation powered pulsars and results from the Energetic Gamma-Ray Experiment Telescope p 2739 N95-29671

STELLAR MASS
Nobeyama Radio Observatory report, no. 382: The mass of a star formed in a cloud core: Theory and its application to the Orion A cloud p 2731 N95-29100
The dynamics of FU Orionis outbursts: Time-dependent accretion through protostellar disks p 2732 N95-29530
The effects of rotation on the evolution of 15 to 30 solar mass stars p 2734 N95-29673
The search for mass segregation in star clusters of the Magellanic Clouds p 2730 N95-29781

STELLAR MASS ACCRETION
Nobeyama Radio Observatory report, no. 382: The mass of a star formed in a cloud core: Theory and its application to the Orion A cloud p 2731 N95-29100
The dynamics of FU Orionis outbursts: Time-dependent accretion through protostellar disks p 2732 N95-29530
Models of accretion-powered x-ray pulsars p 2728 N95-29667

STELLAR MASS EJECTION
Dust formation in stellar outflows: A time-dependent model p 2733 N95-29649

STELLAR MODELS
A pipeline case tool for database design
[AD-A292017] p 2722 N95-29182
Models of accretion-powered x-ray pulsars p 2728 N95-29667
Effects of microscopic diffusion and rotational mixing on stellar models p 2733 N95-29669
The effects of rotation on the evolution of 15 to 30 solar mass stars p 2734 N95-29673

STELLAR ORBITS
Applications of pulsar timing p 2734 N95-29675

STELLAR OSCILLATIONS
Nobeyama Radio Observatory report, no. 380: Detection of the (29)SiO v=1, J=1-0 maser from TX Camelopardalis p 2726 N95-29101

STELLAR RADIATION
The dynamics of FU Orionis outbursts: Time-dependent accretion through protostellar disks p 2732 N95-29530
Gamma radiation from rotation powered pulsars and results from the Energetic Gamma-Ray Experiment Telescope p 2739 N95-29671
X-ray emission from Hybrid stars p 2740 N95-29779

STELLAR ROTATION
X-ray observations of rapidly rotating O stars
[NASA-CR-189423] p 2726 N95-28822
Simultaneous UV and optical study of O star winds and UV and optical covariability of O star winds
[NASA-CR-189424] p 2726 N95-29370
Gamma radiation from rotation powered pulsars and results from the Energetic Gamma-Ray Experiment Telescope p 2739 N95-29671
The effects of rotation on the evolution of 15 to 30 solar mass stars p 2734 N95-29673

STELLAR WINDS
Simultaneous UV and optical study of O star winds and UV and optical covariability of O star winds
[NASA-CR-189424] p 2726 N95-29370
The evolution of binary millisecond pulsars and the formation of planets around them p 2733 N95-29663

STELLARATORS
Transition of radial electric field by electron cyclotron heating in the stellarator plasmas
[AD-B176254L] p 2707 N95-29742

STELLITE (TRADEMARK)
Evaluation of wear resistant ceramic valve seats in gas-fueled power generation engines
[PB95-200218] p 2591 N95-30110

STEREOPHOTOGRAPHY
Modeling foreshortening in stereo vision using local spatial frequency
[AD-A292246] p 2645 N95-28883
STEREOSCOPIC VISION
Modeling foreshortening in stereo vision using local spatial frequency
[AD-A292246] p 2645 N95-28883
Visualization of CAD objects using a stereoscopic display
[AD-A290034] p 2639 N95-29439
STIFFENING
Formulation of an improved smeared stiffener theory for buckling analysis of grid-stiffened composite panels
[NASA-TM-110162] p 2529 N95-30341
STIFFNESS
Dimensional stability of curved panels with cocured stiffeners and cobonded frames p 2515 N95-28836
Impact damage resistance of composite fuselage structure, part 2 p 2516 N95-28838
Design and evaluation of a foam-filled hat-stiffened panel concept for aircraft primary structural applications p 2499 N95-28841
ISPAN (Interactive Stiffened Panel Analysis): A tool for quick concept evaluation and design trade studies p 2517 N95-28846
A biologically-inspired autonomous robot
[AD-A289446] p 2666 N95-30026
Formulation of an improved smeared stiffener theory for buckling analysis of grid-stiffened composite panels
[NASA-TM-110162] p 2529 N95-30341
STIMULATION
Pattern-analysis based models of masking by spatially separated sounds
[AD-A291270] p 2637 N95-29933
STOCHASTIC PROCESSES
International Workshop on Stochastic Filtering Theory
[AD-A291670] p 2661 N95-28788
Stochastic modeling and global warming trend extraction for ocean acoustic travel times
[AD-A292114] p 2608 N95-28922
Stochastic hyperbolic and parabolic partial differential equations
[AD-A290372] p 2669 N95-29229
Simulation methodology
[AD-A290461] p 2674 N95-29491
Theory and experiments on chemical instabilities
[AD-A290773] p 2534 N95-29922
Dynamical instabilities, chaos and spatial complexity in fundamental nonlinear optical interactions
[AD-A291223] p 2588 N95-29980
Applications of Langevin and Molecular Dynamics methods
[DE95-007875] p 2694 N95-30059
Performance evaluation of ATM cell scheduling policies using stochastic petri nets
[PB95-197158] p 2559 N95-30096
Efficient solution of a class of infinite stochastic petri nets: Theory and applications
[PB95-197166] p 2673 N95-30097
STOICHIOMETRY
Fabrication of advanced electrochemical energy materials using sol-gel processing techniques p 2607 N95-30269
STORAGE BATTERIES
High reliability, maintenance-free INS battery development, phase 2
[AD-A291412] p 2566 N95-30070
STORAGE RINGS (PARTICLE ACCELERATORS)
A practical high-energy high-luminosity mu(+)-mu(-) collider
[DE95-006769] p 2696 N95-30009
Prospects for HERMES-spin structure studies at HERA
[DE95-005845] p 2694 N95-30019
STORAGE TANKS
Fuel cell systems for First Lunar Outpost-reactant storage option p 2606 N95-30264
STORM SURGES
Tropical storm database: East and Gulf of Mexico coasts of the United States
[AD-A291406] p 2627 N95-30066
STORMS
The effects of magnetic storm phases on F-layer irregularities from auroral to equatorial latitudes
[AD-A290674] p 2614 N95-29585
STRAIN DISTRIBUTION
Flat rectangular isotropic plates under uniformly distributed normal pressure. Elastic deflections, stresses, and strains, moments and forces, for various forms of edge restraint
[ESDU-94033] p 2593 N95-28801
Three dimensional effects in fiber reinforced composites under compression
[AD-A292027] p 2523 N95-29185
STRAIN ENERGY RELEASE RATE
Master plot analysis of microcracking in graphite/epoxy and graphite/PEEK laminates p 2514 N95-28828
Simplified data reduction methods for the ECT test for mode 3 interlaminar fracture toughness
[NASA-TM-110176] p 2527 N95-29825
STRAIN GAGES
Influence of tooth profile modification on spur gear dynamic tooth strain
[NASA-TM-106952] p 2589 N95-29112
Cable load transducer
[AD-A289548] p 2595 N95-29192
Development of an artificial neural network for real-time classification of cone penetrometer strain gauge data
[AD-A290719] p 2664 N95-29499
STRAIN MEASUREMENT
Cable load transducer
[AD-A289548] p 2595 N95-29192
STRAIN RATE
High field electrostrictive response of polymers
[AD-A292298] p 2539 N95-28864
The study of non-Newtonian contraction flows with a parallel finite element method p 2576 N95-29778
Impact properties of coated engineering plastics
[PB95-197281] p 2547 N95-30201
STRAKES
Pressure based high order TVD methodology for dynamic stall control
[AD-A290149] p 2489 N95-29316
STRATIFIED FLOW
Condensation inside tubes: Condensate film coefficient in horizontal tubes
[ESDU-94041] p 2569 N95-29015
Experimental and theoretical studies of wakes in stratified flows
[AD-A290203] p 2569 N95-29060
Lee vorticity production by tropical mountain ranges p 2622 N95-29701
STRATOCUMULUS CLOUDS
Continental aerosol effects on stratocumulus microphysics during MAST 1994
[AD-A292674] p 2621 N95-29416
A theoretical model of multiple regimes in a stratocumulus-topped boundary layer p 2624 N95-29726
Observations of mesoscale cellular convection from the marine stratocumulus phase of FIRE p 2624 N95-29727
STRATOSPHERE
Numerical studies of the stratospheric aerosol layer under background and perturbed conditions p 2615 N95-29666
A model analysis of the spatial distribution and temporal trends of nitrous oxide sources and sinks p 2609 N95-29804
In situ measurements of ClO and implications for the chemistry of inorganic chlorine in the lower stratosphere p 2618 N95-29830
STREAMS
Measuring variation in ecosystem sensitivity to stress
[AD-A290415] p 2609 N95-29450
STRESS (BIOLOGY)
Measuring variation in ecosystem sensitivity to stress
[AD-A290415] p 2609 N95-29450
STRESS (PHYSIOLOGY)
Improving problem-solving and decision-making skills under stress: Prediction and training
[AD-A292104] p 2638 N95-28918
Flying waivers for history of angioplasty and myocardial infraction
[AD-A292505] p 2635 N95-29161
Human fluid balance and dehydration during cold weather military operations
[AD-A289192] p 2636 N95-29757
STRESS (PSYCHOLOGY)
Improving problem-solving and decision-making skills under stress: Prediction and training
[AD-A292104] p 2638 N95-28918
Coping and adaptation: Theoretical and applied perspectives
[AD-A290513] p 2638 N95-29090
STRESS ANALYSIS
Dimensions, deflections and stresses for Hertzian contacts under combined normal and tangential loading. (Guide to use of computer program A9434.)
[ESDU-94034] p 2593 N95-28711
Flat rectangular isotropic plates under uniformly distributed normal pressure. Elastic deflections, stresses, and strains, moments and forces, for various forms of edge restraint
[ESDU-94033] p 2593 N95-28801
Master plot analysis of microcracking in graphite/epoxy and graphite/PEEK laminates p 2514 N95-28828
Through-the-thickness stresses and failure in the corner radius of a laminated composite section
[ESDU-94019] p 2518 N95-28899
Experimental methods in residual stress measurement using a position-sensitive single-exposure scintillation detection system
[AD-A289803] p 2594 N95-28949
A new methodology for the numerical simulation of strain softening in inelastic solids
[AD-A290295] p 2594 N95-29063
Dynamic decohesion of bimaterial interfaces p 2541 N95-29120
Sensitivity of stress and boundary imperfection of dielectric resonator disks
[AD-A290488] p 2594 N95-29150
Self-stressing structures for wafer-level oxide breakdown to 200 MHz
[DE95-006818] p 2714 N95-29157
Energy theorems and bounds in linearized elasticity with residual stress p 2595 N95-29546
The Stroh formalism for anisotropic elasticity with applications to composite materials
[AD-A290710] p 2527 N95-29763
Investigation of tension-compression fatigue behavior of a notched cross-ply metal matrix composite at elevated temperature
[AD-A291479] p 2527 N95-29770
Analysis of stress concentration in the Dutton groove regions of the Super Lightweight External Tank
[NASA-TM-108490] p 2597 N95-30328
STRESS CONCENTRATION
Stress concentration, stress intensity, and fatigue crack growth along evacuators of pressurized, autofrettaged tubes
[AD-A291920] p 2593 N95-28789
Response of automated tow placed laminates to stress concentrations p 2515 N95-28833
Analysis of stress concentration in the Dutton groove regions of the Super Lightweight External Tank
[NASA-TM-108490] p 2597 N95-30328
STRESS CYCLES
In-phase thermomechanical fatigue mechanisms in an unidirectional SCS-6/Ti 15-3 MMC
[NASA-CR-195482] p 2523 N95-29133
STRESS DISTRIBUTION
Dimensions, deflections and stresses for Hertzian contacts under combined normal and tangential loading. (Guide to use of computer program A9434.)
[ESDU-94034] p 2593 N95-28711
Flat rectangular isotropic plates under uniformly distributed normal pressure. Elastic deflections, stresses, and strains, moments and forces, for various forms of edge restraint
[ESDU-94033] p 2593 N95-28801
Three dimensional effects in fiber reinforced composites under compression
[AD-A292027] p 2523 N95-29185
Unsteady rotational shear flow of power law fluids
[ISBN-0-315-81287-7] p 2575 N95-29718
Toughening mechanisms in mixed-mode interfacial fracture p 2545 N95-29772
The gravitational potential energy of the Earth's lithosphere p 2617 N95-29773
STRESS INTENSITY FACTORS
Stress concentration, stress intensity, and fatigue crack growth along evacuators of pressurized, autofrettaged tubes
[AD-A291920] p 2593 N95-28789
STRESS MEASUREMENT
Experimental methods in residual stress measurement using a position-sensitive single-exposure scintillation detection system
[AD-A289803] p 2594 N95-28949
STRESS TENSORS
Ensemble phase averaged equations for multiphase flows p 2579 N95-30284
STRESS-STRAIN RELATIONSHIPS
Investigation of tension-compression fatigue behavior of a unidirectional metal matrix composite at elevated temperature
[AD-A289394] p 2527 N95-29758
Gradient-dependent plasticity in numerical simulation of localization phenomena
[PB95-197257] p 2596 N95-30049
STRESSES
Contact stress in disc cams with domes of flat-faced followers
[ESDU-94011] p 2589 N95-28901
Investigation of an alternative finite element procedure: A one-step, steady-state analysis
[AD-A290030] p 2670 N95-29311
STRETCH FORMING
Establishing the relationship between manufacturing and component performance in stretch formed thermoplastic composites p 2514 N95-28829
STRINGS
The 2nd European Conference on Smart Structures and Materials
[AD-A290723] p 2550 N95-29579

STRONTIUM OXIDES
Pulsed laser deposition of ferroelectric thin films in conjunction with superconducting oxides
[AD-A290101] p 2585 N95-29208
STRONTIUM TITANATES
Materials science and fabrication of YBCO-SrTi(1-x)Nb(x)O3-YBCO device structures
[AD-A292527] p 2712 N95-28815
Investigation of the characteristics of ferroelectric thin films deposited by pulsed laser ablation
[AD-A292306] p 2540 N95-28963
Growth, characterization and application of KTN family nonlinear optical crystals
[AD-A290330] p 2713 N95-29087
Electrical characteristics of barium strontium titanate-oxide composite films
[AD-A289991] p 2541 N95-29135
Fabrication and characterization of barium strontium titanate and non-ferroelectric oxide composites
[AD-A289994] p 2523 N95-29136
Fabrication and characterization of BSTO and nonferroelectric oxide composites for use in phased array antennas and other electronic devices
[AD-A290070] p 2524 N95-29329
Analysis of the ferroelectric thin films deposited by pulsed laser deposition on oxide and fluoride substrates
[AD-A290088] p 2543 N95-29353
STROUHAL NUMBER
The effects of three-dimensional imposed disturbances on bluff body near wake flows: Effects of taper and splitter plates on the near wake characteristics of a circular cylinder in uniform and shear flow
[AD-A292113] p 2487 N95-28921
STRUCTURAL ANALYSIS
Analysis of static contact in laminated composite plates using damage mechanics
[NASA-CR-198656] p 2513 N95-28809
An efficiency study of the simultaneous analysis and design of structures
[NASA-TM-110168] p 2495 N95-28820
The effects of specimen width on tensile properties of triaxially braided textile composites
p 2513 N95-28825
Impact damage resistance of composite fuselage structure, part 2 p 2516 N95-28838
Buckling analysis of curved composite sandwich panels subjected to inplane loadings p 2517 N95-28845
ISPAN (Interactive Stiffened Panel Analysis): A tool for quick concept evaluation and design trade studies
p 2517 N95-28846
A global/local analysis method for treating details in structural design p 2517 N95-28848
IPACS (Integrated Probabilistic Assessment of Composite Structures): Code development and applications p 2518 N95-28849
Modal interactions and complex responses in weaklyNONLINEAR MULTI-DEGREE-OF-FREEDOM MECHANICAL SYSTEMS
[AD-A292023] p 2594 N95-28853
Advanced composites technology program
p 2519 N95-29032
Test results from large wing and fuselage panels
p 2522 N95-29051
Compressive behavior of thick composite shells: Benchmark solutions for loss of stability and hygroscopic effects p 2595 N95-29424
Structural and electronic properties of adsorbates on semiconductors, metal-semiconductor interfaces and semiconductor heterojunctions
[AD-A291917] p 2715 N95-29438
Examination of dislocation core structures in B2 intermetallic alloys
[AD-A291486] p 2537 N95-29526
Optimization of 100-meter Green Bank Telescope
[NASA-CR-198868] p 2731 N95-30230
STRUCTURAL DESIGN
Design and analysis of the launch vehicle adapter fitting for the petite amateur navy satellite (PANSAT)
[AD-A289693] p 2504 N95-28680
The effects of design details on cost and weight of fuselage structures p 2499 N95-28831
Design and evaluation of a foam-filled hat-stiffened panel concept for aircraft primary structural applications
p 2499 N95-28841
A weight-efficient design strategy for cutouts in composite transport structures p 2516 N95-28843
A global/local analysis method for treating details in structural design p 2517 N95-28848
Analysis of the structural characteristics and intensity evolution of super typhoon flo (1990) in special sensor Microwave/Imager (SSM/I) data
[AD-A292413] p 2619 N95-28989
Advanced composite fuselage technology
p 2519 N95-29034
Design of a fast-tool servo system using magnetic servo levitation
[AD-A290273] p 2663 N95-29183
Programmable materials and structures
[AD-A291807] p 2649 N95-29429
Framework for comparing and controlling number-based design reasoning systems
[PB95-197364] p 2667 N95-30207
Analysis of stress concentration in the Dutton groove regions of the Super Lightweight External Tank
[NASA-TM-108490] p 2597 N95-30328
STRUCTURAL ENGINEERING
Textile composite fuselage structures development
p 2519 N95-29033
Programmable materials and structures
[AD-A291807] p 2649 N95-29429
Development of 'smart' piezothermoelastic laminae: Theory and applications
[AD-A290852] p 2528 N95-29864
Optimization of 100-meter Green Bank Telescope
[NASA-CR-198868] p 2731 N95-30230
Developing a workstation-baaed, real-time simulation for rapid handling qualities evaluations during design
[NASA-CR-198831] p 2499 N95-30335
Formulation of an improved smeared stiffener theory for buckling analysis of grid-stiffened composite panels
[NASA-TM-110162] p 2529 N95-30341
STRUCTURAL FAILURE
An engineering model of woven composites based on micromechanics p 2521 N95-29042
Analytical and experimental studies of the energy absorption behavior of composite structures
p 2524 N95-29411
A three dimensional finite element scheme for fiber microbuckling in thick multidirectional laminated composites p 2525 N95-29512
STRUCTURAL MEMBERS
Mechanical characterization of 2D, 2D stitched, and 3D braided/RTM materials p 2520 N95-29038
STRUCTURAL PROPERTIES (GEOLOGY)
Differentiation in the early Earth: An experimental investigation p 2612 N95-29199
STRUCTURAL RELIABILITY
Health monitoring of operational structures: Initial results
[DE95-008551] p 2597 N95-30210
Fatigue case study and reliability analyses for wind turbines
[DE95-004770] p 2603 N95-30213
STRUCTURAL STABILITY
Precision pointing experiment
[AD-A291015] p 2664 N95-29657
STRUCTURAL VIBRATION
Modal interactions and complex responses in weaklyNONLINEAR MULTI-DEGREE-OF-FREEDOM MECHANICAL SYSTEMS
[AD-A292023] p 2594 N95-28853
Spectral analysis techniques using wavelets as an alternative to Fourier analysis for transient dynamic data
[AD-A289778] p 2556 N95-29459
Broadband control of structural vibration using simultaneous sensing and actuation with nonlinear piezoelectric elements p 2664 N95-29548
A numerical solution method for acoustic radiation from axisymmetric bodies p 2689 N95-30154
STRUCTURAL WEIGHT
The effects of design details on cost and weight of fuselage structures p 2499 N95-28831
STRUCTURED GRIDS (MATHEMATICS)
Surface Modeling, Grid Generation, and Related Issues in Computational Fluid Dynamic (CFD) Solutions
[NASA-CP-3291] p 2478 N95-28723
Automatic blocking for complex three-dimensional configurations p 2480 N95-28734
Block-structured grids for complex aerodynamic configurations: Current status p 2480 N95-28736
Grid related issues for static and dynamic geometry problems using systems of overset structured grids
p 2480 N95-28737
Three-dimensional hybrid grid generation using advancing front techniques p 2481 N95-28745
The National Grid Project: A system overview
p 2482 N95-28749
A 3DGRAPE/AL: The Ames/Langley technology upgrade p 2482 N95-28750
Automatic structured grid generation using Gridgen (some restrictions apply) p 2483 N95-28751
Tuned grid generation with ICEM CFD
p 2483 N95-28752
Automation of three-dimensional structured mesh generation for turbomachinery blade passages
p 2484 N95-28762
A technique for optimizing grid blocks
p 2485 N95-28769
A combined geometric approach for computational fluid dynamics on dynamic grids p 2485 N95-28770
STRUCTURED PROGRAMMING
Structural cut elimination in linear logic
[AD-A292248] p 2645 N95-28886
Garbage collection is fast, but a stack is faster
[AD-A290099] p 2722 N95-29207
Correctness of real-time systems by construction
[PB95-206827] p 2655 N95-30220
STRUTS
Cable load transducer
[AD-A289548] p 2595 N95-29192
Permanent magnet torque/force transfer apparatus
[AD-D017325] p 2682 N95-30051
STUDENTS
Three-D weather displays for aircraft cockpits
[AD-A289759] p 2499 N95-28691
NASA/DOD Aerospace Knowledge Diffusion Research Project. Paper 49: Becoming an aerospace engineer: A cross-gender comparison
[NASA-TM-110731] p 2721 N95-29028
Macroprocesses and adaptive instruction
[AD-A290483] p 2648 N95-29325
US Army aviation epidemiology data register: Gender-specific attrition among the US Army student aviator class of 1987
[AD-A291856] p 2639 N95-29434
Mathematical olympiad summer program (MOSP) 1994
[AD-A290801] p 2672 N95-29647
ADC test support program
[AD-A289445] p 2643 N95-29921
SUBDUCTION (GEOLOGY)
Differentiation in the early Earth: An experimental investigation p 2612 N95-29199
SUBMERGING
Chemically induced passivity of aluminum alloys and Al-based metal matrix composites
[AD-A290778] p 2528 N95-29923
SUBMILLIMETER WAVES
Quasioptical Josephson Oscillator
[AD-A292481] p 2561 N95-28859
Nobeyama Radio Observatory report, no. 381: Parallel connected twin SIS junctions for millimeter and submillimeter wave mixers: Analysis and experimental verification p 2562 N95-29099
Semiconductor film Cherenkov lasers
[AD-A291177] p 2587 N95-29930
SUBROUTINES
Generator of body data (GEBOD) manual
[AD-A289721] p 2640 N95-28683
SUBSIDIARIES
Inhalation Toxicology Research Institute
[AD-A292037] p 2635 N95-29188
SUBSONIC AIRCRAFT
Development of RTM and powder prepreg resins for subsonic aircraft primary structures
p 2521 N95-29044
SUBSONIC FLOW
Finite element vorticity-based methods for the solution of the incompressible and compressible Navier-Stokes equations p 2570 N95-29119
Numerical investigation of surface curvature effects in compressible turbulent flows
[AD-A290114] p 2571 N95-29211
The pressure field of a gust interacting with a flat plate p 2582 N95-30161
Laser doppler velocimeter system for subsonic jet mixer nozzle testing at the NASA Lewis Aeroacoustic Propulsion Lab
[NASA-TM-106984] p 2477 N95-30229
SUBSONIC SPEED
Computer program for estimation of leading-edge suction distribution for plane thin wings at subsonic speeds
[ESDU-94038] p 2477 N95-28708
Leading-edge suction distribution for plane thin wings at subsonic speeds
[ESDU-94037] p 2486 N95-28800
Increments in aerofoil lift coefficient at zero angle of attack and in maximum lift coefficient due to deployment of a plain trailing-edge flap, with or without a leading-edge high-lift device, at low speeds
[ESDU-94028] p 2486 N95-28885
Increments in aerofoil lift coefficient at zero angle of attack and in maximum lift coefficient due to deployment of a trailing-edge split flap, with or without a leading-edge high-lift device, at low speeds
[ESDU-94029] p 2488 N95-29129
Transonic, supersonic and hypersonic wind-tunnel tests on aerodynamic characteristics of reentry body with blunted cone configuration
[ISAS-658] p 2490 N95-29640
The 1995 version of the NSWC aeroprediction code. Part 1: Summary of new theoretical methodology
[AD-A291518] p 2490 N95-29853

SUBSTITUTES
Development of the test kit for fuel acid contamination
[AD-A291953] p 2548 N95-29019
Proceedings of the 11th congress of the international society for artificial cells, blood substitutes and immobilization biotechnology
[AD-A290342] p 2632 N95-29088
SUBSTRATES
Selective attachment of nucleic acid molecules to patterned self-assembled surfaces
[AD-D017379] p 2530 N95-28854
Interface properties of wide bandgap semiconductor structures
[AD-A289817] p 2713 N95-28954
Advanced manufacturing by spray forming: Aluminum strip and microelectromechanical systems
[DE95-008615] p 2536 N95-28959
Analysis of the ferroelectric thin films deposited by pulsed laser deposition on oxide and fluoride substrates
[AD-A290088] p 2543 N95-29353
Structural and electronic properties of adsorbates on semiconductors, metal-semiconductor interfaces and semiconductor heterojunctions
[AD-A291917] p 2715 N95-29438
Compact substrate heater for use in an oxidizing atmosphere
[AD-A290860] p 2502 N95-29522
High T(sub c) superconductor/ferroelectric heterostructures
[AD-A291016] p 2716 N95-29658
Apparatus and method for achieving growth-etch deposition of diamond using a chopped oxygen-acetylene flame
[AD-D017322] p 2718 N95-30164
Thin-film edge field emitter device and method of manufacture therefor
[AD-D017323] p 2567 N95-30165
Impact properties of coated engineering plastics
[PB95-197281] p 2547 N95-30201
Formation and properties of titanium disilicide: A study on the development of stress in Ti-Si thin films
[PB95-197315] p 2538 N95-30205
SUBSTRUCTURES
Substructure-based control of flexible structures
p 2508 N95-29408
SUCROSE
Effect of irradiance, sucrose, and CO2 concentration on the growth of potato (Solanum tuberosum L.) in vitro
[NASA-TM-110654] p 2632 N95-29375
SUCTION
Computer program for estimation of leading-edge suction distribution for plane thin wings at subsonic speeds
[ESDU-94038] p 2477 N95-28708
Leading-edge suction distribution for plane thin wings at subsonic speeds
[ESDU-94037] p 2486 N95-28800
Pressure based high order TVD methodology for dynamic stall control
[AD-A290149] p 2489 N95-29316
SULFATES
Numerical studies of the stratospheric aerosol layer under background and perturbed conditions
p 2615 N95-29666
SULFUR
Chalcogenide superconductors: A search
[AD-A292523] p 2560 N95-28812
SAM1-A new semiempirical method including d-orbitals
[AD-A290903] p 2694 N95-30060
SULFUR OXIDES
Preparation and studies of urazole containing polymers
[AD-A290685] p 2545 N95-29586
SUMMER
An investigation of thunderstorms as a source of short period mesospheric gravity waves
[AD-A289795] p 2611 N95-28697
SUN
A turbulent model of the solar granulation
[AD-A292318] p 2738 N95-29475
Total solar eclipse of 1997 March 9
[NASA-RP-1173] p 2731 N95-30004
Interaction of acoustic oscillations with magnetic flux tubes in the solar photosphere
[PB95-201810] p 2739 N95-30199
SUNLIGHT
Reflectance analysis under solar illumination
[AD-A290489] p 2737 N95-29151
SUNSPOTS
15th NSO/Sac Peak Solar Workshop
[AD-A292297] p 2739 N95-30074
SUPERCOMPUTERS
Graphics supercomputer for computational fluid dynamics research
[AD-A291087] p 2575 N95-29637
SUPERCONDUCTING DEVICES
High Tc superconducting bolometric and nonbolometric infrared (IR) detectors
[NASA-CR-198789] p 2702 N95-30035
SUPERCONDUCTING FILMS
Materials science and fabrication of YBCO-SrTi(1-x)Nb(x)O3-YBCO device structures
[AD-A292527] p 2712 N95-28815
HTS Josephson technology on silicon with application to high speed digital microelectronics
[AD-A290206] p 2562 N95-29061
Processing, fabrication, and demonstration of HTS integrated microwave circuits
[AD-A292480] p 2562 N95-29073
Processing, fabrication, and demonstration of HTS integrated microwave circuits
[AD-A290220] p 2562 N95-29078
The 2nd International Conference on Thin Film Physics and Applications
[AD-A292353] p 2546 N95-29983
High Tc superconducting bolometric and nonbolometric infrared (IR) detectors
[NASA-CR-198789] p 2702 N95-30035
SUPERCONDUCTING MAGNETS
Five-channel SQUID based non-destructive evaluation (NDE) instrument
[AD-A292474] p 2592 N95-29012
Processing and properties of long-lengths of Ag-clad BSCCO superconductors and high-(Tc) magnets
[DE95-005855] p 2716 N95-29984
Flux pinning and stabilizer studies
[DE95-008131] p 2682 N95-30131
SUPERCONDUCTIVITY
Strained-bond semiconductors
[AD-A292524] p 2560 N95-28813
Synthesis and characterization of CuO superconductors with high transient temperatures
[AD-A292478] p 2562 N95-29014
Theoretical investigation of superconductivity in doped fullerenes
[AD-A291942] p 2562 N95-29018
Processing, fabrication, characterization and device demonstration of high temperature superconducting ceramics
[AD-A290183] p 2541 N95-29055
HTS Josephson technology on silicon with application to high speed digital microelectronics
[AD-A290206] p 2562 N95-29061
Optically triggered, superconducting opening switch
[AD-A292642] p 2700 N95-29379
High T(sub c) superconductor/ferroelectric heterostructures
[AD-A291016] p 2716 N95-29658
Flux pinning and stabilizer studies
[DE95-008131] p 2682 N95-30131
SUPERCONDUCTORS (MATERIALS)
Strained-bond semiconductors
[AD-A292524] p 2560 N95-28813
Synthesis and characterization of CuO superconductors with high transient temperatures
[AD-A292478] p 2562 N95-29014
Pulsed laser deposition of ferroelectric thin films in conjunction with superconducting oxides
[AD-A290101] p 2585 N95-29208
New radiation sources through generation and resonant enhancement of Current Driven Plasma Instabilities in lower dimensional solid state systems
[AD-A290669] p 2705 N95-29519
Flux pinning and stabilizer studies
[DE95-008131] p 2682 N95-30131
SUPERCOOLING
Macrosegregation and nucleation in undercooled Pb-Sn alloys
[NASA-TM-102023-REV] p 2535 N95-28701
SUPERCRITICAL FLOW
Supercritical states of two-dimensional wall-bounded shear flow p 2580 N95-30303
SUPERCRITICAL FLUIDS
Photothermal deflection in a supercritical fluid
p 2701 N95-29630
Analysis of factors affecting chemical reactions in supercritical fluids
[AD-A290905] p 2534 N95-30078
Supercritical states of two-dimensional wall-bounded shear flow p 2580 N95-30303
SUPERHIGH FREQUENCIES
Theory of competition between synchronous and nonsynchronous modes in a magnicon output cavity
[AD-A292043] p 2563 N95-29301
SUPERLATTICES
Strained-bond semiconductors
[AD-A292524] p 2560 N95-28813
Novel electric-field effects in quantum wells and superlattices
[AD-A292317] p 2718 N95-28857
Self-Induced Transparency in photonic band structures: Gap solitons near absorption resonances
[AD-A292187] p 2718 N95-28927
The 1.3 micrometer fiber photodetector
[AD-A292462] p 2582 N95-29004
Optoelectronics based on SiGe/Si heterostructures
[AD-A292454] p 2699 N95-29006
Semiconductor science and technology
[AD-A289143] p 2563 N95-29191
New radiation sources through generation and resonant enhancement of Current Driven Plasma Instabilities in lower dimensional solid state systems
[AD-A290669] p 2705 N95-29519
Interfaces in InAsSb/InGaAs strained-layer superlattices grown by MOCVD for use in infrared emitters
[DE95-006323] p 2717 N95-29990
SUPERMASSIVE STARS
Continuum spectra of supermassive accretion disks
p 2732 N95-29252
SUPERNOVA REMNANTS
Far-ultraviolet high-resolution emission line spectroscopy of the Cygnus Loop supernova remnant
p 2729 N95-29710
SUPERPLASTICITY
Superplastic ceramics
[AD-A290817] p 2545 N95-29635
SUPERSONIC AIRCRAFT
A procedure for automating CFD simulations of an inlet-bleed problem p 2485 N95-28768
SUPERSONIC BOUNDARY LAYERS
Numerical investigation of surface curvature effects in compressible turbulent flows
[AD-A290114] p 2571 N95-29211
SUPERSONIC COMBUSTION RAMJET ENGINES
Hydrogen film cooling with incident and swept-shock interactions in a Mach 6.4 nitrogen free stream
[NASA-TM-4603] p 2578 N95-30056
SUPERSONIC FLOW
Numerical investigation of surface curvature effects in compressible turbulent flows
[AD-A290114] p 2571 N95-29211
Research instrumentation for polytechnic university's supersonic wind tunnel facility
[AD-A290232] p 2502 N95-29468
An experimental investigation of the time-dependent separation of tangent bodies in supersonic flow
[AD-A290720] p 2489 N95-29500
One and two fluid numerical investigations of solar wind gas releases p 2738 N95-29704
Cross flow instability of supersonic flow over a 4:1 elliptic cone
[AD-A291128] p 2577 N95-29913
Survey of CFD applications for high speed inlets
[AD-A291365] p 2578 N95-30087
Numerical simulation of stability and stability control of high speed compressible rotating couette flow
[NASA-CR-198832] p 2579 N95-30250
SUPERSONIC INLETS
Survey of CFD applications for high speed inlets
[AD-A291365] p 2578 N95-30087
SUPERSONIC JET FLOW
The spectrum and directivity of turbulent mixing noise from supersonic jets p 2684 N95-29415
SUPERSONIC SPEED
Transonic, supersonic and hypersonic wind-tunnel tests on aerodynamic characteristics of reentry body with blunted cone configuration
[ISAS-658] p 2490 N95-29640
Experimental studies on boundary-layer transition on a reentry vehicle at transonic and supersonic speeds
[ISAS-659] p 2575 N95-29712
The 1995 version of the NSWC aeroprediction code. Part 1: Summary of new theoretical methodology
[AD-A291518] p 2490 N95-29853
An aerodynamic and static-stability analysis of the Hypersonic Applied Research Technology (HART) missile
[DA9426923] p 2491 N95-29965
SUPERSONIC WIND TUNNELS
Research instrumentation for polytechnic university's supersonic wind tunnel facility
[AD-A290232] p 2502 N95-29468
SUPPORT SYSTEMS
Retrieval display and analysis support tool requirements analysis
[AD-A291448] p 2599 N95-29523
SUPPORTS
Adjustable two-axis instrument mount
[AD-D017393] p 2582 N95-29220
SURFACE EMITTING LASERS
Vertical cavity surface emitting lasers for optical signal processing and optical computing applications
[AD-A290626] p 2588 N95-30050

SURFACE FINISHING
Liquefied metal jet program Automation and Robotics Research Institute (ARRI)
[AD-A289781] p 2536 N95-29461
SURFACE LAYERS
Interaction of acoustic oscillations with magnetic flux tubes in the solar photosphere
[PB95-201810] p 2739 N95-30199
SURFACE NOISE INTERACTIONS
The pressure field of a gust interacting with a flat plate p 2582 N95-30161
SURFACE PROPERTIES
Emerging CFD technologies and aerospace vehicle design p 2482 N95-28746
Generating grids directly on CAD database surfaces using a parametric evaluator approach p 2483 N95-28754
Grid generation on trimmed Bezier and NURBS quilted surfaces p 2483 N95-28755
Parametric design and gridding through relational geometry p 2486 N95-28771
GridTool: A surface modeling and grid generation tool p 2486 N95-28773
Intermediate levels of visual processing
[AD-A291569] p 2638 N95-28937
Formation of striped surface phases by short-range forces
[AD-A279962] p 2531 N95-28945
Numerical investigation of surface curvature effects in compressible turbulent flows
[AD-A290114] p 2571 N95-29211
Radar cross section synthesis for planar resistive surfaces
[AD-A290151] p 2555 N95-29318
Fiber-matrix adhesion in single-fiber model composites p 2524 N95-29337
Surface studies of Poly(organophosphazenes) containing dimethylsiloxane grafts
[AD-A291909] p 2543 N95-29355
Molecular spectra and dynamics at interfaces
[AD-A289779] p 2693 N95-29460
Chemically induced passivity of aluminum alloys and Al-based metal matrix composites
[AD-A290778] p 2528 N95-29923
Analysis of factors affecting chemical reactions in supercritical fluids
[AD-A290905] p 2534 N95-30078
SURFACE REACTIONS
Selective attachment of nucleic acid molecules to patterned self-assembled surfaces
[AD-D017379] p 2530 N95-28854
Boronization study for application to large helical device
[AD-B191996L] p 2709 N95-29808
SURFACE ROUGHNESS
100 Hz-10 kHz bottom backscattering model: Generalized treatment of sediment sound propagation, sediment volume scattering and interface-roughness scattering
[AD-A291323] p 2685 N95-29942
Proceedings of the Sixth International Symposium on Long-Range Sound Propagation
[AD-A290920] p 2685 N95-30084
Fundamental studies in cryogenic cooling of power electronics
[AD-A291150] p 2551 N95-30296
SURFACE ROUGHNESS EFFECTS
Growth and development of roughness-induced stationary crossflow vortices p 2492 N95-30294
SURFACE TEMPERATURE
The effect of climate perturbations on extratropical cyclogenesis along the east coast of North America p 2621 N95-29595
Hailstone heat and mass transfer measurements
[ISBN-0-315-86304-8] p 2624 N95-29797
SURFACE TREATMENT
Selection of materials, manufacturing methods and lubricants for cam mechanisms
[ESDU-94017] p 2589 N95-28905
Deposition and surface treatment with intense pulsed ion beams
[DE95-007885] p 2543 N95-29465
SURFACE WATER
Hydrology of the continental United States p 2599 N95-29539
SURFACE WAVES
Long range aircraft detection using high-frequency surface-wave radar
[AD-A290148] p 2555 N95-29313
SURFACTANTS
Surfactant-enhanced in situ biodegradation of strongly sorbing organic substances in soil environments
[AD-A290253] p 2512 N95-29168
SURGERY
Refractive changes during prolonged exposure to altitude following refractive surgery
[AD-A290263] p 2635 N95-29173
SURGES
Cathodic protection system inspection 5
[AD-A289724] p 2592 N95-28684
SURVEILLANCE
Eurasian seismic surveillance - 2D FD seismic synthetics and event discrimination
[AD-A292659] p 2614 N95-29413
Operational test and evaluation (OT&E) integration and operational test plan for fixed ground antenna radome (FGAR)
[AD-A291310] p 2559 N95-29940
SURVEILLANCE RADAR
MATSurv multisensor air traffic surveillance
[AD-A292253] p 2494 N95-28887
A least square real time quality control routine for the North Warning Netted Radar System
[AD-A290063] p 2555 N95-29328
UHF Low Density Radio Communications Link (LDRCL) Operational Test and Evaluation (OT&E) integration and OT&E operational final test report
[AD-A291447] p 2558 N95-29769
Operational test and evaluation (OT&E) integration and operational test plan for fixed ground antenna radome (FGAR)
[AD-A291310] p 2559 N95-29940
SURVEYS
NASA/DOD Aerospace Knowledge Diffusion Research Project. Paper 49: Becoming an aerospace engineer: A cross-gender comparison
[NASA-TM-110731] p 2721 N95-29028
Environmental practice in progam management offices
[AD-A290823] p 2609 N95-29721
Development of an intervention program to encourage shoulder harness use and aircraft retrofit in general aviation aircraft: Phases 1 and 2
[AD-A290966] p 2493 N95-29873
COADE: A framework for cognitive analysis, design, and evaluation
[AD-A291282] p 2720 N95-29935
Parallel rendering
[NASA-CR-195080] p 2655 N95-30306
SURVIVAL EQUIPMENT
Alternative methods for flotation seat cushion use
[DOT/FAA/AM-95/20] p 2493 N95-29448
SWIRLING
Experimental and analytical study of heat transfer and turbulent flow field in tangentially injected swirl flow p 2576 N95-29811
SWITCHES
Optically triggered, superconducting opening switch
[AD-A292642] p 2700 N95-29379
High power switch design
[AD-A291608] p 2565 N95-29601
Fiber compatible acousto-optic modulator using a gradient index lens
[AD-A291164] p 2585 N95-29925
Performance evaluation of ATM cell scheduling policies using stochastic petri nets
[PB95-197158] p 2559 N95-30096
SWITCHING
Optically triggered, superconducting opening switch
[AD-A292642] p 2700 N95-29379
Feature extraction from digital communications signals using wavelet transforms
[AD-A292655] p 2556 N95-29386
High gain, low noise and broadband Raman and Brillouin fiber-optic amplifiers, channel selectors and switches
[AD-A290585] p 2700 N95-29553
SWITCHING CIRCUITS
Low threshold all-optical crossbar switch on GaAs-GaAlAs channel waveguide arrays
[AD-A292483] p 2712 N95-28862
Power measurement and current feedback in a resonant DC link inverter
[AD-A292518] p 2563 N95-29164
Balanced, double-sided calibration circuit for sensor element differential pre-amplifier
[AD-D017326] p 2566 N95-30052
SYMBOLS
Visual and auditory symbols: A literature review
[AD-A290222] p 2641 N95-29908
Multi-dimensional upwind discretization method for the Euler equations on unstructured grids
[PB95-197307] p 2578 N95-30202
SYMMETRY
Ballistic penetration phenomenology of high symmetry single crystals
[AD-A292476] p 2713 N95-29013
Exploiting symmetry in the model checking of relational specifications
[AD-A290230] p 2647 N95-29223
The synthesis of liquid crystalline phophazenes containing chiral mesogens
[AD-A291911] p 2543 N95-29358
Ab initio calculation of vibrational absorption and circular dichroism spectra using density functional force fields
[AD-A291297] p 2720 N95-29936
SYNCHRONISM
An architectural design of a toolkit for synchronous groupware applications
[AD-A290226] p 2642 N95-29146
Performance evaluation of ATM cell scheduling policies using stochastic petri nets
[PB95-197158] p 2559 N95-30096
Efficient solution of a class of infinite stochastic petri nets: Theory and applications
[PB95-197166] p 2673 N95-30097
SYNCHROTRON RADIATION
Drift mobility measurements in thin film boron carbide
[AD-A292510] p 2712 N95-28869
Gamma radiation from rotation powered pulsars and results from the Energetic Gamma-Ray Experiment Telescope p 2739 N95-29671
SYNCHROTRONS
Multiwaveband observations of quasars p 2728 N95-29665
Semiconductor film Cherenkov lasers
[AD-A291177] p 2587 N95-29930
Observation of x ray generation in a proof-of-principle laser synchrotron source experiment
[AD-A291298] p 2588 N95-29937
SYNCOPE
Pulse waveform and pulse amplitude analysis during Lower Body Negative Pressure
[AD-A290521] p 2636 N95-29360
SYNOPTIC METEOROLOGY
Forecast of Atlantic seasonal hurricane activity for 1995 p 2620 N95-29254
The effect of climate perturbations on extratropical cyclogenesis along the east coast of North America p 2621 N95-29595
SYNTAX
Usability: Formalising (un)definedness in typed lambda calculus
[PB95-197190] p 2673 N95-30196
SYNTHESIS (CHEMISTRY)
Synthesis and characterization of (Me3SiCH2)3M(dot)E(SiMe3)3 (M = Ga, E = P or As; M = In, E = P). X-ray crystal structures of (Me3SiCH2)3Ga(dot)P(SiMe3)3 and (Me3SiCH2)3In(dot)P(SiMe3)3
[AD-A291907] p 2715 N95-29444
Synthesis of nanocrystalline indium arsenide and indium phosphide from Indium(III) halides and tris(trimethylsilyl)pnicogens; synthesis, characterization, and decomposition behavior of I3In(dot)P(SiMe3)3
[AD-A291905] p 2715 N95-29486
Bilateral US/Russia Workshop on Self-Propagating High-Temperature Synthesis held in Honolulu, Hawaii on 6-7 November 1993
[AD-A290466] p 2525 N95-29492
Integrated synthesis and post-processing of SiC and AlN
[AD-A290853] p 2537 N95-29724
SYNTHETIC APERTURE RADAR
Optical (LANDSAT/TM) and radar (ERS-1/SAR) imagery sinergism studies applied to land use discrimination
[INPE-5608-TDI/554] p 2598 N95-29433
Evaluation of the utilization of SAR polarimetric images in the survey of land resources in the Amazon area Tapajos Forest Reserve
[INPE-5517-PRE/1792] p 2601 N95-29999
Hi-res SAR data processing report
[AD-A291443] p 2559 N95-30073
Patch diameter limits for tiered subaperture SAR image formation algorithms
[DE95-008816] p 2560 N95-30177
SYNTHETIC APERTURES
A conceptual thermal design study of an electronically scanned thinned array radiometer
[NASA-TM-110173] p 2509 N95-30316
SYNTHETIC FUELS
Introduction to the proceedings of the sixteenth symposium on biotechnology for fuels and chemicals
[DE95-007029] p 2549 N95-30024
SYSTEM EFFECTIVENESS
Transport delays associated with NASA Langley Flight Simulation Facility
[NASA-TM-110150] p 2659 N95-29454
Federal aviation administration plan for research, engineering and development
[AD-A290952] p 2494 N95-29733
SYSTEM IDENTIFICATION
Analysis of multigrid techniques for system modeling with toeplitz approximation
[AD-A289784] p 2644 N95-28694

Fundamental limitations and capabilities of robust identification and adaptive control
[AD-A291085] p 2664 N95-29636
An analytic modeling and system identification study of helicopter dynamics p 2498 N95-29787
Optimal hankel norm identification of dynamical systems
[PB95-197232] p 2672 N95-30046

SYSTEMS ANALYSIS
Modal interactions and complex responses in weaklyNONLINEAR MULTI-DEGREE-OF-FREEDOM MECHANICAL SYSTEMS
[AD-A292023] p 2594 N95-26853
(DEPSCOR-92) acquisition of a metallurgical optical microscope
[AD-A292439] p 2698 N95-28998
Application of optimization technique to control system design for departure prevention and aircraft model estimation through dynamic inversion
p 2501 N95-29156
The generalized railroad crossing: A case study in formal verification of real-time systems
[AD-A290152] p 2648 N95-29319
Prototype stop bar system evaluation at Seattle-Tacoma International Airport
[AD-A290136] p 2495 N95-30031
Tools for Automated Knowledge Engineering (TAKE) system evaluation methodology
[AD-A291145] p 2654 N95-30125
Framework for comparing and controlling number-based design reasoning systems
[PB95-197364] p 2667 N95-30207
A unified matrix inequality approach to linear control design p 2667 N95-30234
Design, analysis and control of large transports so that control of engine thrust can be used as a back-up of the primary flight controls
[NASA-CR-198958] p 2501 N95-30254

SYSTEMS ENGINEERING
Software Design for Reliability and Reuse proof of concept project. Phase 1
[AD-A291690] p 2644 N95-28782
DOD electronic data interchange (EDI) convention: TDCC/EDIA transaction set 210 motor carrier invoice (version 003020). Revision 1
[AD-A292375] p 2720 N95-28797
Proceedings of the Complex Systems Engineering Synthesis and Assessment Technology Workshop (CSESAW 1994)
[AD-A292433] p 2646 N95-28995
Application of optimization technique to control system design for departure prevention and aircraft model estimation through dynamic inversion
p 2501 N95-29156
DOD electronic data interchange (EDI) convention: ASC X12 transaction set 410 Rail Carrier Invoice, version 003020
[AD-A292495] p 2722 N95-29287
Gordon research conference on physical metallurgy: Materials by design
[AD-A290519] p 2524 N95-29326
Design and evaluation of a LQR controller for the bluebird unmanned air vehicle
[AD-A289769] p 2498 N95-29457
Liquefied metal jet program Automation and Robotics Research Institute (ARRI)
[AD-A289781] p 2536 N95-29461
Asymptotically zero energy computing using split-level charge recovery logic
[AD-A290054] p 2564 N95-29478
Retrieval display and analysis support tool requirements analysis
[AD-A291448] p 2599 N95-29523
Applications of machine learning and rule induction
[AD-A292607] p 2664 N95-29577
Modeling spatio-temporal databases to measure the performance of the GPS satellite constellation
p 2494 N95-29596
Equipment resource for MCM technology and system prototyping
[AD-A292492] p 2719 N95-29756
Description and manipulation of method fragments for the assembly of situational methods
[PB95-197133] p 2653 N95-30094
Simulation of robot manipulators
[DE95-008680] p 2654 N95-30189
Structured approach for the methodical and technical integration of heterogeneous CASE tools
[PB95-197653] p 2655 N95-30218
Design, analysis and control of large transports so that control of engine thrust can be used as a back-up of the primary flight controls
[NASA-CR-198958] p 2501 N95-30254
Engineering development program of a closed aluminum-oxygen semi-cell system for an unmanned underwater vehicle: An update p 2606 N95-30266

SYSTEMS MANAGEMENT
Management of speedup mechanisms in learning architectures
[AD-A292206] p 2662 N95-28988

SYSTEMS SIMULATION
R&M design expert system
[AD-A292525] p 2645 N95-28814
Defense Modeling and Simulation Office information/data base technology working group (I/DBTWG) meetings
[AD-A290953] p 2651 N95-29735
SEMINT: Seamless model integration
[AD-A290956] p 2651 N95-29736
Numerical simulation of mechanisms and manipulator robots with flexible links and flexible joints
[PB95-196903] p 2591 N95-30285

SYSTEMS STABILITY
Application of optimization technique to control system design for departure prevention and aircraft model estimation through dynamic inversion
p 2501 N95-29156
Linear matrix inequalities for the problem of absolute stability of control systems p 2501 N95-29680

T

TABLES (DATA)
An atlas of monthly mean distributions of SSMI surface wind speed, AVHRR/2 sea surface temperature, AMI surface wind velocity, TOPEX/POSEIDON sea surface height, and ECMWF surface wind velocity during 1993
[NASA-CR-198880] p 2628 N95-30343

TAIL ASSEMBLIES
Challenges and payoff of composites in transport aircraft: 777 empennage and future applications
p 2519 N95-29031
Low-speed wind-tunnel investigation of the stability and control characteristics of a series of flying wings with sweep angles of 50 deg
[NASA-TM-4640] p 2498 N95-30226

TANDEM MIRRORS
Interchange stability criteria for anisotropic central-cell plasmas in the tandem mirror GAMMA 10
[AD-B176253L] p 2707 N95-29738

TAPERING
Leading-edge suction distribution for plane thin wings at subsonic speeds
[ESDU-94037] p 2486 N95-28800

TARGET ACQUISITION
System and method for rapidly tracking vehicles of special utility in low signal-to-noise environments
[AD-D017378] p 2683 N95-28783
MATSurv multisensor air traffic surveillance
[AD-A292253] p 2494 N95-28887
Design, development and testing of a prototype precision angular positioning control system for a next generation multiplexed imager
[AD-A292585] p 2698 N95-28980
Visualization of improved target acquisition algorithm for Janus (A)
[AD-A290191] p 2646 N95-29056
Unmanned aerial vehicles: No more Hunter systems should be bought until problems are fixed
[AD-A292172] p 2497 N95-29126
Description of the OHGR database
[AD-A290146] p 2722 N95-29221
Offshore next generation weather radar (NEXRAD) test and evaluation master plan (TEMP)
[AD-A291435] p 2559 N95-30072

TARGET RECOGNITION
Automated optical target recognition
[AD-A292397] p 2697 N95-28798
Target aircraft identification, trajectory tracking and prediction using regression-based Kalman filter techniques p 2565 N95-29728

TARGETS
Three-D weather displays for aircraft cockpits
[AD-A289759] p 2499 N95-28691
Conceptual design of a map interactive system for military aircraft cockpits
[AD-A289760] p 2499 N95-28692
A formative evaluation of CU-SeeMe
[AD-A292443] p 2553 N95-29002
Thickness measurement of ammonia targets used in SLAC e143 experiment
[AD-A290215] p 2692 N95-29076
High velocity impact and penetration of thick composite laminates
[AD-A290642] p 2526 N95-29561
Penetration of semi-infinite, bi-element targets by long rod penetrators
[AD-A291176] p 2596 N95-29929
Prospects for HERMES-spin structure studies at HERA
[DE95-005845] p 2694 N95-30019
Development of flame resistant, high efficiency thermal insulation
[AD-A291136] p 2547 N95-30120

TASK PLANNING (ROBOTICS)
Experiments in cooperative manipulation of objects by free-flying robot teams p 2662 N95-29095

TASKS
Conversion of the TRACON operations concepts database into a formal sentence outline job task taxonomy
[DOT/FAA/AM-95/16] p 2493 N95-28819
Ride motion simulator (RMS) testing using human occupants
[AD-A292641] p 2641 N95-29378

TAXONOMY
Automated analysis of zooplankton size and taxonomic composition using the video plankton recorder
[AD-A289725] p 2631 N95-28685
Conversion of the TRACON operations concepts database into a formal sentence outline job task taxonomy
[DOT/FAA/AM-95/16] p 2493 N95-28819
Applicability of neural networks for production planning under uncertainty
[PB95-197406] p 2666 N95-30101

TEARING MODES (PLASMAS)
Turbulent coupling of the magnetosphere-ionosphere through shear-mode Alfven waves p 2615 N95-29687

TECHNOLOGICAL FORECASTING
Grid generation: A view from the trenches
p 2478 N95-28727
Geometry Laboratory (GEOLAB) surface modeling and grid generation technology and services
p 2479 N95-28729
Prospects and expectations for unstructured methods
p 2481 N95-28742
An announcement by Dan Goldin
[NASA-TM-110739] p 2720 N95-29171
Hernandez Engineering: NASA
[NASA-CR-197665] p 2508 N95-29633
Rover story
[NASA-CR-198757] p 2736 N95-29964

TECHNOLOGY ASSESSMENT
Future requirements in surface modeling and grid generation p 2478 N95-28724
Requirements for effective use of CFD in aerospace design p 2478 N95-28725
Application of CFD in aeronautics at NASA Ames Research Center p 2478 N95-28728
Multiblock grid generation with automatic zoning
p 2480 N95-28735
Block-structured grids for complex aerodynamic configurations: Current status p 2480 N95-28736
Grid related issues for static and dynamic geometry problems using systems of overset structured grids
p 2480 N95-28737
The role of overset grids in the development of the general purpose CFD code p 2480 N95-28738
Prospects and expectations for unstructured methods
p 2481 N95-28742
Emerging CFD technologies and aerospace vehicle design p 2482 N95-28746
An assessment of unstructured grid technology for timely CFD analysis p 2482 N95-28747
Evaluation of grid generation technologies from an applied perspective p 2482 N95-28748
Experimental results of Hooper's gravity-electromagnetic coupling concept
[NASA-TM-106963] p 2680 N95-28893
A 1993 review of welding in Japan
[DE95-758701] p 2589 N95-28946
Nanoscience and nanotechnology in Europe
[AD-A290214] p 2562 N95-29075
NASA: The state of the agency
[NASA-TM-110563] p 2720 N95-29170
Unmanned Aerial Vehicle technology
[DSTO-GD-0044] p 2497 N95-29362
Digital video technology, today and tomorrow
[DE95-007689] p 2556 N95-29462
The TEES process cleans waste and produces energy
[DE95-007799] p 2602 N95-29463
Deposition and surface treatment with intense pulsed ion beams
[DE95-007885] p 2543 N95-29465
Hernandez Engineering: NASA
[NASA-CR-197665] p 2508 N95-29633
Japanese remote sensing organizations, research, and technology
[AD-A292420] p 2601 N95-29905
Magnetic fusion commercial power plants
[DE95-007027] p 2711 N95-30023
HIPPI - Gigabit LANS are here today
[DE95-007877] p 2660 N95-30128
Electric and hybrid vehicle program: Site operator program
[DE95-008620] p 2591 N95-30211

Advanced Dependent Pressure Vessel (DPV) nickel-hydrogen spacecraft cell and battery design p 2567 N95-30261
Parallel rendering [NASA-CR-195080] p 2655 N95-30306
CD-ROM preparation: An overview and guide [NASA-CR-198756] p 2655 N95-30307

TECHNOLOGY TRANSFER
Geometry Laboratory (GEOLAB) surface modeling and grid generation technology and services p 2479 N95-28729
Liquefied metal jet program Automation and Robotics Research Institute (ARRI) [AD-A289781] p 2536 N95-29461

TECHNOLOGY UTILIZATION
Future requirements in surface modeling and grid generation p 2478 N95-28724
Requirements for effective use of CFD in aerospace design p 2478 N95-28725
Grid generation: A view from the trenches p 2478 N95-28727
Application of CFD in aeronautics at NASA Ames Research Center p 2478 N95-28728
Geometry Laboratory (GEOLAB) surface modeling and grid generation technology and services p 2479 N95-28729
Research and technology: 1994 annual report of the John F. Kennedy Space Center [NASA-TM-110143] p 2740 N95-28786
Commercial photorefractive device using nonstoichiometric 3-5 semiconductors [AD-A292494] p 2713 N95-28933
Pulse waveform and pulse amplitude analysis during Lower Body Negative Pressure [AD-A290521] p 2636 N95-29360
Unmanned Aerial Vehicle technology [DSTO-GD-0044] p 2497 N95-29362
Development of electrochemical super capacitors for EMA applications p 2568 N95-30270
Solid Oxide Fuel Cell commercialization in the United States [DE95-008210] p 2607 N95-30278

TECTONICS
Channels and valleys on Venus p 2736 N95-29593
The gravitational potential energy of the Earth's lithosphere p 2617 N95-29773

TELECOMMUNICATION
The 1994 IEEE International Workshop on Intelligent Signal Processing and Communication Systems (ISPACS94) [AD-A292312] p 2556 N95-29474
Summary of the 1st International Workshop on Networked Reality in Telecommunication [AD-A292366] p 2558 N95-29862
UMTS network architecture [PB95-206744] p 2558 N95-29919
Delayed choice: An operator for joining message sequence charts [PB95-206710] p 2560 N95-30203
Description of the TV distribution service using MAGIC modelling methods [PB95-206728] p 2560 N95-30219

TELECONFERENCING
Low threshold all-optical crossbar switch on GaAs-GaAlAs channel waveguide arrays [AD-A292483] p 2712 N95-28862

TELEMETRY
High resolution direct digitization and optical telemetry of shipboard antenna signals [AD-A290238] p 2557 N95-29504
Requirement for onboard telemetry equipment p 2506 N95-29625
Data re-formatter program for the topside thermal plasma monitor (PLIESPP) [AD-A290960] p 2616 N95-29737
The topside ionospheric plasma monitor (SSIES, SSIES-2 and SSIES-3) on the spacecraft of the Defense Meteorological Satellite Program (DMSP), user's guide. Volume 3: Program maintenance manual [AD-A290941] p 2617 N95-29765
Balanced, double-sided calibration circuit for sensor element differential pre-amplifier [AD-D017326] p 2566 N95-30052
The topside ionospheric plasma monitor (SSIES, SSIES-2 and SSIES-3) on the spacecraft of the Defense Meteorological Satellite Program (DMSP), user's guide. Volume 2: Programmer's guide for software at AFSFC [AD-A290913] p 2618 N95-30082
The Telemetry Agile Manufacturing Effort [DE95-006177] p 2654 N95-30115

TELEOPERATORS
NASA to use telepresence to explore Antarctic Lakes [NASA-TM-110567] p 2598 N95-29175
Improved operator awareness of teleoperated land vehicle attitude [AD-A290443] p 2641 N95-29359
Telepresence media resource tape [NASA-TM-110648] p 2655 N95-30248

TELEROBOTICS
Experiments in cooperative manipulation of objects by free-flying robot teams p 2662 N95-29095

TELESCOPES
First flight of the Multi-Spectral Solar Telescope Array: Calibration, results and future plans p 2727 N95-29529
The use of charge coupled devices in astronomical speckle imaging p 2727 N95-29545
Low order adaptive optical systems [AD-A291121] p 2701 N95-29766
Advanced research in sky surveillance: A search for low-luminosity objects [AD-A291184] p 2731 N95-29916

TELEVISION SYSTEMS
An investigation of thunderstorms as a source of short period mesospheric gravity waves [AD-A289795] p 2611 N95-28697
Feature-oriented image reconstruction and aero-optic metrology in turbulence [AD-A290269] p 2699 N95-29177
Towards an example-based image compression architecture for video-conferencing [AD-A290041] p 2556 N95-29441
Description of the TV distribution service using MAGIC modelling methods [PB95-206728] p 2560 N95-30219

TELLURIUM
Chalcogenide superconductors: A search [AD-A292523] p 2560 N95-28812

TEMPERATURE CONTROL
EMI Shields made from intercalated graphite composites [NASA-TM-106979] p 2518 N95-28906
Computational methods for the simulation of non-Newtonian flows [AD-A290355] p 2570 N95-29069

TEMPERATURE DEPENDENCE
HTS Josephson technology on silicon with application to high speed digital microelectronics [AD-A290206] p 2562 N95-29061
Theory of pseudo-classical confinement and transmutation to L-mode [AD-B175957L] p 2709 N95-29809
Screening constants for plasma [AD-B179442L] p 2710 N95-29843
Ion beam modification of Tl-Ba-Ca-Cu-O type high temperature superconductors during irradiation [DE95-006807] p 2717 N95-30022
Development and application of fluorescent diagnostics to fundamental droplet and spray problems [AD-A290553] p 2578 N95-30039
Elevated temperature static fatigue of a Nicalon fiber-reinforced SiC composite [DE95-008780] p 2528 N95-30175

TEMPERATURE DISTRIBUTION
Hindcasting changes in thermal structure and acoustic transmission loss in the upper ocean on short time scales with data from MILE and from ocean weather station papa [AD-A292419] p 2629 N95-28991
Unsteady rotational shear flow of power law fluids [ISBN-0-315-81287-7] p 2575 N95-29718
Effects of elevated free-stream turbulence and streamwise acceleration on flow and thermal structures in transitional boundary layers p 2576 N95-29729

TEMPERATURE EFFECTS
Experimental results of Hooper's gravity-electromagnetic coupling concept [NASA-TM-106963] p 2680 N95-28893
Recirculating cavity casing treatment failure [AD-A289330] p 2500 N95-28908
Effects of temperature and humidity cycling on the strengths of textile reinforced carbon/epoxy composite materials p 2520 N95-29037
Effects of thermal and moisture cycling on the internal structure of stitched RTM laminates p 2522 N95-29048
The potential for pulmonary heat injury resulting from the activation of a cabin water spray system to fight aircraft cabin fires [DOT/FAA/AM-95/17] p 2636 N95-29224
Equatorial heating effects on outer plasmasphere evolution p 2616 N95-29716
Unsteady rotational shear flow of power law fluids [ISBN-0-315-81287-7] p 2575 N95-29718
Polyethylene-based polyurethane copolymers and block copolymers [AD-A289996] p 2546 N95-30030
Epitaxial growth of high quality SiC of pulsed laser deposition, phase 1 [AD-A291410] p 2717 N95-30068
Development of LaRC (TM): IA thermoplastic polyimide coated aerospace wiring [NASA-CR-195048] p 2548 N95-30252
A conceptual thermal design study of an electronically scanned thinned array radiometer [NASA-TM-110173] p 2509 N95-30316

TEMPERATURE GRADIENTS
Modeling studies of the Leeuwin current off western and southern Australia [AD-A290158] p 2629 N95-29023
Investigation of the flow turning loss in unstable solid propellant rocket motors p 2510 N95-29331

TEMPERATURE INVERSIONS
Upper-air data collected on Ice Station Weddell [AD-A289707] p 2620 N95-29193

TEMPERATURE MEASUREMENT
Non-coincident multi-wavelength emission absorption spectroscopy [DE95-006480] p 2530 N95-28776
Effects of cooling system parameters on heat transfer in PAFC stack [NASA-CR-198817] p 2570 N95-29131
Comparison of boundary-layer wind and temperature measurements with model estimations [AD-A290471] p 2621 N95-29507
Heat and momentum flux measurements in the planetary boundary layer with a wind profiling radar/radio acoustic sounding system p 2617 N95-29777
Development and application of fluorescent diagnostics to fundamental droplet and spray problems [AD-A290553] p 2578 N95-30039

TEMPERATURE PROFILES
Hindcasting changes in thermal structure and acoustic transmission loss in the upper ocean on short time scales with data from MILE and from ocean weather station papa [AD-A292419] p 2629 N95-28991
A theoretical model of multiple regimes in a stratocumulus-topped boundary layer p 2624 N95-29726
Radiative cooling profiles calculated from ECMWF analyses and ISCCP C1 data, and their application to determination of distributions of apparent convective heating in the equatorial Pacific p 2625 N95-29805

TEMPLATES
Formalizing style to understand descriptions of software architecture [AD-A292237] p 2645 N95-28894

TEMPORAL DISTRIBUTION
Hydrology of the continental United States p 2599 N95-29539
Modeling spatio-temporal databases to measure the performance of the GPS satellite constellation p 2494 N95-29596
Dynamical model of pressure-gradient-driven turbulence and shear flow generation in L-H transition [AD-B195511L] p 2709 N95-29789
A model analysis of the spatial distribution and temporal trends of nitrous oxide sources and sinks p 2609 N95-29804

TEMPORAL RESOLUTION
The Los Alamos Photon Counting Detector Debris Detection Project: An update [DE95-007883] p 2508 N95-29464

TENSILE DEFORMATION
In-phase thermomechanical fatigue mechanisms in an unidirectional SCS-6/Ti 15-3 MMC [NASA-CR-195482] p 2523 N95-29133

TENSILE PROPERTIES
The effects of specimen width on tensile properties of triaxially braided textile composites p 2513 N95-28825
A designed experiment in stitched/RTM composites p 2522 N95-29046
Tensile properties of as-cast iron-aluminide alloys [DE95-005396] p 2538 N95-30216

TENSILE STRENGTH
Effect of open hole on tensile failure properties of 2D triaxial braided textile composites and tape equivalents [NASA-CR-4676] p 2513 N95-28817
Experimental and analytical characterization of triaxially braided textile composites p 2520 N95-29040
The effects of aircraft fuel and fluids on the strength properties of Resin Transfer Molded (RTM) composites p 2522 N95-29047
Measurement of interface strength, intrinsic toughness and their dependence on interfacial segregants [AD-A291798] p 2524 N95-29409
The effects of alloying elements on the strength and cooling rate sensitivity of ultra-low carbon alloy steel weld metals [AD-A290681] p 2537 N95-29759
Measurement of interface strength, intrinsic toughness and their dependence on interfacial segregants [AD-A291169] p 2548 N95-29926

TENSILE STRESS
Measurement of interface strength, intrinsic toughness and their dependence on interfacial segregants
[AD-A291798] p 2524 N95-29409
Structure and orientation behavior of highly oriented polymers under tensile and compressive stresses
p 2546 N95-29822

TENSILE TESTS
Design, analysis, and fabrication of a pressure box test fixture for tension damage tolerance testing of curved fuselage panels p 2516 N95-28839
The effects of alloying elements on the strength and cooling rate sensitivity of ultra-low carbon alloy steel weld metals
[AD-A290681] p 2537 N95-29759

TENSORS
New methods for nonlinear optimization
[AD-A290522] p 2670 N95-29385

TERMINAL BALLISTICS
Ballistic penetration phenomenology of high symmetry single crystals
[AD-A292476] p 2713 N95-29013
Finite element technology for penetration problems
[AD-A290644] p 2671 N95-29516
Robust algorithms for penetration mechanics problems
[AD-A290650] p 2650 N95-29517
High velocity impact and penetration of thick composite laminates
[AD-A290642] p 2526 N95-29561
Penetration of semi-infinite, bi-element targets by long rod penetrators
[AD-A291176] p 2596 N95-29929

TERNARY ALLOYS
Austenite to ferrite transformation kinetics during continuous cooling
[DE95-008582] p 2537 N95-29869

TERRAIN
Statistical properties of bistatic clutter echoes
[AD-A291688] p 2552 N95-28943
Modeling the direct-beam instantaneous spectral surface albedo of a forest landscape using geometric-optics and a distributed parameter approach
p 2599 N95-29540
A full wave study of radar cross sections of rough terrain
[AD-A291227] p 2559 N95-29982
A biologically-inspired autonomous robot
[AD-A289446] p 2666 N95-30026

TEST CHAMBERS
Computational fluid dynamics (CFD) simulation of test chamber and smoke-generating device
[AD-A290199] p 2569 N95-29058
Liquefied metal jet program Automation and Robotics Research Institute (ARRI)
[AD-A289781] p 2536 N95-29461
Experimental study on scaling law of outgassing rate with a pumping parameter
[AD-B191999L] p 2709 N95-29801

TEST FACILITIES
The international fusion materials irradiation facility
[DE95-006536] p 2696 N95-29142
Operational test and evaluation (OT&E) integration and operational test procedures for Fixed Ground Antenna Radome (FGAR)
[AD-A291203] p 2559 N95-29975

TEST RANGES
Crustal deformation measurements in the vicinity of Vandenberg Air Force Base
[AD-A291224] p 2618 N95-29981

TEST STANDS
Boronization study for application to large helical device
[AD-B191996L] p 2709 N95-29808
Inlet flow test calibration for a small axial compressor rig. Part 2: CFD compared with experimental results
[NASA-TM-106999] p 2501 N95-30007

TETHERED SATELLITES
FFT space processing for the ACF of SPREE particle flux measurements
[AD-A290166] p 2507 N95-29026
Spin augmented deployment and retrieval of tethered artificial gravity spacecraft p 2509 N95-30280

TETHERING
Spin augmented deployment and retrieval of tethered artificial gravity spacecraft p 2509 N95-30280

TETRAETHYL ORTHOSILICATE
Cage-like precursor formation from extensive cyclization in sol-gel inorganic condensation polymerization
[AD-A290589] p 2544 N95-29554

TETRAHEDRONS
An assessment of unstructured grid technology for timely CFD analysis p 2482 N95-28747

TEXTILES
Effect of open hole on tensile failure properties of 2D triaxial braided textile composites and tape equivalents
[NASA-CR-4676] p 2513 N95-28817
Third NASA Advanced Composites Technology Conference, volume 1, part 2
[NASA-CP-3178-VOL-1-PT-2] p 2513 N95-28823
Characterization and development of materials for advanced textile composites p 2513 N95-28824
The effects of specimen width on tensile properties of triaxially braided textile composites
p 2513 N95-28825
Novel cost controlled materials and processing for primary structures p 2514 N95-28830
Textile composite fuselage structures development
p 2519 N95-29033
Advanced resin systems and 3D textile preforms for low cost composite structures p 2519 N95-29035
Effects of temperature and humidity cycling on the strengths of textile reinforced carbon/epoxy composite materials p 2520 N95-29037
Performance of resin transfer molded multiaxial warp knit composites p 2520 N95-29039
Experimental and analytical characterization of triaxially braided textile composites p 2520 N95-29040
Cross-stiffened continuous fiber structures
p 2521 N95-29041
Cost model relationships between textile manufacturing processes and design details for transport fuselage elements p 2521 N95-29043
Analytical modeling and sensor monitoring for optimal processing of advanced textile structural composites by resin transfer molding p 2521 N95-29045
Effects of thermal and moisture cycling on the internal structure of stitched RTM laminates
p 2522 N95-29048

THALLIUM COMPOUNDS
Ion beam modification of Tl-Ba-Ca-Cu-O type high temperature superconductors during irradiation
[DE95-006807] p 2717 N95-30022

THEMATIC MAPPERS (LANDSAT)
Monitoring of burning in the Brazilian cerrado region using AVHRR/NOAA data calibrated by TM/Landsat data
[INPE-5490-TDI/507] p 2598 N95-28929

THEMATIC MAPPING
Proposal for a flexible system of phytogeographic classification: Emphasis on the use of multistage remote sensoring
[INPE-5609-PRE/1821] p 2600 N95-29815

THEOREM PROVING
Proving the genericity lemma by leftmost reduction is simple
[PB95-197620] p 2673 N95-30103
Short and elementary proof of the main Bahadur-Kiefer theorem
[PB95-206967] p 2675 N95-30170
Essential structure of the jacopini technique
[PB95-197208] p 2674 N95-30291

THEOREMS
Translation Invariant Operators on Lp-Type Spaces
[PB95-197117] p 2672 N95-30092
Theorem on the existence of solutions of quasi-static moving boundary problems
[PB95-197125] p 2673 N95-30093
Proving the genericity lemma by leftmost reduction is simple
[PB95-197620] p 2673 N95-30103
Usability: Formalising (un)definedness in typed lambda calculus
[PB95-197190] p 2673 N95-30196

THEORETICAL PHYSICS
Photoproduction of hybrid mesons from CEBAF to HERA
[PB95-196218] p 2691 N95-28913
The quantum hydrodynamic model for semiconductor devices
[AD-A291809] p 2564 N95-29430
Modelling of transport phenomena
[AD-B179223L] p 2708 N95-29747
Dynamical model of pressure-gradient-driven turbulence and shear flow generation in L-H transition
[AD-B195511L] p 2709 N95-29789

THERAPY
The effect of bright light and LEET on sleep after a 10-hour phase delay
[AD-A291264] p 2637 N95-29995

THERMAL ANALYSIS
An analysis of B-1B exterior jet blast windshield anti-icing performance using pre-cooled compressor bleed air
[AD-A292522] p 2492 N95-28811
Geothermal heat pumps for heating and cooling
[AD-A292115] p 2602 N95-28858
A conceptual thermal design study of an electronically scanned thinned array radiometer
[NASA-TM-110173] p 2509 N95-30316

THERMAL BOUNDARY LAYER
Effects of elevated free-stream turbulence and streamwise acceleration on flow and thermal structures in transitional boundary layers p 2576 N95-29729

THERMAL CONDUCTIVITY
Thermophysical properties of R-32 (difluoromethane)
[ESDU-94032] p 2530 N95-28802
Thermal conductivity of liquid halogenated aliphatic hydrocarbons. Part 4: Halogenated alkenes and dienes (C1 to C4)
[ESDU-94024-PT-4] p 2511 N95-28803
Thermal conductivity of liquid halogenated aliphatic hydrocarbons. Part 1: Halogenated methanes and azeotropic mixtures
[ESDU-94021-PT-1] p 2511 N95-28804
Thermal conductivity of liquid halogenated aliphatic hydrocarbons. Part 2: Halogenated ethanes
[ESDU-94022] p 2512 N95-29017
HTMIAC/CINDAS silicon properties database. User's guide
[AD-A292602] p 2533 N95-29575
Anomalous transport theory for toroidal helical plasmas
[AD-B192000L] p 2706 N95-29731
Thermal conductivity of liquid halogenated aliphatic hydrocarbons. Part 3: Halogenated higher hydrocarbons (C3 to C16)
[ESDU-94023-PT-3] p 2512 N95-29900

THERMAL CONTROL COATINGS
A simulation technique for predicting thickness of thermal sprayed coatings
[NASA-TM-106939] p 2512 N95-29373

THERMAL CYCLING TESTS
Recirculating cavity casing treatment failure
[AD-A289330] p 2500 N95-28908
In-phase thermomechanical fatigue mechanisms in an unidirectional SCS-6/Ti 15-3 MMC
[NASA-CR-195482] p 2523 N95-29133

THERMAL DECOMPOSITION
Synthesis of nanocrystalline indium arsenide and indium phosphide from Indium(III) halides and tris(trimethylsilyl)pnicogens; synthesis, characterization, and decomposition behavior of I3In(dot)P(SiMe3)3
[AD-A291905] p 2715 N95-29486
The comparative extinguishment performance and thermal decomposition products of halon alternative agents
[AD-A291161] p 2551 N95-29924

THERMAL DIFFUSION
New predictive methods in chaotic fluid dynamics with application to turbulent heat transfer
[AD-A290691] p 2576 N95-29761

THERMAL EMISSION
Some aspects of lunar and martian volcanism as examined with spectral, topographic, and morphologic data derived from spacecraft images p 2736 N95-29594

THERMAL ENERGY
Photothermal deflection in a supercritical fluid
p 2701 N95-29630
High temperature spectroscopy of alkali metal vapors for solar to thermal energy conversion
[AD-A291355] p 2602 N95-29949

THERMAL ENVIRONMENTS
A hybrid electronically scanned pressure module for cryogenic environments
[NASA-TM-110146] p 2583 N95-29453

THERMAL EXPANSION
HTMIAC/CINDAS silicon properties database. User's guide
[AD-A292602] p 2533 N95-29575
Photothermal deflection in a supercritical fluid
p 2701 N95-29630
Formation and properties of titanium disilicide: A study on the development of stress in Ti-Si thin films
[PB95-197315] p 2538 N95-30205

THERMAL FATIGUE
Investigation of tension-compression fatigue behavior of a unidirectional metal matrix composite at elevated temperature
[AD-A289394] p 2527 N95-29758
Elevated temperature static fatigue of a Nicalon fiber-reinforced SiC composite
[DE95-008780] p 2528 N95-30175

THERMAL INSULATION
EMI Shields made from intercalated graphite composites
[NASA-TM-106979] p 2518 N95-28906
Development of flame resistant, high efficiency thermal insulation
[AD-A291136] p 2547 N95-30120

THERMAL PLASMAS
Thermal N(+) in the inner magnetosphere
p 2614 N95-29590
Integrated synthesis and post-processing of SiC and AlN
[AD-A290853] p 2537 N95-29724

Data re-formatter program for the topside thermal plasma monitor (PLIESPP)
[AD-A290960] p 2616 N95-29737

THERMAL PROTECTION
Hydrogen film cooling with incident and swept-shock interactions in a Mach 6.4 nitrogen free stream
[NASA-TM-4603] p 2578 N95-30056

THERMAL RADIATION
The detection of oil slicks at night with airborne infrared imagers
[AD-A289731] p 2598 N95-29281

THERMAL REACTORS
Remote maintenance challenges presented in the ITER engineering design
[DE95-006392] p 2710 N95-29909

THERMAL RESISTANCE
Effects of the cooling system parameters on heat transfer and performance of the PAFC stack during transient operation
[NASA-CR-197654] p 2572 N95-29249

THERMAL STABILITY
Thermally stable organic polymers
[AD-A290755] p 2543 N95-29482
Biological methane activation
[PB95-200705] p 2535 N95-30198

THERMAL STRESSES
Formation and properties of titanium disilicide: A study on the development of stress in Ti-Si thin films
[PB95-197315] p 2538 N95-30205

THERMIONIC EMISSION
Composite material studies for low temperature thermionic emission
[AD-A292159] p 2523 N95-29124

THERMIONIC EMITTERS
Composite material studies for low temperature thermionic emission
[AD-A292159] p 2523 N95-29124

THERMISTORS
XPS study of Ni-Fe manganite thermistor material
[DE95-008778] p 2561 N95-28961

THERMOCHEMICAL PROPERTIES
A thermochemical transport model for analysis of hot-spot formation in energetic materials
[AD-A290441] p 2532 N95-29357

THERMODYNAMIC CYCLES
External combustion engine having an asymmetrical CAM
[AD-D017382] p 2588 N95-28785

THERMODYNAMIC EQUILIBRIUM
Computation of the integrated aerodynamic and propulsive flowfields of a generic hypersonic space plane p 2490 N95-29788
Theory and experiments on chemical instabilities
[AD-A290773] p 2534 N95-29922

THERMODYNAMIC PROPERTIES
Application of a rapid quench thermomagnetic analyzer to austempered ductile iron
[AD-A292261] p 2535 N95-28889
Ferroelectric and piezoelectric properties of nylon 11/Poly(Vinylidene fluoride) bilaminate films
[AD-A292274] p 2539 N95-28891
Micro/Miniature heat pipe analysis
[AD-A292232] p 2570 N95-29127
Effects of critical fluctuations on the thermodynamic properties of fluids and fluid mixtures
p 2719 N95-29216
Gordon research conference on physical metallurgy: Materials by design
[AD-A290519] p 2524 N95-29326
Hot explosive consolidation of W-Ti alloys
[AD-A290880] p 2537 N95-29835
Innovative processing of composites for ultra-high temperature applications, book 1
[AD-A290889] p 2527 N95-29842

THERMODYNAMICS
In-phase thermomechanical fatigue mechanisms in an unidirectional SCS-6/Ti 15-3 MMC
[NASA-CR-195482] p 2523 N95-29133
Effects of critical fluctuations on the thermodynamic properties of fluids and fluid mixtures
p 2719 N95-29216
Consideration of microstructural changes in the study of adiabatic shear bands
[AD-A290398] p 2715 N95-29234
A thermochemical transport model for analysis of hot-spot formation in energetic materials
[AD-A290441] p 2532 N95-29357
Numerical simulation of the genesis of tornado-like vortices p 2625 N95-29806

THERMOELASTICITY
Master plot analysis of microcracking in graphite/epoxy and graphite/PEEK laminates p 2514 N95-28828

THERMOELECTRIC COOLING
Effects of the cooling system parameters on heat transfer and performance of the PAFC stack during transient operation
[NASA-CR-197654] p 2572 N95-29249

THERMOELECTRICITY
US photovoltaic patents: 1991-1993
[DE95-004051] p 2603 N95-30017

THERMOMECHANICAL TREATMENT
Superplastic ceramics
[AD-A290817] p 2545 N95-29635

THERMOMETERS
Development and application of fluorescent diagnostics to fundamental droplet and spray problems
[AD-A290553] p 2578 N95-30039

THERMONUCLEAR REACTIONS
Design of an electronic charged particle spectrometer to measure (rho R), yield, and implosion symmetry on the OMEGA Upgrade
[DE95-006088] p 2695 N95-28930

THERMOPHYSICAL PROPERTIES
Orthobaric densities and molar volumes of liquids. Glycol ethers (cellosolves and carbitols, etc.)
[ESDU-95005] p 2530 N95-28703

THERMOPLASTIC RESINS
Establishing the relationship between manufacturing and component performance in stretch formed thermoplastic composites p 2514 N95-28829
Mechanical characterization of two thermoplastic composites fabricated by automated tow placement p 2515 N95-28834
A study of structurally efficient graphite-thermoplastic trapezoidal-corrugation sandwich and semi-sandwich panels p 2516 N95-28842
Real-time x-ray scattering study of processing of eight performance thermoplastics
[AD-A290374] p 2542 N95-29230
Processing studies on in situ composites based on blends of thermotropic Liquid Crystalline Polymers with thermoplastics
[AD-A290526] p 2544 N95-29494
The 2nd European Conference on Smart Structures and Materials
[AD-A290723] p 2550 N95-29579

THERMOPLASTICITY
Real-time x-ray scattering study of processing of eight performance thermoplastics
[AD-A290374] p 2542 N95-29230
Development of LaRC (TM): IA thermoplastic polyimide coated aerospace wiring
[NASA-CR-195048] p 2548 N95-30252

THERMOREGULATION
Human fluid balance and dehydration during cold weather military operations
[AD-A289192] p 2636 N95-29757

THERMOSETTING RESINS
In situ processing methods for composite fuselage sandwich structures p 2513 N95-28826
Third NASA Advanced Composites Technology Conference, volume 1, part 1
[NASA-CP-3178-VOL-1-PT-1] p 2518 N95-29029
High temperature thermosets and ceramics derived from linear carborane-(siloxane or silane)-acetylene copolymers
[AD-D017400] p 2545 N95-29569

THERMOSPHERE
Studies of thermospheric neutral winds utilizing ground-based optical and radar measurements p 2613 N95-29214
High-latitude electrodynamics: Electromagnetic energy dissipation and neutral wind feedback effects p 2616 N95-29696
SETA/ADS software development
[AD-A291181] p 2651 N95-29932

THICKNESS
Thickness measurement of ammonia targets used in SLAC e143 experiment
[AD-A290215] p 2692 N95-29076
A simulation technique for predicting thickness of thermal sprayed coatings
[NASA-TM-106939] p 2512 N95-29373
Impact properties of coated engineering plastics
[PB95-197281] p 2547 N95-30201

THICKNESS RATIO
Introduction to the estimation of the lift coefficients at zero angle of attack and at maximum lift for aerofoils with high-lift devices at low speeds
[ESDU-94026] p 2491 N95-29899

THIN FILMS
Correlations between micromagnetic, microstructural and microchemical properties in ultrathin epitaxial magnetic structures
[AD-A289705] p 2712 N95-28681
Materials science and fabrication of YBCO-SrTi(1-x)Nb(x)O3-YBCO device structures
[AD-A292527] p 2712 N95-28815
Drift mobility measurements in thin film boron carbide
[AD-A292510] p 2712 N95-28869
Nitride semiconductors for ultraviolet detection
[AD-A289546] p 2712 N95-28910
Proceedings of the 6th Joint Magnetism and Magnetic Materials Intermag Conference
[AD-A286752] p 2681 N95-28923
Proceedings of the 38th Annual Conference on Magnetism and Magnetic Materials
[AD-A286753] p 2681 N95-28924
Thin-film resistor array characterization
[AD-A289806] p 2561 N95-28950
Investigation of the characteristics of ferroelectric thin films deposited by pulsed laser ablation
[AD-A292306] p 2540 N95-28963
Process optimization through discovery and integration of materials and processing properties. phase 1
[AD-A292576] p 2662 N95-28978
Multi-decade time-dependent voltage of polycrystalline thin-film solar cells p 2602 N95-29103
Electrical characteristics of barium strontium titanate-oxide composite films
[AD-A289991] p 2541 N95-29135
Electronic properties of low-temperature grown III/V thin films
[AD-A292521] p 2714 N95-29165
Pulsed laser deposition of ferroelectric thin films in conjunction with superconducting oxides
[AD-A290101] p 2585 N95-29208
The measurement of adhesion at film-substrate interfaces using a constant depth scratch test
[AD-A289940] p 2542 N95-29269
Analysis of the ferroelectric thin films deposited by pulsed laser deposition on oxide and fluoride substrates
[AD-A290088] p 2543 N95-29353
Measurement of interface strength, intrinsic toughness and their dependence on interfacial segregants
[AD-A291798] p 2524 N95-29409
Deposition and surface treatment with intense pulsed ion beams
[DE95-007885] p 2543 N95-29465
Pulsed laser deposition of thin film material for nonlinear waveguides
[AD-A290789] p 2544 N95-29484
Hot electron physics of alternating-current thin-film electroluminescent devices
[AD-A290528] p 2696 N95-29495
Compact substrate heater for use in an oxidizing atmosphere
[AD-A290860] p 2502 N95-29522
High T(sub c) superconductor/ferroelectric heterostructures
[AD-A291016] p 2716 N95-29658
A study of blister tests for film adhesion measurement and fracture efficiency of tests for adhesive bonds p 2545 N95-29799
The 41st Japan Society of Applied Physics Spring Meeting
[AD-A292333] p 2720 N95-29879
Epitaxial growth of high quality SiC of pulsed laser deposition, phase 1
[AD-A291410] p 2717 N95-30068
Thin-film edge field emitter device and method of manufacture therefor
[AD-D017323] p 2567 N95-30165
Formation and properties of titanium disilicide: A study on the development of stress in Ti-Si thin films
[PB95-197315] p 2538 N95-30205
Emissivity measurements in thin metallized membrane reflectors used for microwave radiometer sensors
[NASA-TM-110179] p 2506 N95-30251

THIN WALLS
Severe edge effects and simple complimentary interior solutions for thin-walled anisotropic and composite structures
[AD-A290645] p 2595 N95-29562
Analysis of adiabatic shear bands in thermoviscoplastic materials under combined loading
[AD-A290666] p 2596 N95-29582
Development of LaRC (TM): IA thermoplastic polyimide coated aerospace wiring
[NASA-CR-195048] p 2548 N95-30252

THIN WINGS
Computer program for estimation of leading-edge suction distribution for plane thin wings at subsonic speeds
[ESDU-94038] p 2477 N95-28708
Leading-edge suction distribution for plane thin wings at subsonic speeds
[ESDU-94037] p 2486 N95-28800

THOMSON SCATTERING
Observation of x ray generation in a proof-of-principle laser synchrotron source experiment
[AD-A291298] p 2588 N95-29937

THREADS
Ropes: Support for collective opertions among distributed threads
[NASA-CR-198157] p 2649 N95-29404
THREE DIMENSIONAL BODIES
A grid generation system for multi-disciplinary design optimization p 2484 N95-28763
Relative affine structure: Canonical model for 3D from 2D geometry and applications
[AD-A290085] p 2670 N95-29352
THREE DIMENSIONAL COMPOSITES
Mechanical characterization of 2D, 2D stitched, and 3D braided/RTM materials p 2520 N95-29038
Cross-stiffened continuous fiber structures p 2521 N95-29041
An engineering model of woven composites based on micromechanics p 2521 N95-29042
THREE DIMENSIONAL FLOW
Adaptive hybrid prismatic-tetrahedral grids for viscous flows p 2481 N95-28744
Automation of three-dimensional structured mesh generation for turbomachinery blade passages p 2484 N95-28762
Demonstration of an automated CFD system for three-dimensional flow simulations p 2485 N95-28767
The effects of three-dimensional imposed disturbances on bluff body near wake flows: Effects of taper and splitter plates on the near wake characteristics of a circular cylinder in uniform and shear flow
[AD-A292113] p 2487 N95-28921
A study of fluid problems requiring a direct particle simulation
[AD-A290212] p 2658 N95-29074
Interactions of spanwise and chordwise vorticity associated with three-dimensional dynamic stall over an oscillating wing
[AD-A290546] p 2487 N95-29091
A vorticity-velocity approach for three-dimensional unsteady viscous flow over wings p 2488 N95-29108
Leading edge film cooling effects on turbine blade heat transfer
[NASA-TM-106955] p 2500 N95-29115
Finite element vorticity-based methods for the solution of the incompressible and compressible Navier-Stokes equations p 2570 N95-29119
Molecular mixing in shear layers forced by 2-D and 3-D disturbances
[AD-A290272] p 2571 N95-29181
Numerical investigation of surface curvature effects in compressible turbulent flows
[AD-A290114] p 2571 N95-29211
High-and low-frequency dynamics of isolated blades and rotors with dynamic stall and wake
[AD-A290358] p 2497 N95-29322
The decay of longitudinal vortices shed from airfoil vortex generators
[NASA-CR-198356] p 2489 N95-29402
Direct numerical simulation of compressible turbulent flows, using adaptive spectral element method
[AD-A290115] p 2575 N95-29421
New predictive methods in chaotic fluid dynamics with application to turbulent heat transfer
[AD-A290691] p 2576 N95-29761
Cross flow instability of supersonic flow over a 4:1 elliptic cone
[AD-A291128] p 2577 N95-29913
Experimental research on crossing shock wave boundary layer interactions
[AD-A290764] p 2577 N95-29920
A numerical study of the small scale wing-body junction problem p 2491 N95-30235
Numerical simulation of stability and stability control of high speed compressible rotating couette flow
[NASA-CR-198832] p 2579 N95-30250
THREE DIMENSIONAL MODELS
Marshall Space Flight Center surface modeling and grid generation applications p 2480 N95-28733
Automatic blocking for complex three-dimensional configurations p 2480 N95-28734
Development and application of a 3D Cartesian grid Euler method p 2481 N95-28740
Unstructured Cartesian/prismatic grid generation for complex geometries p 2481 N95-28741
Three-dimensional hybrid grid generation using advancing front techniques p 2481 N95-28745
The National Grid Project: A system overview p 2482 N95-28749
A 3DGRAPE/AL: The Ames/Langley technology upgrade p 2482 N95-28750
Geometry modeling and grid generation using 3D NURBS control volume p 2483 N95-28753
Automatic multi-block grid generation for high-lift configuration wings p 2485 N95-28764
Multilevel elliptic smoothing of large three-dimensional grids p 2485 N95-28765
Parametric design and gridding through relational geometry p 2486 N95-28771
Examples of grid generation with implicitly specified surfaces using GridPro (TM)/az3000. 1: Filleted multi-tube configurations p 2486 N95-28772
Molecular dynamics study of electromigration
[AD-A289811] p 2691 N95-28952
High-and low-frequency dynamics of isolated blades and rotors with dynamic stall and wake
[AD-A290358] p 2497 N95-29322
Simulated imaging properties of a series of magnetic electron lenses
[NASA-CR-195474] p 2564 N95-29406
Visualization of CAD objects using a stereoscopic display
[AD-A290034] p 2639 N95-29439
Load balancing for the parallel adaptive solution of partial differential equations
[AD-A290450] p 2671 N95-29488
A three dimensional finite element scheme for fiber microbuckling in thick multidirectional laminated composites p 2525 N95-29512
The effect of climate perturbations on extratropical cyclogenesis along the east coast of North America p 2621 N95-29595
Quantum mechanical problems in one, two, and three dimensions
[ISBN-0-315-84931-2] p 2719 N95-29677
HIDENEK: An implicit particle simulation of kinetic-MHD phenomena in three-dimensional plasmas
[AD-B176255L] p 2707 N95-29739
Toughening mechanisms in mixed-mode interfacial fracture p 2545 N95-29772
On the topological complexity of the cost function in variational data assimilation p 2724 N95-29798
ANSYS duplicate finite-element checker routine
[NASA-TM-108492] p 2672 N95-29824
Three-dimensional simulation of traveling-wave tube cold-test characteristics using MAFIA
[NASA-TP-3513] p 2566 N95-29998
THREE DIMENSIONAL MOTION
HIDENEK: An implicit particle simulation of kinetic-MHD phenomena in three-dimensional plasmas
[AD-B176255L] p 2707 N95-29739
THRESHOLDS (PERCEPTION)
Improving problem-solving and decision-making skills under stress: Prediction and training
[AD-A292104] p 2638 N95-28918
THRUST
Investigation of wing upper surface flow-field disturbance due to NASA DC-8-72 in-flight inboard thrust-reverser deployment
[NASA-TM-110351] p 2477 N95-28816
THRUST CONTROL
A vehicle health monitoring system for the Space Shuttle Reaction Control System during reentry
[NASA-CR-188370] p 2505 N95-29447
Design, analysis and control of large transports so that control of engine thrust can be used as a back-up of the primary flight controls
[NASA-CR-198958] p 2501 N95-30254
THRUST REVERSAL
Investigation of wing upper surface flow-field disturbance due to NASA DC-8-72 in-flight inboard thrust-reverser deployment
[NASA-TM-110351] p 2477 N95-28816
THUNDERSTORMS
An investigation of thunderstorms as a source of short period mesospheric gravity waves
[AD-A289795] p 2611 N95-28697
Numerical simulation of the genesis of tornado-like vortices p 2625 N95-29806
TIDES
Tidal and lunar data for Point Mugu, San Nicolas Island, and the Barking Sands area during 1995
[AD-A289877] p 2733 N95-29599
TIME
An investigation of thunderstorms as a source of short period mesospheric gravity waves
[AD-A289795] p 2611 N95-28697
An HP-Adaptive method in space and time for parabolic systems
[AD-A292262] p 2668 N95-28890
TIME DEPENDENCE
Sorption and diffusion of moisture in multilayer composite AEM/S sandwich materials
[AD-A289807] p 2518 N95-28951
Multi-decade time-dependent voltage of polycrystalline thin-film solar cells p 2602 N95-29103
Analytical theory of continued fractions and time evolution in many-particle systems
[AD-A290365] p 2692 N95-29227
Vortex element analysis of selected time-dependent flows
[AD-A289944] p 2573 N95-29271
Theory of competition between synchronous and nonsynchronous modes in a magnicon output cavity
[AD-A292048] p 2563 N95-29301
The large discretization step method for time-dependent partial differential equations
[NASA-CR-195068] p 2670 N95-29403
An experimental investigation of the time-dependent separation of tangent bodies in supersonic flow
[AD-A290720] p 2489 N95-29500
The dynamics of FU Orionis outbursts: Time-dependent accretion through protostellar disks p 2732 N95-29530
A new visualization technique to study the time evolution of finite and adaptive mixture estimators
[AD-A291147] p 2673 N95-30126
Second-order numerical solution of time-dependent, first-order hyperbolic equations p 2674 N95-30143
TIME DIVISION MULTIPLE ACCESS
Alternative packet switch architectures for a 30/20 GHz FDMA/TDMA geostationary communication satellite network
[NASA-CR-195470] p 2506 N95-30090
TIME DIVISION MULTIPLEXING
Comparison study of unequal error protection methods for one-dimensional signal constellations
[AD-A290386] p 2554 N95-29231
TIME MARCHING
The large discretization step method for time-dependent partial differential equations
[NASA-CR-195068] p 2670 N95-29403
Reliability enhancement of Navier-Stokes codes through convergence acceleration
[NASA-CR-196635] p 2578 N95-30034
TIME MEASUREMENT
SAO HMC photodetector/event timer engineering model test report
[DE95-007889] p 2582 N95-28917
Applications of pulsar timing p 2734 N95-29675
TIME OPTIMAL CONTROL
Time-optimal multi-axis attitude maneuvers of rigid spacecraft using collocation and nonlinear programming p 2507 N95-29332
TIME SERIES ANALYSIS
Compendium of NASA data base for the global tropospheric experiment's Transport and Atmospheric Chemistry Near the Equator-Atlantic (TRACE-A)
[NASA-TM-110151] p 2608 N95-28717
Stochastic modeling and global warming trend extraction for ocean acoustic travel times
[AD-A292114] p 2608 N95-28922
WinCD: Complex demodulation time-series analysis for windows
[AD-A291550] p 2645 N95-28934
Optimal hankel norm identification of dynamical systems
[PB95-197232] p 2672 N95-30046
TIME SIGNALS
Observation of x ray generation in a proof-of-principle laser synchrotron source experiment
[AD-A291298] p 2588 N95-29937
TIMING DEVICES
SAO HMC photodetector/event timer engineering model test report
[DE95-007889] p 2582 N95-28917
TIN
Macrosegregation and nucleation in undercooled Pb-Sn alloys
[NASA-TM-102023-REV] p 2535 N95-28701
TIP SPEED
Dynamic decohesion of bimaterial interfaces p 2541 N95-29120
TISSUES (BIOLOGY)
Cellular and molecular level responses after radiofrequency radiation exposure, alone or in combination with x rays or chemicals
[AD-A292488] p 2633 N95-28866
TITANIUM
In-phase thermomechanical fatigue mechanisms in an unidirectional SCS-6/Ti 15-3 MMC
[NASA-CR-195482] p 2523 N95-29133
Nippon Steel Research Laboratories, Futtsu, 28 February 1994. and Advanced Materials and Technology Research Laboratories, Kawasaki, 15 June 1994
[AD-A292346] p 2526 N95-29533
A kilohertz femtosecond Ti: Sapphire regeneratie amplifier
[AD-A290591] p 2588 N95-30045
Formation and properties of titanium disilicide: A study on the development of stress in Ti-Si thin films
[PB95-197315] p 2538 N95-30205
TITANIUM ALLOYS
Daido Steel's Shibukawa Plant, Shibukawa City, Gumma Prefecture, Japan, 29 Jul. 1994
[AD-A292343] p 2536 N95-29467

Visit to the Department of Metallurgical Engineering, Tokyo Institute of Technology, 22 Sep. 1994
[AD-A292310] p 2536 N95-29473
Nippon Steel Research Laboratories, Futtsu, 28 February 1994. and Advanced Materials and Technology Research Laboratories, Kawasaki, 15 June 1994
[AD-A292346] p 2526 N95-29533
The Institute for Material Science and Department of Material Science, Tohoku University, Sendai Japan, 2-3 June 1994
[AD-A292348] p 2650 N95-29534
Hot explosive consolidation of W-Ti alloys
[AD-A290880] p 2537 N95-29835
Electrochemical impedance pattern recognition for detection of hidden chemical corrosion on aircraft components, phase 1
[AD-A291345] p 2593 N95-29946

TITANIUM BORIDES
Experimental investigations of wave and fracture phenomena in impacted ceramics and glasses
[AD-A292142] p 2542 N95-29195

TITANIUM OXIDES
Overview of the space debris environment
[AD-A292302] p 2507 N95-28867
Pulsed laser deposition of ferroelectric thin films in conjunction with superconducting oxides
[AD-A290101] p 2585 N95-29208

TOKAMAK DEVICES
Discriminant analysis to predict the occurrence of ELMS in H-mode discharges
[AD-B179183L] p 2708 N95-29746
Theory of pseudo-classical confinement and transmutation to L-mode
[AD-B175957L] p 2709 N95-29809
Carbon sheet pumping
[AD-B179443L] p 2710 N95-29812
Remote maintenance challenges presented in the ITER engineering design
[DE95-006392] p 2710 N95-29909
Magnetic fusion commercial power plants
[DE95-007027] p 2711 N95-30023
Techniques and results of tokamak-edge simulation
[DE95-008075] p 2711 N95-30130

TOLERANCES (MECHANICS)
Design, analysis, and fabrication of a pressure box test fixture for tension damage tolerance testing of curved fuselage panels p 2516 N95-28839
Impact resistance and damage tolerance of composite sandwich panels p 2526 N95-29549

TOMOGRAPHY
Interactive multimedia presentation for applied computer tomography: Impact
[AD-A291955] p 2640 N95-29020
Mapping crust and upper mantle structure beneath southern Eurasia
[AD-A291074] p 2618 N95-29970

TOOLS
Use of quality tools to re-engineer the Aeromedical Evacuation (AE) system p 2676 N95-29605

TOPEX
Data catalog for JPL Physical Oceanography Distributed Active Archive Center (PO.DAAC)
[NASA-CR-198872] p 2631 N95-30231

TOPOGRAPHY
Multi-scale studies of seafloor topography
[AD-A292301] p 2628 N95-28865
XMap: A general purpose mapping program
[AD-A289958] p 2647 N95-29276
Digital mapping, charting, and geodesy analysis program technical review of vector smart map prototypes 1 and 2
[AD-A291217] p 2601 N95-29977
Engineering design of sub-micron topographies for simultaneously adherent and reflective metal-polymer interfaces
[NASA-CR-198845] p 2548 N95-30237

TOPOLOGY
Intermittent energy bursts and recurrent topological change of a twisting magnetic flux tube
[AD-B195513L] p 2708 N95-29755
On the topological complexity of the cost function in variational data assimilation p 2724 N95-29798
Robust testing of cellular neural networks
[AD-A291219] p 2665 N95-29979

TORNADOES
Numerical simulation of the genesis of tornado-like vortices p 2625 N95-29806

TOROIDAL PLASMAS
Anomalous transport theory for toroidal helical plasmas
[AD-B192000L] p 2706 N95-29731
Self-sustained magnetic braiding in toroidal plasmas
[AD-B191998L] p 2706 N95-29734
Comment on a mean field Ohm's law for collisionless plasmas
[AD-B176252L] p 2707 N95-29741
Prandtl number of toroidal plasmas
[AD-B179181L] p 2707 N95-29744
Theory of pseudo-classical confinement and transmutation to L-mode
[AD-B175957L] p 2709 N95-29809
Carbon sheet pumping
[AD-B179443L] p 2710 N95-29812

TORQUE
Shear force, bending moment and torque of rigid aircraft in symmetric steady maneuvering flight
[ESDU-94045] p 2495 N95-28896
Cable load transducer
[AD-A289548] p 2595 N95-29192
Permanent magnet torque/force transfer apparatus
[AD-D017325] p 2682 N95-30051
175Hp contrarotating homopolar motor design report
[AD-A291138] p 2567 N95-30122

TORQUERS
A conceptual design for the attitude control and determination system for the Magnetosphere Imager spacecraft
[NASA-TP-3560] p 2507 N95-28721

TORSION
Analytical investigation of the hygrothermal effects and parametric study of the Edge Crack Torsion (ECT) mode 3 test lay-ups
[NASA-TM-110183] p 2528 N95-30028

TOUGHNESS
The effect of mixed mode precracking on the mode 1 fracture toughness of composite laminates p 2514 N95-28827
High-toughness glass-ceramics
[AD-A290562] p 2541 N95-29071
Correlation of inclusion size and chemistry with weld metal composition and microstructure arc weldments of high strength steels
[AD-A292024] p 2590 N95-29184
Measurement of interface strength, intrinsic toughness and their dependence on interfacial segregants
[AD-A291798] p 2524 N95-29409
Simplified data reduction methods for the ECT test for mode 3 interlaminar fracture toughness
[NASA-TM-110176] p 2527 N95-29825
Measurement of interface strength, intrinsic toughness and their dependence on interfacial segregants
[AD-A291169] p 2546 N95-29926
Analytical investigation of the hygrothermal effects and parametric study of the Edge Crack Torsion (ECT) mode 3 test lay-ups
[NASA-TM-110183] p 2528 N95-30028

TOWING
Cable load transducer
[AD-A289548] p 2595 N95-29192

TOXICITY
Modeling joint effects of mixtures of chemicals on microorganisms using quantitative structure activity relationship techniques, phase 3
[AD-A290153] p 2632 N95-29320

TOXICOLOGY
Inhalation Toxicology Research Institute
[AD-A292037] p 2635 N95-29188

TRACE CONTAMINANTS
A model analysis of the spatial distribution and temporal trends of nitrous oxide sources and sinks p 2609 N95-29804

TRACE ELEMENTS
Effects of microscopic diffusion and rotational mixing on stellar models p 2733 N95-29669

TRACKING (POSITION)
System and method for rapidly tracking vehicles of special utility in low signal-to-noise environments
[AD-D017378] p 2683 N95-28783
MATSurv multisensor air traffic surveillance
[AD-A292253] p 2494 N95-28887
Target aircraft identification, trajectory tracking and prediction using regression-based Kalman filter techniques p 2565 N95-29728
Learning control in linear and nonlinear systems p 2667 N95-30238

TRACKING FILTERS
Target aircraft identification, trajectory tracking and prediction using regression-based Kalman filter techniques p 2565 N95-29728

TRAFFIC
Performance evaluation of ATM cell scheduling policies using stochastic petri nets
[PB95-197158] p 2559 N95-30096

TRAILING EDGE FLAPS
Increments in aerofoil lift coefficient at zero angle of attack and in maximum lift coefficient due to deployment of a plain trailing-edge flap, with or without a leading-edge high-lift device, at low speeds
[ESDU-94028] p 2486 N95-28885
Increments in aerofoil lift coefficient at zero angle of attack and in maximum lift coefficient due to deployment of a trailing-edge split flap, with or without a leading-edge high-lift device, at low speeds
[ESDU-94029] p 2488 N95-29129
Low-speed wind-tunnel investigation of the stability and control characteristics of a series of flying wings with sweep angles of 50 deg
[NASA-TM-4640] p 2498 N95-30226

TRAILING EDGES
Navier-Stokes solution of wing wake structure and its perturbation p 2488 N95-29121
Experimental investigation of aerodynamic devices for wind turbine rotational speed control, phase 1
[DE95-004034] p 2603 N95-30016

TRAINING DEVICES
Applications of digital video and synthetic environments to unmanned aerial vehicles
[AD-A291875] p 2497 N95-29437

TRAINING SIMULATORS
Visualization of improved target acquisition algorithm for Janus (A)
[AD-A290191] p 2646 N95-29056

TRAJECTORIES
Development of a transient internal probe diagnostic
[AD-A292470] p 2704 N95-29011
Continental aerosol effects on stratocumulus microphysics during MAST 1994
[AD-A292674] p 2621 N95-29416

TRAJECTORY ANALYSIS
Effects of small changes on rate of climb
[ESDU-94039] p 2495 N95-28707
Trajectory mapping (TM): A new non-metric scaling technique
[AD-A290036] p 2670 N95-29440
Guidance law development for aeroassisted transfer vehicles using Matched Asymptotic Expansions p 2503 N95-30347

TRAJECTORY MEASUREMENT
Target aircraft identification, trajectory tracking and prediction using regression-based Kalman filter techniques p 2565 N95-29728

TRAJECTORY OPTIMIZATION
Analytical investigations in aircraft and spacecraft trajectory optimization and optimal guidance
[NASA-CR-4672] p 2504 N95-29339

TRAJECTORY PLANNING
Motion planning and sensory processing in a dynamic environment
[AD-A290504] p 2722 N95-29154

TRANSDUCERS
Cable load transducer
[AD-A289548] p 2595 N95-29192
Unitary transducer with variable resistivity
[AD-D017329] p 2566 N95-30055

TRANSFER FUNCTIONS
Multilayer piecewise linear networks. Revision 1
[AD-A289685] p 2658 N95-28955
Adaptive Infinite Impulse Response (IIR) filter system
[AD-D017403] p 2564 N95-29570

TRANSFORMATIONS (MATHEMATICS)
Trajectory mapping (TM): A new non-metric scaling technique
[AD-A290036] p 2670 N95-29440
W-matrices, nonorthogonal multiresolution analysis, and finite signals of arbitrary length
[DE95-005846] p 2652 N95-30020

TRANSIENT RESPONSE
Transient responses of phosphoric acid fuel cell power plant system
[NASA-CR-198948] p 2603 N95-30015

TRANSISTORS
Joint services electronics program
[AD-A292469] p 2561 N95-29010
Interband lateral resonant tunneling transistor
[AD-D017399] p 2564 N95-29568

TRANSITION FLOW
Modelling of transport phenomena
[AD-B179223L] p 2708 N95-29747
Dynamical model of pressure-gradient-driven turbulence and shear flow generation in L-H transition
[AD-B195511L] p 2709 N95-29789

TRANSITION METALS
Transition metal complexes with perfluorinated ligands
[AD-A290250] p 2536 N95-29427
SAM1-A new semiempirical method including d-orbitals
[AD-A290903] p 2694 N95-30060

TRANSITION POINTS
Experimental studies on boundary-layer transition on a reentry vehicle at transonic and supersonic speeds
[ISAS-659] p 2575 N95-29712

TRANSLATING
Acquisition of place knowledge through case-based learning
[AD-A292574] p 2723 N95-29573

Translation Invariant Operators on Lp-Type Spaces
[PB95-197117] p 2672 N95-30092
Enhancing the semantics of federated schemata by translating SQ1-queries into object methods
[PB95-197372] p 2725 N95-30208

TRANSLATORS
NASA-IGES Translator and Viewer
p 2486 N95-28775

TRANSLUNAR INJECTION
Guidance, navigation, and control study for a solar electric propulsion spacecraft
[NASA-CR-198920] p 2509 N95-30357

TRANSMISSION LINES
An electrical and fiber-optic connector
[AD-D017404] p 2589 N95-28791
Finite difference analysis of a cylindrical two conductor microstrip transmission line with truncated dielectrics
[AD-A292592] p 2555 N95-29290

TRANSMISSION LOSS
Hindcasting changes in thermal structure and acoustic transmission loss in the upper ocean on short time scales with data from MILE and from ocean weather station papa
[AD-A292419] p 2629 N95-28991
Emissivity measurements in thin metallized membrane reflectors used for microwave radiometer sensors
[NASA-TM-110179] p 2506 N95-30251

TRANSMISSION RATE (COMMUNICATIONS)
HIPPI - Gigabit LANS are here today
[DE95-007877] p 2660 N95-30128

TRANSMISSIONS (MACHINE ELEMENTS)
Carrier-less, anti-backlash planetary drive system
[NASA-CASE-GSC-13608-1] p 2588 N95-28702
Influence of tooth profile modification on spur gear dynamic tooth strain
[NASA-TM-106952] p 2589 N95-29112
Bell Helicopter Advanced Rotocraft Transmission (ART) program
[NASA-CR-195479] p 2590 N95-29538

TRANSMITTANCE
Broadband Integrated Transmittances (BITS)
[AD-A292176] p 2555 N95-29266
HTMIAC/CINDAS silicon properties database. User's guide
[AD-A292602] p 2533 N95-29575

TRANSMITTER RECEIVERS
Improved interception capability through the use of transform domain processing
[AD-A292231] p 2554 N95-29203

TRANSMITTERS
The design of programmable convolutional encoder using VHDL and an FPGA
[AD-A290048] p 2649 N95-29442

TRANSONIC FLOW
A method for the modelling of porous and solid wind tunnel walls in computational fluid dynamics codes
p 2502 N95-29795
Use of the PARC code to estimate the off-design transonic performance of an over/under turboramjet nozzle
[NASA-TM-106924] p 2491 N95-30091

TRANSONIC SPEED
Excrescence drag levels on aircraft
[ESDU-94044] p 2487 N95-28897
Transonic, supersonic and hypersonic wind-tunnel tests on aerodynamic characteristics of reentry body with blunted cone configuration
[ISAS-658] p 2490 N95-29640
Experimental studies on boundary-layer transition on a reentry vehicle at transonic and supersonic speeds
[ISAS-659] p 2575 N95-29712

TRANSPORT AIRCRAFT
Automated fiber placement: Evolution and current demonstrations p 2514 N95-28832
Effects of cabin pressure on climb and descent rates
[ESDU-94040] p 2496 N95-29016
Advanced composite structural concepts and materials technologies for primary aircraft structures: Advanced material concepts
[NASA-CR-4485] p 2496 N95-29027
Impact of composites on future transport aircraft
p 2519 N95-29030
Advanced composites technology program
p 2519 N95-29032
Textile composite fuselage structures development
p 2519 N95-29033
Cost model relationships between textile manufacturing processes and design details for transport fuselage elements p 2521 N95-29043

TRANSPORT PROPERTIES
Optoelectronics based on SiGe/Si heterostructures
[AD-A292464] p 2699 N95-29006
Transport simulation in spatially modulated low dimensionality systems
[AD-A290486] p 2718 N95-29149
Transport phenomena and noise in real quantum wires
[AD-A290493] p 2714 N95-29152
Tailored microstructures for broadband or selective detection of radiation from the visible to the infrared
[AD-A292097] p 2554 N95-29240
Modelling of transport phenomena
[AD-B179223L] p 2708 N95-29747
New predictive methods in chaotic fluid dynamics with application to turbulent heat transfer
[AD-A290691] p 2576 N95-29761
Theory of pseudo-classical confinement and transmutation to L-mode
[AD-B175957L] p 2709 N95-29809
Molecular probes of gating and open channel conformational transitions of mechanosensitive ion channels
[AD-A291170] p 2637 N95-29927

TRANSPORT THEORY
Anomalous transport theory for toroidal helical plasmas
[AD-B192000L] p 2706 N95-29731
HIDENEK: An implicit particle simulation of kinetic-MHD phenomena in three-dimensional plasmas
[AD-B176255L] p 2707 N95-29739
Comment on a mean field Ohm's law for collisionless plasmas
[AD-B176252L] p 2707 N95-29741
Theory of pseudo-classical confinement and transmutation to L-mode
[AD-B175957L] p 2709 N95-29809
Parameterized spectral distributions for meson production in proton-proton collisions
[NASA-TM-4675] p 2696 N95-30337

TRANSPORTATION
Mode of human image representation and error checking strategies in complex visual displays
[AD-A290107] p 2492 N95-29210
InTlSb as a long-wave infrared (LWIR) material: Defects and transportation properties
[AD-A291218] p 2702 N95-29978

TRANSVERSE LOADS
Simplified data reduction methods for the ECT test for mode 3 interlaminar fracture toughness
[NASA-TM-110176] p 2527 N95-29825

TRANSVERSE WAVES
Collective phenomena in granular fluids
p 2572 N95-29219

TRAPPED PARTICLES
Trapped electron instabilities due to electron temperature gradient and anomalous transport
[AD-B179859L] p 2693 N95-29748
Monte Carlo simulation study of the ICRF minority heating in the large helical device
[AD-B179858L] p 2708 N95-29749
Experiments on nonlinear wave-particle interactions
p 2695 N95-30302

TRAPS
Multi-decade time-dependent voltage of polycrystalline thin-film solar cells p 2602 N95-29103

TRAVELING WAVE AMPLIFIERS
Hybrid harmonic gyrotron traveling wave amplifier
[AD-A292686] p 2564 N95-29417

TRAVELING WAVE TUBES
Studies directed toward new and improved permanent magnet materials
[AD-A290749] p 2681 N95-29481
Three-dimensional simulation of traveling-wave tube cold-test characteristics using MAFIA
[NASA-TP-3513] p 2566 N95-29998

TRAVELING WAVES
Acoustic scattering from ellipses by the modal element method
[NASA-TM-106935] p 2683 N95-29401

TRAYS
Shock resistant optic fiber rotary slice holding device
[AD-D017327] p 2702 N95-30053

TRENDS
An announcement by Dan Goldin
[NASA-TM-110739] p 2720 N95-29171

TRIANGULATION
Algorithms for high aspect ratio oriented triangulations
p 2479 N95-28731
A simple method for range finding via laser triangulation
[AD-A292529] p 2553 N95-29166

TRIBOLOGY
Publications/Patents/Presentations/Honors report: Force and tunneling microscopy studies of atomic level mechanical properties of solids
[AD-A292254] p 2691 N95-28888
Nanoindentation and nanoscratching of hard coating materials for magnetic disks
[DE95-008776] p 2547 N95-30174

TRIGATRONS
High power switch design
[AD-A291608] p 2565 N95-29601

TRIMERS
The synthesis of liquid crystalline phophazenes containing chiral mesogens
[AD-A291911] p 2543 N95-29358

TRIMETHYL COMPOUNDS
Synthesis of nanocrystalline indium arsenide and indium phosphide from Indium(III) halides and tris(trimethylsilyl)pnicogens; synthesis, characterization, and decomposition behavior of I3In(dot)P(SiMe3)3
[AD-A291905] p 2715 N95-29486

TRITIUM
Bubble fusion: Preliminary estimates of spherical micro-implosions in cavitating liquids
[DE95-006260] p 2569 N95-28956

TRIVALENT IONS
ARPA solid state laser and nonlinear materials program
[AD-A289657] p 2564 N95-28678

TROPICAL METEOROLOGY
Forecast of Atlantic seasonal hurricane activity for 1995 p 2620 N95-29254
Lee vorticity production by tropical mountain ranges
p 2622 N95-29701
The tropical atmosphere under convection adjustment
p 2625 N95-29833
The role of diabatic heating, torques and stability in forcing the meridional circulation within cyclones
p 2626 N95-29834

TROPICAL REGIONS
A study of dynamics in the tropical Pacific using satellite data p 2630 N95-29520
The structure of water mass, salt, and temperature transports within intermediate depths of the western tropical Atlantic Ocean p 2631 N95-29541
Radiative cooling profiles calculated from ECMWF analyses and ISCCP C1 data, and their application to determination of distributions of apparent convective heating in the equatorial Pacific p 2625 N95-29805
The tropical atmosphere under convection adjustment
p 2625 N95-29833
The effects of clouds as a feedback mechanism on the Earth's climate in the tropical Pacific
p 2611 N95-30300

TROPICAL STORMS
Typhoon monitoring using passive microwave observations
[AD-A292567] p 2619 N95-28975
Analysis of the structural characteristics and intensity evolution of super typhoon flo (1990) in special sensor Microwave/Imager (SSM/I) data
[AD-A292413] p 2619 N95-29989
Forecast of Atlantic seasonal hurricane activity for 1995 p 2620 N95-29254
A regression model for the western north pacific tropical cyclone intensity forecast
[AD-A290588] p 2627 N95-30044
Tropical storm database: East and Gulf of Mexico coasts of the United States
[AD-A291406] p 2627 N95-30066

TROPOSPHERE
Compendium of NASA data base for the global tropospheric experiment's Transport and Atmospheric Chemistry Near the Equator-Atlantic (TRACE-A)
[NASA-TM-110151] p 2608 N95-28717
Excrescence drag levels on aircraft
[ESDU-94044] p 2487 N95-28897
Analysis of tropospheric propagation characteristics based on regional meteorological data
[AD-A291581] p 2552 N95-28939
Radiative cooling profiles calculated from ECMWF analyses and ISCCP C1 data, and their application to determination of distributions of apparent convective heating in the equatorial Pacific p 2625 N95-29805
Research results on an improved in-situ tropospheric humidity sensor
[AD-A291339] p 2627 N95-29944
Use of ARM data to test an improved parameterization of upper tropospheric clouds for use in climate models
[DE95-009324] p 2610 N95-30181
Extended field observations of cirrus clouds using a ground-based cloud observing system
[NASA-CR-198855] p 2628 N95-30356

TRUNCATION ERRORS
The application of adaptive mesh refinement to the numerical simulation of compressible flow
[AD-A289595] p 2577 N95-30027

TRYPTOPHAN
Reaction field (RF) calculation of the spectral shifts of indole
[AD-A290449] p 2532 N95-29487

TUNABLE LASERS
Laser optics protective device
[AD-D017384] p 2585 N95-29217
Tunable laser for persistent spectral hole burning optical memories
[AD-A292598] p 2586 N95-29292

Molecular spectra and dynamics at interfaces
[AD-A289779] p 2693 N95-29460
Characterisation of a line-tunable He-Xe laser operating at 2.026 and 3.894 micrometers
[AD-A291129] p 2587 N95-29914

TUNGSTEN
Ballistic penetration phenomenology of high symmetry single crystals
[AD-A292476] p 2713 N95-29013
Effects of impurities released from high Z test limiter on plasma performance in TEXTOR
[AD-B191995L] p 2709 N95-29803
Design of a more accurate, higher fidelity, dual-source air mass zero solar simulator
[AD-A291364] p 2603 N95-29953

TUNGSTEN ALLOYS
Characterizing and modeling penetration of ceramic armor
[AD-A292588] p 2542 N95-29288
Hot explosive consolidation of W-Ti alloys
[AD-A290880] p 2537 N95-29835
Processing and properties of extruded tungsten-hafnium and tungsten-steel composites
[DE95-007371] p 2528 N95-30037

TUNNEL JUNCTIONS
Nobeyama Radio Observatory report, no. 381: Parallel connected twin SIS junctions for millimeter and submillimeter wave mixers: Analysis and experimental verification p 2562 N95-29099

TURBINE BLADES
Leading edge film cooling effects on turbine blade heat transfer
[NASA-TM-106955] p 2500 N95-29115
Grid orthogonality effects on predicted turbine midspan heat transfer and performance
[NASA-TM-106931] p 2574 N95-29371
The effects of the thermal boundary condition and turbulence on heat transfer from a cylinder, flat plate, and turbine blade using the transient shroud and heated-coating techniques
[AD-A292646] p 2574 N95-29380

TURBINE ENGINES
Intelligent turbine engines for Army applications
[AD-A290532] p 2500 N95-29496

TURBINE PUMPS
ANSYS duplicate finite-element checker routine
[NASA-TM-108492] p 2672 N95-29824

TURBINE WHEELS
UHB engine fan broadband noise reduction study
[NASA-CR-198357] p 2684 N95-29641

TURBINES
Flow visualization of vorticity cancellation of jets in crossflow
[AD-A292414] p 2569 N95-28990

TURBOCOMPRESSORS
Modeling and control of rotating stall in high speed multi-stage axial compressors p 2500 N95-29244
Inlet flow test calibration for a small axial compressor rig. Part 2: CFD compared with experimental results
[NASA-TM-106999] p 2501 N95-30007

TURBOFAN ENGINES
UHB engine fan broadband noise reduction study
[NASA-CR-198357] p 2684 N95-29641

TURBOFANS
Recirculating cavity casing treatment failure
[AD-A289330] p 2500 N95-28908

TURBOMACHINE BLADES
Automation of three-dimensional structured mesh generation for turbomachinery blade passages p 2484 N95-28762

TURBOMACHINERY
The acoustic characteristics of turbomachinery cavities
[NASA-CR-4671] p 2478 N95-28720
Model development for active control of stall phenomena in aircraft gas turbine engines p 2500 N95-29679

TURBORAMJET ENGINES
Use of the PARC code to estimate the off-design transonic performance of an over/under turboramjet nozzle
[NASA-TM-106924] p 2491 N95-30091

TURBULENCE
Feature-oriented image reconstruction and aero-optic metrology in turbulence
[AD-A290269] p 2699 N95-29177
The effects of the thermal boundary condition and turbulence on heat transfer from a cylinder, flat plate, and turbine blade using the transient shroud and heated-coating techniques
[AD-A292646] p 2574 N95-29380
Effect of Reynolds number on the structure of turbulent boundary layers p 2575 N95-29719
Effects of elevated free-stream turbulence and streamwise acceleration on flow and thermal structures in transitional boundary layers p 2576 N95-29729
The effect of turbulence on vaporization and mixing in fuel sprays
[AD-A291347] p 2577 N95-29948
Numerical simulation and analysis of the hypersonic turbulent flow past a blunt-fin/ramp configuration
[DLR-FB-94-19] p 2492 N95-30349

TURBULENCE EFFECTS
Influence of turbulence parameters, Reynolds number, and body shape on stagnation-region heat transfer
[NASA-TP-3487] p 2568 N95-28719
The effects of the thermal boundary condition and turbulence on heat transfer from a cylinder, flat plate, and turbine blade using the transient shroud and heated-coating techniques
[AD-A292646] p 2574 N95-29380
Turbulent airflow noise production and propagation patterns of a subsonic jet impinging on a flat plate p 2684 N95-29502
Effects of elevated free-stream turbulence and streamwise acceleration on flow and thermal structures in transitional boundary layers p 2576 N95-29729
New predictive methods in chaotic fluid dynamics with application to turbulent heat transfer
[AD-A290691] p 2576 N95-29761
Numerical simulation and analysis of the hypersonic turbulent flow past a blunt-fin/ramp configuration
[DLR-FB-94-19] p 2492 N95-30349

TURBULENCE MODELS
A novel approach to the numerical simulation of turbulent flows
[AD-A290352] p 2569 N95-29068
Interaction of turbulence with complex shock waves
[AD-A290225] p 2571 N95-29145
Grid orthogonality effects on predicted turbine midspan heat transfer and performance
[NASA-TM-106931] p 2574 N95-29371
The decay of longitudinal vortices shed from airfoil vortex generators
[NASA-CR-198356] p 2489 N95-29402
A turbulent model of the solar granulation
[AD-A292318] p 2738 N95-29475
Computation of the integrated aerodynamic and propulsive flowfields of a generic hypersonic space plane p 2490 N95-29788
An aerodynamic and static-stability analysis of the Hypersonic Applied Research Technology (HART) missile
[DA9426923] p 2491 N95-29965
Numerical simulation and analysis of the hypersonic turbulent flow past a blunt-fin/ramp configuration
[DLR-FB-94-19] p 2492 N95-30349

TURBULENT BOUNDARY LAYER
Physical causes of separation shock unsteadiness in shock wave/turbulent boundary layer interactions p 2570 N95-29096
Unsteadiness of shock-induced turbulent boundary layer separation. An inherent feature of turbulent flow or solely a wind tunnel phenomenon
[AD-A290367] p 2572 N95-29228
The decay of longitudinal vortices shed from airfoil vortex generators
[NASA-CR-198356] p 2489 N95-29402
Direct numerical simulation of compressible turbulent flows, using adaptive spectral element method
[AD-A290115] p 2575 N95-29421
Experimental studies on boundary-layer transition on a reentry vehicle at transonic and supersonic speeds
[ISAS-659] p 2575 N95-29712
Effect of Reynolds number on the structure of turbulent boundary layers p 2575 N95-29719
Experimental research on crossing shock wave boundary layer interactions
[AD-A290764] p 2577 N95-29920
Numerical simulations of the flow in the HYPULSE expansion tube
[NASA-TM-110357] p 2503 N95-30228

TURBULENT FLOW
Influence of turbulence parameters, Reynolds number, and body shape on stagnation-region heat transfer
[NASA-TP-3487] p 2568 N95-28719
Computational fluid dynamics (CFD) simulation of test chamber and smoke-generating device
[AD-A290199] p 2569 N95-29058
A novel approach to the numerical simulation of turbulent flows
[AD-A290352] p 2569 N95-29068
Studies in drag reduction p 2487 N95-29094
Interaction of turbulence with complex shock waves
[AD-A290225] p 2571 N95-29145
Numerical investigation of surface curvature effects in compressible turbulent flows
[AD-A290114] p 2571 N95-29211
Unsteadiness of shock-induced turbulent boundary layer separation. An inherent feature of turbulent flow or solely a wind tunnel phenomenon
[AD-A290367] p 2572 N95-29228
Rigorous drag bounds in turbulent shear flow p 2573 N95-29334
Direct numerical simulation of compressible turbulent flows, using adaptive spectral element method
[AD-A290115] p 2575 N95-29421
Turbulent airflow noise production and propagation patterns of a subsonic jet impinging on a flat plate p 2684 N95-29502
Experimental studies on boundary-layer transition on a reentry vehicle at transonic and supersonic speeds
[ISAS-659] p 2575 N95-29712
New predictive methods in chaotic fluid dynamics with application to turbulent heat transfer
[AD-A290691] p 2576 N95-29761
Computation of the integrated aerodynamic and propulsive flowfields of a generic hypersonic space plane p 2490 N95-29788
Dynamical model of pressure-gradient-driven turbulence and shear flow generation in L-H transition
[AD-B195511L] p 2709 N95-29789
Experimental and analytical study of heat transfer and turbulent flow field in tangentially injected swirl flow p 2576 N95-29811
The effect of turbulence on vaporization and mixing in fuel sprays
[AD-A291347] p 2577 N95-29948
Reliability enhancement of Navier-Stokes codes through convergence acceleration
[NASA-CR-196635] p 2578 N95-30034
Survey of CFD applications for high speed inlets
[AD-A291385] p 2578 N95-30087
Numerical simulations of the flow in the HYPULSE expansion tube
[NASA-TM-110357] p 2503 N95-30228
Numerical simulation of stability and stability control of high speed compressible rotating couette flow
[NASA-CR-198832] p 2579 N95-30250
Supercritical states of two-dimensional wall-bounded shear flow p 2580 N95-30303
Numerical simulation and analysis of the hypersonic turbulent flow past a blunt-fin/ramp configuration
[DLR-FB-94-19] p 2492 N95-30349

TURBULENT HEAT TRANSFER
New predictive methods in chaotic fluid dynamics with application to turbulent heat transfer
[AD-A290691] p 2576 N95-29761

TURBULENT MIXING
Molecular mixing in shear layers forced by 2-D and 3-D disturbances
[AD-A290272] p 2571 N95-29181
The spectrum and directivity of turbulent mixing noise from supersonic jets p 2684 N95-29415

TURBULENT WAKES
Experimental and theoretical studies of wakes in stratified flows
[AD-A290203] p 2569 N95-29060
Numerical experiments on the flow past a circular cylinder at sub-critical Reynolds number
[AD-A289937] p 2573 N95-29268

TVD SCHEMES
Pressure based high order TVD methodology for dynamic stall control
[AD-A290149] p 2489 N95-29316

TWISTING
Effects of cutouts on the behavior of symmetric composite laminates subjected to bending and twisting loads p 2517 N95-28844
Intermittent energy bursts and recurrent topological change of a twisting magnetic flux tube
[AD-B195513L] p 2708 N95-29755

TWO DIMENSIONAL BOUNDARY LAYER
Linear stability analysis of hypersonic boundary layers
[AD-A290159] p 2569 N95-29024

TWO DIMENSIONAL FLOW
A combined geometric approach for computational fluid dynamics on dynamic grids p 2485 N95-28770
An extension of the continuum model by Grad's thirteen moment equations for hypersonic rarefied flows p 2488 N95-29118
Finite element vorticity-based methods for the solution of the incompressible and compressible Navier-Stokes equations p 2570 N95-29119
Molecular mixing in shear layers forced by 2-D and 3-D disturbances
[AD-A290272] p 2571 N95-29181
Modeling and control of rotating stall in high speed multi-stage axial compressors p 2500 N95-29244
Application of the space-time conservation element and solution element method to two-dimensional advection-diffusion problems
[NASA-TM-106946] p 2574 N95-29372
Research on bluff-body vortex wakes
[AD-A292650] p 2574 N95-29382
Acoustic scattering from ellipses by the modal element method
[NASA-TM-106935] p 2683 N95-29401

Investigation of Burnett equations for two-dimensional hypersonic flow
[AD-A290233] p 2575 N95-29469
The effects of three dimensional imposed disturbances on bluff body near wake flows
[AD-A290824] p 2575 N95-29654
Supercritical states of two-dimensional wall-bounded shear flow p 2580 N95-30303

TWO DIMENSIONAL MODELS
Marshall Space Flight Center surface modeling and grid generation applications p 2480 N95-28733
A Cartesian, cell-based approach for adaptively-refined solutions of the Euler and Navier-Stokes equations p 2480 N95-28739
The National Grid Project: A system overview p 2482 N95-28749
Algorithms for the automatic generation of 2-D structured multi-block grids p 2483 N95-28757
Examples of grid generation with implicitly specified surfaces using GridPro (TM)/az3000. 1: Filleted multi-tube configurations p 2486 N95-28772
Analytical modeling and sensor monitoring for optimal processing of advanced textile structural composites by resin transfer molding p 2521 N95-29045
Investigation of an alternative finite element procedure: A one-step, steady-state analysis
[AD-A290030] p 2670 N95-29311
Three problems in fluid dynamics
[AD-A290481] p 2573 N95-29324
A simulation technique for predicting thickness of thermal sprayed coatings
[NASA-TM-106939] p 2512 N95-29373
Acoustic scattering from ellipses by the modal element method
[NASA-TM-106935] p 2683 N95-29401
The large discretization step method for time-dependent partial differential equations
[NASA-CR-195068] p 2670 N95-29403
Object oriented segmentation of images
[AD-A290792] p 2671 N95-29485
Quantum mechanical problems in one, two, and three dimensions
[ISBN-0-315-84931-2] p 2719 N95-29677
Experimental investigation of aerodynamic devices for wind turbine rotational speed control, phase 1
[DE95-004034] p 2603 N95-30016
Hydrogen film cooling with incident and swept-shock interactions in a Mach 6.4 nitrogen free stream
[NASA-TM-4603] p 2578 N95-30056

TWO FLUID MODELS
Relativistic effects on large amplitude nonlinear langmuir waves in a two-fluid plasma
[AD-B191980L] p 2710 N95-29841
Ensemble phase averaged equations for multiphase flows p 2579 N95-30284

TWO PHASE FLOW
Three problems in fluid dynamics
[AD-A290481] p 2573 N95-29324
NMR imaging and hydrodynamic analysis of neutrally buoyant non-Newtonian slurry flows
[DE95-005842] p 2578 N95-30187

TYPHOONS
Typhoon monitoring using passive microwave observations
[AD-A292567] p 2619 N95-28975
Analysis of the structural characteristics and intensity evolution of super typhoon flo (1990) in special sensor Microwave/Imager (SSM/I) data
[AD-A292413] p 2619 N95-28989

U

ULTRAHIGH FREQUENCIES
UHF Low Density Radio Communications Link (LDRCL) Operational Test and Evaluation (OT&E) integration and OT&E operational final test report
[AD-A291447] p 2558 N95-29769

ULTRAHIGH VACUUM
Correlations between micromagnetic, microstructural and microchemical properties in ultrathin epitaxial magnetic structures
[AD-A289705] p 2712 N95-28681

ULTRASHORT PULSED LASERS
Topics in high-peak intensity, ultrashort pulse laser-plasma interactions p 2704 N95-29218
Summaries of papers presented at the ultrafast phenomena topical meeting
[AD-A290998] p 2564 N95-29511

ULTRASONIC FLAW DETECTION
Ultrasonic guided waves in cylinders: Theory and experiment p 2685 N95-29826

ULTRASONIC RADIATION
Bubble fusion: Preliminary estimates of spherical micro-implosions in cavitating liquids
[DE95-006260] p 2569 N95-28956
Acoustic imaging of ultrasonic wave propagation
[AD-A290390] p 2683 N95-29232
Ultrasonic guided waves in cylinders: Theory and experiment p 2685 N95-29826

ULTRASONIC TESTS
The development of an interpretive methodology for the application of real-time acousto-ultrasonic NDE technique for monitoring damage in ceramic composites under dynamic loads p 2592 N95-29104
Origins of imperfections in composite materials
[AD-A290261] p 2523 N95-29169
Efficient inversion of Fourier and Laplace domain boundary element solutions for elastodynamic scattering p 2592 N95-29256
Ultrasonic guided waves in cylinders: Theory and experiment p 2685 N95-29826

ULTRASONICS
Conference reports
[AD-A289630] p 2561 N95-28911
Spectral characterization of pulsed ultrasound using neural networks
[AD-A292440] p 2683 N95-28999
Acoustic imaging of ultrasonic wave propagation
[AD-A290390] p 2683 N95-29232

ULTRAVIOLET ASTRONOMY
Simultaneous UV and optical study of O star winds and UV and optical covariability of O star winds
[NASA-CR-189424] p 2726 N95-29370
Space astronomy update
[NASA-TM-110754] p 2731 N95-30317

ULTRAVIOLET DETECTORS
Nitride semiconductors for ultraviolet detection
[AD-A289546] p 2712 N95-28910

ULTRAVIOLET LASERS
Development of distributed feedback dye lasers for generation of high-power 193 nm excimer laser short pulses p 2586 N95-29631

ULTRAVIOLET RADIATION
Study of the space environmental effects on spacecraft engineering materials
[NASA-CR-196638] p 2531 N95-29246
Design of a more accurate, higher fidelity, dual-source air mass zero solar simulator
[AD-A291364] p 2603 N95-29953

ULTRAVIOLET SPECTRA
Continuum spectra of supermassive accretion disks p 2732 N95-29252
Simultaneous UV and optical study of O star winds and UV and optical covariability of O star winds
[NASA-CR-189424] p 2726 N95-29370
Molecular spectra and dynamics at interfaces
[AD-A289779] p 2693 N95-29460
Space astronomy update
[NASA-TM-110754] p 2731 N95-30317

ULTRAVIOLET SPECTROMETERS
A ground support electronic interface for the ionospheric spectroscopy and atmospheric chemistry (ISAAC) ultraviolet spectrograph
[AD-A289761] p 2611 N95-28693

ULTRAVIOLET TELESCOPES
STS-67 mission highlights resource tape
[NASA-TM-110530] p 2504 N95-28715

UMBRAS
Method for the calculation of spacecraft umbra and penumbra shadow terminator points
[NASA-TP-3547] p 2671 N95-29446
Total solar eclipse of 1997 March 9
[NASA-RP-1173] p 2731 N95-30004

UNDAMPED OSCILLATIONS
The one-dimensional bubble: Theory, experiment, and relevance to exposure of divers to low frequency sound, and of lung to lithotripsy
[ISVR-TR-246] *p 2577 N95-29817

UNDERWATER ACOUSTICS
System and method for rapidly tracking vehicles of special utility in low signal-to-noise environments
[AD-D017378] p 2683 N95-28783
Multi-scale studies of seafloor topography
[AD-A292301] p 2628 N95-28865
Stochastic modeling and global warming trend extraction for ocean acoustic travel times
[AD-A292114] p 2608 N95-28922
Airy functions and the recursive ray acoustics algorithm
[AD-A290182] p 2629 N95-29054
Revisions and notes on a model for bubble attenuation in near-surface propagation
[AD-A290312] p 2629 N95-29085
The nature of wavefront fluctuations induced by internal gravity waves in long-range oceanic acoustic pulse transmissions p 2630 N95-29528
The one-dimensional bubble: Theory, experiment, and relevance to exposure of divers to low frequency sound, and of lung to lithotripsy
[ISVR-TR-246] p 2577 N95-29817
A bibliography, with abstracts and annotations, of publications on and related to underwater acoustic fluctuations
[AD-A291342] p 2685 N95-29945

UNDERWATER STRUCTURES
Cable load transducer
[AD-A289548] p 2595 N95-29192

UNDERWATER VEHICLES
Engineering development program of a closed aluminum-oxygen semi-cell system for an unmanned underwater vehicle: An update p 2606 N95-30266

UNIFORM FLOW
The effects of three-dimensional imposed disturbances on bluff body near wake flows: Effects of taper and splitter plates on the near wake characteristics of a circular cylinder in uniform and shear flow
[AD-A292113] p 2487 N95-28921

UNIQUENESS
Discontinuous solutions of semilinear differential-algebraic equations. part 2: Rho-consistency
[AD-A292285] p 2668 N95-28861
Discontinuous solutions of semilinear differential-algebraic equations. part 1: Distribution solutions
[AD-A292286] p 2668 N95-28863

UNITED NATIONS
United Nations aeromedical evacuation operations in the former Yugoslavia p 2676 N95-29607

UNITED STATES
Tidal constituent database: West coast of the United States and eastern North Pacific Ocean
[AD-A292224] p 2630 N95-29198
Bilateral US/Russia Workshop on Self-Propagating High-Temperature Synthesis held in Honolulu, Hawaii on 6-7 November 1993
[AD-A290466] p 2525 N95-29492
Hydrology of the continental United States p 2599 N95-29539
A study of problematic situations and information needs of software managers in the United States and Japan p 2724 N95-29828

UNITS OF MEASUREMENT
SI Handbook for the Lawrence Livermore National Laboratory: Committee on metric transition
[DE95-009329] p 2551 N95-30182

UNIVERSE
Statistics and large-scale structure p 2734 N95-29780

UNIVERSITIES
The 6th Van der Ziel symposium on quantum 1/f noise and other low frequency fluctuations in electronic devices
[AD-A292468] p 2718 N95-29009
Yohkoh Soft X-ray Telescope
[NASA-CR-197655] p 2726 N95-29172
International Space University
[NASA-TM-110646] p 2720 N95-30223
Visit to the Laboratory For Evaluation and Failure Prevention of Materials, Toyohashi University of Technology, 17 Oct 94
[AD-A292340] p 2597 N95-30293

UNIVERSITY PROGRAM
International Space University
[NASA-TM-110646] p 2720 N95-30223

UNIX (OPERATING SYSTEM)
Manual for a workstation-based generic flight simulation program (LaRCsim), version 1.4
[NASA-TM-110164] p 2502 N95-30327

UNSTEADY AERODYNAMICS
Unsteady pressure and inflow velocity on a pitching rotor blade in hover p 2490 N95-29771

UNSTEADY FLOW
The acoustic characteristics of turbomachinery cavities
[NASA-CR-4671] p 2478 N95-28720
A combined geometric approach for computational fluid dynamics on dynamic grids p 2485 N95-28770
External combustion engine having an asymmetrical CAM
[AD-D017382] p 2588 N95-28785
Interactions of spanwise and chordwise vorticity associated with three-dimensional dynamic stall over an oscillating wing
[AD-A290546] p 2487 N95-29091
A vorticity-velocity approach for three-dimensional unsteady viscous flow over wings p 2488 N95-29108
Unsteadiness of shock-induced turbulent boundary layer separation. An inherent feature of turbulent flow or solely a wind tunnel phenomenon
[AD-A290367] p 2572 N95-29228
Investigation of the flow turning loss in unstable solid propellant rocket motors p 2510 N95-29331
Application of the space-time conservation element and solution element method to two-dimensional advection-diffusion problems
[NASA-TM-106946] p 2574 N95-29372

Implicit schemes and parallel computing in unstructured grid CFD
[NASA-CR-195071] p 2671 N95-29451
Research instrumentation for polytechnic university's supersonic wind tunnel facility
[AD-A290232] p 2502 N95-29468
An experimental investigation of the time-dependent separation of tangent bodies in supersonic flow
[AD-A290720] p 2489 N95-29500
Unsteady rotational shear flow of power law fluids
[ISBN-0-315-81287-7] p 2575 N95-29718
Reliability enhancement of Navier-Stokes codes through convergence acceleration
[NASA-CR-196635] p 2578 N95-30034
An interacting boundary layer method for unsteady compressible flows p 2579 N95-30290

UNSTRUCTURED GRIDS (MATHEMATICS)
Surface Modeling, Grid Generation, and Related Issues in Computational Fluid Dynamic (CFD) Solutions
[NASA-CP-3291] p 2478 N95-28723
Grid generation and surface modeling for CFD p 2478 N95-28726
Algorithms for high aspect ratio oriented triangulations p 2479 N95-28731
A Cartesian, cell-based approach for adaptively-refined solutions of the Euler and Navier-Stokes equations p 2480 N95-28739
Unstructured Cartesian/prismatic grid generation for complex geometries p 2481 N95-28741
Prospects and expectations for unstructured methods p 2481 N95-28742
An unstructured-grid software system for solving complex aerodynamic problems p 2481 N95-28743
Three-dimensional hybrid grid generation using advancing front techniques p 2481 N95-28745
An assessment of unstructured grid technology for timely CFD analysis p 2482 N95-28747
The National Grid Project: A system overview p 2482 N95-28749
Tuned grid generation with ICEM CFD p 2483 N95-28752
Demonstration of an automated CFD system for three-dimensional flow simulations p 2485 N95-28767
GridTool: A surface modeling and grid generation tool p 2486 N95-28773
Implicit schemes and parallel computing in unstructured grid CFD
[NASA-CR-195071] p 2671 N95-29451
Computational results for parallel unstructured mesh computations
[DE95-005856] p 2659 N95-29985
Coarsening strategies for unstructured multigrid techniques with application to anisotropic problems
[NASA-CR-198154] p 2674 N95-30227

UPPER ATMOSPHERE
Research results on an improved in-situ tropospheric humidity sensor
[AD-A291339] p 2627 N95-29944

UPSTREAM
Development of a transient internal probe diagnostic
[AD-A292470] p 2704 N95-29011

UPWELLING WATER
A numerical study of the effects of wind forcing on the Chile Current System
[AD-A289808] p 2629 N95-28982

UPWIND SCHEMES (MATHEMATICS)
Results of two new methods for aeroacoustics benchmark problems p 2687 N95-30140

URANIUM
Activities update
[AD-A292431] p 2692 N95-28994
Assay of potentially contaminated propellant
[DE95-006330] p 2549 N95-30345

USER MANUALS (COMPUTER PROGRAMS)
Generator of body data (GEBOD) manual
[AD-A289721] p 2640 N95-28683
A procedure for accessing digital satellites containing amateur payloads
[AD-A289748] p 2506 N95-28686
Dimensions, deflections and stresses for Hertzian contacts under combined normal and tangential loading. (Guide to use of computer program A9434.)
[ESDU-94034] p 2593 N95-28711
Users manual for the improved NASA Lewis ice accretion code LEWICE 1.6
[NASA-CR-198355] p 2492 N95-29132
MapTool version 2. User's manual
[AD-A289470] p 2630 N95-29418
GENAH user's guide and reference manual version 1.0
[AD-A290236] p 2583 N95-29470
AFGWC dial-in subsystem (AFDIS) software users manual, version 3.1
[AD-A291103] p 2651 N95-29639
The topside ionospheric plasma monitor (SSIES, SSIES-2 and SSIES-3) on the spacecraft of the Defense Meteorological Satellite Program (DMSP), user's guide. Volume 3: Program maintenance manual
[AD-A290941] p 2617 N95-29765
Training end-users on database queries: The effectiveness of example format and spatial ability on learing outcomes p 2724 N95-29829
Finite difference ocean acoustic model users guide
[AD-A291544] p 2631 N95-29856
The Scanning Fast Field Program (SCAFFIP) general version 1.0 user's manual
[AD-A291209] p 2618 N95-29976
Software Estimation Program (SWEEP) user manual
[AD-A291137] p 2654 N95-30121
Engineering Design Information System (EDIS), Information Management Services (IMS), Index Function, User's manual: Revision 1
[DE95-009538] p 2725 N95-30194
Manual for a workstation-based generic flight simulation program (LaRCsim), version 1.4
[NASA-TM-110164] p 2502 N95-30327

USER REQUIREMENTS
Future requirements in surface modeling and grid generation p 2478 N95-28724
Requirements for effective use of CFD in aerospace design p 2478 N95-28725
The identification of user criteria of relevance and document characteristics: Beyond the topical approach to information retrieval p 2723 N95-29518
Client-server interactions in multi-server operating systems: The Mach-US approach
[AD-A290431] p 2650 N95-29536
A study of the conceptual symbolics of information system development languages p 2723 N95-29589
Information management in local area networks: Impact on users' perceptions p 2723 N95-29690
DOD listing of approved recurring information requirements
[AD-A291346] p 2724 N95-29947
Retrieval, display, and analysis support tool for earth imagery (RDAST)
[AD-A291366] p 2601 N95-30061

UTILITIES
Interactions between energy efficiency and emission trading under the 1990 Clean Air Act Amendments
[DE95-008649] p 2611 N95-30212

V

VACUUM
Vacuum microelectronic emitters and their applications using compound semiconductor technology
[AD-A291142] p 2567 N95-30124

VACUUM DEPOSITION
Compact substrate heater for use in an oxidizing atmosphere
[AD-A290860] p 2502 N95-29522

VACUUM PUMPS
Carbon sheet pumping
[AD-B179443L] p 2710 N95-29812

VACUUM TUBES
Vacuum microelectronic emitters and their applications using compound semiconductor technology
[AD-A291142] p 2567 N95-30124

VALLEYS
Channels and valleys on Venus p 2736 N95-29593

VALVES
Inflatable life vest
[AD-D017273] p 2641 N95-29600
Evaluation of wear resistant ceramic valve seats in gas-fueled power generation engines
[PB95-200218] p 2591 N95-30110

VANADATES
17O NMR of the structural evolution of V2O5 gels
[AD-A290623] p 2545 N95-29559

VAPOR DEPOSITION
Drift mobility measurements in thin film boron carbide
[AD-A292510] p 2712 N95-28869
Process optimization through discovery and integration of materials and processing properties. phase 1
[AD-A292576] p 2662 N95-28978
The nucleation of crystalline films from vapor phase reactants
[AD-A291122] p 2716 N95-29767
Innovative processing of composites for ultra-high temperature applications, book 1
[AD-A290889] p 2527 N95-29842
Apparatus and method for achieving growth-etch deposition of diamond using a chopped oxygen-acetylene flame
[AD-D017322] p 2718 N95-30164

VAPOR PHASES
Radiative lifetime and quenching rate constants of PF(b(1) Sigma+) and tests for an electronic to vibrational energy transfer quenching mechanism
[AD-A290294] p 2681 N95-29062
Integrated synthesis and post-processing of SiC and AlN
[AD-A290853] p 2537 N95-29724

VAPOR PRESSURE
Vapour pressures and critical points of liquids. Glycols and cyclic diols
[ESDU-95002] p 2534 N95-29897
Vapour pressures and critical points of liquids. Glycol ethers (alkyl cellosolves and carbitols, etc.)
[ESDU-95004] p 2534 N95-29901

VAPORIZING
SCAP spray combustion analysis program
[AD-A289946] p 2532 N95-29273
Semiconductor deposition and etching interactions of laser-generated translationally hot atoms and radicals
[AD-A291824] p 2693 N95-29431
The effect of turbulence on vaporization and mixing in fuel sprays
[AD-A291347] p 2577 N95-29948

VARIABILITY
Ocean Optics XII
[AD-A286734] p 2702 N95-29910

VARIATIONAL PRINCIPLES
Nonlinear mechanics and applied analysis
[AD-A290356] p 2669 N95-29070
The effects of the thermal boundary condition and turbulence on heat transfer from a cylinder, flat plate, and turbine blade using the transient shroud and heated-coating techniques
[AD-A292646] p 2574 N95-29380
On the topological complexity of the cost function in variational data assimilation p 2724 N95-29798

VECTOR PROCESSING (COMPUTERS)
Porting a vector library: A comparison of MPI, paris, CMMD and PVM (or, 'I'll never have to port CVL again')
[AD-A290231] p 2647 N95-29147

VEGETATION
Compendium of NASA data base for the global tropospheric experiment's Transport and Atmospheric Chemistry Near the Equator-Atlantic (TRACE-A)
[NASA-TM-110151] p 2608 N95-28717

VEGETATION GROWTH
Effect of irradiance, sucrose, and CO2 concentration on the growth of potato (Solanum tuberosum L.) in vitro
[NASA-TM-110654] p 2632 N95-29375

VEGETATIVE INDEX
Proposal for a flexible system of phytogeographic classification: Emphasis on the use of multistage remote sensoring
[INPE-5609-PRE/1821] p 2600 N95-29815

VELOCITY DISTRIBUTION
Studies in drag reduction p 2487 N95-29094
PIV investigation of compressibility effects on dynamic stall p 2487 N95-29102
A vorticity-velocity approach for three-dimensional unsteady viscous flow over wings p 2488 N95-29108
Vortex element analysis of selected time-dependent flows
[AD-A289944] p 2573 N95-29271
State resolved differential cross sections for reactions important to the decomposition of energetic materials
[AD-A290718] p 2548 N95-29498
Unsteady rotational shear flow of power law fluids
[ISBN-0-315-81287-7] p 2575 N95-29718
Statistics and large-scale structure p 2734 N95-29780

VELOCITY MEASUREMENT
Joint services electronics program
[AD-A292469] p 2561 N95-29010
Unsteady pressure and inflow velocity on a pitching rotor blade in hover p 2490 N95-29771

VENTILATION
Aeromedical impact of the transportable pressure ventilator in wartime aeromedical evacuation p 2641 N95-29624

VENTILATORS
Aeromedical impact of the transportable pressure ventilator in wartime aeromedical evacuation p 2641 N95-29624

VENUS (PLANET)
Collection of Magellan Venus radar mapping results
[NASA-CR-197656] p 2736 N95-29178
A study of plasma waves arising from the solar wind interaction with Venus p 2704 N95-29215
Channels and valleys on Venus p 2736 N95-29593

VENUS ATMOSPHERE
A study of plasma waves arising from the solar wind interaction with Venus p 2704 N95-29215
Pioneer Venus 12.5 km Anomaly Workshop Report, volume 1
[NASA-CP-3303] p 2737 N95-30058

VENUS PROBES
Pioneer Venus 12.5 km Anomaly Workshop Report, volume 1
[NASA-CP-3303] p 2737 N95-30058
VENUS SURFACE
Collection of Magellan Venus radar mapping results
[NASA-CR-197656] p 2736 N95-29178
Channels and valleys on Venus p 2736 N95-29593
VERTICAL AIR CURRENTS
Development of an improved cloud model for use in cumulus parameterization p 2624 N95-29800
VERTICAL DISTRIBUTION
Radiative cooling profiles calculated from ECMWF analyses and ISCCP C1 data, and their application to determination of distributions of apparent convective heating in the equatorial Pacific p 2625 N95-29805
Short-range precipitation forecasts using assimilation of simulated satellite water vapor profiles and cloud liquid water p 2625 N95-29832
VERTICAL MOTION
Extended field observations of cirrus clouds using a ground-based cloud observing system
[NASA-CR-198855] p 2628 N95-30356
VERTICAL ORIENTATION
Comparison of boundary-layer wind and temperature measurements with model estimations
[AD-A290471] p 2621 N95-29507
VERY LARGE ARRAY (VLA)
Observations and analysis of solar flares at radio and other wavelengths p 2738 N95-29202
VERY LARGE SCALE INTEGRATION
The 6th Van der Ziel symposium on quantum 1/f noise and other low frequency fluctuations in electronic devices
[AD-A292468] p 2718 N95-29009
Computing 3-D motion in custom analog and digital VLSI
[AD-A290270] p 2647 N95-29179
Robust testing of cellular neural networks
[AD-A291219] p 2665 N95-29979
VERY LONG BASE INTERFEROMETRY
Multiwaveband observations of quasars p 2728 N95-29665
VESTS
Inflatable life vest
[AD-D017273] p 2641 N95-29600
VHSIC (CIRCUITS)
The design of programmable convolutional encoder using VHDL and an FPGA
[AD-A290048] p 2649 N95-29442
VIBRATION
Theoretical investigation of superconductivity in doped fullerenes
[AD-A291942] p 2562 N95-29018
The 2nd European Conference on Smart Structures and Materials
[AD-A290723] p 2550 N95-29579
Ab initio calculation of vibrational absorption and circular dichroism spectra using density functional force fields
[AD-A291297] p 2720 N95-29936
VIBRATION DAMPING
Broadband control of structural vibration using simultaneous sensing and actuation with nonlinear piezoelectric elements p 2664 N95-29548
Experimental confirmation of a PDE-based approach to design of feedback controls
[NASA-CR-198167] p 2672 N95-30086
Passive damping to enhance active positioning of a prototype lithography platen
[DE95-008539] p 2655 N95-30209
VIBRATION EFFECTS
Lockheed Stabilizer System for space exercise equipment
[NASA-CR-197657] p 2641 N95-29180
VIBRATION ISOLATORS
Passive damping to enhance active positioning of a prototype lithography platen
[DE95-008539] p 2655 N95-30209
VIBRATION MEASUREMENT
Fibre-coupled remote optical vibrometry
[AD-A291606] p 2698 N95-28932
VIBRATION METERS
Fibre-coupled remote optical vibrometry
[AD-A291606] p 2698 N95-28932
VIBRATIONAL STATES
Studies of energy transfer processes of relevance to chemically and optically pumped lasers
[AD-A290164] p 2585 N95-29025
Research into artificially induced atmospheric disturbances
[AD-A290150] p 2613 N95-29317
VIDEO COMMUNICATION
Towards an example-based image compression architecture for video-conferencing
[AD-A290041] p 2556 N95-29441
VIDEO COMPRESSION
Towards an example-based image compression architecture for video-conferencing
[AD-A290041] p 2556 N95-29441
VIDEO DATA
Towards an example-based image compression architecture for video-conferencing
[AD-A290041] p 2556 N95-29441
VIDEO SIGNALS
Comparison study of unequal error protection methods for one-dimensional signal constellations
[AD-A290386] p 2554 N95-29231
VIEWING
Automated testing of application domains
[AD-A289753] p 2643 N95-28690
Interactive multimedia presentation for applied computer tomography: Impact
[AD-A291955] p 2640 N95-29020
VIKING MARS PROGRAM
The JPL Mars gravity field, Mars50c, based upon Viking and Mariner 9 Doppler tracking data
[NASA-CR-198881] p 2737 N95-30344
VINYL POLYMERS
High field electrostrictive response of polymers
[AD-A292298] p 2539 N95-28864
Ferroelectric and piezoelectric properties of nylon 11/Poly(Vinylidene fluoride) bilaminate films
[AD-A292274] p 2539 N95-28891
Conjugated polymers from cyclohexadienediol monomers
[AD-A290247] p 2544 N95-29505
VIRTUAL REALITY
NASA to use telepresence to explore Antarctic Lakes
[NASA-TM-110567] p 2598 N95-29175
The 2d Eurographics Workshop on Virtual Environments
[AD-A292015] p 2651 N95-29861
Summary of the 1st International Workshop on Networked Reality in Telecommunication
[AD-A292366] p 2558 N95-29862
Telepresence media resource tape
[NASA-TM-110648] p 2655 N95-30248
VISCOELASTICITY
Investigation of an alternative finite element procedure: A one-step, steady-state analysis
[AD-A290030] p 2670 N95-29311
Toughening mechanisms in mixed-mode interfacial fracture p 2545 N95-29772
Passive damping to enhance active positioning of a prototype lithography platen
[DE95-008539] p 2655 N95-30209
Numerical solution of the equations governing non-Newtonian flow at moderate Reynolds numbers p 2579 N95-30233
VISCOPLASTICITY
A thermochemical transport model for analysis of hot-spot formation in energetic materials
[AD-A290441] p 2532 N95-29357
Numerical implementation of a state variable model for friction
[DE95-007844] p 2591 N95-30273
VISCOSITY
Viscosity of liquids: Aliphatic and cyclic ketones
[ESDU-94025] p 2530 N95-28712
Selection of synthetic oils
[ESDU-94020] p 2539 N95-28898
The dynamics of FU Orionis outbursts: Time-dependent accretion through protostellar disks p 2732 N95-29530
VISCOUS DAMPING
Anomalous transport theory for toroidal helical plasmas
[AD-B192000L] p 2706 N95-29731
VISCOUS FLOW
Block-structured grids for complex aerodynamic configurations: Current status p 2480 N95-28736
A Cartesian, cell-based approach for adaptively-refined solutions of the Euler and Navier-Stokes equations p 2480 N95-28739
Adaptive hybrid prismatic-tetrahedral grids for viscous flows p 2481 N95-28744
A combined geometric approach for computational fluid dynamics on dynamic grids p 2485 N95-28770
A vorticity-velocity approach for three-dimensional unsteady viscous flow over wings p 2488 N95-29108
Leading edge film cooling effects on turbine blade heat transfer
[NASA-TM-106955] p 2500 N95-29115
Finite element vorticity-based methods for the solution of the incompressible and compressible Navier-Stokes equations p 2570 N95-29119
Solution of the Navier-Stokes equations on locally refined Cartesian meshes using state-vector splitting p 2571 N95-29197
Collective phenomena in granular fluids p 2572 N95-29219
Direct numerical simulation of compressible turbulent flows, using adaptive spectral element method
[AD-A290115] p 2575 N95-29421
Experimental research on crossing shock wave boundary layer interactions
[AD-A290764] p 2577 N95-29920
Reliability enhancement of Navier-Stokes codes through convergence acceleration
[NASA-CR-196635] p 2578 N95-30034
Coarsening strategies for unstructured multigrid techniques with application to anisotropic problems
[NASA-CR-198154] p 2674 N95-30227
VISCOUS FLUIDS
A novel approach to the numerical simulation of turbulent flows
[AD-A290352] p 2569 N95-29068
Three problems in fluid dynamics
[AD-A290481] p 2573 N95-29324
Rigorous drag bounds in turbulent shear flow p 2573 N95-29334
Attractors of dissipative structure in three dissipative fluids
[AD-B180030L] p 2710 N95-29844
Supercritical states of two-dimensional wall-bounded shear flow p 2580 N95-30303
VISIBILITY
Evaluation of retro-reflective beads in airport pavement markings
[AD-A291065] p 2502 N95-29967
Robust testing of cellular neural networks
[AD-A291219] p 2665 N95-29979
VISION
Reference frames in vision
[AD-A290117] p 2639 N95-29422
VISUAL ACUITY
Variation in visual and near-infrared contrast with a snow background
[AD-A289710] p 2697 N95-28778
VISUAL OBSERVATION
Simultaneous UV and optical study of O star winds and UV and optical covariability of O star winds
[NASA-CR-189424] p 2726 N95-29370
Learning object models from visual observation and background knowledge
[AD-A292606] p 2650 N95-29576
VISUAL PERCEPTION
Variation in visual and near-infrared contrast with a snow background
[AD-A289710] p 2697 N95-28778
Intermediate levels of visual processing
[AD-A291569] p 2638 N95-28937
Large-scale neuronal theories of the brain
[AD-A290200] p 2634 N95-29059
Reference frames in vision
[AD-A290117] p 2639 N95-29422
Visual and auditory symbols: A literature review
[AD-A290222] p 2641 N95-29908
VISUAL SIGNALS
Computer models of retinal function
[AD-A290156] p 2634 N95-29022
Reference frames in vision
[AD-A290117] p 2639 N95-29422
VOIDS
Micromechanics of crack extension in composites p 2529 N95-30276
VOLCANOES
Channels and valleys on Venus p 2736 N95-29593
Some aspects of lunar and martian volcanism as examined with spectral, topographic, and morphologic data derived from spacecraft images p 2736 N95-29594
VOLCANOLOGY
Channels and valleys on Venus p 2736 N95-29593
Numerical studies of the stratospheric aerosol layer under background and perturbed conditions p 2615 N95-29666
VOLUME
Geometry modeling and grid generation using 3D NURBS control volume p 2483 N95-28753
VOLUMETRIC ANALYSIS
Orthobaric densities and molar volumes of liquids. Glycols and cyclic diols
[ESDU-95003] p 2531 N95-28895
VORTEX FILAMENTS
A numerical method for modelling wings with sharp edges maneuvering at high angles of attack p 2496 N95-29122
VORTEX FLAPS
Pressure based high order TVD methodology for dynamic stall control
[AD-A290149] p 2489 N95-29316
VORTEX GENERATORS
The decay of longitudinal vortices shed from airfoil vortex generators
[NASA-CR-198356] p 2489 N95-29402
VORTEX RINGS
Experiments on microbursts p 2620 N95-29110

VORTEX SHEDDING
The acoustic characteristics of turbomachinery cavities
[NASA-CR-4671] p 2478 N95-28720
Research on bluff-body vortex wakes
[AD-A292650] p 2574 N95-29382
The effects of three dimensional imposed disturbances on bluff body near wake flows
[AD-A290824] p 2575 N95-29654
VORTEX SHEETS
A numerical method for modelling wings with sharp edges maneuvering at high angles of attack p 2496 N95-29122
VORTICES
The effects of three-dimensional imposed disturbances on bluff body near wake flows: Effects of taper and splitter plates on the near wake characteristics of a circular cylinder in uniform and shear flow
[AD-A292113] p 2487 N95-28921
A nonintrusive method of quantifying flow visualization data in vortex flow fields
[AD-A289802] p 2568 N95-28948
PIV investigation of compressibility effects on dynamic stall p 2487 N95-29102
Navier-Stokes solution of wing wake structure and its perturbation p 2488 N95-29121
A numerical method for modelling wings with sharp edges maneuvering at high angles of attack p 2496 N95-29122
Numerical investigation of surface curvature effects in compressible turbulent flows
[AD-A290114] p 2571 N95-29211
Parameter study of the statistically steady state of a multi-layer quasi-geostrophic model p 2612 N95-29212
Conversion of an oceanographic expert system to a C-based language
[NASA-CR-198695] p 2630 N95-29237
Dynamic stall of a NACA 0012 airfoil in laminar flow p 2489 N95-29243
Vortex element analysis of selected time-dependent flows
[AD-A289944] p 2573 N95-29271
Research on bluff-body vortex wakes
[AD-A292650] p 2574 N95-29382
The decay of longitudinal vortices shed from airfoil vortex generators
[NASA-CR-198356] p 2489 N95-29402
The effects of three dimensional imposed disturbances on bluff body near wake flows
[AD-A290824] p 2575 N95-29654
Unsteady rotational shear flow of power law fluids
[ISBN-0-315-81287-7] p 2575 N95-29718
Numerical simulation of the genesis of tornado-like vortices p 2625 N95-29806
Cross flow instability of supersonic flow over a 4:1 elliptic cone
[AD-A291128] p 2577 N95-29913
Control of vortex dynamics p 2579 N95-30275
Growth and development of roughness-induced stationary crossflow vortices p 2492 N95-30294
Supercritical states of two-dimensional wall-bounded shear flow p 2580 N95-30303
VORTICITY
Flow visualization of vorticity cancellation of jets in crossflow
[AD-A292414] p 2569 N95-28990
Interactions of spanwise and chordwise vorticity associated with three-dimensional dynamic stall over an oscillating wing
[AD-A290546] p 2487 N95-29091
PIV investigation of compressibility effects on dynamic stall p 2487 N95-29102
A vorticity-velocity approach for three-dimensional unsteady viscous flow over wings p 2488 N95-29108
Finite element vorticity-based methods for the solution of the incompressible and compressible Navier-Stokes equations p 2570 N95-29119
Molecular mixing in shear layers forced by 2-D and 3-D disturbances
[AD-A290272] p 2571 N95-29181
Lee vorticity production by tropical mountain ranges p 2622 N95-29701
Numerical simulation of the genesis of tornado-like vortices p 2625 N95-29806

W

WAKES
Interactions of spanwise and chordwise vorticity associated with three-dimensional dynamic stall over an oscillating wing
[AD-A290546] p 2487 N95-29091
Molecular mixing in shear layers forced by 2-D and 3-D disturbances
[AD-A290272] p 2571 N95-29181
Research on bluff-body vortex wakes
[AD-A292650] p 2574 N95-29382
The effects of three dimensional imposed disturbances on bluff body near wake flows
[AD-A290824] p 2575 N95-29654
Control of vortex dynamics p 2579 N95-30275
WALKING
Dynamic modelling and link mechanism design of four-legged mobile robot p 2591 N95-30277
WALKING MACHINES
Dynamic modelling and link mechanism design of four-legged mobile robot p 2591 N95-30277
WALL FLOW
Finite element vorticity-based methods for the solution of the incompressible and compressible Navier-Stokes equations p 2570 N95-29119
Numerical investigation of surface curvature effects in compressible turbulent flows
[AD-A290114] p 2571 N95-29211
Multifluid nonequilibrium simulation of arcjet thrusters p 2510 N95-29245
New predictive methods in chaotic fluid dynamics with application to turbulent heat transfer
[AD-A290691] p 2576 N95-29761
A method for the modelling of porous and solid wind tunnel walls in computational fluid dynamics codes p 2502 N95-29795
Experimental and analytical study of heat transfer and turbulent flow field in tangentially injected swirl flow p 2576 N95-29811
Supercritical states of two-dimensional wall-bounded shear flow p 2580 N95-30303
WALL PRESSURE
Physical causes of separation shock unsteadiness in shock wave/turbulent boundary layer interactions p 2570 N95-29096
Experimental research on crossing shock wave boundary layer interactions
[AD-A290764] p 2577 N95-29920
WALLS
Effects of impurities released from high Z test limiter on plasma performance in TEXTOR
[AD-B191995L] p 2709 N95-29803
Wave propagation and scattering in computational aeroacoustics p 2689 N95-30152
WAR GAMES
Visualization of improved target acquisition algorithm for Janus (A)
[AD-A290191] p 2646 N95-29056
Software testing toolkit for distributed simulations
[AD-A291867] p 2649 N95-29435
SEMINT: Seamless model integration
[AD-A290956] p 2651 N95-29736
WARFARE
Role of unmanned aerial vehicles in future armed conflict scenarios
[AD-A289777] p 2497 N95-29282
Aeromedical evacuation in combined operations p 2677 N95-29612
Danish aeromedical evacuation efforts during the Gulf War p 2677 N95-29613
Changes in the medevac mission result in an increased role for the flight surgeon p 2680 N95-29628
Sleep during SEAL Delivery Vehicle (SDV)/Dry dock shelter exercises analyzed by a graphic approach
[AD-A290916] p 2637 N95-30083
WARNING SYSTEMS
A least square real time quality control routine for the North Warning Netted Radar System
[AD-A290063] p 2555 N95-29328
WASTE ENERGY UTILIZATION
The TEES process cleans waste and produces energy
[DE95-007799] p 2602 N95-29463
WASTE WATER
In-plant testing of membranes to treat electroplating wastewater
[NASA-CR-198796] p 2532 N95-29250
WATER
Corrosion investigation of multilayered ceramics and experimental nickel alloys in SCWO process environments
[DE95-008666] p 2540 N95-28960
Effects of cooling system parameters on heat transfer in PAFC stack
[NASA-CR-198817] p 2570 N95-29131
Cage-like precursor formation from extensive cyclization in sol-gel inorganic condensation polymerization
[AD-A290589] p 2544 N95-29554
Evaluation of commercial water-in-fuel test kits
[AD-A292135] p 2533 N95-29572
Ocean Optics XII
[AD-A286734] p 2702 N95-29910
Coso monitoring program
[AD-A290604] p 2627 N95-30048
The TMI regenerable solid oxide fuel cell p 2606 N95-30265
WATER COLOR
SeaWiFS technical report series. Volume 24: SeaWiFS technical report series cumulative index, volumes 1-23
[NASA-TM-104556] p 2631 N95-30236
WATER FLOW
The structure of water mass, salt, and temperature transports within intermediate depths of the western tropical Atlantic Ocean p 2631 N95-29541
WATER LOSS
Analysis of wounds by evaporative water loss in man
[AD-A290327] p 2634 N95-29086
WATER POLLUTION
Measuring variation in ecosystem sensitivity to stress
[AD-A290415] p 2609 N95-29450
WATER PRESSURE
Shear reinforcement in deep slabs
[AD-A289528] p 2594 N95-28909
WATER TREATMENT
In-plant testing of membranes to treat electroplating wastewater
[NASA-CR-198796] p 2532 N95-29250
WATER TUNNEL TESTS
Flow visualization of vorticity cancellation of jets in crossflow
[AD-A292414] p 2569 N95-28990
Experimental and theoretical studies of wakes in stratified flows
[AD-A290203] p 2569 N95-29060
Research on bluff-body vortex wakes
[AD-A292650] p 2574 N95-29382
WATER VAPOR
The potential for pulmonary heat injury resulting from the activation of a cabin water spray system to fight aircraft cabin fires
[DOT/FAA/AM-95/17] p 2636 N95-29224
Short-range precipitation forecasts using assimilation of simulated satellite water vapor profiles and cloud liquid water p 2625 N95-29832
Production of a long-term global water vapor and liquid water data set using ultra-fast methods to assimilate multi-satellite and radiosonde observations
[NASA-CR-198955] p 2628 N95-30272
WATERSHEDS
Hydrology of the continental United States p 2599 N95-29539
WATERWAYS
Tidal constituent database: West coast of the United States and eastern North Pacific Ocean
[AD-A292224] p 2630 N95-29198
WAVE DISPERSION
Dispersion analysis and error estimation of Galerkin finite element methods for the numerical computation of waves
[AD-A290296] p 2668 N95-29064
An assessment of artificial damping models for aeroacoustic calculations
[NASA-CR-198354] p 2574 N95-29405
Ultrasonic guided waves in cylinders: Theory and experiment p 2685 N95-29826
Selective multi-chemical fiber optic sensor
[AD-D017409] p 2703 N95-30076
Application of low dissipation and dispersion Runge-Kutta schemes to benchmark problems in computational aeroacoustics p 2687 N95-30139
Solution of acoustic workshop problems by a spectral multidomain method p 2687 N95-30141
Nonlinear wave propagation using three different finite difference schemes (category 2 application) p 2582 N95-30151
Wave propagation and scattering in computational aeroacoustics p 2689 N95-30152
WAVE DRAG
Wave drag coefficient for axisymmetric forecowls at zero incidence (M sub infinity less than or equal to 1.5)
[ESDU-94014] p 2568 N95-28903
Surface pressure coefficient distributions for axisymmetric forecowls at zero incidence (M sub infinity less than or equal to 1.5)
[ESDU-94015] p 2487 N95-28904
WAVE EQUATIONS
Dispersion analysis and error estimation of Galerkin finite element methods for the numerical computation of waves
[AD-A290296] p 2668 N95-29064
A generalized finite element method for solving the Helmholtz equation in two dimensions with minimal pollution
[AD-A290280] p 2669 N95-29080
Finite element solution to the Helmholtz equation with high wave number. Part 2. The h-p version of the FEM
[AD-A290289] p 2669 N95-29084

Stochastic hyperbolic and parabolic partial differential equations
[AD-A290372] p 2689 N95-29229
The large discretization step method for time-dependent partial differential equations
[NASA-CR-195068] p 2670 N95-29403
An assessment of artificial damping models for aeroacoustic calculations
[NASA-CR-198354] p 2574 N95-29405
Eurasian seismic surveillance - 2D FD seismic synthetics and event discrimination
[AD-A292659] p 2614 N95-29413
An extension of the Lighthill theory of jet noise to encompass refraction and shielding
[NASA-TM-110163] p 2684 N95-29452
Multiple dimensional acousto-optic diffraction and multiple dimensional acousto-optic device
[AD-A291037] p 2685 N95-29681
Finite difference ocean acoustic model users guide
[AD-A291544] p 2631 N95-29856
Theory and experiment analysis of two-dimensional acousto-optic interaction
[AD-A291059] p 2685 N95-29951
A compact solution to computational acoustics
p 2686 N95-30138
Interaction of acoustic oscillations with magnetic flux tubes in the solar photosphere
[PB95-201810] p 2739 N95-30199

WAVE FRONT DEFORMATION
Atmospheric wavefront sensing and correction including the stellar phase shifting interferometer
p 2701 N95-29706

WAVE FRONT RECONSTRUCTION
Deconvolution of lateral shear interferograms
p 2699 N95-29222

WAVE FRONTS
Deconvolution of lateral shear interferograms
p 2699 N95-29222
The nature of wavefront fluctuations induced by internal gravity waves in long-range oceanic acoustic pulse transmissions p 2630 N95-29528

WAVE INTERACTION
Solitons in negative ion plasmas p 2706 N95-29668
Turbulent coupling of the magnetosphere-ionosphere through shear-mode Alfven waves p 2615 N95-29687
Aeroacoustic computation of a gust-plate interaction via MacCormack schemes p 2690 N95-30162
Studies of gravity-wave filtering and tidal interaction in the middle atmosphere p 2619 N95-30351

WAVE PACKETS
A compact solution to computational acoustics
p 2686 N95-30138

WAVE PROPAGATION
Systems of hyperbolic partial differential equations
[AD-A290287] p 2669 N95-29083
Acoustic imaging of ultrasonic wave propagation
[AD-A290390] p 2683 N95-29232
Eurasian seismic surveillance - 2D FD seismic synthetics and event discrimination
[AD-A292659] p 2614 N95-29413
Turbulent coupling of the magnetosphere-ionosphere through shear-mode Alfven waves p 2615 N95-29687
Modal analysis of straight and curved integrated optical waveguides: An integral equation approach
[PB95-197265] p 2702 N95-30054
Extreme nonlinearity in rocks: An investigation using elastic pulse wave propagation
[DE95-007879] p 2618 N95-30129
Application of essentially nonoscillatory methods to aeroacoustic flow problems p 2686 N95-30135
Computation of wave propagation in a complex flow
p 2582 N95-30142
Studies of gravity-wave filtering and tidal interaction in the middle atmosphere p 2619 N95-30351

WAVE SCATTERING
Regional seismic event identification and improved locations with small arrays
[AD-A292188] p 2612 N95-29885
Efficient inversion of Fourier and Laplace domain boundary element solutions for elastodynamic scattering
p 2592 N95-29256

WAVE-PARTICLE INTERACTIONS
FFT space processing for the ACF of SPREE particle flux measurements
[AD-A290166] p 2507 N95-29026
A Monte Carlo simulation of Coulomb collisions and wave-particle interactions in space plasma at high latitudes p 2704 N95-29205
Experiments on nonlinear wave-particle interactions
p 2695 N95-30302

WAVEFORMS
Pulse waveform and pulse amplitude analysis during Lower Body Negative Pressure
[AD-A290521] p 2636 N95-29360
Experiments on nonlinear wave-particle interactions
p 2695 N95-30302

WAVEGUIDES
Study of UV bleached channel waveguide performance in NLO polymer films
[AD-A292008] p 2540 N95-29021
Numerical modeling of opto-electronic integrated circuits
[AD-A292096] p 2563 N95-29239
Modal analysis of straight and curved integrated optical waveguides: An integral equation approach
[PB95-197265] p 2702 N95-30054

WAVELET ANALYSIS
Automated optical target recognition
[AD-A292397] p 2697 N95-28798
Wavelets in signal detection and identification comparative signal processing technology evaluation
[AD-A291952] p 2552 N95-28984
Multivariate wavelet representations and approximations
[AD-A290147] p 2670 N95-29312
Feature extraction from digital communications signals using wavelet transforms
[AD-A292655] p 2556 N95-29386
Spectral analysis techniques using wavelets as an alternative to Fourier analysis for transient dynamic data
[AD-A289776] p 2556 N95-29459
W-matrices, nonorthogonal multiresolution analysis, and finite signals of arbitrary length
[DE95-005846] p 2652 N95-30020

WEAPON SYSTEMS
Thermoreactive aircraft coatings (TRAC) program
[AD-A292054] p 2542 N95-29314
Proposed Department of Defense software metrics implementation plan
[AD-A291404] p 2550 N95-29918
Vertical cavity surface emitting lasers for optical signal processing and optical computing applications
[AD-A290626] p 2588 N95-30050

WEAR
The effect of wear on fire-blocking layer material effectiveness
[AD-A291520] p 2493 N95-29855

WEAR RESISTANCE
Evaluation of wear resistant ceramic valve seats in gas-fueled power generation engines
[PB95-200218] p 2591 N95-30110
Nanoindentation and nanoscratching of hard coating materials for magnetic disks
[DE95-008776] p 2547 N95-30174

WEATHER
Three-D weather displays for aircraft cockpits
[AD-A289759] p 2499 N95-28691
On the large scale circulation of the East Asia Mei-Yu fronts and secondary weather dimension disturbances
[AD-A291036] p 2622 N95-29662
Observations of mesoscale cellular convection from the marine stratocumulus phase of FIRE
p 2624 N95-29727

WEATHER FORECASTING
Quality Control of meteorological observations at Fleet Numerical Meteorology and Oceanography Center
[AD-A291577] p 2619 N95-28938
Forecast of Atlantic seasonal hurricane activity for 1995 p 2620 N95-29254
Development and testing of improved techniques for modeling the hydrologic cycle in a mesoscale weather prediction system
[AD-A291243] p 2627 N95-29993

WEATHER STATIONS
Hindcasting changes in thermal structure and acoustic transmission loss in the upper ocean on short time scales with data from MILE and from ocean weather station papa
[AD-A292419] p 2629 N95-28991

WEAVING
Characterization and development of materials for advanced textile composites p 2513 N95-28824
Weavability of dry polymer powder towpreg
p 2519 N95-29036

WEBS (SUPPORTS)
Formulation of an improved smeared stiffener theory for buckling analysis of grid-stiffened composite panels
[NASA-TM-110162] p 2529 N95-30341

WEIGHT REDUCTION
Global cost and weight evaluation of fuselage keel design concepts p 2499 N95-28840
A weight-efficient design strategy for cutouts in composite transport structures p 2516 N95-28843
Effects of chromium picolinate on body composition in a remedial conditioning program
[AD-A292079] p 2636 N95-29238
Bell Helicopter Advanced Rotocraft Transmission (ART) program
[NASA-CR-195479] p 2590 N95-29538
Development of a micro-fiber nickel electrode for nickel-hydrogen cell p 2567 N95-30256
Fuel cell systems for First Lunar Outpost-reactant storage option p 2606 N95-30264

WEIGHTING FUNCTIONS
Finite element vorticity-based methods for the solution of the incompressible and compressible Navier-Stokes equations p 2570 N95-29119

WEIGHTLESSNESS
The influence of space flight on erythrokinetics in man. Space Life Sciences Missions 1 and 2. Experiment E261
[NASA-CR-188368] p 2633 N95-28875
Experiments in cooperative manipulation of objects by free-flying robot teams p 2662 N95-29095
Apollo 14: Shepard hitting golf ball on Moon
[NASA-TM-110538] p 2737 N95-30318

WELD STRENGTH
The effects of alloying elements on the strength and cooling rate sensitivity of ultra-low carbon alloy steel weld metals
[AD-A290681] p 2537 N95-29759

WELD TESTS
The effects of alloying elements on the strength and cooling rate sensitivity of ultra-low carbon alloy steel weld metals
[AD-A290681] p 2537 N95-29759

WELDED JOINTS
Correlation of inclusion size and chemistry with weld metal composition and microstructure arc weldments of high strength steels
[AD-A292024] p 2590 N95-29184

WELDING
A 1993 review of welding in Japan
[DE95-758701] p 2589 N95-28946

WELLS
Coso monitoring program
[AD-A290604] p 2627 N95-30048

WESTERN HEMISPHERE
Large scale fluctuations of the geomagnetic field
p 2617 N95-29796

WHARVES
High-level parallel programming tools for finite element analysis
[AD-A290566] p 2659 N95-29566
Sleep during SEAL Delivery Vehicle (SDV)/Dry dock shelter exercises analyzed by a graphic approach
[AD-A290916] p 2637 N95-30083

WHEELS
Applied Computational Electromagnetics Society Journal, volume 10, number 1, March 1995
[AD-A292069] p 2555 N95-29308

WHISKER COMPOSITES
Composite processing development to improve interlaminar strength using ply interface particles
[NASA-TM-108495] p 2529 N95-30334

WIDTH
The effects of specimen width on tensile properties of triaxially braided textile composites
p 2513 N95-28825

WIGGLER MAGNETS
A finite element analysis of room temperature silicon crystals for the Advanced Photon Source bending-magnet and insertion-device beams
[DE95-005822] p 2718 N95-30184

WIND (METEOROLOGY)
Path resolved optical sensing of atmospheric winds utilizing speckle-turbulence interaction and pseudorandum code modulation
[AD-A290800] p 2621 N95-29497
Comparison of boundary-layer wind and temperature measurements with model estimations
[AD-A290471] p 2621 N95-29507
The high-altitude polar wind: Simulation and observation p 2622 N95-29688
A study of boundary layer aerosol and wind profiles using incoherent Doppler lidar p 2622 N95-29697
Studies of gravity-wave filtering and tidal interaction in the middle atmosphere p 2619 N95-30351

WIND EFFECTS
A numerical study of the effects of wind forcing on the Chile Current System
[AD-A289808] p 2629 N95-28982
Modeling studies of the Leeuwin current off western and southern Australia
[AD-A290158] p 2629 N95-29023
A geotechnical characterization of lunar soils and lunar soil simulants p 2736 N95-29117
High-latitude electrodynamics: Electromagnetic energy dissipation and neutral wind feedback effects
p 2616 N95-29696

WIND MEASUREMENT
Studies of thermospheric neutral winds utilizing ground-based optical and radar measurements
p 2613 N95-29214

WIND PRESSURE
Numerical studies of ablative mass loss from wind accelerated clouds p 2622 N95-29676

WIND PROFILES
A study of boundary layer aerosol and wind profiles using incoherent Doppler lidar p 2622 N95-29697
WIND SHEAR
Path resolved optical sensing of atmospheric winds utilizing speckle-turbulence interaction and pseudorandum code modulation
[AD-A290800] p 2621 N95-29497
Extended field observations of cirrus clouds using a ground-based cloud observing system
[NASA-CR-198855] p 2628 N95-30356
WIND TUNNEL APPARATUS
A hybrid electronically scanned pressure module for cryogenic environments
[NASA-TM-110146] p 2583 N95-29453
WIND TUNNEL MODELS
The effects of the thermal boundary condition and turbulence on heat transfer from a cylinder, flat plate, and turbine blade using the transient shroud and heated-coating techniques
[AD-A292646] p 2574 N95-29380
Experimental investigation of aerodynamic devices for wind turbine rotational speed control, phase 1
[DE95-004034] p 2603 N95-30016
Boundary-layer transition and global skin friction measurement with an oil-fringe imaging technique
[NASA-CR-198814] p 2579 N95-30224
WIND TUNNEL TESTS
Influence of turbulence parameters, Reynolds number, and body shape on stagnation-region heat transfer
[NASA-TP-3487] p 2568 N95-28719
The effects of three-dimensional imposed disturbances on bluff body near wake flows: Effects of taper and splitter plates on the near wake characteristics of a circular cylinder in uniform and shear flow
[AD-A292113] p 2487 N95-28921
A nonintrusive method of quantifying flow visualization data in vortex flow fields
[AD-A289802] p 2568 N95-28948
Interactions of spanwise and chordwise vorticity associated with three-dimensional dynamic stall over an oscillating wing
[AD-A290546] p 2487 N95-29091
Computational Fluid Dynamics (CFD) analysis of a C-135 aircraft with a side-mounted splitter plate (with comparison to wind tunnel data)
[AD-A292029] p 2571 N95-29187
A two element laminar flow airfoil optimized for cruise
[NASA-CR-198580] p 2489 N95-29338
An experimental investigation of the time-dependent separation of tangent bodies in supersonic flow
[AD-A290720] p 2489 N95-29500
Transonic, supersonic and hypersonic wind-tunnel tests on aerodynamic characteristics of reentry body with blunted cone configuration
[ISAS-658] p 2490 N95-29640
The effects of three dimensional imposed disturbances on bluff body near wake flows
[AD-A290824] p 2575 N95-29654
Experimental studies on boundary-layer transition on a reentry vehicle at transonic and supersonic speeds
[ISAS-659] p 2575 N95-29712
Effects of elevated free-stream turbulence and streamwise acceleration on flow and thermal structures in transitional boundary layers p 2576 N95-29729
Hailstone heat and mass transfer measurements
[ISBN-0-315-86304-8] p 2624 N95-29797
Experimental research on crossing shock wave boundary layer interactions
[AD-A290764] p 2577 N95-29920
Experimental investigation of aerodynamic devices for wind turbine rotational speed control, phase 1
[DE95-004034] p 2603 N95-30016
Boundary-layer transition and global skin friction measurement with an oil-fringe imaging technique
[NASA-CR-198814] p 2579 N95-30224
Low-speed wind-tunnel investigation of the stability and control characteristics of a series of flying wings with sweep angles of 50 deg
[NASA-TM-4640] p 2498 N95-30226
Growth and development of roughness-induced stationary crossflow vortices p 2492 N95-30294
WIND TUNNEL WALLS
A method for the modelling of porous and solid wind tunnel walls in computational fluid dynamics codes p 2502 N95-29795
WIND TUNNELS
Unsteadiness of shock-induced turbulent boundary layer separation. An inherent feature of turbulent flow or solely a wind tunnel phenomenon
[AD-A290367] p 2572 N95-29228
Telepresence media resource tape
[NASA-TM-110648] p 2655 N95-30248
WIND TURBINES
Experimental investigation of aerodynamic devices for wind turbine rotational speed control, phase 1
[DE95-004034] p 2603 N95-30016
PREDICHAT: First order performance calculations of windturbine rotors using the method of the acceleration potential
[PB95-206454] p 2603 N95-30200
Fatigue case study and reliability analyses for wind turbines
[DE95-004770] p 2603 N95-30213
WIND VELOCITY
Upper-air data collected on Ice Station Weddell
[AD-A289707] p 2620 N95-29193
Numerical studies of ablative mass loss from wind accelerated clouds p 2622 N95-29676
An air-sea interaction model for stress, sensible heat, latent heat, and sea state, applicable to the full range of wind speeds p 2626 N95-29876
SETA/ADS software development
[AD-A291181] p 2651 N95-29932
A regression model for the western north pacific tropical cyclone intensity forecast
[AD-A290588] p 2627 N95-30044
An atlas of monthly mean distributions of SSMI surface wind speed, AVHRR/2 sea surface temperature, AMI surface wind velocity, TOPEX/POSEIDON sea surface height, and ECMWF surface wind velocity during 1993
[NASA-CR-198680] p 2628 N95-30343
Studies of gravity-wave filtering and tidal interaction in the middle atmosphere p 2619 N95-30351
WIND VELOCITY MEASUREMENT
Comparison of boundary-layer wind and temperature measurements with model estimations
[AD-A290471] p 2621 N95-29507
Heat and momentum flux measurements in the planetary boundary layer with a wind profiling radar/radio acoustic sounding system p 2617 N95-29777
WINDOWS (APERTURES)
High-temperature optical window design
[NASA-TM-106783] p 2596 N95-30008
WINDOWS (COMPUTER PROGRAMS)
WinCD: Complex demodulation time-series analysis for windows
[AD-A291550] p 2645 N95-28934
WINDS ALOFT
Studies of thermospheric neutral winds utilizing ground-based optical and radar measurements p 2613 N95-29214
High-latitude electrodynamics: Electromagnetic energy dissipation and neutral wind feedback effects p 2616 N95-29696
SETA/ADS software development
[AD-A291181] p 2651 N95-29932
WINDSHIELDS
An analysis of B-1B exterior jet blast windshield anti-icing performance using pre-cooled compressor bleed air
[AD-A292522] p 2492 N95-28811
WING OSCILLATIONS
Navier-Stokes solution of wing wake structure and its perturbation p 2488 N95-29121
An interacting boundary layer method for unsteady compressible flows p 2579 N95-30290
WING PANELS
Test results from large wing and fuselage panels p 2522 N95-29051
WING PROFILES
Automatic multi-block grid generation for high-lift configuration wings p 2485 N95-28764
Low-speed wind-tunnel investigation of the stability and control characteristics of a series of flying wings with sweep angles of 50 deg
[NASA-TM-4640] p 2498 N95-30226
WINGS
Investigation of wing upper surface flow-field disturbance due to NASA DC-8-72 in-flight inboard thrust-reverser deployment
[NASA-TM-110351] p 2477 N95-28816
Shear force, bending moment and torque of rigid aircraft in symmetric steady maneuvering flight
[ESDU-94045] p 2495 N95-28896
Advanced composites technology program p 2519 N95-29032
Interactions of spanwise and chordwise vorticity associated with three-dimensional dynamic stall over an oscillating wing
[AD-A290546] p 2487 N95-29091
A vorticity-velocity approach for three-dimensional unsteady viscous flow over wings p 2488 N95-29108
Computational Fluid Dynamics (CFD) analysis of a C-135 aircraft with a side-mounted splitter plate (with comparison to wind tunnel data)
[AD-A292029] p 2571 N95-29187
A two element laminar flow airfoil optimized for cruise
[NASA-CR-198580] p 2489 N95-29338
Boundary-layer transition and global skin friction measurement with an oil-fringe imaging technique
[NASA-CR-198814] p 2579 N95-30224
A numerical study of the small scale wing-body junction problem p 2491 N95-30235
WIRE
Transport phenomena and noise in real quantum wires
[AD-A290493] p 2714 N95-29152
WIRING
Development of LaRC (TM): IA thermoplastic polyimide coated aerospace wiring
[NASA-CR-195048] p 2548 N95-30252
WORDS (LANGUAGE)
Conversion of the TRACON operations concepts database into a formal sentence outline job task taxonomy
[DOT/FAA/AM-95/16] p 2493 N95-28819
US photovoltaic patents: 1991-1993
[DE95-004051] p 2603 N95-30017
WORK-REST CYCLE
Shift work, age, and performance: Investigation of the 2-2-1 shift schedule used in Air Traffic Control facilities I. The sleep/wake cycle
[DOT/FAA/AM-95/19] p 2638 N95-29261
WORKING FLUIDS
Activities update
[AD-A292431] p 2692 N95-28994
WORKLOADS (PSYCHOPHYSIOLOGY)
Improving problem-solving and decision-making skills under stress: Prediction and training
[AD-A292104] p 2638 N95-28918
Task-dependent effects of automation: The role of internal models in performance, workload, and situational awareness in a semi-automated cockpit
[AD-A292538] p 2640 N95-28969
Improved operator awareness of teleoperated land vehicle attitude
[AD-A290443] p 2641 N95-29359
WORKSTATIONS
Interactive multimedia presentation for applied computer tomography: Impact
[AD-A291955] p 2640 N95-29020
Developing a workstation-based, real-time simulation for rapid handling qualities evaluations during design
[NASA-CR-198831] p 2499 N95-30335
WORLD WIDE WEB
Implementing distributed server groups for the World Wide Web
[AD-A292221] p 2658 N95-29196
WOUND HEALING
Analysis of wounds by evaporative water loss in man
[AD-A290327] p 2634 N95-29086
Studies of altered response to infection induced by severe injury
[AD-A288907] p 2634 N95-29139
WOVEN COMPOSITES
Novel cost controlled materials and processing for primary structures p 2514 N95-28830
Cross-stiffened continuous fiber structures p 2521 N95-29041
An engineering model of woven composites based on micromechanics p 2521 N95-29042
Effects of thermal and moisture cycling on the internal structure of stitched RTM laminates p 2522 N95-29048

X

X RAY ANALYSIS
Synthesis and characterization of (Me3SiCH2)3M(dot)E(SiMe3)3 (M = Ga, E = P or As; M = In, E = P). X-ray crystal structures of (Me3SiCH2)3Ga(dot)P(SiMe3)3 and (Me3SiCH2)3In(dot)P(SiMe3)3
[AD-A291907] p 2715 N95-29444
Structure and orientation behavior of highly oriented polymers under tensile and compressive stresses p 2546 N95-29822
X RAY ASTRONOMY
X-ray observations of rapidly rotating O stars
[NASA-CR-189423] p 2726 N95-28822
Yohkoh Soft X-ray Telescope
[NASA-CR-197655] p 2726 N95-29172
A search for cataclysmic variables in globular clusters p 2727 N95-29532
The x-ray scattering halo around Sco-X1 p 2727 N95-29591
The complex broadband x-ray spectra of Seyfert galaxies p 2730 N95-29776
X RAY BINARIES
The evolution of binary millisecond pulsars and the formation of planets around them p 2733 N95-29663

X RAY DIFFRACTION
High T(sub c) superconductor/ferroelectric heterostructures
[AD-A291016] p 2716 N95-29658
X RAY FLUORESCENCE
Experimental studies of electromagnetic propagation at ultrahigh intensities
[AD-A290284] p 2553 N95-29081
Chromium plating and electropolishing solution analyses by online x ray fluorescence spectroscopy
[AD-A290023] p 2541 N95-29138
X RAY IMAGERY
The x-ray scattering halo around Sco-X1
p 2727 N95-29591
X RAY INSPECTION
Impact damage resistance and residual property assessment of (0/+/-45/90)s SCS-6/Timetal 21S
[NASA-TM-110178] p 2529 N95-30340
X RAY IRRADIATION
Thickness measurement of ammonia targets used in SLAC e143 experiment
[AD-A290215] p 2692 N95-29076
X RAY LASERS
Research studies in electromagnetically induced transparency
[AD-A290796] p 2557 N95-29645
X RAY SCATTERING
Real-time x-ray scattering study of processing of eight performance thermoplastics
[AD-A290374] p 2542 N95-29230
The x-ray scattering halo around Sco-X1
p 2727 N95-29591
X RAY SOURCES
X-ray observations of rapidly rotating O stars
[NASA-CR-189423] p 2726 N95-28822
A search for cataclysmic variables in globular clusters
p 2727 N95-29532
The x-ray scattering halo around Sco-X1
p 2727 N95-29591
High T(sub c) superconductor/ferroelectric heterostructures
[AD-A291016] p 2716 N95-29658
X RAY SPECTRA
Si 13 emission lines in solar flare x ray spectra obtained with the P78-1 satellite
[AD-A290000] p 2738 N95-29279
Yohkoh Bragg Crystal Spectrometer light curves for Ca 29(3.1633 - 3.1933 A): 1 October 1993 - 30 September 1994
[AD-A290027] p 2738 N95-29327
The complex broadband x-ray spectra of Seyfert galaxies p 2730 N95-29776
X RAY SPECTROSCOPY
XPS study of Ni-Fe manganite thermistor material
[DE95-008778] p 2561 N95-28961
Chromium plating and electropolishing solution analyses by online x ray fluorescence spectroscopy
[AD-A290023] p 2541 N95-29138
Yohkoh Bragg Crystal Spectrometer light curves for Ca 29(3.1633 - 3.1933 A): 1 October 1993 - 30 September 1994
[AD-A290027] p 2738 N95-29327
Surface studies of Poly(organophosphazenes) containing dimethylsiloxane grafts
[AD-A291909] p 2543 N95-29355
High T(sub c) superconductor/ferroelectric heterostructures
[AD-A291016] p 2716 N95-29658
X RAY STARS
Models of accretion-powered x-ray pulsars
p 2728 N95-29667
X RAY TELESCOPES
Nobeyama Radio Observatory report, no. 361: The radio properties of solar active region soft x-ray transient brightenings p 2737 N95-29098
Yohkoh Soft X-ray Telescope
[NASA-CR-197655] p 2726 N95-29172
X RAYS
Cellular and molecular level responses after radiofrequency radiation exposure, alone or in combination with x rays or chemicals
[AD-A292488] p 2633 N95-28866
Interactive multimedia presentation for applied computer tomography: Impact
[AD-A291955] p 2640 N95-29020
Observations and analysis of solar flares at radio and other wavelengths p 2738 N95-29202
An ultra-high speed incoherent-to-coherent converter for optical computing
[AD-A292658] p 2700 N95-29412
Coherent soft x-ray generation using a powerful subpicosecond laser p 2587 N95-29689
X-ray emission from Hybrid stars
p 2740 N95-29779
Observation of x ray generation in a proof-of-principle laser synchrotron source experiment
[AD-A291298] p 2588 N95-29937
X-31 AIRCRAFT
Evaluation of proposed agility metrics using X-31 vs. F/A-18 flight data
[AD-A292573] p 2496 N95-28977
XENON
Experimental studies of electromagnetic propagation at ultrahigh intensities
[AD-A290284] p 2553 N95-29081
Photothermal deflection in a supercritical fluid
p 2701 N95-29630
Characterisation of a line-tunable He-Xe laser operating at 2.026 and 3.894 micrometers
[AD-A291129] p 2587 N95-29914
XENON LAMPS
Design of a more accurate, higher fidelity, dual-source air mass zero solar simulator
[AD-A291364] p 2603 N95-29953

Y

YAG LASERS
Linewidth-insensitive coherent analog optical links
[AD-A292422] p 2698 N95-28992
Research instrumentation for polytechnic university's supersonic wind tunnel facility
[AD-A290232] p 2502 N95-29468
YBCO SUPERCONDUCTORS
Materials science and fabrication of YBCO-SrTi(1-x)Nb(x)O3-YBCO device structures
[AD-A292527] p 2712 N95-28815
Synthesis and characterization of CuO superconductors with high transient temperatures
[AD-A292478] p 2562 N95-29014
Processing, fabrication, characterization and device demonstration of high temperature superconducting ceramics
[AD-A290183] p 2541 N95-29055
HTS Josephson technology on silicon with application to high speed digital microelectronics
[AD-A290206] p 2562 N95-29061
Processing, fabrication, and demonstration of HTS integrated microwave circuits
[AD-A292480] p 2562 N95-29073
Processing, fabrication, and demonstration of HTS integrated microwave circuits
[AD-A290220] p 2562 N95-29078
High Tc superconducting bolometric and nonbolometric infrared (IR) detectors
[NASA-CR-198789] p 2702 N95-30035
YIELD STRENGTH
The effects of alloying elements on the strength and cooling rate sensitivity of ultra-low carbon alloy steel weld metals
[AD-A290681] p 2537 N95-29759
YTTRIUM OXIDES
Deposition and surface treatment with intense pulsed ion beams
[DE95-007885] p 2543 N95-29465
YUGOSLAVIA
United Nations aeromedical evacuation operations in the former Yugoslavia p 2676 N95-29607
Experiences learned from the Spanish armed forces aeromedical evacuation system in the former Yugoslavia
p 2677 N95-29614

Z

ZERO ANGLE OF ATTACK
Increments in aerofoil lift coefficient at zero angle of attack and in maximum lift coefficient due to deployment of a plain trailing-edge flap, with or without a leading-edge high-lift device, at low speeds
[ESDU-94028] p 2486 N95-28885
Increments in aerofoil lift coefficient at zero angle of attack and in maximum lift coefficient due to deployment of a trailing-edge split flap, with or without a leading-edge high-lift device, at low speeds
[ESDU-94029] p 2488 N95-29129
Increments in aerofoil lift coefficient at zero angle of attack and in maximum lift coefficient due to deployment of various leading-edge high-lift devices at low speeds
[ESDU-94027] p 2490 N95-29898
Introduction to the estimation of the lift coefficients at zero angle of attack and at maximum lift for aerofoils with high-lift devices at low speeds
[ESDU-94026] p 2491 N95-29899
ZINC OXIDES
Overview of the space debris environment
[AD-A292302] p 2507 N95-28867
ZINC TELLURIDES
Raman and photo-modulated reflectivity studies of ZnTe/InAs semiconductor heterostructure under hydrostatic pressure
[AD-A290467] p 2716 N95-29506
Electronic states in Cd(1-x)Zn(x)Te/CdTe strained layer coupled double quantum wells and their photoluminescence
[DE95-006806] p 2716 N95-29814
ZIRCONIUM
Influence of dislocation-solute interactions on the mechanical properties of zirconium-doped NiAl
[DE95-008848] p 2538 N95-30179
ZIRCONIUM OXIDES
High-toughness glass-ceramics
[AD-A290562] p 2541 N95-29071
Alumina reinforced Tetragonal Zirconia (TZP) composites
[DE95-008990] p 2529 N95-30180
ZOOPLANKTON
Automated analysis of zooplankton size and taxonomic composition using the video plankton recorder
[AD-A289725] p 2631 N95-28685

Typical Personal Author Index Listing

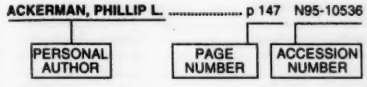

Listings in this index are arranged alphabetically by personal author. The page number helps you locate the citation in the abstract section. The accession number denotes the number by which the citation is identified.

A

AARONS, JULES ..... p 2614 N95-29585
AARTS, E. H. L. ..... p 2666 N95-30101
p 2667 N95-30222
ABATT, F. GEORGE ..... p 2595 N95-29546
ABBASCHIAN, REZA ..... p 2527 N95-29842
ABDOW, DAVID A. ..... p 2595 N95-29192
ABDUL-AZIZ, ALI A. ..... p 2570 N95-29131
ABE, TAKASHI ..... p 2490 N95-29640
p 2575 N95-29712
ABOWD, GREGORY ..... p 2645 N95-28894
ABRAHAM, DOUGLAS A. ..... p 2557 N95-29489
ACKEERMAN, PHILLIP L. ..... p 2638 N95-28918
ACKERMAN, THOMAS P. ..... p 2628 N95-30356
ACKERS, DEANE E. ..... p 2501 N95-30254
ADAMS, GEORGE F. ..... p 2534 N95-29994
ADAN, I. J. B. F. ..... p 2667 N95-30221
ADANUVOR, PROSPER K. ..... p 2511 N95-30257
ADKINS, JAMES D. ..... p 2539 N95-28784
ADLER, DICK ..... p 2553 N95-29159
p 2558 N95-29904
AFTOSMIS, MICHAEL J. ..... p 2481 N95-28740
p 2482 N95-28746
AGGARWAL, ISHWAR D. ..... p 2703 N95-30076
AHMED, R. ..... p 2597 N95-30328
AHN, HYEYEON ..... p 2558 N95-29707
AIFANTIS, E. C. ..... p 2595 N95-29535
AKAISHI, K. ..... p 2709 N95-29808
p 2711 N95-30032
AKAISHI, KENYA ..... p 2709 N95-29801
AKDAG, VEDAT ..... p 2483 N95-28752
AKIYAMA, R. ..... p 2705 N95-29567
p 2707 N95-29742
p 2709 N95-29802
AKSAY, ILHAN A. ..... p 2541 N95-29055
AL-JALAHMA, DAFER R. ..... p 2555 N95-29289
ALAMO, R. G. ..... p 2535 N95-30113
ALBERTODEOLIVEIRA, CARLOS ..... p 2722 N95-29363
ALEM, NABIH M. ..... p 2492 N95-29057
ALEXANDER, EDWARD M. ..... p 2554 N95-29236
ALEXANDER, MILLARD H. ..... p 2692 N95-29082
ALFREY, CLARENCE P. ..... p 2633 N95-28875
ALHO, KARI ..... p 2655 N95-30283
ALLCOCK, HARRY R. ..... p 2543 N95-29355
p 2543 N95-29358
ALLEN, DAVID H. ..... p 2513 N95-28809
ALLEN, MAX J. ..... p 2727 N95-29529
ALLEN, ROBERT ..... p 2645 N95-28894
ALLTOP, W. O. ..... p 2658 N95-28955
ALMAND, KATHLEEN H. ..... p 2526 N95-29598
ALONSO-RODRIGUEZ, C. ..... p 2676 N95-29610
ALSTROEM, PREBEN ..... p 2668 N95-30279
ALTER, STEPHEN J. ..... p 2482 N95-28750
ALURU, NARAYANA R. ..... p 2661 N95-30295
ALVIC, D. R. ..... p 2611 N95-30212
ALWITT, ROBERT S. ..... p 2568 N95-30268
AMANTEA, R. ..... p 2646 N95-29066
AMBROSE, JOSEPH GEORGE ..... p 2699 N95-29222
AMBUR, DAMODAR R. ..... p 2499 N95-28841
p 2517 N95-28847
p 2529 N95-30341
AMER, PAUL D. ..... p 2652 N95-30042
AMERI, A. A. ..... p 2574 N95-29371
AMES, GREGORY ..... p 2589 N95-28791
AMIMOTO, S. ..... p 2504 N95-29992
AMINPOUR, MOHAMMAD A. ..... p 2517 N95-28848
AMIT, YALI ..... p 2675 N95-29634
AMO, HIROYOSHI ..... p 2708 N95-29755
AMZAJERDIAN, FARZIN ..... p 2585 N95-29247
ANDELMAN, RICH M. ..... p 2521 N95-29043
ANDERSH, DENNIS ..... p 2553 N95-29159
p 2558 N95-29904
ANDERSON, C. H. ..... p 2714 N95-29157
ANDERSON, CHARLES R. ..... p 2497 N95-29426
ANDERSON, ELGIN A. ..... p 2487 N95-28921
ANDERSON, FREDERICK ..... p 2499 N95-30335
ANDERSON, JAY ..... p 2731 N95-30004
ANDERSON, O. ..... p 2683 N95-28973
ANDERSON, R. C. ..... p 2601 N95-30061
ANDERSON, SCOTT L. ..... p 2533 N95-29722
ANDO, A. ..... p 2705 N95-29567
ANDREAS, EDGAR L. ..... p 2620 N95-29193
ANDREWS, JOHN M. ..... p 2664 N95-29499
ANGEL, S. M. ..... p 2523 N95-29189
ANGEVINE, WAYNE MERRILL ..... p 2617 N95-29777
ANGLIN, COLIN ..... p 2513 N95-28817
APARICIO, J. ..... p 2677 N95-29611
APERS, P. M. G. ..... p 2725 N95-30208
ARIMOTO, H. ..... p 2707 N95-29742
p 2709 N95-29802
ARNEGARD, MATTHEW ..... p 2609 N95-29450
ARNOLD, FRANCES H. ..... p 2692 N95-29388
ARRIGOTTI, S. ..... p 2535 N95-30111
ARULGNANENDRAN, V. R. ..... p 2632 N95-29320
ASAY, JAMES ..... p 2507 N95-28852
ASCOLI, EDWARD P. ..... p 2484 N95-28762
ASSOUFID, LAHSEN ..... p 2718 N95-30184
ATASSI, HAFIZ M. ..... p 2582 N95-30161
ATHANASSOPOULOS, JOANNA DIMITRIOS EVA
p 2617 N95-29796
ATKINS, HAROLD L. ..... p 2686 N95-30135
ATKINSON, DALE ..... p 2507 N95-28852
ATTENBOROUGH, KEITH ..... p 2685 N95-30084
AUBUCHON, STEVEN R. ..... p 2713 N95-28993
p 2715 N95-29486
AUGI, JOSEPH M. ..... p 2527 N95-29638
AUGL, JOSEPH M. ..... p 2518 N95-28951
AURIAULT, L. ..... p 2674 N95-30145
AVALLONE, LINNEA MARIE ..... p 2618 N95-29830
AVILA, J. H. ..... p 2660 N95-30193
AYERS, ELIZABETH L. ..... p 2552 N95-28936
AZUMI, M. ..... p 2706 N95-29734
p 2707 N95-29741
p 2707 N95-29744
p 2709 N95-29809

B

BABAN, F. ..... p 2504 N95-29992
BABCOCK, S. M. ..... p 2654 N95-30189
BABUSKA, I. ..... p 2668 N95-29065
BABUSKA, IVO ..... p 2668 N95-29064
BABUSKA, IVO M. ..... p 2669 N95-29080
p 2669 N95-29084
BABUSKA, VIT ..... p 2508 N95-29408
BACCARO, I. ..... p 2558 N95-29919
BAEDER, JAMES D. ..... p 2688 N95-30146
BAETEN, J. C. M. ..... p 2673 N95-30106
p 2560 N95-30203
BAGANOFF, DONALD ..... p 2658 N95-29074
BAGOT, KEITH W. ..... p 2502 N95-29967
BAHAR, EZEKIEL ..... p 2559 N95-29982
BAILEY, JOHN ..... p 2644 N95-28807
BAILOR, PAUL ..... p 2653 N95-30080
BAINS, N. J. ..... p 2517 N95-28844
BAIRD, DONALD G. ..... p 2544 N95-29494
BAJAJ, A. K. ..... p 2594 N95-28853
BAK, PER ..... p 2668 N95-30279
BAKER, LEONARD ..... p 2559 N95-29975
BAKER, LEONARD H. ..... p 2559 N95-29940
BAKER, NANCY L. ..... p 2619 N95-28938
BAKER, TIMOTHY J. ..... p 2481 N95-28742
BAKOS, ROBERT J. ..... p 2503 N95-30228
BAKSHI, P. ..... p 2705 N95-29519
BALACHANDRAN, U. ..... p 2716 N95-29984
BALDWIN, RYAN A. ..... p 2715 N95-29444
BANIT, MENASHE ..... p 2733 N95-29663
BANKS, H. T. ..... p 2672 N95-30086
BAOTANG, YANG ..... p 2703 N95-30064
BAR-SHALOM, YAAKOV ..... p 2494 N95-28887
BARAKAT, RICHARD ..... p 2701 N95-29646
BARB, F. D. ..... p 2666 N95-30041
BARCLAY, REBECCA O. ..... p 2721 N95-29028
BARGHOUTHI, IMAD AHMAD ..... p 2704 N95-29205
BARILE, RONALD G. ..... p 2531 N95-29248
BARK, JONG SONG ..... p 2514 N95-28828
BARLOW, JOEL W. ..... p 2527 N95-29732
BARNES, R. ..... p 2642 N95-28818
BARON, M. ..... p 2508 N95-29464
BARRIE, RONALD E. ..... p 2519 N95-29033
BARRIENTOS, J. M. ..... p 2493 N95-29855
BARRY, CAROL LEE ..... p 2723 N95-29518
BARSHTEIN, GREGORY ..... p 2636 N95-29557
BARTELS, ROBERT EDWIN ..... p 2579 N95-30290
BARTOLI, F. J. ..... p 2564 N95-29568
BASCOM, WILLIARD D. ..... p 2514 N95-28827
BASS, H. ..... p 2683 N95-28973
BASSMAN, MITCHELL J. ..... p 2644 N95-28806
BASTIAANSEN, H. J. M. ..... p 2702 N95-30054
BATES, CLAYTON W., JR. ..... p 2523 N95-29124
p 2554 N95-29240
BATIA, SHARON ..... p 2638 N95-29090
BATRA, ROMESH C. ..... p 2715 N95-29234
p 2650 N95-29517
p 2596 N95-29582
BAUCOM, K. C. ..... p 2717 N95-29990
p 2717 N95-30005
BAUER, ERNEST ..... p 2510 N95-29284
BAUER, G. ..... p 2563 N95-29191
BAULDOCK, BARBARA T. ..... p 2723 N95-29449
BAUM, GEORGE N. ..... p 2548 N95-29280
BAUMAN, LESLIE E. ..... p 2530 N95-28776
BAUMEISTER, KENNETH J. ..... p 2683 N95-29401
BAUSCH, MARK J. ..... p 2545 N95-29586
BAYGENTS, JAMES C. ..... p 2565 N95-29968
BAYHA, T. D. ..... p 2519 N95-29035
BAYLOSIS, BENITO E. ..... p 2683 N95-29232
BEAMAN, JOSEPH J. ..... p 2527 N95-29732
BEARMAN, PETER ..... p 2575 N95-29654
BEAUBIEN, DAVID J. ..... p 2627 N95-29944
BEAUDAN, PATRICK ..... p 2573 N95-29268
BEAUSSART, A. J. ..... p 2514 N95-28829
BECHER, P. F. ..... p 2528 N95-30175
BEDAIR, SALAH ..... p 2713 N95-28954
BEER, RANDALL D. ..... p 2666 N95-30026
BEGUELIN, ADAM ..... p 2724 N95-29818
BELIHAR, ROBERT P. ..... p 2677 N95-29612
BELINSKY, STEVEN A. ..... p 2635 N95-29188
BELK, DAVY M. ..... p 2480 N95-28738
BELL, KATHERINE ROBBINS ..... p 2732 N95-29530
BELLE, RICHARD A. ..... p 2526 N95-29598
BELYTSCHKO, TED ..... p 2671 N95-29516
BENFORD, GREGORY ..... p 2703 N95-29001
BENJAMIN, THEODORE G. ..... p 2480 N95-28733
BENSON, VERNON M. ..... p 2514 N95-28832
BENTLEY, J. ..... p 2538 N95-30038
BENTLEY, R. D. ..... p 2738 N95-29327
BENWELL, BRUCE T. ..... p 2551 N95-28687
BERDING, M. A. ..... p 2702 N95-29978
BEREZHIANI, V. I. ..... p 2711 N95-30173
BERGELSON, LEV ..... p 2636 N95-29557
BERGER, ANNMARIE ..... p 2641 N95-29378
BERGER, MARSHA J. ..... p 2481 N95-28740
BERGLUND, C. NEIL ..... p 2715 N95-29267
BERGMAN, KAREN ..... p 2697 N95-28799
BERGSTRA, J. A. ..... p 2673 N95-30106
BERKHEISER, W. E., III ..... p 2608 N95-28920
BERKOFF, TIM ..... p 2699 N95-29283
BERNHOLC, JERRY ..... p 2713 N95-28954
BERNKOPF, JAN ..... p 2556 N95-29472
BERRICK, STEPHEN W. ..... p 2555 N95-29266
BERRY, KENNETH J. ..... p 2620 N95-29254

BERTRAM, JAMES L. p 2521 N95-29044
BERZINS, VALDIS p 2650 N95-29515
BEUTNER, THOMAS JOHN p 2502 N95-29795
BHATTACHARYA, P. p 2712 N95-28874
BIBEAU, MICHAEL p 2553 N95-29002
BICKHAM, JERRY L. p 2646 N95-28968
BIDINGFIELD, RALPH A. p 2682 N95-30051
BIEFELD, R. M. p 2717 N95-29990
p 2717 N95-30005
BIELECKA, DEBORAH E. p 2542 N95-29314
BIEN, FRITZ p 2613 N95-29317
BIEZAD, DANIEL J. p 2499 N95-30335
BILLS, K. C. p 2654 N95-30189
BINDER, MICHAEL P. p 2510 N95-29114
BINFORD, THOMAS O. p 2650 N95-29576
BIRINGEN, SEDAT p 2579 N95-30250
BISBERG, ARTHUR F. p 2627 N95-29944
BISHOP, R. F. p 2694 N95-30065
BIXLER, T. p 2504 N95-29992
BJORNSTAD, S. C. p 2627 N95-30048
BLACKBURN, MICHAEL R. p 2553 N95-29166
BLANCHETTE, MARTIN p 2555 N95-29328
BLANDFORD, G. E. p 2528 N95-29864
BLANKINSHIP, ROSS p 2664 N95-29657
BLANTON, CHRISTOPHER L. p 2635 N95-29173
BLERMAN, GREGORY S. p 2493 N95-28716
BLOOM, E. D. p 2739 N95-29265
BLOOM, STEVEN DAVID p 2728 N95-29665
BLOOMQUIST, CARROLL R. p 2676 N95-29605
BLUME, HANS-JUERGEN C. p 2506 N95-30251
BLUMENTHAL, PHILIP Z. p 2503 N95-30067
BOBB, LLOYD C. p 2703 N95-30166
BODINE, J. B. p 2516 N95-28839
BOERSTOEL, J. W. p 2484 N95-28760
BOGDANOVICH, ALEXANDER E. p 2513 N95-28825
BOHON, HERMAN L. p 2513 N95-28823
p 2518 N95-29029
BOIVIN, LUC p 2697 N95-28799
BOKOR, J. p 2561 N95-29010
BOLEY, MARK S. p 2716 N95-29506
BOLUKBASI, AKIF OKSAL p 2524 N95-29411
BONITO, N. A. p 2507 N95-29026
BONNETT, DAVID p 2532 N95-29357
BONTEKOE, TJ. R. p 2735 N95-29840
BOOKHART, JAMES R., JR. p 2680 N95-29072
BOOZ, JULIETA E. p 2496 N95-28977
BORGES, CARLOS F. p 2648 N95-29304
BORMAN, GARY L. p 2590 N95-29820
BORUCKI, W. p 2737 N95-30058
BOSCHAN, R. S. p 2543 N95-29482
BOSMA, M. p 2547 N95-30201
BOSSI, RICHARD H. p 2640 N95-29020
BOSUA, R. p 2653 N95-30105
p 2655 N95-30218
BOTTONE, STEVEN p 2608 N95-28922
BOUCHARD, M. P. p 2492 N95-28811
BOUGHTON, BRIAN E. p 2550 N95-29307
BOUILLARD, J. X. p 2577 N95-29988
p 2578 N95-30187
BOUNAR, K. H. p 2507 N95-29026
BOURASSA, MARK ALLAN p 2626 N95-29876
BOURASSA, R. J. p 2512 N95-30225
BOURELL, DAVID L. p 2527 N95-29732
BOWER, GLENN R. p 2590 N95-29820
BOWER, W. W. p 2690 N95-30158
BOWERS, J. S. p 2593 N95-29946
BOWLES, M. R. p 2714 N95-29157
BOYCE, D. E. p 2591 N95-30273
BOYER, BRADLEY S. p 2499 N95-28691
BOYER, DON L. p 2569 N95-29060
BOYER, KEITH p 2553 N95-29081
p 2501 N95-29934
BOYLE, CHARLES p 2740 N95-28882
BOYLE, R. J. p 2574 N95-29371
BRAATEN, F. D. p 2721 N95-28958
BRADLEY, PAULA L. p 2635 N95-29188
BRADY, ROBERT F., JR. p 2539 N95-28784
BRANECKY, R. J. p 2591 N95-30110
BRANNON, ROBERT H. p 2677 N95-29612
BRASKI, D. N. p 2561 N95-28961
BRENDLEY, KEITH p 2651 N95-29736
BRENNER, JOSEPH R. p 2621 N95-29416
BRIDGES, JAMES E. p 2477 N95-30229
BRIDGES, SUSAN p 2630 N95-29237
BRIDGES, W. M. p 2720 N95-28797
p 2722 N95-29287
BRIGGS, J. S. p 2502 N95-29522
BRIGGS, MATTHEW E. p 2701 N95-29630
BRINDLEY, WILLIAM J. p 2512 N95-29373
BRINKKEMPER, S. p 2653 N95-30094
p 2653 N95-30105
p 2655 N95-30218
BRISTOW, JOHN p 2644 N95-28805
BRITTON, DORIS L. p 2567 N95-30256
p 2511 N95-30257
BROOKS, KATHY p 2638 N95-29090
BROUSSEAU, N. p 2700 N95-29354
BROWN, CHRISTOPHER A. p 2548 N95-30237
BROWN, D. E. p 2672 N95-30086
BROWN, DAVID GILLESPIE p 2706 N95-29686
BROWN, E. R. p 2564 N95-29384
BROWN, GAIR D. p 2702 N95-30053
BROWN, H. L. p 2591 N95-30211
BROWN, HERBERT C. p 2533 N95-29556
BROWN, JAY L. p 2642 N95-28974
BROWN, JEFF L. p 2681 N95-28987
BROWN, K. D. p 2654 N95-30115
BROWN, KENDALL K. p 2652 N95-30013
BROWN, MICHAEL E. p 2639 N95-29439
BROWN, O. p 2628 N95-30343
BROWN, P. N. p 2711 N95-30130
BROWN, RICHARD B. p 2643 N95-29381
BROWN, ROBERT L. p 2601 N95-29866
BROWN, T. p 2515 N95-28835
BRUCKART, J. E. p 2678 N95-29620
BRYANT, RANDY p 2721 N95-28880
BUB, FRANK LEE p 2631 N95-29541
BUCHNER, STEPHEN p 2584 N95-28892
BUCKLEY, JAMES HENRY p 2739 N95-29531
BUFFMAN, ELIZABETH V. p 2723 N95-29449
BUI, TRONG T. p 2657 N95-30157
BUKHARI, SAMEER ABDULELAH p 2600 N95-29730
BUKUR, DRAGOMIR B. p 2533 N95-29870
BULIK, TOMASZ WOJCIECH p 2728 N95-29667
BURCHELL, M. J. p 2703 N95-30062
BURGE, S. W. p 2577 N95-29988
BURGESS, T. W. p 2710 N95-29909
BURRAHM, R. W. p 2591 N95-30110
BURTON, JOE E. p 2635 N95-29161
BUSSELL, KERRI p 2560 N95-30336
BUTLER, CHRISTOPHER L. p 2629 N95-29023
BUTLER, P. BARRY p 2532 N95-29357
BUTLER, ROBERT J. p 2574 N95-29380
BYME, C. A. p 2546 N95-30030
BYRD, RICHARD H. p 2670 N95-29385
BYRNES, C. I. p 2665 N95-29971

C

CABLE, THOMAS L. p 2606 N95-30265
CAI, BANGWEI p 2584 N95-28679
CAI, FENGYI p 2685 N95-29681
CAI, Y. p 2665 N95-29987
CAIN, A. B. p 2690 N95-30158
CAIRNS, DOUGLAS S. p 2515 N95-28833
CAIRNS, JOHN, JR. p 2609 N95-29450
CALISE, ANTHONY J. p 2504 N95-29339
CALVERT, JEFFREY M. p 2530 N95-28854
CAMERON, JAMES F. p 2542 N95-29272
CAMERON, KEITH p 2497 N95-29362
CAMPBELL, JOHN C. p 2542 N95-29269
CAMPBELL, R. B. p 2711 N95-30130
CAMPILLO, ANTHONY J. p 2585 N95-29217
CANNELL, MICHAEL J. p 2567 N95-30122
CANNON-BOWERS, J. p 2720 N95-29935
CANO, ROBERTO J. p 2520 N95-29037
CANTRELL, CHRIS p 2531 N95-29248
CAPSIMALIS, G. P. p 2594 N95-28949
CARABELL, KEVIN DAVID p 2590 N95-29807
CARLSON, TOBY N. p 2627 N95-29993
CARMODY, MEGHAN A. p 2640 N95-28969
p 2640 N95-28970
CARNE, T. p 2597 N95-30210
CARRINGTON, C. K. p 2507 N95-28721
CARROLL, BONNIE C. p 2723 N95-29449
CARROLL, THOMAS R. p 2600 N95-29754
CARSON, ELIZABETH A. p 2640 N95-28794
CARTER, SUSAN V. p 2598 N95-28931
p 2601 N95-29977
CARTER, W. C. p 2521 N95-29042
CARUTHERS, JOHN E. p 2689 N95-30154
CASPER, JAY p 2690 N95-30159
CASPERSON, D. p 2508 N95-29464
CATES, GORDON D. p 2680 N95-28810
CATTANI, LUIS CARLOS p 2565 N95-29728
CAVIRIS, NICHOLAS P. p 2701 N95-29602
CEBE, PEGGY p 2542 N95-29230
CEPAS, J. p 2677 N95-29611
CERVENKA, PETER O. p 2698 N95-28996
CHABALOWSKI, C. F. p 2532 N95-29487
p 2720 N95-29936
CHABOYER, BRIAN CHARLES p 2733 N95-29669
CHAGANTY, NARASINGA R. p 2669 N95-29233
CHAMIS, C. C. p 2518 N95-28849
CHAN, PUI KING p 2623 N95-29713
CHANDRASEKHAR, H. R. p 2716 N95-29506
CHANDRASEKHAR, MEERA p 2716 N95-29506
CHANDRASEKHARA, M. S. p 2489 N95-29428
CHANG, CHIKUANG p 2667 N95-30238
CHANG, FAY W. p 2658 N95-28879
CHANG, FENGTENG p 2576 N95-29811
CHANG, FU-KUO p 2594 N95-29067
CHANG, HSIAO-LUNG p 2579 N95-30275
CHANG, S. L. p 2577 N95-29988
CHANG, SIN-CHUNG p 2574 N95-29372
CHAPMAN, DEAN R. p 2575 N95-29469
CHAPMAN, J. J. p 2583 N95-29453
CHAWNER, JOHN R. p 2483 N95-28751
CHELLAPPA, RAMA p 2590 N95-29552
CHEN, CHENG-TA p 2620 N95-29206
CHEN, J. T. p 2562 N95-29014
CHEN, LIANG-CHUN p 2630 N95-29237
CHEN, MING-HUEI p 2525 N95-29512
CHEN, PING p 2684 N95-29415
CHEN, S. S. p 2665 N95-29987
CHEN, SHING-BONG p 2548 N95-29019
CHEN, WENSHANG p 2701 N95-29661
CHENG, HUAINING p 2640 N95-28683
CHENG, JOHN p 2662 N95-28988
CHENG, ZHEMING p 2486 N95-28772
CHENNA, RAVI K. p 2590 N95-29369
CHEUNG, K. p 2695 N95-30191
CHIANG, JAMES p 2739 N95-29671
CHIESA, C. C. p 2601 N95-30061
CHILSON, PHILLIP BRUCE p 2627 N95-29877
CHING, CHAN Y. p 2568 N95-28719
CHING, W. Y. p 2681 N95-28923
CHO, CHAHEE P. p 2682 N95-30051
CHO, SE-HYUNG p 2726 N95-29101
CHOATE, TIMOTHY D. p 2510 N95-29584
CHOI, JUNHO p 2552 N95-28939
CHOI, KEEYOUNG p 2595 N95-29419
CHOO, YUNG K. p 2478 N95-28723
p 2479 N95-28732
CHOU, JIN J. p 2486 N95-28775
CHOW, ANDREA W. p 2496 N95-29027
CHOW, CHUEN-YEN p 2574 N95-29372
CHOW, L. C. p 2551 N95-30296
CHRISEY, LINDA A. p 2530 N95-28854
CHRISTE, K. O. p 2533 N95-29581
p 2702 N95-29974
CHRISTENSEN, CARL C. p 2638 N95-29627
CHRISTENSEN, DIANE G. p 2493 N95-29873
CHRISTIE, DAVID R. p 2642 N95-28976
CHRISTODOULOU, CHRISTODOULOS p 2487 N95-29094
CHU, B. p 2546 N95-30030
CHU, C. T. p 2607 N95-30269
CHU, JAN-HWA p 2627 N95-30044
CHU, JAY p 2607 N95-30269
CHU, JEROME T. p 2716 N95-29785
CHU, ROBERT L. p 2519 N95-29033
CHUI, C. J. p 2551 N95-30296
CHUNG, CATHY p 2689 N95-30152
CHUNG, CHANG-BUM p 2595 N95-29424
CHUNG, T. J. p 2575 N95-29421
CHUNG, VICTORIA I. p 2659 N95-29454
CHUNG, Y. W. p 2547 N95-30174
CHYCZEWSKI, THOMAS S. p 2688 N95-30148
CHYU, WEI J. p 2485 N95-28768
CIPOLLO, MICHAEL A. p 2683 N95-28999
CISAR, A. J. p 2605 N95-30263
CITTERIO, M. p 2566 N95-30025
CLAFFEY, KERRY J. p 2620 N95-29193
CLARK, BETH ELLEN p 2733 N95-29672
CLEVER, WILLARD C. p 2483 N95-28755
CLOSE, F. E. p 2691 N95-28913
COATES, DWAINE p 2567 N95-30261
COBLENTZ, DAVID DWIGHT p 2617 N95-29773
COFFEY, H. E. p 2737 N95-28780
p 2737 N95-28781
COFFIN, D. W. p 2514 N95-28829
COHEN, JEROME B. p 2524 N95-29326
COHEN, JUDAH LEVI p 2621 N95-29595
COHEN, ROBERT ALAN p 2623 N95-29714
COHEN, ROBERT E. p 2544 N95-29510
COHENOUR, BERNARD C. p 2733 N95-29599
COHN, DAVID p 2663 N95-29479
COHN, ROBERT W. p 2699 N95-29148
COIRIER, WILLIAM J. p 2480 N95-28739
COLE, J., III p 2478 N95-28720
COLEMAN, HOMER HOWARD, JR. p 2732 N95-29252
COLEMAN, HUGH W. p 2652 N95-30013
COLEMAN, THOMAS F. p 2633 N95-30114
COLLINGS, E. W. p 2682 N95-30131
COLLINS, GREGORY E. p 2512 N95-29052
COLLINS, LINDA BRANT p 2675 N95-30297
COLOSI, JOHN ANTHONY p 2630 N95-29528
COLPIER, L. p 2667 N95-30171
COLUCCI, DNARDO p 2701 N95-29706
COMBES, F. p 2731 N95-29097
COMBS, CYNTHIA L. p 2628 N95-30272
COMFORT, R. H. p 2711 N95-30338
CONCHA, MONICA C. p 2691 N95-28919
CONE, RUFUS L. p 2586 N95-29292

CONLON, E. S. ..... p 2738 N95-29279
CONNELL, STUART D. ..... p 2478 N95-28726
CONNOR, S. B. ..... p 2680 N95-29628
CONSTANTINE, BETSY ..... p 2499 N95-29123
COOK, R. L. ..... p 2531 N95-28916
COOL, ADRIENNE MARGARET .. p 2727 N95-29532
COONEY, JAMIE ..... p 2706 N95-29668
COORAY, A. ..... p 2618 N95-29981
CORNELISON, JONI W. ..... p 2480 N95-28733
CORNELIUS, J. R. ..... p 2616 N95-29737
p 2617 N95-29765
p 2618 N95-30082
COSGROVE, JOSEPH ..... p 2717 N95-30068
COSNER, RAYMOND R. ..... p 2478 N95-28724
COTE, P. J. ..... p 2535 N95-28889
COUGHLAN, SHARON D. ..... p 2598 N95-28931
COURTRIGHT, WILLLIAM V., II. . p 2658 N95-28879
COUTERMARSH, BARRY ..... p 2629 N95-29160
COWARD, JOHN R. ..... p 2648 N95-29356
COX, B. N. ..... p 2521 N95-29042
COZZANI, F. ..... p 2696 N95-29142
CRAIG, R. ..... p 2737 N95-30058
CRANDALL, D. H. ..... p 2696 N95-29142
CRANSTON, ROBERT ..... p 2559 N95-30072
CRAVEN, P. D. ..... p 2711 N95-30338
CRAVEN, PAUL D. ..... p 2614 N95-29590
CRAVEY, ROBIN L. ..... p 2506 N95-30251
p 2560 N95-30336
CRAWFORD, GREGORY KIM ..... p 2704 N95-29215
CRAWFORD, RICHARD H. ..... p 2527 N95-29732
CRIMP, MARTIN A. ..... p 2537 N95-29526
CRISLER, WILLIAM PAUL ..... p 2487 N95-29102
CROCKETT, THOMAS W. ..... p 2655 N95-30306
CRONK, DAVID ..... p 2649 N95-29404
CROSIER, RONALD B. ..... p 2670 N95-29296
CRUZ, CRYSTAL E. ..... p 2638 N95-29261
CRUZ, JUAN R. ..... p 2517 N95-28845
CUCINELL, SAMUEL ..... p 2634 N95-29086
CUCINOTTA, FRANCIS A. ..... p 2696 N95-30337
CUI, YIFENG ..... p 2586 N95-29631
CULSHAW, BRIAN ..... p 2550 N95-29579
CUMNOCK, JUDY ANNE ..... p 2615 N95-29693
CURRAN, DONALD R. ..... p 2542 N95-29288
CUSOLI, F. ..... p 2731 N95-29C97
CUTIONGCO, E. C. ..... p 2547 N95-30174
CYBULSKI, JON ..... p 2551 N95-30299

D

DACOSTAFREITASYANASSE, CORINA
p 2601 N95-29999
DACOSTAPEREIRAJUNIOR, ALFREDO
p 2598 N95-28929
DACRES, CHESTER M. ..... p 2497 N95-29426
DADKHAH, M. S. ..... p 2521 N95-29042
DAGAN, ARIE ..... p 2636 N95-29557
DAGDIGIAN, PAUL J. ..... p 2692 N95-29082
DAHL, PETER H. ..... p 2629 N95-29085
DAHLEH, M. A. ..... p 2664 N95-29636
DAI, S. ..... p 2695 N95-28957
DAIGLE, GILLES A. ..... p 2685 N95-30084
DAINTY, J. C. ..... p 2701 N95-29766
DALANG, ROBERT C. ..... p 2669 N95-29229
DALTON, H. ..... p 2535 N95-30198
DANIEL, RALPH E. ..... p 2655 N95-30307
DANIELS, G. M. ..... p 2598 N95-29281
DANNENHOFFER, JOHN F., III ... p 2480 N95-28734
p 2485 N95-28769
DANNENHOFFER,, JOHN ..... p 2482 N95-28749
DASTIN, S. J. ..... p 2514 N95-28830
DAVIDSON, FREDERIC M. ..... p 2584 N95-28808
DAVIES, P. ..... p 2594 N95-28853
DAVIS, CABELL S. ..... p 2631 N95-28685
DAVIS, D. D., JR. ..... p 2517 N95-28847
DAVIS, H. A. ..... p 2543 N95-29465
DAVIS, JOEL L. ..... p 2634 N95-29059
DAVIS, JOHN G., JR. ..... p 2513 N95-28823
p 2518 N95-29029
p 2519 N95-29032
DAVIS, JOHN S. ..... p 2683 N95-28783
DAVIS, LAWRENCE ..... p 2499 N95-29123
DAVIS, R. C. ..... p 2517 N95-28847
DAVIS, R. F. ..... p 2712 N95-28910
p 2537 N95-29724
DAVIS, ROBERT F. ..... p 2713 N95-28954
DAVIS, ROGER E. ..... p 2555 N95-29266
DAVIS, SANFORD ..... p 2686 N95-30138
DAVIS, SANFORD S. ..... p 2686 N95-30136
DAVIS, T. ..... p 2556 N95-29474
p 2558 N95-29862
DAVISON, B. H. ..... p 2549 N95-30024
DAWSON, L. R. ..... p 2717 N95-30005
DAWSON, ROSAMARY ..... p 2638 N95-29090
DEACON, DAVID A. ..... p 2584 N95-29007
DEATON, JERRY W. ..... p 2515 N95-28834
p 2520 N95-29038
DEB, SOMNATH ..... p 2494 N95-28887
DEBY, R. A. ..... p 2725 N95-30100
DECARVALHO, VITOR CELSODE ..... p 2600 N95-29815
DECOCK, K. M. J. ..... p 2485 N95-28767
DECOUGNY, H. L. ..... p 2671 N95-29488
DEERENBERG, E. ..... p 2597 N95-30206
DEGROH, HENRY C., III ..... p 2535 N95-28701
DEGUCHI, S. ..... p 2735 N95-29837
DEJONG, T. ..... p 2735 N95-29840
DELABARRE, COLETTE MARIE . p 2727 N95-29648
DELCUL, G. D. ..... p 2695 N95-28957
DELLA ROCCO, PAMELA S. ..... p 2638 N95-29261
DELOMBARD, RICHARD ..... p 2509 N95-29643
p 2549 N95-30339
DELONG, KENNETH W. ..... p 2698 N95-28983
DELOREY, DENNIS E. ..... p 2725 N95-30043
DELOZANNE, ALEJANDRO ..... p 2561 N95-29005
DELPOZO, C. ..... p 2677 N95-29611
DELWORTH, THOMAS L. ..... p 2609 N95-29878
DEMAREE, J. D. ..... p 2585 N95-29208
p 2543 N95-29353
DEMETRIOU, CHRIS G. ..... p 2658 N95-28879
DEMOUSTIER, CHRISTIAN ..... p 2628 N95-28796
p 2628 N95-28865
DENG, WEI ..... p 2616 N95-29696
DESPER, C. R. ..... p 2546 N95-30030
DESU, S. B. ..... p 2540 N95-28963
p 2541 N95-29135
DESYLVA, MICHAEL J. ..... p 2681 N95-29000
DEVINE, K. D. ..... p 2671 N95-29488
DEVLIN, F. J. ..... p 2720 N95-29936
DEXTER, H. BENSON ..... p 2520 N95-29039
DICKENS, THOMAS P. ..... p 2484 N95-28761
DICKERMAN, CAREY L. ..... p 2626 N95-29868
DICKINSON, LARRY C. ..... p 2515 N95-28834
p 2522 N95-29046
DICKSON, WILLIAM CHARLES .. p 2662 N95-29095
DIETZ, H. G. ..... p 2658 N95-28965
DIGALAKIS, VASSILIOS ..... p 2557 N95-29564
DIGAVALLI, SASI K. ..... p 2489 N95-29243
DIGBY, SUSAN ..... p 2631 N95-30231
DIGGLE, DAVID WILLIAM ..... p 2494 N95-29542
DING, J. ..... p 2577 N95-29988
DIVECHA, AMARNATH P. ..... p 2560 N95-28855
DOERRY, A. W. ..... p 2560 N95-30177
DOLAND, JERRY ..... p 2645 N95-28821
DOLLING, D. S. ..... p 2572 N95-29228
DONAHUE, RONALD J. ..... p 2590 N95-29820
DONALDSON, WILLIAM R. ..... p 2700 N95-29379
DONG, THOMAS Z. ..... p 2690 N95-30160
DONG, XIAOYI ..... p 2685 N95-29681
DONGPEI, CHEN ..... p 2561 N95-28911
DONNELLY, R. HANK ..... p 2730 N95-29827
DONOHUE, JOHN ..... p 2552 N95-28939
DONOVAN, JAMES G. ..... p 2547 N95-30120
DONOVAN, JOHN F. ..... p 2571 N95-29211
DORFEL, G. ..... p 2720 N95-29935
DORRIS, WILLIAM J. ..... p 2517 N95-28846
DOSKOCIL, DOUG ..... p 2645 N95-28814
DOST, ERNEST ..... p 2513 N95-28826
DOST, ERNEST F. ..... p 2516 N95-28838
DOUGLAS, RANDAL KIRK ..... p 2592 N95-29786
DOW, JOHN D. ..... p 2560 N95-28813
DOW, MARVIN B. ..... p 2522 N95-29047
DOWBEN, PHILIP ..... p 2712 N95-28869
DOWSKI, EDWARD RAYMOND, JR.
p 2700 N95-29543
DOXBECK, M. ..... p 2594 N95-28949
DRAKE, JOHN L. ..... p 2567 N95-30122
DRDA, B. ..... p 2697 N95-28870
DRECHSLER, GENA K. ..... p 2493 N95-28819
DRESSICK, WALTER J. ..... p 2530 N95-28854
DRINGENBURG, NICK ..... p 2536 N95-29461
DRON, LISA ..... p 2647 N95-29179
DROSOPOULOS, ANASTASIOS . p 2722 N95-29221
DUBOIS, PATRICK ..... p 2536 N95-29461
DUBROVIN, L. ..... p 2642 N95-28722
DUDEK, JULIANNE C. ..... p 2492 N95-30253
DUDLEY, KENNETH L. ..... p 2560 N95-30336
DUFF, JAMES W. ..... p 2613 N95-29317
DULIKRAVICH, GEORGE S. ..... p 2578 N95-30034
DUNCANSON, JAMES P. ..... p 2641 N95-29908
DUNNING, T. ..... p 2568 N95-30270
DURAKO, BILL ..... p 2513 N95-28826
DUTTON, ROBERT W. ..... p 2661 N95-30295
DUVA, ANTHONY W. ..... p 2588 N95-28785
DUVALL, LORRAINE MARY ..... p 2724 N95-29828
DWYER, JOSEPH RICHARD ..... p 2740 N95-29705
DYSART, PAUL S. ..... p 2613 N95-29293

E

EAKES, MARK W. ..... p 2590 N95-29184
EATON, W. P. ..... p 2567 N95-30188
EBERHARDT, SCOTT ..... p 2485 N95-28764
EDDINS, WILLIAM R. ..... p 2723 N95-29589
EDWARDS, HENRY O. ..... p 2698 N95-28932
EDWARDS, MARK B. ..... p 2493 N95-28790
EDWARDS, MARSHALL ..... p 2664 N95-29657
EDWARDS, R. ..... p 2611 N95-28697
EFFENHAUSER, RAINER K. ..... p 2636 N95-29360
EGAN, MICHAEL P. ..... p 2733 N95-29649
EGGLETON, CHARLES DIONISIO p 2579 N95-30233
EHRLICH, K. ..... p 2696 N95-29142
EINMAHL, J. H. J. ..... p 2675 N95-30170
EISELE, F. L. ..... p 2501 N95-29764
EISEMAN, PETER R. ..... p 2480 N95-28735
p 2486 N95-28772
p 2486 N95-28774
EISENSTAT, STANLEY C. ..... p 2671 N95-29558
EL-FAKAHANY, ESAM E. ..... p 2635 N95-29153
ELIAS, GLENN ..... p 2645 N95-28814
ELIAS, WILLIAM ..... p 2568 N95-30268
ELLIOTT, D. C. ..... p 2602 N95-29463
ELSHERBENI, ATEF ..... p 2555 N95-29290
ELSMORE, TIMOTHY F. ..... p 2645 N95-28934
EMERY, WILLIAM ..... p 2601 N95-30247
EMMER, D. S. ..... p 2492 N95-28811
EMSLEY, HOWARD T. ..... p 2571 N95-29187
ENG, ANTHONY T. ..... p 2541 N95-29194
ENOME, S. ..... p 2737 N95-29098
ENOMOTO, FRANCIS Y. ..... p 2478 N95-28728
EPSTEIN, ALAN H. ..... p 2500 N95-29496
ERDMAN, PAUL S. ..... p 2602 N95-29949
ERENGIL, M. E. ..... p 2572 N95-29228
ERENGIL, MEHMET ERDAL ..... p 2570 N95-29096
ESAREY, E. ..... p 2588 N95-29937
ESPENAK, FRED ..... p 2731 N95-30004
ESSENS, P. ..... p 2720 N95-29935
EVAN, S. J. ..... p 2725 N95-30100
EVANS, DAVID A. ..... p 2568 N95-30271
EVANS, J. ..... p 2642 N95-28722
EVANS, K. FRANKLIN ..... p 2623 N95-29715
EVANS, N. D. ..... p 2538 N95-30038
EVEKER, KEVIN MICHAEL ..... p 2500 N95-29679
EWEN, JOHN R. ..... p 2521 N95-29041
EZAKI, KAZUHIRO ..... p 2709 N95-29801

F

FADEN, ALAN I. ..... p 2639 N95-29458
FAGHRI, AMIR ..... p 2570 N95-29127
FAHRINGER, THOMAS ..... p 2649 N95-29455
FALCONE, ANTHONY ..... p 2522 N95-29047
FALLESEN, J. ..... p 2720 N95-29935
FAN, J. D. ..... p 2563 N95-29163
FAN, WESLEY C. ..... p 2660 N95-30116
FARGUES, MONIQUE P. ..... p 2556 N95-29386
FARLEY, G. L. ..... p 2517 N95-28847
FARMER, W. S. ..... p 2659 N95-29420
FAROS, NIKOLAOS I. ..... p 2555 N95-29318
FARRIS, MICHAEL HOWARD ..... p 2580 N95-30301
FATH, JEFF ..... p 2553 N95-29159
p 2558 N95-29904
FEARS, SCOTT P. ..... p 2498 N95-30226
FECHETE, A. ..... p 2586 N95-29330
FEDRO, MARK J. ..... p 2520 N95-29040
FELDMANN, ANJA ..... p 2645 N95-28878
FELLEISEN, MATTIAS ..... p 2721 N95-28877
FELSTEIN, STEVEN R. ..... p 2540 N95-28925
FENG, WEI ..... p 2540 N95-29021
FENNER, DAVID B. ..... p 2717 N95-30068
FERKET, P. J. J. ..... p 2672 N95-30088
FERNANDEZ, FELIX E. ..... p 2544 N95-29484
FERNANDO, H. J. ..... p 2569 N95-29060
FERON, ERIC MARIE ..... p 2501 N95-29680
FERRANDO, WILLIAM A. ..... p 2560 N95-28855
FERZIGER, JOEL H. ..... p 2569 N95-29024
FEULNER, MATTHEW ROGER ... p 2500 N95-29244
FIELD, CHRISTOPHER T. ..... p 2584 N95-28808
FIELDS, RENNY A. ..... p 2587 N95-29931
FIFE, DENNIS W. ..... p 2550 N95-29918
FILIPCZAK, ROBERT A. ..... p 2551 N95-29924
FINCANNON, H. J. ..... p 2511 N95-30012
FINN, SCOTT R. ..... p 2516 N95-28838
FIRESTONE, ELAINE R. ..... p 2631 N95-30236
FISCHER, KENNETH WAYNE ..... p 2622 N95-29697
FISCHER, R. ..... p 2588 N95-29937
FISH, D. A. ..... p 2703 N95-30081
FISHER, A. ..... p 2588 N95-29937
FISHER, ALVAN, JR. ..... p 2629 N95-28873
FISHER, CRAIG A. ..... p 2685 N95-29945
FISK, CHARLES J. ..... p 2733 N95-29599
FITERMAN, A. ..... p 2674 N95-30353
FITZPATRICK, C. ..... p 2697 N95-28870
FLAHERTY, J. E. ..... p 2671 N95-29488
FLAHERTY, JOSEPH E. ..... p 2668 N95-28890
p 2650 N95-29480
p 2674 N95-29490
FLEDDERMAN, CHARLES ..... p 2703 N95-29003

FLIFLET, ARNE W. p 2563 N95-29301
FLURY, WALTER p 2507 N95-28852
FLYNN, B. W. p 2515 N95-28836
p 2499 N95-28840
FOGARTY, CHRIS p 2531 N95-29248
FOLEY, BRIAN T. p 2498 N95-29457
FOLLSTAEDT, D. M. p 2717 N95-29990
p 2717 N95-30005
FONG, T. K. p 2698 N95-28992
FONNE, V. M. p 2677 N95-29616
FORNWALL, MARK D. p 2723 N95-29449
FOSTER, CHRISTOPHER C. p 2563 N95-29239
FOSTER, I. T. p 2610 N95-30176
FOSTER, JEFFRY D. p 2489 N95-29402
FOUGERE, G. E. p 2537 N95-30018
FOWLER, CHARLES p 2601 N95-30247
FOX, GEOFFREY C. p 2658 N95-28965
FRANCIS, DOROTHY A. p 2640 N95-28935
FRANGOS, N. p 2669 N95-29229
FRANK, WILLIAM P. p 2677 N95-29615
FRANKLE, S. C. p 2696 N95-30057
FRASER, KEN F. p 2495 N95-28851
FRECHET, JEAN M. p 2542 N95-29270
p 2542 N95-29272
FREEMAN, A. J. p 2715 N95-29438
FREEMAN, ERIC p 2645 N95-28814
FREILICH, M. p 2628 N95-30343
FRERY, ALEJANDRO C. p 2601 N95-29999
FREUND, BEAU J. p 2636 N95-29757
FRIEBELE, JOSEPH p 2699 N95-29283
FRINK, NEAL T. p 2481 N95-28743
FRISCH, M. J. p 2720 N95-29936
FRITSCH, J. M. p 2627 N95-29993
FROHMAN, HAROLD L. p 2720 N95-28797
p 2722 N95-29287
FROST, KENNETH p 2740 N95-28882
FRYLAND, ALBERT p 2552 N95-28939
FU, L. p 2628 N95-30343
FUJIKAWA, GENE p 2508 N95-30011
FUJISAWA, A. p 2707 N95-29745
FUJITA, I. p 2709 N95-29808
FUJIWARA, M. p 2707 N95-29742
FUJIYOSHI, A. p 2735 N95-29839
FUKUYAMA, A. p 2706 N95-29731
p 2706 N95-29734
p 2707 N95-29741
p 2707 N95-29744
p 2709 N95-29809
FUKUYAMA, ATSUSHI p 2708 N95-29747
FULLER, DANA K. p 2493 N95-28790
FUNG, K.-Y. p 2686 N95-30138
FUNKHOUSER, GORDON E. p 2493 N95-29448
FURROW, KEITH W. p 2520 N95-29037

G

GAIER, JAMES R. p 2518 N95-28906
GAITHER, ADAM p 2482 N95-28749
GAITHER, KELLY p 2482 N95-28749
GALHL, JOHN p 2703 N95-29003
GALLAGER, SCOTT M. p 2631 N95-28685
GALLAGHER, D. L. p 2711 N95-30338
GALLAGHER, DENNIS JOSEPH p 2727 N95-29591
GALLARDO, J. p 2696 N95-30009
p 2696 N95-30009
GALLIMORE, JENNIE J. p 2639 N95-29439
GALLUS, WILLIAM ANDREW, JR. p 2623 N95-29725
GANGARAJ, S. K. p 2668 N95-29065
GANNON, BRIAN B. p 2504 N95-28680
GAONKAR, GOPAL H. p 2497 N95-29322
GARCIA-RAMIREZ, RAFAEL p 2546 N95-29822
GARCIA, KAREN M. p 2540 N95-28960
GARDINER, PETER T. p 2550 N95-29579
GARDNER, CARL L. p 2564 N95-29430
GARDNER, DAVID W. p 2700 N95-29412
GARDNER, H. J. p 2707 N95-29743
GARDNER, WILLIAM A. p 2557 N95-29603
GARG, SURESH C. p 2602 N95-28858
GARG, VIJAY K. p 2500 N95-29115
GARLAN, DAVID p 2645 N95-28894
p 2649 N95-29376
GARLAND, MICHAEL p 2658 N95-29196
GARMER, D. R. p 2532 N95-29487
GARNER, ROBERT P. p 2636 N95-29224
GARRETT, S. p 2683 N95-28973
GARRISON, T. J. p 2577 N95-29920
GARVEY, DAVID R. p 2692 N95-29076
GARY, JAMES BENNETT p 2614 N95-29650
GASKIN, DAVID p 2513 N95-28817
GATZKE, TIMOTHY D. p 2483 N95-28754
GAUGLER, RAYMOND E. p 2500 N95-29115
GE, FUYING p 2501 N95-29156
GE, ZHOU p 2583 N95-29656
GEDNEY, STEPHEN D. p 2554 N95-29235
GEHRELS, TOM p 2731 N95-29916
GELSEY, ANDREW p 2484 N95-28758
GEMAN, DONALD p 2675 N95-29634
GEORGE, MARK H. p 2493 N95-29448
GEORGIADIS, NICHOLAS J. p 2492 N95-30253
GERHOLD, THOMAS p 2492 N95-30349
GERIN, M. p 2731 N95-29097
GERREN, DONNA S. p 2501 N95-30254
GESSEL, M. p 2515 N95-28835
GIBSON, GARTH A. p 2658 N95-28879
GILBERT, I. H. p 2659 N95-29420
GILKEY, ROBERT H. p 2637 N95-29933
GILMORE, JUDY C. p 2723 N95-29449
GIROSI, FEDERICO p 2621 N95-29333
GLASS, JEFFREY T. p 2713 N95-28954
GLEGHORN, GEORGE p 2507 N95-28852
GLEICHER, MICHAEL L. p 2647 N95-29125
GLIEBE, PHILIP R. p 2684 N95-29641
GLYNN, PETER W. p 2674 N95-29491
GNACEK, W. J. p 2524 N95-29374
GOCHBERG, LAWRENCE A. p 2503 N95-29351
GOEBEL, MARTIN p 2651 N95-29861
GOEDEKE, A. D. p 2697 N95-28870
GOEDJEN, JOHN G. p 2512 N95-29373
GOERING, JON p 2522 N95-29048
GOFORTH, H. W., JR. p 2637 N95-29846
p 2637 N95-30083
GOLD, STEVEN H. p 2563 N95-29301
GOLDEN, PAUL p 2612 N95-28972
GOLDHABER, GERSON p 2693 N95-29583
GOLE, JAMES L. p 2586 N95-29514
GOLIMOWSKI, DAVID ANDREW p 2728 N95-29651
GOMES, MARIE E. p 2654 N95-30125
GONG, D. p 2591 N95-30285
GONG, KAI F. p 2683 N95-28783
GONZALEZ-MARTIN, A. p 2605 N95-30263
GOOCH, CARL FREDERICK p 2571 N95-29197
GOODDING, J. p 2597 N95-30210
GOODNICK, S. M. p 2696 N95-29495
GOODRICH, JOHN W. p 2689 N95-30155
GOPALAKRISHNA, RAO M. p 2567 N95-30260
GORDON, CLAIRE C. p 2640 N95-28794
GORDON, GEOFFREY J. p 2647 N95-29143
GOULD, D. C. p 2509 N95-30316
GRACE, FRED I. p 2596 N95-29929
GRAF, JOHN CARL p 2736 N95-29117
GRAFTON, ENRICO p 2636 N95-29557
GRAHAM, JOHN R., III p 2659 N95-29760
GRANATA, RICHARD D. p 2540 N95-28925
GRANATSTEIN, V. L. p 2564 N95-29417
GRANGER, MATHEW S. p 2678 N95-29617
p 2506 N95-29625
GRANT, CARROLL G. p 2514 N95-28832
p 2515 N95-28835
GRANT, KENNETH J. p 2587 N95-29914
GRASER, M. p 2697 N95-28912
GRASSIA, SEBASTIAN p 2658 N95-29196
GRAY, HENRY L. p 2608 N95-28922
GRAY, WILLIAM M. p 2620 N95-29254
GREAVES, ROBERT J. p 2558 N95-29875
GREEN, JAMES p 2740 N95-28882
GREEN, ROBERT E., JR. p 2523 N95-29169
p 2596 N95-29580
GREENAN, BLAIR JOHN WILLIAM p 2624 N95-29797
GREENE, TIMOTHY L. p 2513 N95-28824
GREENWALD, ANTON C. p 2587 N95-29912
GREENWALD, THOMAS J. p 2628 N95-30272
GREGG, DANE W. p 2606 N95-30266
GREGORY, D. L. p 2655 N95-30209
GREGORY, GERALD L. p 2608 N95-28717
GREINER, THOMAS M. p 2640 N95-28794
GRICE, M. E. p 2691 N95-28868
GRIEGER, JOHN CLARENCE p 2615 N95-29687
GRIESS, K. H. p 2499 N95-28840
GROCHENIG, K. p 2670 N95-29312
GROLEAU, MICHAEL R. p 2521 N95-29044
GROSNICK, D. P. p 2695 N95-30186
GROTEN, B. p 2535 N95-30111
GRUBBS, ROBERT H. p 2544 N95-29505
GRUCZA, DAVID p 2557 N95-29655
GUANGKAI, GAO p 2632 N95-29263
GUETTER, ALEXANDRE KOLODYNSKIE p 2599 N95-29539
GUEVREMONT, GRANT p 2570 N95-29119
GUNN, WALTER J. p 2493 N95-29873
GUO, H. p 2564 N95-29417
GUPTA, AARTI p 2669 N95-29128
GUPTA, VIJAY p 2546 N95-29926
GUPTIA, VIJAY p 2524 N95-29409
GURNETT, DONALD A. p 2704 N95-29130

H

HAGEMAN, JAMES H. p 2583 N95-29361
HAGER, B. H. p 2618 N95-29981
HAGERTY, JAMES J. p 2566 N95-30052
HAGESTEIJN, G. A. p 2653 N95-30098
HAGMEIJER, R. p 2485 N95-28767
HAHM, O. J. p 2551 N95-30296
HAHN, W. p 2714 N95-29134
HAINES, MATTHEW p 2649 N95-29404
p 2649 N95-29455
HAIRR, JOHN W. p 2517 N95-28846
HALBLEIB, JOHN A., SR. p 2660 N95-30116
HALDAR, P. p 2716 N95-29984
HALE, JACQUELINE p 2679 N95-29622
HALEM, MILTON p 2740 N95-28882
HALL, IAN W. p 2537 N95-29835
HALL, SUSAN E. p 2606 N95-30266
HALPERN, D. p 2628 N95-30343
HAMABE, M. p 2731 N95-29097
HAMADA, Y. p 2707 N95-29745
HAMBLEN, DAVID G. p 2717 N95-30068
HAMID, HEDAYAT U. p 2477 N95-28816
HAMILTON, BRIAN p 2664 N95-29657
HAMLIN, RICHARD D. p 2496 N95-29027
HAMMEL, SHERRY E. p 2683 N95-28783
HAMMER, DANIEL X. p 2585 N95-29274
HAMMOND, SHARON L. p 2634 N95-29086
HAMMOND, VINCENT H. p 2521 N95-29045
HANDEL, PETER H. p 2718 N95-29009
HANGEN, J. p 2516 N95-28843
HANSEN, W. p 2504 N95-29992
HARAS, ZIGO p 2670 N95-29403
HARCHE, F. p 2658 N95-29079
HARDIN, J. C. p 2582 N95-30151
HARDIN, JAY p 2674 N95-30143
HARDIN, JAY C. p 2686 N95-30133
HARDWICK, JONATHAN C. p 2647 N95-29147
HARDY, GORDON p 2477 N95-28816
HARIHARAN, S. I. p 2690 N95-30163
HARIRI, SALIM p 2658 N95-28965
HARMON, MARION p 2648 N95-29285
HARMS, DOUGLAS E. p 2647 N95-29226
HARMSEN, F. p 2653 N95-30094
HAROLD, JAMES BENEDICT p 2738 N95-29704
HARPER, ROBERT p 2721 N95-28877
HARPER, SABRINA p 2549 N95-30014
HARRAND, V. J. p 2489 N95-29316
HARRAND, VINCENT J. p 2482 N95-28748
HARRINGTON, F. p 2504 N95-28718
HARRIS, ALFRED W., JR. p 2721 N95-28907
HARRIS, S. E. p 2557 N95-29645
HARRISON, L. C. p 2608 N95-28920
HARRISON, ROBERT G. p 2588 N95-29980
HART, SEAN M. p 2521 N95-29045
HARTMANN, DIRK ALBRECHT p 2695 N95-30302
HARTNESS, J. TIMOTHY p 2513 N95-28824
HARTRUM, THOMAS C. p 2653 N95-30080
HASE, K. p 2535 N95-30111
HASEGAWA, TETSUO p 2731 N95-29100
HASHIBA, M. p 2709 N95-29808
HASHIMOTO, O. p 2735 N95-29837
HASKO, GREGORY H. p 2520 N95-29039
p 2521 N95-29045
HASSAN, SCOTT E. p 2595 N95-29192
HASTINGS, DANIEL E. p 2602 N95-29200
p 2602 N95-29201
HATAY, FERHAT F. p 2579 N95-30250
HAUS, HERMANN A. p 2697 N95-28799
HAUS, JOSEPH W. p 2718 N95-30298
HAVELOCK, DAVID H. p 2685 N95-30084
HAVERKORT, B. R. p 2559 N95-30096
p 2673 N95-30097
HAWBOLT, E. B. p 2537 N95-29869
HAWKES, N. p 2709 N95-29803
HAYDER, M. EHTESHAM p 2574 N95-29405
p 2582 N95-30149
HAYHOE, MARY M. p 2639 N95-29422
HE, FEIYUE p 2664 N95-29544
HEALEY, G. p 2697 N95-28870
HEARN, CHASE P. p 2506 N95-30251
HEATH, CLEVELAND A. p 2641 N95-29600
HEAVEN, MICHAEL C. p 2585 N95-29025
HECHT, LAURA M. p 2721 N95-29028
HEDRICK, R. L. p 2610 N95-30197
HEGEDUS, CHARLES R. p 2541 N95-29194
HEGGE, F. W. p 2645 N95-28934
HEINRICH, H. p 2563 N95-29191
HEITMEYER, CONSTANCE p 2648 N95-29319
HELBIG, HERBERT F. p 2691 N95-28952
HELMBERGER, DONALD V. p 2618 N95-29970
HEMBREE, G. G. p 2712 N95-28681
HENKE, ANDREA L. p 2661 N95-28926
HENNAGE, DAVID W. p 2564 N95-29511
p 2587 N95-29653
p 2702 N95-29867
HENRY, WENDELL A. p 2646 N95-28964
HENRY, ZACHARY S. p 2590 N95-29538
HERBERT, T. p 2577 N95-29913

HERCHEN, JAMES ..... p 2564 N95-29570
HERNANDESFILHO, PEDRO ..... p 2601 N95-29999
HERNANDEZ, C. ..... p 2677 N95-29611
HERNDON, BRUCE P. ..... p 2661 N95-30295
HERNDON, J. N. ..... p 2710 N95-29909
HERRIN, EUGENE ..... p 2612 N95-28972
HERRING, NANCY ..... p 2550 N95-29537
HERRING, NANCY C. ..... p 2550 N95-29307
HERRING, RODNEY A. ..... p 2713 N95-29013
HERRING, T. A. ..... p 2618 N95-29981
HERRMANN, LEONARD R. ..... p 2670 N95-29311
HETHERINGTON, D. L. ..... p 2718 N95-30214
HEYMAN, EHUD ..... p 2612 N95-28871
p 2612 N95-29140
HICKEY, T. ..... p 2535 N95-28889
HICKS, D. G. ..... p 2695 N95-28930
HILLSMAN, E. L. ..... p 2611 N95-30212
HINDS, W. E. ..... p 2642 N95-28722
HINES, M. L. ..... p 2642 N95-28818
HIPPENSTIEL, RALPH D. ..... p 2556 N95-29386
HIRST, DONALD J. ..... p 2541 N95-29194
HISLOP, DAVID W. ..... p 2722 N95-29154
HJALMARSON, H. P. ..... p 2588 N95-30006
HO, C. Y. ..... p 2533 N95-29575
HO, CHENG ..... p 2508 N95-29464
HO, CHI WING ..... p 2622 N95-29688
HO, CHUNG-RU ..... p 2630 N95-29520
HO, PATRICK Y. ..... p 2684 N95-29641
HOEHN, J. G., JR. ..... p 2716 N95-29984
HOFFMAN, C. A. ..... p 2564 N95-29568
HOFMEISTER, RUDY ..... p 2713 N95-29087
HOJO, HITOSHI ..... p 2707 N95-29738
HOLCOMBE, DAVID ..... p 2567 N95-30124
HOLDER, ANDREW J. ..... p 2694 N95-30060
HOLLANDER, MYLES ..... p 2592 N95-29423
HOLMES, J. F. ..... p 2621 N95-29497
HOLMES, RICHARD B. ..... p 2699 N95-29295
HOMAN, KELLY O. ..... p 2550 N95-29537
HONG, STEVEN W. ..... p 2498 N95-29787
HOOK, JAMES ..... p 2644 N95-28782
HOOKER, R. ..... p 2540 N95-29021
HOOKER, STANFORD B. ..... p 2631 N95-30236
HOOMAN, J. ..... p 2655 N95-30220
HOOVER, MARK D. ..... p 2635 N95-29188
HOPSON, P., JR. ..... p 2583 N95-29453
HORCH, ELLIOTT PIERCE ..... p 2728 N95-29652
HORGAN, C. O. ..... p 2595 N95-29562
HORIE, YASUYUKI ..... p 2682 N95-29588
HORIUCHI, RITOKU ..... p 2709 N95-29810
HORNAK, L. A. ..... p 2719 N95-29756
HORTON, C. M. ..... p 2524 N95-29374
HORTON, RAY E. ..... p 2519 N95-29034
HORTON, W. ..... p 2709 N95-29789
HORWATH, JOHN ..... p 2561 N95-28971
HOSOKAWA, M. ..... p 2707 N95-29742
HOU, MU ..... p 2665 N95-29874
HOU, SHANG ..... p 2712 N95-28815
HOU, X. ..... p 2560 N95-30219
HOUSE, ROBERT S. ..... p 2629 N95-29054
HOUSTON, PAUL L. ..... p 2548 N95-29498
HOVER, G. L. ..... p 2598 N95-29281
HOWARD, JAMIE MICHAEL ..... p 2734 N95-29673
HOWE, R. B. ..... p 2633 N95-28793
HOWELL, JAN M. ..... p 2498 N95-29503
HOWELL, STEVEN ..... p 2646 N95-28995
HOYT, W. ANDES ..... p 2510 N95-29584
HSU, DAVID S. ..... p 2567 N95-30165
HSU, S. M. ..... p 2591 N95-30110
HU, CHIH-PING ..... p 2629 N95-28982
HU, F. Q. ..... p 2687 N95-30139
HU, HONG ..... p 2574 N95-29387
HU, SHOUFENG ..... p 2514 N95-28828
HU, TAIYI ..... p 2685 N95-29681
HUANG, LANJIE ..... p 2577 N95-30027
HUANG, S. L. ..... p 2577 N95-29913
HUDSON, ANNE ..... p 2672 N95-29647
HUDSON, DALE A. ..... p 2661 N95-30150
HUFFORD, GARY S. ..... p 2482 N95-28748
HUGH, MAYLENE K. ..... p 2519 N95-29036
HUGHES, RUSSELL P. ..... p 2536 N95-29427
HUIJBERTS, H. J. C. ..... p 2667 N95-30171
HUISKEN, AMY B. ..... p 2516 N95-28838
HULL, PATRICIA G. ..... p 2696 N95-28695
p 2697 N95-28698
HUMMELS, DONALD M. ..... p 2643 N95-29921
HUMPHREY, R. J. ..... p 2499 N95-28840
HUNT, H. B., III ..... p 2661 N95-30215
HUNT, JEFFREY H. ..... p 2699 N95-29295
HUNT, P. ..... p 2637 N95-30083
HUSEBYE, EYSTEIN S. ..... p 2614 N95-29413
HUSSAINI, M. Y. ..... p 2687 N95-30139
HUSTON, ALAN L. ..... p 2585 N95-29217
HUYNH, H. T. ..... p 2687 N95-30140
HWA, REBECCA ..... p 2499 N95-29123
HWANG, CHANG-JEON ..... p 2686 N95-30137
HYDUK, ROZA ..... p 2637 N95-29995
HYMER, TOM ..... p 2490 N95-29853

I

ICHIGUCHI, K. ..... p 2707 N95-29743
ICHIKAWA, T. ..... p 2731 N95-29097
ICHIMURA, MAKOTO ..... p 2707 N95-29738
IDA, K. ..... p 2707 N95-29742
p 2709 N95-29802
IDEI, H. ..... p 2707 N95-29742
p 2709 N95-29802
IDZENGA, H. P. ..... p 2559 N95-30096
IDZERDA, Y. ..... p 2681 N95-28923
IFJU, PETER G. ..... p 2513 N95-28825
p 2520 N95-29040
IGLEHART, DONALD L. ..... p 2674 N95-29491
IGUCHI, H. ..... p 2707 N95-29742
p 2709 N95-29802
IHLENBURG, FRANK ..... p 2668 N95-29064
p 2669 N95-29080
p 2669 N95-29084
IIYOSHI, A. ..... p 2710 N95-29857
IKEUCHI, KATSUSHI ..... p 2737 N95-29151
ILCEWICZ, LARRY B. ..... p 2515 N95-28833
p 2515 N95-28837
p 2519 N95-29034
INATANI, JUNJI ..... p 2562 N95-29099
INGALIS, PAUL D. ..... p 2685 N95-29942
INGHAM, HOLLY A. ..... p 2647 N95-29276
INGLEFIELD, PAUL T. ..... p 2693 N95-29723
INGRAM, J. EDWARD ..... p 2517 N95-28846
INMAN, DANIEL J. ..... p 2649 N95-29429
INOUE, N. ..... p 2709 N95-29808
p 2711 N95-30032
INUTAKE, MASAAKI ..... p 2707 N95-29738
IRONS, FRED H. ..... p 2643 N95-29921
ITOH, K. ..... p 2706 N95-29731
p 2706 N95-29734
p 2707 N95-29741
p 2707 N95-29744
p 2708 N95-29746
p 2709 N95-29809
ITOH, KIMITAKA ..... p 2708 N95-29747
ITOH, S.-I. ..... p 2706 N95-29731
p 2706 N95-29734
p 2707 N95-29741
p 2707 N95-29744
p 2708 N95-29746
p 2709 N95-29809
ITOH, SANAE-I. ..... p 2708 N95-29747
IVES, DAVID ..... p 2478 N95-28727
p 2483 N95-28756
IWAMOTO, K. ..... p 2709 N95-29808
IWASAKI, TETSUYA ..... p 2667 N95-30234
IYER, A. N. ..... p 2716 N95-29984
IZUMIURA, HIDEYUKI ..... p 2735 N95-29837
p 2735 N95-29838
p 2735 N95-29839
p 2735 N95-29840

J

JACKSON, ANTHONY C. ..... p 2519 N95-29033
JACKSON, DANIEL ..... p 2645 N95-28881
p 2647 N95-29223
JACKSON, DARRELL R. ..... p 2685 N95-29942
JACKSON, E. BRUCE ..... p 2502 N95-30327
JACKSON, H. E. ..... p 2694 N95-30019
JACKSON, MICHAEL ..... p 2645 N95-28881
JACOBS, I. ..... p 2637 N95-29846
JAFFE, JULES S. ..... p 2702 N95-29910
JAFFE, PETER R. ..... p 2512 N95-29168
JAMES, BRIAN D. ..... p 2548 N95-29280
JAMES, G. ..... p 2597 N95-30210
JAMESON, ANTONY ..... p 2491 N95-29972
JAMMY, R. ..... p 2716 N95-29984
JANNSON, TOMASZ ..... p 2712 N95-28862
JANSSEN, W. ..... p 2660 N95-30104
JAQUEZ, R. ..... p 2642 N95-28722
JARBOE, THOMAS R. ..... p 2704 N95-29011
JAUNKY, NAVIN ..... p 2529 N95-30341
JAYARAM, R. ..... p 2538 N95-30179
JEAN, BRIAN ..... p 2482 N95-28749
JECHEL, KURT E. ..... p 2542 N95-29314
JEFF, BYRON ..... p 2659 N95-29915
JEFFERSON, HENRY C. ..... p 2634 N95-29086
JEGLEY, DAWN C. ..... p 2516 N95-28842
JENKINS, JIM ..... p 2591 N95-28682
p 2592 N95-28684
JENSEN, J. O. ..... p 2532 N95-29487
JENSSEN, CARL B. ..... p 2483 N95-28757
JESCHKE, MARK W. ..... p 2655 N95-30307
JIANG, WEI-NAN ..... p 2567 N95-30124
JIANZHONG, ZHANG ..... p 2685 N95-29951
JIN, BO ..... p 2665 N95-29720
JIN, GUO-XIONG ..... p 2719 N95-29216
JISHI, RADI A. ..... p 2562 N95-29018
JOHNSON, CURTIS W. ..... p 2532 N95-29273
JOHNSON, DANIEL L. ..... p 2634 N95-28941
JOHNSON, MARK ..... p 2698 N95-28932
JOHNSON, MARK A. ..... p 2683 N95-28999
JOHNSON, NICHOLAS ..... p 2507 N95-28852
JOHNSON, RICHARD W. ..... p 2619 N95-28872
JOHNSON, W. STEVEN ..... p 2529 N95-30340
JOHNSTON, NORMAN J. ..... p 2519 N95-29036
JONES, M. T. ..... p 2659 N95-29985
JONES, T. E. ..... p 2502 N95-29522
JONES, WESLEY BERGER ..... p 2580 N95-30303
JONES, WILLIAM T. ..... p 2484 N95-28763
JONGSTE, J. F. ..... p 2538 N95-30205
JOSEPH, DANIEL D. ..... p 2573 N95-29324
JOSEPH, SUJOE ..... p 2652 N95-30047
JOSEPHSON, JESSICA L. ..... p 2585 N95-29274
JOSHI, G. C. ..... p 2739 N95-30074
JOSHI, SURESH M. ..... p 2507 N95-29377
JUERGENS, D. ..... p 2737 N95-30058
JULIN, DANIEL P. ..... p 2650 N95-29536
JUNGER, M. ..... p 2478 N95-28720
JUSTUS, BRIAN L. ..... p 2585 N95-29217

K

KADIN, ALAN M. ..... p 2700 N95-29379
KAEDING, THOMAS A. ..... p 2690 N95-28779
KAGEYAMA, AKIRA ..... p 2708 N95-29755
KAHN, MANFRED ..... p 2566 N95-30055
KALKHORAN, IRAJ M. ..... p 2502 N95-29468
KALLIANPUR, G. ..... p 2661 N95-28788
KALLINDERIS, YANNIS ..... p 2481 N95-28744
KALMAN, R. F. ..... p 2698 N95-28992
KAMENY, IRIS M. ..... p 2651 N95-29735
KANAZAWA, CHRISTINE H. ..... p 2542 N95-29288
KANEKO, O. ..... p 2705 N95-29567
KANFER, RUTH ..... p 2638 N95-28918
KANTAR, PHYLLIS ..... p 2651 N95-29736
KAPOOR, D. ..... p 2528 N95-30037
KARALAMANGALA, ARUN S. ..... p 2557 N95-29563
KARDAUN, J. W. P. F. ..... p 2708 N95-29746
KARDAUN, O. J. W. F. ..... p 2708 N95-29748
KARMAN, STEVE L., JR. ..... p 2481 N95-28741
KARR, MONETTE E. ..... p 2619 N95-28872
KASHYAP, VINAY L. ..... p 2740 N95-29779
KASPI, VICTORIA MICHELLE ..... p 2734 N95-29675
KASSAPOGLOU, C. ..... p 2499 N95-28831
KASSLER, MAGGIE ..... p 2720 N95-30223
KATO, SHIGERU ..... p 2710 N95-29843
KATO, T. ..... p 2707 N95-29740
KATOEN, J. P. ..... p 2558 N95-29919
p 2660 N95-30102
KATSIKA, ALEX. ..... p 2638 N95-29629
KATSUMATA, RYOTA ..... p 2707 N95-29738
KATULKA, GARY L. ..... p 2565 N95-29938
KATZ, ERIC ..... p 2495 N95-30031
KAWAMURA, T. ..... p 2710 N95-29812
KAWATA, SHIGEO ..... p 2710 N95-29843
KAY, L. ..... p 2703 N95-30062
KAZOVSKY, L. G. ..... p 2698 N95-28992
KEATING, CHRISTOPHER FRANCIS
p 2614 N95-29524
KEATING, JACK ..... p 2548 N95-30252
KECSKES, LASZLO J. ..... p 2537 N95-29835
KEE, CHANGDON ..... p 2494 N95-29107
KEENAN, CHRIS ..... p 2533 N95-29572
KEENAN, F. P. ..... p 2738 N95-29279
KELKAR, ATUL G. ..... p 2507 N95-29377
KELLER, TEDDY M. ..... p 2545 N95-29569
p 2547 N95-30132
KELLY, KEVIN W. ..... p 2700 N95-29366
KELLY, T. L. ..... p 2637 N95-30083
KELLY, TAMSIN L. ..... p 2637 N95-29995
KEMPA, K. ..... p 2705 N95-29519
KENNEDY, JOHN M. ..... p 2721 N95-29028
KEPPENS, R. ..... p 2739 N95-30199
KERNEY, PAUL T. ..... p 2500 N95-28908
KERR, PATRICIA A. ..... p 2479 N95-28729
KERSEY, ALAN ..... p 2699 N95-29283
KESSLER, DONALD ..... p 2507 N95-28852
KESTER, D. J. M. ..... p 2735 N95-29840
KEWITSCH, ANTHONY ..... p 2713 N95-29087
KHATTAK, C. P. ..... p 2604 N95-30217
KHAWAJA, ALY ..... p 2481 N95-28744
KHER, SHREYAS S. ..... p 2715 N95-29486
KHRUSTALEV, DMITRY ..... p 2570 N95-29127
KIEBURRTZ, RICHARD ..... p 2644 N95-28782
KIGAWA, SEIICHIRO ..... p 2626 N95-29849
KIKUCHI, TADASHI ..... p 2626 N95-29849
KILCOYNE, M. K. ..... p 2588 N95-30050
KILMER, L. C. ..... p 2603 N95-29953
KIM, B. G. ..... p 2559 N95-30096
p 2653 N95-30098

KIM, BYOUNGSOO p 2485 N95-28764
KIM, GOO p 2488 N95-29108
KIM, HAN p 2697 N95-28795
KIM, JAE-WOOK p 2686 N95-30137
KIM, WOO-JIN p 2545 N95-29635
KIMBLE, KENNETH R. p 2556 N95-29459
KINARD, TOM A. p 2482 N95-28747
KINDER, ROBERT H. p 2519 N95-29030
KING, R. W. p 2618 N95-29981
KINGMAN, PAT W. p 2713 N95-29013
KINGON, A. I. p 2537 N95-29724
KIPP, R. L. p 2655 N95-30209
KIRUBARAJAN, T. p 2494 N95-28887
KISER, D. M. p 2591 N95-30211
KISTLER, DAVID p 2644 N95-28805
KITCHEN, ANGELA M. p 2645 N95-28814
KIYOKAWA, SYUJI p 2710 N95-29843
KLEINE, MARVIN LEROY, JR. p 2732 N95-29592
KLINGENBERG, ERIC H. p 2543 N95-29358
KLOPP, RICHARD W. p 2542 N95-29288
KLUEVER, CRAIG A. p 2509 N95-30357
KNAUER, J. P. p 2695 N95-28930
KNAUSS, W. p 2628 N95-30343
KNERR, JEFFREY MATTHEW p 2622 N95-29676
KNIGHT, NORMAN F., JR. p 2529 N95-30341
KNOLL, D. A. p 2711 N95-30130
KNOWLES, STEPHEN p 2507 N95-28852
KO, DUCK-KON p 2686 N95-30137
KOCH, CHRISTOF p 2634 N95-29059
KOCH, W. J. p 2516 N95-28839
KOENDERINK, JAN J. p 2670 N95-29440
KOENEN, L. p 2709 N95-29803
KOHL, THOMAS W. p 2685 N95-29826
KOHLER, BERN p 2698 N95-28983
KOLIAS, JOHN H. p 2687 N95-30141
KOMATSU, GORO p 2736 N95-29593
KOMORI, A. p 2711 N95-30032
KONDOH, YOSHIOMI p 2710 N95-29844
KONOPLIV, ALEXANDER S. p 2737 N95-30344
KOOCHESFAHANI, MANOOCHEHR M. p 2571 N95-29181
KOPRIVA, DAVIS A. p 2687 N95-30141
KORY, CAROL L. p 2564 N95-29406
p 2566 N95-29998
KORYABIN, A. p 2701 N95-29766
KORZEKWA, DAVID A. p 2591 N95-30273
KOSEK, J. A. p 2568 N95-30270
KOSIK, W. p 2585 N95-29208
KOSIK, W. E. p 2543 N95-29353
KOSTER, J. E. p 2549 N95-30345
KOSTRZEWSKI, ANDREW p 2712 N95-28862
KOZACZEK, KRZYSZTOF J. p 2596 N95-29580
KOZAITIS, SAMUEL P. p 2697 N95-28798
KRAABEL, DARREN L. p 2527 N95-29758
KRAKOWSKI, R. A. p 2569 N95-28956
KRAL, LINDA D. p 2571 N95-29211
KRALL, J. p 2588 N95-29937
KRANBUEHL, DAVID E. p 2521 N95-29045
KRAUSS, M. p 2532 N95-29487
KRCHNAVEK, DR. p 2698 N95-28998
KREIDER, KEVIN L. p 2683 N95-29401
KRESS, J. D. p 2652 N95-29989
KRESS, R. L. p 2654 N95-30189
KRISHAN, VINOD p 2738 N95-29475
KRISHNAMURTHY, S. p 2702 N95-29978
KRUG, E. K. p 2610 N95-30197
KRUPAR, MARTIN J. p 2477 N95-30229
KRUSE, N. p 2583 N95-29453
KRUSE, ROBERT J. p 2640 N95-29020
KRUSHELNICK, KARL MICHAEL p 2587 N95-29689
KUBO, S. p 2707 N95-29742
p 2709 N95-29802
KUBOTA, Y. p 2709 N95-29808
p 2711 N95-30032
KUBOTA, YUSUKE p 2709 N95-29801
KUCERA, THERESE ANN p 2738 N95-29202
KUCHAR, F. p 2563 N95-29191
KUDER, STEVE p 2601 N95-29977
KUDER, STEVEN p 2598 N95-28931
KUHN, IRA F., JR. p 2548 N95-29280
KULKARNI, SANJEEV R. p 2666 N95-30040
KULLERD, SUSAN M. p 2520 N95-29038
p 2522 N95-29049
KUMAR, DHARMENDRA p 2496 N95-28928
KUMAR, P. R. p 2648 N95-29310
KUNDU, M. R. p 2737 N95-29098
KUNG, PANG-JEN p 2717 N95-30068
KUNTZ, D. W. p 2538 N95-30176
KUO, CHUNG-I. p 2719 N95-29527
KUPER, J. p 2673 N95-30103
p 2673 N95-30196
p 2674 N95-30291
KUPLICH, TATIANNA MORA p 2598 N95-29433
KURBATSKII, K. A. p 2674 N95-30145
KURIZKI, GERSHON p 2718 N95-28927
KURTZ, S. R. p 2717 N95-29990
p 2717 N95-30005
p 2588 N95-30006
KWON, D. S. p 2654 N95-30189
KWONG, M. K. p 2652 N95-30020

L

LACONTI, A. B. p 2568 N95-30270
LADERA, CELSO L. p 2698 N95-28983
LAFON, PHILIPPE p 2582 N95-30142
LAI, YEH-HUNG p 2545 N95-29799
LAKEOU, SAMUEL p 2702 N95-30035
LAL, MIHIR KUMAR p 2490 N95-29771
LAM, DAVID W. p 2491 N95-30091
LAMBERTSEN, C. J. p 2635 N95-29158
LAMBROS, JOHN p 2541 N95-29120
LAMSON, SCOTT H. p 2478 N95-28726
LANCTO, R. p 2523 N95-29136
p 2524 N95-29329
LANDIS, ABRAHAM L. p 2496 N95-29027
LANDSEA, CHRISTOPHER W. p 2620 N95-29254
LANDY, STEPHEN DANIEL p 2734 N95-29780
LANGER, ROBERT S. p 2632 N95-29088
LANGLEY, PAT p 2649 N95-29456
p 2723 N95-29573
p 2664 N95-29574
p 2650 N95-29576
p 2664 N95-29577
p 2675 N95-29906
LANSING, M. D. p 2524 N95-29374
LANSMAN, JEFFRY B. p 2637 N95-29927
LAPICKI, ADAM p 2533 N95-29722
LAQUER, HENRY L. p 2560 N95-28812
LARSEN, F. K. p 2677 N95-29613
p 2678 N95-29618
LARSON, KEVIN P. p 2651 N95-29932
LARSON, N. R. p 2608 N95-28920
LATUSEK, J. P. p 2591 N95-30110
LAU, KREISLER S. Y. p 2496 N95-29027
LAUFERSWEILER, MARK JOHN p 2624 N95-29726
LAULAINEN, N. S. p 2608 N95-28920
LAW, KINCHO H. p 2661 N95-30295
LAWROW, ALEX p 2698 N95-28932
LEACH, MARTIN JOHN p 2616 N95-29699
LEAL, JAMES p 2540 N95-28925
LEBURTON, J. P. p 2718 N95-29149
LEDLEY, ROBERT S. p 2639 N95-29458
LEE, CHUNGKI p 2553 N95-29106
LEE, DUCK-JOO p 2686 N95-30137
LEE, E. H. p 2547 N95-30190
LEE, EUN YOUNG p 2491 N95-30235
LEE, IDA p 2611 N95-30348
LEE, JAR WHA p 2539 N95-28864
LEE, JIM J. p 2558 N95-29847
LEE, JINHO p 2479 N95-28732
LEE, JUNG KI p 2529 N95-30276
LEE, JUNG M. p 2558 N95-29875
LEE, M. H. p 2692 N95-29227
LEE, PETER C. p 2594 N95-29150
LEE, ROB p 2553 N95-29159
p 2558 N95-29904
LEE, S. L. p 2594 N95-28949
LEE, TA-CHENG p 2488 N95-29121
LEE, WAH-KEAT p 2718 N95-30184
LEGIDAKES, LEO J. p 2477 N95-29414
LEIGHTON, T. G. p 2577 N95-29817
LEISSLER, GEORGE W. p 2512 N95-29373
LEITE, SARA M. p 2702 N95-30053
LELE, SANJIVA p 2571 N95-29145
LEMIRE, GEORGE W. p 2530 N95-28876
LEMMOND, PETER p 2630 N95-29418
LEONARD, ANTHONY p 2576 N95-29761
LEONE, STEPHEN R. p 2693 N95-29431
LEONG, HANK p 2555 N95-29313
LERCH, BRADLEY p 2567 N95-30259
LESMES, DAVID P. p 2558 N95-29875
LETCHER, JOHN S., JR. p 2486 N95-28771
LEUNG, HENRY p 2555 N95-29328
LEUNG, MAN-KIT p 2542 N95-29270
LEVITT, TOD S. p 2650 N95-29576
LEVY, MILTON p 2536 N95-29137
LI, B. Q. p 2700 N95-29366
LI, C. K. p 2695 N95-28930
LI, JIAN p 2527 N95-29825
p 2528 N95-30028
LI, SHAOZHONG p 2682 N95-30232
LI, SHENG S. p 2714 N95-29089
p 2716 N95-29785
LI, SHUXI p 2719 N95-29677
LI, TIESHENG p 2716 N95-29814
LI, Y. J. p 2546 N95-30030
LI, YONG p 2724 N95-29798
LI, YULIN p 2702 N95-29969
LIANG, YUE-MIIN p 2545 N95-29772
LIAW, GOANG S. p 2575 N95-29637
LIBERMAN, D. A. p 2705 N95-29466
LIBERMAN, J. p 2556 N95-29462
LICINA, J. R. p 2678 N95-29620
LIEBERMAN, M. A. p 2561 N95-29010
LIEBERMAN, STEPHEN H. p 2664 N95-29499
LIN, CHICHUNG p 2624 N95-29800
LIN, DAH-SYANG p 2600 N95-29821
LIN, FENGCHIAO JOYCE p 2616 N95-29716
LIN, H. T. p 2528 N95-30175
LIN, SIHAN p 2540 N95-29021
LIN, Z. p 2667 N95-30168
LIND, STEPHANIE p 2654 N95-30125
LINDGREN, ALLEN p 2564 N95-29570
LINTHICUM, K. p 2712 N95-28910
LIU, WING KAM p 2671 N95-29516
LIU, XINBING p 2704 N95-29218
LIU, YANMING p 2568 N95-30268
LIVSHIT, A. I. p 2711 N95-30032
LOELLBACH, JAMES p 2479 N95-28732
LOEWENHAUPT, M. p 2714 N95-29134
LOGAN, MICHAEL A. p 2486 N95-28775
LOH, WEI-YIN p 2671 N95-29578
LOMDAHL, P. S. p 2694 N95-30059
LONDONO, J. D. p 2535 N95-30113
LONG, JOHN P. p 2651 N95-29871
LONG, LYLE N. p 2688 N95-30148
p 2661 N95-30150
p 2661 N95-30156
LONGINO, DANA A. p 2497 N95-29282
LOONG, C. K. p 2714 N95-29134
LOOS, ALFRED C. p 2521 N95-29045
LOPEZ, J. A. p 2677 N95-29611
LOTTS, C. G. p 2517 N95-28847
LOUP, C. p 2735 N95-29840
LOUSTEAU, D. C. p 2710 N95-29909
LOY, R. M. p 2671 N95-29488
LOZYKOWSKI, H. J. p 2716 N95-29814
LU, BAIDA p 2584 N95-28679
LU, CHENG-YI p 2603 N95-30015
LU, NING p 2486 N95-28774
LU, SHIN-YEE p 2697 N95-28912
LU, WENTONG p 2619 N95-30351
LUBE, MICHAEL S. p 2713 N95-28993
p 2715 N95-29486
LUCAS, M. J. p 2478 N95-28720
LUHMAN, THOMAS S. p 2541 N95-29055
LUK, TING SHAN p 2553 N95-29081
LUNDGREN, SCOTT CAMPBELL p 2729 N95-29678
LUNDQUIST, R. C. p 2515 N95-28836
LUO, REN C. p 2722 N95-29154
LYCZKOWSKI, R. W. p 2577 N95-29988
LYDUCH, S. p 2677 N95-29613
p 2678 N95-29618
LYNCH, NANCY p 2648 N95-29319
LYONS, T. J. p 2680 N95-29628
LYZENGA, D. R. p 2559 N95-30073

M

MA, EN p 2700 N95-29366
MA, Z. p 2539 N95-28891
MABSON, G. E. p 2515 N95-28836
MACCORMACK, ROBERT W. p 2575 N95-29469
MACFARLANE, R. E. p 2696 N95-30057
MACQUARRIE, JEFFREY A. p 2611 N95-28693
MACRAE, JOHN D. p 2521 N95-29045
MADAN, RAM C. p 2522 N95-29051
MADDOCKS, JOHN p 2669 N95-29070
MADER, THOMAS p 2635 N95-29173
MADYCH, WOLODYMYR p 2670 N95-29312
MAENNISTOE, TOMI p 2655 N95-30283
MAGGS, BRUCE p 2645 N95-28878
MAHAJAN, S. M. p 2711 N95-30173
MAHER, TIMOTHY P. p 2661 N95-28926
MAHLUM, PHILLIP p 2677 N95-29615
MAIDEN, JANICE R. p 2519 N95-29036
MAIMONE, MARK W. p 2645 N95-28883
MAIXXNER, MICHAEL R. p 2573 N95-29271
MAJUMDAR, BHASKAR S. p 2523 N95-29133
MAKSHTAS, ALEKSANDR P. p 2620 N95-29193
MAKSYMIUK, CATHERINE M. p 2478 N95-28728
MALINAS, N. P. p 2559 N95-30073
MALTE, P. p 2535 N95-30111
MAN, RAYMOND S. O. p 2686 N95-30138
MANDELKERN, L. p 2535 N95-30113
MANI, RAMANI p 2684 N95-29641
MANKBADI, R. p 2690 N95-30163
MANKBADI, REDA R. p 2657 N95-30157
p 2690 N95-30160
MANN, DIANE K. p 2608 N95-28787
MANNING, CAROL A. p 2493 N95-28790
MANSFELD, FLORIAN p 2528 N95-29923
MANTHEY, J. p 2687 N95-30139
MARAN, STEPHEN p 2740 N95-28882
MARATHE, M. V. p 2661 N95-30215
MARCHELLO, JOSEPH M. p 2519 N95-29036

MARCUS, HARRIS L. p 2527 N95-29732
MARGASON, RICHARD J. p 2477 N95-28816
MARISKA, JOHN T. p 2738 N95-29327
MARKOPOULOS, NIKOS p 2504 N95-29339
MARKS, JOE p 2499 N95-29123
MARKS, RONALD C. p 2540 N95-28953
MARKUS, ALAN p 2522 N95-29050
MARKUS, ALAN M. p 2521 N95-29045
MARLIN, DAVE p 2618 N95-29976
MARROCCO, MATTHEW p 2543 N95-29482
MARSDEN, M. A. p 2577 N95-29817
MARTENS, J. p 2593 N95-29941
MARTI, JED p 2651 N95-29736
MARTIN, CHARLES R. p 2539 N95-28850
MARTIN, ELIZABETH L. p 2641 N95-29943
MARTIN, JAMES E. p 2690 N95-30162
MARTIN, PAUL J. p 2629 N95-28991
MARTIN, STEPHEN ALLEN p 2684 N95-29502
MARTINELLI, LUIGI p 2491 N95-29972
MARTINEZ, DEBBIE p 2659 N95-29454
MARTINEZ, RADAME p 2559 N95-30072
MARTINO, WILLIAM R. p 2567 N95-30122
MASELAND, J. E. J. p 2485 N95-28767
MASLANIK, JAMES p 2601 N95-30247
MASON, KEVIN T. p 2634 N95-28940
p 2635 N95-29141
p 2639 N95-29434
MASSA, DERCK p 2726 N95-28822
MASSA, LOU p 2698 N95-28996
MASTERS, JOHN E. p 2513 N95-28825
p 2520 N95-29040
MASTIN, C. WAYNE p 2485 N95-28765
MATARIC, MAJA J. p 2639 N95-29443
MATEER, GEORGE G. p 2579 N95-30224
MATHEW, THOMAS p 2675 N95-29768
MATHEWS, G. J. p 2660 N95-30193
MATSUDA, SHUZO p 2626 N95-29849
MATTA, LAWRENCE MARK p 2510 N95-29331
MATTICK, ARTHUR T. p 2704 N95-29011
MAUDERLY, JOE L. p 2635 N95-29188
MAUW, S. p 2560 N95-30203
MAVRIPLIS, D. J. p 2674 N95-30227
MAXWELL, DAVID R. p 2626 N95-29868
MAYES, R. p 2597 N95-30210
MAYNARD, SHAWN J. p 2521 N95-29044
MAZIASZ, P. J. p 2538 N95-30216
MAZZELLA, ANDREW J., JR. p 2616 N95-29737
p 2617 N95-29765
p 2651 N95-29932
p 2618 N95-30082
MCCANN, C. p 2720 N95-29935
MCCLEARY, SUSAN L. p 2517 N95-28848
MCCLELLAND, GARY M. p 2691 N95-28888
MCCLELLAND, ROBERT S. p 2508 N95-29410
MCCLUSKY, S. p 2618 N95-29981
MCCONNELL, RICHARD A. p 2567 N95-30122
MCCORMICK, A. V. p 2544 N95-29551
p 2544 N95-29554
p 2545 N95-29559
MCCORMICK, PAUL V. p 2609 N95-29450
MCDONACH, ALASTER p 2550 N95-29579
MCDONNELL, J. A. p 2703 N95-30062
MCDONNELL, J. R. p 2665 N95-29831
MCELROY, J. p 2606 N95-30267
MCEWEN, RON S. p 2550 N95-29579
MCFARLANE, ELISABETH ANN p 2612 N95-29199
MCGARRY, FRANK p 2644 N95-28806
MCGILVARY, RANDY p 2629 N95-29160
MCGINN, JOSEPH T. p 2542 N95-29288
MCGINNIS, B. p 2588 N95-30045
MCGINNIS, W. C. p 2502 N95-29522
MCGRATH, JAMES p 2543 N95-29482
MCGUIRE, PATRICK CHARLES p 2726 N95-29204
MCGUIRE, WENDY J. p 2638 N95-29090
MCHUGH, KEVIN M. p 2536 N95-28959
MCHUGH, P. R. p 2711 N95-30130
MCINTYRE, D. C. p 2543 N95-29465
MCINVILLE, ROY M. p 2490 N95-29853
MCKAMEY, C. G. p 2538 N95-30216
MCKENZIE, D. L. p 2738 N95-29279
MCKENZIE, NICK R. p 2568 N95-28696
MCKINLEY, T. p 2644 N95-28777
MCMAHAN, CHRISTOPHER B. p 2646 N95-29008
MCMORRIS, HARLAN p 2481 N95-28744
MCNEIL, W. J. p 2507 N95-29026
MCPHERSON, ARMON p 2553 N95-29081
MCQUAY, P. p 2536 N95-29467
p 2536 N95-29473
p 2525 N95-29476
p 2526 N95-29533
p 2650 N95-29534
p 2597 N95-30293
MEAKIN, ROBERT L. p 2480 N95-28737
MEEKS, ELLEN p 2706 N95-29717
MEHROTRA, PIYUSH p 2649 N95-29404
p 2649 N95-29455
MEI, B. Z. p 2539 N95-28860
MEISSNER, KENITH ERWIN, II p 2705 N95-29632
MELAMED, NAHUM p 2503 N95-30347
MELILLO, MICHAEL R. p 2558 N95-29769
MELLO, JOE p 2670 N95-29311
MELLO, TINA MARIA p 2572 N95-29219
MELMAN, PAUL p 2697 N95-28795
MELSON, THOMAS G. p 2483 N95-28754
MELTON, EDWARD C., III. p 2619 N95-28989
MELTON, GREGORY S. p 2531 N95-29248
MELTON, JOHN E. p 2481 N95-28740
MELTON, LYNN A. p 2578 N95-30039
MELTON, MARA p 2552 N95-28939
MELTZ, MARTIN L. p 2633 N95-28866
MENDEZ, EMILIO E. p 2718 N95-28857
MENDILLO, MICHAEL p 2614 N95-29585
MENTER, FLORIAN R. p 2579 N95-30224
MERKLE, CHARLES L. p 2578 N95-30034
MERRILL, ROBERT T. p 2619 N95-28975
MERRIT, CHARLES D. p 2585 N95-29217
MESHISHNEK, M. J. p 2507 N95-28867
MESICK, HILLARY C. p 2601 N95-29977
MESSICK, FLOYD p 2585 N95-29274
METCALF, D. H. p 2695 N95-28957
METCALF, VERN L. p 2672 N95-30086
METSCHAN, S. L. p 2499 N95-28831
p 2499 N95-28840
METSCHAN, STEPHEN L. p 2521 N95-29043
MEYER, J. R. p 2564 N95-29568
MEYERS, J. A. p 2531 N95-28945
MICHA, DAVID A. p 2693 N95-29460
MICHALAK, RICHARD J. p 2642 N95-28976
MICHALSKY, J. J. p 2608 N95-28920
MICKELSON, ALAN R. p 2540 N95-29021
p 2554 N95-29186
MIDDELHOEK, P. F. A. p 2643 N95-30109
MIDDLETON, MARK E. p 2698 N95-28980
MIELKE, PAUL W., JR. p 2620 N95-29254
MILES, P. p 2676 N95-29610
p 2677 N95-29614
MILHAM, MERILL E. p 2551 N95-28699
MILITZER, M. p 2537 N95-29869
MILLER-GRAZIANO, CAROL L. p 2634 N95-29139
MILLER, ALBERT B. p 2492 N95-29210
MILLER, BRIAN p 2511 N95-30257
MILLER, D. P. p 2501 N95-30007
MILLER, H. V. p 2601 N95-29977
MILLER, JAMES S. p 2722 N95-29207
MILLER, JENNIFER L. p 2529 N95-30340
MILLER, L. S. p 2603 N95-30016
MILLER, M. K. p 2538 N95-30179
MILLER, ROBERT p 2478 N95-28727
MILLER, ROBERT A. p 2512 N95-29373
MILLER, ROBERT N. p 2631 N95-30069
MILLER, SCOTT ALAN p 2510 N95-29245
MILLIS, MARC G. p 2680 N95-28893
MILLS, DENNIS M. p 2718 N95-30184
MILLS, FRANKLIN P. p 2601 N95-29905
MILSTEIN, L. B. p 2554 N95-29203
MINER, PAUL S. p 2659 N95-29823
MINSTER, J. BERNARD p 2612 N95-28985
MISHRA, UMESH K. p 2567 N95-30124
MISLEVY, ROBERT J. p 2639 N95-29432
MITCHELL, CURTIS R. p 2482 N95-28748
MITIN, VLADIMIR p 2714 N95-29152
MIYAJI, T. p 2731 N95-29097
MIYANO, TAKAYA p 2621 N95-29333
MIZIA, RON p 2540 N95-28960
MOBLEY, SCOTT p 2561 N95-28950
MODIANO, DAVID p 2485 N95-28766
MOIN, PARVIZ p 2571 N95-29145
p 2573 N95-29268
MOLONEY p 2585 N95-29053
MOMOTA, H. p 2710 N95-29857
MONACO, PETER p 2557 N95-29564
MONAHAN, J. H. p 2627 N95-30048
MONDOLONI, STEPHANE LUCIEN p 2496 N95-29122
MONG, RENEE L. p 2602 N95-29200
MONK, VIRGINIA C. p 2559 N95-29991
MONROE, ROBERT p 2658 N95-29196
MONSON, DARYL J. p 2579 N95-30224
MONTOYA, ZEFERINO JORGE p 2694 N95-29886
MONTS, D. L. p 2531 N95-28916
MOOLENAAR, ANTOON ALFONS p 2535 N95-30282
MOORE, PETER K. p 2668 N95-28890
MOORE, ROBERT Y. p 2634 N95-28915
MOORE, T. E. p 2711 N95-30338
MOORE, TAMRA p 2647 N95-29278
MORAN, KENNETH JOHN p 2491 N95-29965
MORANO, E. p 2674 N95-30227
MORAVAN, KOU-YING p 2685 N95-29942
MOREAU, P. p 2667 N95-30171
MORENCY, ROGER L. p 2589 N95-28791
MORITA, S. p 2709 N95-29802
MOROSIN, B. p 2717 N95-30022
MORRE, FRANK G. p 2490 N95-29853
MORRELL, WILBERT J., III p 2566 N95-30075
MORRIS, M. R. p 2499 N95-28831
p 2499 N95-28840
MORRIS, PHILIP J. p 2689 N95-30152
MORRIS, W. L. p 2521 N95-29042
MORRISETT, GREG p 2721 N95-28877
MORRISSEY, JAMES F. p 2627 N95-29944
MOSBARGER, NEAL ANTHONY p 2489 N95-29500
MOSSBERG, THOMAS W. p 2693 N95-29555
MOTOJIMA, O. p 2709 N95-29808
p 2710 N95-29812
p 2710 N95-29857
MOTOJIMA, OSAMU p 2709 N95-29801
MOUL, THOMAS M. p 2498 N95-30226
MOULTON, PETER F. p 2584 N95-28678
MOYER, KERRY ALLEN p 2624 N95-29727
MOZER, JOEL BARNEY p 2622 N95-29701
MRAZ, RICHARD T. p 2643 N95-28690
MU, GOUGUANG p 2701 N95-29661
MULLEN, PATRICK p 2556 N95-29472
MUNSON, R. p 2641 N95-29624
MURAKAMI, S. p 2708 N95-29749
MURPHY, DANIEL P. p 2516 N95-28838
MURPHY, MICHAEL C. p 2700 N95-29366
MURPHY, O. J. p 2605 N95-30263
MURVEIT, HY p 2557 N95-29564
MUSEMBI, DAVID KASINA p 2599 N95-29703
MYERS, BRAD A. p 2642 N95-29146
MYHRE, G. p 2677 N95-29616
MYRICK, M. L. p 2523 N95-29189

N

NAIRN, JOHN A. p 2514 N95-28827
p 2514 N95-28828
NAITOH, P. p 2645 N95-28934
p 2637 N95-30083
NAKADA, Y. p 2735 N95-29837
NAKAJIMA, N. p 2708 N95-29749
NAKANO, TAKENORI p 2731 N95-29100
NAKAYAMA, KEN p 2638 N95-28937
NAKIA, N. p 2731 N95-29097
NAKROSHIS, PAUL ANDREW p 2719 N95-29501
NARK, DOUGLAS M. p 2689 N95-30153
NATARAJAN, MOHAN p 2633 N95-28866
NATRAJ, N. R. p 2658 N95-29079
NAU, GREGORY p 2703 N95-30076
NAVAB, NASSIR p 2670 N95-29352
NAVARRO-RUIZ, V. p 2676 N95-29610
p 2677 N95-29614
NEDDERMAN, WILLIAM H. p 2582 N95-29220
NEEL, MICHAEL M. p 2558 N95-29928
NEJOH, YASUNORI p 2710 N95-29841
NELSON, P. A. p 2606 N95-30264
NEMANICH, R. J. p 2713 N95-28954
NESS, JOEL KEVIN p 2592 N95-29256
NETT, E. p 2643 N95-30108
NETTLES, A. p 2529 N95-30334
NEUBAUER, J. C. p 2676 N95-29607
NEUFFER, D. V. p 2696 N95-30009
NEUMEYER, LEO p 2557 N95-29564
NEVISON, CYNTHIA DALE p 2609 N95-29804
NEWAZ, GOLAM M. p 2523 N95-29133
NEWCOMER, P. P. p 2717 N95-30022
NEWMAN, B. A. p 2539 N95-28860
p 2539 N95-28891
NEWMAN, BRIAN A. p 2539 N95-28864
NEWMAN, DANIEL A. p 2554 N95-29231
NG, L. V. p 2544 N95-29554
NGO, E. p 2523 N95-29136
p 2524 N95-29329
NGUEYEN, VINH D. p 2590 N95-29369
NGUYEN, HOA G. p 2553 N95-29166
NIBLETT, D. H. p 2703 N95-30062
NICHOLS, JOY S. p 2726 N95-29370
NICKERSON, GARY R. p 2532 N95-29273
NICOL, D. p 2535 N95-30111
NICOLA, V. F. p 2653 N95-30098
p 2653 N95-30099
NICOLL, JEFFREY F. p 2552 N95-28936
NIELSEN, J. NYBO p 2677 N95-29613
p 2678 N95-29618
NIJHUIS, G. H. p 2484 N95-28760
NIRMALAKHANDAN, N. p 2632 N95-29320
NISHIMOTO, YOSUKE p 2626 N95-29849
NISTLER, CANDY JEAN p 2678 N95-29619
NIX, J. L. p 2681 N95-28924
p 2681 N95-28962
NOACK, RALPH W. p 2481 N95-28745
NOBLE, GEORGE P., III p 2609 N95-29721
NOBLE, JOHN M. p 2618 N95-29976
NODA, N. p 2709 N95-29808
p 2711 N95-30032
NOGUCHI, TAKASHI p 2562 N95-29099

NOLAN, MICHAEL CRAIG ..... p 2732 N95-29255
NOOJIN, GARY D. ..... p 2585 N95-29274
NORBURY, JOHN W. ..... p 2696 N95-30337
NOREEN, R. ..... p 2478 N95-28720
NORMAN, COLIN ..... p 2731 N95-29100
NORMAN, TIMOTHY L. ..... p 2513 N95-28817
NORMAND, EUGENE ..... p 2500 N95-29950
NORTON, MELANIE J. ..... p 2723 N95-29690
NOWAK, ROBERT J. ..... p 2578 N95-30056
NUMBERS, KEITH E. ..... p 2578 N95-30087
NUSCA, MICHAEL J. ..... p 2569 N95-29058

O

OBBINK, B. K. ..... p 2673 N95-30093
OBERGEFELL, LOUISE ..... p 2640 N95-28683
OBRIEN, SUSAN K. ..... p 2531 N95-29246
OBRIEN, T. KEVIN ..... p 2527 N95-29825
p 2528 N95-30028
ODAY, M. E. ..... p 2523 N95-29136
p 2524 N95-29329
OEZYOERUEK, YUSUF ..... p 2661 N95-30156
OGIER, RICHARD G. ..... p 2506 N95-30090
OGILBY, PETER R. ..... p 2692 N95-29092
OHKOUCHI, Y. ..... p 2707 N95-29740
OHNISHI, M. ..... p 2708 N95-29749
p 2710 N95-29857
OHRINER, E. K. ..... p 2528 N95-30037
OHRN, N. Y. ..... p 2693 N95-29460
OHUVAN, SONLINK N. ..... p 2701 N95-29602
OHYABU, N. ..... p 2710 N95-29812
p 2711 N95-30032
OKA, Y. ..... p 2705 N95-29567
OKADA, H. ..... p 2708 N95-29749
OKADA, K. ..... p 2610 N95-30195
OKAMOTO, M. ..... p 2708 N95-29749
p 2710 N95-29857
OKAMOTO, MASAO ..... p 2711 N95-29966
OKAMURA, S. ..... p 2709 N95-29802
OKRASINSKI, RICHARD ..... p 2621 N95-29507
OLIKER, VLADIMIR ..... p 2552 N95-28979
OLIVER, W. C. ..... p 2547 N95-30174
OLSEN, GEORGE C. ..... p 2578 N95-30056
OLSEN, ROBERT ..... p 2621 N95-29507
OLSON, J. C. ..... p 2543 N95-29465
ONAKA, T. ..... p 2735 N95-29837
ONEAL, STEPHANIE L. ..... p 2506 N95-28688
ONINK, MARCEL ..... p 2538 N95-30287
ONO, T. ..... p 2710 N95-29812
ONOZUKA, M. ..... p 2710 N95-29857
ORCUTT, JOHN A. ..... p 2612 N95-28985
ORTEGA, R. ..... p 2672 N95-29824
ORTIZLONGO, CARLOS R. ..... p 2671 N95-29446
ORWOLL, MARK ALEXANDER ..... p 2573 N95-29334
OSBORNE, N. R. ..... p 2561 N95-28961
OSHER, STANLEY ..... p 2553 N95-29176
p 2699 N95-29177
OSWALD, FRED B. ..... p 2589 N95-29112
OTOOLE, B. J. ..... p 2514 N95-28829
OTTENSTEIN, HOWARD ..... p 2740 N95-28882
OTUGEN, M. V. ..... p 2502 N95-29468
OVERDIJK, D. A. ..... p 2597 N95-30169
OZTURA, CAN ..... p 2650 N95-29480
OZTURAN, C. ..... p 2671 N95-29488

P

PACE, PHILLIP E. ..... p 2557 N95-29504
PACKER, MALCOLM ..... p 2552 N95-28986
PAGE, MICHAEL ..... p 2534 N95-29994
PAGE, P. R. ..... p 2691 N95-28913
PAGE, W. C. ..... p 2665 N95-29831
PAIK, ELLEN T. ..... p 2669 N95-29080
PAJERSKI, ROSE ..... p 2644 N95-28806
PALM, T. E. ..... p 2516 N95-28843
PALMER, R. B. ..... p 2696 N95-30009
PAMIN, J. ..... p 2596 N95-30049
PAN, J. ..... p 2698 N95-28992
PANDI, R. ..... p 2537 N95-29869
PANNELL, C. N. ..... p 2565 N95-29925
PANNELL, CHRISTOPHER N. ..... p 2698 N95-28932
PANTALONE, P. A. ..... p 2559 N95-30073
PAPASTOGIANNIDOU, KAL. ..... p 2638 N95-29629
PAPENHAUSEN, PAUL STEPHEN ..... p 2730 N95-29781
PARIKH, PARESH ..... p 2481 N95-28743
PARK, CHUL ..... p 2503 N95-29351
PARK, SUNG-HO ..... p 2591 N95-30277
PARKER, A. P. ..... p 2593 N95-28789
p 2596 N95-30119
PARKER, JAMES F., JR. ..... p 2493 N95-29873
PARKER, L. E. ..... p 2666 N95-30112
PARKS, C. ..... p 2716 N95-29506
PARLETTE, EDWARD B. ..... p 2480 N95-28736
PARTHASARATHY, RANJANI V. ..... p 2539 N95-28850
PASCAL, JEAN-PAUL ..... p 2575 N95-29718
PASTORE, CHRISTOPHER M. ..... p 2513 N95-28825
PASTORE, TRACY HEATH ..... p 2641 N95-29359
PATEL, BHAVIN C. ..... p 2482 N95-28748
PATRICK, MIKE ..... p 2513 N95-28817
PATRICK, SHERYL M. ..... p 2582 N95-30161
PATTERSON, JAMES H., JR. ..... p 2634 N95-28941
PATTERSON, JOHN C. ..... p 2638 N95-29162
PATTINSON, T. J. ..... p 2565 N95-29925
PATTIPATI, KRISHNA R. ..... p 2494 N95-28887
PAUL, D. R. ..... p 2543 N95-29436
PAULK, MARK C. ..... p 2651 N95-29762
PAULSON, DOUGLAS ..... p 2592 N95-29012
PAVAN, VALENTINA ..... p 2612 N95-29212
PAYNE, J. L. ..... p 2538 N95-30178
PEACE, J. ..... p 2632 N95-29320
PEARSON, JOHN ..... p 2665 N95-29863
PEARSON, JOHNNIE A. ..... p 2511 N95-30257
PECK, EUGENE L. ..... p 2600 N95-29754
PECK, LINDAMAE ..... p 2697 N95-28778
PEGGION, GERMANA ..... p 2646 N95-28968
PELTONEN, HANNU ..... p 2655 N95-30283
PENEDO, MARIA H. ..... p 2652 N95-29996
PEPPER, G. T. ..... p 2586 N95-29330
PERALBA-VANO, J. I. ..... p 2676 N95-29610
p 2677 N95-29614

PEREZ, CHRISTOPHER ANTONIO

PERRY, B. ..... p 2729 N95-29709
PERRY, J. P. ..... p 2712 N95-28910
PETERS, FRANK H. ..... p 2714 N95-29157
PETRASSO, R. D. ..... p 2588 N95-30050
PEYGHAMBERIAN, N. ..... p 2695 N95-28930
PFENNING, FRANK ..... p 2588 N95-30045
PFLEGER, KARL ..... p 2645 N95-28886
PHARR, G. M. ..... p 2723 N95-29573
PHILIPPS, V. ..... p 2547 N95-30174
PHILLIPS, K. J. ..... p 2709 N95-29803
PHOOKUN, BIKRAM ..... p 2738 N95-29279
PICKARD, JEB S. ..... p 2729 N95-29774
PICKERING, HOWARD W. ..... p 2635 N95-29161
PIEPER, RONALD J. ..... p 2536 N95-29298
PIHOS, G. ..... p 2557 N95-29504
PIKE, C. D. ..... p 2628 N95-30343
PIKE, E. R. ..... p 2738 N95-29327
PINEDADEGYVEZ, JOSE ..... p 2703 N95-30081
PINELLI, THOMAS E. ..... p 2665 N95-29979
PINKERTON, F. E. ..... p 2721 N95-29028
p 2681 N95-28923
p 2681 N95-28924
p 2681 N95-28962
PINSKY, PETER M. ..... p 2661 N95-30295
PINTZ, ADAM ..... p 2543 N95-29367
PIPES, R. BYRON ..... p 2514 N95-28829
PIPPIN, H. GARY ..... p 2512 N95-30225
PIRZADEH, SHAHYAR ..... p 2481 N95-28743
PLASSMANN, P. E. ..... p 2659 N95-29985
PLOTKIN, SERGE ..... p 2648 N95-29297
PLUZHNIKOV, ANNA ..... p 2675 N95-30297
PODBOY, GARY G. ..... p 2477 N95-30229
POE, C. C., JR. ..... p 2515 N95-28837
POGGIO, TOMAS ..... p 2556 N95-29441
POHLE, L. ..... p 2603 N95-30017
POLITES, M. E. ..... p 2507 N95-28721
POLITZER, PETER ..... p 2691 N95-28868
p 2691 N95-28919
p 2534 N95-30078
POLLAND, D. R. ..... p 2515 N95-28837
POLLY, DAN ..... p 2592 N95-28684
POPE, D. STUART ..... p 2582 N95-30151
POPELAS, JUDY M. ..... p 2550 N95-29918
PORCELLO, JOHN ..... p 2559 N95-30072
PORTANOVA, MARC A. ..... p 2520 N95-29038
p 2529 N95-30340
POSENAU, MARY-ANNE K. ..... p 2479 N95-28729
p 2479 N95-28731
POSPIESZCZYK, A. ..... p 2709 N95-29803
POSTON, WENDY L. ..... p 2675 N95-29819
p 2673 N95-30126
POWELL, KENNETH G. ..... p 2480 N95-28739
POWER, JOHN D. ..... p 2677 N95-29615
POWERS, JOHN P. ..... p 2557 N95-29504
POWERS, ROBERT ..... p 2552 N95-28986
POZARNSKY, G. A. ..... p 2545 N95-29559
PRAHST, P. S. ..... p 2501 N95-30007
PRAKASH, J. ..... p 2632 N95-29320
PRASAD, ADAPA V. ..... p 2633 N95-28866
PRASAD, C. B. ..... p 2517 N95-28844
PREUSS, C. H. ..... p 2516 N95-28839
PRICE, D. L. ..... p 2717 N95-30077
PRIEBE, CAREY E. ..... p 2675 N95-29819
PRIEDHORSKY, W. ..... p 2508 N95-29464
PRIEST, JOHN ..... p 2536 N95-29461
PROSPERETTI, ANDREA ..... p 2549 N95-29550
PRUEGER, GEORGE H. ..... p 2484 N95-28762
PRUSACZYK, W. K. ..... p 2637 N95-29846
PRZEKWAS, A. J. ..... p 2489 N95-29316
PUCKETT, PAUL M. ..... p 2521 N95-29044
PUDLO, G. ..... p 2610 N95-30197
PULLI, JAY J. ..... p 2613 N95-29293
PUREZA, PABLO C. ..... p 2703 N95-30076
PURI, SIDDHARTHA ..... p 2658 N95-29196
PUTMAN, MARTY ..... p 2699 N95-29283
PUTTERMAN, S. ..... p 2683 N95-28973

Q

QIAN, S. ..... p 2531 N95-28916
QIDA, ZHAO ..... p 2685 N95-29951
QIN, LIHONG ..... p 2573 N95-29335
QINQIN, SHENG ..... p 2685 N95-29951
QUATTLEBAUM, M. D. ..... p 2678 N95-29620
QUICK, HOWARD A. ..... p 2498 N95-29445
QUINLIVAN, JOHN ..... p 2519 N95-29031
QUINN, GEORGE ..... p 2547 N95-30118
QUINN, J. M. ..... p 2691 N95-28856

R

RABIER, PATRICK J. ..... p 2668 N95-28861
p 2668 N95-28863
RABITZ, HERSCHEL ..... p 2691 N95-28944
p 2548 N95-29525
RADEKA, V. ..... p 2566 N95-30025
RADEZTSKY, RONALD HENRY, JR.
p 2492 N95-30294
RAGENT, B. ..... p 2737 N95-30058
RAGHAVAN, SRINI ..... p 2540 N95-28925
RAGHAVEN, RAGHU ..... p 2552 N95-28984
RAJ, PRADEEP ..... p 2478 N95-28725
RAMAPRIAN, B. R. ..... p 2487 N95-29091
RAMSEY, PERRY G. ..... p 2625 N95-29805
RAMSEY, ROBERT G. ..... p 2477 N95-29414
RANDALL, D. A. ..... p 2610 N95-30181
RANDEL, DAVID L. ..... p 2628 N95-30272
RANGASWAMY, MURALIDHAR ..... p 2552 N95-28943
RANSOM, JONATHAN B. ..... p 2517 N95-28848
RAO, G. R. ..... p 2547 N95-30190
RAS, ZBIGNIEW W. ..... p 2666 N95-30117
RASMUSSEN, ANDREW PETER ..... p 2729 N95-29710
RASOULI, F. ..... p 2610 N95-30197
RATCLIFF, P. R. ..... p 2703 N95-30062
RAVI, R. ..... p 2661 N95-30215
RAVI, S. S. ..... p 2661 N95-30215
RAVICHANDRAN, V. ..... p 2669 N95-29105
RAVIPRAKASH, G. K. ..... p 2689 N95-30154
RAZVAN, AHMAD ..... p 2525 N95-29513
READ, JULIA M. ..... p 2676 N95-29606
REICHERT, BRUCE A. ..... p 2489 N95-29402
REINKE, DONALD L. ..... p 2628 N95-30272
REISING, JACK D. ..... p 2641 N95-29943
REJ, D. J. ..... p 2543 N95-29465
REMOTIGUE, MICHAEL ..... p 2482 N95-28749
RENO, J. ..... p 2716 N95-29814
RENSINK, M. E. ..... p 2711 N95-30130
REPPLINGER, RON ..... p 2567 N95-30261
RESCIA, S. ..... p 2566 N95-30025
RESNICK, P. J. ..... p 2718 N95-30214
REUSKEN, A. A. ..... p 2672 N95-30088
REUTHER, JAMES ..... p 2491 N95-29972
REX, DIETRICH ..... p 2507 N95-28852
REYNOLDS, DICK ..... p 2513 N95-28826
RHEINBOLDT, WERNER C. ..... p 2668 N95-28861
p 2668 N95-28863
RHOADS, GREGORY L. ..... p 2561 N95-28971
RHODES, CHARLES K. ..... p 2553 N95-29081
RIBNER, HERBERT S. ..... p 2684 N95-29452
RICE, BETSY M. ..... p 2534 N95-29994
RICHA, JULIAN P. ..... p 2601 N95-29977
RICHARD, JULIAN P. ..... p 2598 N95-28931
RICHARDS, WHITMAN ..... p 2670 N95-29440
RICHARDSON, L. ..... p 2641 N95-29624
RICKMAN, STEVEN L. ..... p 2671 N95-29446
RIDHA, RABI M. J. ..... p 2572 N95-29249
RIESTER, L. ..... p 2547 N95-30190
RIMLINGER, MARK J. ..... p 2485 N95-28768
RINGERUD, MARK A. ..... p 2628 N95-30272
RIOS-TEJADA, F. ..... p 2676 N95-29610
p 2677 N95-29614
RISHE, NAPHTALI ..... p 2722 N95-29182
RISTORCELLI, J. RAY ..... p 2686 N95-30133
RIZER, ANNETTE ..... p 2640 N95-28683
RO, PAUL I. ..... p 2663 N95-29183
ROBBINS, KATHLEEN ..... p 2567 N95-30260
ROBERTSON, HERBERT ..... p 2612 N95-28972
ROBINSON, D. W. ..... p 2673 N95-30204
ROBINSON, GERALD D. ..... p 2588 N95-30050
ROBINSON, MARK SOUTHWICK ..... p 2736 N95-29594
ROBINSON, WILLIAM ..... p 2585 N95-29274
RODGERS, M. D. ..... p 2641 N95-29365
RODGERS, MARK D. ..... p 2493 N95-28819

RODRIGUES, EDUARDO ALVES p 2663 N95-29251
ROE, M. P. p 2565 N95-29925
ROEDER, H. p 2652 N95-29989
ROELOFFS, NORMAN p 2596 N95-30008
ROGERS, MELISSA J. B. p 2509 N95-29643
p 2549 N95-30339
ROGNLIEN, T. D. p 2711 N95-30130
ROHWER, KIM p 2522 N95-29050
ROMERO, M. p 2677 N95-29611
ROSE-PEHRSSON, SUSAN p 2512 N95-29052
ROSE, TODD S. p 2587 N95-29931
ROSELLO, ANTHONY DAVID p 2505 N95-29447
ROSENKRANTZ, D. J. p 2661 N95-30215
ROSENTHAL, PETER p 2562 N95-29061
ROSENTHAL, PETER A. p 2717 N95-30068
ROSHKO, ANATOL p 2574 N95-29382
ROSKAM, JAN p 2501 N95-30254
ROSS, HOLLY M. p 2498 N95-30226
ROSS, JOHN p 2534 N95-29922
ROSSITER, ROBERT J. p 2587 N95-29914
ROTE, D. M. p 2665 N95-29987
ROUNDY, LANCE p 2522 N95-29048
ROUSE, M. p 2517 N95-28844
ROWSHANAEE, MEHDI E. p 2648 N95-29321
ROY, MAURICE W. p 2641 N95-29600
ROZAS, GUILLERMO J. p 2722 N95-29207
RUDIN, LEONID p 2553 N95-29176
p 2699 N95-29177
RUPERT, NEVIN L. p 2596 N95-29929
RUPP, P. L. p 2515 N95-28836
RUSSELL, S. G. p 2516 N95-28843
RUSSELL, S. S. p 2524 N95-29374
RUTTEN, F. p 2676 N95-29608
RUUD, BENT O. p 2614 N95-29413
RUUD, CLAYTON O. p 2596 N95-29580
RYDER, DANIEL F., JR. p 2716 N95-29658
RYG, MORTEN p 2638 N95-29627
RYMAN, DAVID p 2637 N95-29995

S

SAATCHI, HOSSEIN p 2513 N95-28826
SABERI, A. p 2667 N95-30168
SABERI, HOSSEIN p 2496 N95-28928
SABIDO, D. J. p 2698 N95-28992
SACHTJEN, S. p 2593 N95-29941
SADATI, SEYED HOSSEIN p 2663 N95-29241
SADOVNIK, LEV p 2698 N95-28914
SAENGER, ARLEEN M. p 2642 N95-29626
SAGARA, A. p 2709 N95-29808
p 2710 N95-29812
p 2711 N95-30032
SAGE, STEPHANIE p 2664 N95-29574
p 2675 N95-29906
SAIEDI, A. p 2558 N95-29919
SAIYED, NASEEM H. p 2477 N95-30229
SAJDA, PAUL p 2665 N95-29863
SAKURAI, TAKAYUKI p 2730 N95-29782
SALINAS, C. E. p 2605 N95-30263
SALT, J. W. p 2700 N95-29354
SAMAREH-ABOLHASSANI, JAMSHID
p 2484 N95-28763
p 2486 N95-28773
SAMM, U. p 2709 N95-29803
SAMMELLS, A. F. p 2593 N95-29946
SANCHEZ-SANCHEZ, Z. G. p 2676 N95-29610
p 2677 N95-29614
SANCHEZ, J. p 2544 N95-29554
SANCHEZCASTELLANOS, ARMANDO R.
p 2506 N95-28700
SANDERFORD, VICKI p 2561 N95-28950
SANETRIK, MARK D. p 2480 N95-28736
SANGHERA, JASBINDER p 2703 N95-30076
SANKAR, ANANTH p 2557 N95-29564
SANKAR, L. N. p 2688 N95-30147
SANTANNA, SIDNEI J. S. p 2601 N95-29999
SANTARE, MICHAEL H. p 2514 N95-28829
SANTAVICCA, DOMENIC A. p 2577 N95-29948
SANUKI, H. p 2707 N95-29742
p 2709 N95-29802
SASAKI, S. p 2707 N95-29740
SASALA, RICHARD ANTHONY p 2602 N95-29103
SASLOW, W. M. p 2681 N95-28924
p 2681 N95-28962
SATO, TETSUYA p 2708 N95-29755
p 2709 N95-29810
SATO, YOICHI p 2737 N95-29151
SAUSA, ROSARIO C. p 2530 N95-28876
SAUTER, STEFAN A. p 2669 N95-29080
SAVAGE, P. D. p 2642 N95-28722
p 2642 N95-28818
SAWKA, MICHAEL N. p 2636 N95-29757
SCANLON, R. D. p 2683 N95-28999
SCHAAF, CRYSTAL LYNN BARKER
p 2599 N95-29540
SCHABOWSKI, DEANNE M. p 2482 N95-28747
SCHAEFER, HENRY F., III p 2693 N95-29865
SCHAMILOGLU, EDI p 2703 N95-29003
SCHEIBE, J. p 2553 N95-29174
SCHEINBEIM, J. I. p 2539 N95-28860
p 2539 N95-28891
SCHEINBEIM, JERRY I. p 2539 N95-28864
SCHEINFEIN, MICHAEL R. p 2712 N95-28681
SCHELL, DONNA J. p 2608 N95-28787
SCHERNER, MICHAEL J. p 2506 N95-30251
SCHLEMMER, J. A. p 2608 N95-28920
SCHMID, F. p 2604 N95-30217
SCHNABEL, ROBERT B. p 2670 N95-29385
SCHNEIDER, JOHN P. p 2696 N95-30337
SCHNEIDER, N. S. p 2546 N95-30030
SCHOENFELD, THILO p 2483 N95-28757
SCHOENWALD, D. A. p 2654 N95-30189
SCHOFIELD, ANDREW N. p 2582 N95-28966
SCHOLFIELD, DAVID W. p 2586 N95-29425
SCHRAMM, M. R. p 2499 N95-28840
SCHROCK, S. L. p 2710 N95-29909
SCHROEDER, LYLE C. p 2506 N95-30251
SCHROEDL, CHRISTOPH p 2678 N95-29621
SCHROER, JAMES A. p 2655 N95-30307
SCHUBERT, W. K. p 2604 N95-30217
SCHUSTER, GARY B. p 2716 N95-29493
SCHWAN, KARSTEN p 2659 N95-29915
SCHWARTING, ALAN p 2702 N95-30053
SCHWARZ, R. K. p 2725 N95-30194
SCHWEER, B. p 2709 N95-29803
SCHWEICKART, DANIEL p 2561 N95-28971
SCOLES, DARREN p 2567 N95-30258
SCOTT, A. DONALD, JR. p 2608 N95-28717
SCOTT, J. N. p 2690 N95-30163
SCOTT, JEFF W. p 2588 N95-30050
SCOTT, W. S. p 2549 N95-30345
SCRIVENER, SANDRA LYNN p 2507 N95-29332
SEAMAN, LYNN p 2542 N95-29288
SEDENQUIST, FRED W. p 2559 N95-29991
SEGALMAN, D. J. p 2655 N95-30209
SEHMBEY, M. S. p 2551 N95-30296
SEI, VINCENT J. p 2568 N95-28948
SEIFF, A. p 2737 N95-30058
SELIGMAN, ERIK p 2724 N95-29818
SELVIN, S. p 2654 N95-30183
SEMINARIO, JORGE M. p 2691 N95-28919
SENF, H. p 2542 N95-29195
SENGUPTA, L. C. p 2541 N95-29135
p 2523 N95-29136
p 2585 N95-29208
p 2524 N95-29329
SENGUPTA, S. p 2543 N95-29353
p 2540 N95-28963
p 2541 N95-29135
p 2585 N95-29208
p 2543 N95-29353
SETSER, D. W. p 2681 N95-29062
SETTLES, G. S. p 2577 N95-29920
SEYFARTH, BENJAMIN R. p 2646 N95-28968
SGALL, JIRI p 2645 N95-28878
SHAFER, STEVEN A. p 2645 N95-28883
SHAH, BHARAT M. p 2517 N95-28846
SHAH, D. B. p 2532 N95-29250
SHAH, JAYANT p 2671 N95-29485
SHAH, PATRICIA L. p 2674 N95-30143
SHANEYFELT, M. R. p 2718 N95-30214
SHANKAR, PRASHANTH p 2514 N95-28827
SHANNON, SAMUEL G. p 2639 N95-29434
SHANNON, T. E. p 2696 N95-29142
SHARPLESS, GARRETT C. p 2521 N95-29043
SHASHUA, AMNON p 2670 N95-29352
SHAW, KEVIN B. p 2598 N95-28931
SHAW, MARY p 2649 N95-29376
SHEARER, MICHAEL p 2669 N95-29083
SHEFFIELD, J. p 2711 N95-30023
SHELDON, BRIAN W. p 2716 N95-29767
SHEN, H. p 2674 N95-30145
SHEN, JIANXIONG p 2577 N95-30027
SHENG, QIUQIN p 2685 N95-29681
SHEPARD, W. S. p 2531 N95-28916
SHEPHARD, MARK S. p 2674 N95-29490
SHEPHERD, WILLIAM T. p 2493 N95-29873
SHEPPARD, ERIC JAMES p 2705 N95-29547
SHER, A. p 2702 N95-29978
SHERBY, OLEG D. p 2545 N95-29635
SHETTY, D. K. p 2529 N95-30180
SHI, SHENG-CAI p 2562 N95-29099
SHIAO, MICHAEL C. p 2518 N95-28849
SHIBASAKI, K. p 2737 N95-29098
SHIEBER, STUART p 2499 N95-29123
SHIELDS, JANET E. p 2619 N95-28872
SHIFFLER, DONALD p 2703 N95-29003
SHIH, MING-HSIN p 2483 N95-28753
SHIH, TOM I.-P. p 2485 N95-28768
SHIMIZU, T. p 2737 N95-29098
SHIMIZU, YOSHINOBU p 2626 N95-29849
SHOCKEY, DONALD A. p 2542 N95-29288
SHOLL, P. L. p 2660 N95-30193
SHOOK, D. MICHAEL p 2486 N95-28771
SHUART, M. J. p 2517 N95-28844
p 2517 N95-28847
SHUKLA, J. G. p 2519 N95-29035
SHULER, S. F. p 2514 N95-28829
SHYPRYKEVICH, PETER p 2498 N95-29565
SI, GONGWANG p 2622 N95-29662
SIDDONS, WILLIAM p 2478 N95-28727
SIEGEL, H. J. p 2658 N95-28965
SIEGEL, R. W. p 2717 N95-29986
p 2537 N95-30018
SIKKA, V. K. p 2528 N95-30037
SILCOX, R. J. p 2672 N95-30086
SILVA, L. J. p 2602 N95-29463
SILVER, R. N. p 2652 N95-29989
SIMEONSSON, JOSEF B. p 2530 N95-28876
SIMMERMACHER, T. p 2597 N95-30210
SIMMONDS, J. G. p 2595 N95-29562
SIMO, J. C. p 2597 N95-30123
SIMO, JUAN C. p 2594 N95-29063
SIMON, HERBERT A. p 2664 N95-29577
SIMON, WILLIAM E. p 2590 N95-29369
SIMONEAU, ROBERT J. p 2568 N95-28719
SIMPSON, ANTHONY G. p 2569 N95-28990
SIMPSON, JACK, II p 2677 N95-29615
SIMPSON, S. F. p 2605 N95-30263
SINCELL, MARK WILLIAM p 2610 N95-29885
SINGH, A. K. p 2537 N95-29724
SINGH, J. p 2712 N95-28874
SINGHAL, S. C. p 2607 N95-30281
SINTON, S. W. p 2578 N95-30187
SIRKIS, JIM p 2699 N95-29283
SISTI, FRANK J. p 2652 N95-30047
SITARAMAN, MURALI p 2647 N95-29226
SJOGREN, WILLIAM L. p 2737 N95-30344
SKOCH, GARY J. p 2582 N95-29113
SLATER, JOHN W. p 2479 N95-28732
p 2485 N95-28770
SLEATOR, DANIEL D. p 2645 N95-28878
SMITH, CHARLES p 2555 N95-29290
p 2536 N95-29461
SMITH, DAWN E. p 2543 N95-29355
SMITH, DON p 2644 N95-28805
SMITH, ERIC P. p 2609 N95-29450
SMITH, G. R. p 2711 N95-30130
SMITH, GERALD A. p 2692 N95-28994
SMITH, GUY A. p 2531 N95-29246
SMITH, J. H. p 2567 N95-30188
SMITH, J. S. p 2713 N95-28967
SMITH, L. p 2712 N95-28910
SMITH, MARILYN JONES p 2572 N95-29242
SMITH, P. J. p 2516 N95-28839
p 2499 N95-28840
SMITH, PETER J. p 2519 N95-29034
SMITH, R. MARSHALL p 2659 N95-29454
SMITH, RALPH C. p 2672 N95-30086
SMITH, RANDALL WILLIAM p 2575 N95-29719
SMITH, RICHARD C. p 2664 N95-29657
SMITH, ROBERT E. p 2479 N95-28729
p 2479 N95-28730
SMITH, S. J. p 2693 N95-29521
SMITH, W. p 2606 N95-30267
SMOLANOFF, JASON p 2533 N95-29722
SNELGROVE, ANDREW H. p 2649 N95-29442
SNELL, HILARY EDMUND p 2608 N95-29213
SNYDER, E. S. p 2714 N95-29157
SOBANIK, JOHN BERTRAM p 2580 N95-30304
SOBER, JANET S. p 2478 N95-28726
SOBIESKI, JAROSLAW p 2495 N95-28820
SODERQUIST, JOE p 2498 N95-29565
SOFFEN, GERALD p 2740 N95-28882
SOFUE, Y. p 2731 N95-29097
SOHN, CHANG W. p 2550 N95-29307
p 2550 N95-29537
SOLDI, JAMES D., JR. p 2602 N95-29200
p 2602 N95-29201
SOLKA, JEFFREY L. p 2675 N95-29819
p 2673 N95-30126
SOLLFREY, WILLIAM p 2651 N95-29736
SON, DAVID Y. p 2545 N95-29569
p 2547 N95-30132
SONG, JIN-JOO p 2702 N95-29973
SONI, BHARAT p 2482 N95-28749
SONI, BHARAT K. p 2483 N95-28753
p 2484 N95-28759
SONNENBERG, N. p 2540 N95-28963
SOPOK, SAMUEL p 2541 N95-29138
SORENSON, REESE L. p 2482 N95-28750
SOUTHERLAND, L. D. p 2478 N95-28720
SOWA-RESAT, MARIANNE p 2533 N95-29722
SOZUER, H. SAMI p 2718 N95-30298
SPADAFORA, STEPHEN J. p 2540 N95-28925
SPANGLER, RONALD L., JR. p 2664 N95-29548
SPARROW, VICTOR W. p 2687 N95-30144

SPEKREIJSE, S. P. ..... p 2484 N95-28760
SPENCE, CLAY ..... p 2665 N95-29863
SPENCER, I. ..... p 2499 N95-29623
SPEZIO, ANTHONY E. ..... p 2554 N95-29236
SPIESS, FRED N. ..... p 2628 N95-28865
SPOONER, CHAD M. ..... p 2557 N95-29603
SPRAVKA, JOHN J. ..... p 2654 N95-30125
SPRIGGS, RICHARD M. ..... p 2525 N95-29492
SPRINGSTEEN, BETH ..... p 2550 N95-29918
SPROUSE, J. K. ..... p 2627 N95-30048
SROMOVSKY, L. ..... p 2737 N95-30058
STAALHAGEN, L. ..... p 2560 N95-30219
STAHL, GARY A. ..... p 2599 N95-29523
STANFORD, EDWARD ROSEMOND ..... p 2586 N95-29336
STANGLE, GREGORY C. ..... p 2525 N95-29492
STARK, MIKE ..... p 2644 N95-28807
STARKEY, MIKE ..... p 2721 N95-28880
STASSINOPOULOS, DIMITRIS ..... p 2668 N95-30279
STAVOLA, MICHAEL ..... p 2714 N95-29209
STEEDMAN, R. S. ..... p 2582 N95-28966
STEELHAMMER, JEFF ..... p 2645 N95-28814
STEEN, GREGORY GLEN ..... p 2489 N95-29338
STEFANESCU, G. ..... p 2673 N95-30106
STEHLE, ROY ..... p 2506 N95-30090
STEHOUWER, H. P. ..... p 2666 N95-30101
STEHOUWER, P. H. P. ..... p 2667 N95-30222
STEIN, MICHAEL L. ..... p 2675 N95-30297
STEINBRENNER, JOHN P. ..... p 2481 N95-28745
..... p 2483 N95-28751
STEINTHORSSON, ERLENDUR ..... p 2485 N95-28766
STEN, J. C. E. ..... p 2673 N95-30172
STEPHENS, GRAEME L. ..... p 2628 N95-30272
STEPHENS, P. J. ..... p 2720 N95-29936
STEUTEL, F. W. ..... p 2666 N95-30167
STEVENS, WILLIAM G. ..... p 2552 N95-28943
STEVENSON, J. MARK ..... p 2650 N95-29536
STINNETT, R. W. ..... p 2543 N95-29465
STINSON, MICHAEL R. ..... p 2685 N95-30084
STODOLSKY, DANIEL ..... p 2658 N95-28879
STOECKLIN, SARA ..... p 2648 N95-29285
STOEN, JEFFREY DONALD ..... p 2509 N95-30280
STOLL, JOHN C. ..... p 2508 N95-30036
STOORVOGEL, A. A. ..... p 2672 N95-30046
..... p 2667 N95-30168
..... p 2668 N95-30288
STOUT, PETER D. ..... p 2658 N95-28884
STOWELL, S. ..... p 2541 N95-29135
..... p 2523 N95-29136
..... p 2524 N95-29329
STRAIN, DOUGLAS ..... p 2731 N95-30230
STRANICK, S. J. ..... p 2531 N95-28945
STRASSBURGER, E. ..... p 2542 N95-29195
STRAWN, GREGORY ..... p 2492 N95-29057
STRIZ, ALFRED G. ..... p 2495 N95-28820
STROUBOULIS, T. ..... p 2668 N95-29065
STROUD, DAVID G. ..... p 2700 N95-29560
STRUIJS, R. ..... p 2578 N95-30202
STUCKERT, G. K. ..... p 2577 N95-29913
STWALLEY, WILLIAM C. ..... p 2602 N95-29949
SU, J. ..... p 2539 N95-28891
SUAREZ, JIM A. ..... p 2521 N95-29041
SUCIU, DAN ..... p 2659 N95-29225
SUDO, S. ..... p 2710 N95-29857
SUENAGA, M. ..... p 2716 N95-29984
SUGAMA, H. ..... p 2709 N95-29789
SUGIYAMA, T. ..... p 2610 N95-30195
SUI, P. C. ..... p 2591 N95-30110
SULLIVAN, WALTER ..... p 2740 N95-28882
SULONEN, REIJO ..... p 2655 N95-30283
SULTAN, PETER JARED ..... p 2708 N95-29783
SUN, B. ..... p 2632 N95-29320
SUN, C. T. ..... p 2526 N95-29561
SUN, PANG-CHEN ..... p 2583 N95-29508
SUN, WEI ..... p 2722 N95-29182
SUN, XIAOLI ..... p 2584 N95-28808
SUNDARAM, R. ..... p 2661 N95-30215
SUSSMAN, MYLES A. ..... p 2503 N95-30228
SUTHERLAND, HERBERT J. ..... p 2603 N95-30213
SUZUKI, H. ..... p 2711 N95-30032
SUZUKI, KOJIRO ..... p 2490 N95-29640
..... p 2575 N95-29712
SVOBODA, JAMES S. ..... p 2508 N95-30011
SWAB, JEFFREY J. ..... p 2547 N95-30118
SWANSON, G. D. ..... p 2499 N95-28831
..... p 2515 N95-28836
..... p 2499 N95-28840
SWANSON, S. E. ..... p 2714 N95-29157
SWARD, MARCIA P. ..... p 2672 N95-29647
SWENSON, JAMES S. ..... p 2587 N95-29931
SWIFT, G. ..... p 2683 N95-28973
SYPHERS, M. ..... p 2696 N95-30021
SZEWCZYK, ALBIN A. ..... p 2487 N95-28921
SZYMANSKI, BOLESLAW K. ..... p 2650 N95-29480

T

TAASAN, SHLOMO ..... p 2670 N95-29403
TABER, ALLEN H. ..... p 2500 N95-29950
TADEPALLI, SRINIVAS. ..... p 2569 N95-29024
TAGGART, BRIAN C. ..... p 2497 N95-29426
TAKAMURA, S. ..... p 2707 N95-29740
TAKATA, SACHIO ..... p 2626 N95-29849
TAKEIRI, Y. ..... p 2705 N95-29567
TALISA, S. H. ..... p 2562 N95-29073
..... p 2562 N95-29078
TALU, ORHAN ..... p 2532 N95-29250
TALVACCHIO, J. ..... p 2562 N95-29073
..... p 2562 N95-29078
TAM, CHRISTOPHER K. W. ..... p 2686 N95-30133
..... p 2686 N95-30134
..... p 2674 N95-30145
TAM, CLEMENT K. ..... p 2483 N95-28755
TAMIL, LAKSHMAN S. ..... p 2556 N95-29383
TAN, DE-TONG ..... p 2587 N95-29660
TANABE, T. ..... p 2709 N95-29803
TANAKA, MOTOHIKO ..... p 2707 N95-29739
..... p 2710 N95-29813
TANAKA, TOSHIHARU ..... p 2626 N95-29849
TANG, LEI ..... p 2688 N95-30146
TANG, P. T. P. ..... p 2652 N95-30020
TANNEN, VAL ..... p 2659 N95-29225
TANNER, D. M. ..... p 2714 N95-29157
TARANTO, NICK ..... p 2596 N95-30008
TASKE, LEO E. ..... p 2513 N95-28824
TATARCHUK, BRUCE ..... p 2511 N95-30257
TAUCHERT, T. R. ..... p 2528 N95-29864
TAYEBATI, PARVIZ ..... p 2713 N95-28933
TAYLOR, M. J. ..... p 2611 N95-28697
TAYLOR, PALMER ..... p 2534 N95-30085
TAYLOR, V. ..... p 2611 N95-28697
TENBRINK, S. C. ..... p 2660 N95-30128
TERELST, A. F. M. ..... p 2673 N95-30204
TERRY, JENNIFER ..... p 2518 N95-28906
TERZUOLI, ANDY ..... p 2553 N95-29159
..... p 2558 N95-29904
TEWARSON, ARCHIBALD ..... p 2523 N95-29277
TEWKSBURY, S. K. ..... p 2719 N95-29756
THALLER, L. H. ..... p 2567 N95-30262
THIEDING-CANCEL, D. ..... p 2636 N95-29238
THOMAS, DANIEL D. ..... p 2702 N95-30053
THOMAS, MARY L. ..... p 2640 N95-28792
THOMAS, ROBERT J. ..... p 2716 N95-29506
THOMPSON, DONALD L. ..... p 2534 N95-29994
THOMPSON, G. L. ..... p 2658 N95-29079
THOMPSON, JOE ..... p 2482 N95-28749
THOMPSON, P. ..... p 2544 N95-29554
THOMPSON, RICHARD C. ..... p 2532 N95-29483
THORNTON, W. P. ..... p 2676 N95-29607
THORPE, THOMAS P. ..... p 2718 N95-30164
THRASH, PATRICK ..... p 2522 N95-29050
THUAN, TRINH X. ..... p 2735 N95-29917
THUMMA, KASPAL REDDY ..... p 2526 N95-29597
TIAN, GUOGUANG ..... p 2701 N95-29571
TIBBALS, THOMAS F. ..... p 2556 N95-29459
TIEMSIN, PACITA I. ..... p 2560 N95-30336
TIEN, H. T. ..... p 2632 N95-29155
TIERNEY, THOMAS P. ..... p 2492 N95-30253
TILS, P. ..... p 2714 N95-29134
TIMON, R. P. ..... p 2718 N95-30214
TING, A. ..... p 2588 N95-29937
TING, T. C. T. ..... p 2527 N95-29763
TIPTON, FRANKLIN J. ..... p 2497 N95-29437
TIWARI, ANIL ..... p 2592 N95-29104
TOBIAS, SIGMUND ..... p 2648 N95-29325
TODA, SUSUMU ..... p 2507 N95-28852
TODOROKI, JIRO ..... p 2711 N95-30033
TOELG, SEBASTIAN ..... p 2556 N95-29441
TOKSOEF, M. N. ..... p 2558 N95-29875
TOLLES, WILLIAM A. ..... p 2562 N95-29075
TOLMIE, D. E. ..... p 2660 N95-30128
TOMASIC, ANTHONY SLAVKO ..... p 2725 N95-30286
TOMBAZIS, NICHOLAS ..... p 2575 N95-29654
TOMITA, Y. ..... p 2710 N95-29857
TOMKINS, ANDREW ..... p 2645 N95-28878
TOMLINSON, JOHN J. ..... p 2550 N95-29307
TOMOZANA, MINORU ..... p 2541 N95-29071
TOONEN, B. R. ..... p 2610 N95-30176
TORTORELLI, P. F. ..... p 2528 N95-30175
TOTH, L. M. ..... p 2695 N95-28957
TOWNSEND, DENNIS P. ..... p 2589 N95-29112
TRAPP, ROBERT JEFFREY ..... p 2625 N95-29806
TREBINO, RICK ..... p 2698 N95-28983
TRENT, L. K. ..... p 2636 N95-29238
TRIPP, LLOYD D., JR. ..... p 2636 N95-29360
TRUSZLOWSKI, WALTER ..... p 2740 N95-28882
TSAI, TAI-PING ..... p 2576 N95-29778
TSANG, PUI HO WILSON ..... p 2526 N95-29549
TSEDILINA, ELENE E. ..... p 2612 N95-28871
..... p 2612 N95-29140
TSITSIKLIS, J. N. ..... p 2664 N95-29636
TSITSOPOULOS, PAUL ..... p 2552 N95-28986
TSOU, PO-YU ..... p 2662 N95-29109
TSUI, T. Y. ..... p 2547 N95-30174
TSUMORI, K. ..... p 2705 N95-29567
TUIJN, CHRIS ..... p 2725 N95-30289
TURKEL, E. ..... p 2674 N95-30353
TURNER, JAMES C. ..... p 2570 N95-29069
TURNER, JAMES C., JR. ..... p 2569 N95-29068
TURNER, MITCHELL K. ..... p 2649 N95-29435
TURNQUIST, DAVID V. ..... p 2565 N95-29601
TYLER, W. A. ..... p 2601 N95-30061
TZOU, H. S. ..... p 2528 N95-29864

U

UCHIDA, SHIGEO ..... p 2626 N95-29849
UEDA, Y. ..... p 2709 N95-29803
UENOSONO, C. ..... p 2710 N95-29857
UHLMANN, DONALD R. ..... p 2547 N95-30071
UKITA, N. ..... p 2735 N95-29837
..... p 2735 N95-29839
UKITA, NOBUHARU ..... p 2726 N95-29101
ULLMAN, JEFFREY D. ..... p 2650 N95-29509
UNDERWOOD, J. H. ..... p 2593 N95-28789
..... p 2596 N95-30119
UNTERBERG, B. ..... p 2709 N95-29803
UPADHYAY, C. S. ..... p 2668 N95-29065
URANKAR, EDWARD J. ..... p 2542 N95-29270
URBAUER, CRAIG L. ..... p 2678 N95-29617
..... p 2506 N95-29625

V

VAIDYANATHAN, H. ..... p 2567 N95-30260
VALETT, JON ..... p 2645 N95-28821
VANBUSSEL, G. J. W. ..... p 2603 N95-30200
VANDALSEM, WILLIAM R. ..... p 2478 N95-28728
VANDENABEELE, KOEN E.-A. ..... p 2618 N95-30129
VANDENBERG, K. G. ..... p 2653 N95-30095
VANDENBROEK, P. M. ..... p 2653 N95-30095
VANDENBUSSCHE, JAN GILBERT ..... p 2722 N95-29116
VANDERBURG, J. W. ..... p 2485 N95-28767
VANDERMEULEN, ROBERT P. ..... p 2676 N95-29609
VANDRESAR, N. T. ..... p 2511 N95-29642
VANDRIEL, W. ..... p 2731 N95-29097
VANDYKE, KEVIN ..... p 2478 N95-28727
VANEIJNDHOVEN, S. J. L. ..... p 2672 N95-30092
VANFOSSEN, G. JAMES ..... p 2568 N95-28719
VANHARN, K. ..... p 2666 N95-30167
VANHOUTUM, G. J. ..... p 2667 N95-30221
VANLOUSDEN, A. J. ..... p 2676 N95-29608
VANSCHILFGAARDE, M. ..... p 2702 N95-29978
VARGA, L. ..... p 2563 N95-29275
VASSILAROS, M. G. ..... p 2537 N95-29759
VATSA, V. ..... p 2674 N95-30353
VATSA, VEER N. ..... p 2480 N95-28736
VEERS, PAUL S. ..... p 2603 N95-30213
VENIAMINOV, STANISLAV ..... p 2507 N95-28852
VENKATAKRISHNAM, V. ..... p 2671 N95-29451
VENKATAKRISHNAN, V. ..... p 2674 N95-30227
VENKATAPATHY, ETHIRAJ ..... p 2503 N95-29351
VERDERAIME, V. ..... p 2504 N95-28718
VEREIJKEN, J. J. ..... p 2672 N95-30089
VERKOULEN, P. A. C. ..... p 2725 N95-30100
VERMEER, M. W. W. ..... p 2725 N95-30208
VERNON, FRANK L. ..... p 2612 N95-28985
VICTORA, R. H. ..... p 2681 N95-28924
..... p 2681 N95-28962
VIEIRADUTRA, LUCIANO ..... p 2601 N95-29999
VIJAY, D. P. ..... p 2540 N95-28963
..... p 2541 N95-29135
VISWANATHAN, K. ..... p 2688 N95-30147
VISWANATHAN, S. ..... p 2538 N95-30216
VLADIMIRSKY, OLGA ..... p 2700 N95-29366
VLADIMIRSKY, YULI ..... p 2700 N95-29366
VOLDMAN, MIKE ..... p 2522 N95-29051
VOLK, JOHN S., III ..... p 2644 N95-28694
VONDERHAAR, THOMAS H. ..... p 2628 N95-30272
VONHERMANN, PIETER ..... p 2543 N95-29367
VORTAC, O. U. ..... p 2493 N95-28790
VOTER, A. F. ..... p 2652 N95-29989
VRANISH, JOHN M. ..... p 2588 N95-28702
VUTETAKIS, DAVID G. ..... p 2566 N95-30070

W

WAAGEN, D. E. ..... p 2665 N95-29831
WACKERMAN, C. C. ..... p 2559 N95-30073
WACOGNE, B. ..... p 2565 N95-29925
WADA, M. ..... p 2709 N95-29803
WADAWADIGI, GANESH ..... p 2490 N95-29788
WAGANAAR, W. J. ..... p 2543 N95-29465

WAGER, J. F. p 2696 N95-29495
WAGNER, G. R. p 2562 N95-29078
WALDRON, WAYNE L. p 2726 N95-28822
WALIGORA, SHARON p 2644 N95-28807
WALKER, JEFF p 2522 N95-29048
WALKER, TOM p 2515 N95-28833
WALKER, TOM H. p 2515 N95-28837
WALLACE, W. E. p 2681 N95-29481
WALSH, JOHN E. p 2587 N95-29930
WALTER, TODD p 2584 N95-29664
WANG, CHENGHAO p 2684 N95-29659
WANG, DAHENG p 2701 N95-29571
WANG, J. T. p 2517 N95-28847
WANG, KANG L. p 2699 N95-29006
WANG, L. M. p 2717 N95-30022
WANG, PAUL S. p 2659 N95-29566
WANG, WANJUN p 2700 N95-29366
WANG, XIAO-YEN p 2574 N95-29372
WANG, Y. p 2528 N95-29923
WANG, Z. J. p 2489 N95-29316
WANG, ZHAO p 2702 N95-29969
WANG, ZHAOQI p 2701 N95-29661
WANG, ZUOQING p 2684 N95-29659
WARNER, THOMAS T. p 2627 N95-29993
WARREN, MICHAEL S. p 2734 N95-29775
WARREN, W. L. p 2718 N95-30214
WASHBURN, KARL B. p 2583 N95-29470
WATANABE, T. p 2711 N95-30032
WATANABE, TSUGUHIRO p 2707 N95-29738
WATERS, L. B. F. M. p 2735 N95-29840
WATSON, B. W. p 2654 N95-30107
WATSON, R. E. p 2654 N95-30107
WEATHERFORD, CHARLES A. p 2692 N95-28981
WEATHERILL, NIGEL p 2482 N95-28749
WEAVER, KIMBERLY ANN p 2730 N95-29776
WEBER, E. p 2713 N95-28967
WEBER, EICKE p 2714 N95-29165
WEEKS, W. p 2712 N95-28910
WEGMAN, EDWARD J. p 2675 N95-29819
p 2653 N95-30063
p 2673 N95-30126
WEGNER, BRIAN W. p 2565 N95-29601
WEIGEL, RUSSELL C. p 2632 N95-29375
WEILAND, S. p 2672 N95-30046
WEILER, B. p 2643 N95-30108
WEIMER, RONALD A. p 2718 N95-30164
WEINERFELT, PER p 2483 N95-28757
WEINGART, M. p 2654 N95-30183
WEISS, P. S. p 2531 N95-28945
WEITSMAN, O. V. p 2612 N95-28871
WEITSMAN, Y. J. p 2523 N95-29185
WELCH, CHUCK p 2504 N95-28715
WELLS, RICHARD L. p 2713 N95-28993
p 2715 N95-29444
p 2715 N95-29486
WENDT, BRUCE J. p 2489 N95-29402
WENGER, LOWELL E. p 2562 N95-29014
WENGLER, MICHAEL J. p 2561 N95-28859
WENTZ, F. p 2628 N95-30343
WENZ, CRAIG J. p 2499 N95-28692
WENZEL, K. W. p 2695 N95-28930
WERBLIN, FRANK p 2634 N95-29022
WERNET, JUDITH H. p 2582 N95-29113
WERNET, MARK P. p 2582 N95-29113
WESSELS, J. p 2666 N95-30101
p 2667 N95-30221
p 2667 N95-30222
WESTON, ED p 2664 N95-29657
WHEELER, RAYMOND M. p 2632 N95-29375
WHETSEL, ELWIN p 2536 N95-29461
WHISNANT, PAM p 2497 N95-29426
WHITE, ANITA ROSE p 2724 N95-29829
WHITE, KEVIN J. p 2565 N95-29938
WHITE, MICHAEL J. p 2683 N95-29077
WHITE, P. R. p 2577 N95-29817
WHITE, PETER S. p 2713 N95-28993
p 2715 N95-29444
p 2715 N95-29486
WHITE, S. M. p 2737 N95-29098
WHITEHEAD, BRUCE A. p 2510 N95-29584
WHITES, KEITH W. p 2554 N95-29235
WHITMIRE, JOHN p 2482 N95-28749
WHITNEY, MARK R. p 2646 N95-29056
WIEDENHOEFT, PAUL E. p 2657 N95-28689
WIEMAN, C. E. p 2693 N95-29521
WIFFEN, F. W. p 2696 N95-29142
WIGGINS, STEPHEN p 2576 N95-29761
WIGNALL, G. D. p 2535 N95-30113
WILDEN, KURTIS S. p 2521 N95-29043
WILLDEN, KURTIS p 2513 N95-28826
p 2515 N95-28835
WILLIAMS, BILL p 2548 N95-29019
WILLIAMS, H. E., III p 2549 N95-30345
WILLIAMS, MARK C. p 2607 N95-30278
WILLIAMS, R. p 2504 N95-29992
WILLIAMS, ROBERT W. p 2480 N95-28733
WILLIAMS, WILLIAM R. p 2533 N95-29572
WILLIAMSON, GARY SCOTT p 2680 N95-28893
WILLSON, C. G. p 2542 N95-29272
WILSON, B. p 2705 N95-29486
WILSON, GREGORY J. p 2503 N95-30228
WILSON, J. R. p 2660 N95-30193
WILSON, JEFFREY D. p 2566 N95-29998
WILSON, KENT R. p 2698 N95-28983
WILSON, TIMOTHY M. p 2498 N95-29911
WILSON, W. W. p 2533 N95-29581
p 2702 N95-29974
WINELAND, D. J. p 2693 N95-29521
WINOKUR, P. S. p 2718 N95-30214
WITHERELL, M. D. p 2535 N95-28889
WITTMEYER, IAN L. p 2628 N95-30272
WOAN, CHUNG-JIN p 2483 N95-28755
WON, YOUNGIN p 2613 N95-29214
WONG, ERIC Y. p 2488 N95-29118
WONG, LEON p 2663 N95-29477
WONG, MICHAEL D. p 2481 N95-28740
WOO, EDMUND P. p 2521 N95-29044
WOODSON, STANLEY C. p 2594 N95-28909
WOODWARD, WAYNE A. p 2608 N95-28922
WORKMAN, GARY L. p 2531 N95-29246
p 2549 N95-30014
WRIGHT, DOUG p 2567 N95-30261
WRIGHT, TED p 2511 N95-29784
WRIGHT, WILLIAM B. p 2492 N95-29132
WU, CARL p 2566 N95-30055
WU, CHANG-HUEI p 2509 N95-29794
WU, PEIJONE p 2721 N95-29093
WU, XIAOHUA p 2625 N95-29832
WU, ZHIJUN p 2633 N95-30114
WU, ZHIQI p 2495 N95-28820
WULF, ARMIN p 2483 N95-28752
WYNN, W. M. p 2566 N95-30079

X

XIAOYI, DONG p 2685 N95-29951
XU, KUANMAN p 2610 N95-30181
XU, S. p 2523 N95-29185

Y

YAGI, M. p 2706 N95-29731
p 2706 N95-29734
p 2707 N95-29741
p 2707 N95-29744
p 2709 N95-29809
YAKURA, S. J. p 2720 N95-29879
p 2546 N95-29983
YAMADA, H. p 2707 N95-29742
p 2709 N95-29802
p 2709 N95-29808
YAMAGISHI, T. p 2693 N95-29748
YAMAGUCHI, S. p 2710 N95-29857
YAMAJI, K. p 2610 N95-30195
YAMAMOTO, H. p 2610 N95-30195
YAMAMOTO, KAZUO p 2626 N95-29849
YAMAMURA, I. p 2735 N95-29837
YAMANOUCHI, JIRO p 2626 N95-29849
YANG, FU-MIN p 2587 N95-29660
YANG, H. Q. p 2489 N95-29316
YANSHENG, TENG p 2632 N95-29263
YAO, JIE p 2620 N95-29110
YAO, KE-THIA p 2484 N95-28758
YAO, YI-SHENG p 2590 N95-29552
YARIV, AMNON p 2713 N95-29087
YATES, R. K. p 2660 N95-30192
YE, QIAN p 2613 N95-29253
YEDDANAPUDI, MURALI p 2494 N95-28887
YEDGAR, SAUL p 2636 N95-29557
p 2637 N95-29872
YEE, BRADLEY p 2549 N95-28686
YELON, W. B. p 2681 N95-28923
p 2681 N95-28924
p 2681 N95-28962
YIMO, ZHANG p 2583 N95-29656
YING, JACKIE Y. p 2546 N95-29939
YIP, PERCY p 2662 N95-28978
YOCUM, MATTHEW W. p 2527 N95-29770
YODA, NOBUHISA p 2642 N95-29146
YOKOSAWA, A. p 2695 N95-30185
YOON, K. T. p 2575 N95-29421
YOON, YONGHYUN p 2484 N95-28759
YORIO, NEIL C. p 2632 N95-29375
YOSHIDA, S. p 2731 N95-29097
YOUNG, R. E. p 2737 N95-30058
YOUNIS, SAED G. p 2564 N95-29478
YU, BIN p 2675 N95-29587
YU, CHRISTOPHER C. p 2554 N95-29231
YU, CHUNG p 2700 N95-29553
YU, JIA-YUH p 2625 N95-29833
YU, L. p 2667 N95-30207
YU, TZU-YI p 2483 N95-28753
YUAN, HE p 2549 N95-29550
YUAN, YING p 2555 N95-29290
YUAN, ZHUOJIAN p 2626 N95-29834
YULONG, MA p 2561 N95-28911
YUN, SEUNGHEE p 2524 N95-29337
YUVARAJAN, SUBBARAYA p 2563 N95-29164

Z

ZABIELSKI, CHESTER V. p 2536 N95-29137
ZADNIK, JEROME A. p 2727 N95-29545
ZAIN, SAADO p 2566 N95-30055
ZAKOUT, WAEL MOHAMED p 2494 N95-29596
ZBIB, H. p 2595 N95-29535
ZEMANKOVA, MARIA p 2666 N95-30117
ZHANG, DUAN ZHONG p 2579 N95-30284
ZHANG, X.-C. p 2582 N95-29004
ZHANXIANG, REN p 2685 N95-29951
ZHAO, JINGXIA p 2615 N95-29666
ZHAO, MINGJUN p 2702 N95-29969
ZHAO, QIDA p 2685 N95-29681
ZHENG, HAIXING p 2607 N95-30269
ZHENGPING, LAN p 2703 N95-30064
ZHENYL, MA p 2539 N95-28864
ZHOU, DADONG p 2576 N95-29729
ZHU, S. p 2665 N95-29987
ZIJM, W. H. M. p 2667 N95-30221
ZIMMERMAN, A. H. p 2567 N95-30262
ZIMMERMAN, ALBERT H. p 2531 N95-28942
ZINGARELLI, R. A. p 2631 N95-29856
ZINKLE, S. J. p 2538 N95-30038
ZISKIN, DANIEL CHARLES p 2611 N95-30300
ZURBUCHEN, J. M. p 2561 N95-28961
ZWIETERING, P. J. p 2667 N95-30222

Typical Corporate Source Index Listing

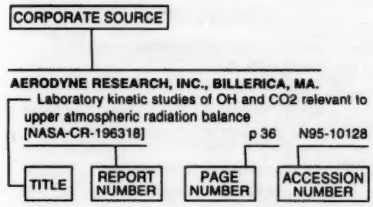

Listings in this index are arranged alphabetically by corporate source. The title of the document provides the user with a brief description of the subject matter. The report number helps to indicate the type of document cited (e.g., NASA report, translation, NASA contractor report). The accession number denotes the number by which the citation is identified. The page number helps you locate the citation in the abstract section. The titles are arranged under each corporate source in ascending accession number order.

A

ADAPTIVE SOLUTIONS, INC., BEAVERTON, OR.
High performance hardware and software for pattern recognition and image processing
[AD-A292307] p 2646 N95-28964

ADVANCED FUEL RESEARCH, INC., EAST HARTFORD, CT.
HTS Josephson technology on silicon with application to high speed digital microelectronics
[AD-A290206] p 2562 N95-29061
Epitaxial growth of high quality SiC of pulsed laser deposition, phase 1
[AD-A291410] p 2717 N95-30068

ADVANCED ROTORCRAFT TECHNOLOGY, INC., MOUNTAIN VIEW, CA.
Application of parallel processing technology in complex helicopter analysis. Phase 1
[NASA-CR-197850] p 2496 N95-28928

ADVISORY GROUP FOR AEROSPACE RESEARCH AND DEVELOPMENT, NEUILLY-SUR-SEINE (FRANCE).
AGARD flight test techniques series. Volume 13: Reliability and maintainability
[AGARD-AG-300-VOL-13] p 2498 N95-29503
Recent Issues and Advances in Aeromedical Evacuation (MEDEVAC)
[AGARD-CP-554] p 2676 N95-29604

AEROHYDRO, INC., SOUTHWEST HARBOR, ME.
Parametric design and gridding through relational geometry p 2486 N95-28771

AEROSPACE CORP., EL SEGUNDO, CA.
Overview of the space debris environment
[AD-A292302] p 2507 N95-28867
The effects of platinum on nickel electrodes in the nickel hydrogen cell
[AD-A291607] p 2531 N95-28942
Si 13 emission lines in solar flare x ray spectra obtained with the P78-1 satellite
[AD-A290000] p 2738 N95-29279
High-efficiency longitudinal diode bar pumping of solid-state lasers
[AD-A291180] p 2587 N95-29931
Design of a more accurate, higher fidelity, dual-source air mass zero solar simulator
[AD-A291364] p 2603 N95-29953
Performance evaluation of bolt-cutter system on first Taurus launch
[AD-A291237] p 2504 N95-29992

AEROSPACE CORP., WASHINGTON, DC.
Electrolyte management considerations in modern nickel hydrogen and nickel cadmium cell and battery designs p 2567 N95-30262

AI WARE, INC., CLEVELAND, OH.
Process optimization through discovery and integration of materials and processing properties. phase 1
[AD-A292576] p 2662 N95-28978

AIR FORCE INST. OF TECH., WRIGHT-PATTERSON AFB, OH.
Automated testing of application domains
[AD-A289753] p 2643 N95-28690
Three-D weather displays for aircraft cockpits
[AD-A289759] p 2499 N95-28691
Conceptual design of a map interactive system for military aircraft cockpits
[AD-A289760] p 2499 N95-28692
The effect of viscous attenuation on shock tube performance
[AD-A289793] p 2568 N95-28696
Using object-oriented database technology to develop a multiple domain capability for domain-oriented application composition systems
[AD-A289244] p 2721 N95-28907
A nonintrusive method of quantifying flow visualization data in vortex flow fields
[AD-A289802] p 2568 N95-28948
New tetraarylborate and ethyldibutylstannane reagents
[AD-A289813] p 2540 N95-28953
Analysis of the structural characteristics and intensity evolution of super typhoon flo (1990) in special sensor Microwave/Imager (SSM/I) data
[AD-A292413] p 2619 N95-28989
Flow visualization of vorticity cancellation of jets in crossflow
[AD-A292414] p 2569 N95-28990
Hybrid fuzzy logic control to stabilize an inverted pendulum from arbitrary initial conditions
[AD-A292441] p 2681 N95-29000
A formative evaluation of CU-SeeMe
[AD-A292443] p 2553 N95-29002
The effects of the thermal boundary condition and turbulence on heat transfer from a cylinder, flat plate, and turbine blade using the transient shroud and heated-coating techniques
[AD-A292646] p 2574 N95-29380
An experimental investigation of the time-dependent separation of tangent bodies in supersonic flow
[AD-A290720] p 2489 N95-29500
Investigation of tension-compression fatigue behavior of a unidirectional metal matrix composite at elevated temperature
[AD-A289394] p 2527 N95-29758
Parallelization of the 2D Roe Scheme on the Intel Paragon
[AD-A290690] p 2659 N95-29760
Investigation of tension-compression fatigue behavior of a notched cross-ply metal matrix composite at elevated temperature
[AD-A291479] p 2527 N95-29770
An aerodynamic and static-stability analysis of the Hypersonic Applied Research Technology (HART) missile
[DA9426923] p 2491 N95-29965
The application of adaptive mesh refinement to the numerical simulation of compressible flow
[AD-A289595] p 2577 N95-30027
A formal extension to object oriented analysis using Z
[AD-A290911] p 2653 N95-30080

AIR FORCE SYSTEMS COMMAND, WRIGHT-PATTERSON AFB, OH.
Propagation and transformation properties of axicon optical systems for laser beams
[AD-A289661] p 2584 N95-28679
Conference reports
[AD-A289630] p 2561 N95-28911
Research on PGI2 and TXA2 effects at times of hyperbaric oxygenation of domestic rabbits with acute cerebral ischemia reirrigation damage
[AD-A289606] p 2632 N95-29263
Multi-focal length and multi-channel holographic optical element
[AD-A291011] p 2583 N95-29656
The angular spread of the deflected acoustic beam diffracted by a Bragg grating out of a surface acoustic wave
[AD-A291018] p 2684 N95-29659
The laser ranging of etalon satellites
[AD-A291019] p 2587 N95-29660
Intensity optical correlation through optical differentiation preprocessing
[AD-A291020] p 2701 N95-29661
On the large scale circulation of the East Asia Mei-Yu fronts and secondary weather dimension disturbances
[AD-A291036] p 2622 N95-29662
Multiple dimensional acousto-optic diffraction and multiple dimensional acousto-optic device
[AD-A291037] p 2685 N95-29681
Progress and trends of multi-valued logic research
[AD-A290997] p 2665 N95-29874
Theory and experiment analysis of two-dimensional acousto-optic interaction
[AD-A291059] p 2685 N95-29951
Brief introduction to state key physics laboratories and division open laboratories
[AD-A291064] p 2682 N95-29952
Photorefractive Bi12SiO20 spatial light modulator
[AD-A291070] p 2702 N95-29969
Distortion-invariant optical pattern recognition by correlative matrix feature criterion
[AD-A291389] p 2703 N95-30064

AIR UNIV., MAXWELL AFB, AL.
Role of unmanned aerial vehicles in future armed conflict scenarios
[AD-A289777] p 2497 N95-29282

AKRON UNIV., AKRON, OH.
Fiber-matrix adhesion in single-fiber model composites p 2524 N95-29337
Structure and orientation behavior of highly oriented polymers under tensile and compressive stresses p 2546 N95-29822

ALABAMA A & M UNIV., NORMAL, AL.
Graphics supercomputer for computational fluid dynamics research
[AD-A291087] p 2575 N95-29637

ALABAMA UNIV., HUNTSVILLE, AL.
Study of the space environmental effects on spacecraft engineering materials
[NASA-CR-196638] p 2531 N95-29246
Analysis of measurements for solid state laser remote lidar system
[NASA-CR-196640] p 2585 N95-29247
Direct numerical simulation of compressible turbulent flows, using adaptive spectral element method
[AD-A290115] p 2575 N95-29421
Thermal N(+) in the inner magnetosphere p 2614 N95-29590
A generalized semikinetic (GSK) model for mesoscale auroral plasma transport p 2706 N95-29686
The high-altitude polar wind: Simulation and observation p 2622 N95-29688
Equatorial heating effects on outer plasmasphere evolution p 2616 N95-29716
Impact of uncertainty on modeling and testing
[NASA-CR-196637] p 2652 N95-30013
Reduce Fluid Experiment System: Flight data from the IML-1 Mission
[NASA-CR-196639] p 2549 N95-30014

ALABAMA UNIV., TUSCALOOSA, AL.
Dynamic modelling and link mechanism design of four-legged mobile robot p 2591 N95-30277

ALASKA UNIV., FAIRBANKS, AK.
Studies of gravity-wave filtering and tidal interaction in the middle atmosphere p 2619 N95-30351
ALBANY INTERNATIONAL RESEARCH CORP., MANSFIELD, MA.
Development of flame resistant, high efficiency thermal insulation
[AD-A291136] p 2547 N95-30120
ALLIED-SIGNAL AEROSPACE CO., KANSAS CITY, MO.
Digital video technology, today and tomorrow
[DE95-007689] p 2556 N95-29462
The Telemetry Agile Manufacturing Effort
[DE95-006177] p 2654 N95-30115
AMERICAN INST. OF PHYSICS, NEW YORK, NY.
Proceedings of the 6th Joint Magnetism and Magnetic Materials Intermag Conference
[AD-A286752] p 2681 N95-28923
Proceedings of the 38th Annual Conference on Magnetism and Magnetic Materials
[AD-A286753] p 2681 N95-28924
Proceedings of the 38th Annual Conference on Magnetism and Magnetic Materials
[AD-A286751] p 2681 N95-28962
Semiconductor science and technology
[AD-A289143] p 2563 N95-29191
ANALEX CORP., BROOK PARK, OH.
Simulated imaging properties of a series of magnetic electron lenses
[NASA-CR-195474] p 2564 N95-29406
APPLIED RESEARCH CORP., LANDOVER, MD.
X-ray observations of rapidly rotating O stars
[NASA-CR-189423] p 2726 N95-28822
ARGONNE NATIONAL LAB., IL.
Crystal field and exchange interactions in DyT4Al8 (T = Fe and Mn)
[DE95-007131] p 2714 N95-29134
Technology development goals for automotive fuel cell power systems
[DE95-008764] p 2548 N95-29280
Processing and properties of long-lengths of Ag-clad BSCCO superconductors and high-(Tc) magnets
[DE95-005855] p 2716 N95-29984
Computational results for parallel unstructured mesh computations
[DE95-005856] p 2659 N95-29985
What do we really know about the atomic scale structures of nanophase materials?
[DE95-005858] p 2717 N95-29986
Magnetic damping for Maglev
[DE95-005861] p 2665 N95-29987
State-of-the-art review of computational fluid dynamics modeling for fluid-solids systems
[DE95-005865] p 2577 N95-29988
Mechanical properties of nanophase metals
[DE95-005408] p 2537 N95-30018
Prospects for HERMES-spin structure studies at HERA
[DE95-005845] p 2694 N95-30019
W-matrices, nonorthogonal multiresolution analysis, and finite signals of arbitrary length
[DE95-005846] p 2652 N95-30020
Neutron scattering from amorphous, disordered and nanocrystalline materials
[DE95-005848] p 2717 N95-30077
Parallel continuation-based global optimization for molecular conformation and protein folding
[DE95-005880] p 2633 N95-30114
Load-balancing algorithms for the parallel community climate model
[DE95-008795] p 2610 N95-30176
A finite element analysis of room temperature silicon crystals for the Advanced Photon Source bending-magnet and insertion-device beams
[DE95-005822] p 2718 N95-30184
Sea and gluon spin structure function measurements at RHIC
[DE95-005823] p 2695 N95-30185
Measurements of (Delta)(sigma)(sub L)(pp) and (Delta)(sigma)(sub L)((bar p)p) at 200 GeV/c
[DE95-005837] p 2695 N95-30186
NMR imaging and hydrodynamic analysis of neutrally buoyant non-Newtonian slurry flows
[DE95-005842] p 2578 N95-30187
Fuel cell systems for First Lunar Outpost-reactant storage option p 2606 N95-30264
ARIZONA STATE UNIV., TEMPE, AZ.
Correlations between micromagnetic, microstructural and microchemical properties in ultrathin epitaxial magnetic structures
[AD-A289705] p 2712 N95-28681
Strained-bond semiconductors
[AD-A292524] p 2560 N95-28813
Experimental and theoretical studies of wakes in stratified flows
[AD-A290203] p 2569 N95-29060
Analytical and experimental studies of the energy absorption behavior of composite structures p 2524 N95-29411
Carbon isotope abundance ratios in comets p 2732 N95-29592
Growth and development of roughness-induced stationary crossflow vortices p 2492 N95-30294
ARIZONA UNIV., TUCSON, AZ.
Exact physical models and methods for stabilization and control of reflection-induced instabilities in semiconductor lasers
[AD-A292437] p 2585 N95-29053
Differentiation in the early Earth: An experimental investigation p 2612 N95-29199
Low-background balloon-borne direct search for ionizing massive particles as a component of the dark galactic halo matter p 2726 N95-29204
Deconvolution of lateral shear interferograms p 2699 N95-29222
Closed loop control of guided missiles using neural networks p 2663 N95-29241
Delivery of meteorites from the asteroid belt p 2732 N95-29255
Channels and valleys on Venus p 2736 N95-29593
High-density plasma dynamics in semiconductors p 2705 N95-29632
Lee vorticity production by tropical mountain ranges p 2622 N95-29701
Atmospheric wavefront sensing and correction including the stellar phase shifting interferometer p 2701 N95-29706
The gravitational potential energy of the Earth's lithosphere p 2617 N95-29773
Advanced research in sky surveillance: A search for low-luminosity objects
[AD-A291184] p 2731 N95-29916
The onset of electrohydrodynamic instability in isoelectric focusing
[NASA-CR-198805] p 2585 N95-29968
A kilohertz femtosecond Ti: Sapphire regeneratie amplifier
[AD-A290591] p 2588 N95-30045
Ceramics derived from organo-metallic precursors
[AD-A291434] p 2547 N95-30071
ARMSTRONG LAB., BROOKS AFB, TX.
Test and evaluation of the Impact Instrumentations, Inc. Uni-Vent model 750M ventilator
[AD-A292321] p 2640 N95-28792
A discrete-event simulation model of myocardial electrical activity: Mathematical electrophysiology
[AD-A292323] p 2633 N95-28793
Flying waivers for history of angioplasty and myocardial infraction
[AD-A292505] p 2635 N95-29161
Astronaut selection (NASA-MIPR)
[AD-A292512] p 2638 N95-29162
A compact universal power supply for laser diodes
[AD-A289950] p 2585 N95-29274
ARMY AEROMEDICAL RESEARCH LAB., FORT RUCKER, AL.
Military flying and aeromedical evaluation of cardiac arrhythmias
[AD-A291595] p 2634 N95-28940
Actual effectiveness of hearing protection in high level impulse noise
[AD-A291604] p 2634 N95-28941
Biodynamic simulation of pilot interaction with a helicopter multiairbag restraint system
[AD-A290196] p 2492 N95-29057
A comparison of the aeromedical administration requirements for US Air Forces and major allies
[AD-A290137] p 2635 N95-29141
US Army aviation epidemiology data register: Gender-specific attrition among the US Army student aviator class of 1987
[AD-A291856] p 2639 N95-29434
First medical test of the UH-60Q and equipment for use in US Army medevac helicopters p 2678 N95-29620
ARMY ARMAMENT RESEARCH, DEVELOPMENT AND ENGINEERING CENTER, WATERVLIET, NY.
Stress concentration, stress intensity, and fatigue crack growth along evacuators of pressurized, autofrettaged tubes
[AD-A291920] p 2593 N95-28789
Application of a rapid quench thermomagnetic analyzer to austempered ductile iron
[AD-A292261] p 2535 N95-28889
An HP-Adaptive method in space and time for parabolic systems
[AD-A292262] p 2668 N95-28890
Experimental methods in residual stress measurement using a position-sensitive single-exposure scintillation detection system
[AD-A289803] p 2594 N95-28949
Spectral characterization of pulsed ultrasound using neural networks
[AD-A292440] p 2683 N95-28999
Chromium plating and electropolishing solution analyses by online x ray fluorescence spectroscopy
[AD-A290023] p 2541 N95-29138
Fatigue life analysis and tests for thick-walled cylinders including effects of overstrain and axial grooves
[AD-A290931] p 2596 N95-30119
ARMY AVIATION BRIGADE, MENDIG (GERMANY).
The large-capacity rescue-helicopter CH-53 G p 2678 N95-29621
ARMY COLD REGIONS RESEARCH AND ENGINEERING LAB., HANOVER, NH.
Variation in visual and near-infrared contrast with a snow background
[AD-A289710] p 2697 N95-28778
Analyzing the stability of floating ice floes
[AD-A292149] p 2629 N95-29160
Upper-air data collected on Ice Station Weddell
[AD-A289707] p 2620 N95-29193
ARMY CONSTRUCTION ENGINEERING RESEARCH LAB., CHAMPAIGN, IL.
The Environmental Assessment and Management (TEAM) guide
[AD-A286748] p 2608 N95-28787
Estimating attenuation and propagation of noise bands from a distant source using the lookup program and data base
[AD-A290218] p 2683 N95-29077
Alternative refrigerant performance: Field test of a nonchlorofluorocarbon chiller at Fort Leonard Wood, MO
[AD-A292052] p 2550 N95-29307
Use of chlorofluorocarbon-based refrigerants in USArmy facility air-conditioning and refrigeration systems: Recommendations for the interim period 1994-2000
[AD-A290432] p 2550 N95-29537
ARMY ENGINEER WATERWAYS EXPERIMENT STATION, VICKSBURG, MS.
Shear reinforcement in deep slabs
[AD-A289528] p 2594 N95-28909
Tidal constituent database: West coast of the United States and eastern North Pacific Ocean
[AD-A292224] p 2630 N95-29198
Tropical storm database: East and Gulf of Mexico coasts of the United States
[AD-A291406] p 2627 N95-30066
ARMY MEDICAL CENTER, AURORA, CO.
Analysis of wounds by evaporative water loss in man
[AD-A290327] p 2634 N95-29086
ARMY MEDICAL COMMAND (18TH), (18TH).
Medical evacuation: A training priority p 2678 N95-29617
Requirement for onboard telemetry equipment p 2506 N95-29625
ARMY MEDICAL RESEARCH AND DEVELOPMENT COMMAND, FORT DETRICK, MD.
Human fluid balance and dehydration during cold weather military operations
[AD-A289192] p 2636 N95-29757
ARMY MISSILE COMMAND, REDSTONE ARSENAL, AL.
Thin-film resistor array characterization
[AD-A289606] p 2561 N95-28950
Computational complexity and encryption
[AD-A291910] p 2648 N95-29356
High-frequency radar target modeling
[AD-A290965] p 2559 N95-29991
ARMY NATICK RESEARCH AND DEVELOPMENT COMMAND, MA.
An analysis of anthropometric differences among occupational groups in the US Army
[AD-A292326] p 2640 N95-28794
ARMY RESEARCH LAB., ABERDEEN PROVING GROUND, MD.
Spectrometric studies of selected nitrocompounds using laser-induced photofragmentation/photoionization at 193 nm
[AD-A289947] p 2530 N95-28876
Ballistic penetration phenomenology of high symmetry single crystals
[AD-A292476] p 2713 N95-29013
Computational fluid dynamics (CFD) simulation of test chamber and smoke-generating device
[AD-A290199] p 2569 N95-29058
XMap: A general purpose mapping program
[AD-A289958] p 2647 N95-29276
Reaction field (RF) calculation of the spectral shifts of indole
[AD-A290449] p 2532 N95-29487
Hot explosive consolidation of W-Ti alloys
[AD-A290880] p 2537 N95-29835
Penetration of semi-infinite, bi-element targets by long rod penetrators
[AD-A291176] p 2596 N95-29929

Ab initio calculation of vibrational absorption and circular dichroism spectra using density functional force fields
[AD-A291297] p 2720 N95-29936
A study of power diode failure mechanisms in the US Army research laboratory 30-mm solid propellant electrothermal-chemical (SPETC) gun facility
[AD-A291300] p 2565 N95-29938
Analytical potential energy surface for methylene nitramine (CH2NNO2)
[AD-A291247] p 2534 N95-29994

ARMY RESEARCH LAB., ADELPHI, MD.
Characterizing the electromagnetic environment produced by the army's repetitive electromagnetic pulse simulator (REPS)
[AD-A289739] p 2551 N95-28687

ARMY RESEARCH LAB., WATERTOWN, MA.
Investigation of the characteristics of ferroelectric thin films deposited by pulsed laser ablation
[AD-A292306] p 2540 N95-28963
Electrical characteristics of barium strontium titanate-oxide composite films
[AD-A289991] p 2541 N95-29135
Fabrication and characterization of barium strontium titanate and non-ferroelectric oxide composites
[AD-A289994] p 2523 N95-29136
Corrosion in methylphosphonic difluoride
[AD-A289995] p 2536 N95-29137
Pulsed laser deposition of ferroelectric thin films in conjunction with superconducting oxides
[AD-A290101] p 2585 N95-29208
Fire hardening assessment (FHA) technology for composite systems
[AD-A289964] p 2523 N95-29277
Fabrication and characterization of BSTO and nonferroelectric oxide composites for use in phased array antennas and other electronic devices
[AD-A290070] p 2524 N95-29329
Analysis of the ferroelectric thin films deposited by pulsed laser deposition on oxide and fluoride substrates
[AD-A290088] p 2543 N95-29353
Polyethylene-based polyurethane copolymers and block copolymers
[AD-A289996] p 2546 N95-30030
Fractography of advanced structural ceramics: Results from the VAMAS round robin exercise
[AD-A290930] p 2547 N95-30118

ARMY RESEARCH LAB., WHITE SANDS MISSLE RANGE, NM.
The Scanning Fast Field Program (SCAFFIP) general version 1.0 user's manual
[AD-A291209] p 2618 N95-29976

ARMY TANK-AUTOMOTIVE COMMAND, WARREN, MI.
Ride motion simulator (RMS) testing using human occupants
[AD-A292641] p 2641 N95-29378

ARMY TANK-AUTOMOTIVE RESEARCH AND DEVELOPMENT COMMAND, WARREN, MI.
Development of the test kit for fuel acid contamination
[AD-A291953] p 2548 N95-29019

ARMY TANK-AUTOMOTIVE SYSTEMS DEVELOPMENT CENTER, WARREN, MI.
Evaluation of commercial water-in-fuel test kits
[AD-A292135] p 2533 N95-29572

ARNOLD ENGINEERING DEVELOPMENT CENTER, ARNOLD AFS, TN.
Spectral analysis techniques using wavelets as an alternative to Fourier analysis for transient dynamic data
[AD-A289776] p 2556 N95-29459

ASIAN OFFICE OF AEROSPACE RESEARCH AND DEVELOPMENT, APO SAN FRANCISCO, CA.
Daido Steel's Shibukawa Plant, Shibukawa City, Gumma Prefecture, Japan, 29 Jul. 1994
[AD-A292343] p 2536 N95-29467
Visit to the Department of Metallurgical Engineering, Tokyo Institute of Technology, 22 Sep. 1994
[AD-A292310] p 2536 N95-29473
The 1994 IEEE International Workshop on Intelligent Signal Processing and Communication Systems (ISPACS94)
[AD-A292312] p 2556 N95-29474
A turbulent model of the solar granulation
[AD-A292318] p 2738 N95-29475
Center for Advanced Aerospace Materials (CAAM), Seoul National University, 29 June 1994
[AD-A292344] p 2525 N95-29476
Nippon Steel Research Laboratories, Futtsu, 28 February 1994, and Advanced Materials and Technology Research Laboratories, Kawasaki, 15 June 1994
[AD-A292346] p 2526 N95-29533
The Institute for Material Science and Department of Material Science, Tohoku University, Sendai Japan, 2-3 June 1994
[AD-A292348] p 2650 N95-29534
Summary of the 1st International Workshop on Networked Reality in Telecommunication
[AD-A292366] p 2558 N95-29862
The 41st Japan Society of Applied Physics Spring Meeting
[AD-A292333] p 2720 N95-29879
Japanese remote sensing organizations, research, and technology
[AD-A292420] p 2601 N95-29905
The 2nd International Conference on Thin Film Physics and Applications
[AD-A292353] p 2546 N95-29983
15th NSO/Sac Peak Solar Workshop
[AD-A292297] p 2739 N95-30074
Visit to the Laboratory For Evaluation and Failure Prevention of Materials, Toyohashi University of Technology, 17 Oct 94
[AD-A292340] p 2597 N95-30293

B

BASF STRUCTURAL MATERIALS, INC., CHARLOTTE, NC.
Characterization and development of materials for advanced textile composites p 2513 N95-28824

BATTELLE COLUMBUS LABS., OH.
Flux pinning and stabilizer studies
[DE95-008131] p 2682 N95-30131

BATTELLE MEMORIAL INST., COLUMBUS, OH.
In-phase thermomechanical fatigue mechanisms in an unidirectional SCS-6/Ti 15-3 MMC
[NASA-CR-195482] p 2523 N95-29133
High reliability, maintenance-free INS battery development, phase 2
[AD-A291412] p 2566 N95-30070

BAYLOR COLL. OF MEDICINE, HOUSTON, TX.
The influence of space flight on erythrokinetics in man. Space Life Sciences Missions 1 and 2. Experiment E261
[NASA-CR-188368] p 2633 N95-28875

BIOTECHNOLOGY, INC., FALLS CHURCH, VA.
Development of an intervention program to encourage shoulder harness use and aircraft retrofit in general aviation aircraft: Phases 1 and 2
[AD-A290966] p 2493 N95-29873

BOEING CO., SEATTLE, WA.
Cooperative solutions coupling a geometry engine and adaptive solver codes p 2484 N95-28761
Impact damage resistance of composite fuselage structure, part 2 p 2516 N95-28838
Challenges and payoff of composites in transport aircraft: 777 empennage and future applications p 2519 N95-29031

BOEING COMMERCIAL AIRPLANE CO., SEATTLE, WA.
The effects of design details on cost and weight of fuselage structures p 2499 N95-28831
Manufacturing scale-up of composite fuselage crown panels p 2515 N95-28835
Dimensional stability of curved panels with cocured stiffeners and cobonded frames p 2515 N95-28836
Design, analysis, and fabrication of a pressure box test fixture for tension damage tolerance testing of curved fuselage panels p 2516 N95-28839
Global cost and weight evaluation of fuselage keel design concepts p 2499 N95-28840
Advanced composite fuselage technology p 2519 N95-29034
Cost model relationships between textile manufacturing processes and design details for transport fuselage elements p 2521 N95-29043

BOEING DEFENSE AND SPACE GROUP, SEATTLE, WA.
Interactive multimedia presentation for applied computer tomography: Impact
[AD-A291955] p 2640 N95-29020
Processing, fabrication, characterization and device demonstration of high temperature superconducting ceramics
[AD-A290183] p 2541 N95-29055
Investigation and characterization of SEU effects and hardening strategies in avionics
[AD-A291058] p 2500 N95-29950
Effects of space exposure on metals flown on the Long Duration Exposure Facility
[NASA-CR-4662] p 2512 N95-30225

BOSTON COLL., CHESTNUT HILL, MA.
New radiation sources through generation and resonant enhancement of Current Driven Plasma Instabilities in lower dimensional solid state systems
[AD-A290669] p 2705 N95-29519
PASP plus time history data base file structures
[AD-A290587] p 2725 N95-30043

BOSTON UNIV., MA.
Modeling the direct-beam instantaneous spectral surface albedo of a forest landscape using geometric-optics and a distributed parameter approach p 2599 N95-29540
The effects of magnetic storm phases on F-layer irregularities from auroral to equatorial latitudes
[AD-A290674] p 2614 N95-29585
Multiwaveband observations of quasars p 2728 N95-29665
Chemical release experiments to induce F region ionospheric plasma irregularities at the magnetic equator p 2708 N95-29783

BOUNDARY TECHNOLOGIES, INC., BUFFALO GROVE, IL.
Hermetically sealed aluminum electrolytic capacitor p 2568 N95-30268

BROOKHAVEN NATIONAL LAB., UPTON, NY.
A practical high-energy high-luminosity mu(+)-mu(-) collider
[DE95-006769] p 2696 N95-30009
Lattice/beam dynamics working group
[DE95-006774] p 2696 N95-30021
Radiation effects on front-end electronics for noble liquid calorimetry
[DE95-007304] p 2566 N95-30025
Self-organization in a simple brain model
[DE95-008312] p 2668 N95-30279

BROWN UNIV., PROVIDENCE, RI.
The nucleation of crystalline films from vapor phase reactants
[AD-A291122] p 2716 N95-29767

C

CALIFORNIA INST. OF TECH., PASADENA, CA.
Theoretical investigation of superconductivity in doped fullerenes
[AD-A291942] p 2562 N95-29018
Large-scale neuronal theories of the brain
[AD-A290200] p 2634 N95-29059
Growth, characterization and application of KTN family nonlinear optical crystals
[AD-A290330] p 2713 N95-29087
Dynamic decohesion of bimaterial interfaces p 2541 N95-29120
Research on bluff-body vortex wakes
[AD-A292650] p 2574 N95-29382
Symposium on Metal-Mediated Molecular Architectures
[AD-A290427] p 2692 N95-29388
Conjugated polymers from cyclohexadienediol monomers
[AD-A290247] p 2544 N95-29505
New predictive methods in chaotic fluid dynamics with application to turbulent heat transfer
[AD-A290691] p 2576 N95-29761
Mapping crust and upper mantle structure beneath southern Eurasia
[AD-A291074] p 2618 N95-29970

CALIFORNIA POLYTECHNIC STATE UNIV., SAN LUIS OBISPO, CA.
Developing a workstation-based, real-time simulation for rapid handling qualities evaluations during design
[NASA-CR-198831] p 2499 N95-30335

CALIFORNIA UNIV., BERKELEY, CA.
Studies of lattice-mismatched and Low-Temperature-Grown semiconductor multiple-phase systems
[AD-A292536] p 2713 N95-28967
Joint services electronics program
[AD-A292469] p 2561 N95-29010
Computer models of retinal function
[AD-A290156] p 2634 N95-29022
Electronic properties of low-temperature grown III/V thin films
[AD-A292521] p 2714 N95-29165

CALIFORNIA UNIV., BERKELEY. LAWRENCE BERKELEY LAB, CA.
Tables of SU3 isoscalar factors
[DE95-009375] p 2690 N95-28779
From the (psi) to charmed mesons
[DE95-006564] p 2693 N95-29583
Nearest neighbor analysis in one dimension
[DE95-009378] p 2654 N95-30183

CALIFORNIA UNIV., DAVIS, CA.
Investigation of an alternative finite element procedure: A one-step, steady-state analysis
[AD-A290030] p 2670 N95-29311

CALIFORNIA UNIV., IRVINE, CA.
High power, high frequency radiation from beam-plasma interactions
[AD-A292442] p 2703 N95-29001

CALIFORNIA UNIV., LOS ANGELES, CA.
Optoelectronics based on SiGe/Si heterostructures
[AD-A292464] p 2699 N95-29006
A study of plasma waves arising from the solar wind interaction with Venus p 2704 N95-29215
Turbulent airflow noise production and propagation patterns of a subsonic jet impinging on a flat plate p 2684 N95-29502

An investigation into the existence of asteroids at Saturn's triangular Lagrangian points
p 2727 N95-29648
Numerical studies of the stratospheric aerosol layer under background and perturbed conditions
p 2615 N95-29666
Development of an improved cloud model for use in cumulus parameterization p 2624 N95-29800
Experimental and analytical study of heat transfer and turbulent flow field in tangentially injected swirl flow
p 2576 N95-29811
Training end-users on database queries: The effectiveness of example format and spatial ability on learing outcomes p 2724 N95-29829
The tropical atmosphere under convection adjustment
p 2625 N95-29833
Control of vortex dynamics p 2579 N95-30275
Micromechanics of crack extension in composites
p 2529 N95-30276
The physics of the collisionless bow shock
p 2580 N95-30301

CALIFORNIA UNIV., SAN DIEGO, CA.
Collective phenomena in granular fluids
p 2572 N95-29219
Experiments on nonlinear wave-particle interactions
p 2695 N95-30302

CALIFORNIA UNIV., SAN DIEGO, LA JOLLA, CA.
Improved interception capability through the use of transform domain processing
[AD-A292231] p 2554 N95-29203
The 5th International Meeting on Cholinesterase
[AD-A291253] p 2534 N95-30085

CALIFORNIA UNIV., SAN FRANCISCO, CA.
Molecular probes of gating and open channel conformational transitions of mechanosensitive ion channels
[AD-A291170] p 2637 N95-29927

CALIFORNIA UNIV., SANTA BARBARA, CA.
Experimental cosmology using fast parallel N-body methods p 2734 N95-29775
Large scale fluctuations of the geomagnetic field
p 2617 N95-29796
Vacuum microelectronic emitters and their applications using compound semiconductor technology
[AD-A291142] p 2567 N95-30124

CALIFORNIA UNIV., SANTA CRUZ, CA.
The nature of wavefront fluctuations induced by internal gravity waves in long-range oceanic acoustic pulse transmissions p 2630 N95-29528
The dynamics of FU Orionis outbursts: Time-dependent accretion through protostellar disks
p 2732 N95-29530
The properties of local poor Abell clusters and instrumentation for the study of clustered objects
p 2730 N95-29827

CANADIAN FORCES AIR COMMAND, WINNIPEG (MANITOBA).
The Canadian experience in UN airevac Sarajevo airlift: April 1993-October 1994 p 2676 N95-29606

CARNEGIE-MELLON UNIV., PITTSBURGH, PA.
Abstract models of memory management
[AD-A292238] p 2721 N95-28877
Competitive analysis of call admission algorithms that allow delay
[AD-A292242] p 2645 N95-28878
The scotch parallel storage systems
[AD-A292243] p 2658 N95-28879
Using ordered binary-decision diagrams for compressing images and image sequences
[AD-A292244] p 2721 N95-28880
Problem decomposition for reuse
[AD-A292245] p 2645 N95-28881
Modeling foreshortening in stereo vision using local spatial frequency
[AD-A292246] p 2645 N95-28883
Wax: A wide-area computation system
[AD-A292247] p 2658 N95-28884
Structural cut elimination in linear logic
[AD-A292248] p 2645 N95-28886
Formalizing style to understand descriptions of software architecture
[AD-A292237] p 2645 N95-28894
Management of speedup mechanisms in learning architectures
[AD-A292206] p 2662 N95-28988
Solving linear programs using distributed parallel computing
[AD-A290221] p 2658 N95-29079
A differential approach to graphical interaction
[AD-A292165] p 2647 N95-29125
Inductive boolean function manipulation: A hardware verification methodology for automatic induction
[AD-A292236] p 2669 N95-29128
Stable function approximation in dynamic programming
[AD-A290224] p 2647 N95-29143
An architectural design of a toolkit for synchronous groupware applications
[AD-A290226] p 2642 N95-29146
Porting a vector library: A comparison of MPI, paris, CMMD and PVM (or, 'I'll never have to port CVL again')
[AD-A290231] p 2647 N95-29147
Reflectance analysis under solar illumination
[AD-A290489] p 2737 N95-29151
Implementing distributed server groups for the World Wide Web
[AD-A292221] p 2658 N95-29196
Exploiting symmetry in the model checking of relational specifications
[AD-A290230] p 2647 N95-29223
Characteristics of higher-level languages for software architecture
[AD-A292215] p 2649 N95-29376
Studies directed toward new and improved permanent magnet materials
[AD-A290749] p 2681 N95-29481
Client-server interactions in multi-server operating systems: The Mach-US approach
[AD-A290431] p 2650 N95-29536
A comparison of ISO 9001 and the Capability Maturity Model for Software
[AD-A290697] p 2651 N95-29762
High-level fault tolerance in distributed programs
[AD-A290430] p 2724 N95-29818
Software risk evaluation method version 1.0
[AD-A290597] p 2652 N95-30047

CASE WESTERN RESERVE UNIV., CLEVELAND, OH.
A genetic algorithm approach to scheduling resources for a space power system p 2511 N95-29784
A biologically-inspired autonomous robot
[AD-A289446] p 2666 N95-30026

CENTRAL CONNECTICUT ENGINEERING, INC., ROCKY HILL, CT.
High power switch design
[AD-A291608] p 2565 N95-29601

CENTRAL RESEARCH INST. OF ELECTRIC POWER INDUSTRY, TOKYO (JAPAN).
Analysis of global economic instruments for CO2 emission reduction: Equity and efficiency
[DE95-764057] p 2610 N95-30195

CENTRAL STATE UNIV., WILBERFORCE, OH.
A novel approach to the numerical simulation of turbulent flows
[AD-A290352] p 2569 N95-29068

CENTRE EUROPEEN RECHERCHE ET DE FORMATION ADVANCE EN CALCUL SCIENTIFIC, TOULOUSE (FRANCE).
Algorithms for the automatic generation of 2-D structured multi-block grids p 2483 N95-28757

CFD RESEARCH CORP., HUNTSVILLE, AL.
Evaluation of grid generation technologies from an applied perspective p 2482 N95-28748
Pressure based high order TVD methodology for dynamic stall control
[AD-A290149] p 2489 N95-29316

CHEMAT TECHNOLOGY, INC., NORTHRIDGE, CA.
Fabrication of advanced electrochemical energy materials using sol-gel processing techniques
p 2607 N95-30269

CIVIL ENGINEERING RESEARCH FOUNDATION, WASHINGTON, DC.
Materials for tomorrow's infrastructure: A ten-year plan for deploying high-performance construction materials and systems
[AD-A289782] p 2526 N95-29598

CHICAGO UNIV., CHICAGO, IL.
Fluxes and relative abundances of light cosmic ray nuclei at energies above 40 GeV/n p 2739 N95-29531
Randomized inquiries about shape: An application to handwritten digit recognition
[AD-A290812] p 2675 N95-29634
The energy spectrum and flux of cosmic ray helium at high energy p 2740 N95-29705
X-ray emission from Hybrid stars
p 2740 N95-29779
Improvement of inter-event distance tests of randomness in spatial point processes
[AD-A291151] p 2675 N95-30297

CHRISTOPHER NEWPORT COLL., NEWPORT NEWS, VA.
Aeroacoustic computation of a gust-plate interaction via MacCormack schemes p 2690 N95-30162

CINCINNATI UNIV., OH.
Periodic and nonsmooth optimal control problems governed by partial differential equations
p 2664 N95-29544

CITY COLL. OF THE CITY UNIV. OF NEW YORK, NY.
Macroprocesses and adaptive instruction
[AD-A290483] p 2648 N95-29325

CIVIL AEROMEDICAL INST., OKLAHOMA CITY, OK.
Conversion of the TRACON operations concepts database into a formal sentence outline job task taxonomy
[DOT/FAA/AM-95/16] p 2493 N95-28819

CLARK UNIV., WORCESTER, MA.
Molecular level characterization by NMR of the transport and structural environment of gases and condensed penetrante
[AD-A290831] p 2693 N95-29723

CLARKSON UNIV., POTSDAM, NY.
Rigorous drag bounds in turbulent shear flow
p 2573 N95-29334

CLEMSON UNIV., SC.
Effects of elevated free-stream turbulence and streamwise acceleration on flow and thermal structures in transitional boundary layers p 2576 N95-29729
A study of precipitation using dual-frequency and interferometric Doppler radars p 2627 N95-29877

CLEVELAND STATE UNIV., OH.
Effects of cooling system parameters on heat transfer in PAFC stack
[NASA-CR-198817] p 2570 N95-29131
Effects of the cooling system parameters on heat transfer and performance of the PAFC stack during transient operation
[NASA-CR-197654] p 2572 N95-29249
In-plant testing of membranes to treat electroplating wastewater
[NASA-CR-198796] p 2532 N95-29250
Ceramic material life prediction: A program to translate ANSYS results to CARES/LIFE reliability analysis
[NASA-CR-198795] p 2543 N95-29367
Transient responses of phosphoric acid fuel cell power plant system
[NASA-CR-198948] p 2603 N95-30015

COGNITECH, INC., SANTA MONICA, CA.
Accurate feature detection and estimation using nonlinear and multiresolution analysis
[AD-A290267] p 2553 N95-29176
Feature-oriented image reconstruction and aero-optic metrology in turbulence
[AD-A290269] p 2699 N95-29177

COLORADO STATE UNIV., FORT COLLINS, CO.
Polymeric microcapsule arrays
[AD-A291937] p 2539 N95-28850
Multi-decade time-dependent voltage of polycrystalline thin-film solar cells p 2602 N95-29103
Forecast of Atlantic seasonal hurricane activity for 1995 p 2620 N95-29254
Microwave remote sensing algorithms for cirrus clouds and precipitation p 2623 N95-29715
The dynamics of circulations within the stratiform regions of squall lines p 2623 N95-29725
Use of ARM data to test an improved parameterization of upper tropospheric clouds for use in climate models
[DE95-009324] p 2610 N95-30181

COLORADO UNIV., BOULDER, CO.
Study of UV bleached channel waveguide performance in NLO polymer films
[AD-A292008] p 2540 N95-29021
An investigation of the channel crosstalk in optical heterodyne controlled phased array radars
[AD-A292028] p 2554 N95-29186
Observations and analysis of solar flares at radio and other wavelengths p 2738 N95-29202
New methods for nonlinear optimization
[AD-A290522] p 2670 N95-29385
Semiconductor deposition and etching interactions of laser-generated translationally hot atoms and radicals
[AD-A291824] p 2693 N95-29431
The 14th International Conference on Atomic Physics
[AD-A290726] p 2693 N95-29521
Passive ranging with an incoherent optical system
p 2700 N95-29543
The x-ray scattering halo around Sco-X1
p 2727 N95-29591
Depicting dust and sand storm signatures through the means of satellite images and ground-based observations for Saudi Arabia p 2600 N95-29730
Heat and momentum flux measurements in the planetary boundary layer with a wind profiling radar/radio acoustic sounding system p 2617 N95-29777
Ultrasonic guided waves in cylinders: Theory and experiment p 2685 N95-29826
Sea ice motions in the Central Arctic pack ice as inferred from AVHRR imagery
[NASA-CR-198835] p 2601 N95-30247
Numerical simulation of stability and stability control of high speed compressible rotating couette flow
[NASA-CR-198832] p 2579 N95-30250

COLUMBIA UNIV., NEW YORK, NY.
The effect of climate perturbations on extratropical cyclogenesis along the east coast of North America
p 2621 N95-29595

Interlaminar fracture mechanics and mechanisms: Linear and nonlinear aspects p 2526 N95-29597
The evolution of binary millisecond pulsars and the formation of planets around them p 2733 N95-29663
Far-ultraviolet high-resolution emission line spectroscopy of the Cygnus Loop supernova remnant p 2729 N95-29710
Learning control in linear and nonlinear systems p 2667 N95-30238

COMMISSARIAT A L'ENERGIE ATOMIQUE, VILLENEUVE-SAINT-GEORGES (FRANCE).
The 2d Eurographics Workshop on Virtual Environments
[AD-A292015] p 2651 N95-29861

COMMISSION OF THE EUROPEAN COMMUNITIES, BRUSSELS (BELGIUM).
Functionally specified distributed transactions in co-operative scenarios
[PB95-197380] p 2725 N95-30100

COMPUTER SCIENCES CORP., CALVERTON, MD.
Simultaneous UV and optical study of O star winds and UV and optical covariability of O star winds
[NASA-CR-189424] p 2726 N95-29370

COMPUTER SCIENCES CORP., HAMPTON, VA.
A grid generation system for multi-disciplinary design optimization p 2484 N95-28763
GridTool: A surface modeling and grid generation tool p 2486 N95-28773

COMPUTER SCIENCES CORP., MOFFETT FIELD, CA.
NASA-IGES Translator and Viewer p 2486 N95-28775

COMPUTER TECHNOLOGY ASSOCIATES, INC., MCKEE CITY, NJ.
Visual and auditory symbols: A literature review
[AD-A290222] p 2641 N95-29908

CONCORD SCIENCE AND TECHNOLOGY, INC., KNOXVILLE, TN.
Novel photoelectric sensing technology for environmental monitoring, phase 1
[AD-A292026] p 2611 N95-30348

CONCORDIA UNIV., MONTREAL (QUEBEC).
Finite element vorticity-based methods for the solution of the incompressible and compressible Navier-Stokes equations p 2570 N95-29119

CONDUCTUS, INC., SUNNYVALE, CA.
The mm-wave resonant methods for the detection of corrosion, phase 1
[AD-A291315] p 2593 N95-29941

CONNECTICUT UNIV., STORRS, CT.
MATSurv multisensor air traffic surveillance
[AD-A292253] p 2494 N95-28887
Multivariate wavelet representations and approximations
[AD-A290147] p 2670 N95-29312
The fluid mechanics of a high aspect ratio slot with an impressed pressure gradient and secondary injection p 2580 N95-30304

CORETEK, INC., WALTHAM, MA.
Commercial photorefractive device using nonstoichiometric 3-5 semiconductors
[AD-A292494] p 2713 N95-28933

CORNELL UNIV., ITHACA, NY.
Photogenerated amines in the design of imaging materials: The radiation-induced imidization of functionalized polystyrenes bearing amide-ester side chains
[AD-A289943] p 2542 N95-29270
Photogenerated amines in polymer curing and imaging: Design and synthesis of (3', 5'-dimethoxybenzoinyl)oxycarbonyl carbamates as novel photoprecursors of amines
[AD-A289945] p 2542 N95-29272
State resolved differential cross sections for reactions important to the decomposition of energetic materials
[AD-A290718] p 2548 N95-29498
A multi-wavelength study of rotation-driven pulsars p 2729 N95-29678

CRYOPOWER ASSOCIATES, LOS ALAMOS, NM.
Chalcogenide superconductors: A search
[AD-A292523] p 2560 N95-28812

D

DACCO SCI, INC., COLUMBIA, MD.
The use of electrochemistry and ellipsometry for identifying and evaluating corrosion on aircraft
[AD-A290249] p 2497 N95-29426

DARTMOUTH COLL., HANOVER, NH.
Measurement of interface strength, intrinsic toughness and their dependence on interfacial segregants
[AD-A291798] p 2524 N95-29409
Transition metal complexes with perfluorinated ligands
[AD-A290250] p 2536 N95-29427
Measurement of interface strength, intrinsic toughness and their dependence on interfacial segregants
[AD-A291169] p 2546 N95-29926
Semiconductor film Cherenkov lasers
[AD-A291177] p 2587 N95-29930
Supercritical states of two-dimensional wall-bounded shear flow p 2580 N95-30303

DAVID SARNOFF RESEARCH CENTER, PRINCETON, NJ.
OEIC ultra. A new approach to OEIC CAD
[AD-A290349] p 2646 N95-29066
Hybrid pyramid/neural network vision system
[AD-A290565] p 2665 N95-29863

DAYTON UNIV., OH.
An analysis of B-1B exterior jet blast windshield anti-icing performance using pre-cooled compressor bleed air
[AD-A292522] p 2492 N95-28811
Distance estimation training with night vision goggles under low illumination
[AD-A291338] p 2641 N95-29943

DEACON RESEARCH, PALO ALTO, CA.
Doubled diode laser. phase 1
[AD-A292465] p 2584 N95-29007

DEFENCE RESEARCH ESTABLISHMENT OTTAWA, OTTAWA (ONTARIO).
Description of the OHGR database
[AD-A290146] p 2722 N95-29221
SOSDOR: Solid-state device simulator code
[AD-A289954] p 2563 N95-29275
Long range aircraft detection using high-frequency surface-wave radar
[AD-A290148] p 2555 N95-29313
A least square real time quality control routine for the North Warning Netted Radar System
[AD-A290063] p 2555 N95-29328
Characterization and calibration of a pulsed laser system for single event upset simulation
[AD-A290075] p 2586 N95-29330
A comparison of three pedestal removal techniques for an optical time-integrating correlator
[AD-A290092] p 2700 N95-29354
Wideband I/Q demodulators: Measurement technique and matching characteristics
[AD-A291505] p 2558 N95-29847

DEFENCE SCIENCE AND TECHNOLOGY ORGANISATION, CANBERRA (AUSTRALIA).
Helicopter life substantiation: Review of some USA and UK initiatives
[AD-A290045] p 2495 N95-28851
Characterisation of a line-tunable He-Xe laser operating at 2.026 and 3.894 micrometers
[AD-A291129] p 2587 N95-29914

DEFENCE SCIENCE AND TECHNOLOGY ORGANISATION, MELBOURNE (AUSTRALIA).
Unmanned Aerial Vehicle technology
[DSTO-GD-0044] p 2497 N95-29362
Estimation of aerodynamic load distributions on the F/A-18 aircraft using a CFD panel code
[DSTO-TR-0147] p 2498 N95-29445

DEFENSE INFORMATION SYSTEMS AGENCY, ARLINGTON, VA.
Software systems reengineering process model, version 2.0
[AD-A289968] p 2647 N95-29278

DEFENSE SYSTEMS MANAGEMENT SCHOOL, FORT BELVOIR, VA.
Environmental practice in progam management offices
[AD-A290823] p 2609 N95-29721

DELAWARE STATE COLL., DOVER, DE.
Mode of human image representation and error checking strategies in complex visual displays
[AD-A290107] p 2492 N95-29210

DELAWARE UNIV., NEWARK, DE.
Establishing the relationship between manufacturing and component performance in stretch formed thermoplastic composites p 2514 N95-28829
A study of dynamics in the tropical Pacific using satellite data p 2630 N95-29520
Formal design of communication protocols using Estelle
[AD-A290584] p 2652 N95-30042

DEPARTMENT OF DEFENSE, WASHINGTON, DC.
DOD listing of approved recurring information requirements
[AD-A291346] p 2724 N95-29947

DEPARTMENT OF ENERGY, MORGANTOWN, WV.
Solid Oxide Fuel Cell commercialization in the United States
[DE95-008210] p 2607 N95-30278

DEPARTMENT OF ENERGY, WASHINGTON, DC.
Scientific and technical information policy implementation under OMB Circular A-130. Report of agency findings and recommendations
[DE-95-11601] p 2723 N95-29449

DEPARTMENT OF THE AIR FORCE, BROOKS AFB, TX.
Civil Reserve Air Fleet-Aeromedical Evacuation Shipset (CRAF-AESS) p 2678 N95-29619
International access to aeromedical evacuation medical equipment assessment data p 2679 N95-29622
Aeromedical impact of the transportable pressure ventilator in wartime aeromedical evacuation p 2641 N95-29624

DEPARTMENT OF THE AIR FORCE, SCOTT AFB, IL.
Use of quality tools to re-engineer the Aeromedical Evacuation (AE) system p 2676 N95-29605
Re-engineering support to the patient movement process p 2677 N95-29615
Care in the air: A system analysis of clinical outcomes in aeromedical evacuation p 2642 N95-29626

DEPARTMENT OF THE AIR FORCE, SHAW AFB, SC.
United Nations aeromedical evacuation operations in the former Yugoslavia p 2676 N95-29607

DEPARTMENT OF THE AIR FORCE, WRIGHT-PATTERSON AFB, OH.
Applied optics laboratory
[AD-A292006] p 2701 N95-29571

DEPARTMENT OF THE NAVY, WASHINGTON, DC.
Lightweight battery electrode and method of making it
[AD-D017389] p 2560 N95-28855
In-line fiber etalon strain sensor
[AD-D017266] p 2699 N95-29283
Permanent magnet torque/force transfer apparatus
[AD-D017325] p 2682 N95-30051
Balanced, double-sided calibration circuit for sensor element differential pre-amplifier
[AD-D017326] p 2566 N95-30052
Shock resistant optic fiber rotary slice holding device
[AD-D017327] p 2702 N95-30053
Unitary transducer with variable resistivity
[AD-D017329] p 2566 N95-30055
A system for conveniently providing load testing termination of an AC power source having at least one battery
[AD-D017408] p 2566 N95-30075
Selective multi-chemical fiber optic sensor
[AD-D017409] p 2703 N95-30076
Linear carborane-(siloxane or silane)-acetylene based copolymers
[AD-D017321] p 2547 N95-30132
Apparatus and method for achieving growth-etch deposition of diamond using a chopped oxygen-acetylene flame
[AD-D017322] p 2718 N95-30164
Thin-film edge field emitter device and method of manufacture therefor
[AD-D017323] p 2567 N95-30165
Method of measuring liquid level with a thermal interface detection
[AD-D017341] p 2703 N95-30166

DETROIT UNIV., MI.
Target aircraft identification, trajectory tracking and prediction using regression-based Kalman filter techniques p 2565 N95-29728

DEUTSCHE FORSCHUNGS- UND VERSUCHSANSTALT FUER LUFT- UND RAUMFAHRT, GOETTINGEN (GERMANY).
Numerical simulation and analysis of the hypersonic turbulent flow past a blunt-fin/ramp configuration
[DLR-FB-94-19] p 2492 N95-30349

DIRECTED TECHNOLOGIES, INC., ARLINGTON, VA.
Technology development goals for automotive fuel cell power systems
[DE95-008764] p 2548 N95-29280

DISTRICT OF COLUMBIA UNIV., WASHINGTON, DC.
High Tc superconducting bolometric and nonbolometric infrared (IR) detectors
[NASA-CR-198789] p 2702 N95-30035

DONMAR LTD., NEWPORT BEACH, CA.
Cost effective, dual-purpose machine vision-based detectors for (1) smoke and flame detection, and (2) engine overhead/burn-through and flame detection
[AD-A292284] p 2697 N95-28870

DOUGLAS AIRCRAFT CO., INC., LONG BEACH, CA.
Impact of composites on future transport aircraft p 2519 N95-29030
Effects of thermal and moisture cycling on the internal structure of stitched RTM laminates p 2522 N95-29048
Progress in manufacturing large primary aircraft structures using the stitching/RTM process p 2522 N95-29050
Test results from large wing and fuselage panels p 2522 N95-29051

DOW CHEMICAL CO., MIDLAND, MI.
Development of RTM and powder prepreg resins for subsonic aircraft primary structures p 2521 N95-29044

DRAPER (CHARLES STARK) LAB., INC., BOSTON, MA.
Performance analysis of a GPS interferometric attitude determination system for a gravity gradient stabilized spacecraft
[NASA-CR-188372] p 2508 N95-30036
DRAPER (CHARLES STARK) LAB., INC., CAMBRIDGE, MA.
Error modeling for differential GPS
[NASA-CR-188367] p 2493 N95-28716
A vehicle health monitoring system for the Space Shuttle Reaction Control System during reentry
[NASA-CR-188370] p 2505 N95-29447
DREXEL UNIV., PHILADELPHIA, PA.
An air stream analysis of the occluded cyclone
p 2623 N95-29714
DUKE UNIV., DURHAM, NC.
Synthesis and complete characterization of a Gallium-Mixed-Pnicogen four-membered ring compound: I2GaAs(SiMe3)(sub 2)Ga(I)2P(SiMe3)(sub 2)
[AD-A292423] p 2713 N95-28993
The quantum hydrodynamic model for semiconductor devices
[AD-A291809] p 2564 N95-29430
Synthesis and characterization of (Me3SiCH2)3M(dot)E(SiMe3)3 (M = Ga, E = P or As; M = In, E = P). X-ray crystal structures of (Me3SiCH2)3Ga(dot)P(SiMe3)3 and (Me3SiCH2)3In(dot)P(SiMe3)3
[AD-A291907] p 2715 N95-29444
Synthesis of nanocrystalline indium arsenide and indium phosphide from Indium(III) halides and tris(trimethylsilyl)pnicogens; synthesis, characterization, and decomposition behavior of I3In(dot)P(SiMe3)3
[AD-A291905] p 2715 N95-29486
DYNAFLOW, INC., COLUMBUS, OH.
Cross flow instability of supersonic flow over a 4:1 elliptic cone
[AD-A291128] p 2577 N95-29913

E

EAGLE-PICHER INDUSTRIES, INC., COLORADO SPRINGS, CO.
Magnum(R) NiCd advanced nickel-cadmium battery cells p 2567 N95-30258
EAGLE-PICHER INDUSTRIES, INC., JOPLIN, MO.
Advanced Dependent Pressure Vessel (DPV) nickel-hydrogen spacecraft cell and battery design
p 2567 N95-30261
EDGERTON, GERMESHAUSEN AND GRIER, INC., IDAHO FALLS, ID.
Austenite to ferrite transformation kinetics during continuous cooling
[DE95-006582] p 2537 N95-29869
EDGEWOOD RESEARCH DEVELOPMENT AND ENGINEERING CENTER, ABERDEEN PROVING GROUND, MD.
Electromagnetic scattering by magnetic spheres: Theory and algorithms
[AD-A289798] p 2551 N95-28699
Some new saturated two-level designs
[AD-A292627] p 2670 N95-29296
EDUCATIONAL TESTING SERVICE, PRINCETON, NJ.
Test theory reconceived
[AD-A291836] p 2639 N95-29432
EG AND G ENERGY MEASUREMENTS, INC., PLEASANTON, CA.
An image cancellation approach to depth-from-focus
[DE95-007625] p 2697 N95-28912
EG AND G ROCKY FLATS, INC., GOLDEN, CO.
Management of meteorological data at a former nuclear weapons facility
[DE95-007619] p 2626 N95-29868
ELECTRICITE DE FRANCE, CLAMART (FRANCE).
Computation of wave propagation in a complex flow
p 2582 N95-30142
ELTRON RESEARCH, INC., BOULDER, CO.
Electrochemical impedance pattern recognition for detection of hidden chemical corrosion on aircraft components, phase 1
[AD-A291345] p 2593 N95-29946
EMORY UNIV., ATLANTA, GA.
Studies of energy transfer processes of relevance to chemically and optically pumped lasers
[AD-A290164] p 2585 N95-29025
ENERGY INTERNATIONAL, INC., BELLEVUE, WA.
Investigation of laminar methane flames with emphasis on kinetics elucidation and NOx reduction
[PB95-200531] p 2535 N95-30111
ENGINEERING RESEARCH AND CONSULTING, INC., TULLAHOMA, TN.
Automated Propulsion Data Screening demonstration system
[NASA-CR-196636] p 2510 N95-29584
ENVIRONMENTAL RESEARCH INST. OF MICHIGAN, ANN ARBOR, MI.
Retrieval, display, and analysis support tool for earth imagery (RDAST)
[AD-A291366] p 2601 N95-30061
Hi-res SAR data processing report
[AD-A291443] p 2559 N95-30073
ESDU INTERNATIONAL LTD., LONDON (ENGLAND).
Orthobaric densities and molar volumes of liquids. Glycol ethers (cellosolves and carbitols, etc.)
[ESDU-95005] p 2530 N95-28703
Ejectors and jet pumps: Computer program for design and performance for steam/gas flow
[ESDU-94046] p 2495 N95-28704
Selection and costing of heat exchangers. Air-cooled type
[ESDU-94043] p 2550 N95-28705
Selection and costing of heat exchangers. Shell-and-tube type
[ESDU-94042] p 2550 N95-28706
Effects of small changes on rate of climb
[ESDU-94039] p 2495 N95-28707
Computer program for estimation of leading-edge suction distribution for plane thin wings at subsonic speeds
[ESDU-94038] p 2477 N95-28708
The prediction of sound attenuation as a result of propagation close to the ground
[ESDU-94036] p 2682 N95-28709
The correction of measured noise spectra for the effects of ground reflection
[ESDU-94035] p 2683 N95-28710
Dimensions, deflections and stresses for Hertzian contacts under combined normal and tangential loading. (Guide to use of computer program A9434.)
[ESDU-94034] p 2593 N95-28711
Viscosity of liquids: Aliphatic and cyclic ketones
[ESDU-94025] p 2530 N95-28712
Leading-edge suction distribution for plane thin wings at subsonic speeds
[ESDU-94037] p 2486 N95-28800
Flat rectangular isotropic plates under uniformly distributed normal pressure. Elastic deflections, stresses, and strains, moments and forces, for various forms of edge restraint
[ESDU-94033] p 2593 N95-28801
Thermophysical properties of R-32 (difluoromethane)
[ESDU-94032] p 2530 N95-28802
Thermal conductivity of liquid halogenated aliphatic hydrocarbons. Part 4: Halogenated alkenes and dienes (C1 to C4)
[ESDU-94024-PT-4] p 2511 N95-28803
Thermal conductivity of liquid halogenated aliphatic hydrocarbons. Part 1: Halogenated methanes and azeotropic mixtures
[ESDU-94021-PT-1] p 2511 N95-28804
Increments in aerofoil lift coefficient at zero angle of attack and in maximum lift coefficient due to deployment of a plain trailing-edge flap, with or without a leading-edge high-lift device, at low speeds
[ESDU-94028] p 2486 N95-28885
Orthobaric densities and molar volumes of liquids. Glycols and cyclic diols
[ESDU-95003] p 2531 N95-28895
Shear force, bending moment and torque of rigid aircraft in symmetric steady maneuvering flight
[ESDU-94045] p 2495 N95-28896
Excrescence drag levels on aircraft
[ESDU-94044] p 2487 N95-28897
Selection of synthetic oils
[ESDU-94020] p 2539 N95-28898
Through-the-thickness stresses and failure in the corner radius of a laminated composite section
[ESDU-94019] p 2518 N95-28899
Lubricant film thickness between disc cams and followers
[ESDU-94008] p 2539 N95-28900
Contact stress in disc cams with domes of flat-faced followers
[ESDU-94011] p 2589 N95-28901
NACA 1-series geometry representation for computational fluid dynamics
[ESDU-94013] p 2568 N95-28902
Wave drag coefficient for axisymmetric forecowls at zero incidence (M sub infinity less than or equal to 1.5)
[ESDU-94014] p 2568 N95-28903
Surface pressure coefficient distributions for axisymmetric forecowls at zero incidence (M sub infinity less than or equal to 1.5)
[ESDU-94015] p 2487 N95-28904
Selection of materials, manufacturing methods and lubricants for cam mechanisms
[ESDU-94017] p 2589 N95-28905
Condensation inside tubes: Condensate film coefficient in horizontal tubes
[ESDU-94041] p 2569 N95-29015
Effects of cabin pressure on climb and descent rates
[ESDU-94040] p 2496 N95-29016
Thermal conductivity of liquid halogenated aliphatic hydrocarbons. Part 2: Halogenated ethanes
[ESDU-94022] p 2512 N95-29017
Increments in aerofoil lift coefficient at zero angle of attack and in maximum lift coefficient due to deployment of a trailing-edge split flap, with or without a leading-edge high-lift device, at low speeds
[ESDU-94029] p 2488 N95-29129
Vapour pressures and critical points of liquids. Glycols and cyclic diols
[ESDU-95002] p 2534 N95-29897
Increments in aerofoil lift coefficient at zero angle of attack and in maximum lift coefficient due to deployment of various leading-edge high-lift devices at low speeds
[ESDU-94027] p 2490 N95-29898
Introduction to the estimation of the lift coefficients at zero angle of attack and at maximum lift for aerofoils with high-lift devices at low speeds
[ESDU-94026] p 2491 N95-29899
Thermal conductivity of liquid halogenated aliphatic hydrocarbons. Part 3: Halogenated higher hydrocarbons (C3 to C16)
[ESDU-94023-PT-3] p 2512 N95-29900
Vapour pressures and critical points of liquids. Glycol ethers (alkyl cellosolves and carbitols, etc.)
[ESDU-95004] p 2534 N95-29901
EVANS CO., EAST PROVIDENCE, RI.
High energy density electrolytic capacitor
p 2568 N95-30271

F

FEDERAL AVIATION ADMINISTRATION, ATLANTIC CITY, NJ.
Aircraft advanced materials research and development program plan
[AD-A290542] p 2498 N95-29565
UHF Low Density Radio Communications Link (LDRCL) Operational Test and Evaluation (OT&E) integration and OT&E operational final test report
[AD-A291447] p 2558 N95-29769
The effect of wear on fire-blocking layer material effectiveness
[AD-A291520] p 2493 N95-29855
The comparative extinguishment performance and thermal decomposition products of halon alternative agents
[AD-A291161] p 2551 N95-29924
Operational test and evaluation (OT&E) integration and operational test plan for fixed ground antenna radome (FGAR)
[AD-A291310] p 2559 N95-29940
Evaluation of retro-reflective beads in airport pavement markings
[AD-A291065] p 2502 N95-29967
Operational test and evaluation (OT&E) integration and operational test procedures for Fixed Ground Antenna Radome (FGAR)
[AD-A291203] p 2559 N95-29975
Prototype stop bar system evaluation at Seattle-Tacoma International Airport
[AD-A290136] p 2495 N95-30031
Offshore next generation weather radar (NEXRAD) test and evaluation master plan (TEMP)
[AD-A291435] p 2559 N95-30072
FEDERAL AVIATION ADMINISTRATION, OKLAHOMA CITY, OK.
Automation and cognition in air traffic control: An empirical investigation
[AD-A291932] p 2493 N95-28790
The potential for pulmonary heat injury resulting from the activation of a cabin water spray system to fight aircraft cabin fires
[DOT/FAA/AM-95/17] p 2636 N95-29224
Shift work, age, and performance: Investigation of the 2-2-1 shift schedule used in Air Traffic Control facilities I. The sleep/wake cycle
[DOT/FAA/AM-95/19] p 2638 N95-29261
A human factors evaluation of the operational demonstration flight inspection aircraft
[DOT/FAA/AM-95/18] p 2641 N95-29365
Alternative methods for flotation seat cushion use
[DOT/FAA/AM-95/20] p 2493 N95-29448
FEDERAL AVIATION ADMINISTRATION, WASHINGTON, DC.
Federal aviation administration plan for research, engineering and development
[AD-A290952] p 2494 N95-29733
Terminal area forecasts-fiscal years 1993-2010
[AD-A290835] p 2495 N95-29880

FLORIDA AGRICULTURAL AND MECHANICAL UNIV., TALLAHASSEE, FL.
AB initio studies of electron and positron scattering from non-linear molecules
[AD-A292586] p 2692 N95-28981
ADA in introductory courses
[AD-A292219] p 2648 N95-29285
FLORIDA ATLANTIC UNIV., BOCA RATON, FL.
High-and low-frequency dynamics of isolated blades and rotors with dynamic stall and wake
[AD-A290358] p 2497 N95-29322
FLORIDA INST. OF TECH., MELBOURNE, FL.
Automated optical target recognition
[AD-A292397] p 2697 N95-28798
FLORIDA INTERNATIONAL UNIV., MIAMI, FL.
A pipeline case tool for database design
[AD-A292017] p 2722 N95-29182
FLORIDA STATE UNIV., GAINESVILLE, FL.
PIV investigation of compressibility effects on dynamic stall p 2487 N95-29102
FLORIDA STATE UNIV., TALLAHASSEE, FL.
The spectrum and directivity of turbulent mixing noise from supersonic jets p 2684 N95-29415
Continuation of research in the statistical aspects of reliability, availability, and maintainability
[AD-A290126] p 2592 N95-29423
Benchmark problems and solutions p 2686 N95-30134
Solution of acoustic workshop problems by a spectral multidomain method p 2687 N95-30141
Solutions of the benchmark problems by the dispersion-relation-preserving scheme p 2674 N95-30145
FLORIDA UNIV., FORT LAUDERDALE, FL.
Investigation of a normal incident high performance P-type strained layer In(0.3)Ga(0.7)As/In(0.52)Al(0.48)As quantum well infrared photodetector
[AD-A290946] p 2716 N95-29785
FLORIDA UNIV., GAINESVILLE, FL.
Development of ultra-low dark current, high performance 3-5 quantum well infrared photodetectors (QWIPs) for focal plane arrays staring imaging sensor systems
[AD-A290343] p 2714 N95-29089
Molecular spectra and dynamics at interfaces
[AD-A289779] p 2693 N95-29460
Innovative processing of composites for ultra-high temperature applications, book 1
[AD-A290889] p 2527 N95-29842
FRAUNHOFER-INST. FUER KURZZEITDYNAMIK, WEIL AM RHEIN (GERMANY).
Experimental investigations of wave and fracture phenomena in impacted ceramics and glasses
[AD-A292142] p 2542 N95-29195
FUKUI INST. OF TECH. (JAPAN).
Trapped electron instabilities due to electron temperature gradient and anomalous transport
[AD-B179859L] p 2693 N95-29748

G

GAS RESEARCH INST., CHICAGO, IL.
Evaluation of wear resistant ceramic valve seats in gas-fueled power generation engines
[PB95-200218] p 2591 N95-30110
Nitrogen dioxide measurement method characterization at the GRI conventional research house
[PB95-200549] p 2610 N95-30197
Biological methane activation
[PB95-200705] p 2535 N95-30198
GENERAL ACCOUNTING OFFICE, WASHINGTON, DC.
Unmanned aerial vehicles: No more Hunter systems should be bought until problems are fixed
[AD-A292172] p 2497 N95-29126
GENERAL ELECTRIC CO., CINCINNATI, OH.
UHB engine fan broadband noise reduction study
[NASA-CR-198357] p 2684 N95-29641
GENERAL ELECTRIC CO., SCHENECTADY, NY.
Grid generation and surface modeling for CFD p 2478 N95-28726
GENETICS SOCIETY OF AMERICA, BETHESDA, MD.
Genetics and the unity of biology
[DE95-006484] p 2633 N95-29471
GEORGE MASON UNIV., FAIRFAX, VA.
A contribution to the theory of robust estimation of multivariate location and shape: EID
[AD-A290435] p 2675 N95-29819
Huge data sets and the frontiers of computational feasibility
[AD-A291384] p 2653 N95-30063
A new visualization technique to study the time evolution of finite and adaptive mixture estimators
[AD-A291147] p 2673 N95-30126
GEORGIA INST. OF TECH., ATLANTA, GA.
Communication protocols in multi-hop radio networks p 2553 N95-29106
A vorticity-velocity approach for three-dimensional unsteady viscous flow over wings p 2488 N95-29108
A fourth order Euler/Navier-Stokes prediction method for the aerodynamics and aeroelasticity of hovering rotor blades p 2572 N95-29242
Investigation of the flow turning loss in unstable solid propellant rocket motors p 2510 N95-29331
Analytical investigations in aircraft and spacecraft trajectory optimization and optimal guidance
[NASA-CR-4672] p 2504 N95-29339
Compressive behavior of thick composite shells: Benchmark solutions for loss of stability and hygroscopic effects p 2595 N95-29424
The use of charge coupled devices in astronomical speckle imaging p 2727 N95-29545
Model development for active control of stall phenomena in aircraft gas turbine engines p 2500 N95-29679
Unsteady pressure and inflow velocity on a pitching rotor blade in hover p 2490 N95-29771
DPARTS. A dynamic parallel adaptive multiprocess or real-time scheduler
[AD-A291160] p 2659 N95-29915
Guidance law development for aeroassisted transfer vehicles using Matched Asymptotic Expansions p 2503 N95-30347
GEORGIA TECH RESEARCH INST., ATLANTA, GA.
Development of continuous visible chemical laser amplifiers and oscillators from the Na3-X(Cl, Br, I) reactions and their analogs and energy transfer pumping from efficiently produced metastable states
[AD-A290999] p 2586 N95-29514
Measurements of ions formed in jet engine exhaust plumes
[AD-A290940] p 2501 N95-29764
GEORGIA UNIV., ATHENS, GA.
Analytical theory of continued fractions and time evolution in many-particle systems
[AD-A290365] p 2692 N95-29227
Fundamental studies of oxygen rings and other high energy density molecular systems
[AD-A290875] p 2693 N95-29865
GESELLSCHAFT FUER MATHEMATIK UND DATENVERARBEITUNG, SAINT AUGUSTIN (GERMANY).
Speedlog: The key architectural element to provide efficient log management
[PB95-198453] p 2643 N95-30108
GINER, INC., WALTHAM, MA.
Development of electrochemical super capacitors for EMA applications p 2568 N95-30270
GORDON RESEARCH CONFERENCES, INC., KINGSTON, RI.
Gordon research conference on point defects, line defects, and interfaces in semiconductors
[AD-A290103] p 2714 N95-29209
GRUMMAN AIRCRAFT ENGINEERING CORP., BETHPAGE, NY.
Novel cost controlled materials and processing for primary structures p 2514 N95-28830
Cross-stiffened continuous fiber structures p 2521 N95-29041
GTE LABS., INC., WALTHAM, MA.
Methods and components for optical contention resolution in high speed networks
[AD-A292331] p 2697 N95-28795
GUNMA UNIV., KIRYU (JAPAN).
Attractors of dissipative structure in three dissipative fluids
[AD-B180030L] p 2710 N95-29844

H

HACHINOHE INST. OF TECH. (JAPAN).
Relativistic effects on large amplitude nonlinear langmuir waves in a two-fluid plasma
[AD-B191980L] p 2710 N95-29841
HAMPTON UNIV., VA.
Computational methods for the simulation of non-Newtonian flows
[AD-A290355] p 2570 N95-29069
Development of a rotary wing Navier-Stokes CFD code based on TLNS3D code
[AD-A290421] p 2574 N95-29387
HARVARD UNIV., CAMBRIDGE, MA.
Intermediate levels of visual processing
[AD-A291569] p 2638 N95-28937
A search for cataclysmic variables in globular clusters p 2727 N95-29532
In situ measurements of ClO and implications for the chemistry of inorganic chlorine in the lower stratosphere p 2618 N95-29830
HAWAII UNIV., HONOLULU, HI.
Some aspects of lunar and martian volcanism as examined with spectral, topographic, and morphologic data derived from spacecraft images p 2736 N95-29594
Spectral reflectance studies and optical surface alteration in the search for links between meteorites and asteroids p 2733 N95-29672
HEBREW UNIV., JERUSALEM (ISRAEL).
Membrane fluidity and shape of human red blood cells are altered by physiological levels of hydrostatic pressure
[AD-A290595] p 2636 N95-29557
Effect of mild hydrostatic pressure on red blood cells
[AD-A290520] p 2637 N95-29872
HELLENIC AIR FORCE GENERAL HOSPITAL, ATHENS (GREECE).
Flight nurse school in the Hellenic Air Force p 2638 N95-29629
HELSINKI UNIV. OF TECHNOLOGY, ESPOO (FINLAND).
Static field solutions and image theory for a conducting sphere with radial anisotropy
[PB95-207171] p 2673 N95-30172
Product configurations: An application for prototype object approach
[PB95-192589] p 2655 N95-30283
HERCULES AEROSPACE CO., MAGNA, UT.
Automated fiber placement: Evolution and current demonstrations p 2514 N95-28832
Response of automated tow placed laminates to stress concentrations p 2515 N95-28833
HERIOT-WATT UNIV., EDINBURGH (SCOTLAND).
Dynamical instabilities, chaos and spatial complexity in fundamental nonlinear optical interactions
[AD-A291223] p 2588 N95-29980
HOSPITAL DEL AIRE, MADRID (SPAIN).
Critical evaluation of aeromedical evacuation in a multinational forces scenario p 2676 N95-29610
Experiences learned from the Spanish armed forces aeromedical evacuation system in the former Yugoslavia p 2677 N95-29614
HUGHES AIRCRAFT CO., TUCSON, AZ.
Zero Discharge Organic Coatings: Powder paint. UV curable paint. E-coat
[AD-A292180] p 2540 N95-28925
HUMAN RESOURCES RESEARCH ORGANIZATION, ALEXANDRIA, VA.
Coping and adaptation: Theoretical and applied perspectives
[AD-A290513] p 2638 N95-29090
HUMAN SYSTEMS DIV., BROOKS AFB, TX.
Aeromedical evacuation in combined operations p 2677 N95-29612
HYDEX CORP., VIENNA, VA.
Remote sensing of hydrologic variables in boreal areas
[NASA-CR-189422] p 2600 N95-29754

I

IBM WATSON RESEARCH CENTER, YORKTOWN HEIGHTS, NY.
Novel electric-field effects in quantum wells and superlattices
[AD-A292317] p 2718 N95-28857
ICEM CFD ENGINEERING, BERKELEY, CA.
Tuned grid generation with ICEM CFD p 2483 N95-28752
ILLINOIS INST. OF TECH., CHICAGO, IL.
Data migration policies for distributed database systems p 2721 N95-29093
ILLINOIS UNIV., CHICAGO, IL.
Experimental studies of electromagnetic propagation at ultrahigh intensities
[AD-A290284] p 2553 N95-29081
The Stroh formalism for anisotropic elasticity with applications to composite materials
[AD-A290710] p 2527 N95-29763
ILLINOIS UNIV., URBANA, IL.
Performance and robustness of self-tuning and adaptation algorithms for identification, filtering and control
[AD-A292070] p 2648 N95-29310
Transitions in liquid crystals initiated with circularly polarized light
[AD-A290525] p 2716 N95-29493
Signal processing for high-resolution image formation
[AD-A290648] p 2557 N95-29563
ILLINOIS UNIV., URBANA-CHAMPAIGN, IL.
Energy theorems and bounds in linearized elasticity with residual stress p 2595 N95-29546
ILLINOIS UNIV. AT URBANA-CHAMPAIGN, SAVOY, IL.
Transport simulation in spatially modulated low dimensionality systems
[AD-A290486] p 2718 N95-29149
IMITECH, INC., SCHENECTADY, NY.
Development of LaRC (TM): IA thermoplastic polyimide coated aerospace wiring
[NASA-CR-195048] p 2548 N95-30252

IMPERIAL COLL. OF SCIENCE AND TECHNOLOGY, LONDON (ENGLAND).
The effects of three dimensional imposed disturbances on bluff body near wake flows
[AD-A290824] p 2575 N95-29654
Low order adaptive optical systems
[AD-A291121] p 2701 N95-29766
INSTITUT FUER FESTKOERPERFORSCHUNG, JUELICH (GERMANY).
Crystal field and exchange interactions in DyT4Al8 (T = Fe and Mn)
[DE95-007131] p 2714 N95-29134
INSTITUTE FOR COMPUTER APPLICATIONS IN SCIENCE AND ENGINEERING, HAMPTON, VA.
The large discretization step method for time-dependent partial differential equations
[NASA-CR-195068] p 2670 N95-29403
Ropes: Support for collective opertions among distributed threads
[NASA-CR-198157] p 2649 N95-29404
An assessment of artificial damping models for aeroacoustic calculations
[NASA-CR-198354] p 2574 N95-29405
Implicit schemes and parallel computing in unstructured grid CFD
[NASA-CR-195071] p 2671 N95-29451
On the utility of threads for data parallel programming
[NASA-CR-198155] p 2649 N95-29455
Experimental confirmation of a PDE-based approach to design of feedback controls
[NASA-CR-198167] p 2672 N95-30086
Parallel rendering
[NASA-CR-195080] p 2655 N95-30306
Pressure updating methods for the steady-state fluid equations
[NASA-CR-198163] p 2674 N95-30353
INSTITUTE FOR DEFENSE ANALYSES, ALEXANDRIA, VA.
An algorithm fusion approach to IRST signal processing (III): Nongaussian-corrected filter fusion
[AD-A291565] p 2552 N95-28936
Estimates of probability of a cloud-free line of sight for RAPTOR TALON
[AD-A291908] p 2510 N95-29284
Proposed Department of Defense software metrics implementation plan
[AD-A291404] p 2550 N95-29918
INSTITUTE FOR THE STUDY OF LEARNING AND EXPERTISE, PALO ALTO, CA.
Workshop on Fielded Applications of Machine Learning
[AD-A280168] p 2649 N95-29456
Acquisition of place knowledge through case-based learning
[AD-A292574] p 2723 N95-29573
Oblivious decision trees and abstract cases
[AD-A292577] p 2664 N95-29574
Learning object models from visual observation and background knowledge
[AD-A292606] p 2650 N95-29576
Applications of machine learning and rule induction
[AD-A292607] p 2664 N95-29577
Induction of selective Bayesian classifiers
[AD-A292690] p 2675 N95-29906
INSTITUTE OF AVIATION MEDICINE, OSLO (NORWAY).
Effect of hypoxia on arterial blood gases in subjects with lung dysfunction p 2638 N95-29627
INSTITUTE OF ELECTRICAL AND ELECTRONICS ENGINEERS, PISCATAWAY, NJ.
Conference proceedings: IEEE Nonlinear Optics, Materials, Fundamentals, and Applications
[AD-A292438] p 2698 N95-28997
INSTITUTO DE PESQUISAS ESPACIAIS, SAO JOSE DOS CAMPOS (BRAZIL).
Monitoring of burning in the Brazilian cerrado region using AVHRR/NOAA data calibrated by TM/Landsat data
[INPE-5490-TDI/507] p 2598 N95-28929
Interface for the translation of sentences in a natural language into a geometrical representation language
[INPE-5467-PRE/1775] p 2722 N95-29363
Optical (LANDSAT/TM) and radar (ERS-1/SAR) imagery sinergism studies applied to land use discrimination
[INPE-5608-TDI/554] p 2598 N95-29433
Proposal for a flexible system of phytogeographic classification: Emphasis on the use of multistage remote sensoring
[INPE-5609-PRE/1821] p 2600 N95-29815
Evaluation of the utilization of SAR polarimetric images in the survey of land resources in the Amazon area Tapajos Forest Reserve
[INPE-5517-PRE/1792] p 2601 N95-29999
INTERFACE VIDEO SYSTEMS, INC., WASHINGTON, DC.
Rover story
[NASA-CR-198757] p 2736 N95-29964
Life sciences program
[NASA-CR-197658] p 2633 N95-30292
INTERNATIONAL BUSINESS MACHINES CORP., SAN JOSE, CA.
Publications/Patents/Presentations/Honors report: Force and tunneling microscopy studies of atomic level mechanical properties of solids
[AD-A292254] p 2691 N95-28888
INTERNATIONAL SOCIETY FOR OPTICAL ENGINEERING, BELLINGHAM, WA.
Ocean Optics XII
[AD-A286734] p 2702 N95-29910
IOWA STATE UNIV. OF SCIENCE AND TECHNOLOGY, AMES, IA.
Solution of second order nonlinear boundary value problems by the boundary element method p 2669 N95-29105
Efficient inversion of Fourier and Laplace domain boundary element solutions for elastodynamic scattering p 2592 N95-29256
Computation of the integrated aerodynamic and propulsive flowfields of a generic hypersonic space plane p 2490 N95-29788
An interacting boundary layer method for unsteady compressible flows p 2579 N95-30290
IOWA UNIV., IOWA CITY, IA.
Solar system plasma waves
[NASA-CR-198767] p 2704 N95-29130
A thermochemical transport model for analysis of hot-spot formation in energetic materials
[AD-A290441] p 2532 N95-29357
Hydrology of the continental United States p 2599 N95-29539
Solitons in negative ion plasmas p 2706 N95-29668
Radioastronomical measurements of plasma characteristics of the solar corona and the solar wind p 2730 N95-29782

J

JAPAN WELDING SOCIETY, TOKYO (JAPAN).
A 1993 review of welding in Japan
[DE95-758701] p 2589 N95-28946
JET PROPULSION LAB., CALIFORNIA INST. OF TECH., PASADENA, CA.
Collection of Magellan Venus radar mapping results
[NASA-CR-197656] p 2736 N95-29178
Optimization of 100-meter Green Bank Telescope
[NASA-CR-198868] p 2731 N95-30230
Data catalog for JPL Physical Oceanography Distributed Active Archive Center (PO.DAAC)
[NASA-CR-198872] p 2631 N95-30231
An atlas of monthly mean distributions of SSMI surface wind speed, AVHRR/2 sea surface temperature, AMI surface wind velocity, TOPEX/POSEIDON sea surface height, and ECMWF surface wind velocity during 1993
[NASA-CR-198880] p 2628 N95-30343
The JPL Mars gravity field, Mars50c, based upon Viking and Mariner 9 Doppler tracking data
[NASA-CR-198881] p 2737 N95-30344
JOHNS HOPKINS UNIV., BALTIMORE, MD.
Receiver design, performance analysis, and evaluation for space-borne laser altimeters and space-to-space laser ranging systems
[NASA-CR-198655] p 2584 N95-28808
The interaction of group 3A atoms with small molecules
[AD-A290285] p 2692 N95-29082
Origins of imperfections in composite materials
[AD-A290261] p 2523 N95-29169
A theoretical study on ignition mechanisms of liquid propellants
[AD-A290569] p 2549 N95-29550
Coronagraphic imaging of protoplanetary-disk candidate stars using adaptive optics p 2728 N95-29651
Statistics and large-scale structure p 2734 N95-29780
Induced Compton scattering by relativistic electrons in magnetized astrophysical plasmas p 2610 N95-29885
Physical modeling and design of semiconductor heterostructures for optical and electronical applications p 2682 N95-30232
Ensemble phase averaged equations for multiphase flows p 2579 N95-30284
The effects of clouds as a feedback mechanism on the Earth's climate in the tropical Pacific p 2611 N95-30300
JOINT INST. FOR ADVANCEMENT OF FLIGHT SCIENCES, HAMPTON, VA.
The use of staggered scheme and an absorbing buffer zone for computational aeroacoustics p 2689 N95-30153

K

KANSAS STATE UNIV., MANHATTAN, KS.
Radiative lifetime and quenching rate constants of PF(b(1) Sigma+) and tests for an electronic to vibrational energy transfer quenching mechanism
[AD-A290294] p 2681 N95-29062
KANSAS UNIV., LAWRENCE, KS.
Navier-Stokes solution of wing wake structure and its perturbation p 2488 N95-29121
KANSAS UNIV. CENTER FOR RESEARCH, INC., LAWRENCE, KS.
Application of optimization technique to control system design for departure prevention and aircraft model estimation through dynamic inversion p 2501 N95-29156
Design, analysis and control of large transports so that control of engine thrust can be used as a back-up of the primary flight controls
[NASA-CR-198958] p 2501 N95-30254
KENT STATE UNIV., OH.
High-level parallel programming tools for finite element analysis
[AD-A290566] p 2659 N95-29566
KENT UNIV., CANTERBURY (ENGLAND).
Investigation of optical damage, energy partitioning and scaling laws at extremely high velocities
[AD-A291368] p 2703 N95-30062
KENTUCKY UNIV., LEXINGTON, KY.
High performance electromagnetic simulation tools
[AD-A290405] p 2554 N95-29235
Development of 'smart' piezothermoelastic laminae: Theory and applications
[AD-A290852] p 2528 N95-29864
Fundamental studies in cryogenic cooling of power electronics
[AD-A291150] p 2551 N95-30296
KINGS COLL., LONDON (ENGLAND).
Diffraction limited imaging using aberrated optics
[AD-A290912] p 2703 N95-30081
KOREA ADVANCED INST. OF SCIENCE AND TECHNOLOGY, TAEJON (REPUBLIC OF KOREA).
Comparative study of numerical schemes of TVD3, UNO3-ACM and optimized compact scheme p 2686 N95-30137
KOREA AIR FORCE ACADEMY, CHEONG-JU (KOREA).
Optimal domain decomposition strategies p 2484 N95-28759

L

LAMAR UNIV., BEAUMONT, TX.
Damage tolerance in filament-wound graphite/epoxy pressure vessels
[NASA-CR-198804] p 2590 N95-29369
LAWRENCE LIVERMORE NATIONAL LAB., LIVERMORE, CA.
Insights on the local density approximation plasma polarization shift as provided by the optimum potential method
[DE95-008078] p 2705 N95-29466
Techniques and results of tokamak-edge simulation
[DE95-008075] p 2711 N95-30130
SI Handbook for the Lawrence Livermore National Laboratory: Committee on metric transition
[DE95-009329] p 2551 N95-30182
Requirements for a portable parallel I/O library for scientific computation
[DE95-009383] p 2660 N95-30192
Massively parallel fast elliptic equation solver for three dimensional hydrodynamics and relativity
[DE95-009385] p 2660 N95-30193
LOCKHEED AERONAUTICAL SYSTEMS CO., MARIETTA, GA.
Requirements for effective use of CFD in aerospace design p 2478 N95-28725
An assessment of unstructured grid technology for timely CFD analysis p 2482 N95-28747
ISPAN (Interactive Stiffened Panel Analysis): A tool for quick concept evaluation and design trade studies p 2517 N95-28846
Advanced composite structural concepts and materials technologies for primary aircraft structures: Advanced material concepts
[NASA-CR-4485] p 2496 N95-29027
Textile composite fuselage structures development p 2519 N95-29033
Advanced resin systems and 3D textile preforms for low cost composite structures p 2519 N95-29035
Thermally stable organic polymers
[AD-A290755] p 2543 N95-29482
A comparative study of upwind and MacCormack schemes for CAA benchmark problems p 2688 N95-30147

LOCKHEED ENGINEERING AND SCIENCES CO., HAMPTON, VA.
The effects of specimen width on tensile properties of triaxially braided textile composites p 2513 N95-28825
Experimental and analytical characterization of triaxially braided textile composites p 2520 N95-29040
A designed experiment in stitched/RTM composites p 2522 N95-29046
The combined effect of glass buffer strips and stitching on the damage tolerance of composites p 2522 N95-29049
LOCKHEED ENGINEERING AND SCIENCES CO., WASHINGTON, DC.
Lockheed Stabilizer System for space exercise equipment
[NASA-CR-197657] p 2641 N95-29180
LOCKHEED-FORT WORTH CO., FORT WORTH, TX.
Unstructured Cartesian/prismatic grid generation for complex geometries p 2481 N95-28741
LOCKHEED IDAHO TECHNOLOGIES CO., IDAHO FALLS, ID.
Advanced manufacturing by spray forming: Aluminum strip and microelectromechanical systems
[DE95-008615] p 2536 N95-28959
Corrosion investigation of multilayered ceramics and experimental nickel alloys in SCWO process environments
[DE95-008666] p 2540 N95-28960
Electric and hybrid vehicle program: Site operator program
[DE95-008620] p 2591 N95-30211
LOCKHEED MISSILES AND SPACE CO., ALBUQUERQUE, NM.
Precision pointing experiment
[AD-A291015] p 2664 N95-29657
LOCKHEED MISSILES AND SPACE CO., HUNTSVILLE, AL.
Surface conversion techniques for low energy neutral atom imagers
[NASA-CR-196604] p 2691 N95-28856
LOCKHEED MISSILES AND SPACE CO., PALO ALTO, CA.
Wavelets in signal detection and identification comparative signal processing technology evaluation
[AD-A291952] p 2552 N95-28984
LOGICON TECHNICAL SERVICES, INC., DAYTON, OH.
Tools for Automated Knowledge Engineering (TAKE) system evaluation methodology
[AD-A291145] p 2654 N95-30125
LOGISTICS MANAGEMENT INST., BETHESDA, MD.
DOD electronic data interchange (EDI) convention: TDCC/EDIA transaction set 210 motor carrier invoice (version 003020). Revision 1
[AD-A292375] p 2720 N95-28797
DOD electronic data interchange (EDI) convention: ASC X12 transaction set 410 Rail Carrier Invoice, version 003020
[AD-A292495] p 2722 N95-29287
LORAL DEFENSE SYSTEMS, AKRON, OH.
Engineering development program of a closed aluminum-oxygen semi-cell system for an unmanned underwater vehicle: An update p 2606 N95-30266
LOS ALAMOS NATIONAL LAB., NM.
SAO HMC photodetector/event timer engineering model test report
[DE95-007889] p 2582 N95-28917
Bubble fusion: Preliminary estimates of spherical micro-implosions in cavitating liquids
[DE95-006260] p 2569 N95-28956
The Los Alamos Photon Counting Detector Debris Detection Project: An update
[DE95-007883] p 2508 N95-29464
Deposition and surface treatment with intense pulsed ion beams
[DE95-007885] p 2543 N95-29465
Polynomial approximations for materials simulations
[DE95-006168] p 2652 N95-29989
Testing of the ENDF/B-VI neutron data library ENDF60 for use with MCNP(trademark)
[DE95-007858] p 2696 N95-30057
Applications of Langevin and Molecular Dynamics methods
[DE95-007875] p 2694 N95-30059
HIPPI - Gigabit LANS are here today
[DE95-007877] p 2660 N95-30128
Extreme nonlinearity in rocks: An investigation using elastic pulse wave propagation
[DE95-007879] p 2618 N95-30129
Bicriteria network design problems
[DE95-005261] p 2661 N95-30215
Numerical implementation of a state variable model for friction
[DE95-007844] p 2591 N95-30273
Assay of potentially contaminated propellant
[DE95-006330] p 2549 N95-30345
LOUISIANA STATE UNIV., BATON ROUGE, LA.
An integrated optical CO2 sensor. Phase 0: Design and fabrication of critical elements
[NASA-CR-198792] p 2700 N95-29366
LOUISVILLE UNIV., KY.
Testbed for precision characterization of spatial light modulators and optical processors
[AD-A290484] p 2699 N95-29148
LOVELACE BIOMEDICAL AND ENVIRONMENTAL RESEARCH INST., ALBUQUERQUE, NM.
Inhalation Toxicology Research Institute
[AD-A292037] p 2635 N95-29188
LYNNTECH, INC., COLLEGE STATION, TX.
A novel unitized regenerative proton exchange membrane fuel cell p 2605 N95-30263

M

MADIGAN ARMY MEDICAL CENTER, TAKOMA, WA.
Refractive changes during prolonged exposure to altitude following refractive surgery
[AD-A290263] p 2635 N95-29173
MAGNASCREEN CORP., PITTSBURGH, PA.
Low voltage, high resistance, Polymer Dispersed Liquid Crystal
[AD-A291946] p 2556 N95-29472
MAINE UNIV., ORONO, ME.
ADC test support program
[AD-A289445] p 2643 N95-29921
MANCHESTER UNIV. (ENGLAND).
Proceedings of the 18th International Workshop on Condensed Matter Theories
[AD-A291396] p 2694 N95-30065
MARTIN MARIETTA CORP., MOORESTOWN, NJ.
R&M design expert system
[AD-A292525] p 2645 N95-28814
MARTIN MARIETTA LABS., BALTIMORE, MD.
Laser simulation of single-event effects: A state of the art review
[AD-A292308] p 2584 N95-28892
MARYLAND UNIV., BALTIMORE, MD.
Statistical inference problems in some multivariate linear models with applications to multivariate calibration and meta-analysis
[AD-A291125] p 2675 N95-29768
MARYLAND UNIV., COLLEGE PARK, MD.
Dispersion analysis and error estimation of Galerkin finite element methods for the numerical computation of waves
[AD-A290296] p 2668 N95-29064
Pollution error in the h-version of the finite element method and the local quality of the recovered derivatives
[AD-A290297] p 2668 N95-29065
Nonlinear mechanics and applied analysis
[AD-A290356] p 2669 N95-29070
A generalized finite element method for solving the Helmholtz equation in two dimensions with minimal pollution
[AD-A290280] p 2669 N95-29080
Finite element solution to the Helmholtz equation with high wave number. Part 2. The h-p version of the FEM
[AD-A290289] p 2669 N95-29084
Effects of critical fluctuations on the thermodynamic properties of fluids and fluid mixtures p 2719 N95-29216
Inhibition of mode competition in free-electron laser oscillators p 2586 N95-29336
Hybrid harmonic gyrotron traveling wave amplifier
[AD-A292686] p 2564 N95-29417
A three dimensional finite element scheme for fiber microbuckling in thick multidirectional laminated composites p 2525 N95-29512
Estimation of unstabilized components in vehicular motion
[AD-A290580] p 2590 N95-29552
Photothermal deflection in a supercritical fluid p 2701 N95-29630
Development of distributed feedback dye lasers for generation of high-power 193 nm excimer laser short pulses p 2586 N95-29631
One and two fluid numerical investigations of solar wind gas releases p 2738 N95-29704
A study of one-armed spiral galaxies p 2729 N95-29774
The complex broadband x-ray spectra of Seyfert galaxies p 2730 N95-29776
The construction of high-accuracy schemes for acoustic equations p 2688 N95-30146
MARYLAND UNIV. BALTIMORE COUNTY, CATONSVILLE, MD.
A study of the conceptual symbolics of information system development languages p 2723 N95-29589
MASSACHUSETTS INST. OF TECH., CAMBRIDGE, MA.
Interferometric measurement with squeezed light
[AD-A292402] p 2697 N95-28799
Design of an electronic charged particle spectrometer to measure (rho R), yield, and implosion symmetry on the OMEGA Upgrade
[DE95-006088] p 2695 N95-28930
Proceedings of the 11th congress of the international society for artificial cells, blood substitutes and immobilization biotechnology
[AD-A290342] p 2632 N95-29088
A numerical method for modelling wings with sharp edges maneuvering at high angles of attack p 2496 N95-29122
Computing 3-D motion in custom analog and digital VLSI
[AD-A290270] p 2647 N95-29179
Arcing mitigation and predictions for high voltage solar arrays
[AD-A292227] p 2602 N95-29200
Arcing predictions for PASP PLUS solar arrays
[AD-A292230] p 2602 N95-29201
Garbage collection is fast, but a stack is faster
[AD-A290099] p 2722 N95-29207
Real-time x-ray scattering study of processing of eight performance thermoplastics
[AD-A290374] p 2542 N95-29230
Dynamic stall of a NACA 0012 airfoil in laminar flow p 2489 N95-29243
Modeling and control of rotating stall in high speed multi-stage axial compressors p 2500 N95-29244
Multifluid nonequilibrium simulation of arcjet thrusters p 2510 N95-29245
The detection of oil slicks at night with airborne infrared imagers
[AD-A289731] p 2598 N95-29281
Forecasting global temperature variations by neural networks
[AD-A290081] p 2621 N95-29333
Relative affine structure: Canonical model for 3D from 2D geometry and applications
[AD-A290085] p 2670 N95-29352
Trajectory mapping (TM): A new non-metric scaling technique
[AD-A290036] p 2670 N95-29440
Towards an example-based image compression architecture for video-conferencing
[AD-A290041] p 2556 N95-29441
Interaction and intelligent behavior
[AD-A290049] p 2639 N95-29443
Automated reasoning about classical mechanics
[AD-A290052] p 2663 N95-29477
Asymptotically zero energy computing using split-level charge recovery logic
[AD-A290054] p 2564 N95-29478
Neural network exploration using optional experiment design
[AD-A290058] p 2663 N95-29479
Intelligent turbine engines for Army applications
[AD-A290532] p 2500 N95-29496
Synthesis morphology and properties of semicrystalline block copolymers
[AD-A290475] p 2544 N95-29510
Ionizational nonequilibrium and ignition in plasma accelerators p 2705 N95-29547
Broadband control of structural vibration using simultaneous sensing and actuation with nonlinear piezoelectric elements p 2664 N95-29548
Impact resistance and damage tolerance of composite sandwich panels p 2526 N95-29549
Fundamental limitations and capabilities of robust identification and adaptive control
[AD-A291085] p 2664 N95-29636
Development of improved geophysical imaging techniques for environmental site characterization
[AD-A291003] p 2558 N95-29875
Nanocrystalline processing and interface engineering of Si3N4-based ceramics
[AD-A291302] p 2546 N95-29939
Crustal deformation measurements in the vicinity of Vandenberg Air Force Base
[AD-A291224] p 2618 N95-29981
Probabilistic modeling and statistical inference for random fields and space-time processes
[AD-A289956] p 2672 N95-30029
MASSACHUSETTS INST. OF TECH., LEXINGTON, MA.
Novel high-power solid-state sources for the millimeter-wave region
[AD-A292653] p 2564 N95-29384
The mesh synchronous processor MeshSP (trademark)
[AD-A289875] p 2659 N95-29420
MASSACHUSETTS UNIV., AMHERST, MA.
A search for a composition-dependent gravitational force p 2719 N95-29501
Scheduling algorithms for mobile packet radio networks p 2558 N95-29707

MASSACHUSETTS UNIV. MEDICAL CENTER, WORCESTER, MA.
Studies of altered response to infection induced by severe injury
[AD-A288907] p 2634 N95-29139
MATHEMATICAL ASSOCIATION OF AMERICA, INC., WASHINGTON, DC.
Mathematical olympiad summer program (MOSP) 1994
[AD-A290801] p 2672 N95-29647
MATIS, INC., DECATUR, GA.
Development of the theory and algorithms for synthesis of reflector antenna systems
[AD-A292579] p 2552 N95-28979
MAX-PLANCK-INST. FUER PLASMAPHYSIK, GARCHING (GERMANY).
Discriminant analysis to predict the occurrence of ELMS in H-mode discharges
[AD-B179183L] p 2708 N95-29746
MCDONNELL-DOUGLAS AEROSPACE, SAINT LOUIS, MO.
Future requirements in surface modeling and grid generation p 2478 N95-28724
Numerical investigation of surface curvature effects in compressible turbulent flows
[AD-A290114] p 2571 N95-29211
MCDONNELL-DOUGLAS CORP., SAINT LOUIS, MO.
Generating grids directly on CAD database surfaces using a parametric evaluator approach p 2483 N95-28754
Comparison of spatial numerical operators for duct-nozzle acoustics p 2690 N95-30158
MCMASTER UNIV., HAMILTON (ONTARIO).
Quantum mechanical problems in one, two, and three dimensions
[ISBN-0-315-84931-2] p 2719 N95-29677
MDA ENGINEERING, INC., ARLINGTON, TX.
Three-dimensional hybrid grid generation using advancing front techniques p 2481 N95-28745
METEOROLOGICAL SATELLITE CENTER, TOKYO (JAPAN).
Meteorological Satellite Center technical note, no. 28, 1994
[JTN-95-80926] p 2626 N95-29849
METSAT, INC., FORT COLLINS, CO.
Production of a long-term global water vapor and liquid water data set using ultra-fast methods to assimilate multi-satellite and radiosonde observations
[NASA-CR-198955] p 2628 N95-30272
MICHIGAN STATE UNIV., EAST LANSING, MI.
Electrical and electronic properties of self-assembled lipid bilayers
[AD-A290507] p 2632 N95-29155
Molecular mixing in shear layers forced by 2-D and 3-D disturbances
[AD-A290272] p 2571 N95-29181
Examination of dislocation core structures in B2 intermetallic alloys
[AD-A291486] p 2537 N95-29526
MICHIGAN TECHNOLOGICAL UNIV., HOUGHTON, MI.
A geotechnical characterization of lunar soils and lunar soil simulants p 2736 N95-29117
Theoretical, experimental and computational studies in plasticity
[AD-A290428] p 2595 N95-29535
MICHIGAN UNIV., ANN ARBOR, MI.
Epitaxial growth and characterization of Si(1-x)Ge(x) materials and devices
[AD-A292528] p 2712 N95-28874
Development of a multiplex Fabry-Perot interferometer and measurement of atmospheric HF and HCl p 2608 N95-29213
Studies of thermospheric neutral winds utilizing ground-based optical and radar measurements p 2613 N95-29214
Topics in high-peak intensity, ultrashort pulse laser-plasma interactions p 2704 N95-29216
Research and development of a high performance GaAs microcomputer system
[AD-A292647] p 2643 N95-29381
The role of the coherence function in holographic imaging p 2583 N95-29508
High-latitude electrodynamics: Electromagnetic energy dissipation and neutral wind feedback effects p 2616 N95-29696
A study of boundary layer aerosol and wind profiles using incoherent Doppler lidar p 2622 N95-29697
MINNESOTA UNIV., MINNEAPOLIS, MN.
Improving problem-solving and decision-making skills under stress: Prediction and training
[AD-A292104] p 2638 N95-28918
Studies in drag reduction p 2487 N95-29094
Experiments on microbursts p 2620 N95-29110
Coupling of brain muscarinic receptors to second messengers
[AD-A290498] p 2635 N95-29153
Three problems in fluid dynamics
[AD-A290481] p 2573 N95-29324
Dynamics of simple chemically reactive fluids p 2573 N95-29335
Recent progress in the study of the kinetics of sol-gel SiO2 synthesis reactions
[AD-A290570] p 2544 N95-29551
Cage-like precursor formation from extensive cyclization in sol-gel inorganic condensation polymerization
[AD-A290589] p 2544 N95-29554
17O NMR of the structural evolution of V2O5 gels
[AD-A290623] p 2545 N95-29559
Turbulent coupling of the magnetosphere-ionosphere through shear-mode Alfven waves p 2615 N95-29687
MISSION RESEARCH CORP., SANTA BARBARA, CA.
Stochastic modeling and global warming trend extraction for ocean acoustic travel times
[AD-A292114] p 2608 N95-28922
MISSISSIPPI STATE UNIV., MISSISSIPPI STATE, MS.
The National Grid Project: A system overview p 2482 N95-28749
Geometry modeling and grid generation using 3D NURBS control volume p 2483 N95-28753
Non-coincident multi-wavelength emission absorption spectroscopy
[DE95-006480] p 2530 N95-28776
Development of Laser Optogalvanic Spectroscopy as a probe of alkali atoms in an MHD environment
[DE95-006481] p 2531 N95-28916
Conversion of an oceanographic expert system to a C-based language
[NASA-CR-198695] p 2630 N95-29237
MISSISSIPPI UNIV., UNIVERSITY, MS.
Physical acoustics summer school, 1994. volume 1. transcript
[AD-A292552] p 2683 N95-28973
Finite difference analysis of a cylindrical two conductor microstrip transmission line with truncated dielectrics
[AD-A292592] p 2555 N95-29290
Proceedings of the Sixth International Symposium on Long-Range Sound Propagation
[AD-A290920] p 2685 N95-30084
MISSOURI UNIV., COLUMBIA, MO.
The redox chemistry of some peroxo and superoxo metal ion complexes
[AD-A290761] p 2532 N95-29483
Raman and photo-modulated reflectivity studies of ZnTe/InAs semiconductor heterostructure under hydrostatic pressure
[AD-A290467] p 2716 N95-29506
Maize yield estimation through the simulation of radiation penetration into the canopy p 2599 N95-29703
MISSOURI UNIV., KANSAS CITY, MO.
SAM1-A new semiempirical method including d-orbitals
[AD-A290903] p 2694 N95-30060
Guidance, navigation, and control study for a solar electric propulsion spacecraft
[NASA-CR-198920] p 2509 N95-30357
MISSOURI UNIV., ROLLA, MO.
Consideration of microstructural changes in the study of adiabatic shear bands
[AD-A290398] p 2715 N95-29234
Robust algorithms for penetration mechanics problems
[AD-A290650] p 2650 N95-29517
Analysis of adiabatic shear bands in thermoviscoplastic materials under combined loading
[AD-A290666] p 2596 N95-29582
MISSOURI UNIV., SAINT LOUIS, MO.
The 6th Van der Ziel symposium on quantum 1/f noise and other low frequency fluctuations in electronic devices
[AD-A292468] p 2718 N95-29009
MODERN TECHNOLOGIES CORP., MIDDLEBURG HEIGHTS, OH.
The decay of longitudinal vortices shed from airfoil vortex generators
[NASA-CR-198356] p 2489 N95-29402
MONTANA STATE UNIV., BOZEMAN, MT.
Tunable laser for persistent spectral hole burning optical memories
[AD-A292598] p 2586 N95-29292
Changes in microstructural parameters of snow during deformation
[AD-A290887] p 2601 N95-29866

N

NAGAOKA TECHNOLOGICAL UNIV. (JAPAN).
Screening constants for plasma
[AD-B179442L] p 2710 N95-29843
NAGOYA UNIV., NAGOYA (JAPAN).
Effective emission and ionization rate coefficients of atomic carbons in plasmas
[AD-B175932L] p 2707 N95-29740
NASA CENTER FOR AEROSPACE INFORMATION, LINTHICUM HEIGHTS, MD.
CD-ROM preparation: An overview and guide
[NASA-CR-198756] p 2655 N95-30307
NATIONAL ACADEMY OF SCIENCES - NATIONAL RESEARCH COUNCIL, WASHINGTON, DC.
Orbital debris: A technical assessment
[NASA-CR-198639] p 2507 N95-28852
NATIONAL AERONAUTICS AND SPACE ADMINISTRATION, WASHINGTON, DC.
NASA: The state of the agency
[NASA-TM-110563] p 2720 N95-29170
An announcement by Dan Goldin
[NASA-TM-110739] p 2720 N95-29171
High resolution microwave survey
[NASA-TM-110566] p 2553 N95-29174
NASA to use telepresence to explore Antarctic Lakes
[NASA-TM-110567] p 2598 N95-29175
Aerospace medicine and biology: A continuing bibliography with indexes (supplement 403)
[NASA-SP-7011(403)] p 2636 N95-29190
Space astronomy update
[NASA-TM-110754] p 2731 N95-30317
NATIONAL AERONAUTICS AND SPACE ADMINISTRATION. AMES RESEARCH CENTER, MOFFETT FIELD, CA.
Experiment kits for processing biological samples inflight on SLS-2
[NASA-TM-4685] p 2642 N95-28722
Application of CFD in aeronautics at NASA Ames Research Center p 2478 N95-28728
Grid related issues for static and dynamic geometry problems using systems of overset structured grids p 2480 N95-28737
Development and application of a 3D Cartesian grid Euler method p 2481 N95-28740
Emerging CFD technologies and aerospace vehicle design p 2482 N95-28746
A 3DGRAPE/AL: The Ames/Langley technology upgrade p 2482 N95-28750
A procedure for automating CFD simulations of an inlet-bleed problem p 2485 N95-28768
Investigation of wing upper surface flow-field disturbance due to NASA DC-8-72 in-flight inboard thrust-reverser deployment
[NASA-TM-110351] p 2477 N95-28816
An inflight refill unit for replenishing research animal drinking water
[NASA-TM-4684] p 2642 N95-28818
Bibliography of Doctor Chul Park
[NASA-TM-110353] p 2503 N95-29351
Pioneer Venus 12.5 km Anomaly Workshop Report, volume 1
[NASA-CP-3303] p 2737 N95-30058
Computational aeroacoustics using hyperbolic wave primitives p 2686 N95-30136
A compact solution to computational acoustics p 2686 N95-30138
Boundary-layer transition and global skin friction measurement with an oil-fringe imaging technique
[NASA-CR-198814] p 2579 N95-30224
Numerical simulations of the flow in the HYPULSE expansion tube
[NASA-TM-110357] p 2503 N95-30228
Telepresence media resource tape
[NASA-TM-110648] p 2655 N95-30248
NATIONAL AERONAUTICS AND SPACE ADMINISTRATION. GODDARD SPACE FLIGHT CENTER, GREENBELT, MD.
Carrier-less, anti-backlash planetary drive system
[NASA-CASE-GSC-13608-1] p 2588 N95-28702
Collected software engineering papers, volume 12
[NASA-CR-189409] p 2644 N95-28713
An overview of the Software Engineering Laboratory
[NASA-CR-189410] p 2644 N95-28714
Annotated bibliography of software engineering laboratory literature
[NASA-CR-189406] p 2644 N95-28805
Software measurement guidebook
[NASA-CR-189407] p 2644 N95-28806
Impact of Ada and object-oriented design in the flight dynamics division at Goddard Space Flight Center
[NASA-CR-189412] p 2644 N95-28807
C style guide
[NASA-CR-189408] p 2645 N95-28821
The 1994 research and technology report at the Goddard Space Flight Center
[NASA-TM-110623] p 2740 N95-28882
Total solar eclipse of 1997 March 9
[NASA-RP-1173] p 2731 N95-30004

SeaWiFS technical report series. Volume 24: SeaWiFS technical report series cumulative index, volumes 1-23
[NASA-TM-104556] p 2631 N95-30236
Effect of KOH concentration and anions on the performance of Ni-H2 battery positive plate
p 2567 N95-30260

NATIONAL AERONAUTICS AND SPACE ADMINISTRATION. JOHN F. KENNEDY SPACE CENTER, COCOA BEACH, FL.

Research and technology: 1994 annual report of the John F. Kennedy Space Center
[NASA-TM-110143] p 2740 N95-28786
Precision cleaning verification of fluid components by air/water impingement and total carbon analysis
[NASA-TM-110742] p 2531 N95-29248
Effect of irradiance, sucrose, and CO2 concentration on the growth of potato (Solanum tuberosum L.) in vitro
[NASA-TM-110654] p 2632 N95-29375

NATIONAL AERONAUTICS AND SPACE ADMINISTRATION. LYNDON B. JOHNSON SPACE CENTER, HOUSTON, TX.

STS-67 mission highlights resource tape
[NASA-TM-110530] p 2504 N95-28715
Apollo 11: For all mankind
[NASA-TM-110622] p 2503 N95-29407
Method for the calculation of spacecraft umbra and penumbra shadow terminator points
[NASA-TP-3547] p 2671 N95-29446
The JSC research and development annual report 1993
[NASA-TM-104787] p 2740 N95-29816
STS-71 Shuttle/Mir flight: Day 1
[NASA-TM-110744] p 2505 N95-29954
STS-71 Shuttle/Mir flight: Day 2
[NASA-TM-110745] p 2505 N95-29955
STS-71 Shuttle/Mir flight: Day 3
[NASA-TM-110746] p 2505 N95-29956
STS-71 Shuttle/Mir flight: Day 4
[NASA-TM-110747] p 2505 N95-29957
STS-71 Shuttle/Mir flight: Day 5
[NASA-TM-110748] p 2505 N95-29958
STS-71 Shuttle/Mir flight: Day 6
[NASA-TM-110749] p 2505 N95-29959
STS-71 Shuttle/Mir flight: Day 7
[NASA-TM-110750] p 2505 N95-29960
STS-71 Shuttle/Mir flight: Day 8
[NASA-TM-110751] p 2505 N95-29961
STS-71 Shuttle/Mir flight: Day 9
[NASA-TM-110752] p 2506 N95-29962
STS-71 Shuttle/Mir flight: Day 10
[NASA-TM-110753] p 2506 N95-29963
Lunar/Mars exploration for synthesis group
[NASA-TM-110647] p 2737 N95-30249
Apollo 14: Shepard hitting golf ball on Moon
[NASA-TM-110638] p 2737 N95-30318

NATIONAL AERONAUTICS AND SPACE ADMINISTRATION. LANGLEY RESEARCH CENTER, HAMPTON, VA.

Compendium of NASA data base for the global tropospheric experiment's Transport and Atmospheric Chemistry Near the Equator-Atlantic (TRACE-A)
[NASA-TM-110151] p 2608 N95-28717
Geometry Laboratory (GEOLAB) surface modeling and grid generation technology and services
p 2479 N95-28729
Rapid Airplane Parametric Input Design (RAPID)
p 2479 N95-28730
Algorithms for high aspect ratio oriented triangulations
p 2479 N95-28731
Block-structured grids for complex aerodynamic configurations: Current status p 2480 N95-28736
An unstructured-grid software system for solving complex aerodynamic problems p 2481 N95-28743
Multilevel elliptic smoothing of large three-dimensional grids p 2485 N95-28765
An efficiency study of the simultaneous analysis and design of structures
[NASA-TM-110168] p 2495 N95-28820
Third NASA Advanced Composites Technology Conference, volume 1, part 2
[NASA-CP-3178-VOL-1-PT-2] p 2513 N95-28823
Mechanical characterization of two thermoplastic composites fabricated by automated tow placement
p 2515 N95-28834
Tension fracture of laminates for transport fuselage. Part 2: Large notches p 2515 N95-28837
Design and evaluation of a foam-filled hat-stiffened panel concept for aircraft primary structural applications
p 2499 N95-28841
A study of structurally efficient graphite-thermoplastic trapezoidal-corrugation sandwich and semi-sandwich panels p 2516 N95-28842
Effects of cutouts on the behavior of symmetric composite laminates subjected to bending and twisting loads p 2517 N95-28844
Buckling analysis of curved composite sandwich panels subjected to inplane loadings p 2517 N95-28845
Technology integration box beam failure study
p 2517 N95-28847
A global/local analysis method for treating details in structural design p 2517 N95-28848
NASA/DOD Aerospace Knowledge Diffusion Research Project. Paper 49: Becoming an aerospace engineer: A cross-gender comparison
[NASA-TM-110731] p 2721 N95-29028
Third NASA Advanced Composites Technology Conference, volume 1, part 1
[NASA-CP-3178-VOL-1-PT-1] p 2518 N95-29029
Advanced composites technology program
p 2519 N95-29032
Weavability of dry polymer powder towpreg
p 2519 N95-29036
Effects of temperature and humidity cycling on the strengths of textile reinforced carbon/epoxy composite materials p 2520 N95-29037
Mechanical characterization of 2D, 2D stitched, and 3D braided/RTM materials p 2520 N95-29038
Performance of resin transfer molded multiaxial warp knit composites p 2520 N95-29039
The effects of aircraft fuel and fluids on the strength properties of Resin Transfer Molded (RTM) composites
p 2522 N95-29047
Robust control of nonlinear flexible multibody systems using quaternion feedback and dissipative compensation
[NASA-TM-109099] p 2507 N95-29377
An extension of the Lighthill theory of jet noise to encompass refraction and shielding
[NASA-TM-110163] p 2684 N95-29452
A hybrid electronically scanned pressure module for cryogenic environments
[NASA-TM-110146] p 2583 N95-29453
Transport delays associated with NASA Langley Flight Simulation Facility
[NASA-TM-110150] p 2659 N95-29454
Defining the IEEE-854 floating-point standard in PVS
[NASA-TM-110167] p 2659 N95-29823
Simplified data reduction methods for the ECT test for mode 3 interlaminar fracture toughness
[NASA-TM-110176] p 2527 N95-29825
Analytical investigation of the hygrothermal effects and parametric study of the Edge Crack Torsion (ECT) mode 3 test lay-ups
[NASA-TM-110183] p 2528 N95-30028
Hydrogen film cooling with incident and swept-shock interactions in a Mach 6.4 nitrogen free stream
[NASA-TM-4603] p 2578 N95-30056
ICASE/LaRC Workshop on Benchmark Problems in Computational Aeroacoustics (CAA)
[NASA-CP-3300] p 2686 N95-30133
Application of essentially nonoscillatory methods to aeroacoustic flow problems p 2686 N95-30135
Second-order numerical solution of time-dependent, first-order hyperbolic equations p 2674 N95-30143
Nonlinear wave propagation using three different finite difference schemes (category 2 application)
p 2582 N95-30151
Low-speed wind-tunnel investigation of the stability and control characteristics of a series of flying wings with sweep angles of 50 deg
[NASA-TM-4640] p 2498 N95-30226
Coarsening strategies for unstructured multigrid techniques with application to anisotropic problems
[NASA-CR-198154] p 2674 N95-30227
Emissivity measurements in thin metallized membrane reflectors used for microwave radiometer sensors
[NASA-TM-110179] p 2506 N95-30251
A conceptual thermal design study of an electronically scanned thinned array radiometer
[NASA-TM-110173] p 2509 N95-30316
Manual for a workstation-based generic flight simulation program (LaRCsim), version 1.4
[NASA-TM-110164] p 2502 N95-30327
Dielectric property measurements in the Electromagnetic Properties Measurement Laboratory
[NASA-TM-110147] p 2560 N95-30336
Parameterized spectral distributions for meson production in proton-proton collisions
[NASA-TM-4675] p 2696 N95-30337
Impact damage resistance and residual property assessment of (0/+/-45/90)s SCS-6/Timetal 21S
[NASA-TM-110178] p 2529 N95-30340
Formulation of an improved smeared stiffener theory for buckling analysis of grid-stiffened composite panels
[NASA-TM-110162] p 2529 N95-30341

NATIONAL AERONAUTICS AND SPACE ADMINISTRATION. LEWIS RESEARCH CENTER, CLEVELAND, OH.

Macrosegregation and nucleation in undercooled Pb-Sn alloys
[NASA-TM-102023-REV] p 2535 N95-28701
Influence of turbulence parameters, Reynolds number, and body shape on stagnation-region heat transfer
[NASA-TP-3487] p 2568 N95-28719
Surface Modeling, Grid Generation, and Related Issues in Computational Fluid Dynamic (CFD) Solutions
[NASA-CP-3291] p 2478 N95-28723
Surface modeling and grid generation for aeropropulsion CFD p 2479 N95-23732
A Cartesian, cell-based approach for adaptively-refined solutions of the Euler and Navier-Stokes equations
p 2480 N95-28739
Advanced methodology for simulation of complex flows using structured grid systems p 2485 N95-28766
A combined geometric approach for computational fluid dynamics on dynamic grids p 2485 N95-28770
IPACS (Integrated Probabilistic Assessment of Composite Structures): Code development and applications p 2518 N95-28849
Experimental results of Hooper's gravity-electromagnetic coupling concept
[NASA-TM-106963] p 2680 N95-28893
EMI Shields made from intercalated graphite composites
[NASA-TM-106979] p 2518 N95-28906
Influence of tooth profile modification on spur gear dynamic tooth strain
[NASA-TM-106952] p 2589 N95-29112
Demonstration of a stabilized alumina/ethanol colloidal dispersion technique for seeding high temperature air flows
[NASA-TM-106945] p 2582 N95-29113
Leading edge film cooling effects on turbine blade heat transfer
[NASA-TM-106955] p 2500 N95-29115
Grid orthogonality effects on predicted turbine midspan heat transfer and performance
[NASA-TM-106931] p 2574 N95-29371
Application of the space-time conservation element and solution element method to two-dimensional advection-diffusion problems
[NASA-TM-106946] p 2574 N95-29372
A simulation technique for predicting thickness of thermal sprayed coatings
[NASA-TM-106939] p 2512 N95-29373
Acoustic scattering from ellipses by the modal element method
[NASA-TM-106935] p 2683 N95-29401
Prediction of pressurant mass requirements for axisymmetric liquid hydrogen tanks
[NASA-TM-106973] p 2511 N95-29642
Summary Report of mission acceleration measurements for STS-66. Launched November 3, 1994
[NASA-TM-106914] p 2509 N95-29643
Three-dimensional simulation of traveling-wave tube cold-test characteristics using MAFIA
[NASA-TP-3513] p 2566 N95-29998
Inlet flow test calibration for a small axial compressor rig. Part 2: CFD compared with experimental results
[NASA-TM-106999] p 2501 N95-30007
High-temperature optical window design
[NASA-TM-106783] p 2596 N95-30008
Test results of a 20 GHz, low noise downconverter for USAT applications
[NASA-TM-106892] p 2508 N95-30011
Analysis of shadowing effects on spacecraft power systems
[NASA-TM-106994] p 2511 N95-30012
Use of the PARC code to estimate the off-design transonic performance of an over/under turboramjet nozzle
[NASA-TM-106924] p 2491 N95-30091
Results of two new methods for aeroacoustics benchmark problems p 2687 N95-30140
Application of a new finite difference algorithm for computational aeroacoustics p 2689 N95-30155
Category 5 problem solution using an unstructured finite volume algorithm p 2657 N95-30157
Numerical simulations of small amplitude acoustic wave propagation in a converging-diverging nozzle
p 2690 N95-30160
Evaluation of numerical schemes for the analysis of sound generation by blade-gust interaction
p 2690 N95-30163
Laser doppler velocimeter system for subsonic jet mixer nozzle testing at the NASA Lewis Aeroacoustic Propulsion Lab
[NASA-TM-106984] p 2477 N95-30229
Grid resolution and turbulent inflow boundary condition recommendations for NPARC calculations
[NASA-TM-106959] p 2492 N95-30253
Space Electrochemical Research and Technology. Abstracts
[NASA-CP-10172] p 2604 N95-30255
Development of a micro-fiber nickel electrode for nickel-hydrogen cell p 2567 N95-30256

High performance nickel electrodes for space power applications p 2511 N95-30257
Bending properties of nickel electrodes for nickel-hydrogen batteries p 2567 N95-30259
Summary report of mission acceleration measurements for STS-65, launched 8 July 1994
[NASA-TM-106871] p 2549 N95-30339

NATIONAL AERONAUTICS AND SPACE ADMINISTRATION. MARSHALL SPACE FLIGHT CENTER, HUNTSVILLE, AL.

Test load verification through strain data analysis
[NASA-TP-3558] p 2504 N95-28718
A conceptual design for the attitude control and determination system for the Magnetosphere Imager spacecraft
[NASA-TP-3560] p 2507 N95-28721
Marshall Space Flight Center surface modeling and grid generation applications p 2480 N95-28733
Probability of detection of defects in coatings with electronic shearography
[NASA-TM-108493] p 2524 N95-29374
ANSYS duplicate finite-element checker routine
[NASA-TM-108492] p 2672 N95-29824
International Space University
[NASA-TM-110646] p 2720 N95-30223
Analysis of stress concentration in the Dutton groove regions of the Super Lightweight External Tank
[NASA-TM-108490] p 2597 N95-30328
Composite processing development to improve interlaminar strength using ply interface particles
[NASA-TM-108495] p 2529 N95-30334
On the azimuthal variation of the equatorial plasmapause
[NASA-CR-198929] p 2711 N95-30338

NATIONAL AEROSPACE LAB., AMSTERDAM (NETHERLANDS).

Elliptic surface grid generation on minimal and parmetrized surfaces p 2484 N95-28760
Demonstration of an automated CFD system for three-dimensional flow simulations p 2485 N95-28767

NATIONAL BIOMEDICAL RESEARCH FOUNDATION, WASHINGTON, DC.

Georgetown Institute for Cognitive and Computational Sciences
[AD-A289775] p 2639 N95-29458

NATIONAL CENTER FOR ATMOSPHERIC RESEARCH, BOULDER, CO.

Interaction of acoustic oscillations with magnetic flux tubes in the solar photosphere
[PB95-201810] p 2739 N95-30199

NATIONAL GEOPHYSICAL DATA CENTER, BOULDER, CO.

Solar-geophysical data number 605, January 1995. Part 2 (comprehensive reports): Data for July 1994 and miscellaneous
[PB95-190997] p 2737 N95-28780
Solar-geophysical data number 605, January 1995. Part 1 (prompt reports): Data for December, November 1994 and late data
[PB95-191003] p 2737 N95-28781

NATIONAL INST. FOR FUSION SCIENCE, NAGOYA (JAPAN).

Development of an intense negative hydrogen ion source with a wide-range of external magnetic filter field
[AD-B195514L] p 2705 N95-29567
Anomalous transport theory for toroidal helical plasmas
[AD-B192000L] p 2706 N95-29731
Self-sustained magnetic braiding in toroidal plasmas
[AD-B191996L] p 2706 N95-29734
HIDENEK: An implicit particle simulation of kinetic-MHD phenomena in three-dimensional plasmas
[AD-B176255L] p 2707 N95-29739
Comment on a mean field Ohm's law for collisionless plasmas
[AD-B176252L] p 2707 N95-29741
Transition of radial electric field by electron cyclotron heating in the stellarator plasmas
[AD-B176254L] p 2707 N95-29742
Free-boundary equilibrium studies for the Large Helical Device
[AD-B175931L] p 2707 N95-29743
Prandtl number of toroidal plasmas
[AD-B179181L] p 2707 N95-29744
Theoretical study of cylindrical energy analyzers for MeV range heavy ion beam probes
[AD-B17200L] p 2707 N95-29745
Modelling of transport phenomena
[AD-B179223L] p 2708 N95-29747
Monte Carlo simulation study of the ICRF minority heating in the large helical device
[AD-B179858L] p 2708 N95-29749
Intermittent energy bursts and recurrent topological change of a twisting magnetic flux tube
[AD-B195513L] p 2708 N95-29755
Dynamical model of pressure-gradient-driven turbulence and shear flow generation in L-H transition
[AD-B195511L] p 2709 N95-29789
Experimental study on scaling law of outgassing rate with a pumping parameter
[AD-B191999L] p 2709 N95-29801
Formation of positive radial electric field by Electron Cyclotron Heating in Compact Helical System
[AD-B191994L] p 2709 N95-29802
Boronization study for application to large helical device
[AD-B191996L] p 2709 N95-29808
Theory of pseudo-classical confinement and transmutation to L-mode
[AD-B175957L] p 2709 N95-29809
Collisionless driven magnetic reconnection
[AD-B178946L] p 2709 N95-29810
Carbon sheet pumping
[AD-B179443L] p 2710 N95-29812
The origin of collisionless dissipation in magnetic reconnection
[AD-B178949L] p 2710 N95-29813
Hydrogen production in fusion reactors
[AD-B180028L] p 2710 N95-29857
Lecture note on the bases of plasma physics
[NIFS-PROC-15] p 2711 N95-29966
Innovative divertor concepts for LHD
[AD-B191997L] p 2711 N95-30032
Averaged resistive MHD equations
[AD-B178947L] p 2711 N95-30033

NATIONAL RENEWABLE ENERGY LAB., GOLDEN, CO.

Experimental investigation of aerodynamic devices for wind turbine rotational speed control, phase 1
[DE95-004034] p 2603 N95-30016
US photovoltaic patents: 1991-1993
[DE95-004051] p 2603 N95-30017
Solar heating and you
[DE95-004012] p 2603 N95-30127

NATO DEFENCE RESEARCH GROUP, BRUSSELS (BELGIUM).

COADE: A framework for cognitive analysis, design, and evaluation
[AD-A291282] p 2720 N95-29935

NAVAL AIR WARFARE CENTER, CHINA LAKE, CA.

Multilayer piecewise linear networks. Revision 1
[AD-A289885] p 2658 N95-28955
Electrically small archimedian spiral method of moment analysis
[AD-A291171] p 2558 N95-29928

NAVAL AIR WARFARE CENTER, POINT MUGU, CA.

Tidal and lunar data for Point Mugu, San Nicolas Island, and the Barking Sands area during 1995
[AD-A289877] p 2733 N95-29599

NAVAL AIR WARFARE CENTER, WARMINSTER, PA.

Task-dependent effects of automation: The role of internal models in performance, workload, and situational awareness in a semi-automated cockpit
[AD-A292538] p 2640 N95-28969
Current issues in the measurement of military aircrew performance: A consideration of the relationship between available metrics and operational concerns
[AD-A292539] p 2640 N95-28970
Evaluation of proposed agility metrics using X-31 vs. F/A-18 flight data
[AD-A292573] p 2496 N95-28977

NAVAL AIR WEAPONS STATION, CHINA LAKE, CA.

Coso monitoring program
[AD-A290604] p 2627 N95-30048

NAVAL BIODYNAMICS LAB., NEW ORLEANS, LA.

Operating procedures for Anthropometry and Initial Conditions Photogrammetric Program
[AD-A291553] p 2640 N95-28935

NAVAL COMMAND, CONTROL AND OCEAN SURVEILLANCE CENTER, SAN DIEGO, CA.

Analysis of historical oceanographic data on a minicomputer: Program WAHOO
[AD-A292530] p 2629 N95-28873
A simple method for range finding via laser triangulation
[AD-A292529] p 2553 N95-29166
Improved operator awareness of teleoperated land vehicle attitude
[AD-A290443] p 2641 N95-29359
Development of an artificial neural network for real-time classification of cone penetrometer strain gauge data
[AD-A290719] p 2664 N95-29499
Compact substrate heater for use in an oxidizing atmosphere
[AD-A290860] p 2502 N95-29522
Neural network construction using evolutionary search
[AD-A290862] p 2665 N95-29831

NAVAL FACILITIES ENGINEERING SERVICE CENTER, PORT HUENEME, CA.

Cathodic protection system inspection 6
[AD-A289720] p 2591 N95-28682
Cathodic protection system inspection 5
[AD-A289724] p 2592 N95-28684
Liquid pressure amplification and liquid injection in air conditioning and refrigeration systems
[AD-A289738] p 2549 N95-28686
Geothermal heat pumps for heating and cooling
[AD-A292115] p 2602 N95-28858

NAVAL HEALTH RESEARCH CENTER, SAN DIEGO, CA.

WinCD: Complex demodulation time-series analysis for windows
[AD-A291550] p 2645 N95-28934
Effects of chromium picolinate on body composition in a remedial conditioning program
[AD-A292079] p 2636 N95-29238
Adaptations to three weeks of aerobic/anaerobic training in west coast U.S: Navy Sea-Air-Land personnel (SEAL's)
[AD-A291500] p 2637 N95-29846
The effect of bright light and LEET on sleep after a 10-hour phase delay
[AD-A291264] p 2637 N95-29995
Sleep during SEAL Delivery Vehicle (SDV)/Dry dock shelter exercises analyzed by a graphic approach
[AD-A290916] p 2637 N95-30083

NAVAL POSTGRADUATE SCHOOL, MONTEREY, CA.

Design and analysis of the launch vehicle adapter fitting for the petite amateur navy satellite (PANSAT)
[AD-A289693] p 2504 N95-28680
A procedure for accessing digital satellites containing amateur payloads
[AD-A289748] p 2506 N95-28688
Analysis of the naval postgraduate school computer network architecture
[AD-A289749] p 2657 N95-28689
A ground support electronic interface for the ionospheric spectroscopy and atmospheric chemistry (ISAAC) ultraviolet spectrograph
[AD-A289761] p 2611 N95-28693
Analysis of multigrid techniques for system modeling with toeplitz approximation
[AD-A289784] p 2644 N95-28694
A layman's look at orbital debris
[AD-A289801] p 2506 N95-28700
Design, development and testing of a prototype precision angular positioning control system for a next generation multiplexed imager
[AD-A292585] p 2698 N95-28980
A numerical study of the effects of wind forcing on the Chile Current System
[AD-A289808] p 2629 N95-28982
NPSNETIV: An object-oriented interface for a three-dimensional virtual world
[AD-A292467] p 2646 N95-29008
Modeling studies of the Leeuwin current off western and southern Australia
[AD-A290158] p 2629 N95-29023
Airy functions and the recursive ray acoustics algorithm
[AD-A290182] p 2629 N95-29054
Visualization of improved target acquisition algorithm for Janus (A)
[AD-A290191] p 2646 N95-29056
Thickness measurement of ammonia targets used in SLAC e143 experiment
[AD-A290215] p 2692 N95-29076
The 10th Annual Review of Progress in Applied Computational Electromagnetics, volume 1
[AD-A286796] p 2553 N95-29159
Correlation of inclusion size and chemistry with weld metal composition and microstructure arc weldments of high strength steels
[AD-A292024] p 2590 N95-29184
Acoustic imaging of ultrasonic wave propagation
[AD-A290390] p 2683 N95-29232
Numerical modeling of opto-electronic integrated circuits
[AD-A292096] p 2563 N95-29239
The measurement of adhesion at film-substrate interfaces using a constant depth scratch test
[AD-A289940] p 2542 N95-29269
Vortex element analysis of selected time-dependent flows
[AD-A289944] p 2573 N95-29271
Methods of generating low redundancy direction finding array configurations
[AD-A292590] p 2555 N95-29289
The (in)complete compendium of computational curiosities: Givens' rotations
[AD-A292050] p 2648 N95-29304
Applied Computational Electromagnetics Society Journal, volume 10, number 1, March 1995
[AD-A292069] p 2555 N95-29308
Radar cross section synthesis for planar resistive surfaces
[AD-A290151] p 2555 N95-29318

A friendly editing environment for computer-sided rapid prototyping of hard real-time systems
[AD-A290154] p 2648 N95-29321
Feature extraction from digital communications signals using wavelet transforms
[AD-A292655] p 2556 N95-29386
Spacecraft attitude control system performance using pulse-width pulse-frequency modulated thrusters
[AD-A291803] p 2508 N95-29410
An analysis of the impact of ASPA on organizational and depot level maintenance
[AD-A292670] p 2477 N95-29414
Continental aerosol effects on stratocumulus microphysics during MAST 1994
[AD-A292674] p 2621 N95-29416
Compressibility effects on and control of dynamic stall of oscillating airfoil
[AD-A291804] p 2489 N95-29428
Software testing toolkit for distributed simulations
[AD-A291867] p 2649 N95-29435
Applications of digital video and synthetic environments to unmanned aerial vehicles
[AD-A291875] p 2497 N95-29437
The design of programmable convolutional encoder using VHDL and an FPGA
[AD-A290048] p 2649 N95-29442
Design and evaluation of a LQR controller for the bluebird unmanned air vehicle
[AD-A289769] p 2498 N95-29457
High resolution direct digitization and optical telemetry of shipboard antenna signals
[AD-A290238] p 2557 N95-29504
Automatically combining changes to software systems
[AD-A290628] p 2650 N95-29515
The 10th Annual Review of Progress in Applied Computational Electromagnetics, volume 2
[AD-A286799] p 2558 N95-29904
An operational comparison of the CH-46E and HH-60H as Navy combat support helicopter replacement options using the Simulated Mobility Modeling and Analysis Toolbox (SMMAT)
[AD-A288494] p 2498 N95-29911

NAVAL RESEARCH LAB., BAY SAINT LOUIS, MS.
A comprehensive analysis of Navy and Marine corps digital mapping, charting, and geodesy requirements for modeling and simulation
[AD-A291601] p 2598 N95-28931
Hindcasting changes in thermal structure and acoustic transmission loss in the upper ocean on short time scales with data from MILE and from ocean weather station papa
[AD-A292419] p 2629 N95-28991
Finite difference ocean acoustic model users guide
[AD-A291544] p 2631 N95-29856
A bibliography, with abstracts and annotations, of publications on and related to underwater acoustic fluctuations
[AD-A291342] p 2685 N95-29945
Digital mapping, charting, and geodesy analysis program technical review of vector smart map prototypes 1 and 2
[AD-A291217] p 2601 N95-29977

NAVAL RESEARCH LAB., MONTEREY, CA.
Quality Control of meteorological observations at Fleet Numerical Meteorology and Oceanography Center
[AD-A291577] p 2619 N95-28938
A regression model for the western north pacific tropical cyclone intensity forecast
[AD-A290588] p 2627 N95-30044

NAVAL RESEARCH LAB., WASHINGTON, DC.
Analysis of tropospheric propagation characteristics based on regional meteorological data
[AD-A291581] p 2552 N95-28939
Nanoscience and nanotechnology in Europe
[AD-A290214] p 2562 N95-29075
Comparison study of unequal error protection methods for one-dimensional signal constellations
[AD-A290386] p 2554 N95-29231
Theory of competition between synchronous and nonsynchronous modes in a magnicon output cavity
[AD-A292048] p 2563 N95-29301
The generalized railroad crossing: A case study in formal verification of real-time systems
[AD-A290152] p 2648 N95-29319
Yohkoh Bragg Crystal Spectrometer light curves for Ca 29(3.1633 - 3.1933 A): 1 October 1993 - 30 September 1994
[AD-A290027] p 2736 N95-29327
GENAH user's guide and reference manual version 1.0
[AD-A290236] p 2583 N95-29470
Observation of x ray generation in a proof-of-principle laser synchrotron source experiment
[AD-A291298] p 2588 N95-29937

NAVAL SURFACE WARFARE CENTER, BETHESDA, MD.
Sorption and diffusion of moisture in multilayer composite AEM/S sandwich materials
[AD-A289807] p 2518 N95-28951
The effects of alloying elements on the strength and cooling rate sensitivity of ultra-low carbon alloy steel weld metals
[AD-A290681] p 2537 N95-29759
175Hp contrarotating homopolar motor design report
[AD-A291138] p 2567 N95-30122

NAVAL SURFACE WARFARE CENTER, DAHLGREN, VA.
Proceedings of the Complex Systems Engineering Synthesis and Assessment Technology Workshop (CSESAW 1994)
[AD-A292433] p 2646 N95-28995
Nonlinear calibration of an infrared radiometer
[AD-A292436] p 2698 N95-28996
The 1995 version of the NSWC aeroprediction code. Part 1: Summary of new theoretical methodology
[AD-A291518] p 2490 N95-29853

NAVAL SURFACE WARFARE CENTER, PANAMA CITY, FL.
Complete analysis of electrode-terminated cables in two-layer conductor bounded above by air: Current density, magnetic field, and magnetic field gradient
[AD-A290907] p 2566 N95-30079

NAVAL SURFACE WARFARE CENTER, SILVER SPRING, MD.
Use of finite element analysis for transient moisture diffusion studies in multilayer composite AEM/S system sandwich materials
[AD-A291092] p 2527 N95-29638

NAVAL UNDERSEA WARFARE CENTER, NEW LONDON, CT.
Adaptive block sequential detection of abrupt signal changes
[AD-A290456] p 2557 N95-29489

NEBRASKA UNIV., LINCOLN, NE.
Drift mobility measurements in thin film boron carbide
[AD-A292510] p 2712 N95-28869
A full wave study of radar cross sections of rough terrain
[AD-A291227] p 2559 N95-29982

NEW HAMPSHIRE UNIV., DURHAM, NH.
The structure of water mass, salt, and temperature transports within intermediate depths of the western tropical Atlantic Ocean p 2631 N95-29541

NEW MEXICO STATE UNIV., LAS CRUCES, NM.
Modeling joint effects of mixtures of chemicals on microorganisms using quantitative structure activity relationship techniques, phase 3
[AD-A290153] p 2632 N95-29320
The (HMI9293) acquisition of a 200 MHz nuclear magnetic resonance spectrometer
[AD-A291913] p 2583 N95-29361
Comparison of boundary-layer wind and temperature measurements with model estimations
[AD-A290471] p 2621 N95-29507

NEW MEXICO UNIV., ALBUQUERQUE, NM.
HBCU/MI instrumentation for the Pulsed Power Plasma Sciences Laboratory at the University of New Mexico, FY92-93
[AD-A292444] p 2703 N95-29003
Characterization of excited state oxygen-organic molecule complexes
[AD-A290548] p 2692 N95-29092

NEW ORLEANS UNIV., LA.
Computational investigation of the stabilities of some N, O, F ions
[AD-A292305] p 2691 N95-28868
Molecular dynamics simulation of liquid nitromethane shocked to 143 kbar
[AD-A292107] p 2691 N95-28919
Analysis of factors affecting chemical reactions in supercritical fluids
[AD-A290905] p 2534 N95-30078

NEW YORK STATE COLL. OF CERAMICS, ALFRED, NY.
Bilateral US/Russia Workshop on Self-Propagating High-Temperature Synthesis held in Honolulu, Hawaii on 6-7 November 1993
[AD-A290466] p 2525 N95-29492

NOBEYEMA SOLAR RADIO OBSERVATORY (JAPAN).
Nobeyama Radio Observatory report, no. 378: The polar ring spiral galaxy NGC 660 p 2731 N95-29097
Nobeyama Radio Observatory report, no. 361: The radio properties of solar active region soft x-ray transient brightenings p 2737 N95-29098
Nobeyama Radio Observatory report, no. 381: Parallel connected twin SIS junctions for millimeter and submillimeter wave mixers: Analysis and experimental verification p 2562 N95-29099
Nobeyama Radio Observatory report, no. 382: The mass of a star formed in a cloud core: Theory and its application to the Orion A cloud p 2731 N95-29100
Nobeyama Radio Observatory report, no. 380: Detection of the (29)SiO v=1, J=1-0 maser from TX Camelopardalis p 2726 N95-29101
Nobeyama Radio Observatory report, no. 379 p 2735 N95-29636

NONVOLATILE ELECTRONICS, INC., EDINA, MN.
Low cost writable RFID tag with MRAM memory
[AD-A292553] p 2642 N95-28974

NORFOLK STATE UNIV., VA.
Proceedings of the 12th Annual National Conference on Ada Technology
[AD-A290693] p 2651 N95-29644

NORTH CAROLINA AGRICULTURAL AND TECHNICAL STATE UNIV., GREENSBORO, NC.
High gain, low noise and broadband Raman and Brillouin fiber-optic amplifiers, channel selectors and switches
[AD-A290585] p 2700 N95-29553

NORTH CAROLINA STATE UNIV., RALEIGH, NC.
Nitride semiconductors for ultraviolet detection
[AD-A289546] p 2712 N95-28910
Interface properties of wide bandgap semiconductor structures
[AD-A289817] p 2713 N95-28954
Motion planning and sensory processing in a dynamic environment
[AD-A290504] p 2722 N95-29154
Design of a fast-tool servo system using magnetic servo levitation
[AD-A290273] p 2663 N95-29183
Short term visits for collaborative research
[AD-A290704] p 2682 N95-29588
The interactive role of clouds and radiative transfer in maintaining atmospheric circulation p 2616 N95-29699
Integrated synthesis and post-processing of SiC and AlN
[AD-A290853] p 2537 N95-29724

NORTH CAROLINA UNIV., CHAPEL HILL, NC.
International Workshop on Stochastic Filtering Theory
[AD-A291670] p 2661 N95-28788
Numerical studies of ablative mass loss from wind accelerated clouds p 2622 N95-29676

NORTH CAROLINA UNIV., RALEIGH, NC.
Systems of hyperbolic partial differential equations
[AD-A290287] p 2669 N95-29083

NORTH DAKOTA STATE UNIV., FARGO, ND.
Power measurement and current feedback in a resonant DC link inverter
[AD-A292518] p 2563 N95-29164

NORTHEASTERN UNIV., BOSTON, MA.
Object oriented segmentation of images
[AD-A290792] p 2671 N95-29485

NORTHROP CORP., HAWTHORNE, CA.
A weight-efficient design strategy for cutouts in composite transport structures p 2516 N95-28843

NORTHWESTERN UNIV., EVANSTON, IL.
Structural and electronic properties of adsorbates on semiconductors, metal-semiconductor interfaces and semiconductor heterojunctions
[AD-A291917] p 2715 N95-29438
Finite element technology for penetration problems
[AD-A290644] p 2671 N95-29516

NOTRE DAME UNIV., IN.
The effects of three-dimensional imposed disturbances on bluff body near wake flows: Effects of taper and splitter plates on the near wake characteristics of a circular cylinder in uniform and shear flow
[AD-A292113] p 2487 N95-28921
The pressure field of a gust interacting with a flat plate p 2582 N95-30161

NYMA, INC., BROOK PARK, OH.
A transient model of the RL10A-3-3A rocket engine
[NASA-CR-195478] p 2510 N95-29114
Users manual for the improved NASA Lewis ice accretion code LEWICE 1.6
[NASA-CR-198355] p 2492 N95-29132
A PC program for estimating measurement uncertainty for aeronautics test instrumentation
[NASA-CR-198361] p 2503 N95-30067

O

OAK RIDGE INST. FOR SCIENCE AND EDUCATION, TN.
Summary report for cooperative research and development agreement between Oak Ridge Associated Universities and Interactive Presentation Systems
[DE95-006874] p 2644 N95-28777

OAK RIDGE K-25 SITE, TN.
Engineering Design Information System (EDIS), Information Management Services (IMS), Index Function, User's manual: Revision 1
[DE95-009538] p 2725 N95-30194

OAK RIDGE NATIONAL LAB., TN.
Molten fluoride fuel salt chemistry
[DE95-007025] p 2695 N95-28957
XPS study of Ni-Fe manganite thermistor material
[DE95-008778] p 2561 N95-28961
The international fusion materials irradiation facility
[DE95-006536] p 2696 N95-29142
Remote maintenance challenges presented in the ITER engineering design
[DE95-006392] p 2710 N95-29909
Magnetic fusion commercial power plants
[DE95-007027] p 2711 N95-30023
Introduction to the proceedings of the sixteenth symposium on biotechnology for fuels and chemicals
[DE95-007029] p 2549 N95-30024
Processing and properties of extruded tungsten-hafnium and tungsten-steel composites
[DE95-007371] p 2528 N95-30037
Analytical electron microscopy of precipitates in ion-implanted MgAl2O4 spinel
[DE95-007406] p 2538 N95-30038
ALLIANCE: An architecture for fault tolerant multi-robot cooperation
[DE95-008658] p 2666 N95-30112
The morphology of blends of linear and branched polyethylenes in solid state by SANS
[DE95-008675] p 2535 N95-30113
Nanoindentation and nanoscratching of hard coating materials for magnetic disks
[DE95-008776] p 2547 N95-30174
Elevated temperature static fatigue of a Nicalon fiber-reinforced SiC composite
[DE95-008780] p 2528 N95-30175
Influence of dislocation-solute interactions on the mechanical properties of zirconium-doped NiAl
[DE95-008848] p 2538 N95-30179
Simulation of robot manipulators
[DE95-008880] p 2654 N95-30189
Depth-independent hardness improvements in ion irradiated polystyrene
[DE95-008882] p 2547 N95-30190
Interactions between energy efficiency and emission trading under the 1990 Clean Air Act Amendments
[DE95-008649] p 2611 N95-30212
Tensile properties of as-cast iron-aluminide alloys
[DE95-005396] p 2538 N95-30216

OFFICE OF NAVAL RESEARCH, ARLINGTON, VA.
System and method for rapidly tracking vehicles of special utility in low signal-to-noise environments
[AD-D017378] p 2683 N95-28783
Epoxy pipelining composition and method of manufacture
[AD-D017380] p 2539 N95-28784
External combustion engine having an asymmetrical CAM
[AD-D017382] p 2588 N95-28785
An electrical and fiber-optic connector
[AD-D017404] p 2589 N95-28791
Selective attachment of nucleic acid molecules to patterned self-assembled surfaces
[AD-D017379] p 2530 N95-28854
The fluorescent detection of hydrazine, monomethylhydrazine, and 1,1-dimethylhydrazine by derivalization with aromatic dicarboxaldehydes
[NAVY-CASE-75451] p 2512 N95-29052
Cable load transducer
[AD-A289548] p 2595 N95-29192
Epoxy self-priming topcoats
[AD-D017383] p 2541 N95-29194
Laser optics protective device
[AD-D017384] p 2585 N95-29217
Adjustable two-axis instrument mount
[AD-D017393] p 2582 N95-29220
A method and apparatus for signal filtering
[AD-D017268] p 2554 N95-29236
Interband lateral resonant tunneling transistor
[AD-D017399] p 2564 N95-29568
High temperature thermosets and ceramics derived from linear carborane-(siloxane or silane)-acetylene copolymers
[AD-D017400] p 2545 N95-29569
Adaptive Infinite Impulse Response (IIR) filter system
[AD-D017403] p 2564 N95-29570
Inflatable life vest
[AD-D017273] p 2641 N95-29600
Variable rate optical iterative processing of optical information
[AD-D017397] p 2701 N95-29602

OHIO AEROSPACE INST., CLEVELAND, OH.
Evaluation of high order schemes for nonlinear wave computations p 2582 N95-30149

OHIO STATE UNIV., COLUMBUS, OH.
On-line damage identification and motion control of adaptive structures: An intelligent control approach p 2662 N95-29109
Theories of the nonlinear optical properties of composite media: Applications to phthalocyanine dyes
[AD-A290640] p 2700 N95-29560
A numerical study of the small scale wing-body junction problem p 2491 N95-30235

OHIO UNIV., ATHENS, OH.
An investigation into the use of satellite-based positioning systems for flight reference/autoland operations p 2494 N95-29542

OKLAHOMA STATE UNIV., STILLWATER, OK.
Sensor protection portion of the development of nonlinear optical materials and processes for laser hardening of sensors
[AD-A291200] p 2702 N95-29973

OKLAHOMA UNIV., NORMAN, OK.
On the topological complexity of the cost function in variational data assimilation p 2724 N95-29798
Numerical simulation of the genesis of tornado-like vortices p 2625 N95-29806

OLD DOMINION UNIV., NORFOLK, VA.
Large deviation limit theorems, with applications
[AD-A290392] p 2669 N95-29233
Application of low dissipation and dispersion Runge-Kutta schemes to benchmark problems in computational aeroacoustics p 2687 N95-30139

OPTICAL CONCEPTS, INC., LOMPOC, CA.
Vertical cavity surface emitting lasers for optical signal processing and optical computing applications
[AD-A290626] p 2588 N95-30050

OPTICAL SOCIETY OF AMERICA, WASHINGTON, DC.
Summaries of papers presented at the ultrafast phenomena topical meeting
[AD-A290998] p 2564 N95-29511
Laser applications to chemical analysis: Summaries of papers presented at the laser applications to chemical analysis topical meeting
[AD-A290738] p 2587 N95-29653
Diffractive optics: Design, fabrication, and applications
[AD-A290942] p 2702 N95-29867

OREGON GRADUATE INST. OF SCIENCE AND TECHNOLOGY, BEAVERTON, OR.
Software Design for Reliability and Reuse proof of concept project. Phase 1
[AD-A291690] p 2644 N95-28782
Path resolved optical sensing of atmospheric winds utilizing speckle-turbulence interaction and pseudorandum code modulation
[AD-A290800] p 2621 N95-29497

OREGON GRADUATE INST. OF SCIENCE AND TECHNOLOGY, PORTLAND, OR.
Low temperature materials growth and processing development for flat panel display technology applications
[AD-A292177] p 2715 N95-29267

OREGON STATE UNIV., CORVALLIS, OR.
The spatial-scale dependence of the observed anisotropy of reflected and emitted radiation p 2613 N95-29253
Hot electron physics of alternating-current thin-film electroluminescent devices
[AD-A290528] p 2696 N95-29495
Numerical modeling of synoptic scale ocean dynamics
[AD-A291411] p 2631 N95-30069

OREGON UNIV., EUGENE, OR.
Experimental studies of fundamental one- and two-photon lasing processes
[AD-A290593] p 2693 N95-29555

OSAKA UNIV., SUITA (JAPAN).
Effects of impurities released from high Z test limiter on plasma performance in TEXTOR
[AD-B191995L] p 2709 N95-29803

OSLO UNIV. (NORWAY).
Eurasian seismic surveillance - 2D FD seismic synthetics and event discrimination
[AD-A292659] p 2614 N95-29413

P

PACIFIC NORTHWEST LAB., RICHLAND, WA.
Measurement of the seasonal and annual variability of total column aerosol in a northeastern US network
[DE95-007259] p 2608 N95-28920
The TEES process cleans waste and produces energy
[DE95-007799] p 2602 N95-29463

PDA ENGINEERING, COSTA MESA, CA.
Thermoreactive aircraft coatings (TRAC) program
[AD-A292054] p 2542 N95-29314

PENNSYLVANIA STATE UNIV., UNIVERSITY PARK, PA.
Formation of striped surface phases by short-range forces
[AD-A279962] p 2531 N95-28945
Activities update
[AD-A292431] p 2692 N95-28994
Prediction of hydrogen entry and permeation in metals and alloys
[AD-A292047] p 2536 N95-29298
Time-optimal multi-axis attitude maneuvers of rigid spacecraft using collocation and nonlinear programming p 2507 N95-29332
Surface studies of Poly(organophosphazenes) containing dimethylsiloxane grafts
[AD-A291909] p 2543 N95-29355
The synthesis of liquid crystalline phophazenes containing chiral mesogens
[AD-A291911] p 2543 N95-29358
Proceedings of the 6th International Conference on Nondestructive Characterization of Materials
[AD-A290727] p 2596 N95-29580
Models of accretion-powered x-ray pulsars p 2728 N95-29667
Energy budget in the Asian monsoon region p 2623 N95-29713
Neural network-based decision support for incomplete databases p 2665 N95-29720
A theoretical model of multiple regimes in a stratocumulus-topped boundary layer p 2624 N95-29726
Observations of mesoscale cellular convection from the marine stratocumulus phase of FIRE p 2624 N95-29727
Experimental research on crossing shock wave boundary layer interactions
[AD-A290764] p 2577 N95-29920
The effect of turbulence on vaporization and mixing in fuel sprays
[AD-A291347] p 2577 N95-29948
Development and testing of improved techniques for modeling the hydrologic cycle in a mesoscale weather prediction system
[AD-A291243] p 2627 N95-29993
Reliability enhancement of Navier-Stokes codes through convergence acceleration
[NASA-CR-196635] p 2578 N95-30034
Lattice gas methods for computational aeroacoustics p 2687 N95-30144
Application of traditional CFD methods to nonlinear computational aeroacoustics problems p 2688 N95-30148
Time accurate application of the MacCormack 2-4 scheme on massively parallel computers p 2661 N95-30150
Wave propagation and scattering in computational aeroacoustics p 2689 N95-30152
Computational aeroacoustics on massively parallel computers p 2661 N95-30156
Extended field observations of cirrus clouds using a ground-based cloud observing system
[NASA-CR-198855] p 2628 N95-30356

PENNSYLVANIA UNIV., PHILADELPHIA, PA.
Efficient compilation of high-level data parallel algorithms
[AD-A290362] p 2659 N95-29225

PENNSYLVANIA UNIV. MEDICAL CENTER, PHILADELPHIA, PA.
CO2-O2 interactions in extension of tolerance to acute hypoxia
[NASA-CR-198575] p 2635 N95-29158

PHILLIPS LAB., EDWARDS AFB, CA.
High temperature spectroscopy of alkali metal vapors for solar to thermal energy conversion
[AD-A291355] p 2602 N95-29949

PHILLIPS LAB., KIRTLAND AFB, NM.
Investigation of the Paschen curve of nitrogen via the application of nanosecond pulsed electromagnetic radiation
[AD-A290129] p 2586 N95-29425

PHYSICAL OPTICS CORP., TORRANCE, CA.
Low threshold all-optical crossbar switch on GaAs-GaAlAs channel waveguide arrays
[AD-A292483] p 2712 N95-28862
Fourier Synthesis Lithographic Machine for large panel display fabrication
[AD-A291921] p 2698 N95-28914

PITTSBURGH UNIV., PITTSBURGH, PA.
Discontinuous solutions of semilinear differential-algebraic equations. part 2: Rho-consistency
[AD-A292285] p 2668 N95-28861
Discontinuous solutions of semilinear differential-algebraic equations. part 1: Distribution solutions
[AD-A292286] p 2668 N95-28863
Organization of the human circadian system
[AD-A286223] p 2634 N95-28915

POINTWISE, INC., BEDFORD, TX.
Automatic structured grid generation using Gridgen (some restrictions apply) p 2483 N95-28751

POLYTECHNIC UNIV., FARMINGDALE, NY.
Research instrumentation for polytechnic university's supersonic wind tunnel facility
[AD-A290232] p 2502 N95-29468
PRATT AND WHITNEY AIRCRAFT, EAST HARTFORD, CT.
Grid generation: A view from the trenches
p 2478 N95-28727
Geometric grid generation p 2483 N95-28756
PRINCESS ALEXANDRA HOSPITAL, SWINDON (ENGLAND).
A generic specification for Special Purpose Aeromedical Equipment p 2499 N95-29623
PRINCETON UNIV., NJ.
Prospects and expectations for unstructured methods
p 2481 N95-28742
The physics of spin polarized gases
[AD-A292511] p 2680 N95-28810
Optimal control of molecular motion
[AD-A291919] p 2691 N95-28944
Sensitivity of stress and boundary imperfection of dielectric resonator disks
[AD-A290488] p 2594 N95-29150
Surfactant-enhanced in situ biodegradation of strongly sorbing organic substances in soil environments
[AD-A290253] p 2512 N95-29168
Sensitivity of the simulated global climate to perturbations in low cloud microphysical properties
p 2620 N95-29206
Parameter study of the statistically steady state of a multi-layer quasi-geostrophic model
p 2612 N95-29212
Retrieval display and analysis support tool requirements analysis
[AD-A291448] p 2599 N95-29523
Quantum dynamical studies of the decomposition of energetic materials containing defect structures
[AD-A291456] p 2548 N95-29525
Applications of pulsar timing p 2734 N95-29675
Coherent soft x-ray generation using a powerful subpicosecond laser p 2587 N95-29689
Effect of Reynolds number on the structure of turbulent boundary layers p 2575 N95-29719
Microwave remote sensing of surface soil moisture and its application to hydrologic modeling
p 2600 N95-29821
Computational algorithms for aerodynamic analysis and design
[AD-A291084] p 2491 N95-29972
Workshop on computing and intelligent systems
[AD-A290581] p 2666 N95-30040
Distributed queries and incremental updates in information retrieval systems p 2725 N95-30286
PROGRAM DEVELOPMENT CORP., WHITE PLAINS, NY.
Multiblock grid generation with automatic zoning
p 2480 N95-28735
Examples of grid generation with implicitly specified surfaces using GridPro (TM)/az3000. 1: Filleted multi-tube configurations p 2486 N95-28772
Interactive high quality grid generation
p 2486 N95-28774
PUERTO RICO UNIV., MAYAGUEZ.
Pulsed laser deposition of thin film material for nonlinear waveguides
[AD-A290789] p 2544 N95-29484
PURDUE UNIV., WEST LAFAYETTE, IN.
Modal interactions and complex responses in weaklyNONLINEAR MULTI-DEGREE-OF-FREEDOM MECHANICAL SYSTEMS
[AD-A292023] p 2594 N95-28853
Linear and nonlinear discrete-time state-space modeling of dynamic systems for control applications
p 2663 N95-29251
Super hydrides
[AD-A290594] p 2533 N95-29556
High velocity impact and penetration of thick composite laminates
[AD-A290642] p 2526 N95-29561
HTMIAC/CINDAS silicon properties database. User's guide
[AD-A292602] p 2533 N95-29575
Radiative cooling profiles calculated from ECMWF analyses and ISCCP C1 data, and their application to determination of distributions of apparent convective heating in the equatorial Pacific p 2625 N95-29805
An air-sea interaction model for stress, sensible heat, latent heat, and sea state, applicable to the full range of wind speeds p 2626 N95-29876
A unified matrix inequality approach to linear control design p 2667 N95-30234

R

RADEX, INC., BEDFORD, MA.
FFT space processing for the ACF of SPREE particle flux measurements
[AD-A290166] p 2507 N95-29026
RADIX SYSTEMS, INC., ROCKVILLE, MD.
Two-dimensional signal processing for regional seismic event identification
[AD-A292601] p 2613 N95-29293
RAND CORP., SANTA MONICA, CA.
Defense Modeling and Simulation Office information/data base technology working group (I/DBTWG) meetings
[AD-A290953] p 2651 N95-29735
SEMINT: Seamless model integration
[AD-A290956] p 2651 N95-29736
RDP, INC., WALTHAM, MA.
Data re-formatter program for the topside thermal plasma monitor (PLIESPP)
[AD-A290960] p 2616 N95-29737
The topside ionospheric plasma monitor (SSIES, SSIES-2 and SSIES-3) on the spacecraft of the Defense Meteorological Satellite Program (DMSP), user's guide. Volume 3: Program maintenance manual
[AD-A290941] p 2617 N95-29765
SETA/ADS software development
[AD-A291181] p 2651 N95-29932
The topside ionospheric plasma monitor (SSIES, SSIES-2 and SSIES-3) on the spacecraft of the Defense Meteorological Satellite Program (DMSP), user's guide. Volume 2: Programmer's guide for software at AFSFC
[AD-A290913] p 2618 N95-30082
RENSSELAER POLYTECHNIC INST., TROY, NY.
The 1.3 micrometer fiber photodetector
[AD-A292462] p 2582 N95-29004
High-toughness glass-ceramics
[AD-A290562] p 2541 N95-29071
Scalable software tools for adaptive scientific computation
[AD-A290446] p 2650 N95-29480
Load balancing for the parallel adaptive solution of partial differential equations
[AD-A290450] p 2671 N95-29488
Parallel adaptive techniques for transient partial differential equations
[AD-A290460] p 2674 N95-29490
Dust formation in stellar outflows: A time-dependent model p 2733 N95-29649
Photonic band structures for optoelectronics
[AD-A291154] p 2718 N95-30298
RGB ASSOCIATES, INC., WAYLAND, MA.
Unconventional image recovery techniques
[AD-A290799] p 2701 N95-29646
RHODE ISLAND UNIV., KINGSTON, RI.
Gordon research conference on physical metallurgy: Materials by design
[AD-A290519] p 2524 N95-29326
ROCHESTER UNIV., NY.
Quasioptical Josephson Oscillator
[AD-A292481] p 2561 N95-28859
Optically triggered, superconducting opening switch
[AD-A292642] p 2700 N95-29379
Reference frames in vision
[AD-A290117] p 2639 N95-29422
Inertial fusion program and national laser users facility program
[DE95-008202] p 2711 N95-30274
ROCKWELL INTERNATIONAL CORP., CANOGA PARK, CA.
Automation of three-dimensional structured mesh generation for turbomachinery blade passages
p 2484 N95-28762
Inorganic halogen oxidizers
[AD-A290747] p 2533 N95-29581
Inorganic halogen oxidizers
[AD-A291201] p 2702 N95-29974
ROCKWELL INTERNATIONAL CORP., HUNTSVILLE, AL.
Photon-counting spatial light modulator technology development
[AD-A292619] p 2699 N95-29295
ROCKWELL INTERNATIONAL CORP., SEAL BEACH, CA.
Grid generation on trimmed Bezier and NURBS quilted surfaces p 2483 N95-28755
ROCKWELL INTERNATIONAL SCIENCE CENTER, THOUSAND OAKS, CA.
An engineering model of woven composites based on micromechanics p 2521 N95-29042
ROLAND HOUSE, ARLINGTON, VA.
Hernandez Engineering: NASA
[NASA-CR-197665] p 2508 N95-29633
ROME LAB., GRIFFISS AFB, NY.
Statistical properties of bistatic clutter echoes
[AD-A291688] p 2552 N95-28943
N4 processor
[AD-A292571] p 2642 N95-28976
Advanced presort process
[AD-A291010] p 2557 N95-29655
ROYAL NETHERLANDS AIR FORCE, THE HAGUE (NETHERLANDS).
Civil military co-operation: A ten year experience of an affiliative aeromedical evacuation programme of the Netherlands Armed Forces and a civilian repatriation organization p 2676 N95-29608
Aeromedical evacuation by RNLAF - work according to protocol p 2676 N95-29609
ROYAL NORWEGIAN INST. OF AVIATION MEDICINE, OSLO (NORWAY).
The impact of occupational cultures on coordination of emergency medical service crew p 2677 N95-29616
RUTGERS - THE STATE UNIV., NEW BRUNSWICK, NJ.
Intelligent automated surface grid generation
p 2484 N95-28758
The search for mass segregation in star clusters of the Magellanic Clouds p 2730 N95-29781
RUTGERS - THE STATE UNIV., PISCATAWAY, NJ.
Ferroelectric polarization mechanism of the odd-numbered nylons
[AD-A292276] p 2539 N95-28860
High field electrostrictive response of polymers
[AD-A292298] p 2539 N95-28864
Ferroelectric and piezoelectric properties of nylon 11/Poly(Vinylidene fluoride) bilaminate films
[AD-A292274] p 2539 N95-28891
RUTHERFORD APPLETON LAB., OXFORD (ENGLAND).
Photoproduction of hybrid mesons from CEBAF to HERA
[PB95-196218] p 2691 N95-28913

S

SANDIA NATIONAL LABS., ALBUQUERQUE, NM.
Self-stressing structures for wafer-level oxide breakdown to 200 MHz
[DE95-006818] p 2714 N95-29157
Electronic states in Cd(1-x)Zn(x)Te/CdTe strained layer coupled double quantum wells and their photoluminescence
[DE95-006806] p 2716 N95-29814
Encryption and networking applications
[DE95-009587] p 2651 N95-29871
Interfaces in InAsSb/InGaAs strained-layer superlattices grown by MOCVD for use in infrared emitters
[DE95-006323] p 2717 N95-29990
Ordering and bandgap reduction in InAs(1-x)Sb(x) alloys
[DE95-006324] p 2717 N95-30005
Auger rates in mid-IR InAsSb laser structures
[DE95-006325] p 2588 N95-30006
Ion beam modification of Tl-Ba-Ca-Cu-O type high temperature superconductors during irradiation
[DE95-006807] p 2717 N95-30022
Distributed multitasking ITS with PVM
[DE95-006821] p 2660 N95-30116
Patch diameter limits for tiered subaperture SAR image formation algorithms
[DE95-008816] p 2560 N95-30177
Simulation of powder metal fabrication with high pressure gas atomization
[DE95-008820] p 2538 N95-30178
A CMOS-compatible, surface-micromachined pressure sensor for aqueous ultrasonic application
[DE95-008538] p 2567 N95-30188
Passive damping to enhance active positioning of a prototype lithography platen
[DE95-008539] p 2655 N95-30209
Health monitoring of operational structures: Initial results
[DE95-008551] p 2597 N95-30210
Fatigue case study and reliability analyses for wind turbines
[DE95-004770] p 2603 N95-30213
Defect centers in chemical-mechanical polished MOS oxides
[DE95-004777] p 2718 N95-30214
High-efficiency solar cells using HEM silicon
[DE95-005424] p 2604 N95-30217
SANDIA NATIONAL LABS., LIVERMORE, CA.
Measurement of ultrashort pulses with a non-instantaneous nonlinearity
[DE95-006500] p 2698 N95-28983
SCHOFIELD (ANDREW N.) AND ASSOCIATES LTD., CAMBRIDGE (ENGLAND).
Coordination of operations for centrifuge quality control. phase 3C
[AD-A292533] p 2582 N95-28966

SCHWARTZ ELECTRO-OPTICS, INC., CONCORD, MA.
ARPA solid state laser and nonlinear materials program
[AD-A289657] p 2584 N95-28678
SCIENCE AND TECHNOLOGY CORP., HAMPTON, VA.
Broadband Integrated Transmittances (BITS)
[AD-A292176] p 2555 N95-29266
SCIENCE APPLICATIONS INTERNATIONAL CORP., STOW, MA.
Electromagnetic antenna modeling (EAM) system
[AD-A292194] p 2552 N95-28986
SCRIPPS INSTITUTION OF OCEANOGRAPHY, LA JOLLA, CA.
Backscatter data acquisition for Hydrosweep DS aboard RV Ewing
[AD-A292332] p 2628 N95-28796
Multi-scale studies of seafloor topography
[AD-A292301] p 2628 N95-28865
Upgrading the Day/Night whole sky imager from Manual/Interactive to full automatic control
[AD-A292296] p 2619 N95-28872
Regional seismic event identification and improved locations with small arrays
[AD-A292188] p 2612 N95-28985
SEU-061, MADRID (SPAIN).
Experience in helicopter aeroevacuation in the community of Madrid, Spain p 2677 N95-29611
SILICON MOUNTAIN DESIGN, INC., COLORADO SPRINGS, CO.
An ultra-high speed incoherent-to-coherent converter for optical computing
[AD-A292658] p 2700 N95-29412
SOCIETY OF INSTRUMENT AND CONTROL ENGINEERS, TOKYO (JAPAN).
Proceedings of the 33d SICE (the Society of Instrument and Control Engineers) Annual Conference, part 1
[DE95-758947] p 2632 N95-28947
Proceeding of the 33rd SICE Annual Conference
[DE95-758943] p 2662 N95-29144
SOFTWARE AND ENGINEERING ASSOCIATES, INC., CARSON CITY, NV.
SCAP spray combustion analysis program
[AD-A289946] p 2532 N95-29273
SOFTWARE PRODUCTIVITY CONSORTIUM, HERNDON, VA.
Software Estimation Program (SWEEP) user manual
[AD-A291137] p 2654 N95-30121
SOUTH CAROLINA UNIV., COLUMBIA, SC.
Fiber optic Raman and micro Raman measurements of bonding agents at interface during the curing process
[AD-A292042] p 2523 N95-29189
SOUTHAMPTON UNIV. (ENGLAND).
Fibre-coupled remote optical vibrometry
[AD-A291606] p 2698 N95-28932
The one-dimensional bubble: Theory, experiment, and relevance to exposure of divers to low frequency sound, and of lung to lithotripsy
[ISVR-TR-246] p 2577 N95-29817
Fiber compatible acousto-optic modulator using a gradient index lens
[AD-A291164] p 2565 N95-29925
SOUTHERN METHODIST UNIV., DALLAS, TX.
Design, evaluation and construction of TEXESS and LUXESS, and research in mini-array technology and use of data from single stations and sparse networks
[AD-A292546] p 2612 N95-28972
SOUTHERN UNIV., BATON ROUGE, LA.
Computer simulation study of high t(sub c) superconductor structure
[AD-A292513] p 2563 N95-29163
SPACE RESEARCH ORGANIZATION NETHERLANDS, GRONINGEN (NETHERLANDS).
SiO maser survey of the IRAS bulge sources p 2735 N95-29837
Observational properties of SiO masers in the galactic bulge IRAS sources p 2735 N95-29838
Extended dust shells around carbon stars resolved by HIRAS p 2735 N95-29840
SPECTRAL SCIENCES, INC., BURLINGTON, MA.
Research into artificially induced atmospheric disturbances
[AD-A290150] p 2613 N95-29317
SPIRE CORP., BEDFORD, MA.
Ion doped quantum well lasers
[AD-A290937] p 2587 N95-29912
SPRINGER-VERLAG G.M.B.H. AND CO. K.G., NEW YORK, NY.
Methodologies for intelligent systems
[AD-A290901] p 2666 N95-30117
SRI INTERNATIONAL CORP., MENLO PARK, CA.
Molecular dynamics study of electromigration
[AD-A289811] p 2691 N95-28952
Characterizing and modeling penetration of ceramic armor
[AD-A292588] p 2542 N95-29288
High-performance speech recognition using consistency modeling
[AD-A290655] p 2557 N95-29564
High T(sub c) superconductor/ferroelectric heterostructures
[AD-A291016] p 2716 N95-29658
InTISb as a long-wave infrared (LWIR) material: Defects and transportation properties
[AD-A291218] p 2702 N95-29978
Alternative packet switch architectures for a 30/20 GHz FDMA/TDMA geostationary communication satellite network
[NASA-CR-195470] p 2506 N95-30090
STANFORD LINEAR ACCELERATOR CENTER, MENLO PARK, CA
GLAST
[DE95-008596] p 2739 N95-29265
STANFORD UNIV., CA.
Linewidth-insensitive coherent analog optical links
[AD-A292422] p 2698 N95-28992
Linear stability analysis of hypersonic boundary layers
[AD-A290159] p 2569 N95-29024
A new methodology for the numerical simulation of strain softening in inelastic solids
[AD-A290295] p 2594 N95-29063
Effect of nose shape and mass of the impactor on impact damage of laminated composites
[AD-A290351] p 2594 N95-29067
A study of fluid problems requiring a direct particle simulation
[AD-A290212] p 2658 N95-29074
Experiments in cooperative manipulation of objects by free-flying robot teams p 2662 N95-29095
Wide Area Differential GPS (WADGPS) p 2494 N95-29107
Composite material studies for low temperature thermionic emission
[AD-A292159] p 2523 N95-29124
Interaction of turbulence with complex shock waves
[AD-A290225] p 2571 N95-29145
Solution of the Navier-Stokes equations on locally refined Cartesian meshes using state-vector splitting p 2571 N95-29197
Tailored microstructures for broadband or selective detection of radiation from the visible to the infrared
[AD-A292097] p 2554 N95-29240
Numerical experiments on the flow past a circular cylinder at sub-critical Reynolds number
[AD-A289937] p 2573 N95-29268
Research in graph algorithms and combinatorial optimization
[AD-A292630] p 2648 N95-29297
An impact load identification method using distributed sensor measurements p 2595 N95-29419
Investigation of Burnett equations for two-dimensional hypersonic flow
[AD-A290233] p 2575 N95-29469
Simulation methodology
[AD-A290461] p 2674 N95-29491
Design and implementation of logical database languages
[AD-A290474] p 2650 N95-29509
First flight of the Multi-Spectral Solar Telescope Array: Calibration, results and future plans p 2727 N95-29529
Superplastic ceramics
[AD-A290817] p 2545 N95-29635
Research studies in electromagnetically induced transparency
[AD-A290796] p 2557 N95-29645
Speckle imaging with the multi-anode microchannel array detector p 2728 N95-29652
A gyroscope clock for a null gravitational redshift experiment p 2584 N95-29664
Gamma radiation from rotation powered pulsars and results from the Energetic Gamma-Ray Experiment Telescope p 2739 N95-29671
Linear matrix inequalities for the problem of absolute stability of control systems p 2501 N95-29680
Observational signatures of rotating black holes p 2729 N95-29709
Modeling the boundary layer interactions between weakly ionized plasmas and cooled, planar electrodes in stagnation-point flows p 2706 N95-29717
DC electrostatic gyro suspension system for the Gravity Probe B experiment p 2509 N95-29794
A method for the modelling of porous and solid wind tunnel walls in computational fluid dynamics codes p 2502 N95-29795
A model analysis of the spatial distribution and temporal trends of nitrous oxide sources and sinks p 2609 N95-29804
Theory and experiments on chemical instabilities
[AD-A290773] p 2534 N95-29922
Mathematical modeling and numerical simulation of the dynamics of flexible structures undergoing large overall motions
[AD-A291139] p 2597 N95-30123
Numerical solution of the equations governing non-Newtonian flow at moderate Reynolds numbers p 2579 N95-30233
Spin augmented deployment and retrieval of tethered artificial gravity spacecraft p 2509 N95-30280
Parallel adaptive finite element: Software for semiconductor device simulation
[AD-A291149] p 2661 N95-30295
STATE UNIV. OF NEW YORK, BUFFALO, NY.
Programmable materials and structures
[AD-A291807] p 2649 N95-29429
STATE UNIV. OF NEW YORK, STONY BROOK, NY.
Materials science and fabrication of YBCO-SrTi(1-x)Nb(x)O3-YBCO device structures
[AD-A292527] p 2712 N95-28815
A cluster beam study of boron, boron oxide and B(x)O(y)H chemistry with hydrogen fluoride
[AD-A290826] p 2533 N95-29722
STATISTICAL SIGNAL PROCESSING, INC., YOUNTVILLE, CA.
Cyclic feature analysis, design and exploitation
[AD-A290639] p 2557 N95-29603
STERLING SOFTWARE, INC., BELLEVUE, NE.
AFGWC dial-in subsystem (AFDIS) software users manual, version 3.1
[AD-A291103] p 2651 N95-29639
STOTTLER HENKE ASSOCIATES, INC., BELMONT, CA.
Artificial intelligence techniques for parts obsolescence prediction
[AD-A292185] p 2661 N95-28926
STRATHCLYDE UNIV., GLASGOW (SCOTLAND).
The 2nd European Conference on Smart Structures and Materials
[AD-A290723] p 2550 N95-29579
SUNDSTRAND AVIATION-ROCKFORD, IL.
In situ processing methods for composite fuselage sandwich structures p 2513 N95-28826
SYRACUSE UNIV., NY.
Rome laboratory software engineering cooperative virtual machine
[AD-A292396] p 2658 N95-28965
The identification of user criteria of relevance and document characteristics: Beyond the topical approach to information retrieval p 2723 N95-29518
A study of problematic situations and information needs of software managers in the United States and Japan p 2724 N95-29828
SYSTEMS RESEARCH LABS., INC., DAYTON, OH.
Generator of body data (GEBOD) manual
[AD-A289721] p 2640 N95-28683
Pulse waveform and pulse amplitude analysis during Lower Body Negative Pressure
[AD-A290521] p 2636 N95-29360

T

TECHNISCHE UNIV., DELFT (NETHERLANDS).
Digital control of distributed parameter systems: A state-space approach
[PB95-197216] p 2666 N95-30041
Gradient-dependent plasticity in numerical simulation of localization phenomena
[PB95-197257] p 2596 N95-30049
Modal analysis of straight and curved integrated optical waveguides: An integral equation approach
[PB95-197265] p 2702 N95-30054
Transformational design of a direction detector for the progressive scan conversion processor
[PB95-198487] p 2643 N95-30109
PREDICHAT: First order performance calculations of windturbine rotors using the method of the acceleration potential
[PB95-206454] p 2603 N95-30200
Impact properties of coated engineering plastics
[PB95-197281] p 2547 N95-30201
Multi-dimensional upwind discretization method for the Euler equations on unstructured grids
[PB95-197307] p 2578 N95-30202
Formation and properties of titanium disilicide: A study on the development of stress in Ti-Si thin films
[PB95-197315] p 2538 N95-30205
Elastoplastic buckling analysis of cylindrical shells using a semi-analytical formulation
[PB95-197349] p 2597 N95-30206
Framework for comparing and controlling number-based design reasoning systems
[PB95-197364] p 2667 N95-30207
A Pr-141 Moessbauer study of praseodymium com pounds
[PB95-192449] p 2535 N95-30282

Numerical simulation of mechanisms and manipulator robots with flexible links and flexible joints
[PB95-196903] p 2591 N95-30285
Decomposition of hypo-eutectoid iron carbon austenites
[PB95-196945] p 2538 N95-30287

TECHNISCHE UNIV., EINDHOVEN (NETHERLANDS).
UMTS network architecture
[PB95-206744] p 2558 N95-29919
Optimal hankel norm identification of dynamical systems
[PB95-197232] p 2672 N95-30046
Comparison of the local defect correction iteration and the fast adaptive composite grid iteration
[PB95-206769] p 2672 N95-30088
Fischer's protocol in timed process algebra
[PB95-206777] p 2672 N95-30089
Translation Invariant Operators on Lp-Type Spaces
[PB95-197117] p 2672 N95-30092
Theorem on the existence of solutions of quasi-static moving boundary problems
[PB95-197125] p 2673 N95-30093
Applicability of neural networks for production planning under uncertainty
[PB95-197406] p 2666 N95-30101
Process algebra with feedback
[PB95-206819] p 2673 N95-30106
Boyer-moore type algorithm for regular expression pattern matching
[PB95-198131] p 2654 N95-30107
Infinite divisibility and the waiting-time paradox
[PB95-206934] p 2666 N95-30167
H(sub 2) almost disturbance decoupling problem with internal stability
[PB95-206942] p 2667 N95-30168
Boundary element algorithms for Somigliana's identity
[PB95-206959] p 2597 N95-30169
Short and elementary proof of the main Bahadur-Kiefer theorem
[PB95-206967] p 2675 N95-30170
Factorization and input-output decoupling by static output feedback for nonlinear control systems
[PB95-206975] p 2667 N95-30171
Delayed choice: An operator for joining message sequence charts
[PB95-206710] p 2560 N95-30203
Spectral estimates for positive Rockland operators
[PB95-206751] p 2673 N95-30204
Description of the TV distribution service using MAGIC modelling methods
[PB95-206728] p 2560 N95-30219
Correctness of real-time systems by construction
[PB95-206827] p 2655 N95-30220
Precedence relation method for deriving flexible bound models for queueing systems
[PB95-206835] p 2667 N95-30221
Neural networks for combinatorial optimization
[PB95-206843] p 2667 N95-30222
H infinity control problem with zeros on the boundary of the stability domain
[PB95-197042] p 2668 N95-30288

TECHNISCHE UNIV., TWENTE (NETHERLANDS).
Description and manipulation of method fragments for the assembly of situational methods
[PB95-197133] p 2653 N95-30094
Static analysis of functional programs
[PB95-197141] p 2653 N95-30095
Performance evaluation of ATM cell scheduling policies using stochastic petri nets
[PB95-197158] p 2559 N95-30096
Efficient solution of a class of infinite stochastic petri nets: Theory and applications
[PB95-197166] p 2673 N95-30097
Fast simulation of the leaky bucket algorithm
[PB95-197174] p 2653 N95-30098
Checkpointing and the modeling of program execution time
[PB95-197182] p 2653 N95-30099
Causal behaviours and nets
[PB95-197612] p 2660 N95-30102
Proving the genericity lemma by leftmost reduction is simple
[PB95-197620] p 2673 N95-30103
Layers as knowledge transitions in the design of distributed systems
[PB95-197638] p 2660 N95-30104
Realisation of an integrated software engineering environment through heterogeneous CASE-tool integration
[PB95-197646] p 2653 N95-30105
Usability: Formalising (un)definedness in typed lambda calculus
[PB95-197190] p 2673 N95-30196
Enhancing the semantics of federated schemata by translating SQ1-queries into object methods
[PB95-197372] p 2725 N95-30208
Structured approach for the methodical and technical integration of heterogeneous CASE tools
[PB95-197653] p 2655 N95-30218
Essential structure of the jacopini technique
[PB95-197208] p 2674 N95-30291

TECHNOLOGY MANAGEMENT, INC., CLEVELAND, OH.
The TMI regenerable solid oxide fuel cell
p 2606 N95-30265

TEL-AVIV UNIV., RAMAT-AVIV, TEL-AVIV (ISRAEL).
Correlation and gradient characteristics of ionospheric parameters in europe
[AD-A292295] p 2612 N95-28871
Correlation and gradient characteristics of ionospheric parameters in Europe
[AD-A290135] p 2612 N95-29140

TENNESSEE STATE UNIV., NASHVILLE, TN.
Predicting polarized light scattering by marine micro-organism
[AD-A289790] p 2696 N95-28695
Predicting polarized light scattering by marine micro-organisms
[AD-A289796] p 2697 N95-28698

TENNESSEE UNIV., KNOXVILLE, TN.
Three dimensional effects in fiber reinforced composites under compression
[AD-A292027] p 2523 N95-29185

TENNESSEE UNIV. SPACE INST., TULLAHOMA, TN.
A numerical solution method for acoustic radiation from axisymmetric bodies p 2689 N95-30154

TEXAS A&M UNIV., COLLEGE STATION, TX.
Analysis of static contact in laminated composite plates using damage mechanics
[NASA-CR-198656] p 2513 N95-28809
A two element laminar flow airfoil optimized for cruise
[NASA-CR-198580] p 2489 N95-29338
Development of precipitated iron Fischer-Tropsch catalysts
[DE95-009334] p 2533 N95-29870
Robust testing of cellular neural networks
[AD-A291219] p 2665 N95-29979

TEXAS INSTRUMENTS, INC., DALLAS, TX.
Liquefied metal jet program Automation and Robotics Research Institute (ARRI)
[AD-A289781] p 2536 N95-29461

TEXAS STATE UNIV., AUSTIN, TX.
Phase coupling and morphology generation in engineering polymer alloys
[AD-A291868] p 2543 N95-29436

TEXAS UNIV., AUSTIN, TX.
Adaptive hybrid prismatic-tetrahedral grids for viscous flows p 2481 N95-28744
Nanofabrication of electronic devices with the scanning tunneling microscope
[AD-A292463] p 2561 N95-29005
The development of methods and techniques to detect and model the underlying structure of chaotic systems
[AD-A292435] p 2680 N95-29072
Physical causes of separation shock unsteadiness in shock wave/turbulent boundary layer interactions
p 2570 N95-29096
Unsteadiness of shock-induced turbulent boundary layer separation. An inherent feature of turbulent flow or solely a wind tunnel phenomenon
[AD-A290367] p 2572 N95-29228
Continuum spectra of supermassive accretion disks
p 2732 N95-29252
Substructure-based control of flexible structures
p 2508 N95-29408
Solid freeform fabrication symposium
[AD-A290949] p 2527 N95-29732
Toughening mechanisms in mixed-mode interfacial fracture p 2545 N95-29772
Robust fault detection filter design
p 2592 N95-29786
Heavy light bullets in electron-positron plasma
[DE95-008751] p 2711 N95-30173
Inclusive hadronic production of the B(sub c) meson via heavy quark fragmentation
[DE95-008739] p 2695 N95-30191

TEXAS UNIV., DALLAS, TX.
Characterization of the geometries of the high-latitude ionospheric convection pattern p 2614 N95-29524
Application of Poynting flux measurements to the determination of energy transfer rates in the high-latitude ionosphere p 2614 N95-29650

TEXAS UNIV. AT DALLAS, RICHARDSON, TX.
Spectral inverse scattering theory for dielectric media: Application to optical devices
[AD-A292651] p 2556 N95-29383
The high latitude ionospheric convection pattern during northward interplanetary magnetic field
p 2615 N95-29693
Development and application of fluorescent diagnostics to fundamental droplet and spray problems
[AD-A290553] p 2578 N95-30039

TEXAS UNIV. HEALTH SCIENCE CENTER, SAN ANTONIO, TX.
Cellular and molecular level responses after radiofrequency radiation exposure, alone or in combination with x rays or chemicals
[AD-A292488] p 2633 N95-28866

TEXTRON BELL HELICOPTER, FORT WORTH, TX.
Bell Helicopter Advanced Rotocraft Transmission (ART) program
[NASA-CR-195479] p 2590 N95-29538

TICA TECHNOLOGIES, INC., CAMBRIDGE, MA.
Optimizing cockpit display configurations with a genetic algorithm system
[AD-A289799] p 2499 N95-29123

TOKYO GAKUGEI UNIV., KOGANEI (JAPAN).
Aperture synthesis observation of HCN J = 1-0 emission from Y Canum Venaticorum p 2735 N95-29839

TOKYO UNIV. (JAPAN).
Yohkoh Soft X-ray Telescope
[NASA-CR-197655] p 2726 N95-29172
Transonic, supersonic and hypersonic wind-tunnel tests on aerodynamic characteristics of reentry body with blunted cone configuration
[ISAS-658] p 2490 N95-29640
Experimental studies on boundary-layer transition on a reentry vehicle at transonic and supersonic speeds
[ISAS-659] p 2575 N95-29712

TORONTO UNIV. (ONTARIO).
Hailstone heat and mass transfer measurements
[ISBN-0-315-86304-6] p 2624 N95-29797

TRISTAN TECHNOLOGIES, INC., SAN DIEGO, CA.
Five-channel SQUID based non-destructive evaluation (NDE) instrument
[AD-A292474] p 2592 N95-29012

TRW SYSTEMS GROUP, REDONDO BEACH, CA.
PSEE architecture report: Architectures and models for next generation process-based software engineering environments
[AD-A291268] p 2652 N95-29996

TSUKUBA UNIV. (JAPAN).
Interchange stability criteria for anisotropic central-cell plasmas in the tandem mirror GAMMA 10
[AD-B176253L] p 2707 N95-29738

TUFTS UNIV., MEDFORD, MA.
Stochastic hyperbolic and parabolic partial differential equations
[AD-A290372] p 2669 N95-29229
Quantum fluctuations and semiclassical gravity theory
p 2719 N95-29527

U

ULLEVAAL HOSPITAL, OSLO (NORWAY).
Effect of hypoxia on arterial blood gases in subjects with lung dysfunction p 2638 N95-29627

UNITED STATES AIR FORCES IN EUROPE, APO NEW YORK, NY.
Changes in the medevac mission result in an increased role for the flight surgeon p 2680 N95-29628

UNITED TECHNOLOGIES CORP., WINDSOR LOCKS, CT.
SPE(R)-OBOGS: On-board oxygen generating system
p 2606 N95-30267

UNITED TECHNOLOGIES RESEARCH CENTER, EAST HARTFORD, CT.
Automatic blocking for complex three-dimensional configurations p 2480 N95-28734
A technique for optimizing grid blocks
p 2485 N95-28789

UNIVERSIDAD NACIONAL AUTONOMA DE MEXICO, MEXICO CITY (MEXICO).
Calculation of shielding parameters
[DE95-608735] p 2694 N95-29886

UNIVERSITAIRE INSTELLING ANTWERPEN, WILRIJK (BELGIUM).
Formal aspects of object identity in database manipulation p 2722 N95-29116
Data modeling from a categorical perspective
p 2725 N95-30289

UNIVERSITY OF NORTH TEXAS, DENTON, TX.
Information management in local area networks: Impact on users' perceptions p 2723 N95-29690

UNIVERSITY OF SOUTHERN CALIFORNIA, LOS ANGELES, CA.
An extension of the continuum model by Grad's thirteen moment equations for hypersonic rarefied flows
p 2488 N95-29118

UNIVERSITY OF SOUTHERN CALIFORNIA, UNIVERSITY PARK, CA.
Chemically induced passivity of aluminum alloys and Al-based metal matrix composites
[AD-A290778] p 2528 N95-29923

UNIVERSITY OF SOUTHERN ILLINOIS, CARBONDALE, IL.
Preparation and studies of urazole containing polymers
[AD-A290685] p 2545 N95-29586
UNIVERSITY OF SOUTHERN MISSISSIPPI, BAY SAINT LOUIS, MS.
Glenda software design
[AD-A292537] p 2646 N95-28968
UNIVERSITY OF WESTERN ONTARIO, LONDON (ONTARIO).
Unsteady rotational shear flow of power law fluids
[ISBN-0-315-81287-7] p 2575 N95-29718
UTAH STATE UNIV., LOGAN, UT.
An investigation of thunderstorms as a source of short period mesospheric gravity waves
[AD-A289795] p 2611 N95-28697
A Monte Carlo simulation of Coulomb collisions and wave-particle interactions in space plasma at high latitudes p 2704 N95-29205
UTAH UNIV., SALT LAKE CITY, UT.
The effect of mixed mode precracking on the mode 1 fracture toughness of composite laminates p 2514 N95-28827
Master plot analysis of microcracking in graphite/epoxy and graphite/PEEK laminates p 2514 N95-28828
Alumina reinforced Tetragonal Zirconia (TZP) composites
[DE95-008990] p 2529 N95-30180

V

VAERLOESE AIR BASE, VAERLOESE (DENMARK).
Danish aeromedical evacuation efforts during the Gulf War p 2677 N95-29613
Flying ambulances: The approach of a small air force to long distance aeromedical evacuation of critically injured patients p 2678 N95-29618
VIGYAN RESEARCH ASSOCIATES, INC., HAMPTON, VA.
High-order essentially non-oscillatory methods for computational aeroacoustics p 2690 N95-30159
VIRGINIA POLYTECHNIC INST. AND STATE UNIV., BLACKSBURG, VA.
Analytical modeling and sensor monitoring for optimal processing of advanced textile structural composites by resin transfer molding p 2521 N95-29045
The development of an interpretive methodology for the application of real-time acousto-ultrasonic NDE technique for monitoring damage in ceramic composites under dynamic loads p 2592 N95-29104
Measuring variation in ecosystem sensitivity to stress
[AD-A290415] p 2609 N95-29450
Processing studies on in situ composites based on blends of thermotropic Liquid Crystalline Polymers with thermoplastics
[AD-A290526] p 2544 N95-29494
Fiber fracture in continuous-fiber reinforced composite materials during cyclic loading p 2525 N95-29513
A study of blister tests for film adhesion measurement and fracture efficiency of tests for adhesive bonds p 2545 N95-29799
VIRGINIA UNIV., CHARLOTTESVILLE, VA.
Severe edge effects and simple complimentary interior solutions for thin-walled anisotropic and composite structures
[AD-A290645] p 2595 N95-29562
The 12 UM contribution of nearby galaxies to the infrared background
[AD-A291185] p 2735 N95-29917

W

WASHINGTON STATE UNIV., PULLMAN, WA.
Interactions of spanwise and chordwise vorticity associated with three-dimensional dynamic stall over an oscillating wing
[AD-A290546] p 2487 N95-29091
WASHINGTON UNIV., SAINT LOUIS, MO.
(DEPSCOR-92) acquisition of a metallurgical optical microscope
[AD-A292439] p 2698 N95-28998
Nonlinear control systems
[AD-A291083] p 2665 N95-29971
WASHINGTON UNIV., SEATTLE, WA.
Automatic multi-block grid generation for high-lift configuration wings p 2485 N95-28764
Development of a transient internal probe diagnostic
[AD-A292470] p 2704 N95-29011
Revisions and notes on a model for bubble attenuation in near-surface propagation
[AD-A290312] p 2629 N95-29085
100 Hz-10 kHz bottom backscattering model: Generalized treatment of sediment sound propagation, sediment volume scattering and interface-roughness scattering
[AD-A291323] p 2685 N95-29942
Feasibility of a jet-stirred reactor for evaluating replacements for halon fire retardants
[AD-A291155] p 2551 N95-30299
WAYNE STATE UNIV., DETROIT, MI.
Synthesis and characterization of CuO superconductors with high transient temperatures
[AD-A292478] p 2562 N95-29014
Transport phenomena and noise in real quantum wires
[AD-A290493] p 2714 N95-29152
WEIZMANN INST. OF SCIENCE, REHOVOT (ISRAEL).
Self-Induced Transparency in photonic band structures: Gap solitons near absorption resonances
[AD-A292187] p 2718 N95-28927
WEST VIRGINIA UNIV., MORGANTOWN, VA.
Effect of open hole on tensile failure properties of 2D triaxial braided textile composites and tape equivalents
[NASA-CR-4676] p 2513 N95-28817
An introduction to the principles of computer science: A reuse-oriented philosophy
[AD-A290364] p 2647 N95-29226
Equipment resource for MCM technology and system prototyping
[AD-A292492] p 2719 N95-29756
WESTINGHOUSE ELECTRIC CORP., PITTSBURGH, PA.
Advances in tubular solid oxide fuel cell technology
[DE95-008361] p 2607 N95-30281
WESTINGHOUSE HANFORD CO., RICHLAND, WA.
QUEST2: System architecture deliverable set
[DE95-008427] p 2721 N95-28958
WESTINGHOUSE SCIENCE AND TECHNOLOGY CENTER, PITTSBURGH, PA.
Processing, fabrication, and demonstration of HTS integrated microwave circuits
[AD-A292480] p 2562 N95-29073
Processing, fabrication, and demonstration of HTS integrated microwave circuits
[AD-A290220] p 2562 N95-29078
WISCONSIN UNIV., MADISON, WI.
Typhoon monitoring using passive microwave observations
[AD-A292567] p 2619 N95-28975
Bootstrap and partitioning methods
[AD-A290662] p 2671 N95-29578
Optimal universal coding and density estimation
[AD-A290694] p 2675 N95-29587
Modeling spatio-temporal databases to measure the performance of the GPS satellite constellation p 2494 N95-29596
The study of non-Newtonian contraction flows with a parallel finite element method p 2576 N95-29778
Air/fuel ratio visualization in a diesel spray p 2590 N95-29807
Cylinder-averaged histories of nitrogen oxide in a DI diesel with simulated turbocharging
[AD-A290568] p 2590 N95-29820
Short-range precipitation forecasts using assimilation of simulated satellite water vapor profiles and cloud liquid water p 2625 N95-29832
The role of diabatic heating, torques and stability in forcing the meridional circulation within cyclones p 2626 N95-29834
Soil wetness and climate variability p 2609 N95-29878
WOODS HOLE OCEANOGRAPHIC INST., MA.
Automated analysis of zooplankton size and taxonomic composition using the video plankton recorder
[AD-A289725] p 2631 N95-28685
MapTool version 2. User's manual
[AD-A289470] p 2630 N95-29418
WORCESTER POLYTECHNIC INST., MA.
Engineering design of sub-micron topographies for simultaneously adherent and reflective metal-polymer interfaces
[NASA-CR-198845] p 2548 N95-30237
WRIGHT LAB., EGLIN AFB, FL.
The role of overset grids in the development of the general purpose CFD code p 2480 N95-28738
WRIGHT LAB., WRIGHT-PATTERSON AFB, OH.
Emerging CFD technologies and aerospace vehicle design p 2482 N95-28746
Recirculating cavity casing treatment failure
[AD-A289330] p 2500 N95-28908
Corona tests of prototype connector
[AD-A292542] p 2561 N95-28971
High resolution, large scale measurement processes
[AD-A292200] p 2681 N95-28987
Computational Fluid Dynamics (CFD) analysis of a C-135 aircraft with a side-mounted splitter plate (with comparison to wind tunnel data)
[AD-A292029] p 2571 N95-29187
Survey of CFD applications for high speed inlets
[AD-A291365] p 2578 N95-30087
WRIGHT RESEARCH DEVELOPMENT CENTER, WRIGHT-PATTERSON AFB, OH.
Characterization of stall inception in high-speed single-stage compressors
[AD-A291275] p 2501 N95-29934
WRIGHT STATE UNIV., DAYTON, OH.
Micro/Miniature heat pipe analysis
[AD-A292232] p 2570 N95-29127
Visualization of CAD objects using a stereoscopic display
[AD-A290034] p 2639 N95-29439
Pattern-analysis based models of masking by spatially separated sounds
[AD-A291270] p 2637 N95-29933
WYLE LABS., INC., ARLINGTON, VA.
The acoustic characteristics of turbomachinery cavities
[NASA-CR-4671] p 2478 N95-28720

Y

YALE UNIV., NEW HAVEN, CT.
Linear algebraic computation on distributed memory parallel machines
[AD-A290615] p 2671 N95-29558
Effects of microscopic diffusion and rotational mixing on stellar models p 2733 N95-29669
The effects of rotation on the evolution of 15 to 30 solar mass stars p 2734 N95-29673
An analytic modeling and system identification study of helicopter dynamics p 2498 N95-29787
YANKEE ENVIRONMENTAL SYSTEMS, INC., TURNERS FALLS, MA.
Research results on an improved in-situ tropospheric humidity sensor
[AD-A291339] p 2627 N95-29944

Typical Contract Number Index Listing

AF- AFOSR-0090-93 ..... p 173 N95-10812

CONTRACT NUMBER | PAGE NUMBER | ACCESSION NUMBER

Listings in this index are arranged alphanumerically by contract number. Under each contract number the accession numbers denoting documents that have been produced as a result of research done under that contract are arranged in ascending order. The page number helps to locate the citation in the abstract section. The accession number denotes the number by which the citation is identified.

AF PROJ. 230-4 ..... p 2552 N95-28943
AF PROJ. 2305 ..... p 2564 N95-29384
AF PROJ. 2307 ..... p 2501 N95-29934
AF PROJ. 2404 ..... p 2571 N95-29187
p 2578 N95-30087
AF PROJ. 3152 ..... p 2586 N95-29425
AF PROJ. 3484 ..... p 2719 N95-29756
AF PROJ. 7476 ..... p 2541 N95-29055
AF PROJ. 7659 ..... p 2618 N95-30082
AF PROJ. 7755 ..... p 2635 N95-29161
AF PROJ. 7757 ..... p 2585 N95-29274
AF-AFOSR-0048-91 ..... p 2592 N95-29423
AF-AFOSR-0196-91 ..... p 2634 N95-29022
AF-AFOSR-0206-91 ..... p 2633 N95-28866
AF-AFOSR-0215-91 ..... p 2534 N95-29922
AF-AFOSR-0226-91 ..... p 2665 N95-29971
AF-AFOSR-0227-91 ..... p 2536 N95-29427
AF-AFOSR-0233-90 ..... p 2561 N95-28859
AF-AFOSR-0241-91 ..... p 2576 N95-29761
AF-AFOSR-0255-90 ..... p 2703 N95-29001
AF-AFOSR-0285-90 ..... p 2586 N95-29514
AF-AFOSR-0286-91 ..... p 2588 N95-29980
AF-AFOSR-0289-91 ..... p 2637 N95-29933
AF-AFOSR-0311-90 ..... p 2670 N95-29312
AF-AFOSR-0313-91 ..... p 2699 N95-29006
AF-AFOSR-0314-91 ..... p 2571 N95-29181
AF-AFOSR-0315-89 ..... p 2577 N95-29920
AF-AFOSR-0321-91 ..... p 2714 N95-29165
AF-AFOSR-0327-91 ..... p 2713 N95-28967
AF-AFOSR-0332-91 ..... p 2639 N95-29422
AF-AFOSR-0337-91 ..... p 2563 N95-29163
AF-AFOSR-0339-90 ..... p 2618 N95-29981
AF-AFOSR-0349-91 ..... p 2712 N95-28874
AF-AFOSR-0357-91 ..... p 2716 N95-29767
AF-AFOSR-0363-91 ..... p 2692 N95-29082
AF-AFOSR-0368-91 ..... p 2664 N95-29636
AF-AFOSR-0379-91 ..... p 2609 N95-29450
AF-AFOSR-0391-91 ..... p 2491 N95-29972
AF-AFOSR-0394-91 ..... p 2632 N95-29320
AF-AFOSR-0406-91 ..... p 2698 N95-28932
AF-AFOSR-0418-91 ..... p 2560 N95-28813
AF-AFOSR-0435-91 ..... p 2512 N95-29168
AF-AFOSR-0437-91 ..... p 2523 N95-29169
AF-AFOSR-0467-89 ..... p 2735 N95-29917
AF-AFOSR-91-1-0334 ..... p 2562 N95-29014
AF-AFOSR-93-C-0014 ..... p 2561 N95-29010
ARO-MIPR-103-94 ..... p 2489 N95-29428
ARO-MIPR-111-94 ..... p 2716 N95-29493
ARO-MIPR-130-94 ..... p 2557 N95-29645
ARPA ORDER 8343 ..... p 2652 N95-29996
ARPA ORDER 128 ..... p 2612 N95-28985
p 2613 N95-29293
ARPA ORDER 6324 ..... p 2702 N95-29973
ARPA ORDER 7476 ..... p 2541 N95-29055
ARPA ORDER 7509 ..... p 2643 N95-29381
ARPA ORDER 7932 ..... p 2562 N95-29073
p 2562 N95-29078
ARPA ORDER 7933 ..... p 2552 N95-28984
ARPA ORDER 9328 ..... p 2536 N95-29461
ARPA ORDER 9339 ..... p 2697 N95-28795
ARPA ORDER-A128 ..... p 2612 N95-28972
ARPA ORDER-8313 ..... p 2721 N95-28877
ARPA ORDER-9328 ..... p 2540 N95-28925
ARPA ORDER-9376 ..... p 2608 N95-28922
ARPA-63-93-C-0064 ..... p 2484 N95-28758
DA PROJ. M02-B-2-FR-21-ABJ ..... p 2535 N95-28889
DA PROJ. NAV-P ..... p 2561 N95-28971
DA PROJ. 1A1-1-Z-1-CANMBJ ..... p 2593 N95-28789
DA PROJ. 1L1-61102-AH-43 ..... p 2530 N95-28876
p 2532 N95-29487
p 2534 N95-29994
DA PROJ. 1L1-61102-AH-45 ..... p 2512 N95-29373
DA PROJ. 1L1-6221-A-47-A ..... p 2590 N95-29538
DA PROJ. 1L1-62211-A-47-A ..... p 2589 N95-29112
DA PROJ. 1L1-62618-AH-80 ..... p 2596 N95-29929
DA PROJ. 1O1-61102-A-71-A ..... p 2670 N95-29296
DA PROJ. 1O1-62622-A-552 ..... p 2551 N95-28699
DA PROJ. 301-62787-A-878 ..... p 2635 N95-29141
p 2639 N95-29434
DA PROJ. 4A1-62720-A-896 ..... p 2683 N95-29077
DA PROJ. 4A1-62784-AT-41 ..... p 2550 N95-29537
DA PROJ. 4A1-62784-AT-45 ..... p 2550 N95-29307
DA PROJ. 402-6 ..... p 2619 N95-28975
DA PROJ. 460-0 ..... p 2642 N95-28976
DA PROJ. 775-5 ..... p 2633 N95-28793
DA PROJ. 793-0 ..... p 2640 N95-28792
DAAB07-88-C-F407 ..... p 2702 N95-29973
DAAD07-89-C-0003 ..... p 2555 N95-29266
DAAH04-83-G-0513 ..... p 2569 N95-29068
DAAH04-93-C-0001 ..... p 2588 N95-30050
DAAH04-93-C-0019 ..... p 2646 N95-29066
DAAH04-93-G-0081 ..... p 2594 N95-29150
DAAH04-93-G-0255 ..... p 2682 N95-29588
DAAH04-93-G-0259 ..... p 2705 N95-29519
DAAH04-93-G-0264 ..... p 2524 N95-29326
DAAH04-93-G-0409 ..... p 2549 N95-29550
DAAH04-93-G-0416 ..... p 2718 N95-30298
DAAH04-93-G-0419 ..... p 2590 N95-29552
DAAH04-93-G-0453 ..... p 2554 N95-29235
DAAH04-93-G-0467 ..... p 2699 N95-29148
DAAH04-93-G-0515 ..... p 2525 N95-29492
DAAH04-94-C-00029 ..... p 2698 N95-28914
DAAH04-94-C-0007 ..... p 2718 N95-28857
DAAH04-94-C-0032 ..... p 2642 N95-28974
DAAH04-94-G-0006 ..... p 2737 N95-29151
DAAH04-94-G-0008 ..... p 2645 N95-28883
DAAH04-94-G-0009 ..... p 2666 N95-30040
DAAH04-94-G-0024 ..... p 2722 N95-29182
DAAH04-94-G-0038 ..... p 2500 N95-29496
DAAH04-94-G-0039 ..... p 2685 N95-30084
DAAH04-94-G-0046 ..... p 2587 N95-29653
DAAH04-94-G-0077 ..... p 2661 N95-28788
DAAH04-94-G-0080 ..... p 2702 N95-29867
DAAH04-94-G-0104 ..... p 2564 N95-29511
DAAH04-94-G-0267 ..... p 2653 N95-30063
p 2673 N95-30126
DAAH04-94-G-0355 ..... p 2555 N95-29290
DAAK60-92-C-0035 ..... p 2547 N95-30120
DAAL-92-G-0289 ..... p 2540 N95-29021
DAAL01-93-M-S403 ..... p 2523 N95-29277
DAAL03-89-C-0031 ..... p 2659 N95-29225
DAAL03-89-D-0003 ..... p 2722 N95-29154
DAAL03-89-G-0111 ..... p 2692 N95-28981
DAAL03-89-K-0131 ..... p 2537 N95-29724
DAAL03-90-C-0026 ..... p 2643 N95-29381
DAAL03-90-G-0046 ..... p 2545 N95-29586
DAAL03-90-G-0151 ..... p 2595 N95-29535
DAAL03-90-G-0213 ..... p 2544 N95-29484
DAAL03-90-G-0220 ..... p 2594 N95-28853
DAAL03-91-C-0018 ..... p 2557 N95-29603
DAAL03-91-C-0025 ..... p 2533 N95-29581
p 2702 N95-29974
DAAL03-91-C-0174 ..... p 2553 N95-29081
DAAL03-91-G-0007 ..... p 2497 N95-29322
DAAL03-91-G-0013 ..... p 2526 N95-29561
DAAL03-91-G-0016 ..... p 2671 N95-29516
DAAL03-91-G-0020 ..... p 2532 N95-29357
DAAL03-91-G-0022 ..... p 2595 N95-29562
DAAL03-91-G-0023 ..... p 2572 N95-29228
DAAL03-91-G-0024 ..... p 2533 N95-29556
DAAL03-91-G-0026 ..... p 2487 N95-29091
DAAL03-91-G-0027 ..... p 2681 N95-29481
DAAL03-91-G-0032 ..... p 2671 N95-29558
DAAL03-91-G-0033 ..... p 2578 N95-30039
DAAL03-91-G-0039 ..... p 2653 N95-30063
p 2673 N95-30126
DAAL03-91-G-0041 ..... p 2671 N95-29485
DAAL03-91-G-0052 ..... p 2718 N95-29149
DAAL03-91-G-0059 ..... p 2524 N95-29409
p 2546 N95-29926
DAAL03-91-G-0060 ..... p 2621 N95-29497
DAAL03-91-G-0062 ..... p 2632 N95-29155
DAAL03-91-G-0063 ..... p 2649 N95-29429
DAAL03-91-G-0065 ..... p 2528 N95-29864
DAAL03-91-G-0071 ..... p 2554 N95-29203
DAAL03-91-G-0082 ..... p 2527 N95-29763
DAAL03-91-G-0084 ..... p 2715 N95-29234
DAAL03-91-G-0086 ..... p 2652 N95-30042
DAAL03-91-G-0087 ..... p 2594 N95-29067
DAAL03-91-G-0101 ..... p 2674 N95-29491
DAAL03-91-G-0102 ..... p 2648 N95-29297
DAAL03-91-G-0105 ..... p 2532 N95-29483
DAAL03-91-G-0107 ..... p 2675 N95-29587
DAAL03-91-G-0108 ..... p 2692 N95-29227
DAAL03-91-G-0111 ..... p 2671 N95-29578
DAAL03-91-G-0118 ..... p 2557 N95-29563
DAAL03-91-G-0122 ..... p 2669 N95-29083
DAAL03-91-G-0125 ..... p 2548 N95-29498
DAAL03-91-G-0128 ..... p 2543 N95-29436
DAAL03-91-G-0132 ..... p 2542 N95-29230
DAAL03-91-G-0137 ..... p 2577 N95-29948
DAAL03-91-G-0146 ..... p 2564 N95-29430
DAAL03-91-G-0149 ..... p 2659 N95-29566
DAAL03-91-G-0151 ..... p 2670 N95-29385
DAAL03-91-G-0161 ..... p 2567 N95-30124
DAAL03-91-G-0166 ..... p 2544 N95-29494
DAAL03-91-G-0172 ..... p 2545 N95-29635
DAAL03-91-G-0177 ..... p 2650 N95-29509
DAAL03-91-G-0179 ..... p 2669 N95-29233
DAAL03-91-G-0181 ..... p 2573 N95-29324
DAAL03-91-G-0182 ..... p 2648 N95-29310
DAAL03-91-G-0189 ..... p 2587 N95-29930
DAAL03-91-G-0191 ..... p 2693 N95-29431
DAAL03-91-G-0204 ..... p 2559 N95-29982
DAAL03-91-G-0207 ..... p 2693 N95-29723
DAAL03-91-G-0211 ..... p 2541 N95-29071
DAAL03-91-G-0215 ..... p 2650 N95-29480
p 2671 N95-29488
p 2674 N95-29490
DAAL03-91-G-0237 ..... p 2570 N95-29069
DAAL03-91-G-0242 ..... p 2696 N95-29495
DAAL03-91-G-0301 ..... p 2700 N95-29553
DAAL03-91-G-0305 ..... p 2713 N95-29087
DAAL03-91-G-0310 ..... p 2601 N95-29866
DAAL03-91-G-0316 ..... p 2693 N95-29555
DAAL03-91-G-0321 ..... p 2692 N95-29092
DAAL03-91-G-0329 ..... p 2637 N95-29927
DAAL03-91-G-0337 ..... p 2635 N95-29153
DAAL03-92-C-0021 ..... p 2543 N95-29482
DAAL03-92-C-0045 ..... p 2701 N95-29846
DAAL03-92-G-0044 ..... p 2714 N95-29152
DAAL03-92-G-0122 ..... p 2590 N95-29820
DAAL03-92-G-0131 ..... p 2596 N95-29582
DAAL03-92-G-0142 ..... p 2703 N95-30081
DAAL03-92-G-0263 ..... p 2700 N95-29560
DAAL03-92-G-0315 ..... p 2650 N95-29517
DAAL03-92-G-0316 ..... p 2523 N95-29189
DAAL03-92-G-0322 ..... p 2675 N95-29634
p 2675 N95-30297
DAAL03-92-G-0333 ..... p 2669 N95-29229
DAAL03-92-G-0381 ..... p 2716 N95-29506
DAAL03-92-G-0412 ..... p 2647 N95-29226
DAAL03-92-G-0415 ..... p 2648 N95-29285
DAAL03-92-G-0416 ..... p 2574 N95-29387
DAAL03-92-K-0004 ..... p 2542 N95-29288
DABT63-92-C-0039 ..... p 2564 N95-29478
DABT63-93-C-0054 ..... p 2658 N95-28879
p 2658 N95-28884
p 2650 N95-29536
p 2724 N95-29818
DAJA45-90-C-0053 ..... p 2542 N95-29195
DAJA45-93-C-0021 ..... p 2582 N95-28966
DAMD17-92-C-2033 ..... p 2634 N95-29139
DAMD17-93-V-3018 ..... p 2639 N95-29458
DAMD17-94-J-4010 ..... p 2534 N95-30085
DAMD17-94-J-4017 ..... p 2632 N95-29088
DARPA ORDER 8961 ..... p 2699 N95-29295

DARPA ORDER 9806 ..... p 2670 N95-29312
DASG60-94-C-0102 ..... p 2611 N95-30348
DASW01-94-C-0054 ..... p 2552 N95-28936
p 2510 N95-29284
DE-AC02-78CH-00016 ..... p 2696 N95-30009
p 2696 N95-30021
p 2566 N95-30025
p 2668 N95-30279
DE-AC02-80ET-15601 ..... p 2530 N95-28776
p 2531 N95-28916
DE-AC02-86ER-40296 ..... p 2682 N95-30131
DE-AC03-76SF-00098 ..... p 2690 N95-28779
p 2693 N95-29583
p 2654 N95-30183
DE-AC03-76SF-00515 ..... p 2739 N95-29265
DE-AC04-76DP-00613 ..... p 2556 N95-29462
p 2654 N95-30115
DE-AC04-76EV-10103 ..... p 2635 N95-29188
DE-AC04-94AL-85000 ..... p 2698 N95-28983
p 2714 N95-29157
p 2716 N95-29814
p 2651 N95-29871
p 2717 N95-29990
p 2717 N95-30005
p 2588 N95-30006
p 2717 N95-30022
p 2660 N95-30116
p 2560 N95-30177
p 2538 N95-30178
p 2567 N95-30188
p 2655 N95-30209
p 2597 N95-30210
p 2603 N95-30213
p 2718 N95-30214
p 2604 N95-30217
DE-AC05-76OR-00033 ..... p 2538 N95-30038
DE-AC05-84OR-21400 ..... p 2695 N95-28957
p 2561 N95-28961
p 2696 N95-29142
p 2710 N95-29909
p 2711 N95-30023
p 2549 N95-30024
p 2528 N95-30037
p 2538 N95-30038
p 2666 N95-30112
p 2535 N95-30113
p 2547 N95-30174
p 2528 N95-30175
p 2538 N95-30179
p 2654 N95-30189
p 2547 N95-30190
p 2725 N95-30194
p 2611 N95-30212
p 2538 N95-30216
DE-AC06-76RL-01830 ..... p 2608 N95-28920
p 2602 N95-29463
DE-AC06-87RL-10930 ..... p 2721 N95-28958
DE-AC07-94ID-13223 ..... p 2536 N95-28959
p 2540 N95-28960
p 2591 N95-30211
DE-AC08-93NV-11265 ..... p 2697 N95-28912
DE-AC22-94PC-93069 ..... p 2533 N95-29870
DE-AC34-90DP-62349 ..... p 2626 N95-29868
DE-AC36-83CH-10093 ..... p 2603 N95-30016
p 2603 N95-30017
p 2549 N95-30024
p 2603 N95-30127
DE-FC03-92SF-19460 ..... p 2711 N95-30274
DE-FC05-85ER-25000 ..... p 2687 N95-30141
DE-FC07-93ID-13205 ..... p 2537 N95-29869
DE-FC21-91MC-28055 ..... p 2607 N95-30281
DE-FG02-86ER-45229 ..... p 2537 N95-30018
DE-FG02-87ER-45312 ..... p 2529 N95-30180
DE-FG02-88ER-25053 ..... p 2481 N95-28740
DE-FG02-90ER-61072 ..... p 2608 N95-28920
DE-FG02-91ER-54109 ..... p 2695 N95-28930
DE-FG02-92ER-61363 ..... p 2610 N95-30181
DE-FG03-93ER-40757 ..... p 2695 N95-30191
DE-FG05-80ET-53088 ..... p 2711 N95-30173
DE-FG05-88ER-60672 ..... p 2633 N95-29471
DLA900-88-D-0392 ..... p 2599 N95-29523
p 2601 N95-30061
DLA900-93-D-5002 ..... p 2533 N95-29575
DNA-MIPR-92-501 ..... p 2500 N95-29950
DNA001-89-C-0066 ..... p 2542 N95-29314
DTFA02-91-C-91089 ..... p 2493 N95-28790
F04606-89-D-0034 ..... p 2566 N95-30070
F04701-88-C-0089 ..... p 2531 N95-28942
p 2738 N95-29279
p 2587 N95-29931
F04701-93-C-0094 ..... p 2507 N95-28867
p 2603 N95-29953
p 2504 N95-29992
F08630-93-C-0074 ..... p 2481 N95-28745
F11623-92-D-0003 ..... p 2651 N95-29639
F19628-89-C-0079 ..... p 2616 N95-29737

F19628-90-C-0002 .....
F19628-90-C-0003 .....
F19628-91-C-0168 .....
F19628-92-K-0016 .....
F19628-93-C-0052 .....
F19628-93-C-0057 .....
F19628-93-C-0060 .....
F19628-93-C-0069 .....
F19628-93-C-0091 .....
F19628-93-C-0165 .....
F19628-93-C-0171 .....
F19628-93-K-0018 .....
F19628-93-K-0019 .....
F19628-93-K-0021 .....
F19628-93-K-0027 .....
F19628-94-C-0064 .....
F19628-95-C-0002 .....
F29601-89-C-0015 .....
F29601-91-C-0099 .....
F30602-91-C-0098 .....
F30602-91-C-0141 .....
F30602-91-C-0159 .....
F30602-91-D-0001 .....
F30602-92-C-0150 .....
F30602-93-C-0090 .....
F30602-94-C-0008 .....
F33615-88-C-5404 .....
F33615-89-C-0574 .....
F33615-90-C-0005 .....
F33615-91-C-1758 .....
F33615-91-C-2152 .....
F33615-92-C-1907 .....
F33615-92-C-2276 .....
F33615-92-C-3400 .....
F33615-93-1-1330 .....
F33615-94-C-3402 .....
F33615-94-C-5417 .....
F33615-94-C-5805 .....
F41624-94-D-6000 .....
F49620-90-C-0079 .....
F49620-91-C-0004 .....
F49620-91-C-0048 .....
F49620-91-C-0097 .....
F49620-92-C-0009 .....
F49620-92-C-0012 .....
F49620-92-C-0026 .....
F49620-92-C-0047 .....
F49620-92-C-0064 .....
F49620-92-C-0070 .....
F49620-92-J-0005 .....
F49620-92-J-0016 .....
F49620-92-J-0047 .....
F49620-92-J-0051 .....
F49620-92-J-0066 .....
F49620-92-J-0073 .....
F49620-92-J-0076 .....
F49620-92-J-0093 .....
F49620-92-J-0111 .....
F49620-92-J-0118 .....
F49620-92-J-0128 .....
F49620-92-J-0211 .....
F49620-92-J-0275 .....
F49620-92-J-0361 .....
F49620-92-J-0374 .....
F49620-92-J-0401 .....
F49620-92-J-0470 .....
F49620-92-J-0483 .....
F49620-92-J-0510 .....
F49620-93-C-0025 .....
F49620-93-C-0069 .....
F49620-93-1-0001 .....
F49620-93-1-0007 .....
F49620-93-1-0020 .....
F49620-93-1-0025 .....
F49620-93-1-0142 .....
F49620-93-1-0143 .....
F49620-93-1-0161 .....
F49620-93-1-0162 .....
F49620-93-1-0198 .....
F49620-93-1-0244 .....
F49620-93-1-0306 .....
p 2617 N95-29765
p 2651 N95-29932
p 2618 N95-30082
p 2598 N95-29281
p 2649 N95-29376
p 2652 N95-30047
p 2721 N95-28877
p 2602 N95-29200
p 2602 N95-29201
p 2613 N95-29317
p 2612 N95-28972
p 2613 N95-29293
p 2644 N95-28782
p 2507 N95-29026
p 2611 N95-28697
p 2658 N95-29196
p 2501 N95-29764
p 2725 N95-30043
p 2612 N95-28985
p 2558 N95-29875
p 2627 N95-29944
p 2659 N95-29420
p 2664 N95-29657
p 2532 N95-29273
p 2552 N95-28986
p 2698 N95-28992
p 2645 N95-28814
p 2691 N95-28952
p 2716 N95-29658
p 2658 N95-28965
p 2494 N95-28887
p 2697 N95-28798
p 2640 N95-29020
p 2636 N95-29360
p 2641 N95-29943
p 2651 N95-29644
p 2551 N95-30296
p 2556 N95-29472
p 2570 N95-29127
p 2492 N95-28811
p 2645 N95-28878
p 2721 N95-28880
p 2645 N95-28881
p 2645 N95-28894
p 2662 N95-28988
p 2669 N95-29128
p 2647 N95-29147
p 2658 N95-29196
p 2647 N95-29223
p 2649 N95-29376
p 2697 N95-28870
p 2717 N95-30068
p 2662 N95-28978
p 2654 N95-30125
p 2541 N95-29055
p 2553 N95-29176
p 2597 N95-30123
p 2552 N95-28984
p 2552 N95-28979
p 2571 N95-29211
p 2592 N95-29012
p 2712 N95-28862
p 2699 N95-29295
p 2489 N95-29316
p 2569 N95-29024
p 2638 N95-28937
p 2693 N95-29865
p 2731 N95-29916
p 2557 N95-29645
p 2585 N95-29025
p 2691 N95-28944
p 2669 N95-29070
p 2712 N95-28815
p 2627 N95-29993
p 2571 N95-29145
p 2680 N95-28810
p 2681 N95-29062
p 2523 N95-29124
p 2692 N95-28994
p 2562 N95-29018
p 2618 N95-29970
p 2544 N95-29505
p 2614 N95-29413
p 2560 N95-28812
p 2587 N95-29912
p 2675 N95-29768
p 2561 N95-29005
p 2575 N95-29421
p 2704 N95-29011
p 2694 N95-30060
p 2658 N95-29074
p 2582 N95-29004
p 2564 N95-29417
p 2672 N95-30086
p 2634 N95-28915
p 2585 N95-29053
F49620-93-1-0323 .....
F49620-93-1-0487 .....
F49620-93-1-0494 .....
F49620-93-1-0530 .....
F49620-93-1-0534 .....
F49620-93-1-0582 .....
F49620-93-1-0585 .....
F49620-93-1-0588 .....
F49620-93-1-0591 .....
F49620-93-1-0601 .....
F49620-93-1-0608 .....
F49620-94-C-0037 .....
F49620-94-C-0039 .....
F49620-94-C-0042 .....
F49620-94-C-0043 .....
F49620-94-C-0049 .....
F49620-94-C-0053 .....
F49620-94-C-0054 .....
F49620-94-1-0018 .....
F49620-94-1-0024 .....
F49620-94-1-0055 .....
F49620-94-1-0099 .....
F49620-94-1-0118 .....
F49620-94-1-0132 .....
F49620-94-1-0230 .....
GRI-5089-260-1826 .....
GRI-5091-288-2319 .....
GRI-5093-260-2657 .....
GRI-5094-250-3084 .....
MDA903-78-C-2042 .....
MDA903-82-C-0353 .....
MDA903-89-C-0003 .....
MDA903-90-C-0004 .....
MDA903-90-C-0006 .....
MDA903-91-C-0006 .....
MDA972-92-J-1018 .....
MDA972-93-C-0020 .....
MDA972-93-C-0021 .....
MDA972-93-C-0035 .....
MDA972-93-C-0057 .....
MDA972-93-1-0012 .....
MIPR-FY7121-91-00003 .....
MIPR-PRJORD-94004 .....
MIPR-92MM2583 .....
MR00-97 .....
MR04101 .....
NAGW-1356 .....
NAGW-1630 .....
NAGW-2948 .....
NAGW-3414 .....
NAG1-1067 .....
NAG1-1095 .....
NAG1-1103 .....
NAG1-1154 .....
NAG1-1257 .....
NAG1-1367 .....
NAG1-1381 .....
NAG1-1407 .....
NAG1-1459 .....
NAG1-1476 .....
NAG1-1479 .....
NAG1-1522 .....
NAG1-1600 .....
NAG1-237 .....
NAG1-343 .....
NAG1-922 .....
NAG2-645 .....
NAG2-789 .....
NAG3-1267 .....
NAG3-1516 .....
NAG3-1566 .....
NAG3-1581 .....
NAG3-879 .....
NAG5-2232 .....
NAG5-2348 .....
NAG8-239 .....
NAG8-909 .....
NAG9-597 .....
NAG9-698 .....
NASA ORDER S-14626-F .....
NASW-4584 .....
NASW-4715 .....
NAS1-18224 .....
NAS1-18580 .....
NAS1-18833 .....
NAS1-18840 .....
NAS1-18841 .....
NAS1-18842 .....
NAS1-18883 .....
NAS1-18888 .....
NAS1-18889 .....
p 2669 N95-29070
p 2703 N95-30062
p 2565 N95-29925
p 2586 N95-29292
p 2563 N95-29164
p 2583 N95-29361
p 2703 N95-29003
p 2502 N95-29468
p 2698 N95-28998
p 2575 N95-29637
p 2492 N95-29210
p 2713 N95-28933
p 2584 N95-29007
p 2497 N95-29426
p 2593 N95-29946
p 2593 N95-29941
p 2577 N95-29913
p 2699 N95-29177
p 2712 N95-28869
p 2716 N95-29814
p 2575 N95-29469
p 2547 N95-30071
p 2664 N95-29577
p 2481 N95-28740
p 2718 N95-29009
p 2535 N95-30198
p 2591 N95-30110
p 2535 N95-30111
p 2610 N95-30197
p 2638 N95-29090
p 2648 N95-29325
p 2550 N95-29918
p 2651 N95-29735
p 2651 N95-29736
p 2720 N95-28797
p 2722 N95-29287
p 2651 N95-29736
p 2654 N95-30121
p 2540 N95-28925
p 2608 N95-28922
p 2536 N95-29461
p 2697 N95-28795
p 2675 N95-29634
p 2619 N95-28975
p 2608 N95-28787
p 2634 N95-29086
p 2640 N95-28935
p 2645 N95-28934
p 2578 N95-30034
p 2711 N95-30338
p 2601 N95-30247
p 2507 N95-28852
p 2519 N95-29036
p 2628 N95-30356
p 2579 N95-30250
p 2696 N95-30337
p 2504 N95-29339
p 2661 N95-30156
p 2513 N95-28817
p 2513 N95-28809
p 2481 N95-28744
p 2548 N95-30237
p 2661 N95-30150
p 2689 N95-30152
p 2489 N95-29338
p 2672 N95-30086
p 2521 N95-29045
p 2521 N95-29045
p 2504 N95-29339
p 2484 N95-28758
p 2501 N95-30254
p 2674 N95-30145
p 2689 N95-30154
p 2574 N95-29372
p 2509 N95-30357
p 2543 N95-29367
p 2584 N95-28808
p 2702 N95-30035
p 2711 N95-30338
p 2565 N95-29968
p 2635 N95-29158
p 2590 N95-29369
p 2726 N95-28822
p 2655 N95-30307
p 2628 N95-30272
p 2512 N95-30225
p 2522 N95-29048
p 2514 N95-28828
p 2521 N95-29042
p 2521 N95-29044
p 2516 N95-28843
p 2514 N95-28827
p 2496 N95-29027
p 2519 N95-29033
p 2499 N95-28831
p 2515 N95-28835

NAS1-18954 ..... p 2522 N95-29047
NAS1-19000 ..... p 2482 N95-28750
p 2517 N95-28848
p 2522 N95-29046
p 2522 N95-29049
p 2582 N95-30151
NAS1-19247 ..... p 2512 N95-30225
NAS1-19317 ..... p 2517 N95-28848
NAS1-19480 ..... p 2670 N95-29403
p 2649 N95-29404
p 2671 N95-29451
p 2649 N95-29455
p 2672 N95-30086
p 2687 N95-30139
p 2674 N95-30143
p 2674 N95-30227
p 2655 N95-30306
p 2674 N95-30353
NAS1-19672 ..... p 2690 N95-30159
NAS1-198167 ..... p 2672 N95-30086
NAS1-20102 ..... p 2688 N95-30147
NAS1-20121 ..... p 2548 N95-30252
NAS10-11943 ..... p 2531 N95-29248
NAS13-330 ..... p 2630 N95-29237
NAS2-14052 ..... p 2499 N95-29123
NAS2-14084 ..... p 2496 N95-28928
NAS3-25455 ..... p 2590 N95-29538
NAS3-25776 ..... p 2564 N95-29406
p 2566 N95-29998
NAS3-25934 ..... p 2506 N95-30090
NAS3-26617 ..... p 2684 N95-29641
NAS3-26715 ..... p 2606 N95-30266
NAS3-26822 ..... p 2523 N95-29133
NAS3-27186 ..... p 2510 N95-29114
p 2492 N95-29132
p 2512 N95-29373
p 2503 N95-30067
NAS3-27377 ..... p 2489 N95-29402
NAS5-32336 ..... p 2600 N95-29754
NAS5-32473 ..... p 2726 N95-29370
NAS7-1260 ..... p 2731 N95-30230
p 2631 N95-30231
p 2628 N95-30343
p 2737 N95-30344
NAS8-37360 ..... p 2478 N95-28720
NAS8-38609 ..... p 2531 N95-29246
p 2585 N95-29247
p 2652 N95-30013
p 2549 N95-30014
NAS8-38861 ..... p 2578 N95-30034
NAS8-39184 ..... p 2510 N95-29584
NAS8-39782 ..... p 2510 N95-29584
NAS8-39950 ..... p 2691 N95-28856
NAS9-18024 ..... p 2633 N95-28875
NAS9-18426 ..... p 2493 N95-28716
p 2505 N95-29447
p 2508 N95-30036
NAS9-58779 ..... p 2704 N95-29130
NAS9-59193 ..... p 2704 N95-29130
NCA2-707 ..... p 2686 N95-30138
NCC2-5055 ..... p 2700 N95-29366
NCC2-800 ..... p 2499 N95-30335
NCC3-17 ..... p 2572 N95-29249
p 2603 N95-30015
NCC3-233 ..... p 2582 N95-30149
NCC3-301 ..... p 2532 N95-29250
NCC3-317 ..... p 2518 N95-28906
NCC3-370 ..... p 2574 N95-29405
NGT-51118 ..... p 2688 N95-30148
NR PROJ. A60-070 ..... p 2557 N95-29489
NR PROJ. RJ3-5-C-51 ..... p 2685 N95-29945
NR PROJ. R19-87 ..... p 2601 N95-29977
NR PROJ. ZW4-4 ..... p 2502 N95-29522
NR PROJ. ZW6-7 ..... p 2665 N95-29831
NR PROJ. 042-04 ..... p 2639 N95-29432
NRL PROJ. R03-5-E-72 ..... p 2619 N95-28938
NSF ADT-88-09616 ..... p 2693 N95-29583
NSF ASC-93-57677 ..... p 2481 N95-28744
NSF BES-94-02439 ..... p 2647 N95-29143
NSF CCR-88-20279 ..... p 2668 N95-29065
NSF CCR-89-20694 ..... p 2650 N95-29480
NSF CCR-91-09469 ..... p 2649 N95-29376
NSF CCR-91-12880 ..... p 2649 N95-29376
NSF CCR-92-09793 ..... p 2484 N95-28758
NSF CCR-93-03383 ..... p 2645 N95-28886
NSF CCR-94-57766 ..... p 2645 N95-28878
NSF DMR-92-22976 ..... p 2681 N95-28923
NSF DMS-92-17655 ..... p 2675 N95-29634
NSF DMS-94-04322 ..... p 2687 N95-30141
NSF ECS-90-15752 ..... p 2540 N95-29021
NSF MIP-91-17724 ..... p 2647 N95-29179
NSF NCR-89-19038 ..... p 2724 N95-29818
NSF-CCR91-09469 ..... p 2645 N95-28894
NSF-CCR92-03488 ..... p 2668 N95-28861
p 2668 N95-28863
NSF-CCR93-08726 ..... p 2645 N95-28881
NSF-ECD89-07068 ..... p 2658 N95-28879
N00014-82-K-0612 ..... p 2539 N95-28850
N00014-85-K-0124 ..... p 2647 N95-29179
N00014-85-K-0198 ..... p 2658 N95-29079
N00014-86-K-0509 ..... p 2554 N95-29240
N00014-88-C-0419 ..... p 2691 N95-28888
N00014-89-D-0142 ..... p 2619 N95-28872
N00014-89-J-1290 ..... p 2715 N95-29438
N00014-89-J-1545 ..... p 2713 N95-28993
p 2715 N95-29444
p 2715 N95-29486
N00014-89-J-1754 ..... p 2614 N95-29585
N00014-89-J-32022 ..... p 2722 N95-29207
N00014-90-C-0235 ..... p 2584 N95-28678
N00014-90-J-1025 ..... p 2668 N95-28861
p 2668 N95-28863
N00014-90-J-1030 ..... p 2668 N95-29065
N00014-90-J-1125 ..... p 2631 N95-30069
N00014-90-J-1545 ..... p 2666 N95-30026
N00014-90-J-1556 ..... p 2523 N95-29185
N00014-90-J-1589 ..... p 2574 N95-29382
N00014-90-J-1621 ..... p 2630 N95-29418
N00014-90-J-1781 ..... p 2628 N95-28796
N00014-90-J-1910 ..... p 2537 N95-29526
N00014-90-J-4063 ..... p 2569 N95-29060
N00014-90-J-4083 ..... p 2487 N95-28921
p 2575 N95-29654
N00014-91-C-0112 ..... p 2562 N95-29078
N00014-91-J-1004 ..... p 2672 N95-30029
N00014-91-J-1021 ..... p 2675 N95-29634
N00014-91-J-1041 ..... p 2528 N95-29923
N00014-91-J-1045 ..... p 2544 N95-29510
N00014-91-J-1078 ..... p 2539 N95-28860
p 2539 N95-28884
p 2539 N95-28891
N00014-91-J-1095 ..... p 2628 N95-28865
N00014-91-J-1194 ..... p 2543 N95-29355
p 2543 N95-29358
N00014-91-J-1209 ..... p 2548 N95-29525
N00014-91-J-1338 ..... p 2542 N95-29270
p 2542 N95-29272
N00014-91-J-1630 ..... p 2531 N95-28945
N00014-91-J-1698 ..... p 2564 N95-29478
N00014-91-J-1880 ..... p 2637 N95-29872
N00014-91-J-1893 ..... p 2544 N95-29551
p 2544 N95-29554
p 2545 N95-29559
N00014-91-J-1897 ..... p 2534 N95-30078
N00014-91-J-1976 ..... p 2714 N95-29089
N00014-91-J-4038 ..... p 2670 N95-29440
p 2639 N95-29443
p 2663 N95-29477
N00014-91-J-4072 ..... p 2573 N95-29268
N00014-91-J-4075 ..... p 2527 N95-29842
N00014-91-J-4101 ..... p 2639 N95-29432
N00014-91-J-4159 ..... p 2638 N95-28918
N00014-92-C-0154 ..... p 2557 N95-29564
N00014-92-J-1030 ..... p 2556 N95-29383
N00014-92-J-1190 ..... p 2540 N95-29021
p 2554 N95-29186
N00014-92-J-1202 ..... p 2533 N95-29722
N00014-92-J-1284 ..... p 2696 N95-28695
p 2697 N95-28698
N00014-92-J-1302 ..... p 2697 N95-28799
N00014-92-J-1303 ..... p 2675 N95-29819
N00014-92-J-1477 ..... p 2713 N95-28954
N00014-92-J-1720 ..... p 2712 N95-28910
N00014-92-J-1879 ..... p 2621 N95-29333
p 2670 N95-29352
p 2556 N95-29441
N00014-92-J-1993 ..... p 2700 N95-29379
N00014-92-J-4096 ..... p 2639 N95-29439
N00014-92-J-4112 ..... p 2646 N95-28968
N00014-93-C-0091 ..... p 2702 N95-29978
N00014-93-C-0202 ..... p 2665 N95-29863
N00014-93-C-0234 ..... p 2646 N95-28964
N00014-93-I-0131 ..... p 2668 N95-29064
p 2669 N95-29080
p 2669 N95-29084
N00014-93-I-0209 ..... p 2649 N95-29456
N00014-93-J-0385 ..... p 2670 N95-29440
p 2556 N95-29441
N00014-93-1-0099 ..... p 2712 N95-28681
N00014-93-1-0122 ..... p 2693 N95-29460
N00014-93-1-0312 ..... p 2715 N95-29267
N00014-93-1-0385 ..... p 2621 N95-29333
p 2670 N95-29352
N00014-93-1-0527 ..... p 2675 N95-29819
N00014-93-1-0553 ..... p 2596 N95-29580
N00014-93-1-0602 ..... p 2631 N95-28685
N00014-93-1-0783 ..... p 2659 N95-29915
N00014-93-1-0827 ..... p 2716 N95-29785
N00014-93-1-1007 ..... p 2643 N95-29921
N00014-94-C-0137 ..... p 2559 N95-30073
N00014-94-C-0241 ..... p 2700 N95-29412
N00014-94-C-0261 ..... p 2562 N95-29061
N00014-94-I-0086 ..... p 2536 N95-29298
N00014-94-WX-35177 ..... p 2558 N95-29928
N00014-94-1-0333 ..... p 2693 N95-29521
N00014-94-1-0383 ..... p 2672 N95-29647
N00014-94-1-0401 ..... p 2563 N95-29191
N00014-94-1-0468 ..... p 2683 N95-28973
N00014-94-1-0505 ..... p 2723 N95-29573
p 2664 N95-29574
p 2664 N95-29577
N00014-94-1-0516 ..... p 2665 N95-29979
N00014-94-1-0546 ..... p 2546 N95-29939
N00014-94-1-0578 ..... p 2714 N95-29209
N00014-94-1-0746 ..... p 2650 N95-29576
p 2664 N95-29577
p 2675 N95-29906
N00014-94-1-0799 ..... p 2668 N95-30117
N00014-94-1-0813 ..... p 2692 N95-29388
N00014-95-1-0028 ..... p 2691 N95-28868
p 2691 N95-28919
N00014-95-1-0194 ..... p 2713 N95-28993
N00039-91-C-0072 ..... p 2629 N95-29085
p 2685 N95-29942
N00039-95-C-0017 ..... p 2652 N95-29996
N00167-95-C-0003 ..... p 2486 N95-28771
N00600-94-C-1827 ..... p 2661 N95-28926
N47408-91-C-1217 ..... p 2594 N95-29063
N60921-94-C-A345 ..... p 2565 N95-29601
N66001-94-C-6037 ..... p 2642 N95-29146
N68171-94-C-9081 ..... p 2718 N95-28927
N68171-94-C-9119 ..... p 2612 N95-28871
p 2612 N95-29140
N68171-94-M-5711 ..... p 2694 N95-30065
PROJ. RA ..... p 2542 N95-29314
PROJ. X15-98 ..... p 2630 N95-29237
PROJS. GARD-A1-197 ..... p 2610 N95-30197
RTOP 106-30-02 ..... p 2642 N95-28722
p 2642 N95-28818
RTOP 199-45-16-12 ..... p 2696 N95-30337
RTOP 233-01-01-05 ..... p 2507 N95-29377
RTOP 233-01-03-06 ..... p 2506 N95-30251
RTOP 233-01-06-01 ..... p 2509 N95-30316
RTOP 233-03-02-02 ..... p 2512 N95-30225
RTOP 235-01-0E ..... p 2508 N95-30011
RTOP 235-01-00 ..... p 2564 N95-29406
RTOP 242-10-80 ..... p 2503 N95-29351
RTOP 242-70-04 ..... p 2510 N95-29114
p 2511 N95-29642
RTOP 242-80-01-02 ..... p 2504 N95-29339
RTOP 307-51-00 ..... p 2680 N95-28893
RTOP 370-24-01 ..... p 2737 N95-30058
RTOP 464-54-03-70 ..... p 2608 N95-28717
RTOP 478-12-10 ..... p 2511 N95-30012
RTOP 505-59-52-01 ..... p 2684 N95-29452
RTOP 505-59-53 ..... p 2477 N95-28816
RTOP 505-59-54-02 ..... p 2583 N95-29453
RTOP 505-62-10 ..... p 2501 N95-30007
RTOP 505-62-36 ..... p 2589 N95-29112
p 2590 N95-29538
RTOP 505-62-50 ..... p 2582 N95-29113
RTOP 505-62-52 ..... p 2568 N95-28719
p 2478 N95-28723
p 2500 N95-29115
p 2574 N95-29371
p 2574 N95-29372
p 2683 N95-29401
p 2489 N95-29402
RTOP 505-62-82 ..... p 2503 N95-30067
RTOP 505-63-12 ..... p 2523 N95-29133
RTOP 505-63-50-04 ..... p 2527 N95-29825
p 2528 N95-30028
p 2529 N95-30340
RTOP 505-63-50-08 ..... p 2495 N95-28820
RTOP 505-63-52 ..... p 2512 N95-29373
RTOP 505-64-10-13 ..... p 2659 N95-29823
RTOP 505-64-52-01 ..... p 2502 N95-30327
RTOP 505-64-52-04 ..... p 2560 N95-30336
RTOP 505-68-10 ..... p 2492 N95-29132
RTOP 505-68-30-01 ..... p 2498 N95-30226
RTOP 505-70-62 ..... p 2491 N95-30091
p 2503 N95-30228
RTOP 505-90-5K ..... p 2574 N95-29405
RTOP 505-90-52-01 ..... p 2670 N95-29403
p 2649 N95-29404
p 2671 N95-29451
p 2649 N95-29455
p 2672 N95-30086
p 2686 N95-30133
p 2674 N95-30227
p 2655 N95-30306

	p 2674	N95-30353
RTOP 505-90-53-02	p 2659	N95-29454
RTOP 506-41-21	p 2604	N95-30255
RTOP 506-41-41	p 2518	N95-28906
RTOP 506-43-11-01	p 2548	N95-30252
RTOP 506-43-31-03	p 2578	N95-30056
RTOP 506-43-61-01	p 2512	N95-30225
RTOP 506-72-21	p 2506	N95-30090
RTOP 510-02-11-07	p 2513	N95-28817
RTOP 510-02-12-01	p 2529	N95-30341
RTOP 510-02-13-01	p 2513	N95-28823
	p 2496	N95-29027
	p 2518	N95-29029
RTOP 537-02-20	p 2596	N95-30008
RTOP 537-02-23	p 2492	N95-30253
RTOP 538-03-11	p 2684	N95-29641
	p 2477	N95-30229
RTOP 674-25-05	p 2535	N95-28701
RTOP 963-60-OD	p 2509	N95-29643
	p 2549	N95-30339
RTOP 973-22-60-54-90	p 2731	N95-30230
W-31-109-ENG-38	p 2714	N95-29134
	p 2548	N95-29280
	p 2716	N95-29984
	p 2659	N95-29985
	p 2717	N95-29986
	p 2665	N95-29987
	p 2577	N95-29988
	p 2537	N95-30018
	p 2694	N95-30019
	p 2652	N95-30020
	p 2717	N95-30077
	p 2633	N95-30114
	p 2610	N95-30176
	p 2718	N95-30184
	p 2695	N95-30185
	p 2695	N95-30186
	p 2578	N95-30187
	p 2606	N95-30264
W-7405-ENG-36	p 2582	N95-28917
	p 2569	N95-28956
	p 2508	N95-29464
	p 2543	N95-29465
	p 2652	N95-29989
	p 2696	N95-30057
	p 2694	N95-30059
	p 2660	N95-30128
	p 2618	N95-30129
	p 2661	N95-30215
	p 2591	N95-30273
	p 2549	N95-30345
W-7405-ENG-48	p 2705	N95-29466
	p 2551	N95-30182
	p 2660	N95-30192
	p 2660	N95-30193

Typical Report Number Index Listing

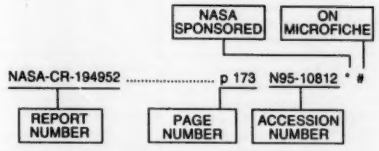

Listings in this index are arranged alphanumerically by report number. The accession number denotes the number by which the citation is identified. The page number helps to locate the citation in the abstract section. An asterisk (*) indicates that the item is a NASA report. A pound sign (#) indicates that the item is available on microfiche.

A-950015 ..... p 2642 N95-28818 * #
A-950016 ..... p 2642 N95-28722 * #
A-950043 ..... p 2737 N95-30058 * #
A-950060 ..... p 2477 N95-28816 * #
A-950065 ..... p 2503 N95-29351 * #
A-950072 ..... p 2503 N95-30228 * #

AAV-1427 ..... p 2598 N95-29175 *
AAV-1432 ..... p 2553 N95-29174 *

AD-A279962 ..... p 2531 N95-28945
AD-A280168 ..... p 2649 N95-29456
AD-A286734 ..... p 2702 N95-29910 #
AD-A286748 ..... p 2608 N95-28787 #
AD-A286751 ..... p 2681 N95-28962 #
AD-A286752 ..... p 2681 N95-28923 #
AD-A286753 ..... p 2681 N95-28924 #
AD-A286796 ..... p 2553 N95-29159 #
AD-A286799 ..... p 2558 N95-29904 #
AD-A288223 ..... p 2634 N95-28915
AD-A288494 ..... p 2498 N95-29911 #
AD-A288877 ..... p 2512 N95-29052
AD-A288899 ..... p 2496 N95-28928 *
AD-A288907 ..... p 2634 N95-29139
AD-A289143 ..... p 2563 N95-29191
AD-A289192 ..... p 2636 N95-29757 #
AD-A289244 ..... p 2721 N95-28907
AD-A289330 ..... p 2500 N95-28908
AD-A289394 ..... p 2527 N95-29758 #
AD-A289445 ..... p 2643 N95-29921 #
AD-A289446 ..... p 2666 N95-30026 #
AD-A289470 ..... p 2630 N95-29418
AD-A289528 ..... p 2594 N95-28909
AD-A289546 ..... p 2712 N95-28910
AD-A289548 ..... p 2595 N95-29192
AD-A289595 ..... p 2577 N95-30027 #
AD-A289606 ..... p 2632 N95-29263
AD-A289630 ..... p 2561 N95-28911
AD-A289657 ..... p 2584 N95-28678
AD-A289661 ..... p 2584 N95-28679
AD-A289693 ..... p 2504 N95-28680
AD-A289705 ..... p 2712 N95-28681
AD-A289707 ..... p 2620 N95-29193
AD-A289710 ..... p 2697 N95-28778
AD-A289720 ..... p 2591 N95-28682
AD-A289721 ..... p 2640 N95-28683
AD-A289724 ..... p 2592 N95-28684
AD-A289725 ..... p 2631 N95-28685
AD-A289731 ..... p 2598 N95-29281
AD-A289738 ..... p 2549 N95-28686
AD-A289739 ..... p 2551 N95-28687
AD-A289748 ..... p 2506 N95-28688
AD-A289749 ..... p 2657 N95-28689
AD-A289753 ..... p 2643 N95-28690
AD-A289759 ..... p 2499 N95-28691
AD-A289760 ..... p 2499 N95-28692
AD-A289761 ..... p 2611 N95-28693
AD-A289769 ..... p 2498 N95-29457
AD-A289775 ..... p 2639 N95-29458
AD-A289776 ..... p 2556 N95-29459
AD-A289777 ..... p 2497 N95-29282
AD-A289779 ..... p 2693 N95-29460
AD-A289781 ..... p 2536 N95-29461
AD-A289782 ..... p 2526 N95-29598
AD-A289784 ..... p 2644 N95-28694
AD-A289790 ..... p 2696 N95-28695
AD-A289793 ..... p 2568 N95-28696
AD-A289795 ..... p 2611 N95-28697
AD-A289796 ..... p 2697 N95-28698
AD-A289798 ..... p 2551 N95-28699
AD-A289799 ..... p 2499 N95-29123 *
AD-A289801 ..... p 2506 N95-28700
AD-A289802 ..... p 2568 N95-28948
AD-A289803 ..... p 2594 N95-28949
AD-A289806 ..... p 2561 N95-28950
AD-A289807 ..... p 2518 N95-28951
AD-A289808 ..... p 2629 N95-28982
AD-A289811 ..... p 2691 N95-28952
AD-A289813 ..... p 2540 N95-28953
AD-A289817 ..... p 2713 N95-28954
AD-A289875 ..... p 2659 N95-29420 #
AD-A289877 ..... p 2733 N95-29599
AD-A289885 ..... p 2658 N95-28955
AD-A289937 ..... p 2573 N95-29268 #
AD-A289940 ..... p 2542 N95-29269 #
AD-A289943 ..... p 2542 N95-29270 #
AD-A289944 ..... p 2573 N95-29271 #
AD-A289945 ..... p 2542 N95-29272 #
AD-A289946 ..... p 2532 N95-29273 #
AD-A289947 ..... p 2530 N95-28876
AD-A289950 ..... p 2585 N95-29274 #
AD-A289954 ..... p 2563 N95-29275 #
AD-A289956 ..... p 2672 N95-30029 #
AD-A289958 ..... p 2647 N95-29276 #
AD-A289964 ..... p 2523 N95-29277 #
AD-A289968 ..... p 2647 N95-29278 #
AD-A289991 ..... p 2541 N95-29135 #
AD-A289994 ..... p 2523 N95-29136 #
AD-A289995 ..... p 2536 N95-29137 #
AD-A289996 ..... p 2546 N95-30030 #
AD-A290000 ..... p 2738 N95-29279 #
AD-A290023 ..... p 2541 N95-29138 #
AD-A290027 ..... p 2738 N95-29327 #
AD-A290030 ..... p 2670 N95-29311 #
AD-A290034 ..... p 2639 N95-29439 #
AD-A290036 ..... p 2670 N95-29440 #
AD-A290041 ..... p 2556 N95-29441 #
AD-A290045 ..... p 2495 N95-28851
AD-A290048 ..... p 2649 N95-29442 #
AD-A290049 ..... p 2639 N95-29443 #
AD-A290052 ..... p 2663 N95-29477 #
AD-A290054 ..... p 2564 N95-29478 #
AD-A290058 ..... p 2663 N95-29479 #
AD-A290063 ..... p 2555 N95-29328 #
AD-A290070 ..... p 2524 N95-29329 #
AD-A290075 ..... p 2586 N95-29330 #
AD-A290081 ..... p 2621 N95-29333 #
AD-A290085 ..... p 2670 N95-29352 #
AD-A290088 ..... p 2543 N95-29353 #
AD-A290092 ..... p 2700 N95-29354 #
AD-A290099 ..... p 2722 N95-29207 #
AD-A290101 ..... p 2585 N95-29208 #
AD-A290103 ..... p 2714 N95-29209 #
AD-A290107 ..... p 2492 N95-29210 #
AD-A290114 ..... p 2571 N95-29211 #
AD-A290115 ..... p 2575 N95-29421 #
AD-A290117 ..... p 2639 N95-29422 #
AD-A290126 ..... p 2592 N95-29423 #
AD-A290129 ..... p 2586 N95-29425 #
AD-A290135 ..... p 2612 N95-29140 #
AD-A290136 ..... p 2495 N95-30031 #
AD-A290137 ..... p 2635 N95-29141 #
AD-A290146 ..... p 2722 N95-29221 #
AD-A290147 ..... p 2670 N95-29312 #
AD-A290148 ..... p 2555 N95-29313 #
AD-A290149 ..... p 2489 N95-29316 #
AD-A290150 ..... p 2613 N95-29317 #
AD-A290151 ..... p 2555 N95-29318 #
AD-A290152 ..... p 2648 N95-29319 #
AD-A290153 ..... p 2632 N95-29320 #
AD-A290154 ..... p 2648 N95-29321 #
AD-A290156 ..... p 2634 N95-29022 #
AD-A290158 ..... p 2629 N95-29023 #
AD-A290159 ..... p 2569 N95-29024 #
AD-A290164 ..... p 2585 N95-29025 #
AD-A290166 ..... p 2507 N95-29026 #
AD-A290182 ..... p 2629 N95-29054 #
AD-A290183 ..... p 2541 N95-29055 #
AD-A290191 ..... p 2646 N95-29056 #
AD-A290196 ..... p 2492 N95-29057 #
AD-A290199 ..... p 2569 N95-29058 #
AD-A290200 ..... p 2634 N95-29059 #
AD-A290203 ..... p 2569 N95-29060 #
AD-A290206 ..... p 2562 N95-29061 #
AD-A290212 ..... p 2658 N95-29074 #
AD-A290214 ..... p 2562 N95-29075 #
AD-A290215 ..... p 2692 N95-29076 #
AD-A290218 ..... p 2683 N95-29077 #
AD-A290220 ..... p 2562 N95-29078 #
AD-A290221 ..... p 2658 N95-29079 #
AD-A290222 ..... p 2641 N95-29908 #
AD-A290224 ..... p 2647 N95-29143 #
AD-A290225 ..... p 2571 N95-29145 #
AD-A290226 ..... p 2642 N95-29146 #
AD-A290230 ..... p 2647 N95-29223 #
AD-A290231 ..... p 2647 N95-29147 #
AD-A290232 ..... p 2502 N95-29468 #
AD-A290233 ..... p 2575 N95-29469 #
AD-A290236 ..... p 2583 N95-29470 #
AD-A290238 ..... p 2557 N95-29504 #
AD-A290247 ..... p 2544 N95-29505 #
AD-A290249 ..... p 2497 N95-29426 #
AD-A290250 ..... p 2536 N95-29427 #
AD-A290253 ..... p 2512 N95-29168 #
AD-A290261 ..... p 2523 N95-29169 #
AD-A290263 ..... p 2635 N95-29173 #
AD-A290267 ..... p 2553 N95-29176 #
AD-A290269 ..... p 2699 N95-29177 #
AD-A290270 ..... p 2647 N95-29179 #
AD-A290272 ..... p 2571 N95-29181 #
AD-A290273 ..... p 2683 N95-29183 #
AD-A290280 ..... p 2669 N95-29080 #
AD-A290284 ..... p 2553 N95-29081 #
AD-A290285 ..... p 2692 N95-29082 #
AD-A290287 ..... p 2669 N95-29083 #
AD-A290289 ..... p 2669 N95-29084 #
AD-A290294 ..... p 2681 N95-29062 #
AD-A290295 ..... p 2594 N95-29063 #
AD-A290296 ..... p 2668 N95-29064 #
AD-A290297 ..... p 2668 N95-29065 #
AD-A290312 ..... p 2629 N95-29085 #
AD-A290327 ..... p 2634 N95-29086 #
AD-A290330 ..... p 2713 N95-29087 #
AD-A290342 ..... p 2632 N95-29088 #
AD-A290343 ..... p 2714 N95-29089 #
AD-A290349 ..... p 2646 N95-29066 #
AD-A290351 ..... p 2594 N95-29067 #
AD-A290352 ..... p 2569 N95-29068 #
AD-A290355 ..... p 2570 N95-29069 #
AD-A290356 ..... p 2669 N95-29070 #
AD-A290358 ..... p 2497 N95-29322 #
AD-A290362 ..... p 2659 N95-29225 #
AD-A290364 ..... p 2647 N95-29226 #
AD-A290365 ..... p 2692 N95-29227 #
AD-A290367 ..... p 2572 N95-29228 #
AD-A290372 ..... p 2669 N95-29229 #
AD-A290374 ..... p 2542 N95-29230 #
AD-A290386 ..... p 2554 N95-29231 #
AD-A290390 ..... p 2683 N95-29232 #
AD-A290392 ..... p 2669 N95-29233 #
AD-A290398 ..... p 2715 N95-29234 #
AD-A290405 ..... p 2554 N95-29235 #
AD-A290415 ..... p 2609 N95-29450
AD-A290421 ..... p 2574 N95-29387 #
AD-A290427 ..... p 2692 N95-29388 #
AD-A290428 ..... p 2595 N95-29535 #
AD-A290430 ..... p 2724 N95-29818
AD-A290431 ..... p 2650 N95-29536 #
AD-A290432 ..... p 2550 N95-29537 #
AD-A290435 ..... p 2675 N95-29819
AD-A290441 ..... p 2532 N95-29357 #

AD-A290443 ..... p 2641 N95-29359 #
AD-A290446 ..... p 2650 N95-29480 #
AD-A290449 ..... p 2532 N95-29487 #
AD-A290450 ..... p 2671 N95-29488
AD-A290456 ..... p 2557 N95-29489
AD-A290460 ..... p 2674 N95-29490 #
AD-A290461 ..... p 2674 N95-29491 #
AD-A290466 ..... p 2525 N95-29492 #
AD-A290467 ..... p 2716 N95-29506 #
AD-A290471 ..... p 2621 N95-29507 #
AD-A290474 ..... p 2650 N95-29509 #
AD-A290475 ..... p 2544 N95-29510 #
AD-A290481 ..... p 2573 N95-29324 #
AD-A290483 ..... p 2648 N95-29325 #
AD-A290484 ..... p 2699 N95-29148 #
AD-A290486 ..... p 2718 N95-29149 #
AD-A290488 ..... p 2594 N95-29150 #
AD-A290489 ..... p 2737 N95-29151
AD-A290493 ..... p 2714 N95-29152 #
AD-A290498 ..... p 2635 N95-29153 #
AD-A290504 ..... p 2722 N95-29154 #
AD-A290507 ..... p 2632 N95-29155 #
AD-A290513 ..... p 2638 N95-29090 #
AD-A290519 ..... p 2524 N95-29326 #
AD-A290520 ..... p 2637 N95-29872 #
AD-A290521 ..... p 2636 N95-29360 #
AD-A290522 ..... p 2670 N95-29385 #
AD-A290525 ..... p 2716 N95-29493 #
AD-A290526 ..... p 2544 N95-29494 #
AD-A290528 ..... p 2696 N95-29495 #
AD-A290532 ..... p 2500 N95-29496 #
AD-A290542 ..... p 2498 N95-29565 #
AD-A290546 ..... p 2487 N95-29091 #
AD-A290548 ..... p 2692 N95-29092 #
AD-A290553 ..... p 2578 N95-30039 #
AD-A290562 ..... p 2541 N95-29071 #
AD-A290565 ..... p 2665 N95-29863 #
AD-A290566 ..... p 2659 N95-29566 #
AD-A290568 ..... p 2590 N95-29820 #
AD-A290569 ..... p 2549 N95-29550 #
AD-A290570 ..... p 2544 N95-29551 #
AD-A290580 ..... p 2590 N95-29552 #
AD-A290581 ..... p 2666 N95-30040 #
AD-A290584 ..... p 2652 N95-30042 #
AD-A290585 ..... p 2700 N95-29553 #
AD-A290587 ..... p 2725 N95-30043 #
AD-A290588 ..... p 2627 N95-30044 #
AD-A290589 ..... p 2544 N95-29554 #
AD-A290591 ..... p 2588 N95-30045 #
AD-A290593 ..... p 2693 N95-29555 #
AD-A290594 ..... p 2533 N95-29556 #
AD-A290595 ..... p 2636 N95-29557 #
AD-A290597 ..... p 2652 N95-30047 #
AD-A290604 ..... p 2627 N95-30048 #
AD-A290615 ..... p 2671 N95-29558 #
AD-A290623 ..... p 2545 N95-29559 #
AD-A290626 ..... p 2588 N95-30050 #
AD-A290628 ..... p 2650 N95-29515 #
AD-A290639 ..... p 2557 N95-29603 #
AD-A290640 ..... p 2700 N95-29560 #
AD-A290642 ..... p 2526 N95-29561 #
AD-A290644 ..... p 2671 N95-29516 #
AD-A290645 ..... p 2595 N95-29562 #
AD-A290648 ..... p 2557 N95-29563
AD-A290650 ..... p 2650 N95-29517 #
AD-A290655 ..... p 2557 N95-29564 #
AD-A290662 ..... p 2671 N95-29578 #
AD-A290666 ..... p 2596 N95-29582
AD-A290669 ..... p 2705 N95-29519 #
AD-A290674 ..... p 2614 N95-29585 #
AD-A290681 ..... p 2537 N95-29759 #
AD-A290685 ..... p 2545 N95-29586 #
AD-A290690 ..... p 2659 N95-29760 #
AD-A290691 ..... p 2576 N95-29761 #
AD-A290693 ..... p 2651 N95-29644 #
AD-A290694 ..... p 2675 N95-29587 #
AD-A290697 ..... p 2651 N95-29762 #
AD-A290704 ..... p 2682 N95-29588 #
AD-A290710 ..... p 2527 N95-29763 #
AD-A290718 ..... p 2548 N95-29498 #
AD-A290719 ..... p 2664 N95-29499 #
AD-A290720 ..... p 2489 N95-29500 #
AD-A290723 ..... p 2550 N95-29579 #
AD-A290726 ..... p 2693 N95-29521 #
AD-A290727 ..... p 2596 N95-29580 #
AD-A290738 ..... p 2587 N95-29653
AD-A290747 ..... p 2533 N95-29581 #
AD-A290749 ..... p 2681 N95-29481 #
AD-A290755 ..... p 2543 N95-29482
AD-A290761 ..... p 2532 N95-29483 #
AD-A290764 ..... p 2577 N95-29920 #
AD-A290773 ..... p 2534 N95-29922 #
AD-A290778 ..... p 2528 N95-29923 #
AD-A290789 ..... p 2544 N95-29484 #
AD-A290792 ..... p 2671 N95-29485 #
AD-A290796 ..... p 2557 N95-29645 #
AD-A290799 ..... p 2701 N95-29646 #
AD-A290800 ..... p 2621 N95-29497 #
AD-A290801 ..... p 2672 N95-29647 #
AD-A290812 ..... p 2675 N95-29634 #
AD-A290817 ..... p 2545 N95-29635 #
AD-A290823 ..... p 2609 N95-29721 #
AD-A290824 ..... p 2575 N95-29654 #
AD-A290826 ..... p 2533 N95-29722 #
AD-A290831 ..... p 2693 N95-29723 #
AD-A290835 ..... p 2495 N95-29880 #
AD-A290852 ..... p 2528 N95-29864 #
AD-A290853 ..... p 2537 N95-29724 #
AD-A290860 ..... p 2502 N95-29522 #
AD-A290862 ..... p 2665 N95-29831 #
AD-A290875 ..... p 2693 N95-29865 #
AD-A290880 ..... p 2537 N95-29835 #
AD-A290887 ..... p 2601 N95-29866 #
AD-A290889 ..... p 2527 N95-29842 #
AD-A290901 ..... p 2666 N95-30117 #
AD-A290903 ..... p 2694 N95-30060 #
AD-A290905 ..... p 2534 N95-30078 #
AD-A290907 ..... p 2566 N95-30079 #
AD-A290911 ..... p 2653 N95-30080 #
AD-A290912 ..... p 2703 N95-30081 #
AD-A290913 ..... p 2618 N95-30082 #
AD-A290916 ..... p 2637 N95-30083 #
AD-A290920 ..... p 2685 N95-30084 #
AD-A290930 ..... p 2547 N95-30118 #
AD-A290931 ..... p 2596 N95-30119 #
AD-A290937 ..... p 2587 N95-29912 #
AD-A290940 ..... p 2501 N95-29764 #
AD-A290941 ..... p 2617 N95-29765 #
AD-A290942 ..... p 2702 N95-29867 #
AD-A290946 ..... p 2716 N95-29785 #
AD-A290949 ..... p 2527 N95-29732 #
AD-A290952 ..... p 2494 N95-29733 #
AD-A290953 ..... p 2651 N95-29735 #
AD-A290956 ..... p 2651 N95-29736 #
AD-A290960 ..... p 2616 N95-29737 #
AD-A290965 ..... p 2559 N95-29991 #
AD-A290966 ..... p 2493 N95-29873 #
AD-A290997 ..... p 2665 N95-29874 #
AD-A290998 ..... p 2564 N95-29511 #
AD-A290999 ..... p 2586 N95-29514 #
AD-A291003 ..... p 2558 N95-29875 #
AD-A291010 ..... p 2557 N95-29655 #
AD-A291011 ..... p 2583 N95-29656 #
AD-A291015 ..... p 2664 N95-29657 #
AD-A291016 ..... p 2716 N95-29658 #
AD-A291018 ..... p 2684 N95-29659 #
AD-A291019 ..... p 2587 N95-29660 #
AD-A291020 ..... p 2701 N95-29661 #
AD-A291036 ..... p 2622 N95-29662 #
AD-A291037 ..... p 2685 N95-29681 #
AD-A291058 ..... p 2500 N95-29950 #
AD-A291059 ..... p 2685 N95-29951 #
AD-A291064 ..... p 2682 N95-29952 #
AD-A291065 ..... p 2502 N95-29967 #
AD-A291070 ..... p 2702 N95-29969 #
AD-A291074 ..... p 2618 N95-29970 #
AD-A291083 ..... p 2665 N95-29971 #
AD-A291084 ..... p 2491 N95-29972 #
AD-A291085 ..... p 2664 N95-29636 #
AD-A291087 ..... p 2575 N95-29637 #
AD-A291092 ..... p 2527 N95-29638 #
AD-A291103 ..... p 2651 N95-29639 #
AD-A291121 ..... p 2701 N95-29766 #
AD-A291122 ..... p 2716 N95-29767 #
AD-A291125 ..... p 2675 N95-29768 #
AD-A291128 ..... p 2577 N95-29913 #
AD-A291129 ..... p 2587 N95-29914 #
AD-A291136 ..... p 2547 N95-30120 #
AD-A291137 ..... p 2654 N95-30121 #
AD-A291138 ..... p 2567 N95-30122 #
AD-A291139 ..... p 2597 N95-30123 #
AD-A291142 ..... p 2567 N95-30124 #
AD-A291145 ..... p 2654 N95-30125 #
AD-A291147 ..... p 2673 N95-30126 #
AD-A291149 ..... p 2661 N95-30295 #
AD-A291150 ..... p 2551 N95-30296 #
AD-A291151 ..... p 2675 N95-30297 #
AD-A291154 ..... p 2718 N95-30298 #
AD-A291155 ..... p 2551 N95-30299 #
AD-A291160 ..... p 2659 N95-29915 #
AD-A291161 ..... p 2551 N95-29924 #
AD-A291164 ..... p 2565 N95-29925 #
AD-A291169 ..... p 2546 N95-29926 #
AD-A291170 ..... p 2637 N95-29927 #
AD-A291171 ..... p 2558 N95-29928 #
AD-A291176 ..... p 2596 N95-29929 #
AD-A291177 ..... p 2587 N95-29930 #
AD-A291180 ..... p 2587 N95-29931 #
AD-A291181 ..... p 2651 N95-29932 #
AD-A291184 ..... p 2731 N95-29916 #
AD-A291185 ..... p 2735 N95-29917 #
AD-A291200 ..... p 2702 N95-29973 #
AD-A291201 ..... p 2702 N95-29974 #
AD-A291203 ..... p 2559 N95-29975 #
AD-A291209 ..... p 2618 N95-29976 #
AD-A291217 ..... p 2601 N95-29977 #
AD-A291218 ..... p 2702 N95-29978 #
AD-A291219 ..... p 2665 N95-29979 #
AD-A291223 ..... p 2588 N95-29980 #
AD-A291224 ..... p 2618 N95-29981 #
AD-A291227 ..... p 2559 N95-29982 #
AD-A291237 ..... p 2504 N95-29992 #
AD-A291243 ..... p 2627 N95-29993 #
AD-A291247 ..... p 2534 N95-29994 #
AD-A291253 ..... p 2534 N95-30085 #
AD-A291264 ..... p 2637 N95-29995 #
AD-A291268 ..... p 2652 N95-29996 #
AD-A291270 ..... p 2637 N95-29933 #
AD-A291275 ..... p 2501 N95-29934 #
AD-A291282 ..... p 2720 N95-29935 #
AD-A291297 ..... p 2720 N95-29936 #
AD-A291298 ..... p 2588 N95-29937 #
AD-A291300 ..... p 2565 N95-29938 #
AD-A291302 ..... p 2546 N95-29939 #
AD-A291310 ..... p 2559 N95-29940 #
AD-A291315 ..... p 2593 N95-29941 #
AD-A291323 ..... p 2685 N95-29942 #
AD-A291338 ..... p 2641 N95-29943 #
AD-A291339 ..... p 2627 N95-29944 #
AD-A291342 ..... p 2685 N95-29945 #
AD-A291345 ..... p 2593 N95-29946 #
AD-A291346 ..... p 2724 N95-29947 #
AD-A291347 ..... p 2577 N95-29948 #
AD-A291355 ..... p 2602 N95-29949 #
AD-A291364 ..... p 2603 N95-29953 #
AD-A291365 ..... p 2578 N95-30087 #
AD-A291366 ..... p 2601 N95-30061 #
AD-A291368 ..... p 2703 N95-30062 #
AD-A291384 ..... p 2653 N95-30063 #
AD-A291389 ..... p 2703 N95-30064 #
AD-A291396 ..... p 2694 N95-30065 #
AD-A291404 ..... p 2550 N95-29918 #
AD-A291406 ..... p 2627 N95-30066 #
AD-A291410 ..... p 2717 N95-30068 #
AD-A291411 ..... p 2631 N95-30069 #
AD-A291412 ..... p 2566 N95-30070 #
AD-A291434 ..... p 2547 N95-30071 #
AD-A291435 ..... p 2559 N95-30072 #
AD-A291443 ..... p 2559 N95-30073 #
AD-A291447 ..... p 2558 N95-29769 #
AD-A291448 ..... p 2599 N95-29523 #
AD-A291456 ..... p 2548 N95-29525 #
AD-A291479 ..... p 2527 N95-29770 #
AD-A291486 ..... p 2537 N95-29526 #
AD-A291500 ..... p 2637 N95-29846 #
AD-A291505 ..... p 2558 N95-29847 #
AD-A291518 ..... p 2490 N95-29853 #
AD-A291520 ..... p 2493 N95-29855 #
AD-A291544 ..... p 2631 N95-29856 #
AD-A291550 ..... p 2645 N95-29934
AD-A291553 ..... p 2640 N95-28935
AD-A291565 ..... p 2552 N95-28936
AD-A291569 ..... p 2638 N95-28937
AD-A291577 ..... p 2619 N95-28938
AD-A291581 ..... p 2552 N95-28939
AD-A291595 ..... p 2634 N95-28940
AD-A291601 ..... p 2598 N95-28931
AD-A291604 ..... p 2634 N95-28941
AD-A291606 ..... p 2698 N95-28932
AD-A291607 ..... p 2531 N95-28942
AD-A291608 ..... p 2565 N95-29601
AD-A291670 ..... p 2661 N95-28788
AD-A291688 ..... p 2552 N95-28943
AD-A291690 ..... p 2644 N95-28782
AD-A291798 ..... p 2524 N95-29409 #
AD-A291803 ..... p 2508 N95-29410 #
AD-A291804 ..... p 2489 N95-29428 #
AD-A291807 ..... p 2649 N95-29429 #
AD-A291809 ..... p 2564 N95-29430 #
AD-A291824 ..... p 2693 N95-29431 #
AD-A291836 ..... p 2639 N95-29432 #
AD-A291856 ..... p 2639 N95-29434 #
AD-A291867 ..... p 2649 N95-29435 #
AD-A291868 ..... p 2543 N95-29436 #
AD-A291875 ..... p 2497 N95-29437 #
AD-A291905 ..... p 2715 N95-29486 #
AD-A291907 ..... p 2715 N95-29444 #
AD-A291908 ..... p 2510 N95-29284 #
AD-A291909 ..... p 2543 N95-29355 #
AD-A291910 ..... p 2648 N95-29356 #
AD-A291911 ..... p 2543 N95-29358 #
AD-A291913 ..... p 2583 N95-29361 #
AD-A291917 ..... p 2715 N95-29438 #
AD-A291919 ..... p 2691 N95-28944 #
AD-A291920 ..... p 2593 N95-28789 #
AD-A291921 ..... p 2698 N95-28914 #
AD-A291932 ..... p 2493 N95-28790 #
AD-A291937 ..... p 2539 N95-28850 #

AD-A291942 ..... p 2562 N95-29018 #
AD-A291946 ..... p 2556 N95-29472 #
AD-A291952 ..... p 2552 N95-28984 #
AD-A291953 ..... p 2548 N95-29019 #
AD-A291955 ..... p 2640 N95-29020 #
AD-A292006 ..... p 2701 N95-29571 #
AD-A292008 ..... p 2540 N95-29021 #
AD-A292015 ..... p 2651 N95-29861 #
AD-A292017 ..... p 2722 N95-29182 #
AD-A292023 ..... p 2594 N95-28853 #
AD-A292024 ..... p 2590 N95-29184 #
AD-A292026 ..... p 2611 N95-30348 #
AD-A292027 ..... p 2523 N95-29185 #
AD-A292028 ..... p 2554 N95-29186 #
AD-A292029 ..... p 2571 N95-29187 #
AD-A292037 ..... p 2635 N95-29188 #
AD-A292042 ..... p 2523 N95-29189 #
AD-A292047 ..... p 2536 N95-29298 #
AD-A292048 ..... p 2563 N95-29301 #
AD-A292050 ..... p 2648 N95-29304 #
AD-A292052 ..... p 2550 N95-29307 #
AD-A292054 ..... p 2542 N95-29314 #
AD-A292069 ..... p 2555 N95-29308 #
AD-A292070 ..... p 2648 N95-29310 #
AD-A292076 ..... p 2630 N95-29237 * #
AD-A292079 ..... p 2636 N95-29238 #
AD-A292096 ..... p 2563 N95-29239 #
AD-A292097 ..... p 2554 N95-29240 #
AD-A292104 ..... p 2638 N95-28918 #
AD-A292107 ..... p 2691 N95-28919 #
AD-A292113 ..... p 2487 N95-28921 #
AD-A292114 ..... p 2608 N95-28922 #
AD-A292115 ..... p 2602 N95-28858 #
AD-A292135 ..... p 2533 N95-29572 #
AD-A292142 ..... p 2542 N95-29195 #
AD-A292149 ..... p 2629 N95-29160 #
AD-A292159 ..... p 2523 N95-29124 #
AD-A292165 ..... p 2647 N95-29125 #
AD-A292172 ..... p 2497 N95-29126 #
AD-A292176 ..... p 2555 N95-29266 #
AD-A292177 ..... p 2715 N95-29267 #
AD-A292180 ..... p 2540 N95-28925 #
AD-A292185 ..... p 2661 N95-28926 #
AD-A292187 ..... p 2718 N95-28927 #
AD-A292188 ..... p 2612 N95-28985 #
AD-A292194 ..... p 2552 N95-28986 #
AD-A292200 ..... p 2681 N95-28987 #
AD-A292206 ..... p 2662 N95-28988 #
AD-A292215 ..... p 2649 N95-29376 #
AD-A292219 ..... p 2648 N95-29285 #
AD-A292221 ..... p 2658 N95-29196 #
AD-A292224 ..... p 2630 N95-29198 #
AD-A292227 ..... p 2602 N95-29200 #
AD-A292230 ..... p 2602 N95-29201 #
AD-A292231 ..... p 2554 N95-29203 #
AD-A292232 ..... p 2570 N95-29127 #
AD-A292236 ..... p 2669 N95-29128 #
AD-A292237 ..... p 2645 N95-28894 #
AD-A292238 ..... p 2721 N95-28877 #
AD-A292242 ..... p 2645 N95-28878 #
AD-A292243 ..... p 2658 N95-28879 #
AD-A292244 ..... p 2721 N95-28880 #
AD-A292245 ..... p 2645 N95-28881 #
AD-A292246 ..... p 2645 N95-28883 #
AD-A292247 ..... p 2658 N95-28884 #
AD-A292248 ..... p 2645 N95-28886 #
AD-A292253 ..... p 2494 N95-28887 #
AD-A292254 ..... p 2691 N95-28888 #
AD-A292261 ..... p 2535 N95-28889 #
AD-A292262 ..... p 2668 N95-28890 #
AD-A292274 ..... p 2539 N95-28891 #
AD-A292276 ..... p 2539 N95-28860 #
AD-A292284 ..... p 2697 N95-28870 #
AD-A292285 ..... p 2668 N95-28861 #
AD-A292286 ..... p 2668 N95-28863 #
AD-A292295 ..... p 2612 N95-28871 #
AD-A292296 ..... p 2619 N95-28872 #
AD-A292297 ..... p 2739 N95-30074 #
AD-A292298 ..... p 2539 N95-28864 #
AD-A292301 ..... p 2628 N95-28865 #
AD-A292302 ..... p 2507 N95-28867 #
AD-A292305 ..... p 2691 N95-28868 #
AD-A292306 ..... p 2540 N95-28963 #
AD-A292307 ..... p 2646 N95-28964 #
AD-A292308 ..... p 2584 N95-28892 #
AD-A292310 ..... p 2536 N95-29473 #
AD-A292312 ..... p 2556 N95-29474 #
AD-A292317 ..... p 2718 N95-28857 #
AD-A292318 ..... p 2738 N95-29475 #
AD-A292321 ..... p 2640 N95-28792 #
AD-A292323 ..... p 2633 N95-28793 #
AD-A292326 ..... p 2640 N95-28794 #
AD-A292331 ..... p 2697 N95-28795 #
AD-A292332 ..... p 2628 N95-28796 #
AD-A292333 ..... p 2720 N95-29879 #
AD-A292340 ..... p 2597 N95-30293 #
AD-A292343 ..... p 2536 N95-29467 #
AD-A292344 ..... p 2525 N95-29476 #
AD-A292346 ..... p 2526 N95-29533 #
AD-A292348 ..... p 2650 N95-29534 #
AD-A292353 ..... p 2546 N95-29983 #
AD-A292366 ..... p 2558 N95-29862 #
AD-A292375 ..... p 2720 N95-28797 #
AD-A292396 ..... p 2658 N95-28965 #
AD-A292397 ..... p 2697 N95-28798 #
AD-A292402 ..... p 2697 N95-28799 #
AD-A292413 ..... p 2619 N95-28989 #
AD-A292414 ..... p 2569 N95-28990 #
AD-A292419 ..... p 2629 N95-28991 #
AD-A292420 ..... p 2601 N95-29905 #
AD-A292422 ..... p 2698 N95-28992 #
AD-A292423 ..... p 2713 N95-28993 #
AD-A292431 ..... p 2692 N95-28994 #
AD-A292433 ..... p 2646 N95-28995 #
AD-A292435 ..... p 2680 N95-29072 #
AD-A292436 ..... p 2698 N95-28996 #
AD-A292437 ..... p 2585 N95-29053 #
AD-A292438 ..... p 2698 N95-28997 #
AD-A292439 ..... p 2698 N95-28998 #
AD-A292440 ..... p 2683 N95-28999 #
AD-A292441 ..... p 2681 N95-29000 #
AD-A292442 ..... p 2703 N95-29001 #
AD-A292443 ..... p 2553 N95-29002 #
AD-A292444 ..... p 2703 N95-29003 #
AD-A292462 ..... p 2582 N95-29004 #
AD-A292463 ..... p 2561 N95-29005 #
AD-A292464 ..... p 2699 N95-29006 #
AD-A292465 ..... p 2584 N95-29007 #
AD-A292467 ..... p 2646 N95-29008 #
AD-A292468 ..... p 2718 N95-29009 #
AD-A292469 ..... p 2561 N95-29010 #
AD-A292470 ..... p 2704 N95-29011 #
AD-A292474 ..... p 2592 N95-29012 #
AD-A292476 ..... p 2713 N95-29013 #
AD-A292478 ..... p 2562 N95-29014 #
AD-A292480 ..... p 2562 N95-29073 #
AD-A292481 ..... p 2561 N95-28859 #
AD-A292483 ..... p 2712 N95-28862 #
AD-A292488 ..... p 2633 N95-28866 #
AD-A292492 ..... p 2719 N95-29756 #
AD-A292494 ..... p 2713 N95-28933 #
AD-A292495 ..... p 2722 N95-29287
AD-A292505 ..... p 2635 N95-29161 #
AD-A292510 ..... p 2712 N95-28869 #
AD-A292511 ..... p 2680 N95-28810 #
AD-A292512 ..... p 2638 N95-29162 #
AD-A292513 ..... p 2563 N95-29163 #
AD-A292518 ..... p 2563 N95-29164 #
AD-A292521 ..... p 2714 N95-29165 #
AD-A292522 ..... p 2492 N95-28811 #
AD-A292523 ..... p 2560 N95-28812 #
AD-A292524 ..... p 2560 N95-28813 #
AD-A292525 ..... p 2645 N95-28814 #
AD-A292527 ..... p 2712 N95-28815 #
AD-A292528 ..... p 2712 N95-28874 #
AD-A292529 ..... p 2553 N95-29166 #
AD-A292530 ..... p 2629 N95-28873 #
AD-A292533 ..... p 2582 N95-28966 #
AD-A292536 ..... p 2713 N95-28967 #
AD-A292537 ..... p 2646 N95-28968 #
AD-A292538 ..... p 2640 N95-28969 #
AD-A292539 ..... p 2640 N95-28970 #
AD-A292542 ..... p 2561 N95-28971 #
AD-A292546 ..... p 2612 N95-28972 #
AD-A292552 ..... p 2683 N95-28973 #
AD-A292553 ..... p 2642 N95-28974 #
AD-A292567 ..... p 2619 N95-28975 #
AD-A292571 ..... p 2642 N95-28976 #
AD-A292573 ..... p 2496 N95-28977 #
AD-A292574 ..... p 2723 N95-29573 #
AD-A292576 ..... p 2662 N95-28978 #
AD-A292577 ..... p 2664 N95-29574 #
AD-A292579 ..... p 2552 N95-28979 #
AD-A292585 ..... p 2698 N95-28980 #
AD-A292586 ..... p 2692 N95-28981 #
AD-A292588 ..... p 2542 N95-29288 #
AD-A292590 ..... p 2555 N95-29289 #
AD-A292592 ..... p 2555 N95-29290 #
AD-A292598 ..... p 2586 N95-29292 #
AD-A292601 ..... p 2613 N95-29293 #
AD-A292602 ..... p 2533 N95-29575 #
AD-A292606 ..... p 2650 N95-29576 #
AD-A292607 ..... p 2664 N95-29577 #
AD-A292619 ..... p 2699 N95-29295 #
AD-A292627 ..... p 2670 N95-29296 #
AD-A292630 ..... p 2648 N95-29297 #
AD-A292641 ..... p 2641 N95-29378 #
AD-A292642 ..... p 2700 N95-29379 #
AD-A292646 ..... p 2574 N95-29380 #
AD-A292647 ..... p 2643 N95-29381
AD-A292650 ..... p 2574 N95-29382 #
AD-A292651 ..... p 2556 N95-29383 #
AD-A292653 ..... p 2564 N95-29384 #
AD-A292655 ..... p 2556 N95-29386
AD-A292658 ..... p 2700 N95-29412 #
AD-A292659 ..... p 2614 N95-29413 #
AD-A292670 ..... p 2477 N95-29414 #
AD-A292674 ..... p 2621 N95-29416 #
AD-A292686 ..... p 2564 N95-29417 #
AD-A292690 ..... p 2675 N95-29906 #

AD-B17200L ..... p 2707 N95-29745 #
AD-B175931L ..... p 2707 N95-29743 #
AD-B175932L ..... p 2707 N95-29740 #
AD-B175957L ..... p 2709 N95-29809 #
AD-B176252L ..... p 2707 N95-29741 #
AD-B176253L ..... p 2707 N95-29738 #
AD-B176254L ..... p 2707 N95-29742 #
AD-B176255L ..... p 2707 N95-29739 #
AD-B178946L ..... p 2709 N95-29810 #
AD-B178947L ..... p 2711 N95-30033 #
AD-B178949L ..... p 2710 N95-29813 #
AD-B179181L ..... p 2707 N95-29744 #
AD-B179183L ..... p 2708 N95-29746 #
AD-B179223L ..... p 2708 N95-29747 #
AD-B179442L ..... p 2710 N95-29843 #
AD-B179443L ..... p 2710 N95-29812 #
AD-B179858L ..... p 2708 N95-29749 #
AD-B179859L ..... p 2693 N95-29748 #
AD-B180028L ..... p 2710 N95-29857 #
AD-B180030L ..... p 2710 N95-29844 #
AD-B191980L ..... p 2710 N95-29841 #
AD-B191994L ..... p 2709 N95-29802 #
AD-B191995L ..... p 2709 N95-29803 #
AD-B191996L ..... p 2709 N95-29808 #
AD-B191997L ..... p 2711 N95-30032 #
AD-B191998L ..... p 2706 N95-29734 #
AD-B191999L ..... p 2709 N95-29801 #
AD-B192000L ..... p 2706 N95-29731 #
AD-B195511L ..... p 2709 N95-29789 #
AD-B195513L ..... p 2708 N95-29755 #
AD-B195514L ..... p 2705 N95-29567 #

AD-D017266 ..... p 2699 N95-29283
AD-D017268 ..... p 2554 N95-29236
AD-D017273 ..... p 2641 N95-29600
AD-D017321 ..... p 2547 N95-30132 #
AD-D017322 ..... p 2718 N95-30164 #
AD-D017323 ..... p 2567 N95-30165 #
AD-D017325 ..... p 2682 N95-30051 #
AD-D017326 ..... p 2566 N95-30052 #
AD-D017327 ..... p 2702 N95-30053 #
AD-D017329 ..... p 2566 N95-30055 #
AD-D017341 ..... p 2703 N95-30166
AD-D017378 ..... p 2683 N95-28783
AD-D017379 ..... p 2530 N95-28854
AD-D017380 ..... p 2539 N95-28784
AD-D017382 ..... p 2588 N95-28785
AD-D017383 ..... p 2541 N95-29194
AD-D017384 ..... p 2585 N95-29217
AD-D017389 ..... p 2560 N95-28855
AD-D017393 ..... p 2582 N95-29220
AD-D017397 ..... p 2701 N95-29602
AD-D017399 ..... p 2564 N95-29568 #
AD-D017400 ..... p 2545 N95-29569 #
AD-D017403 ..... p 2564 N95-29570 #
AD-D017404 ..... p 2589 N95-28791 #
AD-D017408 ..... p 2566 N95-30075 #
AD-D017409 ..... p 2703 N95-30076 #

AEDC-TR-94-17 ..... p 2556 N95-29459

AFGWC/TN-95-001 ..... p 2651 N95-29639 #

AFIT/CI/CIA-94-004 ..... p 2569 N95-28990 #
AFIT/CI/CIA-94-042D ..... p 2643 N95-28690
AFIT/CI/CIA-94-044D ..... p 2540 N95-28953
AFIT/CI/CIA-94-158 ..... p 2499 N95-28692
AFIT/CI/CIA-94-166 ..... p 2499 N95-28691
AFIT/CI/CIA-94-168 ..... p 2568 N95-28696
AFIT/CI/CIA-94-170 ..... p 2568 N95-28948
AFIT/CI/CIA-94-173 ..... p 2619 N95-28989 #
AFIT/CI/CIA-94-174 ..... p 2681 N95-29000 #
AFIT/CI/CIA-95-001D ..... p 2574 N95-29380 #
AFIT/CI/CIA-95-007 ..... p 2553 N95-29002 #

AFIT/DS/AA/94-7 ..... p 2489 N95-29500 #

AFIT/EN/TR-94-07 ..... p 2653 N95-30080 #

AFIT/GAE/ENY/94D-6 ..... p 2527 N95-29758 #
AFIT/GAE/ENY/94D-8 ..... p 2527 N95-29770 #

AFIT/GCS/ENG-94D-07 ..... p 2721 N95-28907

AFIT/GCS/ENG/94D-04 ..... p 2659 N95-29760 #

AFOSR-0020TR ..... p 2489 N95-29316 #

AFOSR-94-0206TR ..... p 2633 N95-28866 #
AFOSR-94-0682TR ..... p 2634 N95-28915
AFOSR-95-0002TR ..... p 2609 N95-29450
AFOSR-95-0004TR ..... p 2544 N95-29505 #
AFOSR-95-0005TR ..... p 2492 N95-29210 #
AFOSR-95-0006TR ..... p 2670 N95-29312 #
AFOSR-95-0011 ..... p 2669 N95-29070 #
AFOSR-95-0012TR ..... p 2585 N95-29025 #
AFOSR-95-0013TR ..... p 2634 N95-29022 #
AFOSR-95-0015TR ..... p 2632 N95-29320 #
AFOSR-95-0016TR ..... p 2512 N95-29168 #
AFOSR-95-0017TR ..... p 2536 N95-29427 #
AFOSR-95-0019TR ..... p 2693 N95-29865 #
AFOSR-95-0021TR ..... p 2639 N95-29422 #
AFOSR-95-0038TR ..... p 2553 N95-29176 #
AFOSR-95-0041TR ..... p 2699 N95-29177 #
AFOSR-95-0043TR ..... p 2692 N95-29082 #
AFOSR-95-0044TR ..... p 2681 N95-29062 #
AFOSR-95-0046TR ..... p 2592 N95-29423 #
AFOSR-95-0048TR ..... p 2502 N95-29468 #
AFOSR-95-0049TR ..... p 2575 N95-29469 #
AFOSR-95-0050TR ..... p 2523 N95-29169 #
AFOSR-95-0051TR ..... p 2575 N95-29421 #
AFOSR-95-0052TR ..... p 2571 N95-29211 #
AFOSR-95-0054TR ..... p 2571 N95-29145 #
AFOSR-95-0055TR ..... p 2658 N95-29074 #
AFOSR-95-0056TR ..... p 2569 N95-29024 #
AFOSR-95-0057TR ..... p 2571 N95-29181 #
AFOSR-95-0064TR ..... p 2586 N95-29514 #
AFOSR-95-0066TR ..... p 2534 N95-29922 #
AFOSR-95-0072TR ..... p 2694 N95-30060 #
AFOSR-95-0073TR ..... p 2577 N95-29920 #
AFOSR-95-0075TR ..... p 2576 N95-29761 #
AFOSR-95-0077TR ..... p 2577 N95-29913 #
AFOSR-95-0078TR ..... p 2675 N95-29768 #
AFOSR-95-0079TR ..... p 2597 N95-30123 #
AFOSR-95-0080TR ..... p 2665 N95-29971 #
AFOSR-95-0081TR ..... p 2731 N95-29916 #
AFOSR-95-0082TR ..... p 2491 N95-29972 #
AFOSR-95-0083TR ..... p 2618 N95-29981 #
AFOSR-95-0085TR ..... p 2716 N95-29767 #
AFOSR-95-0086TR ..... p 2627 N95-29993 #
AFOSR-95-0088TR ..... p 2575 N95-29637 #
AFOSR-95-0090TR ..... p 2618 N95-29970 #
AFOSR-95-0095TR ..... p 2583 N95-29361 #
AFOSR-95-0097TR ..... p 2691 N95-28944 #
AFOSR-95-0098TR ..... p 2552 N95-28984 #
AFOSR-95-0099TR ..... p 2593 N95-29941 #
AFOSR-95-0101TR ..... p 2664 N95-29636 #
AFOSR-95-0103TR ..... p 2735 N95-29917 #
AFOSR-95-0104TR ..... p 2637 N95-29933 #
AFOSR-95-0105TR ..... p 2547 N95-30071 #
AFOSR-95-0106TR ..... p 2593 N95-29946 #
AFOSR-95-0110TR ..... p 2638 N95-26937
AFOSR-95-0111TR ..... p 2562 N95-29018 #
AFOSR-95-0112TR ..... p 2523 N95-29124 #
AFOSR-95-0115TR ..... p 2698 N95-28998 #
AFOSR-95-01154TR ..... p 2692 N95-28994 #
AFOSR-95-0116TR ..... p 2585 N95-29053 #
AFOSR-95-0117TR ..... p 2703 N95-29001 #
AFOSR-95-0118TR ..... p 2563 N95-29164 #
AFOSR-95-0120TR ..... p 2561 N95-28859 #
AFOSR-95-0121TR ..... p 2712 N95-28869 #
AFOSR-95-0124TR ..... p 2713 N95-28967 #
AFOSR-95-0126TR ..... p 2704 N95-29011 #
AFOSR-95-0126TR ..... p 2562 N95-29014 #
AFOSR-95-0127TR ..... p 2713 N95-28933 #
AFOSR-95-0128TR ..... p 2564 N95-29417 #
AFOSR-95-0129TR ..... p 2563 N95-29163 #
AFOSR-95-0132TR ..... p 2560 N95-28812 #
AFOSR-95-0133TR ..... p 2560 N95-28813 #
AFOSR-95-0135TR ..... p 2714 N95-29165 #
AFOSR-95-01377R ..... p 2712 N95-28815 #
AFOSR-95-0138TR ..... p 2719 N95-29756 #
AFOSR-95-0141TR ..... p 2712 N95-28874 #
AFOSR-95-0142TR ..... p 2592 N95-29012 #
AFOSR-95-0143TR ..... p 2561 N95-29010 #
AFOSR-95-0144TR ..... p 2586 N95-29292 #
AFOSR-95-0147TR ..... p 2712 N95-28862 #
AFOSR-95-0149TR ..... p 2699 N95-29295 #
AFOSR-95-0153TR ..... p 2699 N95-29006 #
AFOSR-95-0154TR ..... p 2718 N95-29009 #
AFOSR-95-0155TR ..... p 2584 N95-29007 #
AFOSR-95-0159TR ..... p 2582 N95-29004 #
AFOSR-95-0160TR ..... p 2561 N95-29005 #
AFOSR-95-0164TR ..... p 2680 N95-28810 #
AFOSR-95-0165TR ..... p 2703 N95-29003 #
AFOSR-95-0175TR ..... p 2614 N95-29413 #
AFOSR-95-0180TR ..... p 2552 N95-28979 #
AFOSR-95-0237TR ..... p 2564 N95-29384 #
AFOSR-95-05TR ..... p 2703 N95-30062 #

AGARD-AG-300-VOL-13 ..... p 2498 N95-29503 #

AGARD-CP-554 ..... p 2676 N95-29604 #

AI-M-1468 ..... p 2670 N95-29440 #
AI-M-1489 ..... p 2670 N95-29352 #
AI-M-1494 ..... p 2556 N95-29441 #

AI-TR-1495 ..... p 2639 N95-29443 #
AI-TR-1498 ..... p 2647 N95-29179 #
AI-TR-1500 ..... p 2564 N95-29478 #

AIAA PAPER 95-1797 ..... p 2489 N95-29402 * #
AIAA PAPER 95-2167 ..... p 2574 N95-29405 * #
AIAA PAPER 95-2601 ..... p 2680 N95-28893 * #
AIAA PAPER 95-2613 ..... p 2492 N95-30253 * #
AIAA PAPER 95-2616 ..... p 2491 N95-30091 * #
AIAA PAPER 95-2787 ..... p 2477 N95-30229 * #
AIAA PAPER 95-2964 ..... p 2511 N95-29642 * #
AIAA PAPER 95-2968 ..... p 2510 N95-29114 * #
AIAA PAPER 95-3037 ..... p 2501 N95-30007 * #
AIAA PAPER 95-3050 ..... p 2589 N95-29112 * #
AIAA PAPER 95-3072 ..... p 2503 N95-30067 * #

AIM-1447 ..... p 2621 N95-29333 #
AIM-1462 ..... p 2722 N95-29207 #
AIM-1491 ..... p 2663 N95-29479 #

AL-AO-TN-1995-0001 ..... p 2638 N95-29162 #

AL/AO-TM-1995-0001 ..... p 2635 N95-29161 #

AL/AO-TP-1994-0014 ..... p 2633 N95-28793 #

AL/CF-TE-1994-0051 ..... p 2640 N95-28683

AL/CF-TR-1994-0091 ..... p 2636 N95-29360 #
AL/CF-TR-1994-0112 ..... p 2640 N95-28792 #
AL/CF-TR-1994-0113 ..... p 2654 N95-30125 #

AL/HR-TR-1994-0138 ..... p 2641 N95-29943 #

AL/OE-TR-1994-0079 ..... p 2585 N95-29274 #

AMSMI-RD-SS-94-16 ..... p 2561 N95-28950

AMSMI/RD-SE-95-2 ..... p 2648 N95-29356 #

ANL-HEP-CP-94-63 ..... p 2695 N95-30186 #
ANL-HEP-CP-94-70 ..... p 2695 N95-30185 #

ANL-94/44 ..... p 2548 N95-29280 #

ANL/ES/CP-82070 ..... p 2577 N95-29988 #

ANL/ES/PP-79002 ..... p 2578 N95-30187 #

ANL/ET/CP-82419 ..... p 2665 N95-29987 #
ANL/ET/CP-83565 ..... p 2716 N95-29984 #

ANL/IPNS/CP-83322 ..... p 2714 N95-29134 #

ANL/MCS-TM-190 ..... p 2610 N95-30176 #

ANL/MCS/CP-83621 ..... p 2633 N95-30114 #
ANL/MCS/CP-84114 ..... p 2652 N95-30020 #
ANL/MCS/CP-84514 ..... p 2659 N95-29985 #

ANL/MSD/CP-79956 ..... p 2717 N95-29986 #
ANL/MSD/CP-83455 ..... p 2537 N95-30018 #
ANL/MSD/CP-84502 ..... p 2717 N95-30077 #

ANL/PHY/CP-84488 ..... p 2694 N95-30019 #

ANL/XFD/CP-82848 ..... p 2718 N95-30184 #

ANS/A-26-03-R-009 ..... p 2582 N95-28966 #

AOARD-TR-94-10 ..... p 2720 N95-29879 #
AOARD-TR-94-12 ..... p 2546 N95-29983 #
AOARD-TR-94-13 ..... p 2650 N95-29534 #
AOARD-TR-94-14 ..... p 2601 N95-29905 #
AOARD-TR-94-16 ..... p 2526 N95-29533 #
AOARD-TR-94-21 ..... p 2558 N95-29862 #
AOARD-TR-94-27 ..... p 2525 N95-29476 #
AOARD-TR-94-31 ..... p 2536 N95-29467 #
AOARD-TR-94-32 ..... p 2536 N95-29473 #
AOARD-TR-94-33 ..... p 2597 N95-30293 #
AOARD-TR-94-36 ..... p 2739 N95-30074 #
AOARD-TR-94-37 ..... p 2738 N95-29475 #
AOARD-TR-94-39 ..... p 2556 N95-29474 #

APL-UW-TM-1-94 ..... p 2685 N95-29942 #

APL-UW-TR-9411 ..... p 2629 N95-29085 #

AR-008-372 ..... p 2497 N95-29362
AR-008-420 ..... p 2498 N95-29445
AR-10154.01 ..... p 2587 N95-29912 #

ARC-R95-236 ..... p 2726 N95-28822 * #

ARC-1272 ..... p 2726 N95-28822 * #

ARCCB-TR-94036 ..... p 2594 N95-28949
ARCCB-TR-94037 ..... p 2541 N95-29138 #
ARCCB-TR-94038 ..... p 2596 N95-30119 #
ARCCB-TR-94044 ..... p 2535 N95-28889 #
ARCCB-TR-94045 ..... p 2668 N95-28890 #
ARCCB-TR-94046 ..... p 2593 N95-28789 #
ARCCB-TR-94048 ..... p 2683 N95-28999 #

ARI-RN-95-06 ..... p 2638 N95-29090 #
ARI-RN-95-08 ..... p 2648 N95-29325 #

ARL-CR-112 ..... p 2621 N95-29507 #
ARL-CR-178 ..... p 2523 N95-29277 #
ARL-CR-214 ..... p 2542 N95-29195 #
ARL-CR-238 ..... p 2590 N95-29538 * #

ARL-MR-233 ..... p 2582 N95-29113 * #
ARL-MR-234 ..... p 2527 N95-29825 * #

ARL-TR-273-2 ..... p 2555 N95-29266 #
ARL-TR-306 ..... p 2551 N95-28687
ARL-TR-545 ..... p 2618 N95-29976 #
ARL-TR-628 ..... p 2530 N95-28876
ARL-TR-649 ..... p 2546 N95-30030 #
ARL-TR-651 ..... p 2536 N95-29137 #
ARL-TR-652 ..... p 2524 N95-29329 #
ARL-TR-654 ..... p 2585 N95-29208 #
ARL-TR-655 ..... p 2543 N95-29353 #
ARL-TR-656 ..... p 2547 N95-30118 #
ARL-TR-657 ..... p 2523 N95-29136 #
ARL-TR-663 ..... p 2569 N95-29058 #
ARL-TR-666 ..... p 2596 N95-29929 #
ARL-TR-669 ..... p 2537 N95-29835 #
ARL-TR-671 ..... p 2647 N95-29276 #
ARL-TR-677 ..... p 2532 N95-29487 #
ARL-TR-680 ..... p 2534 N95-29994 #
ARL-TR-681 ..... p 2541 N95-29135 #
ARL-TR-682 ..... p 2540 N95-28963 #
ARL-TR-695 ..... p 2720 N95-29936 #
ARL-TR-698 ..... p 2565 N95-29938 #
ARL-TR-700 ..... p 2713 N95-29013 #
ARL-TR-762 ..... p 2512 N95-29373 * #
ARL-TR-778 ..... p 2589 N95-29112 * #
ARL-TR-807 ..... p 2528 N95-30028 * #

ARO-117-93 ..... p 2650 N95-29515 #
ARO-26673.9-MS-A ..... p 2537 N95-29724 #
ARO-26779.37-MA-AI ..... p 2659 N95-29225 #
ARO-26840.9-CH ..... p 2693 N95-29723 #
ARO-27256.4-PH-SAH ..... p 2692 N95-28981 #
ARO-27300.10-EG ..... p 2594 N95-28853 #
ARO-27409.12-EG ..... p 2595 N95-29535 #
ARO-27445.6-CH ..... p 2545 N95-29586 #
ARO-27567.3-MA ..... p 2722 N95-29154 #
ARO-27580.7-MA ..... p 2692 N95-29227 #
ARO-27754.4-EL ..... p 2554 N95-29203 #
ARO-27790.6-MA ..... p 2671 N95-29485 #
ARO-27894.27-EG ..... p 2489 N95-29428 #
ARO-27917.21-EL-S ..... p 2557 N95-29603 #
ARO-28007.13-MA ..... p 2671 N95-29558 #
ARO-28040.1-GS ..... p 2601 N95-29866 #
ARO-28102.1-GS ..... p 2621 N95-29497 #
ARO-28123.10-EG ..... p 2497 N95-29322 #
ARO-28143.6-MA ..... p 2648 N95-29297 #
ARO-28148.17-MS ..... p 2681 N95-29481 #
ARO-28159.9-EG ..... p 2487 N95-29091 #
ARO-28185.3-PH-SAH ..... p 2544 N95-29484 #
ARO-28250.3-EG ..... p 2578 N95-30039 #
ARO-28253.1-EG ..... p 2594 N95-29067 #
ARO-28283.22-EG ..... p 2715 N95-29234 #
ARO-28293.4-EG ..... p 2572 N95-29228 #
ARO-28307.7-EG ..... p 2526 N95-29561 #
ARO-28310.3-EG ..... p 2532 N95-29357 #
ARO-28319.4-CH ..... p 2716 N95-29493 #
ARO-28320.8-MA ..... p 2671 N95-29516 #
ARO-28325.50-EL ..... p 2643 N95-29381
ARO-28354.5-MA ..... p 2650 N95-29509 #
ARO-28369.5-MS ..... p 2542 N95-29230 #
ARO-28399.15-EG ..... p 2595 N95-29562 #
ARO-28406.11-EL ..... p 2718 N95-29149 #
ARO-28427.1-EG ..... p 2577 N95-29948 #
ARO-28476.8-MA-SDI ..... p 2557 N95-29563
ARO-28480.17-MS ..... p 2524 N95-29409 #
ARO-28486.10-CH ..... p 2532 N95-29483 #
ARO-28499.19-PH ..... p 2553 N95-29081 #
ARO-28506.7-EL ..... p 2652 N95-30042 #
ARO-28525.12-CH ..... p 2543 N95-29436 #
ARO-28528.9-CH ..... p 2533 N95-29556 #
ARO-28560.29-MS ..... p 2544 N95-29494 #
ARO-28561.7-PH ..... p 2693 N95-29431 #
ARO-28569.2-PH ..... p 2567 N95-30124 #
ARO-28577.10-MS ..... p 2541 N95-29071 #

ARO-28606.9-MA ..... p 2527 N95-29763 #
ARO-28628.5-CH ..... p 2692 N95-29092 #
ARO-28653.1-EL-SAH ..... p 2700 N95-29553 #
ARO-28655.24-CH ..... p 2533 N95-29581 #
ARO-28679.15-MA ..... p 2671 N95-29578 #
ARO-28700.3-CH ..... p 2548 N95-29498 #
ARO-28701.10-MA ..... p 2670 N95-29385 #
ARO-28702.5-MA ..... p 2669 N95-29083 #
ARO-28709.5-MA-SAH ..... p 2570 N95-29069 #
ARO-28718.25-MA ..... p 2648 N95-29310 #
ARO-28722.17-MA ..... p 2675 N95-29587 #
ARO-28750.1-LS-SM ..... p 2632 N95-29155 #
ARO-28754.30-EG-SM ..... p 2528 N95-29864 #
ARO-28755.3-EG-SM ..... p 2649 N95-29429 #
ARO-28761.1-MS ..... p 2545 N95-29635 #
ARO-28797.1-MA ..... p 2573 N95-29324 #
ARO-28799.9 ..... p 2564 N95-29430 #
ARO-28809.18-MA-SDI ..... p 2674 N95-29491 #
ARO-28852.25-PH ..... p 2696 N95-29495 #
ARO-28908.4-MA ..... p 2659 N95-29566 #
ARO-28978.31-PH ..... p 2557 N95-29645 #
ARO-29015.5-PH ..... p 2693 N95-29555 #
ARO-29053.8-MA-SDI ..... p 2669 N95-29233 #
ARO-29167.10-MA ..... p 2650 N95-29480 #
ARO-29167.19-MA ..... p 2674 N95-29490 #
ARO-29167.25-MA ..... p 2671 N95-29488
ARO-29321.3-PH ..... p 2713 N95-29087 #
ARO-29541.13-EL ..... p 2714 N95-29152 #
ARO-29594.1-LS ..... p 2635 N95-29153 #
ARO-29682.4-PH ..... p 2716 N95-29506 #
ARO-29907.1-EG-AAS ..... p 2596 N95-29582
ARO-30072.9-MA ..... p 2669 N95-29229 #
ARO-30108.1-MS ..... p 2700 N95-29560 #
ARO-30167.6-MA ..... p 2675 N95-29634 #
ARO-30167.7-MA ..... p 2675 N95-30297 #
ARO-30284.7-EG ..... p 2650 N95-29517 #
ARO-30340.25-EG-URI ..... p 2590 N95-29820 #
ARO-30357.2-MS ..... p 2543 N95-29482
ARO-30390.1-MA-SDI ..... p 2703 N95-30081 #
ARO-30450.5-MS-41P ..... p 2523 N95-29189 #
ARO-30488.3-MS ..... p 2542 N95-29288 #
ARO-30606.1-MA-SDI ..... p 2701 N95-29646 #
ARO-30695-EL-SB2 ..... p 2588 N95-30050 #
ARO-30697.1-EG-H ..... p 2574 N95-29387 #
ARO-30935.1-PH ..... p 2705 N95-29519 #
ARO-30993.5-MA ..... p 2594 N95-29150 #
ARO-30998.4-MA ..... p 2647 N95-29226 #
ARO-30999.1-MA ..... p 2648 N95-29285 #
ARO-31184.1-MS-CF ..... p 2524 N95-29326 #
ARO-31500.2-EL ..... p 2646 N95-29066 #
ARO-31572.1-EG ..... p 2549 N95-29550 #
ARO-32156.1-MS ..... p 2682 N95-29588 #
ARO-32287.1-PH ..... p 2718 N95-28857 #
ARO-32357.1-MA-CF ..... p 2661 N95-28788
ARO-32361.1-MA-CF ..... p 2666 N95-30040 #
ARO-32365.3-MA ..... p 2590 N95-29552 #
ARO-32378.1-EL-DPS ..... p 2554 N95-29235 #
ARO-32402.1-PH-DPS ..... p 2699 N95-29148 #
ARO-32412.1-MA-H ..... p 2569 N95-29068 #
ARO-32427.1-MA-SDI ..... p 2722 N95-29182 #
ARO-32561.1-MS-CF ..... p 2525 N95-29492 #
ARO-32664.1-GS-CF ..... p 2685 N95-30084 #
ARO-32824.1-EL-CF ..... p 2564 N95-29511 #
ARO-32826.1-PH-CF ..... p 2587 N95-29653
ARO-32828.1-PH-CF ..... p 2702 N95-29867 #
ARO-3305.1-EG-CF ..... p 2500 N95-29496 #
ARO-33571.1-EL-SBI ..... p 2642 N95-29974 #
ARO-33577.1-EL-SBI ..... p 2698 N95-29914 #
ARO-33869.1-EL-DPS ..... p 2555 N95-29290 #

AU-ARI-92-12 ..... p 2497 N95-29282

AVC-91-091 ..... p 2736 N95-29178 *

BC-ISR-94-04 ..... p 2725 N95-30043 #

BN-1174 ..... p 2668 N95-29064 #
BN-1179 ..... p 2669 N95-29080 #

BNL-61266 ..... p 2696 N95-30009 #
BNL-61287 ..... p 2696 N95-30021 #
BNL-61327 ..... p 2566 N95-30025 #
BNL-61443 ..... p 2668 N95-30279 #

BRF1343A ..... p 2505 N95-29954 *
BRF1343B ..... p 2505 N95-29955 *
BRF1343C ..... p 2505 N95-29956 *
BRF1343D ..... p 2505 N95-29957 *
BRF1343E ..... p 2505 N95-29958 *
BRF1343F ..... p 2505 N95-29959 *
BRF1343G ..... p 2505 N95-29960 *
BRF1343H ..... p 2505 N95-29961 *
BRF1343I ..... p 2506 N95-29962 *
BRF1343J ..... p 2506 N95-29963 *

CAP-110-MUON-94C ..... p 2696 N95-30009 #

CAR-TR-735 ..... p 2590 N95-29552 #

CARDIVNSWC-TR-61-93/12 ..... p 2537 N95-29759 #
CARDIVNSWC-TR-81-94/25 ..... p 2567 N95-30122 #
CARDIVNSWC-TR-94/018 ..... p 2518 N95-28951
CARDIVNSWC-TR-94/024 ..... p 2698 N95-28996 #

CARDIVNSWC/TR-94/019 ..... p 2527 N95-29638 #

CBCL-M-100 ..... p 2556 N95-29441 #

CBCL-101 ..... p 2621 N95-29333 #
CBCL-97 ..... p 2670 N95-29352 #
CBCL-98 ..... p 2670 N95-29440 #
CBCL-99 ..... p 2663 N95-29479 #

CERF-94-5011 ..... p 2526 N95-29598

CERL-FE-95/09 ..... p 2550 N95-29307 #

CERL-SR-EC-95/05 ..... p 2608 N95-28787 #

CERL-94/12 ..... p 2683 N95-29077 #

CMU-CS-94-108 ..... p 2669 N95-29128 #
CMU-CS-94-191 ..... p 2650 N95-29536 #
CMU-CS-94-200 ..... p 2647 N95-29147 #
CMU-CS-94-210 ..... p 2649 N95-29376 #
CMU-CS-94-217 ..... p 2647 N95-29125 #
CMU-CS-94-219 ..... p 2647 N95-29223 #
CMU-CS-94-221 ..... p 2737 N95-29151
CMU-CS-94-222 ..... p 2645 N95-28886 #
CMU-CS-94-223 ..... p 2724 N95-29818
CMU-CS-94-226 ..... p 2642 N95-29146 #
CMU-CS-94-230 ..... p 2658 N95-28884 #
CMU-CS-95-102 ..... p 2645 N95-28878 #
CMU-CS-95-103 ..... p 2647 N95-29143 #
CMU-CS-95-104 ..... p 2645 N95-28883 #
CMU-CS-95-105 ..... p 2721 N95-28880 #
CMU-CS-95-107 ..... p 2658 N95-28879 #
CMU-CS-95-108 ..... p 2645 N95-28881 #
CMU-CS-95-110 ..... p 2721 N95-28877 #
CMU-CS-95-111 ..... p 2645 N95-28894 #
CMU-CS-95-112 ..... p 2662 N95-28988 #
CMU-CS-95-114 ..... p 2658 N95-29196 #

CMU/SEI-94-TR-12 ..... p 2651 N95-29762 #
CMU/SEI-94-TR-19 ..... p 2652 N95-30047 #

CONF-8808142-PT-3 ..... p 2633 N95-29471 #
CONF-931108-114 ..... p 2717 N95-29986 #
CONF-931133-VOL-1 ..... p 2681 N95-28924 #
CONF-931133 ..... p 2681 N95-28962 #
CONF-9405143-10 ..... p 2538 N95-30216 #
CONF-940526-SUMM ..... p 2549 N95-30024 #
CONF-940580-24 ..... p 2711 N95-30130 #
CONF-9406163-2 ..... p 2531 N95-28916 #
CONF-9406163-3 ..... p 2530 N95-28776
CONF-9406191-2 ..... p 2668 N95-30279 #
CONF-940629-VOL-1 ..... p 2681 N95-28923 #
CONF-940681-13 ..... p 2696 N95-30009 #
CONF-940704-5 ..... p 2537 N95-29869 #
CONF-9407128-PT-1 ..... p 2696 N95-30021 #
CONF-940714-52 ..... p 2718 N95-30184 #
CONF-9407157-4 ..... p 2693 N95-29583 #
CONF-9407170-1 ..... p 2652 N95-30020 #
CONF-9407173-PT-1 ..... p 2632 N95-28947 #
CONF-9407173-PT-2 ..... p 2682 N95-29144 #
CONF-9408211-2 ..... p 2717 N95-30077 #
CONF-9408218-2 ..... p 2694 N95-30059 #
CONF-9409103-15 ..... p 2694 N95-30019 #
CONF-9409103-17 ..... p 2695 N95-30185 #
CONF-9409103-18 ..... p 2695 N95-30186 #
CONF-9409255-3 ..... p 2608 N95-28920 #
CONF-9409268-8 ..... p 2566 N95-30025 #
CONF-9409308-1 ..... p 2711 N95-30023 #
CONF-940933-35 ..... p 2696 N95-29142 #
CONF-941006-4 ..... p 2697 N95-28912 #
CONF-9410213-6 ..... p 2528 N95-30037 #
CONF-9410300-2 ..... p 2556 N95-29462 #
CONF-9410308-1 ..... p 2739 N95-29265 #
CONF-9410311-1 ..... p 2714 N95-29157 #
CONF-9410314-1 ..... p 2705 N95-29466 #
CONF-941039-4 ..... p 2537 N95-30018 #
CONF-9411151-3 ..... p 2536 N95-28959 #
CONF-941118-10 ..... p 2633 N95-30114 #
CONF-9411194-2 ..... p 2665 N95-29987 #
CONF-9411205-1 ..... p 2659 N95-29985 #
CONF-941142-32 ..... p 2577 N95-29988 #
CONF-941144-101 ..... p 2538 N95-30179 #
CONF-941144-80 ..... p 2714 N95-29134 #
CONF-941144-81 ..... p 2716 N95-29814 #
CONF-941144-82 ..... p 2717 N95-30022 #
CONF-941144-90 ..... p 2547 N95-30174 #
CONF-941144-91 ..... p 2561 N95-28961 #
CONF-941144-92 ..... p 2538 N95-30038 #

CONF-941144-93 ..... p 2547 N95-30190 #
CONF-941144-95 ..... p 2528 N95-30175 #
CONF-941176-3 ..... p 2716 N95-29984 #
CONF-941203-18 ..... p 2604 N95-30217 #
CONF-950145-3 ..... p 2695 N95-28957 #
CONF-950167-2 ..... p 2717 N95-30005 #
CONF-950167-3 ..... p 2717 N95-29990 #
CONF-950167-4 ..... p 2588 N95-30006 #
CONF-950170-1 ..... p 2569 N95-28956 #
CONF-950201-7 ..... p 2543 N95-29465 #
CONF-950216-114 ..... p 2549 N95-30345 #
CONF-950228-2 ..... p 2567 N95-30188 #
CONF-950228-3 ..... p 2655 N95-30209 #
CONF-950232-26 ..... p 2654 N95-30189 #
CONF-950232-30 ..... p 2710 N95-29909
CONF-950279-1 ..... p 2602 N95-29463 #
CONF-9503103-1 ..... p 2660 N95-30128 #
CONF-9503107-1 ..... p 2508 N95-29464 #
CONF-9503109-1 ..... p 2654 N95-30115
CONF-950336-16 ..... p 2603 N95-30213 #
CONF-950402-5 ..... p 2535 N95-30113 #
CONF-950439-9 ..... p 2652 N95-29989 #
CONF-950444-2 ..... p 2597 N95-30210 #
CONF-950472-3 ..... p 2560 N95-30177 #
CONF-9505191-2 ..... p 2651 N95-29871 #
CONF-9505195-1 ..... p 2606 N95-30057 #
CONF-950540-7 ..... p 2698 N95-28983 #
CONF-950558-1 ..... p 2538 N95-30178 #
CONF-950801-3 ..... p 2660 N95-30116 #
CONF-9506105-1 ..... p 2718 N95-30214 #
CONF-9506141-1 ..... p 2618 N95-30129 #
CONF-9506143-1 ..... p 2607 N95-30278 #
CONF-9506144-1 ..... p 2591 N95-30273
CONF-950644-1 ..... p 2661 N95-30215 #
CONF-950646-5 ..... p 2626 N95-29868
CONF-950683-1 ..... p 2607 N95-30281 #

CPA-94-02 ..... p 2560 N95-28812 #

CR-95.001 ..... p 2670 N95-29311 #

CRIE-Y-93015 ..... p 2610 N95-30195 #

CRREL-SR-94-25 ..... p 2620 N95-29193
CRREL-SR-94-28 ..... p 2697 N95-28778

CRREL-94-13 ..... p 2629 N95-29160 #

CS-TR-3349 ..... p 2590 N95-29552 #

CSDL-T-1241 ..... p 2493 N95-28716 * #
CSDL-T-1250 ..... p 2505 N95-29447 * #
CSDL-T-1253 ..... p 2508 N95-30036 * #

CSS/TR-94/32 ..... p 2566 N95-30079 #

CSU-TR-101 ..... p 2539 N95-28850 #

DA9426923 ..... p 2491 N95-29965

DE-95-11601 ..... p 2723 N95-29449 #

DE95-004012 ..... p 2603 N95-30127 #
DE95-004034 ..... p 2603 N95-30016 #
DE95-004051 ..... p 2603 N95-30017 #
DE95-004770 ..... p 2603 N95-30213 #
DE95-004777 ..... p 2718 N95-30214 #
DE95-005261 ..... p 2661 N95-30215 #
DE95-005396 ..... p 2538 N95-30216 #
DE95-005408 ..... p 2537 N95-30018 #
DE95-005424 ..... p 2604 N95-30217 #
DE95-005822 ..... p 2718 N95-30184 #
DE95-005823 ..... p 2695 N95-30185 #
DE95-005837 ..... p 2695 N95-30186 #
DE95-005842 ..... p 2578 N95-30187 #
DE95-005845 ..... p 2694 N95-30019 #
DE95-005846 ..... p 2652 N95-30020 #
DE95-005848 ..... p 2717 N95-30077 #
DE95-005855 ..... p 2716 N95-29984 #
DE95-005856 ..... p 2659 N95-29985 #
DE95-005858 ..... p 2717 N95-29986 #
DE95-005860 ..... p 2633 N95-30114 #
DE95-005861 ..... p 2665 N95-29987 #
DE95-005866 ..... p 2577 N95-29988 #
DE95-006088 ..... p 2695 N95-28930 #
DE95-006168 ..... p 2652 N95-29989 #
DE95-006177 ..... p 2654 N95-30115
DE95-006260 ..... p 2569 N95-28956 #
DE95-006323 ..... p 2717 N95-29990 #
DE95-006324 ..... p 2717 N95-30005 #
DE95-006325 ..... p 2588 N95-30006 #
DE95-006330 ..... p 2549 N95-30345 #
DE95-006392 ..... p 2710 N95-29909
DE95-006480 ..... p 2530 N95-28776
DE95-006481 ..... p 2531 N95-28916 #
DE95-006484 ..... p 2633 N95-29471 #

DE95-006500 ..... p 2698 N95-28983 #
DE95-006536 ..... p 2696 N95-29142 #
DE95-006564 ..... p 2693 N95-29583 #
DE95-006769 ..... p 2696 N95-30009 #
DE95-006774 ..... p 2696 N95-30021 #
DE95-006806 ..... p 2716 N95-29814 #
DE95-006807 ..... p 2717 N95-30022 #
DE95-006818 ..... p 2714 N95-29157 #
DE95-006821 ..... p 2660 N95-30116 #
DE95-006874 ..... p 2644 N95-28777 #
DE95-007025 ..... p 2695 N95-28957 #
DE95-007027 ..... p 2711 N95-30023 #
DE95-007029 ..... p 2549 N95-30024 #
DE95-007131 ..... p 2714 N95-29134 #
DE95-007259 ..... p 2608 N95-28920 #
DE95-007304 ..... p 2566 N95-30025 #
DE95-007371 ..... p 2528 N95-30037 #
DE95-007406 ..... p 2538 N95-30038 #
DE95-007619 ..... p 2626 N95-29868
DE95-007625 ..... p 2697 N95-28912 #
DE95-007689 ..... p 2556 N95-29462 #
DE95-007799 ..... p 2602 N95-29463 #
DE95-007844 ..... p 2591 N95-30273
DE95-007858 ..... p 2696 N95-30057 #
DE95-007875 ..... p 2694 N95-30059 #
DE95-007877 ..... p 2660 N95-30128 #
DE95-007879 ..... p 2618 N95-30129 #
DE95-007883 ..... p 2508 N95-29464 #
DE95-007885 ..... p 2543 N95-29465 #
DE95-007889 ..... p 2582 N95-28917
DE95-008075 ..... p 2711 N95-30130 #
DE95-008078 ..... p 2705 N95-29466 #
DE95-008131 ..... p 2682 N95-30131 #
DE95-008202 ..... p 2711 N95-30274 #
DE95-008210 ..... p 2607 N95-30278 #
DE95-008312 ..... p 2668 N95-30279 #
DE95-008361 ..... p 2607 N95-30281 #
DE95-008427 ..... p 2721 N95-28958 #
DE95-008538 ..... p 2567 N95-30188 #
DE95-008539 ..... p 2655 N95-30209 #
DE95-008551 ..... p 2597 N95-30210 #
DE95-008582 ..... p 2537 N95-29869 #
DE95-008596 ..... p 2739 N95-29265 #
DE95-008615 ..... p 2536 N95-28959 #
DE95-008620 ..... p 2591 N95-30211 #
DE95-008649 ..... p 2611 N95-30212 #
DE95-008658 ..... p 2666 N95-30112
DE95-008666 ..... p 2540 N95-28960 #
DE95-008675 ..... p 2535 N95-30113 #
DE95-008680 ..... p 2654 N95-30189 #
DE95-008682 ..... p 2547 N95-30190 #
DE95-008739 ..... p 2695 N95-30191 #
DE95-008751 ..... p 2711 N95-30173 #
DE95-008764 ..... p 2548 N95-29280 #
DE95-008776 ..... p 2547 N95-30174 #
DE95-008778 ..... p 2561 N95-28961 #
DE95-008780 ..... p 2528 N95-30175 #
DE95-008795 ..... p 2610 N95-30176 #
DE95-008816 ..... p 2560 N95-30177 #
DE95-008820 ..... p 2538 N95-30178 #
DE95-008848 ..... p 2538 N95-30179 #
DE95-008990 ..... p 2529 N95-30180 #
DE95-009324 ..... p 2610 N95-30181 #
DE95-009329 ..... p 2551 N95-30182 #
DE95-009334 ..... p 2533 N95-29870 #
DE95-009375 ..... p 2690 N95-28779 #
DE95-009378 ..... p 2654 N95-30183 #
DE95-009383 ..... p 2660 N95-30192 #
DE95-009385 ..... p 2660 N95-30193 #
DE95-009538 ..... p 2725 N95-30194 #
DE95-009587 ..... p 2651 N95-29871 #
DE95-608735 ..... p 2684 N95-29886 #
DE95-758701 ..... p 2589 N95-28946
DE95-758943 ..... p 2662 N95-29144 #
DE95-758947 ..... p 2632 N95-28947 #
DE95-764057 ..... p 2610 N95-30195 #

DLR-FB-94-19 ..... p 2492 N95-30349 #

DNA-TR-94-123 ..... p 2500 N95-29950 #
DNA-TR-94-59 ..... p 2542 N95-29314 #

DOD-8910.1-L ..... p 2724 N95-29947 #

DODA-AR-008-924 ..... p 2495 N95-28851
DODA-AR-008-943 ..... p 2587 N95-29914 #

DOE/CH-10093/272 ..... p 2603 N95-30127 #

DOE/ER-40296/T3 ..... p 2682 N95-30131 #
DOE/ER-40757/065 ..... p 2695 N95-30191 #
DOE/ER-45312/7 ..... p 2529 N95-30180 #
DOE/ER-54109/T4 ..... p 2695 N95-28930 #
DOE/ER-61363/3 ..... p 2610 N95-30181 #

DOE/ET-53088/696 ..... p 2711 N95-30173 #

DOE/MC-28055/95/C0447 ..... p 2607 N95-30281 #

DOE/METC-C/95/7170 ..... p 2607 N95-30278 #

DOE/OSTI-11686 ..... p 2723 N95-29449 #

DOE/PC-93069/3 ..... p 2533 N95-29870 #

DOE/SF-19460/52 ..... p 2711 N95-30274 #

DOT/FAA/AM-95/16 ..... p 2493 N95-28819 #
DOT/FAA/AM-95/17 ..... p 2636 N95-29224 #
DOT/FAA/AM-95/18 ..... p 2641 N95-29365 #
DOT/FAA/AM-95/19 ..... p 2638 N95-29261 #
DOT/FAA/AM-95/20 ..... p 2493 N95-29448 #
DOT/FAA/AM-95/2 ..... p 2493 N95-29873 #
DOT/FAA/AM-95/9 ..... p 2493 N95-28790 #

DOT/FAA/CT-TN-94/37 ..... p 2641 N95-29908 #

DOT/FAA/CT-TN94/16 ..... p 2493 N95-29855 #
DOT/FAA/CT-TN94/48 ..... p 2559 N95-30072 #
DOT/FAA/CT-TN94/56 ..... p 2558 N95-29769 #
DOT/FAA/CT-TN94/63 ..... p 2559 N95-29940 #
DOT/FAA/CT-TN94/65 ..... p 2559 N95-29975 #

DOT/FAA/CT-94/106 ..... p 2498 N95-29565 #
DOT/FAA/CT-94/120 ..... p 2502 N95-29967 #
DOT/FAA/CT-94/58 ..... p 2551 N95-29924 #
DOT/FAA/CT-94/62 ..... p 2495 N95-30031 #

DREO-TN-94-14 ..... p 2722 N95-29221 #
DREO-TN-94-16 ..... p 2700 N95-29354 #

DREO-1235 ..... p 2563 N95-29275 #
DREO-1241 ..... p 2586 N95-29330 #
DREO-1242 ..... p 2558 N95-29847 #
DREO-1245 ..... p 2555 N95-29313 #
DREO-1251 ..... p 2555 N95-29328 #

DSMC-TR-1-95 ..... p 2609 N95-29721 #

DSTO-GD-0022 ..... p 2587 N95-29914 #
DSTO-GD-0044 ..... p 2497 N95-29362

DSTO-TR-0062 ..... p 2495 N95-28851
DSTO-TR-0147 ..... p 2498 N95-29445

DU/DC/TR-47 ..... p 2715 N95-29444 #
DU/DC/TR-48 ..... p 2715 N95-29486 #
DU/DC/TR-49 ..... p 2713 N95-28993 #

E-4759-REV ..... p 2535 N95-28701 * #
E-8882 ..... p 2568 N95-28719 * #
E-9192 ..... p 2566 N95-29998 * #
E-9236 ..... p 2596 N95-30008 * #
E-9458 ..... p 2478 N95-28723 * #
E-9490 ..... p 2549 N95-30339 * #
E-9536 ..... p 2508 N95-30011 * #
E-9609 ..... p 2604 N95-30255 * #
E-9622 ..... p 2509 N95-29643 * #
E-9638 ..... p 2491 N95-30091 * #
E-9652 ..... p 2574 N95-29371 * #
E-9656 ..... p 2506 N95-30090 * #
E-9663 ..... p 2683 N95-29401 * #
E-9667 ..... p 2512 N95-29373 * #
E-9678 ..... p 2564 N95-29406 * #
E-9680 ..... p 2582 N95-29113 * #
E-9681 ..... p 2574 N95-29372 * #
E-9691 ..... p 2589 N95-29112 * #
E-9702 ..... p 2510 N95-29114 * #
E-9705 ..... p 2500 N95-29115 * #
E-9708 ..... p 2590 N95-29538 * #
E-9711 ..... p 2492 N95-30253 * #
E-9716 ..... p 2523 N95-29133 * #
E-9719 ..... p 2680 N95-28893 * #
E-9728 ..... p 2574 N95-29405 * #
E-9729 ..... p 2492 N95-29132 * #
E-9730 ..... p 2489 N95-29402 * #
E-9734 ..... p 2511 N95-29642 * #
E-9740 ..... p 2684 N95-29641 * #
E-9743 ..... p 2518 N95-28906 * #
E-9753 ..... p 2477 N95-30229 * #
E-9759 ..... p 2503 N95-30067 * #
E-9770 ..... p 2511 N95-30012 * #
E-9778 ..... p 2501 N95-30007 * #

ECE/GWOL-63 ..... p 2540 N95-29021 #

EGG-EP-11237-QTR-3 ..... p 2591 N95-30211 #

EGG-M-94157 ..... p 2536 N95-28959 #
EGG-M-94205 ..... p 2537 N95-29869 #

EGG-11265-4012 ..... p 2697 N95-28912 #

EOARD-TR-95-03 ..... p 2701 N95-29766 #
EOARD-TR-95-04 ..... p 2565 N95-29925 #
EOARD-TR-95-08 ..... p 2698 N95-28932

ERC-R-94-082 ..... p 2510 N95-29584 * #

ERDEC-TR-207 ..... p 2551 N95-28699
ERDEC-TR-225 ..... p 2670 N95-29296 #

ERIM-253850-4-T ..... p 2599 N95-29523 #
ERIM-253850-5-0 ..... p 2601 N95-30061 #
ERIM-265400-2-F ..... p 2559 N95-30073 #

ESC-TR-94-019 ..... p 2652 N95-30047 #
ESC-TR-94-12 ..... p 2651 N95-29762 #

ESDU-94008 ..... p 2539 N95-28900
ESDU-94011 ..... p 2589 N95-28901
ESDU-94013 ..... p 2568 N95-28902
ESDU-94014 ..... p 2568 N95-28903
ESDU-94015 ..... p 2487 N95-28904
ESDU-94017 ..... p 2589 N95-28905
ESDU-94019 ..... p 2518 N95-28899
ESDU-94020 ..... p 2539 N95-28898
ESDU-94021-PT-1 ..... p 2511 N95-28804
ESDU-94022 ..... p 2512 N95-29017
ESDU-94023-PT-3 ..... p 2512 N95-29900
ESDU-94024-PT-4 ..... p 2511 N95-28803
ESDU-94025 ..... p 2530 N95-28712
ESDU-94026 ..... p 2491 N95-29899
ESDU-94027 ..... p 2490 N95-29898
ESDU-94028 ..... p 2486 N95-28885
ESDU-94029 ..... p 2488 N95-29129
ESDU-94032 ..... p 2530 N95-28802
ESDU-94033 ..... p 2593 N95-28801
ESDU-94034 ..... p 2593 N95-28711
ESDU-94035 ..... p 2683 N95-28710
ESDU-94036 ..... p 2682 N95-28709
ESDU-94037 ..... p 2486 N95-28800
ESDU-94038 ..... p 2477 N95-28708
ESDU-94039 ..... p 2495 N95-28707
ESDU-94040 ..... p 2496 N95-29016
ESDU-94041 ..... p 2569 N95-29015
ESDU-94042 ..... p 2550 N95-28706
ESDU-94043 ..... p 2550 N95-28705
ESDU-94044 ..... p 2487 N95-28897
ESDU-94045 ..... p 2495 N95-28896
ESDU-94046 ..... p 2495 N95-28704
ESDU-95002 ..... p 2534 N95-29897
ESDU-95003 ..... p 2531 N95-28895
ESDU-95004 ..... p 2534 N95-29901
ESDU-95005 ..... p 2530 N95-28703

ESM95-2.0-CM ..... p 2523 N95-29185 #

ETDE-JP-MF-95-758701 ..... p 2589 N95-28946

FAA-APO-94-11 ..... p 2495 N95-29880 #

FR-950106 ..... p 2627 N95-29944 #

FR7060-001 ..... p 2496 N95-28928 *

F49620-93-1-0334 ..... p 2562 N95-29014 #
F49620-93-1-0543 ..... p 2719 N95-29756 #

GAO-NSIAD-95-52 ..... p 2497 N95-29126 #

GMD-248 ..... p 2643 N95-30108 #

GMU-TR-110 ..... p 2653 N95-30063 #

GRI-94/0411 ..... p 2591 N95-30110 #
GRI-94/0440 ..... p 2535 N95-30198 #
GRI-95/0009 ..... p 2535 N95-30111 #
GRI-95/0056 ..... p 2610 N95-30197 #

HQ-91-03N ..... p 2641 N95-29180 *
HQ-92-03L ..... p 2726 N95-29172 *
HQ-92-04-0371 ..... p 2508 N95-29633 *

IAEA-CN-60/D-P-I-11 ..... p 2709 N95-29789 #
IAEA-CN-60/D-3-3 ..... p 2706 N95-29731 #
IAEA-CN-60/F-2-II-5 ..... p 2696 N95-29142 #

ICASE-95-25 ..... p 2670 N95-29403 * #
ICASE-95-28 ..... p 2671 N95-29451 * #
ICASE-95-31 ..... p 2655 N95-30306 * #
ICASE-95-34 ..... p 2674 N95-30227 * #
ICASE-95-35 ..... p 2649 N95-29455 * #
ICASE-95-36 ..... p 2649 N95-29404 * #
ICASE-95-40 ..... p 2674 N95-30353 * #
ICASE-95-42 ..... p 2672 N95-30086 * #

ICMA-94-190 ..... p 2668 N95-28863 #
ICMA-94-191 ..... p 2668 N95-28861 #

ICOMP-95-11 ..... p 2574 N95-29405 * #

IDA-D-1442 ..... p 2510 N95-29284 #
IDA-D-1619 ..... p 2552 N95-28936

IDA-P-3019 ..... p 2550 N95-29918 #

IFSR-696 ..... p 2711 N95-30173 #

INEL-94-0017 ..... p 2540 N95-28960 #
INEL-94/0072-QTR-3 ..... p 2591 N95-30211 #

INIS-MF-14395 ..... p 2694 N95-29886 #

INPE-5467-PRE/1775 ..... p 2722 N95-29363 #
INPE-5490-TDI/507 ..... p 2598 N95-28929 #
INPE-5517-PRE/1792 ..... p 2601 N95-29999 #
INPE-5608-TDI/554 ..... p 2598 N95-29433 #
INPE-5609-PRE/1821 ..... p 2600 N95-29815 #

ISAS-658 ..... p 2490 N95-29640 #
ISAS-659 ..... p 2575 N95-29712 #

ISBN-0-309-05125-8 ..... p 2507 N95-28852 * #
ISBN-0-315-81287-7 ..... p 2575 N95-29718
ISBN-0-315-84931-2 ..... p 2719 N95-29677
ISBN-0-315-86304-8 ..... p 2624 N95-29797
ISBN-0-7844-0059-8 ..... p 2526 N95-29598
ISBN-0-856-70912-2 ..... p 2530 N95-28712
ISBN-0-856-79911-4 ..... p 2511 N95-28803
ISBN-0-856-79920-3 ..... p 2593 N95-28801
ISBN-0-856-79922-X ..... p 2683 N95-28710
ISBN-0-856-79923-8 ..... p 2682 N95-28709
ISBN-0-856-79925-4 ..... p 2477 N95-28708
ISBN-0-856-79926-2 ..... p 2495 N95-28707
ISBN-0-856-79927-0 ..... p 2496 N95-29016
ISBN-0-856-79928-9 ..... p 2569 N95-29015
ISBN-0-856-79929-7 ..... p 2550 N95-28706
ISBN-0-856-79930-0 ..... p 2550 N95-28705
ISBN-0-856-79931-9 ..... p 2487 N95-28897
ISBN-0-85678-914-9 ..... p 2490 N95-29898
ISBN-0-85679-895-9 ..... p 2539 N95-28900
ISBN-0-85679-898-3 ..... p 2589 N95-28901
ISBN-0-85679-900-9 ..... p 2568 N95-28902
ISBN-0-85679-901-7 ..... p 2568 N95-28903
ISBN-0-85679-902-5 ..... p 2487 N95-28904
ISBN-0-85679-904-1 ..... p 2589 N95-28905
ISBN-0-85679-906-8 ..... p 2518 N95-28899
ISBN-0-85679-907-6 ..... p 2539 N95-28898
ISBN-0-85679-908-4 ..... p 2511 N95-28804
ISBN-0-85679-909-2 ..... p 2512 N95-29017
ISBN-0-85679-910-6 ..... p 2512 N95-29900
ISBN-0-85679-913-0 ..... p 2491 N95-29899
ISBN-0-85679-915-7 ..... p 2486 N95-28885
ISBN-0-85679-916-5 ..... p 2488 N95-29129
ISBN-0-85679-919-X ..... p 2530 N95-28802
ISBN-0-85679-924-6 ..... p 2486 N95-28800
ISBN-0-85679-932-7 ..... p 2495 N95-28896
ISBN-0-85679-933-5 ..... p 2495 N95-28704
ISBN-0-85679-936-X ..... p 2534 N95-29897
ISBN-0-85679-937-8 ..... p 2531 N95-28895
ISBN-0-85679-938-6 ..... p 2534 N95-29901
ISBN-0-85679-939-4 ..... p 2530 N95-28703
ISBN-0-956-79921-1 ..... p 2593 N95-28711
ISBN-1-563-96337-X ..... p 2681 N95-28962 #
ISBN-1-56396-337-X ..... p 2681 N95-28924 #
ISBN-1-56396-348-5 ..... p 2693 N95-29521 #
ISBN-1-56396-403-1 ..... p 2681 N95-28923 #
ISBN-90-370-0117-3 ..... p 2591 N95-30285 #
ISBN-90-407-1042-2 ..... p 2596 N95-30049 #
ISBN-90-5269-164-9 ..... p 2667 N95-30207 #
ISBN-90-72125-41-X ..... p 2702 N95-30054 #
ISBN-90-73861-20-9 ..... p 2535 N95-30282 #
ISBN-90-9007614-X ..... p 2597 N95-30206
ISBN-92-836-1012-1 ..... p 2676 N95-29604 #
ISBN-92-836-1014-8 ..... p 2498 N95-29503 #
ISBN-951-22-2217-5 ..... p 2673 N95-30172 #

ISLE-TR-94-1 ..... p 2664 N95-29574 #
ISLE-TR-94-2 ..... p 2675 N95-29906 #
ISLE-TR-94-4 ..... p 2650 N95-29576 #
ISLE-TR-95-1 ..... p 2664 N95-29577 #
ISLE-TR-95-2 ..... p 2723 N95-29573 #

ISVR-TR-246 ..... p 2577 N95-29817

ITRI-144 ..... p 2635 N95-29188 #

IW-93069R ..... p 2603 N95-30200 #

JB-0-06-0272 ..... p 2736 N95-29964 *

JPL-PUBL-90-49-REV-6 ..... p 2631 N95-30231 * #
JPL-PUBL-95-3 ..... p 2628 N95-30343 * #
JPL-PUBL-95-5 ..... p 2737 N95-30344 * #

JPL-94-6 ..... p 2731 N95-30230 * #

JSC-1478 ..... p 2504 N95-28715 *

JTN-95-80926 ..... p 2626 N95-29849 #

K/CSD/TM-101-REV-1 ..... p 2725 N95-30194 #

KCP-613-5524 ..... p 2556 N95-29462 #
KCP-613-5542 ..... p 2654 N95-30115

L-17167A-VOL-1-PT-1 ..... p 2518 N95-29029 * #
L-17167B-VOL-1-PT-2 ..... p 2513 N95-28823 * #
L-17367 ..... p 2578 N95-30056 * #
L-17427 ..... p 2498 N95-30226 * #
L-17464 ..... p 2696 N95-30337 * #
L-17497 ..... p 2686 N95-30133 * #

LA-UR-94-4088 ..... p 2661 N95-30215 #
LA-UR-95-176 ..... p 2549 N95-30345 #
LA-UR-95-211 ..... p 2569 N95-28956 #
LA-UR-95-437 ..... p 2652 N95-29989 #
LA-UR-95-438 ..... p 2694 N95-30059 #
LA-UR-95-476 ..... p 2660 N95-30128 #
LA-UR-95-511 ..... p 2618 N95-30129 #
LA-UR-95-554 ..... p 2508 N95-29464 #
LA-UR-95-570 ..... p 2543 N95-29465 #
LA-UR-95-600 ..... p 2582 N95-28917
LA-UR-95-627 ..... p 2696 N95-30057 #
LA-UR-95-784 ..... p 2591 N95-30273

LBL-36431 ..... p 2693 N95-29583 #
LBL-36659 ..... p 2690 N95-28779 #
LBL-36888 ..... p 2654 N95-30183 #

LC-94-31335 ..... p 2526 N95-29598
LC-94-70636 ..... p 2553 N95-29159 #
LC-94-70636 ..... p 2558 N95-29904 #
LC-94-70649 ..... p 2681 N95-28924 #
LC-94-70649 ..... p 2681 N95-28962 #
LC-94-73219 ..... p 2693 N95-29521 #
LC-94-79021 ..... p 2681 N95-28923 #
LC-95-18686 ..... p 2507 N95-28852 * #

LG94ER0129 ..... p 2543 N95-29482

LIDS-FR-2285 ..... p 2672 N95-30029 #

LMI-DF301LN2 ..... p 2720 N95-28797 #
LMI-DF301LN4 ..... p 2722 N95-29287

LMSC-P412291 ..... p 2552 N95-28984 #

M-778 ..... p 2478 N95-28720 * #
M-783 ..... p 2504 N95-28718 * #
M-784 ..... p 2507 N95-28721 * #

MAA-1994-MOSP ..... p 2672 N95-29647 #

MDC-94X0041 ..... p 2571 N95-29211 #

MEMO-COSOR-94-23 ..... p 2667 N95-30168 #
MEMO-COSOR-94-24 ..... p 2666 N95-30167 #
MEMO-COSOR-94-25 ..... p 2597 N95-30169 #
MEMO-COSOR-94-26 ..... p 2675 N95-30170 #
MEMO-COSOR-94-27 ..... p 2667 N95-30221 #
MEMO-COSOR-94-28 ..... p 2667 N95-30171 #
MEMO-COSOR-94-29 ..... p 2667 N95-30222 #
MEMO-COSOR-94-32 ..... p 2666 N95-30101 #
MEMO-COSOR-94-38 ..... p 2672 N95-30046 #
MEMO-COSOR-94-39 ..... p 2668 N95-30288 #

MEMO-INF-94-44 ..... p 2558 N95-29919 #
MEMO-INF-94-45 ..... p 2560 N95-30219 #
MEMO-INF-94-52 ..... p 2653 N95-30094 #
MEMO-INF-94-53 ..... p 2653 N95-30095 #
MEMO-INF-94-60 ..... p 2673 N95-30097 #
MEMO-INF-94-61 ..... p 2559 N95-30096 #
MEMO-INF-94-64 ..... p 2643 N95-30109 #
MEMO-INF-94-65 ..... p 2653 N95-30098 #
MEMO-INF-94-66 ..... p 2653 N95-30099 #
MEMO-INF-94-67 ..... p 2673 N95-30196 #
MEMO-INF-94-68 ..... p 2674 N95-30291 #
MEMO-INF-94-69 ..... p 2673 N95-30103 #
MEMO-INF-94-70 ..... p 2660 N95-30102 #
MEMO-INF-94-71 ..... p 2660 N95-30104
MEMO-INF-94-72 ..... p 2725 N95-30100 #
MEMO-INF-94-73 ..... p 2653 N95-30105 #
MEMO-INF-94-74 ..... p 2655 N95-30218 #
MEMO-INF-94-82 ..... p 2725 N95-30208 #

MIT-AI-TR-1488 ..... p 2663 N95-29477 #

MPL-U-140/94 ..... p 2619 N95-28872 #
MPL-U-141/94 ..... p 2628 N95-28796 #
MPL-U-17/95 ..... p 2628 N95-28865 #

MRC-R-1488 ..... p 2608 N95-28922 #

MS-CIS-94-17 ..... p 2659 N95-29225 #

NAIC-ID(RS)T-0310-93 ..... p 2632 N95-29263
NAIC-ID(RS)T-0367-94 ..... p 2561 N95-28911
NAIC-ID(RS)T-0368-94 ..... p 2684 N95-29659 #
NAIC-ID(RS)T-0371-94 ..... p 2685 N95-29951 #
NAIC-ID(RS)T-0372-93 ..... p 2622 N95-29662 #
NAIC-ID(RS)T-0387-94 ..... p 2703 N95-30064 #
NAIC-ID(RS)T-0389-94 ..... p 2702 N95-29969 #
NAIC-ID(RS)T-0390-94 ..... p 2583 N95-29656 #
NAIC-ID(RS)T-0391-94 ..... p 2701 N95-29661 #
NAIC-ID(RS)T-0397-94 ..... p 2685 N95-29681 #
NAIC-ID(RS)T-0399-94 ..... p 2685 N95-29874 #
NAIC-ID(RS)T-0409-94 ..... p 2701 N95-29571 #
NAIC-ID(RS)T-0413-94 ..... p 2682 N95-29952 #
NAIC-ID(RS)T-0556-94 ..... p 2587 N95-29660 #
NAIC-ID(RS)T-0705-94 ..... p 2584 N95-28679
NAIC-ID(RS)T-0921-92 ..... p 2577 N95-30027 #

NAS 1.15:102023-REV ..... p 2535 N95-28701 * #
NAS 1.15:104556 ..... p 2631 N95-30236 * #
NAS 1.15:104787 ..... p 2740 N95-29816 * #
NAS 1.15:106783 ..... p 2596 N95-30008 * #
NAS 1.15:106871 ..... p 2549 N95-30339 * #
NAS 1.15:106892 ..... p 2508 N95-30011 * #
NAS 1.15:106914 ..... p 2509 N95-29643 * #
NAS 1.15:106924 ..... p 2491 N95-30091 * #
NAS 1.15:106931 ..... p 2574 N95-29371 * #
NAS 1.15:106935 ..... p 2683 N95-29401 * #
NAS 1.15:106939 ..... p 2512 N95-29373 * #
NAS 1.15:106945 ..... p 2582 N95-29113 * #
NAS 1.15:106946 ..... p 2574 N95-29372 * #
NAS 1.15:106952 ..... p 2589 N95-29112 * #
NAS 1.15:106955 ..... p 2500 N95-29115 * #
NAS 1.15:106959 ..... p 2492 N95-30253 * #
NAS 1.15:106963 ..... p 2680 N95-28893 * #
NAS 1.15:106973 ..... p 2511 N95-29642 * #
NAS 1.15:106979 ..... p 2518 N95-28906 * #
NAS 1.15:106984 ..... p 2477 N95-30229 * #
NAS 1.15:106994 ..... p 2511 N95-30012 * #
NAS 1.15:106999 ..... p 2501 N95-30007 * #
NAS 1.15:108490 ..... p 2597 N95-30328 * #
NAS 1.15:108492 ..... p 2672 N95-29624 * #
NAS 1.15:108493 ..... p 2524 N95-29374 * #
NAS 1.15:108495 ..... p 2529 N95-30334 * #
NAS 1.15:109099 ..... p 2507 N95-29377 * #
NAS 1.15:110143 ..... p 2740 N95-28786 * #
NAS 1.15:110146 ..... p 2583 N95-29453 * #
NAS 1.15:110147 ..... p 2560 N95-30336 * #
NAS 1.15:110150 ..... p 2659 N95-29454 * #
NAS 1.15:110151 ..... p 2608 N95-28717 * #
NAS 1.15:110162 ..... p 2529 N95-30341 * #
NAS 1.15:110163 ..... p 2684 N95-29452 * #
NAS 1.15:110164 ..... p 2502 N95-30327 * #
NAS 1.15:110167 ..... p 2659 N95-29823 * #
NAS 1.15:110168 ..... p 2495 N95-28820 * #
NAS 1.15:110173 ..... p 2509 N95-30316 * #
NAS 1.15:110176 ..... p 2527 N95-29825 * #
NAS 1.15:110178 ..... p 2529 N95-30340 * #
NAS 1.15:110179 ..... p 2506 N95-30251 * #
NAS 1.15:110183 ..... p 2528 N95-30028 * #
NAS 1.15:110351 ..... p 2477 N95-28816 * #
NAS 1.15:110353 ..... p 2503 N95-29351 * #
NAS 1.15:110357 ..... p 2503 N95-30228 * #
NAS 1.15:110623 ..... p 2740 N95-28882 * #
NAS 1.15:110654 ..... p 2632 N95-29375 * #
NAS 1.15:110731 ..... p 2721 N95-29028 * #
NAS 1.15:110742 ..... p 2531 N95-29248 * #
NAS 1.15:4603 ..... p 2578 N95-30056 * #
NAS 1.15:4640 ..... p 2498 N95-30226 * #
NAS 1.15:4675 ..... p 2696 N95-30337 * #
NAS 1.15:4684 ..... p 2642 N95-28818 * #
NAS 1.15:4685 ..... p 2642 N95-28722 * #
NAS 1.21:7011(403) ..... p 2636 N95-29190 *
NAS 1.26:188368 ..... p 2633 N95-28875 * #
NAS 1.26:188370 ..... p 2505 N95-29447 * #
NAS 1.26:188372 ..... p 2508 N95-30036 * #
NAS 1.26:189406 ..... p 2644 N95-28805 * #
NAS 1.26:189407 ..... p 2644 N95-28806 * #
NAS 1.26:189408 ..... p 2645 N95-28821 * #
NAS 1.26:189409 ..... p 2644 N95-28713 * #
NAS 1.26:189410 ..... p 2644 N95-28714 * #
NAS 1.26:189412 ..... p 2644 N95-28807 * #
NAS 1.26:189422 ..... p 2600 N95-29754 * #
NAS 1.26:189423 ..... p 2726 N95-28822 * #
NAS 1.26:189424 ..... p 2726 N95-29370 * #
NAS 1.26:195048 ..... p 2548 N95-30252 * #
NAS 1.26:195071 ..... p 2671 N95-29451 * #
NAS 1.26:195080 ..... p 2655 N95-30306 * #
NAS 1.26:195470 ..... p 2506 N95-30090 * #
NAS 1.26:195474 ..... p 2584 N95-29406 * #
NAS 1.26:195478 ..... p 2510 N95-29114 * #
NAS 1.26:195479 ..... p 2590 N95-29538 * #
NAS 1.26:195482 ..... p 2523 N95-29133 * #

NAS 1.26:196604 ..... p 2691 N95-28856 * #
NAS 1.26:196635 ..... p 2578 N95-30034 * #
NAS 1.26:196636 ..... p 2510 N95-29584 * #
NAS 1.26:196637 ..... p 2652 N95-30013 * #
NAS 1.26:196638 ..... p 2531 N95-29246 * #
NAS 1.26:196639 ..... p 2549 N95-30014 * #
NAS 1.26:196640 ..... p 2585 N95-29247 * #
NAS 1.26:197654 ..... p 2572 N95-29249 * #
NAS 1.26:197850 ..... p 2496 N95-28928 *
NAS 1.26:198068 ..... p 2670 N95-29403 * #
NAS 1.26:198154 ..... p 2674 N95-30227 * #
NAS 1.26:198155 ..... p 2649 N95-29455 * #
NAS 1.26:198157 ..... p 2649 N95-29404 * #
NAS 1.26:198163 ..... p 2674 N95-30353 * #
NAS 1.26:198167 ..... p 2672 N95-30086 * #
NAS 1.26:198354 ..... p 2574 N95-29405 * #
NAS 1.26:198355 ..... p 2492 N95-29132 * #
NAS 1.26:198356 ..... p 2489 N95-29402 * #
NAS 1.26:198357 ..... p 2684 N95-29641 * #
NAS 1.26:198361 ..... p 2503 N95-30067 * #
NAS 1.26:198575 ..... p 2635 N95-29158 * #
NAS 1.26:198580 ..... p 2489 N95-29338 * #
NAS 1.26:198639 ..... p 2507 N95-28852 * #
NAS 1.26:198655 ..... p 2584 N95-28808 * #
NAS 1.26:198656 ..... p 2513 N95-28809 * #
NAS 1.26:198695 ..... p 2630 N95-29237 * #
NAS 1.26:198756 ..... p 2655 N95-30307 * #
NAS 1.26:198767 ..... p 2704 N95-29130 * #
NAS 1.26:198789 ..... p 2702 N95-30035 * #
NAS 1.26:198792 ..... p 2700 N95-29366 * #
NAS 1.26:198795 ..... p 2543 N95-29367 * #
NAS 1.26:198796 ..... p 2532 N95-29250 * #
NAS 1.26:198804 ..... p 2590 N95-29369 * #
NAS 1.26:198805 ..... p 2565 N95-29968 * #
NAS 1.26:198814 ..... p 2579 N95-30224 * #
NAS 1.26:198817 ..... p 2570 N95-29131 * #
NAS 1.26:198831 ..... p 2499 N95-30335 * #
NAS 1.26:198832 ..... p 2579 N95-30250 * #
NAS 1.26:198835 ..... p 2601 N95-30247 * #
NAS 1.26:198845 ..... p 2548 N95-30237 * #
NAS 1.26:198855 ..... p 2628 N95-30356 * #
NAS 1.26:198868 ..... p 2731 N95-30230 * #
NAS 1.26:198872 ..... p 2631 N95-30231 * #
NAS 1.26:198880 ..... p 2628 N95-30343 * #
NAS 1.26:198881 ..... p 2737 N95-30344 * #
NAS 1.26:198920 ..... p 2509 N95-30357 * #
NAS 1.26:198929 ..... p 2711 N95-30338 * #
NAS 1.26:198948 ..... p 2603 N95-30015 * #
NAS 1.26:198955 ..... p 2628 N95-30272 * #
NAS 1.26:198958 ..... p 2501 N95-30254 * #
NAS 1.26:288367 ..... p 2493 N95-28716 * #
NAS 1.26:4485 ..... p 2496 N95-29027 * #
NAS 1.26:4662 ..... p 2512 N95-30225 * #
NAS 1.26:4671 ..... p 2478 N95-28720 * #
NAS 1.26:4672 ..... p 2504 N95-29339 * #
NAS 1.26:4676 ..... p 2513 N95-28817 * #
NAS 1.55:10172 ..... p 2604 N95-30255 * #
NAS 1.55:3178-VOL-1-PT-1 ..... p 2518 N95-29029 * #
NAS 1.55:3178-VOL-1-PT-2 ..... p 2513 N95-28823 * #
NAS 1.55:3291 ..... p 2478 N95-28723 * #
NAS 1.55:3300 ..... p 2686 N95-30133 * #
NAS 1.55:3303 ..... p 2737 N95-30058 * #
NAS 1.60:3487 ..... p 2568 N95-28719 * #
NAS 1.60:3513 ..... p 2566 N95-29998 * #
NAS 1.60:3547 ..... p 2671 N95-29446 * #
NAS 1.60:3558 ..... p 2504 N95-28718 * #
NAS 1.60:3560 ..... p 2507 N95-28721 * #
NAS 1.61:1369 ..... p 2731 N95-30004 * #

NASA-AAV-1387 ..... p 2655 N95-30248 *

NASA-CASE-GSC-13608-1 ..... p 2588 N95-28702 *

NASA-CP-10172 ..... p 2604 N95-30255 * #
NASA-CP-3178-VOL-1-PT-1 ..... p 2518 N95-29029 * #
NASA-CP-3178-VOL-1-PT-2 ..... p 2513 N95-28823 * #
NASA-CP-3291 ..... p 2478 N95-28723 * #
NASA-CP-3300 ..... p 2686 N95-30133 * #
NASA-CP-3303 ..... p 2737 N95-30058 * #

NASA-CR-166367 ..... p 2493 N95-28716 * #
NASA-CR-166368 ..... p 2633 N95-28875 * #
NASA-CR-166370 ..... p 2505 N95-29447 * #
NASA-CR-166372 ..... p 2508 N95-30036 * #
NASA-CR-189406 ..... p 2644 N95-28805 * #
NASA-CR-189407 ..... p 2644 N95-28806 * #
NASA-CR-189408 ..... p 2645 N95-28821 * #
NASA-CR-189409 ..... p 2644 N95-28713 * #
NASA-CR-189410 ..... p 2644 N95-28714 * #
NASA-CR-189412 ..... p 2644 N95-28807 * #
NASA-CR-189422 ..... p 2600 N95-29754 * #
NASA-CR-189423 ..... p 2726 N95-28822 * #
NASA-CR-189424 ..... p 2726 N95-29370 * #
NASA-CR-195048 ..... p 2548 N95-30252 * #
NASA-CR-195068 ..... p 2670 N95-29403 * #
NASA-CR-195071 ..... p 2671 N95-29451 * #
NASA-CR-195080 ..... p 2655 N95-30306 * #
NASA-CR-195470 ..... p 2506 N95-30090 * #
NASA-CR-195474 ..... p 2564 N95-29406 * #
NASA-CR-195478 ..... p 2510 N95-29114 * #
NASA-CR-195479 ..... p 2590 N95-29538 * #
NASA-CR-195482 ..... p 2523 N95-29133 * #
NASA-CR-196604 ..... p 2691 N95-28856 * #
NASA-CR-196635 ..... p 2578 N95-30034 * #
NASA-CR-196636 ..... p 2510 N95-29584 * #
NASA-CR-196637 ..... p 2652 N95-30013 * #
NASA-CR-196638 ..... p 2531 N95-29246 * #
NASA-CR-196639 ..... p 2549 N95-30014 * #
NASA-CR-196640 ..... p 2585 N95-29247 * #
NASA-CR-197654 ..... p 2572 N95-29249 * #
NASA-CR-197655 ..... p 2726 N95-29172 *
NASA-CR-197656 ..... p 2736 N95-29178 *
NASA-CR-197657 ..... p 2641 N95-29180 *
NASA-CR-197658 ..... p 2633 N95-30292 *
NASA-CR-197665 ..... p 2508 N95-29633 *
NASA-CR-197850 ..... p 2496 N95-28928 *
NASA-CR-198154 ..... p 2674 N95-30227 * #
NASA-CR-198155 ..... p 2649 N95-29455 * #
NASA-CR-198157 ..... p 2649 N95-29404 * #
NASA-CR-198163 ..... p 2674 N95-30353 * #
NASA-CR-198167 ..... p 2672 N95-30086 * #
NASA-CR-198354 ..... p 2574 N95-29405 * #
NASA-CR-198355 ..... p 2492 N95-29132 * #
NASA-CR-198356 ..... p 2489 N95-29402 * #
NASA-CR-198357 ..... p 2684 N95-29641 * #
NASA-CR-198361 ..... p 2503 N95-30067 * #
NASA-CR-198575 ..... p 2635 N95-29158 * #
NASA-CR-198580 ..... p 2489 N95-29338 * #
NASA-CR-198639 ..... p 2507 N95-28852 * #
NASA-CR-198655 ..... p 2584 N95-28808 * #
NASA-CR-198656 ..... p 2513 N95-28809 * #
NASA-CR-198695 ..... p 2630 N95-29237 * #
NASA-CR-198756 ..... p 2655 N95-30307 * #
NASA-CR-198757 ..... p 2736 N95-29964 *
NASA-CR-198767 ..... p 2704 N95-29130 * #
NASA-CR-198789 ..... p 2702 N95-30035 * #
NASA-CR-198792 ..... p 2700 N95-29366 * #
NASA-CR-198795 ..... p 2543 N95-29367 * #
NASA-CR-198796 ..... p 2532 N95-29250 * #
NASA-CR-198804 ..... p 2590 N95-29369 * #
NASA-CR-198805 ..... p 2565 N95-29968 * #
NASA-CR-198814 ..... p 2579 N95-30224 * #
NASA-CR-198817 ..... p 2570 N95-29131 * #
NASA-CR-198831 ..... p 2499 N95-30335 * #
NASA-CR-198832 ..... p 2579 N95-30250 * #
NASA-CR-198835 ..... p 2601 N95-30247 * #
NASA-CR-198845 ..... p 2548 N95-30237 * #
NASA-CR-198855 ..... p 2628 N95-30356 * #
NASA-CR-198868 ..... p 2731 N95-30230 * #
NASA-CR-198872 ..... p 2631 N95-30231 * #
NASA-CR-198880 ..... p 2628 N95-30343 * #
NASA-CR-198881 ..... p 2737 N95-30344 * #
NASA-CR-198920 ..... p 2509 N95-30357 * #
NASA-CR-198929 ..... p 2711 N95-30338 * #
NASA-CR-198948 ..... p 2603 N95-30015 * #
NASA-CR-198955 ..... p 2628 N95-30272 * #
NASA-CR-198958 ..... p 2501 N95-30254 * #
NASA-CR-4485 ..... p 2496 N95-29027 * #
NASA-CR-4662 ..... p 2512 N95-30225 * #
NASA-CR-4671 ..... p 2478 N95-28720 * #
NASA-CR-4672 ..... p 2504 N95-29339 * #
NASA-CR-4676 ..... p 2513 N95-28817 * #

NASA-RP-1173 ..... p 2731 N95-30004 * #

NASA-SP-7011(403) ..... p 2636 N95-29190 *

NASA-TM-102023-REV ..... p 2535 N95-28701 * #
NASA-TM-104556 ..... p 2631 N95-30236 * #
NASA-TM-104787 ..... p 2740 N95-29816 * #
NASA-TM-106783 ..... p 2596 N95-30008 * #
NASA-TM-106871 ..... p 2549 N95-30339 * #
NASA-TM-106892 ..... p 2508 N95-30011 * #
NASA-TM-106914 ..... p 2509 N95-29643 * #
NASA-TM-106924 ..... p 2491 N95-30091 * #
NASA-TM-106931 ..... p 2574 N95-29371 * #
NASA-TM-106935 ..... p 2683 N95-29401 * #
NASA-TM-106939 ..... p 2512 N95-29373 * #
NASA-TM-106945 ..... p 2582 N95-29113 * #
NASA-TM-106946 ..... p 2574 N95-29372 * #
NASA-TM-106952 ..... p 2589 N95-29112 * #
NASA-TM-106955 ..... p 2500 N95-29115 * #
NASA-TM-106959 ..... p 2492 N95-30253 * #
NASA-TM-106963 ..... p 2680 N95-28893 * #
NASA-TM-106973 ..... p 2511 N95-29642 * #
NASA-TM-106979 ..... p 2518 N95-28906 * #
NASA-TM-106984 ..... p 2477 N95-30229 * #
NASA-TM-106994 ..... p 2511 N95-30012 * #
NASA-TM-106999 ..... p 2501 N95-30007 * #
NASA-TM-108490 ..... p 2597 N95-30326 * #
NASA-TM-108492 ..... p 2672 N95-29824 * #
NASA-TM-108493 ..... p 2524 N95-29374 * #
NASA-TM-108495 ..... p 2529 N95-30334 * #
NASA-TM-109099 ..... p 2507 N95-29377 * #
NASA-TM-110143 ..... p 2740 N95-28786 * #
NASA-TM-110146 ..... p 2583 N95-29453 * #
NASA-TM-110147 ..... p 2560 N95-30336 * #
NASA-TM-110150 ..... p 2659 N95-29454 * #
NASA-TM-110151 ..... p 2608 N95-28717 * #
NASA-TM-110162 ..... p 2529 N95-30341 * #
NASA-TM-110163 ..... p 2684 N95-29452 * #
NASA-TM-110164 ..... p 2502 N95-30327 * #
NASA-TM-110167 ..... p 2659 N95-29823 * #
NASA-TM-110168 ..... p 2495 N95-28820 * #
NASA-TM-110173 ..... p 2509 N95-30316 * #
NASA-TM-110176 ..... p 2527 N95-29825 * #
NASA-TM-110178 ..... p 2529 N95-30340 * #
NASA-TM-110179 ..... p 2506 N95-30251 * #
NASA-TM-110183 ..... p 2528 N95-30028 * #
NASA-TM-110351 ..... p 2477 N95-28816 * #
NASA-TM-110353 ..... p 2503 N95-29351 * #
NASA-TM-110357 ..... p 2503 N95-30228 * #
NASA-TM-110530 ..... p 2504 N95-28715 *
NASA-TM-110563 ..... p 2720 N95-29170 *
NASA-TM-110566 ..... p 2553 N95-29174 *
NASA-TM-110567 ..... p 2598 N95-29175 *
NASA-TM-110622 ..... p 2503 N95-29407 *
NASA-TM-110623 ..... p 2740 N95-28882 * #
NASA-TM-110638 ..... p 2737 N95-30318 *
NASA-TM-110646 ..... p 2720 N95-30223 *
NASA-TM-110647 ..... p 2737 N95-30249 *
NASA-TM-110648 ..... p 2655 N95-30248 *
NASA-TM-110654 ..... p 2632 N95-29375 * #
NASA-TM-110731 ..... p 2721 N95-29028 * #
NASA-TM-110739 ..... p 2720 N95-29171 *
NASA-TM-110742 ..... p 2531 N95-29248 * #
NASA-TM-110744 ..... p 2505 N95-29954 *
NASA-TM-110745 ..... p 2505 N95-29955 *
NASA-TM-110746 ..... p 2505 N95-29956 *
NASA-TM-110747 ..... p 2505 N95-29957 *
NASA-TM-110748 ..... p 2505 N95-29958 *
NASA-TM-110749 ..... p 2505 N95-29959 *
NASA-TM-110750 ..... p 2505 N95-29960 *
NASA-TM-110751 ..... p 2505 N95-29961 *
NASA-TM-110752 ..... p 2506 N95-29962 *
NASA-TM-110753 ..... p 2506 N95-29963 *
NASA-TM-110754 ..... p 2731 N95-30317 *
NASA-TM-4603 ..... p 2578 N95-30056 * #
NASA-TM-4640 ..... p 2498 N95-30226 * #
NASA-TM-4675 ..... p 2696 N95-30337 * #
NASA-TM-4684 ..... p 2642 N95-28818 * #
NASA-TM-4685 ..... p 2642 N95-28722 * #

NASA-TP-3487 ..... p 2568 N95-28719 * #
NASA-TP-3513 ..... p 2566 N95-29998 * #
NASA-TP-3547 ..... p 2671 N95-29446 * #
NASA-TP-3558 ..... p 2504 N95-28718 * #
NASA-TP-3560 ..... p 2507 N95-28721 * #

NATICK-TR-95/013 ..... p 2547 N95-30120 #

NATICK/TR-95/016 ..... p 2640 N95-28794 #

NATO-AC/243(PANEL 8)TR/17 .. p 2720 N95-29935 #

NAVY-CASE-73922 ..... p 2701 N95-29602
NAVY-CASE-73983 ..... p 2595 N95-29192
NAVY-CASE-74851 ..... p 2564 N95-29568 #
NAVY-CASE-75355 ..... p 2589 N95-28791 #
NAVY-CASE-75451 ..... p 2512 N95-29052
NAVY-CASE-75498 ..... p 2564 N95-29570 #
NAVY-CASE-75558 ..... p 2541 N95-29194
NAVY-CASE-75646 ..... p 2641 N95-29600
NAVY-CASE-75667 ..... p 2554 N95-29236
NAVY-CASE-75785 ..... p 2585 N95-29217
NAVY-CASE-75894 ..... p 2567 N95-30165 #
NAVY-CASE-76081 ..... p 2530 N95-28854
NAVY-CASE-76105 ..... p 2539 N95-28784
NAVY-CASE-76256 ..... p 2683 N95-28783
NAVY-CASE-76289 ..... p 2588 N95-28785
NAVY-CASE-76290 ..... p 2582 N95-29220
NAVY-CASE-76338 ..... p 2545 N95-29569 #

NAWC-WPNS-TP-8065 ..... p 2733 N95-29599
NAWC-WPNS-TP-8217-REV-1 ..... p 2658 N95-28955
NAWC-WPNS-TP-8245 ..... p 2558 N95-29928 #

NAWCADWAR-94139-60 ..... p 2640 N95-28970 #
NAWCADWAR-94140-60 ..... p 2640 N95-28969 #
NAWCADWAR-95012-4.3 ..... p 2496 N95-28977 #

NAWS-CL-TP-006 ..... p 2627 N95-30048 #

NBDL-93R010 ..... p 2640 N95-28935

NCAR/CT-155 ..... p 2739 N95-30199 #

NFESC-CR-95-002 ..... p 2594 N95-29063 #

NFESC-TDS-2002-SHR ..... p 2592 N95-28684
NFESC-TDS-2003-SHR ..... p 2591 N95-28682
NFESC-TDS-2004-ENG ..... p 2602 N95-28858 #
NFESC-TDS-2005-ENG ..... p 2549 N95-28686

NHRC-TD-94-4D ..... p 2645 N95-28934

NHRC-94-20 ..... p 2636 N95-29238 #
NHRC-94-23 ..... p 2637 N95-29995 #
NHRC-94-28 ..... p 2637 N95-29846 #
NHRC-94-30 ..... p 2637 N95-30083 #

NIFS-PROC-15 ..... p 2711 N95-29966 #

NIFS-222 ..... p 2707 N95-29738 #
NIFS-224 ..... p 2707 N95-29739 #
NIFS-228 ..... p 2707 N95-29740 #
NIFS-229 ..... p 2707 N95-29741 #
NIFS-230 ..... p 2707 N95-29742 #
NIFS-231 ..... p 2707 N95-29743 #
NIFS-231 ..... p 2709 N95-29809 #
NIFS-233 ..... p 2709 N95-29810 #
NIFS-234 ..... p 2707 N95-29744 #
NIFS-235 ..... p 2710 N95-29843 #
NIFS-236 ..... p 2707 N95-29745 #
NIFS-237 ..... p 2710 N95-29812 #
NIFS-242 ..... p 2708 N95-29746 #
NIFS-243 ..... p 2708 N95-29747 #
NIFS-244 ..... p 2711 N95-30033 #
NIFS-245 ..... p 2710 N95-29813 #
NIFS-247 ..... p 2693 N95-29748 #
NIFS-248 ..... p 2710 N95-29844 #
NIFS-249 ..... p 2708 N95-29749 #
NIFS-253 ..... p 2710 N95-29857 #
NIFS-288 ..... p 2706 N95-29734 #
NIFS-289 ..... p 2710 N95-29841 #
NIFS-290 ..... p 2711 N95-30032 #
NIFS-291 ..... p 2709 N95-29802 #
NIFS-292 ..... p 2709 N95-29808 #
NIFS-293 ..... p 2709 N95-29803 #
NIFS-294 ..... p 2709 N95-29801 #
NIFS-296 ..... p 2706 N95-29731 #
NIFS-300 ..... p 2709 N95-29789 #
NIFS-307 ..... p 2705 N95-29567 #
NIFS-309 ..... p 2708 N95-29755 #

NONP-NASA-VT-95-45998 ..... p 2720 N95-29170 *
NONP-NASA-VT-95-45999 ..... p 2720 N95-29171 *
NONP-NASA-VT-95-46000 ..... p 2726 N95-29172 *
NONP-NASA-VT-95-46001 ..... p 2553 N95-29174 *
NONP-NASA-VT-95-46002 ..... p 2598 N95-29175 *
NONP-NASA-VT-95-46003 ..... p 2736 N95-29178 *
NONP-NASA-VT-95-46004 ..... p 2641 N95-29180 *
NONP-NASA-VT-95-46006 ..... p 2633 N95-30292 *
NONP-NASA-VT-95-46019 ..... p 2508 N95-29633 *
NONP-NASA-VT-95-50092 ..... p 2504 N95-28715 *
NONP-NASA-VT-95-51757 ..... p 2503 N95-29407 *
NONP-NASA-VT-95-56567 ..... p 2505 N95-29954 *
NONP-NASA-VT-95-56568 ..... p 2505 N95-29955 *
NONP-NASA-VT-95-56569 ..... p 2505 N95-29956 *
NONP-NASA-VT-95-56570 ..... p 2505 N95-29957 *
NONP-NASA-VT-95-56571 ..... p 2505 N95-29958 *
NONP-NASA-VT-95-56572 ..... p 2505 N95-29959 *
NONP-NASA-VT-95-56573 ..... p 2505 N95-29960 *
NONP-NASA-VT-95-56574 ..... p 2505 N95-29961 *
NONP-NASA-VT-95-56575 ..... p 2506 N95-29962 *
NONP-NASA-VT-95-56622 ..... p 2731 N95-30317 *
NONP-NASA-VT-95-56623 ..... p 2506 N95-29963 *
NONP-NASA-VT-95-56825 ..... p 2736 N95-29964 *
NONP-NASA-VT-95-56871 ..... p 2737 N95-30318 *
NONP-NASA-VT-95-57868 ..... p 2720 N95-30223 *
NONP-NASA-VT-95-57872 ..... p 2655 N95-30248 *
NONP-NASA-VT-95-57873 ..... p 2737 N95-30249 *

NPS-EC-94-016 ..... p 2557 N95-29504 #

NPS-MA-95-001 ..... p 2648 N95-29304 #

NPS-OC-94-007 ..... p 2629 N95-28982
NPS-OC-94-009 ..... p 2629 N95-29023 #

NPSEC-95-001 ..... p 2556 N95-29386

NRAD-TD-2734 ..... p 2553 N95-29166 #

NRAD-TR-1659 ..... p 2641 N95-29359 #
NRAD-TR-1682 ..... p 2664 N95-29499 #
NRAD-TR-2727 ..... p 2629 N95-28873 #

NREL/SP-410-7689 ..... p 2603 N95-30017 #

NREL/TP-441-6913 ..... p 2603 N95-30016 #

NRL-FR/7240-94-9449 ..... p 2630 N95-29237 * #

NRL/FR/1003-94-9755 ..... p 2562 N95-29075 #

NRL/FR/7322-93-9429 ..... p 2629 N95-28991 #
NRL/FR/7441-93-9435 ..... p 2598 N95-28931
NRL/FR/7531-94-9451 ..... p 2619 N95-28938
NRL/FR/8120-95-9736 ..... p 2554 N95-29231 #

NRL/MR/5540-94-7619 ..... p 2648 N95-29319 #
NRL/MR/6790-95-7647 ..... p 2588 N95-29937 #
NRL/MR/6793-95-7639 ..... p 2563 N95-29301 #
NRL/MR/7130-95-7649 ..... p 2583 N95-29470 #
NRL/MR/7176-94-7563 ..... p 2685 N95-29945 #
NRL/MR/7181-94-7533 ..... p 2631 N95-29856 #
NRL/MR/7441-94-7516 ..... p 2601 N95-29977 #
NRL/MR/7541-94-7215 ..... p 2627 N95-30044 #
NRL/MR/7673-94-7642 ..... p 2738 N95-29327 #
NRL/MR/8140-95-7654 ..... p 2552 N95-28939

NSWCDD/MP-94-122 ..... p 2646 N95-28995 #

NSWCDD/TR-94/379 ..... p 2490 N95-29853 #

NUWC-NL-TD-10785 ..... p 2557 N95-29489

NV-94-C11 ..... p 2702 N95-29973 #

ORISE-95006874 ..... p 2644 N95-28777 #

ORNL/CON-400 ..... p 2611 N95-30212 #

ORNL/TM-12920 ..... p 2666 N95-30112

PB95-190997 ..... p 2737 N95-28780
PB95-191003 ..... p 2737 N95-28781
PB95-192449 ..... p 2535 N95-30282 #
PB95-192589 ..... p 2655 N95-30283 #
PB95-196218 ..... p 2691 N95-28913
PB95-196903 ..... p 2591 N95-30285 #
PB95-196945 ..... p 2538 N95-30287 #
PB95-197042 ..... p 2668 N95-30288 #
PB95-197117 ..... p 2672 N95-30092 #
PB95-197125 ..... p 2673 N95-30093 #
PB95-197133 ..... p 2653 N95-30094 #
PB95-197141 ..... p 2653 N95-30095 #
PB95-197158 ..... p 2559 N95-30096 #
PB95-197166 ..... p 2673 N95-30097 #
PB95-197174 ..... p 2653 N95-30098 #
PB95-197182 ..... p 2653 N95-30099 #
PB95-197190 ..... p 2673 N95-30196 #
PB95-197208 ..... p 2674 N95-30291 #
PB95-197216 ..... p 2666 N95-30041 #
PB95-197232 ..... p 2672 N95-30046 #
PB95-197257 ..... p 2596 N95-30049 #
PB95-197265 ..... p 2702 N95-30054 #
PB95-197281 ..... p 2547 N95-30201 #
PB95-197307 ..... p 2578 N95-30202 #
PB95-197315 ..... p 2538 N95-30205 #
PB95-197349 ..... p 2597 N95-30206
PB95-197364 ..... p 2667 N95-30207 #
PB95-197372 ..... p 2725 N95-30208 #
PB95-197380 ..... p 2725 N95-30100 #
PB95-197406 ..... p 2666 N95-30101 #
PB95-197612 ..... p 2660 N95-30102 #
PB95-197620 ..... p 2673 N95-30103 #
PB95-197638 ..... p 2660 N95-30104
PB95-197646 ..... p 2653 N95-30105 #
PB95-197653 ..... p 2655 N95-30218 #
PB95-198131 ..... p 2654 N95-30107 #
PB95-198453 ..... p 2643 N95-30108 #
PB95-198487 ..... p 2643 N95-30109 #
PB95-200218 ..... p 2591 N95-30110 #
PB95-200531 ..... p 2535 N95-30111 #
PB95-200549 ..... p 2610 N95-30197 #
PB95-200705 ..... p 2535 N95-30198 #
PB95-201810 ..... p 2739 N95-30199 #
PB95-206454 ..... p 2603 N95-30200 #
PB95-206710 ..... p 2560 N95-30203 #
PB95-206728 ..... p 2560 N95-30219 #
PB95-206744 ..... p 2558 N95-29919 #
PB95-206751 ..... p 2673 N95-30204 #
PB95-206769 ..... p 2672 N95-30088 #
PB95-206777 ..... p 2672 N95-30089 #
PB95-206819 ..... p 2673 N95-30106 #
PB95-206827 ..... p 2655 N95-30220 #
PB95-206835 ..... p 2667 N95-30221 #
PB95-206843 ..... p 2667 N95-30222 #
PB95-206934 ..... p 2666 N95-30167 #
PB95-206942 ..... p 2667 N95-30168 #
PB95-206959 ..... p 2597 N95-30169 #
PB95-206967 ..... p 2675 N95-30170 #
PB95-206975 ..... p 2667 N95-30171 #
PB95-207171 ..... p 2673 N95-30172 #

PDA-TR-94-1161-54-13 ..... p 2542 N95-29314 #

PFC/RR-94-11 ..... p 2695 N95-28930 #

PL-TR-94-1014 ..... p 2664 N95-29657 #

PL-TR-94-1125 ..... p 2586 N95-29425 #
PL-TR-94-2206 ..... p 2613 N95-29317 #
PL-TR-94-2225 ..... p 2612 N95-28985 #
PL-TR-94-2230 ..... p 2507 N95-29026 #
PL-TR-94-2233 ..... p 2602 N95-29200 #
PL-TR-94-2234 ..... p 2602 N95-29201 #
PL-TR-94-2235 ..... p 2613 N95-29293 #
PL-TR-94-2242 ..... p 2725 N95-30043 #
PL-TR-94-2253 ..... p 2501 N95-29764 #
PL-TR-94-2258 ..... p 2612 N95-28972 #
PL-TR-94-2267 ..... p 2558 N95-29875 #
PL-TR-94-2270 ..... p 2618 N95-30082 #
PL-TR-94-2271 ..... p 2617 N95-29765 #
PL-TR-94-2278 ..... p 2616 N95-29737 #
PL-TR-94-2279 ..... p 2651 N95-29932 #
PL-TR-94-3000 ..... p 2602 N95-29949 #
PL-TR-94-3032 ..... p 2532 N95-29273 #
PL-TR-95-07 ..... p 2588 N95-29980 #
PL-TR-95-2001 ..... p 2611 N95-28697
PL-TR-95-2012 ..... p 2619 N95-28975 #

PNL-SA-25348 ..... p 2608 N95-28920 #
PNL-SA-25504 ..... p 2602 N95-29463 #

POLY-AE-94-02 ..... p 2502 N95-29468 #

PSU-LEPS-94-15 ..... p 2692 N95-28994 #

R/D-7100-EN-01 ..... p 2582 N95-28966 #
R/D-7216-EE-01 ..... p 2612 N95-28871 #
R/D-7216-EE-01 ..... p 2612 N95-29140 #
R/D-7342-PH-03 ..... p 2694 N95-30065 #
R/D-7345-PH-01 ..... p 2716 N95-28927 #

RAL-94-122 ..... p 2691 N95-28913

RANA-94-12 ..... p 2672 N95-30088 #
RANA-94-13 ..... p 2673 N95-30204 #
RANA-94-18 ..... p 2672 N95-30092 #
RANA-94-20 ..... p 2673 N95-30093 #

RAND/MR-403-OSD/A ..... p 2651 N95-29736 #

RAS-F ..... p 2552 N95-28979 #

RDP-TR-9401-VOL-2 ..... p 2618 N95-30062 #
RDP-TR-9402-VOL-3 ..... p 2617 N95-29765 #
RDP-TR-9403 ..... p 2616 N95-29737 #
RDP-TR-9404 ..... p 2651 N95-29932 #

REPT-H355 ..... p 2600 N95-29754 * #

REPT-130-6601-RPT-1 ..... p 2548 N95-29525 #
REPT-153-1072 ..... p 2693 N95-29521 #
REPT-3176 ..... p 2712 N95-28862 #
REPT-39 ..... p 2699 N95-29177 #
REPT-4-20-95 ..... p 2635 N95-29158 * #
REPT-442427-22518 ..... p 2713 N95-28967 #
REPT-5-27959 ..... p 2639 N95-29422 #
REPT-526033 ..... p 2717 N95-30068 #
REPT-60458 ..... p 2558 N95-29875 #
REPT-731/2 ..... p 2612 N95-28871 #
REPT-93-549/4 ..... p 2665 N95-29979 #
REPT-94-01 ..... p 2638 N95-28918 #
REPT-94-9SL2-LAFIL-R2 ..... p 2562 N95-29078 #
REPT-95-C-SRA-001 ..... p 2593 N95-29941 #
REPT-95-005 ..... p 2680 N95-29072 #
REPT-95-1 ..... p 2555 N95-29290 #
REPT-95-9SL2-LAFIL-R1 ..... p 2562 N95-29073 #
REPT-95B00092 ..... p 2631 N95-30236 * #
REPT-95B00100 ..... p 2731 N95-30004 * #

RI/RD94-271 ..... p 2533 N95-29581 #
RI/RD94-271 ..... p 2702 N95-29974 #
RI/RD95-106 ..... p 2699 N95-29295 #

RL-TR-94-186 ..... p 2557 N95-29655 #
RL-TR-94-210 ..... p 2691 N95-28952
RL-TR-94-219 ..... p 2642 N95-28976 #
RL-TR-94-221 ..... p 2658 N95-28965 #
RL-TR-94-222 ..... p 2698 N95-28992 #
RL-TR-94-224 ..... p 2552 N95-28986 #
RL-TR-94-228 ..... p 2697 N95-28798 #
RL-TR-94-231 ..... p 2716 N95-29658 #
RL-TR-94-232 ..... p 2645 N95-28814 #
RL-TR-94-42 ..... p 2552 N95-28943
RL-TR-95-4 ..... p 2494 N95-28887 #

RPI-94-8 ..... p 2671 N95-29488

RR-94-2-ONR ..... p 2639 N95-29432 #

S-757 ..... p 2740 N95-29816 * #
S-800 ..... p 2671 N95-29446 * #

SAND-94-1588C ..... p 2604 N95-30217 #

SAND-94-1731C ..... p 2717 N95-30022 #
SAND-94-2146C ..... p 2567 N95-30188 #
SAND-94-2288C ..... p 2717 N95-30005 #
SAND-94-2292C ..... p 2717 N95-29990 #
SAND-94-2407C ..... p 2655 N95-30209 #
SAND-94-2451C ..... p 2560 N95-30177 #
SAND-94-2619C ..... p 2718 N95-30214 #
SAND-94-2704C ..... p 2603 N95-30213 #
SAND-94-2784C ..... p 2588 N95-30006 #
SAND-95-0140C ..... p 2660 N95-30116 #
SAND-95-0146C ..... p 2714 N95-29157 #
SAND-95-0168C ..... p 2716 N95-29814 #
SAND-95-0345C ..... p 2597 N95-30210 #
SAND-95-0493C ..... p 2538 N95-30178 #
SAND-95-0590C ..... p 2651 N95-29871 #
SAND-95-8460C ..... p 2698 N95-28983 #

SBA-0474-93-2-00007 ..... p 2510 N95-29584 * #

SBIL-C-94 ..... p 2533 N95-29722 #

SDG-605-PT-1 ..... p 2737 N95-28781
SDG-605-PT-2 ..... p 2737 N95-28780

SDL/94-090 ..... p 2611 N95-28697

SEL-82-1306 ..... p 2644 N95-28805 * #
SEL-94-002 ..... p 2644 N95-28806 * #
SEL-94-003 ..... p 2645 N95-28821 * #
SEL-94-004 ..... p 2644 N95-28713 * #
SEL-94-005 ..... p 2644 N95-28714 * #
SEL-95-001 ..... p 2644 N95-28807 * #

SMC-TR-94-47 ..... p 2738 N95-29279 #
SMC-TR-95-3 ..... p 2504 N95-29992 #
SMC-TR-95-4 ..... p 2531 N95-28942
SMC-TR-95-5 ..... p 2587 N95-29931 #
SMC-TR-95-6 ..... p 2603 N95-29953 #
SMC-TR-95-9 ..... p 2507 N95-28867 #

SPC-92017-CMC ..... p 2654 N95-30121 #

SR-1 ..... p 2611 N95-28697
SR-1 ..... p 2612 N95-28985 #
SR-1 ..... p 2507 N95-29026 #
SR-1 ..... p 2602 N95-29200 #
SR-1 ..... p 2501 N95-29764 #
SR-1 ..... p 2725 N95-30043 #
SR-2 ..... p 2602 N95-29201 #
SR-I ..... p 2617 N95-29765 #
SR-5 ..... p 2616 N95-29737 #

SRI-PYU-3673 ..... p 2542 N95-29288 #

SSI-TR-246 ..... p 2613 N95-29317 #

SSM-94-06 ..... p 2665 N95-29971 #

STC-TR-2927 ..... p 2628 N95-30272 * #

SU-SLAC-PUB-95-6738 ..... p 2739 N95-29265 #

SWRI-4770 ..... p 2591 N95-30110 #

TARDEC-TR-13613 ..... p 2533 N95-29572 #
TARDEC-TR-13617 ..... p 2548 N95-29019 #
TARDEC-TR-13660 ..... p 2641 N95-29378 #

TF-62 ..... p 2573 N95-29268 #

TKO-B118 ..... p 2655 N95-30283 #

TN-BN-1173 ..... p 2669 N95-29084 #

TR-BN-1180 ..... p 2668 N95-29065 #

TR-RD-AS-95-2 ..... p 2559 N95-29991 #

TR-009(6945-01)-1 ..... p 2531 N95-28942
TR-1004 ..... p 2659 N95-29420 #
TR-106 ..... p 2675 N95-29819
TR-114 ..... p 2673 N95-30126 #
TR-14 ..... p 2531 N95-28945
TR-2 ..... p 2542 N95-29270 #
TR-3-95 ..... p 2646 N95-28968 #
TR-31 ..... p 2539 N95-28891 #
TR-32 ..... p 2539 N95-28864 #
TR-33 ..... p 2539 N95-28860 #
TR-384 ..... p 2675 N95-30297 #
TR-36 ..... p 2553 N95-29176 #
TR-401 ..... p 2675 N95-29634 #
TR-4 ..... p 2544 N95-29554 #
TR-6 ..... p 2670 N95-29312 #
TR-6 ..... p 2544 N95-29551 #
TR-79 ..... p 2691 N95-28868 #
TR-83 ..... p 2691 N95-28919 #
TR-92(2925)-1 ..... p 2587 N95-29931 #
TR-93(3940)-14 ..... p 2738 N95-29279 #
TR-94(4508)-1 ..... p 2504 N95-29992 #
TR-94(4524)-1 ..... p 2603 N95-29953 #
TR-95(5231)-3 ..... p 2507 N95-28867 #
TR-9 ..... p 2545 N95-29559 #

UCB-PTH-95/01 ..... p 2690 N95-28779 #

UCRL-ID-119527 ..... p 2660 N95-30192 #
UCRL-ID-119803 ..... p 2660 N95-30193 #
UCRL-ID-119971 ..... p 2551 N95-30182 #

UCRL-JC-115909 ..... p 2711 N95-30130 #
UCRL-JC-119340 ..... p 2705 N95-29466 #

UDR-TR-94-94 ..... p 2492 N95-28811 #

UIME-PBB-94-003 ..... p 2532 N95-29357 #

UK-ME-94-01 ..... p 2551 N95-30296 #

US-PATENT-APPL-SN-040944 ..... p 2567 N95-30165 #
US-PATENT-APPL-SN-087002 ..... p 2560 N95-28855
US-PATENT-APPL-SN-147276 ..... p 2588 N95-28702 *
US-PATENT-APPL-SN-159962 ..... p 2703 N95-30166
US-PATENT-APPL-SN-207448 ..... p 2541 N95-29194
US-PATENT-APPL-SN-233562 ..... p 2564 N95-29570 #
US-PATENT-APPL-SN-296881 ..... p 2566 N95-30055 #
US-PATENT-APPL-SN-296883 ..... p 2554 N95-29236
US-PATENT-APPL-SN-302013 ..... p 2699 N95-29263
US-PATENT-APPL-SN-316709 ..... p 2641 N95-29600
US-PATENT-APPL-SN-319709 ..... p 2566 N95-30052 #
US-PATENT-APPL-SN-321642 ..... p 2567 N95-30165 #
US-PATENT-APPL-SN-322655 ..... p 2682 N95-30051 #
US-PATENT-APPL-SN-322668 ..... p 2595 N95-29192
US-PATENT-APPL-SN-324639 ..... p 2683 N95-28783
US-PATENT-APPL-SN-326518 ..... p 2512 N95-29052
US-PATENT-APPL-SN-331231 ..... p 2566 N95-30075 #
US-PATENT-APPL-SN-332294 ..... p 2703 N95-30076 #
US-PATENT-APPL-SN-334088 ..... p 2718 N95-30164 #
US-PATENT-APPL-SN-337012 ..... p 2547 N95-30132 #
US-PATENT-APPL-SN-337013 ..... p 2545 N95-29569 #
US-PATENT-APPL-SN-338842 ..... p 2564 N95-29568 #
US-PATENT-APPL-SN-345049 ..... p 2589 N95-28791 #
US-PATENT-APPL-SN-345716 ..... p 2702 N95-30053 #
US-PATENT-APPL-SN-348688 ..... p 2588 N95-28785
US-PATENT-APPL-SN-349656 ..... p 2582 N95-29220
US-PATENT-APPL-SN-351070 ..... p 2585 N95-29217
US-PATENT-APPL-SN-352126 ..... p 2530 N95-28854
US-PATENT-APPL-SN-355581 ..... p 2539 N95-28784
US-PATENT-APPL-SN-359757 ..... p 2701 N95-29602

US-PATENT-CLASS-F16H-1/28 .. p 2588 N95-28702 *

US-PATENT-CLASS-250-577 ..... p 2703 N95-30166
US-PATENT-CLASS-475-342 ..... p 2588 N95-28702 *

US-PATENT-5,362,580 ..... p 2560 N95-28855
US-PATENT-5,367,175 ..... p 2703 N95-30166
US-PATENT-5,409,431 ..... p 2588 N95-28702 *

USAARL-94-48 ..... p 2634 N95-28941
USAARL-95-12 ..... p 2639 N95-29434 #
USAARL-95-3 ..... p 2492 N95-29057 #
USAARL-95-5 ..... p 2635 N95-29141 #
USAARL-95-7 ..... p 2634 N95-28940

USACERL-TR-FE-95/05 ..... p 2550 N95-29537 #

USAMRMC-T95-4 ..... p 2636 N95-29757 #

USCG-D-30-94 ..... p 2598 N95-29281

UTD/CAO/35 ..... p 2556 N95-29383 #

VAMAS-TR-19 ..... p 2547 N95-30118 #

VJSC-1207 ..... p 2737 N95-30318 *

WES-TN-DRP-1-17 ..... p 2627 N95-30066 #

WES/TN/DRP-1-19 ..... p 2630 N95-29198 #

WES/TR/SL-94-24 ..... p 2594 N95-28909

WHC-SD-GN-CSWD-20010 ..... p 2721 N95-28958 #

WHOI-7800-35/8687-1 ..... p 2631 N95-28685
WHOI-94-17 ..... p 2630 N95-29418

WL-TR-93-2058 ..... p 2501 N95-29934 #
WL-TR-94-1086 ..... p 2556 N95-29472 #
WL-TR-94-2085 ..... p 2570 N95-29127 #
WL-TR-94-2092 ..... p 2500 N95-28908
WL-TR-94-2097 ..... p 2566 N95-30070 #
WL-TR-94-2100 ..... p 2551 N95-30296 #
WL-TR-94-2120 ..... p 2561 N95-28971 #
WL-TR-94-3089 ..... p 2571 N95-29187 #
WL-TR-94-3129 ..... p 2492 N95-28811 #
WL-TR-94-3131 ..... p 2578 N95-30087 #
WL-TR-94-4099 ..... p 2640 N95-29020 #
WL-TR-94-5045 ..... p 2681 N95-28987 #
WL-TR-95-4019 ..... p 2662 N95-28978 #

ZDOC/9404 ..... p 2540 N95-28925 #

APPENDIX

NASA SCIENTIFIC AND TECHNICAL INFORMATION OFFICE PRODUCTS AND SERVICES

The NASA Scientific and Technical Information (STI) Office provides for the collection and announcement of aerospace-related reports and literature obtained worldwide through agreements and exchanges. The result of the collection is the comprehensive NASA STI Database that covers aeronautics, space, and supporting disciplines.

The STI Database, documents generated or obtained by NASA, and products and services derived from or supporting the database are made available to the NASA research community and to the public. Descriptions and sources of these items are presented in the following pages.

Scientific and Technical Aerospace Reports (STAR) is an abstract journal, listing citations with abstracts for aerospace-related reports obtained from worldwide sources. *STAR* is issued on the first of each month, and announces current documents that have been entered into the NASA STI Database during the previous month. The reports are of the following types:

- NASA, NASA contractor, and NASA grantee reports;
- Reports issued by other U.S. Government agencies, domestic and foreign institutions, universities, and private firms;
- Translations in report form;
- NASA-owned patents and patent applications
- Other U.S. Government agency and foreign patents and patent applications
- Domestic and foreign dissertations and theses.

Journal, book, and conference literature, journal translations, and certain foreign dissertations having the same subject scope as *STAR* are announced in a companion journal, *NASA Open Volumes on Aerospace (NOVA). NOVA* is issued on the 15th of each month and is available from the NASA Center for AeroSpace Information, at the address below.

ELIGIBILITY AND REGISTRATION FOR NASA STI PRODUCTS AND SERVICES

Organizations of the type listed below that have registered with NASA can receive products and services.

- NASA offices and installations, contractors, subcontractors, grantees, and consultants;
- Other U.S. Government agencies and their contractors;
- Libraries in the United States that have arrangements with NASA to maintain collections of NASA documents for public reference;
- Other organizations in the United States having a need for NASA documents in work related to aeronautics and space research;
- Organizations abroad that have established reciprocal documents exchange arrangements with NASA.

The central service points—central points of document acquisition and control within qualified organizations—or individuals are eligible to register for NASA STI products and services. Domestic organizations or individuals may be eligible to receive various classes of NASA publications and services and should address their requests for registration or further information to:

ATTN: Registration Services
NASA Center for AeroSpace Information
800 Elkridge Landing Road
Linthicum Heights, MD 21090-2934
301-621-0390

Organizations abroad should direct requests to:

National Aeronautics and Space Administration
Scientific and Technical Information Office (JT)
International STI Office
Washington, DC 20546-0001
USA
703-271-5640

SUBJECT SCOPE

The subject scope of *STAR* and *NOVA* includes all aspects of aeronautics and space research and development, supporting basic and applied research, and applications. Aerospace aspects of Earth resources, energy development, conservation, oceanography, environmental protection, urban transportation, and other topics of high national priority are also covered.

HOW TO USE *STAR* SUBJECT CATEGORIES

Abstracts in *STAR* are categorized by 10 major subject divisions that are divided further into 76 specific subject categories. The subject divisions and categories are listed in the Table of Contents together with a note for each that defines its scope and provides any cross-references. For example:

> **16 SPACE TRANSPORTATION**
>
> Includes passenger and cargo space transportation, e.g., shuttle operations; and space rescue techniques. For related information see also *03 Air Transportation and Safety* and *18 Spacecraft Design, Testing and Performance*. For space suits see *54 Man/System Technology and Life Support*.

CROSS-REFERENCES

Individual *STAR* abstracts are not ordinarily cross-referenced, except for certain conference reports or book translations that have had separate abstracts written for their component papers or chapters. Citations and abstracts of the components follow immediately after those of the parent document. When the subject content of a component differs sufficiently from the general content of the parent, a cross-reference citation also is printed at the end of the category to which it normally would have been assigned if it were independent.

DOCUMENTS ON MICROFICHE

Documents available on microfiche are designated by a pound sign (#) following the accession number.

LIMITED REPRODUCIBILITY

A note of limited reproducibility appears in the citation, if there are factors affecting the reproducibility of more than 20% of the document. These factors include faint or broken type, color photographs, black and white photographs, foldouts, dot matrix print, or some other factor that limits the reproducibility of the document. This notation also appears on the microfiche header.

NASA PATENTS AND PATENT APPLICATIONS

Patents and patent applications owned by NASA are announced in *STAR* under appropriate subject categories and are referenced in the *STAR* indexes. In the Report Number Index, patents are indexed by the NASA Case Number, and the U.S. Patent Class. Patent applications are indexed by the NASA Case Number and the U.S. Patent Application Serial Number.

Printed copies of patents (which are not microfiched) are available for purchase from the U.S. Patent and Trademark Office.

When ordering patents, the U.S. Patent Number should be used, and payment must be remitted in advance, by money order or check payable to the Commissioner of Patents and Trademarks. Prepaid purchase coupons for ordering are also available from the U.S. Patent and Trademark Office.

NASA patent application specifications are sold in both paper copy and microfiche by the NASA Center for AeroSpace Information (CASI). The N accession number should be used in ordering either paper copy or microfiche from CASI.

The patents and patent applications announced in *STAR* are owned by NASA and are available for royalty-free licensing. Requests for licensing terms and further information should be addressed to:

National Aeronautics and Space Administration
Associate General Counsel for Intellectual Property
Code GP
Washington, DC 20546-0001

SOURCES FOR DOCUMENTS

One or more sources from which a document announced in *STAR* is available to the public is ordinarily given on the last line of the citation. The most commonly indicated sources and their acronyms or abbreviations are listed below, and their addresses are listed on page A-6. If the publication is available from a source other than those listed, the publisher and his address will be displayed on the availability line or in combination with the corporate source line.

Avail: CASI. Sold by the NASA Center for AeroSpace Information. Prices for hard copy (HC) and microfiche (MF) are indicated by a price code following the letters HC or MF in the *STAR* citation. Current values for the price codes are given in the tables on page A-7.

NOTE ON ORDERING DOCUMENTS: When ordering publications from NASA CASI, use the N accession number or other report number. It is also advisable to cite the title and other bibliographic identification.

Avail: SOD (or GPO). Sold by the Superintendent of Documents, U.S. Government Printing Office, in hard copy.

Avail: BLL (formerly NLL): British Library Lending Division, Boston Spa, Wetherby, Yorkshire, England. Photocopies available from this organization at the price shown. (If none is given, inquiry should be addressed to the BLL.)

Avail: DOE Depository Libraries. Organizations in U.S. cities and abroad that maintain collections of Department of Energy reports, usually in microfiche form, are listed in *Energy Research Abstracts*. Services available from the DOE and its depositories are described in a booklet, *DOE Technical Information Center - Its Functions and Services* (TID-4660), which may be obtained without charge from the DOE Technical Information Center.

Avail: ESDU. Pricing information on specific data, computer programs, and details on Engineering Sciences Data Unit (ESDU) topic categories can be obtained from ESDU International Ltd. Requesters in North America should use the Virginia address while all other requesters should use the London address, both of which are on page A-6.

Avail: Fachinformationszentrum Karlsruhe. Gesellschaft für wissenschaftlich-technische Information mbH 76344 Eggenstein-Leopoldshafen, Germany.

Avail: HMSO. Publications of Her Majesty's Stationery Office are sold in the U.S. by Pendragon House, Inc. (PHI), Redwood City, CA. The U.S. price (including a service and mailing charge) is given, or a conversion table may be obtained from PHI.

Avail: Issuing Activity, or Corporate Author, or no indication of availability. Inquiries as to the availability of these documents should be addressed to the organization shown in the citation as the corporate author of the document.

Avail: NASA Public Document Rooms. Documents so indicated may be examined at or purchased from the National Aeronautics and Space Administration (JBD-4), Public Documents Room (Room 1H23), Washington, DC 20546-0001, or public document rooms located at NASA installations, and the NASA Pasadena Office at the Jet Propulsion Laboratory.

Avail: NTIS. Sold by the National Technical Information Service. Initially distributed microfiche under the NTIS SRIM (Selected Research in Microfiche) are available. For information concerning this service, consult the NTIS Subscription Section, Springfield, VA 22161.

Avail: Univ. Microfilms. Documents so indicated are dissertations selected from *Dissertation Abstracts* and are sold by University Microfilms as xerographic copy (HC) and microfilm. All requests should cite the author and the Order Number as they appear in the citation.

Avail: US Patent and Trademark Office. Sold by Commissioner of Patents and Trademarks, U.S. Patent and Trademark Office, at the standard price of $1.50 each, postage free. (See discussion of NASA patents and patent applications on page A-3.)

Avail: (US Sales Only). These foreign documents are available to users within the United States from the National Technical Information Service (NTIS). They are available to users outside the United States through the International Nuclear Information Service (INIS) representative in their country, or by applying directly to the issuing organization.

Avail: USGS. Originals of many reports from the U.S. Geological Survey, which may contain color illustrations, or otherwise may not have the quality of illustrations preserved in the microfiche or facsimile reproduction, may be examined by the public at the libraries of the USGS field offices whose addresses are listed on page A-6. The libraries may be queried concerning the availability of specific documents and the possible utilization of local copying services, such as color reproduction.

FEDERAL DEPOSITORY LIBRARY PROGRAM

In order to provide the general public with greater access to U.S. Government publications, Congress established the Federal Depository Library Program under the Government Printing Office (GPO), with 53 regional depositories responsible for permanent retention of material, inter-library loan, and reference services. At least one copy of nearly every NASA and NASA-sponsored publication, either in printed or microfiche format, is received and retained by the 53 regional depositories. A list of the regional GPO libraries, arranged alphabetically by state, appears on page A-8. These libraries are *not* sales outlets. A local library can contact a regional depository to help locate specific reports, or direct contact may be made by an individual.

PUBLIC COLLECTION OF NASA DOCUMENTS

An extensive collection of NASA and NASA-sponsored publications is maintained by the British Library Lending Division, Boston Spa, Wetherby, Yorkshire, England for public access. The British Library Lending Division also has available many of the non-NASA publications cited in *STAR*. European requesters may purchase facsimile copy or microfiche of NASA and NASA-sponsored documents, those identified by both the symbols # and * from ESA — Information Retrieval Service European Space Agency, 8-10 rue Mario-Nikis, 75738 CEDEX 15, France.

SUBMITTING DOCUMENTS

All users of this abstract service are urged to forward reports to be considered for announcement in *STAR*. This will aid NASA in its efforts to provide the fullest possible coverage of all scientific and technical publications that might support aeronautics and space research and development. If you have prepared relevant reports (other than those you will transmit to NASA, DOD, or DOE through the

usual contract- or grant-reporting channels), please send them for consideration to the NASA Center for AeroSpace Information, 800 Elkridge Landing Road, Linthicum Heights, MD 21090-2934.

Reprints of journal articles, book chapters, and conference papers are also welcome. These will be considered for announcement in *STAR's* companion journal, *NOVA*.

You may specify a particular source to be included in a report announcement if you wish; otherwise the report will be placed on a public sale at the NASA Center for AeroSpace Information. Copyrighted publications will be announced but not distributed or sold.

PURCHASE OF *STAR*

STAR is publicly available on annual subscription from the NASA Center for AeroSpace Information (CASI). 1995 *STAR* subscription prices are $100.00/domestic and $125.00/foreign. Single copy prices: $33.00/domestic, $41.00/foreign.

An annual, cumulative *STAR Index* is also available at $70.00/domestic and foreign.

STAR is available to registered users on annual subscription from the NASA Center for AeroSpace Information, ATTN: Registration Services, 800 Elkridge Landing Road, Linthicum Heights, MD 21090-2934.

ADDRESSES OF ORGANIZATIONS

British Library Lending Division
Boston Spa, Wetherby, Yorkshire
England

Commissioner of Patents and Trademarks
U.S. Patent and Trademark Office
Washington, DC 20231

Department of Energy
Technical Information Center
P.O. Box 62
Oak Ridge, TN 37830

European Space Agency-
Information Retrieval Service ESRIN
Via Galileo Galilei
00044 Frascati (Rome) Italy

Engineering Sciences Data Unit International
P.O. Box 1633
Manassas, VA 22110

Engineering Sciences Data Unit
International, Ltd.
251-259 Regent Street
London, W1R 7AD, England

Fachinformationszentrum Karlsruhe
Gesellschaft für wissenschaftlich-technische
Information mbH
76344 Eggenstein-Leopoldshafen, Germany

Her Majesty's Stationery Office
P.O. Box 569, S.E. 1
London, England

NASA Center for AeroSpace Information
800 Elkridge Landing Road
Linthicum Heights, MD 21090-2934

National Aeronautics and Space Administration
Scientific and Technical Information Office
(JT)
Washington, DC 20546-0001

National Technical Information Service
5285 Port Royal Road
Springfield, VA 22161

Pendragon House, Inc.
899 Broadway Avenue
Redwood City, CA 94063

Superintendent of Documents
U.S. Government Printing Office
Washington, DC 20402

University Microfilms
A Xerox Company
300 North Zeeb Road
Ann Arbor, MI 48106

University Microfilms, Ltd.
Tylers Green
London, England

U.S. Geological Survey Library National Center
MS 950
12201 Sunrise Valley Drive
Reston, VA 22092

U.S. Geological Survey Library
2255 North Gemini Drive
Flagstaff, AZ 86001

U.S. Geological Survey
345 Middlefield Road
Menlo Park, CA 94025

U.S. Geological Survey Library
Box 25046
Denver Federal Center, MS914
Denver, CO 80225

NASA CASI PRICE CODE TABLE

(Effective January 1, 1995)

CASI PRICE CODE	NORTH AMERICAN PRICE	FOREIGN PRICE
A01	$ 6.00	$ 12.00
A02	9.00	18.00
A03	17.50	35.00
A04-A05	19.50	39.00
A06-A09	27.00	54.00
A10-A13	36.50	73.00
A14-A17	44.50	89.00
A18-A21	52.00	104.00
A22-A25	61.00	122.00
A99	Call For Price	Call For Price

IMPORTANT NOTICE

For users not registered at the NASA CASI, prepayment is required. Additionally, a shipping and handling fee of $1.00 per document for delivery within the United States and $9.00 per document for delivery outside the United States is charged.

For users registered at the NASA CASI, document orders may be invoiced at the end of the month, charged against a deposit account, or paid by check or credit card. NASA CASI accepts American Express, Diners' Club, MasterCard, and VISA credit cards. There are no shipping and handling charges. To register at the NASA CASI, please request a registration form through the NASA Access Help Desk at the numbers or addresses below.

RETURN POLICY

Effective June 1, 1995, the NASA Center for AeroSpace Information will gladly replace or make full refund on items you have requested if we have made an error in your order, if the item is defective, or if it was received in damaged condition and you contact us within 30 days of your original request. Just contact our NASA Access Help Desk at the numbers or addresses listed below.

NASA Center for AeroSpace Information
800 Elkridge Landing Road
Linthicum Heights, MD 21090-2934
Telephone: (301) 621-0390
E-mail: help@sti.nasa.gov
Fax: (301) 621-0134

FEDERAL REGIONAL DEPOSITORY LIBRARIES

ALABAMA

AUBURN UNIV. AT MONTGOMERY LIBRARY
Documents Dept.
7300 University Dr.
Montgomery, AL 36117-3596
(205) 244-3650 Fax: (205) 244-0678

UNIV. OF ALABAMA
Amelia Gayle Gorgas Library
Govt. Documents
P.O. Box 870266
Tuscaloosa, AL 35487-0266
(205) 348-6046 Fax: (205) 348-0760

ARIZONA

DEPT. OF LIBRARY, ARCHIVES, AND PUBLIC RECORDS
Research Division
Third Floor, State Capitol
1700 West Washington
Phoenix, AZ 85007
(602) 542-3701 Fax: (602) 542-4400

ARKANSAS

ARKANSAS STATE LIBRARY
State Library Service Section
Documents Service Section
One Capitol Mall
Little Rock, AR 72201-1014
(501) 682-2053 Fax: (501) 682-1529

CALIFORNIA

CALIFORNIA STATE LIBRARY
Govt. Publications Section
P.O. Box 942837 - 914 Capitol Mall
Sacramento, CA 94337-0091
(916) 654-0069 Fax: (916) 654-0241

COLORADO

UNIV. OF COLORADO - BOULDER
Libraries - Govt. Publications
Campus Box 184
Boulder, CO 80309-0184
(303) 492-8834 Fax: (303) 492-1881

DENVER PUBLIC LIBRARY
Govt. Publications Dept. BSG
1357 Broadway
Denver, CO 80203-2165
(303) 640-8846 Fax: (303) 640-8817

CONNECTICUT

CONNECTICUT STATE LIBRARY
231 Capitol Avenue
Hartford, CT 06106
(203) 566-4971 Fax: (203) 566-3322

FLORIDA

UNIV. OF FLORIDA LIBRARIES
Documents Dept.
240 Library West
Gainesville, FL 32611-2048
(904) 392-0366 Fax: (904) 392-7251

GEORGIA

UNIV. OF GEORGIA LIBRARIES
Govt. Documents Dept.
Jackson Street
Athens, GA 30602-1645
(706) 542-8949 Fax: (706) 542-4144

HAWAII

UNIV. OF HAWAII
Hamilton Library
Govt. Documents Collection
2550 The Mall
Honolulu, HI 96822
(808) 948-8230 Fax: (808) 956-5968

IDAHO

UNIV. OF IDAHO LIBRARY
Documents Section
Rayburn Street
Moscow, ID 83844-2353
(208) 885-6344 Fax: (208) 885-6817

ILLINOIS

ILLINOIS STATE LIBRARY
Federal Documents Dept.
300 South Second Street
Springfield, IL 62701-1796
(217) 782-7596 Fax: (217) 782-6437

INDIANA

INDIANA STATE LIBRARY
Serials/Documents Section
140 North Senate Avenue
Indianapolis, IN 46204-2296
(317) 232-3679 Fax: (317) 232-3728

IOWA

UNIV. OF IOWA LIBRARIES
Govt. Publications
Washington & Madison Streets
Iowa City, IA 52242-1166
(319) 335-5926 Fax: (319) 335-5900

KANSAS

UNIV. OF KANSAS
Govt. Documents & Maps Library
6001 Malott Hall
Lawrence, KS 66045-2800
(913) 864-4660 Fax: (913) 864-3855

KENTUCKY

UNIV. OF KENTUCKY
King Library South
Govt. Publications/Maps Dept.
Patterson Drive
Lexington, KY 40506-0039
(606) 257-3139 Fax: (606) 257-3139

LOUISIANA

LOUISIANA STATE UNIV.
Middleton Library
Govt. Documents Dept.
Baton Rouge, LA 70803-3312
(504) 388-2570 Fax: (504) 388-6992

LOUISIANA TECHNICAL UNIV.
Prescott Memorial Library
Govt. Documents Dept.
Ruston, LA 71272-0046
(318) 257-4962 Fax: (318) 257-2447

MAINE

UNIV. OF MAINE
Raymond H. Fogler Library
Govt. Documents Dept.
Orono, ME 04469-5729
(207) 581-1673 Fax: (207) 581-1653

MARYLAND

UNIV. OF MARYLAND - COLLEGE PARK
McKeldin Library
Govt. Documents/Maps Unit
College Park, MD 20742
(301) 405-9165 Fax: (301) 314-9416

MASSACHUSETTS

BOSTON PUBLIC LIBRARY
Govt. Documents
666 Boylston Street
Boston, MA 02117-0286
(617) 536-5400, ext. 226
Fax: (617) 536-7758

MICHIGAN

DETROIT PUBLIC LIBRARY
5201 Woodward Avenue
Detroit, MI 48202-4093
(313) 833-1025 Fax: (313) 833-0156

LIBRARY OF MICHIGAN
Govt. Documents Unit
P.O. Box 30007
717 West Allegan Street
Lansing, MI 48909
(517) 373-1300 Fax: (517) 373-3381

MINNESOTA

UNIV. OF MINNESOTA
Govt. Publications
409 Wilson Library
309 19th Avenue South
Minneapolis, MN 55455
(612) 624-5073 Fax: (612) 626-9353

MISSISSIPPI

UNIV. OF MISSISSIPPI
J.D. Williams Library
106 Old Gym Bldg.
University, MS 38677
(601) 232-5857 Fax: (601) 232-7465

MISSOURI

UNIV. OF MISSOURI - COLUMBIA
106B Ellis Library
Govt. Documents Sect.
Columbia, MO 65201-5149
(314) 882-6733 Fax: (314) 882-8044

MONTANA

UNIV. OF MONTANA
Mansfield Library
Documents Division
Missoula, MT 59812-1195
(406) 243-6700 Fax: (406) 243-2060

NEBRASKA

UNIV. OF NEBRASKA - LINCOLN
D.L. Love Memorial Library
Lincoln, NE 68588-0410
(402) 472-2562 Fax: (402) 472-5131

NEVADA

THE UNIV. OF NEVADA LIBRARIES
Business and Govt. Information Center
Reno, NV 89557-0044
(702) 784-6579 Fax: (702) 784-1751

NEW JERSEY

NEWARK PUBLIC LIBRARY
Science Div. - Public Access
P.O. Box 630
Five Washington Street
Newark, NJ 07101-7812
(201) 733-7782 Fax: (201) 733-5648

NEW MEXICO

UNIV. OF NEW MEXICO
General Library
Govt. Information Dept.
Albuquerque, NM 87131-1466
(505) 277-5441 Fax: (505) 277-6019

NEW MEXICO STATE LIBRARY
325 Don Gaspar Avenue
Santa Fe, NM 87503
(505) 827-3824 Fax: (505) 827-3888

NEW YORK

NEW YORK STATE LIBRARY
Cultural Education Center
Documents/Gift & Exchange Section
Empire State Plaza
Albany, NY 12230-0001
(518) 474-5355 Fax: (518) 474-5786

NORTH CAROLINA

UNIV. OF NORTH CAROLINA - CHAPEL HILL
Walter Royal Davis Library
CB 3912, Reference Dept.
Chapel Hill, NC 27514-8890
(919) 962-1151 Fax: (919) 962-4451

NORTH DAKOTA

NORTH DAKOTA STATE UNIV. LIB.
Documents
P.O. Box 5599
Fargo, ND 58105-5599
(701) 237-8886 Fax: (701) 237-7138

UNIV. OF NORTH DAKOTA
Chester Fritz Library
University Station
P.O. Box 9000 - Centennial and University Avenue
Grand Forks, ND 58202-9000
(701) 777-4632 Fax: (701) 777-3319

OHIO

STATE LIBRARY OF OHIO
Documents Dept.
65 South Front Street
Columbus, OH 43215-4163
(614) 644-7051 Fax: (614) 752-9178

OKLAHOMA

OKLAHOMA DEPT. OF LIBRARIES
U.S. Govt. Information Division
200 Northeast 18th Street
Oklahoma City, OK 73105-3298
(405) 521-2502, ext. 253
Fax: (405) 525-7804

OKLAHOMA STATE UNIV.
Edmon Low Library
Stillwater, OK 74078-0375
(405) 744-6546 Fax: (405) 744-5183

OREGON

PORTLAND STATE UNIV.
Branford P. Millar Library
934 Southwest Harrison
Portland, OR 97207-1151
(503) 725-4123 Fax: (503) 725-4524

PENNSYLVANIA

STATE LIBRARY OF PENN.
Govt. Publications Section
116 Walnut & Commonwealth Ave.
Harrisburg, PA 17105-1601
(717) 787-3752 Fax: (717) 783-2070

SOUTH CAROLINA

CLEMSON UNIV.
Robert Muldrow Cooper Library
Public Documents Unit
P.O. Box 343001
Clemson, SC 29634-3001
(803) 656-5174 Fax: (803) 656-3025

UNIV. OF SOUTH CAROLINA
Thomas Cooper Library
Green and Sumter Streets
Columbia, SC 29208
(803) 777-4841 Fax: (803) 777-9503

TENNESSEE

UNIV. OF MEMPHIS LIBRARIES
Govt. Publications Dept.
Memphis, TN 38152-0001
(901) 678-2206 Fax: (901) 678-2511

TEXAS

TEXAS STATE LIBRARY
United States Documents
P.O. Box 12927 - 1201 Brazos
Austin, TX 78701-0001
(512) 463-5455 Fax: (512) 463-5436

TEXAS TECH. UNIV. LIBRARIES
Documents Dept.
Lubbock, TX 79409-0002
(806) 742-2282 Fax: (806) 742-1920

UTAH

UTAH STATE UNIV.
Merrill Library Documents Dept.
Logan, UT 84322-3000
(801) 797-2678 Fax: (801) 797-2677

VIRGINIA

UNIV. OF VIRGINIA
Alderman Library
Govt. Documents
University Ave. & McCormick Rd.
Charlottesville, VA 22903-2498
(804) 824-3133 Fax: (804) 924-4337

WASHINGTON

WASHINGTON STATE LIBRARY
Govt. Publications
P.O. Box 42478
16th and Water Streets
Olympia, WA 98504-2478
(206) 753-4027 Fax: (206) 586-7575

WEST VIRGINIA

WEST VIRGINIA UNIV. LIBRARY
Govt. Documents Section
P.O. Box 6069 - 1549 University Ave.
Morgantown, WV 26506-6069
(304) 293-3051 Fax: (304) 293-6638

WISCONSIN

ST. HIST. SOC. OF WISCONSIN LIBRARY
Govt. Publication Section
816 State Street
Madison, WI 53706
(608) 264-6525 Fax: (608) 264-6520

MILWAUKEE PUBLIC LIBRARY
Documents Division
814 West Wisconsin Avenue
Milwaukee, WI 53233
(414) 286-3073 Fax: (414) 286-8074

*U.S. GOVERNMENT PRINTING OFFICE:1995-387-253/20012

SCAN Goes Electronic!

If you have NASA Mail or if you can access the Internet, you can get biweekly issues of *SCAN* delivered to your desktop absolutely free!

Electronic SCAN takes advantage of computer technology to alert you to the latest aerospace-related, worldwide scientific and technical information that has been published.

No more waiting while the paper copy is printed and mailed to you. You can review *Electronic SCAN* the same day it is released! And you get all 191—or any combination of—subject areas of announcements with abstracts to browse at your leisure. When you locate a publication of interest, you can print the announcement or electronically add it to your publication order list. Start your free access to *Electronic SCAN* today.

Electronic SCAN
Timely
Flexible
Complete
Free!

Over 1,000 announcements of new reports, books, conference proceedings, journal articles . . . and more—delivered to your computer every two weeks.

For instant access via Internet:

ftp.sti.nasa.gov
gopher.sti.nasa.gov
listserv@sti.nasa.gov

For additional information:

e-mail: help@sti.nasa.gov
scan@sti.nasa.gov

(Enter this address on the "To" line. Leave the subject line blank and send. You will receive an automatic reply with instructions in minutes.)

Phone: (301) 621-0390 Fax: (301) 621-0134

Write: NASA Access Help Desk
NASA STI Office
NASA Center for AeroSpace Information
800 Elkridge Landing Road
Linthicum Heights, MD 21090-2934

Home Page: http://www.sti.nasa.gov/STI-homepage.html

National Aeronautics and Space Administration
Scientific and Technical Information Office

7/95

National Aeronautics and
Space Administration
Code JT
Washington, DC 20546-0001